

Technical Report

TR-21-01

December 2022



Post-closure safety for the final repository
for spent nuclear fuel at Forsmark

Main report, PSAR version

Volume I

Volume II

Volume III

SVENSK KÄRNBRÄNSLEHANTERING AB

SWEDISH NUCLEAR FUEL
AND WASTE MANAGEMENT CO

Box 3091, SE-169 03 Solna
Phone +46 8 459 84 00
skb.se

SVENSK KÄRNBRÄNSLEHANTERING

ISSN 1404-0344

SKB TR-21-01

ID 1900477

December 2022

**Post-closure safety for the final repository
for spent nuclear fuel at Forsmark**

Main report, PSAR version

Svensk Kärnbränslehantering AB

Keywords: PSAR, Safety assessment, Post-closure safety, Final repository,
Spent nuclear fuel, Forsmark.

This report is published on www.skb.se

© 2022 Svensk Kärnbränslehantering AB

**Post-closure safety for the final repository
for spent nuclear fuel at Forsmark**

Main report, PSAR version

Volume I

Contents

Volume I

S1	Purposes and general prerequisites	13
S2	Achieving safety in practice – the properties of the site and the design and construction of the repository	16
	S2.1 Safety principles	16
	S2.2 The Forsmark site	17
	S2.3 The site adapted repository reference design	19
S3	Analysing safety – the safety assessment	23
	S3.1 Introduction	23
	S3.2 Step 1: Processing of features, events and processes (FEPs)	24
	S3.3 Step 2: Description of the initial state	25
	S3.4 Step 3: Description of external conditions	25
	S3.5 Step 4: Compilation of processes reports	25
	S3.6 Step 5: Definition of safety functions, safety function indicators and safety function indicator criteria	26
	S3.7 Step 6: Compilation of input data	27
	S3.8 Step 7: Definition and analyses of reference evolution	28
	S3.9 Step 8: Selection of scenarios	33
	S3.10 Step 9, part 1: Analysis of containment potential for the selected scenarios	34
	S3.11 Step 9, part 2: Analysis of the retardation potential for the selected scenarios	36
	S3.12 Step 10: Additional analyses and supporting arguments	40
S4	Conclusions of the PSAR post-closure safety assessment	41
	S4.1 Overview of results	41
	S4.2 Demonstration of compliance	44
	S4.3 Feedback from the analyses in the PSAR	49
	S4.4 Confidence in the results of the assessment	51
S5	Overview of the main report	52
1	Introduction	53
1.1	Licensing of the KBS-3 system in Sweden	53
1.2	Purpose of the safety assessment project	54
1.3	Feedback from the review of post-closure safety in SKB's application for a permit for the final repository	55
	1.3.1 Introduction	55
	1.3.2 The OECD Nuclear Energy Agency, NEA	55
	1.3.3 The Swedish Radiation Safety Authority, SSM	56
	1.3.4 The Land and Environmental Court	57
	1.3.5 The Swedish Government	57
1.4	Regulations	57
	1.4.1 Regulations for final disposal of spent nuclear fuel, SSMFS 2008:37	58
	1.4.2 Regulations concerning safety in final disposal of nuclear waste, SSMFS 2008:21	58
1.5	Relation to the SR-Site reporting	59
1.6	Related activities	59
	1.6.1 Site investigations and site modelling	59
	1.6.2 Repository engineering	61
	1.6.3 Canister development	61
2	Methodology	63
2.1	Introduction	63
2.2	Safety	64
	2.2.1 Safety principles for the KBS-3 repository	64
	2.2.2 Safety functions and measures of safety	65

2.3	System boundary	66
2.4	Time scales	66
2.4.1	Regulatory requirements and guidance	66
2.4.2	Time scale covered by the safety assessment	67
2.4.3	Time scales relevant for repository evolution	68
2.5	Methodology in eleven steps	69
2.5.1	Step 1: FEP processing	69
2.5.2	Step 2: Description of the initial state	70
2.5.3	Step 3: Description of external conditions	71
2.5.4	Step 4: Description of processes	71
2.5.5	Step 5: Definition of safety functions, safety function indicators and safety function indicator criteria	72
2.5.6	Step 6: Compilation of data	73
2.5.7	Step 7: Analysis of reference evolution	73
2.5.8	Step 8: Selection of scenarios	74
2.5.9	Step 9: Analysis of selected scenarios	77
2.5.10	Step 10: Additional analyses and supporting arguments	79
2.5.11	Step 11: Conclusions	79
2.5.12	Report hierarchy in the PSAR	79
2.6	Approach to risk calculations	81
2.6.1	Regulatory requirements and guidance	81
2.6.2	Application in the PSAR	81
2.6.3	Alternative safety indicators	84
2.7	BAT and optimisation	86
2.7.1	Introduction	86
2.7.2	Regulatory requirements	86
2.7.3	General issues regarding optimisation and best available technique	87
2.7.4	Optimisation vs BAT	87
2.7.5	Conclusions relating to methodology for the PSAR	87
2.8	Overall information/uncertainty management	87
2.8.1	Classification of uncertainties	88
2.8.2	Need for stylised examples	89
2.8.3	Uncertainty management; general	89
2.8.4	Integrated handling of uncertainties	91
2.8.5	Formal expert elicitations	94
2.9	Quality assurance	94
2.9.1	General	94
2.9.2	QA procedure for the PSAR assessment of post-closure safety	95
2.9.3	Expert judgements	95
2.9.4	Peer review	96
3	FEP processing	97
3.1	Introduction	97
3.2	SKB FEP database	97
3.3	SR-Site FEP catalogue	98
3.4	Couplings	101
3.5	Developments after the SR-Site assessment	103
4	The Forsmark site	105
4.1	Introduction	105
4.2	The Forsmark area	107
4.2.1	Setting	107
4.2.2	Target area for the repository	107
4.3	Rock domains and their associated thermal and rock mechanics properties	110
4.3.1	Rock composition and division into rock domains	111
4.3.2	Mineral resources	113
4.3.3	Thermal properties	113
4.3.4	Strength and other mechanical properties of intact rock	115
4.4	Deformation zones, fracture domains and fractures	115
4.4.1	Formation and reactivation through geological time	116

4.4.2	Deterministic deformation zones	118
4.4.3	Fracture domains, fractures and DFN models	120
4.4.4	Fracture mineralogy	122
4.4.5	Mechanical properties of deformation zones and fractures	123
4.5	Rock stress	124
4.5.1	Stress evolution	124
4.5.2	Stress model	124
4.6	Bedrock hydraulic properties	126
4.6.1	Evolution	126
4.6.2	Hydraulic properties of deformation zones and fracture domains	126
4.7	Integrated fracture domain, hydrogeological DFN and rock stress models	130
4.8	Groundwater	131
4.8.1	Evolution during the Quaternary period	131
4.8.2	Groundwater composition and water – rock interactions	133
4.8.3	Groundwater flow and consistency with groundwater signatures	137
4.9	Bedrock transport properties	138
4.9.1	Rock matrix properties	138
4.9.2	Flow related transport properties	139
4.10	The surface system	140
4.10.1	Evolution during the Quaternary period	140
4.10.2	Description of the surface system	141
4.10.3	Human population and land use	144
5	Initial state of the repository	145
5.1	Introduction	145
5.1.1	Relation to Technical design requirements, Production reports and Data report	146
5.1.2	Overview of system	147
5.1.3	Initial state FEPs	149
5.2	Site adapted repository – the underground openings	151
5.2.1	Technical design requirements relating to post-closure safety	151
5.2.2	Repository design and resulting layout	152
5.2.3	Initial state of underground openings	155
5.3	Initial state of the fuel and the canister cavity	165
5.3.1	Requirements on the handling of the spent nuclear fuel	165
5.3.2	Fuel types and amounts	165
5.3.3	Handling of spent fuel	166
5.3.4	Initial state	167
5.4	Initial state of the canister	171
5.4.1	Technical design requirements relating to post-closure safety	171
5.4.2	Reference design and production procedures	173
5.4.3	Initial state	180
5.5	Initial state of the buffer	184
5.5.1	Technical design requirements	184
5.5.2	Reference design and production procedures	185
5.5.3	Initial state	191
5.6	Initial state of the deposition tunnel backfill	194
5.6.1	Technical design requirements	195
5.6.2	Reference design and production procedures	195
5.6.3	Initial state	199
5.7	Initial state of repository sealing and additional engineered parts of the repository	201
5.7.1	Technical design requirements	202
5.7.2	Reference design and production procedures	202
5.7.3	Initial state	208
5.8	Summary; Key initial state properties for the safety assessment	209
5.8.1	The fuel	209
5.8.2	The canister	209
5.8.3	The buffer	209

5.8.4	The deposition tunnel backfill	210
5.8.5	The site adapted repository	210
5.9	Monitoring	210
5.9.1	Monitoring purposes	210
5.9.2	Monitoring programme	211
5.9.3	Control programme for repository construction and operation	213
5.9.4	Monitoring after waste emplacement	214
5.9.5	Monitoring after repository closure	214
6	Handling of external conditions	215
6.1	Introduction	215
6.2	Climate-related issues	217
6.2.1	General climate evolution	217
6.2.2	Impact on repository safety	220
6.2.3	Handling the uncertain long-term climatic evolution	220
6.2.4	Documentation	222
6.3	Future human actions	223
7	Handling of internal processes	225
7.1	Introduction	225
7.1.1	Identification of processes	225
7.1.2	Biosphere processes	226
7.2	Format for process representations	226
7.3	Format for process documentation	228
7.4	Process mapping/process tables	232
7.4.1	Fuel and canister interior	233
7.4.2	Canister	235
7.4.3	Buffer	239
7.4.4	Backfill in deposition tunnels	243
7.4.5	Geosphere	246
7.4.6	Additional system parts	251
7.5	Assessment model flow charts, AMFs	252
8	Safety functions and safety function indicators	259
8.1	Introduction	259
8.1.1	Differentiated safety functions in the PSAR	259
8.1.2	Approach to dilution	260
8.2	Safety functions, safety function indicators and safety function indicator criteria; general	260
8.3	Safety functions for containment	264
8.3.1	Canister	264
8.3.2	Buffer	267
8.3.3	Backfill in deposition tunnels	272
8.3.4	Geosphere	273
8.3.5	Summary of safety functions related to containment	276
8.4	Safety functions for retardation	279
8.4.1	Fuel	279
8.4.2	Canister	280
8.4.3	Buffer	280
8.4.4	Deposition tunnel backfill	281
8.4.5	Geosphere	281
8.4.6	Summary of safety functions related to retardation	282
8.5	Factors affecting temporal evolution of safety function indicators – FEP chart	283
9	Compilation of input data	287
9.1	Introduction	287
9.2	Objectives of the Data report	287
9.3	Inventory of data	288
9.4	Instructions on supplying data	288

9.4.1	Suppliers, customers and Data report team	288
9.4.2	Implementation of the instructions	289
9.5	Qualification of input data	289
9.6	Final control of data used in calculations/modelling	292

Volume II

10	Analysis of a reference evolution for a repository at the Forsmark site	295
10.1	Introduction	295
10.1.1	Detailed prerequisites	298
10.1.2	Structure of the analysis	299
10.1.3	Hydrogeological modelling in the PSAR	301
10.2	The excavation and operation phases	303
10.2.1	Thermal evolution of the near field	303
10.2.2	Mechanical evolution of near-field rock due to excavation	304
10.2.3	Hydrogeological evolution	307
10.2.4	Evolution of buffer, backfill and plug	313
10.2.5	Chemical evolution in and around the repository	323
10.2.6	Effects of operational activities on completed parts of the repository	331
10.2.7	Summary of the excavation/operation phase	331
10.3	The initial period of temperate climate after closure	334
10.3.1	Introduction	334
10.3.2	External conditions	334
10.3.3	Biosphere	335
10.3.4	Thermal evolution of the near field	339
10.3.5	Mechanical evolution of the rock	343
10.3.6	Hydrogeological evolution	351
10.3.7	Chemical evolution in and around the repository	372
10.3.8	Saturation of buffer and backfill	385
10.3.9	Swelling and swelling pressure	398
10.3.10	Buffer and backfill chemical evolution	415
10.3.11	Colloid release from buffer and backfill	431
10.3.12	Evolution of the buffer with the bottom plate and backfill with plug after the thermal period	442
10.3.13	Canister evolution	452
10.3.14	Evolution of the central area, the top seal and the borehole plugs	469
10.3.15	Summary of the first 1 000 years after closure	471
10.3.16	Safety functions for the initial temperate period after closure	473
10.4	The remaining part of the reference glacial cycle	479
10.4.1	Reference long-term evolution of climate related conditions	479
10.4.2	Biosphere	494
10.4.3	Thermal evolution	496
10.4.4	Rock mechanics	500
10.4.5	Canister failure due to rock shear movements	507
10.4.6	Hydrogeological evolution	536
10.4.7	Geochemical evolution	559
10.4.8	Effects on buffer and backfill	574
10.4.9	Effects on canister	579
10.4.10	Evolution of other parts of the repository system	583
10.4.11	Safety functions at the end of the reference glacial cycle	583
10.5	Subsequent glacial cycles	588
10.5.1	Safety functions at the end of the assessment period	589
10.6	Global warming variant	593
10.6.1	External conditions	593
10.6.2	Biosphere	598
10.6.3	Repository evolution	599
10.6.4	Safety function indicators for the global warming variant	600
10.7	Conclusions from the analysis of the reference evolution	600

Volume III

11	Selection of scenarios	609
11.1	Introduction	609
11.2	Scenarios derived from safety functions – selection and structuring for analysis	610
11.2.1	Selection of additional scenarios	610
11.2.2	Structure for analysis of the additional scenarios	612
11.2.3	Template for assessment of scenarios based on safety functions	614
11.3	Amendments to scenario selection and analyses in response to SSM's review of SR-Site	616
11.4	Summary of scenario selection	616
12	Analyses of containment potential for the selected scenarios	619
12.1	Introduction	619
12.1.1	General	619
12.1.2	Definition of the main scenario	620
12.1.3	Climate development for the scenario analyses	620
12.2	Buffer advection	622
12.2.1	Introduction	622
12.2.2	Quantitative assessment of routes to buffer advection	625
12.2.3	Conclusions	630
12.2.4	Special case of advective conditions – Canister sinking	631
12.3	Buffer freezing	632
12.3.1	Introduction	632
12.3.2	Quantitative assessment of routes to buffer freezing	633
12.3.3	Conclusions	641
12.4	Buffer transformation	642
12.5	Conclusion from analyses of buffer scenarios	647
12.6	Canister failure due to corrosion	647
12.6.1	Introduction	647
12.6.2	Quantitative assessment of corrosion – general	648
12.6.3	Quantitative assessment of corrosion – potential for early failures	661
12.6.4	Conclusions	664
12.7	Canister failure due to isostatic load	666
12.7.1	Introduction	666
12.7.2	Glacial load	667
12.7.3	Buffer swelling pressure	670
12.7.4	Canister strength	671
12.7.5	Canister resilience to creep	672
12.7.6	Combined assessment	679
12.8	Canister failure due to shear load	680
12.8.1	Introduction	680
12.8.2	Quantitative assessment of routes to canister failure by shear load	681
12.8.3	Conclusions	684
12.9	Summary and combinations of analysed scenarios	685
12.9.1	Summary of results of the analyses	685
12.9.2	Assessment of containment potential for the main scenario	685
12.9.3	Combinations of analysed scenarios and phenomena	686
13	Analysis of retardation potential for the selected scenarios	691
13.1	Introduction	691
13.2	Biosphere assessments and derivation of <i>Landscape dose conversion factors</i>	692
13.2.1	Approaches and central concepts in the biosphere assessments	695
13.2.2	Identification, location and development of biosphere objects	697
13.2.3	The radionuclide model for the biosphere	699
13.2.4	Resulting LDF values	706
13.2.5	Approach and methods for assessment of radiological effects on the environment	710

13.2.6	Uncertainties and cautiousness in the LDF approach	711
13.2.7	Summary and conclusions	714
13.3	Criticality	715
13.3.1	Consequences of a postulated criticality event in the final repository	716
13.4	Models for radionuclide transport and dose calculations	717
13.4.1	The near-field model COMP23	717
13.4.2	The far-field models FARF31 and MARFA	719
13.4.3	Biosphere representation	720
13.4.4	Simplified analytical models	720
13.4.5	Selection of radionuclides	721
13.5	Canister failure due to corrosion	721
13.5.1	Introduction	721
13.5.2	Conceptualisation of transport conditions	722
13.5.3	Input data to transport models	724
13.5.4	Calculation of the central corrosion case	726
13.5.5	Analysis of potential alternative transport conditions/data	731
13.5.6	Calculation of alternative cases	740
13.5.7	Doses to non-human biota for the corrosion scenario	751
13.5.8	Alternative safety indicators for the corrosion scenario	752
13.5.9	Summary of results of calculation cases for the corrosion scenario	756
13.5.10	Calculations with the analytical models	757
13.5.11	Sensitivity analyses	759
13.6	Canister failure due to shear load	764
13.6.1	Conceptualisation of transport conditions	764
13.6.2	Consequence calculations	765
13.6.3	Combination of the shear load and the buffer advection scenarios	770
13.6.4	Analysis of potential alternative transport conditions/data	771
13.6.5	Doses to biota, alternative safety indicators, analytical calculations and collective dose	775
13.7	Hypothetical, residual scenarios to illustrate barrier functions	776
13.7.1	Canister failure due to isostatic load	776
13.7.2	The growing pinhole failure in a single canister	777
13.7.3	Additional cases of hypothetical, early canister failures	784
13.7.4	Additional cases to illustrate barrier functions	790
13.8	Radionuclide transport in the gas phase	801
13.9	Risk summation	802
13.9.1	Introduction	802
13.9.2	Risk associated with the corrosion scenario	802
13.9.3	Risk associated with the shear load scenario	805
13.9.4	Risk contributions from fuel residues and damaged fuel	805
13.9.5	Risk dilution	805
13.9.6	Extended discussion of risk for the initial 1 000 years	807
13.9.7	Conclusions	809
13.10	Summary of uncertainties affecting the calculated risk	811
13.10.1	Summary of main uncertainties affecting the calculated risk	811
13.10.2	Candidate issues for formal expert elicitations	814
13.11	Conclusions	816
14	Additional analyses and supporting arguments	817
14.1	Introduction	817
14.2	Scenarios related to future human actions	818
14.2.1	Introduction	818
14.2.2	Principles and method for handling FHA scenarios	818
14.2.3	Technical and societal background	820
14.2.4	Choice of representative cases	822
14.2.5	Assessment of the drilling case	823
14.2.6	Assessment of the rock excavation or tunnel case	831
14.2.7	Assessment of a mine in the vicinity of the Forsmark site	833
14.2.8	Incompletely sealed repository	834

14.2.9	New knowledge since SR-Site assessment	841
14.2.10	Assessment of potential impact of updated information	843
14.3	Analyses required to demonstrate optimisation and use of best available technique	845
14.3.1	Introduction	845
14.3.2	Potential for corrosion failure	845
14.3.3	Potential for shear failure	849
14.3.4	Design related factors that do not contribute to risk	850
14.4	Verification that FEPs omitted in earlier parts of the assessment are negligible in light of the completed scenario and risk analysis	854
14.4.1	Introduction	854
14.4.2	Fuel	856
14.4.3	Canister	857
14.4.4	Buffer	859
14.4.5	Backfill	861
14.4.6	Geosphere	863
14.5	A brief account of the time period beyond one million years	866
14.6	Natural analogues	868
14.6.1	The role of natural analogue studies in safety assessments	868
14.6.2	Analogues of repository materials and processes affecting them	869
14.6.3	Transport and retardation processes in the geosphere	874
14.6.4	Model testing and method development	877
14.6.5	Concluding remarks	878
15	Conclusions	881
15.1	Introduction	881
15.2	Overview of results	883
15.2.1	Compliance with regulatory risk criterion	883
15.2.2	Issues related to altered climate conditions	884
15.2.3	Other issues related to barrier performance and design	884
15.2.4	Confidence	886
15.3	Demonstration of compliance	886
15.3.1	Introduction	886
15.3.2	The safety concept and allocation of safety	887
15.3.3	Compliance with SSM's risk criterion	888
15.3.4	Effects on the environment from release of radionuclides	892
15.3.5	Optimisation and best available technique, BAT	892
15.3.6	Confidence	895
15.3.7	Bounding cases, robustness	897
15.3.8	Additional, general requirements on the safety assessment	898
15.4	Design basis cases	899
15.4.1	General	899
15.4.2	Canister – Isostatic load	901
15.4.3	Canister – Shear movements	901
15.4.4	Canister – Corrosion load	903
15.4.5	Buffer	904
15.5	Feedback to assessed reference design and related technical design requirements	904
15.5.1	Introduction	904
15.5.2	Canister mechanical stability – withstand isostatic load	905
15.5.3	Canister mechanical stability – withstand shear movement	906
15.5.4	Provide corrosion barrier – Copper thickness	907
15.5.5	Canister material etc	907
15.5.6	Durability of the hydromechanical properties of the buffer material	907
15.5.7	Installed buffer mass	909
15.5.8	Buffer thickness	910
15.5.9	Content of impurities in the buffer	910
15.5.10	Deposition hole bottom plate	911
15.5.11	Deposition tunnel backfill	911

15.5.12	Selecting deposition holes – mechanically stable conditions	912
15.5.13	Selecting deposition holes – hydrological and transport conditions	912
15.5.14	Hydraulic properties in deposition hole wall	913
15.5.15	Canister positions – adapted to the thermal conditions	914
15.5.16	Controlling the Excavation Damage Zone (EDZ)	914
15.5.17	Engineered and residual materials	915
15.5.18	Repository depth	915
15.5.19	Closure of main tunnels, transport tunnels, access tunnels, shafts and central area	916
15.5.20	Sealing of boreholes	916
15.6	Feedback to detailed investigations and site modelling	917
15.6.1	Further characterisation of the deformation zones with potential to generate large earthquakes	918
15.6.2	Further develop the means to bound the size of fractures intersecting deposition holes	918
15.6.3	Reduce the uncertainty of DFN models	918
15.6.4	Identifying connected transmissive fractures	918
15.6.5	Hydraulic properties of the repository volume	919
15.6.6	Verifying the conformity to the EDZ technical design requirement	919
15.6.7	Rock mechanics	919
15.6.8	Thermal properties	920
15.6.9	Hydrogeochemistry	920
15.6.10	Surface ecosystems	920
15.7	Feedback to RD&D Programme	921
15.7.1	Spent fuel	921
15.7.2	Canister	922
15.7.3	Buffer and backfill	922
15.7.4	Geosphere	924
15.7.5	Biosphere	926
15.7.6	Climate	927
15.8	Conclusions regarding the safety assessment methodology	927
	References	929
Appendix A	Applicable regulations relating to post-closure and SKB's implementation of these in the PSAR	969
Appendix B	Glossary of abbreviations and specialised terms used in this report	985
Appendix C	Topography and place names in the Forsmark area	991

Summary

This document is the main report of the assessment of post-closure safety in the Preliminary Safety Assessment Report (PSAR) for a spent fuel repository at the Forsmark site in the municipality of Östhammar. An approval of the PSAR by SSM is required for SKB to start construction of the repository.

The central conclusion of the post-closure safety assessment is that a KBS-3 repository built at the Forsmark site according to the specifications in the PSAR can be expected to fulfil the requirements of post-closure safety expressed in SSM's relevant regulations.

This conclusion is reached because the favourable properties of the Forsmark site ensure the required long-term durability of the barriers of the KBS-3 repository. In particular, the copper canisters with their cast iron inserts have been demonstrated to provide a sufficient resistance to the mechanical and chemical loads to which they may be subjected in the repository environment.

The conclusion is underpinned by:

- The reliance of the KBS-3 repository on i) a geological environment that exhibits long-term stability with respect to properties of importance for post-closure safety, i.e. mechanical stability, low groundwater flow rates at repository depth and the absence of high concentrations of detrimental components in the groundwater, and ii) the choice of naturally occurring materials (copper and bentonite clay) for the engineered barriers that are sufficiently durable in the repository environment to provide the barrier longevity required for safety.
- The understanding, through decades of research at SKB and in international collaboration, of the phenomena that may affect post-closure safety, resulting in a mature knowledge base for the safety assessment.
- The understanding of the characteristics of the site through several years of surface-based investigations of the conditions at depth and of scientific interpretation of the data emerging from the investigations, resulting in a mature model of the site, adequate for use in the safety assessment.
- The detailed specifications of the engineered parts of the repository and the demonstration of how components fulfilling the specifications are to be produced in a quality assured manner, thereby providing a quality assured initial state for the safety assessment.

The detailed analyses demonstrate that canister failures in a one million year perspective are rare. Even with a number of pessimistic assumptions regarding detrimental phenomena affecting the buffer and the canister, they would be sufficiently rare that their cautiously modelled radiological consequences are well below one percent of the natural background radiation, meaning that they are also well below the Swedish regulatory risk criterion.

S1 Purposes and general prerequisites

The purpose of the present assessment of post-closure safety is to investigate whether a spent fuel repository built at the Forsmark site according to the specifications in the PSAR can be expected to fulfil the requirements of post-closure safety expressed in SSM's relevant regulations. The Forsmark site in the municipality of Östhammar has been selected based on findings emerging from several years of surface-based investigations of the conditions at depth at the site.

Several decades of research and development has led SKB to put forward the KBS-3 method for the final stage of spent nuclear fuel management. In this method, copper canisters with a cast iron insert containing spent nuclear fuel are surrounded by bentonite clay and deposited at approximately 500 m depth in groundwater saturated, granitic rock, see Figure S-1. The purpose of the KBS-3 repository is to isolate the nuclear waste from man and the environment for very long times. Around 12 000 tonnes of spent nuclear fuel is forecasted to arise from the currently approved Swedish nuclear power programme (where the last of the 6 operating reactors is planned to end operation in 2045), corresponding to roughly 6 000 canisters in a KBS-3 repository.

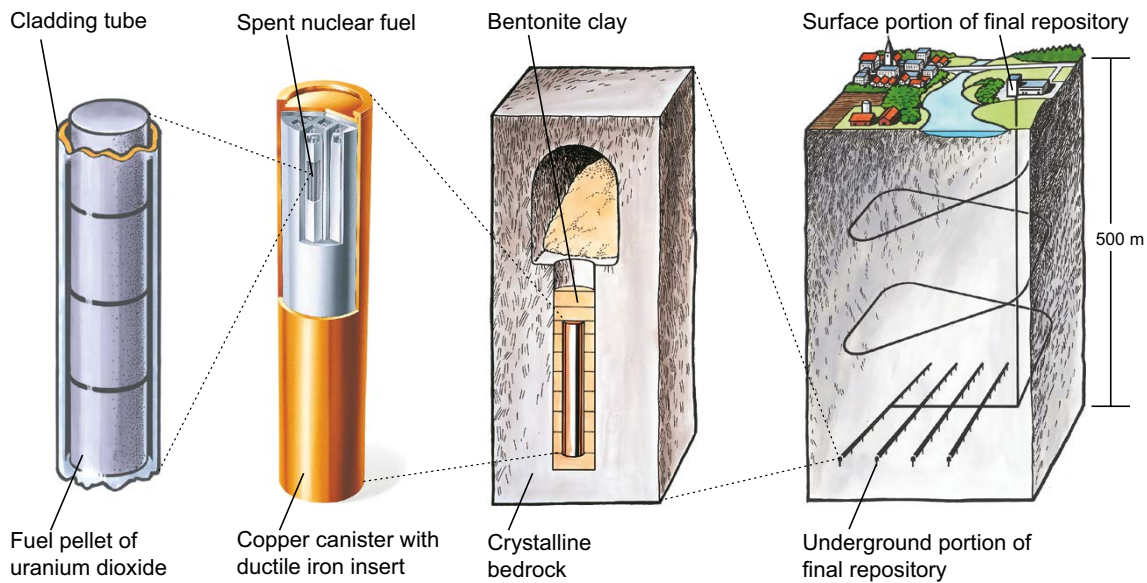


Figure S-1. The KBS-3 concept for disposal of spent nuclear fuel.

The main purposes of the PSAR post-closure safety assessment project are:

- To assess the safety, as defined in applicable Swedish regulations, of the proposed KBS-3 repository at Forsmark.
- To provide feedback to design development, to SKB's RD&D Programme, to detailed site investigations and to future safety assessment projects.

The present report is an update of the SR-Site main report, that provided the assessment of post-closure safety for SKB's applications in 2011 for permissibility according to the Environmental Code and a permit according to the Act on Nuclear Activities for a repository at Forsmark. Material for the update, in addition to results from SKB's continuing RD&D programme, is provided by the findings in the review of the SR-Site assessment by the Swedish Radiation Safety Authority (SSM) and in the trial of the assessment by the Land and Environmental Court.

Regulations

Society's requirements on post-closure safety of nuclear waste repositories are ultimately expressed in legal regulations. Two detailed regulations are issued by the Swedish Radiation Safety Authority (SSM) under the Nuclear Activities Act and the Radiation Protection Act, respectively:

- "The Swedish Radiation Safety Authority's regulations concerning safety in final disposal of nuclear waste" (SSMFS 2008:21).
- "The Swedish Radiation Safety Authority's Regulations concerning the Protection of Human Health and the Environment in connection with the Final Management of Spent Nuclear Fuel or Nuclear Waste" (SSMFS 2008:37).

These two documents are reproduced in their entirety in Appendix A to this report. The way in which this report addresses the requirements is indicated by references to relevant sections of this report, as inserts in the regulatory texts in the Appendix.

The principal acceptance criterion, expressed in SSMFS 2008:37, concerns the protection of human health and requires that "the annual risk of harmful effects after closure does not exceed 10^{-6} for a representative individual in the group exposed to the greatest risk". "Harmful effects" refers to cancer and hereditary effects. The risk limit corresponds to an effective dose limit of about 1.4×10^{-5} Sv/yr. This, in turn, corresponds to around one percent of the effective dose due to natural background radiation in Sweden. Furthermore, the regulation SSMFS 2008:21 require descriptions of the evolution of the biosphere, geosphere and repository for selected scenarios; and evaluation of the environmental impact of the repository for selected scenarios, including the main scenario, with respect to defects in engineered barriers and other identified uncertainties.

The timeframe for the assessment – one million years

In the General Guidance to SSM 2008:37, it is indicated that the time scale of a safety assessment for a final repository for spent nuclear fuel should be one million years after closure. A detailed risk analysis is required for the first thousand years after closure. Also, for the period up to approximately one hundred thousand years, the reporting is required to be based on a quantitative risk analysis.

For the period beyond one hundred thousand years, the General Guidance states that a strict quantitative comparison of calculated risk in relation to the criterion for individual risk in the regulations is not meaningful. Rather, it should be demonstrated that releases from both engineered and geological barriers are limited and delayed as far as reasonably possible using calculated risk as one of several indicators.

The hazard of the waste

After approximately 100 000 years, the radiotoxicity of the spent nuclear fuel is comparable with that of the natural uranium ore once used to produce the fuel. Furthermore, the sum of toxicity of all fractions originating from the nuclear fuel cycle (the daughter nuclides separated from the uranium prior to enrichment, the depleted uranium arising in the enrichment process and the spent fuel) is comparable to that of the utilised uranium ore after 100 000 years, see Figure S-2.

It is also noted that the initially very high dose rates from potential exposure to direct, external radiation from the spent fuel decrease substantially within a few thousand years. In the long term, these dose rates will however remain at levels requiring shielding from humans practically indefinitely, since the long-term direct radiation levels is determined by U-238 progeny.

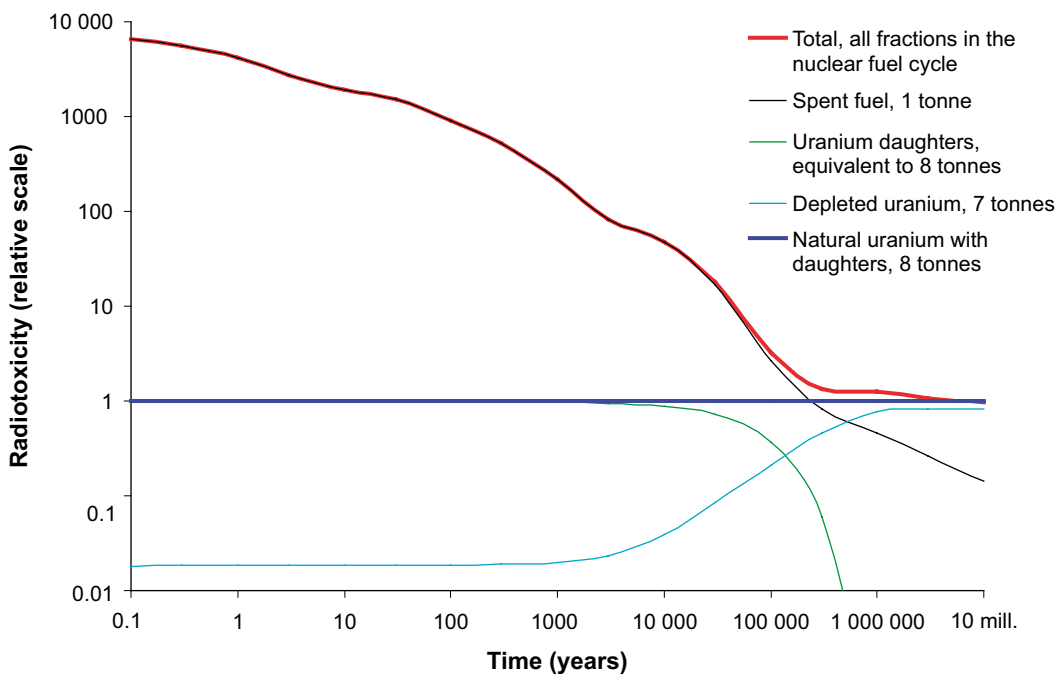


Figure S-2. Radiotoxicity on ingestion of uranium and daughters in ore (blue line), and of the sum of all fractions that arise when the same quantity of uranium is used in the nuclear fuel cycle (red line). The time refers to the time after reactor operation. The different fractions comprise the spent fuel (38 MWd thermal energy/kg U of type SVEA 64 BWR), the depleted uranium and the uranium daughters that are separated in the uranium mill.

The stepwise development of the repository programme

The design and safety evaluation of a repository concept for geological disposal like the KBS-3 system is developed in steps, where a safety evaluation in one step provides feedback to the development of the repository design. The developed design is then evaluated in a subsequent safety assessment, which provides refined feedback to the further development of the design, etc. Likewise, the understanding of natural processes of importance to post-closure safety is developed in an R&D programme and the emerging findings are evaluated in an iterative interaction with safety assessment projects. Another important aspect of this iterative nature of the development is the external reviewing, by authorities and international experts, of the safety assessments.

SKB has conducted research and development of the KBS-3 system for four decades and both the repository design and the scientific knowledge is adequate and mature for the requirements of the safety assessment, as manifested by the facts that no major design changes have occurred in recent years and that the identified set of processes of importance for post-closure safety is stable, although the knowledge base for some processes has been developed further.

SKB has established a technically feasible reference design and layout of the KBS-3 repository and showed that this conforms to the established design premises, see below, but technical development will continue. Detailed designs adapted to an industrialised process designed to fulfil specific requirements on quality, cost and efficiency need still be developed. The repository layout needs to be adapted to the local conditions found when constructing the repository at depth. These, potentially more optimal solutions, must of course also fulfil all requirements on post-closure safety.

The feedback to design development from the preceding SR-Site assessment has provided a basis for updated technical design requirements, and served as input to specifications of the reference design and facilitated the evaluation of the appropriateness of the design with respect to post-closure safety.

S2 Achieving safety in practice – the properties of the site and the design and construction of the repository

S2.1 Safety principles

Since work on the Swedish final repository project commenced at the end of the 1970s, SKB has established a number of principles for the design of a final repository. The principles can be said to constitute the safety philosophy behind the KBS-3 concept. They are summarised below.

- By placing the repository at depth in a long-term stable geological environment, the waste is isolated from the human and near-surface environment. This means that the repository is not strongly affected by either societal changes or the direct effects of long-term climate change at the ground surface.
- By locating the repository at a site where the host rock can be assumed to be of no economic interest to future generations, the risk of human intrusion is reduced.
- The spent fuel is surrounded by several engineered and natural safety barriers.
- The primary safety function of the barriers is to contain the fuel within a canister.
- Should containment be breached, the secondary safety function of the barriers is to retard a potential release from the repository.
- Engineered barriers shall be made of naturally occurring materials that are stable in the long term in the repository environment.
- The repository shall be designed and constructed so that temperatures that could have detrimental effects on the long-term properties of the barriers are avoided.
- The repository shall be designed and constructed so that radiation induced processes that could have detrimental effects on the long term behaviour of the engineered barriers or of the rock are avoided.
- The barriers should be passive, i.e. they should function without human intervention and without artificial supply of matter or energy.

Together with many other considerations, like the geological setting in Sweden and the requirement that the repository must be feasible to construct from a technical point of view, these principles have led to the development of the KBS-3 system for spent nuclear fuel.

In practice, safety is achieved through the selection of a site with favourable properties for post-closure safety and through the design and construction of a repository that fulfils requirements related to post-closure safety. The site conditions today and the design and layout of the KBS-3 repository at Forsmark constitute the initial state of the safety assessment. These are also the aspects that are controlled by the implementer, through the choice of the site and through the design and site adaptation of the repository.

S2.2 The Forsmark site

The Forsmark site is located in the northern part of the county of Uppland within the municipality of Östhammar, about 120 km north of Stockholm. The Forsmark area consists of crystalline bedrock that belongs to the Fennoscandian Shield and formed 1.85 to 1.89 billion years ago. Tectonic lenses, in which the bedrock is less affected by ductile deformation, are enclosed in between ductile high-strain belts. The candidate area is located in the north-westernmost part of one of these tectonic lenses. This lens extends from north-west of the Forsmark nuclear power plant south-eastwards to the area around Öregrund (Figure S-3).

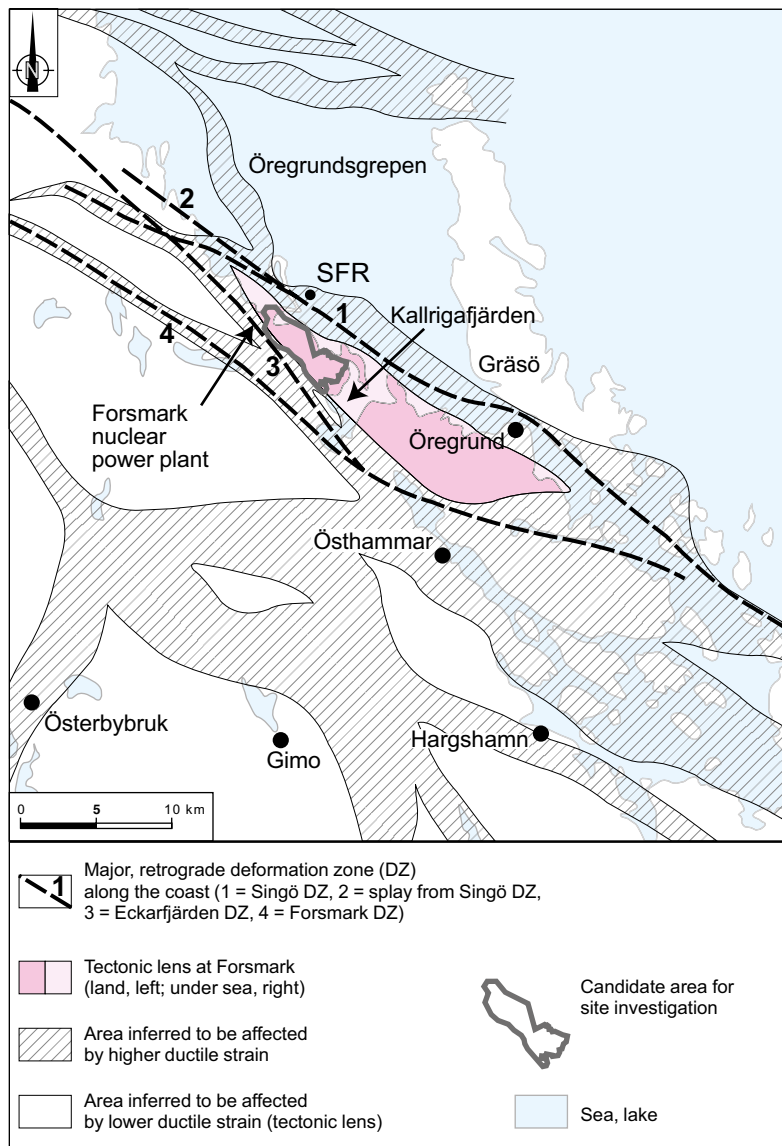


Figure S-3. Tectonic lens at Forsmark and areas affected by strong ductile deformation in the area close to Forsmark.

Three major sets of deformation zones with distinctive orientations have been recognized. In addition to vertical and steeply dipping zones, there are also gently south-east- and south-dipping zones. These gently dipping zones are more frequent in the south-eastern part of the candidate bedrock volume and have higher hydraulic transmissivity than vertical and steeply dipping deformation zones at the site. The frequency of open and partly open fractures is very low below approximately 300 m depth compared to what is observed in the upper part of the bedrock in the north-western part of the candidate volume, which is the target volume for the repository. In addition, the rock stresses are relatively high compared to typical values of the Swedish bedrock. The upper 100 to 150 m of the bedrock overlying the target volume contains many highly transmissive fractures in the horizontal plane and in good hydraulic contact over long distances, whereas at depth the rock has very low permeability with few transmissive fractures. At repository depth (ca 470 m) the average distance between transmissive fractures is more than 100 m.

Groundwaters in the uppermost 100 to 200 m of the bedrock display a wide chemical variability, with chloride concentrations in the range 200 to 5000 mg/L suggesting influence of both brackish marine water and meteoric waters. At depths between 200 and 300 m, the salinity remains fairly constant (5000–6000 mg/L) and the water composition indicates remnants of water from the Littorina Sea that covered Forsmark between 9500 and 5000 years ago. Between 300 m and 800 m the water is brackish to saline and of non-marine origin. At depths between 800 and 1000 m, the salinity increases to higher values.

Data from site investigation to safety assessment

The site investigation at Forsmark, including processing of the emerging data and site modelling, was carried out between 2002 and 2008. The gathering of information and its transfer from the site investigations at Forsmark to the safety assessment application involved several steps.

- Field data have been obtained from various investigation activities like airborne and ground-based geophysics, borehole drilling and borehole testing. After quality control, the data have been entered into the SKB data bases.
- The field data have been interpreted and evaluated into a cross-disciplinary site descriptive model (SDM), being a synthesis of geology, rock mechanics, thermal properties, hydrogeology, hydro-geochemistry, bedrock transport properties and surface system properties, see Figure S-4. The SDM provides a description of the understanding of the present-day site properties within the different disciplines and it also provides an assessment of the uncertainty in these descriptions. The SDM for the Forsmark site at the completion of the surface-based investigations is reported in a main site-description report and a number of supporting reports.
- The site description and references therein cannot always be used directly in the safety assessment. There is a need to also consider non-site specific information, to add judgements on how to handle the uncertainties identified in the site description and to make final selections of model input data. For this reason, all site data used in the PSAR post-closure safety assessment are assessed in the PSAR Data report, using the SDM as input. The role of the Data report is explained in Section S3.7.

As part of the site-descriptive modelling, the uncertainty and confidence in the Forsmark site description were assessed. This assessment comprised exploring confidence in the site characterisation data, key remaining uncertainties in the site description, alternative models and their handling, consistency between disciplines and the main reasons for confidence or lack of confidence in the site descriptive model. The overall outcome of this assessment was that the site properties of importance for both repository constructability and post-closure safety are sufficiently bounded by quantitative uncertainty estimates or alternative models.

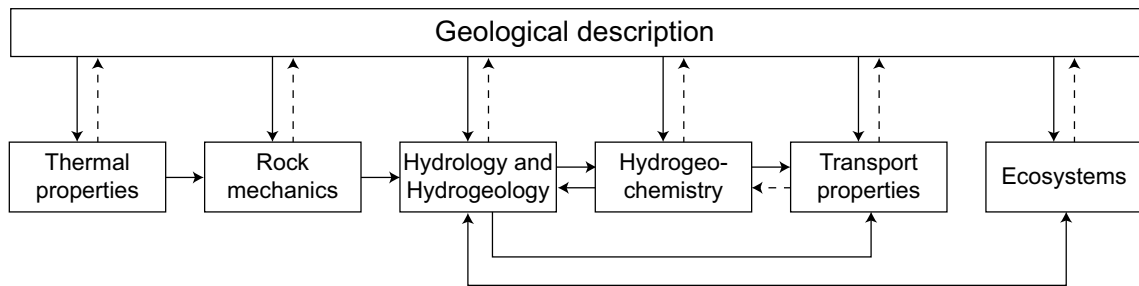


Figure S-4. The different discipline descriptions in the SDM are interrelated with several feedback loops and with geology providing the essential geometrical framework.

In summary, the main safety related features of the Forsmark site are:

- A low frequency of water conducting fractures at repository depth, which is beneficial for both bentonite erosion, corrosion processes and radionuclide retention.
- Favourable chemical conditions, in particular reducing conditions at repository depth, (which is generally found at depth in granitic rocks in Sweden) and salinity that would ensure stability of the bentonite clay buffer.
- The absence of potential for metallic and industrial mineral deposits within the candidate area at Forsmark.

In addition, the relatively high thermal conductivity at the site facilitates an efficient use of the rock volume and the rock mechanics and other properties of importance for a safe and efficient construction of the repository are also favourable.

The assessment of post-closure safety in the PSAR is based on the same SDM as the SR-Site assessment since assessment of monitoring data and the few additional borehole investigations made since the data freeze for the SDM in 2008 have been deemed not to affect the outcome of the assessment and hence not to warrant an update of the model.

S2.3 The site adapted repository reference design

A comprehensive description of the initial state of the repository system is one of the main bases for the safety assessment. The initial state in the PSAR is defined as the state at the time of deposition/installation for the engineered barrier system and the natural, undisturbed state at the time of beginning of excavation of the repository for the geosphere and the biosphere. (Excavation induced impacts on the geosphere and the biosphere are analysed as part of the safety assessment.)

Technical design requirements, reference design and Production reports

The KBS-3 repository concept has been continuously developed since it was first introduced. The current design is based on the design originally presented in the KBS-3 report in 1983. Feedback from assessments of post-closure safety is a key input to the refinement of the design. The PSAR technical design requirements have been established based primarily on feedback from SR-Site, the Finnish safety assessment Turva-2012 and the technology development until 2016, as compiled in a joint Posiva SKB report from 2017.

Design requirements typically concern specification on what mechanical loads the barriers must withstand, restrictions on the composition of barrier materials or acceptance criteria for the various underground excavations. A range of technical design requirements on the canister, buffer, deposition holes, deposition tunnels and backfill and on the main tunnels, transport tunnels, access tunnels, shafts, central area and closure are now established. The design requirements constitute design constraints, which, if all fulfilled, form a good basis for demonstrating repository safety.

A reference design conforming to the design premises has been developed and is reported in a number of so-called **Production reports**. These reports covering the spent fuel, the canister, the buffer, the tunnel backfill, the deposition tunnel plug, the repository closure and the underground openings contain the information required for the PSAR assessment of engineered components of the repository system.

Each report gives an account of i) the technical design requirements to be fulfilled, ii) the reference design selected to achieve the requirements, iii) verifying analyses that the reference design does fulfil the design requirements, iv) the production and control procedures selected to achieve the reference design, and v) verifying analyses that these procedures, if implemented, would achieve the reference design. The initial state of the engineered components is then derived based on the contents of the **Production reports** relevant to post-closure safety.

The initial state provides quantitative information on key inputs to the safety assessment. These are critically evaluated in the **Data report** where the formal qualification of input data to the safety assessment occurs based on an evaluation of uncertainties affecting the initial state data.

The following is a brief account of key features of the repository design.

Fuel

The major part of the nuclear fuel to be deposited consists of spent fuel from the operation of the twelve Swedish nuclear power plants, which are either of boiling water reactor (BWR) type or pressure water reactor (PWR) type. The fuel types and amounts are derived from the spent fuel stored in Clab (31 December 2015) and a reference scenario for the future operation of remaining power plants. In the reference scenario the operating times are set to 60 years for the six remaining reactors; two at Ringhals, three at Forsmark, and one at Oskarshamn. The two reactors in Barsebäck were closed down after approximately 24 years and 28 years of operation, respectively, and in total four reactors have been closed at Oskarshamn (after 39 and 45 years of operation) and Ringhals (after 44 and 45 years of operation). The majority of the fuel used in the reactors consists of uranium oxide fuel (UOX). From Oskarshamn, there will be minor amounts of mixed oxide fuel (MOX). There are also minor quantities of miscellaneous fuels, e.g. from research and the early part of the nuclear power programme, and damaged fuel from the regular operation that are all to be deposited in the KBS-3 repository after adapted containment measures.

Canister

The reference design of the canister consists of a tight, 5 cm thick corrosion barrier of copper and a load-bearing insert of nodular cast iron. The sealed canister has a total length of 4835 mm and a diameter of 1050 mm, see Figure S-5.

In a **Canister production report**, it is demonstrated how canisters are to be manufactured and quality assured in order to fulfil the specifications of the reference design. The report also demonstrates that the reference design conforms to the design requirements for the canister, by referring to a comprehensive design analysis. Probabilistic mechanical analyses based on data from test manufacturing of canister inserts show that these are resilient to isostatic and shear loads specified in the technical design requirements. These and other results in the production report suggest that the reference design together with the proposed production and control methods has prospects of yielding a manufactured canister that conforms to the design requirements. One important implication of this is that all the 6000 canisters are tight at deposition.

Buffer

The main function of the clay buffer is to restrict water flow around the canister. This is achieved by choosing a buffer material with a low hydraulic conductivity after water saturation. This makes diffusion the dominant transport mechanism for water constituents through the buffer. The material should also have a sufficient swelling pressure, making the buffer self-sealing. The clay material's montmorillonite content is a key property for the performance of the buffer.

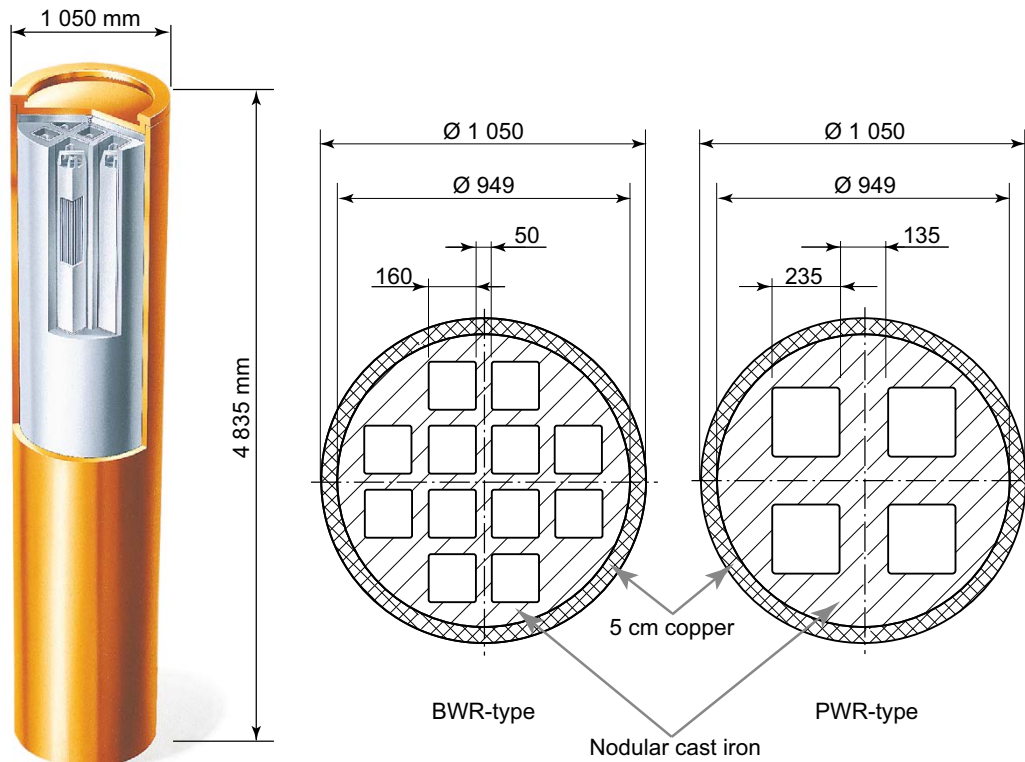


Figure S-5. Left: The reference design with a corrosion resistant outer copper shell and a load-bearing insert of nodular cast iron. Right: Cross section of insert designs of the BWR and PWR types.

In the PSAR one example material, MX-80, that conforms to the technical design requirements is assessed. This material is from a large deposit and is mined by a large bentonite supplier. The buffer reference design includes a thin copper plate placed at the bottom of the deposition hole. Its function is to facilitate the installation of the buffer.

The **Buffer production report** demonstrates how the buffer is to be manufactured and emplaced in a quality assured manner, in order to fulfil the specifications of the reference design.

Deposition tunnel backfill material

The main function of the deposition tunnel backfill is to limit advective transport in the deposition tunnels. This is achieved by choosing a backfill material with a low hydraulic conductivity and a sufficient swelling pressure. The backfill should also contribute to keeping the buffer in place, i.e. it should restrict upwards buffer expansion. This is primarily achieved with a sufficient compressibility of the backfill material.

In the PSAR, one example bentonite material, named Asha 2012, that conforms to the design premises is assessed.

The **Backfill production report** demonstrates how the deposition tunnel backfill is to be manufactured and emplaced in a quality assured manner, in order to fulfil the specifications of the reference design.

Additional engineered components in the repository

For the purpose of the assessment of post-closure safety in the PSAR, the additional engineered components in the repository are defined as:

1. Deposition tunnel plugs: Presented in the **Deposition tunnel plug production report**.
2. Central area: Presented in the **Closure production report**.
3. Top seal: Presented in the **Closure production report**.

4. Bore hole seals: Presented in the **Closure production report**.
5. Closure of main tunnels and transport tunnels: Presented in the **Closure production report**.
6. Closure of ramp and shafts below the top sealing: Presented in the **Closure production report**.
7. Plugs (other than deposition tunnel plugs): Presented in the **Closure production report**.

In the PSAR the closure of all tunnels at repository level as well as the ramp and shaft below the top sealing are similar to the tunnel backfill, in accordance with the current reference design.

The purposes of the closure components are generally to restrict groundwater flow through the underground openings, to provide mechanical restraint and to obstruct unintentional intrusion into the repository.

Underground openings

In all phases of underground design, uncertainties with regard to site conditions must be anticipated. In order to establish a final layout for deposition tunnels and deposition holes, a large volume of rock will have to be characterised, and this characterisation could only effectively be carried out from underground openings. This means that the characterisation will develop as the construction work proceeds. As regards repository layout, details of the access tunnels and central area have been altered compared to the design assessed in SR-Site, whereas the design and layout of the deposition areas are the same as for SR-Site except for an additional transport tunnel passing centrally. These alterations are assessed to be of no importance for post-closure safety and, therefore, the hydrogeological model and the hydrogeological assessments have not been updated since SR-Site. Supplementary studies concerning uncertainties associated with the hydrogeological analyses have, however, been conducted.

The depth established for the reference design is a compromise arising from design requirements on post-closure safety and constructability of the deposition tunnels and deposition holes of the repository facility. Below the depth of 400 m the frequency of water conducting fractures is very low, while the rock stress is still acceptable, justifying that the maximum depth of the repository facility is located at elevation –470 metres (floor of transport tunnel exit from the central area) with a minimum depth (some deposition tunnel roof) at elevation –457 metres.

The thermal properties of the site are used to design a minimum spacing of canisters as to ensure that the maximum peak temperature in the buffer is < 100 °C.

The layout is adapted to meet the technical design requirements relating to mitigating earthquake hazard by ensuring that all deposition holes are placed outside the respect distances to deformation zones large enough to potentially host future earthquakes. Furthermore, large fractures are not allowed to intersect deposition positions. In the PSAR, the same Extended Full Perimeter Intersection Criterion (EFPC) as in SR-Site is used to reject unsuitable deposition holes. It is noted though that findings after the completion of SR-Site suggests that this is a cautious criterion that is likely to be replaced by a more efficient criterion when data from the detailed underground investigations become available. The EFPC criterion requires that a canister position must not be intersected by a fracture that also fully intersects the deposition tunnel perimeter. Furthermore, canister positions that are intersected by fractures that also intersect four or more adjacent positions are rejected.

Potential deposition holes with high inflows are not accepted for deposition. In the PSAR, this is primarily addressed by applying a modified version of the EFPC to avoid deposition positions with potential for high future groundwater flow. Also this criterion is likely to be refined when underground detailed data become available and assessed.

The orientation of the deposition tunnels is related to the orientation of the maximum principal stress in order to mitigate the potential for spalling. Some construction materials in the rock or on rock surfaces, e.g. originating from rock support and from grouting, will remain in the repository after closure.

Summary

In summary, the following are among the most important safety related features of the initial state of the repository:

- The canisters' 5 cm copper shell providing a corrosion barrier.
- The canisters' ability to withstand isostatic loads, provided by the mechanical properties of the cast iron insert.
- The canisters' ability to withstand shear loads, also provided by the mechanical properties of the cast iron insert.
- The deposited buffer density, and the quality assured material composition of the buffer that ensures the development of the buffer into a diffusion barrier when water saturated.
- The deposited density and material composition of the deposition tunnel backfill.
- The general layout of the repository, with respect distances to fracture zones that can potentially host large earthquakes and with a distance between deposition holes that, together with the limitations on thermal output from the deposited canisters, ensure that the temperature of the repository is below 100 °C with a sufficient margin.
- Acceptance of deposition positions according to established criteria, which reduces the likelihood that deposition positions are intersected by large and/or highly water conducting fractures.

S3 Analysing safety – the safety assessment

S3.1 Introduction

The repository system will evolve over time. Future states will depend on

- the initial state,
- internal processes, i.e. a number of radiation related, thermal, hydraulic, mechanical, chemical and biological processes acting internally in the repository system over time, and
- external factors acting on the system.

Internal processes are e.g. the decay of radioactive material, leading to the release of heat and the subsequent warming of the fuel, the engineered barriers and the host rock. Groundwater movements and chemical processes affecting the engineered barriers and the composition of groundwater are other examples. External factors include effects of future climate and climate-related processes, such as glaciations and land uplift.

The initial state, the internal processes and the external factors and the way they together determine repository evolution, can never be fully described or understood. There are thus uncertainties of various types associated with all aspects of the repository evolution and hence with the evaluation of safety. A central theme in any safety assessment methodology must therefore be the management of all relevant types of uncertainty. This management amounts to identifying, classifying and describing uncertainties, as well as handling them in a consistent manner in the quantification of the repository evolution and of the radiological consequences to which it leads. A methodological approach also implies comparing the results of the assessment with regulatory criteria in such a way that appropriate allowance is made for the uncertainties associated with the assessment.

The methodology for the analysis of post-closure safety applied in the PSAR consists of eleven main steps. Figure S-6 is a graphical illustration of the steps. The methodology followed in the first ten steps of the assessment is described in the following subsections, together with key results from each step. The outcome of the final step, the compilation of conclusions, is described in Section S4.

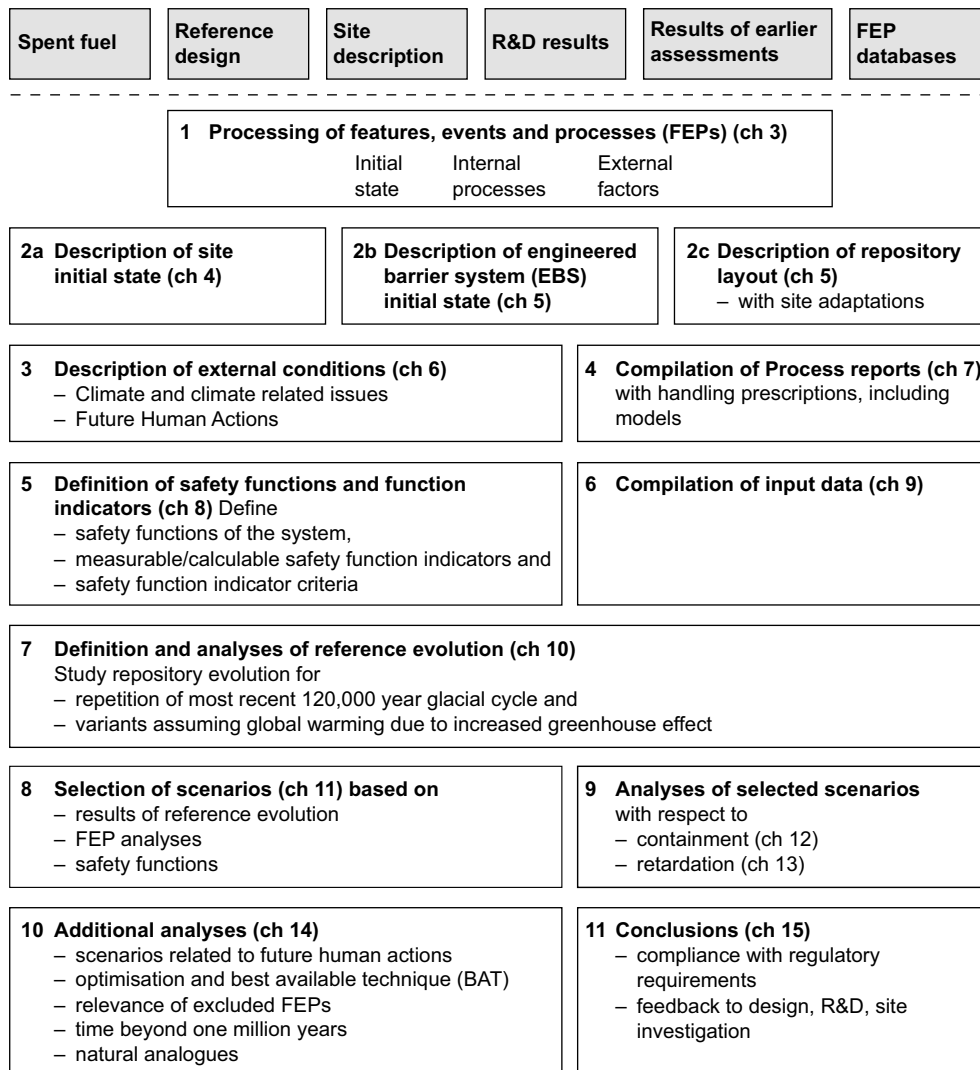


Figure S-6. An outline of the eleven main steps of the PSAR safety assessment. The boxes at the top above the dashed line are inputs to the assessment. The chapters in the main report where the steps are further documented are also indicated.

S3.2 Step 1: Processing of features, events and processes (FEPs)

This step consists of identifying all the factors that need to be included in the analysis. Experience from earlier safety assessments and KBS-3 specific and international databases of relevant features, events and processes (FEPs) influencing post-closure safety is utilised. An SKB FEP database is developed where the great majority of FEPs are classified as being either i) initial state FEPs, ii) internal processes or iii) external FEPs. Remaining FEPs are either related to assessment methodology in general or determined to be irrelevant for the KBS-3 concept. Based on the results of the FEP processing, a FEP catalogue, containing FEPs to be handled in the assessment of post-closure safety, was established within the safety assessment SR-Site. For the PSAR, a review of the development of relevant international FEP databases since the publication of the SR-Site assessment was made, with the conclusion that the FEP handling and the FEP report in SR-Site are valid also for the PSAR. The further handling of the three FEP categories is described in the three subsequent steps of the methodology.

This step of FEP processing is fully documented in the SR-Site **FEP report**¹.

¹ The **FEP report** is one of several principal references in this main report. They are referenced with short-names in bold. The same nomenclature is used in the main text.

S3.3 Step 2: Description of the initial state

The initial state of the system is described, based on the descriptive model of the repository site, the KBS-3 repository design with its different components and a site-specific layout applying this design to the site. The initial state of the geosphere and the biosphere is that of the natural system prior to excavation. The initial state of the fuel and the engineered components is that immediately after deposition.

The initial state of the system is a fundamental input to the assessment and needs thorough substantiation. For the site, this is provided by the site descriptive model of the Forsmark site, in the **Site description Forsmark** report, i.e. the results of the surface-based site investigation and the modelling of the site based on the site investigation data. The Forsmark site model is a fundamental reference to the PSAR assessment of post-closure safety.

The initial state of engineered components of the repository system are derived from information given in the **Production reports** covering the canister, the buffer, the tunnel backfill, the deposition tunnel plug, the repository closure and the underground openings constructions, respectively. The **Spent fuel report** is a main source for describing the initial state of the fuel. See further Section S2.3.

S3.4 Step 3: Description of external conditions

Factors related to external conditions are handled in the three categories “climate related issues”, “large-scale geological processes and effects” and “future human actions”, FHA. The handling of these factors is described in the **Climate report**, the **Geosphere process report**, and the **FHA report**, respectively.

A key point in the handling of external conditions is the establishment of reference external conditions for the subsequent analysis. These reference external conditions postulate a repetition of the last 120 000 year glacial cycle, the Weichselian, as a base case. In addition to the base case, a *global warming climate case*, which takes into account future greenhouse-gas emissions, is analysed. In addition, physically possible climate conditions that would have the most severe impact on repository safety are sought for use in the scenario selection in a later step of the assessment.

Future human actions are handled according to a methodology established in the SR-Site assessment, with most of the account being identical to that in SR-Site. Based on a structured account of a large number of FEPs relating to FHA, a selection of stylised cases for further analyses is made.

S3.5 Step 4: Compilation of processes reports

The identification and handling of processes of importance for the long-term evolution and safety of the repository is a key element in the safety assessment. The identification of processes is based on earlier assessments and FEP screening. All identified processes within the system boundary relevant to the long-term evolution of the system are described in three dedicated **Process reports**, one for the fuel and canister, one for the buffer, backfill and repository closure and one for the geosphere. Short-term geosphere processes/alterations due to repository excavation are included in the **Geosphere process report** and are taken into account in the assessment.

Each process is documented in the **Process reports**, following a template with fixed headings. The documentation concludes with establishing how the process will be handled in the safety assessment, constituting the key result from the **Process reports**. The **Process reports** thus provide a “recipe” for the handling of the various processes in the assessment.

The handling of all processes in a process report is summarised in a *process table* describing if the process is neglected, if it is quantitatively modelled or if the choice between neglect and modelling is subject to a specified condition that may or may not be fulfilled as the repository system evolves.

Several of the processes are thus handled through quantitative modelling, where each model in general includes several interacting processes, often occurring in different system parts and hence described in different process reports. The models form a network, where results from one model are used as input to another. The network is described graphically by two *Assessment Model Flowcharts, AMFs*, and two associated *AMF tables* linking the processes in the process tables, the models in the AMFs and the reporting of the modelling exercise in this main report.

S3.6 Step 5: Definition of safety functions, safety function indicators and safety function indicator criteria

A central element in the methodology of the assessment of post-closure safety is the definition of a set of *safety functions* that the repository system should ideally fulfil over time. Here, the overall safety functions containment and retardation are differentiated into a number of lower level functions for the canister, the buffer, the deposition tunnel backfill and the host rock. The evaluation of the safety functions over time is made possible by associating every safety function with a *safety function indicator*, i.e. a measurable or calculable property of the repository component in question. For several functions, it is also possible to associate a *safety function indicator criterion* such that if the safety function indicator fulfils the criterion, then the safety function in question is upheld.

The ability of the canister to resist isostatic load is an example of a safety function. The associated indicator is the isostatic load on the canister and the criterion is the isostatic load that the canister has been demonstrated to sustain.

It is important to note that the safety function indicator criteria are not the same as design criteria, formally described as technical design requirements in the PSAR. The former should ideally be upheld throughout the assessment period whereas the design requirements should be fulfilled initially. In general, the design requirements should assure that the system is robust to the extent that the safety functions indicator criteria are fulfilled over time. For example, the copper canister must be designed such that its initial thickness (the technical design requirement) ensures that it will sustain corrosion for a very long time, i.e. such that the thickness is non-zero (the function indicator criterion) during this time.

The set of safety functions in itself provides understanding of the safety features of the system and a list of key issues to evaluate over time in the assessment. The safety functions are explicitly used in later steps of the assessment to evaluate safety in a structured manner over different time frames when analysing a reference evolution. A key use of the safety functions is their role in the selection of a number of scenarios whereby uncertainties related to the safety of the system are evaluated in a structured manner.

The safety functions in the PSAR are based on those in the SR-Site assessment, updated with regard to the joint Posiva SKB design requirements and findings in SSM's review of SR-Site, the latter having led to the introduction of canister safety function indicators relating to copper creep.

All safety functions, safety function indicators and safety function indicator criteria related to containment are summarised in Figure S-7. Each function is briefly discussed in connection with the account of the results of the reference evolution below. Safety functions related to retardation have also been developed and they are summarised in a figure similar to Figure S-7. Many of the criteria for retardation are related to those for containment. This applies in particular to the functions of the geosphere to provide favourable chemical and hydrologic/transport conditions.

When the safety functions have been defined, a *FEP chart* is developed, showing how initial state factors and processes in the long-term evolution of the repository are related to the safety functions.

Safety functions related to containment

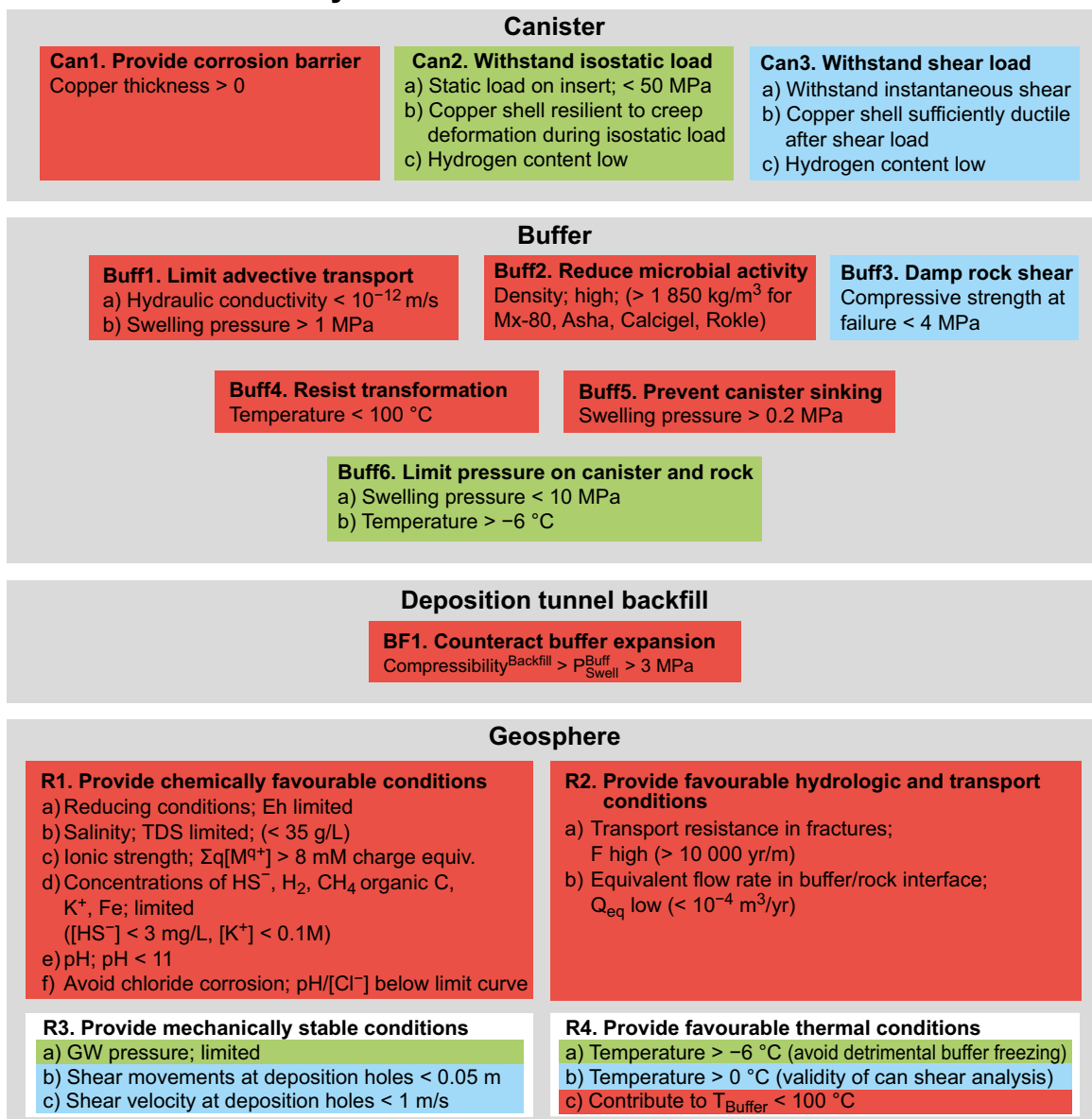


Figure S-7. Safety functions (bold), safety function indicators and safety function indicator criteria related to containment. When quantitative criteria cannot be given, terms like “high”, “low” and “limited” are used to indicate favourable ranges of the safety function indicators. (For some of these, values indicating desired performance are given within parentheses.) The colour coding shows how the functions contribute to the canister safety functions Can1 (red), Can2 (green) and Can3 (blue).

S3.7 Step 6: Compilation of input data

In this step, data to be used in the quantification of repository evolution and in dose calculations are selected using a structured procedure. The process of selection and the data values adopted are reported in a dedicated **Data report**. The process follows a template for discussion of input data quality and uncertainties. The instructions concern two parties, the supplier and the customer. The suppliers are the teams providing the data. The customer is in broad terms the team that is responsible for performing the PSAR post-closure safety assessment. The models for which data are required are given in the AMF described in step 4 above. The formal procedures followed for data auditing and storage contribute to quality assurance in the PSAR.

S3.8 Step 7: Definition and analyses of reference evolution

In this step, a reference evolution of the repository system that follows from the reference external conditions defined in step 3 is defined and analysed. The purpose is to gain an understanding of the overall evolution of the system and of uncertainties affecting the evolution, for the scenario selection and scenario analyses that follow in the two subsequent steps. The evolution is an important basis for the later definition of a main scenario.

Focus is on the containment capacity of the system. Two cases of the reference evolution are analysed.

1. A base case in which the external conditions during the first 120 000 years after closure are assumed to be those reconstructed for the last cycle, that includes the Weichselian glaciation. Thereafter, seven repetitions of that cycle are assumed to cover the entire 1 000 000 year assessment period.
2. A global warming variant in which the future climate and hence external conditions are influenced by anthropogenic greenhouse gas emissions during the first 120 000 years after closure. This analysis is related to that of the base case.

For both these, the initial state with its uncertainties is assumed, all internal processes, with their uncertainties, are handled according to the specification given in the **Process reports**, and data with their uncertainties are taken from the **Data report**.

The presentation of the analysis of the base case of the reference evolution is divided into four time frames:

- The excavation/operational period.
- The first 1 000 years after repository closure and the initial period of temperate domain from the reference glacial cycle.
- The remaining part of the glacial cycle.
- Subsequent glacial cycles up to one million years after repository closure.

For each time frame, issues are presented in the following order:

- Climate issues.
- Biosphere issues.
- Thermal, mechanical, hydraulic and chemical issues in the geosphere.
- Thermal, mechanical, hydraulic and chemical issues for the engineered barrier system (canister, buffer and backfill).

The discussion of each of the issues is concluded with an account of identified uncertainties to be propagated to later stages of the reference evolution and to subsequent parts of the safety assessment.

The commentary on each time frame concludes with a discussion of the expected status of the safety function indicators during and at the end of the time frame.

General development of the reference evolution

A considerable part of the material presented in the reference evolution is results from simulation studies, as established when the handling of processes was determined and as represented graphically in the AMFs.

Initially, the evolution is characterised by a transient caused by the excavation of the host rock and the construction and presence of the repository. In the long term, the evolution is characterised by changes induced by the changing external conditions. Figure S-8 and Figure S-9 show key aspects of the external conditions for the reference evolution, in the form of the modelled reconstruction of the Weichselian glacial cycle.

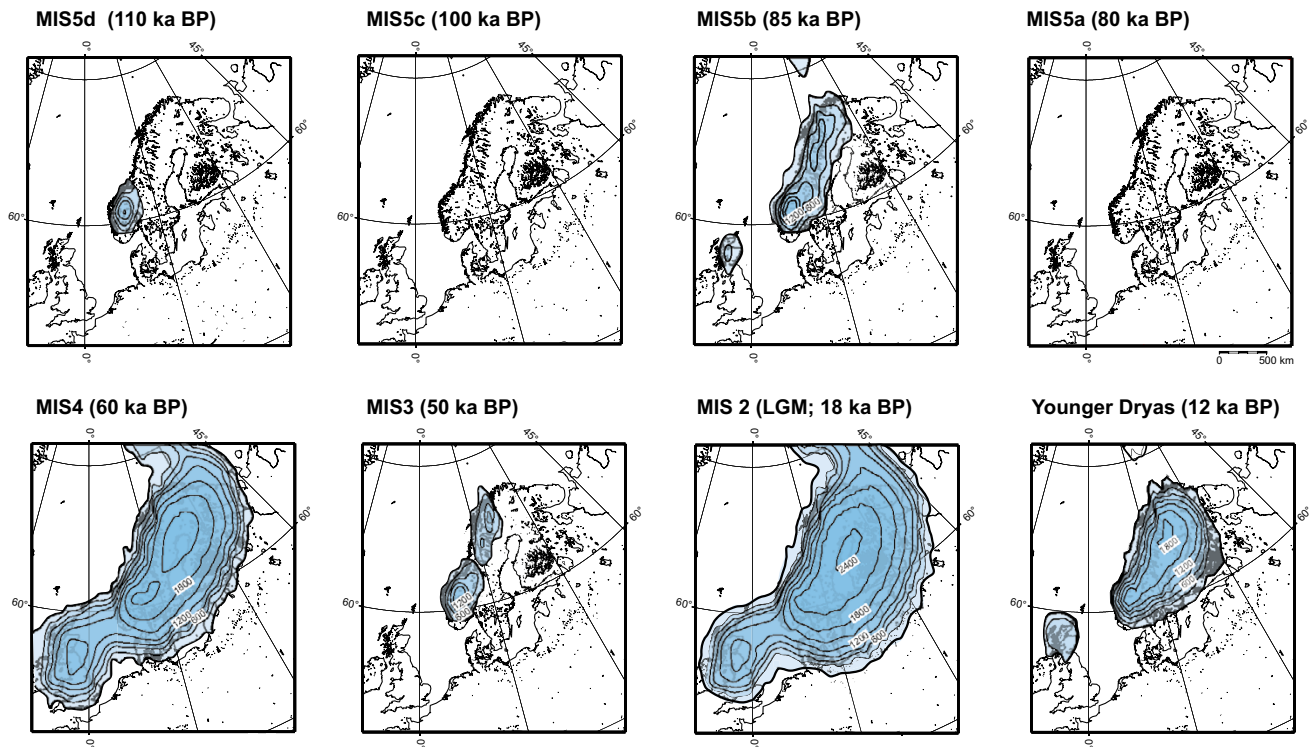


Figure S-8. Selected maps of modelled ice sheet configurations from the reconstruction of the Weichselian ice sheet. Contour lines show ice surface elevation with a 300 m interval. All maps show the present day shore-line position. BP stands for 'before present'.

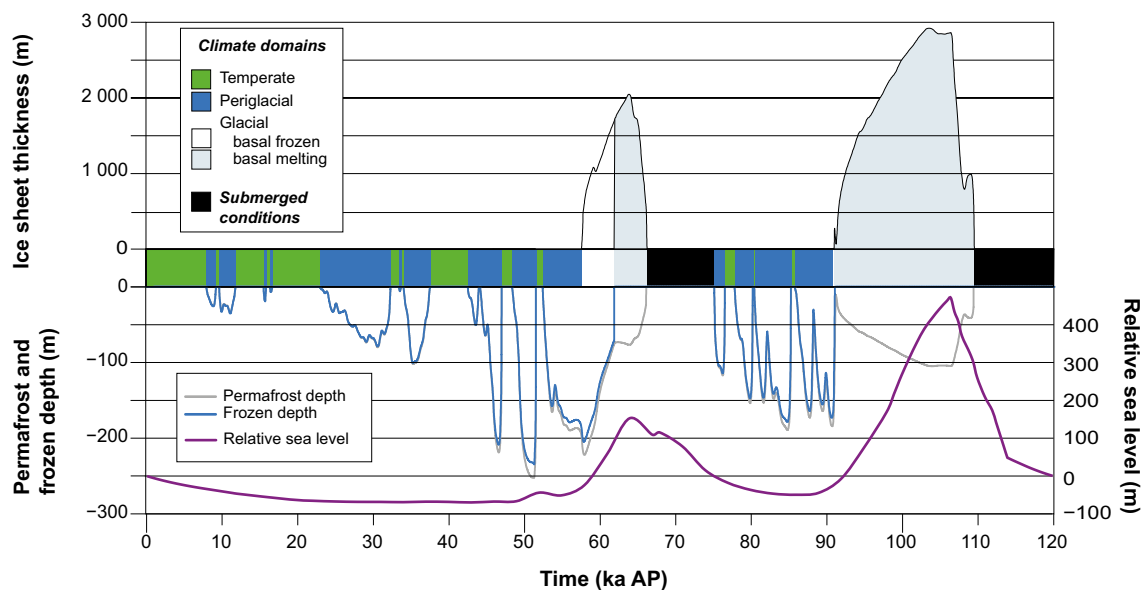


Figure S-9. Reference glacial cycle evolution of important climate-related variables for the Forsmark repository location.

The repository thermal evolution is characterised by a quick temperature increase due to the heat production in the spent fuel, with peak temperatures in the canister, the buffer and the wall of the deposition hole occurring after a few tens of years. The temperature will return to the background temperature of the host rock (about 11 °C at Forsmark) in tens of thousands of years for temperate climate conditions. For glacial and in particular permafrost climate conditions the temperature at repository depth will decrease, but will be above 0 °C throughout the reference evolution.

Mechanically, a damaged zone, in particular below the floors of the deposition tunnels is expected to form during excavation, although it is unlikely that it will form a hydraulically connected pathway, and the initial thermal transients may cause thermally induced spalling of limited extent in the walls of the deposition holes. In the long term, the mechanical conditions are characterised by stability. Large earthquakes in major fracture zones in the vicinity of the repository cannot be excluded, and the layout of the repository is designed to avoid canister failures in such events.

Hydraulically, the repository is drained during construction and operation. The times required for water saturation of the deposition tunnel backfill and of the buffer will vary considerably between different parts of the repository and are likely to range from a few tens of years to several thousand years, as a consequence of the rock properties at Forsmark. In the long term, the flow conditions in the rock are controlled by changing external conditions.

Chemically, initial transients are expected. These include the consumption of initially entrapped oxygen in the repository by microbes and minerals in the rock, in the backfill and the buffer, and reactions involving construction and stray materials in the repository. The transients are followed by slowly varying conditions during the initial period of temperate climate and changes controlled by changing external conditions in the long term.

Safety and safety functions during the reference evolution

For the majority of the 6000 deposition positions, all safety functions relating to the canister, the buffer, the deposition tunnel and the host rock are assessed to be satisfactorily upheld during the reference evolution. The following results and conclusions regarding safety functions emerged from the analysis of the reference evolution. The nomenclature for the safety functions is that used in Figure S-7.

The rock

The results from the studies of the *hydrogeochemical development* over the reference evolution imply the following.

- Reducing conditions (safety function R1a) are upheld throughout the reference evolution, once they have been established shortly after repository closure. Local, temporary penetration of oxygen to repository depth cannot be excluded during hydrologic transients caused by the passage of an ice sheet margin but the potential effects are too small to influence safety.
- The salinity (R1b) is limited to below 0.35 M in terms of chloride, which is below concentrations where the function of the buffer or backfill could be impaired. The highest salinities occur as a result of upconing i) during the initial geochemical transient caused by the draining and subsequent resaturation of the rock and ii) during transients caused by the passage of an ice sheet margin above the repository.
- The ionic strength (R1c) is above 8 mM charge equivalents, required for exclusion of buffer colloid release/erosion/sedimentation, for the majority of deposition positions throughout the reference evolution. However, it cannot be ruled out that a few percent of the deposition positions, those intersected by fractures with the highest flow rates, are exposed to dilute waters such that buffer erosion and sedimentation could occur after thousands of years of temperate or glacial conditions or during short transients caused by the passage of an ice sheet margin above the repository.
- Concentrations of agents detrimental for the buffer and canister (R1d) are as follows.
 - Concentrations of HS^- are expected to not exceed present day concentrations.
 - Concentrations of H_2 are expected to remain below 0.1 mM. Hydrogen produced by the corrosion of steel and iron repository components is expected to either diffuse away or be used in microbial processes.
 - Concentrations of CH_4 and organic C will remain below ~ 0.1 mM and ~ 1 mM, respectively.
 - Concentrations of K^+ and Fe will remain below ~ 5 mM and 0.1 mM, respectively.
- The pH of the groundwater (R1e) is below 11 and above 6.3.
- The conditions required to avoid chloride assisted corrosion (R1f) are satisfied given the limited chloride concentration (< 0.35 M) and the pH values of the groundwaters (> 6.3).

The results from the studies of the *hydrogeological development* over the reference evolution imply the following.

- The equivalent flow rates in the buffer/rock interface (R2b) are low. Almost 5 000 of the 6 000 canister positions are not intersected by water bearing fractures according to the distribution of fracture sizes and intensities in the hydrogeological model. Among the intersected fractures, most have a very low equivalent flow rate. However, the span in flow rates is wide when the entire ensemble of deposition positions is considered and the highest percentile of the flow rate distribution is such that they can contribute to long-term detrimental effects on the buffer and the canister.
- The integrated transport resistance in the network of fractures connecting deposition positions to the surface (R2a) is high for most deposition positions, contributing to efficient retention of radionuclides in the rock. However, the span in transport resistances is wide when the entire ensemble of deposition positions is considered and the lowest percentile of distribution is such that retention in the rock may be poor. Furthermore, transport paths with low transport resistances often have a high flow rate at the deposition position.

Regarding the *mechanical stability* of the host rock, the following is concluded.

- The groundwater pressure (R3a) is usually in the order of 5 MPa, but may increase if the site is covered by an ice sheet. During glacial conditions, the pressure will depend on the thickness of the ice. For the modelled reference evolution, the pressure stays below 26 MPa.
- Shear movements at deposition holes (R3b) exceeding 5 cm are extremely rare, due to the low probability of occurrence of large magnitude earthquakes in the vicinity of the repository, due to the use of respect distances to major fracture zones in selecting deposition areas and in the application of acceptance criteria in the selection of individual deposition positions.
- Shear velocities at deposition holes (R3c) are, for the same reasons as above, below 1 m/s.

Regarding the *thermal development* of the rock, the temperature at repository depth at Forsmark is above 0 °C with a large margin in the reference evolution, i.e. detrimental buffer freezing is avoided (R4a) and the shear analyses of the canister are valid (R4b).

The deposition tunnel backfill

Regarding the deposition tunnel backfill, the compressibility is assessed to be sufficient to counteract buffer expansion (BF1) with the initially installed mass and also when taking losses over time into account.

The buffer

In the majority of deposition holes, the buffer is expected to maintain a density over time such that, given the initial state properties of the buffer, the favourable composition of the groundwater over time and the limited peak temperatures achieved by an appropriate layout of the repository, all its safety functions are fulfilled, i.e. so that:

- Advective transport is limited through a hydraulic conductivity below 10^{-12} m/s (Buff1a) and a swelling pressure above 1 MPa (Buff1b).
- Microbial activity is suppressed (Buff2).
- Rock shear is damped (Buff3), by ensuring an upper limit on compressive strength, which in turn depends on the installed buffer density for the reference material MX-80.
- Buffer transformation is avoided (Buff4) through an upper limit on the temperature.
- Canister sinking (Buff5) is avoided through a swelling pressure above 0.2 MPa.
- The pressure on the canister and the host rock is limited (Buff6) through a swelling pressure below 10 MPa and a rock temperature above -6 °C.

However, as a sufficiently high ionic strength (R1c) is not ensured in the long term for the deposition positions intersected by the fractures with the highest flow rates, it cannot be ruled out that the buffer in these positions will be eroded. The calculated erosion and sedimentation rates are such that advective

conditions could arise in around five percent of the deposition holes during the one million year assessment period. For these holes, the safety functions Buff1 and Buff2 are violated.

The canister

Regarding the canister's role as a corrosion barrier (Can1), the analyses in the reference evolution show that at most a few mm of the 5 cm thick copper shell will be corroded in one million years if the buffer is in place with its safety functions maintained. However, for the few deposition positions where the buffer may be lost due to erosion such that advective conditions arise in the deposition hole, the corrosion rate is enhanced. The quantitative analyses show that, as a statistical average, up to around one canister may have failed due to corrosion under such circumstances at the end of the one million year assessment period.

Regarding the canister's ability to withstand isostatic loads (Can2), the quantitative assessments show that the total isostatic pressure, also during a maximum glacial phase, is below the 50 MPa design requirement of the canister, meaning that this safety function of the canister is maintained.

Regarding the canister's ability to withstand shear loads, the analysis shows that the probability of one such failure having occurred at the end of the one million year assessment periods in the ensemble of 6000 canisters is 0.08, with a number of pessimistic assumptions regarding both the host rock and the canister.

Uncertainties identified in the analysis of the reference evolution

The uncertain issues that need to be propagated to scenario analyses are essentially connected within two groups: issues related to canister failure due to corrosion (safety function Can1) and issues related to canister failure due to shear loads (safety function Can3), whereas canister failures due to isostatic load (Can2) are ruled out according to the assessments in the reference evolution. It is, however, noted that for the latter, the detailed evaluation of copper creep (Can2b,c) is propagated to the analysis of the "Canister failure due to isostatic load" scenario.

The issues relating to canister failure due to corrosion are as follows:

- Groundwater flow over the glacial cycle.
- Groundwater salinity over the glacial cycle.
- Buffer erosion, determined by groundwater flow, fracture apertures and salinity, and the assessment of which is also affected by the incomplete conceptual understanding of buffer erosion.
- Buffer sedimentation, determined by fracture apertures (and indirectly by salinity and flow through the penetration of dilute waters), the assessment of which is also affected by the incomplete conceptual understanding of buffer sedimentation.
- Groundwater sulphide concentrations over the glacial cycle.
- Canister corrosion under advective conditions, requiring buffer erosion to the extent that advective conditions arise in the deposition hole, and then determined by groundwater flow and sulphide concentrations.

The issues relating to canister failure due to shear load are as follows:

- The occurrence of earthquakes of a sufficient magnitude to cause secondary shear movements in fractures intersecting deposition holes.
- The extent of detrimental secondary shear movements given sufficiently large earthquakes.
- The impact of secondary shear movements on the buffer/canister system.

By definition, the external conditions for the reference evolution are constrained either to a development compatible with a repetition of the Weichselian glacial cycle (the base case) or to one compatible with the global warming variant. There are uncertainties within these constraints, leading to uncertainties within the reference evolution, as listed above. There are also significant uncertainties due to the fact that external conditions other than those defining the Weichselian base case or the global warming variant can be conceived. The latter are handled in the scenario analyses.

S3.9 Step 8: Selection of scenarios

Method for scenario selection

A key feature in managing uncertainties in the future evolution of the repository system is the reduction of the number of possible evolutions to analyse by selecting a set of representative scenarios. The selection focuses on addressing the safety relevant aspects of the evolution expressed at a high level by the safety functions ‘containment’ and ‘retardation’ which are further characterised by reference to safety function indicators.

The selected scenarios should cover all reasonable future evolutions. Furthermore, it should be possible to logically calculate the risk associated with the presence of the repository as a sum of risk contributions from the set of scenarios.

There are also several issues concerning applicable regulations that have to be taken into account in the selection of scenarios. Given the regulatory requirements and the general considerations above, a method for the selection of scenarios in five steps has been developed as explained below.

1. Definition of the main scenario

A *main scenario* is defined, based on the reference evolution and in accordance with SSMFS 2008:21. The main scenario is split into two variants, based on the two variants of the reference evolution, i.e. the Weichselian base case and the global warming variant.

2. Selection of additional scenarios based on potential loss of safety functions

A main factor governing scenario selection is the concern that the safety functions relating to containment should be upheld. Therefore, these safety functions are used to structure the selection of additional scenarios. This is the main approach for addressing the issue of *less probable scenarios*, in SSMFS 2008:21.

There are three canister safety functions related to containment: to provide a corrosion barrier, to withstand isostatic load and to withstand shear load. Three distinct canister failure modes, due to corrosion, isostatic pressure and shear movement, respectively, can thus be derived from the safety functions. Therefore, three scenarios, one for each canister failure mode, are generated. Three ‘failed’ states of the buffer; advective, frozen and transformed, are also considered as scenarios. The canister scenarios are systematically combined with the buffer scenarios.

For each selected scenario, uncertainties related to initial state factors, processes and external conditions that are not covered in the main scenario are considered. In e.g. the case of canister failure due to isostatic overpressure, inadequacies in the manufacturing of the load-bearing canister insert, higher than reference buffer swelling pressures and maximum thick ice sheets yielding higher groundwater pressures are considered.

An assessment of whether each scenario is to be considered as “less probable” or “residual” is made. In the former case, the likelihood of the scenario is normally pessimistically set to one, whereas the assessed limited likelihoods of its characteristic FEPs, e.g. large earthquakes, are taken into account in the risk calculation associated with the scenario.

These scenarios also cover many of the residual scenarios required by SSM’s Regulations and General Guidance to analyse *the significance of barriers and barrier functions*. To obtain a deeper understanding of barrier functions, a number of residual scenarios are defined illustrating, from the point of view of radionuclide transport, hypothetical situations where one or several barriers are assumed to be initially lost.

The selection of additional scenarios in the PSAR is identical to that in the safety assessment SR-Site. The analyses of canister failure scenarios have, however, been expanded in response to considerations in SSM’s review of SR-Site. Thus, in the PSAR, the analyses of the early, unsaturated phase of the repository evolution is more emphasised as is the analysis of copper creep, reflecting the introduction of creep related canister safety function indicators in step 8 of the PSAR assessment.

3. Scenarios related to future human actions

A set of scenarios related to future human actions was also defined and analysed. Human intrusion scenarios resulting in a degradation of system performance are to be considered as “less probable scenarios” according to SSMFS 2008:21, but not included in the risk summation according to the General Guidance to SSMFS 2008:37. SSM requires residual scenarios to illustrate *damage to humans intruding into the repository* and cases to illustrate the consequences of an *unclosed repository that is not monitored*.

4. Other residual scenarios, etc.

Any other scenarios that are, for any reason, considered necessary in order to obtain an adequate set of scenarios are also to be defined. These could include scenarios directly identified in the FEP analysis but not according to the criteria above. No such issues have been identified in the PSAR.

5. Combination of scenarios

For the scenario selection to be comprehensive, combinations of the scenarios must be considered. This is done when all the scenarios have been selected and analysed. Related to the issue of combination of scenarios is that of different event sequences. The sequence in which different events or aspects of the evolution occur may be important for the evolution of the repository. This is explicitly addressed within each scenario.

Summary

In summary, the scenario methodology is an investigation of all routes to the three identified canister failure modes aiming at ruling them out or at quantifying them, considering all conceivable evolutions of the system. The safety functions of the repository components and the understanding of the development of the repository system emerging from the analysis of the reference evolution form the basis for exhaustive evaluations of such routes.

Selected scenarios

The following scenarios are selected in the PSAR.

- A main scenario, corresponding to the reference evolution.
- A buffer advection scenario exploring the routes to and quantitative extent of advective conditions in the deposition hole.
- A buffer freezing scenario exploring the routes to buffer freezing.
- A buffer transformation scenario exploring the routes to buffer transformation.
- A scenario exploring the routes to and quantitative extent of canister failures due to corrosion.
- A scenario exploring the routes to and quantitative extent of canister failures due to shear load.
- A scenario exploring the routes to canister failures due to isostatic load.
- Hypothetical, residual scenarios to illustrate barrier functions.
- Scenarios related to future human actions.

S3.10 Step 9, part 1: Analysis of containment potential for the selected scenarios

Method

The analysis of the selected scenarios is divided in two steps: analysis of containment potential and of retardation potential.

The containment potential is not further analysed in the main scenario; the results from the reference evolution in step 7 are adopted.

The additional scenarios are analysed by focussing on the factors potentially leading to situations in which the safety function in question is not maintained. In most cases, these analyses are carried out by comparison with the evolution for the main scenario, meaning that they only encompass aspects of repository evolution for which the scenario in question differs from the main scenario.

A common template, with a set of fixed headings, is followed in the analysis and documentation of the additional scenarios.

Results

In summary, the following conclusions were reached when the containment potential of the selected scenarios was analysed. (For the hypothetical residual scenarios containment failures are postulated and FHA scenarios are analysed with a different methodology.)

- Buffer advection: This situation may occur in the reference evolution. The additional analyses within the buffer advection scenario, considering conceptual uncertainties and additional interpretations of the hydraulic properties of the sites, suggest a range in the possible extent of buffer advection. *These consequences were propagated to the canister corrosion scenario.*
- Buffer freezing: Detrimental effects from buffer freezing was ruled out in the reference evolution, including freezing in buffer erosion cavities. The additional analyses within the buffer freezing scenario also led to the conclusion that detrimental freezing of an intact buffer is ruled out and hence should be considered as a residual scenario. This applies also to the freezing of water in cavities of a partially eroded buffer. *The possibility of detrimental buffer freezing was, therefore, not propagated to the canister scenarios.*
- Buffer transformation: The analyses of a high buffer temperature, or other circumstances leading to the transformation of the buffer material within the buffer transformation scenario led to the conclusion that this should be considered as a residual scenario. *The possibility of buffer transformation was, therefore, not propagated to the canister scenarios.*
- Canister failure due to corrosion: This failure mode is included in the reference evolution, where it occurs for the case of advective transport through an eroded buffer and with sulphide in the groundwater as the important corroding agent. In the canister corrosion scenario, all mechanisms for canister corrosion were revisited. It was confirmed that chloride assisted copper corrosion, requiring high chloride concentrations and very low pH compared to what can be expected in the repository, can be ruled out. The additional analyses in the canister corrosion scenario, with input from the buffer advection scenario, led to the conclusion that advective conditions in the buffer is indeed the main potential cause of corrosion failures. It was also concluded that sulphide in the groundwater is the only corroding agent that has the potential to cause canister failures and then only under advective conditions. Evaluating all the advective situations and other uncertainties related to corrosion led to a range of potential extents of corrosion failure. *These are propagated to the analysis of consequences for the corrosion scenario.*
- Canister failure due to isostatic load: This failure mode was ruled out in the reference evolution. The analysis in the isostatic load scenario, taking into account isostatic pressures caused by maximum thick ice sheets and accounting in more detail for copper creep, led to the conclusion that it should be considered as a residual scenario. Consequences for a hypothetical case of canister failure due to isostatic load are nevertheless analysed.
- Canister failure due to shear load: This failure mode was analysed in the reference evolution, where it had a low probability of occurrence even with a number of pessimistic assumptions. This conclusion remains after the additional analyses in the shear load scenario. *The pessimistically estimated frequency of canister failures due to shear load is propagated to the analyses of consequences for the shear load scenario.*
- The analysis of combinations of scenarios led to the conclusion that relevant combinations and gradual developments of phenomena either have been addressed in earlier parts of the assessment and in some cases propagated to consequence calculations, or can, with relatively simple complementary arguments, be shown not to give rise to additional cases for further consideration. The only exception concerns a case where a shear failure is followed by buffer erosion. This case was also propagated to consequence calculations.

S3.11 Step 9, part 2: Analysis of the retardation potential for the selected scenarios

This second step of the scenario analyses encompasses calculations of radionuclide release, transport and dose impacts for potential failure modes of canisters identified for each scenario in the analysis of containment potential. The purpose is to assess the retardation properties of the system for these scenarios and to quantify risk. Full documentation of the consequence calculations is provided in the **Radionuclide transport report**.

Criticality

If a canister failure occurs, the issue of nuclear criticality has to be considered, since, if this occurred, it could have a strong influence on the further development of the failed canister. The conclusion of criticality analyses in the PSAR is that the canister remains subcritical in the repository for all reasonably conceivable cases.

Biosphere

Over the time scales of relevance for the safety assessment, the biosphere will undergo considerable changes, in particular due to the long-term climate variation involving glacial cycles and the associated shoreline displacement. In the case of releases of radionuclides from the repository, the potential activity concentrations in surface water are expected to increase as the site continues to emerge from the sea and radionuclides which may have accumulated in sediments can enter into the terrestrial food web in existing or agriculturally converted wetlands. Thus, the potentially highest exposure of humans and other organisms to radionuclides from the repository is expected when release locations of the site have emerged from the sea. In the PSAR, adopting results from the SR-Site assessment, the development of the landscape at the Forsmark site is modelled in detail for an interglacial climate period. The landscape is divided into a number of objects, for each of which the detailed development over time is modelled. Unit release rates of relevant nuclides are then fed to each object and the resulting time dependent turnover of radionuclides is determined. Each object is pessimistically assumed to be populated by humans to the extent that it can just wholly feed its inhabitants, meaning that they will eat only contaminated food. Humans are assumed to cover their drinking water demand by equal contributions from a contaminated well, and from the surface water in the lake or stream passing through the object. The time dependent radionuclide distribution in each object leads to annual doses to its inhabitants that vary in time. For each nuclide, the peak annual dose over the entire interglacial and over all objects is determined, yielding a peak annual dose per unit radionuclide release rate to the landscape. These landscape dose conversion factors (LDFs) are used in converting release rates from the repository to annual doses. The approach relies on the fact that releases from the repository in general vary slowly over the time scale of an interglacial. The use of the same LDF values as in the SR-Site assessment is seen as justified, based on an evaluation of additional data and knowledge emerging since the completion of the SR-Site assessment.

Results of radionuclide transport and dose for risk contributing scenarios

There are two scenarios for which canister failures cannot be excluded according to the analysis of the containment potential; the corrosion scenario and the shear load scenario.

For the corrosion scenario, a set of cases covering the range of potential extents of corrosion failure from the analysis of the containment potential is considered. The calculated mean doses are at least one order of magnitude below the dose corresponding to the regulatory risk limit, see Figure S-10. In the most pessimistic variants of this scenario, the first canister failures and hence the first releases occur after around 60 000 years. In these variants, the mean dose is about two orders of magnitude below the regulatory limit at 100 000 years and about one order of magnitude below the limit at one million years. For a more reasonable *central corrosion case* (light blue curve) the mean dose is at least two orders of magnitude below the limit throughout the assessment time.

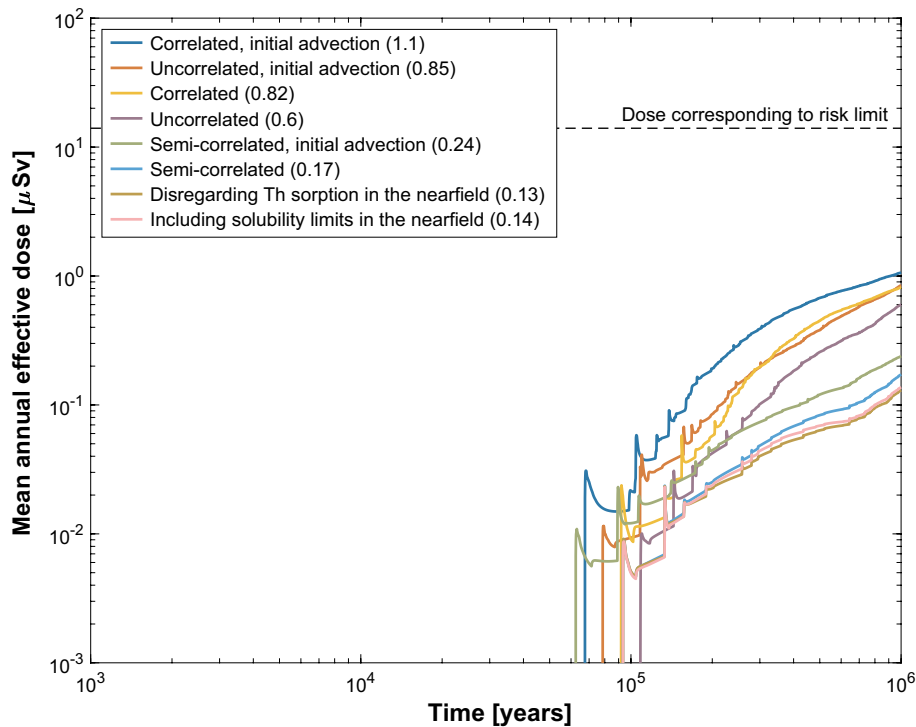


Figure S-10. Summary of far-field mean annual effective dose for all probabilistic calculations performed for the corrosion scenario. The peak doses are given in parentheses in μSv . In the legend, ‘Correlated’, ‘Uncorrelated’ and ‘Semi correlated’ refer to three variants of the hydrogeological model used in the PSAR. The three ‘initial advection’ cases put upper bounds on the possible consequences of buffer loss due to erosion and sedimentation.

Different extents of canister failures in the corrosion scenario propagated from the analysis of containment potential led to variations in calculated mean doses within one order of magnitude. Also uncertainties in the conceptualisation of the near field transport conditions have a similarly limited impact on the calculation results.

For the shear load scenario, the pessimistically derived frequencies of canister failures due to shear load from the analysis of containment potential are used in the consequence calculations. The calculated mean dose for the initial 1 000 years is negligible in comparison to the dose corresponding to the regulatory risk limit. Between 1 000 and 100 000 years, the calculated mean dose is about three orders of magnitude below the limit and then increases to become about two orders of magnitude below the limit at one million years, see Figure S-11.

Sensitivity analyses of the probabilistic calculation results show that input uncertainties for the fuel dissolution rate, the failure time of the canister and the flow related transport resistance in the geosphere account for most of the uncertainty of the calculated dose. Additional uncertainties are addressed through the formulation of variant calculation cases regarding e.g. different conceptual hydrogeological models or through pessimistic assumptions regarding, e.g. the likelihood of canister failure due to shear load. The influences of all important uncertainties on the calculated risk are evaluated based on the outcome of the risk summation, and possibilities of reducing the uncertainties are discussed as feedback from the assessment.

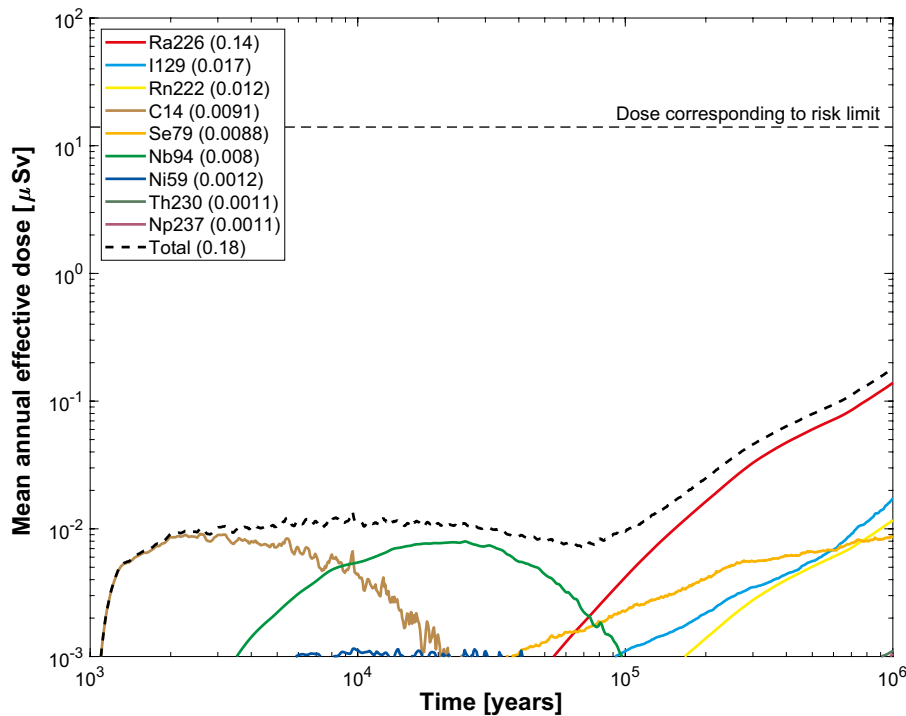


Figure S-11. Probabilistically calculated consequences of shear failure, for the period between 1 000 years and one million years. The legends are sorted according to descending peak mean annual effective dose over one million years (given in brackets in μSv).

Calculation cases with hypothetical complete loss of barrier functions

To illustrate the role of the barriers and as a basis for the discussion of the safety concept, a set of calculation cases with hypothetical, complete losses of barrier functions have also been analysed. The following cases of barrier deficiencies are postulated:

- A. An initial absence of enough buffer causing advective conditions in the deposition hole for all 6 000 deposition holes.
- B. An initial pinhole in the copper shell for all 6 000 canisters.
- C. An initial, large opening in the copper shell and in the cast iron insert for all 6 000 canisters.
- D. A combination of cases A and C, i.e. an initial large opening in all canisters and advective conditions due to loss of buffer for all 6 000 deposition holes.
- E. A combination of case C with an assumption of fast fuel dissolution and fast corrosion of metal parts. An initial, large opening in every canister is combined with the assumption of a complete fuel dissolution and metal corrosion in only 100 years.

A loss of the radionuclide retention capability of the rock is combined with each of the five cases, yielding a total of ten release situations. The cases without geosphere retention are denoted A* through E*.

In all cases it is assumed that the backfill and closure are installed and perform as expected. Also, all aspects of the rock other than those related to retention, e.g. the near-field groundwater flow, which is generally low and with only about one sixth of the deposition holes connected to a water conducting fractures, as well as the stable and favourable groundwater composition in the near-field, are assumed to be present. Elemental solubilities are imposed on concentrations of radionuclides in the canister void volume only if the buffer is in place. This is the same approach as used in the analyses of the corrosion and shear load scenarios. The summed dose for each case is given in Figure S-12.

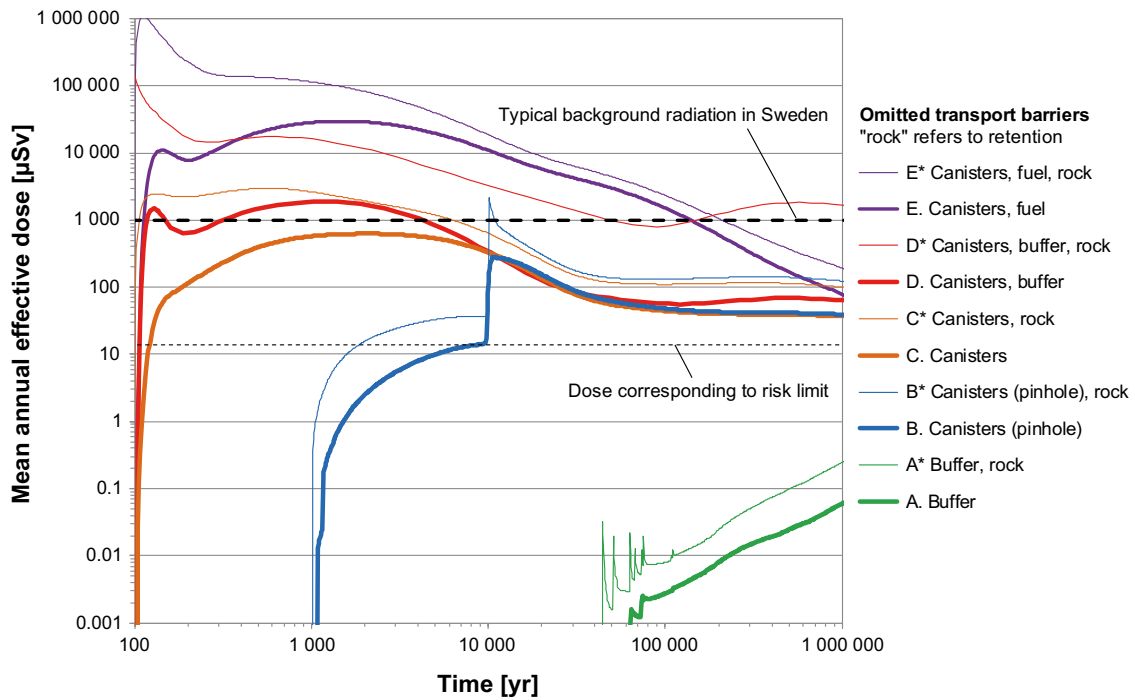


Figure S-12. Results of stylised and hypothetical cases to illustrate loss of barrier functions. Note that an omission of the “rock” barrier in these cases refers to omission of retention of radionuclides in the rock fractures only, whereas the favourable, low flow rate at repository depth and the favourable geochemical conditions are still taken into account.

After about 10 000 years, the doses for all cases are below the dose caused by typical background radiation in Sweden, except the case where retention properties of canisters, buffer and rock are all disregarded (case D*) and that with rapid conversion of the waste form in combination with failed canisters (cases E and E*). The low flow and favourable groundwater chemistry of the rock and the presence of backfill and closure of repository tunnel thus provide substantial protection from a waste with unaltered dissolution rate.

A set of cases of hypothetical, early canister failures, in addition to those discussed above, have been analysed in the PSAR as a response to comments in SSM’s review of the SR-Site assessment. These show that hypothetically postulating initial failure of all canisters and adopting a more reasonable representation of the biosphere for the early development of the system leads to peak doses about a factor of two above the dose corresponding to the regulatory risk criterion in a base case. The doses from the base case thus correspond to about three percent of those from the natural background radiation in Sweden. A number of even more pessimistic sensitivity cases yield doses within an order of magnitude above those of the base case.

Additional results

Further results from the radionuclide and dose calculations are presented in the conclusions section below. These include a summation of risk contributions from scenarios which could not be ruled out from the assessment, the calculations of doses to non-human biota, calculations with alternative, simplified analytical models, and the use of alternative safety indicators.

S3.12 Step 10: Additional analyses and supporting arguments

Overview

In this step of the assessment, a number of additional analyses, required to complete the safety assessment, are carried out.

- Analyses of scenarios related to future human actions.
- Analyses required to demonstrate optimisation and use of best available technique, BAT.
- Verification that FEPs omitted in earlier parts of the assessment are of negligible significance in the light of the completed scenario and risk analysis.
- A brief account of the time period beyond one million years.
- Use of natural analogues.

Only results from the first point are given below. Results of the remaining points are summarised as appropriate in the conclusion section of this summary.

Scenarios related to future human actions

Based on generally accepted principles and SSM's Regulations, the future human actions considered are restricted to global pollution and actions that are carried out after the sealing of the repository, take place at or close to the repository site, are unintentional, and impair the safety functions of the repository's barriers. A systematic approach including a technical analysis, an analysis of societal factors, a choice of representative cases and, finally, scenario descriptions and consequence analysis of the chosen cases is adopted. The main conclusions of these analyses are summarised below.

- For a stylised case where a drilling team unintentionally penetrates a canister and part of spent fuel is brought to the surface, the following is found.
 - The dose rate that a member of the drilling personnel would be exposed to while working in the highly contaminated area can be quite high. However, if the drilling occurs at ca 5 000 years after repository closure, the dose rate will have decreased to a value below 1 mSv/hour.
 - The total dose from using the borehole in the drilling case as a well 300 years after repository closure is below background radiation.
 - The maximum total annual effective dose from agricultural use of soil contaminated by fuel debris is very high, but it is noted that there are a number of simplified, pessimistic assumptions made in the calculations.
- The impacts of an open investigation borehole on the groundwater flow and on the long-term properties of the backfill in the deposition tunnel in the vicinity of the borehole are assessed as negligible.
- A tunnel constructed in the upper part of the bedrock would not affect the groundwater flow at repository depth such that the presence of the tunnel violates the safety functions of the deep repository.
- Exploitation of potential mineral resources in the vicinity of the Forsmark site would not impact the safety functions of the repository.
- Abandoning the repository without backfilling and sealing all parts of the repository may, according to the analysis of a stylised FHA scenario for the Weichselian glacial cycle, imply that backfill in the deposition tunnels is lost and that the safety functions for containment are violated for deposition holes located close to the entrance of the deposition tunnels. Without backfill in parts of the system, no canister failures are expected during the first period of temperate climate conditions. During the subsequent glacial period, assumed to last until 66 000 years after present, corrosion breakthrough may occur and the calculated annual effective dose from radionuclides in the failed canisters exceeds the regulatory risk limit. Considering the large uncertainties and cautious assumptions made in the analysis, the result is seen as a simplified illustration of possible consequences, pointing to the necessity of properly backfilling and sealing the repository.

S4 Conclusions of the PSAR post-closure safety assessment

As mentioned initially, the central conclusion of the PSAR post-closure safety assessment is that a KBS-3 repository built at the Forsmark site according to the specifications in the PSAR can be expected to fulfil the requirements of post-closure safety expressed in SSM's relevant regulations.

This conclusion is reached since the favourable properties of the Forsmark site ensure the required long-term durability of the barriers of the KBS-3 repository. In particular, the copper canisters with their cast iron insert have been demonstrated to provide a sufficient resistance to the mechanical and chemical loads to which they may be subjected in the repository environment.

The detailed analyses, performed systematically according to a well-defined methodology, demonstrate that canister failures in a one million year perspective are rare. Even with a number of pessimistic assumptions regarding detrimental phenomena affecting the buffer and the canister, they would be sufficiently rare that their cautiously modelled radiological consequences are well below one percent of the natural background radiation, meaning that they are also well below the Swedish regulatory risk criterion.

S4.1 Overview of results

Compliance with regulatory risk criterion

A repository at Forsmark is assessed to comply with the regulatory risk criterion

The analyses carried out in the PSAR show that a KBS-3 repository at Forsmark constructed in accordance with the current reference design will comply with the regulatory risk criterion issued by SSM.

The likelihood of canister failures during the initial one thousand years, is assessed as negligible

The pessimistically calculated mean number of canisters failing due to earthquakes during the initial one thousand years is of the order of one in a hundred thousand. All other failure types are assessed as ruled out for this period. Furthermore, the evaluations of the canister sealing procedure, have led to the conclusion that all canisters will be tight at deposition.

In a one million year time perspective, there is a small risk contribution from canister failures due to enhanced corrosion following buffer erosion and sedimentation

Loss of buffer may occur from exposure to low ionic strength waters but the extent is uncertain. The Forsmark site has a large potential to maintain a sufficient ionic strength at repository depth over a glacial cycle. Loss of buffer mass due to erosion, to the extent that advective conditions arise in the deposition hole, may, however, occur in a 100 000 year perspective for typically less than ten deposition positions with high flow rates. Estimates of buffer loss due to sedimentation, based on pessimistic extrapolation to repository conditions of early experimental results, suggest that this process may lead to similar, or at most an order of magnitude higher, losses.

Advective conditions in a deposition hole will enhance the canister corrosion rate. In a one million year time perspective, this may lead to failures of a few canisters when applying the most pessimistic of the hydraulic interpretations made of the Forsmark site, with cautious assumptions regarding concentrations of corrosive agents and deposition hole acceptance rules.

With pessimistic assumptions regarding buffer erosion, buffer sedimentation, copper corrosion and radionuclide transport conditions, the radiological risk from such canister failures is pessimistically calculated to be around 1/100 of the regulatory limit in a 100 000 year perspective and around 1/10 of the regulatory limit in a one million year time perspective.

In a one million year time perspective, there is a small risk contribution from canister failures due to earthquakes

Canister failures due to large earthquakes cannot be categorically ruled out. However, the probabilistic analyses imply that, on average, it would take considerably more than one million years for even one such canister failure to occur.

The contribution to radiological risk from earthquakes is pessimistically calculated to be less than 1/100 of the regulatory limit in a 100 000 year perspective and less than 1/10 of the regulatory limit in a one million year time perspective. Studies performed since the SR-Site assessment further substantiate the pessimistic nature of this calculation as regards the likelihood of detrimental rock shear movements.

Issues related to altered climate conditions

Several issues of importance for post-closure safety are related to future glacial, periglacial or warmer climate conditions. A number of conclusions regarding effects of such conditions can be drawn.

Detrimental freezing of the buffer is ruled out – even for very pessimistically chosen climate conditions

According to the analyses, detrimental freezing of the buffer clay is ruled out, even for the most pessimistic periglacial climate conditions considered, which includes the large uncertainties related to future climate development. Also freezing of a deposition tunnel backfill material or of a water-filled cavity in an eroded buffer is ruled out for the most pessimistic climate development at Forsmark. The temperature at which a frozen buffer could cause detrimental effects on a canister is assessed to be $-6\text{ }^{\circ}\text{C}$ in the PSAR, giving even higher safety margins than for the $-4\text{ }^{\circ}\text{C}$ freezing criterion applied in the SR-Site assessment.

Canister failure due to isostatic load is ruled out – even for very pessimistically chosen climate conditions

According to the analyses, canister failure due to isostatic load is ruled out for the most severe future glacial conditions considered based on the glacial development of the past two million years. New studies conducted since the SR-Site assessment imply that the pessimistically estimated peak glacial load at the Forsmark site may be 20 % higher than assessed in SR-Site. Updated design requirements, however, imply a lowered maximum buffer swelling pressure and an increased canister resilience to isostatic loads. The updated design analysis of the canister suggests that the current design will sustain the estimated peak load at Forsmark with a considerable margin. This applies to both the static load on the insert and to long-term creep in the copper shell.

Oxygen penetration is very unlikely – even for very pessimistically chosen climate conditions – and the consequences are small

Oxygen penetration to canister positions is ruled out, except for enhanced flow situations occurring during the unlikely event when an ice sheet margin is temporarily stationary above the repository in combination with several other pessimistic assumptions. Even in such a case, the consequences in terms of canister corrosion are small.

Repository safety for a prolonged period of warm climate before the next glacial period is assessed as comparable to safety for a climate unperturbed by enhanced global warming

A prolonged period of warm climate (global warming due to an enhanced greenhouse effect) at the expense of the duration of glacial conditions is expected to lead to decreased buffer erosion and sedimentation.

The occurrence of large earthquakes is likely to increase during deglaciation, and this effect is thus delayed by a prolonged initial period of warm climate.

Other issues related to barrier performance and design

The reference design, forming the basis for the assessed initial state in the PSAR, yields a safe repository when implemented at the Forsmark site

Since the analyses in the PSAR show that the regulatory risk criterion is fulfilled, it is concluded that the assessed reference design implemented through the selected production and control procedures will yield a safe repository. The design requirements, the reference design and the production and

control procedures have been substantially updated since the SR-Site assessment. Conclusions regarding design issues important for post-closure safety yielding feedback to future refinement of the design have been drawn.

It is crucial to avoid deposition positions intersected by large or highly water conductive fractures and the low frequency of water conducting fractures allows efficient application of such rejection criteria

The risk contributors are related to the occurrence of large and/or highly conductive fractures intersecting deposition holes. This applies to the buffer colloid release process and the impact of major earthquakes in the vicinity of the repository. These two phenomena are related to canister failures due to canister corrosion and to secondary rock shear movements, respectively. As also the retention in large, highly transmissive fractures is small, such failures are in general associated with high consequences. Accordingly, such fractures need to be avoided once identified.

Cautious assumptions regarding the likelihood of occurrence of such fractures and regarding deposition hole rejection criteria are adopted in the PSAR. The results of the analysis are sensitive to these assumptions. It is important to continue the development of acceptance criteria for deposition holes as a basis for future assessments. This needs to be studied both by simulation of the effects of applying potential criteria and by exploring the practicability of applying the criteria.

The heat from the canister will likely fracture the rock in the deposition hole wall, which would enhance the in- and outward transport of dissolved substances, but this has little impact on risk

Thermally induced spalling around deposition holes at Forsmark cannot be ruled out and may have a considerable impact on mass exchange between the flowing groundwater and the buffer as long as diffusion is the dominant transport mechanism in the buffer. For diffusive conditions, there is, however, a considerable margin to canister failures even when spalling is pessimistically assumed in all deposition positions at Forsmark. If advective conditions prevail in the buffer, the effects of spalling are much less pronounced because it adds little to the already increased flow rate. In consequence, the overall effect on the calculated risk is small.

The importance of the excavation damaged zone in the rock around the deposition tunnels as a transport path for radionuclides is limited

The importance of the excavation damaged zone (EDZ) around deposition tunnels is limited in comparison to other transport routes for radionuclides. Very pessimistic assumptions about the EDZ in relation to the reference excavation method could affect the extent of canister corrosion for advective conditions.

This confirms the suitability of the cautious reference excavation methods adopted in the reference design of the repository.

In most deposition holes groundwater will not reach the canister for thousands of years due to the favourable rock properties at Forsmark

The saturation times for both backfill and buffer are likely to range from a few tens of years to several thousand years, as a consequence of the rock properties (matrix hydraulic conductivity and presence and characteristics of fractures) at Forsmark. The majority of deposition holes are not intersected by water conducting fractures, yielding slow saturation (with water from the deposition tunnel and the buffer) and slow inflow of e.g. corrosive agents in the groundwater both during unsaturated and saturated conditions. Transport of corrosive agents within the bentonite will be very limited and diffusion-dominated also during the unsaturated phase. Since the groundwater flow during saturation is towards the deposition holes, no erosion of the bentonite can occur during the unsaturated period. The effects of the unsaturated period on the geochemical, mineralogical and thermal property changes in the buffer have been investigated. They are found to be small and without any significant impact on long-term performance. Compared to the SR-Site assessment, considerable additional attention has been paid to the early conditions with particular focus on canister integrity.

S4.2 Demonstration of compliance

Introduction

This section summarises the most important aspects of the demonstration of compliance with applicable SSM regulations. A complete account of how the PSAR post-closure safety report meets these requirements is given in Appendix A, where the regulations are reproduced and where references are given to sections in this report where each issue is addressed.

The safety concept and allocation of safety

As an introduction to the discussion of compliance, a brief account of the safety concept, evaluated by results from the post-closure safety assessment is given. The main safety function of the KBS-3 concept is containment and the secondary safety function, mobilised if the containment function is not upheld, is retardation.

Containment for a KBS-3 repository at Forsmark

The containment function is provided by an intact copper shell of the canister. The extent to which this function is upheld is dependent on the buffer's function of limiting advective transport between the host rock and the canister and on favourable mechanical, hydrogeological and geochemical properties of the host rock: i) limited flow rates and a minimum charge concentration of the groundwater to avoid erosion of the buffer ii) limited flow rates and low groundwater concentrations of sulphide to limit corrosion, in particular if the buffer has been eroded, and iii) a low probability of large fractures intersecting deposition holes in order to limit the potential impact on the canister of large earthquakes in the vicinity of the repository.

The analyses in the PSAR indicate that containment is maintained even in the one million year perspective for a vast majority of canisters. Deterioration of the barrier system to the extent that containment is lost is assessed to only occur, as a statistical average, for less than one canister due to buffer mass loss leading to advective conditions and enhanced corrosion. The other failure mode that could not be ruled out, that due to earthquake-induced secondary shear movements in fractures intersecting deposition holes, is even less likely and affects on average considerably less than one canister when this failure mode is evaluated statistically with a number of pessimistic assumptions. This means that containment is assessed to be maintained for the vast majority of the 6 000 canisters throughout the assessment period.

All safety functions related to containment are shown in Figure S-7. Many of these, like the canister's ability to withstand isostatic loads or the "ability" of the host rock to provide a favourable rock temperature, are assessed as upheld throughout the assessment period.

It is also noted that the consequences of a postulated, complete loss of containment for all canisters decrease with time, and are about a factor of 3 higher than the regulatory risk limit at the end of the assessment period (hypothetical case C in Figure S-12).

Retardation for a KBS-3 repository at Forsmark

Both failure mechanisms that could not be ruled out are of the common mode type, i.e. the canister, the buffer and the rock are all affected, either through a detrimental shear movement or through a high flow rate in the geosphere, affecting both erosion and corrosion. The causes of the failures affect also the retention properties through high flow rates and, in the case of erosion, through the absence of the buffer after failure. Hence the retarding potential of the repository is limited in these particular cases, for the canisters that have failed. Instead, safety is to a considerable extent achieved through the slow dissolution of the fuel and, to a lesser extent, through the limited corrosion rate of radionuclide-containing metallic structural parts of the fuel elements.

For the canisters that maintain their containment potential, retardation is a latent safety function throughout the assessment period. A more general view of the retarding potential of the buffer and the host rock is obtained from the analyses of hypothetical, complete losses of barrier functions above.

Retention in the buffer is important for the initial 1 000 years and limited in longer time frames (compare cases C and D in Figure S-12). The latter is due to the fact that the total dose in the long term is dominated by non-sorbing or very long-lived nuclides. However, a nuclide specific comparison reveals that the buffer has a considerable retention function for sorbing nuclides also in the long term, masked in the total dose by the dominance of the non-sorbing species.

The role of retention in the rock is similar; it is important for the initial 1 000 years and limited in longer time frames (compare cases C and C* in Figure S-12) as concerns total dose, again since total dose is then dominated by nuclides that do not sorb in the rock. A nuclide specific comparison reveals that the rock has a considerable retention function for sorbing nuclides also in the long term, masked in the total dose by the dominance of the non-sorbing species. The low flow rates at repository depth also play an important role in limiting the release rate of radionuclides to the rock.

Summary

In summary, containment is the primary safety function of the KBS-3 repository and it is demonstrated to be efficiently upheld at the Forsmark site throughout the assessment period, directly through the properties of the canister and indirectly by the favourable hydrogeological and geochemical properties of the host rock. For the rare failures of containment, retardation is of limited importance due to the common mode nature of the failure mechanisms in question and since only very long-lived nuclides remain when these failures occur. As a latent function, retardation is significant for hypothetical releases of, in particular, sorbing species throughout the assessment period. For hypothetical failure modes affecting the canister only, retardation of sorbing nuclides is significant in the buffer and in the host rock.

Compliance with SSM's risk criterion

Compliance for the first 1 000 years

Of the three identified failure modes of the canister, i.e. failure due to corrosion, due to shear load and due to isostatic loads, corrosion and isostatic load induced failures can be ruled out with large margins for the first 1 000 years, as demonstrated in the reference evolution and the analyses of the corrosion and isostatic load scenarios. It is noted that the discussion on early canister failures has been extended substantially, in particular for the corrosion scenario, compared to the SR-Site assessment.

Shear loads on the canister may occur as a consequence of large earthquake induced secondary shear movements in fractures intersecting deposition holes. Although the likelihood for large earthquakes is higher during periods of tectonic stress, for example during glacial rebound, it cannot be entirely ruled out that a detrimental earthquake would occur during the initial 1 000 years.

The probability that one out of the 6 000 canisters has failed at the end of the initial 1 000 year period is pessimistically estimated at 2.4×10^{-5} , i.e. hypothetically 40 000 repositories, each with 6 000 canisters would have to be constructed in order for there to be an expectation of one failure during the initial 1 000 years. Despite this extremely low probability, a risk contribution was calculated for the first 1 000 years, with the result that the mean annual dose is at most around $0.001 \mu\text{Sv/yr}$ corresponding to a risk of $10^{-10}/\text{yr}$. This analysis builds on a detailed modelling of the biosphere development and radionuclide transport in the developing landscape during the initial 1 000 years, as required by SSM's Regulations.

It is, therefore, concluded that the analysed repository at Forsmark complies with the regulatory risk criterion during the initial 1 000 years after closure.

In hypothetical cases of initially defective canisters, there are several properties of the barrier system that provide protection, some of which are not important, or more difficult to claim, in longer time frames. Some of these would, with cautious assumptions, alone prevent any releases during the initial 1 000 years for an initially defective canister. This relates particularly to the time required for water to get into contact with the fuel elements and the integrity of the Zircaloy cladding.

Compliance for the time beyond the first 1 000 years

The bounding, dashed curve in Figure S-13 is the sum of the risk associated with the shear load scenario and that associated with the corrosion scenario. Each scenario is here pessimistically represented by the calculation case that yields the highest risk.

Other scenarios did not yield any contributions to the calculated risk. In the account of combinations of scenarios and phenomena it was concluded that the consequences of a shear load failure followed by buffer erosion needs to be assessed and this is done in the bounding case of the shear load scenario. All relevant risk contributions are, therefore, assessed to be included in Figure S-13.

Since the bounding curve in Figure S-13 is below the risk limit for the duration of the one million year assessment period, the analysed KBS-3 repository at the Forsmark site is assessed to fulfil the regulatory risk criterion. Risk dilution was shown not to challenge this conclusion.

It is furthermore concluded that a more realistic risk may be anywhere in the area below the bounding curve, down to zero risk based on the zero results of the three cases with no erosion and a situation where no canisters would fail due to shear movements induced by large earthquakes, which could be reached if somewhat less pessimistic assumptions could be defended for the shear load scenario.

It is also noted that through the use of LDF factors to transform releases to doses, it is in the risk assessment implicitly assumed that the landscape to which the releases occur is always fully populated, including the object where the highest dose is calculated to occur and during the point in time when this occurs. Furthermore, long periods of glacial and submerged conditions are expected where no doses to humans occur since the site is not habitable. This has not been taken into account in the risk summation. Rather, temperate conditions yielding the highest doses are assumed.

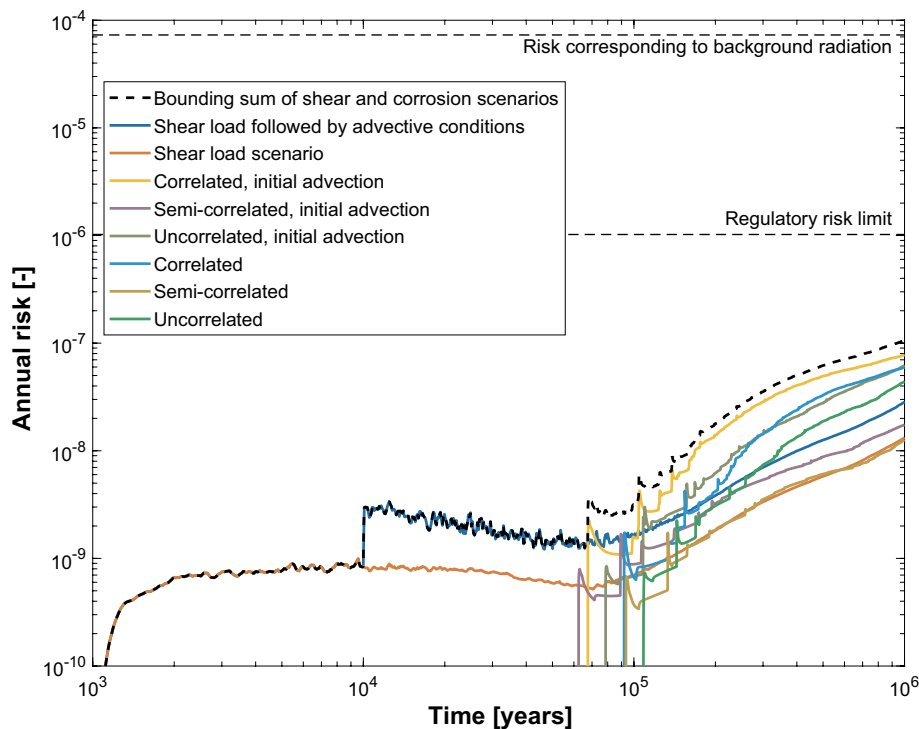


Figure S-13. Risk curves, expressed as annual individual risk. Several alternatives for the corrosion scenario are shown, and two for the shear load scenario. The bounding, dashed curve is the sum of the curve for the shear load failure followed by advective conditions (blue) and the curve for the variant of the corrosion scenario yielding the highest risk (orange). The risk associated with the main scenario is subsumed under the corrosion scenario as it is equal to the semi-correlated case (dark brown).

The time beyond one million years

Although the rocks, the ductile deformation and the brittle deformation zones at Forsmark all formed at least one billion years ago, the increasing uncertainties regarding the external conditions makes it not meaningful to predict the development of the site and of the repository for time periods beyond one million years.

It is noted that the hypothetical case in Section S3.11, where all canisters are failed, where the buffer is absent and where retention in the rock is disregarded, yields releases that correspond to dose consequences that are comparable to the natural background radiation after one million years. The releases are in that case controlled by the groundwater flow at repository depth and the inventory of radionuclides, the latter of which decreases with time and is dominated by radionuclides that also occur in natural ore bodies.

Finally, the scientific understanding of the fuel dissolution process suggests that the longevity of the spent fuel matrix is several million years in the repository environment. Furthermore, uranium ores that are many millions and even billions of years old are known through geological observations. This indicates that, in the case of stable tectonics and maintained reducing conditions in the repository, the uranium oxide which constitutes the fuel matrix can be stable for many millions of years.

Alternative safety indicators

In particular for times far into the future, the calculated risk becomes less useful as an indicator of repository safety, and SSM's Regulations suggest that alternative indicators should, therefore, also be evaluated. Four alternative indicators to risk are used in the PSAR. The following results emerged for the central corrosion case (brown curve in Figure S-13).

- Peak releases of activity from the geosphere are about three orders magnitude below the activity constraints issued by the Finnish regulator STUK.
- The peak radiotoxicity flux from the geosphere is more than three orders of magnitude lower than the reference value for the radiotoxicity flux from the geosphere suggested by the EU SPIN project.
- Calculated radionuclide peak concentrations in ecosystems at Forsmark from repository releases of Ra-226 are about three orders of magnitude below measured concentrations of naturally occurring Ra-226 at Forsmark.
- Peak geosphere fluxes caused by Ra-226 releases from the repository are about two orders of magnitude below naturally occurring fluxes of Ra-226 at the site, as estimated from site data; the difference is larger for U-234 and U-238, see Figure S-14. The total release of all repository derived nuclides converted to dose is also around two orders of magnitude lower than the summed dose from fluxes of the three mentioned naturally occurring nuclides.

The results are readily applicable to other corrosion cases, for most indicators by simply scaling with the release of Ra-226, which is at most one order of magnitude higher than that for the central corrosion case. Similar conclusions are reached for the shear load scenario.

In summary, the application of alternative indicators shows that releases from the repository are orders of magnitude below the adopted reference values for the indicators. This suggests that the future radiological consequences on man and on the environment of releases from the repository are negligible, independent of assumptions in the biosphere model.

Uncertainties linked to the risk calculation for different time periods

Uncertainties that have a significant influence on the calculated risk have been identified for the corrosion and the shear load scenarios. The handling of the uncertain factors in the PSAR is summarised together with references to plans for the reduction of these uncertainties. Most of the uncertain factors have been treated pessimistically, whereas some have been included as probability distributions in the risk calculations, where their full uncertainty range is used in the determination of mean annual doses, the relevant metric for determining the calculated risk.

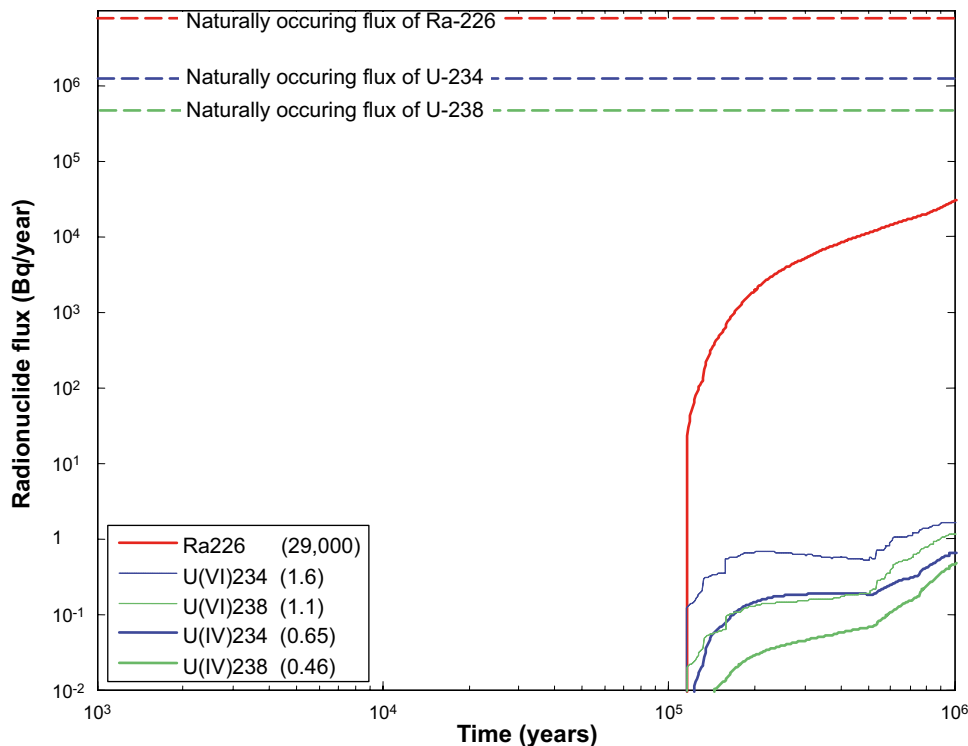


Figure S-14. Far-field release rates (Bq/year) of U-238, U-234 and Ra-226 in the central corrosion case compared to the naturally occurring fluxes at Forsmark.

The combination of pessimistic handling of uncertainties for which probability distributions could not be determined with the probabilistic handling of quantified uncertainties means that the total risk as determined in the risk summation is claimed to represent an upper bound on risk. Since this upper bound is below the risk limit throughout the one million year assessment period, there are no uncertainties of critical importance to resolve with respect to risk.

Effects on the environment from release of radionuclides

Doses to non-human biota for the central corrosion case have been calculated. The highest dose rates to organisms in marine, freshwater and terrestrial ecosystems in Forsmark, both in total and for the dose-dominating radionuclides are well below the screening dose rate (10 μ Gy/h) recommended in the ERICA Integrated Approach. It is therefore concluded that radionuclide releases predicted for this case will not lead to significant detrimental biological effects on individuals of species found, or projected to occur in future, at the site. In consequence, there will be no detrimental impact on populations, communities or ecosystems. The conclusion is applicable to all other cases included in the risk summation.

The use of best available technique, BAT

According to Swedish legislation, a licence application for a final repository needs to address the issue of best available technique (BAT). While a general account of the use of BAT is a broad issue spanning from the selection of method for the management of nuclear waste to fine details of the selected method, a limited part of this issue can and should be addressed in the safety assessment of the preferred method. Feedback can be given whether alterations in relation to the analysed reference design could lead to reductions in risk or in reduction in uncertainties that potentially could affect risk. For aspects of the design where no such reduction in risk or uncertainty in fulfilment of safety functions can be seen to be realistically obtainable, the solution is claimed to be optimal and BAT in the PSAR. However, the PSAR is not an assessment of all conceivable technical solutions. SKB will continue technical development of several aspects of the design in order to further simplify construction and implementation, adopting these developments provided that they comply with all other requirements on post-closure safety. The following is concluded regarding BAT.

- There seems to be little need to alter the *canister design* from a safety perspective. However, the ability of the cast iron insert to withstand shear load depends mainly on the occurrence of surface defects in the insert. While it is concluded in the **Canister production report** that the current canister reference design conforms to the stated design premises, it is also noted that rigorous requirements on manufacturing and NDT (non-destructive testing) capability are needed.
- While there still is uncertainty with regard to modelling of colloid formation and subsequent erosion and sedimentation of the buffer material and the modelling approach thus tends to be pessimistic, it cannot with the current understanding, be defensibly mitigated by e.g. selection of another buffer material. A continued R&D programme on buffer erosion and sedimentation mechanisms is needed.
- There possibly could be improvements in the backfill design from an installation point of view, but there does not seem to be a need to change the design to further improve its safety functions.
- The application of deposition acceptance criteria in the form of EFPC provides adequate protection against shear failure, but there is reason to continue efforts to find critically large fractures by other means, since the EFPC unnecessarily implies rejection of many holes only intersected by short fractures. Finding other means of identifying large fractures could increase the efficiency in the criterion without loss of safety and also increase the safety level since the focus on the detailed investigations would be on the few fractures of potential concern. Application of EFPC is also important for protection against corrosion failures, but there appears to be a potential for further enhancing safety by avoiding deposition holes with high inflows.
- The selected repository depth is adequate and changing the depth is not deemed to reduce the calculated risk. Furthermore, a shallower depth, e.g. above the 400 m level might increase the risk, since the frequency of water conducting fractures is higher there. Placing the repository some 100 m deeper would probably result in a risk contribution similar to the one obtained from the selected depth, whereas much deeper locations would imply that additional factors, such as very high stress levels, might need to be considered.

S4.3 Feedback from the analyses in the PSAR

Technical design requirements

A sufficient level of safety for a repository at Forsmark constructed in accordance with the reference design and conforming to the technical design requirements is demonstrated in the PSAR. Furthermore, the current design requirements are based, among other things, on feedback from the SR-Site assessment, whereas much of the analyses, in particular those related to the performance of the geosphere, have not been updated since essentially no new data for the host rock is available. Thus, some of the current design requirements and associated reference designs are judged adequate based on conclusions in the SR-Site assessment, and for others new feedback can be given only in the next stage of the repository programme when additional geosphere data are available. The following new conclusions can, however, be drawn from the assessment of post-closure safety in the PSAR.

- The current technical design requirements on isostatic load are adequate based on the findings in the PSAR.
- The current design requirements related to shear loads on the canister are adequate from the point of view of post-closure safety. However, the result depends in a complex way on a number of factors related to the canister, the buffer and the host rock. These have been evaluated with varying degree of pessimism in the PSAR and an optimisation including all the concerned design requirements could be of value, in order to achieve a balanced set of requirements on a system level, thereby facilitating the further design development.
- The updated technical design requirement on buffer swelling pressure is judged adequate.
- The updated technical design requirements on the deposition tunnel backfill are judged adequate. There is, however, a need to further elaborate the requirement on compressibility and possibly a need to better define the maximum content of potentially harmful impurities.
- The updated design of the bottom plate in the deposition holes is judged adequate, and it is concluded that no technical design requirement is needed for this component since it does not affect risk.

Detailed site investigations

In the safety assessment SR-Site, it was concluded that while the confidence in the site understanding was judged adequate and remaining uncertainties were sufficiently constrained to allow bounding risk estimates, the repository might still be further optimised with respect to efficiency and risk reduction. Feedback to the detailed site investigations and site modelling was given in order to prioritise and further specifying the development needs. This feedback has been taken into account in SKB's plans for detailed site investigations in the coming stage of the repository programme. Since essentially no new site modelling has been performed in the PSAR, no additional feedback is provided to the detailed site investigations as regards the host rock.

For the surface system, additional data has been collected since the SR-Site assessment and it is concluded that collection of additional data on element concentrations in different media are required as well as more data and understanding of sediment accumulation and erosion, mire development and a detailed stratigraphy of discharge areas.

Research on processes of relevance for post-closure safety

In accordance with a proper safety culture, general research on processes of importance for safety should continue, even if current knowledge is sufficient to demonstrate post-closure safety. More specifically, there are some issues for which the PSAR assessment show that the basis for the assessment can be improved through more R&D and where the results could lead to a reduction of the calculated risk.

- For the spent fuel, such issues include continued efforts to understand spent fuel dissolution mechanisms, to quantify the gap and grain boundary inventory and to improve the characterisation and the understanding of dissolution behaviour of the small amounts of irregular fuel types.
- Understanding copper corrosion is fundamental for the safety concept. Further understanding could e.g. allow less pessimistic assessments of localised corrosion and of the role of the buffer and the backfill for corrosion processes, particularly for unsaturated conditions. Understanding the deformation of cast iron is essential for confidence in the assessment of the impact of mechanical load on the canister. The ongoing development work on the design, manufacturing and testing of cast iron inserts, needs to continue in order to determine material requirements and specifications, and to ensure that all quality requirements can be fulfilled. Understanding of copper deformation under external pressure is also essential for confidence in the assessment of the impact of mechanical load on the canister, including the unlikely impact of hydrogen embrittlement. Conditions for stress corrosion cracking are not judged to occur in the repository, but the basic research focusing on identifying the necessary conditions needed for stress corrosion cracking to occur on copper should continue.
- Regarding the buffer, additional research on water transport, gas composition in unsaturated bentonite, piping/erosion, homogenisation and self-healing, montmorillonite alteration and the studies on rheological effects of cementation should be continued. From the studies of buffer mass loss due to erosion/colloid release and sedimentation it has been concluded that these processes cannot easily be excluded and that a continued R&D programme is needed. Further studies could reduce the degree of pessimism currently adopted.
- Much of the R&D related to the geosphere is covered by the detailed investigation programme, but research on some processes should continue. Research areas of interest include efforts to handle and mitigate thermally induced spalling, continued research on coupled thermo-hydro-mechanical processes in rock, assessing the potential for earthquakes including further development of the earthquake simulation tools, developing the DFN methodology, better bounding of the expected evolution of sulphide at the Forsmark site, the role of microbial activity for maintaining a low and stable redox potential, for sulphide formation and oxygen consumption, the quantification of penetration of dilute groundwater for different climate conditions and the role of channelling for radionuclide migration.

There are also a number of issues regarding the biosphere and future climate of interest to take forward in the RD&D Programme.

S4.4 Confidence in the results of the assessment

The assessment of post-closure safety is a key part of the PSAR. An approval of the PSAR by SSM is required for SKB to start construction of the final repository. The PSAR thus forms an important basis for a major decision point in SKB's programme for the management of spent nuclear fuel. A statement on the confidence in the results obtained in the PSAR is, therefore, appropriate. The confidence in the results obtained is assessed as sufficient for the decision at hand based on the following.

- The knowledge of the Forsmark site from the completed, surface-based investigations is sufficient for the assessment of post-closure safety. The site has favourable conditions for safety and no site-related issues requiring resolution in order to demonstrate safety have been identified. Confidence in the site-descriptive model and in the understanding of the site is obtained by a systematic and quality assured programme for site investigations and site modelling. The confidence in the site model is assessed in detail and documented in the **Site description Forsmark** report.
- There is a well-established reference design with specified and achievable production and control procedures yielding an initial state of the repository system with properties favourable for post-closure safety at the Forsmark site. The engineered parts of the repository system are to a large extent based on demonstrated technology and established quality assurance procedures to achieve the initial state of the system. This is systematically documented in the **Production reports** and their underlying references. Examples of important aspects of the initial state of the engineered barriers include:
 - a. The copper canister sealing quality.
 - b. The cast iron insert casting quality.
 - c. Buffer characteristics such as installed mass and material properties.
 - d. Backfill properties ensuring its ability to keep the buffer in place and to swell.
 - e. The approach to adapt the repository to the detailed conditions found underground and the quality of the excavation technique.
 - f. The quality of the deposition technique.

There is potential for additional optimisation when this reference design is developed and implemented.

- The scientific understanding of issues relevant for post-closure safety is mature as a result of decades of research both within the Swedish and other national programmes and in international collaboration projects. The R&D efforts to understand repository evolution and safety have led to the understanding of key processes like copper corrosion, shearing of canisters and other potential canister failure causes, and of key phenomena controlling retardation. This knowledge is, in the PSAR, systematically documented in several reports in a format suitable for use in the safety assessment.
- The present PSAR post-closure safety report and its supporting documents have undergone comprehensive peer reviewing. In particular the scientific basis of the safety assessment has undergone review by recognised experts in the relevant fields of science.
- A complete analysis of issues identified as relevant to post-closure safety has been carried out in the PSAR according to an established assessment methodology, comprising e.g. cautious approaches when addressing uncertainties.
 - The understanding of safety is built on a systematic identification of safety functions and criteria for the safety functions.
 - Repository evolution is analysed with a structured approach in several time frames, addressing in each of these the processes that have been identified as relevant and with the safety of the system, as expressed by the safety functions, as a focus. Data uncertainties and data quality are assessed and documented according to a pre-established template. Quality assurance of models and modelling is achieved by following procedures documented in a **Model summary report**. The assessment is then broken down into a set of scenarios to exhaustively scrutinise all possible ways in which the identified safety functions could be impaired and consequences of such situations. Additional arguments and analyses are provided according to Section S3.12.

- Confidence in the key results of radionuclide transport and risk calculations is enhanced by the fact that they can often be closely reproduced with simple, analytical models, using the same input data as the fully qualified numerical models.
- The key results of radionuclide transport and risk calculations are overestimates since a number of pessimistic assumptions were made in the analyses, both regarding the extent of canister failures and regarding their consequences.
- Documented quality assurance routines have been applied in the assessment of the initial state, in the development of the site description and in the analysis of post-closure safety. This is part of the overall methodology followed in the assessment.

S5 Overview of the main report

Following the introductory Chapter 1, this report outlines the methodology for the PSAR assessment in Chapter 2, and presents in Chapter 3 the handling of features, events and processes, of importance for post-closure safety. Chapter 4 presents the site and Chapter 5 the initial state of the constructed repository. Chapters 6 and 7 present the plans and methods for handling external influences and internal processes, respectively. Safety functions and safety function indicators are discussed in Chapter 8. The collection of input data for the assessment is described in Chapter 9. The material presented in the first nine chapters is utilised in the analysis of the reference evolution in Chapter 10, focussing on the containment potential of the repository. Scenarios for the further evaluation of safety are selected in Chapter 11. The selected scenarios are analysed in Chapter 12 with respect to containment potential and in Chapter 13 with respect to retardation potential, through radionuclide transport and dose assessments. Additional analyses supporting the safety assessment are presented in Chapter 14. Conclusions and feedback are provided in Chapter 15.

A list of references is given in after the main text. Appendix A is an account of how applicable regulations are addressed in the assessment. A glossary of abbreviations and specialised terms used in the PSAR is found in Appendix B and topography and place names in the Forsmark area are provided in Appendix C.

1 Introduction

1.1 Licensing of the KBS-3 system in Sweden

Radioactive waste from nuclear power plants in Sweden is managed by the Swedish Nuclear Fuel and Waste Management Co., SKB. Within SKB's programme for the management of spent nuclear fuel, an interim storage facility and a transportation system are today (December 2022) in operation. Several decades of research and development has led SKB to put forward the KBS-3 method for the final stage of spent nuclear fuel management. In this method, copper canisters with a cast iron insert containing spent nuclear fuel are surrounded by bentonite clay and deposited at approximately 500 m depth in groundwater saturated, granitic rock, see Figure 1-1. The purpose of the KBS-3 repository is to isolate the nuclear waste from man and the environment for very long times, see further Section 2.4. Around 12 000 tonnes of spent nuclear fuel is forecasted to arise from the currently approved Swedish nuclear power programme (where the last of the 6 operating reactors is planned to end operation in 2045), corresponding to roughly 6 000 canisters in a KBS-3 repository.

Two principal remaining tasks in the programme are to build and operate i) the final repository and ii) an encapsulation plant in which the spent fuel will be emplaced in canisters to be deposited in the final repository.

In March 2011, SKB applied for a permit to build a KBS-3 repository for spent nuclear fuel at the Forsmark site in the municipality of Östhammar and an encapsulation plant in the municipality of Oskarshamn. The application for the final repository was, among a wealth of additional material, based on findings from several years of surface based site investigations at the site. Post-closure safety for the repository was analysed in the so called SR-Site report (SKB 2011). After several years of reviewing of the application by the Swedish Radiation Safety Authority (SSM) under the Act on Nuclear Activities and a Swedish Land and Environmental Court under the Environmental Code (see Section 1.3 for a brief summary of the review process), the Swedish Government approved the application in January 2022.

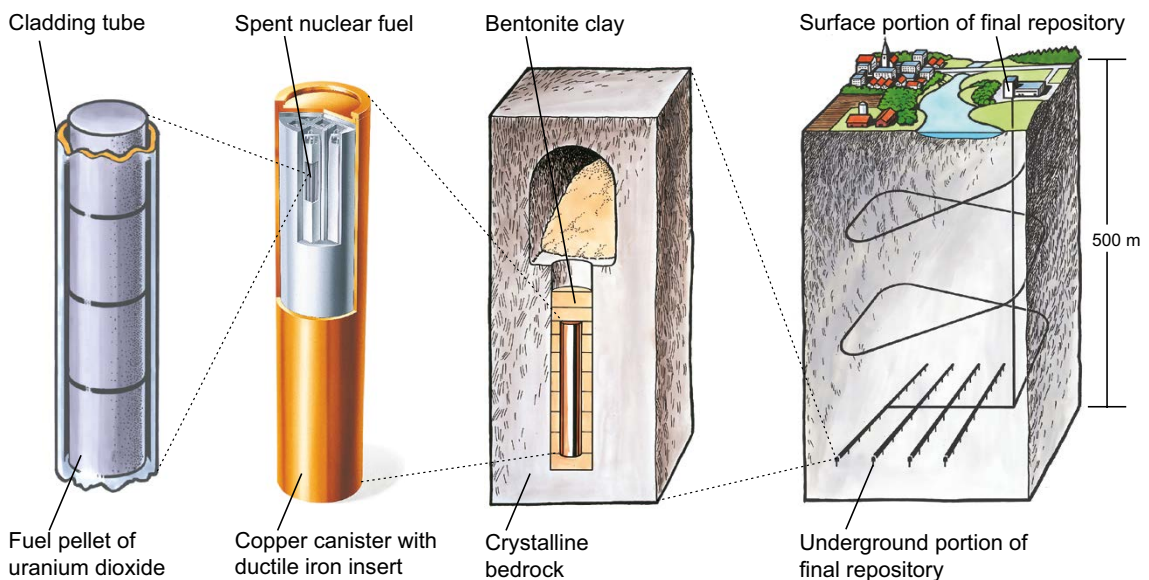


Figure 1-1. The KBS-3 concept for disposal of spent nuclear fuel.

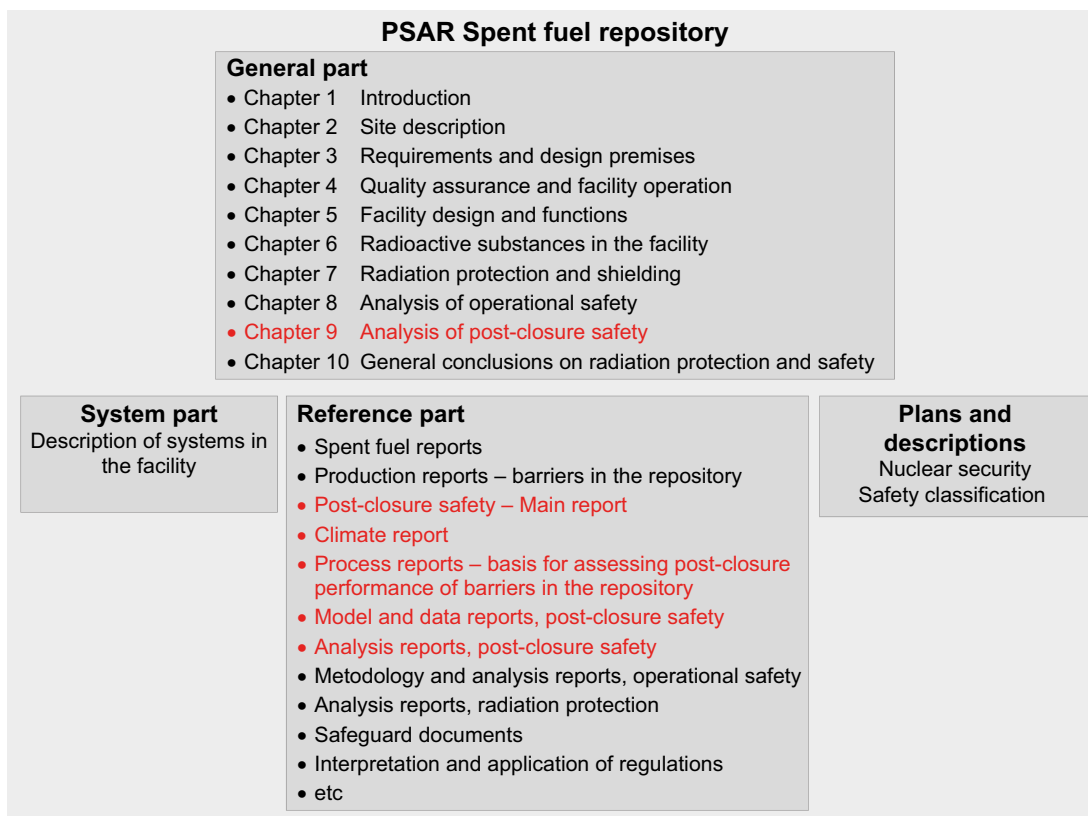


Figure 1-2. Structure of the Preliminary Safety Analysis Report, PSAR, showing all its components, the titles of the 10 chapters of the general part and some important references. Red text indicates documents related to post-closure safety.

In order to start the construction of the final repository, SKB is required, under the Act on Nuclear Activities, to obtain an approval of a Preliminary Safety Analysis Report (PSAR). The PSAR is submitted to and tried by SSM. The PSAR consists of 10 chapters, see Figure 1-2. Chapter 9 of the PSAR addresses post-closure safety and the present report is the main reference to Chapter 9.² The role of Chapter 9 of the PSAR and of the present report is to demonstrate that a final repository built according to the specifications in the PSAR can be expected to fulfil the requirements of post-closure safety expressed in SSM’s relevant regulations, when the safety assessment has been further updated to a Safety Analysis Report (SAR) in an operation license application, required in a forthcoming step of the licensing. The present report was produced as part of the overall PSAR project.

1.2 Purpose of the safety assessment project

The purpose of the safety assessment project in which the present report is produced is to investigate whether a safe repository can be built at Forsmark. If safety is demonstrated, then this report can serve its intended purpose in the PSAR.

² The present report is published some time before the submission of the PSAR. In case the need for any changes of the contents of this report arises between its publication and the submission of the PSAR, a report of these changes will be provided in the PSAR. Also, a few references to this report are currently (December 2022) in preparation and therefore appear as footnotes rather than in the list of references. Full references to these documents will be provided in the PSAR.

The main purposes of the PSAR post-closure safety assessment project are:

- To assess whether a spent fuel repository built at the Forsmark site according to the specifications in the PSAR can be expected to fulfil the requirements of post-closure safety expressed in SSM's relevant regulations.
- To provide feedback to design development, to SKB's RD&D Programme, to detailed site investigations and to future safety assessment projects.

While SKB has established a technically feasible reference design and layout of the KBS-3 repository and shown that this conforms to stated technical design requirements (see further Chapter 5), technical development will continue. Detailed designs adapted to an industrialised process designed to fulfilling specific requirements on quality, cost and efficiency need to be further developed. The layout needs to be adapted to the local conditions found when constructing the repository at depth. These, potentially more optimal solutions, must of course also fulfil all requirements on post-closure safety.

Safety assessments at various stages of the programme will draw on the information available at that particular stage. Information on all the system components is needed at every stage, since safety depends on all these elements. The focus of a particular assessment, however, will be determined not only by the information available but also by the purpose of the assessment, i.e. the decision or decisions that it is intended to support.

The present report is a key basis for the PSAR, of which an approval is required to start repository construction. The objective of the report is to investigate whether the KBS-3 method has the potential of fulfilling regulatory safety criteria at the Forsmark site, with the host rock conditions determined from the surface based site investigations. The assessment is based on a reference design of the engineered parts of the repository, including reference methods to achieve the specified design, taking into account methods of controlling that the specifications of the reference design have been achieved. Another important purpose is to give feedback for further developments to that specification, essentially by commenting on the adequacy of the design premises in the light of the outcome of the assessment. The further development of the design premises is beyond the scope of the present report.

1.3 Feedback from the review of post-closure safety in SKB's application for a permit for the final repository

1.3.1 Introduction

The Swedish Radiation Safety Authority (SSM) tried SKB's applications for the final repository and the encapsulation plant under the Act on Nuclear Activities and a Swedish Land and Environmental Court tried them under the Environmental Code. The purposes of these reviews were to provide statements to the Swedish Government on which it, having first consulted with the two concerned municipalities, could make decisions on permissibility according to the Environmental Code, and on permits according to the Act on Nuclear Activities. In addition, as part of the review under the Act on Nuclear Activities, the Swedish Government asked the OECD Nuclear Energy Agency (NEA) to conduct a review of the application for a spent nuclear fuel repository, with a focus on post-closure safety.

1.3.2 The OECD Nuclear Energy Agency, NEA

According to the Terms of Reference for the NEA review, the peer review should provide the Swedish Government with a statement, from an international perspective, on the sufficiency and credibility of SKB's post-closure radiological safety case for the licensing decision at hand. The review was conducted between May 2011 and June 2012. SKB provided answers to more than 300 written questions, and took part in a hearing by the NEA review team in December 2011. The main high level conclusion in the NEA review report (NEA 2012a) was "From an international perspective, SKB's post-closure radiological safety analysis report, SR-Site, is sufficient and credible for the licensing decision at hand. SKB's spent fuel disposal programme is a mature programme – at the same time innovative and implementing best practice – capable in principle to fulfil the industrial and safety-related requirements that will be relevant for the next licensing steps". A number of additional conclusions and

recommendations for future steps of SKB's program were also provided in the NEA report. The findings in the NEA review were taken into account in SSM's review work and are, therefore, not elaborated here.

1.3.3 The Swedish Radiation Safety Authority, SSM

SSM conducted a thorough review of SKB's licence applications from the spring of 2011. The authority engaged a range of internal and external experts for in-depth reviews of various scientific and technical issues concerning mostly post-closure safety. Based on the findings in these reviews, SSM requested, for several issues, additional material from SKB, and the material submitted by SKB in response to these requests was also reviewed and taken into account before SSM reached its conclusions concerning SKB's application. SSM also offered other stakeholders the opportunity to provide comments on the applications and considered these comments when forming its conclusions.

In its statement to the Government in January 2018, SSM recommended the Government to approve a license for the final repository. It also pointed to a number of issues that SKB needs to develop or resolve in coming phases of the step-wise licensing process under the Act on Nuclear Activities, among them some canister related issues that SKB needs to address in more detail in the Preliminary Safety Assessment Report (the PSAR, to which the current report is a key reference).

SSM also required SKB to submit, in conjunction with the PSAR, a set of plans for the development of repository programme in the coming stage, leading up to an operation license application. These include plans for the development of the engineered components of the repository, for detailed site investigation, for the continued research on issues of relevance for post-closure safety and for the development of the safety assessment. The results of the assessment of post-closure safety in the PSAR provides input to the formulation of such plans as further discussed in Sections 15.5–15.8.

As an Appendix to its review statement, SSM published a 900 page technical documentation of its review of the post-closure safety of the final repository (SSM 2018, available in Swedish only). SKB has considered the contents of SSM's review report in detail and SKB's handling of the issues raised in the report is documented in tabulated form.³ Part of the issues are addressed in the PSAR whereas for others, plans for their handling in the preparation of the forthcoming operation license application have been formulated, as part of the plans mentioned in the preceding paragraph. The handling of the contents of SSM's review report has been conducted in accordance with the QA plan for the overall PSAR project (see further Section 2.9). Key issues relating to post-closure safety where SSM expressed a need for a development in the PSAR include the following (Section 9.2.2 in SSM 2018).

- SSM identifies a need to include a scenario that evaluates the likelihood of early canister failures and points to a number of processes that may occur at early stages of the repository evolution and that should be included in such an evaluation. SSM stresses the need for such an evaluation at the Forsmark site where unsaturated conditions are expected to remain in the clay system for up to thousands of years in some parts of the repository due to the low frequency of water bearing fractures at repository depth at the Forsmark site. The greater hazard of the spent fuel at early times is a further reason to consider early failures in more detail. The handling of this issue in the PSAR is described in Section 11.3.
- The processes potentially related to early canister failures explicitly mentioned by SSM are local corrosion due to sulphide, stress corrosion cracking due to sulphide, creep deformation, and general corrosion for high chloride concentrations, but also other potentially detrimental processes need to be considered. SSM recognises that these processes have been addressed by SKB in the license application, but sees a need for a more in-depth treatment in the PSAR. The issues overlap with some of the canister related issues where the Land and Environmental Court identified a need for supplementary information, see below. The updated basis for addressing these processes is documented in the PSAR version of the **Fuel and canister process report**⁴ and integrated in the safety assessment in the present main report on post-closure safety.

³ "Hantering av SSM:s granskning kopplat till Kärnbränsleförvaret". (In Swedish.) (Internal document.) *In prep.*

⁴ The **Fuel and canister process report** is one of several principal references in this **Post-closure safety report**. See Section 2.5.12 for a complete list and nomenclature for referencing in terms of short-names in bold.

- Another scenario related issue raised by SSM concerns the need for safety functions related to copper creep and to hydrogen embrittlement of copper (see further Section 8.3.1).
- The analyses of consequences of early failures need to be developed further. Also, the analyses of consequences of postulated early canister failures have been expanded (see further Section 13.7.3).

1.3.4 The Land and Environmental Court

The Court's review, after being based on written exchanges with SKB and other stakeholders in a preparatory step, consisted of a thorough, public hearing in the autumn of 2017 where SKB presented its case and where other stakeholders could challenge it.

In its statement to the Government in January 2018, the Land and Environmental Court approved large parts of the application for the final repository; parts relating to the choice of Forsmark as the site for the repository, post-closure aspects related to the rock and the buffer and the environmental impact assessment. It also considered that supplementary information regarding five issues related to the long-term integrity of the copper canisters should be presented and evaluated before a permit is considered. The five issues overlap in part with those pointed out by SSM as prioritised for the PSAR. The Land and Environmental Court then had no role in the continued process leading to a decision by the Government, i.e. the Court had no part in assessing the supplementary material.

1.3.5 The Swedish Government

The supplementary information on canister integrity was requested by the Government and submitted by SKB to the Government in April 2019. The scientific and technical material on which the submission was based is documented in SKB (2019c), and much of that information has subsequently been included in the updated **Fuel and canister process report**, and in the present report. In the review of that information, SSM considered that it strengthened SKB's arguments for post-closure safety and repeated its recommendation that a license be granted by the Government.

In January 2022, the Government approved SKB's license applications for an encapsulation plant at Oskarshamn and a final repository for spent nuclear fuel at Forsmark.

1.4 Regulations

The form and content of a safety assessment, and above all the criteria for judging the safety of the repository, are defined in regulations issued by SSM. The regulations are based on various pertinent components of framework legislation, the most important being the Nuclear Activities Act and the Radiation Protection Act. Guidance on radiation protection matters is provided by a number of international bodies, and national legislation is often, as in the case of Sweden, influenced by international recommendations.

Regarding post-closure safety of nuclear waste repositories, there are two more detailed regulations of particular relevance, issued under the Nuclear Activities Act and the Radiation Protection Act, respectively:

- "The Swedish Radiation Safety Authority's Regulations concerning the Protection of Human Health and the Environment in connection with the Final Management of Spent Nuclear Fuel or Nuclear Waste" (SSMFS 2008:37).
- "The Swedish Radiation Safety Authority's regulations concerning safety in final disposal of nuclear waste" (SSMFS 2008:21).

These two documents are reproduced in their entirety in Appendix A to this report. The way in which this report addresses the requirements is indicated by references to relevant sections of this report, as inserts in the regulatory texts in the Appendix.

Potential risks to human health and the environment due to chemically toxic materials in the repository are addressed in the Environmental Impact Assessment accompanying SKB's application in 2011 on permissibility for the final repository according to the Environmental Code. This assessment has not been updated in the PSAR.

1.4.1 Regulations for final disposal of spent nuclear fuel, SSMFS 2008:37

The parts of SSMFS 2008:37 most relevant to an assessment of post-closure safety imply the following:

- Protection of human health shall be demonstrated by compliance with a risk criterion that states that “the annual risk of harmful effects after closure does not exceed 10^{-6} for a representative individual in the group exposed to the greatest risk”. “Harmful effects” refer to cancer and hereditary effects. The risk limit corresponds, according to SSM, to an effective dose limit of about 1.4×10^{-5} Sv/yr.⁵ This, in turn, corresponds to around one percent of the natural background radiation in Sweden.⁶
- Regarding environmental protection, biological effects of ionising radiation due to releases of radioactive materials from the repository in living environments and ecosystems of relevance shall be described, based on available knowledge.
- The consequences of intrusion into a repository shall be reported and the protective capability of the repository after intrusion shall be described.
- SSM requires a more detailed assessment for the first 1 000 years following repository closure than for later times.

SSM has also issued General Guidance concerning the application of SSMFS 2008:37. There, more detailed information regarding the above aspects is given. The General Guidance is also reproduced in Appendix A.

In the General Guidance, it is indicated that the time scale of a safety assessment for a final repository for spent nuclear fuel should be one million years after closure (see further Section 2.4). A detailed risk analysis is required for the first thousand years after closure. Also, for the period up to approximately one hundred thousand years, the reporting is required to be based on a quantitative risk analysis.

For the period beyond one hundred thousand years, the General Guidance to SSM 2008:37 states that a strict quantitative comparison of calculated risk in relation to the criterion for individual risk in the regulations is not meaningful. Rather, it should be demonstrated that releases from both engineered and geological barriers are limited and delayed as far as reasonably possible using calculated risk as one of several indicators. The demonstration of this is in the regulation seen as part of the demonstration of the use of best available technique, BAT.

1.4.2 Regulations concerning safety in final disposal of nuclear waste, SSMFS 2008:21

The parts of SSMFS 2008:21 most relevant to an assessment of post-closure safety imply the following requirements.

- A safety assessment shall take into account features, events and processes (FEPs) that can lead to the dispersion of radioactive substances after closure.
- A safety assessment shall cover as long a period as barrier functions are required, but at least ten thousand years.
- Reporting of
 - analysis methods for system description and evolution,
 - analysis methods for the selection of scenarios (including a main scenario that takes into account the most probable changes in the repository and its environment),
 - the applicability of models, parameter values and other conditions used in the analyses,
 - handling of uncertainties and sensitivity analyses.

⁵ ICRP’s updated and somewhat lower conversion factor between dose and risk has not yet been formally implemented in Swedish regulations, meaning that this older and somewhat lower dose limit is still applied in the PSAR.

⁶ The natural background radiation in Sweden is around 1 mSv/yr (SSI 2007).

- Regarding analysis of post-closure conditions, SSM requires descriptions of the evolution of the biosphere, geosphere and repository for selected scenarios; and evaluation of the environmental impact of the repository for selected scenarios, including the main scenario, with respect to defects in engineered barriers and other identified uncertainties.

SSM has also issued General Recommendations concerning the application of SSMFS 2008:21. There, more detailed information regarding e.g. classification of scenarios and uncertainties is given. Excerpts from the Recommendations, relevant to an assessment of post-closure safety, are also given in Appendix A, along with a statement of how this post-closure safety report addresses the requirements.

1.5 Relation to the SR-Site reporting

The reporting of post-closure safety in the PSAR is an update of the SR-Site reporting. The reporting hierarchy (see Section 2.5.12), is unchanged. It consists of this main report, 10 main references, 7 production reports and a number of additional references. The PSAR versions of this main report, 7 of the main references and all production reports are updates of the SR-Site versions where the following has been considered.

- Information supplementary to the SR-Site material requested by SSM in the review of SR-Site has been integrated into the updated reports.
- SSM's findings (SSM 2018) in the review of SR-Site have been considered in detail. These findings and comments concern development needs for both the PSAR and the forthcoming SAR reporting of post-closure safety, meaning that a portion of the findings are addressed in the PSAR. Plans for addressing remaining findings are submitted to SSM in parallel to the PSAR submission.
- Results presented in SKB's report (SKB 2019c) regarding supplementary information on canister integrity issues, requested by the Government in 2018, have been integrated into the report.
- New findings in SKB's continuing RD&D programme, and other relevant results emerging from the scientific community, have been included.
- New results from SKB's continued development of the engineered parts of the repository have been included.

The extent of the update varies between the individual main references to this report, depending on the amount of new material that has emerged since the SR-Site assessment. Three main references are not updated, and comments on minor amendments on the matter covered by those references are provided here in the main report. Others are thoroughly updated with a wealth of new findings in the subject area of concern. The extent of these updates are summarised in the introductory chapter of the report in question.

The extent to which each of the following Chapters in this main report has been updated is indicated in the introductory Section of each chapter, often pointing to particular sections where substantial updates have been made.

1.6 Related activities

The safety assessment is dependent on and provides feedback to site investigation and engineering activities at SKB, see Figure 1-3.

1.6.1 Site investigations and site modelling

A considerable part of the basis for the analysis of post-closure safety in the PSAR is provided from SKB's completed site investigation in the municipality of Östhammar.

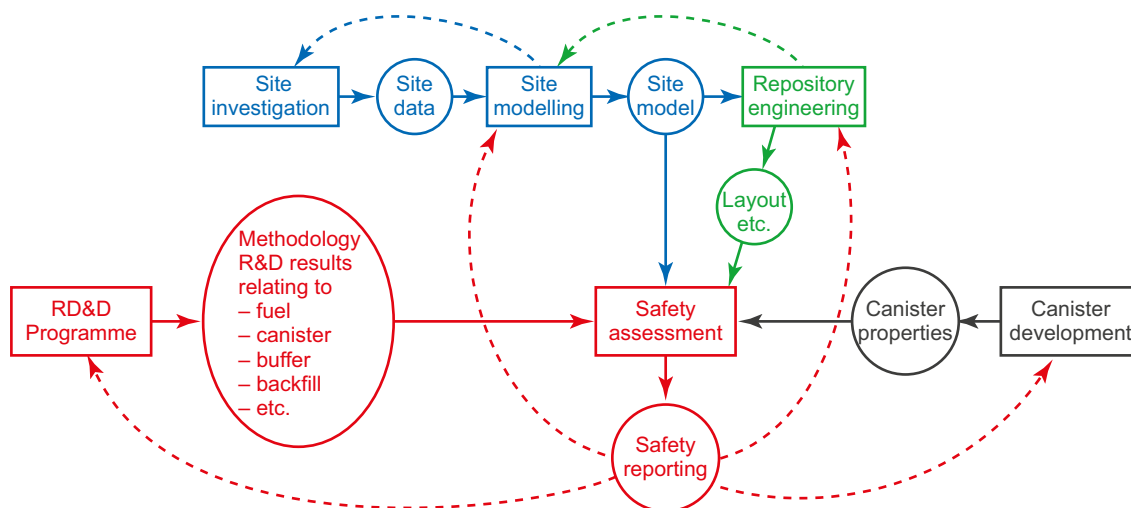


Figure 1-3. Relations to related activities. Activities are shown as rectangles and products as circles or ellipses. As indicated by the dashed lines, the safety report provides feedback to repository engineering concerning e.g. layout issues and choice of backfill materials and to site investigations, via the site model, concerning detailed site investigation needs. The latter type of feedback is also given by the site modelling group independent of the safety assessment. Feedback is also given from the safety assessment to SKB's RD&D Programme.

Field data from the site investigation were analysed, within the site investigation project, by a site analysis team that produced a sequence of site descriptive models of the geosphere and the biosphere. The team consisted of several groups specialising in different disciplines. The site descriptive model is a synthesis of observations of the current state of the site and of the understanding of past and ongoing e.g. hydraulic and geochemical, processes driven by phenomena such as land uplift and climate change. Model simulations of the historical evolution of the site are an important part of the synthesis work carried out by the site analysis group. The resulting geosphere 3D model of current conditions provides thermal, hydraulic, mechanical, chemical and transport properties of the rock, within a geometrical and geological framework describing major structures at the site. The biosphere part of the model includes a description of the ecosystems at the site and is developed to be coherent with the geosphere model. The site descriptive model is accompanied by a comprehensive description of the inter-disciplinary analysis and interpretation work underpinning it.

The site descriptive model of the Forsmark site provides descriptions of the present geosphere and biosphere conditions for the safety assessment. The model is the same as the one used for the SR-Site assessment. A more detailed account is given in Chapter 4. There, also an account of the very limited additional data obtained for the host rock since the SR-Site assessment is given and it is demonstrated that these data do not alter the properties of the site descriptive model in any way that is significant for post-closure safety.

The model describes the situation prior to rock excavation for the final repository. Analyses of how the excavation activities will affect the undisturbed, natural state of the rock are also needed. Parts of this work were undertaken by a repository engineering group, using the site description and in cooperation with the site model experts, in conjunction with their determination of a suitable repository layout in the site model. The results of these analyses are part of the input to the PSAR and are described in relevant parts of this report, in particular in Section 5.2. Additional analyses of the mechanical, hydrogeological and chemical evolution due to the excavation and operational period are made as part of the post-closure safety assessment in the PSAR and are presented in Section 10.2.

Apart from providing descriptions of the geosphere and the biosphere, the site descriptive model gives an understanding of past and ongoing processes at the site. This information is useful for the description and modelling of the future development of the site and repository, the results of which have to be compatible with the understanding of the site history.

The safety assessment uses the hydrogeological simulation models set up by the site analysis group. Whereas these are essentially used to simulate the site history by the site analysis group, the future evolution is in focus in the safety assessment.

Data for the PSAR provided by the site model are, in the present analysis of post-closure safety, assessed according to established procedures for the handling of all input data and data uncertainties (see further Chapter 9). The assessment of confidence in the site descriptive model made by the site modelling group as part of the documentation of the model provides important input to the data assessment in the PSAR.

The results of the safety assessment provide input to the planning of detailed site investigations in connection with repository excavation and to further design developments.

1.6.2 Repository engineering

A reference repository concept that is practically achievable while providing the required safety functions was developed for SR-Site and has been updated for the PSAR. The reference concept includes basic dimensions of the facilities as well as reference technical solutions for buffer and backfill. Using the reference concept and based on the site description, site-adapted layouts of the final repository are developed. During the work, feedback has been given to the continued site modelling and site investigation work. For the needs of the PSAR, the reference concepts, the site adapted repository layout and the methods for achieving these are documented in a number of so called **Production reports**, as further described in Chapter 5. These reports are updates of the versions that provided input to SR-Site.

1.6.3 Canister development

Techniques for canister production and sealing have been further developed and documented since the SR-Site assessment resulting in updated input to the PSAR in terms of canister properties. For the needs of the PSAR, the reference canister and the production methods for achieving it are documented in the **Canister production report**, see further Section 5.4.

2 Methodology

2.1 Introduction

This chapter outlines the methodology that has been used for the analysis of post-closure safety in the PSAR. The methodology follows closely that used in the SR-Site assessment. All central methodological elements are explained in Section 2.5 in sufficient detail to provide a self-contained overview of the assessment methodology.

In broad terms, the methodology development for the SR-Site assessment and the preceding SR-Can assessment (SKB 2006a) was influenced and inspired by several safety assessment studies in e.g. Switzerland (Nagra 2002), Finland (Vieno and Nordman 1999), Belgium (ONDRAF/NIRAS 2001), Japan (JNC 2000), the U.S. (BSC 2003), Canada (Gierszewski et al. 2004) and France (Andra 2005) and by international cooperation in the area organised by the OECD Nuclear Energy Agency (NEA 1997a, 1999a, 2001, 2004a, b, 2009).

SKB has actively followed the international developments within the field of post-closure safety assessments after the submission of the SR-Site assessment, both as outcomes of international cooperation projects, e.g. NEA (2012b), and in the form of published safety cases, e.g. Posiva's assessment in support of the organisation's operation license application (Posiva 2021). Such developments were also discussed at NEA symposia organised in 2013 (NEA 2013) and in 2018 (NEA 2022) in which SKB contributed. SSM, in its review of the SR-Site report, raised no major concerns as regards the overall methodology, but pointed to room for improvement concerning details in the implementation. Therefore, the description of the methodology in general terms in the present Chapter is largely identical to that in the corresponding Chapter in the SR-Site Main report, whereas some details in the implementation in subsequent Chapters differ from that in the SR-Site assessment, as explained in those Chapters. Factual updates have been made in Sections 2.5.6 and 2.8.5. Some text in Section 2.7 has been deleted since it is not relevant for the present step in the development of the final repository. The Quality assurance Section 2.9 has been updated to reflect the fact that much of the material in the present assessment is identical to that in the SR-Site assessment.

The main purpose of a safety assessment of a final repository is to investigate whether the repository can be considered radiologically safe over time. In principle, this is established by comparing estimated releases of repository derived radionuclides and associated radiation doses with regulatory criteria (see Section 1.4 and Appendix A). For a KBS-3 repository, the primary safety function is to completely contain the waste for hundreds of thousands of years, see further Section 2.4. An important purpose of this safety assessment is, therefore, also to analyse the repository's potential for containing the wastes under a wide range of circumstances and for a very long time.

Appropriate scientific and technical support for all statements made and data selected is essential to give confidence in the calculated results. Demonstrating understanding of the disposal system and its evolution is thus a crucial component in any safety assessment.

The repository system, broadly defined as the deposited spent nuclear fuel, the engineered barriers surrounding it, the host rock and the biosphere in the proximity of the repository, will evolve over time. Future states of the system will depend on:

- its initial state,
- internal processes, i.e. a number of radiation related, thermal, hydraulic, mechanical, chemical and biological processes acting internally in the repository system over time, and
- external factors acting on the system.

Internal processes are e.g. the decay of radioactive material, leading to the release of heat and the subsequent warming of the fuel, the engineered barriers and the host rock. Groundwater movements and chemical processes affecting the engineered barriers and the composition of groundwater are other examples. External factors include effects of future climate and climate-related processes, such as glaciations and land uplift. Another example is the build-up of mechanical energy due to plate tectonic movements. Also, future human actions may influence the repository.

The initial state, the internal processes and the external influences and the way they together determine repository evolution, can never be fully described or understood. There are thus uncertainties of various types associated with all aspects of the repository evolution and hence with the evaluation of safety. A central theme in any safety assessment methodology must therefore be the management of all relevant types of uncertainty. This management amounts to identifying, classifying and describing uncertainties, as well as handling them in a consistent manner in the quantification of the repository evolution and of the radiological consequences to which it leads. It also implies comparing the results of the assessment with regulatory criteria in such a way that appropriate allowance is made for the uncertainties associated with the assessment.

The primary safety function of the KBS-3 system described in Figure 1-1 is to completely contain the spent nuclear fuel within the copper/iron canisters over the entire assessment period. Should a canister be damaged, the secondary safety function is to ensure that any releases from the canister are retarded sufficiently to ensure that the resultant radionuclide concentrations are reduced to levels that do not cause unacceptable consequences. The two issues of containment and retardation are, therefore, principal considerations throughout the assessment.

In the next Section 2.2, safety principles for the KBS-3 repository are discussed in more detail. Thereafter the boundary of the repository system is established in Section 2.3 and the relevant time scales for the assessment are given in Section 2.4.

With these fundamentals established, an account of the methodology applied in the SR-Site and the PSAR assessments is given in Section 2.5. Some details of the methodology are best explained as they are applied, meaning that the reader is sometimes referred to subsequent chapters for details.

Methodological aspects of the risk calculation are addressed in Section 2.6.

The safety assessment has an important role in the demonstration of use of best available technique, BAT. This role and how it is fulfilled is discussed in Section 2.7.

The handling of uncertainties permeates the safety assessment and is thus an integral part of the methodology described in Section 2.5. Section 2.8 gives a more thorough account of the identification, classification and handling of uncertainties in the PSAR assessment. This is important since a rigorous handling of uncertainties is closely related to the confidence in the results of the assessment.

Also, quality assurance measures concern all aspects of the assessment. The quality assurance plan for PSAR is presented in Section 2.9.

2.2 Safety

2.2.1 Safety principles for the KBS-3 repository

Since work on the Swedish final repository project commenced at the end of the 1970s, SKB has established a number of principles for the design of a final repository. The principles can be said to constitute the safety philosophy behind the KBS-3 concept. They are summarised below.

- By placing the repository at depth in a long-term stable geological environment, the waste is isolated from the human and near-surface environment. This means that the repository is not strongly affected by either societal changes nor the direct effects of climate change at the ground surface.
- By locating the repository at a site where the host rock can be assumed to be of no economic interest to future generations, the risk of human intrusion is reduced.
- The spent fuel is surrounded by several engineered and natural safety barriers.
- The primary safety function of the barriers is to contain the fuel within a canister.
- Should containment be breached, the secondary safety function of the barriers is to retard a potential release from the repository.
- Engineered barriers shall be made of naturally occurring materials that are stable in the long term in the repository environment.

- The repository shall be designed and constructed so that temperatures that could have significant detrimental effects on the long-term properties of the barriers are avoided.
- The repository shall be designed and constructed so that radiation induced processes that could have significant detrimental effects on the long term behaviour of the engineered barriers or of the rock are avoided.
- The barriers should be passive, i.e. they should function without human intervention and without artificial supply of matter or energy.

Together with many other considerations, like the geological setting in Sweden and the requirement that the repository must be feasible to construct from a technical point of view, these principles have led to the development of the KBS-3 system for spent nuclear fuel management.

2.2.2 Safety functions and measures of safety

The key safety related features of the KBS-3 disposal system can be summarised in the safety functions containment and retardation.

The fuel is placed in corrosion-resistant copper canisters with a cast iron insert providing mechanical strength. The copper canisters are surrounded by bentonite clay in deposition holes at a depth of approximately 500 m in the host rock (see Figure 1-1). The bentonite clay protects the canisters from minor rock movements and limits the inflow of the low concentrations of corrosive agents in the groundwater. The host rock provides a long-term chemically, mechanically, thermally and hydro-geologically stable environment for the canisters and the bentonite clay. The canisters, therefore, constitute a containing barrier with a very long life-time in the environment provided by the buffer and the host rock.

The fuel, the canister, the buffer and the host rock contribute to retarding any potential release of radionuclides should a canister be damaged. The fuel matrix is in itself very stable in the reducing environment at repository depth. Many of the most hazardous radionuclides have a very low solubility in groundwater and thereby have a limited potential for outward transport. Both the cast iron insert and the copper canister limit the inflow of water even if damaged. The buffer limits the inflow of water to a damaged canister. It also limits the release of radionuclides by limiting water flow and through sorption. The groundwater moves slowly in the fracture system of the rock nearest to the canisters and many radionuclides have a strong propensity for diffusion into, and sorption in, the host rock matrix.

The fundamental criterion regarding safety is expressed in SSM's regulation SSMFS 2008:37 where it is stated that the aim is to ensure that "the annual risk of harmful effects after closure does not exceed 10^{-6} for a representative individual in the group exposed to the greatest risk". The risk criterion corresponds to effective doses that are roughly one percent of those due to naturally occurring background radiation. As mentioned in Section 1.4.1, effects on living environments and ecosystems shall also be described.

Results of risk calculations in the safety assessment are compared with this criterion in order to assess compliance. However, the risk results depend in a complex fashion on a large number of factors. In a safety assessment, it is necessary to not only assess compliance with an overall criterion, but also to demonstrate how safety is related to key properties of the barriers and how these properties vary over time. An obvious property is the integrity of the copper canisters. This in turn depends on a number of factors like the buffer properties and the chemical environment of the repository.

In Chapter 8, a number of safety function indicators for the barriers are presented and discussed. Criteria are provided for properties like buffer temperature and buffer and backfill density, hydraulic conductivity and swelling pressure. Demonstrating compliance with these criteria provides arguments that the barriers will function as intended as the repository system evolves. Conversely, should a safety function indicator criterion be breached, this signals that safety in one way or the other is potentially jeopardised and that the consequences need to be further considered. However, it does not automatically imply that overall system performance is unacceptable.

Section 2.6.3 provides a discussion of alternative “top level” indicators to the risk criterion. The alternative criteria are more directly related to releases from the geosphere and do not require detailed assumptions about biosphere conditions or human habits.

2.3 System boundary

The repository system encompasses the spent nuclear fuel, the canisters, the buffer, the backfilled deposition tunnel and other repository cavities, the geosphere and the biosphere in the proximity of the repository, see Figure 1-1. In the development of the SR-Can database of features, events and processes, FEPs, (SKB 2006b), the system boundary was defined in more detail. The following key aspects are taken from that definition.

- In general, a strict boundary definition is neither possible nor necessary, and the same boundaries will not necessarily be relevant to all parts of the safety assessment. The following definitions were the basis for the FEP sorting – and thus have affected the system description.
- Roughly, the portion of the biosphere studied in the site investigations, i.e. an area of the order of 100–300 km² above the repository, is regarded as part of the system, whereas the biosphere on a larger scale is regarded as external. The analysis of the biosphere extends downward to the rock surface in this assessment. Depending on the analysis context this definition may be somewhat modified.
- Roughly the corresponding portion of the geosphere down to a depth of about 1 000 m is regarded as part of the system. Depending on the analysis context, this definition may also be modified. For example, the local groundwater model, which is the scale most relevant to safety, has a smaller projected surface area than 100 km², whereas e.g. larger areas than 300 km² and greater depths than 1 000 m may be required for regional groundwater modelling. Boundary conditions for the local groundwater model are provided from such a larger regional model. Likewise, the modelling of bedrock temperature for the analyses of permafrost development is conducted down to a depth of 10 km.
- Future human behaviour on a local scale is internal to the system, but not issues related to the characteristics and behaviour of future society at large.

2.4 Time scales

A time scale for the safety assessment needs to be established since this provides a general limit on the scope of the assessment and also cut-off times for e.g. radionuclide transport calculations. The issue is addressed in applicable regulations as cited below.

2.4.1 Regulatory requirements and guidance

The SSM regulations SSMFS 2008:21 state that the safety assessment should cover the period during which the barrier functions are needed, though to at least 10 000 years after closure. The recommendations accompanying the regulation suggest that the time scale of an assessment should be related to the hazard posed by the inventory in comparison with naturally occurring radionuclides. In the recommendations it is also noted that “...it should also be possible to take into consideration the difficulties of conducting meaningful analyses for extremely long time-periods, beyond one million years”.

SSM’s regulation 2008:37 state that “For the first thousand years following repository closure, the assessment of the repository’s protective capability shall be based on quantitative analyses of the impact on human health and the environment.” “For the period after the first thousand years following repository closure, the assessment of the repository’s protective capability shall be based on various possible sequences for the development of the repository’s properties, its environment and the biosphere.”

The General Guidance to SSMFS 2008:37 states the following regarding a repository for spent nuclear fuel: “...the risk analysis should at least include approximately one hundred thousand years or the

period for a glaciation cycle to illustrate reasonably predictable external strains on the repository. The risk analysis should thereafter be extended in time as long as it provides important information about the possibility of improving the protective capability of the repository, although at the longest for a time period of up to one million years”.

Regarding the quantitative risk analysis for the first 100 000 years the General Guidance state the following: “Supplementary indicators of the repository’s protective capability, such as barrier functions, radionuclide fluxes and concentrations in the environment, should be used to strengthen the confidence in the calculated risks.”

For the time beyond approximately one hundred thousand years, the guidance furthermore states: “A strict quantitative comparison of calculated risk in relation to the criterion for individual risk in the regulations is not meaningful. The assessment of the protective capability of the repository should instead be based on reasoning on the calculated risk together with several supplementary indicators of the protective capability of the repository such as barrier functions, radionuclide fluxes and concentrations in the environment.”

2.4.2 Time scale covered by the safety assessment

Apart from the obvious necessity of fulfilling regulatory requirements, arguments relating to the radiotoxicity of the spent nuclear fuel can also be considered when a time scale for a safety assessment is determined.

After approximately 100 000 years, the radiotoxicity of the spent nuclear fuel is comparable with that of the natural uranium ore once used to produce the fuel (Hedin 1997). Also the sum of toxicity of all fractions originating from the nuclear fuel cycle (the daughter nuclides separated from the uranium prior to enrichment, the depleted uranium arising in the enrichment process and the spent fuel) is comparable to that of the utilised uranium ore after 100 000 years, see Figure 2-1. The latter comparison is equivalent to comparing the radiotoxicity of the amount of natural U-235 and U-238 consumed in the reactor, to the radiotoxicity of the amounts of the new products created in the reactor (fission products and actinides) remaining after 100 000 years.

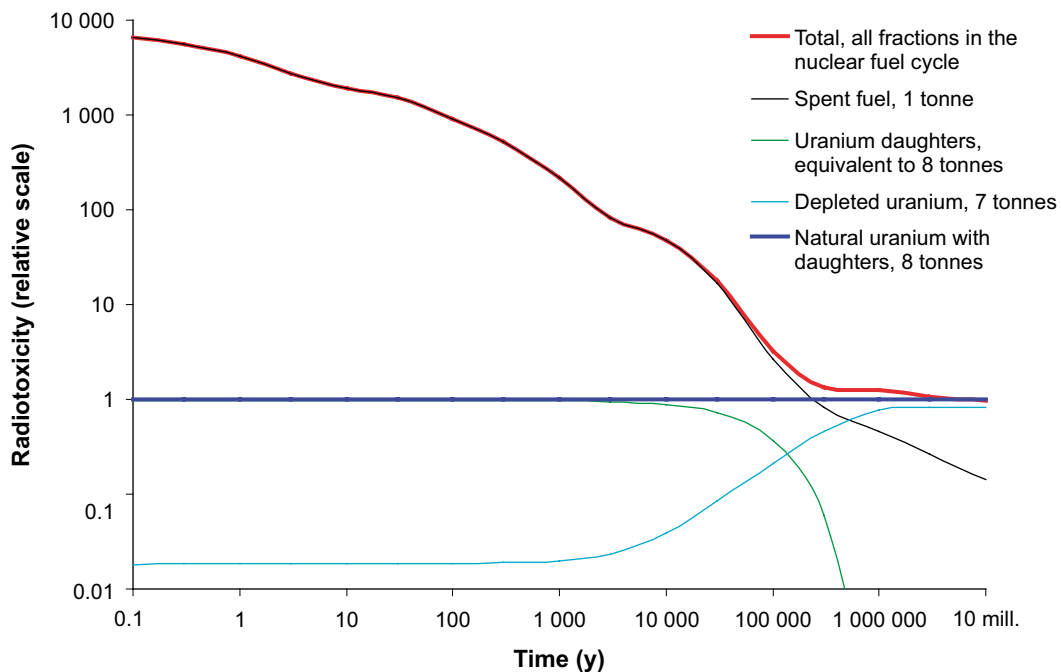


Figure 2-1. Radiotoxicity on ingestion of uranium and daughters in ore (blue line), and of the sum of all fractions that arise when the same quantity of uranium is used in the nuclear fuel cycle (red line). The time refers to the time after reactor operation. The different fractions comprise the spent fuel (38 MWd thermal energy/kg U of type SVEA 64 BWR), the depleted uranium and the uranium daughters that are separated in the uranium mill. From Hedin (1997).

Another criterion that may be considered to justify a time scale for a safety assessment is that the period analysed should go beyond the point in time at which peak doses from the repository occur. However, on long time scales, the peak dose often occurs at the end of the typically one million year assessment period due to in-growth of the naturally occurring nuclide Ra-226 from disposed U-238 combined with the fact that the barrier system inevitably deteriorates over time. This was the case in the SR-Site assessment. Since the KBS-3 concept is aiming at complete containment of the waste for time periods very far into the future through encapsulation, the peak dose criterion is not considered an appropriate criterion for defining the assessment time scale.

In the PSAR, as in the SR-Site assessment, the time scale for the assessment is one million years. This time scale is in accordance with the suggestions in the recommendations and general guidance cited above. It is furthermore longer than that needed to reduce the radiotoxicity of the inventory to a level comparable with that of the corresponding amount of natural uranium ore. It is also noted that the key radionuclides remaining in the waste beyond one million years are also those, such as U-238, associated with natural uranium ore.

As expressed in the guidance to SSMFS 2008:37, the quantitative risk criterion is applicable as a quantitative regulatory limit during approximately the first one hundred thousand years, and thereafter as a basis for discussing the protective capability of the repository. The risk calculations in the PSAR therefore extend to one million years, and the results are used in accordance with SSM's General Guidance in the compliance discussion in Chapter 15. The risk calculations are complemented with calculations of supplementary indicators of repository safety (see further Section 2.6.3).

However, a brief general discussion of the evolution beyond one million years is also given, to demonstrate the effects of a continued development of important processes in the repository and also since a strict cut-off time for the analysis of the general evolution of the system cannot be derived from the regulations.

Regarding the regulatory requirement of a more detailed analysis during the initial 1 000 years after closure, motivated both by the high radiotoxicity of the spent fuel during this period and the better ability to predict this relatively near future, this is partly fulfilled as the initial, transient stages of the repository evolution are analysed, mainly in the reference evolution described in Chapter 10. To fully fulfil the regulatory requirement of a more detailed analysis for the initial 1 000 years, the functioning of the barrier system during this period is revisited later in the report, covering also hypothetical early barrier failure (see Section 13.9.6).

For times beyond one million years, a qualitative account of the repository evolution, based on the quantitative analyses up to one million years, is provided. No risk calculation is presented for these time scales.

2.4.3 Time scales relevant for repository evolution

There are a number of time scales relevant to repository evolution as summarised below.

- A fundamental time scale is that relevant for the decrease of the radiotoxicity of the waste as shown in Figure 2-1. At the time of deposition, the radiotoxicity has decreased by roughly a factor of ten compared with the situation one month after reactor operation, and then continues to decrease by about a factor of ten for every ten-fold increase in time. As mentioned above, after 100 000 years the radiotoxicity of a certain amount of spent nuclear fuel is comparable with the radiotoxicity of the amount of natural uranium ore once used to produce the fuel.
- It is also noted that the initially very high dose rates from potential exposure to direct, external radiation from the spent fuel decrease substantially within a few thousand years. In the long term, these dose rates will however remain at levels requiring shielding from humans practically indefinitely, since the long-term direct radiation level is determined by U-238 progeny. For post-closure safety, direct radiation to humans is only a concern in scenarios addressing unintentional intrusion into the repository. (Processes relating to radiation effects in an undisturbed repository are included in the analysis of repository evolution.)
- The time scale of long-term geological processes, occurring over millions of years, including tectonic movements of continental plates and associated ridge push caused by these movements.

- Climate change occurs on time scales of a few tens of years up to more than one million years. One main time scale relates to the length of glacial cycles, which for the past approximately 700 000 years evolved in ~100 000 year cycles. In the region where Forsmark is now located each cycle includes several episodes of permafrost and glacial conditions. The mechanical, hydraulic and groundwater chemical conditions in the host rock vary in consequence of the climate evolution, in particular as a result of ice sheet overriding. It is likely that such cycles are re-introduced after the perturbation.
- There are a number of time scales on which biological evolution occurs; e.g. man has evolved considerably during the past several hundred thousand years.
- The natural development of ecosystems in general could lead to considerable changes in a 1 000 year perspective. This is e.g. the case for coastal ecosystems in Sweden, which are strongly affected by land-uplift.
- Most aspects of society have changed substantially over the past 100 years and significant changes may occur abruptly or over only a few years. Historical records of humanity cover a few thousand years.
- The residual power of the fuel results in peak temperatures in the near field of the repository after of the order of ten years, and elevated temperatures in the host rock for a few thousand years.
- The resaturation of the buffer, the backfill and the host rock typically requires tens to hundreds of years for Swedish conditions.
- The chemical conditions in the host rock after excavation and operation of a final repository are expected to have largely returned to natural conditions in a 100 or 1 000 year perspective. The chemical conditions in the buffer will change to some degree during the initial period of elevated temperatures. Canister corrosion under typical repository conditions requires millions of years to cause canister failures.

Time scales is a recurring issue in this report, e.g. in the context of process descriptions, Section 7.3, and when analysing repository evolution, Chapter 10. The issue of time scales in safety assessments has also been addressed in an NEA Workshop (NEA 2004a) in which SKB participated. Approaches used in the PSAR regarding e.g. the focussing on complementary indicators to dose and risk for long time scales and the use of scenarios to cover a range of possible evolutions of future external conditions are in agreement with the findings of the NEA workshop.

2.5 Methodology in eleven steps

The evaluation of post-closure safety in the PSAR, as in the SR-Site assessment consists of eleven main steps. Figure 2-2 is a graphical illustration of the steps. The methodology followed in the eleven steps is described in the following subsections. Inevitably, some details of the methodology are best explained as they are applied and the reader is therefore sometimes referred to subsequent chapters for these details.

2.5.1 Step 1: FEP processing

This step consists of identifying all the factors that need to be included in the analysis. Experience from earlier safety assessments and KBS-3 specific and international databases of relevant features, events and processes (FEPs) influencing post-closure safety are utilised. An SKB FEP database is developed where the great majority of FEPs are classified as being either i) initial state FEPs, ii) internal processes or iii) external FEPs. Remaining FEPs are either related to assessment methodology in general or determined to be irrelevant for the KBS-3 concept.

In the SR-Site assessment, based on the results of the FEP processing, an SR-Site FEP catalogue, containing FEPs to be handled in SR-Site, was established. The same catalogue was utilised in the PSAR, as motivated in Chapter 3.

The further handling of the three FEP categories is described in the three subsequent steps of the methodology.

This step of FEP processing is further described in Chapter 3 and fully documented in the SR-Site **FEP report**, that serves as the main source of FEP reporting also in the PSAR.

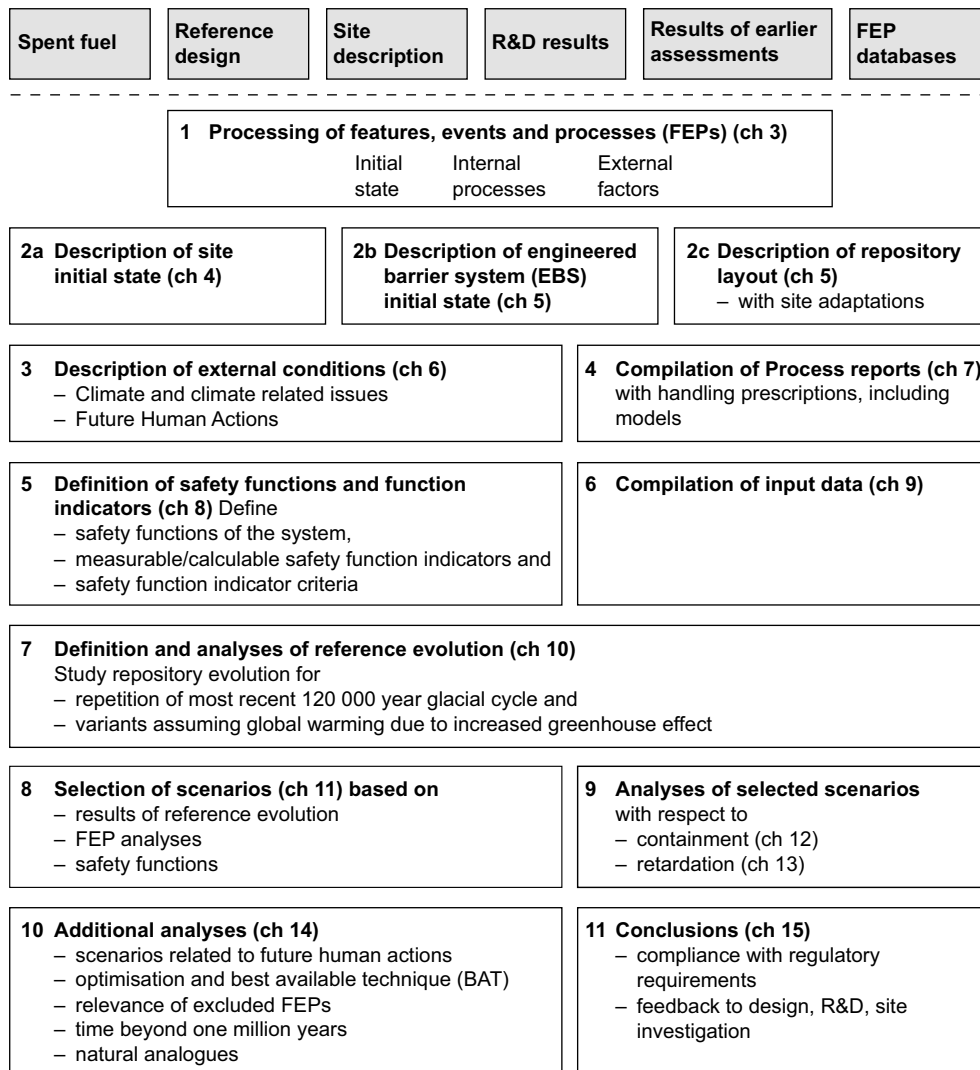


Figure 2-2. An outline of the eleven main steps of the PSAR assessment of post-closure safety. The boxes at the top above the dashed line are inputs to the assessment. The products of each step are described in detail in the main text. Together, the eleven steps represent the box “Safety assessment” in Figure 1-3.

2.5.2 Step 2: Description of the initial state

The initial state of the system is described, based on the descriptive model of the repository site, the KBS-3 repository design with its different components and a site-specific layout applying this design to the site. The initial state of the geosphere and the biosphere is that of the natural system prior to excavation. The initial state of the fuel and the engineered components is that immediately after deposition. The choice of time for the initial state is further elaborated in Section 5.1.

The initial state of the system is a fundamental input to the assessment and needs thorough substantiation. For the site, this is provided by the site descriptive model of the Forsmark site (SKB 2008a), i.e. the results of the surface based site investigation and the modelling of the site based on the site investigation data. The Forsmark site model is a fundamental reference to the PSAR and a summary of the site description, with a focus on aspects relevant for post-closure safety is given in Chapter 4.

The spent fuel types and amounts to be deposited are described in the **Spent fuel report**. From that report and a report on the handling of the fuel prior to deposition, fuel properties relevant for post-closure safety and valid at the time of deposition in the repository are derived in Chapter 5. The engineered components of the repository system are described in a number of so called **Production reports** covering the canister, the buffer, the tunnel backfill, the deposition tunnel plug, the repository closure and the underground openings constructions, respectively. The last report contains a description

of the repository layout after site adaptation. Each production report gives an account of i) technical design requirements derived from the SR-Site assessment and additional sources, ii) the reference design selected to achieve the requirements, iii) verifying analyses that the reference design does fulfil the technical design requirements, iv) the production and control procedures selected to achieve the reference design, and v) verifying analyses that these procedures, if implemented, would achieve the reference design. The initial state of the engineered components is then derived as reported in Chapter 5, based on the contents of the **Production reports** relevant to post-closure safety.

The FEP processing in step 2 resulted in a number of FEPs related to the initial state. Most of these are covered through the descriptions of the initial state and the subsequent use of this information in the assessment. A few initial state FEPs, relating for example to an incomplete closure of the repository require separate treatment in the scenario analysis in later stages of the assessment. Such FEPs are accounted for in Section 5.1.3.

2.5.3 Step 3: Description of external conditions

Factors related to external conditions are handled in the three categories “climate related issues”, “large-scale geological processes and effects” and “future human actions”, FHA. The handling of these factors is described in the **Climate report**, the **Geosphere process report**, and the **FHA report**, respectively.

A key point in the handling of external conditions is the establishment of reference external conditions for the subsequent analysis. These reference external conditions postulate a repetition of the last 120 000 year glacial cycle, the Weichselian, as a base case. In addition to the base case, a *global warming climate case*, which takes into account anthropogenic greenhouse-gas emissions, is analysed. In addition, physically possible climate conditions that would have the most severe impact on repository safety are sought for use in the scenario analyses in a later step of the assessment. The handling of climate related issues is described in more detail in Section 6.2.

Future human actions are handled according to a methodology established in the SR-Site assessment, with most of the account being identical to that in SR-Site. Based on a structured account of a large number of FEPs relating to FHA, a selection of stylised cases for further analyses is made. This is described in the analysis of FHA scenarios, Section 14.2.

2.5.4 Step 4: Description of processes

The identification and handling of processes of importance for the long-term evolution and safety of the repository is a key element in the safety assessment. The identification of processes is based on earlier assessments and FEP screening. All identified processes within the system boundary relevant to the long-term evolution of the system are described in three dedicated **Process reports**, one for the fuel and canister, one for the buffer, backfill and repository closure and one for the geosphere. Short-term geosphere processes/alterations due to repository excavation are included in the **Geosphere process report** and are taken into account in the assessment.

Each process is documented in the Process reports, following a template with the following headings:

- Overview/general description.
- Dependencies between process and system variables.
- Boundary conditions.
- Model studies/experimental studies.
- Natural analogues/observations in nature.
- Time perspective in which the process is relevant.
- Handling in the PSAR.
- Handling of uncertainties in the PSAR.

The description of boundary conditions (third heading) points to interactions with processes in other process reports when relevant. The material under the last two headings, where it is established how the process will be handled in the safety assessment, constitutes the key output from the **Process reports**. The **Process reports** thus provide a “recipe” for the handling of the various processes in the assessment.

The handling of all processes in a process report is summarised in a process table describing if the process is neglected, if it is quantitatively modelled or if the choice between neglect and modelling is subject to a specified condition that may or may not be fulfilled as the repository system evolves.

Several of the processes are thus handled through quantitative modelling, where each model in general includes several interacting processes, often occurring in different system parts and hence described in different process reports. The models form a network, where results from one model are used as input to another. The network is described graphically by two Assessment Model Flowcharts, AMFs, and two associated AMF tables linking the processes in the process tables, the models in the AMFs and the reporting of the modelling in this main report.

The handling of processes is described in more detail in Chapter 7, where the process tables (Section 7.4.4), the AMFs and the AMF tables (Section 7.5) are also provided.

2.5.5 Step 5: Definition of safety functions, safety function indicators and safety function indicator criteria

A central element in the methodology of the PSAR is the definition of a set of *safety functions* that the repository system should ideally fulfil over time. Here, the overall safety functions containment and retardation are differentiated into a number of lower level functions for the canister, the buffer, the deposition tunnel backfill and the host rock. The evaluation of the safety functions over time is made possible by associating every safety function with a *safety function indicator*, i.e. a measurable or calculable property of the repository component in question. For several functions, it is also possible to associate a *safety function indicator criterion* such that if the safety function indicator fulfils the criterion, then the safety function in question is upheld.

The ability of the canister to resist isostatic load is an example of a safety function. The associated indicator is the isostatic load on the canister and the criterion is the isostatic load that the canister has been demonstrated to sustain.

All safety functions, indicators and criteria are provided in Chapter 8 where a more elaborated description of the methodology behind the safety functions is also given. Detailed safety functions for containment and retardation are given in Sections 8.3 and 8.4, respectively.

It is important to note that the safety function indicator criteria are not the same as design criteria, formally described as technical design requirements in the PSAR. The former should ideally be upheld throughout the assessment period whereas the technical design requirements should be fulfilled initially. In general, the technical design requirements should assure that the system is robust to the extent that the safety functions indicator criteria are fulfilled over time. For example, the copper canister must be designed such that its initial thickness (the technical design requirement) ensures that it will sustain corrosion for a very long time, i.e. such that the thickness is non-zero (the function indicator criterion) during this time.

The set of safety functions in itself provides understanding of the safety features of the system and a list of key issues to evaluate over time in the assessment. The safety functions are explicitly used in later steps of the assessment to evaluate safety in a structured manner over the different time frames when analysing a reference evolution. A key use of the safety functions is their role in the selection of a number of scenarios whereby uncertainties related to the safety of the system are evaluated in a structured manner (see further Section 2.5.8).

Based on the defined safety functions, a FEP chart is developed, showing how initial state factors and processes in the long-term evolution of the repository are related to the safety functions.

2.5.6 Step 6: Compilation of data

In this step, data to be used in the quantification of repository evolution and in dose calculations are selected using a structured procedure. The process of selection and the data values adopted are reported in a dedicated **Data report**. The process follows a template, developed and applied in the SR-Site assessment, for discussion of input data uncertainties. The template is given in Chapter 9 and the selected data are provided in the **Data report**. The models for which data are required are given in the AMF described in step 4 (Section 2.5.4).

While the data types used in the PSAR are essentially the same as those used in the SR-Site assessment, data values or value intervals differ between the assessments for some data types. For data types where new values are used in the PSAR, the full template is reported in the PSAR Data report. For data types where it has been assessed that the same values as in SR-Site can be used, the data qualification from the SR-Site assessment is reproduced.

2.5.7 Step 7: Analysis of reference evolution

In this step, a reference evolution of the repository system that follows from the reference external conditions defined in step 3 is defined and analysed. The purpose is to gain an understanding of the overall evolution of the system and of uncertainties affecting the evolution, for the scenario selection and scenario analyses that follow in the two subsequent steps. The evolution is an important basis for the later definition of a main scenario, see Section 2.5.8.

Focus is on the containment capacity of the system. Two cases of the reference evolution are analysed.

1. A base case in which the external conditions during the first 120 000 years after closure are assumed to be those reconstructed for the last cycle, that includes the Weichselian glaciation. Thereafter, seven repetitions of the Weichselian/Holocene cycle are assumed to cover the entire 1 000 000 year assessment period.
2. A global warming variant in which the future climate and hence external conditions during the first 120 000 years after closure are influenced by human-induced greenhouse gas emissions. This analysis is related to that of the base case.

For both these, the initial state with its uncertainties described in Chapter 5 is assumed, all internal processes, with their uncertainties, are handled according to the specification given in the **Process reports**, as summarised in Chapter 7 and data with their uncertainties are taken from the **Data report** as summarised in Chapter 9.

The presentation of the analysis of the base case of the reference evolution is divided into four time frames:

- The excavation/operational period.
- The first 1 000 years after repository closure and the initial period of temperate climate conditions from the reference glacial cycle.
- The remaining part of the glacial cycle.
- Subsequent seven glacial cycles up to one million years after repository closure.

For each time frame, issues are presented in the following order:

- Climate issues.
- Biosphere issues.
- Thermal, mechanical, hydraulic and chemical issues in the geosphere.
- Thermal, mechanical, hydraulic and chemical issues for the engineered barrier system (canister, buffer and backfill).

The discussion of each of the issues is concluded with an account of identified uncertainties to be propagated to later stages of the reference evolution and to subsequent parts of the safety assessment.

The commentary on each time frame concludes with a discussion of the expected status of the safety function indicators defined in Chapter 8 during and at the end of the time frame.

A considerable part of the material presented is results from simulation studies, mentioned in step 4 (Section 2.5.4) and graphically represented in the assessment model flow charts, AMFs.

After the analysis of the base case, the global warming variant is analysed under the headings “External conditions”, “Biosphere”, “Repository evolution” and “Safety functions”, essentially as comparisons to analyses of the base case.

2.5.8 Step 8: Selection of scenarios

A key feature in managing uncertainties in the future evolution of the repository system is the reduction of the number of possible evolutions to analyse by selecting a set of representative scenarios. The selection focuses on addressing the safety relevant aspects of the evolution expressed at a high level by the safety functions ‘containment’ and ‘retardation’ which are further characterised by reference to safety function indicators in Chapter 8.

The selected scenarios should cover all reasonable future evolutions. Furthermore, it should be possible to logically calculate the risk associated with the presence of the repository as a sum of risk contributions from the set of scenarios, as discussed further in Section 2.6.2, subheading “Scenario disaggregation”.

Regulatory requirements and recommendations

There are several issues concerning applicable regulations that have to be taken into account in the selection of scenarios. The quantitative criterion for repository safety in Swedish regulations is a risk limit and from the analyses of the defined scenarios it must therefore be possible to draw conclusions regarding risk.

SSM’s Regulations SSMFS 2008:21 require that scenarios be used to describe future potential evolutions of the repository and that among these, there should be a main scenario that takes into account the most likely changes within the repository and its surroundings.

The General Recommendations concerning SSMFS 2008:21 describe a scenario in the safety assessment as comprising “a description of how a given combination of external and internal conditions affect repository performance”.

The General Recommendations describe three types of scenarios: the main scenario, which includes the expected evolution of the repository system; less probable scenarios, which include alternative sequences of events to the main scenario and also the effects of additional events; and residual scenarios, which evaluate specific events and conditions to illustrate the function of individual barriers. For these categories SSM’s Recommendations state the following:

“The main scenario should be based on the probable evolution of external conditions and realistic, or where justified, pessimistic assumptions with respect to the internal conditions. It should comprise future external events which have a significant probability of occurrence or which cannot be shown to have a low probability of occurrence during the time covered in the safety assessment. Furthermore, it should be based, as far as possible, on credible assumptions with respect to internal conditions, including substantiated assumptions concerning the occurrence of manufacturing defects and other imperfections, and which allow for an analysis of the repository barrier functions (it is, for example, not sufficient to always base the analysis on leak-tight waste containers, even if this can be shown to be the most probable case). The main scenario should be used as the starting point for an analysis of the impact of uncertainties (see below), which means that the analysis of the main scenario also includes a number of calculation cases.

Less probable scenarios should be prepared for the evaluation of scenario uncertainty (see also below). This includes variations on the main scenario with alternative sequences of events as well as scenarios that take into account the impact of future human activities such as damage inflicted on barriers. (Damage to humans intruding into the repository is illustrated by residual scenarios, see below).

The analysis of less probable scenarios should include analyses of such uncertainties that are not evaluated within the framework of the main scenario.

Residual scenarios should include sequences of events and conditions that are selected and studied independently of probabilities in order to, inter alia, illustrate the significance of individual barriers and barrier functions. The residual scenarios should also include cases to illustrate damage to humans intruding into the repository as well as cases to illustrate the consequences of an unclosed repository that is not monitored.”

Regarding scenario probabilities, the SSM Recommendations state: “The probabilities that the scenarios and calculation cases will actually occur should be estimated as far as possible in order to calculate risk.”

SSM’s General Guidance on application of SSMFS 2008:37 defines a scenario as a “description of the development of the repository given an initial state and specified conditions in the environment and their development”.

Regarding the choice of scenarios, SSM’s General Guidance states the following:

“The assessment of the protective capability of the repository and the environmental consequences should be based on a set of scenarios that together illustrate the most important courses of development of the repository, its surroundings and the biosphere.

Taking into consideration the great uncertainties associated with the development of future climate and to facilitate the interpretation of the risk to be calculated, the risk analysis should be simplified to include a few possible climate evolutions.

A realistic set of biosphere conditions should be associated with each climate evolution. The different climate evolutions should be selected so that they together illustrate the most important and reasonably foreseeable sequences of future climate states and their impact on the protective capability of the repository and the environmental consequences.”

“The risk from the repository should be calculated for each assumed climate evolution by summing the risk contributions from a number of scenarios that together illustrate how the more or less probable courses of development in the repository and the surrounding rock affect the repository’s protective capability and environmental consequences. The calculated risk should be reported and evaluated in relation to the criterion of the regulations for individual risk, separately for each climate evolution.”

SSM’s General Guidance states: “A number of scenarios for inadvertent human impact on the repository should be presented. The scenarios should include a case of direct intrusion in connection with drilling in the repository and some examples of other activities that indirectly lead to a deterioration in the protective capability of the repository, for example by changing groundwater chemistry or the hydrological conditions in the repository or its surroundings. The selection of intrusion scenarios should be based on present living habits and technical prerequisites and take into consideration the repository’s properties.

The consequences of the disturbance of the repository’s protective capability should be illustrated by calculations of the doses for individuals in the most exposed group, and reported separately apart from the risk analysis for the undisturbed repository. The results should be used to illustrate conceivable countermeasures and to provide a basis for the application of best available technique”.

SSM’s General Guidance to SSMFS 2008:37 states the following: “An account need not be given of the direct consequences for the individuals intruding into the repository.” It is noted that this is contrary to the view expressed in SSMFS 2008:21, where these situations are included among the residual scenarios.

The guidance to SSMFS 2008:37 also mention “special scenarios”: “... an analysis of a conceivable loss, during the first thousand years after closure, of one or more barrier functions of key importance for the protective capability should be made separately from the risk analysis. The intention of this analysis should be to clarify how the different barriers contribute to the protective capability of the repository.”

Method for scenario selection

Given the regulatory requirements and the general considerations discussed above, a method for the selection of scenarios in five steps has been developed as explained below.

1. Definition of the main scenario

A main scenario is defined, based on the reference evolution and in accordance with SSMFS 2008:21. The main scenario is split into two variants, based on the two variants of the reference evolution, (the Weichselian base case and the global warming variant). (The reference evolution corresponding to the main scenario is explained in general terms in step 7, and the handling of uncertainties within the reference evolution is further developed in Section 2.8.4.)

(It is noted that SSM uses “climate evolutions” as a hierarchical level above the scenarios. In order to not complicate the description further, the different types of climate evolution mentioned in SSM’s General Guidance are handled as variants of scenarios.)

2. Selection of additional scenarios based on potential loss of safety functions

A main factor governing scenario selection is the concern that the intended safety functions relating to containment (Chapter 8) should be upheld. Therefore, these safety functions are used to structure the selection of additional scenarios. This is the main approach for addressing the issue of less probable scenarios, in relation to SSMFS 2008:21.

There are three canister safety functions related to containment: to provide a corrosion barrier, to withstand isostatic load and to withstand shear load. Three distinct canister failure modes, due to corrosion, isostatic pressure and shear movement, respectively, can thus be derived from the safety functions. Therefore, three scenarios, one for each canister failure mode, are generated. Three ‘failed’ states of the buffer; advective, frozen and transformed, are also considered as scenarios. The canister scenarios are systematically combined with the buffer scenarios.

For each selected scenario, uncertainties related to initial state factors, processes and external conditions that are not covered in the main scenario are considered. In e.g. the case of canister failure due to high isostatic pressure, inadequacies in the manufacturing of the load-bearing canister insert, higher than reference buffer swelling pressures and maximum thick ice sheets yielding high groundwater pressures are considered.

The FEP chart, see step 5 (Section 2.5.5), aids in ensuring that all conceivable routes to deficiencies in containment are captured. Systematic analyses of initial state factors, long-term processes and external conditions possibly contributing to each of these scenarios are made. The results of the analysis of the main scenario, with all the coupled FEPs and uncertainties considered there, is an important starting point for this assessment.

Based on this information, an assessment of whether each scenario is to be considered as “less probable” or “residual” is made. In the former case, the likelihood of the scenario is normally pessimistically set to one, whereas the assessed limited likelihoods of its characteristic FEPs, e.g. large earthquakes, are taken into account in the risk calculation associated with the scenario.

These scenarios also cover many of the residual scenarios required by SSM’s Regulations and General Guidance to analyse the significance of barriers and barrier functions. To obtain a deeper understanding of barrier functions, a number of residual scenarios are defined illustrating, from the point of view of radionuclide transport, hypothetical situations where one or several barriers are assumed to be initially lost (see further Sections 13.7.3 and 13.7.4). Also a scenario where criticality occurs in a failed canister is analysed in this context.

The selection of additional scenarios is described in detail in Section 11.2. Amendments to the selection following SSM’s review of the SR-Site assessment are described in Section 11.3.

The analyses of the selected additional scenarios are described in Chapter 12, from Section 12.2 onward.

3. Scenarios related to future human actions

A set of scenarios related to future human actions was also defined and analysed. Human intrusion scenarios resulting in a degradation of system performance are to be considered as “less probable scenarios” according to SSMFS 2008:21, but not included in the risk summation according to the General Guidance to SSMFS 2008:37. SSM requires residual scenarios to illustrate damage to humans intruding into the repository and cases to illustrate the consequences of an unclosed repository that is not monitored.

The selection and consequence analyses of scenarios related to future human actions are reported in Section 14.2, as part of the documentation of additional analyses in Chapter 14. The FHA scenarios are reported separately from the main scenario and the additional scenarios based on potential loss of safety functions, since the methodology for the definition of FHA scenarios as well as the analyses of containment and retardation differs from the approaches for other scenarios.

4. Other residual scenarios, etc.

Any other scenarios that are, for any reason, considered necessary in order to obtain an adequate set of scenarios are also to be defined. These could include scenarios directly identified in the FEP analysis but not according to the criteria above.

No such issues have been identified in the PSAR. There are, therefore, no residual scenarios in addition to those defined according to the procedure described in steps 2 and 3 above.

An additional task for the safety assessment is to contribute to the demonstration that best available technique, BAT, has been applied in the repository design. This requires a number of dedicated calculation cases that are not included among the selected scenarios. See further Section 2.7.

5. Combination of scenarios

For the scenario selection to be comprehensive, combinations of the scenarios and variants must be considered. This is done when all the variants and residual scenarios have been selected and analysed. The number of possible combinations could become large, even considering that mutually exclusive scenarios should not be combined, and a practical approach for handling this situation has to be adopted. The problem is further compounded by the fact that each variant may be investigated through a number of calculation cases.

Related to the issue of combination of scenarios is that of different event sequences. The sequence in which different events or aspects of the evolution occur may be important for the evolution of the repository. This is explicitly addressed within each scenario.

The evaluation of combinations of scenarios is described in Section 12.9.

2.5.9 Step 9: Analysis of selected scenarios

The analysis of the selected scenarios is divided in two steps: Analysis of containment potential and of retardation potential.

Analysis of containment potential

The results of the analysis of the containment potential in the reference evolution in step 7 (Section 2.5.7) are essentially adopted for the main scenario. A more detailed definition of what is covered in terms of containment potential in the main scenario is given after the analysis of the additional scenarios, see Section 12.9.2.

The additional scenarios are analysed by focussing on the factors potentially leading to situations in which the safety function in question is not maintained. In most cases, these analyses are carried out by comparison with the evolution for the main scenario, meaning that they only encompass aspects of repository evolution for which the scenario in question differs from the main scenario.

A common template is followed in the analysis of the additional scenarios. The headings in the template are the following:

- Safety function indicator(s) considered.
- Treatment of this issue in the reference evolution.
- Qualitative description of routes to this situation.
- Quantitative assessment of routes to this situation.
- Categorisation as “less probable” or “residual” scenario.
- Conclusions.

The analysis of the containment potential is carried out in Chapter 12, with the exception of scenarios related to future human actions that are analysed in Section 14.2.

Analysis of the retardation potential

This second step of the scenario analyses encompasses calculations of radionuclide release, transport and dose impacts for potential failure modes of canisters identified for each scenario in the analysis of containment potential. The purpose is to assess the retardation properties of the system for these scenarios and to quantify risk.

In general, a number of calculation cases are defined for each scenario, except for the main scenario for which consequences are encompassed by the cases analysed for the additional scenarios. The calculation cases are formulated to account for uncertainties relating to both the containment potential and the retardation potential.

Uncertainties relating to retardation potential are not included as factors in the selection and analysis of scenarios described above. Therefore, for each scenario, the safety functions related to retardation are treated in a similar manner to that in which the functions related to containment were treated in the scenario analysis described above, in order to get a comprehensive coverage of uncertainties relating to retardation. This is done through application of a similar template as for the containment potential. The number of cases this yields for each scenario is limited to a manageable number since for the most important scenarios i) the cases are similar between the scenarios, and ii) the identified failure modes in a scenario often imply that one or several barriers are impaired to the extent that they are short-circuited so yielding a reduction in the number of uncertain factors. For example, one scenario addresses the loss of containment due to corrosion. In that scenario, a risk contribution is obtained only in cases where the buffer is lost. For this situation, a calculation base case for radionuclide transport and dose is defined, and then all safety functions contributing to retardation are examined through the mentioned template to derive additional calculation cases covering uncertainties relating to retardation. The fact that the buffer is lost in this scenario reduces the number of calculation cases considerably.

The calculated risks from the main scenario and from the additional scenarios that are categorised as “less probable” (but not “residual”) are summed to obtain a total risk over time for the repository.

Sensitivity analyses of the output of the probabilistic calculations to uncertainties in input data are carried out mainly by i) calculation of standardised rank regression coefficients for the evaluation of probabilistic results and ii) the formulation of a tailored regression model, based on the mathematical model used in the risk calculation. Additional methods are applied to key calculation results, in order to further elucidate sensitivities.

The central results of the consequence calculations are presented in Chapter 13 whereas details are provided in the **Radionuclide transport report**.

2.5.10 Step 10: Additional analyses and supporting arguments

In this step, a number of additional analyses, required to complete the safety assessment, are carried out. These comprise:

- The selection and analysis of FHA scenarios, including a brief description of the methodology for the selection.
- Analyses required to demonstrate optimisation and use of best available technique.
- Verification that FEPs omitted in earlier parts of the assessment are negligible in light of the completed scenario and risk analysis.
- A brief account of the time period beyond one million years.
- Natural analogues.

See further Chapter 14.

2.5.11 Step 11: Conclusions

This step includes integration of the results from the various scenario analyses, development of conclusions regarding safety in relation to regulatory criteria and feedback concerning repository design, detailed site investigations and SKB's RD&D Programme.

The discussion of compliance with the regulatory risk limit is a central part of the conclusions. This is associated with a confidence statement, discussing the confidence in the various aspects of the assessment on which the risk calculations are built.

This step also contains conclusions and feedback regarding the design of the engineered barriers and the repository. Specifically, a set of design basis cases is presented, based on the risk contributing scenarios, in agreement with applicable regulations. These take the form of specifications of loads that the repository system should withstand over time. These updated design basis cases, together with other findings from the PSAR, are used to assess the need for updating the technical design requirements related to post-closure safety used for developing the current design for long term safety. In addition to the design basis cases and other input to revision of the technical design requirements, feedback is given regarding a number of detailed aspects of the design. Conclusions are also drawn regarding best available technique, BAT. This is, however, a many-faceted issue for which only part of the basis for conclusions comes from the safety assessment and in particular from the calculated risks.

See further Chapter 15.

2.5.12 Report hierarchy in the PSAR

As indicated in the previous Section, several of the steps carried out in the PSAR result in specific reports that are of central importance for the conclusions and analyses in this main report. Table 2-1 lists these *main references* and defines the abbreviations by which they are identified in the text hereinafter. The report with the full title "Post-closure safety for the final repository for spent nuclear fuel at Forsmark – Model summary report, PSAR version" is e.g. referred to as the **Model summary report**. There are also about 80 *additional references*, treating narrower issues, and that support either the main report or one of the main references. The report hierarchy is illustrated in Figure 2-3. All these reports can be downloaded from www.skb.se.

Furthermore, as mentioned in Section 1.6, one of the most fundamental input documents to the SR-Site and PSAR assessments is the site descriptive model of the Forsmark site (SKB 2008a). This report is briefly identified as **Site description Forsmark**. (In other contexts, the report is in brief referred to as SDM-Site Forsmark.)

Table 2-1. Main references in the reporting of post-closure safety in the PSAR. All technical reports (TR) are available at www.skb.se.

Abbreviation used when referenced in this main report	Full reference (as given in reference list)
Backfill production report	Backfill production report, 2022. Produktionsrapport Återfyllning. SKBdoc 1525864 ver 4.0, Svensk Kärnbränslehantering AB. (In Swedish.) (Internal document.)
Biosphere synthesis report	Biosphere synthesis report, 2010. Biosphere analyses for the safety assessment SR-Site – synthesis and summary of results. SKB TR-10-09, Svensk Kärnbränslehantering AB.
Buffer, backfill and closure process report	Buffer, backfill and closure process report, 2022. Post-closure safety for the final repository for spent nuclear fuel at Forsmark – Buffer, backfill and closure process report, PSAR version. SKB TR-21-03, Svensk Kärnbränslehantering AB.
Buffer production report	Buffer production report, 2022. Produktionsrapport Buffert. SKBdoc 1392269 ver 5.0, Svensk Kärnbränslehantering AB. (In Swedish.) (Internal document.)
Canister production report	Canister production report, 2022. Produktionsrapport Kapsel. SKBdoc 1407944 ver 2.0, Svensk Kärnbränslehantering AB. (In Swedish.) (Internal document.)
Climate report	Climate report, 2020. Post-closure safety for the final repository for spent nuclear fuel at Forsmark – Climate and climate-related issues, PSAR version. SKB TR-20-12, Svensk Kärnbränslehantering AB.
Closure production report	Closure production report, 2022. Produktionsrapport Förslutning. SKBdoc 1387771 ver 3.0, Svensk Kärnbränslehantering AB. (In Swedish.) (Internal document.)
Data report	Data report, 2022. Post-closure safety for the final repository for spent nuclear fuel at Forsmark – Data report, PSAR version. SKB TR-21-06, Svensk Kärnbränslehantering AB.
Deposition tunnel plug production report	Deposition tunnel plug production report, 2022. Produktionsrapport Valvplugg. SKBdoc 1562518 ver 3.0, Svensk Kärnbränslehantering AB. (In Swedish.) (Internal document.)
FEP report	FEP report, 2010. FEP report for the safety assessment SR-Site. SKB TR-10-45, Svensk Kärnbränslehantering AB.
FHA report	FHA report, 2010. Handling of future human actions in the safety assessment SR-Site. SKB TR-10-53, Svensk Kärnbränslehantering AB.
Fuel and canister process report	Fuel and canister process report, 2022. Post-closure safety for the final repository for spent nuclear fuel at Forsmark – Fuel and canister process report, PSAR version. SKB TR-21-02, Svensk Kärnbränslehantering AB.
Geosphere process report	Geosphere process report, 2022. Post-closure safety for the final repository for spent nuclear fuel at Forsmark – Geosphere process report, PSAR version. SKB TR-21-04, Svensk Kärnbränslehantering AB.
Model summary report	Model summary report, 2022. Post-closure safety for the final repository for spent nuclear fuel at Forsmark – Model summary report, PSAR version. SKB TR-21-05, Svensk Kärnbränslehantering AB.
Radionuclide transport report	Radionuclide transport report, 2022. Post-closure safety for the final repository for spent nuclear fuel at Forsmark – Radionuclide transport report, PSAR version. SKB TR-21-07, Svensk Kärnbränslehantering AB.
Site description Forsmark	Site description Forsmark, 2008. Site description of Forsmark at completion of the site investigation phase – SDM-Site Forsmark. SKB TR-08-05, Svensk Kärnbränslehantering AB.
Spent fuel report	Spent fuel report, 2021. Använt kärnbränsle att hantera i KBS-3-systemet. SKBdoc 1380282 ver 3.0, Svensk Kärnbränslehantering AB. (In Swedish.) (Internal document.)
Underground openings construction report	Underground openings construction report. Produktionsrapport Bergutrymmen, Svensk Kärnbränslehantering AB. (In Swedish.) (Internal document.) <i>In prep.</i>

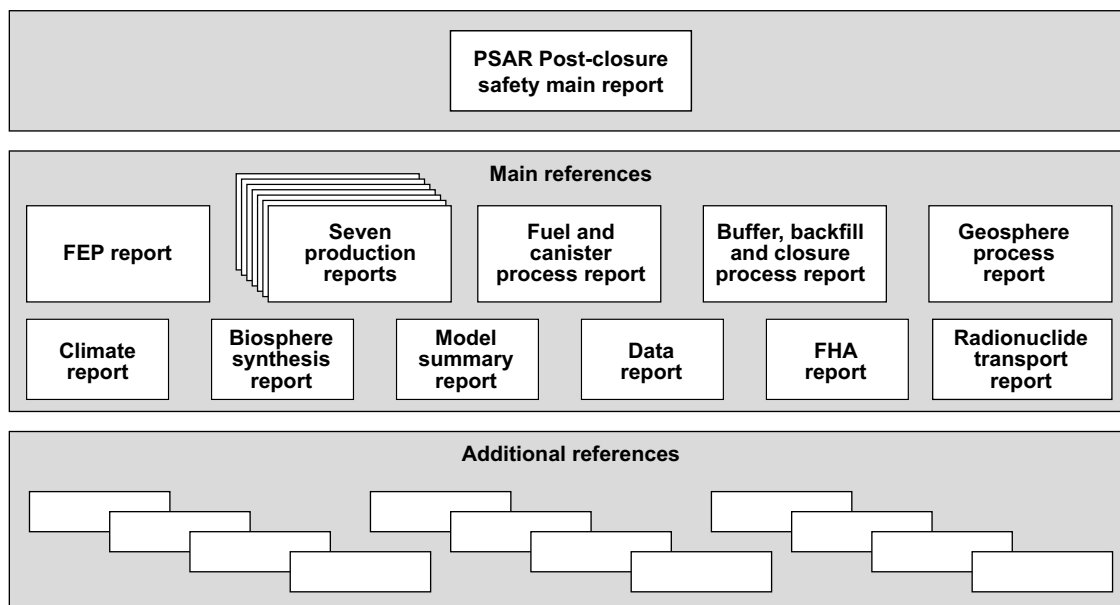


Figure 2-3. The hierarchy of the main and additional references to the PSAR. The main references support the main report. The additional references may either support the main report directly or one of the main references. The seven Production reports include the *Spent fuel report* and the *Underground openings construction report*.

2.6 Approach to risk calculations

2.6.1 Regulatory requirements and guidance

The quantitative acceptance criterion in Sweden for post-closure safety of a nuclear waste repository is a limit on annual risk. SSMFS 2008:37 states the following: “A repository for spent nuclear fuel or nuclear waste shall be designed so that the annual risk of harmful effects after closure does not exceed 10^{-6} for a representative individual in the group exposed to the greatest risk.” The conversion between effective dose and risk is to be carried out using ICRP’s probability coefficient for cancer and hereditary effects of 0.073 per Sievert. An annual risk limit of 10^{-6} thus corresponds to an effective dose limit of about 1.4×10^{-5} Sv/yr. (ICRP’s coefficient has been updated and is now slightly lower, but this has not yet been formally implemented in the Swedish regulations.)

SSM’s General Guidance state the following: “The individual risk should be calculated as an annual average on the basis of an estimate of the lifetime risk for all relevant exposure pathways for every individual.”

As already mentioned in Section 2.4, according to the guidance to SSM’s Regulations, the quantitative risk criterion is applicable as a quantitative regulatory limit during approximately the first one hundred thousand years, and thereafter as one of several indicators forming a basis for discussing the protective capability of the repository.

It is furthermore important to note that scenarios relating to future human actions should not be included in the risk calculation according to SSM’s General Guidance.

2.6.2 Application in the PSAR

This section describes some basic aspects of how compliance with SSM’s risk criterion is demonstrated in the PSAR. The same approach was used in SR-Site and prior to that, most of the material below was presented and discussed at an NEA Workshop on the role of risk in safety assessments (NEA 2005) and at an international conference on probabilistic safety assessment and management (Hedin 2004a).

Scenario disaggregation

In principle, the product of dose consequences and likelihoods of all possible future evolutions of the repository should be weighed together and presented as a time-dependent risk. The spectrum of possible evolutions is, however, very wide and cannot be captured in a detailed sense. This is also recognised in SSM's Regulations and associated General Guidance.

The usual approach taken in safety assessments, and also in the PSAR, is to work with scenarios and variants that are designed to capture the broad features of a number of representative possible future evolutions. Together, these are intended to give a reasonable coverage of possible future exposure situations. In principle, conditional risks could be calculated for each scenario and variant and then weighed together using the probability for each scenario/variant. However, in practice, scenario probabilities often have to be pessimistically overestimated, see further the subsection "*Overestimation of risk*" below. Furthermore, each variant, represented by a specific calculation case, may be evaluated probabilistically in order to determine the mean exposure given the data uncertainties for the particular variant.

The approach of calculating risk as a sum of risk contributions from a number of scenarios constrains the way in which scenarios are selected and defined. It must be possible to logically explain the summation and the set of scenarios should be comprehensive in the sense that all relevant future evolutions are covered.

A "normal evolution" scenario with a high probability of occurrence must e.g. contain initially defective canisters and other barrier insufficiencies, if such are likely when the entire ensemble of canisters and deposition holes in the repository is considered.

Since SSM's General Guidance states that the risk criterion concerns a repository undisturbed by man, scenarios involving direct intrusion into the repository are excluded from the risk summation. Also human actions that disturb the immediate environment of the repository, e.g. the local groundwater flow field, are considered in the treatment of future human actions in Section 14.2, but excluded from the risk summation.

Overestimation of risk

The formulation of scenarios, variants and calculation cases, and the subsequent weighing together of these to give a total risk aims at an over prediction of risk. SSM's regulation requires that the annual risk should be less than 10^{-6} . There are a number of uncertainties that cannot be managed quantitatively in any other rigorous manner from the point of view of demonstrating compliance than by pessimistic assumptions.

Another situation in which risk has to be overestimated concerns scenario probabilities. Regarding e.g. future climate, both repetitions of conditions reconstructed for the past 120 000 year glacial cycle and an alternative where this development is considerably perturbed by a global warming effect can be envisaged. Although the two are mutually exclusive, both must be regarded as possible when considering both a 100 000 and one million year time perspective. In the risk summation, the logical position is adopted that the summed consequence of a set of mutually exclusive scenarios can, at any point in time, never exceed the maximum of the individual scenario consequences. For scenarios and variants where defensible probabilities are difficult to derive, a scenario or variant giving high consequences can pessimistically be assigned unit probability and other scenarios and variants yielding lower dose impacts can be "subsumed" under the one with the more severe consequences.

Although the primary aim with risk calculations is to demonstrate compliance, there is also the clear ambition of clarifying the sensitivities of the calculation results. For this aim, the calculation cases should be, in principle, as realistic as possible in capturing uncertainty. One quantitative tool for this is the use of probabilistic evaluations of calculation cases followed by sensitivity analyses of the results.

It is concluded that pessimistic simplifications should be avoided where a sound scientific basis exists for a quantitative treatment and further that the pessimistically neglected features of the system should be included in a discussion of sensitivities.

Size of the exposed group

The size of the group to which the above risk limit is to be applied must be defined in order to evaluate compliance with the risk criterion. No detailed definition is given in SSMFS 2008:37. In its General Guidance SSM however states the following: “One way of defining the most exposed group is to include the individuals that receive a risk in the interval from the highest risk down to a tenth of this risk. If a larger number of individuals can be considered to be included in such a group, the arithmetic average of individual risks in the group can be used for demonstrating compliance with the criterion for individual risk in the regulations. One example of such exposure situation is a release of radioactive substances into a large lake that can be used as a source of drinking water and for fishing.

If the exposed group only consists of a few individuals, the criterion of the regulations for individual risk can be considered as being complied with if the highest calculated individual risk does not exceed 10^{-5} per year. An example of a situation of this kind might be if consumption of drinking water from a drilled well is the dominant exposure path. In such a calculation example, the choice of individuals with the highest risk load should be justified by information about the spread in calculated individual risks with respect to assumed living habits and places of stay.”

The detailed application of these two options in the PSAR is further developed in connection with the consequence calculations in Chapter 13.

Time frames

Risk calculations are carried out for a one million year time frame in the PSAR. In accordance with SSM’s General Guidance, strict compliance with the risk limit is evaluated in a 100 000 years’ time frame. For longer times, also in accordance with SSM’s General Guidance, the results of the risk calculation are used to discuss the protective capability of the repository and how this capability can be improved.

Time dependent risk or peak over entire assessment period?

An upper bound on the peak of the time dependent risk may be calculated by determining the peak annual effective dose⁷ over the one million year assessment period in each realisation. The mean value of the determined distribution of peak doses is then compared with the effective dose criterion. While this is a correct way of putting an upper bound on risk, it is more informative and also in agreement with the SSM’s Regulations to calculate the mean annual effective dose at each point in time and require that this quantity never exceeds the effective dose corresponding to the risk criterion of 10^{-6} . The two methods are sometimes referred to as “the mean of the peaks” and “the peak of the mean”. The “peak of the mean” interpretation is meaningful in the sense that all exposure pathways to hypothetical individuals living in the future are considered whereas the “mean of the peaks” concept is more difficult to interpret. In the PSAR, risk as a function of time is presented by weighing together the time-dependent mean annual effective doses from each scenario to obtain a time-dependent risk.

Risk dilution

The term “risk dilution” is sometimes used to denote a situation where a higher degree of uncertainty in input parameters, i.e. a broader input distribution, leads to a lower mean value of an output quantity e.g. mean dose or risk (NEA 1997b). A seemingly paradoxical situation arises where less knowledge implies a safer repository if the mean value to a highly exposed individual at a certain point in time is used as the safety indicator. Less knowledge will spread the dose over more individuals and over longer times. The total exposure to all individuals over all times could be the same or larger, whereas more precise knowledge will “concentrate” the risk to fewer individuals and shorter periods of time. This can e.g. be the case when there is uncertainty concerning the time of an event that would lead to canister rupture. The dose consequence for a given time could then depend strongly on the assumed time at which the rupture occurred. Averaging over alternative situations in which canister rupture

⁷ The annual effective dose is the sum of the annual effective dose from external exposure and the annual committed effective dose from internal exposure.

and thus peak dose occurs at different points in time would reduce the resulting mean value at any point in time and more so the larger the span of possible rupture times.

This effect is inherent in the concept of risk as defined in SSM's regulation and is thus an inevitable consequence of a risk criterion which is to be applied as a function of time and where the quantity to be determined is the mean value considering all relevant uncertainties. Therefore, SSM's General Guidance also requires that the issue of risk dilution is addressed when the consequences of releases from the repository are assessed.

A related phenomenon concerns biosphere development during the expected long periods of periglacial or glacial conditions. To illustrate this, it is assumed that appreciable doses to man could occur only during temperate climate periods, and that these periods in this example would prevail in total during about ten percent of the time, but that the temporal location of these temperate intervals cannot be predicted beyond, say 10 000 years into the future. In principle, this situation could be handled by simulating a number of future situations where the onsets of the temperate periods are allowed to vary beyond 10 000 years based on e.g. different carbon emission scenarios. Averaging over all these results would, at each point in time beyond 10 000 years, yield a dose consequence a factor of ten smaller than that obtained during a temperate climate period. This simplistic example demonstrates another type of risk dilution, again caused by an uncertainty in the point in time of the occurrence of a phenomenon, which could in principle be compatible with the Swedish risk criterion. The effect is however avoided in the safety assessment e.g. by assuming the same temporal sequence of climate types in each simulation or by assuming today's biosphere.

For the PSAR several conclusions are drawn from the above, as set out below.

- A broader input data distribution is not necessarily pessimistic, not even if it is broadened towards the high consequence end. Thus, care must be taken in assigning input data distributions so that input data distributions that might influence the calculation end-point in this way are not unduly broadened.
- Disaggregated calculations and disaggregated discussions of the results of more integrated calculations are necessary from the point of view of capturing risk dilution and such calculations and discussions are, therefore, included in the PSAR. A simple but effective means of avoiding risk dilution when its cause has been identified is to illustrate the effect by replacing probabilistic input data of e.g. canister rupture times with a fixed time. This is one approach taken in the PSAR.
- For certain situations with short-term releases, a method suggested in Appendix 1 to SSMFS 2008:37 is used to address risk dilution.
- Another option for capturing risk dilution effects is to complement a "peak of the mean" calculation with a "mean of the peaks" calculation, as described in the previous section. This is, however, used only for illustrative purposes in the PSAR since the result of such a calculation is difficult to interpret, as discussed above.

2.6.3 Alternative safety indicators

The dose/risk safety indicator provides a measure of radiological impact on future humans due to the existence of the repository. Several aspects of biosphere development are highly uncertain, even over a relatively short time perspective. The evaluation of safety depends on a number of assumptions made in order to handle these uncertainties. It is, therefore, of interest to complement both the dose/risk indicator and the evaluation of impacts on non-human biota with alternative indicators that do not require detailed assumptions about the biosphere or concerning human habits.

The recommendations accompanying SSMFS 2008:21 mention that, for distant futures, the dose indicator can be complemented with other safety indicators, e.g. concentrations in groundwaters or near-surface waters of radionuclides from the repository or the calculated fluxes of radionuclides to the biosphere.

A problem with alternative indicators is that there is, in general, no obvious criterion with which the calculated quantities can be compared. In some cases, calculation results can be compared with natural concentrations or fluxes at the site or elsewhere. However, such criteria do not provide points of reference for man-made radionuclides. The problem can be partly overcome by comparing naturally

occurring sum concentrations/fluxes of α - and β -emitters to the corresponding repository related quantities, or by comparing overall toxicities by scaling by dose per unit intake values.

It is also noted that the safety function indicators (Chapter 8) are a type of alternative safety indicator related to barrier conditions, rather than to concentrations and fluxes, with the indicator criteria being reference values with which to compare the outcome of an analysis of the condition in question. However, whereas the safety function indicators relate to the functioning of sub-systems, the safety indicators provide a measure of the overall system performance.

EU SPIN Project

An EU project (Becker et al. 2002) concludes that two alternative indicators could preferably be used to complement the dose indicator. These are:

- Radiotoxicity concentration in biosphere water: preference for medium time frames, i.e. several thousand to several tens of thousands of years.
- Radiotoxicity flux from the geosphere: preference for later time frames.

The project also reports on reference values that could tentatively be used for comparisons to calculated concentrations and fluxes of radionuclides from the repository. Regarding radiotoxicity flux from the geosphere, an indicative reference value of 60 Sv/y for a typical area of 200 km² was suggested.

Finnish activity release constraints

The Finnish Radiation and Nuclear Safety Authority STUK has issued activity release constraints to the environment (STUK 2014).

These nuclide specific constraints are defined for long-lived radionuclides only. The effects of their short-lived progeny have been taken into consideration in the constraints defined for the long-lived parents. The nuclide-specific release rate constraints are:

- 0.03 GBq/y for the long-lived α -emitting isotopes of Ra, Th, Pa, Pu, Am and Cm,
- 0.1 GBq/y for Se-79, Nb-94, I-129, and Np-237,
- 0.3 GBq/y for C-14, Cl-36, Cs-135, and the long-lived isotopes of U,
- 1 GBq/y for Sn-126,
- 3 GBq/y for Tc-99,
- 10 GBq/y for Zr-93,
- 30 GBq/y for Ni-59,
- 100 GBq/y for Pd-107.

The constraints apply to activity releases that arise from the expected evolution scenarios and that may enter the environment after several thousands of years, whereas dose rate constraints are applied in the shorter term. In applying the above constraints, the activity releases can be averaged over 1 000 years at the most. The sum of the ratios between the nuclide-specific activity releases and the respective constraints shall be less than one. It should be noted that the Finnish regulator has derived these constraints partly based on a set of reference biospheres considered possible in the future at the planned disposal site, Olkiluoto at the coast of the Baltic Sea, and partly on natural fluxes of radionuclides established for similar environments. The reference values of the Finnish regulatory guide are thus not directly applicable for other disposal concepts and sites (Becker et al. 2002). However, both the disposal concept and the sites considered in Sweden are similar to those for which the Finnish activity release constraints have been developed.

Other studies

An SKI/SSI study (Miller et al. 2002) compiled from the published literature a substantial database of elemental abundances in natural materials and, using these data, calculated a range of elemental and activity fluxes arising due to different processes at different spatial scales. The authors conclude that these fluxes should be comparable to results from safety assessment calculations.

IAEA has published a study entitled “Safety Indicators in Different Time Frames for the Safety Assessment of Underground Radioactive Waste Repositories” (IAEA 1994) and a research report on natural concentrations and fluxes (IAEA 2005).

Implications for the PSAR

Four alternative indicators to risk are used in the PSAR; release of activity from the geosphere, radiotoxicity flux from the geosphere, concentrations of radionuclides in ecosystems and fluxes of radionuclides. The following reference values are used when evaluating these indicators:

- The Finnish activity constraints. These constraints are strictly applicable only in the Finnish regulatory context, but nevertheless are deemed useful as reference values for the PSAR.
- The reference value for radiotoxicity flux from the geosphere suggested by the SPIN project.
- Measured concentrations of naturally occurring radionuclides in ecosystems at the Forsmark site or other, comparable sites.
- Naturally occurring fluxes of radionuclides at the site, in particular of U-238 and Ra-226.

2.7 BAT and optimisation

2.7.1 Introduction

To comply with the detailed regulations regarding post-closure safety issued by SSM, some aspects of the demonstration of best available technique (BAT) need to be addressed in the assessment of post-closure safety supporting the PSAR. The following is a more detailed account of these requirements and of the approach to addressing them.

2.7.2 Regulatory requirements

Regarding optimisation and best available technique, the General Guidance to SSMFS 2008:37 states the following:

“The regulations require that optimisation must be performed and that best available technique should be taken into account. Optimisation and best available technique should be applied in parallel with a view to improving the protective capability of the repository.

Measures for optimisation of a repository should be evaluated on the basis of calculated risks.

Application of best available technique in connection with final disposal means that the siting, design, construction, operation and closure of the repository and appurtenant system components should be carried out so as to prevent, limit and delay releases from both engineered and geological barriers as far as is reasonably possible. When striking balances between different measures, an overall assessment should be made of their impact on the protective capability of the repository.

In cases where considerable uncertainty is attached to the calculated risks, for instance, in analyses of the repository a long time after closure, or analyses made at an early stage of the development work with the repository system, greater weight should be placed on best available technique.

In the event of any conflicts between application of optimisation and best available technique, priority should be given to best available technique.

Experiences from recurrent risk analyses and the successive development work with the repository should be used in the application of optimisation and best available technique.”

SSMFS 2008:21 states that the “barrier system shall be designed and constructed taking into account the best available technique” and refers to the Swedish Environmental Code. In the General Recommendations related to SSMFS 2008:21, it is stated that “The use of the best available technique means that the technology, from a technical and economic standpoint, shall be industrially feasible for application within this area. This means that the technique must be available and not merely at the experimental stage. However, the technique does not have to be available in Sweden (see bill 1997/98:45, Part I, p 215 ff for details)”.

2.7.3 General issues regarding optimisation and best available technique

A general account of the use of best available technique (BAT) is a broad issue spanning from the selection of method for the management of nuclear waste to fine details of the selected method. Only a limited part of this broad issue can and should be addressed in the safety assessment of the selected method applied at the selected site. Here, the account of BAT is, therefore, confined to the KBS-3 method, using copper/cast iron canisters, buffer and backfill at the selected Forsmark site.

The issue of BAT is also closely related to that of feedback to repository design, as also stated in the General Guidance to SSMFS 2008:37. As also acknowledged in the regulations, the development of a repository system is carried out in steps, with safety evaluations at appropriate points of the development. This means that the developer is not in a position to finally claim optimisation and use of BAT until much of the iterative development work has been finalised. At earlier stages, the account of optimisation and BAT is rather a framework for discussing feedback to remaining development needs. The discussion conducted in relation to the SR-Site assessment is to a considerable extent an example of the latter role for optimisation and BAT.

2.7.4 Optimisation vs BAT

In the General Guidance to SSMFS 2008:37, optimisation is emphasised more for the initial period after closure. It is also stated that optimisation should be carried out with respect to calculated risks. As evidenced by the account of the calculated risk in the SR-Site assessment (SKB 2011, Section 15.3.3), the assessed risk is negligible for tens of thousands of years into the future, suggesting that optimisation is of limited relevance during this initial period that is emphasised in the regulations. However, as also mentioned in the regulations, the considerations of optimisation and BAT should be applied in parallel. In fact, it is often difficult to clearly distinguish the two. The discussion of BAT, when based on results from the safety assessment of the preferred method, is frequently ‘reduced’ to an account of optimisation of the selected solution, since there are in general no alternative techniques to choose between or analyse in the safety assessment. (The term “optimisation” is used in the same sense as in SSMFS 2008:37, i.e. “keeping the radiation doses to mankind as low as reasonably achievable, economic and social factors taken into account”, the so called ALARA principle.)

In the General Guidance to SSMFS 2008:37, it is noted that, for the time period between 100 000 years and one million years, the results of the risk calculation should be used to discuss measures to improve the protective capability of the repository if the risk limit is exceeded.

2.7.5 Conclusions relating to methodology for the PSAR

Based on the above, it is concluded that the calculated risk results in the assessment of post-closure safety need to be evaluated from the point of view of BAT.

To achieve this, analyses of the sensitivity of the risk with respect to important barrier dimensions, layout rules, repository depth etc. are carried out as part of the additional analyses following the risk calculation, see further Section 14.3.

Based on the results of the sensitivity analyses, a discussion of the compliance with this aspect of BAT is also provided, in Section 14.3.

2.8 Overall information/uncertainty management

A safety assessment handles a vast amount of information of qualitative and quantitative nature, including the uncertainties associated with that information. This section gives an overview of issues related to information and uncertainty management in the PSAR. Since this issue permeates the entire analysis, the overview is, in part, a summary of the different steps of the methodology described in Section 2.5, but with emphasis on information/uncertainty management. In all management of uncertainty, it is important to consider the significance of the uncertain issue relative to the purposes of the safety assessment.

As a background, Section 2.8.1 gives a brief description of the different types of uncertainty that have to be managed in the safety assessment.

2.8.1 Classification of uncertainties

There is no unique way in which to classify uncertainties in a safety assessment. The classification adopted below is, however, compatible with international practice (NEA 1991, 1997a) in this type of analysis. SKB has previously discussed the classification and nature of uncertainties in detail, see e.g. SKB (1995, Section 3.4), Andersson (1999, Section 2.1) and the SR-Can main report (SKB 2006a, Section 2.7) of which the following is an update, identical to that presented in the SR-Site main report (SKB 2011, Section 2.8.1). Here, only a brief outline is given, setting the context for the presentation of the management plan in Section 2.8.3.

The safety assessment is built on the analysis of how a system with an initial state evolves as a result of actions on the system by a number of internal processes and external influences/events. From this description, a number of issues regarding uncertainties can be identified, as listed below.

- How well is the initial state known, qualitatively and quantitatively, i.e. are all important aspects of the initial state identified and how well can they be quantitatively described?
- Have all relevant internal processes been identified in the relevant time frames? How well are the process mechanisms understood?
- Have all relevant external events and phenomena been identified? How well can they be quantified?
- How can a representative account of the system evolution be given, taking into account all the types of uncertain factors mentioned above? How well can the internal processes be represented mathematically to give a realistic account of the system evolution? How well are all the input data necessary for the quantification of the system evolution known?

In defining a structure for a rigorous approach to the above issues, it is customary (NEA 1997a) to describe uncertainty in the categories; system/scenario uncertainty, conceptual uncertainty and data uncertainty. A general conclusion from international collaboration efforts in the area of assessment methodology is that there is no unique or correct way to describe or classify uncertainty. Rather, in any safety assessment, it is important to make clear definitions of the use of different terms in this area, in the light of the results from international efforts such as the compilation of lessons learnt from ten performance assessment studies (NEA 1997a).

In the PSAR, the following broad definitions are used.

System uncertainty concerns comprehensiveness issues, i.e. the question of whether all aspects important for the safety evaluation have been identified and whether the analysis is capturing the identified aspects in a qualitatively correct way, e.g. through the selection of an appropriate set of scenarios. In short, have all factors, FEPs, been identified and included in a satisfactory manner or has their exclusion been appropriately justified?

Conceptual uncertainty essentially relates to the understanding of the nature of processes involved in repository evolution. This concerns not only the mechanistic understanding of a process or set of coupled processes, but also how well they are represented, and what is not represented, in a possibly considerably simplified mathematical model of repository evolution.

Data uncertainty concerns all quantitative input data used in the assessment. There are a number of aspects to take into account in the management of data uncertainty. These include correlations between data, the distinction between uncertainty due to lack of knowledge (epistemic uncertainty) and due to natural variability (aleatoric uncertainty) and situations where conceptual uncertainty is treated through a widened range of input data. The input data required by a particular model is in part a consequence of the conceptualisation of the modelled process, meaning that conceptual uncertainty and data uncertainty are to some extent intertwined. Also, there are several conceivable strategies for deriving input data. One possibility is to strive for pessimistic data in order to obtain an upper bound on consequences in compliance calculations. Another option is the full implementation of a probabilistic assessment requiring input data in the form of probability distributions. These aspects are further discussed in Chapter 9 and in the **Data report**.

The plan presented in Section 2.8.3 demonstrates how all the discussed types of uncertainty are managed in the safety assessment.

2.8.2 Need for stylised examples

The management of uncertainties is most comprehensive for the behaviour of the inner parts of the system, which provide the containment and retardation safety functions. The biosphere and the external conditions are handled in a more stylised manner, i.e. through simplified representations where the important aspects of these sub-systems are captured, often in a pessimistic fashion. These latter parts do not incorporate principal safety related features of the system and they are too complex to be modelled in detail in the safety assessment.

The local biosphere is by definition a part of the system, i.e. it lies within the system boundaries and biosphere uncertainties should thus be managed in the same way as for other internal parts. However, in the biosphere, the list of processes determining the system development is long and the system in which they occur is highly inhomogeneous, including a number of different ecosystems each with a large number of components. Furthermore, the time scale on which the biosphere changes is in general considerably shorter than for other parts of the system, and the interactions with humans are stronger and associated with partly irreducible, large uncertainties. Although some aspects of the development of the biosphere at a particular location can be reasonably forecast in maybe a 1 000 year perspective, a large part of the description, particularly of human behaviour has to be through stylised examples (see further Section 13.2).

Also in relation to the effects of external conditions, uncertainty management largely has to be through stylised examples devised to cover the range of possible future evolutions, e.g. regarding climate change. A detailed treatment of all the processes involved in climatic development is outside the scope of the safety assessment. Climate research is furthermore a rapidly evolving field of science, where uncertainties are fundamental. The approach is instead to follow the development of the field, and from an exemplified future reference glacial cycle derive a number of complementary stylised possible evolutions that together bound the possibilities of what could be expected in the future. In particular, extreme conditions that could have a negative effect on repository safety are captured in these examples. These conditions include:

- Maximum glacial overburden and the resulting hydraulic/mechanical pressures and hydraulic/mechanical loads on the bedrock.
- Intrusion of waters of extreme composition, such as oxygenated glacial melt water of low ionic strength.
- Extreme surface boundary conditions for groundwater flow possibly leading to high groundwater fluxes at repository level or groundwater movements that could cause intrusion of deeply lying saline groundwaters.
- Conditions leading to maximum permafrost depths.
- Maximum long period of temperate climate conditions, exclusively with meteoric groundwater recharge reducing groundwater salinity.

2.8.3 Uncertainty management; general

The purpose of the safety assessment affects the management of uncertainties. In this context, the purpose of the assessment is essentially two-fold:

- To assess compliance with Swedish regulations.
- To give feedback to design, research and development and further detailed site investigations as the repository is constructed.

The first purpose can, if there are sufficient safety margins, be largely accomplished by a pessimistic handling of many uncertainties. The second, however, requires more sophisticated management in order to determine quantitatively which uncertain factors and open design issues affect safety most.

In the following, the broad features of the management of uncertainties in the PSAR are outlined. QA aspects of the handling are further discussed in Section 2.9.

System uncertainty

System uncertainty is generally handled through the proper management of FEPs in the FEP database according to the routines described in the **FEP report** and summarised in Chapter 3 of this report.

The database structure and FEP management routines have been set up to assure that the following information is obtained.

- A sufficient set of initial conditions. This is obtained by including all initial state FEPs in the database. These are, however, often formulated in general terms and have to be expressed in a way that is specific to the KBS-3 system. This is done through the systematic documentation of a reference initial state in accordance with the description in the **Production reports** and by using that initial state as a starting point for alternative initial states, where relevant.
- A sufficient set of internal, coupled processes. This is obtained by including in the assessment all relevant process FEPs in the database. It is important to note that the database already from the start includes the result of several earlier exercises aiming at process identification for the KBS-3 concept. This is further described in Section 7.1.1. Influences between processes are handled, in the **Process reports**, by systematically going through a set of defined physical variables that could mediate influences and by the systematic treatment of boundary conditions for each process. These procedures are further described in Section 7.3. Hence, in addition to including FEPs describing influences and couplings, the procedures for process documentation are set up in a way that enforces a systematic search for such influences.
- A sufficient set of external influences. This is obtained by including in the assessment all relevant external FEPs and by structuring the documentation of these in the **Climate report** in a format similar to that used for the internal processes (see further Chapter 6).

Scenario selection

Another aspect of system uncertainty concerns the selection of a sufficient set of scenarios, through which all relevant FEPs are considered in an appropriate way in the analysis. The selection of scenarios is a task of a subjective nature, meaning that it is difficult to propose a method that would guarantee the correct handling of all details of scenario selection. However, several measures have been taken to build confidence in the selected set of scenarios:

- A structured and logical approach to the scenario selection, see further Chapter 11.
- The use of safety function indicators in order to focus the selection on safety relevant issues, see Chapter 8.
- The use of bounding calculation cases to explore the robustness of the system to the effects of alternative ways of selecting scenarios, including unrealistic scenarios that can put an upper bound on possible consequences.
- QA measures to ensure that all FEPs have been properly handled in the assessment.
- The use of external reviews.

Conceptual uncertainty

The handling of conceptual uncertainty for internal processes is essentially described in the **Process reports**. For each process, the knowledge base, including remaining uncertainties, is described and, based on that information, a handling of the process in the safety assessment is established. (Uncertainty regarding influences between processes can be seen as either system uncertainty or conceptual uncertainty; it is described as system uncertainty above.)

Through the use of a defined format for all process descriptions (see Section 7.3), it is assured that the processes and their associated conceptual uncertainties are described in a consistent manner. External reviews of central parts of the process documentation have also been performed.

Conceptual uncertainty for external influences is handled in a more stylised manner, essentially through the definition of a sufficient set of scenarios and by using state-of-the-art models for the quantification of external influences. Another method is the use of bounding cases that ensure that the consequences are overestimated.

Data uncertainty

Data uncertainties are handled according to the routines described in Chapter 9 and further in the **Data report**.

Quality assurance is obtained through the use of a template for data uncertainty documentation, through clearly defined roles for participating experts and generalists and by the use of external reviews prior to finally establishing input data for the assessment.

Modelling

An essential part of the assessment concerns the quantification of both repository evolution and dose and risk consequences through mathematical modelling. Apart from requiring appropriately defined models that represent relevant conceptualisations of the processes to be modelled and quality assured input data, this step requires:

- Good model documentation, including results of code verification and results of benchmarking against other models.
- Procedures to detect and protect against human error in the execution of the models.

A dedicated **Model summary report**, compiled according to a pre-established template describes models used in the assessment and provides references to more detailed descriptions of the models, including quality assurance aspects. The mapping of processes to models (see Chapter 7), provides an overview of the models used. A guiding principle is that models and data should be documented in sufficient detail to allow calculations to be reproduced and audited.

Human errors can be minimised e.g. by formal procedures for checking that input data are correct and by the use of alternative, often simplified, models for crucial aspects of quantification. An example of the latter is given in calculations of radionuclide transport and dose in Chapter 13.

2.8.4 Integrated handling of uncertainties

As mentioned above, uncertainties can be broadly categorised as system uncertainty, conceptual/model uncertainty and data uncertainty. It needs to be assured that all these uncertainties are appropriately handled in the assessment. Since the distinction between the main scenario and additional scenarios is largely related to uncertainties and the likelihood of occurrence of relevant phenomena, the overall strategy for handling of uncertainties is closely related to the selection of scenarios.

The general discussion on handling of uncertainties is further developed below, based on the process of scenario selection.

A first step of integration: The reference evolution

The analysis of the reference evolution is divided into a number of sub-analyses covering different time frames and various, essentially thermal, mechanical, hydraulic and chemical, aspects of the evolution within a particular time frame.

Many of the analyses in the reference evolution aim at demonstrating that a certain criterion is met, i.e. they are bounding analyses, establishing favourable conditions for subsequent parts of the assessment. The results of these analyses essentially facilitate subsequent parts of the assessment and do not, in general, require any further evaluation of uncertainties. For example, the peak buffer temperature is calculated in a bounding fashion and demonstrated to lie below the safety function indicator of 100 °C with all uncertainties considered, thus allowing the exclusion of mineral transformations in the buffer.

Other analyses lead to results that need to be considered in a more profound and often quantitative fashion in subsequent analyses. For examples, the result of the hydrogeological analyses point to both conceptual and data uncertainties that need to be considered in, e.g. radionuclide transport calculations.

Thus, in terms of uncertainties, the analyses in the reference evolution aim at reducing the number of uncertainties requiring further consideration and at identifying and quantifying uncertainties that need to be propagated to subsequent parts of the assessment.

To obtain a systematic handling of uncertainties in the reference evolution, each sub-analysis is concluded with a reporting of uncertainties in the results. The need for propagation of any uncertainties to subsequent parts of the safety assessment is also reported.

After completion of the analysis of the reference evolution, an account of the identified uncertainties is given in table format for subsequent use in the selection of scenarios and calculation cases for consequence analysis of the scenarios.

The main scenario

As mentioned in Section 2.5.8, the main scenario is based on the reference evolution analysed in Chapter 10 and thus covers a reference initial state, based on a realistic description of the repository system immediately after closure and a realistic description of the site with uncertainties, based on the results of site investigations and subsequent site descriptive modelling. Furthermore, all processes identified as relevant for post-closure safety are addressed in the main scenario, in accordance with documentation in the **Process reports**. The main scenario also covers reference external conditions, essentially a repetition of conditions reconstructed for the last glacial cycle and a variant with an extended period of temperate climate caused by an increased greenhouse effect. Future human actions, like drilling or other use of or influences on the host rock are, by definition, not included in the main scenario.

The following is a brief account of how the three classes of uncertainty defined in Section 2.8.1 are addressed in the reference evolution and hence in the main scenario.

General evolution

System uncertainty, FEPs included: All identified internal processes are considered and included in accordance with prescriptions developed in the **Process reports** and summarised in Table 7-2 through Table 7-6. External conditions are included as a base case in the form of a model reconstruction of the last glacial cycle, the Weichselian and the Holocene, and in a global warming variant of the main scenario. This means that *all external, climate related processes/phenomena are considered* in the main scenario. The extent to which the processes and phenomena are addressed is, however, limited to the range covered by the two variants, meaning that e.g. larger glacial loads than those in the reference evolution are not considered. FEPs related to future human actions, FHA, are by definition excluded from the main scenario, as are FEPs related to altered initial states like an abandoned repository that has not been completely backfilled and sealed.

Conceptual uncertainty: Models are selected, taking into consideration conceptual uncertainty, according to prescriptions in the **Process reports** (summarised in Table 7-2 through Table 7-6) and the **Climate report**. In many cases, conceptual uncertainties are handled pessimistically. They may also be addressed by formulating variant representations, as in the case for groundwater flow models. These models constitute the reference conceptual models for the repository evolution in the PSAR. They are summarised in the **Model summary report**.

Data uncertainty: Input data for modelling, with uncertainties, are taken from the **Data report** for many of the calculations related to the general evolution in the main scenario. Reference initial state data, which can imply a range of conditions, are used in accordance with the definition of the main scenario.

Radiological consequences

All situations where radiological consequences occur are treated more exhaustively in the additional scenarios. Radiological consequences of the main scenario, including uncertainties, are subsumed under relevant cases covering the additional scenarios, see below.

Additional scenarios based on potential loss of safety functions

A main purpose of the selection and analysis of a number of additional scenarios based on the potential loss of safety functions is to evaluate the effect of uncertainties not covered in the main scenario and, if appropriate, to include additional scenarios in the overall risk summation if this additional uncertainty analysis so requires.

In each of these additional scenarios, the handling of relevant aspects in the main scenario is revisited and the handling of relevant system, conceptual and data uncertainties is extended or modified, as appropriate.

General evolution

System uncertainty, FEPs included: All relevant FEPs potentially affecting the safety function under consideration are included, based on the FEP chart and the SR-Site FEP catalogue.

Conceptual uncertainty: Conceptual uncertainty beyond that covered by the reference conceptual models used in the main scenario is considered.

Data uncertainty: Input data beyond those used in the main scenario are considered, e.g. initial state conditions beyond the reference initial state and external conditions beyond those covered by the two variants of the main scenario.

As only those aspects of the general evolution relevant for the safety function(s) under consideration are considered, the analysis of the general evolution is much less extensive than that in the main scenario.

Radiological consequences

System uncertainty, FEPs included: All FEPs considered in the general evolution are included indirectly, since data for the consequence calculations are derived from the result of the analysis of the system evolution. All FEPs directly related to radionuclide transport in the engineered barriers and in the geosphere are included in accordance with prescriptions in the **Process reports** (summarised in Table 7-2 through Table 7-6). The biosphere models used in SR-Site are discussed in Andersson (2010), Löfgren (2010), Aquilonius (2010) and Lindborg (2010). Developments after SR-Site are summarised in Section 13.2.

Conceptual uncertainty: Models for radionuclide transport are selected, taking into consideration conceptual uncertainty, according to prescriptions in the **Process reports** (summarised in Table 7-2 through Table 7-6). In many cases, conceptual uncertainties are handled pessimistically. They may also be addressed by formulating variant representations, as is the case for groundwater flow models. These models constitute the reference conceptual models for the radiological consequence calculations in the PSAR. They are summarised in the **Model summary report**.

Conceptual uncertainties for the biosphere models used in SR-Site are discussed in Avila et al. (2010) and the **Biosphere synthesis report**. Developments after SR-Site are summarised in Section 13.2.

Data uncertainty: All data for the consequence calculations are given in the **Data report**. In most cases, input data uncertainties, frequently also those originating from conceptual uncertainties, are quantified in the form of a set of input data distributions. Correlations between these distributions are considered and included as appropriate. Uncertainty of input data to the biosphere modelling is considered in Nordén et al. (2010), Andersson (2010), Löfgren (2010), Aquilonius (2010) and Lindborg (2010). Developments after SR-Site are summarised in Section 13.2.

If the altered evolution does not imply canister failures, then failures related to the safety function under consideration are postulated and the scenario is classified as a residual scenario. The consequence calculations for such cases often provide bounding estimates e.g. in a case where all canisters are assumed to fail at a specific time.

FHA scenarios

FHA scenarios obviously include FHA FEPs that are, by definition, not included in the main scenario. The aspects of the general evolution that are not affected by the FHA FEPs are assumed to develop as in the main scenario, meaning that conceptual and data uncertainty for these aspects are handled as in the main scenario. Aspects related to the FHA FEPs are handled in a stylised manner that gives a reasonable coverage of uncertainties. The case of an open, abandoned repository is treated similarly.

2.8.5 Formal expert elicitations

A formal expert elicitation is a tool for assessing uncertainty in input to a safety assessment. In planning SR-Site, an evaluation of candidate issues for expert elicitations was made and the following criteria were used to determine whether an issue could be considered for an elicitation:

- The issue should be associated with large uncertainties that have a considerable impact on the assessed level of safety.
- A formal expert elicitation can be deemed to contribute to the reduction of these uncertainties in addition to what is achievable through other means established in the methodology for the assessment (evaluation of conceptual uncertainties in the **Process reports**, of data uncertainty in the **Data report**, through quality assured modelling, etc. all of these leading to a well-motivated and often pessimistic handling of the issue in the assessment).

The conclusion of the evaluation was that, although a number of uncertainties could in principle be amenable to a formal expert elicitation, no issue was identified for which both the above criteria apply.

The procedures established for the qualification of processes and data in SR-Site, the considerable and concerted research activities on critical issues, the comprehensive site modelling by expert groups including thorough evaluation of uncertainties and the formulation of a confidence statement, the reviewing by external experts, and the pessimistic handling of many factors in the assessment all contribute to this conclusion.

Based on the sensitivity analyses of the calculated risk in SR-Site, the evaluation of candidate issues for expert elicitations was updated (Section 13.10.2 of SKB 2011), forming input to future handling of uncertain issues of importance for post-closure safety. There, it was concluded that, although a number of uncertainties could in principle be amenable to a formal expert elicitation, no issue was identified for which both i) the calculated risk was highly sensitive to the uncertainty and ii) the uncertainty could be expected to be significantly reduced through a formal expert elicitation. Therefore, formal expert elicitations have not been employed in the PSAR, with the exception of a reference to a study regarding the likelihood of large earthquakes occurring in the vicinity of the repository (Hora and Jensen 2005). The result of that limited study is used as one of several inputs to determine this likelihood in the PSAR.

2.9 Quality assurance

2.9.1 General

In broad terms, Quality assurance (QA) procedures for a post-closure safety assessment of a spent nuclear fuel repository aid in assuring that all relevant factors for post-closure safety have been appropriately included and handled in the safety assessment. Although no QA system will rigorously prove that this is the case, purpose-designed procedures will assist the implementer in carrying out the safety assessment in a structured and comprehensive manner and aid a reviewer in judging the quality and comprehensiveness of the assessment. Quality assurance measures are one important element in building confidence in the fact that e.g. a model representation of a site or of a process is an adequate and sufficient representation of reality for the purposes of the safety assessment.

A principal purpose of a safety assessment of a final repository is to investigate whether the repository can be considered radiologically safe over time. In principle, this is established by comparing estimated releases and associated radiation doses and risks with regulatory criteria.

A large number of factors affecting post-closure safety need to be addressed in the assessment in a quality-assured manner. These factors – or features, events and processes, FEPs – are collected in a database that is also used as a QA instrument. The FEP database and underlying reports demonstrate how specific FEPs are included in the assessment or why they have been excluded.

The handling of many of the FEPs occurs in modelling of the repository evolution. This requires a scientific evaluation of the understanding of the processes involved in the modelling, the formulation of mathematical models that simulate the process or system of coupled processes based on the understanding of the phenomena, the translation of the mathematical model into a computer code, the derivation of input data and execution of the code. All these aspects need to be documented and quality assured.

More specifically, QA procedures aid in demonstrating:

- That all factors relevant for post-closure safety occurring in earlier versions of SKB databases and in the international NEA FEP database have been considered in the assessment.
- That the exclusion of any of these factors is well motivated by an identifiable expert.
- That the handling of included factors is well justified by identifiable experts.
- How quantitative aspects of the assessment are handled by mathematical models and how the models (computer codes) and the uses of the models have been quality assured.
- How appropriate data for quantitative aspects of the assessment have been derived and used in the assessment in a quality assured and traceable manner.
- How the safety assessment reports have been properly reviewed and approved for correct and complete content.

2.9.2 QA procedure for the PSAR assessment of post-closure safety

In accordance with SKB's procedures for project management, described in the management system, quality assurance plans for the PSAR project were developed and implemented.

The assessment of post-closure safety for the PSAR is produced as part of the overall PSAR project, as explained in Section 1.1. The post-closure safety assessment has, therefore, been produced under the quality assurance routines applicable for the overall PSAR project. These routines are all part of SKB's management system and concern e.g. project management and documentation routines, and routines for report production and report reviewing.

Much of the material in the assessment of post-closure safety for the PSAR was produced within the SR-Site assessment and was hence produced under the QA plan of that project, see further Section 2.9 in SKB (2011). In addition to the general SKB routines for report production, templates with instructions regarding contents and structure were developed for several of the main references to the SR-Site main report, as described in the SR-Site QA plan. These templates, with minor modifications, have been applied also for the reports that have been updated to PSAR versions. This concerns the PSAR versions of the **Fuel and canister process report**, the **Buffer, backfill and closure process report**, the **Geosphere process report**, the **Climate report**, the **Data report** and the **Model summary report**. The templates are given in the introductory chapters of the reports in question. As further developed in Section 3.5, the SR-Site version of the **FEP report** has not been updated for the PSAR, since a review of the international development in the area of FEPs of relevance for a KBS 3 repository since the publication of the SR-Site report demonstrated only minor changes. Therefore, the PSAR is based on the SR-Site assessment as regards the several QA aspects of the development of an encompassing FEP database and the handling of relevant FEPs in the post-closure safety assessment.

Information on storage of input data and modelling results is given in the **Model summary report**.

As explained in Section 1.3.3, a key input to the production of this post-closure safety report is the findings in SSM's review of the SR-Site report. An important aspect of the QA procedures for the present report is, therefore, the routines followed to ensure that the issues in the review are adequately addressed. As mentioned in Section 1.3.3, SKB's handling of the issues raised in SSM's report is documented in tabulated form.⁸ Part of the issues are addressed in the PSAR whereas for others, plans for their handling in the preparation of the forthcoming operation license application have been formulated.

2.9.3 Expert judgements

Information based on expert judgements of various kinds permeates safety assessments. Expert judgements can include anything from a scientist's interpretation of a result of a straightforward experiment to an expert's judgement on the impact of an increased greenhouse effects on the future climate evolution or to an assessment of the likelihood of the occurrence of a particular process/phenomenon that could have an impact on repository evolution. A judgement could consist of

⁸ "Hantering av SSM:s granskning kopplat till Kärnbränsleförvaret". (In Swedish.) (Internal document.) *In prep.*

anything from a well-justified quantitative or qualitative statement in a report, to an exhaustive and formal questioning of a carefully selected panel of experts using an approved elicitation protocol.

Furthermore, there are issues on which different experts have differing views. In cases where a consensus view or statement cannot be achieved, it is necessary to take the differing views into account in the assessment. This can be done e.g. through the formulation of several calculation cases or by choosing the most pessimistic approach, if such an approach can be shown to exist.

Most of the information based on expert judgements in the PSAR is provided either in the form of reports written by one or several experts or as decisions made by generalists in e.g. the screening of FEPs, the selection of scenarios or the formulation of calculation cases. Formal questioning of a panel of experts has not been employed in the PSAR (see further Section 2.8.5).

Documentation of expert judgements

For the traceability of the assessment, it is important to clearly state where expert judgements are made and by whom. For this purpose, all important experts providing, in one way or another, expert judgements for the PSAR are accounted for in a dedicated document. This document contains information on the role of the experts in the PSAR, a motivation for their selection as experts and references to where at SKB the credentials of the experts are filed. The document will not be published, but will be made available to reviewing authorities on request.

Also, the present and other reports have been subject to scrutiny within SKB and by external reviewers, as documented in the review protocols (see Section 2.9.4). These reviewers are also included in the list of experts.

Selecting experts

In general, no formal rules for the selection of experts have been applied. The core team of the assessment provide a large fraction of the expert judgements and these individuals have been working with the safety of the KBS-3 system for a number of years and are, therefore, among the most experienced individuals available on the various aspects of the analysis of the system. This does, however, also imply a risk of bias, stressing the importance of external reviews of the material developed within the project (see further Section 2.9.4).

Regarding experts for the documentation of process understanding, for the selection of models or of input data for the quantitative aspects of the assessment, the ambition has been to contract leading experts in the field. These reviewers should be recognised experts (i.e. qualified and experienced, as reflected by their research publication record) in the relevant scientific field. The merits of these experts are documented, providing a sufficient justification for their involvement.

2.9.4 Peer review

Peer reviewing with subsequent handling of review comments is an important method for broadening the basis on which expert opinions/judgements are formed in a safety assessment. All reports produced in the PSAR post-closure safety project have therefore been subject to peer review prior to being finalised, according to a SKB's routine for reviewing of technical documents. This routine defines the document that should be provided to the reviewers, general criteria for acceptance of a report, requirements on reviewers' competence and how the review documents shall be handled. The review routine further prescribes that a review instruction is produced for each report subject to review in which the general as well as report-specific acceptance criteria are specified together with the selected reviewers and their competence.

A template for review comments is used and this template also requires the author of the report to document how each comment is handled when the report is finalised. These review statements are filed in SKB's internal documentation system SKBdoc to ensure traceability of the review process.

3 FEP processing

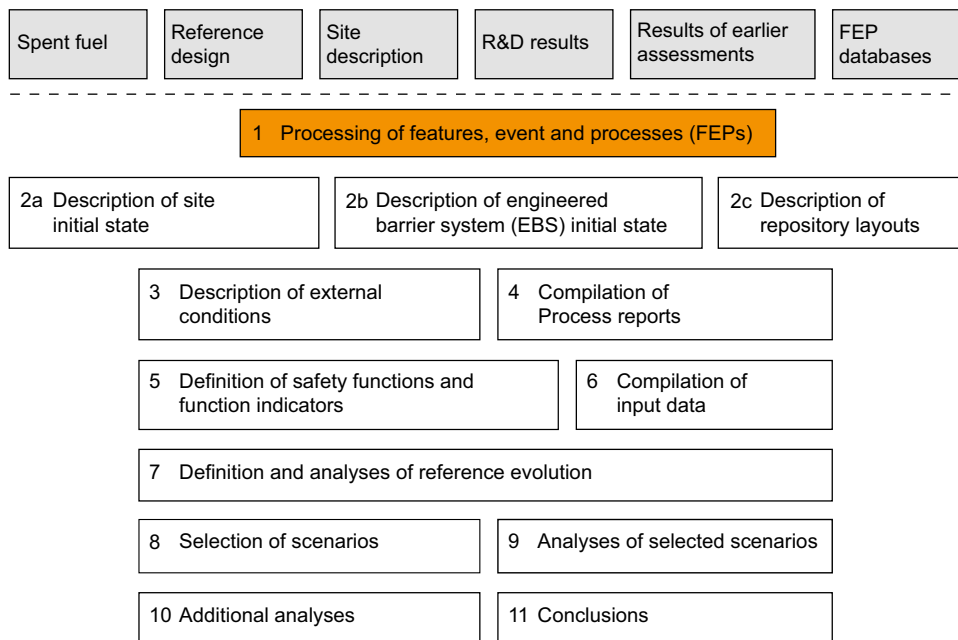


Figure 3-1. The PSAR methodology in eleven steps (Section 2.5), with the present step highlighted.

3.1 Introduction

Much of the methodology described in the previous section is related to the handling of FEPs (Features, Events, Processes) through the different steps of the safety assessment. This section describes in more detail how FEPs are handled throughout the assessment and the various tools used to ensure systematic and comprehensive handling.

A main aim in the FEP handling was to establish a catalogue of FEPs that needed to be addressed in the PSAR. The text in Sections 3.2 to 3.4 relates to the SR-Site assessment and is relevant also to the PSAR, since, as explained in Section 3.5, the developments after the SR-Site assessment have led to only minor changes of the set of FEPs to be addressed in the assessment and since all procedures for the handling of FEPs are unchanged. The text in Sections 3.2 to 3.4 is identical to that in Sections 3.2 to 3.4 in the SR-Site main report (SKB 2011).

3.2 SKB FEP database

An important and formal tool for ensuring that all relevant factors have been considered in the safety assessment is provided by available databases of features, events and processes relevant to post-closure safety of nuclear waste repositories. An SKB FEP database has been developed for SR-Site, as described in the **FEP report**. This FEP database builds on the outcome of the FEP work conducted in SKB’s two most recent major safety assessments for the spent fuel repository, the SR-Can and SR 97 assessments, as reported in the SR-Can FEP report (SKB 2006b), the SR 97 Process report (SKB 1999b) and the supporting documentation on the Interaction matrices developed for a deep repository of the KBS-3 type (Pers et al. 1999).

In the SR 97 Process report (SKB 1999b), comprehensive sets of long-term processes relevant to repository safety for each of the system components, i.e. fuel, canister, buffer/backfill and geosphere, were identified. For each component, a set of variables needed to describe the evolution of the state of the component over time was also established. As a first step in the development of the SKB FEP database, these identified processes and variables were collected in an SR 97 FEP database, forming an important starting point for the SR-Can FEP handling.

The SR 97 database was then systematically compared with other national databases included in version 1.2 of the NEA international FEP database (NEA 1999b), to ensure that all relevant factors were taken into account. In the SR-Can version of the SKB FEP database, all items were classified as one of the following:

- Processes within the system boundaries relevant to post-closure safety and the system component specific variables required to describe the state of the component at a specified point in time.
- Factors affecting the initial state of the repository, either directly related to a specific aspect or to the initial state in general.
- External factors relevant to post-closure safety, e.g. evolution of climate and climate related issues, and human intrusion.

Most FEPs in version 1.2 of the NEA database could be mapped to one of these categories. All other FEPs were characterised as general methodology issues or determined to be irrelevant for the KBS-3 system.

Since the completion of the FEP work within SR-Can, an updated electronic version, version 2.1, of the NEA FEP database has become available (NEA 2006). Compared to version 1.2 of the NEA FEP database, version 2.1 contains FEPs from two more projects. As part of SR-Site, all new project FEPs in version 2.1 of the NEA FEP database have been mapped according to the methodology adopted in SR-Can resulting in an SR-Site version of the SKB FEP database. The present SKB FEP database thus encompasses the SR 97 version, the SR-Can version and the SR-Site version of the FEP database. The SR 97 version contains the SR 97 processes and variables. The SR-Can and SR-Site versions contain all FEPs in the NEA database and in the national databases linked to the NEA database, versions 1.2 and 2.1, respectively, including the classification and characteristics of these FEPs. A more detailed description of the SKB FEP database, in particular the SR-Site version, is provided in the **FEP report**.

3.3 SR-Site FEP catalogue

Based on the FEP processing conducted for SR-Can and briefly described above, an SR-Can FEP catalogue was established. This FEP catalogue contains all FEPs that needed to be handled in SR-Can and is thus fundamentally a subset of FEPs in the SKB FEP database. However, some of the system components were not treated in detail in SR-Can, and for these system components preliminary FEPs were included in the SR-Can FEP catalogue. These components were tunnel plugs, backfill materials for cavities other than the deposition tunnels, the bottom plates in the deposition holes and borehole seals. Furthermore, biosphere processes were not included in the SR 97 Process report and there was, therefore, not the same basis for updating these descriptions in SR-Can as for the engineered barriers and the geosphere. Therefore, the SR-Can FEP catalogue contains provisional biosphere FEPs corresponding to the sub-components of the biosphere system, to which biosphere FEPs in the NEA FEP database are mapped.

The SR-Site FEP catalogue is a developed version of the SR-Can FEP catalogue. For the system components not treated in detail in SR-Can, as well as for the biosphere, SR-Site FEPs have been defined and included in the FEP catalogue. The mapping of NEA Project FEPs made to the preliminary and provisional FEPs for these system components in SR-Can has been revisited and a new mapping has been made to the FEPs now included in the SR-Site FEP catalogue. The categories of FEPs in the SR-Site catalogue are listed below.

- Initial state FEPs.
- Processes in fuel, canister, buffer, backfill, tunnel plug, central area, top seal, bottom plate in deposition holes, borehole seals and geosphere.
- Variables in fuel, canister, buffer, backfill, tunnel plug, central area, top seal, bottom plate in deposition holes, borehole seals and geosphere.
- Biosphere FEPs.
- External FEPs.
- Methodology issues.

In addition, there is a possibility to enter in the FEP catalogue any issue that is, for whatever reason, identified as relevant for the safety assessment. For SR-Can, some site-specific issues identified in the preliminary safety evaluation of the sites were included. For Forsmark these issues concerned the potential impact of nearby nuclear power plants and the power cable to Finland and the effect of a deep mine excavation near, but outside, the tectonic lens at Forsmark. For SR-Site, no additional issues that are not covered by FEPs already included in the SR-Site FEP catalogue were identified.

In the following, each category is briefly described.

Initial state FEPs

This category describes deviations from the intended initial state as a consequence of undetected mishaps, sabotage, repository left open, etc. These are propagated to the selection of scenarios described in Chapter 11. The initial state FEPs in the SR-Site FEP catalogue are in essence the same as those in the SR-Can FEP catalogue. The only exception is that two initial state FEPs defined for backfill of other repository parts in the SR-Can catalogue, in the SR-Site catalogue are replaced by two initial state FEPs defined for the central area and two for the top seal.

It should be noted that the intended initial state with tolerances, the reference initial state, is one of the bases for the main scenario. The reference initial state for the different system components is described in Chapter 5 based on information in the **Production reports** and in the **Underground openings construction report**. In the FEP catalogue, each variable record, see below, contains also a reference to the description of the reference initial state for that variable.

Processes

These FEPs are long-term processes relevant to repository safety for each of the system components fuel, canister, buffer, backfill, tunnel plug, central area, top seal, bottom plate in deposition holes, borehole seals and geosphere. All internal processes are comprehensively documented in a number of **Process reports**, see further Chapter 7. The handling of all processes in the fuel, canister, buffer, backfill and geosphere is summarised in process tables, given in Chapter 7. There are typically around 20 processes for each system component.

A few modifications in the list of internal processes for the system components fuel, canister, buffer, backfill and geosphere have been made compared to the list of processes included in SR-Can. These modifications were not initiated by the complementary mapping of new project FEPs in version 2.1 of the NEA FEP database, but have been made to improve the structure and logic of the descriptions. For example, to improve the handling of uncertainties in the geochemical evolution of the buffer, some mechanisms included in integrated descriptions in SR-Can are in SR-Site included as separate processes, e.g. iron-bentonite interactions and cementation. Another example concerns a modification in the list of geosphere processes. In SR-Can, surface erosion and weathering was described in the Geosphere process report (SKB 2006d), but in SR-Site the description of these mechanisms is included in the **Climate report** and also addressed and considered in the biosphere analyses and reporting. For the system components not treated in detail in SR-Can, i.e. tunnel plugs, central area, top seal, bottom plate in deposition holes and borehole seals, process FEPs have been established largely based on the list of processes defined for the system components buffer and backfill. The outcome of the mapping in SR-Site of FEPs in the NEA FEP database was used to check that no relevant processes are missing in the set of processes for these system components.

Variables

These FEPs are the variables needed to describe the evolution of the state of the fuel, canister, buffer, backfill, tunnel plugs, central area, top seal, bottom plate in deposition holes, borehole seals and geosphere over time. They are thus essentially tables with definitions. The identification of variables has been done by the experts responsible for the documentation of the processes relevant for post-closure safety. The sets of variables were established in conjunction with the documentation of the processes, since it had to be ensured that the variable sets were suited to describe all conceivable alterations of the barrier properties as a result of the long-term processes. There are typically around 10 variables for each system component. In the FEP catalogue, each variable record contains a reference to the description of the reference initial state for that variable.

The handling of influences between processes and variables is described in Section 3.4.

Biosphere FEPs

Biosphere processes were not included in the SR 97 Process report (SKB 1999b) and there was not the same basis for updating these descriptions in SR-Can as for the engineered barriers and the geosphere. In SR-Can, provisional biosphere FEPs were defined and included in the SR-Can FEP catalogue. For SR-Site, a biosphere process report was developed. That report contains general descriptions of the processes considered to be of importance for the safety assessment, whereas the site-specific aspects of the processes and how these are handled in the safety assessment are provided in the various ecosystem reports developed for SR-Site (Andersson 2010, Aquilonius 2010, Löfgren 2010) (see Section 7.1.2). In the SR-Site FEP catalogue, a FEP record is included for each biosphere process defined in the biosphere process report. These FEP records contain references to the corresponding process description in the biosphere process report as well as to the report where the handling of the process in SR-Site is documented.

External FEPs

FEPs in the NEA database defined as external FEPs in SR-Can were subdivided into the categories listed below. The complementary mapping of new project FEPs in the NEA FEP database version 2.1 carried out for SR-Site did not point out any need to modify the categorisation of external FEPs. Consequently, the categories of external FEPs in SR-Can and in SR-Site are:

- climate related issues,
- large-scale geological processes and effects,
- future human actions,
- other.

Climate issues and their handling are described in the **Climate report**. In SR-Can, ten climate FEPs were defined to represent the climate issues described in the SR-Can Climate report (SKB 2006c). The NEA Project FEPs associated with these SR-Can climate FEPs and their handling in SR-Can were documented in the SR-Can FEP catalogue. The SR-Site FEP catalogue contains essentially the same climate FEPs as the SR-Can FEP catalogue, although somewhat restructured, but also one additional FEP, “Denudation”. This additional FEP corresponds to the SR-Can geosphere process “Surface weathering and erosion”, which in SR-Site has been categorised as a climate related and biosphere issue rather than a geosphere process. In SR-Site, the handling of each NEA Project FEP has been revisited and updated as appropriate, including new NEA Project FEPs in version 2.1 of the NEA FEP database that are mapped to these climate FEPs.

Large-scale geological processes and effects were covered in SR-Can by two FEPs in the SR-Can FEP catalogue and described in the SR-Can Geosphere process report (SKB 2006d). As with the climate-related issues, it was checked that relevant aspects of the NEA Project FEPs mapped to these large-scale geological process FEPs were covered in the descriptions of these processes in the Geosphere process report. The outcome of this check was documented in the SR-Can FEP catalogue. In SR-Site, the documentation in the SR-Can FEP catalogue has been revisited and updated as appropriate, considering also new NEA Project FEPs in version 2.1 of the NEA FEP database that are mapped to these large-scale geological process FEPs.

Future human actions and how these are handled in the safety assessment are described in the **FHA report**. In SR-Can, seven FHA FEPs were defined to represent future human actions described in the SR-Can FHA report (SKB 2006e). Each NEA Project FEP mapped to these SR-Can FHA FEPs and their handling in SR-Can was documented in the SR-Can FEP catalogue. The same seven FHA FEPs are included in the SR-Site FEP catalogue. However, the documentation of the handling of each NEA Project FEP mapped to these SR-Site FEPs was revisited and updated as appropriate, considering also new NEA Project FEPs in version 2.1 of the NEA FEP database that are mapped to these SR-Site FHA FEPs.

In the category “other”, only meteorite impact was identified in SR-Can, but excluded from further analysis, see Section 6.1. However, meteorite impact was still defined as a FEP in the SR-Can FEP catalogue for documentation purposes and the justification for excluding this FEP from further analysis was documented in the FEP record in the SR-Can FEP catalogue. The audit of the new NEA Project FEPs in version 2.1 of the NEA FEP database has not indicated any need for modifications. Therefore, for documentation purposes, the FEP was maintained in the SR-Site FEP catalogue.

The handling of external FEPs is further addressed in Chapter 6.

Methodology issues

A number of relevant issues relating to the factual basis for the assessment and to the methodology of the assessment were identified in the NEA FEP database. Most of these are of a very general nature, but were for the sake of comprehensiveness also included in the SR-Can FEP catalogue. The audit of the new NEA Project FEPs in version 2.1 of the NEA FEP database has not resulted in any need for modifications. Therefore, the SR-Site FEP catalogue contains the same methodology FEPs as the SR-Can FEP catalogue.

3.4 Couplings

FEPs are coupled in several ways and on several levels. Couplings between processes and variables occur within a system component and the system components influence each other in several ways. The following is a description of different types of couplings and tools used to document and visualise them.

Influence tables

Within a system component, each process is influenced by one or several of the variables describing the state of the component and the process, in turn, influences one or several of the variables. These couplings within a system component are described by influence tables, one for each process in the **Process report**. A distinction is made between influences that exist in principle but are sufficiently insignificant to be neglected in the safety assessment and those that require a detailed treatment. The handling of the latter category is explicitly mentioned as the handling of the process in question is established in the **Process reports**. See Section 7.3 for an example of an influence table. The influence tables are fed back to the FEP catalogue from the **Process reports**. Couplings across system components are described in the process descriptions in the **Process reports** under the heading “Boundary conditions”, see further Section 7.3.

Process diagrams

Based on the sets of variables and processes and the influences between them, a process diagram can be constructed for each system component. This is done in the FEP database. The diagram essentially takes the form of a table with the processes as lines and the variables as columns. The table matrix consists of arrows visualising the presence of influences between processes and variables and a colour coding of the arrows displaying if the influence is handled or not in the assessment.

AMF, Model summary report

When evaluating repository evolution, a number of coupled or interacting models are utilised. This set of models and the dependencies/interactions between them are described by two assessment model flow charts, AMFs. One concerns the excavation/operation and initial temperate period and one represents periglacial and glacial conditions. These are further described in Section 7.5. A **Model summary report** describes the models represented in the AMFs. The AMFs are also included in the FEP database as well as the process tables and the tables that links the AMF and process tables, see Sections 7.4 and 7.5, respectively.

FEP chart

On a higher level, it is desirable to have an instrument providing an overview of how critical initial state factors, variables, processes and external factors influence the safety functions of the repository. To serve this purpose, a FEP chart has been developed. This is further described in Section 8.5, following a discussion on repository safety and the definition of a number of safety function indicators. The FEP chart is also included in the FEP database with links to the process table that also is included in the FEP database.

Handling of couplings

The overwhelming majority of the large number of couplings that are in principle present in the system are not directly included in any of the models used to quantify the development of the system. Justification for the neglect of couplings is provided e.g. in the **Process reports** where i) some processes, and thereby also their couplings, are argued to be negligible, and ii) where the inclusion or neglect of internal couplings is justified in conjunction with the influence tables, see Section 7.3.

Furthermore, in many cases, a modelling effort results in a bounding value on a certain property of the system, and this result is then used to put bounds on related phenomena of relevance for safety, without a detailed coupled model. The near-field temperature is an example: By modelling, it is demonstrated that the buffer temperature never exceeds a certain limit and this result is used to argue that long-term mineral alterations in the buffer can be neglected, i.e. the coupling between temperature and chemical reactions is addressed without a fully coupled model. In this example, a further detail concerns the handling of the thermal properties of the buffer for which it is assumed that the buffer is unsaturated, which maximises the calculated peak temperatures, i.e. the coupling between buffer saturation and temperature is taken into account from the point of view of safety without a coupled model. Many of these relationships are demonstrated in the process tables, Table 7-2 to Table 7-6 in Chapter 7.

The modelling and couplings are thus not in all respects aiming at a realistic representation of the system, but at one that is adequate for the argumentation in the safety assessment, an approach that in many cases allows considerable simplifications to be made.

The detailed justification of the approach is provided through the collected information behind modelling approaches and assumptions regarding all the particular issues, informed by the understanding of the safety relevant aspects of the system.

The handling of FEPs in SR-Site is summarised in Figure 3-2.

- a. The starting points for the SR-Site FEP handling are FEPs in the SR-Can version of the SKB FEP database including the SR-Can FEP catalogue and associated SR-Can reports, and the two national data bases that are new in the NEA international FEP database version 2.1 as compared with version 1.2, which was the starting point for the SR-Can version of the SKB FEP database.
- b. FEPs are sorted into three main categories: i) initial state, ii) internal process and iii) external FEPs. FEPs are also categorised as irrelevant or as being related to methodology at a general level.
- c. Initial state FEPs are either i) included in the initial state description in SR-Site, i.e. the reference description of the KBS-3 repository, the site description or the site-specific layout of the repository or ii) categorised as initial state deviations to be further handled in scenario selection.
- d. Process FEPs are used to update the SR-Can set of internal processes for the EBS (Engineered Barrier System) and the geosphere. The resulting SR-Site set of processes are documented in the SR-Site **Process reports**. Biosphere FEPs are defined in the **Biosphere process report** and the handling of each process is described in various biosphere reports.
- e. The handling of external FEPs related to long-term climate changes is documented in the **Climate report**. The few external, large-scale geosphere FEPs are addressed in the **Geosphere process report**.
- f. The handling of external FEPs related to future human actions (FHA) is developed in the **FHA report**. The only “other” external FEP, meteorite impact, was dismissed in SR-Can as being extremely unlikely and this applies also for SR-Site. No new “other” external FEPs have been identified for SR-Site.
- g. The FEPs handled in the yellow boxes constitute the SR-Site FEP catalogue.
- h. The reference initial state, all long-term processes and a reference external evolution are used to define a reference evolution for the repository system. This evolution is an important basis for specifying a comprehensive main scenario. A set of additional scenarios address e.g. deviations from the reference initial state and from the reference external evolution as well as situations related to FHA.

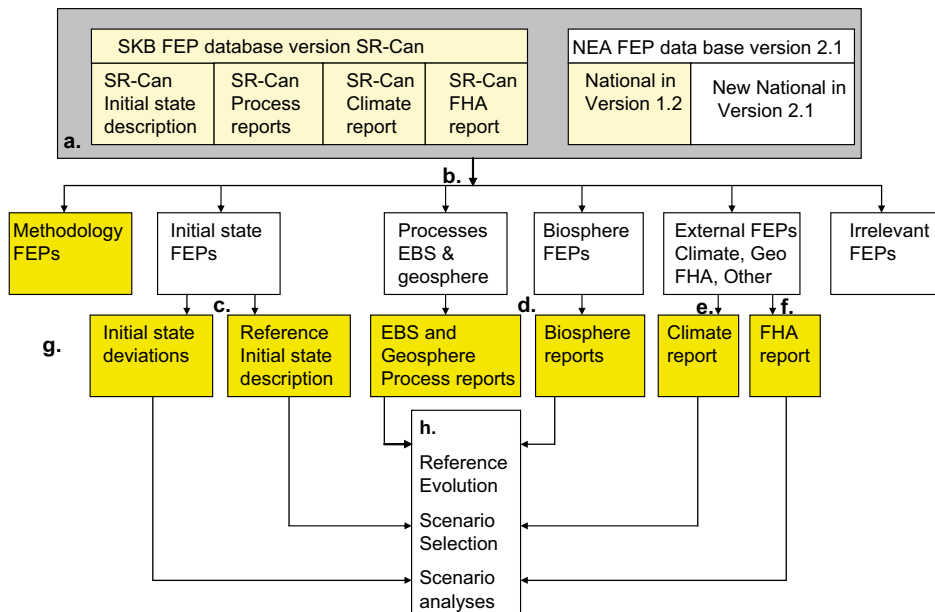


Figure 3-2. The handling of FEPs in SR-Site.

3.5 Developments after the SR-Site assessment

Since the SR-Site assessment, additional FEP lists from other relevant radioactive waste disposal projects have become available. In the FEP analysis carried out within the ongoing safety assessment for the SFR repository, SR-PSU (PSAR), these new FEP lists were checked against the content of the already established SR-PSU FEP catalogue. The following FEP lists were included in the analysis:

- *NEA International FEP (IFEP) List version 3.0* (NEA 2019), which the NEA released in 2019 together with a new web-based FEP Database (version 2.0) that has been subject to a major revision. The IFEP List has been revised both in terms of its structure and its content in comparison with the 2000 IFEP List (NEA 2000). Consistent with many of the more recent project specific FEP (PFEP) Lists (e.g. those from Sweden, Finland and Japan), the new IFEP List is structured around a classification scheme based on external factors and disposal components (waste package, repository, geosphere and biosphere), rather than on the 2000 IFEP List scheme that used external, environment and contaminant factors. Each FEP contains a description, category, commentary on its relevance to performance and safety, and mapping to related FEP(s) in the previous public version of the IFEP List. 268 IFEPs (including FEP groups and subgroups) are contained within version 3.0 of the NEA IFEP List.
- *Posiva's LILW repository* (Nummi et al. 2012), which is the FEP list for Posiva's safety case in support of the construction licence application for a geologic disposal facility situated at Olkiluoto, limited to the repository for the low and intermediate level waste.
- *OPG's LILW repository* (NWMO 2011), which is the FEP list for the post-closure safety assessment for Ontario Power Generation's proposed deep geologic repository for low and intermediate level waste at the Bruce nuclear site in Canada. It should be noted that the geological environment at the Bruce site differs significantly from the Forsmark site. The OPG repository is planned to be located in Ordovician age sediments overlaid by Silurian sediments. This important difference was kept in mind when comparing the FEP lists.
- *Posiva's SNF and LILW repositories* (unpublished FEP-list), which is the preliminary version of the FEP list for SC-OLA, which is Posiva's safety case in support of the operating licence application for a geologic disposal facility situated at Olkiluoto. This facility comprises a repository for disposal of spent nuclear fuel based on the KBS-3V design and a repository for the low and intermediate level waste arising from the operation and decommissioning of the encapsulation plant for the spent nuclear fuel.

The review did not result in any changes being made to the SR-PSU FEP catalogue and no formal documentation of the outcome of the review was added to the SKB FEP database. For the current PSAR for the spent fuel repository, much of the required review of these FEP lists in terms of actual content is provided by the above account. However, to ascertain that the development regarding all FEPs relevant to a KBS 3 spent fuel repository, in particular canister related FEPs, is captured, a dedicated effort with this focus was undertaken (Marsic et al. 2020). The outcome of this work is, in brief, that no additional FEPs were found.

Since the NEA IFEP List version 3.0 has undergone a major revision also in terms of structure, in future safety assessments (i.e. SAR), it may be relevant to reconsider the structure of the SKB FEP database and in particular the mapping made to other project-specific FEP lists (PFEPs). Also, since the new NEA IFEP list has only recently been released, it is considered best at this stage to wait for any updates that might follow before performing a revision of the SKB FEP database.

The SR-Site **FEP report**, amended with the documentation of the KBS 3 specific evaluation (Marsic et al. 2020) constitutes the documentation of the FEP handling in the PSAR. In addition, the SKB FEP database has been updated to reflect a couple of changes in the differentiation of processes for the canister and for the clay system (see Chapter 7 for the PSAR versions of the process tables). The SR-Site FEP report has thus not been updated and, as explained in Section 2.5.12, the short name **FEP report** refers in this PSAR post-closure safety report to the SR-Site FEP report.

4 The Forsmark site

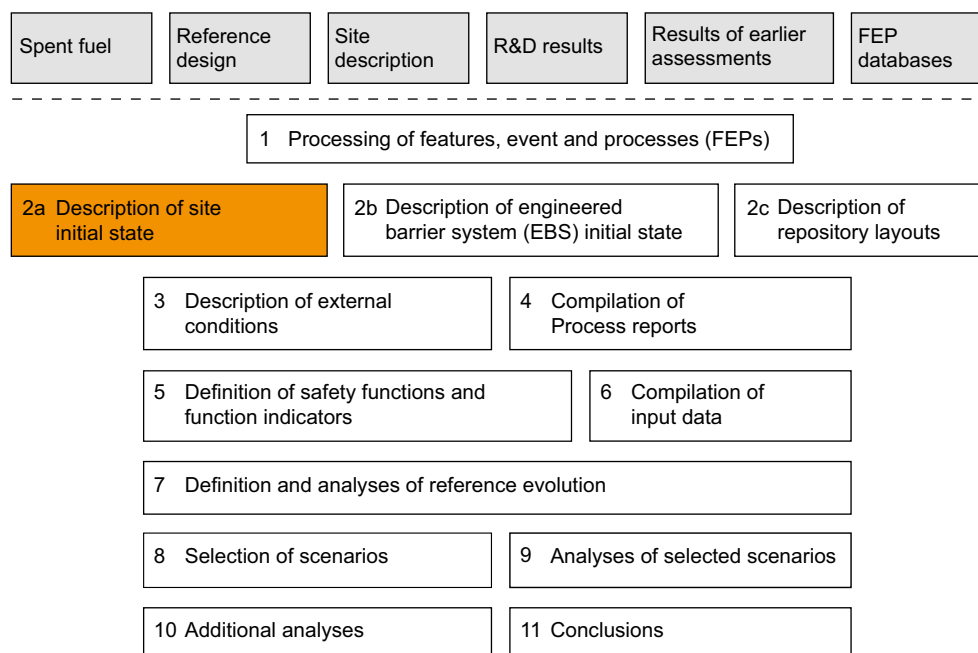


Figure 4-1. The PSAR methodology in eleven steps (Section 2.5), with the present step highlighted.

4.1 Introduction

A comprehensive description of the initial state of the repository system is one of the main bases for the safety assessment (Section 2.5.2), and is also the basis for development of repository design. For the geosphere and the biosphere, the state at the time of beginning of excavation of the repository is a natural starting point, since the knowledge of this relatively undisturbed state is available through the site-descriptive models that are derived from site investigation data. Furthermore, the short-term evolution of the host rock from the undisturbed state to that after excavation has to be considered in a safety assessment that is based on observations made prior to excavation.

Based on these considerations, the initial state of the geosphere and biosphere in the PSAR is defined as the natural, undisturbed state at the time of beginning of excavation of the repository, see further Section 5.1. A repository design, including a site-specific layout, is also developed based on the undisturbed state documented in the site description, see Section 5.2. Short-term geosphere processes or alterations due to repository excavation are documented in the **Geosphere process report**, see Chapter 7, and in the **Underground openings construction report**, Section 5.2. This means that the evolution of the natural system, including the potential evolution of an excavation damaged zone, EDZ, will be followed from the time of beginning of excavation of the repository, see Section 10.2.

The information transfer from the site investigations at Forsmark to the safety assessment application has involved several steps.

- Field data have been obtained from various investigation activities like airborne and ground geophysics, borehole drilling and borehole testing. After quality control, the data have been entered into the SKB data bases Sicada and GIS.
- The field data have been interpreted and evaluated into a cross-disciplinary site descriptive model (SDM), being a synthesis of geology, rock mechanics, thermal properties, hydrogeology, hydrogeochemistry, bedrock transport properties and surface system properties, see Figure 4-2. The SDM provides a description of the understanding of the site properties within the different disciplines and it also provides an assessment of the uncertainty in these descriptions. The SDM for the Forsmark site at the completion of the surface-based investigations is reported in a main site-description report, **Site description Forsmark**, and a number of supporting reports.

- **Site description Forsmark** has been used to develop a site-specific design of the repository, in accordance with stated technical design requirements. This is described in the **Underground openings construction report**, and discussed in Section 5.2 of this report.
- The site description and references therein cannot always be used directly in the safety assessment. There is a need to also consider non-site specific information, to add judgements on how to handle the uncertainties identified in the site description and to make final selections of model input data. For this reason, all site data used in the PSAR are assessed in the **Data report**, using the SDM as input. The role of the **Data report** is explained in Section 2.5.6 and the format of the **Data report** is further discussed in Chapter 9.

Site description Forsmark is based on the surface-based investigations that were completed in 2007. Since then, some sampling and investigations of the surface system as well as monitoring in some existing boreholes have continued. In addition, investigations in preparation for the construction of the repository facility have been carried out (Follin 2019). These preparatory investigations were conducted in the area where the access ramp and shafts of the repository facility are planned to be located. Data from eleven core-drilled boreholes and from three percussion-drilled boreholes, each less than 200 m deep, were collected with the focus to evaluate geological and hydrogeological conditions in the shallow bedrock. To gain more information from depth in the access area, investigations have also been conducted in a core-drilled borehole reaching a depth of 540 m. The evaluation and modelling of the results from these investigations conducted since the completion of the surface-based investigations have added more detailed information to the description of the area where the investigations were conducted, but have not justified an update of the site descriptive model (Follin 2019). Therefore, the analyses of post-closure safety in the PSAR is, likewise to SR-Site, based on **Site description Forsmark**.

In short, the quantitative site-specific input to the analysis of post-closure safety in the PSAR is handled in the **Data report**, and is not repeated here. There is, however, a need to outline the main characteristics and current understanding of the site. The remainder of this chapter provides an overview with this in mind, largely extracted from the site synthesis provided in Chapter 11 of the **Site description Forsmark**, but also addressing results from a few, more recent studies related to the understanding of groundwater composition (see Section 4.8). The overview of the surface system provided in Section 4.10 is, in addition to the **Site description Forsmark** report, based on the surface system description report (Lindborg 2008), one of the main background reports to the **Site description Forsmark**.

As part of the site-descriptive modelling, the uncertainty and confidence in the Forsmark site description were assessed. This assessment comprised exploring confidence in the site characterisation data, key remaining uncertainties in the site description, alternative models and their handling, consistency between disciplines and the main reasons for confidence or lack of confidence in the site descriptive model. The overall outcome of this assessment was that it was found that the site properties of importance for both repository constructability and post-closure safety are sufficiently bounded by quantitative uncertainty estimates or alternative models. A summary of the assessment is provided in Chapter 11 of the **Site description Forsmark** and more extensively reported in SKB (2008b). In the remainder of this chapter, the confidence and remaining uncertainties in the site characteristics are qualitatively addressed as part of demonstrating the current understanding of the site.

Since, as described above, both the PSAR and the SR-Site assessment are based on the same **Site description Forsmark**, the remainder of this Chapter is virtually unchanged relative to the corresponding text in the SR-Site Main report. Exceptions are an updated description of the understanding of the uranium concentrations in the groundwater at the site in Section 4.8.2, subsection “*On-going reactions*” based in part on updated text on uranium minerals in Section 4.4.4, and minor editing of the text in Sections 4.8 and 4.10.2 to improve clarity.

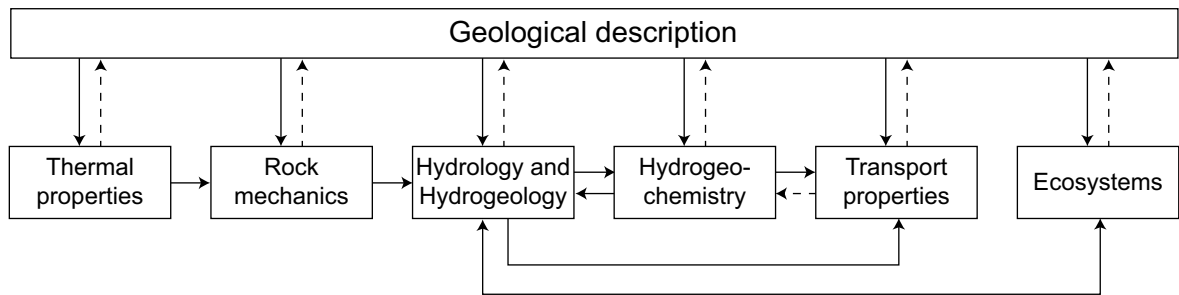


Figure 4-2. The different discipline descriptions in the SDM are interrelated with several feedback loops and with geology providing the essential geometrical framework.

4.2 The Forsmark area

4.2.1 Setting

The Forsmark area is located in northern Uppland within the municipality of Östhammar, about 120 km north of Stockholm (Figure 4-3). The candidate area for site investigation, approximately 6 km long and 2 km wide, is located along the shoreline of Öregrundsgrepen, a funnel-shaped bay of the Baltic Sea. The candidate area extends from the Forsmark nuclear power plant and the access road to the SFR-facility, an existing repository for low- and intermediate level radioactive waste, in the north-west to Kallrigafjärden in the south-east (Figure 4-3 and map in Appendix C).

The current ground surface in the Forsmark region forms a part of the sub-Cambrian peneplain in south-eastern Sweden (Hall et al. 2019). This peneplain represents a relatively flat topographic surface with a gentle dip towards the east that formed more than 540 million years ago. The candidate area at Forsmark is characterised by a small-scale topography at low altitude (Figure 4-4). The most elevated areas to the south-west of the candidate area are located at ca 25 m above current sea level. The whole area is located below the highest coastline associated with the last glaciation, and large parts of the candidate area emerged from the Baltic Sea only during the last 2 000 years. Both the flat topography and the ongoing shore-line displacement of ca 4 mm per year (see the **Climate report**) strongly influence the current landscape (Figure 4-4). The sea floor is continuously transformed into new terrestrial areas or freshwater lakes, and lakes and wetlands are successively covered by peat.

4.2.2 Target area for the repository

The north-western part of the candidate area has been selected as the target area for the repository (Figure 4-5 and map in Appendix C). Characterisation of the bedrock in the target area and the surroundings has been undertaken by both surface investigations and by investigations in boreholes, see Figure 4-5. Surface investigations have included geological mapping, different ground and airborne geophysical investigations, surface ecological investigations and monitoring of, for example, meteorological parameters and water levels in lakes and in the Baltic Sea. Borehole data in support of the Forsmark site description come from 25 core-drilled boreholes at 12 drill sites Figure 4-5. These boreholes range in depth down to ca 1 000 m and have a total borehole length of ca 17 800 m. The database also contains results from investigations in 38 percussion-drilled boreholes, with a total borehole length of ca 6 500 m, and more than 100 monitoring wells in the Quaternary cover, so-called soil wells. The site information available for establishing the site description for Forsmark is fully set out in the **Site description Forsmark**.

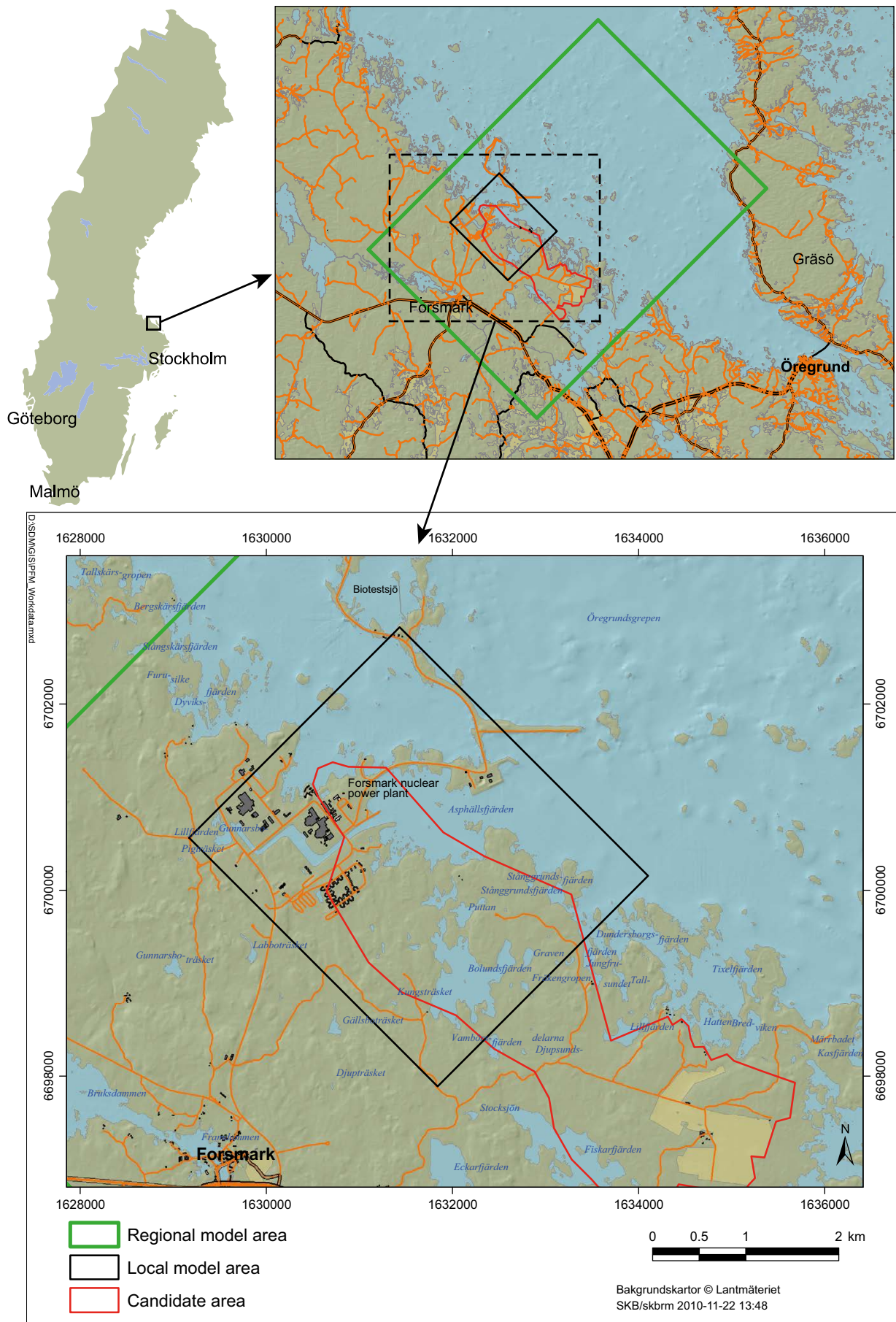


Figure 4-3. Location of the Forsmark candidate area (red) for site investigation.



Figure 4-4. Photographs from Forsmark showing the flat topography and the low-gradient shoreline with recently isolated bays due to land uplift (Figure 1-6 in the *Site description Forsmark*).

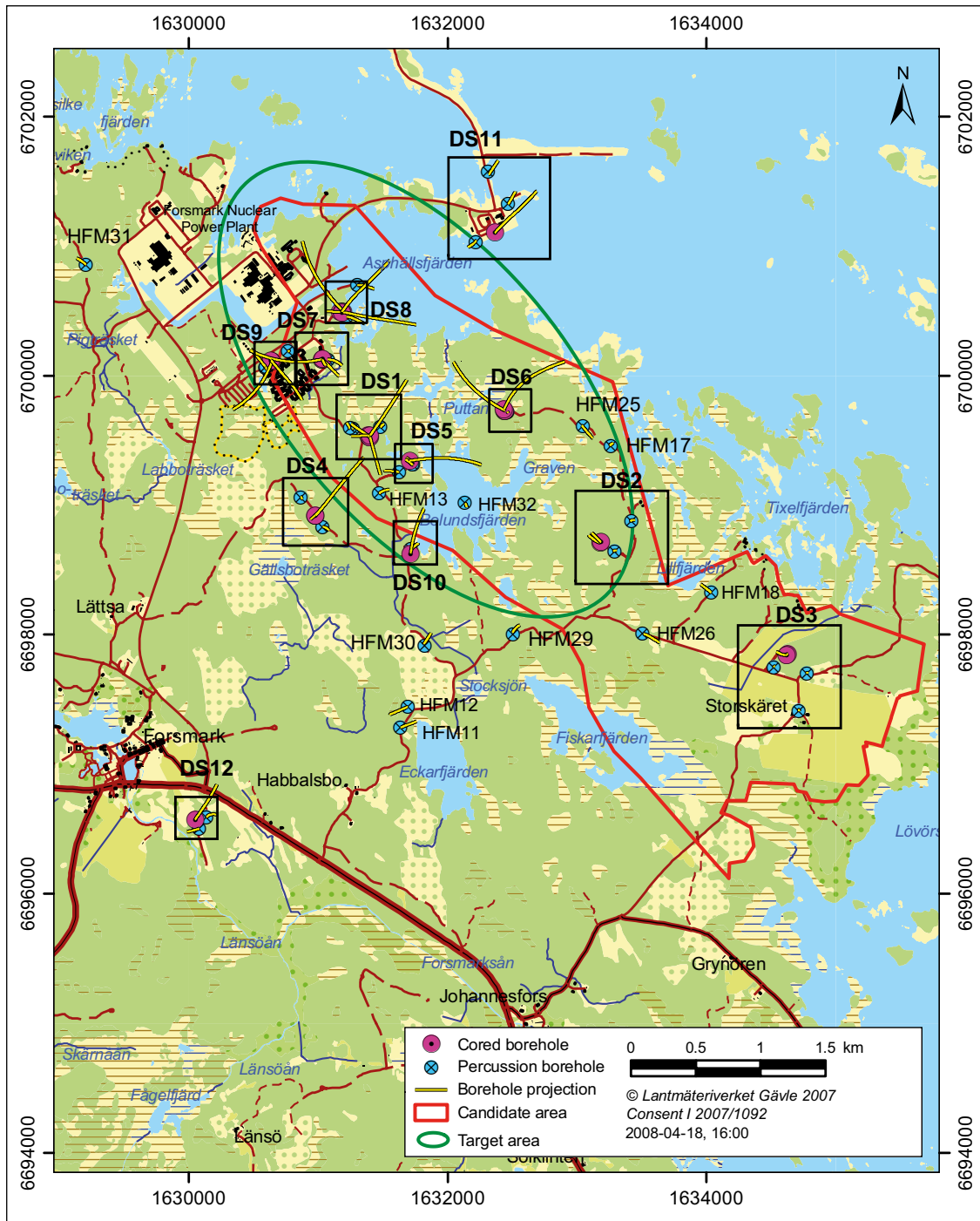


Figure 4-5. The Forsmark candidate area with the target area in the north-western part (ringed in green) and the location of the drill sites (Figure 11-1 in the *Site description Forsmark*).

4.3 Rock domains and their associated thermal and rock mechanics properties

The site lithology, i.e. the occurrence and distribution of rock types, reveals important aspects of the homogeneity of the site. Furthermore, it is directly related to the potential for mineral resources as well as thermal and rock mechanics properties of the intact rock. In the site descriptive model, the lithology is described in terms of rock domains, defined on the basis of composition, grain size, homogeneity, and style and degree of ductile deformation.

4.3.1 Rock composition and division into rock domains

The Forsmark area consists of crystalline bedrock that belongs to the Fennoscandian Shield and formed between 1.89 and 1.85 billion years ago during the Svecokarelian orogeny. The bedrock has been affected by both ductile and brittle deformation. The ductile deformation has resulted in large-scale, ductile high-strain belts and more discrete high-strain zones. Tectonic lenses, in which the bedrock is less affected by ductile deformation, are enclosed in between the ductile high-strain belts. The candidate area is located in the north-westernmost part of one of these tectonic lenses. This lens extends from north-west of the nuclear power plant south-eastwards to the area around Öregrund (Figure 4-6).

Rock domains in the target volume

Due to its internal homogeneity, most of the lens in the candidate area can be described in terms of two rock domains referred to as RFM029 and RFM045 (Figure 4-7). These are also the two rock domains that define the rock in the target volume. The dominant rock type in rock domain RFM029 is a medium-grained metagranite (74 % of the domain volume). Subordinate rock types are pegmatitic granite or pegmatite (13 %), fine- to medium-grained metagranitoid (5 %) and amphibolite and other minor mafic to intermediate rocks (5 %). With the exception of amphibolite that contains little or no quartz, the dominant and subordinate rock types have high quartz content (ca 20–50 %).

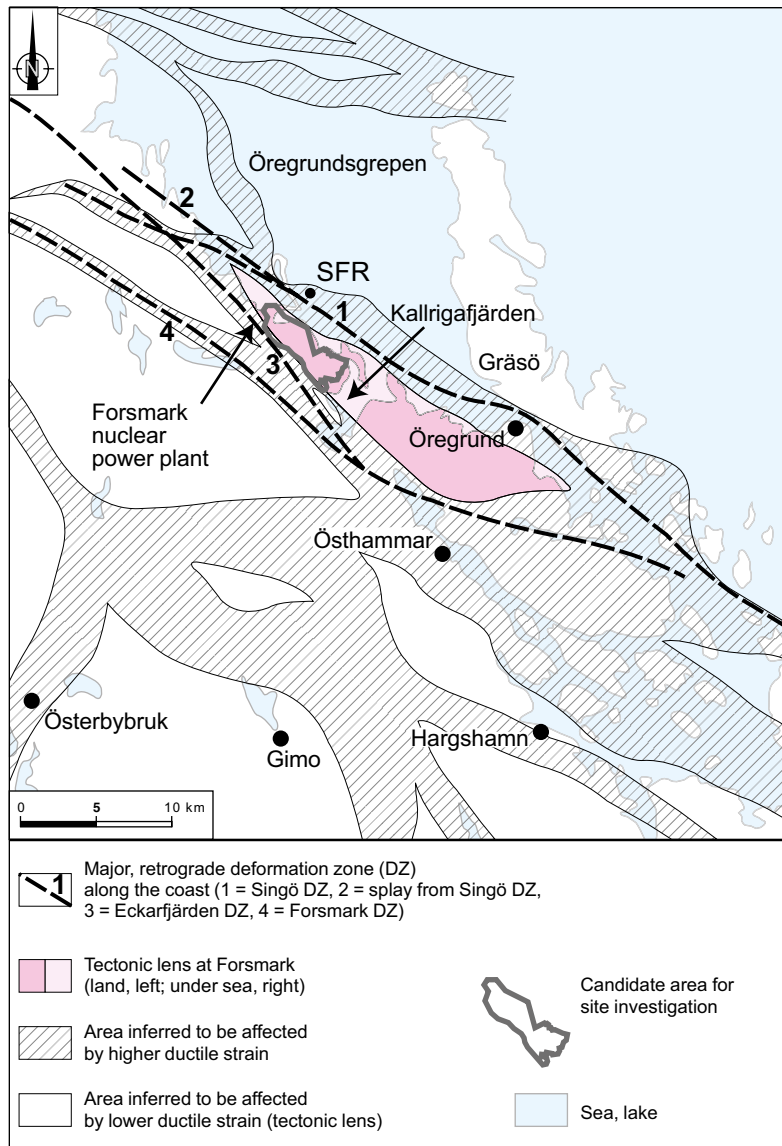


Figure 4-6. Tectonic lens at Forsmark and areas affected by strong ductile deformation in the area close to Forsmark (Figure 1-5 in the *Site description Forsmark*).

Rock domain RFM045 is surrounded by rock domain RFM029 in the target volume (Figure 4-7) and has a constricted rod-like geometry that plunges moderately to steeply to the south-east (Figure 4-8). Aplitic metagranite and medium-grained metagranite similar to the dominant rock type in domain RFM029 are the dominant rock types (67 %) in this domain. More subordinate rock types include pegmatite, and pegmatitic granite (14 %), fine- to medium-grained metagranitoid (9 %) and amphibolite and other minor mafic to intermediate rocks (7 %).

Rock domains outside the target volume

Rock domains outside the tectonic lens and target volume dip steeply towards the south-west, following the trend of the coastal deformation belt (Figure 4-8). They are dominated by different types of granitoid, predominantly felsic volcanic rocks and quartz-poor or quartz-deficient diorite to gabbro. More inhomogeneous bedrock is conspicuous in domains RFM018 and RFM021, on both sides of the tectonic lens (Figure 4-7).

Confidence

Confidence in both the geometry and properties of rock domains within and immediately around the target volume is high down to a depth of 1 000 m, whereas significant uncertainties remain concerning the character and geometry of rock domains outside the target volume, e.g. in the sea area.

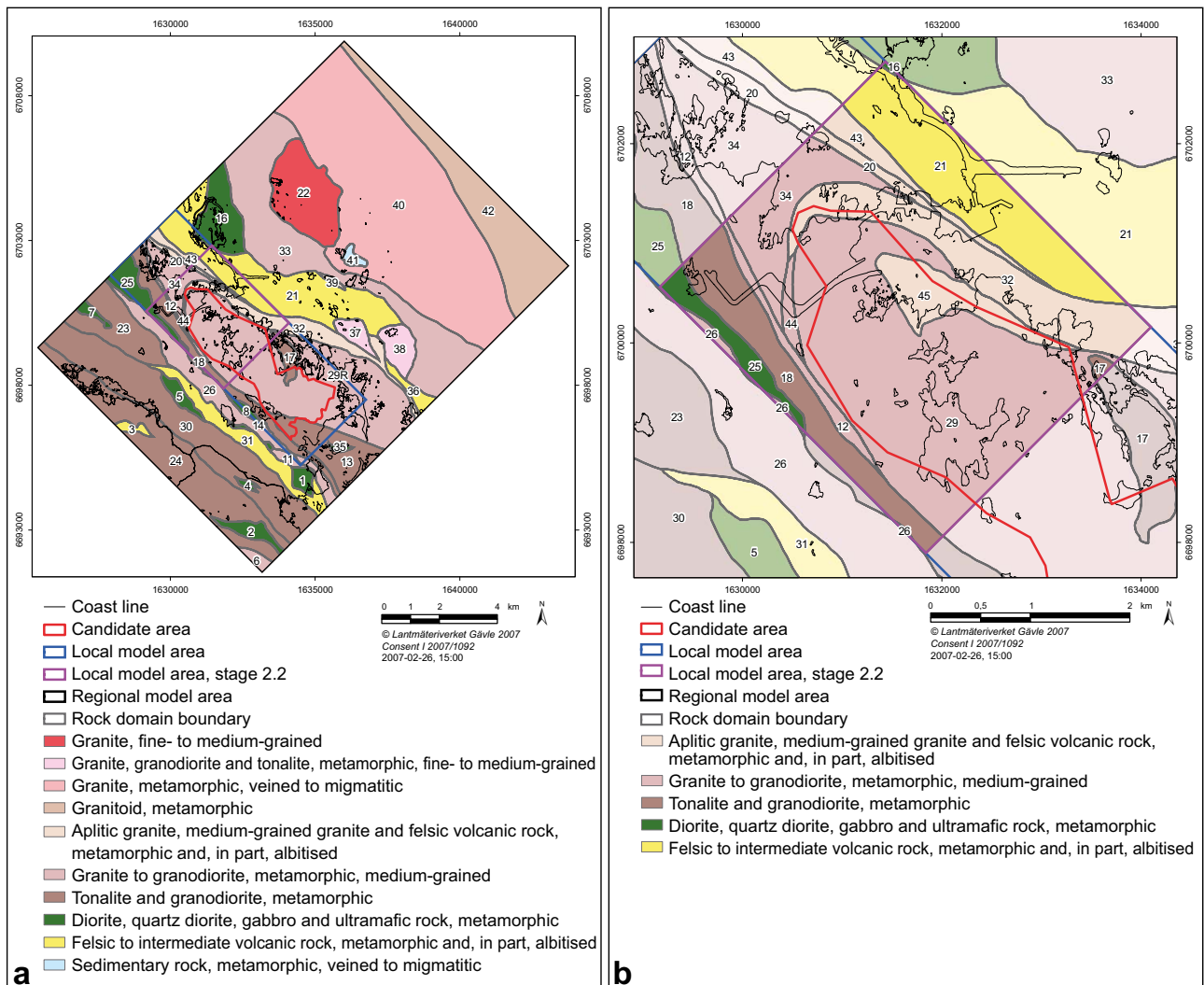


Figure 4-7. Rock domains included in the two dimensional models at the ground surface. a) Model inside the regional model area. b) Model inside the local model area (darker colours). The different colours represent the dominant rock type in each domain (Figure 5-24 in the *Site description Forsmark*).

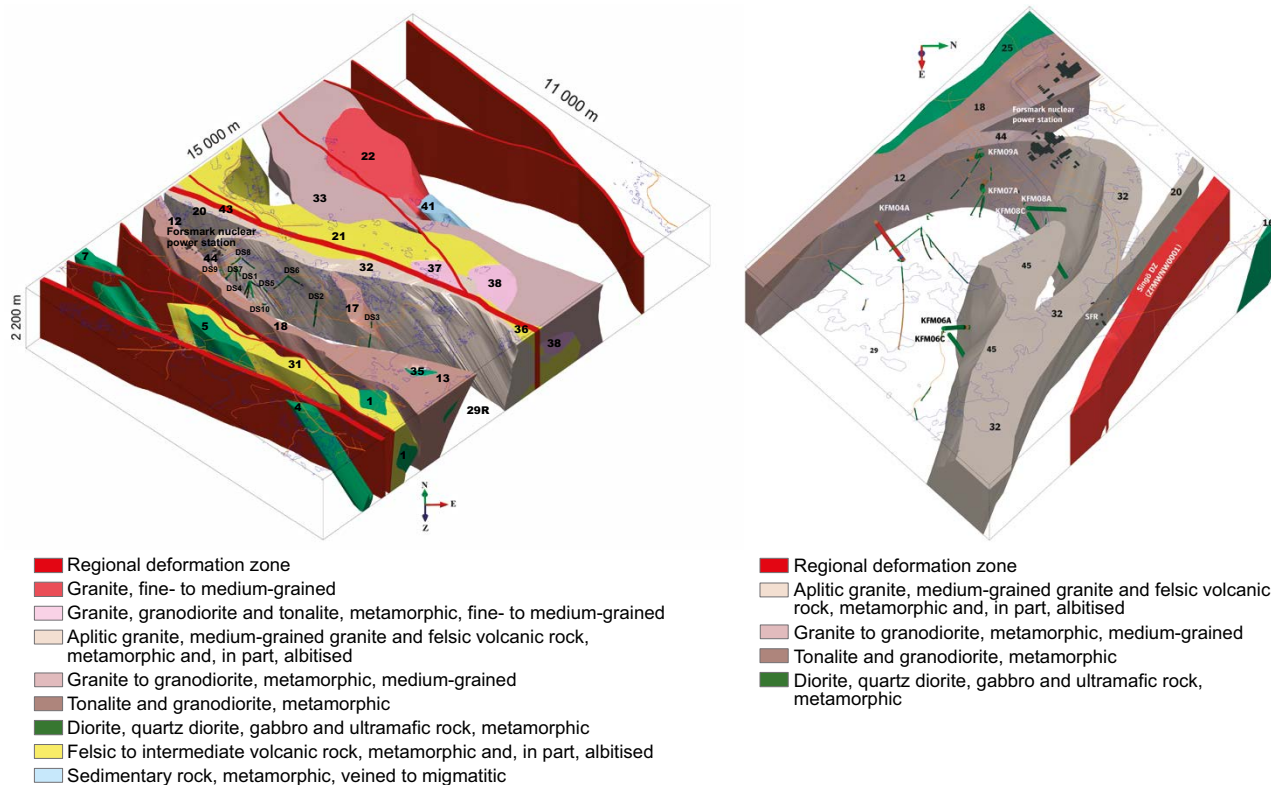


Figure 4-8. Three dimensional model for rock domains (numbered) and regional deformation zones (red colour). Several domains, including RFM029, are unshaded in order to display the structural style at the Forsmark site and in the tectonic lens. The dominant rock type in each domain is illustrated with the help of different colours (see legend). Left: Regional model showing the modelled, south-eastern elongation of several domains (Figure 4-15 in Stephens et al. 2007). Right: Rock domains in the target volume in the north-western part of the candidate area, viewed to the west from approximately the position of SFR (Figure 4-6 in Stephens et al. 2007).

4.3.2 Mineral resources

The ore potential in the coastal area in northern Uppland is correlated to the rock types and their characteristics. An assessment of the ore potential came to the conclusion that there is no potential for metallic and industrial mineral deposits within the candidate area at Forsmark. A potential for iron oxide mineralisation was recognised in an area south-west of the candidate area, predominantly in the felsic to metavolcanic rock, but the mineral deposits are small and have been assessed to be of no current economic value (Lindroos et al. 2004). Felsic to metavolcanic rock is also dominant in rock domain RFM021, located north and offshore of the candidate area (Figure 4-7). There is no documented iron mineralisation in data available from the islands, but since most of this rock domain is located beneath the Baltic Sea from where no mineralogical data exist, the potential for iron oxide mineralisation in rock domain RFM021 cannot be totally excluded.

4.3.3 Thermal properties

The thermal properties, i.e. thermal conductivity and heat capacity, of the rock are closely related to the lithology, since these properties depend on the mineral composition. The thermal conductivity of the rock has been assessed from direct measurements and by calculations based on mineral composition from modal analyses. Relationships between density and thermal conductivity determined from site-specific data support the use of borehole density logging data for modelling the spatial correlation of thermal conductivity within a rock type. These relationships have been shown to be consistent with the results of theoretical calculations of density and thermal conductivity based on the mineralogy of different rock types. The heat capacity has been determined from calorimetric measurements and also indirectly from measurements of thermal conductivity and diffusivity.

Thermal conductivity, heat capacity and temperature

The rock types in rock domain RFM029 have typically high quartz content (ca 20–50 %), which implies high values of thermal conductivity. Measurements at the cm-scale show values in the range 3.2 to 4.0 W/(m·K) for the medium-grained metagranite, the dominant rock type in rock domain RFM029. The altered granitic rocks that dominate in rock domain RFM045 also have high thermal conductivity, with measured values in the range 3.6 to 4.0 W/(m·K). However, subordinate rock types in these rock domains yield significantly lower values, e.g. amphibolite in the range 2.2 to 2.5 W/(m·K). Amphibolite occurs as narrow, dyke-like tabular bodies and irregular inclusions that are elongate in the direction of the mineral stretching lineation. Although some bodies are more than a few metres in thickness, most are inferred to be minor rock occurrences, i.e. thin geological entities. Measured and calculated conductivities also indicate that rocks affected by the alteration referred to as oxidation have higher thermal conductivity than their unaltered equivalents.

The variability in thermal conductivity within each rock type and between rock types is incorporated into stochastic modelling at a domain level by the use of spatial statistical models of lithology and thermal conductivity. The mean value of the thermal conductivity from the stochastic simulations is ca 3.6 W/(m·K) at the 5 m scale at a temperature of 20 °C, both in rock domain RFM029 and RFM045. The impact of low conductivity rock, mainly the subordinate rock type amphibolite, but also the fine- to medium-grained metagranitoid, is particularly conspicuous in RFM045, a feature displayed by the pronounced lower tail in the resulting histogram of thermal conductivity at the 5 m scale (Figure 4-9).

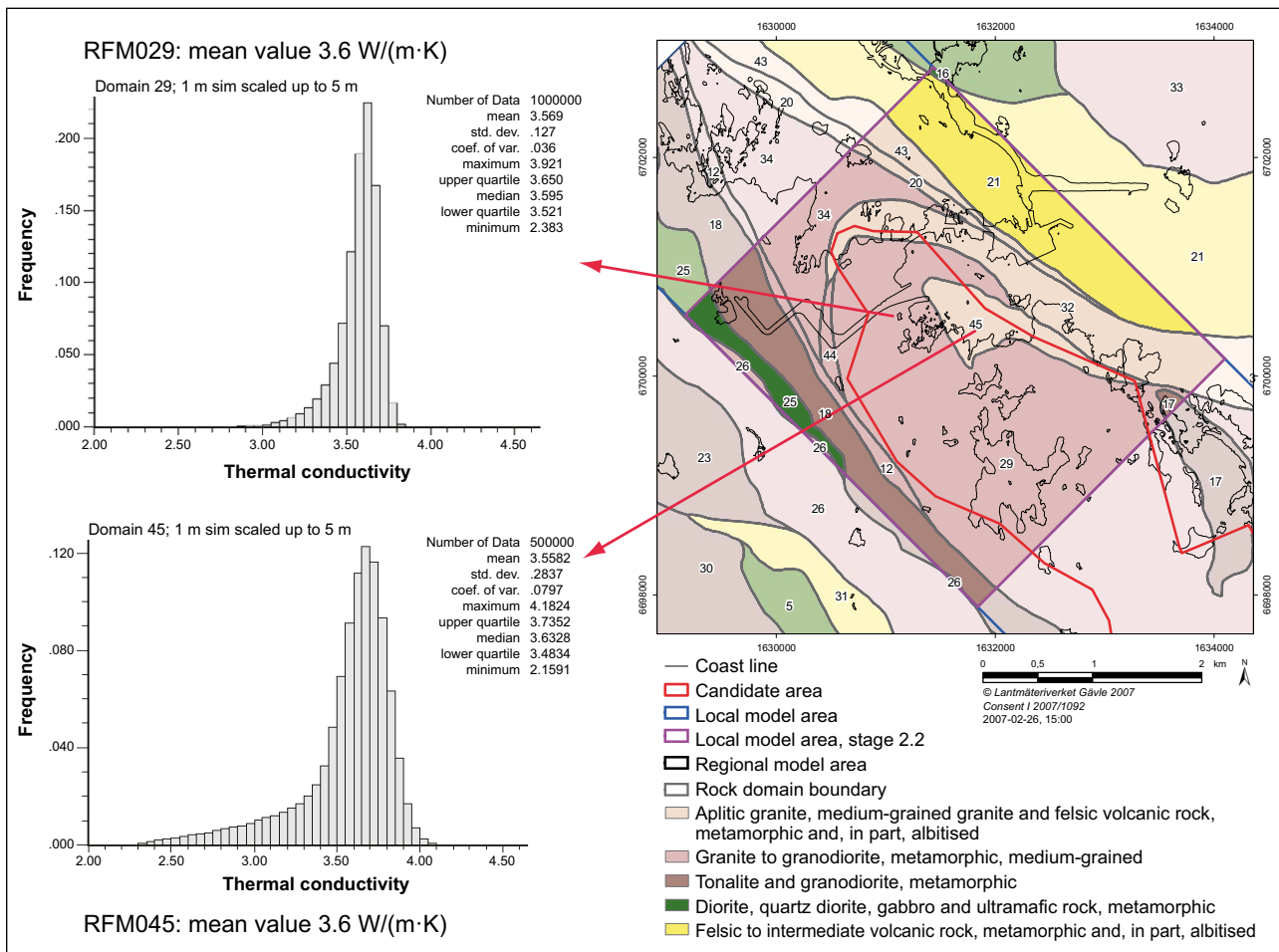


Figure 4-9. Modelled thermal conductivity at the 5 m scale. The lower tail of the distribution is mainly due to the subordinate rock type amphibolite (Figure 11-10 in the **Site description Forsmark**).

The mean value of the heat capacity assessed from measurements and from simulated thermal conductivity is 2.1 MJ/(m³·K), both in rock domain RFM029 and RFM045. This value is valid at a temperature of 20 °C, but it does not vary much over the temperature range of interest. The mean value of the heat capacity of the dominant rock type metagranite increases by about 29 % per 100 °C temperature increase. The *in situ* temperature constitutes the initial temperature condition for a repository. The current mean temperature at 500 m depth is estimated to be 11.6 °C, based on measurements in 8 boreholes.

Confidence

There is generally high confidence in the modelled distribution of thermal properties, due to the large amount of thermal data for the homogeneous rock mass. The thermal conductivity distribution is more uncertain for rock domain RFM045 than for rock domain RFM029. For domain RFM045, these uncertainties concern both the overall distribution and its lower tail, and are related to uncertainties associated with the output of the geological simulations, in particular, the proportions of rock types and the spatial and size distribution of amphibolite. Although the geological simulations performed have managed to model much of the heterogeneity observed in the boreholes, it is still somewhat unclear to what extent the borehole information is representative of the geology in domain RFM045. The reason for this is the small number of boreholes combined with the more heterogeneous distribution of amphibolite in this rock domain.

4.3.4 Strength and other mechanical properties of intact rock

Lithology also directly affects the thermal expansion, mechanical strength and deformation properties of the unfractured (intact) rock. The mechanical strength and deformation properties of the rock are evaluated from results of measurements on samples from the dominant rock types in RFM029 and RFM045, and also from the subordinate rock type pegmatite.

Thermal expansion

The mean value of the measured thermal expansion coefficient for the main metagranitoid rock types within the target volume varies between 7.5×10^{-6} and 7.8×10^{-6} m/(m·K). The mean of the measurements for the dominant medium-grained metagranite in RFM029 is 7.7×10^{-6} m/(m·K), and the corresponding value for the altered metagranite, which dominates in RFM045, is 7.5×10^{-6} m/(m·K). Domain modelling has not been performed, but the small differences in measured values suggest a mean coefficient of thermal expansion of $7\text{--}8 \times 10^{-6}$ m/(m·K) for the different rock domains.

Strength and deformation modulus

The uniaxial compressive strength (UCS) and Young's Modulus (E) of the intact rock show that the rock types in rock domains RFM029 and RFM045 are strong (UCS > 200 MPa) and stiff (E > 70 GPa). The results for samples taken inside or in the vicinity of deformation zones are in the same range as the results for samples taken in the host rock outside deformation zones.

Confidence

There is generally a high confidence in the strength and deformation properties of the dominant rock types in rock domains RFM029 and RFM045. Some uncertainties remain in the uniaxial compressive strength of the subordinate rock types amphibolite and fine- to medium-grained metagranitoid in these rock domains. However, the proportions of these rock types in rock domains RFM029 and RFM045 inside the target volume are small.

4.4 Deformation zones, fracture domains and fractures

Deformation zones and fractures are themselves important characteristics of the site as they affect the possible location of the repository, the mechanical stability of the rock and the groundwater flow. Furthermore, the deformation history and the geometry of the deformation zones affect the rock stress distribution and thereby also the properties of fractures in the volume.

4.4.1 Formation and reactivation through geological time

Four sets of deformation zones have been identified with high confidence at the Forsmark site (Figure 4-10). Vertical and steeply, SW-dipping zones with subsets referred to as WNW and NW show complex, ductile and brittle deformation. Regional zones longer than 10 km that occur outside the candidate volume (e.g. the Forsmark, Singö and Eckarfjärden deformation zones) are restricted to this set (Figure 4-6). The deformation zones in the remaining three sets only display brittle deformation and can be referred to as fracture zones. Vertical and steeply dipping fracture zones with sub-sets referred to as ENE (NE) and NNE transect the tectonic lens and occur frequently inside the target volume Figure 4-10. These zones formed in the brittle regime and are dominated by sealed fractures and sealed fracture networks. Gently dipping fracture zones occur more frequently in the south-eastern part of the candidate area, i.e. outside the target volume. Relative to the other three sets, there is an increased frequency of open fractures, including crush zones, along the gently dipping set. The fourth set consists of vertical and steeply dipping fracture zones referred to as NNW that are dominated again by sealed fractures. On the basis of their low frequency of occurrence, these are judged to be of lower significance relative to the other three sets of zones at Forsmark.

Low-temperature geochronological data, dating of fracture minerals, kinematic data and consideration of deformation in a regional perspective have been used to establish a conceptual model for the formation and reactivation of deformation zones in the context of changes in the stress regime from the later part of the Svecokarelian orogeny, ca 1.85 to 1.75 Ga, until the Quaternary. This conceptual model suggests that the different sets and sub-sets of deformation zones in the Forsmark area had formed and had already been reactivated during Proterozoic time, in connection with several tectonic events prior to 900 Ma (Figure 4-11). The termination pattern of surface lineaments and the occurrence of ductile deformation indicate that the steeply dipping zones referred to as WNW and NW form the oldest discrete structures at the site. It is inferred that they formed in response to bulk crustal shortening in a NW-SE to N-S direction, during the later part of the Svecokarelian orogeny. The size of several of these zones (e.g. Forsmark, Singö and Eckarfjärden) confirms that they comprise the master set. The formation of some steeply dipping NNW structures is also inferred to have occurred at this stage in the tectonic evolution. Displacement along steep NW zones as well as along steep ENE and NNE zones is inferred to be related to approximately N-S compression during the latest part of the Svecokarelian orogeny. Conjugate relationships between steeply dipping ENE and NNW structures are related to approximately NE-SW compression and the younger Gothian tectonic event (1.7–1.6 Ga).

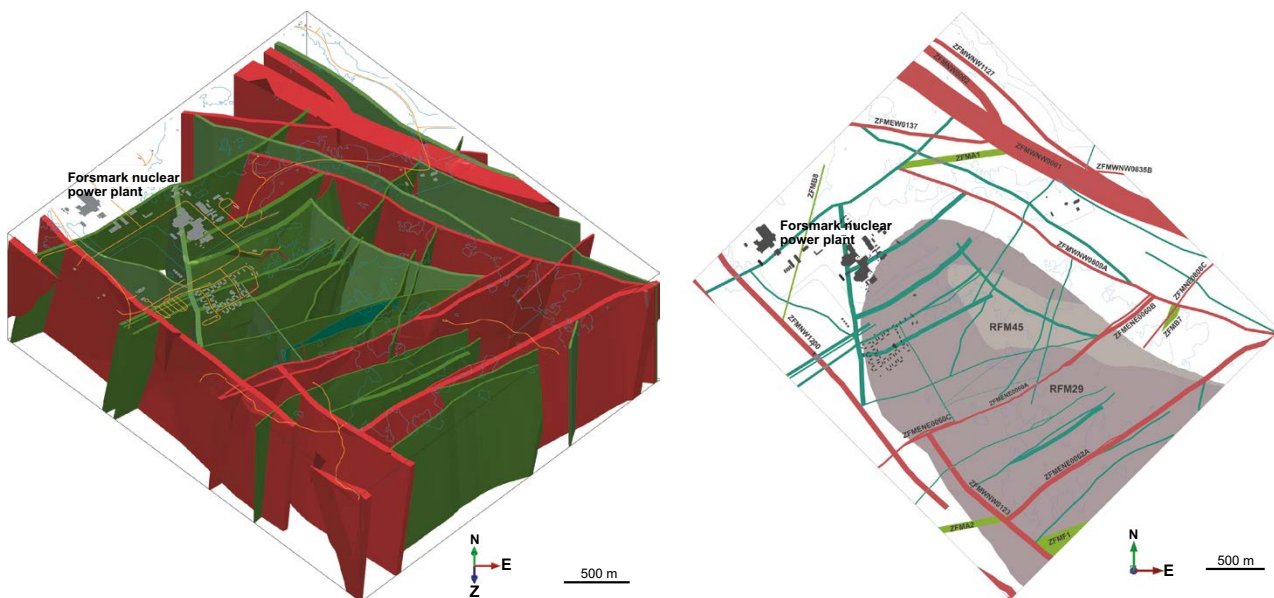


Figure 4-10. Three dimensional model that shows all the vertical and steeply dipping zones in the local model volume (Figure 4-3) (a) and a two dimensional horizontal surface at -500 m elevation in the local model volume including all zones (b) (Figures 5-12 and 5-13 in Stephens et al. 2007). Zones marked in red have a trace length at the surface longer than 3 000 m and zones marked in green (a) or blue-green (b) are shorter than 3 000 m in length. Zones marked in pale green (b) are gently dipping.

It is suggested that the compressive deformation along the gently dipping zones occurred during these tectonic episodes. In such a conceptual model, it can be expected that the gently dipping zones both terminate against the steeply dipping ENE and NNE structures and are displaced by them. The seismic reflection data provide some support to both these statements. Data also demonstrate that the bedrock at Forsmark has been strongly affected by the Sveconorwegian orogenic event (1.1–0.9 Ga).

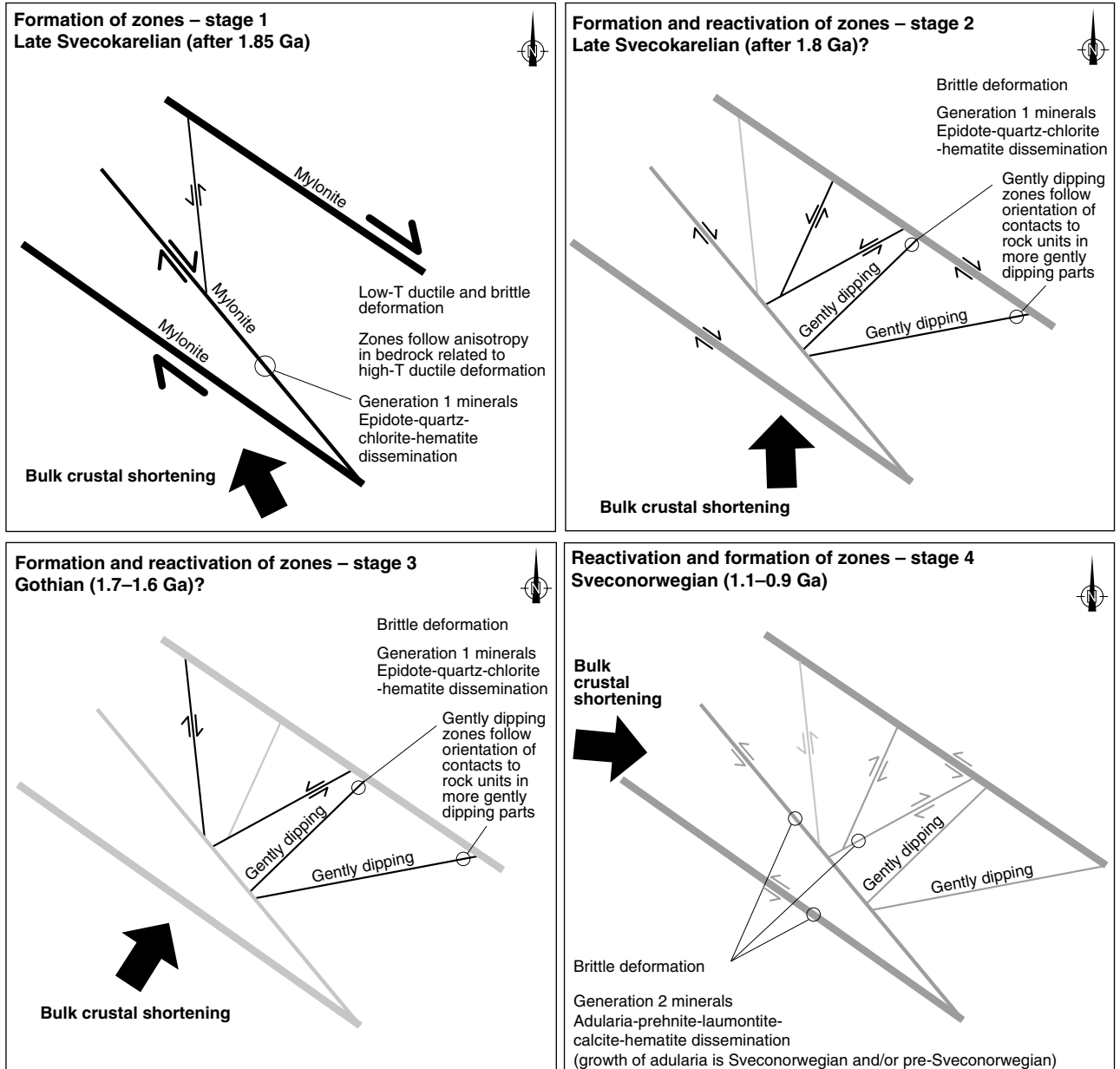


Figure 4-11. Two-dimensional cartoons illustrating the regional scale geodynamics during the formation and reactivation of the different sets of deformation zones at the Forsmark site. This includes late Svecokarelian, low-T ductile and brittle deformation (stage 1), late Svecokarelian brittle deformation (stage 2), Gothian brittle deformation (stage 3), and a major phase of brittle reactivation during the Sveconorwegian orogeny (stage 4). Formation of fractures and fracture zones during stage 4 cannot be ruled out. The different colour shadings along the zones indicate an inferred variable degree of response (strongest is black, intermediate is grey, weakest is pale grey) in each tectonic regime (Figure 5-26 in the *Site description Forsmark*).

As the effects of tectonic activity, for the most part, waned, the effects of loading and unloading increased in significance. The latter occurred in connection with the deposition of sedimentary rocks and the subsequent erosion of these rocks with exhumation of the crystalline bedrock. In this respect, the formation of sedimentary basins during the time interval ca 1.5 to 1.3 Ga and after 900 Ma, an episode of glaciation during the latest part of the Precambrian around ca 650 Ma, the development of a passive continental margin during the Early Palaeozoic, and numerous glaciations during the Quaternary period are examples of loading events during the geological development of central Sweden. It is also suggested that sedimentary loading is a process that, besides tectonic events, gave rise to the build-up of high rock stress in the bedrock. By contrast, unloading resulted in reactivation, especially of gently dipping structures, in the form of extensional failure and the development of dilatational joints. New fractures that are oriented sub-parallel to the topographic surface at the time of unloading and lack alteration associated with hydrothermal alteration, i.e. sheet joints, would also have formed (see Section 4.10 and Figure 4-24). These features occurred in response to a release of stress in the bedrock. They are most conspicuous close to the surface interface, where the differential stress ($\sigma_1 - \sigma_3$) at the time of unloading was high, and, especially, in the vicinity of ancient gently dipping zones.

The Baltic Shield is currently affected by two large-scale deformation processes; plate tectonics and glacial isostatic adjustment due to retreat of the most recent Fennoscandian ice sheet, see further the **Geosphere process report** and the **Climate report**. The plate tectonic component includes ridge push from the west due to seafloor spreading at the Mid-Atlantic Ridge and compression from the south due to the Eurasia-Africa plate collision. The current tectonic stress field in the Forsmark region is dictated by the Mid-Atlantic Ridge push (see also Section 4.5.2).

4.4.2 Deterministic deformation zones

In the geological model, structures that are 1 000 m or longer are included in the deterministic deformation zone model, whereas structures shorter than 1 000 m are described in statistical terms in the geological DFN (discrete fracture network) model (see Section 4.4.3). The deterministic deformation zone model builds on the integration of the understanding of the deformational history in the region, magnetic lineament and seismic reflection data, as well as fracture orientation, fracture mineralogical and alteration data, especially from the cored boreholes. Low magnetic lineaments derived from both high-resolution ground magnetic data and airborne helicopter data inside and immediately around the target area are the main surface data that support the occurrence of steeply dipping deformation zones. Geometrical constraints on the occurrence of gently dipping fracture zones are provided by surface reflection seismic data and borehole seismic data (VSP). Reflectors that dip to the SSE and SE are prominent in the candidate volume, with a much stronger concentration in the upper 2 km of the bedrock in the south-eastern part relative to that observed in the north-western part, i.e. the target volume (Figure 4-12). Borehole data show that several of the gently dipping fracture zones in the south-eastern part of the candidate volume occur along or close to the contact between subordinate rock types, in particular amphibolite, and the dominant host rock metagranite. Since the amphibolite contacts follow the orientation of the tectonic foliation, it is proposed that the more frequent occurrence of gently dipping zones in the south-eastern part is related to the gentler, south-east dip of the amphibolite, the tectonic foliation and the mineral stretching lineation in this part of the candidate volume.

The local model, which contains the target volume (Figure 4-3), includes 60 deterministically modelled deformation zones, and the majority of these zones (> 60 %) are judged to have a high confidence of existence (Figure 4-10). Only two steeply dipping zones with a surface trace length longer than 3 000 m intersect the target volume (zones ENE0060A and ENE0062A with their attached branches) and a further twenty-two steeply dipping zones, which either show a trace length at the ground surface between 1 000 and 3 000 m or form minor splays or attached branches to such zones, are present at 400 to 600 m depth inside the repository volume. Five gently dipping zones, including zones A2 and F1, are also present at 400 to 600 m depth inside or immediately above the repository volume.

The regional model includes 72 deterministically modelled deformation zones of which 29 are present in the local model. The minority of the zones in the regional model (27) are judged to have a high confidence of existence. The remainder lack corroborative geological and geophysical data from boreholes or excavations and are judged to have a medium confidence of existence. As in the local model, vertical and steeply dipping deformation zones (48) dominate over gently dipping zones (24). However, there is an inherent bias in the evaluation of the occurrence of gently dipping zones, since reflection seismic data are not available over the north-eastern half of the regional model volume.

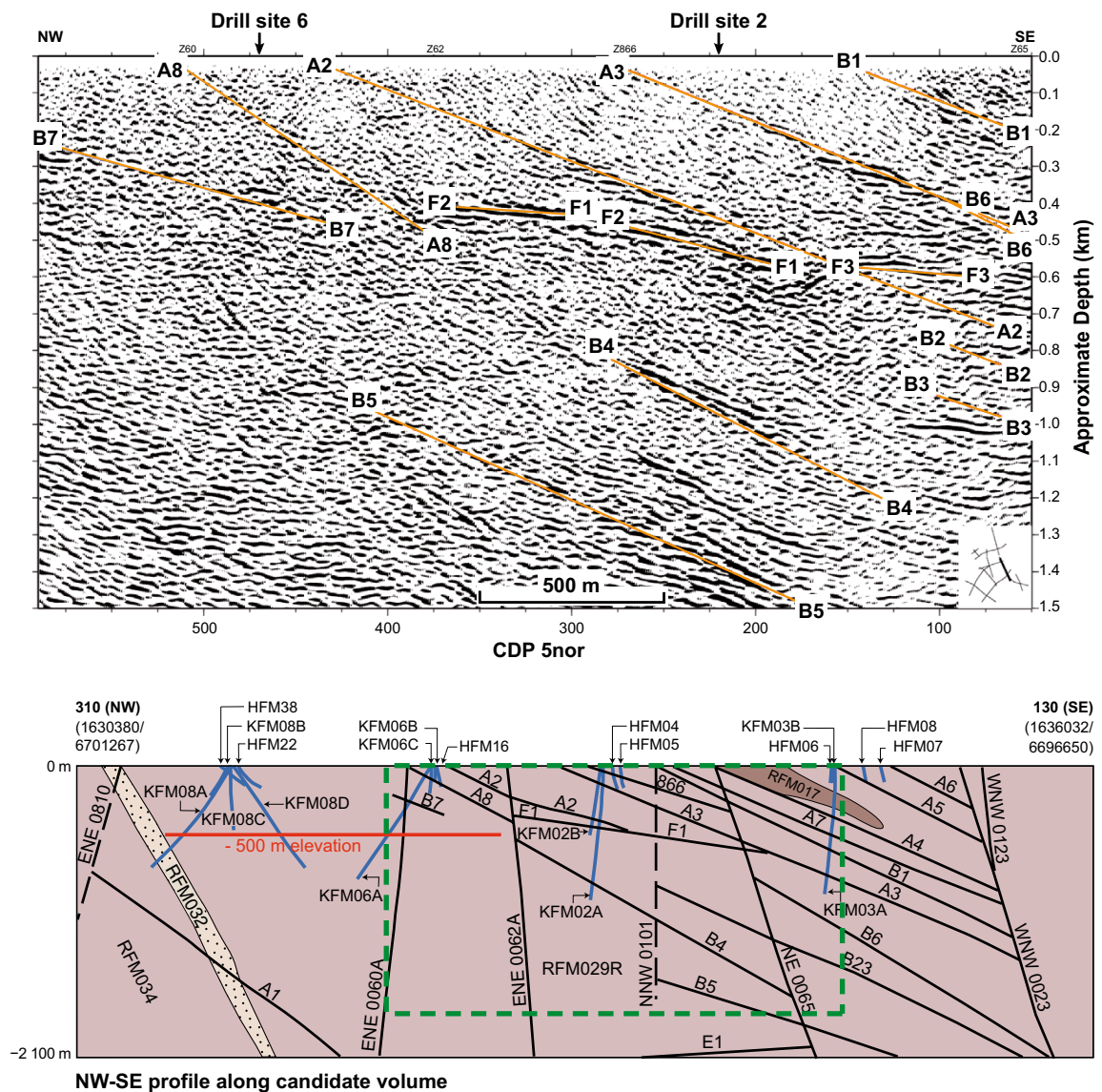


Figure 4-12. Confidence in the gently dipping fracture zones is enhanced by combining reflection seismic data with borehole data. The upper insert shows gently dipping seismic reflectors in the south-eastern part of the candidate volume. The lower insert is a NW-SE cross-section through the candidate volume in the structural model showing rock domains and deformation zones. The approximate location of the upper insert is indicated by green dashed lines in the lower insert. The cross-sections are not identical (Figure 11-13 in the *Site description Forsmark*).

Confidence

Confidence in the occurrence of deterministic deformation zones in the target volume is high and the occurrence of undetected deformation zones longer than 3 000 m is judged unlikely. It is considered that the deterministic model for deformation zones has now attained acceptable stability, in both the local and regional model volumes. The predictability of the occurrence and character of different sets or sub-sets of deformation zones is related to the large-scale bedrock anisotropy that was established over 1.85 billion years ago, when the bedrock was situated at mid-crustal depths and was affected by penetrative, ductile deformation under high-temperature metamorphic conditions.

The principal remaining uncertainty in the deterministic deformation zone model concerns the size of the gently dipping fracture zones. However, it is judged that this uncertainty is sufficiently bounded, since the approach for termination of these zones has been to extend them to the nearest steeply dipping zone. Furthermore, this uncertainty is not fundamental to the conceptual understanding of the site. Another remaining uncertainty concerns the orientation and size of the possible deformation zones

that have not been modelled deterministically. Since it has not been possible to link these geological features to low magnetic lineaments or seismic reflectors and since they commonly occur along short borehole intervals, it is judged that they are predominantly minor zones.

4.4.3 Fracture domains, fractures and DFN models

Analyses of fracture data have indicated a large degree of spatial variability in the size, intensity and properties of fractures between different rock domains, and also within rock domain RFM029. Based on a systematic assessment of the variation in the frequency of fractures with depth along each borehole, the bedrock between deterministically modelled deformation zones has been divided into fracture domains. Thus, fracture domains and deterministically modelled deformation zones are mutually exclusive volumes, whereas rock domains contain both fracture domains and deterministically modelled deformation zones.

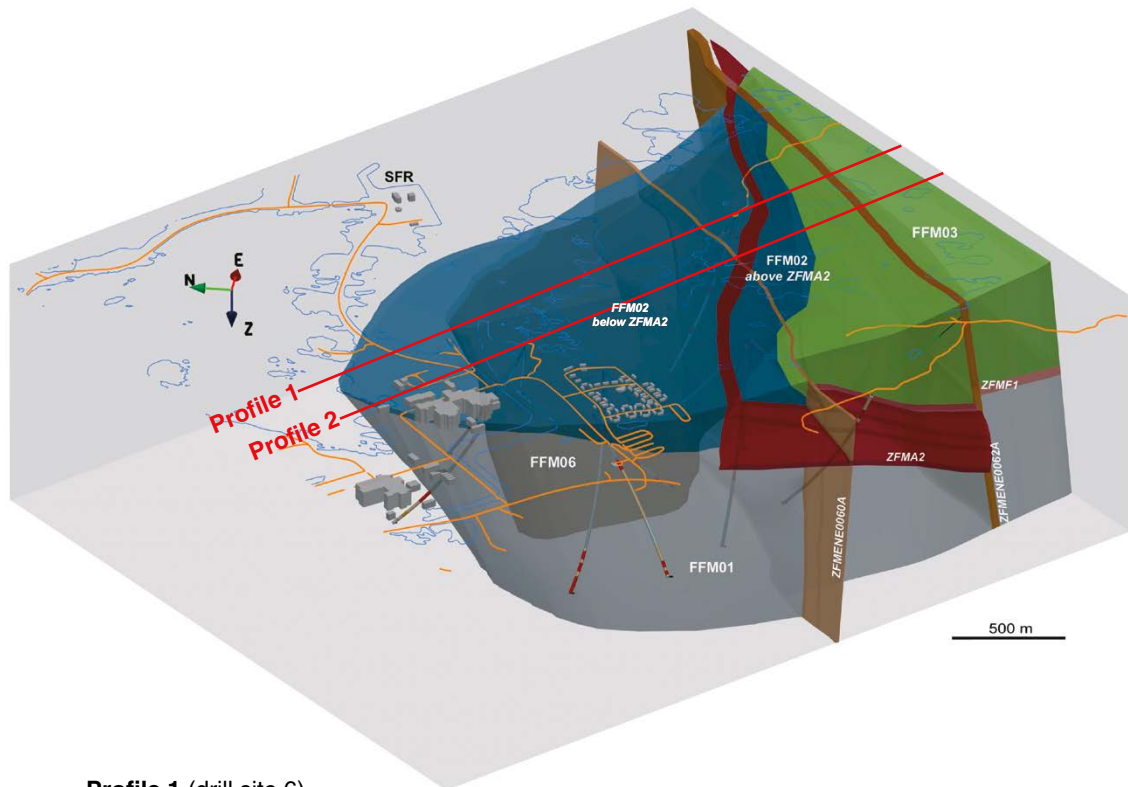
Fracture domains

Fracture domain FFM01 forms the bedrock at depth in the target volume, north-west of and in the footwall of the gently dipping zone A2 (Figure 4-13). This fracture domain forms the main component in rock domain RFM029. Fracture domain FFM02 comprises the bedrock close to the surface, above fracture domain FFM01, predominantly in the same footwall bedrock segment. Fracture domain FFM02 is located in both rock domains RFM029 and RFM045. The bedrock in FFM01 shows a low frequency of open and partly open fractures, whereas the bedrock in FFM02 is characterised by a complex network of sub-horizontal or gently dipping, open and partly open fractures, which, locally, merge into minor zones. The sub-horizontal or gently dipping fractures are oriented at a large angle to the current, minimum principal (vertical) stress in the bedrock. The rock volume south-east of the target volume, in the hanging wall of zone A2, is defined as fracture domain FFM03. It is situated in rock domains RFM029 and RFM017. Open and partly open fractures in this domain are more evenly distributed from surface down to 1 000 m depth than in the rock north-west of zone A2, and the domain is spatially associated with a high frequency of gently dipping fracture zones containing both open and sealed fractures. A fourth fracture domain, FFM06, is defined in the target volume. In the same manner as fracture domain FFM01, it lies in the footwall of zone A2 and beneath FFM02. It forms the main component in rock domain RFM045. It was distinguished from FFM01 simply on the basis of the widespread occurrence of fine-grained, altered (albitised) granitic rock, with slightly higher contents of quartz compared with unaltered granitic rock.

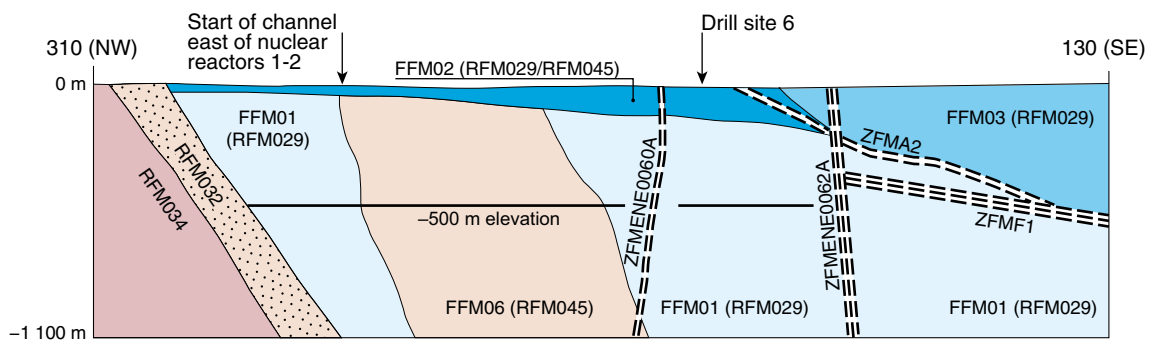
Borehole data have revealed that the orientation and mineralogy of fractures inside fracture domains FFM01 and FFM06, as well as in FFM03, are similar to that in the adjacent fracture zones. However, this correlation breaks down in domain FFM02, where there is an important contribution from sub-horizontal and gently dipping fractures, but relatively few gently dipping zones. It is inferred that tectonic processes during the geological history of the region have determined the fracturing at depth in fracture domains FFM01 and FFM06, whereas the fracturing in the near-surface bedrock in fracture domain FFM02 is the result of a combination of tectonic processes and processes related to stress release.

Discrete fracture network models

Fractures and minor fracture zones, not covered by the deformation zone model, are handled in a statistical way through discrete fracture network (DFN) models. The geological DFN model captures all fractures (open, partly open and sealed), since the sealed fractures are also assumed to be potential planes of weakness and could possibly be planes where there exist flow channels. However, many of the sealed fractures are mechanically and hydrogeologically indistinguishable from the intact rock. The model is presented as a mathematical description of fractures and fracture zones shorter than 1 km, not as a 3D object model or realisation. Thus, the derived model parameters can be used to stochastically model these fractures in various applications.



Profile 1 (drill site 6)



Profile 2 (drill sites 8 and 2)

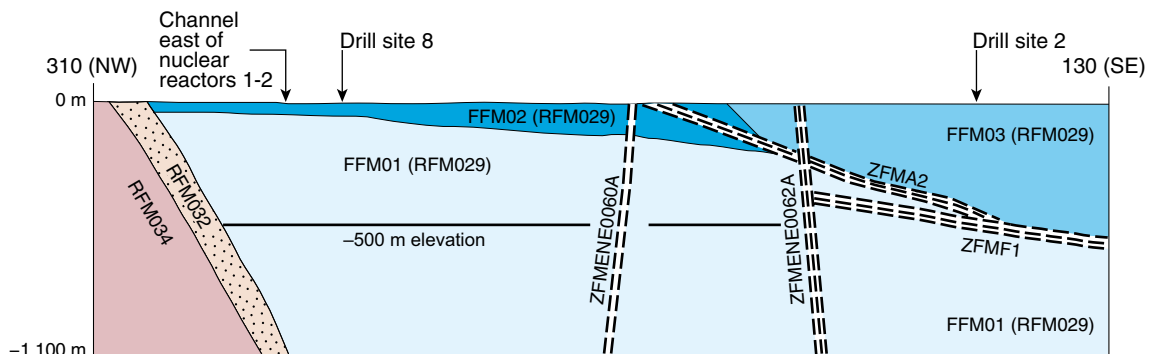


Figure 4-13. View to the ENE (upper) and vertical profiles in a NW-SE direction (middle and lower) showing the fracture domains and their relation to the gently dipping deformation zones ZFMA2 and ZFMF1 and the steeply dipping zones ZFMENE0060A and ZFMENE0062A that are longer than 3000 m (Figure 11-14 in the Site description Forsmark). The profiles are approximately 4500 m long.

DFN models are produced for each fracture domain in the target volume, i.e. fracture domains FFM01, FFM02 and FFM06, and also for fracture domain FFM03, based on fracture trace length data observed in outcrop, data derived from the interpretation of magnetic lineaments, data derived from the lengths of the intercepts of the mid-planes of the deterministic deformation zones and fracture intensity data from boreholes. The influence of different geological processes at depth and close to the surface causes difficulties in applying coupled size-intensity geological DFN models, which are based on surface data, to the two fracture domains at repository depth that do not outcrop, FFM01 and FFM06. There are also uncertainties regarding whether the fractures represented by deformation zones and magnetic lineaments are part of the same fracture population represented by fractures in outcrop or measured in boreholes. These difficulties are captured by alternative size-intensity models for the distribution of fractures. Details of these alternative models and their associated uncertainties are described in the Data report, Section 6.3.

Confidence

There is high confidence in the occurrence of different fracture characteristics in the bedrock outside deformation zones in the target volume and, consequently, in the division of this bedrock into a more fractured near-surface volume, fracture domain FFM02, above less fractured rock volumes, fracture domains FFM01 and FFM06. This division is also supported by hydrogeological and hydrogeochemical data (see Sections 4.6 and 4.8), although the position of the boundary between FFM02 and the fracture domains beneath is still associated with uncertainties. However, the most important remaining uncertainty concerns the DFN model for prediction of the size-intensity relationship of fracturing in the potential repository volume, i.e. fracture domains FFM01 and FFM06. The main reason for this is the lack of data on fracture sizes in these sub-surface domains. Direct data on fracture sizes in these domains can only be obtained from underground mapping, i.e. when the repository excavation has reached relevant depths. This uncertainty as well as the question of tectonic continuity at different size scales has been addressed with the help of alternative DFN models. These alternatives cover a broad range and the uncertainties are judged to be bounded by them.

4.4.4 Fracture mineralogy

Detailed studies of fracture mineralogy and wall rock alteration have provided information on the character and frequency of fracture minerals at Forsmark. Calcite and chlorite, partly associated with corrensite, are by far the most common minerals. Other common minerals are laumontite, adularia, quartz, albite and hematite, whereas prehnite, pyrite, clay minerals and epidote are less common. Rare occurrences of e.g. asphaltite and goethite are also observed.

The older generations of minerals, including epidote, which formed prior to 1.1 Ga, and adularia, which formed around 1.1 Ga or is older, show no depth dependence. In a similar manner, the wall-rock alteration associated with these mineral generations and referred to as oxidation also shows no depth dependence. These features are consistent with the conclusion that these minerals and the associated alteration formed a long time ago when this part of the bedrock was situated at considerably greater depths. The younger mineral asphaltite, which probably formed between ca 500 and 250 million years ago, occurs almost entirely in the upper part of the bedrock along open fractures. This is also the case for clay minerals and goethite that belong to the youngest generation of minerals, except for some occurrences at greater depths along individual fractures in deformation zones. Since the current bedrock surface is situated close in height to the surface of the former sub-Cambrian peneplain (Hall et al. 2019), this distribution of fracture minerals with depth suggests that the near-surface bedrock, i.e. including fracture domain FFM02 in the target volume, has been affected by near-surface processes inferred to be related to loading and unloading cycles during the last ca 500 million years.

A variety of uranium minerals and amorphous phases have been found in some of the pegmatites and fracture coatings at Forsmark (Krall et al. 2015, 2019). U-Pb and Pb-Pb isotope analyses indicate that primary minerals, uraninite and uranothorite, were deposited in pegmatites at ~1.8 Ga. Thereafter, these primary grains were altered during episodic hydrothermal fluid circulation that facilitated the precipitation of secondary uraninite (~1.6 Ga) and at least two generations of U(VI)-bearing minerals, haiweeite and uranophane (1.25 Ga and 400–300 Ma). In two drill cores, the U(VI) minerals had been altered by carbonate-rich fluids and showed recent or on-going Pb loss. U-Pb isotope geochronology, together with the mineral chemistry and petrographic relations, suggest that local U(IV) was oxidized early in the geologic history of the Forsmark site (~1.2 Ga), that the U(VI) minerals formed at that

time persist in the bedrock, and that some of these U(VI) minerals have recently interacted with fluids or groundwaters. Notably, the altered and oxidized uranium was principally found in the deformation zones located outside of the target volume, whereas episodic or recent alteration was not evident in the uraninite found in the target volume (borehole KFM01D). Therefore, field-scale observations support the notion that U(IV) was oxidized during the early tectonothermal evolution of Forsmark and, more generally, the Fennoscandian Shield (see Section 4.8).

Fractures without mineral coating or filling have been observed in the near-surface realm in the bedrock, but are also present at greater depths. The significance and origin of these fractures have been the focus of a specific study (Claesson Liljedahl et al. 2010). A subset of fractures from different depths, rock domains and located outside deformation zones were selected for a more detailed investigation. This revealed that the majority of the investigated fractures contain fracture minerals, but that fractures without minerals (5.7 % of the inspected fractures) are present in the bedrock above 300 metres depth. Most of these fractures without minerals have been recorded as water bearing and are also sub-parallel to nearby fractures. Some of these nearby fractures are open, but their size is very small and they are often not connected all the way through the drill core, leaving the drill core unbroken.

There is currently no unambiguous process explaining the formation of these fractures without minerals. One hypothetical possibility is that they were formed during opening of fractures or that they represent parts of fracture surfaces that were opened up recently, and therefore have not had enough time to allow for mineral precipitation to occur on the fracture surface. Another possibility is that the non-mineralised fractures represent the fronts of larger fracture surfaces where mineral precipitation may have been prevented by insignificant flow of saturated fluids along the peripheral parts of the fractures. It is not possible to determine the formation age of these fractures. However, given that some of the fracture samples with similar characteristic very small fractures contain hydroxyapophyllite, typical for Palaeozoic generation 3 fracture minerals (Sandström et al. 2008, 2009), it is possible that the non-mineralised fractures represent reactivation of Palaeozoic fractures. Given the fresh appearance and lack of fracture minerals, it is unlikely that these fractures have been water conductive during the main events of fluid migration in the area, which caused abundant precipitation of fracture minerals. Thus, these fractures have most likely not been open before 277 Ma. Given the sub-horizontal orientation of the identified fractures, it is likely that they have been reactivated due to denudation associated with sediment erosion and/or post-glacial rebound.

4.4.5 Mechanical properties of deformation zones and fractures

Evaluation of the results from laboratory testing of the mechanical properties of fractures has shown that the deformability and strength properties of open discrete fractures are similar for different fracture sets. Furthermore, the properties of open fractures in fracture domain FFM01 and in deformation zones are quite similar. Empirical and numerical analyses of the data show that the deformation modulus and strength properties of the rock mass (including fractures) in fracture domains FFM01 and FFM06 are almost equal and representative of a stiff and strong rock (Figure 4-14).

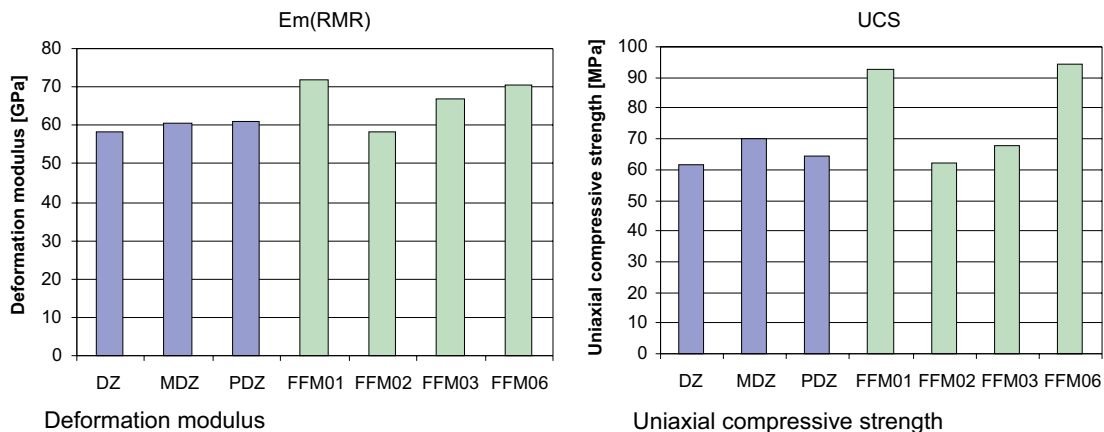


Figure 4-14. Mean values of deformation modulus and strength properties of the rock mass in fracture domains and deformation zones as evaluated by an empirical approach (Figure 11-16 in *Site description Forsmark*). DZ = deformation zone, MDZ = minor deformation zone (shorter than 1 000 m), PDZ = possible deformation zone.

Confidence

The confidence in the derived mechanical properties of the rock mass is in general high, due to the large amount of data in support of the model and the small changes in values caused by the addition of new data during the various modelling stages. In addition, the results are consistent with the understanding of the geology at the site. The largest remaining uncertainty concerns the large-scale mechanical properties of fractures, since the model is based on test results on small samples.

4.5 Rock stress

4.5.1 Stress evolution

The stress evolution is closely related to the deformational history of the site. According to the conceptual understanding (Section 4.4), the different sets and sub-sets of deformation zones at the site formed and had already been reactivated more than 900 million years ago in response to stress conditions affected by different tectonic events along active continental margins. This, in combination with loading and unloading cycles connected with the burial and denudation of sedimentary rocks and glaciation and deglaciation, has most likely played an important role in the evolution of the stress in the bedrock in the Forsmark area, and specifically the bedrock inside the target volume.

The character of the bedrock close to the surface in the target volume, FFM02, is related to the unloading of the rock and the release of *in situ* stress. Reactivation of ancient fractures and even formation of new fractures (sheet joints) is apparent, at least close to the surface, during the Quaternary. The rock in the south-eastern part of the candidate area, FFM03, is spatially associated with a high frequency of gently dipping fracture zones containing both open and sealed fractures. These structural features are consistent with a general stress-released region.

4.5.2 Stress model

The assessment of the *in situ* stress state at the Forsmark site is based on both direct measurements and indirect observations. Data from direct measurements by overcoring, hydraulic fracturing and hydraulic tests on pre-existing fractures are available from a number of boreholes in fracture domains FFM01, FFM02 and FFM03. Indirect observations from boreholes in the same fracture domains include observations of core dinking and borehole breakouts in ca 10 km of borehole walls down to depths of 1 000 m. In addition, estimates of the micro-crack porosity in samples from boreholes were used as indirect indicators in the evaluation of stress. Direct measurements as well as indirect observations all indicate a general orientation of the maximum horizontal stress in the range of N120° to 150°. This major principal stress orientation is consistent with the orientation of regional compression derived from seismic studies, as well as with the overall trend for NW Europe due to the Mid-Atlantic Ridge push.

The stress model for the target volume (Figure 4-15) is developed on the basis of data from overcoring measurements and evaluations of indirect observations, combined with the understanding of the geological conditions at the site and an evaluation of other external influencing factors such as topography, glacial rebound and crustal thickness. As shown by data and supported by findings from regional seismicity studies and the understanding of the deformational history at the site, the magnitudes of both the maximum and minimum horizontal stresses are greater than the vertical stress. The increase in the horizontal stress magnitudes with depth in fracture domain FFM01 appears to correlate with the decrease in frequency of open fractures with depth and a corresponding increase in the rock mass stiffness. The stress model implies a most likely value of the maximum horizontal stress of ca 41 MPa and ca 23 MPa for the minimum horizontal stress at 500 m depth in fracture domain FFM01 in the target volume. The estimated vertical stress at this depth in fracture domain FFM01 is ca 13 MPa. No stress measurements have been carried out in FFM06, but the *in situ* stress state is expected to be similar to that in FFM01, since it consists of a rock mass with similar stiffness properties and is located next to FFM01, below the gently dipping deformation zone A2.

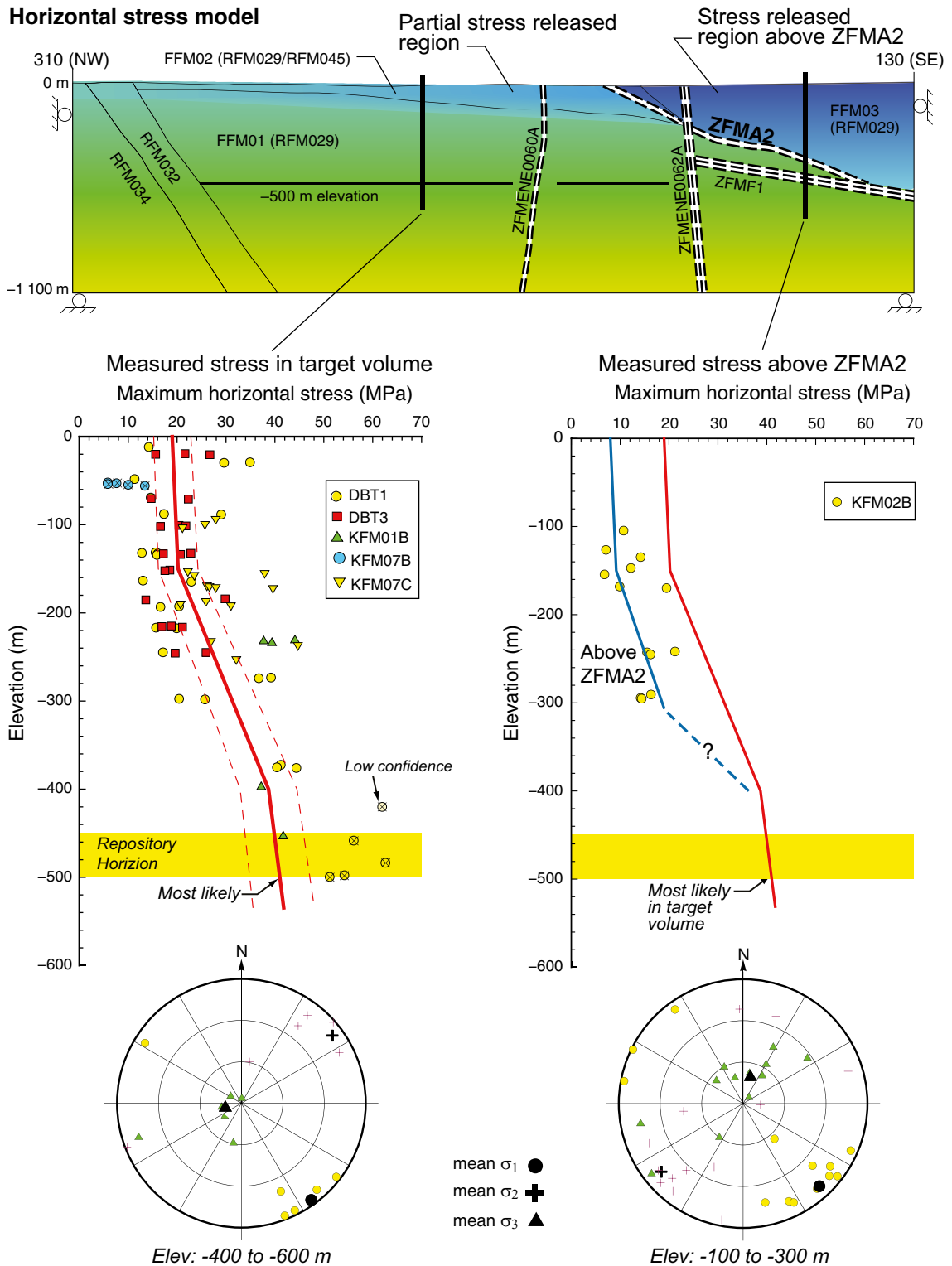


Figure 4-15. Comparison of the measured maximum horizontal stress magnitudes in the target volume with those measured above the gently dipping deformation zone A2 (central insert). The change in slope in the target volume at c. 150 m depth corresponds approximately to the boundary between fracture domains FFM02 and FFM01. An illustration of the distribution of maximum horizontal stresses from numerical modelling is also shown (upper insert), with the blue shades representing reduced stress magnitudes caused by stress release above zone A2 and in fracture domain FFM02 compared with the “normal” stress magnitudes shaded green. The orientations of the measured principal stresses are shown in two lower hemisphere stereonet plots (lower insert). The principal stresses show generally consistent orientations regardless of depth and spatial location (Figure 11-18 in the **Site description Forsmark**).

Based on results of numerical modelling, it is inferred that the steeply dipping deformation zones in the target volume cause only small perturbations in the stress field, whereas the effect of the gently dipping zones A2 and F1 is more pronounced, with significantly higher stress magnitude below relative to that above these zones. The results further show that release of stress in the hanging wall has reached deeper levels south-east of zone A2 relative to that below and north-west of this zone, i.e. in the target volume (Figure 4-15). This is supported by results from overcoring measurements that show an average horizontal stress magnitude approximately 50 % lower in the rock above zone A2 (fracture domain FFM03) compared with the horizontal stress magnitude measured at comparable depths in the target volume. Furthermore, these findings are consistent with the interpretation that the occurrence of the gently dipping zones favoured stress release in the south-eastern part of the candidate volume.

Confidence

The confidence in the orientation of the rock stresses is high due to the consistency in results from the different measuring methods and indirect observations. It also agrees with regional seismic studies. The confidence in the vertical stress magnitude is also high, since measured values and theoretical values based on the weight of the overlying rock cover are in concordance. Uncertainty remains in the magnitude of the horizontal stresses at repository depth. However, an upper bound solution was used to constrain these stress magnitudes and hence it is judged that the uncertainty is sufficiently well constrained.

4.6 Bedrock hydraulic properties

4.6.1 Evolution

Geological data at the site, including the dating of fracture minerals, indicate that a large proportion of the fractures are sealed (ca 75 %) and that the majority of the fractures are ancient structures, especially in the deeper parts of the bedrock in the target volume, i.e. fracture domains FFM01 and FFM06. The youngest generation of calcite occurs in fractures and deformation zones that are currently hydraulically conductive and may have precipitated during a long period including the present. Based on these observations and indications, it is conceptually attractive to envisage that the hydraulic properties of fractures can be correlated with both the brittle deformational history that formed and reactivated the fractures, and with the formation of fracture minerals during different periods in the past. In contrast, an analysis of transmissivity data versus normal stress suggests a poor correlation, if any. Most likely, the processes that occurred during the past 1.85 billion years overshadow any coupling to the current stress field, which has existed for approximately the past 12 million years. Notwithstanding these considerations, the question of correlation may be scale dependent.

4.6.2 Hydraulic properties of deformation zones and fracture domains

Deterministically modelled deformation zones

Detailed information on the position of deterministically modelled deformation zones and water-conductive fractures in between deformation zones combined with results of high-resolution inflow measurements in 22 core-drilled boreholes and pumping tests in 32 percussion-drilled boreholes provide the basis for the assignment of hydraulic properties of deformation zones and fracture domains at the Forsmark site. These data constrain locations of connected flowing fractures with high certainty and values of the integrated transmissivity for the connected fractures down to ca 10^{-9} m²/s. Results from single-hole injection tests and multiple-hole interference tests complement the data base.

Analyses of the hydraulic data have revealed that all deterministically modelled deformation zones, regardless of orientation, are characterised by a substantial decrease in transmissivity with depth, with a contrast of ca 20 000 times over the uppermost 1 000 m of the bedrock (Figure 4-16 upper insert). The lateral heterogeneity at each depth is also substantial, but more irregular, suggesting a channelled flow field within the planes of the deformation zones. Furthermore, the data show that the gently dipping deformation zones, which predominantly occur in the south-eastern part of the candidate volume, are the most transmissive at each depth (Figure 4-16 upper insert). The steeply dipping deformation zones that strike WNW and NW and border the candidate area form structures with a second order of importance as far as transmissivity is concerned. These observations provide

support for the hypothesis that involves a pronounced hydraulic anisotropy on a regional scale, where the largest transmissivities observed are associated with deformation zones that are oriented at a high angle to the minimum principal stress or sub-parallel to the maximum horizontal stress, respectively.

In the model, the observed vertical and lateral heterogeneity in transmissivity of the zones are both honoured. An exponential decrease in transmissivity with depth is assigned based on the depth trend in the data. The lateral heterogeneity in transmissivity is represented statistically as a lognormal distribution at each depth based on the variability observed in the data. This is further quantified in the **Data report**, Section 6.6.

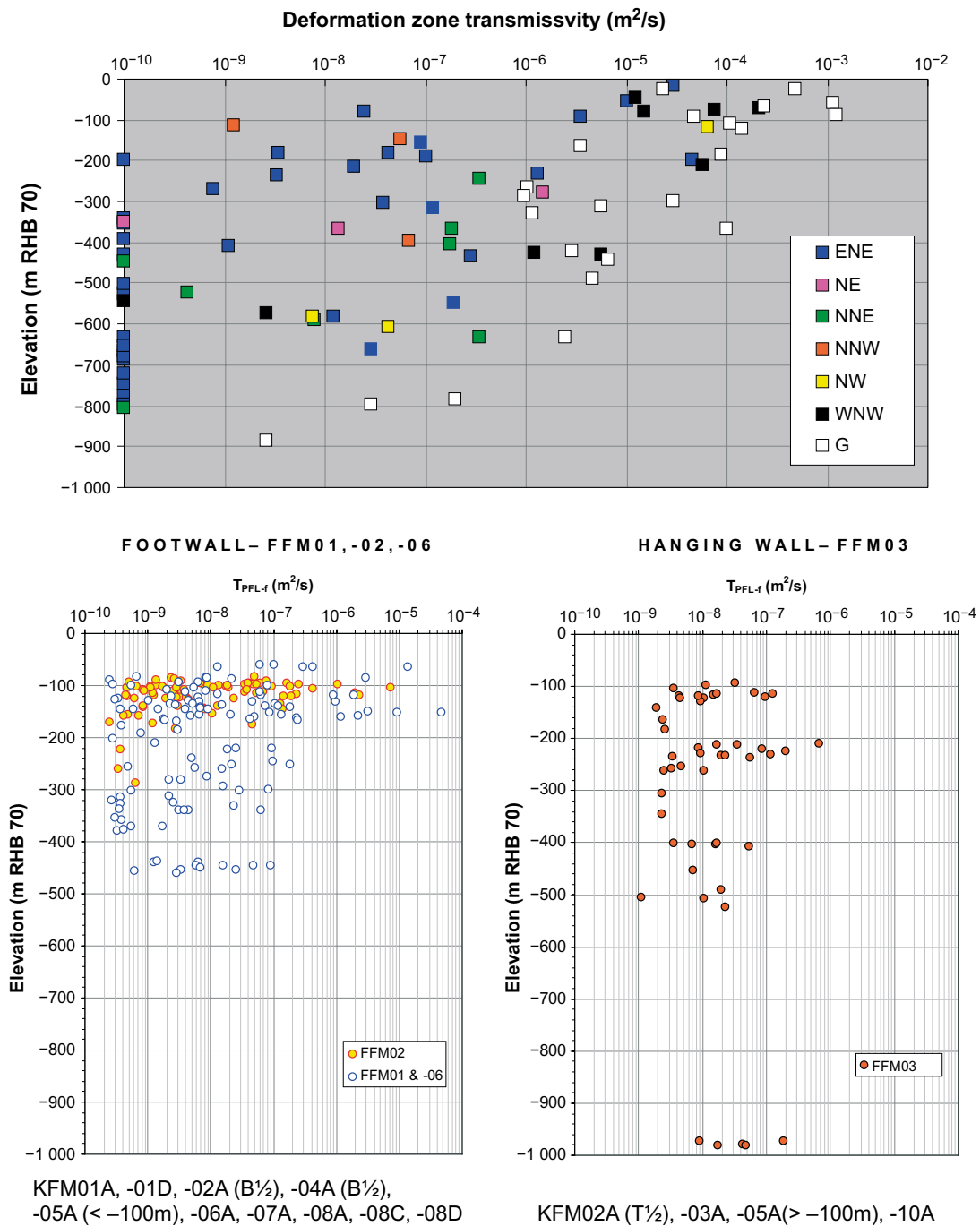


Figure 4-16. Top: Inferred transmissivities of deformation zones with depth and orientation (*G* = gently dipping zones). Bottom: Inferred transmissivities of connected open fractures with depth in FFM01, FFM02 and FFM06 (left) and FFM03 (right) (Figure 11-19 in the *Site description Forsmark*). Note that the bottom left insert contains data from 10 boreholes whereas the bottom right insert contains data from 4 boreholes only (*B*½ = bottom half of the borehole, *T*½ = top half of the borehole).

Fracture domains

The hydraulic characterisation of the rock in between deformation zones supports the division of the bedrock into different fracture domains. In addition, the hydraulic data suggest that the subsurface fracture domain FFM01, located in the target bedrock volume, should be further divided into three depth intervals (Figure 4-16, lower left insert). Below 400 m depth, very few flowing fractures occur, and these are predominantly sub-horizontal fractures with an average spacing of ca 200 m. However, it should be noted that the frequency of flowing fractures below 400 m is so low that it is highly speculative to define an average separation. Above 400 m depth, the frequency of flowing fractures is somewhat higher up to about 200 m depth. Above 200 m depth, there is a significantly higher frequency of flowing fractures, not least fractures with high transmissivities. In FFM03, there are far fewer boreholes to substantiate an analysis of hydraulic subdomains, but as shown in Figure 4-16 (lower right insert), there is also some depth dependence in this domain.

The geometric and hydraulic properties of fractures in the rock between the deterministically modelled deformation zones are represented by DFN models calibrated against fracture frequency data and hydraulic data from boreholes. This calibration is made for fracture domains FFM01, FFM02 and FFM03. Fracture domain FFM06 is inferred to have the same properties as fracture domain FFM01. The division into hydraulic subdomains honours the variation in the intensity and size of open fractures with depth inside fracture domain FFM01. Uncertainties in transmissivity of the connected fracture network are handled by alternative assumptions concerning the possible relationships between fracture transmissivity and size (correlated, semi-correlated and uncorrelated), see **Site description Forsmark**, Section 8.5.2 for details. Although it is difficult to establish which of these models may best reflect reality, all three models yield similar ranges of transmissivities for fractures in the size range 10 to 100 m. For this reason, the three models are likely to show similar flow characteristics. The hydraulic DFN models and their uncertainties are further quantified and discussed in the **Data report**, Section 6.6.

Uppermost part of the bedrock

There are three pieces of evidence that indicate a well-connected network of highly transmissive structures in the uppermost ca 150 m of the bedrock in the target volume where fracture domain FFM02 occurs: 1) exceptionally high water yields in the percussion-drilled boreholes (Figure 4-17), 2) the nearly uniform groundwater levels in the uppermost part of the bedrock, and 3) the extensive and rapid transmission of fluid pressure changes during the large-scale interference tests conducted within the target volume. These structures are inferred to be large sub-horizontal fractures, so-called sheet joints, which are known to exist close to the surface (Figure 4-24). The network is found to short circuit the recharge from above as well as the discharge from below. This is hydrogeologically conceptualised as a shallow, anisotropic, bedrock aquifer on top of a thicker segment of bedrock with aquitard type properties (Figure 4-18). Based on the occurrence of high transmissivities, the lateral extent of this bedrock aquifer is envisaged to correspond approximately to the lateral extent of fracture domain FFM02. However, the hydrogeological data indicate that this network of structures probably extends to the north-east as far as the Singö deformation zone.

Confidence

In general, there is a high confidence in the bedrock hydrogeological model of the site and the assignment of hydraulic properties. The main reason for this assertion is the consistency between different types of hydraulic data, which all support the presence of anisotropic hydrogeological conditions in the area. These conditions are: 1) high transmissivity in the gently dipping fracture zones outside the target volume, 2) few flowing fractures at depth in the target volume (FFM01 and FFM06), and 3) a highly transmissive system of fractures, including sheet joints, in the near-surface realm inside the target volume (FFM02), which are connected over long distances. The various types of hydraulic data are also consistent with the understanding of the geology and the rock stresses at Forsmark and are also supported by the groundwater chemical data (see Section 4.8).



Figure 4-17. Two key features of the bedrock in the target area at Forsmark. Left: High water yields are often observed in the uppermost c. 150 m of the bedrock. Right: The large number of unbroken drill cores gathered at depth support the observation of few flowing test sections in the deeper bedrock (Figure 8-51 in the *Site description Forsmark*).

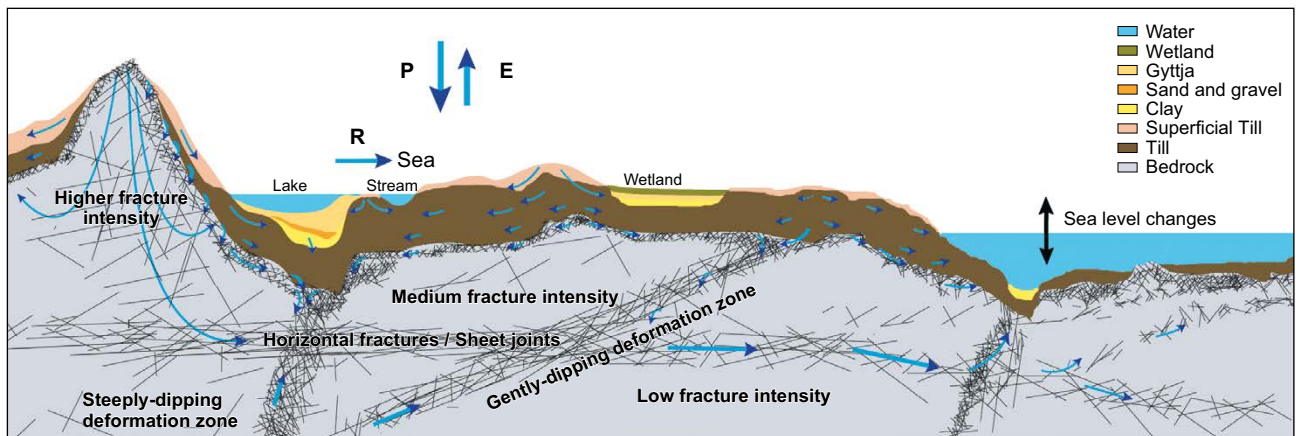


Figure 4-18. Cross-section cartoon visualising the notion of a shallow bedrock aquifer and its envisaged impact on the groundwater flow system in the uppermost part of the bedrock within the target area. The shallow bedrock aquifer is probably hydraulically heterogeneous but at many places it is found to be very anisotropic causing a short circuit of the recharge from above. The shallow bedrock aquifer is conceived to constitute an important discharge horizon for the groundwater flow in outcropping deformation zones. P = precipitation, E = evapotranspiration, R = runoff (Figure 3-21 in Follin et al. 2007a).

Uncertainties remain in the hydraulic properties of deformation zones and fractures south-west and north-east of the tectonic lens and target volume. The most important of these concerns the hydraulic character of the regional Singö deformation zone close to the north-eastern border of the tectonic lens, and the hydraulic properties further downstream of the target volume. Although interference tests conducted show no hydraulic contact between the north-eastern part of the target volume and the bedrock on the north-eastern side of the Singö deformation zone, where the SFR repository is situated, it cannot be excluded that such hydraulic connections exist at other locations along this regionally significant zone.

The implementation of the geometry and hydraulic properties of fracture domains and deformation zones and the shallow bedrock aquifer into a numerical model have revealed that the model can be matched to results of large-scale interference tests, to observed natural point-water heads in percussion holes and soil pipes, and to the concentrations of various species measured in groundwater samples from boreholes. However, there is some concern whether the measured groundwater levels (point-water heads) are natural or disturbed, e.g. disturbed by the abstraction of drainage water at SFR. Even though the abstraction of drainage water in the SFR repository is an uncertain boundary condition that may affect the natural groundwater levels, it is concluded that the hydraulic stresses (drawdowns) induced by the cross-hole tests run in the target volume are sufficiently strong to allow for a fair calibration of the hydraulic properties. The magnitudes of the hydraulic gradients derived from the groundwater flow model using these calibrated properties are quite reasonable, whereas the gradients inferred from the field measurements of the natural groundwater flow in deep boreholes are much higher and generally exceed the maximum possible topographic gradient at the site by orders of magnitude. Conversely, *in situ* measurements of flow rates in fractures by tracer dilution techniques give flow rates that are sometimes much larger than what is expected considering the apparent transmissivity of the same fracture and reasonable hydraulic gradients. The reason for this behaviour is not fully understood, although is likely to be related to the simplifying assumptions necessary to make such scoping calculations on the level of individual flow conductors. The flow rates as a whole, however, are comparable to hydraulic modelling results obtained using the hydraulic network models.

4.7 Integrated fracture domain, hydrogeological DFN and rock stress models

Fracture domain FFM03 in the hanging wall to the gently dipping zones ZFMA2 and ZFMF1 (Figure 4-19) was defined on the basis of an inferred even distribution of open fractures with depth and is contiguous with a bedrock volume containing abundant gently dipping fracture zones. This contrasts sharply with the bedrock further to the north-west in the footwall to these gently dipping zones. Modelling work has shown that connected open fractures are also more evenly distributed in the hanging wall to the gently dipping zones A2 and F1 (Figure 4-19). Furthermore, the maximum horizontal stress is reduced in this domain relative to that in the bedrock volume further to the north-west (Figure 4-19). The even distribution of open fractures and the occurrence of gently dipping fracture zones are consistent with a general stress-released volume. Indeed, the fracture characteristics may have inhibited a more significant build-up of horizontal stresses in this bedrock volume.

The bedrock in the footwall to the gently dipping zones ZFMA2 and ZFMF1 (Figure 4-19) is far more inhomogeneous especially with respect to the distribution of open fractures. This attribute, together with some consideration for increased alteration (albitization) in fracture domain FFM06, formed the basis for the recognition of three different fracture domains in this volume (FFM01, FFM02 and FFM06). An increased intensity of connected open fractures and reduced maximum horizontal stress characterise the upper part of the bedrock in the footwall to zone A2, and this volume corresponds more or less to fracture domain FFM02 (Figure 4-19). A striking consistency between the different models concerns how the intensity of connected open fractures and the stress-released volume conform to the increased thickness of domain FFM02 as the gently dipping zone A2 is approached (Figure 4-19). It is suggested that this change with respect to zone A2 is related to the increased frequency of sub-horizontal and gently dipping fractures in the vicinity of this zone. Since these structures are oriented at a high angle to the vertical stress, which corresponds to the minimum principal stress, there is a more favourable environment for the modification of the aperture of ancient fractures and even formation of new stress-release joints and, consequently, the more pronounced release of stress closer to the A2 zone.

In contrast, the major part of fracture domains FFM01 and FFM06 inside the target volume, including especially the repository volume around 500 m depth, is characterised by relatively few open fractures, a compartmentalised pattern close to the percolation threshold for the connected open fractures and higher maximum horizontal stress. It is inferred that the low intensity of open fractures favoured a more significant build-up of horizontal stresses. The character of the connected open fractures in this volume implies restricted groundwater circulation.

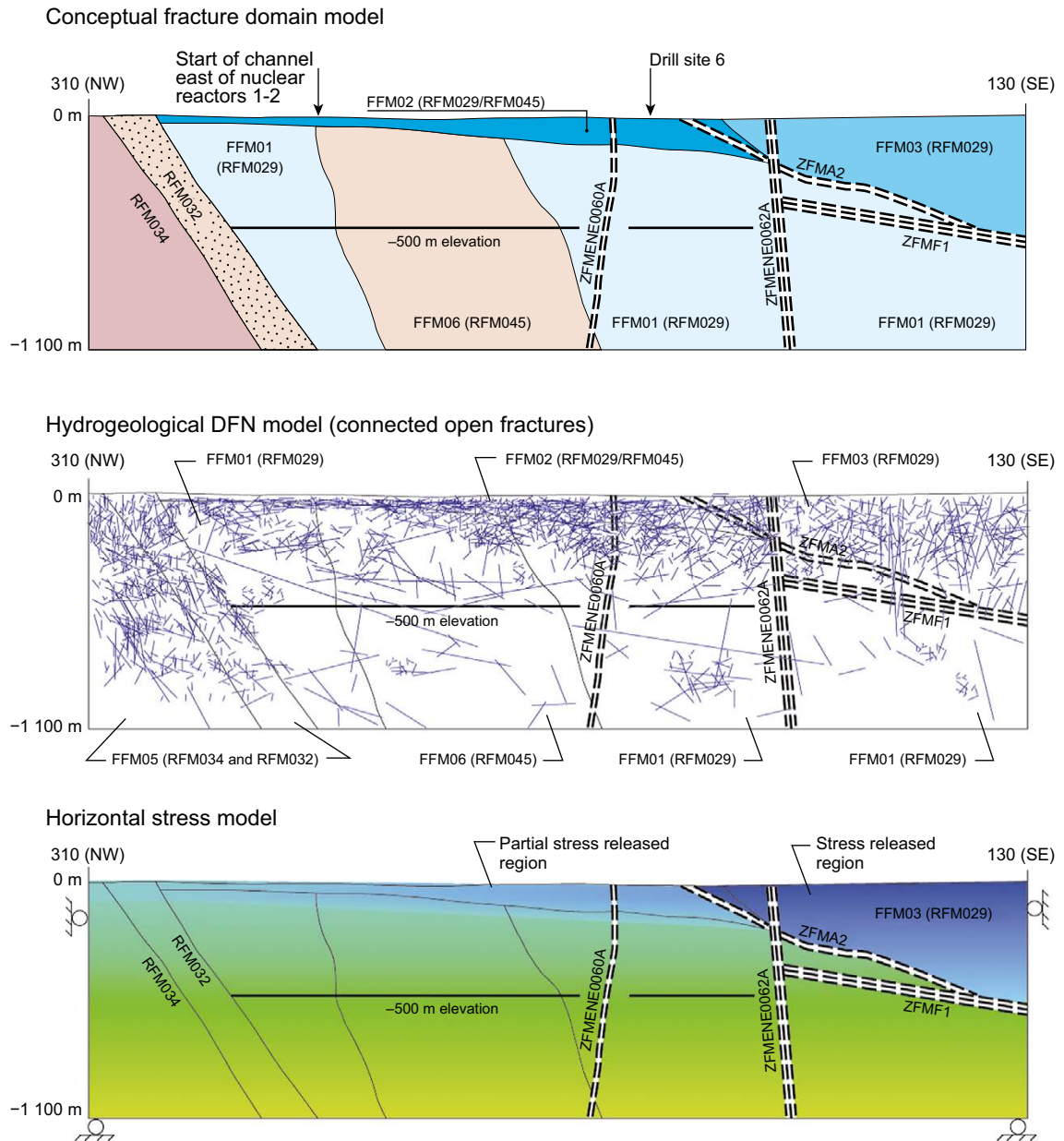


Figure 4-19. Comparison of fracture domain, hydrogeological DFN and maximum horizontal stress models along a NW-SE profile in the north-western part of the candidate volume (Figure 11-21 in the *Site description Forsmark*).

In summary, a bedrock volume where there is a limited number of open fractures and, by corollary, a low permeability is consistent with higher rock stresses. However, the properties of such bedrock are affected by the stress-released conditions in the near-surface realm and close to gently dipping ancient structures.

4.8 Groundwater

4.8.1 Evolution during the Quaternary period

Several water types which are now present in the bedrock can be associated with past climatic events during the Quaternary period (ca 2.5 Ma), including glacials and interglacials, and associated changes in shore-line in connection with transgressions and regressions. Among these, the last glaciation and the present interglacial (the Holocene starting 10 000 years ago) are the most important for the groundwater development in the Fennoscandian Shield, especially in terms of land uplift and shoreline displacement, as well as the post-glacial development of the Baltic Sea.

The Baltic Sea post-glacial development during the Holocene (Figure 4-20) reveals that when the Weichselian ice sheet melted and retreated from the Forsmark area around 8800 BC, glacial meltwater had been hydraulically injected under pressure into the bedrock. The exact penetration depth is unknown and is also dependent on the geometry and heterogeneity of the system. However, chemical and isotopic data indicate penetration depths of about 1000 metres southeast of the target area adjacent to the gently dipping deformation zones, whereas cold climate signature has been found down to about 400 m in the low-conductive target volume of the rock.⁹ Since the deglaciation of the Forsmark region coincided with the end of the Yoldia period, there are no signs of Yoldia Sea water in the bedrock. The Ancylus Lake (8800 to 7500 BC) was lacustrine and developed after the deglaciation. This period was followed by the brackish Littorina Sea (after 7500 BC). During the Littorina Sea stage, the salinity varied and was considerably higher than at present (maximum of about 15 ‰) in the period 4500 to 3000 BC. Dense brackish seawater from the Littorina Sea penetrated the bedrock, resulting in a density intrusion that affected the groundwater in the more conductive parts of the bedrock. When the first parts of the Forsmark region subsequently emerged from the sea, starting ca 500 years BC, recharge of meteoric water subsequently formed a freshwater layer on top of the saline water because of its lower density. As a result of the flat topography of the Forsmark area and of the short period that has elapsed since it emerged from the sea, the out-flushing of saline water has been limited, and consequently a freshwater layer is only present at shallow depth.

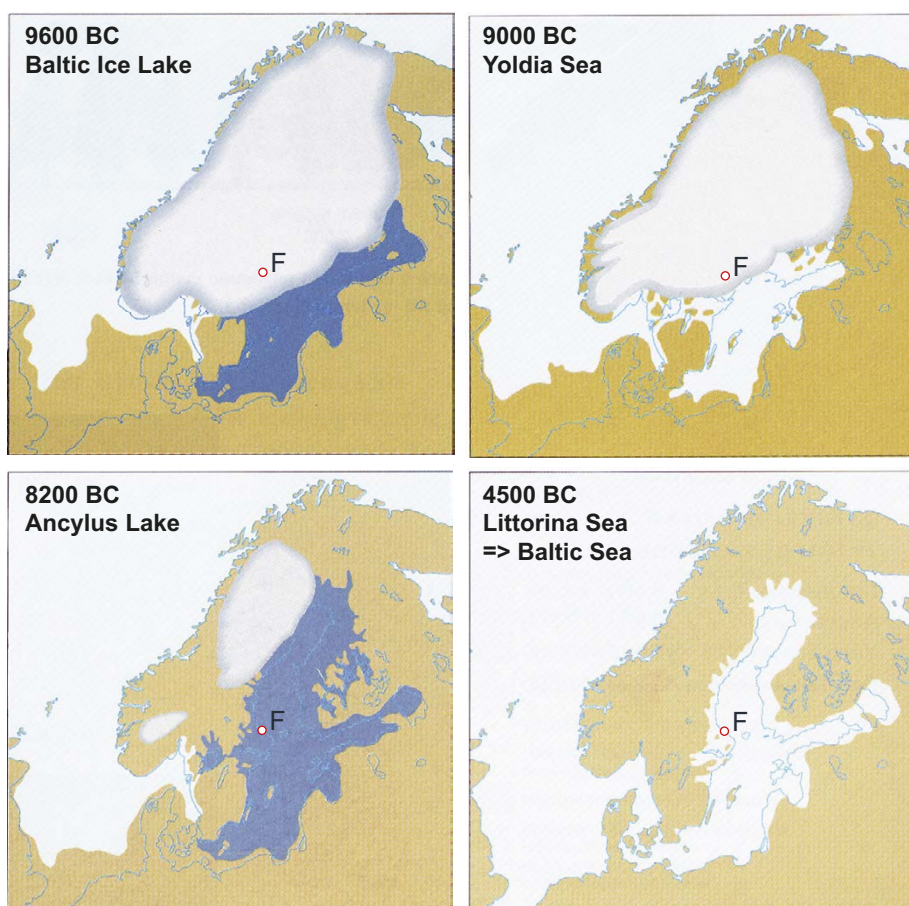


Figure 4-20. Map of Fennoscandia with some important stages during the Holocene interglacial period. Four main stages characterise the development of the aquatic systems in the Baltic basin since the latest deglaciation: the Baltic Ice Lake (13 000–9500 BC), the Yoldia Sea (9500–8800 BC), the Ancylus Lake (8800–7500 BC) and the Littorina Sea 7500 BC–present). Fresh water is symbolised with dark blue and marine/brackish water with pale blue. The Forsmark area (notated 'F') was probably at or close to the rim of the retreating ice sheet during the Yoldia Sea stage (Figure 11-22 in the *Site description Forsmark*).

⁹ The depths 1000 m and 400 m have been corrected relative to the SR-Site report, where shallower maximum penetrations depths were reported. This correction has no bearing on the conclusions drawn from the data in question.

The Quaternary evolution has affected the groundwater chemistry at Forsmark, especially in the more conductive parts of the bedrock, but, as described above, changes in groundwater chemistry are not restricted to post-glacial time. There is groundwater and porewater evidence that indicates the presence of old (pre-Holocene) meteoric water that originated during a temperate climate. The age of this component is unknown, but possibilities include pre-Quaternary or even older. The hydrogeochemistry of the Forsmark area cannot be explained without recognising this older component. The present groundwaters therefore are a result of mixing and reactions over a long period of geological time. The interfaces between different water types are not sharp due to molecular diffusion, but reflect variability in the structural-hydraulic properties.

4.8.2 Groundwater composition and water – rock interactions

Explorative analyses of groundwater chemistry data measured in samples from cored boreholes, percussion boreholes and soil boreholes, and hydrogeochemical modelling have been used to evaluate the hydrogeochemical conditions at the site in terms of origin of the groundwater and the processes that control the water composition. Although the data set is rather limited, the results have revealed that the current groundwater composition in general supports the occurrence of different hydrogeological regimes in the candidate volume, i.e. the bedrock at depth in the target volume, the uppermost part of the bedrock in the target volume and the rock south-east of the gently dipping zone A2 with its swarm of gently dipping fracture zones.

Groundwater in fractures

Groundwaters in the uppermost 100 to 200 m of the bedrock display a wide range of chemical variability, with chloride concentrations in the range 200 to 5000 mg/L (Figure 4-21 and Figure 4-22) suggesting influence of both brackish marine water (i.e. old Littorina Sea and possibly some recent Baltic Sea relicts) and meteoric waters. In the bedrock in the footwall to zone A2 including fracture domain FFM02, this shallow system is controlled by flow along highly transmissive, sub-horizontal fractures and sheet joints (i.e. the shallow bedrock aquifer), which is still in the process of flushing out residual brackish marine (Littorina) groundwaters. Furthermore, a sharp decrease in tritium content at about 150 m depth, as well as carbon-14 data (Figure 4-21), indicate that these shallow groundwaters have short residence times that are in the order of only a few decades to a few hundred years.

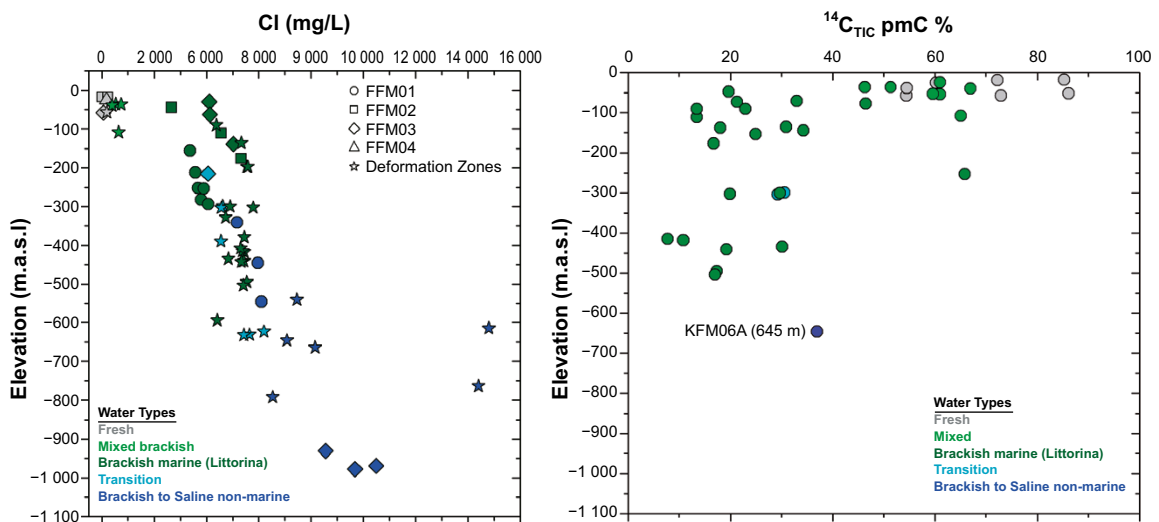


Figure 4-21. Left: Cl concentration as a function of elevation as measured in groundwater from the different fracture domains and from deformation zones (from Figure 9-5 in the *Site description Forsmark*). Right: $^{14}\text{C}_{\text{TIC}}$ as a function of elevation. The only sample of brackish non-marine groundwater type analysed indicated contamination during sampling (Figure 9-20 in the *Site description Forsmark*).

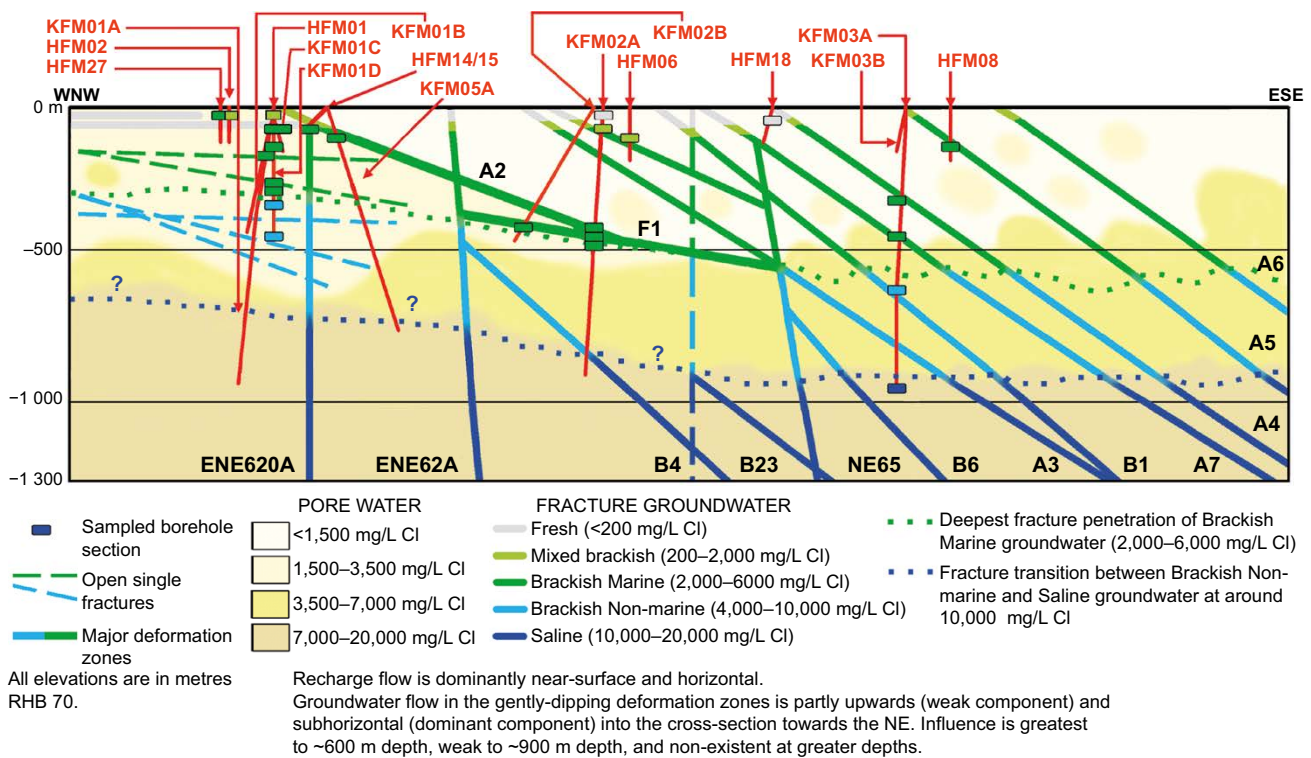


Figure 4-22. Illustration of the groundwater composition along a WNW-ESE cross-section through the candidate area at Forsmark as interpreted from hydrogeochemical data. The location of the boreholes and the sections that have been sampled are shown together with the main fracture groundwater types that characterise the site. The chloride distribution with depth along the fracture zones and single open fractures, as well as the subdivisions of the rock matrix porewater based on chloride concentration are also shown. The dotted lines in different colours crossing the section represent the approximate depths of penetration of the major groundwater types along hydraulically-active fracture zones (Figure 11-23 in the *Site description Forsmark*).

At depths greater than ca 200 m, the water composition is indicative of brackish marine water with chloride concentrations in the range 2 000 to 6 000 mg/L and with a clear Littorina Sea component (Figure 4-21 and Figure 4-22), as indicated by concentrations of magnesium and the ratio of bromide to chloride concentrations. This water type is recognised down to 600 to 700 m depth in the transmissive gently dipping fracture zones in the south-eastern part of the candidate volume, contiguous with fracture domain FFM03, whereas the penetration depth in fracture domain FFM01 in the target volume, where the frequency of water-conducting fractures is low, is restricted to ca 300 m. Below these depths in FFM01, the water composition indicates brackish to saline non-marine groundwaters (i.e. an absence of Littorina Sea influence), reflecting processes which have occurred prior to the intrusion of the Littorina Sea waters. These deep waters further show an increase in calcium with depth, which is a well recognised trend and indicative of water/rock interactions that occur under steadily decreasing flow to stagnant groundwater conditions with increasing depth.

Composition of rock matrix porewater

Analyses of the composition of rock matrix porewater (Waber et al. 2009) also support the occurrence of low groundwater turnover in fracture domain FFM01. Porewater from this domain generally has a lower chloride content compared with the fracture groundwaters, indicating a transient state between the porewater and groundwater down to at least 650 m depth (Figure 4-22). The data suggest that these porewaters have evolved from an earlier, very long lasting circulation of old dilute groundwaters in a few fractures. This is also consistent with the still prevailing transient state between this porewater and fracture groundwaters from equivalent depths which, based on chlorine-36 and helium-4 dating, have residence times of more than 1 Ma.

South-east of the target volume in the hanging wall rock to zone A2, a situation close to steady-state is suggested between porewater and fracture groundwater down to about 200 m below the surface, reflecting the high frequency of water conducting, gently dipping fracture zones, and the rapid circulation of significant volumes of water in this area (Figure 4-22). At greater depth, the porewater has lower chloride contents than the fracture groundwater indicating a transient state down to approximately 650 m depth. The significantly negative $\delta^{18}\text{O}$ values preserved in some samples taken far from the water-conducting fractures suggest that this cold-climate signature relates to glacial water circulating for a considerable period in the fractures at these depths. Chloride, magnesium and oxygen-18 in porewaters sampled closer to the conducting fractures suggest that since the last deglaciation, the porewater signature has become overprinted with a brackish marine water (probably Littorina).

On-going reactions

Whilst mixing (both advection-dispersion and molecular diffusion) is the major process giving rise to present-day groundwater compositions, the role of reactions has also been addressed. In particular, the alkalinity and redox buffering capacity of the bedrock is of key importance for groundwater composition and future changes due to, for example, potential infiltration of dilute and oxygen-rich water.

The presence of limestone (calcite) and extensive biogenic activity in the Quaternary overburden give rise to pH values usually above 7, calcium concentrations mostly between 50 and 200 mg/L and bicarbonate concentrations in the range 200 to 900 mg/L in the near-surface waters (down to ca 20 m depth). Concentrations then decrease to very low values at greater depths. However, bicarbonate is relatively high in most of the brackish marine groundwaters hosted in the upper 600 m of the gently dipping fracture zones south-east of the target volume, whereas brackish non-marine groundwaters below 300 m in fracture domain FFM01 have low bicarbonate contents.

The pH buffering capacity in Forsmark groundwaters at depths greater than 100 m appears to be controlled by the calcite system, and modelling indicates that this water is in equilibrium with calcite. Investigation of fracture minerals shows that calcite in fractures is abundant and that no extensive leaching has occurred in response to past glaciation/deglaciation events.

According to data analyses and modelling of the redox system, reducing conditions currently prevail at depths greater than ca 20 m. Most of the Eh values determined in brackish groundwaters (at depths between 110 and 646 m) seem to be controlled by the occurrence of an amorphous iron oxyhydroxide with higher solubility than a truly crystalline phase. This indicates that the iron system is disturbed. This conclusion is supported by mineralogical investigations that have identified the presence of fine-grained amorphous to poorly crystalline phases now evolving towards more crystalline phases. Dissolved sulphide concentrations are systematically low, possibly due to the precipitation of amorphous Fe(II) monosulphides, linked to the activity of sulphate-reducing bacteria (SRB). At depths greater than 600 m, the dissolved sulphide concentrations increase, which is consistent with the occurrence of SRB and with the active precipitation of Fe(II) monosulphides. The iron system at these depths is believed to be limited by crystalline oxides, mainly hematite. The sulphide values recorded during the complete chemical characterization sampling are generally low compared with those measured when monitoring has been carried out subsequently in the same sections. A discussion and evaluation of the sulphide data, including monitoring after the site investigation, is found in Tullborg et al. (2010). Further studies regarding sulphide related issues support the conclusions of that evaluation.

Elevated concentrations of uranium have been detected in some of the groundwaters with a Littorina Sea component and the highest concentrations are found in waters in the gently dipping fracture zones south-east of the target volume. Thermodynamic calculations, performed using groundwater geochemical data from more than twenty borehole sections, which varied by groundwater-type and uranium concentration, indicate that the uranium speciation is sensitive to whether the redox values are set by the Fe(III)/Fe(II) or the S(-II)/S(VI) redox couple. Speciation-solubility calculations fixed by the Fe(III)/Fe(II) redox couple ($\text{pe-value} < -4.4$) suggest that elevated uranium concentrations are a thermodynamic anomaly, but the higher pe-values associated with the S(-II)/S(VI) redox couple (up to -3.7) indicate a predominance of the $\text{Ca}_2\text{UO}_2(\text{CO}_3)_3^0$ aqueous complex (Krall et al. 2020).

Crystalline U(IV) minerals, uraninite and coffinite, are strongly oversaturated in the groundwaters, and amorphous U(IV) phases are close to equilibrium. Therefore, a prerequisite for elevated U(VI) concentrations in these low redox groundwaters is the presence of a U(VI)-bearing solid phase in the system. U(VI) minerals and amorphous solids, including the uranophane and haiweeite minerals found in the Forsmark drill cores that preserved evidence of recent water-rock interaction, are undersaturated in all of the groundwaters (Section 4.4.4). Therefore, the uranium minerals that were oxidized during the early tectonothermal evolution of Forsmark are the probable source of U(VI) to the present groundwaters. Dissolved U(VI) may be reduced and precipitate as U(IV) in groundwaters that contain sufficient reducing agents, although aqueous U(VI) may be in state of quasi-equilibrium in the young (< 10 000 yr) groundwaters that show disequilibrium between the iron, sulphur, and uranium redox systems and contain calcium and bicarbonate (Krall et al. 2020).

The presence of goethite (FeOOH) in some hydraulically active fractures and fracture zones in the upper part of the bedrock, mainly within the gently dipping fracture zones A2 and F1, indicates circulation of oxygenated fluids during some period in the past (potentially during the Quaternary). However, the presence of pyrite in the same zones suggests that the circulation of oxygenated fluids has been concentrated along channels in which different redox micro environments may have been formed.

The analyses of the current redox system at Forsmark have consistently indicated that sampling (or drilling-induced) perturbation may have altered the original redox conditions of the hydrogeochemical system. Examples include oxygen intrusion and precipitation of amorphous iron oxyhydroxides, as indicated by the colloidal composition (see section below) and mineralogical determinations. Despite these potential disturbances, the buffer capacity of the system maintains a substantially reducing character. As far as the potential redox buffering capacity of the fracture system is concerned, it is concluded that previous oxidising episodes have not been intense enough to exhaust the reducing capacity of fracture-filling minerals, which are still present in the shallow system (for example chlorite and pyrite). Any potential build-up of reducing capacity in the fracture minerals during recent periods of reducing groundwater conditions is difficult to estimate, but it can be concluded that the amounts of recent (Quaternary) minerals formed is small.

Dissolved gas and colloids

Analyses of gas dissolved in groundwater at Forsmark have shown that the gas content increases with depth, but the waters are far from being oversaturated by gas at the depths from which they were sampled. The major gas components are nitrogen and helium. In addition, argon, methane and carbon dioxide have also been detected. Methane concentrations are small (less than 0.2 mL/L), and it is currently unknown whether it is of biogenic or non-biogenic origin.

Colloid amounts in Forsmark groundwater are comparable to those found in other granitic environments. The colloids are composed mainly of iron and sulphur compounds. Uranium associated with the colloids has been found in boreholes KFM02A and KFM06A, in line with the high groundwater uranium concentrations found in these boreholes. The uranium content of the colloids is approximately 10 % of the uranium concentration in the groundwater and colloidal transport is, therefore, a result, but not the origin, of the high uranium content in the groundwater.

Confidence

There is generally high confidence in the description and understanding of the current spatial distribution of groundwater composition, mainly due to the consistency between different analyses and modelling of the chemical data, but also due to the agreement with the hydrogeological and structural geological understanding of the area. The distribution of Fe-minerals (goethite and pyrite) in the near-surface fractures and the common occurrence of calcite suggest that there is buffering capacity against the effects of penetration of dilute groundwater. One remaining uncertainty concerns the increase in sulphide concentrations measured in the on-going monitoring programme. The groundwater sampling procedure for the monitoring programme may have disturbed the system or may have facilitated sulphate reduction. Details of the groundwater composition and associated uncertainties and the implications for PSAR are provided in the **Data report**, Section 6.1.

4.8.3 Groundwater flow and consistency with groundwater signatures

The Holocene evolution of groundwater composition at Forsmark during the last ca 10 000 years, has been simulated and the results compared with measured concentrations of different elements in the boreholes. The conceptual model for the present-day distribution is illustrated in Figure 4-23 and should be compared with the hydrogeochemical site descriptive model described in Figure 4-22.

The initial conditions for the paleo-hydrogeological simulations that start at 8000 BC are defined in terms of the presence of mixtures of different reference waters in the bedrock. These conditions are derived on the basis of analyses of present-day water composition in fractures and matrix porewater, which reveal that there must have been old meteoric waters derived from both warm and cold climate events in the bedrock in the Forsmark area before the injection of glacial meltwater during the last deglaciation.

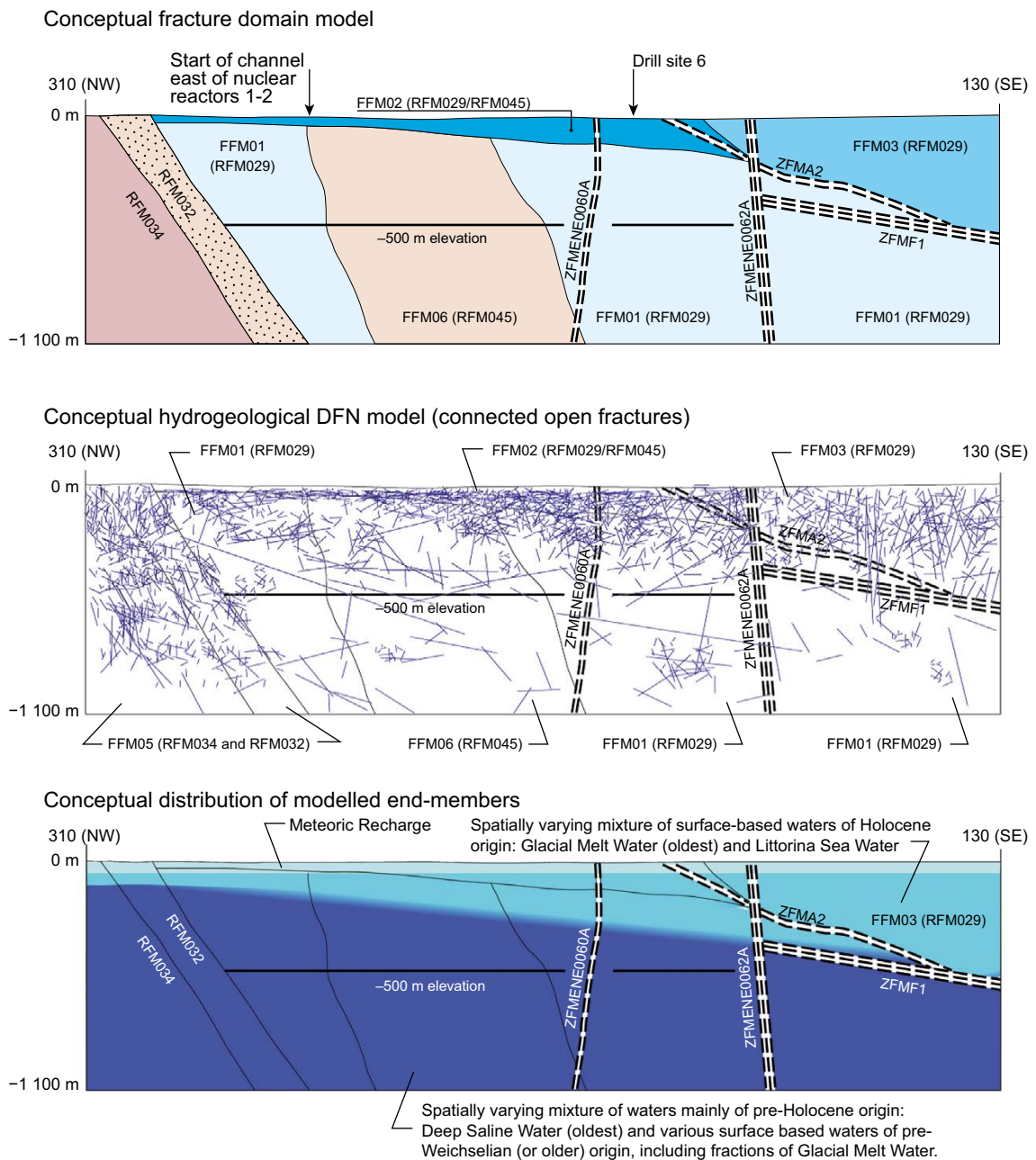


Figure 4-23. Comparison of conceptual models for fracture domains, hydrogeological DFN and the present-day distribution of different end members along a NW-SE profile in the north-western part of the candidate volume (Figure 11-25 in the *Site description Forsmark*).

The results of the simulation with the hydrogeological model show fair agreement with measured concentrations of chloride, the bromide/chloride ratio, $\delta^{18}\text{O}$ and bicarbonate concentrations in the boreholes (Figure 8-46 to 8-50 in the **Site description Forsmark**). Furthermore, the model predicts deeper penetration of Littorina Sea water along the gently dipping fracture zones intersecting fracture domain FFM03 south-east of the target volume (down to ca 500 to 600 m depth) than in steeply dipping deformation zones intersecting fracture domain FFM01 inside the target volume (down to ca 300 to 400 m depth). Although not matching the exact concentrations, the model also predicts higher salinity in the fracture water than in the rock matrix porewater, which is consistent with the field observations (Figure 4-22).

The paleo-hydrogeological simulations also support the hydrochemical observations in surface water and shallow groundwaters, which indicate that there is probably no ongoing discharge of deep saline water into the freshwater surface system (the uppermost ca 150 m of the bedrock). Furthermore, the simulation results are consistent with the field observations of relict marine remnants, which also include deep saline signatures, in the groundwaters in the Quaternary deposits in small areas outside the network of fractures and sheet joints in the upper part of the bedrock. One such area is Lake Gällsboträsket, which coincides with the Eckarfjärden deformation zone (see also Section 4.10).

A comprehensive uncertainty analysis with focus on hydraulic parameter heterogeneity within the target volume was performed and the results demonstrate that model calibration against hydrochemical data is sensitive to parameter heterogeneity in the bedrock hydrogeological properties, which is expected in a sparsely fractured rock mass.

4.9 Bedrock transport properties

4.9.1 Rock matrix properties

The bedrock retardation model in the site description is comprised of a qualitative identification and description of typical fracture types and deformation zones at the Forsmark site with regard to processes of relevance for transport of environmental solutes and radionuclides. Furthermore, it builds on quantitative data describing material properties and the relative abundance and spatial distribution of the different geological materials comprising the rock matrix, as well as relevant alteration types and secondary minerals found in association with fractures and deformation zones.

The input data for the retardation model consist of formation factors for solute transport in the rock matrix, matrix porosities, specific surface areas of internal micro-surfaces, cation exchange capacities (CEC), and sorption properties of rock in contact with synthetic groundwater of varying composition. Formation factors are obtained from *in situ* measurements under natural stress conditions, derived from high spatial resolution geophysical logging in the site investigation boreholes, together with data from laboratory studies.

The limited data available for the different rock masses indicate that there are generally no significant differences in the retardation properties between the rock types present in the rock domains RFM029 and RFM045. Furthermore, taking variations in the parameter values into account, there are very few indications of significant differences between the different rock types. As far as key fracture classes are concerned, either a thin layer of fracture coating or no coating at all have been identified as being of importance, since these classes are likely to be associated with a lower degree of retardation.

The deformation zone structural elements for which retardation properties have been tabulated are all comparatively heterogeneous in their structure. From the material properties data, these structural elements are identified as potentially strong sinks for radionuclides transported from a leaking repository. However, this should be considered in the context of the possibly lower hydrodynamic transport resistance of these zones set against their increased micro-structural complexity including additional diffusion-accessible surface area.

Confidence

The porosity and effective diffusivity of the rock matrix appear to be relatively well constrained for the main rock types. Although there is evidence for *in situ* compression of pore spaces in the unaltered matrix rock, the effect upon material properties can be quantitatively bounded. Sorption uncertainty is only semi-quantitatively established and is large for many species and specific groundwater compositions. Sorptivities of certain radionuclides in contact with specific groundwaters and rock types are not known or are not supported by sufficiently large sample sizes to be considered statistically quantified. Sorptivities of U and Np under strongly reducing conditions are likely to be underestimated owing to difficulties in maintaining appropriately low redox conditions in the laboratory. There is uncertainty in the distribution and thickness of altered rock surrounding flow paths. However, the importance of this feature depends on the differences in the material properties of these materials relative to unaltered rock. The data suggest that altered rock is generally associated with increased retention for most radionuclides and therefore this uncertainty can be bounded by the retention properties of unaltered rock. A further quantification of the retardation properties and their associated uncertainties for the purpose of the PSAR assessment is provided in the **Data report**, Section 6.7.

4.9.2 Flow related transport properties

Flow related transport properties are evaluated as part of the PSAR assessment, see Section 10.3.6. However, as a support to the selection of processes and parameters to be considered in the safety assessment modelling, analyses of flow related transport properties were also carried out as part of the site-descriptive modelling and reported in the **Site description Forsmark**.

Molecular diffusion and sorption within the rock matrix is considered to be an important transport retardation mechanism limiting the migration of escaping radionuclides. A key parameter describing this process is the ratio of the surface area in contact with flowing water (the flow-wetted surface) and the flow rate. In general, the greater surface area in contact with flowing water for a given flow rate, the greater the interaction will be with both the fracture surface itself and the rock matrix. The flow-wetted surface to flow ratio is commonly referred to as the flow related transport resistance or (F), see Section 10.3.6 for details.

Numerical simulations of flow and migration provided indications of median F values for “typical” flow paths on the 100 m scale to be on the order of 10^6 y/m at depths larger than 400 metres in fracture domain FFM01. The simulations further demonstrate that less than 4 % of the hydrogeological DFN realisations for FFM01 below 400 m depth exhibit hydraulic connectivity of any kind. Simulations of other fracture domains (upper regions of FFM01, FFM02, and FFM03) give indications of substantially smaller F values as compared with FFM01 at depths below 400 m. An analytical model analysis reveals that flow paths within gently dipping zones such as ZFMA2 are associated with F values of less than 10^3 y/m for transport from repository depth to the near surface. Steeply dipping deformation zones, on the other hand, (for example zone ZFMENE0060A) are found to have F values on the order of 10^5 y/m.

Scoping calculations of the effects of flow channelling on the interpretation of hydraulic borehole data indicate that channelling would not be severe enough to cast doubt on the utility of the hydrogeological models produced based on the site data. It is further concluded that additional physical mechanisms enhancing solute uptake, such as radial diffusion from channels of limited extent and diffusion into stagnant zones with concomitant matrix diffusion, may increase transport retardation substantially. Flow channelling may therefore possibly have an overall beneficial effect.

Confidence

Uncertainty in hydrogeological DFN parameters and the role of channelling phenomena may lead to underestimation of flow channel frequency in the target volume. However, the overall F values for typical flow paths through the repository volume should not be greatly different, provided that the fracture transmissivity model is determined to be reasonable (i.e. it yields the approximately correct order of magnitude in flow predictions). The hydrogeological DFN fitting parameters for fractures within the repository volume can only be properly constrained by statistics from mapping of open

fractures in tunnels. Nevertheless, it is judged that the current hydrogeological DFN, with its alternative descriptions of the transmissivity size correlation, provides adequate bounds on the uncertainty of the flow-related transport properties. These uncertainties are further discussed in the **Data report**, Section 6.6.

4.10 The surface system

The Forsmark area is special in many ways and does not represent a typical Swedish Baltic Sea site. Post-glacial uplift, in combination with the flat topography, results in a relatively fast shoreline displacement, which has resulted in a very young terrestrial system that contains a number of young lakes and wetlands. Shallow and with sediments rich in calcium, the oligotrophic hardwater lakes are unique to northern Uppland.

4.10.1 Evolution during the Quaternary period

The character of the current surface system has been strongly influenced by the climate evolution during the Quaternary period under which the Forsmark area has repeatedly been covered by ice sheets. There have been in the order of 50 glacial/interglacial cycles during the Quaternary and there is evidence for several periods during the Weichselian glacial when large parts of Sweden were ice free, see the **Climate report**. Deposition of sediments at Forsmark occurred during the Weichselian glacial and during the period following deglaciation. In the western part of the candidate area, a silty-clayey till with an extremely high degree of consolidation is present. Based on its stratigraphical position and pollen composition, it is concluded that the deposit is older than the latest ice overriding. In addition, sediment-filled open fractures beneath till in the upper bedrock have been recognised (Figure 4-24). The deposition of these sediments is dated back to a late stage of the glacial phase, when large amounts of sediment-loaded meltwater were concentrated below and within the retreating ice. These fractures formed or were reactivated during a late stage of the local deglaciation and are inferred to be sheet joints formed in connection with the release of stress in the bedrock. During further retreat of the ice, glacial clay was deposited in low topographic areas. The deposition of this glacial clay at Forsmark is dated to the Yoldia Sea stage.

The development of the Baltic Sea after the latest glaciation has been characterised by ongoing shoreline displacement. The highest shore level in north-eastern Uppland developed during the Yoldia Sea stage (9500–8800 BC) of the Baltic Sea development and was located ca 100 km to the west of Forsmark. At that time, the Forsmark area was covered by ca 150 m of water. Since then, the shoreline displacement has been continuously regressive and most of the Forsmark area has emerged from the Baltic Sea during the last 2 500 years. The shoreline displacement has had a large impact on the distribution and relocation of fine-grained Quaternary deposits. Wave washing and bottom currents have eroded, transported and re-deposited sand, gravel and post-glacial clay.



Figure 4-24. a) Laminated silt in an open fracture in the north-western part of the excavated area at drill site 5. The site was originally covered with till that has been removed. b) Horizontal fractures along the more than 1 km long canal between the Baltic Sea and the nuclear power reactors in Forsmark. These fractures are inferred to be sheet joints formed in connection with the release of stress in the bedrock (Figure 11-2 in the **Site description Forsmark**).

The recent emergence of the Forsmark area from the Baltic Sea implies that peat formation has affected the area for a relatively short period of time. The shoreline displacement continuously transforms sea floor to new terrestrial areas or to freshwater lakes. Lakes and wetlands are successively covered by fen peat, which at some locations is covered by bog peat. At Forsmark, rich fens form the dominant type of peat. Bogs do occur, but they are few and still young. Peat is found most frequently in the most elevated south-western part of the area, i.e. in the area that has been above sea level for a sufficiently long time for infilling of basins and for peat to form.

The post-glacial development of the ecosystems at Forsmark is strongly correlated to climate changes and the shoreline displacement, but also to human activities during the last ca 2000 years, as discussed in Section 4.10.3.

Detailed investigations to evaluate the occurrence of paleoseismic activity during the latest part of and after the Weichselian glaciation in and around the Forsmark area have been carried out in the context of the site investigation work. None of the morphological lineaments that have been recognised have been inferred to represent late- or post-glacial faults. Furthermore, no deformational features in Quaternary sediment have been unambiguously related to seismic activity. On the basis of these results, there is no evidence in the geological record for major (magnitude > 7 on the Richter scale) earthquakes.

4.10.2 Description of the surface system

The relatively flat bedrock relief at Forsmark has its origin in the Sub-Cambrian peneplain, a denudation surface formed prior to ca 540 million years ago. Today the bedrock surface dips gently towards the east. The candidate area (Figure 4-3) is almost entirely located less than 20 m above current sea level. The modest topography is partly explained by the flat morphology of the bedrock surface and partly by the thicker Quaternary deposits that fill the small scale depressions of the bedrock surface (see below).

Quaternary deposits

More than 90 % of the regional model area is covered by Quaternary deposits, with till as the dominant deposit, especially in the terrestrial part. Post-glacial clay, including clay gyttja, is predominantly found in the deeper parts of valleys on the sea floor and only minor occurrences have been documented in the terrestrial area. Post-glacial gravel and sand are frequently superimposed on glacial clay. The thickness of the Quaternary deposits is generally larger in the marine area (average ca 8 m) than in the terrestrial part (average ca 4 m). Clay gyttja is frequent in the surface of the wetlands located at low altitudes, e.g. along the shores of Lake Fiskarfjärden and Lake Gällsboträsket. Gyttja is formed in lakes and consists mainly of remnants from plants that have grown in the lake.

Lakes and water courses

The lakes at Forsmark are small (at most ca 0.6 km²) and shallow, with maximum depths in the range 0.4 to 2 m. The largest lakes in the area are Lake Fiskarfjärden, Lake Bolundsfjärden and Lake Eckarfjärden (Figure 4-3). Flows of sea water into the most low-lying lakes have been registered during events of very high seawater levels. Furthermore, interpretation of data suggests that the lakes sometimes act as recharge sources to till aquifers in the riparian zone during summer, because of water losses from this zone by evapotranspiration. The annual precipitation and runoff are 560 and 150 mm, respectively.

No major water courses flow through the central part of the area. The streams downstream of Lake Gunnarsboträsket, Lake Eckarfjärden and Lake Gällsboträsket carry water most of the year, but can be dry for long periods during dry years such as 2003 and 2006. Many brooks in the area have been deepened for considerable distances for drainage purposes.

Hydraulic properties of Quaternary deposits

Hydraulic data show that the horizontal hydraulic conductivity within the till is significantly higher than the vertical conductivity and that the groundwater levels in the Quaternary deposits are shallow and closely correlated to the topography. These groundwater levels are significantly higher than the

levels in the uppermost part of the bedrock within the target area, where the gradients in groundwater level are very small. This suggests that local, small-scale recharge and discharge areas, involving groundwater flow systems restricted to the Quaternary deposits, overlie the larger-scale flow systems associated with groundwater flow in the bedrock. In contrast, outside the target area and the tectonic lens, for example in the area around Lake Eckarfjärden, groundwater levels in the bedrock are well above those in the Quaternary deposits and imply that flow systems involving the bedrock may have local discharge areas.

The lake sediments and the underlying till have low vertical hydraulic conductivities. This is indicated by lake-water/groundwater level relationships and the presence of relict marine chemical signatures beneath the lakes, which contrast with fresh groundwaters in the riparian zone.

Hydrogeochemistry

The till and the glacial clay are rich in calcium carbonate (CaCO_3), originating from Palaeozoic limestone that outcrops on the sea floor north of the Forsmark area. This, together with the recent emergence of the area above sea level, affects the chemistry of both surface water and shallow groundwater, causing high pH and high contents of calcium and bicarbonate. Furthermore, the surface waters are high in nitrogen and low in phosphorous. This is a characteristic feature of the oligotrophic hardwater lakes that are typical of the Forsmark area.

Interpretation of hydrochemical data from surface water and groundwater in Quaternary deposits supports the conclusion from the hydrological model evaluation that discharge of deeper groundwater occurs around Lake Eckarfjärden. In addition, this interpretation suggests that water sampled at the edge of Lake Gällsboträsket also has a signature indicating an influence from deep saline water. Furthermore, a mass balance calculation of chloride suggests that there must be an additional source of chloride in the water to that stored in the Quaternary deposits, possibly from discharging deep groundwater. The discharge of more saline deep groundwater at Lake Gällsboträsket is consistent with results of the hydrogeological model that predicts discharge of deep groundwaters both at Lake Eckarfjärden and Lake Gällsboträsket (Section 4.8). Both these lakes lie along the outcrop of the regional Eckarfjärden deformation zone (see Section 4.4).

Terrestrial ecosystems

The terrestrial vegetation is strongly influenced by the characteristics of the Quaternary deposits and by human land use. The calcareous influence is manifested in the flora by herbs and broad-leaved grasses, along with a number of orchid species. The long history of continuous forestry in the area is seen today as a fairly high proportion of younger and older clear-cuts. Forests cover 73 % of the land area at Forsmark and are dominated by Scots pine and Norway spruce growing mainly on wave-washed till. Wetlands are frequent and cover 10 to 20 % of the three major catchment areas of the site (Gunnarsbo-Lillfjärden-Labboträsk, Bolundsfjärden and Fiskarfjärden). A major part of the wetlands comprises coniferous forest wetlands and open mires. Agricultural land covers hardly 5 % of the land area and is mainly located in the south-eastern part of the area. It consists of arable land and grasslands. Some arable land and to a large extent semi-natural grasslands (intensively used grassland with a long management tradition) in the area have been abandoned following the nationwide general regression of agricultural activities during the past 60 years.

The quantification of pools and fluxes of carbon has revealed that the vegetation is the largest store for organic material. The exception is the wetlands which are of significant importance for accumulation of organic matter, in the soil organic pool. In particular, the reed-dominated wetlands surrounding many of the lakes accumulate large amounts of organic matter and accompanying elements, such as phosphorus. This wetland type is one step in the succession of a lake to a terrestrial area that could potentially be drained and cultivated.

Lake ecosystems

The lakes are all shallow and classified as oligotrophic hardwater lakes. These lakes contain high calcium levels, but low levels of nutrients, as phosphorus is precipitated together with the calcium. These characteristics have a strong impact on the limnic ecosystem. Due to the shallow depth, all

lake bottoms are reached by sunlight, and vegetation occurs at all depths. The dominant vegetation is stoneworts, which harbour various kinds of benthic fauna and also function as refuges for smaller fish. Common fish species are perch and roach, as well as tench and crucian carp. This last species survives low oxygen levels and is the only fish species present in the smaller lakes, where oxygen levels can be very low during winter.

Modelling results show that, contrary to typical Swedish lakes, primary production exceeds respiration in many lakes in the Forsmark area. Primary production in the larger lakes involves large amounts of carbon compared with the amounts entering the lakes from the surrounding catchment. Consequently, there is a large potential for carbon entering these lakes from the surroundings to be incorporated into the lake food web. However, according to the modelling, only a minor portion (7–10 %) of the carbon incorporated into primary producers is transported upwards in the food chain. This means that most of the carbon incorporated into primary producers circulates within the microbial food web and is transported back into the abiotic carbon pools. In the larger lakes, there is a large degree of sediment accumulation and this sediment can be a permanent sink of pollutants and radionuclides.

Marine ecosystems

The marine ecosystem in the Forsmark area is relatively productive in a region of otherwise fairly low primary production. This is due to up-welling along the mainland. The salinity of the seawater is low (ca 5 ‰) due to large freshwater run-off to the semi enclosed Baltic Sea. The low salinity strongly affects the marine environment, as most organisms are adapted to either freshwater or saltwater and not to brackish conditions. Therefore, a mix of few freshwater and marine species is found in the Forsmark area. The marine biota in the area is dominated by benthic organisms such as macroalgae, vascular plants and benthic microalgae. Detritivores, snails and mussels feeding on dead material, dominate both hard and soft bottom substrates. The fish community is dominated by the marine species herring in the pelagic area, whereas limnic species, especially perch, dominate in the coastal areas and in the secluded bays.

Modelling results show that transport from land, lakes and streams gives only a minor contribution of organic matter to the marine ecosystem. The major fluxes of organic matter in the marine ecosystem are governed by water movements, and the advective flow of carbon is several orders of magnitude larger than any other flux, such as photosynthesis by primary producers, runoff from the adjacent terrestrial environment and burial. Even though parts of the coastal area are heterotrophic, the mean character of the whole area is autotrophic, i.e. more carbon is fixed in biomass by primary producers than is mineralised by all organisms. The major pool of carbon in the ecosystem is the sediment, followed by the pools present in the dissolved phase (DIC and DOC) and in biota. The sediment content of carbon is around 20 times larger than that in the other pools.

Confidence

Generally, the site descriptive model for the surface system is based on a wealth of site data. Uncertainties associated with the sub-models have been thoroughly evaluated, and descriptions and model results are, in most cases, consistent with regional/generic data and/or with the results from alternative models. The principal remaining uncertainties are associated with the description of the spatial distribution of the thickness of the overburden and the hydraulic properties of the shallow bedrock, especially in areas covered by the sea today where landscape modelling is needed to estimate the properties in future lakes, wetlands and agricultural areas. The hydraulic description of the shallow bedrock is part of the hydrogeological bedrock model, but determines where deep groundwater discharges and thus contributes to uncertainty in where potential releases of radionuclides to the biosphere could occur. Other remaining uncertainties concern the chemical composition of biota, the spatial variation of chemistry in the regolith, as well as the impact of chemical processes on transport of elements and quantitative estimates of processes, such as plant uptake and respiration. Most of these remaining uncertainties are judged to be of relatively minor importance for post-closure safety, except that the uncertainties in chemical processes affecting the transport of elements contribute significantly to uncertainties in the assessment of doses to humans and to the environment (cf. Section 13.2).

4.10.3 Human population and land use

The Forsmark region was not permanently settled until the end of Sweden's prehistoric period (1100 AD). During the medieval period (1100–1550 AD), the region was characterised by small villages and new settlements were created in the areas peripheral to the older ones. At the end of the medieval period, the majority of the farms in the region belonged to freeholders, and only a few farms belonged to the church or the nobility. During the early modern period (1550–1750 AD), the establishment of the iron industry in the Forsmark region dramatically affected the surrounding landscape. Production was geared towards the needs of this industry; charcoal production, mining and the production of fodder for animals used in the industry. There was a strong population expansion and many crofts were established in the forested areas, inhabited by people involved in the production of charcoal.

During the 18th century, the number of freehold farms decreased, both due to the partitioning of farms and to the fact that large estates expanded. The population increased dramatically up to the late 19th century. At the turn of the century the increase ceased and, during the latter part of the 20th century, the rural population decreased. The number of people involved in agriculture decreased and, in contrast, the number of people employed in industry and crafts increased.

At the present day, the Forsmark parish is sparsely populated and the Forsmark model area has no permanent inhabitants. However, the nuclear power plant, situated immediately northwest of the planned repository, is a large industry with around 1 000 employees, which leave its mark on the area today. Besides this, there is a small holiday population manifested by the presence of five holiday cottages. The land use in the parish is dominated by forestry, and wood extraction is the only significant outflow of biomass from the area. The agriculture in the parish is limited in extent and there is only one agricultural enterprise in operation within the Forsmark area, situated at Storskäret.

5 Initial state of the repository

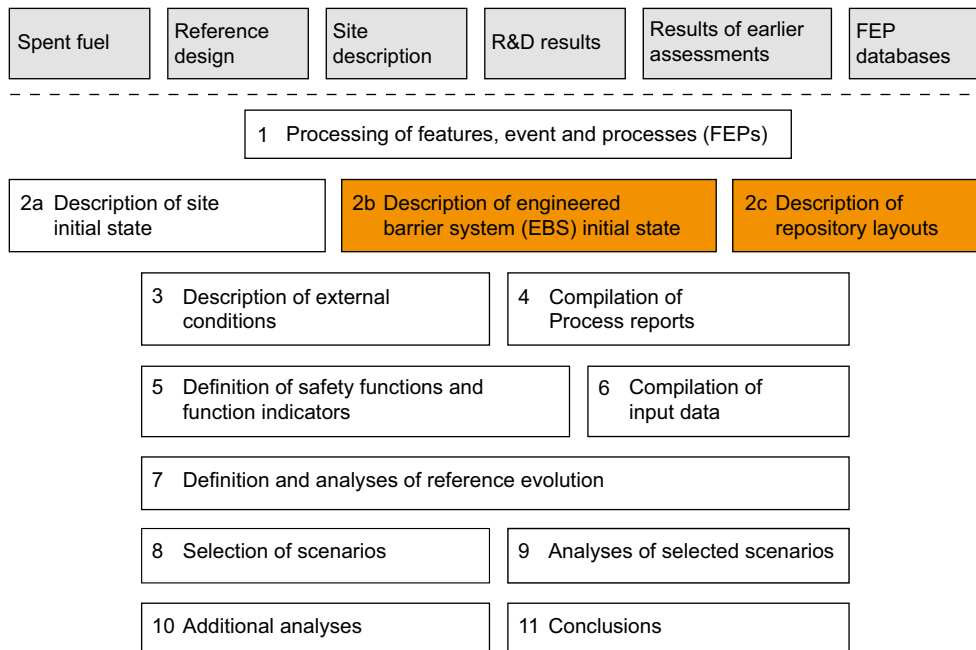


Figure 5-1. The PSAR methodology in eleven steps (Section 2.5), with the present step highlighted.

5.1 Introduction

As mentioned in Section 2.5, a comprehensive description of the initial state of the repository system is one of the main bases for the safety assessment.

There is no obvious definition of the time of the initial state. For the geosphere and the biosphere, the state at the time of beginning of excavation of the repository is a natural starting point, since knowledge of this relatively undisturbed state is available through the site descriptive model that is derived from site investigation data. An alternative would be to consider, for each deposition hole, the state of the surrounding host rock at the time of deposition. Irrespective of which alternative is chosen, the short-term evolution of the host rock from the undisturbed state to that after excavation has to be considered in a safety assessment that is based on observations made prior to excavation. For the biosphere, the problem is less pronounced, since it will be less affected by the excavation of the repository. It is noted that for the post-closure safety assessment supporting the operation license application, i.e. the next step in the step-wise licensing of the final repository, data from the then partially excavate rock will be available and utilised in the assessment.

For the engineered barrier system, the time of deposition/installation is a natural starting point when a specific part of the system is concerned, e.g. an individual deposition hole with its canister and buffer. However, if the entire ensemble of deposition holes is considered, there is no unique time of deposition. Neither is the time of repository closure a suitable choice for the engineered barrier system, since different parts of the repository will, at that time, have reached different stages of e.g. thermal and hydraulic evolution depending on the time of deposition and on spatial variability of rock conditions within the repository. The most reasonable approach is, therefore, judged to be to define the time of the initial state as that of deposition for each deposition hole with its canister, buffer and backfill, and then to describe the common evolution that all deposition holes will go through, taking spatial variability into account. For some aspects of the evolution, e.g. the thermal development, the deposition sequence has to be considered.

Based on these considerations, the initial state in the PSAR is defined as the state at the time of deposition/installation for the engineered barrier system and the natural, undisturbed state at the time of beginning of excavation of the repository for the geosphere and the biosphere. The evolution of the natural system is, therefore, at least in some aspects, followed from the time of beginning of excavation in the safety assessment. Short-term geosphere processes/alterations due to repository excavation are, therefore, documented in the **Geosphere process report**. An integrated description of the evolution driven by these processes is given in the excavation/operation phases of the reference evolution, Section 10.2.

The initial state of the engineered parts of the repository system is largely obtained from the design specifications of the repository, including allowed tolerances or deviations. Also the manufacturing, excavation and control methods have had to be described in order to adequately discuss and handle hypothetical initial states outside the allowed limits in the design specifications. The basis for establishing the initial state of the engineered parts of the repository system for the PSAR is compiled in a number of dedicated **Production reports**, see further Section 5.1.1.

The initial state of the geosphere and the biosphere is, as mentioned, determined by site investigations. Field data from the site investigations are analysed, within the site investigation project, to produce a site descriptive model of the geosphere and the biosphere for the Forsmark site, as reported in the **Site description Forsmark** and summarised in Chapter 4.

The present chapter contains a description of the initial state with uncertainties, based on information on the engineered components and the repository layout from the **Production reports**, and the results of the FEP analyses reported in the **FEP report**. The level of detail in this chapter is meant to be sufficient for understanding the remaining parts of the safety report without reading the above reference documents.

Most of the text from Section 5.2 and onwards has been substantially updated compared to the SR-Site version of the text, reflecting the development of the repository design and construction procedures since the publication of the SR-Site assessment.

5.1.1 Relation to Technical design requirements, Production reports and Data report

Feedback from assessments of post closure safety is a key input to the refinement of the design of the KBS-3 repository. Feedback on the assessed reference design and related design requirements were given in the SR-Site main report (SKB 2011, Section 15.5) and received regulatory feedback.

The feedback was further developed through a reassessment and compilation of technical design requirements based on feedback from SR-Site, the Finnish safety assessment Turva-2012 and the technology development until 2016. The work was published as a joint Posiva SKB report (Posiva SKB 2017). Technical design requirements specify characteristics that can be inspected and verified in the production. They are based on the assessment of the post-closure evolution of the repository and available technology. In addition the development of the design, methods, processes and technical systems to produce and quality assure a KBS-3 repository have proceeded on the basis of the results of the safety assessments. The justification of the design requirements and the implications for verification and design are documented in the report (Posiva SKB 2017). The general approach to the updating of the technical design requirements is described in Posiva SKB (2017, Section 2.1). In this approach, the safety functions (see further Chapter 8) are a key link between post-closure safety and repository design.

The methodology was applied and resulted in 5 technical design requirements on the underground openings, 6 on the canister, 8 on the buffer, 5 on the deposition tunnel backfill and 3 on the deposition tunnel plug. Additional technical design requirements have been specified for the backfill in the main tunnels, transport tunnels, access tunnels, shafts, central area and closure in the **Closure production report**. The technical design requirements constitute design constraints, which, if all fulfilled in an updated design, should form a sound basis for demonstrating repository safety.

This feedback has been a key input to the latest refinement cycle of the KBS-3 repository design.

The spent fuel types and amounts to be deposited are described in the **Spent fuel report** from which fuel properties relevant for post-closure safety and valid at the time of deposition in the repository can be derived. The engineered components of the repository system are described in a number of so called **Production reports** covering the canister, the buffer, the deposition tunnel backfill, the deposition tunnel plug, the repository closure and the underground openings constructions, respectively. The last report contains a description of the repository layout after site adaptation. This layout of the deposition area is basically the same as that assessed in SR-Site.

Each production report gives an account of i) technical design requirements primarily from Posiva SKB (2017), ii) the reference design selected to achieve the requirements, iii) verifying analyses that the reference design does fulfil the technical design requirements, iv) the production and control procedures selected to achieve the reference design, and v) verifying analyses that these procedures, if implemented, would achieve the reference design. The initial state of the engineered components is then derived as reported in subsequent sections of this Chapter, based on the contents of the **Production reports** relevant to post-closure safety.

It is possible that the selected reference design and the production and control procedures yield an assessed initial state more favourable for post-closure safety than one that just fulfils the technical design requirements. In PSAR, credit is generally not taken for this, “better-than-demanded” performance although it is the expected outcome of the production of the actual reference design that is assessed. An exception is the requirement the copper thickness of the canisters, which according to the technical design requirements shall be ≥ 40 mm at deposition with acceptable local reductions to a thickness of 35 mm for 10 % of the copper shell. The copper thickness used in the analysis is based on results from test production and exceeds the values in the design requirements.

Furthermore, if the reference design is significantly better than demanded by the design requirements, it is argued that this may form the basis for future revision of the design requirements. Generally, the design requirements may be modified in future stages of SKB’s programme. Reasons for such modifications include results of analyses based on more detailed site data and a more developed understanding of processes of importance for post-closure safety. Feedback on current design requirements is given in Section 15.4.

The initial state, as given in this Chapter provides quantitative information on key inputs to the safety assessment. These are critically evaluated in the **Data report** where the formal qualification of input data to the safety assessment occurs based on an evaluation of uncertainties affecting the initial state data.

5.1.2 Overview of system

The repository system is based on the KBS-3 method, in which corrosion resistant copper canisters with a load-bearing cast iron insert containing spent nuclear fuel are surrounded by bentonite clay preventing groundwater flow and deposited at approximately 500 m depth in groundwater saturated, granitic rock, see Figure 5-2. The facility design with rock caverns, tunnels, deposition positions etc. is based on the design originally presented in the KBS-3 report (SKBF/KBS 1983a) which has since been developed and described in more detail. The deposition tunnels are linked by main tunnels for transport and communication. One ramp and several shafts connect the surface facility to the underground repository. The ramp is used for heavy and bulky transports and the shafts are used for utility systems, ventilation and for transport of excavated rock, backfill and staff. The different parts of the final repository are outlined in Figure 5-3.

Around 54 000 spent fuel assemblies corresponding to around 12 000 tonnes (heavy metal – initial weight) of spent nuclear fuel are forecast to arise from the Swedish nuclear power programme (see the **Spent fuel report**), corresponding to roughly 6 000 canisters in the repository. These figures are based on assumed reactor operational times of 50–60 years. The PSAR is, therefore, based on a repository with 6 000 canisters, corresponding to around 12 000 tonnes of fuel.

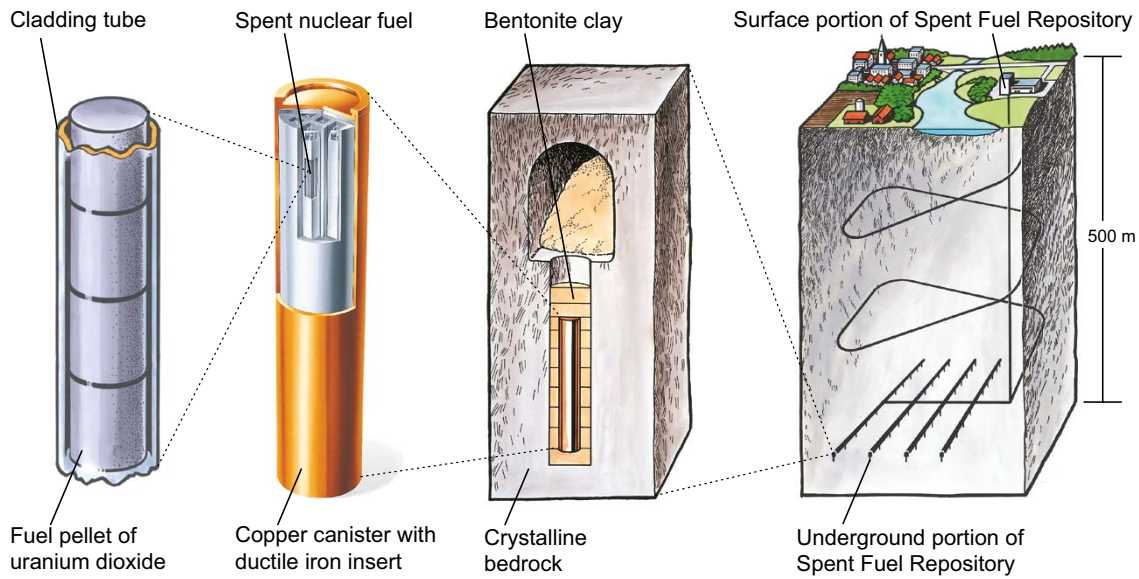


Figure 5-2. The KBS-3 concept for disposal of spent nuclear fuel.

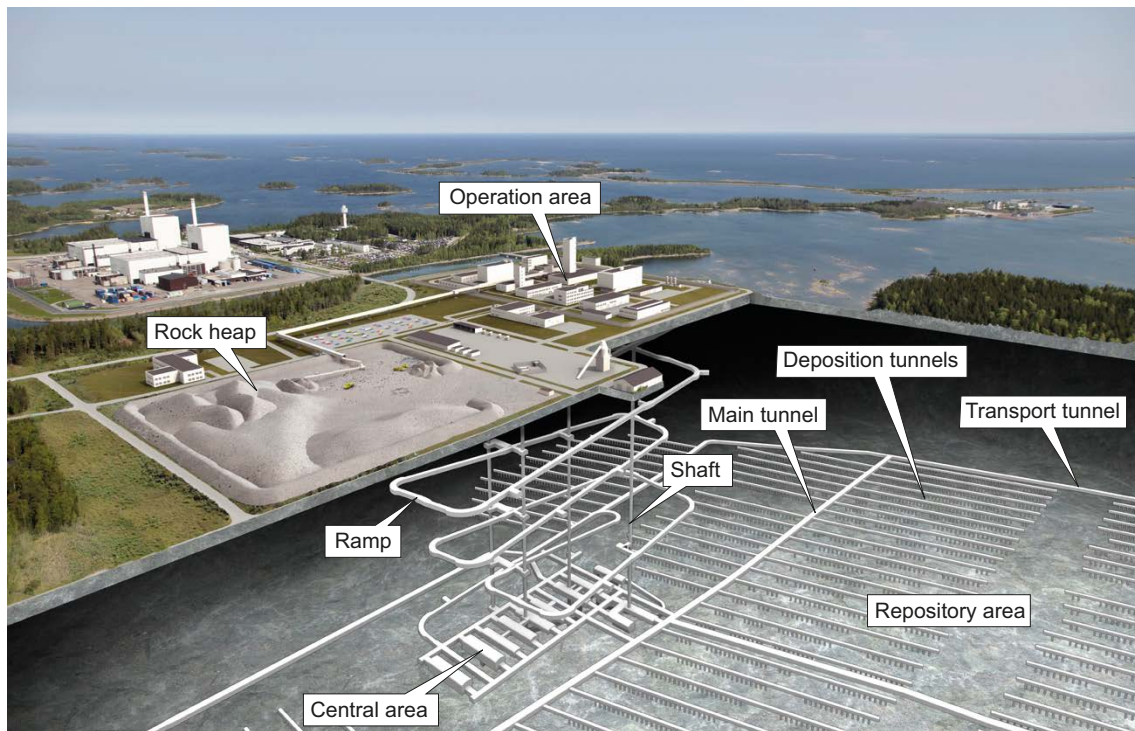


Figure 5-3. General repository layout showing the location of the underground functional areas (Access ramp, Central and Repository area with deposition tunnels and the surface facilities in the operation area).

For the purposes of the safety assessment, the final repository system has been sub-divided into a number of components or sub-systems. These are:

- The host rock, see Chapter 4.
- The biosphere, see Chapter 4.
- The site adapted repository layout including descriptions of all underground openings, i.e. deposition holes, deposition tunnels, transport tunnels, the central underground area and access shafts and ramp, see Section 5.2.

- The fuel, (also including cavities in the canister since strong interactions between the two occur if the canister is ruptured), see Section 5.3.
- The copper canister with a cast iron insert , see Section 5.4.
- The buffer in the deposition hole, see Section 5.5.
- The backfill material in the deposition tunnel, see Section 5.6.
- Closure and additional engineered parts of the repository, see Section 5.7:
 - The closure backfill materials in transport tunnels, the central underground area, shafts and ramp.
 - Plugs.
 - Investigation boreholes with their means of sealing.

This particular sub-division is dictated by the desire to define components that are as homogeneous as possible without introducing an unmanageable multitude of components. Homogeneity facilitates both characterisation of a component and the structuring and handling of processes relevant to its long-term evolution. Also, the importance of a particular feature for safety has influenced the resolution into components. In principle, components close to the potential source term, i.e. the spent fuel, and those that play an important role for safety are treated in more detail than peripheral components.

Key initial state properties for the most safety relevant components of the system are summarised in Section 5.8.

5.1.3 Initial state FEPs

As mentioned in Chapter 3, the SR-Site FEP catalogue is used in the PSAR. (As also noted in Chapter 3, additional FEP lists from other relevant radioactive waste disposal projects have become available since the SR-Site assessment. These contain no information that affects the initial state FEPs for the current assessment.) Initial state FEPs in the SR-Site FEP catalogue, also used in the PSAR, are either related to an initial state in conformity to the specification given for the reference design or to deviations from the reference design. The former of these are handled in the category of variables in the SR-Site FEP catalogue.

The initial state FEPs in the SR-Site FEP catalogue that are related to deviations from the reference design of the canister, the buffer and the backfill of the deposition tunnels, or to more general deviations, are compiled in Table 5-1. One such FEP of more general character is related to severe mishaps not expected to occur during the operational phase, like fires, explosions, sabotage and severe flooding or other events occurring prior to closure. Such events are excluded from the scenario selection. The reasons for this are i) the probabilities for such events are low and ii) if they occur, they shall be reported to SSM, their consequences assessed and correcting or mitigating actions made accordingly.

Another FEP in the SR-Site FEP catalogue refers the effects of phased operation. This affects mainly the geosphere and the subsequent development of the entire repository. The hydrological state of the bedrock is perturbed as soon as repository excavation starts (a smaller perturbation even occurs earlier during site investigations). Different parts of the repository, completed at different times, will be exposed to different hydrological conditions, affecting e.g. the saturation of the buffer and backfill. Possible upconing of saline water could also vary between different parts of the repository due to phased operation. Other factors to consider are the effects of blasting and underground traffic on completed parts of the repository. All these issues are part of the expected evolution of the repository, but are not automatically captured in the system of processes describing the repository evolution over time or by the initial state descriptions. As they need to be adequately included in the discussion of the repository evolution, they are propagated to the analysis of the reference evolution in Section 10.2.6.

Other FEPs in the FEP catalogue concern the effects of an abandoned, not completely sealed repository or open monitoring boreholes or shafts. These issues are also propagated to the scenario selection in Chapter 11.

FEPs relating to effects detrimental for post-closure safety caused by monitoring are excluded from further analysis since monitoring activities that could disturb the repository safety functions will not be accepted.

Several FEPs concern design deviations due to undetected mishaps during manufacturing, transportation, deposition and repository operations etc. Measures to avoid or mitigate such deviations during excavation, manufacturing, handling, deposition etc. are described in the **Production reports**. To the extent that such mishaps may still occur, these issues are addressed in the scenario selection and the scenario analyses described in Chapters 11 and 12, respectively. Only such FEPs defined for the canister, buffer and the backfill of repository tunnels are included in Table 5-1. In addition to these FEPs, the FEP catalogue contains corresponding initial state FEPs for the remaining system components, i.e. a thin copper bottom plate in the deposition holes, plugs, borehole seals and closure in the central area, ramp shafts and tunnels other than deposition tunnels. Since these system components are not of primary importance for the safety of the repository, no safety functions have been assigned to them. Therefore, the consequences of deviations in their initial state are not analysed in detail, but are addressed in the analysis of the reference evolution (Chapter 10) and, if relevant, considered in subsequent parts of the assessment.

Table 5-1. Initial state FEPs in the SR-Site FEP catalogue and how they are handled in the PSAR.

Initial state FEP		Handling in the PSAR	FEP chart item (see Section 8.5)	Comment
ISGen1	Major mishaps/ accidents/sabotage	Excluded. The probabilities for such events are low. If they occur, this will be known prior to repository sealing so mitigation measures and assessments of possible effects on post-closure safety can be based on the specific real event.		
ISGen2	Effects of phased operation	Assessed based on thermal, rock mechanics and transient hydro-geological simulations for an open repository.		See Section 10.2.6
ISGen3	Incomplete closure	Considered in scenario selection.		See Section 11.2 (scenario selection) and 14.2 (scenario analysis)
ISGen4	Monitoring activities	Excluded. Monitoring activities that could disturb the repository safety functions will not be accepted.		
ISC1	Mishaps – canister	Considered in the selection of scenarios based on safety function indicators related to canister integrity.	Copper thickness Canister design analysis	See Sections 11.2 (scenario selection) and 12.6 to 12.8 (scenario analyses).
ISC2	Design deviations – canister	Considered in the selection of scenarios based on safety function indicators related to canister integrity.	Copper thickness Canister design analysis	See Sections 11.2 (scenario selection) and 12.6 to 12.8 (scenario analyses).
ISBu1	Mishaps – buffer	Considered in the selection of scenarios based on safety function indicators related to buffer performance.	Density Geometry	See Sections 11.2 (scenario selection) and 12.2 to 12.4 (scenario analyses).
ISBu2	Design deviations – buffer	Considered in the selection of scenarios based on safety function indicators related to buffer performance.	Density Geometry	See Sections 11.2 (scenario selection) and 0 to 12.4 (scenario analyses).
ISBfT1	Mishaps – backfill in tunnels	Considered in the selection of scenarios based on safety function indicators.	Density Geometry	See Sections 11.2 (scenario selection) and 12.2 (scenario analyses). Transport properties of defective backfill addressed in Section 13.7.
ISBfT2	Design deviations – backfill in tunnels	Considered in the selection of scenarios based on safety function indicators.	Density Geometry	See Sections 11.2 (scenario selection) and 12.2 (scenario analyses). Transport properties of defective backfill addressed in Section 13.7.

5.2 Site adapted repository – the underground openings

The underground openings are the cavities constructed in the rock that are required to accommodate the sub-surface part of the final repository facility. The underground openings comprise:

- The actual geometry and location of the excavations.
- Engineered materials for sealing and rock reinforcement, and residual materials from performance of activities in the final repository facility which, at deposition, backfilling or closure, remain in and on the rock that surrounds the openings.

The underground openings as such do not contribute to the safety of the KBS-3 repository and do not have any barrier functions. However, the locations of the deposition areas and deposition holes with respect to the thermal, hydrological, mechanical and chemical properties of the rock are important for the utilization of the rock as a barrier and thus for the safety of the repository. Furthermore, the potential Excavation Damaged Zone (EDZ) and engineered and stray materials that remain in the rock may impact the barrier functions of the rock and/or the engineered barriers, and must therefore be known when assessing the post-closure safety of the repository.

5.2.1 Technical design requirements relating to post-closure safety

To guide the design and production of the underground openings, technical design requirements on characteristics that can be inspected and verified have been established (Posiva SKB 2017). The design of the underground openings must also be based on design decisions affecting different parts of the repository facility and the more general principles stated by SKB in the **Underground openings construction report** and with some additional clarifications in Chapter 8 of SKB (2021b).

In establishing rules for the selection of positions for the various underground openings, three classes of critical structures (CS) and critical volumes (CV) are defined in the **Underground openings construction report** (Section 3.1.2):

“CS1/CV1 are structures/volumes with properties such that they cannot be accepted within the repository footprint i.e. shall not intersect any tunnels or shafts belonging to the repository system. Thus they steer the location of the repository and set boundary limits for the repository.

CS2/CV2 are structures/volumes with properties such that they cannot be accepted within deposition tunnels. Thus they influence the layout of the repository and steer the locations of deposition tunnels.

CS3/CV3 are structures/volumes with properties such that they cannot be accepted to intersect deposition holes. Thus they steer the location of deposition holes.”

The details of the classification procedure, i.e. of how the observed rock properties are used in classifying the structures and volumes in the repository are described in Section 3.1 in the **Underground openings construction report**.

Selecting repository depth: The repository volumes and depth need to be selected where it is possible to find large volumes of rock fulfilling the specific requirements on deposition holes. The minimum depth is prescribed to be as specified for a KBS-3 repository i.e. at least 400 m.

Placement of deposition areas: Deposition areas must not be placed within critical volumes of class 1.

Placement of deposition areas in relation to the chemical conditions at the site: The deposition areas should be placed so that the salinity (TDS), pH and sulphide content of the groundwater are within the limits of their performance targets, salinity (TDS < 35 g/L, whereas temporarily up to 70 g/L can be accepted), pH (5–11) and sulphide content ($[HS^-] < 3$ mg/L).

Placement of deposition tunnels and holes in relation to critical structures and volumes: The critical structures and critical volumes are geological structures or rock volumes in their vicinity with properties such that they can negatively impact the post-closure safety of a KBS-3 repository. For example, deformation zones that form main groundwater flow routes or that can transmit movements generated by earthquakes large enough to induce canister-breaching secondary displacements, are considered as critical structures. Deposition holes should be, as far as reasonably possible, selected such that they do not have potential for shear larger than the canister can withstand. To achieve this,

deposition tunnels must not be placed within critical volumes of class 1 or class 2 and deposition holes must not be placed within critical volumes of class 1, class 2 or class 3.

Placement of deposition holes in relation to hydrological and transport conditions at the site: Favourable hydrogeological conditions with limited transport of solutes are required to support the performance of the engineered barrier system and to limit radionuclide transport in the case of release from a breached canister. Limitation of the flow rate around the deposition holes contributes to limit changes in the groundwater chemistry in the vicinity of the deposition holes and restricts the mass transfer between the groundwater and the buffer. Thereby deposition holes shall be placed where the transmissivity of the pilot hole drilled in deposition hole position is less than a limit that will be selected when data from repository level has been obtained, see further the **Underground openings construction report**, Section 4.2.4.

Placement of deposition holes in relation to thermal conditions at the site: Buffer geometry (e.g. void spaces), water content and distances between deposition holes should be selected such that the temperature in the buffer never exceeds 100 °C. (The maximum thermal output from the canister is limited to 1 700 W).

Inflow to underground openings to ensure proper initial state: The groundwater inflow to the underground openings shall be less than the site-specific limits listed in the **Underground openings construction report**, Section 3.3. The potential extent of changes in the groundwater composition due to up-coning of groundwater with high salinity has been analysed in SR-site (SKB 2011, Svensson and Follin 2010) and is expected to be very low during construction and operation. This implies that the inflow requirement will be governed by the need to minimize the environmental impact due to groundwater drawdown.

As noted in the introduction, Section 5.1, the design of the underground openings as well as the as-built and inspected underground openings are required to conform to the above technical design requirements.

5.2.2 Repository design and resulting layout

The reference design of the underground openings is described in the **Underground openings construction report**, Chapter 3, and a more detailed description and justification of the design is provided in SKB (2018b). Details of the access tunnels and central area have been altered compared to the design assessed in SR-Site, whereas the design and layout of the deposition areas, are the same as for SR-Site except for an additional transport tunnel passing centrally. Moreover, the present design has no ventilation shafts outside the access area. The basis for the reference design is site-specific geotechnical information which has been interpreted and evaluated in a Site engineering report (SER) (SKB 2009c), building on the extensive surface-based site investigations and their evaluation and modelling presented in the **Site description Forsmark**, and the stated technical design requirements with respect to post-closure safety and other technical design requirements, as specified in the **Underground openings construction report**. A part of the design work has been to assess the risk of practically achieving this design in relation to the current confidence and remaining uncertainty in the **Site description Forsmark**, see SKB (2009b, Chapter 8). This risk assessment concluded that none of the consequences from these uncertainties would render the repository unsuitable for the purpose intended. However, several uncertainties were identified that should be resolved during the next design step and/or during construction of the repository accesses (ramp and shafts).

The objective of rock engineering is to ensure that the layout of the repository facility

- is well adapted to the site conditions, and that it
- conforms to the design requirements in any phase of design and construction as well as after the construction is completed.

Design stages

In all phases of underground design, uncertainties with regard to site conditions are anticipated. In order to establish a final layout for deposition tunnels and deposition holes, a large volume of rock will have to be characterised, but this characterisation can only effectively be carried out from existing underground openings. This means that the characterisation will develop as the construction work proceeds.

The primary uncertainties that will influence the final layout are the spatial location and variability of the geological setting and the potential behaviour of the rock mass with respect to excavation also considering the effects of rock support and grouting measures. These uncertainties and the scale of the repository volume emphasize that the methodology used to adapt the final layout of the repository to the site conditions must be integrated with the construction activities required to develop the repository.

The development of a final layout for the repository facility based on site adaptation requires the use of an iterative design process. In particular the orientation of the deposition tunnels and the exact location of deposition tunnels and deposition holes will be selected based on the findings from the detailed investigations and site modelling to ensure that the underground openings conform to the stated technical design requirements, see further Chapter 5 of the **Underground openings construction report**. This adaptation has similarities with the *Observational Method*, which is a risk-based approach to underground design and construction that employs adaptive management, including advanced monitoring and measurement techniques, for designing the mechanical support and grouting needed but is formally not part of the observational method.

The design assessed in the PSAR is preliminary. As more knowledge is attained during the excavation and connected detailed characterisation, more refined designs will be developed. Rock engineering for the underground openings in the final repository facility will therefore be divided into several stages prior to construction as described in Chapter 3 of the **Underground openings construction report**. In this context, the current Reference Design in the **Underground openings construction report** documents the results from a design stage which established the feasibility of the repository facility. The design of the deposition area assessed in PSAR is essentially the same as in SR-Site. In later stages, when the design is developed into the detailed and final stages, relevant parts of the safety assessment may need to be updated.

During construction, site adaption will continue and is foreseen to primarily concern rock support, grouting activities and the final positioning of deposition tunnels and deposition holes. The latter decision will require a characterisation of the rock mass on location, something which is a major topic for the investigation, inspection and monitoring programme¹⁰. Finally, verifying that the drilled deposition holes conform to all design requirements such that they can be used as intended may require additional input from monitoring and inspections carried out during the period between completion of excavation and deposition.

Repository depth

The depth established for the reference design is a compromise arising from design requirements on post-closure safety and constructability of the deposition tunnels and deposition holes of the repository facility. According to the design requirements the depth should be selected “where it is possible to find large volumes of rock fulfilling the specific requirements on deposition holes” and the premises also state a minimum depth of 400 m. A rationale for identifying suitable rock volumes for deposition as well as depth intervals for the final repository facility are outlined in appendix 4 in the **Underground openings construction report**. This rationale has been used to establish a depth interval where it is possible to find rock volumes that fulfil the specific requirements for deposition holes and deposition tunnels with regard to:

- Available space.
- Fracture frequency and frequency of connected transmissive fractures.
- Groundwater pressure.
- *In situ* stress magnitudes and orientation.
- Initial temperature and thermal properties of the rock.
- Salinity and up-coning.
- Chemical conditions.
- Lengths and transport resistances of hydraulic travel paths to and from the repository.

¹⁰ Kärnbränsleförvaret – Preliminärt detaljundersökningsprogram för deponeringsområden. SKBdoc 1600833. (In Swedish.) (Internal document.) *In prep.* Program för övervakning av Kärnbränsleförvaret med avseende på säkerheten efter förslutning. SKBdoc 1584443. (In Swedish.) (Internal document.) *In prep.*

These factors are assessed in Appendix 4 in the **Underground openings construction report**, using the information in the **Site description Forsmark**. At Forsmark, it is mainly the hydraulic conditions of the site, i.e. frequency and occurrence of transmissive fractures and their dependency on depth that are of importance for safety, while the constructability is mainly related to rock mechanics issues, e.g. the likelihood and extent of spalling in deposition holes prior to emplacement. Below the minimum depth of 400 m it is found that the main conditions of importance are the frequency of water conducting fractures and the *in situ* stress magnitude, whereas other factors show little or moderate change with depth. While the frequency of water conducting fractures is already low at depth, this frequency dramatically drops at depths greater than 400 m pointing to a potential major advantage for depths below 450 m. Below 300 m depth, there appears to be little evidence that the horizontal stress magnitudes in fracture domain FFM01 increase significantly with depth. Hence placing the repository at 400 m or 500 m depth does not significantly increase the risk for excavation-induced spalling in the deposition holes. For these reasons, the repository at Forsmark is suggested to be located at a depth range of between 450 m and 500 m, see Appendix 4 in the **Underground openings construction report**.

In the preliminary design developed, the maximum depth of the repository facility is located at elevation -470 metres, i.e. where the transport tunnels (tunnel floor) exit from the central area. The minimum depth (tunnel roof) of the reference design is located at elevation -457 metres, i.e. in some deposition tunnels. The respective locations of minimum and maximum depth for the repository facility will be based on the drainage system requirements. During the course of the detailed investigations carried out in conjunction with the construction of the repository access (shaft and ramp) the repository depth may be adjusted as outlined in Appendix 4 of the **Underground openings construction report**. This adjustment will be within the limits of the volumes stipulated in the construction license according to the Environmental Code.

Thermal dimensioning – distance between deposition holes

The basis of the thermal dimensioning for the reference design are: A fixed deposition hole spacing, a canister maximum thermal power of 1 700 W, a minimum deposition hole spacing of 6 m, a deposition tunnel spacing of 40 m and a maximum allowed peak temperature in the buffer of 100 °C. The latter is in accordance with the design requirement that the distance between deposition holes must be sufficiently large to achieve a temperature in the buffer < 100 °C.

The design methodology to meet this requirement is presented in Hökmark et al. (2009). The minimum spacing between deposition holes for the reference design at Forsmark is given in Table 3-3 in the **Underground openings construction report** and was evaluated in the SER (SKB 2009c, Appendix A) and the analysis gave provision for a minimum centre-to-centre spacing for deposition holes equal to 6.0 m in rock domain RFM029 and 6.8 m in rock domain RFM045.

Site adaptation with respect to critical structures and volumes

The layout is adapted to meet the design requirements relating to mitigating earthquake hazard, see Section 5.2.1. Within the target volume there are only four deformation zones that are large enough to potentially require a respect distance: the three steeply dipping zones of critical structure class 2 ZFMENE060A, ZFMENE062 and ZFMNW0123, and the gently dipping zone ZFMA2, see Chapter 3 and Chapter 4 of the **Underground openings construction report**.

Deposition holes must not be placed within critical volumes of class 1, class 2 or class 3.

According to SKB (2009b, Section 3.6.4) the loss of positions could range between 10 to 25 % depending on which DFN model is used, but it is also stated that the actual loss of positions is judged much smaller, since prospects are good of finding more efficient means of identifying fractures that are too large.

Adaptation to hydrogeological conditions

Several design requirements concern limitations on inflow of water to different parts of the repository facility. In the design this is handled by not accepting deposition holes with too high inflows, by layout adjustments of other parts and by means of grouting. Grouting measures need in turn follow the restrictions on grouting material and placement of grouting holes. The composition and the amounts of the materials used for ground support and for grouting are given in Table 8-3 of the **Underground construction report**.

Resulting layout

The major site adaptation issues for the reference design layout discussed above are:

- Repository depth.
- The distance between deposition holes based on thermal dimensioning.
- Respect distance relative to modelled locations of critical structures of class 1, 2 and 3.
- The alignment of deposition tunnels in relation to the direction of maximum horizontal stress.
- The disqualification of unsuitable deposition hole positions.

Considering these issues, a reference design layout for Forsmark was developed, see Figure 5-4, with the aim of maximising the gross capacity relative to potential deposition positions. The reference layout includes provision for all deterministic deformation zones identified in the site descriptive model. In addition, there is a respect distance of 100 m for deformation zones with a trace length longer than 3 km. There are no deposition hole positions in any of these zones in the layout. Furthermore, there are no deposition hole positions intersecting known deterministic minor deformation zones. The gross capacity of the reference design layout is 7818 deposition hole positions and allows for a 23 % loss of deposition hole positions relative to the about 6000 canisters that are planned for the final repository facility, i.e. more than is expected to be needed. The reference design layout for the final repository facility is shown in Figure 5-4.

The reference layout of the deposition areas is, as mentioned above, basically the same as was assessed in the safety assessment SR-Site (SKB 2011), since new underground data on which to base update are not available at the present stage. The layout will be adapted to the findings of the detailed investigations carried out as an integral part of the construction of the repository, as outlined in Chapter 4 of the **Underground openings construction report**. Furthermore, since there are essentially no new underground data since the publication of **Site description Forsmark** the design rules described in Chapter 3 of the **Underground openings construction report** regarding acceptance or rejection of individual deposition holes have not been fully applied yet.

The reference design does not include any spare areas for deposition, in addition to the allowable 23 % loss of positions, but recognises the fact that utilising other potentially suitable rock volumes would offer additional deposition positions. The reference design also acknowledges that the justification of spare capacity would require additional site investigations and modelling.

Since there is a need to maintain segregation between construction and emplacement zones during operation, a stepwise methodology for the successive extension of deposition areas is envisaged. A tentative stepwise development of the repository facility is presented in Section 3.1 of SKB (2018b).

5.2.3 Initial state of underground openings

Chapter 8 of the **Underground openings construction report** is an assessment of the projected initial state of the openings at the time when deposition starts. This assessment is based on an evaluation of the adequacy of current design tools and planned excavation techniques together with an evaluation of the efficiency of potential control measures and contingency actions during and after construction. A formal assessment of the adequacy of these data is made in the **Data report**; the findings given in this Section are for information only.

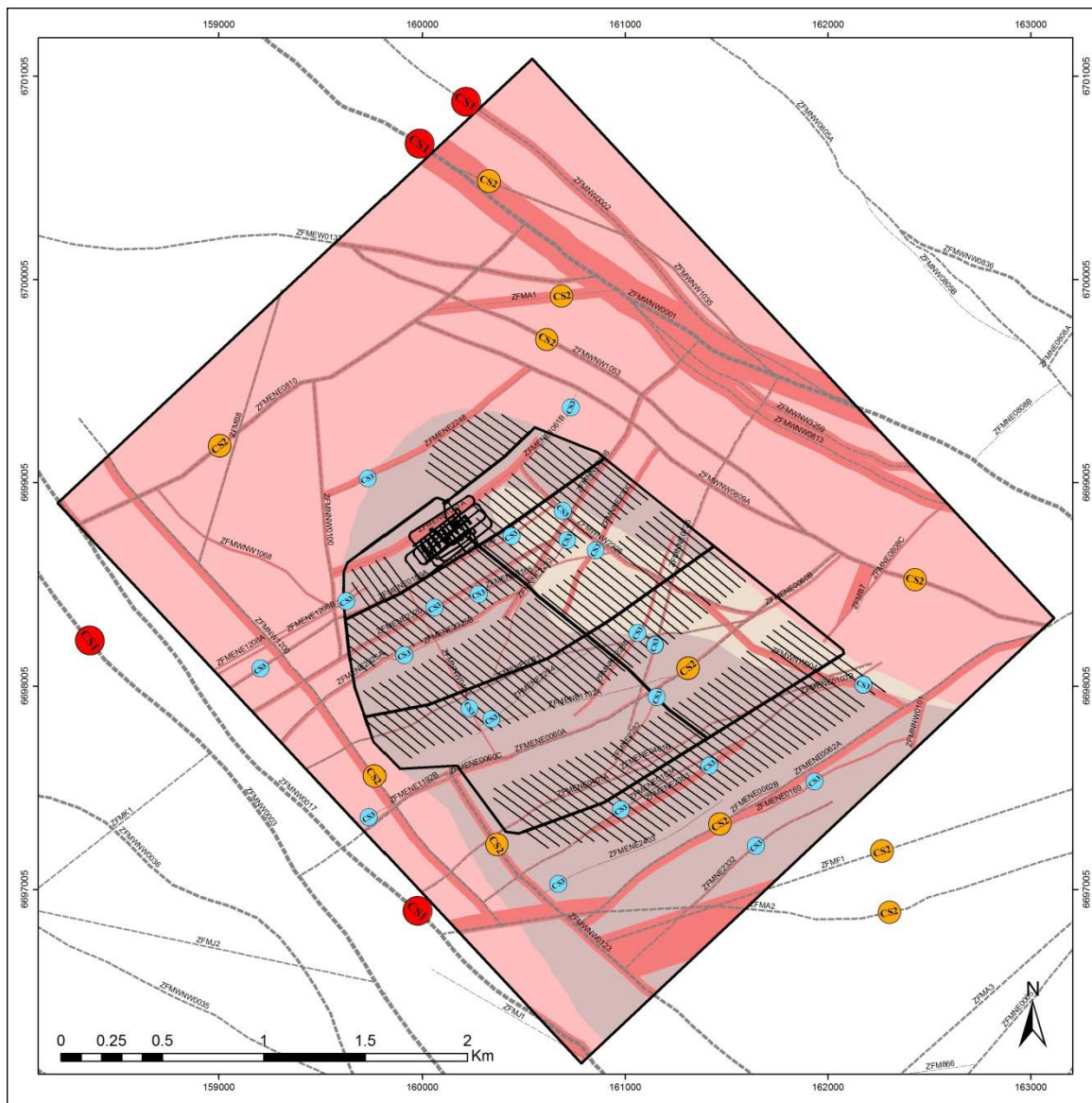


Figure 5-4. Reference design layout for the repository at Forsmark at depth 470 m, also showing respect distances and critical structures of class 1,2 and 3 (Figure 3-1 in the *Underground openings construction report*). The three classes of critical structures described in Section 5.1.2 are marked: CS1 with red dots, CS2 with yellow dots and CS3 with blue dots.

Repository depth and repository areas

The repository design with its reference layout is justified and presented in the previous section.

It is judged that remaining uncertainties in the geological description can be sufficiently resolved using methods and techniques that were implemented during the site investigations and would only require minor re-adjustments of the available areas. Uncertainties in the orientation of maximum horizontal stress can only be significantly reduced by *in situ* tests at depth during access construction. The finding may necessitate a re-orientation of the deposition tunnels, but would not affect the overall suitability of the designated depth and repository areas.

Chemical conditions at the site

The site and layout of the repository is selected to conform to the stated design requirements on the chemical conditions. Assessment of the actual chemical conditions, and more importantly their future evolution together with an assessment of the safety importance, is part of the PSAR and is presented in Chapter 10 of this report.

Thermal conditions

For the reference design, the minimum centre-to-centre spacing for the deposition tunnels is 40 m and the minimum centre-to-centre spacing for the deposition holes is 6 m in RFM029 and 6.8 m in RFM045. While there is no experience of heating large volumes of rock, the analytical and numerical techniques used to predict heat transfer are well established and the smaller scale experiments have validated the approaches used to verify the distance between deposition holes in the reference design (Hökmark et al. 2009). There is high confidence in the thermal dimensioning methodology used for the reference layout and it is also recognised that there is a good potential for refining the design, once underground data are available, for further reducing the repository footprint. The adequacy of the current design is re-assessed in Section 10.3.4, using thermal data and other properties qualified in Sections 6.2 and 6.4 of the **Data report**.

An effective way of ensuring that the thermal properties are determined correctly is to combine geological mapping with measurement techniques. The measurement technologies and instruments utilised to determine thermal properties of the rock are well established. Details of the approach to developing tools for measuring and evaluating the thermal properties are presented in the programmes for detailed investigations¹¹.

Mitigating earthquake hazard

The reference design was developed in accordance with the stated design requirements and considers all the deterministic deformation zones and respect distances for the deformation zones with a trace length exceeding 3 km. Deposition positions are not located in any of the deterministic zones, nor inside the given respect distances.

The effective way of determining the extent of discriminating fractures and critical deformation zones in underground openings would be to combine geological mapping with investigations in pilot holes, see programmes for detailed investigations¹² and the **Underground openings construction report**, Section 5.5. The methodology for analysis of the effects of earthquakes on a KBS-3 repository has developed since its first application in conjunction with SR-Site (Fälth 2018, Hökmark et al. 2019). The results of this research effort suggest that the critical radii, i.e. the smallest fractures that can endanger safety after closure, are significantly larger than previously accounted for. The critical radii in all parts of the repository have been found to be in excess of ca 200 m. Hence, in practice those structures/fractures that are critical for canister integrity (Class 3, per Munier and Mattila 2015) are in fact small deformation zones which are assumed to be readily identified through the use of standard mapping and investigation methods presented in the programmes for detailed investigations.

The location of discriminating fractures intersecting deposition holes cannot be determined deterministically at this stage, but the locations are judged to be sufficiently known after deposition tunnels are excavated and characterised according to the programme for detailed investigations.¹³

¹¹ Kärnbränsleförvaret – Detaljundersökningsprogram för tillfarter och centralområde. SKBdoc 1862104. (In Swedish.) (Internal document.) *In prep.* Kärnbränsleförvaret – Preliminärt detaljundersökningsprogram för deponeringsområden. SKBdoc 1600833. (In Swedish.) (Internal document.) *In prep.*

¹² Kärnbränsleförvaret – Detaljundersökningsprogram för tillfarter och centralområde. SKBdoc 1862104. (In Swedish.) (Internal document.) *In prep.* Kärnbränsleförvaret – Preliminärt detaljundersökningsprogram för deponeringsområden. SKBdoc 1600833. (In Swedish.) (Internal document.) *In prep.*

¹³ Kärnbränsleförvaret – Detaljundersökningsprogram för tillfarter och centralområde. SKBdoc 1862104. (In Swedish.) (Internal document.) *In prep.*

At the present stage, the cautious approach of applying the same deposition position rejection criteria as in the SR-Site assessment, the so called full perimeter intersection criterion, FPC, and the extended full perimeter intersection criterion, EFPC (see Figure 5-5), is adopted in the assessment of earthquake hazard in Section 10.4.5. The FPC and EFPC are defined as follows (SKB 2011, Section 5.2.2):

- Deposition positions being intersected by a fracture that intersects the full tunnel perimeter and that also is projected to intersect the canister location in the deposition hole, are rejected (FPC).
- Deposition positions intersected by a fracture intersecting four or more additional potential deposition positions are rejected.

The same criterion with a minor alteration is used, as was done in SR-Site, in the hydrogeological analyses. The variation concerns the FPC criterion where tunnel intersecting fractures projected to intersect the deposition hole (rather than the canister position) are rejected.

Based on the above mentioned findings obtained after the SR-Site assessment, it is judged that this approach overestimates the residual probability that a canister position would be intersected by a fracture sufficiently large to undergo a secondary movement that could damage a canister in the event of a large earthquake near the repository, see further Section 10.4.5.

Hydraulic conditions around deposition holes

Favourable hydrogeological conditions with limited transport of solutes are required to support the performance of the engineered barrier system and to limit radionuclide transport in the case of release from a breached canister. Limitation of the flow rate around the deposition holes contributes to limit changes in the groundwater chemistry in the vicinity of the deposition holes and restricts the mass transfer between the groundwater and the buffer. Thereby, the risk of erosion and loss of the safety functions of the buffer is reduced. Results by Joyce et al. (2013) and Hartley et al. (2014) show that there is a limited correlation between inflows to deposition holes during open repository conditions and the post-closure flow rates. This means that identification of deposition holes with post-closure flow rates higher than a proposed limit value cannot be achieved to the quality desired based solely on inflow during open conditions. According to the results by Joyce et al. (2013), a potentially better indicator of the post-closure flow rates is the specific capacity (outflow divided by head change) observed in injection tests and further, that there is also a reasonable correlation between the specific capacity (a proxy for transmissivity) and the sum of transmissivities of the fractures intersecting the injection hole. This suggests that injection test results could be used for defining technical design requirements for deposition hole positions. It is also noted that conditioning of the underlying DFN models used in hydrogeological modelling according to a recently developed

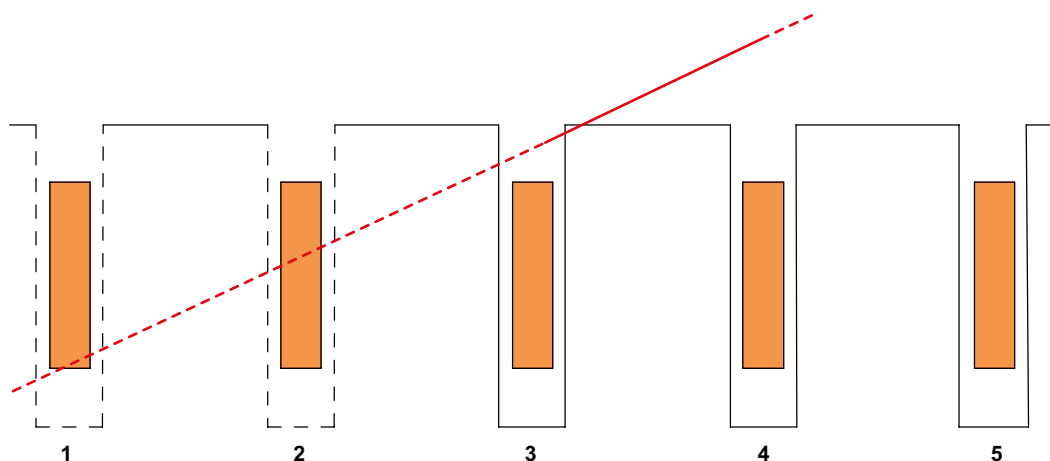


Figure 5-5. The EFPC criterion applied in earthquake analyses that deposition positions being intersected by a fracture that intersects the full tunnel perimeter and that also is projected to intersect the canister location in the deposition hole, are rejected (i.e. positions 1 and 2). For potentially water bearing fractures slightly different criterion applies (i.e. position 3 is also rejected).

methodology (Appleyard et al. 2018) likely results in better correlations between the various entities as exemplified when applied to real data in the ONKALO facility (Baxter et al. 2018). In the PSAR, hydraulic acceptance/rejection criteria based on the studies above are not assessed, but are planned to be used for the SAR.

The design methodologies used to estimate groundwater inflow into underground excavations are well established in hydrogeology. Analytical and numerical methods were used in SR-Site to estimate the inflows for the reference design (the same study is that referred to in Section 10.2.3 of the present report). These numerical models were calibrated with respect to hydrogeology measurements for the site and hence there is confidence in the estimated inflows to the underground openings.

The total volume of water flowing into an accepted deposition hole, between buffer installation and the time when the buffer has saturated, must be less than 150 m³ to ensure that the buffer mass loss due to piping erosion is limited. For the current reference design it is judged that this design requirement is met if only potential deposition holes with inflows less than 0.1 L/min are accepted according to the **Buffer production report**. The most likely situation is that very few additional deposition holes will be rejected due to high inflows. This is because most of the few high flow positions are likely to be already screened out since deposition holes are not allowed in critical volumes class 3. At the most extreme, i.e. assuming that this screening did not capture any such holes, an additional 6 % could be rejected due to observed inflows higher than 0.1 L/min. It is also noted that deposition holes with inflows larger than 0.1 L/min can be identified statistically based on correlations between inflows in deposition holes and injection tests done in the pilot holes of the deposition holes (Joyce et al. 2013) according to the same approach as described above. Thus, limit values in specific capacity (proxy for transmissivity) can be established both for inflows to deposition holes and for post-closure flows (as discussed above).

It is relatively straightforward to monitor the inflow to deposition holes and to evaluate the initial state, see the **Underground openings construction report**, Section 5.11. Should the measured inflow not conform to the design requirement the deposition hole will be rejected. Details of the programme to select measurement techniques for evaluating the inflows of water to deposition holes and how these flows will be measured and evaluated are presented in the programme for detailed investigations¹⁴.

The deposition hole selection criteria will also affect the groundwater flow conditions applicable to deposition holes after closure. This applies both to the requirement to not allow deposition holes to be placed in critical volume class 3, introduced to mitigate the earthquake hazard and the omission of deposition holes with high inflows.

At this stage, as a proxy for more developed hydrological selection criteria in coming stages, application of the FPC and EFPC used in the mitigation of earthquake hazard mentioned above is assumed also for the hydrogeological simulations, i.e. deposition holes intersected by flowing fractures that fulfil FPC or EFPC are omitted.

A transmissivity related rejection criterion is also assumed according to the following: An inflow of 0.1 L/min would be produced by a large fracture and with a transmissivity of 4×10^{-9} m²/s (Smith et al. 2008, Appendix B2). However, considering that inflow may be reduced by e.g. intersecting fractures and local skin effects it is judged to be too optimistic to assume that all fractures of this transmissivity or higher would be found when applying the inflow criterion and thereby avoided when selecting deposition hole positions. It is, however, assessed as justified to assume that very large and very transmissive fractures would be detected. It is thus assumed that fractures, or rather minor deformation zones, with a radius larger than 250 m and with efficient transmissivity larger than 10^{-6} m²/s, will be detected by the detailed investigations so that potential deposition positions intersecting such fractures would be avoided. Such fractures would have the potential of an inflow in the order of 25 L/min. Furthermore, they would also be easy to recognize by local geophysics and other tools applied within the detailed investigation programme. The size limit of 250 m is the same as that applied when assessing critical deposition positions regarding shear movements, see Section 10.4.5. The transmissivity limit of 10^{-6} m²/s is seen as cautious considering the characteristics of such a

¹⁴ Kärnbränsleförvaret – Preliminärt detaljundersökningsprogram för deponeringsområden. SKBdoc 1600833. (In Swedish.) (Internal document.) *In prep.*

fracture discussed above. In all hydrogeological calculations, this transmissivity/fracture length (T/L) criterion is implicitly included in the EFPC criterion, see SKB (2010, Sections 4.2.2 and 4.2.3), unless otherwise stated. (It is demonstrated in Section 14.3 that this additional T/L criterion has a much more limited impact than the ‘pure’ EFPC criterion.)

It is foreseen that the deposition hole selection criteria applied in the safety assessment will be revised for the forthcoming SAR assessment, see further Section 15.5.13.

Rock mechanics and rock support

General engineering guidelines, listed in the SER (SKB 2009c), were considered in the reference design with regard to rock mechanics issues. These guidelines cover feasibility for both construction and deposition. Furthermore, the buffer and backfill imposes design requirements on the acceptable geometry of the deposition holes and tunnels (see the **Underground construction report**, Chapter 2). Potential alterations of the geometry from spalling as well as the capability of the drilling and excavation methods need to be considered when verifying the conformity to these design requirements.

According to the design report (SKB 2009b, Section 9.4) the *in situ* stress conditions at Forsmark at the depth of the repository are not expected to be sufficient to cause extensive stress-induced stability problems in the form of spalling in the deposition tunnels, using the “most likely” stress model and for the current layout and tunnel orientations. However, there is uncertainty regarding this design parameter. Some evidence points to lower stress magnitudes while other evidence points to higher stress magnitudes. The evaluation of all possible stress models indicates that mitigation measures using reinforcement, tunnel orientation and opening shape should be enough to maintain the spalling at acceptable levels also for the access ramp, the central area, the main tunnels and the transport tunnels, even if these latter parts cannot always be aligned with the orientation of the maximum principal stress. The reference design includes quantities of rock support specifically aimed at reducing structurally-related overbreak, i.e. rock fallout beyond the theoretical contour, to an acceptable level.

Martin (2005) showed that the likelihood of spalling in deposition tunnels could be significantly reduced – if not eliminated – by aligning the deposition tunnels parallel to the maximum horizontal stress. Such alignment would also reduce the potential for thermally induced spalling. According to the guideline given in the SER the deposition tunnels shall be aligned within ± 30 degrees of the trend of the maximum horizontal stress to significantly reduce the risk of spalling. A three dimensional elastic stress analysis, presented in the design report (SKB 2009b, Appendix C), confirms this guideline.

For deposition holes, the three dimensional elastic analyses showed that for the “most likely” stress model, only the deposition tunnels aligned greater than 30 degrees to the maximum horizontal stress will produce tangential stress concentrations that are higher than the spalling strength, and in these situations the spalling will occur above the top of the canister. In the case of the “most likely” stress model, the results indicate that some 100–200 deposition holes (out of 6000) would sustain a spalling depth (overbreak) that exceeds 5 cm, provided the deposition tunnels are aligned between 0 and 30 degrees to the maximum horizontal stress. For the “unlikely maximum” stress model, the deposition tunnel must be aligned parallel to the maximum horizontal stress, but the number of deposition holes that can sustain a spalling depth in excess of 5 cm is approximately the same, see Figure 5-6. Moreover, loose rock debris from localised spalling that remains on the rock walls in deposition holes can be scaled off to achieve compliance with the requirement for associated effective transmissivity.

In order to use space efficiently, the deposition tunnels in the reference design are aligned between azimuths 123 to 140 degrees. Should the “unlikely maximum” stress conditions be found when the excavation reached the repository level, these alignments must be adjusted.

In order to prevent minor spalling from being an operational safety issue, roof support with shotcrete is included in the reference design for all underground openings except in the deposition tunnels where continuous shotcrete is not allowed.

Some material in the rock or on rock surfaces e.g. originating from rock support will remain in the repository after closure. The assessed quantities are given in the **Underground openings construction report**, Table 4-1.

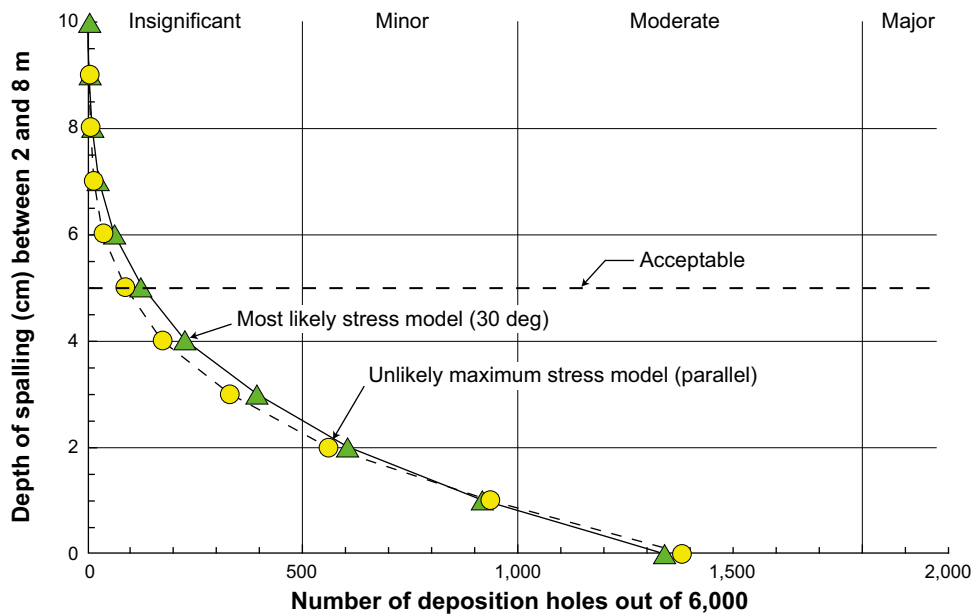


Figure 5-6. Estimated depth of spalling in deposition holes for the “most likely” and the “unlikely maximum” stress models. For the “most likely” case deposition tunnels are assumed to be aligned between 0 and 30 degrees to the maximum horizontal stress, whereas for the “unlikely maximum case” deposition tunnels are assumed exactly parallel to the maximum horizontal stress (Figure 8-4 in SKB 2009b). The classification of number of holes affected being “insignificant”, “minor”, “moderate” and “major” relates to the design risk assessment presented in SKB (2009b).

Deposition tunnel and deposition hole geometry

In the **Underground openings construction report**, it is concluded that the design requirements on tunnel geometry, imposed by the backfill, are likely to be fulfilled using existing technology. This conclusion is based on the results from excavation of deposition tunnels at Äspö Hard Rock Laboratory (HRL) (Johansson et al. 2013, Karlzén and Johansson 2010). However, deviations cannot be totally excluded and means of inspecting the geometry and handling the potential deviations are needed. Measuring techniques are well established and demonstrated to be fit for measuring the geometry of deposition tunnels after excavation (see the **Underground construction report**, Sections 8.3). Should the as-built dimensions not conform to the design requirements, the current contingency measure for maximum cross-sectional area and maximum volume is to apply shotcrete and smooth out the rock surface to cope with any irregularity or rock fall out. Should the design requirement for minimum cross section not be fulfilled due to occurrences of underbreak, the contingency measure is to remove it by using standard mechanical equipment. The ultimate contingency measure is to reject the deposition tunnel.

The results from full face down-hole drilling of deposition holes at the Äspö HRL (Andersson and Johansson 2002) and in Onkalo (Railo et al. 2016, 2017) were used to investigate the performance for excavating deposition holes. The variability of the mean cross-section diameter relative to the mean diameter of the deposition hole is well within the current geometrical tolerances.

The effective way of ensuring that the geometrical tolerances are fulfilled would be to combine quality assurance in the execution of works with measuring techniques to determine the as-built dimensions. There are methods and instruments that are potentially fit for measuring the geometry of deposition holes after excavation, e.g. laser scanning, photogrammetry and geodetic methods. However, the current methods are considered to be conceptual and although they are based on proven technology, a certain degree of new technology and innovation is likely to be required to develop a suitable field method, as discussed in Section 6.5 of the **Underground openings construction report**.

Properties of the excavation damaged zone (EDZ)

Over the years SKB has carried out extensive studies on the presence and physical properties of an excavation damaged zone, the so called EDZ, which may surround a tunnel. Blast damages in the tunnel floor exhibit a zonation with respect to the bottom charge and the column charge. Both blast-induced and stress-induced fractures will form sub-parallel to the tunnel contour. The connectivity of the most transmissive fractures is short and is normally connected to the tunnel floor. Based on experience from the excavation of the TASQ tunnel at the Äspö H RL (Olsson et al. 2004), TASS tunnel (Olsson et al. 2009) and TAS04 tunnel (Ericsson et al. 2009) it is possible to design and control the drilling and blasting of tunnels such that continuous fracturing along the axial direction of the tunnel will not develop. Blast-induced fractures are dominantly radial in direction and such fractures are not continuous along the axial direction of the tunnel over any significant distance.

If a connected zone at all develops, a reasonable value for the hydraulic conductivity of the damage zone is in the order of 10^{-8} m/s. The properties of a damaged zone surrounding an underground opening change if spalling has occurred. The results of the major experiments suggest that the hydraulic conductivity will be in the order of 10^{-6} m/s and that such a zone extends a couple of decimetres into the rock surrounding the underground opening (Bäckblom 2009).

Currently, there is no reliable direct method that can quantify the connected effective transmissivity along a tunnel, apart from judging the likelihood that no continuous EDZ has developed at all. The full extent and connectivity of the fractures can only be explored by indirect methods, such as hydraulic testing in boreholes or the use of geophysical methods in addition to geological mapping (Ericsson et al. 2009). SKB plans to develop several procedures for ensuring that the damage in deposition tunnels conforms to the design requirement. Procedures to control and inspect the drilling, charging and ignition sequences will be developed and included in the monitoring and control programmes for the underground openings as discussed in Section 5.7.2 of the **Underground openings construction report**.

Should the connected effective transmissivity caused by EDZ not conform to the design requirement, the contingency action is to remove any loose rock debris that remains on the rock walls. The wire sawing of the floor will also mitigate occurrence of EDZ in the floor. The ultimate contingency measure is to reject the deposition tunnel. In addition, the local stress reduction close to the tunnel may open fractures parallel to it, as is further assessed in Section 10.2.2. Further discussion on these matters, together with input data for the PSAR, is found in the **Data report**, Section 6.5.

Findings from a comprehensive literature study (Bäckblom 2009) indicate that for mechanical excavation techniques in elastic rock conditions, i.e. full face down-hole drilling, the depth of the excavation damaged zone (EDZ) is limited to a few centimetres in the rock surrounding the deposition hole. The hydraulic conductivity in such a zone is in the order of 10^{-10} m/s or less. There is high confidence that elastic rock conditions prevail for the reference design and consequently that the transmissivity of the EDZ in deposition holes, if such a zone exists at all, would be less than 10^{-10} m²/s.

The magnitude of the connected effective transmissivity may be altered due to occurrences of spalling. While there is high confidence in the design methodology utilised to assess the spalling potential for the reference design, there are uncertainties relating to the *in situ* stress conditions and the rock properties. This restricts the capability of modelling the extent of spalling and the associated change in transmissivity at this stage. It was assessed that approximately 100–200 deposition holes (out of the about 6 000) would be subject to overbreak that exceeds 5 cm, see Figure 5-6. Because the design methodology is empirically based, additional investigations will be needed at the repository level to confirm the design assumptions. Details of the programme to develop means for evaluating the stress at the repository level are presented in the programme for detailed investigations¹⁵. Furthermore, the probability of spalling is reduced in the design as the deposition tunnels are aligned sub-parallel to the major horizontal stress.

¹⁵ Kärnbränsleförvaret – Preliminärt detaljundersökningsprogram för deponeringsområden. SKBdoc 1600833. (In Swedish.) (Internal document.) *In prep.*

Should spalling occur, loose rock debris from localised spalling on the rock walls would be removed. The ultimate contingency action is to reject the deposition hole. In conclusion, spalling prior to deposition would not affect the geometry of accepted deposition holes outside the stated margins.

Grouting, reinforcement and stray materials

The compositions, amounts and locations of the engineered and residual materials have to be accepted considering their impact on the favourable chemical conditions in the repository. The pH of the ground-water in the host rock shall be less than 11 for the buffer to fulfil its intended performance. The main source of increased pH is grouting and rock reinforcement, therefore the pH of the leachates shall be limited and not increase the pH of water in contact with the buffer or backfill to values higher than 11. In practice, this is controlled by using low-pH cements with low Ca:Si ratios or non-cementitious grouts.

The need for grouting and a rationale for assessing the quantities of cement, silica sol and additives for the reference design, including both the total amount and the amount remaining in the rock, is presented in Brantberger and Janson (2009, Section 7.3). In fracture domain FFM02, located within the upper 100–200 m of the rock, the rock has a relatively high frequency of transmissive fractures and relatively extensive grouting measures would be needed in this part of the rock. Below 200 m the frequency of transmissive fractures is generally low and decreases with depth and the grouting can be carried out as selective pre-grouting, with probe hole investigations, when passing deformation zones and where discrete water-bearing fractures are encountered. Below a depth of approximately 400 m, the observed frequency of flowing features is very low and grouting of flowing fractures and zones will be localised and not result in continuous grouting holes outside the deposition tunnel perimeter. On average, less than 2 % of the 20 m sections between deformation zones will require grouting (Brantberger and Janson 2009, Section 3.5).

When grouting is required at repository level, it is anticipated that cement-based grouting will be adequate to achieve the required sealing efficiency. However, for some water-bearing fractures and deformation zones in deposition tunnels it may not be practical to use cement-based grouts. In order to achieve the required sealing efficiency in such cases, options were included in the reference design for the use of new technologies such as silica sol, which has been tested at the Äspö HRL (Funehag and Emmelin 2011). Quantities of stray material that remain in the rock from grouting activities will form part of the final repository facility. The assessed quantities on completion of the final repository facility are given in Table 8-3 of the **Underground openings construction report**. The estimated quantities contain cement, silica fume, silica sol and additives.

Well established and reliable, empirical, analytical and numerical design methodologies were used to assess the stability of underground openings and the rock support required for the underground openings in the reference design layout. The assessment of the deposition tunnels concludes that continuous shotcrete is not required for the foreseen rock qualities. The assessed composition and amounts of engineered materials associated with elements of rock support are presented in Table 8-3 of the **Underground openings construction report**.

Currently, there are no quantitative technical design requirements for other materials or characteristics. The composition and amount of these materials as well as locations, where these materials are used, shall be documented. The so far estimated compositions, amounts and locations, see Table 8-2 of the **Underground openings construction report**, have been concluded to be acceptable with respect to post-closure safety.

The deposition holes shall not be grouted. By grouting, the hydraulic properties of the host rock and fractures can be enhanced locally and temporarily e.g. to limit inflows. However, as the grout degrades with time, grouted fractures can become of importance as flow routes and enhance the flows around the deposition holes and thereby jeopardise the safety function of the host rock to provide favourable hydrogeological conditions in the long term. Further, the interaction of the grout and its degradation products with the buffer may impair the characteristics of the buffer. In some cases, even if the deposition hole itself is not grouted, signs of grout may be observed in fractures intersecting the deposition hole. Such observations are used as input for assessing the importance of the fracture as a hydraulic connection and considered in the classification of the structure.

Deposition tunnels can be intersected by structures that are acceptable in terms of long-term behaviour of the repository, but provide an inflow that needs to be limited in order to allow the installation of the backfill. For this reason, some sections of the deposition tunnels may need to be grouted. Further water handling measures, e.g. use of geotextiles, may need to be applied, if grouting is not efficient. Such methods can have local effects on the performance of the backfill. These effects and the potential impacts on the buffer performance in the long term need to be evaluated. Deposition holes shall not be emplaced along sections of the tunnel where grouting or other water handling measures are applied, if these measures may impair the backfill performance e.g. by reducing the density of the installed buffer so that it cannot maintain its safety functions above the deposition hole.

Location with respect to other underground openings

The construction of the underground openings must not impair the safety functions of the host rock. The excavation works will generate mechanical disturbances such as vibrations. In addition, depending on the rock strength with respect to prevailing rock stresses, spalling may occur in the underground openings. Increased fracturing around the underground openings will affect the groundwater flow and transport of solutes. In order to avoid creating hydraulic connections between the surface and the underground openings, there needs to be a distance between existing investigation holes connected to the surface and underground openings where the hydraulic conductivity must be limited after closure of the repository. This required distance depends on the kind of underground opening, e.g. deposition hole, deposition tunnel, other tunnel or shaft, and on the properties of the host rock. Investigation holes in this context mean boreholes and drill holes made either for investigation or construction purposes.

Construction works shall not disturb the canisters and buffer already emplaced in the deposition holes and the backfill and plugs already installed. In order to avoid mechanical disturbances caused by the excavation and the potential hydraulic and hydrogeochemical disturbances caused by the adjacent underground openings, there must be a sufficient distance between the backfilled deposition tunnels and other underground openings and construction work. Further, the heat produced by the emplaced canisters may induce spalling and mechanical instability and therefore there needs to be sufficient distance between the emplaced canisters and open tunnels. These distances depend on the properties of the host rock at the site and to some extent on the time for which specific tunnels remain open, and need to be assessed considering the site-specific conditions and disposal schedule.

The deposition tunnel plug shall be placed in a location that allows it to perform as specified. This means that the quality of the rock shall be good and, therefore, plugs shall not be constructed within critical volumes of class 1, 2 or 3. There needs to be a sufficient distance between the plug and the intersection of the deposition tunnel and central, or main, tunnel in order to limit rock damage caused by redistribution of stresses around the excavated tunnels and to ensure the tightness of the plug. Further requirements, e.g. on the inflows, and on the plug location may arise based on the ongoing plug tests.

Deposition tunnel inflows

In SKB (2010, Section 6.3.2) it is concluded that the open flowing fracture frequency at the repository level, assessed to be around 0.005/m, indicates that, on average, less than 2 % of the 20 m sections between deformation zones will require grouting (Brantberger and Janson 2009). However, there are uncertainties associated with the grouting methods and the level of effort to locate the water-bearing fractures, particularly if they have relatively small apertures with channelised flow. The estimated grout quantities required to reduce the inflows to acceptable levels are based on combining cement based grout mixes and solution grouting with silica sol. Based on the measured inflow of the deposition tunnel there are several developed water handling methods to be used before installing the backfill (Sandén et al. 2018b). Details of the programme for measuring and evaluating inflow of water to deposition tunnels are presented in the programme for detailed investigations¹⁶.

¹⁶ Kärnbränsleförvaret – Preliminärt detaljundersökningsprogram för deponeringsområden. SKBdoc 1600833. (In Swedish.) (Internal document.) *In prep.*

5.3 Initial state of the fuel and the canister cavity

All spent fuel from the currently approved Swedish nuclear programme shall be deposited in the KBS-3 repository. Information about the amounts and the characteristics of the fuel to be handled in the KBS-3-system and deposited in the final repository is described in the **Spent fuel report**.

Only spent fuel in oxide form (UOX or MOX) is accepted for deposition in the KBS-3 repository. Furthermore, the maximum allowed enrichment is 5 % and the maximum average assembly burnup is 60 MWd/kgU for spent fuel in interim storage.

5.3.1 Requirements on the handling of the spent nuclear fuel

The handling of the fuel in the facilities, and the requirements on the handling related to its final disposal in the repository, is presented in SKB (2021a). The most important handling requirements and criteria related to post-closure safety are the following.

- The fuel assemblies to be encapsulated in any single canister shall be selected with respect to burnup and age so that the total decay power in the canister will not result in temperatures exceeding the maximum allowed in the buffer. The total decay power in each canister must not exceed 1 700 W at the time of deposition.
- The fuel assemblies to be encapsulated shall be selected with respect to enrichment, burnable absorbers (BA), burnup, geometrical configuration and materials in the canister so that criticality will not occur during the handling and storage of canisters even if the canister is filled with water. The effective multiplication factor (k_{eff}) must not exceed 0.95 including uncertainties.
- Before the fuel assemblies are placed in the canister they shall be dried so that it can be justified that the allowed amount of water stated as a technical design requirement for the canister is not exceeded. The amount of water left in any one canister shall be less than 600 g.
- Before the canister is finally sealed, the atmosphere in the insert shall be changed so that acceptable chemical conditions can be ensured. The atmosphere in a canister insert shall consist of at least 90 % argon.
- It shall be verified that the radiation dose rate on the canister surface will not exceed the level used as a premise in the assessment of the post-closure safety. The radiation dose rate at the surface of the canister must not exceed 1 Gy/h.

5.3.2 Fuel types and amounts

BWR and PWR fuel

The major part of the nuclear fuel to be deposited consists of spent fuel from the operation of the twelve Swedish nuclear power plants, which are either of boiling water reactor (BWR) type or pressurised water reactor (PWR) type.

The data in the scenario for the operation of the Swedish nuclear power plants that are used to determine the set of fuel elements and the total amount of fuel to handle and deposit are summarized in Table 5-2. For the time period after 31 December 2015, the scenario is based on the prognosis and the planned year for shutdown for each reactor. It is noted that the then planned shutdown years of the reactors O1 (2017), R1 (2020) and R2 (2019) are in agreement with the actual years of shutdown.

The majority of the fuel used in the reactors consists of uranium oxide fuel (UOX). From Oskarshamn, there will be three fuel assemblies with mixed oxide fuel (MOX).

The number of fuel assemblies discharged from the Swedish nuclear power plants stored in the interim storage facility (Clab) at the end of 2015, and the estimated total number of assemblies for the scenario for future operation of the reactors are given in Table 5-3 together with the corresponding estimated amount of uranium or heavy metal expressed as tonnes initial weight. As seen in the table, the total amount of fuel generated in the reference scenario is around 11 500 tonnes (expressed as tonnes of U or heavy metal (HM) in initial fuel). It is noted that this is slightly less than the 12 000 tonnes (U or HM) which is the estimate used in the licence application in 2011 and in the PSAR.

Table 5-2. The scenario for the operation of the Swedish nuclear power plants.

Reactor	First year of operation	Last year of operation	Total time of operation
B1	1975	1999	24
B2	1977	2005	28
F1	1980	2040	60
F2	1981	2041	60
F3	1985	2045	60
O1	1972	2017	45
O2	1974	2013	39
O3	1985	2045	60
R1	1975	2020	45
R2	1975	2019	44
R3	1981	2041	60
R4	1983	2043	60

Table 5-3. Spent fuel from operation of the nuclear power plants stored in the interim storage facility, Clab, and total amounts estimated for the scenario for the operation of the power plants.

Fuel type	Number in interim storage (31 December 2015)	Total number for scenario for the operation of the nuclear power plants	Total initial weight for the scenario for the operation (tonnes of U or heavy metal HM)
BWR assemblies from operation of the NPP at Barsebäck, Oskarshamn, Forsmark and Ringhals	28 931 ¹⁾	47 314	8 367.5 ²⁾
PWR assemblies from operation of the NPP at Ringhals	3 834	6 793	3 125.0 ³⁾

¹⁾ Including 3 BWR MOX assemblies from Oskarshamn nuclear power plant.

²⁾ Assumed 176.8 kg U/HM per assembly.

³⁾ Assumed 460.0 kg U per assembly.

Miscellaneous fuels

There are minor quantities of spent fuel from research and the early part of the nuclear power programme to be deposited in the KBS-3 repository. Leaking fuel pins stored at the nuclear power plants have been removed from their assemblies and put in water tight and air tight boxes. All these fuels are in the following referred to as *miscellaneous fuels*. The amount of miscellaneous fuel and, if applicable, the number of fuel assemblies in the interim storage facility as well as the estimated total amount of uranium or heavy metal, expressed as tonnes initial weight, is presented in Table 5-4.

5.3.3 Handling of spent fuel

The handling of the spent fuel comprises the following main steps:

- Transport and deliveries of the fuel assemblies from the power plant to the interim storage facility, Clab (later Clink).
- Interim storage for typically 30–40 years.
- Selection of assemblies for encapsulation, transport to the encapsulation building and drying of the assemblies.
- Encapsulation consisting of placement in the canister and exchange of atmosphere in the canister insert prior to sealing of the copper canister.

The interim storage and encapsulation of the spent nuclear fuel will take place in Clink (Central interim storage and encapsulation plant). The Clink facility will consist of the current interim storage facility (Clab) and the encapsulation plant to be constructed in connection to Clab.

Table 5-4. Miscellaneous oxide fuels stored in the interim storage facility, Clab, and total amounts estimated for the scenario of the operation of the power plants.

Fuel type	Number in interim storage 31 December 2015	Total number for the scenario for the operation of the nuclear power plants	Total initial weight for the reference scenario (tonnes of U or HM)
Fuel assemblies from the dismantled pressurised Ågesta heavy water reactor	222 (1 unirradiated)	222 (1 unirradiated)	20.3
Swap MOX assemblies ¹⁾	217	217	23.4
Rod cassettes ²⁾	65	-	10.0
Fuel residues in special boxes from Studsvik	20	Approximately 37	3.9
Tight boxes for leaking fuel pins	-	33 (existing) + ca 30 (prognosis)	2.3 (existing) + ca 2 (prognosis)

¹⁾ Some spent fuel from Ringhals and Barsebäck was earlier sent to La Hague for reprocessing. This spent fuel was exchanged in 1986 for spent German MOX fuel in equivalent amounts of plutonium.

²⁾ Dismounted fuel rods placed in rod cassettes.

5.3.4 Initial state

Encapsulated spent fuel is the spent nuclear fuel encapsulated for deposition in the KBS-3 repository. Gases and liquids in the cavities of the canister and fuel assemblies are considered together with the encapsulated spent fuel. The initial state of the encapsulated spent fuel refers to the properties of the spent fuel and the gases and liquids in the cavities of the canister when the canister is finally sealed and no further handling of the individual fuel assemblies is possible.

Radionuclide inventory

At closure of the final repository, the burn-up, irradiation and power history and age of the assemblies in each canister will be known and the radionuclide inventory can be calculated for each canister individually. However, at the present stage it is not possible to calculate the inventory in individual canisters.

Based on the premise that the decay power of a canister shall not exceed 1700 W in the repository, various combinations of fuel elements are possible in a canister. Using a simple simulation of the encapsulation process over time (**Spent fuel report**), the individual canisters are found to vary in both average burnup and decay time (age of the fuel element). In a long-term perspective, the age of the fuel at deposition is of minor importance for the radionuclide inventory since the short lived nuclides of importance for the decay power will have decayed away. Thus, assuming all canisters will be fully utilised, burnup will be the most important parameters for the radionuclide inventory. The variability in radionuclide content in the canisters has been estimated using canisters of low average burnup, medium average burnup and high average burnup. These canister types provide a reasonable description, from the point of view of post-closure safety, of how the radionuclide content can be expected to vary between canisters.

The selected burn-ups of the assemblies in these canisters are based on the results of a simulation of the encapsulation procedure. The following canisters have been used to illustrate the variation in radionuclide content between canisters:

- BWR Low: representing BWR canisters with an average burnup of 30 MWd/kgU.
- BWR Medium: representing BWR canisters with an average burnup of 40 MWd/kgU.
- BWR High: representing BWR canisters with an average burnup of 50 MWd/kgU.
- PWR Low: representing PWR canisters with an average burnup of 35 MWd/kgU.
- PWR Medium: representing PWR canisters with an average burnup of 45 MWd/kgU.
- PWR High: representing PWR canisters with an average burnup of 55 MWd/kgU.

In the current safety assessment, dose and risk calculations are based on the estimated radionuclide content in an average canister. The use of the average canister is suitable for the probabilistic approach adopted in the calculations, and corresponds to the total radionuclide inventory divided by the number of canisters in the repository (5689), including the projected number of canisters needed for the future operation of the nuclear power plants, see **Spent fuel report**. Note that the assessment of post-closure safety is made based on 6 000 average canisters, as this is the amount of fuel in the application for construction of the final repository.

The radionuclide inventory in different canisters of some of the more important radionuclides is presented in Table 5-5. The full inventory for radionuclide transport calculations for the average canister is given in Table 5-6 and in the in the **Data report**. The radionuclides in the inventory are found in the fuel rods, construction materials in the fuel assembly, crud (a deposit on the cladding), and control rods (PWR canisters).

The radionuclide inventory is located in different parts of the fuel assembly: Fuel pellets, cladding and other construction materials (metal alloys), in the gap between fuel and cladding, and in the crud. These different fractions of the inventory are assumed to be released at different rates in the event of a canister failure. Certain elements, originally formed in the fuel matrix, have a sufficiently high mobility that a fraction of the inventory will transfer to the fuel/cladding gap. This fraction is expected to be released rapidly and is an important part of the Instant Release Fraction (IRF). The size of this fraction can, for some elements, be estimated from measured and calculated fission gas (Xe, Kr) release (FGR). The FGR is correlated to the linear heat generation rate, which in turn will depend on the thermal effect of the nuclear reactor, the number of assemblies and configuration of the assemblies in the reactor core and on how the fuel assemblies are utilized during operation. Thus, using the calculated FGR for existing BWR and PWR assemblies, the average FGR is used to determine the IRF of some radionuclides in the average canister.

Of all relevant radionuclides Cl-36 is among the most mobile and the fraction of Cl-36 in the fuel/cladding gap is about three times the FGR. Most significantly, the fraction of the mobile radionuclides I-129, Cs-135, and Cs-137 is found to have an IRF which is, at most, equal to the FGR. Other, less mobile radionuclides originally formed in the fuel matrix (e.g. Sr-90, Tc-99, Pd-107, Sn-126) are also found to have an IRF; however, available leaching data indicate that this fraction is very small and not correlated to FGR. The actual IRF values used in the safety assessment modelling for all nuclides are given in the **Data report**.

Table 5-5. The inventories (Bq) of thirteen radionuclides of importance for decay power, radio-toxicity and calculated long-term risk in different canisters and total inventory of the radionuclides in the repository (calculated for the calendar year 2045). Note that the calculations of post-closure safety include many more nuclides than those listed in this table. The full inventory is provided in the Data report and supporting documents (Spent fuel report).

Radio-nuclide	BWR Low	BWR Medium	BWR High	PWR Low	PWR Medium	PWR High	Average canister	Total for reference scenario
Am-241	2.11×10^{14}	2.54×10^{14}	2.85×10^{14}	2.68×10^{14}	3.13×10^{14}	3.52×10^{14}	2.74×10^{14}	1.56×10^{18}
C-14	1.14×10^{11}	1.27×10^{11}	1.59×10^{11}	7.12×10^{10}	8.88×10^{10}	1.06×10^{11}	1.15×10^{11}	6.57×10^{14}
Cl-36	4.83×10^8	4.83×10^8	5.42×10^8	1.28×10^8	1.44×10^8	1.59×10^8	3.79×10^8	2.15×10^{12}
Cs-137	3.37×10^{15}	4.47×10^{15}	5.52×10^{15}	3.45×10^{15}	4.36×10^{15}	5.25×10^{15}	4.41×10^{15}	2.51×10^{19}
I-129	1.94×10^9	2.61×10^9	3.21×10^9	2.03×10^9	2.57×10^9	3.11×10^9	2.59×10^9	1.47×10^{13}
Nb-94	8.53×10^9	8.50×10^9	1.09×10^{10}	5.42×10^{11}	6.88×10^{11}	8.30×10^{11}	2.11×10^{11}	1.2×10^{15}
Pu-238	1.26×10^{14}	2.14×10^{14}	3.25×10^{14}	1.60×10^{14}	2.71×10^{14}	4.02×10^{14}	2.30×10^{14}	1.31×10^{18}
Pu-239	2.00×10^{13}	2.11×10^{13}	2.18×10^{13}	2.34×10^{13}	2.50×10^{13}	2.62×10^{13}	2.23×10^{13}	1.27×10^{17}
Pu-240	4.01×10^{13}	4.84×10^{13}	5.37×10^{13}	3.85×10^{13}	4.40×10^{13}	4.87×10^{13}	4.73×10^{13}	2.69×10^{17}
Pu-241	1.42×10^{15}	1.71×10^{15}	1.90×10^{15}	1.83×10^{15}	2.10×10^{15}	2.35×10^{15}	1.82×10^{15}	1.03×10^{19}
Sr-90	2.25×10^{15}	2.89×10^{15}	3.57×10^{15}	2.23×10^{15}	2.81×10^{15}	3.37×10^{15}	2.85×10^{15}	1.62×10^{19}
U-238	2.53×10^{10}	2.50×10^{10}	2.47×10^{10}	2.18×10^{10}	2.15×10^{10}	2.12×10^{10}	2.39×10^{10}	1.36×10^{14}

Table 5-6. Inventory for radionuclide transport calculations as mol per average canister at year 2045 (Data report, Section 3.1). The radionuclides marked with (*) are not explicitly included in the PSAR radionuclide transport calculations, but their inventories are included in those of their progeny nuclides.

Radionuclide	Inventory [mol/canister]	Radionuclide	Inventory [mol/canister]
Ac-227	1.85×10^{-9}	Pa-231	4.71×10^{-6}
Ag-108m	1.60×10^{-1}	Pa-233 (*)	1.64×10^{-7}
Am-241	8.98	Pa-234m (*)	3.98×10^{-12}
Am-242 (*)	9.37×10^{-8}	Pb-210	1.13×10^{-10}
Am-242m	7.25×10^{-3}	Pd-107	5.74
Am-243	1.60	Pu-238	1.53
C-14	4.99×10^{-2}	Pu-239	40.8
Cd-113m	3.40×10^{-4}	Pu-240	23.5
Cl-36	8.64×10^{-3}	Pu-241 (*)	1.97
Cm-242 (*)	1.89×10^{-5}	Pu-242	6.66
Cm-243 (*)	1.84×10^{-3}	Ra-226	2.74×10^{-8}
Cm-244 (*)	1.56×10^{-1}	Rn-222	-
Cm-245	2.42×10^{-2}	Se-79	1.67×10^{-1}
Cm-246	3.50×10^{-3}	Sm-151	1.47×10^{-1}
Cs-135	6.45	Sn-121m	2.77×10^{-3}
Cs-137	10.1	Sn-126	8.97×10^{-1}
Eu-152	9.44×10^{-5}	Sr-90	6.21
H-3	7.25×10^{-3}	Tc-99	19.9
Ho-166m	7.49×10^{-4}	Th-229	1.34×10^{-8}
I-129	3.08	Th-230	1.64×10^{-4}
Mo-93	8.81×10^{-4}	Th-232	4.39×10^{-5}
Nb-93m	7.75×10^{-2}	Th-234 (*)	1.20×10^{-7}
Nb-94	3.25×10^{-1}	U-233	1.17×10^{-4}
Ni-59	2.25	U-234	1.76
Ni-63	3.18×10^{-1}	U-235	42.1
Np-237	4.75	U-236	39.3
Np-238	1.34×10^{-9}	U-237 (*)	6.10×10^{-8}
Np-239 (*)	1.39×10^{-6}	U-238	8110
		Zr-93	21.3

Some radionuclides, such as Nb-94, are found mainly in the construction parts of the fuel, and these are released at the rate of corrosion of these metals. Thus, this fraction is called Corrosion Release Fraction (CRF).

In addition to regular fuel assemblies, containers with fuel residues from Studsvik and failed fuel rods will be encapsulated and deposited. These containers represent a very small fraction of the total radionuclide inventory. Since the properties of the fuel residues and the failed fuel differ from those of the regular fuel, their potential contribution to the calculated long-term risk for the repository must nevertheless be assessed.

Criticality

The assemblies must not under any circumstances be encapsulated if the criticality criteria cannot be met. Reported calculations (Johansson et al. 2019) show that the criteria can be met for all postulated events in the first one million years in the repository. The analysis is based on the required amount of burnable absorber (Gd) in BWR fuel and the required burnup of PWR fuel. The criticality calculations are based on the canister reference design, which is constrained by design requirements related to criticality and expressed as requirements on geometry and material composition, see Section 5.4.

They also take into account the possible geometry changes in a failed copper canister in the post-closure repository environment (Spahiu and Agrenius 2016). If an individual assembly does not conform to the acceptance criteria in this check, a canister specific calculation of criticality will be made where a specific set of assemblies will be selected. If it cannot be shown that a canister specific calculation conforms to the criticality criteria, even if the assembly is loaded alone in the canister, the assembly will be loaded together with a long term resistant neutron absorber. The ultimate measure will be to alter the geometry, i.e. to reconstruct the assembly.

Variables for the spent fuel

In the **Fuel and canister process report** the spent fuel is described by the variables in Table 5-7, which together characterise the spent fuel in a suitable manner for the safety assessment. The description applies not only to the spent fuel itself, but also to the cavities in the canister. This Section presents the initial condition values for the variables.

Geometry

The BWR fuel assemblies contain about 60 up to ca 100 fuel rods. The fuel rods consist of zirconium alloy tubes filled with cylindrical fuel pellets. The rods are arranged in square arrays enclosed in a fuel channel. The cross-sectional area of the fuel assemblies is about $0.141 \times 0.141 \text{ m}^2$ and the total length can be up to about 4.4 m. The PWR fuel assemblies contain 204 or 264 fuel rods, arranged in square arrays. The cross-sectional area is about $0.214 \times 0.214 \text{ m}^2$ and the total length is about 4.3 m.

Table 5-7. Variables for fuel/cavity in canister.

Variable	Definition
Geometry	Geometric dimensions of all components of the fuel assembly, such as fuel pellets and Zircaloy cladding. Also includes the detailed geometry, including cracking, of the fuel pellets.
Radiation intensity	Intensity of alpha, beta, gamma and neutron radiation as a function of time and space in the fuel assembly.
Temperature	Temperature as a function of time and space in the fuel assembly.
Hydrovariables (pressure and flow)	Flows, volumes and pressures of water and gas as a function of time and space in the cavities in the fuel and canister.
Mechanical stresses	Mechanical stresses as a function of time and space in the fuel assembly.
Radionuclide inventory	Occurrence of radionuclides as a function of time and space in the different parts of the fuel assembly. The distribution of the radionuclides between the pellet matrix, gap between cladding and pellet, construction materials and crud (a surface deposit) is also described here.
Material composition	The materials of which the different components in the fuel assembly are composed, excluding radionuclides.
Water composition	Composition of water (including any radionuclides and dissolved gases) in the fuel and canister cavities.
Gas composition	Composition of gas (including any radionuclides) in the fuel and canister cavities.

Radiation intensity

Given that canisters in the repository will not exceed 1 700 W, the dose rate on the canister surface for such canisters were calculated (SKB 2010e). The results show that for a PWR element with a burn-up of 42.2 MWd/kgU after 34.1 years, the source strength of neutrons is $1.2 \times 10^8/\text{s}$ and of photons $6.8 \times 10^{14}/\text{s}$. A canister with four such elements (1 700 W) will have a maximum dose rate on the canister surface of 115 mSv/h and a maximum neutron dose rate of 2.9 mSv/h.

Dose rates have also been calculated for canisters with higher residual power. These calculations are used for design of the radiation shielding in both Clink and the final repository, and are based on canisters with a residual power of ca 2200 W. Results from these calculations show that also for these hypothetical canisters, containing one high-burnup fuel assembly with short decay time (e.g.

60 MWd/kgU BWR with a decay time of 5 years), the dose rate is dominated by the gamma dose, and will not exceed 1 Gy/h (**Spent fuel report**).

Temperature, Hydrovariables (pressure and flow) and Mechanical stresses

The initial conditions of these variables are dependent on the external environment and are assessed where appropriate in the PSAR. Only the temperature is of relevance for an intact canister.

Material composition

Certain elements in the fuel construction materials are important for determining the content of radio-nuclides relevant for the safety assessment. One example is niobium (Nb) which, through neutron capture during operation, forms the long-lived radioactive isotope Nb-94 (see Table 5-5 for activity in the various canisters). Additionally, the composition and dimensions of the metal parts of the fuel affect the corrosion rate and therefore the release rate of the CRF. Therefore, the chemical composition, including the content of some impurities (Cl, N), of the construction materials for PWR and BWR fuels are used as input for the inventory calculations. The dimensions, most importantly the thinnest part, of these construction materials are used as input for the radionuclide transport calculations.

More information concerning construction materials is provided in the **Spent fuel report**.

Water and gas composition

The content of gases and liquids in the canister depends on the result of the drying of fuel elements and the exchange of air with argon in the canister insert. Based on the chosen procedures, described in SKB (2020a), there is no reason to believe that the water content in the canisters will exceed the 600 g given as a premise or that the argon content will be below the acceptable level of at least 90 %. The requirement on the production system for the canister states that the canister shall be filled with 99 % argon (Ljungberg 2021), giving a considerable margin to the 90 % technical design requirement.

5.4 Initial state of the canister

The initial state of the canister for the spent nuclear fuel in the repository is based on the canister design including the choice of materials, and is further affected by the manufacturing, testing and handling.

The **Canister production report** presents the technical design requirements, the canister reference design, verifying analyses showing that the reference design fulfils the technical design requirements, and the production and testing procedures selected to achieve the reference design. The report also includes an account of the achieved results from test manufacturing and an overview of the transportation and deposition of the canister with spent fuel. The following sections give a summary of the contents of the **Canister production report** and in particular give a specification of the initial state.

In a KBS-3 repository, the function of the canister is to maintain containment. Containment is achieved by making and keeping the canister leak-tight. As long as the copper shell is not breached, the containment is maintained. In a KBS-3 repository, the canister shall maintain the containment and contribute to the main safety functions of the repository by:

- withstanding corrosion,
- withstanding mechanical loads,
- maintaining sub-criticality of the encapsulated spent nuclear fuel.

5.4.1 Technical design requirements relating to post-closure safety

To guide the design and production of the canister, technical design requirements on characteristics that can be inspected and verified in the production are stated in the **Canister production report**, with justification in Posiva and SKB (2017) and some additional clarifications in Chapter 3 of SKB (2021b). The technical design requirements are based on earlier assessments of the post-closure evolution of the canister in the repository and available technology and shall be fulfilled at initial state.

The copper shell, after sealing, shall give a completely tight canister. The thickness of the copper shell shall be sufficient to withstand corrosion processes that may occur in the final repository and keep the canister tight for as long as is necessary with regard to the repository's radiation safety. The following is stated in the **Canister production report**:

- The copper material shall be high purity copper. To avoid grain boundary corrosion the oxygen contents shall be ≤ 5 wt-ppm.
- At deposition the copper thickness shall be ≥ 40 mm. Local reductions to a thickness of 35 mm is acceptable for 10 % of the copper shell.
- The copper shell shall remain leak tight and the canister shall maintain its ability to resist loads for an isostatic pressure of 50 MPa.
- The copper shell shall remain tight and the canister shall maintain its ability to resist loads for 5 cm rock displacements at all angles and a rate of 1 m/s, exerted on the canister by a buffer with an unconfined compressive strength at failure lower than 4 MPa at a deformation rate of 0.8 %/min.
- The copper shell shall remain tight and the canister shall maintain its ability to resist loads for bending of the canister resulting from asymmetric loads according to Figure 5-7 and Figure 5-8:
 - Maximum swelling pressure from buffer $\sigma_1 = 10$ MPa.
 - Minimum swelling pressure from buffer $\sigma_2 = 3$ MPa.
 - Repository hydrostatic water pressure, 5 MPa, is added to σ_1 and σ_2 .
- To limit gamma radiation caused hardness and brittleness in the cast iron the Cu-content of the insert material shall be < 0.05 %.
- The quantity of nitric acid that can be formed in the insert shall be limited and therefore the atmosphere in the insert shall consist of > 90 % argon. The maximum permissible content of water in a sealed canister is 600 g. No organic materials in insert components are allowed.
- To maintain sub-criticality the material composition and the dimensions of the canister shall lie within the limits for the validity of the criticality analyses. The alterations of the canister materials in a breached canister, and their resulting corrosion products and substances acting to increase reactivity shall be predictable (see also Section 5.2.1).
- The radiation attenuation over the canister components shall, given the encapsulated spent fuel assemblies and their radiation emission rate, yield a dose rate at the canister surface < 1 Gray/h (see Section 5.2.1.)

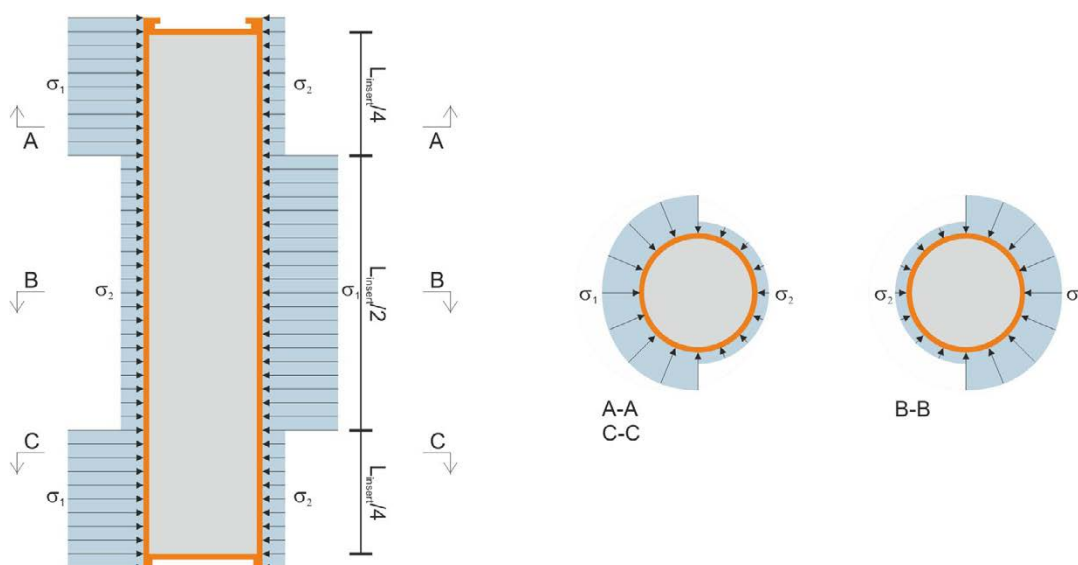


Figure 5-7. Bending of the canister, σ_1 is the maximum swelling pressure and σ_2 the minimum swelling pressure of the buffer; i.e. 10 and 3 MPa respectively. To σ_1 and σ_2 the hydrostatic pressure at repository depth, 5 MPa added.

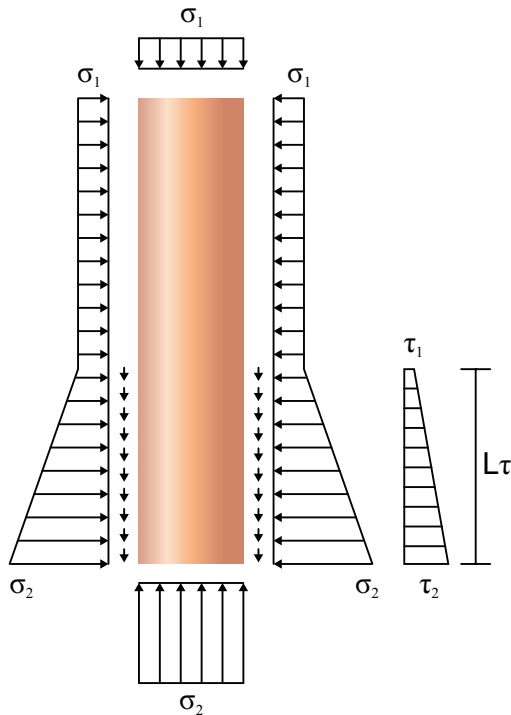


Figure 5-8. Shearing of the copper canister induced by a buffer swelling pressure between 10 MPa (σ_1) and 3 MPa (σ_2). The hydrostatic pressure at repository depth, 5 MPa, shall be added to σ_1 and σ_2 . The parameters τ_1 and τ_2 are the resulting shear stresses that act along the length L_τ of the surface of the canister.

5.4.2 Reference design and production procedures

The reference design shall conform to the technical design requirements and be demonstrated as technically feasible to produce by the methods for production and the methods applied for encapsulation, transportation and deposition. The reference design is given in detail in Chapter 3 of the **Canister production report** and the production and inspection procedures are described in Chapter 5 in the same report.

Reference design and verifying analyses

The reference design is described by a set of design parameters for which nominal values and acceptable variations are given. In short, the current reference design of the canister consists of a tight corrosion barrier of copper and a load-bearing insert of nodular cast iron. The sealed canister has a total length of 4 835 mm and a diameter of 1 050 mm, see Figure 5-9. The copper shell thicknesses with acceptable tolerance for the reference design are:

- Copper tube: $49^{+1.35}_{-0.85}$ mm
- Welds: 48.5 ± 0.7 mm
- Lid: 50 ± 1.0 mm
- Base: 50 ± 1.0 mm.

Two reference canister designs have been developed, one for 12 BWR fuel assemblies and one for 4 PWR fuel assemblies, Figure 5-9. The maximum total weight of the canister, including fuel, is 24 600 kg for BWR and 27 000 kg for PWR. Other types of fuel assemblies, see Section 5.3.2, for example swap MOX assemblies and fuel assemblies from Ågesta, can be accommodated in these canister designs.

The canister comprises the cast iron insert with a steel tube cassette with positions for each fuel element, the steel lid, the copper tube, the copper lid and the copper base, see Figure 5-10.

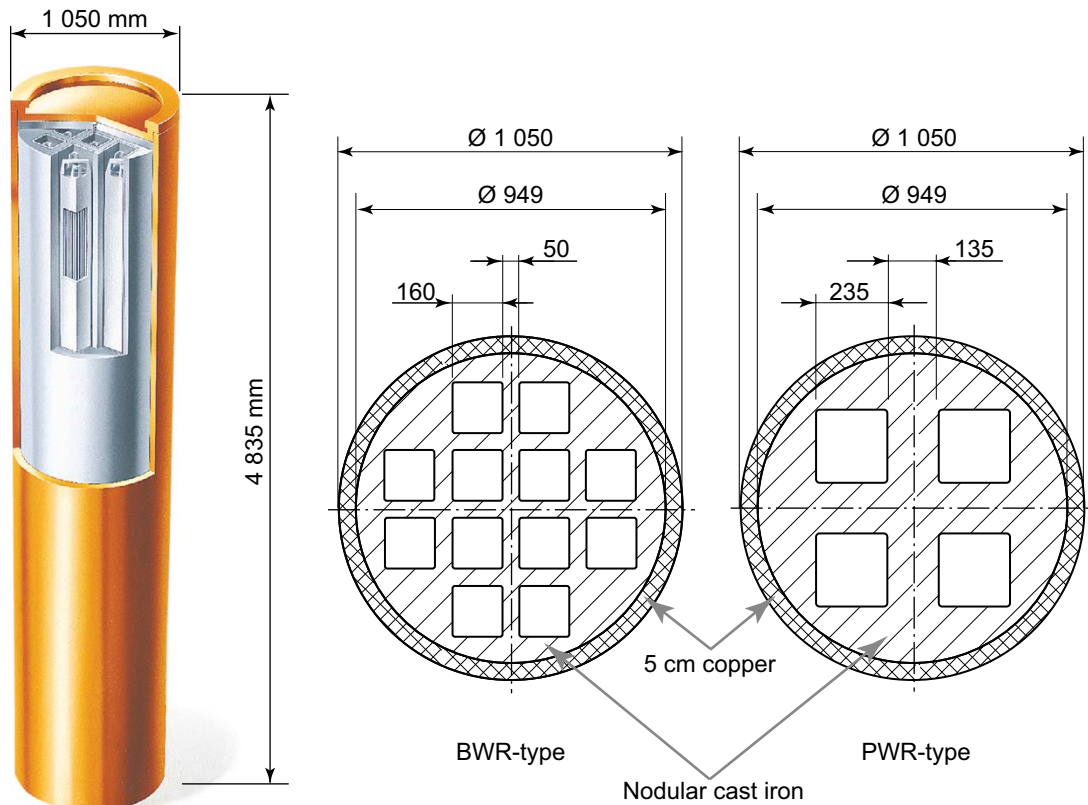


Figure 5-9. Left: The reference design with a corrosion resistant outer copper shell and a load-bearing insert of nodular cast iron. Right: Cross Section of insert designs of the BWR and PWR types.



Figure 5-10. Exploded view of the canister components (from left: copper base, copper tube, insert, steel lid for insert and copper lid).

In order to remain tight for a long time, the reference design of the canister has a copper shell that is almost 5 cm thick. To resist corrosion the shell shall be made of a high purity oxygen-free copper. The copper shell also needs to be ductile to remain tight despite the deformations that occur due to the mechanical loads in the repository. Phosphorus improves the copper ductility. Therefore phosphorus is added during casting of the ingot, see Table 5-8. In contrast, sulphur affects the copper ductility negatively and its content is limited in high purity copper. The strength and the ductility are affected by the average grain size of the copper and is therefore limited to $< 800 \mu\text{m}$ in the copper shell.

The density of copper decreases with defects and most of the impurities and shall be $8900 \pm 50 \text{ kg/m}^3$.

Table 5-8. Copper shell material composition.

Design parameter	Material composition	Justification
Copper (Cu)	$\geq 99.99 \text{ wt.}\%$	High purity oxygen-free copper to resist corrosion
Phosphorus (P)	30–100 wt-ppm	Added to obtain good creep ductility
Sulphur (S)	$< 12 \text{ wt-ppm}$	Limited to obtain good creep ductility
Hydrogen (H)	$< 0.6 \text{ wt-ppm}$	Limited to avoid embrittlement
Oxygen	$< 5 \text{ wt-ppm}$	Limited to avoid corrosion in grain boundaries

The verifying analyses discussed in Chapter 4 of the **Canister production report**, have been used to identify which of the canister properties are important for the different load cases and to specify values of the related design parameters for which the reference design conforms to the technical design requirements. For the isostatic load, these include the yield strength and the misalignment of the channel tubes. For the shear load important examples are elongation at rupture and the fracture toughness.

The deterministic collapse load for the cylindrical part of a canister (without defects) was calculated to 90 MPa and 109 MPa for BWR and PWR inserts, respectively (Jonsson et al. 2018).

In addition, for both the isostatic and the shear load cases, damage tolerance analyses are carried out on the reference design to assess sensitivity to damages in different parts of the insert and to establish acceptable sizes of defects in the materials. It must then be demonstrated that the production and inspection procedures yield canisters conforming to these specifications.

For the isostatic load, the deterministic analyses demonstrate that the insert is insensitive to large, postulated spherical damages in various positions outside the channel tubes and to substantial losses of material between the tubes. Also, the damage tolerance analyses show that defect sizes of 20 mm are acceptable in the outer part of the insert. Larger defects are acceptable in the interior part along the entire length since such defects do not grow in a way that jeopardises the integrity of the insert for an isostatic load of 50 MPa. There are no requirements on defect sizes for the bottom part of the insert.

For the shear load, the maximum accepted depth for crack-like surface defects in the circumferential direction is 9 mm for a semi-elliptical shape. The insert is less sensitive to internal defects, allowing much larger defects between the channel tubes. The analyses also show that the results are dependent on the buffer density. A lower buffer density means that larger defects can be accepted in the insert.

Production and inspection of the inserts and steel lid

The inserts are cast with 12 channels for BWR assemblies or 4 channels for PWR assemblies. Materials testing and geometric inspection is performed to determine the important properties identified in the verifying analyses. The eccentricity of the cassette in the insert is inspected by measuring the position of the cassette, in relation to the insert envelop surface (see Figure 5-9), at both the top and the bottom of the insert. Exterior machining and ultrasonic testing are performed in steps to inspect the inserts, followed by a final surface inspection.

As regards the eccentricity, the specified edge distance for BWR inserts is 33 ± 10 mm and for PWR inserts 37 ± 10 mm. Maximum measured misalignments in trial manufacturing are 8 mm. The misalignment under normal production is assumed to be ± 5 mm. The probability of exceeding the specified ± 10 mm is regarded as negligible based on the fact that the eccentricity of the cassette is inspected by ultrasonic testing after casting, and again after machining if the cassette was not centred.

The damage tolerance analysis of the shear load case results in the highest demands on the NDT capability for the insert. According to Section 5.6.4 of the **Canister production report**, there are good prospects of detecting crack like defects of required sizes according to the damage tolerance analyses with ultrasound for the surface of the insert and for the internal region outside the channel tubes, provided that the material is sufficiently homogeneous. The sensitivity of the ultra sound technique to pore clusters is limited and it has not been fully demonstrated that the requirements on finding such defects can be met. It also remains to be demonstrated how well defects can be detected between the channel tubes. It is, however, also noted that, according to the above, the function of the canister is insensitive to defects between the tubes.

The steel lids will be manufactured from steel plates and delivered with certificates that verify that the yield tensile strength conforms to the design parameter specifications.

Probabilistic analyses of the manufactured insert

As mentioned in Section 7.1.2 of the **Canister production report** development work remains in demonstrating that the stated manufacturing requirements can be achieved in an industrial production of canister inserts. To evaluate the properties of canisters emerging from trial production as documented

in the **Canister production report**, probabilistic analyses of the isostatic and shear load cases with material properties measured on manufactured canisters have been performed, as reported in Jonsson et al. (2018). The purpose was to assess the robustness of the canisters and to provide a base for the analysis of the two load cases in the safety assessment. These analyses have aimed at being as realistic as possible as regards input data and model assumptions. They are seen as the most adequate when characterising the initial state of the canister in the assessment of post-closure safety.

“As-manufactured” data for the analyses were taken from testing of the mechanical properties of specimens of manufactured inserts. Specimens were taken from various parts of the inserts, yielding a model of the insert differentiated with respect to key mechanical properties. The data show that the properties of the inner regions of the insert are less favourable than those of the outer parts. The deterioration of the inner parts is due to the flow pattern of the melt during casting and to chemical interactions, involving mainly carbon, between the nodular cast iron and the non-alloyed steel in the cassette. Also observed fractures and defects were included in the model. No filtering of the data to simulate the effects of non-destructive testing was done. Most of the data was taken from the BWR inserts I53–I57, a series for which the intention was to give an indication of what could be achieved in a serial production of canister inserts.

The results from the probabilistic analyses (Jonsson et al. 2018) of the robustness of the insert to carry isostatic load are summarised in Figure 5-11. The analyses are based on data from the BWR inserts trial production and the parameters yield strength, idealised crack-like defects, edge distance and outer channel tube radius were used as probabilistic parameters. The calculated probability of a global plastic collapse is $< 10^{-20}$ when the isostatic load is less than 75 MPa. The PWR insert has a higher capacity to carry an isostatic load than the BWR insert. The results show that the probability that manufactured inserts will not withstand the isostatic load of 50 MPa is negligible and independent of defect detection, i.e. without any assumptions on NDT procedures. The fracture frequencies and sizes (including pore clusters) derived for the probabilistic analyses from test specimens from manufactured inserts gives a completely negligible probability of fracture initiation for pressures far above 100 MPa. It is noted that, according to Section 2.4 in Dillström and Manngård (2017), data for the channel tubes with deteriorated properties after casting of the inserts were used; these data are further discussed in Section 4.6 of the Canister design analysis (Jonsson et al. 2018). It is also noted that long, axial fractures between the channel tubes have been discovered in some inserts after the probabilistic analyses were carried out. These are thus not included. The deterministic damage tolerance analyses have, however, shown that the insert’s isostatic collapse load is insensitive to substantial losses of material between the channel tubes. It, therefore, appears reasonable that fractures of such a size that they would significantly influence the outcome of the probabilistic modelling would be readily detected by NDT.

The results from the probabilistic analyses (Jonsson et al. 2018) of the robustness of the insert to carry shear load are summarised in Figure 5-12. The figure shows that the calculated probability of a canister failure as a result of a 5 cm rock shear displacement is at most around 2×10^{-3} . The corresponding probability for a 4 cm displacement is less than 10^{-5} . Again, no defect detection is assumed. The probabilistic modelling of the shear load case was carried out before the above mentioned data on deteriorated properties of the inner parts of the inserts were available. Therefore, the sensitivity of the probabilistic shear load results to deteriorated inner properties was assessed as part of Hernelind and Börgesson (2019), with the conclusion that these altered properties have a negligible impact on the canister’s ability to withstand shear loads.

Pressure tests of inserts

Two destructive pressure tests have been performed using two BWR canisters with insert lengths of 700 mm; the diameter was that of the current reference design. The tested inserts were covered by a copper tube and lids with a normal thickness. In a full length, 5 m, canister the lids are welded to the copper tube and the bottom part of the insert is homogeneous, which provides a stiffening effect at the ends of the canister. Since the mock-up is substantially shorter than a full size KBS-3 canister, the “end effects” would be larger if the same design were used at the ends of the mock-up. To alleviate such end-effects, the lids were attached to both ends of the insert by one large bolt and the lid to the copper tube by 16 smaller bolts (Nilsson et al. 2005).

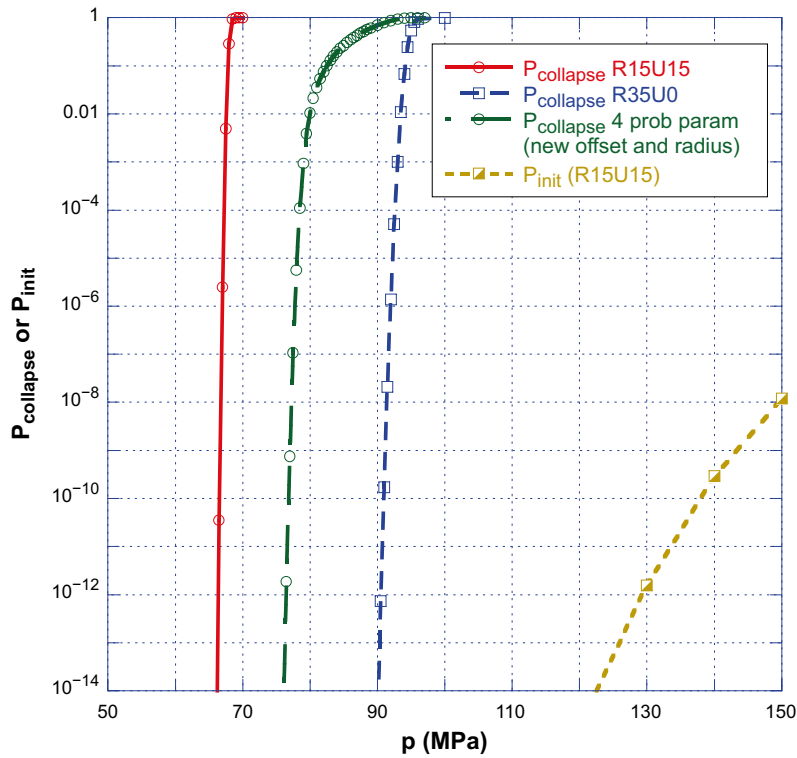


Figure 5-11. The probability of global plastic collapse (green, dashed curve) and the probability of the initiation of axial crack growth (light brown, dashed curve) as a function of the magnitude of the isostatic load (Jonsson et al. 2018). The effect of assuming that the outer channel tube radius and the edge distance is set to the least favourable values for safety (red curve) and to the most favourable values (blue, dashed curve) are also shown.

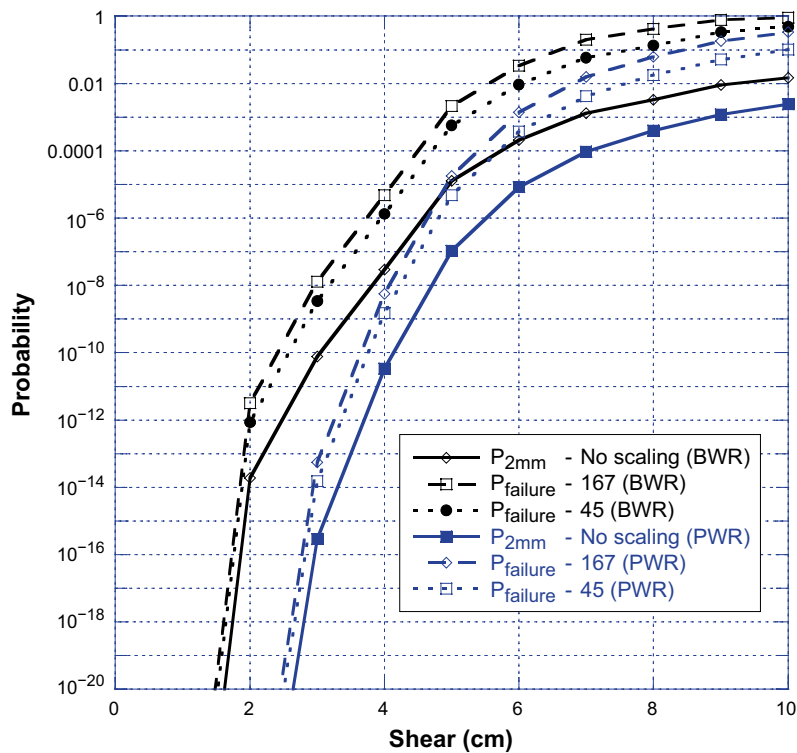


Figure 5-12. The probability of failure of an insert as a function of the size of the rock shear displacement. Sensitivity analysis using defect distributions from BWR or PWR inserts. The “no scaling” curves show results before scaling to defect frequencies relevant to an entire canister. The scaling has been done with two methods denoted “167” and “45”, respectively. See Chapter 8 of Dillström (2014) for details.

The first sample was a knowingly poorly cast sample, which contained large defects, and the machining was performed with a 12 mm offset (eccentric) so that the steel cassette was not placed centrally. The second sample was one of the best available samples at that time (2004–2005). The later developed BWR series (I53-I57) had better quality (Leskinen and Ronneteg 2013). The first sample was pressurised in a pressure chamber until reaching a large plastic deformation of 20 mm at an external pressure of 130 MPa, and the second sample was pressurised until reaching full plastic collapse and rupture at an external pressure of 139 MPa. The testing was documented and reported in Nilsson et al. (2005).

The pressure tests were simulated with various FE-analyses and were found to match. This showed that the collapse pressure of the canister was remarkably high and that the strength of the canister insert could be predicted and simulated using numerical methods with good accuracy and reliability.

The pressure tests and verification strength analyses are summarised in Dillström (2009) and Martin et al. (2009). The pressure test results show that the calculated collapse load results are pessimistic and thus verify the analysis models and reliability of the calculation methods for this type of analysis.

Production and inspection of the copper components

The copper tubes and lids are manufactured by hot forming; the tubes by extrusion and the lids by forging. An alternative hot forming process for the tubes is piercing and drawing. Possible hot forming defects are laps (Kopp et al. 1988) and the tubes are tested with eddy current testing for detection of such defects. After final machining the surfaces are inspected. The machining of the copper components is performed in two stages with intermediate non-destructive testing.

Machining is a well-known and proven industrial process. The dimensions, including the copper wall thickness, can be measured either by conventional laser tracker systems or by use of ultrasonics. In Section 5.5.4 in the **Canister production report** the resulting wall thicknesses for a number of manufactured copper components are presented. Based on these data, the minimum copper thickness after machining in normal operations is judged to be 48.1 mm for the tube, 48.9 for the base, 48.3 for the lid, including a 1 mm deep identity marking, and 47.5 mm for the welds. Therefore, the overall minimum thickness in normal operation is 47.5 mm, see Table 5-9.

Furthermore, it cannot be excluded that one percent of the canisters might have areas where the minimal copper thickness is reduced to 45 mm due to disturbed operation, Table 5-9. This value is based on the fact that deviations larger than this will be detected when the components are handled, assembled and the canister is sealed and these deviations will thereby lead to rejection of the canister. Experience indicates that such large deviations in dimensions will be detected during measuring. The probability that any canister will have a minimum thickness after machining of less than 45 mm is therefore judged as negligible.

To test the mechanical properties of the copper, samples will be taken from components before final machining and tested with conventional destructive methods.

Welding and inspection of the welding

The copper canisters will be sealed with solid state welding by friction stirring (FSW). The lids and the bases are welded onto the tube with the same method. The bases are welded before the canister components are dispatched to the encapsulation plant.

Control of a set of process parameters in connection to the welding ensures that it has been conducted within a so-called process window, which has been shown to result in welds according to specification. The welding process has relatively few process parameters, and it has been proved possible to both control and monitor them. The process is normally very stable with a high level of repeatability since the process is adaptive, i.e. the important tool temperature is measured constantly and the input parameters are adjusted in order to keep the temperature within a given range. An optimisation of the welding tool and regulation of the welding depth has reduced the occurrence of root defects (Cederqvist et al. 2018). The welding is done in an atmosphere of argon to reduce the occurrence of oxides in the welds.

The occurrences of defects in the welds have been investigated based on the results of welding demonstration series under normal operational conditions performed at the SKB Canister Laboratory. Normal operation during welding means that both input and output welding variables are within a defined “process window” that must be met in order for a weld to be considered approved. The only type of defect that has been detected in the welds made in normal operation is joint line hooking and incomplete penetration. The cavity type of defect (near-surface discontinuity) has only been seen outside normal operations for the weld.

Table 5-9. Minimum thicknesses of the copper shell after machining, i.e. a copper shell without defects is at least this thick over its entire surface. Defects can locally reduce the thickness. Further information is given in Sections 5.5.4, 5.7.3 and 7.1.1 of the Canister production report.

Design parameter Thickness (mm)	Reference design (mm)	Initial state value (all dimensions in mm)
– tube	49 ^{+1.35} _{-0.85}	Minimum > 47.5 Fraction of canisters > 99 %
– lid	50 ⁺¹ ₋₁	
– base	50 ⁺¹ ₋₁	
– welds	48.5 ^{+0.7} _{-0.7}	
		45–47.5* Fraction of canisters: 1 %
		Minimum < 45* Fraction of canisters: negligible
Local reduction in thickness due to defects (mm)	–	< 5 Fraction of canisters: > 97 % welds > 99 % tubes, lids, base
		5–10* Fraction of canisters: 3 %
		> 10* Fraction of canisters: negligible

* Values occurring only in disturbed operations considering both the manufacturing processes and inspection.

In the first demonstration series, the largest detected defects were of the order of a few millimetres with the largest one being 5.4 mm in radial direction. The second series was performed with an improved welding tool and resulted in smaller defects with the largest one being 1.5 mm.

The probability for disturbed operations resulting in one or more of the process variables are outside the process window is estimated to be low; 97 % of the welds are free from joint line hooking defects (Cederqvist et al. 2018). The results from probability-of-detection studies of the NDT methods show a 90 % detection capability for a 5 mm joint line hooking defect and a capability of almost 100 % for defects larger than 10 mm, see Table 5-9.

The probability that the process variables are such that they cause defects that exceed 5 mm and that this occurs simultaneously with a failure of the control system, is at the present stage of development judged to be less than 3 % of the canisters. This statement is based on the fact that the developed welding process is very reliable and reproducible. If these disturbed operations do occur, the maximum reduction of the copper thickness is estimated not to exceed 10 mm. See Table 5-9.

For the copper shell components (the base, the lid and the tube), there are few possible defects, forging laps being one example. Such defects can be avoided by proper manufacturing. Further, the defects can be detected by non-destructive testing (van den Bos 2018). Forging laps can be detected by eddy current testing. Since the possible defects in the copper components are expected to mainly extend parallel to the surface of the corrosion barrier and since no metallurgical defects have been found in the canister components, the welds are presently considered to be the potentially thinnest parts of the copper shell. The results of inspections of manufactured copper components indicate that there will remain no defects in the extruded tubes or forged lids and bases that remain after the final machining.

Reductions may also occur as a result of surface damage during transportation, handling and deposition of the canister. Available information on the occurrence of surface damage during these stages is limited since full-scale tests, which focus on this issue using relevant handling equipment and transport casks, remain to be performed. The probability for critical reduction of the corrosion barrier due to transportation damage is, however, considered negligible since the canister is protected by a transport cask. In addition, the canister is inspected for surface damage when it is lifted from the transport cask into the radiation shield of the deposition machine in the reloading station at repository depth.

The material composition is determined by the manufacturing of the copper ingots together with the subsequent hot-forming and welding processes. The copper quality used in the ingots is a high purity oxygen-free copper of a standard quality. The material composition in the welds is determined primarily from the basic material. The machining of the components and welds has no influence on the material composition.

Analyses of the copper ingot performed during the test manufacturing shows that the oxygen content in the ingots is well below the design requirement of maximum 5 ppm.

As previously mentioned, the copper canisters will be welded in an argon gas shield. Test of the welding in argon shield shows that the oxygen pick-up is negligible and that no oxygen inclusions are formed during welding. The highest measured oxygen content in the welds produced in argon gas was 2 wt-ppm and the mean oxygen content (with standard deviation) was 1.8 ± 0.4 wt-ppm (Björck et al. 2017, Cederqvist et al. 2018). By introduction of a tool coating, contaminants from the tool material have been reduced. The tool coating is chromium nitride (CrN) applied with PVD (physical vapour deposition). The levels of Ni, Co and Cr are all less than 1 wt-ppm to be compared to the mean levels when using non-coated tools (18 samples from 3 welds) of Ni, Co and Cr of 6.0 wt-ppm, 1.8 wt-ppm and 1.6 wt-ppm, respectively.

A corrosion study (Gubner and Andersson 2007) on the weld zones from welds made in air and with non-coated tools was performed and concluded that the FSW tool is cathodic compared to the copper – small particles in the weld are cathodic protected by surrounding copper, resulting in a very small cathode compared to the large copper anode. The good corrosion resistance of the FSW tool material will even further reduce the risk of corrosion of the surrounding weld material. Therefore, small metallic particles from the FSW tool do not pose a risk for accelerated corrosion of the welds. The study also concluded that a negative effect of copper oxides close to the surface could not be detected.

Encapsulation and inspection of encapsulated canisters

The encapsulation of spent nuclear fuel is performed in the planned encapsulation plant. The nuclear fuel assemblies are selected and dried before being placed in the canister. The insert steel lid is mounted and the atmosphere in the insert is replaced with argon. Thereafter the canister is sealed by welding of the copper lid. The welds are inspected before the canister leaves the encapsulation plant. The canister is placed in a transport cask and transported to the final repository, where it is transferred to a deposition machine and placed in the deposition hole.

5.4.3 Initial state

The initial state refers to the properties of the canisters once they have been deposited in the final repository and will not be further handled within the repository facility, see Section 5.1. The conclusions regarding results from trial production of canisters, in particular conclusions regarding conformity to the design requirements are derived in several steps in the **Canister production report**.

In a first step, the conformity of the reference design to the design requirements is evaluated through a number of analyses compiled in Jonsson et al. (2018) and summarised in Chapter 4 in the **Canister production report**. In a second step the capability of the canister production line to produce canisters that conform to the reference design is evaluated. The canister production line consists of the manufacturing of canisters, the encapsulation of spent fuel as well as the transportation and deposition of the canisters. These activities are summarised in Chapters 5 and 6 in the **Canister production report**, respectively.

Finally, conclusions from trial production and the conformity of the expected outcome of canisters to the reference design are evaluated in Chapters 7 of the **Canister production report**.

Isostatic load in the repository

The design requirement states that the canister copper shall remain leak tight and that the canister shall maintain its ability to resist an isostatic load of up to 50 MPa. The maximum isostatic load comprises the sum of maximum buffer swelling pressure, and maximum groundwater pressure in the repository under future glacial conditions.

It is stated in the **Canister production report** Section 4.2, that the robustness of the canister is high for an external overpressure, therefore the probability that the canister would not fulfil the design requirements related to isostatic loads is insignificant. The basis for this judgement can be summarised as follows.

- The deterministic collapse load for the cylindrical part of a canister (without defects) has been calculated to be 90 MPa and 109 MPa for BWR and PWR inserts, respectively (Jonsson et al. 2018). Results from pressure tests of real canisters show that the collapse load for the canister is 130 MPa (Nilsson et al. 2006).
- An analysis of the reference design of the canister where the variability of the material data (yield stress, ultimate strength and fracture toughness) was treated probabilistically shows that the likelihood for global plastic collapse or initiation of crack growth due to variation in material properties is insignificant. The calculated probability of global plastic collapse or initiation of crack growth is below 1×10^{-50} at an isostatic load of 50 MPa. The probabilistic analysis also shows very low calculated collapse probabilities (1×10^{-20}) for loads up to 75 MPa (Jonsson et al. 2018). No credit for non-destructive testing was taken in these analyses. The results of the probabilistic analysis are seen as the most adequate data when characterising the initial state of the canister as regards its resilience to isostatic loads in the assessment of post-closure safety.
- The prospects of achieving the specified requirement on limited misalignment of the insert are good, whereas development work remains as regards the NDT of defects. It is noted here *i*) that the probabilistic analysis does not take any credit for NDT and *ii*) that isostatic failure due to fracture initiation at defects is completely negligible for observed fracture frequencies and sizes.

Canister isostatic load resistance data for use in the PSAR are formally qualified in the **Data report**, based on the same sources as cited here.

Shear load in the repository

The canister shall also withstand shear loads that may occur when fractures intersecting the deposition hole experience secondary shear movement as a result of potential, large earthquakes in the vicinity of the repository. The design requirement states that the copper corrosion barrier should remain intact after a 5 cm rock shear movement at 1 m/s by a buffer with an unconfined compressive strength at failure lower than 4 MPa at a deformation rate of 0.8 %/min. This applies for all locations and angles of the shearing fracture in the deposition hole, and for temperatures down to 0 °C. The insert should maintain its pressure-bearing properties to isostatic loads after such shear movements.

Regarding the fulfilment of the design requirement for shear movements, the following is concluded.

- Strength calculations of the canister's resistance to shear load (Jonsson et al. 2018) verify that a canister with properties in conformity to the specification for the reference design withstands the design basis shear load.
- Probabilistic analysis of the shear load case yielded a calculated probability of a canister failure as a result of a 5 cm rock shear displacement is around 2×10^{-3} . No credit for non-destructive testing was taken in these analyses. It is also noted that a very small fraction of canisters was assessed to be exposed to this load in the post-closure safety assessment SR-Site (SKB 2011). The results of the probabilistic analysis are seen as the most adequate data when characterising the initial state of the canister as regards its resilience to shear loads in the assessment of post-closure safety.
- The results from inspections of manufactured canister components show that the specified values for fracture toughness and yield tensile strength in the manufactured series of inserts are obtained in the outer part of the insert where the stresses are highest, and elongation and creep ductility in the copper shells conform to the reference design (values given in the **Canister production report**).

- According to the damage tolerance analyses the maximum acceptable depths for surface defects in the circumferential direction is 9 mm for semi-elliptical shape (**Canister production report**). The insert is less sensitive to internal defects, allowing much larger defects. The analyses also show that the results are clearly dependent on the buffer density. A lower buffer density means that larger defects can be accepted in the insert.
- The damage tolerance analysis gives acceptable defect sizes that put rigorous requirements on manufacturing and NDT capability for the insert. Development work remains as regards the NDT of defects. It is noted i) that the probabilistic analysis does not take any credit for NDT and ii) that relatively large defects are acceptable between the channel tubes, i.e. in the volumes where it is more difficult to apply an efficient NDT.

Canister shear load resistance data for use in the PSAR are formally qualified in the **Data report**, based on the same sources as cited here.

Uneven pressure from bentonite buffer swelling

The canister may be subjected to asymmetric loads during different phases of the repository evolution. This could temporarily occur due to uneven water saturation in the buffer. Permanent asymmetric loads may occur due to uneven density distribution of the saturated buffer due to irregularities in the geometry of the deposition holes. The resulting bending stresses in the cast iron insert have been evaluated (Jonsson et al. 2018) and are lower than the yield strength.

An evaluation of the uneven swelling loads based on the FE simulation in Jonsson et al. (2018) was performed with respect to the damage tolerance of the insert. The crack sensitivity at the most stressed location on the insert surface was estimated for asymmetric loads representing the technical design requirements and the maximum acceptable radial crack size depth was equal to 21.1 mm compared with a 9.0 mm acceptable radial crack size depth in the rock shear case.

The uneven pressure from the buffer leads to small deformations in the copper casing due to the direction of the load and the load bearing support from the insert. The plastic elongation in the copper is estimated to be about 4 %, which is considerably less than the deformation caused by the shear load case.

In conclusion, the probability that the canister will not withstand the loads is deemed negligible based on Jonsson et al. (2018).

Corrosion load

A main function of the canister is to provide a corrosion barrier, and one parameter is the copper thickness, also considering the welds. The copper in the canister should be of high purity (> 99.99 % Cu) and to avoid corrosion coupled to grain boundaries the oxygen content shall be less than 5 wt-ppm.

According to the technical design requirements the copper thickness shall be ≥ 40 mm at deposition with acceptable local reductions to a thickness of 35 mm for 10 % of the copper shell. The copper thicknesses of the tube, welds, lid and base according to the reference design exceeds these values. The minimum acceptable thickness in the reference design is 48.1 mm for the tube, defects not considered. The reference design fulfils, through its specification, the requirement on maximum oxygen content in the copper shell.

The quality of the corrosion barrier is determined by the thickness and the material composition of the copper shell. The thickness of the copper shell of a deposited canister is determined by:

- The thickness according to the reference design.
- The efficiency of the manufacturing of the canister's components and welds.

The thickness can be reduced locally by deviations and defects due to:

- The occurrence of surface damage during transportation, handling in the facilities and at deposition.
- The occurrences of defects induced during hot-forming and welding processes.

Therefore, measurement, testing and inspection of the copper shell are necessary to ensure that the thickness of the copper shell conforms to the reference design and that the copper shell does not contain unacceptable defects.

The copper thickness for the initial state is thus determined by all possible causes of reduction of the corrosion barrier. Conclusions regarding this aspect of the initial state are based on experience from test production as described in the **Canister production report** and briefly discussed in Section 5.4.2.

The minimum copper thickness at the initial state is given in Table 5-9. This is the manufactured and inspected thickness of the corrosion barrier after the final machining of the canister components. The initial state thickness also takes the occurrence of local internal defects in the copper shell into consideration. The initial state data is input to the further assessment of corrosion processes in the PSAR.

Defects may also occur during handling and transportation of the canister that could possibly weaken the overall mechanical integrity of the canister and cause premature failure of the copper shell as reported in Jonsson et al. (2018). The maximum acceptable indentation depth is 5 mm. Several indentions are acceptable if they can be considered local, which means that the acceptable distance between them depends on their size. Indentions with a depth of less than 1 mm are always acceptable.

The oxygen content in the copper shell is well below 5 wt-ppm. The oxygen content in welds produced with argon gas shield does not differ from the base material and the welds have low or not measurable levels of oxide inclusions.

Storing the copper canisters for extended periods of time before disposal will have a negligible effect on their service life after disposal. The total corrosion attack even after two years' storage is expected to be less than 1 µm, see the **Fuel and canister process report**, Section 3.5.4.

Copper thickness data for use in the PSAR are formally qualified in the **Data report**, based on the same sources as quoted here.

Criticality

The canister shall prevent criticality and the analysis of the propensity for criticality of the encapsulated spent fuel assemblies are based on the reference canister design, see Section 5.3.4. The analysis has been carried out for the most pessimistic choice regarding tolerances for canister material compositions and geometric dimensions.

Reactivity increases e.g. when the assemblies are located close together towards the centre of the canister. The distance between the channel tubes of 30 mm for the BWR insert and 110 mm for the PWR insert is specified in the reference design. Hereby, the reference design conforms to the design requirements in criticality respect. The distance between the channel tubes measured in three manufactured PWR-inserts at three positions (top, middle and bottom) shows that the requirement is fulfilled.

Of the elements occurring in nodular iron, a high content of manganese (Mn) results in a lower reactivity. Therefore, the calculations have been performed at the lowest tolerance value in the material specification, i.e. 0.05 %. Both carbon (C) and silicon (Si) are more potent neutron reflectors than iron. The content of these substances shall be kept below 4 % (C) and 2.8 % (Si) according to the reference design. Analyses of the material composition of the nodular cast iron used for the five serial-manufactured BWR inserts and three PWR inserts show that the manganese content is > 0.12 % and the carbon and silicon contents are below 3.7 % (C) and 2.4 % (Si) respectively in the manufactured inserts.

Material composition and structure, and the environment within the sealed canister

The **Canister production report** shows that the specification of the reference design with regard to the material composition and structure, and to the environment within the sealed canister, will be fulfilled for the inspected canisters leaving the encapsulation plant. In summary:

- The maximum copper content of < 0.05 % of the insert is verified by conventional material analysis during production. This will guarantee the conformity to this requirement.
- The material composition of the copper shell regarding content of sulphur, phosphorus and hydrogen is verified by conventional material analysis during production. The destructive inspections during manufacturing and the subsequent ultrasonic inspection verify that the average grain size in the copper shell will be below 360 µm. This will guarantee the conformity to this requirement.

- The design of the system for drying the fuel and change of atmosphere in the insert in the encapsulation plant will guarantee that the maximum water content will conform to the design requirement.
- The temperature on the copper shell surface shall be < 100 °C with respect to long-term stability of the buffer in the repository. In addition, the material models used in the design and tolerance analysis are in general valid in the temperature interval 0–125 °C. The acceptable surface temperature has to be considered in the instructions for handling the canister in the facilities and during transportation as well as in the detailed design of the canister transport cask. As the temperature is a parameter that is relatively trivial to measure, the conformity to this design requirement can be verified.
- The highest obtained radiation dose rate on the canister surface as stated in SKB (2010g) is 0.18 Gy/h on limited areas of the canister. Since the decay power and the radiation are related to the radioactivity of the assemblies, it can be concluded that the radiation dose rate on the canister surface will be well below the acceptable 1.0 Gy/h as long as the fuel assemblies selected for encapsulation conform to the decay power criterion.
- Residual stresses induced in the material during manufacturing processes like casting, hot-deformation, welding or machining, are secondary stresses. They do not have any external driving force that would cause them to prevail after yielding or thermal stress relief treatment of the material. Measurements of residual stresses in inserts show that these have no practical influence on limit load or other higher loads that cause yielding, because the manufacturing-based residual stresses are expected to vanish when the material yields, see Section 7.4.2 in Jonsson et al. (2018). The significance of residual stresses in copper shells is primarily related to the possibility that stress corrosion cracking might appear for unforeseen reasons or that elastic deformation might take place. It can be concluded (Section 6.2.10 in Raiko et al. 2010) that the primary stresses are more important for analysing stress corrosion cracking than the secondary residual stresses.

5.5 Initial state of the buffer

The **Buffer production report** presents the technical design requirements, the reference design of a bentonite buffer, verifying analyses showing that the reference design fulfils the design requirements and the production and control procedures selected to achieve the reference design. The report also includes an account of the achieved results from test manufacturing and buffer installation. The following sections give a summary of the contents of the **Buffer production report** and a specification of the Initial state.

The main function of the buffer is to restrict water flow around the canisters. This is achieved by a low hydraulic conductivity, which makes diffusion the dominant transport mechanism, and a swelling pressure, which makes the buffer self-sealing. The buffer should also keep the canisters in position in the deposition holes, mitigate impact of rock shear movements and maintain its properties for the time scale of the assessment. The buffer should, furthermore, limit microbial activity in the buffer and on the canister surface and filter colloidal particles. The buffer should not significantly impair the functions of the other barriers.

The water saturation and swelling processes form part of the long-term evolution of the buffer; hence the result of these processes cannot be inspected at installation. Based on analyses of these processes, the ability of the buffer, as specified in the reference design, to provide the above functions can be evaluated.

5.5.1 Technical design requirements

To guide the design and production of the buffer, technical design requirements on characteristics that can be inspected and verified in the production are stated in the **Buffer production report** with justification in Posiva and SKB (2017) and with some additional clarifications in Chapter 4 of SKB (2021b). The technical design requirements are based on the assessment of the post-closure evolution of the buffer in the repository and available technology and shall be fulfilled at initial state.

- The following shall be *determined* for the selected buffer material:
 - the maximum dry density yielding a swelling pressure < 10 MPa when determined with a specified laboratory test procedure.
 - the minimum dry density yielding a swelling pressure > 3 MPa when determined with a specified laboratory test procedure.
 - the minimum dry density yielding a hydraulic conductivity in saturated state < 10^{-12} m/s when determined with a specified laboratory test procedure.
 - the maximum dry density yielding an unconfined compressive strength at failure < 4 MPa at a deformation rate of 0.8 %/min when determined with a specified laboratory test procedure, and for material specimens in contact with waters with less favourable characteristics than site-specific groundwater, i.e. deionised water and water with a salinity of 1 M CaCl₂ respectively to cover uncertainties with a margin.
- The buffer volume shall be cylindrical and determined from its cross sectional area in the deposition hole and its height, i.e. the sum of its thickness above and below the canister and the distance between the surface of the canister lid and bottom, minus the canister volume.
- The buffer thickness shall be
 - at least 50 cm below the canister,
 - at least 50 cm above the canister,
 - at least 30 cm around the canister.
- The installed buffer material mass shall in average in the buffer volume (Figure 5-10) result in
 - a dry density \geq the lowest required material-specific dry density determined for the specific buffer material,
 - a dry density \leq the highest allowed dry density determined for the specific buffer material.
- The installed dry density shall be > 1 000 kg/m³, to filter colloids.
- Acceptable contents of impurities:
 - Organic carbon should be less than 1 wt.%.
 - Sulphide should be less than 0.5 wt.% of the total mass, corresponding to approximately 1 wt.% of pyrite.
 - Total sulphur, including the sulphide, should be less than 1 wt.%.

Furthermore, the thermal conductivity over the installed buffer shall, given the allowed decay power in the canister, the thermal properties of the canister and the rock and the canister spacing, yield a buffer temperature < 100 °C.

5.5.2 Reference design and production procedures

Reference design

The reference design of the buffer is described by a set of *design parameters* for which nominal values and acceptable variations are given. The design parameters will be inspected in the production to confirm that the installed buffer conforms to the reference design and to provide an estimate of the actual properties of the buffer at the initial state.

The buffer material is a bentonite clay with a high content of smectites (swelling minerals), mostly montmorillonite, to uphold and maintain the required minimum swelling pressure, maximum hydraulic conductivity and allowed stiffness. In addition, the content of harmful accessory minerals has to be low. The properties of bentonite from different sources differ as is discussed in Svensson et al. (2017, 2019). The natural variation is handled in the design of the buffer (Luterkort et al. 2017) as some design parameters for buffer blocks and pellets need to be adapted to the specific bentonite, as described in Section 5.5.1. Therefore, no buffer material is specified in the reference design.

The reference geometry of the buffer in the deposition hole is shown in Figure 5-13.

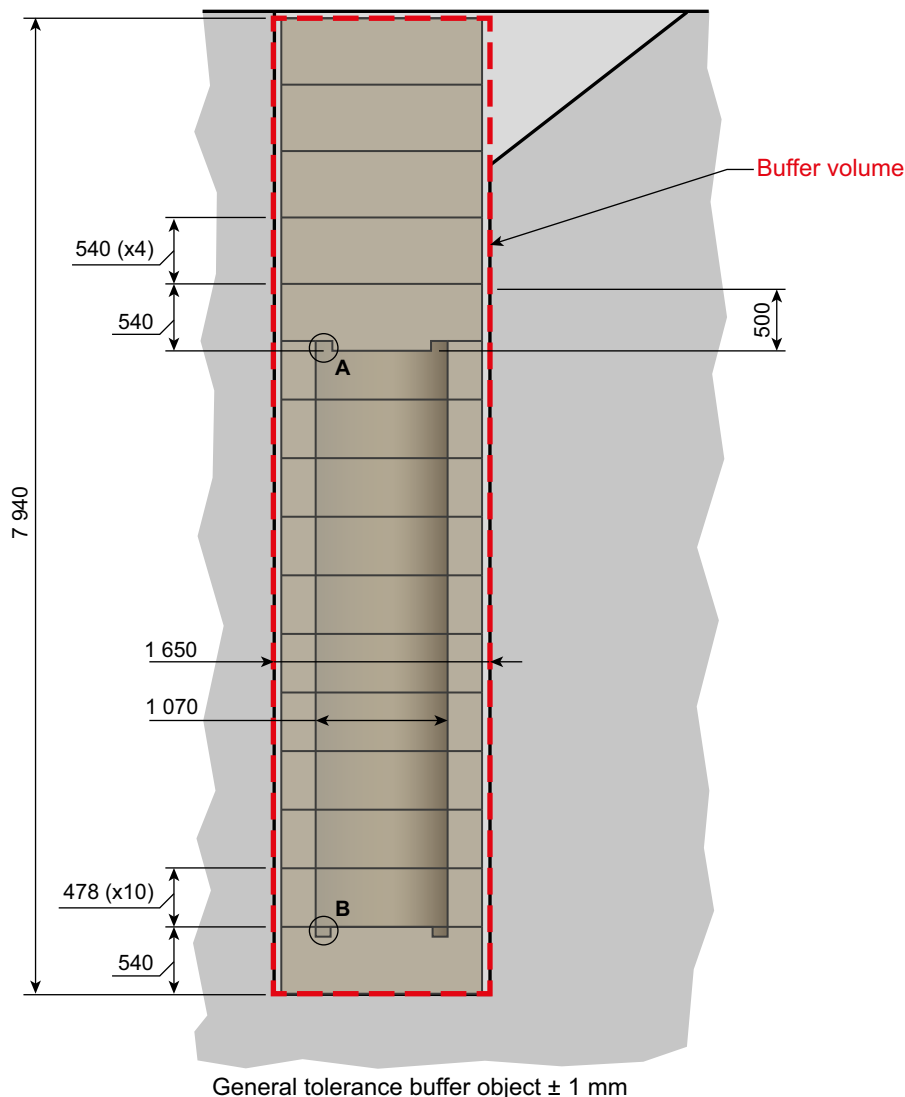


Figure 5-13. The geometrical configuration of the buffer in the deposition hole (Buffer production report).

The bentonite is installed in the deposition holes in compacted form (blocks and pellets). The reference design of the buffer consists of specifications of:

- The material ready for compaction.
- The fabricated blocks and pellets.
- The installed buffer.

MX-80, a bentonite from a large deposit that is mined by a large bentonite supplier can be seen as one relevant illustration of a possible bentonite to be used in the repository. For bentonite material that has been investigated by SKB it is the correlation between swelling pressure and dry density that determine the acceptable dry density range. Figure 5-14 shows the relation between swelling pressure and dry density for MX-80 exposed to extreme cases of groundwater composition, deionised water and 1M CaCl₂ solutions, respectively. The figure shows that the dry density of a buffer of MX-80 may vary between about 1 453–1 558 kg/m³ in order to fulfil the governing design requirement which states that the swelling pressure should be between 3 MPa and 10 MPa.

The reference designs of the blocks and pellets are presented in Table 5-10, respectively. The densities in the table are given as material specific dry densities for MX-80, whereas the bulk densities (installed mass) will be inspected in the production.

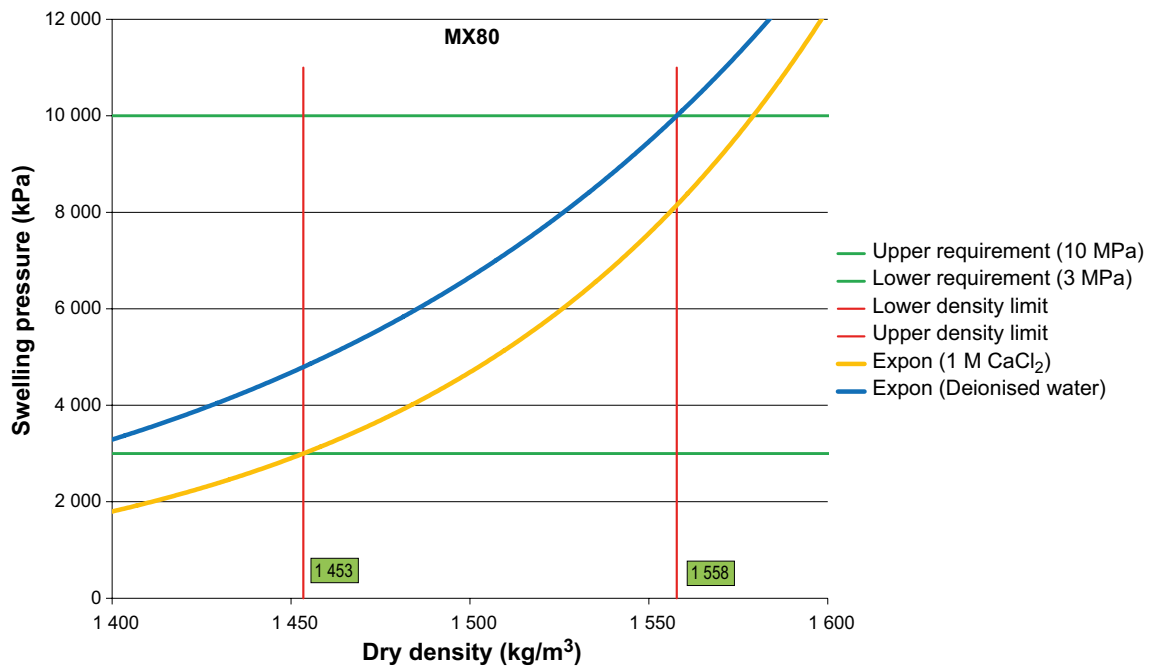


Figure 5-14. MX-80 swelling pressure vs dry density for deionized water and 1 M CaCl₂ solution. The green lines indicate the technical design requirement interval 3–10 MPa and the red lines show the acceptable dry density (1 453–1 558 kg/m³) that has been selected as the target for the reference design.

The density and homogeneity of compacted blocks and pellets will depend on the granule size distribution and water content of the material to be compacted and on the compaction pressure. To achieve high reliability in the production, the granule size distribution and water content must be specified for the selected material.

The buffer volume that needs to be designed to adapt to the specific bentonite to fulfil the design requirements consists of one solid bottom block, ten ring-shaped blocks around the canister and one solid block on top of the canister. Four more solid blocks are part of the buffer. The bevel is filled with backfill pellets, see Section 5.6.2. The centre line of the buffer blocks shall coincide with the centre line of the deposition hole. The gap between the blocks and the rock surface of the deposition hole is filled with bentonite pellets. The buffer thickness around the canister (i.e. the radial distance from the canister surface to the wall of the deposition hole) will, after saturation, depend on the diameter of the deposition hole and its variation along the hole and on the position of the ring-shaped blocks within it. The buffer thickness will also be affected by the position of the canister within the ring-shaped blocks and the diameter of the canister.

The canister lids and bottoms are not flat but contain hollows and edges, see Section 5.4.2. These volumes must be filled with bentonite. This is done by specially machined solid blocks.

The buffer takes up additional water after installation and will develop a swelling pressure at the end of the water saturation process. This will lead to an upward expansion of the buffer and a corresponding compaction of the overlying deposition tunnel backfill until an equilibrium is reached. The reference design, in particular the installed mass and installed dry density, has been determined with regard to this swelling process, so that the required swelling pressure, hydraulic conductivity and unconfined compressive strength is obtained also after swelling.

An upward swelling of the buffer is expected to occur due to buffer water uptake, resulting in a compression of the backfill. Expansion calculations show that the buffer reference design fulfils the design requirements also after 175 mm upheave, see the **Buffer production report**. As the expansion process is part of the long-term evolution, it is further accounted for in Section 10.3.9 of the present report.

After installation of blocks and pellets of MX 80 in a deposition hole with dimensions as specified in Figure 5-13 and densities as specified in Table 5-10, the calculated nominal average dry density is 1 547 kg/m³.

The reference method for drilling deposition holes will not accomplish a completely flat bottom in the deposition holes. In order to limit the water uptake in the bottom block during installation, a plate of copper is installed. In the reference design the bottom plate consists of a thin copper plate that covers the bottom and the lower part of the mantle surface of the bottom bentonite block, see Figure 5-15. The bottom plate is attached to the bottom bentonite block prior to installation. The purpose of the bottom plate is to limit the water uptake in the bottom block during the installation of the buffer.

Table 5-10. Reference buffer blocks and pellets. The parameters where the material is specified are material-specific, the others are independent of material.

Design parameter	Nominal design	Accepted variation
Solid blocks		
Bulk density MX-80 (kg/m ³)	1 930	±20
Dry density (kg/m ³)	1 650	
Water content MX 80 (wt.%)	17 <i>As in the material ready for compaction.</i>	± 1 <i>As in the material ready for compaction.</i>
Dimensions (mm)	Height: 540 Outer diameter: 1 650	± 1
Ring-shaped blocks		
Bulk density MX-80 (kg/m ³)	1 995	±20
Dry density (kg/m ³)	1 675	
Water content MX-80 (wt.%)	17 <i>(As in the material ready for compaction.)</i>	± 1 <i>(As in the material ready for compaction.)</i>
Dimensions (mm)	Height: 478 Outer diameter: 1 650 Inner diameter: 1 070	± 1
Pellets		
Dimensions (mm)	16 × 16 × 8	
Bulk density loose filling MX-80 (kg/m ³)	1 000	±40
Water content MX-80 (wt.%)	15 <i>(As in the material ready for compaction.)</i>	± 1 <i>(As in the material ready for compaction.)</i>
Installed buffer		
Dry density, buffer volume with design adapted to specific bentonite	1 550	1 540–1 554
Dry density, buffer surrounding the canister MX-80 (kg/m ³)	1 510	1 501–1 517
Dry density, buffer above and below canister MX-80 (kg/m ³)	1 580	1 576–1 592

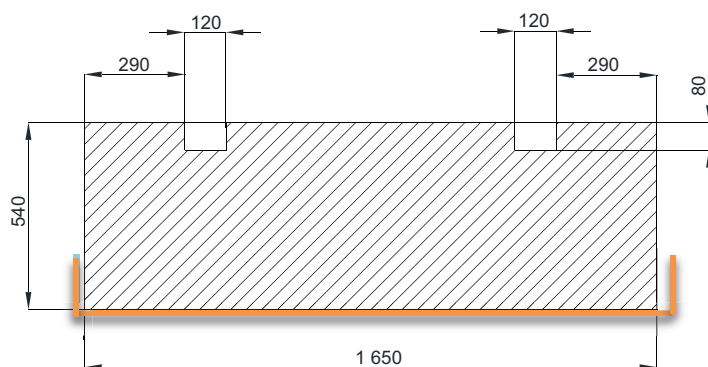


Figure 5-15. The bottom plate of copper in the deposition hole.

Production and installation

The production line for the buffer consists of four main parts:

- Purchase, excavation and delivery.
- Quality control at delivery.
- Manufacturing of blocks and pellets.
- Handling and installation.

Details about the production can be found in the **Buffer production report**.

Bentonite deposits exist at many places around the world and excavation and delivery can be made by alternative companies. The desired material properties will be specified at ordering. Each shipment of bentonite will be accompanied by a protocol from the supplier that describes the actual composition of the delivered material.

The delivered material is inspected as a basis for the acceptance of the delivery. Inspections for the production comprise content of impurities, water content and granule size distribution of the delivered material and measurement of its total weight. Material specific design parameters of importance for the functions of the buffer are the relationships between dry density and hydraulic conductivity, swelling pressure and compressive strength, respectively. These relationships are determined with specific procedures, see the **Buffer production report**.

Before compaction, the bentonite is crushed and dried and the granule size distribution and water content is adjusted. The reference method for pressing of blocks is uniaxial compaction. The pressure applied determines the block density and has to be adapted to the specific bentonite material. The compacted blocks are machined to specified dimensions in order to achieve a well-aligned stack of blocks in the deposition hole and the required installed dry density. The weight and dimensions (height, inner and outer diameter) of each block are inspected to check that the density is within the specified range. The reference method to manufacture pellets is to compact the conditioned material to small briquettes. The water content, granule size distribution and setting of press parameters for different materials are based on tests performed during material characterization.

Over 300 blocks and rings have been manufactured for use in SKB's full-scale experiments since the late 1990's. Full-scale manufacturing and laboratory tests show that the pressing of block is a robust process. The dry density, in 22 manufactured blocks after machining, had a standard deviation of 9.2 kg/m^3 (Johannesson 2014). These blocks were furthermore manufactured at several occasions and since it takes a couple of blocks to adjust the press parameters it is expected that the standard deviation will be considerably lower during series production.

Based on the manufacturing of components for the Prototype repository and the geometries obtained for the deposition holes in the Prototype repository the calculated average dry density was 1597 kg/m^3 in the buffer around the canister and 1633 kg/m^3 in the buffer below and above the canister. A standard deviation of 6 kg/m^3 in installed dry density is obtained. It is reasonable to assume that the corresponding variation or lower installed density can be achieved in a proven industrial production and installation in a repository at Forsmark.

The installation of the buffer is based on the fact that deposition holes, according to specifications, are provided from the underground opening production line. The excavation and inspection of deposition holes is described in the **Underground openings construction report**.

The installation of buffer starts with the lower base block. Then the annular blocks are installed and it is checked that the blocks are placed horizontally and in the correct position. The copper canister is thereafter deposited. Finally the buffer blocks on top of the canister and pellets in the slot between the blocks and the rock are emplaced.

The thickness of the saturated buffer around the canister is determined by the dimensions of the deposition hole, the position of the installed ring-shaped blocks, the position of the canister in the buffer, and the diameter of the canister. The bottom block is installed and centred with respect to the geometry of the deposition hole. Thereafter the ring shaped blocks are installed on top of each other and the position of the rings are measured to inspect that they are placed horizontally and with a straight and centred hole for deposition of the canister in the middle and a distance of at least 25 mm from the deposition hole walls.

The canister can then be deposited as described in the **Canister production report**.

When the canister has been deposited the four top buffer blocks are installed as well as the buffer pellets. The installed average bulk density is determined based on the total installed buffer mass and the volumes of the deposition hole and the canister. Finally, the top buffer block is installed, which has an appropriate height for the specific deposition hole. The gap around the top block and bevel is filled with backfill pellets. Pellets are filled into the gap by placing a conical hood on top of the last installed bentonite block and pouring the pellets into the deposition hole.

The backfill in the deposition tunnel prevent swelling and expansion (up-lift) of the buffer and the buffer installation sequence needs to be adapted to the inflow of groundwater to the deposition holes. Therefore, buffer and canisters are first installed in relatively dry deposition holes in a deposition tunnel, i.e. where the heaving of the buffer is slow. Deposition holes that are not approved for disposal of canisters are in parallel backfilled with solid buffer blocks and buffer pellets. The deposition holes where the water inflow is approved, but relatively large, are left empty. The installation of buffer and canisters in these deposition holes are done in connection with the installation of the backfill in the deposition tunnel.

Installing the blocks in a deposition hole with an average diameter of $1\,750 \pm 5$ mm results in the calculated installed density presented in Table 5-10.

The positions for installed buffer blocks and deposited canisters have not been registered in SKB's full scale tests. On the basis of measurements made on drilled deposition holes, the standard deviation of the diameter of the holes has been estimated at 2.02 mm on average (Birgersson and Johannesson 2006). Assuming nominal values for the diameter of the deposition holes (1 750 mm) and the diameter of the canister (1 050 mm) and that both the buffer block and the canister can be placed centrally in the deposition holes, a 95 % confidence interval for the average thickness of the saturated buffer can be estimated at 350 ± 2 mm. The thickness of the buffer under and above the canister depends on the variation in height of the installed, solid buffer blocks.

Two full-scale installation tests have been performed to study the buffer heaving that may occur before the backfill in the deposition tunnel has been installed (Luterkort et al. 2017). The evaluation of the test shows that the installation is robust for water inflows less or equal to the inflow into the test hole (8×10^{-4} l/min). The technique to fill the outer gap with pellets has been used in several large scale tests at Äspö HRL with good results.

The techniques for loading, transportation and storage of the buffer blocks and pellets are well known from similar industrial applications. SKB has such experience from the Äspö HRL. Blocks have been stored placed on pallets with an air tight hood for several months without showing any changes in weight or water content.

5.5.3 Initial state

The initial state of the buffer is the state when the auxiliary equipment used during installation is removed and all buffer components are installed in the deposition hole. Inflow of groundwater to the deposition hole and its impact on the buffer is not accounted for in the initial state.

The properties of the buffer to be designed to conform to the design requirements for post-closure safety are:

- Material composition.
- Installed dry density.
- Buffer geometry.

These properties are to some extent interdependent. The design density, for example, is based on a selected material. In the **Buffer, backfill and closure process report**, the buffer is characterised by a number of variables. Most of the initial state values for these variables are determined by the design properties. This is illustrated in Table 5-11.

Table 5-11. Relation between the designed buffer properties and the variables used in the safety assessment. References to where, or how, initial state values of the variables not related designed buffer properties can be found or derived are also given.

Variable	Buffer property	Initial state values
Water content	Material composition	
Gas content		
Bentonite composition		
Montmorillonite composition		
Porewater composition		
Hydrovariables (pressure and flows)	Material composition	
Stress state	Installed density	
Pore geometry	Installed density	
Buffer geometry	Installed dimensions and geometrical configuration	
Radiation intensity	–	
Temperature	–	Calculated
Structural and stray materials	–	Bottom plate (see Figure 5-15) and material and dimensions according to the reference design Underground openings construction report , Section 3.2.

Material composition

Maximum inventories of certain impurities are specified among the design requirements (see Section 5.5.1). Regarding these requirements, it is concluded that the specified limitations on organic carbon, sulphide and sulphur are fulfilled at the initial state. This conclusion is based on the presented analyses of the compositions of MX-80 which is used as an example material and of the handling and inspection procedures outlined in the description of the production of the buffer.

To evaluate the long term performance of the buffer, a more detailed characterization of the material is needed. Important parameters in the description of the materials are:

- Chemical composition.
- Mineralogical composition.
- Grain density.
- Specific surface area.
- Grain size distribution.
- Water content.

In addition to this the clay fraction of the material is characterized by:

- Structural formula including:
 - Layer charge.
 - Charge distribution.
- Cation exchange capacity.
- Original exchangeable cations.
- Charge distribution.

These parameters are further described in the **Buffer, backfill and closure process report** and are defined as the Bentonite composition and the Montmorillonite composition variables.

In natural bentonite, the charge compensating cations are usually a mixture of mono- and divalent ions. The swelling properties are to a large extent dependant on the magnitude and the position of the layer charge, but also on the type of charge compensating cation. The dominating cation is therefore often used to describe the type of bentonite, e.g. sodium bentonite, although the content of other ions may be quite large. High-quality commercial bentonites normally contain over 80 % of montmorillonite, which is expected to give various bentonite products similar sealing properties. However, the other minerals in bentonite may vary substantially within, and especially between, different quarries. Typical accessory minerals are other clays, feldspars, quartz, cristobalite, gypsum, calcite and pyrite. There are quantitative limits for sulphide, total sulphur and organic carbon, see Section 5.5.1. The mineralogical composition of the material (MX-80) used for the PSAR is presented in Table 5-12.

For the purpose of the calculation of radiation shielding as well as the check on the maximum contents of sulphur and organic carbon it is important to determine the total chemical composition of the bentonite. The mean chemical composition of the bulk material from Table 5-13 expressed as oxides is shown in Table 5-12 for MX-80. The initial conditions of other parameters for bentonite and montmorillonite composition, together with their relevance for the post closure performance, are discussed in Svensson et al. (2017, 2019).

Table 5-12. Mineralogy in Wyoming MX-80 batches as determined by XRD/Siroquant. SD(n), n = number of measurements used for calculation of standard deviation (Svensson et al. 2017, 2019).

MX-80 batch	Mineralogy (%)									
	Montmorillonite	Quartz	Anorthite	Cristobalite	Calcite	Albite	Pyrite	Mica/illite	Gypsum	Tridymite
MX80 2015	85.43	4.18	0.00	1.15	0.43	2.03	0.35	4.63	0.85	0.95
SD(4):	0.73	0.38	0.00	0.10	0.10	0.26	0.06	1.52	0.40	0.06
MX80 2012	86.15	4.56	0.37	0.35	0.23	1.41	0.33	5.27	0.49	0.83
SD(10):	1.83	0.81	0.99	0.05	0.14	0.47	0.00	0.74	0.08	0.08
MX80 2006	83.9	2.7	0	2.1	0.2	3.3	0.2	6	0.5	1.1
MX80 2002	83.90	4.23	0.77	1.37	0.17	1.47	0.30	5.73	0.87	1.13
SD(3):	0.85	0.15	0.83	0.12	0.21	0.42	0.00	0.40	0.12	0.06
MX80 1993	82.83	3.13	0.57	1.97	0.17	3.27	0.13	5.70	0.87	1.30
SD(3):	0.83	0.25	0.60	0.12	0.12	0.65	0.06	0.56	0.06	0.00

Table 5-13. Overview of the chemical content in the bentonite batches (Svensson et al. 2017).

MX-80 batch	Chemical composition expressed as oxides (%)											
	Na ₂ O	MgO	Al ₂ O ₃	SiO ₂	Fe ₂ O ₃	P ₂ O ₅	SO ₃	Cl	K ₂ O	CaO	TiO ₂	MnO
MX80 2015	1.87	2.44	22.28	66.09	4.39	0.00	0.58	0.01	0.59	1.54	0.19	0.01
MX80 2012	1.91	2.59	22.42	64.44	4.95	0.02	0.81	0.01	0.72	1.86	0.25	0.02
MX80 2006	1.67	2.52	21.55	66.71	4.35	0.01	0.83	0.01	0.55	1.60	0.18	0.01
MX80 2002	1.56	2.45	21.87	66.64	4.75	0.00	0.46	0.00	0.46	1.66	0.14	0.01
MX80 1993	1.69	2.33	21.32	67.21	4.93	0.01	0.41	0.01	0.52	1.39	0.16	0.01

Water content, gas content and porewater composition

There are no specific design requirements with regard to gas content and porewater composition, but these properties need to be known for the subsequent analysis. In the reference design with MX-80, the initial water content in blocks is selected to be 17 % and 15 % in pellets. Water content is determined by a standard geotechnical method. The original water content in the buffer material is adjusted to facilitate the manufacturing process. All porosity not filled with water contains air. The initial porewater composition may be calculated but not directly measured. The calculated content of installed mass and volume of water and air in a deposition hole is presented in Table 5-14.

Table 5-14 Buffer Volume-canister +bevel, installed total mass and volume of buffer material, water and air in a deposition hole + bevel, assuming nominal blocks and pellets and nominal dimensions of the deposition hole.

	Mass (ton)	Volume (m ³)
Full dep hole + Bevel – canister		17.21
Solid Buffer vol + top 4 + bevel	25.37	9.09
Water Buffer vol + top 4 + bevel	4.31	4.31
Air Buffer vol + top 4 + bevel	~0	3.81
Total	29.69	17.21

Installed dry density

The initial state represents the installed buffer blocks and pellets with dry densities given by the manufacturing process. The parameters in the initial state should produce a saturated buffer that lies within the required swelling pressure, hydraulic conductivity and compressive strength after saturation for every cross-section that mechanically can affect the canister in the deposition hole, neglecting the effects of incomplete homogenization.

The average installed buffer dry density will depend on the density and dimensions of the installed blocks and pellets, i.e. the installed buffer mass, and the volumes of the deposition hole and canister. The impact of the variations of volume of the canister and dimensions of the blocks on the installed buffer density can be neglected. The important parameters are the installed density of the blocks and pellets and the volume of the deposition hole.

A simulation of the adapted buffer reference design (MX-80) including 10 000 deposition holes and nominal data with tolerances on blocks, pellets and deposition holes has been performed. The process is iterated aiming at an average swelling pressure of 10 MPa in the buffer volume. The results are presented in Table 5-15 and Table 5-16. The swelling pressure is within the acceptance interval (3–10 MPa) in the ring section around the canister. The swelling pressure in the block section above the canister will be higher, which is acceptable.

Table 5-15. Results of simulation of variation between deposition holes of average key buffer properties within a hole. Resulting dry densities with standard deviation and 95 % confidence. Corresponding minimum (1M CaCl₂ solutions) and maximum (deionised water) swelling pressures are given.

Without heave	Dry density (kg/m ³)	Std dev	Dry density min (kg/m ³)	Dry density max (kg/m ³)	Swelling pressure min, CaCl ₂ (kPa)	Swelling pressure max, Deion (kPa)
Average deposition hole	1547.1	3.3	1540.5	1553.6	6906	9711
Block section	1584.0	3.7	1576.8	1591.3	9772	12664
Ring section	1509.3	4.0	1501.6	1517.0	4756	7504

Table 5-16. Additional data.

Parameter	Value
Dry mass, pellets	2.12 tonnes
Dry mass, blocks	21.1 tonnes
Water ratio, pellets	0.15
Water ratio, blocks	0.17

In the **Buffer production report** it is concluded that the methods for producing the buffer will yield installed average densities that fulfil the specification of the reference design.

Geometry

The thickness of the saturated buffer around the canister is determined by the dimensions of the deposition hole, the position of the installed ring-shaped blocks, the position of the canister in the buffer, and the diameter of the canister. The impact of the variation in canister placement and canister diameter on the buffer thickness can be neglected. The actual deposition hole diameter will deviate from the nominal. Analysis of measurements of diameters from the Prototype Repository (see Section 5.5.2) shows that the standard deviation of the average diameter of the deposition hole is 2.02 mm. Assuming a nominal value of the deposition hole diameter of 1750 mm and a nominal diameter of canister of 1050 mm, and that both buffer blocks and canisters can be centrally placed in the deposition holes results in a 95 % confidence interval for the average buffer thickness (after saturation) of 350 ± 2 mm.

The thickness of the buffer below and above the canister depends only on the variation in height of the installed, solid buffer blocks.

5.6 Initial state of the deposition tunnel backfill

The **Backfill production report** presents the technical design requirements, the reference design, verifying analyses that the reference design does fulfil the design requirements, the production and control procedures selected to achieve the reference design, verifying analyses that these procedures do achieve the reference design and an account of the achieved initial state of the deposition tunnel backfill. The following sections give a summary of the contents of the **Backfill production report** and in particular of the Initial state.

The deposition tunnel backfill is the material installed in deposition tunnels to fill them. The purpose and function of the backfill in deposition tunnels is to keep the buffer in place and to restrict groundwater flow through the deposition tunnels. Further, the backfill shall not significantly impair the other barriers and it shall maintain its barrier function during long times. In the PSAR, the main tunnels and the transportation tunnels at the repository level as well the ramp and shaft up to the level of -370 m are at this stage assumed to be filled with bentonite.

The water saturation and swelling processes form part of the long-term evolution of the backfill and cannot be inspected at the initial state. Based on analyses of these processes, the ability of the backfill, as specified in the reference design, to provide the above functions can be evaluated.

5.6.1 Technical design requirements

To guide the design and production of the deposition tunnel backfill, technical design requirements on characteristics that can be inspected and verified in the production are stated in the **Backfill production report** with justification in Posiva and SKB (2017) and with some additional clarifications in Chapter 5 of SKB (2021b). The technical design requirements are based on the assessment of the post-closure evolution of the backfill in the repository and available technology and shall be fulfilled at initial state.

- The following shall be determined for the specific backfill material:
 - the minimum dry density yielding a hydraulic conductivity $< 10^{-10}$ m/s determined according to a specified test procedure.
 - the minimum dry density yielding a swelling pressure > 1 MPa determined according to a specified test procedure.
- The installed backfill material mass shall in average in the tunnel volume between two deposition holes result in a dry density \geq the lowest required material-specific dry density determined for the backfill material.
- The overall deformation of the installed backfill both in dry and saturated state shall resist the swelling pressure from the buffer and maintain the buffer swelling pressure > 3 MPa on average over the buffer volume

Furthermore, the **Backfill production report** also states the general requirement that the backfill should not significantly impair the barrier functions of the buffer or canister, therefore:

- The backfill material shall not contain substances that constitute a significant source of sulphide that can corrode the canister.

Except for the design requirement related to the backfill's long-term functions there are currently no design requirements set for the backfill by the other barriers.

5.6.2 Reference design and production procedures

Reference design

The reference design of the backfill is described by a set of *design parameters* for which nominal values and acceptable variations are given. The design parameters will be inspected in the production to confirm that the installed backfill conforms to the reference design and to provide an estimate of the actual properties of the backfill at the initial state.

The backfill material is a bentonite clay and the potential to meet the design requirements on hydraulic conductivity and swelling pressure depends to a large extent on the montmorillonite content.

The backfill is installed as blocks and pellets, pellets as a bottom bed, blocks stacked in the tunnel and the additional space between the stack and the rock is filled with pellets. The reference backfill geometry is presented in Figure 5-16.

A bentonite from Ashapura Minechem Ltd. delivered to SKB 2012, named Asha 2012 is used as an example of a backfill material (Fritzell 2017). In addition, some information from a 2010 delivery called Asha 2010 is used.

SKB's strategy is to have the opportunity to use several different types of bentonite from different suppliers. The reference design of the backfill is therefore not based on a specific bentonite material. A process to adapt the reference design and the production to different materials has been developed. It is the correlation between swelling pressure and dry density that determine the acceptable dry density range, see the **Backfill production report**. Figure 5-17 shows the relation between swelling pressure and dry density for Asha 2012 exposed to extreme cases of groundwater composition, deionised water and 1M CaCl₂ solutions, respectively. The figure shows that the dry density of a backfill of Asha 2012 shall be > 1360 kg/m³ to fulfil the governing design requirement which states that the swelling pressure should be > 1 MPa.

The hydraulic conductivity and swelling pressure of the reference backfill material, at the installed density, will thus conform to the design requirements, and there will be a margin for density losses.

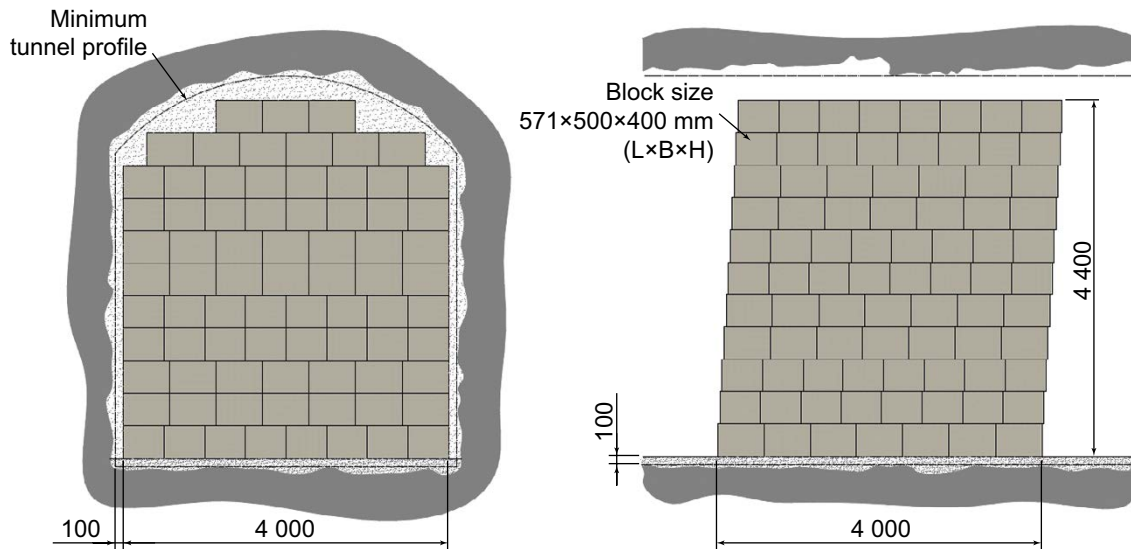


Figure 5-16. Reference geometry of the installed backfill in a tunnel showing vertical cross sections perpendicular (left) and along (right) the tunnel.

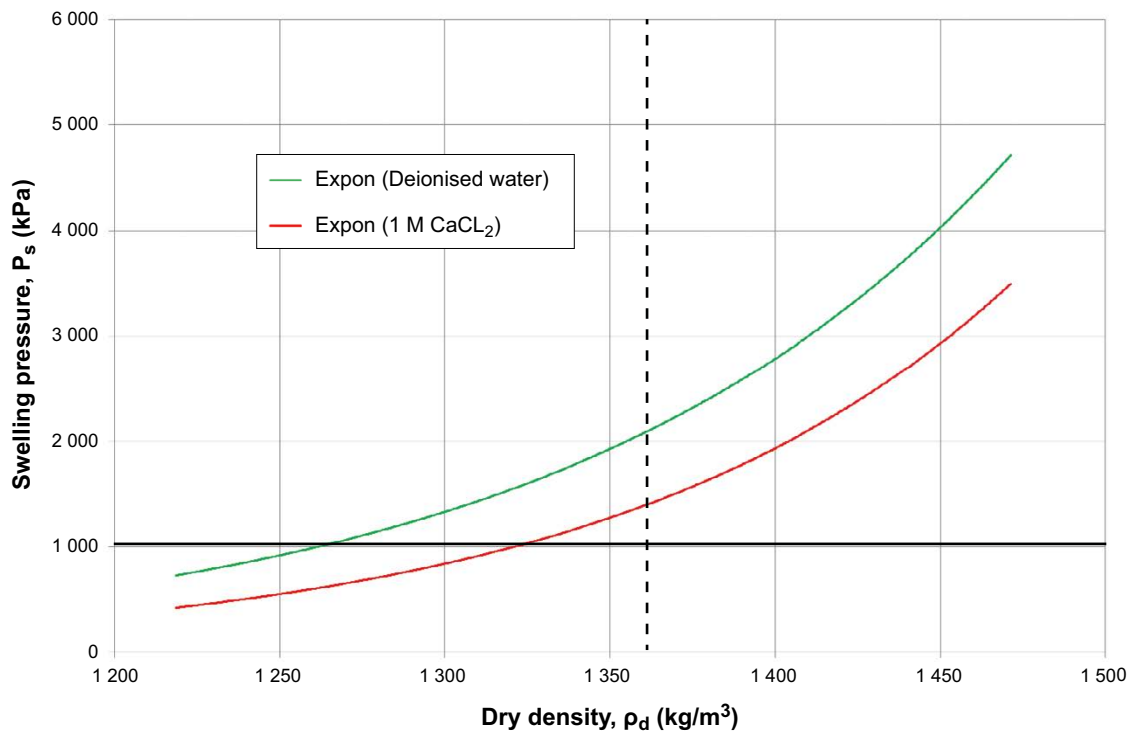


Figure 5-17. Asha 2012 swelling pressure vs dry density for deionized water and 1 mol CaCl₂ solution. The solid black line indicates the Technical Design Requirement of 1 MPa and the dotted black line shows the minimum acceptable dry density (1361 kg/m³) that has been selected as the target for the reference design.

The reference designs of the blocks and pellets are given in Table 5-17 and the design parameters specifying the installed backfill properties that the components shall have when they are installed are given in Table 5-18.

Pellets around the blocks are needed as a buffering volume to absorb groundwater flow from the surrounding rock that otherwise could erode the bentonite blocks. The acceptable water content in the backfill pellets is designed to contribute to the water storage properties.

The installed dry density of the backfill will depend on the volume of the deposition tunnel and the mass of backfill material installed in the tunnel. The installed density is calculated per tunnel section, defined as the average distance between two deposition holes, i.e. about 6 m. The calculated installed density for the reference design of backfill components according to Table 5-17 and the installed backfill according to Table 5-18, are set out in Table 5-19.

The calculated average dry density in a backfilled tunnel section is reported in the **Backfill production report**. The calculated dry density of Asha 2012 is 1 488 kg/m³ if the design parameters for the backfill have their nominal values and the excavated tunnel volume including the expected average of 18 % overbreak. At 30 % overbreak, the corresponding calculated average density is 1 437 kg/m³. At both these values, the interval of acceptance for Asha 2012 on installed dry density is achieved. Even the lowest calculated density that can be obtained with the present design, that is when all design parameters have their lowest accepted value, meets the interval of acceptance.

Table 5-17. Reference blocks and pellets ready for installation (based on Asha 2012).

Design parameter	Nominal design	Accepted variation
Blocks		
Dry density Asha 2012 (kg/m ³)	1 725	≥ 1 650
Water content (%)	20 (As in the material ready for compaction)	± 1.5 (As in the material ready for compaction)
Dimensions (mm ³)	500 × 571 × 400	± 1 × 1 × 2
Tensile strength (kPa)	–	> 200
Pellets		
Dry density Asha 2012 (kg/m ³)	900	≥ 850
Dimensions (mm ³)	Ø 6 L: 6-22	–
Water content		< 20 %
Pellet durability		Sufficient to have less than 10 % fine material in the pellets filling

Table 5-18. Reference design of installed backfill (based on Asha 2012).

Design parameter	Nominal design	Accepted variation
Blocks		
Geometry	According to Figure 5-16	The number of blocks must not be changed
Free space between blocks and nominal tunnel profile (mm)	100	≥ 100
Pellet filling in gap between blocks and tunnel walls		
Pellet-filled proportion of free space between block and tunnel wall (%)	94	≥ 90
Percentage of fine material in the installed pellet filling (%)	–	< 10
Pellet bottom bed		
Thickness (above theoretical floor above deposition hole (mm)	100	± 20
Surface roughness (mm)	Perfectly even	± 5
Calculated installed average dry density between deposition holes		
Dry density Asha 2012 (kg/m ³)	1 488	≤ 1 361

¹⁾ In the reference design buffer blocks are used and the design parameters are the ones specified for solid blocks in the **Buffer production report**, Table 3-4.

²⁾ In the reference design the same kind of pellets are used for the bottom bed and the gap between the blocks and tunnel walls. This may be changed.

Table 5-19. Calculated average installed backfill dry density for reference design with Asha 2012.

Design parameter	Value, average overbreak (V _r =136.5 m ³)	Value, highest acceptable overbreak (V _r =150.4 m ³)
Dry density blocks	1 725 kg/m ³	1 725 kg/m ³
Volume, block stack incl. space between blocks	100.7 m ³	100.7 m ³
Dry density, pellets	980 kg/m ³	980 kg/m ³
Volume, free space between blocks and tunnel profile	30.2 m ³	44.1 m ³
Volume, pellets bottom bed	5.6 m ³	5.6 m ³
Volume, pellets bevel in deposition hole	1.9 m ³	1.9 m ³
Degree of filling, pellets between block stack and rock	94 %	94 %
Degree of filling, pellets bottom bed and bevel	100 %	100 %
Average dry density in tunnel section with one deposition hole.	1 488 kg/m ³	1 437 kg/m ³

Production and installation

The production line for the backfill comprises the following three main parts:

- Purchase, excavation and delivery.
- Manufacturing of blocks and pellets.
- Handling and installation.

Details about the production can be found in the **Backfill production report**.

Purchase, excavation and delivery of the backfill bentonite are similar to that for the buffer, see Section 5.5.2. The bentonite material needs to be characterized with the aim to determine whether the material can meet the design requirements. This includes determination of required dry density and investigations of the material composition as well as compaction, tests, manufacturing tests of blocks and pellets and tests of block strength.

The bentonite material is dried and subsequently crushed prior to compaction to blocks and pellets and the water content is then adjusted by adding water. The blocks are manufactured using uniaxial compression which gives homogeneous blocks and the cylindrical pellets are produced by extrusion. These processes determine the dry density, dimensions and strength of the products.

Of all blocks manufactured for the full-scale experiment in Äspö HRL, 58 were taken for measurement and the height of these blocks were all within the tolerance of 2 mm. The average height was 399.8 mm with standard deviation 0.7 mm (Sandén et al. 2015). Similar results are expected in industrial production.

The installation of backfill in the deposition tunnel needs to be co-ordinated with the installation of the buffer and of the canisters. The backfill pellets in the bevel of the deposition hole and around the upper buffer blocks are installed in conjunction with the installation of the buffer. After this, the spread of backfill pellets in the bottom bed begins and the pellet mass and the position and surface evenness of the bottom bed surface are measured. The dry density and thickness of the pellet bed is calculated from the gathered data on the bed, data from laser scanning of the actual tunnel profile and the pellet water content after extrusion. An industrial robot equipped with a control system stacks the backfill blocks. The stacking of the blocks can be carried out with accuracy and the robot has a measurement system where information about the mass of the blocks, positions in the block stack, the distance between the blocks and the rock are recorded. Installation of pellets in the space between the block stack and the rock walls of the tunnel can be done by blowing pellets with pressurized air. During the installation of pellets, the installed pellet mass is recorded. Backfill blocks have been manufactured during trial production. The dry densities in the blocks were about 1 740 kg/m³ at a compaction pressure of 25 MPa and 1 787 kg/m³ at a compaction pressure of 50 MPa (Sandén et al. 2016). It is therefore likely that blocks can be produced with a density of around 1 725 kg/m³, i.e. the nominal dry density for Asha 2012.

SKB has carried out a full-scale trial installation of backfill in a 12 m long tunnel in Äspö HRL (Arvidsson et al. 2015). Prototypes of most of the equipment planned to be used in the final repository was used. The bottom bed was, however, spread manually and levelled with a screed. The block stack met all requirements except that the proportion of voids in the stack was 2.5 % whereas the requirement was 2 % and the free space between the block stack and the tunnel wall was not 100 mm everywhere. These quality deficiencies are deemed to be readily corrected through improvements to the industrial robot's control system.

5.6.3 Initial state

The initial state of the backfill is the state when the entire deposition tunnel is backfilled. Inflow of groundwater to the deposition tunnel and its impact on the backfill is not accounted for in the initial state. The presented initial state of the backfill is the outcome of the design parameters that can be expected based on the experience and results from the test production.

The properties of the backfill to be designed to conform to the design requirements for post-closure safety are:

- Material composition.
- Installed density.

In the **Buffer, backfill and closure process report**, the backfill is characterised by a number of variables. Most of the initial state values for these variables are determined by the design properties. The relation between the variables and the design parameters are basically the same as for the buffer, see Table 5-11.

Material composition

According to the design requirements the backfill material must not contain substances that may cause harmful buffer degradation or canister corrosion. This entails that the backfill material must not be a significant source of sulphide that can corrode the copper canister. Currently, no limits are given as design requirement from the assessment of the post-closure safety.

As a check on the maximum contents of sulphur and organic carbon it is important to determine the total chemical composition of the bentonite. The mean chemical composition of the bulk material expressed as oxides are given in Table 5-20 for Asha 2012. Descriptive statistics on the exchangeable cations are given in Table 5-21. The total carbon content of five samples of Asha 2012 ranges from 0.54 to 0.70 % C. The acid-soluble carbon content is systematically somewhat lower, which suggests that carbon sources other than carbonates may exist. If so, a probable source is organic matter. The remnant carbon content (i.e. total minus acid-soluble carbon) is 0.24 % C at a maximum (Sandén et al. 2014).

Based on the specifications of the example bentonite material (Asha 2012), the impact of the backfill material composition on buffer degradation and canister corrosion is assessed in the PSAR.

Table 5-20. Overview of the chemical composition of the bentonite samples from the batch Asha 2012. Major elements by ICP-AES, S and C by evolved gas (Sandén et al. 2014).

Bentonite	Chemical composition (%)														
	SiO ₂	Al ₂ O ₃	Fe ₂ O ₃	MgO	CaO	Na ₂ O	K ₂ O	TiO ₂	P ₂ O ₅	MnO	Cr ₂ O ₃	LOI	C _{tot}	S _{tot}	CO ₂
Asha 2012 mean (N=5)	47.62	18.54	14.50	2.71	3.29	1.64	0.10	1.03	0.11	0.15	0.034	10.0	0.60	0.12	1.61
Standard dev	0.82	0.87	1.78	0.07	0.30	0.15	0.01	0.02	0.01	0.03	0.004	0.3	0.07	0.05	0.11

Table 5-21. Descriptive statistics on the exchangeable cations in Asha 2012 (Sandén et al. 2014).

Bentonite	Cation	Mean meq/100 g	Std.dev.	Max. value meq/100 g	Min. value meq/100 g
Asha 2012 (N=5)	Ca	30.5	3.67	35	26.0
	Mg	13.4	0.75	15	13
	K	0.5	0.03	0.6	0.5
	Na	46.9	4.21	53	43
	Sum	91	1.7	93	90

Water content, gas content and porewater composition

There are no specific design requirements with regard to gas content and porewater composition, but these properties need to be known for the subsequent analysis of post-closure safety. In the reference design with Asha, the initial water content in blocks is selected to be 20 % and 19 % in pellets. Water content is determined by a standard geotechnical method. All porosity not filled with water contains air. The initial porewater composition may be calculated but not directly measured. The calculated content of installed mass and volume of water and air in a deposition hole is presented in Table 5-22.

Table 5-22. Backfill, installed total mass and volume of backfill material, water and air in a deposition tunnel section (6.0 m), assuming nominal and nominal dimensions of the deposition tunnel, blocks and pellets.

	Mass (tons)				Volume (m ³)			
	Total	Solid	Water	Air	Total	Solid	Water	Air
6 m tunnel	239.61	199.95	39.66	~0	134.02	68.66	39.66	25.70

Installed density

The installed dry density in the backfill shall be $> 1361 \text{ kg/m}^3$ on average between two deposition holes, see Figure 5-14. This limit is valid for the reference material in the PSAR. Another backfill material would most likely have another density limit. The density of the installed backfill blocks and pellets can be found in Table 5-17. The installed blocks and pellets with dry densities given by the manufacturing process shall also fulfil the required properties after saturation.

The average installed backfill dry density will depend on the density and dimensions of the installed blocks and pellets, i.e. the installed buffer mass and the backfill geometry which is dependent on the excavated tunnel volumes. The dimensions of the tunnel and the installed mass will be registered during installation and the average installed dry density calculated to ensure that the properties at initial state fulfil the reference design.

Based on the initial state values of the design parameters of the backfill and the deposition tunnel volumes the installed dry density, mass and porosity to be used in the PSAR have been calculated, the results are presented in Table 5-23. The reference design values are given as comparison.

During operation some backfill material in already completed and plugged deposition tunnels may be lost by piping and erosion. Material may also be lost in the future during the assessment period both during and after saturation of the backfill. Countermeasures related to piping erosion during installation due to water inflow have been taken in the reference design of the pellets surrounding the block pile, see the **Backfill production report**.

Table 5-23. The backfill design parameters at the initial state.

Design parameter	Reference design and initial state	Acceptable tolerances
Dry density of blocks (Asha 2012) (kg/m ³) <ul style="list-style-type: none"> • Tunnel section 	1725	≥ 1650
Dry density of pellet filling (kg/m ³) <ul style="list-style-type: none"> • Bottom bed • Between blocks and rock wall • Bevel in deposition hole 	980	≥ 950
Geometry	Nominal: Figure 5-16	
Average dry density in deposition tunnel (Asha 2012)*	1437*–1488	≥ 1361

* Interval is given by variations in the tunnel volume (18 to 30 % overbreak).

5.7 Initial state of repository sealing and additional engineered parts of the repository

Once all spent nuclear fuel has been disposed the repository can be closed. The **Closure production report** presents the technical design requirements, the reference design of the closure, verifying analyses that show that the reference design does fulfil the technical design requirements and the production and control procedures selected to achieve the reference design. The report also includes achieved results from test manufacturing and installation.

The following sections give a summary of the contents of the **Closure production report** and a specification of the Initial state.

The closure includes:

1. Main tunnels and transport tunnels
2. Central area
3. Ramp and shafts below the top sealing
4. Top seal
5. Plugs (other than deposition tunnel plugs)
6. Investigation boreholes from the ground surface and boreholes from the underground openings in the repository.

The other engineered parts referred to in the present Section are the plugs in the deposition tunnels as described in the **Deposition tunnel plug production report**.

The purpose and function of the closure is i) to limit groundwater flow and migration of radionuclides through the tunnels and other openings, ii) to significantly obstruct unintentional intrusion into the final repository, iii) to prevent collapse of the rock structure and iv) to prevent the expansion of bentonite into connecting rock spaces. This means that all rock spaces need to be backfilled.

The closure backfill material in different underground openings have different purposes e.g. to restrict groundwater flow through the underground opening, to provide mechanical restraint and to obstruct unintentional intrusion into the repository as further discussed in Chapter 7 of SKB (2021b). An outline of the different kinds of closure and plugs and their functions is shown in Table 5-24.

Table 5-24. Functions of the closure parts.

Part of closure	Material	Function				
		Prevent collapse	Keep other parts in place	Resist bentonite expansion	Restrict water flow	Prevent intrusion
Main tunnels	Bentonite	X	X	X	X	
Transport tunnels	Bentonite	X	X	X	X	
Central area	Crushed rock	X	X	X		
Lower part of ramp (-470 m to -370 m)	Bentonite	X	X		X	
Lower part of shaft (-470 m to -370 m)	Bentonite	X	X		X	
Upper part of ramp (-370 to -50 m)	Crushed rock	X	X			
Upper part of shaft (-370 to -50 m)	Crushed rock	X	X			
Top seal (-50 m to 0 m)	Crushed rock	X	X			X
Boreholes	Bentonite, sand, concrete	X	X		X	
Plugs (other than deposition tunnel plugs)	Concrete		X	X	X	

5.7.1 Technical design requirements

To guide the design and production of the closure the design requirements of the backfill materials used for closure are stated. The technical design requirements are based on the assessment of the post-closure evolution of the closure in the repository and available technology and shall be fulfilled at initial state.

Technical design requirements on the closure have been formulated according to the following in the **Closure production report** with additional clarifications in Chapter 7 of SKB (2021b).

- The integrated effective connected hydraulic conductivity of the backfill in main and transport tunnels, in the lower part (-470 to -370 m) of ramp and shafts must be less than 10^{-8} m/s. This value need not be upheld in sections where e.g. the tunnel or ramp passes highly transmissive zones.
- There is no restriction on the hydraulic conductivity in the central area, upper part (-370 to -50 m) of the ramp and shafts and in the top seal. These shall, however, be backfilled.
- Boreholes must be sealed such that they do not unduly impair containment or retention properties of the repository. For boreholes in hydraulic contact with the repository this is achieved if the hydraulic conductivity of the borehole seal is $< 10^{-8}$ m/s, which is ensured if the swelling pressure of the seal is > 0.1 MPa. This value need not be upheld in sections where e.g. the hole passes highly transmissive zones. The hydraulic conductivity shall be $< 10^{-6}$ m/s in the other boreholes.
- Accepted pH value of leaching products from materials below the level of -200 m: $\text{pH}_{\text{leach}} < 11$.

The main functions of the deposition tunnel plugs are to keep the backfill in the deposition tunnels in place and prevent water flow past the plug until the main tunnel has been backfilled and the material is water saturated. Technical design requirements for the deposition tunnel plugs are given in Chapter 6 of SKB (2021b).

5.7.2 Reference design and production procedures

This section describes the reference design of the closure and the other engineered parts, see Figure 5-18.

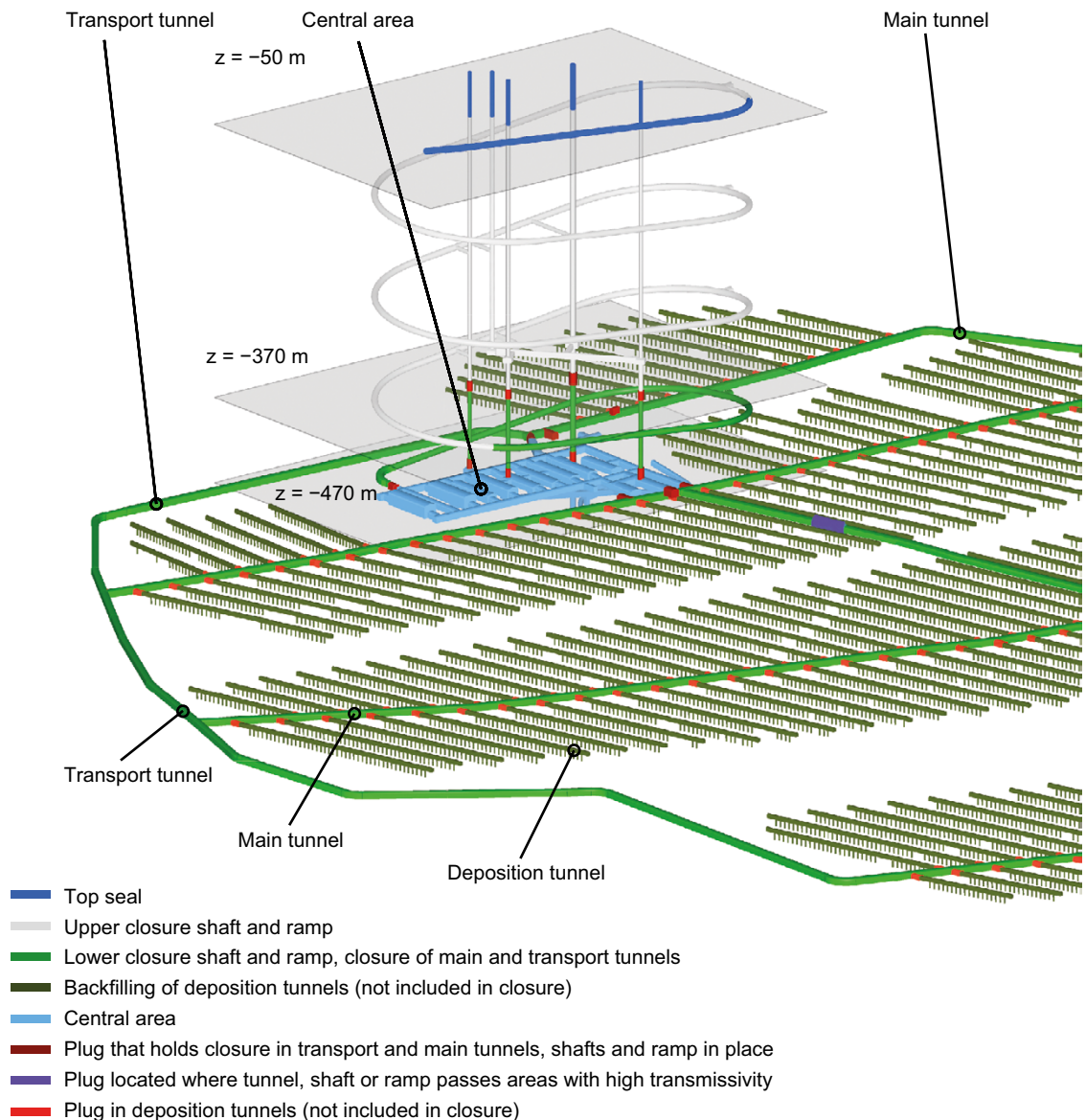


Figure 5-18. General outline of the reference designs of closure and plugs in the underground openings.

Deposition tunnel plug

The deposition tunnel plugs are here referred to as engineered parts in the repository. They are especially designed with respect to the properties and function of the buffer and backfill. The plug consists of several parts that in different ways will contribute to maintaining its functions during the curing phase, the sealing phase and the post-closure phase of its lifetime, see the **Deposition tunnel plug production report**.

The plug has a water tight seal of highly compacted bentonite and a concrete dome installed into a slot deepened from the excavated tunnel contour with a non-damaging technique. The dome is sufficiently deep to cut off all possible flow paths caused by excavation disturbance. The backfill, the bentonite seal and the concrete dome are separated by different materials. The concrete dome is cast from low-pH concrete without reinforcement but it contains cooling pipes to limit the temperature during curing. The bentonite seal consists of compacted bentonite blocks and pellets. The parts of the deposition tunnel plug are illustrated in Figure 5-19 and the materials, dimensions and volumes of the different parts of the deposition tunnel plug are given in Table 5-25.

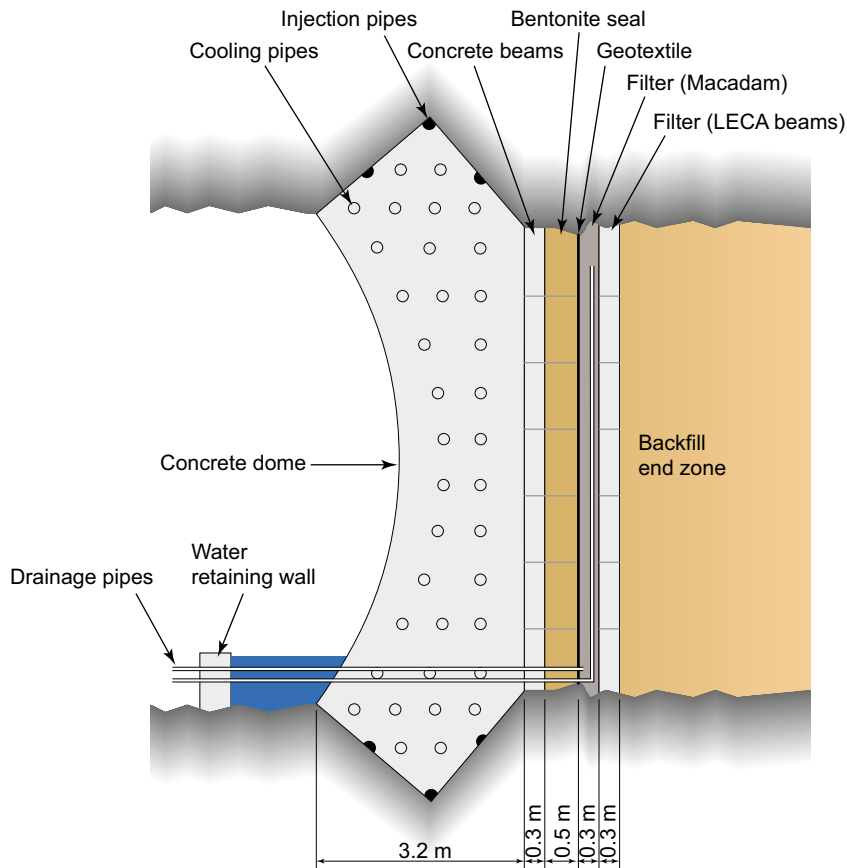


Figure 5-19. Schematic Section of the reference design of the plug.

Table 5-25. The main components and design parameters of the installed deposition tunnel plug.

Component	Material	Volume (m ³) or weight (kg)	Length (m)	Density (kg/m ³)
Concrete dome	Low pH-concrete B200	93 m ³	ca 3.2 m (contact zone between dome and rock)	2 170–2 260
Concrete beam	Low pH-concrete B200	6 m ³	0.3 m	2 170–2 260
Bentonite seal	Bentonite	11 m ³	0.5 m	1 560
Filter (Macadam)	Macadam 2–4 mm	7 m ³	0.3 m	1 400
Filter (LECA beams*)		5.2 m ³	0.3 m	660
Reinforcement	Carbon steel	2 500 kg	-	-
Cooling pipes	Copper	150 kg	-	-
Drainage pipes	Stainless steel	25 kg	-	-

* Reinforced lightweight concrete, e.g. from LECA®.

Other plugs

Plugs in the repository, other than the deposition tunnel plugs, have different purposes. They separate closed and open underground openings by keeping the closure material in place until the opening on the other side of the plug is filled with closure material and it is fully water saturated. The design of the different types of plugs depends on the properties of the surrounding rock.

The plugs contain no materials that can impair the functions of other barriers and the concrete used for all plugs has the same composition as the concrete in the deposition tunnel plugs.

Main tunnels and transport tunnels

To conform to the design requirements, the design of the closure of the main tunnels and transport tunnels at repository level will be based on a similar principle as the backfill in deposition tunnels with pre-compacted bentonite but the material quality and density will be different. An outline of the reference design is given in Section 5.6.2.

According to current guidelines, the closure in the main tunnels and the transport tunnels should have a similar conceptual design as the backfill in the deposition tunnels (**Backfill production report**). It involves the use of bentonite material in some form to backfill the tunnels. Figure 5-18 shows main tunnels and transport tunnels.

In practice, the requirements on the material composition and the installed density in the main and transport tunnels are relaxed compared to those for the deposition tunnels. For example, there is no need to prevent buffer expansion and the acceptable hydraulic conductivity is higher.

Central area

The only function of the closure of the cavities in the central area, Figure 5-18, is to occupy the space with no other design requirement than to prevent substantial convergence and subsidence of the surrounding rock. With respect to this, the reference design is crushed rock that will be placed in horizontal compacted layers. Table 5-26 shows examples of densities of filling masses.

Table 5-26. Achieved dry densities of filling masses – results from road and dam constructions and backfill experiments at Äspö HRL

Material	Dry density (kg/m³)
Horizontal layers (packed with 5-ton vibration roller)	
Raw TBM muck	2 390–2 470
Crushed rock from blasting and TBM muck	2 100–2 300
Road	2 050–2 200
Dam construction (6-ton vibration roller)	2 000
Inclined layers	
Raw TBM muck, no compaction	1 600–2 120
Raw TBM muck, compacted	2 210–2 330
Crushed rock from blasting and TBM muck	2 110–2 210

Ramp and shafts

The final repository is in contact with the ground via a ramp and three types of shafts; skip shaft, elevator shaft and ventilation shaft. The shaft has circular cross sections. In the closure reference design the ramp and shafts, from level –470 m up to level –370 m, are backfilled with compacted bentonite blocks and pellets in accordance with the current reference design for the backfill in the deposition tunnels, see Section 5.6.2. All bentonite sections end with plugs and stabilizing plugs are installed where the ramp and shaft passes water-carrying zones.

From the level of –370 m up to the level of –50 m, the ramp and shaft are sealed with crushed rock.

Top seal

The top seal is in the uppermost 50 meters of the shaft and ramp. To conform to the requirement that “closure in the upper part of the ramp, shafts and boreholes shall hinder unintentional intrusion into the repository” the ramp and shafts, from –50 m depth to ground level, is filled with fairly well fitted rock blocks and the crushed rock compacted by its own weight. Alternatively, cast concrete could be used as top-seal.

The reference design for sealing the upper part of the ramp and shafts is indicated in Figure 5-18.

Investigation boreholes

A number of investigation boreholes, drilled both from the surface and from underground openings, have to be sealed at the closure of the repository. The layout of the repository is adapted to the locations of deep investigation boreholes, to ensure that boreholes connected to the surface do not intersect underground openings. Furthermore, deposition holes must not be intersected by any investigation boreholes.

The length of surface-based boreholes ranges from a few metres to more than 1 000 metres and the diameter ranges from 56 to 120 mm. The tunnel-based boreholes are expected to have a length of a few hundred metres and a diameter of 56 to 76 mm. The shallowest parts of the boreholes may have larger diameters and some boreholes may be more or less horizontal.

The geometry of a borehole seal is mainly determined by the dimensions of the drilled holes. The applied borehole seal concept, the Sandwich-concept, means that the main part of a borehole is filled with granular material, sand, while sealing sections consisting of highly compacted bentonite, are positioned in selected borehole sections with good rock quality i.e. there are no water bearing fractures present.

The boreholes are divided into three classes (class 1–3) depending on depth and distance from the repository, and whether the boreholes are in hydraulic contact with the repository. Each borehole class will be sealed by one or more methods of closure. Schematic sketches of the borehole seals related to the three classes are shown in Figure 5-20.

Class 1 (BHC1) includes shallow boreholes, 0–75 m deep, either in soil or in both soil and rock. These boreholes do not pass water-bearing fracture zones that have contact with the repository. These boreholes are sealed with bentonite pellets to prevent infiltrating surface water from spreading into the groundwater. A quartz-based concrete plug (top seal) is cast in the upper part of the rock layer.

Class 2 (BHC2) includes boreholes with depth between 75 and > 1 000 m that are located relatively far from the repository (> 400 m). These boreholes do not pass water-bearing fracture zones that have contact with the repository. The part of the borehole that passes through the soil layer is sealed with bentonite pellets, the part that passes through rock is filled with sand or quartz-based concrete. A quartz-based concrete plug (top seal) is cast in the upper part of the rock layer.

Class 3 (BHC3) includes boreholes with depth between 75 and > 1 000 m that are located relatively close to the repository (\leq 400 m). This class also includes other boreholes, with different depths and distances from the repository, that are judged to cross water-bearing fracture zones that have hydraulic contact with the repository. Most of these boreholes are sealed with bentonite pellets in the soil layer part and with layers of sand and bentonite in the rock part. Bentonite is used where the rock has good quality. Concrete plugs and copper expanders are installed between the layers of sand and the bentonite to prevent mixing of them.

Boreholes drilled for grouting or rock bolts are filled with grout or bolts and cement, consequently no sealing actions are required.

Production procedures

Closure of the repository will, with the exception of the plugs in the deposition tunnels and some boreholes that have to be closed earlier, not take place until all canisters have been deposited. The installation of the plugs in the deposition tunnels starts as soon as the deposition tunnel is backfilled.

This means that the closure activities lie well into the future. So far SKB has prioritised the development of the backfill and plugs in deposition tunnels. The production of closure for main tunnels and transport tunnels and the ramp and shafts below the level of the top sealing have not yet been developed in detail, but it will most likely resemble production of closure for deposition tunnels. For that reason, this section refers to the **Backfill production report**.

Prior to closure of any underground opening, construction features such as road beds and building components and installations will, as part of the decommissioning, be removed and the underground opening cleaned. Routines for these activities have not yet been specified.

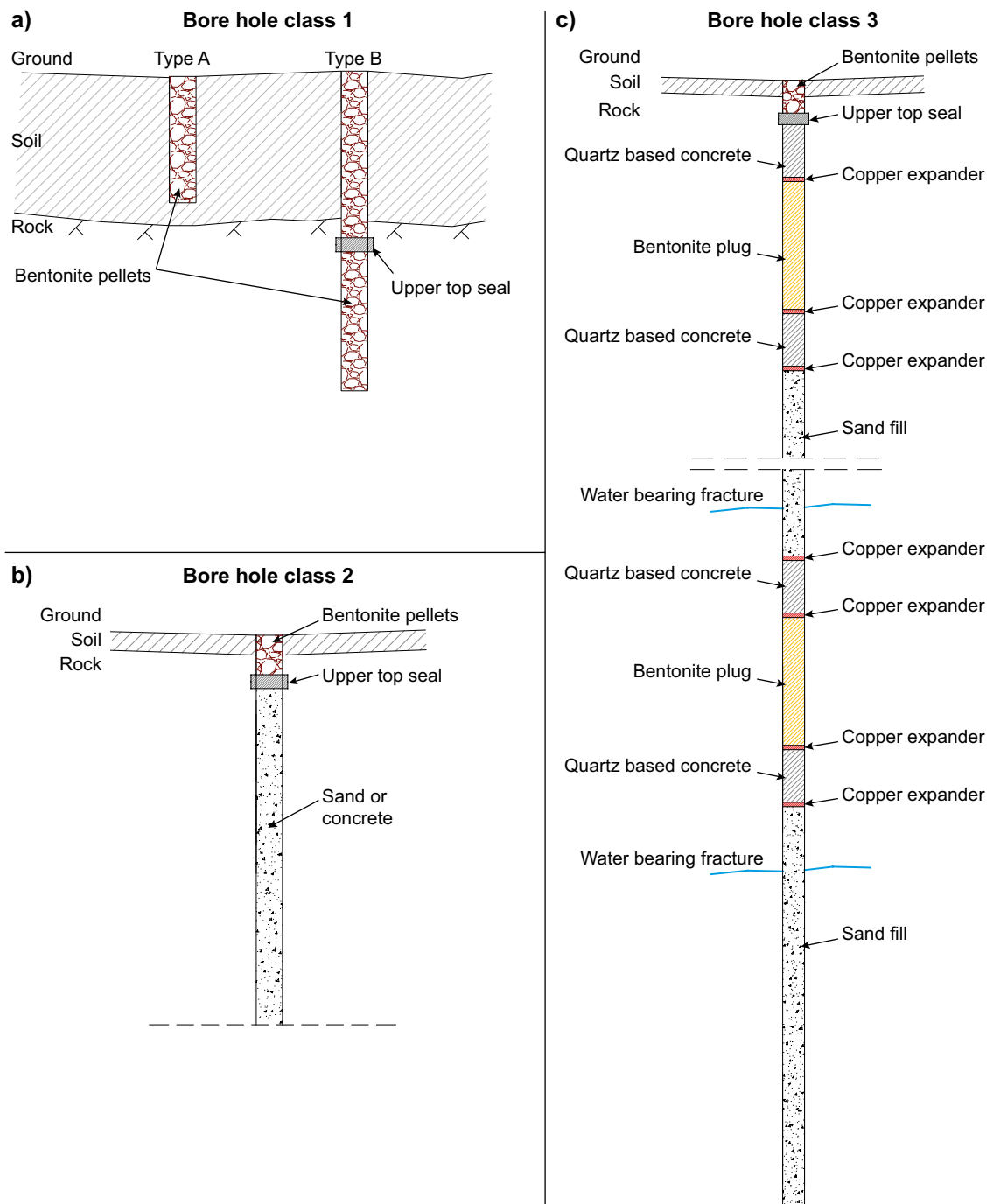


Figure 5-20. Schematic sketch of the borehole seals.

Besides decommissioning, the main stages for closure of the repository are:

- Backfilling and, if necessary, installation of plugs in any ventilation shaft far away from the central area.
- Backfilling and, where necessary, installation of plugs in main tunnels and transport tunnels.
- Installation of plugs where the transport tunnels connect to the central area.
- Backfilling of the central area.
- Installation of plugs where the central area connects to shafts and the ramp.
- Backfilling and, where necessary, installation of plugs in the ramp and remaining shafts.
- Installation of the top seal.

Borehole seals are installed at suitable locations before or during the other closure activities.

5.7.3 Initial state

The initial state of the closure is the state when all closure material in a specific underground opening or borehole is installed and the borehole, rock cavity, shaft or tunnel has been closed. Inflow of groundwater to an underground opening or a borehole and its impact on the closure is not accounted for in the initial state, but is assessed as part of the PSAR, see Chapter 10.

In the **Buffer, backfill and closure process report**, the closure components numbered 1–6 in Section 5.7 are characterised by a set of variables. Most of the initial state values for these variables are determined by the design properties. For the clay-filled parts the relationships between the variables and the design parameters are basically the same as for the buffer (see Table 5-11).

Material composition, installed density, installed geometry

Regarding the backfill in main tunnels, ramp and shaft (below level –370 m), the same material and similar production procedures as for the deposition tunnel backfill will be used. Since the maximum allowed hydraulic conductivity in the deposition tunnel backfill is two orders of magnitude lower than that in the main tunnels, ramp and shaft, and since technical design requirements on the deposition tunnel backfill are assumed to be met according to Section 5.6.3, it is assumed that the premises are met also for the main tunnels, ramp and shaft.

The Central area and the upper parts of the shafts and ramp are backfilled with crushed rock that will provide the properties required, mainly density but also the mineral composition, to fulfil the requirements. Table 5-26 shows examples of achieved dry densities of filling masses.

The initial states of the other closure components in the underground openings and boreholes are presented in Table 5-27. At this stage of development, the closure properties are described as a compilation of reasonable values of some main parameters that can be estimated based on the current results and experience.

Table 5-27. The initial state of the closure in the different underground openings and boreholes.

Underground openings	Material	Volume (m ³)	Installed dry density (kg/m ³)	Dry weight of installed closure (ton)	Integrated hydraulic conductivity (m/s)
Main and transport tunnels	Bentonite	842 000	1500	1 263 000	< 10 ⁻⁸
Central area	Crushed rock	215 000	1900	408 000	-
Ramp, lower part (-470 m to -370 m)	Bentonite	50 000	1500	75 000	< 10 ⁻⁸
Shafts, lower part (-470 m to -370 m)	Bentonite	9 600	1500	14 400	< 10 ⁻⁸
Ramp, upper part (-370 to -50 m)	Crushed rock	160 000	1900	304 000	-
Shafts, upper part (-370 to -50 m)	Crushed rock	31 000	1900	58 900	-
Top seal (-50 m to 0 m)	Crushed rock	30 000	1900	57 000	-
Boreholes	Bentonite, sand, concrete	For geometry see Section 5.7.2			< 10 ⁻⁶ < 10 ⁻⁸ *
Plugs (other than Deposition tunnel plugs)	Concrete				

* in boreholes in hydraulic contact with the repository, this value need not be upheld in sections where e.g. the hole passes highly transmissive zones.

The initial state of the bottom plate is given by the reference design in Section 5.7.2. The main components of the installed deposition tunnel plug and the design parameters that shall be inspected in its production are presented in Table 5-22 and the dimensions are shown in Figure 5-20.

There is currently no specification on the number of boreholes. It is however judged that the tightness of the sealed boreholes only marginally affect the groundwater flow at repository depth. Regarding closure of the boreholes, SKB has developed concepts for sealing of long and short boreholes. The sandwich concept is judged to work in both steeply and gently plunging boreholes (Sandén et al. 2018a) to fulfil the requirement on hydraulic conductivity.

5.8 Summary; Key initial state properties for the safety assessment

This section summarises initial state properties of particular relevance for the safety assessment. Some key properties for the analyses presented later in this report are given for the fuel, the canister, the buffer, the deposition tunnel backfill and the site adapted repository. The summary can be seen as a guide to the necessary fuller descriptions given earlier in this Chapter and in references therein.

5.8.1 The fuel

For the fuel, key initial state properties are

- The amount of regular spent fuel to be deposited, see Table 5-3.
- The radionuclide inventory of the regular fuel as given in Table 5-5.
- The fractions of the regular fuel inventory that resides outside the fuel matrix as the instant release fraction (IRF) and the corrosion release fraction (CRF), see Section 5.3.4 and, for details, Section 3.2 of the **Data report**.
- The amount of miscellaneous fuels, as specified in Table 5-4.
- Material properties and dimensions of the metal parts of the fuel housing radioactive activation products, see further Section 5.3.4.

5.8.2 The canister

For the canister, key initial state properties are:

- The reactivity of the sealed, fuel containing canister, as described in Section 5.3.4.
- The residual power of the fuel in the loaded canister as well as the intensity of gamma and neutron radiation at the outer canister surface, see further Section 5.3.4.
- The thickness of the copper shell as specified in Table 5-9.
- The ability of the canister to withstand shear and isostatic loads, including copper creep, as discussed in Section 5.4.3.

5.8.3 The buffer

For the buffer, key initial state properties are:

- The installed buffer mass and its distribution in the deposition hole, ensuring that the buffer obtains its intended properties after water saturation in the repository, see Table 5-14 and Table 5-15.
- The material composition of the buffer including amounts of impurities, see Table 5-12.

5.8.4 The deposition tunnel backfill

For the deposition tunnel backfill, key initial state properties are

- The installed backfill mass and its distribution in the deposition tunnel, ensuring that the backfill obtains its intended properties after water saturation in the repository, see Table 5-22 and Table 5-23.
- The chemical composition of the backfill including amounts of impurities, see Table 5-20.

5.8.5 The site adapted repository

For the site adapted repository, the layout as shown in Figure 5-4 is a key initial state property. Of particular importance are the layout of the deposition tunnels and the locations of the deposition holes, after applying relevant deposition position rejection criteria. (Key properties of the host rock at the site are described in Chapter 4.)

5.9 Monitoring

Repository construction and operation will cause disturbances of the site. Aspects relevant to safety will be handled in the assessment. Monitoring the disturbances will be important for advancing the understanding of the site and the repository. As a part of the application to start underground construction SKB has presented a monitoring programme¹⁷ for the final repository for spent nuclear fuel. Some basic aspect of this is described below.

5.9.1 Monitoring purposes

Monitoring of the repository site has been ongoing since the conclusion of the site investigations at Forsmark, forming a baseline of understanding the temporal variation of e.g. groundwater pressure and hydrogeochemistry for conditions undisturbed by construction activities. Furthermore, SKB has a long experience of conducting experiments where monitoring methods have been developed and utilized. The purpose of these experiments was to increase the knowledge of the host rock and barriers as input to barrier design, repository design, barrier installation method and to the assessment of post closure safety. This knowledge and experience is essential for planning the specifics of the monitoring programme for the construction and operational phase of the final repository.

Confidence in the post-closure safety assessment rests upon:

- A sufficient understanding of the THMCB processes determining the evolution of the repository system, thereby providing a necessary basis for demonstrating the repository's ability to provide adequate containment and retention; and
- Demonstration that the installed engineered barriers and the underground construction work conforms to stated technical design requirements.

For the former, the thorough process understanding achieved by decades of research will be complemented by a research programme tailored to the specific conditions at the chosen site and to the need to analyse the wealth of high-resolution rock data expected from the underground site characterization. For the latter, a quality control programme is being developed and described in the **Production reports** as outlined in previous subsections in this chapter. This implies possibilities to find potential manufacturing or installation errors or other deviations in material, equipment and handling. Before and during waste emplacement, quality control provides the main source for ensuring that the as-built stage complies with stated design requirements.

In addition, monitoring aspects of the evolution during operation may provide further insights. While monitoring results essentially never can relate to direct safety impacts, a management structure will be developed to handle situations when monitoring results deviate from expectations.

¹⁷ Program för övervakning av Kärnbränsleförvaret med avseende på säkerheten efter förslutning. SKBdoc 1584443. (In Swedish.) (Internal document.) *In prep.*

Hence the objectives of the SKB monitoring programme related to post closure safety are:

- Check that the basic assumptions made for the assessment of post closure safety are not challenged.
- Further increase the confidence in SKB's handling and understanding of repository evolution.
- Contribute to the search for earlier unknown features, events and processes.

5.9.2 Monitoring programme

The monitoring programme¹⁸ describes monitoring related to post closure safety, follow up of monitoring data, compilation of decision bases and response plans. The parameters suitable for inclusion in the monitoring programme need to be identified and their relevance to post-closure safety explained. Furthermore, a strategy is needed to deal with the results of the monitoring.

Selection of monitoring parameters

The question of which parameters should be monitored has been one of the main tasks within the international project Modern2020 (White and Scourfield 2019). As part of this project, partners from various nuclear waste organizations (including SKB), regulatory authorities and social scientists from different European countries developed a generic methodology for developing and maintaining an appropriate and motivated set of parameters that should be monitored from the perspective of post closure safety. Based on Modern2020 a simplified illustration of the screening methodology to identify parameters worth monitoring is outlined in the IAEA document *Use of Monitoring Programmes in the Safe Development of Geological Disposal Facilities for Radioactive Waste*.¹⁹

- The starting point of the methodology is a list of the processes that are of potential interest for monitoring. In the case that detailed safety functions have been defined, these processes would be taken from the assessed list of processes affecting these safety functions. Furthermore, additional processes of interest may be put forward, e.g. by people outside the safety assessment team;
- The next step is to assess whether a suggested process is considered relevant for safety. If found not relevant, the process should still be listed (parked), such that its relevance can be reassessed in later iterations or by other stakeholders;
- If a process is judged relevant the next step is to consider which parameters describe or affect the process. For each such parameter it is considered i) what are the potential technical means of monitoring the parameter or a proxy representing the parameter, ii) which, if any of the monitoring methods is judged practical within the constraints of the repository programme and iii) if impacts on safety and environment are judged acceptable. If no practical means of monitoring the parameter is found, the parameter should still be documented in the monitoring programme (parked) such that this judgement can be reassessed in later iterations.
- For the remaining set of parameters with monitoring methods found feasible it is judged whether monitoring these would provide sufficient support for confidence in the assessment of the considered process. If the answer is yes, the parameters and the means of monitoring them should be added to the monitoring programme. If the answer is no, even considering other means of verifying the elements of a safety case, the monitoring strategy or the safety case may need to be revised, or R&D efforts on monitoring to be put in place.

SKB has adopted this methodology on the basis of the conditions and work already done in previous safety analyses. SKB's experiences from measurements and test at the Äspö HRL have also been used in developing the programme.

¹⁸ Program för övervakning av Kärnbränsleförvaret med avseende på säkerheten efter förslutning. SKBdoc 1584443. (In Swedish.) (Internal document.) *In prep.*

¹⁹ IAEA. Use of monitoring programmes in the safe development of geological disposal facilities for radioactive waste. Vienna: International Atomic Energy Agency. *In prep.*

Limitations and risks that need to be considered

The monitoring must not interfere with the repository safety functions. The safety of the nuclear fuel repository is based on passive barriers. Therefore, introducing monitoring equipment into a barrier always involves a risk of safety impact. This is also clearly expressed in the Swedish Radiation Safety Authority's regulations and general advice. According to SSMFS 2008: 21 § 8: "*The impact on the safety of measures taken to facilitate monitoring or withdrawal of deposited nuclear material or nuclear waste from the final repository or to make it more difficult access to the final repository shall be analysed and reported to the Radiation Safety Authority.*" In the general advice to this section it is stated that: "*It should be stated in the safety report for the facility according to § 9 that the measures either have a small and negligible impact on the safety of the final repository or that the measures result in an improvement of the safety, compared to the case that the measures were not taken*". This significantly limits the choice of technology, location and time frames to perform the monitoring. Any use of monitoring equipment in the technical barriers must be taken into account in the post closure safety analysis.

The risk of incorrect signals that could be misinterpreted must also be taken into account. Incorrect signals could, in the worst case, lead to unjustified decisions on various measures, such as recovering already deposited canisters associated with high costs and radiological risks.

At least on the basis of the monitoring technology available today, this means that SKB does not plan to place monitoring equipment directly in backfilled deposition tunnels or deposition holes. However, there are opportunities for monitoring that can provide more relevant information about the development of the barriers at the repository site, without compromising safety. One such possibility is to install long-term in situ tests of varying scope and character, focusing on the most important aspects of the technical barriers at representative locations in the repository. Some of these tests can be decommissioned and evaluated at various times during the operational period to provide the basis for updating the current safety report (SAR). Prior to closure, all such tests should be completed and evaluated to provide the basis and confidence for the decision to close the repository.

Follow up and evaluation of monitoring results

When a parameter is deemed to be included in the monitoring programme, a forecast must be made regarding its expected development. Depending on which parameter is intended, such forecasts can be made qualitatively or taken from quantitative results from models. Reasoning about probable and possible alternative developments together with descriptions of what can cause these should be done if knowledge is available. The level of ambition for these forecasts is based on reasoning about the type of evolution that could affect the analysis of post closure safety and types of evolutions that have no impact.

The data from the monitoring can be evaluated continuously and be combined with measurements at decommissioning. The evaluation can be made both regarding individual specific data and periodic evaluation of the entire dataset. If monitoring results deviate from what is expected, action needs to be taken.

Deviations in the monitoring programme are planned to be followed up by a special unit termed "Safety in the project Nuclear fuel repository (SIP-K)" (SKB 2020b). The function of this unit is to support the construction organization and later operational management in matters relating to nuclear safety during construction as well as post closure safety.

The SIP-K function consists of a group of people who, when necessary and depending on the issue, call on relevant subject area specialists. It is primarily SIP-K that follows up deviations in the results of the monitoring.

SIP-K works in a solution-oriented manner, i.e. the deviations between predicted and measured results that are noticed shall be accompanied by proposals for concrete measures to deal with the deviations. The process starts when a question is reported to function SIP-K, for example, if the results of the monitoring deviate from the range of predicted parameter values. The work is conducted in the following steps:

- The SIP-K function performs an analysis and assesses whether the question is a safety issue or not.
- In cases where this is not a safety issue, this is documented and the function does not take any other measures.
- In cases where it is considered a security issue, the function begins to break down the issue. If necessary, SIP-K calls for the resources and competencies needed, depending on the nature of the question.
- When designated persons are convened, a new analysis is carried out, the need for action and possible solution proposals are determined, as well as the consequences of the action.

All work done in function SIP-K is documented in protocols or memos. Depending on the nature of the question, this is also reported to SSM.

The continuous evaluation of the results of the monitoring is to compare the results with the expected variation of the parameter values in time and space. SKB's plans for this management are in line with the recommendations given in the project Modern 2020 (White and Scourfield 2019) and in the previously mentioned IAEA document.

In addition to continuous evaluation of individual parameter values, the results of the monitoring will be included in more comprehensive analyses of location understanding and safety. Such analyses are always done in conjunction with planned updates to the safety report, but can also be done more often if needed.

Contents of the monitoring programme

As for the host rock, the surface-based monitoring activities at Forsmark will continue complemented with monitoring of hydrogeological, geochemical, thermal and rock mechanics parameters from boreholes or other installations underground. The monitoring of buffer, backfill and plugs is described and so is monitoring of copper corrosion. Considering the EBS, the work is currently aimed at designing single or multiple barrier component tests that can focus on processes that are relevant to post closure safety, see also the monitoring programme²⁰. The design and planning for such tests have recently been initiated based on SKB's comprehensive experience of in situ tests. Work is also directed at developing models to increase the accuracy for predictions of parameter evolution.

In some cases the transients during construction and operation of the repository have been assessed to have no or very marginal influence on the post closure safety. Hence little effort has previously been put into modelling and predicting the parameter evolution for these short transients.

SKB do not intend to apply monitoring that could disturb or jeopardize the EBS function. Hence neither emplaced waste nor EBS components (canister, buffer and backfill) will be directly monitored.

5.9.3 Control programme for repository construction and operation

A control program has been developed and is outlined in the **Production reports**. The control programme has the objective of ensuring that the technical design requirements and other requirements on the construction work and on the operations are fulfilled. The control programme will consider:

- Material deliveries.
- Workmanship.
- Control of the as built and operated facility relative to the design and specification of operational activities.

The control programme with its quality documentation is the basis for assessing whether the construction and operational work conform to the stated technical design requirements and requirements on efficiency and quality. The objectives and contents of the control programme are defined, but will evolve and be adjusted in response to experience gained.

²⁰ Program för övervakning av Kärnbränsleförvaret med avseende på säkerheten efter förslutning. SKBdoc 1584443. (In Swedish.) (Internal document.) *In prep.*

5.9.4 Monitoring after waste emplacement

Repository closure is a stepwise process from consecutively closing a deposition tunnel to closing one or several deposition areas before the whole repository is closed. Monitoring is planned to continue until all waste has been emplaced and closure of the repository facility is commenced. At closure monitoring systems will be decommissioned successively. At that time it must be considered to what extent the closure process itself needs to be monitored.

5.9.5 Monitoring after repository closure

There is no legal requirement for monitoring after repository closure. According to the IAEA Guide *Geological Disposal Facilities for Radioactive Waste, SSG-14*, regarding the post-closure period, *“the geological disposal facility should be of a passively safe design and should not require or rely on a post-closure monitoring programme to provide assurance of safety. Post-closure monitoring may be performed to provide public assurance, if required, by the government or the regulatory body, but should not compromise the passively safe design.”*. However, it is also noted in the SSG-14 that. *“IAEA policy for geological disposal facilities is that safeguards requirements will continue even after the waste has been sealed in a geological disposal facility. In the post-closure period, IAEA nuclear safeguards might, in practice, be applied by remote means (e.g. satellite monitoring, aerial photography, micro-seismic surveillance) although simpler administrative arrangements could also be adequate. “Intrusive methods, which might compromise safety after closure, have to be avoided”*.

One of the basic requirements is that a final repository should fulfil its function without maintenance and monitoring. The assessment of post-closure safety and compliance with applicable regulations is made under these assumptions. Consequently the PSAR gives no consideration to monitoring after waste emplacement, and it is also assumed that such monitoring, were it to be performed, would not have any detrimental impact on post-closure safety. However, if monitoring after closure is considered the applicable regulations by SSM should be considered. (SSMFS 2008:21 8§ *The impact on safety of such measures that are adopted to facilitate the monitoring or retrieval of disposed nuclear material or nuclear waste from the repository, or to make access to the repository difficult, shall be analysed and reported to the authority*). Furthermore, the recommendation to this paragraph states: *“The safety report for the facility, in accordance with 9 § should show that these measures either have a minor or negligible impact on repository safety, or that the measures result in an improvement of safety, compared with the situation that would arise if the measures were not adopted.”*

6 Handling of external conditions

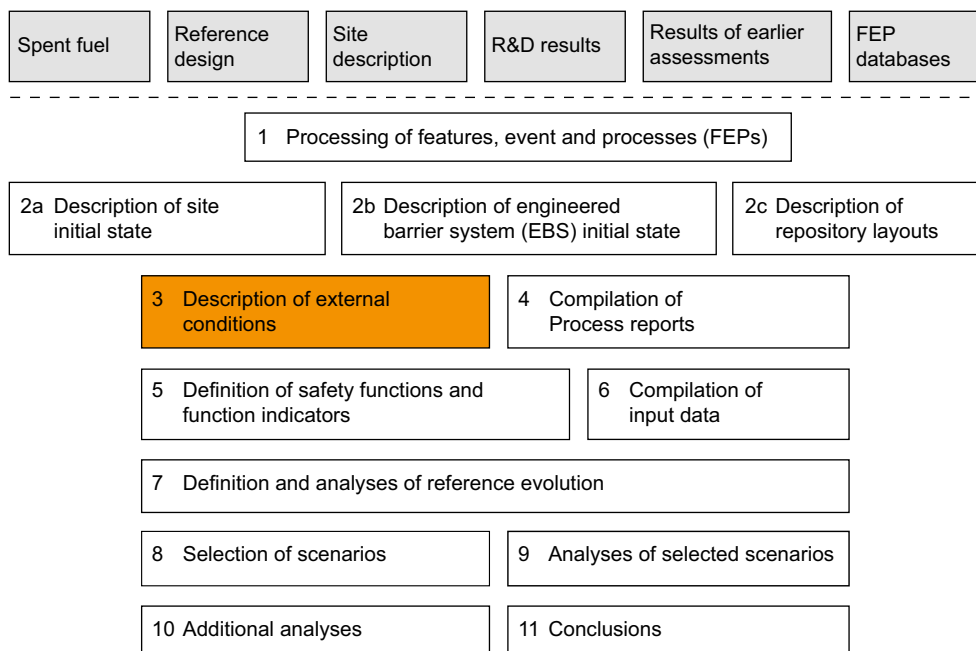


Figure 6-1. The PSAR methodology in eleven steps (Section 2.5), with the present step highlighted.

6.1 Introduction

The contents of the present chapter is quite similar to that of the corresponding chapter 6 of the SR-Site main report (SKB 2011). Substantial updates have, however, been made to the descriptions of denudation in the present Section 6.1 and of human-induced climate change in Section 6.2.1.

The external conditions at the repository site are expected to change considerably over the time scale of the safety assessment. External FEPs are one of the main categories in the SR-Site FEP catalogue, see Chapter 3 and the **FEP report**. The external FEPs are further sorted into the following groups.

1. Climate related issues.
2. Large-scale geological processes and effects.
3. Future human actions.
4. Other (only meteorite impact is identified in this group).

The geological processes that can be regarded as external include weathering, erosion, deposition and tectonic uplift (other than induced by glacial loading and unloading, see below) and plate tectonics. In very long time perspectives, millions to hundreds of millions of years, plate tectonic movements, uplift or downwarping, including denudation of the bedrock surface through weathering and erosion, will affect both the geosphere and the Earth climate system.

The tectonic uplift events that formed the present large-scale Fennoscandian topography mainly occurred in the Tertiary (1.8–65 Ma ago), events that raised the Scandinavian mountain range and the South Swedish Dome centred over the Småland county (e.g. Lidmar-Bergström and Näslund 2002). Although the uplift centres were located mainly west of Forsmark, the site was probably to some extent affected by the uplift. Through increased erosion and weathering, the Tertiary uplift events and Quaternary glacial erosion resulted in a re-exposure of an ancient smooth bedrock surface formed in crystalline bedrock prior to the Cambrian period. Although this smooth bedrock surface, called the Sub-Cambrian peneplain, is dissected along major fracture zones in the Forsmark region (e.g. Grigull et al. 2019), it has been subject to relatively stable large-scale tectonic conditions during the past 1.8 million years (e.g. Lidmar-Bergström and Näslund 2002, Hall et al. 2019). During this period, isostatic changes due to glacial loading and unloading have dominated the vertical displacement of the site.

Estimates of past and future depths of total denudation of bedrock, including glacial erosion, in the Forsmark region have been provided by Hall et al. (2019), see also the **Climate report**, Section 3.5.4), using a detailed multi-methodological approach including e.g. geomorphological analyses and cosmogenic nuclide exposure dating. Quartz in 32 surface basement bedrock samples was analysed for paired cosmogenic ^{10}Be and ^{26}Al nuclide concentrations. The results yield a mean range (25 and 75 % percentiles) of total denudation depths of basement rock of 1.6 m to 3.5 m for the last glacial cycle (last ~100 000 years), with full range values ranging between 0 m and 8.6 m. The corresponding ranges for the last one million years are 12–29 m and 2–61 m. As expected, these ranges mostly reflect the spatial variation in past denudation across the investigated area, but also (to a lesser extent) reflect uncertainties in assumptions adopted regarding different modes of glacial erosion in the calculations of erosion depths (see Hall et al. 2019). The geomorphological analyses provided similar estimates on depths of erosion over the past one million years (Hall et al. 2019). Therefore, the overall conclusion from this study is that typical total denudation depths of basement rock at Forsmark over the past one million years, including glacial erosion, has been restricted, from a few metres up to almost 30 m (see also the **Climate report**, Section 3.5.4).

Lord et al. (2019) provided a first-order estimate of the timing and durations of ice sheet coverage over Forsmark for the coming one million years, based on e.g. IPCC greenhouse-gas emission scenarios. Hall et al. (2019) concluded that if typical glacial erosion depths for Forsmark over the past one million years are assumed to be representative for erosion depths during the future ice covered periods modelled by Lord et al. (2019), then erosion rates over the coming one million years will also be restricted. Adopting this approach, the estimated depth of total denudation, including glacial erosion, of basement rock over the coming 100 000 years is less than 1 m for the Forsmark site and for the location of the repository. Over the coming one million years, the mid-range (25 and 75 % percentiles) of total denudation depths is 5–28 m, whereas a full range is 2–43 m (Hall et al. 2019). Again, the ranges mostly reflect spatial variations in erosion across the Forsmark site and adjacent regions (i.e. differences between the 32 examined sites). All in all, the Hall et al. (2019) results indicate that total maximum denudation of basement rock, including glacial erosion, at Forsmark over the coming one million years, will be less than 50 m (see also **Climate report**, Section 3.5).

The evolving surface topography will change the stress field locally in terms of magnitude and orientation due to the change in overburden weight, shape of the free surface and rearrangement of the groundwater pressure (Moon et al. 2020). This may, in turn, affect the groundwater flow. The main effects will be rather superficial i.e. 100–250 m below the surface. Effects at repository depth are expected to be negligible. A maximum of 50 m reduction in bedrock thickness over the coming 1 Ma will have a corresponding reduction on solute transport characteristics such as groundwater flow path lengths and travel times, but a much smaller effect on transport resistance (which largely controls radionuclide transport) since most of the transport resistance is accumulated in the first parts of flow paths. However, if this reduction in bedrock thickness were to form locally such that surface relief were to increase correspondingly, also hydraulic gradients may increase. This may further reduce transport times and transport resistance, but the changes are estimated to be small relative to other uncertainties.

Another effect of the lowering of the ground surface is that permafrost reaches closer to the repository during periods of periglacial climate conditions that follows glacial periods. However, given the temperature criteria for detrimental effects of freezing of the buffer (Section 8.3.2) and backfill (Section 8.4.4) materials and the estimated depths of the corresponding isotherms in the relevant future climate cases (Sections 10.4.1 and 12.3), the alterations of external conditions caused by erosion and weathering are of minor importance for repository safety within the assessment period. Their impact on the geosphere in the vicinity of the repository and on the current state of the Baltic Shield are reported in the **Climate report** and in the **Geosphere process report** and are not further discussed in this chapter.

Climate changes or climate-related changes, such as the ongoing changes in relative sea level, are the most important external factors affecting the repository in a time perspective from tens of years to hundreds of thousands of years. Most of the safety relevant long-term processes occurring in the biosphere and the geosphere are affected by climate and climate-related changes. A safety assessment therefore must address the potential impact of climate change on repository safety. Climate-related issues are further discussed in Section 6.2.

Another main category of external FEPs that may impact the repository is future human actions. These can be divided into actions at or close to the repository site like utilisation of resources from the bedrock and regional or global actions, e.g. those resulting in severe pollution. Future human actions are further discussed in Section 6.3.

The third group of external FEPs in the FEP catalogue contains only the FEP “Meteorite impact”. Meteorite impacts have been excluded from further analyses, since the probability is very low that a meteorite, large enough to damage the repository, will actually impact Earth, e.g. on the order of one collision every 500 000 year for objects of roughly 1 km in size (Morbidelli et al. 2002) and about one collision every 10 000 years for objects causing craters larger than 1 km in diameter (Melosh 1989). The probability that the hit actually occurs at the repository site is then significantly lower; e.g. an estimated frequency in the order of 10^{-13} per km² per year for impacts causing craters larger than 1 km in diameter has been reported by Hartmann (1965). Since the depth of a crater is about one third of its diameter (Melosh 1989), the crater has to be larger than 1 km in order to expose the repository, but the rock would likely be fractured at repository depth due to somewhat smaller impacts. Furthermore, such an impact event would cause substantial damage to the local and regional biosphere, including humans (Collins et al. 2005), and these direct effects of a meteorite impact are deemed to be much more severe than its possible radiological consequences.

6.2 Climate-related issues

6.2.1 General climate evolution

Natural climate change is caused by factors external to the Earth’s climate system and by the complex response of the climate system’s components and internal dynamics to those forces. Examples of external natural factors affecting climate in the time perspective of interest for the safety assessment are changes in insolation due to variations of the Earth’s orbital parameters, volcanism and solar variability. Another factor affecting climate is anthropogenic activities such as burning of fossil fuel, which increases the concentrations of greenhouse gases in the atmosphere. Internal dynamics affecting the climate include those associated with atmospheric and ocean circulation, the waxing and waning of ice sheets and feedback processes such as those relating to temperature – water vapour, ice – albedo, vegetation – albedo and vegetation – precipitation.

The Earth climate system is also closely linked to the carbon cycle, i.e. the continued exchange and reactions of carbon in the terrestrial biosphere, atmosphere, hydrosphere, and sediments, the latter including fossil fuels. There are important feed-back mechanisms in the carbon transfer processes between these carbon reservoirs, many of which have an impact on climate.

Past climate

For the past ~2.5 million years, several cycles of growth and decay of ice sheets have occurred on Northern Hemisphere mid- to high latitudes. Periods during which ice sheets grow and decay are known as glacials. Periods with warm climate when the ice sheets decay to an extent similar to that at the present day are called interglacials. A glacial cycle consists of a glacial and an interglacial. Glacial cycles also include colder and warmer stages termed stadials and interstadials, respectively. Within the glacial phases, the extent of the ice sheets may vary significantly.

Over the last 700 000 years about 100 000 years long glacial-interglacial cycles have dominated climate variability. These cycles consist, generally speaking, of a long period of, in phases, progressively colder conditions followed by a fast transition back to a warm interglacial climate. During the glacial periods, ice sheets and glaciers have successively – by repeated advances and decays – grown to a maximum extent, followed by the transition to a warm climate during which the ice sheets rapidly melted away to extents similar to that of the present. At the maximum extent during these cold periods, ice sheets covered about one third of the total land area of Earth (nearly 47 million km²), compared to at present with ice sheets and glaciers covering about 10 % (15 million km²) of the land surface. One example of proxy data for global climate change during the past 700 000 years is shown in Figure 6-2.

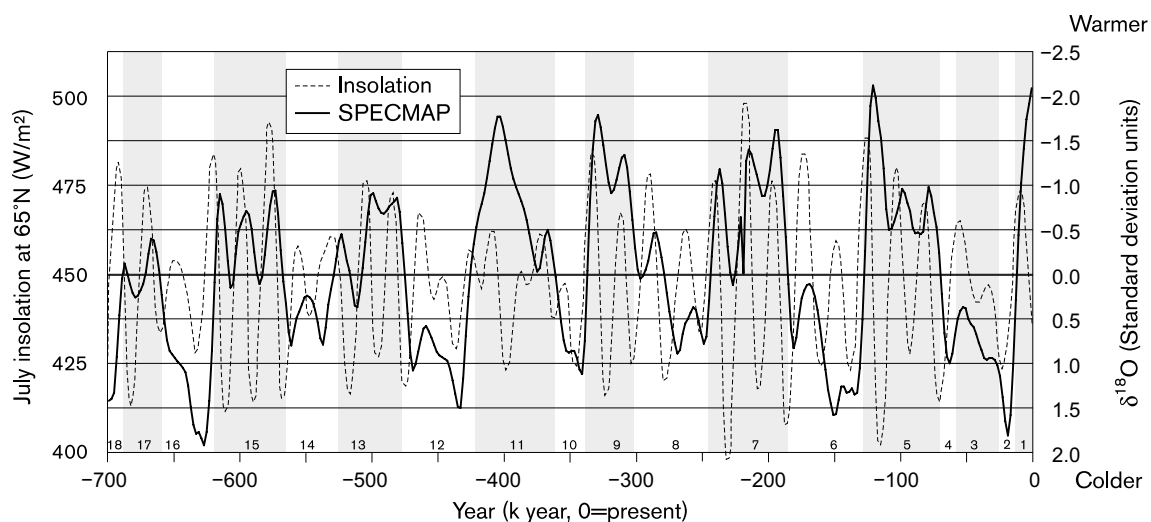


Figure 6-2. $\delta^{18}\text{O}$ variation from five drill cores of deep sea sediments expressed as number of standard deviations from the long-term mean. From Imbrie et al. (1984). $\delta^{18}\text{O}$ variations reflect the temperature of the sea and the volume of water that has been bound in land-based ice sheets and glaciers all over the world. The grey and white fields indicate warm and cold periods.

Glacials in Sweden

During glacial periods, mountain glaciers in the Scandinavian mountain range expand, eventually forming ice caps that in turn expand into an ice sheet. Due to the cold climate, permafrost typically developed in the landscape prior to ice sheet overriding. During the last glacial cycle, the ice sheet grew to its maximum extent at around 20 000 years ago, generally speaking, in a series of ice expansions interrupted by warm interstadials with considerably more restricted ice sheet coverage, see the **Climate report**, Section 4.2.

As the ice sheet grows, the weight of the ice causes an isostatic depression of the Earth's crust. For an overview of the process of glacial isostatic adjustment see the **Climate report**, Section 3.3, Lund and Näslund (2009) and Whitehouse (2009). Simultaneously as ice sheets and glaciers expand globally, an eustatic lowering of global sea level occurs as water is moved from the oceans to the land-based ice masses. The net result of the eustatic component (sea level fluctuations) and isostatic component (vertical changes of the lithosphere) gives a particular development of relative sea level. Depending on the relative rate of the eustatic and isostatic processes, the shore-level can either rise or fall, which in turn gives a transgression or regression, respectively. During a deglaciation after a period of major ice sheet coverage, large portions of the coastal regions of Sweden experience a dominant isostatic recovery component with a general regression as a result, interrupted by shorter periods of sea transgressions.

The changes in the position of the shore-line due to the eustatic and isostatic processes will alter the hydrological conditions at the Forsmark site. The ice load and isostatic process will also alter rock stresses. Changes in the stress state introduced by glacial loading and unloading may in places in Sweden lead to bedrock instability (e.g. Lund et al. 2009) and glacially induced faulting (e.g. Fälvh et al. 2010).

Further, the basal conditions of the ice sheet are important for the hydrological boundary conditions as well as for effective stresses. Figure 6-3 shows a simplified view of the course of events as an ice sheet grows and decays along a transect from the Norwegian coast towards east.

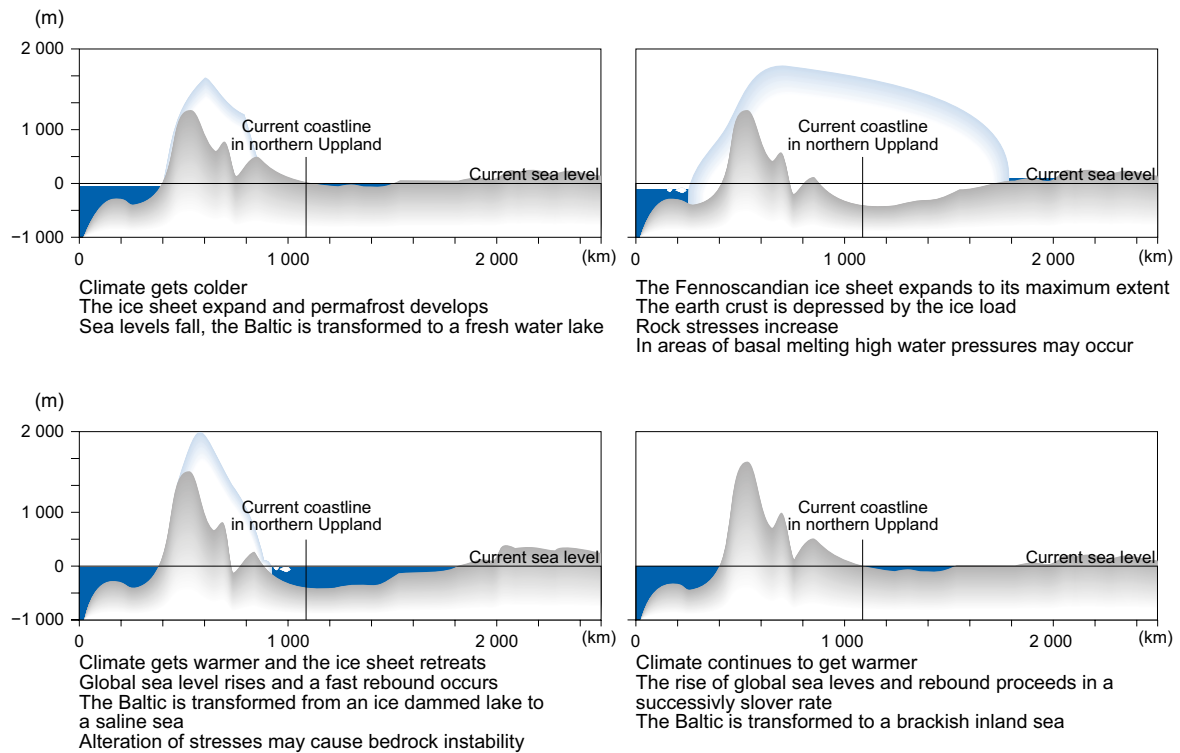


Figure 6-3. The course of events as an ice sheet expands and decays along a schematic transect from the Norwegian coast towards the east. Note that there is a strong vertical exaggeration of the scale of the y-axis.

Human-induced climate change

In addition to naturally occurring processes, the climate is also influenced by human activities, most importantly by anthropogenic emissions of CO₂ and other greenhouse gases. As a result of these emissions, the global-mean surface air temperature has currently increased by approximately 1 °C since the pre-industrial era (e.g. IPCC 2018). This warming will continue also in the future until net emissions are cut to zero (e.g. IPCC 2013, 2018). The anthropogenic influence on the air temperature will remain until the emitted CO₂ has been removed by natural processes from the surface ocean-atmosphere system. This process is projected to take several tens of thousands of years, if not hundreds of thousands of years, depending on the size of the emissions. Therefore, future anthropogenic greenhouse-gas emissions, as well as current levels of atmospheric CO₂, largely influence the climate also on very long time scales, including the length of the current interglacial. Most modelling studies on long-term climate change suggest that the current interglacial will last for another 50 000 years under low future anthropogenic greenhouse-gas emissions, but likely for 100 000 years or longer under higher emissions (Lord et al. 2019, Liakka et al. 2021, see also the **Climate report** Section 5.1.1).

In order to account for the uncertainties related to the magnitude and extent of the anthropogenic influence on climate, two climate cases that describe different levels of anthropogenic greenhouse-gas emissions, and hence different degrees of global warming, are included in the analysis.

- The *global warming climate case* is applied in a variant of the PSAR main scenario (as a complement to the Base case based on the reference glacial cycle). In this climate case, the initial climate evolution is assumed to be influenced by medium future greenhouse-gas emissions, comparable to the Intergovernmental Panel on Climate Change (IPCC) Representative Concentrations Pathway 4.5 (RCP4.5). This assumption results in increased air temperatures and annual precipitation, as well as potentially large changes in the relative sea level at the Forsmark site during the initial 10 000 years and beyond (Section 10.6.1 and Climate report Section 5.1). In the global warming climate case, it is assumed that the current interglacial will be extended by 50 000 years compared to the reference glacial cycle. To that end, the length of the current interglacial in the *global warming climate case* is shorter than suggested by most modelling studies under medium emissions (Liakka et al. 2021, **Climate report**, Section 5.1.1). The choice of a shorter initial period of temperate conditions

is however considered to be pessimistic, as it allows for an earlier occurrence of colder climate conditions and ice-sheet development at the Forsmark site. The possibility of a longer initial period of temperate conditions is covered by the *extended global warming climate case*, see below.

- The *extended global warming climate case* is included as one of the additional safety assessment scenarios to cover the possibility of a longer interglacial than assumed in the *global warming climate case*. In the *extended global warming climate case*, the initial climate evolution is assumed to be influenced by high future greenhouse-gas emissions, comparable to IPCC RCP8.5. This assumption results in higher air temperatures, annual precipitation and relative sea level at the Forsmark site during the initial 10 000 years compared to the *global warming climate case*. In the *extended global warming climate case* (**Climate report** Section 5.2), it is assumed that the current interglacial will be extended by 100 000 years compared to the reference glacial cycle.

6.2.2 Impact on repository safety

Climate-related changes such as shore-line displacement, development of permafrost and the growth and decay of ice sheets will alter not only surface but also subsurface conditions. Freezing, shore-line displacement and the presence of ice sheets will change bedrock permeability, water turnover, groundwater pressures, groundwater flow and composition. The ice load will alter rock stresses and during different phases of a glaciation the principal stresses will change in magnitude. At depths corresponding to the repository depth, the glacial stresses are large enough to change the direction of principal stresses, while this is not the case at large depths. In general, the integrated effects of continuous climatic evolution need to be considered, but there are also a number of more specific phenomena of importance for repository safety that require special attention. Based on the results of earlier assessments, these include:

- The maximum hydrostatic pressure and rock stress occurring at repository depth for glacial conditions.
- The permafrost and freezing depth, affecting freezing of the repository and groundwater flow patterns.
- The possible penetration of oxygen-rich groundwater to repository depth during glacial conditions.
- The possible penetration of dilute groundwaters to repository depth during glacial and temperate conditions, potentially causing erosion of buffer and backfill.
- The groundwater salinity occurring at repository depth, both during glacial, periglacial and temperate climate conditions, the latter including also a period of global warming.
- Glacially induced reactivation of faults.
- Factors affecting retardation in the geosphere, such as high groundwater fluxes and mechanical influences on permeability.

6.2.3 Handling the uncertain long-term climatic evolution

The timing and extent of future climate changes are uncertain due to the complexity of the climate system, see the **Climate report**. Additional uncertainty regarding climate evolution is introduced by the uncertain impact and duration of human influence on the climate. It is not possible to predict a single future climate evolution with the confidence needed for assessments of post-closure repository safety. However, the *range* within which the climate and climate related processes in Sweden may vary in the future can be estimated with reasonable confidence. Rather than focussing on a most likely climate development, the approach to handling climate uncertainty in the safety assessment is to focus on identifying, describing and analysing this range including its bounding end-members. Within these limits, characteristic climate conditions can be identified. The conceivable climate conditions can be represented as climate-driven process domains (Boulton et al. 2001), where such a climate domain is defined as *a climatically determined environment in which a set of characteristic processes of importance for repository safety appear*. The identified domains relevant for the site of the deep repository are:

- A temperate climate domain.
- A periglacial climate domain.
- A glacial climate domain.

The purpose of identifying climate domains is to create a framework for the assessment of climate-related processes of importance for repository safety associated with a particular climatically determined environment. The extent of each climate domain will vary in time and the specific conditions within it will vary both with time and location. The duration of each climate domain depends both on global climate changes and more regional and local factors. The succession of climate domains during a typical glacial cycle will, generally described, follow a cyclic pattern, see Figure 6-4. If a repository for spent nuclear fuel fulfils the safety requirements independent of the prevailing climate domain, and the possible transitions between them, then the uncertainty regarding their extent in time and space is of less importance.

Even if it is not possible to make predictions of the future long-term climate with enough confidence for safety assessment, it is highly likely that the three climate domains will appear repeatedly during the one million year assessment period, i.e. any reasonable future evolution will have to cover them. It is furthermore possible to put bounds on the conditions that plausibly could occur during each of the climate domains. The main scenario of the safety assessment includes a reasonable succession of the identified climate domains.

For compliance purposes, it is particularly important to include sequences covering external conditions yielding, with a high likelihood, the highest risk during the assessment period for a specified scenario of radionuclide release from the repository. Based on results of earlier analyses, the highest risks are likely to occur during temperate periods. Typical situations are i) a terrestrial system that has accumulated radionuclide releases over a long time, possibly in sea sediment prior to its emergence and that is later used for agriculture and ii) a well intruding into the host rock and used for domestic purposes.

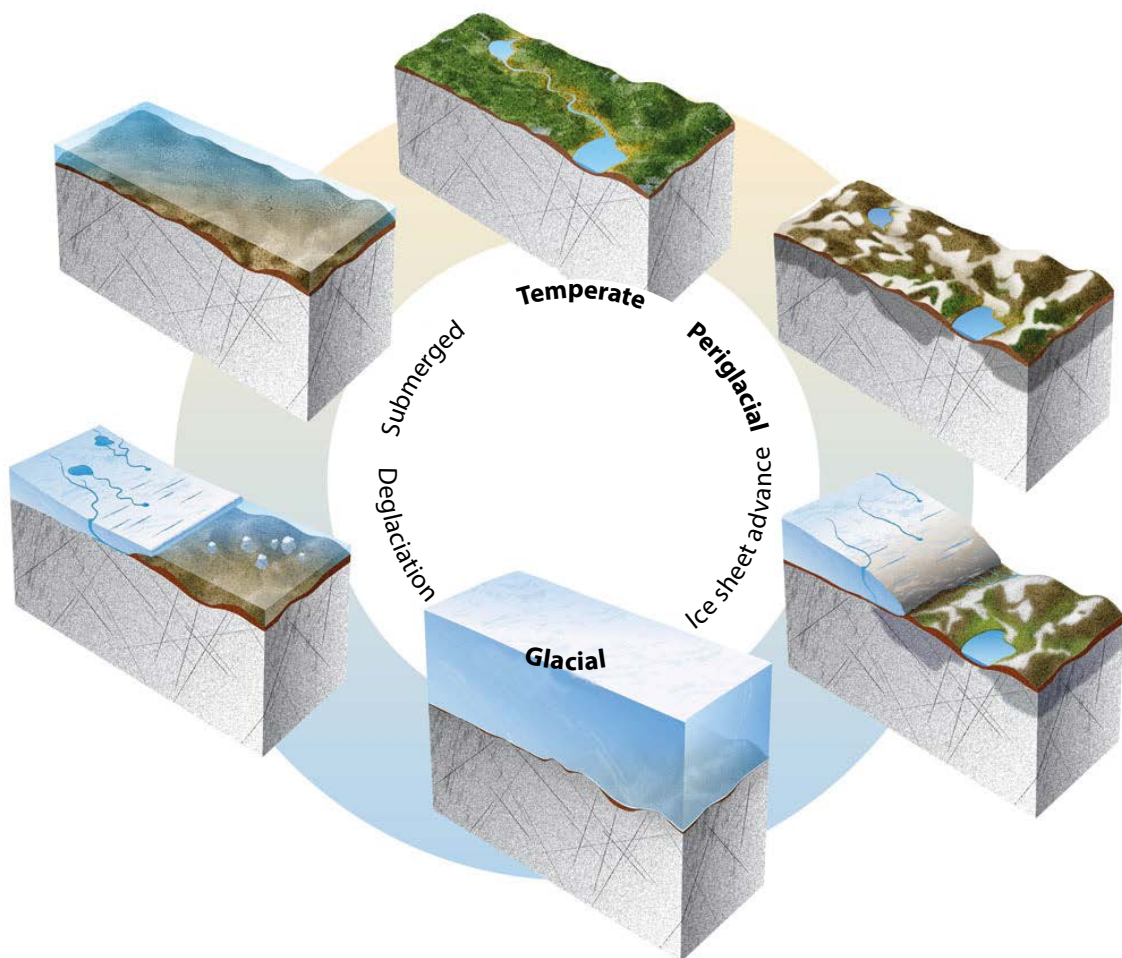


Figure 6-4. The temperate, periglacial and glacial climate domains succeed each other in a cyclic pattern. For the analyses in the safety assessment, this picture is refined to include a more complex and realistic variability.

It is also important to include the climate domains and sequences that have the greatest impact on repository safety through impairment of barrier safety functions. Phenomena that may impact barrier safety functions are mentioned above; the most severe potential effects are related to the development of permafrost and the advance and decay of ice sheets.

The handling of the climate evolution in the PSAR is further developed in Chapter 11 in conjunction with scenarios and in Section 12.1.3 as an introduction to the analyses of the selected scenarios.

6.2.4 Documentation

The climate-related conditions and processes identified as relevant for the post-closure safety of a KBS-3 repository are identified and described in the **Climate report**, one of the supporting documents for the PSAR assessment, see Section 2.5.12. The purpose of the **Climate report** is to provide a concise description of the climate system and to document the scientific knowledge of the climate-related conditions and processes relevant for the post-closure safety of a KBS-3 repository to a level required for an adequate treatment in the safety assessment. The report includes five main parts/chapters:

- Introduction.
- Present and near-future climate in Sweden and Forsmark.
- Climate and climate-related issues.
- Climate and climate-related conditions for the PSAR safety assessment, including a reference glacial cycle.
- Additional climate cases for the safety assessment PSAR with a potentially larger impact on the post-closure safety of a KBS-3 repository than the reference glacial cycle.

The climate-related issues relevant to the post-closure safety of a KBS-3 repository are identified, such as ice sheet growth, ice sheet hydrology, variations in relative sea level, and development of permafrost. These are documented in Chapter 3 “Climate and climate-related issues” to a level required for an adequate treatment in the safety assessment. In Chapter 4, a future 120 000 years long reference glacial cycle, including a characterisation of identified climate-related issues of importance for repository safety, is presented. Finally, relevant complementary climate cases, with a potentially larger impact on repository safety than the reference glacial cycle, are presented in Chapter 5. These cases describe for example situations of expected maximum ice load or maximum permafrost depth. The **Climate report** also includes a description of surface denudation processes (erosion and weathering) as well as a detailed description of the strategy to accommodate long-term climate changes in line with the presentation above.

As further described in the **FEP report**, the content of the **Climate report** has been audited through comparisons with FEP databases compiled in other assessment projects. The **Climate report** follows as far as possible the template for documentation of processes regarded as internal to the repository system, see Section 7.3. However, rather than single processes, a number of more comprehensive climate related *issues* are treated. The issues are i) development of ice sheets, ii) development of permafrost, iii) isostatic adjustment and relative sea level change, iv) glacial hydrology, and v) surface denudation. Each climate-related issue includes a set of processes together resulting in the behaviour of a system or feature. For instance “development of ice sheets” is the result of several thermal, hydrological and mechanical processes.

6.3 Future human actions

A great number of external FEPs related to future human actions (FHA) were identified as a result of an audit against the NEA international database conducted for SR-Can and the complementary audit carried out for SR-Site (described in Chapter 3), see further the **FEP report**. These include actions like rock drilling, mining, severe pollution, underground excavations in relation to urbanisation and intentional or inadvertent repository intrusion. In SR-Can, the identified FEPs were briefly audited against the results of the analyses of scenarios based on future human actions carried out in the SR 97 assessment (SKB 1999a). The majority of the identified FEPs were included in the SR 97 analyses. The latter study was carried out without reference to the NEA database.

The strategy for managing and analysing future human actions in SR-Can (SKB 2006e) was built on the strategy developed for SR 97 and experience from SR 97, the FEP audit in SR-Can and review of some relevant literature published after SR 97. Some further developments have been made for SR-Site based on experience from SR-Can and more recent literature, whereas the complementary FEP audit carried out in SR-Site did not contribute any new information that needed to be considered. The development of the strategy for handling future human actions in SR-Site is described in the **FHA report** together with the analyses of some representative cases. A summary is provided in Section 14.2, where also new developments after SR-Site are reported.

7 Handling of internal processes

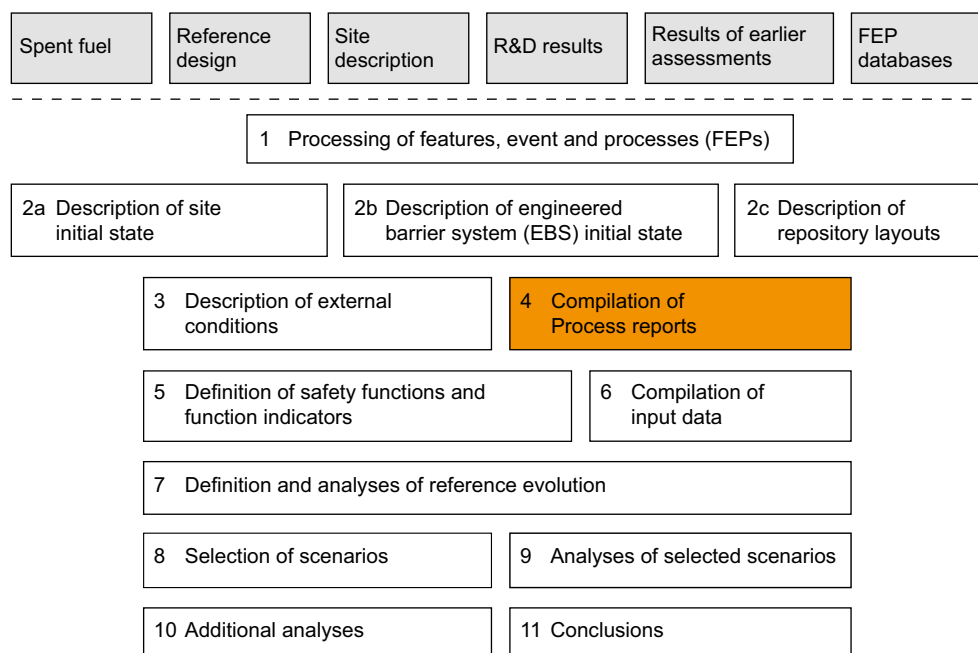


Figure 7-1. The PSAR methodology in eleven steps (Section 2.5), with the present step highlighted.

7.1 Introduction

A thorough understanding and handling of the processes occurring over time in the repository system is a fundamental basis for the safety assessment. The basic sources of information for this are the results of decades of R&D efforts by SKB and other organisations. In a broader sense, these are based on the knowledge accumulated over centuries of scientific and technological development. The R&D efforts have led to the identification and understanding of a number of processes occurring in the engineered barriers and the natural systems relevant to post-closure safety. For the purpose of the safety assessment, the relevant process knowledge for the engineered barriers and the host rock is compiled in a number of **Process reports** which also, for each process, contain a prescription for its handling in the safety assessment. Also short-term geosphere processes/alterations due to repository excavation are included.

This chapter describes how processes are documented in the PSAR **Process reports**, including the principles for their handling in the safety assessment taking into account relevant uncertainties. Formats for graphically illustrating the system of coupled processes are discussed in Section 7.2. The format for process documentation in the PSAR **Process reports** is described in Section 7.3. Section 7.4 gives an overview of the handling of all processes in the PSAR, based on the material in the **Process reports**.

The contents of the present chapter is quite similar to that of the corresponding chapter 7 of the SR-Site main report (SKB 2011). The format for process documentation described in Section 7.3 is identical except that the handling of unqualified references in the SR-Site version is now obsolete, as explained in Section 7.3. The process tables in Section 7.4 and the tables and flow charts in Section 7.5 have been updated to some extent, reflecting differences in process handling compared to the SR-Site assessment.

7.1.1 Identification of processes

The identification of relevant processes has been a continuing effort over many years, based on R&D results, findings in earlier safety assessments etc. In the SR 97 assessment, an identification of the set of processes to be managed in the safety assessment was made (Pers et al. 1999) and this set was the starting point for process identification in SR-Can, the assessment preceding the SR-Site assessment.

As mentioned in Chapter 3, in an audit against the contents of the international FEP database carried out for the SR-Can assessment, a large number of FEPs were mapped to the set of relevant processes in the SKB database leading also to the identification of a few additional processes relevant to the engineered barriers or the geosphere. The updated audit for SR-Site did not lead to the identification of new processes. As mentioned in Section 3.5, the renewed audit for the PSAR did not lead to the identification of any new processes, but the need to include hydrogen embrittlement of copper as a canister process was identified in the R&D work on canister materials. This need was also pointed out in SSM's review of the SR-Site assessment.

In the SR-Can assessment, the division of the system into components was revised and refined, yielding the division given in Section 5.1.2. The deposition tunnel backfill was included as a distinct system component, rather than being described together with the buffer as in SR 97. Also, the components "bottom plate in deposition hole", "plugs", "borehole seals" and "backfill of other repository cavities" were added, but no process reports were developed for them as they are in general not crucially linked to safety. In the PSAR as in SR-Site they are included in the **Buffer, backfill and closure process report**.

7.1.2 Biosphere processes

An interaction matrix for the biosphere was developed in the SAFE project (Kautsky 2001). The result of that work and its further development has been used when setting up the site investigation programme, and it has also provided important input for the development of models for radionuclide transport and exposure to humans. As mentioned in Section 3.3, biosphere processes were not included in the SR 97 Process report and there was not the same basis for updating these descriptions in SR-Can as for the engineered barriers and the geosphere.

For SR-Site, a biosphere process report has been developed (SKB 2010c). This report contains general descriptions of the processes considered to be of importance for the safety assessment, whereas the site-specific aspects of the processes and how these are handled in the safety assessment are provided in the various ecosystem reports developed for SR-Site (Andersson 2010, Aquilonius 2010, Löfgren 2010).

7.2 Format for process representations

For the purpose of the safety assessment, the repository system is divided into several system components and each component is characterised by a number of specified time-dependent physical variables, Section 3.3. Within a specific system component, a number of processes act over time to alter the state of the system, i.e. changing the variables. Examples from the buffer are heat transport, water uptake, swelling, chemical decomposition and ion exchange.

The coupling between the processes is expressed by the network of connected processes and variables and the system of coupled processes needs to be managed in the safety assessment. Couplings between system components are, if required, handled via the time-dependent boundary conditions at the component interfaces.

Variables, processes and their dependencies may be graphically represented in different ways. In SR 97, the representation was in the form of Process Diagrams, one for each system component. Figure 7-2 shows the SR 97 process diagram for the buffer. The diagram also shows which variables influence each process as well as the influences a particular process has on the set of variables. Also, interactions across the boundaries of the system component are described. Another example of graphical representation is the Interaction Matrix (e.g. Skagius et al. 1995). Both these representations condense a vast amount of information graphically. Both interaction matrices and process diagrams have historically and in SR-Site been used to force the analyst to work in a structured way in identifying relevant processes and barrier properties and their dependencies.

The benefits of the structured treatment of processes and variables in the process diagrams are utilised in the process documentation in the PSAR **Process reports**. For each process, a table is given describing, for each variable in the system component, if it influences or is influenced by the process in question, see further Section 7.3. For a given process, the table will thus correspond to the arrows for that process in Figure 7-2. The table format also allows comments to be included and thus gives a fuller description than the arrows in the diagram. In conjunction with the table, the influences are documented.

Buffer/Backfill

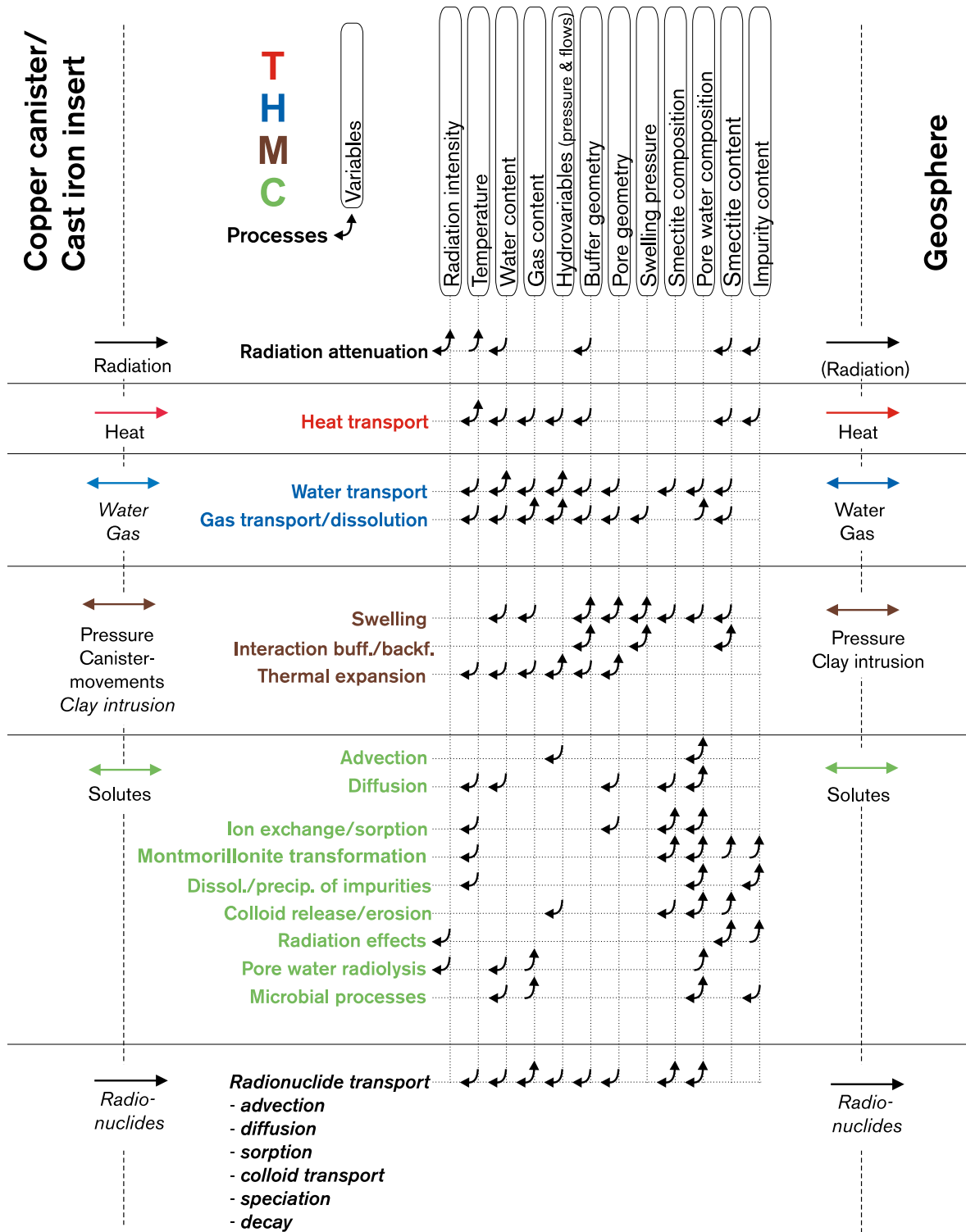


Figure 7-2. The SR 97 version of the process diagram for the buffer. Thermal, hydraulic, mechanical and chemical processes are listed in the left column, the variables are given in the top row. Influences between variables and processes are shown by arrows in the diagram. Processes and interactions in italics only occur if containment by the copper canister is lost.

Both interaction matrices and process diagrams do, however, share a difficulty: It is difficult to grasp system evolution by studying these graphical representations. The graphical information in the diagrams or matrices has, therefore, not been utilised directly in the safety assessment, e.g. for illustrating the evolution of the system. The interaction matrices and the process diagrams convey a (true) impression of complexity, but often with no clear guidance as to the relative importance of different traits of system evolution. This is partly related to the lack of distinction between the different time frames of repository evolution. Most processes and influences on barrier properties are only relevant in some of the several time frames that need to be considered in the safety assessment. The SR-Site FEP catalogue can generate process diagrams, and, if required, be developed so that interaction matrices can also be generated, but neither of these representations has a central role in the further analyses in the PSAR.

The graphical representation of processes in the PSAR is in the form of tables, where the handling of the processes in different time frames is explained. This mode of presentation is further developed in Section 7.4.

7.3 Format for process documentation

The PSAR **Process reports** document all processes in the fuel, the canister, the buffer, the backfill and the host rock identified as relevant for post-closure safety of a KBS-3 repository as discussed in Section 7.1.1. In addition, processes for the system components bottom plate in deposition holes, tunnel plugs, central area, top seal and borehole seals, which were not included in the process reports in SR-Can, are in SR-Site and the PSAR documented in the **Buffer, backfill and closure process report**. As mentioned in Section 7.1.2, biosphere processes are treated in various biosphere reports and the process descriptions do not follow the format applied in the process reports for the other system components. The main reason for this discrepancy is that the description of processes in the biosphere involves a number of different scientific disciplines, in contrast to the discipline-specific descriptions in the geosphere.

The purpose of the **Process reports** is to document the scientific knowledge of the processes to a level required for an adequate treatment in the PSAR. Therefore, from a scientific point of view, the documentation is not fully comprehensive or highly detailed, since such a treatment is neither necessary for the purposes of the safety assessment nor possible within the scope of an assessment.

The purpose is further to determine an approach to the handling of each process in the safety assessment and to demonstrate how uncertainties are taken care of given the adopted handling.

Generally, all arguments including bases for decisions, and underpinning references are provided in the process description under the appropriate headings.

All identified processes are documented using a template, where, in essence, all of the headings are the same as those used in the SR-Can versions of the reports. The template is provided below.

Overview/General description

Under this heading, a general description of the knowledge regarding the process is given. For most processes, a basis for this is the contents of the SR-Can version of the process reports, but reviewed and updated as necessary.

Dependencies between process and variables

For each system component, a set of physical variables that defines the state of the system is specified (see Section 3.3). For each process identified according to Section 7.1.1, a table is presented under this heading with documentation of how the process is influenced by the specified set of physical variables and how the process influences the variables. In addition, the handling of each influence in the PSAR is indicated in the table. In all cases where an influence is present, but not handled in the analyses, a justification for the neglect is provided in the table, and/or in the process description. In the latter case, a reference to the text is included in the table. An example of an influence table is provided in Table 7-1.

Table 7-1. Influence table for the process “heat transport” in the geosphere.

Variable	Variable influence on process			Process influence on variable		
	Influence present? (Yes/No Description)	Time period/ Climate domain	Handling of influence (How/If not – Why)	Influence present? (Yes/No Description)	Time period/ Climate domain	Handling of influence (How/If not – Why)
Temperature in bedrock	Yes. Temperature gradients are the driving force for heat transport. Thermal conductivity and heat capacity are temperature dependent.	Excavation/ operation.	Heat transport neglected (see Section 2.1.7 in the Geosphere process report).	Yes.	Excavation/operation	Heat transport neglected (see Section 2.1.7 in the Geosphere process report).
		Temperate.	Site-specific temperature and thermal properties. Dependence of thermal properties on temp accounted for in dimensioning calculations. Otherwise thermal properties for constant temp.		Temperate	Output from calculations.
		Periglacial Glacial.	See Temperate above and the Climate report .		Periglacial Glacial	Output from calculations, see also Section 2.2 in the Geosphere process report and the Climate report
Groundwater flow	Yes.	Excavation/ operation.	Heat transport neglected (see Section 2.1.7 in the Geosphere process report).	No. But indirectly through temperature.	–	See Section 3.1 Groundwater flow in the Geosphere process report .
		Temperate Periglacial Glacial.	Influence of convection neglected; small contribution compared with thermal conduction.			
Groundwater pressure	Yes.	Excavation/ operation.	Heat transport neglected (see Section 2.1.7 in the Geosphere process report).	No. But indirectly through temperature.	–	See Section 3.1 Groundwater flow in the Geosphere process report .
		Temperate.	Influence neglected; little significance compared with other influences.			
		Periglacial Glacial.	See Temperate above and the Climate report .			
Gas phase flow	Yes.	Excavation/ operation.	Heat transport neglected (see Section 2.1.7 in the Geosphere process report).	No. But indirectly through temperature.	–	See Section 3.2 Gas flow/dissolution in the Geosphere process report .
		Temperate.	Influence neglected; little significance compared with other influences.			
		Periglacial Glacial.	See Temperate above and the Climate report .			
Repository geometry	Yes. Affects heat flux from repository. Canister spacing particularly important in the near field.	Excavation/ operation.	Heat transport neglected (see Section 2.1.7 in the Geosphere process report).	No.	–	–
		Temperate	Included in model.			
		Periglacial Glacial.	Included in permafrost model (see the Climate report).			

Variable	Variable influence on process			Process influence on variable		
	Influence present? (Yes/No Description)	Time period/ Climate domain	Handling of influence (How/If not – Why)	Influence present? (Yes/No Description)	Time period/ Climate domain	Handling of influence (How/If not – Why)
Fracture geometry	Yes.	Excavation/ operation.	Heat transport neglected (see Section 2.1.7 in the Geosphere process report).	No. But indirectly through rock stresses and temperature.		See mechanical processes in Chapter 4 in the Geosphere process report .
		Temperate.	Influence neglected; little significance compared with other influences.			
		Periglacial Glacial.	Influence neglected; little significance compared with other influences.			
Rock stresses	No.	–	–	No. But indirectly through temperature.		See mechanical processes in Chapter 4 in the Geosphere process report .
Matrix minerals	Yes. Determines thermal properties.	Excavation/ operation.	Heat transport neglected (see Section 2.1.7 in the Geosphere process report).	No.	–	–
		Temperate.	Use of site-specific thermal properties.			
		Periglacial Glacial.	Use of site-specific thermal properties in permafrost model (see the Climate report).			
Fracture minerals	Yes. Marginally and locally.	Excavation/ operation.	Heat transport neglected (see Section 2.1.7 in the Geosphere process report).	No. But indirectly through temperature and groundwater composition.	–	See chemical processes in Chapter 5 in the Geosphere process report .
		Temperate.	Influence neglected; little significance compared with other influences.			
		Periglacial Glacial.	Influence neglected; little significance compared with other influences (see the Climate report).			
Groundwater composition	No.	–	–	No. But indirectly through temperature.	–	See chemical processes in Chapter 5 in the Geosphere process report .
Gas composition	No.	–	–	No.	–	–
Structural and stray materials	No.	–	–	No.	–	–
Saturation	Yes. Affects scope and extent of convective heat transport.	Excavation/ operation.	Heat transport neglected (see Section 2.1.7 in the Geosphere Process report).	No. But, indirectly through temperature.	–	–
		Temperate.	Influence neglected; little significance compared with other influences.			
		Periglacial Glacial.	See Temperate above and the Climate report .			

Several reasons for neglect of an influence can be distinguished. These include:

- Little intrinsic significance.
- Little significance compared with other influences.
- Can be subsumed into another influence (without necessarily judging which is the more significant).

Boundary conditions

The boundary conditions for each process are discussed. These refer to the boundaries of the relevant system part. For example, for buffer processes the boundaries are the buffer interfaces with the canister, the walls of the deposition hole, the backfill and the bottom plate in the deposition hole. The processes for which boundary conditions need to be described are, in general, related to transport of material or energy across the boundaries. For example, for chemical processes occurring within a system component, like illitisation in the buffer, the discussion of boundary conditions relates to the boundary conditions of the relevant transport processes occurring in the buffer, i.e. advection and diffusion.

Model studies/experimental studies

Model and experimental studies of the process are summarised. This documentation constitutes the major source of information for many of the processes.

Natural analogues/observations in nature

If relevant, natural analogues and/or observations in nature regarding the process are documented under this heading.

Time perspective

The time scale or time scales on which the process occurs are documented, if such time scales can be defined.

Handling in the PSAR

Under this heading, the handling in the PSAR is described. Typically, the process is either;

- neglected on the basis of the information under the previous headings,
- neglected provided that a particular condition is fulfilled, e.g. that the buffer density is within a specific range, or
- included by means of modelling.

The following aspects are covered, although no prescribed format for the documentation is given.

Time periods: Over what time periods is the process relevant for the system evolution? In e.g. the case of the buffer, relevant time periods might be:

- The resaturation phase extending from the time of deposition until the time when the buffer is fully water saturated.
- The so called thermal phase extending from the time of deposition and throughout the approximately 1 000 year time period of elevated temperature in the buffer. or
- The long-term time scale extending throughout the one million year assessment period and including the varying conditions in the bedrock caused by long-term climate and other environmental variations.

By documenting the relevance of the process for applicable time periods, the process system can be simplified by omitting the process in time periods during which it is not relevant.

Boundary conditions: How are the boundary conditions handled? Are e.g. spatially and temporally varying chemical and hydraulic conditions considered?

Influences and couplings to other processes: The handling of the influences documented according to the above description is discussed as are couplings to other processes within the system component.

The special cases of a failed canister and of earthquakes altering deposition hole or tunnel geometry: These special cases imply altered conditions that could influence many processes in particular for the fuel, the canister, the buffer and the backfill and they therefore need to be discussed separately. Canister failures and earthquakes of a magnitude that could affect the deposition hole or tunnel geometry are not expected during the several thousands of years after deposition when temperate conditions are likely to prevail, meaning that the special cases are not relevant for many “early” processes.

As a result of the information under this subheading, a mapping of all processes to method of treatment and, in relevant cases, applicable models is produced, see further Section 7.4.

Handling of uncertainties in the PSAR

Given the adopted handling of each process in the PSAR, the handling of different types of uncertainties associated with the process is summarised.

Uncertainties in mechanistic understanding: The uncertainty in the general understanding of the process is discussed based on the available documentation and with the aim of answering the question: Are the basic scientific mechanisms governing the process included and understood to a level necessary for the adopted handling? Alternative models are sometimes used to illustrate this type of uncertainty.

Model simplification uncertainties: In most cases, the quantitative representation of a process contains simplifications. These may result in a significant source of uncertainty in the description of the system evolution. Alternative models or alternative approaches to simplification for a particular conceptual model are sometimes used to illustrate this type of uncertainty.

Input data uncertainties: The set of input data necessary to quantify the process for the suggested handling is documented. The further treatment of important input data and input data uncertainties is described in the **Data report**, to which reference is made if relevant.

References

A list of references used in the process documentation is given at the end of the reports. In the SR-Site version of the reports, each process also had the sub-heading “Adequacy of the references supporting the handling in SR-Site”. Under that heading, statements were provided concerning the adequacy of the references in a quality assurance perspective, since some references were not qualified according to the requirements in the SR-Site QA plan. Some of those references are used also in the PSAR versions, without repeating the qualification statement from the SR-Site assessment. All new references in the PSAR versions are qualified according to the SKB management system. The mentioned sub-heading is thus obsolete and is not used in the PSAR version.

7.4 Process mapping/process tables

To summarise the handling of processes in the safety assessment, a table showing the handling of each process has been produced, based on the handling documented in the **Process reports**. The description is broken down in different time frames where relevant. One table per system component is provided. In the table, the process is either “mapped” to a model by which it is quantified or associated with a brief description of how it is handled. The PSAR process tables for the fuel, the canister, the buffer, the deposition tunnel backfill and the geosphere are presented in Sections 7.4.1 to 7.4.5.

In Section 7.5, two flow charts demonstrate how the different modelling activities are connected.

7.4.1 Fuel and canister interior

Table 7-2. Process table for the fuel and canister interior describing how fuel processes and processes occurring in the canister interior are handled for intact canisters and in the special cases of failed canisters (italicised text). Green fields denote processes that are neglected or irrelevant for the period of interest. Red fields denote processes that are quantified by modelling in the safety assessment. Orange fields denote processes that are neglected subject to a specified condition. Motives for the adopted handling are given in the Fuel and canister process report. An overview of all modelling activities, with references to sections in this main report where the results are discussed, is given in Section 7.5. Much of this information is also given in the last column in the table.

	Intact canister	FEP chart item intact can (see Section 8.5)	Failed canister	Reference to sections in this report (if relevant) and other notes
F1. Radioactive decay	Thermal model.	Decay, heat generation.	COMP23.	In thermal calculation, see Section 10.3.4, in nuclide transport calculations Section 13.4.1.
F2. Radiation attenuation/heat generation	Radiation attenuation: Initial radiation levels given in (SKB 2010e). Heat generation: Included in integrated modelling of thermal evolution.	Decay, heat generation.	Neglected when releases occur after period of elevated temperatures.	See Sections 5.3.4 (initial radiation levels) and 10.3.4 (thermal evolution).
F3. <i>Induced fission (criticality)</i>	Neglected since there will be insufficient amounts of moderator inside the canister prior to failure.	–	Neglected since the probability is negligibly small if credit is taken for the burn-up of the fuel.	See further Section 13.3.
F4. Heat transport	Included in integrated modelling of thermal evolution.	Heat conduction.	Neglected when releases occur after period of elevated temperatures.	In thermal calculation, see Section 10.3.4.
F5. <i>Water and gas transport in canister cavity, boiling/condensation</i>	Not relevant.	–	Description in the Fuel and canister process report , Section 2.3.1, integrated with other relevant processes yielding simplified, pessimistic assumptions on retardation in failed canister depending on failure mode.	See the Radionuclide transport report .
F6. Mechanical cladding failure	Not relevant.	–	Pessimistic assumption.	
F7. Structural evolution of fuel matrix	Not relevant.	–	Negligible for the fuel types and burnup relevant for the PSAR.	
F8. <i>Advection and diffusion</i>	Not relevant.	–	Description in the Fuel and canister process report , Section 2.3.1, integrated with other relevant processes yielding simplified, pessimistic assumptions on retardation in failed canister depending on failure mode.	Refers to diffusion and advection in the canister interior, see Chapter 13. See also process F17.
F9. Residual gas radiolysis/acid formation	Neglected since only small amounts of corrodents are produced.	–	Not relevant.	See Sections 10.2.5 and 15.5.5.

	Intact canister	FEP chart item intact can (see Section 8.5)	Failed canister	Reference to sections in this report (if relevant) and other notes
F10. <i>Water radiolysis</i>	Neglected.	–	Neglected except for fuel dissolution, see that process.	Initial water consumed by nitric acid formation or cast iron corrosion.
F11. <i>Metal corrosion</i>	Not relevant.	–	Modelled in COMP23.	See Section 13.4.1 and 13.5.2, subheading "Release of activation products".
F12. <i>Fuel dissolution</i>	Not relevant.	–	Modelled as constant, pessimistic dissolution rate in COMP23.	Chapter 13.
F13. <i>Dissolution of gap inventory</i>	Not relevant.	–	Pessimistic, instantaneous.	See Section 13.4.1.
F14. <i>Speciation of radionuclides, colloid formation</i>	Not relevant.	–	COMP23.	Precipitation/dissolution handled by COMP23, concentration limits provided in the Data report . See Chapter 13.
F15. Helium production	Neglected since the amount of helium produced will not increase the pressure inside the canister enough to affect its mechanical stability.	–	Not relevant.	See the Fuel and canister process report , Section 2.5.8.
F16. Chemical alteration of the fuel matrix	Not relevant.		Neglected since it is not deemed to increase the dissolution rate of the fuel.	
F17. <i>Radionuclide transport</i>	Not relevant.		COMP23.	Canister interior treated as mixed tank in all transport calculations reported in Chapter 13.

7.4.2 Canister

Table 7-3. Process table for the canister describing how canister processes are handled for intact canisters and in the special case of failed canisters (italicised text). Green fields denote processes that are neglected or irrelevant for the period of interest. Red fields denote processes that are quantified by modelling in the safety assessment. Orange fields denote processes that are neglected subject to a specified condition. Motives for the adopted handling are given in the Fuel and canister process report. An overview of all modelling activities, with references to sections in this main report where the results are discussed, is given in Section 7.5. Much of this information is also given in the last column in the table.

	Intact canister	FEP chart item intact can (see Section 8.5)	Failed canister	Reference to sections in this report (if relevant) and other notes
C1. Radiation attenuation/heat generation	Radiation attenuation: Initial radiation levels given in SKB (2010g). Heat generation: Included in integrated modelling of thermal evolution.	Decay, heat generation.	Neglected when releases occur after period of elevated temperatures.	See Sections 5.3.4 (initial radiation levels) and 10.3.4 (thermal evolution).
C2. Heat transport	Included in integrated modelling of thermal evolution.	Heat conduction.	Neglected when releases occur after period of elevated temperatures.	See Section 10.3.4.
C3. Deformation of cast iron insert	Isostatic and shear loads modelled in design analysis of canister, see Section 5.4.3. (Uneven loads from uneven swelling and lack of straightness of the deposition hole included.) Considered as cause for failure when isostatic or shear loads on canister exceed technical design requirements loads.	Isostatic load. Rock shear.	Description in the Fuel and canister process report , Section 3.4.2, integrated with other relevant processes yielding simplified, pessimistic assumptions on retardation in failed canister depending on failure mode.	See Sections 10.3.13 (temperate period), 10.4.5 (large earthquakes) and 10.4.9 (isostatic pressure for glacial load).
C4. Deformation of copper canister from external pressure	Isostatic and shear loads modelled in design analysis of canister, see Section 5.4.3. (Uneven loads from uneven swelling and lack of straightness of the deposition hole as well as creep in copper included.) Considered as cause for failure when isostatic or shear loads on canister exceed technical design requirements loads.	Isostatic load. Rock shear.	Neglected.	See in particular Section 10.4.5 (large earthquakes) and Section 12.7.5 (copper creep due to isostatic load).
C5. Thermal expansion (both cast iron insert and copper canister)	Neglected since the thermal expansion will cause negligible strains in the materials.	–	Neglected.	

	Intact canister	FEP chart item intact can (see Section 8.5)	Failed canister	Reference to sections in this report (if relevant) and other notes
C6. <i>Deformation from internal corrosion products</i>	Not relevant due to limited amount of water.	–	Description in the Fuel and canister process report , Section 2.3.1 and 3.4.5, integrated with other relevant processes yielding simplified, pessimistic assumptions on retardation in failed canister depending on failure mode.	See the Radionuclide transport report .
C7. Radiation effects	Neglected based on the specified limit on Cu content for the insert. (Cu impurities promote radiation damage.) Radiation effect on the copper shell neglected due to negligible changes in the material.	–	Neglected.	
C8. <i>Corrosion of cast iron insert</i>	Neglected due to limited amount of water giving negligible corrosion effects.	–	Description in the Fuel and canister process report , Section 2.3.1 and 3.5.1, integrated with other relevant processes yielding simplified, pessimistic assumptions on retardation in failed canister depending on failure mode.	See the Radionuclide transport report .
C9. <i>Galvanic corrosion</i>	Not relevant.	–	Neglected, as influence of galvanic corrosion under oxygen-free, reducing conditions lies within the margins of error for the corrosion rate of the iron insert.	See the Radionuclide transport report .
C10. Stress corrosion cracking of cast iron insert	Neglected since stress corrosion cracking is considered unlikely and even if it occurred it would have no consequences for stability of the insert.	–	Neglected.	

	Intact canister	FEP chart item intact can (see Section 8.5)	Failed canister	Reference to sections in this report (if relevant) and other notes
C11. Corrosion of copper canister	<p>Generally, corrosion is modelled based on mass balance (entrapped O₂) and transport capacity considerations (H₂S(g) and HS⁻(aq)) whereas reaction rates are disregarded.</p> <p>Sulphide from pyrite in buffer and backfill modelled based on transport capacity. Microbially generated sulphide in buffer (after buffer loss) and backfill pessimistically bounded by supply of nutrients for microbes. Entrapped O₂ in buffer and backfill: Pessimistically assumed that all O₂ corrodes copper neglecting consumption by pyrite in buffer, rock minerals and microbial activity. Potentially intruding O₂ during glaciation: Integrated handling of rock, backfill and buffer conditions.</p> <p>Localised O₂ corrosion: Assessed with probabilistic model and data from field tests. Localised sulphide corrosion: described as micro-galvanic corrosion, only possible for very high sulphide fluxes.</p> <p>Corrosion due to radiation: Negligible corrosion depths and minor localised corrosion, based on experimental studies and modelling.</p> <p>Chloride assisted corrosion neglected as long as the combinations of pH and chloride concentration is below (the right-hand side of) the limiting curve (i.e. a total copper concentration in solution of less than 10⁻⁶ mol/kg).</p> <p>Effects of different corrosion behaviour of cold worked or welded material neglected due to small effects (if any) on fundamental corrosion properties.</p> <p>Corrosion by water disregarded based on thermodynamic considerations and laboratory tests.</p>	Corrosion.	Not relevant for failed canister.	See Sections 10.2.5, 10.3.13 and 10.4.9.

	Intact canister	FEP chart item intact can (see Section 8.5)	Failed canister	Reference to sections in this report (if relevant) and other notes
C12. Stress corrosion cracking, copper canister	<p>For aerobic conditions the possible concentrations of SCC promoting agents close to the canister surface are compared with the threshold concentrations where SCC has been noticed in laboratory experiments.</p> <p>For radiolytic conditions, neglected due to low dose rate and thus insignificant effect on corrosion potential, material defect structure and mechanical properties.</p> <p>For reducing sulphidic conditions, the sulphide flux is compared with experimental threshold values for observed interfacial cracking.</p>	Corrosion	Neglected.	See Section 10.3.13
C13. Earth currents – stray current corrosion	Negligible increase in corrosion from external electrical field from natural earth currents or present HVDC installations. Future installations mentioned as a stylised case of future human action, with negligible consequences.	–	Neglected.	See Section 14.2.1.
C14. Deposition of salts on canister surface	Neglected due to small consequences (and only relevant during bentonite saturation phase).	–	Neglected.	
C15. Radionuclide transport	Not relevant.	–	COMP23.	See Chapter 13.
C16. Hydrogen embrittlement of copper	<p>Embrittlement due to reduction of oxides neglected since the concentration of oxygen in Cu-OFP is sufficiently low, and since welding under inert gas has been shown as efficient to avoid enhanced oxide concentrations in the weld.</p> <p>The levels of hydrogen potentially absorbed by copper under the H₂ flux generated at the canister surface by radiolysis and sulphide corrosion, are compared with the initial concentration of H in Cu-OFP and/or the concentrations of H known to experimentally affect the material properties and tendency to crack under tensile stress.</p>	Substantial H ingress in Cu	Neglected.	See Section 10.3.13.

7.4.3 Buffer

Table 7-4. Process table for the buffer describing how buffer processes are handled in different time frames and for the special case of an earthquake. Green fields denote processes that are neglected or not relevant for the period of interest. Red fields denote processes that are quantified by modelling in the safety assessment. Orange fields denote processes that are neglected subject to a specified condition. Motives for the adopted handling are given in the Buffer, backfill and closure process report. An overview of all modelling activities, with references to sections in this main report where the results are discussed, is given in Section 7.5. Much of this information is also given in the last column in the table.

	Resaturation/"thermal" period	Long-term after saturation and "thermal" period	Earthquakes	FEP chart item (see Section 8.5)	Reference to sections in this report (if relevant) and other notes.
Intact canister					
Bu1. Radiation attenuation/heat generation	Neglected since dose rate is too low to be of importance for the buffer	Neglected since dose rate is too low to be of importance for the buffer	Not relevant	–	
Bu2. Heat transport	System model	System model	Not relevant	Heat conduction.	See Section 10.3.4.
Bu3. Freezing	Neglected, since temperatures causing detrimental freezing effects cannot occur during this period	Neglected if buffer temperature > –6 °C. Otherwise bounding consequence calculation	Not relevant	Freezing, expansion.	Repository temperature in long term obtained from permafrost depth modelling, see Section 10.4.3.
Bu4. Water uptake and transport for unsaturated conditions	THM model	Not relevant by definition	Not relevant	Saturation.	See Section 10.3.8.
Bu5. Water transport for saturated conditions	Neglected by definition under unsaturated conditions. For saturated conditions the treatment is the same as for "Long-term"	Neglected if hydraulic conductivity < 10 ⁻¹² m/s since diffusion would then dominate	Consider pressure transients	Advection.	Regarding consequences of buffer colloid release, see Section 10.4.9, subheading "Canister corrosion for a partially eroded buffer".
Bu6. Gas transport/dissolution	Through dissolution/THM model	(Through dissolution) No gas phase is assumed to be present	(Through dissolution) No gas phase is assumed to be present	–	
Bu7. Piping/erosion	Model study	Not relevant, see also Bu18	Not relevant	Piping/erosion.	See Section 10.2.4.

	Resaturation/"thermal" period	Long-term after saturation and "thermal" period	Earthquakes	FEP chart item (see Section 8.5)	Reference to sections in this report (if relevant) and other notes.
Bu8. Swelling/Mass redistribution	THM modelling including interaction buffer/backfill and thermal expansion System model (final swelling)	Integrated evaluation of erosion, convergence, corrosion products, creep, swelling pressure changes due to ion exchange and salinity, canister sinking	Part of integrated assessment of buffer/canister/rock	Swelling.	Initial saturation/swelling: See Section 10.3.9. Long-term temperate conditions: Section 10.3.12. Effects on swelling pressure from salinity are discussed in Sections 10.3.9, 10.4.8 and 12.2.2. The effect of ion-exchange on swelling pressure is discussed in Section 12.2.2. Earthquakes: See Section 10.4.5. Consequences of buffer colloid release (erosion) discussed in Section 10.4.9, subheading "Canister corrosion for a partially eroded buffer" and covered by stylised case reported in Section 10.3.9. Canister sinking is discussed in Section 10.4.8 and 12.2.4.
Bu9. Liquefaction	Not relevant in an unsaturated material	Neglected since liquefaction from a short pulse cannot occur in a high density bentonite, due to high effective stresses	Neglected since liquefaction from a short pulse cannot occur in a high density bentonite, due to high effective stresses		See Section 10.4.8, subheading "Liquefaction".
Bu10. Advective transport of species	Simplified assumptions of mass transport of dissolved species during saturation	Neglected if hydraulic conductivity $< 10^{-12}$ m/s	Consider pressure transients	Advection.	See process Bu5.
Bu11. Diffusive transport of species	Chemistry model (thermal, saturated phase; unsaturated phase disregarded)	Chemistry model	Consider altered geometry (diffusion pathways)	Diffusion.	Thermal phase: Section 10.3.10 Long-term temperate: Section 10.3.12 Glacial cycle: Section 10.4.8, subheading "Chemical evolution of buffer and backfill for altered groundwater compositions".

	Resaturation/"thermal" period	Long-term after saturation and "thermal" period	Earthquakes	FEP chart item (see Section 8.5)	Reference to sections in this report (if relevant) and other notes.
Bu12. Sorption (including ion-exchange)	Chemistry model (thermal, saturated phase; unsaturated phase disregarded)	Chemistry model	Not specifically treated	Reactions in porewater, gas and clay, sorption.	See process Bu11.
Bu13. Alterations of impurities	Chemistry model (thermal, saturated phase; unsaturated phase disregarded)	Chemistry model	Not specifically treated	Reactions in porewater, gas and clay, sorption.	See process Bu11.
Bu14a. Aqueous speciation and reactions	Chemistry model (thermal, saturated phase; unsaturated phase disregarded)	Chemistry model	Not specifically treated	Reactions in porewater, gas and clay, sorption.	See process Bu11.
Bu14b. Gaseous speciation and reactions	Included as a partial pressure in geochemical modelling Included in corrosion estimates Neglected in THM modelling	Not relevant by definition	Not specifically treated	Reactions in porewater, gas and clay, sorption.	See process Bu11.
Bu15. Osmosis	Evaluation through comparison with empirical data.	Evaluation through comparison with empirical data	Not specifically treated	Osmosis.	Initial saturation/swelling: See Section 10.3.9. Long-term temperate: Section 10.3.12. Glacial cycle: Section 10.4.8, subheading "Effects of saline water on buffer and backfill".
Bu16. Montmorillonite transformation	Model calculations (thermal, saturated phase; unsaturated phase disregarded)	Estimate based on evidence from nature	Part of integrated assessment of buffer/canister/rock	Reactions in porewater and clay, sorption.	Thermal phase: See Section 10.3.10, subheading "Mineral transformation", covers also long-term temperate phase.
Bu17. Iron-bentonite interaction	Neglected since no iron will be in contact with the bentonite	Only considered for failed canister. Possible loss of buffer efficiency	Only considered for failed canister. Possible loss of buffer efficiency		
Bu18. Montmorillonite colloid release	Neglected if total cation charge is > 8 mM. Otherwise modelled	Neglected if total cation charge is > 8 mM. Otherwise modelled	Not specifically treated	Colloid release.	Long-term temperate: Section 10.3.12 Glacial cycle: Section 10.4.8, subheading "Colloid release from buffer and backfill".
Bu19. Radiation-induced transformations	Neglected since dose rate outside canister is too low to have any effect	Neglected since dose rate outside canister is too low to have any effect	Neglected since dose rate outside canister is too low to have any effect	–	

	Resaturation/"thermal" period	Long-term after saturation and "thermal" period	Earthquakes	FEP chart item (see Section 8.5)	Reference to sections in this report (if relevant) and other notes.
Bu20. Radiolysis of porewater	Neglected since dose rate outside canister is too low to have any effect	Neglected since dose rate outside canister is too low to have any effect	Neglected since dose rate outside canister is too low to have any effect	–	
Bu21. Microbial processes	Neglected under unsaturated conditions, in this case the unsaturated part of the buffer, since the extent of aqueous reactions is limited. For saturated conditions the treatment is the same as for "Long-term"	Neglected if buffer density is sufficient. Quantitative estimate of sulphate reduction, limited by supply of microbe nutrients in groundwater	Not specifically treated	Corrosion.	Sulphate reduction included in corrosion calculation, Section 10.4.9.
Bu22 Cementation	Discussed together with Process Bu16 "Montmorillonite transformation"	Discussed together with Process Bu16 "Montmorillonite transformation"	Part of integrated assessment of buffer/canister/rock		
Failed canister					
Bu6. Failed canister. Gas transport/dissolution	Quantitative estimate based on empirical data (<i>no failures are expected this period</i>)	Quantitative estimate based on empirical data	Quantitative estimate based on empirical data	–	See Section 13.8.
Bu19. Failed canister. Radiation-induced transformations	Neglected since dose rate outside canister is too low to have any effect	The effect of α -radiation from nuclides from a failed canister is estimated	The effect of α -radiation from nuclides from a failed canister is estimated	–	The effect of α -radiation from nuclides is estimated in the Buffer, backfill and closure process report , Section 3.5.12. There, it is concluded that the consequences can be neglected.
Bu23. Colloid transport	Neglected if dry density > 1000 kg/m ³ , otherwise bounding calculation (<i>no failures are expected this period</i>)	Neglected if dry density > 1000 kg/m ³ , otherwise bounding calculation	Neglected if dry density > 1000 kg/m ³ , otherwise bounding calculation	–	See Section 13.5.3.
Bu24. Speciation of radionuclides	No failures are expected this period	Assumptions based on empirical data	Assumptions based on empirical data	–	See Chapter 13.
Bu25. Transport of radionuclides in water phase	No failures are expected this period	COMP23	COMP23 Reduced diffusion path	–	See Chapter 13. Earthquake: See Section 13.6.
Bu26. Transport of radionuclides by a gas phase	No failures are expected this period	Quantitative estimate	Quantitative estimate	–	See Section 13.8.

7.4.4 Backfill in deposition tunnels

Table 7-5. Process table for the backfill describing how backfill processes are handled in different time frames. Green fields denote processes that are neglected or not relevant for the period of interest. Red fields denote processes that are quantified by modelling in the safety assessment. Orange fields denote processes that are neglected subject to a specified condition. Motives for the adopted handling are given in the Buffer, backfill and closure process report. An overview of all modelling activities, with references to sections in this main report where the results are discussed, is given in Section 7.5.

	Resaturation/"thermal" period	Long-term after saturation and "thermal" period	FEP chart item (see Section 8.5)	Reference to Sections in this report (if relevant) and other notes
Intact canister				
BFT1. Heat transport	Simplified assumption	Simplified assumption	–	
BFT2. Freezing	Neglected, since this requires permafrost conditions	Neglected if backfill temperature > –6 °C. Otherwise discussed	Not included since freezing in backfill relates to retardation.	Less severe consequences than for buffer.
BFT3. Water uptake and transport for unsaturated conditions	THM model	Not relevant by definition	Saturation.	The pellets are included in the model.
BFT4. Water transport for saturated conditions	Neglected under unsaturated conditions, for saturated conditions the treatment is the same as for "Long-term"	Included in geosphere modelling	Advection.	Evaluate effects on conductivity of chemical evolution and mass redistribution/loss and of possible changes of hydraulic gradients for permafrost and glaciation.
BFT5. Gas transport/dissolution	THM model	(Through dissolution)		The presence of a trapped gas phase is considered in the modelling of the saturation of the backfill (not the case for the buffer).
BFT6. Piping/erosion	Quantitative estimate with an empirical model	Not relevant, see also BFT16	Piping/erosion.	See also water transport for saturated conditions.
BFT7. Swelling/Mass redistribution	THM modelling including interaction buffer/backfill and homogenisation in tunnel	Integrated evaluation of erosion, convergence, creep, swelling pressure changes due to ion exchange and salinity and transformation	Swelling (buffer).	Deviations in amount of buffer and backfill initially deposited and buffer saturating before tunnel backfill is discussed in Section 10.3.9. The effect of salinity is discussed in Section 10.3.9 and 10.4.8. The effect of erosion is discussed in Section 10.4.8.
BFT8. Liquefaction	Not relevant	Not relevant	–	Less severe consequences than for buffer. Discussed in Section 10.4.8.

	Resaturation/"thermal" period	Long-term after saturation and "thermal" period	FEP chart item (see Section 8.5)	Reference to Sections in this report (if relevant) and other notes
BFT9. Advective transport of species	Simplified assumptions of mass transport of dissolved species during saturation	Included in geosphere modelling. Cases without the backfill path will be considered	Advection.	See "Water transport for saturated conditions".
BFT10. Diffusive transport of species	The early stage is not studied specifically, since the conditions in the backfill will be about the same as for the long-term evolution	Chemistry model	Diffusion.	Thermal phase: Section 10.3.10 Long-term temperate: Section 10.3.12 Glacial cycle: Section 10.4.8, subheading "Chemical evolution of buffer and backfill for altered groundwater compositions"
BFT11. Sorption (including ion-exchange)	The early stage is not studied specifically, since the conditions in the backfill will be comparable to those for the long-term evolution	Chemistry model	Reactions in porewater and clay, sorption.	See process BFT10. See also osmosis.
BFT12. Alterations of impurities	The effect on inorganic reduction of oxygen is modelled	Chemistry model	Reactions in porewater and clay, sorption.	See process BFT10.
BFT13. Aqueous speciation and reactions	The early stage is not studied specifically, since the conditions in the backfill will be about the same as for the long-term evolution	Chemistry model	Reactions in porewater and clay, sorption.	See process BFT10.
BFT14. Osmosis	Included as a partial pressure in geochemical modelling Included in corrosion estimates Neglected in THM modelling	Not relevant by definition	Osmosis.	Handling of long-term intrusion of saline water.
BFT15. Montmorillonite transformation	Hydraulic conductivity in THM model chosen so as to handle osmosis	Evaluation through comparison with empirical data	Reactions in porewater and clay, sorption.	
BFT16. Colloid release	Model calculations (thermal, saturated phase; unsaturated phase disregarded)	Model calculations	Colloid release.	Loss of backfill is discussed in Section 10.4.8.
BFT17. Radiation-induced transformations	Neglected if total cation charge is > 8 mM Otherwise modelled	Neglected if total cation charge is > 8 mM Otherwise modelled	–	
BFT18. Microbial processes	Neglected, since dose rate in backfill is too low to have any effect	Neglected, since dose rate in backfill is too low to have any effect		

	Resaturation/"thermal" period	Long-term after saturation and "thermal" period	FEP chart item (see Section 8.5)	Reference to Sections in this report (if relevant) and other notes
Failed canister				
BFT5 Failed can. Gas transport/dissolution	Neglected, since gas volumes (from buffer) assumed to be too low to reach backfill during this period	Neglected, pessimistically since transport would delay radioactive releases and decrease buffer pressure. The backfill would act as a sink for gas.	–	Gas release from canister.
BFT19. Colloid formation and transport	See geosphere (no failures are expected this period)	See geosphere	–	Called "colloid transport" for buffer. Reference to corresponding geosphere process.
BFT20. Speciation of radionuclides	Assumptions based on empirical data (no failures are expected this period)	Assumptions based on empirical data	–	See Chapter 13.
<i>BFT21. Transport of radionuclides in water phase</i>	COMP23 (no failures are expected this period)	COMP23	–	See Chapter 13.
<i>BFT22. Transport of radionuclides by a gas phase</i>	By-passed (no failures are expected this period)	By-passed	–	See Section 13.8.

7.4.5 Geosphere

Table 7-6. Process table for the geosphere describing how processes are handled in different time frames/climate domains and in the special case of earthquakes. Green fields denote processes that are neglected or irrelevant. Red fields denote processes that are quantified by modelling in the safety assessment. Orange fields denote processes that are neglected subject to a specified condition. Motives for the adopted handling are given in the Geosphere process report. An overview of all modelling activities, with references to sections in this main report where the results are discussed, is given in Section 7.5. Much of this information is also given in the last column in the table. Model acronyms are explained in Table 7-7.

Process	Excavation/operation	Temperate	Periglacial	Glacial	Earthquakes	FEP chart item (see Section 8.5)	Reference to sections in this report (if relevant) and other notes
Ge1. Heat transport	Neglected since sensitivity studies show that it takes very specific excavation/deposition sequences for heat generation to influence.	Modelling of peak canister temperature, assessment of distribution of peak temperature among the canisters and temperature distribution in rock.	Site-specific 2-D estimations of temperature distribution with depth.	Site-specific 1-D estimations of sub-glacial permafrost and freezing depths.	Not relevant.	Row "Temperature".	Temperate: Section 10.3.4. Permafrost and glacial: Section 10.4.3.
Ge2. Freezing	Not relevant.	Not relevant.	Site-specific 2-D estimations of permafrost and freezing depths.	Site-specific 1-D estimations of sub-glacial permafrost and freezing depths.	Not relevant.	Row "Temperature".	Section 10.4.3.
Ge3. Groundwater flow	Modelling of inflow, water table drawdown, and salt water upconing assuming saturated groundwater flow using DarcyTools. MIKE SHE used for simulating water table drawdown effects in detail.	Modelling of backfill resaturation using DarcyTools and saturated groundwater flow on different scales using ConnectFlow.	Modelling of saturated groundwater flow on a super-regional scale using DarcyTools.	Modelling of saturated groundwater flow on a super-regional scale during advance and retreat of ice sheets, with and without permafrost, using DarcyTools.	Impact on groundwater flow not specifically addressed but simplified calculations of radionuclide transport carried out (see Ge24).	Row "GW flow".	Excavation/operation: Section 10.2.3. Temperate: Section 10.3.6. Permafrost and glacial: Section 10.4.6.
Ge4. Gas flow/dissolution	Neglected based on arguments supporting the assumption of small effects of unsaturated regions on inflows to tunnels.	Included in a simplified manner in the backfill resaturation calculations.	Neglected based on considerations that gas that may be trapped below permafrost will have a similar effect on groundwater flow to a slightly thicker permafrost layer. Also, gas may escape through taliks if present.	Neglected based on the assumption that gas generated in the repository can rapidly escape through the geosphere without causing a pressure build-up (if permafrost is not present).	Not relevant.	(Row "GW flow".)	Section 13.8.
		Neglected for other calculations due to quantitative estimates based on empirical data.					
Ge5. Displacements in intact rock	3DEC modelling of near-field effects of excavation of tunnels and deposition holes.	3DEC modelling of thermal stresses and deformations in the near field and in the far field.	3DEC modelling of horizontal stress reduction caused by cooling.	3DEC stress modelling of near field. ABAQUS modelling of far field.	Included in the modelling of shear movements.	Row "Rock stresses"	Excavation/operation: Section 10.2.2. Temperate: Section 10.3.5 Permafrost and glacial: Section 10.4.4

Process	Excavation/operation	Temperate	Periglacial	Glacial	Earthquakes	FEP chart item (see Section 8.5)	Reference to sections in this report (if relevant) and other notes
Ge6. Reactivation – displacement along existing discontinuities	3DEC modelling of construction-induced reactivation.	3DEC modelling of reactivation due to thermal load (near field). Assessment of reactivation based on 3DEC stress evolution (far field). Estimation of earthquake probability (consequence analysis, see Earthquake).	3DEC modelling of fracture reactivation caused by thermal stress reduction, fore-bulge stress conditions and pore overpressure under impermeable permafrost layer (near field). Assessment of reactivation based on ABAQUS stress evolution, 3DEC thermal stress reduction and pore overpressure estimates (far field). Estimation of earthquake probability (consequence analysis, see Earthquake).	3DEC modelling of ice-load induced reactivation (near field). Assessment of reactivation based on ABAQUS stress model and pore overpressure estimates. Estimation of earthquake probability (consequence analysis, see Earthquake).	Apply design rules (respect distances and canister spacing). Assessment of residual probability for canister failure due to shear displacement.	Row “Fracture structure”	See process Ge5. Integrated handling of effects of earthquakes in Section 10.4.5
	Construction-induced seismicity neglected since it may only potentially cause local and limited construction-induced instability					Row “Fracture structure”	
Ge7. Fracturing	Assessment of EDZ. 3DEC modelling of potential for spalling. Observations (APSE) of size and shape of fractured (spalled) zone around deposition holes.	3DEC modelling of potential for spalling. Observations of size and shape of fractured (spalled) zone around deposition holes.	Thermal effects modelled and neglected provided that only marginal changes in mechanical state occur.	3DEC modelling of potential for fracturing induced by ice load (near field). Assessment of risk for hydraulic fracturing.	Neglected based on lack of observations at relevant distances from earthquake faults of earthquake-induced damage around open tunnels at shallow depth.	Row “Fracture structure”	See process Ge5.
			Assessment of hydraulic fracturing under impermeable permafrost layer.				
Ge8. Creep	Not relevant. Covered by construction-induced reactivation.	Neglected because of insignificant convergence of deposition holes at expected rock stresses.	Neglected because of insignificant convergence of deposition holes at expected rock stresses.	Neglected because of insignificant convergence of deposition holes at expected rock stresses.	Not relevant.	–	See also Section 10.3.5.
Ge9. Surface weathering and erosion	Not relevant. Too short time period for surface weathering and erosion processes to be of relevance.	Included in the estimates of denudation (surface weathering and erosion) for the climate cases.	Included in the estimates of denudation (surface weathering and erosion) for the climate cases where periglacial conditions occur.	Included in the estimates of denudation (surface weathering and erosion) for the climate cases where glacial conditions occur.	Not relevant	–	See sections 6.1, 14.3.4, 14.4.1 and 14.5.

Process	Excavation/operation	Temperate	Periglacial	Glacial	Earthquakes	FEP chart item (see Section 8.5)	Reference to sections in this report (if relevant) and other notes
Ge10. Erosion/ sedimentation in fractures	Neglected because of too low flow rates in non-grouted fractures.	Neglected because expected hydraulic gradients and shear stresses are too low to cause significant erosion.	Neglected because expected hydraulic gradients and shear stresses are too low to cause significant erosion.	Neglected because expected hydraulic gradients and shear stresses are too low to cause significant erosion.	Not relevant.	–	–
Ge11. Advective transport/ mixing of dissolved species	Advection and dispersion of salt included in saturated groundwater flow modelling using DarcyTools. Composition of mixtures assessed based on the groundwater flow modelling and site understanding.	Advection and dispersion of salt and reference waters included in saturated groundwater flow modelling using ConnectFlow. Composition of mixtures assessed based on the groundwater flow modelling and site understanding.	Advection and dispersion of salt included in saturated groundwater flow modelling using DarcyTools. Composition of mixtures assessed based on the groundwater flow modelling and site understanding.	Advection and dispersion of salt included in saturated groundwater flow modelling using DarcyTools. Composition of mixtures assessed based on the groundwater flow modelling and site understanding. Modelling of oxygen penetration based on the groundwater flow modelling, matrix diffusion and reactions with matrix minerals.	Not relevant.	Rows “GW flow and GW salinity”.	Excavation/operation: Section 10.2.5. Temperate: Section 10.3.7. Permafrost and glacial: Section 10.4.7.
Ge12. Diffusive transport of dissolved species in fractures and rock matrix	Diffusion of salt between mobile and immobile groundwater included in saturated groundwater flow modelling using DarcyTools.	Diffusion of salt between mobile and immobile groundwater included in saturated groundwater flow modelling using ConnectFlow.	Diffusion of salt between mobile and immobile groundwater included in saturated groundwater flow modelling using DarcyTools.	Diffusion of salt between mobile and immobile groundwater included in saturated groundwater flow modelling using DarcyTools. Modelling of oxygen penetration based on the groundwater flow modelling, matrix diffusion and reactions with matrix minerals.	Not relevant.	(Row “GW composition”).	See process Ge11.
Ge13. Speciation and sorption	Not relevant.	Simplified K_d -approach for modelling sorption of radionuclides. Speciation considered in the selection of K_d values.	Simplified K_d -approach for modelling sorption of radionuclides. Speciation considered in the selection of K_d values.	Simplified K_d -approach for modelling sorption of radionuclides. Speciation considered in the selection of K_d values.	Not relevant.	Row “GW composition”.	See the Data report .
Ge14. Reactions groundwater/ rock matrix	Neglected since reactions are considered to be insignificant compared with the effects of reactions with fracture-filling minerals.	Neglected since reactions are considered to be insignificant compared with the effects of reactions with fracture-filling minerals.	Neglected since reactions are considered to be insignificant compared with the effects of reactions with fracture-filling minerals.	Modelling of oxygen penetration based on the groundwater flow modelling, matrix diffusion and reactions with matrix minerals.	Not relevant.	Row “GW composition”.	Glacial: Section 10.4.7, subheading “Glaciation”; Redox condition”

Process	Excavation/operation	Temperate	Periglacial	Glacial	Earthquakes	FEP chart item (see Section 8.5)	Reference to sections in this report (if relevant) and other notes
Ge15. Dissolution/precipitation of fracture-filling minerals	Composition of groundwater in fractures modelled based on results of the groundwater flow modelling, assumed local mineral equilibria and site understanding.	Composition of groundwater in fractures modelled based on results of the groundwater flow modelling, assumed local mineral equilibria and site understanding.	Composition of groundwater in fractures modelled based on results of the groundwater flow modelling, assumed local mineral equilibria and site understanding.	Composition of groundwater in fractures modelled based on results of the groundwater flow modelling, assumed local mineral equilibria and site understanding.	Not relevant.	Row "GW composition".	See process Ge11.
Ge16. Microbial processes	Modelling of diffusive transport of methane and hydrogen, mass balance calculations of organic matter and assessment of potential for microbial processes.	Modelling of diffusive transport of methane and hydrogen, mass balance calculations of organic matter and assessment of potential for microbial processes.	Modelling of diffusive transport of methane and hydrogen, mass balance calculations of organic matter and assessment of potential for microbial processes.	Modelling of diffusive transport of methane and hydrogen, mass balance calculations of organic matter and assessment of potential for microbial processes.	Not relevant.	Row "GW composition".	Excavation/operation: Section 10.2.5. Temperate: Section 10.3.7.
Ge17. Degradation of grout	Neglected since expected effects will occur during Temperate period.	Generic modelling of effects on chemistry of fractures and changes of hydraulic conductivity in grouting boreholes.	Not specifically handled. Extrapolation of results from Temperate period.	Not specifically handled. Extrapolation of results from Temperate period.	Not relevant.	Row "GW composition".	Temperate: Section 10.3.7
Ge18. Colloid processes	Neglected because of insignificant impact on geochemical conditions.	Neglected because of insignificant impact on geochemical conditions.	Neglected because of insignificant impact on geochemical conditions.	Neglected because of insignificant impact on geochemical conditions.	Impact of earthquake on colloidal processes not addressed, but simplified calculations of radionuclide transport carried out (see Ge24).	–	See the Geosphere process report .
	Impact on radionuclide transport not relevant because of intact barriers.	Bounding calculations of colloid-facilitated radionuclide transport.	Bounding calculations of colloid-facilitated radionuclide transport.	Bounding calculations of colloid-facilitated radionuclide transport.		–	–
Ge19. Formation/dissolution/reaction of gaseous species	Composition of mixtures modelled based on the groundwater flow modelling, assumed local mineral equilibria and site understanding. This affects the concentrations of dissolved CO ₂ .	Modelling of diffusive transport of methane and hydrogen.	Modelling of diffusive transport of methane and hydrogen.	Included in modelling of oxygen consumption. Modelling of diffusive transport of methane and hydrogen.	Not relevant.		Glacial: Section 10.4.7, subheading "Glaciation; Redox condition"

Process	Excavation/operation	Temperate	Periglacial	Glacial	Earthquakes	FEP chart item (see Section 8.5)	Reference to sections in this report (if relevant) and other notes
Ge20. Methane hydrate formation	Not relevant.	Not relevant.	Neglected based on site understanding coupled with assessment of the potential for hydrate formation.	Neglected based on site understanding coupled with assessment of the potential for hydrate formation.	Not relevant.	Row "GW composition".	–
Ge21. Salt exclusion	Not relevant.	Not relevant.	Modelling of transport of outfrozen salt.	Not relevant.	Not relevant.	Row "GW salinity"	Permafrost: Section 10.4.7, subheading "Evolution during periglacial conditions"
Ge22. Radiation effects (rock and grout)	Neglected because of too low radiation fluxes.	Neglected because of too low radiation fluxes.	Neglected because of too low radiation fluxes.	Neglected because of too low radiation fluxes.	Not relevant.	–	See Geosphere process report .
Ge23. Earth currents	Effect on the geosphere neglected since expected electrical potential fields are too small to affect groundwater flow or solute transport	Effect on the geosphere neglected since expected electrical potential fields are too small to affect groundwater flow or solute transport.	Effect on the geosphere neglected since expected electrical potential fields are too small to affect groundwater flow or solute transport.	Effect on the geosphere neglected since expected electrical potential fields are too small to affect groundwater flow or solute transport.	Not relevant.	–	See Geosphere process report .
Ge24. Transport of radionuclides in the water phase	Not relevant since engineered barriers are intact.	Advection, dispersion, matrix diffusion, sorption, and radioactive decay included in integrated modelling using FARF31 and MARFA.	Advection, dispersion, matrix diffusion, sorption, and radioactive decay included in integrated modelling using FARF31 and MARFA.	Advection, dispersion, matrix diffusion, sorption, and radioactive decay included in integrated modelling using FARF31 and MARFA.	No credit taken for radionuclide retardation in the geosphere i.e. geosphere far field is short-circuited.	Not explicitly included in present version.	See Chapter 13, in particular Section 13.4.2.
Ge25. Transport of radionuclides in the gas phase	Not relevant since engineered barriers are intact.	Assessed by neglecting the geosphere as a barrier.	Assessed by neglecting the geosphere as a barrier.	Assessed by neglecting the geosphere as a barrier.	Not relevant.	Not explicitly included in present version.	Section 13.8.

7.4.6 Additional system parts

Process tables for the tunnel plugs, the central underground area, the top seal, the bottom plate in the deposition hole and the borehole seals have also been developed and are included in the **Buffer, backfill and closure process report**. Since these components are less important for safety, these process tables are not presented here in the main report. The following is a summary of how processes in the additional system parts are handled in the PSAR.

Deposition tunnel plug

The purpose of the deposition tunnel plug is to restore the hydraulic conditions in a deposition tunnel once the canisters have been installed and the tunnel has been backfilled. It is important that the plug can withstand the pressure gradient and restrict any flow of water out from deposition tunnel to the open transport tunnel. The saturation and the mechanical evolution of the plug during the operational phase are treated in the THM-modelling of the buffer and backfill. The concrete part will eventually degrade and it cannot be excluded that a more porous local volume will be formed. The mechanical effect of the intrusion of backfill into the volume is also covered in these THM-calculations. The hydraulic effect of the volume is not treated in the PSAR, since it will be sealed off with backfill on both sides. The degradation of the concrete will also give an effect on the geochemical conditions in the repository. This is treated in the modelling of the geochemical evolution.

Central area

The saturation of the central area after the closure of the repository is included in the buffer and backfill THM-modelling. After saturation most processes are of little or no concern for the repository performance. The geochemical evolution, especially the effect of reinforcements, is discussed as well as the mechanical interaction between the central area backfill and the plugs in the transport tunnels.

Top seal

The processes in the top seal are of limited concern for the performance of the repository. The saturation time is estimated in the THM-modelling. The mechanical interaction with the backfill below is not modelled specifically, but the process is handled in the same fashion as the interaction between the tunnel plug and backfill.

Bottom plate in deposition hole

The bottom plate serves no purpose apart as an aid for the installation of the canister and buffer. The bottom plate may however affect the buffer mechanically. The mechanical effects may occur only during the saturation phase. This is considered in the buffer and backfill THM-modelling.

Borehole seals

The borehole seals are in many respects similar to the buffer. The processes that are of particular concern and thus treated in the PSAR are:

1. Freezing, the upper part of the seals will under all circumstances experience low temperatures.
2. Water uptake, assessment of time scale of seal hydration.
3. Homogenisation during saturation.
4. Homogenisation after a local loss of bentonite – in the case of bentonite colloid formation.

The chemical interactions between bentonite and concrete are not treated specifically. The same reasoning as for the interaction between tunnel plug and backfill is utilised.

7.5 Assessment model flow charts, AMFs

To give an overview of the models used in the evaluation of repository evolution, the dependencies/interactions between them, and data used in the modelling, two assessment model flow charts, AMFs, have been developed. One AMF concerns the excavation/operation and initial temperate period, Figure 7-3 and one represents periglacial and glacial conditions, Figure 7-4.

In the AMFs, the modelling tasks are displayed as rounded rectangles, data to/results from model studies are displayed as rectangles and assessments of data for further modelling based on model output and other information are displayed as boxes. Data that are qualified in the **Data report** are indicated with blue colouration and modelling tasks presented in the **Model summary report** are indicated with yellow colouration.

The **Model summary report** describes the models represented in the AMFs. Table 7-7 and Table 7-8 provides links between the processes in the process tables, the modelling activities described by the AMFs and the section of the reference evolution (Chapters 10, 12 and 13) where the modelling is reported.

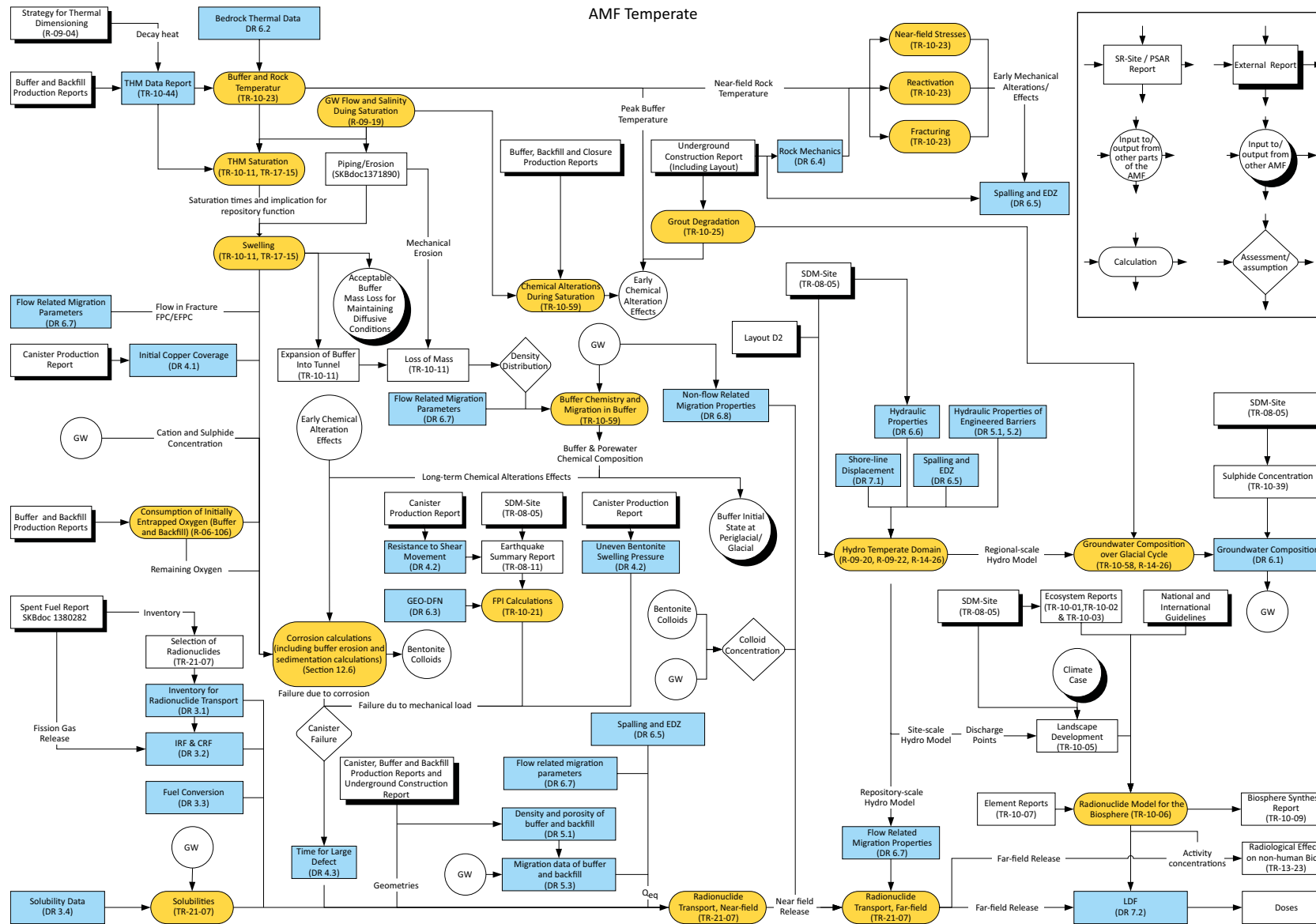


Figure 7-3. The assessment model flow chart for the excavation/operation period and the initial temperate period after closure. See main text for further explanations.

AMF Periglacial and Glacial

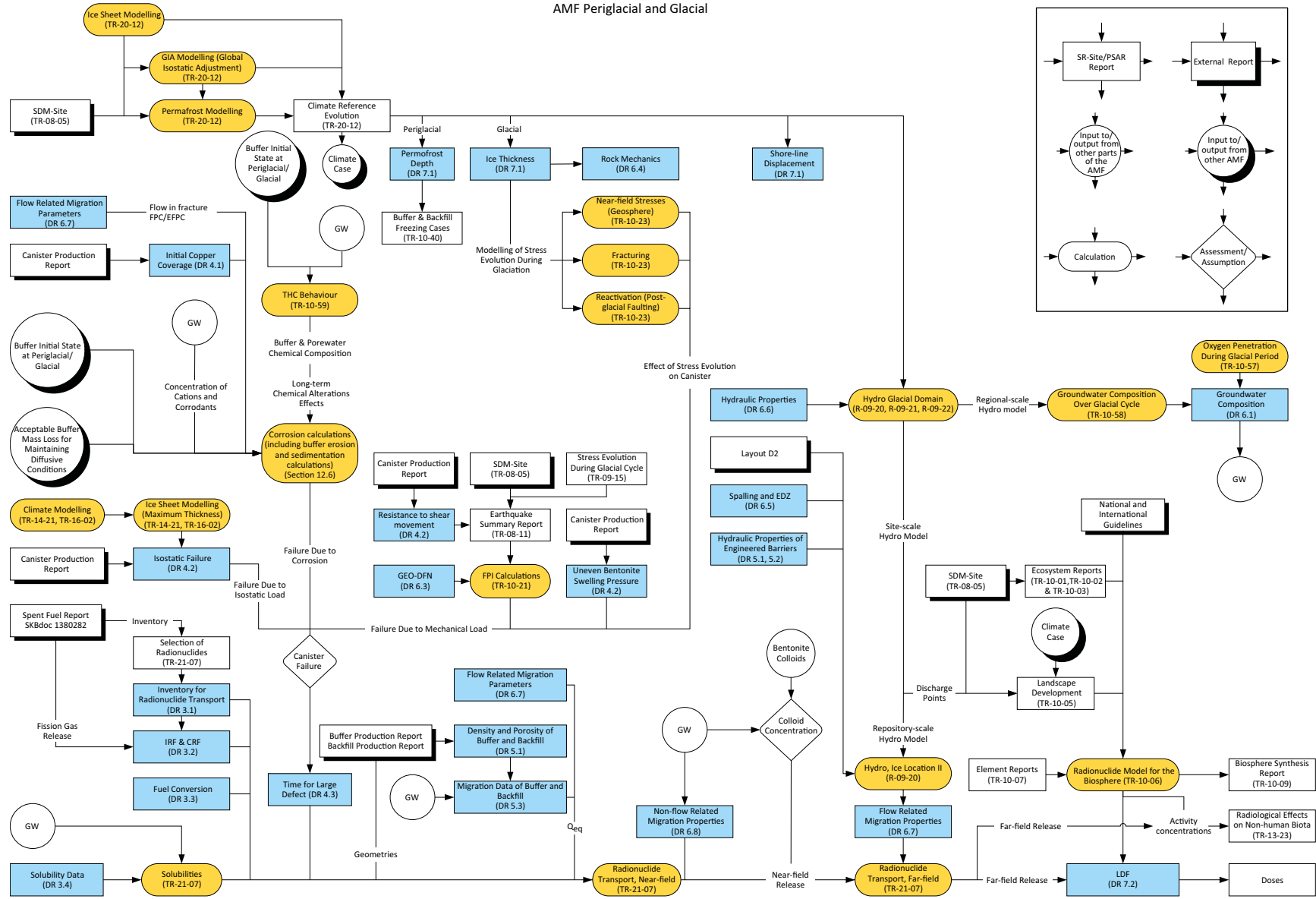


Figure 7-4. The assessment model flow chart for periglacial and glacial conditions. See main text for further explanations.

Table 7-7. Links between process tables, AMF (Figure 7-3) and reporting in this main report. Excavation/operation and temperate periods. The modelling activities in the left column correspond to yellow objects in Figure 7-3.

Modelling activity in AMF	Included processes, as indexed in process tables in Section 7.4	Code	Section(s) where modelling is reported	Note	Modelling report	
					Reference	In AMF
Buffer and rock temperature	F1, F2, Bu1, Bu2, Ge1	3DEC	10.3.4	Decay and heat generation modelled as exponential expressions fitted to results of detailed calculations	Hökmark et al. 2010	TR-10-23
THM saturation (buffer and backfill)	Bu2, Bu4, BfT3	ABAQUS	10.3.8		Åkesson et al. 2010a Sellin et al. 2017	TR-10-11 TR-17-15
Near-field stresses (geosphere)	Ge5	3DEC	10.2.2 (Excavation/operation) 10.3.5 (Initial temperate)		Hökmark et al. 2010	TR-10-23
Reactivation	Ge6	3DEC	10.2.2 (Excavation/operation) 10.3.5 (Initial temperate)		Hökmark et al. 2010	TR-10-23
Fracturing (spalling)	Ge7	3DEC	10.2.2 (Excavation/operation) 10.3.5 (Initial temperate)		Hökmark et al. 2010	TR-10-23
FPI calculations; calculation of the occurrence of Full Perimeter Intersecting fractures in deposition tunnels (see Section 5.2.2)	Initial state issue	Matlab	10.4.5		Munier 2010	TR-10-21
Chemical alterations during saturation (geosphere)	Ge13, Ge15	PHAST	10.2.5		Sena et al. 2010b	TR-10-59
Grout degradation	Ge17	CodeBright	10.3.7 (Initial temperate) (Mentioned also in 10.2.5 Excavation/operation)		Grandia et al. 2010a	TR-10-25
Groundwater flow and salinity during saturation	Ge3	DarcyTools	10.2.3		Svensson and Follin 2010	R-09-19
Swelling	Bu8, BfT7	ABAQUS, CodeBright	10.3.9		Åkesson et al. 2010a Sellin et al. 2017	TR-10-11 TR-17-15
Buffer chemistry and migration in buffer	Bu11, Bu12, Bu13, Bu14	PHAST	10.3.10 (elevated temperatures) 10.3.12 (long-term)		Sena et al. 2010b	TR-10-59
Consumption of initially entrapped oxygen (buffer and backfill)	BfT12	PHAST	10.2.5		Grandia et al. 2006	TR-06-106

Modelling activity in AMF	Included processes, as indexed in process tables in Section 7.4	Code	Section(s) where modelling is reported	Note	Modelling report	
					Reference	In AMF
Corrosion calculations (including buffer erosion and sedimentation calculations)	Bu18, C11	Analytical expressions (Excel)	10.2.5 (excavation/operation) 10.3.13 (initial temperate) 12.6		Section 12.6	Section 12.6
Hydro temperate domain	BfT4, Ge3, Ge11	Connect-Flow	10.3.6		Joyce et al. 2010 Selroos and Follin 2010 Joyce et al. 2015	R-09-20 R-09-22 R-14-26
Groundwater composition over glacial cycle	Ge13, Ge14, Ge15, Ge19	PhreeqC	10.3.7 (temperate period)		Salas et al. 2010 Joyce et al. 2015	TR-10-58 R-14-26
Solubilities	F14	"Simple functions"			Radionuclide transport report	TR-21-07
Radionuclide transport, near-field	F17, Bu25, BfT21 (The above three include, as sub-processes, F1, F12, F13, F14, Bu11, Bu12, BfT9, BfT10 and BfT11)	COMP23	Chapter 13		Radionuclide transport report	TR-21-07
Radionuclide transport, far-field	Ge24, consisting of sub-processes Ge11, Ge12, Ge13 and F1	FARF31 MARFA	Chapter 13		Radionuclide transport report	TR-21-07
Radionuclide Model for the Biosphere	Biosphere processes	Ecolego, MIKE_SHE, Pandora,	13.2		Avila et al. 2010	TR-10-06

Table 7-8. Links between process tables, AMF, Figure 7-4 and reporting in in this main report. Periglacial and glacial periods. The modelling activities in the left column correspond to yellow objects in Figure 7-4.

Modelling activity in AMF	Included processes, as indexed in process tables in Section 7.4	Code	Section(s) where modelling is reported	Note	Modelling report	
					Reference	In AMF
Permafrost modelling	F1, F2, Ge1	Numerical permafrost model	10.4.1, 10.4.3		In the Climate report , details in Hartikainen et al. 2010	In TR-10-49, details in TR-09-17
Ice sheet modelling	External processes, see the Climate report	UMISM	10.4.1		In the Climate report	In, TR-10-49, details in TR-09-19
Ice sheet modelling (maximum thickness)		Grisli			Colleoni et al. 2014 Quiquet et al. 2016	TR-14-21 TR-16-02
GIA modelling; (Global Isostatic Adjustment)	External processes, see the Climate report	Numerical GIA model	10.4.1		In the Climate report , details in SKB 2006c	In, TR-20-12, details in TR-06-23
FPI calculations; calculation of the occurrence of Full Perimeter Intersecting fractures in deposition tunnels (see Section 5.2.2)	Initial state issue	Matlab	10.4.5		Munier 2010	TR-10-21
Near-field stresses (geosphere)	Ge5	3DEC	10.4.4		Hökmark et al. 2010	TR-10-23
Reactivation	Ge6	3DEC	10.4.4		Hökmark et al. 2010	TR-10-23
Fracturing	Ge7	3DEC	10.4.4		Hökmark et al. 2010	TR-10-23
Groundwater composition over glacial cycle	Ge3, Ge11, Ge12, Ge21	PhreeqC	10.4.7		Salas et al. 2010	TR-10-58
Hydro, glacial domain	Ge3, Ge11	DarcyTools	10.4.6		Joyce et al. 2010 Vidstrand et al. 2010 Selroos and Follin 2010	R-09-20 R-09-21 R-09-22
Hydro, ice location II	Ge3, Ge11	ConnectFlow	10.4.6		Joyce et al. 2010	R-09-20
Oxygen penetration during glacial period	Ge11, Ge15	PhreeqC, PHAST, analytical expressions	10.4.7		Sidborn et al. 2010	TR-10-57
Buffer and backfill freezing cases	Bu3, BfT2		10.4.8		Birgersson et al. 2010	TR-10-40
THC behaviour	Bu11, Bu12, Bu13, Bu14	PHAST	10.4.8		Sena et al. 2010b	TR-10-59

Modelling activity in AMF	Included processes, as indexed in process tables in Section 7.4	Code	Section(s) where modelling is reported	Note	Modelling report	
					Reference	In AMF
Corrosion calculations (including buffer erosion and sedimentation calculations)	Bu18, C11	Analytical expressions (Excel)	12.6		Section 12.6	Section 12.6
Solubilities	F14	"Simple functions"			Radionuclide transport report	TR-21-07
Radionuclide transport, near-field	F17, Bu25, BfT21 (The above three include, as sub-processes, F1, F12, F13, F14, Bu11, Bu12, BfT9, BfT10 and BfT11)	COMP23	Chapter 13		Radionuclide transport report	TR-21-07
Radionuclide transport, far-field	Ge24, consisting of sub-processes Ge11, Ge12, Ge13 and F1.	FARF31 MARFA	Chapter 13		Radionuclide transport report	TR-21-07
Radionuclide Model for the Biosphere	Biosphere processes	Ecolego, MIKE_SHE, Pandora,	13.2		Avila et al. 2010	TR-10-06
Radiological Effects on Non-human Biota		ERICA			Jaeschke et al. 2013	TR-13-23

8 Safety functions and safety function indicators

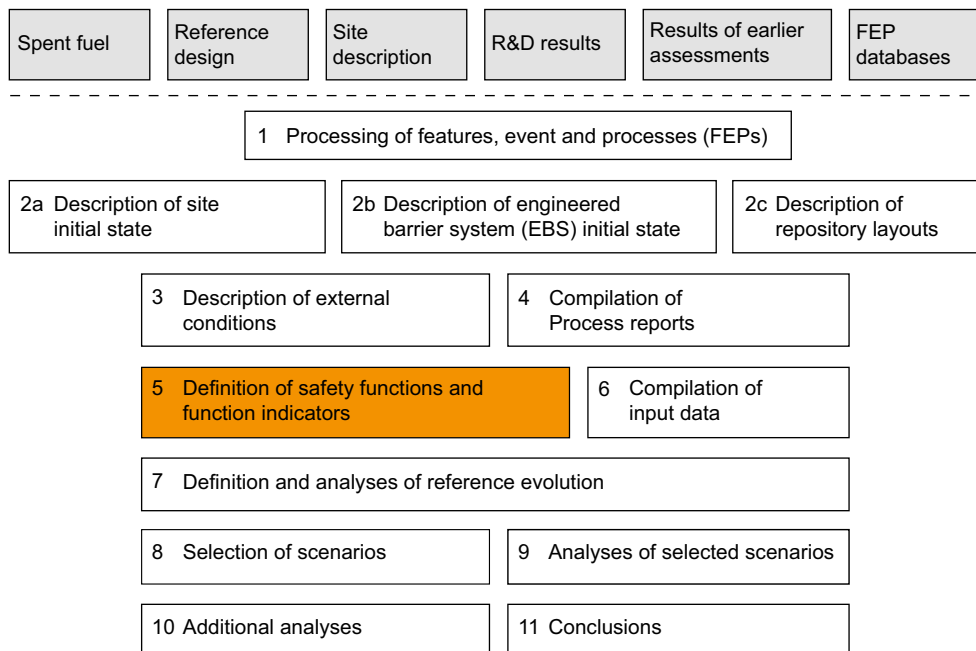


Figure 8-1. The PSAR methodology in eleven steps (Section 2.5), with the present step highlighted.

8.1 Introduction

8.1.1 Differentiated safety functions in the PSAR

As mentioned in Section 2.1, the primary safety function of the KBS-3 concept is to completely contain the spent nuclear fuel within copper canisters over the entire assessment period, which is one million years in the PSAR. Should a canister be damaged, the secondary safety function is to retard any releases from the canisters. The two issues of containment and retardation are thus of primary importance throughout the assessment. It should be noted that the containment function is more prominent in the KBS-3 concept than in many other repository concepts for spent nuclear fuel or high level waste (e.g. Nagra 2002, Andra 2005). This is also reflected in the methodology and structure of the safety assessment, which focuses to a comparatively large extent on the containing capacity of the repository.

In the safety assessment SR-Can, more differentiated safety functions for a KBS-3 repository were introduced and used to focus the assessment on important factors for post-closure safety, for giving a structured account of the reference evolution and as a basis for scenario selection. The approach was seen as a positive development in the review of the SR-Can assessment (Dverstorp and Strömberg 2008) and is also well in line with international developments in the area of safety assessment methodology (NEA 2009). The approach was further developed in the SR-Site assessment, taking considerations in the review of SR-Can into account. In its review of the SR-Site assessment, SSM reiterated a positive view of the approach and also pointed to specific issues seen as requiring development for the PSAR. These concern details in the safety functions for the canister.

This chapter deals with differentiation of safety functions for a KBS-3 repository for the PSAR, building on the work in the SR-Can and the SR-Site assessments and considerations in the reviews of these. Another key input for the development since the SR-Site assessment is the conclusions and recommendations of a joint Posiva-SKB working group on Safety functions, performance targets and technical design requirements for a KBS-3V repository (Posiva SKB 2017). In the few cases where there are substantial deviations in the present report from the safety functions, indicators and criteria suggested in Posiva SKB (2017), this is pointed out and discussed in this chapter.

The contents of this Chapter are an expansion and a modification of the contents of the corresponding Chapter in the SR-Site main report. In particular the discussion of the safety functions related to containment for the canister, for the buffer and for the backfill in Section 8.3 have been developed since the SR-Site assessment.

Safety function indicators and criteria for these indicating safe conditions in the repository are introduced in Section 8.2. Safety function indicators and criteria related to containment and retardation are developed in Sections 8.3 and 8.4, respectively. In Section 8.5, a FEP chart is developed. The chart describes the connections between important initial state conditions, long-term processes and safety functions and thus integrates much of the information given in this chapter, Chapters 5 and 7, and external factors described in Chapter 6.

The safety functions and their indicators and criteria are used to structure the evaluation of safety when the long-term evolution of the repository is evaluated in Chapter 10. They also play a key role in the selection and analyses of scenarios in Chapters 11 and 12, respectively.

8.1.2 Approach to dilution

Dilution is sometimes seen as a safety function in the context of waste management. Dilution is, however, not seen as a safety function for the KBS-3 system. The main reasons for this are that dilution essentially cannot be controlled by the design of the repository and only to some extent by site selection. Nevertheless, dilution will play an essential role in a realistic estimate of the consequences of a potential release from the repository. A coastal site can be expected to be submerged for extended periods of time and dilution of potential releases in sea water could dramatically lower the calculated annual effective doses and thus the associated radiological risks.

The future evolution of climate and climate-related conditions, which will be determining factors for dilution, is however uncertain; many climate-related parameters may vary by several orders of magnitude. Although marine discharges can be predicted to exist for long periods, these will also be interrupted by periods during which releases occur to terrestrial ecosystems, or when earlier releases accumulated in marine sediments will be present in terrestrial systems due to shore-line displacement. The terrestrial conditions will likely be associated with the highest individual risks. The compliance discussion for a repository has to be based on these unfavourable but, in a long-term perspective, not unlikely conditions.

Inevitably, dilution has to be included in quantitative assessments of wells but also in this case the situations that will occur are not amenable to control by repository design or site considerations.

A related phenomenon concerns the fact that the repository is distributed in space and that the host rock and the near-surface hydrological systems will redistribute potential releases from the repository before they cause human exposure. These phenomena have to be included in the quantification of consequences of potential releases. The redistribution effects cannot however be straightforwardly described as positive or negative.

8.2 Safety functions, safety function indicators and safety function indicator criteria; general

The overall criterion for evaluating repository safety is the risk criterion issued by SSM, which states that “the annual risk of harmful effects after closure does not exceed 10^{-6} for a representative individual in the group exposed to the greatest risk”. This is a “top level” criterion that requires input from numerous analyses on lower levels, and where the final risk calculation is the integrated result of various model evaluations using a large set of input data.

Safety functions

A detailed and quantitative understanding and evaluation of repository safety requires a more elaborated description of how the main safety functions of containment and retardation are maintained by the components of the repository. Based on the understanding of the properties of the components and

the long-term evolution of the system, a number of subordinate safety functions to containment and retardation can be identified.

In this context, a *safety function* is defined qualitatively as a role through which a repository component contributes to safety. For example, canisters should resist isostatic loads in the repository without the containment function being breached. A safety function related to the canister and subordinate to containment would therefore be the ability of the canister to *resist isostatic loads*.

Safety function indicators

In order to quantitatively evaluate safety, it is desirable to relate the safety functions to measurable or calculable quantities, often in the form of barrier conditions.

For the canister's function of resisting isostatic loads in the repository, the total isostatic load with contributions from the buffer swelling pressure and the hydrostatic pressure is a suitable quantity to use in order to evaluate the extent to which this safety function is fulfilled. The isostatic load is said to be a *safety function indicator*²¹ for the mentioned canister safety function. A safety function indicator is thus a measurable or calculable quantity through which a safety function can be quantitatively evaluated.

Safety function indicator criteria

In order to determine whether a safety function is maintained or not, it is desirable to have quantitative criteria against which the safety function indicators can be evaluated over the time period covered by the safety assessment.

The situation is however different from safety evaluations of many other technical or industrial systems in an important sense: The performance of the repository system or parts thereof do not, in general, change in discrete steps, as opposed to e.g. the case of a pump or a power system that could be characterised as either functioning or not (possibly in addition to intermediate states of partial functioning). The repository system will evolve continuously and in many respects there will be no sharp distinction between acceptable performance and a failed system on a sub-system level or regarding detailed barrier features.

There are thus many safety function indicators on which no limit for acceptable performance can be given. The groundwater concentrations of canister corroding agents or agents detrimental to the buffer are examples of this kind of factor related to containment. Usually, they enter in more complex analyses where a number of parameters together determine, e.g. the corrosion rate of the canister. Most of the factors determining retardation are also of this nature.

Nevertheless, as will be demonstrated in this chapter, there are some crucial barrier properties on which quantitative limits for safe functioning can be put. Regarding containment, an obvious condition is the requirement that the copper canister should nowhere have a penetrating defect, i.e. there should, over the entire surface of the canister, be a non-zero copper thickness. In addition to this direct measure of containment performance, a number of quantitative supplementary criteria can also be defined. These relate, for example, to the peak temperature in the buffer and to requirements on buffer density and buffer swelling pressure giving favourable buffer properties for maintaining containment. Most of them determine whether certain potentially detrimental processes can be excluded from the assessment. Relating to the above example of isostatic loads in the repository, the design analysis of the canister has demonstrated that the canister withstands an isostatic load of 50 MPa. The requirement that the isostatic load should not exceed 50 MPa is thus a *safety function indicator criterion* in this case. It is noted that safety function indicator criteria are termed performance targets in Posiva SKB (2017).

²¹ In choosing the term "function indicator", it was observed that the two terms "performance indicator" and "safety indicator" in this context normally refer to releases of radionuclide or resulting dose consequences (Becker et al. 2002). Those terms were thus avoided.

Relation between global safety and individual safety functions

It is emphasised that the breaching of a safety function indicator criterion does not mean that the repository is unsafe, but rather that more elaborate analyses and more extensive data are needed in order to evaluate safety.

The criteria are an aid in determining whether safety is maintained. If the criteria are fulfilled, the safety evaluation is facilitated. If all criteria related to canister failures are fulfilled, this implies that the overall risk criterion is fulfilled, provided that all canister failure modes have been identified. Fulfilment of all criteria related to the buffer, the backfill and the host rock is not a guarantee for compliance with the overall risk criterion, since the canister could still be failed so that releases of radionuclides could occur. On the other hand, compliance with the risk criterion could well be compatible with a violation of one or several of the criteria. A violation would be an implication of caution; further analyses could be required in order to determine the consequences on a sub-system level or a system level.

An example is the criterion that the charge concentration of groundwater cations should exceed 8 mM, $\Sigma q[M^{g+}] > 8 \text{ mM}$, in order for buffer erosion to be excluded. If this criterion is breached, buffer erosion must be quantitatively evaluated and its consequence, in terms of reduced buffer density, needs to be propagated to assessments of buffer swelling pressure and hydraulic conductivity. Alterations of the latter factors could, in turn, influence e.g. canister corrosion. A chain of assessments is thus initiated by the breaching of the first safety function, but the final outcome of a possibly increased corrosion rate is not necessarily an unacceptable impact on containment.

Another example concerns the initial period of repository evolution when the buffer and backfill are not yet water saturated. This means that in particular the buffer has not yet achieved its intended safety functions. As a consequence, the development of the near field during this phase must be given careful attention in the analysis of e.g. canister corrosion.

Approach to margins

Related to the above, a criterion may be defined so that it includes a considerable margin to unacceptable performance.

The peak temperature criterion for the buffer, set to 100 °C in order to avoid mineral transformations, is an example of a criterion with a considerable margin as documented in the **Buffer, backfill and closure process report**, Section 3.5.9. One reason for this is that the extent of mineral transformation increases gradually with temperature and it is not possible to determine a sharp limit below which no transformation occurs. Rather, a criterion is determined below which transformation can, for all practical purposes and for long time spans, be neglected in the safety assessment.

An example of a criterion with a smaller margin is the requirement that the total groundwater charge concentration of cations should exceed 8 mM in order to rule out erosion/colloid formation of the buffer. Here, a sharper onset of the safety function exists and it is possible to formulate the criterion with a smaller margin.

For the safety function indicator criteria used in the PSAR, there has been no systematic approach to margins when determining the criteria. The only requirement applicable to all safety function indicator criteria is that the safety function to which it relates should be fulfilled if the criterion is satisfied, based on the scientific understanding of the phenomenon in question. For application in the safety assessment, the margin for each indicator is of interest. Therefore, discussions of margins for all defined indicator criteria related to containment and retardation are given in Sections 8.3.5 and 8.4.6, respectively.

Quantities for safety function indicators

There is, for some safety functions, a certain degree of freedom in the choice of quantities for the indicators used to represent the safety function.

For example, in the presently developed version, the indicator used to quantify the buffer safety function “prevent colloid transport through buffer” is the buffer density, whereas one could also have

chosen the buffer pore size, a more direct measure of the safety function. For a specific bentonite material, the pore size is however directly related to the density and the buffer density is of interest in many other aspects of the safety assessment. Therefore, the density was chosen as the safety function indicator in this case.

There are other similar examples, in particular for the buffer for which many characteristics are dependent and thus to some degree interchangeable.

Derivation of safety functions, indicators and criteria

For the set of safety functions, their indicators and criteria to be useful in the evaluation of safety, they need to be sufficiently comprehensive. It is therefore important to have a systematic approach to the derivation of these entities.

The pillars on which the derivation of safety functions is built are:

- The two principal safety functions containment and retardation on which the design of the KBS-3 repository is based.
- The scientific understanding of the long-term evolution of a KBS-3 repository.

Throughout the decades of research related to the post-closure safety of a KBS-3 repository, safety functions or barrier requirements have been discussed and established successively.

In the PSAR, the results of these efforts have been utilised. Also, all canister and buffer processes identified as relevant for post-closure safety and documented in the **Process reports** have been considered with the aim of determining if a safety function relating to the process could be defined, ideally accompanied by an indicator and a criterion, see further Sections 8.3.1 and 8.3.2, sub-headings “Additional considerations”.

As for the set of processes identified as important for post-closure safety, completeness can never be unequivocally claimed for the set of safety functions in the evaluation of safety. The set of safety functions can be more or less mature, as a reflection of the maturity of the scientific understanding of the system analysed. The safety of the KBS-3 system has been studied for decades and new detrimental processes, that could form a basis for the formulation of additional safety functions, have not been identified in recent years. Furthermore, the principle of designing a relatively simple system using naturally occurring materials with well-known long-term properties, as in the case of KBS-3, favours the derivation of a comprehensive and mature set of safety functions. The level of differentiation of the functions can, however, be a matter of consideration. For example, SSM considered in its review of the SR-Site assessment that the mechanical safety functions of the canister need to be further differentiated to include also functions relating to copper creep ductility.

Safety function indicator criteria are not the same as technical design requirements

It is noted that safety function indicator criteria are not the same as design criteria, formalised into design requirements as discussed in Chapter 5. Safety function indicator criteria are meant to be fulfilled throughout the one million year assessment period, whereas technical design requirements relate to the initial state of the repository. Technical design requirements need to be defined with sufficient margin to allow deterioration of the system components over the assessment period so that safety is still fulfilled, i.e. so that, ideally, all the safety function indicator criteria are fulfilled also at the end of the assessment period. A clear example of this is the copper thickness of the canister: It is designed with a 5 cm copper thickness to allow for corrosion, whereas the safety function indicator criterion requires that it is nowhere zero, as this is the criterion for the breaching of containment.

There are also a number of technical design requirements relating to limits on content of detrimental agents in the engineered components of the repository, e.g. the oxygen content of the copper and the pyrite content of the buffer. These properties are determined by the production and control procedures relating to the component in question and given as initial state conditions for the safety assessment. They need to be included in the analysis of relevant detrimental processes in the assessment; for the two above examples this would be in the analysis of canister corrosion. They are, however, not necessarily suited as safety function indicators since they do not change over time other than by being consumed in the analysed detrimental processes.

The situation is, however, different for the corresponding safety function indicators and criteria related to future geosphere conditions, e.g. groundwater concentrations of solutes detrimental to the buffer or the canister. These can only to a limited extent be controlled by design or siting choices and are thus more relevant to include as function indicators for post-closure safety.

Relations between safety functions

The safety functions are related. All safety functions of the buffer either support a safety function of the canister, or contribute to retardation in the buffer. For example, the safety function “limit advective transport” in the buffer supports the canister safety function “provide corrosion barrier”, and also contributes to retardation in the buffer since advection is a more efficient transport mechanism than diffusion. Similarly, all safety functions of the host rock either support a safety function of the canister directly or indirectly via a buffer safety function, or contribute to retardation in the rock.

Summary

The following definitions have been introduced:

- A safety function is a role through which a repository component contributes to safety.
- A safety function indicator is a measurable or calculable property of a repository component that indicates the extent to which a safety function is fulfilled.
- A safety function indicator criterion is a quantitative limit such that if the safety function indicator to which it relates fulfils the criterion, the corresponding safety function is maintained.

Safety functions are an aid in the evaluation of safety, but the fulfilment of all safety function indicator criteria is neither necessary nor sufficient to argue safety. The different safety function indicator criteria are furthermore determined with varying margins to acceptable performance.

Safety function indicator criteria are related to, but not the same as, technical design requirements. Whereas the latter relate to the initial state of the repository and primarily to its engineered components, the former should be fulfilled throughout the assessment period and relate, in addition to the engineered components, to the natural system.

The set of safety functions used in the PSAR has been derived based on the documented experience accumulated over decades of research related to the post-closure safety of the KBS-3 repository.

8.3 Safety functions for containment

Safety functions, function indicators and, where applicable, function indicator criteria for containment are presented below. All defined entities are summarised in Figure 8-3 at the end of this section using the function labelling introduced in the subheadings in the following sections (Can1, Can2 etc.). The criteria presented below are often selected from a cautious perspective and further studies and engineering development may show that some of the criteria could be relaxed for future safety assessments. Also, additional criteria may be added.

8.3.1 Canister

Can1. Provide corrosion barrier

The canister integrity can be threatened either mechanically or chemically. An obvious requirement regarding canister integrity is that the copper shell of the canisters should not be penetrated. This can be expressed such that the minimum copper thickness taken over the entire canister surface shall be larger than zero:

$$d_{\min}^{\text{Can}} > 0$$

As long as this criterion is strictly fulfilled for all canisters, containment is complete and no releases occur.

Can2. Withstand isostatic load

Static load on insert

A key safety function of the canister is its ability to withstand isostatic loads in the repository.

Maximum isostatic pressures in a repository were, in the SR-Site assessment, estimated at around 50 MPa, composed of the bentonite swelling pressure and the hydrostatic pressure at the repository depth during a glaciation (SKB 2011). Since the SR-Site assessment, the estimated maximum hydrostatic pressure during a glaciation (from ice load and repository depth) has increased from 34.5 MPa to 40.5 MPa (Section 12.7.2) whereas the design requirement on the buffer implies lowering of the maximum swelling pressure from 15 MPa to 10 MPa. Based on this, and the fact that the two pressures result in a total pressure that is lower than their sum (see Section 12.7.3), a technical design requirement that the canister should withstand a 50 MPa isostatic load was established, see further Section 5.4.1. The evaluation of the design and manufacturing procedures for the ensemble of deposited reference canisters led to the conclusion that they will fulfil this technical design requirement, Section 5.4.3.

The isostatic load on the canister is, therefore, used as a safety function indicator in the PSAR and the technical design requirement of 50 MPa is used as the corresponding safety function indicator criterion. This does, however, not necessarily mean that a canister will fail if the load exceeds 50 MPa, since, in the design analyses of the canister, pessimistically chosen criteria are used when assessing the results of the underlying strength calculations and damage tolerance analyses. This is reflected by the results of two pressure tests of canister mock-ups where collapse occurred around 130 MPa (Jonsson et al. 2018).

In the PSAR, it is, therefore, strictly assumed that canisters withstand isostatic loads up to 50 MPa, based on the results of the design analysis. For potential loads exceeding 50 MPa, a more detailed scrutiny of the results of the design analysis is required.

Copper creep

In the assessment of the canister's ability to withstand an isostatic load, also the creep deformation behaviour and the creep ductility of the copper shell must be taken into consideration, since stresses that could cause thermally activated copper creep may be present during long periods of time. The deformation is analysed and compared with the creep ductility in the design analysis, for the isostatic load cases expected in the repository.

To ensure that creep properties are duly assessed in the evaluation of post-closure safety, a safety function relating to copper creep is appropriate, as also pointed out in SSM's review of the SR-Site assessment. In the PSAR, it is therefore stated that *the copper shell shall maintain its ductile properties for all relevant isostatic loads in the repository*. No quantitative indicator is formulated for this function. Rather, for all relevant isostatic loads, creep phenomena need to be evaluated. In this evaluation, all phenomena that may affect the long-term ductility of the copper material need to be considered. One such phenomenon concerns potential hydrogen embrittlement. Therefore, a dedicated safety function related to the hydrogen content of the copper material is also introduced, stating that *the hydrogen content of the material should be low*. (It is not sufficient to formulate this as a technical design requirement since hydrogen could in principle be introduced into the copper due to corrosion and other processes occurring in the repository.)

The adoption of the above three safety functions (relating to the load itself, to ductility and to hydrogen content) thus implies a differentiation of the single safety function related to isostatic loads in the SR-Site assessment.

Can3. Withstand shear load

Another key safety function of the canister is its ability to withstand shear movements in fractures intersecting the canister's deposition hole.

The technical design requirement related to shear movements is given in Section 5.4.1: “The copper shell shall remain tight and the canister shall maintain its ability to resist loads for 5 cm rock displacements at all angles and a rate of 1 m/s, exerted on the canister by a buffer with an unconfined compressive strength at failure lower than 4 MPa at a deformation rate of 0.8 %/min.”

The evaluation of the design and manufacturing procedures for the ensemble of deposited reference canisters led to the conclusion that they will fulfil this technical design requirement, Section 5.4.3.

No safety function indicator criterion for the canister relating to shear movements is formulated since no further detailed mechanical analyses of the canister are carried out in the safety assessment. Rather, the findings in the design analysis of the canister are adopted and lead to the following safety function indicators and criteria on other parts of the system:

- For the buffer, the safety function indicator and the safety function indicator criterion can be derived from the canister design analysis. In this case the criterion coincides with the Technical Design Requirement. This has been set to be the maximum dry density yielding an unconfined compressive strength at failure < 4 MPa at a deformation rate of 0.8 %/min when determined with a specific laboratory test procedure, and for material specimens in contact with waters with less favourable characteristics than site-specific groundwater should be considered (and is in fact what 1 560 kg/m³ represents for an MX-80 bentonite).
- For the geosphere, that the magnitude of shear movements in fractures intersecting deposition holes should not exceed 5 cm and that their velocity should not exceed 1 m/s. Furthermore, the temperature in the repository should not be below 0 °C when such shear movements occur for the calculations in the design analysis to be strictly applicable.

If these conditions are fulfilled, then it is assumed in the safety assessment that the canister will not fail due to shear movements. Should any of the conditions be violated, a more detailed scrutiny of the results of the design analysis is required.

A safety function relating to copper creep ductility is formulated as follows. “The copper shell shall maintain its ductile properties both for the instantaneous displacement controlled deformation and the time-dependent relaxing deformation resulting from all relevant shear loads in the repository.” No quantitative indicator is formulated for this function. Rather, for all relevant shear loads, creep phenomena need to be evaluated. As for isostatic loads, all phenomena that may affect the long-term ductility of the copper material, must also be considered when evaluating this safety function. One such phenomenon concerns potential hydrogen embrittlement. Therefore, as for the isostatic load, a dedicated safety function related to the hydrogen content of the copper material is also introduced, stating that the hydrogen content of the material should be low.

Additional considerations

A brief examination of all long-term canister processes was carried out to check whether any additional safety functions could be identified based on processes of relevance for post-closure safety. The following resulted.

- The canister attenuates the radiation from the fuel and thereby reduces the radiation levels exterior to the canister (process C1 in Table 7-3). A function relating to this property could in principle be defined. This was not done since the attenuation function is fulfilled initially and is therefore trivially fulfilled in the long-term as long as the canister is intact (radiation levels decrease rapidly with time whereas the extent of attenuation in the canister is intact). The radiation effects outside the canister are related to processes that impact on the containment function, meaning that they are essentially irrelevant for a failed canister.
- The canister transports heat from its interior to the exterior (process C2 in Table 7-3). Efficient heat transfer ensures limited peak temperatures in the canister interior, whereas the heat transfer does not influence the exterior temperatures, as these are determined by properties of the buffer and the rock and also by the heat output from the waste. A function relating to this property could in principle be defined. This was not done since peak temperatures in the canister interior are reached typically ten years after deposition, a time during which the heat transfer properties of the canister do not change. It is therefore not relevant to use this property as a long-term safety function.

- The following processes are related to safety functions:
 - C3 “Deformation of cast iron insert” through functions Can2 and Can3 (see Figure 8-3).
 - C4 “Deformation of copper canister from external pressure” through functions Can2 and Can3.
 - C6 “Copper deformation from internal corrosion products” through function Can4, defined in Section 8.4.2 and Figure 8-4.
 - C8 “Corrosion of cast iron insert” through function Can4.
 - C9 “Galvanic corrosion” through function Can4.
 - C11 “Corrosion of copper canister” through function Can1.
 - C12 “Stress corrosion cracking, copper canister” through function Can1.
 - C13 “Earth currents – stray current corrosion” through function Can1 (mentioned as a future human action case in Section 14.2.1).
 - C15 “Radionuclide transport” through function Can4.
- The following processes have not led to the definition of safety functions since they were deemed as insignificant for post-closure safety in the evaluation in the **Fuel and canister process report**:
 - C5 “Thermal expansion (both cast iron insert and copper canister)”.
 - C7 “Radiation effects”.
 - C10 “Stress corrosion cracking of cast iron insert”.
 - C14 “Deposition of salts on canister surface”.

For these processes, the following is noted:

- The basis for neglecting these processes is revisited in Section 14.4 where it is sought to verify that FEPs omitted in earlier parts of the assessment are negligible in light of the completed scenario and risk analysis.
- None of these processes, even if they were to have a significant impact on safety, would generate new safety functions. They would rather lead to the introduction of additional safety function indicators and possibly criteria for these for already existing functions. For example, the process C14 “Deposition of salts on canister surface” has a (negligible) impact on the existing function Can1 “Provide corrosion barrier”. Had it been deemed important for post-closure safety, then it would be evaluated in the following analyses together with other processes threatening the function Can1.

As long as the containment is intact, the possibility of criticality is ruled out. Therefore, no safety function related to criticality is formulated for an intact canister. See further Section 8.4.

There are also a number of technical design requirements related to the material composition of the copper shell and of the cast iron insert. These include limits on the oxygen and phosphorous contents in the copper and on the copper content in the cast iron. All these technical design requirements are evaluated in the determination of the initial state of the repository and the results of that evaluation are then used as premises in the analysis of the long-term evolution. Their values do not change in time and they are thus not suitable as indicators of safety. In addition, all these premises are related to processes that impact on existing functions.

8.3.2 Buffer

Buff1. Limit advective mass transfer

An important safety function of the buffer is to limit transport of dissolved copper corroding agents to the canister and potential radionuclide releases from the canister. The material of the buffer surrounding the canister has been chosen so as to prevent advective transport in the deposition hole. A guideline is that the hydraulic conductivity of the buffer should fulfil, see the **Buffer, backfill and closure process report**, Section 3.3.2:

$$k^{Buff} < 10^{-12} \text{ m/s}$$

The requirement refers to all parts of the buffer, i.e. the variability within the buffer must be such that the requirement is everywhere fulfilled.

For any reasonable hydraulic gradient in the repository, this condition will mean that transport in the buffer will be dominated by diffusion. The hydraulic conductivity is strongly related to the density of the buffer, to the adsorbed ionic species and to the ionic strength of the surrounding groundwater.

To ensure diffusive transport, the swelling pressure in the buffer shall be such that it has capability to self-seal conductive features, e.g. remnants from the saturation process such as erosion channels and dead angle locations in the buffer blocks or in the pellet-filled space between the buffer and the rock. Unless such features are sealed, advective transport through or along the buffer may occur. The buffer homogeneity is ensured partially by the fact that the buffer is made of a clay material that swells when water saturated. A swelling pressure criterion is therefore formulated, see the **Buffer, backfill and closure process report**, Section 3.4.1:

$$P_{Swell}^{Buff} > 1 \text{ MPa}$$

The requirement refers to all parts of the buffer, i.e. the variability within the buffer must be such that the requirement is everywhere fulfilled.

Diffusion controlled transport in the buffer in combination with the buffer being in tight contact with the wall of the deposition hole, which is obtained if the swelling pressure criterion is fulfilled, contributes to increasing the transport resistance in the buffer/rock interface, see further Section 8.3.4.

Buff2. Reduce microbial activity

The buffer shall have the ability to limit microbial activity (Posiva SKB 2017).

The sulphide production by sulphate reducing bacteria present initially in the buffer is, in the long-term, normally bounded to insignificant levels by their reliance on nutrients present in the groundwater.

In certain transient situations, the access to nutrients could be significant, e.g. due to degradation of construction and stray materials in the repository. In such cases, the buffer has the function of reducing the activity of initially present microbes. There is a limit to the rate of microbial sulphide corrosion that must not be exceeded. This rate is defined by the thickness of the canister and is based on the assumption that sulphide corrosion of copper is of a non-pitting type. Based on the results in Bengtsson et al. (2017a, b) which show that sulphide production drop from high to very low or below detection in the saturated density interval 1 740–1 880 kg m⁻³ for the MX-80, Asha, Calcigel and Rogle bentonites, microbial sulphide production can be treated as an on-off process. If the buffer density is sufficient the process can be neglected. If the buffer density is too low the rate of microbial sulphide production will depend on the availability and diffusion rate of nutrients and sulphate from groundwater.

In Posiva SKB (2017) the swelling pressure was used as the safety function indicator (performance target). According to the results from Bengtsson et al. (2017b) this may be ambiguous. An increasing swelling pressure will inhibit the microbial sulphide production at some point, but there are other factors active as well. A swelling pressure criterion could be defined for a given material, but since the laboratory tests use density (saturated in Bengtsson et al. 2017b) this is a more direct indicator than the swelling pressure. A safety function indicator, expressed as density, can be derived from experiments for any buffer material. The value will be the lowest dry density where no microbial sulphate reduction is observed.

In the PSAR, MX-80 bentonite is used as reference material. According to Bengtsson et al. (2017b) the interval for the limit for microbial sulphide production for MX-80 is a saturated density of 1 750–1 847 kg/m³ for that material. Hence, a saturated density of 1 850 kg/m³ is selected as the safety function indicator criterion in the PSAR. The technical design requirement of a swelling pressure above 3 MPa is compatible with this density criterion for MX-80, including a margin.

The above concerns microbes initially present in the buffer. To prevent additional microbes from intruding, a buffer density much less than the reference density is sufficient.

Buff3. Damp rock shear movements

The buffer shall mitigate the impact of rock shear on the canister (Posiva SKB 2017).

Depending on the mechanical properties of the buffer, the rock shear movements may cause the insert to collapse or deform to such extent that the deformation of the copper shell will result in a breach and loss of containment. The less the buffer deforms in the deposition hole the higher the stresses that will be transmitted to the canister, i.e. the higher the shear strength of the buffer, the higher the stresses in the canister. To maintain containment, the shear strength of the buffer must not result in a load larger than the load the canister can withstand for the shear movements expected to occur in a deposition hole. The buffer shall be designed such that a shear movement in the deposition hole with 5 cm displacement at the rate of 1 m/s, will not cause excessive shear strain on the canister. This implies that the buffer must not be too stiff, and it must not be stiffer than in the canister design analyses (Jonsson et al. 2018).

The safety function indicator and the safety function indicator criterion can be derived from the canister design analysis. In this case the criterion coincides with the Technical Design Requirement.

The shear strength in the technical design requirement is expressed as the unconfined compressive strength at failure, since it is this strength that is measured in the test. Since the shear strength will also depend on the rate of strain, this also needs to be considered in the technical design requirement. The rate of 0.8 %/min is selected based on generally applied experimental practices. Since the shear strength increases with swelling pressure, the technical design requirement for shear strength should for most materials be fulfilled for the dry density yielding a swelling pressure of 10 MPa. The aim is to verify this by testing that the technical design requirement for shear strength is fulfilled at the dry density that corresponds to a swelling pressure of 10 MPa for a fully Ca-exchanged material. If the tested unconfined compressive strength at failure exceeds 4 MPa at a swelling pressure of 10 MPa and a deformation rate of 0.8 %/min when determined for fully Ca-exchanged material specimens, the dry density, and thus the swelling pressure, that fulfils the unconfined compressive strength technical design requirement shall be determined. The unconfined compressive strength at failure should be less than 4 MPa for this situation (see also Section 5.5.1).

Buff4. Resist transformations (requirement on temperature)

The buffer shall maintain its barrier functions and have long-term durability in the environment expected in the final repository (Posiva SKB 2017).

The buffer must resist transformation in order to maintain its safety functions in a long-term perspective. At elevated temperatures, chemical alterations of the swelling clay material acting to decrease the development of swelling pressure would occur (Leupin et al. 2014). With respect to the temperature increase resulting from the disposal of the spent nuclear fuel, the buffer shall retain its favourable characteristics at temperatures up to 100 °C. Also the alkalinity of the groundwater is of importance for the stability of the buffer material, see further Section 8.3.4.

$$T^{Buffer} < 100 \text{ °C}$$

An additional reason to requiring this maximum buffer temperature is that the extent of abiotic sulphate reduction increases with temperature and will become non-negligible at some temperature above 100 °C (e.g. Machel 2001), whereas it is negligible below 100 °C (**Fuel and canister process report**, Section 3.5.4).

Buff5. Keep the canister in position

The buffer shall keep the canister in its centred position in the deposition hole as long as required with respect to the safety of the final repository (Posiva SKB 2017).

The buffer's main role is to reduce the potential negative interactions between the canister and the host rock including the groundwater. If the buffer density is too low, it will deform under the weight of the canister and thus allowing the canister either to sink or to tilt so that the surrounding buffer thickness is reduced or the canister even touches the walls or bottom of the deposition hole. The main determinant of the creep rate and the resulting canister sinking is the magnitude of the

mobilised shear strength (shear stress divided by shear strength), which results in an increased canister sinking. The shear strength decreases with decreasing swelling pressure. Analyses (Åkesson et al. 2010a) of canister sinking in a deposition hole for a range of buffer densities and hence swelling pressures indicate that the total sinking will be less than 2 cm for swelling pressures down to 0.1 MPa, see further the **Buffer backfill and closure process report**, Section 3.4.1. Based on these calculations, the following safety function indicator criterion is cautiously formulated:

$$P_{Swell}^{Buff} > 0.2 \text{ MPa (Prevent canister sinking.)}$$

Buff6. Limit pressure on canister and rock

a. Swelling pressure limit

The swelling pressure of the buffer needs to be limited so that neither the canister nor the rock is exposed to loads they cannot withstand. High pressures on the canister may result in breach of the copper shell and loss of containment, and high pressures on the rock may cause cracking that in turn may result in increased transmissivity around the deposition hole. The maximum acceptable buffer swelling pressure in the deposition hole is restricted by the acceptable isostatic load on the canister. A previous performance target used in SR-Site for the isostatic load on the canister was determined under the assumption that the buffer swelling pressure will not exceed 15 MPa. The now specified safety function indicator criterion (< 10 MPa) is selected based on feed-back from the design analyses of the mechanical loads on the canister (Jonsson et al. 2018) and the need of tolerances in design and installation of the buffer.

$$P_{Swell} < 10 \text{ MPa}$$

b. Buffer freezing

The key issue for the freezing process is when the pressure generated from the volume expansion of the ice can be harmful for the canister and the rock. According to Posiva SKB (2017) the performance target for the canister is that it should withstand isostatic load ≤ 50 MPa. The mean crack initiation stress level for the main rock type in Forsmark is 116 MPa and the minimum is 60 MPa (SKB 2008a).

According to the Clausius-Clapeyron equation (**Buffer, backfill and closure process report**, Section 3.2.2), 50 MPa is generated when ice is cooled by 3.7 °C below the freezing point of water. This pressure would be reached in a deposition hole at atmospheric pressure filled with pure water at -3.7 °C. The bentonite swelling pressure will lower the freezing point of water, thus lowering the temperature when the pressure from the ice will be 50 MPa.

The freezing process in a bentonite buffer is studied in Birgersson et al. (2010). The temperature when ice starts to form can be predicted with an empirical approach. Using the lowest swelling pressure value for the technical design requirement in Posiva SKB (2017) of 3 MPa, the critical temperature according to the **Buffer, backfill and closure process report**, Section 3.2.2, is -2.5 °C. The most pessimistic value for when freezing causes a pressure above 50 MPa is therefore $-2.5-3.7$ °C = -6.2 °C. Based on this -6 °C is selected as the safety function indicator criterion for the safety function “Limit pressure on canister and rock – Buffer freezing”.

In a situation with ice formation in the deposition hole, no hydrostatic pressure and no swelling pressure needs to be considered.

$$T^{Buffer} > -6 \text{ °C}$$

It is noted that this temperature criterion is lower than that in Posiva SKB (2017). The lower temperature adopted here is justified by a more in-depth analysis of the behaviour of the buffer under freezing conditions, and its relation to the 50 MPa isostatic load criterion for the canister.

If the buffer freezes, the pressure exerted on the canister and the rock may increase, an issue requiring separate analyses.

Other requirements

The content of canister corroding agents in the buffer should be low. Apart from unavoidable initial amounts of oxygen, the pyrite content could pose a long-term problem, as pyrite, if not oxidised by initially present or intruding oxygen, will release sulphide, a canister corroding agent. There is, however, no absolute criterion placed on this amount; the corrosion effects of measured amounts will have to be evaluated quantitatively. As pyrite could also act as a scavenger for any initially present or intruding oxygen in the repository, the evaluation of the effects of the presence of this material in the buffer is complex.

It is also noted that the technical design requirements for the buffer include a limit on the sulphide content of 0.5 weight percent of the total mass, corresponding to approximately 1 % of pyrite.

Additional considerations

A brief examination of all long-term buffer processes was carried out to check whether any additional safety functions could be identified based on processes of relevance for post-closure safety, in the same manner as described for the canister in Section 8.3.1. The following resulted:

- The water saturation of the buffer described in the process “Water uptake and transport for unsaturated conditions”, process Bu4 in Table 7-4 is a pre-requisite for the safety function “Limit advective transport” to be fulfilled. However, as long as the buffer is unsaturated the safety function is not needed. Hence, no separate safety function can be defined for this process.
- The process Bu11 “Diffusive transport of species” controls both the corrosion rate of the canister and the possible transport of radionuclides. However, the key issue is if diffusion is the dominating transport mechanism, which is covered by the safety function “Limit advective transport”. No separate safety function for the diffusion process itself has therefore been defined.
- The process “Sorption (including ion-exchange)” is important for the retardation of radionuclides from a failed canister. This process has the potential to generate a safety function. This is further discussed in Section 8.4.3.
- The processes “Alterations of impurities” and “Aqueous speciation and reactions” are critical for the determination of the chemistry in the buffer. In this way they will affect a number of other processes. However, there is no direct impact on the safety from these processes and no safety function has been defined.
- The following processes are related to safety functions:
 - “Heat transport” through function Buff4 (see Figure 8-3).
 - “Freezing” through functions Buff6 and R4.
 - “Water transport under saturated conditions” through function Buff1.
 - “Piping” through function Buff1 (indirectly).
 - “Gas transport/dissolution” through the retardation function Buff9 (Figure 8-4).
 - “Swelling/mass redistribution” through functions Buff1, Buff2 and Buff5.
 - “Advective transport of species” through function Buff1.
 - “Montmorillonite alteration” through functions Buff4 and R1.
 - “Colloid formation” through function R1.
 - “Microbial processes” through function Buff2.
 - “Colloid filtration” through the retardation function Buff7 (Figure 8-4).
 - “Cementation” includes “stiffening” through Buff3.
- The following processes have not led to the definition of safety functions since they were deemed as insignificant for post-closure safety in the evaluation in the **Buffer, backfill and closure process report**:
 - “Radiation attenuation/heat generation”.
 - “Radiolysis of porewater”.
 - “Radiation-induced transformations”.
 - “Liquefaction”

For these processes, the following is noted:

- The basis for neglecting these processes is revisited in Section 14.4 where it is sought to verify that FEPs omitted in earlier parts of the assessment are negligible in light of the completed scenario and risk analysis.
- None of these processes, even if they were to have a significant impact on safety, would generate new safety functions. They would rather lead to the introduction of additional safety function indicators and possibly criteria for these for already existing functions.

There are also a number of technical design requirements related to the material composition of the buffer. These include a limit on the sulphide, total sulphur and organic content. All these technical design requirements are evaluated in the determination of the initial state of the repository and the results of that evaluation are then used as premises in the analysis of the long-term evolution. Their values do not change in time and they are thus not suitable as indicators of safety. In addition, all these premises are related to processes that impact on existing functions.

8.3.3 Backfill in deposition tunnels

BF1. Counteract buffer expansion

The buffer swelling will cause an upward expansion with a resulting compression of the backfill. This needs to be counteracted by the backfill in order to keep the buffer density within the desired limits and to maintain the buffer safety functions related to swelling pressure and density. The mechanical interaction between the buffer and the backfill is dependent on many factors. The process is treated in the **Backfill production report** and in the THM modelling of the buffer, backfill and other components (Åkesson et al. 2010a). This function is evaluated as part of the analysis of the buffer's long-term ability of limiting advective transport, which includes studies of the buffer's density loss through its upward swelling into the backfill. The buffer indicators relating to limiting advective transport are thus used to evaluate this backfill function. In general terms, it is advantageous if the backfill density is high for this function to be fulfilled, but since there are many factors affecting this process, no single criterion can be defined.

In Posiva SKB (2017) this safety function was expressed as “The backfill shall restrict upward buffer swelling/expansion in the deposition holes” and the safety function indicator criterion/performance target was “backfill deformation shall be sufficiently limited to keep the buffer swelling pressure > 2 MPa in average over the buffer volume”. This formulation appears to be a mistake in the report. An average swelling pressure of 2 MPa could give very low local swelling pressures in the part of the buffer where the swelling actually occurs. A safety function for the backfill that is expressed in buffer properties may also be somewhat awkward to evaluate.

In the PSAR version of the **Backfill production report** the technical design requirement, which in this case is identical to the safety function indicator criterion, states that the total compressibility of the installed backfill, in a dry as well as in a saturated state, should resist the expansion of the buffer and maintain a swelling pressure in the buffer which is higher than 3 MPa in a specified buffer volume. This volume extends from 50 cm above the canister to 50 cm below the canister.

$$\text{Compressibility}^{\text{Backfill}} > P_{\text{Swell}}^{\text{Buff}} > 3 \text{ MPa}$$

This technical design requirement is to be further evaluated.

The expansion of the buffer into the backfill will directly affect the buffer safety functions Buff1, Buff2 and Buff5 and needs to be considered when those safety functions are evaluated.

Other requirements

The concentration of canister-corroding agents in the backfill should be low. As for the buffer, a certain amount of initially entrapped oxygen is unavoidable in the backfill, and the pyrite concentration could pose a long-term problem. There is, however, no specific constraint placed on this concentration; the corrosive effects of the measured concentrations will have to be evaluated quantitatively.

8.3.4 Geosphere

Many aspects of the host rock safety functions cannot generally be captured by simple criteria but require more complex analyses where the combined effect of a number of factors determine the outcome. Still it is possible to identify conditions that should be favourable with regard to containment, as well as retardation, and conditions that would ultimately be detrimental to the safety functions of the engineered barriers. This was, for example, discussed in the report on geoscientific suitability indicators and criteria for siting and site evaluation (Andersson et al. 2000) and additional conclusions were made in the SR-Can main report (SKB 2006a, Sections 13.6 and 13.7).

In the following, host rock safety functions and function indicators relating to chemical, mechanical, hydrogeological and thermal conditions are discussed qualitatively and quantitative limits on indicators are provided where possible.

R1. Provide chemically favourable conditions

Several characteristics of the groundwater composition are essential for providing chemically favourable conditions for the repository.

a. Reducing conditions

A fundamental requirement is that of reducing conditions. A necessary condition is the absence of dissolved oxygen, because any evidence of its presence would indicate oxidising conditions. The presence of reducing agents that react quickly with O₂, such as Fe²⁺ and sulphide is sufficient to indicate reducing conditions. Other indicators of redox conditions, like negative redox potential, are not always well defined and thus less useful as a basis. Nevertheless, redox potential is a measure of the availability of all kinetically active oxidising species, and therefore a useful measure of the available reducing intensity.

This requirement ensures that canister corrosion due to oxygen dissolved in the groundwater is avoided. Furthermore, should a canister be penetrated, reducing conditions are essential to ensure a low dissolution rate of the fuel matrix, to ensure favourable solubilities of several radioelements and, for some elements, also to ensure redox states favourable for sorption in the buffer, the backfill and the host rock.

In addition to dissolved O₂, other oxidising groundwater components could be considered, for example nitrate and sulphate. However nitrate and sulphate can only be reactive by the intervention of microbes, which require both nutrients and reduced species such as dissolved hydrogen, methane or organic matter in order to be able to reduce nitrate or sulphate, whereas dissolved oxygen may react directly e.g. with the copper canister or the spent fuel.

b, c. Ionic strength, salinity

The salinity of the groundwater should neither be too high, nor too low. The total charge concentration of cations should exceed 8 mM in order to avoid colloid release from buffer and backfill, hence, (see the **Buffer, backfill and closure process report**, Section 3.5.11):

$$\Sigma q[M^{q+}]^{GW} > 8 \text{ mM}$$

A criterion based on charge equivalents and not on separate concentrations for different ionic species has the advantage that the effect of ion exchange equilibrium is incorporated in a single criterion. Furthermore, modelling by Neretnieks et al. (2009) shows that during the transient of ion exchange, the concentration of Ca²⁺ in the seeping water drops at the bentonite-groundwater interface, whereas charge neutrality requires that the equivalent charge concentration remains constant.

Groundwaters of high ionic strengths would have a negative impact on the buffer and backfill properties, in particular on the backfill swelling pressure and hydraulic conductivity. In general, ionic strengths corresponding to NaCl concentrations of approximately 35 g/L (0.6 M NaCl) are an upper limit for maintaining backfill properties whereas the corresponding limit for the buffer is around 100 g/L (1.7 M NaCl). These requirements are also in line with the limit on total dissolved solids (TDS)

given as a performance target in Posiva SKB (2017) as 35 g/L with acceptable short-term transients up to 70 g/L. The limit of tolerable ionic strength is, however, highly dependent on the material properties of these components, (see Section 5.5.3 and, for details, Karnland et al. 2006).

Colloid concentrations: The concentration of natural colloids should be low to avoid transport of radionuclides mediated by colloids. The stability of colloids is much decreased if the charge concentration of cations exceeds some millimole per litre. The condition discussed above for the stability of the buffer and backfill ($\Sigma q[M^{q+}]^{GW} > 8 \text{ mM}$) is therefore also sufficient to keep the concentration of colloids suspended in groundwaters to a low level.

d. Concentrations of detrimental agents

Regarding canister corrosion, there should be low groundwater concentrations of other canister-corroding agents, in particular sulphide, HS^- . In addition, the groundwater should also have low concentrations of nutrients that may be used by sulphate reducing bacteria to produce sulphide. These are dissolved hydrogen, methane and organic carbon. For sulphide in the groundwater to pose a problem, earlier assessments demonstrated that, for an intact buffer, considerably higher concentrations than have ever been observed in Swedish groundwaters would be required. The quantitative extent of such corrosion also depends on the groundwater flow around the deposition hole and on the transport properties of fractures intersecting the hole. Posiva SKB (2017) gives an upper of limit 3 mg/L $\approx 10^{-4} \text{ M}$ as a performance target for sulphide concentrations in the groundwater.

Furthermore, low groundwater concentrations of agents detrimental to long-term stability of the buffer and backfill, in particular potassium and iron, are desirable, see the **Buffer, backfill and closure process report**, Section 3.5.10. Posiva SKB (2017) gives an upper of limit 0.1 M as a performance target for K^+ concentrations in the groundwater.

e. pH

Regarding pH, a criterion can be formulated from the point of view of buffer and backfill stability, see the **Buffer, backfill and closure process report**, Section 3.5.8:

$$pH^{GW} < 11$$

This is fulfilled for any natural groundwater in Sweden. However, construction and stray materials in the repository, in particular concrete, could contaminate the groundwater such that high pH values are reached. In addition, Posiva SKB (2017) suggests a pH-value above 5 as a performance target. The scientific basis for this value is however weak and very low pH is not expected in the water in Forsmark.

f. Avoiding chloride assisted corrosion

A further requirement is that the combination of low pH values and high chloride concentrations should be avoided in order to exclude chloride assisted corrosion of the canister. In quantitative terms, the requirement is expressed as being below (at the right-hand side of) a curve of chloride concentration as a function of pH, see Figure 8-2. The basis for this criterion is documented in the **Fuel and canister process report**, Section 3.5.4 and Appendix A4.

R2. Provide favourable hydrogeologic and transport conditions

For the host rock to provide favourable hydrogeologic and transport conditions, the flow-related transport resistance (F) of flow paths leading into and out of the repository should be sufficiently high. Limited transmissivity of the water conducting fractures in combination with low hydraulic gradients yields limited flows and high transport resistance in the water conducting fractures.

Furthermore, the geosphere has an important function in controlling the transport resistance in the buffer/rock interface. This property is dependent on three factors: i) diffusive conditions in the buffer, ii) limited flow in the rock fractures intersecting the deposition hole, and iii) a favourable (limited) intersection area over which the exchange of solutes can occur. The first two factors are expressed by the safety functions relating to transport conditions in the buffer and the rock expressed above.

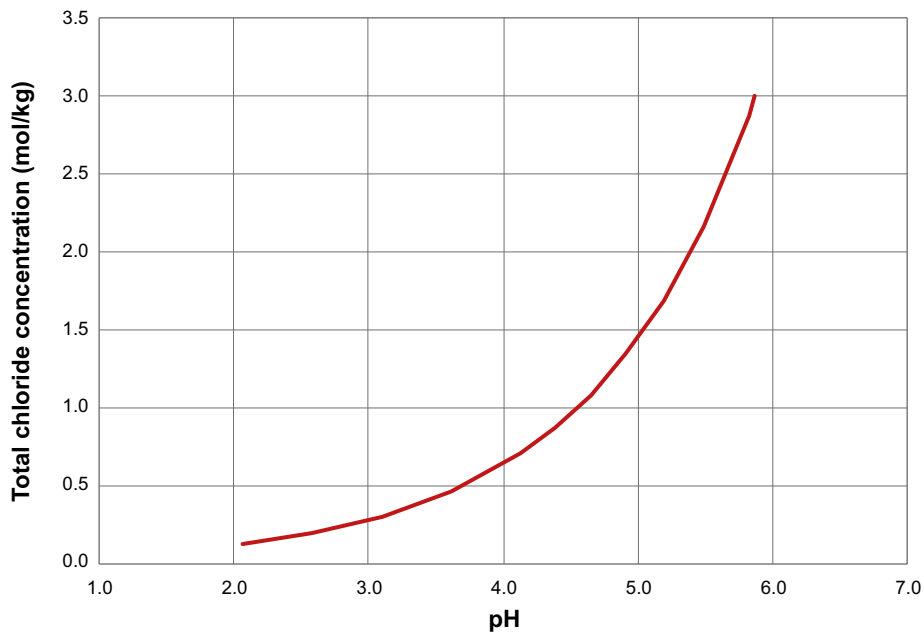


Figure 8-2. The limiting curve for combinations of chloride concentration and pH for which chloride-assisted corrosion needs to be taken into account (total copper concentration in solution 10^{-6} mol/kg).

The third factor is obtained by i) an intact buffer in tight contact with the wall of the deposition hole, which, in turn, is achieved through the buffer swelling pressure, and ii) limited aperture in the fractures intersecting the deposition hole. The latter factor can increase considerably through thermally induced spalling of the rock wall of the deposition hole. A suitable indicator for this safety function is the equivalent flow rate, Q_{eq} , which is an integrated measure of all the above factors.

In summary, for the host rock to have favourable hydrogeologic and transport conditions, it should have:

- a) High flow-related transport resistance, F , in flow paths (connected fractures) from the surface environment to the repository and in flow paths leading away from the repository.
- b) Low equivalent flow rate in the buffer/rock interface, Q_{eq} .

On neither of these indicators is it possible to put quantitative limits, but they require integrated analyses of site specific hydrogeologic conditions and evolution. As rules-of-thumb, F -values above 10^4 yr/m and Q_{eq} -values below 10^{-4} m³/yr can be regarded as favourable. These values are compatible with performance targets given in Posiva SKB (2017).

R3. Provide mechanically stable environment

The mechanical stability of the host rock cannot, in most respects, be simply evaluated. However, two main reasons for potential mechanical failure of the canisters can be identified. These are collapse due to isostatic load and failure due to earthquakes causing secondary movements on fractures intersecting deposition holes, see Section 8.3.1. A strongly contributing factor to the former could be high groundwater pressures during glaciation.

Addressing the latter failure mode requires a complex evaluation of shear movements for a range of mechanical load situations. For assessing the consequences of such movements the following conditions regarding secondary shear displacements and velocities in fractures at deposition holes have, through the canister technical design requirements and the design analysis of the canister (see above) been established:

$$d_{shear} < 5 \text{ cm}$$

$$v_{Shear} < 1 \text{ m/s.}$$

R4. Provide favourable thermal conditions

The safety evaluation is simplified if water in the various components of the repository does not freeze. It is, however, not a global requirement that freezing does not occur. For example, freezing is part of the expected evolution for the groundwater down to typically 100–200 m depth for permafrost conditions, during which also the closure in the access shaft and ramp is expected to freeze.

The temperature at which the groundwater freezes at repository depth is determined by the groundwater composition and the hydrostatic pressure. Groundwater freezing *per se* is, however, not necessarily negative for post-closure safety. An exception concerns the possibility of long-term buffer erosion to the extent that a water-filled cavity forms in the deposition hole. The freezing of water in such a cavity could lead to an increased pressure on the canister. The freezing temperature of distilled water at a hydrostatic pressure corresponding to a repository depth of 450 m is -0.3 °C.

As mentioned in Section 8.3.2, the safety function indicator for detrimental buffer freezing is -6 °C. The rock temperature at repository depth should thus not fall below this value.

Furthermore, as also mentioned above, the analyses of the mechanical impact of shear movements is carried out for material properties valid for temperatures down to 0 °C, which is thus set as another indicator criterion, that it is necessary to evaluate in the context of consequences of fracture shear movements.

The rock, through its current background temperature at repository depth and its thermal conductivity, affects the peak temperature in the buffer. A low background temperature and a high thermal conductivity is favourable for keeping the buffer temperature below the required 100 °C.

Additional considerations

The overall safety functions for the host rock, expressed as providing favourable chemical, mechanical, hydrological and thermal conditions, are general in nature. The safety function indicators and, where applicable, indicator criteria, to a large extent stem from canister or buffer processes, except for the indicators related to hydrogeology and transport, which are derived from intrinsic host rock properties.

A scrutiny of the geosphere processes is thus not expected to generate additional safety functions to the general categories already identified since all geosphere processes belong to one of these categories and also since the geosphere processes themselves do not, in general, provide indicators and indicator criteria. This was also the result of a brief scrutiny of the geosphere processes.

Safety functions relating to the prevention of future human actions (FHA) with detrimental effects on the host rock, and in particular intrusion into the repository were considered. However, properties of the host rock related to the likelihood of future human actions (mineral or thermal energy resources) and to the efforts/resources required for an intrusion of the repository (depth, sealing) are considered in the siting and design of the repository and are not factors that change over time in the post-closure safety assessment. These factors are included in the analysis of FHA scenarios, but are not seen as suitable for the formulation of safety functions.

8.3.5 Summary of safety functions related to containment

The safety function, and associated indicators and criteria derived in the preceding sections are summarised in Figure 8-3. Table 8-1 gives a summary of the margins to appropriate functioning for the safety function indicator criteria for containment, see also Section 8.2, subheading “Approach to margins”.

Safety functions related to containment

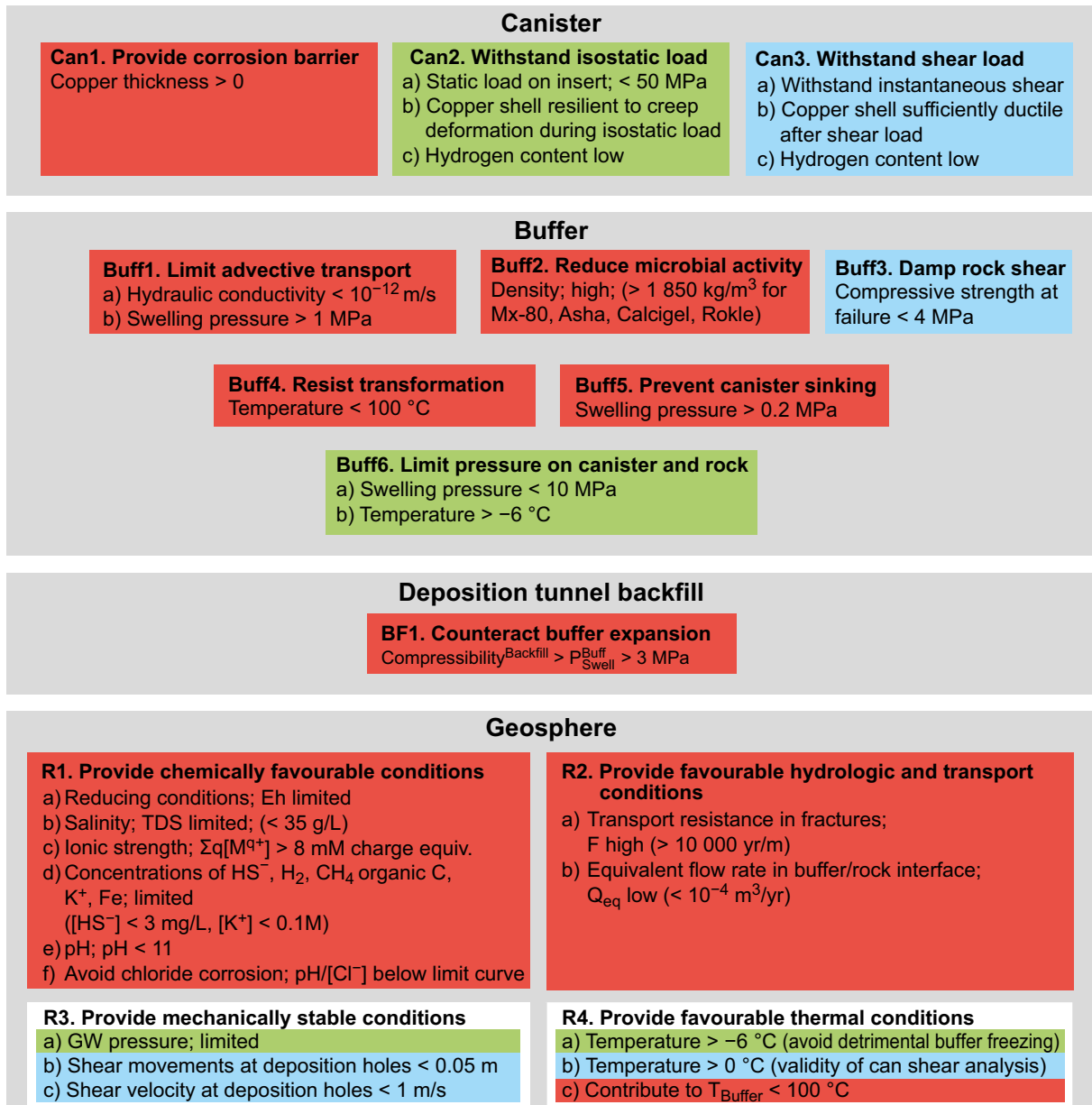


Figure 8-3. Safety functions (bold), safety function indicators and safety function indicator criteria related to containment. When quantitative criteria cannot be given, terms like “high”, “low” and “limited” are used to indicate favourable ranges of the safety function indicators. (For some of these, values indicating desired performance are given within parentheses.) The colour coding shows how the functions contribute to the canister safety functions Can1 (red), Can2 (green) and Can3 (blue).

Table 8-1. Summary of margins for safety function indicator criteria for containment.

Indicator	Criterion	Notes on margin
Minimum copper coverage	0	No margin, for trivial reasons.
Isostatic load on canister	50 MPa	Criterion from technical design requirements. Shown in design analysis to be fulfilled with a margin that could possibly be considerable (up to roughly 100 MPa) for global collapse. See further Jonsson et al. (2018).
Shear: Fracture shear distance Maximum buffer uniaxial compression strength Shear velocity Minimum temperature	5 cm 4 MPa 1 m/s 0 °C	Set of criteria from Technical design requirements. Shown in design analysis to be fulfilled, but 5 cm shear is without a margin to calculated failure for the most unfavourable fracture locations and angles with the maximum buffer density. For buffer densities obtained in the evaluation of the reference design, the margin may be considerable in many situations, although these were not fully evaluated in the design analysis. See further Jonsson et al. (2018).
Buffer hydraulic conductivity	10^{-12} m/s	The margin is related to the hydraulic gradient and the diffusivity of species in question. The margin is considerable.
Buffer swelling pressure	1 MPa	As the swelling pressure drops, the possibility for pathway formation in the buffer increases. There is an effect of the hydraulic gradient and possibly of salinity. Laboratory samples show piping at ~60 kPa, i.e. the margin to observed malfunction is considerable.
Buffer maximum temperature	100 °C	The extent of mineral transformations in the buffer is related to both the temperature and to the duration of the thermal pulse. Since the duration of the thermal pulse is short (on a geological time scale) the margin is considerable.
Buffer maximum swelling pressure (to limit isostatic load on canister)	10 MPa	Contributes to isostatic load on canister. See above for a discussion of margins on limits for isostatic load.
Detrimental buffer freezing temperature	-6 °C	For a given temperature drop below the freezing point of water, only a portion of the water in the bentonite turns into ice, i.e. any possible pressure build-up occurs gradually with decreasing temperature and will be less than 13.5 MPa/°C, which defines the phase boundary between ice and liquid bulk water. Furthermore, the lowering of the freezing point of water in the buffer will have additional contributions from the hydrostatic pressure at repository depth as well as from any dissolved salts in the ground water. The criterion is derived from when the ice causes an isostatic load of 50 MPa on the canister. See above for a discussion of margins on limits for isostatic load
Buffer minimum swelling pressure (to prevent canister sinking)	0.2 MPa	Modelling has been done for swelling pressures down to 80 kPa, a value for which the consequences of canister sinking could be considered to be acceptable.
Groundwater ionic strength (avoid buffer erosion)	$q[M^{n+}] > 8$ mM	The experimental margin on this value is a factor of two. However, there could be other factors that could limit erosion.
Groundwater pH	< 11	The value is a practical limit. The duration of the conditions with increased pH and mass balances of involved reactions need to be evaluated when consequences are analysed.
Groundwater pH and chloride concentration (to avoid chloride assisted corrosion of copper)	$pH/[Cl^-]^{GW}$ below limiting curve	No margin to onset of chloride assisted corrosion, but considerable margin to conditions ever expected in groundwater at repository depth at Forsmark.

8.4 Safety functions for retardation

Several of the above safety functions and associated indicators and criteria are related only to the containment properties of the system. This is particularly the case for the three canister functions Can1–Can3.

Should a canister be breached, a number of additional phenomena and processes related to the release and transport of radionuclides, i.e. relating to the retarding function of the system, become relevant.

Should a canister failure occur, release limitation and retardation is provided by functions, function indicators and, where applicable, function indicator criteria according to the following. All defined entities are summarised in Figure 8-4 at the end of this section.

8.4.1 Fuel

F1. Contain radionuclides

The fuel matrix cannot be controlled in the design of the repository. Nevertheless, the fuel types to be deposited have a matrix structure that is very stable in a repository environment and therefore provide an important function by containing radionuclides. The fuel dissolution rate is a suitable indicator for this safety function. The dissolution rate is less for reducing conditions, hence providing reducing conditions is a safety function of the host rock also from the point of view of retardation.

Also the structural metal parts of the fuel elements contain radionuclides. The corrosion rate of these metals is, therefore, also an indicator for the containment function of the fuel. Posiva SKB (2017) suggests a target value for the fractional dissolution rate of structural metal parts of $< 10^{-3}/\text{yr}$.

F2. Precipitation

Many of the most hazardous radionuclides have limited solubilities in a repository environment, hereby providing an important limitation on radionuclide releases from a failed canister. The elemental solubilities are suitable indicators for this safety function.

Many elemental solubilities are lower for reducing conditions, hence providing reducing conditions is a safety function of the host rock also in this respect.

F3. Avoid criticality

The fuel properties and geometrical arrangement in the canister should be such that criticality is avoided if water should enter a defective canister, but there is no meaningful simple criterion to use for such an evaluation. Qualitatively, the fuel reactivity should be low and it is a technical design requirement that the effective multiplication factor (k_{eff}) for the encapsulated fuel in a water-filled canister should not exceed 0.95 including uncertainties.

The canister insert should have a favourable geometry and material composition with respect to prevention of criticality. This is reflected in geometrical constraints on the canister design and on limitations on the contents of C and Si in the cast iron insert.

Furthermore, for altered geometries and materials acting to increase the reactivity, in both cases as consequences of the development in the canister after a potential breach of containment, the reactivity should not exceed 0.98.

8.4.2 Canister

Can4. Provide transport resistance

After a canister failure, water must reach the fuel and radionuclides must be transported through the canister for a release to occur. The nature of the failure will determine whether there are remaining physical hindrances in the canister to transport of water and radionuclides. Although the canister is not designed to provide such transport resistances, they may provide a considerable limitation on release rates, at least over a limited time span after failure.

The delay after failure to an onset of a release (t_{delay}) and a time for expansion of an initial failure to the extent that all transport resistances have been lost (t_{large}) may, for some failure types, be used as indicators for this safety function.

Can5. Avoid fuel criticality

As mentioned above, the canister geometry and material composition should be such that they contribute to the prevention of criticality.

8.4.3 Buffer

Functions in common with containment functions

Also for retardation, the buffer has an important function in limiting advective transport. The criteria on hydraulic conductivity and swelling pressure hence apply also for retention. In order to keep its favourable properties, the buffer should also resist transformation for which there is a criterion on temperature and it should prevent canister sinking that could short-circuit the buffer, ensured through a criterion on swelling pressure.

Buff7. Filter colloids

The buffer should furthermore be dense enough to prevent transport of colloids through it. This requirement is put on the buffer so that fuel colloids should not be able to escape a defective canister. Thereby, the releases of several key radionuclides will be limited by their solubilities. This requirement has led to the following criterion, see the **Buffer, backfill and closure process report**, Section 3.5.12.

$$\rho_{\text{Dry}}^{\text{Buff}} > 1\,000 \text{ kg/m}^3$$

Buff8. Sorb radionuclides

Limited advection in the buffer so that diffusion is the dominant transport mechanism is of primary importance also for radionuclide transport and ensured by the same safety functions as for containment. In addition, the sorption of radionuclides in the buffer may provide a significant limitation on the outward transport of radionuclides. The movement of water through the buffer is strongly limited, through the diffusion dominated transport in an intact buffer. In comparison to water, the transport of radionuclides is further retarded:

- By slower diffusion, which may be caused by a smaller diffusion coefficient in free water and by the electrostatic influence on apparent diffusion-available porosity (anion exclusion).
- By interaction with the clay surface, leading to sorption (expressed as K_d).

The element specific effective diffusion coefficients (D_e) and sorption coefficients (K_d) are suitable indicators for this safety function.

Buff9. Allow gas passage

The buffer should allow gas produced within a potentially damaged canister to escape. The gas transport properties are related to the buffer swelling pressure, where a lower swelling pressure is an advantage, but quantitative limits for favourable buffer function in this respect cannot be formulated at this stage. A limit would be related to the potential damage to the repository from the pressure or release of an overpressurised gas. The buffer issues related to gas transport are dealt with in the assessment of the evolution of a defective canister in Section 13.8.

8.4.4 Deposition tunnel backfill

BF2. Limit advective transport

The backfill shall limit the flow of water (advective transport) in deposition tunnels (Posiva SKB 2017). For this to be fulfilled the backfill should have a certain swelling pressure to assure tightness and homogeneity and a limited hydraulic conductivity. The quantitative criteria are the following:

$$P_{Swell}^{Backfill} > 0.1 \text{ MPa}$$

and

$$k^{Backfill} < 10^{-10} \text{ m/s}$$

The basis for these criteria is documented in the **Buffer, backfill and closure process report**, Sections 4.3.1 and 4.2.2, respectively.

There is also a requirement that the freezing of the backfill in the deposition tunnels should not lead to excessive pressures on the surrounding rock. The mean crack initiation stress level for the main rock type in Forsmark is 116 MPa and the minimum is 60 MPa (SKB 2008a). According to the Clausius-Clapeyron equation, 60 MPa is generated when ice is cooled by 4.4 °C below the freezing point of water. As for the buffer, the critical temperature is dependent on the swelling pressure. The swelling pressure of the installed backfill at average density of 1 488 kg/m³ is > 4 MPa and the swelling pressure for the minimum backfill density 1 361 kg/m³ is ~2 MPa for deionised water (Figure 5-17 and Fritzell 2017). A swelling pressure of 2 MPa would yield a critical temperature of -1.6 °C. Based on this a freezing criterion can be formulated:

$$T^{Backfill} > -6 \text{ °C} (= -4.4 - 1.6)$$

This is based on pure water and the salinity at the Forsmark site may reduce the freezing temperature further. For the deposition tunnel backfill, this requirement is primarily related to the retardation function, since i) freezing may damage the walls of the tunnel thus creating new transport paths for radionuclides and ii) the transport properties of a frozen and thawed backfill may be less favourable than those before freezing. It is, finally, noted that there is no temperature criterion related to the safety function BF2 in Posiva SKB (2017).

BF3. Sorb radionuclides

As for the buffer, sorption of radionuclides in the deposition tunnel backfill may provide a limitation on the outward transport of radionuclides. The sorption coefficients (K_d) are suitable indicators for this safety function.

8.4.5 Geosphere

Functions in common with containment functions

The geosphere safety functions concerning retardation are related to favourable i) chemical and ii) hydrologic and transport conditions and most of the relevant functions and function indicators are the same as for containment:

- A criterion related to the groundwater composition is that of reducing conditions which is of particular importance for maintaining a stable fuel matrix and low solubilities. In addition, indicators relating to ionic strength play a role, mainly in order to ensure favourable conditions for the retarding buffer.
- Regarding hydrologic and transport conditions, requirements on high transport resistances and low equivalent flow rates are common to the corresponding functions for containment.

R2c. Matrix diffusion and sorption

Matrix diffusion and sorption give important contributions to retardation of radionuclides in the geosphere. The element specific effective diffusivities (D_e) and sorption coefficients (K_d) are suitable function indicators.

R2d. Low colloid concentrations

Colloids travelling with the flowing water in fractures may transport radionuclides sorbed to their surfaces, thereby preventing retention of these nuclides by matrix diffusion and sorption. It is therefore favourable if colloid concentrations are low.

8.4.6 Summary of safety functions related to retardation

The safety functions, and associated indicators and criteria derived in the preceding sections are summarised in Figure 8-4. Table 8-2 gives a summary of the margins with which the safety function indicator criteria for containment have been determined.

Safety functions related to retardation

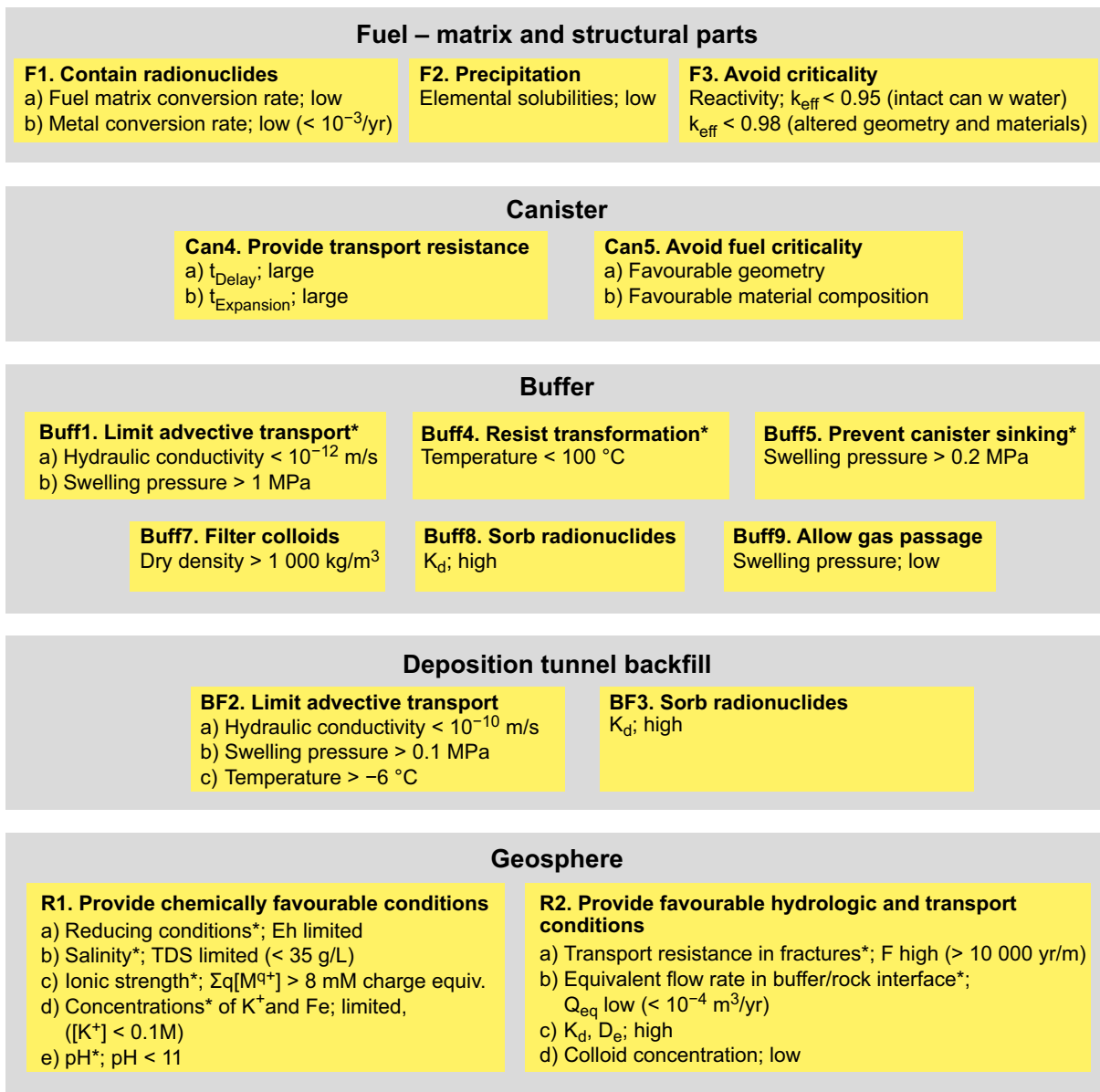


Figure 8-4. Safety functions (bold), safety function indicators and safety function indicator criteria related to retardation. When quantitative criteria cannot be given, terms like “high”, “low” and “limited” are used to indicate favourable ranges of the safety function indicators. (For some of these, values indicating desired performance are given within parentheses. Safety functions marked with an asterisk (*) apply also to containment, see Figure 8-3.

Table 8-2. Summary of margins for safety function indicator criteria for retardation.

Indicator	Criterion	Notes on margin
Fuel reactivity	$k_{\text{eff}} < 0.95$	Established according to principles generally applied for handling of nuclear fuel, see further the Spent fuel report .
Backfill hydraulic conductivity	$k < 10^{-10}$ m/s	The criterion is defined to ensure limited overall transport (not to guarantee diffusion). The margin is largely dependent on the characteristics of the rock.
Backfill swelling pressure	$P_{\text{sw}} > 0.1$ MPa	Piping has been observed at ~60 kPa, however at gradients much higher than those projected to occur in the repository.
Backfill temperature	> -6 °C	According to Table 5-23 the minimum allowed density in the backfill will be 1361 kg/m ³ . According to Figure 2-9 in the Buffer backfill and closure process report this would give a swelling pressure of ~2 MPa and a critical temperature of -1.6 °C together with the freezing point depression of water of 4.4 °C at 60 MPa this yields a criterion of -6 °C. The average density and the mean crack initiation stress are expected to be much higher and would allow for a temperature of ~-12 °C.

8.5 Factors affecting temporal evolution of safety function indicators – FEP chart

As mentioned earlier, the general evolution of the repository system, and that of the safety function indicators in particular, is determined by the initial state of the system, by a number of coupled, internal processes and by external influences on the system.

For the purposes of the safety assessment, it is desirable to have an overview of all these factors and their interdependencies. This was, in the SR-Site assessment, obtained through the development of a FEP chart, of which a slightly modified version is presented below.

A FEP chart contains important initial state properties, important processes, external influences, safety function indicators and the relations between these.

Figure 8-5 shows a FEP chart for a KBS-3 repository, covering factors of importance for containment. The figure shows initial state factors (e.g. the initial copper thickness), processes (e.g. corrosion), safety function indicators (e.g. copper thickness over time) and the safety function indicator criterion (e.g. thickness > 0). Dashed lines indicate influences that occur if a safety function indicator criterion is violated.

The FEP chart contains the following components.

- All variables defined as containment related safety function indicators and their criteria, i.e. those given in Figure 8-3. However, all variables that express a component of the groundwater composition are collectively described as “groundwater composition” in the FEP chart, rather than being listed individually.
- Additional variables necessary to describe system evolution and safety, but which are not regarded as safety function indicators, e.g. the porewater pressure of the buffer.
- All identified fuel, canister, buffer and backfill processes related to containment, except those which may be neglected according to the Process reports. However, some processes in the process tables are lumped into a single process, as indicated in the last columns of the process tables, Table 7-2 to Table 7-5.
- Geosphere processes and variables lumped into a limited number of phenomena that control the system evolution. The lumping is described in the geosphere process table, Table 7-6. The lumping also includes external influences on the system through the division of geosphere process descriptions into those applicable in the temperate, periglacial and glacial climate domains.
- Couplings and influences between the variables and the processes.

The FEP chart is useful in providing an overview of all major safety related factors related to containment, e.g. in the selection (Chapter 11) and analysis (Chapter 12) of scenarios based on safety function indicators.

The biosphere is not represented in the FEP chart since no safety functions are associated with the biosphere. The geosphere is less detailed than the engineered parts of the system since most of the safety function indicator criteria are related to the engineered parts. Factors related purely to retardation are not included. Most retardation factors are, however, important also for containment and are therefore included.

In summary, the FEP chart provides an overview of the relationships between initial state factors, variables, processes and safety function indicators. It aids an expert in analysing the system qualitatively, and is used, in combination with other sources, for scenario selection and analysis in the PSAR.

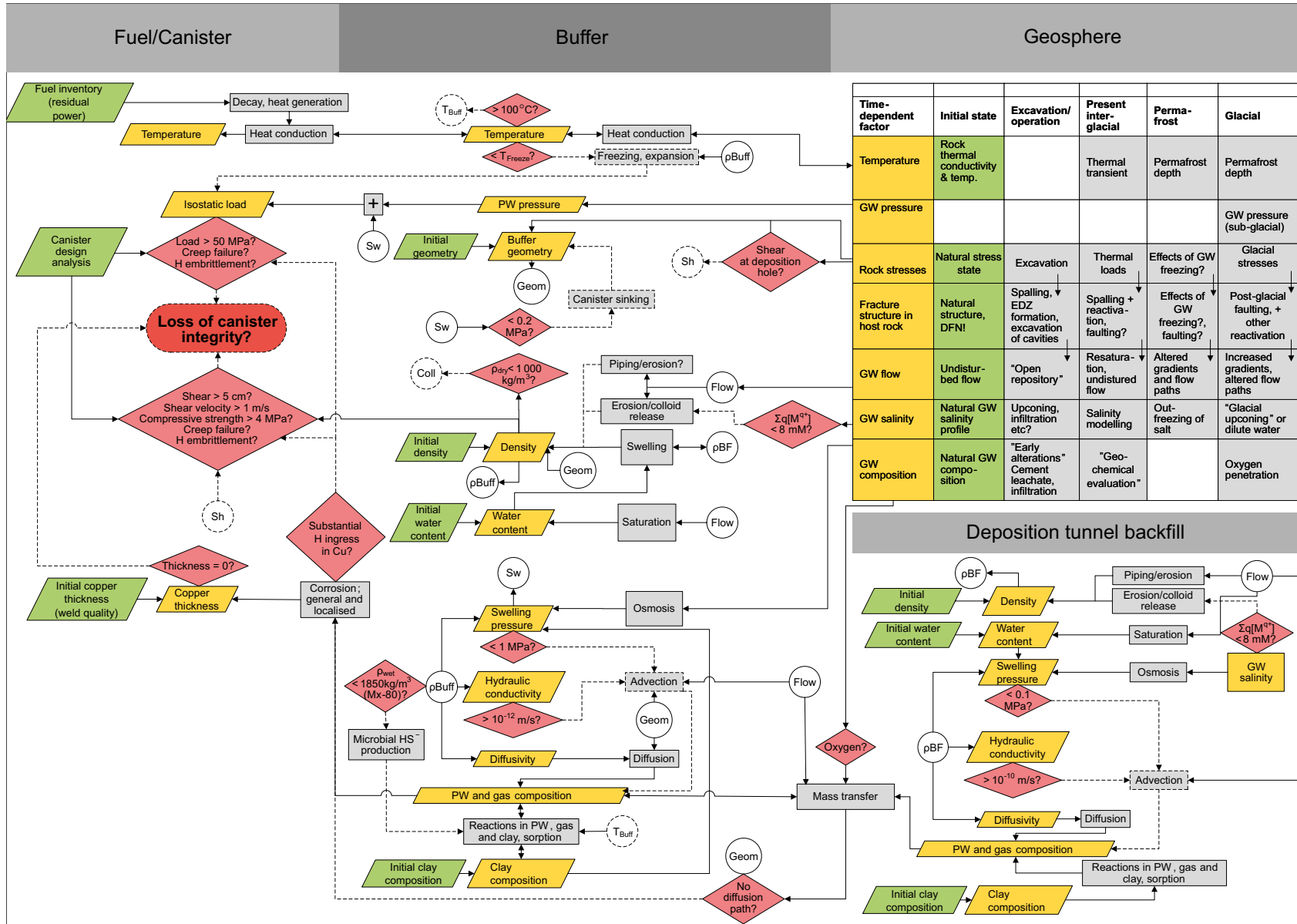


Figure 8-5. The PSAR FEP chart, covering factors of relevance for containment. Colour coding: Initial state factors, Variables, Processes, Safety function indicators. Solid lines: Influences that always occur. Dashed lines: Influences if there is safety function indicator violation. Circles: Interrupted influence lines (to increase readability).

9 Compilation of input data

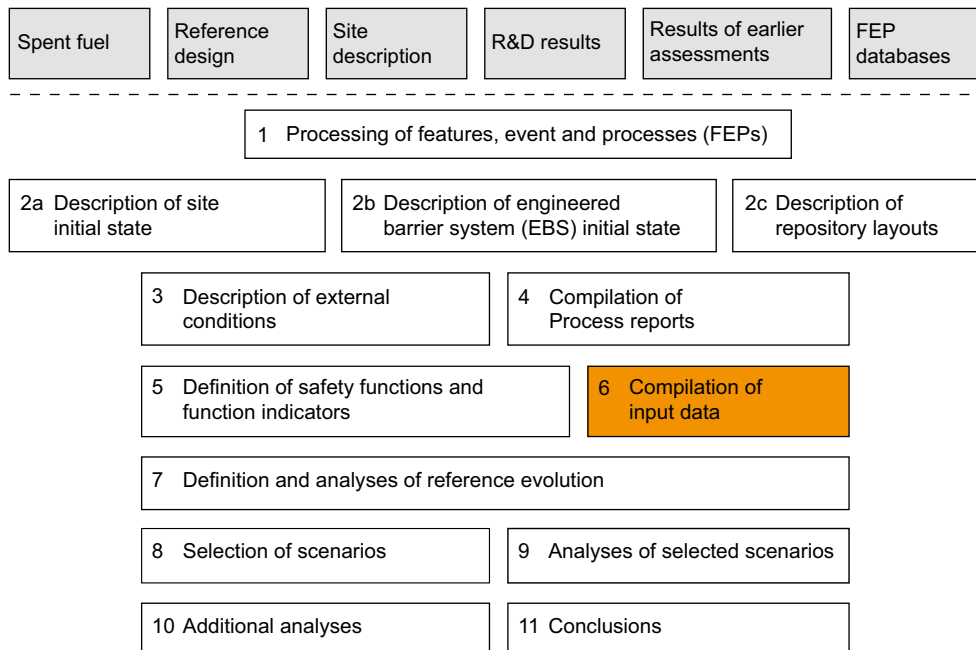


Figure 9-1. The PSAR methodology in eleven steps (Section 2.5), with the present step highlighted.

9.1 Introduction

The main purpose of a safety assessment of a final repository is to investigate whether the repository can be considered radiologically safe over time. In principle, this is established by comparing estimated releases of repository derived radionuclides and associated radiation doses with regulatory criteria. All input data used in quantitative aspects of the safety assessment have uncertainties. The quality of the results of any calculation in the assessment will, among other factors, depend on the quality of the input data and on the rigor with which input data uncertainties have been handled. A methodological approach for the determination of input data with uncertainties and the subsequent handling of the uncertainties is, therefore, required.

The set of input data parameters for the safety assessment is very large. Some input data uncertainties will have a substantial influence on output uncertainty, whereas others will essentially not influence output uncertainty at all. An example of the latter are transport properties of those radionuclides that never give a significant contribution to the radiological risk. It is thus appropriate to identify input data to which output is sensitive and use these insights in allocating resources to the determination and, where feasible, reduction of input data uncertainties. It is also important to have a high degree of confidence in the data that are used to conclude that particular nuclides will never contribute to risk.

9.2 Objectives of the Data report

The objective of the **Data report** is to compile input data, with uncertainty estimates, for the assessment calculations for a wide selection of conditions. Data have been assessed through standardised procedures, adapted to the importance of the data, aiming at identifying the origins of uncertainties and where data obtained through scientific methods is clearly distinguished from judgements made by the assessment team. Versions of the Data report have formed part of SKB's assessments of post-closure safety for the final repository since the safety assessment SR 97 published in 1999.

A specific instruction on “*Supplying data for the SR-Site Data report*” was developed as part of the Quality assurance plan for the safety assessment SR-Site. The same approach has been used when updating the SR-Site version to the PSAR version see further Section 2.3 of **Data report**. This instruction has been written to facilitate methodical and traceable data qualification, where comments made by the authorities form a basis for the improvements in the data qualification methodology.

In the PSAR version of the **Data report**, only data that has been updated since the SR-Site assessment are qualified. For data that has not been updated the material from the SR-Site Data report is reproduced, and an indication of this is given in the heading of a reproduced text. The text may still be slightly modified in that references to the PSAR report hierarchy rather than to that of SR-Site may occur as appropriate. Also, experiences from the modelling in SR-Site have been taken into account when evaluating all data sets, irrespective of whether they are updated or not.

The remainder of this Chapter 9 is essentially unchanged compared to the SR-Site version of the chapter.

9.3 Inventory of data

The mapping of safety relevant processes to models, see Section 7.4, yields a set of models that are used to quantify the system evolution, including models for radionuclide transport and risk calculations. In principle, data requirements of these models constitute the input data inventory to be managed in the safety assessment. The importance of the various parameters, however, differs markedly. While data for all the several hundred input parameters must be quality assured, only a limited sub-set are uncertain to an extent critical to the safety assessment, thus requiring a detailed quantification of uncertainty. These data are identified by sensitivity analyses of calculation results often from earlier assessments. For the PSAR, the SR-Site assessment results have predominantly been used for the sensitivity analysis.

A number of calculation end-points regarding both containment and retardation have been considered and sensitivities of these to input parameter uncertainty and natural variability have been determined. This study has not resulted in any new parameters of relevance for the assessment.

In many cases, input data to modelling are provided as probabilistic distributions. Experience from previous safety assessments provides information on which part of the distribution contributes most to the radiological risk. Most often it is the upper or lower tail of the data distribution that contributes. This is an aid in the determination of input data, since it informs the analyst that as long as the relevant tail is carefully described, details in the shape of the remaining distribution are less important, or even insignificant.

9.4 Instructions on supplying data

9.4.1 Suppliers, customers and Data report team

The instructions concern two parties, the suppliers and the customer.

- The suppliers supply data that are qualified in the **Data report**. The suppliers are the teams originating the sources of data, as described in the Site descriptive model report, **Production reports**, and other supporting documents. The author producing text for the **Data report** on behalf of the supplier is called the supplier representative. The supplier representatives should represent the teams, and not rely solely upon their own opinions.
- The customer is in broader terms the team that is responsible for performing the safety assessment. However, the entire team is not generally involved in each subject area but it is rather embodied by a group of persons with special knowledge and responsibility. The author producing text for the **Data report** on behalf of the assessment team is called the customer representative. The customer representatives should represent the assessment team, and not rely solely upon their own opinions.

A Data report team, being a subgroup to the assessment team administers the **Data report**, and writes the general text in the **Data report** that does not concern specific data. The persons identified as supplier representatives, customer representatives, and members of the Data report team and of the assessment team, responsible for different subject areas, are listed among the experts used in the assessment, see Section 2.9.3. The customer, supplier, and/or Data report team can in certain cases be represented by the same individual. If so, steps are taken to involve the groups they represent, or other experts, in the handling of the text.

9.4.2 Implementation of the instructions

Upon identification of the supplier and customer representatives for the specific Data report section, and after they have accepted their tasks, the instructions for a specific Data report section are normally presented during a meeting between the supplier and customer representatives and a member of the Data report team. The section and the associated data are then developed in steps:

- The customer writes the sections specifying the task and experience from SR-Site etc. according to the instructions.
- After approval by the Data report team these sections are then sent to the supplier, who should then supply the text concerning data and their variability and uncertainties, according to the instructions.
- Several iterations of these steps may occur.
- Finally, part of the assessment team and the supplier convene at a meeting to discuss the entire subject area delivery. This meeting, which is formally recorded, is called a Data qualification meeting. At this meeting the data that are recommended for use in the safety assessment modelling are formally decided upon. This meeting may also give rise to review comments that should be handled by the supplier or customer.

9.5 Qualification of input data

Data that are closely associated in the context of the safety assessment are categorised into one of many different subject areas. For each subject area, the data qualification process comprises a sequence of stages resulting in a text of a standard outline. According to the instructions, some of the sections in these steps are written by the customer, whereas others are written by the supplier. The steps are outlined in the following (for further detail, see the **Data report**). These steps have been applied consistently in qualifying the input data for the assessment.

Modelling

In this section, the *customer* defines what data are requested from the supplier and gives a brief explanation of how the data for the subject area are used in the assessment. This information is provided for precisely defining the input data and explaining the context in which the data are to be used. Justification for the use of these models in the assessment is formally given in the **Model summary report**. If the modelling in the PSAR assessment agrees with that in SR-Site, the SR-Site Data report is referenced.

Experience from SR-Site

In this section the *customer* gives a brief summary on how the data for the subject area were used in SR-Site. The experience from SR-Site should function as one of the bases for defining the input data required in the PSAR modelling. It should be noted that the teams undertaking the SR-Site and the PSAR safety assessments largely are the same, so transferring experience from SR-Site to PSAR has not presented any substantial problem. The summary of how the data were used in SR-Site should conform to the following outline;

- modelling in SR-Site,
- conditions for which data were used in SR-Site,

- sensitivity of assessment results in SR-Site,
- alternative modelling in SR-Site,
- correlations used in SR-Site modelling,
- identified limitations of the data used in SR-Site modelling.

More detailed guidance regarding what should be included in the summary in relation to each of these bullets is given in the instructions.

Supplier input on use of data

In this section the *supplier* has the opportunity to comment on the two above sections. The focus for the supplier should be to help the assessment team in choosing an appropriate modelling approach, and avoid repeating errors and propagating misconceptions from SR-Site or from earlier safety analyses. Even if a single individual has the roles as both supplier and customer, he or she may still make comment upon the use of data in previous assessments.

Sources of information and documentation of data qualification

This section, as provided by the *supplier*, is devoted to presenting the most important sources of data, as well as categorising different data sets on the basis of their traceability and transparency, and scientific adequacy. Sources of data may include SKB reports, SKB databases, and public domain material. Documents of importance for the data qualification may also consist of SKB internal documents. All underlying documents should be properly cited throughout the **Data report**.

The supplier should categorise data as either qualified data or supporting data. Qualified data have been produced within, and/or in accordance with, the current framework of data qualification, whereas supporting data have been produced outside, and/or not in conformance with, the framework. Data may also be categorised as supporting if they are not entirely representative for the Forsmark site or KBS-3 repository. Data taken from peer-reviewed literature have a special position in that they may be considered as qualified even though they are produced outside the SKB framework of data qualification. However, such data are not by necessity categorised as qualified, as they may be non-representative or lack in some other aspect. Data recently produced by SKB, for example in the site investigations, should *a priori* be considered as qualified. However, before the data are formally categorised as qualified, a number of considerations need to be addressed, as described in detail in the instructions. Data produced outside the data qualification framework should *a priori* be considered as supporting data.

Conditions for which data are supplied

The data for the different subject areas are likely affected by different conditions. Conditions refer to initial conditions, boundary conditions, barrier states, and other circumstances, which potentially may affect the data to be estimated. In the process of qualifying data for subsequent use in safety assessment, an important consideration is to account for the conditions for which data were acquired, and to compare these conditions with those of interest for the safety assessment. The *supplier* has to provide this information.

Conceptual uncertainty

Here, the *supplier* discusses the conceptual uncertainty of the subject area data. Two types of conceptual uncertainty should be discussed. The first concerns how well the data, and the models wherein it is used, represent the physical reality, and the second concerns conceptual uncertainties introduced by the acquisition, interpretation, and refinement of the data.

Data uncertainty due to precision, bias, and representativity

Here, the *supplier* discusses data uncertainty in terms of precision, bias, and representativity. Such uncertainty is associated both with the acquisition of data, for example in the site investigations,

and subsequent refinement of data, for example in the site descriptive modelling. Data uncertainty includes neither conceptual uncertainty nor natural variability.

Spatial and temporal variability

Here, this *supplier* deals with the spatial and temporal variability of the data. The natural variability should as far as possible be separated from data uncertainty, discussed in the above section.

Correlations

An appropriate treatment of probabilistic input data requires that any correlations and functional dependencies between those data are identified and quantified. If such exist, they are described by the *supplier*. However, in the extensive work with the FEP database and the **Process reports**, most correlations and functional dependencies between parameters have been identified. Where appropriate, these correlations and functional dependencies have usually also been implemented in the safety assessment models. Correlations and functional dependencies may also have been used when acquiring, interpreting, and refining data. For example, concerning sorption partition coefficients, data have not been acquired for all relevant radionuclides. For elements for which there is a lack of observations, the supplied sorption partition coefficient will have been estimated from data obtained for one or more analogue elements.

Results of supplier's data qualification

In this section the *supplier* presents data that are considered to be appropriate as a basis for selecting input data for use in the assessment. The general process of reducing data, valuing different data sets, and finally selecting the recommended data for delivery to the assessment team should be fully accounted for. The main instructions are as follows.

- If data qualification has already been performed and accounted for in supporting documents, it is sufficient to briefly summarise the process of selecting the delivered data. In other cases the data presented in supporting documents may need reinterpretation and further refinement, in the light of this instruction and/or other information. If so, the process of reinterpretation and data refinement should be fully documented.
- The data sets that the supplier recommends to the assessment team should be in the form of single point values, probability distributions, mean or median values with standard deviations, percentiles, and/or ranges, or as otherwise appropriate.
- If no probability distribution can be supplied, but where the data have significant variability and/or uncertainty, the spread in data could instead be described as a range. However, the meaning of the range has to be provided, e.g. does it represent all possible values, all “realistically possible” values or just the more likely values?
- It should be noted that in many cases, at some stage probability distributions must be assigned to numerical data being the input to probabilistic safety assessment modelling. If the supplier feels inadequate to deliver a defined distribution, but for example delivers a best estimate, an upper, and a lower limit for data, it may fall on the assessment team to transform such information into probability distributions. This is justified as the assessment team may have a better understanding of how the shape of the assigned distributions (especially in their tails) affects the modelling results. The assessment team may also, in some cases, have a better understanding of the underlying statistics of the suggested distribution.
- If it is impossible to express the uncertainty by means other than a selection of alternative data sets or by pessimistic assumptions, this is allowed, as long as the supplier clearly documents this together with the motivation for adopting this approach.
- Unless published elsewhere, the numerical values relating to the individual data sets and/or data points should be stored in a database.

For details see the instructions.

Judgements by the assessment team

In this section, the *customer* documents the examination of the delivery provided by the supplier, and makes judgment on the data qualification. This text should be produced in close cooperation with persons in the assessment team with special knowledge and responsibility. In the case of unresolved issues, the final phrasing should be decided upon by the assessment team.

If the assessment team needs to suggest probability distributions based on data supplied in the previous sections, this is justified here. Typical choices made are whether to suggest a distribution in the log space or in normal space, whether to use a truncated or non-truncated distribution, and selecting the shape of the distribution. The base, shape, and truncation of the distribution may affect the calculated risk as well as the influence of extreme values on the assessment results. Therefore it is important to be cautious in selecting such a distribution. For crucial data, where the choice of distribution significantly affects assessment results, the suggested distribution is communicated with those performing the subsequent modelling, with the larger assessment team, and with the experts of the supplier team.

Data recommended for use in the assessment

Based on all the available information, but also on modelling needs, the assessment team makes a final choice of data, often in form of well-defined probability distributions, including natural variability, data uncertainty and other uncertainty. In some cases where the spread in data is small, single point values may be chosen. The choice should be fully documented and the resulting data should be tabulated. Also guidelines for how to use the data in subsequent modelling should be given, as required. Justifications and guidelines are required to be kept short so that this section mainly contains tabulated data that are easily extractable for the safety assessment modelling.

In the process of making the final choice of data, the supplier is consulted one more time in a *data qualification meeting*. Here the formal decision on the data recommended for use in modelling is taken, and records of the meeting are made as part of the SKB quality assurance system. The formal decision is acknowledged by those representing the supplier team and those representing the assessment team.

9.6 Final control of data used in calculations/modelling

The supplied, quality assured input data must also be used in a correct manner in the modelling. Common errors that may appear in the usage of data are that i) the final version of the data set is not used ii) errors and misprints are made in inputting the data in the program code iii) an incorrect data set is used (for example groundwater composition for temperate climate conditions instead of glacial conditions).

After the completion of the **Data report**, it falls upon the modeller to check that the final data sets have been used. In doing this, the modeller also checks that there are no errors or misprints from inputting the data in the code.

**Post-closure safety for the final repository
for spent nuclear fuel at Forsmark**

Main report, PSAR version

Volume II

10 Analysis of a reference evolution for a repository at the Forsmark site

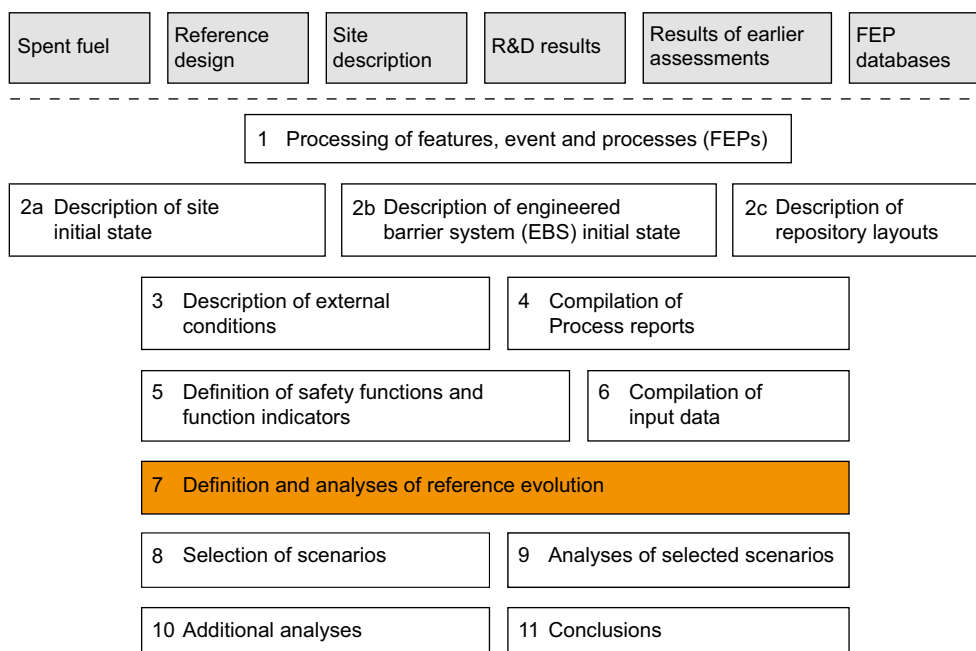


Figure 10-1. The PSAR methodology in eleven steps (Section 2.5), with the present step highlighted. This chapter deals with the definition of the reference evolution and with the analysis of the containment potential. Retardation is treated in Chapter 13 (step 9 in the figure).

10.1 Introduction

This chapter describes a reference evolution of a KBS-3 repository at the Forsmark site over the entire one million year assessment period. The purpose is to gain an understanding of the overall evolution of the system, for the scenario selection and scenario analyses that follow in Chapters 11, 12 and 13. The ambition is to assess the impacts of processes affecting the containment safety functions and to describe a reasonable evolution of the repository system over time. The reasonable evolution is an important basis for the definition of a main scenario, see Chapter 11 and, for details, Section 12.1.2.

Focus is on the containment capacity; consequences in terms of radionuclide releases are not analysed. Chapter 13 describes radionuclide transport and dose consequences for canister failure modes identified in all scenarios, of which the main scenario is closely related to the reference evolution described below.

Two cases of the reference evolution are analysed.

1. A base case in which the external conditions during the first 120 000 years after closure are assumed to be those reconstructed for the most recent glacial cycle, that includes the Weichselian glaciation. Thereafter, seven repetitions of that cycle are assumed to cover the entire 1 000 000 year assessment period. The base case is analysed in Sections 10.2 through 10.5.
2. A global warming variant in which the future climate and hence external conditions are influenced by anthropogenic greenhouse gas emissions during the first 120 000 years after closure. This analysis is related to that of the base case and is presented in Section 10.6.

For both cases, the initial state described in Chapter 5 is assumed and all internal processes are handled according to the specification given in the **Process report**, as summarised in Chapter 7.

In order to fulfil its requirements, the chapter covers a substantial number of issues and subject areas to a rather detailed level, where the level of detail is to a large extent a reflection of the safety relevance of the issue in question. In fact a large part of all the analyses conducted within the PSAR post-closure safety project are summarised and put into perspective in this chapter. Also, for reasons explained below, the chapter is divided into different time frames. This structuring makes the chapter longer since the same process needs to be discussed at several occurrences. However, it is preferred, since it helps to demonstrate the comprehensiveness of the analysis and compliance with regulatory criteria, as well as making the approach transparent.

Substantial updates of the contents of the present Chapter have been made compared to the SR-Site version of the text, as summarised in Table 10-1. The structure of the chapter is, however, unchanged.

Table 10-1. Summary of main factual updates in Chapter 10.

Level 3 Section	Heading of Level 4 Section with substantially updated text	Further specification of update (Empty cell indicates that entire Level 4 Section is updated)
10.2.2	New fracturing induced near the tunnel by the excavation work – formation of an “EDZ”	
10.2.3	Identified uncertainties and their handling in the PSAR	Sub-section “Inflow rejection criteria”
10.2.4	Water saturation of the plug and its sealing ability	
	Piping erosion	
	Identified uncertainties and their handling in the subsequent analysis	
10.2.5	Nitrogen compounds from blasting activities	
	Effects of organic materials and microbial processes	
	Oxygen consumption in backfill	
	Canister corrosion	
	Identified uncertainties and their handling in the subsequent analysis	
10.2.7		10.2.7 updated to reflect changes in preceding parts of Section 10.2
10.3.6	Methodology	Figure 10-23 and associated bulk text.
	Penetration of dilute water	
	Uncertainties related to the DFN model and its input data	
10.3.7	Modelling	Texts relating to Puigdomenech (2013) and Auqué et al. (2013); Discussion of DOC; Sub-heading “Nitrogen compounds”
	Effects of grout, shotcrete and concrete on pH	
10.3.8	The Sauna effect	
	Saturation of the backfill	Sub-heading “Additional evaluation of uncertainties in Åkesson et al. (2010b)”
	Application to hydraulic conditions at the Forsmark site	
	Identified uncertainties and their handling in the subsequent analysis	
10.3.9	Buffer homogenisation	Sub-heading “Additional assessment of water saturation phases”
	Buffer upward expansion	
	Homogenisation after loss of bentonite mass	Sub-heading “Potential for microbial sulfate reduction”
	Identified uncertainties and their handling in the subsequent analysis	Updated to reflect changes in preceding parts of Section 10.3.9

Level 3 Section	Heading of Level 4 Section with substantially updated text	Further specification of update (Empty cell indicates that entire Level 4 Section is updated)
10.3.10	Unsaturated phase and period of elevated temperatures	
	Interaction with copper corrosion products	
	Sulphate reduction under saturated conditions	
	Composition of water in the buffer/canister interface	
	Identified uncertainties and their handling in the subsequent analysis	Updated to reflect changes in preceding parts of Section 10.3.10
10.3.11		Entire section 10.3.11 re-written
10.3.12	Chemical and mechanical interaction bottom plate/buffer	
10.3.13		Entire section 10.3.13 re-written
10.3.14	Evolution of the borehole seals	Sub-heading "Analysis of time scale of borehole seal hydration"
	Identified uncertainties and their handling in the subsequent analysis	Updated to reflect changes in preceding parts of Section 10.3.14
10.3.15		Minor updates to reflect changes in preceding parts of Section 10.3
10.3.16		Minor updates to reflect changes in preceding parts of Section 10.3
10.4.1	Ice sheet evolution and modelling	Sub-headings "Glacial hydrological conceptual model", "Amount of water produced by melting", "Spatial perspective on the subglacial hydrological system", "Temporal perspective on the subglacial hydrological system"
	Relative sea level and GIA modelling	
10.4.3		Minor factual updates in entire Section 10.4.3
10.4.5		Entire Section 10.4.5 updated
10.4.6	Penetration of glacial melt water	
10.4.7	Glaciation	Sub-heading "General"
10.4.8	Freezing Colloid release from buffer and backfill	
10.4.9	Canister failure due to isostatic load	
	Canister corrosion for a partially eroded buffer	
10.4.11		Updated to reflect changes in preceding parts of Section 10.4
10.5		Updated to reflect changes in first glacial cycle
10.6.1		Entire Section re-written
10.6.3		Entire Section updated
10.7		Updated to reflect changes in preceding Section of Chapter 10

10.1.1 Detailed prerequisites

Initial state of engineered barriers

The initial state encompasses the entire repository with all 6 000 deposition holes and the initial state relates to the conditions expected in the entire ensemble of deposition holes. The initial state, as given in Chapter 5, is the expected result of the production of the engineered components of the repository, including the application of relevant control procedures (see further Section 5.1.1). For example, the initial state of the canister includes welding defects (Table 5-9 in Section 5.4.3) and variations in initial buffer density that were derived taking imperfections in deposition hole geometry, variations in raw material composition and imperfections in the manufacturing process into account (Table 5-15 in Section 5.5.3).

Possible deviations from the initial state given in Chapter 5 are further addressed in the selection of scenarios in Chapter 11.

Geosphere and biosphere initial state

The initial state for the geosphere and the biosphere is that given by the site descriptive model, including uncertainties and possible variants as described in Chapter 4 and quantified for the purposes of the PSAR in the **Data report**. The site-specific layouts are those described in Section 5.2.2.

Process system

The set of processes governing repository evolution is handled according to the information given in the **Process reports** for the fuel/canister, the buffer/backfill/closure, the geosphere and the biosphere. Uncertainties in process understanding and/or model representation are handled according to the procedures established in those reports.

It should be noted that all identified processes are considered in the evolution. If, after consideration, a process is excluded, this exclusion is justified in the Process report. The handling is summarised in Table 7-2 through Table 7-6 in Chapter 7. Data uncertainty as identified in the **Data report** is also considered.

External conditions – base case

As mentioned in Section 6.2, it is not possible to predict a single future climate evolution in a long-term perspective with enough confidence for a safety assessment. It is very likely though that the repository site in the long-term will experience periods of all the identified climate domains and all the associated transitions. The reference evolution should, therefore, include periods of temperate conditions including shore-level displacement, both regression and transgression, at different rates, as well as permafrost and glaciation of different extent and also the possible transitions between the domains. A relatively well known evolution including all the mentioned components is the one covered by the Weichselian glacial and the Holocene interglacial, i.e. the evolution from the end of the Eemian (Marine Isotope Stage 5e, see Figure 10-101, Section 10.4.1) at about 120 000 years ago to the present time. In this assessment, this last glacial cycle has been chosen to constitute a reference evolution of climate-related conditions at the Forsmark site.

The selected external conditions of the reference evolution are regarded as one example of a credible development during a glacial cycle. The description in the reference evolution is not an attempt to predict a “most probable” future development. Instead the purpose of the reference evolution is to construct a scientifically reasonable starting point for the analysis of potential climate related impacts on repository safety. It is only necessary to capture the major aspects of the last glacial cycle, since even if for instance the ice sheet development were to be constructed in more detail for the site, the impact of any future glaciation will differ at such a detailed level. Instead, the reference glacial cycle is complemented by additional climate cases that describe more extreme conditions, with for example larger and smaller ice sheets. It is, furthermore, noted that even with the greenhouse warming committed to date, the reference evolution with a repeat of the Weichselian cycle is unlikely, hence the need for a greenhouse-warmed variant (see below).

The analysis of the evolution is initiated by a 1 000 year long period within which the development is based on extrapolation of current evolution and trends. Thereafter, the analysis is based on a repetition of conditions reconstructed for the Weichselian glacial cycle from 120 000 years ago until the present day. At 120 000 years ago, the climate-related conditions are, in a broad sense, considered to have been similar to those existing at the present. For the remainder of the assessment period, this 120 000 years long glacial cycle is assumed to be repeated.

The reason for choosing the reconstruction of Weichselian conditions as the reference evolution is twofold. Firstly, it is the best known of the past glacial cycles and the evolution and variability of climate-related conditions can be investigated by reference to associated geological information. Secondly, the available geological information makes it possible to test or constrain the supporting analysis and modelling efforts aimed at process understanding and the studies of the, often complex, coupled processes related to climate changes. For more information on the approach of using reconstructed last glacial cycle conditions as one example of a future development of climate related issues at Forsmark, see the **Climate report**.

External conditions – global warming variant

An additional factor related to future climate evolution is introduced by the impact and duration of human influence on climate due to emissions of greenhouse gases. Therefore, as a variant of the evolution based on the repetition of the last glacial cycle, a global warming variant comprising a 50 000 year long period of temperate domain, followed by the first, relatively mild, 70 000 years of the base case is analysed, see further Section 10.6 and the **Climate report**, Section 5.1. In addition, a complementary case with more severe global warming is described and analysed, see the **Climate report**, Section 5.2.

10.1.2 Structure of the analysis

The presentation of the analysis of the base case of the reference evolution is divided into four time frames:

- The excavation/operational period, Section 10.2.
- The first 1 000 years after closure and the initial period of temperate domain from the reference glacial cycle, Section 10.3.
- The remaining part of the glacial cycle, Section 10.4.
- Subsequent glacial cycles up to one million years after closure, Section 10.5.

In Section 10.6, the global warming variant is analysed over an entire glacial cycle.

For each time frame, issues are presented in the following order:

- Climate issues.
- Biosphere issues.
- Thermal, mechanical, hydraulic and chemical issues in the geosphere.
- Thermal, mechanical, hydraulic and chemical issues for the engineered barrier system (canister, buffer, backfill and other repository components).

The commentary on each time frame concludes with a discussion of the expected status of the safety function indicators defined in Chapter 8 during and at the end of the time frame.

A considerable part of the material presented results from simulation studies. An overview of these studies is given in the assessment model flow chart, AMF, for the excavation/operation period, the first 1 000 years after closure and a continued warm period, Section 7.5 and Figure 7-3. Table 7-7 explains how the modelling activities in the AMF are documented and the processes that are handled by each model. An AMF for periglacial and glacial conditions is given in Figure 7-4, with the associated Table 7-8.

Figure 10-2 shows the safety functions of the repository system and the safety function indicators used to evaluate whether the safety functions are maintained, as defined in Chapter 8. The safety functions in Figure 10-2 are referred to in the following sections, to explain the safety-related purposes of the analyses undertaken in the evaluation of the reference evolution.

Safety functions related to containment



Figure 10-2. Safety functions (bold), safety function indicators and safety function indicator criteria. When quantitative criteria cannot be given, terms like “high”, “low” and “limited” are used to indicate favourable ranges of the safety function indicators. (For some of these, values indicating desired performance are given within parentheses.) The colour coding shows how the functions contribute to the canister safety functions Can1 (red), Can2 (green) or Can3 (blue). See Section 8.3 for details.

10.1.3 Hydrogeological modelling in the PSAR

The systems approach in hydrogeological modelling used by SKB in the **Site description Forsmark** and in the PSAR is to divide the geosphere into three hydraulic domains denoted by HCD, HRD and HSD, where:

- HCDs (Hydraulic Conductor Domains) represent the deterministically modelled deformation zones.
- HRDs (Hydraulic Rock mass Domains) represent the less fractured bedrock in between the deformation zones.
- HSDs (Hydraulic Soil Domains) represent the regolith (Quaternary deposits).

The approach and its implementation is the same as in the SR-Site assessment.

Figure 10-3 shows an overview of the three flow modelling studies made with respect to the safety functions related to the bedrock domains, i.e. HCDs and HRDs (Svensson and Follin 2010, Joyce et al. 2010, Vidstrand et al. 2010). The modelling methodology, numerical setups including description of utilised data, and summary of results in a PSAR context of these studies are provided in Selroos and Follin (2010). A summary of the results is given in Sections 10.2.3, 10.3.6 and 10.4.6.

Any release of radionuclides reaching the surface system from the bedrock will be directed to the deeper parts of the regolith (i.e. HSD). From there, radionuclides will be distributed up to and within the surface ecosystems by near-surface groundwater and surface water flow systems. In order to support the modelling of radionuclide transport in the surface system, detailed hydrological modelling of the surface system during periods with temperate and periglacial climate conditions has been conducted by Bosson et al. (2010). A summary of the results is given in the **Biosphere synthesis report**. Studies of the effects of groundwater withdrawal during the excavation and operational phases on hydrological and near-surface hydrogeological conditions (including groundwater in the HSD) are reported by Mårtensson and Gustafsson (2010). These results are used as an input to analyses of ecological and other types of consequences during the mentioned phases, as a basis for the Environmental Impact Assessment (EIA) (SKB 2010a, Werner et al. 2010).

Figure 10-3 indicates the time period handled by each bedrock flow modelling study and where the results are presented in the present report. The three studies employ different computer codes and modelling teams. The studies conducted by Svensson and Follin (2010) and Vidstrand et al. (2010) were made with DarcyTools, whereas the study by Joyce et al. (2010) was made with ConnectFlow. The studies share the same systems approach and hydrogeological input to support conceptual integration, to allow for consistency checks of the reported flow simulations and to provide a good modelling strategy.

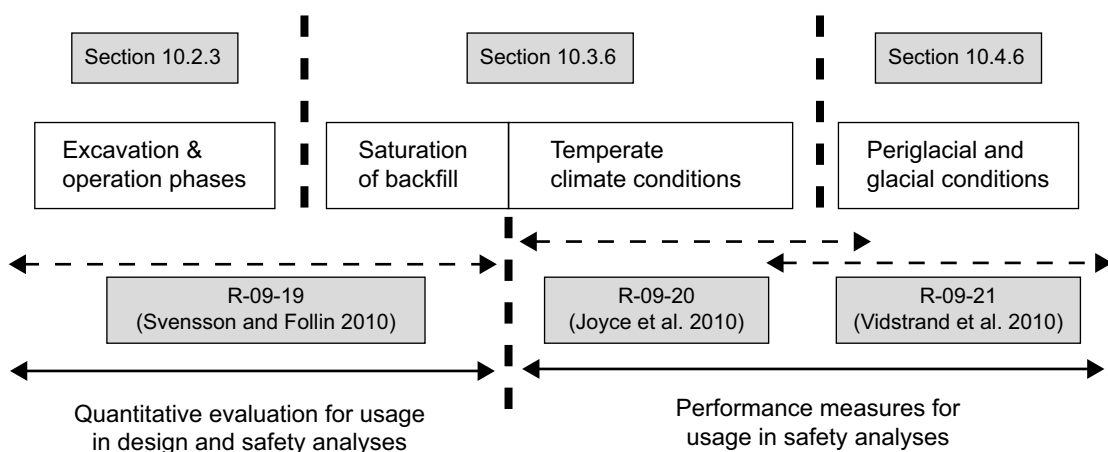


Figure 10-3. Overview of flow modelling made with respect to the safety functions related to the bedrock.

In Figure 10-4, the relation between the hydrogeological model presented in the **Site description Forsmark** and in more detail in Follin (2008), i.e. the Base model simulation, and the models used in the PSAR are exemplified. The term ‘SDM-Site’ in Figure 10-4 and in the discussions on hydrogeology in the present report is used synonymously with the **Site description Forsmark**.

A Hydrogeological base case model is derived within the temperate phase modelling. This model is essentially identical to the SDM-Site model, which also was derived using the modelling tool ConnectFlow, but with slight modifications to incorporate features specific to the PSAR. This model is in turn exported to the other two phases, and modified on two accounts. First, modifications are made specific to the other modelling tool DarcyTools, and second, modifications and/or additional parameterisations are made specific to the problems addressed. Within these other phases, the central cases studied are denoted Base cases in order to clearly distinguish them from the central ConnectFlow case (hydrogeological base case) used within the temperate period simulations.

The spatial distribution of waters of different salinities is modelled during all phases since the variation in fluid density affects the flow field and the interactions between waters of different chemical compositions. In particular, the transport of fresh water from the top boundary down to repository depth and the upconing of saline water from below are analysed in detail. The transport of fresh water from the surface during the Temperate and Glacial time periods is important to describe since dilute water conditions over a long period of time affects repository performance.

SDM-Site concluded that the occurrence of horizontal sheet joints of high transmissivities in the uppermost 100 m of bedrock have a profound effect on the percolation depth of the fresh water recharge that started approximately 1 100 years ago as a result of the ongoing shoreline displacement. In effect, the salinity of the fracture water in the uppermost 100 m of bedrock is generally lower than the salinity of the fracture water below this depth. The increase in fracture water salinity is fairly moderate between –100 and –800 m elevation, where the fracture water salinity is approximately 1 % by weight (ca 10 g of total dissolved solids per litre). Below this elevation, the fracture water salinity could be expected to increase significantly with depth. In the PSAR, the salinity at the elevation –2 000 m is set to be about 7 % by weight based on data acquired in the 1 660 m deep borehole KLX02 at Laxemar, see Selroos and Follin (2010) and Vidstrand et al. (2010) for details.

The chemical composition of near-surface groundwater samples gathered in the uppermost 100 m of bedrock reveals that chemical reactions (water-rock interactions) have a profound effect on the composition of the infiltrating rain water. Therefore, the chemical composition of rain water considered in the palaeohydrological groundwater flow modelling is substituted by a modified water composition called Altered Meteoric water. The characteristic composition of this reference water is described in Laaksoharju et al. (2008) and in Salas et al. (2010).

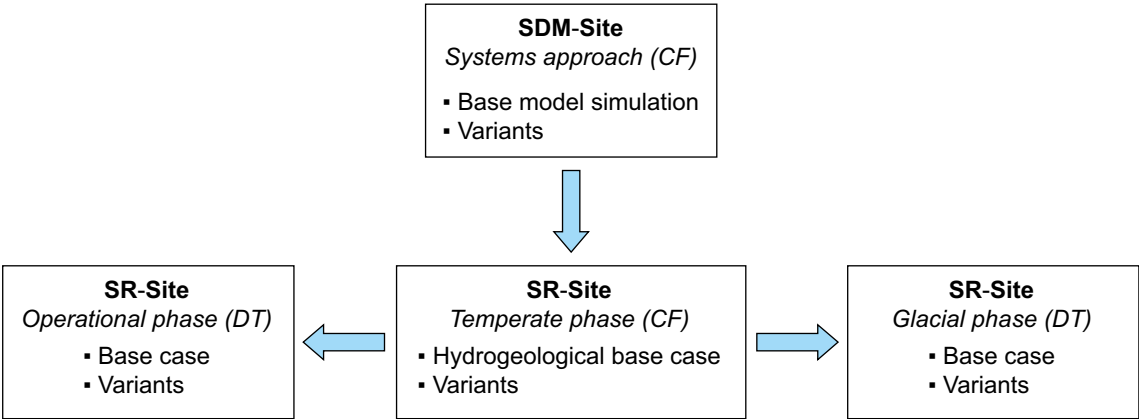


Figure 10-4. Relation between SDM-Site model, Hydrogeological base case, Base cases and variants. CF and DT denote ConnectFlow and DarcyTools, respectively. The modelling structure is the same as in the SR-Site assessment, as indicated in the boxes in the lower row.

Besides reactions, the transport of Altered Meteoric water is also affected by matrix diffusion. The matrix porewater data used for modelling come from three boreholes drilled in the target volume, see Section 4.8.2 (or Laaksoharju et al. 2008, Waber et al. 2009 for details). The key bedrock matrix transport properties governing the penetration length (depth) of a non-sorbing fracture water component are the effective diffusivity and matrix porosity. Albeit an important process for radionuclide transport modelling, particularly for sorbing radionuclides, the penetration into the matrix of Altered Meteoric (or Glacial) water from a flowing fracture nearby is probably not very deep during a glacial cycle. During a period of about 10 000 years, the penetration into the matrix of Altered Meteoric (or Glacial) fracture water could be expected to be on the metre scale, see Selroos and Follin (2010).

The interaction between the fracture water salinity and the matrix porewater salinity is also dependent on the spacing between the flowing fractures. At Forsmark, the intensity (frequency) of conductive (flowing) fractures varies considerably with depth within the target volume, see the **Data report**; the fracture intensity is very high above –100 m elevation, whereas it is very low below –400 m elevation. The two types of water, the fracture water and the matrix porewater, should be more alike in the densely fractured bedrock close to surface than in the sparsely fractured bedrock at repository depth, and this is also what the data show as described in the references cited above. At even larger depths, the water circulation is low and the system may become diffusion controlled. Hence, the fracture water and the matrix porewater are more alike.

SDM-Site concluded that the initial hydrochemical conditions of the fracture water at the start of the flow simulations at 8000 BC can be modelled by mimicking the present-day depth trends in matrix porewater salinity within the target volume and outside this volume, respectively, see Section 4.8.2 and Follin (2008) for details. This simplification is accepted in the PSAR since the key changes in the top boundary conditions during Holocene time between 8000 BC and 2000 AD are sufficient to create differences between the fracture water and matrix porewater that resemble the observed differences (Follin 2008). The key hydrological changes are the intrusion of Littorina Sea water, that began approximately 6500 BC, and the subsequent flushing by Altered Meteoric water that started approximately 900 AD (see Follin 2008 for details). In principle, these palaeohydrological phenomena have a greater effect on the near-surface fracture water salinity than on the matrix porewater salinity at repository depth.

10.2 The excavation and operation phases

The analyses for the excavation, construction and operation phases of the repository have mainly focused on disturbances of the mechanical, hydrological and chemical conditions induced by the excavation/operational activities.

The duration of this stage can be assumed to be several tens up to a hundred years, depending on the progress of the excavation/operational activities and the total number of canisters to be disposed.

10.2.1 Thermal evolution of the near field

The undisturbed rock temperature at repository depth is around 11.2 °C, see the **Data report**, Section 6.2. As the rock is excavated, this temperature will be slightly affected by ventilation of the excavated volumes. This effect is small and of negligible significance compared with the thermal impact of the residual radioactivity of the gradually deposited spent nuclear fuel. This will alter the rock temperature for thousands of years and is, therefore, handled in more detail in Section 10.3.4, which is part of the description of repository evolution during the initial period of temperate climate after closure.

Since the repository is gradually excavated and operated, the thermal impact of the residual radioactivity will also be potentially important during the excavation/operational phase. The safety relevant issue is, however, the peak temperatures over time. According to the thermal analyses by Hökmark et al. (2010), THM-report Chapter 5, peak buffer temperature is underestimated by less than 0.2 °C if simultaneous deposition is assumed, compared to a case where canisters are deposited in a sequential fashion (i.e. panel by panel) at a rate of 2 or 4 days per canister. However, certain deposition sequencing, although possibly non-practical, may result in higher temperatures for a few canisters. This issue is further discussed in Section 10.3.4.

Identified uncertainties and their handling in the subsequent analysis

As already stated, the discussion on thermal evolution during the excavation phase is found in Section 10.3.4.

10.2.2 Mechanical evolution of near-field rock due to excavation

The rock mass at repository depth is under a pre-stressed condition, namely the in situ rock stress. Repository excavation, i.e. removal of rock, creates a localised readjustment of the in situ stresses. This raises several rock mechanics concerns for the construction work, such as the risk of breakouts into excavated volumes, spalling and/or key block instability. These engineering-related rock mechanics issues are evaluated within the framework of the repository design work and reported in the design report (SKB 2009b), and are to a large extent not of importance for long term safety. However, as further discussed in Chapter 5 and fully assessed in the **Underground openings construction report**, the design and construction of the underground openings must follow specific technical design requirements provided from a long term safety perspective (SKB 2009a).

The following mechanical processes related to the excavation and the open phase could have potential safety implications (the safety functions refer to Figure 10-2):

- Development of an Excavation Damaged Zone (EDZ) and other impacts on rock permeability (safety function R2ab, see Figure 10-2).
- Spalling, (safety function R2b and also safety functions of the buffer that either directly or indirectly depend on buffer density).
- Reactivation of fractures (safety function R2ab and R3b).
- Induced seismicity (safety function R3bc).

These issues are assessed in the **Underground openings construction report** and the resulting initial state is summarised in Section 5.2.3. However, for transparency the safety relevant conclusions are repeated in the following subsections, together with the assessed implications for the safety functions.

Deposition hole EDZ and spalling

Drilling of deposition holes is not judged to result in any significant damage to the surrounding intact rock. As stated in Section 5.2.3 and in the **Underground openings construction report**, Chapter 6, findings from a comprehensive literature study (Bäckblom 2009) suggest that for mechanical full face down-hole drilling techniques in competent rock the depth of damaged zone (EDZ) is limited to less than a few centimetres in the rock surrounding the deposition hole. The hydraulic conductivity in such a zone is in the order of 10^{-10} m/s or less. Hence there is high confidence that competent rock conditions prevail for the reference design and consequently that the EDZ axial transmissivity in deposition holes would be less than 10^{-10} m²/s. However, the magnitude of the connected effective transmissivity may be altered due to occurrences of spalling.

If the initial, pre-excavation, stresses are sufficiently high, spalling may occur during the operational phase in response to the stress redistribution caused by excavation. The **Underground openings construction report** states, based on analyses by Martin (2005) and a three dimensional elastic stress analysis, presented in the repository design report (SKB 2009b), that in the case of the “most likely” stress model, some 100–200 deposition holes (out of 6 000) would experience a spalling depth (overbreak) that exceeds 5 cm, provided the deposition tunnels are aligned between 0 and 30 degrees to the maximum horizontal stress. Due to uncertainty in stress an alternative, “unlikely maximum” stress model is also considered. For the “unlikely maximum” stress model, the deposition tunnel must be aligned parallel to the maximum horizontal stress, but the number of deposition holes that can sustain a spalling depth in excess of 5 cm is approximately the same.

If spalling were to occur prior to waste emplacement, the current reference method stated in the **Underground openings construction report**, would be to remove loose rock debris from localised spalling on the rock walls. Larger overbreak would need to be filled with, for instance, pieces of bentonite or with bentonite pellets before or during installation of the bentonite buffer. The ultimate

contingency action is to reject the deposition hole. Thereby it should be ensured that deposition holes will always have negligible EDZ prior to waste emplacement. In conclusion, there are no safety related impacts of the few cases of spalling prior to canister emplacement expected provided the action envisaged in the **Underground openings construction report** is implemented.

New fracturing induced near the tunnel by the excavation work – formation of an “EDZ”

The possibility that the damage done to the rock using the drill-and-blast excavation method will result in zones of increased axial permeability has long been considered. For the PSAR the EDZ is defined as *the part of the rock mass closest to the underground opening that has suffered irreversible deformation where shearing of existing fractures as well as propagation or development of new fractures has occurred*, since this is the long term safety relevant issue of concern for repositories in crystalline rock. It is recognised that other definitions of the EDZ exist that may be more appropriate for other disposal concepts. Clearly, there may also be reversible effects that, together with pure hydrodynamical changes, may impact on the inflow to open tunnels. However, these “skin effects” are of limited importance for the long term safety functions since they only relate to conditions when the repository is open.

As stated in Section 5.2.3 and in the **Underground openings construction report**, Section 8.2 it is possible to control the drill and blasting of the tunnels such that a continuous fracturing along the axial direction of the tunnel will not develop. This was already stated in SR-Can based on experience from the excavation of the TASQ tunnel at Äspö HRL (Olsson et al. 2004) and was confirmed by the results from the demonstration trial of smooth blasting techniques at the Hard Rock Laboratory in Äspö (Olsson et al. 2009, Ericsson et al. 2009). These observations have been further confirmed in a subsequent project at the TASS04 tunnel at Äspö HRL in which a characterization method to confirm the initial state regarding the extent of excavation induced fractures and the characterization of the hydraulic properties of the EDZ has been developed and demonstrated (Ericsson et al. 2015). Furthermore, available literature suggests that the hydraulic conductivity in drilled and blasted tunnels is in the order of 10^{-8} m/s (Bäckblom 2009) although this conductivity could possibly be very local and may not necessarily be created by the excavation activities. It should be added that further reduction of the potential EDZ can be made by either wire sawing the deposition tunnel floor (Ericsson et al. 2015) or by mechanical excavation. However, existing fractures parallel to the tunnel may be reactivated as discussed in the next section.

It is concluded that there is ample evidence that the fractures induced by the drill-and-blast construction work, will not result in a connected zone along the tunnel with a transmissivity above the maximum allowed transmissivity as set out in the technical design requirements. In fact, data suggest that a continuous EDZ would not develop at all. However, given that the occurrence of the EDZ currently can only be assessed by indirect measurements such as hydraulic testing in boreholes or the use of geophysical methods in addition to geological mapping (Ericsson et al. 2015), it seems justified to consider an EDZ according to the technical design requirements, i.e. with an axial transmissivity of 10^{-8} m²/s as a basic assumption for further analyses. This may however be a too pessimistic assumption given other methods for excavation.

Furthermore, it also seems justified to explore how transmissive an EDZ needs to be in order to significantly impact other safety functions as well as exploring the impact of no axially continuous EDZ at all. A more rigorous discussion of these matters, together with input data for the PSAR, is found in the **Data report**, Section 6.5.

Reactivation of fractures

The stress redistribution resulting from the tunnel excavation may reactivate some existing near-field fractures. The process has been modelled in a set of numerical analyses (Hökmark et al. 2010), building on the experience of a similar approach used for SR-Can (Hökmark et al. 2006). In short the three-dimensional discontinuum programme 3DEC is used to determine stress redistribution effects in fractured near-field rock, and then the results are used to estimate possible permeability changes caused by shear and extensional fracture deformations. The numerical analysis covers a series of events ranging from excavation of the tunnel to the mechanical effects of glacial loading and unloading

with the boundary stresses resulting from large-scale three-dimensional simulations of mechanical ice/crust/mantle interactions. Relevant changes, i.e. changes that extend more than a couple of metres from the openings, only occur after the thermal load is applied, e.g. starting from the initial temperate phase. More details of the modelling are thus provided later, e.g. starting from Section 10.3.5.

The analysis shows that the normal stress on fractures parallel to the tunnel and close to the tunnel wall or to the tunnel floor will decrease to a few MPa over significant distances, whereas fractures intersecting the tunnel at an angle of a few tens of degrees will show significant stress reductions only very close to the tunnel. However, since gently dipping fractures already have relatively low normal stress, the impact on relative transmissivity of a horizontal fracture is quite small, see Figure 10-5 (left). Furthermore, in reality, large fractures that connect to the flowing fracture network will not be persistently parallel to the tunnel where there are deposition holes, especially since deposition holes intersected by fractures intersecting more than four deposition holes will be rejected according to the EFPC, see Section 5.2.2. For steeply dipping fractures almost parallel to the tunnel, the transmissivity change is, at most, a factor of 6–7 on the intersecting fracture, Figure 10-5 (right), but it is confined to a limited area. This means that this effect can be discarded, or at least captured within the EDZ assumption of 10^{-8} m²/s along the tunnel.

Induced seismicity

The excavation activities may induce seismicity through the generation of new fractures or reactivation of pre-existing fractures. However, as argued in the **Geosphere process report**, neither of these possibilities needs further consideration in the PSAR. As further discussed in the **Geosphere process report**, Section 4.3.7, seismic events that could impair the integrity of the already deposited canisters, would require an induced earthquake of approximately magnitude 5. To host such an earthquake, the structure must have a rupture area exceeding a square kilometre and it is unlikely that such a structure would remain undetected after tunnel mapping. Furthermore, there is no evidence that present-day deviatoric stresses in Swedish bedrock at repository depth are sufficient to power seismic events of magnitude 5.

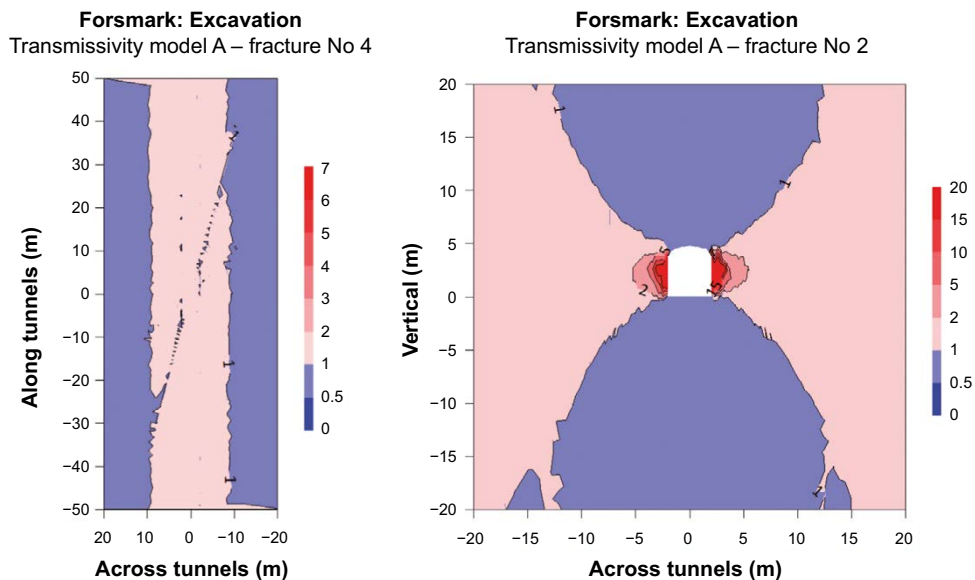


Figure 10-5. Relative transmissivity change due to stress impact from the tunnel boundary in a fracture (left) parallel to the tunnel floor and (right) a vertical fracture intersecting the tunnel at a small angle. See Figure 10-19 for an illustration on how the modelled fractures intersect the deposition tunnel. Modified after Figures 8-16 and 8-12 in Hökmark et al. (2010).

Identified uncertainties and their handling in the subsequent analysis

The discussion above is used to draw a set of conclusions regarding the uncertainties and their subsequent handling in the PSAR analyses related to the mechanical evolution during the excavation phase.

- There are no safety related impacts of the few cases of *spalling prior to canister emplacement* expected provided the action envisaged in the **Underground openings construction report** is implemented. Heating from already deposited canisters may increase stress and cause spalling in and additional loss of holes prior to canister emplacement. This allows the exclusion of the phenomenon in question in the risk calculation.
- There is ample evidence that an *EDZ formed during excavation* will be kept below the maximum allowed transmissivity as set out by the technical design requirements and data suggest that a continuous EDZ would not develop at all. However, given that the occurrence of the EDZ currently can only be assessed by indirect measurements, it seems justified to consider an EDZ according to the technical design requirements, i.e. with an axial transmissivity of 10^{-8} m²/s as a basic assumption for further analyses. Furthermore, it also seems justified to explore how transmissive an EDZ would need to be in order to significantly impact other safety functions as well as exploring the impact of no axially continuous EDZ at all. A more rigorous discussion on these matters, together with input data for the PSAR, is found in the **Data report**, Section 6.5, which propagates this uncertainty into a set of distinct calculation cases for the hydrogeological assessment.
- *Reactivation of fractures* caused by the stress redistribution only results in insignificant increases of transmissivity in near-field fractures, apart from very locally close to the tunnel. These limited fields of increased transmissivity will have little importance, unless the fracture is located close to the tunnel floor and approximately parallel to it. However, in reality large fractures connected to the flowing fracture network will not be persistently parallel to the tunnel where there are deposition holes, especially since deposition holes intersected by fractures intersecting more than four deposition holes will be rejected according to the EFPC. This means that this effect can be discarded, or at least captured within the EDZ assumption of 10^{-8} m²/s along the tunnel.
- *Induced seismicity*: The implications of induced seismicity can be excluded in the risk calculation.

10.2.3 Hydrogeological evolution

During the excavation and operational phases, the tunnels will be at atmospheric pressure and the inflow of water to the open repository will depend on the hydraulic properties of the intersecting, water conducting fractures. The inflow may result in a redirection of flow and in changes of the groundwater flow pattern, potentially resulting in drawdown of the water table, infiltration of near-surface waters into the deeper parts of the bedrock, and in upconing of saline water from depth. The actual impacts primarily depend on the permeability distribution of the rock, the repository layout and on the tightness of the underground construction, which in turn depends on the grouting efficiency. In order to assess the magnitude of these impacts, groundwater flow simulations, based on the hydrogeological models developed as part of the **Site description Forsmark**, are performed. The overall objective is to assess the effects of an open repository on site hydrogeochemical and hydrogeological conditions, i.e. safety functions R1 and R2 in Figure 10-2.

The expected effects of the operational phase with relevance for post-closure safety are related to changes in groundwater flow and chemistry. Inflow rates into tunnels and deposition holes during the operational phase are relevant both for construction issues and post-closure safety. Near-surface effects such as lowering of the groundwater table are of primary interest for the environmental impact assessment.

Methodology

The groundwater flow modelling of the excavation and operational phases conducted by Svensson and Follin (2010) using the DarcyTools modelling tool has the following key components.

- An unstructured grid that allows for a spatially varying resolution of the computational grid. For the PSAR, a fine resolution is used in the proximity of the repository.
- A tunnel routine that allows for detailed inflow simulations to the repository, including analyses of grouting efficiency and canister failures.
- A phreatic surface algorithm that allows for a spatially varying elevation of the groundwater table. For the PSAR, the disturbance of the water table (drawdown) as a function of the grouting efficiency is analysed.
- Variable-density flow. For the PSAR, the potential for upconing of more saline water present at depth is analysed.
- An approach for studying the saturation of backfilled tunnels. For the PSAR, the hydration process of the initially unsaturated backfill material is analysed in several ways. The results reported by Svensson and Follin (2010) are presented in Section 10.3.6.
- Spatially varying equivalent continuous porous medium (ECPM) properties. For the PSAR, the ECPM properties were derived through up-scaling of deformation zone and discrete fracture network (DFN) realisations generated in the groundwater flow modelling of temperate climate conditions using the ConnectFlow modelling tool (Joyce et al. 2010), see Section 10.3.6.

The traditional approach in ECPM modelling is to assign a low value of the hydraulic conductivity to all parts of the computational grid that do not contain fractures. Besides using the ECPM model grid, Svensson and Follin (2010) also provide results for an alternative approach where grid cells not intersected by fractures are deleted, i.e. an equivalent discontinuous porous medium (EDPM) is created. Selroos and Follin (2010) conclude that the EDPM model grid is of particular interest for the inflow rejection calculations, see below for details.

Performed analyses and usage within the PSAR

The different cases that Svensson and Follin (2010) performed with relevance for the excavation and operational phases are listed below. It is indicated where the results produced by each case are used within the subsequent analyses in the PSAR.

- **Drawdown of the groundwater table, infiltration of shallow surface water, and upconing of deep saline groundwater.** The operational phase of the repository with tunnels at atmospheric pressure, i.e. water will flow into the tunnels, implies a drawdown of the groundwater table with a possible change of water composition at repository depth. Upconing may also change water composition at repository depth. The drawdown results are used as an input to analyses of ecological and other types of environmental consequences during the mentioned phases, see Section 10.1.3. The upconing results are used as an input to analyses of the groundwater chemistry at repository depth during the mentioned phases, see Section 10.2.5.
- **Inflow calculations.** Since the tunnels are maintained at atmospheric pressure during the operational phase, the natural hydraulic gradients are affected and redirected towards the tunnels. Depending on which tunnels are kept open and which are closed, and also depending on the grouting efficiency achieved, the inflow distribution and magnitude will vary in space and time. The results of these analyses are used primarily within Repository Engineering (SKB 2009b), but also in the assessment of buffer and backfill (mechanical) erosion during backfilling of the deposition holes and tunnels, see Section 10.2.4.
- **Inflow rejection criteria.** The deposition holes associated with the highest groundwater flow (Darcy flux) during saturated conditions yield the most severe consequences in terms of erosion of the buffer and copper corrosion, see Sections 10.3.11, 10.3.13, 10.4.8 and 10.4.9. Since some degree of correlation in flow characteristics exists between the open conditions and later saturated conditions and it is desirable to avoid deposition hole positions with high Darcy fluxes during saturated conditions, an assessment is conducted concerning the merits of applying inflow rejection criteria during the operational phase (see Selroos and Follin 2010 for details). The potential benefits of inflow rejection criteria are further discussed in Section 14.3.

Drawdown of the groundwater table, infiltration of shallow surface water, and upconing of deep saline groundwater

Three different stages of operation, A–C, are considered, see Figure 10-6. The three stages are run in sequence, where the first stage, stage A, lasts for 15 years, stage B lasts for 15 years and stage C lasts for 20 years. Hence, the total operational time is 50 years. The different stages imply that different parts of the repository are kept open while the other parts are not yet excavated or are already backfilled. Furthermore, for each stage, three different levels of grouting efficiency are assessed. These are:

- Level I: The hydraulic conductivity of all cells in contact with the repository has a maximum value of 10^{-7} m/s.
- Level II: The hydraulic conductivity of all cells in contact with the repository has a maximum value of 10^{-8} m/s.
- Level III: The hydraulic conductivity of all cells in contact with the repository has a maximum value of 10^{-9} m/s except where the modelled ungrouted hydraulic conductivity is 10^{-6} m/s or greater. At these positions the hydraulic conductivity has a maximum value of 10^{-8} m/s.

Results are produced for all combinations above. However, here only a set of key illustrations are presented for operation stage C and grouting level II.

Operation stage C implies the largest inflows and hence the strongest perturbation of the initial salinity field. Also, since operation stage C is the last stage, the chemical conditions have already to some extent been perturbed during the first two operational stages. The modelled drawdown is relatively small with maximum values around one metre except for the central area (CA) of the repository, where a drawdown of around ten metres is obtained (Svensson and Follin 2010).

Comparing the salinity for conditions prior to the construction of the repository with conditions during operation stage C, it is observed that a dilution occurs around most parts of the repository. That is, fresh water is drawn towards repository depth since the groundwater table is lowered as a result of water draining into the repository due to the induced hydraulic gradient. A corresponding upconing occurs, but water with higher salinity is found only around the central area with ramp and shafts. It is also noted that surface water with a higher salt content may infiltrate into the bedrock from the brackish Baltic Sea.

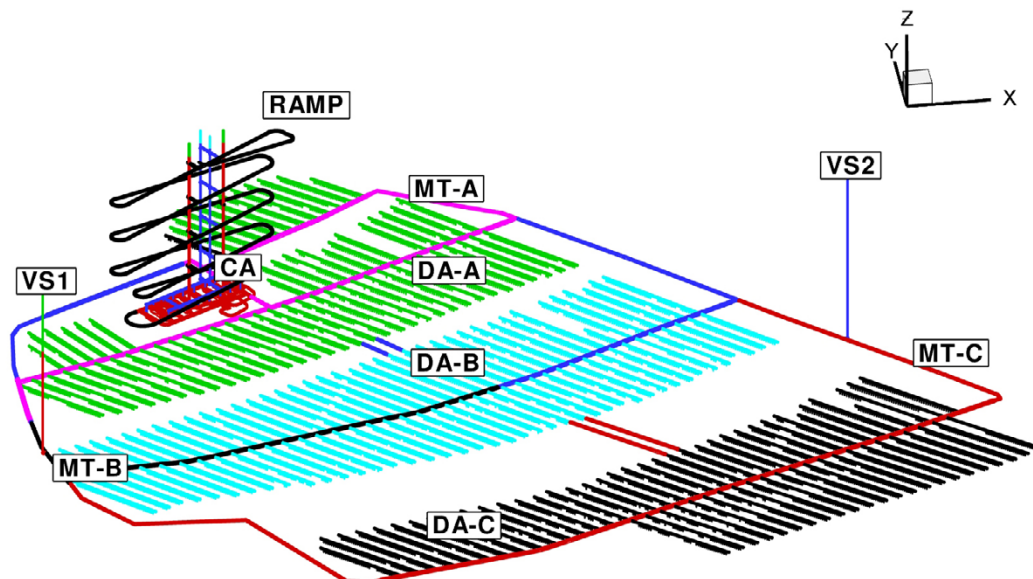


Figure 10-6. Definition of different parts of the studied repository layout. The modelling considers three operational stages (A–C) and three possible grouting levels for each stage. The three stages are indicated by green, turquoise and black colours. DA = deposition area, MT = transportation and main tunnel, VS = ventilation shaft, CA = central area.

The recharge area for water entering the repository is assessed by backward particle tracking. The results in Svensson and Follin (2010) indicate that most of the recharge to the repository is located right above the facility, i.e. within a small radius of influence as expected.

The spent fuel repository and the SFR²² facility will likely be in operation simultaneously. Svensson and Follin (2010) simulate various operational cases of the two repositories as a means to investigate their hydraulic contact. In summary, during the time when both repositories are in operation, the recharge area of the deep repository does not include the SFR facility. This is due to several reasons, e.g. the SFR facility is located beneath the sea floor, the existence of the thick, steeply dipping, regional Singö deformation zone that strikes perpendicular to the cross-section between the two repositories, and the fact that a water divide forms due to the pumping needed to keep both repositories open.

Inflow calculations

The calculated inflow during the different operational stages and grouting levels using the ECPM model grid are presented in Table 10-2. The total inflows vary from 8 to 51 L/s depending on the stage of operation (A–C) and the level of grouting efficiency (I–III). For the case discussed above, i.e. operation stage C and grouting level II, the inflow is 28 L/s. The inflows mainly occur at the boundaries of the repository. This is due to the fact that the largest gradients are found at the boundaries between the repository and the outside rock volumes. Also of interest to note is that for grouting level I, i.e. the lowest grouting efficiency, the main inflows occur in the ramp. The ramp penetrates the transmissive sheet joints encountered at shallow depths in Forsmark (Follin 2008); hence, large inflows occur for the case with a low grouting efficiency.

The sensitivity to inflow is tested by applying a second realisation of the underlying fracture network combined with heterogeneous deformation zones (see Svensson and Follin 2010 for details). In this comparison, grouting level II is used in combination with the condition that the whole repository is kept open. It is noted that in the base case realisation, each deformation zone has a unique but homogeneous value of hydraulic conductivity including a constant depth trend. Thus, the resulting values using the second realisation are not directly comparable to Table 10-2. The base case realisation yields a total inflow rate of 31.2 L/s, whereas the second realisation yields a total inflow rate of 33.4 L/s. The magnitude of the total inflow rates as well as the variability in inflow rate between the two realisations is considered small.

Table 10-2. Calculated inflow rates (L/s) to different parts of the repository for three levels of grouting efficiency (I–III) and three stages of operation (A–C). CA = central area, DA = deposition area, MT = transportation and main tunnels, VS = ventilation shaft.

Part of repository	Grouting level I			Grouting level II			Grouting level III		
	Operation stage			Operation stage			Operation stage		
	A	B	C	A	B	C	A	B	C
CA	4	4	5	2	2	2	1	1	1
DA-A	6	–	–	4	–	–	3	–	–
DA-B	–	8	–	–	6	–	–	3	–
DA-C	–	–	9	–	–	8	–	–	4
RAMP	16	17	17	6	6	6	2	2	2
MT-A	6	6	7	4	4	5	2	2	2
MT-B	–	1	1	–	1	1	–	0	0
MT-C	–	–	9	–	–	5	–	–	2
VS1	1	1	1	1	1	0	0	0	0
VS2	–	2	2	–	1	1	–	0	0
Total	33	39	51	17	21	28	8	8	11

²² The SFR facility for low and intermediate waste is located outside the target area approximately one kilometre to the north of the final repository at approximately 50–100 m depth below the Baltic Sea.

Inflow rejection criterion

According to the technical design requirements (SKB 2009a) “The total volume of water flowing into a deposition hole, for the time between when the buffer is exposed to inflowing water and saturation, should be limited to ensure that no more than 100 kg of the initially deposited buffer material is lost due to piping/erosion. This implies, according to the present knowledge, that this total volume of water flowing into an accepted deposition hole must be less than 150 m³”.

In the reference design, see Section 5.2.3, it is judged that this technical design requirement is met if

- Potential deposition holes with inflows greater than 0.1 L/min are avoided (inflow criterion #1 in Svensson and Follin 2010).

As explained above, it is also of interest to evaluate to what extent high inflow rates during the operational phase are correlated to deposition holes with high Darcy fluxes during saturated conditions. If this is the case, avoiding deposition holes with high inflow rates would also have potential advantageous implications for long term safety. In order to investigate this, the EDPM approach in Svensson and Follin (2010) is used. The inflow rejection criteria are applied for the inflow calculations for the operational phase analyses described above, and then recording the impact on the distribution of equivalent flow rates and flow-related transport resistance for the remaining deposition holes.

Figure 10-7 shows the positions of the deposition holes failing inflow criterion #1 using the base case realisation and the EDPM model grid. The number of failing deposition hole positions is 88 out of 6916.

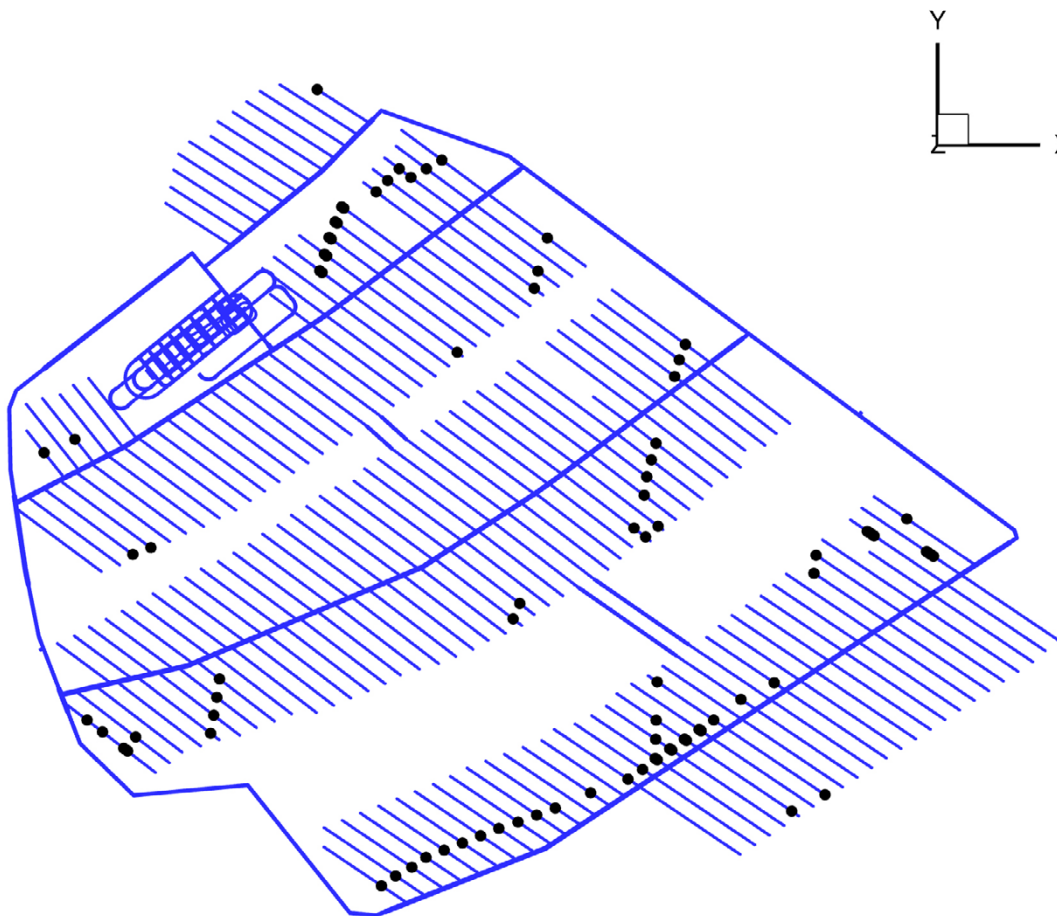


Figure 10-7. Illustration of the 88 deposition hole positions, out of 6916 deposition hole positions, failing inflow criterion #1 in Svensson and Follin (2010) using the equivalent discontinuous porous medium (EDPM) approach for the base case realisation.

In Selroos and Follin (2010), an analysis is conducted to assess whether the inflow rejection criteria are able to identify deposition hole positions with unfavourable characteristics for long term safety; i.e. deposition holes with a high Darcy flux during saturated conditions. Based on the correlation found between deposition hole inflows during open repository conditions and the Darcy flux at deposition hole positions during saturated conditions, it is concluded that inflow rejection criteria should be able to identify deposition holes with unfavourable characteristics for long term safety. Furthermore, the inflow rejection criteria appear as a good complement to the EFPC criterion in terms of identifying hydraulically unfavourable deposition hole positions. The outcome of this analysis is further assessed in Section 14.3.

Identified uncertainties and their handling in the PSAR

General uncertainties related to the hydrogeological modelling, specifically the use of discrete fracture network (DFN) modelling within hydrogeological modelling, are discussed in more detail in the **Data report**, Section 6.6 and in Selroos and Follin (2010). Here, a set of conclusions regarding the uncertainties in the hydraulic evolution during the excavation and operational phases and their subsequent handling in the PSAR analyses are drawn based on the discussion in the above sub-sections.

Drawdown of the groundwater table, infiltration of shallow surface water and upconing of deep saline groundwater

The results of the analysis of drawdown of the water table, infiltration of shallow water and upconing of saline water from depth are used for assessing the chemical evolution in and around the repository during the operational period, see Section 10.2.5. The results are also used as a starting point for assessing the groundwater flow during resaturation, see Section 10.3.6.

Detailed calculations of the near-surface effects of an open repository are carried out with MIKE SHE (Mårtensson and Gustafsson 2010) as part of the analyses of ecological and other types of consequences during the mentioned phases, as a basis for the Environmental Impact Assessment (EIA) (SKB 2010a, Werner et al. 2010), see Section 10.1.3. Based on this comparison, it is noted that the near-surface effects, including the changes in advective (fracture water) salinity around the repository reported by Svensson and Follin (2010) may be too large. In conclusion, in the subsequent PSAR analyses, no further action to handle these uncertainties is needed as the calculated water chemistry perturbation is exaggerating the probable effect of salinity dilution.

Inflow to the repository

The calculated inflow to the repository is used as the input for assessing the evolution, mainly piping and erosion of the buffer and the backfill on the already sealed deposition tunnels during the operational phase, see Section 10.2.4. The inflows are also used as input for assessing the saturation of buffer and backfill, see Section 10.3.8.

The tunnel routines implemented in the DarcyTools modelling tool have been verified against an analytical solution and shown to be accurate within 10 % (Svensson and Follin 2010). However, the ECPM approximation may imply an overestimation relative to the discrete system. A comparison has also been performed between DarcyTools and the MIKE SHE modelling tool for a tunnel located in a porous medium. The difference in total inflow to the open repository is also here found to be within 10 % (Mårtensson and Gustafsson 2010). In the subsequent PSAR analyses, no further action is needed as the calculated water inflow likely is an overestimation of the true inflow.

Inflow rejection criterion

Selroos and Follin (2010) conclude that the EDPM approach described in Svensson and Follin (2010) should be applied in future analyses if inflow rejection criteria were to be evaluated. It may be noted that the inflow rejection calculations have been verified by later independent explicit DFN simulations in Joyce et al. (2013); here the number of rejected positions is roughly a factor two to five lower than reported for the EDPM approach in Svensson and Follin (2010).

The potential benefits in applying hydraulically based deposition hole rejection criteria are discussed in Section 14.3 and the findings made there are in turn used as input for the discussion on the need to revise the technical design requirements in Section 15.5.

10.2.4 Evolution of buffer, backfill and plug

During the operational phase the already installed buffer, backfill and plugs may be affected by the groundwater flow seeping into the open repository. This affects the safety functions in the following ways:

- When the canisters have been emplaced and the deposition tunnels have been backfilled, a plug is placed at the end of deposition tunnel (see Figure 5-19). The plug is required for the backfill in the deposition tunnel to maintain its barrier function. The performance of the plug affects the flow of water in the backfill and potentially the buffer during the operational phase of the repository when high hydraulic gradients are present. The plug should also restrict the transport of air from the central tunnel into the deposition tunnel. Inflow of air in gaseous form into the deposition tunnel could increase canister corrosion, at least in the deposition hole closest to the plug. A well-performing plug is needed to ensure that the safety functions related to canister corrosion as well as buffer and backfill density, swelling pressure and hydraulic conductivity (Can1, Buff1, Buff2, Buff3, Buff5, Buff6 and BF1) are upheld.
- As long as the buffer and the backfill have not developed a sufficient swelling pressure there is a potential for piping and associated erosion effects in these components. Piping may lead to erosion of bentonite. Erosion is a redistribution of material within the repository. This may lead to a lowered density in certain parts of the buffer and backfill and will affect the safety functions related to buffer and backfill density (Buff1, Buff2, Buff3, Buff5, Buff6 and BF1).
- The swelling properties of bentonite make the buffer and backfill material swell and close open gaps or channels to form a more homogeneous buffer or backfill. Homogenisation of buffer and backfill is crucial to fulfil the safety functions related to buffer and backfill density (Buff1, Buff2, Buff3, Buff5, Buff6 and BF1).
- The reference bottom plate consists of a copper plate (see Figure 5-15). The only purpose of the bottom plate in the deposition holes is to facilitate the installation of the canister and the buffer. As soon as the buffer is installed in the deposition hole, no more performance is expected from the bottom plate. This, however, does not mean that the bottom plate can be neglected in the long term assessment of the repository.

These issues are assessed in the following subsections.

Water saturation of the plug and its sealing ability

The purpose of the plug is to seal the deposition tunnel and keep the backfill in place during the operational phase until the transport tunnels have been backfilled and water saturated, and have regained their hydrostatic water pressure. It should also limit the flow of water out from the backfilled deposition tunnel to the transport tunnel in order to minimise the effects of piping and subsequent erosion. The design of the plug is presented in Figure 5-19, Section 5.7.2. The discussion in this section concerns the performance of the current design of the plug, but was not covered in the **Buffer, backfill and closure production report** forming the basis for the reference design in Section 5.7.

The water saturation of the bentonite seal in the plug has been modelled (Åkesson et al. 2010a). In these models the seal, with a thickness of 0.7 m and located between the concrete plug and the filter, was made of bentonite blocks and pellets in a similar configuration to the backfill. Under the condition that there is good availability of water at the plug, either natural or artificial, then the saturation process is a fairly simple one-dimensional hydration problem. If the pellets filling the seal were to seal quickly, then the hydration would only occur from one side, and this process would take around twenty years. If, on the other hand, there were a sustained piping through the pellet filling, then the hydration would be two-sided, resulting in a saturation time of around five years.

To define the required plug performance, the maximum allowed cumulative leakage through the plug is considered to be a certain fraction of the available pore volume of the pellet-filled slots in the

entire tunnel. A value of 10 % is used as an example in the PSAR. Moreover, although the seal constitutes the main resistance, it will require access to water and time to develop a high flow resistance. During this period the sealing ability will rely on the plug itself (or actually the low transmissivity between the concrete and the rock). These circumstances thus imply a relation between: i) the maximum allowed leakage, ii) the flow resistance of the plug and, iii) the time needed for the seal to become functional.

The analysis of needed sealing abilities for the plug and the bentonite (Åkesson et al. 2010a) shows that an aperture smaller than $\sim 5 \mu\text{m}$ in the contact zone between the concrete plug and the rock surface is required in order to obtain a sufficiently high flow resistance in the concrete plug/rock interface itself if the entire water pressure gradient is taken by the concrete plug without considering the sealing ability of the clay seal. A larger aperture can nevertheless be acceptable if the hydraulic conductivity of the pellet-filled slot in the clay seal is taken into account. If this conductivity is lower than approx. 10^{-10} m/s , then there is no need to rely on the plug/rock interface. It is noted that this value is much higher than the hydraulic conductivity at the expected density of the homogenised seal.

Gas tightness for the plug is defined as the ability to restrict the transport of gas in a gas phase. It does not apply to gases dissolved in water. The reference design of the plug is presented in Figure 5-19. The plug must be able to restrict gas transport into the sealed deposition tunnel from the central tunnel until the central tunnel is water filled. This is important not just to restrict the ingress of oxygen, but also to limit the outflow of water vapour. This is especially important for deposition tunnels with low water inflow that can be expected to be “dry” during the operational period of the repository. In practice, this requirement is expected to be fulfilled by the design of the plug.

At the commissioning of the plug the filter will be water filled from the outside through the drainage. The bentonite seal can thereby be artificially water saturated, which means that the transport of water vapour will be efficiently restricted. Transport of oxygen is only possible by diffusion of dissolved oxygen in the porewater of the bentonite seal. This will be extremely limited due to the low solubility and diffusivity in the porewater, the geometrical restriction and the relatively short duration of the operational phase. The gas seal is needed as long as the central tunnel remains open. The saturated bentonite seal is expected to retain its properties much longer than this.

In the deposition tunnels that are not expected to be water filled during the operational period the pellets will remain dry and the transport capacity for gas in the tunnels will be significant. If the tunnel plug is not gas tight the consequences are:

1. Air from the central tunnels is transported in, which could increase canister corrosion.
2. Vapour is transported out, which will dry out the backfill and enable water transport from the buffer to the backfill. This could decrease the thermal conductivity of the buffer.

This is however not expected to occur, since the filter will be water filled.

In SR-Site there was an assumption that no gas transport took place through the plug.

The consequences of a failed gas seal on canister corrosion are assessed in Lilja et al. (2014). With the assumption that all oxygen originally present in the tunnels is consumed and eventually replaced by nitrogen from air in the central tunnel the total amount of oxygen that can enter is 3700 moles which is an addition of 25 % to what was originally present. If this oxygen pessimistically is assumed to corrode copper and only corrode the canister closest to the plug the corrosion depth will be 6 mm evenly distributed on the canister surface or 120 mm if all corrosion occurs on the lid (this is more than the thickness of the lid).

If the seal is failed, oxygen could also be transported by diffusion. With the assumption of an open slot of 10 mm around the entire plug, diffusive flux could be 360 mol/year (Lilja et al. 2014). A slot of 10 mm is unrealistic, but the flux scales linearly with the slot width.

Out-diffusion of vapour can be calculated the same way, but this is more complex, since assumptions about the relative humidity needs to be made.

Even though the calculations presented should be seen as pessimistic, they clearly show that the transport capacity for oxygen in a gas phase is high and the requirement for a tight gas seal needs to be fulfilled.

Piping erosion

An additional hydraulic issue during the operational phase concerns piping and associated erosion effects in the buffer and backfill. Water inflow into the deposition hole will take place mainly through fractures and will contribute to the wetting of the buffer. However, if the inflow is localised to fractures that carry more water than the swelling bentonite can adsorb, there will be a water pressure in the fracture acting on the buffer. Since the swelling bentonite is initially a gel, which increases its density with time as the water goes deeper into the bentonite; the gel may be too soft to stop the water inflow. The results may be piping in the bentonite, formation of a channel and a continuing water flow and a consecutive erosion of bentonite particles. There will be a competition between the swelling rate of the bentonite and the flow and erosion rate of the buffer. The process can be further divided into three sub-processes, which can be described separately (see Figure 10-8).

- Piping is regarded as a hydraulic process with water transport through a pipe or channel that is maintained as long as the pore pressure is equal to or exceeds the swelling pressure in the surrounding bentonite. The flow rate is assumed to be related to the hydraulic gradient and the radius of the pipe in accordance with the Hagen–Poiseuille equation.
- The sealing process is regarded as a hydro-mechanical process that includes water uptake in the surrounding bentonite, which in turn leads to swelling. The first step in describing the process is to define a density profile for the bentonite around the pipe. The shape of the profile should yield a relationship between the radius of the pipe, the mass of lost material and the distance to a saturation front. The idea of such an approach is that it could make it possible to simulate a pipe that is sealed and the cessation of piping.
- Loss of material is regarded as a complex process that includes erosion of bentonite out into an aqueous phase, sedimentation and advective transport of bentonite. Erosion is generally assumed to be controlled by the shear strength of the bentonite and the shear forces exerted by the flowing water. Sedimentation is also assumed to have a significant impact on the bentonite concentration in eroding water, since observed concentrations in vertical erosion tests are considerably lower than equivalent concentrations in horizontal erosion tests. The first step in describing this process is to formulate and analyse a mass balance with expressions for erosion and sedimentation.

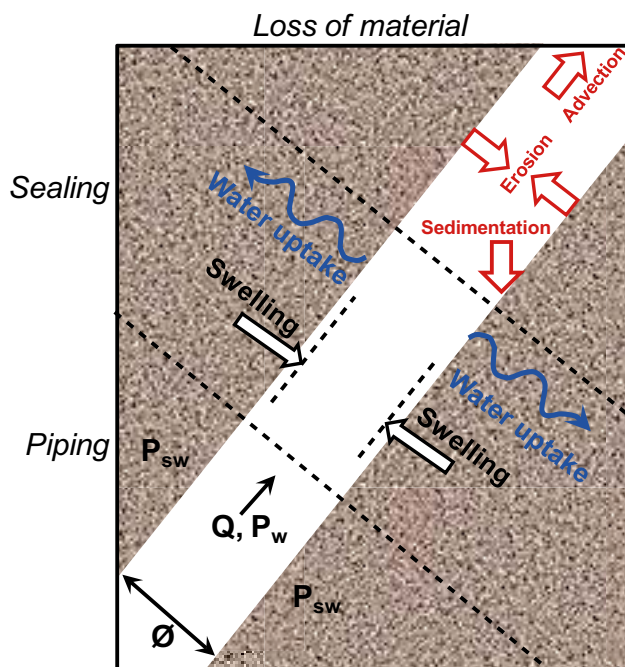


Figure 10-8. Schematic illustration of piping, sealing and loss of material.

This is further discussed in the **Buffer, backfill and closure process report**.

Piping will take place and the pipes remain open if the following three conditions are fulfilled at the same time:

1. the water pressure p_{wf} in the fracture, when the water flow is prevented, is higher than the sum of the counteracting total pressure from the clay and the shear resistance of the clay,
2. the hydraulic conductivity of the clay is so low that water flow into the clay is sufficiently prevented so as to keep the water pressure at p_{wf} ,
3. there is a downstream location available for the flowing water and the removal of eroded materials in order for the pipe to stay open.

Erosion will take place if the drag force on the clay particle from the water movement is higher than the sum of the friction and attraction forces between the particle and the clay structure.

Erosion can occur both as a consequence of channels caused by piping and over the long-term at the interface between the clay and the fractures in the rock. Since the water flow rate in the latter case is very low, erosion will only be important for colloids leaving the clay gel that has penetrated into the fractures.

The consequence of piping will be a channel leading the flowing water out to dry or unfilled parts of the repository. Since the clay swells, the channel will reduce in size with time, but on the other hand the erosion will counteract and tear off bentonite particles and thus increase the size of the channel. There is thus a competition between swelling clay and eroding clay. If the inflow is low and the increase in water pressure slow the pipe may seal before water pressure equilibrium has been reached.

The consequence of piping is always that there will be erosion of material that has been torn off from the pipes. That material is transported in the pipes out into either a stagnant part of the backfill where the eroded material may settle or out from the backfill into the open transport tunnel.

After completed water saturation and homogenisation of the buffer and backfill and re-establishment of the hydrostatic water pressure, the water pressure can be separated from the swelling pressure according to the effective stress theory. The pipes or openings caused by the erosion will thus be healed and a swelling pressure established if the density and resulting swelling pressure are high enough to overcome the internal friction. After the initial stage, there is very little risk that piping will occur again, since piping requires a strong and fast increase in water pressure gradient locally in the rock at the contact with the buffer or backfill.

Problem description

There are some general understandings of how flowing water interacts with bentonite after installation at repository depth that are important for the behaviour of the buffer material in the deposition hole after exposure to the natural ground water inflow.

- Before swelling the pellet filling cannot stop the water inflow since the water pressure that will occur if the water inflow is stopped is in the order of several MPa and the swelling pressure of the pellet filling is initially only about 100 kPa.
- It will take several years for the buffer and even more for the backfill to generate a swelling pressure that is high enough to stop the water inflow.
- The consequence of this is that, when the tunnel is filled with water after installing the plug, new channels that distribute the water to empty parts will steadily be formed until the slots are filled with water. When the slots are filled the water pressure in the tunnel will start to rise and the hydraulic gradients will be taken by the plug instead of by the bentonite and the inflow will be strongly reduced.
- Since the pellet filling cannot stop the water inflow there may consequently be channels in the pellet filling in the deposition hole leading to the tunnel. However, this will only be the case if there is an inflow of water in the deposition hole.

- Numerous measurements of water flowing in channels in bentonite pellets or on the surface of bentonite blocks show that the discharging water contains bentonite collected on the way through the channels due to erosion. Water flowing in channels out from the deposition hole will thus transport bentonite from the deposition hole into the backfill.

Since piping and subsequent erosion cannot be prevented by the pellet filling in the buffer or the backfill it is important to try to estimate the amount of bentonite material lost by erosion especially from the buffer in a deposition hole.

In SR-Can the loss was estimated with a simple expression based on a description by Börgesson and Sandén (2006). A loss of 1–10 g dry mass of bentonite per litre eroding water was used as an estimate.

Hydromechanical modelling of erosion processes expected during the operational phase has not been done due to lack of models and tools. However, measurements show that limits can be set to the effect of the erosion. An empirical model of the erosion rate has been developed and is used to estimate the erosion for different cases.

Erosion estimates in deposition holes; generic example

The erosion from a deposition hole out to the tunnel and to some extent possibly out through the plug is to a large degree a function of the total volume of eroding water. If the water inflow is strong, water will at first fill up the open pore space in the pellet filling both in the buffer and in the backfill before any significant amount of water is absorbed by the buffer or backfill blocks since there is no resistance against water flow in the pellets while the very low hydraulic conductivity in the blocks limits the water uptake rate in the blocks. Thus the volume of the open pore space available for water in the pellet filling is an important parameter, but also the unsaturated voids in the blocks and the possible leakage through the plug is of relevance. The voids in the blocks cannot be neglected if the total inflow to the tunnel is relatively low.

The total empty pore volume in the buffer and the backfill in a 300 metres long tunnel with 50 deposition holes was estimated to be ~1 050 m³ in SR-Site. The value may be slightly lower with the backfill and tunnel design presented in chapter 5, but the SR-Site value is still used in this example. Some leakage through the plug cannot be ruled out, depending on the tightness of the plug. It is presently not known how tight these plugs can be made. As an illustration, it is assumed that additionally 20 % of the total volume in the tunnel will leak out through the plug. This yields a *total possible water volume that could flow into the tunnel*, V_t , of ~1 250 m³.

A large number of erosion tests have been performed. The results from some of these are presented in Sandén et al. (2008). Different materials, flow rates and flow lengths have been used for the tests but all those tests were done with horizontal flow directions. A number of additional tests have recently been performed in order to simulate erosion in a deposition hole that mainly takes place in the vertical direction in the pellet filling (Sandén and Börgesson 2010). Based on the tests an exponential erosion model has been suggested (Sandén et al. 2008, Sandén and Börgesson 2010). According to the model the accumulated mass of eroded bentonite is related to the accumulated mass of eroding water. Based on the tests an exponential erosion model described by the equation below has been suggested:

$$m_s = \beta \cdot (m_w)^\alpha$$

where

m_s = accumulated mass of eroded bentonite (g)

m_w = accumulated mass of eroding water (g)

β = 0.02–2.0 (general), 0.02–0.2 (vertical piping) = parameter defined by the level of erosion at a certain accumulated water flow

α = 0.65 = parameter defined by the inclination of the straight line relation between m_s and m_w .

As stated above a total volume of about 1 250 m³ = 1.25 × 10⁹ g water is expected to flow into the tunnel before it is filled with water and sealed including possible leakage through the plug. In an extreme case where all water to the entire tunnel comes from one single deposition hole the eroding

mass of bentonite will according to the model be 16.4–164 kg of bentonite. For deposition holes where the inflow is at the limit value for acceptance in accordance with the technical design requirements (see Section 5.2.1) of 150 m³ the models yields an erosion of 4–41 kg of bentonite. In fact, most of the inflow of water into a deposition tunnel will occur through the periphery of the tunnel itself and not through the deposition holes. The reasons for this are that the volume and surface area of the tunnel are much larger, which means that it is more likely to intersect fractures and that the deposition holes should preferably be placed in locations with limited inflow of water.

For the case when the total inflow of water to a deposition tunnel (including deposition holes) is very low, or not measurable, it is difficult to claim that the accumulated inflow to a single deposition hole will be less than 150 m³. However, in this case the first condition for piping, described in the first paragraph in this section, will not be fulfilled and neither piping nor erosion will occur. The bentonite will have time to absorb all water that enters the deposition hole and the water pressure p_{wf} in the fracture will remain low. The lower inflow limit, when piping cannot occur is still not clearly defined.

Erosion estimates in deposition holes; example calculation for the Forsmark site

The extent of buffer loss caused by piping and erosion can be estimated using the quantitative model for mass loss from SR-Site (presented above) together with calculated data for water inflows in deposition tunnels and deposition holes in an open repository (Andersson 2013). To illustrate probability the reference case without EDZ from Joyce et al. (2013) is used. The data needed are:

1. Total inflow to the respective deposition tunnel. Data are provided for 207 tunnels. In the data delivered, the inflow to the deposition holes is not included in the total tunnel flow.
2. Total inflow to deposition holes (6916 deposition holes are analysed in total the calculations) in the respective deposition tunnel.
3. The flow to all the deposition holes in each tunnel.
4. The total void volume in each deposition tunnel. Here it is simplified to assume that all tunnels are identical and the total volume is the same as specified in the section above, 1 250 m³, which includes a leakage of 20 % through the plug.
5. The erosion expression described above: $m_s = \beta \cdot (m_w)^\alpha$

The time to fill a tunnel and restore the hydraulic gradient can be calculated from the void volume of the tunnel and the total inflow (tunnel and deposition holes). The results show that the variability is very large: 18 tunnels are filled in less than a month, 66 in less than one year, while it takes more than 100 years for 31 tunnels.

The accumulated mass of eroding water passing through a deposition hole is obtained by multiplying the time to fill a tunnel with the inflow to the deposition hole. Erosion is calculated using the accumulated mass of eroding water and the erosion model in point 5 above. The mass loss for the deposition holes to which the inflow exceeds 10 % of the total inflow to the tunnel are tabulated in Andersson (2013). The limit was chosen because a 10 % share means a mass loss of about 35 kg, which gives a margin for the requirement of 100 kg. These 71 deposition holes are the ones that have the highest calculated extents of erosion, out of the total of 6 000 holes.

The maximum erosion in a single channel is slightly above 160 kg and this occurs when the entire tunnel inflow (1250 m³) takes place through a single point in a single deposition hole. The total erosion in a deposition hole may be greater, but this requires that the hole has several inflow points and the erosion will then be distributed over several channels. In total there are five deposition holes out of 6916 where the erosion exceeds the requirement of 100 kg. Of these, one hole has such a high inflow that it would not be accepted for deposition and one such a low inflow (6 µL/min) that piping would hardly occur. Of the 43 deposition holes where the inflow exceeds 10 % of the total inflow to the tunnel, there are however a number of holes where the inflow is so low that it can be difficult to detect (< 0.1 L/min), and therefore it cannot be excluded that mass losses of the order of 35–100 kg will occur in individual holes in around 30 different deposition tunnels. The distribution of mass loss is shown in Table 10-3.

Table 10-3. Distribution of deposition holes with different mass loss. The calculation is based on the reference case without EDZ in Joyce et al. (2013).

Mass loss (kg)	Number of holes
< 0.01	5 890
0.01–1	474
1–10	345
10–35	136
35–100	66
> 100	5

Today SKB has requirements for:

1. A maximum inflow of 0.1 L/min to a deposition hole (13 of the 43 holes in the above example would hereby be avoided).
2. The deposition sequence, that avoids that water leaves the tunnel before the plug is in place.
3. The sealing ability of the plug, to minimize the total amount of water that can cause erosion.

Some of the deposition holes with mass loss over 100 kg in the above example have such large inflows that they can be easily detected, and thus avoided. However, there are a few deposition holes: 3 holes of 6916 in the example simulation, where a mass loss of more than 100 kg occurs as a result of piping and where there will be hardly any opportunities to avoid this. These holes have such low inflows, that they are impossible to detect, but at the same time they are placed in extremely dry deposition tunnels, which means that a major part of the inflow to the tunnel still comes from the respective deposition holes. In these holes it cannot be guaranteed that the performance target for the swelling pressure will be upheld. The mass loss is still significantly less than what is needed before the diffusion barrier is lost (see further Section 10.3.9). The calculation result also show that the Darcy flows and the equivalent flow rates are relatively low in these holes. This means that the “piping holes” do not belong to the group of deposition holes where mass loss from chemical erosion (see Section 10.3.11) can be expected.

Eroded mass in a deposition tunnel

The erosion model described above can be used for the deposition tunnel as well. With a total volume of 1 250 m³, the largest possible erosion will be 1 640 kg. Erosion in the backfill will basically mean that material is redistributed within the tunnel itself. According to Table 5-22 the total mass of backfill in a 300 m tunnel will be ~10 200 tonnes. Considering the large mass of backfill in the tunnel, a redistribution of 1 640 kg is assessed to have no impact at all on the backfill performance.

Homogenisation after loss of bentonite mass

The swelling properties of bentonite make the buffer and backfill material swell and close open gaps or channels to form a more homogeneous medium. Homogenisation of buffer and backfill is crucial to fulfil the safety functions related buffer and backfill density (swelling pressure and hydraulic conductivity).

Erosion caused by piping will not be prevented by the bentonite as long as water flow and high water pressure gradients persist in the deposition tunnel. This will be the case until the flow and gradients are limited by the tunnel plug. If the erosion is strong, large openings of missing bentonite may locally be formed. The swelling and sealing of bentonite cannot take place unhindered since there is a resistance to swelling caused by friction both internally in the bentonite and between the bentonite and the surrounding fixed walls represented by the rock surface and in some cases the canister.

In order to investigate how well the buffer material seals the openings resulting from the mentioned processes a number of finite element calculations with the code Abaqus have been performed (Åkesson et al. 2010a).

As described above, erosion during and after installation of the buffer may cause significant loss of bentonite under unsatisfactory conditions.

Two different geometrical cases have been considered:

- The bentonite is lost in the shape of a half torus at the rock surface.
- The bentonite is lost in the shape of a half sphere at the rock surface.

The half torus shape around the deposition hole has been selected to maximise the mass loss around the canister. A more likely geometry would be a vertical half pipe going up towards the deposition tunnel. The geometry and the element mesh of the half torus case are shown in Figure 10-9. This geometry has been used to study the influence of:

- The water supply; water can be supplied from the rock surface, the inside space and the backfill.
- The radius of the half torus, which was varied from 0.034 m to 0.134 m (15–240 kg). (Note that the estimation of buffer loss due to piping erosion shows that for the maximum allowed inflow to the deposition hole (150 m^3) an erosion of up to 41 kg can occur).
- Combinations of the above.

The results from the variations of the water supply show that the final swelling pressure varies very little as a function of the water supply. However, the time for saturation and sealing of a pipe with radius of 67 mm (61 kg) varies from 2.2 years for the case where the water is supplied from rock surface, the inside space and the backfill to 42 years when water is only supplied from the backfill. The final swelling pressure in the original hole (pipe) is around 1.2 MPa. Variations of the radius of the half torus also yielded very similar final swelling pressures, even though 240 kg of bentonite is lost when the radius is increased.

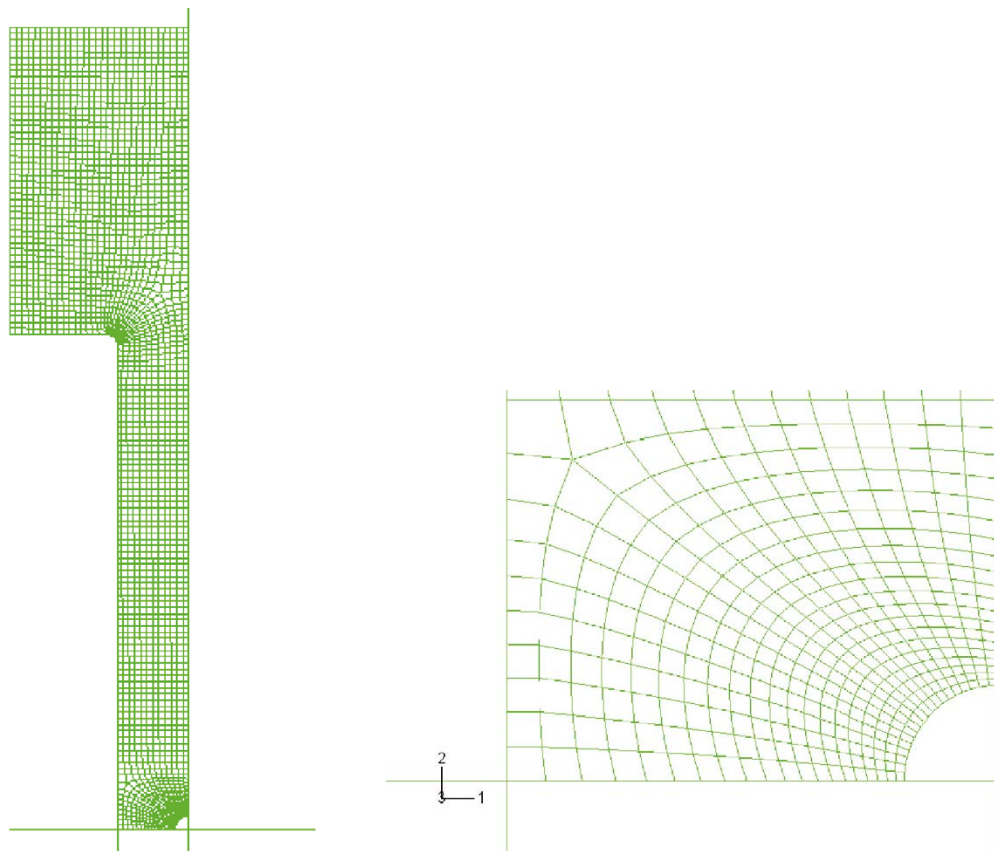


Figure 10-9. Element mesh of the calculation of a case with a half torus and radius 0.067 m. The mesh is axially symmetric around the left side and the bottom plane is a symmetry plane. The whole mesh and an enlargement of the part with the empty torus are shown (Åkesson et al. 2010a).

As an illustration of the significance of the piping geometry, a case where water enters the deposition hole at one point, at e.g. a fracture intersection, and where the erosion is very local around the inflow spot, which could be imagined as a loss of bentonite in a half sphere like configuration, has been evaluated (Figure 10-10). This is a more severe case than the torus case since bentonite is lost locally instead of distributed around the canister.

The results show that the swelling process is similar to the case with the half torus. Due to the friction against the rock there is very little swelling along the rock surface. Instead, the bentonite between the canister and the hole swells and seals the hole. Due to the rather thin buffer left between the canister and the spherical hole, the resulting void ratio after completion is rather high (> 1.5), which yields a swelling pressure below 1 MPa in about 1/3 of the buffer. This piping geometry would then violate the safety function criteria for the buffer. However, this case does not reflect a possible piping situation, since there is no exit point for the flow. It is noted that, even though the safety function is violated, the mass loss is not sufficient to lead to advective conditions (see Section 10.3.9).

Hydraulic interaction bottom plate/package

In order to achieve a sufficiently flat bottom of the deposition hole, a bottom plate is installed in each deposition hole (Figure 5-15). In the case where water can enter the deposition hole under the bottom plate, there might be a possibility that the water pressure generated may be sufficient to lift the entire buffer-canister package.

Åkesson et al. (2010a) have studied the potential lifting of the buffer/canister package during the period from the termination of the drainage to the installation of the backfill. This was done for a case in which a water-bearing fracture intersects the deposition hole beneath the bottom plate. In the **Buffer, backfill and closure process report**, it was observed that the contact zones between the concrete and both the copper plate and the rock are not tight, and that this implies that a water pressure can act on the entire surface area.

The current design of the bottom plate does not include a concrete component. The copper plate is however still there and the process description from Åkesson et al. (2010a) is still valid.

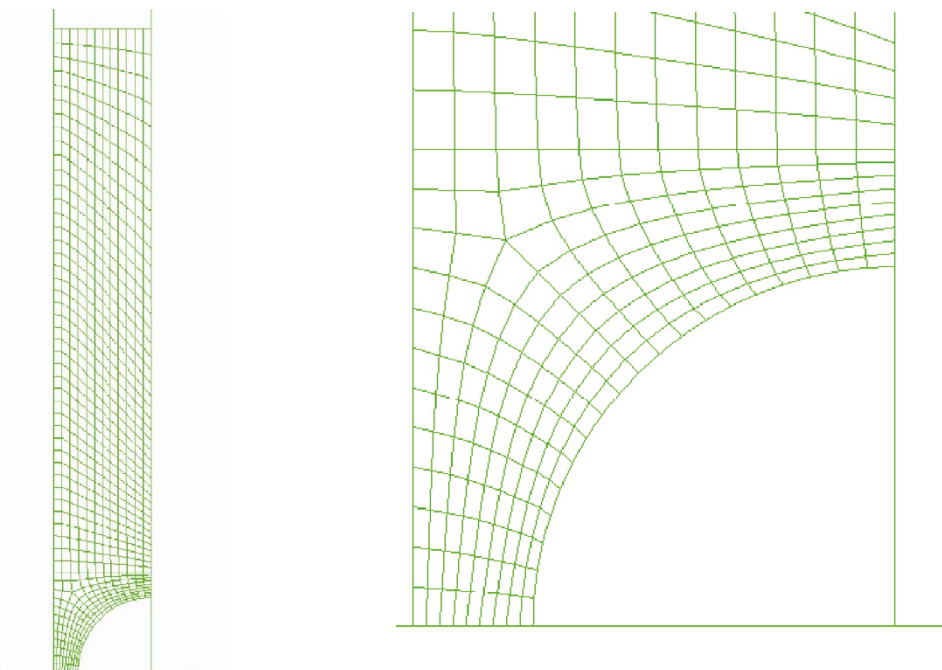


Figure 10-10. Element mesh for the case with a half sphere with radius 0.263 m. The mesh is axially symmetric around the bottom side. The whole mesh and an enlargement of the empty part are shown (Åkesson et al. 2010a).

This is a complex process which is related to the phenomenon of piping and a key issue is how fast the build-up of the swelling pressure can be. The assumption that pellets cannot stop inflowing water until all slots are filled due to piping is pessimistic in other cases, such as for the tunnel plug, but it disregards the build-up of pore pressure upstream. So in this case it is optimistic since such a build-up is unfavourable.

A tailored solution has been developed based on the following assumptions:

1. The hydration varies with time and distance from the bottom plate.
2. The build-up of swelling pressure is proportional to the hydration.
3. The water pressure beneath the package equals the swelling pressure at the bottom.

The build-up of the lifting forces is concurrent with the build-up of the frictional forces along the rock wall. Details of the calculations can be found in Åkesson et al. (2010a). These calculations indicate that the time to reach lifting conditions is approximately one week. And the model also suggests that an inflow higher than approximately 100 litres per day will avoid lifting conditions, due to the rapid build-up of the frictional force along the rock wall. The time scales to reach lifting conditions at low inflows are given directly by the adopted swelling pressure evolution, and the weight of the package, which corresponds to a pressure of 0.2 MPa. The swelling pressure should therefore not be allowed to reach this level as long as the backfill has not been installed.

The empirical data on the initial swelling pressure build-up in large-scale experiments is quite scattered. The chosen swelling pressure evolution in the presented model can nevertheless be regarded to be fairly rapid. This suggests that there should not be any risk of lifting conditions before the installation of the backfill, if a bottom plate is used in a deposition hole with a water-bearing fracture beneath. Still, due to the uncertainty in data, and to some extent also in conceptual understanding, it has not been possible to make any definitive judgment concerning the use of the bottom plate in such holes.

Identified uncertainties and their handling in the subsequent analysis

The function of the plug is to limit the flow of water out from the backfilled tunnel. The primary reason for this is to minimise the effect of piping and subsequent erosion in the buffer and backfill. A secondary reason is to limit the transport of gas (oxygen in air) from the main tunnel into the sealed deposition tunnel. A certain sealing capability is therefore needed from the bentonite seal within the plug.

The current plan is to pre-saturate the seal component of the plug through the drainage tubes. This means that the seal will be saturated faster than the tunnel backfill and this will efficiently limit gas and water transport through the plug. Piping and subsequent water flow from a fracture into a deposition hole and further out into the deposition tunnel cannot be excluded if the inflow rate is higher than the rate of water absorption of the buffer material, since the pellet filling and the bentonite blocks cannot stop the water inflow until the deposition holes and the tunnel are water filled and the hydraulic gradient occurs over the end plug. Erosion tests have shown that the dry mass of eroded bentonite can be modelled as a function of the total volume of inflowing water according to the model discussed in this section. The results shows that piping followed by erosion generally is a limited problem, but rare combinations of inflows to deposition holes and tunnels may cause erosion of up to around 150 kg in a few deposition holes. The model is purely empirical and it is difficult to theoretically derive a model. However, many geotechnical models are empirical (e.g. strength and friction angle relations) for the same reason and have successfully been used for numerous geotechnical design works.

The analysis of homogenisation processes occurring in the buffer after erosion yielding a half torus-shaped pipe indicates a strong decrease in density and swelling pressure in the analysed volume due to the friction in the bentonite. However, the swelling pressure after complete homogenisation is above 1 MPa for the analysed cases with torus radius varying from 3.4 cm to 13.4 cm. The influence of the radius seems to be insignificant due to the long distance to the bentonite boundaries. For the cases when the piping occurs as a half torus (or half pipe) the conclusion is thus that more 100 kg of dry bentonite may be lost from one deposition hole due to erosion without violating the safety function of the buffer. The uncertainty in the assessment of the eroded volume has been considered when the technical design requirements for acceptable inflow to deposition holes was revisited.

It is expected that most of the inflow of water into a deposition tunnel will occur through the wall of the tunnel itself and not through the deposition holes. The largest possible erosion will be 1 640 kg. Erosion in the backfill will basically mean that material is redistributed within the tunnel itself. Considering the large mass of backfill in the tunnel a redistribution of 1 640 kg can be assumed to have no impact on the backfill performance.

The design of the bottom plate has changed since SR-Site. The potential for lifting of the entire package described in this section is however still an issue. This process does however require that most of the inflow into the deposition hole is in the bottom and that the pellets filling close to the bottom of the deposition hole quickly develops a sufficient swelling pressure to restrict piping, while the rest of the pellets filling in the slot between the bentonite block and the rock wall remains dry. If those pellets starts to swell, the frictional force will prohibit lifting of the package. The possibility for lifting of the buffer/canister package is related to the properties of the pellets and may still put a stricter requirement on the inflow into the deposition hole, especially into the floor of the deposition hole.

10.2.5 Chemical evolution in and around the repository

Introduction

During the excavation and relatively long operational period, hydraulic conditions will change as described in Section 10.2.3. The changed hydraulic conditions may alter the groundwater composition around the repository. Some of these changes will be induced by the presence of the repository, but also shore-line displacement and climate variations may cause more limited alterations. As a consequence, the salinity in some parts of the repository may decrease due to an increased infiltration of dilute waters of meteoric origin, whereas in other regions the corresponding up-coning or the infiltration of Baltic seawater might instead induce an increase in salinity. This involves the safety function indicators R1b and R1c in Figure 10-2, and in extreme cases it might affect the swelling of the backfill, see Section 10.3.9 or enhance colloidal erosion of the buffer during deposition, see Section 10.3.11.

In addition to the groundwater changes caused by hydrological processes, other chemical aspects need to be considered during this period. It is to be expected that the excavation will be accompanied by grouting, and the chemical influence of the grout on groundwater must be considered. In general, cementitious grouts will increase the pH of the water, involving the safety function indicator R1e. During the operational phase, it is necessary to assess the role of stray materials such as nitrogenous compounds from the use of explosives, as well as the influence of any other process that could possibly change the chemical conditions in the repository, such as the precipitation or dissolution of minerals, corrosion of metal in rock bolts, etc. These processes might, for example, affect the safety function indicators R1d and R1e in Figure 10-2, that is, the generation of colloids and the sorption properties of minerals. Nitrite, ammonium and acetate are compounds that would increase the possibility of stress corrosion cracking of the copper canister.

When deposition tunnels are backfilled and plugged, air will be trapped in the porous buffer and backfill, and processes consuming oxygen must be evaluated. Air will also cause some initial corrosion of the copper canisters until anoxic conditions are reached. All these chemical processes are related to the safety indicators Can1 (copper canister thickness) and R1a (reducing conditions) in Figure 10-2.

Other chemical processes taking place in the buffer and backfill occur on longer time scales than the relatively short operational phase, and they are discussed in Section 10.3.10.

Natural groundwater conditions at the site

The chemical characteristics of groundwater at Forsmark prior to the construction of the repository are set out in detail in the **Site description Forsmark** and supporting documents (Laaksoharju et al. 2008). A brief account is provided in Chapter 4.

Salinity (upconing effects)

The groundwater salinity and composition in the vicinity of the repository will be affected during the excavation and operational phases because of the inflow into open tunnel sections. This will cause an

unnatural infiltration of meteoric and Baltic seawater, and as a consequence groundwater drawdown and upconing may occur. This phenomenon has been observed for example in some boreholes at Äspö. In extreme cases, if the groundwaters at larger depth have high salinities, the upconing of these waters might decrease the swelling pressure of the backfill, safety function indicator R1b. However, no such highly saline groundwaters have been found at the deepest sampling points at Forsmark. A quick inflow of Baltic seawater would increase the potassium concentrations of the groundwaters, involving the safety function indicator R1d in Figure 10-2.

The inflow to the tunnels will be reduced by injecting grout into the surrounding fractures. This will prevent the depression of groundwater levels near the ground surface and the corresponding inflow of meteoric water and seawater, as well as the upconing of saline waters.

The hydraulic effect of grouting has been modelled, see Section 10.2.3. The results obtained using the code DarcyTools indicate that limited upconing and, therefore, limited salinity increases are to be expected during construction and operation of a repository located at Forsmark. Other groundwater parameters, such as pH, are expected to be practically unaffected by groundwater upconing. Further details are given in Section 10.2.3 and references therein. Once the repository has been backfilled and closed it is expected that groundwater salinities will return to normal conditions after some time. For example saline groundwaters that had moved upwards due to upconing will then sink due to their higher density.

Redox conditions

Even with moderate inflows to the open tunnels, see Section 10.2.3, large amounts of superficial waters are predicted to percolate when considering the whole period of repository operation. Infiltrating waters will initially be equilibrated with oxygen in the atmosphere, whether they are marine, lake, stream or meteoric in origin. It could be contended that the redox stability of the rock volume on top of the repository area might be challenged at the time of repository closure by the large amounts of infiltrating O₂-rich waters.

However, microbial oxygen consumption takes place in the overburden and in the first metres of rock, as well as in lacustrine, fluvial and marine sediments. Therefore infiltrating waters are free of dissolved O₂. Oxygen consumption in saturated soils is well documented, see for example Drew (1983), Silver et al. (1999) and Pedersen (2006). The Äspö Redox Zone experiment (Banwart 1999, Molinero-Huguet et al. 2004) also showed that microbial respiration in the upper metres of a fracture zone effectively consumes the oxygen in infiltrating waters. In addition, groundwater samples from Äspö (Banwart et al. 1999, Luukkonen 2008) and Stripa (Nordstrom et al. 1989) are always found to contain dissolved Fe²⁺ indicating that groundwaters remain reducing even after prolonged periods of inflow into the tunnels.

Concerning nitrate and nitrogen compounds, data from Äspö suggest that although during the excavation period nitrogen compounds may accumulate in the groundwater draining into the tunnel and in the waters percolating through rock debris, these waters are pumped out, and fracture groundwaters appear to be unaffected (Mathurin 2018).

In conclusion, the reducing capacity of transmissive fracture zones is not affected during the excavation and operational periods, because consumption of oxygen in infiltrating waters takes place in soils, sediments as well as in the upper metres of fractures by microbial processes.

Effects of grout, shotcrete and concrete on pH

Injection of grout into fractures surrounding the repository tunnels will be necessary to avoid inflow of groundwater. Traditionally, cement-based grout is used when excavating tunnels. Standard Portland cement paste has porewater that is highly alkaline (pH ≈ 12.5). In order to avoid detrimental effects from porewater diffusing out of the cement matrix, cement recipes with porewaters having pH ≤ 11 will be used in deposition tunnels, see the **Underground openings construction report**. It is to be expected that the development of recipes for such materials will be an ongoing process both at SKB and elsewhere during the whole period of repository operation. Although the effects of these porewaters are much smaller, they must be considered, because it is possible that relatively large quantities of cement will be used in some repository areas. In general only limited amounts of grouting will be needed at Forsmark due to the low permeability of the rock.

The distribution of shotcrete and concrete in the repository will probably be spatially limited and their potential impact during the excavation and operational phases will be restricted. The exact shotcreting needs will not be known until the construction itself. Most of the leaking porewaters from these materials will be mixed with groundwater infiltrating into the tunnel and pumped away. A small part of the cement materials will be in contact with the backfill, and cement porewaters could migrate and diffuse into the bentonite. As long as low-alkalinity cement materials are used, the consequences on the performance of the backfill may be neglected.

On the other hand, grout could have a large impact on the geosphere conditions, as it is widely and diffusely distributed in the fracture system. Grouting is, however, necessary to avoid a large groundwater drawdown (increased meteoric water influx) and the corresponding up-coning of saline waters. Grouting is also needed for construction purposes; the ingress of water needs to be limited for the engineering installation and for worker safety. Two types of grout are envisaged in the vicinity of the deposition tunnels in the final repository, (see the **Underground openings construction report**): low-pH cement based grouts and suspensions of nano-sized silica particles (silica sol). The solidified silica sol grout is similar in its properties to the silica present in large quantities in the rock and fracture fillings, and may, therefore, be ignored in a post-closure safety context. Cement-based grouts on the other hand have chemical properties quite different from the surrounding rock, and their effects have to be considered.

Boreholes crossing cement grouted fractures at the Olkiluoto site in Finland have yielded waters with elevated pH values since sampling started (Arenius et al. 2008). The more limited experience from Äspö (Nilsson and Sandberg 2017) shows that a pulse of alkaline solution (pH up to 11.3) may be detected in the immediate vicinity of the grouted fractures during the first few days after injection. This pulse of alkaline waters is believed to be due to two factors: porewater released while the liquid grout solidifies; and erosion and dilution of grout by flowing groundwater in the outer edge of the grouted volume. These effects in the grouted fractures at Äspö were transitory, and after a few days the chemical composition of the groundwater returned to its original state (pH \approx 7.5). The pH values were sufficiently low as to indicate that substantial dilution had occurred. The data from Olkiluoto indicates that the intensity of this short alkaline pulse will be decreased by the use of “low-pH” cement. Because of its short duration, the effects of a pulse with pH \approx 11 are negligible.

After the excavation and operational phases grout will start to react with circulating groundwater, and a slightly alkaline plume will develop downstream in the grouted fractures (Luna et al. 2006, Nilsson and Sandberg 2017). This process is, however, relatively slow and it is, therefore, discussed in Section 10.3.7 in connection with the evolution of the repository during the initial temperate period after closure.

Precipitation/dissolution of minerals

During the operational phase, inflow of groundwater into the tunnel and mixing of groundwaters of different origin within rock fractures will result in precipitation or dissolution of minerals. These processes could only indirectly affect the safety function indicators. Precipitation and dissolution may be observed at the tunnel walls of the Äspö Hard Rock Laboratory (HRL). Simulations indicate that calcite and iron(III)oxyhydroxide may precipitate at the tunnel/backfill boundary (Domènech et al. 2006) but that this process does not influence the performance of the repository negatively.

Nitrogen compounds from blasting activities

As the explosives used in tunnel construction have a large proportion of nitrogen, the possibility of groundwater contamination by nitrogenous compounds originating from the nitrogen-based explosives has to be considered. Nitrite and ammonium would increase the risk of stress corrosion cracking for the copper canisters. During tunnel excavation at Äspö, groundwater data was collected to evaluate the influence of blasting (Håkansson 2016, Mathurin 2018). No significant concentration increase of nitrogen compounds in the groundwater was observed. This is supported by a study at the Kiruna iron ore mine (Nilsson and Widerlund 2017) which suggests that groundwater contamination by nitrogenous compounds from blasting activities at the site (using nitrogen-based explosives) primarily originates from secondary leaching of undetonated explosives in rock piles at the ground surface (above the mine), rather than direct dissolution of nitrogenous compounds in groundwater at the site of application.

Effects of organic materials and microbial processes

Remaining organic materials in the repository include microbial biofilms, plastics, cellulose, hydraulic oil, surfactants and cement additives. Most of these organic compounds can be degraded by microorganisms, initially via aerobic degradation pathway as long as there is oxygen, and later via anaerobic biodegradation pathways. The degradation products will increase the reducing capacity of the near field of the repository. There will also be a potential for formation of organic material by autotrophic microorganisms using the energy in H_2 that can be produced in anaerobic corrosion of steel constructions like rock support left in the rock at closure of the repository. Apart from the possibility of acting as reductants in aerobic or anaerobic biodegradation, organic materials might also be detrimental during later periods in enhancing the potential for radionuclide transport in groundwater after repository closure, for example by the formation of organic complexing compounds and organic colloids (safety function indicator R1d in Figure 10-2). In addition, acetate would increase the risk of stress corrosion cracking for the copper canisters.

The largest pool of organic material is potentially the organic carbon in the bentonite clay, which according to specifications is less than 0.25 weight %, although the design criterion is < 1 %, see the **Buffer production report**. This organic material is assumed to be mostly humic and fulvic acids, i.e. presumably plant-derived waxes and highly aromatic carbon with low contributions from small molecules (Marshall et al. 2015). It is not known how much of it will be subject to biodegradation. However, in the study by Marshall et al. (2015) it was concluded that since the majority of the natural organic matter in the bentonite clay is recalcitrant and already diagenetically altered, it is unlikely to serve as microbial substrate. Due to the low concentration of water-extractable organic carbon, which was less than 0.01 %, of the total organic amount, the bioavailability of these compounds in the repository will be low. The low solubility of organic carbon was also confirmed by Maanoja et al. (2020).

An inventory of organic materials and an assessment of their impact on microbial processes has been compiled (Hallbeck 2010). This study concluded that it is to be expected that microbial degradation of organic materials will contribute: a) to quick consumption of any oxygen left in the repository; and b) by a combination of processes, involving anaerobic degradation and sulphate-reduction, to sulphide production in the vicinity of the deposition holes. Some of the sulphide could reach the canister and may cause corrosion. The possible increase in acetate concentration has been found to be of no significance (Appendix A in Hallbeck 2010).

The real amount of organic carbon in the bentonite is expected to be ~ 0.20 – 0.25 % by weight in both the buffer and the backfill material in PSAR, and furthermore it is deemed as highly improbable that all of it could be used by microbial sulphate reduction given its non-reactive nature. In the deposition holes, the bentonite density is such that microbial sulphate reduction sustained by the organic matter in the bentonite is not expected to take place to any great extent (see Section 10.3.9). If the bentonite buffer were to be eroded away then the corresponding amounts of organic matter would also be eroded and although microbial sulphate reduction would then become possible, the dissolved organic carbon in the incoming groundwater would have to be used.

Marshall et al. (2015) found that the water-extractable organic content in MX-80 was 0.0095 % of total organic carbon. A deposition hole contains about 15 000 kg of bentonite (Section 5.5) with a content of organic carbon of 0.2 % (Svensson et al. 2019). Assuming a content of water-extractable organics of 0.01 % gives 3 g of organic carbon that is readily available for sulphate reduction. This corresponds to 0.25 mol carbon.

The organic content of the Ashapura backfill in PSAR is 0.24 % at a maximum (Section 5.6.3). This corresponds well with the value of 0.15 % measured by Maanoja et al. (2020) for “Indian bentonite”. The solid mass in a 6 m tunnel section, corresponding to one canister position is 200 tonnes (Table 5-23). The maximum content of organic carbon in this section is 40 kmol. As for the buffer material, most of this carbon is not soluble and readily available for microbial reactions. Maanoja et al. (2020) concludes that only a small part of the bentonite organic matter (0.01–0.06 % TOC w/w) can be readily soluble to a water phase. Using the highest value, it can be estimated that the backfill can supply 24 moles of organic carbon to each canister position.

The amount of organic carbon with the bentonite excluded is 5.2×10^3 kg in the deposition tunnels and 7.2×10^3 kg in the other areas, which if all of it were to be used for microbial sulphate reduction, the resulting sulphide, if evenly distributed, would correspond to about 35 mol per canister (SKB 2011).

Rock bolts and other iron components will remain in the deposition tunnels, and the highest theoretical amount of sulphide that can be produced with H₂ from anaerobic iron corrosion coupled with sulphate-reduction in Forsmark is about 685 mol per canister as calculated from the amounts of steel in **Underground openings construction report**, Tables 8-2 and 8-3. The amount of sulphide produced from biodegradation of rock biofilms in the deposition tunnels could be estimated with the assumptions as in Hallbeck (2010): biofilm thickness 1 mm, density 75 kg/m³ and a biofilm coverage of tunnel walls and ceilings of 5 %. With all organic matter in a biofilm available for microbial activity and a carbon content of 50 % by mass (Fagerbakke et al. 1996), this gives 13 moles sulphide per canister (for 6 m canister spacing, and tunnel dimensions as in Appendix B of the **Fuel and canister process report**). These are highly uncertain values and are based on the presumption that no cleaning of the rock surfaces is undertaken before closure. Steel corrosion will proceed slowly and the total values are reported here for reference only. It is to be expected that the hydrogen produced by corrosion will diffuse and be mixed with circulating waters, and that only a small fraction will reach any deposition hole. If the corrosion products are not dispersed, then there is no contribution to dissolved sulphide because steel corrosion also produces iron compounds which react with sulphide.

In conclusion, the largest pool of organic carbon in the repository is the organic matter included in the bentonite. Organic matter and hydrogen from iron/steel corrosion could contribute to canister corrosion if it was available for microbial sulphate reduction, and this is further evaluated in Section 10.3.13. The organic matter in the deposition holes can be ruled out as long as the buffer density is sufficient, but that in the backfill could potentially be used in microbial sulphate reduction.

Intrusion of sulphide

In the groundwater at repository depth a certain level of microbial sulphate reduction can be expected. This is the main source for sulphide at the conditions found in deep groundwaters. In the safety assessment, SR-Site, a distribution based on measured sulphide levels during the site investigations at Forsmark, was assessed using the median value of 1 mM and the highest value of 120 mM (Section 4.3.5. in SKB 2010d).

During undisturbed conditions, microbial activity, sulphate reducing bacteria (SRB) in this case, is limited by, e.g. the supply of energy sources (electron donors) such as organic carbon and hydrogen.

Both metallic and organic materials in the borehole equipment can provide electron donors to stimulate sulphide production by SRB (Chukharkina et al. 2016, 2017, Nilsson et al. 2017). These types of instrumentation materials will not be present after the closure, but sulphide production favoured by these and similar materials may cause high concentrations of sulphide during the construction of the repository.

The excavation itself will change the groundwater flow pathways compared to the situation prior to the tunnel system. The created head differences allow groundwater flow along open boreholes due to the drawdown towards the tunnel system (Posiva 2012). This results in mixing of different water types which most likely will stimulate microbial activity.

During the repository's operating time and the time shortly thereafter, meteoric water from the surface could reach repository depth. Such water may be sufficiently rich in suitable organic carbon for sulphate reducing bacteria and thereby constitute the limiting factor for sulphide production. This type of organic carbon is quickly consumed in the groundwater and thus the elevated levels of organic carbon at repository depth will only exist as long as the groundwater flow in the rock is elevated as a result of the construction and operation of the repository, i.e. during the first 100 years. This will apply only for the parts of the repository where groundwater flows are expected to be high during the operational time. Large parts of the repository are expected to have limited turnover of groundwater also during operating time. During excavation, H₂ from the rock matrix may be released which likely will result in an increased activity of SRB. However, monitoring and modelling results indicate that elevated sulphide concentrations tend to disappear within a few years (Wersin et al. 2014). The reason may be depletion of energy sources (e.g. H₂) or precipitation of insoluble iron sulphides.

Pessimistically, the concentration of sulphate in the penetrating water can be used as an upper limit for the concentration of sulphide at repository depth. Thus, the maximum sulphate content is then constituted by an undiluted pulse of surface water to repository depth, although it is likely that it

will be diluted on the way. The highest measured sulphate concentrations at the surface are in the millimolar range (SKB 2014a). A sulphate concentration of 1 mM could therefore be set as the upper limit of what could occur at repository depth during 100 years after construction has been initiated. Accordingly, 1 mM is the maximum sulphide concentration that could occur under these conditions (SKB 2014a).

Interactions with SFR

The conclusions from the study (Svensson and Follin 2010) are that an expanded SFR in operation appears to have little or no impact on the groundwater inflow rates to a final operating repository in the target volume at Forsmark. The case with SFR closed (but existing in the model) and a deep spent fuel repository open has not been fully analysed in Svensson and Follin (2010), but the simulations indicate that some pressure response is transmitted from the deep repository to boreholes close to SFR. Thus, some interactions between a closed SFR and an operating deep repository cannot be excluded.

Although the plans at present are that SFR will be kept open during the excavation and operational periods of the spent fuel repository, the possibility of early closure cannot be ignored. If that was to happen, anaerobic microbial processes in the BLA vault of SFR, that contains large amounts of cellulose and other organic compounds, would result in porewaters that could have a large content of organic matter. These organic matter rich porewaters could then find their way to the operating deep repository, where microbial sulphate reduction would generate locally high sulphide concentrations.

Even if microbial consumption of the organic matter along the pathway between SFR and the deep repository and mixing of groundwaters are disregarded, the consequences for the performance of the canisters can be neglected. This is due to the short time period involved (at most ~100 years) and to the fact that during this period all canisters will be surrounded by an intact buffer that will act as a diffusion barrier.

Oxygen consumption in backfill

Air will be trapped in the porous buffer and backfill when deposition tunnels are plugged. Most of the oxygen in this air will be in the backfill because of its larger volume. This oxygen could potentially diffuse to the canister surface and cause some initial corrosion until anoxic conditions are achieved, and, therefore, it is valuable to estimate the reducing capacity of the backfill. Chemical reactions and microbial activities are both expected to consume oxygen to a degree which depends on the saturation and water content of the clay.

Numerical calculations (Grandia et al. 2006, Yang et al. 2007) coupling chemical processes consuming oxygen with the hydrodynamic saturation of the backfill have been used to estimate the time scale for reaching anoxic conditions in the tunnels of the repository. These studies show that several inorganic O₂ consumption processes may take place with the accessory minerals present in the bentonite in the buffer and in the backfill. These reactions are, in order of decreasing rate, the dissolution of Fe²⁺ containing carbonates, the oxidation of pyrite, and the oxidation of Fe²⁺ bearing silicates such as mica and montmorillonite. The calculated oxygen consumption times are highly dependent on the postulated value for the surface area of the reacting minerals. Nevertheless, it may be concluded that anoxic conditions are likely to be reached after a period of the order of one month after the backfill becomes completely water saturated.

As noted in Section 10.3.8, it may take several thousand years for some parts of the repository to reach full saturation. It can thus not be excluded that the density of the backfill is low enough to allow some microbial activity, at least before it is fully homogenised in all parts, i.e. a combination of a saturated pellets filling together with partially saturated blocks, and the effect of microbial activity could be to shorten the time to reach anoxic conditions in the backfill. Diffusion of oxygen to the surrounding granite would also be an effective mechanism for oxygen consumption by aerobic bacteria populations that could develop in the backfill/granite interface. The REX experiment in the Äspö HRL showed that oxygenated water in contact with a granite surface will be reduced in a few weeks. The rock wall will most likely be an efficient sink for oxygen if there is a sufficient supply of water. The case with a very dry rock surface is more uncertain.

In the Prototype Repository Project at the Äspö Hard Rock Laboratory, a programme was in progress for sampling and analysing gases at different locations in the buffer and backfill. One of the specific aims is to monitor the consumption of oxygen (Pedersen et al. 2004). The two sections of the Prototype Repository were sealed in September 2001 and September 2003, respectively. Results have been published for the samplings in 2004 and 2007 (Eriksson 2007). The resulting oxygen content in the gas phase ranged from almost zero to that present in the atmosphere, although there is a general decreasing trend with time. However, for technical reasons the backfill was not completely water saturated in all parts, and the two sections were not fully sealed off, which prevents the drawing of unequivocal conclusions about the processes responsible for the decrease of oxygen. These data, however, provide further indications that the oxygen consumption will be rapid when the water content of the clay is high enough.

Giroud et al. (2018) report experiments where open glass vials were filled with granulated bentonite and placed into the stainless-steel bottles that were subsequently sealed airtight. All bottles were kept at laboratory temperature (~23 °C). The partial pressure of oxygen decreased by a few percent over a time period of 15 days, however, the same pressure drop was seen also for “inert” gases like nitrogen and argon and the results were therefore interpreted as sorption and not reaction.

Similarly, Birgersson and Goudarzi (2018) reported a test that was conducted in isothermal (room temperature or 50 °C), isolated conditions, and involved only bentonite pellets. The test showed no noticeable oxygen consumption at room temperature and very little at 50 °C over a period of 1 year.

In conclusion, both inorganic reactions and microbial processes may consume O₂ in the air trapped in the backfill. There are however experimental results indicating that the consumption rate may be low at the temperatures that prevail in the backfill, at least for an unsaturated conditions. In the case of a partially saturated backfill, it can therefore not be ruled out that the majority of the oxygen in the backfill either diffuses into the buffer and reaches the surface of a canister or possibly diffuses to the rock in the tunnel wall. In the case of a rapidly saturated backfill, it is more likely that the main part of the dissolved oxygen will react with minerals present in the backfill.

Colloid formation

During the excavation and operational phases, substantial amounts of colloids may be formed due to microbial activities, and microbes themselves may act as colloids. In addition, bentonite erosion by fresh waters may generate colloids as may the precipitation of amorphous Fe(III) hydroxides, etc. These colloids are expected to be short-lived, mainly because colloids will aggregate and sediment in moderately saline waters, see for example (Degueldre et al. 1996).

Other processes contributing to the elimination of colloids are microbial decomposition of organics, and the recrystallisation and sedimentation of amorphous materials.

In conclusion, possible increased formation of colloids during the excavation and operational phases is not expected to affect the performance of the repository in the long-term, because the colloid concentrations will quickly resume the natural values under the saline water conditions that will prevail.

Canister corrosion

During operation, before deposition in the final repository, the canister will be subject to atmospheric corrosion, at slightly elevated temperatures, and most probably at a varying relative humidity (canisters stored in and cooled by circulating indoor air), see the **Fuel and canister process report**, Section 3.5.4. Under these conditions, the maximum corrosion is estimated to be less than 1 µm even after a storage period of two years.

In the **Fuel and canister process report**, Section 3.5.4 it is further described how the total extent of corrosion under aerobic conditions will be limited by the available amount of oxygen, i.e. the oxygen trapped in the repository after closure. After backfilling the tunnels, the available trapped oxygen can be calculated to be about 277 moles oxygen gas per canister. Due to the large difference in volume between the buffer in one deposition hole and the amount of backfill that can be assigned to each deposition hole, only a small part of the oxygen (36 moles) comes from the buffer, and the remainder from the backfill. Although there may be other sinks for O₂ than corrosion, e.g. microbial activity

and oxidation of rock surfaces and minerals in the clay, the efficiency of these sinks has not been quantified. It is therefore pessimistically assumed that all O₂ in the buffer and backfill is available for corrosion of the copper canisters. The entrapped 277 moles of oxygen from the backfill corresponds to a corrosion depth of 446 µm if evenly distributed on the canister surface. In this estimate, it is pessimistically assumed that Cu₂O is the only corrosion product formed.

The corrosion from the oxygen in the buffer corresponds to a corrosion depth of 64 µm if all oxygen diffuses inward to be consumed by corrosion, and other sinks in the clay or at the rock surface are neglected as for the backfill. Adding the corrosion depths from O₂ in the buffer and backfill, and accounting for a differential corrosion depth due to the diffusion geometry from the backfill to the deposition hole (resulting in a maximum corrosion depth of 891 µm), it is estimated that the total corrosion depth will be less than 1 mm anywhere on the canister surface. During the time period when the oxygen concentration and potential is sufficiently high, pitting corrosion is conceivable. In probabilistic assessments of pitting of copper under initially oxygenated repository conditions the maximum pit depth is estimated to be less than 1.22 mm, but the overwhelming majority (87 %) of the pits are predicted to be less than 100 µm deep. Experimentally, the deepest pits observed on copper exposed to initially unsaturated repository like environments is a few tens or nearly 100 µm. Adding up these contributions of localised corrosion during initially aerobic unsaturated and saturated conditions gives a maximum pit depth of less than 1.5 mm, see further the **Fuel and canister process report**, Section 3.5.4.

In conclusion, the corrosion depth from the atmospheric and initially entrapped oxygen is pessimistically assessed to be less than 2.5 mm including pits, which is small compared to the minimum copper coverage of the canisters.

As concluded in the **Fuel and canister process report**, Section 3.5.5, for the case of water present in the interior of the canister, also the possible overlapping time periods with radiolytic formation of NH₃ while water still is present, needs to be considered as the ammonium ion is one of the species that could cause stress corrosion cracking in the copper. If pessimistically assuming initial water (600 g) and gas (90 % argon) contents according to the technical design requirements a limited period of overlap between wet conditions and presence of ammonium cannot be excluded (Henshaw and Spahiu 2021). Such an overlap is one of several prerequisites for ammonium to have any detrimental effect on the copper, see the **Fuel and canister process report**, Section 3.5.4. An overlap does not appear if an initial argon content of 99 %, in accordance with the requirement on the production system (see Section 5.3.4), is assumed. The results of the modelling in Henshaw and Spahiu (2021), behind these conclusions, are preliminary, but the consequences (and need for further assessment) could be reduced by increasing the initial argon content in the technical design requirements on the initial gas content in the canister interior.

Identified uncertainties and their handling in the subsequent analysis

Several uncertainties are identified when considering the different chemical aspects of the evolution of the repository during the operational period:

- There is a large degree of uncertainty in the detailed salinity distribution around the repository. However, the salinity will not become so high or so low as to affect the performance of the repository during this period or when considering its future evolution. The distributions of salinity, pH and other groundwater characteristics obtained from the modelling of the temperate conditions at 2000 AD, described in Section 10.3.7, is wide enough to include the small changes caused by the operation of the repository.
- The corrosion effects of sulphide produced by microbial activity with organic matter in bentonite and man-made materials, and anaerobic corrosion of iron and steel as an energy source is further discussed in Section 10.3.13. The corrosion from intrusion of groundwater with high initial content of sulphide is likewise evaluated in Section 10.3.13.
- Although various assumptions can be made for other sinks for oxygen in the buffer and backfill than corrosion, e. g. microbial activity and oxidation of clay and/or rock minerals, the efficiency of these have not been possible to quantify. It is thus pessimistically assumed that all oxygen in the buffer and backfill is available for corrosion of the copper canisters. A pessimistic assessment of the corrosion depth can be estimated to less than 1 mm from a mass-balance assuming that all

oxygen available in the buffer and backfill is distributed as general corrosion, but only on the upper part of the canister in the deposition hole (**Fuel and canister process report**, Section 3.5.4 and Appendix A2).

- Initially entrapped oxygen in the repository will lead to uneven general corrosion, although some localised corrosion cannot be excluded early when the potential is high. In the **Fuel and canister process report**, Section 3.5.4, the upper limit of localised corrosion was estimated to less than 1.5 mm by adding the maximum pit depths observed under unsaturated conditions (100 µm) with the maximum pit depths predicted probabilistically for saturated conditions (1.22 mm).
- The corrosion depth from the atmospheric and initially entrapped oxygen is thus pessimistically assessed to be less than 2.5 mm (including pits), which is small compared to the minimum copper coverage of the canisters. Here, several uncertainties have been handled pessimistically, most importantly regarding the efficiency of sinks other than corrosion, which may consume O₂ during unsaturated conditions in the backfill.
- Preliminary results suggest that radiolysis in the interior of the canister could cause the formation of NH₃ for pessimistic assumption on remaining water and air. The potential extent of this could be reduced or avoided by decreasing the maximum amount of remaining air allowed in the canister. See further Section 15.5.5.

10.2.6 Effects of operational activities on completed parts of the repository

In the repository design, a minimum of 80 m separation between a deposition tunnel under construction and a backfilled deposition tunnel is applied. A study has been conducted (Jonsson et al. 2009) exploring whether this separation is sufficient to ensure there will be no vibration damage from the blasting over such a distance. According to Jonsson et al. (2009) the most vulnerable stage from a vibration point of view is when the bentonite buffer is placed in the deposition hole but the canister has not yet been placed. During this stage, a hollow column of bentonite blocks remains free to vibrate inside the deposition hole. A three dimensional model in 3DEC, capable of capturing the dynamic behaviour of the bentonite buffer was set up and calibrated to recorded vibrations from the TASQ tunnel at Äspö HRL. It was concluded that when conducting blasting activities at 30 m distance with 4 kg of loading, the bentonite buffer will likely encounter a displacement which is less than 0.5 mm.

These analyses imply that the continued excavation and operation of the repository, provided the blasting activities are separated a minimum of 80 m away from the completed parts, will not imply any detrimental impacts on the completed part of the repository. Furthermore, analyses suggest that this minimum distance can probably be shorter without any loss in safety.

As stated in Section 10.2.4 piping followed by erosion of buffer and backfill in already deposited tunnels cannot be ruled out in the PSAR. About 100 kg of dry bentonite may be lost from a deposition hole by erosion without jeopardizing the function of the buffer. The potential effect is substantial, but the case of point erosion rather unlikely. This situation is handled by avoiding potential deposition hole positions with too high an inflow, and need thus not be further considered in the risk assessment. Since the inflow to the backfill cannot be higher than the available void volume in the deposition tunnel, the largest possible erosion of the backfill will be 1 640 kg. Considering the large mass of backfill in the tunnel, about 34 000 kg per m tunnel (see Table 5-22), a redistribution of 1 640 kg can be assumed to have no impact at all on the backfill performance.

10.2.7 Summary of the excavation/operation phase

Summary of system evolution

The state of the repository system at the start of the excavation/operational phase is the initial state described in Chapter 5.

The evolution of the system during this phase is dominated by the excavation/operational activities. The evolution is thus different in nature from that at later stages, since the latter is essentially driven by naturally occurring processes. In principle, this evolution also depends on how the repository excavation and emplacement proceeds, but this is not specified in the current phase of the repository layout and design work. Several conclusions can be drawn without this more detailed specification.

The duration of this stage can be assumed to be several tens up to a hundred years depending on the progress of the excavation/operational activities and the total number of canisters.

Radiologically, the radiation intensity from each deposited canister will decrease during this period. This has a direct impact on the residual radioactive decay heat from the deposited canisters.

The thermal evolution will be dominated by the heat output from the canisters and some parts of the engineered barrier system will reach their peak temperatures during the excavation/operational phase as this occurs after typically a few tens of years. This evolution is treated in more detail in the next section, as it continues for thousands of years and as the local peak temperatures are insensitive to details of the operational sequence. See Section 10.2.1.

The mechanical evolution is dominated by the excavation of the host rock. An obvious mechanical impact is the creation of rock cavities for the repository. According to Section 10.2.2, the following conclusions regarding additional mechanical consequences can be drawn.

- There are no safety related impacts of the few cases of spalling prior to canister emplacement expected provided the actions envisaged in the **Underground openings construction report** are implemented. This allows the exclusion of the phenomenon in question in the risk assessment.
- There is ample evidence that a potential EDZ formed during excavation will be kept below the maximum allowed transmissivity as set out by the technical design requirements and data suggest that a continuous EDZ would not develop at all. However, given that the occurrence of the EDZ currently can only be assessed by indirect measurements, it seems justified to consider an EDZ according to the technical design requirements, i.e. with an axial transmissivity of 10^{-8} m²/s as a basic assumption for further analyses. Furthermore, it also seems justified to explore how transmissive an EDZ needs to be in order to significantly impact other safety functions as well as exploring the impact of no axially continuous EDZ at all.
- Reactivation of fractures caused by the stress redistribution only results in insignificant increases of transmissivity in near-field fractures, apart from fractures that are parallel, and very close, to the tunnel. However, in reality fractures will not be persistently parallel to the tunnel where there are deposition holes, especially since deposition holes intersected by fractures intersecting more than four deposition holes will be rejected according to the EFPC criterion. This means that this effect can be discarded, or at least captured within the EDZ assumption of 10^{-8} m²/s along the tunnel.
- Induced seismicity: The implications of induced seismicity can be excluded in the risk calculation.

Hydraulically, the evolution is dominated by upconing and drawdown effects of the repository excavation. The hydrogeology studies presented in Section 10.2.3 show that salinities generally will decrease at repository level due to the drawdown of shallow waters, apart from a few locations where salinities slightly increase due to upconing. The inflow to the repository is very small, but it should be noted that groundwater will seep into the already plugged deposition tunnels, thus affecting the potential for piping and erosion of the buffer and the backfill in these tunnels.

The drainage of water into the opened part of the repository affects the hydraulic evolution of the buffer, backfill and plug in already deposited tunnels. The plug needs to be able to limit the flow of water out from the backfilled tunnel, primarily to minimise the effect of piping in the buffer and backfill. Modelling has shown that it will take 5–20 years to saturate the bentonite seal within the plug. This means that either the plug/rock interface or the pellet filling in the seal need to limit the flow during that period. Precise requirements on the seal capacity are not yet defined but the plug design will under all circumstances be adjusted to meet the requirements when specified. Since the only function of the plug is to ensure the initial state before closure, failed plug performance is not assessed in the PSAR.

- Piping and subsequent water flow from a fracture into a deposition hole and further out into the deposition tunnel cannot be excluded if the inflow rate is higher than the rate of water absorption of the buffer material, since the pellet filling and the bentonite blocks cannot stop the water inflow until the deposition holes and the tunnel are water filled and the hydraulic gradient is taken by the end plug. Erosion tests have shown that the dry mass of eroded bentonite can be modelled as a function of the total volume of inflowing water.

- The calculations of the swelling and homogenisation of a half torus resulting from erosion show that the swelling yields a strong decrease in density and swelling pressure in the eroded volume due to the friction in the bentonite. About 100 kg of dry bentonite may be lost due to erosion without jeopardizing the function of the buffer. The results of the assessment of likelihood of piping and erosion presented in section 10.2.4 shows that piping followed by erosion generally is a limited problem, but rare combinations of inflows to deposition holes and tunnels may cause erosion of up to around 150 kg in a few deposition holes. However, the uncertainty in the assessment of the eroded volume needs to be considered when revising the technical design requirements for acceptable inflow to deposition holes, see further Section 15.5.

During the excavation/operational phase, the chemical evolution mainly arises from the disturbance to the natural conditions caused by the presence of the repository. According to the results presented in Section 10.2.5, the following conclusions can be drawn.

- There is a large uncertainty in the detailed salinity distribution around the repository. However, the salinity will not become so high or so low as to affect the performance of the repository during this period or when considering its future evolution. The distributions of salinity, pH and other groundwater characteristics obtained from the modelling of the temperate conditions at 2000 AD, described in Section 10.3.7, is wide enough to include the small changes caused by the operation of the repository.
- A short alkaline pulse in the groundwater from low-pH cement, shotcrete and concrete is likely to form, but its effects will be negligible.
- An increased precipitation of calcite and iron(III)-oxyhydroxides will occur at the tunnel wall during operations, but this process is evaluated as being of no consequence for the performance of the repository.
- Organic stray materials will be consumed by microbes, with the main effects being an increased rate of oxygen consumption and possibly also of sulphate reduction. This could contribute to canister corrosion if it could be made available for microbial sulphate reduction. This is considered in the canister corrosion assessment during the initial temperate period, see Section 10.3.13.
- An increased formation of colloids during the excavation and operational phases will not affect the performance of the repository in the long-term, because the colloid concentrations will quickly resume their natural values.
- Both inorganic reactions and microbial processes may consume O₂ in the air trapped in the backfill. In the case of a partially saturated backfill, it can however not be ruled out that the majority of the oxygen in the backfill will either diffuse into the buffer and reach the surface of a canister or possibly diffuse to the rock in the tunnel wall. In the case of a rapidly saturated backfill, it is more likely that the main part of the dissolved oxygen will react with minerals present in the backfill.
- Canister corrosion depths from the atmospheric and initially entrapped oxygen are pessimistically assessed to be less than 2.5 mm (including pits), which is small compared to the minimum copper coverage of the canisters.

Safety function indicators at the end of the excavation/operation phase

Due both to the gradual excavation of the repository and the spatial variability of rock conditions, the state of the system at the end of the excavation/operational phase will vary e.g. between deposition holes.

Also, several safety function indicators are defined only for a water saturated repository, meaning that several safety function indicators are not meaningful to discuss at this stage.

Therefore, the detailed discussion of safety functions and status of safety function indicators is postponed until the end of the account of the initial temperate period, see Section 10.3.16. There also, the development during the excavation/operational phase is taken into account.

10.3 The initial period of temperate climate after closure

10.3.1 Introduction

The initial period of temperate climate can be expected to last several thousand years after repository closure. From a compliance point of view, the initial 1 000 years after closure are of particular interest, since SSM's regulations require a more detailed account of repository evolution for this period. Since many of the initial phenomena in the repository system occur within a 1 000 year period, a more detailed account of this time period is automatically obtained as every phenomenon is studied on the time scale appropriate to its nature. Examples of such phenomena are the resaturation of the host rock, the saturation of the buffer and the backfill and the thermal transient with its induced mechanical effects. Biosphere development is explicitly divided into an initial 1 000 year period and a subsequent period of development extending to the end of the temperate domain.

10.3.2 External conditions

The development of external conditions over the first 1 000 years after present is based on current knowledge of the Forsmark site and extrapolation of present trends, e.g. of changes in relative sea level. The development of climate-related processes for the remaining part of the initial period of temperate climate domain is based on model reconstructions of ice sheet-, relative sea level-, and permafrost development for the last glacial cycle, including the Weichselian glacial, i.e. from 120 000 years ago up to present, see further Section 10.4.1. In the reference glacial cycle, the initial period of temperate climate domain after repository construction is ca 8 000 years long. Note that this initial temperate period subsequently has been revised to have a duration of at least ca 17 000 years (SKB 2014b, Brandefelt et al. 2013). However, for the purpose of the safety assessment for the spent nuclear fuel repository, the exact duration of this period is not essential. For the assessment period of 1 million years, several identical reference glacial cycles, 120 000 years long, are envisaged to follow each other. In this process, each of the following full interglacial periods locally defined for Forsmark are ~20 000 years long. During these future interglacials, the repository location is submerged by the Baltic Sea for about half of the time, resulting in the repository being exposed to temperate climate conditions for almost 8 000 years in each interglacial, see the **Climate report**, Section 4.4.4.

In the reference glacial cycle, the long-term climate trend is assumed to be affected only by natural climate variability, and not by anthropogenically enhanced global warming. Therefore, palaeoclimate data depicting natural climate variability and trends can be used to assess the reference glacial cycle climate during the initial 1 000 years of temperate climate conditions. Climate variability in Sweden during the past millennium has experienced changes both in air temperature and precipitation (Moberg et al. 2006), but the changes have not been large. If a 30 year smoothing filter on simulated air temperature data is applied, then, for southern Sweden, including the Forsmark region, annual air temperature variability was up to around ± 1 degree C for variations slower than ca 30 years (Moberg et al. 2006, Figure 6-1). Therefore, in the reference glacial cycle it is assumed that the temperate climate variability, in terms of temperature and precipitation, during the first 1 000 years after present is also relatively small, and, in line with the basic assumption, that climate trends during this period follow the patterns of natural climate variability.

The reference glacial cycle has been produced by applying palaeoclimate interpretations and regional Fennoscandian climatic- and topographical conditions for modelling of ice sheet, permafrost and relative sea level changes, see the **Climate report**. This approach results in the timing and durations of all following periods of climate domains during the reference glacial cycle (Section 10.4.1). In the ice-sheet modelling, a paleotemperature curve obtained from central Greenland is used in the absence of a continuous long-term climate proxy record from Fennoscandia. However, even though the Greenland paleotemperature curve, and its use for Fennoscandian conditions, involve major uncertainties, see the **Climate report**, Appendix 1, this is not a drawback considering the general approach adopted; namely to first develop a reference glacial cycle for the coming 120 000 years, and subsequently construct other complementary climate cases covering a broader range of possibilities of future climate developments with a potentially larger impact on repository safety.

A climate case that includes global warming, as a result of an increase in atmospheric greenhouse gases from anthropogenic activity, is described in Section 10.6.

10.3.3 Biosphere

Processes of importance for long-term biosphere development

Long-term landscape development in the Forsmark area is dependent on two main, and partly inter-dependent factors, *climate variations* and *shoreline displacement*. These two factors in combination strongly affect a number of processes, which in turn determine the development of ecosystems. Some examples of such processes are erosion and sedimentation, groundwater recharge and discharge, soil formation, primary production, and decomposition of organic matter. These processes are discussed in relation to landscape development in more detail in Lindborg (2010). According to results from the hydrogeological modelling (Joyce et al. 2010), discharge of deep groundwater will almost exclusively take place at low points in the landscape, i.e. in lakes, wetlands, streams and in near-shore areas of the sea. Thus the focus in the description of landscape development is on these areas where accumulation of potentially released radionuclides may occur.

Periodically, the shoreline displacement has strongly affected the Forsmark area, both before and after the latest deglaciation. At the time of the latest deglaciation around 8800 BC, the area was covered by approximately 150 m of glacio-lacustrine water and the nearest shoreline was situated some 100 km west of Forsmark, see Chapter 3 in Söderbäck (2008). Thereafter, the isostatic rebound has been continuous and slowly declining. The rate of rebound in Forsmark has decreased from ca 3.5 m/100 years directly after the deglaciation to a present rate of ca 0.6 m/100 years, and it is predicted to decrease further to become insignificant around 30 000 AD (see Figure 10-106).

The present regression of the shoreline will continuously bring new areas of the sea floor above the wave base. This will expose sediments to wave erosion and resuspended fine-grained particles will be transported out of the area into the Bothnian Sea, or re-settle on deeper bottoms within the study area (Brydsten and Strömberg 2010). Accordingly, the relocation of sediments may have important implications for transport and accumulation of radionuclides potentially originating from a future repository.

When new areas of the present seafloor are raised above the sea level, weathering of the calcium-rich Quaternary deposits is initiated. Most of the easily weathered calcite in the upper regolith will be dissolved and washed out within a period of some thousands of years (Tröjbom and Grolander 2010). This means that the strong influence of the calcium-rich deposits on the terrestrial and limnic ecosystems will be reduced over time. For instance, the oligotrophic hardwater lakes that are characteristic for the coastal area in Forsmark will likely be transformed to more dystrophic (low pH, brown-water) conditions within some thousand years after isolation from the sea (see Andersson 2010).

The shoreline displacement will also cause a continuing and predictable change in the abiotic environment, e.g. in water depth and nutrient availability. It is therefore appropriate to describe the origin and succession of major ecosystem types in relation to shoreline displacement. One example of this is the isolation of a sea bay into a lake, followed by the ontogeny of the lake and its development into a wetland. As the lake is ageing, sediment and organic matter are accumulating due to sedimentation and vegetation growth, and eventually all lakes are transformed to wetlands. The rate of sedimentation decreases with decreasing lake volume (Brydsten 2004), whereas the colonisation of littoral plants requires shallow water (< 2 metres). Thus, the rate of lake infilling is mainly dependent on lake depth, area and volume (Brydsten and Strömberg 2010). Mires may also develop on newly emerged land without a preceding lake stage (Kellner 2003).

The initial 1 000 years after closure of the repository

The vertical component of the shoreline displacement is projected to be around 4 m during the next 1 000 years, assuming no change in the rate of sea level rise (2.6 mm/year) and an almost constant isostatic rebound rate of 6.7 mm/year (see the **Climate report**). Based on this scenario, a likely development of the site is described below.

The shoreline displacement results in a horizontal transfer of the coastline to a location ca 1 km east of the repository at 3000 AD, which means that parts of the present seafloor becomes land. Some of the coastal bays becomes isolated and transformed to lakes (see Figure 10-11). The ongoing shoreline regression causes a succession pattern, where the shore vegetation, dominated by herbs, sedges and grasses, are replaced by forest vegetation. The types of dominating vegetation communities during

this succession are mainly determined by the composition of the underlying Quaternary deposits, which, in turn, depends on the extent of previous wave exposure of the shallow coast.

The newly isolated lakes are occasionally affected by flooding with brackish water from the Bothnian Sea during periods of high sea water levels, in the same way that can be seen in low-elevation present-day lakes in the area.

All present-day lakes in the Forsmark area are small and shallow. This means that large parts of the lakes are transformed to wetlands during the coming 1 000 years (Brydsten and Strömgren 2010). For example, two of the smaller lakes, Lake Puttan and Norra Bassängen, situated close to the planned repository, are almost completely transformed to wetlands, whereas a minor part of the larger Lake Bolundsfjärden remains as open water in the year 3000 AD (see Appendix C for a map of the Forsmark area today).

The human-made, deep inlet canal for cooling water to the nuclear power plants, situated immediately north of the planned repository, is isolated from the sea around 2500 AD (Lindborg 2010). If it is left unaltered after decommissioning of the power plants, it probably remains as a lake far beyond the initial 1 000 years. Moreover, two new, relatively large lakes situated north of the repository and west of the present “Biotest basin”, are isolated from the sea in the latter part of the period (see Figure 10-11).

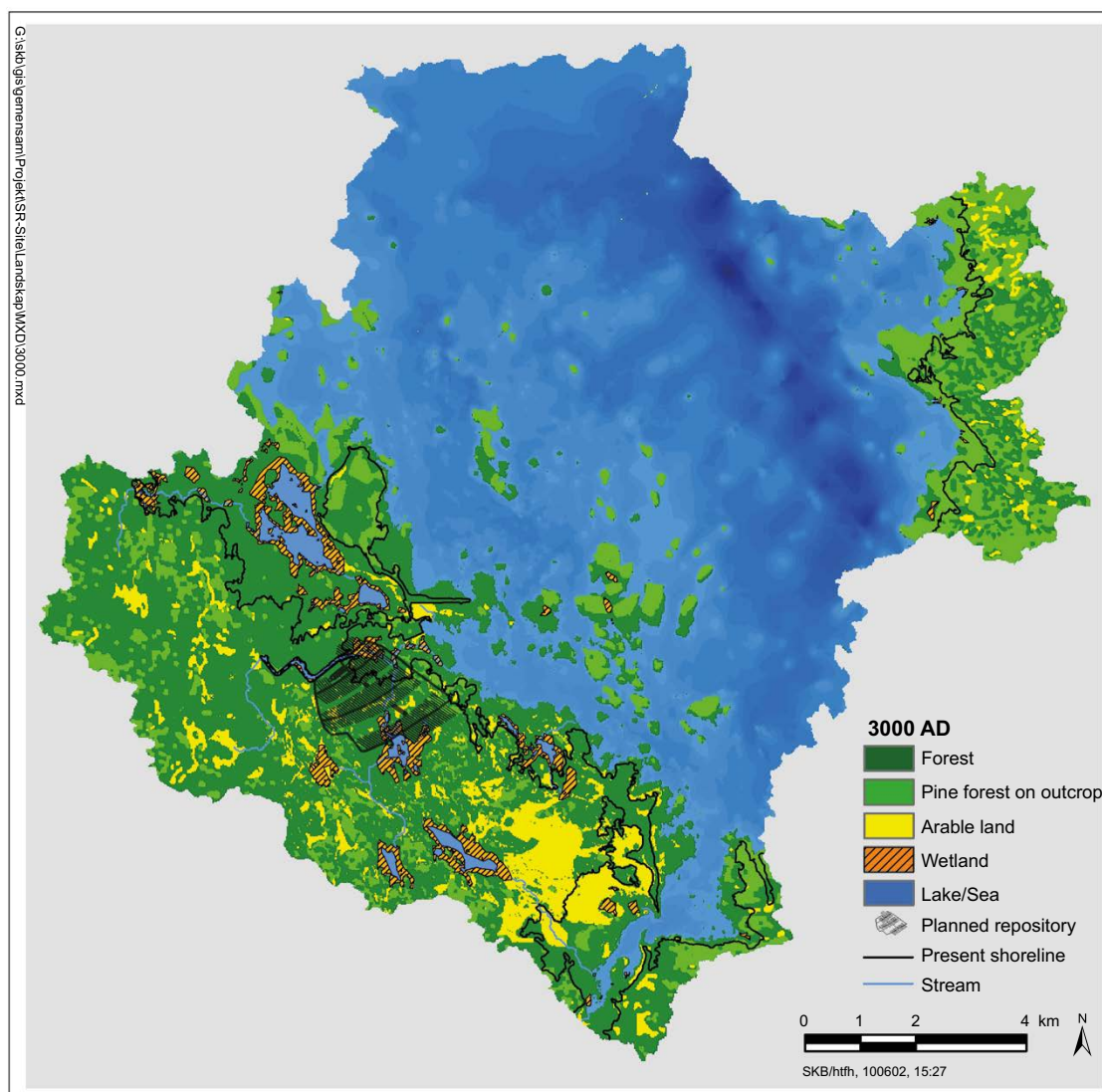


Figure 10-11. Modelled distribution of vegetation and land use in Forsmark at 3000 AD. All areas that potentially can be cultivated are represented on the map as arable land (see Chapter 4 in Lindborg 2010). The present shoreline is marked as a black line and darker shades of blue represent deeper sea.

As the seafloor close to the coast gets shallower, erosion occurs on wave-exposed sea-floor. Some sheltered areas inside a developing, denser archipelago show accumulation for a short period (Brydsten 2009). The circulation in Öregrundsgrepen remains essentially the same as today (Karlsson et al. 2010). The salinity of the Bothnian Sea decreases slightly to around 4.8 ‰ during the initial 1 000 years, assuming unaltered runoff to the Bothnian Sea (Gustafsson 2004).

The potential for sustainable human exploitation of food resources in the area over the coming 1 000 years does differ much from the situation today. Only minor parts of the newly formed land have the potential for cultivation due to the boulder-rich sediments in the former sea and lake areas, but also due to problems with draining the low-elevation new areas (Lindborg 2010). New areas are, however, available for grazing by livestock.

The potential water supply for humans is fairly unaltered during this period. Lakes existing in the area today, e.g. Bolundsfjärden and Puttan, contain bad-tasting water due to fringing mires and occasionally high salinity. The deep canal north of the repository has potential as a freshwater reservoir when the salinity decreases, and also the stream through Bolundsfjärden may potentially be used for freshwater supply. New wells may be drilled in the bedrock or dug in the regolith in the area which is land today, whereas the new land is too young for wells if current practises are sustained (Kautsky 2001). However, the water quality of drilled wells in this area is poor and few wells are today used for drinking water (Ludvigsson 2002).

In summary, the biosphere at the site during the next 1 000 years is here assumed to be quite similar to the present situation. The most important changes are the natural infilling of lakes and a slight withdrawal of the sea with its effects on the near-shore areas and the shallow coastal basins.

Biosphere development after 1 000 years until the end of the initial period of a temperate domain at Forsmark

According to the PSAR reference glacial cycle, see Section 10.4.1, temperate climate conditions persists in Forsmark until 9400 AD. During this period, the regressive shoreline displacement continues, but at a gradually declining rate (Lindborg 2010) (see further Section 10.4.1). Initially, the coastline is subject to a horizontal transfer of approximately 1 km per 1 000 years. This strongly influences the landscape, especially during the first part of the period, and eventually results in a situation where the planned repository has an inland rather than a coastal setting (see Figure 10-12).

The strait at Öregrund, south of the modelled area, is cut off about 3000 AD, and Öregrundsgrepen turns into a bay. This affects the water circulation, and, due to the continued narrowing of the bay, the water turnover is further restricted. However, at the beginning of the period it is not longer than a couple of weeks, except for minor sub-basins which are near isolation (Karlsson et al. 2010, Engqvist and Andrejev 2000). During the period from 3000 to 5000 AD, a semi-enclosed archipelago develops northeast of the repository. Around 5000 AD, many straits in this archipelago are closed and a number of lakes are isolated from the sea.

At 5000 AD, the coastline has withdrawn ca 5 km from the repository. A small stream drains the area above the repository, and some small and shallow lakes are situated along the stream. This small stream joins a large stream in the south-east at about 5000 AD. This large stream consists of the merged Forsmarksån and Olandsån, draining a large part of Northern Uppland (drainage area 1.3×10^3 km²). During the period from 3000 AD to 10 000 AD, the Öregrundsgrepen bay gradually shrinks to finally form a short and narrow bay along the island of Gräsö (Figure 10-12).

In the modelled area, a large number of lakes are isolated from the sea during the period from 3000 AD to 10 000 AD. Most of the new lakes are small and shallow, and are infilled and transformed into mires within a period of 2 000 to 6 000 years (Brydsten and Strömngren 2010). Around 10 000 AD, almost all lakes in the area have been infilled and only some initially relatively large and deep lakes near Gräsö island are expected to remain (Figure 10-12).

The salinity of the sea continuously decreases due to the isostatic rebound of the shallow sills at Åland between the Bothnian Sea and the Baltic Proper. Around 6000 AD, the salinity have decreased to 3–4 ‰, which means that an ecosystem similar to that in the Northern Kvarn today, with lower abundance of marine species and higher of freshwater species, have developed.

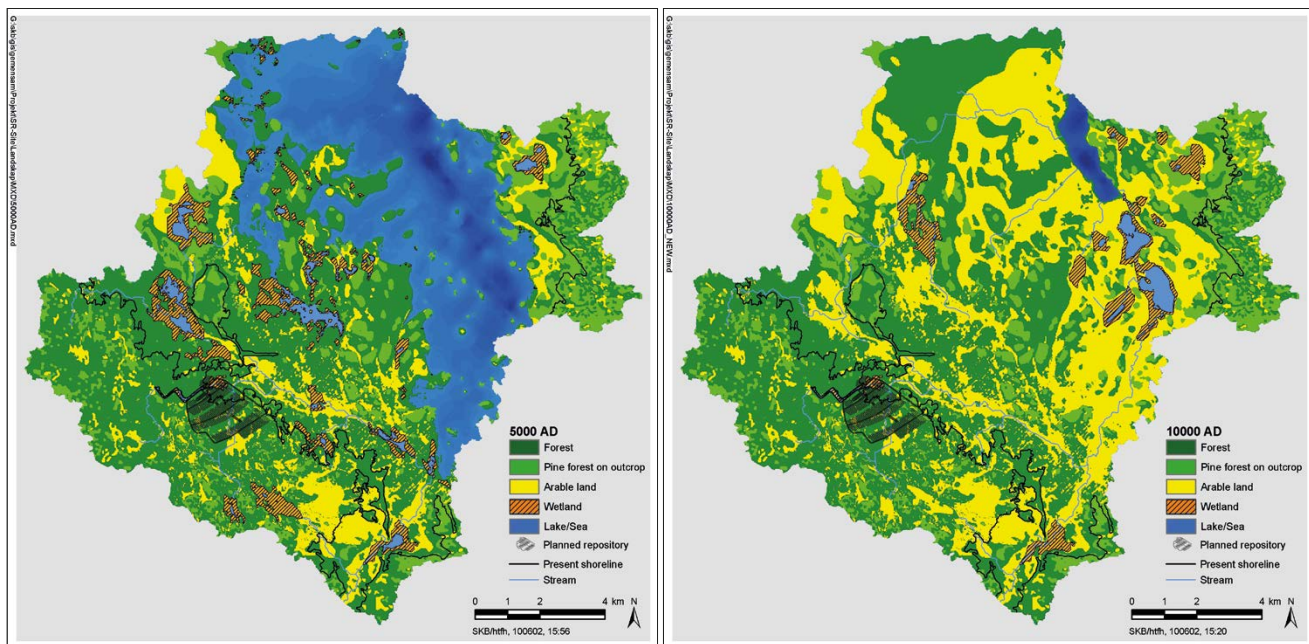


Figure 10-12. Modelled distribution of vegetation and land use in Forsmark at 5000 AD and at 10000 AD. All areas that potentially can be cultivated are represented on the map as arable land (see Chapter 4 in Lindborg 2010). The present shoreline is marked as a black line and darker shades of blue represent deeper sea.

According to Brydsten (2009), accumulation of sediments may occur both on bottoms at large water depths and on shallow bottoms that are sheltered from wave exposure inside a belt of the skerries. Erosion occurs mainly on shallow bottoms exposed to waves. Transport bottoms can be found in all places between these two extremes, i.e. at intermediate depth with moderate wave exposure. This means that the seafloor in the model area will show a characteristic evolution over time, beginning with a period of accumulation due to large water depth early after deglaciation. Then comes a period with transport, after which erosion dominates when the water depth decrease even more. Finally, transport and accumulation may occur in sheltered locations during a short period before the sea bottom becomes land. This means that there are very limited parts of the model area that will show continuous accumulation of sediments throughout the whole marine period. The small areas that potentially may show continuous accumulation since the latest deglaciation are situated in the deepest parts of Öregrundsgrepen (Brydsten and Strömberg 2010).

Much of the newly formed land are unsuitable for farming due to boulder- and stone-rich deposits (see Lindborg 2010), but there are large areas in central Öregrundsgrepen with fine-grained sediments that can be cultivated. Also patches of organic soils on previous lakes/mires may be cultivated, but presumably these soils can be sustainably utilised only for limited periods since compression and oxidation of the organic material lowers the ground surface and cause problems with the draining (see Lindborg 2010).

The food productivity in agricultural areas is several hundred times higher than that in aquatic or non-cultivated terrestrial areas (Andersson 2010, Aquilonius 2010, Löfgren 2010). Since the proportion of land that it is possible to cultivate increases as new land areas are formed, this means that the potential food productivity in the total modelled area is increasing during the period. However, the number of people that potentially can be sustained by food produced within the Forsmark area is strongly dependent on the degree to which land is used for farming.

The availability of freshwater for human supply gradually increases. As mentioned above, new lakes and streams form, but most of the lakes are short-lived due to their shallowness. New groundwater, potentially useful as drinking water, is available when the shoreline moves eastwards. Among already existing geological formations, the Börstilåsen esker, situated ca 4 km southeast of the planned repository, may provide groundwater of drinking-water quality, but there are no indications in the hydrogeological modelling results that this aquifer will have contact with discharging groundwater from the repository (Joyce et al. 2010).

Identified uncertainties and their handling in the subsequent analysis

The description of the landscape development during the initial temperate period is associated with three major uncertainties:

1. The configuration of the landscape, e.g. location and size of future lakes and streams, and depth and stratigraphy of the deepest regolith layers (that are assumed to be marginally affected by landscape development).
2. The rates at which processes that influence the landscape operates, e.g. the rates of; relative sea level change, wave erosion, sedimentation and lake infilling.
3. The timing of different events, e.g. the time of lake isolation and the time for completion of lake ingrowth.

Uncertainties in the development of the landscape configuration in Forsmark are not handled explicitly in the modelling. Thus, the modelled landscape development should be seen as an example of a possible future, based on understanding of present-day geometries and an expected shoreline displacement. The topography is not expected to vary significantly during the period, and the main uncertainties in the future landscape configuration are associated with the locations of thresholds for future lakes.

The landscape can be subdivided into drainage areas, delimited by water divides. In the SR-Site assessment, low-lying areas that, according to the hydrogeological modelling (Joyce et al. 2010), potentially will be affected by discharge of deep groundwater, are identified and described over time (see further the discussion of biosphere objects in Section 13.2). Each biosphere object will typically go through a similar succession, from being part of the open sea, over a sea bay phase, to a lake which eventually will transform to a wetland (or agricultural land). Thus, the biosphere objects encompass considerable variation, both in size (the area range is almost two orders of magnitude) and in the timing and rate of succession events.

Uncertainties associated with the depth and development of regolith layers, the infilling of lakes, the future surface hydrology and the properties of species and communities that may inhabit the future landscape, are handled either as parameter uncertainties or in systematic studies of alternative scenarios in the modelling of radionuclide transport and accumulation in the surface system (see Section 13.2, and Sections 5.3.1 and 5.3.2 in Avila et al. 2010).

The annual water balances for a suite of lakes in the area, which vary with respect to size, ontogeny and depth of underlying sediments, have been used to set reasonable boundaries on the hydrology of future lakes. In addition, natural variations of biomass and primary productivity in temperate aquatic and wetland ecosystems similar to those observed in Forsmark today (or expected to develop in the area) have been used to characterize uncertainties in the properties of communities that may inhabit the future landscape.

In the biosphere assessment, the worst case (i.e. highest risk) for each radionuclide during an interglacial period is selected from a number of biosphere objects in a dynamic landscape, covering landscape configurations from a fully submerged to an entirely terrestrial landscape. Thus, even though the exact future landscape development is difficult to predict, the systematic landscape analysis and the approach for estimating doses encompasses a broad array of future landscape configurations. Further details of the landscape modelling are given in Section 13.2.

10.3.4 Thermal evolution of the near field

Introduction

The thermal evolution of the near field is of importance as general input information to the mechanical, chemical and hydrological processes. The direct safety relevant thermal criterion concerns the buffer peak temperature, safety function indicator Buff4 (Figure 10-2) that requires that this temperature does not exceed 100 °C, chosen pessimistically in order to avoid, with a margin of safety, mineral transformations of the buffer.

The thermal evolution of the repository depends on the thermal properties of the rock and the initial temperature at the site being considered, on the repository layout, i.e. canister spacing and tunnel spacing, and the canister power. For the thermal evolution in the interior of the deposition holes the

properties of the bentonite buffer and of possible air-filled gaps are additional parameters. These properties depend strongly on the water supply, i.e. on the degree of saturation and may differ from one deposition hole to another depending on the local hydraulic conditions.

The peak buffer temperature occurs some 5-15 years after deposition. At this time, approximately 50 % of the local temperature increase is caused by the heat from the canister itself and 50 % by the heat contribution from all the other canisters. This means that the local rock heat transport properties are particularly important to the peak temperature for the individual canisters and that, therefore, the low tail of the conductivity distribution, the spatial variability and the scale of variation are important for the dimensioning issue.

The SR-Site assessment of the thermal evolution is based on dimensioning guidelines and calculation schemes established by Hökmark et al. (2009) and on results in the Site engineering report (SKB 2009c) regarding layout D2 for the Forsmark site obtained applying those guidelines as described in the **Underground openings construction report**, see also Section 5.2.2. The current layout is not exactly the same as the D2 layout. This does, however, not affect the deposition areas and therefore the SR-Site analysis is valid also for the PSAR.

As far as demonstrating that the 100 °C safety assessment requirement is met for all canisters, the numerical calculations in the Site engineering report (SKB 2009c) are adequate and sufficient. These calculations do however concern only the first 20 years after deposition and apply only to canisters deposited in rock volumes dominated by low thermal conductivity rocks. They cannot be used to estimate the number of canisters that actually will have peak temperatures close to the design threshold. It should be noted that the majority of the canisters will be deposited in rock with properties approximately equal to the domain mean values and consequently have lower peak temperatures. The dimensioning calculations do not capture the overall large-scale and long-time thermal evolution of the repository host rock. To account for this additional thermal assessments have been made and reported in detail by Hökmark et al. (2010, Chapter 5), using data from the **Data report**, Section 6.2.

Distribution of peak buffer temperatures

An estimate of the distribution of peak buffer temperatures in *both dry and wet* deposition holes can be made by use of an analytical solution (Hökmark et al. 2009) and the distributions of thermal conductivity in each rock domain as provided by the **Data report**, Section 6.2.

In dry deposition holes the maximum buffer temperature is found at the top of the canister where the bentonite is in direct contact with the copper surface, see Figure 10-13 (left). Note that the hottest point on the canister surface is located at canister mid-height. In wet deposition holes, the air-filled gap between the canister and bentonite blocks will be closed at the time of the peak temperature, and the bentonite will also be in direct thermal contact with the copper shell at points on the vertical canister surface. In this case the maximum buffer temperature will coincide with the hottest point on the canister surface, i.e. at mid-height, see Figure 10-13 (right).

The analytical model does not take spatial variations of the thermal properties into account, i.e. it is assumed that the thermal properties are uniform everywhere. Therefore, the peak buffer temperatures calculated using thermal conductivity values from the low end of the distribution are overestimated, whereas the corresponding temperatures at the high end of the distribution are underestimated. A temperature correction term, T_{corr} , that accounts for the variability of the thermal properties is therefore added. It should be noted that the temperature correction is an approximate way of accounting for the inhomogeneity in rock thermal properties. The method was, however, compared to numerical analyses modelling the spatial variability and the correction was found to forecast the spacing values finally established in the Site engineering report (SKB 2009c) with good accuracy.

Figure 10-14 shows the peak temperature distribution using the canister spacing in the layout. There are two cases: with and without the temperature correction above. Without the correction there are temperature over- and underestimates, for canisters associated with the low- and high conductivity parts of the distributions, respectively.

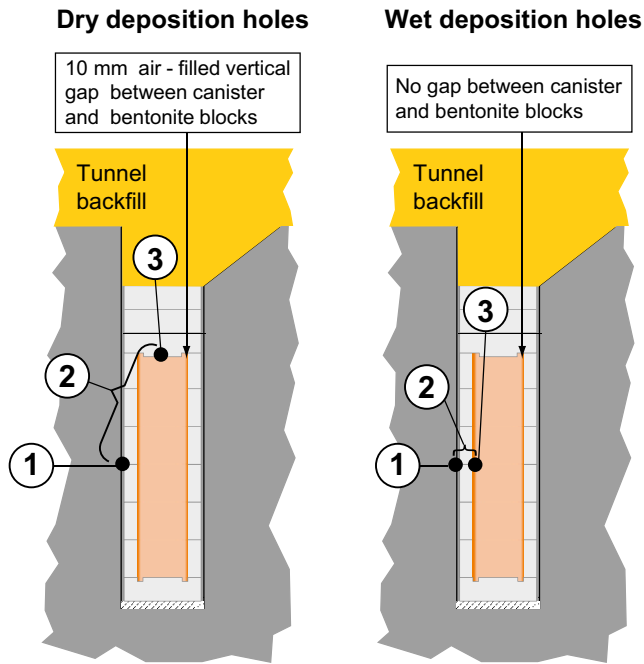


Figure 10-13. Rock wall temperature (1), temperature drop across bentonite (2), maximum bentonite temperature (3) located at the top of the canister in dry deposition holes and at canister mid-height in wet deposition holes. Modified from Hökmark et al. (2009).

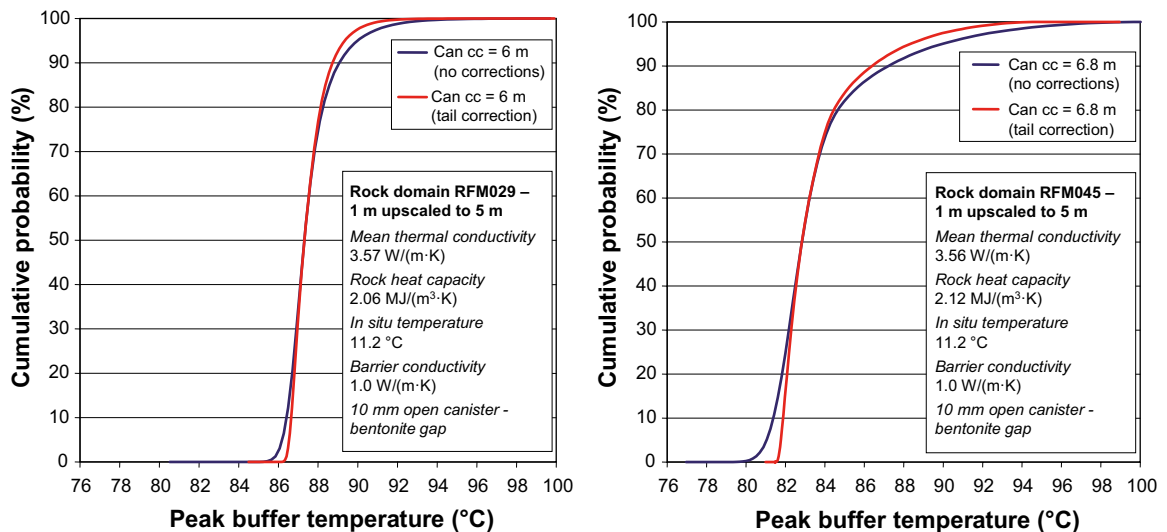


Figure 10-14. Distribution of buffer peak temperature in rock domains RFM029 (left) and RFM045 (right), with and without correction for spatial variability. Modified from Hökmark et al. (2010, Figure 5-6).

On average, less than one canister position, out of 6 000 canister positions, would have a peak buffer temperature larger than 95 °C meaning that the design requirement would be satisfied with a margin of 5 °C, based on this analysis. A very large majority of the canisters, about 98 %, will have a margin of 10 °C or more. Furthermore the peak temperatures are overestimated because of the following considerations.

- All canisters are assumed to be deposited with the nominal canister spacing everywhere, whereas some deposition holes in reality will be discarded. Canisters neighbouring rejected positions will have lower temperatures.
- All canisters are assumed to be deposited in the central parts of the deposition areas while in reality about 1 000 canisters will be deposited close enough to the tunnel ends to get reduced peak temperatures.

- All canisters are assumed to be completely dry with a 10 mm air-filled gap between canister and bentonite, while in reality there will be a variation in the degree of saturation. A fraction of the holes will be sufficiently close to saturation that the wet hole model rather than the dry hole model applies, Figure 10-13. This will reduce the peak temperatures.

Importance of deposition sequence

In assessing the peak temperature it is assumed that all canisters are deposited simultaneously. Analytical temperature calculations by Hökmark et al. (2009) show that if the canisters are deposited in an orderly fashion (i.e. panel by panel) at a rate of 2 or 4 days per canister, the increase in temperature at the time of peak buffer temperature is less than 0.2 °C, and this approximation is justified. However, it is possible to envisage deposition sequences, e.g. when a canister is deposited centrally in a panel where all other positions were deposited several years before, where the resulting temperature would be much higher. Such situations will, however, always be avoided, but this observation highlights the need for careful thermal management of the disposal sequence.

Thermal evolution

Hökmark et al. (2010, Chapter 5) numerically assess the thermal evolution of the repository both in the large and near-field scale. In the large-scale, covering the entire repository with surrounding rock, all the canisters are represented by point sources of heat.

Since no information can be given regarding how the loss of canister positions is distributed across the repository region, Hökmark et al. (2010) uniformly removed every 8th canister position across the repository in order to achieve the approximate thermal load on a large scale. Contour plots of the calculated mean rock temperature increase at repository level after 50 and 1 000 years are shown in Figure 10-15 assuming simultaneous deposition. Corresponding contour plots of the temperature increase valid at other times with and without account being taken of the deposition sequence are provided in Hökmark et al. (2010).

In the near-field temperature calculations, i.e. the temperature at the wall of a deposition hole at canister mid-height, surrounding canisters are represented in the same way as in the large-scale calculations but the local canister and its six nearest neighbours (in the same tunnel segment) are replaced by more detailed representations of canisters. Also all available canister positions are assumed to be filled, which consequently may overestimate the temperature.

Figure 10-16 shows the resulting rock wall and buffer temperatures in two different positions, considering both dry and wet deposition holes. The peak buffer temperature occurs approximately 5–15 years after deposition (Hökmark et al. 2010) and the peak rock wall temperature occurs approximately 50 years after deposition.

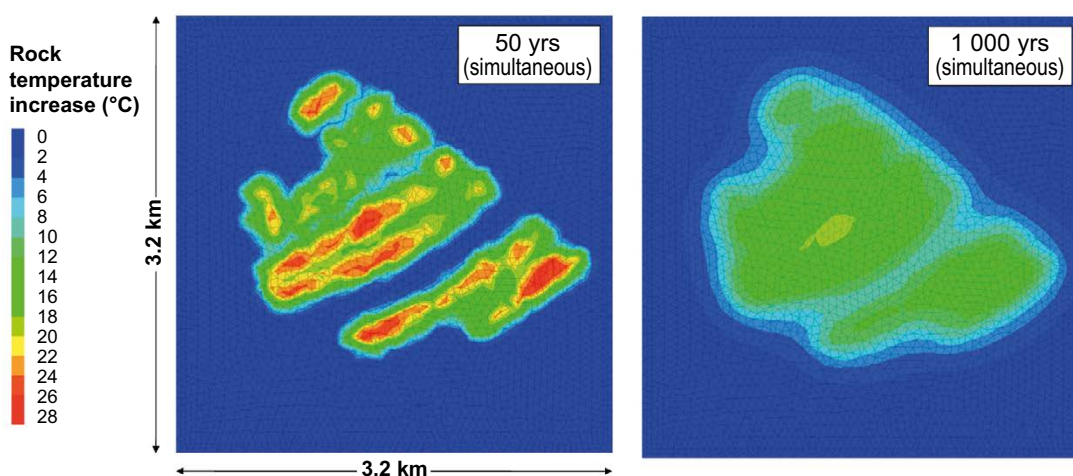


Figure 10-15. Contour plots of the rock temperature increase at repository level (460 m) at Forsmark. Point sources representing canisters are placed 5 m below. "Simultaneous" implies that all canisters are assumed to be emplaced simultaneously. From Hökmark et al. (2010, Figure 5-12).

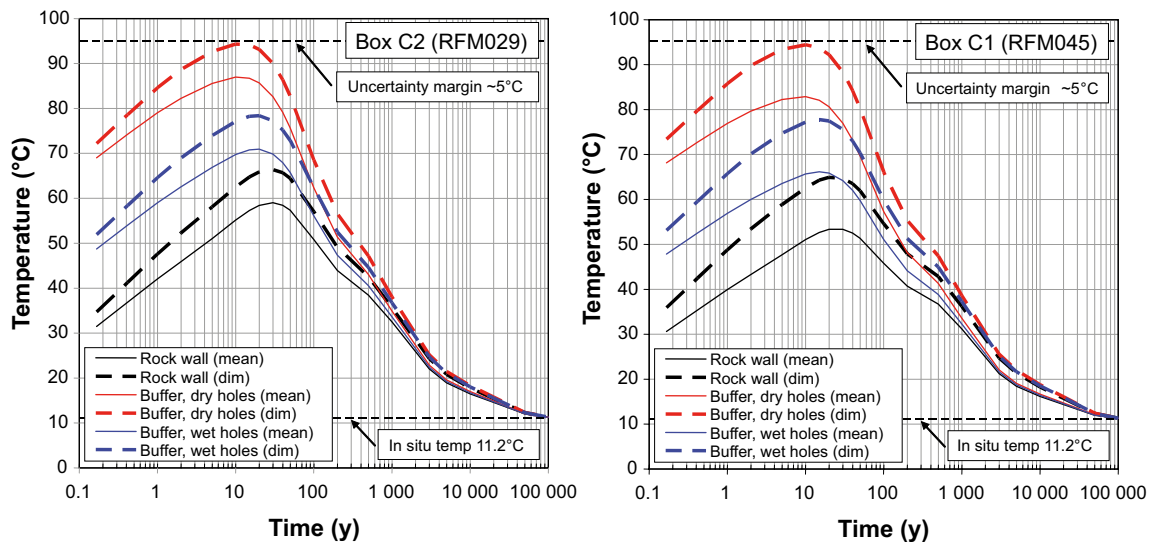


Figure 10-16. Rock wall temperature at canister mid-height and peak buffer temperature, considering mean and dimensioning (“worst case”) thermal conductivity, both dry deposition and wet deposition holes for central locations in rock domain RFM029 (left) and in rock domain RFM045 (right). Note that the shapes of the peak temperature distributions are direct reflections of the shapes of the conductivity distributions, which are different in the two domains. From Hökmark et al. (2010, Figure 5-15).

Identified uncertainties and their handling in the subsequent analysis

The discussion above can be used to draw a set of conclusions regarding the uncertainties and their subsequent handling in the PSAR analyses.

- For the *thermal evolution during the initial temperate period* there is an adequate margin to the peak temperature criterion for the buffer, even when the spatial variability of the rock thermal properties is taken into account and with other data essential for computing the result chosen pessimistically. However, the thermal evolution is input to other assessments of the reference evolution. Only a representative thermal evolution without uncertainty is propagated for use in these assessments since the uncertainty in the thermal evolution is sufficiently small that it would not impact these other parts of the assessment.
- It is possible to envisage *deposition sequences*, e.g. when a canister is deposited centrally in a panel where nearby positions were deposited several years before, where the resulting temperature in the buffer would exceed the maximum allowed. Such situations will, however, always be avoided, but this observation highlights the need for careful thermal management of the disposal *sequence*. This will be further considered in providing feedback to current technical design requirements, see Section 15.5.

10.3.5 Mechanical evolution of the rock

After deposition, backfilling and closure, the mechanical evolution, e.g. rock stress changes, rock expansion/compression and fracture aperture reductions/expansions, is controlled by the heat generation from the spent fuel, by the swelling pressure of the bentonite buffer in the deposition holes, and by the gradual restoration of the groundwater pressure, which will locally reduce the effective stress and the fracture shear strength. The time scale for the thermal effects can be predicted in detail as demonstrated in Section 10.3.4 and numerous other analyses of the thermal development of the repository. The time scale for the development of the swelling pressure depends on the local permeability conditions around the individual deposition hole and on the general repository-scale restoration of the groundwater pressure.

Furthermore, as further explained in the **Geosphere process report**, Section 4.1, the Baltic Shield is continuously subject to a horizontal compression or “ridge push” due to seafloor spreading from the Mid-Atlantic Ridge at the western tectonic plate boundary which initiated approximately 15 million years ago (Muir Wood 1993). The compression is an important factor for the development of the state

of stress currently prevailing in the Swedish bedrock (see Chapter 4) where the maximum principal stress tends to be horizontal and oriented NW-SE, i.e. in the ridge-push direction.

The following mechanical processes related to the initial temperate period after repository closure, could have potential safety implications.

- Reactivation of fractures in the near field due to thermal load, including fracture aperture reductions due to temperature increase expanding the intact rock, that could affect the mechanical stability (safety function R3bc, see Figure 10-2) and the fracture transmissivity and thus the transport resistance in the near-field rock (safety functions R2ab).
- Reactivation of fractures in the far field that could affect fracture transmissivity and thus the transport resistance (safety function R2a).
- Reactivation due to the crustal strain resulting from the mid-Atlantic ridge push that could affect the mechanical stability of the deposition holes (safety function R3bc).
- Fracturing of the rock that could affect the deposition hole geometry (safety function Buff1) and migration between buffer and rock (related to safety function R2a).
- Potential for creep deformation that could affect deposition hole geometry (related to safety functions Buff3 and Buff6). Here the term creep is also used for cases in which the mechanical load is not constant over time, i.e. when the shear strain successively relaxes the stresses.

These issues are assessed in the following subsections.

Modelling approach

Most of the above issues are assessed by integrated numerical modelling (Hökmark et al. 2010) applying the distinct element code 3DEC (3 Dimensional Distinct Element Code) (Itasca 2007) on a large scale and on near-field models. This modelling produces stress changes resulting from the thermal (and later glacial) loads. These stress changes, in turn, are used to assess potential changes in fracture or fracture zone transmissivity by assuming certain relationships between stress change and transmissivity.

The large-scale model is represented by rectangular blocks with dimensions $8 \times 7.4 \times \sim 3$ km, see Figure 10-17. Average values of the thermo-mechanical properties judged to be relevant in the entire modelled domain are used to represent the properties of the rock mass as further specified in the **Data report**, Section 6.4. The heat sources are positioned in the models according to Layout D2, where the loss of canister positions is assumed to be uniformly distributed across the repository region. Boundary conditions for the subsequent near-field modelling are obtained from the displacements on pre-defined cut-planes representing the near-field model boundaries and are evaluated as the expansion/contraction relative to the centre of the near-field model as a function of time.

Two types of and sizes of near-field models are used:

- One tunnel segment with seven heat generating canisters (for spalling analyses), but with only three of the deposition holes explicitly included. Model dimensions are 40 m (across tunnels) and 50 m (vertically), see Figure 10-18.
- Five tunnel segments each with 33 potential canister positions (shearing, normal stress variations and transmissivity changes of fractures). None of the deposition holes are explicitly included. Similarly to the approach taken by Hökmark et al. (2006) and Fälth and Hökmark (2007) the fracture system is stylised considering a model in which the fracture orientations are based on site-data in fracture domain FFM01 (Fox et al. 2007) and a model with one fracture orientated such that the potential for shear failure is large, see Figure 10-19. Model dimensions are 200 m (across tunnels) and 200 m (vertically).

Based on the transmissivity data for fracture domain FFM01 at Forsmark (Follin et al. 2007b) and fracture normal stiffness data given in the **Data report**, Hökmark et al. (2010) apply two different models for the relation between stress and transmissivity changes, see Figure 10-20. As further discussed in the **Data report**, the strength of the hydromechanical coupling is highly uncertain, but it is judged that the range of these models captures, or at least overestimates, this coupling.

Hökmark et al. (2010) also assessed, using analytical solutions of the thermo-mechanical evolution of an elastic medium subject to time dependant thermal loads, whether the calculated stresses depend on the deposition sequence. As with the analyses for the temperatures they show that the assumption that all canisters are deposited simultaneously produces very similar stresses to those produced in the models where the impact of the deposition sequence is considered, unless very specific sequences are used (for instance starting and finishing the deposition in neighbouring tunnels or very nearby deposition areas). Given a proposed deposition sequence, it can easily be checked (e.g. by use of the analytical solution) whether or not the approximation of simultaneous deposition still gives valid results.

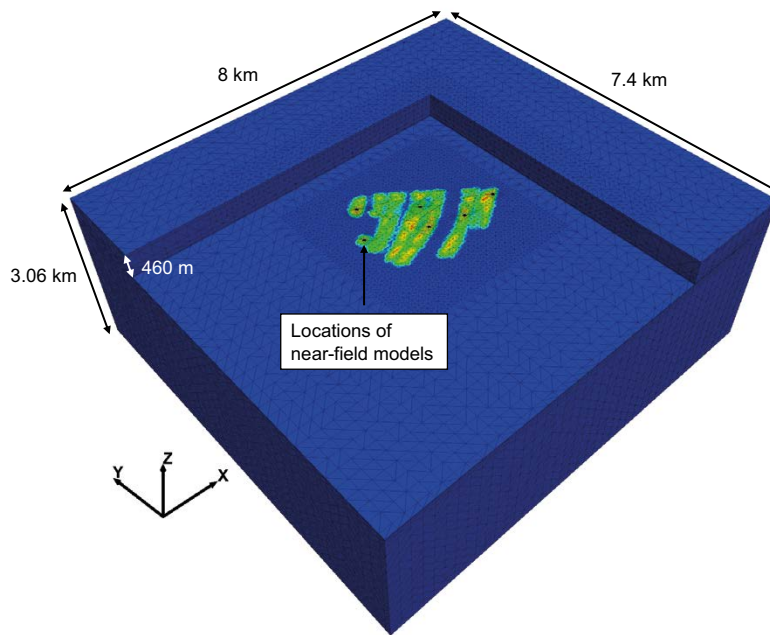


Figure 10-17. Outline of Forsmark large-scale 3DEC model. Note that parts of the model are hidden from view. (Figure 6-13 in Hökmark et al. 2010).

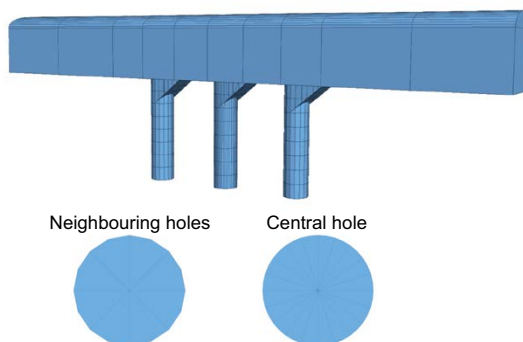
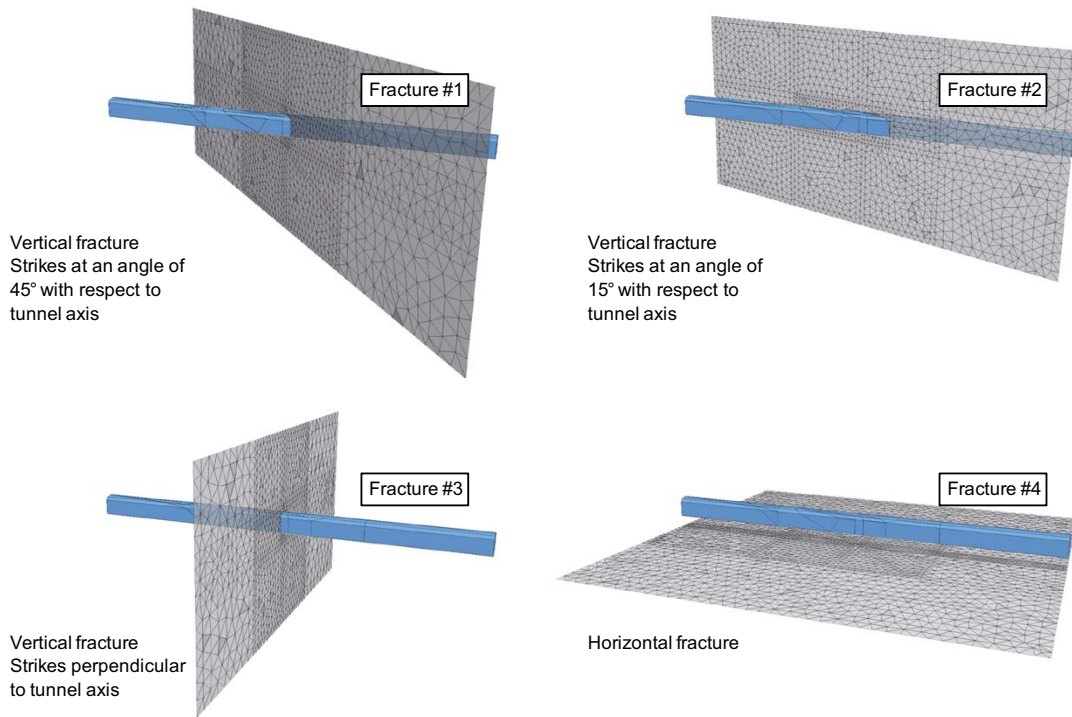


Figure 10-18. The detailed near-field model representation of three central deposition holes. From Hökmark et al. (2010).

Model 1a



Model 2a

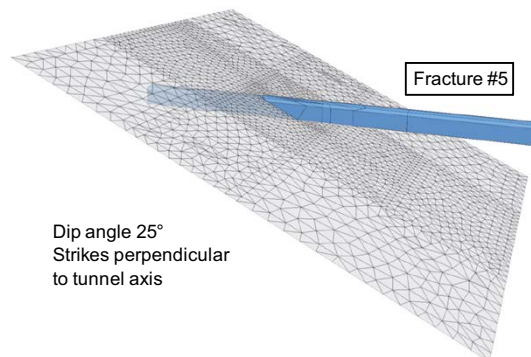


Figure 10-19. Fracture configurations in the medium size near-field model. All 5 orientations are based on site data, but the orientation of fracture 5 is selected in order to maximize shear failure. The dip direction of fracture 5 is SE and the tunnel trends NW-SE i.e. parallel to the direction of the present day maximum principal stress which is linked to the Atlantic ridge push. From Hökmark et al. (2010, Figure 8-6).

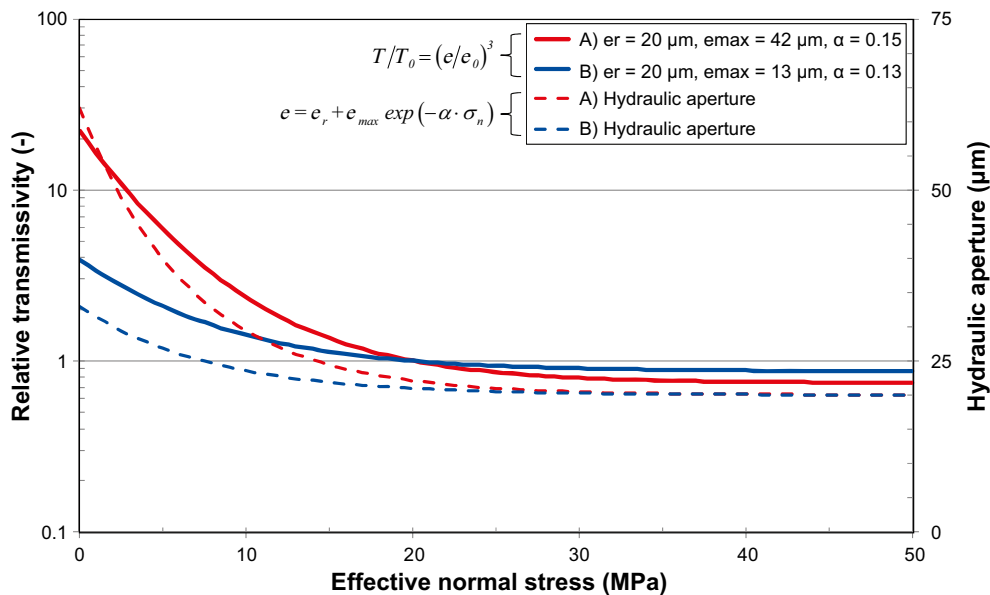


Figure 10-20. The two stress-transmissivity models (A and B) and related stress-hydraulic aperture models adopted for the Forsmark site. T is transmissivity, e hydraulic aperture and σ_n normal stress. The range of these models captures, or at least overestimates, the stress coupling. From Hökmark et al. (2010, Figure 4-9).

Reactivation of fractures in the far field

A complete set of results from the numerical modelling of the impact of the thermal load is provided by Hökmark et al. (2010, Chapter 6). In the far field, the numerical modelling shows that for fractures perpendicular to the major horizontal in situ stress there are only negligible variations in relative transmissivity. For vertical fractures oriented perpendicular to the minor horizontal in situ stress and located above the repository panels, the reductions in effective normal stress in the upper 100 m of rock result in an increase in relative transmissivity by at most a factor 2.5 (model A) and 1.5 (model B). Below a depth of 200 m there are only negligible changes in relative transmissivity for both stress-transmissivity models, see Figure 10-21. Between repository panels and just outside the repository there is a decrease in vertical stress leading to transmissivity increases for sub-horizontal fractures by, at most, a factor 1.5 to 2 at the repository level, depending on which stress versus relative transmissivity curve is used, but there is no such increase inside the panels.

The large scale thermally induced horizontal stresses are aligned with the deposition geometry, i.e. oriented perpendicular and parallel to the deposition tunnels, respectively. Since the tunnels are approximately parallel to the major horizontal stress, the resulting net background stress field is approximately oriented as the *in situ* stress field such that the stability and response of differently oriented fractures can be easily deduced from the results of the large-scale thermo-mechanical models using analytical expressions. However, the analytical expression assumes fractures to be perfectly planar with uniform properties, meaning that effects of large scale undulations, local in-plane asperities and other irregularities that are not captured by the laboratory scale tests used to provide shear strength data to the model are not accounted for. The actual slip will, therefore, probably be less due to the actual fracture cohesion. The analysis, presented by Hökmark et al. (2010, Sections 7.5 and 8.4), suggests that fractures dipping approximately 27° in the direction of the major horizontal in situ stress and passing through non-heated regions appear to have the largest potential for instability. For a fracture with 150 m radius at 450 m depth, outside the deposition area, the maximum slip at the fracture centre is less than 27 mm according to the applied analytical expression. Because of the accompanying reduction of the normal stress, the transmissivity is likely to increase. The scope of that increase is, however, very uncertain. Fractures intersecting the heated deposition areas are significantly more stable. For a fracture with 150 m radius at 450 m depth, inside the deposition area, the maximum slip would be around 6–7 mm – again according to the analytical expression. The slip movement is accompanied by a normal stress increase, due to the heat load, which means that the transmissivity might decrease rather than increase. It should also be noted that the slip, and transmissivity impacts, will be much less for fractures with other orientations.

In conclusion, the transmissivity changes induced by the thermal load are judged too small to require any further consideration in the far-field hydrogeological analyses.

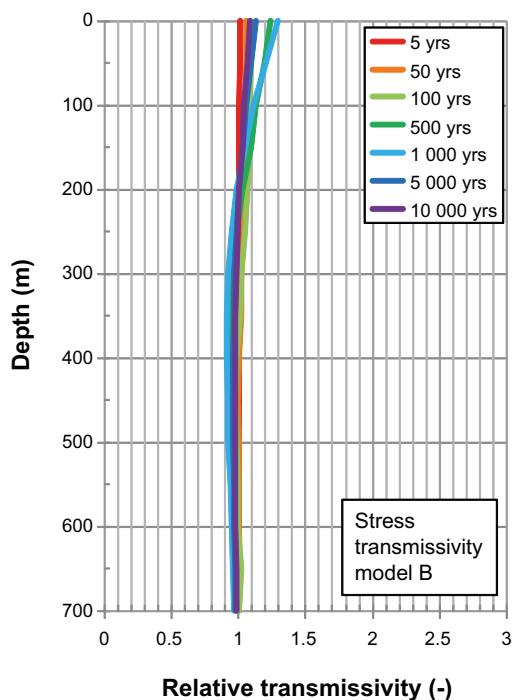
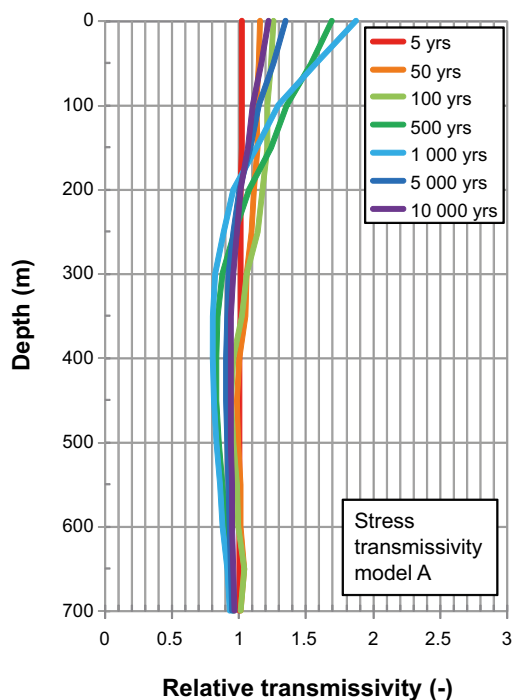
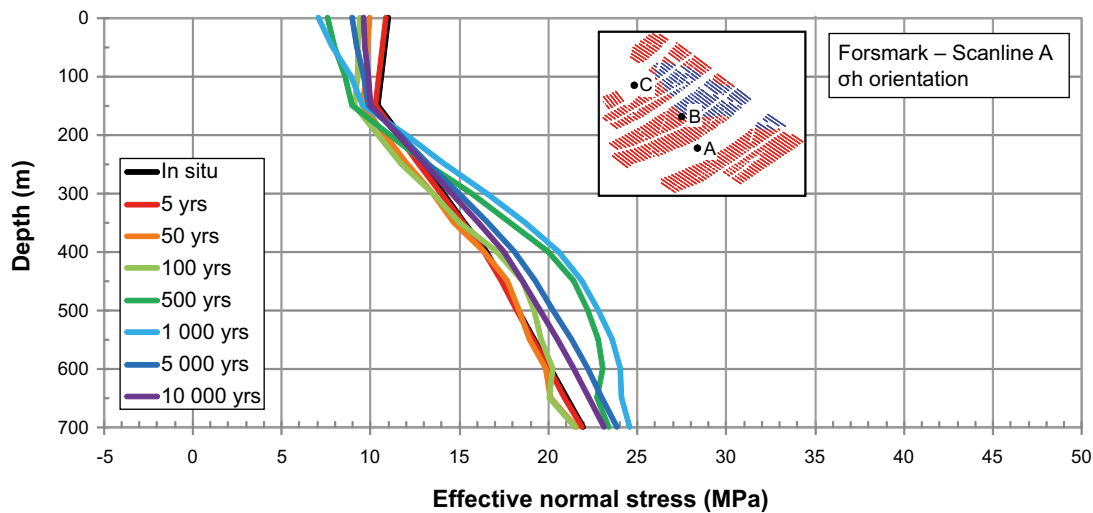


Figure 10-21. Top: Effective stress along a scan-line in the direction of σ_h . Here compression is positive. Bottom: Relative transmissivity of fractures perpendicular to σ_h . From Hökmark et al. (2010, Figure 6-21).

Reactivation of near-field fractures

Results from the intermediate scale near-field model suggest that during the thermal phase the normal stresses for the site specific fracture orientations generally increase, leading to small reductions of the transmissivity of the modelled fractures. Also, the transmissivity increase close to the tunnel resulting from the excavation, see Figure 10-5, is much reduced compared with that during the period of excavation. There may be regions very close to the openings where local transmissivity effects could be significant, for instance because of thermally induced shear displacements along fractures in very low compression. According to Hökmark et al. (2010) these effects do, however, not extend more than about a metre into the rock from the wall. As already judged for the excavation phase these impacts are too local to warrant further consideration. Transmissivity effects in the immediate surroundings of the opening peripheries are judged be adequately covered by the schematic representation of the EDZ.

In general, the shear displacements are small, apart from gently dipping fractures with unfavourable orientations with regard to shear stability. The conclusions are the same as those for the far field.

In conclusion, since the impact on fracture transmissivity during the heating phase is small, and very local to the deposition tunnel, there is no reason to assess the implications of these changes in the hydraulic modelling.

Reactivation due to tectonic compression and/or glacial isostatic adjustment

The tectonic conditions in the Baltic Shield have been stable for the past 2 million years (Muir Wood 1995). In addition to ridge push, the shield suffered shorter-term loading and unloading because of repeated glaciations and deglaciations. The potential for future seismicity during the temperate period needs thus to be handled as a part of the assessment of seismicity during the glacial cycle. This is discussed in Section 10.4.5. There, it is shown that between 9.3×10^{-6} and 2.2×10^{-5} canisters may be sheared 50 mm or more due to earthquakes within the 1 000-year time frame. In short, while the seismic activity is generally very low in Sweden, earthquakes leading to potential canister damage cannot be totally ruled out even during the initial temperate period.

Fracturing of the rock – thermally induced spalling

Even if the initial rock stress magnitudes may not be sufficient to produce spalling in deposition holes, there is still the possibility that spalling may occur later due to the additional thermal load. The potential occurrence of spalling is site and repository design specific, as it depends on the *in situ* stress, the strength of the intact rock, its thermo-mechanical properties, and on the repository layout. This is the only fracturing mechanism identified as relevant during the initial temperate period.

Hökmark et al. (2010) have revised the assessment of the potential for thermally induced spalling presented in SR-Can, using the detailed near-field model geometry that incorporates one tunnel segment with seven canisters, three of which have explicitly modelled deposition holes, see Figure 10-18. The model calculates the tangential stress at the wall of the deposition hole during the period of thermal load. This stress is compared with the spalling strength of the rock. The latter is assumed to lie somewhere between 52 and 62 % of the Uniaxial Compressive Strength (UCS) of the rock, cf. Section 6.4 in the **Data report**. The following is found, see also Figure 10-22.

- The spalling strength is likely to be reached in all deposition holes during the thermal phase even when the lower limit of the stress magnitudes and most favourable tunnel orientations are considered. Hökmark et al. (2010) also assess the major principal stress at the centre of the tunnel roof. As opposed to the stresses in the deposition hole walls, the stresses at the centre of the tunnel roof will not reach the spalling strength during the heated phase.
- For the most unfavourable stress orientation and upper limit of stress magnitudes, it is possible that the lower limit of the spalling strength (52 % of UCS) will be reached from the tunnel floor down to a depth of around 7.9 m (both values of the thermal conductivity) after 50 years. The upper limit of the spalling strength (62 % of UCS) will be reached after 50 years, from the tunnel floor to a depth of 7.3 m (mean value of the thermal conductivity) and 7.6 m (dimensioning value of the thermal conductivity), respectively.

In addition, SKB has conducted field tests at Äspö HRL (Glamheden et al. 2010) to assess the support for mitigating spalling by adding small counter pressures. However, while the project findings supports the possibility that the counter pressure exerted by bentonite pellets in the slot between buffer and rock wall may suppress the spalling, or at least keep the spalled slabs in place and by this minimize the hydraulic transmissivity of the spalled damage zone, current results are inconclusive. For the PSAR, it is judged necessary to assume that thermally induced spalling is likely to occur, and this needs to be considered when assessing the migration across the rock-buffer interface. This does not mean that efforts to handle and mitigate thermally induced spalling should not continue, since suppressing the spalling will enhance this safety function. There is plenty of evidence in the literature to show that a small amount of confining stress has a significant effect on increasing the compressive strength of a rock, but numerically strict rules for how much counter pressure is needed to suppress the spalling are lacking.

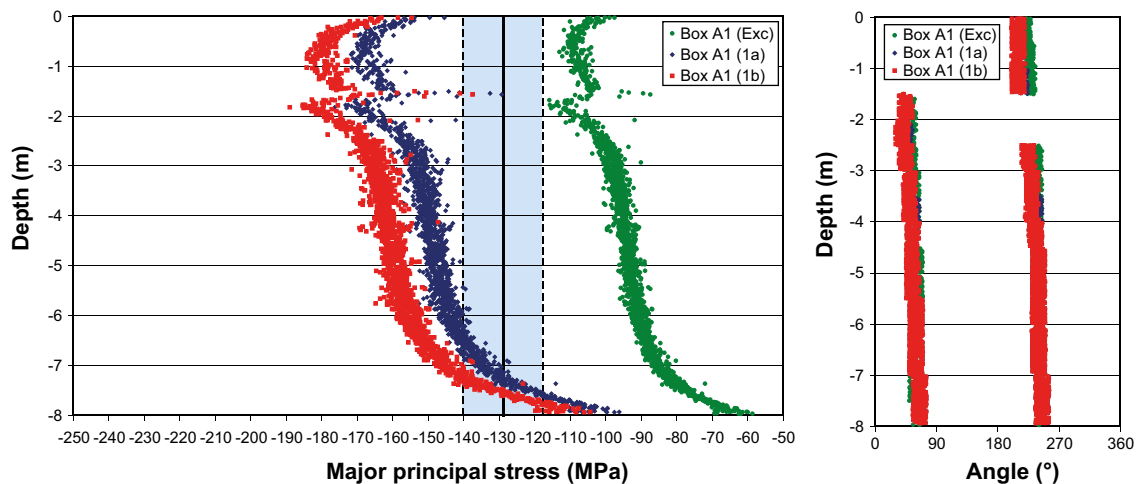


Figure 10-22. Left: Simulated maximum tangential stress after excavation (green) and 50 years (for two different thermal conductivities- red and blue) along deposition hole wall. Blue area represents spalling strength in fracture domain FFM01 (52–62 % of UCS). Right: Location and orientation of maximum stress on deposition hole perimeter. (Figure 9-8 of Hökmark et al. 2010).

Hökmark et al. (2010) also assessed whether or not the order of deposition of canisters influences the risk of spalling during the construction of a local tunnel and its deposition holes or if the deposition sequence would influence the magnitudes of the thermally induced stress concentrations. Their results show that the construction-deposition sequence approximation made in all models in their report, i.e. that all excavation work has been completed prior to deposition and that all canisters are deposited simultaneously, is valid unless very specific sequences are used (for instance excavating or depositing late, close to regions of early deposition). Given a proposed construction-deposition sequence, it will easily be checked (e.g. by use of the thermo-mechanical analytical solution demonstrated in Hökmark et al. (2010)) that these approximations hold also for that specific case.

Potential for creep – time dependent deformation

The concept of creep implies that a material has inherent time-dependent mechanical properties so that movements take place without additional loading, due to already active stresses. The consequence of extensive creep movement along fractures would be that fracture shear stresses would relax and that the stress state would tend to be less deviatoric over time. However, there is no evidence, anywhere in the world where deep mining is carried out in hard rocks that such a condition exists, i.e. substantial deviatoric stresses are recorded at all mine sites. Based on this, it was argued in SR-Can that the relative importance of creep, i.e. in comparison to movements calculated to take place in direct response to changes in mechanical load and pore pressure, are small enough that effects of creep can be neglected.

These conclusions are strongly supported by a study by Damjanac and Fairhurst (2010) assessing whether there is a lower bound to the long-term strength of rocks. The analysis demonstrates that there is always a stress threshold for confined conditions, because confinement acts to suppress the tensile stresses associated with crack growth. Furthermore, even under unconfined conditions, the internal structure and heterogeneity of the rock, with grains several orders of magnitude tougher than the interface, results in blunting of the fracture tip and arrest of the fracture, even when the fracture toughness is reduced to zero (i.e. assuming that the stress-corrosion activation energy is zero). The actual magnitude of the lower bound to the long-term strength, when the stress-corrosion activation energy is assumed to be zero, will depend on a number of parameters, including pre-existing fracture sizes, their spacing, grain size and magnitude of confining stress.

If spalling occurs and a notch forms, the stress adjustments that can occur at the notch tip may cause additional time-dependent/creep deformations. The monitoring of the unconfined open notch in the APSE Experiment showed that the majority of the new displacements occurred in the existing notch (Andersson 2007). Martin and Kaiser (1996) reported that the displacements for an unconfined spalled zone/notch in the AECL Mine-by Test Tunnel Canada were monitored for a 13 day period

and that the creep related displacements amounted to between 0.6 and 1.4 % of the total displacements measured over that period. They concluded from their field experiment that changes in the measured displacements over time generally can be attributed to changes in boundary conditions and that these time-dependent displacements occur in the unconfined damaged zone around the test tunnel. As shown by the APSE experiment a small confining stress is often sufficient to suppress spalling (Andersson 2007). When the spalled notch is confined, any time-dependent deformations are expected to be insignificant, compared with the deformations that formed the notch.

It can also be noted that the effects of fracture creep, in terms of fracture displacement under constant shear load because of time-dependent material strength properties, can be estimated using the modeling approach for fracture reactivation described in Hökmark et al. (2010). This would be the same as the effects of a slow decrease in fracture shear strength, i.e. some additional stress relaxation and a corresponding amount of additional movement. Even if the strength is reduced to zero over the entire fracture plane, only very minor fracture displacements would occur.

Creep deformation and related issues like “sub-critical crack growth” are, therefore, not further considered in the PSAR.

Identified uncertainties and their handling in the subsequent analysis

The discussion above can be used to draw a set of conclusions regarding the uncertainties and their subsequent handling in the PSAR analyses in relation to the mechanical evolution during the initial temperate period.

- *Reactivation of fractures in the near field* due to thermal load that could affect the mechanical stability and the fracture transmissivity in the near-field rock are excluded from further analysis since the calculated impacts on fracture transmissivity during the heating phase are small, and very local to the deposition tunnel.
- *Reactivation of fractures in the far field* that could affect fracture transmissivity is excluded from further analyses since the calculated transmissivity changes induced by the thermal load are judged too small to require any further consideration in the far-field hydrogeological analyses.
- *Reactivation due to tectonic compression* that could affect the mechanical stability of the deposition holes (safety function R3a) cannot be totally ruled out even during the temperate period. This is further assessed in Section 10.4.5.
- *Fracturing of the rock, i.e. thermally induced spalling*, is likely to occur but the counter pressure exerted by bentonite pellets in the slot between buffer and rock wall, may suppress the spalling, or at least keep the spalled slabs in place and minimize the hydraulic transmissivity of the spalled damage zone. A set of distinct calculation cases, assuming no spalling or spalling in all deposition holes, are propagated for further assessment. This does not mean that efforts to handle and mitigate thermally induced spalling should not continue since suppressing the spalling will enhance this safety function. The potential for spalling may also depend on the deposition sequence, but only for very specific ones. Nevertheless this may need consideration for the detailed design of deposition areas, see further Section 15.5.15.
- There is no potential for *creep deformation* that significantly could affect deposition hole geometry, allowing the exclusion of the phenomenon.

10.3.6 Hydrogeological evolution

In the PSAR, no new hydrogeological groundwater flow modelling of the site is performed. Thus, the same analyses and results as in SR-Site are re-used. However, during the review of SR-Site a number of questions for clarification and demands for additional analyses were requested by SSM. The PSAR text below has been updated with relevant parts of those responses and additional analyses. Furthermore, completely new analyses and calculations have been performed for the penetration of dilute water as reported below.

In the PSAR, the hydrogeological evolution during the temperate period after repository closure involves two distinct time intervals. The first is that for saturation of the repository once pumping of the open tunnels has stopped. The subsequent time interval deals with the evolution of the saturated

repository up to the start of the next glacial period. The actual impacts primarily depend on the permeability distribution of the bedrock (fracture network connectivity and hydraulic properties of the fractures), the repository layout and the associated permeability of the backfilled tunnels, and the prevailing initial and boundary conditions. At Forsmark, the primary hydraulic driving force for groundwater flow during the temperate period considered in the PSAR is the flushing due to precipitation; the ongoing shoreline displacement implies a continuous change in the flushing pattern. In order to assess the magnitude of these impacts, groundwater flow simulations, based on the hydrogeological models developed as part of the **Site description Forsmark**, have been performed. These models start at 8000 BC, i.e. at a time when the Forsmark area was submerged under approximately 100 m of water.

The overall objective is to assess the effects of a temperate climate on site hydrogeochemical and hydrogeological conditions in the presence of a backfilled repository, i.e. safety functions R1 and R2 in Figure 10-2. The expected effects with relevance for post-closure safety are mainly related to the composition of groundwater and the performance measures (PM) of groundwater flow at repository depth and the so-called flow-related transport properties.

Methodology

In order to meet the requirements of SR-Site, Joyce et al. (2010) adopted a methodology where a mixture of discrete media (DFN) and continuous porous media (ECPM and CPM) flow concepts using the ConnectFlow modelling tool are used in a sequence. Furthermore, due to computational constraints that arise from using large amounts of high resolution data within a large model domain, three “model scales” are used in ConnectFlow; regional scale, repository scale and site scale.

In the *regional-scale* model, variable-density pressure solutions are derived for a transient flow model based on continuous porous media concepts. The advective transport of salt is subject to a dual-porosity rock matrix diffusion (RMD) process. Between 8000 BC and 1000 AD, the repository area is submerged and for a long period covered by marine water (Littorina Sea). Between 1000 AD and 12 000 AD, terrestrial conditions prevail and the groundwater is subjected to a flushing by meteoric water. The shoreline displacement between today and 12 000 AD results in a total vertical displacement of the area of about 40 m upwards. Thus, the modelling methodology used for SR-Site is identical to that used for SDM-Site, except that the regional-scale modelling in SDM-Site halted at 2000 AD.

To exemplify and visualize the hydraulic properties of the developed model, ECPM properties calculated by upscaling the Forsmark Hydro-DFN model for cuboid blocks of fixed scale of 5 m, 20 m and 100 m have been calculated (SKB 2013a, b). The results are presented graphically in Figure 10-23 for fracture domains FFM01/06. It has to be noted that in this case the effective hydraulic conductivity is calculated for each fracture domain and depth in isolation, and so the up-scaled properties are not calculated in the structural context of the more conductive volumes above or surrounding FFM01/06 or deformation zones that can produce more conductive fractures or connected fractures protruding into FFM01/06.

In Figure 10-23, the bars compare the geometric mean horizontal hydraulic conductivity calculated by upscaling on 5, 20 and 100 m scales, and the bars show the standard deviation in log (hydraulic conductivity). The modelled values are also scaled by the percentage of active blocks to take account of the significant numbers of blocks for which flow does not percolate through the fracture network (the percentages shown on the bars). For the PSS data, the values are scaled by the number of intervals with hydraulic conductivity above the detection limit (also shown as percentages on the bars) to account for e.g. borehole intervals that were not tested on the 5m scale, because there was no flow detected over the 20 m interval spanning that interval. Horizontal hydraulic conductivity is compared with estimates from PFL and PSS data since the vertical component of hydraulic conductivity is not really measured directly in the predominantly vertical boreholes.

Both data and model values show the expected reduction in mean hydraulic conductivity for a reduced length scale, but an increase in variability. The variations in modelled hydraulic conductivities typically span the measured values. Modelled and measured values show reasonable consistency in the upper two depth zones.

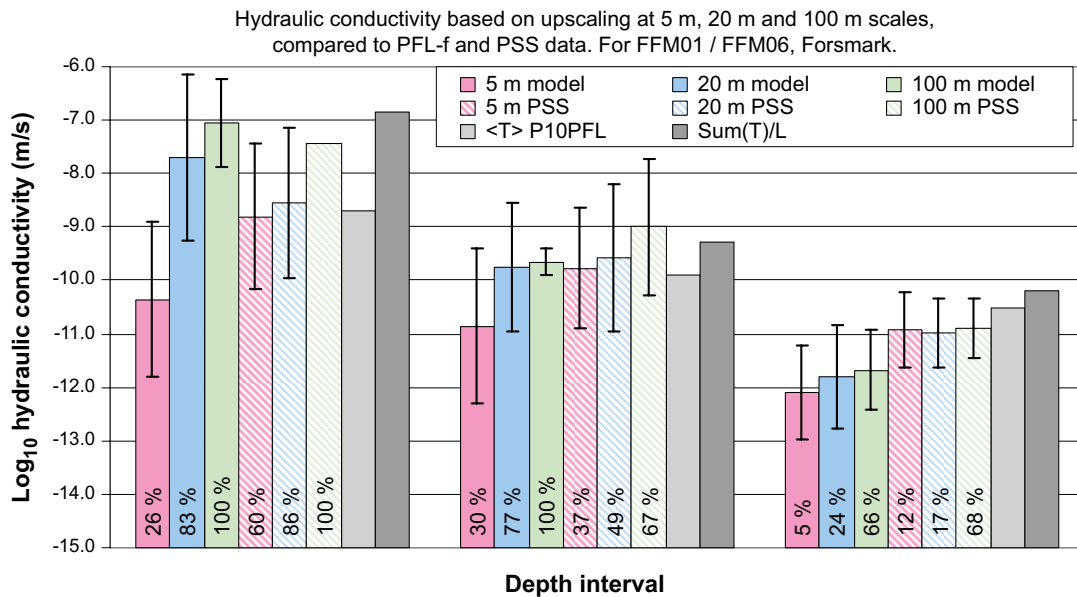


Figure 10-23. A comparison of upscaled mean horizontal hydraulic conductivities for 5 m, 20 m, and 100 m blocks predicted by the base case DFN model against hydraulic conductivities measured by the PSS method with 5 m, 20 m, and 100 m borehole sections and PFL-f data. The percentages are explained in the text while $\langle T \rangle * P10PFL$ denotes the geometric mean specific capacity multiplied by the Terzaghi corrected frequency of PFL-f fractures and $Sum(T)/L$ denotes the sum of all measured specific capacities divided by the length of borehole tested. The comparison is for FFM01 / FFM06 (based on parameters from Follin et al. 2007b, Table 11-20.) and is discussed in more detail in Hartley and Roberts (2012).

The usage in SR-Site of the results from the regional-scale flow modelling between 2000 AD and 12000 AD is based on the assumption that there is no remaining impact from the excavation and operational phases on the groundwater salinity or the variable-density flow during the initial period of temperate climate after closure. Given that this assumption is justified, the regional-scale flow modelling between 2000 AD and 12000 AD is representative for the initial period of temperate climate after closure. In the reference evolution of the PSAR, the initial temperate period is assumed to end at 9400 AD; thus the hydrogeological modelling covers a slightly longer period. The choice of 12000 AD is made in order to assess the effects of the shoreline displacement up to the point in time when the shoreline retreats beyond the model domain.

The output from the regional-scale model consists of pressure, salinity, concentrations of groundwater constituents, fractions of reference waters, and fluid density at predefined time slices between 8000 BC and 12000 AD. The salinity and fractions of reference waters are used as input to the analysis of the chemical conditions in the proximity to the repository during the initial period of temperate climate after closure, i.e. between 2000 AD and 9000 AD (Section 10.3.7), as well as during the submerged conditions following forthcoming periglacial and glacial conditions, i.e. based on results from the modelled period between 8000 BC and 1000 AD (Section 10.4.7). The simulated pressures and densities are used to define initial and boundary conditions of the groundwater flow modelling carried out on the more detailed model scales, i.e. repository scale and site scale, during the initial period of temperate climate after closure, i.e. between 2000 AD and 9000 AD. Thus, the temperate period is assumed to last until 9000 AD in both the hydrogeochemical analyses and the hydrogeological analyses at the most detailed scale.

In the *repository-scale* model, steady state pressure solutions are derived for predefined time slices between 2000 AD and 12000 AD treated in the regional-scale model. The pressure solutions assume fixed pressures on the model domain boundaries and a fixed, but spatially varying, density field throughout the model domain. Hence, there is no advective transport of salt and no matrix diffusion in the repository-scale model; i.e. the salinity field is fixed.

The physical dimensions of the repository-scale model domain are limited because of the computational constraints involved. Therefore, three repository blocks are used. For each repository block, the derived pressure solution is based on a discrete fracture network (DFN) medium representation of the fractured bedrock surrounding the repository. It is noted that in the repository-scale model, some of the implemented repository features are modelled in a discrete fashion, i.e. ramp, shafts, central area and transport tunnels, whereas others are modelled as continuous porous media, i.e. deposition holes, deposition tunnels and main tunnels.

The output from the repository-scale model consists of two types of performance measures with regard to safety functions R2a and R2b, see Figure 10-2.

1. Cumulative advective travel times (t_w [T]) and flow-related transport resistances²³ (F [TL⁻¹]) of the released particles.
2. Darcy fluxes (q [LT⁻¹]) and equivalent flow rates (Q_{eq} [L³T⁻¹]) at the deposition-hole positions.

The Darcy fluxes and equivalent flow rates are used as input to buffer erosion-corrosion analyses (Sections 10.3.11 and 10.3.13) as well as input for the near-field radionuclide transport calculations (Chapter 13). The advective travel times and flow-related transport resistances are used as input for the far-field radionuclide transport calculations (Chapter 13). In the transport calculations, three release paths, Q1, Q2 and Q3, for radionuclide release are considered, see also Figure 13-12:

1. A fracture intersecting the deposition hole, i.e. the Q1 path.
2. The excavation damaged zone (EDZ), if such a zone exists, located below the floor of the deposition tunnel that runs above the deposition holes, i.e. the Q2 path.
3. A path through the backfilled tunnel and into a fracture intersecting the deposition tunnel, i.e. the Q3 path. The Darcy flux associated with this path is the flux in a fracture intersecting the deposition tunnel.

Individual particles are released for each canister deposition hole and release path, i.e. three particles per deposition hole (see Joyce et al. 2010 for details). It is noted that for the Q3 release path, the fracture intersecting the deposition tunnel is identified through particle tracking of a particle released in the tunnel above the deposition hole. The cumulative values of t_w and F of each particle together with its exit location on the side of the repository-scale block are propagated to the site-scale model for continued particle tracking to the biosphere.

The *site-scale* model domain is as large as the regional-scale model domain, but a mixture of the flow concepts described above is used. However, the mixture of flow concepts is a bit different from that of the repository-scale model as the scale is different. It is noted that the flow concepts are formally coupled through an embedding approach where continuity of both pressure and mass flux is ensured by the use of constraint equations (see Joyce et al. 2010 for details).

In the site-scale model, steady state pressure solutions are derived for predefined time slices in the same fashion as in the repository-scale model. Thus, there is no advective transport of salt and no matrix diffusion in the site-scale model in contrast to the regional-scale model.

In the repository-scale model, particles are also back-tracked from the deposition hole positions in order to assess recharge pathways. The particle paths extend into the site-scale model in a corresponding manner to the discharge pathways. An assessment of the potential for penetration of dilute waters to repository depth is made by Joyce et al. (2010, Appendix F). The assessment is based on the recharge paths and an analytical solution for solute transport.

²³ The flow-related transport resistance is an entity, integrated along a flow path, that quantifies the flow-related aspects of the possible retention of a solute transported in fractures. A description of how the flow-related transport resistance is calculated in the present analysis is given in Joyce et al. (2010) and summarised in both the **Data report** and in Selroos and Follin (2010). A comprehensive, and more general, description of the flow-related transport resistance is given in e.g. Crawford and Sidborn (2009).

Performed analyses and usage within the PSAR

Below, the different cases that Joyce et al. (2010) performed with relevance for the periods with temperate climate conditions are listed. In addition, the saturation calculation of Svensson and Follin (2010) is included. Finally, it is indicated where the results produced by each case are used within the subsequent analyses of SR-Site and the PSAR.

- **Saturation.** In the simulations of Joyce et al. (2010), the back-filled repository is assumed saturated. However, the analysis of the temperate period formally starts when the repository is closed; i.e. prior to full saturation. In order to assess the simplification of assuming full saturation, an assessment of the saturation process is conducted. The results of the saturation calculations are also used in Section 10.3.8.
- **Hydrogeochemical evolution.** The groundwater chemistry, here represented as fractions of different reference waters, is calculated in the regional-scale model utilising a porous medium representation of the discrete fracture network (Joyce et al. 2010). Due to the shoreline displacement process and infiltration of meteoric water, the groundwater chemistry changes with time. The results are used within the hydrogeochemistry assessment in Section 10.3.7.
- **Discharge locations in the biosphere.** The discharge locations of particles transported advectively through the system from all deposition hole positions are calculated. The analysis is first performed in the site-scale model for every 1 000 years (i.e. from 0 AD to 12 000 AD) in order to support the identification of discharge locations in the biosphere, see Section 10.3.3 for details. Furthermore, discharge locations are calculated in the combined repository and site-scale models (by performing particle tracking in the repository scale model, and continuing in the site scale model) including a detailed representation of the repository structures for a few selected snapshots-in-time. These flow paths are used when flow-related migration properties are calculated, see bullet point below. Due to the shoreline displacement process, the discharge locations move in time and generally follow the retreating shoreline.
- **Performance measures.** The main performance measures used in the subsequent radionuclide transport calculations are the Darcy flux (and associated equivalent flow rates) and flow-related migration properties along flow paths. These are calculated for each deposition hole position (Darcy flux and equivalent flow rates) and associated flow path from deposition hole position to the biosphere (flow-related transport resistance and advective travel time). Due to the shoreline displacement, these measures also change with time. The results are used as input for the buffer erosion and canister corrosion analyses (Sections 10.3.11 and 10.3.13) and for radionuclide transport calculations, see Chapter 13.
- **Penetration of meteoric water.** The recharge of meteoric water in combination with the shoreline displacement implies a gradual dilution of the originally more saline water. As dilute water has negative effects on the buffer and backfill stability, it is of interest to assess the possibilities of dilute water reaching repository depth considering the hydrogeological flow and transport conditions. This is done using the flow-related migration properties described above in conjunction with analytical transport estimates. The results are used within the hydrogeochemistry assessment in Section 10.3.7 and subsequently in the assessment of buffer erosion and sedimentation in Section 10.3.11.
- **EDZ, crown space and spalling.** The intended properties of the repository are defined in the **Underground openings construction report** and the **Backfill production report**; however, it is of interest to assess consequences in terms of the performance measures if the intended repository properties are not achieved. The results of these sensitivity analyses are mainly used in Chapter 13.
- **SDM-Site related model variants.** The hydrogeological base case properties of the geosphere are defined through SDM-Site Forsmark (Follin 2008). However, it is of interest to assess consequences in terms of the performance measures if the geosphere is assumed to be characterised by other cases or properties identified as relevant in the SDM-Site work. The results of these sensitivity analyses are used for the buffer erosion and canister corrosion analyses (Sections 10.3.11 and 10.3.13) and for radionuclide transport, see Chapter 13.

- **Unsealed boreholes.** Boreholes are drilled in close proximity to or into the repository rock volume both during the characterisation phase and during construction. In case the sealing of these boreholes does not function as intended, or if a borehole is abandoned and forgotten, the boreholes may affect the groundwater flow and transport characteristics. Variant cases incorporating completely unsealed boreholes are performed to bound the importance of such boreholes. The results of this analysis are also used as input to the Future Human Action scenario, see Section 14.2.

Saturation

The time scale of saturation is estimated using the DarcyTools code based on the methodology described above (Svensson and Follin 2010). The inflow is calculated separately for each operational stage A–C; for an explanation of the different phases, see Section 10.2.3.

In Figure 10-24, the inflow is shown as a function of time for stage A. A high initial inflow rate is followed by an asymptotic regime where the inflow gradually decreases. Based on the calculations, Svensson and Follin (2010) conclude that it will take several hundred years for the repository to reach full saturation. The temperate period is on the order of 10 000 years; hence this initial period of unsaturated conditions covers only a small part of it, and the assumption of saturated conditions within the rest of the simulations of the temperate period can be motivated.

In order to study differences in saturation characteristics between different parts of the repository, an analysis is made where slow, intermediate and fast tunnel sections, in terms of saturation, are identified based on the pressure distribution after 100 days of saturation. The result is shown in Figure 10-25 in terms of integrated inflow per metre of tunnel. Approximately 4.1 m³/m of water is needed to fully saturate the void space of the backfill in the tunnels. The results indicate that after 50 years the fast tunnel section has reached 3.7 m³/m, whereas the slow tunnel section has reached 2.9 m³/m. The intermediate tunnel section has reached 3.1 m³/m.

The water that saturates the backfilled repository structures originates predominantly from the top of the model domain. The reasoning behind this conclusion is twofold. First, the only available free source of water in the model is the recharge at the surface. This enters the model either as net precipitation (meteoric water with an altered chemical composition) or as water from the Baltic Sea (sea water with an altered chemical composition). Second, the permeability of the bedrock is much lower below repository depth than above. In principle, the contrast in kinematic porosity between the backfill and the bedrock suggests that the entire volume of mobile water in the bedrock above repository depth equals the volume of water required to reach full saturation.

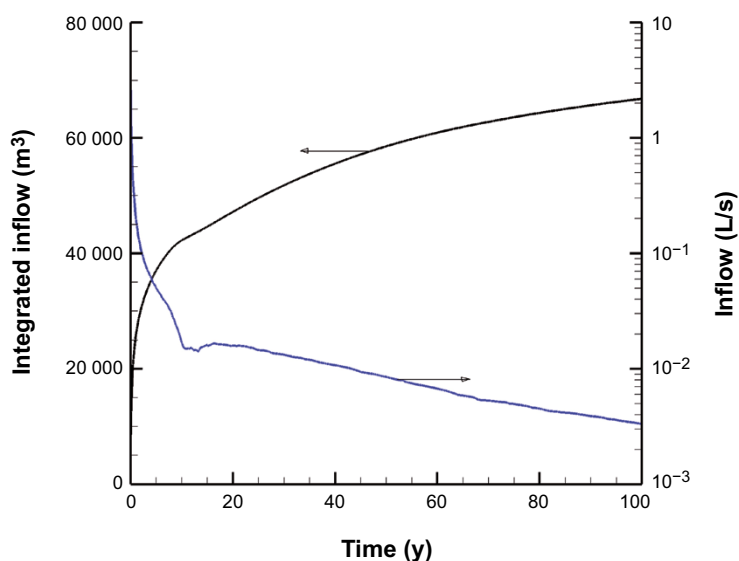


Figure 10-24. Inflow rate [L/s] and cumulate inflow [m³] for operational stage A.

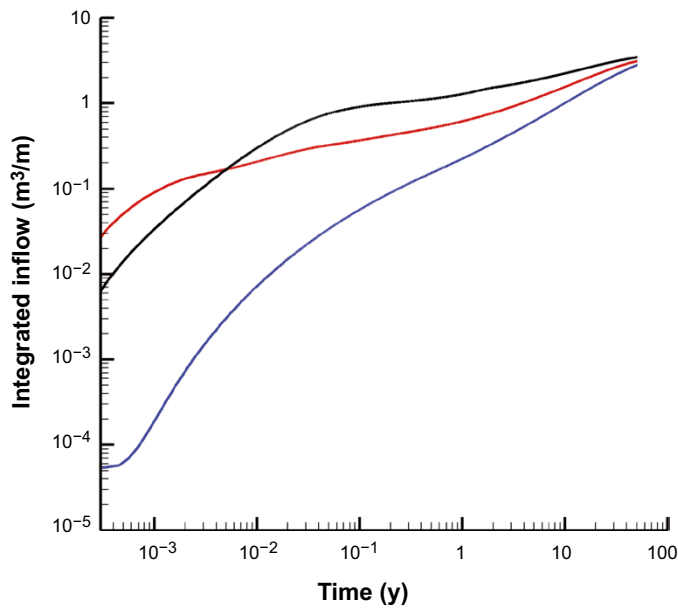


Figure 10-25. Integrated inflow [m^3/m] for three tunnel sections with different saturation rates; black = fast, red = intermediate, and blue = slow.

Hydrogeochemical evolution

The evolution of groundwater flow and hydrogeochemistry for the temperate period from 8000 BC to 12000 AD is modelled (note that results only up till 9000 AD are used in the geochemical analyses, see Section 10.3.7). The initial condition is expressed in terms of reference waters which are assumed to contribute to the groundwater composition in the Forsmark area. The chosen initial condition is Deep Saline water at depth, with the less saline groundwater above being a mixture of Deep Saline water, Old Meteoric waters and Glacial Melt water.

Figure 10-26 shows the location of a slice through the regional-scale model domain; in Figure 10-27, the distribution of Altered Meteoric water at 2000 AD and 9000 AD is shown for this vertical slice. The important deformation zones ZFMA2 and ZFMENE0060 in the region of the repository and the repository structures are also shown for context.

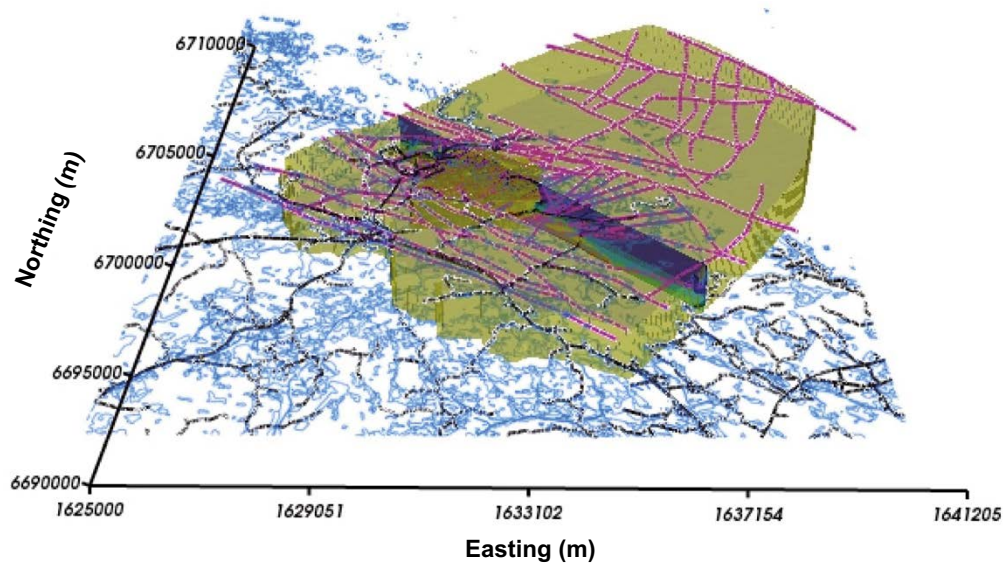


Figure 10-26. The location of the north-west to south-east vertical slice used in the fractional distribution plots in Figure 10-27.

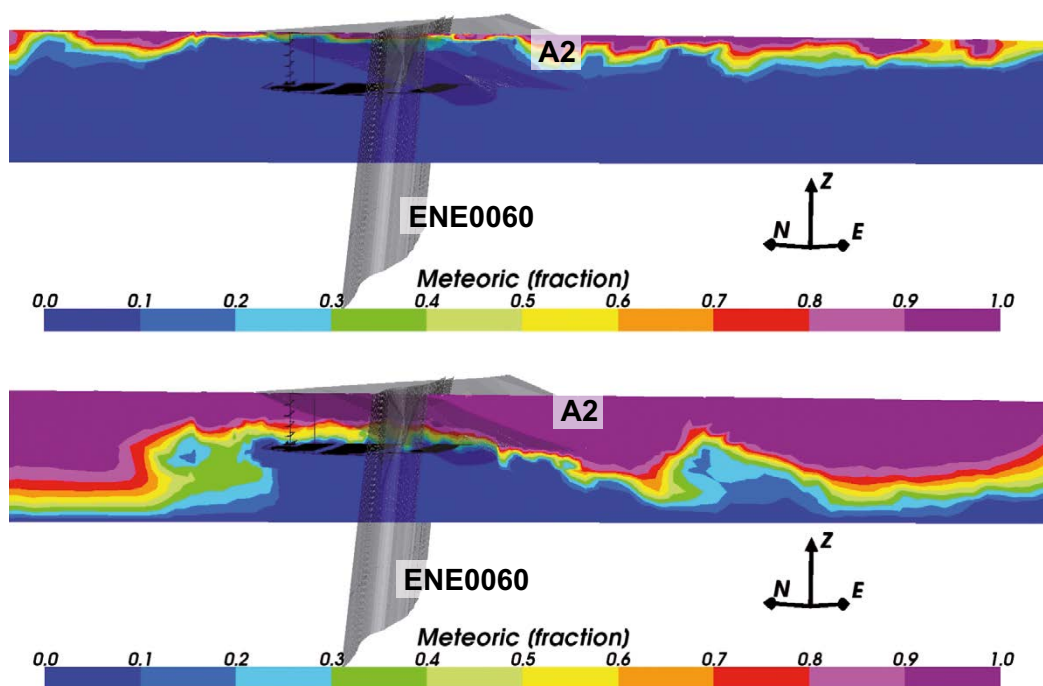


Figure 10-27. Vertical slices (north-west to south-east) of the fractional distributions of the Altered Meteoric water for the regional-scale model. From the top: Distributions at 2000 AD and 9000 AD. The model depth is 1 200 m. The profile is seen in Figure 10-26.

In Figure 10-27, the distribution of concentrations of Altered Meteoric water at 2000 AD is comparable to that found in the Site descriptive model, with concentrations (maximum concentration fraction of over 0.9) highest at the very top of the slice. The depth of the highest concentrations increases steadily from 2000 AD through to 9000 AD until it reaches the full depth of the model. Thus, it can be concluded that the domain over time will also be subject to more dilute water conditions at depth. This will have implications on repository performance as discussed below.

Discharge locations in the biosphere

Figure 10-28 shows the discharge point evolution in time. Particles are released in steady-state velocity fields at times from 0 AD to 12 000 AD in the site-scale model. The repository is included in a simplified manner expressed as equivalent fractures. The discharge points of particles released at earlier times (0 AD, 1000 AD and 2000 AD) are located onshore near the repository and show a very slight migration toward the 2000 AD shoreline with release time. The near-future exit points (3000 AD, 4000 AD and 5000 AD) follow the retreating shoreline. The far-future exit points (6000 AD through to 12 000 AD) congregate on the north-eastern model boundary. This may be interpreted such that the model domain should be extended further to the northeast. However, the boundary is consistent with the boundary of the SDM-Site model (Follin 2008) and also corresponds to a bathymetric depression in the terrain. Thus, extending the model domain would not necessarily change the discharge location pattern. Furthermore, as discussed in Section 13.2.2, a minor change in discharge locations would not affect the derived biosphere discharge areas used in subsequent dose calculations.

In Joyce et al. (2010), it is shown that the Darcy flux in the starting locations, and properties along the flow paths (travel time and flow-related transport resistance) are essentially unchanged between different release times.

Performance measures

The performance measures are calculated for four steady-state velocity fields at different times; these are 2000 AD, 3000 AD, 5000 AD and 9000 AD. A multitude of results are available in Joyce et al. (2010) for multiple times and realisations representing the hydrogeological base case presented. In addition, the effect of branching along flow paths is assessed in a variant calculation by the use of

multiple particles per start position. Furthermore, results can be analysed in terms of spatial variability among different particle start locations within the same realisation. Here, only a small subset of the results is presented for illustrative purposes.

In Figure 10-29, the flow-related transport resistance (F) is shown at the starting location for the released particles; i.e. the final F value at the end of the path is shown at the start location. No clear trend of more or less favourable conditions within the repository is readily discerned.

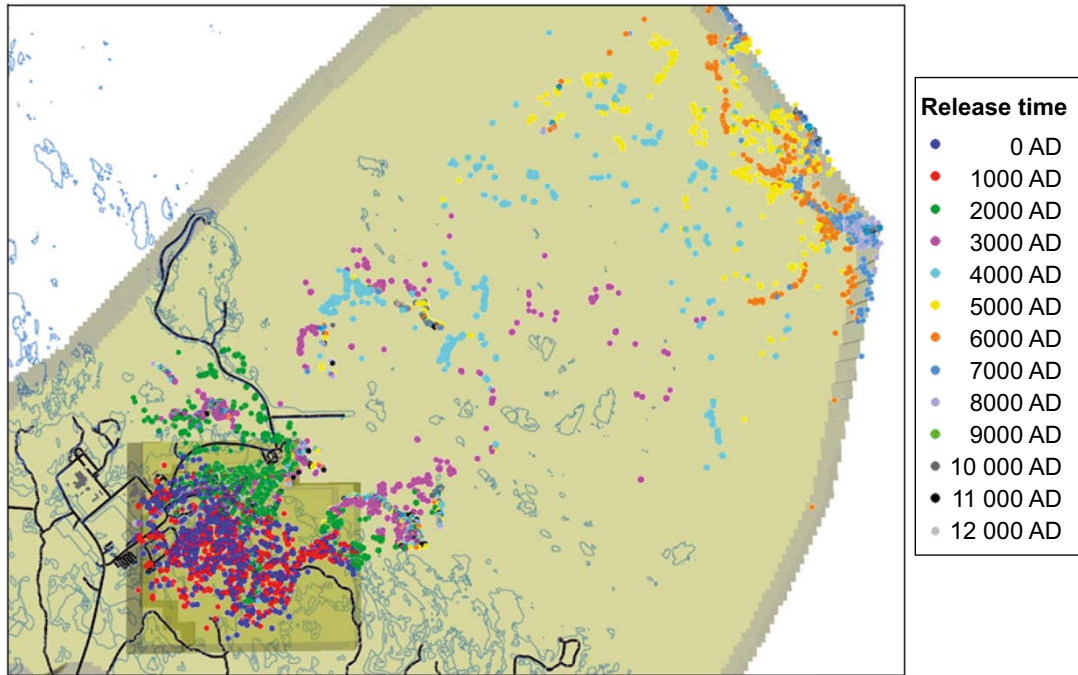


Figure 10-28. Discharge locations for particles ($Q2$ path) successfully reaching the top boundary of the site-scale hydrogeological base case model (89 %–97 %) for releases every 1 000 years from 0 AD to 12 000 AD. The model domain is shown in beige.

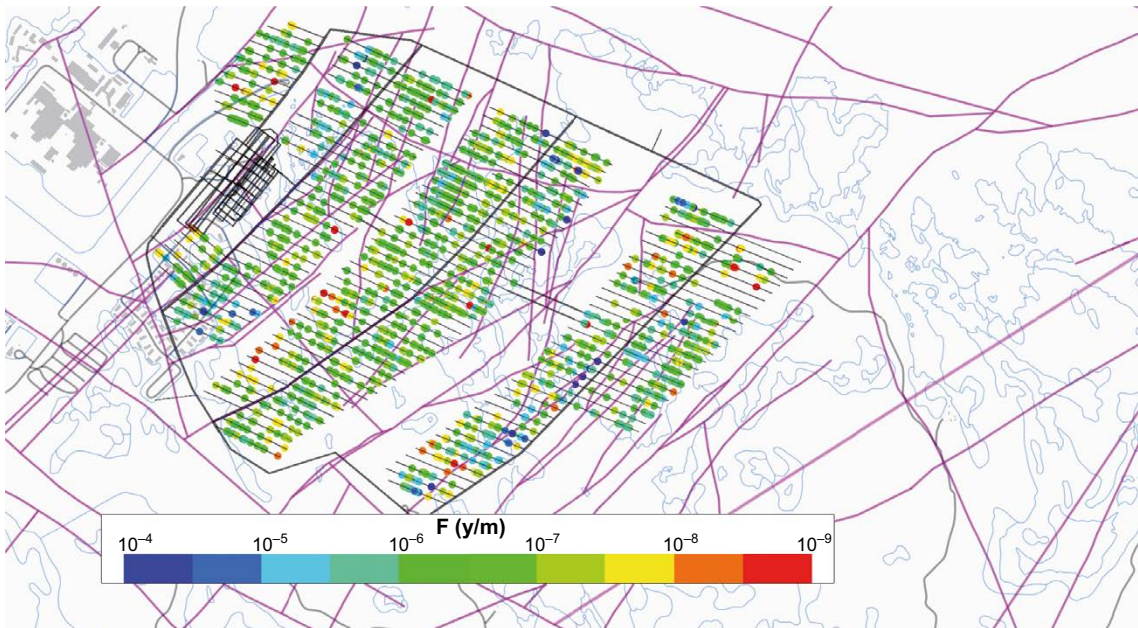


Figure 10-29. Starting locations coloured by $\log_{10}(F)$ for particles released at 2000 AD ($Q1$ path) and successfully reaching the top boundary (24 %). The HCD model at $z = -470m$ (purple), roads and buildings (black) and shoreline (blue) are also shown.

As indicated above when assessing discharge locations, flow paths tend to become longer as the shoreline is displaced. This generally implies longer travel times and larger flow-related transport resistance values with time as indicated in Figure 10-30.

The definition of the flow-related transport resistance (F) is straight forward in a discrete model; in a continuum model, additional assumptions need to be made. Thus it is of interest to assess how much contribution to the overall F is accumulated in the continuum representation (ECPM+CPM) part of the domain. Figure 10-30 shows that for the later release times, the F values are shifted to somewhat higher values when the continuum representation is included. However, for the subsequent radionuclide transport calculations, only the discrete contribution is included.

As indicated in Section 5.2.2, deposition hole rejection criteria based on the Extended Full Perimeter Criterion (EFPC) are adopted within SR-Site. In Figure 10-31, the effect of the application of this criterion is illustrated for the Darcy flux in fractures intersecting deposition holes. The figure illustrates that roughly 70 percent of deposition holes do not have a flowing fracture intersecting the deposition hole. When the criterion is applied, only about 20 percent of the remaining deposition holes are intersected by a flowing fracture; i.e. the criterion leads to rejection of roughly 10 percent of the deposition holes. Also seen in the figure is that the remaining distribution is shifted towards lower Darcy flux values. Hence, the application of the criterion will have positive consequences for subsequent assessment calculations.

In the hydrogeological base case realisation, all deformation zones are assumed to have a depth trend of transmissivity, but otherwise constant properties. However, the discrete fracture network is stochastic. In additional realisations, the deformation zone properties are also assumed to be characterised by spatial variability. In Figure 10-32, box and whisker plots of the flow-related transport resistance (F) for the Q3 path are shown for the base case realisation and ten additional realisations. It is seen that the median and upper percentiles are quite stable between realisations, whereas some realisations, e.g. r1, r5 and r9, are characterised by a lower tail, i.e. a lower 5th percentile. Corresponding results are observed for the advective travel time; however, the Darcy flux is more stable between realisations. Also, for all performance measures, the Q1 path is characterised by less variability between realisations than the Q2 and Q3 paths. The reason is the large stochastic fractures intersecting the deposition tunnels and hence determining the Q2 and Q3 paths in individual realisations.

In order to assess the effect of branching along the flow paths on the advective travel time and flow-related transport resistance, multiple particles (ten) have been released per start point in the particle tracking. Only the 25 percent of start points with highest Darcy flux were used in the comparison. The ten particles choose different flow paths due to a stochastic choice (weighted by flow rate) at each fracture intersection. The results indicate that the branching has negligible effects on the ensemble statistics of the analysed performance measures.

Penetration of dilute water

In principle, the future groundwater chemistry is provided by the regional scale groundwater flow simulation reported above. However, the regional scale simulation only covers the temperate period and, furthermore, has a fairly coarse discretisation which does not allow an assessment of the groundwater chemistry evolution on a deposition hole scale. Thus, an alternative assessment of the evolution of the groundwater chemistry, and specifically the potential for penetration of dilute water, is made since dilute groundwater may cause erosion of the buffer and the backfill.

In order to assess the potential for penetration of dilute water, a simplified approach is adopted. An injection of water representative of current soil water conditions along those recharge pathways that originate close to the surface within the combined repository-scale and site-scale models is considered; it is assumed that the infiltrating water has a salinity of 0.4 g/L, see Appendix J of the **Radionuclide transport report** for a motivation of the chosen value. As also shown in the Appendix, a salinity of 0.4 g/L corresponds to a cation concentration of about 3 mM. Also, in this simplified calculation, it is assumed that the matrix and fracture water salinity is in equilibrium at the start of the simulations; the relevance of this assumption is discussed in Section 10.1.3 and in Section 5.3 of Salas et al. (2010). The flow field and recharge flow paths of year 2000 AD are used, specifically the flow-related transport resistance and advective travel times along these paths are used as input for the calculations (note that advective travel time and flow-related transport resistance are accounted for only in the part of the model with an explicit DFN representation). Along the flow paths, the only mitigating process considered is the out-diffusion of matrix water affecting the penetration of the meteoric water front.

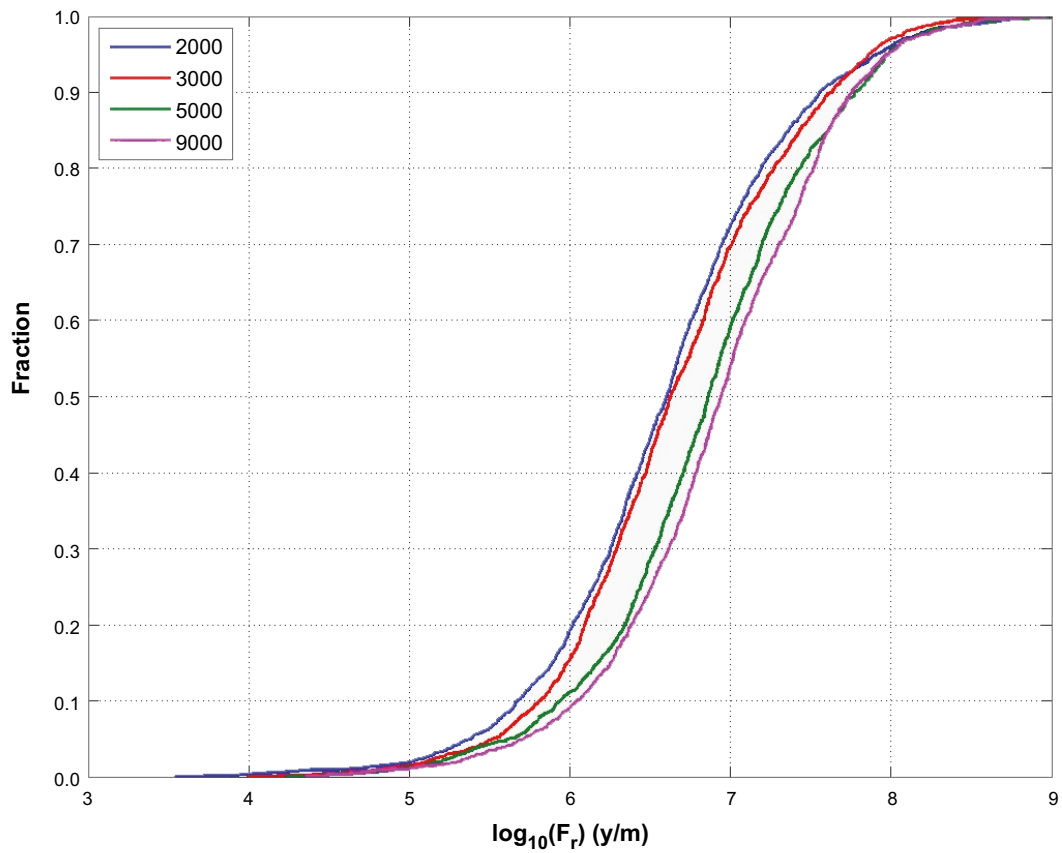
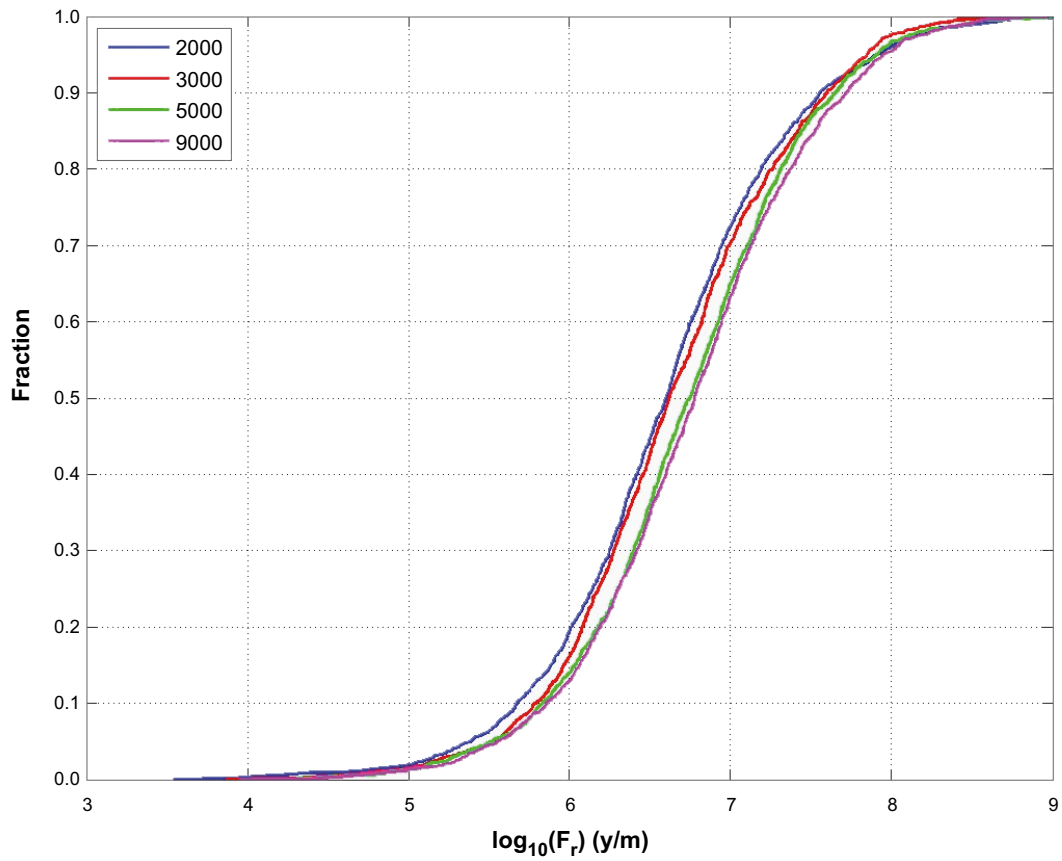


Figure 10-30. Cumulative distribution function plots of flow-related transport resistance (F) for the Q1 path for the particles successfully reaching the model top boundary (24 %) released at 2000 AD, 3000 AD, 5000 AD and 9000 AD. The top plot shows the contribution from the DFN part of the model only, whereas the bottom figure includes the contribution also from the ECPM and CPM parts.

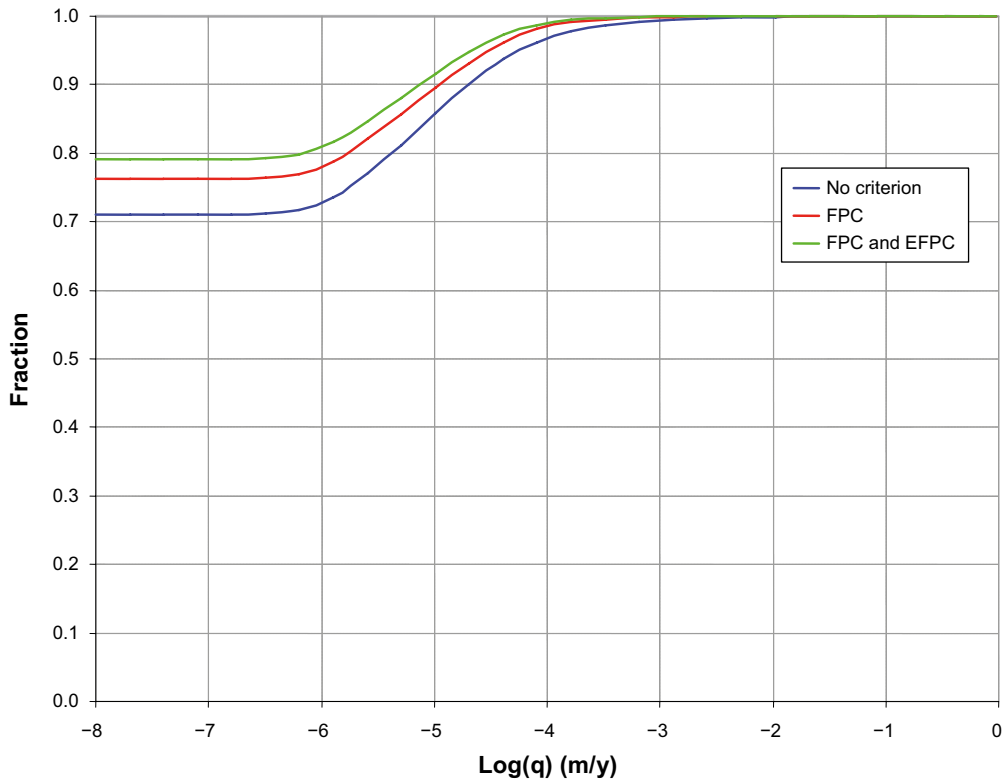


Figure 10-31. Cumulative distribution plot of Darcy flux (q) for the $Q1$ path for all deposition hole positions at 2000 AD for different rejection criteria. (Modified after Figure 6-15 in Joyce et al. 2010).

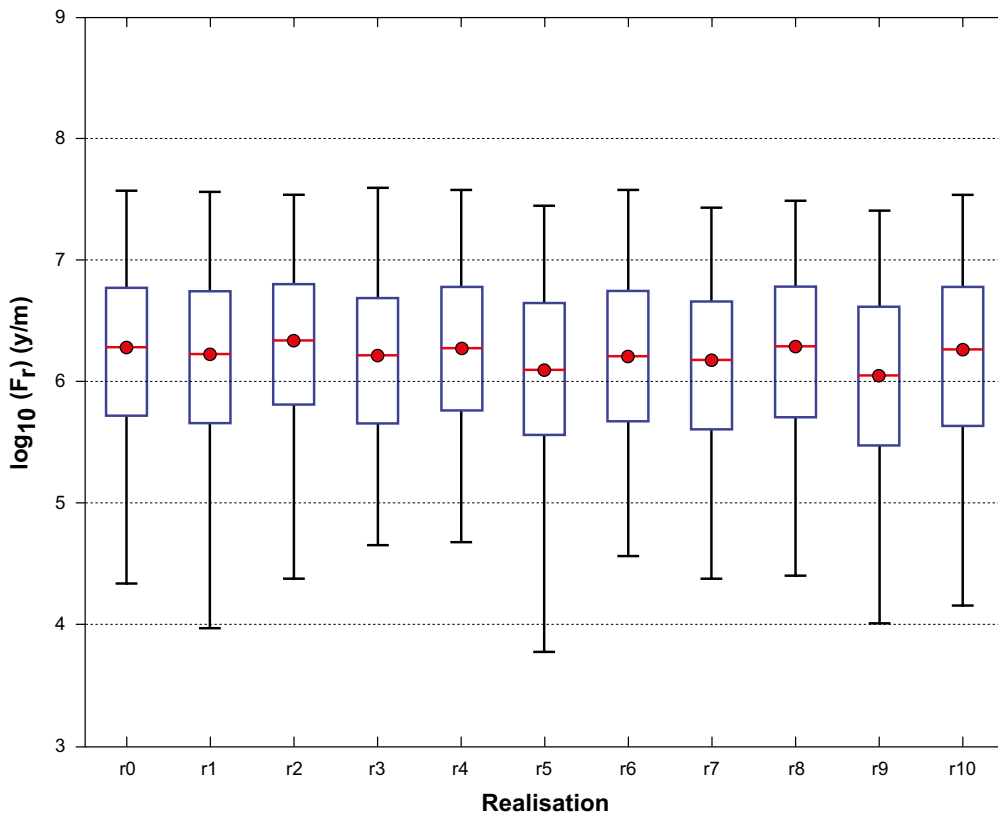


Figure 10-32. Box and whisker plots of flow-related transport resistance (F) for the $Q3$ path in the hydro-geological base case realisation ($r0$) and the 10 stochastic realisations of the HCD and HRD ($r1$ to $r10$) for the particles successfully reaching the model top boundary released at 2000 AD. The statistical measures are the median (red), 25th and 75th percentile (blue box) and the 5th and 95th percentile (black “whiskers”).

For each deposition hole, the time required for the groundwater salinity to be equal or fall below six percent of the initial water concentration is calculated. Figure 10-33 shows the distribution of these times for all deposition hole positions. The present day salinity at the site is approximately 10 g/L; six percent of the initial concentration thus corresponds to 0.6 g/L, which is equal to the criterion which is assumed to represent dilute conditions with potential buffer erosion, see Section 10.3.7. The vertical lines represent the assumed approximate duration of the temperate period; i.e. 10 000 years for the base case, and 60 000 years for the Global warming variant (see Section 10.6 and Joyce et al. 2015). The pink curve in the figure represents the case where matrix diffusion only between the flowing water and its adjacent rock matrix is considered. It is observed that less than one half of a percent of the deposition hole positions experience dilute conditions within the Global warming variant, whereas only one quarter of a percent experience dilute conditions during the first ten thousand years of the initial temperate period. In Table 10-4, the exact ratios of deposition hole positions experiencing dilute conditions are provided.

Table 10-4. Fraction of deposition hole positions experiencing dilute conditions at 10 000 and 60 000 years, for the case without stagnant zones and different assumptions on the width of stagnant zones.

Time (y)	$W_s = 0.0$ m	$W_s = 0.1$ m	$W_s = 1.0$ m	$W_s = 5.0$ m
10 000	0.0024	0.0020	0.0011	5.8×10^{-4}
60 000	0.0043	0.0038	0.0020	0.0010

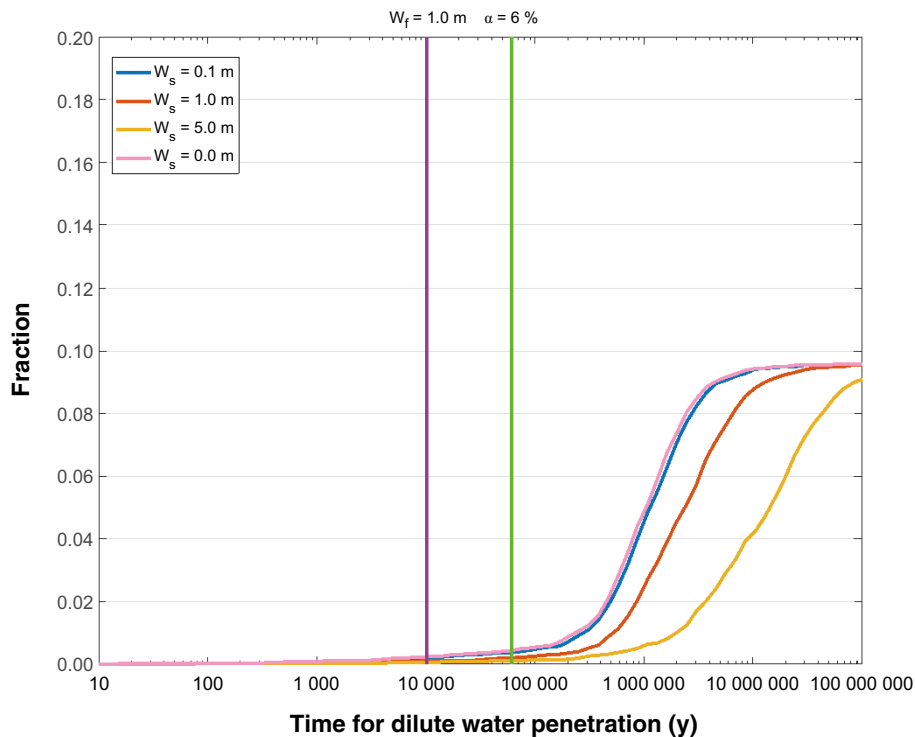


Figure 10-33. Temporal distribution for all deposition hole positions to obtain six percent of the initial water salinity concentration. The green line shows that approximately one half of a percent of the deposition holes experience dilute conditions within the Global warming variant. The purple line shows that approximately one quarter of a percent of the deposition holes experience dilute conditions during the first ten thousand years of the initial temperate period. The pink curve represents the case without stagnant water, while the other curves assume additional stagnant water zones being available. The calculated fractions of deposition holes experiencing dilute conditions at the times 10 000 and 60 000 years are also given in Table 10-4.

The other curves in the graph assume that matrix diffusion also takes place into stagnant water volumes (in the fracture plane) surrounding the flowing water channels, with subsequent mass exchange (diffusion) between the stagnant and flowing water. The development and verification of the modelling tool and methodology employed here is described in more detail in Appendix K of the **Radionuclide transport report**. In the PSAR each fracture is modelled as having a uniform aperture (i.e., no internal aperture heterogeneity), and hence channelling effects of the flow field are not fully accounted for, even though some channelling emerges due to network effects. The solution employed here thus re-introduces the effect of the neglected channelling for solute (salt) transport.

The process of diffusion through the stagnant zones provides an additional source of salinity, and hence the curves are shifted to even lower ratios of deposition hole positions experiencing dilute conditions. For the illustrative examples, a flowing channel width of 1 m is considered, while the half-width of the distance between flowing channels ($2W_s$) is set at 0.2, 2, and 10 m, respectively. It is noted that the sparser the flowing channels, the stronger is the effect of the stagnant water zones between the flowing channels. However, for the smallest stagnant water zone considered ($2W_s = 0.2$), the effect is minimal.

In the PSAR, the additional mitigating effect of stagnant water zones is not employed. Clearly, in a sparsely fractured network such as the one characteristic of the Forsmark site, flowing water channels will also be sparse and an exchange of mass with the more or less stagnant, surrounding water will take place. However, it is challenging to conceptualize (and parameterize) exactly how such stagnant water will manifest itself along a complete flow path from surface to repository depth (Zou et al. 2017, Zou and Cvetkovic 2020). It is thus here pessimistically assumed that this mitigating effect is not active. In an overall discussion of repository safety, however, this additional process may well be acknowledged.

Uncertainties in the F-factor have been quantified (SKB 2014c) to address several recognised uncertainties in the site description or in performance of the closure design in Joyce et al. (2010). In summary, most variants were within an envelope of about a factor two of the base case, but some realisations with a correlated transmissivity could be a factor five lower. In SKB (2014), a pessimistic case where the F-factor and advective travel times are reduced by a factor of five, compared to the base case of SR-Site, is discussed and the fraction of holes that experience dilute waters is illustrated. The results show that the numbers of locations affected are about two to three times higher than the values reported within SR-Site in the figure corresponding to Figure 10-33. It is emphasized that this is a pessimistic representation of the uncertainty effect since several of the uncertainties imply also higher F-factors.

It should be noted that for the results in Figure 10-33, it was found that the travel time and flow-related transport resistance distribution are very similar for each of Q1, Q2 and Q3 for forward path (downstream discharge) from the repository, see Figures E-26 and E-27 in Joyce et al. (2010), for example. The results of these 1D dilution pathway calculations would therefore be expected to be similar for Q1, Q2 and Q3. Q1 was considered to be most relevant to chemical erosion processes since it represents those deposition holes with a direct interface between buffer in the deposition holes and fracture water. More indirect paths for dilute water via the EDZ and tunnel and their significance to buffer erosion processes were beyond the scope of this simple 1D approach. These paths are, however, much less significant since the dilute water would in these cases interact with the clay system at locations much farther away from the canister than the Q1 fracture (cautiously assumed in the subsequent erosion/sedimentation analyses to be located at canister mid height).

EDZ and crown space in deposition tunnels

As concluded in Section 10.2.2 there is ample evidence that a potential excavation damaged zone (EDZ) formed during excavation will be kept below the maximum allowed transmissivity as set out by the technical design requirements. Furthermore, data suggest that a continuous EDZ will not develop at all. However, given that the occurrence of the EDZ currently can only be assessed by indirect measurements, it is justified to consider an EDZ according to the technical design requirements, i.e. with an axial transmissivity of 10^{-8} m²/s as a basic assumption for further analyses. Furthermore, it also seems justified to explore how transmissive an EDZ needs to be in order to significantly impact other safety functions as well as exploring the impact of no axially continuous EDZ at all.

In the hydrogeological base case model, a continuous excavation damaged zone is implemented in all tunnels (deposition, main, transport and access tunnels) under the tunnel floor. The EDZ has a transmissivity value of $T = 1 \times 10^{-8} \text{ m}^2/\text{s}$ and a thickness of 0.3 m. In order to assess the sensitivity of performance measures to tunnel properties, four alternative cases are analysed. Two of these have higher EDZ transmissivities ($T = 1 \times 10^{-7} \text{ m}^2/\text{s}$ and $T = 1 \times 10^{-6} \text{ m}^2/\text{s}$, respectively), one case has no EDZ, and the final case has the base case EDZ properties, but is combined with a crown space under the tunnel ceiling. The crown space results from a consolidation of the backfill material. In the model, the crown space is implemented as a 0.1 m thick zone with a high conductivity value ($K = 1 \times 10^{-3} \text{ m/s}$) and a porosity equal to unity.

The Darcy flux (q) for the Q2 path of the particles successfully reaching the model top boundary is shown in Figure 10-34. Since the Q2 path corresponds to the EDZ path, no result exists by definition for the case with the EDZ removed. The figure clearly shows, as expected, that an increase in the EDZ transmissivity implies an increase in the associated Darcy flux. The crown space, on the other hand, implies no change in the Darcy flux in the EDZ. The same holds true for the other release paths; i.e. the crown space has only a marginal influence on the estimated Darcy fluxes.

Concerning the flow-related transport resistance (F), the case with no EDZ provides the most favourable conditions. The reason is that with no EDZ present, particles tend to travel more in the fractured rock, and hence accumulate their F values (no retention is assumed in the EDZ). Conversely, with an increased EDZ transmissivity or a crown space, less favourable conditions prevail and the flow-related transport resistance distributions are shifted towards lower values. The effect of EDZ and crown space on the flow-related transport resistance is most pronounced for the Q3 path.

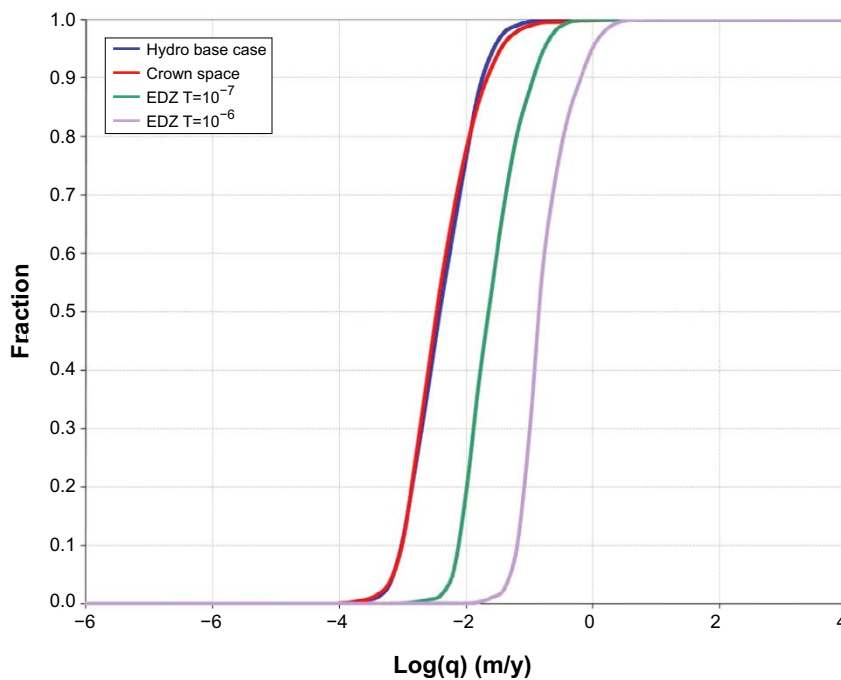


Figure 10-34. Cumulative distribution function plot of the Darcy flux (q) for the Q2 release path for the hydrogeological base case model, the crown space model, the EDZ $T = 1 \times 10^{-7} \text{ m}^2/\text{s}$ case, and the EDZ $T = 1 \times 10^{-6} \text{ m}^2/\text{s}$ case for the deposition holes with particles successfully reaching the model top boundary, released at 2000 AD. (Modified after Figure E-49 in Joyce et al. 2010).

Effects of spalling

In Section 10.3.5 the mechanical effects of spalling in deposition holes induced by the additional stress caused by the heat from the spent fuel are discussed. The spalling also results in changed conditions for mass exchange between the buffer and the fracture intersecting the deposition hole, in the form of an altered Q_{eq} for the Q1 path. To take into account spalling in deposition hole walls, a special model was developed for use in SR-Can (Neretnieks 2006a), with an altered equivalent flow rate for the Q1 path due to the damaged zone caused by spalling. This model has been updated for use in SR-Site (Neretnieks et al. 2010). The altered equivalent flow rate in the damaged zone is obtained as being proportional to the square root of the flow rate in the fractures around the deposition hole, with the proportionality factor being a function of the deposition hole tortuosity (-), porosity (-), width and thickness (m) of the spalled zone, if such a zone occurs (see the **Data report**, Table 6-69). These data are obtained from the modelling results of Hökmark et al. (2010) presented in Section 10.3.5 and data from experiments carried out at the Äspö HRL, as further described in the **Data report**, Section 6.5. In Figure 10-35 the effects of spalling are illustrated. The results indicate that spalling may increase the equivalent flow rate for the Q1 path by more than an order of magnitude, but the other paths are not affected.

SDM-Site related model variants

A number of variants related to site characteristics and motivated in the SDM-Site report (Follin 2008) are also assessed within SR-Site. These are briefly summarised below.

Alternative DFN transmissivity-size relationships

The hydrogeological DFN modelling for SDM-Site (Follin et al. 2007b) treated three kinds of transmissivity-size correlation models; fully correlated, uncorrelated and semi-correlated. It was found that the fully correlated and semi-correlated models reproduced the numbers and shapes of distributions of specific capacities measured with the Posiva Flow Log reasonably well, giving a wedge shaped distribution characteristic of having some kind of transmissivity-size correlation, whereas the simulated distribution for the uncorrelated model was flatter and less representative. For this reason, the hydrogeological base case in SR-Site is based on the semi-correlated relationship between transmissivity and size as propagated by SDM-Site. However, to quantify uncertainties, the alternative relationships, i.e. the fully correlated and the uncorrelated models, are also investigated in SR-Site as variant cases, see Figure 10-36.

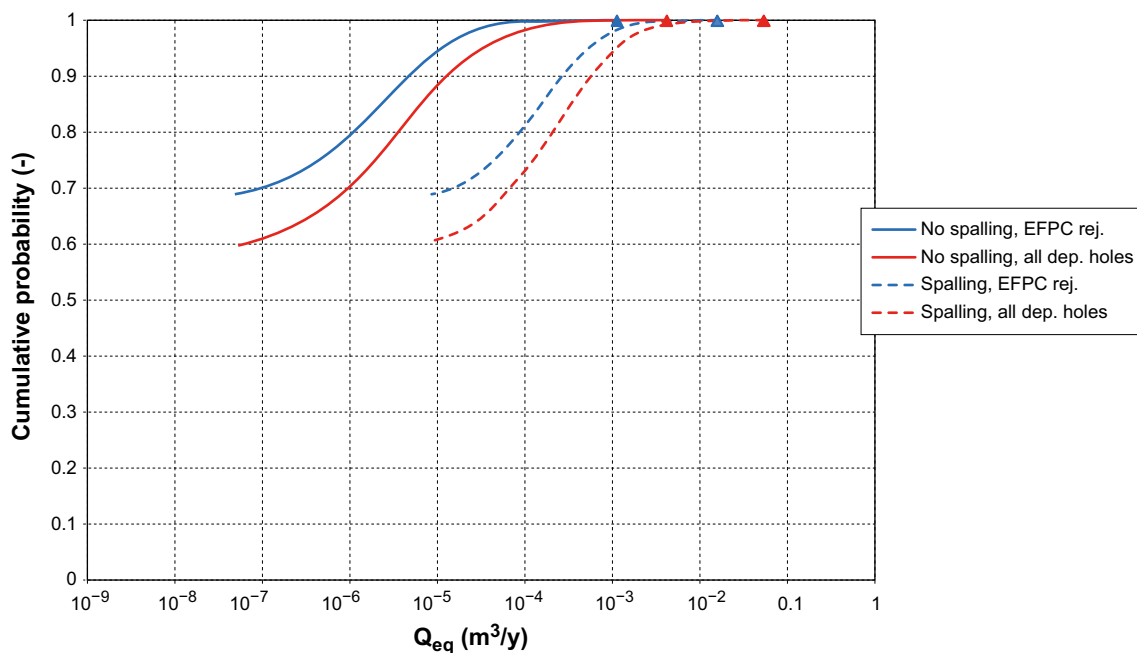


Figure 10-35. Cumulative distribution plots of Q_{eq} for path Q1 at time 2020 AD in Forsmark for conditions with and without spalling, considering application and no application of the EFPC rejection. The triangles mark the maximum values of the distributions.

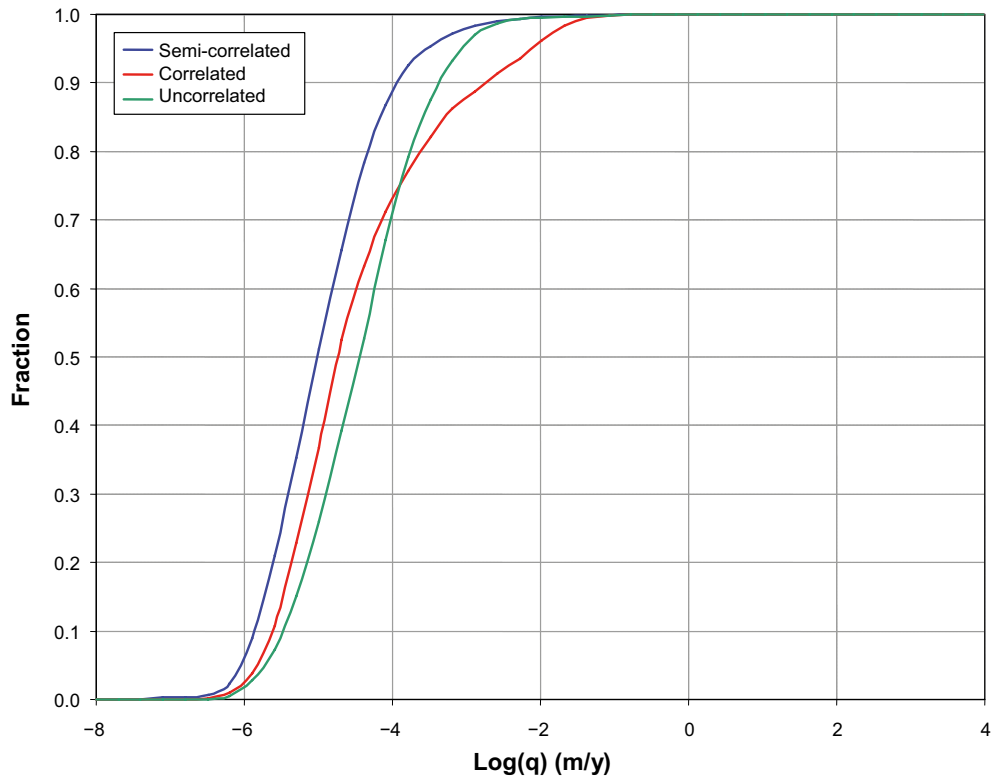


Figure 10-36. Cumulative distribution function plots of the Darcy flux (q) for the correlated and uncorrelated transmissivity-size relationships compared to the hydrogeological base case (semi-correlated) for the Q1 release path at 2000 AD for deposition holes with particles successfully reaching the model top boundary. (Modified after Figure 6-28 in Joyce et al. 2010.)

The particle tracking results reported by Joyce et al. (2010) indicate that the performance measures (Darcy flux and the flow-related transport resistance) are dependent on the chosen transmissivity-size relationship with up to about half an order of magnitude variation between variants.

Possible deformation zones

As a variant case for SR-Site, four possible deformation zones (PDZ) identified in SDM-Site were added to the HCD model and treated in the same way as the deterministically modelled deformation zones. These were combined with the corresponding realisations of the HCD and HRD fractures generated for the hydrogeological base case. Figure 10-37 shows the possible deformation zones relative to the repository structures. Some of them intersect the repository structures and may provide potential flow pathways.

The simulated exit locations for the three PDZ realisations show little variation between realisations and are similar to those for the hydrogeological base case. The modelled possible deformation zones have little effect on the performance measures.

Unmodified vertical hydraulic conductivity

During the calibration and confirmatory testing of the SDM-Site base model simulation, the vertical hydraulic conductivity of the ECPM representation of the HRD above an elevation of -400 m was reduced by a factor of ten in order to provide a better fit to chemistry and interference test data. This modification was also used for the ECPM representation in the regional and site-scale hydrogeological base case models for SR-Site. However, no corresponding change was made to the properties of the fractures in the DFN representation in the site-scale model, leading to a possible inconsistency in flows between the DFN and ECPM in the site-scale model. Therefore, as a variant case for SR-Site, the modification of the vertical hydraulic conductivity of the ECPM representation used in the regional and site-scale models was removed.

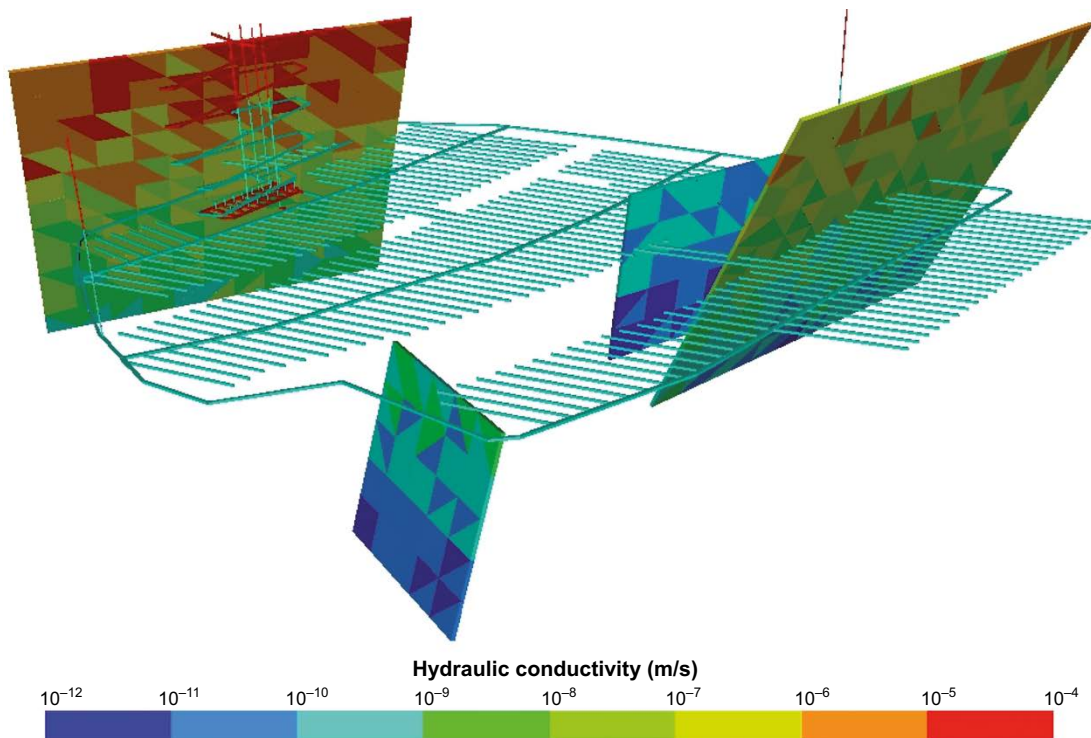


Figure 10-37. Realisation 1 of the possible deformation zones in relation to the repository structures.

The simulated exit locations for the unmodified vertical hydraulic conductivity variant case are similar to those for the hydrogeological base case. The cumulative distribution function plots showing the Darcy flux and the flow-related transport resistance compare well with the corresponding plots for the hydrogeological base case suggesting that the site-scale model is insensitive to changes in the vertical hydraulic conductivity in the ECPM.

Extended spatial variability

The HRD model developed for SDM-Site essentially covers the repository site area. Outside this area, there was little or no information available to support any elaborated HRD modelling. Therefore, the bedrock outside the repository area was modelled as a CPM with homogeneous and isotropic properties for each depth zone. The hydrogeological base case in SR-Site is no different in this regard.

As a model variant for SR-Site, the area treated as a CPM in the hydrogeological base case was replaced by an elaborated HRD. The additional DFN data required for this variant case come from the investigations at SFR (Öhman and Follin 2010). This information is used to provide a full ECPM representation for the regional-scale and site-scale models. In addition, the area of the DFN in the site-scale model was extended northwards beyond the Singö deformation zone, which may provide an important discharge location. Both models retain the existing HSD. The repository-scale model is not included in the analysis.

For the extended spatial variability case, more particles seem to exit closer to the repository, which is reasonable given the improved representation of discrete features (flow paths). However, the cumulative distribution function plots showing the Darcy flux and the flow-related transport resistance do not differ significantly from the corresponding plots for the hydrogeological base case, thus suggesting that the extended spatial variability case has only a moderate effect on performance measures.

Unsealed boreholes

The results indicate that the presence of an open borehole has some effect on the flow field. However, in most simulations only a small subset of released particles enter the boreholes. As a maximum, 23 % of the released particles enter a borehole in one simulation.

The statistical analysis of the complete ensemble of the released particles shows that there is little change in performance measures. The change in performance measures generally stays within 20 % comparing the borehole case to the hydrogeological base case. The performance measures behave as expected; the Darcy flux is slightly increased while the advective travel time and flow-related transport resistance are somewhat decreased in the borehole cases.

When the statistical analysis is performed on only the particles that enter the boreholes and the results are compared to the same subset of particles in the hydrogeological base case, the effect on the performance measures is larger. However, the changes still remain within a factor of four and in the same direction for the different performance measures as before.

Thus, it can be concluded that including a borehole in the hydrogeological base case model does not have a major effect on the performance measures even if the groundwater flow pattern is affected and the flow paths of the released particles change.

Identified uncertainties and their handling in the PSAR

General uncertainties of the results presented in this section are related to the derived hydrogeological discrete fracture network (DFN) model used in the hydrogeological base case. A comprehensive discussion of these uncertainties, including the relation between the hydrogeological DFN and geological DFN models, is presented in the **Data report**, Section 6.6. Below, specific uncertainties related to the performed analyses are discussed.

Saturation. Based on their calculations, Svensson and Follin (2010) conclude that it will take several hundreds of years for the repository to reach full saturation, with a relatively short period of rapid initial inflow followed by an asymptotic regime where the inflow gradually decreases. The time scale for saturation is probably overestimated in DarcyTools considering the adopted simplified handling of capillary suction (Enssle and Poppei 2010). The saturation times reported by Svensson and Follin (2010) are within the range of values obtained from modelling where the hydrology of the backfill is treated in more detail and where also the buffer is included (see Section 10.3.8).

Hydrogeochemical evolution. The uncertainties related to the hydrogeochemical evolution are mainly related to the chosen initial and boundary conditions. Thus, the evolution of the proportions of individual reference waters is associated with an uncertainty comparable to the uncertainty in initial and boundary condition specification. The evolution of salinity, which depends on the reference water composition, is hence also associated with some uncertainty; however, it is argued that this uncertainty is smaller than the uncertainty related to the individual reference waters since the salinity is an integrated entity (summation of individual reference water constituents). The modelled salinity development of generally more dilute conditions during the temperate period is considered an evolution with a high degree of certainty.

Discharge locations in the biosphere. Due to the continuum representation in the outer parts of the domain where particles tend to discharge at later times, the discharge locations may be excessively dominated by the location of the shoreline. For a discrete representation, the exit locations may be more influenced by outcropping deformation zones or fractures. This issue is examined in the extended spatial variability variant case, see SDM-Site related model variants below for details.

Multiple realisations and branching. The uncertainty in performance measures is addressed both through multiple realisations and multiple particles per start location. The results indicate that branching (assessed by multiple particles per start location) implies no additional uncertainty, whereas there is some variability between realisations. Thus, multiple realisations need to be assessed in subsequent analyses.

Choice of conceptual model. The uncertainty in results due to the conceptual model chosen, i.e. a discrete representation where the parameterisation of the discrete model has been done according to the methodology developed as part of the site descriptive modelling (Follin 2008), has been assessed by adopting a different conceptual model representation. In Liu et al. (2010), the channel network modelling tool CHAN3D has been applied to the temperate conditions of the Forsmark site, and the corresponding performance measures as in Joyce et al. (2010) have been calculated. In CHAN3D, the model is parameterised using the statistics of block-conductivity values resulting from up-scaling of

the original hydrogeological DFN model. The results indicate that the reported median performance measures are very similar, whereas the spread of results is smaller in CHAN3D than in the ConnectFlow application. These results are consistent with findings in an earlier assessment (SR 97) as reported by Selroos et al. (2002); i.e. discrete models tend to exhibit more spreading than continuum representations.

Kinematic porosity. Out of the different performance measures, only the advective travel time is dependent on porosity (or aperture in a discrete model). In Joyce et al. (2010) the effect of this uncertainty is considered, and a comprehensive evaluation is presented in Selroos and Follin (2010). The conclusion is that this uncertainty is of limited importance for the applications within SR-Site since advective travel time has only a minor impact on hydrogeochemical and radionuclide transport simulations.

Penetration of dilute water. The assessment of penetration of dilute water should be considered an approximate quantification. First, the flow field at 2000 AD is used; i.e. the temporal development in flow characteristics is not accounted for. Second, no mixing or water-rock interactions are considered, which clearly may affect the water chemistry evolution. Thus, the reported numbers should be seen as very rough estimates rather than predictions of a future evolution. However, the presented numbers of deposition holes experiencing dilute conditions are deemed appropriate for use in subsequent analyses of buffer erosion and canister corrosion as they are likely pessimistic estimates. The site understanding presented in Section 10.1.3, based on collected data, indicates that dilute waters do not penetrate to repository depth. However, as the simplified analysis conducted here indicates, it is hard to defend a position that not even a few deposition holes will experience dilute conditions.

EDZ, crown space and spalling. The extent of the crown space is purely hypothesised. In reality, a crown space is considered unlikely or even impossible to develop with a swelling backfill, see Section 10.3.8. The implemented properties of the EDZ are also assessed to be pessimistic, see Section 10.2.2. Thus, the cases addressed are pessimistic variants, and no additional uncertainties relative to the simulations with base case repository properties are identified. However, the cases with modified repository related properties are of interest to propagate to subsequent radionuclide transport calculations since system performance is affected.

SDM-Site related model variants. The uncertainty in performance measures of the SDM-Site related hydrogeological base case parameterisation is addressed through a number of model variant simulations. Among the four variant cases studied, it is primarily the “Alternative DFN transmissivity-size relationship” variant cases that suggest any substantial additional variability (uncertainty). The results for these variant cases indicate that the performance measures of the semi-correlated relationship utilised in the hydrogeological base case model in general are more favourable than the other two correlation models. Thus it is important to propagate the other correlation models to assessment calculations. The results of the extended spatial variability variant case indicate that the effect of representing the full domain in a discrete fashion changes the discharge location pattern to a certain extent. Specifically, the incorporation of the additional discretely modelled fractures causes more particles to exit close to the repository. However, since the base case parameterisation already contains discharge locations close to the repository, it is argued that this variant does not warrant further consideration in the subsequent analyses.

In summary, the uncertainty in transmissivity-size relationship implies that all three correlation models need to be propagated for subsequent analyses of buffer erosion, canister corrosion and radionuclide transport. The other SDM-Site related variants do not warrant further consideration in the assessment.

Channeling. The calculated flow-related transport resistance (F) values can be used unmodified in subsequent radionuclide transport and oxygen penetration calculations. In SR-Can, F values were divided by a factor of ten to account for channelling. In SR-Site no such channelling factor is used based on motivations provided in the **Radionuclide transport report**. First, fracture-to-fracture variability is generally larger than within-fracture variability in aperture. Second, fluid can only enter and leave fractures on a limited area, significantly constraining the meander of flow paths. Third, substantial portions of the non-contacting fracture surface area outside of the dominant flow channels may still be accessible by diffusion within the fracture pore space and thus provide additional surface area for radionuclides to interact with the rock matrix.

The results obtained using the alternative conceptual model inherent in CHAN3D, see Choice of conceptual model above, also support the use of an unmodified flow-related transport resistance (F) value. In CHAN3D, the flow-wetted surface is not given through the discrete fractures in the model but rather estimated based on fracture frequency. Thus, similar estimates of F in both modelling tools indicate that the distribution of the flow-related transport resistance should not be modified in the discrete application.

Uncertainties related to the DFN model and its input data

A number of uncertainties in the underlying DFN model were discussed during SSM's review of SR-Site. In SKB (2013b, c) these are listed and discussed in detail. Below, a short summary is provided. Also, in Hartley and Roberts (2013) a more general and comprehensive evaluation of the adopted Hydro-DFN methodology is provided. Plans for future DFN modelling is briefly discussed in Section 15.6.3.

PFL measurement accuracy. It is concluded that the conditions at Forsmark are favourable for hydraulic tests using the PFL tool and the operations of the PFL measurements were of high quality. This permitted for the base level of flow (lower measurement limit) to be low ca 10^{-9} m²/s and sometimes even lower.

Sensitivity of model calibration to PFL measurement accuracy. If more flow-conducting fractures were apparent at a lower detection limit, the connectivity of the system would increase, implying more deposition holes would connect with the natural fracture system and have a Q1 path. However, the flow rates in these fractures would be less than those in the assumed connected EDZ at the top of the deposition hole; estimates of initial equivalent flux would be less than median values calculated in SR-Site, and estimates of flow-related transport resistance would be higher than median values in SR-Site. Therefore, the assessment of the integrity of the engineered barrier system is not considered sensitive to the presence of additional flow conducting fractures below the PFL detection limit. It is noteworthy that such additional low transmissivity fractures would provide an increased surface area for sorption and rock matrix diffusion as well as higher kinematic porosity without significantly affecting bulk hydraulic conductivity, and hence would have some beneficial effects on radionuclide transport calculations.

Representativeness of borehole data for the target area. Uncertainty related to bias in boreholes is deemed negligible. This is primarily based on the findings from the drilling of in total 25 core drilled and 38 percussion drilled boreholes at the site during the site investigations. Even if the different boreholes had different objectives (e.g. to confirm individual deformation zones and volumes in between), they provide a consistent conceptual view of the site. In short, the upper part of the bedrock is highly fractured, whereas the lower part has very few conductive fractures.

Sensitivity to fracture shape. The key parameter to measure at sites to determine hydraulic fracture connectivity is the flow conducting surface area per unit volume (for some threshold on fracture transmissivity suitable to safety assessment, see above), which can be inferred from the fracture intensity (Terzaghi corrected for orientation bias (Terzaghi 1965)) of flow measurements detected by the PFL method. Fracture shape is considered to be of secondary importance. It is expected that calibration of model variants including different aspect ratio shapes against observed connectivity and flow distributions in boreholes will yield models with similar connected fracture surface areas per unit volume. A number of studies summarized in SKB (2013c) support this conclusion; however, results in Hartley et al. (2018) indicate that the issue may be more complex. Specifically, when models with different aspect ratios were calibrated against the same data and compared (aspect ratio 1:1 vs. 3:1) it was observed that connectivity increased and flow became more directional with more pronounced transport anisotropy in the model with higher aspect ratio. However, the models used in Hartley et al. (2018) employed a so-called chequerboard approach where fractures are partially closed, and hence results may not be directly comparable to the PSAR approach.

Sensitivity to channelisation of flow within fractures. It is expected that were alternative DFN models calibrated with greater spatial variability within fractures (e.g., internal aperture variability) rather than between fractures, then the connected fracture surface area with specific capacity above the PFL detection limit would remain similar to that derived in SDM-Site. The calibration of specific capacity on the PFL flow distribution would also be expected to constrain the predicted distribution

of initial equivalent flux around the deposition holes to be similar to that derived in SR-Site. Likewise, flow-related transport resistance would be expected to be largely unchanged since it depends on flow conducting surface area, which can be estimated from PFL fracture intensity, and on flow rate which distribution is measured by the PFL tool itself.

Sensitivity to spatial distribution. The Geo-DFN analysis concludes that a Euclidean spatial distribution is appropriate at scales greater than 30 m; furthermore, PFL-detected flowing fractures are spaced on the order of a hundred meters or more at repository depth. Thus, with the current data sets, there is limited scope or basis for applying alternative spatial models to Hydro-DFN modelling of the deep bedrock.

Sensitivity to interpreted depth trend in deformation zone transmissivity to spatial distribution. Alternative transmissivity models were not developed in SDM-Site. Instead, focus was put on conditioning the propagated transmissivity model against measured data. The overall depth trend in transmissivity of deformation zones is based on an interpretation of site data of the observed decrease in maximum and geometric mean transmissivity with depth. This pattern is consistent with the expected sensitivity of effective hydraulic aperture to the increase of *in situ* stress with depth. There is also a large lateral heterogeneity in transmissivity, equating to a 95 % confidence interval spanning 2.5 orders of magnitude. The same magnitude of variation in the geometric mean occurs over 600 m of depth according to the interpreted trend, i.e. from the surface to below the repository, and so the realisations will create transmissivities at repository depth equal to those at the surface at some places in each realisation. The propagated model has been found to reproduce observed hydraulic responses at about 600–700 m depth during the conducted interference tests. The ten realisations in SR-Site (on which also the PSAR is based) including lateral heterogeneity in the deformation zones can thus be considered a proxy for uncertainties in the depth trend also.

Sensitivity to intensity-scaling (spatial model). A sensitivity analysis of spatial model was not performed since it is believed that uncertainties in intensity-size scaling relationships are of greater significance to safety assessment than the spatial model. Specifically, it was not considered representative to adopt alternative intensity-size concepts developed in the Geo-DFN, in which no depth trend in intensity was interpreted, while a huge decrease with depth of the intensity of flow conducting fractures was detected by the PFL method. This feature of the system is in the current study implemented using discrete depth zones.

10.3.7 Chemical evolution in and around the repository

Introduction

During the initial temperate period after closure, the infiltration of meteoric waters, the displacement of the Baltic shore line and changes in annual precipitation will influence the hydrology of the site as described in Section 10.3.6. These phenomena induce changes in the geochemical composition of groundwater around the repository.

One of the questions to be addressed for this period is whether the chemical environment will remain favourable for the containment function after repository closure. The most important parameters, as discussed in Sections 8.3 and 8.4, are redox properties (safety function R1a in Figure 10-2) and salinity (safety function R1b and R1c). Other factors to consider are the groundwater content of potassium, sulphide and iron(II), as they might affect the chemical stability of the buffer and the canister (safety function R1d) and the effect of grouting in the geosphere and cement materials in the engineered barriers that could affect groundwater pH (safety function R1e).

Modelling

Groundwater compositions are modelled through advection, mixing and chemical reactions with fracture-filling minerals. The results of the regional-scale groundwater flow modelling are used as input to a geochemical mixing and reaction model. The aim has been to obtain equivalent groundwater models for hydrogeology and geochemistry. The loose coupling of the two models also allows a description of the geochemical heterogeneity, which otherwise would be hard to attain. Indirectly the matrix diffusion effects are also accounted for because the regional-scale model considers the diffusion of salt in and out of the rock matrix (see Joyce et al. (2010) and Section 5.3 in the **Geosphere process report** as well as Section 10.1.3). This influences the fractions of end members used to assess the chemistry evolution.

The groundwater flow modelling is described in Section 10.3.6. One of the processes modelled is the transport of fractions of selected reference waters (altered meteoric, marine, glacial, brine and an older meteoric water). By this approach, the proportions of these waters may be obtained at any time for the different parts of the studied rock volume, as illustrated in Figure 10-38. The driving forces for groundwater flow during this temperate period are the topographic gradient and the density differences between overlying water bodies.

The waters of meteoric origin entering the modelled system are essentially rain, but due to their chemical reactivity these waters react quickly in the overlying soil layers, if there are any, and with the bedrock minerals in the initial few metres (perhaps some tens) of their pathways. Microbial activities contribute substantially to these processes. As a result, meteoric waters quickly obtain small amounts of solutes which may be seen for example in groundwaters sampled both at Forsmark and Laxemar in the upper ≈ 100 m of rock. This has been reflected in the composition chosen for the reference water labelled “Altered Meteoric” in the mixing calculations.

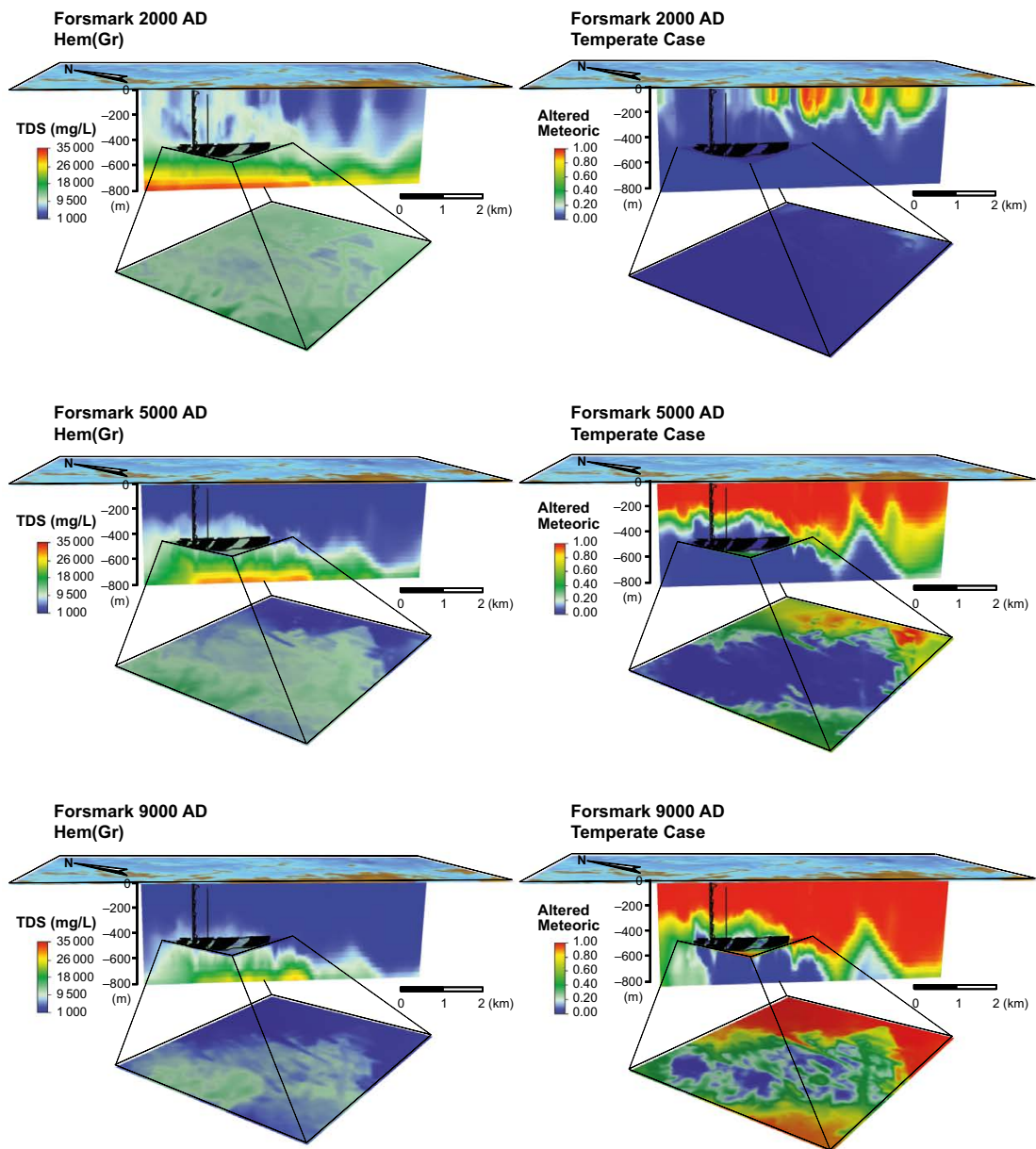


Figure 10-38. Distribution of TDS (total dissolved solids, mg/L, left) and Altered Meteoric fraction (right) for Forsmark in vertical slices and in an enlarged horizontal slice showing the repository area at times equal to (from top to bottom) 2000 AD, 5000 AD and 9000 AD. From Salas et al. (2010). The figure shows the gradual inflow of Altered Meteoric water (defined in the text), and the corresponding decrease in TDS.

Some groundwater components behave as “conservative”, that is, they do not participate to a large extent in chemical reactions, and they are mostly affected by groundwater mixing. Examples are the water isotopes such as deuterium and ^{18}O , as well as chloride, and, to some degree, sodium and calcium. However, most of the groundwater chemical components are reactive, for example Fe^{2+} and Fe^{3+} , H^+ , and bicarbonate. Sodium and calcium may participate in ion-exchange processes and calcium participates readily in the precipitation and dissolution of calcite (see Section 5.4 of **Geosphere process report** and Auqué et al. 2013), but in spite of this, the buffer capacity of the saline waters is such that these elements behave almost as conservatively. Sulphate may be reduced to sulphide under hydrothermal conditions, that is, at high pressure and temperature. At lower temperatures, as are applicable in this context, sulphate can only be reduced to sulphide by microbially mediated reactions with organic matter.

Due to the factors mentioned above, the evolution of groundwater components cannot be dealt with through calculations involving only groundwater mixing, and it has instead been modelled by using the results from the hydrogeological model as input to fully coupled chemical mixing and reaction calculations. The computer code PhreeqC (Parkhurst and Appelo 1999) was used for that purpose. The results of this modelling are reported in the **Data report**, Section 6.1, and in Salas et al. (2010) and Joyce et al. (2015). The minerals calcite, quartz, hydroxyapatite and either a Fe(III) oxyhydroxide or an amorphous Fe(II) sulphide have been equilibrated with the mixtures at all points in space and time.

The type of results that can be obtained using this procedure are illustrated in Figure 10-39, which shows a comparison between the calculated pH and the concentration of Ca as a function of depth with the data obtained in the site investigation programme. Figures comparing the model results to site observations for Mg and PO_4^{3-} can be found in Section 6.1.2 of Salas et al. (2010) and for most of the remaining major groundwater constituents (TDS, alkalinity, Al, Br, Cl, Eh, F, Fe_{Total} , Li, Mn, K, Si, Na, Sr, sulphate, and sulphide) in Puigdomenech (2013). Modelling of other major groundwater constituents is not performed, either because they do not affect safety function indicators (e.g. iodine) or because their distribution is mainly controlled by microbial activity (DOC, TOC, NO_2^- , NO_3^- , and NH_4^+) and so are problematic to quantitatively model following the approach of Salas et al. (2010). Nevertheless, a qualitative assessment in Section 8 of Salas et al. (2010) shows that their concentrations over a glacial cycle are not expected to affect post-closure safety; this is further discussed in corresponding sub-sections below.

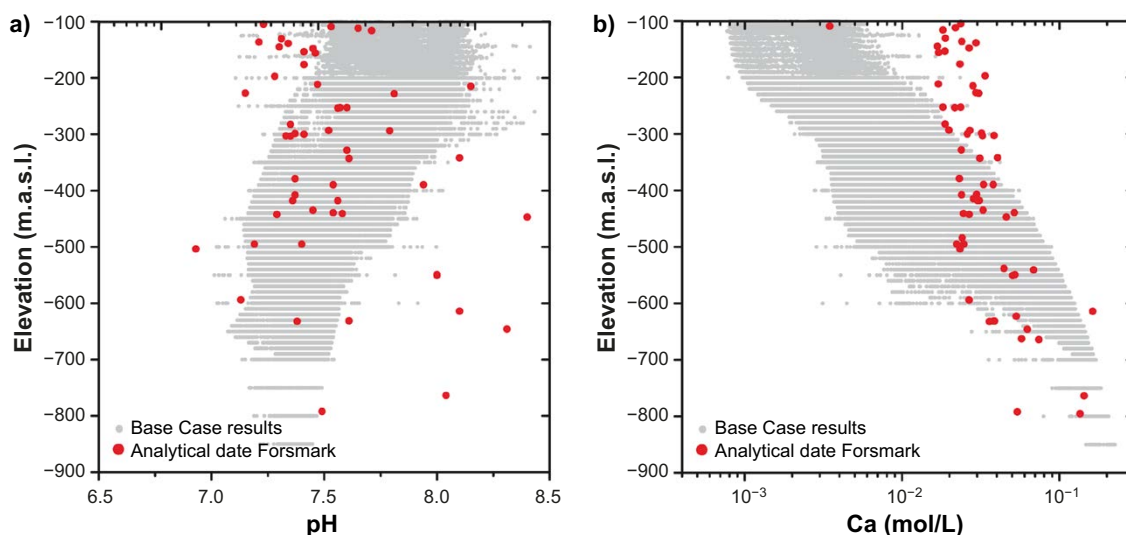


Figure 10-39. The pH and the concentration of calcium in groundwaters sampled in boreholes at the Forsmark site (red dots) compared with values calculated using the proportions of reference waters obtained from the hydrogeological model as input for chemical mixing and reactions, including, among others, calcite dissolution and precipitation (grey dots). From Salas et al. (2010). The groundwater data of category 3 or better (Laaksoharju et al. 2008) have been plotted. The calculated values correspond to the vertical slice shown in Figure 10-38.

Several approximations have been used in this modelling strategy. The minerals chosen to be at equilibrium with the groundwater mixtures are reasonable in that they include relatively fast groundwater/rock interactions, as in the case of calcite, or characterize the silica levels observed in the groundwaters, as in the case of quartz. However, they are a limited subset of those likely to be present. Nevertheless, even if other solid phases could be stipulated, it would not be possible to justify their selection and the minerals selected effectively represent the chemical effects observed in the reactive components discussed here. The upper part of the simulated domain, less than ≈ 100 m depth, is more affected by groundwater flow, mixing and infiltrating waters that are chemically more aggressive and the assumption of chemical equilibrium with the selected minerals is possibly less well justified than at greater depths.

As Figure 10-39 shows, the combination of the hydrogeological model results with the geochemical equilibrium assumption results in depth trends that do not fully correspond with the observed concentrations. The mismatch in the calcium concentrations, for example, indicates either insufficiencies in the mixing proportions obtained from the hydrogeological model (e.g. Section 5.2 of the **Geosphere process report**), or it shows that some of the processes that have not been included in the present model have a significant influence in the concentration of the individual groundwater chemical components. The model results show better consistency with the observed concentrations of most of the other groundwater constituents (Puigdomenech 2013). One of the limitations in the geochemical modelling strategy followed within SR-Site is that the composition of the marine reference water should vary with time as the waters change from a Littorina Sea composition at ≈ 4000 BC to the present Baltic Sea composition, which will be further diluted in the future. This has been properly taken into account in the hydrogeological model, but for the geochemical modelling the Littorina salinity has been assumed as the reference water used in mixing calculations. This assumption is justified by the fact that less saline marine waters do not displace the Littorina component, which is denser, whereas meteoric waters displace the denser marine waters due to topographic effects.

A full propagation of uncertainties, from the hydrogeological modelling into the geochemical calculations, has not been performed. In addition, the natural variability and other uncertainties in the compositions of the reference waters used for mixing (altered meteoric, marine, glacial and brine) have not been propagated to the mineral reaction calculations (see Section 5.2 in the **Geosphere process report**). It is, therefore, probable that at any given time the real variability in the chemical compositions of groundwaters is somewhat larger than that seen in the model results presented here.

Evolution of salinity

As mentioned previously in Sections 10.2.3 and 10.2.5, the salinity distribution may initially be affected during repository operation by perturbations in the hydraulic conditions, although in the case of Forsmark this perturbation is small due to the low hydraulic conductivity. After repository closure, the backfilled tunnels will become water saturated. The modelling discussed briefly in Section 10.3.6 suggests it will take several hundred years for the repository to reach full saturation, with a relatively short period of rapid initial inflow followed by an asymptotic regime during which the inflow gradually decreases. The effects of the open repository on groundwater salinities at Forsmark, which will be minor, are expected to disappear during the resaturation period.

As explained in the introduction to this subsection, during the remaining part of the initial temperate period after repository closure, groundwaters will be affected by increasing amounts of waters of meteoric origin, see Figure 10-38. On a regional scale this corresponds to a gradual decrease of the groundwater salinity, especially in the upper part of the modelled rock volume. The salinity distribution for this time period has been calculated using the ConnectFlow model presented in Section 10.3.6. Figure 10-40 presents the calculated distribution of salinities at Forsmark at (470 ± 20) m depth at four time steps. Towards the end of the modelled period 25 % of the groundwaters in the repository volume have less than 3 g/L of dissolved salts at repository depth, whereas all the groundwaters had salinities above 6 g/L at the start of the simulation, that is, at repository closure.

In conclusion, the salinities during the first temperate period following repository closure will remain limited at Forsmark, ensuring that the swelling properties of the buffer and backfill are not negatively affected, cf. the safety function indicator R1b.

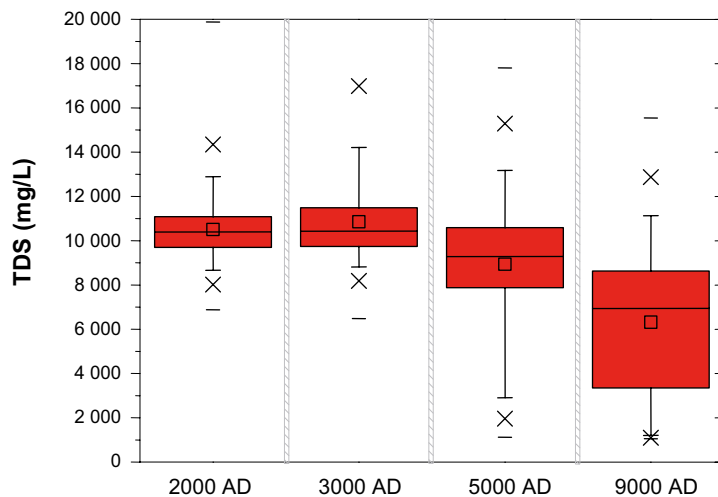


Figure 10-40. Box-and-whisker plots showing the statistical distribution of the calculated TDS (total dissolved solids) at the Forsmark repository depth. The statistical measures are the median, the 25th and 75th percentile (box), the mean (square), the 5th and 95th percentile (“whiskers”), the 1st and 99th percentile (crosses) and the maximum and the minimum values. The figure shows the effect at repository depth of the gradual inflow of meteoric water.

Evolution of concentrations of other natural groundwater components

The increasing proportions of groundwaters of meteoric origin will decrease the overall salt content of the groundwaters as discussed in the previous sub-section. However, the effects on the individual chemical constituents will depend on their reactivity. The evolution of the different chemical properties of groundwaters has been estimated by coupling the results from the hydrological calculations with a mixing and chemical reaction model, as described in the introduction to this section. The final objective has been to check if, during its evolution, the chemical environment around the repository fulfils at all times the safety function indicator criteria R1a to R1e. In this sub-section, the results are discussed for cations (safety function indicator R1c), potassium, sulphide and iron (R1d), and alkalinity and pH (R1e). The results for salinity (R1b) are discussed in the previous sub-section, whereas the results for redox conditions are presented in the following sub-section.

Cations

The concentration of cations (safety function indicator R1c) is important in that their presence decreases the stability of colloids (see the discussion on colloids later in this section). In groundwaters that are too dilute, colloids might enhance the transport of radionuclides. In addition, as the buffer swells into fractures, montmorillonite colloids may be released and transported away by dilute groundwaters. The criterion for the safety function indicator R1c is expressed in charge equivalents as $\Sigma q[M^{q+}] > 8 \text{ mM}$, as available experimental data suggests that montmorillonite colloids are not stable at cation concentrations above this limit (Birgersson et al. 2009).

The cations contributing with the highest charge concentrations in the groundwaters at Forsmark are calcium and sodium, and to a much lesser extent magnesium and potassium. Because the concentration of calcium has double the weight of sodium in the safety function indicator, $\Sigma q[M^{q+}]$, calcium is the most important element in this context. The groundwaters sampled at Forsmark, Laxemar and Simpevarp show a good correlation between $\Sigma q[M^{q+}]$ and the total dissolved solids (TDS). The safety function indicator criterion $\Sigma q[M^{q+}] > 8 \text{ mM}$ corresponds to $\text{TDS} > 0.61 \text{ g/L}$, that is, a salinity $> 0.061 \%$ for these waters.

Calcium participates in water-rock interactions as carbonates and may be released from the weathering of feldspar. The other major divalent cation is magnesium, which is normally regulated in granitic groundwaters by the precipitation and dissolution of chlorite, a mineral that may have a wide range of compositions. In general, magnesium concentrations in groundwaters are much lower than those of calcium, and because of the low solubility of chlorites and the uncertainty in the composition of this mineral, the modelling of Mg concentrations is much more uncertain than that of Ca.

The calcium concentrations observed at present at Forsmark increase rapidly with depth in the top ≈ 100 m of the bedrock, see Figure 10-39. The selected meteoric reference water for Forsmark in the mixing and reaction calculations corresponds to groundwaters sampled at 50 to 150 m depth, which have the composition expected for a rain water that has travelled a short distance in the fractures of the granite at Forsmark.

The results of coupling the hydrogeological model results with the mixing and reaction calculations, including equilibrium with calcite, are shown in Figure 10-41, which illustrates the gradual dilution of the groundwaters at repository depth due to the inflow of superficial waters of meteoric origin. It should be noted that the Ca concentrations in groundwaters found at present in the upper 200 m vary between 0.2 and 30 mM, according to the data shown in Figure 10-39. This spread of the data is not included in the meteoric reference water used in the mixing calculations, and, therefore, the variability shown in Figure 10-41 is probably underestimated.

It may be concluded from these modelling results that for the whole temperate period following repository closure cation charge concentrations at repository depth at Forsmark will, in general, remain higher than 8 mM, that is, above to the limit where montmorillonite colloids start to become unstable. However, this analysis based on the hydrogeological simulations described in Section 10.3.6, does not consider the impact of the most extreme pathways from the surface to the repository, and additional calculations were performed to investigate this issue, see Section 10.3.6, subsection “*Penetration of dilute water*”. As seen from the results depicted in Figure 10-33 and in Table 10-4, about 0.24 percent of the deposition holes may actually experience dilute conditions during the first ten thousand years. Ion exchange processes are also excluded from the models, but calculations by Auqué et al. (2013) show that their inclusion would not change the results of the cation charge concentrations.

Potassium, sulphide, iron, H₂, CH₄ and dissolved organic carbon

Potassium concentrations are generally low in the groundwaters sampled at Forsmark, as observed also in other Fennoscandian sites in granitic rocks. Solubility control by sericite has been proposed as a mechanism controlling the maximum concentrations of potassium (Nordstrom et al. 1989), but ion-exchange processes cannot be ruled out. Even though the exact mechanism is not known, all available groundwater data indicate that the increased infiltration of waters of meteoric origin will not increase the potassium concentrations found at present. The reaction modelling performed within SR-Site is not well suited to constrain potassium concentrations because, as mentioned, there is not enough information available on the possible reactions that could control this element. The mixing calculations give maximum values of [K⁺] below 4 mM at any time for Forsmark. Auqué et al. (2013) reached the conclusion that unrealistic results for potassium may be obtained when combining some aluminosilicate equilibrium reactions.

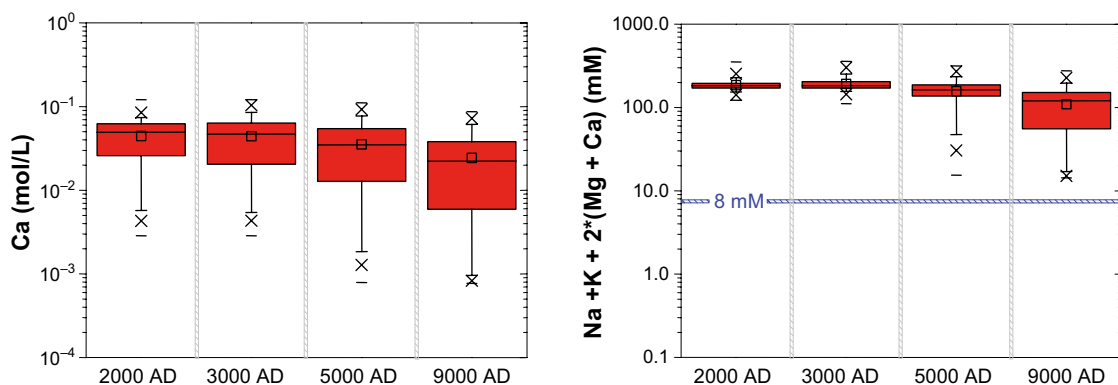
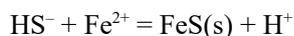


Figure 10-41. Box-and-whisker plots showing the statistical distribution of the calculated Ca concentrations and the safety function indicator $\Sigma q[Mq^+]$ for the positions located within the candidate repository volume at Forsmark. The statistical measures are the median, the 25th and 75th percentile (box), the mean (square), the 5th and 95th percentile (“whiskers”), the 1st and 99th percentile (crosses) and the maximum and the minimum values.

The content of sulphide in groundwaters is controlled by a steady state between microbial sulphate reduction and the processes that remove sulphide: oxidation and precipitation with metals. Under oxidising conditions, for example in superficial waters, sulphide is quickly oxidised to sulphate. Under reducing conditions, dissolved Fe^{2+} is normally present and the maximum sulphide concentrations are regulated by the precipitation of Fe(II) sulphide according to



with $\log_{10}K = \log_{10}([\text{H}^+]/([\text{Fe}^{2+}][\text{HS}^-])) \approx 3$. At a pH between 7 and 8 one obtains $\log_{10}([\text{Fe}^{2+}][\text{HS}^-]) \approx -10$ to -11 . In most groundwaters $\log_{10}[\text{Fe}^{2+}] \geq -6$ which sets the maximum $\log_{10}[\text{HS}^-]$ in the range -4 to -5 .

Sulphide concentrations were analysed during the site characterisation process and during the subsequent groundwater monitoring. The data are often below the detection limit of the analysis procedure, but in some borehole sections sulphate reduction has taken place during the monitoring period and relatively high sulphide concentrations have been observed. This process has been studied and the conclusion is that accumulated organic gunge and biofilm in the standing monitoring equipment can result in microbial sulphate reduction. It is still not known why this occurs only in some of the monitored sections. When groundwater pumping is initiated for sampling during monitoring, large enough volumes of groundwater must be allowed to rinse the borehole section, tubing and standpipe in order to obtain a representative sample for the fracture groundwater. This cannot be controlled unless a time series is analysed. Although monitoring sampling procedures have now been modified to take this into account, some of the earlier monitoring groundwater analyses were of dubious quality, as discussed by Tullborg et al. (2010).

To address this problem a careful review of all sulphide data has been performed (Tullborg et al. 2010) and in order to avoid bias due to having many samples in some borehole sections and a few in other locations, a group of samples representing the sulphide concentrations in the different sampling points has been selected, cf. Figure 10-42. The maximum sulphide value for Forsmark is 1.2×10^{-4} M from KFM01D at 343 metres depth. This is, however, an exception and, for practically all of the groundwaters, the sulphide concentration is below 1.3×10^{-5} M. No correlation was found between hydrogeological information on the fractures being sampled and the sulphide data.

Because sulphide in groundwaters is mainly produced by bacterial sulphate reduction, it is essential to have data on the reductants (electron donors) to evaluate the potential for sulphide production over long periods of time. Dissolved hydrogen, H_2 , methane, CH_4 , and organic carbon, DOC, are potential reductants that may be used in many microbial processes, including sulphate reduction. It must be noted that the sulphide concentrations found at present in Forsmark's groundwaters, Figure 10-42, already reflect the steady state between the microbial sulphide production that is achieved with the present levels of H_2 , CH_4 and DOC, and the consequent formation of sulphide minerals (see Section 5.7 of the **Geosphere process report**).

The overall reactions with methane or hydrogen are:



In Figure 10-43 it is seen that the maximum possible contribution to sulphate reduction from H_2 is modest, given the concentrations of this gas found in the groundwaters. If all hydrogen was quantitatively used by microbes in sulphate reduction, at most the sulphide concentration would increase to $10^{-5.6}$ M. Methane can be used by bacterial consortia to achieve sulphate reduction. Figure 10-43 shows that methane concentrations are as a rule below 10^{-5} M. The "outlier" in Figure 10-43 corresponds to borehole KFM01D at 445 metres depth. As shown in Section 10.2.5, the corrosion of iron materials left in deposition tunnels is a potential source of hydrogen. However, because of the simultaneous production of iron corrosion products that will react with sulphide, if bacterial sulphate reduction takes place, the corrosion of Fe-materials is not expected to contribute significantly to the dissolved sulphide contents of the groundwaters around the repository.

The contribution from methane and hydrogen to microbial sulphate reduction, and hence, to the observed sulphide concentrations is deemed to be minor because the estimated flows of these gaseous species are $< 3 \times 10^{-10}$ mol/($\text{m}^2 \cdot \text{y}$) (Delos et al. 2010).

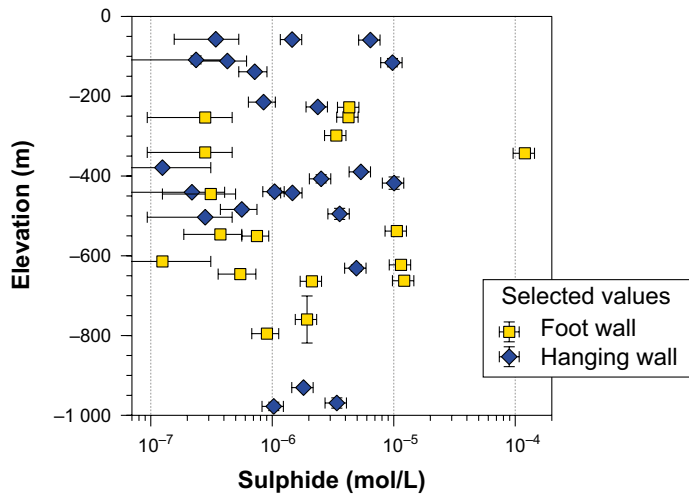


Figure 10-42. Selected set of sulphide concentrations in contemporary groundwaters of the Forsmark area below 50 m depth (Tullborg et al. 2010). In general only one value has been selected for any given borehole section for cases where several analyses have been reported. Data below the detection limit of the analyses, which is between 9×10^{-7} and 6×10^{-8} M, are not shown in this diagram. “Foot wall” data refer to sampling points below 100 m depth and below the A2 and F1 fracture zones, while “Hanging wall” are the remaining data.

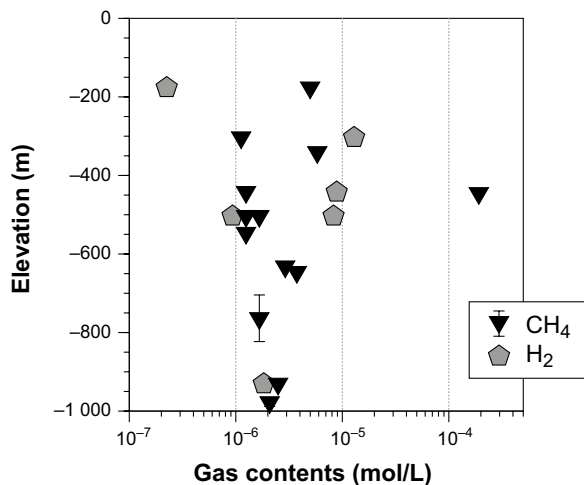


Figure 10-43. Methane and hydrogen concentrations in contemporary groundwaters in the Forsmark area. Samples having hydrogen values below the detection limit have not been plotted.

Dissolved organic carbon (DOC) in groundwaters can, at least in principle, be involved in microbial processes. In a study by Osterholz et al 2022 it is shown that the DOC that reaches the deep continental fractures are mainly terrigenous in origin and the vast majority of the DOC is recalcitrant to degradation. Acetate, which can increase the risk of stress corrosion cracking, is a minor part of the DOC, and the evaluation in Salas et al. (2010) indicates that its concentration during temperate periods is expected to be in the micromolar range. The theoretical potential for sulphate reduction, in terms of amount of dissolved carbon, is quite large as seen in Figure 10-44. Given the relatively large sulphate concentrations, at least in the upper ~500 m, if there was any fraction of the DOC that could be used in bacterial sulphate reduction, then that organic carbon would be quickly consumed, and it can thus be concluded that the observed DOC concentrations correspond mainly to organic matter that is not readily accessible for sulphate-reducing bacteria or to fermenting bacteria that produce the small organic acids needed by sulphate-reducing bacteria. Pedersen et al. (2012) and Bengtsson et al. (2019) have shown that upon addition of energy sources such as acetate and hydrogen, further sulphide production in groundwaters is stimulated. This further supports that the observed DOC is not bioavailable. Therefore the sulphide concentration distributions used in the copper corrosion modelling, see Sections 10.3.12 and 10.4.8, have not been increased to take into account dissolved organic carbon.

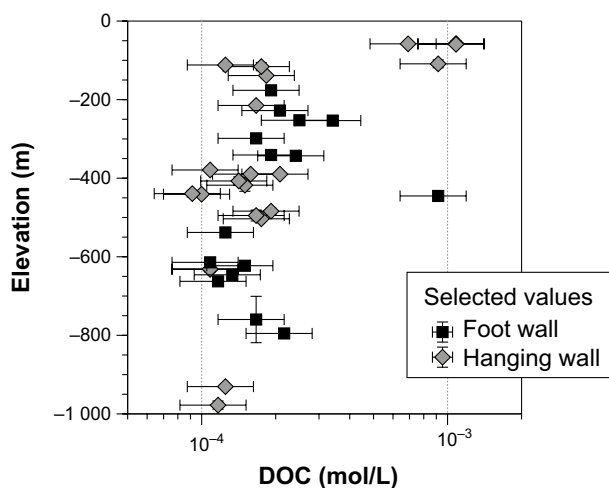


Figure 10-44. Dissolved organic carbon in groundwaters analysed in Forsmark and obtained from below 50 m depth. Values below the detection limit have not been plotted. “Foot wall” data refer to sampling points below 100 m depth and below the A2 and F1 fracture zones, while “Hanging wall” are the remaining data.

For the assessment of microbial sulphide production in a partially eroded buffer and its potential consequences for copper corrosion (Section 10.3.13) it is, however, warranted to seek an upper bound on the concentration of bioavailable DOC. Bacterial sulphate reduction preferentially uses small organic molecules such as acetate, formate and propionate (Glombitza et al. 2015), which constitute only a fraction of the DOC analysed. Shen et al. (2015) conducted a long-term study of groundwater in a fractured-rock aquifer in the Carolina slate belt in the U.S in order to monitor bioavailability of DOC. It was concluded that only 4–12 % of the DOC in groundwater is bioavailable. Thus, a reasonable estimate to use as the portion of bioavailable organic carbon in groundwater is taken to be 10 % of the analysed DOC which is at most 1 mmol/L (Figure 10-44). The exact fraction of the DOC that will be available to sulphate-reducing bacteria over very long time scales cannot be established. As mentioned above, the sulphide concentrations found at present in Forsmark’s groundwaters, Figure 10-42, already reflect the steady state between the microbial sulphide production that is achieved with the present levels of H_2 , CH_4 and DOC, and the consequent formation of sulphide minerals (see Section 5.7 of the **Geosphere process report**).

In the reaction modelling performed within SR-Site, apart from the “marine” and “deep-saline” components, the reference waters used in the mixing calculation were assumed to contain no sulphide. The marine waters infiltrating in the rock may be relatively rich in organic matter, and observations at Äspö have shown that some sulphate reduction takes place in these groundwaters. Therefore, the “marine” component was assumed to be in equilibrium with solid Fe(II) sulphide.

The results of mixing the marine component with the other reference waters are shown Figure 10-45, illustrating the decrease in sulphide values as meteoric waters become increasingly dominant with time. In the calculations, equilibrium with Fe(III) oxyhydroxide has been imposed. A comparison with Figure 10-42 indicates that the mixing/reaction calculations have very limited validity for sulphide which is instead affected by microbial sulphate reduction.

From the sulphide data in Figure 10-42, from the results of the hydrogeological and geochemical modelling described above, and from the understanding of the microbial sulphate reduction processes and the data relating to it on CH_4 , H_2 and DOC, it is concluded that during the initial temperate period following repository closure the sulphide concentrations in the groundwaters will remain at the levels found at present in Forsmark. Sulphide concentrations in a given fracture are expected to vary over a temperate period, but it cannot be concluded that the temporal variations in that fracture will be sufficiently large that the time averaged concentration in the fracture would correspond to the average of sulphide concentrations sampled at Forsmark today.

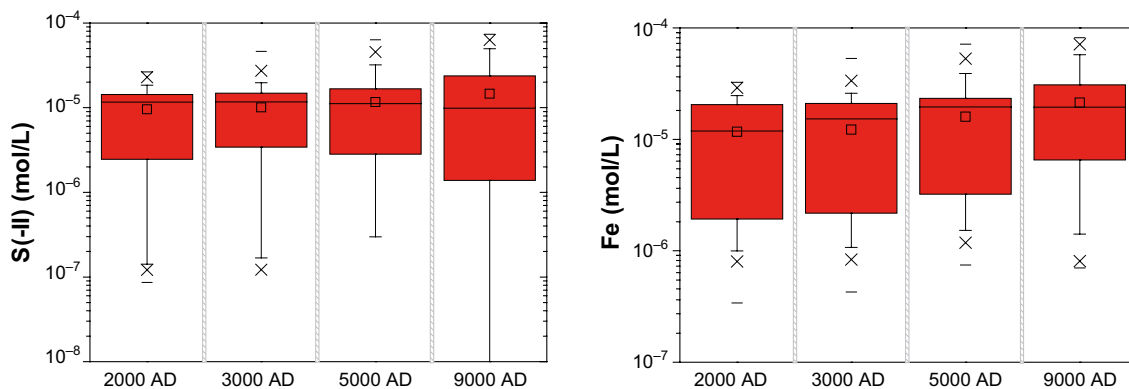


Figure 10-45. Box-and-whisker plots showing the statistical distribution of the calculated total sulphide and total iron concentrations for the positions located within the candidate repository volume at Forsmark. The statistical measures are the median, the 25th and 75th percentile (box), the mean (square), the 5th and 95th percentile (“whiskers”), the 1st and 99th percentile (crosses) and the maximum and the minimum values.

The conclusion reached here concerning sulphide concentrations in groundwaters is propagated in later sections of this chapter to the other time periods of the reference evolution, that is, periglacial and glacial. Although microbial sulphide production might increase during the expectedly short periods when the repository area at Forsmark is submerged under marine waters, especially at depths above ~300 m where there is at present some evidence of past infiltration of marine waters, the sulphide concentrations observed at present already reflect the enhanced sulphide production during the relatively recent Littorina sea stage. On the other hand, during the expectedly long periods when the repository area is covered by an ice sheet, the sulphide levels would decrease because of low levels of sulphate, H₂, CH₄ and DOC in the glacial meltwaters, and selecting the present sulphide concentrations during the glacial periods is judged to be a pessimistic approach.

The concentration of Fe²⁺ is regulated by a complicated set of reactions including the slow dissolution of Fe(II) silicates, such as chlorite and biotite, the precipitation of Fe(II) sulphides and redox reactions. The concentrations of Fe³⁺ are in general negligible in granitic groundwaters, as the oxyhydroxides of Fe³⁺ are quite insoluble and they precipitate quickly. The results from the reaction modelling in SR-Site are displayed in Figure 10-45, which shows that the calculated Fe concentrations of groundwaters at repository level are expected to increase with time as waters of meteoric origin, assumed to have [Fe] ≈ 10⁻⁵ mol/L, become increasingly dominant.

In conclusion, during the initial temperate domain following repository closure, the potassium concentrations are expected to remain ≤ 0.004 mol/L, sulphide concentrations are expected to remain at the levels found at present, that is, ≤ 10⁻⁵ mol/L for most deposition positions with a probability that for some deposition holes the surrounding groundwaters will have sulphide concentrations as high as 10^{-3.9} M, as shown in Figure 10-42, and iron concentrations are expected to gradually increase but to remain below 10⁻⁴ mol/L.

pH and bicarbonate

Acidity, expressed as pH, is a master variable controlling most chemical processes. Too low or too high values would affect, among others, the corrosion of the canister, the dissolution of the spent fuel, the solubility limit of several radionuclides, etc. Bicarbonate, HCO₃⁻, is also an important parameter that can affect spent fuel dissolution and solubility limits. For pH and bicarbonate, the mixing and reaction calculations are dominated by the precipitation and dissolution of calcite. The results show that the pH values remain approximately in the range 6.5 to 8, and that bicarbonate values increase with time being up to about 0.0075 mol/L at 9000 AD, see Figure 10-46. Sensitivity analyses indicate that, if weathering of aluminosilicate minerals and ion exchange (see Section 5.7 of the **Geosphere process report**) were incorporated into the geochemical evolution simulations, the groundwater pH might increase to a maximum of 9 by 9000 AD in certain cases (Auqué et al. 2013). It may be shown that the calculated partial pressures of dissolved carbon dioxide increase with time, as it is assumed in the modelling that the infiltrating meteoric waters have a higher CO₂ content than the other waters in the system. The conclusion is that the criterion for the safety function indicator R1e (pH < 11) is fulfilled during the whole temperate period following repository closure.

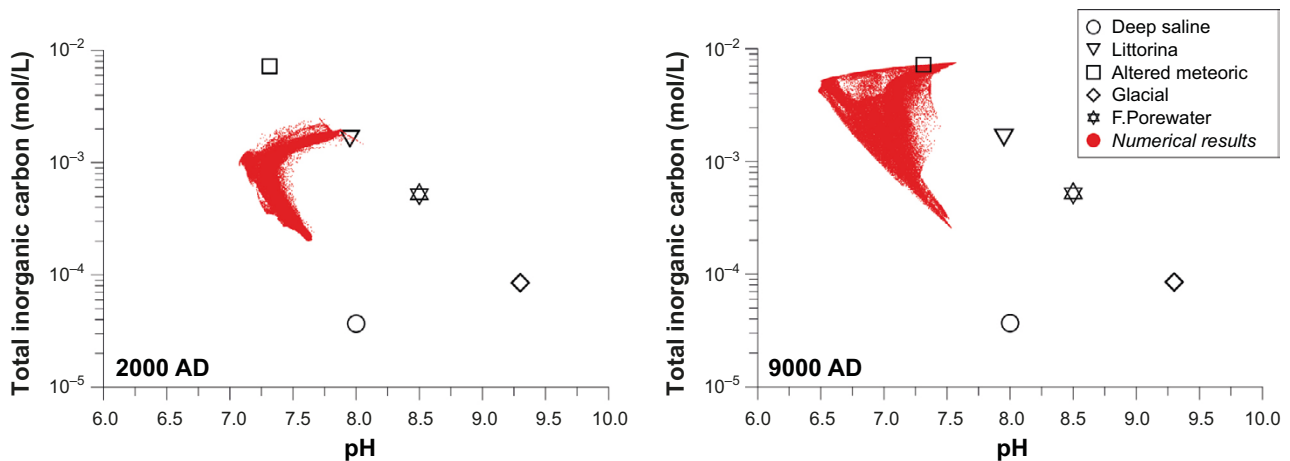


Figure 10-46. Correlation and evolution of the calculated pH values and the concentrations of the total inorganic carbon for the positions located within the candidate repository volume at Forsmark corresponding to 2000 AD (left) and 9000 AD (right).

Chloride and sulphate

Chloride concentrations below 2 M imply that chloride assisted corrosion of the canister can be excluded (safety function indicator R1f). Chloride concentrations are also relevant when selecting radionuclide transport properties (sorption coefficients). Sulphate is important when determining the solubility limits for radium, although not a safety function indicator. These two components behave almost conservatively, i.e. they participate in chemical reactions only to a very limited extent, and they have been modelled by mixing calculations in SR-Site. Figure 10-47 shows that the groundwater concentrations of chloride and sulphate at repository level tend to decrease with time as waters of meteoric origin become increasingly dominant. Details on these results may be found in Salas et al. (2010).

Nitrogen compounds

Nitrite and ammonium would increase the risk of stress corrosion cracking for the copper canisters. The evaluation presented in Salas et al. (2010) indicates that nitrite concentrations are expected to be below $\approx 10^{-7}$ mol/L, while ammonium concentrations will be below 2×10^{-4} mol/L during this period.

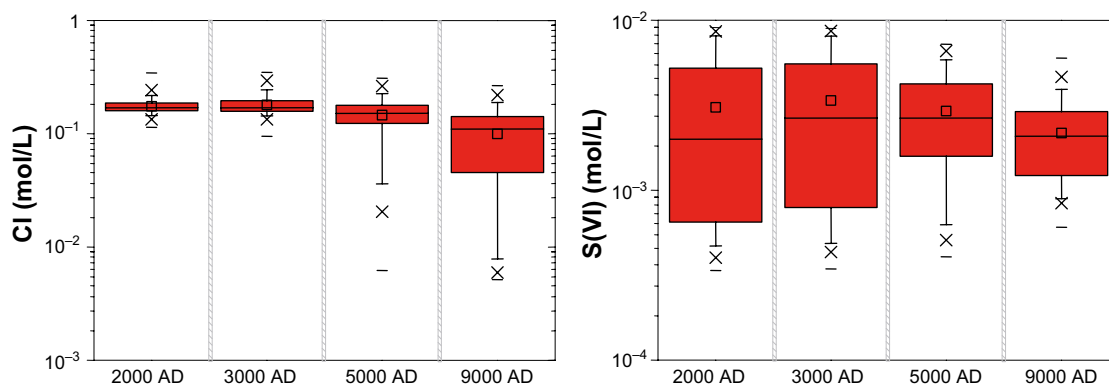


Figure 10-47. Box-and-whisker plots showing the distribution of total chloride concentrations (left) and of total sulphate concentrations (right) in Forsmark at 400 m depth as a function of time. The statistical measures are the median and the 25th and 75th percentile (box) and the 5th and 95th percentile (“whiskers”) the 1st and 99th percentile (crosses) and the maximum and the minimum values.

Colloids

Colloids may sorb irreversibly some radionuclides, and given the appropriate conditions, colloids are transported with the groundwater flow. Because of this, colloids can affect the transport of radionuclides that would otherwise be fully retained in the rock. Colloids are partly stabilised by electric repulsions between charges in their surfaces. Some of these charges arise from the dissociation of acid-base groups, and are, therefore, pH dependent. The presence of cations in the water counteracts these charge effects. The results from the modelling calculations show that colloids will not be especially stable during this temperate period, because the pH values, salinities and cation concentrations will be high enough to destabilise them. The conclusion is that colloid concentrations are expected to remain at the levels that have been measured during the site investigations, i.e. less than 200 µg/L (Hallbeck and Pedersen 2008).

Evolution of redox conditions

Redox conditions are often reported as the value for the redox potential, Eh, and this value is used when selecting radionuclide transport properties (sorption coefficients) and when calculating the solubility limit of many radionuclides. Evidence from the Äspö laboratory and other Swedish sites, shows that anoxic conditions prevail in the host rock even at a short distance from tunnel walls or from the ground surface. Air will be entrapped in the buffer and backfill, but anoxic conditions are expected to be established soon after the tunnels become resaturated, see Section 10.2.5. Even if the buffer or backfill do not become fully saturated during this period (see also the discussion in Section 10.3.8), oxygen consumption processes will take place in the partially saturated materials, as shown from the data obtained at the Febex and Prototype experiments (Jockwer and Wiczorek 2003, Eriksson 2007).

The hydrogeological modelling described in Section 10.3.6 shows that the proportion of waters of meteoric origin at repository depth will increase with time, see Figure 10-38. This evolution is not expected to change the reducing characteristics of the groundwater, as infiltrating meteoric waters become depleted of oxygen by microbial processes in the soil layers, if there are any, or after some tens of metres along fractures in the bedrock, as shown by the data collected within the Rex experiment (Puigdomenech et al. 2001) and from groundwaters sampled at 40 to 70 m depth during the “Redox Zone” experiment at Äspö (Banwart 1999, Banwart et al. 1999).

The results from the hydrogeological model have been coupled with the mixing and reaction calculations, as described in the introduction to this section. The calculations included equilibrium with either an Fe(III) oxyhydroxide or with Fe(II) sulphide. The results are slightly dependent on the solid phase chosen. However, there are no geochemical arguments that can be used to postulate what mineral regulates the measured redox potentials of groundwaters, and therefore the calculated redox potentials from both options are given the same weight in SR-Site. The calculations for Forsmark including equilibrium with either an Fe(III) oxyhydroxide or with Fe(II) sulphide are presented in Figure 10-48 which shows that the redox potentials increase slightly with time but remain well below -50 mV at the end of the simulation period.

It may, therefore, be concluded that the anoxic groundwater conditions now prevailing at repository depth will continue for the whole temperate period following the closure of the repository, in spite of the increasing proportion of meteoric waters with time. The chemical environment surrounding the repository will thus satisfy the criteria for the safety function indicator R1a.

Effects of grout, shotcrete and concrete on pH

The presence of cement materials in the repository is discussed in Section 10.2.5. Cement recipes with porewaters having pH around or below 11 will be used in the vicinity of the deposition tunnels in order to avoid detrimental effects from porewater diffusing out of the cement matrix. The effect of these porewaters is much smaller than that of Standard Portland Cement paste that contains porewater that is highly alkaline (pH ≈ 12.5).

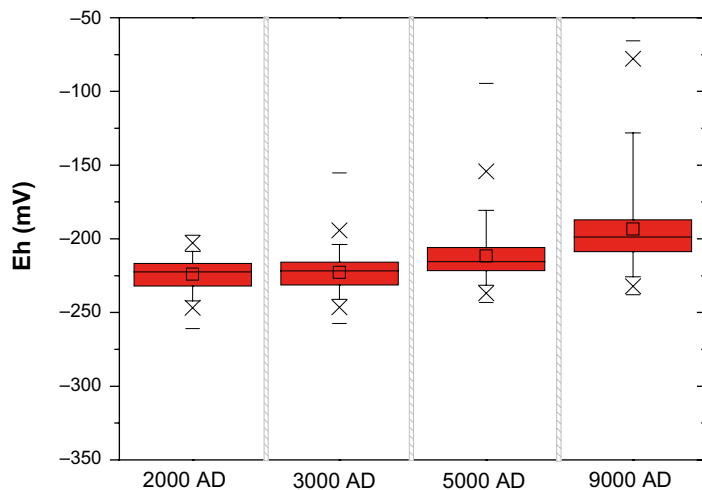


Figure 10-48. Box-and-whisker plots showing the statistical distribution of the calculated Eh (redox potential) taking into account results using either equilibrium with Fe(III) oxyhydroxide or amorphous FeS. The statistical measures have been obtained for the positions located within the candidate repository volume at Forsmark and they are the median, the 25th and 75th percentile (box), the mean (square), the 5th and 95th percentile (“whiskers”), the 1st and 99th percentile (crosses) and the maximum and the minimum values.

At Forsmark, it is expected that only deformation zones and a few single fractures will require grouting to avoid the inflow of groundwater into the tunnels during repository operation. These zones, however, may have a large role in model simulations of radionuclide transport. In deposition tunnels, the average amount of grout in rock fractures is expected to be less than 20 kg per metre of tunnel according to the **Underground openings construction report**, Table 4-3, while shotcrete will only be used in transport tunnels and other cavities in which deposition does not occur. It must be noted that grouting will be concentrated to a few locations in each deposition tunnel and that therefore grout will be unevenly distributed.

After repository closure, grout and shotcrete will start reacting with circulating groundwater, and a slightly alkaline plume is expected to develop downstream in the grouted fractures and fractures intersecting shotcrete. This process has been illustrated through modelling (Luna et al. 2006, Sidborn et al. 2014). The results have shown that a moderately high pH plume ($\text{pH} < 11$) can develop in grouted fractures intersected by the deposition tunnel. The leaching of grout material leads to the precipitation of CSH phases (calcium silicate hydrates) and calcite (CaCO_3) in the fracture and a corresponding decrease of the carbonate concentrations in the groundwater. Depending on the geometry and hydrologic properties of the grouted fracture and on the amount of grout, this process could continue for up to one hundred thousand years.

A consequence of this process is that transport pathways for potentially released radionuclides will include groundwaters that have circulated through a grouting zone and have been modified to higher pH (< 11) and lower carbonate (due to increased calcium concentrations and consequent calcite precipitation). This could affect the retention properties of the transport pathways although calcite precipitation will reduce the transmissivity of the affected fractures.

Groundwater sampled in boreholes drilled in grouted tunnel sections in the upper part of Onkalo (0–100 m) to monitor the influence of cement on groundwater, showed initial high pH values ($\text{pH} > 11$) in some of the sampled fracture waters (Ahokas et al. 2006). In 2019, the pH in the monitoring boreholes had decreased to circumambient values ($\text{pH} \sim 8$). The results from the monitoring of cement influence on groundwater at Onkalo suggest that the model results of Luna et al. (2006) are pessimistic.

The conclusion is, therefore, that the effect of grout in fractures will be to increase the pH in deformation zones for relatively long periods of time, probably lasting throughout the first glacial cycle ($\approx 120\,000$ years). The increased pH values will be, however, within the criterion for the safety function indicator R1e, *i.e.* < 11 . Radionuclide sorption data (see the **Data report**, Section 6.7) have been selected for the pH range 7 to 9, and are therefore adequate as long as “low” pH materials are used for grouting.

Degradation of grout in grouting holes

In order to be able to penetrate small fractures, the cement-based grout has to have a low viscosity. This can be achieved by using a high water/solid material ratio. A grout produced in this way will also have a high porosity and could degrade quickly. Modelling has shown that the degradation of cement-based grout in grouting boreholes is relatively slow in the hydrochemical conditions of Forsmark groundwaters (Galíndez and Molinero 2010, Grandia et al. 2010a). Simulated results have indicated that after 1 000 years grout material in contact with flowing groundwater can be degraded in its outmost 0.5 cm. Precipitation of calcite at the grout/granite interface would decrease the porosity, isolating the grout from the surrounding groundwater or matrix porewater.

In contrast, the natural evolution for silicasol, which is planned to be used if cement based grout is unsuitable, is to slowly recrystallise into thermodynamically more stable forms of silica, and both grouted fractures and grouting holes where silicasol have been used will, therefore, remain sealed. The conclusion is, therefore, that for modelling purposes it may be assumed that cement-based grouting boreholes are filled with a material having a high porosity. Grouting holes are, however, not included as flow paths in the flow and transport modelling in SR-Site and it is expected that their connectivity to flow paths will be limited. Small amounts of organic additives (superplasticizers) included in cement-based grouts will be gradually released during grout degradation and these substances will then be accessible for microbial processes. Their contribution to the concentration of organic carbon in groundwaters will, however, be negligible.

Identified uncertainties and their handling in the subsequent analysis

The following uncertainties are identified when considering the different chemical aspects of the evolution of the repository during the initial temperate period.

- There is a large degree of uncertainty in the detailed salinity distribution around the repository, but in general the salinity will not become so high or so low as to affect the performance of the repository during this period or when considering its future evolution. However, a fraction of a percent of the deposition holes may experience dilute conditions during the first ten thousand years, i.e. violating safety function R1c. The calculated distributions of salinity, pH and other groundwater components obtained from the modelling are used in the analysis of bentonite evolution, see Section 10.3.10 and 10.3.11, and in the radionuclide transport calculations (values for solubility and sorption) described in Chapter 13.
- There is a large degree of uncertainty in the detailed distribution of dissolved sulphide in the groundwaters around the repository. Because no dependency has been found between sulphide and other groundwater geochemical or hydrogeological parameters, the observed distribution of concentrations shown in Figure 10-42 is propagated to the analysis of canister corrosion in Section 10.3.13.

The uncertainties on other chemical aspects, such as redox, etc, have been established to be of no concern for the performance of the repository. In particular the uncertainties in the redox potential are not propagated to subsequent analyses. The anoxic groundwater conditions now prevailing at repository depth will continue for the whole temperate period following the closure of the repository, in spite of the increasing proportion of meteoric waters with time. The chemical environment surrounding the repository will thus satisfy the criteria for the safety function indicator R1a.

10.3.8 Saturation of buffer and backfill

General

The safety functions for the buffer and backfill assumes a fully water saturated state. This should mean that the buffer and backfill need to be saturated to perform properly. However, no performance is needed from the buffer as long as the deposition hole is unsaturated, since no mass-transfer between the canister and the groundwater in the rock can take place in the unsaturated stage. The water saturation process itself has therefore no direct impact on the safety functions of the buffer and backfill. It is still important to understand the water saturation process since it defines the state of the barriers in the early evolution of the repository. Finally, the ventilation of deposition tunnels during significant time spans (prior to filling of the deposition holes and the tunnels) may imply that the surrounding

rock can dehydrate. This air-filled pore-space in the rock could potentially constitute a sink for the water that is associated with the buffer during installation. If a significant amount of this water were to migrate into the rock, then this could potentially cause a significant increase of peak temperatures at the canister surfaces and thus affect safety function Buff 4.

The initial state of the installed buffer and backfill is presented in Sections 5.5.3 and 5.6.3 respectively. Both the buffer and backfill are installed as compacted bentonite blocks combined with bentonite pellets. The buffer blocks will be deposited into the deposition holes with an initial water content of 17 percent (by weight).

During the early stage of the repository evolution, the deposited buffer and backfill blocks will take up water from the surrounding bedrock. The water will expand the mineral flakes and the buffer and backfill will start swelling. The swelling will be restricted by the rock wall and a swelling pressure will develop. The process is dependent on the properties of the buffer as well as on the local hydraulic conditions and the saturation state of the tunnel backfill. The saturation of the backfill is mainly dependent on its material properties and the conditions in the surrounding rock. After final saturation, the hydraulic conductivity of the buffer and backfill will be very low and the swelling pressure will be high. This section describes the general modelling of the processes as well as an application to conditions specific to the Forsmark site. The following is assessed:

- The Sauna effect.
- Saturation of the backfill.
- Saturation of the buffer.
- Moisture redistribution in the dry rock case.
- Application to hydraulic conditions at the Forsmark site.

For the PSAR, saturation of buffer and backfill is based on the assessment in SR-Site and described in Åkesson et al. (2010a). The key focus was there on the evaluation of the importance of different parameters and assumptions in the modelling of the process. The modelling in Åkesson et al. (2010a) was essentially generic and not based on data from the Forsmark site. A more detailed application to hydraulic conditions at the Forsmark site was subsequently made as response to a request during SSM's review of the SR-Site assessment.

The Sauna effect

The Sauna effect is defined as uptake of water in the bentonite, followed by evaporation of water in the vicinity of the hot canister and precipitation of salts from the water in the evaporation zone. This is illustrated in Figure 10-49. This effect requires:

- That only a single (or a few) fracture feeds water to a larger part of the repository; if the repository is locally intersected by many fractures, the saturation time will be short, and the effect is negligible; because it is dependent on vapour transport, the effect requires unsaturated conditions.
- That the fracture(s) enters the repository in a relatively hot part; the effect is dependent on separation of water and (dissolved) salt due to vaporization. Vaporization is only conceivable if it occurs in a relatively hot part from which the vapour subsequently can be transported to a cooler part where it condenses.
- That "escape paths" for vapour remain open; if vapour is taken up by bentonite rather close to the vaporization point to such an extent that the bentonite saturates and seals, there is no longer a driving force for sustaining the process

SKB has for a long time investigated various aspects related to the "Sauna" effect within a KBS-3 repository (Karlund et al. 2000, Birgersson and Goudarzi 2013, 2016, 2017, SKB 2019c). The "Sauna" effect is of interest for the KBS-3 concept, because it constitutes a possible situation where increased corrosion rates of the copper canisters are conceivable.

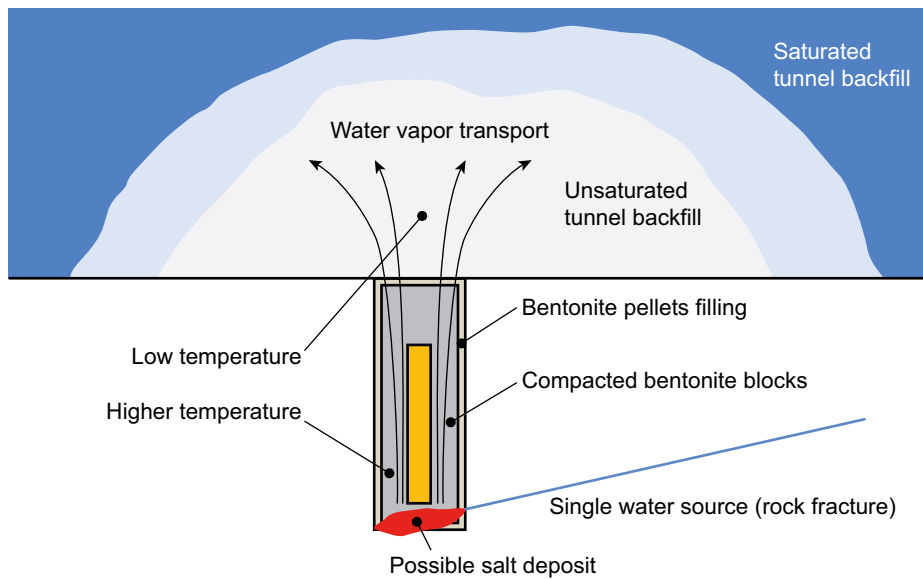


Figure 10-49. Schematics of the “Sauna” effect (Birgersson and Goudarzi 2013).

The residual power in the canister may be as high as 1 700 W at deposition (Section 5.3), which means that the potential for evaporation of water is substantial. Extensive salt enrichment is possible if a large part of the water that enters the deposition hole can leave in the vapour phase. If condensation of vapour occurs in the bentonite within the deposition hole, only a limited part will leave as vapour and the salt enrichment will consequently be limited. If all water that enters the deposition hole condenses, no more salt than what is present in the volume of water needed to saturate the buffer can be enriched in the deposition hole. Water vapour diffusivity in bentonite decreases with increasing degree of saturation and reaches zero at full saturation (at which condition vapour transport does not occur).

Over the last several years SKB has undertaken a number of laboratory experiments specifically focused on the Sauna effect. These experiments are reported in Birgersson and Goudarzi (2013, 2016, 2017). The overall conclusion from the tests performed is that while water vapour may move relatively freely in slots and dry pellets at constant temperature, condensation will occur rapidly in blocks as well as in pellets when a temperature gradient is present. Therefore, water vapour generated in the vicinity of the canister is not expected to ever leave the deposition hole. Since no water vapour is leaving the deposition hole no accumulation of chloride salts will occur.

Conclusions about the Sauna effect can be obtained from available field experiments, although these are not dedicated to this particular phenomenon. In the Prototype (Olsson et al. 2013) and LOT (Karlund et al. 2009) studies, the chloride concentration profiles are flat over the radius of the buffer and the overall chloride content corresponds to, or is lower than, a proportional mixture between the content in the groundwater and the content originally present in the bentonite, thus indicating that no salt enrichment has occurred close to the central heater in these experiments. In the FEBEX study (Fernández et al. 2018), there is an enrichment of chloride close to the heater as well as a concentration gradient from the heater towards the rock. The test was not fully saturated close to the heater. Enrichment of salt due to evaporation/condensation in the remaining unsaturated part of the bentonite may be the reason for the increased concentration at the heater contact. The bulk of the bentonite surrounding the heater in FEBEX is depleted in chloride compared to the initial state. None of the field tests show any accumulation of chloride in the buffer, apart from pure mixing. There is hence no evidence for the existence of the Sauna effect in these tests.

The total void volume in the buffer surrounding the canister (Table 5-14) is 4.34 m³. An additional 1.78 m³ of water is needed for full saturation. The chloride content in the MX-80 bentonite is ~0.1–0.2 mg/g dry weight and the concentration in the present day Forsmark groundwater is 5 500–6 000 mg/L (Laaksoharju et al. 2008). With the assumption that no vapour and no chloride are lost from the buffer, the final amount of chloride in the saturated buffer will be 11.3–13.7 kg from pure mixing at the end of the saturation phase. This would yield a mean concentration of 2 600–3 200 mg/L. If exclusion

effects are accounted for (e.g. Birgersson and Karnland 2009), the mean concentration at full saturation would be lower. A modelling case where a single fracture intersects a deposition hole providing water for saturation of a substantial amount of the bentonite in the hole is considered in Birgersson and Goudarzi (2017), and summarised here. When the temperature in the region where water enters is elevated, evaporation of the water is conceivable, which in turn may result in accumulation of salt. The mere evaporation process, however, is not sufficient for drawing the conclusion that any significant salt accumulation occurs. On the contrary, in order for salt to accumulate to any significant degree, it is necessary that the major part of the incoming water is vaporized and transported as a gas some distance. Only in such a case will there be a significant salt concentration increase in the liquid left behind. As an example, consider a liquid-to-vapour dissolution rate of 90 % of the inflow rate, which would give a 10-fold increase of the concentration of the incoming water, i.e. the solution being transported in liquid form would have a chloride concentration of 2 mol/L, based on a groundwater concentration of 0.2 mol/L. As an evaporation process requires elevated temperatures and temperature gradients, it is expected that possible salt accumulation effects will be influential only in the early stages of the repository lifespan. A maximum bentonite temperature of 90 °C is estimated to be reached in a KBS-3 repository already within 10–20 years after closure, see Figure 10-13, while a peak temperature of approximately 60 °C is expected to be reached at the rock wall at canister mid height after about 30–50 years. After approximately 100 years, the corresponding temperatures are ~65 and ~55 °C, respectively, and after 1 000 years, the difference between these temperatures is only a few degrees, both being close to 40 °C. The saturated vapour pressure at 40 °C is approximately 7 kPa, in comparison with 47 kPa at 80 °C. Thus, this 7-fold decrease of the saturated vapour pressure, combined with the fact that only minor temperature gradients remain after 1 000 years, suggest that possible effects of evaporation will be negligible after this time period. For a given inflow rate (q_{in}), the amount of accumulated chloride in the specified case is:

$$nCl = q_{in} \times c \times t = 1.05 \times 10^8 \text{ mol/L} \times \text{min} \times q_{in}$$

where the inflow rate is given in L/min, $c = 0.2 \text{ mol/L}$ is the chloride concentration in the groundwater, and $t = 1\,000 \text{ years}$ is the assumed total time for the process. Table 10-5 gives the calculated amount of accumulated chloride for the considered range of inflow rates. In the table the amount of accumulated chloride is also given in terms of the corresponding total mass of NaCl, in terms of the corresponding mass fraction of NaCl with respect to the total buffer mass (23 600 kg), and in terms of the total chloride concentration if distributed in a fully saturated buffer (6 450 litres).

Table 10-5. Amount of accumulated chloride in the adopted inflow case for different values of inflow rate (q). The second column lists the total amount of water during the 1 000 year duration. The third column lists the calculated amount of chloride accumulated, and the fourth and fifth columns lists the corresponding mass of NaCl, in absolute terms and as a mass fraction of the whole buffer dry mass (23 600 kg), respectively. The last column lists the corresponding concentration of chloride if distributed in the entire pore volume of the deposition hole (values in red corresponds to supersaturation with respect to NaCl).

q (L/min)	Total water volume (L)	Amount Cl (mol)	mass NaCl (kg)	mass fraction NaCl	Cl concentration (mol/L)
10^{-7}	5.26×10^1	1.05×10^1	0.61	0	0.00163
10^{-6}	5.26×10^2	1.05×10^2	6.1	0.03	0.0163
10^{-5}	5.26×10^3	1.05×10^3	61	0.26	0.163
10^{-4}	5.26×10^4	1.05×10^4	610	2.6	1.63
10^{-3}	5.26×10^5	1.05×10^5	6 100	26	16.3
10^{-2}	5.26×10^6	1.05×10^6	61 000	260	163
10^{-1}	5.26×10^7	1.05×10^7	610 000	2 600	1 630

In the saturated state, salt which may have precipitated locally during the saturation process will relatively quickly diffuse out in the entire buffer region (and eventually out of the entire repository). As a criterion for whether a certain amount of accumulated salt in the considered case poses a problem regarding canister corrosion, the corresponding concentration when the precipitated chloride is distributed in the fully saturated buffer is used – if this concentration is one mol/L or less, the effect of salt accumulation on the corrosion process is negligible. This criterion is solely based on the solubilities

of CaCl_2 and NaCl which both are ~ 6.7 mol/L and the assumption of some concentration gradient within the buffer. Below an average concentration in some mol/L region no precipitation of chloride salts is expected to occur. Using this criterion, Table 10-5 shows that the amount of accumulated salt in the considered case begins to lead to NaCl concentrations approaching NaCl solubility for rates around 10^{-4} L/min. Note that the total amount of water entering the deposition hole at an inflow rate of 10^{-4} L/min during 1 000 years corresponds to the pore volume of approximately eight deposition holes. In order to actually deposit the ~ 600 kg of NaCl given by this analysis, it is thus required that this amount of water is transported exclusively as vapour far out into the overhead tunnel section. Such a process can be judged as highly unlikely by simply noting the strong tendency for vapour condensation occur within the buffer, as observed in many of the tests described in Birgersson and Goudarzi (2013, 2016, 2017). Furthermore, state-of-the-art THM (Thermo-Hydro-Mechanical) simulations of the saturation process from a single fracture intersecting a deposition hole predict that a saturation front reaches the canister within only 2–35 years for water inflows in the range 10^{-5} – 10^{-3} L/min (see **Saturation of the buffer**, later in this section). These simulations thus conclude that possible evaporation effects can, at most, only be active during the first few years after closure, giving negligible salt accumulation.

A study presented in SKB (2019c) indicates that gaps and fractures are of limited importance regarding vapour transport. The main part of the vapour seems to go through the bentonite block even if there is a fracture present. Fractured blocks and block joints will not affect the vapour transport the process.

It is concluded that significant salt accumulation as a consequence of evaporation of inflowing water from a fracture intersecting a deposition hole will not occur in a KBS-3 repository. There are several reasons for this:

- For significant amounts of salt to accumulate, the major part of the inflowing water must transform into vapour, rather than continue to flow in liquid form, since chloride concentration only can be increased if water is evaporated. For the relevant inflow geometry, it is highly unlikely that the liquid flow is suppressed to such an extent. It is also verified in state-of-the-art THM models that significant liquid flow is maintained.
- The experimental results strongly suggest that the vapour transport capacity within a KBS-3 buffer is not large enough to support a significant amount of salt accumulation, since condensation will limit the vapour transport.
- No relevant signs of salt accumulation have been observed in field experiments. In the FEBEX test, there was a chloride concentration gradient in the clay with enrichment close to the heater. There was, however, no accumulation of the total chloride content in the bentonite but rather a redistribution of the initial amount.

In summary, it is concluded that the Sauna effect will be insignificant in a KBS-3 repository at Forsmark and thus this process will not be included in the further analyses of e.g. pitting corrosion and stress corrosion cracking of the canister where salt enrichment could have an impact.

Saturation of the backfill

In Åkesson et al. (2010a) the saturation of the backfill was modelled for a number of different geometries and assumptions about data and boundary conditions. A summary of the investigated variations is given in Table 10-6. The primary purpose of the modelling was to analyse the time needed to saturate the backfill.

40 different cases were investigated in the primary variation, including combinations of tunnel sections, backfill representations, and fracture inflow (or boundary pressure). 25 different cases were investigated in the secondary variations using base case models and modified features including an EDZ, removal of fractures as well as modified permeabilities and retention properties. The approach with primary variations was largely an attempt to map the effects of different combinations of section areas, backfill representations, and fracture inflows (or boundary pressures) for different geometries. The secondary variations were mainly performed with 1D models with altered bentonite properties, and with large plane geometries, with or without fractures, and with altered rock properties.

Table 10-6. Summary of primary and secondary variations.

Variation		
Primary	Tunnel section area Backfill representation Fracture distance and orientation Fracture transmissivity	Two different tunnel sections Two and in some cases three different representations Two different orientations: vertical and horizontal. Two different distances for the vertical orientation Two different transmissivities
Secondary	Rock permeability Presence of EDZ Absence of fractures Water retention in the rock Bentonite permeability Bentonite relative permeability Thermal evolution Hydromechanical processes Bentonite retention Tunnel ventilation	Several cases with different rock permeabilities Two cases with EDZ Five cases with no fracture Two cases with different retention curve Four cases with different permeabilities Two cases with different relative permeability One case with thermal evolution One case with hydromechanical processes Two cases with steeper retention curve One case with 10 years of RH 70 %

The main result of each analysis was the time to fully saturate the backfill, where the time needed for the last node to reach 99 % degree of saturation has been regarded as the saturation time. In general, either the backfill or the rock system can be regarded as the limiting factor for the rate of hydration. Hydration times of approximately 80 to 100 years, given by the one dimensional models, represent the time needed for the backfill, with free access of water, to become fully saturated. Times longer than this represent cases in which the rock system is limiting.

The different tunnel geometries that were represented were:

- One dimensional axisymmetric geometry.
- Two dimensional axisymmetric geometries with different fracture distances (6 m and 24 m).
- A two dimensional plane geometry (Figure 10-50).

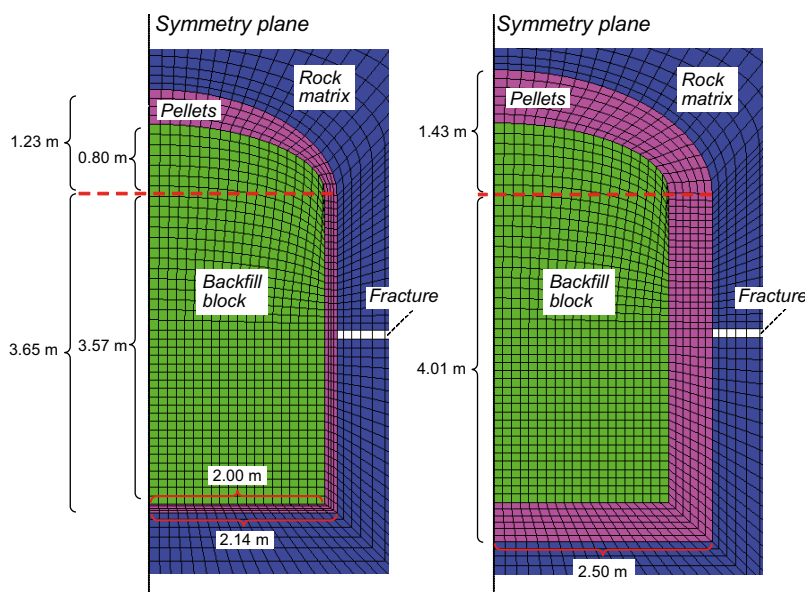


Figure 10-50. The Geometry of 2D plane models analysed. Theoretical section (left) and maximum fallout (right) (Åkesson et al. 2010a).

The effect of uneven tunnel diameter was handled with the Maximum Fallout case, i.e. assuming the largest allowed tunnel cross section according to Figure 5-16, in which a larger proportion of pellets was included.

A selection of the calculated saturation times is compiled in Figure 10-51. The dotted lines represent the base case properties and two different fracture transmissivities. The diagram illustrates the effects of changing the bentonite properties on one hand, and the effects of changing the rock properties and fracture distance on the other. The effects of different bentonite properties and other variations are shown for a situation with free access of water in the top row. The dependence on the rock matrix permeability in a fracture-free condition is shown on the lower row, while the middle rows show results from two different fracture distances. The figure thus demonstrates that the overall influence of the rock on the hydration rate is much higher than the uncertainties related to the bentonite. The calculations for backfill with free access of water result in time scales of approximately 80 years. A case with no fracture and a matrix hydraulic conductivity of 10^{-13} m/s result in time scales of approximately 6 000 years. Since the rock at Forsmark is expected to contain very few water conducting fractures, typically separated by more than 100 m, it is difficult to state that any of the presented cases could be entirely ruled out. In the PSAR it is assumed that the saturation of the backfill can take anything from < 100 years to ~6 000 years depending on the location in the rock and this entire range is likely to arise at Forsmark.

Saturation of the buffer

The buffer water saturation process is externally influenced by the wetting/drying from the rock and backfill and the heating from the canister. Inwards in the buffer, from the rock side, liquid water is transported by “advective” flow in the buffer and outwards, from the canister, vapour is transported by diffusion. The advective flow is driven by the water pressure gradient and the diffusive flow is driven by the vapour concentration gradient.

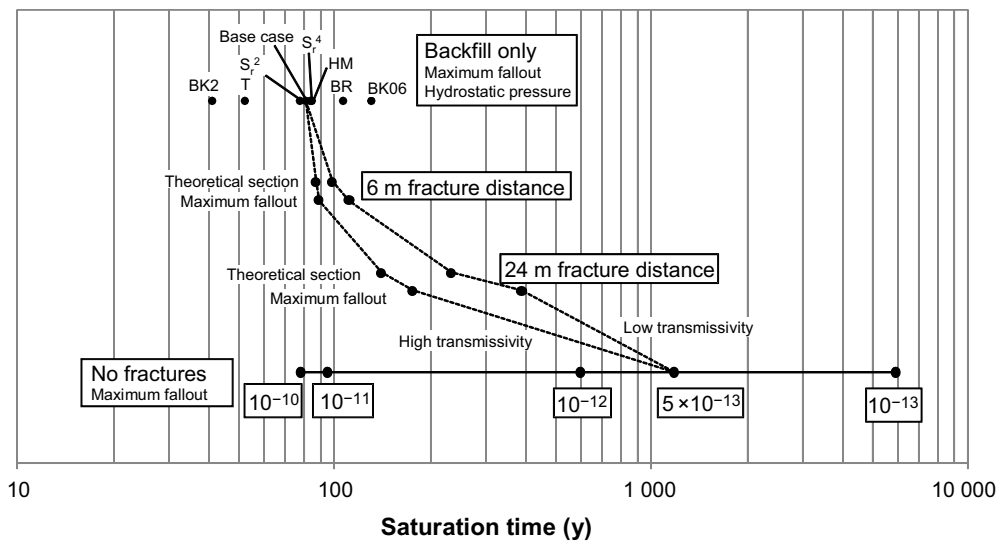


Figure 10-51. Compilation of backfill saturation times for different geometries and cases. Results from 1D models with free access of water shown on the top row (BK2: with doubled backfill permeability; T: with thermal evolution and temperature dependence of the viscosity of water; Sr^2 and Sr^4 : with square and 4th power saturation dependent backfill relative permeability relations – the base case has a cubic dependence; HM: with hydromechanical processes; BR: with steeper backfill water retention curve; BK06: with 40 % lower backfill permeability). Results from 2D axisymmetric models with different fracture representations shown in the middle rows. Results from plane 2D models without fractures shown on the bottom row (numbers indicate rock hydraulic conductivity). The dotted lines represent the base case properties and two different fracture transmissivities (Åkesson et al. 2010a).

The transport properties are dependent on the state of the materials in terms of degree of saturation and temperature. The different retention properties of the buffer constituents (cylinder- and ring-shaped blocks and the pellet filled slot) will also influence the water transport in the buffer. The saturation of the buffer has been calculated in Åkesson et al. (2010a) for a number of cases with different conditions and assumptions:

- Pellets and blocks or a homogenised material.
- Unfractured rock.
- Fractured rock.
- The effect of extremely low rock permeability.
- Rock permeability dependence.
- The effect of higher water retention for the rock.
- The effect of an initially ventilated tunnel.
- The effect of altered block retention.
- The effect of altered buffer permeability.

The cases have been selected based on the identification of important parameters in the **Buffer, backfill and closure process report**.

The buffer saturation times (the time where $S_l \geq 0.99$ (liquid saturation) in the entire buffer), for all Thermo-Hydraulic (TH)-simulations of a deposition hole made in Åkesson et al. (2010a), are shown in Figure 10-52. The horizontal lines represent the cases indicated to the right of the line where also the “mechanical assumption”, where *Homogenised* refers to an initially homogenised buffer material while *Initial state* considers the case with blocks and pellets, is indicated. The concept of using a homogenised and initial state model is to obtain two extreme solutions that are bounding the “true case” (in which mechanics, i.e. the homogenisation process, should be incorporated). Below the lower line (Init. Unfractured rock) the rock conductivity used is indicated. The hatched lines connect models with identical rock conductivities. Close to the lower line, the positions of the models where the buffer was altered are given (unfilled circles). A more detailed description of the cases can be found in Åkesson et al. (2010a).

As presented in Figure 10-52, the results from the calculations show:

- In general, the assumption of a homogenised buffer gives longer saturation times than when pellets and blocks are considered. The exception is when the saturation is very slow, where the homogenised buffer gives a more rapid saturation.
- For an unfractured rock, the conductivity of the rock is very important for the saturation time. For a rock conductivity of 10^{-11} m/s, the saturation time will be in the range of ~ 20 years, whereas it will take > 150 years for a conductivity of 10^{-12} m/s.
- Equipping the unfractured model with a horizontal fracture at either the canister mid-height (CMH) or at the tunnel wall significantly decreases the time for saturation, especially when the conductivity of the rock is low.
- To investigate the effect of a low permeability rock, the unfractured model was assigned a low rock permeability of 10^{-20} m², corresponding to a hydraulic conductivity of $\sim 10^{-14}$ m/s. All of the rock mass surrounding the modelled deposition hole and associated with the tunnel representation was assigned the extremely low permeability. The water entering the backfill and buffer had to come through the rock matrix (no fractures are present) driven by the water pressure gradient. The obtained saturation times were 1 760 and 1 476 years for the block-pellet and homogenised model, respectively.
- For a high permeability rock, i.e. if the rock conductivity $> 10^{-11}$ m/s, the calculations show that the saturation time is more or less independent of rock permeability.
- Using a higher water retention curve for the rock (larger suction given the same water degree of saturation) does not have a significant effect on the buffer saturation time.

- The effects of different relative humidity in the rock were investigated by first modelling the system without the buffer/backfill/canister and then applying the resulting pressure field as an initial condition in the model with all constituents. Two cases were investigated, a drained condition (RH = 100 %) and a ventilated condition (RH = 70 %). The rock permeability influences the effect of the relative humidity on the water saturation of the surrounding rock, and by extension, the saturation time of the bentonite. A low rock permeability implies a smaller volume of rock affected as well as slower resaturation. A significant effect was noted only for the ventilated case, with 70 % RH, for both low and high rock permeability. The saturation times became longer, from 21 to 28 years for a rock with high permeability, and from 177 to 233 years for a rock of low permeability, considering a ventilated condition. The assumption of 70 % relative humidity is, however, a very extreme case.
- The effect of block retention was also investigated. This was done by moderately altering the retention curve. At degrees of saturation higher than the initial state, the curve was lowered, while for lower degrees of saturation the curve was close to the original one. The effect of this was to increase the saturation time for high permeability rock from 21 to 26 years, while for low permeability rock the saturation time increased from 177 to 192 years.
- Changing the buffer permeabilities within a range of 0.6 to 2 times the original value did not have a significant effect on saturation time. The range of permeabilities was selected from an assessment of a relatively large number of experimental data. More about this can be found in the dedicated Data Report for the THM-modelling of the buffer, backfill and other system components (Åkesson et al. 2010b).

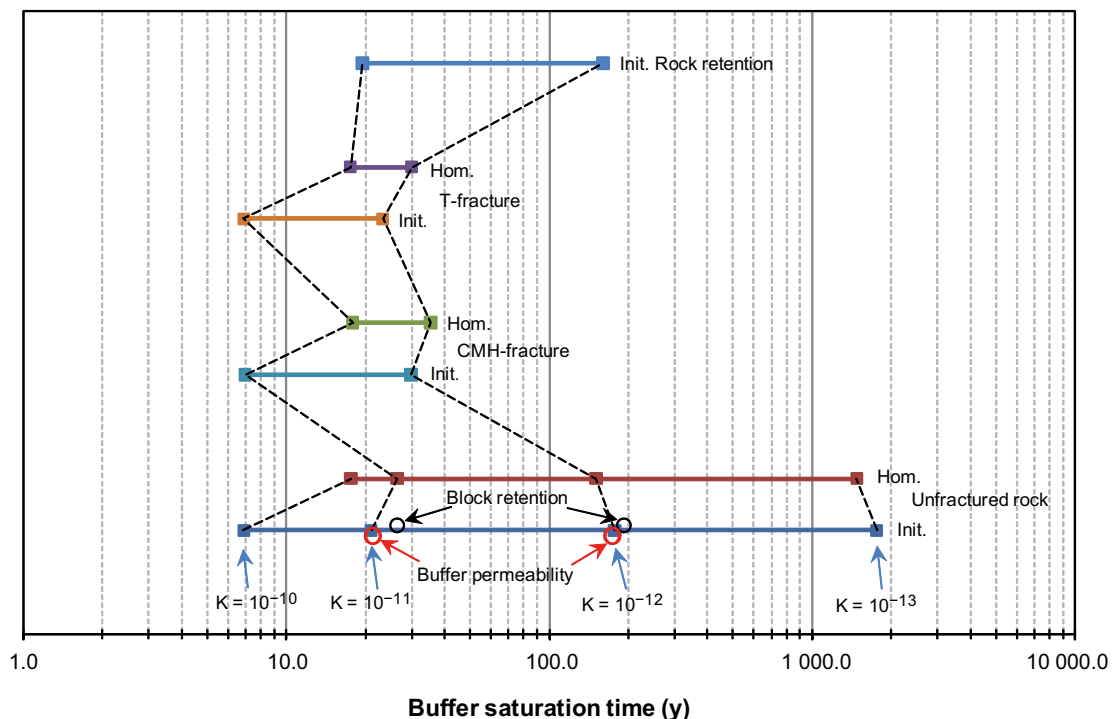


Figure 10-52. Compilation of the buffer saturation times (the time when the liquid saturation $S_l = 0.99$ in the entire buffer) for all TH-simulations of a deposition hole. The text to the right of the lines indicates the representation of the rock: Unfractured rock, CMH-fracture (fracture at canister mid-height), T-fracture (fracture at tunnel) and Rock retention (changed rock water retention curve). In the three first cases (from the bottom up) the buffer has been represented as in the initial state (Init.), where blocks and pellet slot are present, and as in a fully homogenised state (Hom.) as indicated to the left of the corresponding horizontal line. In the Rock retention case only the Init. buffer representation has been used. The results obtained using the same rock conductivity, indicated below the bottom line, are connected by hatched lines. The results from changing the Buffer permeability or Block retention are indicated by red or black circles, respectively. (Åkesson et al. 2010a).

Apart from the investigated cases there are some additional uncertainties in the description of the saturation process:

- The effect of the assumed axial symmetry, reducing the problem to two dimensions, has not been investigated.
- The inner slot (between the vertical canister boundary and the bentonite blocks), present in the buffer initially, has been omitted in the models. This effect, however, is included in the description of the thermal evolution (Section 10.3.4).
- The relation between the saturation responses for TH-models and Thermo-Hydro-Mechanical (THM)-models has only been investigated for rapid saturation processes.
- Regarding the distance to the hydraulic pressure boundary, 60 m above the repository, the strategy has been to study data on the rock properties at the Forsmark site and to develop a relevant representation. This distance is based on the distance to a more permeable part of the rock characterised at the Forsmark site.
- The importance of the mesh used in the models has only been investigated to a limited extent.

These uncertainties may influence the calculated time spans, but they are not expected to affect the conclusions and general understanding of the wetting cases.

Additional evaluation of uncertainties in Åkesson et al. (2010b)

Conceptual uncertainties associated with thermal, hydraulic and mechanical processes in the vicinity of a final repository have been investigated for many years, both theoretically and through large scale experiments, in a number of EU projects and in the international DECOVALEX project. The available material has been reviewed (Sellin et al. 2017) and analyses have been done on how the results could affect the resaturation calculations in Åkesson et al. (2010a).

The aims of the study were:

- to provide a description of the FEBEX in situ experiment together with a summary of the modelling of the experiment carried out,
- to provide a description of the FEBEX Mock-up test together with a summary of the modelling of the experiment carried out; An important component here is the description of the three non-standard flow models proposed to describe the experiment (hydraulic threshold, thermo-osmosis and microstructure development),
- to make an analysis of how the models for hydraulic threshold, thermo-osmosis and microstructure development would affect the results in SR-Site analyses, as well as
- to analyse the significance of other identified uncertainties.

Evaluation of alternative models was made with analytical solutions. With a threshold for the hydraulic gradient in Darcy's law, the buffer will never be saturated. However, the significance of this is not great because the final saturation becomes $> 99\%$ even with relatively low gradients. The model results presented in Sánchez and Gens (2006) also show that the time perspective for achieving a stationary state with a threshold gradient is approximately the same as the time to full water saturation without the threshold gradient. This has no significance for the buffer's hydromechanical function in the repository because swelling pressure develops at a much lower degree of saturation.

A thermo-osmosis model also leads to full saturation not being achieved as long as there is a temperature gradient. However, the remaining unsaturation will not be great in that case either. The model results presented in Zheng and Samper (2008) also show that the time perspective for achieving a stationary state with thermo-osmosis is approximately the same as the time to reach full water saturation without thermo-osmosis.

The development of microstructure has been modelled as a reduction in permeability as a function of water saturation. This gives generally slower water absorption. Unlike the models with thermo-osmosis and threshold, the microstructure development model gives final full water saturation. The significance of this process for the estimated water saturation times in Åkesson et al. (2010a) has been analysed by employing adjusted vapour diffusivity. The results indicate that the time of water saturation may have been underestimated in Åkesson et al. (2010a).

For relatively dry rock conditions, the most important transport process is diffusion of vapour, and this is the only way to transfer moisture from hot to cold parts in the models used. Therefore, the potential contribution of natural convection for a more pronounced moisture distribution has been identified as a conceptual uncertainty for the development of the re-saturation. The analysis shows that the natural convection is strongly dependent on the gas permeability of the pellet gap. Figure 10-53 shows the maximum height of natural convection as a function of permeability and gap. Permeability is not systematically measured for bentonite pellets, but with a maximum literature value of 10^{-7} m^2 , the figure shows that the maximum height will be 2 meters for a 5 cm gap and 8 meters for a 10 cm gap. It is therefore not impossible for the process to matter. Assuming that the equilibrium state is a constant vapour pressure throughout the deposition tunnel, a relatively large amount of water will be lost from the buffer around the canister in a case of dry tunnel and deposition holes. This would mean that the heat conductivity of the buffer decreases and that the temperature of the canister surface increases. However, this requires that no condensation or swelling will occur in the pellet filling in the upper part of the deposition hole, whereas the likely development is that vapour will condense in the pellet slab in the upper part of the deposition hole. The pellets in the gap will then swell and seal. Therefore, no transport of vapour to the backfill tunnel is expected.

Experimental data show that the retention properties of bentonite are temperature dependent. The general trend is that relative humidity increases with increasing temperature. However, the analysis in Sellin et al. (2017) shows that the effect of this, for relevant KBS-3 conditions, is very small.

Sellin et al. (2017) reviewed the available data of other possible buffer and backfill materials and assessed how these data could affect the conclusions Åkesson et al. (2010a). Available data refers primarily to measurements of hydraulic conductivity, swelling pressure and retention characteristics from water absorption tests. The various materials compared are buffer materials MX-80, Deponit CA-N and Febex, and the backfill materials Ibeco RWC BF and Friedland. Two different grades and several shipments of Asha material are also included in the study. One of the materials is of buffer and the second of the backfill type. The time scale for resaturation for a particular material is largely determined by the hydromechanical properties of the material in question, but also by the initial dry density and water content. Different materials can therefore exhibit optimum properties with regard to water absorption capacity for different installed initial states (density and water content). A detailed comparison of different bentonite materials with regard to the time scale for water uptake is therefore not straightforward. Instead, evaluated vapour diffusion data can be used to make a simple comparison. The reason for this is that the time scale for water absorption is in principle inversely proportional to diffusivity (e.g. $t_{\text{febex}} \sim t_{\text{mx80}} \times D_{\text{mx80}}/D_{\text{febex}}$). Even though the differences in vapour diffusivity were found to be quite small between different materials, it should be noted that the lowest values were for the MX-80. This means that the time scale for re-saturation for other materials would be slightly shorter than for MX-80 (the decrease would be a factor of $\frac{1}{2}$ for Friedland, and $\frac{1}{3}$ for the other analysed materials). Apart from these observations, it can be noted that the analysis showed a general coherence between different data sets and gave a verification of the material model based on independent measurements. This difference is only relevant under conditions when the bentonite properties control the saturation process, which only will be in a very limited number of deposition holes at the Forsmark site.

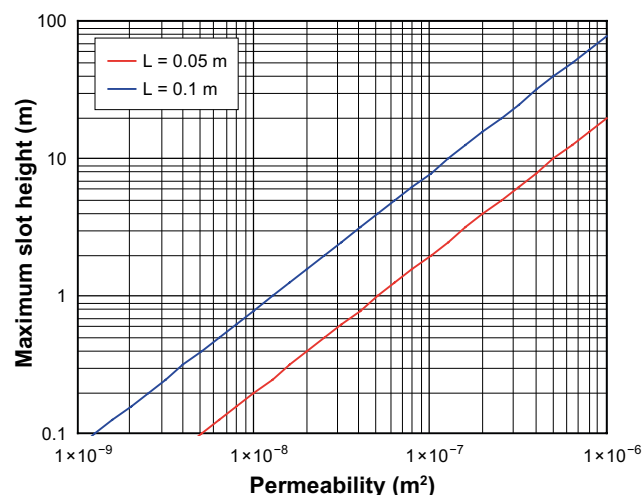


Figure 10-53. Maximum height with sustained natural convection (Sellin et al. 2017).

If several deposition holes share the same water conducting fracture, this could affect the water saturation process. This phenomenon has been described in Sellin et al. (2017). The main effect could be that the upstream hole is “drying out” the fracture and no water reaches the hole downstream. In order for the process to be important, the flow in the fracture must be large enough to affect the water saturation of the buffer, but not greater than that the water absorption capacity of the buffer in a hole will be able to absorb a significant portion of the flow. It is therefore only in the range of inflows between 10^{-3} and 10^{-4} L/min, in open repository conditions, that the interaction may have significance at the Forsmark site. Based on Joyce et al. (2013), 2.6 % of the deposition holes in Forsmark lie in this range. Of these, the fracture is divided between several holes in half the cases. In an extreme case, 1.3 % of the deposition holes may lose some of their inflow from a fracture through hydraulic interaction between deposition holes. In Forsmark, it is likely that most deposition holes will be saturated by flow through the rock matrix. Adding 1.3 % of the deposition holes to this group will not affect the overall picture of the water saturation process.

The sensitivity of the saturation time to the permeability of the rock matrix is very strong. The available data set is also rather limited. Further data should be obtained in the detailed site investigations, see further Section 15.6.

Moisture redistribution in dry rock case

The venting of deposition tunnels during significant time spans (prior to filling of the deposition holes and the tunnels) may lead to dehydration of the surrounding rock. This air-filled pore-space in the rock could potentially constitute a sink for the water that is associated with the buffer at installation. If a significant amount of this water were to migrate into the rock, then this could potentially result in a significant increase of peak temperatures at the canister surfaces.

The moisture redistribution in a deposition hole buffer for a case with a dry surrounding rock mass was studied in Åkesson et al. (2010a). The main reason for the study was to investigate the effect of the water redistribution in the buffer of a dry deposition hole on the thermal conductivities in different parts of the buffer. The result of this investigation (a water saturation field translated into thermal conductivities) was used as one case in the calculations of the thermal evolution (see Section 10.3.4). While the dry conditions imply that temperature increases, these analyses show that temperatures in the buffer remain below the highest accepted value.

Application to hydraulic conditions at the Forsmark site

In Åkesson et al. (2010a), the water saturation process in the buffer was studied for three different “type holes”:

- Hole with a water-conducting fracture.
- Hole without water-conducting fracture, but near a water-conducting fracture in the deposition tunnel.
- Hole without water-conducting fractures either in the hole itself or in the tunnel.

The water saturation in the backfill for different cases was also studied. The cases were chosen to cover all possible ranges of water saturation times. However, there was no attempt to link the different cases to the hydraulic situation in Forsmark and no distribution of saturation times was presented. In SR-Site (SKB 2011, Section 10.3.8), it was, nevertheless, found that the conditions in Forsmark were well covered by the cases in Åkesson et al. (2010a).

Sellin et al. (2017, Chapter 7) has linked the water saturation models in Åkesson et al. (2010a) to the expected inflows in Forsmark based on Joyce et al. (2013). The inflow to the open repository has been used to calibrate the CodeBright model. After that, the buffer and backfill is introduced and water saturation time is calculated. It is noted that:

- Matrix flow is not handled in the hydrogeological model.
- Generally, the flows in the fractures that intersect deposition holes are significantly lower than the assumptions in Åkesson et al. (2010b).
- The distance between most deposition holes and the fractures that intersect the deposition tunnels is longer than in the typical cases in Åkesson et al. (2010a).

The summarized results from the study are shown in Figure 10-54.

The conclusion from the study is that the assumption of the hydraulic conductivity of the rock matrix is crucial for the estimation of water saturation times in Forsmark. Measurements of matrix conductivities show that these are in the order of $K_m = 4 \times 10^{-14} - 5 \times 10^{-12}$ m/s (Vilks 2007). For the values in that range it can be noted:

- $K_m \geq 10^{-11}$ m/s: Only a small proportion of the holes are saturated from fracture flow. The tunnel does not affect the process at all. All holes are saturated within 30 years.
- $10^{-12} > K_m \geq 10^{-13}$ m/s: Between 10 and 30 % of the holes are saturated with water from fractures or from the deposition tunnel. All the other deposition holes are saturated from the rock matrix and these are saturated within a period of between 200 and 2 000 years.
- $10^{-13} > K_m \geq 10^{-14}$ m/s: A significant proportion (30–60 %) of the deposition holes is saturated with water from fractures or from the deposition tunnel. The other deposition holes are saturated from the rock matrix and this may take more than 20 000 years.
- $K_m < 10^{-14}$ m/s: In practice, all deposition holes are saturated with water from fractures or from the deposition tunnel. In tunnels without fractures the saturation will take a very long time. The calculations show times of $> 1\,000\,000$ years.

In the assessment for SR-Site (Åkesson et al. 2010a) 10^{-13} m/s was employed as a “typical” matrix conductivity. With this value, according to Figure 10-54, 65 % of the deposition holes in Forsmark would be saturated in $\sim 2\,000$ years and the largest part of the others in the 300–2 000 year range. Only a small proportion is saturated faster than 100 years. It is obvious that the uncertainty in the estimation of water saturation time is high. The range of matrix conductivities in Vilks (2007) extends over two orders of magnitude, and in principle, this scales linearly with water saturation time, since few holes are saturated from water-conducting fractures.

Based on the results presented here, it is predicted that around 30 % of the deposition holes are saturated from fractures and the saturation time will then be around 1000 years or less. Only a few percent of the deposition holes will be saturated faster than 100 years. The majority of the deposition holes in Forsmark will be saturated from the tunnel or from the rock matrix. This will take a few thousand years with the assumption of a matrix hydraulic conductivity of 10^{-13} m/s.

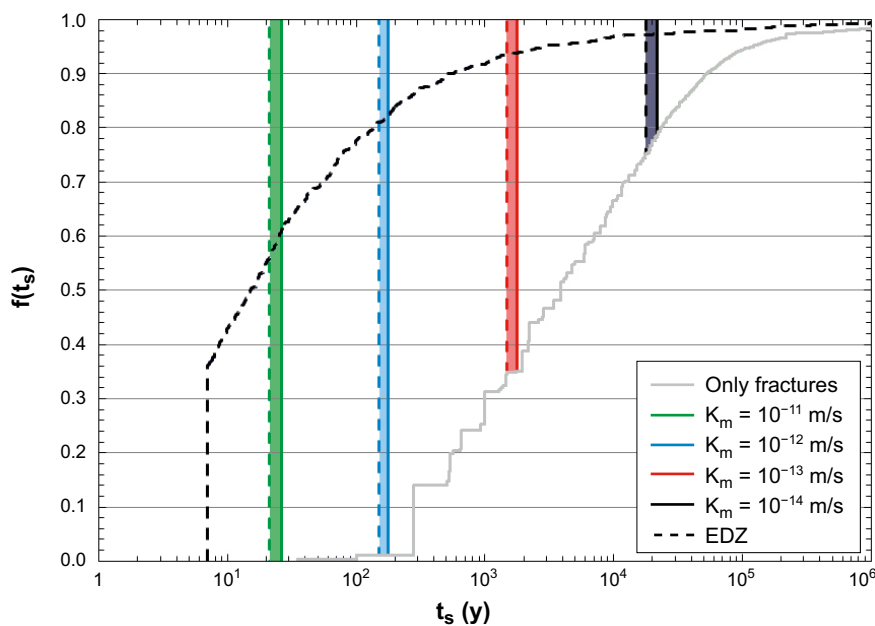


Figure 10-54. The solid grey line identifies the cumulative distribution of saturation times, $f(t_s)$, in the Forsmark repository calculated assuming no matrix flow. The coloured lines identify the time interval within which all deposition holes will reach full saturation if the matrix hydraulic conductivity has the value $K_m = 10^{-exp}$, where $exp = \{11, 12, 13, 14\}$. The dashed black line identifies the distribution of saturation times if no flow resistance was present in the tunnels (see text) (Sellin et al. 2017).

Identified uncertainties and their handling in the subsequent analysis

SKB finds that the Sauna effect will be insignificant in a KBS-3 repository at Forsmark and this phenomenon will not be progressed further into the assessment.

There are a number of identified uncertainties regarding the time for saturation of the buffer as well as the backfill. These have been evaluated and can be divided into different categories:

1. Uncertainties regarding the conceptual models/understanding and additional processes. These may have an impact on the estimated saturation time for deposition holes with relatively high water inflows and will in most cases slow down the saturation process for those holes. Some assumptions, like a threshold I Darcy's law would lead to a situation where the buffer never gets saturated, which is inconsistent with results from field tests.
2. Uncertainties regarding material data and especially the effect of a different buffer/backfill material. Evaluated vapour diffusion data for different materials have been used to make a simple comparison of the effect on the saturation time. Alternative materials to MX-80 will generally saturate faster. This is however only relevant in deposition holes with high inflow of water.
3. Uncertainties in the hydrogeological conditions. The saturation times presented in Figure 10-54 are based on one single realisation with the hydrogeological model. A different realisation would give different results. The general picture is however not expected to change very much.
4. Uncertainties in the hydraulic conductivity of the rock matrix. The buffer in most of the deposition holes in Forsmark will be saturated through the rock matrix, or possibly the backfill, since the holes are unconnected to any water conducting fractures. As seen in Figure 10-54, the matrix conductivity has a strong impact on the saturation time. A matrix conductivity of 10^{-13} m/s would lead to a maximum saturation time of ~2 000 years, while 10^{-14} m/s would give ~20 000 years.

The saturation times for both backfill and buffer range from a few tens of years to several thousand years. Examples from across this entire range are likely to arise at Forsmark, since rock properties (matrix hydraulic conductivity and presence and characteristics of fractures) are the primary controls, with backfill and buffer properties only a secondary consideration.

10.3.9 Swelling and swelling pressure

The primary purpose of the buffer is to ensure that transport of species from the rock to the canister and from the canister to the rock is dominated by diffusion. The swelling pressure in the bentonite is expected to seal all gaps and ensure that there is tight contact between the rock and the buffer. It is, therefore, important that the swelling pressure is maintained. The safety function indicator criterion for ensuring tightness in the buffer is a swelling pressure of 1 MPa (Section 8.3.2), safety function indicator Buff1b in Figure 10-2. A high swelling pressure is needed for reducing microbial activity (Buff2). The required swelling pressure for preventing canister sinking is 0.2 MPa (Buff 5). On the other hand, the swelling pressure must not be higher than 15 MPa in order to limit the pressure on canister and rock (Buff6). The densities needed to meet these values are discussed in Section 5.5.3. To ensure that the buffer density is not lost by buffer swelling into the tunnel backfill, the backfill density needs to be sufficiently high (BF1), see Section 5.6 for actual values.

The reference buffer material MX-80 is assumed to have a dry density interval of 1 450–1 560 kg/m³. The swelling pressure for the reference average dry density in a deposition hole (1 550 kg/m³) will be 7.2–9.9 MPa, see Section 5.5.3. This range includes the expected variability in installed density, but assumes that the buffer material is fully confined to the volume it occupies at deposition. The hydraulic conductivity will be well below 10^{-13} m/s. These values are valid for a rather large range of ground-water salinities. The present day groundwater at Forsmark has a salinity of ~0.9 % or 0.15 M Cl⁻.

For the backfill material with a specified dry density of 1 488 kg/m³, the swelling pressure after full water saturation should be well above 4 MPa, (Figure 5-17). Under these conditions, the hydraulic conductivity should be well below 10^{-12} m/s.

In short this means that if the buffer saturates and swells without loss of buffer material and without expanding into the backfill the above safety function indicators will be within the allowed values. In order to verify that the intended conditions after swelling will be reached, it is, however, necessary to assess more carefully the swelling process with focus on:

- Buffer homogenisation.
- Buffer upward expansion.
- Movement of the canister in the deposition hole.
- Homogenisation after loss of bentonite mass.

The findings of this assessment are presented in the following.

Buffer homogenisation

The initial state of the buffer after placement is unsaturated bentonite blocks and rings with much higher density than the average density for the entire hole and one empty slot at the canister surface and a pellet filled slot with very low density at the rock surface. Due mainly to friction within the material, but also due to hysteresis effects, the swelling and homogenisation that comes with the wetting of the bentonite is not complete and there will remain density differences and swelling pressure differences in the buffer.

In Åkesson et al. (2010a), three different analyses of the natural homogenisation process in the buffer have been carried out. In the first analysis, analytical solutions have been studied. In the second analysis, the finite element code CodeBright has been used for studying the process in more detail. In the third analysis, the finite element code Abaqus has been used for modelling the entire deposition hole.

The important geometrical components of the models are the initial open slot between the canister and the buffer blocks, the buffer blocks themselves and the pellet filled outer slot as shown in Figure 10-55. The key phenomena investigated with the CodeBright, was the influence on the homogenisation and swelling pressure of slot width in a section between the canister and the rock and the wetting sequence. In the study, the slot width was varied from 3 to 9 cm with the other parameters kept constant. Figure 10-56 shows the final swelling pressure in the buffer components as a function of slot width.

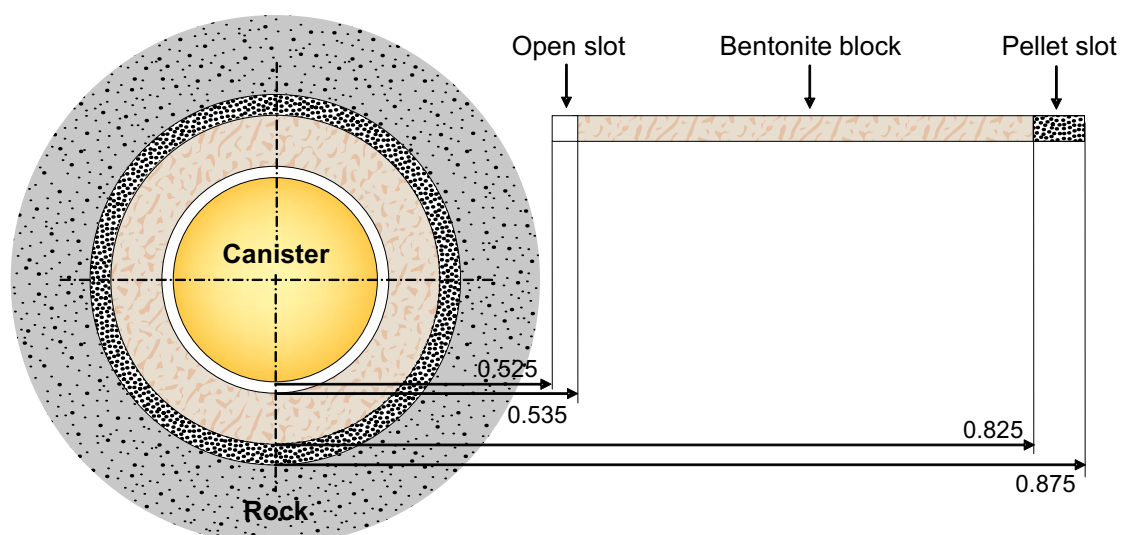


Figure 10-55. Model geometry and constituents (Åkesson et al. 2010a)

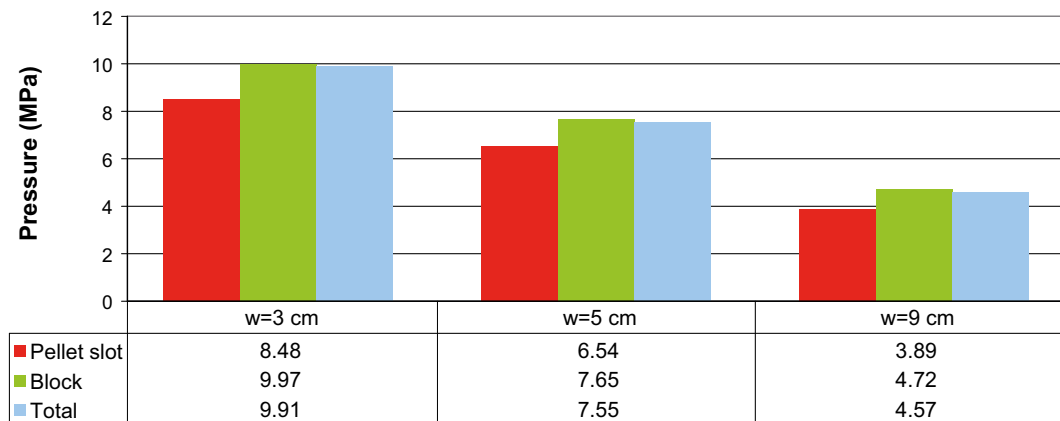


Figure 10-56. Averages of pressure for 3, 5 and 9 cm pellet slot (Åkesson et al. 2010a).

The effect of the wetting sequence was tested by the assumption of either entirely serial or parallel wetting. In the case of serial wetting water uptake comes from the pellet slot, while parallel wetting assumes that both components are swelling simultaneously. The results from the two models have been compared with the results obtained from the Canister Retrieval Test (CRT) (Åkesson et al. 2010a). Compared with CRT results, pure serial wetting produces more heterogeneity in the void ratio field. The parallel wetting process produces less heterogeneity than the CRT measurements. This is illustrated in Figure 10-57.

The finite element code Abaqus was used to model the homogenisation process in an entire deposition hole with identical initial conditions and boundary conditions with those in the CRT. The results shown in Figure 10-58 and Figure 10-59 give an expected final density and stress distribution in a deposition hole covered with a backfill that is compressed about 3 cm.

The only remarkable observation is that there is no obvious density gradient (decrease in density and swelling pressure towards the backfill) in spite of there being an upwards swelling of 3 cm. This result deviates from the results of the calculations of buffer upwards swelling shown later (e.g. Figure 10-61 and Figure 10-62), where initially completely water saturated and homogenised buffer was used.

There are several factors that in combination may explain this difference.

- The buffer material in the swelling calculations presented in the section about buffer upwards expansion, was modelled as being completely saturated and homogenised from the start. This means that the swelling pressure and the friction against the rock were fully developed from the start. This is not the case for the calculation made here where the initially low density of the pellet filling and initially unsaturated buffer blocks result in a lower friction between the rock and the buffer during a large part of the swelling process.
- The upper 75 cm was wetted later, which delayed the mobilization of the friction. The reason for this was the wetting history of CRT and the calculation was a continuation of the CRT modelling.

Modelling of the Canister Retrieval Test (CRT) and comparison with measurements confirm that the material model of unsaturated bentonite blocks and the calculation technique used are relevant for modelling the homogenisation process, since the agreement between modelled and measured density distribution in the buffer between the canister and the rock after full saturation and completed homogenisation was very good. The material model and calculation technique were then used to model the homogenisation process in an entire deposition hole with identical initial conditions and boundary conditions to those in CRT. The results shown in Figure 10-58 and Figure 10-59 gave an expected final density and stress distribution in a deposition hole covered with a backfill that is compressed about 3 cm. Very similar results were reached with the Abaqus and the CodeBright models, as well as with the analytical expression, but the entire test was only modelled with Abaqus.

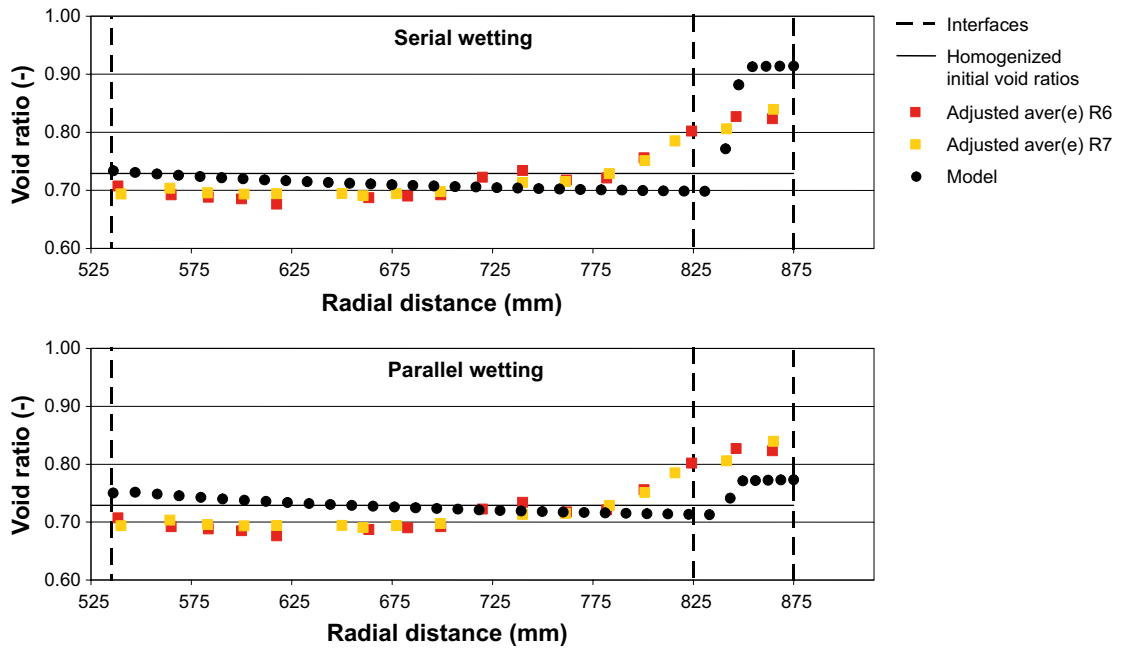


Figure 10-57. Void ratio profiles obtained for serial and parallel wetting. Adjusted average refers to the measured average void ratio (e) for the entire periphery of ring (R) 6 and 7 in the Canister Retrieval Test (Åkesson et al. 2010a).

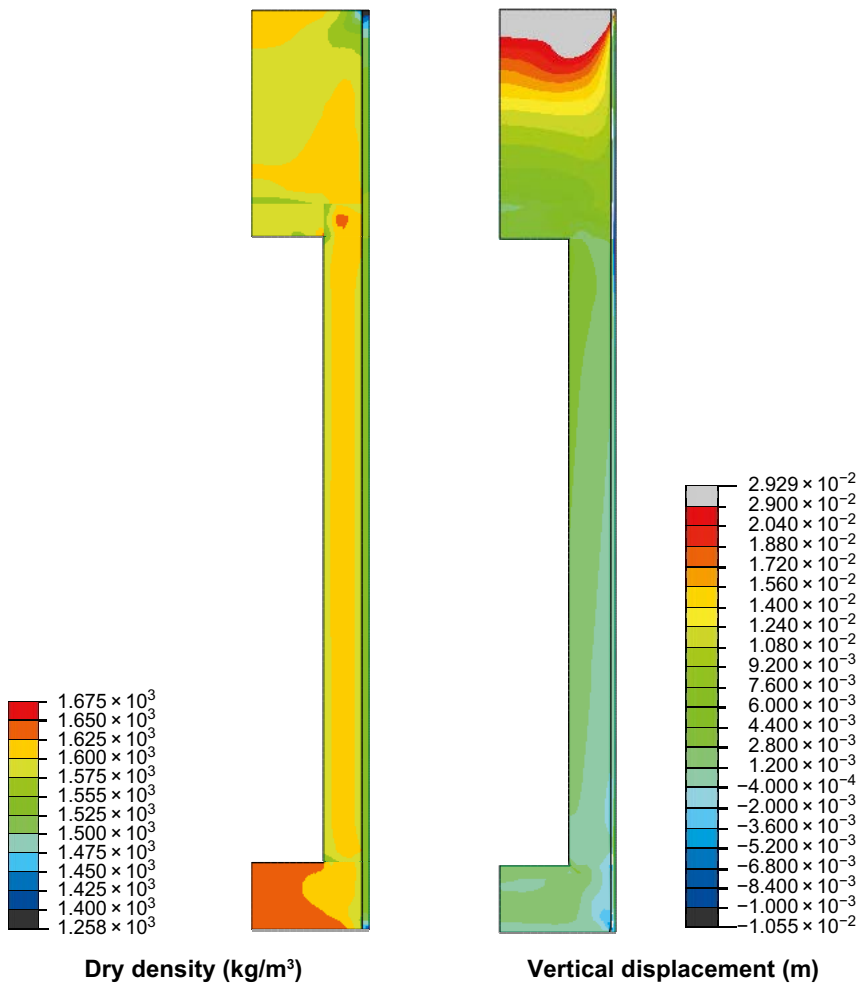


Figure 10-58. Final state of the buffer after full saturation and completed homogenisation. The distribution of the dry density and the vertical swelling is shown (Åkesson et al. 2010a).

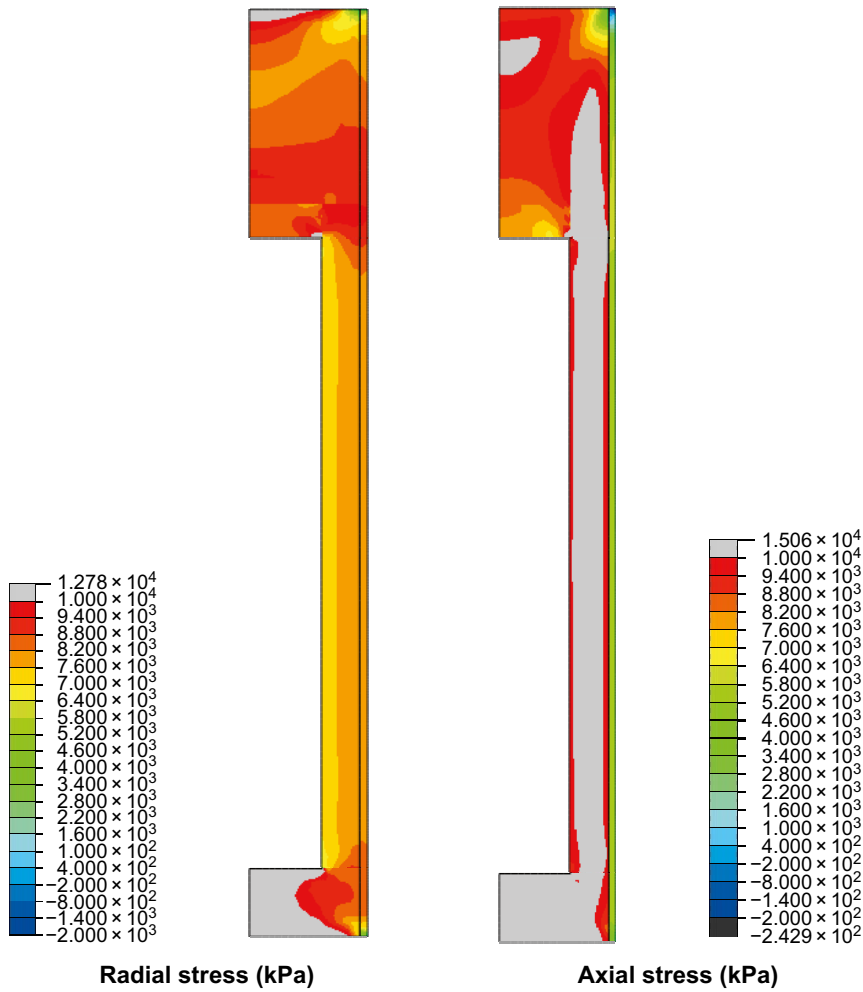


Figure 10-59. Final state of the buffer after full saturation and completed homogenisation. The distribution of radial and axial stress is shown (Åkesson et al. 2010a).

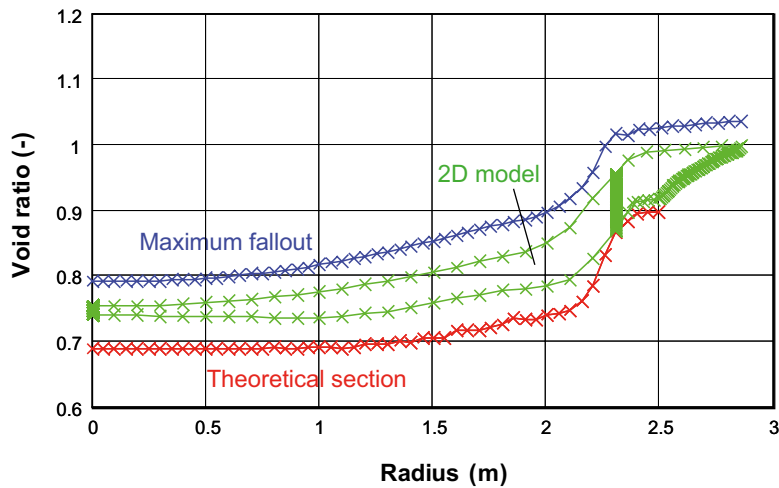


Figure 10-60. Final void ratio distributions in 1D (blue and red crosses) and 2D models (Åkesson et al. 2010a).

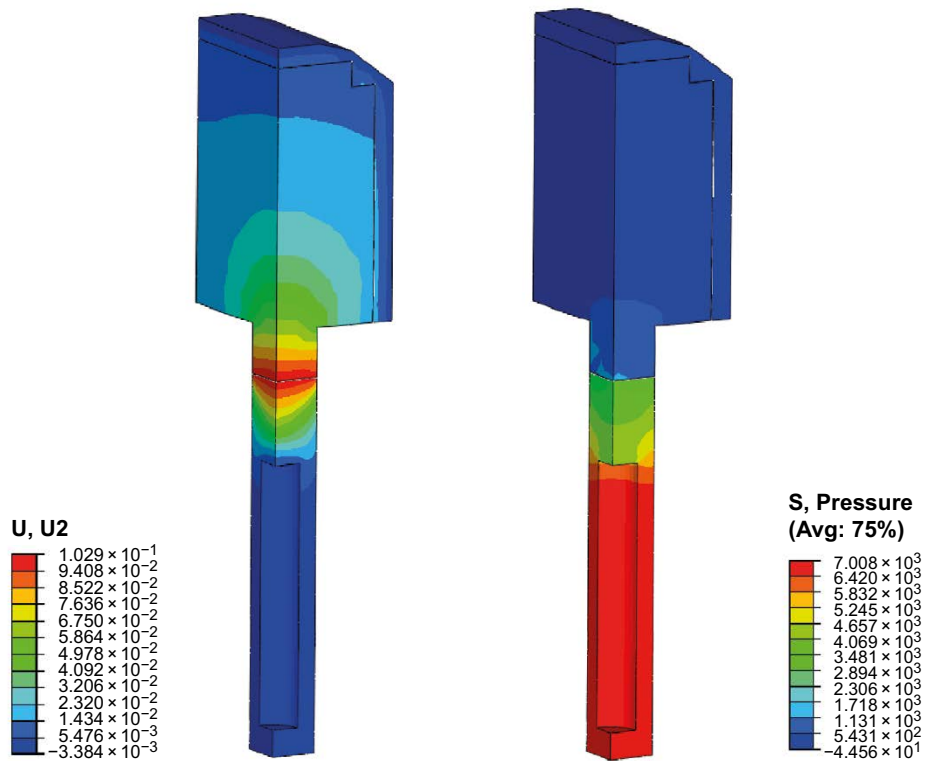


Figure 10-61. Vertical displacements (U , m) and average stress (S , kPa) in the buffer and backfill after completed swelling (Case 1.) U_2 is the direction (vertical) of the displacement U (Börgesson and Hernelind 2009).

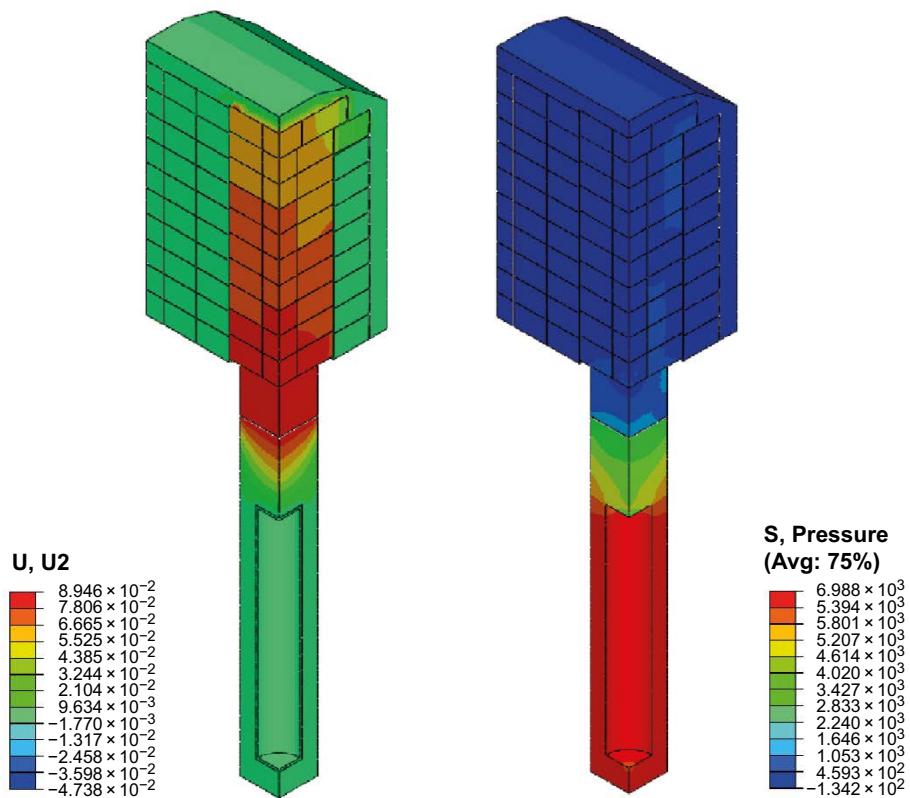


Figure 10-62. Vertical displacements (U , m) and average stress (S , kPa) in the buffer and backfill after completed swelling (Case 2.) U_2 is the direction (vertical) of the displacement U (Börgesson and Hernelind 2009).

The uncertainties are mainly the material models, which are very complicated, and the parameter values. Although they have been verified for the 1D case of swelling and homogenisation of the bentonite rings and pellets between the canister and the rock, the 2D case involves more degrees of freedom for the variables and more interactions like the friction between the bentonite and the rock or canister.

The results show that under expected conditions the buffer density and swelling pressure will homogenise to a situation where the relevant safety functions will be upheld.

Additional assessment of water saturation phases

In Åkesson et al. (2010b) 99 % was defined as “full” water saturation. The reason for this is that it made possible comparisons between different water saturation cases. The value itself has no practical significance. To illustrate the importance of different phases in the water saturation process Sellin et al. (2017, Chapter 8) has studied the safety functions of the buffer as a function of water saturation. The most relevant safety function for water saturation is the swelling pressure. In the PSAR (as in SR-Site), most safety functions are only relevant for a saturated buffer. The conclusions from the study show the following:

- The mechanical material model is process-dependent and must be calibrated for different situations. Slow water saturation was studied, and the mechanical parameters of the pellet filling must therefore be chosen to give a representative density profile at full water saturation.
- The processes in the buffer are heterogeneous. The models show great differences between blocks and pellets, but also internally in the pellets and blocks.
- Degree of water saturation is not a suitable parameter for assessing the pressure in the buffer. The buffer can reach a given pressure for a large range of water saturation levels, absolute or relative. Near the canister, 1 MPa can be reached without any water uptake.
- The safety function indicator criteria of 1–2 MPa is reached heterogeneously in the buffer. The general trend shows that it occurs later in the upper parts of the buffer and in the pellet filling.
- The hydraulic properties of the rock are crucial for the development of the swelling pressure and for the time it takes to reach the performance target.

The deposition holes in Forsmark are expected to be practically dry. In most of the holes there will be no water conducting fractures and in the cases where there are inflows, these are usually small. The significance of a low inflow in a single point in a deposition hole has been studied by Sellin et al. (2017, Chapter 9).

The study is based on a geometry where the water flow occurs at a point in the buffer at the mid-height of the canister. A constant inflow or constant pressure is set as boundary conditions in that point. In the case of flow, this will be adjusted if it requires an unrealistically high water pressure in the rock or if there is a counter pressure from water absorption in the buffer. Generally, it is difficult to get the model to converge and to make an appropriate representation of the pellet gap. Despite this, it is possible to draw some conclusions from the study:

- In order for a point flow to yield heterogeneous conditions, water saturation must be faster than if the buffer is saturated via the rock matrix. With an assumed matrix conductivity of 10^{-13} m/s no uneven saturation will occur for water saturation times longer than $\sim 1\,500$ years.
- The time it takes to fill all empty pores in the buffer is $\sim 3\,500$ years for an inflow of 10^{-6} L/min and ~ 350 years for an inflow of 10^{-5} L/min. The minimum inflow rate of interest lies therefore somewhere in the middle of this range.
- If the flow is so high that the pellet gap is filled before the blocks are saturated, there will also be no heterogeneous saturation since the blocks then will be saturated from a filled gap. It takes 1.55 years to fill the gap at an inflow of 10^{-3} L/min and ~ 2 years to saturate the blocks with free access to water throughout the gap. For flows $> 10^{-3}$ L/min, the saturation always becomes homogeneous.

- According to Joyce et al. (2013), there are approximately 400 deposition holes where the inflow is in the range of 5×10^{-5} to 10^{-3} L/min, which could cause uneven saturation.
- The mechanical analysis also reported by Sellin et al. (2017, Chapter 9) shows that the effect of the inhomogeneities caused is small. However, a small lift of the canister and some local effects around the infusion point can be noted. The effect on the density distribution in the deposition hole is small.

An example of results is shown in Figure 10-63. Even with an extreme case where the buffer get al. water at a single point and the inflow rate is unfavourable, the water is distributed relatively well in the buffer blocks. The risk of an extremely heterogeneously saturated buffer is therefore considered negligible.

However, there are some uncertainties in the mechanical and hydraulic representation of the pellet gap and it is not clear how this affects the results. The significance of alternative models of pellet filling has been evaluated in Sellin et al. (2017, Chapter 9). Figure 10-64 shows calculated pore pressure in the pellet with three different representations of the hydraulic conductivity of the pellet filling.

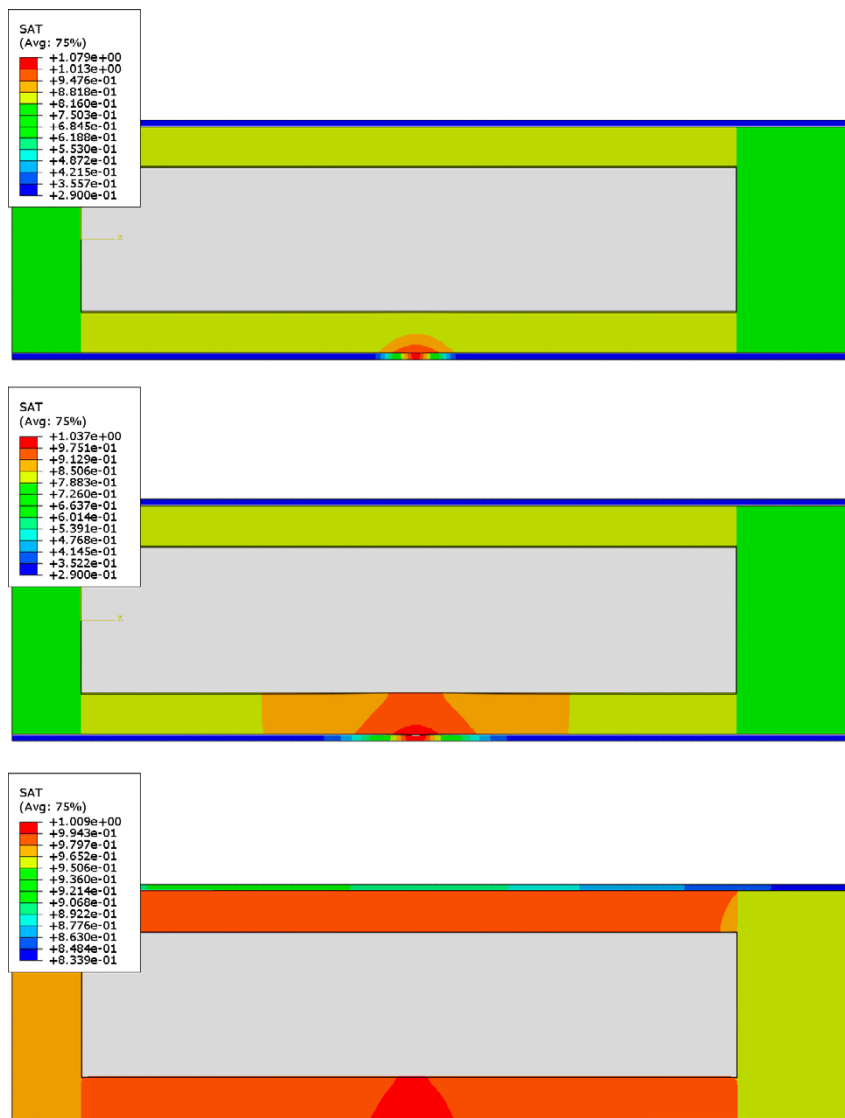


Figure 10-63. HM-modelling of an entire deposition hole with the point inflow rate of 0.0001 L/min. Degree of saturation after 0.32 years (upper), 3.2 years (middle) and 320 years (lower) Sellin et al. (2017).

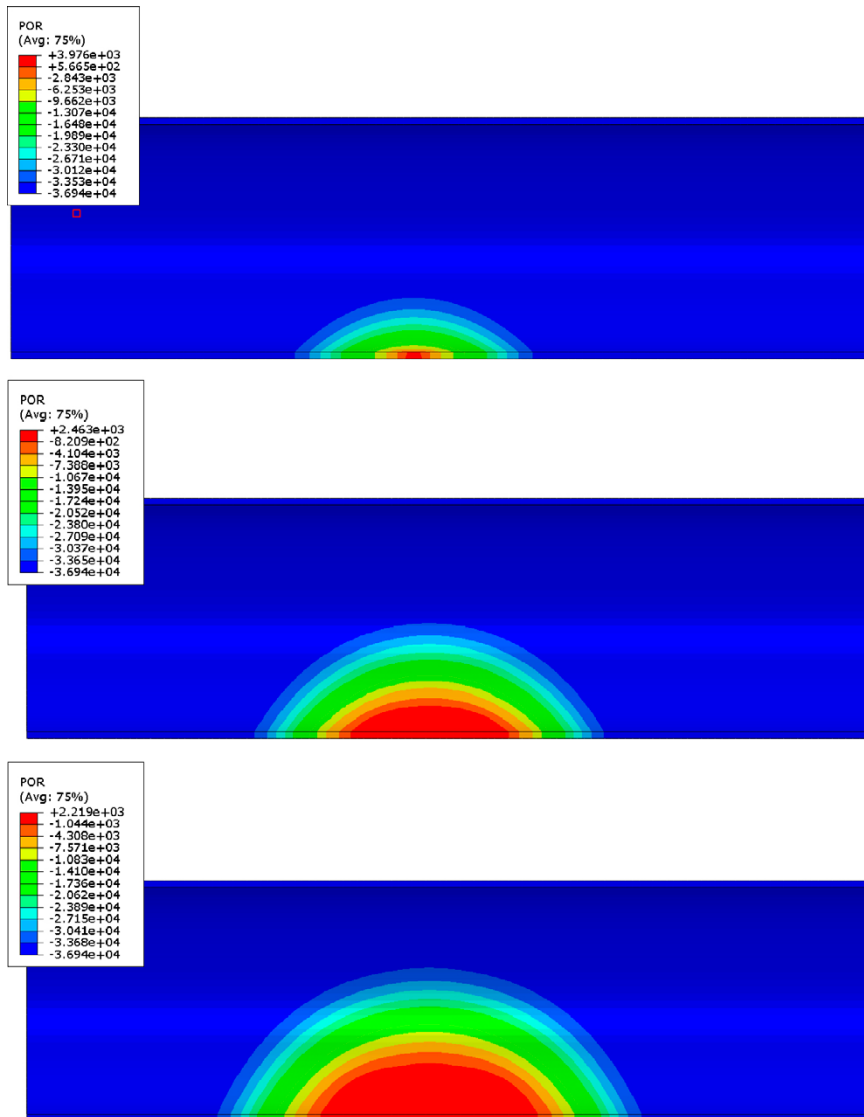


Figure 10-64. H-modelling of pellet filled slot only with the point inflow rate of 0.0001 L/min. The top figure is the reference case, the middle represents a case where the hydraulic conductivity of the pellets fill is increased to 10^{-6} m/s for a degree of saturation of > 90 % and the bottom represents a case where it is increased to 1 m/s for the same condition. Pore-water pressure (kPa) after 3.2 years Sellin et al. (2017).

Backfill homogenisation

The deposition tunnels will have a varying cross section. Since the ratio of backfill blocks/pellets will vary in the installed backfill, density will vary in the axial direction of the tunnel. The homogenisation of the backfill was studied by Åkesson et al. (2010a).

The final void ratio distributions both for 1D and 2D models are shown in Figure 10-60. A general difference between the inner and the outer parts of slightly more than 0.2 in void ratio can be noticed. This is generally in agreement with the experimental findings from the Canister retrieval test (Johannesson 2007). It can be noticed that the distribution in the 2D model falls between the two extreme results obtained with the 1D models.

The models indicate that the backfill material will not be completely homogenised. The remaining heterogeneity is of such a degree that the difference between the inner and the outer parts is slightly more than 0.2 in terms of void ratio, and the reason for this appears to be the hysteretic effects during swelling/compression cycles. The remaining heterogeneity indicates that the final void ratio can be as high as 1.03 which corresponds to a dry density of 1370 kg/m³. This value is substantially lower

than the lowest value in the range presented in Chapter 5 and in the **Backfill production report**, which shows that the homogenisation process needs to be considered in the design of the backfill. However, this is still higher than the dry density of 1 100 kg/m³ that is required for the SR-Site backfill to reach a hydraulic conductivity less than 10⁻¹⁰ m/s which is stated in the **Backfill production report**.

Buffer upward expansion

The mechanical interaction between the buffer material in the deposition hole and the backfill material in the deposition tunnel is an important process in the safety assessment since the primary function of the backfill is to keep the buffer in place and not allow it to expand too much and thereby lose too much of its density and barrier properties.

The process has been analysed through *hydro-mechanical modelling* performed by Börgesson and Hernelind (2009, 2017) and Åkesson et al. (2010a) using the code Abaqus; and by Sandén et al. (2020) using CodeBright. All Abaqus buffer models have used a material model consisting of a porous elastic model and a Drucker-Prager, or a Claytech plastic cap plasticity model, and were described as water saturated from the start of the simulation. In contrast, all CodeBright simulations of the buffer have used a material model based on the Barcelona Basic Model, and were described as unsaturated from start. All parameter values for the buffer material were selected as to describe MX-80 bentonite.

The process has also been analysed through different *experimental work*: i) The Buffer Swelling Test was performed at Äspö HRL, and involved a bentonite buffer block being pushed upward into a full-scale tunnel section filled with backfill blocks and pellets, while simultaneously measuring the vertical force, the displacement and the pressure against the rock surface (Sandén et al. 2017); ii) Tunnel scale-tests (in scale 1:20) involved a tunnel section made of steel and filled with backfill blocks and pellets, and a piston which was pushed upwards into the backfill at a constant rate, while simultaneously measuring the force and the displacement. Different tests were performed after supplying water to the backfill during different time periods: from 0 (dry case) to 52 days (Sandén et al. 2020); and iii) Deposition hole scale-tests (in scale 1:10) involved two deposition holes made of steel which were filled with buffer blocks and pellets, and equipped with springs as the top representing the compressibility of a backfill. The deposition holes were supplied with water through filters at the lateral surface; in one case along the lower buffer block only, and in the second case along the entire lateral surface (Sandén et al. 2020).

The extent of the upward expansion is essentially a *combined effect* of the properties and dimensions of the deposition tunnel and the backfill on one hand, and the deposition hole and the bentonite buffer on the other. The influence of individual factors and their contribution to the upward swelling can be summarized as:

- The tunnels-scale tests clearly showed that the compressibility of the backfill decreased with an increasing *water content*. A dry backfill is therefore the most pessimistic case concerning the buffer upward swelling.
- Models and experimental works clearly showed that the *thickness of the pellets bed on the tunnel floor* has a major influence of the upward swelling of the buffer. They also showed that the current nominal thickness in the reference design (i.e. 100 mm) result in an acceptable displacement.
- Models showed that the *thickness of the pellets layer in the tunnel ceiling* has a rather small influence of the upward swelling.
- Models and experimental works have demonstrated that the use of *overlapping backfill blocks* will lead to a lateral spreading of the pressure from the buffer and will therefore limit the upward swelling. The current reference design is based on a system with overlapping block.
- Models and results from the Buffer Swelling Tests demonstrated the importance of installing *backfill blocks with a sufficiently high compressive strength* in order to limit the upward swelling.
- The *friction angle between the buffer and the rock wall* in the deposition hole will influence whether a specific displacement at the buffer/backfill interface will affect the density in the vicinity of the canister. The representation of wall friction in all presented models has been quite consistent with experimental data from independent tests.

- *The installed dry density of the buffer* will influence the potential for upward swelling. Models have illustrated that a higher density generally results in a larger displacement. However, this does not mean that the final density in the vicinity of the canister is lower. The installed density is therefore not a relevant factor for reducing the upward swelling.
- Models showed that the upward swelling is influenced by the *buffer homogenisation*. This finding therefore demonstrates the importance of taking the initial heterogeneities into account in models, but does not have any real implications for the design.
- Results from the depositions hole scale-tests have demonstrated that a *localised water uptake* can result in a significant localised swelling and a reduction of the dry density in the bentonite block below the canister (corresponding to a swelling pressure < 3 MPa). The average dry density of the buffer volume was, however, high enough to fulfil the swelling pressure requirement (mean swelling pressure 3MPa in the volume from 50 cm below to 50 cm above the canister).
- The *pellets-filled bevel* will aggravate the upward swelling, since the bentonite blocks in the upper part of the deposition hole can swell horizontally, which will lead to a reduction of the dry density in this part. Model results have nevertheless shown that a design with a pellets bed with a thickness of 100 mm would be acceptable in combination with a pellets-filled bevel.

Finally, the buffer upward swelling has implications for the *dimensioning* of the buffer (Luterkort et al. 2017) and the compressive strength of the backfill blocks (Eriksson 2020).

Despite the uncertainties associated with the influence of the pellets-filled bevel and the potential occurrence of localised water uptake, the analyses demonstrate that the displacements and the dry density reduction in the vicinity of the canister will be such that the technical design requirement on buffer swelling pressure will be met, if the thickness of the pellets bed on the tunnel floor is limited to 100 mm and if the compressive strength of the backfill blocks is sufficiently high. Analyses in Eriksson (2020) indicate that 3.8 MPa is a sufficiently high compressive strength to achieve this intended function of the backfill.

Movement of the canister in the deposition hole

One of the safety functions for the buffer is that it should prevent the canister from sinking in the deposition hole since this would render the canister in direct contact with the rock thus short-circuiting the buffer.

Canister settlement consists mainly of four different processes:

1. Consolidation/swelling caused by the canister weight.
2. Volumetric creep caused by the canister weight.
3. Deviatoric creep caused by the canister weight.
4. Stress changes caused by upwards swelling of the buffer/backfill interface
 - a. Consolidation/swelling.
 - b. Volumetric creep.
 - c. Deviatoric creep.

The fourth process can thus be divided into the same processes as the first three processes but the consolidation and creep is caused by the swelling pressure from the buffer on the backfill instead of the weight of the canister.

The settlement of the canister has been modelled in Åkesson et al. (2010a). The calculations include two stages, where the first stage models the swelling and consolidation that takes place in order for the buffer to reach force equilibrium. This stage takes place during the saturation phase and the subsequent consolidation/swelling phase. The second stage models the deviatoric creep in the buffer over 100 000 years. The modelling takes into account all processes except volumetric creep, which thus may cause a slight underestimation of the canister displacement. The motive for excluding volumetric creep is that canister settlement caused by volumetric creep will not change the total mass of bentonite under the canister but will only increase the density and is thus not judged to be a problem.

The base cases in the calculations correspond to the final average density at saturation of 2 000 kg/m³ with the expected swelling pressure 7 MPa in a buffer. In order to study the sensitivity of the system to loss in bentonite mass and swelling pressure seven additional calculations were done with reduced swelling pressure down to 80 kPa corresponding to a density at water saturation of about 1 500 kg/m³. The results of the calculations with fixed backfill boundary and the corresponding friction angle at retained initial swelling pressure are summarized in Table 10-7. The canister settlement shown in column 5 also includes the consolidation settlement, which takes into account that the compressibility increases when the swelling pressure decreases whereas a reduced friction angle with retained swelling pressure will not have an increased compressibility. The settlements at the presented friction angles have for this reason been recalculated as the sum of the settlement of the base case and the creep from respective creep calculation (column 7).

Table 10-7. Summary of results from the calculations with fixed buffer/backfill boundary (Åkesson et al. 2010a).

Calculation No	Density at saturation ρ_m (kg/m ³)	Swelling pressure p (kPa)	von Mises stress at failure q_r (kPa)	Canister settlement (mm)	Friction angle at retained swelling pressure ϕ (°) ¹⁾	Canister settlement at corresponding friction angle and retained swelling pressure (mm) ²⁾³⁾
1 (base case)	2010	7000	2238	0.35	8.8	0.35
2	1950	3500	1312	0.67	5.2	0.47
3	1890	1750	770	1.26	3.1	0.67
4	1840	875	451	2.42	1.8	1.04
5	1780	438	265	4.63	1.1	1.67
6	1720	219	155	8.89	0.63	2.78
7	1690 (1640) ¹⁾	160	122	12.0	0.50	3.51
8	1620 (1470) ¹⁾	80	72	22.5	0.29	5.54

1. For the actual values of void ratio and density at saturation since the void ratio, $e > 1.5$ and equation

$$\phi = \frac{3}{6 p/q_f + 1}$$

2. Derived from the consolidation in the base case (0.20 mm) + the creep from respective creep calculation.

3. The total bottom buffer thickness is 500 mm.

The conclusion is thus that the expected displacement of the canister in a deposition hole from consolidation and creep during 100 000 years is very small. The sensitivity analyses with reduced swelling pressure corresponding to reduced density or reduced friction angle also show that the canister displacement is very insensitive to such phenomena since the total settlement will be less than a few cm even at a buffer density of 1 500 kg/m³ or at a friction angle of 0.3°. The only condition when the safety function could be violated is when there is a large loss of buffer. However, if that situation would occur, many of the other buffer safety functions would be lost long before.

Homogenisation after loss of bentonite mass

Homogenisation of buffer and backfill is crucial to fulfil the safety functions related to buffer and backfill density (swelling pressure and hydraulic conductivity as well as the ability to limit microbial sulphate reduction). The swelling properties of bentonite make the buffer and backfill material swell and close open gaps or channels to form a more homogeneous buffer. These properties are important not only for homogenising the buffer and backfill after installation of the bentonite blocks but also for limiting the potential for the long term formation of openings in the buffer and backfill. Except for the natural slots that exist after installation, which are treated in the Buffer homogenisation section, such spaces may appear for several reasons, as summarised below.

1. The postulated case of missing bentonite rings.
2. Erosion before closure of the repository caused by water inflow into deposition holes and a deposition tunnel until the water flow and high water pressure gradients are stopped by temporary plugs. If the erosion is severe, large openings of missing bentonite may locally be formed.

3. Long term erosion of bentonite by water from fractures intersecting the deposition hole or the deposition tunnel mainly caused by bentonite dispersion and subsequent colloid transportation after fresh water intrusion.

The consequences of erosion before the closure of the repository are discussed in Section 10.2.4.

Loss of buffer

The swelling and sealing of bentonite cannot take place unhindered since there is a resistance to swelling caused by friction both internally in the bentonite and between the bentonite and the surrounding fixed walls represented by the rock surface and in some cases the canister. In order to investigate how well the buffer material seals the openings resulting from the mentioned processes a number of finite element calculations with the code Abaqus have been performed (Åkesson et al. 2010a).

The case that has been modelled represents either a huge loss of bentonite after a long time of erosion or the totally fictional case of one to three bentonite rings at the upper end of the canister, missing. The rings are 50 cm thick and are for the sake of the calculations assumed to be forgotten during the installation. This case can also represent an extreme loss of bentonite by colloid erosion. The calculations comprise cases with an empty space of 0.5 m, 1.0 m and 1.5 m. Additional calculations were also done for each case in order to investigate the influence of the friction against the rock.

Figure 10-65 shows the course of swelling for the base case (two missing rings) assuming a friction angle $j = 8.69^\circ$. After a rather long time the space is almost completely filled with bentonite but there is a small remaining final opening and the void ratio is rather high (1.7) close to that opening. The density is so low that the expected swelling pressure might very well be below 100 kPa at the position closest to the canister. For a case with low friction the lowest swelling pressure case is 300 kPa at the canister.

Variant calculations corresponding to one, two or three missing bentonite blocks were also analysed. In summary, the analyses show that in the case where large amounts of bentonite are lost from a deposition hole or missing from the start the remaining bentonite swells and fills the empty space but the density and resulting swelling pressure will be rather low due to the friction in the buffer and the friction against the rock surface. For a 50 cm vertical opening in a deposition hole, the resulting swelling pressure will be in average 0.5–1 MPa in almost the entire former hole. However, if the rock surface is smooth and the resulting friction against the rock is halved the swelling pressure will be above 1 MPa in a majority of the former space. For a 100 cm opening the swelling pressure will be rather low close to the canister with the pressure below 100 kPa and there may even be an unfilled part left, while the case with low friction yields a minimum swelling pressure of more than 300 kPa. If the opening is 150 cm, a large volume will have a swelling pressure below 100 kPa and may even be unfilled. However, the influence of the friction between the bentonite and the rock and canister is large and with halved friction almost the entire opening will be filled. The homogenisation is enhanced by the swelling of the bentonite above or below the canister, which is shown by comparison with results from the calculations that only consider the buffer around the canister.

Homogenisation after a loss of backfill mass

If a fracture intersects the entire perimeter of the backfilled tunnel there will be no deposition hole at that location, which means that such fractures do not intersect deposition holes. However, it is expected that there will be some such water conducting fractures crossing the tunnel close to deposition holes. If these fractures are hydraulically active they may expose the backfill to colloid erosion. Åkesson et al. (2010a) have investigated how much backfill can be lost before the buffer upwards swelling decreases the density in the deposition hole around the canister to a level where advective conditions have to be considered.

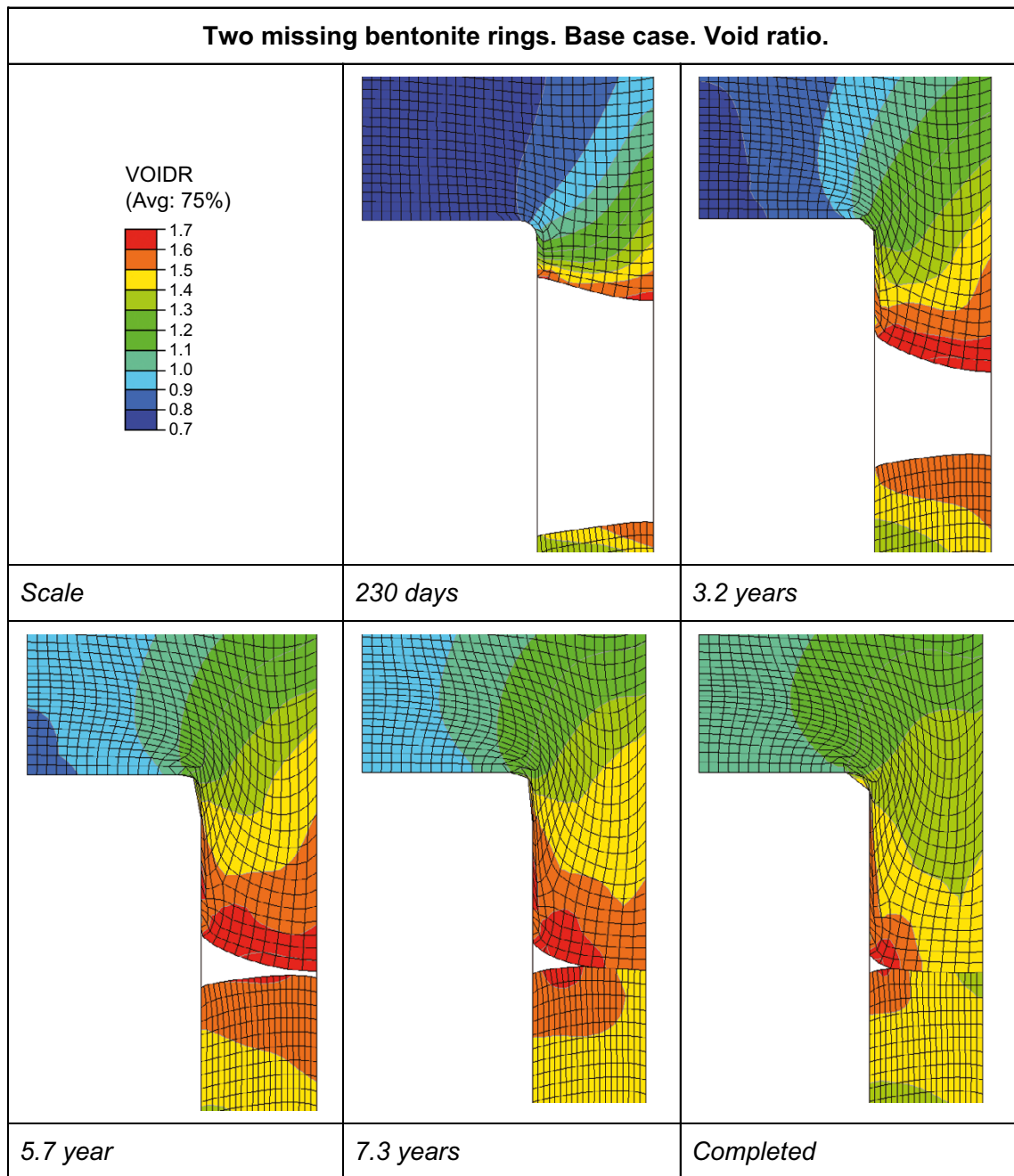


Figure 10-65. Void ratio plotted at different times for the base case with two missing ring (Åkesson et al. 2010a).

In the calculations, the buffer material is considered to completely have lost its sealing ability when the average swelling pressure between the canister and the rock has become lower than 100 kPa, see previous section. Since the swelling of the buffer takes place upwards into the tunnel where the backfill is lost, the swelling pressure will be lower on top of the canister than further down into the deposition hole. The criterion for loss of sealing ability will thus be when the swelling pressure on top of the canister is 100 kPa. Due mainly to friction between the buffer and the rock the swelling pressure is likely to be lower at the opening of the hole than on top of the canister. The aim of the calculations was to study how much backfill can be lost under a range of conditions where a swelling pressure of 100 kPa is still maintained on top of the canister.

A number of calculations for different assumptions and geometries were made to determine the maximum allowed loss of mass. For a bounding case where the backfill is lost directly on top of the canister and no homogenisation whatsoever is considered about 25 tonnes of backfill can be lost before the swelling pressure in the buffer on the canister top drops to 100 kPa. This case is totally unrealistic since the swelling pressures in the remaining buffer and backfill are totally neglected. It is only presented to illustrate the importance of the homogenisation and friction.

Figure 10-66 illustrates a case where both the homogenisation in the backfill in the tunnel and the friction in the deposition hole is considered. Table 10-8 summarises the maximum allowed loss of backfill for this case. Here the homogenisation and the friction in the remaining backfill and the friction in the buffer have been considered. The bevel in the deposition hole has also been considered.

Table 10-8. Total allowed loss for the case illustrated in Figure 10-66.

ϕ (°)	Total loss (t)
10	430
20	220
30	150

It is reasonable to assume that the friction angle will be about 20° for these conditions, since the swelling pressure is lower than 100 kPa (Börgesson et al. 1995). This means that a total of 220 tonnes of backfill can be lost before the swelling pressure on top of the canister drops to 100 kPa.

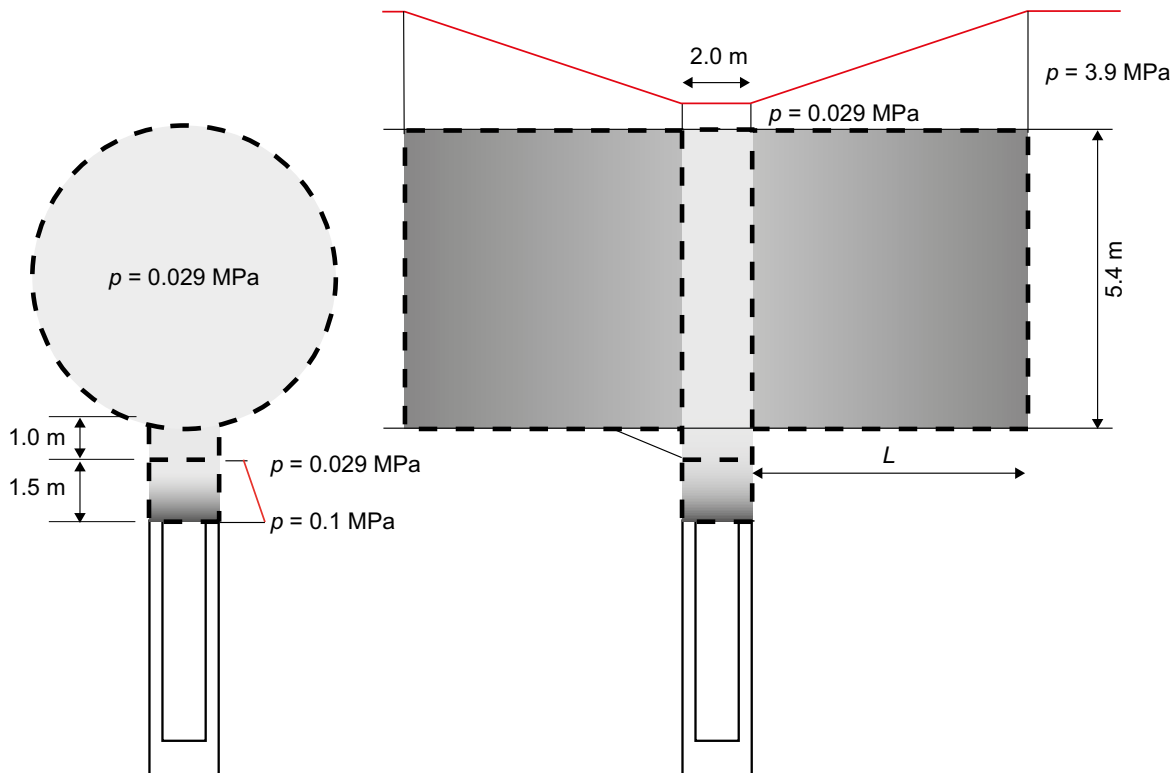


Figure 10-66. The light grey area has lost mass to yield a swelling pressure of 29 kPa. The successive transition from dark grey to light grey illustrates the decrease in swelling pressure and density. The swelling pressure variation in the upper part of the deposition hole and in the deposition tunnel are shown by the red lines (derived from Åkesson et al. 2010a).

Loss of backfill from erosion is important for the properties of the buffer in the deposition hole, but is not expected to have any significant importance for the transport properties itself. There will be a local volume with low swelling pressure and high hydraulic conductivity. However, the main part of the tunnel volume will be unaffected.

Potential for advective conditions

Advective conditions in the buffer can occur if the hydraulic conductivity is sufficiently high. The buffer function indicators prescribe a hydraulic conductivity of 10^{-12} m/s and a swelling pressure of 1 MPa to rule out advection in the buffer. These values do, however, have some safety margins included in them.

Neretnieks (2006b) calculated the conditions under which water is drawn into a deposition hole. He concluded that even for a rock fracture with a very high flow rate (transmissivity 10^{-6} m²/s and hydraulic gradient 0.01), a buffer conductivity of around 3×10^{-6} m/s suffices to prevent advection and causes the water in the fracture to flow around the buffer as if it were impervious. Such conductivity corresponds to a dry density well below 500 kg/m³. However, to ensure that the self-sealing ability is maintained and no channels or pipes will be formed, a certain swelling pressure is also required. The minimum swelling pressure needed will be about 100 kPa. This is based on laboratory investigations in which piping has been observed at ~60 kPa (Karnland et al. 2006). This value is most likely still pessimistic, since the gradients at the site are expected to be very low. However, the effect on the accepted mass loss will be relatively small. To ensure this for all expected groundwater compositions, a minimum dry density of 1 000 kg/m³ is required (Figure 5-14). This corresponds to a void ratio of 1.75. As seen in Figure 10-65 this requirement is still met in almost the entire buffer diameter when two entire bentonite rings are omitted, corresponding to a dry mass loss of 2 400 kg.

For the case when the buffer erodes by colloid formation, the mass loss may be more local compared with the case in which entire blocks are omitted and it is more appropriate to consider the corresponding limit for losses over typically half the circumference, i.e. 1 200 kg, which would also cover the situation when the loss occurs closer to the centre of the canister. This value includes some pessimism since homogenisation in the horizontal direction is neglected. However, at higher mass losses, the swelling pressure cannot be guaranteed and advection in the buffer has to be considered. This is further elaborated for the case of buffer erosion in Section 10.3.11.

For the case when mass loss occurs mainly in the tunnel and only backfill material is lost, a maximum loss of 220 tonnes of backfill can be allowed before advective conditions have to be considered in the buffer in the deposition hole. However, loss of backfill by erosion does not mean that the hydraulic conductivity of the entire tunnel will be affected.

Potential for microbial sulfate reduction

As stated in Section 8.3.2, the buffer density is the safety function indicator for the ability to limit microbial sulphate reduction. The indicator criterion for the reference material in PSAR, MX-80, is a saturated density of 1 850 kg/m³, which corresponds to a void ratio of 1.1. As seen in Figure 10-65, a large part of the buffer has a higher void ratio than this in the case of a mass loss corresponding to two bentonite rings. The calculations of homogenisation in the case of loss of one bentonite ring in Åkesson et al. (2010b) shows that the final void ratio still is higher than 1.1 for this case as well. The maximum mass loss where a void ratio of 1.1 will be reached has not been calculated. It should be somewhat less than the equivalent of one missing ring, based on the results from Åkesson et al. (2010b).

Buffer mass losses of a few hundred kilos may lead to a situation where sulphate reducing bacteria can be active in the deposition hole. As seen in the previous section, this will happen before advective conditions are reached. See also Section 10.3.13.

Identified uncertainties and their handling in the subsequent analysis

If the buffer and backfill is installed as envisaged by the reference design, the buffer density and swelling pressure will homogenise to a situation where the relevant safety functions will be upheld. Modelling of the Canister Retrieval Test (CRT) and comparison with measurements confirm that

the material model of unsaturated bentonite blocks and the calculation technique used are relevant for modelling the homogenisation process. The uncertainties are mainly the material models, which are very complicated, and the parameter values. Although they have been verified for the one-dimensional case of swelling and homogenisation of the bentonite rings and pellets between the canister and the rock, the two-dimensional case involves more degrees of freedom for the variables and more interactions like the friction between the bentonite and the rock or canister.

The overall picture is that the swelling pressure of the buffer and the associated safety functions will be maintained during the expansion of the buffer into the backfill for all possible combinations of buffer and backfill conditions. The safety function concerning the ability to limit microbial activity will also be upheld after buffer saturation and swelling. The indicator criterion for the reference material in PSAR, MX-80, is a saturated density of 1850 kg/m^3 , which corresponds to a dry density of 1327 kg/m^3 , or void ratio of 1.1. As seen in Figure 10-57 and Figure 10-58, the dry density will be higher and the void ratio lower even in the original low density pellets filling in the deposition hole.

However, in the analysis the buffer is modelled as completely water saturated and homogenised from start, which may affect the results such that the modelled density gradient between the canister and the backfill probably is larger than if a heterogeneous unsaturated buffer was modelled. The mechanical behaviour of the horizontal contacts between the backfill blocks has not been measured. The relation used assumes that there is a slot of 4 mm that is closed at the pressure 10 MPa, which is probably pessimistic, since it is reasonable to assume that blocks can be made and piled with better precision. The effect of local crushing of the blocks that may occur close to the floor is not included in the model, but this is not expected to yield any problems. Another uncertainty relates to how the blocks are piled. It is assumed that the blocks are not overlapping each other, which means that there will be no lateral spreading of the pressure. The swelling is expected to be smaller if the blocks are piled with overlaps like masonry.

The safety function for canister settlement in the deposition hole will not be violated as long as there is a reasonable amount of buffer left in the deposition hole. The only condition when the safety function could be violated is when there is a large loss of buffer. However, if that situation were to occur, many of the other buffer safety functions would be lost long before. These buffer loss cases are analysed elsewhere.

When large amounts of bentonite are lost or missing from the start, the bentonite swells and fills the empty space but the density and resulting swelling pressure is rather low due to the friction in the buffer and the friction against the rock surface. For a 50 cm opening the swelling pressure will be on average 0.5–1 MPa in almost the entire former hole in the base case. However, if the rock surface is smooth and the resulting friction against the rock is halved, the swelling pressure will be above 1 MPa in a majority of the former space. For 100 cm opening the swelling pressure will be rather low close to the canister in the base case with a pressure below 100 kPa or even an unfilled part left, whereas the low friction case yields a minimum swelling pressure of more than 300 kPa. If the opening is 150 cm corresponding to three missing bentonite rings, the base case yields that a large volume will have a swelling pressure below 100 kPa and even be unfilled. However, the influence of the friction between the bentonite and the rock and canister is large and with halved friction almost the entire opening will be filled. The homogenisation is enhanced by the swelling of the bentonite above or below the canister, which is shown by comparison with the calculations that do not include that part of the buffer.

Advective conditions in the buffer can occur if the hydraulic conductivity is sufficiently high. The buffer function indicators prescribe a hydraulic conductivity of 10^{-12} m/s and a swelling pressure of 1 MPa to rule out advection in the buffer. These values do, however, have some safety margins included in them, but a minimum dry density of 1000 kg/m^3 is required corresponding to a void ratio of 1.75. This requirement is still met in almost the entire buffer diameter when two entire bentonite rings are omitted, corresponding to a dry mass loss of 2400 kg.

For the case when the buffer erodes by colloid formation, further discussed in Section 10.3.11, the mass loss may be more local compared to when entire blocks are omitted and it is more appropriate to consider the corresponding limit for losses over typically half the circumference, i.e. 1200 kg, which also would cover the situation when the loss occurs closer to the centre of the canister. This value includes some pessimism since homogenisation in the horizontal direction is neglected.

For the case when backfill material is lost, a maximum loss of 220 tonnes can be allowed before advective conditions have to be considered in the deposition hole. However, loss of backfill by erosion does not mean that the hydraulic conductivity of the entire tunnel will be affected.

10.3.10 Buffer and backfill chemical evolution

After deposition, the buffer is subjected to a thermal gradient due to the heat generation from the canister. At the same time there will be a hydraulic gradient caused by the suction in the unsaturated bentonite blocks and the hydrostatic pressure in the surrounding rock. After saturation and cooling of the near field, the interaction of groundwater with the bentonite buffer may result in an evolving distribution of some aqueous species in the bentonite porewater, as well as the redistribution of accessory minerals and the cation exchanger.

Three aspects must be considered regarding the geochemical evolution of the near field:

1. The effect of the thermal period.
2. The processes during the saturation of bentonite.
3. The interaction of the water-saturated bentonite with the local groundwater.

There are no buffer safety functions directly connected to this evolution, but an assessment needs to be made as to whether this evolution indirectly would violate the buffer safety functions.

During the period of bentonite saturation (before 10, 100, 1 000 and 2 000 years, depending on the hydrological model) advection of solutes to the bentonite porewater is the main mechanism of transport between the groundwater and the buffer. The effect of solute diffusion between the inflowing groundwater and the bentonite porewater is negligible in the cases with a high rate of water saturation (10 and 100 years). In the models with low rates of saturation (1 000 and 2 000 years), the effects of the diffusion on the calculated concentrations during the period of saturation are significant. When the bentonite buffer becomes fully saturated, diffusion is the exclusive mechanism of solute transport.

Table 10-9 shows some chemical properties of the groundwaters flowing in the repository volume for different climatic conditions. The table is a summary of the results presented in Sections 10.2.5, 10.3.7 and 10.4.7, and the data are used as boundary conditions when evaluating geochemical properties of the buffer and backfill.

Table 10-9. Maximum chloride concentration, maximum and minimum Ca/Na ratio, pH and carbonate, and maximum ionic strength in the Forsmark groundwaters for all time frames (Salas et al. 2010). The position of the ice front locations IFL 0 to V is defined in Figure 10-135 and associated text and “a” and “r” stand for ice advance and ice retreat, respectively.

	Max Cl (M)	Max Ca/Na	Min Ca/Na	Max pH	Min pH	Max carbonate (M)	Min carbonate (M)	Max Ionic Strength (M)
Temperate (2000 AD)	0.345	1.219	0.024	8.05	7.07	0.0025	0.00020	0.47
Temperate (9000 AD)	0.267	1.127	0.050	7.57	6.48	0.0075	0.00026	0.36
Glacial (IFL IIa)	0.343	1.228	0.600	8.54	6.34	0.0063	0.00026	0.47
Glacial (IFL Vr)	0.078	1.548	1.023	9.42	6.97	0.0022	0.00008	0.11
Permafrost (before onset of glaciation)	0.099	1.036	0.398	7.01	6.52	0.0067	0.00552	0.14
Submerged fresh water	0.091	1.320	1.200	8.99	7.01	0.0015	0.00006	0.13
Submerged seawater	0.276	1.230	0.024	8.03	7.22	0.0018	0.00019	0.38

Unsaturated phase and period of elevated temperatures

At the Forsmark site, the saturation time of the buffer surrounding the canister is expected to vary between a few tens to a few thousands of years, depending on the location in the repository (see Section 10.3.8). In most deposition holes the saturation time is expected to be more than 1 000 years. This means that the canister surface can be exposed to unsaturated conditions for a relatively long time. One issue for canister corrosion is the chemical composition of the gas in the unsaturated bentonite and in the engineering voids in the deposition hole. Of particular interest is the content of oxygen (O₂) and hydrogen sulphide (H₂S). Issues of interest include:

Will O₂ be consumed by the repository components? If yes, what is the reaction rate?

Will H₂S be generated from accessory minerals in the buffer?

Can H₂S be generated microbially in an unsaturated buffer?

These issues are discussed in detail in SKB (2019c).

Experimental and field studies

Two tests have been designed and conducted in order to investigate the possible evolution of gases in the buffer of an unsaturated KBS-3 repository (Birgersson and Goudarzi 2018). One of the tests included a central heater in the form of a copper tube as well as IBECO RWC bentonite blocks and pellets, configured to form a scaled model of an isolated unsaturated KBS-3 buffer (10 cm copper tube, approximately 30 cm bentonite block diameter). The other test was conducted in isothermal (room temperature or 50 °C), isolated conditions, and involved only bentonite pellets. The evolution of the oxygen concentration in the tests was monitored by occasional measurements using an *in situ* system. At the end of the tests, gas was sampled and analysed. The tests were conducted over the course of approximately one year.

Although the bentonite used was chosen due to its rather high sulphur content, no sulphide gas was detected in any of the samples. This result is a strong indication that such gas is not to be expected under semi-dry repository conditions. Furthermore, a pronounced oxygen consumption was noted in the test involving a copper tube – after approximately 50–60 days, the oxygen concentration was about 1 %. In contrast, the test which did not include a copper component showed no noticeable oxygen consumption at room temperature. From this difference in behaviour it can be concluded that oxygen is mainly consumed as a consequence of aerobic copper corrosion. This conclusion is also strengthened by visual proof of copper(I) and copper(II) oxides on the heater after test termination. The gas samples were also analysed for carbon monoxide, methane, and other light hydrocarbons. None of these compounds were detected. A noticeable carbon dioxide level was detected in both tests (above 1 %). A tentative explanation for this is carbonate dissolution as a consequence of pyrite oxidation and associated acidification.

As a comparison, Giroud (2014) present the results of the O₂ monitoring during the backfilling and early heating phases of the Full-scale Emplacement Experiment (FE Experiment) at the Mont Terri underground laboratory Switzerland, as well as the first results of laboratory experiments which aim at identifying the processes controlling O₂ concentrations. The monitoring shows the disappearance of gaseous O₂ and onset of anaerobic corrosion in sections not affected by O₂ inflow from the access tunnel within weeks after backfilling, and even before closure of the drift for the deepest parts of the experiment.

The tests described in Birgersson and Goudarzi (2018) above gave an indication about the evolution of the gaseous phase in an unsaturated bentonite. There are however still uncertainties remaining: no H₂S was detected, either in the temperature gradient test or in the isothermal test. It cannot be ruled out that the reason could have been that the H₂S reacted with the copper in the temperature gradient test and with oxygen in the isothermal test (Johansson 2019).

Åkesson and Laitinen (2022) continued with the same type of tests as Birgersson and Goudarzi (2018). Some of the objectives were to better check the temperature dependence and to use on-line detectors for more gases. Isothermal experiments were performed in an isothermal setup with a glass container in a heating cabinet. The temperature dependence of the rate of O₂ consumption was evaluated from data measured during the initial phase of five of the tests performed in glass container. Two of these

were performed at 70 °C, two at 50 °C and one at 40 °C. The oxygen consumption rates used in the evaluation was simply defined as the concentration decrease per unit time (i.e. %/day). This was deemed to be sufficiently detailed, since the bulk mass and the water content in the different tests were quite similar. From these evolutions, the following consumption rates were evaluated: 4.5, 1 and 0.1 %/day for 70, 55 and 40 °C, respectively. In all tests, relatively high amounts of CO₂, together with measurable quantities of H₂S and SO₂ were detected. The H₂S concentrations were highest at 70 °C, reaching values of ~15 ppm. Since there were no metals in the glass container, and since a clear generation of SO₂ could be measured, it appears evident that oxygen is consumed through pyrite oxidation. This process probably occurs in the presence of water, since the O₂ concentration reduction exceeds by far the concentration of SO₂. The formation of CO₂ indicates the dissolution of calcite. This process requires the formation of H⁺, which in turn also indicates pyrite oxidation in the presence of water. Pyrite oxidation would though not lead to the formation of H₂S, if the sulphur is oxidized. Pyrite dissolution, possibly aided by a local low pH, could be the source of H₂S, and thus both reactions seem operable at the same time.

The observations by Åkesson and Laitinen (2022) are, in some respects, different than the ones from Birgersson and Goudarzi (2018). It is clear that bentonite can consume oxygen if the temperature is sufficiently high. The temperature dependence of the process is however very strong. The temperature in the unsaturated buffer in the early stage of the repository evolution should be sufficient to ensure that practically all oxygen is consumed in a few weeks after the canister is emplaced. H₂S can definitely form in a bentonite containing pyrite. The concentrations can be expected to be low. The bentonites used by Åkesson and Laitinen (2022) and Birgersson and Goudarzi (2018) had higher initial content of both pyrite and total sulphur compared to MX-80, which is the reference material in PSAR. However, MX-80 still contains both pyrite and gypsum and the behaviour is not expected to be vastly different compared to the materials in the experiments.

During water saturation, bentonite expands and builds up a swelling pressure such that once it reaches a pressure greater than approximately 2 MPa, microbes are expected to be inactive due to limited space and generally hostile conditions (Section 8.3.2). The exact condition where microbial activity is inactivated is linked to swelling pressure, but is controlled by other factors as well. Therefore, a material specific dry density limit is used as a safety function indicator criterion. The same is true for dry bentonite, where the water content is too low to allow for microbial activity. However, during the early period of the repository lifetime and before the bentonite is water saturated, there may be a window of opportunity when the bentonite is sufficiently moist for the RH to support SRB activity. Svensson et al. (2020) studied if there is a moisture threshold limit for the bentonite when SRB may produce sulphide. The focus was on experiments with the commercially available *Pseudodesulfovibrio aespoensis* (formerly known as *Desulfovibrio aespoensis*) originally isolated from the Äspö Hard Rock Laboratory with further experiments using cell concentrates from a natural groundwater from the Äspö Hard Rock Laboratory boreholes KA3105A:3 and KA2511A:5. Additionally, one demonstration experiment was performed using a measuring cylinder to investigate if the natural presence of SRB in bentonite could be activated. When gypsum, lactate (serving as both energy and carbon source), nutrients and liquid water were added the SRB reduced sulphate to sulphide regardless of whether bentonite was present or not. This was observed as a black precipitate in the inoculated samples. However, there were strong indications that the bentonite reacted with the sulphide since little (in some samples no) sulphide could be detected in solution when supplemented with bentonite. When replacing the liquid water with only moist air (up to 100 % RH) no sulphate reduction was observed. Hence, the conclusion from these experiments is that 100 % RH alone is insufficient to promote sulphate reduction; both liquid water and an energy source such as lactate in this case, needs to be present. There, hence, seems to be no stage during the saturation of the bentonite in which sulphate reduction can occur.

Transport of sulphide in the clay system

As a part of the analysis of copper corrosion in a KBS-3 repository, it is of interest to understand the transport of sulphide in the clay system. Transport in saturated clay has been extensively studied as evidenced e.g. by the wealth of buffer diffusion data cited in the **Data report**, whereas this is not the case for an unsaturated clay system. Both the accumulated flux of sulphide to the canister surface and the flux as a function of time are of interest. The latter is of importance since the instantaneous flux has an impact on the properties of the copper sulphide film formed on the surface (10.3.13).

Eriksson and Hedin (2019) provide a modelling study of how sulphide diffuses in the gas phase of the unsaturated bentonite backfill and buffer to the copper canister where it is assumed to react with the copper and cause corrosion. Specifically, a case where the initial water content of the clay system is unchanged is considered. This is relevant for low permeability site, as at Forsmark in Sweden, where saturation may take hundreds of years or longer as discussed in Section 10.3.8.

As the bentonite saturates, the physical volume of the gas phase in the bentonite will be reduced and the diffusion of sulphide will slow down and finally, when full saturation is reached, the diffusion in the gas phase will stop. Such a case, with an exemplifying water saturation time of 125 years, is also considered. For modelling purposes, a pessimistic case taking into account only the transport resistance in the buffer and not in the backfill was defined. A detailed model including the pellet filled slot between the buffer and the rock and the slot between the canister and the bentonite was used, see Figure 10-67.

For unsaturated conditions, the main gas phase transport path from the backfill to the canister is through the pellet filled slot between the bentonite and the wall of the deposition hole. The concentration of sulphide is assumed to be zero at the canister surface, i.e. all sulphide that reaches the canister surface will react instantaneously. At the interface between the deposition tunnel and the deposition hole a sulphide concentration of $1.7 \times 10^{-4} \text{ mol/m}^3$ in the gas phase (approximately 4 ppm) is assumed to be upheld. As further explained in Eriksson and Hedin (2019), this value is based on equilibrium with an assumed aqueous concentration of sulphide of 10^{-6} mol/L and a pH of 7 in the backfill immediately above the deposition hole. It is noted that this is a pessimistic assumption, since no measurements of sulphide concentrations in bentonite have exceeded the detection limit of $3 \times 10^{-7} \text{ mol/L}$ in earlier studies and now also corroborated by the findings reported earlier in this section. Also, the pH in bentonite is generally 8 or higher, leading to a further reduction in the sulphide concentration. With the above assumptions and considering the case where no groundwater flows into the system, the highest influx of sulphide to the canister occurs at the top corner of the canister, see Figure 10-68.

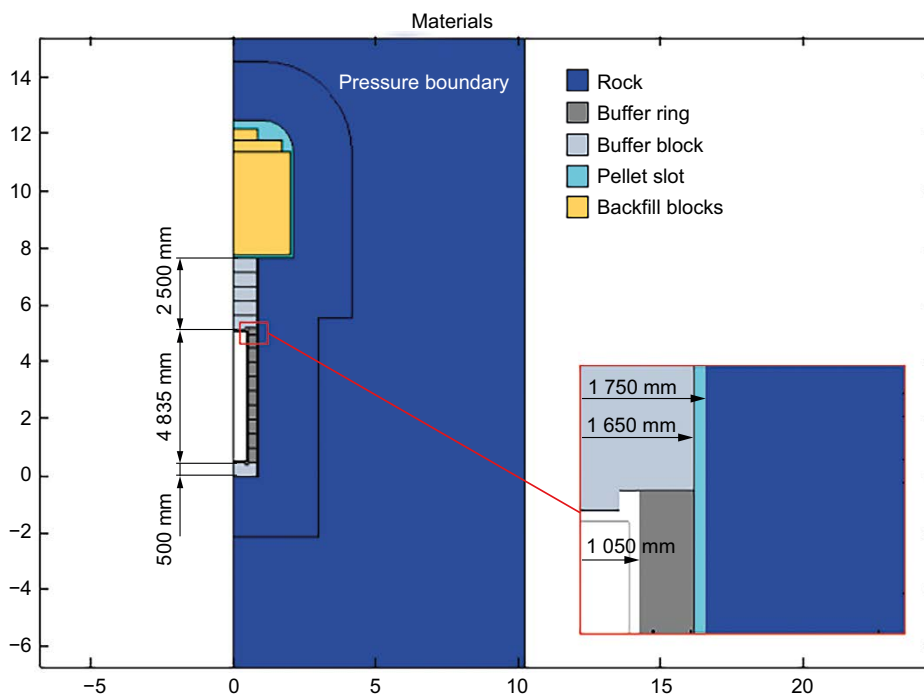


Figure 10-67. Geometry and the different materials used in the model. The x- and y-axes have units of metres (Eriksson and Hedin 2019).

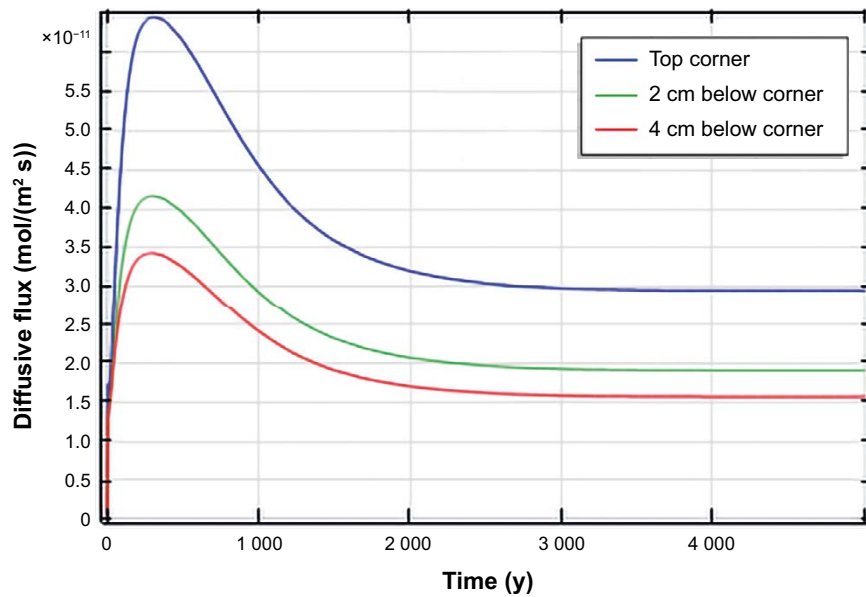


Figure 10-68. The flux of sulphide to the top corner of the canister, 2 centimetres and 4 centimetres below the top corner (Eriksson and Hedin 2019)

As seen in the figure, the peak flux is about $6.5 \times 10^{-11} \text{ mol}/(\text{m}^2 \cdot \text{s})$. The temporal development of the flux is determined essentially by the redistribution of water present initially in the buffer, due to the heating of the system by the residual power of the fuel. It is noted that $10^{-10} \text{ mol}/(\text{m}^2 \cdot \text{s})$ corresponds to a corrosion rate of around $4.5 \times 10^{-6} \text{ cm}/\text{yr}$, i.e. the calculated peak corrosion rates of less than $10^{-10} \text{ mol}/(\text{m}^2 \cdot \text{s})$ would cause negligible general corrosion depths in the 5 cm thick copper canister even if the dry conditions persisted for thousands of years. The exemplifying case where water saturation is assumed to occur in 125 years yields considerably lower peak sulphide concentrations and fluxes. The key result in this study is the peak sulphide flux of $6.5 \times 10^{-11} \text{ mol}/(\text{m}^2 \cdot \text{s})$ for unsaturated conditions. This flux is used in the evaluation of corrosion issues involving sulphide under unsaturated conditions, see Section 10.3.13.

Chemical evolution of the buffer

During the thermal period of the repository, the initially unsaturated compacted bentonite will progressively saturate due to the hydraulic pressure of the surrounding rock (Figure 10-69). Although the main transport mechanism in the low permeability compacted bentonite is diffusion, advective transport will be more important during the saturation stage due to the capillary pressure that is established during this stage.

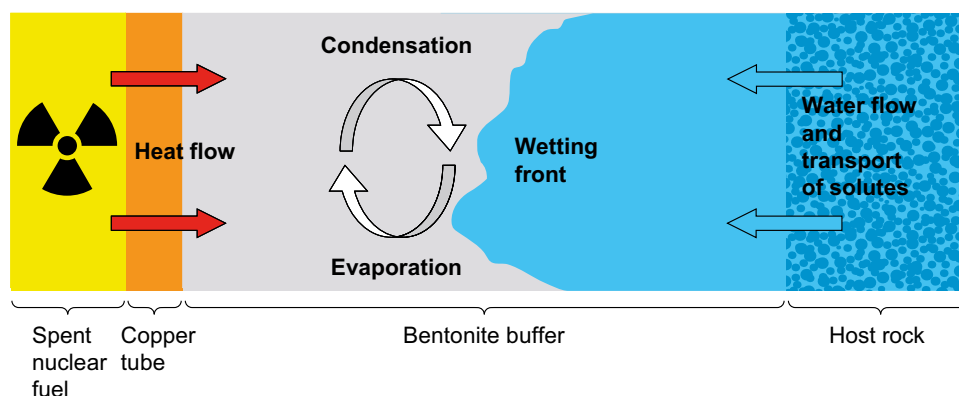


Figure 10-69. Sketch of a vertical cross section of the near field of a KBS-3 repository showing the thermo-hydraulic and transport processes that are believed to occur during the saturation period of the bentonite buffer (Sena et al. 2010b).

The buffer material consists of montmorillonite and accessory minerals (see Table 5-12). In the repository environment these minerals may dissolve and sometimes re-precipitate depending on the prevailing conditions. Sena et al. (2010b) have calculated the redistribution of accessory minerals during the early repository evolution when a thermal gradient is present and the details about the processes and mechanisms in the modelling can be found in the reference. In the calculations the following were tested:

1. The saturation time.
2. The flow rate in a fracture intersecting the deposition hole.

In Sena et al. (2010a) the composition of the original water in a saturated MX-80 bentonite was defined from the water compositions measured in the LOT-A2 experiments (LOT A2-13-1, UniBern (Sena et al. 2010b)). The Forsmark water composition was adjusted by equilibrating the original composition (Laaksoharju et al. 2004, Table 3-4; Forsmark GW, measured) with the minerals identified. This adjustment results in slight variations to the original composition. The compositions can be found in Table 10-10.

Table 10-10. Initial and boundary waters considered in the numerical simulations of the thermal period (concentrations in mol/L) (Sena et al. 2010a).

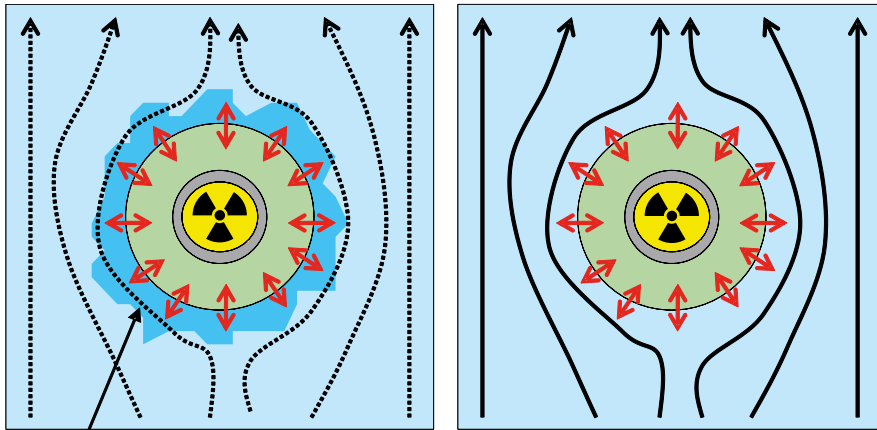
Parameter	Forsmark GW (measured)	MX-80
Temp. (°C)	15	15
pH	7.2	7.86
Alk. (HCO ₃ ⁻)	2.2 × 10 ⁻³	1.05 × 10 ⁻³
Cl	1.53 × 10 ⁻¹	4 × 10 ⁻²
SO ₄ ²⁻	6.8 × 10 ⁻³	9.65 × 10 ⁻²
Ca	2.33 × 10 ⁻²	1.01 × 10 ⁻²
Na	8.88 × 10 ⁻²	2.12 × 10 ⁻¹
K	8.75 × 10 ⁻⁴	1.4 × 10 ⁻³
Mg	9.3 × 10 ⁻³	5.81 × 10 ⁻³
Si	1.85 × 10 ⁻⁴	1.82 × 10 ⁻³

As seen in Table 10-10, the difference in composition between the Forsmark groundwater and the MX80 porewater is not very large. The chloride content is lower in the porewater since the original water, which constitutes about 62 %, in MX-80 is low in chloride. Sulphate is higher in MX-80, since there is gypsum present.

Under a higher flow rate regime within the fracture, the effect of the diffusion of solutes from the bentonite porewater to the granite or vice versa on the chemical conditions of the granite around the deposition hole will be rapidly buffered by the supply of unaffected granitic groundwater. Under these conditions, the geochemical changes induced by the chemical reactions taking place in the buffer will be limited to the buffer itself since any influence of these over the chemical conditions of the granite will be rapidly annulled due to granitic groundwater renewal (Figure 10-70). On the other hand, if the advective flow in the fracture is very low, diffusion will prevail and therefore, the chemical and diffusive processes occurring in the buffer will influence the chemical conditions of the fracture around the deposition hole (Figure 10-70).

In the calculations these parameters have been considered independently. However, a high flow rate would affect the saturation time. Therefore, no combinations of high flow and long saturation have been studied.

Ca-sulphates are originally present in the MX-80 bentonite mineralogy. At the beginning of the thermal period, anhydrite precipitates in the bentonite pores due to the increase of temperature, except close to the outer boundary of the buffer where the granitic groundwater (which is unsaturated with respect to this mineral) flows into the buffer. The dissolution of the primary anhydrite is more efficient for a situation when the saturation is rapid (10 and 100 years in Figure 10-71).



Chemistry in the fracture influenced by diffusive processes around the deposition hole

Legend:

- Fracture plan
- Bentonite
- Copper canister
- HLNW
- Low advective flow in the fracture
- High advective flow in the fracture
- Diffusive flow

Figure 10-70. Sketch of the two different flow cases (Sena et al. 2010b).

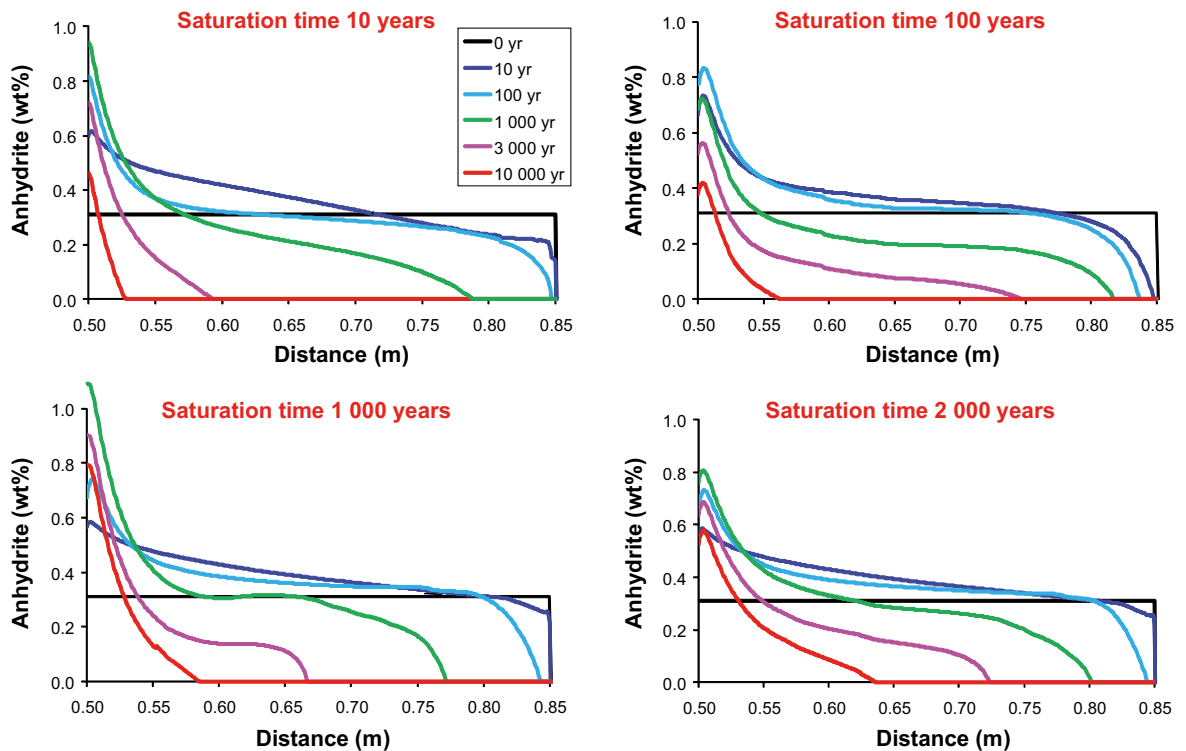


Figure 10-71. Calculated evolution of the amount of anhydrite in the MX-80 bentonite buffer as a function of buffer saturation time (Sena et al. 2010b).

SiO₂(am) is also a primary mineral of the MX-80 bentonite. The primary SiO₂(am) in the bentonite is preferentially dissolved close to the inner surface of the buffer (left side in Figure 10-72). In the case with a relatively fast saturation (10 years), a small amount of SiO₂(am) is also dissolved during the saturation period, close to the contact with the granite. Until 10 years, the SiO₂(aq) concentration progressively increases, both in the bentonite and in the granite due to the solute supply by SiO₂(am) dissolution close to the hot boundary of the system. After 10 years the aqueous SiO₂ concentration decreases due to dilution provided by the inflow of the granitic groundwater, which is depleted in SiO₂(aq) compared to the initial bentonite porewater.

In general, the calculated evolution of the composition in the montmorillonite exchanger in the MX-80 bentonite indicates that the concentration of sodium decreases with time in favour of more calcium adsorbed. The concentration of potassium and magnesium also decreases in the montmorillonite exchanger. Within the same case of advective flow in the fracture intersecting the deposition hole, the calculated evolution of the composition of the exchanger is very similar for the different cases of bentonite saturation.

The comparison between the cases with low and high advective flow in the fracture, for a saturation time of 10 years is shown in Figure 10-73. It is seen that for a high advective flow in the fracture, the final composition of the exchanger has suffered more profound changes than for the case with a low advective flow in the fracture.

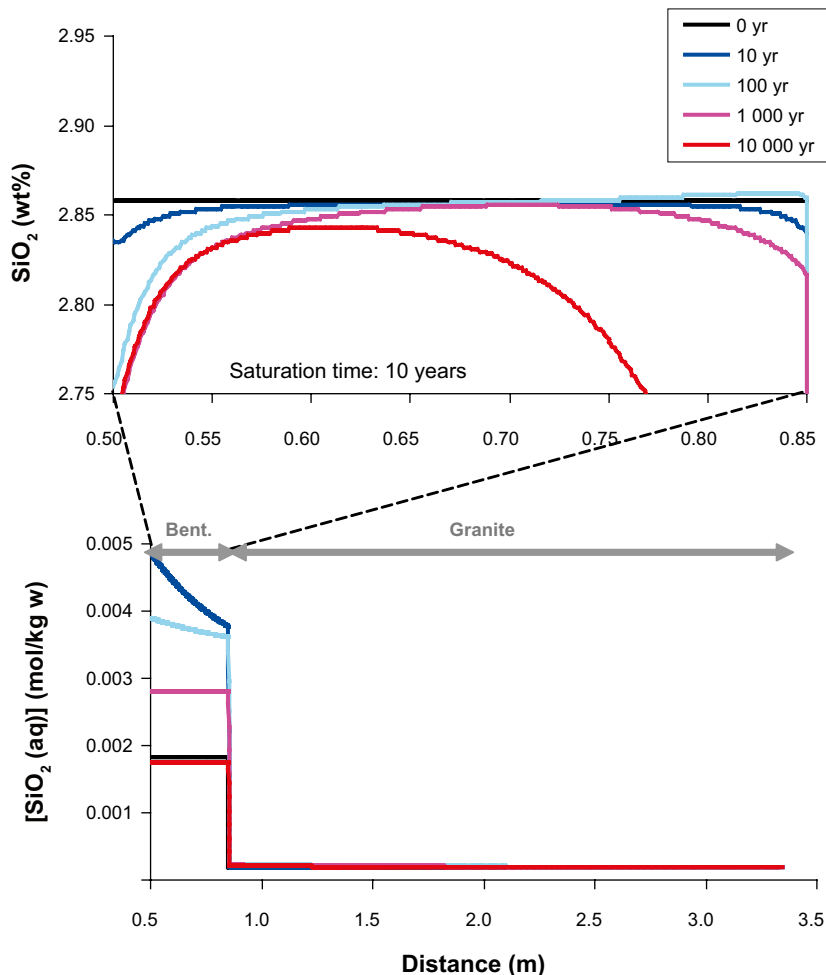


Figure 10-72. Calculated evolution of the amount of SiO₂ in the modelled domain of MX-80 bentonite, for a saturation time of the bentonite of 10 years (Sena et al. 2010b).

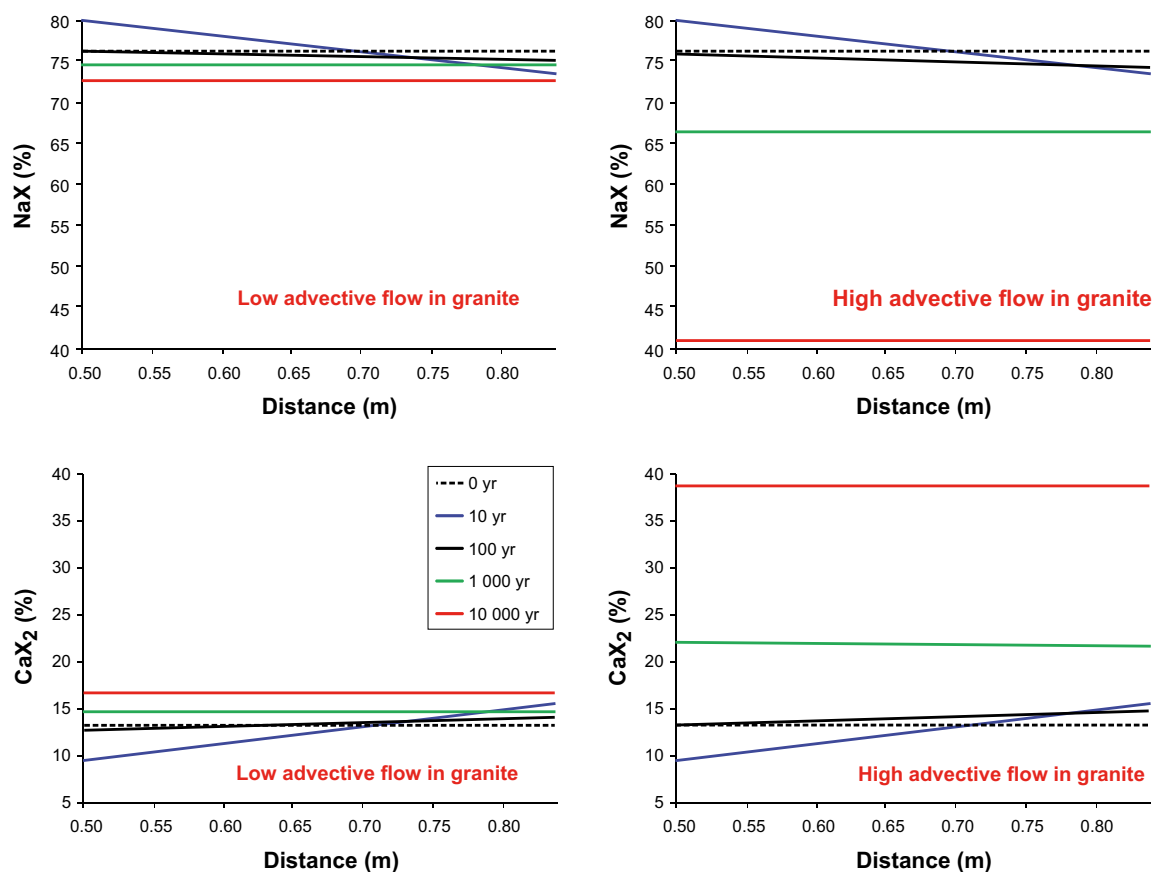


Figure 10-73. Calculated evolution of the concentration of sodium and calcium in the montmorillonite exchanger for the case where the MX-80 bentonite is fully water saturated at 10 years, and for the two scenarios of advective flow in the fracture (low and high) (Sena et al. 2010b).

As a result of the numerical simulations in Sena et al. (2010b), it can be concluded that the main mechanisms controlling the mineralogical changes of the bentonite during the thermal period are related to:

- The dependence of the mineral solubilities on the evolution of the temperature in the near field.
- The solute transport and mass transfer between the groundwater flowing along the fracture and the bentonite porewater.

The evolution of the concentrations obtained for the bentonite porewater is a result of mixing with the local groundwater during the period of bentonite water saturation, whereas thereafter, diffusion of solutes is the dominant mechanism. Simultaneously, mineral reactions (anhydrite and carbonate dissolution and/or precipitation) and cation exchange reactions are the key mechanisms controlling the long term geochemical evolution of the buffer and its porewater. The distribution of the concentration of solutes in the granitic groundwater is a consequence of the ratio between:

- The diffusion rate through the granite-bentonite interface.
- The fluid flow rate along the fracture in contact with the deposition hole.

In this way, the results obtained considering two regimes of groundwater flow rates along the fracture intersecting the deposition hole are substantially different.

- With low flow rates along the fracture, the final composition of the bentonite porewater is different from the Forsmark groundwater. The composition of the buffer porewater has the potential to modify, by diffusion, the composition of the surrounding granitic groundwater.
- With high flow rates along the fracture, the groundwater composition is practically constant during the modelled period, maintaining the gradients of concentrations and the rates of solute transport by diffusion. Consequently, the final composition of the bentonite porewater is similar to the composition of the Forsmark groundwater.

The thermal evolution in the buffer modifies mineral solubilities (Ca-sulphates, carbonates and silica). The silica precipitation and/or dissolution in the bentonite are basically controlled by the changes of solubilities associated with the thermal evolution of the system, modifying slightly the mineralogical composition of the bentonite. The stability of the carbonate phases is the main geochemical difference between the two types of bentonite considered.

During the period of saturation, there will be dissolution/precipitation of accessory minerals like calcium sulphates and amorphous SiO₂. The conclusion is, however, that these effects are too small to have any impact on the long-term performance of the buffer.

Physical properties of the buffer

Slow water saturation generally causes transient conditions and gradients to prevail for a longer period than in the case of rapid water saturation. High temperature conditions could potentially affect the buffer properties in a negative direction, through steam, bacterial activity, transport and enrichment of dissolved species. This is discussed and investigated in both laboratory trials and field trials. Sellin et al. (2017, Chapter 11) has made a summary of the studies available and underway that deal with these processes.

In terms of physical properties such as shear strength, shear elongation, swelling pressure and hydraulic conductivity as a result of short-term (24h) elevated exposure (up to 150 °C) it appears that there is a tendency of increased shear strength and a significant change in maximum strain failure as a result of short-term hydrothermal treatment. However, the effect is equal or greater for samples heated under saturated conditions compared to those heated without an external water pressure.

Swelling pressure and hydraulic conductivity are not affected by short-term heating irrespective of hydraulic conditions. Vapour transport tests in bentonite show that vapour condensed under all investigated conditions, and that water absorption from condensation water totally dominated over water absorption directly from vapour (Leupin et al. 2014). All tests showed that water absorption decreased over time, indicating that the pellet system was sealed and that vapour transport decreased with time. Test series of material exposed to temperatures of up to 200 °C for 7 days at different water saturation levels show no clear differences due to hydrothermal treatment between unsaturated and water-saturated samples with respect to swelling capacity (Figure 10-74). Generally, differences in measured swelling properties due to hydrothermal treatment are negligible in comparison to the differences between sodium-dominated and calcium-dominated materials. The effects of short-term vapour pressure on free swelling are therefore not considered to be a problem for a KBS-3 repository. One study included experiments with bentonite at different degrees of water saturation (0, 50, 85 and 100 %) exposed to temperatures up to 150 °C for 7 days (Leupin et al. 2014). After hydrothermal treatment, the samples were saturated and swelling pressure and hydraulic conductivity were determined both at elevated temperature and at room temperature. In no case was any significant change in the properties compared to the reference materials.

Precipitation of secondary minerals in the buffer, e.g. CaSO₄, in a temperature and water saturation gradient has been observed in field tests. However, these reactions are reversible and the precipitated minerals will be dissolved when water saturation increases. The precipitates are therefore not expected to affect the performance of the buffer. There is nothing in the above-mentioned studies suggesting that there would be changes in the properties caused by mineralogical changes due to short-term exposure to dry or semi-dry conditions at high temperatures. The transport capacity of dissolved species can generally be expected to be lower at low water content than at full water saturation, which counteracts most known transformation processes. SKB estimates based on the above, that the material properties of the buffer will not be adversely affected to an extent that adversely affects post-closure safety by a long water saturation phase.

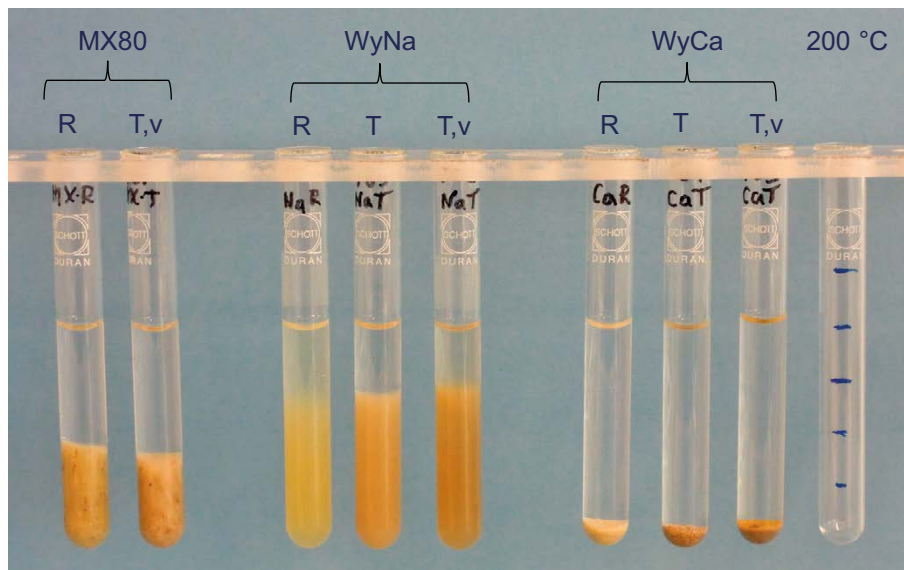


Figure 10-74. Result from free swelling tests. All test tubes contain 1.00 grams of material expanded to the maximum volume. MX-80 bentonite was the starting material for all samples purified for some experiments and ion exchanged into sodium (WyNa) and calcium form (WyCa) respectively. R indicates reference material; T indicates material hydrothermally treated at full water saturation, and T, v indicates material hydrothermally treated in unsaturated state (Leupin et al. 2014).

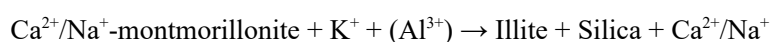
Mineral transformation

The advantageous physical properties of the buffer, e.g. swelling pressure and low hydraulic conductivity, are determined by the ability for water uptake between the montmorillonite mineral layers (swelling) in the bentonite. However, montmorillonite can transform into other naturally occurring minerals of the same principal atomic structure but with less or no ability to swell in contact with groundwater. The transformation processes usually involve several basic mechanisms. At the expected physico-chemical conditions in a repository, the following possible mechanisms are identified:

- congruent dissolution,
- reduction/oxidation of iron in the mineral structure,
- atomic substitutions in the mineral structure,
- octahedral layer charge elimination by small cations,
- replacement of charge compensating cations in the interlayer.

This is discussed further in the **Buffer, backfill and closure process report**.

Transformation from smectite (montmorillonite) to illite, which is the most common alteration observed in natural sediments, is well documented in different geological formations, and has been reproduced under laboratory conditions. The main mineralogical differences being that the illites have approximately one unit charge higher tetrahedral charge, and potassium as the main charge compensating cation. Thus, potassium is a must for the montmorillonite to turn into illite. Simplified, the total illitization reaction may be expressed:



High content of smectite is commonly found in old formations exposed to repository temperatures. For example, Velde and Vasseur (1992) studied the time-temperature space of illitization in seven deep wells in four sedimentary basins in the US, Japan and France. In all wells there was a typical reduction of smectite content with depth, which represents increase in both age and temperature (Figure 10-75).

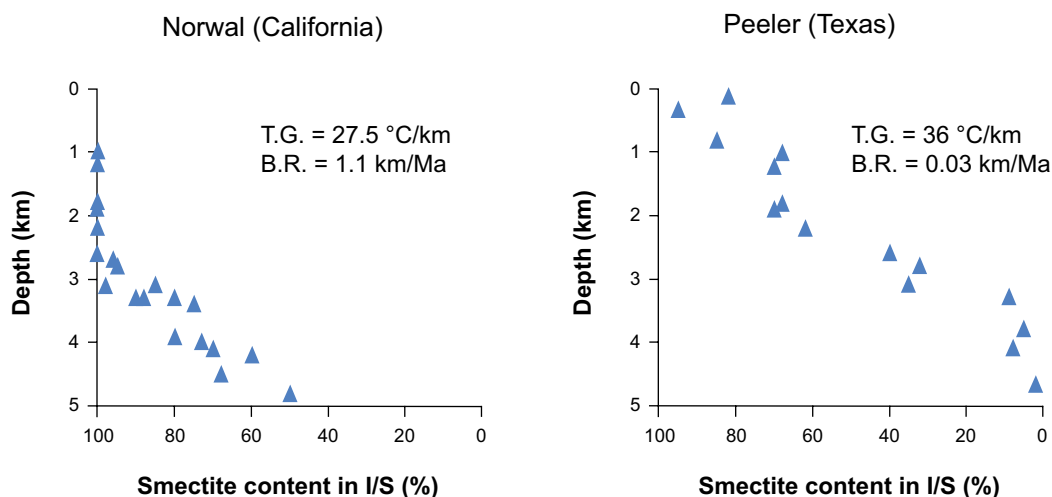


Figure 10-75. Smectite content versus depth in smectite-illite mixed layer material in two sediments representing relatively fast burial rate (left) and slow burial rate (right). T.G. indicates the present temperature gradient and B.R. indicates the burial rate. Redrawn from Velde and Vasseur (1992).

The prerequisites for a transformation are obviously present in the sediments and time and temperature are the governing parameters. A decrease to around 60 % smectite was observed in the Californian Norwal formation after 4.5 million years at a depth of 5 km, representing a final temperature increase of over 100 °C. The same transformation took around 60 million years at a depth of 2 km and a temperature increase of around 70 °C in the Texan Peeler sediments. The reaction rate at these repository relevant temperatures is consequently very slow in relation to the time scale of a repository.

The availability of potassium could also limit alteration rate. According to Karnland and Birgersson (2006) complete illitization requires approximately 850 kg of potassium per deposition hole. The concentration of potassium in the groundwater in Forsmark is low and very limited illitization would occur if the groundwater was the only source. However, the rock in Forsmark may contain a few percent of potassium (Sandström and Stephens 2009). This means that the rock within a short distance (~metre) around the deposition hole would be able to supply sufficient potassium to convert the entire buffer to illite. The critical question is therefore whether the potassium is available for the transformation or not. Both the rate of dissolution of potassium from the granitic minerals as well as the rate of transformation of smectite to illite is very slow at the expected temperatures of the near field. Therefore, there is no need to quantify this process. No credit for limited availability of potassium is taken, since buffer transformation can be ruled out for other reasons.

The silica solubility increases significantly at pH above 9. The tetrahedral silica in the montmorillonite consequently equilibrates at higher concentrations at pH over 9. Diffusive removal of silica or precipitation of new silica minerals thereby lead to a faster increase of the tetrahedral layer charge compared to near neutral conditions. The corresponding increase in concentration of charge compensating cations leads to a change in the interaction with water and thereby to a change in sealing properties. The layer charge may reach the critical value for collapse, which results in total loss of expandability and in principle, to the same consequences as for illitization. At pH 11 the total silica concentration is calculated to be approximately 16 times larger than at neutral pH conditions, and at pH 12.4, representing matured Portland cement, the theoretical increase in total silica solubility is more than 3 orders of magnitude higher than at near neutral conditions. The total silica concentration difference between the bentonite porewater and the groundwater increases approximately by the same factor, assuming the groundwater is in equilibrium with quartz. Huertas et al. (2005) studied the dissolution rate of smectite as a function of pH. Figure 10-76 plots log dissolution rate vs. pH at 25, 50, and 70 °C. In alkaline solutions, the smectite dissolution rate increases as pH increases, showing a steeper slope for pH values higher than 11, which seems to be a critical value for the smectite dissolution and stability. The conclusion from Huertas et al. (2005) is that the results indicate that dissolution rates are strongly affected by pH and temperature. This effect is particularly important for pH values above 11.

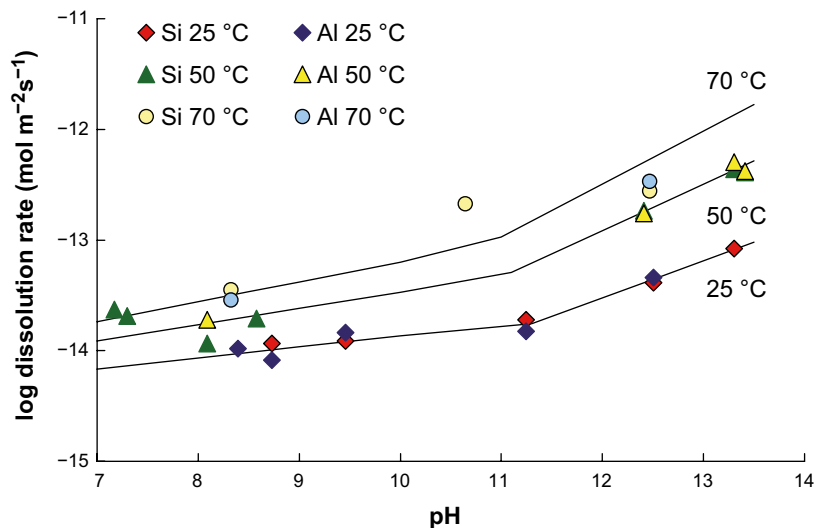


Figure 10-76. Experimental (dots) and estimated (lines) dissolution rates (Huertas et al. 2005).

The effect of the alkaline plumes is especially strong for young cement waters and for high temperatures. In the KBS-3 concept any contact between cement porewater and bentonite will occur at the contact with the bottom plate, plug and fracture grouting where the temperature is relatively low and the pH is restricted to < 11. The bentonite components should therefore be much more stable.

The montmorillonite transformation in a KBS-3 repository is assumed to be small based on the following observations and arguments:

1. The time scale for significant montmorillonite transformation at repository temperatures in natural sediments is orders of magnitude larger than the period of elevated temperature in a KBS-3 repository (e.g. Velde and Vasseur 1992).
2. The bentonite material is close to mineralogical equilibrium to start with (e.g. Fritz et al. 1984).
3. Transformation is limited by transport restrictions (Hökmark et al. 1997).
4. All published kinetic models, based both on natural analogues and laboratory experiments indicate that the transformation rate is very low at repository conditions (e.g. Huang et al. 1993).

Based on this reasoning two safety function indicator criteria have been defined (see also Chapter 8). As long as the maximum temperature is below 100 °C and the pH of the water in the rock is below 11 the montmorillonite in the buffer is assumed to be stable for the time scale for assessment of the repository (1 000 000 years).

In the reference evolution, both the pH and the temperature in the buffer are assumed to be within the given limits and the alteration is not expected to proceed to a level where it will affect the properties of the buffer.

Interaction with copper corrosion products

Interaction between copper corrosion products and bentonite was not explicitly treated in SR-Site, since copper and bentonite were assumed to be “compatible” materials.

From a thermodynamic point of view, the solubility of metallic copper is very low under repository conditions and the amount of copper ions that come into contact with the bentonite have therefore been considered negligible. The main corrosion products in the repository environment are copper sulphides. These have even lower solubility than the metallic copper and are therefore not expected to affect bentonite. However, some copper will corrode by oxygen trapped in the repository with mainly Cu₂O and some copper(II) hydroxides as corrosion products (Karlund et al. 2009, Rosborg 2013, Kober and Wersin 2017, Johansson et al. 2020). These have higher solubility than metallic copper and copper sulphide, but the solubility is still low compared to the concentrations of cations (Na⁺ and Ca²⁺) already present in the bentonite.

Elevated levels of copper in bentonite have been observed in field tests. There are thus mechanisms that, at least at an early stage of the repository evolution, can release copper and make it available for transport into the bentonite buffer as a solute. Reaction with copper would potentially affect the bentonite buffer in the following ways:

1. Ion exchange between copper ions and the original charge-compensating ions. Different cations give different properties of the bentonite. The biggest difference is between mono- and divalent ions, however other characteristics, such as ion radii, may also be important.
2. Precipitation of copper corrosion products in the buffer's pore system. Extensive precipitation would be able to "cement" the buffer and change its hydraulic and mechanical properties.
3. Reaction between copper and montmorillonite. Cu(0) or Cu(I) could reduce Fe(III) to Fe(II) in the clay which could result in increased surface charge and, in the end, potentially collapse of the montmorillonite structure.

However, none of these processes is expected to occur to any significant extent. The reasoning behind this is discussed in more detail in Sellin (2013). Available results from the LOT experiment (Karlund et al. 2009, Johansson et al. 2020) and the Prototype repository (Olsson et al. 2013) indicate that the interaction between copper corrosion products and bentonite is extremely limited. Ion exchange is of minor importance. Solid copper phases have been found in the bentonite, in concentrations up to some weight percent in individual points. However, the phases have not been identified. No influence of copper corrosion products on the hydro-mechanical or mineralogical properties of the buffer properties have been found. There is nothing to indicate that corrosion products are important:

1. The bentonite shear strength, which is important for the shear load drop, is not considered to be affected because the total amount of corrosion products is very low. The changes in the rheological properties of the buffer in the field tests also appear to be mostly related to the heating and not to the precipitation of secondary minerals.
2. The hydraulic conductivity of the bentonite, which is important for, among other things, corrosion calculations is also not considered to be affected because the copper concentrations will be very low and since even a completely copper(II) ion-exchanged bentonite has the same hydromechanical properties as a calcium bentonite.
3. Neither is the presence of microbial activity in the buffer judged to be affected by corrosion of the copper canister for the same reasons as in the previous points: concentrations of copper and the amounts of copper minerals are too low to have any effect on the swelling pressure of bentonite.

These conclusions are based on observations from relatively short term experiments (up to 20 years). However, these experiments do cover periods of thermal, hydraulic and chemical gradients, which will greatly decrease in the long term. They also contain disturbances in the form of trapped air and initial corrosion products on the copper heaters. Therefore, it is likely that the conclusions will be valid in a long-term perspective where the highly insoluble copper sulphides will be the dominant corrosion products.

Effects of salinity

The salinity of the groundwater influences the vapour pressure relation and thereby the water saturation process. However, for the groundwater (Table 10-9) at the Forsmark site the effect is negligible.

Cementation

The term "cementation" has often been used in a broad sense to describe processes that lead to specific changes in rheology and swelling properties of the buffer material. A number of quite different chemical/mineralogical and mechanical underlying processes could conceivably cause such cementation effects. The above sections which address the underlying and related processes, i.e. montmorillonite stability, ion exchange, accessory minerals alteration, diffusive transport etc. are consequently very relevant to the cementation process. There are two main concerns about the effects of cementation on the bentonite buffer; one is an increase in hydraulic conductivity, and the other is an increase of shear strength. This is discussed further in the **Buffer, backfill and closure process report**.

As described earlier in this section there is no reason to believe that there would be mineralogical changes in the buffer that would lead to substantial changes of the mechanical or hydraulic properties over the assessment time scale. The redistribution of soluble accessory minerals calculated in the previous section is rather limited and is not expected to have a significant impact on the buffer properties. However, there are experimental results that show that the mechanical properties of bentonite can be altered if the material is exposed to an elevated temperature in a saturated state (Dueck 2010). This is observed both in field experiments over a number of years as well as in 24-hour laboratory experiments. The maximum deviatoric stress q_{max} (kPa) and corresponding strain e (%) were measured on mainly undisturbed samples as a function of bulk density ρ (kg/m³) for a range of conditions.

Figure 10-77 shows the influence of temperature on the stress-strain behaviour for the reference bentonite MX-80 and the second bentonite from SR-Site, Ibeco RWC, for a saturated density of about 2 000 kg/m³. A tendency towards increasing deviatoric stress at failure with increasing temperature is seen for both MX-80 and Ibeco RWC (Deponit CA-N). However, the influence of temperature is in the same range as the difference between the two bentonites. The strain at failure is approximately the same for MX-80 and Ibeco RWC (Deponit CA-N) at the same density for any particular temperature.

Important observations from Dueck (2010) are that the influence of temperature on the stress/strain behaviour of bentonite can be seen after only a few hours of exposure and that milling and re-compaction after heating restored the original failure behaviour. It is evident that an increased temperature will have an effect on the mechanical properties of the bentonite. The reason behind this is still unknown. The effect is not very pronounced even at 150 degrees and does not seem to progress with time. However, this effect does have to be considered in the evaluation of shear load on the canister.

Sulphate reduction under saturated conditions

One of the safety functions of the buffer is to limit microbial activity (Section 8.3.2). The process in focus is the production of sulphide from sulphate reducing bacteria, since sulphide could act as a corroding agent for the copper canister (Section 10.3.13).

The prerequisites for significant viability of microbes are sufficient availability of free water, nutrients, and space for living cells to grow. Mechanical forces, low water activity and pore size will therefore affect the microbial activity in the buffer. As seen in the previous section, no sulphate reduction is expected as long as the buffer is unsaturated. The presence of sulphate-reducing bacteria (SRB) in commercial bentonite and their potential to be active after exposure to elevated temperature and salinity has been shown in earlier studies (Masurat et al. 2010, Svensson et al. 2011).

There seems to be a correlation between swelling pressure and microbial activity. This correlation has not been sufficiently investigated and it is currently not clear which buffer characteristics limit microbial activity. In the SR-Can safety assessment, the limit for controlling microbial sulphide production was set as a saturated clay density of 1 800 kg/m³. This gives a pore space and swelling pressure that lie close to the low pore space and high swelling pressure reported to suppress microbes in Masurat (2006). (The limit was not further specified in the SR-Site assessment.)

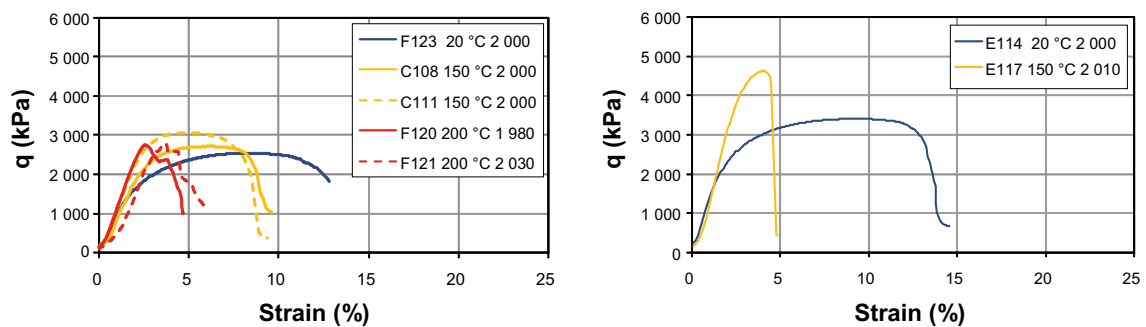


Figure 10-77. Influence of temperature on deviatoric stress at failure as a function of strain of MX-80 (left) and Ibeco RWC (right) with a density about 2 000 kg/m³ (Dueck 2010).

The lower limit of bentonite density and thereby the swelling pressure for which the microbial sulphate reduction can be considered to be insignificant have been studied. Conclusions concerning the swelling pressure and/or dry density and potential additional constraints limiting microbial activity are, however, somewhat incomplete. There are preliminary results that indicate a sharp limit in dry density where microbial sulphate reduction ceases in MX-80 as well as in other bentonites (Bengtsson et al. 2015, 2017a, b). The limit seems to be dependent on the type of bentonite (Figure 10-78). The findings presented in Bengtsson et al. (2017a, b) have been verified by Haynes et al. (2019).

In the PSAR, MX-80 bentonite is used as reference material. According to Bengtsson et al. (2017b) the limit of saturated density to prevent microbial sulphide production for MX-80 lies in the interval 1750–1847 kg/m³ for that material. Hence, a saturated density of 1850 kg/m³ is selected as the safety function indicator criterion in the PSAR (Section 8.3.2). This means that no sulphate reduction will occur in the buffer as long as the saturated density is higher than 1850 kg/m³.

Composition of water in the buffer/canister interface

The composition of the water in the buffer/canister interface is of importance for the corrosion assessment. The initial composition of the porewater in a saturated MX-80 bentonite, based on experimental data, is given in Table 10-10. The concentrations given are based on the entire pore volume of the buffer. There are, however, different conceptual approaches to the description of bentonite porewater. These are described in detail in the **Buffer, backfill and closure process report**, Section 3.5.2. In short, the porewater can be described with a single porosity, Donnan-equilibrium model, or with a multi-porosity model, which differs between bulk, diffuse double-layer and interlayer water. However, the models should give the same results for the buffer/canister interface if it is assumed to be an external reservoir.

In the case of saturated conditions, the chloride concentration in the interface should be very close to the concentration in the groundwater. The sulphate concentration is controlled by gypsum/anhydrite solubility for at least 10 000 years according to Figure 10-71. The carbonate concentration in the interface can be assumed to be similar to the groundwater concentration, since the calcite content in MX-80 can be low. The same is true for trace groundwater components with low original contents in the bentonite, like nitrite and ammonium, which will be mixed into the porewater during the saturation process. After saturation the exchange of dissolved components between the porewater and the ground water will be diffusion controlled and is expected to be very slow.

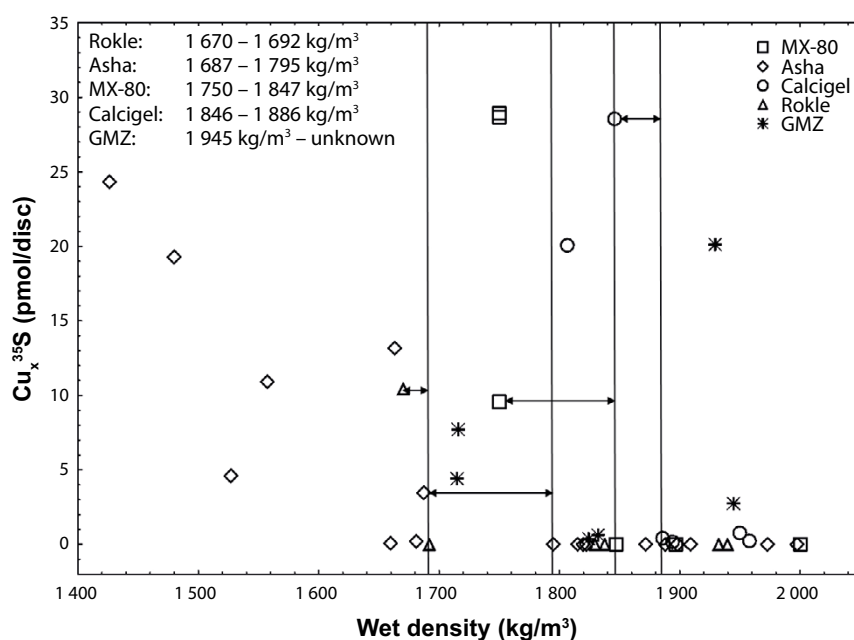


Figure 10-78. Accumulated Cu_2^{35}S on copper discs (pmol) over wet density. The respective intervals where sulphide-production shifts from high to low are indicated with arrows. The corresponding analysed wet density intervals are inserted, for GMZ all tested wet densities shows high sulphide production. (Bengtsson et al. 2017c).

The situation during the saturation process is much more complex. Due to evaporation, there will be very little water in the interface as long as the thermal output from the fuel is high. The evaporation-condensation process illustrated in Figure 10-69 will also redistribute dissolved species from the cold to the hot side of the buffer. The accumulation in the interface is strongly dependent on the diffusivity of the species in question. This effect has not been evaluated in PSAR.

Identified uncertainties and their handling in the subsequent analysis

- A long saturation phase is not expected to have any significant effect on the long-term properties of the buffer after full saturation.
- One issue for canister corrosion is the chemical composition of the gas in the unsaturated bentonite. Of particular interest is the content of oxygen (O₂) and hydrogen sulphide (H₂S). Based on the experimental results of oxygen consumption with a copper heater it is realistic to assume that all oxygen initially present in the gas phase will be consumed by reaction with the copper canister before full buffer saturation is reached. This is true even for canister positions with the highest water inflows. This means that aerobic and saturated conditions will not occur simultaneously. The same is true for a backfill in dry tunnel sections. If the saturation of the tunnel is rapid, it is likely that the dissolved oxygen will react with minerals in the backfill or in the interface between the backfill and the tunnel wall.
- No gaseous H₂S above the detection limit of 0.1 ppm has been detected in the gas phase in unsaturated bentonite. The assumed gaseous concentration (~4 ppm) in the modelling can therefore be seen as pessimistic.
- Interaction between bentonite and copper corrosion products is not expected to have any influence on the properties of the barrier.
- The geochemical changes in the buffer during the period of saturation and thermal gradient are small and are not considered to have any significant impact on the long-term performance.
- In the reference evolution, both the pH and the temperature in the buffer are assumed to be within the given limits and mineral alteration is not expected to proceed to a level where it will affect the properties of the buffer.
- The salinity of the groundwater influences the vapour pressure relation and thereby the water saturation process, but for the groundwater at the Forsmark site the effect is negligible.
- An increased temperature will have an effect on the mechanical properties of the bentonite, but the effect is not very pronounced even at 150 degrees and does not seem to progress with time. However, this effect does have to be considered in the evaluation of shear load on the canister, see Section 10.4.5.

10.3.11 Colloid release from buffer and backfill

The uptake of water and resulting swelling of the bentonite buffer is hindered by the walls of the deposition hole, and a swelling pressure is developed in the bentonite. If fractures intersect the deposition hole, rigid swelling restrictions are not present everywhere, and localised swelling continues into the fractures until equilibrium or steady state is reached. This free swelling may lead to separation of individual montmorillonite layers (dispersion) and part of the buffer could thereby be transported away with the groundwater. This would directly affect safety functions Buff1, Buff2 and Buff5.

The maximum free swelling of the bentonite is strongly dependant on the valence and concentration of the ions in the interlayer space. At low solute concentrations in groundwater, the interlayer distance between the individual montmorillonite layers may increase enough to give the clay/water system a sol character, i.e. single or small groups of montmorillonite layers act as individual colloidal particles.

Expansion of bentonite into fractures will lead to mass loss in the deposition hole. Colloids that are generated at the clay/water interface may be transported away with the flowing water (erosion), which leads to an additional mass loss. In vertical, or sloping fractures, colloids may flocculate and sediment by gravity downwards in the fracture, which also leads to mass loss.

Conditions when colloid release can occur

For simple model systems such as charged spheres or parallel extended flat charged surfaces, the concept of a critical coagulation concentration (CCC) is readily defined within the DLVO theory as the salt/electrolyte concentration where the energy barrier for particle-particle association approaches zero (e.g. Evans and Wennerström 1999). At the CCC and higher salt concentrations the attractive van der Waals forces dominate the system and colloidal particles will be held together and not disperse spontaneously.

A CCC may be determined for monovalent systems and used as a pessimistic concentration limit for spontaneous colloid particle release. Governing variables are the concentration and the layer charge of the montmorillonite. Laboratory results have shown that montmorillonite extracted from MX-80 bentonite and ion-exchanged to Na⁺-state has a CCC of around 25 mM in NaCl solution, i.e. an attractive gel is formed (Birgersson et al. 2010). For systems with only divalent counterions the CCC concept is not really valid, and the CCC may be considered zero, i.e. no excess ions are needed in order to prevent colloidal sol formation of colloidal particles as demonstrated in e.g. Chapter 4 in Birgersson et al. (2010) or from theoretical considerations (Kjellander et al. 1988). Although it has been demonstrated that a CCC value for clay/water systems containing both mono and divalent counterions cannot be defined in terms of a single, aqueous cation concentration due to ion exchange (Birgersson et al. 2009), erosion tests on such mixed electrolyte systems can be used to establish stability. A number of tests were conducted for which measurable erosion was observed (Schatz et al. 2013). For most of these tests erosion was observed to begin almost immediately upon contact between the compacted material and the dilute solution and continue throughout the experiments.

Water with cation content higher than 4–8 mM charge equivalents is considered to prevent colloidal sol formation provided that the calcium content in the montmorillonite is above 20 %, irrespective of whether the montmorillonite is of Wyoming, Milos or Kutch type (see the **Buffer, backfill and closure process report**, Section 3.5.11). Ion exchange processes during the operation of the repository may alter the counterion content relative to the initial state. The content of calcium in the exchanger is, however, not expected to fall below 20 %, since the ion-exchange to a calcium form is promoted at low concentrations. Thus the process of colloidal sol formation can be neglected during operation of the repository. Present day groundwater at the Forsmark site fulfils this condition as does Baltic Sea water. During glacial conditions the cation content may possibly fall below 4–8 mM charge equivalents, and colloidal sol formation can therefore not be excluded. It is also possible that deposition positions intersected by fractures with prolonged high groundwater flow rates during temperate conditions could be exposed to sufficiently dilute groundwaters that erosion and sedimentation occurs.

The route to dilute water in the buffer/groundwater interface

Erosion of the bentonite may start once the concentrations of cations in the bentonite drops below the 8 mM. Soon after the dilute water reaches the buffer, leaching of soluble salts in the short term from the buffer towards the fracture will affect the salinity of the water in the vicinity of the buffer. The leaching has been studied by Pont et al. (2020) using two different modelling approaches: an optimistic one corresponding to the Donnan model, which limits the solute transport to cation exchange processes, and a more pessimistic Fickian diffusion through free porosity, which does not account for the compensation of structural negative charge. This simplified Fickian approach does account for the initial leaching of ions stored in the free porewater, but does not provide any retention mechanism in terms of mineral or cation exchange reactions. The Donnan equilibrium model proposed by Birgersson and Karnland (2009) considers only the interlayer porosity to represent interconnected porosity in compacted bentonite. The interlayer concentrates most of the positive charge of the system. However, the transport is restricted by the bentonite electroneutrality, which assumes that the interlayer will always retain most of this charge in order to compensate the excessive negative surface. This means that a very small charge can be effectively leached, which corresponds to the cations compensating the negative charge of the mobile anions present in the interlayer. Thus, most of the ionic transport will correspond to cation exchange processes with the external water. This retention capacity will also lead to the presence of a concentration jump at the bentonite/water interface, the so-called Donnan equilibrium. None of the models consider dissolution of accessory minerals and both can therefore be seen as pessimistic.

The results show that it will take somewhere between a few hundred (Fickian/high flow) to close to 10 000 years (Donnan/low flow) for the cation concentration in the groundwater close to the buffer to drop below 8 mM. The conclusion is that there will always be a delay between an intrusion of dilute water and the onset of erosion, but this delay will be short in relation to the time periods with dilute water for temperate conditions (Section 10.3.6). For glacial conditions the delay is likely short compared to the durations of glacial conditions, but not compared to durations of ice margin passages with increased flow (Section 10.4.6). The potential benefit of the latter is, however, pessimistically disregarded in the PSAR analyses.

Quantification of buffer loss

There are three fundamental processes that may contribute to the loss of buffer mass in this respect:

1. Expansion: the expansion of bentonite into a fracture is caused by the water uptake and swelling. This process is not related to colloid release, but will still contribute to mass loss from the deposition hole.
2. Erosion: erosion is caused by sol formation in the bentonite/groundwater interface in a fracture. Colloidal particles are generated at the interface and can be transported away with the flowing groundwater.
3. Sedimentation: For stable sols gravity has a negligible effect (Neretnieks et al. 2009). However, experiments have shown that colloids form flocs under the effect of gravity and that the flocs are strongly affected by gravity (e.g. Schatz et al. 2013). The effect of gravity can therefore not be neglected in PSAR.

Expansion

According to Neretnieks et al. (2017) for ion strengths above CCC, the expansion only depends on time as the loss at the rim is zero. Furthermore it is assumed that the loss is small compared to the total amount of clay in the deposition hole so that the volume fraction of clay in the deposition hole is essentially constant. The approach is the same as that in Liu et al. (2009) and in Neretnieks et al. (2009). The radius r_R (metres) of the expanded clay sheet in the assumed circular fracture after time t (years) can then be well fitted by the following expression:

$$r_R(t) = 1.300 + 0.3428\sqrt{t} - 0.0000335t \quad (10-1)$$

According to Equation (10-1) the expansion would extend to > 100 m in a period of 100 000 years even for groundwater concentrations above CCC. The reason for this is that wall friction between the bentonite and the rock surface is assumed to be zero. This approach is in conflict with the view of Börgesson et al. (2018), where experimental evidence for wall friction is clearly demonstrated and a theory is developed for the bentonite penetration into a horizontal fracture. The penetration depth is analysed in terms of the equilibrium situation where the swelling is completed, and the swelling pressure is balanced by the friction against the fracture walls.

There are several ways of estimating the friction angle at the low dry densities relevant for the non-swelling gel. Depending on the approach taken and the swelling pressure chosen the evaluated friction angles show large variations; from 0.5° to 30° (Börgesson et al. 2018). By using these large variations in the sensitivity analyses it was possible to show that the penetration into a 100 µm wide fracture is anyway limited to < 80 mm at the lowest friction angle. Alonso et al. (2019) presents a number of experiments with different clays, fracture apertures and water compositions. All erosion experiments carried out within narrow fractures with apertures smaller than 1 mm, showed that clay extrusion in the fracture was stopped at some time at both dilute and more saline conditions. Clay expansion was favoured within fractures of wider apertures. In general, Na-rich bentonites (Nanocor® or Na-exchanged MX-80) exhibited longer extrusion distances than raw MX-80 or Ibeco. Extrusion distances measured for Ca-exchanged bentonites, or other clays as saponite, were clearly shorter, but not zero.

As regards expansion of clay into a fracture for above CCC conditions, the approach by Börgesson et al. (2018) is used in the PSAR, since all experimental evidence supports that approach rather than the one put forward in Neretnieks et al. (2017). *Expansion is thus assumed to be negligible above CCC.*

The approach by Börjesson et al. (2018) is not valid at conditions below CCC, since it contains an assumption about the formation of a stable gel. However, as stated in the previous paragraph, experimental results, e.g. Alonso et al. (2019), show that expansion is restricted even at dilute conditions. *Therefore, in the PSAR, it is assumed that expansion will be limited to 5 cm for all conditions.* A more detailed discussion of the matter is found in the **Buffer, backfill and closure process report**, Section 3.5.11.

Erosion

The erosion model used in the SR-Site assessment has been improved. A modified solution method was developed where two regions were considered; the expanding clay region and the rim region (Neretnieks et al. 2017). The latter was, using some simplifying assumptions, solved by a technique that can resolve the details in the rim zone with very high accuracy.

The erosion rate at the rim depends on water velocity, aperture, radius to the rim and ion concentration.

A transition period starts after dilute water intrusion. After some time a steady state is reached where the intrusion rate from the deposition hole is equal to the erosion rate at the rim. The distance to the rim stabilises and the loss rate from the deposition hole becomes constant. The time to reach this steady state is short when erosion is large. The model is described in detail in Neretnieks et al. (2017) and also in the **Buffer, backfill and closure process report**, Section 3.5.11.

Figure 10-79 shows loss rate as function of water velocity as predicted by the model for different ion concentrations for a 0.1 mm aperture fracture and for a fixed expansion of 5 cm (see above). Steady state is well reached for $u_0 > 10^{-7}$ m/s in 1 000 years. The dashed line shows the old model results from Neretnieks et al. (2009) that was used in the SR-Site assessment for all cation charge concentrations below 4 mM. In Neretnieks et al. (2017, Appendix 2) the model is tested against some experimental results. The ability to reproduce the mass loss as a function of ion concentration is in general good.

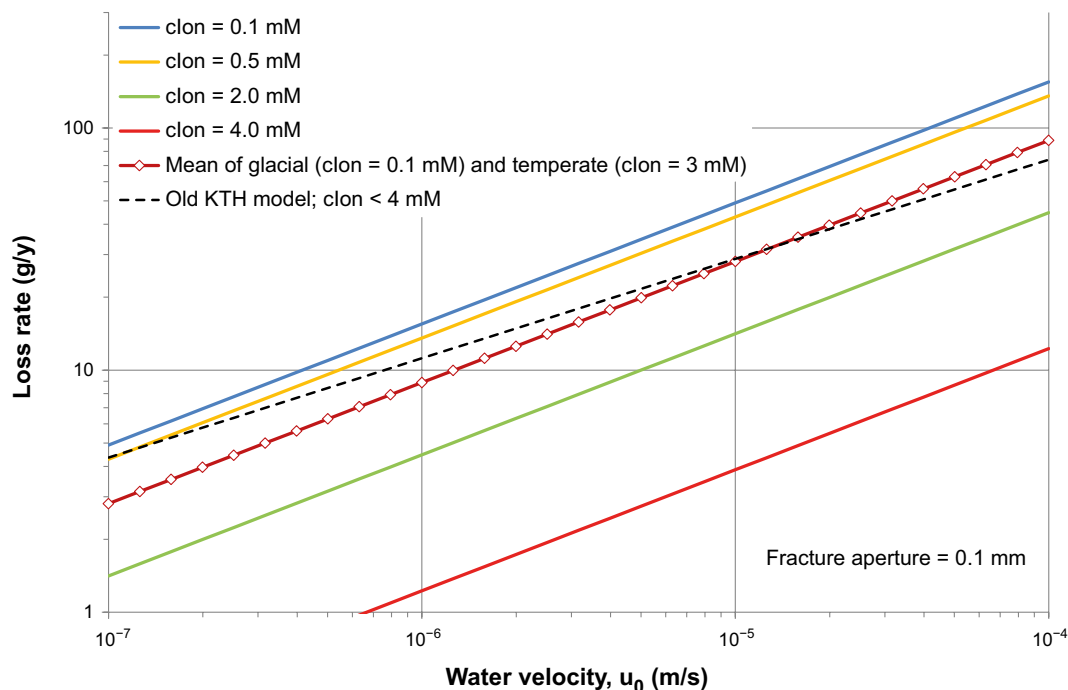


Figure 10-79. Loss rate as function of water velocity for different ion concentrations (c_{Ion}) in mM for a 0.1 mm aperture fracture. The dashed line shows results with the old model used in SR-Site. Also shown is the mean loss rate of for glacial and temperate intruding waters, see text further details.

For use in later Sections of this report, the Figure also shows a curve with the average loss rate for groundwater cation concentrations of 0.1 mM and 3 mM. The values represent infiltrating water during glacial and temperate conditions, respectively. Since such conditions are expected roughly equal periods of time during a reference glacial cycle, the average represents a mean loss rate during glacial and temperate conditions of a cycle. As seen in the Figure, this average loss rate happens to be quite similar to that calculated with the old model presented in Neretnieks et al. (2009). Further details on the analysis of erosion over a glacial cycle are provided in Section 10.4.8.

As is evident from the discussion in the preceding sections, erosion is a complex phenomenon dependent on a number of material specific and environmental factors. In the PSAR a thorough analysis of the extent of mass loss due to erosion given site specific, spatially and temporally varying data is required. In terms of models for the safety assessment, the simpler model in Neretnieks et al. (2009) and the more detailed model in Neretnieks et al. (2017), taking also ion concentration into account, are available. As seen in Figure 10-79 the two give fairly similar results for cation concentrations around 1–2 mM.

Sedimentation

In the description and modelling of erosion no account is taken of gravity effects. This is because it was found that in stable soils gravity has a negligible effect (Neretnieks et al. 2009). However, in the simulated fracture experiments mentioned above it was seen that when the fracture was turned vertical the flocs sedimented and new flocs were released from the expanding clay, also for non-flowing water. The erosive loss was comparable to or larger than that in the horizontal fractures (Schatz et al. 2013) with flowing water. Based on Schatz and Akhanoba (2017) it appears that, irrespective of whether mass loss occurs in a horizontal or 45° sloped fracture, at cation charge concentrations ≥ 8.6 meq/L the rate of mass loss for all of the tested materials is effectively zero assuming that the small amounts of mass loss detected in some of the cases can be ascribed to slaking (or other phenomena not associated with a continuous mass loss process).

A simple model was devised that accounts for the sedimentation rate of small floc particles in a fluid in a fracture (Neretnieks et al. 2017). The model is a pessimistic upper bound on the formation and release of agglomerates. However, at present it is only possible to use direct experimental results on the loss rate from small cylindrical sources and assume that these results can be extrapolated to much larger dimensions. Experiments in sloping fractures show that in low ionic strength waters tiny smectite agglomerates are constantly released and they sediment in the fracture (Schatz et al. 2013, Schatz and Akhanoba 2017)²⁴. The results can be summarised according to Equation (10-2) for 45° and 90° slopes from the horizontal. The release rate is proportional to the circumference of the extruded clay ($2\pi r_{RSS}$), the aperture (δ), and the projection of the fracture normal on the horizontal plane ($\sin\alpha$).

$$N_{Exp} = J_{Exp} \delta 2\pi r_{RSS} \sin \alpha \quad (10-2)$$

J_{Exp} was found to be 850 and 1 550 kg/(m²·y) by Schatz and Akhanoba (2017) for different clays in mainly 1 mm fractures with slopes of 90 and 45° from horizontal. More recent, still preliminary and unpublished tests performed in stagnant water and 0.2 mm aperture showed significantly lower J_{Exp} (< 30 kg/(m²·y) for MX-80 and several other bentonites). Two values of J_{Exp} , representing the two sets of experiments, will therefore be used in assessments of sedimentation in the PSAR: 30 kg/(m²·y) and 1000 kg/(m²·y), respectively. As mentioned, the former was obtained for 0.2 mm apertures and the latter for 1 mm apertures. Virtually all fractures intersecting deposition holes at the Forsmark site have apertures smaller than 0.1 mm, see Figure 10-80, meaning that the lower value of 30 kg/(m²·y) could be a more reasonable representation but that also this value is quite pessimistic for the great majority of intersecting fractures. In reality the fracture aperture will vary over the intersection, but this effect was not evaluated in the treatment. For the estimate of mass loss sedimentation in PSAR it is assumed that the expansion into the fracture is limited to 5 cm (see subsection “Expansion” above).

It also needs to be considered whether the smectite can be transported away in the fracture as an agglomerate fluid at the rate it is being released. Neretnieks et al. (2017) provide a model for quantitative analysis of the sedimentation rate. The report also demonstrates how the lower of the release rate and the sedimentation rate determines the rate of mass loss due to sedimentation.

²⁴ Schatz and Akhanoba do not account for the angle in their summary of results. Without access to the detailed data the effect of slope is omitted in Equation (10-2).

Figure 10-80 shows the buffer loss rate due to sedimentation as a function of aperture size for the two values of J_{Exp} discussed above. For aperture sizes below $\sim 2 \mu\text{m}$, the rate of agglomerate fluid transport limits the loss rate in both cases, and it continues to limit in the case of $J_{Exp} = 1000 \text{ kg}/(\text{m}^2 \cdot \text{y})$ up to $\sim 15 \mu\text{m}$. For higher aperture sizes the rate of smectite release is determining the loss rate.

The loss due to sedimentation occurs even without any flow in the sloping fractures, provided the sediments can move away continuously. Such further movement may not be assured if the sediments have a non-zero friction angle and cannot move on at intersections with fractures with slopes less than the friction angle.

Erosion due to sedimentation cannot be neglected in the safety assessment, given the current understanding of the phenomenon. The only available quantitative model is that described in Neretnieks et al. (2017), as discussed above. The extent of mass loss due to sedimentation according to this model is illustrated for site specific, spatially and temporally varying data in the following subsection.

The route to advection in the buffer

Erosion

As discussed in Section 10.3.9, a loss of 1 200 kg of buffer or 220 000 kg backfill material from one deposition hole position will lead to cases where advective transport in the buffer needs to be considered (loss of the diffusive barrier). The rate of loss can be calculated with the models described and discussed above. The information needed for each canister position is:

- The duration of conditions with a groundwater composition with a positive charge concentration of less than 8 mM, requiring a determination of the groundwater composition, in particular the concentrations of Na^+ and Ca^{2+} .
- The actual concentration of cations in the groundwater.
- The water velocity around a deposition hole/tunnel.
- The fracture aperture and slope.

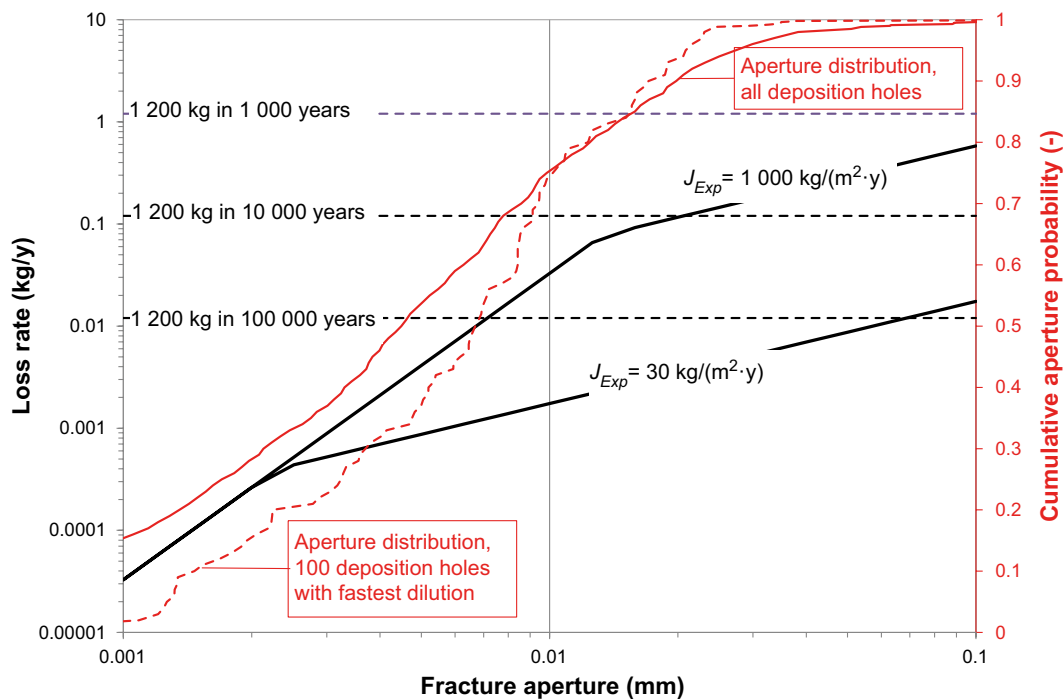


Figure 10-80. Loss rate of smectite due to gravitational effects (thick black lines) according to two sets of experiments. For small apertures, the sedimentation rate in the fracture limits the loss, whereas for larger apertures the release rate of agglomerates from the clay determines the loss. The figure also shows the distribution of apertures intersecting deposition holes at the Forsmark site, for the base case of the semi-correlated hydrogeological model (solid red line). The aperture distribution of the 100 deposition holes with the fastest dilution during temperate conditions is also shown (dashed red line).

As concluded in Section 10.3.7 the ionic strength of the groundwater; $\Sigma q[M^{q+}]$, could fall below 8 mM charge equivalents, i.e. violating safety indicator criterion R1c, for typically 0.24 percent of the deposition holes after 10 000 years of temperate conditions and 0.46 percent after 60 000 years of such conditions. This means that colloid release may occur from these holes and from deposition holes, if any, located under sections of the backfill losing their density.

It should be noted that the mechanical model (Section 10.3.9) used for the determination of the buffer and backfill loss in the analyses of the swelling period, is deliberately inconsistent with the model used for the rate of loss presented in this section. The mechanical model in Section 10.3.9 is based on buffer/backfill data determined for conditions where the ionic strength of the groundwater; $\Sigma q[M^{q+}]$ is above 8 mM charge equivalent and the swelling will be restricted mainly due to friction. The model used for the rate of loss on the other hand, is based on a situation where $\Sigma q[M^{q+}]$ is below 8 mM charge equivalent and then the swelling will be sufficient for colloidal particles to form. If this latter model were to be used for the homogenisation in the deposition hole/tunnel the acceptable mass loss would be larger. It could be argued that this could be defended, since the erosion only occurs for dilute conditions. However, in PSAR the more pessimistic values of maximum mass losses from the mechanical model have been used throughout the assessment. One important reason for this approach is the fact that the temporal variations in groundwater composition will lead to both spatial and temporal variations in the buffer porewater composition that are difficult to take into account in a strict sense in these analyses, other than through the adopted pessimistic approach.

To illustrate the loss of buffer mass due to erosion during the initial temperate period, it is noted that the cation concentration is never expected to fall below 3 mM, as this is the pessimistically estimated cation concentration of the infiltrating water that is expected to dilute the groundwater at repository depth during a temperate period, see Section 10.3.6. Using the modelling approach described above and the flow rates from the semi-correlated base case of the hydrogeological DFN model (Section 10.3.6), the resulting distribution of erosion rates, once this lower limit of charge concentration has been reached, is seen in Figure 10-81. It is obvious that only a small number of deposition holes will reach advective conditions, even in 10^6 years. Using the EFPC rejection criterion and assuming that “dilute” conditions occur 100 % of the time, 5 deposition holes reach advective conditions. Furthermore, as indicated in Section 10.3.6 only a fraction of a percent (0.24 %) of the deposition hole positions are likely to have dilute conditions after 10 000 years of the initial temperate period, and as will be shown in Section 10.4.6, less than 5 percent of the deposition hole positions are likely to have dilute conditions during a glacial cycle, and they will only have these conditions a fraction of the time. Given the slow buffer erosion rate, no deposition holes are expected to reach advective conditions during the initial temperate period of the base case. This applies also for the Global warming case of an extended temperate period of 60 000 years.

The above erosion model is valid when the gel/sol interface occurs in the flowing fracture. If erosion has proceeded to the extent that a sol filled cavity has formed in the deposition hole, then the erosion rate is more adequately expressed as

$$R_{\text{Erosion}} = q \cdot C_{\text{Clay}}$$

where q is the volumetric flow through the deposition hole cavity and C_{Clay} is the concentration of clay particles in the cavity, valid for most flow rates of concern here. The expression is the same as that used for the exchange of a solute in a deposition hole with a cavity (see Neretnieks 2006b for details). No additional studies have been done for this issue since SR-Site and the expression used for calculating mass loss remains the same. This is a considerably higher erosion rate than that valid when the release to the groundwater occurs in the fracture. The crucial issue to evaluate is when advective conditions arise in the deposition hole, whereas the further evolution of the erosion is of secondary importance. Therefore, the development past the situation when a cavity has arisen is not further addressed here.

Sedimentation

The basis for quantitative assessments of buffer sedimentation is currently not well developed and a pessimistic approach, based on the account given above, is therefore taken. A basic requirement for sedimentation to occur is a groundwater cation charge concentration below 8 mM. As seen in the example calculation in Section 10.3.6, around 0.24 percent, or 14 deposition positions, are expected

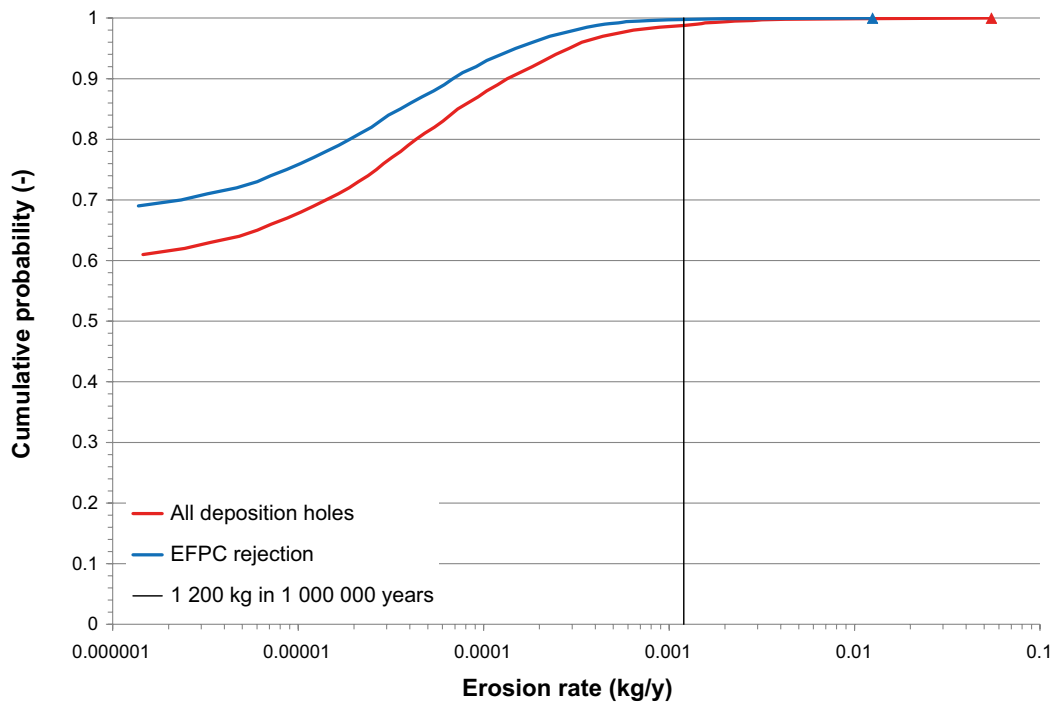


Figure 10-81. Distribution of erosion rates for the semi-correlated base case of the hydrogeological DFN model, with the EFPC rejection criterion used and for all deposition holes. The erosion rate required to achieve advective conditions in a deposition hole are given as a vertical line, for a groundwater cation concentration of 3mM (solid line) in all deposition holes. Only a fraction of a percent of the deposition holes is expected to be exposed to dilute conditions during the initial temperate period.

to experience such concentrations after 10 000 years of temperate conditions and around 0.43 percent (26 positions) after 60 000 years. The only additional host rock related factors determining the rate of mass loss due to sedimentation are the fracture aperture and slope. (The charge concentration of cations in the groundwater could potentially be another factor that determines the loss rate, in the same way as for the erosion process. There are however currently no data available that support this.) Most fractures at repository depth at the Forsmark site are oriented vertically according to current understanding, meaning that the slope angle in Equation (10-2) above is close to 90°. As for apertures, it is of interest to consider the apertures of fractures intersecting the fraction of deposition holes that reach dilute conditions during the initial temperate period. As seen in Figure 10-80, the distribution of fracture apertures in these deposition holes is similar to that when all holes are considered. Also, there is no pronounced correlation between the time to reach dilute conditions and aperture size. The aperture required to reach advective conditions due to sedimentation in 10 000 years of dilute conditions is around 0.02 mm assuming a J_{Exp} -value of 1 000 kg/m²/yr and for both the aperture distributions shown in Figure 10-80 more than 90 percent of the deposition holes have apertures smaller than this value. Of the calculated 14 positions reaching dilute conditions after 10 000 years, typically one could possibly reach advective conditions during the initial temperate period. For an extended temperate period of 60 000 years, typically half of the 26 positions experiencing dilute conditions could lose sufficient material due to sedimentation to become advective, disregarding pessimistically that the dilute conditions would for most positions take a considerable part of the 60 000 years to arise. For the more reasonable J_{Exp} -value of 30 kg/m²/yr, no deposition holes would experience advective conditions due to sedimentation in either of these time periods.

The loss due to sedimentation occurs even without any flow in the sloping fractures, provided the sediments can move away continuously. Such further movement may not be assured if the sediments have a non-zero friction angle and cannot move on at intersections with fractures with slopes less than the friction angle. Also, at some point the sedimenting material will reach the bottom of the fracture. At this point the fracture will start to fill up and the material will eventually reach the expanded front in the deposition hole. At this point, sedimentation will stop. The fractures are generally limited in volume and the sedimented material is low in density, which means that the bentonite mass that can

be accommodated is low. This means that the maximum mass loss from sedimentation in a stagnant system should be low. However, if the sedimented material in the fracture is in contact with flowing water (e.g. an intersecting fracture) erosion may occur. The magnitude of this erosion process is dependent on the flow rate in the fractures and the geometry of the fracture intersections. This process has not been studied and is not possible to quantify at present. Although this process may have a significant effect on mass loss of buffer from sedimentation, it is pessimistically neglected in the PSAR.

Further analyses of the extent of erosion and sedimentation, including studies of sensitivities to a number of uncertain factors are given in the analysis of the remaining part of the reference glacial cycle, Section 10.4.8, and in the buffer advection scenario, Section 12.2.

Erosion of deposition tunnel backfill

In SR-Site, the erosion rate of the deposition tunnel backfill was calculated with the same model as that used for buffer erosion with the following modification: The loss rate is increased by a factor of 2 to account for the increase in diameter of the interface between the fracture and the tunnel (diameter 5 m) compared to the deposition hole (diameter 1.75 m). The rate hence scales more slowly than linearly with the diameter (Moreno et al. 2010).

Fracture aperture and Darcy flux data were taken from the hydrogeological calculation results for the semi-correlated case without EDZ, to ensure that the analysis only included “true” tunnel intersecting fractures. Water velocities were determined from the Darcy fluxes with the same procedure as used for buffer erosion (Joyce et al. 2010). The results from the hydro analyses show the fracture apertures and water velocities for structures where particles released in the deposition tunnels immediately above each deposition hole escape to the rock. Several of these structures are in fact deformation zones that intersect the tunnel system far away from any canister position. Such data should thus be excluded from the analysis when the aim is to establish whether tunnel erosion could affect the conditions near a deposition hole.

The result of the calculation is shown in Figure 10-82. As indicated in the Figure, none of the tunnel intersecting single fractures will cause erosion to the extent that the criterion is violated, i.e. that more than 220 tonnes (Section 10.3.9) is lost in one million years if erosion occurs 25 % of the time. For a few positions where the particle escapes to a deformation zone, potentially more than 220 tonnes could be lost, but this is not relevant from the point of view of canister integrity. For an unrealistic, bounding case of erosion occurring 100 % of the time, five tunnel intersecting single fractures experience losses just above 220 tonnes in one million years. The loss of 220 tonnes of backfill indicates that advective conditions may not be excluded in the deposition hole closest to the tunnel intersecting fracture. Considering that canister corrosion is a process requiring hundreds of thousands of years to cause failure of the canister's containment for advective conditions with high sulphide concentrations, and that 220 tonnes of tunnel backfill are lost in only five positions with the unrealistic, bounding assumption of erosion 100 % of the time, the contribution of loss of deposition tunnel backfill to the possible generation of advective conditions in deposition holes is considered negligible.

Sedimentation of tunnel backfill material could in principle be handled the same way as what is done for the buffer. One considerable difference is however the amount of material lost before the safety function is violated. The 220 tonnes of backfill lost before advective conditions starts, means that the fate of the sedimented material, which was neglected for the buffer, becomes a real issue. It is unlikely that the fracture system in the rock can accommodate this amount of material unless flow and erosion are severe. A rough mass balance calculation with the assumption that the density of the sedimented material is 30 kg/m³ and the available porosity in the rock is 10⁻⁴ gives that the rock volume needed to accommodate 200 tonnes is 7.3 × 10⁷ m³, which corresponds to a cube with a side of 420 m. The backfill erosion model from SR-Site used above actually represents both an expansion and erosion and can, at least in a simplified fashion, be said to represent a situation with a combination of erosion and sedimentation. The consequences of sedimentation in the buffer will be more severe than in the backfill under almost all circumstances and since the uncertainties regarding sedimentation are still large, the mass loss in the backfill is handled the same way in the PSAR as in SR-Site.

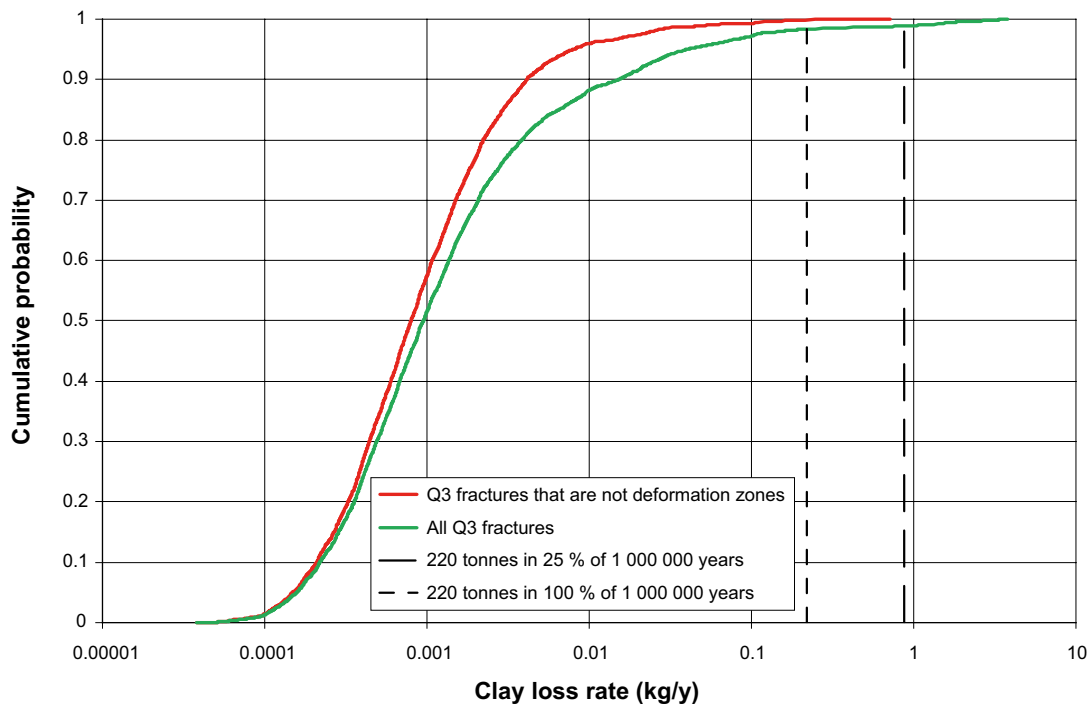


Figure 10-82. Calculated distribution function of clay loss rate in deposition tunnels for the semi-correlated hydro case and assuming dilute conditions.

It should also be noted that the calculated local loss of backfill does not mean that the other safety functions of the backfill are lost. 220 tonne represents only a small part of the backfill in one deposition tunnel. Loss of backfill will lead to an open void only in a part of the tunnel while the main part will retain its hydraulic and mechanical properties (Section 10.3.9).

The saturation period

During the water filling and saturation period of the repository (Section 10.3.6), the water that enters the repository originates predominantly from the surface, either as meteoric water or water from the Baltic Sea. In the case of meteoric water it cannot be excluded that $\Sigma q[M^{eq}]$ will be below 8 mM charge equivalents. This means that the risk of erosion needs to be considered for this period. However, during this period additional factors need to be considered.

1. The buffer and backfill will be in a state of suction in this situation. The direction of the water flow will be in towards the buffer and backfill. The water uptake will compete with the clay expansion into fractures.
2. The accessory minerals in the clay will be present. The presence of calcium sulphates (gypsum), in particular, increases the cation concentration in the buffer and thus restricts the release of colloids.
3. The duration of this period is relatively short.

The results that are presented in Svensson and Follin (2010) show that the salinity in certain parts of the repository will decrease from 0.8 to ~0.3 % during the operational period. This would have no effect on the bentonite stability, since 0.3 % salinity still is above the limit for colloid stability. Svensson and Follin (2010) also show that some parts of the repository will get an inflow of brackish water from the Baltic during the operational period. After the repository closure, the natural hydrostatic pressure field will be reset and the natural groundwater flow will be restored, which will have an impact on the salt content of groundwater in the repository volume. Matrix diffusion will also affect the salt content of the groundwater in the fractures. The land uplift, and the accompanying shoreline displacement during the first temperate period will slowly increase the inflow of meteoric water to the repository level, as shown in, for example, Salas et al. (2010). These processes are expected to overshadow the effects of the operational period, even if the respective time scales are different.

Erosion before saturation is only possible if the water flow in the deposition hole is higher than what the installed buffer can take up by itself, as discussed in Lilja et al. (2014). This situation is represented by a saturation time of 20 years or less. According to Figure 10-52 this will occur in very few deposition holes in Forsmark. If the flow is lower, the bentonite will take all the water and no material can be transported away. If the groundwater that comes into contact with the buffer is sufficiently diluted and the flow is higher than what the buffer can absorb, there are conditions for chemical erosion in an unsaturated buffer as well. At an early stage, the accessory minerals in the bentonite will affect the erosion, but it is not possible to unambiguously show that the process would not occur. However, the deposition holes where this would be relevant are placed in deposition tunnels with such high inflows that the tunnel is expected to fill quickly and the hydraulic gradients will be restored. Tunnels with high inflows can be water filled on a monthly scale and after this the hydraulic gradient can be assumed to be restored. Water exchange in the deposition holes is then expected to be at the same level as in the undisturbed conditions. When the repository is closed and the groundwater chemistry is restored, the erosion, if any had occurred, will cease. Since the operational period is short, the erosion is then expected to be insignificant compared to that occurring due to long-term diluted groundwater.

Identified uncertainties and their handling in the subsequent analysis

Knowledge concerning colloidal sol formation and colloid stability is good concerning the effects of mono- and divalent ions. However, modelling of the correlation effects caused by divalent ions is demanding. The prevention of sol formation at low ionic strength when the calcium content in the montmorillonite is above 20 % has been verified experimentally. Detailed understanding of this effect is less well developed and handling edge-face interactions in modelling is complicated. The force-balance model is based on parallel layers and furthermore only tested versus vertical swelling experiments and for short swelling times, up to 5 weeks.

The possible transport of colloids by diffusive and flow transport is less well known. The effects of mechanical erosion of loose gels close to sol forming conditions have not been fully examined. Experiments show that montmorillonite does not penetrate filters with pore-sizes of 0.5 mm. However, it has not been shown that accessory minerals could actually form an effective filter in the fractures. The understanding of the effect of pH on colloidal sol formation is incomplete.

The role of friction between the expanding clay paste and the fracture surface is also an important uncertainty. Börgesson et al. (2018) demonstrates well the role of friction for groundwater concentrations > CCC. However, the importance below CCC has not currently been assessed more than by experimental observations.

Sedimentation of clay particles in sloping fractures below CCC is an area where the mechanistic understanding is very limited. So far only empirical models are available.

There is a large uncertainty in the J_{Exp} values used in the empirical expression. The values in Schatz and Akhanoba (2017) range between 850 and 1 550 kg/m²/year for fracture apertures of 1 mm, while more recent, still unpublished, experiments show much lower values when more narrow apertures are used.

The experimental observations are not always consistent, which makes interpretation as well as verification or validation of models difficult.

None of the tunnel-intersecting single fractures will cause erosion to the extent that this will cause such a loss of swelling pressure above deposition holes that these in turn would enter an advective condition, even when the entire one million year assessment period is considered. For a few positions where the particles escape to a deformation zone, potentially more than 220 tonnes could be lost, but this is not relevant from the point of view of canister integrity. Furthermore, loss of backfill will lead to an open void only in a part of the tunnel while the main part will retain its hydraulic and mechanical properties.

10.3.12 Evolution of the buffer with the bottom plate and backfill with plug after the thermal period

The barriers in the repository are designed to prevent the intrusion of groundwater into the canisters and, in case of canister failure, to retard radionuclides on their way to the geosphere. In addition to the colloid formation discussed in the previous section, groundwater interactions with the components of the barriers will modify the composition of the groundwater that will eventually reach the canister. Knowledge of its composition, especially of the master variables, is important since it may affect:

- The solubility of radionuclides in case of containment failure.
- The hydraulic and mechanical behaviour of the buffer.
- The chemical stability of the buffer.
- The corrosion of the canister.
- The sorption of radionuclides in case of isolation failure.

Sena et al. (2010b) described the chemical evolution in the repository for a range of conditions and assumptions. The focus of the calculations has been on:

- pH.
- Amount of calcite, gypsum, dolomite.
- Concentration of calcium in the aqueous phase and in the montmorillonite interlayer.

In the study, no calculations of the evolution of either the iron system or the redox conditions have been made. The redox system is instead treated by equilibrium considerations or mass balance in the PSAR. For example, oxidation of sulphide in the buffer is pessimistically neglected and all sulphide is assumed to be available for canister corrosion (see Section 10.3.13). The details of the processes and mechanisms represented in the modelling are presented in Sena et al. (2010b).

While no performance is required from the deposition tunnel plug after closure since the transport tunnels will be backfilled, the concrete in the plug cannot be assumed to be stable over the entire assessment timeframe and therefore its degradation needs to be described.

Geochemical evolution in a buffer connected to a water conductive fracture

For a deposition hole intersected by a water conductive fracture, the geochemical evolution in the buffer was calculated for a number of cases based on the geometry presented in Figure 10-83. The geochemical simulations for the water-saturated period have been performed with the reactive transport code PHAST (Parkhurst et al. 2004). This code is the result of coupling a transport code and a geochemical code. PHAST is able to simulate multicomponent, reactive solute transport in three-dimensional saturated groundwater flow systems. The reference case for the sensitivity study is the bentonite composition according to Table 5-12, and a typical Forsmark groundwater.

The variations considered have been the magnitude of the water inflow and the composition of the groundwater. Figure 10-84 shows an example of a calculation of the evolution of pH in the buffer as a function of the composition of the groundwater. The variations considered were sulphate content (S(VI)), calcium/sodium ratio (Ca/Na), carbonate concentration (C(IV)) and pH.

Table 10-11 shows a summary of the main results obtained in the sensitivity analysis.

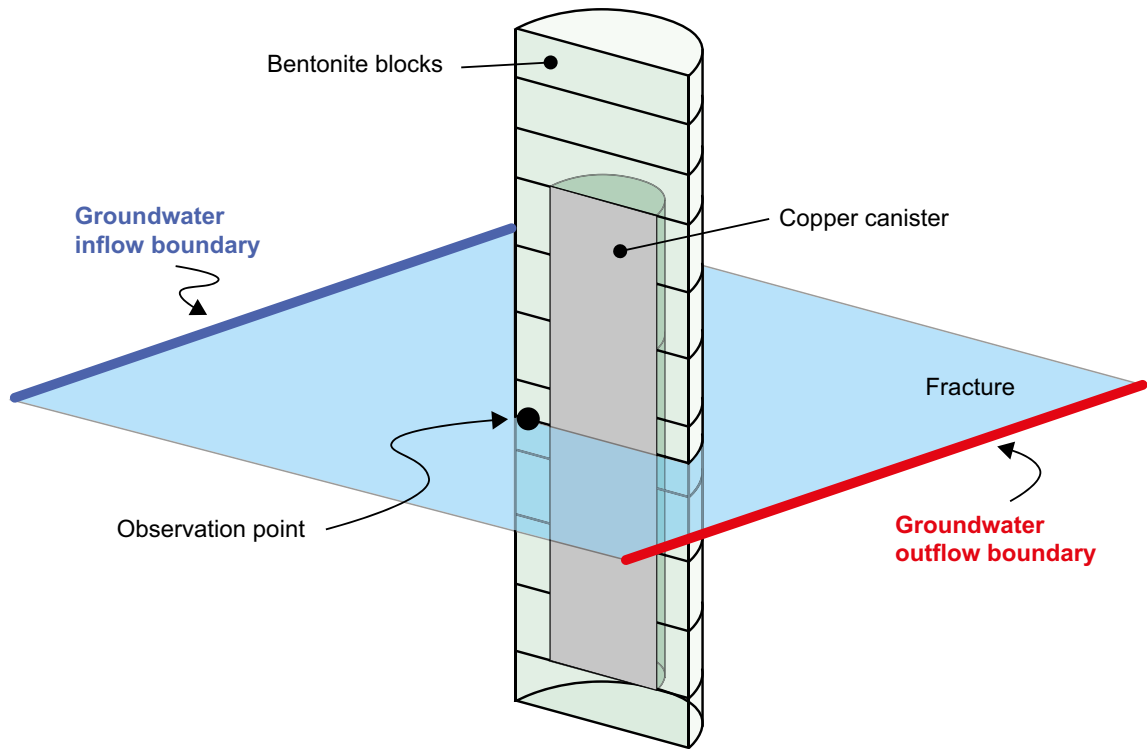


Figure 10-83. Location of the observation point inside the buffer where the computed time evolution of selected chemical parameters has been analysed for the sensitivity cases considered (Sena et al. 2010b).

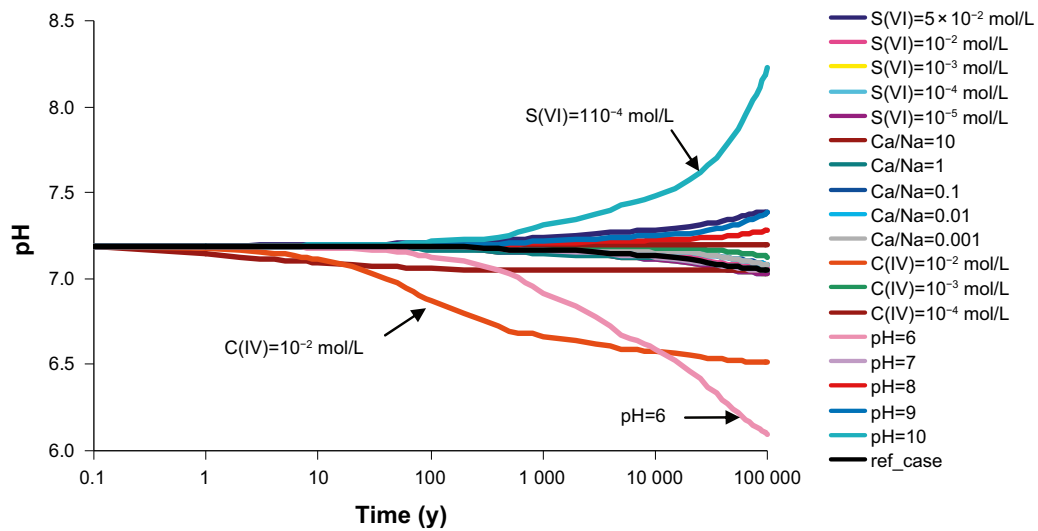


Figure 10-84. Calculated time evolution of pH at the observation point located in the bentonite (see Figure 10-83) for nineteen inflow water compositions for a flow rate of $0.1 \text{ m}^3/\text{yr}$, MX-80 bentonite (Sena et al. 2010b).

Table 10-11. Summary of the main results obtained for MX-80 in the sensitivity analysis performed for the chemical composition of the groundwater (Sena et al. 2010b).

Flow rate (m ³ /yr)	Variable	Value	Sensitivity case
10 ⁻³	Maximum pH	7.30	pH = 10
	Minimum pH	6.63	C(IV) = 10 ⁻² mol/L
	Maximum amount of calcite	3.19 × 10 ⁻² wt. %	C(IV) = 10 ⁻² mol/L
	Fastest gypsum exhaustion	At 50 000 yr	Ca/Na = 0.001
	Maximum amount of gypsum	1 wt. %	Ca/Na = 10
	Maximum [Ca(aq)]	1 mol/L	Ca/Na = 10
	Maximum [CaX ₂]	71.2 %	Ca/Na = 10
	Minimum [CaX ₂]	20.0 %	Ca/Na = 0.001
10 ⁻¹	Maximum pH	8.22	pH = 10
	Minimum pH	6.09	pH = 6
	Maximum amount of calcite	2.79 × 10 ⁻² wt. %	C(IV) = 10 ⁻² mol/L
	Fastest gypsum exhaustion	At 400 yr	Ca/Na = 0.001
	Maximum amount of gypsum	5.32 wt. %	S(VI) = 5 × 10 ⁻² mol/L
	Maximum [Ca(aq)]	1 mol/L	Ca/Na = 10
	Maximum [CaX ₂]	84.0 %	Ca/Na = 10
	Minimum [CaX ₂]	7.6 %	Ca/Na = 0.001

The overall conclusions from the sensitivity study of the geochemical evolution in the buffer were as follows.

- For higher flow rates in the fracture, more pronounced geochemical changes occur. In both bentonite types analysed, gypsum is exhausted earlier in the cases with a higher flow rate. More calcite precipitates in these cases.
- The lowest pH value computed for the MX-80 bentonite buffer is 6.10 which is reached in the case where the inflowing groundwater has a pH of 6. The computed pH drop is mainly related to the lack of carbonate minerals in this type of bentonite.
- The highest pH value computed for the MX-80 bentonite is 8.23, which is reached in the case where the inflowing groundwater has a pH of 10, and the flow rate along the fracture is 0.1 m³/yr.
- When the inflowing water has a Ca/Na of 10, the excess of calcium in the bentonite buffer leads to the highest amount of calcite precipitated, and the highest concentration of calcium in the aqueous phase and in the montmorillonite interlayer.
- The population of calcium in the exchanger depends on the initial bentonite composition, the flow in the fracture intersecting the deposition hole and the relation between calcium and sodium in the groundwater. The highest calculated proportion is 71 % and the lowest is 7.6 %, see Table 10-11.

By comparing the results calculated for the thermal period and the water-saturated period (Figure 10-71), it is seen that the evolution of the amount of Ca-sulphate in the buffer is similar for both periods. Ca-sulphate minerals tend to dissolve due to the inflow of Forsmark groundwater. Nevertheless, during the warming period, anhydrite is predicted to precipitate close to the copper canister, but as soon as the temperature drops it will tend to dissolve. When the reference Forsmark groundwater is considered, secondary calcite precipitation in the MX-80 bentonite is predicted to be very small and temporary in both periods analysed.

Geochemical evolution in the backfill and in a buffer not connected to a water conductive fracture

The results of the calculations of the geochemical evolution in the buffer in the previous section only consider the situation when the deposition hole is intersected by a fracture with flowing water. In Forsmark many deposition holes will not be intersected by any water conducting fractures and in those positions the geochemistry in the buffer will be conditioned by the tunnel backfill. To evaluate the effect of the backfill on the geochemical evolution in the buffer, a similar sensitivity study to the

one discussed in the previous section was performed (Sena et al. 2010b). The geometry and sections where the evolutions have been calculated is shown in Figure 10-85. In this case groundwater is supplied through a hypothetical fracture at the edge of the backfill.

Figure 10-86 shows the calculated pH along the backfill (Section 1 in Figure 10-85) for the same set of different groundwaters as was considered in the previous section. The initial pH of the backfill porewater is 7.16. At the end of the simulation period, almost all the cases lead to a pH profile equal or slightly higher than the initial value. Exceptions occur for two cases (Figure 10-86):

- [C(IV)] of the groundwater entering through the fracture is 1×10^{-2} mol/L,
- Ca/Na of the groundwater entering through the fracture is 10.

When the carbonate content of the groundwater entering through the fracture is 1×10^{-2} mol/L, the final pH in the mid-height of the tunnel is around 7. The calculated pH decrease with respect to the initial value of 7.16 is mainly due to the fact that the pH of the inflowing water is relatively low. When the Ca/Na ratio of the groundwater entering through the fracture is 10, a considerable amount of calcite is predicted to precipitate in the backfilled tunnel, and therefore, the pH of the backfill porewater decreases to 6.7 (Figure 10-86), at the end of the simulation period.

Figure 10-87 shows the pH profile along a vertical section through the backfill and buffer (Section 2 in Figure 10-85). The initial pH of the backfill and MX-80 bentonite was 7.16 and 7.19, respectively. The final pH computed along Section 2 for the case with the MX-80 bentonite, is between 6.69 and 7.29 (Figure 10-87). Although a relatively wide range of pH values (between 6 and 10) is considered for the groundwater entering through the fracture, the continuous mixing between the fracture groundwater and the backfill porewater, together with the geochemical reactions triggered by such mixing are able to buffer the pH perturbation induced by the groundwater entering through the fracture, so that the final pH of the bentonite buffer does not change much with respect to its original value.

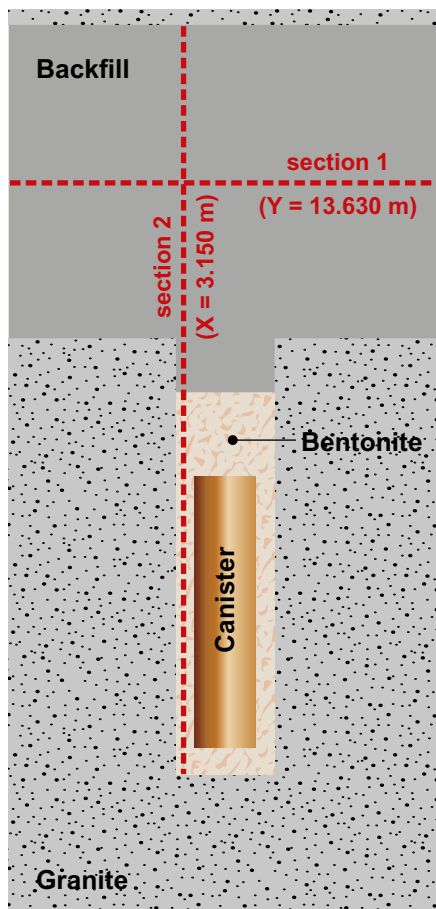


Figure 10-85. Location of the two sections of where the geochemical evolution has been calculated for the different sensitivity cases. Water enters from the left side in the backfill (Sena et al. 2010b).

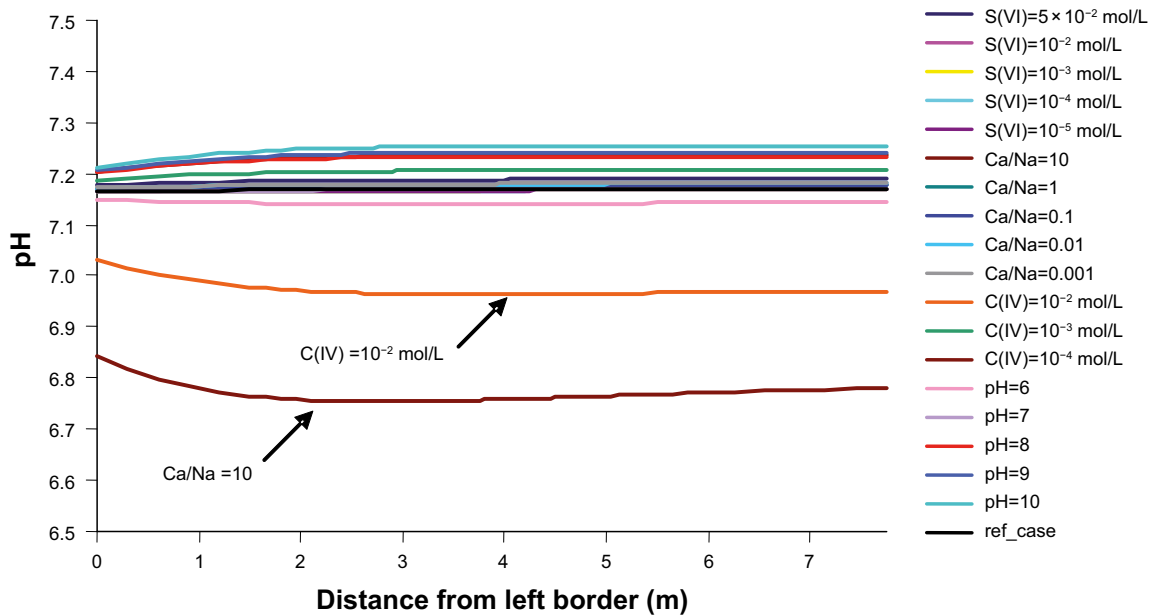


Figure 10-86. Calculated pH profiles along Section 1 (see Figure 10-85) for the sensitivity cases, at the end of the simulation period (100 000 years) (Sena et al. 2010b).

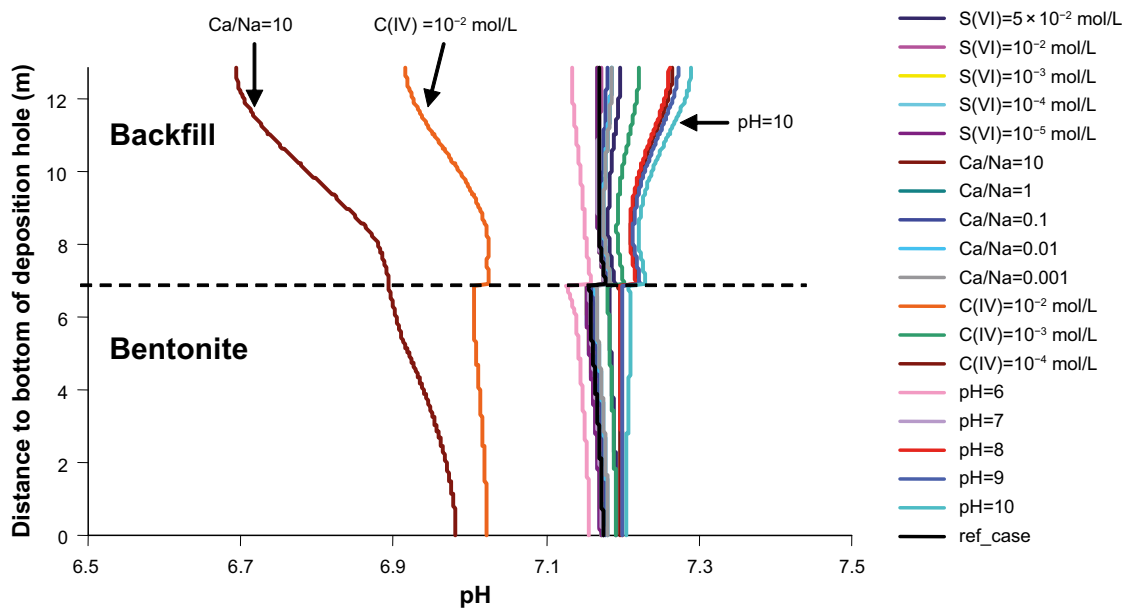


Figure 10-87. Calculated pH profiles along Section 2 (see Figure 10-85) for the sensitivity cases, at the end of the simulation period (100 000 years), MX-80 bentonite buffer (Sena et al. 2010b).

Table 10-12 presents a summary of the main results obtained in the sensitivity analysis developed for backfill/buffer. The values are calculated for the observation point in Figure 10-83. Although a wide range of pH values, from 6 to 10, has been considered in the sensitivity analysis by Sena et al. (2010b), the final pH in the bentonite buffer does not reach such extreme values. These results show that geochemical changes in the bentonite buffer, induced by inflows of the different groundwaters considered, are less pronounced in the case with supply through the backfill than in the case where water is supplied directly from a fracture in the rock.

Table 10-12. Summary of the MX-80 results of the sensitivity cases for the backfill/buffer interaction (Sena et al. 2010b).

Variable	Value	Sensitivity Case
Maximum pH	7.21	pH = 10
Minimum pH	6.91	Ca/Na = 10
Maximum amount of calcite	2.88×10^{-2} wt.%	Ca/Na = 10
Minimum amount of gypsum	0.33 wt.%	Ca/Na = 0.001
Maximum amount of gypsum	1.85 wt.%	Ca/Na = 10
Maximum [Ca(aq)]	9.4×10^{-2} mol/L	Ca/Na = 10
Maximum [CaX ₂]	50.0 %	Ca/Na = 10
Minimum [CaX ₂]	29.3 %	[S(VI)] = 5×10^{-2} mol/L

In summary, the sensitivity cases developed for the backfill result in the following conclusions.

- The geochemical evolution of the bentonite buffer is similar to that computed for the case where water is supplied from a fracture, but it evolves at a much slower rate, since mixing of the groundwater entering through the fracture with the backfill porewater buffers the disturbing effect of the inflowing “foreign” groundwater.
- The geochemical evolution of the backfill does not change much regardless of the type of bentonite considered in the deposition hole.
- Calcite is predicted to precipitate in the backfilled tunnel in all the sensitivity cases considered. The highest amounts of calcite precipitated are computed in the cases where the inflowing water has a Ca/Na > 1. Therefore, the lowest pH computed for the backfill is 6.76, in the case where the inflowing water has a Ca/Na of 10.
- The highest concentration of calcium in the backfill (1.4×10^{-1} mol/L), at the end of the simulation period, is computed for the case with Ca/Na of 10.

Application to geochemical conditions at the Forsmark site

The various cases that are described in this section and for which the results are summarised in Table 10-11 and Table 10-12 show that the backfill/bentonite is rather stable from a geochemical point of view and no dramatic changes of the geochemical conditions in the buffer can be expected. A comparison of the input data in Table 10-11 and Table 10-12 with the expected geochemical evolution at the Forsmark site presented in Table 10-9 shows that the expected evolution is covered well within the cases considered.

Chemical and mechanical interaction bottom plate/buffer

One conclusion from the SR-Site assessment was that the design of the bottom plate at that time required further consideration. The present bottom plate only consists of copper. The chemical interactions with the surroundings can therefore be considered to be negligible.

The mechanical interaction between the bottom plate and a water pressure under the plate is also less likely. Since there is no tight connection between the plate and the rock, water from a fracture under the plate will move the pellets instead of lifting the plate.

Degradation of the concrete in the deposition tunnel plug

Grandia et al. (2010b) have evaluated the degradation of the concrete part of the plug. The conceptual description of the plug can be found in Figure 10-88.

The rock is not considered physically as a rock in the model. Instead, a flowing groundwater of Forsmark-type composition is considered. The reason behind this selection is the slow kinetics of the granite mineralogy which is not expected to undergo significant changes in spite of the diffusion of alkaline fluids from concrete alteration. Low-reactivity aggregate is predicted to be present in a defined fraction of the volume in the hydrated cement mixture. The remaining porosity is ~30 %;

however, this value includes all pore sizes, most of them are unconnected. Figure 10-89 and Figure 10-90 show the calculated water composition, porosity and pH in the concrete and the backfill for 1 and 100 years of simulation.

The results from reactive transport simulations predict that the effect of low-pH concrete alteration on the stability of backfill materials is low. Dissolution of Ca-Si-hydrates (CSH phases) causes an initial hyperalkaline plume (pH > 11) penetrating ~6 cm into the backfill. This plume is transient since in a few years (< 10 y), pH decreases back to more neutral values. The main process governing geochemistry in the backfill-concrete boundary is the quick loss of porosity due to ettringite precipitation. The model predicts insignificant modifications in the geochemistry of the system from 10 years and on, since porosity has already been clogged at both concrete boundaries decreasing the diffusion between material pores. CSH phases keep replacing from Ca-rich to Si-rich intermediates. Since CSH replacement is controlled by kinetics, Si-rich CSH will form until complete equilibrium with porewater is achieved, regardless of the fluid renewal. Alkaline pH does not affect the composition of the granitic groundwater, mainly because of the rate of water renewal specified in the fracture.

Backfill swelling after tunnel plug disintegration

As described in the previous section, the cement and other substances in the concrete plugs may be dissolved with time and transported away, which means that the stiffness and strength of the plugs will be dramatically reduced. This disintegration will affect the backfill material on both sides of the plug. When the plug cannot withstand the swelling pressure of the backfill it will be compressed and the backfill will swell, which leads to a loss in density and swelling pressure of the backfill. Since there is friction against the rock surface the loss in density may be significant close to the plug but will be reduced with distance from the plug. In order to understand how this affects the backfill and the location of the first deposition hole a number of finite element calculations have been carried out (Åkesson et al. 2010a). The main purpose of the calculations was to find how much the backfill density will decrease in order to put a limit on how close to the plug the deposition hole can be located. Since no detailed knowledge of the plug status after disintegration is required only a very simplified model of the plug was used. The geometry used in the calculations is shown in Figure 10-91.

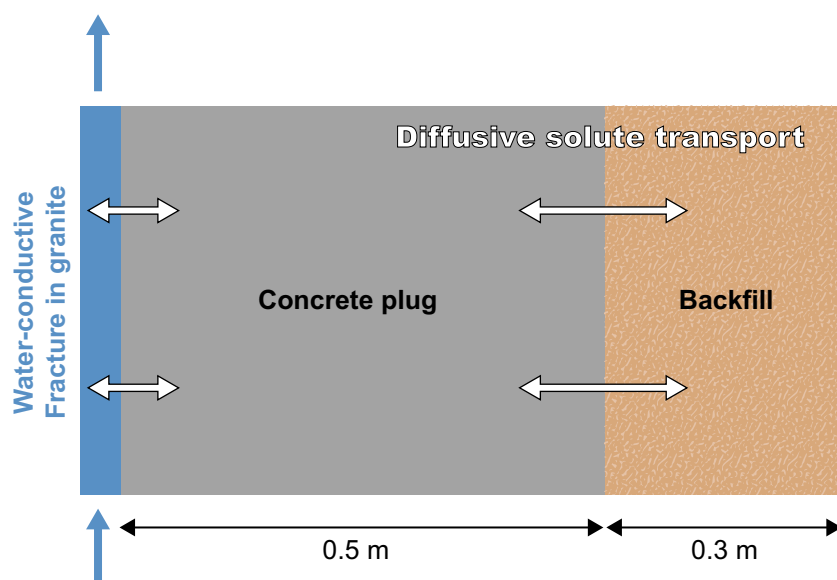


Figure 10-88. Domain selected in the reactive transport simulations (Grandia et al. 2010b). The actual plug design is more complex and has a tight bentonite filled seal, see Figure 5-19. However, these details are judged insignificant for the modelling.

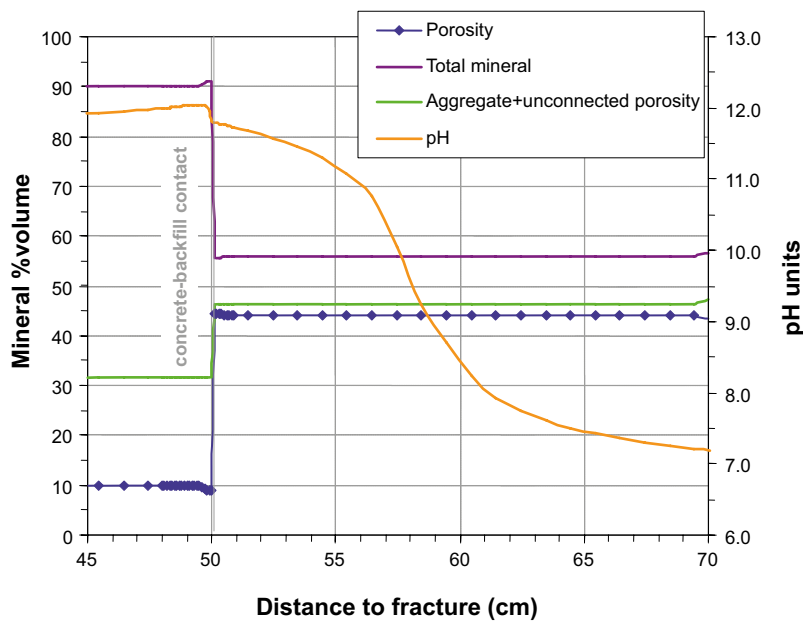
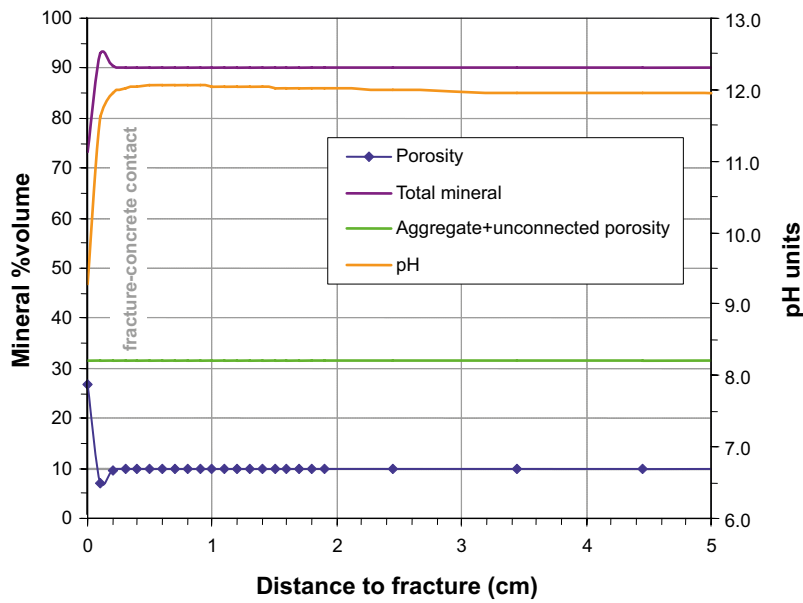


Figure 10-89. Predicted composition of porewater, porosity and pH in concrete and backfill after 1 year of simulation in fracture-concrete and concrete-backfill contacts. Unconnected porosity and non-reactive aggregates in the concrete and backfill are plotted together (Grandia et al. 2010b).

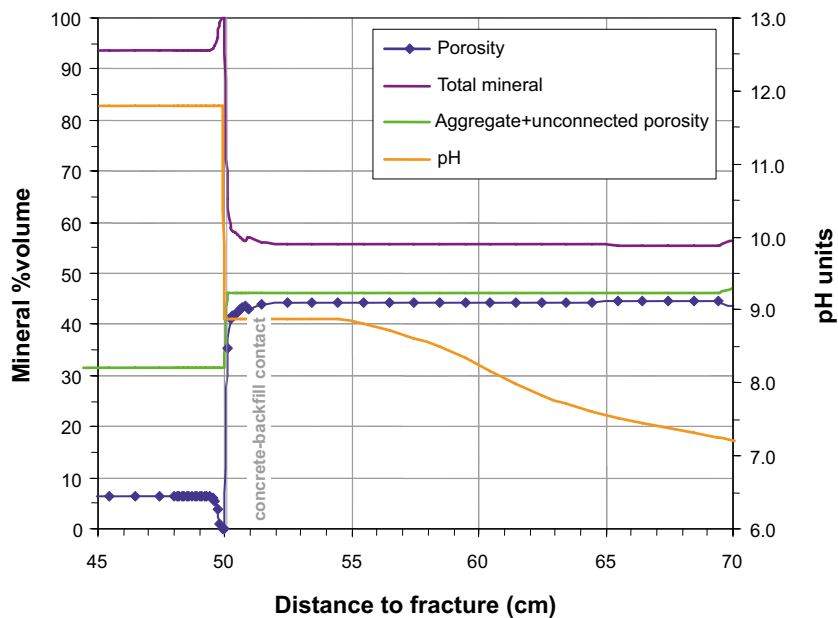
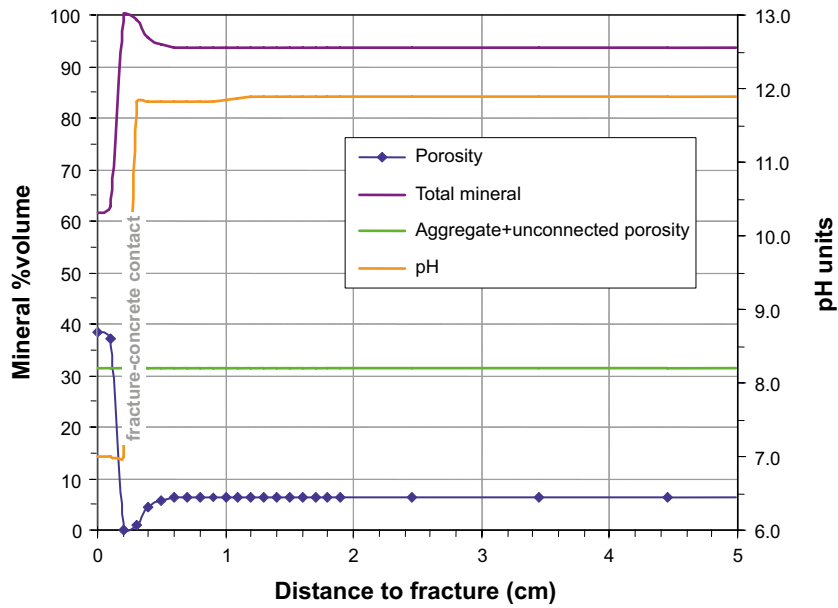


Figure 10-90. Predicted composition of porewater, porosity and pH in concrete and backfill after 100 years of simulation in fracture-concrete and concrete-backfill contacts. Unconnected porosity and non-reactive aggregates in the concrete and backfill are plotted together (Grandia et al. 2010b).

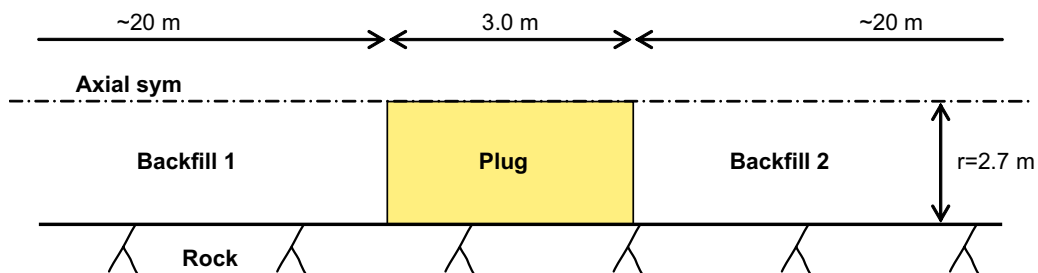


Figure 10-91. Schematic drawing of the model. Backfill 1 is located inside the plug and Backfill 2 outside (Åkesson et al. 2010a).

Different sensitivity cases, varying the E-modulus, the pressure and the void ratio have been studied (Åkesson et al. 2010a).

A typical example of a result from the calculations can be found in Figure 10-92. The results show that case *Plug1* yields a swelling of only 7 cm, which is the smallest swelling of the investigated cases due to the low initial swelling pressure of the backfill and the high E-modulus of the plug. The entire swelling corresponds to a compression of half the plug since the same backfill is assumed to be present outside the plug. The void ratio and the swelling pressure are only changed marginally except for a small zone at the rock/plug/backfill contact.

Table 10-13 is a compilation of the most important results of the different calculations.

Table 10-13. Compilation of results from the cases presented in Åkesson et al. (2010a). The calculations with names beginning with Plug1 have bentonite backfill on both sides of the plug while calculations with names beginning with Plug2 have crushed rock outside the plug. Suffix -2 refers to calculations with the high dry density $\rho_d = 1600 \text{ kg/m}^3$ and high swelling pressure of the bentonite backfill, while the names without suffix refer to calculations with the low dry density $\rho_d = 1450 \text{ kg/m}^3$ and low swelling pressure.

Calculation	Displacements (m)		Maximum void ratio	Minimum swelling pressure (MPa)	Remarks
	Backfill1/Plug	Backfill2/Plug			
Plug1	0.03–0.07	–(0.03–0.07)	1.0	2.0	Locally at corner
Plug1b	0.15–0.27	–(0.15–0.27)	1.1	1.3	
Plug1-2	0.08–0.17	–(0.08–0.17)	0.86	5.7	
Plug1b-2	0.30–0.58	–(0.30–0.58)	0.99	3.0	
Plug2	0.10–0.15	0.05–0.07	1.1	1.7	Locally at corner
Plug2b	0.35–0.50	0.20–0.28	1.2	0.8	
Plug2-2	0.24–0.32	0.13–0.17	0.98	3.0	
Plug2b-2	0.70–1.05	0.40–0.58	1.2	1.0	

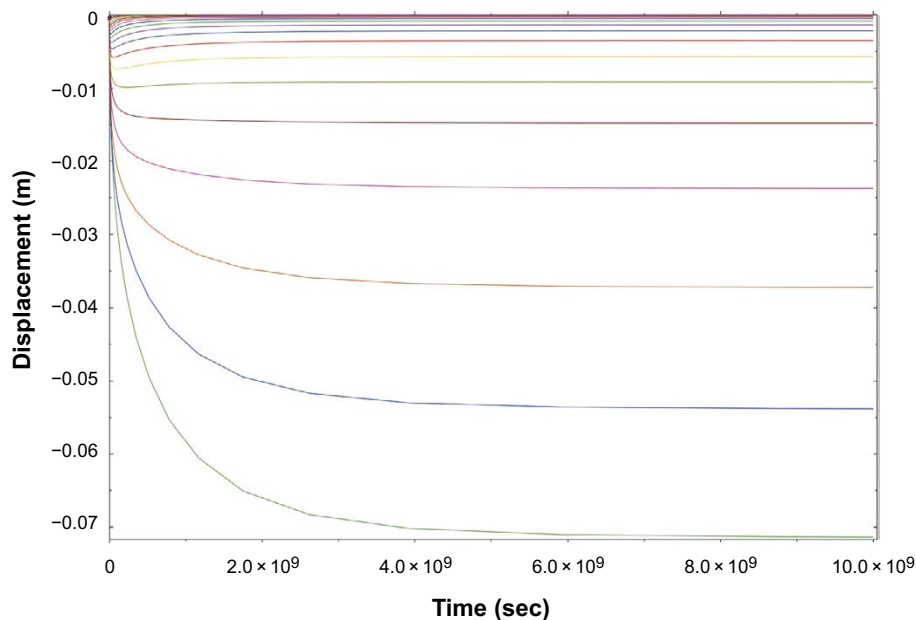


Figure 10-92. *Plug1.* Axial displacements of the centre nodes in Backfill 1 as a function of time. The lowest curve represents the contact backfill/plug and the consecutive lines represent 10 cm, 20 cm, 30 cm etc. axial distance from the contact (Åkesson et al. 2010a).

According to Table 10-13, the highest resulting void ratio at the backfill/plug interface is 1.2. Since this is within the limits set for the backfill above a deposition hole ($e < 1.22$) the conclusion from the calculations is that the disintegration of the plug has no detrimental effect on the backfill above the first deposition hole and no restrictions caused by plug disintegration on the location of the first deposition hole are needed.

There are of course several uncertainties particularly regarding the data applicable to the plug after disintegration. There are also uncertainties regarding the initial density and properties of the backfill. However, the properties of the plug are very pessimistically set and in spite of this the results are far from critical for the buffer in the first deposition hole.

Canister sinking

Apart from the few deposition holes losing buffer through colloid release, as assessed in Section 10.3.11, the buffer in other deposition holes will not be affected by any processes that may alter its swelling properties in a way that the swelling pressure would sink below the value needed to retain the canister in position ($P > 0.2$ MPa, see Section 8.3.2). Furthermore, in deposition holes losing buffer due to colloid sol formation, creation of advective conditions would occur long before the canister sinking could happen, making this issue irrelevant also for these cases.

Osmotic effects on the buffer and backfill

According to Table 10-9, the maximum chloride concentration of any time frame is < 0.4 M at repository level in the Forsmark groundwater. As seen in Figure 5-14 this is not expected to have any impact on the properties of the buffer material. This conclusion is valid for the entire repository evolution period.

Identified uncertainties and their handling in the subsequent analysis

The various cases described in this section show that the chemical conditions in the buffer and the backfill are rather stable and no dramatic changes of the geochemical conditions can be expected. The expected conditions in the Forsmark groundwater (Table 10-9) are well within the range of the parameters used in the sensitivity study for all future evolutions. As seen in the right side of Figure 10-73 the buffer (MX-80) is expected to have about equal populations of sodium and calcium in the exchanger for a typical Forsmark groundwater. The sensitivity study presented in Table 10-11 shows a range of 7–84 % for the calcium population, but the minimum and maximum values in the range are both for Ca/Na ratios that are far away from what is expected in the Forsmark water for any condition (Table 10-9).

The model predictions indicate that the durability of backfill materials is not expected to be affected by the potential alkaline plumes developed from concrete alteration of the plug. Hence, the effect on the backfill properties will be small and can be neglected in the subsequent analysis. Also calculations show that the disintegration of the plug, which means that the backfill could then swell into the voids created, has no detrimental effect on the backfill above the first deposition hole and no restrictions on the location of the first deposition hole are needed.

10.3.13 Canister evolution

One of the main safety functions of the canister is to provide a corrosion barrier, safety function Can1 in Figure 10-2. Processes that could cause deterioration of the copper shell during the temperate phase need thus be assessed.

Thermal evolution

The thermal evolution of the buffer is analysed in Section 10.3.4 where it is shown that the buffer temperature will always stay below 100 °C. This analysis can also be used to assess the temperature on the canister. For dry deposition holes the maximum temperature at the canister surface and at canister mid-height is about 2 degrees higher than the maximum buffer temperature, i.e. at the very most 102 °C for a few canisters. At the canister top and bottom, the temperature is at most 100 °C under these dry conditions, since there the canister is in direct contact with the buffer. If there is

water in the deposition hole such that the buffer swells, there will be direct contact between buffer and canister everywhere and the temperature at the canister surface, and in the buffer, will be much lower (up to a 20 degree decrease relative to the dry case). 3D modelling of the internal temperature distribution in the canister showed that the temperature of the insert becomes at most 105 °C, see the **Fuel and canister process report**, Section 3.2.1. This is well below the earlier design requirement of a maximum temperature of 125 °C for the insert. There are thus no consequences for the integrity of the canister. (Currently, no design requirement is defined for this entity.)

Mechanical impact of buffer swelling

After emplacement of the canister and the buffer, water will enter the deposition holes via the water conductive fractures that intersect the holes, and, to some extent, via diffusive transport of water through the rock. This leads to wetting and swelling of the buffer. After some time, the buffer will stop the water inflow through the fractures and the groundwater pressure will start to build up, which may lead to flow paths opening around the deposition holes in the superficial excavation-disturbed zone, where the flow resistance is expected to be lowest. This will tend towards a more uniform wetting of the bentonite and a more uniform pressure build-up. The size of this effect is, however, uncertain. It is, therefore, reasonable to assume that there will be inhomogeneities in the pressure build-up.

Furthermore, if the canister is slightly tilted or inclined in the emplacement hole, or if the rock is uneven, permanent pressure disequilibrium can exist in the bentonite even after water saturation. This can also occur due to swelling of the buffer at the top of the hole. Temporarily, asymmetric loads may thus occur due to uneven water saturation in the buffer. Permanent asymmetric loads may also occur due to a non-uniform density distribution of the saturated buffer caused by irregularities in the geometry of the deposition holes.

The external outer pressure resulting from the buffer swelling forces the copper shell to deform against the insert, which thereafter supports the copper shell and limits further deformation. However, radial swelling on the copper lid flange and uneven stresses caused by density gradients in the buffer can result in deformation in the copper (Jonsson et al. 2018). The buffer swelling along the canister also creates shear forces on the outer surface of the copper shell. The resulting local deformations based on an elastic-plastic material model were compared with creep model results and both give similar plastic strains around 1 % (Hernelind 2015, 2017), which is well below the creep strain at rupture for the copper canister material. Uneven stresses caused by vertical density gradients in the buffer were investigated in Hernelind and Börgesson (2019). The shear stress of $\tau = 0.77$ MPa gives no plastic strain in the copper shell. A more detailed assessment of creep for these cases is given in Section 12.7.5.

As described above and in Section 5.4.3, the probability that the canister would not withstand the load from uneven swelling of the bentonite is negligible. In short, buffer swelling will not pose a threat to the safety function indicators Can2 and Can3 in Figure 10-2.

Copper corrosion – general

Overview

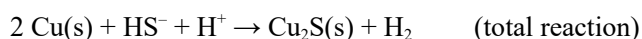
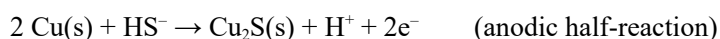
A range of studies over several decades (see the **Fuel and canister process report**) has identified the following substances as capable of corroding the copper canister material under repository conditions, after the operating period:

- Oxygen transported to the canister surface from the buffer and backfill, or from the groundwater bearing fractures in the deposition hole via the buffer.
- Nitric acid formed by gamma radiolysis of nitrogen compounds in moist air in the gap between canister and buffer.
- Oxidants formed by radiolysis of condensed water at the canister surface or bentonite pore water in contact with the canister.
- Sulphide transported to the canister surface from the buffer and backfill or from the groundwater in fractures intersecting the deposition hole and via the buffer.

Even though the kinetics of certain corrosion processes can be affected by temperature, due to transport limitations, the extent of corrosion is marginally affected by the changes in temperature expected in the final repository. The results of corrosion are formation of corrosion products and a reduction of the thickness of the copper shell.

As argued in the **Fuel and canister process report**, the influence on corrosion of chemical and mechanical conditions of the copper material (welded area, cold worked material), corrosion of copper in pure O₂-free water, the effects of deposition of salts and the effect of natural earth currents as well as earth currents from the present HVDC installation (Fenno-Skan, with its electrode 25 km from Forsmark), are deemed to be negligible.

After the entrapped oxygen has been consumed, sulphide will be the remaining corroding agent present in the repository. The sources of sulphide could be dissolution of sulphide minerals in the buffer and backfill (different iron sulphides, possibly also pyrite), sulphide formed by microbial sulphate reduction in the buffer and backfill and dissolved sulphide in the groundwater (either from dissolution of sulphide minerals in the rock or as a result of microbial reduction of sulphates in the groundwater-rock system). The corrosion of copper by sulphide will proceed with formation of copper sulphide (for simplicity written as Cu₂S even though other non-stoichiometric forms are possible, e.g. Cu_{1.8}S or Cu_{1.96}S) and molecular hydrogen. This is also the most pessimistic stoichiometry from a corrosion point of view (2 copper atoms are oxidised per sulphide).



The extent of general corrosion is then for the most part assessed with transport rate modelling, as the upper limit for general copper corrosion by sulphide is given by the sulphide influx to the canister surface, for the case where sulphide is immediately consumed at the surface. As the flux also influences the nature of the sulphide corrosion (the morphology of the formed copper sulphide film and the possibilities for different forms of localised corrosion) the sulphide flux at the canister surface is compared with threshold fluxes from corrosion experiments.

Stress corrosion cracking, which requires not only a specific corrosive environment, but also tensile stresses in the material, is evaluated in different ways depending on the redox conditions. For oxidising conditions the environmental concentrations of specific ions (ammonium, acetate and nitrite) are compared to estimated threshold concentrations for stress corrosion cracking to appear in laboratory experiments. Under sulphidic conditions, the sulphide flux at the canister surface is compared to threshold fluxes for transport limited sulphide corrosion, which cannot sustain cracking at a crack tip.

Although some initial corrosion due to the entrapped oxygen is expected in the repository, the copper oxides formed are not stable in sulphide solution and will be transformed to copper sulphides when sulphide exposure commences. This further means that the electrochemical properties of the canister surface that are established under the initially oxygenated conditions (possibly passivity) do not prevail and the long-term corrosion morphology is instead controlled by the copper sulphide film, see further in the **Fuel and canister process report**, Section 3.5.4.

Localised corrosion in sulphide solution

If the corrosion is sulphide transport limited it means that the sulphide is consumed as soon as it reaches the canister surface, and no interfacial concentration of sulphide at the canister surface can build up. This is the result of the balance between flux to the surface and the kinetics of the corrosion reactions involving sulphide.

The corrosion of copper in sulphide solution has been studied by SKB for a long period, mainly at the University of Western Ontario, Canada. Copper from SKB (Cu-OFP) has been exposed to sulphide solutions with different concentrations and/or fluxes at the electrode surface. By studying the properties and growth of copper sulphide films formed during corrosion knowledge can be gained about the corrosion mechanisms. This work is described in more detail in Section 3.5.4 of the **Fuel and canister process report**. A summary was compiled in Section 5.3 of SKB (2019c), and, here with a few new references added, the main findings were:

- In experiments under natural corroding conditions (no externally applied potential) it is the sulphide flux at the canister surface that determines the type of film formed. At a low flux, the film becomes porous, while a higher flux gives a compact film (Chen et al. 2014).
- The same dependence of sulphide flux on the film type formed is observed in experiments with an applied potential, so that a high sulphide flux (achieved by using a rotating electrode) is required to get a compact film, while otherwise a porous film is formed (Martino et al. 2017).
- If other anions are present in the solution (as in groundwater), they will influence the film formation process, in at least two ways (Chen et al. 2017, Martino et al. 2020). Increasing the ionic strength (higher concentration of Cl^- , SO_4^{2-} or HCO_3^-), decreases the electric field and thus the resistance at the copper-electrolyte interface at the pore bottom, which in turn shifts the control of further film growth to the reaction kinetics of the anodic dissolution, rather than mass-transport. Another effect is from the competition for adsorption sites on the copper surface, and thereby lessened formation of the intermediate $\text{Cu}(\text{SH})_{\text{ads}}$, which is necessary for the Cu_2S film formation. Although the sulphide concentration influences the morphology of the formed film (e.g. if the film is compact or porous, and in the latter case if the pores are narrow or wider), the presence of other anions can also have an effect, and the ratio $[\text{HS}^-]/[\text{X}^n]$ needs to be taken into consideration in the subtleties of the film formation process.
- In the literature it is claimed that the sulphide films formed during electrochemical experiments are passive (e.g. Mao et al. 2014, Dong et al. 2016, Kong et al. 2018), with the sharp increase of the current at higher potentials being the breakdown potential. Other experimental work (Martino et al. 2019a, Guo et al. 2019, 2020) shows that the increase in current is the onset potential for active dissolution of copper, and not breakdown of a passive film. Another argument for passivity is the use of the Point Defect Model (PDM) to describe and interpret the film formation, e.g. in experiments with sulphate-reducing bacteria (Huttunen-Saarivirta et al. 2018), but this has also been criticised (Martino et al. 2019b), rebutted (Huttunen-Saarivirta et al. 2019a) and corrected with an erratum (Huttunen-Saarivirta et al. 2019b). As the PDM is developed to describe a passive film, the interpretation is biased by the inherent assumption of passivity. In Huttunen-Saarivirta et al. (2019a) it is argued that Cu-OFP has a lower pitting susceptibility than pure copper without phosphorus. Similar conclusions were drawn in Bai et al. (2023). Taxén and Sparr (2014) compared the nobility of copper with different amounts of added phosphorus (under oxidising conditions), and found minor differences.

Thus, the results from natural corrosion as well as polarization experiments show that the formation of a passive, and thus protecting film, requires a high interfacial concentration of sulphide at the film/electrolyte interface, where the film formation takes place.

Also, it can be noted that the observations of “pits” on copper in sulphide solutions show features that are not growing extensively deeper with time, but rather becomes wider, and these are attributed to micro-galvanic coupling, rather than true pitting. This is consistent with a system that is largely transport-limited, and which cannot sustain a localised corrosion process with a penetration depth significantly ahead of the general corrosion front, as the interfacial sulphide concentration at the canister surface is close to zero. The transport resistance for the sulphide is further increased by the precipitation of corrosion products in pits, and the latter is also seen in cracks appearing in tensile stress experiments (Taxén et al. 2019).

As described in the **Fuel and canister process report**, Section 3.5.4, at sulphide fluxes below $3 \times 10^{-10} \text{ mol}/(\text{m}^2 \cdot \text{s})$ the film growth is controlled by the transport of sulphide in solution (and in the pores of the film), giving only general corrosion. For sulphide fluxes higher than that, localised features (resulting from micro-galvanic coupling) need to be taken into account.

Stress corrosion cracking in sulphide solution

Stress corrosion cracking (SCC) on copper in sulphide solution has been investigated in several studies during the last decade. The test method has mainly been slow strain rate testing, at various conditions, but the results have not been fully consistent. Taniguchi and Kawasaki (2008) noted small superficial cracks, but several other observations point to the possibility that this could have been attacks in the grain boundaries and not traditional stress corrosion cracking. Bhaskaran et al. (2013) tried to repeat the Japanese experiments, but in spite of aggressive laboratory conditions and

variation of many experimental parameters, no cracks were observed. Also a group at VTT Technical Research Centre of Finland tried to repeat the experiments, but found no evidence for SCC (Sipilä et al. 2014). The first results published (Arihata et al. 2011) inferred sulphide would quickly go into the copper material, but the authors concluded in a later publication (Sipilä et al. 2014) that the cause of the observed sulphur ingress was an unsuitable method for specimen analysis.

Tests have been done at Studsvik AB (Becker and Öijerholm 2017, Becker et al. 2020, Forsström et al. 2021), with another type of specimen (tapered), and as a departure from the earlier test conditions, a phosphate buffer was used to keep the pH stable. In the first study (Becker and Öijerholm 2017) some small fractures were observed at a high the sulphide concentration (10^{-3} mol/L), but with a lower strain rate (Becker et al. 2020) corrosion in grain boundaries rather than cracks were found. The grain boundaries had opened (especially high angle boundaries) and were often filled with corrosion products. Mechanically unloaded specimens were also exposed to the same solution, but no similar surface defects were found. Material from the exposed test specimens at Studsvik has also been analysed at Aalto University in Finland (Forsström et al. 2017, 2021, Becker et al. 2020) for the concentration of hydrogen in the different samples. The authors noted higher concentrations of hydrogen in copper after exposure to the sulphide solution, and the strained samples had a higher concentration than the unloaded samples, exposed to the same sulphide concentration. The authors concluded that the surface defect formation on the grain boundaries is most likely related to corrosion of Cu, rather than hydrogen embrittlement of the grain boundaries.

Further repetitions of these experiments were performed (Taxén et al. 2018, 2019) with varying specimen design, level of cold work in the material, temperature and sulphide concentration. The later work also introduced a phosphate buffer. After rupture of the specimen, the fracture surface indicated a ductile rupture, and there were signs of corrosion attacks in the grain boundaries. When a phosphate buffer was present, superficial cracks were observed at high sulphide concentrations ($\geq 10^{-3}$ mol/L), but not at low concentration (2×10^{-5} mol/L).

It is clear that superficial cracks have been observed in some strain experiments with copper in high concentration sulphide solutions, but this does not lead to the conclusion that “classical” stress corrosion cracking has occurred. As concluded above (with further details in Section 3.5.4 in SKB (2019c)), a passive sulphide film has only been observed in laboratory experiments with high sulphide flux, and not under natural corroding conditions. This means that mechanisms requiring the presence of a passive film are not applicable.

In Taxén et al. (2019) a mechanistic description is presented that tries to encompass the results from that study as well as the earlier studies by the same and other researchers. The process leading to the observed corrosion morphology is described as an intergranular corrosion aggravated by strain. The tensile stress breaks the sulphide film and corrosion (anodic dissolution) initiates at susceptible grain boundaries and produces small cavities. (The copper atoms in the grain boundary would require somewhat less energy to be oxidised than atoms in the bulk copper matrix.) The intergranular corrosion is aggravated by strain that pulls apart the grains that form the flanks of the cavity. The primary corrosion products are the dissolved copper sulphide complexes, $\text{CuHS}(\text{aq})$, $\text{Cu}(\text{HS})_2^-$, $\text{Cu}_2\text{S}(\text{HS})_2^{2-}$, and the anodic corrosion process produces a concentration of dissolved Cu(I). This concentration will increase with increasing temperature and decreasing pH, and if the transport of copper sulphide species is less effective, e.g. at the tip of a crack in the film or on convex surfaces on a rounded test specimen, the increased concentration of copper will promote the precipitation of $\text{Cu}_2\text{S}(\text{s})$, i.e. as a secondary corrosion product. The precipitation will occur preferably at growing copper sulphide particles, often outside the crack, but also inside. The growth of solid corrosion products will thus tend to block the crack and hence reduce the transport of sulphide to the crack tip, and the process will be self-limiting. Further, these superficial cracks are only seen for experiments where the bulk sulphide concentration is 10^{-3} mol/L or higher, and the sulphide flux is high enough to give a compact sulphide film (see above). The porous type of film formed at lower concentrations will not support cracking according to the mechanistic understanding, and thus the stress and strain effects are not operating. With the experimental results and the mechanistic description at hand, it is concluded that strain-induced grain boundary corrosion (rather than SCC) only takes place at a bulk sulphide concentration of 10^{-3} mol/L or higher. This corresponds to a sulphide flux of the order of 10^{-6} mol/($\text{m}^2 \cdot \text{s}$), assuming a diffusion layer of 1 mm and a diffusivity in bulk solution of 10^{-9} m^2/s .

The possibility that the so called Aaltonen mechanism could be an operable SCC mechanism has been revisited (Huutilainen et al. 2018). This mechanism is based on the concept that excess vacancies in the metal can activate dislocations within the material leading to strain localisation at the crack tip and further to crack propagation. There is no intrinsic reason why excess vacancies could not be generated in copper exposed to a sulphide solution and that atomic hydrogen liberated in the corrosion process could enter the material, but observations of effects in laboratory experiments have only been seen at applied currents of the order of 1 mA/cm², which would correspond to corrosion at a sulphide flux of 10⁻⁴ mol/(m²·s).

The combined effects of irradiation and tensile stresses have been deemed negligible due to the low dose rates at the canister surface in the repository, this is further described in the **Fuel and canister report**, Section 3.5.5.

Copper corrosion – unsaturated conditions

Corrosion from oxygen and from radiolysis products

As concluded in Section 10.3.8 the saturation will take longer time than the oxygen consumption, so that aerobic and saturated conditions will not occur simultaneously. There will though be an unsaturated phase, when the chemical composition of the gas in the unsaturated bentonite is important from a corrosion point of view.

Atmospheric corrosion and corrosion caused by oxygen initially present in the buffer and the backfill was discussed in Section 10.2.5 and the corrosion depth was shown to be less than 2.5 mm (including pits). The chemical conditions in the repository are then expected to be reducing for the period of temperate climate, see Section 10.3.7, i.e. no further corrosion due to oxygen is expected.

During the unsaturated phase, nitric acid formed by gamma radiolysis of moist air will contribute to the corrosion attack during this period. It can be shown, however, that the amount of nitric acid formed corresponds to a corrosion depth of a few nanometre only, see the **Fuel and canister process report**, Section 3.5.4.

Corrosion depths from the radiolysis of water is estimated to ca 3 µm, considering modelling of general corrosion depth and experimental observations of localised corrosion features. The available information shows that there is no indication for shifted corrosion potentials or significantly enhanced corrosion rates caused by gamma radiation at the low dose rates representative for the repository see the **Fuel and canister process report**, Section 3.5.4.

Stress corrosion cracking under oxidising conditions

As described in the **Fuel and canister process report**, Section 3.5.5, the presence of high enough concentrations of specific ions is one of the prerequisites for stress corrosion cracking to occur at the canister surface. There are, however, few threshold values for the concentrations of ions causing SCC, and it may not be enough to consider just the SCC-causing ion in itself, as e.g. also chloride may play a role in the mechanism. There are though laboratory tests showing that ammonium concentrations of approximately 0.1 mol/L (Kinnunen and Varis 2011) or nitrite concentrations of 0.001 mol/L (Benjamin et al. 1988) are required to cause stress corrosion cracking in copper under oxidising conditions. For acetate there is less experimental data available, but according to Ikäläinen et al. (2021), stress corrosion cracking did not occur even when the acetate concentration was as high as 0.4 mol/L.

For assessing corrosion it is the composition of the water close to the canister that is important. The water composition in the pore water is not very different from the groundwater as the bentonite buffer will not interact to any substantial degree with the incoming water, see further Section 10.3.10, and the concentrations of these anions in the groundwater can be used to assess SCC of the copper. In Section 10.3.7 groundwater concentrations are stated to be below 2 × 10⁻⁴ and 10⁻⁷ mol/L for ammonium and nitrite respectively, while the acetate would be in the micromolar range. During the operational phase nitrogen-containing compounds, like nitrite and ammonium may remain from the blasting of the tunnels, or acetate may be formed from organic material, but the increase of these compounds will be insignificant (Section 10.2.5).

Comparing the maximum groundwater concentrations with the threshold values from SCC experiments, it can be concluded that the concentration of SCC-assisting ions is too low, by 2–3 orders of magnitude for SCC to occur under oxidising conditions.

Sulphide corrosion

The dryness of the Forsmark site, resulting from relatively few water-bearing fractures and low advective flow of groundwater, is in principle an inherent limitation for corrosion. In order for a galvanic cell to establish, water must be present and serve as an electrolyte, but liquid water also transports corrosive agents like sulphide to the canister surface. During the very earliest period of the unsaturated phase the temperature on the outer canister surface may rise to ca 95 °C for some canisters (see Figure 10-16) and with low relative humidity (Malmberg and Åkesson 2020), meaning that there might be a period when the canister surface is sufficiently dry so that electrochemical corrosion is not supported. Under such conditions the reaction between gaseous sulphide species and the copper surface is feasible, but different reaction mechanisms are suggested in the literature (King and Kolář 2019). The period of such dry conditions is however relatively short. Furthermore, as the copper surface initially will have an oxide layer, the first reaction to occur is the exchange of the oxides in the film into copper sulphide.

When the temperature falls, a liquid film will form on the canister surface due to humidity and condensation. Since full saturation of the bentonite clay may take hundreds or even thousands of years in the deposition holes in the driest parts of the repository, there will be a period during which hydrogen sulphide gas (H_2S) is the only sulphide species which can be transported through the clay system. This sulphide gas will dissolve in the water film at the canister surface and the flux of sulphide at the canister surface is then controlled by the transport of gaseous sulphide through the unsaturated clay system. Since there is no evidence for the generation of H_2S from microbial processes in experiments with unsaturated bentonite (Section 10.3.10), the only source of sulphide during the unsaturated phase will be the transport of H_2S from the $\text{H}_2\text{S}/\text{HS}^-$ equilibrium in the groundwater.

The possibilities of transport of gaseous sulphide, $\text{H}_2\text{S}(\text{g})$, during the unsaturated phase is discussed in Section 10.3.10, under the assumption of a constant aqueous sulphide concentration of 10^{-6} mol/L in the backfill porewater (or rather at the top of the buffer). From this a highest flux of $\text{H}_2\text{S}(\text{g})$ that could possibly be established in the unsaturated repository environment is about 6.5×10^{-11} mol/($\text{m}^2 \cdot \text{s}$). This is about a factor 4 lower than the threshold sulphide flux of 3×10^{-10} mol/($\text{m}^2 \cdot \text{s}$), where the film growth is controlled by the transport of sulphide in solution (and in the pores of the film).

The mass transport control of the corrosion also means the interfacial concentration will be close to zero, which verifies the boundary condition assumed in the analysis of sulphide fluxes in Eriksson and Hedin (2019). The concentration for which localised corrosion of copper in sulphide solution has been observed can thus not be maintained, and only general sulphide corrosion needs to be assessed for corrosion from sulphide transported in gas phase.

In the same way the sulphide flux of 6.5×10^{-11} mol/($\text{m}^2 \cdot \text{s}$) under unsaturated conditions can be compared to the sulphide flux of 10^{-6} mol/($\text{m}^2 \cdot \text{s}$) in experiments where superficial cracking (interpreted as intergranular corrosion or possibly SCC) has been observed. There is thus a margin of several orders of magnitude. The margin is ever larger for the effects interpreted as by the Aaltonen mechanism, where crack like effects have only been observed at sulphide concentrations corresponding to sulphide fluxes of 10^{-4} mol/($\text{m}^2 \cdot \text{s}$).

The excavation of the repository will change the groundwater flow pathways compared to the situation prior to establishment of the tunnel system, so that meteoric water from the surface could reach repository depth through drawdown in open boreholes. Such water may be sufficiently rich in suitable organic carbon for sulphate reducing bacteria and thereby constitute the limiting factor for sulphide production (see Section 10.2.5). This type of organic carbon is quickly consumed in the groundwater and thus the elevated levels of organic carbon at repository depth will only exist as long as the groundwater flow in the rock is elevated as a result from the construction and operation of the repository, i.e. during the first 100 years. This will further apply only for the parts of the repository where groundwater flows are expected to be high during the operational phase.

For a bounding estimate of the corrosion caused by this possible initial high sulphide concentration, the concentration of sulphate in the penetrating water can be used as an upper limit for the concentration of sulphide at repository depth during the first 100 years after construction has been initiated. The highest measured sulphate concentration at the surface is about 10^{-3} mol/L, and from that a maximum concentration of 10^{-3} mol/L sulphide is assumed (see Section 10.2.5).

This water rich in sulphide is pessimistically assumed to fill the entire pore volume in the buffer and backfill, and the corrosion is estimated by a mass balance (Lilja et al. 2014), resulting in less than 10 μm corrosion from the buffer pore water. The sulphide in the pore water in 6 m of the deposition tunnel (corresponding to one canister) would cause about 500 μm of corrosion on the canister lid, but it is totally unrealistic as this sulphide concentration cannot be upheld in the pore water (see Section 10.3.10) for a time long enough to allow for the sulphide to reach the canister by diffusion.

Corrosion from organic material left during construction is treated below, together with other organic material and other sources of electron donors for SRB activity.

From the evaluation of sulphide fluxes at the canister surface it can be concluded that neither localised corrosion in the form of micro-galvanic coupling, nor stress corrosion cracking processes will occur during the unsaturated phase. The general corrosion is evaluated through the mass transport of sulphide to the canister, assessed as two components depending on the source of the sulphide. The corrosion from the sulphide in the groundwater for saturated conditions is evaluated below. The additional sulphide from gas transport from the backfill, with the assumed maximum concentration of 10^{-6} mol/L sulphide, would give pessimistically 6000 years (maximum saturation time) of the sulphide flux of 6.5×10^{-11} mol/($\text{m}^2 \cdot \text{s}$), which in turn will give a corrosion depth of approximately 175 μm .

For the case of initial high sulphide concentrations, the corrosion is assessed with a mass balance, under the pessimistic assumption that water with a sulphide concentration of 10^{-3} mol/L could be maintained for 100 years. The flux could be crudely evaluated at steady-state (assuming a sulphide concentration of 10^{-3} mol/L outside the buffer) with the same model as for intact buffer (see below for saturated conditions in subsection “*Sulphide fluxes from the groundwater – intact buffer*”). Such an analysis gives a flux of 1.4×10^{-10} mol/($\text{m}^2 \cdot \text{s}$). This is below, but not so far from, the threshold sulphide flux of 3×10^{-10} mol/($\text{m}^2 \cdot \text{s}$), where the film growth is controlled by the transport of sulphide in solution (and in the pores of the film). In this estimate, it should be noted that the case is very pessimistically set up and that no other sinks for sulphide in the bentonite are taken into account. The probabilities for localised corrosion phenomena are therefore deemed negligible. These fluxes are further also below those in experiments where superficial cracking (interpreted as intergranular corrosion or possibly SCC) or vacancy injection (the Aaltonen mechanism) has been observed (10^{-6} and 10^{-4} mol/($\text{m}^2 \cdot \text{s}$) respectively). While the buffer is initially too dry to allow microbial activity, and eventually develops a swelling pressure and environment that effectively suppresses microbial activity (safety function Buff2), there could in principle be a transient period during which microbial activity is supported by the buffer environment. However, experimental studies of unsaturated bentonite have shown that high relative humidity is not sufficient for bacterial sulphate reduction to occur during the bentonite saturation process. This is discussed further in Section 10.3.10, where it was concluded that microbial sulphate reduction is not expected to occur in the bentonite buffer at any time during the unsaturated phase.

Hydrogen embrittlement

Inherent in the process of sulphide corrosion of copper is the liberation of hydrogen gas, which could decompose into atomic hydrogen and possibly enter the copper material and influence its properties; hydrogen embrittlement. The issue of hydrogen embrittlement is described in the **Fuel and canister process** report, Section 3.4.7, with more details in SKB (2019c). Superficial defects are observed in experiments, though under conditions far more aggressive than in the repository environment. The introduction of hydrogen in copper and associated mechanical effects under repository conditions are evaluated in SKB (2019c), considering both the possibility that hydrogen simply diffuses through the material and a situation where an excess of hydrogen in the metal matrix leads to the formation of pores in the material. With the maximum estimated flux of sulphide in the order of 10^{-10} mol/($\text{m}^2 \cdot \text{s}$) for unsaturated conditions, lasting at a maximum for a few thousand years, and taking into account

the fact that only a small fraction of the generated hydrogen is expected to enter the metal, the maximum inflow of hydrogen is estimated at 1×10^{-14} mol/(m²·s) for unsaturated conditions. For a canister wall with a thickness of 50 mm, such an inflow is estimated to produce an additional 1.7×10^{-4} wt.ppm of hydrogen near the entry surface when a stationary flow through the canister is reached, and assuming no pore formation. For saturated conditions with the buffer in place, the concentration would be an order of magnitude lower and for the small fraction of canisters that can be expected to experience advective conditions due to buffer loss, it is an order of magnitude higher. This is totally negligible compared to the initial content of hydrogen in the Cu-OFP (Table 5-8). The fraction of generated hydrogen entering the metal is uncertain and was here assumed to be 10^{-4} . As discussed in SKB (2019c) this is a value for which there is some support both experimentally (Martinsson and Sandström 2012) and theoretically (Lousada and Korzhavii 2020). Assuming instead in a pessimistic sensitivity case a factor of 10^{-1} still leads to peak near-surface hydrogen levels that are assessed to be of no concern for the canister (SKB 2019c). If pore formation is considered, both experiments at much higher hydrogen inflow rates than in the repository and modelling of such situations, suggest that increased hydrogen content with possible impact on mechanical properties would only occur in the outermost up to 100 micrometres of the material, and thus be of no concern under repository conditions (SKB 2019c).

Corrosion in high chloride concentrations

This process is mainly of concern during saturated conditions. It is briefly discussed also for unsaturated conditions at the end of the next subsection.

Copper corrosion – saturated conditions

Corrosion in high chloride concentrations

High chloride concentration in combination with very low pH could cause copper corrosion in oxygen-free water by reduction of H⁺ to H₂ (hydrogen gas evolution), as described in the **Fuel and canister process report**, Section 3.5.4. That low pH in itself is not sufficient to induce corrosion of copper in anoxic environments is shown by the Pourbaix diagram for copper in water, in which the stability region for copper metal extends over the whole pH scale at low redox potentials (Pourbaix 1974, Beverskog and Puigdomenech 1997). Corrosion at low pH is possible if driven by the formation and transport away of copper(I) chloro complexes, which require sufficiently high chloride concentration (Lilja et al. 2021). A safety function indicator is defined (see Section 8.3.4), for which a maximum concentration of dissolved copper is set to 10^{-6} mol/kg (or mol/L). This limit has been verified not to cause failure by corrosion either for intact or eroded buffer, using the same transport models as for sulphide from groundwater, see the **Fuel and canister process report**, Section 3.5.4. As described there, the speciation calculation is more elaborate than in SR-Site and takes into account a more complete set of thermodynamic data for copper-chloride complexes, an initially low hydrogen pressure and the uncertainties in the activity coefficient models. The result is a limiting curve in a chloride concentration – pH plot, see Figure 8-2, and chloride assisted corrosion is not considered significant as long as the pH and chloride concentration is below (at the right-hand side of) the limiting curve.

In the same way as for the ions assisting stress corrosion cracking under oxidising conditions, also pH and chloride concentrations will be rather unaffected by the bentonite buffer (Section 10.3.10, Table 10-9), so that groundwater conditions can be used to describe the environment close to the canister.

The expected chemical groundwater conditions in the repository are described in Section 10.3.8, and calculated values for combinations of pH and chloride concentration are taken from Salas et al. (2010) and plotted together with the limiting curve in Figure 10-93. All data are within the repository volume at 450–490 m depth. Groundwater changes during different climate periods are illustrated with data from both temperate and glacial periods (further described in Section 10.4.7). It is concluded that all expected combinations of pH and chloride concentrations are such that chloride-assisted corrosion can be disregarded with a considerable margin.

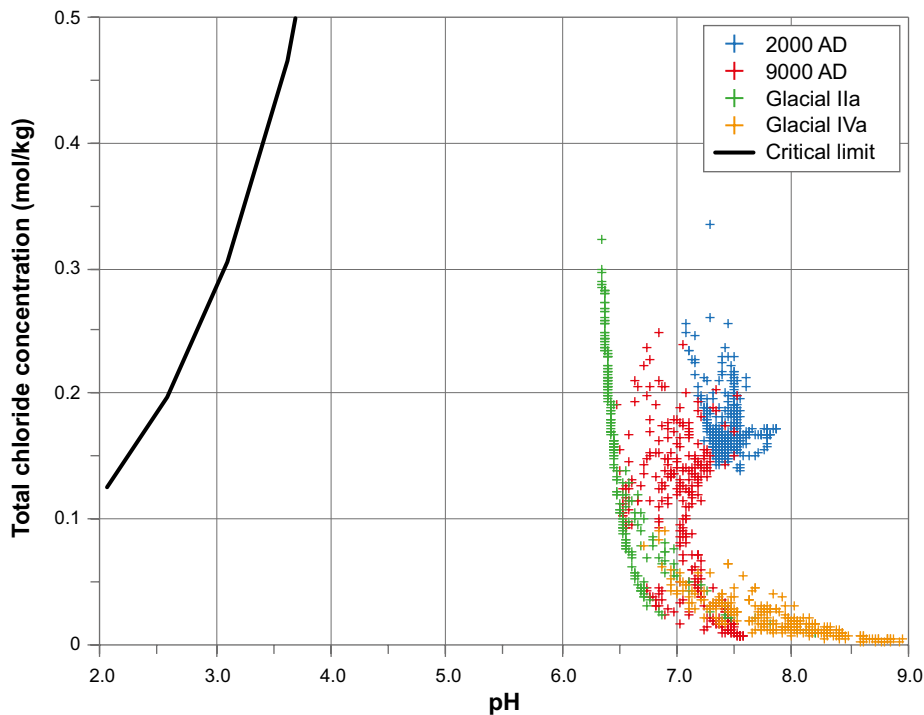


Figure 10-93. The limiting curve for combinations of chloride concentration and pH for which chloride-assisted corrosion needs to be taken into account (total copper concentration in solution 10^{-6} mol/kg), together with calculated values of pH and chloride concentration, from different times in the repository evolution.

During the excavation and operational phase upconing of groundwaters with higher chloride concentrations may occur, but as concluded in Section 10.2.5 only limited changes in salinity are to be expected during construction and operation of a repository located at Forsmark. It is further stated that other groundwater parameters, such as pH, are expected to be practically unaffected by groundwater upconing, which is why this phase does not need to be assessed separately.

The distribution of salt, including chloride, during the early phase with the saturation of the bentonite, is described in Section 10.3.8. Continuous enrichment of chloride would only be possible through inflow of water, which counteracts any increase in concentration. It is further concluded that there is no Sauna effect possible with evaporation of water from the deposition hole. Therefore, neither of the enrichment effects on chloride concentrations need to be taken into account.

Sulphide from pyrite in buffer and backfill

Dissolution of sulphide minerals in the bentonite could be a source of dissolved sulphide, which will corrode the canister if and when it reaches the canister surface. The design requirements specify the maximum allowed sulphide to be 0.5 weight-%, corresponding to approximately 1 weight-% pyrite (FeS_2), see Section 5.5.1.

Iron sulphides are relatively insoluble, especially under the redox condition and pH expected in the repository. The solubility of the metastable iron sulphides mackinawite and greigite has been measured, while the solubility of the even more insoluble pyrite (FeS_2) could be derived with a thermodynamic approach. In this way the sulphide concentration is found to be in the order of 1×10^{-12} to 6.3×10^{-12} mol/L in bentonite pore water at 25 °C and pH 8 (King 2013) for congruent dissolution of pyrite, i.e. no other source of iron(II) in the solution. With other iron minerals dissolving and determining the iron concentration to higher values, the sulphide from dissolution of pyrite will decrease to even lower levels. Duro et al. (2006) estimated the concentration of $\text{H}_2\text{S}/\text{HS}^-$ from dissolution of pyrite by equilibrating groundwater containing sulphide with pyrite. The precipitation of pyrite resulted in a $\text{H}_2\text{S}/\text{HS}^-$ concentration of 1.17×10^{-11} mol/L (considering a total iron concentration of 3.31×10^{-5} mol/L), which is in fair agreement with the sulphide concentration estimated in King (2013).

Corrosion due to sulphide from pyrite initially present in the buffer can be bounded by a mass balance estimate, see SKB (2010d). If all initially present pyrite in the buffer sections surrounding the canister side attacks the canister side as sulphide, corrosion of 0.1 mm copper is obtained for MX-80 bentonite. The corresponding values for pyrite in the top part of the buffer attacking the canister lid is 0.4 mm.

In SKB (2010d) it is further described how a less pessimistic estimate of corrosion should include the dissolution of pyrite and the diffusion transport of the sulphide from the pyrite. The time required for complete depletion of this sulphide from the pyrite can be estimated with a transport expression involving the diffusivity and the concentration limit of sulphide in the buffer (Hedin 2004b, SKB 2010d). The diffusivity of anions is estimated to have an upper limit of $3.0 \times 10^{-11} \text{ m}^2/\text{s}$ (Ochs and Talerico 2004), while the solubility of sulphide from pyrite is estimated to $1.17 \times 10^{-11} \text{ mol/L}$ from Duro et al. (2006). This would give corrosion depths of less than 1 μm even for the highest allowed pyrite content in the buffer for a 10^6 year assessment period, see Table 10-14. These small corrosion depths are nearly independent of geometry, rendering the same corrosion depth at the side and the top. The depletion front penetrates less than 2 cm (even for the lowest pyrite content as in MX-80), thus only pyrite in the very close vicinity of the canister can reach the copper surface.

Both the diffusivity and the pyrite solubility are uncertain. Assuming very pessimistically a diffusivity of $1.2 \times 10^{-10} \text{ m}^2/\text{s}$ (corresponding to uncharged H_2S , diffusing as HTO, tritium labelled water) and a solubility of $3.84 \times 10^{-9} \text{ mol/L}$ (assuming a very low iron content in the bentonite, $1 \times 10^{-10} \text{ mol/L}$ as estimated in Duro et al. 2006) the bentonite at the side of the canister would be depleted of pyrite. The pyrite on top of the canister would not be depleted in one million years as the depletion front reaches at a maximum 40 cm, and thus not allowing time for any pyrite in the backfill to reach the canister. The corrosion depth would be at a maximum 114 μm , even including a factor of 3 for the deposition hole being approximately 3 times larger than the canister top.

The sulphide flux to the canister surface will decrease as the depletion front moves further out, but initially it could be estimated to not exceed $4.6 \times 10^{-13} \text{ mol}/(\text{m}^2 \cdot \text{s})$, using a diffusion distance of 1 mm, comparable to diffusion layer thickness in stagnant solution (King et al. 2017), and the pessimistic diffusivity and solubility values above. This is far below the threshold for mass transport limitation of sulphide corrosion ($3 \times 10^{-10} \text{ mol}/(\text{m}^2 \cdot \text{s})$), and only general corrosion needs to be considered.

In conclusion, even in a million year perspective, corrosion caused by initially present pyrite in the buffer and backfill has a negligible effect on the copper thickness.

Table 10-14. Corrosion depth caused by pyrite initially present in the buffer, using a 1-D diffusion model, for different pyrite contents in the bentonite, for an assessment period of 10^6 years.

		Mx-80	Maximum allowed sulphide content in the buffer (Buffer production report)
Pyrite and sulphide contents			
Pyrite (FeS_2)		0.07 wt. %	
Sulphide content		0.0374 wt. %	0.5 wt. %
Corrosion depth			
Estimated pyrite solubility, upper limit of sulphide diffusivity.		0.3 μm	1.0 μm
Pessimistic case pyrite solubility at low iron content (10^{-10} mol/L), and diffusivity as uncharged H_2S	Canister side	9.5 μm depleted in 773 ky	38 μm
	Straight on canister top	10.4 μm	38 μm
	Also considering cylinder with width of dep. hole	31 μm	114 μm

Sulphide from sulphate reducing bacteria (SRB) in buffer and backfill

The buffer shall have the ability to limit microbial activity, which has led to the derivation of the safety function indicator criteria Buff2, which states that no microbial activity would occur as long as the saturated density of the buffer is higher than 1850 kg/m³ for the analysed buffer material (Section 8.3.2). In Section 10.3.9 it is concluded that the overall picture is that the swelling pressure of the buffer and the associated safety functions will be maintained during the expansion of the buffer into the backfill for all possible combinations of buffer and backfill conditions, and the safety function concerning the ability to limit microbial activity will be upheld after buffer saturation and swelling. Sulphide production in the buffer is thus excluded for the subsequent corrosion analysis (for the case of bentonite erosion causing buffer mass loss and eventually advective conditions, see further below, subsection “*Impact of buffer loss in the deposition hole*”). However, for the backfill, no assessment of microbial sulfate reduction has been done, and the process can therefore not be excluded.

As discussed in Section 10.2.5, there are several different types of organic matter with different origins that could be degraded by microorganisms and thus be a source of energy for sulphate reducing bacteria. The largest pool of organic material in the repository at closure is potentially the organic material in the bentonite in buffer and backfill. The character of this material is not known in detail but it probably consists to a large extent of humic and fulvic acids. Most of this material is probably very closely attached to the clay, with a low solubility and unlikely to serve as microbial substrate. In Section 10.2.5 estimates of the organic carbon readily available for sulphate reduction are given as 0.25 and 24 mol per canister for the buffer and backfill (6 m tunnel) respectively.

There could be other sources of organic matter in the repository (Hallbeck 2010). As further described in Section 10.2.5, the organic matter in deposition tunnels and other areas excluding the bentonite organics, which if all of it were to be used for microbial sulphate reduction, if evenly distributed corresponds to about 35 moles sulphide per canister. Biofilms formed on the rock surfaces, assuming that no cleaning is undertaken before repository closure, would correspond to 13 moles of sulphide per canister from the deposition tunnels. Anaerobic corrosion of rock bolts and other iron components remaining in the repository gives hydrogen gas that could give sulphide via sulphate reducing bacteria, as described in the subsection “*Effects of organic materials and microbial processes*” in Section 10.2.5. The maximum amount of sulphide produced is estimated to be 685 moles sulphide per canister, if the sulphide is pessimistically assumed to be directly available for corrosion and no account is taken of hydrogen gas diffusion away to the groundwater or the precipitation of sulphide with the corroded iron as iron(II) sulphide. Again, for illustration purposes these maximum values of possibly produced sulphide can be converted to corrosion depths, assuming corrosion on the canister lid and 10 % of the cylindrical surface, and with all transport processes neglected. In such a comparison 685 moles of sulphide per canister corresponds to a corrosion depth of 4 mm, and 35 moles sulphide corresponds to 0.2 mm.

In this evaluation of sulphide from SRB activity the electron donor in the form of organic matter (or hydrogen gas) is assumed to be limiting, with an excess of sulphate. It can further be pointed out that the hydrogen generated when sulphide is corroding copper will not lead to an ever increasing process, but at a maximum an increased corrosion by a factor of 4/3 (SKB 2010d).

The extent of corrosion caused by sulphide from SRB using organic material or hydrogen from corrosion of iron and steel is pessimistically estimated with mass balance considerations, disregarding the limitations caused by transport of both organic matter to the microbes and sulphide to the canister. All of these sources of electron donors are located outside the buffer (except the minute amount of sulphide from organic matter in the buffer). The maximum fluxes of sulphide to the canister surface could be estimated by calculating the diffusive sulphide flux from the tunnel floor to the canister top. A bounding concentration would be obtained by assuming that the sulphide from these sources is instantaneously dissolved in the backfill porewater, but a more reasonable value would be to use a sulphide concentration of 10⁻⁶ mol/L (no measurements of sulphide concentrations in bentonite have exceeded the detection limit of 3 × 10⁻⁷, see Section 10.3.10). With a sulphide diffusivity of 3 × 10⁻¹¹ m²/s (SKB 2010d), and the diffusion length of 1.5 m saturated bentonite on top of the canister (Lilja et al. 2014), the sulphide flux would be 2 × 10⁻¹⁴ mol/(m²·s), which is below the

threshold flux, $3 \times 10^{-10} \text{ mol}/(\text{m}^2 \cdot \text{s})$, where the film growth is controlled by the transport of sulphide in solution (and in the pores of the film), and no localised corrosion needs to be taken into account for these sulphide sources. The margin is even larger for the fluxes in experiments where superficial cracking (interpreted as intergranular corrosion or possibly SCC) or vacancy injection (the Aaltonen mechanism) has been observed (10^{-6} and $10^{-4} \text{ mol}/(\text{m}^2 \cdot \text{s})$ respectively).

Sulphide fluxes from the groundwater – intact buffer

When the bentonite buffer has become fully saturated the sulphide concentration at the canister/clay interface is determined by the sulphide concentration in the groundwater, the transport of the sulphide ions from the groundwater into and through the dense clay, and the rate of sulphide consumption by corrosion of the copper surface. Here it is pessimistically assumed there are no other sinks for sulphide, such as e.g. the precipitation of iron(II) sulphide.

The hydrogeochemical assessment presented in Section 10.3.7 concludes that the anoxic groundwater conditions now prevailing at repository depth will continue for the whole temperate period following the closure of the repository, in spite of the increasing proportion of meteoric waters with time. The chemical environment surrounding the repository will thus satisfy the criterion for safety function indicator R1a.

For sulphide in groundwater, the transport of the sulphide to the canister surface determines the corrosion rate. The transport resistance consists of different parts, having different importance under different flow conditions. The concept of equivalent flow, Q_{eq} , is the main feature in the conceptual model for the transport for an intact buffer.

The mass transfer between the intact buffer and a flowing fracture intersected by the buffer is schematically depicted in Figure 10-94. The transport description depends on the existence of a thermally induced spalling zone in the rock or not as e.g. shown in Figure 10-35. In summary the transport resistance is modelled as follows. The Q_{eq} derived from the hydrogeological DFN modelling described in Section 10.3.6 is common to both cases (this transport path to/from the deposition hole is nominated Q1 in the hydrogeological modelling as well as in radionuclide transport calculations). Without spalling this resistance is a series with a geometric term accounting for the diffusion in different directions in the bentonite. With spalling, the Q_{eq} is modified such that it takes into account the diffusion in the zone with higher conductivity, which reduces the transport resistance between buffer and flowing fracture. A diffusive transport resistance is then added in series to represent diffusion in the rest of the buffer. For the derivation of the equations describing the transport in mathematical terms, see SKB (2010d). The amount of sulphide reaching the canister is calculated from the equivalent flow and the sulphide concentration in the groundwater.

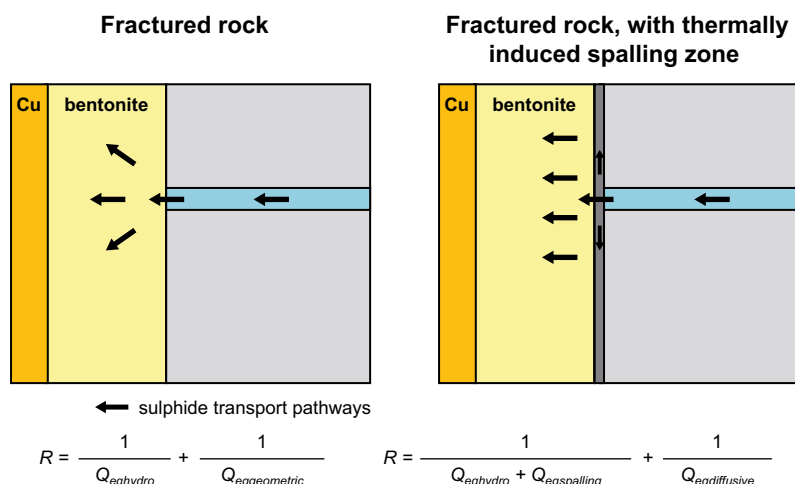


Figure 10-94. Schematic description of the different transport resistances, for fractured rock and fractured rock with a thermally induced spalling zone.

The corrosion rate (assuming general corrosion) is then derived from the amount of sulphide acting on the surface area that is set to the cylindrical part of the canister. Due to the vertical spread of the sulphide in the buffer the sulphide will be more concentrated near the fracture, meaning that the part of the canister surface nearest the fracture will be most exposed. Compared to an even spread of sulphide over the entire canister surface, the point of highest exposure will be about 7 times more exposed. This is taken into account in the calculations by applying a so called buffer concentration factor, $BCF = 7$, see further SKB (2010d).

The transport models are then applied for the flow distributions derived from the hydrogeological DFN modelling described in Section 10.3.6. In Figure 10-95 the distribution of corrosion rates for the semi-correlated, uncorrelated and fully correlated hydrogeological base cases are shown, with and without thermally induced spalling. The sulphide concentration is set to 1×10^{-5} mol/L, which is the 90-percentile of the sulphide distribution measured in Forsmark, see Section 10.3.6. The highest calculated corrosion rate (for the fully correlated hydrogeological DFN base case, including spalling) corresponds to a corrosion depth of about 0.6 mm in one million years. It must be remembered that the sulphide concentration is set constant over time in these calculations. Even if the highest measured sulphide concentration (1.2×10^{-4} mol/L) is used for all the deposition holes, the corrosion depth would be at the most 7.8 mm for the one million year assessment period. This is, however, a totally unrealistic case.

The corrosion rates giving corrosion depths of 0.6 and 7.8 mm respectively as above, correspond to sulphide fluxes of 1.4×10^{-12} mol/(m²·s) and 1.7×10^{-11} mol/(m²·s), which are below the threshold for mass transport limitation of sulphide corrosion (3×10^{-10} mol/(m²·s)), and thus only general corrosion needs to be considered. These fluxes are further also below those in experiments where superficial cracking (interpreted as intergranular corrosion or possibly SCC) or vacancy injection (the Aaltonen mechanism) has been observed (10^{-6} and 10^{-4} mol/(m²·s) respectively), and those processes are concluded not to occur under saturated conditions with an intact buffer.

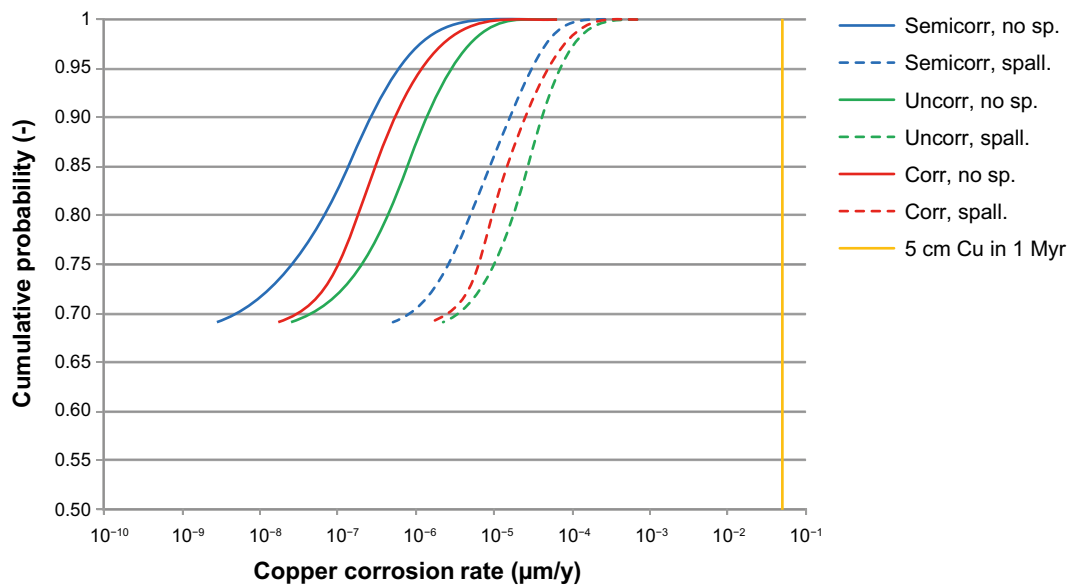


Figure 10-95. Distribution of corrosion rates for the different Hydrogeological DFN models. The effect of a thermally induced spalling zone is shown. The sulphide concentration is set to 1×10^{-5} mol/L, which is the 90-percentile of the sulphide distribution at Forsmark. Note that nearly 70 % of the deposition holes do not have a connected Q1 fracture at all.

The following should also be noted regarding the intersection of water bearing fractures with deposition holes.

- If several fractures intersect the deposition hole, the equivalent flow rates for these have been added, which is pessimistic since a partition between several fractures would spread the corrosion attack over the canister area. A realistic approach would be to consider the flow in the immediate vicinity of a failure point in the canister. This is likely to involve only a single fracture, which could have a low flow and/or low contact area in the calculation of Q_{eq} . Considering the greater flow and contact area associated with all the fractures that intersect the deposition hole provides a larger Q_{eq} to the near-field model.
- All fractures are assumed to intersect the part of the deposition hole where the canister is located.

Impact of buffer loss in the deposition hole

Corrosion under advective conditions in the deposition holes is assessed in Section 10.4.9. According to Section 10.3.11 no deposition holes are likely to lose so much buffer mass by colloid release or sedimentation due to dilute groundwaters such that advective conditions must be assumed during the initial temperate period. (Even if such conditions were to occur, it is shown in Section 10.4.9, that the corrosion is not fast enough to create any failures of the copper shell during the first 100 000 years.)

However, the buffer mass loss during the process of colloid release could cause the void ratio in the buffer to exceed 1.1 (dry density of 1327 kg/m^3) where the safety function Buff2 is lost and microbial sulphate reduction in the buffer cannot be excluded (see Section 10.3.9). Unless the mass loss is so large that Buff1 is lost as well, the transport in the buffer will still be diffusion controlled. The volume of the buffer where sulphate reduction actually can occur will be limited. The rate of sulphate reduction will be determined by the rate of supply of sulphate and nutrients to the low density region in the buffer. The transport rate of sulphide to the canister will be determined by the rate of sulphate reduction together with the rate of transport from the low density region to the canister. This is a complex coupled system, which has not been fully assessed in the PSAR. A simplified pessimistic approach is to look at the supply of nutrients only. As described in Section 10.2.5 the MX-80 bentonite buffer contains organic carbon, but only a part is water-extractable and available for SRB to produce sulphide. This corresponds to 0.25 mol carbon per deposition hole. This is still pessimistic as even if the environment in the buffer after a certain amount of buffer mass loss makes it possible for microbial activity (from pressure, space and water activity aspects), it is pessimistic to assume the microbes are still viable. The FEBEX project indicated that the rather hostile environment prevailing in the mid sections around the heater, with high density and temperatures slightly above $100 \text{ }^\circ\text{C}$ during 18 years, seems to have exhausted the cells in such a way that they cannot be recovered enough to be cultivated (Bengtsson et al. 2017c). The resulting corrosion would, with a mass balance, correspond to $0.2 \text{ }\mu\text{m}$.

To this should be added the amount of nutrients that can be supplied by the groundwater. This can be determined by groundwater concentrations and the equivalent flowrate in the deposition hole in question. With this approach all transport resistances within the bentonite itself are neglected, as well as all interactions between the bentonite and the produced sulphide. In Section 10.3.7 an upper bounding estimate of the concentration of dissolved organic carbon in groundwater is given as $1 \times 10^{-3} \text{ mol/L}$, but with only 10 % bioavailable for sulphate reduction. For the stoichiometry for the sulphate reduction, acetate could be used as a model substrate for a bioavailable molecule, which gives $\frac{1}{2}$ mol sulphide formed per mol DOC, see the **Geosphere process report**, Section 5.7.1. The corrosion from this sulphide could be estimated with the model as for sulphide from groundwater for an intact buffer, as the buffer is still limiting the transport. Using the maximum available dissolved organic concentration in groundwater of $0.10 \times 10^{-3} \text{ mol/L} = 10^{-4} \text{ mol/L}$, which will form sulphide at a concentration of $5 \times 10^{-5} \text{ mol/L}$ gives a corrosion depth of 3.2 mm, including thermally induced spalling as in the calculations for intact buffer, see above.

For the case of a partially eroded buffer, that has not reached advective conditions, the corrosion is thus pessimistically estimated to $0.2 \text{ }\mu\text{m}$ and 3.2 mm, from the organic matter in the buffer and the groundwater respectively. The corrosion rate giving a corrosion depth of 3.2 mm, corresponds to a sulphide flux of $7.2 \times 10^{-12} \text{ mol}/(\text{m}^2 \cdot \text{s})$, which is below the threshold for mass transport limitation (only general corrosion), and far below those where superficial cracking interpreted as intergranular corrosion or possibly SCC) or vacancy injection (the Aaltonen mechanism) has been observed. Thus no localised corrosion processes need to be taken into account for this case.

It is also noted that the above mass balance and flux considerations apply irrespective of how the microbes are distributed in the buffer, i.e. also if the possibility of a biofilm being established on the canister surface would be considered.

Hydrogen embrittlement

The discussion above regarding hydrogen embrittlement for unsaturated conditions is applicable also for saturated conditions. The sulphide fluxes from the groundwater through intact buffer is at least an order of magnitude smaller than the highest flux for unsaturated conditions, with a negligible hydrogen ingress into the copper.

Summary of copper corrosion analysis

For the corrosion processes analysed for the initial temperate period, the corrosion depth is much smaller than the copper shell thickness. This is the case also for an assessment time of 10^6 years, as summarised in Table 10-15 and Figure 10-96. Several processes give corrosion depths less than 200 μm , and no processes give corrosion depths larger than a few mm.

Table 10-15. Estimates of corrosion depths from different corrosion processes conceivable in the repository, for an assessment time of 10^6 years. The bases for the assessments are given, with pessimistic values for all processes and more realistic assumptions for a few (where calculations are available).

	Corrosion depth		Assessment	
	More realistic	Pessimistic	Based on	Limited by
Gamma radiation air		7 nm	Mass balance	Gamma dose, 1 cm air filled gap.
Radiolysis of water		3 μm	Mass balance + empirical	Modelled general corrosion (limited by dose) + empirically measured pits.
Atmospheric		1 μm	Corrosion rate	Empirical corrosion rate (maximum 2 years).
Remaining oxygen		2.5 mm	Mass balance + max pit depths	Mass balance oxygen (general corrosion) + probabilistically modelled max pit depth + max measured pit depths.
Pyrite in buffer/backfill	0.3 μm	114 μm	Mass transport and depletion	Amount pyrite in buffer (more realistic: values of solubility and diffusivity).
HS in groundwater, initially high		500 μm	Mass balance	Max concentration of sulphate measured at surface, filled in pore volume of buffer and backfill.
HS through gas transport		175 μm	Mass transport	Constant concentration of sulphide in backfill pores, for a maximum saturation period of 6000 years.
SRB, org in buffer/backfill		0.1 mm	Mass balance	Amount of organic carbon in backfill (and buffer), available for SRB.
SRB, other organics		0.2 mm	Mass balance	Amount of other organic material, in deposition tunnels.
SRB, rock biofilm		75 μm	Mass balance	Amount of rock biofilm, in deposition tunnels.
SRB, iron/steel corrosion		4 mm	Mass balance	Amount of iron and steel, in deposition tunnels.
SRB, during erosion	0.3 mm	3.2 mm	Mass transport	Max concentration of dissolved organics, existence of spalling (more realistic: no thermal spalling).
HS in groundwater, intact buffer	0.06 mm	0.6 mm	Mass transport	Sulphide concentration, hydrology model data, existence of spalling (more realistic: no thermal spalling).

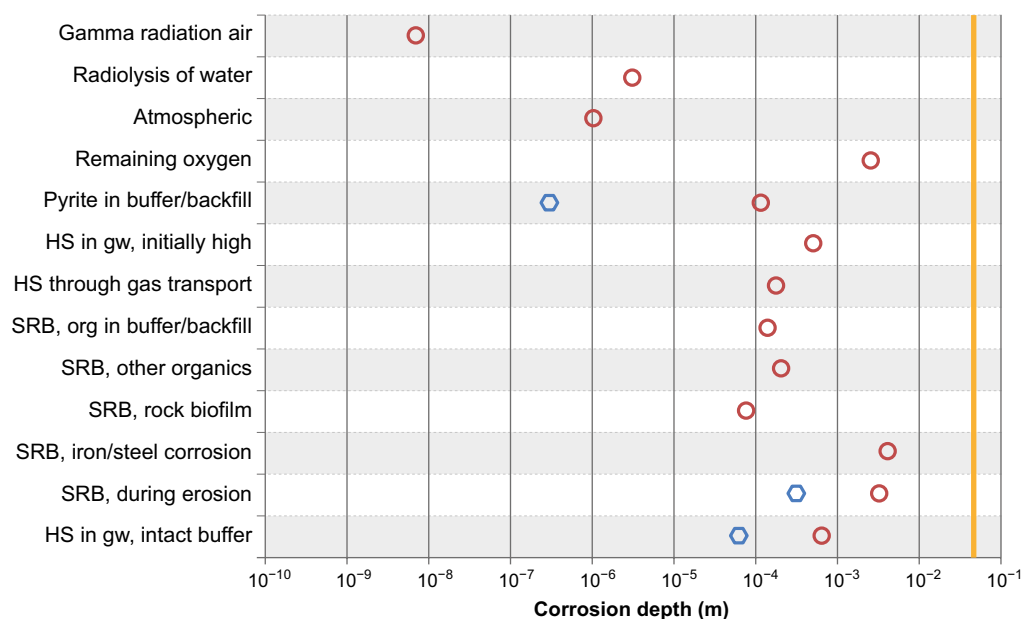


Figure 10-96. Estimates of corrosion depth from different corrosion processes conceivable in the repository, for an assessment time of 10^6 years. Red circles represent pessimistic assumptions, whereas blue hexagons represent more realistic assumptions (where calculations are available), see Table 10-15. The yellow line indicates the copper thickness of 5 cm.

Identified uncertainties and their handling in the subsequent analysis

The following conclusions are reached regarding copper corrosion during the temperate period.

- The total amount of copper corrosion during the excavation and operational phases and the first 1 000 year period can be estimated to be less than 2.5 mm (including pits). The largest contribution to this estimate comes from the initially entrapped oxygen. This contribution is propagated to subsequent long-term analyses of corrosion in Section 10.4.9.
- Copper corrosion by contaminants in the buffer, backfill or groundwater does not pose a threat to canister integrity for the initial temperate period. Even during the one million year overall assessment period, expected corrosion of the canister for an assumed temperate climate would cause corrosion depths of the order of a few millimetres, even for the most unfavourable deposition positions at Forsmark. The largest contribution to this estimate comes from the very pessimistic mass balance estimate of sulphide production from hydrogen from corrosion of rock reinforcements made of iron and steel in the deposition tunnels. This contribution (4 mm) is propagated to subsequent long-term analyses of corrosion in Section 10.4.9.
- No deposition holes will lose so much buffer mass by colloid release due to dilute groundwaters such that advective conditions must be assumed, meaning that corrosion under advective conditions can be ruled out during the initial temperate period. If buffer is lost to such an extent that microbial activity is possible in the buffer, the sulphide produced is limited by the dissolved organic material from groundwater (the available amount of organic material from the buffer itself is negligible) and would cause corrosion depths of a few mm, even for the most unfavourable deposition positions at Forsmark.

No canister failures due to corrosion are thus expected during the initial thermal period of the reference evolution.

10.3.14 Evolution of the central area, the top seal and the borehole plugs

The only function of the closure of the cavities in the central area is to occupy the space with no other technical design requirement than to prevent substantial convergence and subsidence of the surrounding rock. The only purposes of the backfill in the upper part of the ramp and shaft are to hinder unintentional intrusion into the repository and to keep the lower backfill in place. Both these areas are filled with crushed rock with an assumed high hydraulic conductivity.

To ensure that they do not act as preferential transport paths, a number of investigation boreholes, holes drilled both from the surface and from underground openings have to be sealed, at the closure of the deep repository. The design of the borehole seals is provided in the **Closure production report** and outlined in Section 5.7.2. The basic idea is to use bentonite as a seal in the intact rock and low-pH concrete plugs where the boreholes are intersected by fractures.

Central area and top seal

For these areas, in SR-Site, only an assessment of the time scale of the saturation was done. Two different axisymmetric 2D geometries were used: with a true ramp section area and with a true ramp volume, Figure 10-97. The spiral shaped inclined ramp is simply represented with vertical cylinders. In the geometry with a true ramp section area, the section area of the cylinder in the model is the same as in the ramp (33 m²). However, this also means that the volume of the cylinder in the model is only a tenth of the ramp volume since the ramp has a 10 % inclination. A correct ramp volume is therefore represented in the second geometry in which the section area of the modelled cylinder is ten times larger than the actual section area of the ramp.

The first material to reach saturation is the crushed rock in the ramp. The crushed rock in the central area is the second, and the backfill is the last material to get saturated.

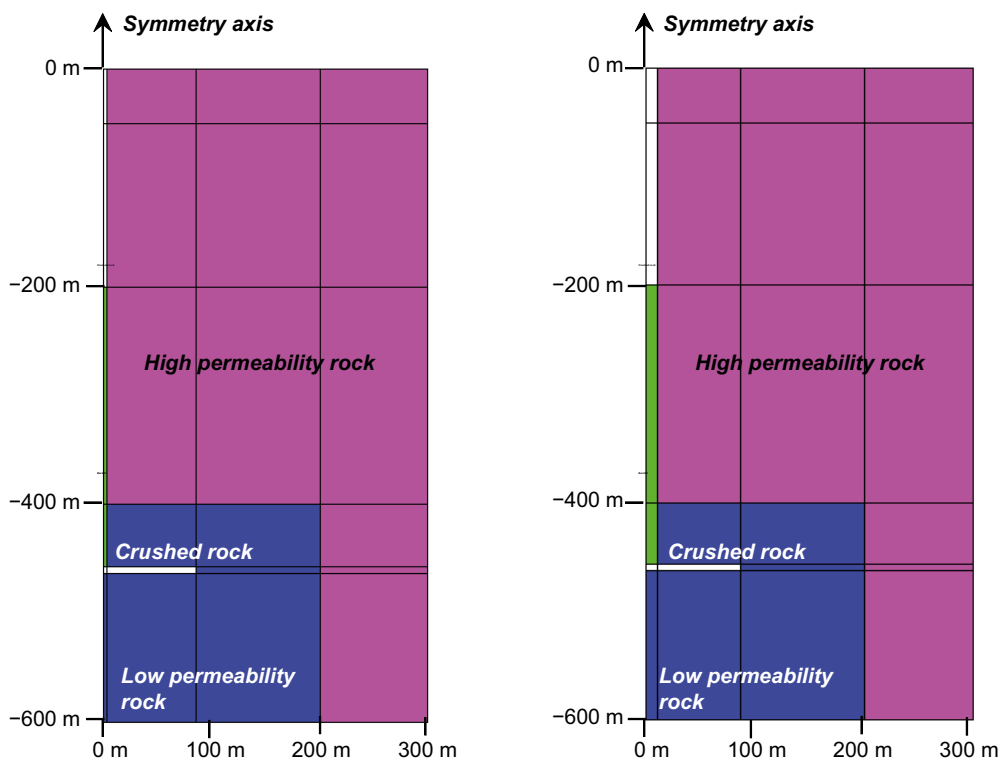


Figure 10-97. Axisymmetric geometries for the central area and ramp showing true ramp section area (left) and true ramp volume (right) (Åkesson et al. 2010a).

According to the chosen approach, the true section area model is relevant for parts in which the filling material limits the inflow, since in this case the hydration is mainly governed by the properties of the filling material and the dimensions of the ramp section. In contrast, the true section volume model is relevant for parts in which the rock limits the inflow, since in this case the main process is basically the transfer of a specific water volume through a large rock volume. With this approach and the available results the following observations can be made.

- The time to saturate the crushed rock in the ramp is mainly governed by the rock. The most relevant time scale for this is therefore given by the true section volume model, i.e. approximately 20 years.
- The time to saturate the crushed rock in the central area is also mainly governed by the rock. The most relevant time scale for this is therefore also given by the true section volume model (although the difference is smaller) i.e. approximately 150 years.
- Finally, the time to saturate the backfill in the ramp is mainly governed by the backfill. The most relevant time scale for this is therefore given by the true section area model, i.e. approximately 200 years.

At the Forsmark site, the time scale for saturating the central area is governed by the flow conditions in the rock, see Section 10.3.6 and Figure 10-24.

Evolution of the borehole seals

Chemical interaction concrete/bentonite

The interaction between the bentonite and the concrete in the borehole seals can be described in the same way as the interaction between the tunnel plugs and the backfill, see Section 10.3.12. The conclusion is that there will be an increase in the pH in the bentonite closest to the concrete, but the duration of the pH pulse and the penetration depth will be small. The cement part of the concrete will degrade with time, but the ballast material will remain. Thereby, the loss of bentonite to the flowing water in the fracture can be assumed to be limited.

According to Table 10-9, the maximum chloride concentration of any time frame is $< 0.4 \text{ kmol/m}^3$ in the Forsmark groundwater. As seen in Figure 5-14 this is not expected to have any impact on the properties of the bentonite material. This conclusion is valid for the entire repository evolution period.

Analysis of time scale of borehole seal hydration

Åkesson et al. (2010a) has calculated the time for water saturation of the bentonite in the seals as a function of the permeability of the surrounding rock. Figure 10-98 shows the saturation time at the 100 m level. At 500 m the time will be even shorter, because of the greater hydraulic pressure.

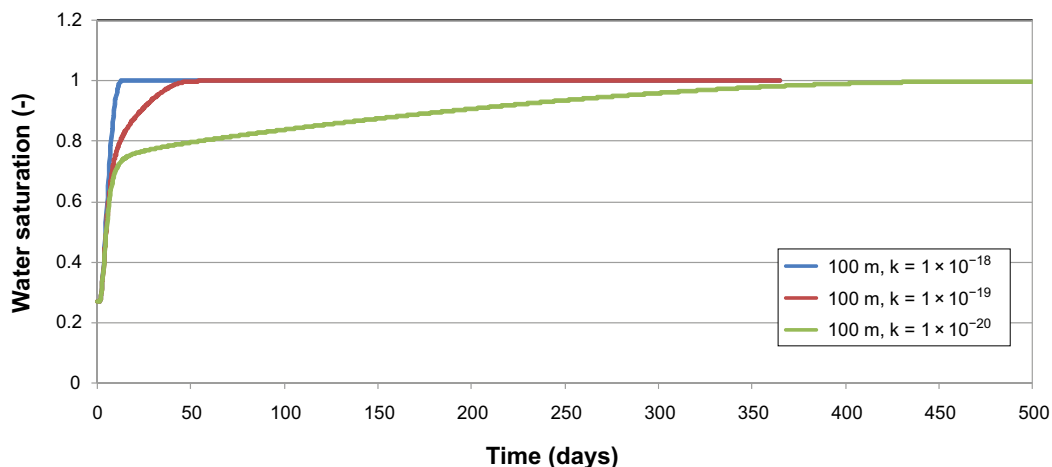


Figure 10-98. Water saturation evolution of bentonite borehole seals for different rock permeability (m^2), 100 m depth model with a radius to water bearing boundary of 600 m.

Even if the rock mass is unfractured, with extremely low permeability, the models indicate that the plug is saturated rapidly. Given that rapid saturation is desirable, the model is assessed to be rather pessimistic in the sense that the time until water saturation is probably overestimated for the lower rock conductivity. It is very unlikely that a disc with 600 m radius has such low rock permeability and is not cut by any fractures. Also, the hydraulic water pressure boundary is located quite far from the borehole (600 m). The adopted model is 1D (radially symmetric) and only radial flow is permitted. Prescribing hydrostatic pressure 600 m away from the borehole induces a very low water pressure gradient which in turn is the only driving force for saturating the borehole seal. Finally, no axial flow is allowed in the borehole, i.e. saturated parts of the seal cannot contribute to the wetting of close unsaturated parts. A less pessimistic assumption with a smaller distance to the boundary would imply faster saturation of the bentonite seal.

The modelling in Åkesson et al. (2010a) is based on the old design of the borehole seals. The conclusion that the bentonite part will be rapidly saturated under all circumstances is however valid for the current design as well.

Identified uncertainties and their handling in the subsequent analysis

The saturation time for the central area and the ramp and shaft are not used further in the assessment. The aim of the calculations reported in this section was to get a reasonable estimate of the duration of the process.

The reference design of the borehole seals is expected to yield the intended performance, since the saturation is relatively rapid, full saturation can be expected in less than a year even in a very dry part of the rock.

10.3.15 Summary of the first 1 000 years after closure

The heat from the spent fuel results in a fast temperature increase in the buffer, with the peak temperature occurring some 5–15 years after deposition, followed by a slow reduction of the temperature due to the decay of the heat source. The analyses presented in Section 10.3.4 show that there is an adequate margin to the peak temperature criterion for the buffer, even when the spatial variability of the rock thermal properties is taken into account and with other data essential for computing the result chosen pessimistically. This conclusion is valid provided there is thermal management of the disposal sequence, such that the influence of already deposited canisters would not unduly affect the thermal evolution of canisters deposited later, see also Section 15.5.15. Such management is judged fully feasible and there is no need to consider a situation with a buffer above the peak thermal criterion in the PSAR.

The mechanical evolution of the host rock is dominated by effects of the thermal load from the canisters and, to a minor extent, the developing swelling pressure from the buffer and the backfill. The long-term impact of the rock stress field need also to be taken into account. According to Section 10.3.5, the following conclusions concerning the mechanical evolution can be drawn.

- *Reactivation of fractures in the near field as well in the far field* due to thermal load that could affect the mechanical stability and the fracture transmissivity in the rock are excluded from further analysis since the calculated impacts on fracture transmissivity during the heating phase are small, and very local to the deposition tunnel.
- *Reactivation due to ongoing Mid-Atlantic Ridge push* that could affect the mechanical stability of the deposition holes (safety function R3a) cannot be totally ruled out even during the temperate period. According to the earthquake analysis presented in Section 10.4.5, on average between 9.3×10^{-6} and 2.2×10^{-5} canisters may be sheared 50 mm or more due to earthquakes within the 1 000-year time frame.
- *Fracturing of the rock, i.e. thermally induced spalling*, is likely to occur but the counter pressure exerted by bentonite pellets in the slot between buffer and rock wall, may suppress the spalling, or at least keep the spalled slabs in place and minimize the hydraulic transmissivity of the spalled damage zone. A set of distinct calculation cases, assuming no spalling or spalling in all deposition holes, are propagated for further assessment. The potential for spalling might to some extent depend on the deposition sequence and other aspects of the design, see further Section 15.5.15.

- Literature evidence suggests that there is no potential for *creep* deformation that could significantly affect deposition hole geometry, allowing the exclusion of the phenomenon from the safety assessment.

Analyses of the hydraulic evolution of the system indicate that after repository closure a rapid initial inflow is followed by an asymptotic regime where the inflow gradually decreases. It will take several hundreds of years for the repository to reach full saturation.

Detailed regional and repository scale groundwater flow analyses for the saturated host rock indicate that the Forsmark site has favourable properties in terms of performance measures related to groundwater flow and transport, using either of the models. Specifically, the transport resistance of the host rock, the so called *F*-factor, ranges between 10^4 and 10^9 y/m depending on the spatial location, and about 90 % of all potential deposition holes have *F* values above 10^6 y/m. Distributions of Darcy fluxes and equivalent flow rates for use in subsequent analyses have also been obtained and show favourable properties. It can be noted that at least 70 % of all potential deposition holes are not connected to any water bearing fractures, which implies that the hydraulic contact with these holes primarily is by diffusion to the EDZ (if present) and to the deposition tunnel. The models also yield salinity distributions and handle mixing of different water types yielding concentrations of other relevant non-reacting components of the groundwater. All these results are propagated to subsequent analyses of engineered barrier performance and radionuclide transport.

The analysis of the evolution of the geochemical conditions at the site has resulted in the following conclusions.

- Anoxic conditions are expected to be re-established shortly after closure and will continue for the whole temperate period following the closure of the repository, in spite of the increasing proportion of meteoric waters with time.
- The maximum salinity is expected during operations and immediately after closure. The salt content is expected to decrease slightly during the first 1 000 years due to the progressive inflow of waters of meteoric origin.
- Cation charge concentrations at repository depth at Forsmark will, in general, remain higher than 0.004 mol/L, i.e. above to the limit where montmorillonite colloids start to become unstable, but a fraction of a percent of the deposition holes may experience dilute conditions during the first ten thousand years.
- The effect of grout in fractures will be to increase the pH in deformation zones for relatively long periods of time, probably lasting throughout the first glacial cycle ($\approx 120\,000$ years).

Since the rock at Forsmark is expected to contain very few water conducting fractures, typically separated by more than 100 m, the saturation of the backfill can be anything from < 100 years to $\sim 6\,000$ years, the longer times being for positions far away from the flowing fractures. As for the saturation of the backfill, the time for the saturation of the buffer is strongly dependent on the local hydraulic conditions. The presence of a water conducting fracture in, or in the vicinity of, the deposition hole will lead to a relatively rapid saturation, while a position where the water is supplied solely by the rock may stay partially saturated for hundreds of years. Given the expected very low frequency of water conducting fractures at Forsmark the saturation of the buffer can be anything from < 10 years to $\sim 1\,000$ years, the longer times for holes not connected to water conducting fractures. Furthermore, the moisture redistribution in the buffer in deposition holes with a dry surrounding rock mass affects the thermal conductivity of the buffer. This is considered in the assessment of the thermal evolution of the buffer.

If the buffer and backfill are installed as envisaged in the reference design, the buffer density and swelling pressure will homogenise to a situation where the relevant safety functions will be upheld. The saturation of the buffer will result in the establishment of a swelling pressure of typically 7–10 MPa. The pressure will be somewhat reduced in the upper part of the buffer, but this effect is calculated to be too small to jeopardise any of the buffer safety functions.

The geochemical changes in the buffer during the period of saturation and thermal gradient are small and are not considered to have any significant impact on the long-term performance. There will be dissolution/precipitation of accessory minerals like calcium sulphates and amorphous SiO_2 .

In the reference evolution, both the pH and temperature in the buffer are assumed to be within the given limits on the basis of our assessment and the alteration in these characteristics is not expected to proceed to a level where it will affect the properties of the buffer.

The model predictions indicate that the durability of backfill materials is not expected to be affected by the potential alkaline plumes developed from concrete alteration of the deposition tunnel plug. Even if the plug eventually disintegrates this has no detrimental effect on the backfill above the first deposition hole and no restrictions caused by plug disintegration on the location of the first deposition hole are needed.

The saturation time for the central area and the ramp and shaft are not used further in the assessment. The aim of calculations performed in this section was to get a reasonable estimate of the duration of the process.

The reference design of the borehole seals will perform as intended. The saturation is relatively rapid, full saturation can be expected in less than a year even in a very dry part of the rock. A loss of bentonite in the range of a few metres in the seals will lead to a total loss of performance in that section. However, the rest of the seal will be virtually unaffected.

Both asymmetric and symmetric mechanical loads on the canisters from the swelling buffer and the groundwater pressure is far too low to jeopardise canister integrity. Both the strength of the insert and the ability of the copper shell to withstand creep are sufficient to withstand the loads during the initial temperate period.

Canister corrosion from initially present oxygen and sulphide, from corroding agents formed by radiolysis and from sulphide in ingressing groundwater, has been found to be less than 2.5 mm based on pessimistic assessments.

10.3.16 Safety functions for the initial temperate period after closure

The following is an account of the development of all safety functions in Figure 10-2 during the initial temperate period after repository closure. Also the development during the excavation/operational period is considered where relevant.

Rock safety functions

R1. Provide chemically favourable conditions

a) Reducing conditions; Eh limited.

The analyses have led to the conclusion that the chemical conditions will be reducing shortly after deposition in individual deposition holes and deposition tunnels and shortly after closure in the repository as a whole. This is of fundamental importance for the post-closure safety of the repository and no process has been identified that challenges this conclusion during the initial temperate period after closure.

b) Salinity; TDS limited.

The salinity at the Forsmark site has, through model studies, been demonstrated to be below 12 g/L, corresponding to 0.2 M [Cl⁻]. Upcoming effects on salinity during the excavation/operational phase have also been studied and found to be negligible.

c) Ionic strength; $\Sigma q[M^{q+}] > 8$ mM charge equivalent.

For the whole temperate period following repository closure, the cation charge concentrations at repository depth at Forsmark will, in general, remain higher than 8 mM. However, a fraction of a percent of the deposition holes may experience dilute conditions during the first ten thousand years.

d) Concentrations of HS⁻, H₂, CH₄, organic C, K⁺ and Fe; limited.

During the initial temperate domain following repository closure, the potassium concentrations are expected to remain ≤ 0.004 mol/L, sulphide concentrations are expected to be $\leq 10^{-5}$ mol/L for most deposition positions, including the possible contributions from bacterial sulphate reduction using dissolved methane, hydrogen and organic carbon. Iron concentrations are expected to gradually increase up to 10^{-4} mol/L.

- e) pH; pH 5–11.

The effect of grout in fractures will be to increase the pH in deformation zones for relatively long periods of time, probably lasting throughout the first glacial cycle ($\approx 120\,000$ years).

- f) Avoid chloride assisted corrosion; combinations of pH and $[\text{Cl}^-]$ below limiting curve.

The hydrogeochemical analysis shows that this safety function indicator criterion is fulfilled throughout the initial temperate period.

R2. Provide favourable hydrologic and transport conditions

- a) Transport resistance in fractures, F ; high.

The transport resistance essentially depends on the connected fracture transmissivity and the hydraulic gradient. As demonstrated in Chapter 4 there are few transmissive water conducting fractures at repository depth at Forsmark. Currently, hydraulic gradients are low since they are controlled by the very flat topography at Forsmark. This means that transport resistance is generally high although there are a few flow paths of lower transport resistance. The calculated transport resistance of the host rock ranges between 10^4 and 10^9 y/m depending on the spatial location, and about 90 % of all potential deposition holes have F values above 10^6 y/m.

During excavation there is a potential for inducing new fractures forming an “EDZ”. However, provided that mechanical excavation is used and that blasting is well controlled, there is ample evidence that a potential EDZ formed during excavation will be kept below the maximum allowed transmissivity as set out in the technical design requirements and data suggest that a continuous EDZ would not develop at all. It seems justified to consider an EDZ according to the technical design requirements, but also to explore how transmissive an EDZ would need to be in order to significantly impact other safety functions as well as exploring the impact of no axially continuous EDZ at all. There is some reactivation of fractures due to thermal load but the impact on the fracture transmissivity is small and can be neglected from further analysis. As a base case it is assumed that the EDZ has a transmissivity of 10^{-8} m²/s. Assuming no EDZ implies an increase in F of about half an order of magnitude. Assuming a much more transmissive EDZ (10^{-6} m²/s) decreases F by about an order of magnitude.

- b) Equivalent flow rate in buffer/rock interface, Q_{eq} ; low.

The equivalent flow rate in the buffer/rock interface essentially depends on the groundwater flow around the deposition hole and the local geometry of the flow. The former is affected by the same things that affect the transport resistance; there is thus also a need to consider changes of the local geometry of the flow around deposition holes. It can be noted that at least 70 % of all potential deposition holes are not connected to any water bearing fractures, which implies that the hydraulic contact with these holes primarily is by diffusion to the EDZ (if it exists) and to the deposition tunnel.

As for the transport resistance, it thus seems justified to consider an EDZ according to the technical design requirements, but also to explore how transmissive an EDZ need to be in order to significantly impact other safety functions as well as exploring the impact of no axially continuous EDZ at all. Naturally, only release path Q2, i.e. through the potential EDZ, is affected by the transmissivity of the EDZ. Roughly, Q_{eq} for this release path is proportional to the square root of the EDZ transmissivity.

For assessing Q_{eq} it is also necessary to consider the impact from fracturing (spalling) in the deposition hole wall. This can occur either as a direct result of the mechanical impact resulting from the process of excavation, in which case it can be mitigated, or as a consequence of the thermal load from the spent fuel after deposition. It has been concluded that thermally induced spalling is likely to occur, but the counter pressure exerted by bentonite pellets in the slot between buffer and rock wall may suppress the spalling, or at least keep the spalled slabs in place and minimize the hydraulic transmissivity of the spalled damage zone. A set of distinct calculation cases, assuming no spalling or spalling in all deposition holes, are propagated for further assessment and must be considered in all quantitative treatments of mass transfers between buffer and rock. Spalling affects Q_{eq} only if there is a water conducting fracture intersecting the deposition hole, i.e. the migration path Q1. Spalling implies that Q_{eq} for the Q1 path increases by about a factor of 100.

R3. Provide mechanically stable conditions

- a) GW pressure; limited.

The groundwater pressure is determined by repository depth for temperate climate conditions. It is hence around 4.5 MPa at the repository depth, which, from the point of view of post-closure safety, is not problematic.

- b) Shear movements at deposition holes < 0.05 m.

According to the earthquake analysis presented in Section 10.4.5, large seismic events are highly improbable, but cannot be totally excluded even during the thermal period. Based on the analyses presented, on average between 9.3×10^{-6} and 2.2×10^{-5} canisters may be sheared 50 mm or more due to earthquakes within the 1 000-year time frame, i.e. there is a chance of at most about 1 in 40 000 that one out of the 6 000 canisters will be sheared by an earthquake within 1 000 years. This frequency will be similar for the remaining part of the initial temperate period, i.e. the expected number of potentially sheared canisters scales linearly with time.

- c) Shear velocity at deposition holes < 1 m/s

This criterion will always be upheld, as is further justified in Section 10.4.5.

R4. Provide thermally favourable conditions

- a) Temperature > -6 °C (avoid detrimental buffer freezing)

- b) Temperature > 0 °C (validity of canister shear analysis)

Since a temperate climate similar to the current is assumed to prevail during the temperate period under consideration, there is no possibility that these criteria would not be fulfilled.

Buffer safety functions

Several of the buffer safety functions are related to the buffer density. The initially allowed range of dry density of 1 450–1 560 kg/m³ for MX-80 may potentially alter during the initial temperate period due to erosion related to piping during the resaturation of the buffer and backfill, upward expansion of the buffer as a consequence of swelling and colloid release in the long-term.

For the majority of deposition holes, no losses due to piping are expected since the inflow of groundwater is expected to be too low to cause piping. For holes with a significant inflow of groundwater during saturation the losses will be higher. The calculations of the swelling and homogenisation of a half torus resulting from erosion show that the swelling yields a strong decrease in density and swelling pressure in the eroded volume due to the friction in the bentonite. However, the swelling pressure after completed homogenisation is in none of the cases with torus radius varying from 3.4 cm to 13.4 cm below 1 MPa. The influence of the radius seems to be insignificant due to the long distance to the bentonite boundaries. If half a sphere is created instead of a torus the consequences are more severe, since the radius of the sphere is larger for the same amount of bentonite and thus the mass of bentonite left between the half sphere and the canister much less. However, in 2/3 of the distance between the canister and the rock the buffer has a swelling pressure higher than 1 MPa for the case corresponding to the volume of the 3.4 cm radius half torus. The conclusion is thus that about 100 kg of dry bentonite may be lost due to erosion without jeopardising the function of the buffer. The effect is strong, but the case of point erosion rather unlikely. Losses larger than 100 kg of dry bentonite are not possible since potential deposition holes with too high inflow are avoided, see Section 5.2.1, and need thus not be further assessed in the PSAR. However, the uncertainty in the assessment of the eroded volume needs to be considered when revising the technical design requirements for acceptable inflow to deposition holes.

All deposition holes are expected to experience some loss of buffer density due to swelling and upward expansion of the buffer. This phenomenon has been analysed through a number of calculations that demonstrate that buffer density at the canister top will remain within the reference interval of 1 450–1 560 kg/m³ after buffer swelling and expansion.

At the later part of the initial temperate period, i.e. after around 7000 years, a fraction of a percent of the deposition hole positions may experience dilute conditions such that buffer colloids are formed and released. However, given the slow erosion rate, no deposition holes are expected to reach advective conditions during the initial temperate period.

Buff1. Limit advective transport

a) Hydraulic conductivity $< 10^{-12}$ m/s.

For deposition holes with reference design buffer density, the hydraulic conductivity criterion is fulfilled with ample margin for the range of groundwater salinities that can be expected during the initial temperate period.

b) Swelling pressure > 1 MPa.

For deposition holes with reference design buffer density, the swelling pressure criterion is fulfilled with ample margin, again for the range of groundwater salinities that can be expected during the initial temperate period.

These conclusions also hold for deposition holes affected by piping.

Buff2. Reduce microbial activity

For this safety function to be fulfilled it is required that the saturated buffer density is higher than 1850 kg/m^3 for the reference buffer material Mx-80. For the initial temperate period, the analyses of possible loss of buffer mass and groundwater salinities have demonstrated that the buffer density will remain sufficiently high, as long as the buffer is installed according to the reference design.

Buff3. Damp rock shear

For this safety function to be fulfilled it is required that the buffer has a maximum dry density yielding an unconfined compressive strength at failure < 4 MPa at a deformation rate of 0.8 %/min . According to Figure 6-5 in Svensson et al. (2019), 4 MPa is reached for MX-80 at a dry density of around 1640 kg/m^3 which is substantially higher than the installed density. No relevant processes that would increase the buffer density have been identified, so it is concluded that this safety function is fulfilled for all deposition holes. It is also noted for the analyses of canister resilience to shear load reported in Section 10.4.5 that the maximum unconfined compressive strength at failure of the buffer is assessed to be around 2.5 MPa for MX-80 according to Svensson et al. (2019), meaning that canister design calculations based on the technical design requirement of 4 MP are pessimistic in this sense.

Buff4. Resist transformation

For this safety function to be fulfilled, it is required that the buffer temperature is less than $100 \text{ }^\circ\text{C}$. It has been demonstrated that there is an adequate margin to the peak temperature criterion for the buffer, even when the spatial variability of the rock thermal properties is taken into account and with other data essential for computing the result chosen pessimistically.

Buff5. Prevent canister sinking

For this safety function to be fulfilled, it is required that the buffer swelling pressure exceeds 0.2 MPa. This is less than the fulfilled criterion (> 1 MPa) for Buff1b and the canister sinking criterion is thus fulfilled with ample margin.

Buff6. Limit pressure on canister and rock

a) Swelling pressure < 10 MPa.

With buffer and backfill selected and installed according to the reference design, the swelling pressure may vary between 7 and 10 MPa, with account taken for the allowed variations in density and provided that the buffer material is fully confined to the volume it occupies at deposition. Since no process is identified where the buffer material will be added during the initial temperate stage the maximum swelling pressure criterion will be upheld.

b) Temperature > -6 °C.

Since a temperate climate similar to the current is assumed to prevail during the time period under consideration, there is no possibility that this criterion would not be fulfilled.

Backfill safety functions

BF1. Counteract buffer expansion

For this safety function to be fulfilled it is required that the compressibility of the backfill material is sufficiently high. The assessment reported in Section 10.3.9 implies that the backfill fulfils the safety function for an installed backfill mass according to the reference design. As shown in Section 10.2.4, the largest possible erosion due to piping will be 1 640 kg. Erosion in the backfill will basically mean that material is redistributed within the tunnel itself. Considering the large mass of backfill in the tunnel a redistribution of 1 640 kg can be assumed to have no impact at all on the backfill performance.

Even though dilute conditions may occur in some of the more transmissive single fractures intersecting a deposition tunnel, at the later part of the initial temperate period, these conditions will not cause erosion to the extent that this will result in such a loss of swelling pressure above deposition holes that these in turn would enter an advective condition.

Canister safety functions

Can1. Provide corrosion barrier

For this safety function to be fulfilled, it is required that the minimum copper coverage exceeds zero. This safety function will be upheld throughout the initial temperate period. The total amount of copper corrosion during the excavation and operational phases and the first 1 000 year period can pessimistically be estimated to be less than 2.5 mm, when taking into account the contributions from residual oxygen in the repository, from corroding agents formed by radiolysis and from possible microbial sulphate reduction as well as the contribution from sulphides in the bentonite and backfill. Copper corrosion by contaminants in the buffer, backfill or groundwater does not pose a threat to canister integrity for the initial temperate period and, even during the one million year overall assessment period, expected corrosion of the canister for an assumed temperate climate would cause corrosion depths of the order only of a few millimetres, even for the most unfavourable deposition positions at Forsmark. No deposition holes will lose so much buffer mass by colloid release due to dilute groundwaters that advective conditions must be assumed, meaning that corrosion under advective conditions can be ruled out during the initial temperate period.

Can2. Withstand isostatic load

For this safety function to be fulfilled, it is required that the canister withstands isostatic loads up to 50 MPa, Can2a. The fulfilment of this safety function is assured by the design of the canister, see Section 5.4.3 and the **Canister production report** for further details. It may also be noted that during the initial temperate period, the isostatic loads consist of the groundwater pressure of 4–5 MPa and the swelling pressure of the buffer that is estimated at maximally 10 MPa for the reference buffer density interval. This is considerably less than 50 MPa, i.e. no canisters will fail due to isostatic load.

Also, the copper shell must be resilient to creep deformation during the expected isostatic loads, Can2b. The mechanical modelling of the canister has shown this to be the case.

Related to Can2b, it is required that the hydrogen content of the copper shell is low, to ensure its ductile properties in the long term, Can2c. Bounding calculations have demonstrated negligible ingress of hydrogen in the copper material as a consequence of copper corrosion.

Can3. Withstand shear loads

The canister is designed to withstand a fracture shearing of 50 mm (see Section 5.4.3 and the **Canister production report** for further details, Can3a). As further discussed in Section 10.4.5, on average between 9.3×10^{-6} and 2.2×10^{-5} canisters may be sheared 50 mm or more due to earthquakes within the 1 000-year time frame.

Also, the copper shell must remain sufficiently ductile after expected shear loads, Can3b. The mechanical modelling of the canister has shown this to be the case, as further discussed in Section 10.4.5. Regarding low content of hydrogen, Can3c, the same conclusion as for Can2c above applies.

Status of buffer/backfill after the thermal and saturation phase

The buffer and, to a lesser extent, the backfill goes through a unique transient thermal and saturation phase in the first few hundred years after deposition. The status of these components after this transient phase is not expected to change much thereafter, meaning that the initial state, in combination with the alterations occurring during the transient phase, to a large degree determine the long-term properties of the buffer and the backfill. Therefore, a specific account of the expected status of the buffer and the backfill after the thermal and saturation phase is given here.

The buffer and the backfill will be deposited as blocks and the gaps between the blocks and the rock are assumed to be filled with bentonite pellets. Water from the rock will enter into the pellets and come into contact with the blocks. The bentonite will take up water and swell. From the time of deposition, the residual heat from the waste will increase the temperature in the near field of the repository. Temperature differences of up to 20 degrees will occur across the buffer for typically 100 years. Elevated temperatures in the near field are expected for about 1 000 years. During this period, the buffer and backfill are expected to evolve as described earlier in this section. The expected final state after the thermal and saturation phase is as set out below.

- After a period of < 100 years to ~6 000 years the buffer is expected to be fully saturated. During the period over which saturation is achieved, the buffer will swell and exert a swelling pressure on the canister, the rock and the backfill. The pressure is too low to have any effect on the canister and rock, but the backfill will deform to a certain extent. This will lead to a small loss of swelling pressure in the top of the deposition holes, but the pressure exerted by the buffer around the canister is expected to remain at its initial value.
- The hydraulic gradients in the unsaturated repository may cause piping and erosion of the buffer and backfill. This may lead to a loss or redistribution of material, but the losses will not jeopardize the function of the buffer nor the backfill.
- The increased temperature in, and the thermal gradient over, the buffer may lead to redistribution of minerals. CaCO_3 and anhydrite could be enriched close to the canister. The movement of compounds of silica is expected to be negligible.
- The maximum temperature increase and the maximum duration of increased temperature are well below the limits that might cause any significant transformation of the montmorillonite.
- Groundwater from the site will enter into the buffer and mix with the original porewater. This will yield a new composition for the buffer water. Both the composition of the original bentonite and the water from the site are sufficiently well known that the new composition can be estimated.
- At the later part of the initial temperate period, i.e. after 10 000 years, a fraction of a percent of the deposition hole positions may have dilute conditions such that buffer colloids are formed and released. However, given the time it takes for such erosion, no deposition holes will reach advective conditions during the initial temperate period.

- Even if dilute conditions may occur in some of the more transmissive single fractures intersecting a deposition tunnel, at the later part of the initial temperate period, none of them will cause erosion to the extent that this will cause such loss of swelling pressure above deposition holes that these in turn would enter an advective condition. For a few positions where the fracture is connected to a deformation zone, potentially more than 220 tonnes could be lost in a million year perspective, but this is not relevant from the point of view of canister integrity.

In summary, for all identified processes occurring in the buffer and backfill during the saturation and thermal phase the consequences have been estimated. The conclusion is that none of these phenomena will jeopardize the long term performance of the buffer and backfill.

Conclusions for radionuclide transport

The following conclusions for radionuclide transport have been drawn.

1. Large earthquakes cannot totally be ruled out even for the initial temperate period. There is a chance of at most about 1 in 40 000 that one out of the 6 000 canisters will be sheared by an earthquake within 1 000 years, see Section 10.4.5. This frequency will be similar for the remaining part of the initial temperate period, i.e. the expected number of potentially sheared canisters scales linearly with time.
2. The EDZ developed during construction needs to be considered in the radionuclide transport analyses.
3. The hydrogeological analyses have provided distributions of F , t_w and Q_{eq} to be used in radionuclide transport calculations.
4. The geochemical assessments have provided geochemical conditions for which retention properties in the host rock for radionuclide transport can be derived.
5. The buffer assessments have provided buffer conditions for which retention properties in the buffer for radionuclide transport can be derived.
6. Spalling may affect the equivalent flow rates, Q_{eq} , in deposition holes.
7. The pH increase from cement leaching may affect geosphere retention in larger, grouted fractures.

10.4 The remaining part of the reference glacial cycle

This section presents the evolution for the remaining part of the 120 000 year long reference glacial cycle, essentially a repetition of the conditions reconstructed for the Weichselian. It is important to note that the model reconstruction of the Weichselian, constituting the reference evolution, should be regarded as one example of a credible evolution during a glacial cycle. The description is not an attempt to predict a most probable future evolution. It is a simplified 'best estimate' of the Weichselian evolution, focusing on aspects of relevance for repository safety, and used as a scientifically defensible starting point for the analysis of climate impacts on repository safety. It is complemented by additional climate cases with a potentially larger impact on repository safety, analysed in other safety assessment scenarios.

Figure 7-4 in Section 7.5 shows the assessment model flow chart, AMF, for periglacial and glacial conditions giving an overview of the modelling and other assessment studies for these periods.

10.4.1 Reference long-term evolution of climate related conditions

Model reconstructions of last glacial cycle conditions, including the Weichselian ice sheet, are chosen as reference glacial cycle and reference evolution in the PSAR main scenario, see Figure 10-99. The rationale for this is given in Section 10.1.1 and in Chapter 11. The evolution of the repository is mainly affected by the evolution of climate-related conditions e.g. variations in relative-sea level and development of permafrost and ice sheets, whereas the climate as such at the ground surface is of

secondary importance for repository safety. On the basis of conditions and processes of importance for repository safety, three characteristic *climate domains* (see further Section 6.2.3) that can be expected to occur in Sweden in a 100 000-year time perspective were identified:

- Temperate climate domain.
- Periglacial climate domain.
- Glacial climate domain.

In addition, periods when the ground above the repository is submerged, either by the Baltic Sea or by a freshwater lake, can be expected. During submerged periods, the climate conditions can either be temperate or periglacial, the latter yielding permafrost development in areas not covered by the sea/lake. The evolution of climate-related conditions is described as time series of climate domains and submerged periods.

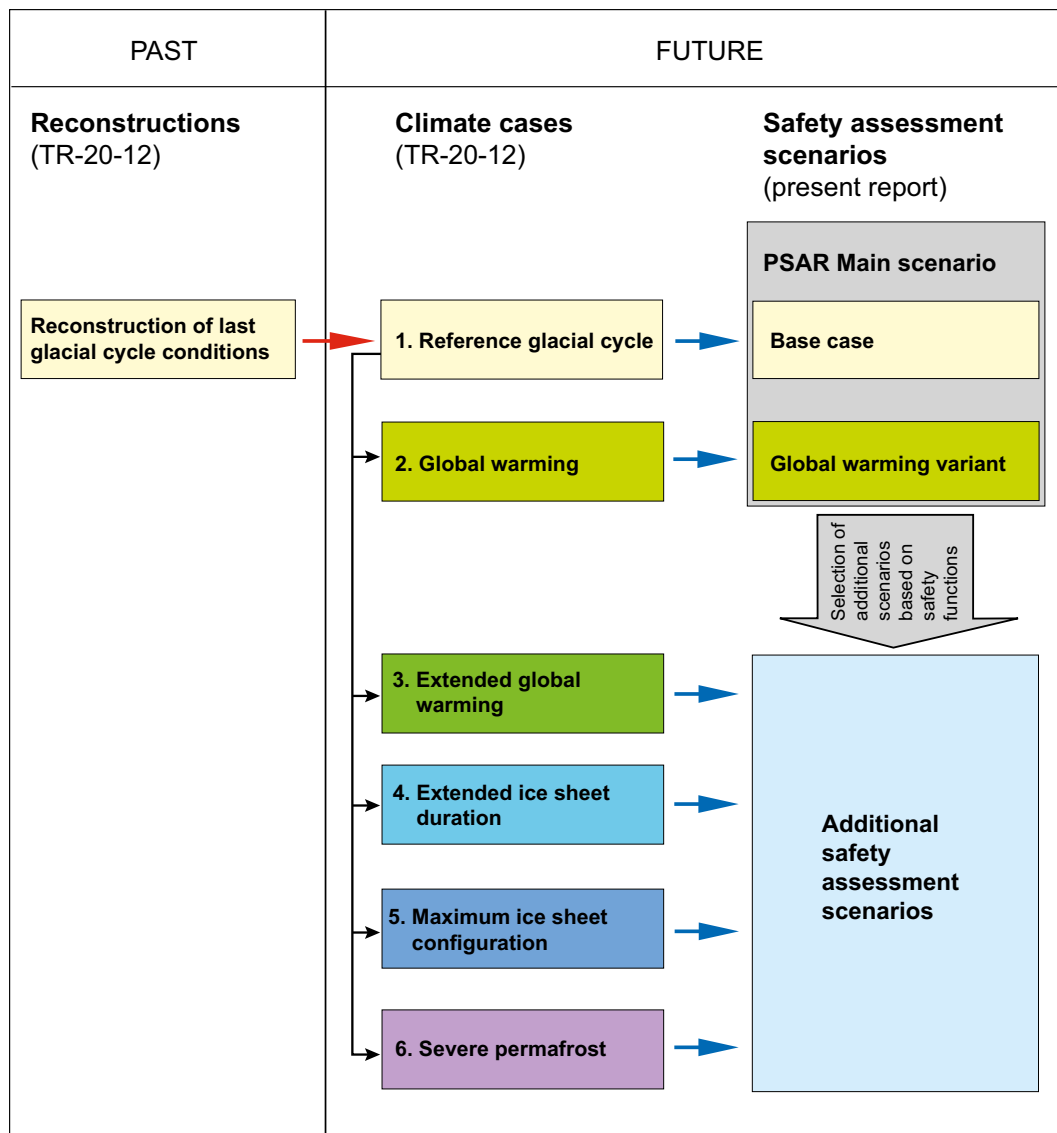


Figure 10-99. Relationship between the reconstruction of last glacial cycle conditions, the reference glacial cycle, additional climate cases, and the corresponding PSAR safety assessment scenarios. Figure modified from the Climate report.

To first reconstruct last glacial cycle conditions, and subsequently to generate the future reference glacial cycle, three models have been used; a dynamic ice sheet model, a Glacial Isostatic Adjustment (GIA) model, and a permafrost model, see the **Climate report**, Sections 3.1, 3.3 and 3.4. Details and references relating to the models are found in the **Climate report**, Chapter 3 and in the **Model summary report**.

The basis for the reference evolution of climate-related conditions is a reconstruction of the evolution of the Fennoscandian ice sheet during the Weichselian, employing the ice sheet model. The generated ice sheet evolution has been used as input to the GIA model. The third main component in the modelling of the reference evolution is the permafrost model, yielding an evolution of permafrost depth given the evolution of air temperature, ice sheet extent and thickness, shore level and vegetation. The main data flows between the ice sheet, GIA and permafrost models are shown in Figure 10-100.

Ice sheet evolution and modelling

The dynamic ice sheet model (Figure 10-100) is capable of simulating realistic ice sheets that constantly are trying to adapt their size and shape to a changing climate. Derived ice temperatures, together with density variations with depth, control ice viscosity and ice flow. The thermo-dynamic calculation accounts for vertical diffusion, vertical advection, and heating caused by internal shear. The model has been developed over an extended period (Fastook and Chapman 1989, Fastook 1994, Fastook and Holmlund 1994, Johnson 1994) and model outputs are similar to other major ice-sheet models (e.g. Payne et al. 2000).

Inputs to the dynamic ice sheet model are:

- Topography.
- Geothermal heat flux.
- Global sea level variations.
- Thermo-mechanical properties of the ice.
- Isostatic properties of the Earth's crust.
- Annual air temperature at sea level, and its variation over time.

For the reconstruction of the Weichselian ice sheet, the temperature pattern over the Fennoscandian model domain is changed according to a palaeo-temperature curve for the modelled time period, resulting in changes in the distributed precipitation and ice sheet surface mass balance. In the absence of a long-term paleo-temperature climate curve from Fennoscandia, the simulation of the Weichselian ice sheet used the temperature curve from the GRIP ice core (Figure 10-101), obtained from central Greenland (e.g. Dansgaard et al. 1993). This is a typical method used in modelling of the Weichselian ice sheet (see the **Climate report**, Section 3.1).

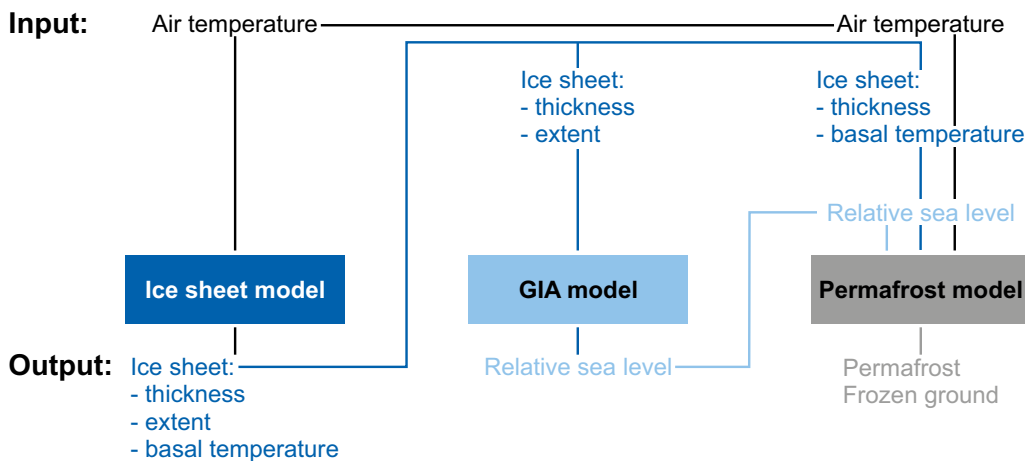


Figure 10-100. Models used to provide data for the description and analysis of the reference glacial cycle. Only input and output data shared between the models used to generate the results are shown.

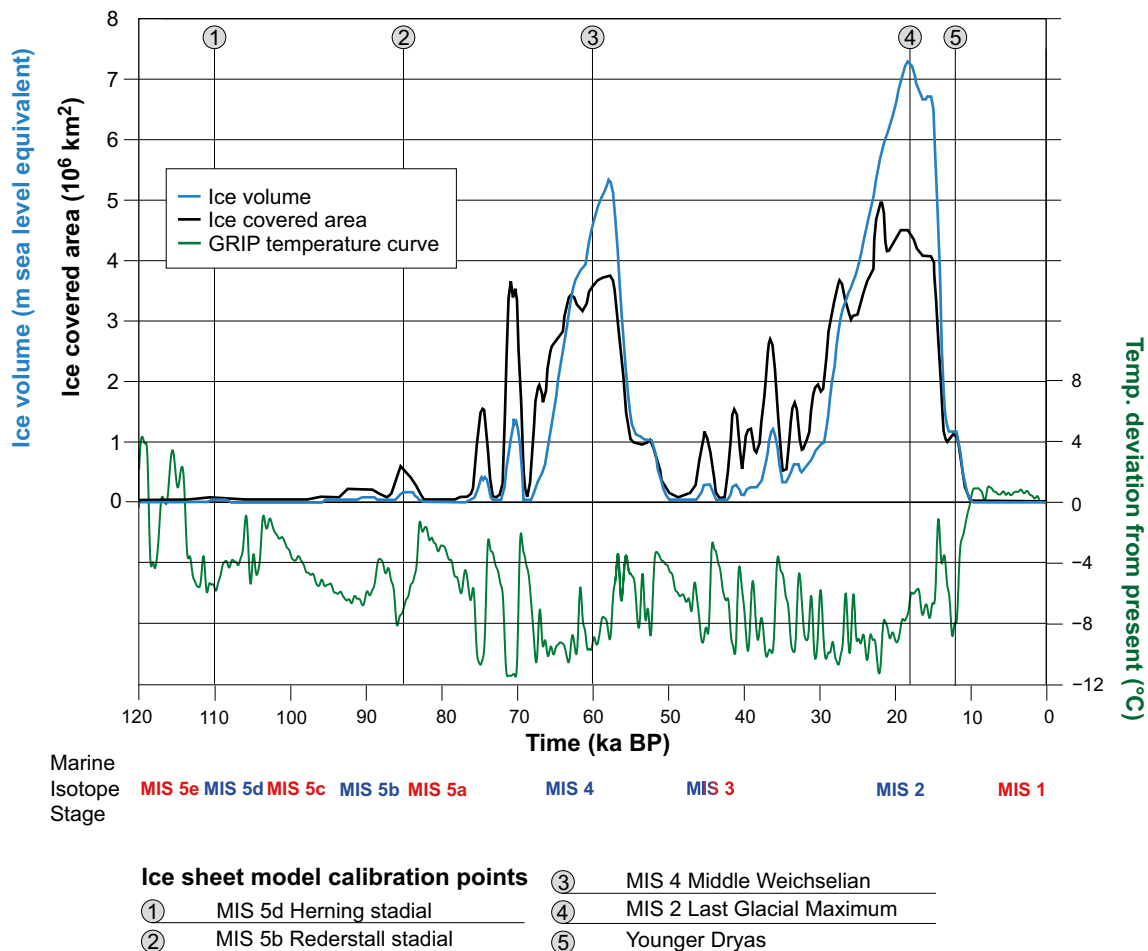


Figure 10-101. Reconstructed ice-covered area and ice volume for the Weichselian ice sheet. The GRIP proxy temperature curve and times of model calibration are also shown, as well as Marine Isotope Stages (warm stages in red and cold stages in blue). Since the growth of continental ice sheet results in a lowering of global sea level, the changes in ice sheet volume are expressed as m sea level equivalents.

The modelled ice sheet evolution starts at the end of the penultimate interglacial (the Eemian), in a situation when ice sheet extent and relative sea level are assumed to have been similar to the present. The geothermal heat flow and its spatial variation has been shown to be of importance for obtaining realistic modelled basal ice temperatures and basal ice melt rates (e.g. Waddington 1987, Näslund et al. 2005). Basal temperatures and basal water production are in turn important for the overall ice flow and ice dynamics. A detailed dataset of geothermal heat flux, based on national measurements of gamma emission in Sweden and Finland, was therefore compiled (Näslund et al. 2005) and used as input to the ice sheet model.

Modelled ice sheet configurations were calibrated against geological information on the Weichselian glaciation history (e.g. Lokrantz and Sohlenius 2006) and the **Climate report**, Section 4.2. For details on the ice sheet modelling (see the **Climate report**, Section 3.1.4).

The resulting evolution of ice-covered area and ice volume during the past 120 000 years are shown in Figure 10-101, together with times at which geological information was used to constrain ice sheet evolution. The modelled ice configurations for these times are shown in Figure 10-102. During the glacial cycle, the ice sheet grows progressively larger in a number of distinct growth phases. Between these phases, the ice sheet is thinner. The Last Glacial Maximum, as reflected in peak ice volume, is reached around 18 000 years before present. The overall behaviour of the ice sheet can be characterised as dynamic throughout the glacial cycle (Figure 10-101 and Figure 10-102), as suggested also by several recent studies of the last glacial cycle (see the **Climate report**, Section 4.2 and references therein). The reconstruction of the Weichselian ice sheet is described in more detail in the **Climate report**, Sections 3.1.4 and 4.4.1.

In the reference glacial cycle, the ice sheet over Forsmark was, as expected, at its thickest at around 18000 years ago, during the Last Glacial Maximum. The largest ice thickness over the Forsmark region was at that time ~2900 metres. Figure 10-103 shows extracted ice thickness variations over Forsmark, when projecting the reconstructed last glacial cycle ice sheet development into the future reference glacial cycle.

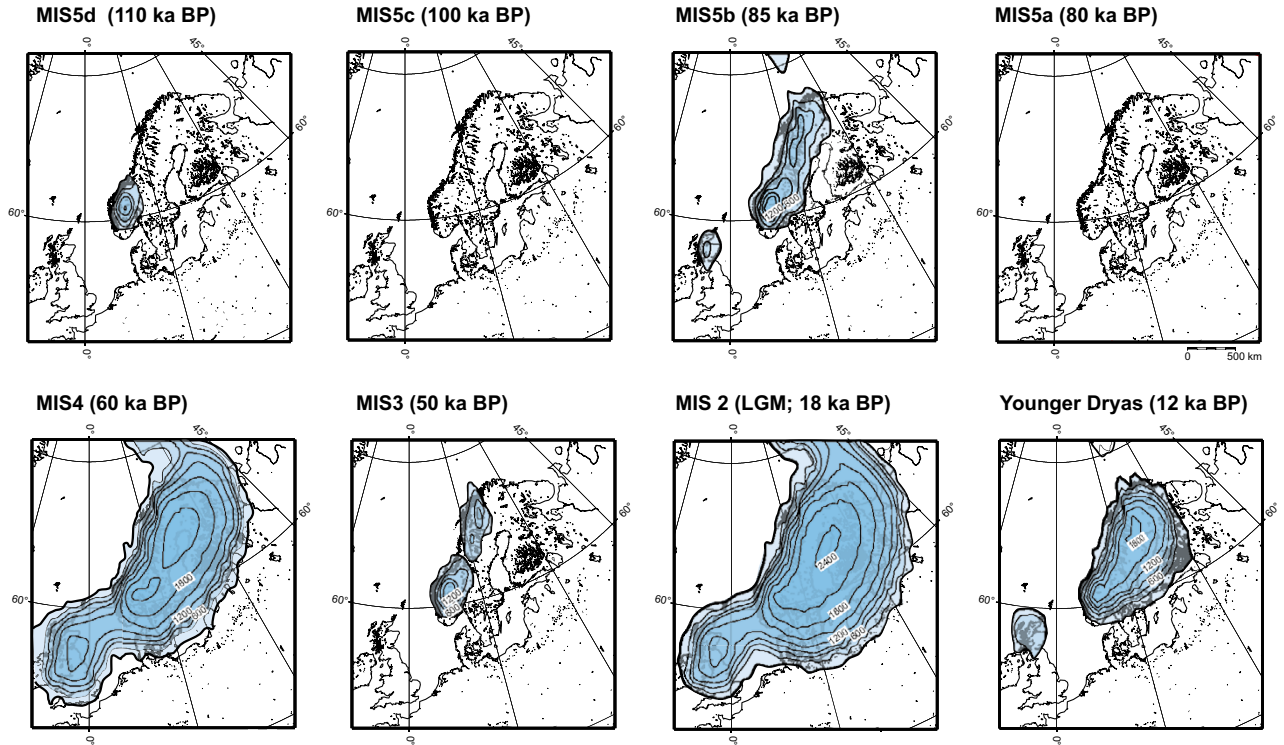


Figure 10-102. Selected maps of modelled ice sheet configurations at major stadials and interstadials from the reconstruction of the Weichselian ice sheet. Contour lines show ice surface elevation with a 300 m interval. All maps show present day shore-line position.

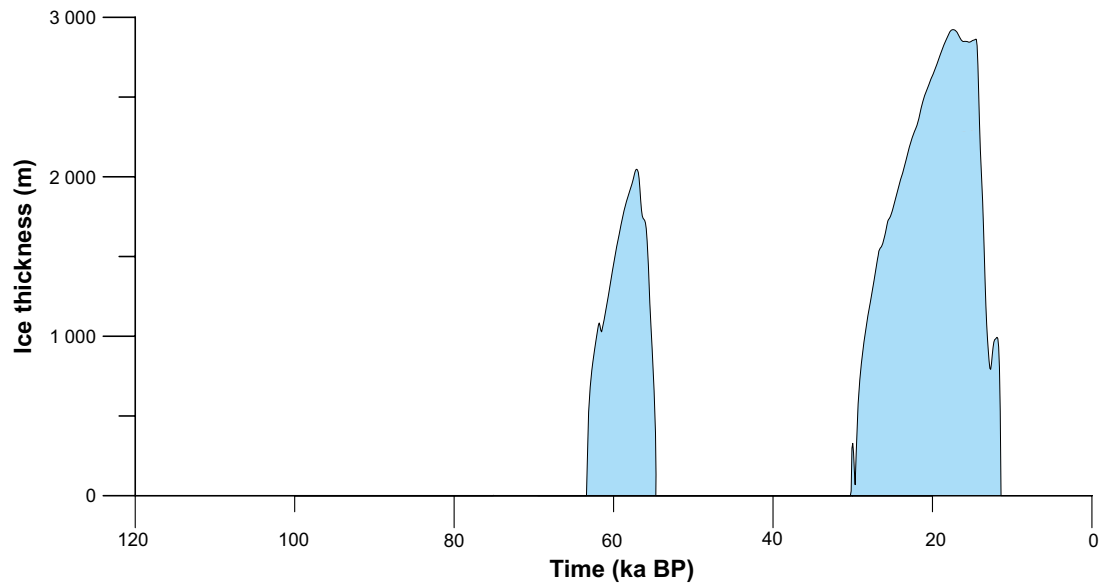


Figure 10-103. Development of ice sheet thickness at the Forsmark site in the PSAR reference glacial cycle. Note that even though an ice sheet is present in Fennoscandia during most of the glacial cycle, the Forsmark site, located in south-central Sweden, is not covered by the ice sheet for the majority of the time.

The groundwater pressure at repository depth is, for non-glacial conditions, determined by the repository depth and, for glacial conditions, by the repository depth as well as an additional pressure induced by the ice load. The ice sheet thickness sets a limit on the maximum hydrostatic pressure that may occur at the ice sheet/bed interface. In the reference glacial cycle, the additional hydrostatic pressure related to the maximum thickness at Forsmark is 26 MPa. This value is listed in Table 12-2, Section 12.7.2, together with estimates of *maximum* expected ice loads and associated *maximum* expected hydrostatic pressures, discussed in Section 12.7.2.

Figure 10-104 shows a selected ice sheet surface profile modelled for the deglaciation phase of the reference glacial cycle, compared with a steeper theoretical steady-state ice sheet profile. The ice sheet profiles were used for calculations of e.g. hydraulic pressure gradients during glacial conditions (Vidstrand et al. 2010). The hydraulic gradients associated with the steep frontal part of the theoretical profile are seen in Table 10-16.

The duration of hydraulic conditions with steep gradients depends on i) what gradients are considered as steep, ii) the assumed ice sheet profile, iii) the velocity of the ice sheet margin during advance and retreat, and iv) the size of the area of interest. For example, the theoretical profile (Figure 10-104) has been analysed together with ice sheet model data and is considered a proper representation of an advancing ice sheet over Forsmark (for details see the **Climate report**, Appendix 2). If steep gradients for instance are defined as larger than 10°, the first ~3 km of the theoretical ice sheet profile has a steep gradient (Table 10-16). If advancing ice sheet conditions similar to the last glacial cycle are assumed, the ice margin advance rate is ~50 m/a (see the **Climate report**). This results in the steep gradients in this example prevailing for ~60 years during each ice advance over any given location within the repository. However, it should be noted that at the time of ice sheet advance in the reference glacial cycle, the Forsmark site is subject to continuous permafrost conditions, see below. This indicates that the steep gradient from the ice sheet is not the only process that governs the hydrogeological conditions, see Section 10.4.6 and Vidstrand et al. (2010).

For a detailed description of the ice sheet profiles, and the motivation for selecting and using them in SR-Site, see the **Climate report**, Appendix 2.

Table 10-16. Hydraulic gradients calculated from the theoretical ice sheet profile, averaged over various distances from the ice sheet margin.

Length from margin (m)	Hydraulic gradient (m/m)	Hydraulic gradient (degrees)
100	1.49	56
200	0.96	44
400	0.62	32
1000	0.35	19
2000	0.23	13
4000	0.15	8.5

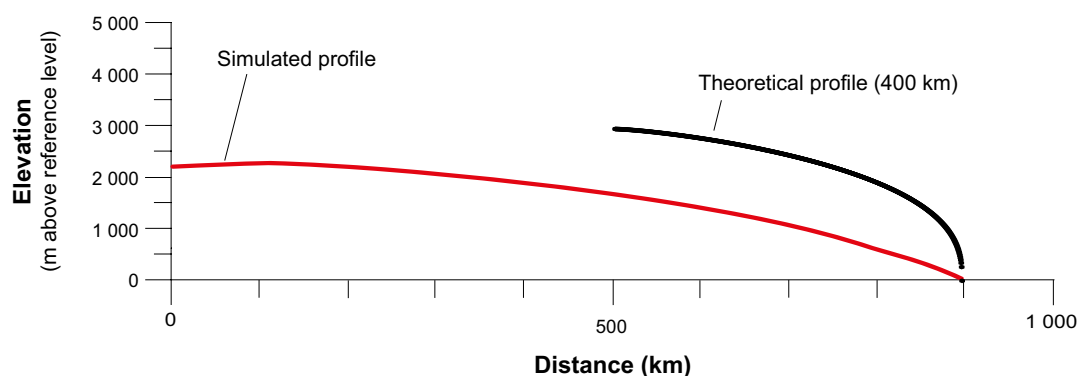


Figure 10-104. Ice surface topography for a simulated ice profile during the last deglaciation phase of the reference glacial cycle, and a theoretical steady-state profile. For descriptions of the profiles, see the text and the **Climate report**, Appendix B.

Glacial hydrological conceptual model

The hydrological system of an ice sheet consists of three parts; the supraglacial system (on the ice-sheet surface), englacial system (within the ice) and subglacial system (at the bed). A schematic section through an ice sheet is shown in Figure 10-105. Water from surface melting is produced over a large area, even above the equilibrium line (ELA) which defines the altitude of net-zero surface mass balance. In the ablation area, i.e. below the ELA, surface streams are common features during the melt season. These often end in crevasses or moulins, through which the surface water enters the en- and subglacial systems. At the ice margin, part of the surface melt water leaves the ice sheet directly by channelized surface flow, without entering into the ice sheet and reaching the ice sheet bed.

In the conceptual model, a zone of basal melting extends some hundreds of km inward from the margin, see Figure 10-105. In interior parts of the ice sheet, basal ice is frozen to the bed and no basal melting occurs. One of the most important characteristics of the en- and subglacial hydrological systems is that they are highly dynamic. They adjust their transport capacity to any prevailing input of melt water at the ice-sheet surface. Because of the seasonal and intra-seasonal variations in water input, and the continuously ongoing ice deformation, both the en- and subglacial conductive features experience major seasonal and intra-seasonal variations in size and capacity (Claesson-Liljedahl et al. 2016, Harper et al. 2016). For this reason, there is no limit to the transport capacity of these hydrological systems, given enough time for them to develop. Further information on the supra- sub- and englacial systems are found in the **Climate report**, Section 3.2 and references therein.

Amount of water produced by melting

In the reference glacial cycle, surface melt water production for the modelled Weichselian ice sheet typically varies up to 4–8 m of water per year in the ablation area. This can be compared with observed present average ablation rates of the Greenland ice sheet of a few metres/year and up to more than 10 m/year (Claesson-Liljedahl et al. 2016, Harper et al. 2016). During the deglaciation of the Weichselian ice sheet, melt rates up to values higher than 10 m/year occurred (Humlum and Houmark-Nielsen 1994). Basal melt rates are typically a few mm/a, and can be regarded as constant over the year (Claesson-Liljedahl et al. 2016).

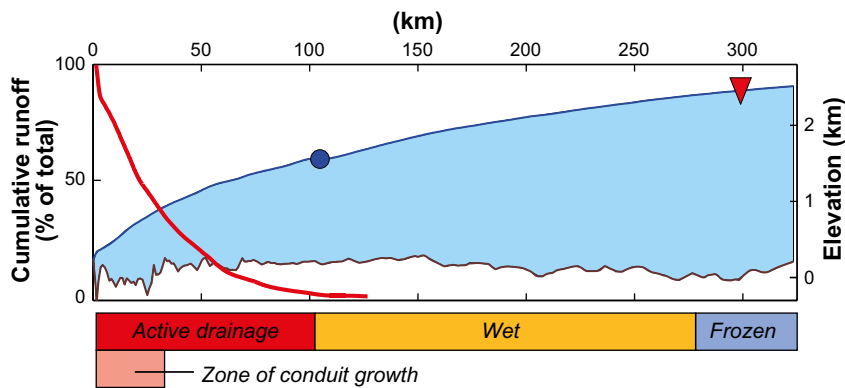


Figure 10-105. Conceptual view of the thermal and hydrological system of an ice sheet. Melted basal conditions extend beyond the Equilibrium Line Altitude (ELA) (represented by the blue circle). Below the ELA surface melt increases such that cumulative runoff increases exponentially towards the ice-sheet margin (red curve). An active drainage system develops in response to surface melt routing to the bed. Basal melt conduit development in the drainage network is limited to a region near the ice-sheet margin where sufficient melt energy promotes conduit growth during the melt season. Left y-axis refers to the red runoff curve. Red triangle refers to the inland limit of surface melting. The conceptual schematic is developed based on the GAP project transect in western Greenland (Claesson-Liljedahl et al. 2016, Harper et al. 2016).

Spatial perspective on the subglacial hydrological system

Basal thermal conditions define the maximum spatial extent of active drainage system processes and meltwater recharge to the groundwater system. The inland extent of melted basal conditions depends on the magnitude of processes acting to increase (geothermal heat flux, strain heating) or decrease (vertical advection of cold ice from the surface) the basal ice temperature. These depend on ice-flow processes that are subject to change in time (see the **Climate report**, Section 3.2). Current consensus is that in Greenland the boundary between frozen and melted conditions generally extends well beyond the ELA. Temperate basal conditions persist from this inland boundary to the ice-sheet margin (Figure 10-105). Beneath the ablation zone, substantial water is seasonally input to the bed from the surface, leading to drainage system/sliding speed interactions. As the surface can generate as much meltwater in one day as is generated in one year at the bed by basal melt, the surface conditions have a substantial impact on bed conditions across this reach.

Collectively, model results and in situ pressure observations in Greenland support a view of the basal drainage system beneath the ablation zone in which basal melt conduits grow in response to seasonal surface melt routed to the ice-sheet bed, but the extent of conduit growth is limited to within 20–25 km of the margin. Further inland, a conductive linked cavity system likely remains stable, transporting basal and surface-derived melt towards the margin. The water flux across a large portion of this region has been observed to be relatively large and fast flowing. Rare conduits may extend deeper beneath the ablation zone if, for instance substantial englacial storage provides a water source preventing complete conduit shutdown during the winter, or if the closure of conduits is impeded by pinching off of the conduit closer to the margin in response to some unconstrained process. Alternatively, a linked cavity system could maintain stability if its conductivity (and therefore transmissivity) increased during the melt season, as may occur from increasing connectivity along the bed in response to substantial basal melt fluxes. Such processes enhancing conduit or linked cavity stability are without modelled or observed evidence, however, and therefore remain speculative.

Temporal perspective on the subglacial hydrological system

The time perspective of glacier hydrology can be divided in two main categories: time scales under which the ice-sheet undergoes significant changes in volume and extent and where the associated hydrological conditions change with the ice-sheet; and time scales under which the ice-sheet can be considered constant in volume and extent and where the variability of the acting processes dominates.

Seen in the perspective of an entire glaciation, the hydrological system varies spatially with the size of the ice-sheet. This means that different parts of the bed are either temperate or cold and can be associated with hydrological systems of different overall structure and parameterisation. The distribution of cold and temperate basal conditions changes in time and also in location with the waxing and waning ice-sheet. From this perspective, a possible repository site will experience changing conditions of active hydrology under thawed bed conditions or cold frozen bed conditions. With changing ice-sheet configuration, the basal hydraulic conditions also vary so that shifts in location of drainage pathways occur. How much time a specific location is subjected to either condition is determined by the large-scale fluctuations of the ice volume and extent.

The processes in the hydrological system of an ice-sheet exhibit variations ranging from diurnal (in the case of temperature-dependent melt variations), or possibly even shorter duration (in the case of rainfall-induced variations), to seasonal variations that depend on long-term temperature variations. Since variations in temperature-induced melting and liquid precipitation alter the input to the hydrological system, they also yield subglacial water pressure oscillations on similar time scales. This means that the base of an ice sheet will exhibit variations on a diurnal and subdaily time scale superimposed on longer-term variations due to changing air masses and seasonal temperature fluctuations.

For further information on the hydrological system of ice sheets, see the **Climate report**, Section 3.2.

Relative sea level and GIA modelling

In Sweden, the evolution of the Fennoscandian ice sheet has been the principal factor governing changes in relative sea level since the last deglaciation. Hence, Glacial Isostatic Adjustment (GIA) has dominated shore-level changes during this time. GIA-induced shore-level changes depend on the following factors:

- The depth and extent of the oceans.
- The location and thickness of ice sheets over time.
- The structure and properties of the solid Earth and its response to surface loading.

The GIA model used for generating the reference glacial cycle was developed by Mitrovica and Milne (2003). The global ice-loading function used in the study is modified from the ICE3G deglaciation history (Tushingham and Peltier 1991), and has been calibrated using far-field (i.e. far from the margin of the ice sheet) relative sea level data. The near-field ice load history is taken from the ice sheet modelling described above. A eustatic curve has been used to tune the mass of ice contained within far-field ice sheets. The Earth model is based on Maxwell rheology with a 1D radial three-layer structure. For details on the GIA modelling, see the **Climate report**, Section 3.3.

The relative sea level curve for the reference glacial cycle is shown in Figure 10-106. The first ~8000 years of the future period are based on an extrapolation of the reconstructed relative sea level of the Holocene (**Climate report**, Section 4.5.2 and Appendix D), whereas from about 8000 years after present to the end of the reference glacial cycle, the relative sea level evolution is based on GIA-modelling.

During the initial phase of the glacial cycle, when climate is becoming gradually colder and ice sheets expand globally, sea levels fall. At the same time, the rate of isostatic rebound from the previous glaciation decreases. However, even if the rate is low, the amount of remaining uplift until the Earth reaches a relaxed state is significant. The remaining uplift at Forsmark is estimated to ~70 m from the GIA simulations.

During a glacial cycle, the shore-level of the Baltic Sea is constrained by the variations in ice sheet extent and by relative sea levels at its sills. The Baltic may at times constitute a freshwater lake, with a surface level determined by the contemporary level of either the Darss sill, located in the southern Baltic between Denmark and Germany, or for the northern part of the Baltic (the Bothnian Sea), the Southern Kvarn sill, located between Åland and Sweden.

In the GIA model results (Figure 10-106), the Baltic is cut off from the Atlantic and is transformed into a lake after about 9000 years after present. However, due to the uncertainties in the GIA modelling relating to the assumption of a 2D Earth structure, Earth rheology, and ice load input, it is likely that this result underestimates the time at which isolation of the Baltic occurs in the reference evolution (see further the **Climate report**, Section 4.4). After the first major ice sheet advance over Fennoscandia, around 60000 years after present, the Baltic is re-formed during a period around 70000 years after present. This period of the reference glacial cycle corresponds to Marine Isotope Stage 3 of the Weichselian, during which the Baltic may have formed a fresh water lake (Lambeck et al. 2010).

Later in the reference glacial cycle, following the deglaciation of the second and larger ice sheet coverage at around 110000 years after present, the Baltic is in contact with the Atlantic and hence forms a brackish inland sea. Given that the reference glacial cycle is based on the repetition of conditions reconstructed for the last glacial cycle (including the Holocene epoch of the last ca 10000 years), the development of the Baltic for this future post-glacial period is envisaged to follow the Holocene development, which included both saline and freshwater stages. After this deglaciation, large parts of southern Sweden are submerged by a predominantly saline Baltic Sea. At the end of the reference glacial cycle, and as isostatic rebound proceeds, the Baltic Sea is again transformed to an inland brackish sea, similar to today's situation.

During periods of maximum salinity in the Baltic Sea, which generally develop some time after periods of maximum glaciation, the Forsmark site is submerged. A more detailed description of the development of salinity in the Baltic Sea for this submerged period of the reference glacial cycle is found in Lindborg (2010).

The most important factor affecting the GIA modelled relative sea level change is the Earth model and the ice loading history, in particular the near-field history. 3D GIA modelling performed for Fennoscandia, described in Whitehouse (2009) has shown that the assumption of a laterally homogenous earth structure over Fennoscandia, used for the construction of Figure 10-106, probably resulted in an over-prediction of the isostatic response to ice sheet load and present-day uplift rates. The relation between the Earth model structure and the ice loading history, as well as the assumption of a laterally homogenous earth structure, are further discussed in the **Climate report**, Section 3.3.

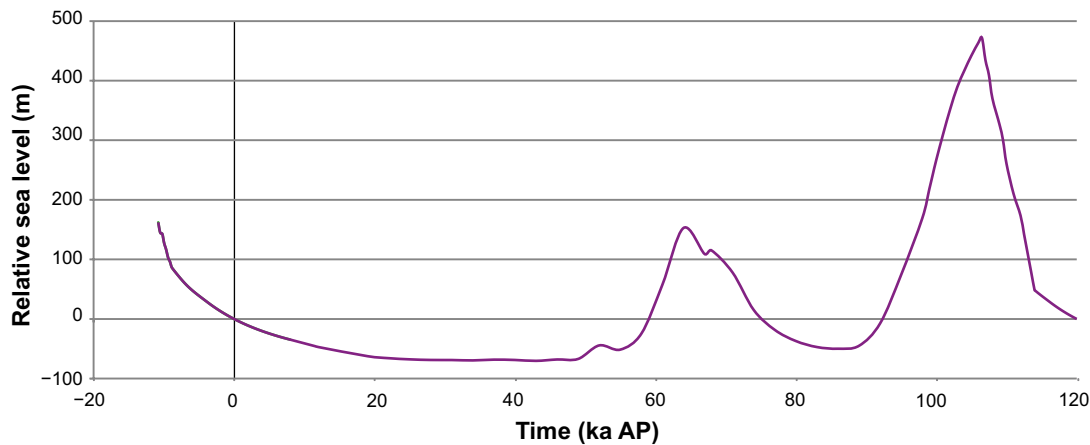


Figure 10-106. Relative sea level at Forsmark for the reference glacial cycle. The first ~8000 years of the future period are based on observed relative sea level data (Climate report Section 4.5.2 and Appendix D) whereas the following part of the curve is constructed from Glacial Isostatic Adjustment modelling. A detailed description of how the relative sea level curve was constructed is provided in the Climate report, Appendix D. The relative sea level is expressed relative to the contemporary Baltic sea level. Positive numbers indicate that the site is submerged and vice versa. Note that for most of the time when the figure shows submerged conditions, the site is covered by an ice-sheet.

The uncertainty in modelled relative sea level relates mainly to the fact that reported values could be too large as a result of an overestimation of isostatic depression in response to the ice load. The size of the uncertainty varies over the modelled glacial cycle. Postulating that the ice sheet evolution is correct, the *mean* overestimation of isostatic depression, over the whole glacial cycle, may be up to 45 metres. For details on uncertainties in modelled relative shore-levels see the **Climate report**, Section 3.3.

Permafrost development and modelling

Permafrost is defined as ground where the temperature remains below 0 °C for more than a year while perennially frozen ground is defined as ground that remains frozen for at least two consecutive years. Therefore, the presence of permafrost does not necessarily mean that the ground is frozen. Depending on the pressure and composition of groundwater, and on adsorptive and capillary properties of ground matter, groundwater may freeze at a temperature below 0 °C.

Permafrost originates from the ground surface and grows downwards as a result of a complex heat exchange across the atmosphere/ground boundary layers and the geothermal heat flow from the Earth's interior. In the reference glacial cycle, permafrost occurs in the periglacial climate domain, as well as beneath parts of the ice sheet in the glacial climate domain (see the **Climate report**, Sections 3.4.4 and 4.5). Generally, an ice sheet isolates the ground from the cold climate and therefore the presence of an ice sheet prevents the development of permafrost to great depth in cold climates. Instead, the ice sheet typically results in degradation of pre-existing permafrost.

The development of permafrost depends on:

- The climate conditions; mainly air temperature at the ground surface but also on precipitation and wind.
- The topography; air temperature decreases with increasing altitude and, in northern latitudes, slopes with a southern aspect are more exposed to solar irradiation than slopes with a northern aspect.
- The presence of a soil cover and its porosity, saturation and thermal properties.
- The presence and type of vegetation.
- The presence of water bodies of substantial extent (lakes, sea, major rivers).
- The presence of ice sheets and the basal ice temperature.
- The bedrock thermal, mechanical and hydraulic properties.
- The geothermal heat flow.

As a general rule for a majority of surface covers, permafrost can build from the ground surface if the annual mean air temperature is lower than a value ranging between -9 and -1 °C (Washburn 1979, Yershov 1998, French 2007).

For the reconstruction of the last glacial cycle conditions and the construction of the reference glacial cycle, 1D permafrost modelling was performed for the repository location, see SKB (2006c) and the **Climate report**, Section 3.4.4. In addition, 2D permafrost modelling was performed for a section of the Forsmark site (see Hartikainen et al. (2010) and the **Climate report**, Sections 3.4.4 and 5.5). The main objective with the 1D modelling was to study the evolution and depth of permafrost and perennially frozen ground for the full glacial cycle specifically at the repository location, whereas the 2D simulations were made to study the spatial development of permafrost and frozen ground, including talik formation, freeze-out of salt and groundwater flow along a profile over the Forsmark site. The 2D model was also used for extensive sensitivity experiments on uncertainties in subsurface- and surface conditions, as well as in climate parameters, including air temperature. Figure 10-107 shows the results when projecting the reconstructed last glacial cycle permafrost and perennially frozen ground conditions into the future reference glacial cycle. For further presentations of the results of the permafrost modelling, see Section 10.4.3, the **Climate report**, Section 3.4.4, and Hartikainen et al. (2010).

Permafrost growth is a progressive process, starting with sporadic permafrost at the most exposed areas and, if climate allows, ending with a continuous spatial coverage of permafrost. Examples of permafrost development from the reference glacial cycle along the profile investigated with the 2D permafrost model are seen in Figure 10-108. Note that heat from the repository is included in these simulations. At time 8 500 yrs (8.5 kyrs) after present (Figure 10-108 upper panel), the temperature effect from the repository has a clear impact on the temperature of the surrounding bedrock.

At time 25 000 years after present, two unfrozen taliks have formed through the frozen ground beneath lakes located at $\sim 9\,000$ and $\sim 15\,000$ m in the profile (Figure 10-108 Second panel). Groundwater recharge and discharge may take place in the taliks but not in the surrounding frozen terrain. The size of the water body required to retain a talik was investigated by permafrost modelling. For the results of these calculations, see the **Climate report**, Section 3.4.

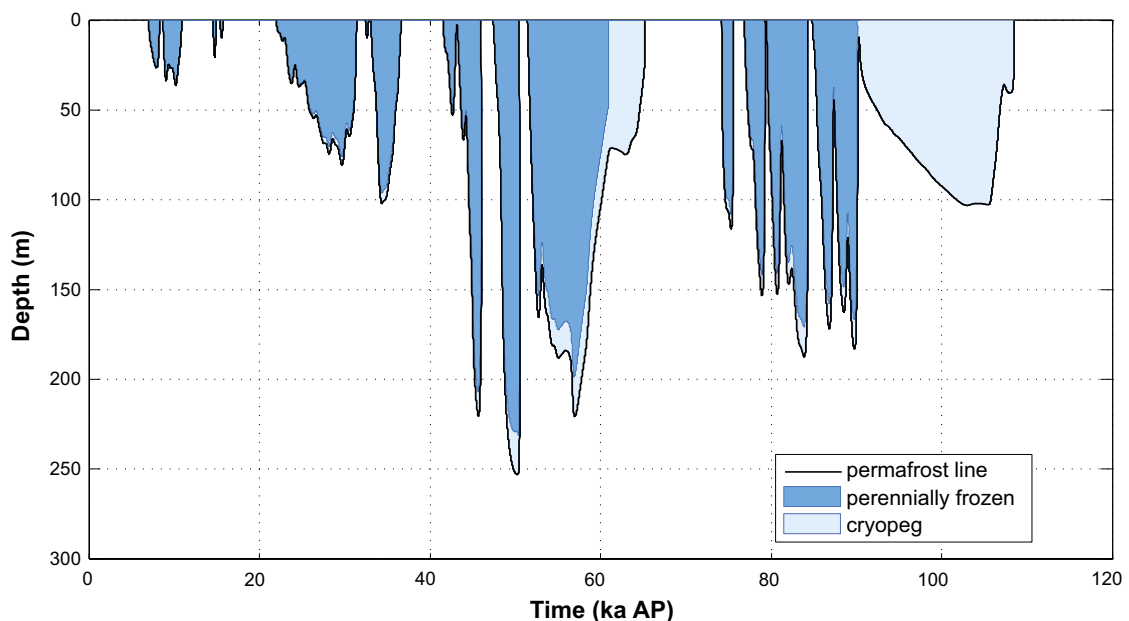


Figure 10-107. Evolution of permafrost and perennially frozen ground depth for the reference glacial cycle. The curve shows the development specifically at the repository location, obtained from 1D modelling. Due to the high pressure, a thick unfrozen cryopeg exists within the permafrost (defined by the 0 °C isotherm) for periods with ice sheet coverage around 60 000 years and 100 000 years after present. The largest permafrost depth is -260 m.

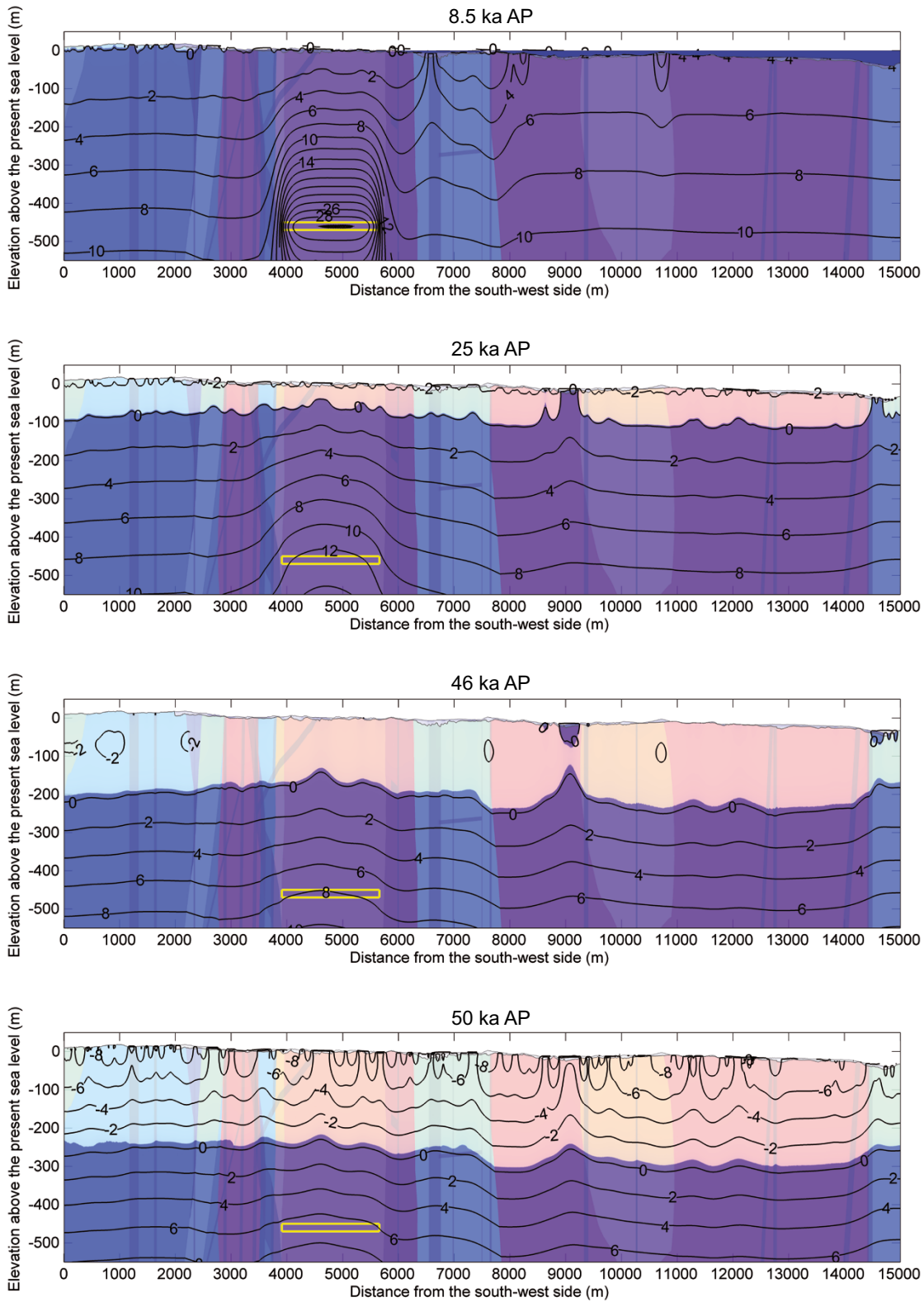


Figure 10-108. Examples of temperature contours in (°C) and the extent of perennially frozen ground (light colour) and permafrost (0 °C isotherm), obtained from 2D modelling, at times 8.5, 25, 46 and 50 kyrs after present in the reference glacial cycle. Blue colour on the top of the profile at 8.5 kyrs after present shows the Baltic Sea. The yellow rectangle indicates the location of the repository. The profile follows the general regional topographic gradient, approximately in a SW-NE direction.

At time 46 000 years after present (Figure 10-108 third panel), the taliks are closed by the developing permafrost. The lower panel in Figure 10-108 shows the permafrost distribution for the situation with deepest permafrost in the reference glacial cycle. At this time, 50 000 years after present, the permafrost depth over the repository is 259 m. The perennially frozen depth is a few metres shallower, 246 m.

Some of the input data for the permafrost simulations are associated with significant uncertainties, see the **Climate report**, Sections 3.4.4 and 5.5. The largest uncertainty relates to the air temperature curve reconstructed for the Forsmark site for the last glacial cycle, which is estimated to be uncertain by up to ± 6 °C (see the **Climate report**, Appendix 1, the **Data report** and Hartikainen et al. 2010). If this uncertainty in air temperature is combined with the uncertainty in climate humidity, the uncertainty range for the permafrost depth (e.g. 0 °C isotherm depth) for the reference glacial cycle reaches a maximum depth of ~ 410 m, whereas the uncertainty range for the perennially frozen ground reaches ~ 380 m (Figure 10-109).

Uncertainties related to other surface conditions (vegetation type, surface wetness, snow cover) and subsurface conditions (thermal conductivity and diffusivity, and geothermal heat flow) have a smaller impact on the simulated permafrost results. If they all are combined with the uncertainty in climate humidity (still excluding the uncertainty in air temperature), they result in a permafrost uncertainty interval between ~ 170 and ~ 290 m depth (Figure 10-110).

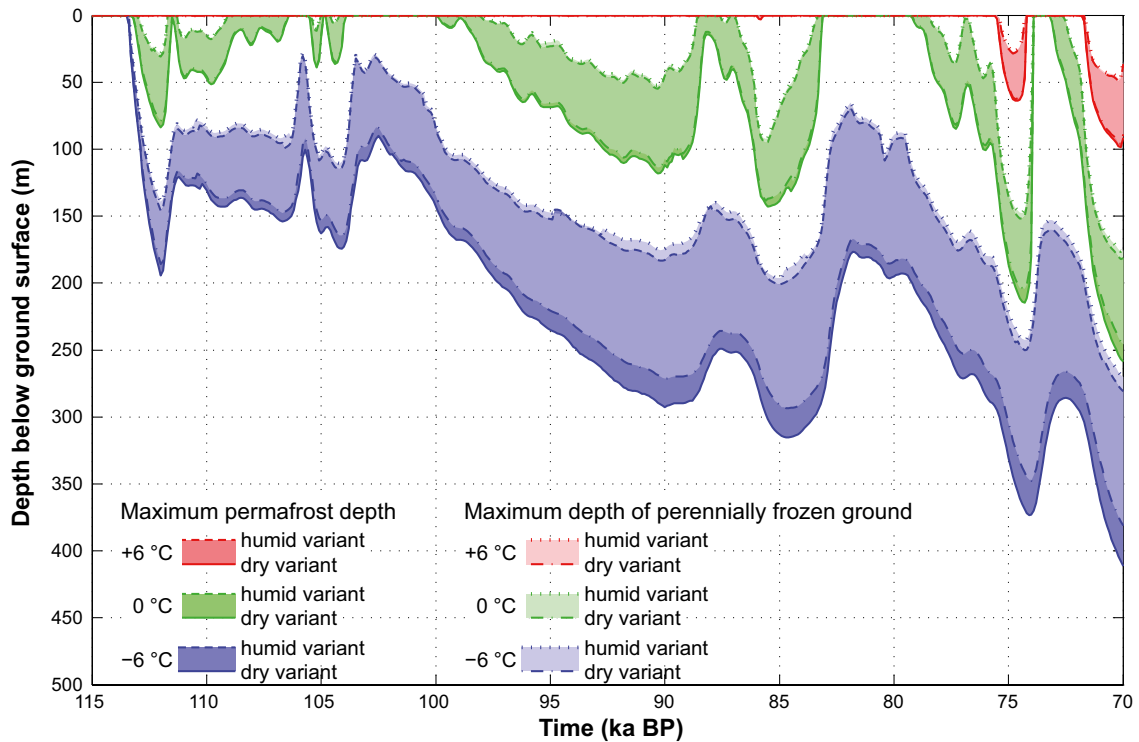


Figure 10-109. Result of sensitivity experiment on uncertainty in air temperature and climate humidity for the first 50 000 years of the reference glacial cycle. Evolution of maximum permafrost depth (solid lines) and maximum depth of perennially frozen ground (dashed lines) over the repository location considering mean thermal properties and the air temperature curve changed by -6 , 0 and $+6$ °C. The shaded areas in blue and red represent the range when considering the dry and humid climate variants. Note that the results for permafrost and perennially frozen ground overlap to a large degree. It should also be mentioned that changes of the buffer and backfill clay properties during freezing, if freezing would occur, are reversed following thawing.

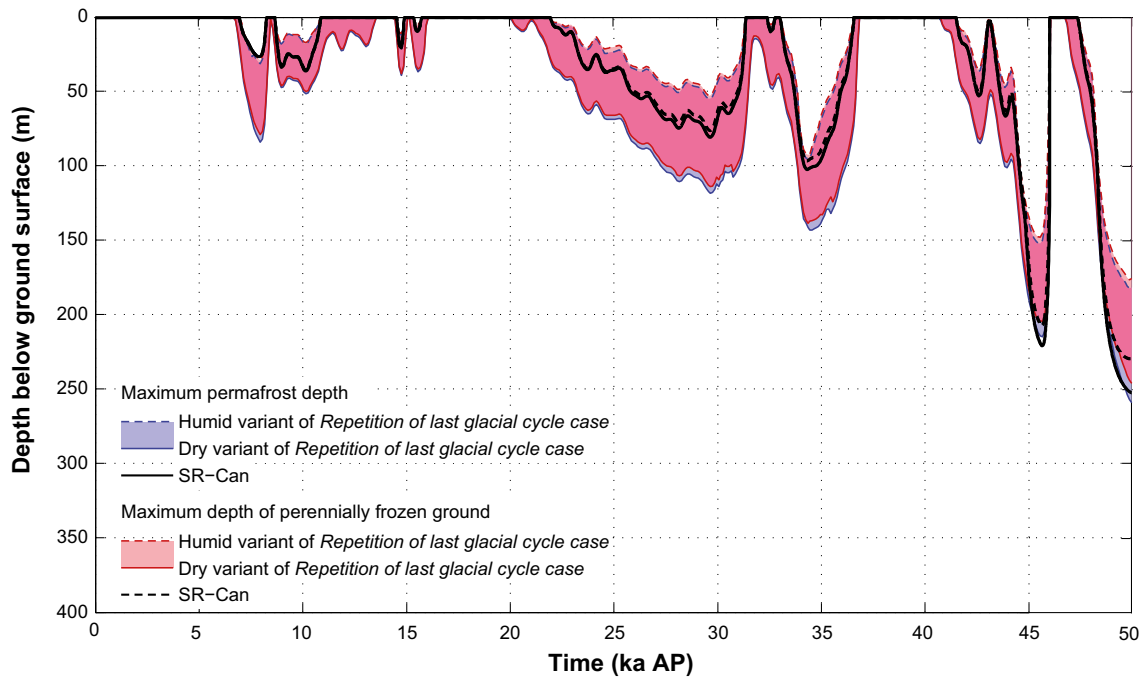


Figure 10-110. Evolution of maximum permafrost depth and maximum depth of perennially frozen ground over the repository for the reference glacial cycle considering combined uncertainties in all surface conditions (except air temperature) and bedrock thermal properties (including geothermal heat flow). The figure shows the first 50 000 years of the reference glacial cycle as simulated by the SR-Site 2D modelling. The shaded areas in blue and red represent the range when considering dry and humid climate variants. Note that the areas overlap to a large extent (lilac colour). Corresponding 1D results from SR-Can are also shown.

With all known uncertainties (e.g. in air temperature, climate humidity, surface wetness, vegetation, snow cover, bedrock thermal conductivity and diffusivity, and geothermal heat flux) in their most extreme setting favourable for permafrost growth, the permafrost uncertainty range reaches a maximum depth of 463 m, whereas the uncertainty range for the perennially frozen ground reach a maximum depth of 422 m (see the **Climate report** Table 4-4). It must be noted, however, that this most extreme combination of uncertainties is quite unrealistic. Given that the uncertainty in the maximum depth of perennially frozen ground does not reach 450 m depth even in this most extreme unrealistic combination of all uncertainties, freezing of groundwater at repository depth is excluded in the reference glacial cycle. For a more detailed description of e.g. individual contributions of uncertainty from various parameters affecting permafrost growth, see the **Climate report**, Section 3.4.4 and Hartikainen et al. (2010).

Reference evolution at Forsmark

Based on the results of the ice sheet-, GIA- and permafrost modelling, the reference glacial cycle evolution of climate-related conditions at Forsmark is described as a time series of future climate domains and submerged periods (Figure 10-111).

The time series and the identification of main processes and conditions of importance for repository safety are the basis for the subsequent identification and construction of additional possible future climate cases for the SR-Site safety assessment (Figure 10-99).

Periods of temperate climate domain occupy ~28 000 years (24 %) of the reference glacial cycle at Forsmark. It occurs in the initial phase of the reference glacial cycle, during the interstadial between the two major ice advances, and during the interglacial period following the glacial maximum (Figure 10-111). During the end of the present interglacial and during following early phases of the reference glacial cycle, the periods of temperate climate domain are generally longer than those occurring during the interstadial in the later part of the glacial.

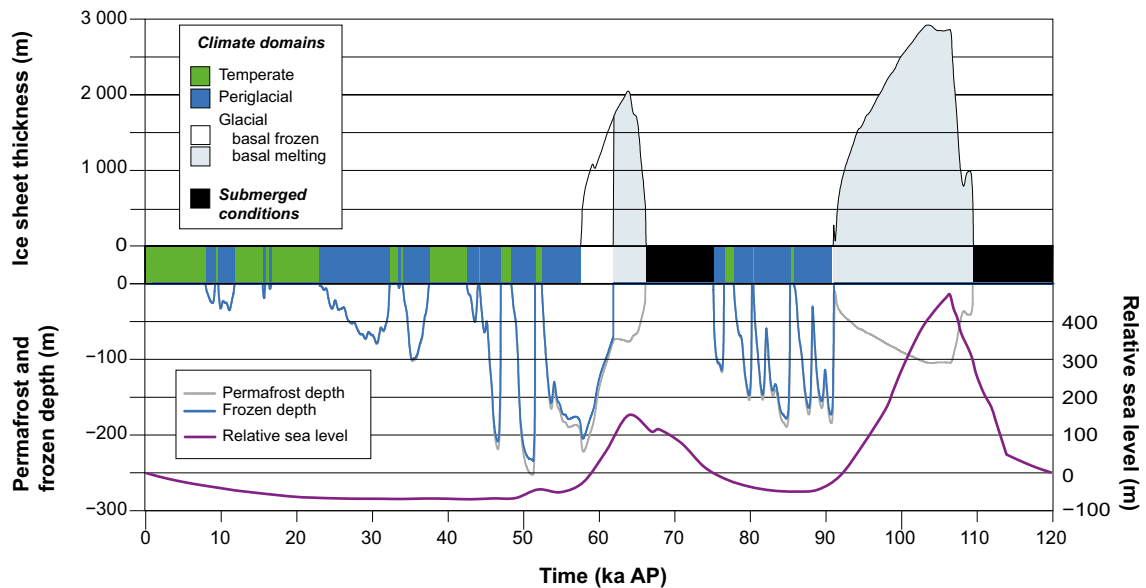


Figure 10-111. Evolution of important climate-related variables at Forsmark for the coming 120 ka in the PSAR reference glacial cycle.

During the first 50 000 years of the reference glacial cycle, and in the interstadial period between the two glacial phases, the increasingly colder climate results in progressively longer periods of periglacial climate domain and correspondingly shorter periods of temperate climate domain (Figure 10-111). The total duration of the periglacial climate domain is ~46 000 years (38 % of reference glacial cycle). The calculated permafrost depth at the repository location for the most severe permafrost period of the reference glacial cycle is ~250 m. As described in the discussion on uncertainties above, freezing of groundwater at repository depth is excluded in the reference glacial cycle.

Forsmark is exposed to two major ice advances and retreats during the reference glacial cycle, the first around 60 000 years after present and the second at around 90 000 to 110 000 years after present (Figure 10-111). Prior to both of these glaciated periods, the Forsmark site is situated above sea level with prevailing continuous permafrost conditions (more than 90 % spatial permafrost coverage) when the ice sheet advances towards and over the site.

A period of basal frozen conditions, ~4 000 years long, initiates the first major stadial of glacial climate domain. During this period, there is deep sub-glacial permafrost. As the ice sheet continues to grow over the site, it insulates the subsurface from the cold climate and in time induces basal melting conditions. Also the sub-glacial permafrost starts to decay once the ice sheet has overridden the site, with very fast permafrost melting once warm-based ice sheet conditions form (Figure 10-111). The total length of periods of glacial domain in the reference glacial cycle is about 27 000 years (23 % of reference glacial cycle). During this time, ice sheet basal melting conditions dominate.

Table 10-17 summarises the durations of the climate domains for the reference glacial cycle. It is again emphasized that the reference evolution is not an expected or predicted climate evolution. It is *one example* of a climate evolution covering the climate-related conditions that could occur in a 100 000 year time perspective. The example is subsequently used in the process of identifying other climate cases with a potentially larger impact on repository safety.

Climate-related factors of importance for safety

During periods of temperate climate domain, the main factor of importance for repository safety is changes in relative sea level and groundwater salinity. When the site is submerged, a diminished groundwater flow will be driven by prevailing differences in groundwater density, and, when not submerged, the gradients for groundwater flow will be constrained by landscape topography. During periods of periglacial climate domain, the main factor of importance for repository safety is the

development of permafrost and frozen ground. Frozen ground will affect groundwater flow and composition, and cause freezing of backfill material in the ramp and shaft. If freezing temperatures were to occur at repository depth, the backfill in deposition tunnels and buffer would freeze.

The advance and retreat of an ice sheet over the Forsmark site brings about the largest climate-related change the repository will experience during a glacial cycle. The main factors of importance for repository safety in the glacial climate domain are the maximum hydrostatic pressure, the penetration of oxygen rich and/or dilute glacial melt waters to great depth, the possible up-coning of saline waters from below the repository, the alteration of rock stresses, the occurrence of glacially induced faulting and the alteration of flow properties of the bedrock.

The evolution of climate-related conditions of importance for repository safety is illustrated by the succession of climate domains and by the evolution of important climate-related variables in Figure 10-111. In this climate succession, the temperate climate domain is always followed by the periglacial climate domain. The periglacial climate domain can either be followed by the temperate or glacial climate domain. In the reference glacial cycle, the Forsmark site is submerged by the Baltic after periods of major glaciation. The subsequent transition from submerged conditions to land can take place either during periods of periglacial climate domain, or, as at present, during periods of temperate climate domain.

Table 10-17. Duration of climate domains in the SR-Site reference glacial cycle.

Climate domain	Duration (% of reference glacial cycle)	Duration (years)
Temperate climate domain	24 %	28 200
Periglacial climate domain	38 %	46 000
Glacial climate domain	23 %	27 300
Submerged conditions	15 %	18 500

10.4.2 Biosphere

The PSAR uses a reconstruction of the last glacial cycle as a starting point for describing possible future changes in climate and climate-related processes (see Section 10.4.1). This reconstruction is used as an example of a future evolution that, in a realistic way, covers all relevant climate-related changes that can be expected in a 120 000-year perspective. The reconstruction divides the period into climate-driven process domains (in short: climate domains). In reality when looking at the entire modelled area at Forsmark, changeover from one climate domain to another is a smooth transition (see the **Climate report**, Section 4.5.4). In addition, it takes time for the environment and its predominant processes to adapt even to an abrupt change in climate (cf. Chapter 3 in Lindborg 2010).

For the modelled area at Forsmark it takes time for a change in environmental conditions to propagate from one end to the other. For instance, this is true for the changeover after the deglaciation, from submerged conditions to an entirely terrestrial and temperate domain. This transition is caused by shoreline displacement, which takes ~ 12 000 years to transfer the whole area from fully submerged just before the first islet emerges from the sea (1000 BC), until the last marine embayment is turned into a lake (around 11 000 AD). During two periods in the later part of the reference evolution, Forsmark is covered by an ice sheet (Section 10.4.1). Directly after the deglaciation of these ice sheets, the site is submerged, and thereafter the transfer from submerged conditions to an entirely terrestrial area is assumed to be repeated.

Periods of temperate climate domain

The temperate climate domain corresponds to 26 % of the reference glacial cycle, Section 10.4.1. After the initial temperate period, which according to the reference glacial cycle ends around 9400 AD, a relative short period of periglacial conditions follows, and thereafter temperate conditions again dominate until ca 23 000 AD. Another temperate period lasting for about 5 000 years occurs around 40 000 AD.

During future periods of temperate conditions before the next glaciation, Forsmark is assumed to show biosphere characteristics similar to those of the later parts of the initial temperate period, i.e. the landscape will consist of terrestrial ecosystems, mainly forests and mires, with few or no lakes and no sea. Parts of the area, especially those with fine-grained sediments in central Öregrundsgrepen (see Figure 10-12), can potentially be used for long-term agriculture (cf. Chapter 4 in Lindborg 2010). Patches with mainly organic soils may also be cultivated for limited periods. Higher altitude areas with outcrops of bedrock will be forested with pine. Also the pattern for discharge of deep groundwater, as well as the conditions determining transport and accumulation of radionuclides in the landscape, are expected to be similar to those prevailing during the late part of the initial temperate period (cf. Chapters 4 and 5 in Lindborg 2010).

Periods of periglacial climate domain

Periods of periglacial conditions, which are characterised by tundra vegetation and permafrost features, correspond to 34 % of the reference glacial cycle. Although the periglacial domain constitutes the largest share of the reference glacial cycle, it often occurs during relatively short periods interrupted by other climate domains. The longest uninterrupted period of periglacial conditions starts around 23 000 AD and continues for ca 10 000 years.

The vegetation period in the periglacial domain is short. Nevertheless, primary production may be high in some environments, e.g. in shallow lakes (Andersson 2010). The terrestrial vegetation consists of sedges, herbs and shrubs. At more exposed and dryer localities, lichens dominate, whereas wet ground is dominated by mosses. The precipitation will likely be lower than during temperate conditions, due to the limited evapotranspiration transporting water to the atmosphere (Kjellström et al. 2009). The low evapotranspiration means that wet ground is prevalent, because surplus water is unable to infiltrate into the ground (Bosson et al. 2010, French 2007). This may result in larger areas of wetlands compared with a temperate climate, but on the other hand the peat formation rate is lower, partly because the terrestrial plant productivity is low.

Even on gentle slopes, the soil creeps downhill with the peat cover on top. Other processes typical of periglacial conditions are upward migration of stones induced by freeze-thaw processes, so called cryoturbation, causing tundra-polygons (patterned ground whose mesh is tetragonal, pentagonal or hexagonal) and thermokarsts (topographic features produced by thawing permafrost and associated settling of the ground). Thus, there are many processes disturbing the soil and also exposing it to erosion.

Taliks are unfrozen areas, often occurring under lakes or rivers in the permafrost region (e.g. Hartikainen et al. 2010). The talik features are the only spots in the periglacial landscape where radionuclides released from the repository can be transported up to the biosphere (Bosson et al. 2010). Given that lakes and streams often are locations for human settlement and land use, taliks can potentially be locations where humans are exposed to high radionuclide concentrations during periglacial conditions. However, the generally low productivity in the permafrost region requires utilisation of a larger area to supply the resources needed by even a small community. Therefore, even if radionuclides are discharged into a talik in such an area, this does not necessarily imply that the average concentrations in the food consumed by humans living in the area will be particularly high.

Periods of glacial climate domain

Forsmark is covered by an ice sheet during 24 % of the reference glacial cycle, mainly during the later part of this cycle. On the ice surface, microbes, algae and some insects can exist. At the ice-margin, a productive aquatic community may exist, which can sustain fish populations that may be exploited by humans and by animals living on the ice (e.g. birds, polar foxes, polar bears) and in the sea (e.g. seals and whales).

Any larger vertebrates or humans living on the ice are likely to migrate over large areas due to low food production and severe weather conditions. In most cases, a human population will probably comprise occasional visitors, due to the harsh environment. The only situation under glacial conditions when humans or other biota may be exposed to high concentrations of radionuclides from the repository is when the retreating ice-front is situated near the Forsmark area and the area is submerged. Under

these conditions, it is possible that a human population could be present for longer periods and live on fish taken from close to the ice margin.

During periods of glacial climate domain, no long-term accumulation of radionuclides is assumed to occur in the regolith due to the short turnover time of this potential reservoir. It is only during short periods of the glacial climate domain that radionuclides discharged from underground sources may accumulate as under periglacial conditions. However, since the Forsmark site will be depressed below the sea level during most of the glacial periods, fast water turnover in the open sea along the ice margin will probably dilute any released radionuclides and prevent the accumulation of high concentrations in sediments and organisms.

Periods with submerged conditions

In the reference glacial cycle, two periods of submerged conditions at Forsmark are present, representing 16 % of the total reference glacial cycle. These periods always follow directly after the ice sheet has withdrawn as a result of the bedrock being depressed by the ice load. After the last glaciation which ended at 8800 BC in Forsmark, the first terrestrial areas appeared around 1000 BC and the last marine embayment in the modelled area is turned into a lake around 11 000 AD. This means that the submerged conditions in the modelled area may be divided into two phases; one first phase of ca 8 000 years when the whole area is submerged, and another that continues during 12 000 years when the sea gradually withdraws and the land area expands accordingly. This description of the temporal succession is not seen in the description in the reference glacial cycle (see Figure 10-111) since the latter is valid specifically for a point above the repository target area, but it gives a more realistic picture of the succession for the whole landscape (see also the section on transitions between climate domains in the **Climate report**, Section 4.5.4).

Submerged conditions are not defined as a climate domain in the PSAR (see the **Climate report**). Instead, it is a state when the processes and properties related to the marine conditions are dominant. The marine ecosystem is not expected to change dramatically from today as a result of changes in climate, except for the long-term variations in salinity. Therefore, the submerged future landscape is treated as corresponding to the historical and present aquatic ecosystems at Forsmark, and the prerequisites for transport and accumulation of radionuclides are assumed to be similar to those in the present marine ecosystem.

Identified uncertainties and their handling in the subsequent analysis

The main uncertainties in the landscape development during the remaining part of the reference glacial cycle are essentially the same as those dominating during the initial temperate period, i.e. 1) the configuration of the landscape, 2) the timing of different events, and 3) the composition and properties of species and communities inhabiting the future landscape (cf. Section 10.3.3). Even though it is impossible to describe in detail the landscape development during a complete glacial cycle, the systematic landscape analysis and the approach for estimating doses encompasses most of the potential future landscape configurations for the reference glacial cycle.

10.4.3 Thermal evolution

The decreasing temperature and in particular the presence of permafrost and perennially frozen ground may impact the buffer clay, backfill material and copper canister. Primarily it is the safety function R4, see Figure 10-2, that may be affected, since it a) states that the temperature in the buffer should > -6 °C in order to avoid detrimental effect of a frozen buffer on the canister and b) that the buffer temperature should be > 0 °C to ensure the validity of the canister shear analysis. Furthermore, there is also a temperature related safety function for retention (BF2c) stating that the backfill temperature > -6 °C, since this is the temperature at which a frozen backfill may have detrimental effects on the surrounding host rock. Presence of permafrost also affects the hydromechanical conditions (potential for hydraulic jacking) as is further discussed in Section 10.4.4. It is therefore important to analyse i) the depths of permafrost, or more specifically, the depth of perennially frozen ground, ii) the depth of the isotherm corresponding to the temperature criterion used for buffer clay freezing, iii) the depth of the isotherm corresponding to the temperature criterion used for freezing of the backfill material, and iv) the freeze-out of salt that may result in a zone with higher salinity beneath the perennially frozen ground.

Permafrost development

The depth of permafrost is defined by the depth of the 0 °C isotherm (see the **Climate report**, Section 3.4). However, the depth of the perennially frozen ground is often shallower, depending on the prevailing hydrostatic pressure, chemical composition of groundwater and on adsorptive and capillary properties of ground matter. These factors result in the possibility that groundwater may freeze at temperatures below 0 °C (see e.g. the **Climate report**, Section 3.4). The temperature criterion used in the PSAR for detrimental buffer freezing is –6 °C, see Section 8.3.2 and the above paragraph. The temperature criterion used for the backfill material is –6 °C, see Section 8.4.4 and the above paragraph.

The prevailing surface conditions, such as air temperature and surface cover, are the main factors governing the spatial and temporal development of permafrost and perennially frozen ground at Forsmark (see the **Climate report**, Section 3.4.4). Subsurface conditions, such as bedrock thermal properties, geothermal heat flow, groundwater salinity and heat produced by the repository, modify the spatial and temporal development, but are of secondary importance compared to surface conditions. For a description of the development of permafrost during the reference glacial cycle, see Section 10.4.1 and the **Climate report**, Section 4.4.3.

Permafrost modelling

The evolution of permafrost and perennially frozen ground has been investigated by means of numerical modelling in 1D and 2D (SKB 2006c, Hartikainen et al. 2010). The related mathematical models are based on the theory of mixtures and basic principles of continuum mechanics and thermodynamics considering the freezing ground as an elastic porous medium of soil or rock skeleton saturated by saline groundwater and ice. The models are capable of describing the heat- and mass transfer in a porous medium, freezing of groundwater being affected by groundwater pressure and salt concentration, and freezing-induced groundwater flow (cryogenic-suction). The numerical 2D model also describes the exclusion of salt during freezing and the density dependent groundwater flow in unfrozen and partially frozen ground. The continuum approach is adequate for modelling of permafrost and perennially frozen ground development, since these processes are primarily governed by heat conduction and only secondarily by groundwater flow (Hartikainen et al. 2010).

The 1D modelling approach could, in certain situations, result in somewhat higher temperatures than would be calculated using a multi-dimensional model. However, a comparison between the results from the 1D model and the 2D model shows that the results from both are very similar (see the **Climate report**, Section 3.4.4). Since lateral groundwater flow has only a minor role in permafrost development (e.g. Hartikainen et al. 2010) it is likely that modelling including 3D groundwater flow would only contribute minor changes to the permafrost and perennially frozen depths. Furthermore, the anisotropy of thermal properties is not a problem in 1D, since one can choose a combination of thermal properties that would give lowest temperatures, or at least very close to the lowest temperatures. Therefore, it is not likely that 3D permafrost simulations would yield notably lower temperatures than the range obtained by the full series of 1D and 2D sensitivity modelling simulations that have been performed (see the **Climate report**, Section 3.4.4, and Hartikainen et al. 2010). A description of the 1D permafrost model is found in Hartikainen (2004) and the 2D model in Hartikainen et al. (2010).

For describing the depths of permafrost and perennially frozen ground, specifically at the repository location and for the full reference glacial cycle, the 1D modelling approach was applied (Hartikainen 2004, SKB 2006c). The 2D modelling approach was used to simulate the temporal- and spatial (along the profile) development of permafrost and frozen ground for the first ~ 50 000 years of the reference glacial cycle for a section of the entire Forsmark site. This time period includes the time with deepest permafrost for the full reference glacial cycle. The 2D modelling approach was also used to perform a broad range of sensitivity experiments covering all known uncertainties in input data for the permafrost simulations (see the **Climate report**, Section 3.4.4 and Hartikainen et al. 2010).

The air temperature curve reconstructed for the last glacial cycle, Figure 10-112, was used to calculate ground surface temperatures using among other things assumptions regarding ground surface coverage (vegetation and snow) (for details see the **Climate report**, Section 3.4.4 and Hartikainen et al. 2010). The influence of vegetation and surface snow cover have been considered using an empirical relationship between air and ground temperatures for different kinds of vegetation and topographic wetness index (see SKB 2006c, Hartikainen et al. 2010).

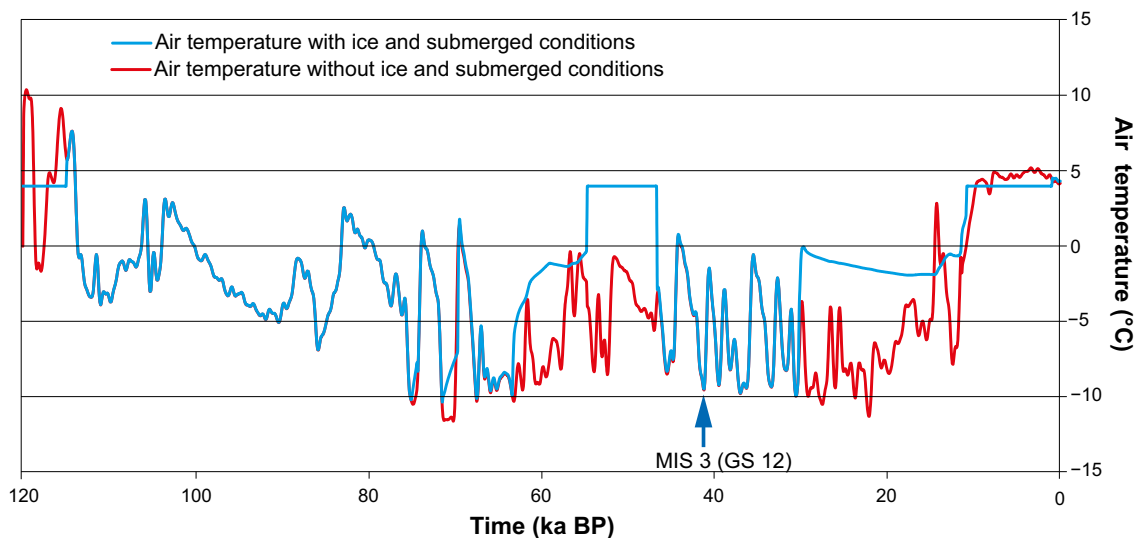


Figure 10-112. Reconstructed air temperature curve for the Forsmark region for the past 120 000 years. The red line shows reconstructed last glacial cycle air temperatures without a presence of an ice sheet and submerged periods. The blue line includes periods of ice sheet coverage and submerged periods, i.e. it shows simulated basal ice temperatures for glaciated periods and air temperatures for ice free periods. A temperature of +4 °C has been estimated for the submerged periods of the Eemian, Mid-Weichselian and Holocene. The construction of the temperature curve and its uncertainties are described and discussed in the Climate report, Appendix A.

For the permafrost modelling, the soil type and depth (full depth of unconsolidated Quaternary deposits), thermal and mechanical properties of rock domains and soil types, geothermal heat flow, chemical characteristics of groundwater and development of future lakes were obtained from the site descriptive models, see further SKB (2006c) and Hartikainen et al. (2010). For examples of modelled ground surface temperatures for different stages of the reference glacial cycle (Boreal, Sub-arctic and Arctic settings), see Hartikainen et al. (2010).

The results of the calculations of permafrost depth (0 °C isotherm) and depth of perennially frozen ground at the repository site for the full glacial cycle, projected into the future for the reference glacial cycle, are seen in Figure 10-107. The evolution of the maximum depth of the 0 °C, -2 °C and -4 °C isotherms, as well as the perennially frozen ground, obtained from the 2D permafrost simulations are seen in Figure 10-113. The figure illustrates the first ~50 000 years of the reference glacial cycle, including the time with deepest permafrost at around 50 000 years after present. As seen in the figure, and further discussed in Section 10.4.1, the 0 °C isotherm (permafrost) reaches a maximum depth of 259 m whereas the -2 and -4 °C isotherms reach maximum depths of 200 m and 150 m, respectively, in the reference glacial cycle. However, these numbers do not account for all uncertainties in the input data.

As also mentioned in Section 10.4.1, the input data for the permafrost modelling have quite large uncertainties. The consequences of these uncertainties for the simulated depths of permafrost and perennially frozen ground were analysed in detail in Hartikainen et al. (2010). The largest uncertainty relates to air temperature. By setting *all* known uncertainties (e.g. in air temperature, climate humidity, surface wetness, vegetation, snow cover, bedrock thermal conductivity and diffusivity, and geothermal heat flux) in their most extreme setting favourable for permafrost growth, the uncertainty range for the permafrost reaches a maximum depth of 463 m and for the perennially frozen ground a depth of 422 m (see the **Climate report** Table 4-4). At the same time, the uncertainty ranges for the -2 and -4 °C isotherms reach maximum depths of 388 and 316 m, respectively (see the **Climate report**, Table 4-4). This most extreme combination of uncertainties is quite unrealistic. These results conclusively show that the -4 °C isotherm does not reach repository depth in the reference glacial cycle. During permafrost periods with cold climate conditions, an isotherm for a lower bedrock temperature is located at a shallower depth than an isotherm for a higher temperature (that is, bedrock temperatures

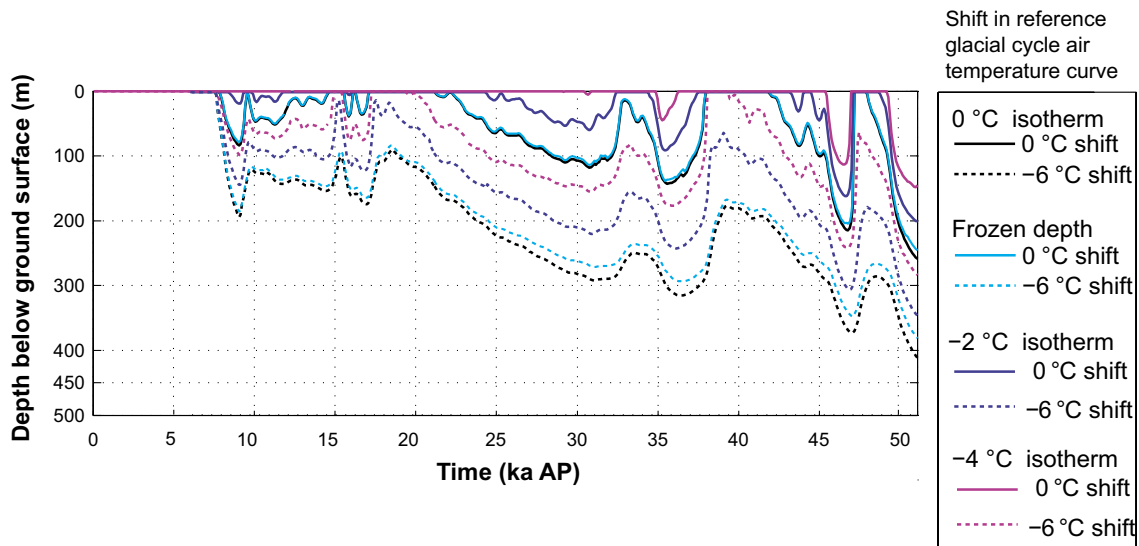


Figure 10-113. Evolution of the 0 °C isotherm (permafrost depth), perennially frozen ground, and the -2 °C and -4 °C isotherms at the Forsmark repository location. The results show the first ~50 000 years of the reference glacial cycle, including the period with deepest permafrost. Solid lines show reference glacial cycle. Dashed lines show the lower boundaries of the corresponding uncertainty intervals when considering the maximum uncertainty in air temperature (± 6 °C) (see the Climate report, Appendix 1). The results are from the dry climate variant with deeper permafrost (see the Climate report, Section 3.4.4).

are lowest towards the ground surface). Therefore, it can also be concluded that the -6 °C isotherm, i.e. the temperature relevant for detrimental buffer freezing (see Section 12.3), does not reach repository depth in the reference glacial cycle. Furthermore, since the uncertainty interval for the perennially frozen ground does not reach 450 m depth, even in this most extreme combination of all uncertainties, freezing of groundwater at repository depth is excluded in the reference glacial cycle. In this most extreme situation, the lowest temperature at the 450 and 470 m depths are approximately -0.5 °C and 0 °C respectively.

In the reference glacial cycle, the maximum freezing depth is reached prior to the ice sheet overriding. This means that for this glacial cycle, glacial erosion will not reduce the repository depth so that it affects the conclusion on freezing. In addition, the total amount of surface denudation, i.e. the combined effect of surface erosion (including glacial erosion) and weathering, is expected to be within the range 1.6–3.5 m for the Forsmark site for the reference glacial cycle (see the **Climate report**, Section 4.5). Here it is also worth mentioning that the *actual* denudation at the Forsmark site over the coming 100 000 years is estimated to be considerably smaller than this range based on last glacial cycle conditions. Given the carbon emission scenarios of IPCC (see the **Climate report** Sections 5.2 and 5.3 and Appendix E and F), and the resulting associated reduction in length of glaciated periods at Forsmark (Lord et al. 2019), the total denudation of bedrock at Forsmark may be less than 1 m (see the Climate report Section 3.5.4). Over the coming one million years, the total amount of bedrock denudation at the Forsmark site has been estimated to be less than 50 m (see the Climate report, Section 3.5).

The reconstruction of permafrost for the reference glacial cycle is described in detail in the **Climate report**, Sections 3.4.4 and 4.4.3.

Identified uncertainties and their handling in the subsequent analysis

Based on the above results, and on the buffer and backfill concept presented in Chapter 5, freezing of water, buffer clay and backfill material at repository depth does not occur in the reference evolution. Further evaluations of the uncertainties involved in this issue, including analyses of climate conditions favouring the occurrence of permafrost, are given in a dedicated scenario, see Section 12.3.

10.4.4 Rock mechanics

If the buffer or backfill were to freeze under permafrost conditions, this would imply a mechanical load on the surrounding rock. However, based on the analyses in Section 10.4.3, freezing is not included in the reference evolution.

Glaciations will alter rock stresses compared with present-day conditions. The nature of glacially induced stresses depends not only on the ice-load, but also on the crust/mantle characteristics and interactions between the two. Whereas estimating the added vertical stress component is relatively straightforward, it is more complex to assess the horizontal stress components, as they will depend on the evolution and properties of the ice sheet, the thickness and mechanical properties of the crust and the properties of the viscoelastic material that the crust is assumed to rest on. However, any shear stress applied by the ice sheet at the ice-rock interface will not be significant.

The load imposed by the ice sheet on the underlying bedrock leads, on the large scale, to downwarping under the ice sheet and upwarping at the margins of the depression (forebulge). This results in an increase of compressional stresses in the crust below the ice and extensional stresses in the forebulge. On a small scale, the transient load of the ice sheet will cause an overall increase in total stresses, and an increased confinement due to the associated increase in horizontal stress. The combination of load from the ice sheet and increased pore pressures means that the effective stress is affected in two counteracting ways:

- An increase in total stress due to the mechanical loading by the ice sheet leads to an increase in effective stress, but
- an increase in pore pressure due to glaciation leads to a decrease in effective stress.

The resulting hydro-mechanical impacts will thus largely depend upon how the load of the ice sheet is transmitted to the underlying rock.

The following processes related to the glaciation cycle could have potential safety implications.

- Reactivation of fractures that could affect fracture transmissivity and transport resistance in the far field (safety function R2a) and in the near field (safety function R2b).
- Fracturing – potential for hydraulic jacking that could affect fracture transmissivity and the aperture of the deposition hole fracture interface and thus the buffer/rock interface transport resistance (safety function R2b).
- Potential for creep deformation, that could affect the geometry of the deposition holes (safety function R3), which in turn indirectly could affect several of the buffer and canister safety functions.
- Seismicity and faulting that could imply shear movement of fractures intersecting deposition holes (safety function R3b) and also increase the transmissivity of the sheared fracture (safety function R2b).

The safety implications of these processes except seismicity and faulting are assessed in the following sub-sections. Seismicity and faulting are treated in a dedicated Section 10.4.5, which also includes an assessment of the effects on the buffer and canister.

Stress changes during the glacial cycle

The ice sheet will increase the mechanical load on the repository, both through the additional weight of the ice itself and through the flexural response of the Earth's lithosphere. This will, on a large scale, result in a depression beneath the load, where crustal flexure will give an additional slow increase in horizontal stresses in the upper crust. Outside the ice sheet margin crustal flexure will result in an up-warping peripheral bulge in which the horizontal stresses are reduced. The magnitude of the induced bending stresses depends on the thickness of the ice sheet and on the duration the area is covered by ice. As the ice sheet retreats during deglaciation, the depressed lithosphere will experience isostatic rebound, which is a much slower process than the ice load removal process. Consequently, high horizontal stresses remain in the lithosphere for a significant amount of time after the ice sheet induced vertical stress has disappeared, resulting in increased stress anisotropy.

In addition to the glacially induced stress variations, the ice sheet will increase the water pressure in the rock below the ice or beneath an impermeable permafrost layer in front of the advancing ice. The increased pore pressure, in combination with the increased stress anisotropy, may cause the rock to fail, thereby causing disturbances ranging from increased fracture permeability to large earthquakes, such as those associated with the endglacial faults of northern Sweden (e.g. Lagerbäck 1979).

Lund et al. (2009) studied how stresses induced by a realistic model of the Weichselian ice sheet evolve in time and space, and how those stresses interact with, and affect, the regional state of stress in Scandinavia. Lund et al. (2009) used the three-dimensional Weichselian ice sheet reported in SKB (2006c), which is the reference ice sheet scenario for the PSAR, in combination with both simple, horizontally layered Earth models and more complex 3D representations of the Earth. The resulting displacement fields were compared to available GPS data. In order to investigate the interaction of the glacial stresses with the background stress field the authors constructed models of the background field and showed how the combined stress field evolves. Using the combined stress field, Lund et al. (2009) estimated how the stability of faults is affected by the glaciation, giving particular attention to the Forsmark and Laxemar sites and, for comparison, the Pärvie fault in northern Sweden, the largest of the known glacially reactivated faults.

Hökmark et al. (2010) use the results of Lund et al. (2009) to estimate the stress changes in the far field as well as the near field. Figure 10-114 shows the temporal evolution of the total principal stresses at repository depth (460 m) during the glacial phase at Forsmark. Similarly to the repository heated period of the temperate phase, the temperature changes introduced during permafrost conditions will alter the stresses in the rock mass. However, as opposed to the temperate phase the temperature reduction during permafrost conditions affects much larger volumes of the rock mass meaning that thermo-mechanical properties on a larger scale have to be considered, i.e. accounting for surrounding rock with lower stiffness and the presence of deformation zones, which will effectively reduce the deformation modulus of the rock mass. Based on estimates of the rock mass deformation modulus, in the range 40–45 GPa, suggested to be valid for large scale models of the bedrock surrounding the Forsmark site, the results from the present modelling work are scaled to an effective deformation modulus of 40 GPa. Figure 10-115 shows the resulting reduction in horizontal stress as a function of depth. Furthermore, Hökmark et al. (2010) make two alternative assumptions regarding the glacially induced pore pressure at different depths.

1. It is assumed to follow the hydrostatic pressure at the ice bed interface, i.e. 98 % of the increase in vertical stress due to the glacier, at all times and at all depths. However, as the ice margin is passing over the site or in combination with proglacial permafrost as the ice is advancing, this approach may underestimate the excess pore pressure at large depths.
2. Estimates of the residual pore overpressure as a function of depth as the ice margin is passing over the site are established in 2D using a simplified ice sheet profile (Paterson 1994) with the suggested ice frontal retreat rate at Forsmark (SKB 2006a) and with depth-dependent hydraulic properties of the rock mass (Follin et al. 2007b, Vidstrand et al. 2010). The estimate of the overpressure that could exist under an impermeable proglacial permafrost layer is based on worst case assumptions of the permafrost melting rate, i.e. on a case that maximizes the potential jacking depth under the advancing margin (Lönnqvist and Hökmark 2010). For the latter pore pressure estimate, the seasonal pressure variations are taken into account.

Reactivation of fractures during glacial cycle – hydraulic impacts in the far field

Using the modelling approach outlined in Section 10.3.5, Hökmark et al. (2010) assess the transmissivity effects for five instances in time, the first glacial maximum (12 000 years after the first mechanical impact due to the ice), ice margin passing over the site in connection with the first episode of ice frontal retreat (after 15 000 years), stress reductions due to forebulge (after 39 000 years), second glacial maximum (after 54 500 years) and ice margin passing over the site in connection with the second episode of ice frontal retreat (58 000 years after the first mechanical impact).

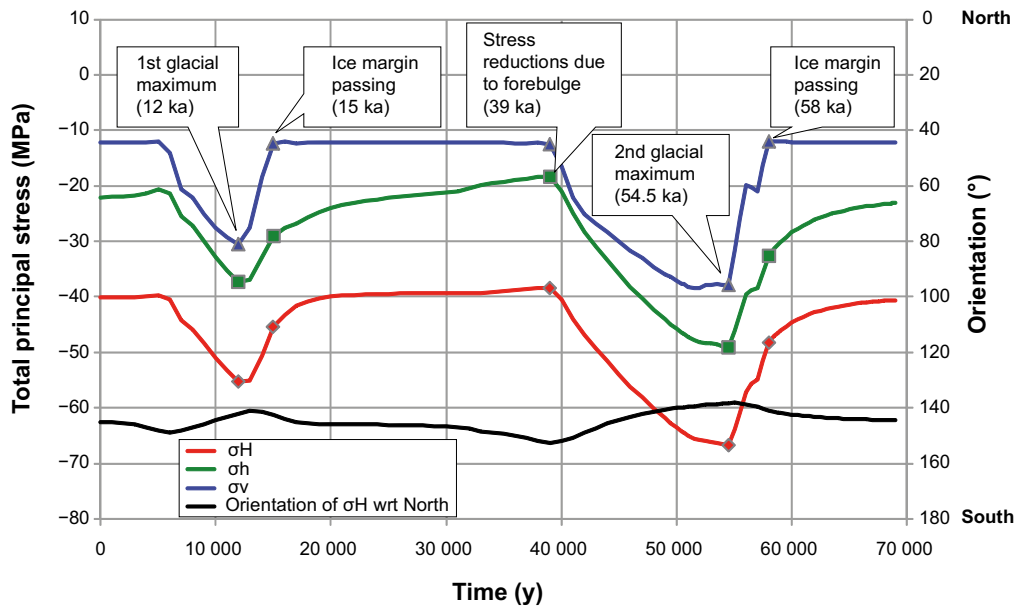


Figure 10-114. Total principal (σ_H , σ_h , σ_v) stress magnitudes at repository depth during the glacial phase at Forsmark. Note that time = 0 in the figure is the time when glacial mechanical effects begin, i.e. about 50 000 AP, according to the reference glacial cycle. The orientation of major horizontal stress with respect to North is also shown. The glacially induced stresses at 500 m depth are taken from Lund et al. (2009). In this diagram compression is negative. From Hökmark et al. (2010, Figure 7-14).

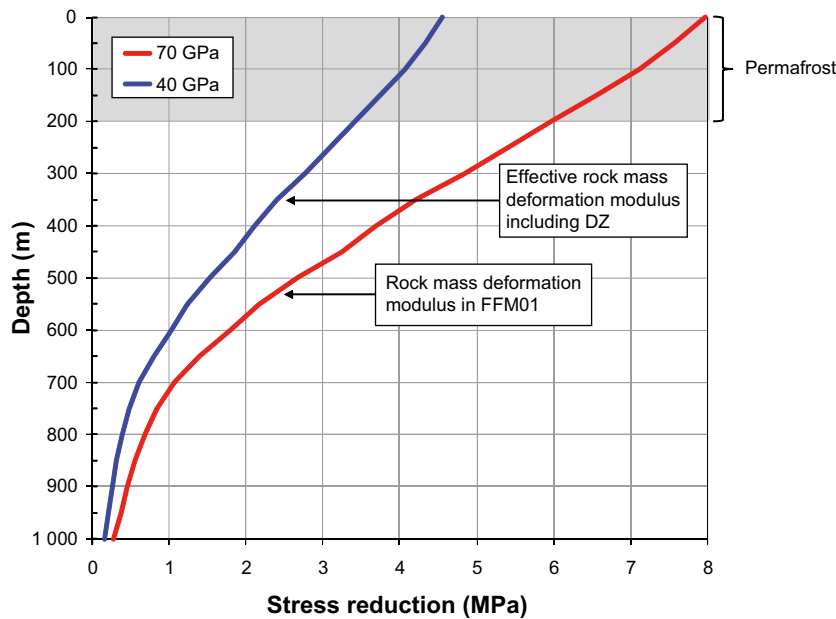


Figure 10-115. Horizontal stress reduction (i.e. reduction of compression) during permafrost conditions. The red line is the calculation result based on a local scale rock mass stiffness of 70 GPa. For use in subsequent analyses this stress reduction is revised, shown in the blue line, such that it represent the rock mass stiffness for relevant large-scale elastic properties, i.e. a rock mass stiffness of 40 GPa. From Hökmark et al. (2010, Figure 7-6).

The results are sensitive to the assumptions regarding the magnitude of the pore pressures. Two cases, described in the text above, regarding the glacially induced pore pressure are considered. In addition to variations in pore pressure, the impact of the potential reduction of the horizontal stress components by thermo-mechanical effects due to permafrost are also considered. The following is found:

- On fractures or fracture zones perpendicular to the major horizontal *in situ* stress, there are only negligible variations in relative transmissivity below a depth of around 200 m, regardless of the pore pressure assumption or potential reductions of the horizontal stress components during permafrost.
- On fractures and fracture zones oriented perpendicular to the present-day minor horizontal *in situ* principal stress, the relative transmissivity is increased during the first glacial maximum (after 12 000 years) and during the forebulge (after 39 000 years), whereas it is reduced as the ice margin passes (after 15 000 and 58 000 years) and during the second glacial maximum (after 54 500 years). This applies for both assumptions regarding the pore pressure. The maximum increase in relative transmissivity occurs during the forebulge (after 39 000 years). Without considering an increase in pore pressure due to permafrost, the relative transmissivity is increased by a factor around 2 (model A according to Figure 10-20) at shallow depths and less than 30 % at repository depth and below, see Figure 10-116 (left). In combination with proglacial permafrost (after 39 000 years), the increase in pore pressure results in an increase in relative transmissivity by a factor around 2–3 (model A) at repository level and above. For model B (see Figure 10-20), no increase in relative transmissivity larger than a factor 1.6 was found. The additional reduction in the effective horizontal stresses during permafrost conditions results in a substantial increase in relative transmissivity at shallow depths (a factor about 7) but the increase at repository level is a factor around 2.5 (model A) (see Hökmark et al. 2010, Figure 7-10). The corresponding range for model B is 1.5–2.5.
- The effective vertical stress is unaffected or marginally increased at all times and at all depths when residual or permafrost induced pore pressures are not considered, resulting in only negligible variations in the relative transmissivity of horizontal fractures, see Figure 10-117. As the ice front is retreating (after 15 000 and 58 000 years), the maximum increase in relative transmissivity is in the range 1.5–2.1 (model A). For model B the maximum increase is less than a factor 1.4 at all depths. In combination with proglacial permafrost (39 000 years), the maximum increase in relative transmissivity is a factor 2.3 directly below the permafrost and decreases with depth (model A). For model B the maximum increase is less than a factor 1.5 at all depths.

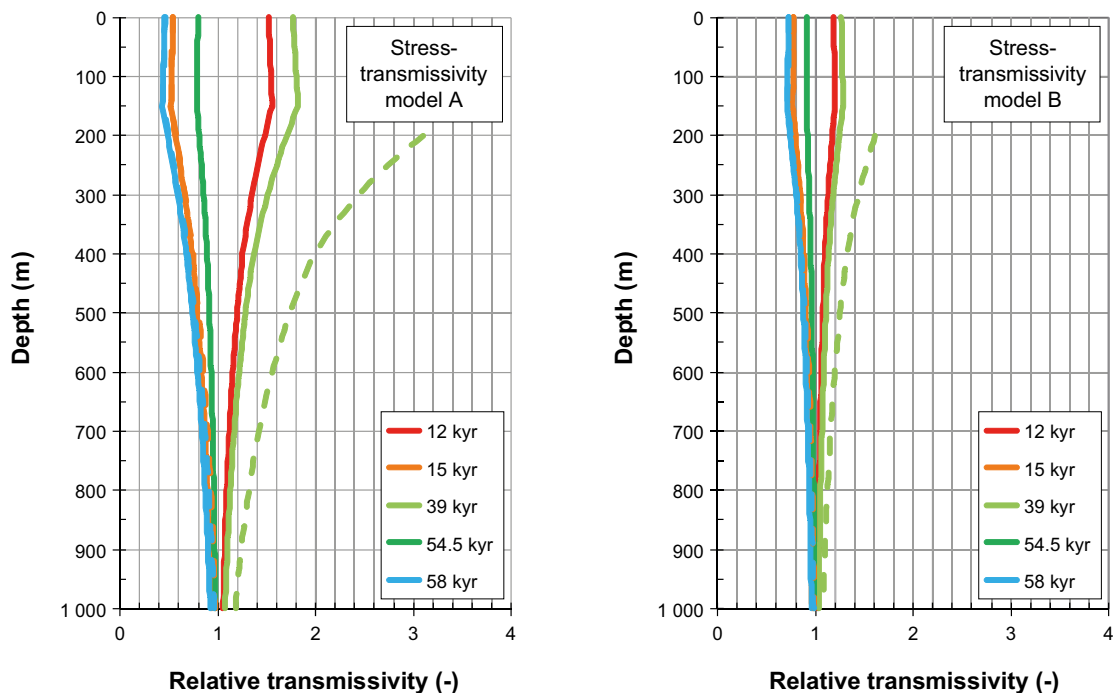


Figure 10-116. Relative transmissivity of vertical fractures perpendicular to the present-day minor horizontal *in situ* principal stress, σ_h . Effects due to residual pore pressures are marked with dashed lines. From Hökmark et al. (2010, Figure 7-9).

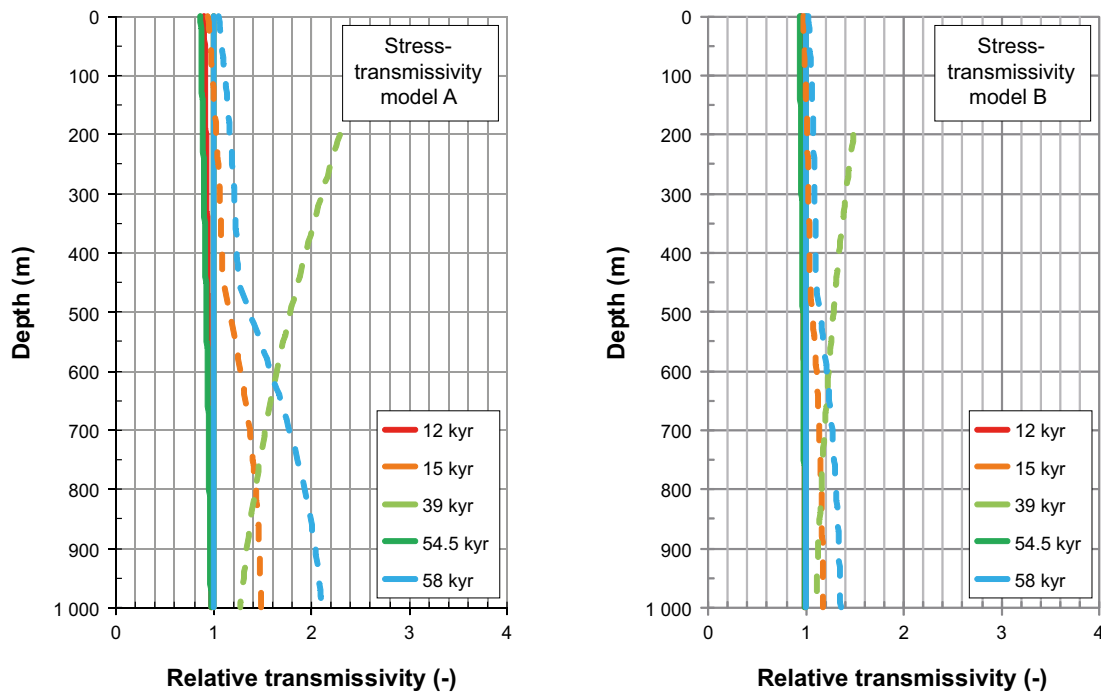


Figure 10-117. Relative transmissivity of horizontal fractures. Effects due to residual pore pressures are marked with dashed lines. From Hökmark et al. (2010, Figure 7-11).

In conclusion, the potential transmissivity increases during the glacial cycle are very moderate, especially in relation to other uncertainties in the flow model, and there seems to be little reason to assess their impacts on the groundwater flow during this period.

Hökmark et al. (2010, Section 7–5) also assess the potential for shearing during the glacial cycle and draw the following conclusions.

- The largest shear displacements occur in connection with the second episode of ice frontal retreat. A 100 m radius fracture with the most favourable orientation, with regard to slip, might slip at maximum about 12 mm assuming the largest possible residual pore pressure considered (about 1 MPa at repository depth). Without any residual excess pore pressure, the corresponding maximum slip is about 8 mm. Smaller fractures slip correspondingly less. The effective normal stresses are reduced but are still around 12–14 MPa for the most unstable fractures, i.e. high enough to suppress dilation. It is therefore assumed that the resulting changes in transmissivity are negligible.
- For fractures dipping more than 45°, the shear displacement is less than 2–3 mm regardless of strike. Fracture with radii larger than 100 m will move correspondingly more. The effective normal stress is significantly increased, which will mean that the resulting transmissivity is likely to be reduced rather than increased regardless of the magnitude of the displacement.

These findings should be regarded as upper bound estimates of the impact of stress changes. All results are based on numerical and analytical solutions that approximate fractures with perfectly planar slip planes. This means that, for given stress conditions, the amount of slip scales with fracture size. In reality, slip along large fractures probably would be controlled by variations in fracture orientation, large scale irregularities etc. There is, however, no defensible way of accounting for these effects and it cannot be excluded that some fractures could be close to being perfectly planar.

In conclusion, while there are some mechanical impacts on fracture transmissivity during the glacial cycle, these impacts are judged too small to require further assessment in the PSAR.

Reactivation of fractures – potential hydraulic impacts in the near field

The transmissivity impacts discussed in the previous section also apply to the near field. However, to complement these analyses for the near-field scale, the 3DEC near-field rock mechanics analysis of

Hökmark et al. (2010), see Section 10.3.5, explored the effects of the glacial load regarding transmissivity impacts due to variations in effective normal stress, see also Figure 10-118:

- The largest reductions in effective normal stress occur during the two glacial maxima (12 000 and 54 500 years).
- Steeply dipping fractures striking perpendicular to the deposition tunnel, and approximately to σ_H , have sufficiently high compressions that the resulting variations in relative transmissivity are only marginal.
- For other steeply dipping fractures, the changes in transmissivity could be as high as a factor of 20, but these would be concentrated in a limited region around the tunnel. The size of the fracture is not important. Note that the stress-transmissivity relation becomes very uncertain as the effective normal stress approaches zero, i.e. when the transmissivity becomes indefinite. However, Hökmark et al. (2010) argue that, for fractures in compression of a few MPa, the stress-transmissivity relations are relevant as upper bound estimates of the sensitivity to variations in effective normal stress.
- If the fracture is less than 2 m from the tunnel and almost parallel to the tunnel periphery, then the high-transmissivity part of the fracture may be large, i.e. extend along large distances of the tunnel. In this case, the size of the fracture will become important.
- At distances larger than approximately 2 m from the tunnel, there are only marginal changes in relative transmissivity.

Conclusions that can be drawn from the analyses of shear displacements coincide with those for the far-field fractures. However, there may be regions very close to the openings where local transmissivity effects could be significant, for instance because of shear displacements along fractures in very low compression.

- For steeply dipping fractures there are only very limited shear displacements close to the tunnel regardless of whether transient pore pressure effects during the glacial phase are considered or not. These small shear displacements are judged not to have any implications for the overall transmissivity of fractures intersecting the tunnels.
- Gently dipping fractures are more likely to shear, but the impact depends on the assumptions made on pore pressures. The amount of shearing will depend on the size of the fracture and its strike orientation. For the 50 m-radius fracture assessed by Hökmark et al. (2010), the maximum shear displacement was around 8–9 mm.

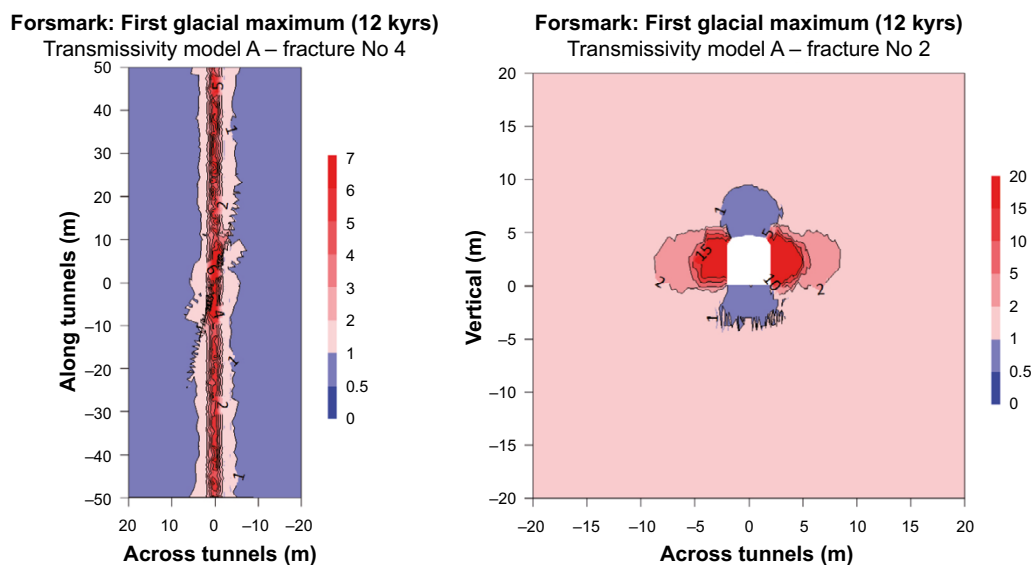


Figure 10-118. Relative transmissivity change for at the first glacial maximum (after 12 ka) in a fracture (left) parallel to the tunnel floor and (right) a vertical fracture intersecting the tunnel at a small angle projected onto the vertical plane perpendicular to the deposition tunnel. Modified after Figures 8-16 and 8-12 in Hökmark et al. (2010).

In summary, when taking transmissivity impacts originating from both variations in effective normal stress and shearing into account, Hökmark et al. (2010) concluded that the results obtained for SR-Can (Hökmark et al. 2006, Figure 5-8) give an adequate description of the transmissivity increase of differently oriented fractures intersecting the near field. Hökmark et al. (2006) estimated that the transmissivity might increase by two orders of magnitude in a region of around 1–2 m from the tunnel periphery.

Fracturing – potential for hydraulic jacking

Hydraulic jacking is a phenomenon that theoretically occurs when the pore pressure in a fracture exceeds both the normal stress acting on the fracture and the fracture's tensile strength. This is the same mechanism as hydraulic fracturing, which is a standard operation in the petroleum industry carried out in wells for improving oil or gas recovery from reservoir rocks and in rock stress measurement. Hydraulic jacking could potentially be initiated during a glacial period when high pore pressures must be assumed to build up in the rock beneath the permafrost in front of an advancing ice sheet or below the ice sheet. As the ice sheet retreats at the end of the glacial phase, the pore pressure may remain high for a long time after the ice is gone. When jacking occurs, the fracture surfaces separate from each other and the fracture aperture may be very large. Jacking can be expected to continue as long as the conditions driving tensile conditions in the fracture exist. Except for horizontal or sub-horizontal fractures close to the ground surface where the overlying rock can potentially be lifted, the maximum aperture resulting from the process is limited by the deformation potential of the rock mass surrounding the dilating fractures.

The present understanding is that the horizontal stress components due to the ice are of the same magnitude or greater than the corresponding vertical stress component and that they exist outside the ice (Lund et al. 2009). In a reverse stress field ($\sigma_H > \sigma_h > \sigma_v$), which is the case at Forsmark (Glamheden et al. 2007), this implies that hydraulic jacking is mainly of concern for sub-horizontal fractures.

Possible indications of hydraulic jacking events, in the form of sediment-filled fractures, have been found at Forsmark, to depths of a few tens of metres. However, hydraulic jacking may, in theory, also be initiated at substantially larger depths (Talbot 1999, Hökmark et al. 2006). Therefore, a special study on the potential for hydraulic jacking during a glacial cycle (Lönnqvist and Hökmark 2010) has been conducted. It shows that:

- In the absence of proglacial permafrost, hydraulic jacking in front of an advancing ice sheet is unlikely to be initiated at depths greater than about 30 m if the rock can be treated as a continuous and relatively homogeneous porous medium. The possibility that a few highly transmissive fractures in otherwise low permeable rock may transfer high pressures from large distances under the ice to the ice front and thereby cause hydraulic jacking can also be discarded. Analytical estimates indicate that in order to initiate hydraulic jacking at 400 m depth a fracture at least 7.6 km long in otherwise impermeable rock is needed. There are no indications of the existence of such fractures at Forsmark.
- For the case of proglacial permafrost in front of an advancing ice, hydraulic jacking below the permafrost could only be seen for permafrost melting rates much higher than those established for the reference glaciation cycle. Note that the pore pressure beneath the permafrost is completely determined by the pressure at the melting zone, the diffusivity of the rock and the time-frame of the frontal advance, which implies that the initial permafrost thickness will not influence the maximum jacking depth. The worst cases studied had an initial permafrost depth of 200 m with melting rates between 0.5 and 1 m/year and this condition gave maximum jacking depths of around 330–350 m. However, this depth was reduced to about 175–210 m, considering the seasonal variations in the boundary hydrostatic pressure. The reference melting rate resulted in increased pore pressure levels corresponding to jacking depths of less than 10 m. A potential occurrence of open taliks near the repository would further decrease the maximum jacking depth.
- For a retreating ice sheet, the key factors are the frontal retreat rate of the ice and the hydraulic diffusivity of the rock. The maximum jacking depth was established for two assumptions regarding the frontal retreat rate: A much faster frontal retreat rate (500 m/year) suggested by Talbot (1999) and the retreat rate of 300 m/year considered to be more relevant for Forsmark (SKB 2006a). A maximum jacking depth less than 100 m results even for the fastest retreat speed. For the retreat speed relevant for Forsmark (300 m/year) the maximum jacking depth is around 50 m.

In conclusion, hydraulic jacking due to the impacts of the glacial cycle, below 200 m depth is judged highly unlikely. At more shallow depths it may happen, and the highly transmissive subhorizontal fractures near surface at Forsmark may be evidence of this occurring in the past. However, given the already very high, and potentially jacking-induced, near surface horizontal permeability, this effect is already captured in the hydrogeological models used.

Fracturing of the rock due to the glacial load

Hökmark et al. (2010) also assess the potential for spalling in the deposition tunnel walls due to the glacial load. The stresses at the centre of the tunnel roof will not exceed the spalling strength during the temperate phase. During the second glacial maximum (54.5 ka) the major principal stress at the centre of the tunnel roof reaches a maximum of about 95 MPa, i.e. well below the spalling threshold, but the spalling strength might be exceeded in the corners. Potentially, this can be avoided by rounding the corners, but the possibility needs to be considered as a potential mechanism for generating enhanced rock permeability near the roof.

Potential for creep deformation

As further discussed in Section 4.5 of the **Geosphere process report**, and supported by the recent study by Damjanac and Fairhurst (2010), creep deformation of the rock mass may be neglected for the mechanical loads that may occur during permafrost or glaciation. The process is neglected for the same reasons as for the temperate periods, see Section 10.3.5.

Identified uncertainties and their handling in the subsequent analysis

The discussion above is used to draw a set of conclusions regarding the uncertainties, and their subsequent handling in the PSAR analyses, on the mechanical changes in the bedrock projected to occur during the remaining part of the reference glacial cycle.

- The *transmissivity increases due to reactivation of fractures* during the forebulge period of the glacial cycle are relatively moderate, especially in relation to other uncertainties, and it is judged not to be justified to assess their impacts on the groundwater flow during this period, apart from the transmissivity increase that would occur for fractures close to and parallel with the tunnel floor. However, this case is already covered by the assumptions made for the EDZ (see further the **Data report**).
- *Hydraulic jacking* below 200 m, due to the impacts of the glacial cycle is judged highly unlikely. At shallower depths it may happen, and the highly transmissive gently dipping fractures near surface at Forsmark may be evidence of this occurring in the past. Given the already very high, and potentially jacking-induced, near surface horizontal permeability, this effect is already captured in the hydrogeological models used and the phenomenon is excluded from further analysis.
- *Fracturing of the rock due to the glacial load*. During the second glacial maximum (54 500 years after first mechanical impact of the ice) the spalling strength might be exceeded in the corners of the tunnel roof. Potentially, this can be avoided by rounding the corners, but the possibility should be considered as having the potential for enhanced rock permeability near the roof. However, the permeability increase would be much smaller than the “crown space” case considered in the hydrogeological assessment, see Section 10.4.6 and there is no need for a special calculation case for assessing the importance of this effect.
- Literature evidence suggests that there is no potential for *creep deformation* that could significantly affect deposition hole geometry, allowing exclusion of the phenomenon from the safety assessment.

10.4.5 Canister failure due to rock shear movements

Sweden is located in the Fennoscandian Shield (Koistinen et al. 2004) far from plate boundaries and active volcanism. Though its rocks bear witness of a violent tectonic past that includes several orogenies and failed rifts, the bedrock is now seismically stable. However, glacially triggered faults (Kujansuu 1964, Lundquist and Lagerbäck 1976, Olesen et al. 2000), commonly referred to as “post-glacial faults” and traditionally abbreviated “PGF”, occur in glaciated regions in response to changes in the glacial load, either as a result of deglaciation (crustal unloading) or glacial advance (crustal

loading). Glacially induced faulting has been reported from northwest Europe (Norway, Sweden, Finland, Russia, Eire, Germany and Scotland) and North America (eastern Canada, New England, and possibly California and Montana). To date, all examples of glacially induced faults have been recorded in regions of low to moderate seismicity, namely passive margin, failed rift, or intraplate/craton environments such as Sweden.

The postglacial faults in northern Sweden are convincing examples of such glacially induced faulting. Although there have been numerous claims of such faulting in mid- to southern Sweden (Mörner 1989, 2003, 2004), many have been disregarded or questioned as such (SKB 1990, Carlsten and Strähle 2000, Wänstedt 2000, Lagerbäck and Sundh 2008). A nation-wide inventory of scarps using LiDAR (Mikko et al. 2014, 2015) revealed a few, previously unknown, minor scarps of which the one at Bollnäs, about 150 km NW of Forsmark, is the most prominent. Within the framework of the site investigations, Lagerbäck et al. (2005, 2006) investigated large areas in the vicinity of the Forsmark and the Laxemar sites and came to the conclusion that large, glacially induced earthquakes cannot be positively demonstrated. This was also confirmed by a recent study using high resolution LiDAR (Öhrling et al. 2018). Still, as also emphasised by Lagerbäck and Sundh (2008), this does not exclude the possibility of smaller earthquakes having occurred, nor the possibility of future, large earthquakes in the investigated areas. The latter argument is a major rationale for including an earthquake scenario in the post-closure safety assessment.

Earthquakes have been recognised to potentially threaten post-closure safety since the early days of the Swedish nuclear waste programme (SKBF/KBS 1977, 1983b). Using probabilistic arguments, these assessments concluded that “block movement” indeed could be induced by earthquakes also in cratonic bedrock, but also concluded that such movements would be very small, in the order of less than a mm over a million years, and with very low probability of occurrence. These conclusions were supported by the instrumental record of Scandinavian earthquakes and by findings that tunnels are very much more resistant to earthquakes than surface structures (e.g. Dowding and Rozan 1978). Altogether, therefore, the impact of earthquakes on repository safety was, then, regarded insignificant.

This view also prevailed in the following safety assessment, SKB 91 (SKB 1992), in which it was additionally concluded that, based on an analysis by Slunga (1991), “...*the aseismic movements i.e. movements that do not give rise to earthquakes - are probably of greater importance...*” (SKB 1992, p 40). It must be noted, however, that SKB 91 served as a basis for testing a system of efficient procedures for carrying out safety assessments, i.e. a test of methodology for safety assessments rather than a safety assessment proper, using the Finnsjön site as a tentative location for the repository. Some limited modelling efforts (e.g. Barton and Chryssanthakis 1989) were performed to address the impact of glaciations upon fracture stability but these were not in any obvious way included in the safety assessment.

Although findings of large fault scarps indicative of large earthquakes in Scandinavia (example shown in Figure 10-119) were reported early (Du Rietz 1937, Kujansuu 1964), these records passed fairly unnoticed by the geoscientific community or were regarded with a certain degree of scepticism. However, in the late seventies, paleoseismology became an emerging, and accepted, branch of geosciences in Scandinavia, much triggered by the findings of exceptionally impressive fault scarps in Lapland (Lundqvist and Lagerbäck 1976, Mörner 1978, Henkel et al. 1983, Olesen 1985, Johnston 1987). The newly discovered scarps altered the prevailing view on seismicity in cratonic, formerly glaciated, regions. SKB initiated a comprehensive research program to address the paleoseismic records in Sweden (e.g. Bäckblom and Stanfors 1989, Ericsson and Stanfors 1993, Stanfors and Ericsson 1993 and references therein) and a comprehensive earthquake scenario was included in SKB’s SR 97 safety assessment (SKB 1999a).

The potential for fault weakening and/or reactivation at the sites, as a response to future glaciations has, using simulation of advancing and retreating ice sheets, been addressed in a series of reports to SKB (Lund 2005, 2006, Lund et al. 2009) and the effect on a repository, should a large earthquake occur in the vicinity, has been investigated in a series of reports and publications by Fälth and Hökmark (Fälth and Hökmark 2006, Fälth et al. 2007, 2008, Fälth 2018, Hökmark et al. 2019).

It is well known that underground facilities are resistant to earthquakes (e.g. Bäckblom and Munier 2002, and references therein) and the detrimental effects of a large earthquake near the repository can be avoided or considerably lessened by adaptive design involving the use of respect distance (Munier and Hökmark 2004, Munier et al. 2008) and deposition hole rejection criteria (Munier 2006, 2007, Hedin 2008b).



Figure 10-119. The 150 km long Pärvie fault scarp (Lundqvist and Lagerbäck 1976) displays offsets that locally exceed 15 m (Muir-Wood et al. 1989, Lagerbäck and Sundh 2008). Estimates of the magnitude of the associated earthquake range between 7.8 and 8.2 (Muir-Wood et al. 1989, Lagerbäck 1992, Arvidsson 1996, Lindblom et al. 2015). This, and many other similar observations, are compelling evidence that the Baltic shield is indeed seismically active, albeit with longer recurrence rates (Photo Raymond Munier 2012).

Using idealised geometries and pessimistic assumptions, the seismic impact on the canister integrity was addressed by La Pointe et al. (1997, 1999, 2002) in SR 97 (SKB 1999) with the result that earthquakes were recognised to, indeed, impose a potential threat to the canister integrity. Following the initial work of La Pointe et al. (1997), a number of efforts were initiated within the SKB research programme (SKB 2001) to evaluate the pessimistic assumptions (La Pointe et al. 2000), to corroborate modelling results with tunnel observations (Bäckblom and Munier 2002, Bäckblom et al. 2004) and to identify alternative modelling concepts (Munier and Hökmark 2004). This resulted in an intensified research programme (SKB 2004b) to develop adequate methods to compute the seismic impact, to populate the models with realistic and site-specific data and to incorporate the results of these analyses in safety assessments.

For post-closure safety, it was early concluded that the only earthquake-related process that would constitute a risk for the integrity of the buffer-canister system would be shear displacements along fractures intersecting canister positions (Fälth et al. 2010). For instance liquefaction, i.e. the process in which a soil-water system behaves as a liquid because of shaking, stress increases or liquid pressure increases, was early ruled out as a problem because of the high density of the compacted bentonite buffer (SKB 2006f). Other earthquake-related processes that potentially could constitute a risk for the integrity of the canisters, the bentonite buffer and the tunnel backfill material (shaking, rock failure in walls of tunnels and deposition holes, hydraulic disturbances) are discussed, commented and ruled out as realistic risks in Fälth et al. (2010) based on conclusions and observations made by, for instance, Muir-Wood and King (1993), La Pointe et al. (1997), Bäckblom and Munier (2002) and Aydan et al. (2010). The concept of secondary fracture shear displacements that potentially could occur at different distances from an earthquake was consequently the main issue addressed in Fälth et al. (2010). Dynamic simulations of rupturing potential earthquake faults surrounded by differently located and oriented host rock fractures were performed in order to provide input material to the SR-Site handling of the risk associated with shear displacements along fractures intersecting canister positions.

After the publication of SR-Site (SKB 2011), the work on dynamic simulations has been continued with site-specific input and assumptions regarding in-situ stresses, thermal and glacial load additions, fault and fracture geometries to name the most significant additions. Models relevant to the Forsmark site, which also include some models of the Olkiluoto site in Finland, have been analysed and described in a number of studies which have been summarised in Hökmark et al. (2019). Since the publication of SR-Site, it has been possible to take advantage of the steadily ongoing development of the numerical tools and the increasing computer capacity which, in turn, has made it possible to perform advanced benchmarks and to model less schematic, more detailed rupture models. It has also been possible to analyse larger models and to test the impact of different kinds of fault- and fracture inhomogeneities and of different assumptions relevant to, for instance, the impact of shielding from a fracture network.

The so-called *critical radii* is, perhaps, the most important output from the earthquake modelling, introduced in the supporting material to SR-Site. Critical radii are the radii of the smallest structures (e.g. fractures, deformation zones or any weakness planes) that can host shear movement such as to impose a potential threat to the long-term integrity of the canister. Accordingly, structures equal to or larger than the critical radii, so called critical structures (Munier and Mattila 2015), must be avoided in canister positions. The stepwise and systematic approach to challenge the pessimistic approaches of the assessment has, since SR-Site, led to the following main conclusions (Hökmark et al. 2019):

- The critical radii used as input to the SR-Site assessment were indeed pessimistic estimates and the conclusions of SR-Site are still valid, with considerable margins. In particular, the critical radii that would be relevant for earthquakes occurring on deformation zones located > 600 m away from the repository footprint are large enough for these deformation zones to be without importance to the seismic risk assessment (since they are easily identifiable).
- The critical structures are so large that they constitute deformation zones rather than individual fracture planes. This renders the FPI criteria (Munier 2006, 2007, 2010, Hedin 2008) obsolete and the degree-of-utilisation can be considerably improved as the criteria are very pessimistic by design (Munier 2010, Section 8.2). Additionally, the intersection probability between a canister and a critical structure decrease rapidly with structure size. Thus, as compared to SR-Site, far fewer canisters can be located in critical positions.
- Finally, the results suggest that the steep, NE striking deformation zones in the repository footprint (ZFMENE0060A and ZFMENE0062A) should not require any respect distances. This would enable SKB to make the footprint more compact and, in the process, also maximise the utilisation of the rock volume with the lowest seismic risk. These particular zones were actually classified as stable already in the SR-Site background material relevant to the respect distance issue (Fälth et al. 2010). The results in Hökmark et al. (2019) indicate that this is likely to be, for all load scenarios, the case for all local, steeply dipping deformation zones located within or in the immediate vicinity of the repository footprint at Forsmark. This would mean that the only Forsmark zone of any potential concern for the seismic risk issue should be the gently dipping ZFMA2.
- Though some work remains to verify the conclusions regarding the possibility to optimise the layout (Hökmark et al. 2019), the work carried out since the SR-Site assessment *i)* further supports the claim that the results presented in SR-Site regarding long term earthquake related risk are pessimistic, and *ii)* points to the possibility of entirely eradicating seismic impact as a contribution to long term risk by further optimisation of the repository.

The remainder of the text as regards the rock in this section 10.4.5 is largely identical to that in the SR-Site assessment (SKB 2011, Section 10.4.5). At a few places, important developments since the SR-Site assessment are described. Most of these additions or alterations are based on results reported in Hökmark et al. (2019).

Requirement on the canister

One of three identified failure modes of the canister is that due to a rock shear movement across a deposition hole. The safety function Can3 in Figure 10-2 relates to the ability of the canister to withstand such loads. The buffer is designed to damp rock shear and the safety function requirement on the buffer (Buff3) in this context is specified in Section 8.3.2. An integrated evaluation of the response of the buffer and canister to rock shear has led to the criterion that the shear movement should not exceed 5 cm (safety function R3b), and that the shear velocity should be less than 1 m/s (safety function R3c).

Accordingly, earthquake-triggered, fast, shear movements along structures intersecting a canister can potentially affect the containment of the spent fuel assemblies if the amount of slip exceeds 5 cm. Shear velocities higher than 1 m/s have not been observed in any of the simulations conducted to quantify seismically-induced fracture shear displacements at different distances from earthquakes of different magnitudes (Munier and Hökmark 2004, Fälth and Hökmark 2006, 2012, 2015, Fälth et al. 2010). Therefore, the question of whether the containment of the spent fuel could also be affected by very fast shear displacements smaller than 5 cm is not relevant.

Fracture shear displacements occurring during the time between deposition and a future potential earthquake are not judged to impact on the relevance of the 50 mm canister damage criterion established for seismically induced fracture displacements across deposition holes. Thermally-induced loads during the early temperate phase, for instance will not produce fracture shear displacements larger than about 6 mm on optimally oriented 300 m diameter fractures (Hökmark et al. 2010, Figure 6-28). Loads included in the slowly changing load scenario leading up to the end-glacial instability that is the main concern for the seismic issue will not produce fracture displacements larger than, in total, about 18 mm on 300 m diameter fractures. The 18 mm slip estimate is based on worst case assumptions regarding pore pressure and fracture orientation (Hökmark et al. 2010, Fig 7-19). It should be noted that the 18 mm estimate is obtained without account of local stress relaxations associated with previous episodes of slip occurring, for instance, during the thermal period. The 18 mm, or say 20 mm, estimate should, therefore, be taken as the sum of a number of small slip movements distributed over tens of thousands of years of slow loading-unloading. The effects on the buffer-canister system of such minor shear displacements produced by time-continuous variations of the host rock stresses are judged to be irrelevant to the assessment of the seismic risk, i.e. the canister will withstand a 5 cm seismically-induced shear displacement, regardless of whether minor displacements occurred in the past.

In the following, the 5 cm damage threshold is pessimistically applied throughout all assessments of the number of canisters being damaged as a result of seismically-induced shear displacements, regardless of the canister-fracture intersection geometry and the actual shear velocity. At present there is no estimate of the probability that, for instance, a 6, 7 or 10 cm random intersection geometry displacement actually would impact sufficiently that the canister should be regarded as failed. All estimates of the number of failed canisters are thus pessimistic as regards the applied damage threshold.

Probability of future large earthquakes

All tectonic plates have internal stress fields caused by their interactions with neighbouring plates and loading or unloading (e.g. sediments, ice sheets). These stresses may be sufficient to cause failure along existing fault planes, giving rise to earthquakes. Large intraplate earthquakes are rare compared to earthquakes at plate boundaries but, given the very long time frame of this safety assessment, 10^5 – 10^6 years, large earthquakes are anticipated in Sweden. The difficulty lies in estimating where, how large, and how many earthquakes we anticipate over the time frame considered for the PSAR.

The presence of a continental ice sheet, such as Weichsel, tends to promote fault stability (Johnston 1987, Lund et al. 2009) while the retreat of the ice sheet is followed by rapid glacio-isostatic adjustment and is believed to be accompanied by a sudden increase in both frequency and magnitude of earthquakes. The glacially induced stress magnitudes are not large enough (Lund et al. 2009) to initiate large ruptures on their own. However, during some periods in the glacial cycle they are large enough, aided by pore pressure disturbances, to trigger reactivation of pre-existing faults that are close to failure in the background, preglacial, stress field. Figure 10-120 displays historic and recent earthquakes in Sweden from the FENCAT (FENCAT 2007) and SNSN (Böðvarsson 2002, 2009, Böðvarsson et al. 2006) catalogues, respectively.

The relationship between the magnitude and total number of earthquakes in any given region and time period is given by the Gutenberg–Richter law. Prediction of future earthquakes thus essentially concerns our ability to adequately determine the parameters a and b of the Gutenberg–Richter law:

$$\log N = a - bM_L$$

in which N is the number of earthquakes with magnitudes greater than M_L .

There have been few attempts to estimate the earthquake frequency for time periods relevant to the PSAR. To our knowledge, these are restricted to the ones listed in Table 10-18.

Table 10-18. Estimated^{25,26} yearly frequency of earthquakes \geq M5 within a 5 km radius area. These frequencies are distributed (f) along the 30 deformation zones susceptible to reactivation (see Table 10-19 and Fälth et al. 2010), out of the 36 deformation zones intersecting the area (Figure 10-136).

Reference	Earthquake frequency ($M \geq 5$ /year)	
	5 km radius area	Per deformation zone
(Böörvarsson et al. 2006)	2.4×10^{-6}	7.8×10^{-8}
(La Pointe et al. 2000, 2002)	8.7×10^{-7}	2.9×10^{-8}
(Hora and Jensen 2005)	2.5×10^{-6}	8.3×10^{-8}
(Fenton et al. 2006)	2.0×10^{-6}	6.8×10^{-8}

The frequencies shown in Table 10-18 were, for comparative reasons, normalised by averaging the original frequencies predicted by each estimate over the area covered by each assessment and here rescaled to an area corresponding to a circle with 5 km radius. It is emphasised that estimates of anticipated earthquakes at Forsmark, based on frequencies in Table 10-18, are associated with some yet unresolved uncertainties and fundamental assumptions:

- A. Lagerbäck and Sundh (2008) note that the erosional impact of the Weichsel was quite limited, and it could not have erased remnants of post-glacial faults triggered by previous glaciations. The authors hypothesise that glaciations previous to the Weichsel did not generate faulting analogous to the ones during the Weichsel and suggest that the Weichselian ice sheet could have been anomalous in terms of permafrost-related hydraulic overpressures. Nevertheless, in the absence of further knowledge, it is cautiously assumed that the coming glaciations will have the same impact as the Weichsel in terms of fault stability.
- B. All major, unequivocally identified, post-glacial faults are located in the Lapland region although a few minor fault scarps have been identified as far south as Bollnäs, about 150 km NW of Forsmark (Mikko et al. 2015, Malehmir et al. 2016). It is nonetheless cautiously assumed that the estimated frequencies of large earthquakes are applicable to Forsmark. However, whether strain energy release at Forsmark will indeed be dominated by seismic or aseismic slip is an open issue. The lack of markers for large earthquakes at Forsmark (Lagerbäck et al. 2005, Lagerbäck and Sundh 2008, Öhrling et al. 2018) is taken as an indication that faults following the retreat of Weichsel either slipped aseismically, with small magnitudes, or not at all. As aseismic slip is not anticipated to impose any threat to the integrity of the repository, the assumption is pessimistic.
- C. The site proposed for the repository is located in a tectonic lens bounded by regional deformation zones (Figure 10-121) having surface trace lengths exceeding 30 km for the Singö (ZFMWNW0001) and Eckarfjärden (ZFMNW0003) zones, respectively, and exceeding 70 km for the Forsmark (ZFMWNW0004) deformation zone (Table 10-19). It is judged probable that these zones have greater potential to attract future strains than the much smaller zones within the lens, as has been the case for the latest 1.8–1.7 Ga (Stephens et al. 2007). In particular, these are the only zones near the repository that are large enough to host large earthquakes (up to perhaps M7.5). However, as there are no means to know which of the zones will in fact reactivate in the future, we need to pessimistically assume that all zones considered unstable during the reference glacial cycle have equal probability to reactivate. It is, however, clear that these regional deformation zones, as all vertical or subvertical zones, will be more stable under end-glacial conditions than under all other load conditions. Additionally, the work presented in Hökmark et al. (2019) verifies the SR-Site statement that secondary displacements along host rock fractures at distances relevant for these steeply dipping regional deformations (> 600 m) would be, for all load scenarios and with good margins, too small to be of any concern for the safety of the repository. This holds true even

²⁵ The frequency estimates of Hora and Jensen (2005) in Table 10-18 concern earthquakes of magnitude M6 or larger. The references therein were not readily scalable to \geq M5 but, as the slope of the logarithmic G-R relationship is close to unity (Scholz 2002), we increased the frequencies in Table 10-14 by a factor 10 to incorporate earthquakes of magnitude M5 or larger as an approximation.

²⁶ In Fenton et al. (2006) frequency estimates \geq M4.9 were provided and we choose to use the original values rather than rescaling to M5. This will slightly overestimate the frequency.

for assumptions regarding the initial, present-day, stresses at large depths that would maximize the potential instability of these zones. Altogether, the results of the modelling work performed after SR- Site verify that events occurring on faults located at distances > 600 m from the closest canisters will not be a concern for the safety of the repository.

- D. The earthquake catalogue that forms the foundation of any estimate is very short in relation to the assessment, only about 100 years. The inter-glacial seismicity might be cyclic in nature and it is essentially unknown whether the recorded earthquakes can be regarded as representative.
- E. The magnitude-frequency assessment is very much affected by the largest possible earthquake within the area for which the catalogue is defined. Very few attempts have been made to address this aspect and, using Pärvie as the largest event, published estimates of maximum magnitude range between M7.8 and M8.2 (Muir Wood et al. 1989, Arvidsson 1996, Johnston 1996).
- F. In the 100 years of observed seismicity there is significant spatial variation. It is unclear whether the spatial distribution of earthquakes observed during the last century is a stationary feature, or if it will vary with time. The average spatial frequency for Sweden, which is higher than the recorded frequency at Forsmark, has been pessimistically used for the assessment.
- G. Although much is known about the earthquake frequency pulse following the retreat of the ice sheet (Johnston 1987, Muir Wood et al. 1989, Muir Wood 2000, Mörner 2003) the understanding of the nature of the frequency decay with time is incomplete (Bungum et al. 2010). The fundamental assumption that the frequency estimates used for the safety assessment represent an *average* over the glacial cycle is made. This assumption can be somewhat corroborated by checking how well the frequency-magnitude relations predict the largest events. Using the frequency-magnitude relations of Böðvarsson et al. (2006, Section 4.4) about 40 earthquakes \geq M7 and about 6 earthquakes \geq M8 during a glacial cycle are computed, when normalised to the area of Sweden. Despite the vast uncertainties, this number of events seems within an order of magnitude consistent with the number of faults that have unequivocally been designated as post-glacial faults. Additionally, this indicates that though the frequency estimates of Böðvarsson et al. (2006) were targeted for short time frames (\leq 1 000 years) they seem to be adequate for extrapolation to longer time frames.

All earthquakes result in permanent strain and stress relaxation that stabilises the surrounding rock mass for a considerable amount of time. The stabilising effects reach several km from the earthquake (Fälth et al. 2010), in agreement with observed spacing of faults as noted in Munier and Hökmark (2004, Appendix 3). When, or if, an earthquake occurs at Forsmark, the stress relaxation will be sufficiently efficient to encompass the nearest deformation zones at least during the same period of potential instability. Consequently, given the geometry and, in particular, the spacing of deformation zones at Forsmark (Figure 10-122), only one zone will be able to reactivate within such an episode. However, the duration of the stabilising effect is uncertain. This uncertainty relates to the strain rate, determined by large scale tectonic processes. If the tectonic strain rate is high, the background stresses may largely be restored between glacial cycles. This could lead to repeated endglacial earthquakes during following periods of glacial retreat. Intraplate strain rate estimates range between roughly 10^{-12} per year (Anderson 1986, Muir Wood 1995) and roughly $1.5 \cdot 10^{-9}$ per year (Slunga 1991, Sandiford et al. 2004, Scherneck et al. 2010). However, Slunga (1991) argues that most of the strain energy is continuously released aseismically, meaning that only a fraction of the tectonic strain would be effective for accumulating energy and restoring stresses. This implies that the strain rate effective for local stress regeneration is much lower than the large-scale strain rate across the Fennoscandian Shield.

Assuming the average crust deformation modulus (E) to be 64 GPa (Lund et al. 2009) for the upper 15 km, a tectonic strain rate, $\dot{\epsilon}$, of 10^{-10} per year (e.g. Calais et al. 2005, 2006, Mazotti et al. 2005), which is intermediate to those proposed by Muir Wood (1995) and Slunga (1991), and a stress relaxation, D_s , of 3 MPa (Fälth et al. 2010) near (< 1–2 km) the fault, then the time t required to restore the stress field sufficiently for a new earthquake to occur within 1–2 km is approximately $t = 500\,000$ years according to the equation below.

$$t = \frac{\Delta\sigma}{E\dot{\epsilon}}$$

Accordingly, at most two seismic events of magnitude \geq M5 at Forsmark during the assessment period might be expected. It is recalled that the probability for having one large earthquake within the site is very low. The probability of having two or more earthquakes within the same area is very much smaller.

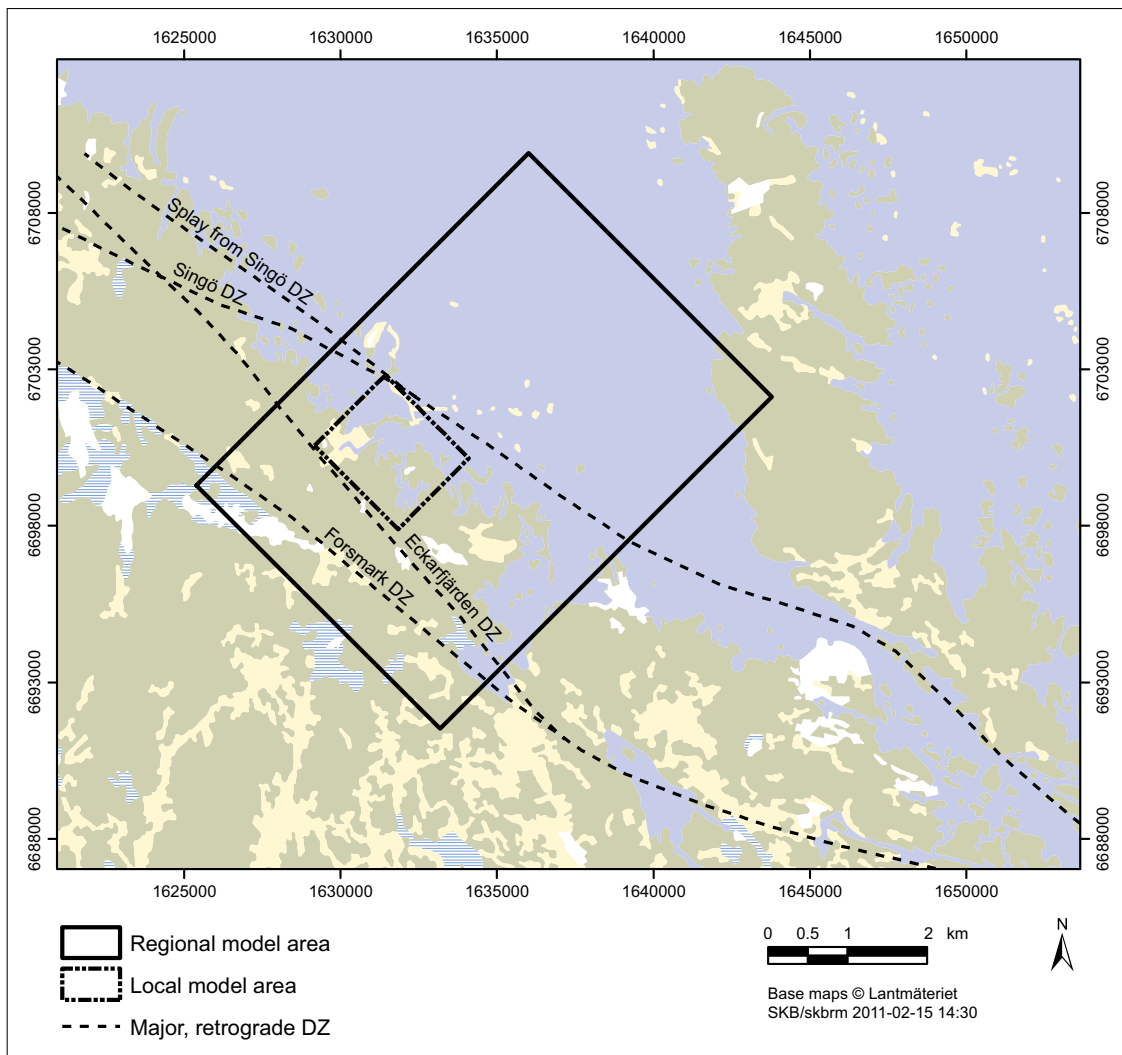


Figure 10-121. Major deformation zones that intersect the regional model area at Forsmark (edited from Stephens et al. 2007).

The probability of any deformation zone hosting an earthquake can be obtained by dividing the probability estimated for the circular area (Figure 10-122) by the number of deformation zones intersecting that area. Using only deformation zones modelled with intermediate to high confidence (Stephens et al. 2007), 36 zones are identified with traces exceeding 3 km (Table 10-19 and Figure 10-122), and judged, therefore, to be able to host earthquakes of magnitude M5 or larger.

The findings of Lund et al. (2009) were used in Fälvh et al. (2010) to identify which of the deformation zones at Forsmark could impact the repository during the glacial evolution. In Figure 10-123 we show the deformation zones that have any part closer than 600 m to any canister position; zones farther away have little means of jeopardising the integrity of the canisters (see next section) provided that canister position rejection criteria are applied. Of these, only five deformation zones are, due to their orientation with respect to stress field, amenable to reactivation (Fälvh et al. 2010) during the glacial evolution; the remaining two are judged stable. All zones classified unstable on Figure 10-123 and in Table 10-19 are judged large enough to host earthquakes of magnitudes exceeding M5 but only one of these zones, ZFMNW0017, is judged large enough to host earthquakes of magnitude up to roughly M6. In the next section we examine the impact of earthquakes on canister integrity.

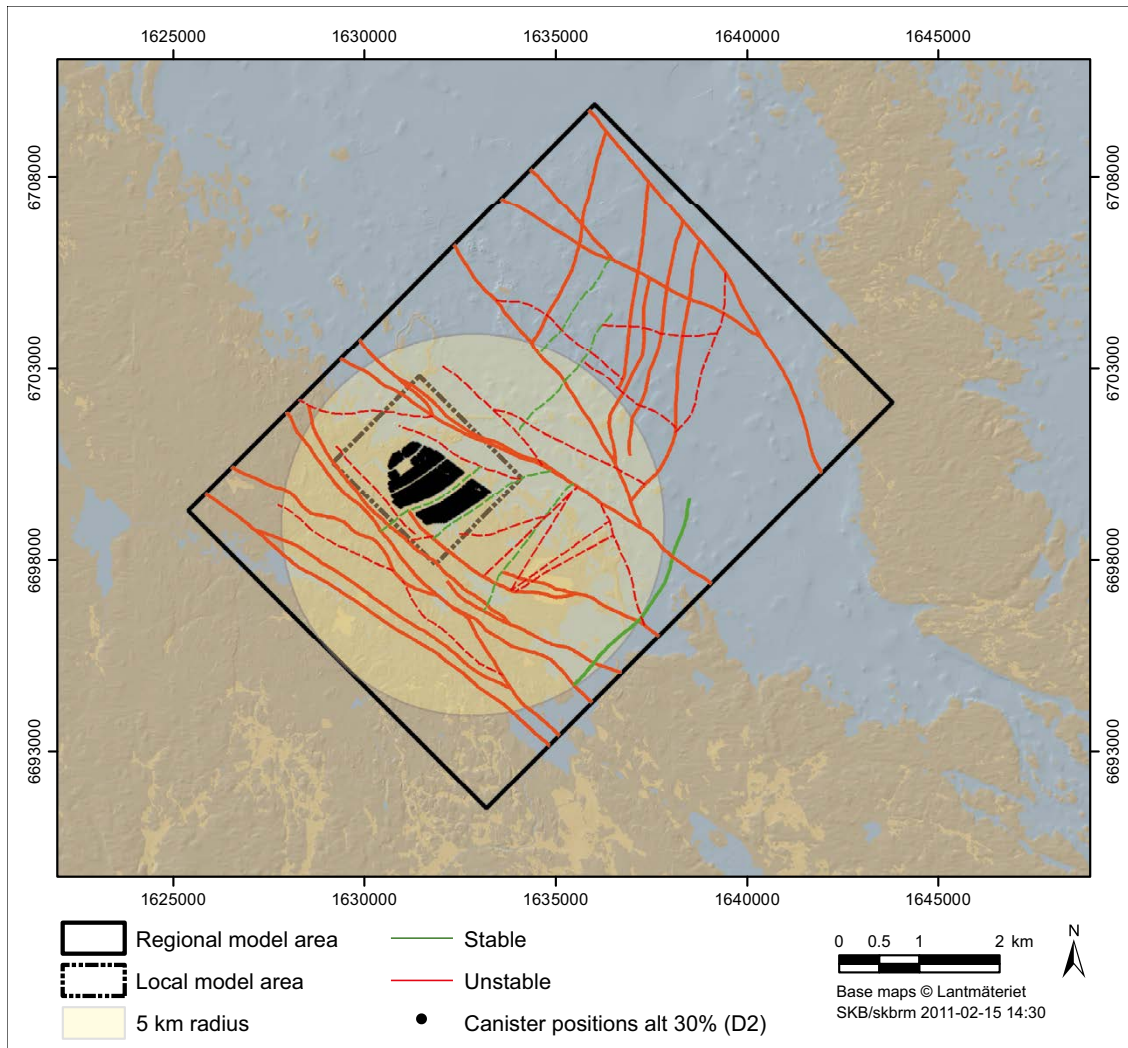


Figure 10-122. Deformation zones at Forsmark. The circle of 5 km radius defines the area for normalisation of earthquake frequencies. Note that surface traces are truncated against the regional model boundary. The zones are classified in terms of stability in a combined strike-slip/reverse regime according to Fälth et al. (2010). The results of the work presented in Hökmark et al. (2019) indicate that all steeply dipping deformation zones located with fault segments within 600 m distance from the repository footprint would be stable under all relevant load conditions. Since earthquakes occurring on deformation zones located at distances > 600 m from the closest canisters have been verified (in agreement with the statements made in SR-Site) to induce only irrelevant shear displacements across canister positions, the only Forsmark deformation zone that appears to be a potential concern would be the ZFMA2 zone.

Table 10-19. Deformation zones intersecting an area corresponding to a 5 km radius circle centred at Forsmark. Attributes stem from Stephens et al. (2007). The thickness includes the fault damage zone. Red = unstable, green = stable in the mixed stress regime (strike-slip/reverse).

ID	Trace length (m)	Confidence	Strike	Dip	“Thickness (m) (incl. damage zone)”
ZFMNW0017	7 923	Medium	135	85	64
ZFMNW0029	3 792	Medium	133	90	30
ZFMNW0805	3 694	High	134	90	10
ZFMNW0806	22 000	Medium	145	90	80
ZFMWNW0836	4 498	Medium	117	90	30
ZFMNW1200	3 121	High	138	85	47
ZFMWNW0001	30 000	High	120	90	200
ZFMWNW0004	70 000	High	125	90	160
ZFMWNW0016	8 060	Medium	123	90	45
ZFMWNW0019	8 760	Medium	116	85	45
ZFMWNW0023	7 665	Medium	111	82	45
ZFMWNW0024	7 986	Medium	124	90	45
ZFMWNW0036	11 000	Medium	123	90	55
ZFMWNW0123	5 086	High	117	82	52
ZFMWNW0809A	3 347	Medium	116	90	25
ZFMWNW1127	5 394	Medium	120	90	35
ZFMWNW0035	3 521	Medium	120	90	25
ZFMA2	3 987	High	80	24	23
ZFMA3	3 234	High	46	22	22
ZFMA4	3 641	High	61	25	37
ZFMB1	3 224	High	32	27	7
ZFMA7	3 510	High	55	23	7
ZFMENE0060A	3 120	High	239	85	17
ZFMENE0062A	3 543	High	58	85	44
ZFMEW0137	4 300	Medium	95	90	30
ZFMNE0065	4 068	High	36	70	26
ZFMNE0808A	4 080	Medium	218	80	30
ZFMNNE0828	5 932	Medium	213	80	35
ZFMNNE0842	3 157	Medium	217	80	25
ZFMNNE0860	5 922	Medium	198	80	35
ZFMNNE0929	5 203	Medium	193	80	35
ZFMNNE1133	6 284	Medium	193	80	40
ZFMNNE1134	7 284	Medium	191	80	40
ZFMNNE0823	3 273	Medium	160	90	25
ZFMNW0002	18 000	High	134	90	74
ZFMNW0003	30 000	High	139	85	53

Prerequisites for shear load by earthquakes

The stress evolution analysed explicitly for the Forsmark site by Lund et al. (2009) verifies that there is a significant increase in fault stability during periods of ice-cover, i.e. when canisters could, potentially, be subjected to high pore overpressures, i.e. to high isostatic loads. This means that shear movements across canisters such as those calculated by Fälth et al. (2010) will not occur in connection with high isostatic loads. At times of ice retreat (Lund et al. 2009) predict a period of reduced fault stability, possibly resulting in end-glacial faulting along suitably-oriented deformation zones and reactivation of host rock fractures. At such times, residual pore overpressures will amount to about one MPa (Hökmark et al. 2010). Therefore, combined effects of isostatic loads and shear movements across canisters are not taken into account.

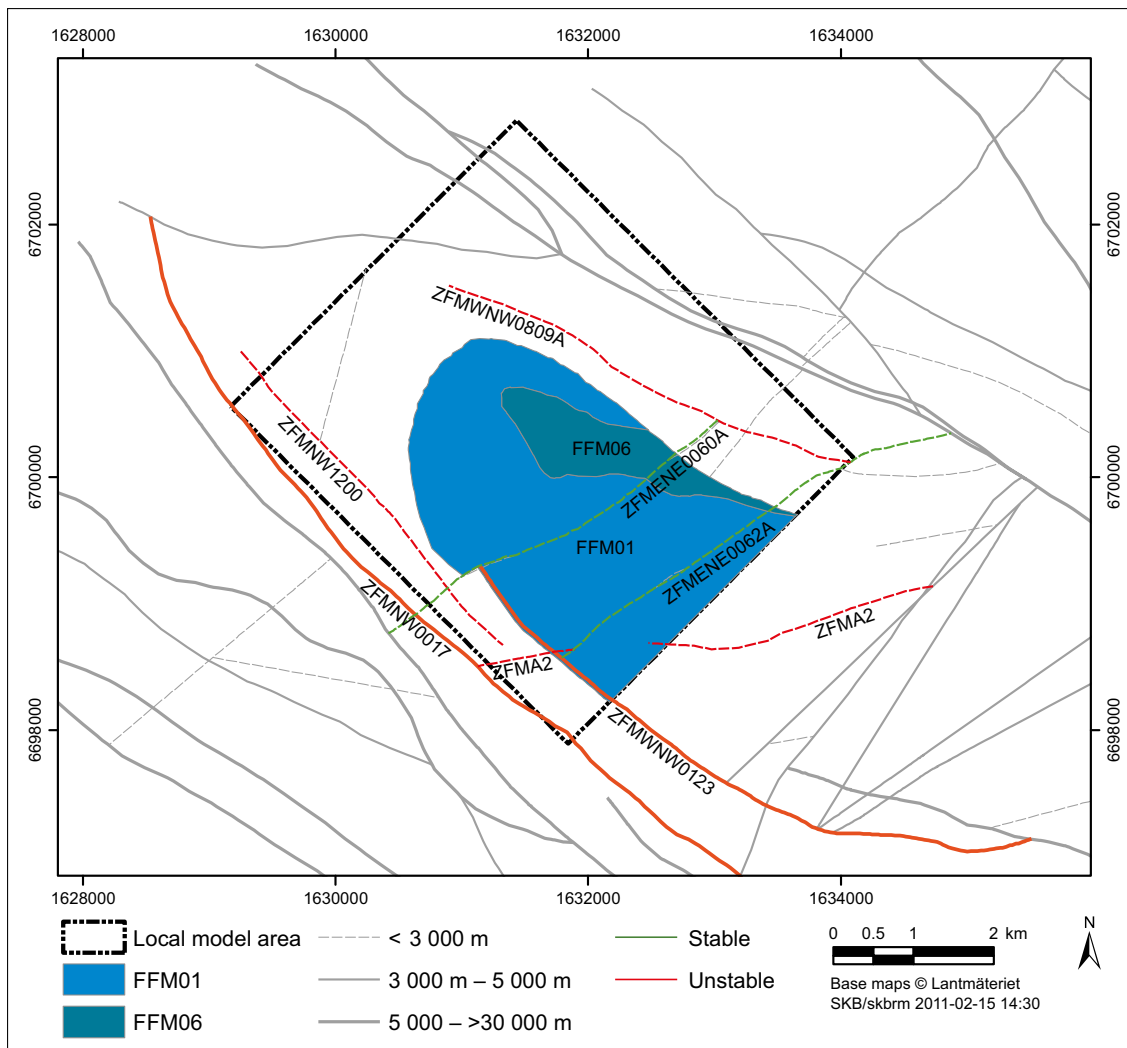


Figure 10-123. Deformation zones (intersections at repository depth) considered in the earthquake hazard assessment, i.e., the Forsmark deformation zones with trace lengths > 3 km and with fault segments located at distances < 600 m from any canister position.

The canister is designed to withstand a shear movement of 5 cm. This means that if cumulative slip exceeding 5 cm along fracture planes that intersect the canisters can be avoided, earthquakes have no means to jeopardise the integrity of the canisters. As the maximum slip that can be hosted by a fracture is related to its size (Cowie and Scholz 1992b), it must be ensured that canisters are not intersected by large fractures to warrant long term safety.

The impact of earthquakes near the repository on host rock fractures (target fractures) within the repository was addressed by Fälvh et al. (2010), who investigated the influence of earthquake magnitude, distance to the fault and target fracture orientation on seismically induced slip on target fractures. Fälvh et al. (2010) conclude that, provided that a distance of 600 m is kept to the boundary of deformation zones, none of the canisters within a repository will be subject to shear loads such that their integrity is jeopardised, regardless of earthquake magnitude (faults corresponding to moment magnitudes up to M7.5 were simulated). This is under the condition that fractures with radii exceeding 225 m are avoided in deposition holes. This has later been verified to hold, with good margins, for all load scenarios (Hökmark et al. 2019). Such fractures are judged to be safely detected during underground mapping (Cosgrove et al. 2006, SKB 2010b) and it may hence be concluded that, beyond 600 m from any deformation zone (≥ 3 km), earthquakes have no impact on canister integrity.

In the interpretation of the simulation results, the deformation zones were divided into two categories: zones 3–5 km able to host minor earthquakes ($\leq M5.5$), and zones exceeding 5 km in trace length

which are able to host large earthquakes ($> M5.5$). If both respect distances and rejection criteria (Munier 2010) are applied, the canisters will avoid the impact of earthquakes even occurring on zones intersecting portions of the repository volume. For this to be valid, however, the following need to be ensured (Figure 10-124).

1. No canister is placed within the damage zone of a deformation zone (fault). The damage zone of a fault is the volume of rock within which the zone may grow (Scholz 2002, Kim et al. 2004, Kim and Sanderson 2008, Choi et al. 2016). This is ensured by repository design (SKB 2009c) and using the site descriptive models (e.g. Stephens et al. 2007, 2008a, b). The boundaries of the deformation zones will be delineated with further detail and less uncertainty during underground mapping and modelling.
2. No canister is intersected by any fracture that is mechanically connected (i.e. splay) to any deformation zone. The risk for this to occur is lessened by the use of 100 m respect distances (Munier and Hökmark 2004, Munier et al. 2008) to the boundary of the deformation zone, defined to include the damage zone (see e.g. Munier et al. 2003 for details). There is an uncertainty, however, as to whether this respect distance is sufficient to include all splays. The splays are smaller than the deterministically modelled zones and ought to consist of fractures or small deformation zones with radii in the order of about 100–500 m. Hence most of them are expected to be detected and characterised by forthcoming underground investigations, see further Section 15.6.2. It is, however, important, during underground investigations, to ensure that such splays do not intersect any deposition hole. The work of Cosgrove et al. (2006) is of particular importance in this context and the detailing of the underground investigation programme (SKB 2010b) will further specify the identification tools.
3. Deposition hole rejection criteria are applied to the rock volumes beyond the 100 m respect distance which depend on Fälth et al. (2010):
 - a. the size of the nearest deformation zone (i.e. the maximum size of anticipated earthquake, should it occur),
 - b. the distance to the deformation zone,
 - c. the orientation of the fracture intersecting the deposition hole,
 - d. the size of the fracture intersecting the deposition hole.

The complex task of determining the absolute size of fractures (Cosgrove et al. 2006) can be avoided by the use of the so called FPI criteria (FPC + EFPC, see Section 5.2.2) which constitute proxies for large fractures (Munier 2010). In practice, therefore, the critical radii of Table 10-20 are used only to obtain a quantitative estimate of the number of critical canister positions for the few cases for which the FPI criteria may fail (see next section).

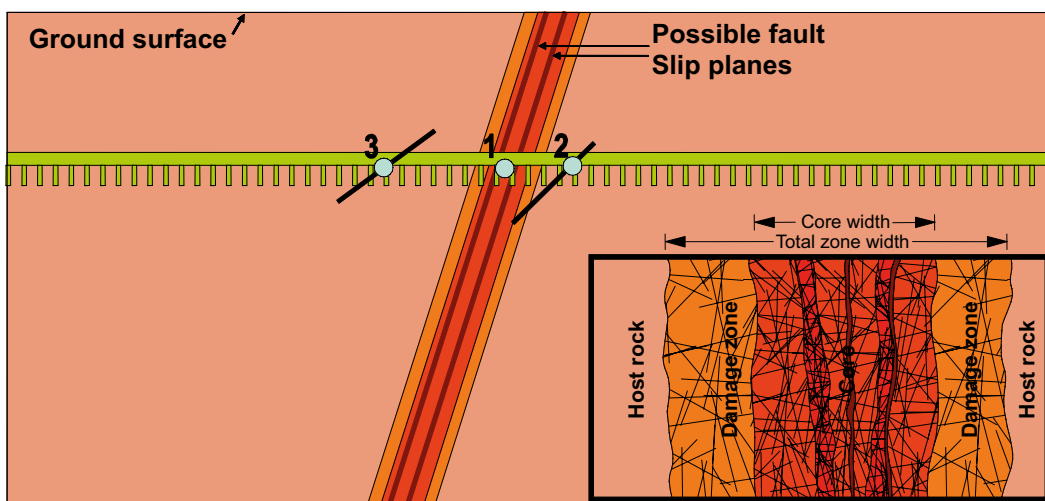


Figure 10-124. Cases to consider regarding slip across canisters. Case #1 = the canister is intersected by a deformation zone. Case #2 = the canister is intersected by a splay from the deformation zone. Case #3 = the canister is intersected by a large fracture at some distance from, and mechanically disconnected from, the zone.

Table 10-20. Summary of critical radii for relevant zone lengths and target fracture dips at Forsmark (from Fälth et al. 2010). The work presented in Hökmark et al. (2019) verifies that these radii are, with good margins, lower bounds.

Zone trace length (km)	Target fracture dip (degree)	Distance from zone (m)	Critical target fracture radius (m)
> 5	0–55	100–200	62.5
> 5	0–55	200–400	125
> 5	0–55	400–600	160
> 5	0–55	> 600	225
> 5	55–90	100–200	85
> 5	55–90	200–400	170
> 5	55–90	400–600	215
> 5	55–90	> 600	> 300
3–5	0–55	100–200	75
3–5	0–55	200–400	150
3–5	0–55	400–600	235
3–5	0–55	> 600	> 300
3–5	55–90	100–200	100
3–5	55–90	200–400	200
3–5	55–90	400–600	> 300
3–5	55–90	> 600	>> 300

Cases of shear load to consider

The impact of earthquakes on the canister/buffer integrity can be avoided by the use of respect distance and deposition hole rejection criteria. In essence, SKB needs to ensure that deposition holes are not intersected by structures large enough to host slip that may exceed the canister failure criterion. As argued by Cosgrove et al. (2006), the vast majority of large fractures (radii \approx 100–500 m) are not anonymous and most display clear and interpretable characteristics (Nordbäck and Mattila 2018). However, we need for the safety assessment a quantification of how many critical positions might escape detection. The full perimeter intersection (FPI) criteria (Munier 2010) have been proposed as a robust proxy for large fractures. By applying the FPI criteria to the Forsmark site, we are able to provide, by simulations, a pessimistic upper estimate on the number of critical positions that may escape detection and, ultimately, an estimate of how many canisters might therefore fail as a result of nearby earthquakes.

Due to the large time spans considered in this assessment, up to 10^6 years, the effect of repeated earthquakes and hence of cumulative slip across canisters must also be considered. The concern is that though the induced slip due to an individual earthquake might be insufficient to damage the canister, the cumulative slip due to several earthquakes, on the same or different faults, might exceed the canister failure criterion of 5 cm.

There are several different cases to consider (Figure 10-125).

- 1) The fracture that intersects the canister is large enough to host a slip exceeding the canister failure criterion. It can either host its maximum possible slip allowed by its size (1c) or slip in smaller increments, one for each seismic event, that accumulates to a value exceeding the failure criterion ($1a + 1b + \dots$).
- 2) The fracture does not initially intersect the canister (2a). Triggered by nearby earthquakes (or itself hosting a small earthquake) the fracture grows into the canister position (2b), thereby enabling slip across the fracture. For large enough a growth, the fracture will eventually be able to host a slip across the canister that exceeds the canister failure criterion (2c).
- 3) The fracture intersects the canister position (3a), but is too small to host a critical slip. The fracture grows (3b) to a size that is able to host a critical (cumulative) slip (3c).

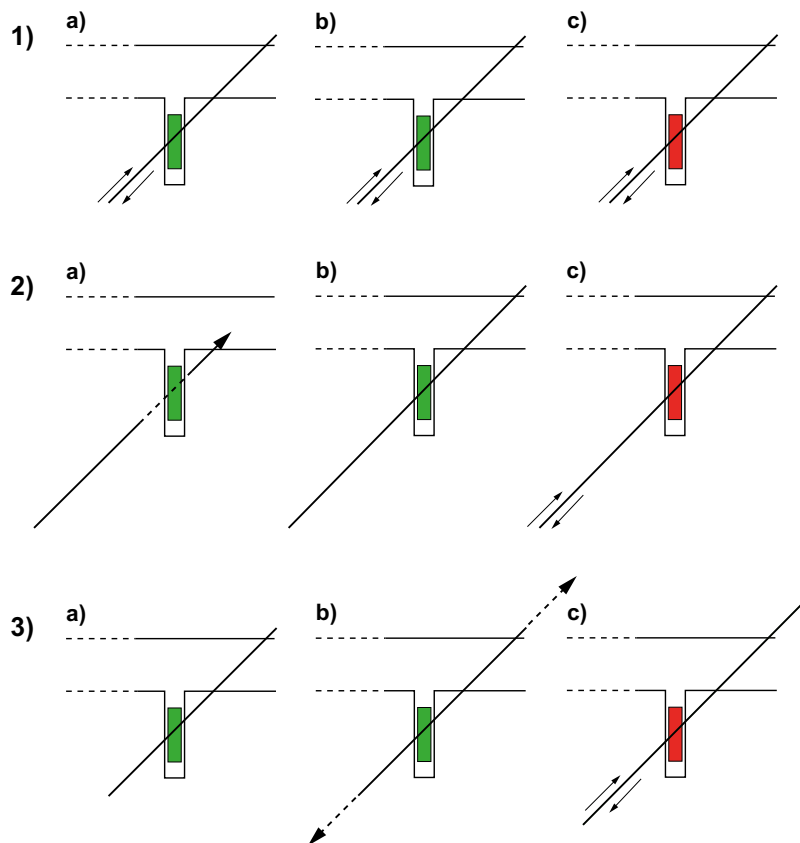


Figure 10-125. Various cases to consider regarding slip across a canister. In “1a–c” we address the effect of cumulative slip. In 2a–c we address growth of a fracture into a deposition hole. In 3a–c we address the growth of a fracture from a subcritical size to a critical size. Red canisters could experience detrimental shear movements.

Whether a fracture slips a distance, D , in a single event or if D is subdivided into several smaller slip distances d_1, d_2, \dots, d_n , is, from a purely geometric point of view, equivalent. Thus, Cases 1a+1b are equivalent to Case 1c. However, for the cumulative slip d_1, d_2, \dots, d_n to equal D , slip vectors need to be perfectly parallel. This essentially requires that the same deformation zone reactivates, with essentially identical dynamics, pore pressure, etc. Additionally, the number of successive slip events is controlled by the frequency of triggering earthquakes, in practice limited to two events during the assessment period (10^6 years) as argued for earlier. Thus, only the possibility of two successive slip events on the same target fracture needs to be considered. The smallest fracture that can host a slip exceeding the canister failure criterion as a consequence of a *single* earthquake is given by Table 10-20 in terms of critical radii. For two seismic events, we need to consider the cumulative slip of fractures with subcritical radii. The smallest fractures that can accumulate 50 mm of slip in two reactivation events have radii equal to half the critical radius of a single event, since slip scales linearly with fracture size (see the **Geosphere process report**, Section 4.3). We thus pessimistically assume that the slip vectors on the subcritical target fractures will indeed be perfectly parallel and neglect stress relaxation effects around the target fractures. Note, further, that slip velocity scales linearly with displacement as shown in Figure 10-126. We thus, pessimistically, also assume that a cumulative slip of 50 mm will have the same impact on the canister as a single, faster, slip of 50 mm. The canister failure criterion has been deduced from high shear velocities (1 m/s (Hernelind 2010)); low shear velocities have a considerably lower impact upon the canister-buffer system. It is likely that the buffer, which is sensitive to shear velocity, has sufficient time to recover between seismic events. This effect is, however, not taken into account and assuming that the cumulative effect of several smaller slip events equals a single larger event is thus additionally pessimistic.

Target fracture shear velocity versus maximum shear displacement

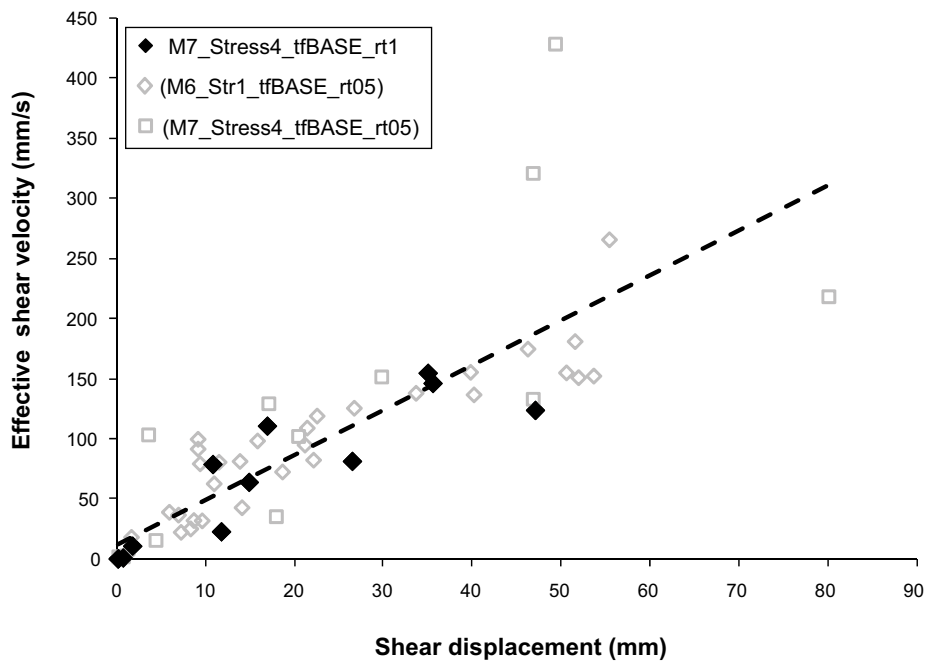


Figure 10-126. Relation between shear velocity and shear displacement on a target fracture (from Fälth et al. 2010). Results are from various earthquake simulations. Unfilled plot symbols denote results from cases that were discarded in the final assessment because the source mechanism was not considered to be representative of real earthquakes.

The growth of fractures by repeated reactivation has been investigated by Cowie and Scholz (1992a). The authors propose that a fracture may, for each seismic event, grow in the range 0.2–2.5 percent of its size as an upper estimate, pessimistically assuming that the entire fracture surface also constitutes the faulting surface. A fracture that grows into a deposition hole, as hypothesised in Case 2, would have the canister located close to its tip. As shown by numerous authors, e.g. Walsh and Watterson (1987, 1989), Marrett and Allmendinger (1990) and Dawers et al. (1993), the displacement profile tapers off from a maximum near the centre of the fracture to zero at its tip (Figure 10-127) where ductile deformation (e.g. growth of damage zone, propagation through damage zone, folding) takes place. For a fracture to grow to such an extent, that a canister’s position is shifted from being near the tip of a fracture to a region in which slip might exceed the canister failure criterion, would require a large number of slip/growth events. For a fracture to slip 0.05 m, the canister needs to be located at the centre of a fracture with a radius of 62.5 m (strictly following simulation results), with the additional conditions that the fracture is located no farther than 200 m from a large (> 5 km) deformation zone and is gently ($\leq 55^\circ$) dipping (see Table 10-20 from Fälth et al. 2010). In any case: Fracture growth consequences are obviously overshadowed by uncertainties in the size and the shape of potentially critical fractures in general and by the pessimistic handling of the multiple slip issue in particular. The results presented in Hökmark et al. (2019) verify the SR-Site critical radii with good margins, lending further support to the statements made here regarding multiple seismic events and fracture growth.

With a growth in the range 0.2–2.5 percent for each seismic event, as proposed by Cowie and Scholz (1992a), it would require about 15 (Cowie and Scholz 1992a, Equation 22) consecutive seismic events on the fracture (n.b. not necessarily triggered by a distant fault) before the canister is located in a critical position, assuming a perfectly elastic material for which Eshelby’s elliptical displacement profile holds (Eshelby 1957, Munier 2010, Equation 27). For fractures located more than 200 m from the fault, many more seismic events are required. The collage of prerequisites for Cases 2 and 3 are judged unlikely, their effects subordinate, and they are therefore not addressed further.

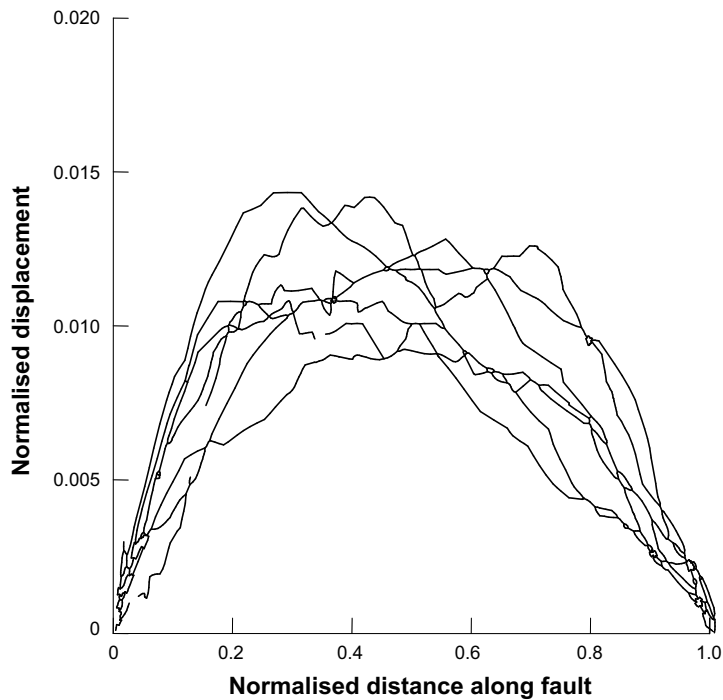


Figure 10-127. Displacement profiles along normal faults of different size, normalised to fault size (redrawn from Dawers et al. 1993).

Number of canisters in critical positions

The detrimental effects of earthquakes on the canister-bentonite packages can be avoided by the application of deposition hole rejection criteria to the design of canister deposition locations. The maximum fracture radii allowed to intersect the deposition hole (Figure 10-128) are provided from simulations in Fälth et al. (2010). Applying the full perimeter intersection criteria on site-specific deformation zone and fracture models, Munier (2010) computed the number of canister positions that escape detection using the FPI criterion, the main results of which are presented in Table 10-21 and Table 10-22 (see Munier 2010 for details²⁷).

In short, the number of critical canisters in Forsmark, i.e. canisters that escaped the FPI rejection criteria and are thus intersected by fractures large enough to host slips exceeding 5 cm, varies between roughly 1.0×10^{-3} (for DFN model “OSM + TFM” and deformation zone ZFMNW0017) and 1.1×10^{-1} (for DFN model “TCM” and deformation zone ZFMA2) canisters depending on DFN model, stress regime and zone assumed to reactivate seismically (Table 10-21). The reverse stress regime (Table 10-22) only affects one deformation zone, ZFMA2, and yields a maximum of 0.11 canisters in critical positions (using DFN model TCM). Note that ZFMA2 is judged unstable also in the mixed stress regime and that this is the zone that affects most canister positions and the maximum number of critical positions is therefore the same (0.11) for the mixed- and the reverse stress regime.

The results in Table 10-21 and Table 10-22 are valid only for the case when exactly one of the deformation zones will reactivate seismically. In Figure 10-128 we display two examples of how critical radii depend on the distance to deformation zones.

²⁷ Since the publication of Munier (2010) more realisations have been added to stabilise the mean values further. As a consequence, there is small difference between the tables in Munier (2010) and those herein.

Table 10-21. Mean number of critical canister positions for various DFN models, assuming mixed stress regime (6 000 canister repository) at Forsmark.

DFN Model	# Crit. Min ¹	# Crit. Max ¹
OSM+TFM	1.0×10^{-3}	6.7×10^{-2}
r0-fixed	3.5×10^{-3}	4.8×10^{-2}
TCM	2.3×10^{-3}	1.1×10^{-1}
Overall	1.0×10^{-3}	1.1×10^{-1}

¹ The number of critical positions (“# Crit. Min”) is obtained by combining the zone which affects the least number of canisters with the DFN model that yields the lowest intersection probabilities and doing the opposite to obtain “# Crit. Max” (Munier 2010).

Table 10-22. Mean number of critical canister positions for various DFN models, assuming reverse stress regime (6 000 canister repository) at Forsmark.

DFN Model	# Crit
OSM+TFM	6.7×10^{-2}
r0-fixed	4.8×10^{-2}
TCM	1.1×10^{-1}

Number of potentially failed canisters by shear load

To compute the number of canisters that may fail within a certain time span, the number of critically emplaced canisters (Table 10-21 and Table 10-22) is multiplied by the earthquake frequencies in Table 10-18. All earthquakes are here projected on the deformation zone ZFMA2 because:

- its geometry is similar to the geometry of the known post-glacial faults,
- it is considered unstable in both the reverse- and combined reverse+strike slip (mixed) stress regimes²⁸,
- it is the deformation zone that affects most canisters.

Additionally the following prerequisites apply.

- For the 1 000-year time frame, only earthquake frequencies given by Böðvarsson et al. (2006) are used. This work was specifically targeted towards short time frames and was therefore judged the most suitable reference in this context. Additionally, as argued for in the **Geosphere process report**, most earthquakes, at least in this time frame, occur at greater depth than is relevant to the context discussed here. Following the reasoning in the **Geosphere process report**, the frequencies are reduced by a factor of 0.5. This is judged to be a quite modest frequency reduction. The work presented in Hökmark et al. (2019) verifies that earthquakes on faults located at distances larger than 600 m from the closest canister position will not be a concern for the repository, meaning that present-day earthquakes occurring below depths of, say, two kilometres should not contribute to the frequencies relevant to the seismic risk issue.
- For the time frame of a glacial cycle, 120 000 years, all references in Table 10-18 are used because, with the exception of Böðvarsson et al. (2006), they all targeted this specific time frame in their assessment. Since extrapolation of Böðvarsson et al. (2006) to 120 000 years produces similar frequencies, we judged it reasonable to include the results of Böðvarsson et al. (2006) in this time frame despite the consideration that their assessment did not target a larger time frame than 1 000 years.
- In contrast to the 1 000 year time frame, we cannot rule out the possibility of shallow, postglacial, earthquakes for the 120 000 and 1 000 000-year time frames. Hence, the frequencies have been used without adjustment for depth.
- For the 1 000 000-year time frame, a maximum of two seismic events $\geq M5$ which is a consequence of an assumed strain rate of $10^{-10} \text{ year}^{-1}$ is postulated.

²⁸ The combination of strike-slip and reverse regime (sometimes referred to as mixed regime) refers to a notion of predominantly strike-slip regime at depth ($> \approx 1 \text{ km}$) and reverse slip at shallower levels (Lund et al. 2009, Fälth et al. 2010)

Following the reasoning in the **Geosphere process report**, Section 4.3, the number of canisters that may fail is computed according to:

$$N_{failed} = 5 \cdot f \cdot t \cdot N_{crit}$$

N_{crit} is the average number of canisters in critical positions (Table 10-21), f is obtained from Table 10-18 and t is the time. The factor 5 is due to the projection of all earthquake frequencies onto ZFMA2.

For the second seismic event, applicable only to the 1 000 000-year time frame, the following expression is used (see the **Geosphere process report**, Section 4.3.1 for details):

$$N_{failed} = \frac{1}{2} \cdot (5 \cdot f)^2 \cdot (10^6 - T)^2 \cdot N_{crit,2nd}$$

in which T stands for relaxation time and $N_{crit,2nd}$ stands for the average number of canisters in critical positions (Table 10-23) using the critical radii of Table 10-20 divided by two.

The main results are summarised in Table 10-24, which should be understood as follows:

Under the assumption that a combination of strike-slip and reverse stress regime will prevail during the assessment period, between 9.3×10^{-6} and 2.2×10^{-5} canisters may fail (averages of probabilistic evaluations) during the 1 000-year time frame. Note that only (Böðvarsson et al. 2006) is used for this assessment even though estimates for all references are supplied. Similarly, on average between 8.3×10^{-4} and 5.7×10^{-3} canisters may fail during a glacial cycle. For the 1 000 000 time frame, two seismic events are assumed and it is estimated that on average between 8.3×10^{-3} and 7.9×10^{-2} canisters may fail. The contribution of the second seismic event is between 20 and 50 percent of the total. Despite a much lower probability for the second event, reducing the critical radii by half dramatically increases the number of canisters in critical positions due to the powerlaw size distribution of the fractures. Since all these average numbers are well below one, the numbers, to a good approximation, are also equal to the calculated probability that canister failure has occurred in the repository at the end of the time periods under consideration.

The above results can be expressed as the frequency of canister failures as a function of time for times beyond the initial 1 000 years. This frequency will be constant during the first 500 000 years when only one large earthquake may occur, and linearly increasing between 500 000 and one million years, when also the possibility of a second earthquake must be taken into account. If, pessimistically, the highest earthquake frequencies (those by Hora and Jensen 2005) and the DFN model yielding the largest numbers of critically emplaced canisters (the TCM model) are used, the frequency during the first 500 000 years is 4.75×10^{-8} per year (the emboldened max value for 120 000 years in Table 10-24 divided by 120 000). The frequency then increases linearly to reach 1.74×10^{-7} per year at one million years, see Figure 10-129. (The latter result is obtained by the requirement that the area under the frequency curve in Figure 10-129 must correspond to the accumulated maximum number of failures from both one and two events given in Table 10-24.) This result is used as input to consequence calculations of the shear load scenario, see further Section 13.6. For the initial 1 000 years the corresponding frequency is 2.4×10^{-8} per year.

Table 10-23. Number of critical canister positions (2nd seismic event) for various DFN models, assuming reverse regime (6 000 canister repository) at Forsmark.

DFN Model	# Crit. 2nd
OSM+TFM	0.7
r0-fixed	0.46
TCM	1.3

Table 10-24. Number of canisters that may fail during different time spans and using different earthquake frequencies. The lowest Min values and the highest Max values in each column are marked with blue and red respectively.

Strike-slip + reverse (mixed) stress regime			Number of potentially failed canisters					
Reference	Earthquake frequency (M ≥ 5/year)		1 000 years		120 000 years		1 000 000 years (2 events)	
	5 km radius area	Per zone (30)	Min	Max	Min	Max	Min	Max
Böðvarsson et al. 2006	2.4×10^{-6}	7.8×10^{-8}	9.3×10^{-6}	2.2×10^{-5}	2.2×10^{-3}	5.4×10^{-3}	2.9×10^{-2}	7.3×10^{-2}
La Pointe et al. 2000, 2002	8.7×10^{-7}	2.9×10^{-8}	3.4×10^{-6}	8.2×10^{-6}	8.3×10^{-4}	2.0×10^{-3}	8.3×10^{-3}	2.0×10^{-2}
Hora and Jensen 2005	2.5×10^{-6}	8.3×10^{-8}	9.9×10^{-6}	2.4×10^{-5}	2.4×10^{-3}	5.7×10^{-3}	3.1×10^{-2}	7.9×10^{-2}
Fenton et al. 2006	2.0×10^{-6}	6.8×10^{-8}	8.1×10^{-6}	1.9×10^{-5}	1.9×10^{-3}	4.7×10^{-3}	2.4×10^{-2}	6.0×10^{-2}

As an illustration of the impact of the work presented in Hökmark et al. (2019), the canister failure frequency has also been calculated using the critical radii emerging from that report, again for the TCM version of the DFN model since this yields the highest frequencies, see Figure 10-130. The repository layout is identical to that used in the SR-Site assessment, i.e. the reduction in respect distances that could tentatively be implemented based on the results in Hökmark et al. (2019) has not been taken into consideration. The calculation was done with the semi-analytic model described in Hedin (2011), that is demonstrated to yield similar results as the more computationally demanding numerical model used to produce Figure 10-129, see benchmark in section 5.14 of Munier (2010). In Figure 10-130, the black curve is taken from Figure 10-129, the blue curve shows the same case as in Figure 10-129 but using the semi-analytic model and the red curve is based on the critical radii in Hökmark et al. (2019), calculated with the semi-analytic model. As seen, the frequencies are reduced by about a factor of 4 throughout the one million year time span when using the new data. As described in Chapter 9 of Hökmark et al. (2019), some additional work remains before the results can be considered fully qualified for use in the safety assessment. Therefore, the further assessments of earthquake induced canister failures in the present report are based on the results in Figure 10-129, rather than those in Figure 10-130.

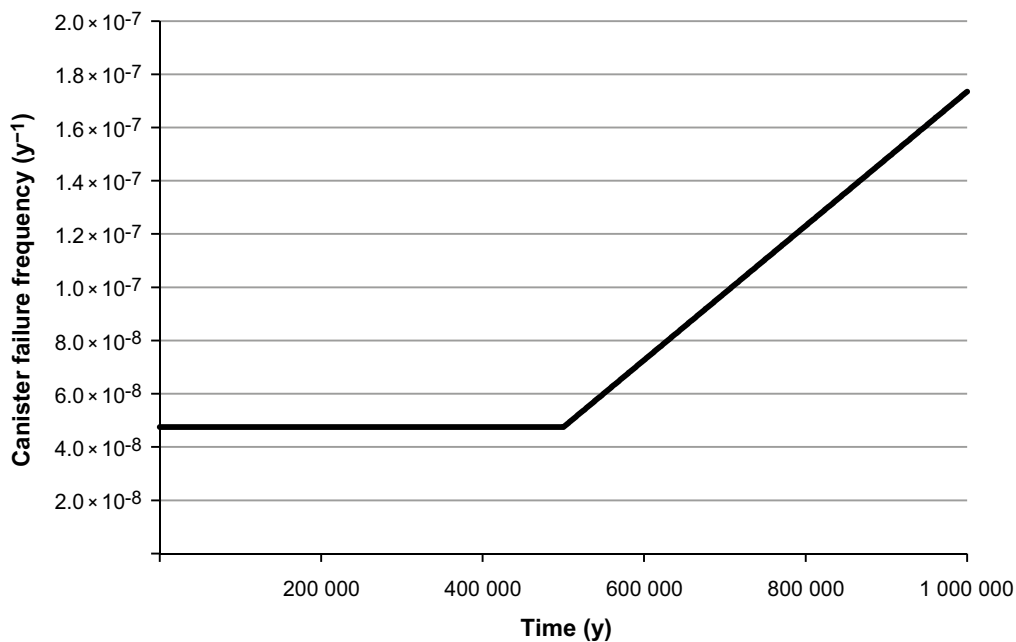


Figure 10-129. Frequency of canister failures due to earthquake-induced shear load as a function of time. The area under the graph yields the mean number of failed canisters at one million years as 0.079, in agreement with Table 10-24.

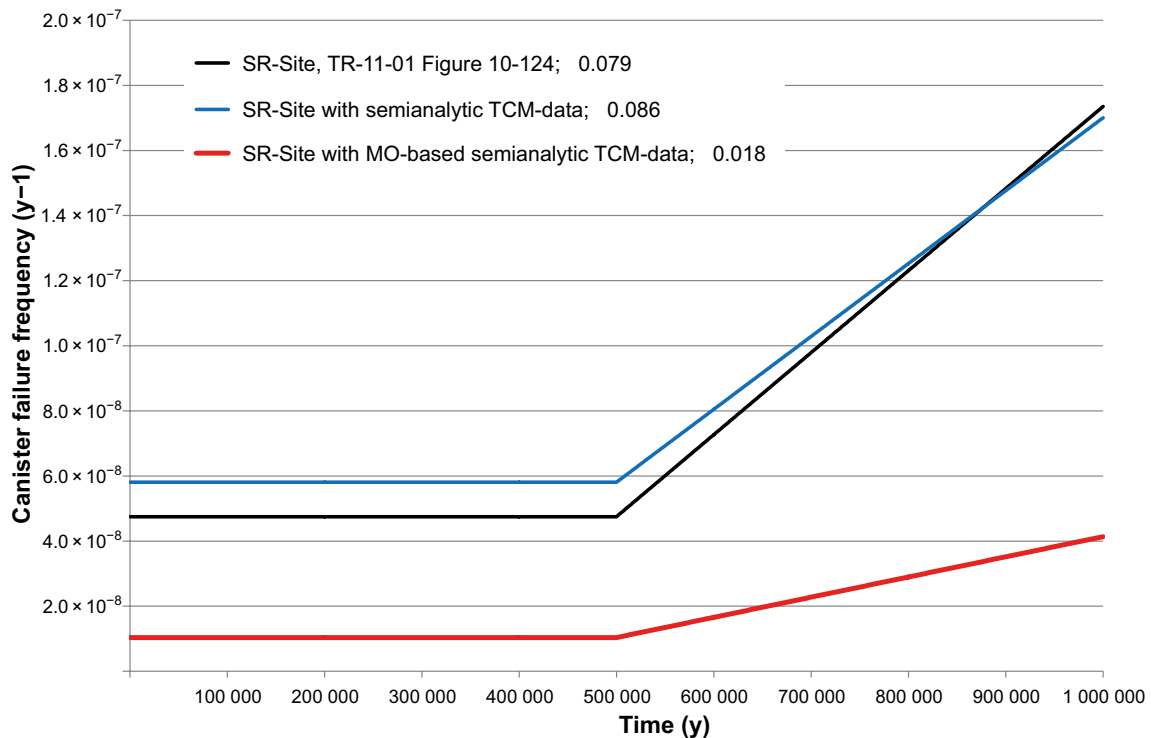


Figure 10-130. Frequency of canister failures due to earthquake-induced shear load as a function of time. Black: taken from Figure 10-129; Blue: same case as in Figure 10-129, but with semi-analytic model; Red: same repository layout as used for Figure 10-129, but with critical radii suggested in Hökmark et al. (2019), semi-analytic model. TCM version of the DFN model in all cases.

Modelling of buffer-canister response to shear movements

The effect on the canister of a shear movement has been assessed as a basis for the **Canister production report**, the supporting documentation being the design analysis of the canister (Jonsson et al. 2018), in turn supported by FEM-modelling of the impact of shear movements on the buffer-canister system by Hernelind (2010, 2014a) and by an analysis of damage tolerance of the canister insert when subjected to shear movements in Dillström and Bolinder (2010), and in Dillström (2015 a, b). As noted in Section 5.4.2, the probabilistic study of the canister’s resilience to shear load (Dillström 2014) is a key input to the analysis of post-closure safety.

The starting point for the canister shear analyses and the design analysis is the technical design requirements given in Posiva SKB (2017) and already cited in Section 5.4.1: For the shear movement the technical design requirements require that the copper corrosion barrier should remain tight and the canister shall maintain its ability to resist loads for 5 cm rock displacements at a rate of 1 m/s, exerted on the canister by a buffer with an unconfined compressive strength at failure lower than 4 MPa at a deformation rate of 0.8 %/min. This applies for all locations and angles of the shearing fracture in the deposition hole, and for temperatures down to 0 °C. The insert should maintain its pressure-bearing properties to isostatic loads after such shear movements.

The overall conclusion of these efforts is that a canister manufactured according to the reference design fulfils the technical design requirements, as already reported in Section 5.4.3. The probabilistic analysis in Dillström (2014) yielded a calculated probability of a canister failure as a result of a 5 cm rock shear displacement of around 2×10^{-3} . No credit for non-destructive testing was taken in these analyses. Based on all the cited results, it is in the PSAR assumed that a canister will sustain shear movements up to 5 cm, and, pessimistically, that any movement exceeding 5 cm leads to canister failure.

The following brief account of the modelling efforts is given to demonstrate the margins to failure, and in particular to evaluate the potential of the canister to withstand a load caused by a 5 cm shearing. In addition, the results are also available for larger shearing amplitudes in Hernelind (2010, 2017b).

There are a number of factors influencing the impact of a postulated shear movement of the buffer and canister. Table 10-25 gives an overview of such factors, their related technical design requirements, the cases analysed as support to the **Canister production report** and their relation to the rock analyses.

The technical design requirement of 5 cm shear is the result of a balance between achievable requirements on the canister and on the layout of the repository, given the understanding of earthquakes and secondary shear movements on the one hand and of the response of the buffer-canister system on the other. A lower technical design requirement shear displacement would give a higher probability for shear with given layout rules, but lower requirements on the canister design and material (especially the non-destructive testing of the insert) and vice versa.

Table 10-25. Overview of factors influencing the calculated impact of a postulated shear movement on the buffer-canister system, and the relations between technical design requirements, buffer-canister response analyses and the rock analyses.

Factor	Technical design requirement	Cases analysed in Hernelind (2010) and Jonsson et al. (2018)
Shear displacement	5 cm	5 cm
Shear velocity	1 m/s	1 m/s Also 0.1 m/s analysed for the base case (horizontal fracture impacting at ¾ height from canister bottom, buffer density 2050 kg/m ³).
Shear plane and angle of intersection	All angles	Shear planes: horizontal, vertical, 22.5° (to the canister axis).
Location of impact	All locations	Centred at mid height or centred on top; not-centred at a quarter of the length or diameter, see Figure 10-131.
Insert material properties	–	Material model derived from test manufacturing (iron) for different strain rates; table data are used for steel tubes.
Copper shell material properties	–	Material model derived from slow strain rate testing of copper material from test manufacturing.
Creep in copper shell	–	Creep model included for cases with bentonite 2050 kg/m ³ .
Buffer properties – density	2050 kg/m ³ Ca-bentonite	1950, 2000 and 2050 kg/m ³ Ca-bentonite; strain-rate dependent elasto-plastic model derived from laboratory testing.
Alteration of material	Temperatures down to 0 °C	Iron material model from testing at 0 °C. Temperature effects on buffer properties negligible.
Combined isostatic and shear loads	The insert should maintain its pressure-bearing properties to isostatic loads after shear movements	<ul style="list-style-type: none"> • Shear movement with isostatic load from ice sheet present. • Shear movement, ice developed afterwards.

Sensitivity analyses

The response of the canister to a shear movement in the rock is analysed in two steps. The first consists of FEM-modelling of buffer and canister response to an applied displacement at the outer boundary of the buffer (Hernelind 2010). As a second step the displacements in the canister from the FEM-modelling are transferred to the damage tolerance analysis, conducted for the part of the canister with the largest displacements and only for the cases with the largest impacts on the canister (Dillström and Bolinder 2010). Results of additional sensitivity modelling and analyses (Hernelind 2014a, Dillström 2015a, b), are summarised in Jonsson et al. (2018) and below.

Sensitivity to buffer density and to location, angle, speed and direction of shear movement

Results for the insert from the buffer-canister modelling are given in Table 10-26. The important parameters are the peak values for the equivalent plastic strain (PEEQ), the effective stress (von Mises) and the maximum axial tension stress (S33). The calculated effective strains and effective stresses all indicate that there is considerable deformation capacity left in the insert structure after shearing. The ultimate tensile strength in the BWR insert from the test manufacturing is at least 391 ± 10 MPa, and the elongation after fracture 13.7 ± 3.7 %. The axial tension stress is important for the fracture resistance analysis.

The shear velocity for the buffer-canister system is pessimistically set to 1 m/s, which is higher than the highest velocities deduced from target fractures (0.3 m/s) in earthquake simulations (Fälth et al. 2010). The shear velocity has only a minor impact on the strains and stresses as seen when comparing the first and penultimate cases in Table 10-26.

The analysed combinations of shear plane and angle of intersection are shown in Table 10-26. In Figure 10-131 the shear planes, angles of intersection and location of impact are illustrated as a)–f). The rock shear cases analysed:

- Shear perpendicular to the axis of the canister, at $\frac{3}{4}$ height and $\frac{1}{2}$ height from the bottom, a) and b).
- With tension of the canister and a shear plane at an angle of 22.5° to the canister axis, at $\frac{1}{4}$ height and at $\frac{1}{2}$ height from the bottom, c) and d).
- With a horizontal movement of a vertical plane, at a $\frac{1}{4}$ of the diameter and through the centre of the canister, e) and f).

Table 10-26. Peak values for the equivalent plastic strain (PEEQ), the effective stress (von Mises) and the maximum axial tension stress (S33) in the insert, for different shear load cases. The tabulated values should be compared to the measured elongation after fracture in the BWR insert from the test manufacturing which is 13.7 ± 3.7 %, and the measured ultimate tensile strength which is at least 391 ± 10 MPa. All models were performed with a slip rate of 1 m/s unless indicated differently (Hernelind 2010).

Model case: Impact angle Impact location Buffer density	Illustrated in part of Figure 10-131	PEEQ [%]		von Mises stress [MPa]		Maximum axial stress, S33 [MPa]	
		5 cm shear	10 cm shear	5 cm shear	10 cm shear	5 cm shear	10 cm shear
Normal $\frac{3}{4}$ height 2050 kg/m ³	a)	0.5	1.6	321	351	333	361
Normal $\frac{3}{4}$ height 2000 kg/m ³	a)	0.2	1.2	309	340	324	354
Normal $\frac{3}{4}$ height 1950 kg/m ³	a)	0.1	0.7	301	320	310	336
Normal Half height 2050 kg/m ³	b)	0.1	0.7	299	315	212	265
22.5° $\frac{1}{4}$ height 2050 kg/m ³	c)	0	0.09	290	297	126	219
22.5° Half height 2050 kg/m ³	d)	0.03	0.2	295	301	177	258
Zero (horizontal) Quarter width 2050 kg/m ³	e)	0.4	0.4	300	303	64	83
Zero (horizontal) Half width 2050 kg/m ³	f)	0.5	0.6	309	311	82	93
Normal $\frac{3}{4}$ height 2050 kg/m ³ Shear velocity 0.1 m/s	a)	0.5	1.7	312	344	327	354
Normal $\frac{3}{4}$ height 2050 kg/m ³ Creep modelling added	a)	0.4	1.5	314	347	336	365

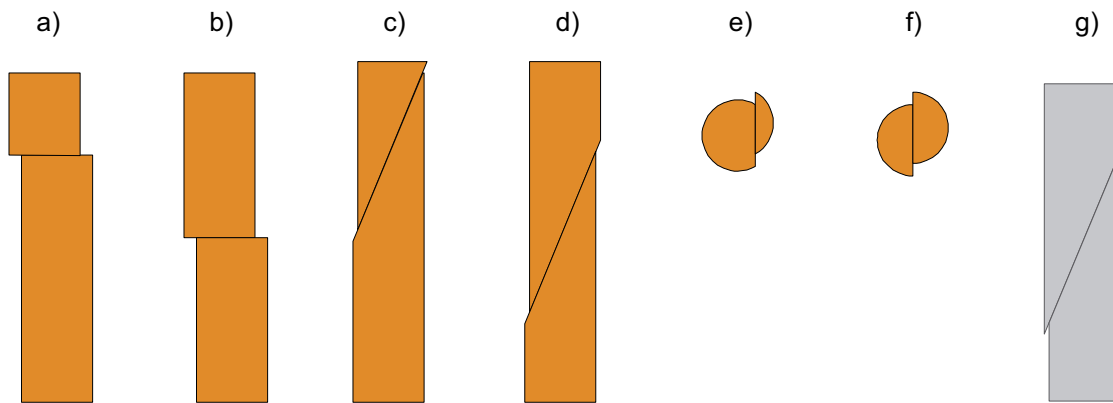


Figure 10-131. a)–f) Shear plane, angle of intersection and location of impact for the analysed cases in Hernelind (2010). The normal shear mode (g) was excluded from analyses (see text for further explanation).

Post-glacial stress conditions at 500 m depth are, as argued by Lund et al. (2009) to be of reverse type. Though some strike-slip component could be deduced from slip vectors on target fractures, the simulation of Fälth et al. (2010) show that all significant displacement on non-horizontal target fractures displayed reverse slip and that none of the target fractures displayed any normal slip. Consequently, analyses of normal faulting (deposition hole shortening) across the canister were excluded, (see g) in Figure 10-131).

The angle of 22.5° as an adverse condition was chosen based on results from previous analyses (SKB 2006a). With the current improved FEM modelling the copper lid fillets and the buffer are modelled more accurately (Hernelind 2010), which causes the inclined shear to give smaller strains and stresses than the shear perpendicular to the canister axis (see Table 10-26). A horizontal shear on a vertical plane through the canister gives strains in the same range as for the perpendicular shear, but considerably smaller stresses.

For several cases with the highest density of buffer, long-term creep in copper was modelled after the fast shear displacements. The stresses and strains in the insert after this sequence are given in Table 10-26, last row. Comparing with the corresponding cases without creep in copper indicates minor effects at 5 cm displacement, as the plastic deformation occurs during the fast shearing phase. For 10 cm shear, higher stresses occur in the insert. The maximum plastic strain in the copper shell appears in fillets (besides regions containing singularities in the model). At the global level the plastic strains are much lower. Creep is thus not a concern since the copper deformation is controlled by the surrounding material, which implies small creep strain rates as soon as the final deformation has been established.

The effect of varying the bentonite density, as well as shear plane and intersection is shown in Table 10-26. The largest effects on the insert (highest strains and stresses) are obtained with shearing perpendicular to the canister axis and with an intersection point $\frac{3}{4}$ of the height from the bottom. Lowering the density to 2000 or 1950 kg/m³ lessens both the strains and stresses.

All results in Table 10-26 are below the measured values of elongation and ultimate tensile strength suggesting that the integrity of the canister would not be jeopardised by such shear loads. The subsequent damage tolerance analysis was performed for the cases with the highest impact on the canister, i.e. for shear perpendicular to the canister axis, at $\frac{3}{4}$ height from the bottom, for different bentonite densities. Four different types of crack-like defects were analysed (semi-circular and semi-elliptical; internal and surface defects). The results were used to formulate requirements on acceptable defects and on the capability of the NDT system for the canister insert, see further Section 5.4. The analysis by Unosson (2016) provides important information in terms of the mechanical response of the insert in the case of a rock shear and the presence of unacceptable defects. The steel channel tubes behave like reinforcing composite bars in the cast iron and prevent the cracks from cutting the insert into separate pieces (Jonsson et al. 2018).

Sensitivity to model discretisation and other model related factors

The framed structure of the insert steel channels was modelled at different levels of detail in the analyses. A simplified geometry is a satisfactory numerical idealisation of the geometry and mechanical response of the insert and canister (Hernelind 2010, Jonsson et al. 2018).

The steel channel offset variation resulting from manufacturing does not influence the mechanical response in the rock shear case or the acceptable defect sizes derived from rock shearing (Hernelind 2017).

The casting of the insert around the steel channel tubes affects the mechanical properties of the steel tubes. Hernelind and Börgesson (2019) investigated the influence of the insert casting on the steel tube properties using the material definitions based on measurements after casting and concluded that the influence of the properties can be considered as negligible in the rock shear case (Jonsson et al. 2018).

The mesh of the modelling can influence the resulting strains and stresses. For example, stress concentrations can be directly related to poorly behaving wedge elements. In all cases, disregarding the elements that behave poorly significantly reduces the locally higher tensile stresses. The global analyses of the rock shear case has also been modelled by other authors using other FE-software programmes. The consistency between the different works shows that uncertainties in the analysis methodology can be considered to be low (Jonsson et al. 2018).

Additional buffer sensitivity cases

Alteration of the buffer material due to cementation yields small effects in the shear analyses. In the shear calculation made for SR-Can (Börgesson and Hernelind 2006) an 8.75 cm thick zone of the buffer material around the canister was assumed to be converted to cement like material, with no swelling pressure, with an E-modulus increased by a factor of 100 and a shear strength increased by a factor of 5 compared to the unaltered buffer. In spite of the high stiffness and strength, the change in effect of a rock shear on the canister was rather small with an increased plastic strain of about a factor of 1.5. This calculation treats much more severe cementation than the case described in Section 10.3.10. With the resulting rather small effects, no new calculations were done either for SR-Site or for the PSAR. In addition, the material model used for the rock shear calculations covers a potential increase in strength since the shear strength values used are about 15 % higher than the average measured values.

Tests on bentonite exposed to high temperatures have shown tendencies of brittle failure as opposed to results from unaffected bentonite, which show smooth or no decrease in strength after maximum shear stress. Figure 10-132 shows an example of such results. The general conclusions from the experiments were that shear strength was not affected, but the failure may be brittle, i.e., abrupt shear strength reduction after maximum shear stress has been achieved. The maximum deviator stress is a measure of shear strength and it depends on the density. In case of brittle failure, a lower strain is also often seen and the surface of the failure may also be vertical. In summary, the shear strength is not affected since the maximum deviator stress at a given density is not considered to be affected by an increased temperature. Since the test results to the left in Figure 10-132 come from three samples that have approximately the same density, but not exactly the same value, it cannot be clearly be determined from this figure whether the deviator stress increases with the temperature. The impact of a rock shear through a deposition hole has been investigated both with laboratory tests which have been the basis for a buffer model and with a number of finite element calculations that have studied the effect of various shear cases on the canister. A number of calculation cases are reported in Sellin et al. (2017, Chapter 10). The bentonite was modelled as an elastoplastic material with strain rate-dependent stress-strain relationships. Four different calculations have been made, a reference calculation with unaffected bentonite, two calculations with brittle bentonite and a fourth calculation of brittle bentonite and the shear plane of the buffer removed to simulate that shear strength has been completely lost in that zone. The material model for the reference case is identical to the material model for bentonite used for SR-Site (Åkesson et al. 2010a). An example of results is shown in Figure 10-133 illustrating the plastic strain in the copper shell. The most obvious difference occurs in case 4 where the shear plane in the buffer is removed and the stress concentrations (as well as the plastic strain in the copper envelope) near the shear plane are greater than in the other cases.

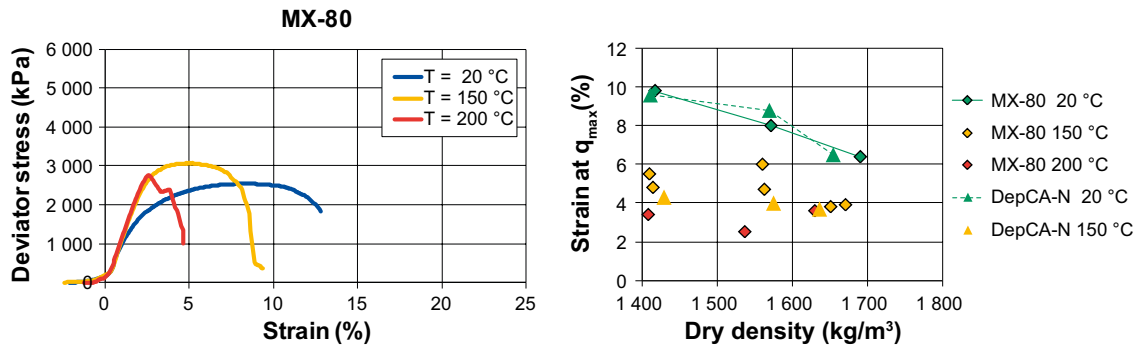


Figure 10-132. Example of brittle failure. The left figure shows example of stress strain relations at uni-axial testing of specimen of bentonite that have been exposed to different temperatures. The right figure shows measured strain until failure as function of dry density for specimen exposed to different temperature (Sellin et al. 2017).

However, the maximum plastic strain is not higher and as a whole the difference between the different cases is small. The overall conclusion is that a brittle behaviour of the buffer will not have a significant effect on the consequences of a shear. This is a logical conclusion, because brittle failure does not mean increased, but instead reduced shear strength with elongation, i.e. shear resistance from the buffer decreases. Earlier calculations of the shear also show that lower shear resistance in the buffer means lower tension in the canister.

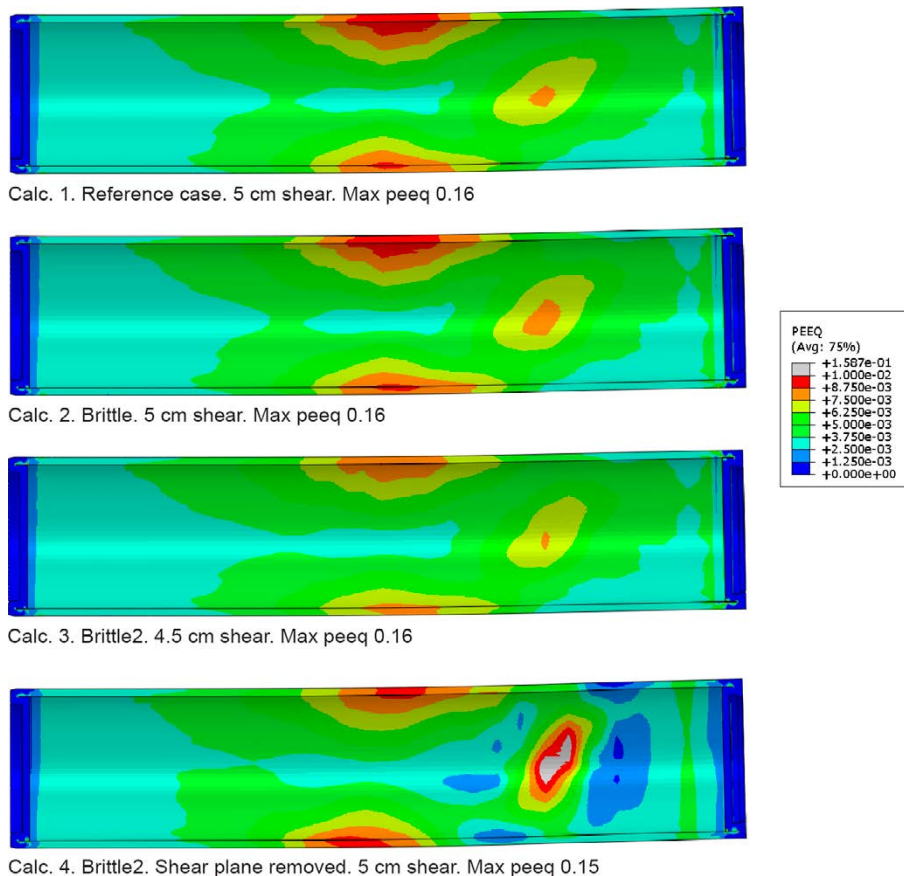


Figure 10-133. Plastic strain (peeq) in the copper (Sellin et al. 2017).

Combined isostatic and shear loads

The analyses of combined shear and isostatic loads were performed for two sequences of events:

- Shear displacements of 5 cm and 10 cm with an additional 30 MPa isostatic load from an ice sheet present. This value is somewhat higher than the assessed maximum ice load of 26 MPa in the reference evolution.
- Shear displacement of 5 cm and 10 cm followed by isostatic loads of 30 MPa. This case is analysed with a simplified model (for convergence reasons) where the buffer is replaced by corresponding reaction forces before applying the pressure of 30 MPa.

The results are summarised schematically in Table 10-27, for 10 cm shear. The axial stress in the insert is decreased, and the strains are decreased or only slightly increased, compared to the case with only shear load. The case with only isostatic load calculated with the same global FEM-model (Hernelind 2010) gives no plastic strains in the insert and von Mises stress at 358 MPa, which is comparable to the values in Table 10-26. The effects on the copper shell of the combined loads are strains slightly higher locally or small changes of the already small strains at the global level (indicated by the values for strain at mid-shell). The strain (equivalent creep strain, CEEQ) in the copper shell for an isostatic load only is at a maximum very locally 16 %, and about 0.1 % at mid height. All the strain values should be compared to the requirements on the design parameters for the copper components that are a minimum elongation of 40 percent and a minimum creep ductility of 15 percent, and with the even higher values achieved for manufactured copper components (see the **Canister production report**).

The following is, therefore, concluded.

- A glacial load of 30 MPa during a shear displacement does not yield a more severe impact on the canister than the corresponding case without isostatic load. Since it was concluded in the subsection “Prerequisites for shear load by earthquakes” above that large earthquakes will not occur in connection with high isostatic loads, this case is, furthermore, seen as unrealistic.
- A glacial load after a shear displacement is to be expected since several glaciations are expected in a 1 000 000 year perspective according to geological evidence and hence have been postulated in the reference evolution. It is therefore important to note that the canister integrity is not jeopardised by a 5 cm shear movement followed by a 30 MPa glacial load.

Table 10-27. The effects on the canister insert and copper shell for combinations of shear load (10 cm shear) and isostatic load. The effects compared to the case with only rock shear are indicated with arrows, ↑ and ↓, for increase and decrease, respectively. Arrows within parentheses indicate small effects.

Case	Plastic strain insert	Axial stress insert	Local strain copper shell		Maximum strain mid copper shell	
			(↑)	%	↑	%
Glacial load during shear	↓	↓	(↑)	17 %	↓	1.4 %
Shear followed by glacial load	(↑)	↓	↑	23 %	↑	2.7 %
For comparison – shear only				16 %		2.0 %

Identified uncertainties and their handling in the subsequent analysis

Figure 10-134 displays a flowchart summarising the relevant steps in the workflow.

The largest uncertainty, and the most difficult to reduce, concerns the expected frequency of earthquakes of various sizes at Forsmark. The literature is sparse and data coverage incomplete both in time and space. However, the frequencies used herein do not underestimate the number of faults that have been unequivocally designated “post-glacial”. As noted by Lagerbäck and Sundh (2008), the erosional effect of the latest glaciation, the Weichselian, was quite limited and could most probably not have erased remnant evidence of fault scarps from previous glaciations. Hence, the frequencies used herein seem representative of at least the latest glacial cycle. The extent, duration and impact of future glaciations are unknown but Weichselian conditions, which promote fault reactivation should sufficient strain be accumulated over time, are assumed. It is also, pessimistically, assumed that each fault will indeed host the largest possible earthquake compatible with its size (area); a single, large

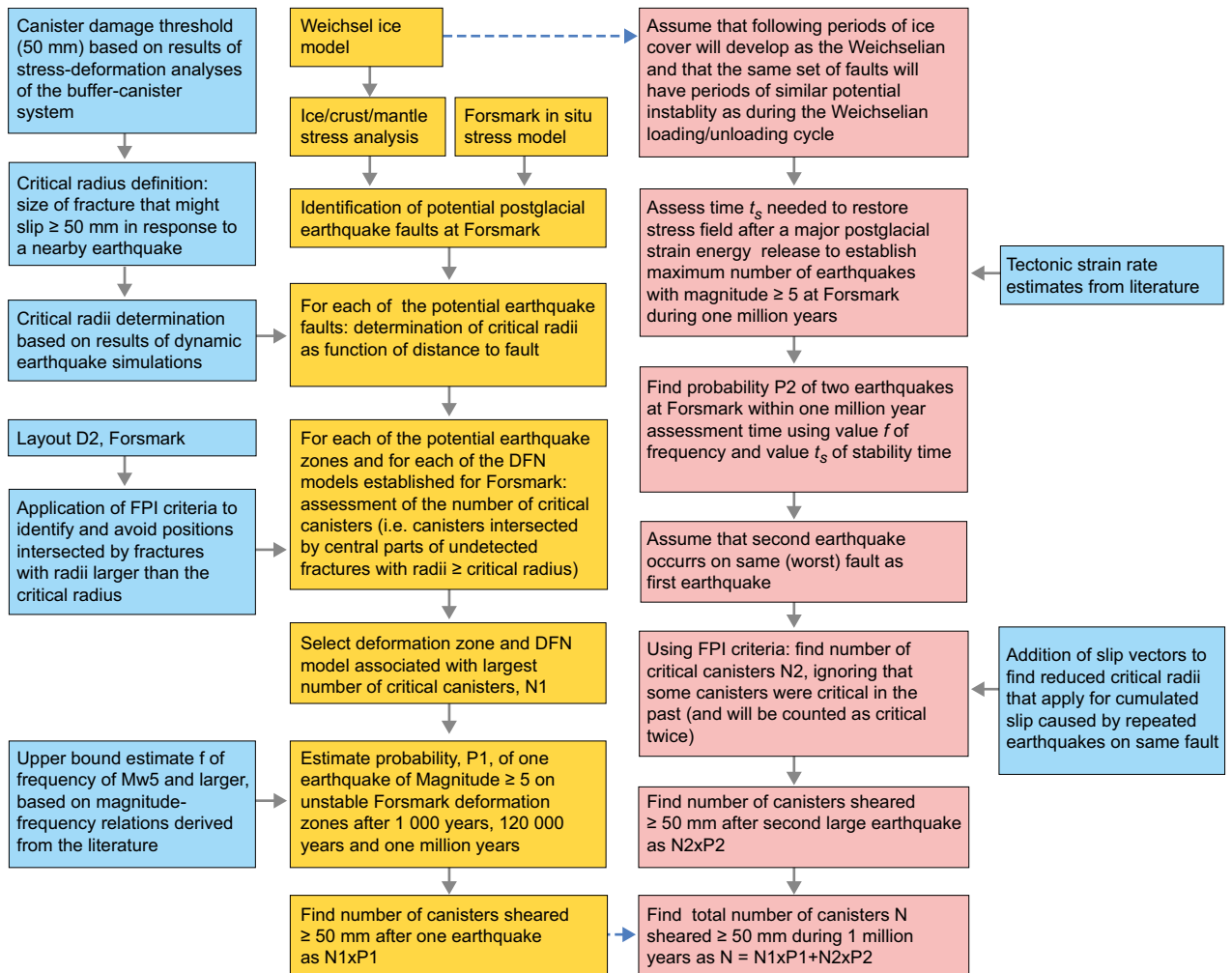


Figure 10-134. Flow diagram showing the various steps needed for the earthquake impact assessment (Figure 4-7 in the Geosphere process report).

earthquake on a fault results in far larger dynamic effects on surrounding host rock fractures than a series of smaller earthquakes releasing the same amount of strain energy. In summary, though the uncertainties are large, cautious or pessimistic assumptions have systematically been chosen.

Another large uncertainty concerns the properties of the deformation zones at Forsmark. Though the site has a thorough description with details on both geometry and properties of both the deformation zones and rock in-between, there is insufficient information on e.g. the strength properties of faults, to forecast the response of the deformation zones to a future deglaciation and insufficiently detailed knowledge on the process itself. Despite the lack of indications of large earthquakes at Forsmark (Lagerbäck et al. 2005, Lagerbäck and Sundh 2008) it is pessimistically assumed that the deformation zones used for this analysis will indeed reactivate seismically.

There is a large uncertainty in the estimate of the strain rate. The strain rate governs the time necessary to build up stresses along faults and, hence, the relaxation time. The latter governs the number of successive earthquakes a fault can host within the time frame considered. Implicitly it is assumed that the strain rate (and orientation of maximum compressional stress) will remain constant for the coming 1 000 000 years. Even though the time frame is very large indeed, this is considered a reasonable assumption.

Consecutive earthquakes have been handled in the simulation of canister/fracture intersections by setting the critical radius to half the critical radius of a single event. This is a consequence of assuming that the second slip event on the target fracture occurs according to the same slip magnitude distribution as the previous one, and in the same direction. The prerequisites for this to occur are unlikely but as

we do not yet possess other means to quantify the net slip this conservatism is judged appropriate. However, it needs to be emphasised that, due to the powerlaw distribution of fracture size, the number of critical fractures increases dramatically which tends to substantially overestimate the number of canisters that may fail. In addition, we do not take into account the fact that slip velocity scales with slip magnitude. Instead, we apply the same 50 mm damage criterion for the total effects of two small low-velocity slip events separated by tens of thousands of years as for one large high-velocity slip event, hence adding further to the pessimism. However, the canister/buffer system is not particularly sensitive to slip velocity.

The number of critical canister positions is influenced by the fracture model of the Forsmark Site (Fox et al. 2007). The uncertainties in the models are discussed thoroughly in the **Data report** and the full argumentation is not repeated here. In short, in this assessment all variants of the Discrete Fracture Network (DFN) models are propagated through all stages of this assessment to cover full uncertainty space given by the model uncertainties.

Finally, there is an uncertainty regarding the damage criterion of 50 mm. Only specific fracture/canister intersection geometries do in fact result in damage at 50 mm; other intersection geometries require larger slip magnitudes for damage to occur. Also, the failure criterion for the canister is the acceptable defect size for surface defects in the insert. The copper shell is assumed to be penetrated at the same moment as this criterion is exceeded. The strains in the copper shell are low (with the exception of model singularities) compared to copper material ductility requirements, though uncertainties arising from a copper thickness of slightly less than 50 mm are not evaluated. As the effects of different intersection geometries have been difficult to quantify and extract from the modelling and experiments on shear across the canister/bentonite package, it has pessimistically been assumed that all canisters that host slips exceeding 50 mm should count as damaged regardless of intersection geometry.

In conclusion, large earthquakes at Forsmark cannot be excluded within any of the safety assessment time frames. The impact of earthquakes, in terms of the number of canisters expected to be sheared 50 mm or more has here been quantified by using a range of earthquake frequency estimates, the Forsmark site description and by applying deposition hole rejection criteria. Using a number of numerical simulations, we identified potentially unstable deformation zones, computed critical radii of host rock fractures and the average number of canisters in critical positions. Finally, we computed the number of canisters that may be sheared 50 mm or more during the assessment time frames.

Between 9.3×10^{-6} and 2.2×10^{-5} canisters may be sheared 50 mm or more due to earthquakes within the 1 000-year time frame. During a glacial cycle, it is estimated that between 8.3×10^{-4} and 5.7×10^{-3} canisters may fail. For the 1 000 000-year time frame, at maximum two seismic events are assumed and it is estimated, using the most pessimistic way of accounting for the combined effects of both, that between 8.3×10^{-3} and 7.9×10^{-2} canisters may be sheared 50 mm or more. Because these expected numbers of sheared canisters are substantially less than one, they can be interpreted as the probability of one or more failed canisters being present at the end of the specified assessment time frame. It has also been demonstrated that these figures can likely be reduced in future assessments. Based on modelling in Hökmark et al. (2019) and with unaltered DFN models, rejection rules and repository layout the reduction is estimated to a factor of about 4.

The issue is further elaborated in the analysis of the scenario ‘canister failure due to shear load’ in Section 12.8.

10.4.6 Hydrogeological evolution

The primary driving force for groundwater flow at repository depth during periods of periglacial (permafrost) and glacial climate conditions is the hydraulic pressure gradient resulting from the presence of an ice sheet. The expected effects of this gradient with relevance for post-closure safety are related to the groundwater chemistry, the performance measures of groundwater flow at repository depth, the advective travel time, and the flow-related transport resistance. In order to assess the magnitude of these impacts, groundwater flow simulations, based on the hydrogeological models developed as part of the **Site description Forsmark**, have been performed (Vidstrand et al. 2010, Joyce et al. 2010). The overall objective of these simulations was to assess the effects of periglacial and glacial climate conditions on site hydrogeochemical and hydrogeological conditions in the presence of a backfilled repository, i.e. safety functions R1 and R2 in Figure 10-2.

Methodology

As described in Section 10.3.6, the groundwater flow modelling conducted for temperate climate conditions by Joyce et al. (2010) considers the period between 8000 BC and 12 000 AD. To a large extent the setup of this modelling follows the specifications of the groundwater flow modelling considered in SDM-Site, which dealt with the evolution between 8000 BC and 2000 AD, i.e. the Holocene interglacial period.

In comparison, the groundwater flow modelling during periglacial and glacial climate conditions conducted by Vidstrand et al. (2010) is less specific with regard to time although the flow modelling as such encompasses periglacial and glacial climate conditions during a time period of approximately 19 000 years. That is, there is no particular start time associated with the flow simulations conducted to represent periglacial and glacial climate conditions. Furthermore, it is noted that Vidstrand et al. (2010) focused on studying the effects of a number of bounding hydraulic assumptions rather than striving for realism in every detail. Although some of the studied assumptions create overly pessimistic premises for the flow simulations, as compared to the reference glacial cycle presented in the **Climate report**, Section 4.5, they are useful for safety assessment applications as they provide bounds on the uncertainties involved.

Based on the reference glacial cycle described in the **Climate report**, the flow modelling in Vidstrand et al. (2010) is divided into three stages referred to as pre-LGM²⁹, LGM, and post-LGM. During the pre-LGM stage, the ice sheet grows and the ice sheet margin moves across the site in a forward (advancing) direction. During the LGM stage, the model domain is completely covered by ice for thousands of years. During the post-LGM stage, the ice sheet melts and its margin moves across the site in a backward (retreating) direction. Hence, the flow modelling of the three stages implies a transient top boundary condition.

It is noted that a repository is not included in the groundwater flow modelling conducted by Vidstrand et al. (2010). However, the influence of the hydraulic characteristics of the backfilled tunnels on the performance measures during periods with glacial climate conditions is accounted for by exporting the simulation results of Vidstrand et al. (2010) to be used as input (boundary conditions) in the groundwater flow modelling conducted by Joyce et al. (2010). The results from the simulations are presented below.

In summary, the following hydraulic conditions (assumptions) are considered in the groundwater flow modelling conducted by Vidstrand et al. (2010).

- **Pre-LGM stage.** Two different azimuth directions of ice sheet movement (advance from northwest and advance from north); three types of periglacial conditions (no permafrost, permafrost in front of the ice sheet margin, and permafrost in front of the ice margin as well as below the tip of the ice sheet margin); two types of permeability conditions (undistorted conditions, i.e. present-day conditions as defined in the **Site description Forsmark**, and distorted conditions, i.e. increased permeability due to hydro-mechanical deformations).
- **LGM stage.** The model domain is completely covered by a thick ice sheet for approximately 17 000 years.
- **Post-LGM stage.** One azimuth direction of ice sheet movement (retreat from southeast); submerged ground conditions in front of the ice sheet margin; undistorted permeability conditions.

The different simulations carried out by Vidstrand et al. (2010) may be grouped as shown in Table 10-28.

Figure 10-135 shows a map of the topography of a NW-SE orientation of the flow model domain. All structural and hydraulic properties inside the model domain are specified in Vidstrand et al. (2010). Inside the target volume, i.e. within the bedrock volume that hosts the repository, a DFN realisation is generated. The DFN realisation is transformed into an equivalent continuous porous medium (ECPM) approximation using the up-scaling methodology implemented in DarcyTools (Svensson et al. 2010). Outside the region of the DFN realisation, a continuous porous medium (CPM) approximation is used.

²⁹ LGM is a standard acronym used to denote the glacial maximum of the last glaciation (Weichsel), cf. the **Climate report**.

Table 10-28. Overview of flow simulations in Vidstrand et al. (2010). The main scenarios, A and B, are divided into five cases (a)–(e). The bullets indicate the particular conditions modelled with each case considered. Case (a) constitutes the Base case in Vidstrand et al. (2010).

A. Glacial conditions without permafrost	
Pre-LGM stage	LGM stage
(a) • Ice sheet movement from northwest. No permafrost in front of the ice sheet margin. Undistorted permeability conditions.	• Entire model domain is covered by an ice sheet. Undistorted permeability conditions. Post-LGM stages. • Submerged conditions in the ice free area. Undistorted permeability conditions.
Variants	
Pre-LGM stage	LGM and Post-LGM stages
(b) • As in (a), but ice sheet movement from north.	• –
(c) • As in (a), but distorted permeability conditions.	
B. Glacial conditions with permafrost	
Pre-LGM stage	LGM and Post-LGM stages
(d) • Ice sheet movement from northwest. Permafrost in front of the ice sheet margin as well as 2 km below the tip (tongue) of the ice sheet margin Undistorted permeability conditions.	• –
Variants	
Pre-LGM stage	LGM and Post-LGM stages
(e) • As in (d), but no permafrost tongue.	• –

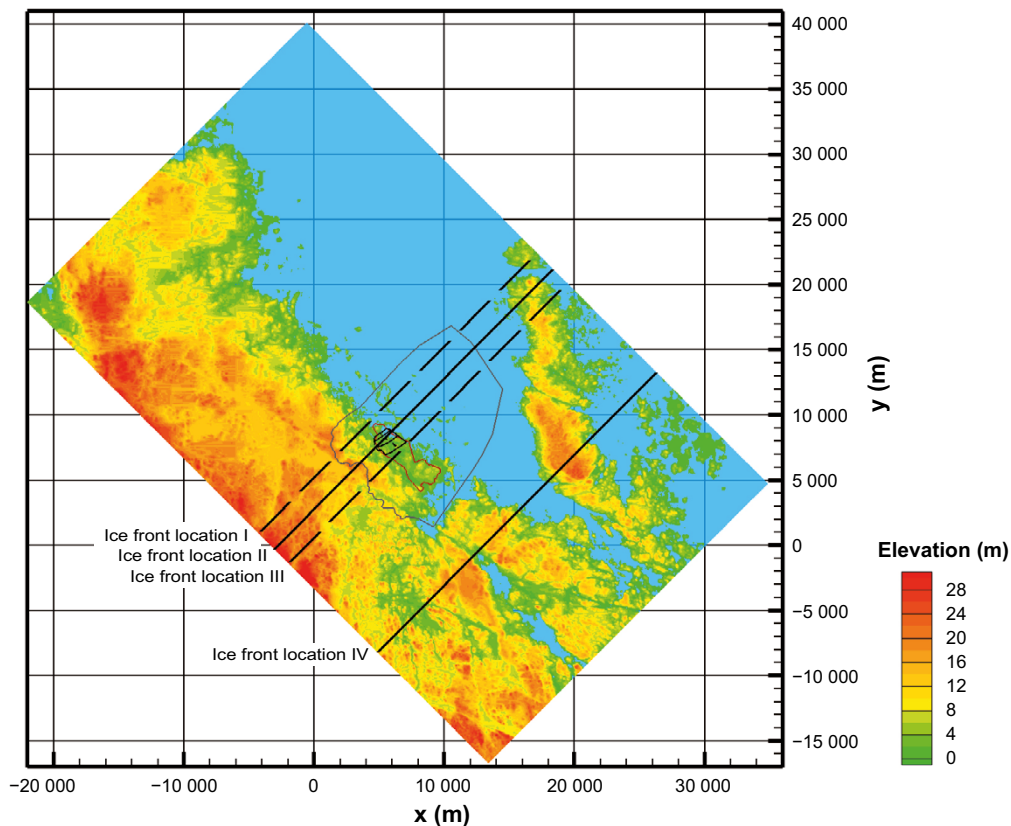


Figure 10-135. Map showing the present-day topography at Forsmark and the positions of ice front locations IFL I–IV for a NW-SE orientation of the flow model domain studied by Vidstrand et al. (2010). The large polygon in the centre shows the model domain used for groundwater flow modelling in SDM-Site. The small, polygon inside the large polygon shows the location of the investigated candidate area. The repository area is located in the north-western part of the small polygon. The y-axis points towards north.

The results of the flow simulations are reported for four ice-front locations denoted by IFL I-IV, see Figure 10-135, and five measurement localities denoted by ML 1–5, see Figure 10-136. IFL II corresponds to a situation when the ice sheet margin is right above the repository; ML 2 corresponds to a position in the centre of the repository layout. In addition to IFL I-IV, two additional ice-front locations are referred to in the flow modelling, IFL 0 and IFL V. These are both located outside the model domain shown in Figure 10-135. IFL 0 is simply the start position of the advancing ice sheet margin and IFL V is the start position of the retreating ice sheet margin. In summary, the advancing ice sheet margin starts at IFL 0 and passes IFL I-IV on its way to IFL V. At IFL V it stops and returns back to IFL 0. Conceptually, IFL 0 represents the temperate (initial) conditions at some time in the future (hence not 2000 AD), whereas IFL V coincides with the LGM.

The output parameters from the flow simulations conducted by Vidstrand et al. (2010) are the pressure (p [$\text{ML}^{-1}\text{T}^{-1}$]), the Darcy flux (q [LT^{-1}]) and the salinity (C [MM^{-1}]) at repository depth, i.e. at ML 1–5 for IFL I–IV. The flow simulations are accompanied by particle tracking simulations. The potential repository considered for modelling contains 6916 deposition hole positions. One particle is released at each deposition hole position when the ice sheet margin reaches ice front locations II and IV during the pre-LGM stage simulations. All particles are tracked backwards and forwards as a means to identify their recharge and discharge locations, respectively. It is noted that the Darcy fluxes are fixed in space and time during the particle tracking, which is a simplification since the boundary conditions at ground surface change with the position of the advancing/retreating ice sheet margin. The output parameters from the particle tracking are the flow path length (L [L]), advective travel time (t_w [T]) and the flow-related transport resistance (F [TL^{-1}]).

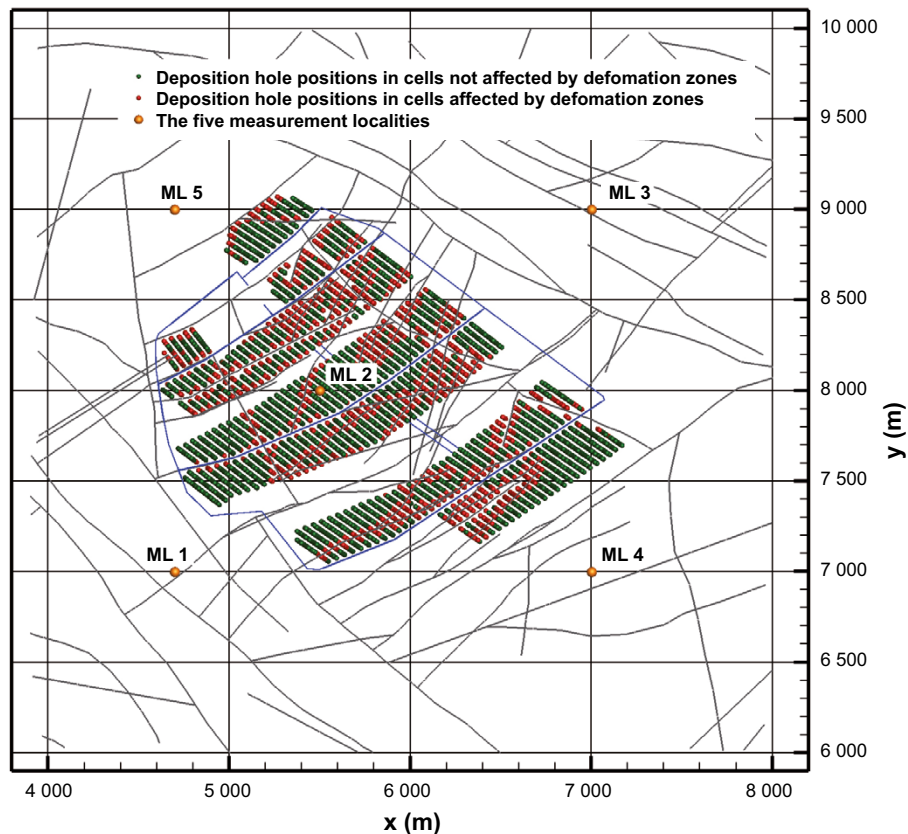


Figure 10-136. Plane view of the repository layout at -465 m elevation (the blue lines represent major tunnels). The repository has 6916 deposition hole positions. These are coloured according their structural location, i.e. whether the computational grid cell in DarcyTools is intersected by a deformation zone (HCD) or is fully inside the rock mass volumes between the deformation zones (HRD). (The deformation zones are shown as grey lines. It is noted that tunnels and deposition holes are not included in the model, but just shown in the figure for context.) The simulated evolution of the Darcy fluxes and the salinities is monitored at five measurement localities denoted by ML 1–5. The y-axis points towards north.

As already mentioned, the pressure and density fields calculated by Vidstrand et al. (2010) are exported to the flow modelling conducted by Joyce et al. (2010), since the repository layout and the excavated damage zone (EDZ) are not explicitly resolved within the flow modelling conducted by Vidstrand et al. (2010). Thus, the flow model presented in Joyce et al. (2010) is also used to calculate performance measures during glacial climate conditions. These results are used as input for the far-field radionuclide transport calculations (Chapter 13). The groundwater flow results are also used as input to buffer erosion-corrosion analyses (Sections 10.4.8 and 10.4.9). Further, in the repository-scale model of Joyce et al. (2010), particles are also back-tracked from the deposition hole positions in order to assess recharge pathways. The particle paths extend into the site-scale model in a corresponding manner as for the discharge pathways. Using the recharge paths and an analytical solution for solute transport, an assessment of potential for penetration of dilute waters to repository depth is made (Joyce et al. 2010, Appendix G).

Finally, the results calculated by Vidstrand et al. (2010) (fracture water and matrix porewater salinities, flow path lengths, advective travel times, and flow-related transport resistances of particles travelling from the surface to repository depth) are exported to the hydrogeochemical modelling carried out by Salas et al. (2010) and Sidborn et al. (2010) to study chemical processes during periglacial and glacial climate conditions, in particular the consumption of oxygen dissolved in recharging water that could potentially reach repository depth, see Section 10.4.7.

Performed analyses and usage within the PSAR

Below, the different cases of Vidstrand et al. (2010) performed with relevance for the periods with periglacial and glacial climate conditions are listed. In addition, the calculations of Joyce et al. (2010) using boundary conditions from the glacial models are included. It is indicated where the results produced by each case are used within the subsequent analyses of SR-Site and the PSAR.

- **Hydrogeological evolution.** In Vidstrand et al. (2010), the hydrogeological evolution for the case without permafrost in front of an advancing ice sheet margin constitutes a base case for a number of other models (variant cases). Thus, results on the hydrogeological evolution for the simulated period (IFL 0 → IFL V → IFL 0) are reported for a number of different cases including a case with permafrost in front of an advancing ice sheet margin, see below. It is noted that the groundwater chemistry in all these flow models is represented by salinity alone and that the results of the simulated hydrogeochemical evolution are discussed in Section 10.4.7.
- **Recharge and discharge locations in the biosphere.** The recharge and discharge locations are identified using forward and backward particle tracking from coordinates representing the deposition hole positions within the repository footprint. The particle tracking is performed for steady-state velocity fields representing different ice front locations relative to the location of the repository. Several cases, including an ice sheet with permafrost, are presented here in a manner corresponding to the hydrogeological evolution above. The performance measures discussed below are related to these deposition hole positions and associated particle tracks. The results on discharge locations in the biosphere are used for the dose calculation in the biosphere.
- **Performance measures.** The performance measures are Darcy flux (q), advective travel time (t_w) and the flow-related transport resistance (F). The advective travel time and flow-related transport resistance are calculated for both the recharge and discharge flow paths in the super-regional scale model. Furthermore, performance measures are obtained from the combined repository-scale and site-scale model including an explicit representation of the repository structures by applying boundary conditions from the super-regional scale model (Joyce et al. 2010). These results are used in radionuclide transport calculations, see Chapter 13.
- **Penetration of glacial meltwater.** The recharge of glacial melt water implies a gradual dilution of the originally more saline water. As dilute water has negative effects on the buffer and backfill stability, it is of interest to assess the possibilities of dilute water reaching repository depth considering the hydrogeological flow and transport conditions. This is done using the flow-related transport properties resulting from the repository-scale and site-scale models described above in conjunction with analytical transport estimates. The results are used in Section 10.4.7.

- **EDZ and crown space.** In the application of glacial boundary conditions in the repository-scale and site-scale models including an explicit representation of the repository, an assessment of modified properties of the excavation damaged zone (EDZ) is performed. Also, an assessment of the impact of a crown space in the tunnels is made. The crown space is caused by a consolidation of the tunnel backfill material. These results are used in radionuclide transport calculations, see Chapter 13.
- **Site related variants.** Some properties of the site, with specific relevance to glacial conditions, as well as the glacial conditions themselves are uncertain. The impacts of alternative parameterisations related to these issues are assessed in order to judge their importance. For example, the transmissivity of all deformation zones and fractures that strike towards northwest is changed based on the results from the rock mechanics modelling conducted for SR-Site (Hökmark et al. 2010, Lönnqvist and Hökmark 2010).
- **Glacial conditions with permafrost.** The reference evolution in the **Climate report** is characterised by permafrost conditions in front of an advancing ice sheet margin. The same set of analyses performed for the case without permafrost in front of an advancing ice sheet margin is repeated for this case. The most important differences are high-lighted. It is noted that boundary conditions for this case cannot be exported to the repository-scale and site-scale models of Joyce et al. (2010) since the hydraulic properties of the geosphere are modified due to the presence of permafrost. It is noted that the hydrogeological evolution and recharge and discharge locations of this case are commented upon above under the specific bullet points dealing with these two issues. Other aspects of this case are treated under this bullet point.
- **Comparison of the Darcy flux at different times during glaciation and deglaciation.** Various model simplifications are made in Vidstrand et al. (2010) and Joyce et al. (2010) that do not conform fully to the expected reference evolution described the **Climate report**. In order to obtain an appreciation of the evolution of groundwater flow for an advancing and retreating ice sheet margin, methods to combine all simulated “climate events” (states) are presented and exemplified. The objective is to find reasonable simplifications of the complex temporal evolution of the Darcy flux for subsequent handling in radionuclide transport calculations within the safety assessment.

Hydrogeological evolution

Figure 10-137 shows Darcy fluxes for a NW-SE vertical cross section through the potential repository area. Three cases are shown. The upper-most cross-section represents temperate conditions (IFL 0). The cross-section in the middle represents an advancing ice sheet margin at IFL II without permafrost in the periglacial area. The bottom-most cross-section represents an advancing ice sheet margin at IFL II with permafrost conditions in the periglacial area.

Figure 10-138 shows the salinity field for a NW-SE vertical cross section through the potential repository area. Three cases are shown. The upper-most cross-section represents temperate conditions (IFL 0). The cross-section in the middle represents an advancing ice sheet margin at IFL II without permafrost in the periglacial area. The bottom-most cross-section represents an advancing ice sheet margin at IFL II with permafrost conditions in the periglacial area. Figure 10-139 shows the same salinity fields but for a horizontal plane placed at -465 m through the target volume.

It is noteworthy that in order to create a stable initial condition for the glacial simulations, a temperate model variant was set up that simulated a pseudo steady-state situation with all current conditions locked as boundary conditions. The model was initiated with the initial salt conditions described in Table 5-2 in Vidstrand et al. (2010). The model was run in 200 time steps of 10 years each, i.e. 2000 years. At this time, the model was in “numerical” steady-state, that is, no further change in pressure and salinity occurred within the numerical criteria set.

In summary, Figure 10-137 and Figure 10-138 show that the hydraulic pressure at the bottom of the ice sheet distorts the temperate conditions and causes glacial meltwater to recharge and flush the advective system. In effect, the more saline water in the fractures is pushed forwards and upwards (upconing). The reason for the high salinity near the ground surface is that the permafrost hinders discharge at the top boundary (cf. the bottom most image in Figure 10-137), except where taliks (unfrozen ground) occur.

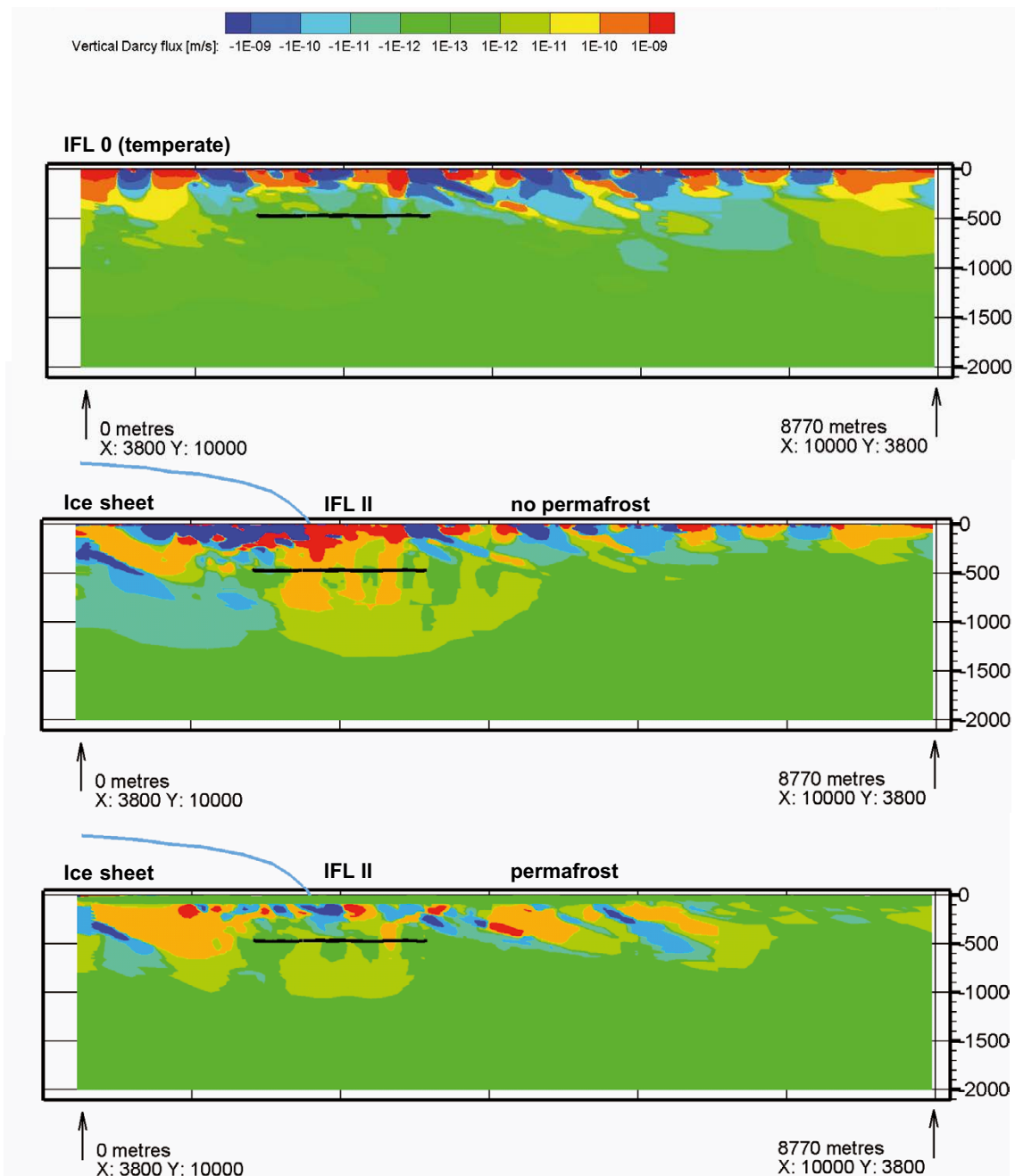


Figure 10-137. Top: Darcy flux during temperate conditions mapped on a cross-section parallel to the direction of the ice sheet movement during glaciation. The images in the middle and at the bottom show the Darcy fluxes when the ice sheet margin is at IFL II for the glacial case without permafrost (middle) and for the glacial case with permafrost (bottom). Negative values represent downward directed fluxes. The position of the ice sheet profile is illustrated with a blue curve.

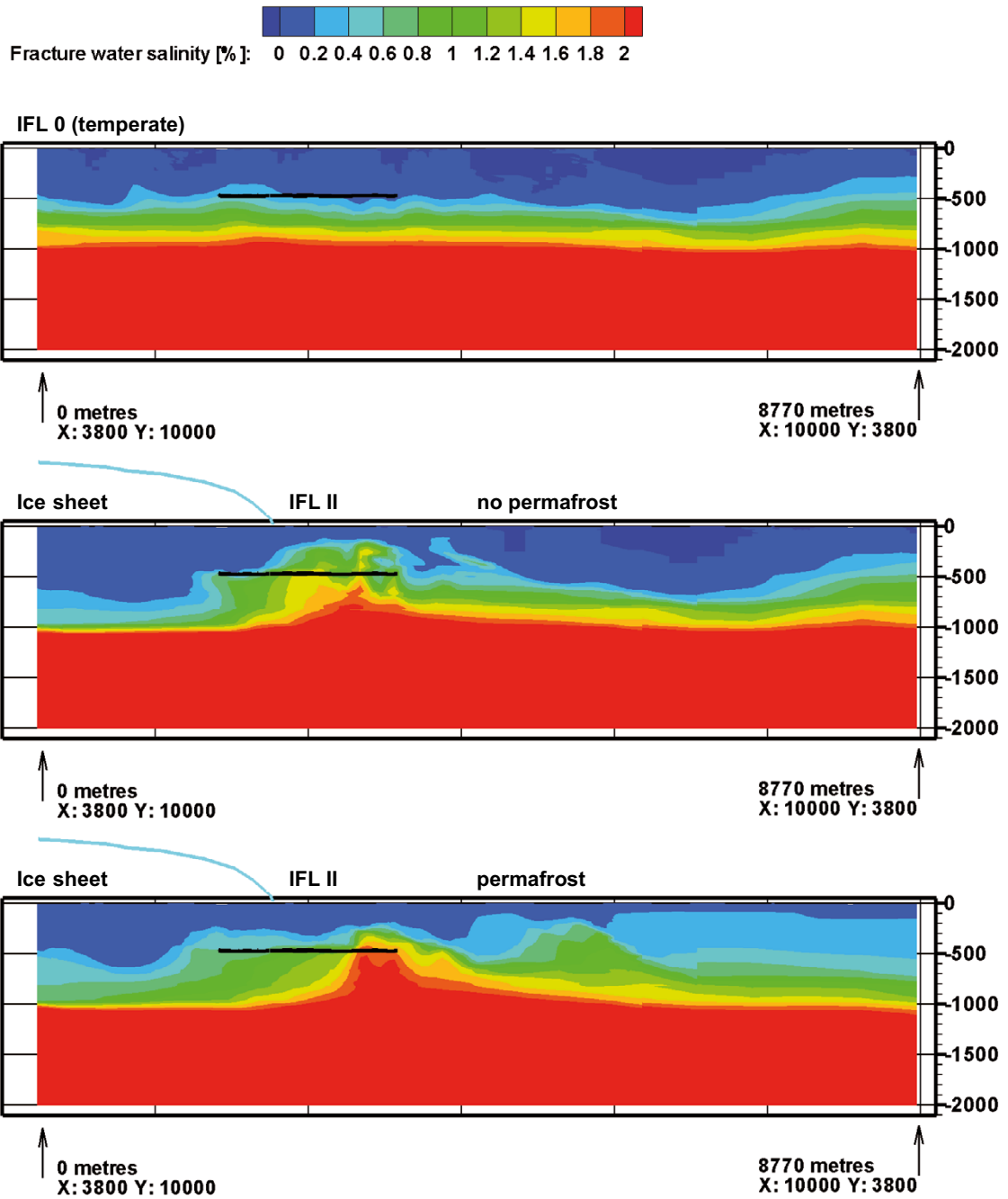


Figure 10-138. Top: Fracture (advective) water salinity during temperate conditions mapped on a cross-section parallel to the direction of the ice sheet movement during glaciation. The images in the middle and at the bottom show the fracture water salinity when the ice sheet margin is at IFL II for the glacial case without permafrost (middle) and for the glacial case with permafrost (bottom). The position of the ice sheet profile is illustrated with a blue curve.

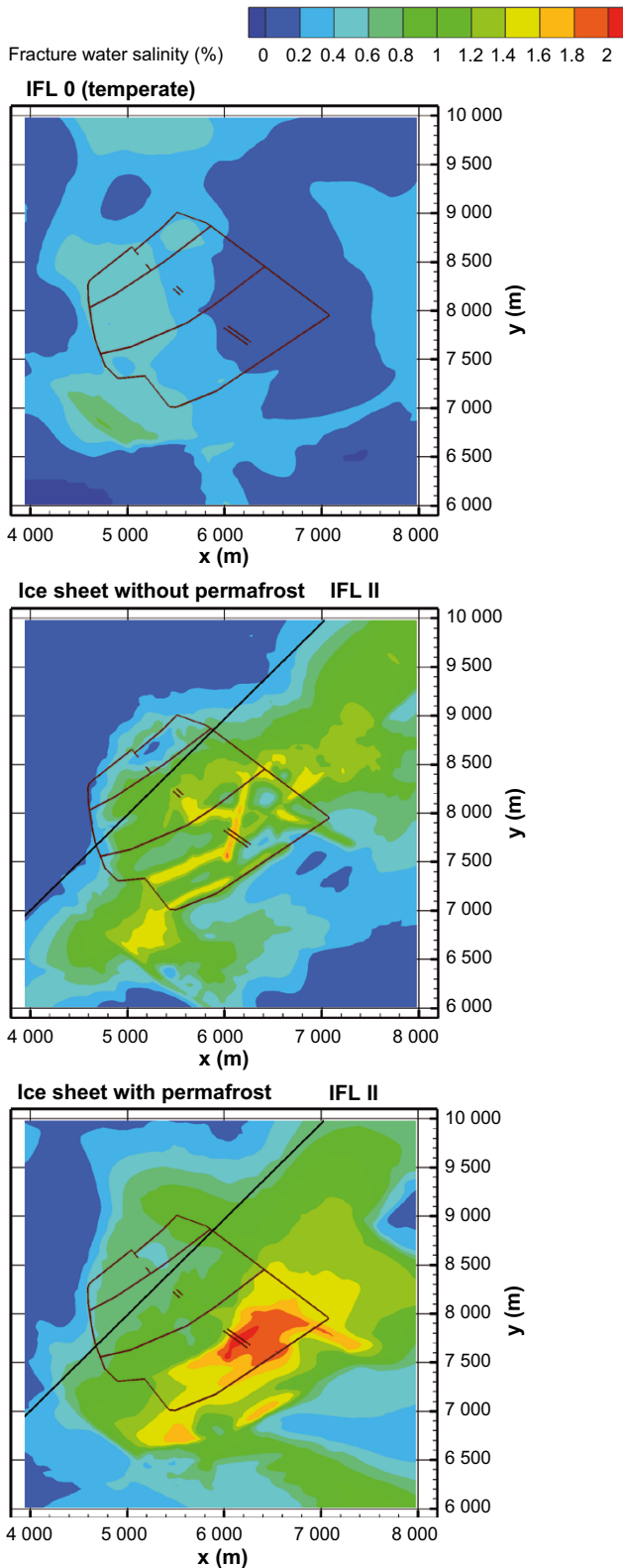


Figure 10-139. Top: Fracture (advective) water salinity during temperate conditions mapped on a horizontal plane located at -465 m. The images in the middle and at the bottom show the fracture water salinity when the ice sheet margin is at IFL II for the glacial case without permafrost (middle) and for the glacial case with permafrost (bottom). The black thin lines represent main repository tunnels.

The changes in Darcy flux and fracture water salinity during the simulated period (IFL 0 → IFL V → IFL 0) are monitored at the five measurement localities ML 1–5 and expressed as ratios relative to the corresponding initial, temperate values, see Figure 10-140 and Figure 10-142. It is recalled that the term temperate in Vidstrand et al. (2010) is not to be understood as 2000 AD, but rather as a time slot in the future when the ice sheet margin is close to, but still outside, the flow model domain, i.e. IFL 0.

In Figure 10-140, it is seen that the Darcy flux increases dramatically during the two ice front passages. The immediate shift to low and constant values at the start of the period of complete ice coverage is an artefact of the instantaneous shift in ice sheet gradient at the same moment. In reality, a more smooth transition is expected. For the glacial case with permafrost, slightly different shapes of the curves are obtained during glacial advance, see Figure 10-141. However, for the remaining parts of the cycle, the curves are identical to those shown in Figure 10-140 as there is no permafrost during these periods.

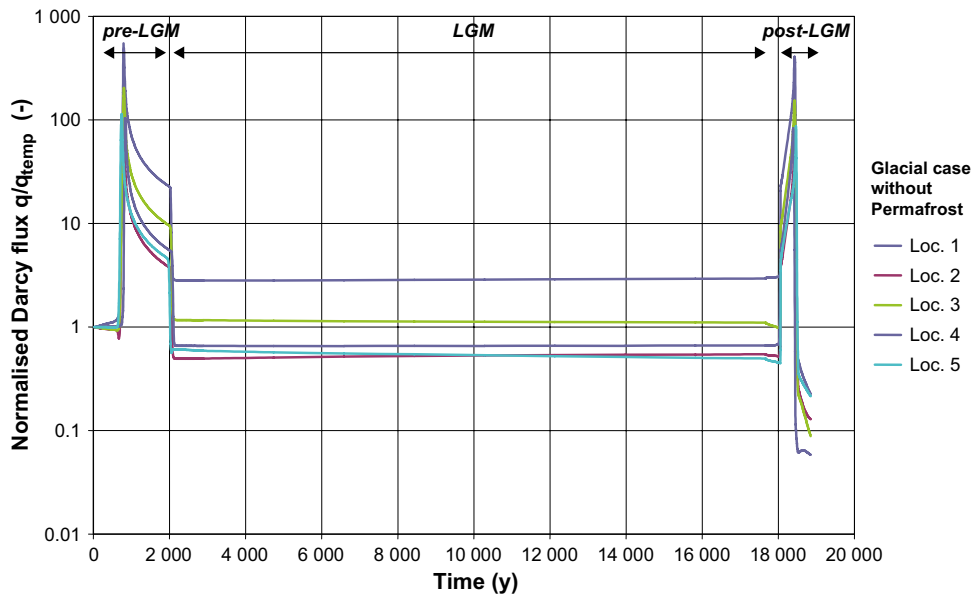


Figure 10-140. Plot showing the normalised change in Darcy flux, (q/q_{temp}), at ML 1–5 during approximately 19 000 years for the glacial case without permafrost. ML 1 is located close to a steeply dipping deformation zone.

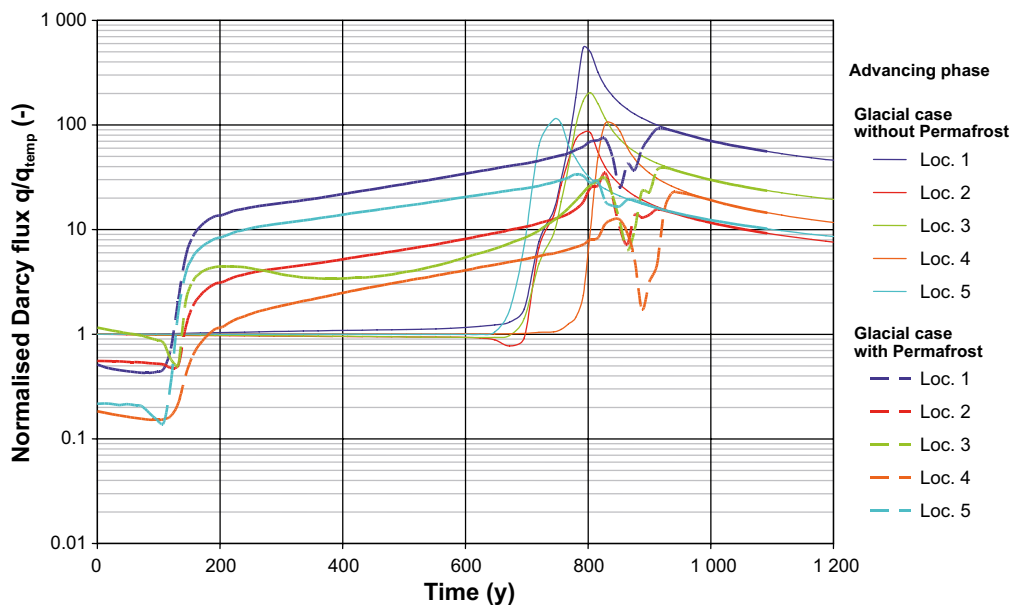


Figure 10-141. Close-up showing the normalised change in Darcy flux, (q/q_{temp}), at ML 1–5 during glaciation (pre-LGM). In addition to the glacial case with permafrost (solid lines), the evolution of the glacial case without permafrost (dashed lines) is shown. Beyond $t = 1000$ years the two cases are alike.

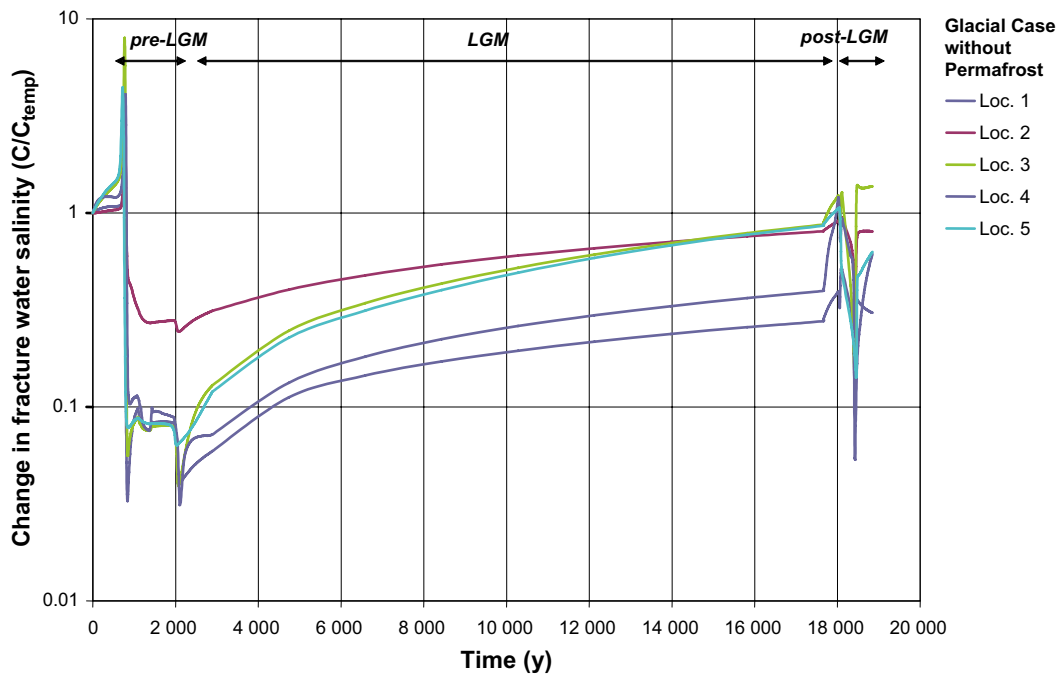


Figure 10-142. Change in concentration, (C/C_{temp}) , during a cycle of approximately 19000 years for the glacial case without permafrost.

The normalised change in the salinity development is shown in Figure 10-142. The glacial passage during advance (pre-LGM) is characterised by an initial upconing followed by an out flushing resulting in lower salinities than during the initial temperate conditions. However, during the subsequent stage, i.e. when the site is completely covered by the ice sheet (LGM), a gradual increase in fracture water salinity at repository depth occurs. This gain of the “salt water interface” is due to an accommodation of the buoyancy forces to the very weak top boundary condition of an almost uniform ice sheet thickness, and to the slow, but continuous advective transport of salt from below. It is recalled that the fracture water salinity at great depth is assumed to be undisturbed (fixed) at all times in the flow model. The data support for this assumption is presented in SDM-Site.

The glacial passage during retreat (post-LGM) is also characterised by an upconing and flushing event, but the effects are considerably smaller than during the advance. The reasons for this are twofold; (i) the speed of the retreating ice sheet margin is twice as fast as the speed of the advancing ice sheet margin (100 m/y versus 50 m/y), and (ii) the subglacial area in front of the retreating ice sheet margin is submerged. These conditions reduce the duration and the magnitude of the hydraulic gradient across the ice sheet margin significantly.

Figure 10-143 shows the simulated difference in flushing as a function of the average speed of the retreating ice sheet margin. A retreat speed of 300 m/y yields less flushing than a retreat speed of 100 m/y. It is noted that the average speed of the retreating ice sheet margin considered for the reference evolution in the Climate report is 300 m/y; i.e. three times the speed considered in Vidstrand et al. (2010). Second, the retreating ice sheet profile considered for the reference evolution in the Climate report is significantly thinner and less steep at the ice sheet margin than the ice sheet profile considered in Vidstrand et al. (2010), which is a theoretical maximum. Thus, the conditions considered by Vidstrand et al. (2010) exaggerate the impact of the ice sheet; still the results indicate that the fracture water salinities are more or less restored during the simulated period (IFL 0 → IFL V → IFL 0).

In conclusion, low fracture water salinities, i.e. dilute conditions, are mainly found in conjunction with the ice front passages. The results presented in Figure 10-142 indicate that fracture water salinities reach values below ten percent of the values in temperate conditions for a limited period of time only.

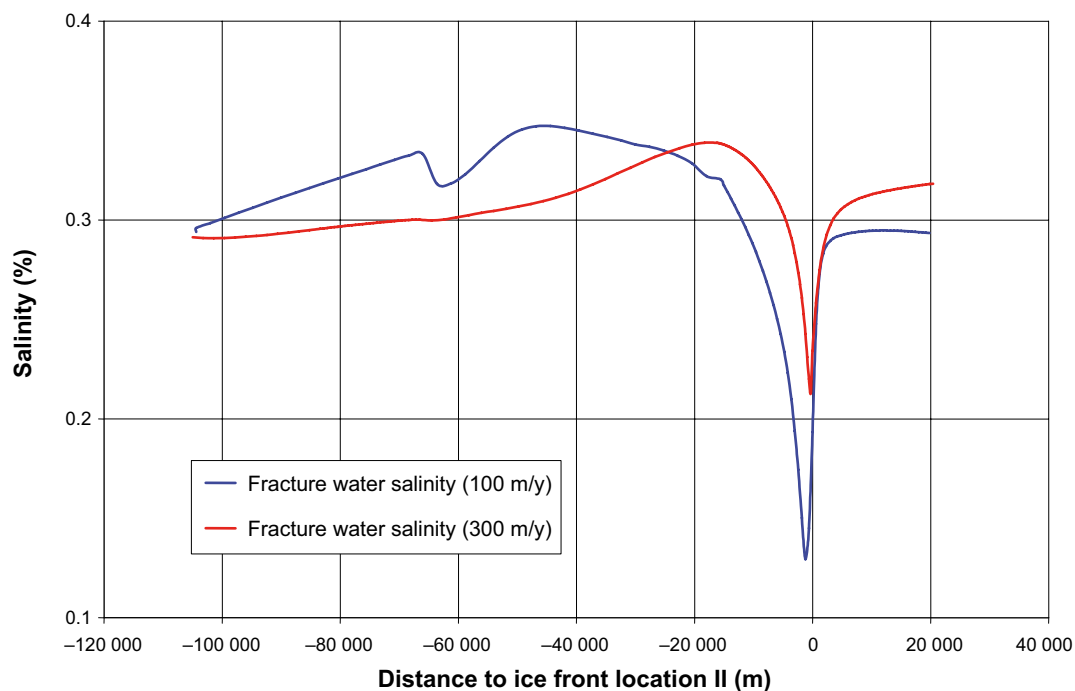


Figure 10-143. Plot showing the difference in flushing as a function of the average speed of the retreating ice sheet margin. A retreat speed of 300 m/y yields less flushing. (The ice sheet margin moves from left to right in this plot.)

Recharge and discharge locations in the biosphere

The top image in Figure 10-144 shows the recharge and discharge locations when the ice sheet margin reaches ice-front location II for an ice sheet without permafrost, and the bottom image in Figure 10-144 shows the corresponding results for an ice sheet with permafrost. For both cases, a number of particles recharge at the upstream boundary of the model domain, which suggests that the model domain is too short to give a fully undisturbed view of all recharge locations for a fixed flow field. Nevertheless, it may be concluded that the present-day topographic water divides, which play an important role in the recharge and discharge during temperate conditions, are significantly diminished in importance during glacial conditions.

In contrast, the discharge locations are predominantly found well within the physical boundaries of the model domain and often very close to the margin of the ice sheet. The differences seen in the discharge pattern between the two glacial cases are largely caused by the varying hydraulic properties and boundary conditions. For an ice sheet with permafrost, there are two centres of discharge:

- The deformation zone model that exists within the regional model domain for SDM-Site Forsmark. In this simulation approximately two percent of the released particles exit along deformation zones.
- The taliks positioned at the topographic lows in front of the ice sheet margin to the east (outside the regional model domain). In this simulation, the taliks catch approximately 98 % of the released particles.

Performance measures

The performance measures of interest are the Darcy flux (and equivalent flow rate) at each deposition hole position, and the flow-related transport properties along flow paths from the deposition hole positions, i.e. the advective travel time and flow-related transport resistance. In principle, these are directly obtained from the super-regional model Vidstrand et al. (2010) for all ice front locations. However, the repository structures are not explicitly included in this model, and hence results for the different release paths Q1, Q2 and Q3 handled in Joyce et al. (2010) and presented in Section 10.3.6 are not obtained. By transferring boundary conditions from the super-regional scale model to the combined repository-scale and site-scale models of Joyce et al. (2010) where the repository is included, all performance measures needed for subsequent radionuclide transport calculations are obtained.

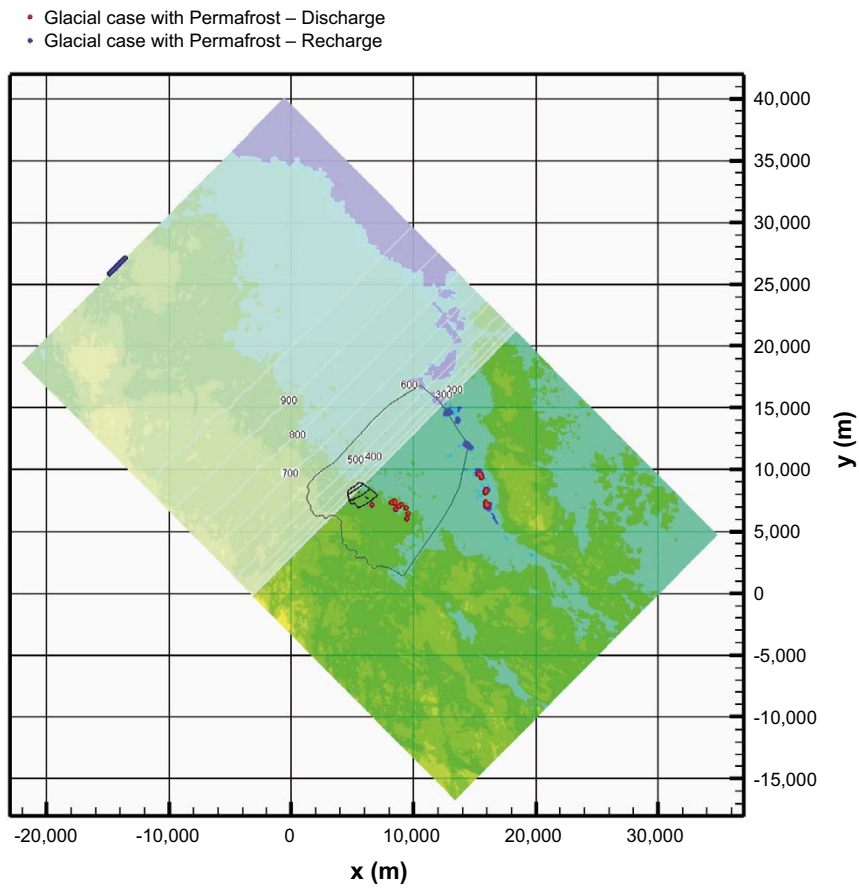
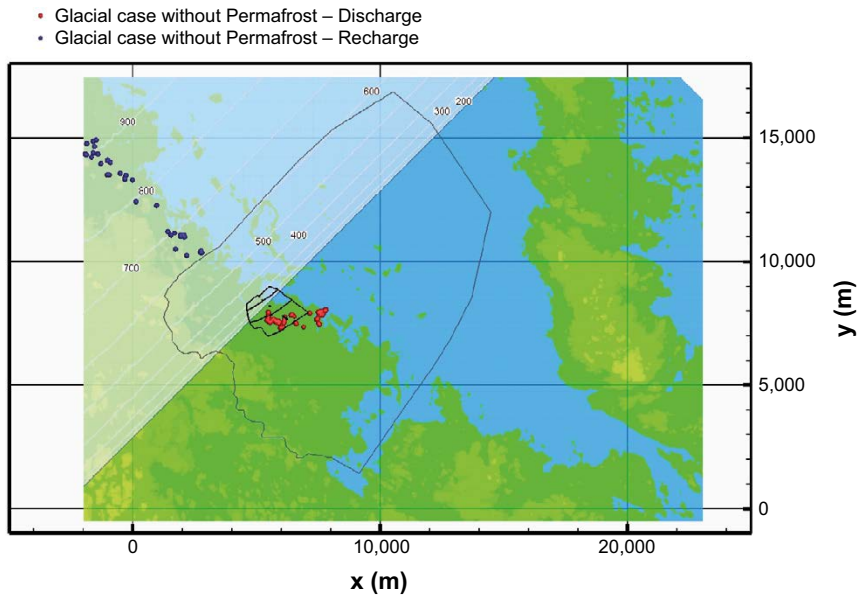


Figure 10-144. Recharge (blue) and discharge (red) locations of the 6916 particles released at repository depth when the advancing ice sheet margin is at ice-front location II. Top: Ice sheet without permafrost. Bottom: Ice sheet with permafrost and taliks. The taliks are positioned in the topographic lows in front of the ice sheet margin to the east (outside the polygon that indicates the SDM-Site model domain).

In Figure 10-145 and Figure 10-146, the Darcy flux and flow-related transport resistance are shown for the Q1 path for the case with an advancing ice sheet margin without permafrost where the ice front is in close proximity to the repository (ice-front location II). It is observed that the median Darcy flux is increased by approximately an order of magnitude. A corresponding decrease of the flow-related transport resistance is observed. Also, the results indicate that the high Darcy fluxes are more influenced by the glacial boundary conditions than the low values; e.g. the 90th percentile is shifted more than the 10th percentile. Thus, it appears that regions with low flow are relatively less affected by the high gradients induced by the ice sheet than regions with high flows.

Penetration of glacial melt water

In principle, the future groundwater chemistry, specifically salinity, is provided by the super-regional scale groundwater flow simulation reported above. However, the super-regional scale model has a fairly coarse discretisation, which does not allow an assessment of the groundwater chemistry evolution on a deposition hole scale. Thus, an alternative assessment of the evolution of the groundwater chemistry, and specifically the potential for penetration of dilute water, is made.

The combined repository-scale and site-scale models of Joyce et al. (2010) with boundary conditions from the super-regional scale model of Vidstrand et al. (2010) are used. The cases with an advancing ice sheet margin without permafrost for ice-front locations II and V are analysed. In order to assess the potential for penetration of dilute water, an injection of glacial melt water along those recharge pathways that originate close to the surface within the regional-scale model is considered for the two ice front locations. Similar simplifying assumptions as used for the temperate period calculations in Section 10.3.6 are adopted here. Along the flow paths, the only mitigating process considered is the out-diffusion of salt from the matrix affecting the penetration of the glacial melt water front. As in Section 10.3.6, also the effect of stagnant water next to the flowing water path is illustrated. Furthermore, it is assumed that the salt concentration of the matrix water is in equilibrium with the fracture water prior to the injection of glacial meltwater with a salt concentration of 0 g/L. The simplifying nature of these assumptions is discussed in Section 10.1.3.

In Figure 10-147 and Figure 10-148, the temporal distribution for deposition holes to obtain twenty percent of the initial water concentration is shown for ice front location II and V, respectively. The initial salt concentration of the fracture water before the onset of the glacial period is estimated to be 3 g/L for both the base case and the global warming variant of the reference evolution (Section 10.4.7 and 10.6.3; Salas et al. 2010, Joyce et al. 2015). The 3 g/L was estimated as typical values extracted from nodes close to the repository volume in the salinity field provided for ice front location II of the glacial period modelling (Vidstrand et al. 2010). Twenty percent of the initial concentration thus corresponds to 0.6 g/L, which coincides with the value assumed to represent dilute conditions with potential buffer erosion. The vertical lines represent the assumed approximate duration of the periods. For ice front location II, i.e. an ice front in close proximity to the repository, the assumed durations are 20 and 100 years. The longer duration is an estimate for an advancing ice front, whereas 20 years is an estimate for a retreating ice front; however, all results presented in the figure are based on a flow field obtained for an advancing ice sheet. For ice-front location V, i.e. the glacial maximum case (LGM), two time durations are assumed, 20 000 and 100 000 years. Considering no stagnant water zones, it is observed that approximately three percent of the deposition holes experience dilute conditions during an advancing ice front, approximately two percent during a retreating ice front (Figure 10-147), and approximately one and two percent during an assumed period of 20 000 and 100 000 years corresponding to different assumptions on glacial maximum conditions (Figure 10-148). The exact fractions of deposition holes experiencing dilute conditions are provided in Table 10-29 and Table 10-30.

Similar to the temperate phase results shown in Section 10.3.6, the inclusion of stagnant water zones between the flowing channels, thus enhancing the out-diffusion of salt, yields more favourable results. However, also here the additional safety implied by the stagnant water is pessimistically not accounted for in the subsequent assessment. For the overall safety discussion, the process of enhanced matrix diffusion through stagnant water may well be included.

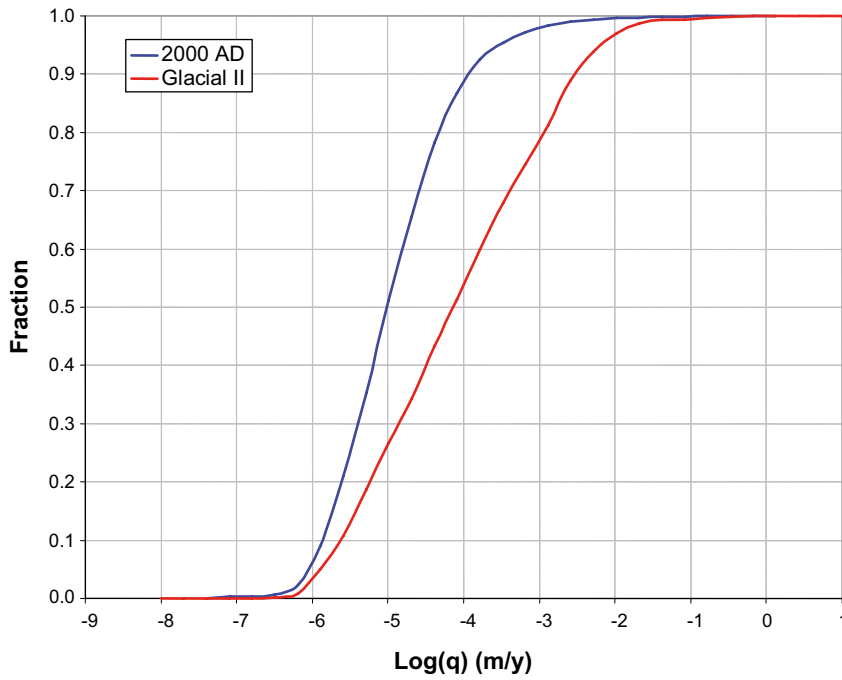


Figure 10-145. Cumulative distribution function plots of Darcy flux (q) for the $Q1$ path for the hydrogeological base case simulation at 2000 AD (2000) and the glacial case without permafrost simulation at ice-front location II (glacial II) for the deposition holes with particles successfully reaching the model top boundary. (Modified after Figure E-51 in Joyce et al. 2010.)

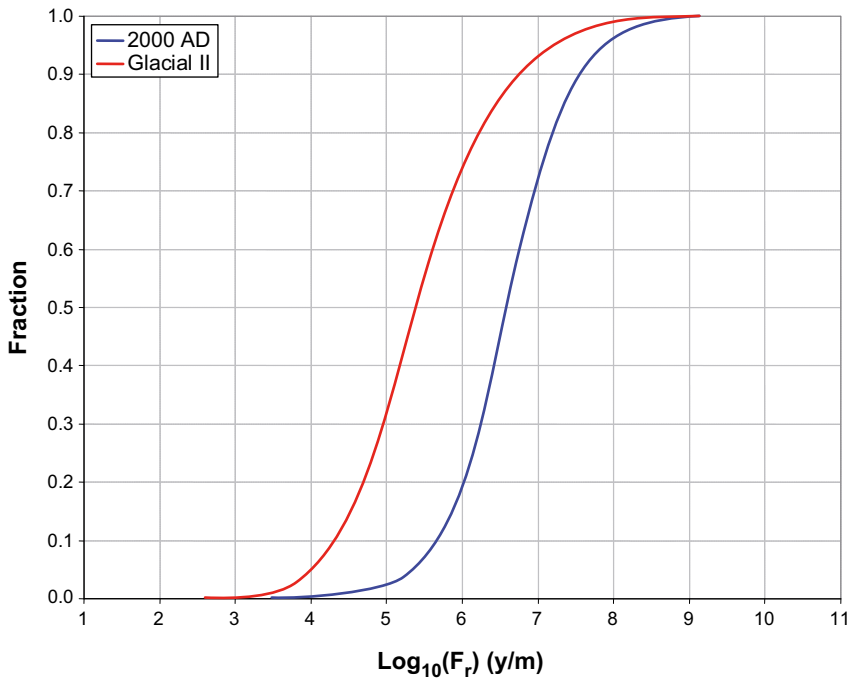


Figure 10-146. Cumulative distribution function plots of flow-related transport resistance (F) for the $Q1$ path for the hydrogeological base case simulation at 2000 AD (2000) and the glacial case without permafrost simulation at ice-front location II (glacial II) for the deposition holes with particles successfully reaching the model top boundary.

Table 10-29. Fraction of deposition hole positions experiencing dilute conditions after 20 years of glacial retreat and 100 years of glacial advance, respectively, for the case without stagnant zones and different assumptions on width of the stagnant zones.

Time (y)	$W_s = 0.0$ m	$W_s = 0.1$ m	$W_s = 1.0$ m	$W_s = 5.0$ m
20	0.0195	0.0173	0.0133	0.0133
100	0.0340	0.0305	0.0242	0.0240

Table 10-30. Fraction of deposition hole positions experiencing dilute conditions after 20 000 and 100 000 years of glacial maximum conditions, respectively, for the case without stagnant zones and different assumptions on width of the stagnant zones.

Time (y)	$W_s = 0.0$ m	$W_s = 0.1$ m	$W_s = 1.0$ m	$W_s = 5.0$ m
20 000	0.0099	0.0082	0.0033	0.0025
100 000	0.0180	0.0168	0.0077	0.0039

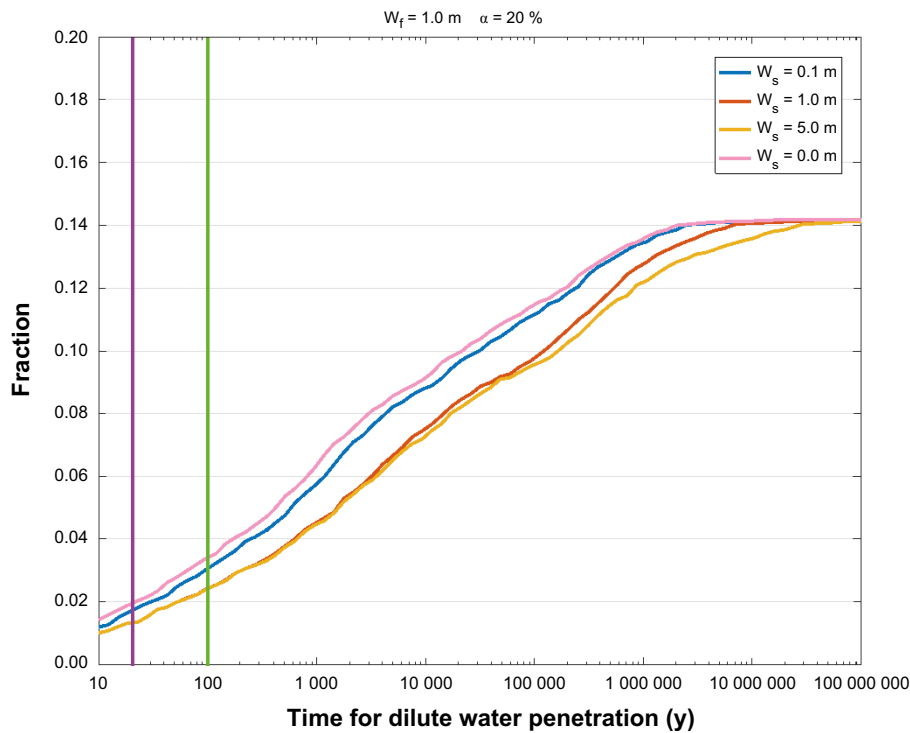


Figure 10-147. Temporal distribution for all deposition hole positions to obtain twenty percent of the initial water concentration with an ice front at ice-front location II. The green line shows that approximately three percent of the deposition holes experience dilute conditions for an advancing ice front that is assumed stationary for 100 years at IFL II and assuming no stagnant water between flowing channels. The pink curve represents the case without stagnant water, while the other curves assume additional stagnant water zones being available. The calculated fractions of deposition holes experiencing dilute conditions at the times 20 and 100 years are also given in Table 10-29.

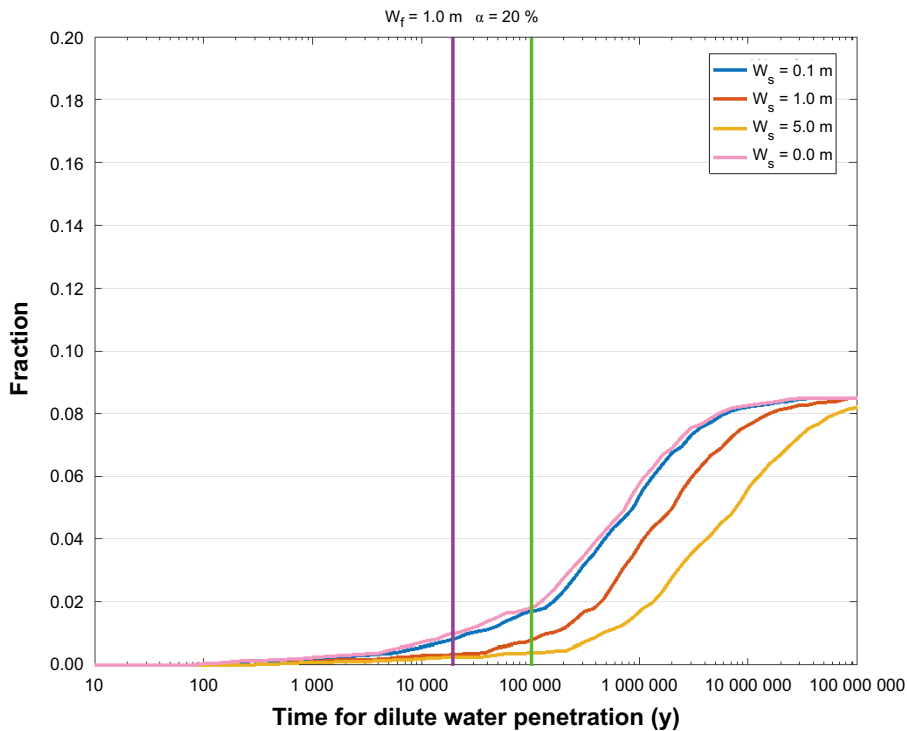


Figure 10-148. Temporal distribution for all deposition hole positions to obtain twenty percent of the initial water concentration for different assumed durations of ice-front location V (glacial maximum) conditions. The green line shows that approximately two percent of the deposition holes experience dilute conditions during an assumed duration of 100 000 years and assuming no stagnant water between flowing channels. The pink curve represents the case without stagnant water, while the other curves assume additional stagnant water zones being available. The calculated fractions of deposition holes experiencing dilute conditions at the times 20 000 and 100 000 years are also given in Table 10-30.

The calculations provided here are bounding estimates; as shown in the results above for the temporal evolution during a glacial cycle, the salinity in the system is in fact restored at repository depth due to up-coning effects. Also, as discussed in Section 10.1.3 but not accounted for here, water-rock interactions will also modify the water chemistry. Thus, penetration of dilute water with zero concentration for an extended period of time is a pessimistic assumption. For the further evaluation of buffer erosion and sedimentation in Section 10.4.8, it is noted that in Appendix K of the **Radionuclide transport report** it is shown that 0.1 mM is a reasonably pessimistic value of the cation concentration of the infiltrating glacial water. Assuming this value rather than zero concentration would, however, have a negligible effect on the above calculation of groundwater dilution at repository depth.

It is noteworthy that although in theory the maximum number of deposition holes that can be subject to dilute groundwater should be dependent only on the number of deposition holes with a connected fracture, for practical reasons Q1 paths were only tracked for locations with initial flowrates per unit length above some threshold. Below this, flows are essentially stagnant, and it was difficult to achieve sufficient local mass balance to track flows through such regions. This is also mentioned on page 46 of Joyce et al. (2010). The numbers are therefore highest for ice front location II (Figure 10-147) with a fraction of approximately 0.14 as this has the highest gradient with an ice margin over the site. The other cases, i.e., ice front location V and temperate conditions (Figure 10-148 and Figure 10-33) with lower gradients have accordingly lower fractions in the range of approximately 0.08-0.10. The reported differences in total fractions between the cases are thus mainly due to numerical reasons (applied threshold values in initial flow rate at deposition holes).

EDZ and crown space

In the hydrogeological base case model, a continuous excavation damaged zone (EDZ) is implemented in all tunnels (both deposition tunnels and other tunnels) under the tunnel floor. The EDZ has a transmissivity value of $T = 1 \times 10^{-8} \text{ m}^2/\text{s}$ and a thickness of 0.3 m. In order to assess the sensitivity in performance measures to tunnel properties, four alternative cases are analysed. Two of these have higher EDZ transmissivities ($T = 1 \times 10^{-7} \text{ m}^2/\text{s}$ and $T = 1 \times 10^{-6} \text{ m}^2/\text{s}$, respectively), one case has no EDZ, and the final case has the base case EDZ properties, but is combined with a crown space under the tunnel ceiling. The crown space represents the effects of consolidation of the backfill material. In the model, the crown space is implemented as a 0.1 m thick zone with a high conductivity value ($K = 1 \times 10^{-3} \text{ m/s}$) and a porosity equal to unity.

The Darcy flux for the Q2 path is shown in Figure 10-149. Since the Q2 path corresponds to the EDZ path, no result exists by definition for the case with the EDZ removed. The figure clearly shows, as expected, that an increase in the EDZ transmissivity implies an increase in the associated Darcy flux in the EDZ. The crown space implies a small reduction of the Darcy flux in the EDZ; i.e. the flow is redistributed to the crown space from the EDZ.

The flow-related transport resistance of the Q3 path is shown in Figure 10-150. It is observed that more favourable results are obtained when the EDZ is removed, whereas all other cases imply less favourable conditions. The existence of a crown space is by far the most unfavourable case. Also worth noticing is that the crown space seems to have a stronger influence during glacial conditions than during temperate conditions (Section 10.3.6). This is likely due to the modified flow direction and larger flows to be accommodated during the glacial flow regime; the flow is thus preferentially directed to the high permeability crown space. With flow paths preferentially going through the crown space, less flow-related transport resistance is accumulated in the fractured rock.

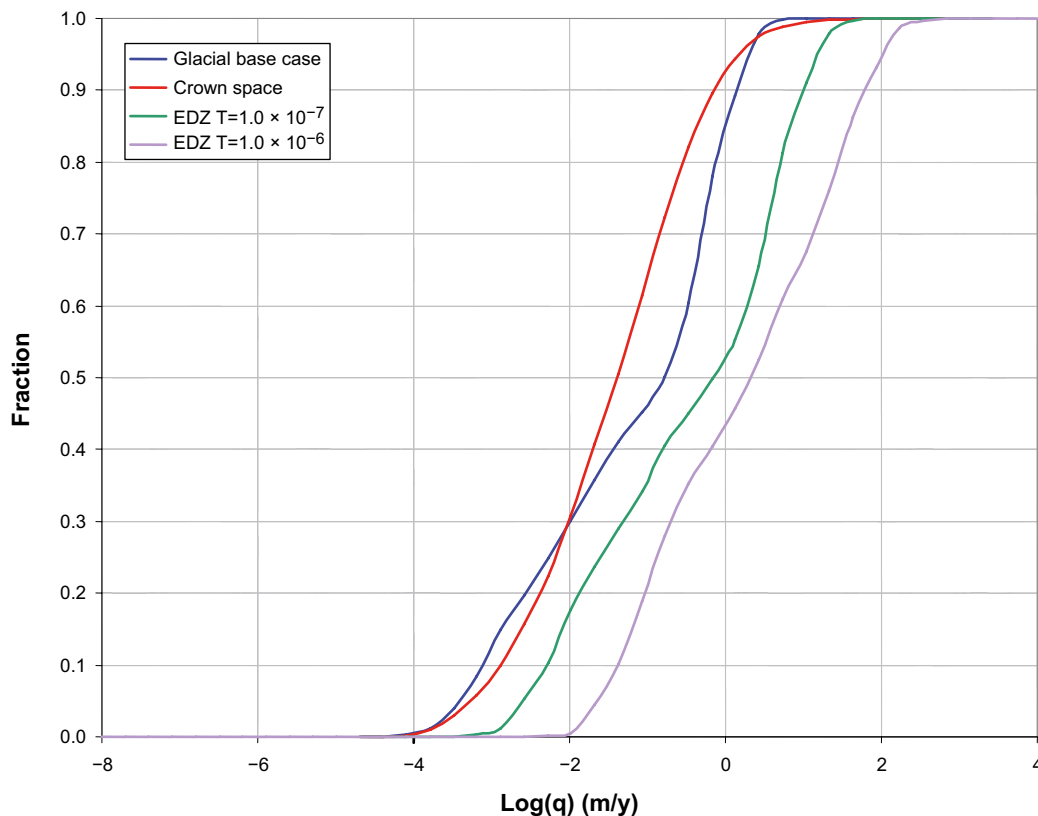


Figure 10-149. Cumulative distribution function plots of Darcy flux (q) at glacial ice front location II for release path Q2 for the hydrogeological base case model (Glacial base case), the crown space model (Crown space), the EDZ $T = 1 \times 10^{-7} \text{ m}^2/\text{s}$ model, and the EDZ $T = 1 \times 10^{-6} \text{ m}^2/\text{s}$ model for the deposition hole locations with particles successfully reaching the model top boundary. (Modified after Figure E-56 in Joyce et al. 2010.)

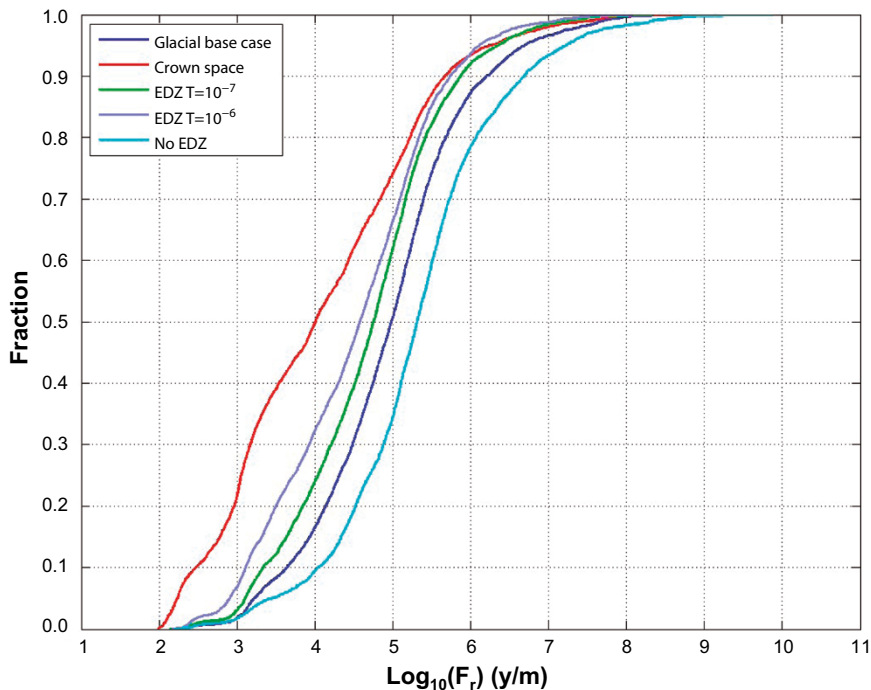


Figure 10-150. Cumulative distribution function plots of flow-related transport resistance (F) at the glacial ice front location II for release path Q3 for the hydrogeological base case model (Glacial base case), the crown space model (Crown space), the EDZ $T = 1 \times 10^{-7} \text{ m}^2/\text{s}$ model, the EDZ $T = 1 \times 10^{-6} \text{ m}^2/\text{s}$ model, and the No EDZ model for the deposition hole locations with particles successfully reaching the model top boundary.

Site related variants

N-S ice advance direction

Based on the historic and modelled data described in the **Climate report**, a NW-SE orientation of the model domain is conceived to be the most appropriate orientation to study for an advancing ice sheet margin. (The most appropriate retreat direction is probably somewhat more parallel to S-N.) The simulations carried out by Vidstrand et al. (2010) include a variant sensitivity test in which a N-S ice advance direction is used. Overall, the simulation results reported by Vidstrand et al. (2010) suggest minor differences of insignificant importance for SR-Site. For example, Figure 10-151 displays the Darcy fluxes at measurement localities 2 and 4 for the two different ice advance directions. The evolutions and magnitudes are similar.

THM properties

Isostasy is not accounted for in the study by Vidstrand et al. (2010) but the potential impact on ground-water flow of an uneven surface loading at the ice sheet terminus (the forebulge phenomenon) is addressed by incorporating a change in fracture transmissivity data as a sensitivity test. It is noted that the change in transmissivity applied by Vidstrand et al. (2010) exceeds the change suggested in the THM modelling within the SR-Site project (Hökmark et al. 2010, Lönnqvist and Hökmark 2010), see Section 10.4.4. However, the simulation results reported by Vidstrand et al. (2010) suggest insignificant differences in the peak values of the Darcy flux also for these exaggerated values. As an example, Figure 10-152 displays the Darcy fluxes at measurement localities 1 to 5. Evidently, the peak values of the undistorted and the distorted simulations are alike.

Another variant case of the model presented in Vidstrand et al. (2010) is studied in SKB (2013d). The structural-hydraulic model in the new case is identical to that used in Vidstrand et al. (2010) except that the additional transmissivity contribution from the three sheet joints is excluded from the model. The results indicate that the exclusion of the sheet joints as modelled in SDM-Site has extremely limited effects on the Darcy fluxes at repository depth in general and at ML2 in particular. This interpretation implies that the differences in fracture intensity (and other discrete fracture network characteristics) with depth by itself is enough to result in the observed lack of sensitivity to the sheet joints (cf. Figure 6-65 in the **Data report**).

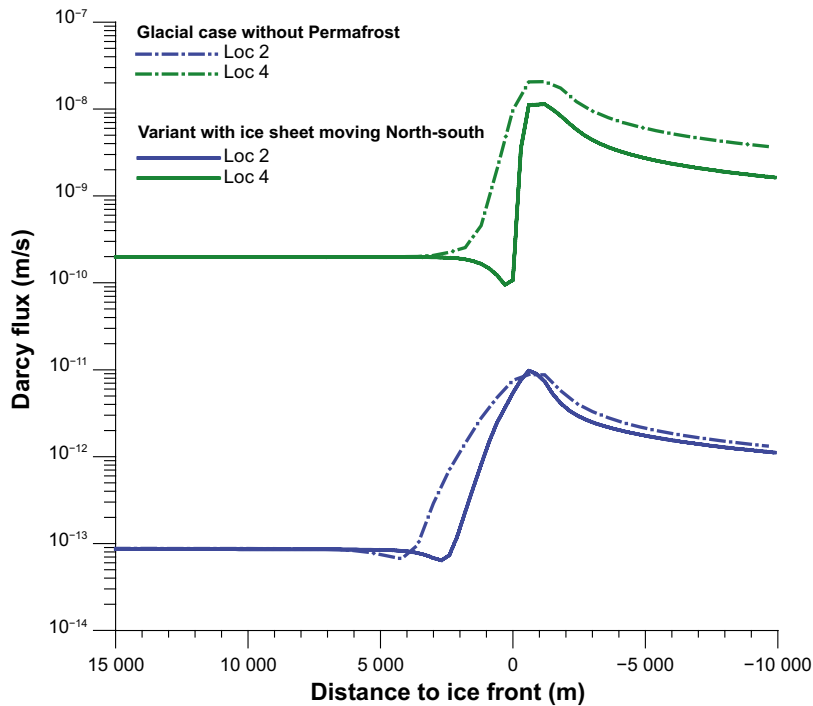


Figure 10-151. Darcy flux at measurement localities 2 and 4 (ML 2 and ML 4) during the advance of the ice sheet margin considered in the NW-SE case (dashed lines) and the N-S case (solid lines). Positive values of “Distance to ice front” mean that the ice sheet margin has not yet arrived to the measurement locality.

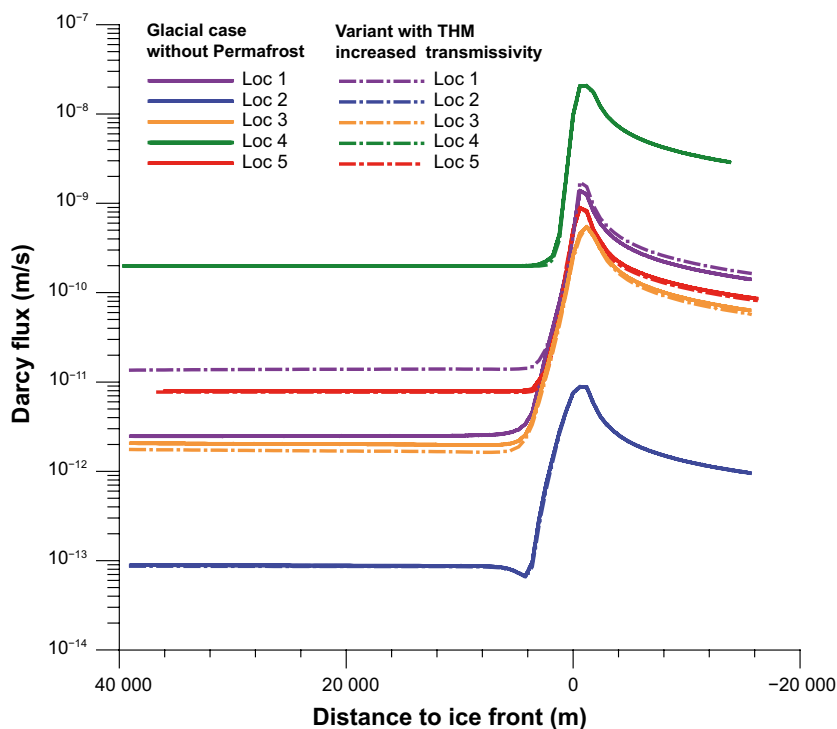


Figure 10-152. Darcy flux at measurement localities 1–5 (ML 1–5) during the advance of the ice sheet margin considered in the undistorted case (solid lines) and the distorted case (dashed lines). Positive values of “Distance to ice front” mean that the ice sheet margin has not yet arrived at the measurement locality.

Glacial case with permafrost

Permafrost is a key process to consider as it reduces the permeability of subsurface materials to water flux. Permafrost does not develop instantaneously. Its development is a transient process. Vidstrand et al. (2010) use a freezing algorithm to modify reported Holocene hydraulic conductivity values in a transient fashion. The input to the permafrost model was obtained from the ground surface temperature time series described in the **Climate report**, Appendix 1.

A discontinuous permafrost layer is considered. This implies that the permafrost layer may contain more or less unfrozen sections depending on the local boundary conditions and material properties. Probable locations for taliks can be estimated from the forecasted landscape development, carried out in the SR-Site project, following the shoreline displacement at Forsmark.

Further, in the model the speed of the advancing ice sheet was set to 50 m/y. The ice sheet acts as a blanket that isolates the frozen ground from further influence of low surface temperatures. The speed of the advancing ice sheet is imagined to be greater than the rate of thawing of the permafrost layer, thus implying a tip (tongue) close to the ice sheet margin with trapped permafrost and cold basal ice conditions. However, as a variant and sensitivity case, no permafrost under the tip close to the ice sheet margin is studied. Figure 10-153 suggests insignificant differences in Darcy flux between the two cases of permafrost conditions at the ice sheet margin. It is noted that the oscillations near the peak reflect transient effects at the top boundary due to the transient hydraulic properties of the permafrost.

Comparison of the Darcy flux at different time slots during glaciation and deglaciation

In Section 10.4.1, the expected hydrogeological evolution during a glacial cycle is described based on present day understanding of relevant processes. In the model studies described in that section, various simplifications are made that do not conform fully to the expected reference evolution. Here, an outline is provided on how the modelling results may be used for subsequent assessment calculations.

Figure 10-154 shows the minimum, median and maximum values of the Darcy flux at all deposition hole positions during the main “climate events” during the simulated period (IFL 0 → IFL V → IFL 0) of periglacial and glacial climate conditions. The main “climate events” are:

- Temperate (used to produce scaled (normalised) quantities for SR-Site).
- Glacial without permafrost.
- Glacial maximum.
- Submerged.
- Permafrost.
- Glacial with permafrost and a 2 km long tongue.
- Glacial with permafrost but no tongue.

The climate condition Glacial without permafrost provides the highest maximum as well as highest median value of all simulated climate events. Relative to the median temperate period value, the median Glacial without permafrost value is almost two orders of magnitude higher. The maximum Glacial without permafrost value is also almost two orders of magnitude higher than the maximum Temperate period value. Conditions when only permafrost prevails or when the domain is submerged provide the smallest Darcy fluxes of all climate situations. The values for these two cases are below the temperate period value.

The results presented by Vidstrand et al. (2010) and Joyce et al. (2010) are utilised in different ways in the radionuclide transport calculations presented in Chapter 13. One approach is to take the flow paths and performance measures obtained from the combined repository-scale and site-scale models, and scale the measures by factors that are obtained by scaling all different periods in Figure 10-154 with the corresponding temperate period values. A second approach is to directly use the performance measures calculated in the combined repository-scale and site-scale models utilising glacial boundary conditions from the super-regional model. However, this approach only provides results for the glacial case without permafrost for the ice front position IFL II. Thus, the second approach is used to assess the effects of glacial conditions on performance measures when different assumptions on repository properties (EDZ crown space) are made, whereas the first approach is utilized when transport calculations incorporating flow changes implied by a glacial cycle are performed.

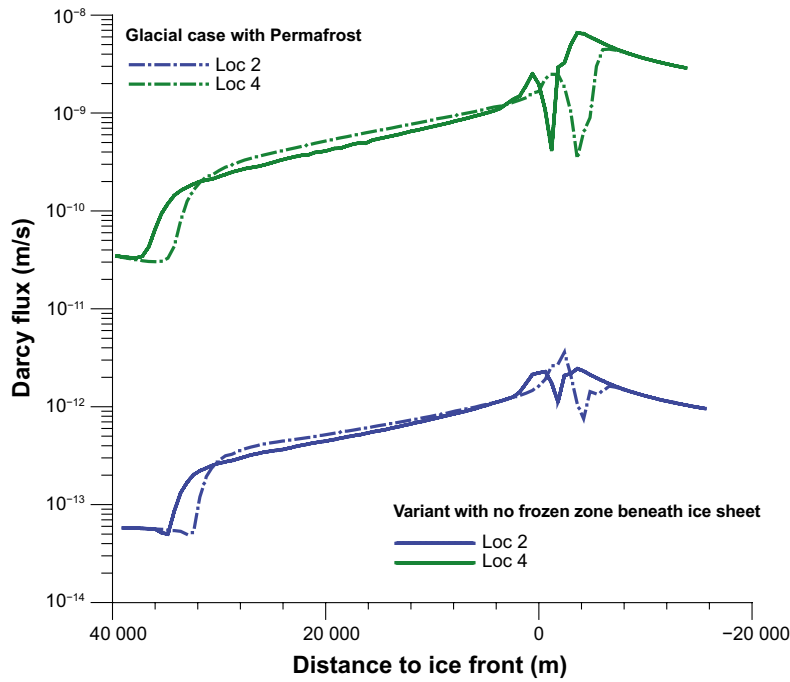


Figure 10-153. Darcy flux at measurement localities 2 and 4 (ML 2 and ML 4) during the advance of the ice sheet margin considered in the two cases with permafrost, i.e. permafrost in front of the ice sheet margin only (dashed lines), and permafrost in front of the ice sheet margin as well as under the tip (tongue) of the ice sheet margin (solid lines). Positive values of “Distance to ice front” mean that the ice sheet margin has not yet arrived to the measurement locality.

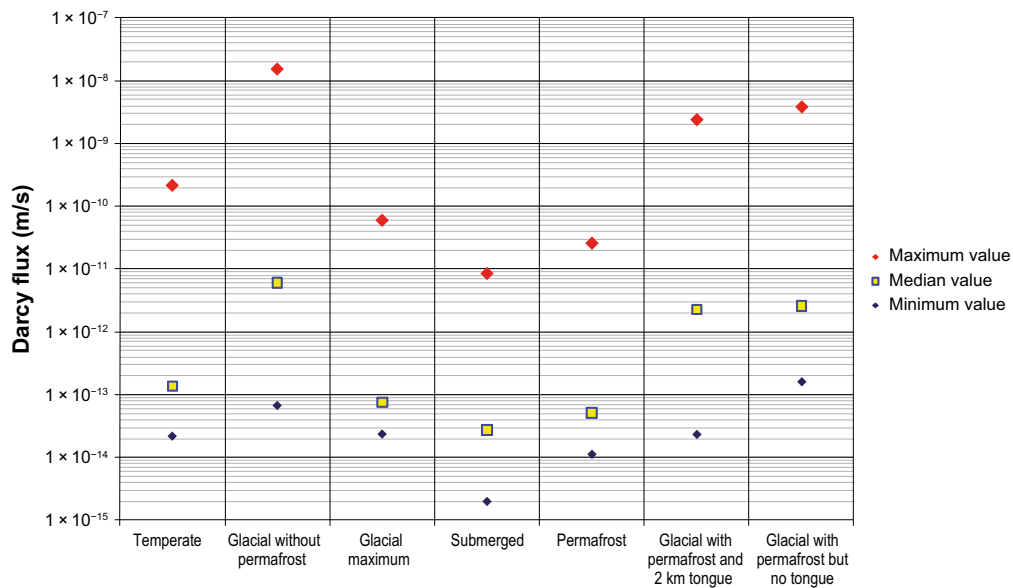


Figure 10-154. Estimated Darcy fluxes for the main climate situations considered during the simulated period (IFL 0 → IFL V → IFL 0) of periglacial and glacial climate conditions.

A similar approach is used for calculations of buffer erosion and canister corrosion over a glacial cycle. Figure 10-155 (based on calculations in Vidstrand et al. 2010) shows normalised average values of the three powers of the Darcy flux that are of interest, (q , $q^{0.41}$, $q^{0.5}$), see Sections 10.4.8 and 10.4.9 for details. The desired values are obtained by averaging the values of “Glacial without permafrost” over a full glacial cycle (120 000 years) and then normalising against the corresponding temperate value (see Selroos and Follin 2010 for details). It is observed that for measurement location ML 2, which is inside the repository footprint, the normalised average value is about 0.8; i.e. the Darcy flux averaged over the 120 000 year glacial cycle is below the corresponding value for the temperate period.

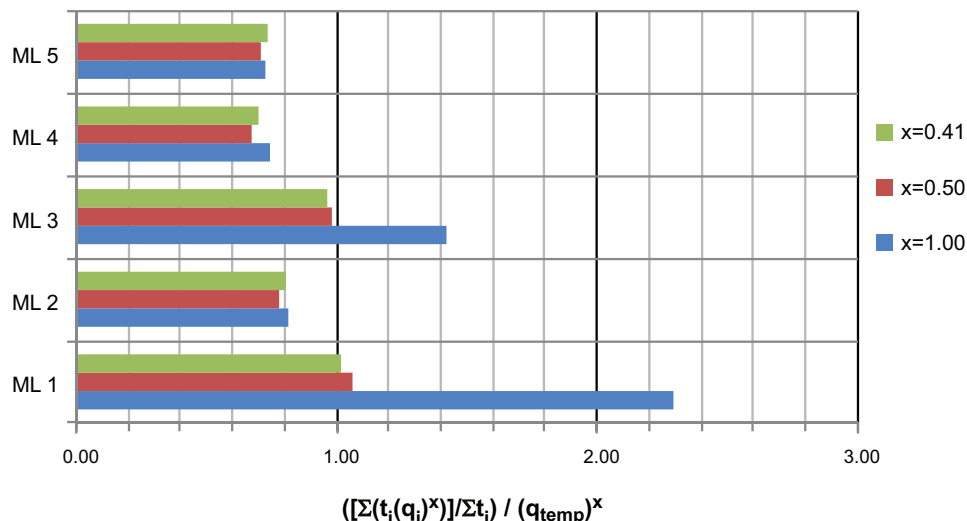


Figure 10-155. Plot of Darcy flux to three different powers (q , $q^{0.41}$, $q^{0.5}$) averaged over a full glacial cycle and normalised against the corresponding temperate value (q , $q^{0.41}$, $q^{0.5}$)temp. The temperate values are used in buffer erosion and canister corrosion calculations, see Sections 10.4.8 and 10.4.9 for details. ML = measurement locality. The glacial period within the glacial cycle is based on the glacial case without permafrost.

Identified uncertainties and their handling in SR-Site and the PSAR

A general uncertainty in all models dealing with groundwater flow during periglacial and glacial conditions is the boundary condition on the top surface. Vidstrand et al. (2010) assume a specified head under the ice sheet, which is a common assumption in this field of science. Nonetheless, it is not clear that the water pressure at the ice-subsurface interface should be related to the ice sheet thickness under all circumstances as it implies an infinite source of water. This implies a general uncertainty of the models utilised. Another general uncertainty is in the particle tracking, which is performed for a steady state flow condition although the boundary conditions are constantly and rapidly changing in comparison to the advective travel times.

- Hydrogeological evolution.** The importance of taking different events during a glacial cycle into account in a groundwater flow model intended for predicting the hydrochemistry in the vicinity of a repository is recognised in NEA (1993) and Bath and Lalieux (1999). An example of an important event at Forsmark during Holocene time that is considered in SDM-Site is the Littorina Sea stage, which began at about 6500 BC and prevailed for several thousands of years. During the Littorina Sea stage, the Forsmark site was submerged by seawater that had a maximum salinity of about 1.2–1.5 % by weight (approximately 12–15 g/L of TDS). According to the chemical analyses, the origin of the salt seen in the fracture water samples acquired today could be remnants from the Littorina Sea stage (Laaksoharju et al. 2008). In comparison, little or no remnants of Littorina Sea water have been observed in the samples that represent matrix porewater from the target volume at repository depth. Furthermore, the less saline matrix porewater is not glacial meltwater but of a pre-Weichselian origin as the low contents of TDS is accompanied by high values of oxygen-18, approximately –5 to –4 ‰ of $d^{18}O$ SMOW. (Glacial meltwater is considered to be much more depleted of oxygen-18, approximately –20 to –16 ‰ of $d^{18}O$ SMOW (Laaksoharju et al. 2008)).

In conclusion, the groundwater flow modelling considered in SDM-Site suggests that it is transients in advective flow rather than matrix diffusion that govern the fracture water salinity. This observation is supported by the modelling conducted by Vidstrand et al. (2010). However, as the scheme of ice sheet movement considered by Vidstrand et al. (2010) does not represent a full glacial cycle, the groundwater salinity after the passage of the retreating ice sheet margin cannot be expected to be equal to the groundwater salinity prior to the passage of the advancing ice sheet margin. Furthermore, water-rock interactions possibly affecting groundwater salinity are neglected, which also implies that the salinity field will not be restored in the model.

- **Recharge and discharge locations in the biosphere.** Regardless of the case studied, an ice sheet without permafrost or an ice sheet with permafrost, a number of particles recharge at the upstream boundary of the model domain, which suggests that the model domain is too short to give a fully undisturbed view of all recharge locations. Nevertheless, it may be concluded that the present-day topographic water divides, which play an important role for the recharge and discharge during temperate conditions, are significantly diminished in significance during glacial conditions. In contrast, the discharge locations are predominantly found well within the physical boundaries of the model domain and often very close to the margin of the ice sheet. The differences seen in the discharge pattern between the two glacial cases are largely caused by the alternative hydraulic properties and boundary conditions. The uncertainty in the occurrence of taliks, which may act as major discharge areas in the case of permafrost in the periglacial area in front of the ice sheet margin, is discussed in the **Climate report**.
- **Performance measures.** The same uncertainties as in the temperate simulations in Section 10.3.6 apply to the simulations based on the combined repository-scale and site-scale models used here. In addition, the transfer of boundary conditions from the super-regional model to these smaller scale models implemented in a different numerical flow code implies uncertainties.
- **Penetration of glacial melt water.** The assessment of penetration of dilute water should be considered an approximate quantification. The same uncertainties as listed for the corresponding analyses performed for temperate conditions in Section 10.3.6 apply here. Specifically, steady-state flow fields are used, and no mixing or water-rock interactions are considered. The results of the analysis of penetration of glacial melt water are propagated for further assessment.
- **EDZ and crown space.** The same uncertainties as listed above for Performance measures apply here. The results of this analysis are propagated for further assessment.
- **Site related variants.** None of the studied site related variants provide significantly different results to those of the base case, i.e. the case with a steep ice sheet profile without permafrost moving from NW to SE. It is noted that the use of the theoretical maximum ice sheet profile during the post-LGM stage is probably a considerable exaggeration compared to the reference evolution ice sheet. Furthermore, it is noted that the applied change in transmissivity in the hydro-mechanical variant case exceeds the change suggested in the THM modelling within the SR-Site project.
- **Glacial case with permafrost.** An advancing ice sheet with permafrost ahead is considered a more realistic case than an ice sheet without permafrost. However, neither of the two permafrost cases studied (cf. Table 10-28) give significantly different results from the base case, i.e. an advancing ice sheet without permafrost. It is noted that the simulations with ice sheet and permafrost combined are stopped at ice front location IV (IFL IV) to avoid numerical instabilities. These arise when the ice sheet margin gets close to the downstream boundary and the discharge at ground surface in the periglacial area is prevented due to the permafrost growth.
- **Comparison of the Darcy flux at different times during glaciation and deglaciation.** The results presented under this heading are merely a different way of illustrating the results. Thus, no additional uncertainties per se are introduced. However, the outlined methodology of using scaling factors for the performance measures representing the different climate regimes clearly is a simplification of the development depicted in the **Climate report**, and hence implies an additional uncertainty. For the subsequent assessment, an ice sheet with permafrost in front of the ice sheet margin is used for the pre-LGM stage, and a retreating ice sheet with submerged ground conditions in front of the ice sheet margin is used for the post-LGM stage. As indicated above, the climate stages of permafrost alone and submerged conditions alone also need to be included in the quantitative assessment.

10.4.7 Geochemical evolution

The successions of temperate, periglacial and glacial climate domains will affect the flow and composition of the groundwaters around the repository. The evolution between climate domains will be gradual, without a clear boundary between them. For example, during a temperate climate period, temperatures may slowly decrease such that permafrost regions slowly develop within parts of the repository region. In SR-Site (and the PSAR) the evaluation of geochemical effects is restricted to

using separate specifications for the different climate domains. It is expected that different groundwater compositions will prevail around the repository as a result of the different types of climate domains and their corresponding hydraulic conditions. This section discusses the groundwater chemistry for periods in which the repository is *below permafrost during periglacial climatic conditions* or *under an ice sheet during glacial conditions*, whereas the conditions expected under a *temperate domain* are discussed in Section 10.3.7. In addition, this section discusses groundwater chemistry for periods in which the repository area is *submerged* either under a glacial meltwater lake, or under more or less saline seawater, such as the Littorina sea water periods in the past.

The following issues, and safety functions according to Figure 10-2, are treated for all the expected conditions during the reference glacial cycle:

- Evolution of salinity and of other relevant natural groundwater components (safety functions R1b and R1c).
- Evolution of redox conditions (safety function R1a).
- Effects of grouting, shotcreting and concrete on pH (safety function R1e).

Modelling

The modelling for the remaining part of the reference glacial cycle is similar to that performed for the initial temperate period described in Section 10.3.7. Groundwater compositions are modelled through advection, mixing and chemical reactions with fracture-filling minerals. The different components of the modelling are not fully coupled: the results of regional-scale groundwater flow modelling are used as input to a geochemical mixing and reaction model. The aim has been to obtain equivalent groundwater models for hydrology and geochemistry.

The groundwater flow modelling of the periglacial and glacial conditions is described in the previous Section 10.4.6. One of the processes modelled is the transport of salts. Contrary to the modelling of the initial temperate period, the models for the periglacial and glacial periods have not included the fractions of selected reference waters. In the geochemical models, either for the glacial scenario without permafrost or in the glacial scenario with permafrost, the rock volume initially contains a mixture of two end-member waters: a deep saline groundwater and a water of meteoric origin. The proportion of these two end-members can be obtained from the salinity at any point. With the advance and retreat of the glacier the proportion of a third mixing end-member, glacial melt-water, is calculated from the decrease in salinity at any point in space.

This strategy is used as well to describe the site submerged by a glacial melt-water lake. For periods when the candidate site is submerged under seawater, however, the results obtained using ConnectFlow (Joyce et al. 2010), see Section 10.3.6, are used. In this case the same model is used as for the initial temperate period, and therefore the hydrogeological results include the mixing proportions of end-member waters.

A process that must be evaluated is the out-freezing of dissolved salts when ice builds up underground during periglacial periods. The groundwater flow modelling described in Section 10.4.6 considers density-driven groundwater flow and transport of salts, but the out-freezing of salts is not included. The process has instead been evaluated using a two-dimensional model set-up (Hartikainen et al. 2010). Examples of temperature contours obtained using this model are shown in Figure 10-108 in Section 10.4.1.

Evolution during periglacial conditions

The periglacial conditions are characterised by perennial freezing of groundwaters, i.e. permafrost, and the frozen areas may be continuous or discontinuous. In any case the permafrost areas will include taliks where sufficiently large lakes are encountered. There is limited information concerning the chemical characteristics of groundwaters under permafrost. This is due to practical difficulties when drilling and sampling at ambient temperatures where freezing of drilling fluids and groundwater samples occurs.

Many geochemical characteristics of groundwaters are expected to be almost unaffected by the permafrost. The studies at the High Lake and at the Lupin Mine in N. Canada (Frape et al. 2004, Ruskeeniemi et al. 2004, Stotler et al. 2009a, b, Holden et al. 2009) may be used to illustrate this. Geologically, the bedrock at Lupin consists of an ancient metamorphosed sedimentary rock sequence dominated by quartz feldspar gneiss/phyllite; these were formed some 2.5 Ga, somewhat older than 1.89–1.85 Ga which was the peak of metamorphism at the Forsmark site, characterised by different types of granitoids with subordinate felsic to intermediate volcanic rocks, diorite or gabbro, pegmatite and amphibolite. Whilst the rock types are certainly not identical, they share enough properties to compare qualitatively the general hydrochemical properties at each site. The pH values for sampled groundwaters at Lupin vary between 6 and 9 and bicarbonate concentrations are found to be below 5×10^{-3} mol/L. For potassium, the concentrations are higher than for the groundwaters sampled at Forsmark or Laxemar: sub-permafrost groundwaters at Lupin have $< 2.6 \times 10^{-3}$ mol/L. For iron, most of the groundwaters sampled at Lupin had $< 5.4 \times 10^{-5}$ mol/L. Thus, the concentrations and pH values found are not far from those for groundwaters sampled elsewhere, for example at Forsmark (see Laaksoharju et al. 2008). A study at Greenland corroborates the notion that geochemical conditions are essentially unaltered by permafrost, see further Section 14.6.3.

Evolution of salinity and relevant natural groundwater components

It is estimated that at Forsmark the ground will be frozen to a depth of 50 m or more for around 30 percent of the time in the glacial cycle of the reference evolution, see Figure 10-111. According to these results, the permafrost will not occur over a continuous period of time, but rather thawing will occur between more or less short periods of permafrost, see also the discussion in Section 10.4.1. Some of these permafrost periods will furthermore coincide with the time when the site is covered by an ice sheet.

When water freezes slowly, the solutes present in the water will not be incorporated in the crystal lattice of the ice. During this process, salts that have been present in the surface waters and groundwaters will tend to accumulate at the propagating freeze-out front. This front is, however, not necessarily sharp, because e.g. freezing will take place over a range of temperatures, depending on the salinity, etc. The freezing process can give rise to an accumulation of saline water at the depth to which the perennially frozen front has reached. The saline waters formed in this manner within fractures and fracture zones will sink rapidly due to density gradients.

The calculations made using a two-dimensional model set-up (Hartikainen et al. 2010) show that when the freezing is extensive (down to several hundred metres depth) a salt front is developed in the calculations. The model also shows that pockets of unfrozen groundwater with high salinity may develop in the perennially frozen rock when the freezing front advances faster than the transport of salt. These results agree qualitatively with the previous generic calculations reported in Vidstrand et al. (2006). It should be noted that the model used in Hartikainen et al. (2010) does not account for matrix diffusion, and the amounts of salts frozen out in the mobile groundwater are only a fraction of the salt contents in whole rock volume.

The concentration of the frozen out salt has been estimated in these calculations assuming that before the onset of the permafrost the salinity distribution is that found at present in Forsmark. Judging from the results in Figure 10-40, Section 10.3.7, it may be that these initial salinities are overestimated, as the groundwaters will become gradually more dilute before the start of the permafrost.

Nevertheless the results of the 2D modelling (Hartikainen et al. 2010) indicate only a very moderate increase in salinities around the repository volume, not exceeding 1 %, for the most extreme permafrost simulation, that is, for the (dry variant of) the repetition of the last glacial cycle with an air temperature decreased by 8 degrees. That is, even for the most extreme permafrost extent simulated, the calculated groundwater salinities in the repository volume do not exceed those found at present.

The possibility of upconing of deep saline groundwater to repository depths during permafrost conditions was addressed in King-Clayton et al. (1997). This may possibly occur in the vicinity of permanent discharge features such as some taliks. Such discharge features mainly occur along more extensive conductive deformation zones. In Forsmark, where the topography is quite flat, the probable location of taliks is at some distance from the candidate repository area, as estimated from the landscape development following the reference evolution shore-level displacement at Forsmark (see the **Climate report**, Section 4.5.2).

When the permafrost melts and decays there will be a release of dilute melt water from the upper highly permeable network of fractures. At this stage the low permeability matrix which has preserved (or accumulated) its salinity, especially at greater depths, will probably be more saline than the surrounding groundwaters. The resulting chemical gradient will then cause a gradual transfer of salinity to the more permeable rock mass. In all probability this will be a relatively slow process and dilution by mixing will occur also within the more permeable rock mass. The more dilute waters will tend to stay in the top layers of the rock mass due to their lower density.

The hydrogeological calculation results obtained in Vidstrand et al. (2010) and described in Section 10.4.6 have produced salinity distributions for the Forsmark area under permafrost simulated by having a constant air temperature of $-4.5\text{ }^{\circ}\text{C}$. These salinities were used to calculate mixing proportions of a deep saline end-member and a meteoric water component, and these mixing proportions were then used as input to the PhreeqC code which imposed equilibrium with calcite, quartz, hydroxyapatite and either Fe(III) oxyhydroxide or amorphous iron sulphide, FeS. As a result, the detailed distribution of compositions was obtained. A full description of the procedure and the results obtained may be found in Salas et al. (2010).

These model results shown in Figure 10-156 indicate that during periglacial conditions, when the Forsmark site is subjected to permafrost, salinities will be limited, satisfying the safety function indicator R1b in Figure 10-2, the concentration of cations expressed as charge, $\Sigma q[M^{q+}]$, will be above 8 mM, satisfying the criterion R1c, the concentrations of chloride, potassium, iron and sulphide will be limited and the pH will be above 5 and below 11, in agreement with the safety function indicators and criteria R1d and R1e. The criterion R1f was evaluated in Section 10.3.13, see Figure 10-93. In addition, colloid concentration levels are expected to remain low because sufficiently high ionic strengths are expected under these conditions.

As for the temperate period discussed in Section 10.3.7, two geochemical assumptions, namely equilibrium with respect to FeS(am) or Fe(III) oxyhydroxide, have been simulated in order to estimate the evolution of the redox potential within the repository domain. The results shown in Figure 10-156 indicate that the redox potentials during a permafrost period should not differ substantially from those during a temperate period, shown in Figure 10-48.

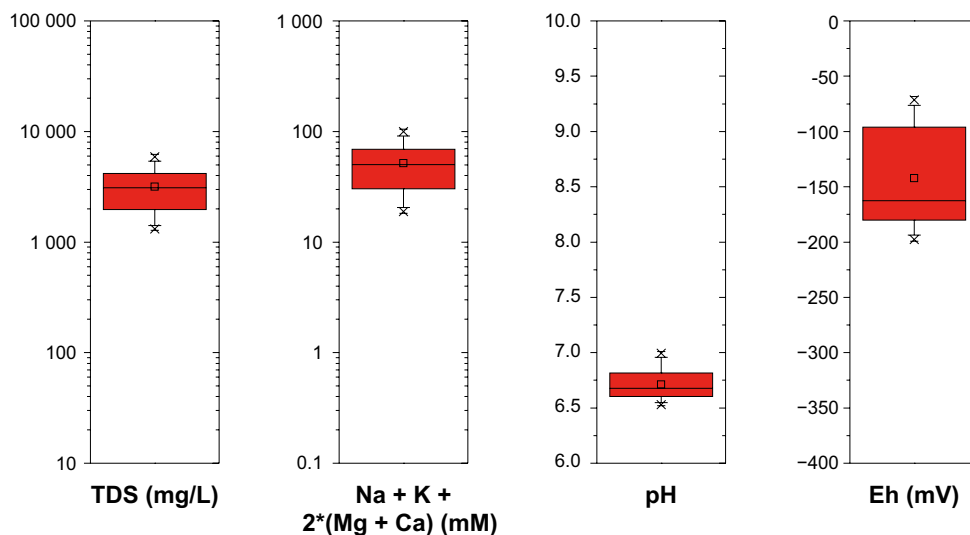


Figure 10-156. Permafrost: Box-and-whisker plots showing the statistical distribution of the calculated TDS (total dissolved solids), $\Sigma q[M^{q+}]$, pH and Eh within the candidate repository volume at Forsmark. The statistical measures are the median, the 25th and 75th percentile (box), the mean (square), the 5th and 95th percentile (“whiskers”), the 1st and 99th percentile (crosses) and the maximum and the minimum values.

Sulphide, H₂, CH₄ and dissolved organic carbon

The rate of production of sulphide due to microbially mediated SO₄²⁻ reduction could possibly decrease due to the lower temperatures. Due to freeze-out of salts, sulphate concentrations might increase as compared with those at the end of a preceding temperate period, when diluted groundwaters of meteoric origin predominate. Reducing agents are required for any sulphate reduction to take place, and under permafrost conditions the inflow of organic matter from the surface will probably decrease. However, SO₄²⁻ reduction could also be sustained by the gaseous groundwater components methane and hydrogen, see the discussion in Section 10.3.7. If microbial sulphide production occurs during this period, it will be limited by the availability of mainly CH₄ and dissolved organic carbon, as discussed in Tullborg et al. (2010). Fluxes and maximum production of methane and hydrogen have been estimated based on the groundwater gas content for three Fennoscandian sites: Forsmark, Laxemar and Olkiluoto (Delos et al. 2010). There is a large uncertainty in estimating the flow of gases in Forsmark because the data are very scarce, but the estimated fluxes are $< 3 \times 10^{-10}$ mol/(m² yr) for CH₄ and H₂. The conclusion is that there is only a minor contribution from the flow of these gases to sustaining microbial sulphide production.

Although sulphide concentrations are obtained as a result of the PhreeqC modelling described in subsection “*Model results*” above, for the reasons outlined in Section 10.3.7, it is believed that the equilibrium solubility constraints applied cannot reflect the variability of sulphide concentrations that can be expected during periglacial conditions. Because of this the sulphide concentrations for periglacial conditions are assumed to be the same as the observed distribution of sulphide in groundwaters during the present temperate conditions, which is after a recent period of intrusion of marine sulphate-rich waters and described in Section 10.3.7. This distribution of sulphide concentrations is used to estimate canister corrosion rates during the periglacial periods. This is a cautious approach: sulphate concentrations in the groundwaters may have been reduced during a preceding long temperate period when the site is subject to the infiltration of meteoric waters, and this would reduce rates of microbial sulphide production. Although freeze-out of salts from ponds and lakes affected by sulphate-rich sea spray might induce locally an accumulation of sulphate, this should not occur at Forsmark because the Baltic Sea will be at some distance from the site during the periglacial periods. Furthermore the input of dissolved organic matter from the surface could be decreased because of the frozen ground layer, and upwards diffusion of methane or hydrogen in Forsmark is too slow. These arguments suggest that sulphide concentrations during periglacial conditions could be generally lower than those observed during the site investigations, which are used in the analysis of canister corrosion.

Given the low estimated flows of methane mentioned above in this subsection, the potential for formation of substantial amounts of methane ice can be discounted in Forsmark (Tohidi et al. 2010).

In conclusion, although groundwaters will become progressively diluted during the temperate period following the closure of the repository, permafrost can move salts to repository depth from the upper parts of the rock. All arguments indicate that groundwaters below permafrost will not become more dilute than under temperate conditions. Rather, saline waters may move downwards within conductive fracture zones. Thus the charge concentration of cations is expected to increase during permafrost periods and satisfy the criterion concerning the safety function indicator R1c in Figure 10-2, $\Sigma q[M^{q+}] > 0.004$ mol/L. Regarding safety function indicator R1b, the concentration of salt at repository level due to freezing out will not become so high as to lower the swelling pressure of the buffer and the backfill, among other reasons because of the downward gravity-driven flow of saline waters. This situation will not be changed during permafrost decay as a transition to a temperate period occurs.

For major groundwater components, such as Cl, Na, Ca and other cations and sulphate the conclusion is that they will follow the trends of salinity discussed above. Other components, such as bicarbonate, potassium, iron sulphide, etc. as well as pH that are controlled by relatively fast chemical reactions are expected to remain mostly unaffected by permafrost. Therefore, the criteria concerning the safety function indicators R1d and R1e in Figure 10-2 are expected to be fulfilled, in that pH will remain < 11 and the concentrations of K and Fe will remain limited. Sulphide concentrations are generally expected to be lower than or at similar levels to those found during the temperate period preceding the periglacial conditions.

Redox conditions

The perennial freezing of rock volumes will effectively shut down the hydraulic circulation in the bedrock, at least locally. In this way, microbial populations within the rock could be isolated from the surface. Some reactive gases such as methane could be trapped as clathrates, especially in soil layers. Microbes present in the upper bedrock and soils will survive in the permafrost and will become active during the subsequent melting. No changes in redox conditions are, therefore, to be expected unless the nutrient sources become exhausted. Because of abundant biological activity in the active layer (Hallbeck 2009) the presence of organic matter at the surface will be maintained at levels similar to those encountered during temperate conditions. All indications are that prior to, during and following permafrost decay, groundwaters will be reducing due to a combination of microbial and geochemical reactions and processes. The results of the modelling presented in previous sections support these statements.

In conclusion, it is not expected that redox conditions will change at repository depth during the formation or decay of permafrost, remaining reducing as demanded by the safety function indicator R1a in Figure 10-2.

Effects of grouting, shotcreting and concrete on pH

The processes described in Section 10.3.7 for the temperate domain following repository closure will continue during permafrost periods. Given enough time all grout will be converted first into calcium silicate hydrates with low calcium to silica ratios, and finally into calcite and silica (Luna et al. 2006, Galíndez and Molinero 2009, Sidborn et al. 2014). The duration of this process will depend on the velocity of the groundwaters flowing around the grouted volumes, but times of the order of 10^4 years are expected.

The conclusion reached in Section 10.3.7 is therefore still valid: the effect of grout in fractures will be to increase the pH in deformation zones for relatively long periods of time. The pH values obtained in the simulations are, however, within the criteria for the safety function indicator R1e in Figure 10-2, that is $\text{pH} < 11$.

Glaciation

General

There is almost no information concerning the chemical characteristics of groundwaters in fractured rock under an ice sheet or even close to the margin of an ice sheet. This is partly due to practical difficulties when drilling and sampling at ambient temperatures where freezing of drilling fluids and groundwater samples occurs.

The composition of glacier melt waters was reviewed in Brown (2002). Although as expected some of these waters are extremely dilute (1 mg/L), others have gained solutes from mineral weathering reactions, reaching salinities up to 0.2 g/L. Other examples of dilute granitic waters are those sampled in Gideå (0.33 g/L) and Grimsel (0.08 g/L). Although dilute, both these waters are close to saturation with calcite. The relatively high pH values, ≈ 9 , originate from the weathering of bedrock minerals.

SKB, together with NWMO (Canada) and Posiva (Finland) have conducted a joint project that sampled groundwaters in an area close to the Greenland Ice Sheet near Kangerlussuaq in Greenland (Claesson Liljedahl et al. 2016, Harper et al. 2016). Three deep boreholes were drilled, one in a talik beneath a lake in a continuous permafrost area, to a depth of ~ 190 m below the top of the borehole; and two near the ice sheet margin down to depths of about 322 and 649 m, respectively, below the top of the borehole. Groundwater samples could only be collected from two boreholes: from the one reaching the talik and from the deepest borehole that reached just under the ice sheet; the third borehole, with intermediate length, was within permafrost-affected rock down to the bottom. The stable water isotopic signatures ($\delta^2\text{H}$ and $\delta^{18}\text{O}$) of the sampled groundwaters indicate that they are of glacial meltwater origin. The groundwaters had relatively low concentrations of Na and Cl, likely originating from water-rock interactions and diffusion from the rock matrix, while Ca and SO_4 in these waters originate from dissolution of gypsum, which occurs as a fracture infill mineral at depths below approximately 300 m. Helium concentrations were preliminarily interpreted to indicate that the deep groundwaters may have residence times exceeding hundreds of thousands of years. Past

penetration of dissolved oxygen in meltwaters into the bedrock has been limited in depth, as indicated by the presence of pyrite in fractures below approximately 50 m; while iron oxyhydroxides are found in fractures only in the upper parts of the rock (down to 60 m), with only a few isolated occurrences of goethite down to 260 m depth. U-series disequilibrium data ($^{230}\text{Th}/^{238}\text{U}$ activity ratios up to 2.97 at 431 m depth), indicate circulation of oxidative water beneath the permafrost only in a few fractures in the last one million years (Drake et al. 2017). Below the permafrost (and/or at depths greater than about 350 m), reducing conditions were interpreted to prevail at present in the study area.

Evolution of salinity and of other relevant natural groundwater components

During the glacial cycle of the reference evolution (about 120 000 years) the Forsmark site is covered by an ice sheet during a few periods with a total duration of about 30 thousand years, see Section 10.4.1. Groundwater flow during the glacial domain has been estimated at the large regional scale including the Forsmark area (Vidstrand et al. 2010). A full description of these calculations is given in Section 10.4.6 and in the original report. The results of that model include evaluations of the salinity distribution beneath an ice sheet, and the modelling included situations where the ice sheet advanced either over an unfrozen terrain or over an area subjected to permafrost.

For the case of advance over an unfrozen ground, a glacial period of 18 850 years has been simulated in 10 time steps, reproducing the advance and the retreat of the ice front. Three hydrological scenarios have been considered: i) when the ice front is advancing to the repository area (2 900 years, approximately), ii) when the repository is entirely covered by a warm-based ice sheet i.e. an ice sheet with basal melting (15 000 years) and, finally, iii) when the ice sheet is retreating (1 200 years) and the area is covered by a 100 m deep melt water lake.

Dilute waters of glacial origin are expected under a warm-based ice sheet. Significant changes in groundwater composition are expected as soon as the ice front advances over the repository area. The calculated results shown in Figure 10-157 indicate that salinities in the upper part of the modelled domain would usually be lower than 2 g/L. The model results also illustrate the upconing of deep saline waters under an advancing and a retreating warm-based ice sheet. The calculated salinities can reach values up to 20 g/L in locations affected by upconing. Because the advance of the ice sheet is a relatively fast process and the retreat even more so, the high salinity conditions are predicted to last only a few centuries at most. The groundwater data sampled at Forsmark during the site investigations indicate a glacial meltwater component at repository depth (Laaksoharju et al. 2008) qualitatively supporting the results shown in the figure.

Figure 10-158 presents the calculated changes with time of the distribution of salinities (total dissolved solids) when an ice sheet advances over unfrozen ground and retreats behind a glacial meltwater lake. The figure shows the results within the candidate repository volume at Forsmark (due to the hydrogeological grid, depths between 432 and 528 m have been included). The computed salinity is not homogeneously distributed; the calculations show groundwaters having salinities between about 0.03 g/L (during and soon after the glacial advance over the repository) and 20 g/L as a consequence of the upconing of deep saline waters when the ice front margin is located on top of the repository.

The hydrogeological calculation results obtained in Vidstrand et al. (2010) and described in Section 10.4.6 have produced salinity distributions for the Forsmark area during an ice sheet advance and retreat. Both an ice sheet advancing over unfrozen and permafrost ground have been modelled. The procedure used to obtain mixing proportions of end-member waters is described in the subsection “*Modelling*”. These mixing proportions were then used as input to the PhreeqC code which imposed equilibrium with calcite, quartz, hydroxiapatite and Fe(III) oxyhydroxide. As a result, the detailed distribution of compositions was obtained. A full description of the results may be found in Salas et al. (2010).

Only the results from one of the modelled cases in Vidstrand et al. (2010) of an ice sheet advancing over a permafrost area have been used for the geochemical modelling described here, namely the model in which there is a permafrost zone remaining below the ice sheet, as it advances. This zone stretches 2 km from the ice margin under the ice. Figure 10-160 shows a comparison between some of the calculation results for the ice sheet advancing over unfrozen ground and results for the advance over permafrost. Full details of the calculation results are provided in Salas et al. (2010). It should be noted that because there are almost no field data on the groundwater chemistry in granitic rocks under or close to an ice sheet, the model results are associated with a large degree of uncertainty.

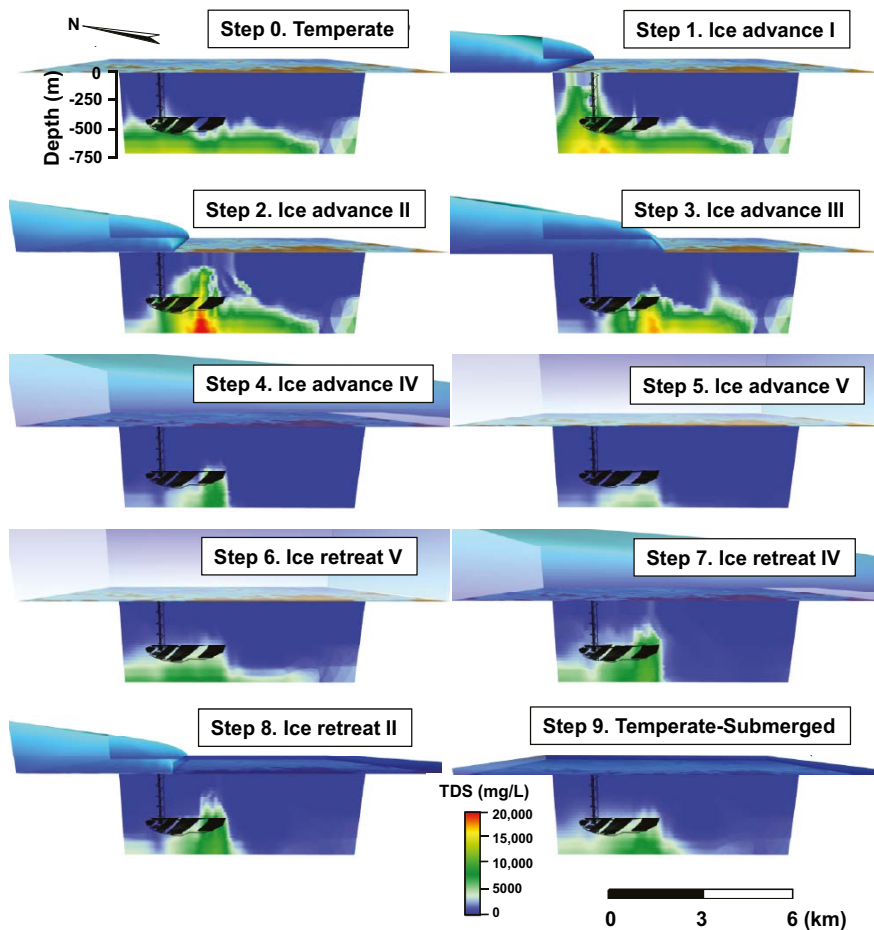


Figure 10-157. Ice sheet advancing and retreating over unfrozen ground: Changes in the distribution of TDS (total dissolved solids, mg/L) shown in vertical slices when an ice sheet advances and retreats over the unfrozen Forsmark area. The figure shows results during the glacial sheet advance (1 to 6) and the glacial retreat (7 to 10) calculated using the model described in Section 10.4.6 (Vidstrand et al. 2010). When the ice sheet retreats the area is covered by a 100 m deep glacial melt water lake.

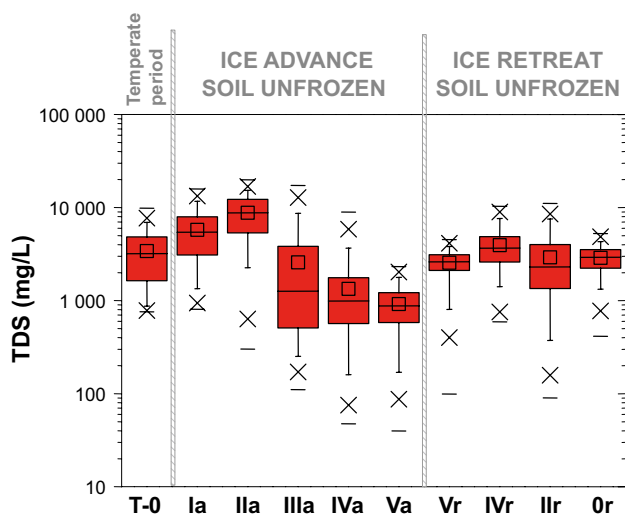


Figure 10-158. Ice sheet advancing and retreating over unfrozen ground: Box-and-whisker plots showing the statistical distribution of the calculated TDS (total dissolved solids) within the candidate repository volume at Forsmark. The figure illustrates the steady-state temperate model (left) and the TDS distribution at different stages of the ice sheet advance over unfrozen ground (ice front locations Ia to Va) and ice sheet retreat (ice front locations Vr to Or). The statistical measures are the median, the 25th and 75th percentile (box), the mean (square), the 5th and 95th percentile (“whiskers”), the 1st and 99th percentile (crosses) and the maximum and the minimum values.

Chemical components not participating extensively in chemical reactions, such as Cl, Na, sulphate, and possibly to some extent Ca, follow the salinity patterns under the ice sheet described above. The calculated $\Sigma q[M^{q+}]$ displayed in Figure 10-159 and Figure 10-160, as well as the results shown in Figure 10-147 and Figure 10-148, indicate that dilute melt waters, with $\Sigma q[M^{q+}] < 8$ mM, may occur within the candidate repository volume for some period of time during the advance and retreat of an ice sheet, violating the criterion for the safety function indicator R1c. For the glacial period, around 3.4 percent of deposition hole locations (see Figure 10-147 and Figure 10-148) experience dilute conditions during an advancing ice front whereas only slightly less than two percent of the deposition holes experience dilute conditions during an assumed period of 100 000 years corresponding to glacial maximum conditions. The proportion of dilute conditions is somewhat larger in Figure 10-159 and Figure 10-160 because they show all groundwaters in the rock volume close to the repository, that is, in the hydrogeological grid at depths between 432 and 528 m. Also, as seen in Figure 10-33, it would take up to 60 000 years of temperate conditions to reach dilute conditions in about 0.5 percent of the deposition hole locations. For permafrost conditions, all arguments indicate that groundwaters below permafrost will not become more diluted than under temperate conditions. The hydrogeological model results described in Section 10.4.6, indicate that after the complete retreat of the ice sheet the salinities, shown in Figure 10-158, and the concentrations of cations, shown in Figure 10-159, are back, approximately, to the levels estimated before the onset of the glacial period, and these results are not in contradiction with the salinities observed now in Forsmark. The overall conclusion is that around 5 percent of the deposition hole positions may pessimistically be assumed to experience dilute conditions during a glacial cycle, and they will only have these conditions for a fraction of the time, see further Section 10.4.8.

Other components, such as bicarbonate, iron, sulphide and pH that are controlled by relatively fast chemical reactions and reactions with minerals can also be affected by the glacial conditions to a lesser extent. The calculated pH values results shown in Figure 10-159 (and in Figure 10-160 for the advance of an ice sheet over permafrost) indicate that glacial conditions may result in a general increase of pH values, an effect which is observed for example in the Grimsel groundwaters (see for example Degueldre et al. 1989). The safety function criteria R1d and R1e in Figure 10-2 will be fulfilled in that pH will remain < 11 and the concentrations of K and Fe will remain limited as shown in the figures in Salas et al. (2010), whereas the groundwater concentrations of sulphide are discussed below.

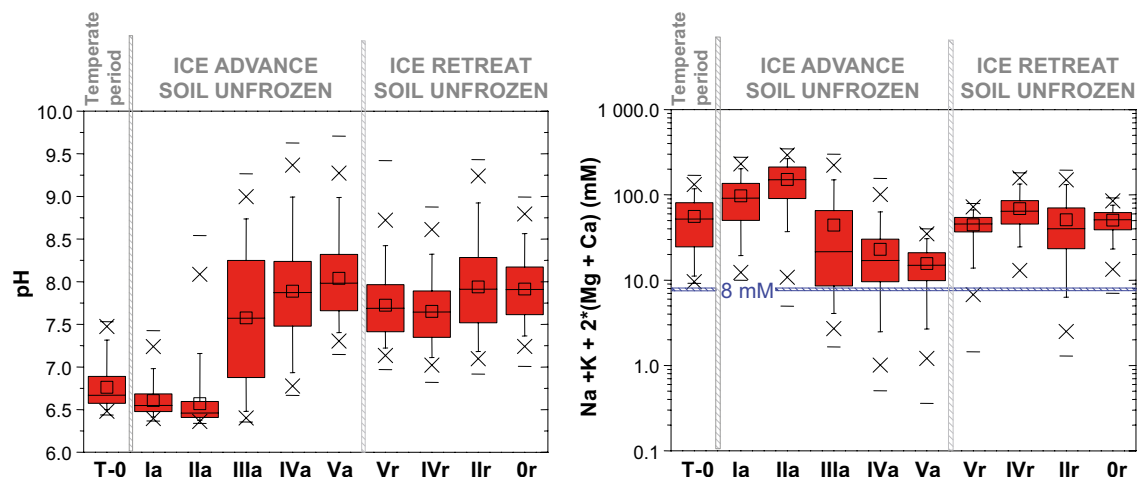


Figure 10-159. Ice sheet advancing and retreating over unfrozen ground: Box-and-whisker plots showing the statistical distribution of calculated pH values (left) and the safety function indicator $\Sigma q[M^{q+}]$ (right) for the positions located within the candidate repository volume at Forsmark. The figure illustrates the steady-state temperate model (T-0 at left) and the distribution of pH or cation concentrations at different stages of the ice sheet advance over unfrozen ground (ice front locations Ia to Va) and ice sheet retreat (ice front locations Vr to Or). The statistical measures are the median, the 25th and 75th percentile (box), the mean (square), the 5th and 95th percentile (“whiskers”), the 1st and 99th percentile (crosses) and the maximum and the minimum values.

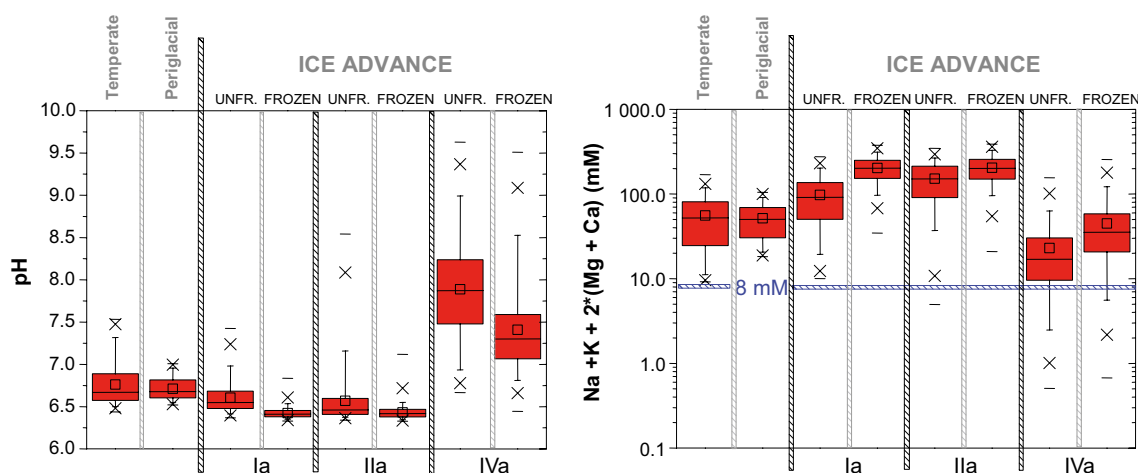


Figure 10-160. Comparison between the advance of an ice sheet over unfrozen terrain with the advance over a permafrost area for different ice front locations: Box-and-whisker plots showing the statistical distribution of pH and the safety function indicator $\Sigma q[M^{n+}]$ for the positions located within the candidate repository volume at Forsmark. The figure illustrates the steady-state permafrost model (left, ice front location "0") and the pH and cation concentrations at different stages of the ice sheet advance over permafrost ground (ice front locations I to IV). The statistical measures are the median, the 25th and 75th percentile (box), the mean (square), the 5th and 95th percentile ("whiskers"), the 1st and 99th percentile (crosses) and the maximum and the minimum values.

Figure 10-160 and other results in Salas et al. (2010) indicate that although the calculated chemical characteristics of the groundwaters in general show a narrower range of values in the case of the ice sheet advancing over permafrost as compared with the ice sheet advancing over an unfrozen area, for a few of the modelled grid points extreme values may occur, for example there is a possibility of having lower cation concentrations in the case of the ice sheet advancing over permafrost.

As for temperate and periglacial conditions, two geochemical assumptions, namely equilibrium with respect to FeS(am) or Fe(III) oxyhydroxide, have been simulated in order to estimate the evolution of the values of Eh (the redox potential) within the repository domain. Because the model is based on chemical equilibrium, it assumes that oxygenated waters are not present. Under equilibrium conditions any infiltrating oxygen with the glacial melt waters would react with the Fe(II) minerals included in the model.

The calculated Eh values in the case where an ice sheet advances and retreats over unfrozen ground are shown in Figure 10-161. Due to the imposed mineral equilibrium, the general variations in the pH values, shown in Figure 10-159, are reflected in corresponding variations in the calculated Eh, as these two variables are inversely related through the reaction $\text{Fe}(\text{OH})_3(\text{s}) + 3\text{H}^+ + \text{e}^- \rightleftharpoons \text{Fe}^{2+} + 3\text{H}_2\text{O}$. Similar values of Eh are obtained from the modelling of the advancement of an ice sheet over permafrost (Salas et al. 2010).

As discussed in Section 10.4.1, immediately after the retreat of an ice sheet, isostatic depression will set the ground surface at the repository site below the Baltic Sea surface level for a period of time, see Section 10.4.1. In the reference evolution, which is a repetition of the last glacial cycle, the Weichselian, the Forsmark site is expected to be below glacial melt water lakes, and sea or brackish waters during a period of time of between a few thousand years up to maybe ten thousand years.

Both the site descriptive modelling of the Forsmark site since the retreat of the last ice sheet to the present day (Laaksoharju et al. 2008) and the SR-Site hydrogeological modelling (Joyce et al. 2010) show a relatively fast turnover of groundwaters, in which glacial melt water is replaced by a succession of waters penetrating from the surface: the Littorina sea gradually evolving into the present day Baltic sea, and finally modern meteoric waters.

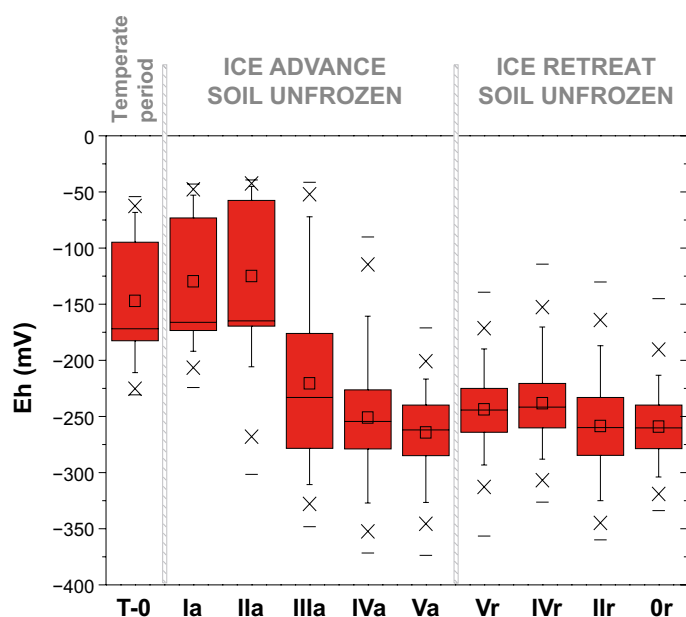


Figure 10-161. Ice sheet advancing and retreating over unfrozen ground: Box-and-whisker plots showing the statistical distribution of calculated Eh (redox potential) for the positions located within the candidate repository volume at Forsmark. The figure illustrates the steady-state temperate model (left) and the calculated Eh values at different stages of the ice sheet advance over unfrozen ground (ice front locations Ia to Va) and ice sheet retreat (ice front locations Vr to Or). The statistical measures are the median, the 25th and 75th percentile (box), the mean (square), the 5th and 95th percentile (“whiskers”), the 1st and 99th percentile (crosses) and the maximum and the minimum values.

The model results presented above indicate that concerning salinity and the concentration of cations, the conditions when the site is submerged under a glacial melt water lake are similar to those found before the onset of the glaciation, see the starting steady state temperate result “T-0” and the ice front locations “Or” in Figure 10-158 and Figure 10-159. Other more reactive groundwater components such as Eh or pH may remain affected, see Figure 10-159 and Figure 10-161, but all groundwater characteristics are expected to satisfy the safety function indicators and criteria R1a to R1f in Figure 10-2.

The possible infiltration for relatively short periods of time of waters of marine origin after a glaciation has been modelled within SR-Site (Joyce et al. 2010, Salas et al. 2010). Within such a period, equivalent to the Littorina sea episode that had its maximum salinity at 4000 BC, the salinity of groundwaters at repository depth could increase due to density driven groundwater flow. The detailed results of the modelled groundwater chemical characteristics are presented in Salas et al. (2010). The results modelled for 3000 BC show that the effects of the marine water intrusion at repository depth are delayed in time and that the proportion of Littorina waters in the repository volume is larger at present than it was then. The calculated groundwater compositions for 3000 BC show that the charge concentration of cations around the repository is well above 0.004 mol/L, corresponding to compliance with the safety function indicator R1c in Figure 10-2. As the salinities are not expected to increase above those of sea water during any period of time, the swelling capacity of the backfill will not be affected, see safety function indicator R1b.

As in the case of permafrost, the intensity of microbially mediated SO_4^{2-} reduction to produce sulphide will probably decrease under an ice sheet due to the lower temperatures. Compared with a preceding permafrost period, sulphate concentrations might increase during the short periods of upconing waters and they will decrease substantially during the longer periods of intrusion of glacial melt waters, although in Forsmark where deep saline waters have low sulphate contents, the upconing process should not increase sulphate concentrations noticeably. In any case, reducing agents are required for any sulphate reduction to take place, and under glacial conditions the inflow of organic matter from the surface will be lower. SO_4^{2-} reduction could still be sustained by the gaseous groundwater components methane and hydrogen, see the discussion in Section 10.3.7. There is a large uncertainty in estimating the flow of CH_4 and H_2 in Forsmark because the data are very scarce, but the estimated

fluxes for these gaseous species are $< 3 \times 10^{-10}$ mol/(m² yr) (Delos et al. 2010). The conclusion is that there is only a minor contribution from the flow of these gases to sustaining microbial sulphide production. Most indications suggest therefore lower sulphide concentrations during a glacial period, see also the discussion in Tullborg et al. (2010).

Although sulphide concentrations may be obtained by considering equilibrium with either FeS(am) or Fe(III) oxyhydroxides, for the reasons outlined in Section 10.3.7, it is believed that the equilibrium solubility constraints applied cannot reflect the variability of sulphide concentrations that can be expected during glacial and submerged conditions. Because of this the sulphide concentrations for the glacial and submerged conditions are assumed to be the same as the observed distribution of sulphide in groundwaters during the present temperate conditions, which is after a recent period of possible intrusion of marine sulphate-rich waters and described in Section 10.3.7. This distribution of sulphide concentrations is used to estimate canister corrosion rates during the glacial and submerged periods. However, it is to be expected that glacial meltwaters will have low concentrations both of sulphate and of reductants such as DOC, methane and hydrogen, and therefore, microbial sulphate reduction during a glacial period should be more restricted than during other climatic conditions. Therefore, the use of the sulphide distribution observed during the site investigations in the analysis of canister corrosion during glacial conditions is pessimistic.

Based on the assessment presented in this subsection the following may be concluded regarding the evolution of salinity and of other relevant natural groundwater components during glacial conditions.

- Dilute melt waters, with $\Sigma q[M^{q+}] < 8$ mM, may occur within the repository volume for some period of time during the advance and retreat of an ice sheet, violating the criterion for the safety function indicator R1c. Upconing of deep seated saline groundwaters during the glacial period is not expected to affect the swelling capacity of the backfill, corresponding to the safety function indicator R1b.
- Major groundwater components, such as Cl, Na, sulphate, and possibly Ca, will follow the salinity trends. Other components, such as bicarbonate, potassium, iron, sulphide and pH that are controlled by relatively fast chemical reactions and mineral dissolution/precipitation are likely to be less affected by the glacial conditions. However, all the evidence points towards dilute waters with relatively high pH. The criteria concerning the safety function indicators R1d and R1e in Figure 10-2 will be fulfilled in that the pH will remain < 11 and the concentrations of K, HS⁻ and Fe will remain limited. Sulphide concentrations are expected to be lower than for temperate conditions.
- As indicated previously, salinity levels are expected in general to decrease during glacial periods. Colloids are known to be strongly destabilised at high ionic strengths, and at high concentrations of divalent cations (Ca²⁺) in particular. Therefore, during periods of glaciation, with predominantly dilute groundwaters, it cannot be excluded that colloids may be generated and transported by groundwater. However, a high potential stability of colloids does not necessarily imply a high colloid concentration. It has, for example, been shown that the granitic groundwaters at Grimsel, which are quite dilute and where colloids, if formed, are quite stable, have low concentrations of colloids (≤ 0.1 mg/L). The reason for this is not clear: there might be some unknown mechanism that removes colloids at that site, or there could be no significant generation of colloids at Grimsel. The conclusion is, therefore, that there is a potential for higher colloid concentrations in groundwaters during a glacial period, especially during the advance and retreat of an ice sheet when groundwater velocities are highest. An upper limit would be the highest colloid concentrations reported in Birgersson et al. (2009), about 40 g/L.

Redox conditions

As discussed in the previous section, temporal changes in groundwater conditions are expected during a glaciation cycle. Short periods of upconing of deep reducing groundwaters will be followed by longer periods with glacial melt water intruding into the rock. After some time the situation may look as in Figure 10-157, i.e. with groundwaters that originate mainly from ice melt water in large volumes of rock. Arguments have been put forward that if glacial melt waters were rich in dissolved atmospheric gases, reducing conditions might no longer prevail at repository depth, infringing the safety function indicator criterion R1a (see e.g. Puigdomenech et al. 2001).

Large changes in hydrogeological conditions are expected when the ice front margin passes over the repository volume as discussed in Section 10.4.6. During these periods, which will be relatively

limited in time, large quantities of glacial melt water may intrude into the rock, owing to the drastic change in hydraulic head gradients. In the remainder of a glaciation cycle, the magnitude of the hydraulic head gradient over the repository volume will be much lower, with groundwater flow rates not considerably different from temperate conditions, and probably lower.

The compaction of snow into glacier ice involves the incorporation of substantial amounts of air (Martinerie et al. 1992). Thus, recharging glacial melt water under the ice may contain dissolved carbon dioxide and oxygen at above the concentrations expected for aerated water. The oxygen concentration in pure water in equilibrium with air is temperature dependent, and approximately 0.25 mM at 20 °C. For glacial melt waters, based on theoretical constraints, the maximum oxygen concentration has been estimated to be 1.4 mM (Ahonen and Vieno 1994). However, it has been noted that much lower values are normally measured in sampled glacial melt waters in the field, in the range 0–0.16 mM (Gascoyne 1999). It may be argued that degassing could have contributed to the observed low oxygen levels of these field samples. Also, photosynthetic and heterotrophic microbial activity on the surface of glaciers may partly be responsible for the low oxygen content (Hallbeck 2009). Furthermore, glacial melt water reacts rapidly with sub-glacial rock minerals and debris (Wadham et al. 2010). The amounts of sulphate found in glacial melt waters (Brown 2002, Cooper et al. 2002) supposedly from pyrite oxidation ($4 \text{ FeS}_2 + 14 \text{ H}_2\text{O} + 15 \text{ O}_2 \rightarrow 16 \text{ H}^+ + 8 \text{ SO}_4^{2-} + 4 \text{ Fe(OH)}_3$) are sufficient to explain the low oxygen concentrations found. It is concluded that a cautious oxygen concentration for infiltrating glacial meltwaters is 0.3 mM (the rounded up value for equilibrium with air).

During temperate conditions the top soil and the uppermost part of the rock contains relatively large amounts of organic material. Mediated by microbes the degradation of the organic substances explains the lack of oxygen below a few metres in the rock at Forsmark. During a period of glaciation, the amount of degradable organic substances is uncertain, although microbial activity is observed at the surface of most glaciers, and in glacial melt water (Hallbeck 2009). The main reducing capacity in the absence of organic material is comprised in ferrous minerals in the rock. Biotite inside the bulk of the rock matrix and chlorite adjacent to fractures has been shown to dominate the reducing capacity in the absence of organic substances. The ferrous iron content in the bulk rock is approximately one percent by weight in the dominant rock types in Forsmark, accessible through diffusion in the pores of the matrix. Fracture minerals directly accessible in flowing fractures have even larger ferrous iron content.

The penetration of oxygen-rich glacial melt waters in fractures in granitic rocks under a warm-based ice sheet has been the subject of several modelling efforts, with an early study by Neretnieks (1986). Guimerà et al. (1999) showed that a change in the redox potential is to be expected at repository depth under certain circumstances. Sidborn and Neretnieks (2003, 2004) considered the possible influence of microorganisms in fractures but concluded that diffusion resistance in pores of the rock matrix eventually controls the consumption rate of oxygen.

The results from these studies along with more recent modelling efforts (Sidborn and Neretnieks 2008, Spiessl et al. 2010, Sidborn et al. 2010) confirm that the flow-wetted surface to flow rate ratio, commonly referred to as the flow-related transport resistance (or *F*-factor) is a key parameter when studying the interaction between dissolved oxygen in the flowing water and minerals in the rock.

For relatively short times when reducing minerals are exposed to the flowing water in the fracture, a pseudo-steady state oxygen concentration profile develops to a certain distance downstream. It may also be shown (Auqué et al. 2006, Sidborn and Neretnieks 2008) that in this case the inflow of oxygen is exactly balanced by the dissolution of reducing minerals at that distance along the flow path. Given the reducing capacity of the bedrock in Forsmark, this pseudo-steady state situation would prevail for more than 1000 years. When eventually the reducing capacity directly exposed to the flowing water along the flow path is substantially decreased, the effect of diffusion resistance in pores of the rock matrix becomes more and more prominent, limiting the rate of oxidation. When diffusion limits the oxidation reaction, the time required for oxygen to reach a certain distance along the flow path is proportional to the square of the corresponding *F*-factor (Sidborn and Neretnieks 2008). The oxygen concentration profile for the pseudo-steady state situation with oxidation rate limited by abiotic chemical kinetics is illustrated by the blue curves in Figure 10-162 for the conditions at Forsmark (Sidborn et al. 2010). These curves are calculated using pessimistic parameters and assumptions, as explained later in Section 12.6.2 and in Sidborn et al. (2010). A cautious oxygen concentration for glacial melt waters is 0.3 mM, and the corresponding pseudo steady state oxygen

profile along a recharge path, using a set of other pessimistic assumptions, is shown as the blue curve in Figure 10-162-b. According to this figure, glacial melt water with a remaining oxygen concentration of $0.1 \mu\text{M}$ may reach a distance along the flow-path corresponding to an F -factor of about $5\,000 \text{ yr/m}$. These generic results for the pseudo-steady state oxygen concentration profiles are coupled with F -factors obtained from site-specific hydrogeological modelling presented in Section 10.4.6. Particle back-tracking results for various glaciation scenarios are reported in Joyce et al. (2010) for complete flow paths from the ground surface to each canister position. The F -factors are calculated using the extended heterogeneity model, see Section 12.6.2 subsection “ F -factors”. Cumulative F -factors for the most pessimistic glacial situation, when the ice front margin is right above the repository volume (ice front location III) are illustrated by the red curve in Figure 10-162. Only 1 184 out of 6 916 flow paths are included in the cumulative distribution in the figure. The remaining particles either did not reach the surface for the simulated time or have inflow outside the modelled domain or the deposition positions are excluded based on the FPC and EFPC criteria.

As can be seen in Figure 10-162 there is a small overlap between the oxygen concentration profile and the F -factors when pessimistic assumptions are made to calculate the oxygen penetration depth, indicating that a few deposition locations may be reached by oxygen at concentrations exceeding $0.1 \mu\text{M}$ under these conditions.

It is important to note that the cumulative result (red curve in Figure 10-162) is obtained for a “snap-shot” of the most pessimistic ice front margin location. During the ice sheet advance or retreat, with a normal rate between 50 and 300 m/yr , the front margin passes over the candidate repository footprint (a few km) in less than 100 years. With such a rate for the ice front movement the hydraulic conditions change considerably according to the hydrogeological model results. The flow pattern evolves so that recharge flow paths for a given ice front location may become discharge flow paths in another, and flow rates and hydraulic gradients change in a manner such that F -factors for recharge flow paths reaching the repository may become orders of magnitude smaller or larger.

In a situation where the ice sheet advances over a periglacial (frozen) area, a comparison of the results obtained by the modelling described in Section 10.4.6 and in Vidstrand et al. (2010) shows that recharge paths in most cases have larger flow-related transport resistances (F -factors). The lowest F -values are increased at least by a factor of 3.6 , depending on the ice front location considered.

If microbial activity and reducing fracture coatings are considered (in addition to an intact rock matrix and abiotic reaction rates), a lower F -value will yield the same oxygen consumption along the flow path. In a flow path region where the reducing minerals in the fracture walls are not yet completely oxidised, the Fe(II) minerals are exposed to the flowing water in the fracture. In such an environment it is likely that microbe populations thrive and mediate the oxidation reaction. It is not possible however to quantify to what extent the reaction rate would increase.

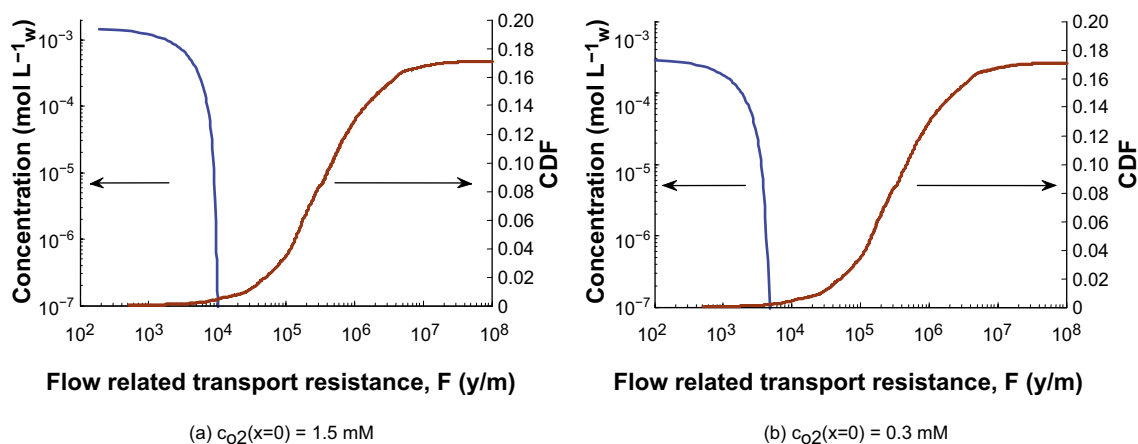


Figure 10-162. Plots of generic pseudo-steady state oxygen concentration profiles (blue curves) and the cumulative distribution function (CDF) of the flow-related transport resistance (or F -factor) for the most pessimistic glacial situation (ice front location III). The recharge oxygen concentration in the melt water (at $F = 0$) is (a) 1.5 mM and (b) 0.3 mM . From Sidborn et al. (2010).

The conclusion is therefore that for situations where the ice sheet advances or retreats at a continuous rate, then oxygen penetration can be discarded, because the calculated blue curve in Figure 10-162b will be shifted to the left if for example fracture filling materials and microbial processes are considered, and the F -values would move to the right in the situation of an ice sheet advancing when the site is affected by permafrost.

Oxygen reduction potential (ORP) measurements in soil pipes have shown that most of the oxygen under present day conditions is depleted within the first few metres at the site (Sidborn et al. 2010) and references therein. Although no general depth trend of oxygen intrusion can be found at depths greater than a few metres, this does not exclude the possibility of greater intrusion depths in transmissive domains such as deformation zones, where only scattered samples have been taken. After the retreat of an ice sheet, during temperate conditions, the reducing conditions of the rock directly exposed to flowing groundwater are restored (Banwart 1999), and therefore a lack of evidence of past intrusions of oxygen-rich glacial meltwaters may be expected. In addition to the investigations made at the Forsmark site, redox transition zones have been investigated in many locations in Scandinavia as well as in various sites throughout the world. Although the historical hydraulic properties at many of the investigated sites are difficult to evaluate, it is relevant to note that traces of oxygen intrusion are seldom found below 200 metres.

In conclusion, based on observations and results from pessimistic modelling, oxygen intrusion to repository depth in highly transmissive deformation zones cannot be discarded. However, the model results for a recharge oxygen concentration of 0.3 mM indicate that more than one thousand years of the worst glacial situation would be needed for oxygen at non-negligible concentrations to reach the canisters in the repository. Since such circumstances do not occur in the reference evolution, it is concluded that reducing conditions will prevail in the repository, satisfying the safety function indicator criterion R1a.

Alternative evolutions, aimed at capturing more pessimistic situations as regards oxygen penetration to repository depth are considered in the corrosion scenario, Section 12.6.2. For example if the ice front advance were to cease for a period of up to about one thousand years, then the penetration of oxygen can be discarded if the ground is frozen or if it is submerged under a melt-water lake. But if the ice sheet is stationary over the repository on unfrozen ground and if the repository area is not submerged, then calculations (Sidborn et al. 2010) indicate that if a pessimistic value for the oxygen content in the glacial melt water is used (1.5 mM) and if several other pessimistic assumptions are made, for example microbial processes and reducing fracture infill are excluded, then oxygen could reach the deposition locations that have the smallest flow-related transport resistance (F -factor). As soon as the ice margin starts to move again, because of the shifting in the flow paths and the associated mixing, anoxic conditions are quickly reached. The consequences of an eventual oxygen intrusion for the corrosion scenario are analysed in Section 12.6.2.

Effects of grouting, shotcreting and concrete on pH

The processes described in Section 10.3.7 for the temperate domain following repository closure will continue during the glaciation periods of the first glacial cycle, although the effects will gradually decrease. Given enough time, all cement in grout will be converted first into calcium silicate hydrates with low calcium to silica ratios, and finally into calcite and silica (Luna et al. 2006, Galíndez and Molinero 2009). The duration of this process will depend on the velocity of the groundwaters flowing around the grouted volumes, but times of the order of 10^4 years are expected.

Therefore, the conclusion reached in Section 10.3.7 is in part still valid here: the effect of grout in fractures will be to increase the pH in deformation zones for relatively long periods of time. It is expected that, with time, the pH will progressively homogenise with the values found in surrounding parts of the rock, and therefore remain within the criteria for the safety function indicator R1e.

Identified uncertainties and their handling in the subsequent analysis

The following uncertainties are identified when considering the different chemical aspects of the evolution of the repository during the period after the initial temperate period, that is, for the remaining part of the reference glacial cycle.

There is a large degree of uncertainty in the detailed salinity distribution around the repository. In addition, the salinities can become sufficiently low in some parts of the candidate repository volume as to affect the performance of the buffer during this period or when considering its future evolution. The calculated distributions of salinity, pH and other groundwater components obtained from the modelling are used in the analysis of bentonite evolution in Section 10.4.8 and for the selection of radionuclide transport related parameters in Chapter 13.

There is a large degree of uncertainty in the detailed distribution of dissolved sulphide in the groundwaters around the repository. Because no dependency has been found between sulphide and other groundwater geochemical or hydrogeological parameters, the observed distribution of concentrations in the Forsmark site at present is propagated to the analysis of canister corrosion in Section 10.4.9. However, it is to be expected that glacial melt waters will have low concentrations of sulphate and of reductants such as DOC, methane and hydrogen, and therefore, microbial sulphate reduction during a glacial period should be more restricted than during other climatic conditions. Therefore, the use of the sulphide distribution observed during the site investigations in the analysis of canister corrosion during glacial conditions is pessimistic.

Based on observations and results from pessimistic modelling, oxygen intrusion to repository depth in highly transmissive deformation zones during the advance or retreat of an ice sheet cannot be discarded. However, model results indicate that hundreds of years of the worst glacial situation, a situation which does not occur in the reference evolution, would be needed for oxygen to reach only a few of the canister positions in the repository. Therefore it is concluded that reducing conditions will prevail in the deposition holes of the repository, satisfying the safety function indicator criterion R1a in Figure 10-2.

10.4.8 Effects on buffer and backfill

Freezing

As concluded in Section 10.4.3, temperatures leading to buffer and backfill freezing do not occur in the reference evolution. Freezing of the upper parts of access tunnels or sealed boreholes could, however, not be excluded. Nevertheless, this section addresses the conditions when freezing may occur and how this affects the clay barriers. This information is then used in Section 12.3 when assessing consequences of more extreme future climates.

General

At temperatures somewhat below 0 °C it can be anticipated that the water in the buffer and the backfill would turn into ice. This is not an issue for the materials themselves since the process is reversible and they will regain their properties after thawing Birgersson et al. (2010). However, the formation of ice could lead to

1. An increased pressure on the canister and rock.
2. Redistribution of material due to ice lens formation.

The key issue for the freezing process is when the pressure generated from the volume expansion of the ice can be harmful for the canister and the rock. According to Posiva SKB (2017) the performance target for the canister is that it should withstand isostatic load ≤ 50 MPa. The mean crack initiation stress level for the main rock type in Forsmark is 116 MPa and the minimum is 60 MPa SKB (2008a). The crack damage stress level is, according to Cai et al. (2004), in between 70 to 90 % of the Unconfined Compressive Strength. This implies that the mean lies between 158 MPa and 203 MPa, with the minimum at 109 MPa. According to the Clapeyron equation 50 MPa is generated when ice is cooled by 3.7 °C below the freezing point of water. This pressure would be reached in a deposition hole filled with pure water at -3.7 °C. The presence of bentonite will lower the freezing point of water, thus lower the temperature when the pressure from the ice will be 50 MPa.

Buffer

The freezing process in a bentonite buffer is studied in Birgersson et al. (2010). The temperature when ice starts to form can be predicted with the empirical approach and a thermodynamic approach

(Buffer, backfill and closure process report). They both predict that no ice will be formed in an intact buffer at standard density at a temperature above $-5\text{ }^{\circ}\text{C}$. Using the lowest swelling pressure value for the technical design requirement in Posiva SKB (2017) of 3 MPa, the critical temperature is $-2.5\text{ }^{\circ}\text{C}$. The most pessimistic value for when freezing causes a pressure above 50 MPa is therefore $-2.5-3.7\text{ }^{\circ}\text{C} = -6.2\text{ }^{\circ}\text{C}$

Backfill

For the freezing of the backfill only pressure exerted on the rock is of concern. The minimum rock strength of 60 MPa corresponds to a temperature of $-4.4\text{ }^{\circ}\text{C}$. The swelling pressure of the backfill is around 2 MPa which would give a critical temperature of $-1.7\text{ }^{\circ}\text{C}$. Freezing of the backfill could potentially damage the rock if the temperature falls below $-6\text{ }^{\circ}\text{C}$.

Ice lens formation

Ice lens formation requires that water is supplied to the growing lens. Since the water in the rock will freeze before the water in the buffer and the backfill, ice lens formation in these components is not possible.

Borehole seals

Ice lens formation in the bentonite component in a bore hole seal was evaluated in the main report of SR-Site (SKB 2011). The conclusion was that the effect was negligible. The updated design of the seal makes ice lens formation even more unlikely. The effect is therefore neglected in the PSAR.

Conclusions

Figure 10-113 shows the predicted evolution of the temperature in and above the repository. Based on this modelling, no component of the repository will be exposed to freezing temperatures in the reference evolution. At some level, the backfill in the ramp and shaft and the borehole seals will be exposed to freezing conditions. This, however, is not expected to have any negative effects on the repository performance.

Chemical evolution of buffer and backfill for altered groundwater compositions

Intrusion of water types other than the present day deep groundwater in the repository area may modify the chemical evolution of the system. In the SR-Can assessment (SKB 2006a) this was assessed by a geochemical simulation of an intrusion of a typical glacial melt water and a high salinity water (Arcos et al. 2006). The conclusion from that study was that none of the waters had any significant impact on the expected performance of the system.

In the SR-Site assessment (SKB 2011), another approach was adopted in order to better support the conclusions from SR-Can. In SR-Site no attempt to simulate the effect of future changes of groundwater chemistry on the chemistry of the buffer and backfill has been made. Instead a sensitivity study of the importance of the groundwater components on the geochemical evolution has been made (Sena et al. 2010b). A summary of results can be found in Section 10.3.10.

Colloid release from buffer and backfill

Erosion

As concluded in Section 10.4.7, the ionic strength of the groundwater; $\Sigma q[\text{M}^{q+}]$, will fall below 8 mM charge equivalent i.e. violating safety indicator criterion R1c, for some deposition holes during some part of the glacial cycle. This means that colloid release may occur from these holes and sections of the backfill similar to the situation during later parts of the temperate period, as discussed in Section 10.3.11. More specifically, it is concluded in Section 10.4.7 that around 5 percent of the deposition hole positions may be assumed to have dilute conditions during a glacial cycle, and they will only have these conditions for a fraction of the time.

Regarding the duration of dilute conditions, Figure 10-33 and Table 10-4 indicate that after 60 000 years of temperate conditions, 0.43 percent of the deposition holes, i.e. those with the highest flow rates, will have been exposed to dilute groundwater. For a glacial advance, Figure 10-147 and Table 10-29 indicate that an additional 3.4 percent of the deposition hole locations will have been exposed to dilute conditions, while Figure 10-148 and Table 10-30 indicate that after 20 000 years of glacial conditions, one percent of the deposition holes will have been exposed to dilute groundwater. Pessimistically assuming that different deposition hole locations will be exposed during the different climate regimes, in total roughly 5 percent of deposition hole locations will be exposed to dilute water during a sequence of a 60 000 year temperate period and a 20 000 year glacial period. This estimate assumes that the same holes will be exposed during a glacial retreat as during a glacial advance. Furthermore, it is reasonable to assume that these same holes will be exposed also at repeated episodes of temperate and glacial conditions and hence during the full Weichselian glacial cycle.

Temperate or glacial conditions occur during about half the reference glacial cycle (see Figure 10-111) and it cannot be excluded that the most exposed deposition holes are exposed to dilute groundwater during large parts of these periods (according to Figure 10-33 and Figure 10-148). Together, these results indicate that a total exposure time of dilute ground water for the deposition holes with the highest flow rates of around 60 000 years, or 50 percent of the time of the glacial cycle is a cautious assumption for the calculations of buffer erosion and sedimentation, although no strict exposure time can be derived from the cited results. However, note that different deposition holes likely will experience different exposure times since the flow field varies in time, particularly between temperate and glacial conditions. Thus, this estimate is cautious in terms of for how long time any single deposition hole will be exposed to dilute conditions. Also, results in earlier sections indicate that the majority of deposition holes will never be exposed to dilute waters during the reference glacial cycle. Assuming that each glacial cycle is a repetition of the reference glacial cycle, the total time of dilute conditions for the assessment time scale is readily obtained.

As already shown in Section 10.3.11, and illustrated in Figure 10-81, it is clear that only a small number of deposition holes will reach advective conditions, even in 10^6 years, when applying the erosion model described in Section 10.3.11 to all deposition holes for temperate conditions with a cation concentration of the infiltrating water of 3 mM. Considering now a full glacial cycle, the following approach is taken.

- The part of the glacial cycle where dilute conditions may occur is simplified as consisting of 30 000 years of temperate conditions and 30 000 years of glacial conditions as suggested above.
- Dilute conditions are assumed to prevail during both the temperate and the glacial domains in the deposition holes experiencing the highest fluxes, as suggested as a pessimistic assumption in Section 10.4.6 and above.
- The groundwater cation concentration at the affected deposition holes is assumed to be 3 mM in the temperate domain (Section 10.3.6) and 0.1 mM in the glacial domain (Section 10.4.6).
- The flow rate is approximated as that of temperate conditions. This is pessimistic according to the averaging of flow related quantities over a glacial cycle discussed in section 10.4.6, see Figure 10-155.

For the base case semi-correlated hydrogeological DFN model and using the EFPC rejection criterion, then no deposition hole reaches advective conditions during the assumed total of 30 000 years of dilute conditions in the first 120 000 year glacial cycle (as already noted above). Summing the effect of temperate conditions for eight such cycles (a total of 240 000 years of temperate conditions) yields advective conditions in 3 deposition holes as the total effect of the temperate domain.

For the glacial domain, the corresponding number of deposition holes is 1 and 34 after one and eight glacial cycles, respectively.

Adding the erosion from the temperate and glacial domains (30 000 years of dilute water during temperate conditions and 30 000 during glacial conditions for each glacial cycle) yields advective conditions in 3 deposition holes after one glacial cycle and in 41 holes after eight cycles, see Table 10-31.

These positions are strongly related to those with the highest Darcy flux. Positions with the highest fluxes are also with high likelihood among the five percent of positions exposed to dilute groundwaters. Since the 41 positions are much less than the five percent of the 6000 positions assumed to be exposed to dilute water, further efforts to reduce the estimate of five percent being exposed to dilute groundwater would not readily yield any further reduction in the number of advective positions due to erosion.

Sedimentation

For the sedimentation process, it is noted that an assumption of dilute conditions in up to 5 percent of the deposition holes during half the glacial cycle is seen as a cautious approach. For the sedimentation process *per se*, the flow conditions are not relevant, but so are the fracture aperture and angle as noted in Section 10.3.11. Using the model discussed in Section 10.3.11 with aperture data from the base case of the semi-correlated hydrogeological model for Forsmark and with a J_{Exp} -value of 30 kg/m²/yr yields advective conditions in 2 deposition holes after a full glacial cycle and in all of the about 5 percent of the holes exposed to dilute conditions, i.e. about 300 holes, after 10⁶ years, see Table 10-31. Using instead the more pessimistic J_{Exp} -value of 1000 kg/m²/yr yields advective conditions in all the 300 holes already during the first full glacial cycle. It is clear that an assessment based on the current limited knowledge of buffer sedimentation yields considerably more buffer loss than the chemical erosion process.

As also found in Section 10.3.11 none of the tunnel intersecting single fractures will cause erosion of the backfill to the extent that it loses so much swelling pressure that advective conditions must be assumed in underlying deposition holes. For a few positions where the tunnel is intersected by a deformation zone, potentially more than 220 tonnes could be lost, but this is not relevant from the point of view of canister integrity since no deposition holes will be located there.

In conclusion, the quantitative evaluations of the erosion process indicate that substantial losses, affecting several of the buffer safety functions negatively, are expected to occur in a few single deposition holes during the first 120 000-year reference glacial cycle, and in a few tens of deposition holes in a million year perspective assuming exposure to dilute groundwater 50 percent of the time. For the sedimentation process, the pessimistic approach taken here indicates that most of the 300 deposition positions estimated to ever be in contact with dilute water could be affected, in the most pessimistic setting already during the first glacial cycle. The buffer erosion and sedimentation calculations are integrated with the calculations of canister corrosion in a million year perspective, see Section 10.4.9, and, in the case of resulting canister failures, to calculations of radionuclide transport in Chapter 13.

Table 10-31. Number of deposition positions estimated to reach advective conditions due to erosion and to sedimentation during one and eight glacial cycles. The numbers are capped at 300 since this is the number of deposition holes expected to ever experience dilute conditions during a glacial cycle.

	Erosion	Sedimentation $J_{Exp} = 30 \text{ kg/m}^2/\text{yr}$	Sedimentation $J_{Exp} = 1000 \text{ kg/m}^2/\text{yr}$
One reference glacial cycle	3	2	~300
Eight reference glacial cycles	41	~300	~300

Liquefaction

Liquefaction, as observed in loose clay and sand, cannot take place in a bentonite with high density, since the effective stress that holds the clay together is high due to the swelling pressure. Furthermore, the **Buffer, backfill and closure process report**, Section 3.4.2, conclusively rules out that a very high hydrostatic pressure during a reference glacial event could reduce the effective stress (swelling pressure) of the buffer to zero. Pressure increases resulting from earthquakes have been demonstrated as not being able to cause liquefaction in the buffer (see the **Buffer, backfill and closure process report**, Section 3.4.2).

Effects of saline water on buffer and backfill

Hydraulic conductivity and swelling pressure of the buffer and backfill, as affected by different groundwater salinities are presented in Section 10.3.9. The conclusion is that the hydraulic properties of the buffer will not be significantly affected by the intrusion of saline water. The conclusions in that section are valid at chloride concentrations of up to 3 M (17.5 % NaCl). The highest expected value at Forsmark is a salinity of TDS = 20 g/L, i.e. about 2 percent, as a consequence of the upconing of deep saline waters when the ice front margin is located on top of the repository, see Section 10.4.7.

Mechanical effects of increased flow

For the case where there are strong hydraulic gradients in a fracture intersecting a deposition hole, it could be imagined that buffer could be lost by shearing of particles from the bentonite gel by seeping water. For physical shearing the cohesiveness of the gel has to be overcome by the friction force on the gel. The yield stress of the gel and the shear stress of the water will determine when this mechanism is active. The non-Newtonian properties, especially the Bingham yield stress must be quantified. Neretnieks et al. (2009) presents a model for the shear stress as a function of the hydraulic gradient and fracture aperture. Figure 10-163 shows the shear stress as a function of the hydraulic gradient based on the output from hydrogeological modelling of the glacial Base case in SR-Site, see Table 10-28 in Section 10.4.6, and aperture.

It is seen from the figure that that even for a gradient as high as 10 % and a large fracture aperture as 1 mm, the shear stress is no more than 0.5 N/m² (0.5 Pa). This is a very low shear stress and is less than the yield stress of cohesive gels as found by Birgersson et al. (2009). They found that the shear strength of MX-80 at a water ratio of 100 ($\phi = 0.0037$) for sodium concentrations of 10 and 100 mM is larger than 5 Pa. This is the concentration range where the gel is expected to be cohesive. Even in distilled water the shear strength is larger than 1 Pa for water ratios below 40 (Birgersson et al. 2009). The mean aperture is also expected to be much less than 1 mm.

The hydrogeological modelling of the “expanding ice front” case in SR-Site shows a similar picture to what is presented by Neretnieks et al. (2009). According to Figure 10-163 the calculated shear stresses are always below 5 Pa and much lower most of the time. It can thus be concluded that the loss of bentonite from shearing of particles can be neglected for all reasonable conditions.

Bentonite particles eroded/sedimented from the buffer/backfill for groundwater charge concentrations below 8 mM could potentially clog fractures and thereby restrict groundwater flow in the vicinity of the repository. Such effects on groundwater flow are pessimistically disregarded since there is currently no robust way of addressing the issue.

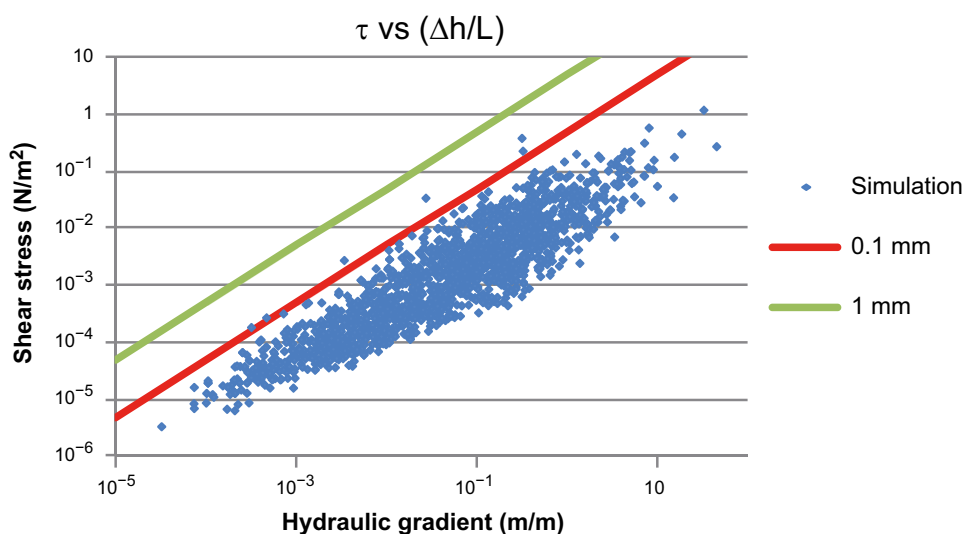


Figure 10-163. Plot of the shear stress at gel/water interface during glaciation as a function of hydraulic gradient for two different aperture values (0.1 mm and 1 mm) using a model in Neretnieks et al. (2009) together with data from Vidstrand et al. (2010). (Selroos and Follin 2010).

Identified uncertainties and their handling in the subsequent analysis

In the reference evolution, no component of the repository will be exposed to freezing temperatures. At some level the backfill in the ramp and shaft and the borehole seals will be exposed to freezing conditions. This however, is not expected to have any negative effects on repository performance. Uncertainties regarding detrimental buffer freezing are further evaluated in a dedicated scenario, Section 12.3.

The quantitative evaluations of the erosion process indicate that substantial losses, affecting several of the buffer safety functions negatively, cannot be ruled out, for less than 2 percent of the deposition holes during the 120 000-year reference glacial cycle. These effects are propagated to calculations of canister corrosion and, in the case of resulting canister failures, to calculations of radionuclide transport.

The loss of bentonite from shearing of particles can be neglected for all reasonable conditions and such effects are therefore not propagated to further analyses.

10.4.9 Effects on canister

Canister failure due to isostatic load

The maximum expected isostatic load on the canister at the Forsmark site is 4.5 MPa hydrostatic pressure, up to 10 MPa isostatic swelling pressure from the bentonite (see Section 5.5.3) and a maximum addition of 26 MPa hydrostatic pressure from a future ice sheet in the reference glacial cycle, see Section 10.4.1. The maximum total isostatic pressure the canister will be subjected to can thus be estimated to be 40.5 MPa. This is less than the design load of 50 MPa. A probabilistic analysis for the BWR insert shows that the risk of failure of the insert is low up to the design pressure of 50 MPa (Dillström 2019). Even at a pressure of 75 MPa (Jonsson et al. 2018), the probability of failure was calculated to be 1×10^{-14} . Copper creep for expected maximum isostatic pressures has been analysed by Hernelind (2015, 2019) and found to not jeopardize canister integrity. A more extensive assessment of creep under isostatic load is given in Section 12.7.5.

As described above and in Section 5.4.3, the probability that the canister would not fulfil the technical design requirements related to isostatic loads is deemed as insignificant. It can thus be concluded that no canisters will fail due to isostatic load, and that the safety function Can2 in Figure 10-2 will not be threatened.

Canister failure due to shear loads

This failure mode is treated in Section 10.4.5.

Canister corrosion for diffusive conditions

In Section 10.3.13, it was concluded that, for an intact buffer, corrosion has an insignificant impact on the copper canister thickness in a 120 000 year perspective, if groundwater flow rates and sulphide concentrations for temperate climate conditions are assumed.

According to Section 10.4.7, sulphide concentrations are expected to be similar or lower for periglacial or glacial conditions compared to those for temperate conditions used in Section 10.3.13. According to Section 10.4.6, the hydrogeological entity controlling the transport of corroding species from the groundwater to the buffer, $q^{1/2}$, is, when averaged over the reference glacial cycle, less than the values for temperate conditions used in Section 10.3.13.

It is thus concluded that corrosion has an insignificant impact on the copper canister thickness in a 120 000 year perspective when variations in geochemical and hydrogeological conditions during the 120 000 year reference glacial cycle are taken into account.

Canister corrosion for a partially eroded buffer

The quantitative evaluations of the hydrogeological evolution cited in Section 10.4.8 indicate that exposure of the buffer to dilute groundwater such that buffer erosion and sedimentation must be considered may occur in the 5 percent of the deposition holes with the highest groundwater flow

rates during the 120 000-year glacial cycle and for up to 50 percent of the time. As demonstrated in Section 10.4.8, in a small fraction of these deposition holes, buffer may be lost to the extent that advective conditions arise. For corrosion when advection occurs in the buffer, Neretnieks (2006b), supplemented by the Appendix to Neretnieks et al. (2010) concluded that, for a very wide range of such conditions the equivalent flow rate, Q_{eq} , used for assessing the migration of corroding agents from the groundwater to the canister should be replaced by q , the water flux through the part of the fracture that intersects the deposition hole. In addition, the water flux is increased due to the lost flow resistance in the void arising from the missing bentonite. Neretnieks (2006b) demonstrated that this effect can be bounded by multiplying the undisturbed flow by a factor of 2.

The rate of corrosion will also depend on the geometry of the eroded buffer section, and in particular on the area of the canister exposed to groundwater, where a smaller area yields a higher corrosion rate. If buffer erosion occurs, it is also likely to continue after part of the canister surface is first exposed, meaning that the exposed area will grow with time. (Also, the erosion rate is expected to increase once a cavity is formed in the deposition hole since the outward transport of clay in solution is more efficient from a cavity than from a fracture, see Section 10.3.11.) It is cautiously assumed that the height of the exposed canister surface is equal to the buffer thickness, $d_{buff} = 0.35$ m, and that this situation does not change with time. The exposed height is set equal to the buffer thickness since buffer is lost to a fracture intersecting the deposition hole and the material for this loss is transported from all directions in the deposition hole, meaning that the eroded volume should be roughly equal in height and depth when the canister is first exposed. Furthermore, buffer loss is assumed along half the circumference of the deposition hole since the up-stream half of the fracture-deposition hole interface is most exposed to erosion. The exposed canister area, A_{corr} , is thus

$$A_{corr} = \pi \cdot r_{can} \cdot d_{buff}$$

where $r_{can} = 0.525$ m is the canister radius. For a more detailed discussion of the corrosion geometry and its uncertainty, see Section 12.6.2.

The copper shell thickness of 47 mm is assumed in these corrosion calculations. This is the reasonable minimum copper coverage derived from the experience of test manufacturing of the canisters. As stated in Table 5-9, one percent of the canisters could though have a minimum copper coverage of 45–47.5 mm after machining. As mentioned in Section 10.2.5, subsection “*Canister corrosion*”, corrosion by atmospheric oxygen before emplacement and from initially entrapped oxygen after emplacement, is expected to cause corrosion depths less than 2.5 mm (including pits), and will thus have a small impact on the minimum copper coverage of the canisters. It is emphasized that adding the depth of the initial corrosion by O_2 with the long-term corrosion due to sulphide, is pessimistic for several reasons. First, the maximum corrosion depth due to entrapped O_2 was derived under the assumption that all O_2 entrapped in the buffer and backfill is consumed by corrosion of copper canisters, while it is likely that at least part of the O_2 in the backfill will be consumed by microbial activity and oxidation of clay and rock minerals before it has had time to diffuse to the deposition holes. Second, it is further pessimistic to assume that the deepest pits predicted probabilistically during the initially aerobic conditions, would coincide with the location of the initiation of the sulphide corrosion.

Furthermore, it is also pessimistic to simply add the corrosion depth caused by O_2 and sulphide, since the sulphidation of Cu_2O to Cu_2S , could act as a transient phase and delay the initiation of the sulphide corrosion. Due to the pessimism invoked both in the derivation of the limit of 2.5 mm corrosion due to entrapped O_2 and its combination with long-term sulphide corrosion, this is not accounted for in the assessment of corrosion here in the reference evolution. Instead, the effect of reducing the initial thickness of the copper shell by 2.5 mm is evaluated as part of the sensitivity analysis made in Section 12.6.2. As further mentioned in Section 10.2.5, subsection “*Canister corrosion*”, corrosion from sulphide produced from hydrogen from corrosion of rock reinforcements made of iron and steel in the deposition tunnels, is evaluated with a mass balance approach to give a maximum corrosion depth of 4 mm. This is highly pessimistic as it disregards any transport (of hydrogen to the location of microbes and sulphide to the canister), as well as precipitation of sulphide with oxidised iron formed in the corrosion process giving hydrogen. Due to these pessimisms this process is not accounted for in the assessment of corrosion here in the reference evolution. In the same way as for the corrosion for initially entrapped oxygen, instead the effect of reducing the initial thickness of the copper shell by 4 mm is evaluated as part of the sensitivity analysis made in Section 12.6.2.

A distribution of sulphide concentrations for present conditions was derived in Section 10.3.7 and it was argued that this distribution can be expected to persist during temperate climate conditions. The values include the potential contribution from methane and hydrogen as nutrients for sulphate reducing bacteria. The dissolved organic carbon is not expected to influence the sulphide concentration in the groundwater.

As described in Section 10.4.7 there could be factors influencing, and in general lowering, the sulphide concentration during other climate conditions but these are difficult to quantify. The overall conclusion is that it is pessimistic to use present day sulphide concentrations for other climate conditions. The observed distribution of sulphide concentrations at the Forsmark site at present is thus used in the corrosion calculations, see Figure 10-42.

As stated in Section 10.4.6, the time averaged flow, q , over the reference glacial cycle is about 80 percent of the values for temperate conditions. This is pessimistically disregarded in the erosion/corrosion calculations, where temperate climate flow rates are used throughout.

Erosion/sedimentation and subsequent corrosion is modelled probabilistically, using distributions of groundwater flow conditions from the hydrogeological DFN modelling and the sulphide distribution for temperate conditions. The corrosion rate distribution for the semi-correlated base case of the hydrogeological DFN model and assuming advective conditions in all deposition holes remaining after rejection according to the EFPC criterion, is given in Figure 10-164. Here, a sulphide concentration of 10^{-5} M is assumed in all deposition holes and all incoming sulphide is assumed to attack the exposed canister surface. Also the result when disregarding EFPC rejection is shown in the figure.

In the combined buffer loss/corrosion calculations the time to canister failure is calculated by adding the corrosion time to the time required to reach advective conditions for each deposition hole with its specific flow and for a sulphide concentration randomly sampled from the sulphide distribution. The central output is the mean number of failed canisters at one million years and a list of failure times and canister positions resulting from the combination of canister specific flow rates with the sampled sulphide concentrations.

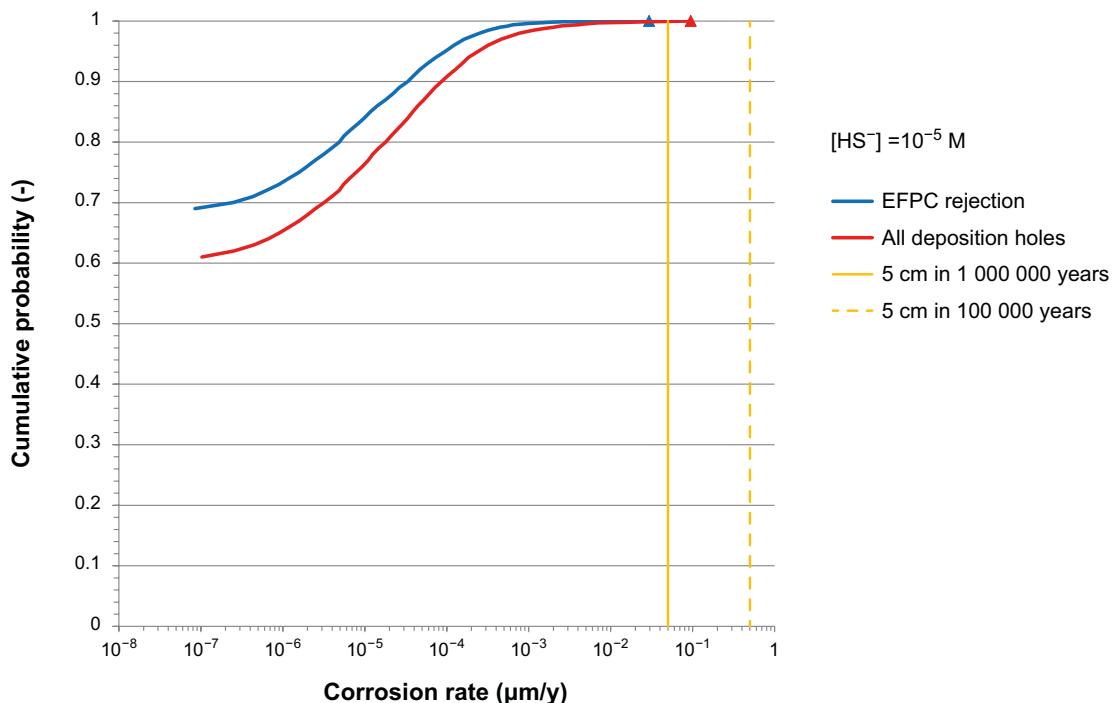


Figure 10-164. Distribution of corrosion rates for the base case semi-correlated hydrogeological DFN model assuming advective conditions. The vertical lines indicate the corrosion rates that correspond to corrosion of 47 mm copper in 10^5 (dashed line) and 10^6 (solid line) years respectively.

In a base case calculation, the semi-correlated base case of the hydrogeological DFN model, deposition hole rejection according to the EFPC criterion, the sulphide concentration distribution for temperate climate conditions and the cautious corrosion geometry are used. This yields a mean number of failed canisters of 0.083 at one million years when the sulphide distribution is randomly combined with the flow rates for all the deposition holes. Only four deposition holes have sufficiently high flow rates for failure to occur within one million years and for all four, the highest concentration of sulphide in the set of discrete values, 1.2×10^{-4} M, is required. The description of the calculation procedures is elaborated in Lilja and Puigdomenech (2012).

Table 10-32 shows the erosion and corrosion times for the four canister positions that could fail within 10^6 years for the base case calculation. It can be seen from the table that the erosion and corrosion times are comparable for this highest sulphide concentration. For lower sulphide concentrations the corrosion times will increase, and thus largely determine the failure times.

If all ten available realisations of the semi-correlated hydrogeological DFN model are evaluated, on average 0.094 canisters fail within one million years. The same calculation with the five realisations of the uncorrelated and correlated hydrogeological DFN models yield on average 0.53 and 0.61 failed canisters, respectively. It is also noted that assuming advective conditions initially in all deposition holes leads to increases of less than a factor of two in the mean number of failed canisters, i.e. uncertainties in the extent of buffer erosion cannot lead to significantly increased occurrences of corrosion failures. For e.g. the semi-correlated hydrogeological DFN model, the mean number of canister failures is 0.13 if advective conditions are assumed initially in all deposition holes. This also puts a strict upper bound on the effects of buffer sedimentation, where the experimental and theoretical understanding is currently less well developed.

More extensive corrosion calculations, including sensitivities to additional factors are given in the corrosion scenario, Section 12.6.2. Documentation of all calculations of buffer loss and subsequent canister corrosion under advective conditions is given in Hedin (2021).

In conclusion, on average less than one canister may fail due to dilute groundwater causing advective conditions in the deposition holes over the entire 10^6 year assessment period. Further assessments of corrosion, including additional sensitivity analyses are made in the corrosion scenario, Section 12.6.

Table 10-32. Flow rate, erosion, corrosion and failure time for the 4 canister positions, that fail within 10^6 years, for the base case of the semi-correlated hydrogeological DFN model and after applying the EFPC criterion. The figures are model data output, with the possible failures sorted with the earliest time listed first. In this case, failures within 10^6 years only occur for the highest sulphide concentration in the distribution, 1.2×10^{-4} M.

Dep. hole ID in DFN hydro model	Flow rate [m ³ /yr]	Erosion time [yr]	Corrosion time [yr]	Failure time [yr]
1978	0.144	49 027	140 414	189 442
411	0.161	60 933	132 880	193 813
6875	0.084	62 927	188 485	251 412
401	0.026	164 551	607 395	771 947

Canister corrosion due to oxygen penetration

As discussed in Section 10.4.7, reducing conditions will prevail in the deposition holes of the repository, during the entire glacial cycle. There is thus no further corrosion caused by oxygen in the analysis of the reference evolution.

Identified uncertainties and their handling in the subsequent analysis

In addition to failure caused by shear movements on fractures intersecting deposition holes, see Section 10.4.5, the only reason for canister failure during the remaining part of the reference glacial cycle is by corrosion due to dilute groundwater causing advective conditions in deposition holes. As further elaborated in the corrosion scenario, Section 12.6, up to around one canister may fail over the

entire 10^6 year assessment period for this reason. The results from the erosion/corrosion calculations in the corrosion scenario are further transferred to the radionuclide transport calculations, giving the time needed for erosion and corrosion specifically for each deposition hole and for each sulphide concentration.

10.4.10 Evolution of other parts of the repository system

Except for freezing of the ramp, shaft and borehole seals, see Section 10.4.8, other repository components are not expected to be affected by the conditions imposed by the remaining part of the reference glacial cycle.

10.4.11 Safety functions at the end of the reference glacial cycle

The following is an account of the development of all safety functions in Figure 10-2 during the reference glacial cycle.

Rock safety functions

R1. Provide chemically favourable conditions

a) Reducing conditions; Eh limited.

The reducing conditions during the initial temperate period are expected to continue to exist throughout the reference glacial cycle. The only identified challenge to this conclusion concerns the possible penetration of oxygenated glacial melt water to repository depth for glacial phases with enhanced groundwater flow. Based on observations and results from pessimistic modelling efforts, oxygen intrusion to repository depth in highly transmissive deformation zones cannot be discarded. Model results indicate that hundreds of years of the worst glacial situation would be needed for oxygen to reach the canisters in the repository. Therefore it is concluded that reducing conditions will prevail in the repository throughout the reference evolution.

b) Salinity; TDS limited.

For temperate climate conditions during the reference glacial cycle, the salinity is not expected to exceed that of the initial temperate period, i.e. the salinities are well within the ranges where the buffer and backfill have favourable properties.

For periglacial conditions, freeze out of salt above the repository may increase the groundwater salinity at repository depth, but the concentration of salt at repository level due to out-freezing will not become high enough to lower the swelling pressure of the buffer and the backfill, among other reasons because of the downward gravity-driven flow of saline waters. This situation will not be changed during permafrost decay as a transition to a temperate climate period occurs.

Upconing of deep saline groundwaters during the glacial period is not expected to affect the swelling capacity of the backfill. The highest expected value at Forsmark is a salinity of TDS = 20 g/L, i.e. about 2 percent, as a consequence of the upconing of deep saline waters when the ice sheet margin is located on top of the repository.

c) Ionic strength; $\Sigma q[M^{q+}] > 8$ mM charge equivalent.

For the glacial period, slightly more than 3 percent of deposition hole locations could experience dilute conditions during a period with an advancing ice front whereas only slightly less than 2 percent of the deposition holes could experience dilute conditions during an assumed period of 100 000 years corresponding to glacial maximum conditions. Also, as seen in Figure 10-33, even after 60 000 years of temperate climate conditions less than 1 percent of the deposition hole locations would have reached dilute conditions in 1 percent. For periglacial conditions, all results indicate that groundwaters below permafrost will not become more diluted than under temperate conditions. Rather, saline waters may move downwards within conductive fracture zones. Thus the charge concentration of cations is expected to increase during periglacial periods. Finally, the hydrogeological analysis indicates that salinities are more or less restored during a glacial cycle. The low salinities, i.e. dilute conditions, are mainly found in conjunction with glacial margin passages. This means that less than 2 percent of the deposition hole positions may have dilute conditions during a reference glacial cycle, and they will only have these conditions for a fraction of the time.

- d) Concentrations of HS^- , H_2 , CH_4 organic C, K^+ and Fe; limited.

Other components, such as bicarbonate, potassium, iron sulphide, etc. that are controlled by relatively fast chemical reactions are expected to remain mostly unaffected by periglacial conditions. These components will also be less affected by glacial conditions, although all the results points towards more dilute waters and hence lower concentrations of these components. Therefore the concentrations of K, HS^- and Fe will remain limited. This means that the potassium concentrations are expected to remain ≤ 0.004 mol/L, sulphide concentrations are expected to be $\leq 10^{-5}$ mol/L for most deposition positions and iron concentrations are expected to gradually increase up to 10^{-4} mol/L. Dissolved organic carbon, methane and hydrogen during periglacial periods will remain at the same levels as during temperate periods, but they are expected to decrease during glacial periods due to the overall dilution by melt waters depleted in these components. For the same reason sulphide concentrations and microbial sulphate reduction will be lower during glacial periods, but they are expected to return to present levels observed at Forsmark after a short submerged period under brackish marine waters.

- e) pH 5–11.

pH is controlled by relatively fast chemical reactions and expected to remain mostly unaffected by permafrost and will also be less affected by the glacial conditions, although all the evidence points towards dilute waters with relatively high pH. The effect of grout in fractures will be to increase the pH in deformation zones for relatively long periods of time. It is expected that, with time, the pH will progressively homogenise with the values found in surrounding parts of the rock.

- f) Avoid chloride assisted corrosion; combinations of pH and $[\text{Cl}^-]$ below limiting curve.

The hydrogeochemical analysis shows that this safety function indicator criterion is fulfilled throughout the assessed period.

R2. Provide favourable hydrologic and transport conditions

The analyses of mechanical evolution for the reference glacial cycle have not given rise to any results that imply any significant change of fracture transmissivity or new fracturing at repository depth. The transmissivity increases due to reactivation of fractures during the forebulge period of the glacial cycle are relatively moderate, apart from the transmissivity increase that would occur for fractures close to and parallel to the tunnel floor. However, this case is already covered by the assumptions made for the EDZ. Hydraulic jacking below 200 m depth, due to the impacts of glacial conditions is judged highly unlikely. At shallower depths it may happen, and the highly transmissive gently dipping fractures near surface at Forsmark is evidence of this occurring in the past (e.g. Hall et al. 2019). Given the already very high, and potentially jacking-induced, near surface horizontal permeability, this effect is already captured in the hydrogeological models used and the phenomenon is excluded from further analysis.

Pessimistically, it is also assumed that if a fracture shears more than 5 cm in a deposition hole, i.e. potentially causing a canister failure, that fracture is assumed to have such large transmissivity that its transport resistance can be neglected.

While changes to the fractures are relatively small during the glacial cycle, there are dramatic effects from the changes of boundary conditions. The Darcy flux increases dramatically, some orders of magnitude, during the ice front passages during ice sheet advance and retreat, while the flux is generally below the temperate climate value during the phase when the repository is covered by ice. Darcy flux is lower, or at the same magnitude as for temperate climate conditions, during periglacial conditions. For submerged conditions, very low flows are expected.

- a) Transport resistance in fractures, F ; high.

Due to changing boundary conditions during the reference glacial cycle, the transport resistance decreases dramatically, some orders of magnitude, during the ice front passages during ice sheet advance and retreat, while it is generally above the temperate value during the phase when the repository is covered by ice. It is higher, or at the same magnitude as for temperate conditions, during permafrost. For submerged conditions, the transport resistance in fractures will be high.

- b) Equivalent flow rate at the buffer/rock interface, Q_{eq} ; low.

No significant changes of the fracturing close to deposition holes are expected during the reference glacial cycle, but the equivalent flow rate will change due to the changing flow boundary conditions during the glacial cycle. It increases dramatically, up to between one and two orders of magnitude, during the ice front passages during ice sheet advance and retreat, while it is generally below the temperate climate value during the phase when the repository is covered by ice. It is below, or at the same magnitude as for temperate conditions, during periglacial conditions. For submerged conditions, very low flows are expected.

R3. Provide mechanically stable conditions

- a) GW pressure; limited.

For temperate climate conditions during the reference glacial cycle, the groundwater pressure is expected to be similar to that of the initial temperate period, i.e. around 4.5 MPa at repository depth at Forsmark.

For periglacial, unglaciated conditions, the same groundwater pressure as for temperate conditions is expected.

For glacial conditions, the maximum groundwater pressure is determined by the thickness of the overlying ice sheet. In the reference glacial cycle, the maximum thickness at Forsmark (ca 2900 m) corresponds to an increase in groundwater pressure of 26 MPa, yielding a total groundwater pressure of around 30 MPa. Furthermore, it is pessimistic to assume that the full ice burden is translated into groundwater pressure.

- b) Shear movements at deposition holes < 0.05 m.

Large earthquakes at Forsmark cannot be excluded within any of the safety assessment time frames. The impact of earthquakes, in terms of the number of canisters expected to be sheared 50 mm or more has here been quantified by using a range of earthquake frequency estimates, the Forsmark site description and by applying deposition hole rejection criteria. During a 120000 year long glacial cycle, it is estimated that between 8.3×10^{-4} and 5.7×10^{-3} canisters may fail. For the 1000000-year time frame, at maximum two seismic events are assumed and, using the most pessimistic way of accounting for the combined effects of both, between 8.1×10^{-3} and 6.9×10^{-2} canisters may be sheared 50 mm or more. As the numbers of failed canisters are substantially less than one, they can be interpreted as the probabilities of a canister failure occurring over the cited time frames.

- c) Shear velocity at deposition holes < 1 m/s

This criterion is upheld, as is further justified in Section 10.4.5.

R4. Provide thermally favourable conditions

For temperate climate conditions during the reference glacial cycle, the rock temperature is envisaged to be similar to that of the initial temperate period, i.e. well above 0 °C at Forsmark. As shown in Section 10.4.3, the 0 °C isotherm reaches a maximum depth of 250 m while the -4 °C isotherm reach a maximum depth of ~150 m in the reference glacial cycle. If also considering a quite unrealistic and most extreme combination of uncertainties, the uncertainty range for the perennially frozen ground reach a maximum depth of ~420 m and at the same time, the uncertainty range for the -4 °C isotherm reach a maximum depth of ~320 m. These results conclusively show that the -4 °C isotherm does not reach repository depth in the reference glacial cycle and since the uncertainty interval for the perennially frozen ground does not reach 450 m depth, even in this most extreme combination of all uncertainties, freezing of groundwater at repository depth is excluded in the reference glacial cycle. In this most extreme situation, the lowest temperature at the 450 and 470 m depths are approximately -0.5 °C and 0 °C respectively. For periods with glacial conditions, the ice sheet acts to insulate the bedrock from the low air temperatures, meaning that permafrost depths are smaller than for periglacial conditions.

- a) Temperature > -6 °C (avoid detrimental effects of buffer freezing)

The thermal modelling shows that this safety function is fulfilled for the reference glacial cycle.

b) Temperature $> 0\text{ }^{\circ}\text{C}$ (validity of can shear analysis)

When not considering the uncertainties related to permafrost growth, the bedrock temperature is well above $0\text{ }^{\circ}\text{C}$ for the reference glacial cycle. In the case of the most extreme, and quite unrealistic, combination of uncertainties related to permafrost growth, the bedrock temperature at repository level may have a temperature marginally below $0\text{ }^{\circ}\text{C}$. However, since this case is considered unrealistic it is anyway judged that the safety function is upheld for the reference glacial cycle. Furthermore, during the first glacial cycle after deposition the residual heat in the spent fuel implies that the temperature in the buffer and inside the canister will be higher than in the rock for at least the first 100 000 years, see e.g. Figure 10-16.

Buffer safety functions

For the initial temperate period, it was concluded that the dry buffer density in deposition holes where piping does not occur will be in the interval allowed for the initial state, i.e. $1\,450\text{--}1\,560\text{ kg/m}^3$ around the canister.

Up to 5 percent of deposition hole positions may experience dilute conditions during a reference glacial cycle, although only for a limited part of the time. Assuming that these positions coincide with the positions of the highest flow, only one out of 6 000 deposition holes is calculated to also lose buffer mass due to erosion to the extent that advective conditions must be assumed during the 120 000 year reference glacial cycle. For the most pessimistic assessment of mass loss due to sedimentation, all the 5 percent of the deposition positions experiencing dilute conditions could become advective.

Buff1. Limit advective transport

a) Hydraulic conductivity $< 10^{-12}\text{ m/s}$

For deposition holes within the initially allowed buffer density range, the hydraulic conductivity criterion is fulfilled with ample margin, also for groundwater salinities that can be expected during the reference glacial cycle, see Section 10.4.8. For a deposition hole that has experienced loss of buffer mass due to erosion/colloid release and to the extent that advective conditions prevail, this safety function can, however, not be guaranteed.

b) Swelling pressure $> 1\text{ MPa}$.

For deposition holes within the initially allowed buffer density range, the swelling pressure criterion is fulfilled with ample margin, also for groundwater salinities that can be expected during the reference glacial cycle, see Section 10.4.8. For a deposition hole that has experienced loss of buffer mass due to erosion/colloid release and to the extent that advective conditions prevail, this safety function can, however, not be guaranteed.

Buff2. Reduce microbial activity

For this safety function to be fulfilled it is required that the saturated buffer density is higher than 1850 kg/m^3 for the MX-80 reference material. For deposition holes within the initially allowed buffer density range, this safety function is fulfilled.

For a deposition hole that has experienced substantial loss of buffer mass due to erosion/colloid release, this safety function can, however, not be guaranteed.

Buff3. Damp rock shear

For this safety function to be fulfilled it is required that the buffer has a maximum dry density yielding an unconfined compressive strength at failure $< 4\text{ MPa}$ at a deformation rate of $0.8\text{ } \%/ \text{min}$. According to Figure 6-5 in Svensson et al. (2019) 4 MPa is reached for MX-80 at a dry density of around $1\,640\text{ kg/m}^3$ which is substantially higher than the installed density. No relevant processes that would increase the buffer density have been identified, so it is concluded that this safety function is fulfilled for all deposition holes.

Buff4. Resist transformation

For this safety function to be fulfilled, it is required that the buffer temperature is less than 100 °C. The peak buffer temperature will occur a few tens of years after deposition. At the start of the reference glacial (almost 10 000 years after deposition), the buffer temperature will be similar to that of the ambient, natural rock temperature. There is thus no conceivable way in which the buffer temperature could exceed 100 °C during the reference glacial cycle.

Buff5. Prevent canister sinking

For this safety function to be fulfilled, it is required that the buffer swelling pressure exceeds 0.2 MPa. For deposition holes within the initially allowed buffer density range, the swelling pressure criterion is fulfilled with ample margin, see above. For a deposition hole that has experienced loss of buffer mass due to erosion/colloid release and to the extent that advective conditions prevail, this safety function cannot be guaranteed. However, if advective conditions prevail, the fact that the canister sinks is of secondary importance.

Buff6. Limit pressure on canister and rock

a) Swelling pressure < 10 MPa

Since no process is identified where the buffer material will be added during the reference glacial cycle, the maximum swelling pressure criterion will be upheld.

b) Temperature > -6 °C.

As mentioned regarding the rock safety function R4 above, the criterion is expected to be fulfilled with ample margin for the reference glacial cycle.

Backfill safety functions

BF1. Counteract buffer expansion

For this safety function to be fulfilled it is required that the density of the backfill material is sufficiently high. As shown in Section 10.2.4, the largest possible erosion due to piping will be 1 640 kg. Erosion in the backfill will basically mean that material is redistributed within the tunnel itself. Considering the large mass of backfill in the tunnel a redistribution of 1 640 kg can be assumed to have no impact at all on the backfill performance.

Even if dilute conditions occur in some of the more transmissive single fractures intersecting deposition tunnel, during the first reference glacial cycle, none of them will cause erosion to the extent that this will result in such loss of swelling pressure above deposition holes that these in turn would enter an advective condition. For a few canister positions where the fracture is connected to a deformation zone, potentially more than 220 tonnes could be lost, but this is not relevant from the point of view of canister integrity.

Canister safety functions

Can1. Provide corrosion barrier

The only reason for canister failure due to corrosion during the remaining part of the reference glacial cycle is by corrosion for advective conditions in the deposition holes, caused by erosion of the buffer when exposed to dilute groundwaters. Up to around one canister may fail over the entire 10⁶ year assessment period for this reason. The results from the erosion/corrosion calculations are further transferred to the radionuclide transport calculations, giving the time needed for erosion and corrosion specifically for each deposition hole and for each sulphide concentration.

Can2. Withstand isostatic load

For this safety function to be fulfilled, it is required that the canister withstands isostatic loads above 50 MPa, Can2a. The fulfilment of this safety function is assured by the design of the canister, see Section 5.4.3 and the **Canister production report**. It may also be noted that the maximum expected

isostatic load on the canister at the Forsmark site is 4.5 MPa hydrostatic pressure, up to 10 MPa isostatic swelling pressure from the bentonite and a maximum additional 26 MPa hydrostatic pressure from a reference glacial cycle ice sheet in the Weichselian reference evolution. The maximum total isostatic pressure to which the canister will be subjected during the reference glacial cycle can thus be estimated to be 40.5 MPa.

The probability for local canister insert damage at 40.5 MPa over-pressure is vanishingly small, as demonstrated by probabilistic calculations, see Section 5.4.3. Furthermore, the criterion for failure is that a global collapse occurs, which is not expected for pressures below 100 MPa, see further Section 5.4.3. As a consequence, no canister failures are expected at the maximum over-pressure that could be experienced at the Forsmark site in the reference evolution.

Also, the copper shell must be resilient to creep deformation during the expected isostatic loads, Can2b. The mechanical modelling of the canister has shown this to be the case.

Related to Can2b, it is required that the hydrogen content of the copper shell is low, to ensure its ductile properties in the long term, Can2c. Bounding calculations have demonstrated negligible ingress of hydrogen in the copper material as a consequence of copper corrosion.

Can3. Withstand shear loads

Canister failures due to future earthquakes are avoided through the use of respect distances and acceptance criteria for deposition holes, adapted to the ability of the canister to resist loads from fracture shear movements. However, it cannot be fully ruled out that such failures will occur, see discussion of rock safety function R3b for estimates of the likelihood of such failures.

Conclusions for consequence calculations

The following conclusions for radionuclide transport can be drawn.

1. The only causes for canister failure that has not been ruled out for the reference glacial cycle are corrosion in a deposition hole with advective conditions and shearing due to a large earthquake. The likelihood of either of these types of failure during the first glacial cycle is low.
2. As for the initial temperate period, the EDZ developed during construction needs to be considered in the RN-transport analyses.
3. The hydrogeological analyses have provided distributions of F , t_w and Q_{eq} to be used in radionuclide transport calculations for temperate periods of the reference glacial cycle. For other climate periods (periglacial-, glacial- and submerged conditions), estimates of these quantities, in many cases as stylised examples, have been derived.
4. The geochemical assessments have provided geochemical conditions for which retention properties in the host rock for radionuclide transport can be derived.
5. The buffer and backfill assessments have provided buffer conditions for which retention properties in the buffer for radionuclide transport can be derived.
6. The effect of a partially eroded backfill needs to be evaluated in radionuclide transport calculations.
7. Spalling may affect the equivalent flow rates, Q_{eq} , in deposition holes.
8. pH increase from cement may affect geosphere retention in larger, grouted fractures, potentially throughout the reference glacial cycle.

10.5 Subsequent glacial cycles

For the reference climate evolution, the first reference glacial cycle is simply assumed to be repeated until the end of the one million year assessment period. This is also in line with suggestions given in SSM's General Guidance. With a cycle period of 120 000 years, this means about seven repetitions of the initial Weichselian glacial cycle, i.e. a total of eight such cycles.

Reversible phenomena like the thermal, hydrogeological and geochemical evolution of the bedrock are essentially expected to follow the cyclic variations of external conditions controlling them, see e.g. the discussion in Section 10.4.6 on the evolution of salinity during a glacial cycle and in Section 10.4.7 on the evolution of redox conditions during a glacial cycle. This is also the case for biosphere development at the site.

Irreversible phenomena like buffer erosion, canister corrosion and possibly earthquake-induced effects are essentially expected to occur to an extent eight times greater than that during the initial glacial cycle. Particular implications of this are listed below.

- Buffer mass loss caused by dilute groundwater that could be a significant phenomenon during the initial glacial cycle, has to be considered for subsequent glacial cycles. Essentially, eight times more erosion could be expected at the end of the one million year assessment period, whereas the extent of mass loss due to sedimentation would not progress beyond the maximum of 5 percent of deposition holes where this is pessimistically assessed to occur during the reference glacial cycle, since the same holes are expected to experience dilute conditions in later cycles.
- The evaluations of canister corrosion for the initial glacial cycle indicate that, for an unaltered buffer, corrosion would not cause canister failures even in a million year perspective. For a buffer that has been partially eroded to the extent that advective conditions must be assumed in the deposition hole on average less than one canister may fail over the entire 10^6 year assessment period for this reason.
- The analysis of canister failures due to earthquakes for the initial glacial cycle is extended to one million years. During a glacial cycle, it is estimated that between 8.3×10^{-4} and 5.7×10^{-3} canisters may fail. For the 1 000 000-year time frame, using the most pessimistic way of accounting for the combined effects of multiple earthquakes, it is estimated that between 8.1×10^{-3} and 6.9×10^{-2} canisters may be sheared 50 mm or more.

There are also phenomena like ion exchange in the buffer that could require millions of years to equilibrate with the average ionic contents of the groundwater over a glacial cycle. Furthermore, the residual power will affect the thermal conditions in the rock only during the initial glacial cycle. Thereafter, the thermal evolution is determined by naturally occurring phenomena.

10.5.1 Safety functions at the end of the assessment period

The following is an account of all safety functions in Figure 10-2 at the end of the one million year assessment time, often as a comparison to the situation after the initial glacial cycle reported in Section 10.4.11.

Rock safety functions

R1. Provide chemically favourable conditions

a) Reducing conditions; Eh limited

No challenges to the conclusion for the initial glacial cycle, that reducing conditions will prevail, have been identified. It is, therefore, concluded that reducing conditions will prevail throughout the assessment period.

b) Salinity; TDS limited.

Repetitions of the same pattern of variations as for the initial glacial cycle are expected, meaning that salinity levels will remain limited.

c) Ionic strength; $\Sigma q[M^{q+}] > 8$ mM charge equivalent.

Repetitions of the same pattern of variations as for the initial glacial cycle are expected, meaning that additional periods of temperate and glacial conditions where this safety function indicator is not fulfilled must be assumed.

d) Concentrations of HS^- , H_2 , CH_4 organic C, K^+ and Fe; limited.

Repetitions of the same pattern of variations as for the initial glacial cycle are expected, meaning that concentrations of K and Fe will remain limited and that sulphide concentrations are expected to be $\leq 10^{-5}$ mol/L for most deposition positions averaged over the time period.

- e) pH; pH 5–11.

Repetitions of the same pattern of natural variations as for the initial glacial cycle are expected, meaning that pH is not expected to exceed 10. Possibly, continued releases of leach water from grout, shotcrete and cement may exhibit pH-values of around 9 even after the initial glacial cycle.

- f) Avoid chloride assisted corrosion; combinations of pH and $[Cl^-]$ below limiting curve.

Repetitions of the same pattern of natural variations as for the initial glacial cycle are expected, which means that this safety function indicator criterion is fulfilled throughout the period.

R2. Provide favourable hydrologic and transport conditions

- a) Transport resistance in fractures, F ; high

Repetitions of the same pattern of variations of gradients and small alterations of fracture transmissivity for different glacial loads as for the initial glacial cycle are expected. This means that the variation in groundwater flow and thus in transport resistance of the initial glacial cycle will also be applicable for the subsequent glacial cycles.

- b) Equivalent flow rate in buffer/rock interface, Q_{eq} ; low.

Repetitions of the same pattern of variations of gradients and small alterations of fracture transmissivity for different glacial loads as for the initial glacial cycle are expected. This means that the variation in groundwater flow and thus in equivalent flow rate of the initial glacial cycle will also be applicable for the subsequent glacial cycles. However, in deposition holes where advective conditions need to be assumed, Q_{eq} should be replaced by the flow in the fracture intersecting the deposition hole, as further discussed in Section 10.4.9.

R3. Provide mechanically stable conditions

- a) GW pressure; limited.

Repetitions of the same pattern of variations as for the initial glacial cycle are expected, meaning that increased pressures will occur for glacial conditions. As for the initial glacial cycle, this yields maximum total groundwater pressures of around 30 MPa.

- b) Shear movements at deposition holes < 0.05 m.

For the 1 000 000-year time frame, using the most pessimistic way of accounting for the combined effects of multiple earthquakes, between 8.1×10^{-3} and 6.9×10^{-2} canisters may be sheared 50 mm or more.

- c) Shear velocity at deposition holes < 1 m/s.

As for the initial glacial cycle it is shown that shear velocities will stay below the 1 m/s limit.

R4. Provide thermally favourable conditions

Repetitions of the same pattern of variations as for the initial glacial cycle are envisaged. For the first glacial cycle it was shown that the -4 °C isotherm reaches a maximum depth of ~ 150 m and if also considering a quite unrealistic and most extreme combination of uncertainties, the uncertainty range for the perennially frozen ground reach a maximum depth of ~ 420 m and at the same time, the uncertainty range for the -4 °C isotherm reach a maximum depth of ~ 320 m. These results conclusively show that the -4 °C isotherm does not reach repository depth in the reference glacial cycle and since the uncertainty interval for the perennially frozen ground does not reach 450 m depth, even in this most extreme combination of all uncertainties, freezing of groundwater at repository depth is excluded in the reference glacial cycle. In this most extreme situation, the lowest temperatures at the 450 and 470 m depths are approximately -0.5 °C and 0 °C, respectively. For periods with glacial conditions, the ice sheet acts to insulate the bedrock from the low air temperatures, meaning that permafrost depths are smaller than for periglacial conditions.

- a) Temperature > -6 °C (avoid detrimental effects of buffer freezing).

This safety function is fulfilled, even considering that the maximum permafrost depths for the reference glacial cycle may increase by up to ca 40 m (see the **Climate report**, Section 4.5.3), when the residual power from the fuel does not counteract the development of permafrost after the initial glacial cycle.

- b) Temperature > 0 °C (validity of can shear analysis).

When not considering the uncertainties related to permafrost growth, the bedrock temperature is well above 0 °C during the first and all following safety assessment period glacial cycles. In the case of the most extreme, and quite unrealistic, combination of uncertainties related to permafrost growth, the bedrock temperature at repository level may have a temperature marginally below 0 °C. However, since this case is considered unrealistic it is anyway judged that the safety function is upheld for the entire assessment period of 1 million years.

Buffer safety functions

As for the initial glacial cycle, quantitative evaluations of the buffer erosion process indicate that substantial losses, affecting several of the buffer safety functions negatively, cannot be ruled out, potentially for a fraction of the deposition holes during the one million year assessment period. These potential losses would be higher than for the initial glacial cycle.

This influences the evaluation of several of the buffer safety function indicators, as discussed below.

Buff1. Limit advective transport

- a) Hydraulic conductivity $< 10^{-12}$ m/s.

For deposition holes within the accepted range of buffer density, the hydraulic conductivity criterion is fulfilled with ample margin, also for groundwater salinities that can be expected during the reference glacial cycle, see Section 10.4.8. For a deposition hole that has experienced loss of buffer mass due to erosion/colloid release and to the extent that advective conditions prevail, this safety function can, however, not be guaranteed.

- b) Swelling pressure > 1 MPa.

For deposition holes within the accepted range of buffer density, the swelling pressure criterion is fulfilled with ample margin, also for groundwater salinities that can be expected during the reference glacial cycle, see Section 10.4.8. For a deposition hole that has experienced loss of buffer mass due to erosion/colloid release and to the extent that advective conditions prevail, this safety function can, however, not be guaranteed.

Buff2. Reduce microbial activity

For this safety function to be fulfilled it is required that the buffer density is high.

For deposition holes within the accepted range of buffer density, this safety function is fulfilled.

For a deposition hole that has experienced substantial loss of buffer mass due to erosion/colloid release, this safety function can, however, not be guaranteed.

Buff3. Damp rock shear

For this safety function to be fulfilled it is required that the buffer has maximum dry density yielding an unconfined compressive strength at failure < 4 MPa at a deformation rate of 0.8 %/min. According to Figure 6-5 in Svensson et al. (2019) 4 MPa is reached for MX-80 at a dry density of around 1 640 kg/m³ which is substantially higher than the installed density. No relevant processes that would increase the buffer density have been identified, so it is concluded that this safety function is fulfilled for all deposition holes.

Buff4. Resist transformation

For this safety function to be fulfilled, it is required that the buffer temperature is less than 100 °C. As for the initial glacial cycle, there is no conceivable way in which the buffer temperature could exceed 100 °C during the assessment period.

Buff5. Prevent canister sinking

For this safety function to be fulfilled, it is required that the buffer swelling pressure exceeds 0.2 MPa.

For deposition holes within the acceptable buffer density range, the swelling pressure criterion is fulfilled with ample margin, see above.

For a deposition hole that has experienced loss of buffer mass due to erosion/colloid release and to the extent that advective conditions prevail, this safety function cannot be guaranteed. However, if advective conditions prevail, the fact that the canister sinks is of secondary importance since corrosion is already accelerated by advective conditions.

Buff6. Limit pressure on canister and rock

a) Swelling pressure < 10 MPa.

Since no process is identified where buffer material will be added during the future glacial cycles, this maximum swelling pressure criterion will be fulfilled.

b) Temperature > -6°.

As mentioned regarding the rock safety function R4, the criterion is expected to be fulfilled with ample margin.

Backfill safety functions

BF1. Counteract buffer expansion

Even though dilute conditions may occur in some of the more transmissive single fractures intersecting deposition tunnels, during the 10⁶ years assessment period, none of them will cause erosion to the extent that this will result in such loss of swelling pressure above deposition holes that these in turn would enter an advective condition. For a few positions where the fracture is connected to a deformation zone, potentially more than 220 tonnes could be lost, but this is not relevant from the point of view of canister integrity since 220 tonnes is a relatively small mass compared with the total mass of the backfill in a deposition tunnel.

Canister safety functions

Can1. Provide corrosion barrier

The only reason for canister failure due to corrosion during future glacial cycles is by corrosion for advective conditions in the deposition holes, caused by to erosion and/or sedimentation of the buffer when exposed to dilute groundwaters. On average less than one canister may fail over the entire 10⁶ year assessment period for this reason. The results from the erosion/sedimentation/corrosion calculations are further transferred to the radionuclide transport calculations, giving the time needed for erosion and corrosion specifically for each deposition hole and for each sulphide concentration.

Can2. Withstand isostatic load

Since repetitions of the maximum loads experienced during the initial glacial cycle are expected for the remainder of the assessment period, it is concluded that this safety function will be upheld also for the one million year assessment time.

Can3. Withstand shear loads

Canister failures due to future earthquakes are avoided through the use of respect distances and acceptance criteria for deposition holes, adapted to the ability of the canister to resist loads due to fracture shear movements. However, it cannot be fully ruled out that such failures will occur, see discussion of rock safety function R3b for estimates of likelihoods of such failures.

Conclusions for consequence calculations

The following conclusions for radionuclide transport can be drawn.

- One cause for canister failure that has not been ruled out for the one million year assessment period is an earthquake caused by changes in the glacial load. The likelihood of this type of failure is low, even when the entire assessment period is considered.
- Failure due to corrosion for advective conditions in a partially eroded buffer must be also considered for the one million year assessment time. On average less than one canister may fail due to this cause.
- All other conclusions regarding consequence calculations drawn for the initial glacial cycle, see Section 10.4.11, are also considered to be valid for repeated glacial cycles.

10.6 Global warming variant

10.6.1 External conditions

There is a large range of potential future climate developments when the combined effect of natural and anthropogenic climate change is considered. One such case is described in the present *Global warming variant*. This variant describes a future climate development influenced by both natural climate variability and climate change induced by anthropogenic emissions of greenhouse gases, with the latter resulting in moderate global warming. This climate case includes the effect of moderate global warming under medium anthropogenic greenhouse-gas emissions, comparable to the IPCC RCP4.5 emissions scenario (see the **Climate report**, Section 5.1 and Appendix E). In order to cover a reasonably broad array of warmer future climate developments based on present knowledge, the *extended global warming case* is also included in the PSAR. This climate case includes the effect of a strong and persistent global warming under high anthropogenic greenhouse-gas emissions, comparable to the RCP8.5 emission scenario (see the **Climate report**, Section 5.2 and Appendix E).

In the PSAR, there are two main reasons for analysing cases of climates warmer than the reference glacial cycle; i) modelling studies of the climate response to increased greenhouse gas emissions, mainly CO₂, indicate that global temperatures will increase in the future under such conditions (e.g. IPCC 2013), and ii) natural long-term climate cycles are believed to be driven mainly by changes in solar insolation (see the **Climate report**, Sections 5.1 and 5.2). The coming 100 000 year period is initially characterised by exceptionally small amplitudes of insolation variations (Berger 1978), suggesting that the present interglacial may be exceptionally long. By considering the known future changes in insolation, several studies (e.g. Loutre and Berger 2000, Berger and Loutre 2002, Lord et al. 2019) suggest that the interglacial may end ~50 000 years after present if atmospheric CO₂ concentrations remain relatively low. Given this insolation forcing, the results suggest that a growth of the Greenland-, Eurasian- and North American ice sheets would not start until after 50 000 years after present even without increased CO₂ levels (Liakka et al. 2021). For high future atmospheric CO₂ concentrations, most studies suggest that the current interglacial will last for another 100 000 years or longer.

In the global warming variant, it is assumed that the present temperate climate domain, albeit with higher initial air temperatures, will prevail for another 50 000 years before the relative mild onset of the next glacial cycle. To that end, the length of the current interglacial in the *global warming climate case* is pessimistically chosen to be shorter than suggested by most modelling studies under medium emissions (Liakka et al. 2021). After the initial 50 000 years of temperate climate domain,

the first 70 000 years of the reference glacial cycle is assumed to follow. Due to the coastal location of Forsmark, the surface conditions at the site are sensitive to changes in relative sea level and shore line position. Such changes are envisaged to follow from global warming, mainly by melting of ice sheets and glaciers and from thermal expansion of ocean water. At present, there are major uncertainties in the estimates of future sea level rise due to global warming. A major part of this uncertainty relates to the response of the cryosphere to increased temperatures. For detailed information on this, see the **Climate report**, Sections 5.1.3 and 5.2.3, and Pellikka et al. (2020). The above sections in the Climate report also present an up-to-date picture on how the Greenland and Antarctic ice sheets may respond to different degrees of global warming.

Pellikka et al. (2020) estimated extreme sea levels that could occur at the Forsmark site up to 2100 AD. The global mean sea level is projected to rise 0.20–2.90 m during this century due to thermal expansion of seawater and melting of land-based ice. The projections have large uncertainties, mainly related to the behaviour of the Antarctic and Greenland ice sheets in a warming climate. In Pellikka et al. (2020) an ensemble of different global mean sea level projections were combined into probability distributions of global mean sea level rise for RCP2.6 (low emissions), RCP4.5 (intermediate emissions), and RCP8.5 (high emissions). Due to gravitational and rotational effects, meltwater from decaying ice sheets are not distributed evenly over the oceans (e.g. Milne et al. 2009). This uneven geographical distribution of global sea level rise was taken into account when estimating the local sea level changes at Forsmark. The isostatic uplift of 0.67 m/century, counteracting the sea level rise, was also included in the projections. The 1 % to 99 % ranges of the projected relative sea level change at Forsmark from 2000 to 2100 AD are –0.57 to +0.12 m for RCP2.6, –0.51 to +0.74 m for RCP4.5, and –0.38 to +1.66 m for RCP8.5 (Pellikka et al. 2020). The study also presents storm surge level probability distributions for Forsmark up to 2100 AD.

The long-term sea level response to global warming, beyond 2100 AD, is naturally associated with major uncertainties, larger than the ones estimated for 2100 AD. It is clear that global sea level will continue to rise far beyond 2100 AD as a response to previous and continued global warming (**Climate report**, Sections 5.1.3 and 5.2.3 and references therein). Complete collapses of the Greenland and West Antarctic ice-sheets are suggested to contribute sea level rises around Fennoscandia of ~0 and ~3 m, respectively (with the 0 m value resulting from equal amounts of isostatic uplift and sea level rise). There are however major uncertainties related to the amount of global warming and the associated amount of ice-sheet disintegration, as well as on the timing of such events.

A compilation of selected global mean sea level projections from 2200 AD up to 12 000 AD for the global warming climate case (RCP4.5 emission scenario) is presented in the **Climate report** Section 5.1.3, Table 5-5. Figure 10-165 shows the sea level projections for the period 2200 to 12 000 AD from the data in the **Climate report**, Table 5-5, as well as the estimated isostatic uplift for the Forsmark site, and the resulting local changes in relative sea level (shore-line displacement).

The lowest sea level rise projection in Figure 10-165 (Levermann et al. 2013, lower blue line), together with the isostatic curve for the Forsmark site from GIA modelling (solid green line), results in the relative sea level curve shown by the lower solid red line. This continued lowering of relative sea level hence describes a future development with a sea regression, similar to today. On the other hand, the highest sea level rise projection in Figure 10-165 (Clark et al. 2016, upper dark blue line), together with the isostatic curve for Forsmark, results in the relative sea level curve shown by the upper solid red line. This line shows an initial major transgression at the Forsmark site, peaking at around 4500 AD at a level of +12.3 m. This is followed by a regression back to the present-day situation at around 9500 AD (Figure 10-165). The transgression thus results in a ~7 500 year long period with a higher relative sea level than at present for the highest sea level projection in the global warming climate case. To estimate the shortest time that a raised relative sea level could prevail, with this eustatic projection, a comparison is given with the linear development of isostatic uplift (hatched green line). The resulting relative sea level is shown by the hatched red line, showing that the period of raised relative sea level caused by the transgression will not end before ~7500 AD (Figure 10-165), given the highest eustatic projection. The areas that would be permanently flooded at around 4500 AD with a relative sea level rise of +12 m are shown in Figure 10-166.

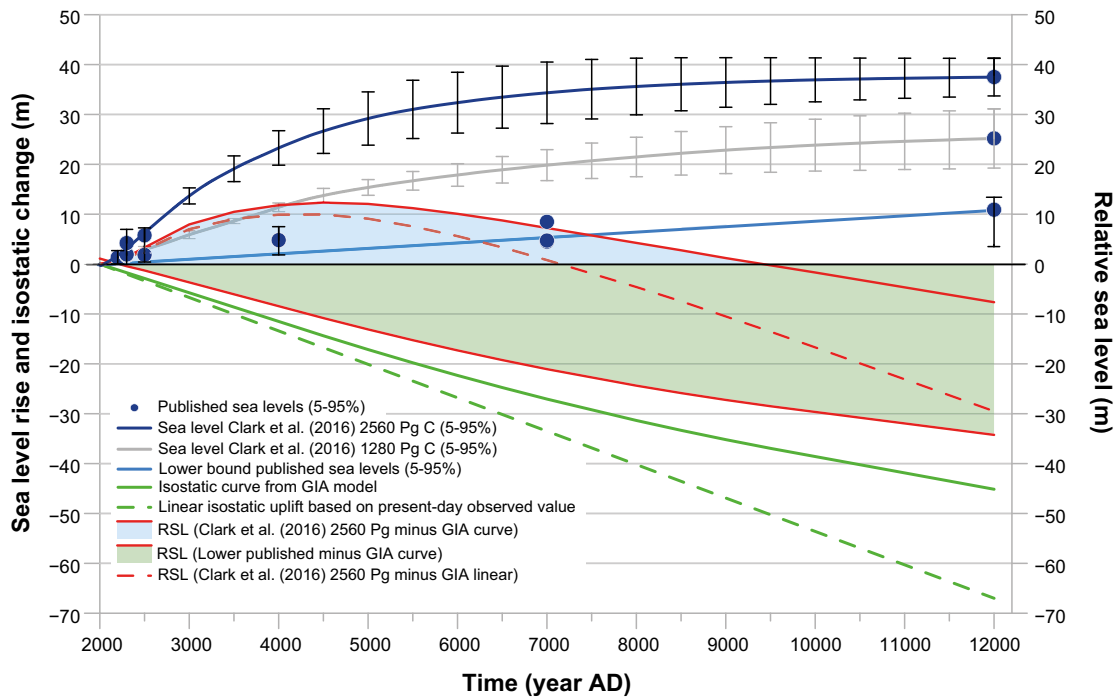


Figure 10-165. Mean sea level rise projections (blue dots) for the period 2200 to 12000 AD (from the Climate report, Section 5.1.3) for the global warming climate case (the IPCC RCP4.5 emission scenario). Median values are shown by blue dots whereas the 5–95 % confidence interval is shown by uncertainty bars. For the highest projected sea level at 12000 AD ($+37.5 \pm 3.8$ m from Clark et al. 2016), the projected sea level development leading up to the maximum level has also been plotted together with the 5–95 % confidence interval (upper dark blue line with black bars). The scenario by Clark et al. (2016) represents the highest long-term sea level projection, whereas Levermann et al. (2013) represents the lowest long-term sea level projection, both under the RCP4.5 emission scenario. The substantial difference between the highest and lowest projections is striking, clearly demonstrating the large uncertainty within the field of future sea level rise in a warming climate caused by moderate carbon emissions. The isostatic uplift rate for the Forsmark site as projected by GIA modelling (see the Climate report, Sections 3.3.4 and 5.1.3) is shown by the solid green line. The evolution of relative sea level at Forsmark, constituting the net effect of the eustatic changes (blue lines) and isostatic changes (green lines) for the global warming climate case are shown in red. The results show that the Forsmark site could either be subject to continued regression (relative sea level lowering) similar to today, or to a substantial transgression (relative sea level rise) shown by the lower and upper solid red lines respectively, depending on which projection of long-term global sea level rise is assumed.

All in all, this shows that the very large spread in long-term projections of future sea level rise for the RCP4.5 emission scenario could result in either a transgression (more than +12 m) at the Forsmark site, giving a higher-than-present relative sea level over the next 5000–7500 years (up until 7000–9500 AD), or at the other end of the uncertainty spectrum, a situation with continued regression at the site for the coming tens of thousands of years. Both evolutions over the coming 10000 years fit within the uncertainty range of long-term future sea level rise for the medium emission scenarios that form basis for the global warming climate case.

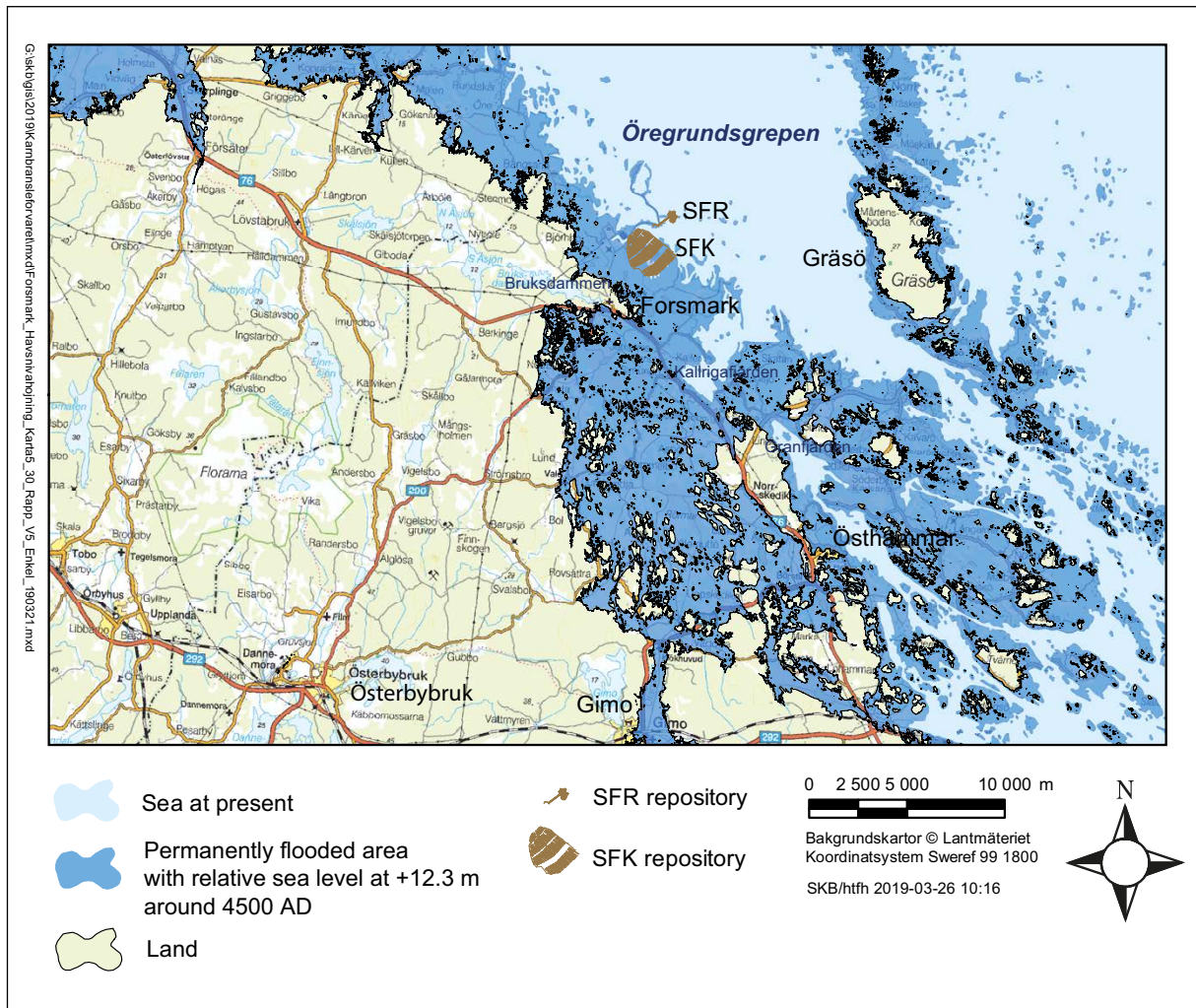


Figure 10-166. Areas in the Forsmark region that will be permanently flooded with a relative sea level at +12.3 m at around 4500 AD. This transgression results from the high long-term projection of global mean sea level rise of Clark et al. (2016) (see Figure 10-165 and the Climate report, Section 5.1.3).

The effects of sea level rise on the development of the Baltic shore level up to 120 000 years after present, under global warming conditions, were investigated by Global Isostatic Adjustment (GIA) modelling (see the **Climate report**, Sections 3.3.4 and 5.1.3). The resulting relative sea level curve from the GIA model was combined with empirical relative sea level data for the Holocene (based on the equations in Pässe and Daniels 2015; see the **Climate report**, Appendix D) in order to connect past relative sea level changes, from the deglaciation of Forsmark (at 10.8 ka BP) to the present-day and the future. In order to also account for the effects of global warming on the relative sea level at Forsmark for the next 120 000 years, the global mean sea level curves from Clark et al. (2016) and Levermann et al. (2013), see Figure 10-165, are added to the combined isostatic curve from GIA modelling and Pässe and Daniels (2015), see Figure 10-167.

The large uncertainties associated with the relative sea level projection for the coming 80, 10 000 and 120 000 years are discussed in detail in the **Climate report**, Section 5.1.3.

The succession of climate domains in the global warming variant of the reference evolution is shown in Figure 10-168. Given the assumption of a prolonged initial period of temperate climate conditions compared to the reference glacial cycle, the temperate climate domain is dominating. Submerged conditions may last for 0 up to 7 500 years (0 to ~6 % of the initial 120 000 years) reflecting the large uncertainty associated with the projected future relative sea level change (Figure 10-165). This means that the temperate climate domain prevails between ~73 500 and ~81 000 years (61 or 68 % of the time, respectively), the periglacial domain for ~28 000 years (23 % of the time) and the glacial domain for ~11 000 years (9 % of the time).

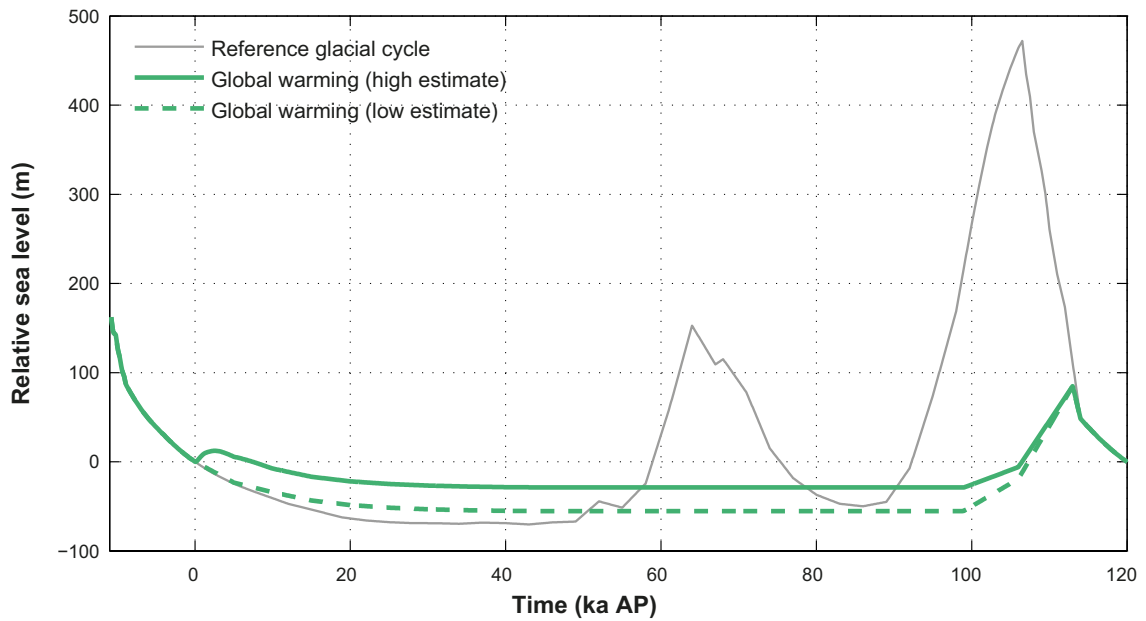


Figure 10-167. Relative sea level change at Forsmark for the global warming variant of the reference evolution, based on IPCC emission scenario RCP4.5 (green curves). For comparison, the corresponding curve for the reference glacial cycle (Section 10.4.1) is also shown (grey curve). The solid green curve represents the high-end relative sea level projection under moderate global warming, based on the highest global mean sea level projection until 12 000 AD (Clark et al. 2016 in Figure 10-165), whereas the dashed green curve represents the low-end relative sea level projection based on the lowest global mean sea level projection until 12 000 AD (Levermann et al. 2013 in Figure 10-165), also under moderate global warming. Negative numbers indicate that the area is situated above the contemporary sea level. Uncertainties in future shore level are discussed in the text.

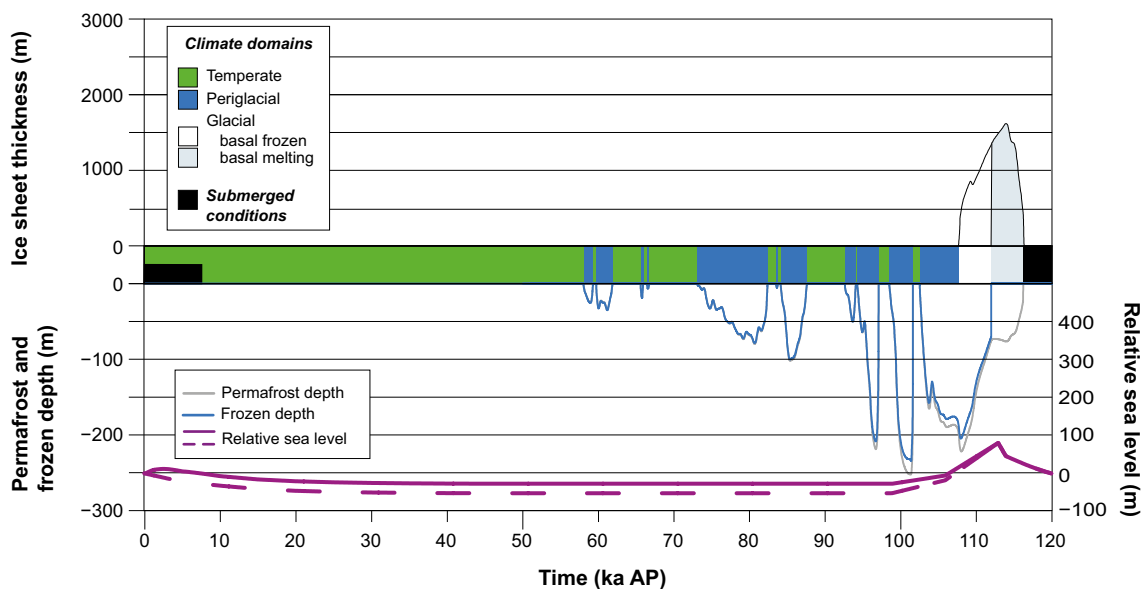


Figure 10-168. Evolution of climate-related conditions at Forsmark as a time series of climate domains and submerged periods for the global warming variant of the reference evolution. Due to the major uncertainties in future sea level rise, the initial temperate period has two variants; with and without submerged conditions during the first 7 500 years.

The climate at Forsmark site is dominated by an initial ~60 000 year long period with temperate climate conditions. The variation in air temperature and precipitation is significant within this period, with the highest air temperatures and annual precipitation amounts occurring within the first thousand years. Within this period, the air temperature at the Forsmark site is projected to increase by a maximum value of 5 °C above the present value, resulting in an annual average air temperature of ~11 °C (**Climate report**, Section 5.1.1). Subsequent to this peak, the air temperature will slowly decline as a result of declining atmospheric CO₂ concentrations. After 10 000 years, the air temperature is estimated to be of similar magnitude to the temperature at 2100 AD, illustrating the slow decline of the surface air temperature over the coming millennia in the Global warming variant. During this initial long warm period, it is likely that climate within the temperate domain will vary significantly, with a range that is larger than that during the preceding parts of the Holocene. Annual precipitation at Forsmark is projected to increase by up to ~20 % as a result of the 5 °C peak temperature increase (**Climate report**, Section 5.1.1). This corresponds to an annual precipitation of almost 700 mm.

The length of the initial period of temperate climate domain in the global warming variant does not constitute a prediction on how a future global warming climate will manifest itself. Given the present state of knowledge, this interglacial period is likely to be even longer than envisaged in the global warming variant (Liakka et al. 2021). One alternative case with a longer duration is described in the extended global warming climate case (see the **Climate report**, Section 5.2).

Between ~60 000 years after present and more than 100 000 years after present, periods of periglacial conditions with permafrost occur and get progressively more severe. The first major ice sheet advance occurs after 100 000 years after present. The maximum ice sheet thickness, around 2 000 m, occurs at around 115 000 years after present.

During the second half of the global warming variant (Figure 10-168), climate varies within the same range as during the first part of the reference evolution, and consequently the climate-related processes will act in the same way as in the reference evolution. The global warming variant reduces the effects of climate-related processes of importance for repository safety that are related to cold climate conditions, i.e. in the periglacial- and glacial climate domains.

In a climate initially dominated by (moderate) global warming, the warmer temperatures at the ground surface would not affect repository safety functions. If precipitation increases, this would not affect groundwater formation significantly, since, on a regional scale, the major part of the groundwater aquifer is filled already by present-day precipitation rates. However, low groundwater salinity due to persistent infiltration of meteoric water during the initial prolonged temperate period in the global warming variant may have a potential effect on the function of the clay buffer, investigated in Section 10.6.3.

10.6.2 Biosphere

Climate change or variability due to increased greenhouse gas-induced warming over the coming 1 000 years, considered in the global warming variant of the reference evolution, is also expected to influence important parameters in the biosphere such as the hydrological cycle, the shore-line position, and the seasonal vegetation period.

Increased precipitation predicted in the global warming variant (see Section 10.6.1) may lead to higher runoff (Bosson et al. 2010), even if partly balanced by increased evapotranspiration due to higher temperatures. The expected changes of sea levels will reduce, stop or, at least for limited periods, even reverse the shoreline displacement and thus maintain the site close to the sea, see the **Climate report**. In that case, water turnover rates close to the repository may be affected by the vicinity of the sea for extended periods. As the areas for discharge of groundwater from the repository are temporally varying and, to some extent, move with the moving shoreline (Joyce et al. 2010), this means that discharge areas near the repository may receive potentially released radionuclides for extended periods, compared with the reference evolution. The predicted increase in runoff to the northern parts of the Baltic Basin will probably decrease salinity in the Bothnian Sea (Gustafsson 2004).

Due to higher winter temperatures (see the **Climate report**, Section 5.1.7 and Appendix F) and longer vegetation period, there may be a shift in species composition, especially in the terrestrial

ecosystem where deciduous trees may be more common. Such changes may also suggest higher biomasses and similar or slightly higher productivity. However, this is not necessarily the case and there are studies from freshwater ecosystems indicating that increased temperatures may disfavour primary producers on lake bottoms, even if total lake productivity remains unaltered (cf. Andersson 2010). Moreover, data describing peat accumulation suggest that the peat accumulation decreases with a warmer temperate climate as it changes from a boreal to a nemoral climate state (cf. Löfgren 2010). In summary, the prerequisites for transport and accumulation of radionuclides in the biosphere during temperate periods of the global warming variant are assumed to be similar to those in the initial temperate period of the reference evolution.

10.6.3 Repository evolution

For the global warming variant, which describes a situation with moderate global warming, atmospheric CO₂ levels increase, temporarily, up to around 750 ppm before starting to decline (see the **Climate report**, Section 5.1), which is approximately three times the pre-industrial value of 280 ppm. Higher levels of atmospheric CO₂ concentrations, and thus stronger global warming, are envisaged for the extended global warming climate case (see the **Climate report**, Section 5.2). In this case, peak atmospheric CO₂ concentration could temporarily be above 1 000 ppm. The consequences of the increased acidity and sulphate contents of superficial waters on a granitic aquifer were analysed in Wersin et al. (1994), where it was concluded that several tens of thousands of years would be necessary to exhaust the calcite present in fracture-filling minerals. In addition, silicate weathering and ion-exchange processes also contribute to neutralise the increased inflow of carbonic acid in infiltrating waters while sulphate is removed by microbial reduction to sulphide.

The implications of a long period of temperate climate for the deep repository were analysed by Joyce et al. (2015) using a hydrogeochemical model similar to that described by Salas et al. (2010), except that temperate conditions were maintained through to 60 000 AD as opposed to 12 000 AD. Five calculation cases, which included variations to end-member groundwater composition and mineral equilibrium, were tested. In addition, the extended temperate evolution model introduced a mechanism for two-way coupling between the step-wise geochemical and the hydrological calculations (Joyce et al. 2015).

The results show that the site geochemistry changes little beyond the temperate climate period considered in the base case of the reference evolution discussed in Section 10.3.6 (up to 9000 AD), and hardly at all beyond 20 000 A.D (Joyce et al. 2015). Redox conditions and salinity exhibited the most notable excursions relative to the reference evolution. Of the five calculation cases, -160 mV was the maximum computed redox potential, but lower potentials prevailed in most of the deposition holes. The median total dissolved solids in the repository volume decreased to ~4 g/L at the end of the simulated period, and about ~5 % of the grid point2 in the repository volume had salinities below ~1 g/L, in qualitative agreement with the results shown in Figure 10-32 for 60 000 AD. Similarly, cation concentrations, expressed as $\Sigma q[M^{q+}]$, remained above the 0.004 mol/L limit for all cases, thus supporting preservation of the buffer and backfill even through an extended temperate period. The median pH shifted by less than 0.4 units between 9000 and 60 000 AD for all calculation cases (Joyce et al. 2015). These results are consistent with those presented by Wersin et al. (1994). The low topographic gradient and low hydraulic conductivity at the Forsmark site also support the notion that the infiltration of meteoric waters down to the repository horizon (below ~400 m) will be limited, even over a prolonged temperate period.

The conclusions are, therefore, similar to those presented in Sections 10.3.7 and 10.4.7. For the whole first temperate period following repository closure, anoxic groundwater conditions will prevail at repository depth, in spite of the increasing proportion of meteoric waters with time, thus satisfying the criterion for the safety function indicator R1a in Figure 10-2. Salinities during this period will be limited, ensuring that the swelling properties of the buffer and backfill are not negatively affected, cf. the safety function indicator R1b in Figure 10-2. Cation concentrations, expressed as charge, $\Sigma q[M^{q+}]$, will be above 0.004 mol/L in the candidate repository volume, although it cannot be excluded that for a fraction of deposition holes the cation concentrations may be below the limit where montmorillonite colloids start to become stable.

The concentration of sulphide, which is another important parameter, is expected to remain at the levels found in the Forsmark groundwaters at present. For colloids, because the salinity is preserved, concentrations are also expected to remain at the levels that have been measured during the site investigations, i.e. less than 200 µg/L (Hallbeck and Pedersen 2008).

Buffer and deposition tunnel backfill

The buffer and deposition tunnel backfill will not be significantly affected by the different evolution in the global warming variant. The main difference is that the temperate period will be longer and glacial conditions will occur later, which will have an effect on the groundwater chemistry, etc. As can be concluded from the analyses in Section 10.4.8, a longer period of temperate condition at the expense of the duration of glacial conditions, is expected to be favourable for the buffer performance in the sense that buffer erosion will be less extensive.

Canister

An initial 60 000 year warm period will have negligible impact on canister performance. The prolonged period before the first occurrence of periglacial conditions is expected to lead to a longer period of exposure to groundwaters of meteoric origin, with some influence at repository depth, but the groundwater conditions will be similar to those of the reference evolution. The concentration of sulphide is expected to remain at the levels found in the Forsmark groundwaters at present.

Consider the canister corrosion analyses presented in Section 10.4.9, for canister failure due to a partially eroded buffer. A somewhat longer period of temperate conditions in the first glacial cycle, than the 25 % of the time in the reference evolution, implies a larger margin to canister failures, since the buffer erosion would be less extensive. This is further elaborated in the sensitivity analyses in Section 12.6.2.

The reduced ice-sheet thickness will lead to a lower mechanical load on the canister during the first 120 000 year glacial cycle. This may also lead to a lowering of the risk for the occurrence of larger earthquakes, but as discussed in Section 10.4.5 it is not trivial to adapt the earthquake frequency estimates to the occurrence of glaciations. This means that the earthquake probability, and the potential shearing of canisters, is cautiously assumed to be the same for the global warming variant, as for the reference glacial cycle.

10.6.4 Safety function indicators for the global warming variant

Based on the contents of Section 10.6.3, the status of the safety function indicators at the end of a prolonged period of temperate climate can be expected to be very similar to those reported for the initial temperate period in Section 10.3.16. Therefore, no detailed account of the safety function indicators is given here.

10.7 Conclusions from the analysis of the reference evolution

Conclusions regarding all the identified safety functions, related to their indicators have been given in Section 10.2.7 for the excavation/operational period, in Section 10.3.16 for the initial period of temperate climate, in Section 10.4.11 for the first glacial cycle and in Section 10.5.1 for the entire assessment period for the base case of the reference evolution. Brief conclusions regarding the global warming variant of the reference evolution are provided in Section 10.6.4. These are not repeated in detail here.

Results and uncertainties related to containment

A number of uncertainties relating to containment have been identified and evaluated in the analysis of the reference evolution, and these are summarised under the headings “Identified uncertainties and their handling in the subsequent analysis” throughout the chapter. Table 10-33 provides an overview of these uncertainties. Issues labelled “red” in the table may affect one or several safety functions related to containment, indicated in the rightmost column of Table 10-33. When relevant, these issues are propagated to analyses of subsequent parts of the reference evolution as also indicated in the table. For example, uncertainties related to groundwater flow for temperate conditions are propagated to evaluations of buffer erosion and canister corrosion.

If propagated uncertainties are found to be insignificant in all their impacts on subsequent parts of the reference evolution, they are not qualified as uncertainties to be considered in the scenario selection as a result of the analysis of the reference evolution.

Most of the uncertainties propagated to subsequent parts of the analyses do have significant impact on the resulting evaluation of containment in the reference evolution. This is e.g. the case for uncertainties related to groundwater flow and in particular the three different fracture transmissivity-size relationships, through their impact on buffer erosion and canister corrosion, ultimately leading to uncertainty in the number of failed canisters in the reference evolution. These uncertainties are propagated to the analyses of scenarios and calculation cases in the subsequent chapters of the report.

The uncertain issues that need to be propagated to scenario analyses are essentially connected within two groups: issues related to canister failure due to corrosion (safety function Can1) and issues related to canister failure due to shear loads (safety function Can3), whereas canister failures due to isostatic load (Can2) are ruled out according to the assessments in the reference evolution. It is, however, noted that for the latter, the detailed evaluation of copper creep (Can2b,c) has been propagated to the analysis of the “Canister failure due to isostatic load” scenario.

The issues relating to canister failure due to corrosion are as follows.

- Groundwater flow over the reference glacial cycle.
- Groundwater salinity over the reference glacial cycle.
- Buffer erosion, determined by groundwater flow, fracture apertures and salinity and the assessment of which is also affected by the incomplete conceptual understanding of buffer erosion.
- Buffer sedimentation, determined by fracture apertures (and indirectly by salinity and flow through the penetration of dilute waters) and the assessment of which is also affected by the incomplete conceptual understanding of buffer sedimentation.
- Pessimistically assessed maximum pit depths (2.5 mm) from oxygen corrosion of copper and maximum general corrosion depth (4 mm) caused by sulphide generated by SRB feeding on hydrogen from degradation of rock reinforcements.
- Groundwater sulphide concentrations over the reference glacial cycle.
- Canister corrosion under advective conditions, requiring buffer erosion to the extent that advective conditions arise in the deposition hole, and then determined by groundwater flow and sulphide concentrations.

The issues relating to canister failure due to shear load are as follows.

- The occurrence of earthquakes of a sufficient magnitude to cause secondary shear movements in fractures intersecting deposition holes.
- The extent of detrimental secondary shear movements given sufficiently large earthquakes.
- The impact of secondary shear movements on the buffer/canister system.

Table 10-33. Summary of issues potentially affecting safety functions and findings from the evaluation made in this chapter. The following colour code is used: **Green: Analysis results indicate either favourable or insignificant conditions with respect to risk allowing the exclusion of the phenomenon in question from further analyses. **Yellow:** Results propagated with no significant uncertainties. **Red:** Results and uncertainties propagated as distributions, range(s) of values or several distinct cases. The rightmost column lists uncertain issues that are assessed to contribute to canister failures in the reference evolution and that are hence of particular importance in the subsequent scenario analysis.**

Subject Section	Issue	Further assessed in analyses of	Canister safety function affected
Excavation/Operational phase			
M-rock 10.2.2	EDZ	Groundwater flow	
	Excavation induced spalling		
	Reactivation of fractures		
	Induced seismicity		
H-rock 10.2.3	Infiltration of shallow water and upconing of saline water		
	Inflow to the repository		
HM-buffer/backfill 10.2.4	Piping/erosion		
C – rock, backfill, buffer 10.2.5	Salinity (upconing effects)		
	Redox conditions		
	Effects of grout, shotcrete and concrete on pH		
	Precipitation/dissolution of minerals		
	Effects of organic materials and microbial processes		
	Oxygen consumption in backfill		
	Colloid formation		
Initial temperate period			
T 10.3.4	Near-field temperature	Buffer mineral alteration, Canister corrosion	
M-rock 10.3.5	Thermally induced spalling (cases with and without)	Groundwater flow	
	Reactivation of fractures – hydraulic impacts		
	Creep		
	Reactivation of fractures (potential for shearing)	Canister shear failure	Can3
H-rock 10.3.6	Groundwater flow – DFN transmissivity-size relationship – EDZ and crown space cases – Cases with and without thermally induced spalling	Salinity, erosion, corrosion	Can1
	Time for saturation	Buffer saturation	
	Branching migration paths Choice of conceptual model Channelling		

Subject Section	Issue	Further assessed in analyses of	Canister safety function affected
C-rock 10.3.7	Salinity – potential for dilute groundwater	Erosion	Can1
	Concentrations of sulphide	Corrosion	Can1
	Redox conditions		
	Effects of grout, shotcrete and concrete on pH		
	Degradation of grout in grouting holes		
HMC-buffer, backfill 10.3.8 10.3.9 10.3.10 10.3.11 10.3.12 10.3.14	Saturation		
	Moisture redistribution	Near field temperature	
	Swelling – if no loss of buffer due to erosion/colloid formation		
	Chemical evolution and effects of salinity		
	Mineral alteration		
	Cementation due to increased temperatures	Canister shear failure	Can3
	Canister sinking		
	Degradation of bottom plate – covered by spalling assumption		
	Degradation of deposition tunnel plug		
	Erosion/colloid formation	Corrosion	Can1
	Saturation time for the central area and the ramp and shaft		
Saturation and swelling of borehole plugs			
Canister 10.3.13	Corrosion		
Remaining part of the reference glacial cycle			
T-rock 10.4.3	Periglacial conditions		
M-rock 10.4.4 10.4.5	Hydraulic jacking		
	Reactivation of fractures – Hydraulic impacts		
	Fracturing of the rock due to the glacial load		
	Earthquakes – Shearing		Can3
H-rock 10.4.6	Groundwater flow – DFN transmissivity-size relationship – EDZ and crown space cases – Cases with and without thermally induced spalling	Salinity, erosion, corrosion	Can1
	Shape of ice profile Development of permafrost and frozen conditions		

Subject Section	Issue	Further assessed in analyses of	Canister safety function affected
C-rock 10.4.7	Salinity ("glacial upconing" effects)		
	Redox conditions		
	Effects of grout, shotcrete and concrete on pH		
	Degradation of grout in grouting holes		
	Salinity – potential for dilute groundwater	Erosion	Can1
	Concentrations of sulphide	Corrosion	Can1
Buffer backfill borehole seals 10.4.8	Freezing of closure material	12.4	
	Erosion/colloid formation	Corrosion	Can1
	Erosion due to high hydraulic gradients		
Canister 10.4.9	Corrosion		Can1
	Canister shear failure		Can3
	Isostatic loads		
Global warming variant			
M-rock 10.6.3	Earthquakes – Shearing	Canister shear failure	Can3
H-rock 10.6.3	Groundwater flow	Erosion, corrosion	Can1
C-rock 10.6.3	Salinity – potential for dilute groundwater	Erosion	Can1
	Concentrations of sulphide	Corrosion	Can1
	Redox conditions		
	Effects of grout, shotcrete and concrete on pH		
	Degradation of grout in grouting holes		
Buffer, backfill 10.6.3	Chemical evolution		
	Erosion/colloid formation	Corrosion	Can1
Canister 10.6.3	Corrosion		Can1
	Canister shear failure		Can3

Results and uncertainties related to retardation

A number of results, with their uncertainties, are relevant for the evaluation of the secondary safety function of the repository, i.e. its retardation potential. These include the following.

- Biosphere conditions and groundwater discharge locations during a glacial cycle, providing input to the derivation of release-to-dose conversion factors.
- Groundwater flow in the geosphere over a glacial cycle, providing direct input to the modelling of radionuclide transport in the geosphere.
- Geochemical conditions in the geosphere over a glacial cycle, providing input to the determination of solubilities of radioelements in the repository near field and of sorption properties in buffer and the geosphere.
- Transport conditions in the near field, e.g. the flow conditions and the relevant properties of the buffer and at the wall of the deposition hole.

These are propagated and further evaluated in the assessment of the retarding potential of the repository in Chapter 13.

Uncertainties related to external conditions

By definition, the external conditions for the reference evolution are constrained either to a development compatible with a repetition of conditions reconstructed for the Weichselian glacial cycle (the base case) or to one compatible with the global warming variant. There are uncertainties within these constraints, leading to uncertainties within the reference evolution. There are also significant uncertainties due to the fact that external conditions other than those defining the reference glacial cycle or the global warming variant can be conceived. The former uncertainties are addressed in the same way as other uncertain factors relating to the reference evolution and the latter are handled in the analyses of additional scenarios in Chapters 12 and 13.

Design issues and feedback to repository engineering and to R&D

A number of issues regarding design options have emerged from the analysis of the reference evolution. Issues specifically mentioned in the conclusions from the various sections of the reference evolution are the following.

- Deposition hole rejection criteria. It is of interest to explore both the effect of variants of the geometric criterion applied in the layout for the PSAR and the impact of potential criteria based on inflow.
- The consequences of alternative excavation techniques in terms of associated differences in EDZ properties affecting the flow conditions in the repository.

Additional conclusions concerning e.g. feedback to repository engineering, to needs of research and development etc. could to some extent be developed based on the findings in the reference evolution. This discussion is, however, postponed to the development of final conclusions in Chapter 15 where a fuller account, also based on results of consequence calculations and of the analyses of additional scenarios, can be given.

**Post-closure safety for the final repository
for spent nuclear fuel at Forsmark**

Main report, PSAR version

Volume III

11 Selection of scenarios

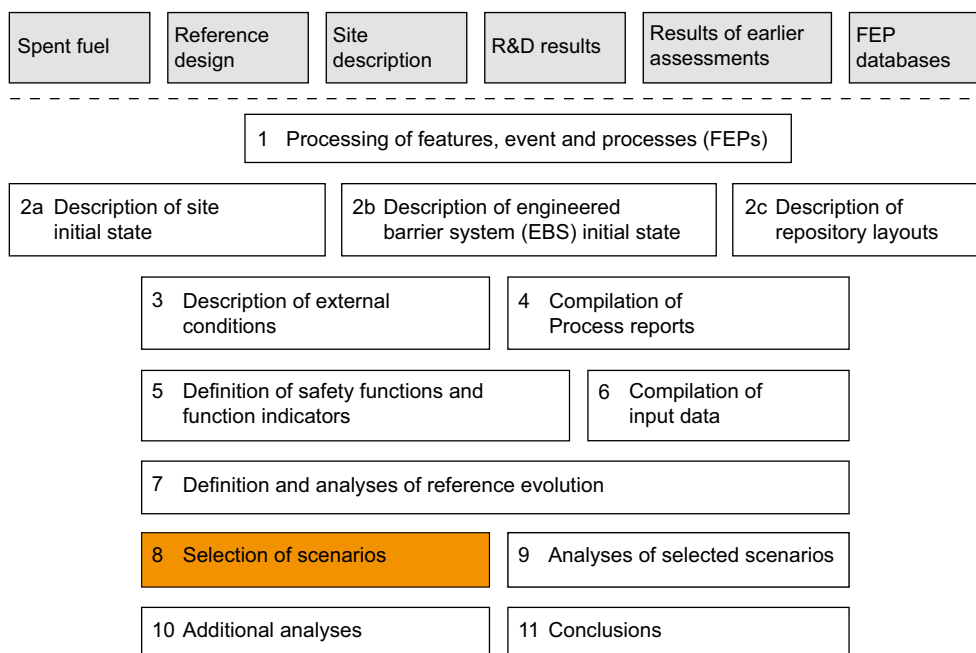


Figure 11-1. The PSAR methodology in eleven steps (Section 2.5), with the present step highlighted.

11.1 Introduction

As mentioned in Section 2.5.8, a key feature in managing uncertainties in the future evolution of the repository system is the reduction of the number of possible evolutions to analyse by selecting a set of representative scenarios.

The selection focuses on addressing the safety relevant aspects of the evolution expressed at a high level by the safety functions containment and retardation which are further characterised by reference to safety function indicators, as discussed in Chapter 8.

In Section 2.5.8 the regulatory requirements in the selection of scenarios were discussed and a general methodology for the selection of scenarios was presented. The methodology explains i) how a main scenario, closely related to the reference evolution, is defined and ii) the principles for selecting a number of additional scenarios, based on safety functions.

In the following, the selection of additional scenarios based on safety functions is carried out in Section 11.2.1, a structure for the further analyses of these scenarios is presented in Section 11.2.2, leading to a template for the account of the analyses given in Section 11.2.3. The selection of additional scenarios is identical to that in the safety assessment SR-Site and the text in Section 11.2 is virtually unchanged. The analyses of canister failure scenarios have, however, been expanded in response to considerations regarding early canister failures in SSM's review of SR-Site. This, and additional issues relating to scenario selection brought up in SSM's review are elaborated in Section 11.3. All selected scenarios are summarised in Section 11.4. A discussion on uncertainties in relation to scenario selection was given in Section 2.8.

11.2 Scenarios derived from safety functions – selection and structuring for analysis

11.2.1 Selection of additional scenarios

Uncertainties not covered by the reference evolution

As discussed above, the main scenario is based on the reference evolution that covers the evolution of the repository system for a **realistic** initial state of the repository and for an example of a **credible** evolution of external conditions over the assessment period.

However, as implied by the terms ‘realistic’ and ‘credible’, significantly different conditions and hence different repository evolutions cannot be ruled out. There are uncertainties regarding the initial state, the processes governing the repository evolution and the external conditions. Not all these uncertainties are covered in the reference evolution on which the main scenario is based and they need to be explored in a set of additional scenarios. The evaluation of uncertainties explores whether more extreme initial state and external conditions need to be included in the analyses, and if uncertainties related to the handling of processes warrant further analyses.

Approach to selection of additional scenarios

A structured selection approach is required in order to obtain a set of additional scenarios that can be argued to be comprehensive. The purpose of the scenarios is to aid in a critical evaluation of repository safety and it is, therefore, natural to use the safety functions and the safety function indicators discussed in Chapter 8 when seeking a structure for scenario selection.

The approach taken in SR-Site and the PSAR is to use the safety functions with their indicators and indicator criteria as expressed in Figure 10-2 to define a set of scenarios that are distinguished by their different status of the safety functions. The scenarios thus consider cases where the possibility and consequences of partially or completely losing one or several of the safety functions are evaluated. Examples are scenarios where canisters fail due to corrosion, to high isostatic pressure or to shear movements in fractures intersecting the deposition hole. The scenarios are defined without consideration of their likelihood.

In the analyses of the selected scenarios, all conceivable routes to the loss of the safety function that defines the scenario are critically examined, in order to evaluate the likelihood of the scenario, its consequences and its potential contribution to the risk summation for the repository. From the understanding of the functioning of the repository system, this examination is focussed on the factors contributing to the particular safety function, thus focussing the evaluation of each scenario on a limited set of uncertain factors. The FEP chart, Figure 8-5, is an aid when identifying such factors. The basis for the evaluation is the analysis of the reference evolution, where all the factors covered in the FEP chart are analysed for reference conditions.

The approach taken when selecting scenarios is thus to ask the question: What characterises a failed repository? The answer to that question is a list of states where one or several safety functions are not upheld, e.g. a situation where advection is the dominant transport mechanism in the buffer. The analyses of the so selected scenarios then focus on identifying and quantifying all conceivable routes to these failed states. The goal, for each scenario, is to either dismiss it, since no credible such route can be identified, or to assess its likelihood and consequences so that it can be included in the risk summation for the repository. For the latter scenarios, it may, as feedback to future design development, be appropriate to consider whether modifications to the design could eliminate or reduce the potential for occurrence of the scenario.

Elaboration of list of safety functions for the scenario selection

The primary safety function of a KBS-3 repository is containment. Therefore, an obvious step when selecting scenarios based on safety functions is to select three **canister scenarios** based on the three safety functions directly related to canister containment, i.e. scenarios characterised by (Figure 10-2)

- A. Canister failure due to corrosion, safety function Can1.
- B. Canister failure due to isostatic load, safety function Can2, considering both static loads on the insert and creep deformation of the copper shell.
- C. Canister failure due shear load, safety function Can3, considering both instantaneous loads and long-term creep ductility.

For the further selection of scenarios, the list of safety functions requires some elaboration, since many of the safety functions are overlapping or inter-connected. The buffer safety function ‘limit advective transport’ is e.g. connected to the canister safety function ‘provide corrosion barrier’ in that corrosion is strongly enhanced if advective conditions prevail in the buffer. A comprehensive evaluation of the canister corrosion scenario must thus encompass also an evaluation of advection in the buffer. In general, each of the above three scenarios related to canister failure needs to be combined with relevant states of the buffer in order to obtain a comprehensive evaluation.

Derivation of critical buffer states

From the safety functions, six buffer states related to safety can be derived:

1. A basic state is the **intact buffer**, where all buffer safety functions are upheld.
2. Another state directly derivable from the safety functions is the **buffer with advective conditions**, relating to loss of the safety functions Buff1a or Buff1b. A special case of advective conditions occurs when the buffer is not able to keep the canister in its intended vertical position so that, in the most extreme case, the canister has sunk to the bottom of the deposition hole. The buffer diffusion barrier is then lost and the mass transfer between the groundwater and the canister is controlled by advection in the surrounding rock and possibly also in the buffer. This relates to the buffer function Buff5 (prevent canister sinking).
3. Another state needing consideration is the **transformed buffer**. This is related to the buffer function Buff4 that concerns the maximum temperature of the buffer. There are, however, a number of additional potential causes for, or routes to, buffer transformation that also need to be considered in order to fully evaluate this buffer state.
4. A **frozen buffer** must be considered, relating to the buffer function Buff6b.
5. A **dense buffer** considers a situation where the density of the buffer is higher than that given in the technical design requirements. This state relates to the buffer function Buff3 (damp rock shear) and Buff6a (limit swelling pressure on the canister).
6. Finally, a **buffer housing active microbes** implies a situation where microbial reduction of sulphate needs to be considered in the buffer itself. This state relates to the function Buff2.

These are six buffer states, five of which that may be characterised as ‘failed’, that emerge from the list of safety functions, and also from the general understanding of the role of the buffer and its evolution over time in a KBS-3 repository. Of these, the first four are treated as distinct buffer scenarios (one intact and three failed). The last two, the dense buffer and the buffer housing active microbes are included in the analyses of the relevant canister scenarios as indicated in Figure 11-2. Both these are related to the buffer density and swelling pressure, and are readily analysed within the appropriate canister scenarios, hereby reducing the number of scenarios and the complexity of the account of the scenarios.

11.2.2 Structure for analysis of the additional scenarios

Approach

The analysis of the additional scenarios uses the reference evolution as a point of departure. The analysis of each of the scenarios then focuses on an evaluation of possible uncertainties of relevance to the particular scenario, including uncertainties that are not addressed in the analysis of the reference evolution. These uncertainties may be related to the initial state of the repository, to processes governing repository evolution or to external influences.

For example, in the analysis of the buffer advection scenario, the following issues are among those addressed.

- Could the initial density of the buffer – density being a critical factor for the occurrence of buffer advection – for any reason be lower than the reference initial density assumed in the reference evolution?
- Are there remaining conceptual uncertainties related to the buffer colloid release/erosion/sedimentation process (leading to loss of density) that are not addressed by the models used to quantify this process in the reference evolution? This includes effects of piping and erosion during the saturation of the repository.
- Could the groundwater composition and flow be less favourable to safety due to the induction of buffer advection than the composition and flow that follow from the reference external conditions, a repetition of the Weichselian glacial cycle, in the reference evolution?

Combination of scenarios related to buffer functions and canister functions

Each of the three failed buffer states is evaluated as a separate scenario, critically examining all identified routes to them, as described under the previous sub-heading. Their consequences in terms of canister failures and release of radionuclides are, however, not evaluated until they are combined with the three canister scenarios defined above. By this procedure, much of the issue of combining scenarios is handled. Figure 11-2 shows schematically how the scenario analysis based on safety functions is carried out. Note that, if the analysis of a particular buffer scenario comes to the conclusion that it is to be considered as residual, then it is not propagated to the canister scenarios defined above.

The safety functions related to the rock are evaluated **within** each of these combinations through the consideration also of uncertainties related to geosphere and external conditions when evaluating both the buffer states and the canister failure modes (see buffer advection example above). This is necessary since e.g. the potential occurrence of advective conditions in the buffer is directly related to the groundwater composition through the safety function R1c (groundwater minimum ionic strength) and the occurrence of canister failures due to rock shear is directly related to rock movements through the safety functions R3b and c, see further Figure 11-2.

Approach to retardation

The approach presented so far concerns direct failure modes of the canister, and how the buffer safety functions relate to these failure modes, i.e. it is related to the primary safety function of the repository. The approach taken to evaluate also the secondary safety function, retardation, is to determine, for each of the canister failure modes, uncertainties related to retardation. This approach is strongly motivated by the fact that each canister failure mode has distinct consequences for retardation, thus requiring a specific evaluation of uncertainties related to this characteristic.

Within each scenario, uncertainties related to the relevant aspects, for that particular scenario, of retardation properties of the fuel, the canister, the buffer, the deposition tunnel backfill and the geosphere are evaluated. Many of the uncertainty issues overlap with those relevant for containment. For example, advective conditions in the buffer are relevant for both containment, through the inward transport of canister corroding agents, and for retardation, in relation to the outward transport of radionuclides. This evaluation is made in Chapter 13, following a similar but simpler approach to that used in the evaluation of scenarios related to containment, see Section 11.2.3.

Analyse a comprehensive reference evolution, used to define the:

Main scenario

For defined
reference initial state, reference handling of processes
and reference external conditions

Select 6 additional scenarios based on safety functions:

3 relating to failed states of the buffer
3 relating to failed states of the canister

Analyse occurrence of:

“Advective” buffer
Buff1ab, Buff5
R1bc, R2ab

Frozen buffer
Buff6b
R4a

Transformed buffer
Buff4
R1de, R2ab

Evaluating, for each:

Relevant uncertainties related to
Initial state, processes and external conditions
not covered by the main scenario

Propagate each of these (descriptions of buffer states) to analysis of each of:

Canister failure
due to corrosion
Can1, Buff1
R1adf, R2ab + §

Canister failure
due to isostatic
load Can2
R3a + §

Canister failure
due to shear load
Can3, Buff3
R3bc + §

§ safety functions related to propagated buffer states included indirectly

Again evaluating, for each:

Relevant uncertainties related to
Initial state, processes and external conditions
not covered by the main scenario

Figure 11-2. The main components of the scenario selection and analysis procedure where safety functions of the canister and the buffer are used to derive the additional scenarios (yellow and orange squares). The safety function indicators of relevance in each scenario are given with the same nomenclature as in Figure 8-3.

Classification as ‘less probable’ or ‘residual’

A key point in the evaluation of the scenarios is to arrive at an assessment of whether there is any possibility of the scenario occurring. If this is the case, the scenario is classified as ‘less probable’ and included in the risk summation, otherwise it is defined as ‘residual’.

There is no numerical limit to the probability below which a scenario is considered as residual in SR-Site or the PSAR. The approach taken is that if it can be argued that a scenario is not physically reasonable, given cautious evaluations of current knowledge of e.g. barrier properties, processes and effects of future climate change, then the scenario is considered as residual.

A more precise definition, covering all possible situations, is not seen as possible or meaningful to formulate; the reader is referred to the implementation in Chapter 12 for detailed applications of the approach.

Common causes affecting several scenarios, combination of scenarios

As mentioned above, through the combination of buffer- and canister-related scenarios, much of the issue of combining scenarios is handled. There are, however, some additional considerations regarding scenario combinations.

Combinations of the canister failure scenarios need to be considered. Are the identified failure modes independent, so that their risk contributions can be added, i.e. are their causes independent? Furthermore, is the response to a particular failure cause independent of whether another cause is acting simultaneously? The combination of isostatic load and loads caused by a rock shear movement on a canister illustrates both these issues: Is the likelihood of an earthquake independent of whether a major ice sheet, generating high groundwater pressures, exists above the repository? If these two load situations can exist simultaneously, is the canister response to an earthquake-induced shear movement independent of the existence of an isostatic overpressure?

Also combinations of the buffer states need to be considered in a similar way. The freezing temperature of the buffer is e.g. dependent on the buffer density which is lowered when advective conditions prevail in the buffer.

When the analyses described in Figure 11-2 are completed, the issue of combinations is revisited through a structured approach aiming at a comprehensive treatment of scenario combinations, see further Section 12.9.

Risk summation

The risk contributions from each of the scenarios form the basis for a risk summation, when the scenario analyses are completed.

Risk contributions from scenarios that are independent are added, if combinations do not lead to higher consequences than the individual scenarios. If combinations may lead to higher consequences, the likelihood and consequences of each such combination are also assessed.

In the summation, it is also observed whether some sub-sets of the scenarios are mutually exclusive, in which case the total consequence of the sub-set cannot exceed that of the scenario with the highest consequence in the sub-set. This is a way of bounding the risk from a set of mutually exclusive scenarios (or cases within a scenario) if the basis for apportioning probabilities among the members of the set is limited.

Relation to reference evolution

For several safety function indicators, criteria exist such that if the criterion is fulfilled, a certain phenomenon, negatively impacting safety, is excluded. Detrimental freezing of the buffer is e.g. excluded if the buffer temperature is above -6 °C. If the criterion was assessed to be fulfilled in the reference evolution, then the evaluation focuses on conceivable routes, beyond those covered by the reference evolution, to a violation of the criterion. Guided by the FEP chart, see Section 8.5, uncertainties related to initial state and external conditions as well as conceptual uncertainties associated with processes are explored.

If the indicator is not associated with a criterion, or if the criterion was assessed to be violated in the reference evolution, then it is evaluated if the value of the safety function indicator could be less favourable for safety than is the case in the reference evolution. Again, uncertainties related to initial state, external conditions and processes are explored.

11.2.3 Template for assessment of scenarios based on safety functions

A common template is followed in the analysis of all scenarios derived from safety function indicators. The template is given below, and, for each heading, a brief description of the information that can be expected under it is given. Minor modifications of the structure for a specific scenario are made as appropriate, but the contents given below are always covered.

Note that the template covers only the analysis of containment potential in Chapter 12. Consequence calculations for the canister failure modes assessed in the scenarios are carried out in Chapter 13, according to procedures described in that chapter.

Safety function indicator(s) considered

The safety function under consideration is stated. If the scenario concerns a safety function for which a criterion of adequate safety function has been determined, it is stated that this criterion is assumed to be violated. The degree to which it is violated is specified as the analysis continues.

In some cases, several safety functions are evaluated within the same scenario, since they all relate to circumstances that are relevant to a common safety issue. If this is the case, all involved functions and their dependencies are explained. The function indicator “buffer hydraulic conductivity” related to the safety function Buff1 is e.g. related to the indicators “buffer swelling pressure”, “minimum ionic strength of groundwater”, “limited salinity” and “backfill density”.

Treatment of this issue in the reference evolution

The treatment in the reference evolution is described briefly.

Qualitative description of routes to this situation

The table of uncertainties derived from the analysis of the reference evolution is revisited, in order to identify uncertainties requiring further treatment in the scenario under consideration. Based on this table and the FEP chart, the factors contributing to the possible occurrence of the scenario are presented. The presentation results in a listing of i) initial state factors, ii) processes within the repository system and iii) external conditions to be considered.

Quantitative assessment of routes to this situation

A critical evaluation of the analysis of the reference evolution is carried out, in order to exhaustively evaluate all conceivable routes to the situation characterising the scenario. Uncertainties possibly remaining after the treatment in the reference evolution are addressed. For example, initial state conditions not covered by the reference initial state are addressed as are external conditions not covered by the reference external evolution. Conceptual uncertainties related to the processes involved are discussed.

An analysis of the importance of the sequence in which different processes or events occur is made.

Unless overridden by assumptions related to this particular scenario, the scenario is analysed for the reference glacial cycle, the global warming variant and other relevant climate cases, to satisfy SSM's requirement that each scenario is to be analysed for several alternative climate evolutions.

Categorisation as “less probable” or “residual” scenario

Based on an assessment of plausibility of the routes to the situation, the scenario is characterised as either a “less probable” scenario if its occurrence cannot be ruled out or otherwise as a “residual” scenario. In the former case, the consequences of the scenario are included in the risk summation for the repository, which means that an assessment of the likelihood of the scenario's occurrence is made. In some cases it is relevant to consider both the probability that a single deposition hole is affected and the probability of all (or many) holes being affected. In the “residual scenario” case, the consequences of the scenario are not included in the risk summation for the repository.

Conclusions

Conclusions, based on the results under the previous headings, are drawn.

11.3 Amendments to scenario selection and analyses in response to SSM's review of SR-Site

As mentioned in Section 1.3.3, SSM in the review of the safety assessment SR-Site identified a need to include a scenario that evaluates the likelihood of early canister failures and points to a number of processes that may occur at early stages of the repository evolution and that should be included in such an evaluation. SSM stresses the need for such an evaluation at the Forsmark site where unsaturated conditions are expected to remain in the clay system for up to thousands of years in some parts of the repository due to the low frequency of water bearing fractures at the Forsmark site. The greater hazard of the spent fuel at early times is a further reason to consider early failures in more detail. The processes explicitly mentioned by SSM are local corrosion due to sulphide, stress corrosion cracking due to sulphide, creep deformation, and general corrosion for high chloride concentrations, but also other potentially detrimental processes need to be considered. As seen in the preceding sections, SKB's method for selection of scenarios is based on safety functions, and the selected scenarios are structured according to the safety functions to which they relate. The methodology is based on potential failure modes, but not in any explicit way on the time at which a failure occurs. Therefore, in order to take SSM's point into account, for each scenario related to a canister failure mode, an explicit discussion of the potential for early failures is provided. Such a discussion is thus provided in the analyses of the scenarios addressing canister failure due to corrosion (Section 12.6.3), due to isostatic load (Section 12.7) and due to shear load (Section 12.8). Most of the discussion is provided in the corrosion scenario (Section 12.6.3), where the potential for combined effects of a number of phenomena are assessed. In addition, early failures are assessed in Section 12.9 addressing combinations of scenarios. Also, the analyses of consequences of postulated early canister failures have been expanded, see further Section 13.7.3.

Other scenario related issues raised by SSM concern the need for safety functions related to copper creep and to hydrogen embrittlement of copper. Such functions were introduced in Section 8.3.1. This has also resulted in an expanded discussion of copper creep and the long-term ductility of the copper material in the isostatic load scenario, Section 12.7.5 and in the shear load scenario, Section 12.8.2.

During the review of the SR-Site assessment, SSM requested an analysis of a residual scenario addressing the consequences of postulated criticality in the final repository. Such an analysis was provided by SKB and is now summarised in the analyses of the repository's retardation potential, since it relates to canisters where the containment has failed, see further Section 13.3.1.

11.4 Summary of scenario selection

Table 11-1 summarises the result of the scenario selection carried out as described in this chapter.

The reference evolution described in Chapter 10, is defined as the main scenario and forms the basis for selection of additional scenarios.

The safety functions are used as a basis for the selection of additional scenarios. These comprise three buffer scenarios, representing 'failed' states of the buffer and three canister scenarios, representing distinct canister failure modes. The buffer scenarios are analysed first and each buffer state is then considered in the analyses of the canister failure modes. Should, however, the analyses of any of the buffer states lead to the conclusion that it can be ruled out, that state is not propagated. The outcome of the analyses in Chapter 12 determines whether a combination is 'less probable' and hence included in the risk summation, or 'residual'.

Scenarios related to future human actions and other scenarios analysed e.g. in order to understand barrier functions are included as necessary if not covered by the results of the already analysed scenarios. These latter points are discussed in Section 2.5.8.

The completeness of the set of selected scenarios is discussed in Chapter 15.

In summary, the scenario methodology is an investigation of all routes to the three identified canister failure modes aiming at ruling them out or at quantifying them, considering all conceivable evolutions of the system. The safety functions of the repository components and the understanding of the development of the repository system emerging from the analysis of the reference evolution form the basis for exhaustive evaluations of such routes.

Table 11-1. Result of scenario selection. Green cells denote conditions for the base case of the main scenario, red cells denote deviations from those conditions.

Main scenario/Reference evolution				
Name	Initial state EBS	Initial state Site	Process handling	Handling of external conditions
Base case.	Reference ± tolerances.	Site descriptive model (with variants/uncertainties).	According to Process reports.	Reference climate (repetitions of Weichselian glacial cycle) No future human actions (FHA).
Global warming variant.	Reference ± tolerances.	Site descriptive model (with variants/uncertainties).	According to Process reports.	Extended temperate climate period No future human actions (FHA).
Additional scenarios based on potential loss of safety functions (“less probable” or “residual” based on outcome of analysis)				
Name	Initial state EBS	Initial state Site	Process handling	Handling of external conditions
Buffer advection.	Scrutinise uncertainties of relevant initial state factors, internal processes and external conditions possibly leading to violation of safety function indicator under consideration. Analysis of reference evolution used as starting point.			
Buffer freezing.	See above.			
Buffer transformation.	See above.			
Consider each of above three buffer states + intact buffer when analysing the three canister scenarios below.				
Canister failure due to isostatic load.	Scrutinise uncertainties of relevant initial state factors, internal processes and external conditions possibly leading to violation of safety function indicator under consideration. Analysis of reference evolution used as starting point.			
Canister failure due to shear load.	See above.			
Canister failure due to corrosion.	See above.			
Hypothetical, residual scenarios to illustrate barrier functions				
Name	Initial state EBS	Initial state Site	Process handling	Handling of external conditions
Several cases, covering together the KBS-3 barriers.	As base case of main scenario, except factors related to the hypothetical loss of barriers. E.g. canister completely failed initially, growing initial pinhole in canister, canister + buffer failed initially, criticality in failed canister.			
Scenarios related to future human actions				
Name	Initial state EBS	Initial state Site	Process handling	Handling of external conditions
Boring intrusion.	As base case of main scenario.	As base case of main scenario.	As base case of main scenario, except processes affected by boring.	Reference climate + boring.
Additional intrusion cases, e.g. nearby rock facility.	As base case of main scenario.	As base case of main scenario.	As base case of main scenario, except processes affected by intrusion.	Reference climate + intrusion activity.
Unsealed repository.	As base case of main scenario, but insufficient sealing.	As base case of main scenario.	As base case of main scenario, modified according to initial state.	Reference climate.

12 Analyses of containment potential for the selected scenarios

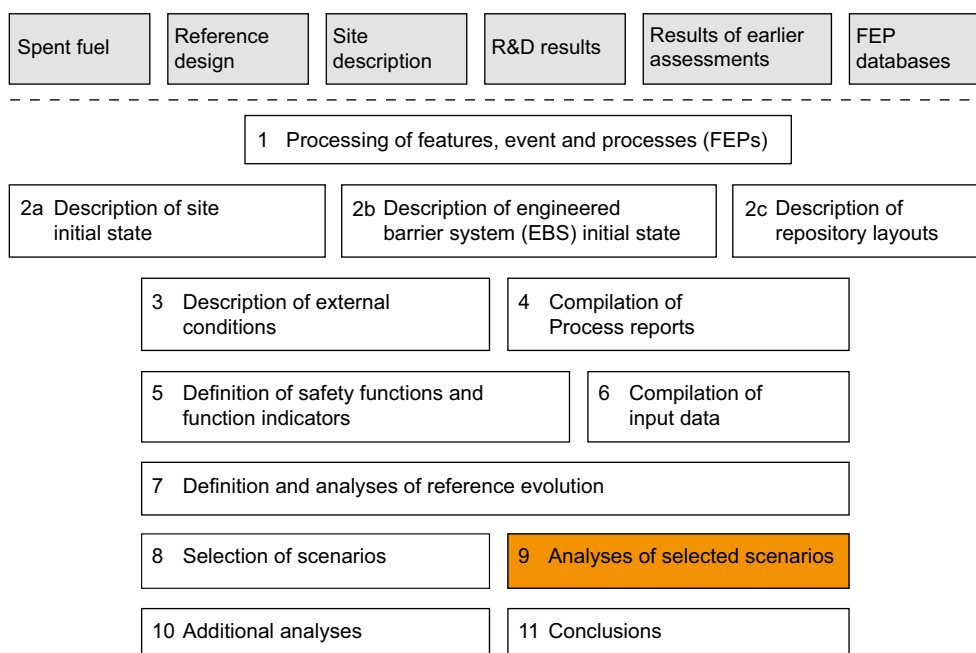


Figure 12-1. The PSAR methodology in eleven steps (Section 2.5), with the present step highlighted. This chapter deals with the analysis of containment potential in step 9. The retardation potential is analysed in Chapter 13.

12.1 Introduction

12.1.1 General

This chapter deals with analyses of the containment potential for most of the scenarios selected in Chapter 11.

Scenarios derived from safety function indicators are analysed in Section 12.2 through 12.8. The three buffer scenarios are treated in Sections 12.2 to 12.4, with conclusions in Section 12.5, and then propagated to the three canister scenarios analysed in Sections 12.6 to 12.8.

The chapter also provides, in Section 12.9, an analysis of possible combinations of the above scenarios.

Analyses of the retardation potential for the scenarios analysed in this chapter are carried out in Chapter 13.

The containment potential of the main scenario is not analysed in detail in this chapter since it is closely related to the containment potential for the reference evolution that was analysed in Chapter 10, see further Section 12.1.2.

Hypothetical, residual scenarios to illustrate barrier functions are also not analysed in this chapter, since the affected barrier properties are postulated and not the outcome of an analysis. Assumptions regarding such barrier states and analyses of consequences are presented in Chapter 13, Section 13.7.

Both containment and retardation potential for FHA scenarios are analysed in Section 14.2, where also an account of the methodology for the analysis of FHA scenarios is given.

Updates relative to the SR-Site assessment

The Buffer advection scenario in Section 12.2 has been updated taking into account the updated buffer erosion model used in the reference evolution and with sedimentation included in the assessment.

The Buffer freezing scenario in Section 12.3 has been updated with respect to the lower buffer freezing temperature of $-6\text{ }^{\circ}\text{C}$ compared to the freezing temperature of $-4\text{ }^{\circ}\text{C}$ in the SR-Site assessment.

The Buffer transformation scenario in Section 12.4 is quite similar to the corresponding scenario in the SR-Site assessment, considered in both assessments as a residual scenario. An additional study of the effect of steam on the properties of bentonite lends further support for ruling this out as a detrimental effect in a KBS-3 repository.

The Canister failure due to corrosion scenario in Section 12.6 has been updated based on the updated corrosion analyses in the reference evolution and with considerations of a biofilm on the canister surface, of hydrogen embrittlement, and of localised corrosion in connection with oxygen intrusion under glacial conditions. The input from the Buffer advection scenario has been updated and an extended discussion of the potential for early canister failures due to corrosion has been added as Section 12.6.3.

The Canister failure due to isostatic load scenario in Section 12.7 has been updated with a new estimate of maximum glacial load in Section 12.7.2, with new buffer swelling pressures in Section 12.7.3, new canister strength calculations in Section 12.7.4 (obtained from the canister design analysis reported in Jonsson et al. 2018)) and a new Section 12.7.5 accounting for the canister's resilience to creep. A brief discussion of on early failures due to isostatic loads is included in Section 12.7.6.

The Canister failure due to shear load scenario in Section 12.8 has been updated based on the updated shear load analyses in the reference evolution. An account of copper creep following a shear load has been added as has a brief discussion of early failures due to shear loads.

12.1.2 Definition of the main scenario

The main scenario corresponds closely to the reference evolution described in Chapter 10. The definition of the main scenario thus includes the detailed prerequisites given for the general evolution in Section 10.1.1. The aim of that description is to present a reasonable evolution of the repository system, and that is also the aim with the main scenario. Therefore, most of the developments and results described in Chapter 10 apply to the main scenario. As for the reference evolution, there are two variants of the main scenario; the Weichselian base case and the global warming variant.

There are also a number of uncertainties associated with the reference evolution. Those uncertainties requiring further consideration regarding containment are compiled in Table 10-33. All these are revisited in the analyses of the additional scenarios in the subsequent sections, where uncertainties are addressed as appropriate for the scenario in question. Therefore, it is not meaningful to assess these uncertainties here to arrive at a more precise judgement on the evolution of the main scenario. Rather, a brief assessment of the containment potential of the main scenario is given in Section 12.9.2, after the analyses of the additional scenarios, when such an assessment can be based on the outcome of the more detailed evaluation of uncertainties in the additional scenarios.

12.1.3 Climate development for the scenario analyses

As mentioned in Section 6.2.4, in addition to the external evolution for the reference scenario, complementary climate cases, with potentially larger impacts on repository safety than the reference glacial cycle, have been analysed as documented in the **Climate report**. These results are utilised as appropriate in the analyses of the containment potential of the additional scenarios. The climate cases are shown in Figure 12-2.

The reference glacial cycle constitutes the external conditions for the reference evolution, analysed in Chapter 10, with the *global warming* climate case as a variant also analysed in Chapter 10.

The longest period of temperate climate conditions for the coming 120 000 years, resulting in the longest period of groundwater formation from precipitation, is found in the *extended global warming* climate case. This case is relevant for the assessment of the extent of buffer erosion potentially leading to advective conditions in the buffer (see Section 12.2).

The most extended period of periglacial climate conditions, with longest periods of permafrost and deepest frozen ground at Forsmark, is found in the *severe permafrost* case. This case is relevant for the analysis of detrimental buffer freezing in Section 12.3.

The longest period of glacial conditions, and associated period of groundwater formation from glacial melt water, is found in the *extended ice sheet duration* case. Also this case is relevant for the assessment of buffer advection in Section 12.2.

The maximum future ice sheet thickness, and resulting largest increase in hydrostatic pressure at repository depth, is found in the *maximum ice sheet configuration* case. This case is not depicted in Figure 12-2. It is relevant for the analysis of canister failure due to isostatic load in Section 12.7.

The six climate cases together cover the expected maximum range within which climate and climate related conditions of importance for post-closure repository safety may vary within the time scales analysed in the PSAR, i.e. over multiple glacial cycles over the coming 1 million years. The *actual* development of climate and climate related processes of importance for a KBS-3 repository at the Forsmark site are expected to lie within the range covered by the six climate cases in Figure 12-2.

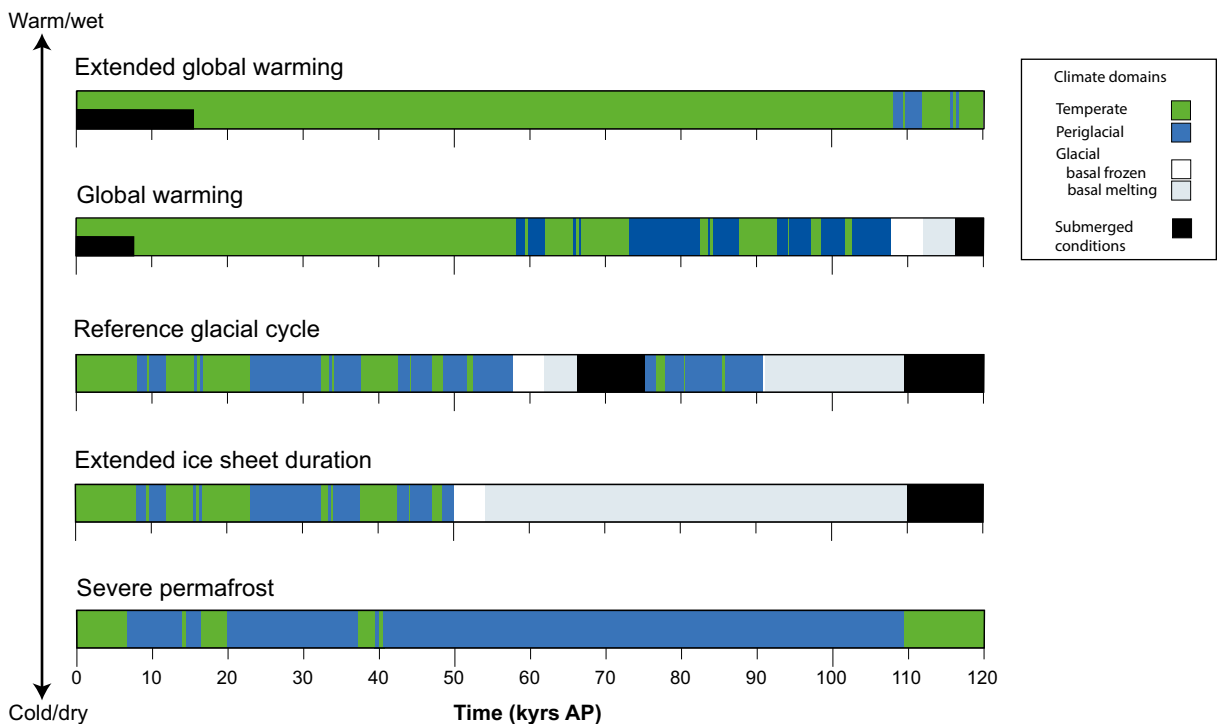


Figure 12-2. Summary of future climate cases analysed in the PSAR assessment. The maximum ice sheet configuration climate case, with maximum ice thicknesses, is not shown. For a description of the climate domains (see the Climate report, Section 1.2.3).

12.2 Buffer advection

12.2.1 Introduction

Safety function indicator(s) considered

A central safety function of the buffer is to prevent advective transport of species between the groundwater and the canister, (safety function indicators Buff1a and b) ensuring that diffusion is the dominant mechanism of transport. In order to maintain this safety function, the buffer must have a sufficiently low hydraulic conductivity. A prerequisite for an appropriate and homogeneous hydraulic conductivity is also a certain minimum buffer swelling pressure, which ensures tightness and self-sealing of the material.

In this scenario, conceivable routes to a violation of the buffer hydraulic conductivity criterion are examined. Basically, there are two routes to a situation where advection could be an important mechanism for transport in the buffer.

- A drop in dry density caused by loss of buffer material which would give a hydraulic conductivity sufficiently high for advection to dominate over diffusion, or too low a swelling pressure to maintain the self-sealing ability.
- Transformation of the montmorillonite in the buffer to another mineral with different hydraulic properties.

The results of these routes could lead to either:

- *High conductivity case:* A case where so much buffer material is lost that water can flow through the buffer,
- *Fracture case:* A case where the buffer has lost its sealing properties and a conductive fracture is formed in it.

For an intact canister, advection concerns the transport of corroding agents to the canister. For a defective canister, transport of radionuclides to the groundwater is affected.

A number of factors influence, directly or indirectly, the buffer hydraulic conductivity. The hydraulic conductivity is directly influenced by the buffer density, and the type of cations in the buffer. These factors also influence the buffer swelling pressure. The swelling pressure is further influenced by the ionic strength of the surrounding groundwater.

There are a number of safety function indicators that can be seen as “sub-indicators” to the “master” indicator buffer hydraulic conductivity. These are all used to evaluate this scenario:

- Buffer swelling pressure > 1 MPa.
- Cation charge concentration in the groundwater $\Sigma q[M^{q+}] > 8$ mM.
- Limited groundwater salinity.

A maximum temperature of 100 °C or a pH of < 11 can also be seen as sub-indicators for this scenario. The consequences of these are evaluated in Section 12.4.

A special case of this scenario is the effect of a sinking canister. This is dealt with in Section 12.2.4.

Treatment of this issue in the reference evolution

In the reference evolution, advection as a transport mechanism in the buffer is assumed to the extent suggested by the results of calculations of the base case for the reference evolution in Sections 10.3.11 and 10.4.8, where 41 out of approximately 6 000 deposition positions are calculated to experience advective conditions due to chemical erosion and up to 300 positions due to sedimentation within one million years for the base case realisation of the semi-correlated hydrogeological DFN model.

Bounding cases

For the reference evolution, the mean number of canisters calculated probabilistically to fail during the one million year assessment period due to buffer colloid release/erosion leading to buffer advection and hence enhanced corrosion is 0.094 for the semi-correlated hydrogeological DFN model, see Section 10.4.9. There, it is also demonstrated that the consequences in terms of canister failures are similar (on average 0.13) if **advection is assumed initially in all deposition positions**. (In both these cases rejection of deposition hole positions according to EFPC is assumed.)

This result is important for the treatment of the buffer advection scenario. Irrespective of the outcome of the complex interplay of a number of uncertain factors influencing the occurrence of buffer advection, the consequences in terms of canister failures are always bounded by the case where advection is assumed for all canisters throughout the assessment period, and these failure rates are similar to those for the reference evolution where only a small fraction of the deposition holes are affected by advective conditions in the buffer. The reason for this simplifying circumstance is that the time taken to erode the buffer to the extent that advection occurs is shorter than that required to cause corrosion failure once the advective conditions are established. For both processes, the groundwater flow rate at the deposition position in question is an important determining factor, and dependence on other factors influencing erosion and corrosion, respectively, is such that the time required to reach advective conditions is, in general, shorter than that required to cause corrosion failure once advective conditions are established. It is also noted again that it is only in the small number of holes that have high advective flow rates in the intersecting fractures that erosion and subsequent enhanced corrosion could lead to canister failures in one million years. The situation regarding buffer loss due to sedimentation is even more pronounced, when applying the model described and quantified in Section 10.3.11, and further quantified for an entire glacial cycle in Section 10.4.8. As mentioned in Section 10.3.11, the model is a pessimistic interpretation of empirical data and yields in general higher buffer loss rates than the chemical erosion process. A case with advective conditions in all deposition holes initially bounds also the effects of the buffer sedimentation process.

As also discussed in the reference evolution Section 10.3.11, a situation where erosion or sedimentation do not occur to the extent that advective conditions arise is also conceivable given the incomplete understanding of the processes as such and uncertainties regarding future groundwater compositions.

Three important cases can therefore be envisaged before this scenario is analysed:

1. a base case where advective conditions occur to the extent given by the erosion model in the reference evolution treated in Chapter 10,
2. a case where advective conditions occur in every deposition hole throughout the assessment period,
3. a case where diffusive conditions are preserved in every deposition hole throughout the assessment period.

The erosion model rather than the sedimentation model is used in case 1 since the understanding of erosion is much more developed than that of sedimentation. Sedimentation is assessed to cause advective conditions in at most around 300 deposition holes in the reference evolution and this case is, in terms of buffer loss, limited with a considerable margin by case 2. These three cases, two of which are bounding, are used as a background for the discussion below.

In terms of consequences for canister corrosion, in a one million year perspective, case 2 is not vastly different from the reference evolution case 1, in particular since advective conditions in the buffer are tolerated by the canister throughout the assessment period for the majority of deposition holes and for around 100 000 years for all holes, according to the calculations in Chapter 10. The three cases can be said to reasonably reflect the current uncertain knowledge of the extent of buffer loss due to colloid release/erosion and due to sedimentation. They are, furthermore, encompassing in the sense that it is difficult to conceive of a worse situation than case 2 or a more favourable situation than case 3.

Qualitative description of routes to buffer advection (including initial state aspects and external conditions)

As mentioned, the buffer density plays a key role for the buffer's ability to prevent advection. The density may decrease due to erosion induced by piping as the buffer saturates, through buffer expansion into the deposition tunnel as a saturated buffer swells or through erosion and/or sedimentation caused by dilute groundwater for predominantly glacial conditions. Buffer expansion into the deposition tunnel will be counteracted by the tunnel backfill material, meaning that factors affecting the density and compressibility of the backfill material could also indirectly influence buffer hydraulic conductivity.

Of these factors, colloid release/erosion and sedimentation caused by dilute groundwater has by far the highest impact on density in the reference evolution and it is the only factor that causes any considerable alteration of buffer density over the one million year assessment period in that evolution.

The overall conclusion from the analysis of the reference evolution is, therefore, that the buffer is expected to function as intended until intruded by dilute groundwater, and, if dilute conditions prevail for tens of thousands of years, there is currently little confidence that advection is prevented in the deposition positions intersected by the fractures with the highest flow rates. At the end of the one million year assessment period, a few tens of deposition positions are calculated to experience advective conditions due to erosion for the base case realisation of the semi-correlated hydrogeological DFN model. For sedimentation a few hundred of deposition holes may be affected, but this is based on a pessimistic application of experimental data obtained for 0.2–1 mm fractures to fractures of considerably smaller dimensions in the repository for which no data are currently available.

The following factors of importance for buffer advection are identified, based on the discussion above, on Table 10-33 describing uncertainties identified in the reference evolution and on the FEP chart, Figure 8-5.

Initial state factors involved

- Buffer density (amount of dry mass deposited).
- Backfill density (amount of dry mass deposited above the deposition hole).

Processes involved

A number of different processes could lead to a drop in buffer density:

- piping/erosion during the early stage,
- swelling/expansion into the backfill,
- buffer erosion/colloid release,
- buffer sedimentation.

For a given density, the hydraulic conductivity and swelling pressure will be determined by the following processes:

- ion exchange,
- osmosis.

The hydraulic conductivity and swelling pressure of the buffer will also be determined by the process of montmorillonite transformation.

External conditions involved

- Geosphere conditions yielding very high or very low ionic strengths of groundwater.
- Geosphere conditions leading to increased flow.

There are thus a large number of factors that need to be considered in the buffer advection scenario.

12.2.2 Quantitative assessment of routes to buffer advection

In the reference evolution, the reference buffer and backfill densities are addressed, as are reasonably high and low ionic strengths and durations of such conditions for a glacial cycle. The possibility for the transformation of the montmorillonite in the buffer is also evaluated.

Initially deposited dry buffer mass

The effect of a variation in the composition of the buffer material is not discussed in the reference evolution. It is expected that the defined delivery and quality control systems will ensure that all material will meet the specified requirements. The accepted variability in material properties has not yet been fully defined. However, considering the very small difference in the important properties between the two reference materials considered in the SR-Site assessment at the target density (see Section 5.5 in SKB 2011), it can be concluded that variation in the material composition will have a rather limited effect on buffer performance. The allowed variability of composition for the selected buffer material will be defined at time of purchase of the buffer. Under all circumstances this variability is expected to be small.

The overall conclusion regarding initially deposited buffer dry mass is that the initial buffer mass and composition is expected to be well within the design specifications.

Initially deposited dry backfill mass

The expected uncertainties in the amount of initially deposited backfill are discussed in Section 5.6. If less backfill is deposited this could potentially lead to buffer swelling into the deposition tunnel and a loss of buffer mass. However, according to the production and control procedures described in Section 5.6, there is no reason to believe that failures in the backfilling process will lead to significant contributions to the generation of advective conditions in the buffer.

Swelling

If the initial density of the tunnel backfill is lower than the design target or if the buffer saturates ahead of the backfill and expands into a pile of dry backfill blocks, the buffer can expand into the backfill which in turn gives a lower average buffer density. These cases have been evaluated in the reference evolution (Section 10.3.9). The extent of the upward expansion is essentially a combined effect of the properties and dimensions of the deposition tunnel and the backfill on one hand, and the deposition hole and the bentonite buffer on the other. Despite the uncertainties associated with the influence of the pellets-filled bevel and the potential occurrence of localised water uptake, the analyses demonstrate that the displacements and the dry density reduction in the vicinity of the canister will be such that the technical design requirement on swelling buffer pressure will be met, if the thickness of the pellets bed on the tunnel floor is limited to 100 mm and if the compressive strength of the backfill blocks is sufficiently high. . Therefore, this issue is not further considered here.

Erosion caused by piping

Erosion caused by piping is discussed in the reference evolution in Section 10.2.4. If the pressure of the water flowing into a deposition hole is higher than the swelling pressure, the buffer will not be able to seal and a channel (pipe) may form. The channel will most likely end in the deposition tunnel. As long as the tunnel is not sealed and the hydrostatic pressure has not been restored, there will be a flow in the pipe. The flow may erode the buffer and some material may be lost. The potential loss can be calculated from the accumulated flow of water.

For the maximum allowed inflow to the deposition hole (150 m³) an erosion of up to 41 kg was calculated (Section 10.2.4). At the dry density of the buffer $\rho_d = 1\,570 \text{ kg/m}^3$, this would correspond to a volume of 0.026 m³.

Overall, the uncertainties in the parameters related to piping are in these circumstances rather limited and it is unlikely that the erosion from piping should be substantially higher than in the reference evolution. This issue is, therefore, not further considered here.

Erosion of backfill

Erosion of backfill material during the operational phase could lead to a local loss of backfill density at the top of a deposition hole. This could, in turn, lead to expansion of buffer material into the backfill and a loss of buffer density. However, as seen in Section 10.2.4, the maximum loss (redistribution) of backfill during this phase is estimated at 1 640 kg which is insignificant compared to the backfill losses that would lead to advective condition in the buffer according to Section 10.3.11 (220 tonnes). This issue is, therefore, not further considered here.

Buffer erosion/sedimentation/colloid release

Buffer colloid formation and release during a glacial cycle is discussed in the reference evolution, Section 10.3.11. Several uncertain aspects of the colloid release process are mentioned in connection with the analysis of the reference evolution. These include the conceptual uncertainty in the erosion model (Neretnieks et al. 2009, 2017), the role of friction between the clay and the rock wall, the quantitative approach for calculation of sedimentation loss, interpretation of experimental results, behaviour of the selected buffer material, the duration of periods of low ionic strength groundwater and the groundwater flow rates during these periods. These uncertainties are the main reason for selecting the bounding cases for the buffer erosion scenario described in Section 12.2.1.

A quantitative treatment of the impact on the extent of erosion of uncertainty in factors affecting the erosion process is given in a subsection below.

Ion-exchange and osmosis

Figure 5-14 shows the swelling pressure for the reference buffer material as a function of dry density for two different water salinities. For the high salinity a 1 M CaCl₂ solution was used, while deionised water was used for the low salinity. Comparing the two salinities gives a good indication on the effect of ion-exchange as well. MX-80 is a Na-bentonite and will remain in a Na-state when exposed to deionised water while the 1 M CaCl₂ solution will convert it into a Ca-state. Neither the exchangeable cation nor the salinity has any major effect on the swelling pressure at the reference density. There is a difference of 1–2 MPa, but the swelling pressure remains high for both salinities. For the salinities expected in Forsmark (Table 10-11), the effect can be neglected for dry densities > 1 000 kg/m³. The ion-exchange characteristics are not important until the density drops to about 1 000 kg/m³, but below that value the effect is very strong.

The groundwater composition, Ca/Na-ratio and total salinity, will determine how much buffer mass can be lost before advection starts to be important.

The effect of groundwater salinity will only be important if large amounts of buffer are lost, i.e. in combination with colloid release. The processes are mutually exclusive since colloid formation only occurs at low calcium concentrations but they could occur in sequence if the groundwater composition is changing.

In conclusion, the uncertainties regarding the effects of increased salinities are unimportant compared to the uncertainties in the colloid formation process.

Montmorillonite transformation

Transformation of the montmorillonite in the buffer to other minerals as an effect of elevated temperature is evaluated in the reference evolution and in the buffer transformation scenario (Section 12.4).

Geosphere conditions

The development of the buffer is dependent on conditions imposed by the geosphere on the buffer. Key parameters are the following.

1. Flows and pressure gradients during the construction phase. These will determine the magnitude of mass loss from piping/erosion.
2. Ionic strength of the groundwater for all time scales. A low charge concentration of cations in the groundwater will make it possible for the buffer to form a colloidal phase that can be transported away with the groundwater. A high ionic strength will affect the buffer hydromechanical properties, which may result in a higher hydraulic conductivity and a lower swelling pressure, in the case where some mass loss has occurred. The Ca/Na ratio will affect the ion-exchange capacity which can affect the buffer properties at very low densities.
3. The groundwater flow will determine how much buffer mass can be transported away in the colloid formation case.

Flows and gradients during the construction phase are treated above under 'Erosion caused by piping'. The latter two factors are treated in the sensitivity analysis immediately below.

Quantitative sensitivity analysis of buffer erosion/colloid release

The following is a quantitative treatment of the impact on the extent of erosion of uncertainty in factors affecting the erosion process.

The extent of buffer erosion is calculated with the model described in Section 10.3.11. As illustrated in Figure 10-79, this model yields, when applied to the sequence of temperate and glacial groundwater conditions described by the reference glacial cycle, very similar results as the SR-Site model. The calculated results are, therefore, also similar to those calculated in the SR-Site assessment.

The calculated extent of erosion will depend on the groundwater composition required for erosion to occur, the fraction of time during the one million year assessment period during which the groundwater has the composition favouring erosion and the quantitative extent of the corrosion process for these conditions. An additional factor of importance is the amount of buffer that is required to be eroded away before advective conditions occur in a deposition hole. The following have been assumed or concluded regarding these factors in the PSAR.

- The *criterion* determining whether the process occurs states that the groundwater cation charge concentration, $\Sigma q[M^{q+}]$, should exceed 8 mM to avoid erosion see Section 10.3.11.
- The *fraction of time* of the one million year assessment period during which erosion occurs was assumed to be 50 percent of the time in the two percent of the deposition holes exposed to the highest flow rates, based on analyses summarised in Section 10.4.8. During half of this time (i.e. during a quarter of the total time), the conditions are assumed to be temperate and during the other half glacial conditions are assumed.
- The *amount of buffer* that needs to be eroded in order for advective conditions to arise in the deposition hole is assumed to be 1 200 kg based on the discussion in Section 10.3.9.
- The *quantitative model* for quantifying the extent of erosion is that described in Section 10.3.11.
- The *groundwater velocity* and the *fracture aperture* are obtained from the groundwater flow calculations. The natural variability of these entities is covered by determining the flow conditions in each of the ensemble of 6 000 deposition position in the repository. The hydrogeological DFN model with semi-correlated relation between fracture length and transmissivity (Section 10.3.6) is used in the calculation.
- The calculation result also depends on the *criteria for deposition hole rejection* applied in the layout and simulated in the hydrogeological modelling. This is not an uncertainty in the same sense as the above factors, but a design choice. In the PSAR (as in SR-Site) it is assumed that deposition holes are rejected according to the EFP criterion and to the transmissivity related criterion described in Section 5.2.2.

With the above assumptions, it is calculated that on average 1.4 deposition holes out of the repository's 6000 experience advective conditions after 100 000 years. At the end of the one million year assessment period, the corresponding number is almost 42, see 'Semi-correlated base case' in Figure 12-3. These results were obtained through averaging over ten realisations of the semi-correlated hydrogeological DFN model. (The earlier cited value of 41 was obtained with the base case realisation of this DFN model.) Each realisation covers the 6000 deposition positions and thus covers spatial variability within that realisation. The variability between realisations is shown by the ranges in Figure 12-3. Documentation of all calculations of buffer loss and subsequent canister corrosion under advective conditions is given in Hedin (2021).

The following sensitivity calculations were carried out, essentially by varying one of the above mentioned factors at a time. Results are shown in Figure 12-3.

- The *amount of buffer* assumed to be required to be eroded away in order for advective conditions to arise in the deposition hole was changed from 1 200 kg by a factor of two up and down, respectively i.e. to i) 600 kg and ii) 2 400 kg. This yielded changes in the calculated number of deposition holes by factors larger than two.
- Uncertainties relating to the nature of the *criterion* determining whether erosion occurs and also to the *fraction of time* during which the criterion is fulfilled is addressed by assuming that erosion occurs throughout the entire one million year assessment period. As seen in Figure 12-3, this causes the number of deposition positions experiencing advective condition to increase by a factor of about 3 in the one million year perspective, yielding approximately 140 deposition holes with advective conditions after one million years. The corresponding number for 100 000 years is approximately 3 out of the 6 000 deposition holes. There are uncertainties in both the factors covered by this variation and neither less nor more extensive erosion than in the base case can be excluded. The sensitivity case calculated here puts an upper bound on the possible variation.
- In the hydrogeological model, fracture apertures (δ) are obtained from the fracture transmissivity (T) according to $\delta = 0.5 \cdot T^{0.5}$, see further Section 10.3.6. An alternative, for buffer erosion more pessimistic, relation was also evaluated: $\delta = 0.28 \cdot T^{0.3}$ (Joyce et al. 2010, Selroos and Follin 2010). This yields an almost 30-fold increase in the calculated number of deposition positions experiencing advective conditions at one million years. However, in the **Data report** the second of the two relationships is shown to be overly pessimistic since the relationship yields fracture apertures larger than those measured at the site using electrical resistivity measurements. Hence, for the quantification of buffer erosion the first relationship is justified for use in the PSAR.
- An important aspect of conceptual uncertainties relating to the *groundwater velocity* in fractures intersecting the deposition holes is illustrated by calculations with the hydrogeological DFN models based on the uncorrelated and fully correlated relations between fracture size and transmissivity (see Section 10.3.6 for details). As seen in Figure 12-3, these both yield a larger extent of buffer erosion. Both the uncorrelated and the fully correlated models represent extremes of the correlation structure. In particular, the uncorrelated model lacks support in observations. The semi-correlated model used as the base case is seen as the most realistic representation, but it is not possible to quantify the degree of correlation in a rigorous manner. Therefore, the span represented by the three models is considered as a reasonable illustration of the conceptual uncertainties associated with the hydrogeological DFN models.

Regarding varying groundwater flow conditions over a glacial cycle, it is demonstrated in Section 10.4.6 that the time averaged value over the reference glacial cycle of $q^{0.41}$, relevant for buffer erosion is around 80 percent of that for temperate conditions, see ML2 data in Figure 10-155. Using the temperate values is thus pessimistic in terms of groundwater flow and gives some margin for alternative evolutions to the reference glacial cycle. The issue of temporal variability is, therefore, not treated further here.

In conclusion, with base case assumptions (Semi-correlated base case), around one of six thousand deposition positions is calculated to be advective at 10^5 years and around two percent at 10^6 years.

The sensitivity cases analysed here show that a considerable variation around the base case calculation result in the extent of erosion is possible. However, less than ten percent of the deposition positions reach advective conditions after one million years even for the most unfavourable cases. Also, the sensitivity cases give far less variation of the extent than the two bounding cases identified at the beginning of this section, i.e. no erosion and advective conditions initially in all deposition holes.

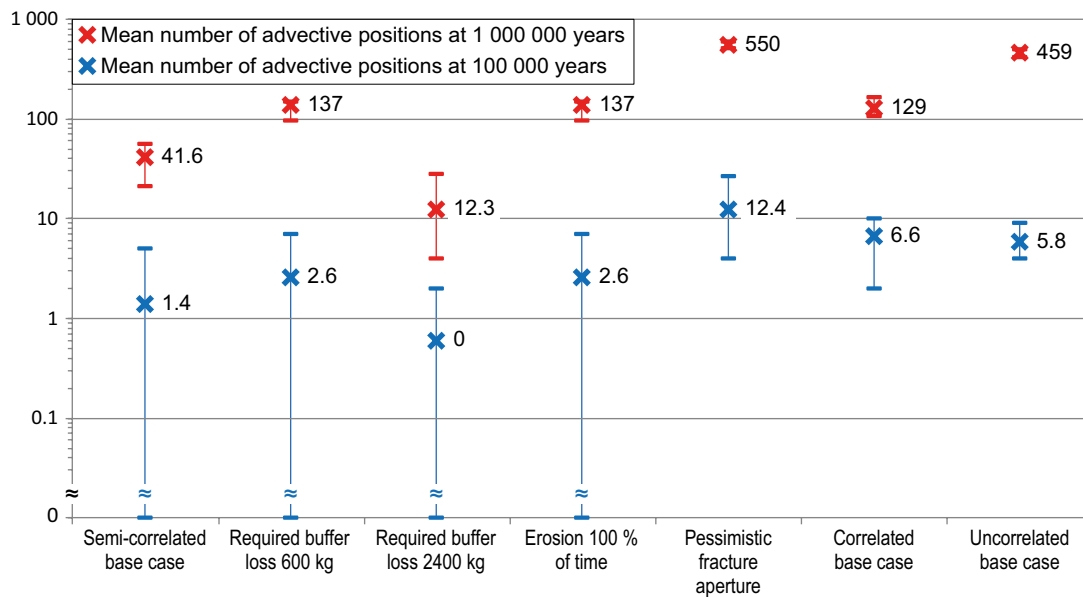


Figure 12-3. Calculated extent of erosion at 100 000 years and at one million years for a number of cases. The crosses denote mean values and the bars denote the variability over the several realisations of the hydrogeological DFN models.

The conceptual model for quantifying the extent of erosion is associated with uncertainties that are difficult to quantify:

- There are potentially mitigating effects like clogging of the water conductive fracture with detritus material from the eroded bentonite (Neretnieks et al. 2009).
- The actual cation concentration in the buffer/groundwater will have an impact on the rate of erosion as seen in Section 10.3.11. This is determined by the concentrations of cations in the groundwater as well as from buffering effects from the cations in the buffer. The effect on erosion of small differences in concentrations can be rather large. There are additional factors that could lead to a decrease in the clay dispersion rate, see further the concluding discussion of uncertainties in Section 10.3.11.
- Wall friction between the extruding clay and the rock in the fractures determines how far the clay front can expand into the fracture. In section 10.3.11 it is assumed that the friction will limit the expansion to 5 cm, while the model in Neretnieks et al. (2009) assumes no friction.

The influences of the sensitivity cases on the extent of corrosion are evaluated in the corrosion scenario, Section 12.6.2.

Uncertainties concerning sedimentation

As discussed in section 10.3.11, the uncertainties regarding the sedimentation process are significant. The combination of the empirical approach and the highest experimental values for J_{Exp} will lead to large mass losses in some deposition holes. There are, however, a number of features and processes that will limit this:

- Most deposition holes (~ 95 % in the reference evolution) are expected to never experience water with a cation concentrations less than 8 mM.
- The mass loss is calculated with an empirical approach based on short term experiments. It is not unlikely that the mass loss rate will decrease with time.
- The J_{Exp} values in the empirical approach has been determined for fractures that have larger apertures than the ones expected at Forsmark. There seem to be a tendency of decreasing (relative to area) mass loss with decreasing aperture. The higher value in section 10.3.11 can therefore be seen as particularly pessimistic.

- The fate of the sedimented material has not been accounted for. The sediment has a low density and the available space in the fracture system in the rock is limited. The fractures are expected to “fill up” with time and after this, material has to be transported away with erosion before sedimentation can progress further.

No quantitative assessment of the uncertainties regarding the sedimentation process has been made in the PSAR. The sedimentation case is pessimistically bounded by the “initial advection” case (Section 12.3.3).

Global warming variant and other climate cases

The occurrence of buffer advection is strongly linked to the presence of low ionic strength groundwaters at repository depth. As demonstrated in the reference evolution Section 10.3.6, an extended initial period of temperate climate conditions could give rise to longer periods of exposure to dilute groundwaters. However, in the global warming variant, the initial temperate period is prolonged at the expense of subsequent glacial periods, for which the erosion rate is assessed to be higher due to the lower ionic strength of the infiltrating water. The overall effect of the global warming variant is, therefore, a decrease in the extent of erosion. This difference relative to the base case applies only for the first glacial cycle, whereas the effects of global warming are assumed to not affect subsequent cycles in the global warming variant. The issue is therefore not further treated in the PSAR for the global warming variant.

Regarding other climate cases, the *extended global warming* case and the *extended ice sheet duration* case (see Section 12.1.3) could imply more extensive intrusion of dilute water than in the reference evolution. Such developments are covered by the bounding case where advection is assumed initially in all deposition holes.

12.2.3 Conclusions

As evidenced by the above account, there are a number of uncertainties regarding the evolution of the buffer density. All conceivable initial states and subsequent developments are however, from the point of view of advection, which is the issue in this scenario, covered by the three cases outlined at the beginning of the analysis of the scenario, Section 12.2.1. This analysis applies to the high conductivity case, see Section 12.2.1.

For the fracture case, see Section 12.2.1, no route leading to this situation has been identified and it is thus considered as a residual scenario. Canister corrosion for a fractured buffer can be illustrated with expressions given in Neretnieks et al. (2010). The life time of the canister is considerably longer for a fractured buffer than for an eroded buffer, for otherwise identical circumstances, see examples in Neretnieks (2006b). No additional such calculation cases have been performed in the PSAR.

Regarding event sequences, the evolution can certainly be affected by the order in which swelling, mass losses, intrusion of various types of groundwater, etc occur. Again, however, these situations are bounded by the three cases considered.

Should transport in the buffer not be controlled by diffusion, corrosion of the canister could ultimately be controlled by advection of corroding agents in the groundwater. This is illustrated in the reference evolution. The extent of corrosion is further treated in the corrosion scenario, Section 12.6, to which the three cases of buffer advection are propagated, i.e. advection as calculated with base case assumptions and the two bounding cases of initial advection in all deposition holes and no advection throughout the assessment period. As concluded above, all three hydrogeological model variants are also propagated to further analyses. This yields the nine cases in Figure 12-4 to consider.

The occurrence of buffer advection cannot be ruled out and the buffer advection scenario is thus considered as a less probable scenario, to be further addressed in combination with the canister scenarios. The probability that the scenario will occur cannot be quantified in an exact way. It is represented by the nine cases in Figure 12-4, in three of which no advective positions occur.

Hydrogeological DFN model		Mean number of advective positions	
		(at 10 ⁵ yrs)	at 10 ⁶ yrs
Uncorrelated	Initial advection	(6 000)	6 000
	PSAR erosion model	(5.8)	459
	No advection	(0)	0
Semicorrelated	Initial advection	(6 000)	6 000
	PSAR erosion model	(1.4)	41.6
	No advection	(0)	0
Fully correlated	Initial advection	(6 000)	6 000
	PSAR erosion model	(6.6)	129
	No advection	(0)	0

Figure 12-4. Erosion cases propagated to further analysis of canister corrosion. The data were obtained in the sensitivity calculations reported in Section 12.2.2, Figure 12-3.

12.2.4 Special case of advective conditions – Canister sinking

Function indicator(s) considered

A central safety function of the buffer is to prevent advective transport of species between the ground-water and the canister. To ensure this, a certain buffer thickness is required. If the canister sinks or tilts in the deposition hole, this minimum thickness cannot be guaranteed. A swelling pressure of 200 kPa is needed to keep the canister in position in the deposition hole (Buff5). This function indicator assumes that the buffer consists of bentonite.

Treatment of this issue in the reference evolution

Since the loss of buffer mass needed for the advective conditions as described in Sections 10.3.9 and 10.3.11 is less than the loss needed to get to a situation where the canister would sink, advective conditions due to canister sinking *per se* can never occur in the reference evolution. Advective condition will already prevail when the canister sinks.

Qualitative description of routes to canister sinking

The swelling pressure could be reduced by:

1. Loss of buffer material,
2. A transformation of the montmorillonite to a non-expandable mineral.

If sufficient buffer mass was lost to bring the average swelling pressure around the canister down to 200 kPa, advection would likely already be the dominant transport mechanism, hence item 1 above is covered in the reference evolution and in the general buffer advection scenario above. Transformation of the montmorillonite in the buffer is discussed in the transformation scenario, Section 12.4.

Quantitative assessment of routes to canister sinking

The routes to loss of swelling pressure are discussed in the scenarios mentioned above.

Categorisation as “less probable” or “residual” scenario

The consequences of the loss of large amounts of buffer material are discussed in the reference evolution and further in the general buffer advection scenario above. Since considerably higher mass losses are required to cause canister sinking than are required for advective conditions, and since advective conditions is the safety related concern also in the case of canister sinking, the occurrence of canister sinking would not lead to consequences beyond those already quantified in Section 12.2.3.

Conclusion

The only way the canister could sink to the bottom of the deposition hole is in the case of a large loss of buffer material. If this happens the diffusive barrier of the buffer is lost long before the canister starts to sink. Therefore, loss of the diffusive barrier caused by canister sinking does not have to be treated as a scenario on its own.

12.3 Buffer freezing

12.3.1 Introduction

Indicator criterion violated

This scenario concerns the criterion of minimum buffer temperature, namely that the temperature in the buffer should not fall below $-6\text{ }^{\circ}\text{C}$ to avoid detrimental freezing effects.

If the buffer minimum temperature criterion is violated, this could potentially affect both containment and retardation. It has previously been shown that the bentonite will retain its properties after a freezing cycle, but containment could be jeopardised through mechanical impact on the canister by a freezing buffer and the retardation potential may be impaired in the case of severe ice lens formation.

Treatment of buffer freezing in the reference evolution

The possibility of buffer freezing was excluded from the reference evolution which is based on a plausible glacial cycle in which permafrost (that is the $0\text{ }^{\circ}\text{C}$ isotherm) develops to a maximum depth of 259 m at Forsmark (Section 10.4.3). When including all known surface and subsurface uncertainties (e.g. uncertainties in air temperature, climate humidity, surface wetness, vegetation, snow cover, bedrock thermal conductivity and diffusivity, and geothermal heat flux) and setting them all in the condition most favourable for permafrost growth, the uncertainty interval for the permafrost reaches a maximum depth of 463 m in the reference evolution. Correspondingly, the uncertainty interval for the perennially frozen ground reaches a maximum depth of 422 m. In the PSAR assessment, the temperature for which detrimental freezing effects on a canister may occur is determined to be $-6\text{ }^{\circ}\text{C}$ or lower, see Section 8.3.2. This is two degrees lower than the buffer freezing criterion used in SR-Site ($-4\text{ }^{\circ}\text{C}$). In the reference evolution, the $-4\text{ }^{\circ}\text{C}$ isotherm reaches a maximum depth of 148 m. Including the most pessimistic combination of all uncertainties relevant for the reference glacial cycle, the uncertainty interval for the $-4\text{ }^{\circ}\text{C}$ isotherm reaches a maximum depth of 316 m (Section 10.4.3). This shows that even in this most pessimistic case, the $-4\text{ }^{\circ}\text{C}$ isotherm does not reach repository depth in the reference evolution. When cold climate conditions results in permafrost growth, an isotherm for a lower bedrock temperature is located at a shallower depth than an isotherm for a higher temperature (that is, bedrock temperatures are lowest towards the ground surface), see e.g. Figure 10-113. Therefore, it can also be concluded that the $-6\text{ }^{\circ}\text{C}$ isotherm, i.e. the temperature at which a frozen buffer could cause detrimental effects on a canister, does not reach repository depth in the reference glacial cycle.

Qualitative description of routes to buffer freezing

The route to this scenario is development of permafrost under periglacial climate conditions.

The following factors of importance for the occurrence of buffer freezing are identified, based on the discussion above, on Table 10-33 describing uncertainties identified in the reference evolution and on the FEP chart Figure 8-5.

Initial state factors

- Thermal conductivity of bedrock.
- Heat capacity of bedrock.
- Geothermal heat flow.
- Hydraulic conductivity of bedrock.
- Groundwater salinity.
- Porosity of bedrock.
- Heat output of the spent fuel, including its diminishing over time.

Processes

- Heat conduction in bedrock.
- Heat conduction in buffer.
- Freezing of buffer.

External conditions

- Periglacial climate conditions leading to lowered temperature at ground surface.
- Soil coverage at ground surface.
- Vegetation coverage at ground surface.
- Snow coverage at ground surface.
- Glacial conditions leading to changes in temperature at ground surface.
- Submerged conditions leading to changes in temperature at ground surface.

For more details on the processes involved in the development of permafrost and perennially frozen ground, see the **Climate report**, Section 3.4.4 and Hartikainen et al. (2010).

12.3.2 Quantitative assessment of routes to buffer freezing

Three types of sensitivity studies were made to investigate if and under what conditions permafrost, perennially frozen ground and sub-zero temperature ground may reach repository depth:

- Lowering of constant ground surface temperatures.
- Lowering of the air temperature curve reconstructed for the last glacial cycle.
- Assumptions of extremely dry conditions during periods of cold climate; e.g. that no ice sheet, sea, vegetation or winter snow exist at the site during a full glacial cycle.

Sensitivity study on lowering of constant ground surface temperatures

Sensitivity tests on the evolution of permafrost for different constant air temperatures were first made. Site-specific data on physical-, thermal-, and hydrological bedrock properties were used (see the **Climate report**, Section 3.4.4). These calculations were made for two cases, with and without the heat contribution from a repository using the 1D permafrost model. The results show that, with heat from the repository included (which corresponds to conditions during the first future glacial cycle), the constant ground surface temperature must be lower than -8 °C for permafrost (0 °C isotherm) to reach repository depth (450 m) (Figure 12-5). If no heat from spent fuel is taken into account (corresponding to subsequent glacial cycles), the 0 °C isotherm reaches repository depth in $\sim 120\,000$ years if the ground temperature is -8 °C (Figure 12-5). At present, the annual mean air temperature at Forsmark is ca $+5.5\text{ °C}$ (see the **Climate report**, Section 2.2). The ground surface temperature is typically a few degrees higher than the air temperature (e.g. Hartikainen et al. 2010). The results thus indicate that an air temperature lowering of more than 13 °C is required to make permafrost develop to repository depth when considering constant air temperatures.

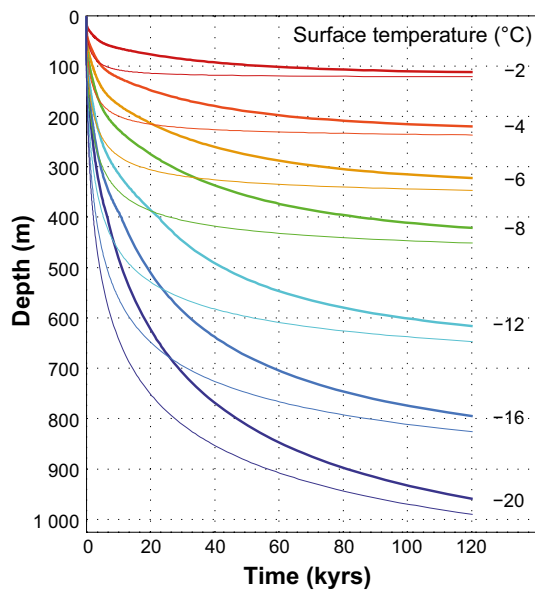


Figure 12-5. Calculated evolution of permafrost depth (defined by the 0 °C isotherm) at the repository location in Forsmark for different constant ground surface temperatures. Bold lines: with repository heat contribution. Thin lines: without repository heat contribution.

Sensitivity study on lowering of the air- and ground surface temperature curves reconstructed for the last glacial cycle

Permafrost simulations were made to investigate how much air- and ground surface temperatures need to be lowered in a more realistic *variable* climate for permafrost, perennally frozen ground, and sub-zero temperatures to develop to repository depth. Specifically, it was investigated how much the local temperature curve used for the assessment of permafrost in the reference evolution, Section 10.4.3, was required to be lowered to get the 0, -2 and -4 °C isotherms to reach the 450 m repository depth. The temperature of 0 °C corresponds to the freezing point of fresh water at atmospheric pressure, as well as the definition of permafrost. The -6 °C temperature is the temperature used in the PSAR for detrimental freezing of the backfill material in the deposition tunnels, see Sections 8.4.4. As previously mentioned, the temperature criteria for detrimental freezing of the buffer clay is also -6 °C in the PSAR, see Section 8.3.2. Lowerings of the temperature curve of 4, 6, 8, 10, 12, 14 and 16 °C were studied in this sensitivity experiment. These sensitivity simulations were made with the 2D permafrost model (see the **Climate report**, Section 3.4.4 and Hartikainen et al. 2010).

In the 2D permafrost simulations performed, the significant uncertainties associated with descriptions of the surface conditions motivated an analysis of two variants, one with humid surface conditions and one with dry conditions (see the **Climate report**, Section 3.4.4 and Hartikainen et al. 2010). As a pessimistic case, the dry variant of the reconstruction of last glacial cycle conditions was used for this sensitivity experiment since it results in deeper permafrost than the humid variant. Mean thermal properties of the subsurface were used. Note that these simulations only cover the initial 50 000 years of the glacial cycle, which however includes the period with deepest permafrost during the glacial cycle (see the **Climate report**, Section 3.4.4).

The resulting temporal evolution of maximum 0, -2 and -4 °C isotherm depths over the repository are shown in Figure 12-6 to Figure 12-8. Figure 12-6 also includes the depth of the perennally frozen ground, which is somewhat shallower than the permafrost depth due to the prevailing pressure- and salinity conditions at depth. The results show that the temperature curve reconstructed for the last glacial cycle needs to be lowered by 8 °C to make permafrost reach the repository depth (Figure 12-6). Furthermore, the results show that a lowering of the reconstructed temperature curve of more than 10 °C and around 14 °C are needed to get the -2 °C and -4 °C isotherms to reach the repository depth (Figure 12-7 and Figure 12-8). In line with this, in order to get the -6 °C isotherm down to repository depth would require a lowering of the air temperature curve several degrees more than 14 degrees (not shown in the figure). These lowerings are large, especially for the -2, -4 and -6 °C isotherms. They

are for instance considerably larger than the estimated maximum uncertainty in the air temperature curve ($\pm 6\text{ }^{\circ}\text{C}$) used as input to the simulations (see Section 10.4.3 and the **Climate report**, Appendix 1 and Section 3.4.4).

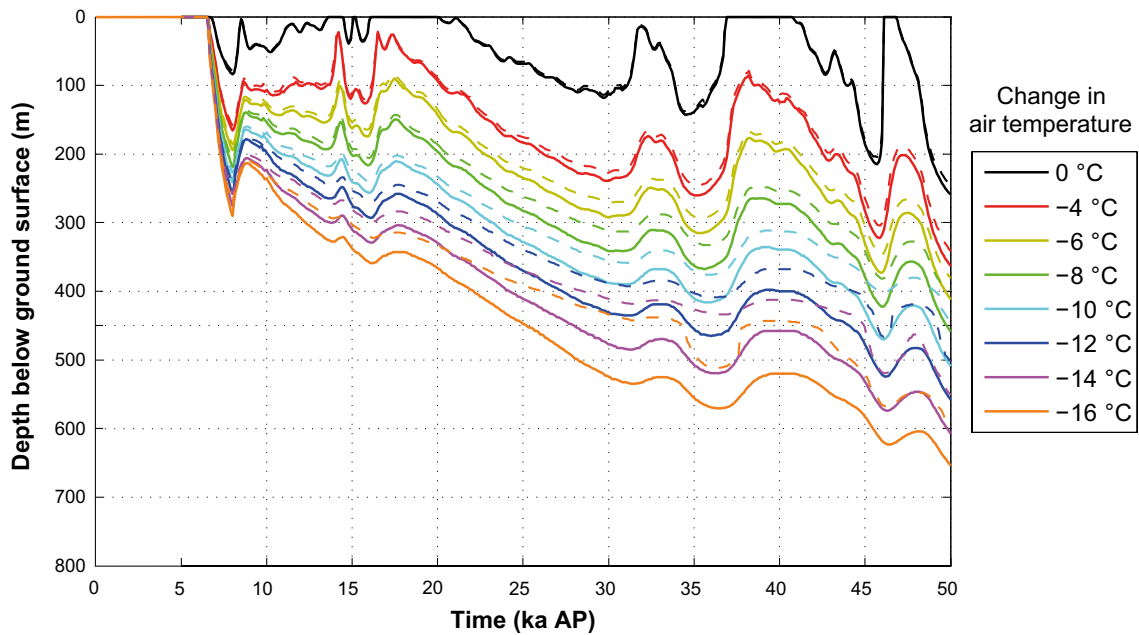


Figure 12-6. Evolution of the 0 °C isotherm (permafrost) depth (solid lines) and depth of perennially frozen ground (dashed lines) at the repository location for the reference glacial cycle (dry climate variant, see the Climate report, Section 3.4.4). The figure also shows corresponding results for simulations where the temperature curve reconstructed for the last glacial cycle has been lowered by -4, -6, -8, -10, -12, -14 and -16 °C. The results are extracted from the 2D permafrost modelling conducted for the Forsmark site (see the Climate report, Sections 3.4.4 and 0 and Hartikainen et al. 2010).

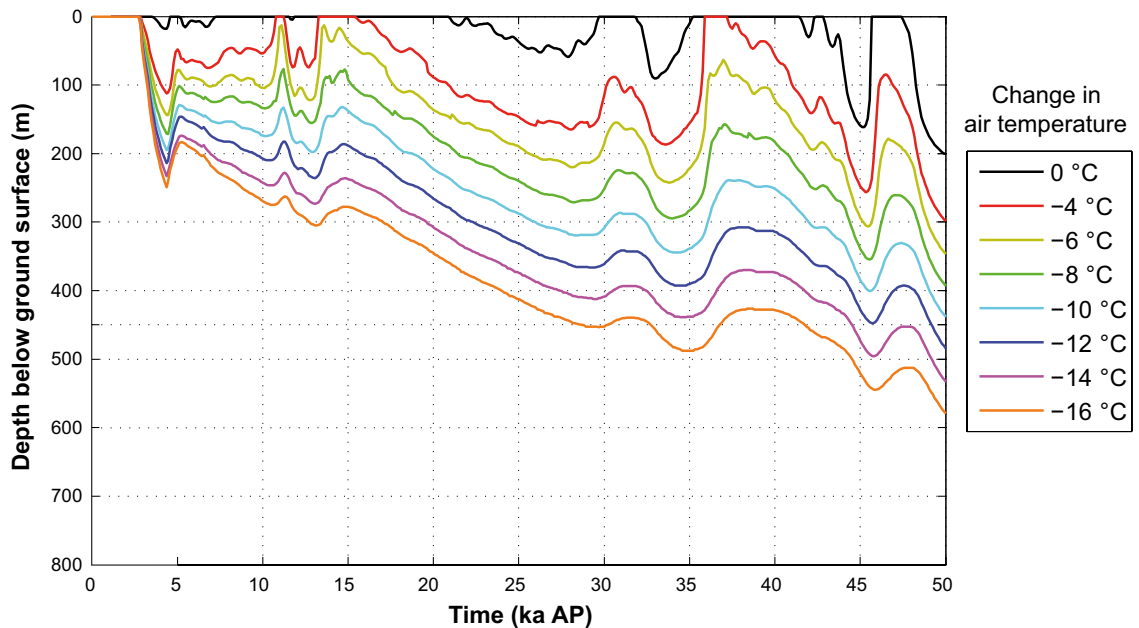


Figure 12-7. Evolution of the -2 °C isotherm depth at the repository location for the reference glacial cycle (dry climate variant). The figure also shows corresponding results for simulations where the temperature curve reconstructed for the last glacial cycle has been lowered by -4, -6, -8, -10, -12, -14 and -16 °C. The results are extracted from the 2D permafrost modelling conducted over the Forsmark site (see the Climate report, Sections 3.4.4 and 0 and Hartikainen et al. 2010).

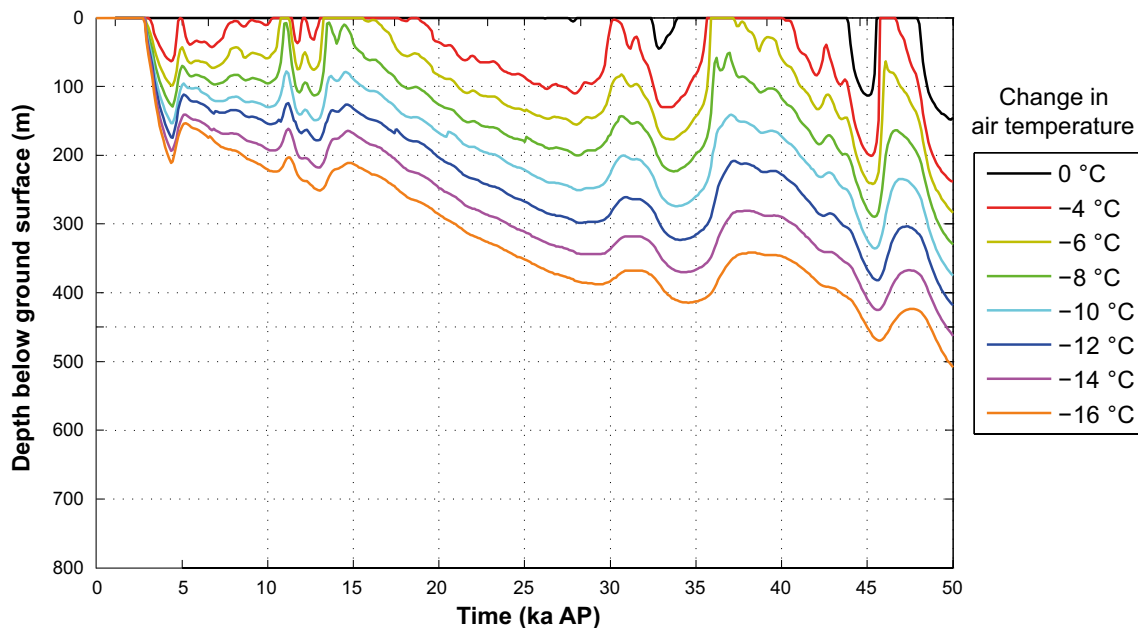


Figure 12-8. Evolution of the $-4\text{ }^{\circ}\text{C}$ isotherm depth at the repository location for the reference glacial cycle (dry climate variant). The figure also shows corresponding results for simulations where the temperature curve reconstructed for the last glacial cycle has been lowered by -4 , -6 , -8 , -10 , -12 , -14 and $-16\text{ }^{\circ}\text{C}$. The results are extracted from the 2D permafrost modelling conducted over the Forsmark site, see the *Climate report*, Sections 3.4.4 and 0 and Hartikainen et al. (2010).

Sensitivity study on assumptions of no ice sheet, sea, vegetation or winter snow during a full glacial cycle (Severe permafrost case)

The main uncertainty in all permafrost simulations conducted for the PSAR is the uncertainty in the input air temperature curve (see the **Climate report**, Section 3.4.4 and Appendix 1). This uncertainty was, together with all other climate-, surface- and subsurface uncertainties relevant for the reference glacial cycle, treated in Section 10.4.3. In the present sensitivity study, the remaining uncertainties, on e.g. ice sheet and sea coverage are treated based on the results of the severe permafrost case (see the **Climate report**, Section 5.5).

The main assumption in the severe permafrost case is that a very dry periglacial climate dominates, a climate not supporting ice sheet growth over the Forsmark site at any time during the glacial cycle. To favour permafrost growth further, the effects of protective snow cover and vegetation were excluded, in line with the assumption of a very dry climate. In addition, the repository location was assumed to always remain above sea level. Heat generated by the repository is however included in the simulation, since it is relevant for the first future glacial cycle. The 2D permafrost model was used for the simulations. For further information on the permafrost models and the setup of these simulations, see Sections 10.4.1 and 10.4.3, **Climate report**, Section 4.5.5 and Hartikainen et al. (2010).

In the severe permafrost case, all known uncertainties compatible with the main assumption of having no ice sheet over Forsmark are included. It should be noted that the main assumption for the severe permafrost case, that is of having no ice sheet over the site, is incompatible with the temperature curve reconstructed for the last glacial cycle, and its uncertainty range towards lower temperatures handled in the reference evolution, Sections 10.4.1 and 10.4.3, since these temperatures do result in an ice sheet over Forsmark (see the **Climate report**, Section 3.1.4). Nevertheless, in order to make a pessimistic choice of temperature curve for the severe permafrost case, air temperatures were assumed to fall according to the reconstructed temperature curve for the reference glacial cycle (Figure 12-9). For further discussion and motivation for this approach, see the **Climate report**, Section 5.5.

The air temperature curve reconstructed for the last glacial cycle was used to calculate ground surface temperatures for the severe permafrost case, see Figure 12-9, using an empirical relationship between air and ground temperatures. For details of this calculation (see Hartikainen et al. 2010).

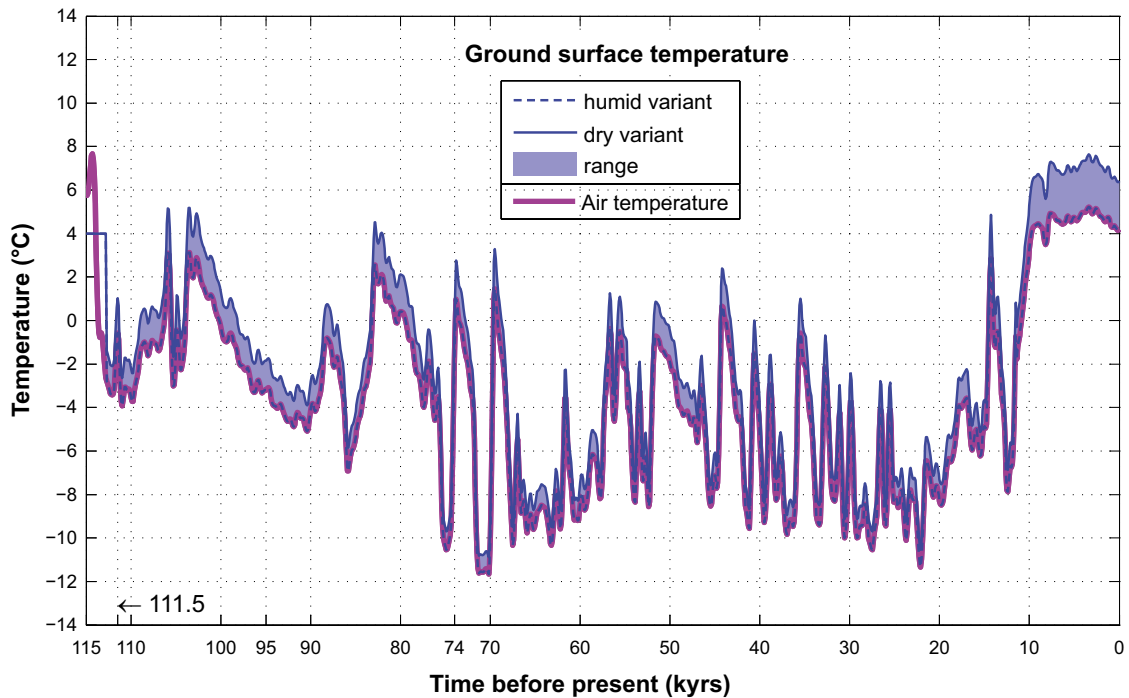


Figure 12-9. Example of evolution of air temperature and modelled ground surface temperatures used for the severe permafrost case. In this plot, the temperature has not been projected into the future. For a description of the modelling of ground surface temperature (see Hartikainen et al. 2010). Note that the air temperature curve typically is located behind the dry variant of the ground surface temperature curve.

Evolution of the depth of permafrost, perennially frozen ground and the -2 and -4 °C isotherms over the repository for the severe permafrost case is shown in Figure 12-10. As one variant of the severe permafrost case, a simulation was made to study the effects of uncertainties in bedrock thermal properties together with uncertainties in surface conditions (except air temperature, see above). In order to obtain the largest uncertainty range, the dry climate variant was combined with the bedrock thermal properties enhancing permafrost development, and the humid climate variant with thermal properties diminishing permafrost development (Figure 12-11).

The results show that the maximum depth of permafrost over the repository in the severe permafrost case is 393 m (Figure 12-10), with the uncertainty interval reaching down to 456 m (Figure 12-11). This occurs after more than 90 000 years into the future. The maximum depth of perennially frozen ground, occurring at the same time, is 359 m with an uncertainty interval down to 408 m. The -2 and -4 °C isotherms reach depths of 311 and 234 m respectively, with the uncertainty intervals reaching down to 359 and 268 m. Since colder bedrock temperatures are found at shallower depths (see above), the -6 °C isotherm would be located at a shallower depth than the -4 °C isotherm (not shown in Figure 12-11). Table 12-1 summarises all results from the severe permafrost case, together with the results from the reference evolution.

The values in Table 12-1 are valid for the first future glacial cycle of the 1 Myr long safety assessment period. For the second and following glacial cycles, the heat from the repository is negligible, resulting in up to 37 m deeper permafrost and frozen ground (see the **Climate report**, Section 4.5.3).

Further results from the 2D permafrost simulations made for the severe permafrost case, regarding e.g. salinity concentrations, ground water flow and vertical temperature profiles for various surface cover types, are found in the **Climate report**, Section 3.4.4 and Hartikainen et al. (2010).

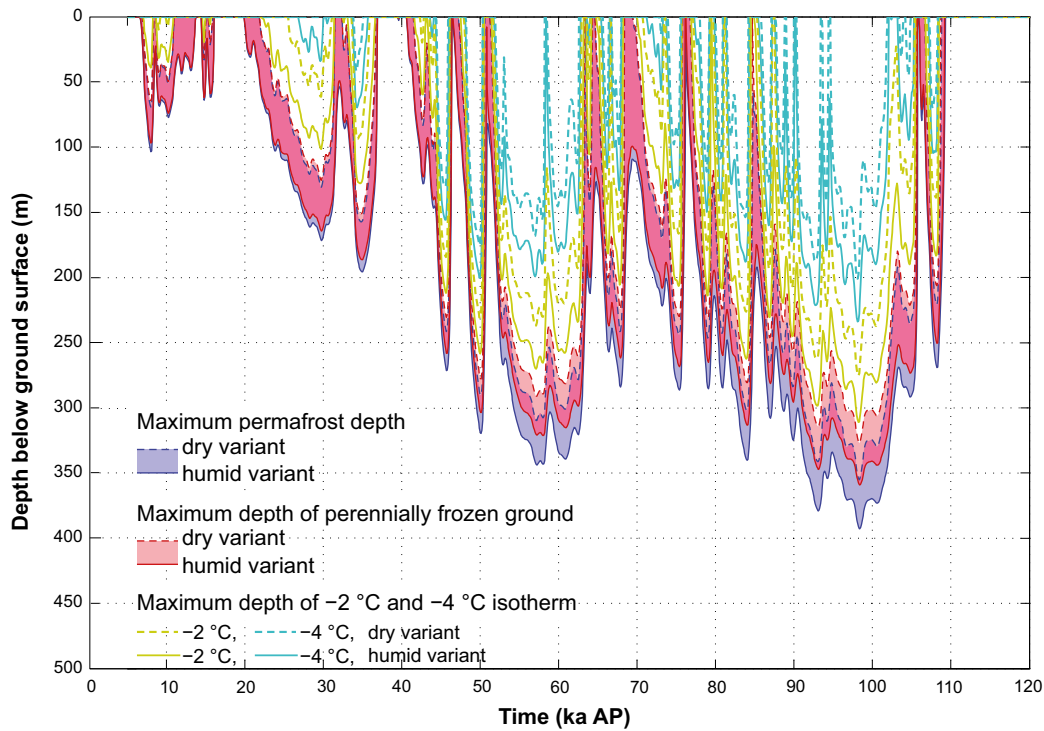


Figure 12-10. Evolution of maximum permafrost depth, maximum depth of perennially frozen ground and maximum depth of -2 and -4 °C isotherms over the repository for the severe permafrost case. The upper permafrost surface, for periods of degradation from above, is not shown. The shaded area in blue and red represents the range when considering the dry and humid climate variants of the severe permafrost case. The lilac colour indicates that the results for permafrost and perennially frozen ground overlap.

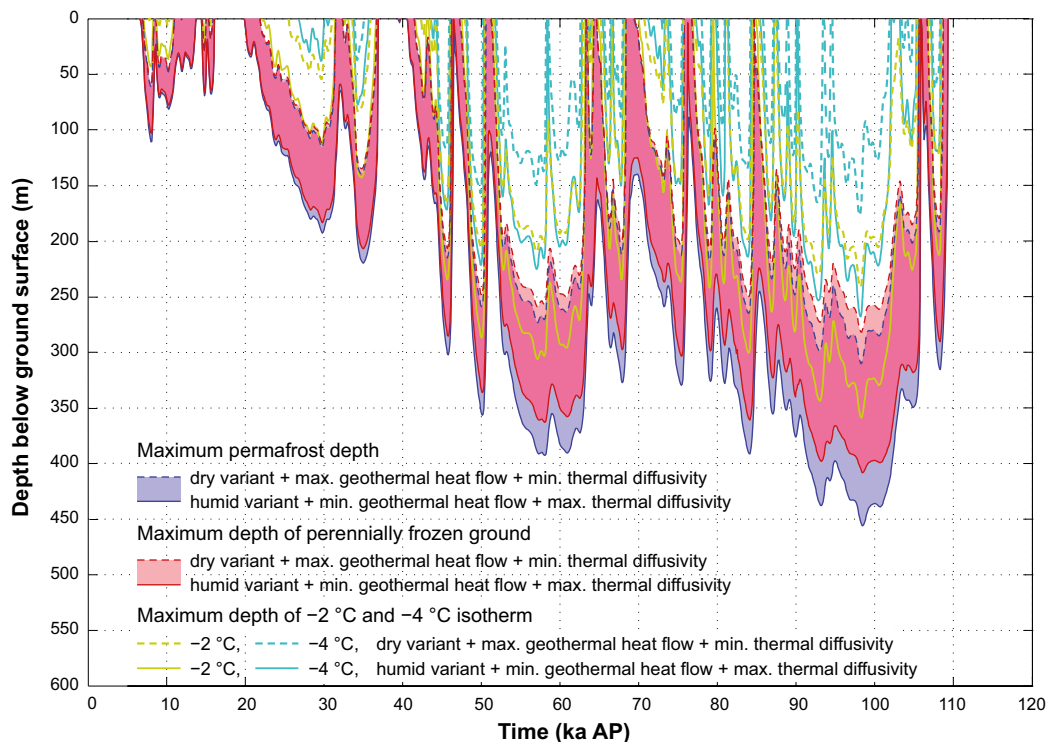


Figure 12-11. Evolution of maximum permafrost depth, maximum depth of perennially frozen ground and maximum depth of -2 and -4 °C isotherms over the repository for the severe permafrost case considering combined uncertainties in surface conditions and thermal properties favourable for permafrost growth. The shaded area in blue and red represents the range when considering the dry and humid climate variants. The lilac colour indicates that the results for permafrost and perennially frozen ground overlap.

The conclusion from the results of the severe permafrost case is that the uncertainties remaining from the analysis of the reference evolution, Section 10.4.3, i.e. mainly the uncertainty in ice sheet and sea coverage, yielded larger depths for the permafrost, perennially frozen ground, -2 and -4 °C isotherms, but with a smaller uncertainty range (Table 12-1). For most parameters, the uncertainty ranges reach maximum depths that are a few tens of metres shallower in the severe permafrost case than in the reference evolution (Table 12-1). The largest depth of perennially frozen ground is achieved not in the severe permafrost case but from making the unrealistic combination of setting all uncertainties relevant for the reference evolution to their values most favourable for permafrost growth, see Table 12-1 and Section 10.4.3. In the analysis of maximum possible freezing depths, the situation is bounded by the consideration of both the reference glacial cycle and severe permafrost case, including their respective uncertainty ranges.

Table 12-1. Maximum depths of permafrost (0 °C isotherm), perennially frozen ground, -2 °C isotherm and -4 °C isotherm for the severe permafrost case and the reference evolution. The uncertainty interval for the reference glacial cycle includes the unlikely combination of having all uncertainties, including air temperature, set to the most pessimistic values favouring permafrost growth. The uncertainty interval for the severe permafrost case includes all relevant uncertainties for this case (set to their most pessimistic settings), which excludes air temperature since lower air temperatures than the reconstructed last glacial cycle air temperature curve are not compatible with the main assumption of having no ice sheet development over the site. Since colder bedrock temperatures are found at shallower depths, the depths of the -6 °C isotherm would be located at a shallower depth than the depth of the -4 °C isotherm (not shown in the table).

	Maximum permafrost depth (0 °C isotherm) [uncertainty interval]	Maximum depth perennially frozen ground [uncertainty interval]	Maximum depth -2 °C isotherm (i.e. freezing temperature of backfill) [uncertainty interval]	Maximum depth -4 °C isotherm (i.e. freezing temperature of buffer clay) [uncertainty interval]
Reference evolution	259 m [down to 463 m]	246 m [down to 422 m]	200 m [down to 388 m]	148 m [down to 316 m]
Severe permafrost case	393 m [down to 456 m]	359 m [down to 408 m]	311 m [down to 359 m]	234 m [down to 268 m]

Can climate get cold enough to cause detrimental buffer freezing?

The difference between the present warm interglacial temperatures and the *coldest* temperatures during the last glacial cycle as recorded in the GRIP ice core from central Greenland is in the order of 12 °C (Figure 12-12). The figure also exemplifies a typical feature of glacial climate archives namely that they show that temperature and climate is highly variable on both long and short time scales (see the **Climate report**, Section 4.3.4), variability for example seen in the GRIP proxy temperature data. When severe very cold conditions occur, these conditions do not persist for long periods of time. Such climate variability is observed also in frequency analyses of climate records (e.g. Moberg et al. 2005, Witt and Schumann 2005).

How low could temperatures have been at Forsmark during the last glacial cycle? Global and regional climate modelling suggest that the proglacial regions, south, southeast and southwest of the Last Glacial Maximum (LGM) ice margin in northern Europe, experienced annual mean air temperatures around 0 to -6 °C (around 9 to 12 degrees colder than at present) (Kjellström et al. 2009, Figure 3-27, Brandefelt and Otto-Bliesner 2009). The LGM model results for the Forsmark area are not relevant to this discussion, since at that time Forsmark was covered by the ice sheet. However, Kjellström et al. (2009) also made a climate simulation for a stadial period during Marine Isotope Stage 3 during the Weichselian, at 44 000 years BP, with postulated ice-free conditions at Forsmark. The resulting cold and dry periglacial climate had an annual mean air temperature in the Forsmark region of ca -7.5 °C (around 13 degrees lower than at present) (Kjellström et al. 2009, Figure 4-4 and Tables 4-2 and 5-1). The annual mean air temperature of -7.5 °C is well in line with the temperature in the reconstructed temperature curve for this specific period (Figure 12-9) which is around -8 °C. The results show a consistency between the independent temperature obtained from the climate model and the temperature curve reconstructed for the last glacial cycle, both showing that during cold last glacial cycle stadials, with restricted duration, temperatures in the Forsmark area often may have dropped to be more than 10 °C colder than at present.

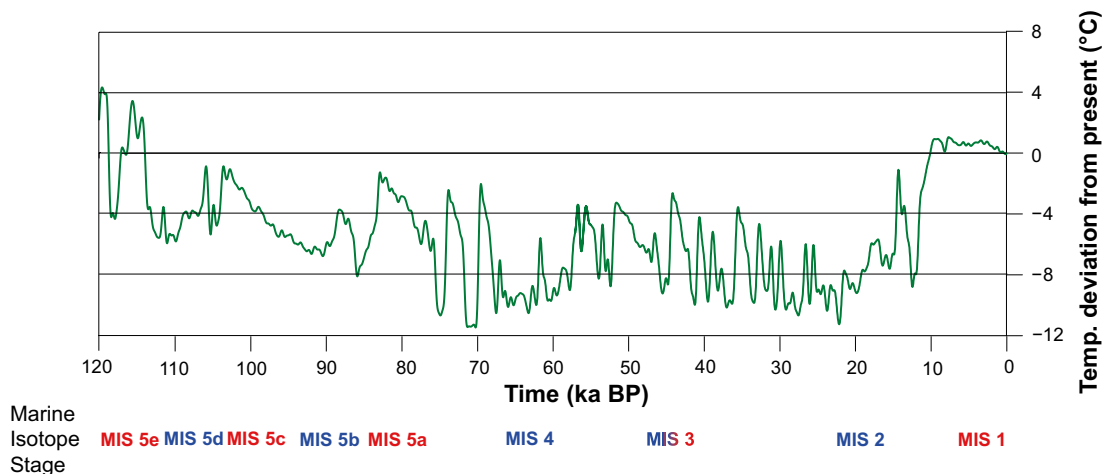


Figure 12-12. GRIP proxy temperature curve. During the last glacial cycle, temperature was highly variable on both long and short time scales. Modified from Dansgaard et al. (1993).

Furthermore, the air temperature curve reconstructed for the last glacial cycle for the Forsmark region (Figure 12-9) suggests that mean annual air temperatures during the *coldest* stadials of the glacial cycle may have been around -11 to -12 °C (about 16 to 18 degrees colder than at present). However, considering the uncertainties in e.g. the transfer functions between ^{18}O and air temperature and the adaptation of the curve for Fennoscandian conditions, temperatures could have been even lower (see the **Climate report**, Appendix 1). In this context, it should also be noted that the mean annual ground surface temperature, relevant for permafrost growth, typically is a few degrees higher than the air temperature, see Figure 12-9.

During the last glacial cycle, really low air temperatures only prevailed during stadials with relatively short duration, typically some thousands of years long (Figure 12-12). This prevented permafrost from developing to great depths (Figure 10-107), and would do so also under even more extreme glacial cycle conditions (Figure 12-10 and Figure 12-11). For more information on the last glacial cycle climate, see the **Climate report**, Section 4.3.

If climate were to shift towards colder glacial cycles, it is unlikely that the variability within the climate system would drastically change. Very cold periods have been short lived in the past and it is very likely that this will be the case also during future glacial cycles. Variability is a characteristic feature of Earth's climate system. However, for a discussion on a less variable climate, see further below.

Assuming a similar climate variability to that during the last glacial cycle, it requires a lowering of the entire last glacial cycle temperature curve by as much as 14 °C in order to make the -4 °C isotherm reach repository depth at Forsmark (Figure 12-8) and several degrees more for the -6 °C isotherm to do the same. Also when considering the significant estimated maximum uncertainty in the reconstructed air temperature curve (± 6 °C), as well as the maximum potential intrinsic permafrost model error of ± 1.5 °C (Hartikainen et al. 2022), this corresponds to an unrealistically large change in glacial climate conditions.

Furthermore, during the coldest phases of glacial cycles, Fennoscandia is typically covered by an ice sheet. Under these coldest periods it is very likely that the Forsmark site is covered by an ice sheet, and under such conditions permafrost either develops at a much lower rate or decreases (see the **Climate report**, Sections 3.4.4 and 4.5). In association with major ice sheet advances over the site, the area is also submerged for a considerable time after deglaciation, which further prevents permafrost development. If future glacial cycles were to be colder than in the past, this would most likely produce larger ice sheets and longer periods of ice sheet coverage at the site, reducing the depth of the permafrost and -4 and -6 °C isotherms.

The effect of an unlikely future climate with considerably less glacial climate variability than during the past 2 million years can be determined by reference to the sensitivity test results presented in Figure 12-5. If the ground temperature is $-8\text{ }^{\circ}\text{C}$ at Forsmark, it would take about 120 000 years for permafrost ($0\text{ }^{\circ}\text{C}$ isotherm) to develop to repository depth (if heat from spent fuel is present). At present, the annual mean air temperature at Forsmark is around $+5.5\text{ }^{\circ}\text{C}$ (see the **Climate report**, Section 2.4.2). Since the air temperature often is a few degrees lower than the ground surface temperature, Figure 12-9 and Hartikainen et al. (2010), the results indicate that an air temperature lowering of more than $13\text{ }^{\circ}\text{C}$ is required to make permafrost develop to repository depth when considering constant temperatures. Such low temperatures could occur occasionally during a glacial cycle (Figure 12-9 and Figure 12-12), but such cold periods prevail for considerably shorter times than 120 000 years (see Section 4.3 and Appendix 1, both in the **Climate report**).

Freezing of backfill

During periglacial periods in the reference evolution, the $-4\text{ }^{\circ}\text{C}$ isotherm reaches down to a maximum depth of 148 m, with an uncertainty interval down to 316 m (Table 12-1). In the severe permafrost climate case, the $-4\text{ }^{\circ}\text{C}$ isotherm reaches a maximum depth of 234 m (Figure 12-10), with an uncertainty interval down to 268 m (Figure 12-11, Table 12-1). The temperature for which a frozen backfill material may start having detrimental effects on the surrounding host rock is $-6\text{ }^{\circ}\text{C}$ (Section 8.4.4). Hence, since the $-6\text{ }^{\circ}\text{C}$ isotherm is located at a shallower depth than the $-4\text{ }^{\circ}\text{C}$ isotherm (cf Figure 10-113), such backfill freezing effects along the ramp and shafts may occur down to depths shallower than the ones indicated for the $-4\text{ }^{\circ}\text{C}$ isotherm above. Possible consequences of this are discussed in Section 10.4.8.

12.3.3 Conclusions

Based on the model studies described above, including sensitivity studies of all known uncertainties, perennially frozen ground and the -4 and $-6\text{ }^{\circ}\text{C}$ isotherms do not reach repository depth in the reference evolution, nor in the severe permafrost case. By adapting the most pessimistic combination of all uncertainties related to permafrost development in the reference evolution, the $0\text{ }^{\circ}\text{C}$ isotherm may reach repository depth. However, this case, which is considered quite unrealistic, does not result in groundwater freezing at repository depth during the first future glacial cycle since the repository heat and the prevailing pressure and salinity conditions at depth counterbalance the freezing process. After repository heat has declined, i.e. for the second future glacial cycle, and for all following glacial cycles in the 1 Myr assessment period, the most pessimistic combination of uncertainties results in water at repository depth freezing. However, it should again be emphasised that this combination of uncertainties is considered quite unrealistic, and consequently, that freezing at repository depth also for these glacial cycles are considered unrealistic.

The temperature criterion for detrimental freezing in the buffer material is $-6\text{ }^{\circ}\text{C}$. The results in Figure 12-10 and Figure 12-11 show that in the pessimistic cold and dry severe permafrost case, there is ample margin before the $-4\text{ }^{\circ}\text{C}$ isotherm would reach repository depth. Consequently, there is an even larger margin before the $-6\text{ }^{\circ}\text{C}$ isotherm would reach repository depth. The results in Figure 12-8 show that the temperature curve reconstructed for the last glacial cycle needs to be lowered by $\sim 14\text{ }^{\circ}\text{C}$ in order for the $-4\text{ }^{\circ}\text{C}$ isotherm reach a depth of 450 m, and consequently that an even larger lowering of the air temperature would be required for the $-6\text{ }^{\circ}\text{C}$ isotherm to reach repository depth. Even when including the significant uncertainty in the reconstructed air temperature curve (see the **Climate report**, Appendix 1 and Hartikainen et al. 2010), and the maximum uncertainty introduced by intrinsic model errors (Hartikainen et al. 2022), such low temperatures are considered unrealistic based on what is known about past climate conditions and climate variability. There is a large margin for detrimental freezing of the buffer clay and repository tunnel back fill for all assessment period glacial cycles, even when adopting the most pessimistic combination of uncertainties. The possibility for detrimental freezing of the buffer clay, under any feasible future climate development, is therefore considered as ruled out. The same conclusion applies for detrimental freezing of the back-fill.

Categorisation as “less probable” or “residual” scenario

Since the conclusion of the analysis of this scenario is that the buffer will not freeze, this is considered as a residual scenario.

Quantitative consequence analysis/discussion – containment and retardation

If the consequences in terms of containment of a postulated freezing were to be analysed, a bounding case would be one where all canisters are damaged due to freezing. This is similar to the situation where all canisters fail due to isostatic over-pressure, analysed as a postulated “what-if” case in Section 13.7.1.

Global warming variant and other climate cases

The occurrence of permafrost is delayed in the Global warming variant, see Section 10.6.1. The delay would also delay the onset of possible buffer freezing and thus any consequences would also be delayed and reduced. Buffer freezing is, therefore, not further treated for the Global warming variant.

Since the severe permafrost climate case (see Section 12.1.3) has been used in the above analysis and since that case was defined to maximise the potential for buffer freezing, no additional climate cases need to be considered.

Combination of buffer erosion and freezing

The results from the permafrost simulations show that, in the reference evolution and in the severe permafrost case, freezing of ground water does not occur at repository depth during the first glacial cycle (although the 0 °C isotherm may reach repository depth under very pessimistic assumptions). Therefore, groundwater in erosion cavities does not freeze during the first glacial cycle when a buffer erosion case is combined with a freezing case based on the reference evolution or severe permafrost case. Such a combined case is therefore not further treated in this report.

For the second future glacial cycle, and all following glacial cycles in the 1 Ma assessment period, the heat from the spent fuel has declined, resulting in the situation that under the most pessimistic and quite unrealistic combination of uncertainties, water may freeze at repository depth during these glacial cycles. Therefore, an analysis of freezing of water in buffer erosion cavities is presented in the **Climate report**, Appendix 3C. The results show that, if freezing were to occur at repository depth, the maximum freezing induced pressure in buffer erosion cavities would be 26–27 MPa, which is considerably lower than the critical pressure for canister collapse described in the scenario treating canister collapse due to isostatic load (Section 12.7.2).

12.4 Buffer transformation

Indicator criterion violated

This scenario concerns all conceivable routes to an alteration of the montmorillonite in the buffer material. This refers to a transformation of the montmorillonite in the buffer to non-expandable minerals (e.g. illite), but also accumulation of impurities that could change the properties of the buffer. This mainly concerns the function indicators on maximum buffer temperature and limited pH:

1. The temperature in the buffer should not exceed 100 °C.
2. The pH of the groundwater should not exceed 11.

There may also be other processes that affect the stability of the montmorillonite. A *temperature gradient over the buffer* may cause transport of silica from the hot to the cold part. Presence of *metallic iron in contact with bentonite* could also alter the montmorillonite.

If the buffer material is transformed, this could possibly affect both containment and retardation by affecting other function indicators. Containment could be jeopardized indirectly through a lack of swelling pressure, which could lead to enhanced sulphide corrosion and create conditions suitable for microbially induced corrosion on the canister surface. Retardation could be affected by an increased hydraulic conductivity in the buffer, or by a loss of swelling pressure, which in turn could lead to the formation of pathways.

Treatment of routes to transformation in the reference evolution

According to Section 10.3.4 there are substantial margins to the 100 °C function indicator even with account taken of uncertainties in the thermal conductivity in the rock. Based on this, temperatures above 100 °C were not considered in the reference evolution.

The movement of silica in the thermal gradient is discussed in Section 10.3.10, see Figure 10-72. The expected thermal gradients gave a very small redistribution of silica.

Contact between metallic iron and the buffer is only possible if there is a defect in the copper shell. This is not addressed in the reference evolution.

Qualitative description of routes to buffer transformation

The following factors of importance for the occurrence of buffer transformation are identified, based on the discussion above, on Table 10-33 describing uncertainties identified in the reference evolution and on the FEP chart, Figure 8-5.

High temperature

This route to the transformation scenario can be due to:

1. a residual power in the canister which is higher than the design value,
2. a misinterpretation of the thermal properties of the rock at the site,
3. a lower initial water content in the buffer than the design value,
4. a drying of the buffer, leading to a decreased thermal conductivity.

The only identified cause for route 4 is ventilation of the deposition hole for an extended period of time. The consequences of drying of the rock and its effect on the thermal properties of the buffer are discussed in Section 10.3.8. There is no foreseen evolution of the near-field that could lead to those conditions and drying of the buffer is not considered further.

High pH

High pH groundwaters in contact with the buffer could occur if the quality control system for repository construction fails or malfunctions. The possible routes could either be a misjudgement of the pH arising from the cement used, or the use of a wrong cement mixture.

Thermal gradient

The thermal gradient is dependent on the thermal power from the canister and the thermal properties of the rock. However, the sensitivity to the parameters is small and the conclusions from the reference evolution are expected to be valid for all possible conditions.

Interaction with metallic iron

This process will occur if the canister insert gets in contact with the buffer material. Laboratory experiments under repository conditions have shown that reactions between montmorillonite and metallic iron in an oxygen-free environment may be relatively fast and in some cases also lead to a general breakdown of the montmorillonite structure (Lantenois et al. 2005).

Another possibility would be if stray equipment or material containing iron or steel was left in a deposition hole during buffer emplacement. However, in the PSAR it is assumed that the QC system will ensure that the deposition holes are cleaned before the buffer is deposited.

Quantitative consequence analysis/discussion

The effect of the thermal period on the buffer is described in Section 10.3.10. The conclusion is that the expected temperature increase will have no significant effect on the buffer properties.

A buffer temperature exceeding the function indicator could lead to the following consequences.

1. A transformation of the montmorillonite in the buffer to non-expandable minerals (illite). This would give a higher hydraulic conductivity and a decrease in swelling pressure.
2. An accumulation of impurities in the buffer on the hot (or cold) side. This would be caused by temperature-dependent solubilities. This accumulation could potentially lead to clogging of the pore space and a change in the rheological or/and the hydraulic properties.

The transformation of montmorillonite to illite is discussed in Section 10.3.10. It is evident that the transformation is very slow even if repository time scales are considered. Karnland and Birgersson (2006) undertook a review of different kinetic models for smectite to illite conversion. Figure 12-13 shows the results from different models. The models of Cuadros (Cuadros and Linares 1996) (Cuadros 1) estimate a much faster alteration rate than the one that was used in the SR-Can assessment (Huang). However, the Cuadros experimental work did not include specific determinations of all rate-determining constants and parameters, as was done by Huang et al. (1993). Cuadros, therefore, used natural analogues to adjust their model (Cuadros 5) in order to represent the conditions in nature, where bentonite persists over geological time scales.

There are two kinds of data uncertainties for this process.

- Uncertainties in the temperature calculation. This is described in the section above.
- Uncertainties in the data used in the alteration calculation (Karnland and Birgersson 2006) and in the reactive transport calculation.

The potentially most critical data uncertainties are in the frequency factor for a first order reaction (Arrhenius equation) and the activation energy in the kinetic expression for the alteration rate.

Using the Huang model, a temperature of 125 °C for 10 000 years would not have any significant effect on the swelling pressure and hydraulic conductivity function indicators (Karnland and Birgersson 2006). However, the experimentally measured model parameters have to be determined at temperatures significantly higher than the maximum repository temperature. The uncertainty in the model predictions is thereby increasing with decreasing temperature. The kinetic model is thereby only used for the justification of the temperature criterion, but not for a detailed long-term prediction of the transformation with attention to the decreasing temperature. As seen in Figure 10-16, the temperature in the warmest part of the buffer decreases below 60 °C already after 200 years. This means that the uncertainties in the kinetic models will only impact a very limited period of the repository evolution.

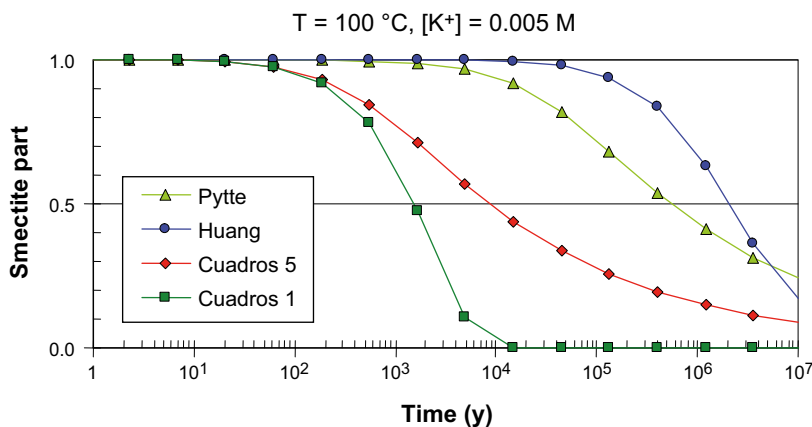


Figure 12-13. Comparison of kinetic models for the smectite to illite transformation. Lines show the calculated remaining proportion of smectite versus time for a constant temperature of 100 °C and a constant potassium concentration of 0.005 M.

Figure 12-14 (Karnland and Birgersson 2006) shows the swelling pressure of the MX-80 buffer material as a function of the dry density. The arrows in the figure indicate the swelling pressure for the reference density, a material with 30 % transformation and a material with 50 % conversion to illite. A conversion of 30 % of the montmorillonite to illite would still give a swelling pressure above the 1 MPa function indicator. Figure 12-13 shows that with the Huang model a temperature of 100 °C for a period of over 1 000 000 years is needed to get a degree of conversion of 30 %. It is evident that the period with elevated temperature under any reasonably postulated set of conditions will never be close to that value. The problem with the kinetic model is not the long time scale but rather a more exact estimation of the effect of the decreasing temperature. The scoping calculation by use of a temperature of 100 °C is though considered useful since it does not lead to significant alteration despite the over-pessimistic temperature assumptions.

An effect of steam on the properties of bentonite has been identified by Couture (1985) and is discussed by Pusch (2000a) and Karnland and Birgersson (2006). There is an observed effect of vapour that could influence the maximum free swelling of the bentonite. However, no obvious mineral alteration was identified by Couture although the experiments were performed at temperatures significantly higher than the maximum temperature in a repository. Laboratory test series with materials that were briefly (7 days) exposed to temperatures of up to 200 °C at different water saturation levels are reported as Leupin et al. (2014). The test series comprised of ten different bentonites, which represent different excavation sites and hence suppliers, as well as various counter-ion compositions. Also tests were made with four different purified montmorillonites as completely ion-exchanged into calcium, sodium and potassium, respectively. The water saturation rate was controlled according to two principles; partly passively via the added amount of water in a closed system, and partly through external control of water activity. The results show no clear differences as a result of hydrothermal treatment between unsaturated and water-saturated samples with respect to swelling capacity. On the other hand, significant differences in sedimentation behaviour of bentonites/montmorillonites that contain calcium as a counter-ion, probably due to structural changes. Furthermore, there are large expected differences between samples dominated by sodium as counter-ion and samples dominated by calcium. Generally, differences in measured swelling properties due to hydrothermal treatment are negligible in comparison to the differences between sodium dominated and calcium-dominated materials. The effects of short-term vapour exposure on free swelling are therefore not considered to be a problem for a KBS-3 repository.

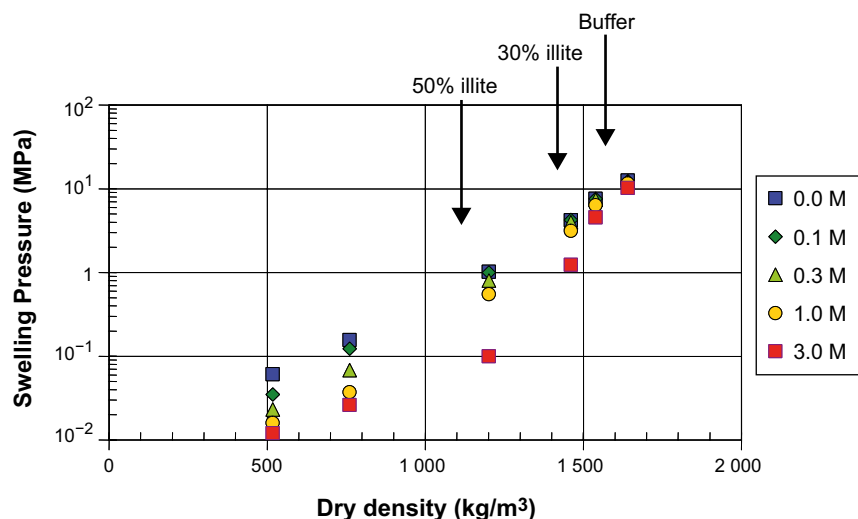


Figure 12-14. Swelling pressure of MX-80 material in contact with pure water and NaCl solutions. Dots show measured values. Buffer indicates the swelling pressure of unaltered buffer material at KBS-3 target density, 30 % illite indicates the pressure at the maximum acceptable transformation, and 50 % illite illustrates the pressure at 50 % illitization.

High pH

If high pH ($\text{pH} > 11$) groundwaters were to contact the buffer, some alteration or dissolution would be expected. The extent of the transformation is dependent on the actual pH of the water, the local hydrologic situation and the amount of cement producing the high pH (mass balance). However, in the PSAR it is assumed that the quality control systems will be sufficient to avoid the introduction of cements that could give rise to high pH waters in the repository.

Thermal gradient

The effect of the temperature gradient on the redistribution of impurities has been calculated by Sena et al. (2010b) and Karnland and Birgersson (2006). This process has been shown to have a very limited effect. The temperature gradient is only affected by the absolute temperature to a limited degree, and the dependence of this process on the temperature is, therefore, limited.

Interaction with metallic iron

Currently, a mechanistic understanding is lacking and a quantitative model does not exist. However, no interaction between buffer bentonite and metallic iron is expected to occur as long as the copper canister is intact.

Summary

Since there still are some uncertainties on the effect of high temperatures on the long-term performance of the buffer, a case with an altered buffer zone next to the canister cannot be entirely excluded. The consequences of such a case would be a loss of swelling pressure next to the canister, and a correlated consolidation of this part due to the swelling pressure in the remaining buffer. However, a major part of the buffer has to be transformed in order for the buffer swelling pressure to fall below the pressure criterion of 1 MPa, where advection conditions need to be considered, which is most unlikely. If such a low pressure occurred, this would mean that it could be possible for sulphate-reducing bacteria to survive and sulphide corrosion to be enhanced.

The interaction between iron and buffer material is still under investigation. It is likely that only the region closest to the insert would be affected, assuming that there was any contact between the insert and the buffer, and the overall transport properties of the buffer would be maintained. However, today it cannot be excluded that the entire diffusion barrier could be lost. This, however, would have consequences only for retardation.

Global warming variant and other climate cases

There is nothing connected to the global warming variant (essentially 60 000 years before the first periglacial period) that would make buffer transformation worse. The climate on the surface has no bearing on any of the processes discussed in this section. The issue is therefore not further treated for the global warming variant. Nor do any of the other climate cases described in Section 12.1.3 have any relevance for the buffer transformation scenario.

Categorisation as “less probable” or “residual” scenario

High temperature, high pH and high temperature gradients are not expected to have any significant effect on buffer stability under any plausible conditions. Transformations of buffer material to such an extent that the beneficial containment and retardation properties are affected are, therefore, considered as a residual scenario.

If the buffer gets in contact with metallic iron some alteration will occur. The extent of this is currently unknown. The process can only occur after copper canister failure. It is not relevant for failures when buffer is missing.

Conclusions

Processes that may alter or transform the montmorillonite, as described above, are not expected to have any significant effect on the important buffer properties. However, since there are uncertainties over the combined effect of elevated temperatures and high pH, a case where the buffer next to the canister is altered and the swelling pressure is lost to a level where bacteria can survive is appropriate to study. This case is treated as a residual scenario.

12.5 Conclusion from analyses of buffer scenarios

From the results of the analyses of the three buffer scenarios above, the following conclusions are drawn regarding propagation of buffer conditions to the analyses of canister scenarios.

- The buffer advection scenario is propagated as three cases to the canister scenarios: i) advective conditions in every deposition hole throughout the assessment period, ii) advective conditions as calculated with base case assumptions in Section 12.2.2, iii) no advective conditions in any deposition hole at any part of the assessment period.
- The buffer freezing scenario is regarded as residual. It is, therefore, not propagated to the canister scenarios in the PSAR.
- The buffer transformation scenario is regarded as residual. It is, therefore, not propagated to the canister scenarios in the PSAR.

In addition to the buffer scenarios treating altered buffer states, also the case of an intact buffer needs to be considered, and this is covered by case iii) in the first bullet point.

12.6 Canister failure due to corrosion

12.6.1 Introduction

Canister corrosion was evaluated for a number of situations in the reference evolution. As demonstrated in Chapter 10, canister corrosion leads to failure only for advective conditions in the buffer, and for such conditions only in the most highly flowing deposition holes, in general after several hundreds of thousands of years.

The buffer conditions are thus crucial for the evaluation of the canister failure due to corrosion scenario. Based on the findings in the analyses of the buffer scenarios, the cases of intact buffer and of advective conditions in the buffer need to be propagated to this corrosion scenario. As described in the analysis of the buffer advection scenario, Section 12.2.3, three cases for buffer advective conditions are propagated for further analyses.

Safety function indicator(s) considered

This scenario concerns the safety function Can1, 'Provide corrosion barrier', that is directly related to the containment potential of the canister.

This is one of the top-level safety functions, meaning that a number of sub-functions must be evaluated in order to fully assess the canister corrosion scenario. Several results from other scenarios, in particular regarding the buffer are, therefore, propagated to this scenario.

Treatment of canister corrosion in the reference evolution

Canister failures due to corrosion occur in the reference evolution, for the case of advective conditions in the buffer. For an intact buffer, the margins protecting against corrosion failures were demonstrated to be considerable.

The two tasks for this corrosion scenario are thus to evaluate i) whether all uncertainties for the corrosion case with advective conditions in the buffer are appropriately addressed in the reference evolution and ii) whether for an intact buffer there are any remaining uncertainties that could challenge the conclusion that corrosion failures will not occur.

Qualitative description of routes to corrosion

The following factors of importance for the occurrence of canister failures due to corrosion are identified, based on the discussion above, on Table 10-33 describing uncertainties identified in the reference evolution and on the FEP chart, Figure 8-5.

Initial state factors involved

- Initial minimum copper coverage.
- Deposition hole rejection criteria.
- Corroding agents in buffer and backfill.

Processes and rock conditions involved

- Copper corrosion.
- Diffusive transport of corroding species through the buffer (for intact buffer).
- Advective transport in a deposition hole with an eroded buffer.
- Groundwater flow.
- Groundwater concentrations of sulphide.
- The possibility of oxygen penetration.

External conditions involved

- Glacial conditions leading to enhanced groundwater flow.
- Glacial conditions leading to changed groundwater composition (oxygen and sulphide).

12.6.2 Quantitative assessment of corrosion – general

Remaining uncertainties regarding each of the factors mentioned above are addressed below followed by corrosion calculations based on the additional uncertainties identified for a buffer in advective conditions.

Initial copper coverage

The initial copper coverage was evaluated in the **Canister production report**, leading to the initial state values cited in Section 5.4.2, Table 5-9. The derivation of the initial state is based on the reference design, production and control methods described in the **Canister production report**, see Section 5.4. This issue is, therefore, not further treated here.

As seen in Table 5-9 the minimum copper thickness is 47.5 mm for more than 99 percent of the canisters, and somewhat lower values may exist for the remaining small fraction. For the corrosion analyses presented in this section, only a limited part of the canister surface is exposed to the corroding agent. For an eroded buffer where advection is the dominant transport process, a height of the canister corresponding to the thickness of the buffer around the canister, 35 cm, is assumed to be corroded (see Section 10.4.9). For an intact buffer, where diffusion is the dominant transport process, the concentration profile in the buffer from species entering through a fracture in the deposition hole will have its maximum over an even smaller area. The probability that the area with (pessimistically) assumed reduced copper thicknesses around the seals will actually be exposed to corrosion is thus small. Therefore, the thickness is assumed to be 47 mm in the corrosion analyses (see the **Data report**, Section 4.1). More sophisticated analyses are not seen as warranted in light of the considerable uncertainties associated with many other factors in the corrosion calculations, in comparison to the rather limited range of values of initial copper coverage discussed here.

Furthermore, a reduction in copper coverage by a small cavity on the outside, say at the mm scale, would not decrease the time required for penetration due to corrosion in proportion to the reduced coverage, as the copper outer surface would be evened out as corrosion proceeds. It is only cavities on the inner surfaces that would result in a proportionate decrease in penetration time.

As mentioned in Section 10.2.5, subsection “*Canister corrosion*”, initial corrosion by atmospheric oxygen before emplacement and from initially entrapped oxygen is expected to cause corrosion depths less than 2.5 mm, including pits, and will thus have a small impact on the minimum copper coverage of the canisters. Due to the pessimisms invoked both in the derivation of the maximum corrosion depth due to O₂, as well as its direct combination with the long-term sulphide corrosion, the corresponding reduction of the initial thickness of the copper shell was neglected in the assessment of corrosion in the reference evolution. As mentioned in Sections 10.4.9 and 10.7, the sensitivity to this assumption is addressed in the present Section. This is done with a sensitivity case with reduced initial copper coverage under the subheading “*Quantitative sensitivity analysis of canister corrosion*” below.

In Section 10.3.13, corrosion caused by sulphide is discussed, for various sources and transport pathways of sulphide, and the maximum corrosion depths are summarised in Table 10-15 and Figure 10-96. The estimated corrosion depths include many pessimistic assumptions. Not all canisters will be affected by initial high sulphide concentrations, through gas transport of sulphide, or increased groundwater flow due to thermally induced spalling (either for intact buffer or corrosion during erosion). For corrosion caused by SRB activity using different substrates, and where hydrogen from corrosion of iron and steel gives the highest corrosion, the processes are evaluated with mass balances ignoring both transport processes (of both hydrogen and sulphide) as well as precipitation of sulphide with Fe²⁺. To set a corrosion allowance for all canisters, and all over the surface, using corrosion depths derived with these very pessimistic assumptions, is, in Chapter 10 deemed overly pessimistic for the reference evolution, and further, the maximum corrosion depths are generally below 1 mm. To illustrate the sensitivity to such assumptions, and in particular to that of a corrosion depth of 4 mm from sulphide generated by SRB feeding on hydrogen from the degradation of rock reinforcements, a case with a reduced initial coverage is analysed under the subheading “*Quantitative sensitivity analysis of canister corrosion*” below.

It is further demonstrated that only general corrosion takes place as long as the sulphide flux at the canister surface is below 3×10^{-10} mol/(m²·s), as the film growth is then controlled by the transport of sulphide in solution (and in the pores of the film). For sulphide fluxes higher than that, localised features (resulting from micro-galvanic coupling) cannot be excluded. In the **Fuel and canister process report**, Section 3.5.4, Subsection “*Localised corrosion in sulphide environment*”, it is summarised that the observations of “pits” on copper in sulphide solutions show features that are not growing extensively deeper with time, but rather become more shallow, if formed at all. This is consistent with a system that is largely transport-limited, and which cannot sustain a localised corrosion process with a penetration depth significantly ahead of the general corrosion front, as the interfacial sulphide concentration at the canister surface is close to zero. The transport resistance for the sulphide is further increased by the precipitation of corrosion products in pits. In Section 10.3.13 the sulphide flux at the canister surface is evaluated for the different sulphide sources, but for all cases shown to be below the threshold flux.

For the safety assessment it is thus reasonable to describe these localised features in terms of a maximum pit depth to be added to the average corrosion depth. As shown in the **Fuel and canister process report** the observed features are in the range of 1–15 µm, but there it was suggested to pessimistically set the maximum pit depth to be ten times deeper than the deepest observation, i.e. 150 µm. However, in analogy to the handling above of pessimistic and localised processes that do not appear all over the surface, no reduction of the initial copper thickness is done. This is in somewhat contrast to the very pessimistic approach of using a pitting factor of 20 (for the canisters that fail within 10⁶ years) as was done in SKB (2019c), but ongoing work suggests a tendency for the ratio of maximum pit depth to average corrosion to decrease with exposure time.

Alternative design copper thicknesses, including halving the thickness to 25 mm, are evaluated as part of the BAT analyses in Section 14.3.2.

Deposition hole rejection criteria

Deposition holes are rejected according to the EFPC criterion in the reference evolution. This is a design decision and it is seen fully feasible to implement the EFPC, see Section 5.2.3. Therefore, rejection according to EFPC is assumed also in the corrosion scenario. Alternative rejection criteria are evaluated as part of the BAT analyses in Section 14.3.2. Alternative criteria are underway (see Section 5.2.3), but have not been implemented in the PSAR.

Buffer and backfill impurities

The analysis of the reference evolution demonstrates that constituents initially present in the buffer and the backfill, i.e. entrapped oxygen and impurities (pyrite, organic matter) as well as other sources of organic matter (rock biofilms) and hydrogen from corroding rock bolts and other iron components contribute negligibly to copper corrosion, see Section 10.3.13. Mass balance considerations lead to the conclusion that corrosion depths from these constituents would, with several pessimistic assumptions, be at most 4 mm and furthermore that time intervals comparable to the one million year assessment period are required for all constituents to reach the canister. Considering that the initial content of these constituents puts a fundamental limit on the extent of corrosion caused by these, and that this extent is limited also with several pessimistic assumptions, this issue is not further considered in this scenario, except as a sensitivity case at the end of this Section 12.6.2.

Copper corrosion

In the analysis of the reference evolution corrosion is evaluated as caused by oxygen (atmospheric, and initially entrapped), sulphide (transported via groundwater, or produced by sulphate reducing bacteria, as mentioned above) as well as corroding agents formed by radiolysis of water or irradiation of nitrogen in humid air. Section 10.3.13 gives the extent of this corrosion as limited to a few mm in the 10⁶ year assessment perspective, and with these margins and most of the processes bounded by mass balance (otherwise by mass transport), these corrosion mechanisms are not further treated in this scenario. However, there is a need to revisit the discussion on corrosion of copper with water under hydrogen gas production, for low pH conditions.

In Section 8.3.4 it is stated that chloride-assisted corrosion of copper is ruled out if pH and chloride concentration are below (at the right-hand side of) the limiting curve, and there is thus a need to analyse additional evolutions to rule out unfavourable pH conditions and high ionic strength conditions. During temperate climate conditions the acidity of groundwaters is highest in the upper parts of the rock where recharge of meteoric waters dominates because rain water is saturated with atmospheric CO₂, which is an acid, and several biological processes produce CO₂ in the soil layers. When these waters penetrate further down in the rock, the acidity is neutralised through several water-rock reactions. Typical pH values for waters at Forsmark are illustrated in Figure 10-46. In addition to the enhanced infiltration of fresh meteoric waters, another process that may result in low-pH groundwaters is the upconing of deep saline groundwaters which results in mixtures with fresh groundwaters. If the mixtures become oversaturated with calcite, the acidity of the mixture increases when calcite precipitates: $\text{Ca}^{2+} + \text{HCO}_3^- \rightarrow \text{CaCO}_3 + \text{H}^+$. This effect is larger when waters of meteoric origin, rich in HCO₃⁻, rather than glacial melt waters are mixed with deep Ca-rich groundwaters. The present-day groundwater data at Forsmark together with sensitivity analysis results of mixing calculations show that the lowest pH that may be attained is around 6.3, and this agrees with the analysis presented in Section 10.3.7. In Section 10.6.3 a transitory rise in atmospheric CO₂ concentrations is discussed. As long as the increased CO₂ levels are limited to a period of hundreds to thousands of years, it would not affect the acidity of groundwaters at repository level. The controls on atmospheric CO₂ concentrations subsequent to a reduction in fossil fuel emissions indicate that although enhanced CO₂ concentration values would persist over such time scales, concentrations would be lower than the peak value (see the **Climate report**, Sections 5.1 and 5.2).

The groundwater data at Forsmark indicate that in volumes of rock outside fracture zones the salinity has been stable during the Weichselian glacial cycle, and large oscillations in groundwater salinities are therefore not expected in the future. The same is anticipated based on simulations of groundwater salinity under periglacial and glacial conditions (see the **Climate report**, Sections 3.4.4 and 5.5.3, and Hartikainen et al. 2010). The analyses of different possible climatic episodes presented in Sections 10.3.7 and 10.4.7 show that salinity can increase due to upconing during the short glacial margin passage above the repository area. The analyses reported in Sections 10.4.6 and 10.4.7 show that the upconing effect is moderate and the resulting ionic strengths in the repository volume are below 0.5 M. Because the most pronounced upconing takes place during an ice advance, when the ice profile is steepest, the analysis of the reference evolution includes the highest salinities that can be expected from upconing at Forsmark. It is therefore concluded that there is no need to analyse consequences of chloride-assisted copper corrosion.

Diffusion in intact buffer

As demonstrated in SKB (2010d) the flow rate controlled transport resistance in the buffer/rock interface determines the rate of transport of species from the groundwater to the canister. The transport resistance due to the buffer diffusivity is negligible in comparison. Therefore, there is no reason to handle buffer diffusion any further in this corrosion scenario for the intact buffer. In the case of advective conditions in the buffer, diffusion of dissolved species in the buffer porewater is, by definition, irrelevant.

Corrosion geometry

For the diffusive case with the buffer present, the corrosion geometry is given by the dimensions of the near-field repository components. There are no significant uncertainties to evaluate in this case.

As discussed in the context of the reference evolution at Section 10.4.9, the corrosion geometry for the case with advective conditions in the deposition hole is uncertain, varying in time and difficult to quantify. In Section 10.4.9 a cautious geometry was used in the calculation examples. An extreme, bounding geometry is evaluated below as a sensitivity case.

The canister is first exposed along a line around half its circumference and this situation does not change with time, see Figure 12-15. Corrosion would then proceed radially in the copper material, corresponding to a corroded area with an equivalent height, h_{corr} , of $\pi \cdot d_{can}/2$, where d_{can} is the thickness of the copper shell. This yields an exposed area of

$$A_{corr} = \frac{1}{2} \cdot \pi^2 \cdot r_{can} \cdot d_{can}$$

This extreme value is about a factor of five smaller than the cautious value in the reference evolution. (A smaller area yields a higher corrosion rate since all incoming sulphide is assumed to react with the exposed canister surface.)

In the corrosion scenario, the cautious geometry is used since it is seen as unrealistic and overly pessimistic to base the calculations in the corrosion scenario on the above extreme geometry. For this extreme geometry to arise and persist would require the erosion to first go on for a long time (hundreds of thousands of years) and then abruptly stop due to changed groundwater conditions at just this eroded position, and then remain in this state for another long time (again hundreds of thousands of years). However, the sensitivity of the corrosion result to the pessimistic corrosion geometry is analysed below.

The geometrical shape for the eroded material is selected to represent a reasonably pessimistic case for the assessment of consequences (Sellin 2013). The geometrical shape is not represented by Figure 12-15, but by the illustration furthest to the right in Figure 12-16. Figure 12-15 shows an extreme bounding case. The bounding case illustrates a situation where the erosion has been going on such that the eroded volume has just reached the canister wall and then stopped. If the erosion would continue according to Figure 12-16, it would only take 20 % more time to go from the 3rd illustration where corrosion can start to the 4th illustration, where corrosion occurs according to the assessment. In all other time intervals the corrosion rate will be less than what is assumed in the calculations. To assume that the erosion will continue up to the situation in the 3rd illustration and then suddenly stop is considered to be unreasonably pessimistic. The sensitivity analysis in SKB (2010d) shows that the selected cautious geometry yields an extent of corrosion that is a factor of 5 lower than with the extreme bounding geometry.

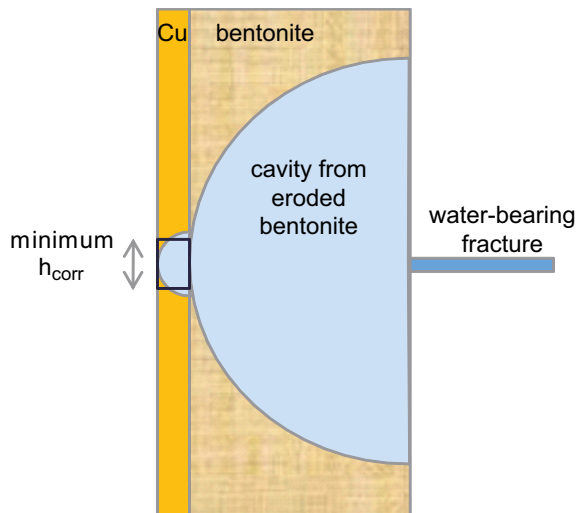


Figure 12-15. Illustration of erosion and corrosion geometry in the erosion/corrosion model. The corroded copper volume is modelled with a constant height, with an extreme, minimum value derived from a growing semi-circular cross section into the copper.

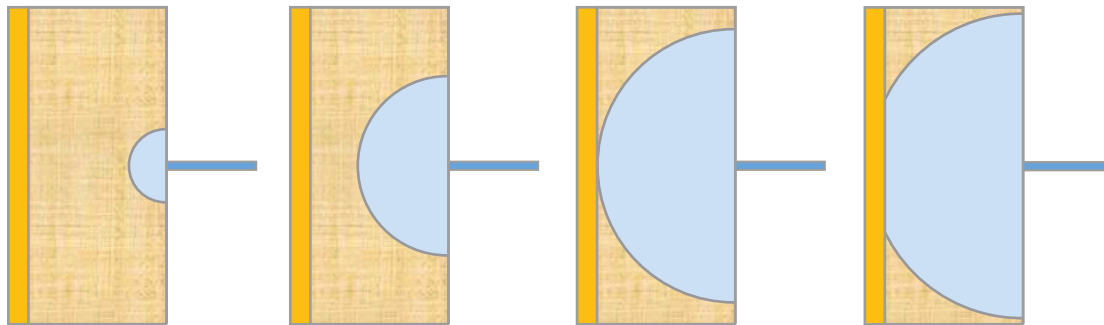


Figure 12-16. Illustration of the geometry for erosion of buffer, with a growing semi-circular cross section. When the copper surface is reached the eroded section will continue to grow, and expose a larger height of the copper surface (SKB 2010d).

Groundwater flow and glacial conditions leading to enhanced groundwater flow

The groundwater flow is one of the factors determining the equivalent flow rates around the deposition holes. In the reference evolution, conceptual uncertainties regarding groundwater flow for temperate climate conditions were evaluated for the advection case, Section 10.4.9, by considering the three fracture size/transmissivity correlation functions treated in the Forsmark hydrogeological DFN model in **Site description Forsmark** and further handled in the uncertainty analysis described in Section 10.3.6. These three variants of the hydro DFN model are used in the further quantitative evaluations of the extent of corrosion below.

Regarding varying groundwater flow conditions over a glacial cycle, it is demonstrated in Section 10.4.6 that the time averaged values over the reference glacial cycle of q (Darcy flux), $q^{1/2}$ and $q^{0.41}$, relevant for copper corrosion under advective conditions, copper corrosion under diffusive conditions and buffer erosion, respectively, are all around 80 percent of the corresponding entities for temperate conditions, see ML2 data in Figure 10-155. Using the temperate values is thus pessimistic and gives some margin for alternative evolutions to the reference glacial cycle.

To address this further, it is noted that increased flow in comparison with temperate conditions occurs when the margin of an advancing ice sheet reaches the repository footprint or the margin of a retreating ice sheet leaves the footprint, see Section 10.4.6. More severe cases of increased flow could thus occur if a margin of an ice sheet came to a halt on top of the repository. This is addressed as follows.

During the deglaciation of the Weichselian ice sheet, the general ice sheet retreat temporarily halted several times. This is seen from dated ice marginal moraines, including the deposits from the Younger Dryas stadial in e.g. southern Sweden (see the **Climate report**, Section 4.2.2). During such halts in the deglaciation, the ice margin either oscillated back and forth or moved slowly within a zone that could be many km wide, in the case of the Younger Dryas several tens of km. During the formation of individual moraine ridges, the ice margin is estimated to have been at stable positions for up to a few hundred years (see the **Climate report**, Section 4.2.2). It has to be assumed that similar types of stillstands may occur also during phases of ice sheet advance.

Although not the case during the last deglaciation and in the SR-Site reference glacial cycle, future periods of frontal stillstands could occur at the Forsmark site during ice advance, maximum or retreat phases, given suitable climate conditions. An extreme case in terms of hydraulic gradients and associated increased groundwater flow would occur if the ice front came to a temporary halt with the frontal part of the ice sheet situated above the repository. According to Vidstrand et al. (2010) there is an approximately two km wide influence zone with significantly increased groundwater flux associated with an ice sheet margin over Forsmark. This situation is valid if there is no permafrost at the Forsmark site. If permafrost is present, which is the case in the reference evolution, and also very likely during a future glaciation of the Forsmark site, a zone of increased groundwater flow is significantly less pronounced (Vidstrand et al. 2010). Using a two km wide near-frontal zone with significantly increased groundwater flux is therefore a pessimistic choice for the analysis of the probability for a future situation with an ice sheet margin stillstand over the repository.

Assuming that future periods of ice margin stillstands would have the same characteristics as the stillstands associated with the most recent deglaciation, briefly described above and in more detail in the **Climate report**, Section 4.2.2, one could make an estimate of the probability of having such a situation occurring at the Forsmark site. By generalising the development of the last deglaciation, one could postulate ten temporary halts of shorter duration and one major halt of longer duration, corresponding to the Younger Dryas event, for a deglaciation of a full-sized ice sheet equivalent to the one of the LGM. Furthermore, for the halts of shorter duration, completely stable ice margin conditions are set to persist for 200 years, while during the major stillstand, a completely stable position of the ice margin is pessimistically set to a full 1 000 years. This is somewhat longer than the time period that the ice margin was located somewhere within the 20–25 km wide Younger Dryas zone in Sweden, which lasted around 900 years. In reality, it is likely that, during such long phases, the ice margin would move slowly and/or oscillate within an ice marginal zone (see the **Climate report**, Section 4.2.2). Nevertheless, in order to cover uncertainties in future ice sheet behaviour, a completely stable margin position for 1 000 years is assumed for the major stillstand. In this way, the major stillstand constitutes a pessimistically chosen case in terms of the duration of a high hydraulic gradient and associated high groundwater fluxes.

The deglaciation of the Weichselian ice sheet, from its LGM position in Poland and Germany to the Scandinavian mountain range, occurred along a distance of ~2 500 km (Fredén 2002). For each of the postulated stillstands, there is a ~2 km wide frontal zone with significantly increased groundwater fluxes (Vidstrand et al. 2010). For each advance or deglaciation phase, the probability of having a 200 year long stillstand at Forsmark is therefore 0.008 ($10 \times 2 \text{ km} / 2\,500 \text{ km}$), while the probability of having the postulated 1 000 year long stillstand at Forsmark is 0.0008 ($2 \text{ km} / 2\,500 \text{ km}$). For a complete glacial cycle with two phases of ice advance and two phases of deglaciation over Forsmark, i.e. a glacial cycle similar to the SR-Site reference glacial cycle, the probabilities for the 200 year and 1 000 year ice margin stillstands at Forsmark are 0.03 ($0.008 \cdot 4$) and 0.003 ($0.0008 \cdot 4$), respectively. For the full assessment period of 1 million years, comprising eight repeated identical glacial cycles, the probabilities grow correspondingly larger.

For the question of increased flow during an ice sheet margin stillstand, also the presence or absence of permafrost should be considered. In the reference glacial cycle, the simulated advancing ice sheet is cold-based, and it advances over permafrost, whereas the ice sheet is warm-based during the deglaciations, see Section 10.4.1. It is mainly the latter situation gives rise to increased flow since frozen ground significantly reduces groundwater flow (e.g. Vidstrand et al. 2010, Hartikainen et al. 2010). In estimating the probability of having an ice margin stillstand over Forsmark, it is reasonable to include also this development. In line with this, it is assumed that half of the stillstands are cold-based and half are warm-based. The resulting probability of having a warm based, 200 year stillstand over the reposi-

tory during one reference glacial cycle is thus estimated at 0.015 (0.03/2), while the probability of a warm based 1 000 year stillstand is estimated at 0.0015 (0.003/2). For the one million year assessment period, these figures should be multiplied by eight, yielding probabilities of 0.12 and 0.012 for 200 year and 1 000 year stillstands, respectively. Hence, it can be concluded that there is a low probability that the ice margin zone, with high groundwater flux, would come to a temporary halt above the repository during the deglaciation, especially when considering the rarer stillstands of long duration. In this context, it is again pointed out that the assumption of a completely stable ice margin over the repository for 1 000 years is a highly pessimistic case compared to what is known from the typical conditions during last deglaciation (see further the **Climate report**, Section 4.2.2).

Intact buffer

For an intact buffer, $q^{1/2}$ is the relevant entity to consider. Assuming according to Figure 10-140 that q is increased by a factor of 100 during the ice margin stillstand, $q^{1/2}$ increases by a factor of ten. A one thousand year stillstand then gives an impact on corrosion corresponding to 10 000 years of temperate flow, which is only one percent of the one million year assessment period. Considering that the probability of this to occur once during one million years is 0.012 leads to the conclusion that this impact is negligible. The same conclusion is reached for the 200 year stillstands.

Advection in buffer

For a buffer with advective conditions, the Darcy flux, q , is normally the relevant entity to consider, but for the high flow rates of concern in this case, the dependence on Darcy flux is as $q^{1/2}$ (Neretnieks et al. 2010) and the effect is thus negligible according to the above. Even with a linear dependence on q , the effect would be negligible considering the low probabilities involved.

In conclusion, the Darcy flux distributions at 2000 AD for the three hydrogeological DFN models do not have to be modified to account for varying flow conditions over a glacial cycle.

Groundwater concentrations of sulphide

For corrosion calculations in the reference evolution, it was assumed that the distribution of groundwater concentrations of sulphide over a glacial cycle is equal to that for temperate conditions reported in Section 10.3.7. This is regarded as a pessimistic assumption, see Section 10.4.7. These concentrations also include effects of microbial sulphate reduction. That is, the availability of the various nutrients that feed sulphate reducing bacteria, such as organic carbon and hydrogen, are also assumed to remain similar to the present temperate period. This is justified by the slow sulphate redox kinetics in the deep groundwater, as interpreted from the co-occurrence of organic carbon and sulphate in groundwaters with residence times on the order of thousands of years or more (Kalinowski 2013). Also, it was pessimistically assumed in the corrosion calculations reported for the reference evolution that sulphide concentrations at a given position in the repository do not vary in time, but a randomly sampled value from the distribution of sulphide concentrations is assumed to prevail throughout the one million years assessment period. As also shown for the reference evolution, assignment of the mean value of the distribution to all deposition holes results in lower consequences in terms of failed canisters at one million years.

No reason to pursue this pessimistic approach any further has been identified. However, some simple studies of the sensitivity of the corrosion result to the properties of the sulphide distribution are presented below. The distribution consists of 46 data points ranging from 1.2×10^{-7} M representing a detection limit, to a maximum value of 1.2×10^{-4} M. It is noted that the second highest value is 1.2×10^{-5} M, i.e. an order of magnitude lower than the highest. Since it is only the combination of high sulphide concentrations and high flow rates that yield corrosion failures, it is of interest to study the sensitivity of the corrosion results to details of the high-end tail of the sulphide distribution. (The corresponding dependence on the high-end tail of the flow distribution is covered by the multiple realisations of the flow models.)

The following sensitivity cases are analysed:

- The highest point in the distribution i.e. $[\text{HS}^-] = 1.2 \times 10^{-4} \text{ M}$ is deleted from the distribution.
- A point with twice the highest, i.e. $[\text{HS}^-] = 2.4 \times 10^{-4} \text{ M}$ is added to the distribution.
- The mean value of $[\text{HS}^-]$ is used for all deposition positions. This is equivalent to saying that $[\text{HS}^-]$ at a given position will vary over time with an average value equal to the mean value of the $[\text{HS}^-]$ distribution = $5 \times 10^{-6} \text{ M}$.

Justification for selecting these $[\text{HS}^-]$ concentrations as parameters for the sensitivity tests are provided in Section 5.7 of the **Geosphere process report** and in Tullborg et al. (2010).

Biofilm at the canister surface

In the case that buffer erosion occurs to the extent that advective conditions are established at the canister surface, the safety function Buff2 is lost and it is in principle possible that a biofilm of active SRB could form directly on the canister surface. In laboratory studies, active SRB biofilms on copper have been reported for nutrient-rich environments, i.e. with high concentrations of sulphate and organics (Stahlén 2018). However, even at lactate concentrations of 14 mM, which is about one order of magnitude higher than the highest concentration of DOC measured at Forsmark (Figure 10-44), the estimated coverage of SRB cells was minimal and at the lower limit for what is considered as a biofilm (Persson et al. 2011). It may be noted that several pessimistic assumptions were made in this estimate and it is further pessimistic to compare the level of lactate with DOC, since only a small fraction of the DOC is typically bio-available (see further Section 10.3.13). Furthermore, even in experiments where the growth media contained as much as 47 mM lactate and corrosion was studied up to average corrosion depths of ca 50 μm , localised corrosion was only about the same depth as the average corrosion giving a pitting factor of 2 (Dou et al. 2018), as discussed further in **the Fuel and canister process report**, Section 3.5.4.

Hydrogen embrittlement

In Section 10.3.13 the possible ingress of hydrogen liberated during corrosion of copper with sulphide is evaluated by modelling and by references to experimental results, and shown to give additions of hydrogen compared to the initial content in the copper that are of no concern for the canister integrity, also in a modelling case with an unrealistically high uptake of generated hydrogen in the copper. It is, therefore, concluded that no realistic route to uptake of hydrogen such that it could affect the mechanical properties of the copper canister detrimentally under repository conditions has been identified.

Oxygen penetration

Penetration of oxygenated groundwater to the deposition holes was ruled out in the reference evolution, see Section 10.4.7. This issue needs, however, to be analysed also for situations with increased flow caused by an ice sheet margin stationary over a repository for longer periods than in the reference evolution.

The understanding of oxygen penetration is discussed in Section 10.4.7. There, it is demonstrated that the degree of oxygen penetration for steady state flow conditions is controlled by:

- the duration of the steady state episode,
- the concentration of oxygen at the inlet of the flow paths,
- the extent to which microbial processes contribute to oxygen consumption,
- the surface area of the reducing minerals in the rock and the kinetics of their reactions with oxygen,
- the F factors of the recharge flow paths connecting the surface to the deposition holes.

In the following, each of these factors is discussed and quantified in order to arrive at a quantitative assessment of the extent of oxygen penetration and potential consequences in terms of corrosion.

Duration

According to the section on glacial conditions leading to enhanced groundwater flow above, situations with 200 year and 1 000 year stillstands can be considered, with probabilities of occurrence in combination with warm-based glaciers, of 0.12 and 0.012, respectively.

Oxygen concentration

According to Section 10.4.7, see also Sidborn et al. (2010), there is a theoretical upper limit on the oxygen concentration of intruding glacial melt water of 1.5 mM. This concentration is pessimistically assumed in the following.

Microbial activity at the surface

As mentioned in Section 10.4.7, during a period of glaciation, the amount of degradable organic substances is uncertain, although microbial activity is observed at the surface of most glaciers, and in glacial melt water (Hallbeck 2009). Microbial activity is pessimistically disregarded here.

Mineral surface area and reaction kinetics

The same data as used in Section 10.4.7 is used here. A cautious value for the specific reactive surface is used based on the size and geometric shape of biotite grains in the rock mass at Forsmark.

The pH of the water is assumed to be equal to 8. Higher pH values would result in increased mineral dissolution rates and homogeneous oxidation rates, and therefore, in an increased oxygen consumption rate, and in a decreased penetration of oxygen both into the rock matrix and along the fracture. The results are however not very dependent on the pH in the range 7 to 8, but this effect begins to be important at pH 8.5. It is indicated in Salas et al. (2010) that groundwaters with a large glacial meltwater component are characterised by pH values around 9, and therefore the pH value assumed here is considered cautious.

No account is taken here for the reducing capacity of fracture filling minerals. Along the fracture path, the oxygen-rich waters will encounter Fe(II) minerals which in Forsmark correspond to a concentration of Fe^{2+} increased by a factor of 3 in a 0.2 mm thick layer of rock adjacent to the fracture surface. This increased reducing capacity close to the fracture surface is pessimistically not included in the calculations. The effect is however discussed in the calculations reported in Sidborn et al. (2010).

Diffusivity and porosity

The penetration of oxygen is evaluated for a rock matrix having the characteristics of intact rock. Close to the fracture surface the porosity is higher, and therefore the diffusion of oxygen and other dissolved substances is faster. Because of this, the diffusion of oxygen into the rock matrix is deeper than in the present calculations, and the penetration along the fracture is shorter. Due to the difficulty of assigning cautious values for the effective diffusivity and porosity in the altered zone close to fractures, values for the bulk rock matrix are used for the base-case calculations in Sidborn et al. (2010), but an example of increased D_e and porosity is included in that report as a parameter sensitivity analysis. The increased rock porosity close to fracture surfaces is pessimistically disregarded here.

F factors

Flow-related transport resistance values for steady state recharge flow conditions with the ice margin right above the repository were reported in Section 10.4.6 and used there for assessments of penetration of dilute water. In these calculations, the flowing fractures in the part of the flow domain that hosts the repository are described with an explicit hydrogeological discrete fracture network model (DFN). This part is surrounded by two successive volumes. Next to the DFN volume, the advective flow system is modelled using an Equivalent Continuous Porous Medium (ECPM) approach based on up-scaling of a DFN representation. Outside of the ECPM, a Continuous Porous Medium (CPM) approach is used with assumed homogeneous properties. In the calculation of penetration of dilute water, only the

explicit DFN part was accounted for. There is, however, no reason to disregard the part of the flow path going through the two continuum representations of the flow domain. The initial part of the recharge flow paths, i.e. close to ground surface, will predominantly be in the CPM part of the domain, and it is desirable to capture the oxygen depletion along the full flow path.

To obtain an ECPM representation of the fractures in the full domain, a variant representation of the groundwater flow model described in Section 10.3.6 was produced, namely the *Extended spatial variability case*. In this variant, an ECPM representation, based on up-scaling of an explicit discrete fracture network representation, is used throughout the regional model domain. However, the repository region is still represented by an explicit DFN, see Section 10.3.6 and Joyce et al. (2010) for details. Recharge particle tracking is done in this model with boundary conditions from the glacial case model presented in Section 10.4.6. Ice front locations II and III, i.e. when the ice front is in close proximity to the repository, are considered. Along the recharge flow paths, advective travel time and flow-related transport resistance are calculated for use in the calculations of oxygen penetration.

It should be noted that the model of Joyce et al. (2010a) underestimates the length of the recharge flow paths due to the finite extent of the domain used. In the super-regional scale model of Vidstrand et al. (2010), recharge paths are obtained, for the corresponding ice front locations, that extend well beyond the upstream boundary of the model domain used in Joyce et al. (2010). Hence, the flow-related transport resistance (F) values used in the present assessment are likely under-predicted.

Extent of oxygen penetration

Using the F -values obtained according to the approach described above, that is, using the *Extended spatial variability case*, for ice front location III and applying the EFPC rejection criterion, 31 deposition positions out of the 6 000 experience oxygen concentrations above 10^{-7} M, and of these, the oxygen concentration is higher than ~ 1 mM for 6 positions. For ice front location II the deposition location most affected (in a different volume of the repository not affected by ice front location III), has an O_2 concentration slightly below 0.15 mM.

Corrosion for diffusive conditions

A 1 000 year exposure to 1.5 mM of O_2 in a fracture intersecting a deposition hole with an intact buffer yields a corrosion of about 0.3 mm in the most exposed deposition hole in the repository, for the flow conditions discussed above and assuming spalling in all deposition holes. Note that i) all deposition holes are included in this calculation, not only those for which the corresponding F factors imply oxygen penetration and ii) the theoretically maximal oxygen concentration is assumed.

Any localised corrosion in connection with oxygen intrusion under glacial conditions would either be in the form of uneven general corrosion due to (rarely) alternating oxic/sulphidic conditions or relatively shallow pitting during oxic conditions, as developed further in the **Fuel and canister process report**, Section 3.5.4. There it was concluded that pitting could be supported for the 6 deposition holes in which the glacial meltwater reaching repository depth possibly could retain ~ 1 mM O_2 , since some of this O_2 could then be retained also after diffusion through the buffer, and since the low chloride content of the meltwater promotes pitting of copper. Applying the same pit growth rate model as for localised corrosion during initially oxygenated conditions (Briggs et al. 2021) gives maximum pit depths of 1.8 mm and 4.6 mm, for ice front standstills of 200 and 1 000 years, respectively.

It is concluded that corrosion due to oxygen penetration with diffusive conditions in the deposition hole can be neglected.

Corrosion for advective conditions

The same corrosion model as used for sulphide corrosion for assumed advective conditions in the deposition hole was applied for the deposition positions to which oxygen was calculated to penetrate as mentioned above. The enhanced flow rates calculated for these positions were used in the corrosion calculation.

The calculations result in a corrosion rate slightly below 6 $\mu\text{m}/\text{yr}$ for the deposition location mostly affected by the high O_2 concentration for ice front location III. The following three most affected positions have corrosion rates of 3.6, 1.7 and 0.9 $\mu\text{m}/\text{yr}$ respectively. This yields corrosion depths after a 1 000 year ice margin stillstand of at most 6 millimetres. A 200 year stillstand would result in a corrosion depth of about 1.2 mm for the position most affected. These corrosion depths do not include surface roughening due to localised corrosion, see below.

The following is noted.

- The particular position for which the high oxygen concentration occurs is not among those predicted to experience advective conditions in the erosion calculations carried out with the same hydrogeological DFN model (the same DFN realisation of the semi-correlated base case). This is because the hydrogeological boundary conditions for the two situations are different.
- Only ice front location III results in substantial oxygen penetration. The distance between ice front location II and III is 1.7 km. It is assumed here that for the 1 000 year duration of the ice front standstill, the ice margin is pessimistically assumed to not oscillate forth and back for distances in the scale of several hundreds of metres. If the ice front should oscillate around its margin position, which is likely during such a stillstand, then the hydrogeological conditions would change in such a way that no single deposition location would be affected by oxygen penetration during any significant period of time.
- Any localised corrosion in connection with oxygen corrosion under glacial conditions would be either in the form of uneven general corrosion, due to (seldomly) alternating redox conditions, or relatively shallow pitting, as developed further in the **Fuel and canister process report**, Section 3.5.4.

Conclusion

With the pessimistic assumptions i) that a theoretical upper limit on oxygen concentration is used, ii) that the reducing potential of fracture filling minerals and microbial processes are neglected, and iii) that no credit is taken for the fact that different canister positions are the most exposed to erosion and corrosion, respectively, and iv) that small oscillations of the ice front during the 1 000 year stillstand are not considered, then the calculated corrosion depths are in the millimetre scale. Furthermore, the probabilities of the 1 000 year and 200 year stillstands occurring during the one million year assessment period are estimated at only 0.012 and 0.12, respectively. Therefore, it is concluded that effects of oxygen penetration can be excluded from the corrosion scenario.

Event sequences

The sequences of events that are considered in this scenario concern the succession of climate domains with their associated variations in groundwater flow and geochemical conditions. As averages over glacial cycles are used for these entities, justified by the fact that corrosion failures generally take several glacial cycles to develop, the detailed event sequences are of secondary importance for estimation of the number and timing of the resulting corrosion failures. Hence one important aspect of the regulatory requirement on treatment of alternative climate evolutions has been addressed.

Quantitative sensitivity analysis of canister corrosion

Intact buffer

For an intact buffer, the analysis of additional uncertainties did not result in any situations that challenge the conclusion from the reference evolution that there are considerable margins to canister failures. Therefore, no additional corrosion calculations are carried out for the case of an intact buffer.

Advection in buffer

In the buffer advection scenario, Section 12.2, three cases to be propagated to the corrosion scenario were identified.

- A case where advective conditions occur to the extent given by the reference evolution treated in Chapter 10.
- A bounding case where advective conditions occur in every deposition hole throughout the assessment period.
- A case where diffusive conditions are preserved in every deposition hole throughout the assessment period.

The third case corresponds to an intact buffer and has been treated above. That case does not represent a situation with advective conditions in the buffer, but is included to represent the conceptual uncertainty regarding buffer colloid release/sedimentation/erosion. Further understanding of that process could lead to the exclusion of colloid release from future assessments. In addition to these three cases, also the sensitivity cases based on *erosion related factors* identified in the buffer erosion scenario are studied from the point of view of corrosion below.

The uncertainty analyses of factors contributing to corrosion above have led to the following conclusions regarding base case assumptions and sensitivity cases for *corrosion related factors*.

- The initial copper coverage is assumed to be 47 mm, as in the reference evolution.
- EFPC rejection of deposition positions is applied.
- Corrosion due to impurities in buffer and backfill is neglected.
- Buffer diffusion is irrelevant for the advection case. However, before advective conditions arise, diffusion controlled sulphide corrosion in a partially eroded buffer will occur. The extent of this corrosion is difficult to quantify. Here, the case with initial advection in all deposition holes puts a bound also on the extent of corrosion with a partially eroded buffer followed by corrosion under advective conditions.
- The cautious corrosion geometry from the reference evolution is used, with the bounding pessimistic geometry as a sensitivity case.
- Regarding flow conditions, the three cases of uncorrelated, semi-correlated and fully correlated relations between fracture length and transmissivity are propagated to corrosion calculations. Temperate flow conditions are pessimistically assumed and ice sheet margin stillstands are disregarded for sulphide corrosion since they give negligible additional contributions.
- As in the reference evolution, present day sulphide concentrations are pessimistically assumed and, also pessimistically, a deposition position is assumed to experience the same, randomly sampled sulphide concentration throughout the assessment period. Three sensitivity cases are defined to study the sensitivity to the properties of the sulphide distribution.
- Corrosion contributions from oxygen penetration are disregarded, since they are unlikely and, also with a number of pessimistic assumptions, limited in extent.

A base case using all ten realisations of the semi-correlated hydrogeological DFN model, the site specific sulphide distribution and base case assumptions regarding buffer erosion yields on average 0.094 failed canisters in one million years as already reported in the reference evolution, Section 10.4.9.

The sensitivity to uncertainties in *erosion related factors* is studied by calculating the number of failed canisters for the sensitivity cases for buffer erosion studied in the buffer advection scenario, Section 12.2.2. The results are shown in Figure 12-17, which thus corresponds to the erosion cases in Figure 12-3 of Section 12.2.2, but where the cases F, H and J with initial advection have been added.

As seen in the figure, the sensitivity to all assumptions regarding buffer erosion is limited. The highest impact is obtained for the different hydrogeological DFN models. It is noteworthy that even assuming advective conditions initially in all deposition holes has a limited impact on the extent of corrosion for a given hydrogeological model variant. This finding justifies the simplification of only propagating the base case and the two bounding cases from the analysis of buffer erosion.

Figure 12-18 shows results of the sensitivity cases based on uncertainties in *corrosion related factors* identified above, i.e. sensitivities related to the distribution of sulphide concentrations and to the corrosion geometry. (The impact of the different hydrogeological DFN models is shown in Figure 12-17). The cases show the following.

- Assuming the mean value of $[HS^-]$ for all deposition positions, which is equivalent to assuming that $[HS^-]$ at a given position will vary over time with an average equal to the mean value of the entire $[HS^-]$ -distribution, i.e. 5×10^{-6} M, yields no corrosion failures for the semi-correlated hydrogeological DFN model. The same result is obtained with the uncorrelated and the fully correlated hydro DFN models (not shown in the Figure). This is a significant result. Although it cannot be justified to assume a temporal variability that is represented by the given sulphide distribution, it is not unreasonable to assume that the sulphide concentrations would vary over time and thus serve to reduce the expected number of canister failures considerably. The result is a reflection of the fact that canister failures occur only when the highest flow rates are combined with the highest sulphide concentrations, and when both these entities are pessimistically assumed to be constant in time over the entire one million year assessment period for a given deposition position.
- Omitting or adding another data point with the highest sulphide concentration, i.e. 0.12 mM, has a significant impact on the result. As mentioned above this point is about one order of magnitude higher than the next highest point in the distribution.
- Assuming the unrealistic, pessimistic corrosion geometry leads to an increase in the mean number of failed canisters by about a factor of six meaning that the dependence is roughly inversely proportional to the exposed canister surface in this case.
- Combining the maximum corrosion depths of 2.5 mm (including pits) caused by entrapped O_2 from the buffer and backfill and of 4 mm caused by sulphide generated by SRB with hydrogen from degradation of rock reinforcements as an energy source, with the long-term sulphide corrosion: This is pessimistic due to assumptions made in the derivation of the general corrosion depth caused by O_2 , and by assuming that the location of the deepest pits predicted probabilistically would coincide with the location of the sulphide corrosion. This case is analysed by pessimistically reducing the initial copper thickness by 10 mm, i.e. more than the 2.5 + 4 mm from the factors mentioned. The case yields a mean number of failed canisters of 0.13, i.e. marginally higher than the base case.

As earlier noted, documentation of all calculations of buffer loss and subsequent canister corrosion under advective conditions is given in Hedin (2021).

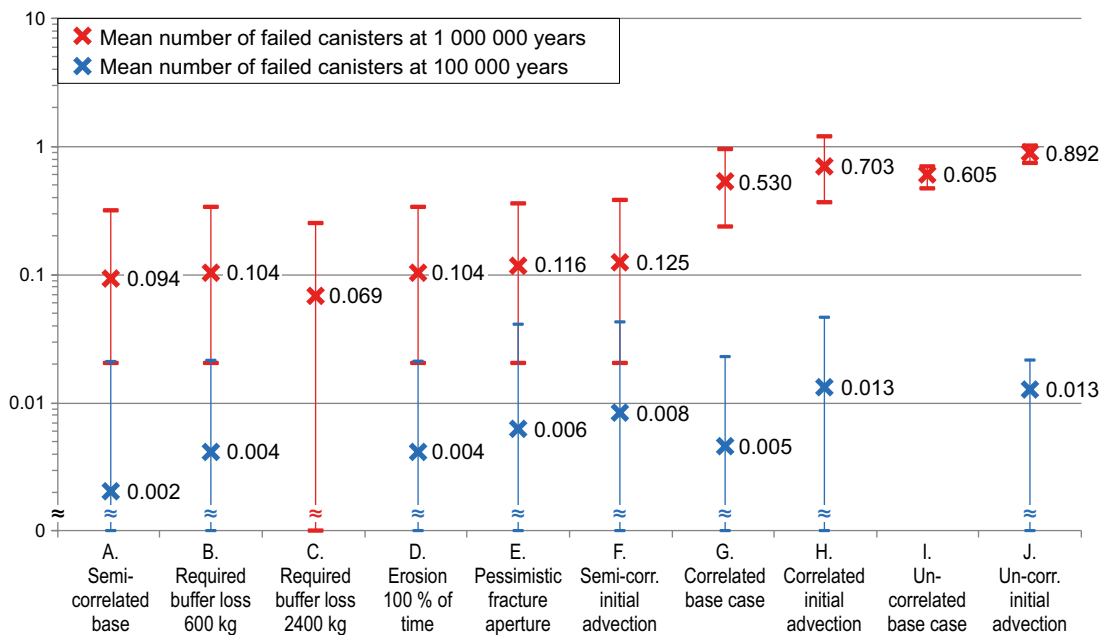


Figure 12-17. Calculated mean number of failed canisters at 100 000 years and one million years for the sensitivity cases identified in the buffer advection scenario, Figure 12-3 in Section 12.2.2, and with base case assumption for corrosion. The crosses denote mean values and the bars denote the variability over the several realisations of the hydrogeological DFN models.

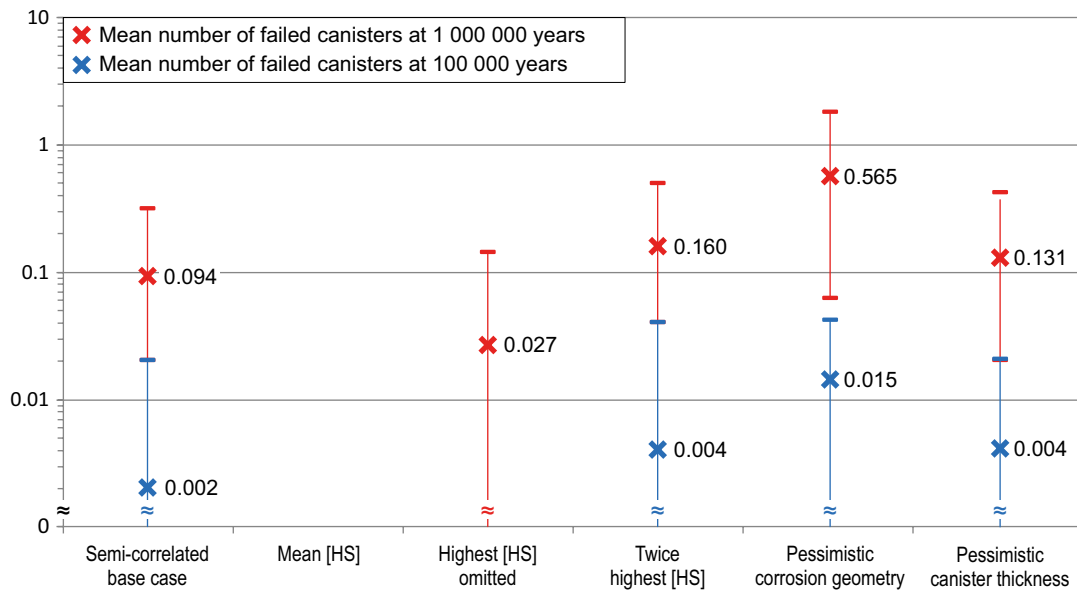


Figure 12-18. Calculated mean number of failed canisters at 100 000 years and one million years for the sensitivity cases identified in the corrosion scenario and with base case assumptions for erosion. The crosses denote mean values and the bars denote the variability over the several realisations of the hydrogeological DFN models.

12.6.3 Quantitative assessment of corrosion – potential for early failures

Introduction

A pronounced feature of the Forsmark site is the scarcity of water bearing fractures at repository depth. As demonstrated in Section 10.3.8, this means that the clay subsystem in some parts of the repository will likely remain unsaturated for long times, even thousands of years. This, in turn, means that the canisters will experience an environment influenced by the transient, unsaturated buffer and backfill conditions for corresponding lengths of time, and it is of interest to elucidate what this means in terms of post-closure safety. Another reason to emphasize early stages in the assessment of the repository evolution is the higher hazard of the spent fuel during this phase. Therefore, a dedicated assessment of the potential for early canister failures due to corrosion and corrosion related phenomena is provided in the present Section, even though the development is essentially covered in the **Fuel and canister process report**, as well as in preceding parts of this report. The need for such an assessment was also identified in SSM's review of the safety assessment SR-Site, see Section 11.3.

The difference of corrosion during the early phase, compared to the longer full assessment period regards the canister environment directly as well as changes in the nature of the corrosion processes. Phenomena that could potentially affect the extent of corrosion under unsaturated conditions include

- The sauna effect and corrosion due to elevated chloride concentrations.
- Initial high sulphide concentrations in the groundwater during operation.
- Corrosion under oxidising conditions, including stress corrosion cracking.
- Corrosion phenomena related to sulphide in the unsaturated buffer.
- Radiation related effects.
- Hydrogen from sulphide corrosion, entering the copper material, potentially causing hydrogen embrittlement.

The sauna effect and corrosion due to elevated chloride concentrations

In Section 10.3.8, the saturation of the buffer and backfill is evaluated, including the buffer specific sauna effect. A more elaborated description of the sauna effect is given in SKB (2019c), summarizing experimental studies, experience from in situ tests as well as modelling.

The sauna effect is defined as uptake of water in the bentonite, followed by evaporation of water in the vicinity of the hot canister and precipitation of salts from the water in the evaporation zone and is illustrated in Figure 10-49. The potential influences of the sauna effect on corrosion processes are a higher chloride concentration close to the canister and deposition of salts at the canister surface.

In Section 10.3.8 it is concluded that significant salt accumulation as a consequence of evaporation of inflowing water from a fracture intersecting a deposition hole will not occur in a KBS-3 repository, with the main reasons being:

- For significant amounts of salt to accumulate, the major part of the inflowing water must transform into vapour, rather than continue to flow in liquid form, since chloride concentration can be increased only if water is evaporated. For the relevant inflow geometry, it is highly unlikely that the liquid flow is suppressed to such an extent. It is also verified in state-of-the-art THM models that significant liquid flow is maintained.
- The experimental results strongly suggest that the vapour transport capacity within a KBS-3 buffer is not large enough to support a significant amount of salt accumulation, since condensation will limit the vapour transport.
- No relevant signs of salt accumulation have been observed in field experiments. In the FEBEX test, there was a chloride concentration gradient in the clay with enrichment close to the heater. There was, however, no accumulation of the total chloride content in the bentonite but rather a redistribution of the initial amount.

In summary, it is found that the sauna effect will be insignificant in a KBS-3 repository at Forsmark. This effect is, therefore, not further considered when discussing corrosion phenomena in the present section.

It is further noted that even though some redistribution of chloride has been observed under field conditions, which could potentially lead to enhanced chloride levels close to the canister surface, continuous enrichment of chloride would only be possible through inflow of water, which counteracts any increase in concentration. With the conclusion above that there is no sauna effect possible with evaporation of water from the deposition hole, this enrichment effect of chloride is not further considered.

During the excavation and operational phase upconing of groundwaters with higher chloride concentrations may occur, but as concluded in Section 10.2.5 only limited changes in salinity are to be expected during construction and operation of a repository located at Forsmark. It is further stated in Section 10.2.5 that other groundwater parameters, such as pH, are expected to be practically unaffected by groundwater upconing, meaning that corrosion due to enhanced chloride concentrations is assessed not to pose a problem during the excavation and operational phase.

It is thus concluded that corrosion driven by high chloride concentrations could be disregarded for the whole unsaturated phase.

Initial high sulphide concentrations in the groundwater during operation

In the early phase of the repository evolution not only the properties of the unsaturated bentonite could influence corrosion, but there could also be changes in the geochemical conditions during the excavation and operation of the repository, leading potentially to sulphide concentrations up to at most 10^{-3} mol/L according to Section 10.2.5. In Section 10.3.13 it is concluded through an unrealistic, bounding mass balance consideration that the corrosion caused by groundwater with such initially high sulphide concentration is at most 500 μm . This phenomenon occurs during the operation phase of the repository and would thus not be extended in time in parts of the repository that remain unsaturated long after the operation phase.

Corrosion under oxidising conditions

Atmospheric corrosion and corrosion caused by oxygen initially present in the buffer and the backfill was discussed in Section 10.2.5 (with details in the **Fuel and canister process report**, Section 3.5.4). The corrosion depth bounded with a mass balance was shown to be less than 2.5 mm, including pits. A more complete discussion of localised corrosion under oxidising conditions is given in the **Fuel and canister process report**, Section 3.5.4.

In Section 10.3.13 it was concluded that the concentration of ions assisting stress corrosion cracking is too low, by 2–3 orders of magnitude for stress corrosion cracking to occur under oxidising conditions. Further details are given in the **Fuel and canister process report**, Section 3.5.5. Nitrogen compounds (nitrite and ammonium) from blasting activities during tunnel construction could possibly contaminate groundwater with increased risk for stress corrosion cracking. In Section 10.2.5 it was shown with data from tunnel excavation at Äspö that no significant concentration increase of nitrogen compounds in the groundwater was observed.

The chemical conditions in the repository are subsequently expected to be reducing for the period of temperate climate, see Section 10.3.7, i.e. no further corrosion due to oxygen is expected.

Corrosion phenomena related to sulphide in the unsaturated buffer

Corrosion of copper by the reaction of sulphide is the most important corrosion process during the long-term assessment period, but needs also to be assessed for the early phase. Especially the unsaturated conditions in the buffer makes transport of sulphide in gaseous form possible, and the potential for microbial activity and formation of a biofilm on the canister needs to be evaluated.

Copper corrosion due to gaseous sulphide for unsaturated buffer conditions needs to be addressed, both as concerns the total extent of this corrosion mode and regarding the peak sulphide flux at the canister surface, in order to evaluate whether this is below the threshold flux where compact film formation (and passivation) may occur. These issues are handled in Section 10.3.13, where both the transport limit and reaction mechanisms are discussed. Transport of gaseous sulphide, $\text{H}_2\text{S}(\text{g})$, during the unsaturated phase is evaluated in Section 10.3.10. Through modelling, the highest flux of $\text{H}_2\text{S}(\text{g})$ at the canister surface that could possibly be established in the unsaturated repository environment is found to be about $6.5 \times 10^{-11} \text{ mol}/(\text{m}^2 \cdot \text{s})$. This is about a factor of 4 lower than the pessimistically evaluated threshold sulphide flux of $3 \times 10^{-10} \text{ mol}/(\text{m}^2 \cdot \text{s})$. Below this threshold, the film growth is controlled by the transport of sulphide in solution (and in the pores of the film) and formation of a compact and possibly passive film is not supported, meaning that localised corrosion mechanisms (pitting or micro-galvanic effects) are not expected.

Neither is any stress corrosion cracking in a sulphide environment supported as the maximum sulphide flux of $6.5 \times 10^{-11} \text{ mol}/(\text{m}^2 \cdot \text{s})$ under unsaturated conditions can be compared to the sulphide fluxes of $10^{-6} \text{ mol}/(\text{m}^2 \cdot \text{s})$ in experiments where superficial cracking (interpreted as intergranular corrosion or possibly SCC) has been observed. There is thus a margin of several orders of magnitude. The margin is ever larger for the effects interpreted as by the Aaltonen mechanism, where crack like effects have only been observed at sulphide concentrations corresponding to sulphide fluxes of $10^{-4} \text{ mol}/(\text{m}^2 \cdot \text{s})$.

In Section 10.3.13, with further details in Section 10.3.10, the potential for microbial activity in unsaturated buffer is discussed. While the buffer is initially too dry to allow microbial activity, and eventually develops a swelling pressure and environment that effectively suppresses microbial activity (safety function Buff2), there could in principle be a transient period during which microbial activity is supported by the buffer environment. However, experimental studies of unsaturated bentonite have shown that high relative humidity is not sufficient for bacterial sulphate reduction to occur during the bentonite saturation process. It is concluded in Section 10.3.10 that microbial sulphate reduction is not expected to occur in the bentonite buffer at any time during the unsaturated phase. As discussed in Section 12.6.2, active biofilms have been observed in laboratory experiments, but only in nutrient-rich environments (i.e. with high concentrations of sulphate and bio-available organics), which is far from the canister environment. The formation of an active biofilm on the canister surface under the unsaturated phase is thus not conceivable.

Radiation related effects

Most of the radiation from the spent fuel is absorbed by the canister materials during the first few hundred years after closure, meaning that radiation effects are of relevance as regards a discussion of potential early canister failures.

The direct effect of radiation on the corrosion direct effects the formation of corrosive species via radiation in humid air and of oxidising species formed during radiolysis of water (see the **Fuel and canister process report**, Section 3.5.4). There, it is shown that the corrosion depths from the radiolysis of water is estimated to ca 3 μm , as derived from modelling of general corrosion depth and experimental observations of localised corrosion features, accounting for the full radiation dose for which the copper canister material is exposed. As described in the **Fuel and canister process report**, Section 3.5.4, the effects of gamma radiation on water close to copper metal has been studied experimentally with the conclusion that molecular O_2 , formed by decomposition of H_2O_2 on the oxide surface, is the dominating oxidant in the copper-water system under radiolysis. There it is shown that ground water components such as chloride, sulphate and bicarbonate, will have minor effects on the extent of radiolytic corrosion, as long as the pH is near neutral or alkaline.

The available information from the scientific literature shows that there are no indications for shifted corrosion potentials or enhanced corrosion rates caused by gamma radiation at the low dose rates representative of the repository. It is further shown that the amount of nitric acid formed corresponds to a corrosion depth of a few nanometres only.

Neutron and gamma radiation from the fuel could potentially give rise to material changes in cast iron insert and in the copper shell. In the **Fuel and canister process report**, Section 3.4.6 it is described how comparison of calculations with experimental data in the literature, leads to the conclusion that the magnitude of any physical property changes (e.g. yield stress, creep rates, enhanced solute segregation, dimensional changes, or brittleness) resulting from exposure to neutron and gamma radiation, even over the one million year time period of the safety assessment, will be negligible for both the copper and the cast iron. Specifically, due to the low dose rates (unaltered corrosion potential) and the negligible effects on the material properties, stress corrosion cracking (SCC) is not expected as a consequence of irradiation.

From this, it is concluded that both direct and indirect effects of radiation are negligible for the canister evolution in general and during early stages in particular.

Hydrogen from sulphide corrosion, entering the copper material

The potential of hydrogen liberated in the corrosion process to enter the copper material is discussed in Section 10.3.13 (with details given SKB (2019)), and found to give negligible amounts compared to the initial content of hydrogen in the Cu-OFP. The properties of the copper material are thus not expected to deteriorate due to hydrogen embrittlement, a conclusion of importance for the analysis of copper creep, see further Section 12.7.5.

Conclusion

The above account of corrosion and corrosion related phenomena under early, unsaturated conditions yields the conclusion that such phenomena will not lead to any canister failures. Also, the reduction of the corrosion barrier due to such phenomena is limited as analysed in particular in Section 10.3.13. Consequences of postulated early canister failures (irrespective of failure mode) are analysed as a residual scenario in Section 13.7.3.

12.6.4 Conclusions

The canister failure due to corrosion scenario is a less probable scenario, since this type of canister failure cannot be ruled out in the one million year assessment period.

For the assessment of consequences in terms of dose and risk, the three buffer cases (no advection, erosion according to the PSAR model, initial advection) need to be combined with the three hydrogeological DFN models, with the base case assumptions used above for other erosion and corrosion related parameters. Evidently, the bounding case where advective conditions occur in every deposition hole throughout the assessment period is unrealistic, but this case is still kept within the scenario, to illustrate the impact of the uncertainties covered by this case.

Figure 12-19 shows the cases that have been formulated for the corrosion scenario. The three hydrogeological DFN model variants of the Forsmark site are included to cover uncertainties in the correlation structure (blue objects). The next branching represents the three cases of buffer advection (red) propagated from the buffer advection scenario. Finally, the mean number of failed canisters calculated for each of the situations is given in orange.

The case with the semi-correlated hydrogeological DFN variant combined with the PSAR model for buffer erosion is seen as a *central corrosion variant*, based on which assessments of radionuclide transport and dose should primarily be made. This position is adopted because of the following considerations.

- The semi-correlated DFN model is more compatible with site data than the other two variants since its description of the relation between fracture size and transmissivity is most consistent with observations.
- The PSAR model for buffer erosion is the best available representation of current knowledge of this process, although there are conceptual uncertainties associated with the model.

The remaining combinations of hydro DFN models and erosion cases are seen as illustrative cases providing bounds on uncertainties in the aspects of corrosion they represent.

The cases discussed above are propagated to analyses of the retardation potential for the corrosion scenario, Section 13.5.

Hydrogeological DFN model		Mean number of advective positions		Mean number of failed canisters	
		(at 10 ⁵ yrs)	at 10 ⁶ yrs	(at 10 ⁵ yrs)	at 10 ⁶ yrs
Uncorrelated	Initial advection	(6 000)	6 000	(0.013)	0.892
	PSAR erosion model	(5.8)	459	(0)	0.605
	No advection	(0)	0	(0)	0
Semicorrelated	Initial advection	(6 000)	6 000	(0.008)	0.125
	PSAR erosion model	(1.4)	41.6	(0.002)	0.094
	No advection	(0)	0	(0)	0
Fully correlated	Initial advection	(6 000)	6 000	(0.013)	0.703
	PSAR erosion model	(6.6)	129	(0.005)	0.530
	No advection	(0)	0	(0)	0

Figure 12-19. Mean number of advective deposition positions and mean number of failed canisters for the calculation cases identified as relevant for the corrosion scenario. The data were obtained in the sensitivity calculations reported in Section 12.6.2, Figure 12-17. Results for 10⁶ years are propagated to consequence calculations. Results for 10⁵ years are shown in parentheses for comparison, demonstrating that the metrics increase non-linearly with time.

Global warming variant and other climate cases

The above conclusions are valid also in relation to the global warming variant of the reference evolution. Such a variant could possibly impact negatively on the extent of erosion during the initial temperate period. In the one million year assessment period, this impact is very limited (see Section 10.3.6 and Joyce et al. 2015) and it is covered by the case with initial advection in all deposition holes. Nor do any of the other climate cases described in Section 12.1.3 have any relevance for the corrosion scenario.

12.7 Canister failure due to isostatic load

12.7.1 Introduction

Safety function indicator(s) considered

This scenario concerns the safety function relating to the canister's ability to withstand isostatic loads, safety function Can2. As seen in Figure 8-3, both static loads on the insert and creep deformation of the copper shell need to be considered.

This safety function is directly related to containment, as the containment is assumed to be breached if the safety function is not maintained.

Treatment of this issue in the reference evolution

Canister failure due to isostatic load was not included in the reference evolution, since peak loads in the reference evolution (43.5 MPa) are below the design load of the canister (50 MPa).

Propagated buffer conditions

According to Section 12.5, three different buffer conditions are propagated to the canister scenarios. Two of these concern advective conditions in the buffer and the third is the intact buffer. Since advective conditions are related to an eroded buffer which has a lower swelling pressure than an intact buffer, such conditions are less likely to induce isostatic collapse.

Furthermore, in Section 12.3, it was concluded that neither an intact buffer nor groundwater in potential buffer erosion cavities will freeze, not even for pessimistic assumptions of future climate conditions at the Forsmark site.

Based on these considerations, only the intact buffer is further treated in the analysis of potential canister failures due to isostatic load.

Qualitative description of routes to canister failure due to isostatic load (including initial state aspects and external conditions)

The evolution in this scenario is assumed to be identical to that of the reference glacial cycle variant of the reference evolution, except for factors related to isostatic collapse of a canister.

According to the FEP chart, this safety function would be jeopardised if the isostatic load on the canister, determined by the groundwater pressure, equal to the buffer porewater pressure, and the buffer swelling pressure, exceeds the design load of 50 MPa.

The groundwater pressure is determined by repository depth for non-glacial conditions. For the Forsmark site, this means pressures of around 4.5 MPa. For glacial conditions the alteration of the hydrostatic pressure due to the presence of the ice sheet is added. This pressure is, in the reference evolution, assumed to correspond to the maximum ice thickness at the site, as it cannot be significantly greater than this. At Forsmark, the additional hydrostatic pressure is 26 MPa, see Section 10.4.1.

The buffer swelling pressure is determined by the buffer density and chemical composition, including the species of adsorbed cation. In the reference evolution, the maximum buffer swelling pressure, corresponding to an unaltered buffer of 1 560 kg/m³ (the upper limit of the reference dry density interval), was determined to 10 MPa.

The following factors of importance for the occurrence of canister failure due to isostatic load are identified, based on the discussion above, on Table 10-33 describing uncertainties identified in the reference evolution and on the FEP chart, Figure 8-5.

Initial state factors involved

- Canister strength.
- Installed buffer mass and buffer swelling properties.
- Repository depth (determining groundwater pressure if no glacial load).

Processes involved

- Deformation of copper canister; creep.
- Buffer swelling.
- Buffer chemical alterations and density losses.
- Convergence of deposition hole.

External conditions involved

- Ice sheet thickness and hydrology.

These factors are discussed quantitatively in the following under the three headings glacial load, buffer swelling pressure and canister strength.

12.7.2 Glacial load

Introduction

As mentioned in Section 10.4.1, for glacial conditions an additional hydrostatic pressure related to the ice sheet thickness is added to the hydrostatic pressure for ice free conditions. The extremes regarding hydrostatic pressure in the glacial climate domain depend on the ice sheet configuration and on its hydraulic systems. Under the Antarctic ice sheet, sub-glacial lakes have been observed. The hydrostatic pressure in these lakes is typically assumed to correspond to the ice overburden pressure. A hydro-thermo-mechanical balance is assumed, where supply of basal melt water, re-freezing and ice deformation result in a hydrostatic equilibrium where the ice sheet rests, or floats, on the water surface (e.g. Pattyn et al. 2004). As further justified below, it is reasonable to assume that also for the Fennoscandian ice sheet, the maximum ice sheet thickness sets a limit to the maximum hydrostatic pressure that may occur at the ice sheet bed-substrate interface.

Methodological approach

To investigate the maximum ice sheet thickness that may occur in Fennoscandia and over Forsmark in the future, ice thicknesses associated with the largest known ice sheet in the region over the past 2 million years have been studied. The results are then used, together with other information, to infer a maximum ice sheet thickness over the Forsmark site for the coming one million years.

Estimate of maximum ice thickness over Forsmark during the past 2 million years

From geological information, it is known that the maximum ice extent of Pleistocene Fennoscandian ice sheets (i.e. those occurring during the past ~2 million years) were larger than that of the Weichselian ice sheet, and occurred during the Saalian glaciation (e.g. Svendsen et al. 1999, 2004, Lambeck et al. 2006, Colleoni et al. 2009). At the peak of the Saalian glaciation, around 140 000 years ago, the ice sheet reached up to ~200 km further south and more than 1 000 km further east than the Weichselian ice sheet (Svendsen et al. 2004).

Most modelling efforts of the peak Saalian ice sheets indicate that the Fennoscandian ice sheet at that time was thicker than during the Last Glacial Maximum (at around 20 000 years ago). For example, Lambeck et al. (2006) simulated a peak Saalian ice thickness of ~3 400 m over the Forsmark region. Similar values can be inferred from Colleoni et al. (2009).

Although the study of Lambeck et al. (2006) provided useful information on the typical ice thickness associated with an extensive glaciation in Fennoscandia, they did not explore the sensitivity of the ice thickness to various uncertainties. Therefore, two dedicated ice-sheet and climate modelling studies were conducted by Colleoni et al. (2014) and Quiquet et al. (2016) (see also the **Climate report**, Section 5.4), in order to analyse the uncertainties related to simulations of the peak Saalian ice-sheet configuration, and their effects on the resulting ice-sheet thickness over Forsmark. Combined, these two studies carried out a large array of sensitivity experiments to investigate the influence of various uncertainty sources on the peak Saalian ice-sheet thickness, including potential errors associated with the initialization of the ice-sheet model and the peak Saalian climate representation (related to the size of the prevailing North American ice sheet). In addition, both studies thoroughly analysed the sensitivity of the ice-sheet thickness to poorly constrained parameters in the ice-sheet model. In Colleoni et al. (2014), the ice thickness sensitivity to the parameter space was analysed by means of uni-variate experiments, whereas in Quiquet et al. (2016), a multi-variate analysis of the parameter space was carried out to investigate the effect on ice-sheet thickness.

The experiments in both studies were integrated to steady-state, i.e. they used a constant-in-time climate forcing of the ice-sheet model instead of a time-dependent, more realistic, climate representation. However, using a steady-state climate representation for a cold period, such as the peak Saalian, likely results in overall thicker ice sheets compared to a time-dependent climate that fluctuates between warmer and colder periods. The steady-state assumption is therefore considered to be pessimistic in terms of maximum ice thickness (see the **Climate report**, Section 5.4.5).

The simulated peak Saalian ice-sheet thickness over Forsmark in Colleoni et al. (2014) and Quiquet et al. (2016) was found to be more sensitive to variations of ice-sheet model parameter values than to other uncertainty sources. The parameter sensitivity experiments therefore also resulted in the thickest ice sheets (see the **Climate report**, Sections 5.4.2 and 5.4.3). In Colleoni et al. (2014), the uni-variate parameter sensitivity experiments resulted in a maximum ice thickness over Forsmark of ~3 500 m. In the multi-variate analysis by Quiquet et al. (2016), the ice-sheet thickness over Forsmark reached at most ~4 000 m in some of the experiments (Figure 12-20).

Based on the sensitivity experiments in Quiquet et al. (2016), and taking uncertainties related to e.g. the steady-state assumption and the peak Saalian climate representation into account, the maximum ice-sheet thickness over Forsmark over the coming 1 million years was set to 4 000 m (see the **Climate report**, Section 5.4.5).

Hydrostatic pressures exceeding ice overburden pressure

The basal hydrostatic pressure from the ice thickness represents estimates of the ice overburden pressure, i.e. the pressure exerted on the basal hydrological system by the local ice thickness. However, there is also the possibility that basal pressures could exceed ice overburden pressure in some specific situations. This has been observed on mountain glaciers with soft (till) beds (e.g. Roberts et al. 2000, Kavanaugh 2009, Kavanaugh et al. 2010).

In order to investigate if basal water pressures higher than overburden pressure can be observed also in an ice-sheet setting, either as short-lived pressure pulses or more persistent high pressures, detailed measurements of basal water pressure were made within the GAP study (Claesson Liljedahl et al. 2016, Harper et al. 2016) and the ICE study (Harper et al. 2019) in a sector of the ablation zone of the Greenland ice-sheet (see also the **Climate report** Sections 3.2.2 and 5.4.7). Over daily to seasonal time scales, they reported that the basal water pressure varied between 0.8 and 1.1 times the overburden pressure. In this context, it is important to note that the measurements were all made in the ablation zone where basal meltwater is abundant. No equivalent measurements have been made in the ice-sheet interior where the ice-sheet is 2 to 3 times thicker than in the more frontal-near ablation zone. However, because there is virtually no surface melt input within the ice-sheet interior areas, it is unlikely that the maximum basal pressures (i.e. pressure above overburden) found in the ablation zone should scale with ice overburden pressure in the ice-sheet interior.

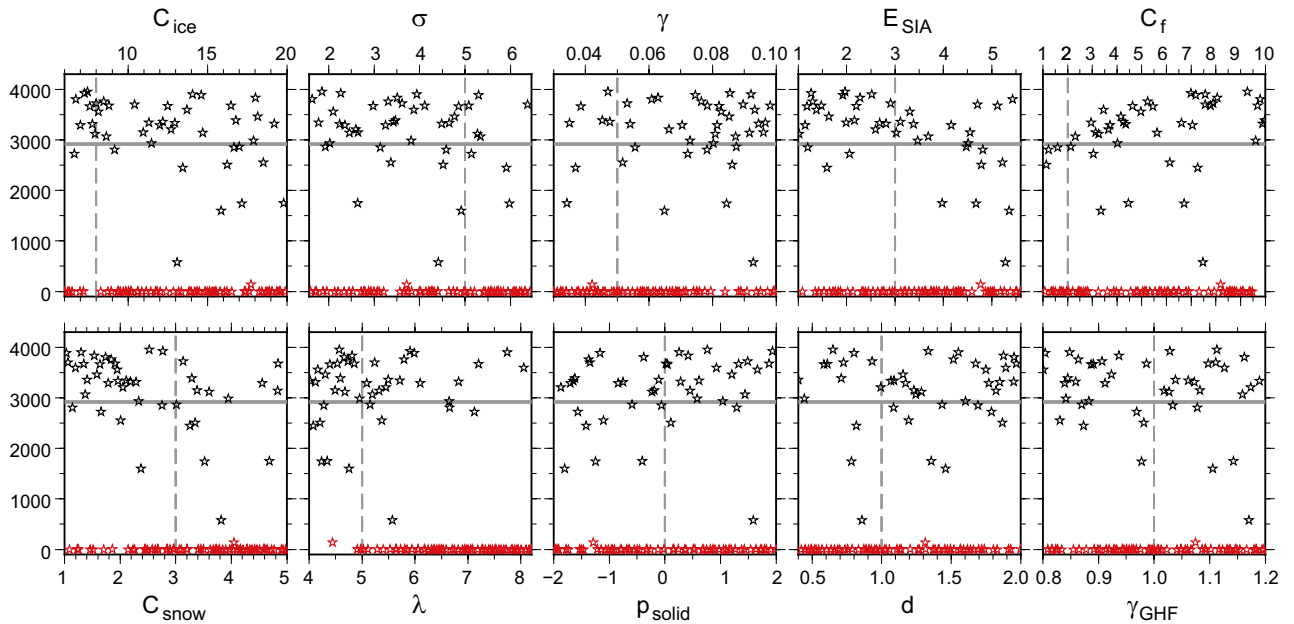


Figure 12-20. Simulated ice sheet thickness over Forsmark during the peak Saalian glacial maximum (about 140 000 years ago) as a function of different parameter combinations in the ice-sheet model (from Quiquet et al. 2016). The black stars represent individual steady-state simulations that resulted in ice thicknesses over Forsmark of at least 500 metres, whereas the red stars represent simulations that yielded no ice sheet or ice sheets thinner than 500 metres. The horizontal lines show the simulated ice thickness according to a reference run (Colleoni et al. 2014), while the vertical lines show the value of each parameter in this reference run. The investigated parameters are: C_{ice} = melting coefficient for ice (unit: $\text{mm } ^\circ\text{C day}^{-1}$), C_{snow} = melting coefficient for snow ($\text{mm } ^\circ\text{C day}^{-1}$), σ = standard deviation of the daily mean air temperature ($^\circ\text{C}$), λ = rate of air temperature decrease with elevation ($^\circ\text{C km}^{-1}$), γ = coefficient controlling the precipitation change with temperature ($^\circ\text{C}^{-1}$), p_{solid} = air temperature at which precipitation changes from snow to rain ($^\circ\text{C}$), E_{sia} = enhancement factor of ice flow (unitless), d = coefficient controlling the amount of refreezing of meltwater (m), C_f = coefficient controlling the ice flow's friction against the ground surface in areas with fast ice flows (unitless) and γ_{GHF} = factor controlling the geothermal heat flow from the ground surface (unitless). For a detailed description of these parameters and the simulations, see Quiquet et al. (2016) and the Climate report, Section 5.4.

Localised regions with water pressure persisting above ice overburden may still be plausible over longer time scales due to increased stress induced by ice flow against steep bedrock bumps. However, to first order, the magnitude of such stress perturbation does not scale with the overlying ice pressure, but rather with the basal shear stress at the bed that the feature must support (Weertman 1957). Hence, there is no physical justification as to why the reported pressures above overburden over daily to seasonal time scales in the ablation zone should also be present in the ice-sheet interior (Harper et al. 2019).

In addition, basal hydrostatic pressures can also occur in the form of pressure pulses over shorter time scales, with a typical a duration of seconds or minutes. The possibility of transient short pressure pulses beneath the Greenland ice sheets was therefore also investigated in two boreholes during the ICE project (Harper et al. 2019). The measurements identified rapid pressure pulses to be exceedingly rare. Importantly, the measured pulses all occurred as *pressure drops* and therefore did not contribute to basal pressures higher than overburden pressure. In addition, none of the pulses were transmitted between the two investigated boreholes, located close to each other. This demonstrates that the measured pressure pulses are localised events that occur over length scales much less than the ice thickness (Harper et al. 2019). Even if extension of the measured high frequency pressure dataset to the broader basal system is hindered by an incomplete understanding of the potential cause(s) of the few measured pulses, the localised characteristics of the pressure pulses detected in the ICE study makes it implausible that a pressure pulse event, even if it were to be positive, could impact a location at 450 m repository depth in bedrock.

Conclusions

For the reference glacial cycle, the additional hydrostatic pressure related to ice thickness over Forsmark is 26 MPa (Table 12-2). The *maximum* expected additional hydrostatic pressure, pessimistically derived from the largest ice sheet configuration during the past 2 million years, as supported by geological observations and ice-sheet model experiments, is 36 MPa. Adding the hydrostatic pressure for ice free conditions, 4.5 MPa, yields a total maximum hydrostatic pressure at Forsmark of 40.5 MPa.

Table 12-2. Maximum ice sheet thickness and associated additional hydrostatic pressure at Forsmark for two Fennoscandian ice sheet configurations.

	Maximum ice thickness (m)	Hydrostatic pressure contribution (MPa)
Reference glacial cycle	2900	26
Largest Fennoscandian ice sheet during past 2 million years (Saalian ice sheet)	4000	36

12.7.3 Buffer swelling pressure

Buffer initial density

The dry density of the buffer is designed to result in a swelling pressure less than 10 MPa, regardless of the bentonite material selected.

The acceptable dry density interval of the buffer consisting of MX-80 bentonite according to the reference design is 1453–1558 kg/m³. The initial diameter of the deposition hole cannot reasonably be smaller than the reference value of 1.75 m since this is determined by the diameter of the boring machine. Furthermore, the diameter of the hole will be inspected before being accepted for deposition, as further described in the **Underground openings construction report**.

The upper reference density limit of 1558 kg/m³ results in around 10 MPa swelling pressure for MX-80 to Figure 5-14.

According to Section 5.5.3, the maximum dry density around the canister will be 1541 kg/m³ if no spalling occurs (spalling will lead to a lower density). The upper swelling pressure of 10 MPa is therefore seen as pessimistic.

It is also noted that the total stress on the canister is not the sum of the bentonite swelling pressure and the hydrostatic pressure. According to Harrington and Birchall (2007) the total stress σ can be expressed as:

$$\sigma = \Pi + \alpha p_w$$

where Π is the original swelling pressure, p_w is the porewater pressure and α a constant of proportionality. Experimentally, α has been found to be in the range of 0.86–0.92. In the experiments by Harrington and Birchall (2007) with MX-80 with an original swelling pressure of ~8 MPa the bentonite retains a proportion of its original swelling ranging between 48 and 67 % at porewater pressures of 46 MPa. There are indications of a reduction in the rate of decline in swelling pressure as backpressure increases, indicative of a rise in α values at high water pressures. Linear regression suggests $\alpha = 1$ at a porewater pressure of around 64 MPa.

Based on the findings by Harrington and Birchall (2007), for a hydrostatic pressure of 40.5 MPa and a swelling pressure of 10 MPa, the total pressure is estimated at around 47.3 MPa (10 MPa + 0.92 × 40.5 MPa).

Buffer compaction

The buffer will have a higher swelling pressure than the backfill in a saturated state. No compaction of the buffer from the swelling of the backfill is therefore expected. However, there is a possibility that the backfill will saturate and develop its swelling pressure ahead of the buffer. This situation has not been directly evaluated in the PSAR, but it is briefly discussed in Börgesson and Hernelind (2009), where it is stated that the case is not of primary interest since there will be very little compression of the buffer blocks and rings and the uniaxial compression strength of the blocks is in the same range as the fully developed swelling pressure from the backfill.

Buffer chemical alterations and density losses

The buffer swelling pressure is determined by the buffer density and chemical composition, including the species of adsorbed cation. All identified chemical changes (ion exchange, osmosis and mineral transformation, see Section 10.3.10) of the buffer result in unaltered or decreased swelling pressure (possibly with the exception of a marginal effect for high density Ca bentonite). It is, therefore, pessimistically assumed that no such changes take place.

According to the FEP chart, the mechanisms through which buffer mass may be lost are piping, erosion or swelling into the deposition tunnel. It is pessimistically assumed that no buffer mass is lost over time due to these processes.

Conceptual uncertainties

No process has been identified that could increase the swelling of the buffer to a higher value than the original starting value. The pressure is expected to be as specified above or lower for all possible conditions.

Convergence of deposition holes

A possible issue is the convergence of deposition holes. No residual uncertainty has been identified that would challenge the conclusion from the reference evolution, namely that convergence effects are negligible, see Section 10.3.5.

12.7.4 Canister strength

As mentioned in Section 5.4.3, extensive analyses of the canister's ability to withstand isostatic load have been undertaken as part of the canister design analysis (Jonsson et al. 2018). These analyses are focussed on demonstrating that the canister can withstand the design load of 50 MPa. It is demonstrated that this is achieved with considerable margin, both as regards avoidance of local plastic collapse of the insert due to variation in material properties and allowed defect sizes in relation to expected and detectable defects. In particular, as noted in Section 5.4.2, the probabilistic evaluation reported in Dillström (2019) demonstrates that the probability both of plastic collapse and of failure due to propagation of fractures from the manufacturing of the insert are vanishingly small ($\sim 10^{-14}$) for pressures up to 75 MPa. In this analysis, fracture occurrences from test manufacturing, without considering subsequent reduction of occurrences when implementing a production control system, were applied. It has also been demonstrated that the insert can be manufactured with a fully sufficient accuracy regarding its critical dimensions relating to isostatic loads.

Also, the global collapse load for the cylindrical part of a canister (without defects) has been calculated to be 99 MPa and 128 MPa for BWR and PWR inserts, respectively (Raiko et al. 2018). Results from pressure tests of real canisters show that the collapse load for the canister is approximately 100 MPa or higher (Jonsson et al. 2018).

Hence, the following conclusions are drawn.

- *Total collapse*, i.e. the criterion for canister failure, of the insert is not expected to occur below at least 90 MPa according to both model calculations and laboratory tests.
- *Local collapse* is excluded for loads up to 50 MPa with a considerable margin.

12.7.5 Canister resilience to creep

General

When a static stress acts on the canister, its metal components can deform *instantaneously* if the stress is higher than the elasticity limit of the metal. The resulting hardening of the metal counteracts further deformation. But even below such limits metals can deform *with time*. Such time-dependent deformation, creep, increases with temperature and at high temperatures the material can recover with time and recrystallize, allowing an increase of the creep deformation before the occurrence of a potential creep induced failure. Copper is softer and has a higher creep rate than iron, but copper also hardens quite strongly with deformation. To lower the creep rate and improve the creep ductility, the canister copper is alloyed with a small amount of phosphorus. Importantly, the deformation of the canister copper shell is also limited by geometrical constraints through the presence of the cast iron insert.

In the repository the stresses on the canister are expected to increase slowly as the buffer swelling pressure is developed, and thereafter remain static for long periods. The pressures and resulting stresses on the canister are moderate compared to the strength of the canister up until a glacial load acts on the repository, which occurs tens of thousands of years into the future in the reference evolution. By that time the copper shell will have cooled down from an estimate average of 75 °C to around 10 °C (Figure 12-21).

Time dependent creep deformation behaviour and underlying fundamental mechanisms are characterized as functions of the ratio of the absolute temperature to the melting point for the metal in question. The melting point for copper is 1356 K, and therefore the final temperature in the copper shell in the repository is about 22 % of that of the melting temperature. For normal industrial applications, this would mean that creep would in principle be negligible, whereas for the time frames applicable for the final repository, the issue still requires consideration.

To explain and predict how much the copper shell deforms (amount of strain), the time to rupture, and whether it deforms in a ductile manner, the creep behaviour of the copper shell in the repository has been studied extensively; fundamental theories have been applied (Sandström 2012), the canister creep deformation has been simulated with finite element methods for repository conditions (Hernelind 2015), and copper from full-sized canister parts has been creep tested (Andersson-Östling 2020).

In general, there are several deformation mechanisms that govern copper creep behaviour, among them gliding and climbing within the grains, and sliding of grain-boundaries. In special cases diffusion of atoms is also of importance. The mechanisms can occur simultaneously and sliding of grain-boundaries requires gliding within the grains to maintain compatibility of the microstructure. It has been assumed that gliding controlled the creep rate for repository temperatures (Honeycombe 1968). In recent years it has, however, been suggested that climb is controlling the creep deformation even at ambient temperatures (Sandström 2017). These new findings can explain why the creep deformation at near to ambient temperatures shows similar behaviour as at elevated temperatures.

The creep rate generally decreases with time, recognized as primary creep during creep testing. Under certain conditions, such as elevated temperature, this may be followed by a secondary, steady state creep, characterised by a constant creep rate. The creep behaviour of canister copper is mainly primary with a decreasing rate until the secondary stage is reached according to observations and SKB's fundamental model for primary creep (Sandström 2012, 2016, Sui and Sandström 2018). The fundamental model for primary creep gives 2 % deformation for an arbitrarily chosen constant temperature of 95 °C and a stress of 60 N/mm² (60 MPa) during 100 000 years.

Creep testing can be performed faster if the temperature is raised, and creep by the climb mechanism is more active at higher temperatures. Also, due to geometric effects the stresses can rise locally. Furthermore, the copper metals can possibly contain impurities or defects if copper manufacturing or the sealing of the canister has not been performed as planned. Therefore, creep testing has been performed at higher temperatures, higher stresses, and included copper without phosphorus, with oxide defects or higher content of impurities (Andersson-Östling 2020).

In the case of high strains or higher temperatures, defects as voids and precipitations, as well as softening of the metal matrix can decrease the ductility of the copper. A high content of sulphur and large grain sizes are detrimental to the creep ductility of copper (Henderson and Sandström 1998).

To improve creep properties, small amounts of alloying elements can be added to counteract time-dependent softening as recovery and recrystallization. Metals such as silver, tellurium, and tin can be used to increase the softening temperature, but also a non-metal element as phosphorus is similar to tin as regards the increasing effect on the softening. The influences of phosphorus on copper's response to deformation are manifold, and is still not understood in detail. Sandström and Wu (2013) computed the effect of phosphorus on the creep ductility of the phosphorus-alloyed canister copper and discussed the mechanisms through which the increased ductility is achieved. The ductility findings have been further substantiated by demonstrating that the creep cavities are initiated by grain boundary sliding and that it is energetically much more difficult to form cavities in phosphorus-alloyed copper in comparison to phosphorus free copper (Sandström et al. 2016b, Sandström and Lousada 2021). The ductility modelling is fully in agreement with measured values for canister copper. In creep tests, the phosphorus-alloyed canister copper shows high creep ductility at temperatures between 75 and 450 °C, higher than that of pure copper without added phosphorus. This has been verified for at least 30 years' of testing (Andersson-Östling 2020), with the longest test lasting for about three years. For creep tests of temperatures up to 125 °C, no evident crack initiation (in a fracture mechanics point of view) could be observed. In tests with deliberately initiated cracks, the ensuing crack growth during creep tests was typical of ductile fracture initiation characterized by void nucleation, growth and coalescence, in which the initial increments of growth often follows the pattern that is predicted by conventional slip line theory. This indicates that fracture growth in the copper shell would halt due stress relaxation. (Björkblad and Faleskog 2018).

Modelling of canister mechanical evolution for slowly varying loads

To identify areas in the copper shell where creep can occur and to calculate the amount of creep strain, finite element simulations of the canister's mechanical response to the isostatic loads expected in a 100 000 year time frame were performed by Hernelind (2015). Several time-dependent boundary conditions in terms of canister temperature and external loads were studied, see Figure 12-21 for an example.

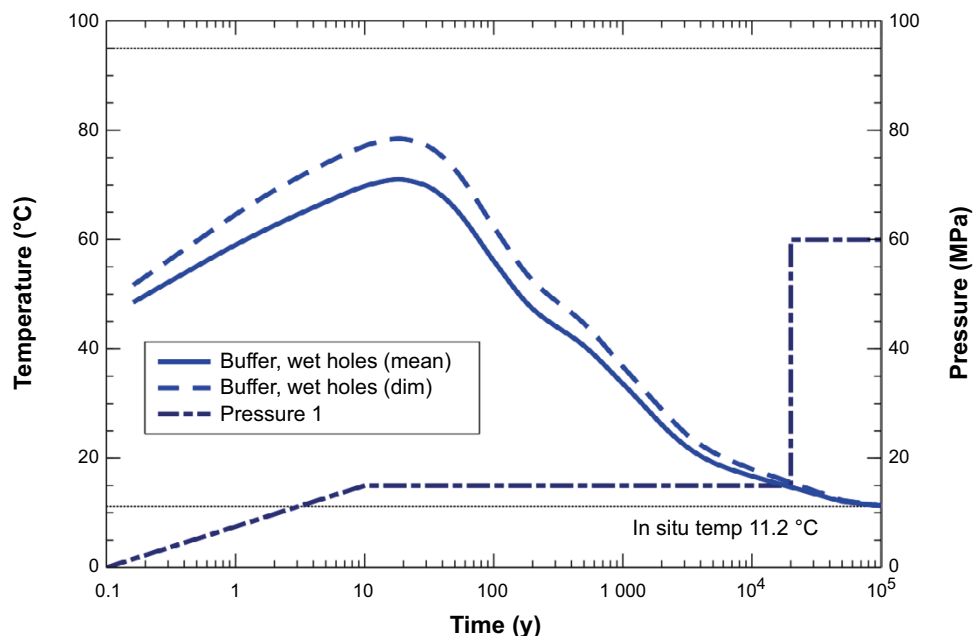


Figure 12-21. Pressure and temperature development used in Hernelind (2015) for deposition holes with short buffer saturation time. The swelling pressure develops in 10 years in this case. Note that values differing from this example for the maximum load and its onset are used in the analysis in the text.

The canister will be heated by the residual power of the fuel when the buffer swelling load of 15 MPa develops (the sum of 5 MPa hydrostatic load and 10 MPa swelling pressure, see Section 10.3.4). The copper temperatures at which this load may occur range from 25 °C up to 90 °C depending on the location of the deposition hole in the repository, due to the spread in saturation times of the buffer at the Forsmark site (Section 10.3.8). Later in the repository evolution when maximum glacial loads may yield total loads of up to almost 50 MPa cannot be excluded (Section 12.7.6) the temperature of the copper shell is expected to be around 10 °C.

Most of the simulations were performed as axi-symmetric analyses to enable a smaller element size and higher resolution with reasonable simulation times. The left part of Figure 12-22 shows how the element size varies through the cross-section of the modelled copper shell and that an increasing number of elements have been meshed close to discontinuities such as the weld and fillets to improve the resolution of anticipated stress concentrations. For comparison, some simulations with a three-dimensional model were also performed. The number of elements for the three-dimensional model was 10 times higher than for the axi-symmetrical model, and the simulation times much longer. Comparisons show that differences in strain are small, and that axi-symmetrical analyses yield pessimistic results compared to the 3D model.

The model based on material physics mechanisms (Sandström 2012) used in Hernelind (2015) included both primary and secondary creep, as further described in Jonsson et al. (2018). In the modelling of the creep behaviour it is assumed that the creep mechanisms are the same over time and that no major structural change such as recrystallization occurs in the copper.

The amount of creep for the main part of the copper shell is controlled by the gap between the shell and the insert. As the external pressure from the swelling buffer is applied to the copper shell, the gap closes and the cylindrical part of the shell is compressed. This compression results, in turn, in tension in parts of the copper lid and base. Most of the copper structure is hence compressed, whereas minor parts of the canister base and lid experience tensile stresses, which may cause creep in the long-term. The evolution of creep can be traced in the finite element model simulation for relevant material volumes by plotting the strain of a specific element over time. The right part of Figure 12-22 shows how the creep strain increases and stabilizes for the anticipated two loads, from the buffer swelling and the glaciation. Element 1155 is indicated in Figure 12-22 and represents a volume where deformation can occur due to outer pressure at the upper flange and disappearance of constraint from the insert close to the top of the copper shell. The buffer swelling with its pressure of 15 MPa (including the hydrostatic pressure of 5 around MPa at repository depth) and decreasing temperature from 75 to 20 °C stabilize at a strain of less than 1 %.

In the case of a subsequent glacial load, the gap between the copper shell and the insert is expected to have already closed. The main effect of this load is, therefore, to potentially increase the strain and tensile stress in the copper base and lid through the additional load on the top and the base of the canister.

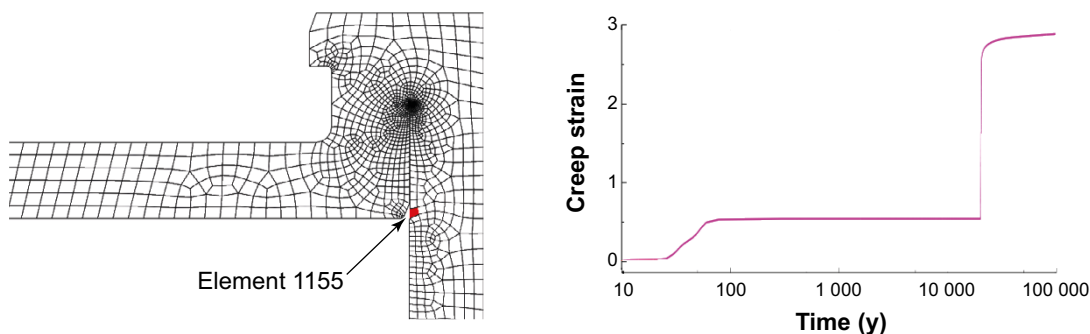


Figure 12-22. Left: Mesh for axi-symmetric finite element model of the copper shell. Element 1155 highlighted with red filling. Right: Simulated creep strain (%) for element 1155 for the time span of buffer swelling and glaciation in the upper part of the copper shell (Hernelind 2015).

For the maximum glacial load, the overall plastic strain in the copper is 1–3 %, and for element 1155 in Figure 12-22 the strain increases to 3 % and the rate is decreasing with time. The strain contour plot in Figure 12-23 shows that the affected volume due to the outer pressure where the disappearance of constraint from the inserts includes element 1155. The highest local strains occur at postulated worst-case discontinuities at the upper weld in the model and are concentrated to a few elements, corresponding to a few mm in spatial extent, and approach 30 % (Jonsson et al. 2018). Similar strains can be expected in the base of the copper shell and are also reported in Hernelind (2015). In comparison, the canister copper alloyed with phosphorus has shown an ability to withstand strains above 40 % without breaking in creep testing (Andersson-Östling 2020). It is also noted that neither of the volumes of strain concentrations extend through the copper coverage of approximately 5 cm.

In the simulation of the evolution of stress/strain in a canister under repository conditions in Hernelind (2015, 2019a, b) tensile stresses (grey-red) occur at the inner part of the lid and these arise because of the bending of the flange into the radial direction as seen at left in Figure 12-24. Also, at the flange at the base there are some areas with tensile stresses. The tensile stresses (axial) penetrating through the wall thickness decrease with the distance from the copper surface by an order of magnitude (Hernelind 2019a, b). Black mapping corresponds to compressive (harmless) stresses. The creep deformation in itself will relax and redistribute the tensile stresses (though not realised in the simulation).

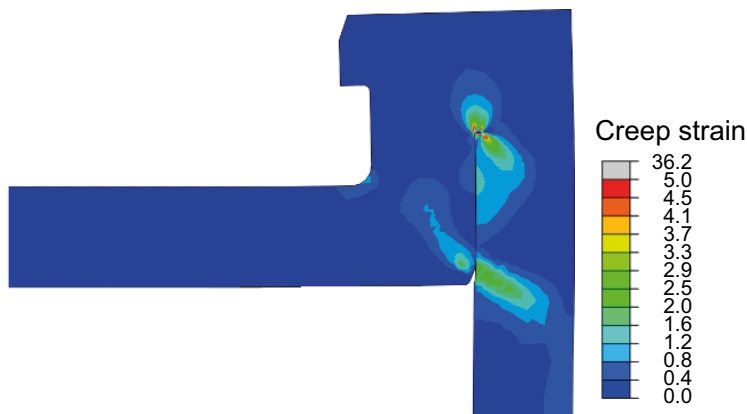


Figure 12-23. Simulated creep strain after buffer swelling and glaciation in the upper part of the copper shell (Hernelind 2015).

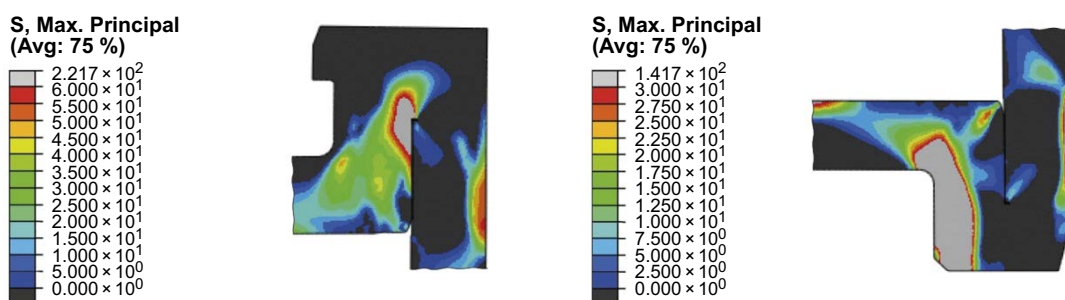


Figure 12-24. Finite element simulation of the maximum principal stresses in the copper lid and base due to the isostatic pressure and creep strain, with zero gap. For clarity, all compressive stresses are shown as black. (Hernelind 2019b).

Discussion of results and uncertainties

Load impact of non-glacial versus maximum glacial conditions

It is evident from Figure 12-22 that both the creep strain rate and the resulting magnitude of creep strain caused by the 15 MPa load after completed buffer swelling are considerably smaller than the 50 MPa maximum load under glacial conditions. The margin to local damage due to creep strain is considerably higher for the swelling pressure load.

Relevance of copper temperature

In principle creep deformation of metals occurs at all temperatures, but in normal applications it is only above 30–50 % of the melting temperature of the metal that creep contributes to permanent strains in the metal. For copper, 30–50 % of the melting temperature corresponds to 130–400 °C, and in the repository the temperature is well below this interval. The extremely long time frame considered in the assessment of post-closure safety, however, still necessitates an analysis of creep.

As mentioned above, the buffer swelling can occur after 10 years, with canister temperatures of 90 °C, as in Hernelind (2015), or after more than 1 000 years when the canister temperature would have cooled down to 20 °C. At both these temperatures primary creep is expected and the amount of creep can be modelled with a physically based logarithmic time law for creep deformation (Honeycombe 1968), as done by Hernelind (2015). Also, the amount of creep can be shown to be proportional to the absolute temperature in such a physically based relation. This would hence result in a large decrease of creep deformation at 20 °C compared to 90 °C since the primary creep rate decreases with decreasing temperature. The possible delay of the buffer swelling is, therefore, not problematic as concerns creep deformation of the copper canister.

Impact of model mesh density

The determination of the creep strain in model simulations is strongly influenced by the element mesh density. Therefore, several mesh densities were tried and compared, and the strains of severely distorted elements were manually evaluated (Hernelind 2015). Since several models were executed with different mesh densities it has been possible to make a comparison and the conclusion is that the mesh in a global sense is accurate.

Conceptual uncertainties regarding the creep model

The creep behaviour has been simulated with fundamental material models for both primary and secondary creep to bridge the extrapolation in time domain from the creep testing to repository time spans. In detail, most of the creep strain comes from primary creep as usually observed at low temperature conditions.

According to Sandström and Wu (2013), Sandström et al. (2016b), and Sandström and Lousada (2021), the beneficial effect of phosphorus on creep ductility is agglomeration of phosphorus in the copper, slowing down the deformation and limiting local deformation of the grain boundaries at intermediate temperatures and most probably throughout the repository time evolution.

Relevance of small regions with elevated creep strain or tensile stresses in the model results

The creep strains and tensile stresses anticipated in the copper shell of the canister are mostly localised to inner parts, the affected volumes are small and do not extend through the copper shell. Therefore, possible damage by excessive shearing or tensile stresses for the glacial load is expected to be local, and further deformation is expected to be ductile and not extend through the copper thickness. Some of the highest creep strains can occur in the weld area, but due to the effects of the friction stir welding on the material properties, the grain sizes of the welds are smaller compared to the structure in the lids and the shell, making the welds even more resistant to deformation or damage.

Creep ductility in a 100 000 year time perspective

The long-term creep behaviour of the canister copper can be assessed from short term tests and theoretical reasoning. The ductile behaviour of the canister copper is facilitated by the phosphorus alloying, and it is essential to evaluate how these beneficial material properties develop over time. It has been verified that the basic creep model can be used to extrapolate the creep rate many orders of magnitude in time to the extent that it can handle the time perspective of the repository (Sandström 2012). This means that the finite element model simulation presented above has a good foundation.

Creep ductility has since the 1930s been determined on plots of *the logarithm of the stress* against the logarithm of rupture time, see Figure 12-25 where copper has been creep tested under constant stress. In such a diagram linear dependencies are usually expected for the short term creep tests, but extrapolation, shown as solid lines in the figure, based on such assumption for longer times is now known to be wrong, giving optimistic predictions.

More importantly, the creep behaviour is strongly dependent on stress and temperature and therefore testing at higher temperatures give possibilities to assess the behaviour at higher stresses and longer times. There are several extrapolation methods in the literature (Penny and Marriott 1995). Standard extrapolation methods have been applied to SKB's creep rupture data, and in Figure 12-25 the dotted lines show extrapolations according to Manson and Haferd (1953) described in Penny and Marriott (1995) with data from Sandström (1999) for longer times and other temperatures than actually creep tested. Even if the method describes the relations between stress, temperature, and creep rupture times, the confidence of the predictions decreases with time, but it gives valuable insights to the general trends of the creep behaviour of copper.

However, the creep behaviour cannot readily be extrapolated to longer times from short term tests since intergranular material damage can occur in the grain boundaries and the microstructure can become coarser. At high temperatures round pores can occur in the grain boundaries, and at high stresses wedge-cracks are possible (Honeycombe 1968, Sandström and Wu 2013).

Relating the results of the Manson-Haferd plots to repository conditions, it is noted that the 50 °C-curve (dashed line) is vertical at a rupture time of 3.15×10^5 years, i.e. this is the predicted rupture time constant of the Manson-Haferd model at 50 °C (and lower), independent of stress. Again, it is noted that in the long-term the repository temperature is 20 °C or lower. The model is applicable for temperatures above ~50 °C and demonstrates that at this temperature the rupture time is extremely long. It is, however, not possible to use the model to predict time spans of hundreds of thousands of years for the repository relevant long-term temperatures, other than noting that at such low temperatures the rupture time would be even longer than for the 50 °C-curve. In fact, the model breaks down mathematically if applied at 20 °C.

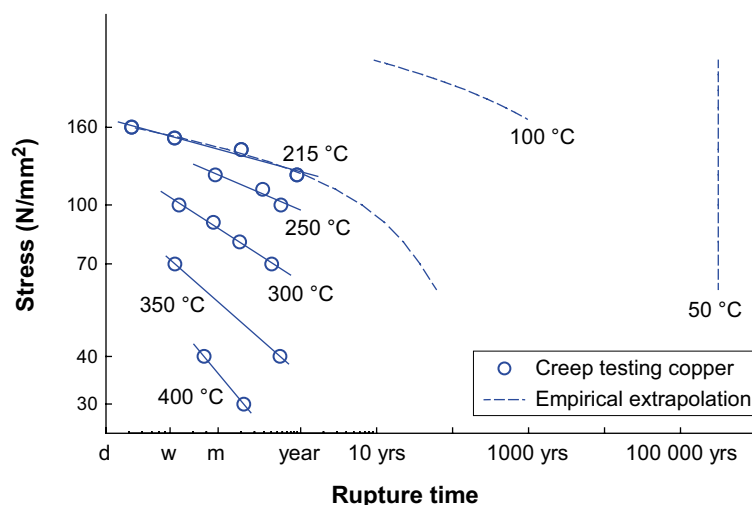


Figure 12-25. Stress as a function of creep rupture time for phosphorus alloyed canister copper. The data for 215–400 °C (Sandström 1999) have been extrapolated according to the Manson-Haferd-method, yielding the two dotted curves.

It is also noted that for a temperature of 215 °C, the Manson-Haferd model predicts a rupture time of the order of 1 000 years. This is also compatible with the results of an analysis by Pettersson (2016), that considered data obtained at 215 °C.

It is finally noted that in the simulation of the evolution of stress/strain in a canister under repository condition in Hernelind (2015), no failure mechanism reflecting the material behaviour according to the Manson-Haferd plots is included. The model produces the amount of creep strain, but not the rupture time depending on tensile stresses. Rather, the creep strain in the modelling is compared to measured creep strains at failure. This does not capture the long-term deterioration in material properties under tensile stresses, whereas this phenomenon is implicitly described by the Manson-Haferd type of plot.

Hydrogen embrittlement

High contents of hydrogen in the copper material can in principle deteriorate its ductile properties (see further the **Fuel and canister process report**, Section 3.4.7). However, as demonstrated in Section 10.3.13 (with details given SKB 2019), no mechanisms through which detrimental amounts of hydrogen could enter the canister material have been identified. Hydrogen embrittlement is, therefore, not expected to occur in the copper material.

Conclusions

The following is concluded.

- Whereas most of the copper shell will be subjected to compressive stresses in the repository, creep due to tensile stresses can be expected to occur in limited regions at the lid and the base of the shell.
- Modelled creep strains are overall considerably lower than the 40 % creep elongation at rupture measured in creep tests
 - For the 15 MPa load after completed buffer swelling the creep strain is around 1 % in exposed regions. This load has been modelled at a copper temperature of around 60 °C, expected if the swelling occurs some tens of years after deposition in the repository. If the swelling is delayed until the temperature has decreased to around 20 °C, this would give slightly lower creep strains compared to the situation with the higher temperature.
 - For the maximum isostatic load of 50 MPa at 20 °C the creep strain is around 3 % in exposed regions.
 - Also for postulated worst case discontinuities, the maximum local strains of 30 % for the maximum glacial load are below the measured critical elongation. The spatial extent of such discontinuities would be a few mm. Even if damage were to occur in such discontinuities, this is expected to be limited to the affected small regions and be of no consequence for canister integrity.
- The conceptual understanding of creep in phosphorous alloyed copper has evolved during the past decade, leading to the development of the model based on material physics mechanisms applied in the mechanical modelling of the canister. Continued research is warranted to further clarify the details of the role of phosphorous for the creep properties of phosphorous alloyed copper.
- The copper material can be expected to maintain its beneficial ductile properties for very long times, also taking temperature activated deterioration of material properties into account in both empirical and physically based models, as demonstrated with an extrapolation technique. The physically based models have been experimentally verified.
- Hydrogen embrittlement is not expected to occur in the copper material, since no mechanisms through which detrimental amounts of hydrogen could enter the canister material have been identified.

The overall conclusion is that copper creep does not jeopardise the integrity of the copper canisters in the final repository.

12.7.6 Combined assessment

According to Section 12.7.3, a maximum swelling pressure of 10 MPa could occur in the buffer.

The groundwater pressure is around 4.5 MPa at Forsmark for ice-free conditions. According to Section 12.7.2, an additional ground water pressure of at most 36 MPa could occur as a result of a maximum glacial load.

This would give a maximum feasible isostatic load on the canister of 50.5 MPa at Forsmark if the hydrostatic and swelling pressures are added. However, applying an α -value of 0.92 in the addition as suggested in Section 12.7.3 results in a total pressure of around 47.3 MPa.

According to Section 12.7.4, local collapse is avoided with substantial margin for 50 MPa, implying that local collapse would be avoided also at 47.3 MPa. In particular, probabilistic evaluations of the canister insert imply that the likelihood of failures due to isostatic loads is vanishingly small for pressures up to 75 MPa. The margin to total collapse (90 MPa), i.e. the criterion for canister failure, is considerable. According to Section 12.7.5, the copper shell will not fail due to creep for isostatic load up to 50 MPa.

Overall, the following conclusions can be drawn.

- Total collapse is the relevant failure criterion since only this type of failure will lead to the release of radionuclides from the canister.
- There is ample margin to prevent canister failure due to isostatic load, even for the most extreme load situations.

Different event sequences

There are no different event sequences to consider in the discussion of this scenario, since pessimistic assumptions are made and maximum effects are sought for all involved factors. During the one million year assessment time, the canister is in the analysis subjected to some eight glaciations leading to repeated load cycles. The number of events is, however, far too low to have any fatigue effect on the mechanical stability of the cast iron insert.

Combination of isostatic load and shear movement

See the shear load scenario, Section 12.8.2, where it is concluded that the combined case can be excluded from consideration.

Global warming variant and other climate cases

The occurrence of high groundwater pressures is directly related to glacial conditions. The delay of glacial conditions in the global warming variant would thus be beneficial for repository safety in this respect. The issue is therefore not further treated for the global warming variant.

Since the *maximum ice sheet configuration* climate case (see Section 12.1.3) has been used in the above analysis and since that case was defined to maximise the isostatic load on the canister, no additional climate cases need to be considered.

Early canister failures due to isostatic loads

As mentioned in Section 11.3, a dedicated analysis of the potential for early failures is provided for each scenario relating to canister failure modes. The need for this analysis is primarily due to the long period of unsaturated conditions expected for a repository at Forsmark. These conditions affect primarily corrosion related processes as analysed in Section 12.6.3. As regards isostatic loads, extended periods of unsaturated conditions would delay the onset of the isostatic load due to buffer swelling. As seen in particularly in Section 12.7.5, this is assessed not to have any negative effects as concerns the creep behaviour of the copper shell. Early failures due to isostatic loads are, therefore, assessed as ruled out. Consequences of postulated early canister failures (irrespective of failure mode) are analysed as a residual scenario in Section 13.7.3.

Categorisation as “less probable” or “residual” scenario

Based on the above assessment, this scenario, i.e. a canister failure due to isostatic load, is considered as “residual”, meaning that its consequences are excluded from the risk summation.

The consequences in terms of radionuclide transport and annual effective dose of a postulated isostatic collapse are addressed in Section 13.7.1.

12.8 Canister failure due to shear load

12.8.1 Introduction

Safety function indicator(s) considered

This scenario primarily concerns the safety function relating to shear loads on the canister. If the shear load on the canister is too large, the canister is assumed to lose its containment capacity (safety function Can3a, b and c). As seen in Figure 8-3, both instantaneous loads and long-term creep ductility need to be considered.

Safety function indicators and criteria relevant to the evaluation of this failure mode are i) the requirement that shearing across the deposition hole should be less than 0.05 m (R3b) and ii) that the buffer has a maximum dry density yielding an unconfined compressive strength at failure < 4 MPa at a deformation rate of 0.8 %/min for the R3b criterion to be applicable (Buff 3). According to Figure 6-5 in Svensson et al. (2019) 4 MPa is reached for MX-80 at a dry density of around 1 640 kg/m³.

This safety function is directly related to containment, as the containment is assumed to be breached if the safety function indicator criterion R3b is violated. Should this occur, also the retarding capacity of the system is affected, since the rock shear event is assumed to affect the retarding properties of the buffer and the rock negatively.

Treatment of failure due to shear load in the reference evolution

The possibility of canister failure due to shear load is of low probability and is, therefore, excluded from the reference evolution, see Section 12.1.2. This is motivated by the results of the analysis of the reference evolution reported in Section 10.4.5.

The analysis below evaluates whether all uncertainties were appropriately considered in the reference evolution and also provides an upper bound on the likelihood for canister failures due to shear load.

This upper bound is related to the result of the pessimistically derived frequency of canister failures due to shear loads in Section 10.4.5 and illustrated in Figure 10-129.

Qualitative description of routes to failure due to shear load

The evolution in this scenario is assumed to be identical to that of the base case of the reference evolution, except for factors related to collapse of the canister due to shear load.

As indicated in the FEP chart, the ability of the cast iron insert to withstand shear loads is determined by the canister design and by the quality of the production and NDT (non-destructive testing). The shear stress on the canister is determined by the nature of the slip along the fracture intersecting the deposition hole and the way in which this shear load is propagated through the buffer. The buffer density affects this propagation, meaning that the initial buffer density must be evaluated. The shear load is determined by the likelihood that the deposition hole is intersected by a fracture of a particular size, which, in turn, depends on the properties of the fracture network within the host rock and the likelihood with which unsuitable fractures can be detected and avoided in deposition holes.

Also the likelihood that earthquakes of a sufficient magnitude will occur during the assessment period needs to be evaluated.

The following factors of importance for possible occurrence of a canister failure due to shear load are identified, based on the discussion above, on Table 10-33 describing uncertainties identified in the reference evolution and on the FEP chart, Figure 8-5.

Initial state factors involved

- Insert strength and the occurrence of defects (casting quality).
- Copper shell mechanical properties.
- Buffer density.
- Buffer material properties.
- Fracture network properties.
- Efficiency in the implementation of deposition hole rejection.

Processes involved

- Canister: Deformation of copper canister; creep.
- Canister: Deformation of cast iron insert.
- Buffer: Swelling/mass redistribution.
- Buffer transformation.
- Geosphere: Reactivation of fractures as a consequence of earthquakes.

External conditions involved

- Earthquakes.

Propagated buffer conditions

According to Section 12.5, three different buffer conditions are propagated to the canister scenarios. Two of these concern advective conditions in the buffer and the third is the intact buffer. Since advective conditions are related to an eroded buffer which has a lowered swelling pressure than an intact buffer, such conditions are of less concern when canister failures due to shearing are evaluated. Therefore, only the intact buffer is further treated in the analysis of canister failures due to shear loads and it is evaluated if the intact buffer may under any circumstances have a higher density than that specified in the initial state. (In addition, the transformed buffer is discussed as a residual case below.)

12.8.2 Quantitative assessment of routes to canister failure by shear load

Canister and buffer response to shear loads

The response of the canister-buffer system to shear loads has been extensively studied within the canister design analysis (Jonsson et al. 2018), forming an important basis for the **Canister production report**. The aim of those studies has been to establish that the canister fulfils the technical design requirement stating that the copper corrosion barrier should remain intact after a 5 cm rock shear movement at 1 m/s for buffer material with maximum dry density yielding an unconfined compressive strength at failure < 4 MPa at a deformation rate of 0.8 %/min. This applies for all locations and angles of the shearing fracture in the deposition hole, and for temperatures down to 0 °C. The insert should maintain its pressure-bearing properties to isostatic loads after such shear movements.

In the design analysis a number of the factors listed above are by necessity taken into account and evaluated. This regards the following factors related to the initial state: the strength of the insert, the copper shell mechanical properties, the buffer density and the buffer material properties. The design analysis also considers deformation of the copper canister and the cast iron insert, including creep in the copper.

The overall conclusion of the design analysis is that the canister fulfils the technical design requirement relating to shear load, as further discussed in Section 5.4.3. In the design analysis report, this conclusion is reached after discussing all relevant uncertainties of the phenomena included in the analysis, i.e. uncertainties in the above mentioned initial state factors and processes have been considered. These are, therefore, not discussed here.

The design analysis considers material properties down to 0 °C in accordance with the technical design requirements. As demonstrated in the buffer freezing scenario, Section 12.3, temperatures below 0 °C at repository depth are not expected for any reasonable assumptions for the Forsmark site. Therefore, the results of the design analysis are considered valid for all relevant temperatures in the repository. (It is also noted that the mechanical properties of the canister do not change abruptly at 0 °C.)

Consequences of alterations of the buffer are discussed in Section 10.4.5, and argued to be of no concern, in a stylised calculation case where a substantial part of the buffer is assumed to be cemented. This, in combination with the fact that buffer alteration is considered to be a residual scenario in Section 12.4, yields the conclusion that buffer alterations are not a concern for the shear load scenario.

In the reference evolution, Section 10.4.5, it is argued that there is a margin in the results obtained in the design analysis such that, in many of the shearing cases analysed, e.g. for different angles of intersection and points of impact, there is evidence that the canister would in fact sustain also the load from a 10 cm shearing. This is further strengthened by the fact that the initial state of the buffer resulting from an analysis of the reference procedures for buffer production and installation yields an upper limit on buffer dry density of 1 541 kg/m³, in the ring section surrounding the canister, which is substantially lower than the density yielding an unconfined compressive strength at failure < 4 MPa at a deformation rate of 0.8 %/min. For MX-80, the shear strength is less than this for dry densities less than ≈ 1 640 kg/m³. Also, the failure criterion for the canister is the acceptable defect size for surface defects in the insert. The copper shell is assumed to be penetrated at the same moment as this criterion is exceeded. The strains in the copper shell are low (with the exception of model singularities) compared to copper material ductility requirements. However, uncertainties due to a copper thickness of slightly less than 50 mm are not evaluated.

Copper creep

As noted above, creep deformation of the copper shell was evaluated in the analysis of shear loads in Section 10.4.5 of the reference evolution. There, it was found that the canister will withstand all aspects of the design shear loads, i.e. also creep deformation in the copper shell.

The shear load deformation of the copper shell will harden the copper by cold working. Cold working results in pronounced substructures within the grains that increase the strength of the material. The cold worked material exhibits much longer creep lifetime, and lower creep strain and creep rate (Wu and Sandström 2018).

A copper creep material model (Jin and Sandström 2008) was used together with an elastic-plastic material model in the shear load analysis by Hernelind (2010), the main reference as regards modelling of the canister's response to shear loads in Section 10.4.5. Using this rate-dependent material model describing creep for the shear load simulation decreases the maximum strain in the copper. The rate-dependency makes the material stiffer like the cold working hardening described above.

According to Jonsson et al. (2018) all relevant shear cases are displacement controlled, meaning that the final mechanical state in the canister can be simulated with elastic-plastic models. This approach obviates the need for a creep model; the final state is calculated directly, without a detailed modelling of the temporal evolution. This latter approach was also used and evaluated in Hernelind (2010), yielding similar strain results as the creep model described above. This finding is seen to imply that the creep model is a relevant description of the creep process since it yields a similar final state as the elastic-plastic model. Also, conceptual uncertainties in the description of creep are of secondary importance since the final strain state is the relevant result, rather than the temporal evolution leading to it.

As for the analysis of creep deformation for isostatic loads, it is noted that high contents of hydrogen in the copper material can in principle deteriorate its ductile properties (see further the **Fuel and canister process report**, Section 3.4.7). However, as demonstrated in Section 10.3.13 (with details given SKB 2019), no mechanisms through which detrimental amounts of hydrogen could enter the canister material have been identified. Hydrogen embrittlement is, therefore, not expected to occur in the copper material.

Based on the analyses presented in Section 10.4.5 and the above discussion, it is concluded that the copper canister will withstand the design shear loads also with respect to copper creep.

Fracture network

The discrete fracture network (DFN) uncertainties are treated by the use of alternative DFN models that together span a wide range of uncertainties (see the **Data report** for details). In the reference evolution (Section 10.4.5), all three DFN models suggested for the Forsmark site were propagated through all calculations, which resulted in a range (min–max) of the number of potentially damaged canisters. In deriving the frequency of canister failures as a function of time in Section 10.4.5, the maximum value of this range was chosen.

Further, for the analyses summarised in Section 10.4.5, all earthquakes were pessimistically assumed to occur on the deformation zone (A2) that affects the largest number of canisters. Also, as argued in Munier (2010), the use of FPI criteria considerably lessens the impact of DFN uncertainties on the number of canisters intersected by potentially critical fractures.

Efficiency in the implementation of deposition hole rejection

The number of canisters that may fail due to shear load during the assessment period depends on the success of detecting and avoiding large fractures in deposition holes. The EFPC deposition hole rejection criterion has been shown to be effective in finding critical structures and enables the detection of > 97 % of the critical canister positions irrespective of DFN model (Munier 2010). The remaining positions are propagated to the assessment of seismic impact (Section 10.4.5). However, the EFPC simulations are based on idealisations of fractures as being perfectly planar, infinitely thin discs for computational convenience. Most real fractures are not so anonymous and, rather, display many properties that can be used as proxies for size (Cosgrove et al. 2006). It is therefore, likely, as argued in Munier (2010), that critical fractures that escaped detection in the simulations used as input for this assessment will indeed be detected by a carefully designed investigation programme, see further Section 15.6.2. Hence, it is likely that the number of potentially damaged canisters will be lower than predicted in this assessment.

Earthquakes, in particular those of post-glacial origin

The largest uncertainty concerns the estimated frequency of earthquakes during different time frames. In the reference evolution (Section 10.4.5) all relevant estimates of long-term earthquake frequencies were considered, thereby enabling the definition of a frequency range. This frequency range was then combined with the range of the number of critically positioned canisters to yield, eventually, a range of numbers of potentially damaged canisters.

In deriving the frequency of canister failures as a function of time in Section 10.4.5, the maximum value of this range was chosen.

Reactivation of fractures as a consequence of earthquakes

Uncertainties regarding the reactivation of fractures as a consequence of earthquakes are discussed in the reference evolution, Section 10.4.5. Several pessimistic approaches are used when quantifying the reactivation of fractures and these are not repeated here.

Combination with isostatic load

As discussed in Section 10.4.5, the stability of fractures in the rock is increased during periods of high isostatic load. This is a consequence of how stresses in the upper crust are expected to develop as a result of a typical future glacial cycle according to analyses of large scale ice-crust-mantle interactions (Lund et al. 2009). Accordingly, the combined effects of high isostatic pressures and shear load across canisters do not have to be further considered.

Cumulative effects of several earthquakes

The induced slip on large fractures, as a response to an earthquake, might be less than the canister failure criterion due to the fracture's position, orientation, local stress field and other properties. However, it is possible that slips along a particular fracture might accumulate to exceed the failure criterion as a response to repeated large earthquakes.

It is questionable if large earthquakes can be treated as independent events, which is implied by the above use of a time-independent, frequency based approach. In fact, large earthquakes within a glacial cycle are most probably *dependent* events such that the release of elastic energy relaxes the fault so that another large earthquake along the same fault is less likely. Similarly, but on another scale, slip relaxes the target fracture such that a repeated slip is less likely, and in particular slip of the same amount and orientation.

By taking strain rate into consideration, the time necessary for a fault to accumulate sufficient stress for a repeated earthquake was estimated in Section 10.4.5. With the assumptions made in Section 10.4.5, it was estimated that a maximum of 2 large seismic events can occur on the same fault within the assessment period of 10^6 years. The slip vectors on the fractures crossing the canisters were then pessimistically assumed to be perfectly parallel which implicitly assumes that the same zone reactivates and that the earthquake mechanism (slip velocity, stress drop, shear mode, etc) is identical. The positive effect of buffer restoration between the seismic events was disregarded and, further, a constant slip velocity (1 m/s) regardless of displacement on target fractures was assumed. Altogether, therefore, the cumulative effect of repeated earthquakes as treated in Section 10.4.5 is judged to yield an upper, pessimistic, estimate of the number of failed canisters.

Global warming variant and other climate cases

The external conditions of relevance to the occurrence of large earthquakes have already been considered in the above analysis.

12.8.3 Conclusions

Categorisation as “less probable” or “residual” scenario

Based on the above assessment, this scenario is considered as “less probable”, meaning that its consequences are to be included in the risk summation.

The above analysis demonstrates that the handling of uncertainties for this scenario was exhaustive in the reference evolution. Therefore, probabilities of canister failures estimated in Section 10.4.5, Figure 10-129, are used for the consequence calculations in Section 13.6 and considered as bounding for the risk contribution from the shear load scenario.

Early canister failures due to shear loads

As mentioned in Section 11.3, a dedicated analysis of the potential for early failures is provided for each scenario relating to canister failure modes. For the case of shear load failures, such an analysis is provided in Section 10.4.5, where it is concluded that this cannot be categorically ruled out, but that the likelihood is very low, according to Table 10-24. Cases of early failures are therefore propagated to the consequence calculations of shear loads in Section 13.6.

12.9 Summary and combinations of analysed scenarios

12.9.1 Summary of results of the analyses

In summary, the following conclusions were reached when the selected scenarios were analysed, as described above.

- Buffer advection: This situation may occur in the reference evolution. The additional analyses in Section 12.2.2, considering conceptual uncertainties and additional interpretations of the hydraulic properties of the sites, suggest a range in the possible extent of buffer advection. *These consequences were propagated to the canister corrosion scenario.*

(Regarding canister sinking to the bottom of the deposition holes, in terms of consequences, this is a special case of buffer advection. The additional analyses in Section 12.2.4 led to the conclusion that canister sinking, if it occurs, is preceded by advective conditions in the buffer due to buffer erosion. The consequences of a possible canister sinking are, therefore, covered by the general treatment of buffer advection.)

- Buffer freezing: Buffer freezing with detrimental effect was ruled out in the reference evolution, also for an eroded buffer. The additional analyses in Section 12.3 also led to the conclusion that freezing of an intact buffer is ruled out and hence should be considered as a residual scenario. This applies also to the freezing of water in cavities of a partially eroded buffer. *The possibility of detrimental buffer freezing was, therefore, not propagated to the canister scenarios.*
- Buffer transformation: The analyses of a high buffer temperature, or other circumstances leading to the transformation of the buffer material in Section 12.4 led to the conclusion that this should be considered as a residual scenario. *The possibility of buffer transformation was, therefore, not propagated to the canister scenarios.*
- Canister failure due to corrosion: This failure mode is included in the reference evolution, where it occurs for the case of advective transport through an eroded buffer. The additional analyses in Section 12.6, with input from the buffer advection scenario, Section 12.2, led to the conclusion that buffer advection is indeed the main potential cause of corrosion failures. Evaluating all the advective situations and other uncertainties related to corrosion led to a range of potential extents of corrosion failure. *These are propagated to the analysis of consequences for the corrosion scenario in Section 13.5.*
- Canister failure due to isostatic load: This failure mode was ruled out in the reference evolution and the analysis in Section 12.7 led to the conclusion that it should be considered as a residual scenario. *Consequences for a hypothetical case of canister failure due to isostatic load are analysed in Section 13.7.1.*
- Canister failure due to shear load: This failure mode was analysed in the reference evolution, where it had a low probability of occurrence even with a number of pessimistic assumptions, Section 10.4.5. This conclusion remains after the additional analyses in Section 12.8. *The pessimistically estimated frequency of canister failures due to shear load is propagated to the analyses of consequences for the shear load scenario in Section 13.6.*

Both the conclusions and the quantitative results propagated to consequence calculations are similar to those in the SR-Site assessment.

12.9.2 Assessment of containment potential for the main scenario

As mentioned in Section 12.1.2, an assessment of the containment potential of the main scenario is postponed until after the analysis of the additional scenarios, so that the assessment can be based on also the evaluation of uncertainties carried out in the analysis of additional scenarios. Since only two of the additional scenarios lead to the conclusion that canister failures cannot be ruled out, and since the uncertainty span for the additional scenarios is broader than that of the main scenario, only these two failure modes need to be considered in the evaluation of the containment potential of the main scenario.

Based on the analyses of the corrosion scenario in Section 12.6.2, the central corrosion variant is seen as representative for the main scenario, since it has an appreciable likelihood of occurrence given the cautious assumptions underpinning it and since it is compatible with the reference evolution of the repository.

Regarding canister failure due to shear load in the main scenario, the probability of shear failure in the reference evolution is low; on average 0.078 canisters in one million years even with a number of pessimistic assumptions regarding earthquake probability, location of earthquakes to fracture zones, extent of secondary movements for a given fracture size, the selection of geological DFN model, assumptions on the implications of the location and angle of shearing fractures on the impact on the buffer/canister system, handling of multiple earthquakes, etc. Therefore, it is seen as justified to exclude this failure mode from the main scenario. Note, however, that this does not reduce the calculated risk since the shear load scenario is based on all the pessimistic assumptions mentioned and no reduction in probability of the shear load scenario is made for these pessimisms when it is propagated to the consequence calculations.

In conclusion, the containment potential for the main scenario is assessed as equal to that of the central corrosion variant in Section 12.6.2.

12.9.3 Combinations of analysed scenarios and phenomena

Combinations of the analysed scenarios need to be considered. However, it is important to note that several such combinations have already been addressed, since, in the methodology for scenario analysis adopted, the buffer scenarios were analysed first. Results of those buffer scenarios that were not found to be residual were then propagated to the analyses of the canister scenarios. Also gradually developing phenomena need to be considered.

According to the summary above, the scenario analyses in this chapter demonstrate that the only appreciable safety related degradations of the engineered barrier system that cannot be ruled out are loss of buffer due to erosion, corrosion of the copper canister when buffer erosion has proceeded to the stage when advective conditions have arisen and canister failure due to shear movements on fractures intersecting the deposition hole. In addition, the canister may be subject to considerable isostatic loads, although not to the extent that canister failures occur. Buffer freezing with detrimental effects and buffer transformation were ruled out.

In the following discussion of combinations, the emphasis is on combinations of physical phenomena rather than on combinations of the formal scenarios. To direct the discussion towards an account of combinations of potentially detrimental phenomena, the thermal, hydraulic, mechanical and chemical impacts on the buffer and on the canister are considered, in light of the results of the analyses of the reference evolution and the scenarios.

- The thermal impact on the canister and the buffer occurs initially in terms of elevated temperatures and during periglacial conditions in terms of the lowest temperatures. As reported in Section 10.3.4, the safety related thermal requirements on the repository are met and no challenge to this conclusion has been identified in the scenario analyses, in particular as regards buffer transformation (Section 12.4). As also mentioned above, buffer freezing with detrimental effects is ruled out in the analysis of the buffer freezing scenario. Thermal aspects are, therefore, not further considered in the following.
- Two mechanical phenomena of relevance for post-closure safety have been identified: canister failure due to shear movements in fractures intersecting the deposition hole and canister failure due to isostatic pressure. Furthermore, thermally induced spalling is included in the transport analyses that it affects. A number of additional mechanical phenomena, mainly related to the host rock are ruled out either in the reference evolution or in the screening in the **Geosphere process report**.
- The hydraulic impact on the buffer and the canister is indirect as part of the buffer erosion and canister corrosion processes, that are considered in the following. Groundwater transport of solvents could also contribute to the deterioration of the buffer, but this process was considered negligible in the analysis of the buffer transformation scenario.
- Also the chemical impact on the buffer and the canister is included as part of the buffer erosion and canister corrosion processes, that are considered in the following.

Phenomena that have been excluded in the **Process reports**, the reference evolution or the scenario analyses are hence not further considered here, but their exclusion is further justified in Section 14.4 where it is verified that FEPs omitted in earlier parts of the assessment are of negligible significance in the light of the completed scenario and risk analysis.

The analyses of the reference evolution and the scenarios hence leave the following processes or phenomena of which combinations need to be considered:

- loss of buffer due to erosion,
- corrosion of the copper canister when buffer erosion has proceeded to the stage that advective conditions have arisen,
- canister failure due to shear movements in fractures intersecting the deposition hole,
- isostatic loads on the canister.

Loss of buffer due to erosion and canister corrosion during advective conditions are already combined in the corrosion scenario and are therefore treated together in the following, leaving three phenomena for which to consider combinations and gradual developments.

Buffer erosion and canister corrosion in combination with shear movement

Impact of erosion on effects of shear movements: If the buffer is eroded, then the likelihood of failures due to shear movements is significantly reduced due to the reduced buffer stiffness, in particular near a potentially shearing fracture. This combination is thus favourable for safety and it is pessimistic to neglect it.

Impact of erosion on radiological consequences of a shear movement failure: Failure due to a shear movement in a deposition hole with an intact buffer that is subsequently eroded is addressed in the consequence analyses of the shear scenario, see Section 13.6. The likelihoods of these two phenomena are not independent since both are positively correlated to fracture size.

Impact of corrosion on canister response to shear movement: It needs to be considered whether a partly corroded canister is more sensitive to shear movements. It is first noted that it is the canister insert that is the load bearing component and that the insert is unaffected by copper corrosion. Furthermore, an intact copper shell sustains a 5 cm shear movement with a large margin. Corrosion has been demonstrated to reduce the copper shell by at most a few mm for an intact buffer, and, considering the large margins for an intact 50 mm canister, it is unreasonable that such a corrosion depth should jeopardise that integrity of the copper shell in the case of a shear movement. Appreciable corrosion could occur if the buffer is eroded. However, erosion of the buffer is favourable as regards the mechanical impact of shear movements on the canister, see above. Therefore, the possible increased sensitivity of a corroded canister to shear movements is counteracted by the fact that the stresses are reduced, particularly in the corroded area where the buffer is lost. As noted in Section 12.8.2, corrosion is not expected to cause detrimental amounts of hydrogen to enter the copper, meaning that hydrogen embrittlement is not seen as a concern as regards shear loads following corrosion. It is noted that the shear analyses are performed for 50 mm copper since the resulting copper thickness after production had not been finally assessed when this analysis was carried out, whereas the corrosion analyses for advective conditions uses a copper coverage of 47 mm; this is considered to be a negligible difference.

Impact of corrosion on radiological consequences of a shear movement failure: Since a canister having experienced a shear movement failure is not assigned any transport resistance for radionuclides, corrosion will, in the analysis, not have a negative impact on the consequences of a shear movement failure.

Impact of shear movements on buffer erosion: Shear movements that do not lead to failure are less than 5 cm in extent, since the canister is designed to resist 5 cm movements. Such minor movements give a limited impact on buffer thickness and thus also on the time required to reach advective conditions according to the sensitivity analyses in Section 12.2.2. A shear movement may also lead to an enhanced flow in the shearing fracture. However, the mean number of deposition holes that are calculated to experience 5 cm shear movements or larger during the one million year assessment period is around 0.08, whereas at least several tens of holes are calculated to experience severe erosion during one million years with the assumptions in the PSAR, see Figure 12-3. Therefore, even if much smaller shear movements were considered to lead to enhanced flow, the overall impact on the extent of buffer erosion in the repository would be small.

Impact of shear movements on corrosion: Shear movements will induce stresses in the copper shell, even if the movement does not cause canister failure. For stresses to have an impact on corrosion (by stress corrosion cracking), high concentrations of detrimental anions are needed (as well as oxidising conditions). Such conditions are not expected in the repository environment (Section 10.2.5) and there is no reason that a shear movement would induce such an environment.

Buffer erosion and canister corrosion in combination with isostatic load

Impact of erosion on isostatic load: Erosion of the buffer leads to a lowered isostatic load on the canister. This combination is thus favourable for safety and it is pessimistic to neglect it.

Impact of corrosion on resilience to isostatic load: A partially corroded canister surface does not influence the canister's resilience to isostatic loads negatively since it is the insert that bears the load.

Impact of isostatic load on erosion and corrosion: There is no reason to assume that an increased isostatic load has a negative impact on the buffer erosion and the canister corrosion processes, other than it is in some situations associated with an increased groundwater flow. This latter phenomenon is included in the analyses of buffer erosion and canister corrosion scenarios.

Shear movement in combination with isostatic load

Impact of isostatic load on shear movement: As concluded in Section 10.4.5, subsection “*Combined isostatic and shear loads*”, an isostatic load during a shear displacement does not yield a more severe impact on the canister than the corresponding case without isostatic load. It was also concluded that, since large earthquakes will not occur in connection with high isostatic loads, this case is unrealistic. An ice load of 30 MPa was used in that analysis, i.e. somewhat lower than the maximum of 36 MPa assessed in Section 12.7.2.

Impact of shear movement on resilience to isostatic load: Also as concluded in Section 10.4.5, subsection “*Combined isostatic and shear loads*” the canister is expected to maintain its resilience to isostatic loads after experiencing a 5 cm shear movement, in accordance with the technical design requirements for the canister.

Gradually developing phenomena

Erosion and corrosion are by their nature gradually developing phenomena and have been analysed as such. However, corrosion is considered in detail for an intact buffer or for a missing buffer. Therefore, also corrosion for an eroding buffer needs to be considered, see below. Shear movements occur as discrete events. However, the accumulated effect of several minor shear movements can be seen as a gradually developing load on the canister. This is already addressed in the analyses of shear movements, see Section 10.4.5, subsection “*Cases of shear load to consider*”. Isostatic loads develop gradually as the buffer swells and, in particular, as ice sheets develop resulting in increased groundwater pressures. These developments are, however, slow and it is the peak loads that need to be considered, as is done in the analyses already reported. There is, therefore, no need to further address gradual developments of isostatic load.

Corrosion for an eroding buffer: Corrosion for an eroding buffer is pessimistically bounded by the case where the buffer is assumed to be lost initially. The consequences in terms of corrosion are not vastly different from the case where the buffer erodes according to the adopted erosion model. Both cases are propagated to the consequence analysis for the corrosion scenario in Section 13.5.

Early canister failures

According to detailed evaluations of the potential for early canister failures due to corrosion related phenomena in Sections 12.6.3, and the conclusion regarding early failures for an isostatic load in Section 12.7.6, early failures will not occur within the corrosion and isostatic load scenarios, whereas there is a very low probability of such failures in the shear load scenario, as concluded already in Section 10.4.5. There is nothing in these evaluations to suggest that combinations according to the above paragraphs would lead to early failures.

Completeness of the scenarios

Combinations of scenarios and phenomena are an important aspect of the discussion of scenario completeness. This discussion is provided as part of the conclusions of the safety assessment, see Section 15.3.6.

Conclusion

The above account demonstrates that relevant combinations and gradual developments of phenomena either have been addressed in earlier parts of the assessment and in some cases propagated to consequence calculations, or can, with relatively simple complementary arguments, be shown to not give rise to additional cases for further consideration. The only exception concerns a case where a shear failure is followed by buffer erosion. This case was also propagated to consequence calculations. The conclusions are similar to those in the SR-Site assessment, also taking into account the added consideration of early canister failures above.

13 Analysis of retardation potential for the selected scenarios

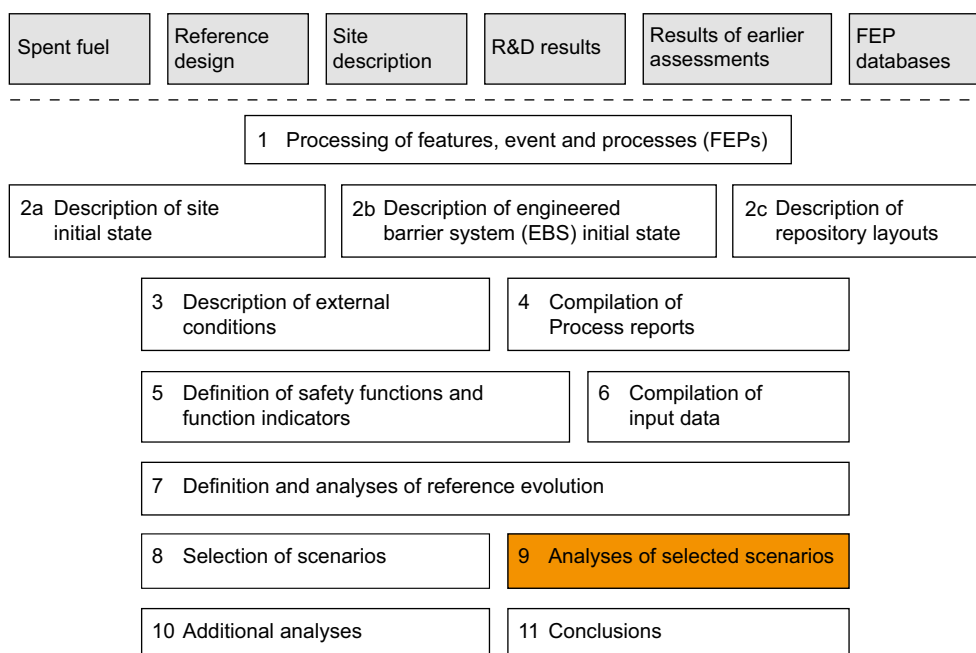


Figure 13-1. The PSAR methodology in eleven steps (Section 2.5), with the present step highlighted. This chapter deals with the analysis of the retardation potential of the repository.

13.1 Introduction

This chapter describes analyses of radionuclide release, transport and dose impacts for the scenarios selected in Chapter 11 and for which the containment potential was analysed in Chapter 12. In terms of safety functions, this chapter contains analyses of the repository's retardation potential.

Two issues related to radionuclide transport and dose calculations that can to a large degree be treated independent of the scenario or the nature of the failure mode of the canister are addressed first in this chapter:

- The modelling of radionuclide transport and dose estimation in the biosphere is described in some detail in Section 13.2.
- The issue of potential criticality for a failed canister is treated in Section 13.3.

The models used for radionuclide transport in the water phase for the near-field and the geosphere are then described in Section 13.4.

The analyses of the two scenarios based on safety functions for which canister failures could not be excluded, i.e. the scenarios 'canister failure due to corrosion' and 'canister failure due to shear load' are described in Sections 13.5 and 13.6, respectively. In the following, these two scenarios are often referred to as the corrosion scenario and the shear load scenario, respectively, for simplicity.

Canister failures in the main scenario occur according to the central corrosion variant of the corrosion scenario and are thus covered by the analysis of this particular variant in Section 13.5.

Analyses of hypothetical, residual scenarios to illustrate barrier functions are presented in Section 13.7. This section also includes the scenario 'canister failure due to isostatic load'. Radionuclide transport in the gas phase is analysed in Section 13.8, common to all scenarios where it can occur.

Finally, a risk summation is provided in Section 13.9.

All modelling and modelling results for the near-field and the far-field are discussed in more detail in the **Radionuclide transport report**. Details of the biosphere modelling are found in references given in Section 13.2.

The overall structure of this Chapter is the same as that of the corresponding Chapter in the SR-Site assessment. The account of the biosphere model in Section 13.2 has in part been substantially updated, reflecting the development since the SR-Site assessment. The same dose conversion factors as in SR-Site are used, as justified in Section 13.2. The account of criticality in Section 13.3 has been extended, and now also includes a reference to a What if scenario analysing postulated criticality in the final repository. New calculation cases have been formulated to broaden the account of hypothetical, early canister failures, Section 13.7.3, and to assess the risk associated with residual fuel types, mentioned in Section 13.9.4.

The transport models for the near and far-field are identical to those used in SR-Site. Also the vast majority of calculated cases are the same as those in SR-Site and the input data to most cases are nearly identical. Therefore, the approach to accounting for radionuclide transport in the PSAR has been to calculate all cases related to compliance with all appropriate updates, whereas much of the cases used for illustrative and completeness purposes have not been recalculated. In Appendix M to the **Radionuclide transport report** a number of recalculated cases are compared to the corresponding SR-Site cases and the minor differences in outcome are discussed, as a justification of the chosen approach. Most of the results shown in the present report have been recalculated, and those that have not have an indication to this effect in their Figure captions.

The **Radionuclide transport report** is quite similar to that of the SR-Site assessment (SKB 2010f). In addition to the new Appendix M mentioned above, two new Appendices related to the penetration of dilute waters have been added and the newly formulated cases related to hypothetical early canister failures and miscellaneous fuels (see Table 5-4) are reported in a new Chapter 7. Remaining parts of the report are virtually identical to the SR-Site version.

13.2 Biosphere assessments and derivation of *Landscape dose conversion factors*

The Swedish regulations state that human health and the environment must be protected from harmful effects of ionising radiation both during operation of the repository and in the future (see Section 1.4). More specifically, harm to humans should be assessed as the mean annual risk of harmful effects over a lifetime to a representative individual of the most exposed group (see Section 2.6.2 for details). For this assessment, the annual effective doses to future inhabitants of the Forsmark area per unit constant release rate or per unit released in a single pulse to potential release areas (biosphere objects) are calculated for each radionuclide with the *Radionuclide model for the biosphere*. These doses are referred to as *Landscape dose conversion factors* (LDFs). Multiplying the maximum LDFs over all biosphere objects and time points with modelled radionuclide release rates or pulse releases to the biosphere under different release scenarios, results in estimates of the annual doses used to assess compliance with the regulatory risk criterion. The results from such calculations are reported for a number of release scenarios later in this chapter (Sections 13.5–13.8).

For the assessment of the effects on the environment, activity concentrations in soil and water are calculated with the *Radionuclide model for the biosphere*, given a geosphere release. From these concentrations whole-body absorbed dose rates to individual organisms are then calculated and compared to a no-effect dose rate. If harmful effects at the level of the individual organisms can be excluded, then this also ensures the sustainability of populations and of ecosystem functions.

Over the time scales of relevance for the safety assessment, the biosphere will undergo considerable changes, in particular due to the long-term climate variation involving glacial cycles and the associated change in the position of the shoreline (see Chapter 10). As the site emerges from the sea, the potential activity concentrations in surface water are expected to increase and radionuclides that accumulate in the regolith can enter the terrestrial food web in wetlands, especially after they have been drained and cultivated. Furthermore, exposure from well water is restricted to periods when well drilling is possible on land above the sea level. Thus, the potentially highest exposure of humans and other organisms

to radionuclides from the repository is expected when at least parts of the site have emerged from the sea. However, at what stage in the ecosystem succession and in what part of the landscape a specific radionuclide release will cause maximum exposure may vary due to the properties of the specific radionuclide and of the potential release location.

Contents of this Section 13.2

In the following subsections, the approach, methods and main results from the biosphere assessment are described. In Section 13.2.1, the approaches and central concepts for the biosphere assessment are presented. The methods to identify and delineate biosphere objects are presented in Section 13.2.2. This section also gives an account of how the biosphere objects are connected to each other and how the *Landscape development model* is used to describe the development of the biosphere objects during a reference glacial cycle. Details of the work concerning biosphere objects and the *Landscape development model* are presented in Lindborg (2010). Section 13.2.3 gives an overview of the *Radionuclide model for the biosphere*, presented in detail in Avila et al. (2010), and presents the methods for calculation of *Landscape dose conversion factor* (LDF values). In Section 13.2.4, the resulting LDF values are presented. Section 13.2.5 gives an overview of methods for estimation of doses to non-human biota with the ERICA assessment tool (Jaeschke et al. 2013) and in Section 13.2.6 the uncertainties in the risk estimates are discussed.

Method development and data updates since the SR-Site assessment

As further developed below, the core of the biosphere assessment performed during SR-Site and the estimated LDF values are seen as sufficient for the PSAR assessment. A comprehensive account of the biosphere assessment can thus be found in the **Biosphere synthesis report** that has not been updated for the PSAR, and the details of this work are presented in a number of technical reports referenced therein.

During the review of the SR-Site assessment, as responses to requests by SSM, SKB provided a number of clarifications and supplementary information about the biosphere assessment, including:

- a more detailed explanation of distributed LDFs (Kautsky 2012, see Section 13.2.3),
- an estimate of an LDF value for Rn-222 for exposure from drilled well water, and thus valid for conditions (i.e. temperate and global warming conditions) where such a well may exist (Hedin and Kautsky 2015, Avila 2013, see Section 13.2.4),
- a revised assessment of potential effects on the environment (Nordén 2013, Jaeschke et al. 2013, see Section 13.2.5),
- the selection and handling of (homogenous) biosphere objects (Hedin and Kautsky 2015, see Section 13.2.6).

The content of this Section 13.2 corresponds to the text in the SR-Site Main report (SKB 2011, Section 13.2), updated e.g. by including the supplementary information listed above.

Although there are issues in SSM's final review report (SSM 2018) for SKB to manage in coming biosphere assessments, SSM's general conclusion was that the estimated LDFs were reasonable at this stage of the application. This conclusion was partly based on the fact that SKB's approach pessimistically combines the maximum LDF values from various radionuclides independent of when (time) or where (biosphere objects) the maximum of the individual radionuclides occurred. The appropriateness of the LDFs was also supported by independent calculations of dose conversion factors initiated by SSM.

Some of SSM's remaining requests have been handled and/or implemented in the biosphere modelling for SR-PSU (SKB 2014d) and more recently in SE-SFL (SKB 2019a). In SR-PSU for example:

- K_d and CR values were updated based on additional site specific data, and the weight on site specific data was increased,
- new exposure pathways for humans, including exposure from a dug well and more reasonable production and human consumption patterns were used,

- object specific hydrological parameters were derived for separate ecosystem states,
- modelling methods for specific radionuclides, including C-14 and Cl-36, were updated,
- an updated atmospheric model was used for C-14,
- the representation of regolith layers in terms of model compartments was improved.

The resulting differences between *LDFs* from SR-Site and SR-PSU were analysed in the SR-PSU Biosphere synthesis report (SKB 2014d, Section 10.4.2). The SR-PSU model was further developed since the SR-Site assessment and included for example potential exposure from a dug well and radionuclide releases to a different set of biosphere objects. Nevertheless, for most radionuclides there was a general agreement between the *LDFs* from the two assessments and the analysis showed that no *LDF* value was more than one order of magnitude larger in SR-PSU than in SR-Site. Among the radionuclides contributing most to the dose in SR-Site, the SR PSU *LDFs* ranged from marginally higher (e.g. 12 % higher for Ra-226), to sometimes substantially smaller in SR-PSU (e.g. Se-79 and I-129, Figure 13-2).

Those results were confirmed in the more recent supplementary report to SSM (SKB 2019a) where the updated K_d and CR values from the SR-PSU were used in time dynamic biosphere modelling of doses for some illustrative “what if” calculation cases for the spent nuclear fuel repository (but not in the *LDF* calculations used for compliance demonstration).

In SE-SFL several additional updates of the biosphere model were introduced and evaluated. These include for example a higher discretisation of deeper regolith layers. The conclusion from SE-SFL was similar to that of the uncertainty analysis presented in SR-Site (Avila et al. 2010, Section 5.2.1). That is, for most radionuclides an increased vertical discretization has a limited or no effect on the *LDF*-values, and this is partly due to the importance of alternative exposure pathways unaffected by the biosphere discretisation (such as the drilled well). However, for a few radionuclides with a long residence time in the lower regolith layers relative to the radionuclide half-life which exposed through accumulation in crops, the coarse resolution used in SR-Site was clearly cautious (e.g. Cs-135).

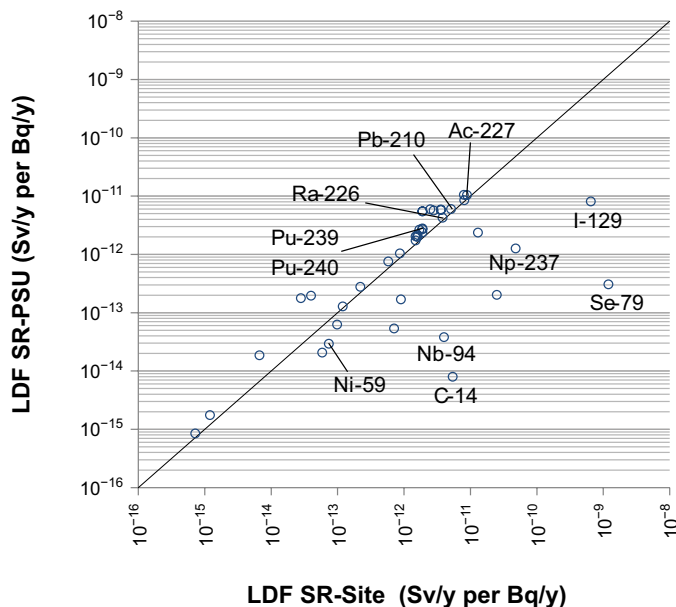


Figure 13-2. *LDF*-values from the SR-PSU plotted versus *LDF*-values from SR-Site (data from Figure 10-1 in SKB 2014d). The *LDF* values for the most dose-contributing radionuclides in the SR-Site compliance scenarios are indicated in the plot and the black line shows the one to one relationship between the two *LDF* datasets.

Based on SSM's conclusion that the SR-Site *LDFs* are reasonable at this stage and that the *LDFs* from SR-PSU are not substantially larger than the original SR-Site *LDF* values, no new estimates (except for Rn-222) were made in the PSAR assessment and the original SR-Site *LDF* values were used (Section 13.4.3). This approach is seen as further justified by the limited effects on results by the model development in SE-SFL.

In the next assessment step for the spent nuclear fuel repository (the SAR), the biosphere analyses will be more thoroughly reassessed and implementation of relevant changes and updates to the radionuclide transport model are planned. These include features mentioned above and already implemented in the SR-PSU and SE-SFL biosphere assessments. See further Sections 15.6.10 and 15.7.5.

The PSAR global warming climate case (Section 12.1.3) includes two alternative variants to capture the range of future relative sea levels; one low-level projection with continued coastline regression (similar to the reference glacial cycle and global warming shore-line developments in SR-Site) and one high-level projection with maximum increasing relative sea level resulting in a longer initial submerged period after repository closure. The main focus of the global warming *LDF* values is to capture potential effects of a longer terrestrial interglacial phase where radionuclides could accumulate in the upper regolith before cultivation and potential exposure. Therefore no new global warming *LDFs* have been estimated based on the longer submerged period but the original SR-Site *LDF* values are used. Besides, since the likelihood for canister failures and also the highest total risk for harmful radiological effects are larger after the first 100 000 years (see Section 13.9), no effects of a longer initial submerged period are expected for the risk compliance scenarios in the PSAR.

13.2.1 Approaches and central concepts in the biosphere assessments

The main objectives of the biosphere assessments in the PSAR are to produce values of the *Landscape dose conversion factors* that allow translation of a potential release from the KBS-3 repository to the exposure of humans inhabiting the Forsmark site in the future, and to assess the exposure of other organisms in the area. The estimated doses in turn, are used in demonstrating compliance with the regulatory criteria.

To accomplish this, areas with potential discharge of deep groundwater from the repository, here called *biosphere objects*, have been identified at the site, and the long-term development of these areas has been modelled. A biosphere object is defined as an area of the landscape that may receive radionuclides released from the repository, either through discharge of deep groundwater or by contaminated surface water, at any time during a glacial cycle. The biosphere at Forsmark is represented by a set of interconnected biosphere objects (see the **Biosphere synthesis report** for an overview and Lindborg (2010) for details).

The transport and accumulation of radionuclides in the biosphere objects throughout a full glacial cycle has then been described with the radionuclide model for the biosphere. The biological uptake of radionuclides by various organisms, some of which are potential food sources for humans, have been calculated from activity concentrations in the environment (air, soil, and water). Finally, assumptions on land use and human habits have been used in combination with activity concentrations in the environment and biota, to calculate *LDFs* for future human inhabitants. The activity concentrations have also been used to assess the potential future exposure of other organisms at the site.

Assessment philosophy

The main purpose of the biosphere assessment is to allow estimations of the radiological risk for humans and the environment that reflect a robust description of the biosphere and a credible handling of associated uncertainties. Thus, the transport model of natural ecosystems aims at being realistic, with respect to model structure, primary transport pathways, landscape development and the associated parameters, based on the knowledge of present-day conditions and of the past and expected future development of the Forsmark site (see Section 4.10). However, the uncertainties with respect to the characteristics of future human inhabitants of the area are large. Thus, the description of exposure has been based on potential exposure pathways, rather than on an attempt to explicitly predict living conditions and habits of generations to come in the Forsmark area.

The LDFs obtained from the biosphere assessment are derived from deterministic simulations. These simulations are the combined results of process understanding, a comprehensive description of the site, and relevant assumptions on the habits of future human inhabitants. In addition, the effects of parameter uncertainties, assumptions and conceptual uncertainties on the estimated LDFs have been addressed through probabilistic simulations, alternative models and informed assumptions. This approach is consistent with recommendations from the ICRP (ICRP 2007) and with the guidelines from the Swedish Radiation Safety Authority (SSM 2008b).

To be able to provide the calculation chain (presented in Section 13.4) with an *a priori* dose conversion factor, the LDFs were calculated for a release rate of 1 Bq/y, i.e. it represents a unit release dose. Because there is no temporal or spatial resolution when this factor is applied on radionuclide releases to the biosphere, the LDFs used in the assessment were cautiously chosen as the maximum value over all times and biosphere objects. Combining these radionuclide specific maximum LDFs (see Figure 13-3) is likely to lead to an overestimation of dose when radionuclides that reach peak levels at different times and/or in different locations are combined. For detailed analysis or interpretations, including e.g. analysis of time varying releases due to transient hydrogeological conditions, the temporal and spatial dimensions of the surface systems should be considered (see further discussion in the **Biosphere synthesis report**).

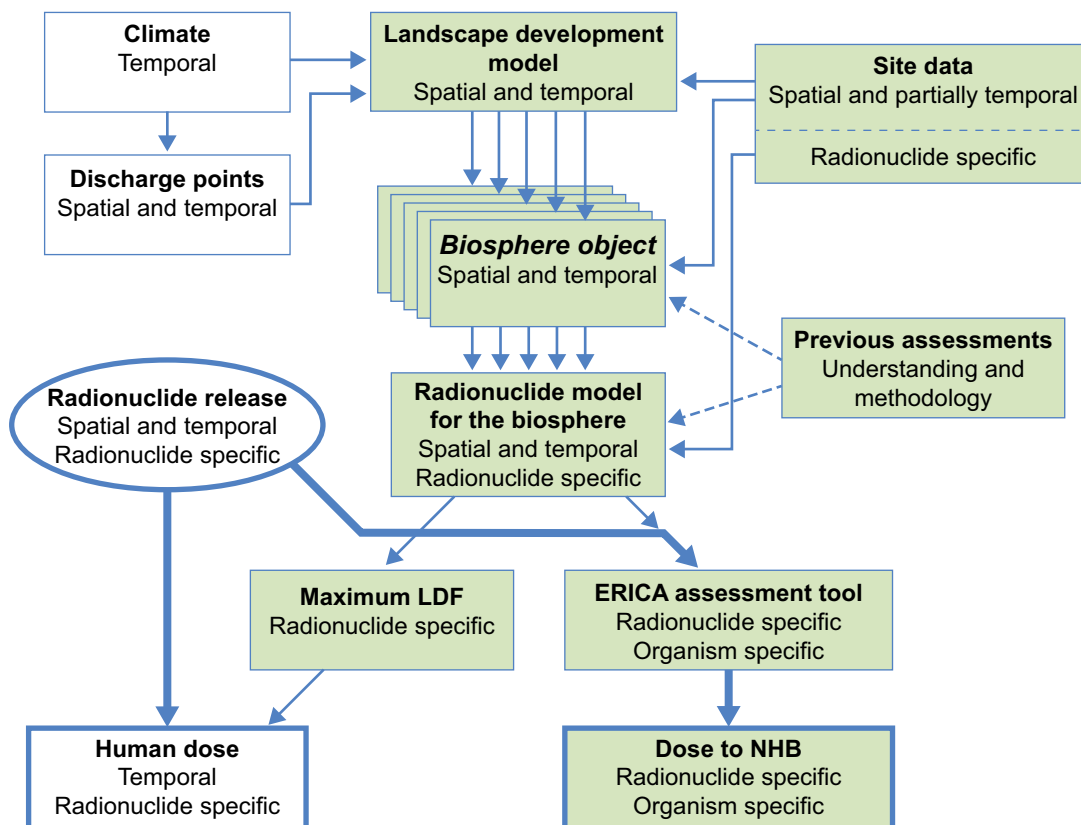


Figure 13-3. Major dependencies and spatial/temporal dimensions of models used in the biosphere assessment (green boxes). Climate scenarios and discharge points provide temporal and spatial information (but no radionuclide specific information), that is used in the Landscape development model to define and describe Biosphere objects. The Radionuclide model for the biosphere provides temporally and spatially resolved environmental radionuclide activity concentrations. The maximum unit release dose (LDF) over all objects and time steps has no temporal or spatial dimension and is used in the SR-Site calculation chain (see Section 13.4) to calculate doses to humans by multiplication with radionuclide releases to the biosphere (thick arrows, which has a temporal, but no spatial dimension). For doses to non-human biota (NHB), maximum environmental activity concentrations from the Radionuclide model for the biosphere based on unit release were multiplied with maximum releases to the biosphere to generate maximum environmental radionuclide activity concentrations that were used by the ERICA assessment tool to estimate dose to NHB. Thicker arrows indicate where radionuclide release information was included in the calculations.

13.2.2 Identification, location and development of biosphere objects

The identification of biosphere objects in the Forsmark area is based on the modelling of flow paths from the repository to the ground surface (Figure 13-4, see further Section 4.2 in Joyce et al. 2010). To locate potential discharge areas of groundwater from the repository, the end positions of flow paths from the particle tracking simulations were assessed. According to Joyce et al. (2010), the discharge pattern is determined mainly by the local topography and deterministic deformation zones, and the pattern does not vary significantly among model realisations of the discrete fracture network. With few exceptions, the discharge points cluster together in space and time into a limited number of areas. Detailed surface hydrological modelling confirmed the overall pattern of the location of discharge areas in Forsmark (Bosson et al. 2010). It was assumed that the location of these clusters indicates areas likely to be affected by discharge of deep groundwater from the repository.

The locations of discharge points in the Forsmark landscape show that: 1) deep groundwater from the repository is primarily attracted to low points in the landscape, e.g. shallow parts of the sea, along the shoreline, and in lakes, streams and wetlands, 2) discharge areas covered by the sea tend to be relatively large, whereas discharge areas above sea level are smaller and primarily located in lake basins (which may be open or infilled), 3) discharge areas are located in a limited number of basins in the Forsmark landscape (Figure 13-4, see further the **Biosphere synthesis report** and Chapter 6 in Lindborg 2010).

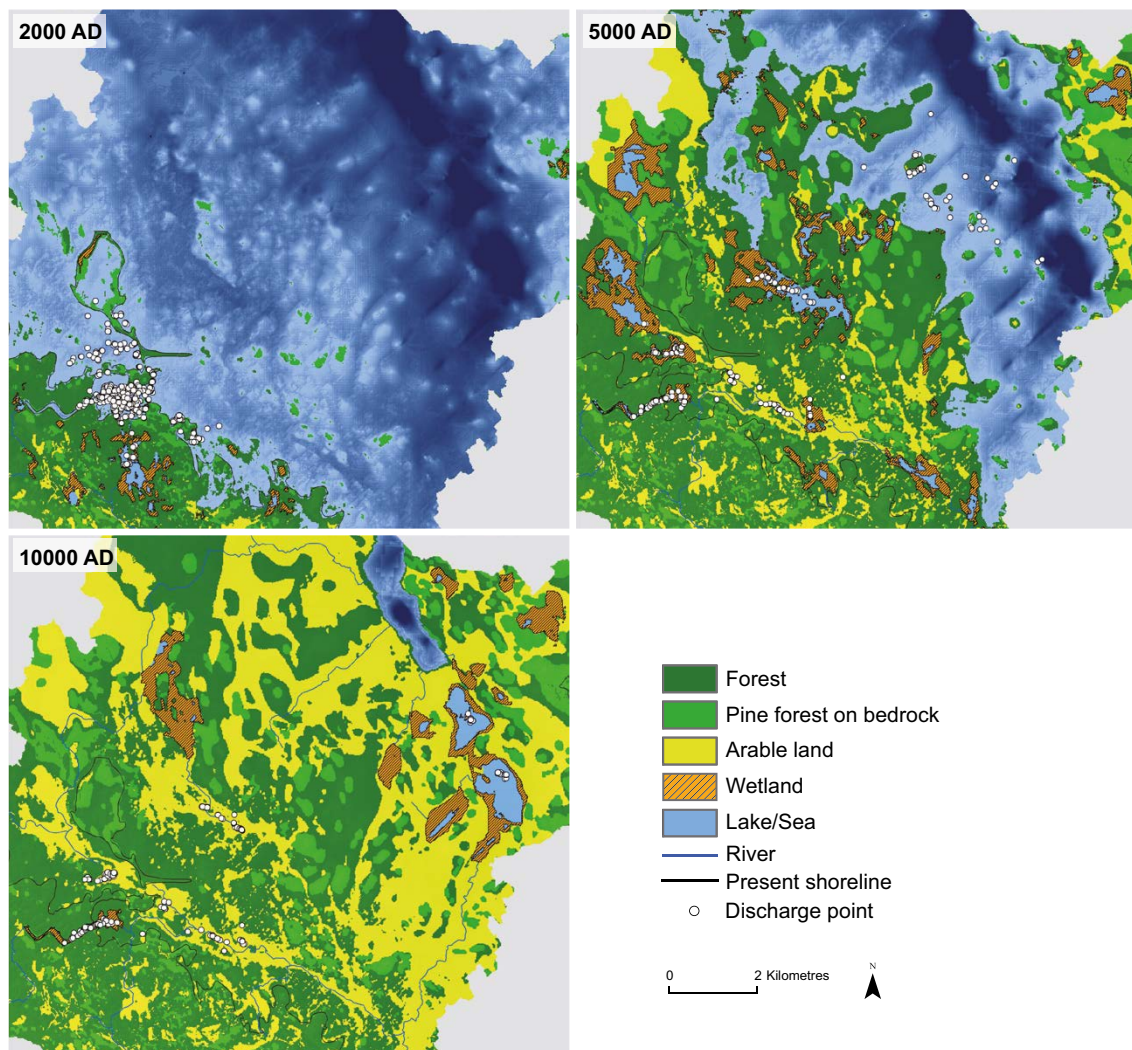


Figure 13-4. Discharge points from the particle tracking simulations (see Section 4.2 in Joyce et al. 2010) at three different times. The discharge points are displayed on maps of the Forsmark landscape at corresponding times, predicted from the Landscape Development Model (see Lindborg 2010).

The long-term development of the site is determined mainly by climate variation, both directly and indirectly through the resulting shoreline displacement (Section 10.3.3, see also the **Biosphere synthesis report**). The shoreline displacement affects the size and position of potential discharge areas in two important ways. First, the size of a discharge area that receives groundwater from the repository over extended periods of time (e.g. areas situated above the repository) decreases substantially when the area emerges from the sea. Secondly, changes in the hydrological forces due to the moving shoreline affect the discharge of deep groundwater. The majority of the discharge points are found close to the repository, but new discharge areas will appear in the emerging landscape and in shallow parts of the sea following the shoreline displacement towards the northeast (Figure 13-4, for more details see Chapter 6 in Lindborg 2010).

During the submerged phase, the outer boundary of each biosphere object was determined from the future sub-catchments (called basins), whereas the shoreline of the lake at the time of isolation from the sea delineates the biosphere object during the lake and terrestrial phases.

In total, ten biosphere objects, containing a discharge area during any period of the present interglacial, were identified. Five additional biosphere objects located downstream of the discharge areas were also defined. Finally, to represent discharge directly into a stream or a wetland without an initial lake stage, the basin of one of the original biosphere objects (object 121) was partitioned into three separate objects (denoted 121_1, 121_2 and 121_3, Figure 13-5). See discussion in the **Biosphere synthesis report** and for details see Lindborg (2010).

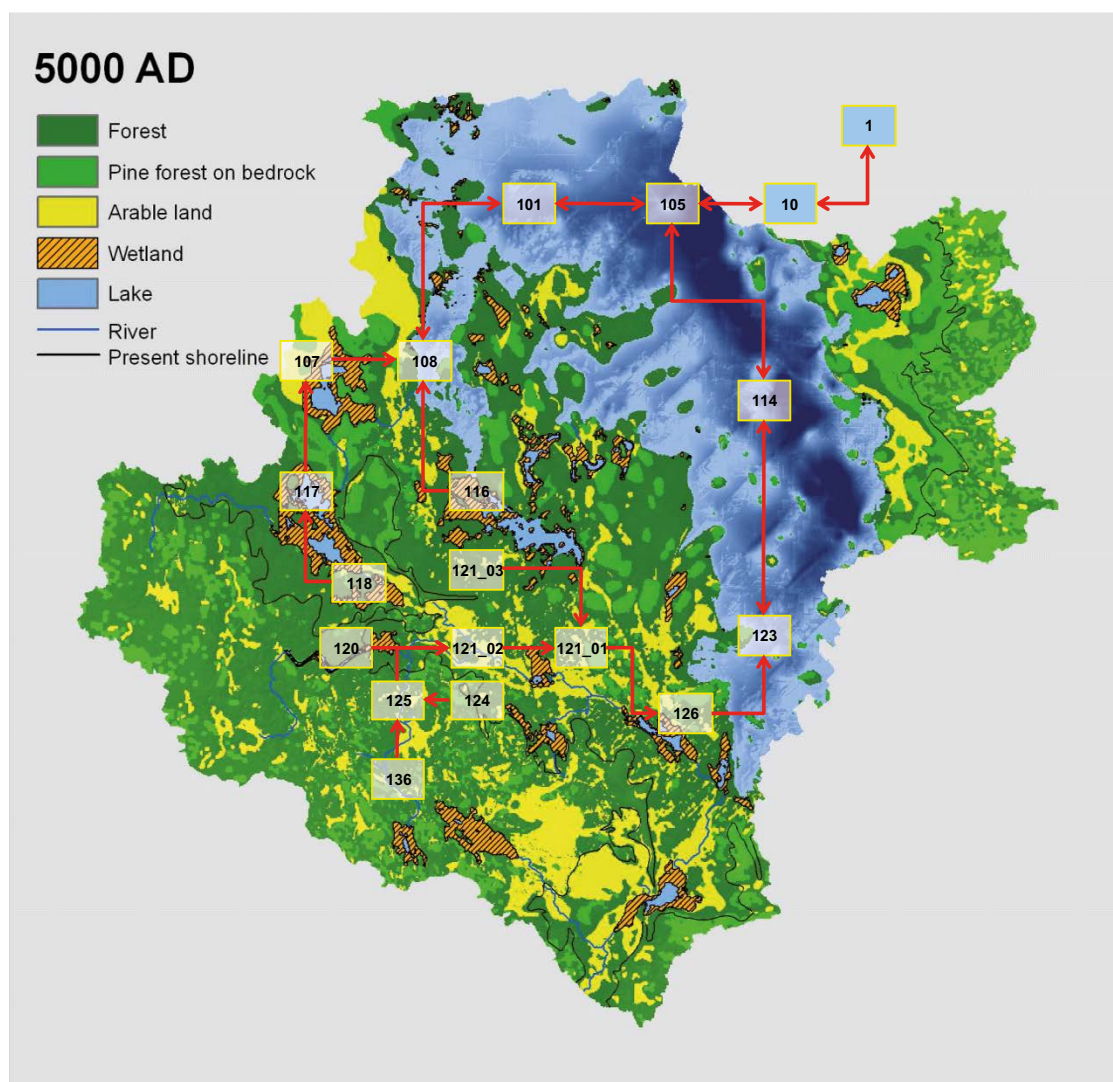


Figure 13-5. The location and hydrological connections of biosphere objects in the SR-Site assessment, displayed on a map of the Forsmark landscape at 5000 AD.

The main features of the landscape relief in the Forsmark area, like the locations of higher and lower altitude areas, are determined mainly by the bedrock topography. The small-scale undulations of the bedrock surface are smoothed by glacial and post-glacial deposits, which, to a limited extent, are redistributed by wave erosion when the shoreline moves over the area (see Section 10.3.3). The bedrock topography is expected to be modestly modified by denudation (erosion and weathering, see Section 6.1 and the **Climate report** Sections 3.5, 4.5, 5.1 and 5.2) and the shoreline displacement is expected to be repeated during future glacial cycles. Therefore, descriptions of the present state and landscape forming processes (in terms of wave erosion and sedimentation, lake infilling and ecosystem succession) are considered to give a general representation of object properties and the landscape development that is sufficient for the assessment of future ice-free periods (see Section 10.3.3).

The information from the contemporary *Regolith depth* (Hedenström et al. 2008) and *Digital elevation* (Strömngren and Brydsten 2008) *models* were combined with the postulated change in relative sea level according to the SR-Site version of the Climate report (SKB 2010g), to describe the development of the Forsmark landscape in the *Coupled regolith-lake development model (RLDM*, Brydsten and Strömngren 2010, see Section 10.3.3). In this context it is worth noting that the SR-Site relative sea level curve is very similar to the updated relative sea level curve constructed for the PSAR (see the **Climate report**). This description of the landscape development, in combination with biotic information from the ecosystem modelling (Andersson 2010, Aquilonius 2010, Löfgren 2010) was then used to extract time-dependent properties of the biosphere objects that were used as input parameters to the radionuclide model for the biosphere (see next section). The information from the RLDM was also combined with assumptions on vegetation and land use to produce maps describing the projected future landscape with a high spatial resolution (20×20 m) (Lindborg 2010).

13.2.3 The radionuclide model for the biosphere

The radionuclide model for the biosphere can handle different types of sources and properties of radionuclides. The relatively coarse resolution of the model was chosen primarily considering long-term release rate of radionuclides. Given a stable long-term release, steady-state conditions are likely to be approached within the time frames of the assessment and these conditions are considered to be sufficiently captured by describing the biosphere object at a coarse spatial scale by average conditions. This chosen approach is flexible and the short simulation times allows for probabilistic approaches and an efficient handling of decay products. The approach is fit for purpose as the radionuclides associated with the highest dose are expected to be released from the fuel matrix and corroded metals in the repository. These releases are in most cases approximately constant over the time scale of the biosphere assessment (i.e. 20 000–70 000 years), as demonstrated in later sections of this chapter.

To assess the potential doses to humans for release scenarios with approximately constant release rates (see Section 13.5 and 13.6), the radionuclide model was used to calculate *basic LDFs*. Those scenarios typically simulate releases from rare failures of individual canisters where the discharge could potentially occur in one or a few individual biosphere objects rather than being distributed over the entire modelled landscape.

The coarse model resolution is less appropriate for short release events where transient spatial dispersion within a biosphere objects may be important, or the influence of within year variation significantly affects transport and accumulation of radionuclides. Nevertheless, the radionuclide model for the biosphere was also used to calculate doses from a release reaching the biosphere as a pulse (*LDF pulse*). This was necessary as the transport of the instantaneously accessible fraction of radionuclides from the fuel is, in some release scenarios, not handled by the near-field and far-field transport models in the PSAR. Instead this fraction is assumed to reach the biosphere instantaneously, see further Section 13.5.2.

The radionuclide model was also used to illustrate the consequences of a number of hypothetical and illustrative release scenarios where losses of barrier functions of the repository are assumed in all canister positions already at deposition (see Sections 13.7.3 and 13.7.4). For these simulations, which are described in more detail in Avila et al. (2010) and Kautsky (2012), two approaches were taken.

1. Releases were multiplied by LDFs obtained with a constant release rate distributed to the biosphere objects in accordance with the time dependent distribution of release points over an interglacial (*distributed LDF*). This is more appropriate than the use of the basic LDFs for these scenarios, since releases would be distributed over several rather than in one single biosphere object, as could not be ruled out for releases from one single canister.
2. Since these situations lead to transient releases that vary significantly over an interglacial, time-dependent dose modelling in the biosphere was also carried out. Here, the modelled time dependent far-field release (instead of a constant unit release) was used as input data to the radionuclide model to calculate annual effective dose to a representative member of the most exposed group. Also here, the release was distributed over all biosphere objects in accordance with the time-dependent density of discharge points in the landscape and the maximum doses over all objects were used.

In addition, dose consequences of releases from rare, early canister failures due to earthquakes, i.e. early failures in the shear load scenario, Section 13.6.2, are handled with time-dependent modelling as in case 2 above. However, here the entire release was input to each landscape object in order to capture the landscape object in which the highest consequences would arise due to release from a single canister.

Radionuclides released from the repository are in the radionuclide model assumed to be transported with groundwater to the deeper parts of the regolith in a biosphere object. Additionally, it is assumed that the released radionuclides also reach a hypothetical well drilled into the bedrock, as soon as a biosphere object has emerged from the sea. The activity concentration in well water (Bq/m³) was calculated by dividing the total release rate to the biosphere (Bq/y) by the well capacity (m³/y). This implies complete capture of the radionuclide plume irrespective of the well abstraction rate and is thus a cautious assumption. The capacity of the well was selected to represent drilled wells in the central part of the site investigation area, where they would have the possibility to receive released radionuclides from the repository (Avila et al. 2010).

Modelling radionuclide transport and accumulation in biosphere objects

The radionuclide model for the biosphere is a compartment model, where system components that are considered internally homogeneous in their properties are represented by distinct compartments. A graphical representation of the conceptual model is shown in Figure 13-6, where each box corresponds to a model compartment. Definitions of the model compartments are presented in Table 13-1.

Table 13-1. Compartments in the radionuclide model for the biosphere used in the conceptual approach adopted Figure 13-6 (for further description see Andersson 2010).

Model name	Description
Regolith Low	The lower part of the regolith overlying the bedrock, primarily composed of till. It is common to the terrestrial and aquatic parts and its origin is from the glaciation.
Aqu Regolith Mid	The middle part of the regolith in the aquatic part of biosphere objects, usually consisting of glacial and postglacial clays, gyttja and finer sediments which originate mainly from the period after the retreat of the ice sheet, or from later resuspended matter with a relatively high organic content.
Aqu Regolith Up	The part of the aquatic regolith with highest biological activity, comprising ca 5–10 cm of the upper aquatic sediments where resuspension and bioturbation can maintain an oxidising environment.
Ter Regolith Mid	The middle part of the terrestrial regolith, containing glacial and postglacial fine material, i.e. former sediments from the seabed and lake bottoms.
Ter Regolith Up	The upper part of the terrestrial regolith which has the highest biological activity, like the peat in a mire, or the ploughing layer in agricultural land.
Litter	Dead plant material overlying the regolith.
Water	The surface water (stream, lake, or sea water).
Aqu Primary Producers	The community of primary producers in aquatic habitats, including macrophytes, microphytobenthos and phytoplankton.
Ter Primary Producers	Terrestrial primary producers.

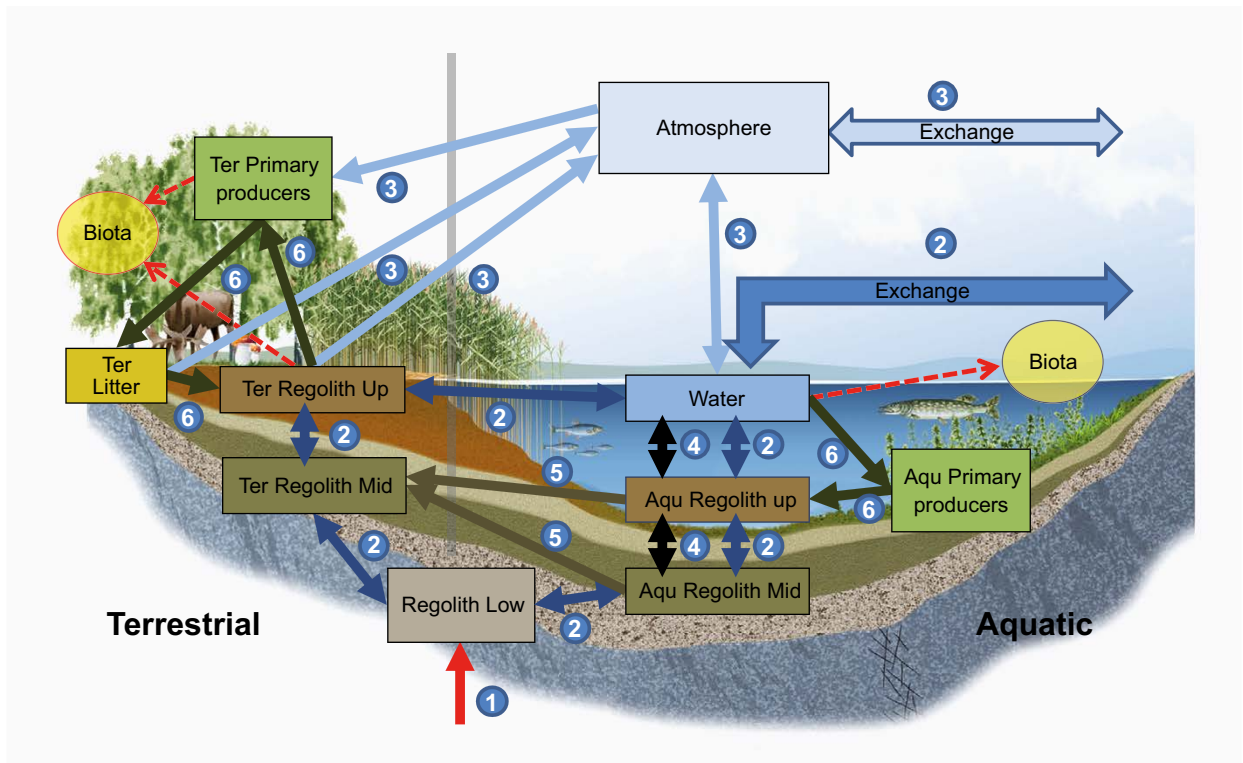


Figure 13-6. Conceptual illustration of the Radionuclide model for the biosphere. Boxes represent compartments, thick arrows fluxes, and dotted arrows concentration computations for non-human biota (these are not included in the mass balance). The model represents one object which contains an aquatic (right) and a terrestrial part (left) with a common lower regolith and atmosphere. The source flux (1 Bq/y) is represented by a red arrow (1). The radionuclide transport is mediated by different major processes, indicated with dark blue arrows for water (2), light blue for gas (3), black for sedimentation/resuspension (4), dark brown for terrestrialisation (5), and green for biological uptake/decomposition (6). Import from and export to surrounding objects in the landscape is represented by arrows marked “exchange”. A detailed explanation can be found in Andersson (2010) and descriptions of the compartments are given in Table 13-1.

The arrows in Figure 13-6 represent radionuclide fluxes between compartments and fluxes into and out of the system. Radionuclide fluxes are linked to the movement of matter in the biosphere, i.e. water flow, particle transport and gas emanation and transport, or to diffusion. Radionuclide transfer mediated by biota, like uptake and release by primary producers, has also been represented. The arrow reaching the lower regolith compartment represents radionuclide releases from the geosphere into the biosphere objects. These releases are directed to the deeper parts of the regolith, which at the site normally consists of glacial till deposited on the bedrock (see Section 4.10.2 and the **Biosphere synthesis report**).

Radionuclides released to the lower regolith compartment are transported to the upper layers of the ecosystems by advection and diffusion. The representation of the waterborne transport of radionuclides between compartments is based on detailed hydrological modelling with MIKE-SHE (Bosson et al. 2010). The effect of radionuclide sorption on the advective and diffusive transport is taken into account by assuming equilibrium between the porewater and the solid phase of the different compartments and is modelled with partitioning coefficients (K_d). The model also considers the transport of radionuclides absorbed to suspended particles, driven by surface water fluxes, sedimentation and resuspension processes (see the **Biosphere synthesis report** and Avila et al. 2010).

The radionuclide transport mediated by biota is, for both terrestrial and aquatic ecosystems, described in the model through fluxes driven by net primary production. It is assumed that equilibrium is established between the activity concentrations of radionuclides in the newly produced biomass and in the corresponding environmental media (upper regolith for terrestrial and water for aquatic ecosystems) and is modelled with concentration ratios (CR). Losses from the upper regolith and surface waters

via degassing processes are cautiously neglected for all radionuclides, except for C-14 for which this process has been explicitly considered since uptake from air through photosynthesis is the dominant pathway for incorporation into terrestrial primary producers in the model (see the **Biosphere synthesis report** and Avila et al. 2010).

Biosphere objects may, beside a release to the lower regolith, also receive radionuclides with surface water from contaminated biosphere objects located upstream or in adjacent marine bays (exchange arrows in Figure 13-6). In initial simulations, the radionuclide model was implemented for each identified biosphere object in a network according to the flux of surface water in the landscape (see Figure 13-5). These simulations showed that the maximum unit release dose was always found in a biosphere object that received a direct release from the geosphere, and that the dose resulting from the indirect release to the same object via an adjacent object was typically an order of magnitude lower (Avila et al. 2010). As the aim of the biosphere assessment is to identify the most exposed group across all biosphere objects, indirect contamination was not considered in the assessment, in order to simplify the analysis with separate simulations for each object (see the **Biosphere synthesis report**).

Temporal development of biosphere objects in the radionuclide model

The radionuclide model has two parts when it is applied to a biosphere objects, one aquatic (right side in Figure 13-6) and one terrestrial (left side). The temporal development of an object is handled by varying the sizes and properties of these two parts in accordance with the simulated natural development of the specific biosphere object (see Lindborg 2010 for details). Thus, most biosphere objects are expected to experience three main stages:

- Sea stage – the biosphere object is a sea bay which, as the landscape emerges from the sea, is continuously reduced in size. During this period the object is totally dominated by the aquatic part, and the fluxes from the deep regolith layers are consequently directed only to the aquatic sediments (mid and upper regolith).
- Lake stage – the surrounding wetland expands into the lake, and the aquatic sediments are gradually covered by a layer of peat. This process is represented by a flux of radionuclides bound to the regolith from the aquatic to the terrestrial regolith layers. The lake stage ends when the lake has been fully transformed into a wetland, intersected by a small stream.
- Terrestrial stage – the biosphere object has reached a mature state and no further natural succession occurs. The end stage is a wetland, generally with a small stream. If the wetland has a suitable size and regolith composition for agriculture (see Lindborg 2010), it may potentially be cultivated at any time in the future and this agricultural use is represented in the model.

The transitional period, when a sea bay becomes isolated and transforms into a lake (or directly into a terrestrial mire system like in e.g. 121_3), typically takes around 500 years in the Forsmark area (Lindborg 2010), and parameter values are changed linearly from sea to lake (or terrestrial) values.

Definition of most exposed group

The most exposed group is defined as the group of individuals that receives the highest exposure across all potential release areas (i.e. biosphere objects) in the landscape. A representative individual of the most exposed group is assumed to spend all his/her time in the contaminated area, and to get his/her full supply of food and water from this area. When the productivity of a biosphere object is insufficient to support one individual, all sustainably produced food in the object is assumed to be consumed by the one individual.

Assumptions on human behaviour and land use

When the wetland in a biosphere object has emerged to sufficiently high elevation above the sea level to avoid periodic seawater flooding (2 m), it can be drained and subsequently used for crop (cereals, root crop, and vegetables) and livestock production (see the **Biosphere synthesis report** and Avila et al. 2010). The organic layers (peat and gyttja) on drained and cultivated wetlands will rapidly become oxidised and compacted, resulting in an agricultural soil that is a mixture of potentially contaminated organic matter and deeper mineral layers (glacial and postglacial deposits) where radionuclides may have accumulated since the early sea stage (cf Chapter 3 in Avila et al. 2010).

The production capacity of human food in a contaminated biosphere object is directly determined by the size of the object and the sustainable yield of natural food and agricultural products. The number of individuals that can be sustained in a biosphere object is thus proportional to the area of the object. It is assumed that all available food sources from both aquatic and terrestrial parts of a biosphere object are utilised by human inhabitants. Additionally, it is assumed that wetlands will at least partly be converted to agricultural land when this is possible. At times when cultivation is not possible, the human diet is directly determined by the potential production of different types of food in the object. However, after the biosphere object can be drained and cultivated it is assumed that a fifth of the terrestrial area of the object remains pristine (as a mire) whereas the rest of the object is used for production of cereal, tubers, vegetables and fodder (for animal husbandry) in equal parts. Biosphere objects that can be drained and cultivated can typically feed a population in the range of 100–1 000 persons, whereas biosphere objects that cannot be cultivated can support approximately 10 individuals during the sea stage and only one or a few individuals during the lake and terrestrial stages (see the **Biosphere synthesis report** and Avila et al. 2010).

Once a wetland is drained, further contamination of the soil through groundwater is assumed to not be of quantitative importance, and any additional contamination will reach the soil only through irrigation with surface water. The highest activity concentrations of radionuclides in agricultural soil are therefore expected in the period directly after drainage. Thus, the 50 years following immediately after drainage are cautiously used to assess the average annual dose from the use of contaminated agricultural soil during a human lifetime. The wetland is assumed to be converted to agricultural land at the point in time when it results in the largest radionuclide specific annual dose, which becomes a cautious assumption when the radionuclide specific doses are summarised into total LDFs (see further explanation in the **Biosphere synthesis report**).

Future humans are assumed to acquire their drinking water by equal contributions from a well drilled into the bedrock, and from the surface water in the lake or stream passing through the object. Livestock are assumed to consume water from the same sources. Exposure from contaminated drinking water is considered from the point in time when a biosphere object has emerged from the sea. Exposure originating from irrigation with contaminated surface water is considered in the production of vegetables. Surface water for irrigation of agricultural soils will be readily available in all considered biosphere objects, and irrigation with water from a drilled well has consequently been deemed unlikely (see the **Biosphere synthesis report** and Avila et al. 2010).

Mathematical implementation

The radionuclide model consists of a system of ordinary differential equations, representing the rate of change of the radionuclide content (Bq) in a model compartment (Figure 13-6 and Table 13-1), as a function of the radionuclide fluxes (Bq/y) into and out from the compartment, of radioactive decay and of ingrowth (Andersson 2010). The model has the same mathematical formulation for all biosphere objects. The differences between biosphere objects are captured by using object-specific parameter values describing the geometry of the biosphere objects, the depth of regolith layers, and the rate and timing of transitions between sea, lake and terrestrial stages.

The radionuclide fluxes are modelled in the same way for all radionuclides. Element-specific values describe e.g. retention (partitioning coefficients, K_d) and biological uptake (concentration ratios, CR). However, for C-14 the uptake by biota is modelled using a specific activity approach (Avila and Pröhl 2008), and gas exchange between the upper regolith/surface water compartments and the atmosphere has also been considered for this radionuclide.

The radionuclide model was implemented in the software package Pandora (Åstrand et al. 2005, Ekström 2011). Pandora is an extension of the codes Matlab and Simulink. A brief description of the development, functionality and features of the Pandora tool is presented in the **Biosphere synthesis report**, and the tool is described in detail in Ekström (2011). The model code was validated by a parallel implementation in the Ecolego software, and probabilistic simulations were run in this software (Section 5.4 in Avila et al. 2010).

Estimating activity concentrations

The radionuclide model was used to dynamically model the inventories in the ten compartments of the biosphere object (see Figure 13-6). The activity concentrations in upper regolith, atmosphere and surface water were used to assess exposure to humans (see below) and to non-human biota (Section 13.5.7). Activity concentrations in human food (Bq/kg C) were calculated from concentrations in environmental media (upper regolith and surface water), assuming equilibrium between the concentrations in food and in the corresponding environmental media (see the **Biosphere synthesis report** and Avila et al. 2010).

Assessment of human exposure

The average exposure over the entire life of individuals was assessed by averaging annual doses over a period of 50 years. Adults have been shown to provide a sufficiently good approximation of the average lifetime exposure (see discussion in Avila et al. 2010). The contributions to human exposure from all relevant pathways were summed as outlined in Avila and Bergström (2006). A brief description of the assumptions and calculations of human exposure from inhalation, external exposure, and consumption of contaminated food and water can be found in the **Biosphere synthesis report** and details are presented in Avila et al. (2010) and Nordén et al. (2010).

Landscape dose conversion factors

Basic LDF and LDF pulse

Potential doses to humans from continuous long-term releases were assessed by multiplying the releases of different radionuclides to the biosphere by a radionuclide specific *Landscape dose conversion factor* (LDF). The basic LDF for each potentially released radionuclide was defined as the mean annual dose to a representative individual of the most exposed group, resulting from a constant release rate of 1 Bq/y of this radionuclide. For each radionuclide, annual doses were calculated by applying a constant unit release to the radionuclide model representation of each object of the biosphere. After the sea stage, when well drilling becomes possible, the same amount (1 Bq/y) was also released into the well. The exposure was averaged over 50 years (approximating the adult lifetime of an individual), and the unit is Sv/y per Bq/y. Since unit releases were made both to each biosphere object in general and to a postulated drilled well in each object, the resulting LDFs cautiously exaggerated the consequences of unit releases. The dose was assessed over time for each biosphere object, and the highest value over time among all objects was chosen to represent the most exposed group.

Beside the basic LDF, a modified LDF was calculated for pulse releases of radionuclides that would be released within a relatively short time after a canister failure (LDF pulse). The modified LDF for a pulse release of each radionuclide was defined as the mean annual dose to a representative individual of the most exposed group, resulting from a pulse release of 1 Bq released during one single year. Time series of doses from pulse releases were simulated for the object with the maximum basic LDF of each radionuclide, and similar to the basic LDFs, the pulse was also released into the drilled well after the sea stage. For each radionuclide considered, three separate simulations with different release times of the pulse, ranging from early marine conditions (~9000 BC) to late terrestrial conditions (9400 AD), were performed. Like for the basic LDFs, the exposure was averaged over 50 years and the unit is Sv/y per Bq. The maximum dose over time from the release time yielding the highest dose was used as the radionuclide specific LDF pulse value. For a further discussion of the LDF concept (see the **Biosphere synthesis report** and details in Avila et al. 2010).

Basic LDF values for different climate conditions

Basic LDF values were calculated for three different periods of the reference glacial cycle; a period of submerged conditions following the deglaciation, the interglacial period, and a prolonged period of periglacial conditions. Additionally, LDFs were calculated for the global warming climate case. The modified LDF values for a pulse release were calculated for the interglacial period only.

The calculation period starts at the time for the deglaciation around 9000 BC, when the landscape is covered by the sea (i.e. *submerged conditions*). The length of the submerged period differs between biosphere objects since it takes almost 10 000 years from the emergence of the first biosphere object from the sea until the shoreline has passed over the whole model area.

The *interglacial period*, i.e. the period from deglaciation to the onset of periglacial conditions (see the **Climate report**), is represented by climate conditions similar to those of today. It is, in accordance with the reference glacial cycle, assumed to prevail for 18400 years (i.e. from –9000 to 9400 AD) and includes both submerged and temperate conditions. As land has emerged sufficiently from the sea, wetlands are assumed to be converted to arable land. Drinking water for humans and livestock during the terrestrial stage of this period is supplied by equal parts from surface water and from a contaminated well drilled into the bedrock (see Chapter 8 in the **Biosphere synthesis report**).

The initial period of temperate climate conditions is followed by a period of *periglacial conditions* in the reference glacial cycle. During this period, the climate is colder than today, with episodes of deep permafrost. For the LDF calculation, periglacial conditions are assumed to prevail until the onset of the next glaciation around 60000 AD. During this period, it is assumed that agriculture is not possible, and drinking water from a contaminated deep drilled well is not accessible (see Chapter 8 in the **Biosphere synthesis report**).

Exposures of humans under *glacial conditions*, when the site is covered by an ice sheet, are unlikely. Nevertheless, if releases occur, humans may be exposed to radionuclides through ingestion of sea food when the ice margin is situated above or close to the repository. As a cautious estimate of the exposure from releases during glacial conditions, the LDFs from the open sea stage during a temperate climate (i.e. submerged conditions) are used in the assessment.

In the PSAR *global warming* climate case, like in the SR-Site assessment, it is assumed that the temperate climate domain is extended by approximately 50000 years compared with the reference glacial cycle (i.e. the temperate climate domain prevails until about 60000 AD, see Section 5.1 in the **Climate report**). Since the main focus of the global warming LDF values was to capture potential effects of a longer terrestrial period for radionuclide accumulation in the mire before cultivation and potential exposure, a submerged period identical to the one in the SR-Site reference glacial cycle was, for simplicity, used. This was done instead of using i) the updated, but very similar, submerged period in the PSAR reference glacial (Climate report, Section 4.5.2), or ii) the new PSAR variants with longer initial submerged periods (Climate report Section 5.1.3 and 5.2.3). Assumptions concerning human usage of the landscape during this period are the same as for the interglacial, i.e. wetlands are converted to arable land when possible and drinking water for humans and livestock is supplied in equal parts from surface water and water from a contaminated well drilled in the rock.

Distributed LDFs

The radionuclide model has also been applied to illustrate the barrier function of the repository for a number of hypothetical release scenarios, where losses of barrier function are assumed in all canister positions already at deposition (see Section 13.7 for details). For such cases, the assumption that the entire release will reach one biosphere object is clearly not valid. Instead it was assumed that the release of radionuclides would be distributed over all identified discharge areas in the landscape in proportion to the fractions of modelled (Joyce et al. 2010) release points in the objects over time.

The *distributed LDFs* were estimated by multiplying the radionuclide specific time series of annual doses in each biosphere object estimated for the *basic LDFs* with time series of the proportion of discharge points to each object (between 9000 BC and 9400 AD) and then summing over objects. The maximum value from these time series was used as the distributed LDF for each radionuclide.

Input data

The radionuclide model for the biosphere relies on nearly 140 input parameters, of which a third represent radionuclide or element specific properties. The input data include physical constants and parameters that describe the development of the individual biosphere objects. Other parameters describe the characteristics of the ecosystems where radionuclides are likely to accumulate, the surface hydrology which drives transport within and between biosphere objects, element distribution between the solid and aqueous phases, and equilibrium concentration ratios for organisms (see the **Biosphere synthesis report** for more details).

A majority of the parameter values have been estimated from field measurements at the site as part of the site investigations, or have been extracted from models of the future development of the site.

These parameter values, which are chosen as typical for the site, are associated with uncertainties due to natural variation and also to the methods used to measure and model them. There are also parameters describing the exposed individuals and the dose coefficients for external exposure, inhalation, and ingestion of food and drinking water. Fixed, slightly cautious values have been chosen for these parameters, in line with international recommendations (ICRP 2007).

Uncertainty analyses

Sensitivity and uncertainty analyses of LDF values were performed for the most dose-contributing radionuclides. Both the effects of parameter uncertainties and conceptual uncertainties were quantified. The results from a selection of these analyses are summarised in Section 13.2.6. The results are further discussed in the **Biosphere synthesis report** and details are presented in Avila et al. (2010).

For the input parameters (summarised in Table 9-1, **Biosphere synthesis report**), a combination of site-specific data, generic data, and expert judgement were used to determine a best estimate, and to characterise the uncertainty in the parameter estimate with a probability density function (see Chapter 9 in the **Biosphere synthesis report** and for details on K_d and CR values in Chapter 2 in Nordén et al. 2010). The parameter uncertainty included natural interannual variation (expected at the site during the interglacial period) and measurement uncertainties. For each selected radionuclide, probabilistic simulations were then performed by applying Monte Carlo simulations for the landscape object that resulted in the highest LDF value in the deterministic simulations.

Some parameters that occur in the model as time series do not vary independently (e.g. the development of the different regolith layers or different parameters describing aquatic production) and were therefore excluded from the probabilistic simulations. Instead, these parameters were varied systematically as a group, preserving their correlation structure.

A number of conceptual uncertainties were addressed with alternative models. These analyses included e.g. evaluation of the pattern of groundwater discharge using particle tracking in hydrogeological models (Bosson et al. 2010). Other analyses included evaluation of the effects on the LDFs of a finer discretisation of the lower regolith compartment, evaluation of the effects of periglacial conditions using an alternative parameter set, evaluation of the effects of irrigation, and evaluation of how assumptions on land use and human diet affect LDFs (Avila et al. 2010).

13.2.4 Resulting LDF values

Maximum LDFs for a constant release rate of radionuclides (1 Bq/year) were calculated for interglacial and periglacial conditions, and for the global warming climate case. Maximum LDFs for submerged interglacial conditions were used as a cautious estimate also for the glacial climate domain. Results for a selection of 19 radionuclides, including the ones that contributed most to human exposure (see, e.g., Sections 13.5 and 13.6) are presented in Figure 13-7. LDFs for the 40 fully assessed radionuclides are described in the **Data report**, Section 7.2, that in turn refers to the SR-Site Data report (SKB 2010h) and Avila et al. (2010). In addition, the Rn-222 LDF value (5.1×10^{-14} Sv Bq⁻¹) reported in Hedin and Kautsky (2015) and based on Avila (2013) is used for conditions where a drilled well may exist (i.e. temperate and global warming conditions).

The LDFs are consistently higher for the interglacial period than for any of the other climate domains in the reference glacial cycle (Figure 13-7). For instance, LDF values for submerged and glacial conditions are in general less than the values for interglacial conditions by two orders of magnitude or more. LDFs for periglacial conditions are also generally lower than the corresponding values for the interglacial period, although they are higher than the LDFs for submerged and glacial conditions. For many radionuclides, the LDFs for the interglacial period differ marginally between the situations with and without agriculture (Figure 13-7). However, for a few radionuclides (i.e. C-14, I-129, Nb-54, Ni-59, Se-79, U-238, Zr-93), the LDFs differ by about an order of magnitude or more between these two situations (see further the **Biosphere synthesis report** and Avila et al. 2010).

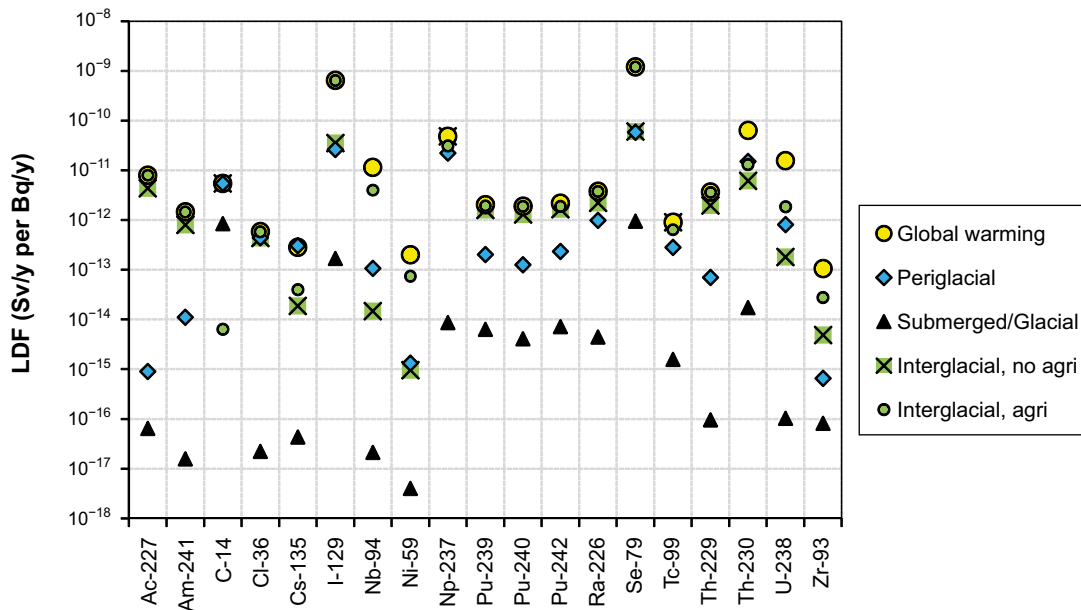


Figure 13-7. Resulting LDFs (i.e. the maximum LDF over time among all biosphere objects) for different climate conditions (Avila et al. 2010). LDFs for the initial submerged period were used to represent glacial conditions in the assessment. The effect on the LDFs of using agricultural products as food is visualised by including and excluding food from arable land during the interglacial period.

Thus, the highest doses from a constant release rate from the repository are expected under interglacial conditions when humans are exposed to radionuclides that have accumulated in a wetland that has been converted to arable land, and when contaminated well water is utilised by human inhabitants and livestock. The most obvious exception is C-14, for which the maximum LDF occurs in an aquatic system that exists during the interglacial period before agriculture is possible. Accordingly, the LDFs for the interglacial period are the maximum values applicable during the reference glacial cycle and have been used for the dose assessments in e.g. the corrosion scenario (see Section 13.5).

The global warming climate case is represented by a 50 000 year extension of temperate conditions. Consequently, radionuclides that do not reach steady state activity concentrations within the initial temperate period (–9000 to 9400 AD) will continue to accumulate during the extended temperate period. However, most radionuclides have approached steady state at 9400 AD, and additional accumulation and the associated increase in LDF is marginal for dose-dominating radionuclides (exemplified for biosphere object 121-3 in Figure 13-8). Therefore, the LDFs for most radionuclides calculated for the global warming case do not differ significantly from those for the reference glacial cycle. However, two radionuclides, Cs-135 and U-238 (the latter not included in the figure), have maximum LDFs approximately an order of magnitude larger in the global warming climate case than under the reference glacial cycle, which can be explained by several factors as discussed in Avila et al. (2010). However, due to the small contributions of Cs-135 and U-238 to the total risk estimate resulting from a long-term release (see Section 13.5.4), this tenfold increase in the LDFs of these radionuclides would not affect the final risk estimates significantly. It is therefore concluded that, from the perspective of the biosphere, the global warming case is not significantly different from the reference glacial cycle.

The LDFs clearly vary among biosphere objects, and the degree of variation depends on the properties of different radionuclides (Figure 13-9). For radionuclides for which food ingestion is the dominant exposure pathway (e.g. C-14, Cl-36, I-129, Nb-94, Ni-59, Np-237, Se-79, and Tc-99, see Table 4-1 in Avila et al. 2010), the LDFs typically vary by two to three orders of magnitude among objects (excluding object 105). However, for radionuclides for which drinking water is an important exposure pathway (e.g. Ac-227, Am-241, Pu-239, Pu-240, Pu-242, Ra-226 and Th-229), the variation in LDFs among objects is typically less than a factor of three. For most radionuclides, the rank order of objects with respect to LDF is similar. The small biosphere object 121-3 yields the highest LDF for a majority of the examined radionuclides, whereas biosphere object 105, which is in the sea stage during the entire interglacial, consistently has three orders of magnitude or more lower LDFs for all radionuclides Avila et al. (2010).

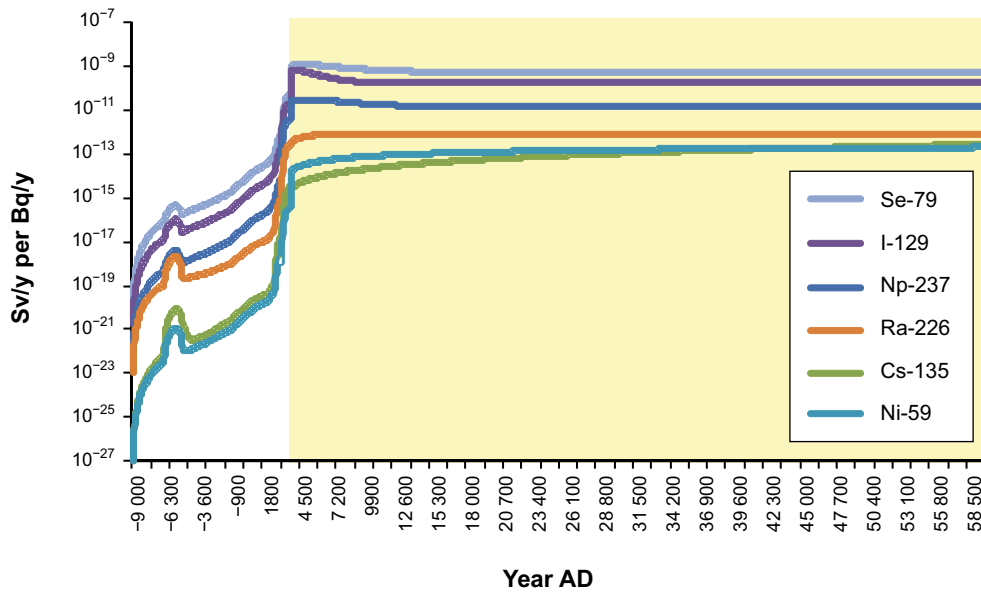


Figure 13-8. Development of the LDF for a number of radionuclides in biosphere object 121-3 in the global warming climate case. Yellow colour indicates when agriculture is possible (Avila et al. 2010).

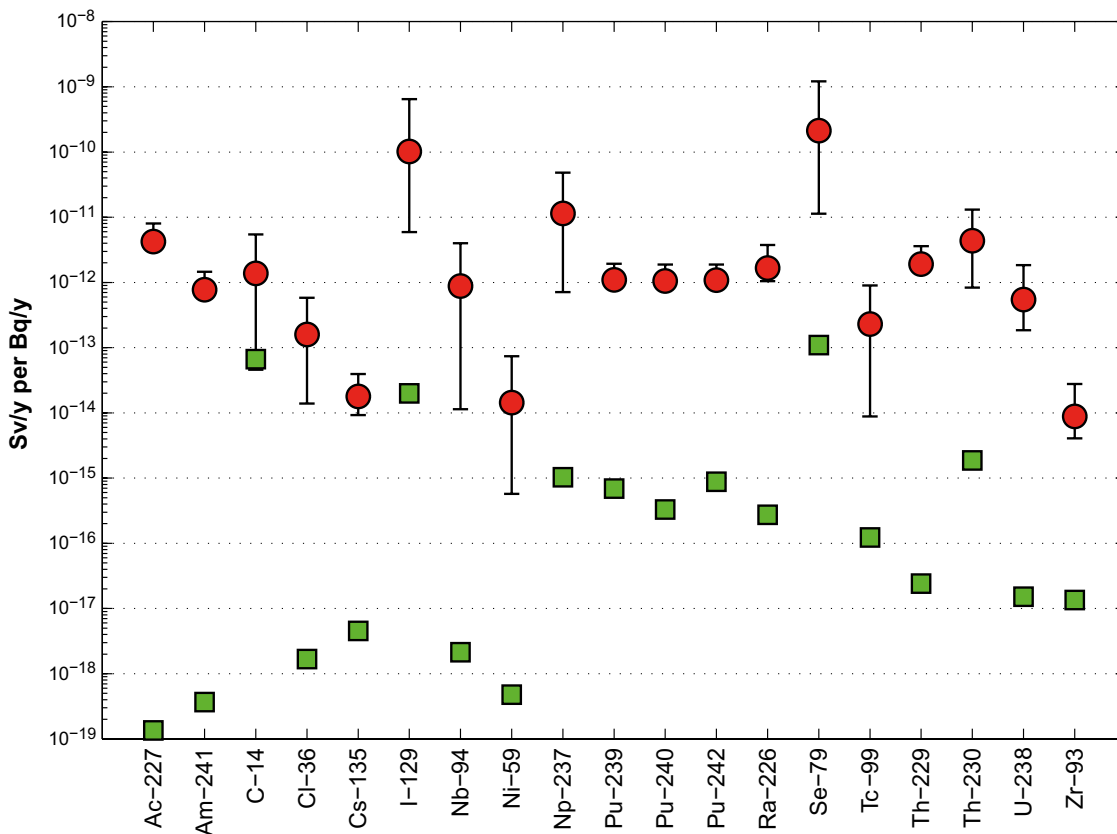


Figure 13-9. Mean (red circles), minimum and maximum (whiskers) LDF for a selection of radionuclides across biosphere objects (excluding object 105). The LDF values for object 105, which is submerged during the whole interglacial, are shown separately (green squares) (Avila et al. 2010).

In e.g. the central corrosion case, a fraction of the inventory in a canister is assumed to be instantaneously released from the fuel upon water contact, propagated through the geosphere, and released to the biosphere as a pulse with duration of years to hundreds of years (see Section 13.5.2). The modified LDF values for radionuclides that may be present in pulse releases are presented in Table 13-2. The values correspond to the maximum annual doses obtained in a simulation with a pulse unit release of 1 year duration, occurring at any time point within a period with temperate conditions. These LDF pulse values were then multiplied with the total activity of the radionuclide specific pulse releases to get the dose contributions from pulse releases.

Table 13-2. Modified *Landscape dose conversion factors* derived for pulse releases (from Avila et al. 2010). Asterisk denotes the radionuclides contributing most to dose in the pulse release cases (see Section 13.5.4).

Radionuclide	LDF pulse (Sv/y per Bq)
Se-79*	9.7×10^{-14}
I-129*	5.6×10^{-14}
Cl-36	4.3×10^{-15}
Tc-99	2.8×10^{-15}
Sn-126	2.3×10^{-15}
Ag-108m	5.1×10^{-16}
Nb-94	3.2×10^{-16}
Cs-135	1.8×10^{-16}
Ni-59	9.7×10^{-18}

Comparison of the SR-Site LDFs with results from other studies

The method used for calculating *Landscape dose factors* in SR-Site was updated in several important ways since the previous two biosphere assessments of a deep repository (i.e. SR-Can, SKB 2006a and SR 97, SKB 1999a), and data from the site were used to modify parameters from values used in the past, with improved justification for the values used in the SR-Site assessment. The changes in methodology and parameter values, and their consequences for exposure, are discussed in detail in Avila et al. (2010).

The maximum values of the Ecosystem specific Dose conversion Factors (EDF) used in SR 97 (Bergström et al. 1999) were systematically higher than the LDFs calculated in the present assessment, with the exception of a few radionuclides (e.g. C-14) (Figure 13-10). These differences are attributable to important methodological differences between the two assessments, including the delineation of the sub-catchment, assumptions on where a release will reach discharge areas and enter the ecosystems, as well as differences in the approach to evaluate the well (Avila et al. 2010).

The methodology applied in SR-Site was based on that developed in SR-Can and a comparison between SR-Can and SR-Site LDFs shows no general tendencies. Differences in LDF values between the two assessments are mainly explained by differences between the generic parameter values (e.g. Kd and CR values) that were used in most cases in SR-Can, and the SR-Site parameters that were more based on site-specific data.

As described in the introduction of this Section 13.2, the biosphere assessment has developed further during the safety assessments SR-PSU (SKB 2014d) and more recently in SE-SFL (SKB 2019a). Since the SR PSU LDFs were generally smaller and never substantially larger than the SR-Site LDFs for any dose dominating radionuclide, the risk of underestimating LDFs and resulting doses is deemed as small. The need for updating the LDFs at this stage was thus seen as limited, but is planned for the next step in the stepwise licensing process. Feedback to coming steps is provided in Sections 15.6.10 and 15.7.5.

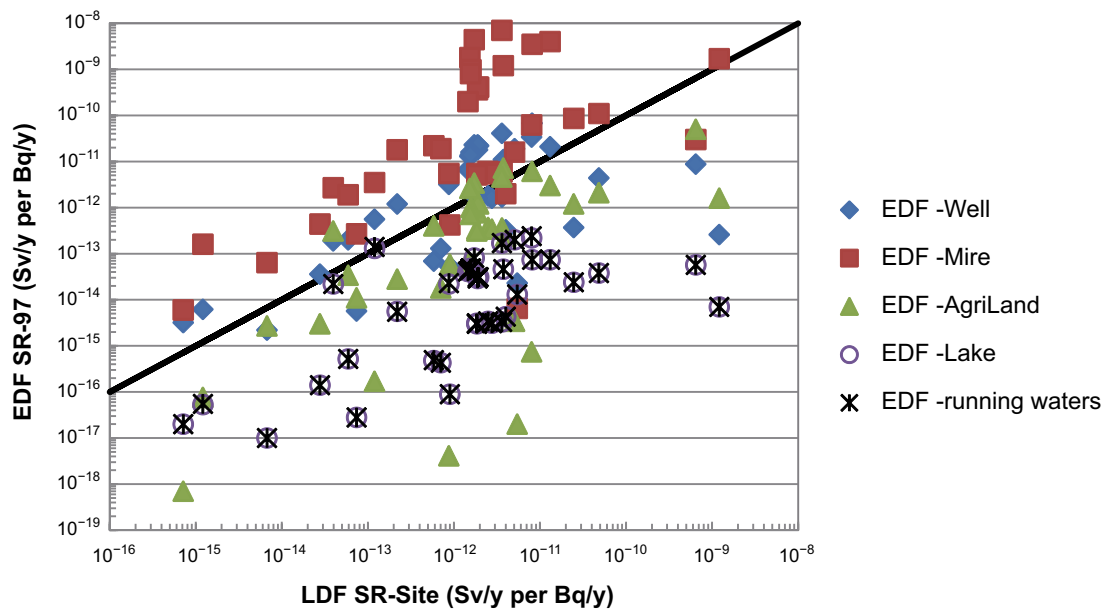


Figure 13-10. Comparison of the SR-Site LDFs with corresponding dose conversion factors (EDF) reported in SR 97 (SKB 1999a). The solid line represents a 1:1 relationship between SR-Site and the SR 97 dose factors, and each point represents a specific radionuclide (Avila et al. 2010).

13.2.5 Approach and methods for assessment of radiological effects on the environment

To ensure the protection of the environment, adverse effects on non-human biota from a potential radionuclide release in the Forsmark area were assessed. Details are presented in Jaeschke et al. (2013). The assessment built upon and further developed the initial SR-Site assessment of radiological effects on the environment by Torudd (2010) and was carried out using the approach recommended by ICRP (ICRP 2007) and developed within the European projects FASSET (FASSET 2004), ERICA (Beresford et al. 2007) and PROTECT (Howard et al. 2010). The potential effects on individual specimens of a variety of organism types occurring at the site were evaluated. This approach is based on the rationale that if there are no detrimental effects at the level of individuals, then negative consequences at the population or ecosystem levels can also be excluded (see Jaeschke et al. 2013).

Unit release rates and unit pulse releases were used in the radionuclide model for the biosphere to estimate unit release activity concentrations of each radionuclide in water and the upper regolith of aquatic and terrestrial ecosystems. The maximum unit release concentrations of each radionuclide over environmental media, ecosystems, biosphere objects and time were multiplied with maximum continuous radionuclide release rates or pulse releases to the surface from the deterministic central corrosion case, where a canister was assumed to fail at 114000 years after deposition (Section 13.5.4). In relation to the probabilistic central corrosion case used to assess doses to humans, using the deterministic case is more pessimistic and assesses the maximum potential impact on the environment in any time period if a canister fails.

The resulting maximum activity concentrations of each radionuclide were used as input in the ERICA tool to estimate the absorbed dose rates, both internal and external, to different types of organisms. The sum of the absorbed dose rates was evaluated against a screening no-effect dose rate of $10 \mu\text{Gy h}^{-1}$ (Andersson et al. 2009). The assessment was performed for a number of reference organisms using predefined settings in the ERICA tool (see Brown et al. 2008), but the main focus was on representative species for the Forsmark area, using concentration ratios (CR values), habitat occupancy data and organism sizes from the site. The representative species included ecologically and economically important species and vulnerable or protected species identified in the Forsmark area. Furthermore, effects on species that could be exposed from a potential release during future warmer climate conditions were assessed and potential effects during future periglacial conditions were estimated. The results from the assessment are summarised in Section 13.5.7.

13.2.6 Uncertainties and cautiousness in the LDF approach

There are three types of uncertainties associated with the final LDFs; parameter uncertainties, model uncertainties and system uncertainties (see Section 2.8 and the **Biosphere synthesis report**). The effect of *parameter uncertainties* on the LDFs can be evaluated through systematic and/or random variations of parameter values (see Avila et al. 2010 and Ekström 2011 and summarised below). Parameters describing biosphere object properties are not independent of each other and therefore more difficult to handle in a traditional uncertainty analysis. Uncertainties in object properties are instead handled cautiously by selecting the maximum LDF from a number of biosphere objects with a wide range of properties. *Model uncertainties* arise either from limited process understanding or from simplified mathematical representation of our understanding. *System uncertainties* arise from our inability to predict the long-term development of the biosphere and the future human behaviour and utilisation of the landscape. Model and system uncertainties were evaluated by using alternative approaches and models, or by discussing the potential outcome of erroneous assumptions.

The effect of these three types of uncertainties differs among radionuclides. To illustrate the approaches used to evaluate uncertainties, the following discussion presents how important sources of uncertainty were handled. The analyses were based on the modelling of a continuous release in the central corrosion case and on the radionuclides contributing most to dose, especially Ra-226 (see Section 13.5.4). A more detailed discussion of uncertainties in the LDF modelling is found in the **Biosphere synthesis report** and in Avila et al. (2010).

Influence of parameter uncertainties on the final LDF estimates

The deterministic LDFs were calculated by selecting input parameters using expert judgement, with an intention that the LDF should reflect a reasonable value, given the uncertainties. This approach should therefore produce results that represent the central tendency of a full analysis of parameter uncertainty. To substantiate this approach, probabilistic simulations were used to propagate parameter uncertainties through the model to establish how they affect the LDF estimates. The LDF distributions calculated in this way were approximately log-normal, with a 90 % confidence interval of LDFs typically spanning two orders of magnitude (Figure 13-11).

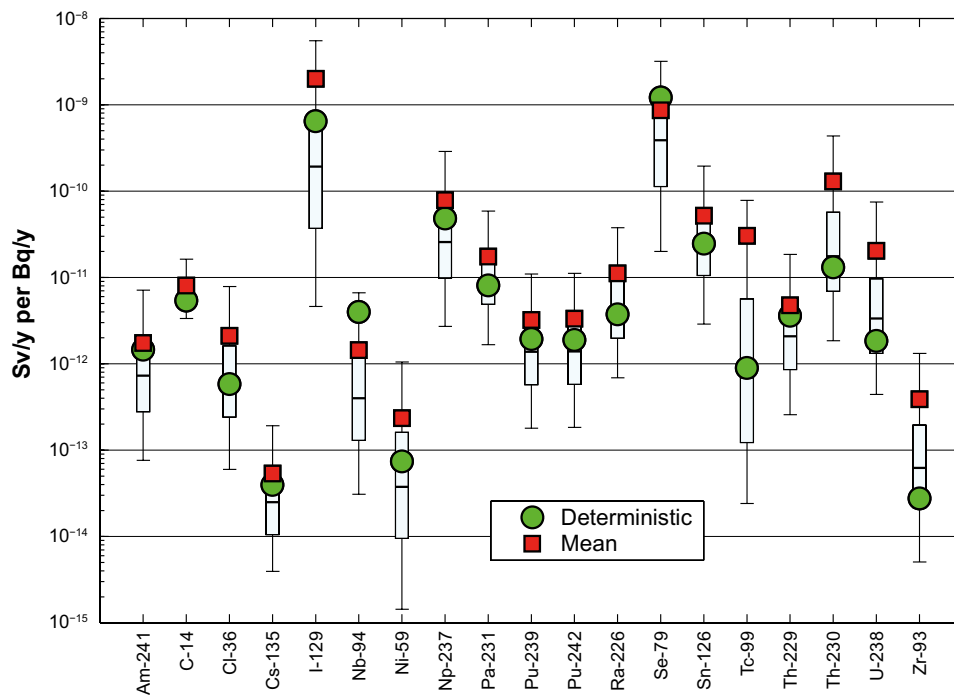


Figure 13-11. Variation in interglacial LDFs obtained from probabilistic simulations for a subset of the analysed radionuclides. The LDF distributions are taken at the time when the median of the probabilistic output reached its peak. The mean (red squares), median, 5 percentile, 25 percentile, 75 percentile and 95 percentile from the probabilistic simulations are shown (box and whiskers). The deterministic LDFs (green circles) are also shown for comparison (from Avila et al. 2010).

The central tendency of distributions that span several orders of magnitude can be thought to be represented by either the median or the mean of the distribution. Due to the log-normal distribution of LDFs, the arithmetic mean was systematically higher than the median value. Because of the nature of information used to establish the input distributions for the probabilistic approach, there is uncertainty whether the probabilistic realisations drawn from a large number of independent distributions represent actual site behaviour.

Nevertheless, the deterministic LDFs were generally close to the median and slightly lower than the mean of the probabilistic simulations, with a few exceptions. For a few radionuclides, the mean from probabilistic simulations would have resulted in LDFs that were an order of magnitude larger than the LDFs used in the safety assessment (e.g. Tc-99, Th-230 and U-238). However, the potential release of these radionuclides to the biosphere is expected to be insignificant (see Section 13.5.4). Thus, it can be concluded that there is reasonable agreement between the deterministic approach to calculating LDFs for use in the safety assessment, and a probabilistic approach that accounts for parameter uncertainties. This is discussed in more detail in the **Biosphere synthesis report** and in Avila et al. (2010).

Parameter uncertainty effects on the LDF of the dose dominating Ra-226 and some other dose dominating radionuclides

The dose from continuous radionuclide releases in the compliance scenarios (the central corrosion and the shear load case, Section 13.3.5 and 13.3.6) was dominated by Ra-226 and thus parameter uncertainty that influences the Ra-226 LDF is of particular interest. The deterministic maximum LDF of Ra-226 was derived from object 121_3 at the end of the initial interglacial. Slightly over 50 % of the exposure was through drinking well water and the rest was through food intake (see Table 4-1 in Avila et al. 2010). The 90 % confidence interval of the LDF due to parameter uncertainty spanned about two orders of magnitude (Figure 13-11). Half of the variation was explained by the well capacity, followed by uptake (the concentration ratio, *CR*) of Ra-226 (explained 6 %) and its decay product Pb-210 (20 %) in vegetables, and sorption in the lowest regolith layer (partitioning coefficient, K_d RegoLow, 5 %). The LDF for Ra-226 would decrease with an increase in well capacity or in the K_d for the lowest regolith layer, and increase with increased uptake in vegetables. Thus for both Ra-226 doses and total doses, uncertainty in parameters influencing both the well water exposure as well as transport and accumulation in, and uptake from the regolith are important. The results were similar for radionuclides with similar properties, like Cs-135. However, for more mobile dose contributing radionuclides like, I-129 and Se-79, where exposure was dominated by food intake and drinking well water was insignificant, accumulation in shallower regolith layers (K_d in RegoMid and RegoUp) were most important.

Uncertainties related to biosphere object properties

The identification, location and temporal development of biosphere objects were described in Section 13.2.2. Several characteristics of the biosphere objects (including area of sub-catchment, timing of emergence from the sea and depth of regolith layers) affect the transport and accumulation of radionuclides. These features are not independent properties, but they vary together in response to the topography and geometry of the landscape. There are uncertainties in the location and configuration of the biosphere objects that are submerged today, associated mainly with uncertainties in the sea floor bathymetry and regolith characteristics. The uncertainty in and model sensitivity to such object properties were not analysed specifically. However, the identified biosphere objects span a wide range in different characteristics, such as topographical location, geometric features and thickness of different regolith layers, and they are therefore assumed to be representative both for the present and the future landscape.

Although there are many characteristics that affect the predicted development of activity concentrations in a discharge area, the steady state activity concentrations in soil and water are primarily determined by the sizes of the watershed and the local drainage area (sub-catchment). The biosphere objects that yield the highest environmental activity concentrations are objects with a small sub-catchment and no inflow of surface water from an upstream watershed. The smallest identified object has an area of about 8 ha, and the smallest local drainage area (sub catchment) only three times larger (24 ha). According to the SR-Site assumptions about food production, those small objects can support approximately 80 individuals. In theory, smaller biosphere objects with smaller sub-catchments, which could sustainably support a group of say 10–20 individuals, would reasonably result in larger activity concentrations

and LDFs. However, based on more realistic assumptions about food production, the SR-PSU analysis suggests that biosphere object areas of about 3 ha would only suffice to support one family and would thus reasonably apply to the risk criteria for a small exposed group (10^{-5} year⁻¹ rather than 10^{-6} year⁻¹) (SSM 2008b, Berglund et al. 2015, SKB 2014d). Besides, a thorough analysis of the Forsmark landscape fails to identify any discharge area with a smaller sub-catchment than 24 ha and a reasonable likelihood of persistent release from the repository (Lindborg 2010).

The biosphere objects are modelled as horizontally homogenous, i.e. that potential releases of radionuclides are spread horizontally over the entire object and effects of possible hot spots are not considered. This assumption is partly supported by simulations of releases from individual canister positions indicating that the particles are generally distributed over areas approximately corresponding to the size of the smallest biosphere objects (Berglund et al. 2015, based on data from Joyce et al. 2010). For water bodies, a horizontal spread of a concentrated release would be relatively fast. Highest exposures from mires occur after they have been drained and cultivated. Such an enterprise requires much work and would for practical reasons most likely involve conversion of the full lake/wetland system for cultivation. Except for the largest biosphere objects, it is not reasonable to assume that a person (or an exposed group) would obtain food from a subarea within the area with the highest concentrations during the entire adult lifetime (50 years). Horizontal mixing due to ploughing, rotation of land, and mixing through storage and processing of crops (e.g. milling), all make it reasonable to average radionuclide concentrations in the diet over the full land area claimed by the draining enterprise. The assumption of horizontally homogenous biosphere objects is a reasonable simplification (Berglund et al. 2015).

The use of maximum LDF values in the calculation chain (see Figure 13-3) disregards the fact that discharges may affect several objects, and that different radionuclides will give maximum LDF values during different successional stages of the biosphere or in different biosphere objects. Thus, the maximum LDF used in the assessment overestimates the potential risk when more than one radionuclide contributes significantly to the dose (see Avila et al. 2010).

It is concluded that the biosphere objects used to represent the future Forsmark landscape give a reasonable representation of the range of discharge areas that may receive contaminated groundwater from the repository, and consequently uncertainties with respect to the properties of future discharge areas have been incorporated in the LDF values used in the safety assessment.

Discretisation of the regolith compartments

Model uncertainty partly relates to the degree of mathematical simplification of the modelled system. In the radionuclide model, the lower regolith is represented by a single compartment. A single-compartment model will tend to produce earlier breakthrough and more dispersion of radionuclides that are accumulating in the regolith, than a model with a finer discretisation. To examine the effect of discretisation on dilution and dispersion, the lower regolith compartment was split into a varying number of compartments, stacked on top of each other (Avila et al. 2010). The analysis showed that a finer discretisation of the lower regolith compartment increases the retention in deeper soil layers, but that this has a limited effect on the calculated LDFs for most radionuclides (including the dose-dominating radionuclides). Moreover, for radionuclides that are significantly affected by decay in the lower regolith, the single-compartment representation used in SR-Site leads to pessimistic LDF estimates as compared to estimates based on finer discretisation of the lower regolith (see the **Biosphere synthesis report** and Avila et al. 2010).

Human behaviour and utilisation of the landscape

System uncertainties, like future human behaviour and utilisation of the landscape, were evaluated by comparing with results using alternative assumptions, or by discussing the potential outcome of erroneous assumptions. A potential release of radionuclides from the repository will reach the biosphere in spatially restricted discharge areas, i.e. biosphere objects. It is concluded that the highest activity concentrations in the landscape over time will be found in biosphere objects that receive direct releases of radionuclides from the geosphere (Avila et al. 2010).

In the assessment it is assumed that the most exposed group spend all of their time in the contaminated area, and get their full supply of food and water from the biosphere object. It is further assumed that a contaminated wetland will be drained and used for agricultural purposes at the point in time which would result in the maximum annual dose for unit release rate. These assumptions are unlikely in a cultural or landscape utilisation perspective. For example, a sustainable agricultural use of the drained organic soils that are typical for the biosphere objects is possible only for a period of 50–100 years (Lindborg 2010). In contrast, the thick and partly continuous layers of clay and sand in the central parts of Öregrundsgrepen can be sustainably cultivated for thousands of years.

Thus, a more realistic scenario for a future self-supporting society in the area is that the mainly lightly contaminated central parts of Öregrundsgrepen will be intensively cultivated and contribute the major part of the food consumed, even by the most exposed group. Some of the small biosphere objects may occasionally be cultivated and may then complement the food produced in the more suitable agricultural areas in Öregrundsgrepen, but probably the biosphere objects will primarily be utilised for extensive collection of naturally produced foods. Thus, the assumption that a representative individual of the most exposed group will spend all his or her time in the contaminated area and get his/her full supply of food and water from this biosphere object is strongly pessimistic.

The effect of uncertainties in the composition of the human diet was investigated in a separate probabilistic simulation. This resulted in a 90 % confidence interval of about one order of magnitude and the arithmetic mean was less than a factor 2 from the deterministic LDF value for the dose dominating Ra-226, suggesting limited effects of uncertainties in diet composition (see Avila et al. 2010).

For the LDF calculations it was assumed that vegetables are irrigated with contaminated surface water. The effects of irrigation with well water and long-term irrigation were explored in separate simulations. Irrigation with well water increased activity concentrations in vegetables somewhat for most examined radionuclides, but the effects on the most dose-contributing radionuclides was at maximum a factor of two. Long-term irrigation of uncontaminated minerogenic soil with contaminated surface water did not result in higher concentrations in vegetables than those resulting from draining and cultivating a wetland in an adjacent contaminated discharge area (Avila et al. 2010). From these simulations it was concluded that assumptions on the origin of contaminated irrigation water did not significantly affect the calculated LDFs, and that long-term irrigation with contaminated surface water would not lead to significantly higher doses than those arising from the initial cultivation of the contaminated organic soil (Avila et al. 2010).

13.2.7 Summary and conclusions

The biosphere assessment is built on knowledge and results from extensive investigations of the site. The site investigations have underpinned the conceptual description of the site and contributed to a systematic mapping of processes that may be important for transport and accumulation of radionuclides in the biosphere, in order to ensure that all relevant processes have been included in the assessment. The investigations have also enabled the use of parameter estimates that correspond to conditions at the site today and in the future, in the different modelling steps.

A number of different biosphere objects have been identified as potential release areas for radionuclides from the repository. The objects are situated in a dynamic landscape, ranging from fully submerged to entirely terrestrial, and they include considerable variation in size, timing of succession and object-specific properties. Even if the exact future landscape development is difficult to predict, the modelled landscape development can be seen as a systematic evaluation of possible futures, based on the understanding of how present-day geometries have developed and an expected shoreline displacement regime.

An ecosystem-based approach has been used to dynamically model the transport and accumulation of radionuclides in the biosphere objects over a 60 000 year ice-free period of the reference glacial cycle. Effects of different climate conditions have also been evaluated in the modelling approach. Human utilisation of natural resources was, in the assessment, based on the productivity of natural and cultivated food in the object. The annual dose to future inhabitants of the Forsmark area was calculated per unit constant release rate to each biosphere object and for each radionuclide. The calculated LDFs have been selected from the biosphere object and point in time which gives the highest radionuclide specific unit release doses, and consequently those maximum LDFs do not necessarily match the same group of exposed individuals with respect to point in time or location in the landscape.

Additional simulations and alternative models have been used to explore how uncertainties and assumptions may affect the final LDF estimates. From these analyses it is concluded that neither object discretisation, nor parameter uncertainties, nor assumptions on human utilisation of natural resources will have significant effects on the calculated LDFs. For parameter uncertainties, this conclusion is conditioned on the comparison of the expected value from probabilistic calculations (i.e. the mean) with that from deterministic calculations. However, the analyses highlighted that a large proportion of LDF uncertainty can be attributed to parameters describing the radionuclide activity in the well water (well capacity), followed by biological uptake (i.e. CR values) and to partitioning of radionuclides between the solid and liquid phases (i.e. K_d values). Consequently, the uncertainties can be reduced by better estimates of these parameters from the site, or by alternative modelling approaches for sorption and uptake of radionuclides that are less sensitive to parameter uncertainties (see further discussion in the **Biosphere synthesis report**).

The intent of the biosphere modelling effort has been to make an assessment of reasonable future conditions by combining the best available knowledge of today's conditions and the past development of the Forsmark site with reasonable and cautious assumptions about the future. A systematic evaluation of the effects of assumptions and other sources of uncertainties on the SR-Site LDFs (equal to the PSAR LDFs) shows that the handling of system and model uncertainties tends to be cautious (see the **Biosphere synthesis report**). Site representative values were used for model parameters, and their uncertainties were not handled pessimistically, whereas the definition of the most exposed group was clearly cautious. However, the effect of quantified uncertainties was limited and is therefore not expected to have a significant effect on the assessment endpoint. Taken together there is confidence that the maximum LDFs used in the PSAR are robust estimates for the most exposed group, reflecting the current process understanding and the most precise description of the site available.

13.3 Criticality

If a canister failure occurs, the issue of nuclear criticality has to be considered, since, if this occurred, it could have a strong influence on the further development of the failed canister and of repository areas in its vicinity.

The possibility of nuclear criticality in the canister interior, process F3 Induced fission (criticality) in the process table for the fuel in Section 7.4.1, has been dismissed in a number of studies, see e.g. the SR-Can report (SKB 2006a). The issue has most recently been analysed by Johansson et al. (2019).

Acceptance criteria for encapsulation of fuel assemblies are defined to ensure that the fuel assemblies shall not, under any circumstances, be encapsulated if the criticality criteria cannot be met, see further Section 5.3.4. This means that the effective neutron multiplication factor k_{eff} , including uncertainties, must not exceed 0.95, or, for events that based on their very low frequency are classified as not expected or improbable, k_{eff} should not exceed 0.98. Previous analyses (Agrenius 2010) showed that credit for burnup has to be taken to demonstrate that the canister remains subcritical in the repository for all reasonably conceivable scenarios. Since then the method for criticality calculations has been updated to include credit for burnup (PWR fuel) and burnable absorber (BWR); however burnup credit is only required for PWR fuel with an initial enrichment higher than 2.3 %. For BWR fuel, credit is taken for burnable absorbers if initial enrichment is higher than 3.4 %. Note, however, that a canister that is dry inside is strongly subcritical with k_{eff} less than 0.4. The reactivity increases in scenarios with a water filled canister, i.e. after canister failure in the repository. All identified uncertainties in the determining parameters such as the manufacturing tolerances, geometry, declared burnup, and more, were taken into account.

In scenarios where the canister has failed in the repository and water has entered, the geometry is likely to change due to corrosion of metal parts inside the canister. This situation was studied in detail by Agrenius and Spahiu (2016) to estimate the effects of canister internal corrosion on reactivity. This study involved formulating a reasonable evolution of the formation of corrosion products inside the canister. Criticality calculations have been performed and Agrenius and Spahiu (2016) show that the highest reactivity is reached when the gap between the corrosion product magnetite and the fuel rods is ca 2 mm. The reactivity increase connected to that situation is included in all the additions to k_{eff} related to uncertainties described by Johansson et al. (2019).

With all fuel element locations occupied in a canister deposited in the repository, surrounded by 35 cm bentonite and filled with water, the following PWR burnup is required to meet the criteria:

3 % enriched: 12 MWd/kgU

4 % enriched: 24 MWd/kgU

5 % enriched: 34 MWd/kgU

The required amount of initial burnable absorber (for BWR) is higher for fuels with higher enrichment. Details are given by Johansson et al. (2019).

The risk of criticality as a result of redistribution of material has been analysed by Behrenz and Hannerz (1978) and by Oversby (1996, 1998). The conclusions were that criticality outside the canister has a vanishingly small probability, requiring several highly improbable events. After the report of a possibility of criticality outside a canister by Bowman and Venneri (1994) that was dismissed in a review by Van Konynenburg (1995), several other studies have concluded that criticality in a geologic repository as a result of redistribution of fissile material is a highly unlikely event.

The possibility of nuclear criticality in the vicinity of the proposed Yucca Mountain repository was explored by Nicot (2008). It was concluded that external nuclear criticality is not a concern at the proposed Yucca Mountain repository for any of the deposited waste. Some of the waste intended for Yucca Mountain contains higher levels of fissile material than what is intended for disposal in a Swedish repository.

In conclusion, as the criticality analyses show that acceptance criteria for encapsulation of fuel assemblies will be met, the canisters remain subcritical in the repository for all reasonably conceivable scenarios (Table 2-3 in the **Fuel and canister process report**). The probability of criticality outside the canister is considered to be negligibly small, based on the results reported in Van Konynenburg (1995), Oversby (1996, 1998) and Nicot (2008).

13.3.1 Consequences of a postulated criticality event in the final repository

During the review of the safety assessment SR-Site, SSM requested an analysis of a residual scenario to illustrate the effects of a postulated criticality in a failed and water-filled canister.

In the analysis of such a scenario (Hedin et al. 2013), it was postulated that a failed canister would become critical when a sufficient amount of water had entered the canister. The further development is determined by the competition between the inflowing water, leading to an increased k_{eff} , and the increasing temperature, yielding a decrease in k_{eff} . Eventually, a steady state is expected to be established at a temperature near the boiling point of water at repository conditions. This temperature is around 264 °C for a hydrostatic pressure of 5 MPa. The further analysis of the scenario led to the following conclusions:

- The power developed in a critical canister is limited by the finite capacity of the rock to carry away the generated heat by thermal conduction. This means that a canister maintained at 264 °C is calculated to develop a power of around 14 kW in the host rock in Forsmark.
- The resulting increase in temperature in the host rock is not sufficient to cause any damage to the bentonite buffer in adjacent deposition positions.
- The fuel dissolution rate in a steady-state criticality situation is judged to possibly be an order of magnitude higher than for sub-critical conditions.
- Using this higher fuel dissolution rate, the radiological consequences for a steady-state criticality situation in a failed canister were calculated to be about a factor of six higher than for the corresponding sub-critical situation.

In summary, the results thus showed that the consequences of a postulated criticality are limited. It is also noted that SSM in its review report (SSM 2018) considered SKB's approach of not including the consequences of criticality scenarios such as the above in the summation of post-closure risk for the final repository, as reasonable.

13.4 Models for radionuclide transport and dose calculations

Figure 13-12 shows the models and data used in the radionuclide transport and dose calculations. In the following, a brief description is given of the near-field model COMP23 in Section 13.4.1 and of the far-field model FARF31 in Section 13.4.2, which also describes a separate model, MARFA, for modelling of varying flow and colloid-facilitated transport in the geosphere. The biosphere representation is briefly described in Section 13.4.3.

Radionuclide transport and dose consequences for some cases have been calculated with simplified, analytical models that yield similar results to the numerical models. The analytical models are briefly explained in Section 13.4.4.

13.4.1 The near-field model COMP23

The near-field radionuclide transport model used in SR-Site as well as in the PSAR to handle radionuclide transport in the water phase is COMP 23 (Cliffe and Kelly 2006, Kelly and Cliffe 2006). This is an updated version of the compartment model used in the SR 97 assessment and it was originally developed from the NUCTRAN code (Romero 1995, Romero et al. 1999). A Matlab/Simulink implementation (Vahlund and Hermansson 2006) is used to solve the COMP23 model instead of the original Fortran implementation.

COMP23 models processes related to radionuclide release and transport in the canister interior, the buffer and the deposition tunnel backfill, i.e. the summary processes F17, Bu25 and BfT21, respectively in the process tables in Section 7.4. These incorporate the processes radioactive decay (F1), metal corrosion (modelled as a constant metal corrosion rate, F11), fuel dissolution (F12), dissolution of gap inventory (modelled as an instantaneous release, F13), speciation of radionuclides (i.e. dissolution/precipitation of nuclides with shared elemental solubilities, F14), diffusion (Bu11) and sorption (Bu12) in the buffer and advection (BfT9), diffusion (BfT10) and sorption (BfT11) in the deposition tunnel backfill. It also handles the release of radionuclides to exit paths from the near-field, see below.

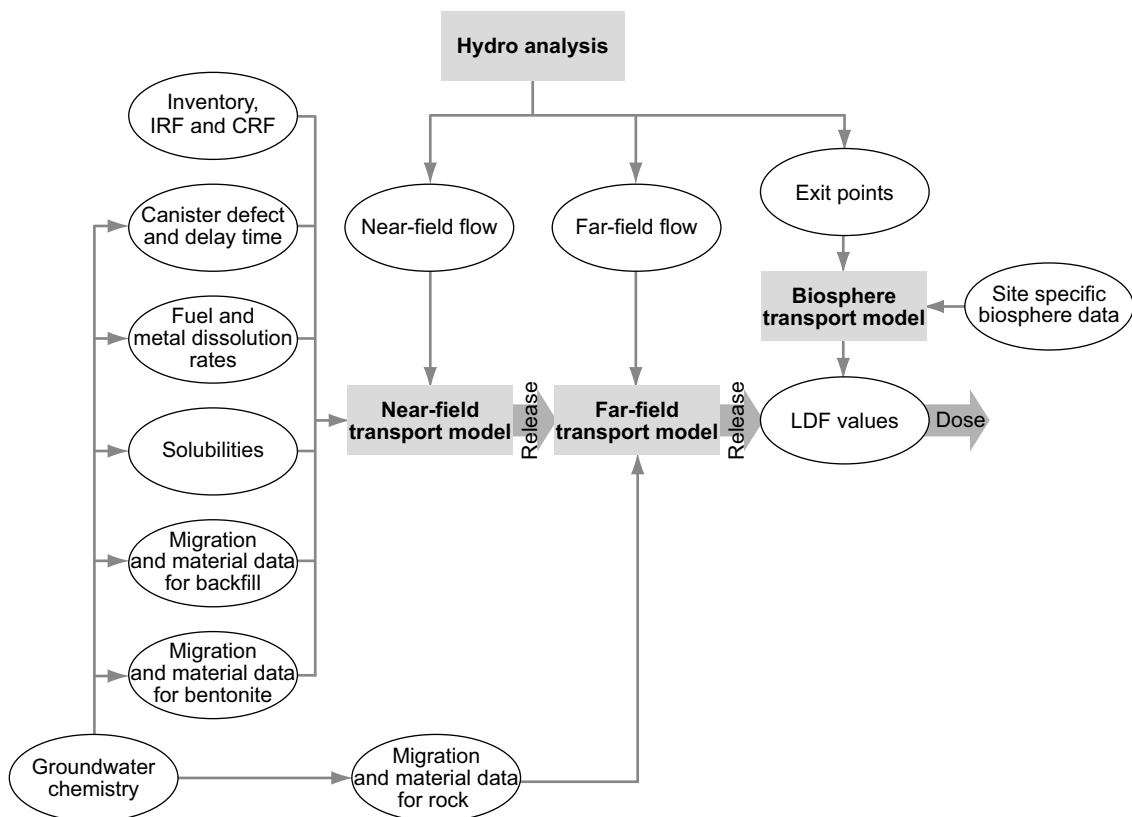


Figure 13-12. Models and data for the consequence calculations.

COMP23 is a multiple-path model that calculates transient nuclide transport in the near-field of a repository by use of a network of coupled resistances and capacitances in analogy with an electrical circuit network. Analytical solutions, instead of fine discretisation, at sensitive zones, for example at the exit point of a small canister hole and at the entrance to fractures, are embedded to enhance calculation speed.

Figure 13-13 shows the canister, deposition hole and the deposition tunnel backfill and how these are modelled by COMP23 in SR-Site and the PSAR. Three exits from the near-field are included: a fracture intersecting the deposition hole at the vertical position of the canister lid, denoted Q1, an excavation damaged zone, EDZ, in the floor of the deposition tunnel (if such a zone is assumed to exist), Q2, and a fracture intersecting the deposition tunnel, Q3. In the hydrogeological modelling, the number of fractures intersecting a deposition hole and the properties of these fractures are determined statistically based on the DFN description of the rock (see further the **Data report**, Section 6.6). If more than one fracture intersects a deposition hole, the transport capacity of the several fractures are added and pessimistically assigned to the single fracture modelled by COMP23. The equivalent flow rate through Q2 is also calculated as an integral part of the hydrogeological modelling. Data on transport properties for the EDZ used in these calculations are given in the **Data report**, Section 6.5. The flow rate in the deposition tunnel and the distance to the nearest Q3 fracture through which radionuclides are released to the geosphere from the tunnel are given by the hydrogeological modelling. Transport by advection/diffusion in the tunnel is included in the near-field simulations and the computational domain is extended in the downstream direction to include the Q3 fracture.

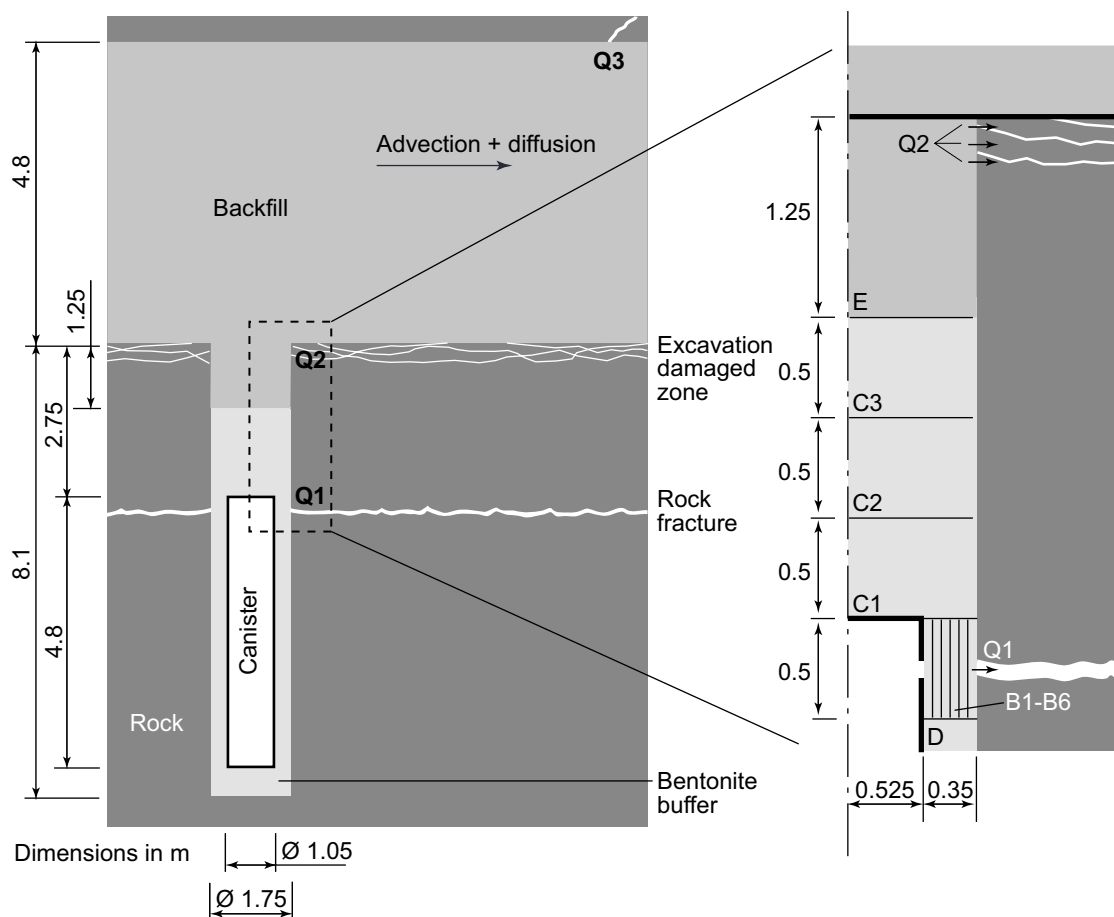


Figure 13-13. The near-field and detail of its model representation as compartments B1–B6, C1–C3, D and E in the model COMP23. The transport paths Q1, Q2 and Q3 to a fracture intersecting the deposition hole, to the excavation damaged zone, and to a fracture intersecting the deposition tunnel, respectively, are also shown. (Potentially a minor EDZ around the deposition hole could exist, but as shown in the Underground construction report such a zone would have very low – if any – connected hydraulic conductivity and is thus not included in the model.) The differentiation of compartments shown in this figure is relevant for a pinhole failure in the canister. All other analysed failure modes require less differentiated representations of the near-field.

Effects of spalling in deposition holes are treated by a modification of the input equivalent flow rates for the transport path Q1, as described in Section 10.3.6 and further in the **Data report**, Section 6.6. The handling of spalling does not require any modification of the numerical model.

Advective conditions in the buffer are simply treated by equating the outflux from the canister interior compartment with the release to Q1. The release paths Q2 and Q3 are not modelled when advective conditions are assumed in the buffer since releases to Q1 completely dominate over those to Q2 and Q3 for such cases.

13.4.2 The far-field models FARF31 and MARFA

The far-field radionuclide transport models used in SR-Site as well as in the PSAR to handle radionuclide transport in the water phase are FARF31 (Norman and Kjellbert 1990, Elert et al. 2004) and MARFA (Painter and Mancillas 2009).

FARF31 has been employed already in earlier assessments, e.g. SR 97 (SKB 1999a) and SR-Can (SKB 2006a), whereas MARFA was developed for use within SR-Site with still on-going development. Development and use of MARFA after SR-Site is discussed in the **Radionuclide transport report**, Sections 3.6.3 and 4.5.7. Within the PSAR, as in SR-Site, MARFA is primarily used for calculations employing code functionality not available in FARF31. The two codes are partially used also in parallel to show that they produce consistent results. The two codes solve migration along one-dimensional paths and handle, using the nomenclature in the process tables in Section 7.4, the process Ge24 ‘Transport of radionuclides in the water phase’, consisting of the sub-processes advection (an aspect of process Ge11), dispersion, matrix diffusion with equilibrium sorption (Ge12 and Ge13), and radioactive decay (F1, including decay chains). MARFA can in addition also handle equilibrium sorption within the flowing phase, i.e. not only within the stagnant water of the matrix.

In FARF31, the equations are solved analytically in Laplace space and subsequently numerically inverted to obtain the breakthrough curves. It is noted that the equations are expressed in terms of accumulated travel time rather than distance along the flow path. This feature makes it easy to calculate travel times in a stand-alone groundwater flow model, see Section 10.3.6, and subsequently radionuclide transport in a decoupled fashion.

FARF31 was originally developed to be used with a groundwater flow model adopting a continuum representation of the rock. In the PSAR, as in SR-Site, groundwater flow is primarily modelled through a discrete fracture network (DFN) where individual fractures are represented explicitly. Here, the conceptualisation of a migration path is slightly different than in a continuum-based groundwater flow model. Rather than macroscopic stream tubes encompassing both rock and flow paths, the equation now describes flow paths through the actual open pore space, i.e. through the connected fracture network (RETROCK 2005). However, the governing equations are identical for the two conceptualisations. The entities calculated in the DFN-based groundwater flow models are the advective travel time (t_w) and flow-related transport resistance (F) along flow paths. FARF31 has been modified to use these inputs directly.

MARFA (Migration Analysis of Radionuclides in the Far-Field) uses a particle-based Monte Carlo method to simulate the transport of radionuclides in a sparsely fractured geological medium. MARFA uses a time-domain random walk algorithm (Painter et al. 2008), wherein noninteracting particles representing packets of radionuclide mass are moved through the system according to rules that mimic the underlying physical transport and retention processes. MARFA is specifically designed to work with output from discrete fracture network (DFN), continuous porous medium (CPM), or nested DFN/CPM flow models.

The main advantage of MARFA relative to FARF31 is that different retention models can be specified for different sub-units of the system, e.g. different models for hydraulic rock, hydraulic conductor (deformation zone), and hydraulic soil domains. Furthermore, also the engineered part of the system, i.e. tunnels, can be assigned retention. Finally, the flow magnitude, but not direction, can be changed along the pathlines. This provides an opportunity to address, in at least an approximate sense, e.g. glacial conditions where flow may be almost stagnant during ice cover, but very high when the ice front passes above the repository.

Immobilisation processes, known to occur in the field, are not readily quantified and not included in the codes. However, in the **Radionuclide transport report**, these processes are evaluated through screening calculations, and their implications on the safety assessment discussed in detail. The exclusion of these processes in the radionuclide transport codes is judged cautious in terms of resulting doses for most relevant situations, with the possible exception of the case in which there is precipitation with subsequent dissolution due to e.g. changed chemical conditions (RETROCK 2005). Radionuclides that exhibit sensitivity to redox conditions are most strongly influenced by such processes on account of the fact that they can undergo transition from being essentially immobile to being in a highly mobile state over very short distances in proximity to a redox front. Situations where this might compromise the safety function of the repository, however, are considered to be unlikely on account of the uncharacteristic configuration of redox boundary conditions that such an accumulation and remobilisation process would require.

A limitation with the flow path concept used in FARF31 is that only steady-state velocity fields can be addressed (adopting the snapshots in time approach for transport modelling), whereas the flow field is expected to evolve in time due to shoreline displacement. In MARFA, changes in flow magnitude can be handled.

Colloid-facilitated transport is not included in FARF31. For rapid reversible sorption/desorption onto colloids, an expression is derived which modifies the MARFA input parameters which quantify radionuclide retention in the host rock matrix. In principle, the same modification could be done in FARF31, but colloid-facilitated transport is chosen to be handled in MARFA since this case is combined with changes in flow conditions.

13.4.3 Biosphere representation

The biosphere is mainly represented by multiplying the radionuclide releases from the near-field or from the geosphere by an appropriate *Landscape dose conversion factor*, i.e. the LDF, derived as explained in Section 13.2.3.

The so obtained doses, or, in the case of the near-field, dose equivalent releases, are the main calculation end-points in the consequence calculations presented in this chapter. The conversion to dose is done to obtain a convenient measure of the impact of the releases, where also a total measure is obtained as the summed dose.

In some release situations, a pulse is rapidly released to the biosphere, and the LDF that is derived for a steady state release, is not a suitable conversion factor. In such cases LDF pulse values described in Section 13.2.4 are applied.

In a few cases of relatively early releases, the LDFs would represent an overestimation of the dose consequences, again since a steady state release situation is far from established. In some of these cases, time dependent releases are transferred to the same biosphere model as used for the derivation of LDFs and a time dependent dose, taking into account both the temporal variation of the release and the development of the landscape, is obtained, see Section 13.2.3.

There are also a few cases, calculated for illustrative purposes, where a large number of canisters are assumed to fail. In such cases, LDF values calculated for a release spread over the biosphere objects in the landscape according to the distribution of release locations over time during the modelled interglacial period are applied, rather than the basic LDFs where the landscape object yielding the highest dose is pessimistically used to represent the biosphere, see Section 13.2.3.

13.4.4 Simplified analytical models

Analytical simplified versions of the near- and far-field transport models have been developed (Hedin 2002b). These models use the same input data as the corresponding numerical models and doses are calculated using the same LDF values as in the numerical approach. The models may be executed probabilistically and yield results in good agreement with the deterministic and probabilistic calculation cases in the SR 97 assessment (Hedin 2002b, SKB 2004a). In the SR-Can assessment they were shown to be in good agreement for the corrosion scenario, for the shear load scenario and for releases from

a pinhole failure of the canister (SKB 2006a). A single realisation with the analytical models executes in around 0.1 second on a single CPU kernel. The corresponding calculation time for the numerical models is of the order of 10 seconds. Both models are well suited for probabilistic calculations, the numerical models in particular when they are executed on multiple kernels.

The analytical models have been benchmarked against the numerical models for several calculation cases in this chapter. The roles of the analytical models are to i) quickly and preliminarily evaluate calculation cases to be used in the planning of the transport calculations, ii) serve as one of several quality assurance measures of the numerical calculations by identifying potential differences in results obtained with the analytical and numerical models and seeking explanations for these (are they due to modelling errors or to differences in the nature of the models?), and iii) demonstrating an understanding of the nature of the models facilitated by the simple nature of the analytic models.

The analytical models have not been quality assured according to the procedures used for the numerical models for radionuclide transport, since they are not a formally approved tool for transport calculations in SR-Site or in the PSAR.

These models are applied in parallel to the numerical models to key variants of the corrosion scenario, Section 13.5.10, and the shear load scenario, Section 13.6.5.

13.4.5 Selection of radionuclides

The selection of radionuclides is based on radiotoxicity, inventory, half-life and shared solubility. The selection is further described in the **Radionuclide transport report**. Some of the selected, short-lived nuclides were omitted in cases where they would have decayed to insignificance at the time of the start of the calculation (see the **Radionuclide transport report**).

The following fission and activation products were selected: Ag-108m, C-14, Cd-113m, Cl-36, Cs-135, Cs-137, Eu-152, H-3, Ho-166m, I-129, Mo-93, Nb-93m, Nb-94, Ni-59, Ni-63, Pd-107, Se-79, Sm-151, Sn-121m, Sn-126, Sr-90, Tc-99 and Zr-93.

The following decay chain nuclides (ordered by chain) were selected: Pu-240, U-236, Th-232, Cm-245, Am-241, Np-237, U-233, Th-229, Cm-246, Am-242m, Pu-242, Pu-238, U-238, U-234, Th-230, Ra-226, Rn-222, Po-210, Pb-210, Am-243, Pu-239, U-235, Pa-231 and Ac-227. Here, Rn-222 and Po-210 have been added since the SR-Site assessment. Some nuclides with short half-lives in comparison to their progeny were only included by adding their initial inventory to that of their progeny. This applies to e.g. Cm-244, Pu-241, Cm-243 and Pa-233.

13.5 Canister failure due to corrosion

13.5.1 Introduction

As reported in Section 12.6, in the ‘canister failure due to corrosion’ scenario (called briefly the corrosion scenario below) canisters fail as a result of enhanced corrosion due to advective conditions in the deposition hole following the loss of buffer through erosion.

For this failure mode, both the canister and the buffer are bypassed, and the rock retention is small since substantial copper corrosion after buffer erosion only occurs in deposition holes with high flow rates, which are in general associated with flow paths to the surface of low geosphere retention.

Six variants yielding varying extents of corrosion failures were identified in the corrosion scenario, see Figure 12-19 in Section 12.6.4, for which radionuclide transport and dose calculations are reported in the following. A *central corrosion variant* was identified as the one on which assessments of radionuclide transport and dose should primarily be made.

In the following, the conceptualisation of the transport conditions including the handling of pulse releases for the instantaneously released fraction of the inventory is accounted for in Section 13.5.2 and input data for these *base case transport assumptions* are given in Section 13.5.3. Data from the central corrosion variant from the corrosion analysis are used with the base case transport data yielding a *central corrosion case* that is analysed in Section 13.5.4.

In Section 13.5.5, reasons to consider alternative transport data are examined. This analysis corresponds to the analysis of containment conditions in Section 12.6.2. Section 13.5.6 presents calculations of alternative cases, both as concerns transport assumptions and data, including findings in Section 13.5.5, and alternative corrosion variants identified in Section 12.6.2. Some cases in Section 13.5.6 are analysed with the MARFA code.

Results of calculations of doses to non-human biota for the central corrosion case are given in Section 13.5.7. Alternative safety indicators for the central corrosion case are given in Section 13.5.8. Section 13.5.9 gives a summary of the results for the corrosion scenario.

13.5.2 Conceptualisation of transport conditions

Evolution of the canister after canister failure

According to the analysis of copper corrosion for advective conditions, Section 10.4.9, a band, 0.35 m high and covering half the circumference of the canister, is assumed to be evenly corroded. This means that when penetration occurs, a large amount of damage must be assumed in the copper shell.

The time required to penetrate the cast iron insert is pessimistically neglected since it is difficult to estimate a reasonable development for this process for this failure mode. Also, because penetration of the copper shell in general occurs after several hundred thousand years for the few canisters exposed to the highest corrosion rates, the additional time to penetrate the cast iron insert is of less importance.

Once the copper canister and the cast iron insert have failed, the void in the insert is assumed to be rapidly filled with water due to the high flow rate and the lack of transport resistances in the absence of the buffer and with a large amount of damage also to the cast iron insert.

Radionuclide release

Advective conditions in the buffer must be assumed also for the consequence calculations for the corrosion scenario. There is no buffer hindering the outward transport of radionuclides meaning that this is controlled by the flow through the deposition hole, q . The following three contributions to the outward transport can be distinguished.

- The instantaneously accessible fraction of radionuclides, IRF, that is assumed to be rapidly dissolved in the water void volume and subsequently flushed out of the canister. This gives rise to a pulse of uncertain duration, the uncertainty stemming from e.g. uncertainties in the detailed development of the canister failure through which the IRF is made accessible.
- A contribution from the corrosion of metal parts in the fuel assemblies and the congruent release of radionuclides embedded in the metal parts. These inventories are collectively called the corrosion release fraction, abbreviated CRF.
- A contribution from fuel dissolution and the congruent release of radionuclides embedded in the fuel matrix.

In a case where the buffer is severely eroded, a colloid filter (buffer function indicator Buff7) cannot be guaranteed. This means that the use of elemental solubilities as a limit for radionuclide release could be questioned, since it cannot be excluded that the solid particles formed by various radionuclides reaching saturation would leave the canister and migrate further. In this case, however, this is of minor concern, since the flow through the deposition hole is often too high for solid phases to precipitate (with the exception of uranium). This is demonstrated in Section 13.5.6 by analysing a case where solubility limits are included.

The release into the fracture is thus controlled by the corrosion rate and the fuel dissolution rate, with two exceptions:

1. For uranium, a concentration limit is still an effective constraint on release, due to the large amount of U-238 present in the fuel. This limits the near-field releases of uranium isotopes, but also leads to increased near-field releases of Th-230, Th-229 and Pa-231 generated by the re-precipitated U-234, U-233 and U-235, respectively.

2. It cannot be excluded that co-precipitation processes and sorption/immobilisation in the remaining bentonite in the deposition hole could confine Th-230 to the near-field. If this is the case, its daughter nuclide, the considerably more mobile Ra-226, would be released. The so generated Ra-226 is assumed to be released to the flowing groundwater in the fracture intersecting the deposition hole. This causes higher releases of Ra-226, since there is a contribution not only directly from the fuel dissolution, but also from the confined Th-230. Since Ra-226 is often the main contributor to dose, this also causes higher total doses. Sorption of Th in the near-field is thus assumed. The effect of disregarding Th sorption is analysed as a separate calculation case.

Furthermore, as the flow rate in the intersecting fracture is high, the retention of the rock is in general limited for these deposition holes.

Release of activation products

The inventory of activation products in the metal parts of the fuel assemblies has often been assigned to the instantaneously accessible fraction, since it has been considered unnecessary to develop a model for the metal parts as nuclides in these are dispersed by the buffer. However, in the corrosion scenario this assumption would lead to unrealistically high releases of e.g. Ni-59 and Nb-94. Therefore, corrosion of metal parts of the fuel assemblies is included in the near-field model, with corrosion rates given in the **Data report**. The geosphere transport and the release-to-dose conversion in the biosphere is done as for the bulk of the nuclides, i.e. with the far-field model FARF31 and using LDF values. The fraction of the inventory for which corrosion of metal parts determines the release rate is called the corrosion release fraction, CRF. The CRF is given in the **Data report**, in the same manner as other fractions of the inventory.

Release of instantaneous release fraction

The fraction of the inventory assumed to be instantaneously released from the fuel upon water contact is expected to be released to the geosphere in a matter of years in the corrosion scenario, since the flow rates at the deposition positions with the eroded buffer and failed canister are high, see further Table 13-4. Since these nuclides are in general non-sorbing and since the flow related retardation properties in the geosphere are poor for the flow paths associated with the deposition positions in question, they are generally released as pulses of durations of tens of years from the geosphere to the biosphere. In this case, the LDF values would yield overly pessimistic estimates of doses, as discussed in Section 13.2.3. Therefore, the LDF pulse values given in Table 13-2 are applied to the total IRF inventory in a canister at the time of canister failure for Cl-36, Ni-59, Se-79, Nb-94, Tc-99, Sn-126, I-129 and Cs-135. A number of nuclides with an IRF, and with half-lives up to 10000 years (e.g. Sr-90, Cs-137, C-14), were excluded from the analysis since they would decay to insignificance before a failure would occur in the corrosion scenario.

Note that it is also pessimistic to apply the pulse LDF approach even though some of the species in some realisations of a probabilistic transport calculation in the geosphere would result in releases to the biosphere of longer duration. This is because the maximum dose for a given mass released to the biosphere is obtained when the entire mass is released at once, noting that the LDF pulse values are by definition taken for the point in time in the landscape development where the consequences are maximal.

Note also that it is pessimistically assumed that the development of the canister failure is such that all the fuel rods become accessible simultaneously, i.e. a sudden breaching of the cladding for all fuel rods is assumed.

The handling of pulse releases assumes that if several canisters fail, no two canisters will affect the same biosphere object simultaneously. This is justified by the fact that on average less than one canister fails due to advection/corrosion and further since calculated failure times are spread over hundreds of thousands of years.

13.5.3 Input data to transport models

Input data to the transport models for the corrosion scenario are summarised in Table 13-3. All data in the table are qualified in the **Data report**, except the failure times that are obtained as output from the erosion/corrosion calculations reported in Section 12.6.2 and in detail in SKB (2010d). However, the input to those latter calculations is qualified in the **Data report**.

Table 13-3. Input data for the corrosion cases.

Entity	Nuclide/ Element specific	Data	Section in Data report
Number of failed canisters	–	As calculated with corrosion model, see Section 12.6.2.	–
Failure times	–	As calculated with corrosion model, see Section 12.6.2.	–
Radionuclide inventory	N	Mean inventory taken over all fuel types.	3.1
Instantaneous release fraction of inventory	N	Distributions according to the Data report .	3.2
Corrosion release fraction of inventory	N	Distributions according to the Data report .	3.2
Corrosion release rate	–	Log-triangular (10^{-4} /yr, 10^{-3} /yr, 10^{-2} /yr)	3.2
Fuel dissolution rate	–	Log-triangular (10^{-8} /yr, 10^{-7} /yr, 10^{-6} /yr)	3.3
Concentration limits	E	Calculated distribution based on distribution of several groundwater compositions*	3.4
Rock porosity	–	Constant = 0.0018	6.8
Rock diffusivities	–	Log-normal distributions; mean values: Cations: 6.6×10^{-7} m ² /yr Anions: 2.1×10^{-7} m ² /yr	6.8
Rock partitioning coefficients	E	Truncated log-normal distributions	6.8
Hydrogeological data related to flow and transport:	–	Correlated distributions from several DFN model calculations propagated from hydrogeological analyses:	6.7
• Darcy flux at deposition hole (U_0)		• Uncorrelated model; base case and 5 additional realisations	
• Rock transport resistance, F , for paths beginning at release point Q1		• Semi-correlated model; base case and 10 additional realisations	
• Rock advective travel time, t_w , for paths beginning at release point Q1		• Fully correlated model; base case and 5 additional realisations	
		Only deposition holes where failures occur are included.	
Rock Peclet number	–	Constant = 10	6.7
Max. penetration depth in rock matrix	–	Constant = 12.5 m	6.7
Biosphere LDF factors	N	Calculated LDF values, see Section 13.2.	7.2

* As noted above, concentration limits are not applied in the central corrosion case, with the exception of U. Concentration limits for U, and for other elements to be used in other calculation cases, are calculated probabilistically by using distributions of groundwater compositions for either temperate, permafrost, glacial or submerged conditions and combining the calculated distributions into the one distribution used in the transport calculation. See further the **Radionuclide transport report**, where also sensitivities to different groundwater types, thermodynamic data etc are analysed.

Hydrogeological data related to flow and transport

Hydrogeological data, obtained from the modelling described in Section 10.3.6 are used. As described in Section 10.3.6, three fracture size/transmissivity correlation functions are considered yielding three variants of the hydrogeological DFN model. Several realisations of each of these three variants are propagated to the corrosion scenario, see Table 13-3. In a probabilistic central corrosion case, data from all the ten additional realisations of the semi-correlated DFN model are used. In all calculations for this scenario, deposition positions are rejected according to the EFPC criterion (Section 5.2.2) in the output from the hydrogeological modelling.

It is only data for the few deposition holes for which canister failures due to corrosion occur that are used for this corrosion case. This means that all deposition holes of relevance experience a high flow rate and in general also a low geosphere transport resistance, since these properties are strongly correlated.

Data for the four deposition holes of relevance for the base case realisation of the semi-correlated DFN model are given as an example in Table 13-4. The advective flow through the deposition hole, q , is obtained from the hydrogeological calculations and multiplied by a factor of two to account for the locally increased flow due to the void from the eroded buffer.

Table 13-4. Data for the four deposition holes where canisters fail due to advection/corrosion for the base case realisation of the semi-correlated DFN model. The ten additional realisations are used in the calculations below.

Time of failure (yr)	Rock transport resistance, F (yr/m)	Advective travel time, t_w (yr)	Advective flow through deposition hole q (m^3/yr)
189442	471800	122.6	0.144
193813	149800	27.54	0.166
251412	11970	23.14	0.084
771947	35890000	1968	0.026

It is noted that the calculated hydraulic and transport properties of these deposition holes are from the extreme tails of distributions derived from a complex hydrogeological model with stochastic components (the generated fracture network). All ten realisations of the semi-correlated model variant are used in order to obtain more reliable representations of these tails. (For the uncorrelated and fully correlated DFN model variants, for which consequences are analysed in Section 13.5.6, all five available realisations are used.)

Figure 13-14 is a graphical representation of failure time versus F -value for the deposition positions where failures occur in three of the cases propagated from the analysis of containment potential for the corrosion scenario. The figure shows results obtained with the base case realisations of the semi-correlated, uncorrelated and fully correlated hydrogeological DFN models, respectively.

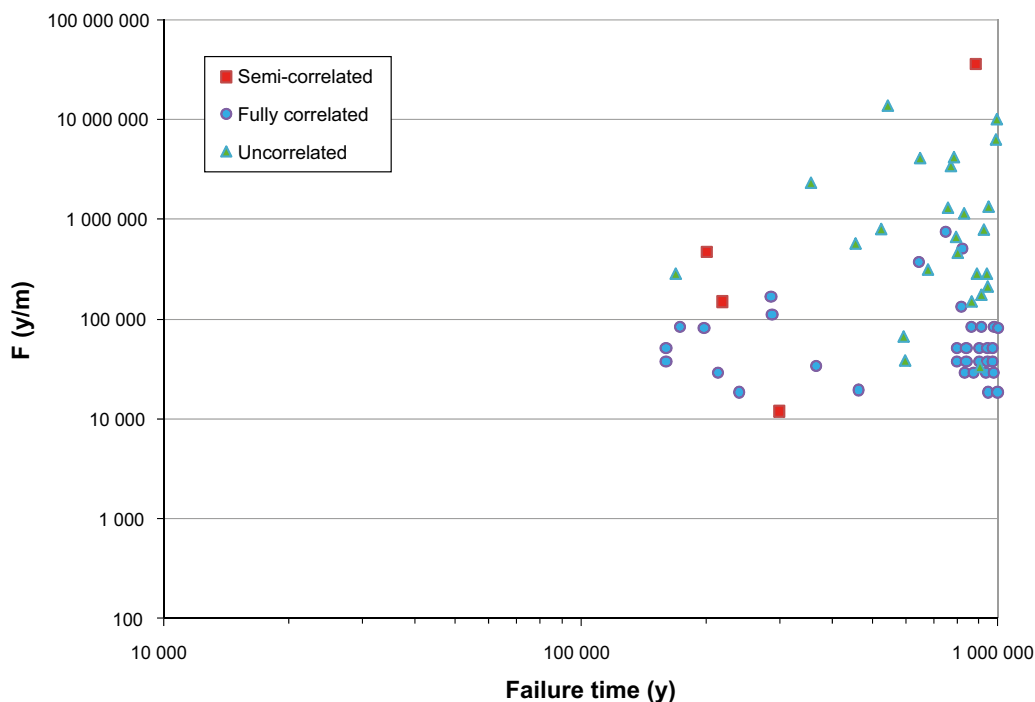


Figure 13-14. Graphical representation of pairs of failure times and F values for base case realisations of the semi-correlated, uncorrelated and fully correlated hydrogeological DFN models propagated from the analysis of containment potential for the corrosion scenario. (From the SR-Site assessment, SKB 2011, Figure 13-14.)

13.5.4 Calculation of the central corrosion case

Deterministic calculations

Figure 13-15 shows near-field releases converted to dose equivalent releases through multiplying the release rate by the LDF-value for each nuclide in a stylised, deterministic case where a canister is assumed to fail at 93 141 years after deposition (the earliest failure time of the analysed realisations). As mentioned in Section 13.4.3, the conversion to dose is done to obtain a convenient measure of the impact of the releases, where also a total measure is obtained as the summed dose. Advection occurs in the buffer void and the dose equivalent releases are primarily determined by the fuel dissolution rate set to 10^{-7} /yr. The contributions from the instantaneously released fraction of nuclides, IRF, are not included in the figure, since it is more convenient to show these separately.

The dose equivalent releases caused by releases from the near-field are dominated by Nb-94, Ni-59 and Ra-226. Most uranium released from the fuel is precipitated in the canister interior, since the concentration limit of uranium always applies because of the large amount of U-238 present, see Section 13.5.2. The precipitated uranium isotopes U-234, U-233 and U-235 generate the daughter nuclides Th-230, Th-229 and Pa-231, respectively.

The dose equivalent releases from the geosphere for the same calculation case are shown in Figure 13-16. The doses caused by releases from the far-field are dominated by Ra-226, Ni-59, Se-79, Rn-222 and Pb-210. It is noted that the peak dose appears at the end of the assessment period in Figure 13-16., indicating that the time of the peak dose is not strongly related to the time of the canister failure. This also indicates that a distribution of failure times will not cause risk dilution, an issue that is addressed further in Section 13.9.5.

The numerical calculation results have been compared to results obtained with analytical models and the agreement is good. This was expected since the situation to model is simple and the release rates straightforward to express analytically. See further Section 13.5.10.

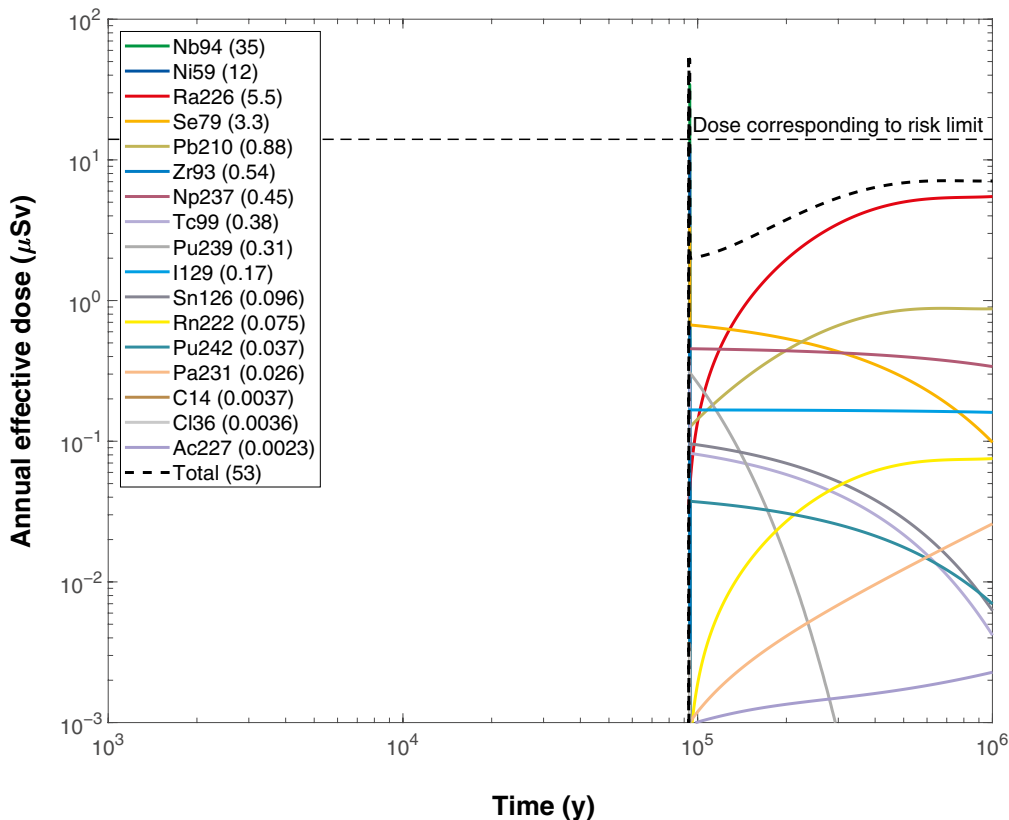


Figure 13-15. Near-field annual effective dose equivalent release for a deterministic calculation of the central corrosion case. The legends are sorted according to descending peak annual effective dose over one million years (given in brackets in µSv). The curves for Nb-94 and Ni-59 are hidden under the curve showing the total dose.

Table 13-5 shows peak annual doses from the pulse releases from the instantaneously released fraction, IRF, for the deterministic calculation. The IRF inventory at 100 000 years has been multiplied by the pulse LDF values given in Table 13-2.

It is noted that these doses are, for some nuclides, higher than the peak doses from the continuous releases in Figure 13-16.

Table 13-5. Peak annual dose from the pulse releases from the instantaneously released fraction, IRF.

Nuclide	Peak annual dose (μSv)	Nuclide	Peak annual dose (μSv)
Cl-36	0.12	Tc-99	7.6 ^{a)}
Ni-59	0.0081	Sn-126	0.032
Se-79	2.5	I-129	4.5
Nb-94	0.012	Cs-135	0.20

^{a)} This value applies to the near-field dose equivalent release only. The far-field pulse release is modelled with the far-field transport model since sorption in the geosphere is considerable for Tc-99. The pulse release of Tc-99 is thus included in the results shown in Figure 13-16.

Finally, Figure 13-17 shows how the time-dependent pulse release compares to the continuous release for the deterministic evaluation of the central corrosion case. This comparison was reported in Hedin and Kautsky (2015) and is based on SR-Site input data, that are similar to the corresponding PSAR data.

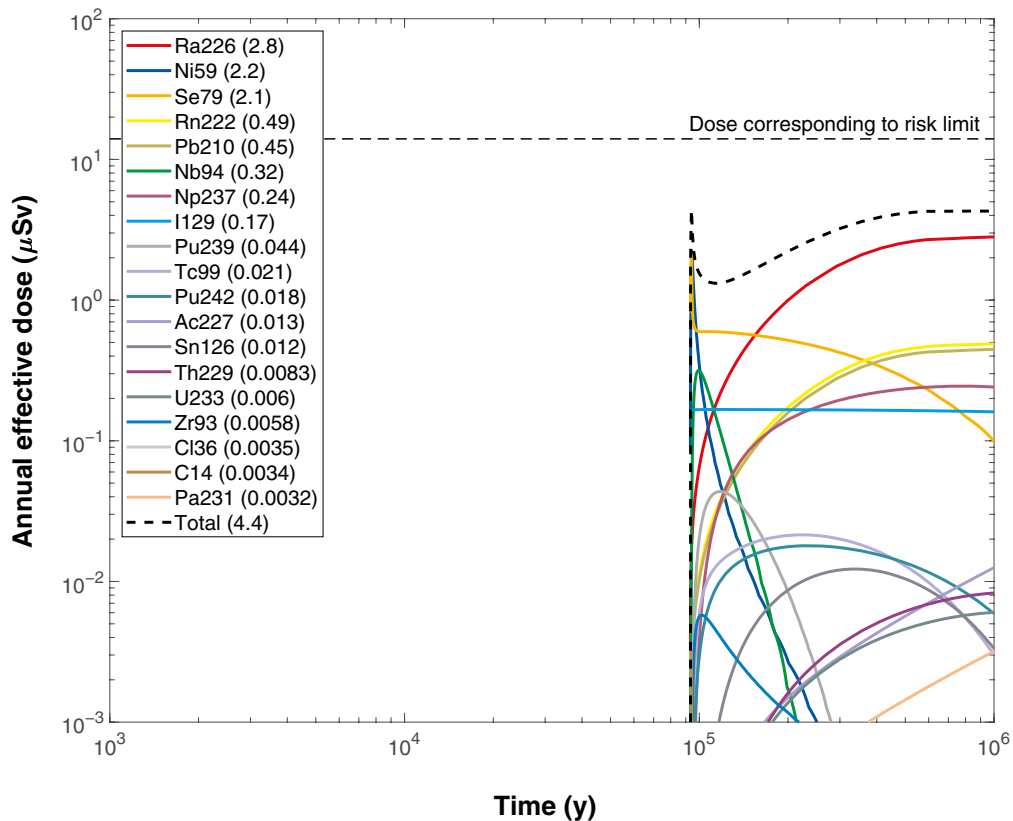


Figure 13-16. Far-field annual effective dose for a deterministic calculation of the central corrosion case. The legends are sorted according to descending peak annual effective dose over one million years (given in brackets in μSv).

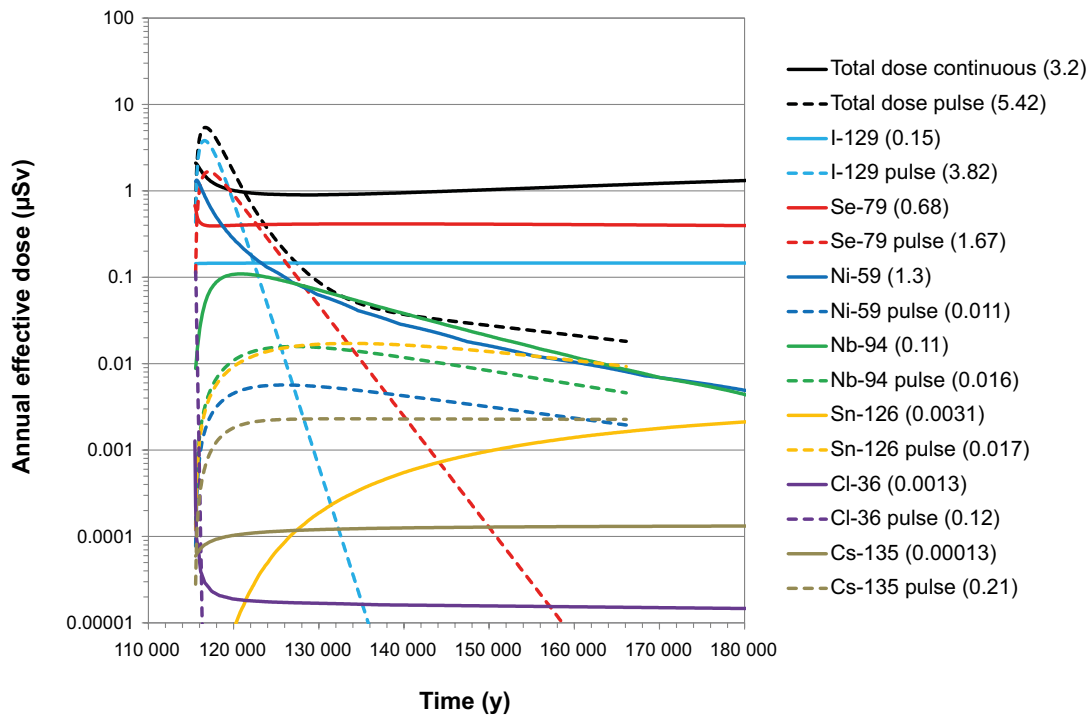


Figure 13-17. Annual effective dose for the deterministic calculation of the central corrosion case, showing the continuous releases (solid lines) and the pulse releases (dashed lines). Only nuclides with a pulse release are shown; the curve showing the total continuous dose does, however, include all nuclides contributing to the continuous release. The figures in brackets give the peak doses for each nuclide; for the continuous release for one million years and for the pulse releases for the 50 000 years during which these releases are calculated. The pulse release of Cl-36 is very short and is therefore not clearly visible in the figure.

Probabilistic calculation

Figure 13-18 shows near-field dose equivalent releases for a probabilistic calculation encompassing 2 250 realisations with input data distributions according to Table 13-3. Input distributions of failure times and geosphere transport data were obtained from the ten realisations of the semi-correlated DFN model, each yielding data for the ensemble of 6 000 canisters. Figure 13-19 shows the corresponding far-field releases. The first releases occur after around 93 000 years when the first canister fails. The average number of failed canisters in the probabilistic calculation of failure times is 0.094, see Section 12.6.2. This is reflected in the calculation results here.

The dose equivalent releases from the near-field and the dose after transport through the geosphere are both dominated by Ra-226. Much of the Ra-226 released from the near-field is transmitted through the geosphere since the failed canisters are located in deposition holes intersected by large, highly transmissive fractures with low retention. The release of Ra-226 from the geosphere is almost exclusively due to Ra released from the near-field and not to in-growth in the geosphere. This, in turn, is related to the fact that the parent nuclide Th-230 is assumed to be confined to the near-field.

The failure times are reflected as distinct features in the release curves, in particular for the near-field. The pulse like features are due to release controlled by corrosion of the metal parts of the fuel assemblies (e.g. Ni-59 and Nb-94). The corrosion times (ranging between 100 and 10 000 years, see Table 13-3) are such that the releases appear as pulses on the time scale of the dose curves.

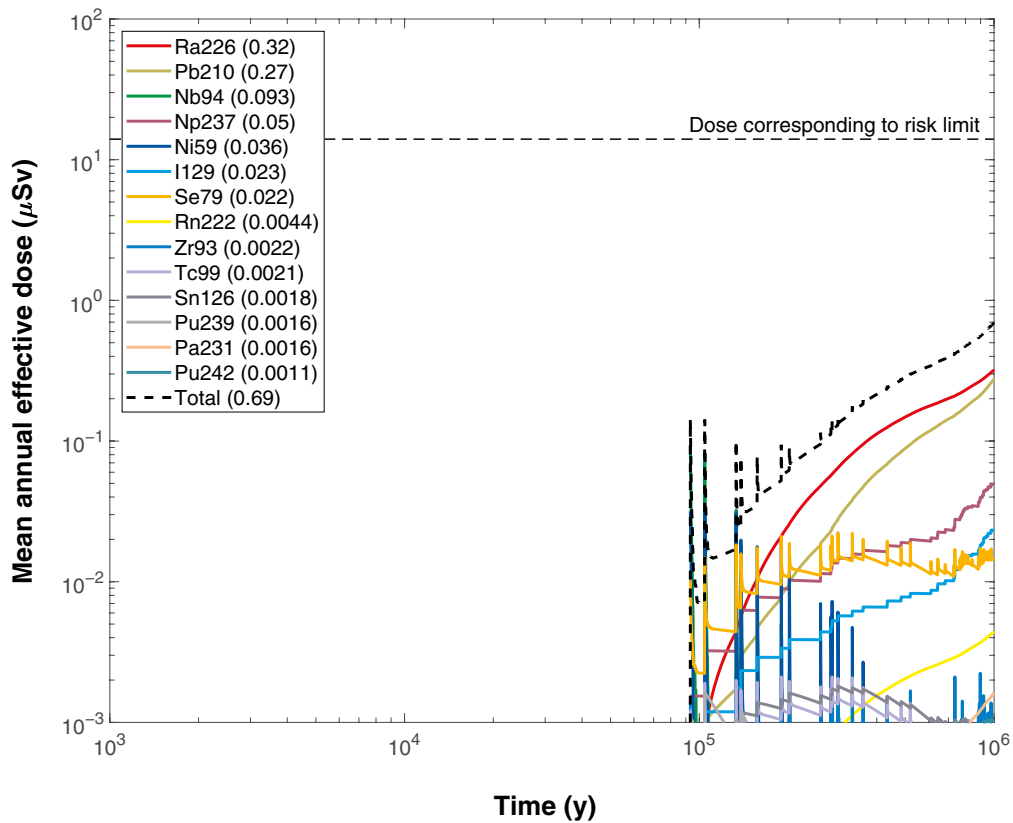


Figure 13-18. Near-field mean annual effective dose equivalent release for a probabilistic calculation of the central corrosion case. The average number of failed canisters is 0.094. The legends are sorted according to descending peak mean annual effective dose over one million years (given in brackets in μSv).

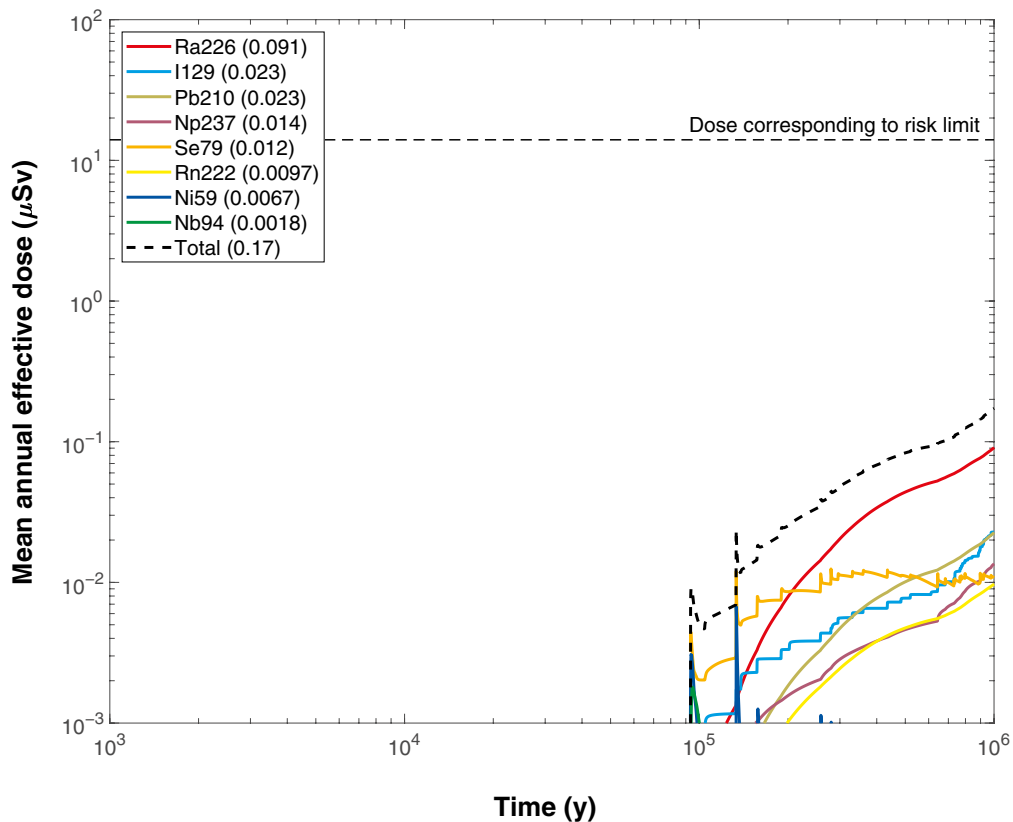


Figure 13-19. Far-field mean annual effective dose for the same case as in Figure 13-18. The legends are sorted according to descending peak mean annual effective dose over one million years (given in brackets in μSv).

Some statistics for the far-field release are shown in Figure 13-20. Note that these are derived only for the realisations of the failure times where failures actually occur in the corrosion calculations. Since the mean number of failed canisters is about 0.094, the most likely outcome of the corrosion calculations is zero failures. This is not reflected in the percentiles in Figure 13-20, other than for the mean value. Taking this into account would bring the 99th and 95th percentiles closer to the mean.

Contribution from the IRF pulse

The contribution from the IRF pulse in the probabilistically calculated mean dose is treated as follows. The probability of canister failure, p_{Fail} , is determined for each 100 000 year interval from the calculated distribution of canister failure times for the central corrosion case. The width of the dose curves in the biosphere is typically 1 000 years. The likelihood that an exposure due to a pulse release, p_{Expo} , is present at a given point in time during the 100 000 year interval is thus $10^{-2} \cdot p_{Fail}$. (The likelihood of overlaps between pulses is very small due to the low probabilities.) The total dose associated with a pulse release $D_{TotPulse}$ is determined at the start of each 100 000 year interval. The probabilistically calculated mean dose is then obtained as $D_{TotPulse} \cdot p_{Expo}$. The result of this procedure for the central corrosion case is shown in Table 13-6. The contents of Table 13-6 is taken from the SR-Site assessment, since all input data to the calculations are quite close to those in the PSAR and since all calculated dose contributions in the table are negligible compared to the dose corresponding to the risk criterion. As seen in the table, the highest mean dose is around $1.0 \times 10^{-3} \mu\text{Sv}$, i.e. more than four orders of magnitude below the dose corresponding to the risk limit. The pulse releases thus give negligible contributions to the probabilistically calculated mean dose. They do, however, need to be considered in the account of risk dilution. This is done in Section 13.9.5. It is also noted that this treatment assumes that temperate conditions are prevailing. Including probabilities of periglacial and glacial climate conditions would reduce the mean dose further.

For other calculation cases of the corrosion scenario, the pulse contribution to the mean dose is not calculated. All cases are, however, considered in the treatment of risk dilution, see Section 13.9.5.

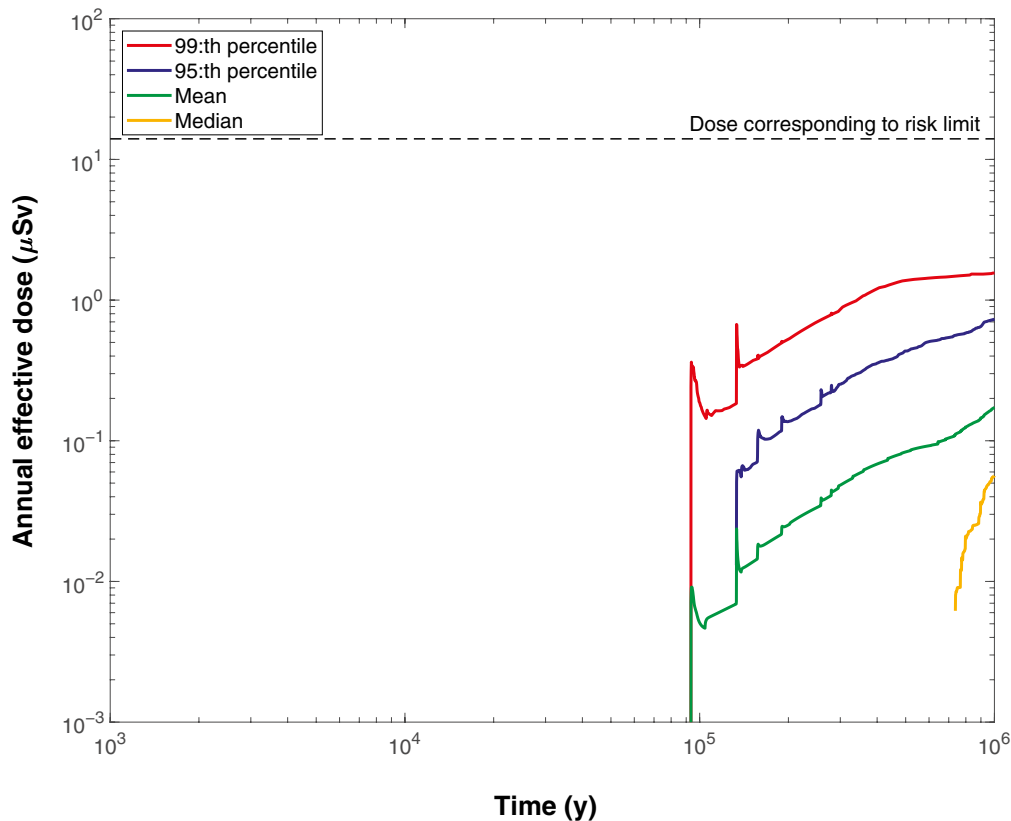


Figure 13-20. Far-field annual effective dose (mean, median, 95th and 99th percentiles) for the probabilistic calculation of the central corrosion case.

Table 13-6. Contribution from the pulse release for the probabilistically calculated mean dose for the central corrosion case. Results from the SR-Site assessment.

Time interval [yr]	P_{Fail}	P_{Expo}	$D_{TotPulse}$ [μSv]	Mean dose [μSv]
0–100 000	0	0	0	0
100 000–200 000	1.25×10^{-2}	1.25×10^{-4}	5.92	7.4×10^{-4}
200 000–300 000	4.17×10^{-3}	4.17×10^{-5}	5.54	2.3×10^{-4}
300 000–400 000	1.04×10^{-2}	1.04×10^{-4}	5.25	5.5×10^{-4}
400 000–500 000	8.33×10^{-3}	8.33×10^{-5}	5.01	4.2×10^{-4}
500 000–600 000	1.46×10^{-2}	1.46×10^{-4}	4.81	7.0×10^{-4}
600 000–700 000	1.46×10^{-2}	1.46×10^{-4}	4.64	6.8×10^{-4}
700 000–800 000	1.25×10^{-2}	1.25×10^{-4}	4.49	5.6×10^{-4}
800 000–900 000	2.29×10^{-2}	2.29×10^{-4}	4.37	1.0×10^{-3}
900 000–1 000 000	1.67×10^{-2}	1.67×10^{-4}	4.26	7.1×10^{-4}

13.5.5 Analysis of potential alternative transport conditions/data

The transport data used in the calculation of the probabilistic central corrosion case are those provided in the **Data report** and presented in Table 13-3. The data have been selected for certain conditions and, in the following, it is analysed i) whether the evolution in the corrosion scenario is compatible with these conditions and ii) whether any alternative evolutions of the system, that could imply less favourable transport conditions, need to be considered.

This analysis corresponds to the analysis of the possible routes to alternative containment conditions in Section 12.6, but is simplified based on the analyses already made in the derivation of data in the **Data report**.

Number of failed canisters and failure times

The number of failed canisters is an outcome of the analysis of the containment potential for the corrosion scenario, and has thus been exhaustively analysed in Section 12.6.2. This led to several corrosion variants for which consequences are analysed in Section 13.5.6.

Radionuclide inventory, IRF and CRF

It is not relevant to include these entities here since they are not affected by external factors, but by conditions determining the initial state. Uncertainties related to the initial state are fully explored in the **Data report**.

Fuel dissolution rate

Introduction

At the time when water enters a failed canister, fuel dissolution is expected to begin. Based on a review of the experimental data available at the time (Werme et al. 2004) suggested a constant fractional dissolution rate with a triangular probability density function in the \log_{10} -space with lower limit, best estimate, and upper limit of 10^{-8} , 10^{-7} , and 10^{-6} per year, respectively. The review of more recent experimental data discussed in the **Fuel and canister process report** and the **Data report**, Section 3.3, support these data and the mentioned distribution is qualified for use in the PSAR although support can be found for even lower values. The arguments for the suggested distribution presented in the **Fuel and canister process report** and the **Data report** are briefly summarised here, as an introduction to the subsequent discussion of its robustness under conditions that lead to the analysed failure scenarios.

For all fuel dissolution studies carried out in the presence of hydrogen or actively corroding iron, the levels of molecular oxidants in the solution or gas phase are below the detection limit and the same holds for oxidised states of all redox sensitive radionuclides. The release rates of non-redox sensitive fission products such as Cs and Sr decrease by more than two orders of magnitude during one year. The absence of oxidised species in the test solutions in spite of the relatively high radiation field of fresh

spent fuel shows that radiolytic oxidants have been consumed either by oxidising the fuel surface or by recombining with hydrogen to give water. Post leaching spectroscopic analysis of fuel surfaces shows no signs of surface oxidation (Ekeröth et al. 2020).

Experimental studies with UO_2 , doped with the alpha-emitters U-233 or Pu-238, have been carried out in the presence of low concentrations of dissolved hydrogen, sulphide ions or actively corroding iron. These experiments with alpha-doped $\text{UO}_2(\text{s})$ indicate clearly that the presence of a small amount of sulphide and strict anoxic conditions are sufficient to cancel any oxidising effect due to α -radiolysis from a few thousand year old fuel. In most tests with U-233-doped UO_2 (0, 5 and 10 %) under inert (N_2) and reducing ($\text{Fe}(\text{s})$) conditions, very low total uranium concentrations were measured, especially in the presence of an iron strip. Estimation of the matrix dissolution rate confirms previously measured low values.

An UO_2 pellet with a high doping level (385 MBq/g corresponding to 50 years old fuel) was also tested (Muzeau et al. 2009), and a very clear effect of α -radiolysis was observed under Ar atmosphere, with U concentrations increasing quickly with time in carbonate solutions. The same system, tested under 1 bar H_2 atmosphere, showed a slight decrease in U concentration. This suppressing effect of hydrogen, indicates that oxidative dissolution (corrosion) of fuel occurs at extremely low rates if at all in an environment similar to that expected in the failed canister.

The following is a summary of conditions for which the range of fuel dissolution rates given in the **Data report** is valid. For each condition, a brief discussion of whether it can be considered as fulfilled for the possible evolutions discussed in the PSAR is provided.

Redox conditions

*Range in which the fuel dissolution rate is valid according to the **Data report**:* In the corrosion scenario, canister failures occur after typically hundreds of thousands of years. In such time frames, the alpha radiation field of the spent fuel is expected to have decreased to such low levels that there will be no measurable effect of alpha radiolysis on fuel dissolution, see the **Fuel and canister process report**. After a canister failure, the hydrogen producing iron corrosion of the insert will continue for tens of thousands of years. As long as there is corroding iron, both hydrogen and Fe^{2+} concentrations will be sufficient to assure reducing conditions. If the groundwaters penetrating the failed canister contain sulphate, microbial sulphate reduction might result in the precipitation of iron sulphide. In the longer perspective, the Fe^{2+} concentrations and the redox potential of groundwaters inside the canister will be determined by equilibrium with magnetite or possibly iron sulphides, while hydrogen concentrations may decrease to those produced by water radiolysis when all metallic iron has corroded.

Hydrogen concentrations inside the canister from corrosion of the cast iron insert has been evaluated by Sellin and Hedin (2013). Calculations of hydrogen concentrations were done for the two canister failure cases in SR-Site: shear and erosion/corrosion. For the canister shear case, it is assumed that generated hydrogen gas can escape by diffusion and the equilibrium concentration inside the damaged canister will be $\sim 2.2 \times 10^{-3} \text{ m}^3 (\text{STP})/\text{m}^3$ ($\sim 10^{-4} \text{ M}$). Transport resistances offered by the damaged copper shell and the rock have been pessimistically neglected. For the case of erosion/corrosion there will be no diffusion barrier and the dissolved hydrogen gas from corrosion will be transported away with the flowing groundwater. With the assumption of a flow of 100 L/year, estimated from Table 13-4, Section 13.5.4 in SKB (2011), is the equilibrium concentration of hydrogen inside the canister is $\sim 1.7 \times 10^{-4} \text{ M}$.

If the reducing conditions in the flowing groundwaters are disturbed by penetration to repository depth of oxidising glacial melt waters, the fuel may dissolve at higher rates. However, the reducing capacity of the canister components needs to be considered since a continuous supply of oxidants is needed to support a higher dissolution rate. About 4×10^{-3} moles of oxygen/year are needed to support a fuel corrosion rate of 10^{-6} /year (neglecting any consumption of oxygen by interaction with magnetite, sulphides or copper). This means that both the redox potential of the groundwater and the mass-balance of oxygen need to be considered. Under oxidising conditions with P_{O_2} up to 0.2 bar, that is, air saturation, the long-term rates measured at the pH interval 7 to 9 (Forsyth and Werme 1992, Forsyth 1997) may be used, and the spent fuel dissolution rate is then in the interval 10^{-4} to 10^{-5} /year. All other environmental parameters (temperature, pH etc) affect in various degrees the dissolution rate under oxic conditions, but they are discussed below only for reducing conditions because limiting rates have been defined for oxidising conditions, as set out above.

Ranges in evolution cases studied: The possibility of oxidising conditions has been extensively studied, since it also would affect canister corrosion negatively, see in particular Section 12.6.2. The conclusion was that oxidising conditions can be ruled out.

Need for assessments of additional evolutions: The analysis of a glacial episode in Section 12.6.2 shows that the penetration of oxygen rich glacial melt waters is a low probability event that is deemed to be possible only if a set of extreme assumptions are made. However, even if these extreme assumptions were to be assumed, and oxygen postulated to reach a breached canister, the large reducing capacity of the remains of the failed copper canister and of the iron insert, would imply that anoxic conditions would prevail inside the canister. Even if the mass transfer of oxygen to the canister were to be higher than 4×10^{-3} moles/year, it is unreasonable that all the oxygen would react with the fuel. The remaining copper and the iron/iron corrosion products would act as a sink and consequently no additional evolutions need to be assessed.

pH

Range in which the fuel dissolution rate is valid according to the **Data report:** $4 < \text{pH} < 11$.

Ranges in evolution cases studied: The possibility of high pH conditions has been extensively studied in the buffer alteration scenario, since it also would affect the buffer negatively, see Section 12.4. There, it is concluded that pH values above 11 can be excluded. The possibility of low pH conditions has been studied in the corrosion scenario, since it also could affect canister corrosion negatively in combination with high chloride concentrations, see Section 12.6. There, it is concluded that pH values below 6.3 can be excluded.

Need for studies of additional evolutions to rule out unfavourable pH conditions: None, since exhaustive such studies have already been performed.

Temperature

Range in which the fuel dissolution rate is valid according to the **Data report:** < 70 °C.

Ranges in evolution cases studied: Elevated temperatures only occur early in the repository evolution, see Section 10.3.4, whereas canister failures in the corrosion scenario occur after typically hundreds of thousands of years. In such time frames, the fuel temperature is close to the background temperature of the host rock, i.e. well below 70 °C.

Need for studies of additional evolutions to rule out unfavourable temperature conditions: None according to the above.

Ionic strength

Range in which the fuel dissolution rate is valid according to the Data report: Up to 1 M ionic strength and there is no indication for increased fuel dissolution rates even at higher ionic strengths.

Ranges in evolution cases studied: The ionic strengths of groundwaters expected during the whole period of repository evolution are lower than 0.5 M.

Need for analyses of additional evolutions to rule out unfavourable ionic strengths: The groundwater data at Forsmark indicate that the salinity has been stable during the Weichselian, and large oscillations in groundwater salinities are therefore not expected in the future. The analysis of different possible climatic episodes presented in Sections 10.4.6 and 10.4.7 shows that salinity can increase due to upconing during the short glacial transit above the repository area. The analyses reported in Sections 10.4.6 and 10.4.7 show that the upconing effect is moderate and the resulting ionic strengths in the repository volume are below 0.5 M. Because the most pronounced upconing takes place during an ice advance, where the ice profile is steepest, the analysis of the reference evolution includes the highest salinities that can be expected at Forsmark, and no additional analyses are required.

Chemical influence of major and minor groundwater components

Range in which the fuel dissolution rate is valid according to the Data report: $\text{HCO}_3^- < 0.01 \text{ M}$. Bicarbonate is an important major component due to the effect of carbonate complexation with uranium. The fuel dissolution rate is valid for relevant carbonate concentrations such as those studied in the laboratory and expected in the repository. Groundwater carbonate concentrations in Forsmark will stay below 0.008 M for the full assessment period (SR-Site Data report table 6-10) and no scenario is expected where the fuel dissolution rate would be invalidated due to high bicarbonate content. Concerning minor components, bromide ions may influence the beneficial effect of molecular hydrogen in homogeneous radiolysis. This effect is based on its reaction with the OH-radical, which converts the very oxidising radical ($\text{OH}\cdot$) to water and a very reducing radical ($\text{H}\cdot$). Bromide ions are strong reductants and react ~ 250 times faster with the OH-radical than the H_2 molecule. It is said that bromide scavenges the OH-radical, thus decreasing the beneficial effect of hydrogen on homogeneous water radiolysis. The radical-rich beta and gamma radiations are expected to have decayed to negligible levels at the time of canister failure in the corrosion scenario. This together with the absence of very saline waters during repository evolution and the very low alpha activity makes any influence of bromide on fuel dissolution very improbable. This conclusion is supported by the results of Ollila et al. presented in the final REDUPP report (Evins et al. 2014, pp 39–53).

Ranges in evolution cases studied: The carbonate concentrations during the whole repository evolution are expected to be below 0.01 M.

Need for analyses of additional evolutions to rule out unfavourable conditions: The total concentration of inorganic carbon, which at pH values close to neutral is close to the concentration of HCO_3^- , is highest in the upper parts of the rock where recharge of meteoric waters dominates, because several biological processes produce CO_2 in the soil. In deep saline waters, rich in Ca^{2+} , the concentration of carbonate is kept low because of equilibrium with calcite. Typical carbonate concentrations for waters at Forsmark are illustrated in Figure 10-46. Thus, the only process that can increase bicarbonate concentrations in groundwaters is the enhanced infiltration of fresh meteoric waters. The data at Forsmark shows that the waters having a large influence of meteoric recharge all have carbonate concentrations around or below 0.01 M, and it is therefore concluded that there is no need to analyse the fuel dissolution rate for higher total carbonate concentrations.

Additional factor identified: Transport of uranium with clay colloids in the groundwater

When the buffer is partially or completely eroded, a cavity filled with a slurry (gel/sol) of water containing colloidal clay particles may exist in the deposition hole. Should the canister be breached under such circumstances, the clay particles are not expected to affect the oxidative fuel dissolution rate. Dissolved U(IV) would, however, be expected to sorb strongly to the clay particles. This sorption increases the amount of U(IV) released into solution from the re-precipitated $\text{UO}_2(\text{s})$ or the fuel matrix. In this case, the amount of U(IV) sorbed on clay particles may be calculated as the K_d value for U(IV) on clay particles multiplied by the U(IV) concentration in solution, determined by $\text{UO}_2(\text{s})$ solubility. The U(IV) release rate from $\text{UO}_2(\text{s})$ is then not limited by only the U(IV) solubility limit in the canister void, but also by the removal of [U(IV)] from solution due to sorption. To calculate this enhanced U release, the values for $\text{UO}_2(\text{s})$ solubility and K_d for U(IV) on clay particles are taken from the **Data report**. Using the solubility limit of U in this case is pessimistic, since it is likely that the U concentration is lower (Grambow et al. 2014). The rate at which the clay particles with sorbed uranium are carried away are set by the concentration of clay particles and water flow rate. These depend on the scenario analysed.

Need for studies of additional evolutions to rule out unfavourable conditions: Fuel dissolution in the presence of a clay slurry needs to be considered. This is done as described below. The eroded void volume of the deposition hole is assumed to be filled with clay particles that enhance the dissolution rate of the UO_2 fuel matrix. The outward transport rate of U, R_U (mole/yr), is then obtained as

$$R_U = C_{\text{Sol}}U \cdot q \cdot (1 + C_{\text{clay}} \cdot K_d)$$

where

$C_{\text{Sol}}U$ is the solubility of U(IV) (mole/m³),

q is the advective flow at the deposition hole (m³/yr),

C_{Clay} is the concentration of clay in the flowing fluid (kg/m^3),

K_d is the partitioning coefficient between solid phase and solution for U in a clay slurry (m^3/kg).

In Birgersson et al. (2009) the void ratio when the transport of bentonite is by colloid dispersion is determined to be 73, which corresponds to a dry density of $37.6 \text{ kg}/\text{m}^3$. This concentration will not be maintained in a large void in the deposition hole, since there will be a concentration gradient from the source of the colloids to the fuel. The location of the source could be remaining bentonite in the deposition hole, the backfill in the tunnel or through a fracture from another deposition hole/tunnel in the repository. Since it is impossible to determine the location of the source, and it may change with time, the value for C_{Clay} cannot be calculated. Instead a fixed value of $10 \text{ kg}/\text{m}^3$ is selected and judged to be a reasonable estimate of an upper bound of the mean value taken over the entire void volume.

Using $C_{\text{Clay}} = 10 \text{ kg}/\text{m}^3$ and distributions of K_d , $C_{\text{Sol}}U$ and q for the central corrosion case, the contribution from U transport on clay particles to the fuel dissolution rate is calculated probabilistically and compared to the probabilistically sampled ordinary fuel dissolution rate for the central corrosion case. The following also applies in the modelling.

- This process is only active during the relatively limited periods when the deposition position is exposed to dilute groundwater such that clay colloids can form. This is not taken into account in the calculation.
- Inflowing groundwater may have U concentrations exceeding $10^{-9} \text{ mol}/\text{L}$, but the influence of the occupation of sorption sites of clay particles by natural uranium present in the groundwater is pessimistically neglected.
- Should sorption to clay colloids be modelled as irreversible and assuming that all sorption sites were to be occupied by U, then a transport rate of the order of $2.5 \times 10^{-3} \text{ moles}/\text{yr}$ is calculated for a sorption site density of $2.0 \times 10^{-6} \text{ moles}/\text{g}$ (Bradbury and Baeyens 2005, cited in Ochs and Talerico 2004), $q = 100 \text{ L}/\text{yr}$, and $C_{\text{Clay}} = 10 \text{ g}/\text{L}$. This, in turn, corresponds to a fuel dissolution rate of approximately $3 \times 10^{-7}/\text{yr}$, i.e. slightly lower than the maximum value of the “ordinary” distribution. An upper limit on the transport rate determined by the product of the sorption site density, q , and C_{Clay} is imposed in the calculation of the distribution in Figure 13-20, curve B. (Irreversible sorption, as well as U occupancy of all available sites is, however, ruled out for the conditions in the deposition hole, based on the description of the sorption process in the **Buffer, backfill and closure process report.**)
- Although advective conditions are assumed to prevail in the deposition hole, there will be parts of the path between the inner parts of the, assumed damaged, fuel elements and the canister exterior where the transport is diffusion controlled. A certain continuous outward, clay assisted transport of UO_2 then requires a corresponding flux of UO_2 over the diffusion controlled path. The geometry for this transport is difficult to assess, but an upper bound can be estimated as follows: Assume a pessimistically high cross sectional area of 0.1 m^2 and a pessimistically low diffusion path length of 1 mm . Taking then the highest U solubility in the distribution used in SR-Site, i.e. $4.2 \times 10^{-4} \text{ mol}/\text{m}^3$, and assuming a U diffusivity in water (at $11 \text{ }^\circ\text{C}$) of $0.01 \text{ m}^2/\text{yr}$, one obtains a maximum U flux of $4.2 \times 10^{-4} \text{ mol}/\text{yr}$, assuming a zero concentration 1 mm away from the fuel. With $8400 \text{ mol U}/\text{canister}$ this corresponds to a fractional dissolution rate of approximately $5 \times 10^{-8}/\text{yr}$. This pessimistic bound suggests that the effect of U transport with clay particles is negligible in the radionuclide transport calculations. A bound using these diffusion data in combination with the distribution of U solubility is imposed in curve A in Figure 13-21.

As seen in Figure 13-21, the clay assisted fuel dissolution rate (curve B) is considerably lower than the “ordinary” dissolution rate (curve C) up to the 90th percentile of the distribution, whereas it is comparable or slightly higher above the 90th percentile. If also the pessimistic diffusion limitation is imposed (curve A), the clay assisted dissolution rate is well below the “ordinary” dissolution rate over the entire range. Inside a failed canister, corrosion of the iron insert and metal parts of the fuel will in ca 10 kyr fill the space inside the canister (Agrenius and Spahiu 2016). Therefore, it is quite clear that diffusion will play a significant role in the transport of U from the fuel to the site where U is transported away by advective flow. This indicates that the contribution from the clay assisted transport can be expected to be less than the pessimistic case described above. Therefore, it is concluded that the contribution to fuel dissolution from U transport with colloids is negligible.

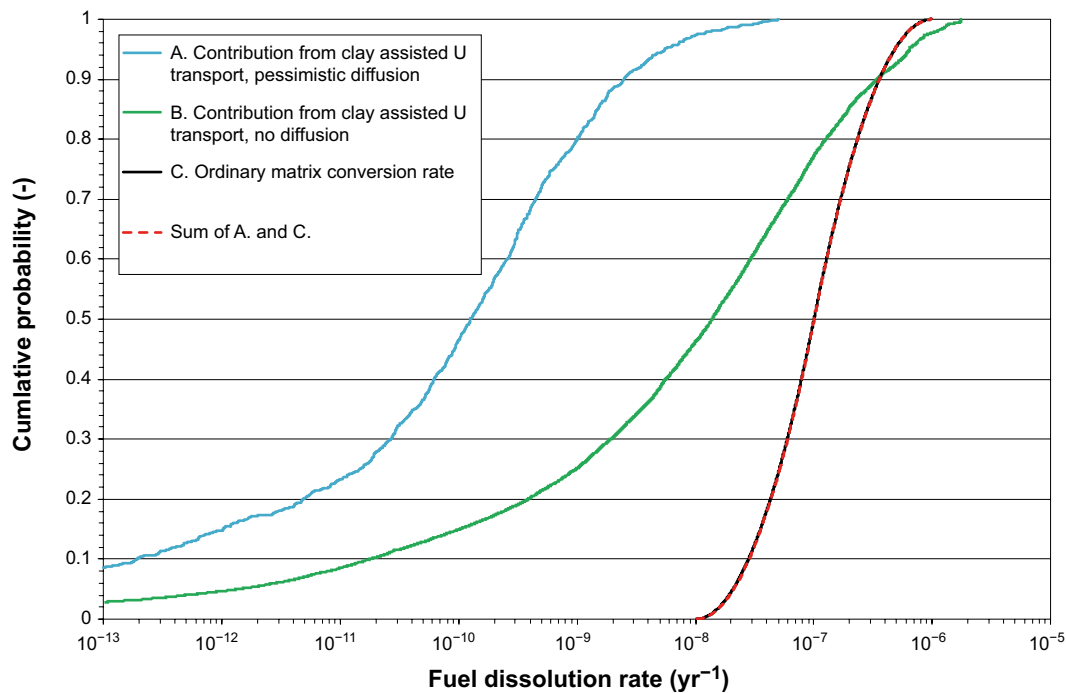


Figure 13-21. Cumulative distributions of fuel dissolution rate. The contribution from clay assisted U transport has a negligible impact on the distribution for the ordinary matrix dissolution rate.

Intrinsic conditions

The following intrinsic conditions/processes have been considered in the **Fuel and canister process report** which provided the bases for the derivation of fuel dissolution data in the **Data report**: Alpha self-irradiation, enhanced diffusion (ASIED), helium build-up and the influence of high burn-up.

Conclusion

Based on the above account, it is concluded that the distribution of fuel dissolution rates given in the **Data report** is valid for all evolutions that need to be considered in the PSAR, even for groundwater conditions in which a clay slurry may contribute to the outward transport of uranium.

Metal corrosion rate

Range in which metal corrosion release rates are valid: The release rates of the activation products from the metallic parts given in the **Data report** are based on a range of corrosion rates for stainless steel under anoxic conditions. These corrosion rates were estimated from a number of relevant studies carried out at temperatures up to 140 °C and salinities up to anoxic sea water. Data concerning silver in the PWR control rods was experimentally obtained at room temperature in repository relevant conditions (anoxic atmosphere and synthetic simplified groundwater). The important parameters are thus salinity (especially chloride concentration) and redox conditions.

Ranges in evolution cases studied: In the corrosion scenario, canister failures occur after typically hundreds of thousands of years. In such time frames, the fuel temperature is close to the background temperature of the host rock, i.e. no increase of corrosion rates due to high temperatures is expected. The highest chloride concentrations expected during the whole repository evolution time are of the order 0.35 mol/L, i.e. much lower than in anoxic sea water. Hence the corrosion rates used in the **Data report** are valid (with a large margin) for the corrosion scenario.

Need for analyses of additional evolutions: The important parameters for the metal corrosion rate are the chloride concentrations and the redox conditions. As stated in the previous section about fuel dissolution, the analysis of the reference evolution includes the highest salinities that can be expected at Forsmark. The analysis of the redox conditions for the reference evolution shows a variability

of redox potentials, always with anoxic conditions. Only the penetration of oxygen rich glacial melt waters can possibly lead to a deviation, and as described in Section 10.4.7 this is a very low probability event that is deemed to be possible only if in addition a set of extreme assumptions are made. Even if extreme assumptions were to be made, and oxygen postulated to reach a breached canister, the large reducing capacity of the remains of the failed copper canister and of the iron insert, would imply that anoxic conditions would prevail inside the canister. It is therefore concluded that there are no additional evolutions that need to be assessed.

Rock porosity, rock diffusivities and rock sorption coefficients

Rock porosity and effective diffusivity

The rock porosity and effective diffusivity provided in the **Data report**, Section 6.8 are valid for all conditions in the host rock during repository evolution. The host rock conditions discussed in the **Data report** are groundwater composition, in situ temperature, and in situ stress. However, it is argued that the effective diffusivity and, especially, the porosity are relatively insensitive to host rock conditions.

Concerning the groundwater composition, which affects the porewater composition, the salinity may affect the degree of anion exclusion in the porous system. This is judged to have an insignificant effect on the porosity but a minor effect on the effective diffusivity. In the **Data report**, this is treated as data uncertainty, and the data provided should encompass not only reasonable groundwater compositions during repository evolution, but also a larger range of groundwaters seen in crystalline rock. Also, anions are transported through the geosphere virtually without retention in the corrosion scenario, i.e. it is not warranted to explore even less favourable cases of anion exclusion.

The in situ temperature affects the diffusivity in free solution, as described by well-known relations, and thus also the effective diffusivity. The data provided are valid for temperatures ranging from somewhat elevated temperatures, compared to present day conditions, to temperatures just above freezing. Within this temperature range, the variation in the effective diffusivity is small. To exemplify, the diffusivity at room temperature is about a factor of two larger than that at temperatures just above freezing. This is treated as data uncertainty in the **Data report**. Since temperatures below freezing are irrelevant and since temperatures above present day values are favourable, there is no reason to explore more extreme cases than those covered by the **Data report**.

The porosity provided in the **Data report** is based on laboratory measurements at atmospheric pressure. However, corrections are made so that the data given should represent in situ stress conditions. The provided effective diffusivity is based on measurements at, and should represent, in situ stress conditions. The in situ stress will change during the glacial cycle, primarily due to the extra load from an ice sheet during glaciation. However, this additional stress is judged to have a very minor effect on the porosity and minor effect on effective diffusivity, and is treated as data uncertainty in the **Data report**. Also, in the 'Canister failure due to isostatic load' scenario, Section 12.7, maximum ice thicknesses were found to be within the range covered by the input to the determination of porosity data in the **Data report**.

Finally, it is seen as unlikely that potential erosion products from the buffer would act as diffusion resistance at the fracture/rock interface, preventing radionuclides from entering the microporous system.

In summary, there is no need for additional studies, as the subject has been exhaustively studied and the data are provided in the **Data report**.

Pore connectivity

An entity closely related to the effective diffusivity is the pore connectivity. In the **Data report** the in situ pore connectivity is suggested to be unlimited on all scales relevant for safety assessment calculations (that is on the scale of at least several tens of metres). During glaciation, the microporous system could be affected by the additional in situ stress originating from the ice sheet. However, this effect is included in the data uncertainty assessment of the effective diffusivity, and even under glaciation unlimited pore connectivity is expected.

Also, for the transport conditions in the corrosion scenario, the pore connectivity would have to be reduced to the centimetre scale before affecting the geosphere retention in any significant way.

Sorption partitioning coefficient

The sorption partitioning coefficient, K_d , is for many radionuclides sensitive to conditions in the host rock. In the **Data report** the groundwater composition is singled out as the most important condition, while in situ temperature and stress are subordinate conditions with a minor or even very minor impact. For radionuclides sorbing by surface complexation, pH, the carbonate concentration and the concentrations of various other ligands that can directly compete to bind radionuclides at the expense of sorption, are of importance. For radionuclides sorbing by cation exchange, the concentrations of competing cations are of importance.

For many nuclides, the K_d value is sensitive to redox conditions, which are determined by the presence of redox controlling pairs such as $\text{Fe}^{2+}/\text{Fe}(\text{OH})_3$ or $\text{SO}_4^{2-}/\text{FeS}_{(\text{am})}$, and is also related to pH and dissolved carbonate concentration. The redox conditions of the host rock are discussed in Section 6.1 of the **Data report**.

In the case of nuclides sorbing by cation exchange, K_d values have been corrected to encompass the range of groundwater compositions projected during repository evolution. Input data for this correction have been modelled groundwater compositions at a great number of locations at the repository, delivered in Section 6.1 of the **Data report**. This has resulted in distributions of K_d values in which the lower tail of the distributions corresponds to unfavourable groundwater conditions. However, for nuclides sorbing by surface complexation, the complexity of the sorption mechanism has prevented making such detailed corrections. Here, based on expert judgment, compiled data have been sorted to be (fairly) representative for the Forsmark host rock, or not. Unrepresentative data have to the extent possible been discarded.

In summary, there are great uncertainties associated with K_d values, which are also reflected in the wide K_d ranges given in the **Data report**. As the lower tails of the distributions imply no geosphere retention for, in particular, the dose determining Ra-226 in the corrosion scenario, and as a wide range of conditions are covered by the data in the **Data report**, it is not deemed warranted to explore additional ranges of K_d values. In addition to the transport conditions for the central corrosion case, where the full range of K_d values for reducing conditions is used, also a case where rock K_d values for oxidising conditions are used when an ice sheet passes above the repository with flow rates also varying in accordance with the changing external conditions, is explored, see Section 13.5.6.

Hydrogeological data related to flow and transport

The hydrogeologic flow-related migration data are presented in the **Data report**, Section 6.7. The different data sets that are of relevance for the corrosion scenario are:

- Equivalent flow rate (Q_{eq}) and Darcy flux (U_0) for the Q1 release path.
- Flow-related transport resistance (F).
- Advective travel time (t_w).
- Peclet number (Pe).
- Maximum penetration depth in rock matrix (x_0).

Canister failures in the corrosion scenario occur when the buffer is lost in the deposition hole. Backfill material from tunnels will also be lost, but it is judged that this loss will be small relative to the total amount of backfilled material (Section 10.3.11) and hence not modify the flow conditions in the tunnels. However, flow in fractures intersecting deposition holes may be changed locally because of the modified properties of the fractures. Specifically, eroded buffer from the deposition holes may fill up the fracture void space and hence change the flow characteristics.

Equivalent flow rate and Darcy flux

If the eroded buffer remains within the fracture close to the deposition hole, it is likely that groundwater flow (and associated equivalent flow rate and Darcy flux) will be decreased. Also, the radionuclide release rate from the near-field is virtually independent of the flow rate for the transport conditions in the corrosion scenario. The flow rate is sufficiently high to carry away all radionuclides released from the spent fuel, and there is thus no need to consider higher flow rates from this point of view. Any reduction in flow rate due to remaining buffer in the fractures is pessimistically disregarded.

Flow-related transport resistance and advective travel time

The flow paths through the geosphere are not believed to be affected by the modified properties implied by the eroded buffer. Darcy flux at deposition hole locations is inversely correlated to flow-related transport resistance and advective travel time. Thus, if the eroded material implies a decrease in flow at deposition hole locations, the flow-related transport resistance and advective travel time will increase. Repository evolutions leading to increased flow rates were explored in the analysis of containment for the corrosion scenario, Section 12.6, leading to the conclusion that no additional cases need to be analysed with respect to corrosion, in which case essentially temperate flow rates were used. However, for the analysis of radionuclide transport, it is warranted to explore the effects of flow varying in accordance with the changing conditions during a glacial cycle. This is done as a variant case, see Section 13.5.6.

Peclet number and maximum penetration depth in rock matrix

The penetration depth of the rock matrix is not assessed to be affected by the presence of buffer material in the fractures, see also discussion on pore connectivity above. Also, the Peclet number is not assessed to be affected by the presence of some buffer material in the fracture network.

No other issues of concern related to the corrosion scenario have been identified. The data presented in the **Data report** are thus judged relevant for the corrosion scenario. Furthermore, no other repository evolutions compatible with the corrosion scenario have been identified that would imply less favourable flow and transport conditions.

Biosphere LDF factors

All climate conditions emerging from the analyses of the evolution of the system are covered by the different sets of LDFs available. LDFs for the interglacial period are used in the central corrosion case.

As concluded in Section 13.2.4, the highest doses from a constant release rate from the repository are expected under temperate conditions when humans are exposed to radionuclides that have accumulated in a wetland that has been converted to arable land, and when contaminated well water is utilised by human inhabitants and livestock. Hence, the LDFs for the interglacial period used in the calculations are maximum values during the reference glacial cycle. For the global warming climate case, LDFs were significantly (about an order of magnitude) larger than under the reference glacial cycle only for Cs-135 and U-238, see Figure 13-7. Since neither of these nuclides contributes significantly to the total annual dose in the corrosion scenario, there is no need to apply any LDFs other than those used in the central corrosion case to cover biosphere uncertainties.

Overall conclusion regarding additional cases to analyse

The analyses in this section demonstrate that i) the evolution in the corrosion scenario is compatible with conditions for which data in the **Data report** have been determined and ii) no alternative evolutions of the system that could imply less favourable transport conditions, need to be considered. However, a case with host rock conditions varying in accordance with the changing conditions during a glacial cycle needs to be explored.

13.5.6 Calculation of alternative cases

Overview of cases

Figure 13-22 gives an overview of calculation cases for the corrosion scenario. The three hydrogeological DFN models (blue) are combined with three erosion cases (red) yielding nine corrosion variants to consider in the derivation of calculation cases for radionuclide transport and dose. Of these, the three 'no advection' variants are not further treated as they do not lead to canister failures.

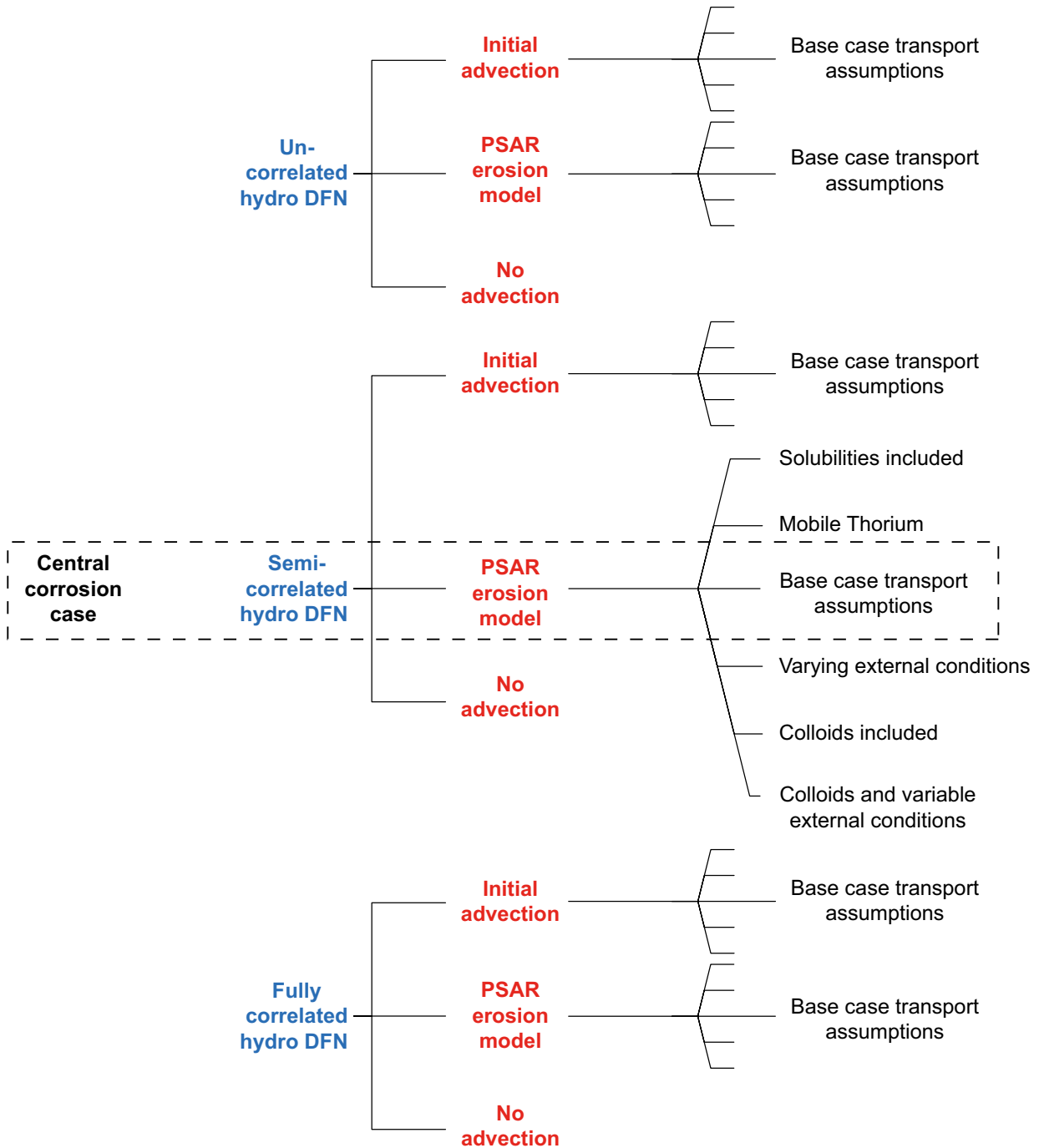


Figure 13-22. Overview of calculation cases for the corrosion scenario.

The central corrosion case consists of the semi-correlated hydrogeological DFN model, the PSAR erosion model and base case transport assumptions and data as presented above. Five cases of alternative transport conditions are analysed for the central corrosion variant:

- A case with solubilities included.
- A case in which Thorium is assumed to be mobile in the near-field.
- A case with varying climate conditions.
- A case with colloid facilitated transport in the geosphere.
- A case with varying climate conditions and colloids in the geosphere.

(The case mentioned in the fourth bullet point is shown only in the **Radionuclide transport report**.) The other four relevant corrosion variants are analysed for the base case transport conditions. Additional corrosion variants are reported in the **Radionuclide transport report**.

Mobile Thorium in the near-field

Figure 13-23 and Figure 13-24 show near-field dose equivalent releases and far-field doses, respectively, for the central corrosion case when disregarding sorption of Thorium in the near-field. Both doses caused by release of Ra-226 and the total dose are lower than in the central case, showing that the assumption of Thorium sorption in the near-field made in the central corrosion case is pessimistic. Note also that considerably less Ra-226 is released from the near-field compared to the central corrosion case (radiological impact 0.0021 versus 0.32 μSv), but that the far-field releases are more similar (0.056 versus 0.091 μSv). This is due to the fact that, in the case where Thorium sorption in the near-field is disregarded, Th-230 is released from the near-field and thus generates Ra-226 in the geosphere rather than in the near-field.

Solubilities included in the near-field

Figure 13-25 and Figure 13-26 show near-field dose equivalent release and far-field annual doses, respectively, for the central corrosion case when including solubilities in the near-field. The near-field dose caused by release of Pb-210 is considerably higher than for the central corrosion case since Ra-226 is confined to the canister interior where it generates Pb-210. The far-field doses are, however, similar to those of the central corrosion case. Pb-210 decays considerably in the geosphere, due to in particular its short half-life.

Uncorrelated and fully correlated hydrogeological DFN model

Far-field annual doses for the central corrosion case but with hydrogeological data for the uncorrelated relation between DFN fracture size and transmissivity used in the calculation of canister failure times and radionuclide transport are shown in Figure 13-27. The corresponding far-field annual doses for the fully correlated DFN model are shown in Figure 13-28. The mean numbers of failed canisters are 0.60 and 0.53, respectively, and the first releases occur after around 100 000 years.

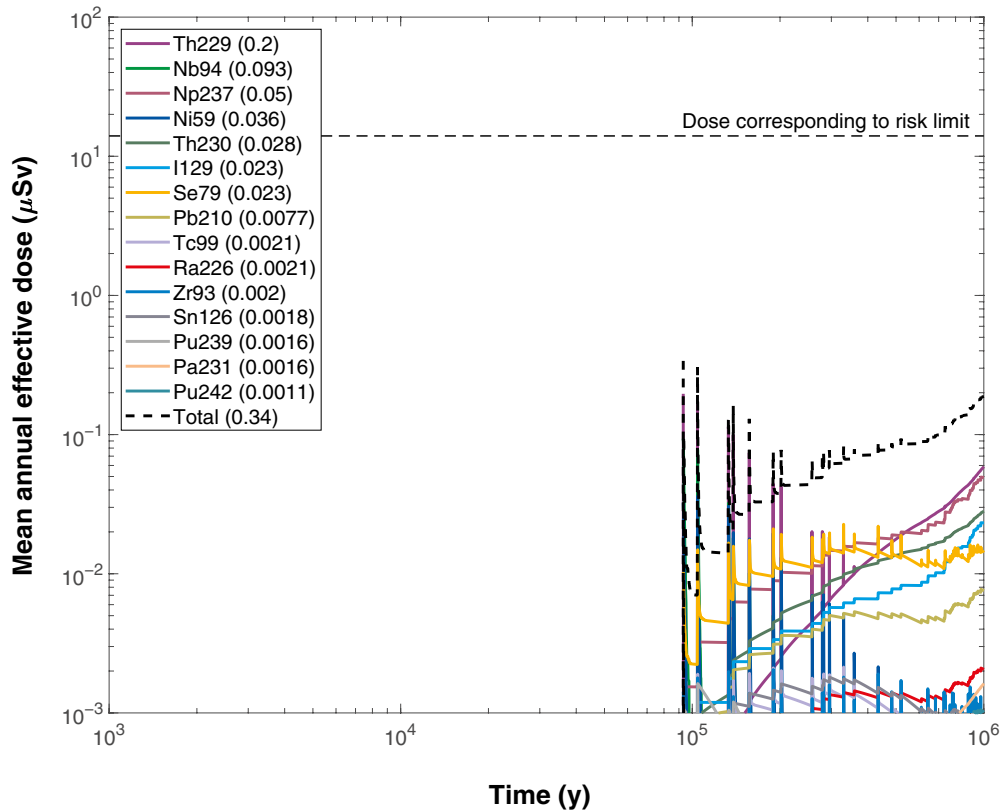


Figure 13-23. Near-field mean annual effective dose equivalent release for the probabilistic central corrosion case, disregarding Th sorption in the near-field. The legends are sorted according to descending peak mean annual effective dose over one million years (given in brackets in μSv).

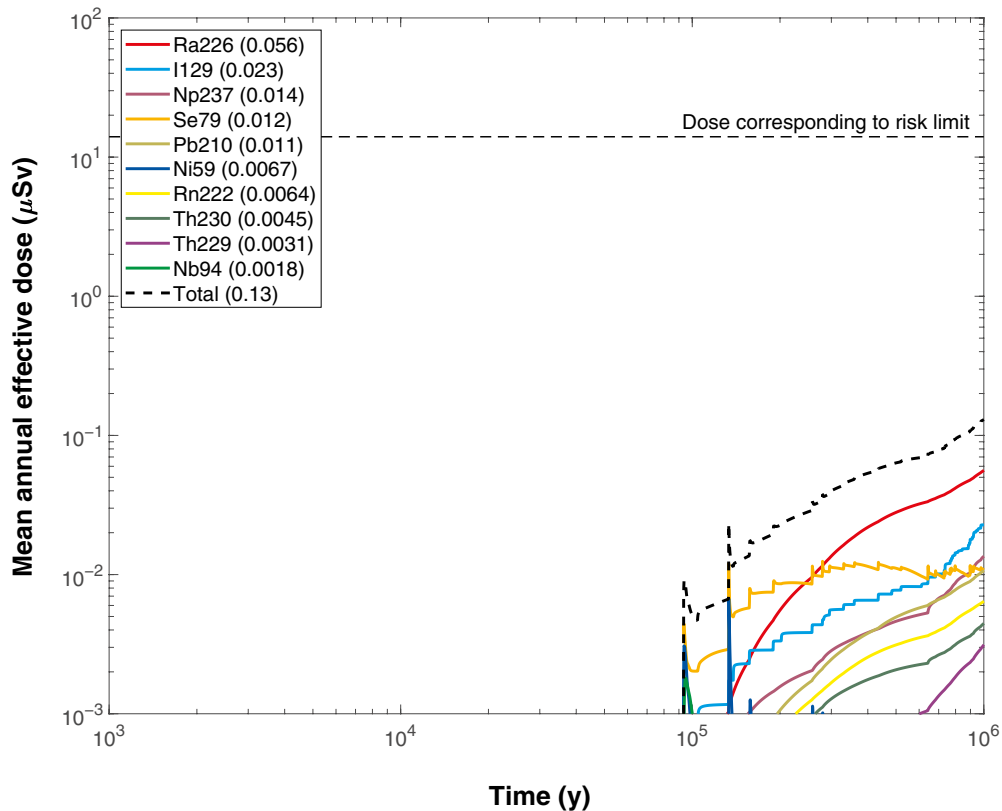


Figure 13-24. Far-field mean annual effective dose for the probabilistic central corrosion case, disregarding Th sorption in the near-field. The legends are sorted according to descending peak mean annual effective dose over one million years (given in brackets in μSv).

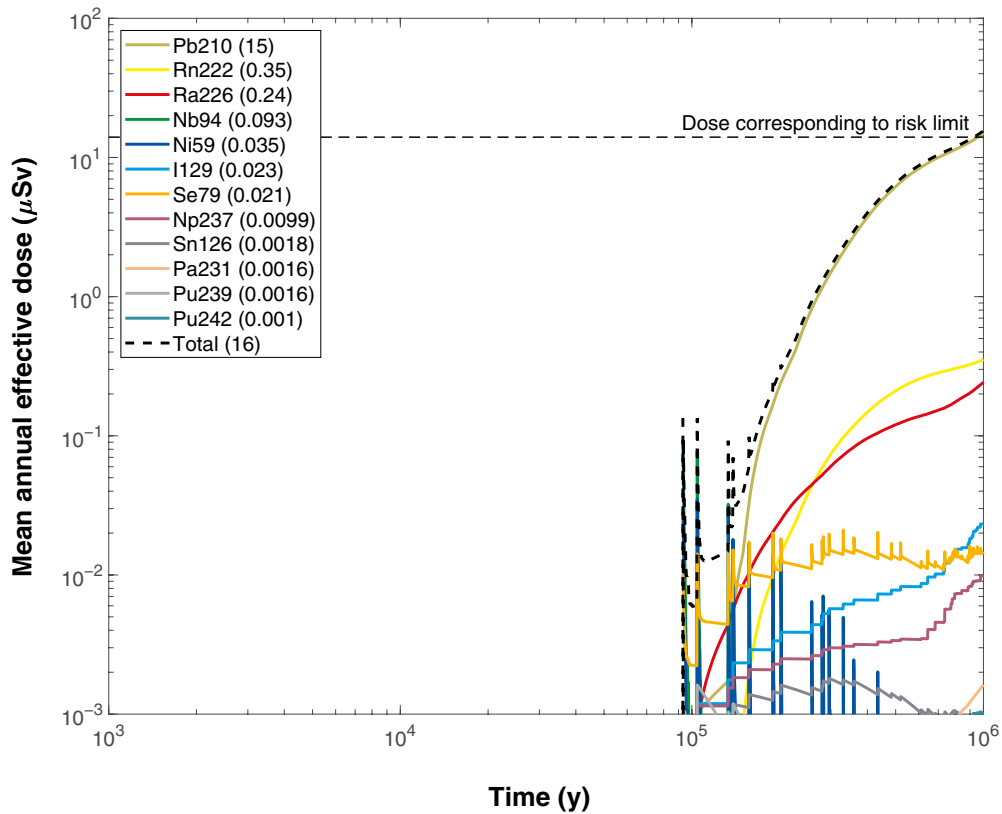


Figure 13-25. Near-field mean annual effective dose equivalent release for the probabilistic central corrosion case, including solubility limits in the near-field. The legends are sorted according to descending peak mean annual effective dose over one million years (given in brackets in μSv).

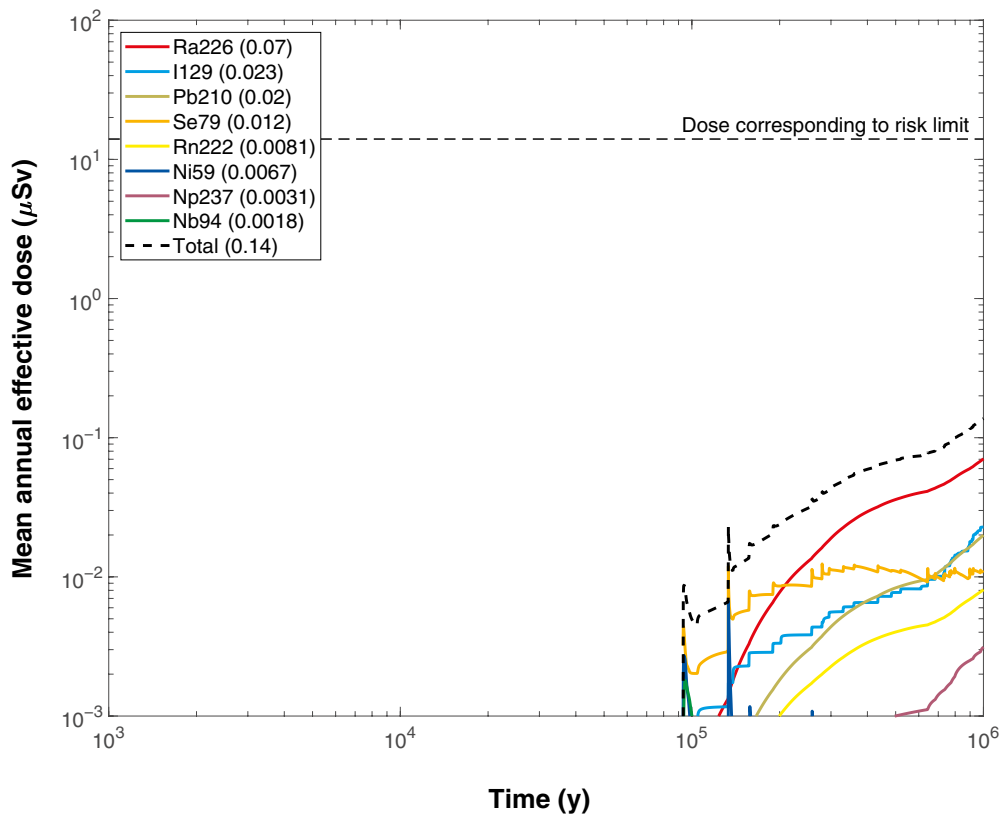


Figure 13-26. Far-field mean annual effective dose for the probabilistic central corrosion case, including solubility limits in the near-field. The legends are sorted according to descending peak mean annual effective dose over one million years (given in brackets in μSv).

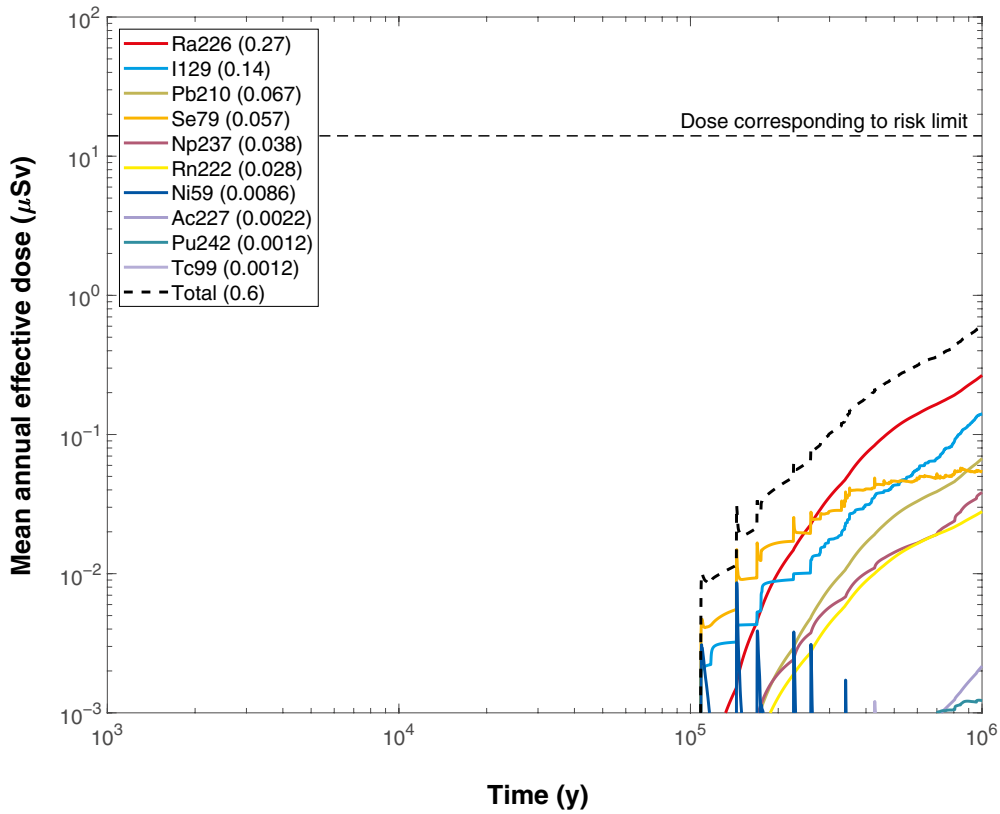


Figure 13-27. Far-field mean annual effective dose for a probabilistic calculation for the corrosion failure with the uncorrelated hydrogeological DFN model. The legends are sorted according to descending peak mean annual effective dose over one million years (given in brackets in μSv).

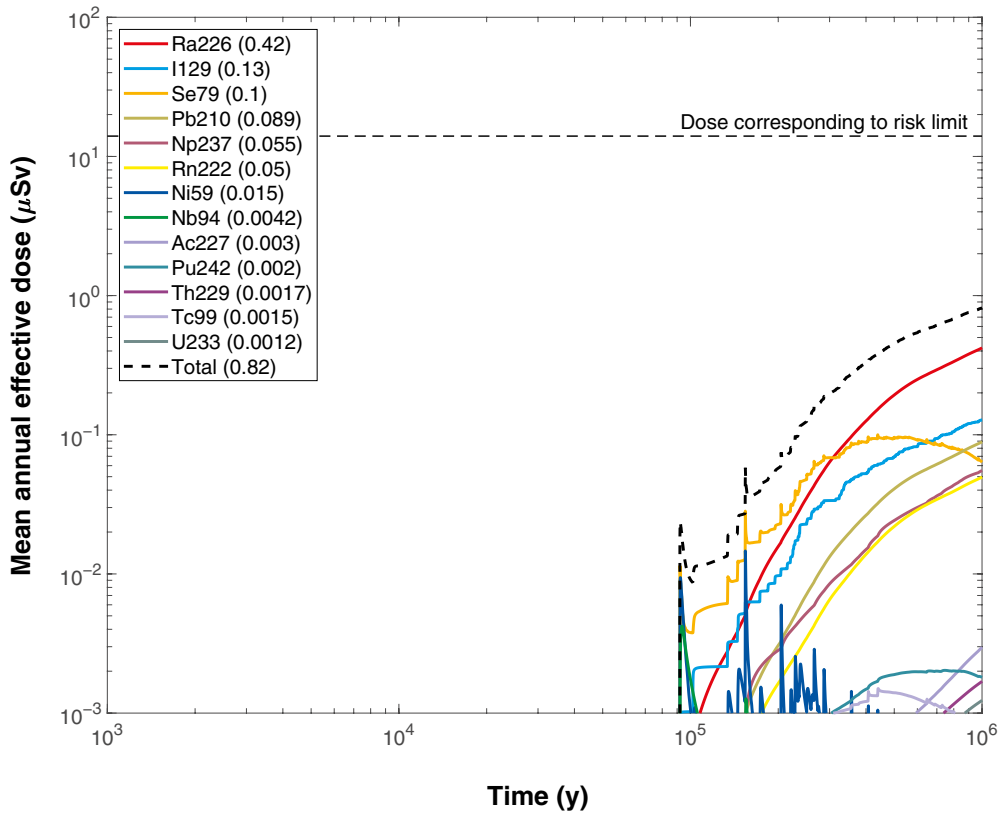


Figure 13-28. Far-field mean annual effective dose for a probabilistic calculation for the corrosion failure with the fully correlated hydrogeological DFN model. The legends are sorted according to descending peak mean annual effective dose over one million years (given in brackets in μSv).

Cases with initial advection in all deposition holes

Consequences for the extreme case assuming initial advection in all deposition holes are shown for the near-field and the far-field in Figure 13-29 and Figure 13-30, respectively. The mean number of failed canisters is 0.12.

The first releases occur after 60 000 years. The dose equivalent releases from the near-field are dominated by pulse release from metal corrosion of Nb-94 and the more continuous releases of Pb-210, Se-79 and Ra-226. The doses caused by releases from the far-field are dominated by the pulse releases from Nb-94 and Ni-59 and the more continuous release of Se-79 and Ra-226.

The relatively small difference between this case and the central corrosion case is due to the fact that most canisters will not fail even if the buffer is missing since the time required to corrode through the canister exceeds the one million year assessment period for the majority of canisters.

The corresponding cases for the uncorrelated and fully correlated hydrogeological DFN models yield similar results (see the **Radionuclide transport report**). Total doses for these cases are also included in the summary of cases given in Figure 13-41 and Figure 13-42 in Section 13.5.9.

Varying external conditions

Flow related transport data for temperate climate conditions are used in the above cases. The effect of varying flow conditions and other climate related geosphere data are analysed with the MARFA model. The analyses in this subsection have not been updated since the SR-Site assessment.

Future climate evolution at the Forsmark site is described in detail in the **Climate report** and summarised in Section 10.4.1. Future glacial cycles will have a significant effect on groundwater flow and chemistry. A pessimistic abstraction of the groundwater flow field evolution is developed to assess the impacts of future glacial cycles on radionuclide transport in the corrosion scenario.

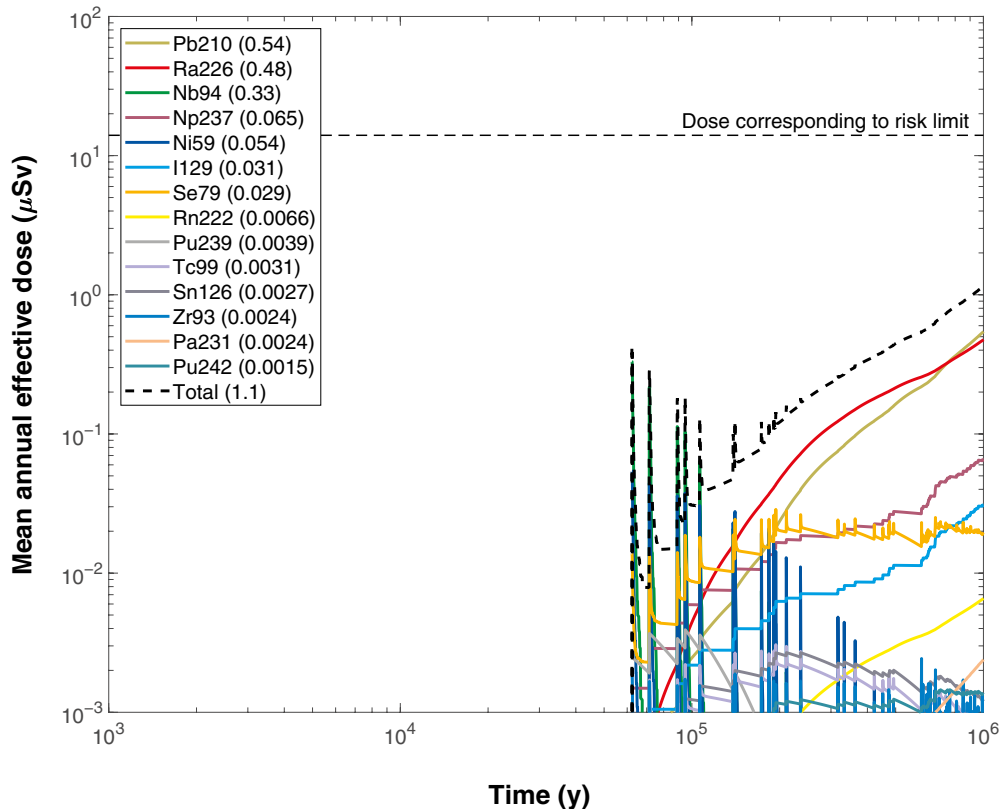


Figure 13-29. Near-field mean annual effective dose equivalent release for a probabilistic calculation for the corrosion failure with initial advection in the buffer and otherwise as the central corrosion case. The legends are sorted according to descending peak mean annual effective dose over one million years (given in brackets in μSv).

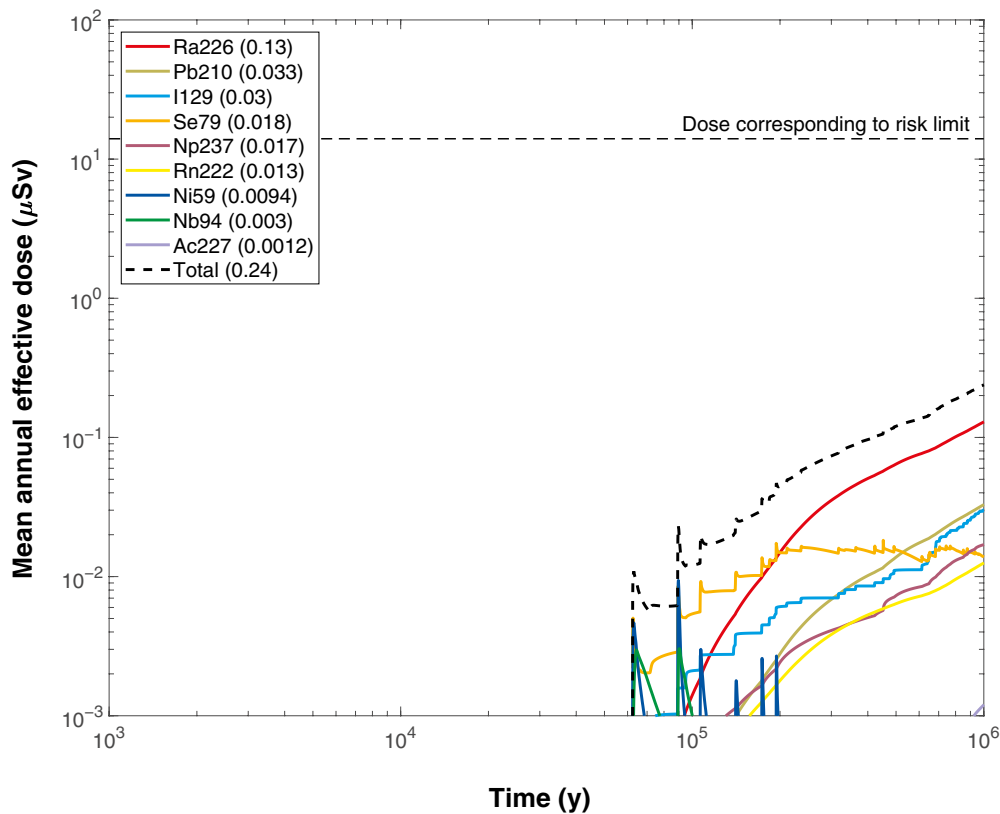


Figure 13-30. Far-field mean annual effective dose for a probabilistic calculation for the corrosion failure with initial advection in the buffer and otherwise as the central corrosion case. The legends are sorted according to descending peak mean annual effective dose over one million years (given in brackets in μSv).

A simplification of the glacial cycle is developed in the **Climate report**, Section 4.5.4 to support the abstraction, see Figure 13-31. The simplified cycle has two temperate periods, three periglacial periods, two glacial periods, and two submerged periods in the 120 000 year cycle. It is noted that the summed percentages of each climate period coincide with the corresponding percentages for the original, non-simplified cycle. In the abstraction, the cycle repeats 8 times in the 1 million year assessment period of interest. Table 13-7 provides times for each flow change in the first 120 000 year cycle.

Detailed simulations of transient flow during a glacial cycle have been undertaken (Vidstrand et al. 2010) and are summarised in Section 10.4.6. These simulations show that both the direction and magnitude of groundwater flow are affected by the glacial cycle. As an alternative to representing the full details of transient groundwater flow fields in the transport simulations, a pessimistic bounding abstraction is developed.

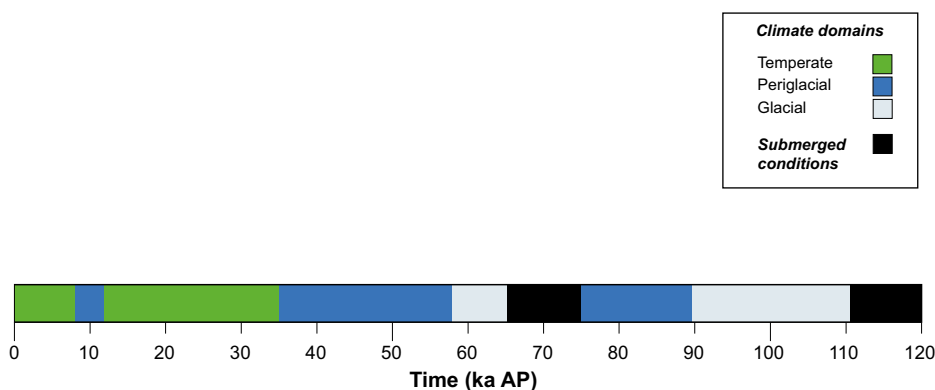


Figure 13-31. Simplified glacial cycle for use in the geosphere transport assessment, see the *Climate report*, Section 4.5.4.

Table 13-7. Duration of each climate period in the simplified 120 000 year cycle. The percentage of each accumulated period is also indicated.

Period	Calendar time (kyrs)	Duration (kyrs)	Accumulated duration (kyrs)
Temperate	0–8	8	8
Periglacial	8–12	4	4
Temperate	12–35	23	8 + 23 = 31 (26 %)
Periglacial	35–58	23	4 + 23 = 27
Glacial	58–65	7	7
Submerged	65–75	10	10
Periglacial	75–89	14	27 + 14 = 41 (34 %)
Glacial	89–111	22	7 + 22 = 29 (24 %)
Submerged	111–120	9	10 + 9 = 19 (16 %)

The abstraction includes changes in flow magnitude, but uses pathlines from the temperate period (Joyce et al. 2010) and ignores changes in flow direction. This abstraction is pessimistic because it greatly overestimates the vertical component of the flow velocity compared with detailed simulations (Vidstrand et al. 2010), and also ignores lengthening of the flow paths that may occur during some of the climate periods.

The glacial periods summarised in Figure 13-31 and Table 13-7 need to be further subdivided into advancing, glacial maximum and retreating phases, because the groundwater velocity will be very different in these three phases. For the advancing ice sheet, it takes 366 years for the ice sheet to move between ice front locations I and IV, see Section 10.4.6 and Vidstrand et al. (2010) for details. For the retreating ice sheet it takes 61 years to move between ice front locations IV and I. As an approximation, it is judged that when the ice front is beyond these ice front locations, the influence of the ice front on the repository will be small, i.e. conditions close to periglacial or submerged will prevail. However, even beyond these times, there is some influence, even if not comparable to the peak, see Figure 13-32 which shows the Darcy flux at repository depth within the repository footprint (measurement locality 2 in Vidstrand et al. 2010). Specifically, during the ice advance, the increase in Darcy flux relative to temperate conditions prevails approximately for 2 000 years. It is decided to represent the glacial advancing period as having duration of 1 800 years, which is much longer than the time to move between ice front locations I and IV, but slightly shorter than the time 2 000 years. The more rapid retreating phase is modelled as having duration of 300 years; i.e. the ratio in duration between advance and retreat phases is maintained. It is also noted that the increase in Darcy flux during the advancing phase is smaller than during the retreating phase. This is due to the fact that the advancing phase is characterised by permafrost in front of the ice sheet, whereas the retreating ice sheet is warm based such that no permafrost is present, see Section 10.4.6 and Vidstrand et al. (2010) for details.

Flow scaling factors for each climate domain are obtained from the calculated Darcy flux distributions at deposition hole locations in the super-regional groundwater flow model of Vidstrand et al. (2010) summarised in Section 10.4.6. In Figure 10-154 the Darcy flux distributions are shown in terms of maximum, median, and minimum values. The median values from Figure 10-154 and the duration of each flow period in Table 13-7 are used to obtain time-dependent flow factors (Figure 13-33). In developing the flow factors, the glacial state without permafrost was assumed for the glacial retreating phase. The latter assumption is regarded as slightly pessimistic because the fluxes in the glacial case without permafrost of Vidstrand et al. (2010) were developed for an advancing ice sheet but applied here for a retreating ice sheet. In the far-field calculations performed with MARFA, the advective travel time and flow-related transport resistance for the temperate period are inversely scaled by the values in Figure 13-33 to obtain corresponding values for other stages in the glacial cycle.

The transport simulations are identical to the temperate period base case described in Section 13.5.4 except for the flow changes shown in Figure 13-33 and the use of sorption K_d -values for oxidising conditions for the redox sensitive elements during ice front passages (i.e. during the time periods when flow scaling factors are 20 and 50, respectively). In addition, different *Landscape dose factors* (LDFs) are applied for different periods in the glacial cycle. The near-field release calculations used as input to the MARFA simulations do not take into consideration the changes in flow. This simplification is based on the fact that releases of radioelements that are not solubility limited will be limited by the rate of fuel dissolution, which is independent of flow rate. It should also be noted that instantaneous release fractions are not included in this simulation.

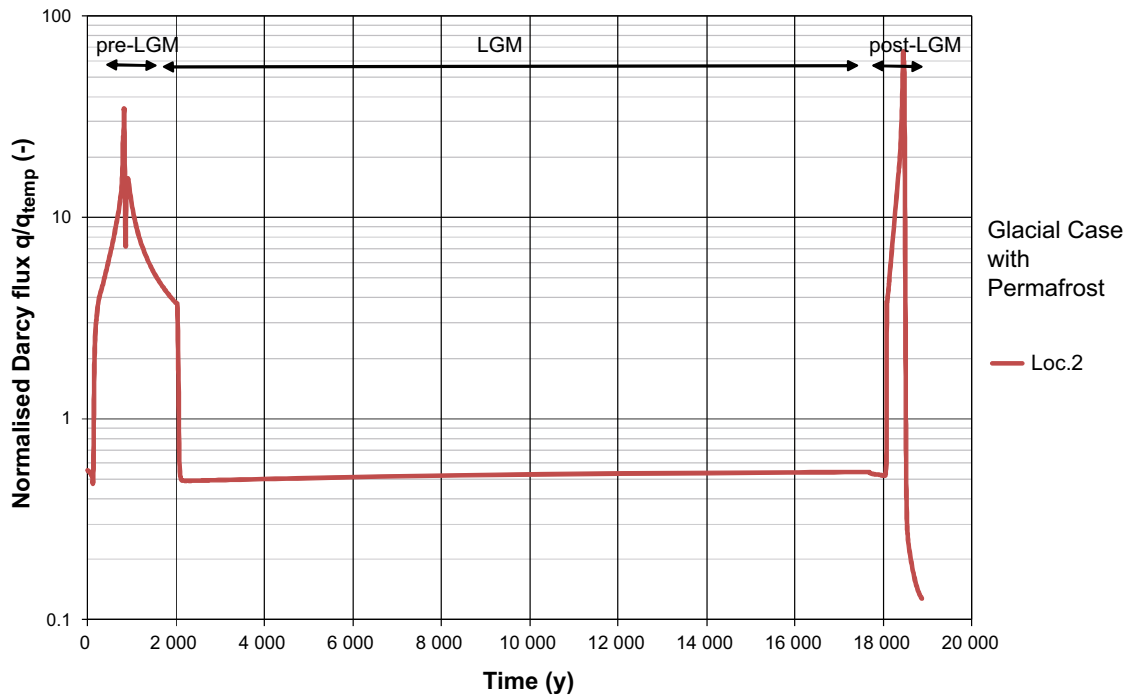


Figure 13-32. Change in Darcy flux relative to the temperate period as the ice sheet advances and retreats over the repository location. Figure is modified after Figure G-12 of Vidstrand et al. (2010).

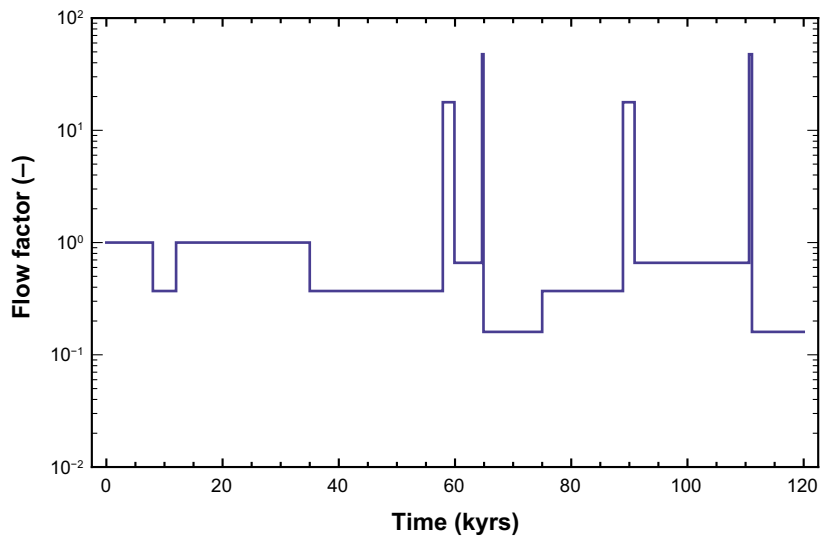


Figure 13-33. Flow scaling factors for one glacial cycle (of eight) for use in far-field radionuclide transport simulations. The spikes at the end of each glacial period have 300 year duration, but are not resolved on the scale of this figure. The scaling factor is defined relative to the Darcy flux in the temperate period.

Expected annual dose versus time for this case is shown in Figure 13-34. Also the case without flow changes, i.e. with temperate flow throughout the assessment period, is shown. The results are based on 2 800 realisations of the central corrosion case where both near-field and far-field parameters follow distributions given in the **Data report**.

The results in Figure 13-34 indicate that the flow, K_d and LDF changes collectively cause no significant increase in peak dose. The main effect is the sharp downward spikes in dose during the time of glacial approach and retreat. Although the radionuclide mass discharge to the biosphere is increased sharply during these periods due to changes in flow and, more importantly, changes in K_d for redox-sensitive radionuclides, this increase is more than compensated by the greatly reduced LDF values during these periods.

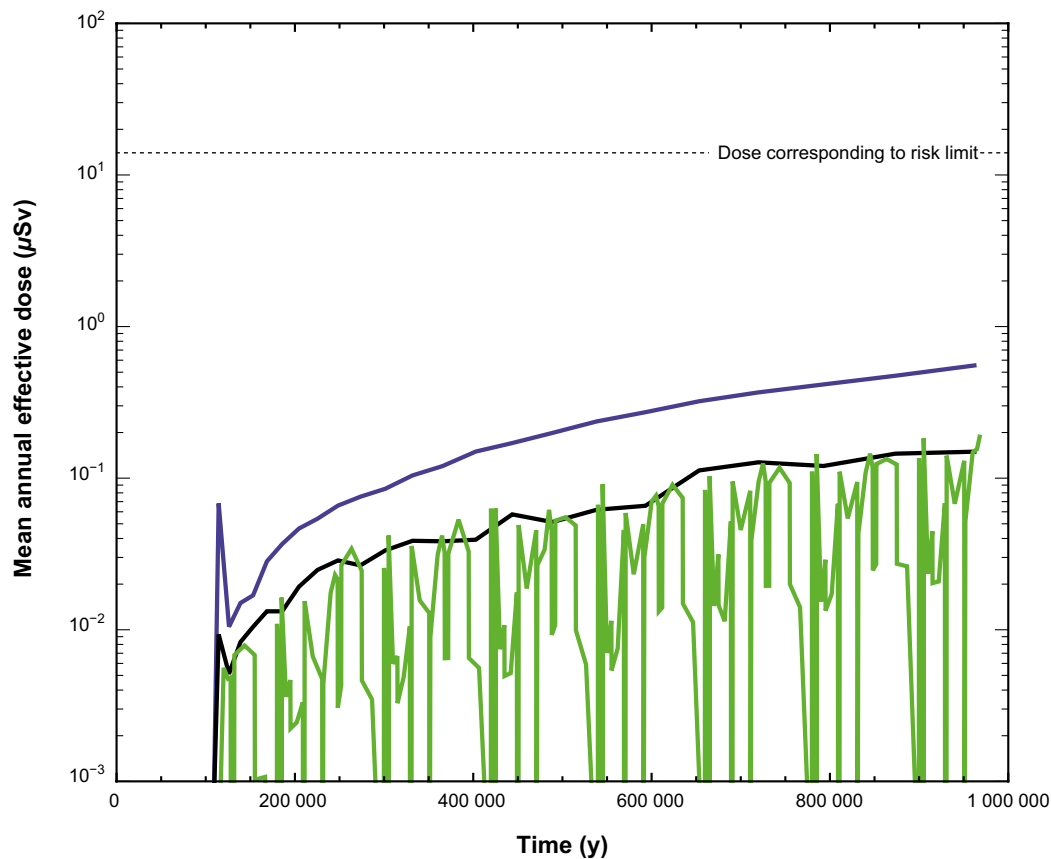


Figure 13-34. Expected doses with and without flow changes. The solid blue curve is the near-field release expressed as an annual effective dose. The black and green curves are far-field annual effective dose without and with flow changes, respectively.

The results without flow changes can also be compared to the corresponding case calculated using FARF31, see Figure 13-19 of Section 13.5.4, showing very similar total dose results.

Colloid facilitated transport

The presence of bentonite material in the deposition tunnel backfill and in the buffer in the deposition hole is expected to result in bentonite colloids in the groundwater near deposition holes and along the geosphere transport pathways. Radionuclides that have a strong affinity for bentonite will sorb onto bentonite colloids and may be transported through the geosphere with reduced interaction with the rock matrix, i.e. with a reduced retention. Colloid facilitated transport involves a complicated combination of processes, many of which can mitigate the transport. Mitigating processes include colloid retardation in fractures, physical filtration (straining) of colloids in fractures, colloid flocculation and sedimentation, radionuclide desorption from colloids, saturation of sorption sites on colloids, and competition for sites on colloids. These processes are uncertain or involve uncertain parameters that are difficult to quantify in short duration experiments. Rather than attempting to develop detailed process models for colloid facilitated transport, potential mitigating processes are ignored so as to place an upper bound on the possible effect. Ignoring these potential mitigating processes and taking into consideration that sorption of radionuclides onto bentonite is understood to be a reversible process on the time scale of geosphere transport (see the **Buffer, backfill and closure process report**), the effect of colloids in facilitating transport may be modelled through the introduction of effective transport parameters, as described in Appendix I of the **Radionuclide transport report**.

Colloid concentrations that can be stably supported are highly sensitive to groundwater chemistry. It has been determined from a review of laboratory and field data (Wold 2010) that 10 mg/L is a reasonably pessimistic value for colloid concentrations for typical groundwater chemistries. However, this value may be much higher during brief periods when highly dilute glacial melt water enters the geosphere.

The maximum concentration of clay colloids in very dilute waters has been determined to be ~40 g/L at the buffer/groundwater boundary (Birgersson et al. 2009, **Geosphere process report**). However, it is unreasonable to assume that this concentration can be maintained throughout the geosphere. For the radionuclide transport calculations a value of 10 g/L has been selected to be a pessimistic value for colloid concentrations in very dilute waters. The pessimistic value for dilute waters (i.e. 10 g/L) is used during periods of glacial retreat/advance and during the second halves of the glacial maximum and temperate periods, to illustrate consequences of periods of potential dilute water intrusion according to the analyses in Chapter 10. The lower value of 10 mg/L is used for other periods.

The partitioning coefficient for sorption onto bentonite colloids K_c may be related to the same parameter for sorption onto bentonite buffer material K_d as $K_c = \gamma K_d$ where γ is a ratio of specific surface areas for colloidal and bulk bentonite. Given that bentonite is a fine-grained material and that equilibrium partitioning coefficients for bentonite are typically measured using colloidal suspensions with particle sizes less than 1 μm , $\gamma \approx 1$ is a reasonable assumption. Thus, K_d distributions from Section 5.3 of the **Data report** were used for K_c .

Results using 2 800 realisations of the central corrosion case are shown in Figure 13-35. By comparison with Figure 13-34, it can be seen that colloids enhance the mean annual dose by a modest factor (< 3) and only during the last halves of the temperate periods. In all cases the mean annual dose is less than the dose-equivalent near-field release. That the mean annual dose would be bounded by the dose-equivalent near-field release is not obvious *a priori* because of the potential for colloid-induced pulse remobilization (i.e. build-up of radionuclide mass in the geosphere during periods of low mobility that is subsequently released during periods of high mobility). The results in Figure 13-35 clearly show that colloid-induced pulse remobilization is not an issue and that the dose-equivalent near-field release can be used as an upper bound on the mean annual dose.

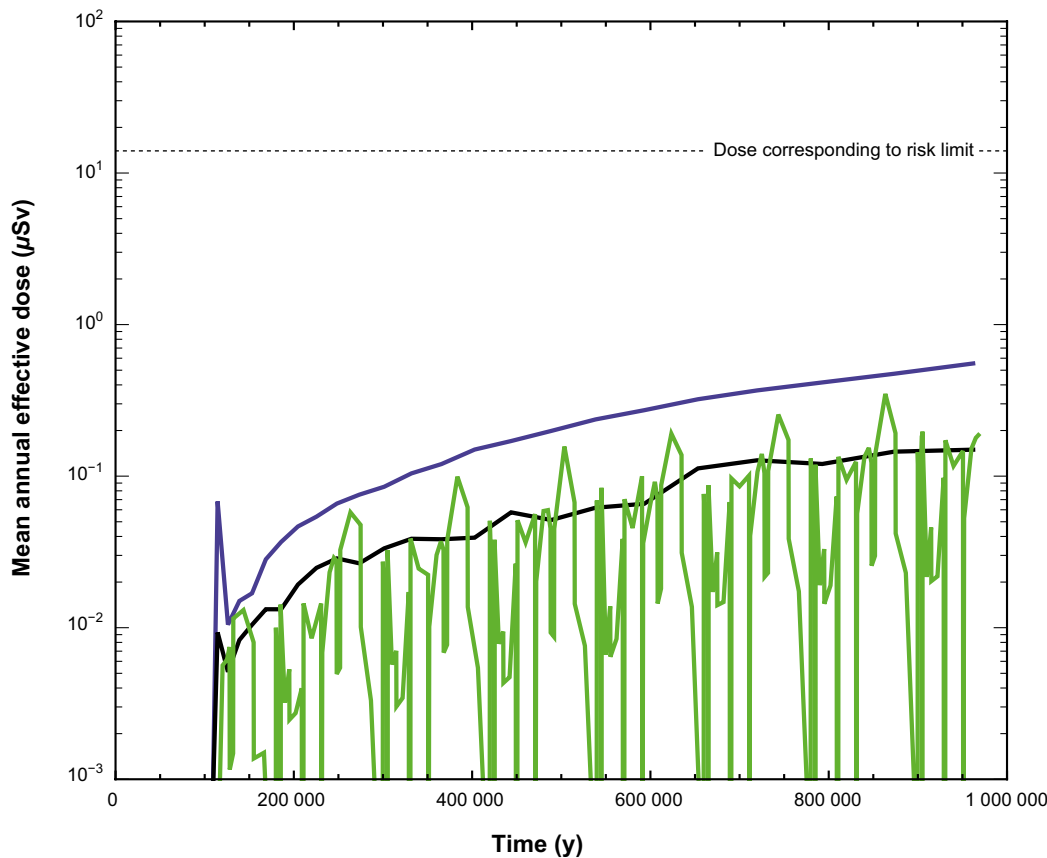


Figure 13-35. Expected dose with unsteady flow and colloid-facilitated transport. The solid blue curve is the near-field release expressed as an annual effective dose. The green curve is far-field annual dose with flow changes and colloid-facilitated transport. The case with no flow changes and no colloid-facilitated transport is shown for comparison purposes (black curve).

13.5.7 Doses to non-human biota for the corrosion scenario

Doses to non-human biota from continuous and pulse releases for the deterministic central corrosion base case, when a canister is assumed to fail at 114000 years after deposition, were calculated according to the methodology described in Section 13.2.5. All total dose rates for the reference species in fresh-water, marine and terrestrial environments, from both continuous and pulse releases, were well below the screening dose rate ($10 \mu\text{Gy h}^{-1}$) recommended in the ERICA Integrated Approach (Beresford et al. 2007, results summarised in Figure 13-36 and details are presented in Jaeschke et al. 2013). Estimated doses to all representative species for the site were also well below the screening value, and differences from the doses to the reference species were explained mainly by the use of site specific concentration ratios and habitat occupancies. Exposure to arctic organisms in a future lake large enough to contain a through talik in a future periglacial landscape were estimated to be higher than in a temperate lake of corresponding size, but well below the screening level (Figure 13-36), while exposures during future warmer climates were assessed not to exceed exposures in the current temperate climate regimes.

It is, therefore, concluded that radionuclide releases predicted for this case will not lead to detrimental biological effects on individuals of species found at the site. As discussed in Section 13.2.5, the lack of biological detriment to individuals is regarded as clear evidence that the ecosystems and populations comprising those individuals are similarly protected.

The results are readily applicable to other corrosion cases, by scaling the releases of the radionuclides in question, which are at most about one order of magnitude higher than those for the central corrosion case. This means that the conclusion for the central corrosion case holds also for all other corrosion cases considered in SR-Site and the PSAR.

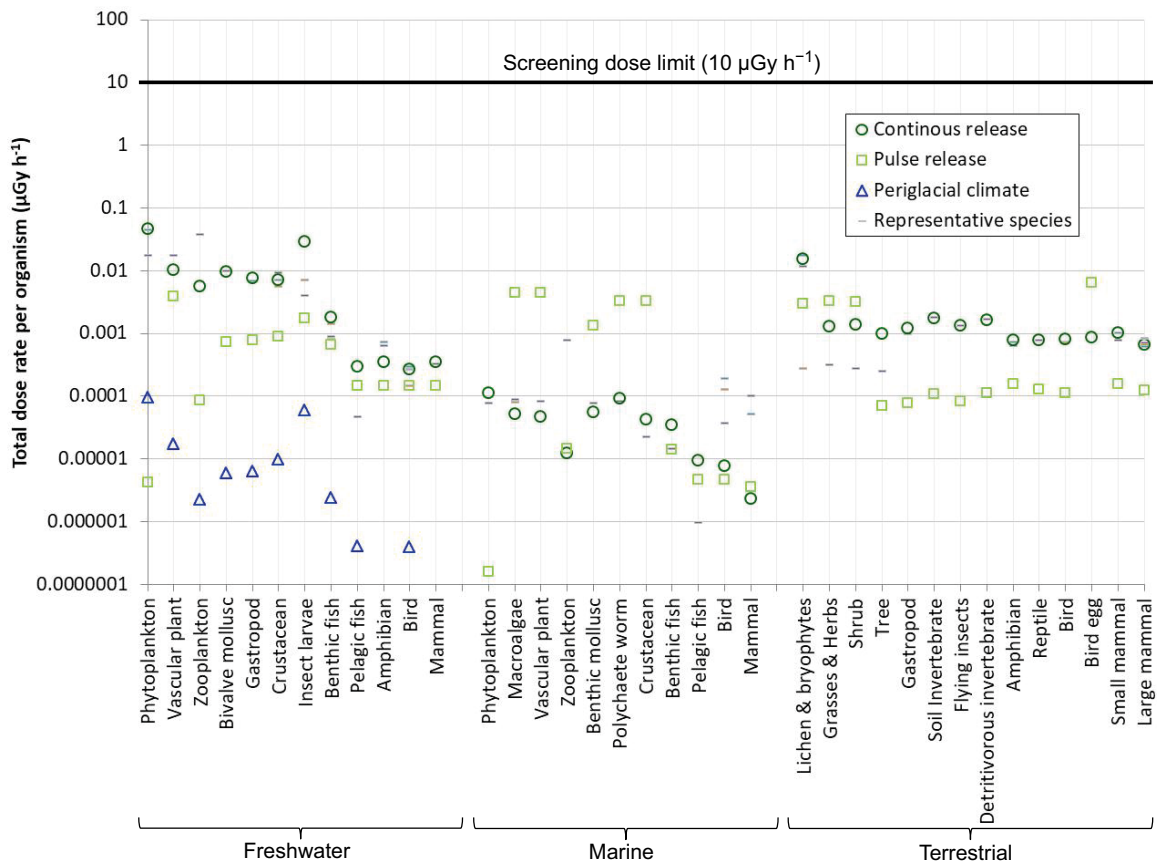


Figure 13-36. Total estimated dose rates to freshwater, marine and terrestrial reference species from continuous and pulse releases in the deterministic central corrosion base case. Estimated dose rates for the corresponding species representative for the Forsmark site and species assumed to become exposed from a potential continuous release in a future periglacial lake are also presented. All dose rates are at least two orders of magnitude below the screening dose limit of $10 \mu\text{Gy h}^{-1}$ (based on results in Jaeschke et al. 2013).

13.5.8 Alternative safety indicators for the corrosion scenario

As mentioned in Section 2.6.3, four alternative indicators to risk are used in the PSAR; release of activity from the geosphere, radiotoxicity flux from the geosphere, concentrations of radionuclides in ecosystems and natural geosphere fluxes of radionuclides. The following reference values are used when evaluating these indicators.

- The Finnish activity constraints. These constraints are strictly applicable only in the Finnish regulatory context, but are nevertheless deemed useful as reference values for the PSAR.
- The reference value for radiotoxicity flux from the geosphere suggested by the EU SPIN project.
- Measured concentrations of naturally occurring radionuclides in ecosystems at the Forsmark site or other, comparable sites.
- Naturally occurring fluxes of radionuclides at the site, in particular of U-238 and Ra-226.

Release of activity from the geosphere

The constraints on activity release from the geosphere issued by the Finnish regulator STUK yield an index calculated as described in Section 2.6.3. Figure 13-37 shows the result of applying this activity constraint to mean releases calculated for the probabilistic central corrosion case (see the **Radionuclide transport report** for details). The releases from the geosphere are around three orders of magnitude lower than the STUK constraint. Figure 13-37 is taken from the SR-Site report. It has been checked that the update of the activity constraints (STUK 2014) does not have any impact on the results.

Radiotoxicity flux from the geosphere

As mentioned in Section 2.6.3, the radiotoxicity flux from the geosphere may be used as an alternative indicator for late time frames. An EU project (Becker et al. 2002) suggests a reference value of 60 Sv/yr for a typical area of 200 km² that could tentatively be used for comparisons to calculated fluxes of radionuclides from the repository.

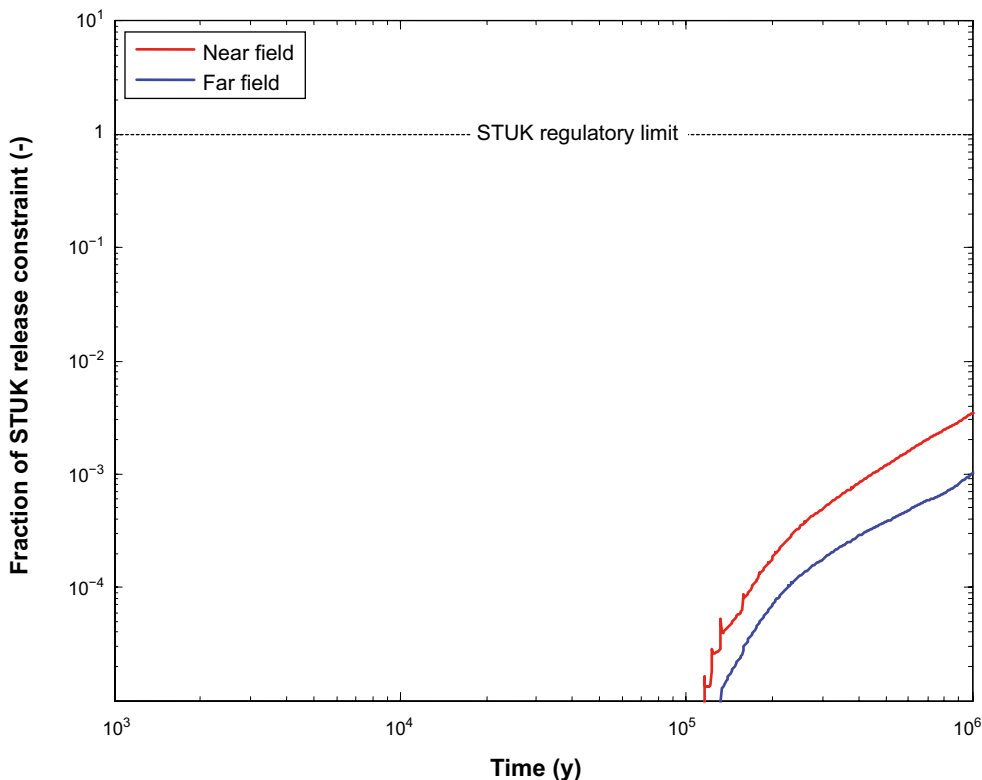


Figure 13-37. Releases as a fraction of the activity release constraint index adopted by the Finnish regulator.

For the probabilistic central corrosion case, the mean activity release for each nuclide was converted to radiotoxicity flux by using ingestion dose coefficients (see further the **Radionuclide transport report**). This yielded the result shown in Figure 13-38. The peak release from the geosphere is around 10^{-2} Sv/yr, i.e. more than three orders of magnitude below the suggested reference value. The IRF pulses are not included in this calculation.

The relevance of the reference value can be argued. It is seen as more significant that for a totally hypothetical situation where an individual alone would ingest all repository-derived radionuclides released from the geosphere in the central corrosion case, the maximum received dose over one million years would only be around one order of magnitude above that caused by typical background radiation in Sweden. It is noted that the result is based on the probabilistic calculation of the central corrosion case, whereas a deterministic calculation not taking into account the probability of 0.12 of this case would yield about one order of magnitude higher dose.

Concentrations in ecosystems

Another alternative indicator is the calculated concentration of radionuclides in the biosphere, which can be compared to the natural content of radionuclides in soil, sediment, groundwater and surface water. This comparison is here made for the most dose-contributing radionuclide Ra-226. In addition, the comparison has been done for all isotopes with measured activity concentrations and is further described and discussed in the **Biosphere synthesis report**.

In the biosphere assessment, maximum activity concentrations of radionuclides are calculated for different environmental media with the radionuclide transport model for the biosphere, given a constant unit release per year of each radionuclide (see Section 13.2.4). These concentration factors (i.e. concentration per Bq/yr) were here multiplied by the maximum activity release rate (Bq/yr) from the geosphere according to the mean release of the probabilistic central corrosion case, to get maximum activity concentrations in different environmental media. The maximum concentration factor and the maximum activity release rate were not coupled in time, giving a pessimistic approach.

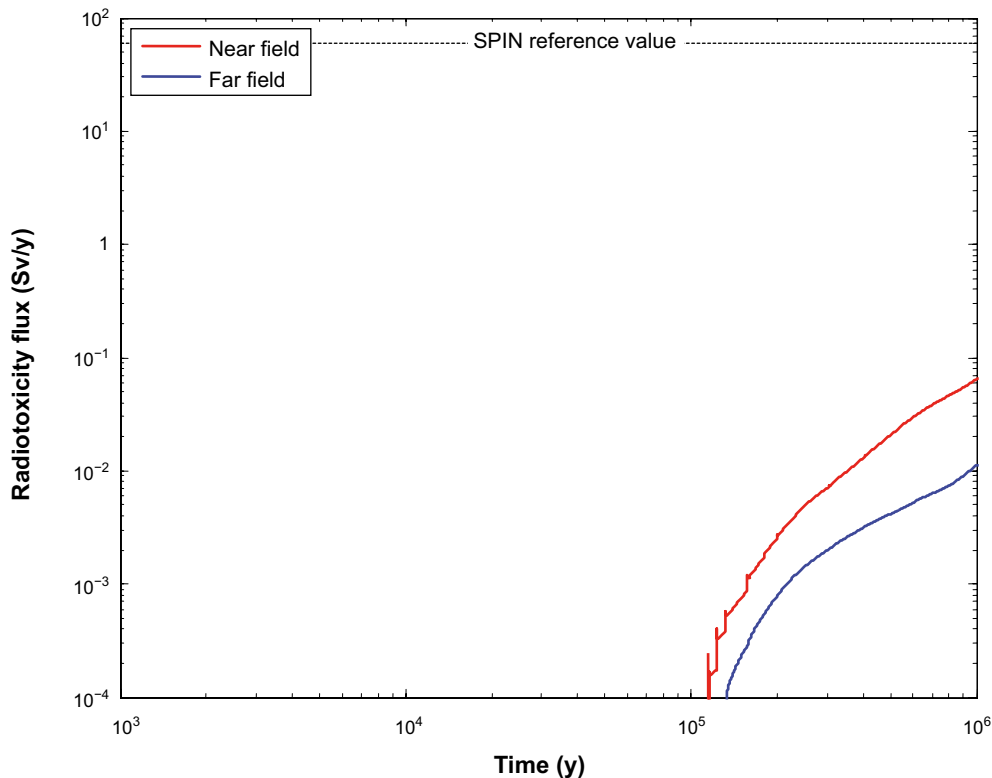


Figure 13-38. Radiotoxicity fluxes from near-field and geosphere for the central corrosion case. Case not recalculated since SR-Site.

Biosphere object 136 (Figure 13-5) was chosen as a representative object for the Forsmark site for the comparison, since the calculated activity concentrations for this object can be compared to the natural content of Ra-226 in different media (soil, sediment, groundwater, lake water and sea water) measured in the basin and in its vicinity as part of the site investigations. The calculated activity concentrations of Ra-226 in different media in this object were of similar magnitude as the highest calculated concentrations among all biosphere objects. The difference was at most 1.6 times lower in object 136 (noted for sediments). As shown in Table 13-8, the calculated activity concentrations for Ra-226 from a release are at least three orders of magnitude lower than the measured background activity concentrations for all the compared environmental media.

Table 13-8. Calculated activity concentration for Ra-226 in different environmental media in Biosphere object 136 (Bolundsfjärden), resulting from the mean release of radionuclides given the probabilistic central corrosion case, compared with measured activity concentrations (median values) from Forsmark. For reference, measured concentrations from Laxemar and from reference sites available in the literature are presented. N represents the number of samples.

	Calculated activity concentration	Measured activity concentration Forsmark (N)	Measured activity concentration Laxemar (N)	Reference sites
Lake water (Bq/l)	4.5×10^{-7}	6.0×10^{-3} (4)		4.6×10^{-4} ¹⁾
Sea water (Bq/l)	3.1×10^{-9}	3.1×10^{-3} (1)		1.1×10^{-3} ¹⁾
Near surface groundwater (Bq/l)	4.2×10^{-5}	7.2×10^{-2} (11)	5.9×10^{-2} (10)	4.2×10^{-3} ²⁾
Limnic sediment (Bq/kg dw)	2.9×10^{-3}	36 (2)	70 (1)	
Marine sediment (Bq/kg dw)	3.5×10^{-4}	8.5 (1)	8.5 (1)	
Top soil (Bq/kg dw)	2.2×10^{-3}	39 (4)	16 (1)	2–1000 ³⁾

¹⁾ Aastrup 1981.

²⁾ Porcelli et al. 2001.

³⁾ UNSCEAR 2008.

Geosphere fluxes of radionuclides

The naturally occurring fluxes of U-238, U-234 and Ra-226, are estimated based on i) measured activities in the groundwater during the site investigations, ii) an estimate of the surface area to which hypothetical releases from the ensemble of deposition positions in the repository would occur for present day conditions, and iii) an estimate of the fraction of the average groundwater discharge originating from repository depth. See Section 2.3 in the **Radionuclide transport report** for details. The resulting natural fluxes are 4.7×10^5 Bq/yr U-238, 1.2×10^6 Bq/yr U-234 and 7.6×10^6 Bq/yr Ra-226.

Figure 13-39 shows the far-field release rates of U-238, U-234 and Ra-226 for the probabilistic central corrosion case compared to the estimated naturally occurring fluxes at Forsmark. The repository derived flux of Ra-226 for the central corrosion case is about two orders of magnitude below the naturally occurring flux of Ra-226. For the U isotopes, the fluxes from the repository are about six orders of magnitude below the natural fluxes, irrespective of whether rock K_d -distributions for U(IV) or U(VI) are used.

It is noted that the releases from the repository could be concentrated to one or a few of the landscape objects in the release area. There are about ten objects in the area used in the derivation of the naturally occurring fluxes, suggesting that the natural fluxes would exceed those from the repository even if all the release from the repository were to occur to a single landscape object.

The naturally occurring fluxes of U-238, U-234 and Ra-226 have been converted to effective dose by using the basic LDF values. The result is shown together with the far-field annual effective dose in the central corrosion case in Figure 13-40. The result is similar to that in Figure 13-39 since the dose is dominated by Ra-226 in the central corrosion case.

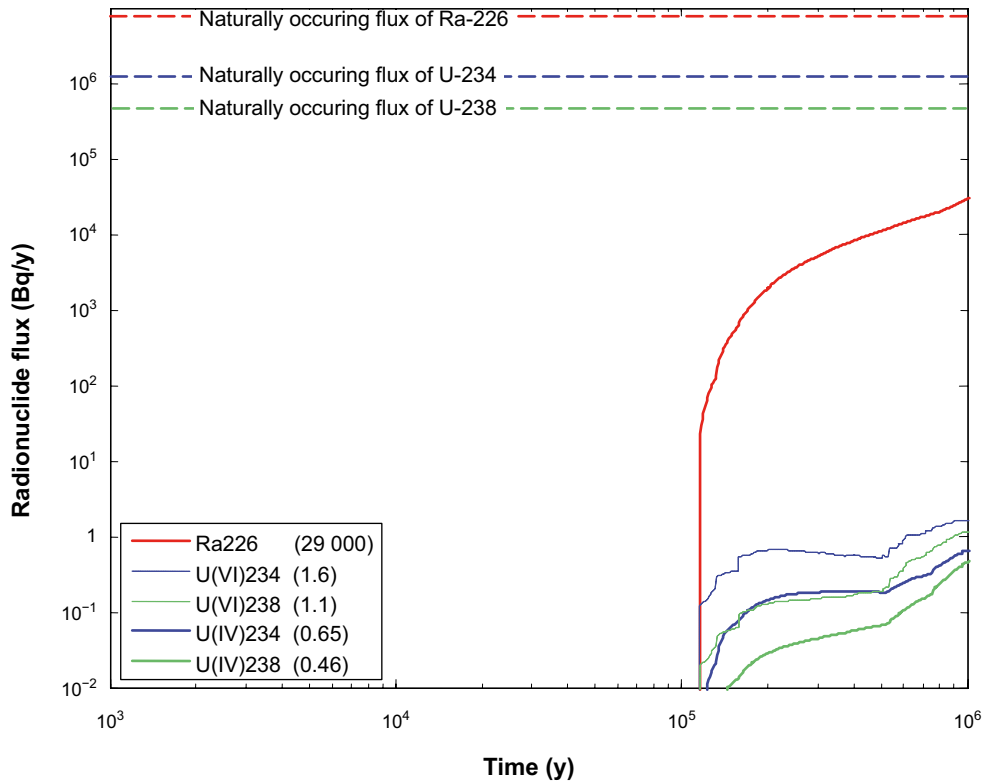


Figure 13-39. Far-field release rates (Bq/year) of U-238, U-234 and Ra-226 in the central corrosion case compared to the naturally occurring fluxes at Forsmark. Case not recalculated since SR-Site.

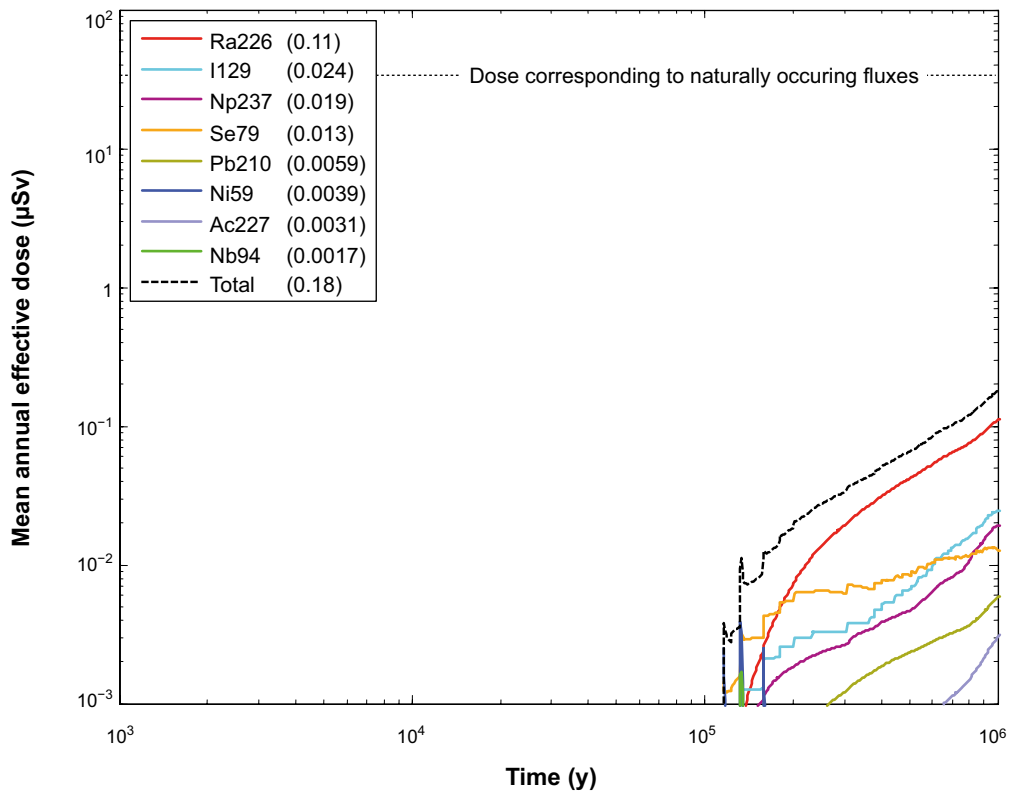


Figure 13-40. Far-field mean annual effective dose in the central corrosion case compared to the annual effective dose coming from naturally occurring fluxes of U-238, U-234 and Ra-226 at Forsmark converted to annual effective dose using the basic LDF values. Case not recalculated since SR-Site.

Conclusions

Four alternative indicators to risk are used in the PSAR, yielding the following results for the central corrosion case:

- Peak releases of activity from the geosphere are about three orders magnitude below the activity constraints issued by the Finnish regulator STUK.
- The peak radiotoxicity flux from the geosphere is more than three orders of magnitude lower than the reference value for the radiotoxicity flux from the geosphere suggested by the EU SPIN project.
- Calculated radionuclide peak concentrations in ecosystems at Forsmark from repository releases of Ra-226 are about three orders of magnitude below measured concentrations of naturally occurring Ra-226 at Forsmark.
- Peak geosphere fluxes caused by Ra-226 releases from the repository are about two orders of magnitude below naturally occurring fluxes of Ra-226 at the site, as estimated from site data; the difference is larger for U-234 and U-238. The total release of all repository derived nuclides converted to dose is also around two orders of magnitude lower than the summed dose from releases of the three mentioned naturally occurring nuclides.

The results are readily applicable to other corrosion cases, for most indicators by simply scaling with the release of Ra-226, which is at most one order of magnitude higher than that for the central corrosion case.

13.5.9 Summary of results of calculation cases for the corrosion scenario

Figure 13-41 (near-field) and Figure 13-42 (far-field) summarise the probabilistic calculations done for the corrosion scenario with COMP23/FARF31. Peak mean annual doses vary roughly within an order of magnitude between the cases.

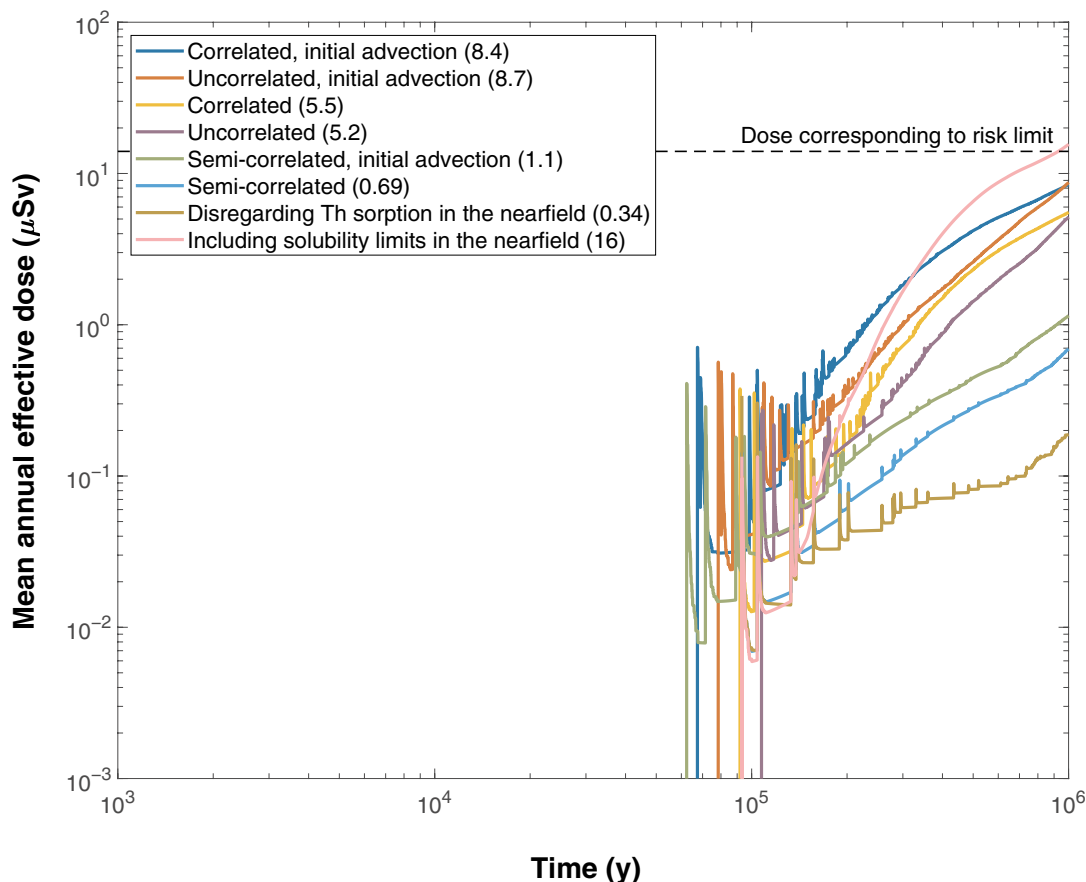


Figure 13-41. Summary of near-field mean annual effective dose equivalent release for all probabilistic calculations performed with COMP23 for the corrosion scenario.

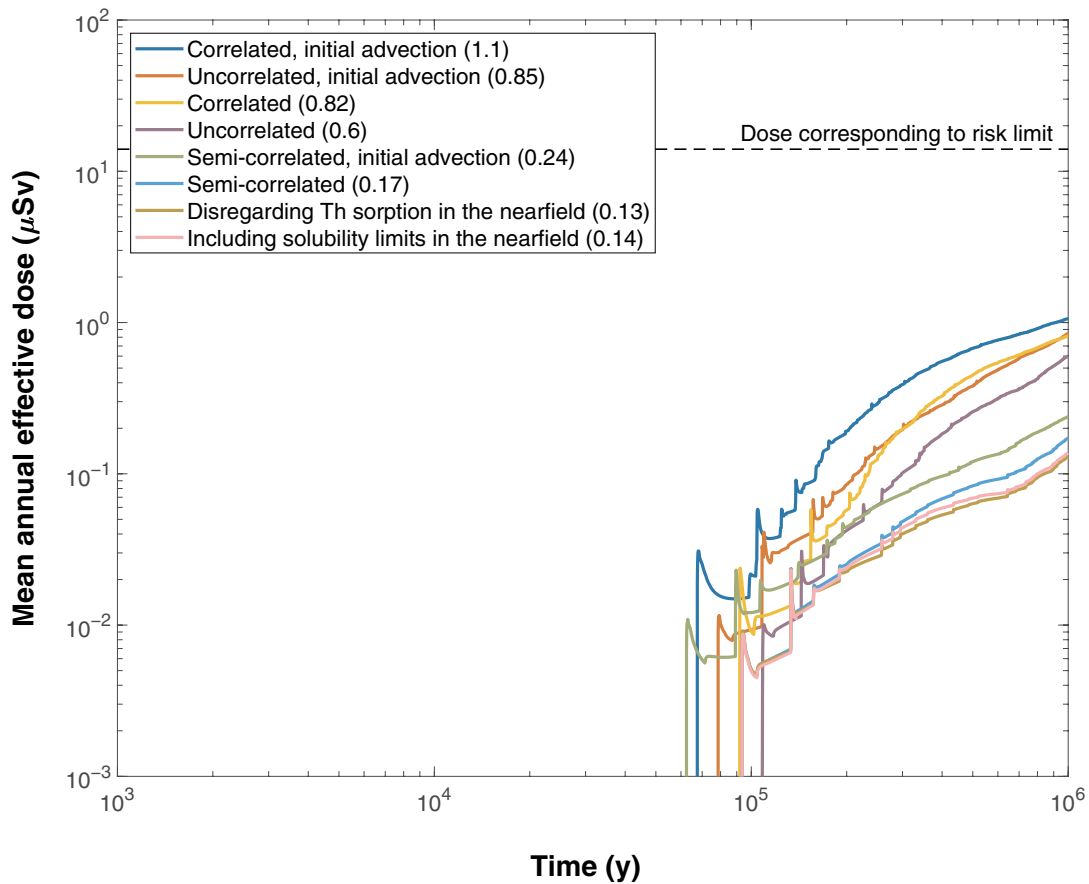


Figure 13-42. Summary of far-field mean annual effective dose for all probabilistic calculations performed with COMP23/FARF31 for the corrosion scenario. The peak doses are given in parentheses in μSv .

13.5.10 Calculations with the analytical models

As mentioned in Section 13.4.4, simplified, analytical models are available for the modelling of radionuclide transport in the near-field and the far-field.

The analytical models have been applied to the six corrosion variants of the corrosion scenario.

Regarding the application of the models to the corrosion scenario, the following, further simplifying, conditions are noted. The near-field release is determined by the rate of radionuclide release to water in the void space because the flow rate in the Q1 fracture is not a limitation (canister failures due to corrosion only occur in the deposition holes with the highest flow rates). Therefore, the release rate from the near-field is simply modelled as the dissolution rate of the fuel, alternatively the corrosion rate of the metal parts, in both cases multiplied by the inventory. As in the numerical models, the IRF is not included but handled separately.

The release rate from the far-field is in most cases calculated as the release rate from the near-field times a geosphere transmission factor (Hedin 2002b). This yields a good approximation in cases of a continuous release over long times.

However, in some cases of relatively short duration, releases caused by corrosion of the metal parts of the fuel, the treatment is overly pessimistic. In such cases the release of the entire inventory in the metal parts, M_0 , as a pulse to the geosphere is also considered. This yields a peak release rate from the geosphere of M_0/τ where τ is obtained from SKB (2006a, Appendix B). Hydrodynamic and molecular dispersion in the flowing fracture are pessimistically neglected when this expression is used. Also, radioactive decay is neglected in the expression since no appreciable decay will take place during the short transients of concern here.

Since both the above approaches overestimate the release rate from the far-field, the smaller of the two is chosen in each realisation.

It is also noted that chain decay in the geosphere is not accounted for when applying the transmission factors for geosphere retention. The theory for a full, analytical treatment of chain decay in transmission factors has been developed, but is not yet implemented in the analytical model. Using the numerical models, it has been demonstrated that chain decay of parent nuclides of Ra-226 in the far-field has a negligible impact on the releases of Ra-226 in the corrosion scenario.

The result of the analytical modelling of the probabilistic central corrosion case is shown in Figure 13-43. As seen by comparing the results in Figure 13-43 with those of the corresponding numerical case in Figure 13-19, the agreement of the peak doses is very good for nuclides emerging from the fuel matrix, whereas doses from nuclides embedded in metal parts (Ni-59 and Nb-94) are somewhat overestimated with the analytical model. This is due to the pessimistic modelling of nuclide release from corrosion of metal parts discussed above.

The modelling results of the six corrosion variants are shown in Figure 13-44. Each case was modelled with 20 000 realisations using Latin Hypercube Sampling. As seen by comparing the results in Figure 13-44 with those in Figure 13-42, which shows far-field annual effective dose for all corrosion cases calculated with FARF31, the agreement between results obtained with the two sets of models is good. All peak doses over one million years are the same to within less than ten percent.

The fact that the numerical calculations are in good agreement with the analytical calculations enhances confidence in the dose equivalent releases provided here and in the **Radionuclide transport report** for two reasons. First, the comparison provides a quality assurance check on the numerical modelling of dose equivalent releases. This check applies not only to the numerical calculations but also to the data/parameter transfers, as the data for the analytical calculations were taken directly from the **Data report** independently of the numerical calculations. Second, it demonstrates that dose equivalent releases for the corrosion cases are controlled by relatively simple processes that are straightforward to understand and model.

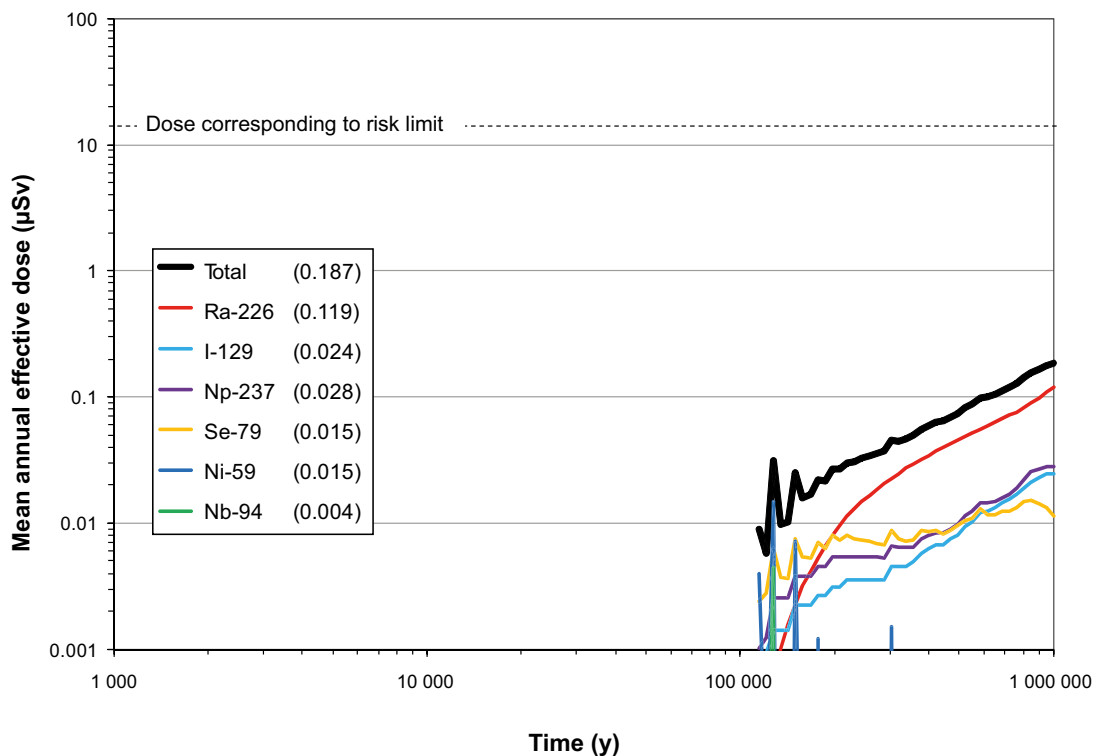


Figure 13-43. Far-field mean annual effective dose for the central corrosion case, obtained with analytical models. The legends are sorted according to descending peak mean annual effective dose over one million years (given in brackets in µSv). Case not recalculated since SR-Site.

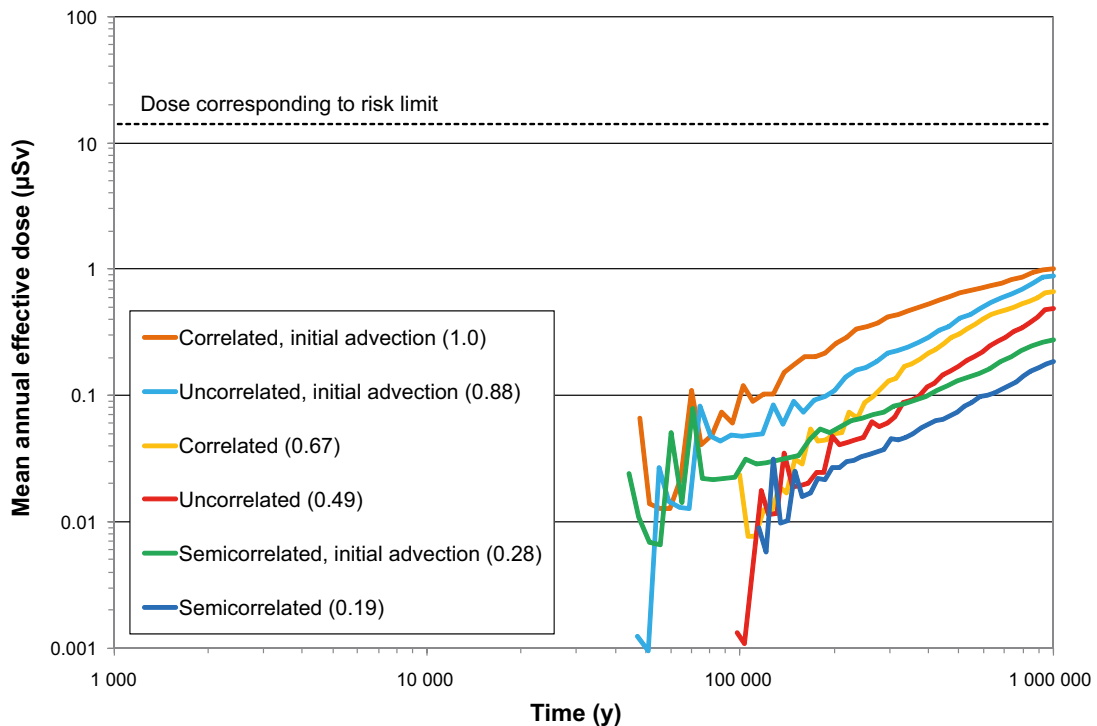


Figure 13-44. Summary of far-field mean annual effective dose for analytical, probabilistic calculations of the six corrosion variants of the corrosion scenario. The peak doses are given in parentheses in μSv . These results can be compared to the corresponding results obtained with numerical models in Figure 13-42. Case not recalculated since SR-Site.

13.5.11 Sensitivity analyses

Introduction

This section presents results of sensitivity analyses of the results of the dose calculations, i.e. the sensitivity of the uncertainty in calculated dose to uncertainties in the input parameters is analysed. All analyses concern the probabilistic calculation of the central corrosion case, Section 13.5.4.

It is of interest to determine i) the variables that correlate with the dose over the entire dose range and ii) the parameter values that are related to high and low doses. Ra-226 dominates the dose in most of the realisations in the central corrosion case and it is thus of particular interest to clarify sensitivities of the Ra-226 dose to input parameters.

The analyses in this Section are based on results from the SR-Site assessment. Most of the analyses are the same as in that assessment, meaning that most of the text is virtually identical to that in SR-Site. In addition, a variance based method for global sensitivity analysis and a graphic method to identify parameters related to high consequences, both employed after the SR-Site assessment, are reported in a dedicated subsection below.

Global sensitivity analysis

The first purpose is thus to perform a so called global sensitivity analysis, i.e. to identify the input parameters that have the greatest influence on the spread of the results. The contribution to output spread depends on both the spread of the input parameter and the model's sensitivity to variations in that particular input parameter. A range of methods for this type of sensitivity analysis exists (Saltelli et al. 2000). Several studies and reviews have demonstrated that standardised rank regression is a suitable method for sensitivity analysis of non-linear systems where the calculation end point is a monotonic function of the input variables (Saltelli et al. 1993, Helton 1993, Hamby 1994, Iman and Conover 1979). This applies to the present non-linear and monotonic system (Hedin 2003), and the standardised rank regression coefficient (SRRC) is, therefore, used for identifying the most important variables contributing to dose uncertainty.

A standardised rank regression analysis of the total dose at 10^6 years on the input variables yields, in descending order, the fuel dissolution rate D_{Fuel} , the transport resistance along the geosphere flow path, F , and the failure time $t_{Failure}$ as the input parameters most affecting dose results, see Figure 13-45. Regressing on Ra-226 dose at 10^6 years yields a similar result due to the dominance of Ra-226. The ranking of the two most important variables is switched in this case and this is consistent with the fact that the fuel dissolution rate, D_{Fuel} , affects all nuclides whereas the F parameter only affects sorbing nuclides and is hence relatively more important for the Ra-226 dose, than for the total dose which is in some of the realisations dominated by the non-sorbing I-129. It is also noted that the three variables F , t_w and $t_{Failure}$ are correlated, meaning that their significance is not necessarily as high as indicated by the SRRC method. This was further investigated with a tailored regression model, as described below. Standardised rank regression analysis on maximum total dose over time yields an almost identical result as regressing on total dose at one million years (not shown in the figure). However, regressing on e.g. peak Ni-59 equivalent dose from the near-field (not shown in the figure) identifies also the corrosion release rate, CRR , as a sensitive input variable. This is consistent with the fact that in some realisations of the central corrosion case, the peak dose of Ni-59 occurs shortly after canister failure and is then caused by the releases congruent with the corrosion of the metal parts of the fuel assemblies.

Main risk contributors

The standardised rank regression analysis identifies the variables that co-vary with the dependent variable, the total dose, over the entire dose range. To determine the variables that are related to the highest doses, a conditional mean value analysis (Hedin 2002a) was carried out. Here, the subsets of input parameter values related to the top percentile of the dose are selected. For each such subset, the mean value of the logarithmically transformed data was determined for each parameter and compared to the corresponding mean value of the entire input distribution. A dimensionless, normalised measure, α_{99} , is obtained by dividing the difference between the two mean values by the standard deviation of the entire distribution.

The so determined conditional mean value identifies variables that take on significantly different values in the top percentile realisations than in the entire dose distribution. In descending order, the $t_{Failure}$, D_{Fuel} , F and t_w parameters were identified as most significant, see Figure 13-46. Similarly, α_{1} -values, relating to the lowest percentile of the dose distribution were determined. Also $\alpha_{99} - \alpha_1$ values were determined to distinguish extreme outcomes from others. The highest ranking variables were here, in descending order, D_{Fuel} , F , t_w , which is strongly correlated to F , and $t_{Failure}$.

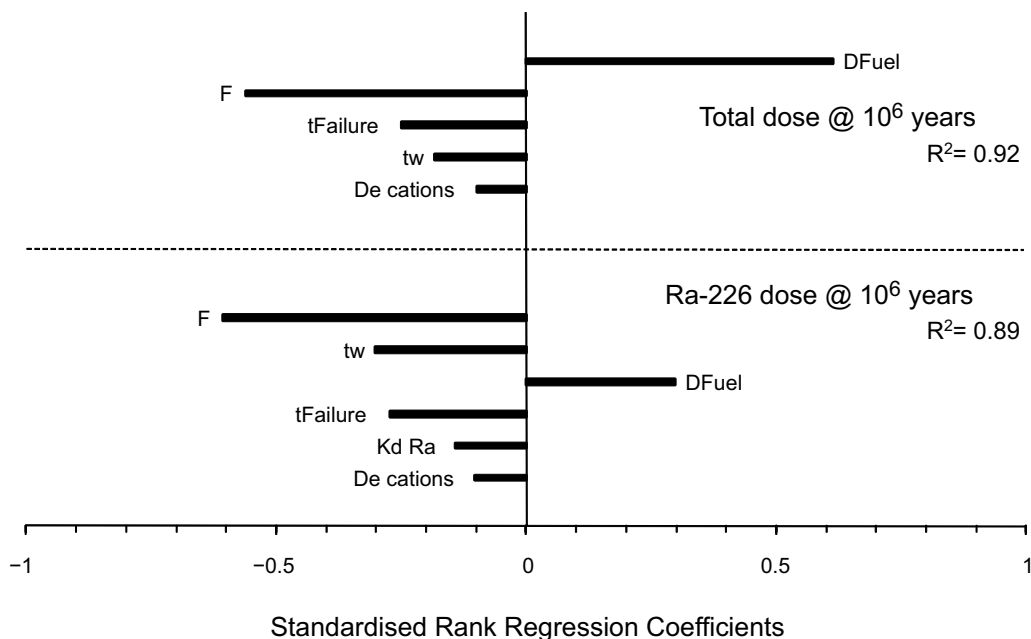


Figure 13-45. Results of standardised rank regression. Regressing on total dose at 10^6 years and on Ra-226 dose at 10^6 years yields similar results due to the dominance of Ra-226.

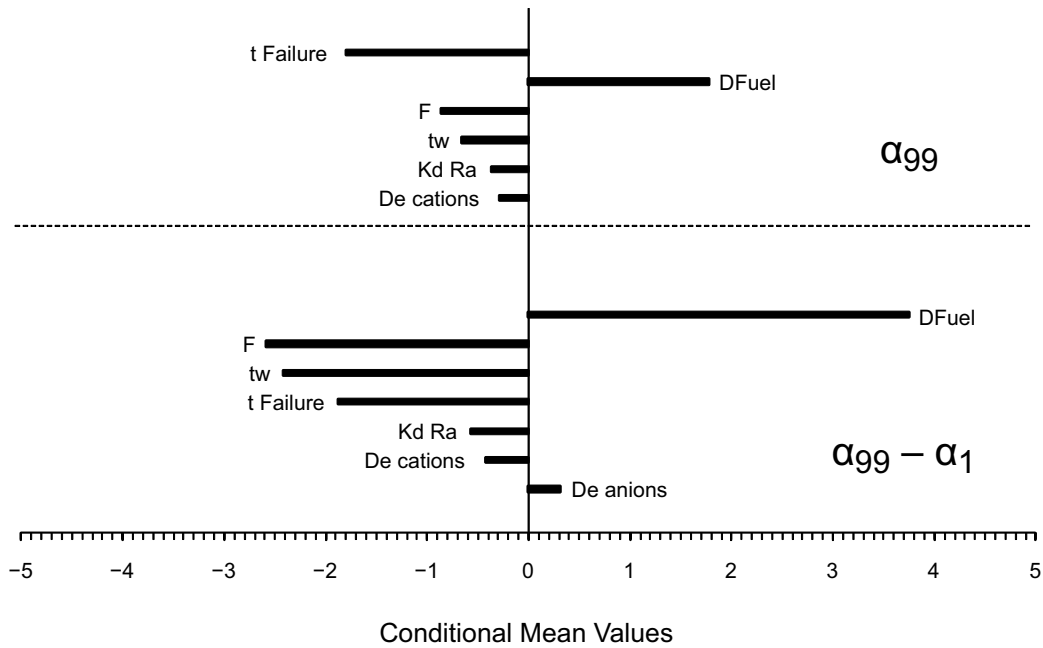


Figure 13-46. Conditional mean values.

Tailored regression model

The understanding and mathematical formulation of the transport models used in the dose calculations can be utilised to further explain the results. The release rate of Ra-226 is determined by the amount of its parent nuclide, Th-230, liberated from the fuel matrix and subsequently assumed to sorb in the near-field. This amount is proportional to the product of the fuel dissolution rate, D_{Fuel} , and the time, t , elapsed between the canister failure and the point in time for which the dose is calculated, i.e. it is proportional to $D_{Fuel} \cdot t$. In the studied case $t = 10^6 - t_{Failure}$. It can further be shown that the released Ra-226 is transported through the geosphere with a certain transmission efficiency, θ , that in its full expression depends in a complex way on all the uncertain parameters relating to geosphere transport (see e.g. Hedin 2002b). However, it can also be demonstrated that most of the variability of θ is captured by the simpler expression (Hedin 2003):

$$\theta \propto \exp(-cF^{0.5} \cdot (K_d D_e)^{0.25})$$

where c is a positive constant determined by well-known properties like the density of the rock and the half-life of Ra-226. This suggests that the Ra-226 dose varies according to

$$\log(DoseRa226) = Constant + \log(D_{Fuel}t) - cF^{0.5} \cdot (K_d D_e)^{0.25}$$

and that a tailored regression model according to the above expression could be successful in explaining the calculated results. Figure 13-47 shows how such a regression model is able to predict the calculated results when successively more terms are included in the model. As seen in the figure, the agreement when all terms are included is good, with an R^2 -value of 0.99.

These expressions also reveal combinations of input variables of importance. Obviously, combinations of high D_{Fuel} and t values and combinations of low values of the three factors occurring in the exponent of the first expression favour high doses. This result also illustrates that the variable t_w , identified as important for the Ra-226 dose by the SRRC method above is not needed to explain the Ra-226 dose. It is concluded that t_w is identified in the SRRC method only since it is correlated to the F parameter. (This can be further analysed through use of partial rank correlations in the SRRC method.)

A partition plot, Figure 13-48, showing how high and low dose results relate to the variable groups $D \cdot t$ and $F^{0.5}(K_d \cdot D_e)^{0.25}$ confirms the explanatory power of these variable groups.

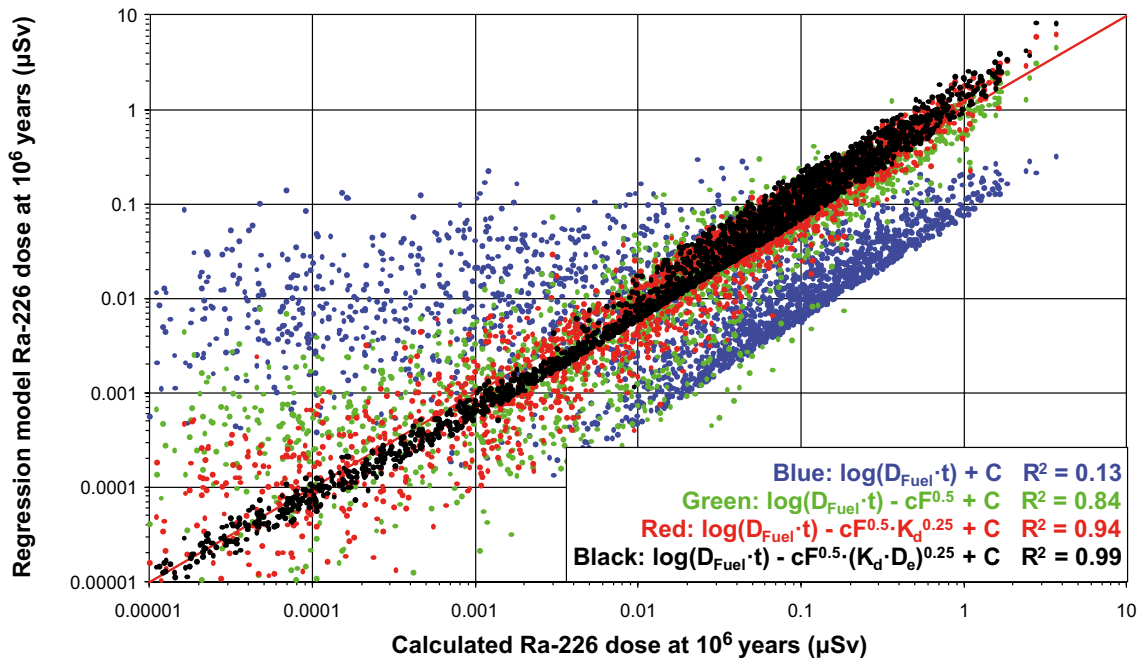


Figure 13-47. Four tailored regression models, including successively more variables, for the Ra-226 dose at one million years.

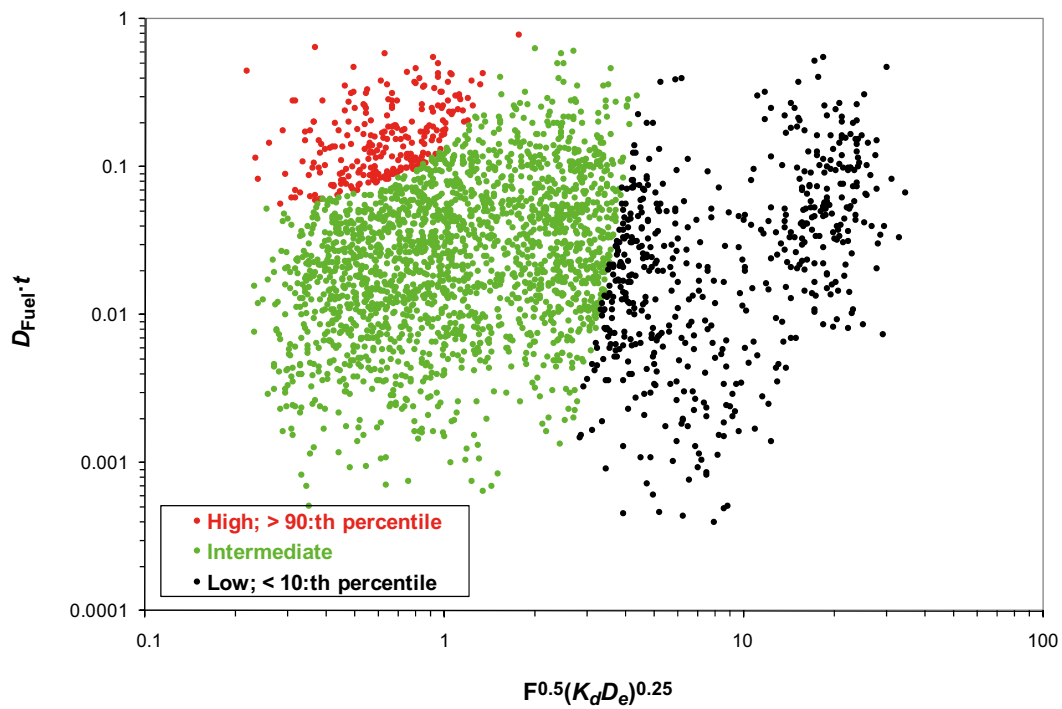


Figure 13-48. Partition plot demonstrating how the two groups of variables on the axes relate to high and low dose results for Ra-226.

Additional methods employed after the reporting of the SR-Site assessment

A variance based sensitivity analysis is a powerful method for global sensitivity analysis, albeit potentially demanding in terms of calculation capacity. Analyses based on the determination of so called Sobol' indices have been at the centre of the development of such methods. Here, variance of the output of a model is decomposed into terms which can be attributed to single input parameters and to combinations of input parameters (Sobol' 1993, Homma and Saltelli 1996). A full set of Sobol' indices for the probabilistically calculated peak Ra-226 dose was determined in Hedin (2013). The analysis confirmed the findings of the simpler SRRC method by identifying, in descending order, the transport resistance along the geosphere flow path, F , the fuel dissolution rate D_{Fuel} , and the failure time $t_{Failure}$ as the three most important parameters. The order of two highest ranking parameters was reversed compared to the SRRC results.

An alternative way of demonstrating how individual parameters or parameter combinations contribute to high or low model output values is through so called cobweb plots (Cooke 1995), a straightforward method of displaying relationships between input and output data for probabilistic modelling results. Figure 13-49 shows a cobweb plot for the peak dose of Ra-226, reproduced from Hedin (2013). On the leftmost vertical axis, output values of the Ra-226 dose are represented in the form of percentiles. The Figure shows the 5 percent highest (red lines) and the 5 percent lowest (black lines) dose values. For each realization represented in the plot, a line is drawn from its output Ra-226 dose on the leftmost axis to the corresponding input value of the F -value on the next vertical axis. Each line continues to the remaining axes, connecting to the input values of the variables represented on these. It is obvious from the figure that high dose results are related to low values of the geosphere transport resistance, high values of the fuel dissolution rate and to low values of the failure time and, to a lesser extent, to low values of the geosphere sorption coefficient of Ra. Low doses are clearly related to high F values and to some extent to high values of the geosphere sorption coefficient of Ra. The outcome is in good agreement with the results of the analysis based on conditional mean values reported above.

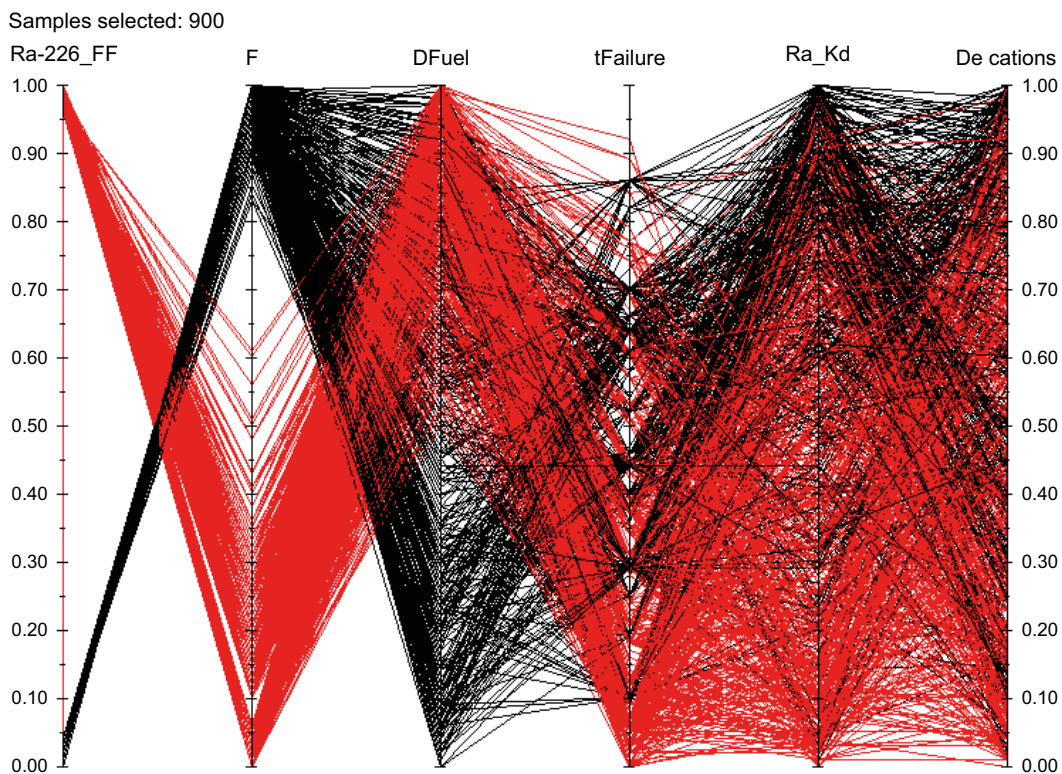


Figure 13-49. Cobweb plot for the peak Ra-226 dose results.

Conclusions

The above analyses show that it is possible to identify the uncertain input parameters to which the probabilistic result is most sensitive with relatively simple methods. This is in part due to the nature of the conceptualisation of the calculation cases in the corrosion scenario, where the buffer is omitted and the near-field release is essentially controlled only by the fuel dissolution rate.

The fuel dissolution rate, D_{Fuel} , and the geosphere transport resistance factor, F , emerge generally as the uncertain input parameters to which the result is most sensitive. The uncertainty in corrosion release rate, CRR , has a significant impact on the result of near-field releases immediately after failure for nuclides that are released congruently with metal corrosion.

It is also noted that a number of different assumptions regarding transport conditions were analysed in Section 13.5.6, where it was found that the sensitivity to these assumptions is low, see Figure 13-41 and Figure 13-42. Similar results are expected for all corrosion variants since they differ from the central corrosion case only through somewhat altered input distributions for the failure times and the hydrogeological transport parameters.

It is noted that, in the corrosion scenario, the canister failure times and positions are determined by the distribution of advective flow at the deposition holes and of the distribution of sulphide concentrations. As concluded in Section 12.6.2, it is only combinations of the highest flows with the highest concentrations that have the potential of yielding canister failures.

Finally, it has been demonstrated that a more advanced method based on variance analysis yields similar sensitivity results as the simpler methods employed in the SR-Site assessment and that a cobweb plots identifies the same parameters related to high dose consequences as the conditional mean value analysis in the SR-Site assessment.

13.6 Canister failure due to shear load

13.6.1 Conceptualisation of transport conditions

Canister failure due to rock shear was demonstrated to have a low probability in the reference evolution. The only identified cause for this failure mode is the event of large earthquakes in the vicinity of the repository, see further Section 10.4.5.

Pessimistic estimates of the extent of this failure mode in Section 10.4.5 indicate that the probability that one out of the 6 000 canisters has failed at the end of the one million year assessment period is 0.079. A failure frequency as a function of time is also provided in Section 10.4.5, Figure 10-129, and this is used in the probabilistic assessment of the canister failure due to shear load scenario, briefly called the shear load scenario in the following.

A calculation case is formulated, based partially on the analyses carried out in Section 10.4.5. The following data and assumptions are used.

- In the affected deposition holes the faulting is supposed to be so large that it causes massive failure of the canister. A delay time of 100 years between failure and the onset of radionuclide transport is assumed, based on a pessimistic estimate of the time required to fill the canister with water (see further the **Data report**). Thereafter, no credit is taken from limited transport resistance in the canister.
- The shear movement will not affect the buffer to the extent that its protection against advective flow will be impaired, but the effective amount of buffer between the canister and the shearing fracture is assumed to be reduced from 35 to 25 cm. In Section 10.4.5, canister failures are pessimistically assumed to occur for shear movements exceeding 5 cm in fractures intersecting deposition holes. The reduction in buffer thickness by 10 cm is selected in relation to this criterion.
- The canister failure location is assumed to fully coincide with the location of the shearing fracture. Furthermore, the shear is assumed to increase the fracture transmissivity significantly. The Q_{eq} value for the intersecting fracture is, therefore, assumed to be sufficiently high ($1 \text{ m}^3/\text{yr}$) that it does not contribute to the transport resistance in the near-field. Nor are any transport resistances

related to the geometric constraint of the fracture intersection with the buffer assumed, meaning that the flux through the buffer is that obtained with a zero concentration of radionuclides on the buffer exterior.

- The shearing fracture is likely to be among the larger in the modelled fracture network and its properties after shearing are difficult to assess. Therefore, no credit for radionuclide retention in the geosphere is taken.
- Solubility limits are imposed since, contrary to case in the corrosion scenario, the buffer is in place in the shear load scenario.

All other data and assumptions are handled probabilistically, with data from the **Data report**. This concerns the radionuclide inventory, the fuel dissolution rate, the metal corrosion rate and buffer sorption and diffusion data.

13.6.2 Consequence calculations

Postulated failure at 100 000 years

Figure 13-50 shows the result of a calculation where the failure of one canister at 100 000 years is postulated. As for the corrosion scenario, the contributions from the instantaneously released fraction of nuclides, IRF, are not included here. Note that the near-field dose equivalent release and the far-field dose are the same since no retention in the far-field is assumed. The total dose is dominated by Ra-226, which is efficiently transferred through the buffer. The solubility of Ra-226 has a very limited impact on the result. The slight decrease of Ra-226 dose at the end of the calculation period is due to the decrease in inventory of U-234 in the fuel matrix.

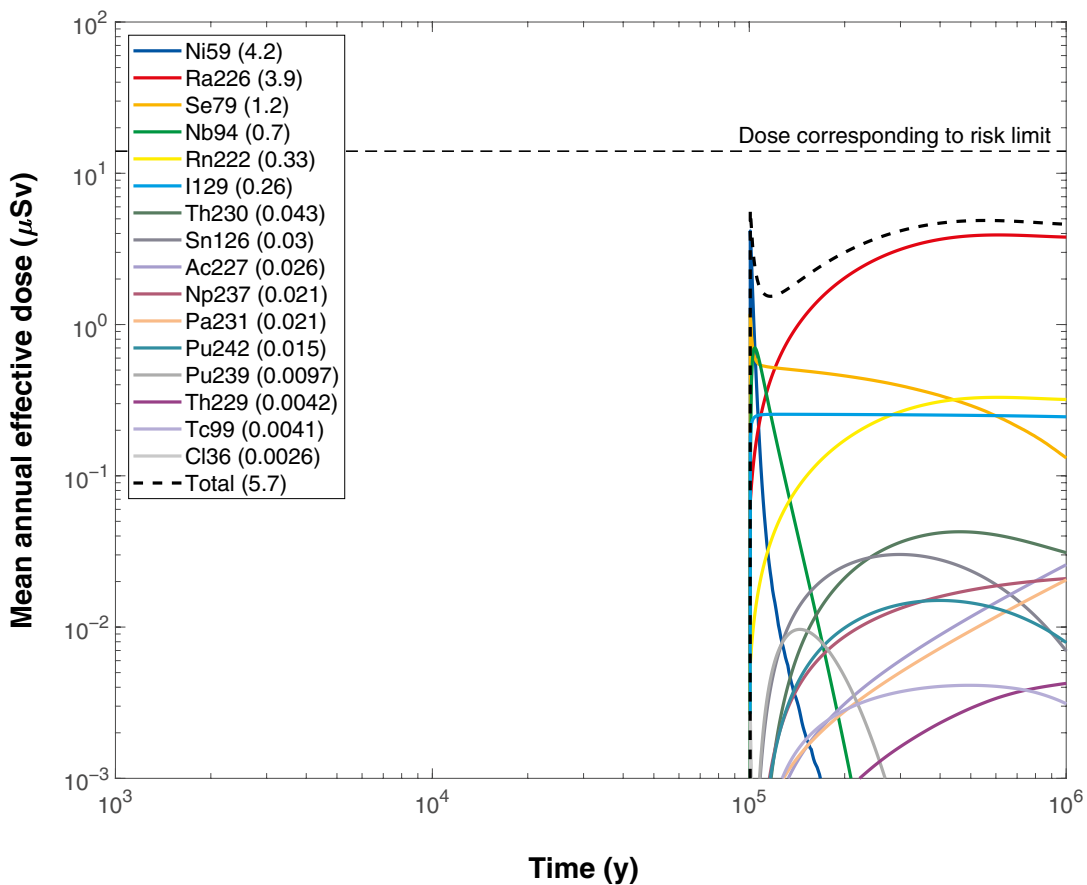


Figure 13-50. Far-field annual effective dose for a probabilistic calculation postulating failure of one canister due to rock shear at 100 000 years.

Distribution of failures between 1 000 and 1 000 000 years

Figure 13-51 shows a probabilistic evaluation of rock shear failures for the period between 1 000 and one million years and using the frequency of canister failures due to shear load from the reference evolution cited above. The doses are dominated by releases of Ra-226 after about 100 000 years. Before that, releases of Nb-94 and C-14 dominate. It is seen that the peak dose of 0.18 μSv , occurring at one million years is about two orders of magnitude below the dose corresponding to the regulatory risk limit, 14 μSv .

Due to the assumed high equivalent flow rate in the Q1 buffer/rock interface, the outward transport capacity from the near-field is in general sufficiently high to carry away all radionuclides released from the fuel, thus rendering solubility limits in the near-field ineffective. As an illustration, a probabilistic case where no credit was taken for co-precipitation of Ra/Ba was calculated, i.e. where the solubility of Ra was increased by a factor of 1 000. This led to an increase of the release rate of Ra by only a factor of about 1.6 (see further the **Radionuclide transport report**).

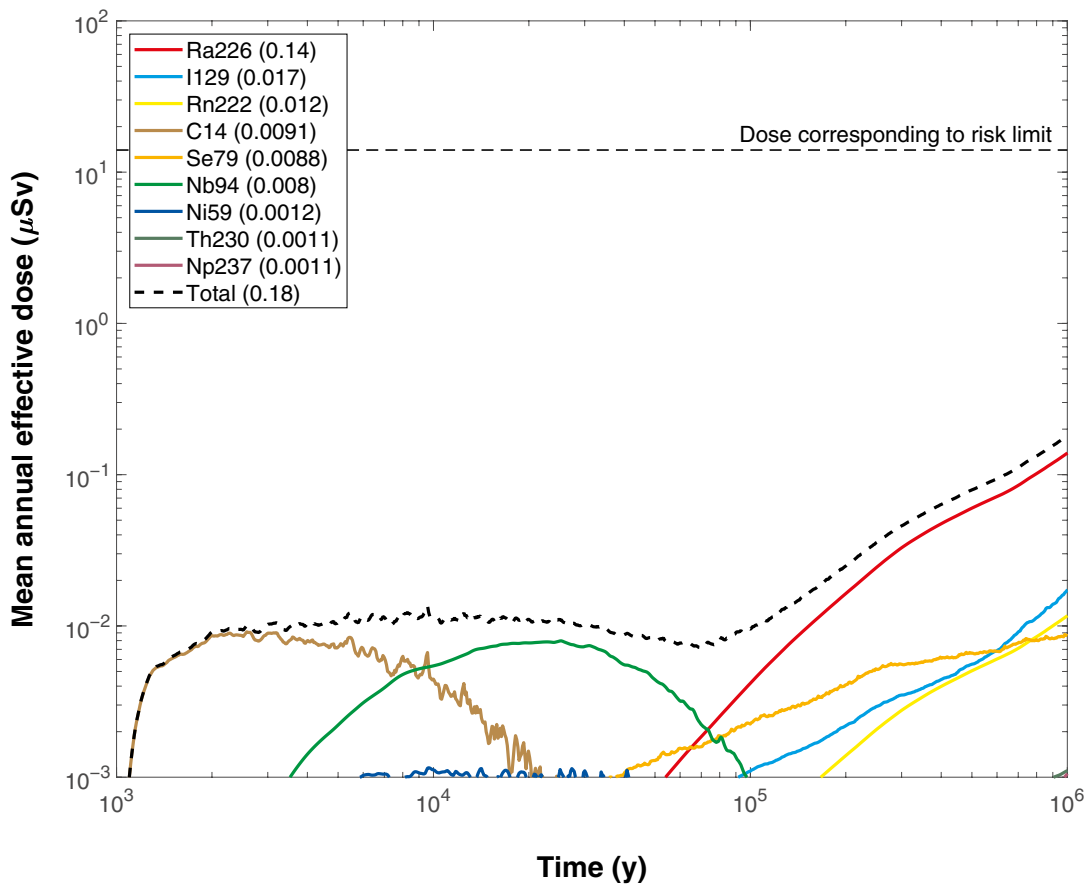


Figure 13-51. Probabilistically calculated consequences of shear failure, for the period between 1 000 years and one million years. The legends are sorted according to descending peak mean annual effective dose over one million years (given in brackets in μSv).

Distribution of failures up to 1 000 years

For times up to 1 000 years after closure, the frequency of earthquakes is assessed to be lower, with a probability that one out of the 6 000 canisters has failed at the end of the initial 1 000 year period being 2.4×10^{-5} , see further Section 10.4.5. Also, the use of LDF values overestimates the doses in this time perspective since i) the LDF is a pessimistic upper bound for releases occurring continuously over an entire interglacial period taking into account accumulation, whereas a large part of the interglacial period has elapsed without any releases when the repository is sealed and ii) it is not meaningful to use the LDF concept for a radionuclide that decays to insignificance over an interglacial period, since the concept is based on a continuous uniform release over the period.

A more detailed calculation of the shear load failure case for the initial 1 000 years was therefore done. In this calculation, releases from the near-field were determined as for all other cases, and also the IRFs were included. Since no credit is taken for geosphere retention in the shear scenario, the near-field releases were used as direct input to the biosphere modelling. Since it is not possible to determine a location of the releases among the identified potential landscape objects, the mean release over all realisations as a function of time was fed to each object and the time dependent development of radionuclide transport and dose in the landscape was calculated for each object. The object giving the highest dose was then determined for each point in time and for each radionuclide. This entity is pessimistically defined as the calculated dose consequence for the case of a shear failure during the initial 1 000 years. A well was included in each landscape object in the same way as for the LDF calculations. The modelling of failures and of consequences in terms of releases and doses was continued to 10 000 years to facilitate comparisons with the LDF results for the one million year time frame presented above.

The peak dose is almost four orders of magnitude lower than that corresponding to the regulatory risk limit, see Figure 13-52. The release of C-14 dominates the initial 1 000 years. (Note the extended dose scale, required as the most of the dose curves lie below the scale used for other figures). The curve shape of C-14 is due to the release dynamics and to the temporal development of the landscape, in particular the transitions from sea to lake occurring at different times for different biosphere objects. The modelling of the dose consequences in the two time frames are compared in Figure 13-53.

As for the corrosion scenario, the calculated consequences of the shear load scenario represent a contribution to the calculated risks associated with releases from the repository. This is further addressed in Section 13.9.

Risk dilution

Risk dilution for the shear load scenario needs to be considered, since canisters fail at probabilistically determined times.

An illustration is obtained by comparing the results in Figure 13-50 (postulated, deterministic failure time) with those in Figure 13-51 (distribution of failure times). If the result in Figure 13-50 is multiplied by the overall probability of the event occurring during the assessment period, i.e. 0.079, then the dose at one million years ($0.31 \mu\text{Sv}$) is close to that obtained at one million years in Figure 13-51 ($0.18 \mu\text{Sv}$).

This is because the consequences are determined i) by in-growth of Ra-226 and ii) by the build-up of Th-230 released from the fuel and precipitated in the canister interior or sorbed in the buffer, and thus in general occur long after the failure time. The in-growth of Ra-226 is essentially controlled by the build-up of its parent nuclide Th-230, that occurs over a time scale comparable to the half-life of Th-230 which is approximately 75 000 years. The build-up of Th-230 occurs over times determined by the fuel dissolution rate which are of the order of one million years.

Risk dilution, including a treatment of the pulse releases, is further discussed in Section 13.9.5.

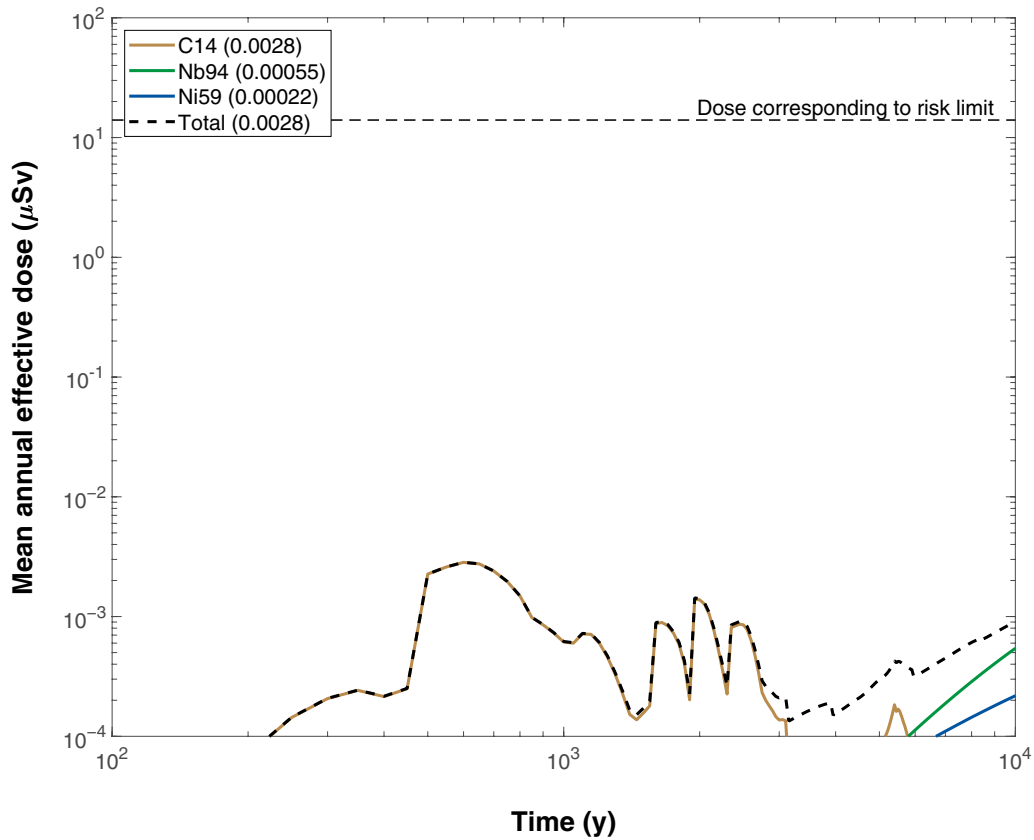


Figure 13-52. Probabilistically calculated consequences of shear failure, occurring for the period up to 10 000 years.

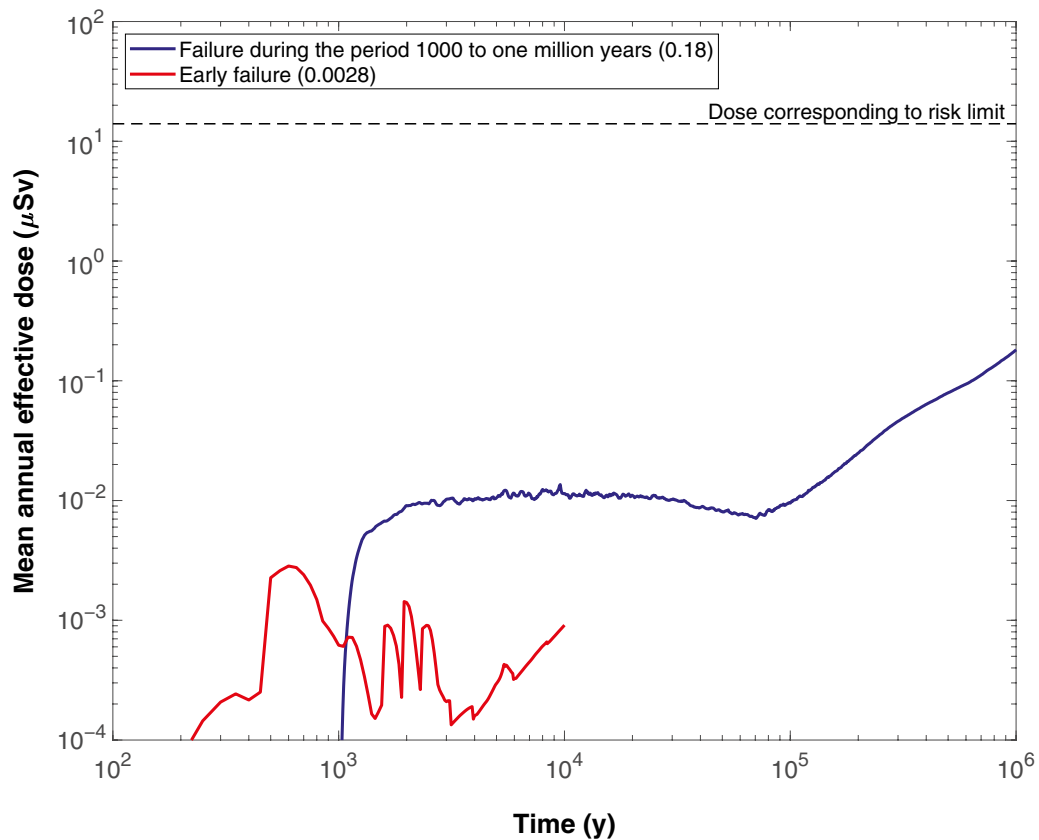


Figure 13-53. A comparison of mean annual effective doses for early shear load failures modelled transiently in the biosphere and failures in the 10^3 – 10^6 year time frame modelled using LDF values.

Global sensitivity analysis

A global sensitivity analysis on the results of the probabilistic shear load case using the SRRC method as for the central corrosion case yields results according to Figure 13-54.

Regressing the total dose at 10^6 years on the input variables yields, in descending order, the fuel dissolution rate D_{Fuel} , the solubilities of Radium and Thorium, and the failure time $t_{Failure}$ as the input parameters most affecting dose results. Regressing on Ra-226 dose at 10^6 years yields a similar result due to the dominance of Ra-226. The significance of the solubility of Thorium is due to decay of Th-230 to Ra-226 in the buffer, where the release of Th-230 to the buffer is controlled by the solubility of Th. A further scrutiny of individual realisations reveals that the significance of the limited solubility overall is due to a relatively limited number of realisations with low solubilities, whereas the total dose is dominated by the larger number of realisations where the solubilities are sufficiently high not to limit the release. Thus solubilities of neither Th nor Ra, where co-precipitation with Ba is taken into account significantly limit the mean release rate of Ra-226. This conclusion is corroborated by the fact that the case with the omitted buffer, where neither sorption in the buffer nor solubility limits are included, see Section 13.6.3 yields increases in Ra-226 mean dose by only a factor of 2.

Regressing instead on the maximum of total dose over time yields the failure time and the corrosion release rate, CRR , as significant variables. This is consistent with the fact that, for early failures, the highest doses occur due to release of e.g. Ni-59 and Nb-94 congruently with the corrosion of structural parts of the fuel elements.

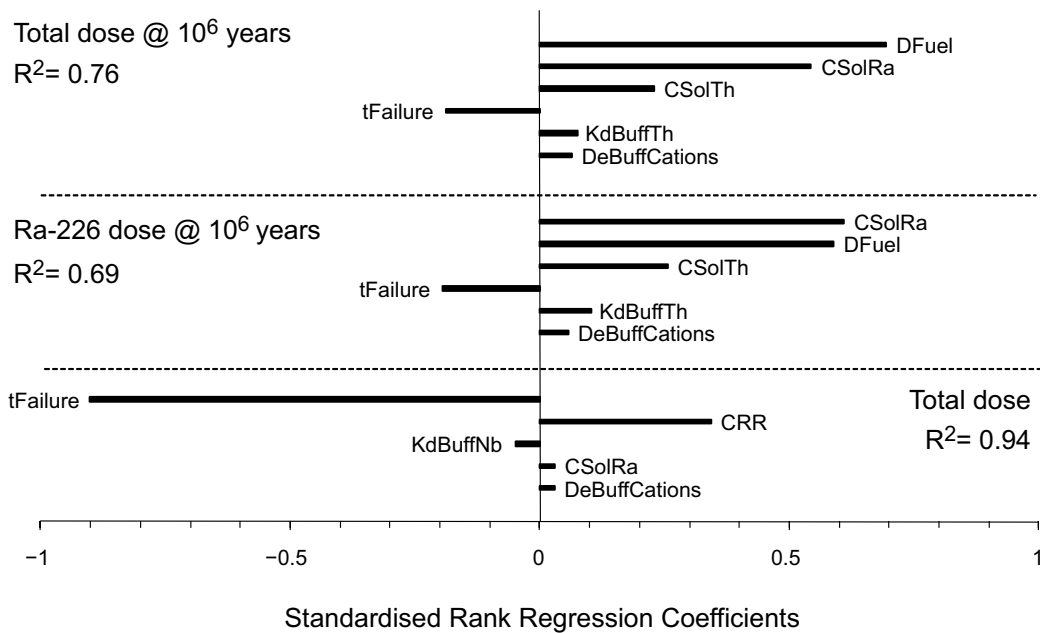


Figure 13-54. Results of standardised rank regression. Regressing on total dose at 10^6 years and on Ra-226 dose at 10^6 years yields similar results due to the dominance of Ra-226. Regression on the maximum of total dose over time identifies CRR as an additional sensitive input parameter. From the SR-Site assessment.

13.6.3 Combination of the shear load and the buffer advection scenarios

As noted in the discussion of buffer erosion in combination with shear movement in Section 12.9.3, the consequences of a shear failure followed by buffer erosion need to be considered, since it is reasonable to assume that the groundwater flow in a fracture that has undergone a major secondary shear movement could be high. Buffer erosion could then ultimately lead to loss of the buffer and its retardation function in the deposition hole with the canister failed due to shearing. A similar situation could arise if the buffer material is transformed through interaction with iron ions from the failed canister, as discussed in the buffer transformation scenario in Section 12.4.

The case with shear failures distributed between 1 000 and one million years was therefore calculated also for near-field conditions with a missing buffer. The conceptualisation of the near-field is thus the same as in the corrosion scenario, but near-field flow data are stylised and geosphere retention is disregarded as in other consequence calculations for the shear load scenario. The results are shown in Figure 13-55.

The result is similar to that where the buffer is present in Figure 13-51, in particular beyond 100 000 years. The peak annual effective dose from Ra-226 increases by a factor of 2 from 0.14 μSv to 0.28 μSv . The retardation in the buffer and the limited solubility of the dose driving Ra-226, both of which contribute to retardation only when the buffer is present, are thus of minor importance in the shear load scenario. This result is also consistent with the limited effect of imposing solubility limits as a variant case in the corrosion scenario, where solubility limits are otherwise not imposed due to the absence of the buffer.

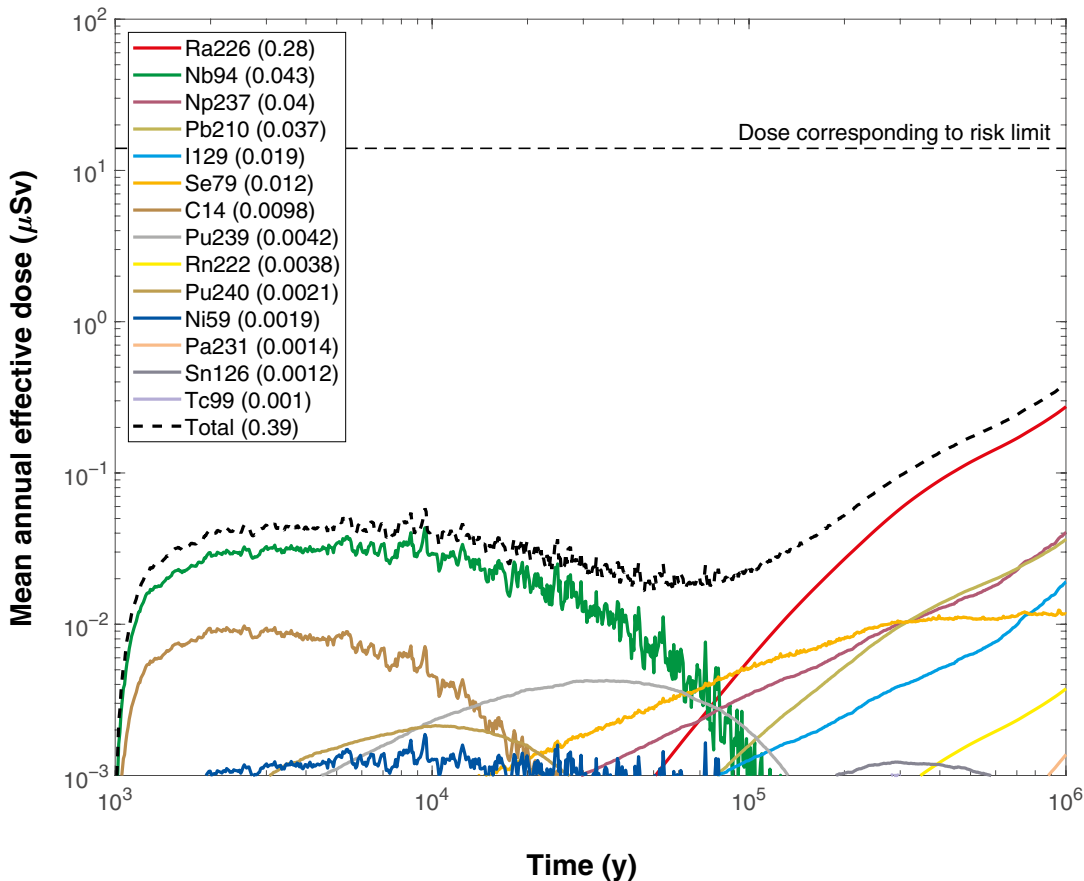


Figure 13-55. Probabilistically calculated consequences of shear failure with advective conditions in the deposition hole, for the period between 1 000 years and one million years. The legends are sorted according to descending peak mean annual effective dose over one million years (given in brackets in μSv).

The main difference for the radionuclides contributing most to dose is for Nb-94, as this is significantly retained in the buffer when it is present. However, Nb-94 contributes to dose mainly before 100 000 years. The above case is only relevant after the buffer has been eroded. Since the near-field hydrogeological conditions are stylised with respect to radionuclide transport in the above case, they are not necessarily relevant for estimating the time taken for buffer erosion to cause advective conditions in the deposition hole. The first advective positions occur after several tens of thousands of years in the buffer advection scenario. However, considering the unknown nature of the hydraulic conditions in the deposition hole after a shear failure, the results in Figure 13-55 are seen as cautiously representative of a combined scenario for times beyond 10 000 years.

This combined case is further considered in the risk summation in Section 13.9.

13.6.4 Analysis of potential alternative transport conditions/data

The transport data used in the calculation of the probabilistic base case calculation are those provided in the **Data report**. The data have been selected for certain conditions and in the following, it is analysed i) whether the evolution in the shear scenario is compatible with these conditions and ii) whether any alternative evolutions of the system, that could imply less favourable transport conditions, need to be considered.

This analysis corresponds to the analysis of the possible routes to alternative containment conditions in Section 12.8.2, but is simplified based on the analyses already done in the derivation of data in the **Data report**.

Number of failed canisters and failure times

This is the outcome of the analysis of the containment potential for the shear load scenario, and has thus been exhaustively analysed in Section 10.4.5.

Radionuclide inventory, IRF and CRF

It is not relevant to include these entities here since they are not affected by external factors, but by conditions determining the initial state. Uncertainties related to the initial state are fully explored in the **Data report**.

Metal corrosion rate

Even for a very early shear failure the temperature is not expected to be above 70 °C for a water filled canister. Therefore, as for the corrosion scenario, see Section 13.5.4, the corrosion rates used in the **Data report** are valid (with a large margin) also for the shear load scenario.

Fuel dissolution rate

In this case the buffer is in place and the expected hydrogen concentrations are relatively high, as discussed later in Section 13.7.2. On the other hand the radioactivity of the fuel may be higher at the time of water contact. However, the iron corrosion will continue for tens of thousands years and during this time fuel activity will decrease to levels below the alpha activity threshold (Muzeau et al. 2009). Even for a very early shear failure the temperature is not expected to be above 70 °C for a water filled canister.

Solubilities

Redox conditions

The solubility of several of the important radionuclides is strongly dependent on the prevailing redox conditions in the near-field of the repository. For example, the solubility of technetium increases by many orders of magnitude for a $p_e > 0$. However, since the redox chemistry inside the canister will be dominated by the iron corrosion products (magnetite), the redox potential is expected to stay low under all circumstances.

Need for studies of additional evolutions to rule out unfavourable redox conditions: None; the vast amounts of iron and its anoxic corrosion products will buffer the redox conditions inside a defective canister.

pH

Natural groundwaters will have a pH in the range of about 6–9. The dissolution of low pH cement used for grouting and plugs could locally give a pH of ~ 11.

Need for studies of additional evolutions to rule out unfavourable pH conditions: As stated in Section 13.5.5, a pH above 11 or below 6.3 can be excluded. This range is already covered in the assessment of solubilities.

Temperature

The most relevant uncertainty associated with the thermodynamic data is the effect of temperature on the stability of aqueous species and solid compounds. In the database used a selection of reaction enthalpy is included, although in some cases no enthalpy data are available. The approach to correct the equilibrium constants for temperature effects follows the Van't Hoff equation, which relates the change in temperature to the change in the equilibrium constant, given that the standard molar enthalpy of reaction ($\Delta_r H^\circ$) is considered constant at all temperatures (Allard et al. 1997, p 434). The calculations in SR-Site (used also in the PSAR) are based on fixed temperature of 25 °C, since it is judged that the small temperature variations that can be expected in the repository when solubility limits are important will have marginal effect on the calculated values.

Need for studies of additional evolutions to rule out unfavourable temperature conditions: Solubility limits are generally only important for the long-term assessment. This means that temperatures above 25 °C are of limited or no concern. Even in the case of an early failure the period with temperatures > 25 °C will be short compared to the assessment time scale. Temperatures between ~0–25 °C may on the other hand be important for solubility. Since there is a scarcity of enthalpy data, no temperature effects have been included in the solubility calculations in SR-Site (used also in the PSAR). Instead a sensitivity study has been made in the documentation of the solubility assessment (Grivé et al. 2010). The conclusion is that the effect of temperature < 25 °C on the elemental solubilities is limited.

Groundwater ionic strength

The treatment of *activity corrections* also represents an uncertainty to the current solubility assessment. The range of ionic strength (I) in the groundwaters used (Duro et al. 2006) is from 10^{-3} to 2 mole/dm³. The most appropriated procedure to conduct activity corrections in this range would be the Specific Interaction Theory (SIT) (Allard et al. 1997, p 331). However, this approach is still not implemented in the geochemical codes used and, therefore, the extended Debye-Hückel approach (Allard et al. 1997, pp 328–329) has been used for activity corrections. The results obtained by using the extended Debye-Hückel approach are comparable with the ones obtained by the SIT for those cases where the comparison is possible. Higher ionic strength than 1 mole/dm³ would lead to an increased uncertainty in the obtained results.

Need for studies of additional evolutions to rule out unfavourable ionic strength conditions: As discussed for the fuel dissolution in Section 13.5.5, the reference evolution includes the highest salinities that can be expected at Forsmark, and no additional analyses are required.

Minor components in groundwaters

The lack of data on phosphate species and solid phases is an important drawback in the prediction of the solubility of some elements, mainly for rare earth elements and trivalent actinides. The consideration of phosphate in the groundwater composition may cause a change in the selected solubility controlling phases as well as in the solubility limits recommended for some of the radionuclides. Inclusion of phosphate phases and species could potentially lead to either higher or lower solubilities for radio-elements.

Need for studies of additional evolutions to rule out unfavourable conditions: There will be a competition for phosphate between the iron together with its corrosion products and the components in the spent fuel. The total concentrations of phosphate in the Forsmark groundwaters are generally low and are therefore not expected to have any significant impact on the solubilities. Therefore, it is concluded that no additional studies of the effect of phosphate on the solubilities are required.

Conclusions

The suggested handling of, and data for, solubilities in the **Data report** are sufficient to cover the shear failure scenario.

Buffer porosities

This case involves no loss of buffer mass. The suggested handling of, and data for, porosities in the **Data report** are, therefore, sufficient to cover the shear failure scenario. Furthermore, as shown in Section 13.6.3, a loss of buffer following shear failure has a limited impact on the consequences.

Buffer diffusivities and buffer partitioning coefficients

Cases leading to decreased retardation of radionuclide transport may be expressed through alterations of the parameters that affect radionuclide interactions with bentonite. These are separated into the following:

Intrinsic or structural parameters:

- Bentonite composition.
- (Assumed) tightness with regard to CO₂ exchange with the host formation.

External or environmental parameters such as:

- Changes in assumed groundwater composition, or pCO₂ imposed by the host formation leading to changes in porewater composition (very high or very low pH, high ionic strength, high concentration of competing cations/complexing ligands).
- Temperature.

The effects of different factors will be different for each radionuclide (or group of radionuclides). The validity range of sorption and diffusion coefficients is dependent on the uncertainties considered to be associated with each parameter in data derivation in the **Data report**. Different assumptions regarding these uncertainties would have led to a different validity range.

Lower buffer density will correspond to higher diffusion coefficients. Sorption will only be affected by the density if the porewater chemistry is significantly changed due to the higher water/solid ratio, but the effect of this ratio is of little importance in comparison to bentonite and groundwater composition. Smectite (montmorillonite) is the principal source of sorption sites; its content determines the magnitude of sorption. K_d values are selected for a CEC of 85 meq/100 g in the **Data report**. Changing this internal factor to a lower value will lead to a lower K_d , but the effect is small considering the range of the K_d values. A lower CEC is easily compensated by e.g. a slight variation of pH within the given uncertainty range. The content of accessory minerals of the bentonite influences porewater composition. Calcite in bentonite is needed to establish carbonate buffering. Absence of calcite would increase the dependency on groundwater composition; the corresponding effects on porewater composition were not quantified in Ochs and Talerico (2004). Absence of salts gives porewater results that lie within the parameter space already considered. Higher salt content is only relevant if it leads to a porewater salt concentration higher than that covered by the parameter space considered (ionic strength up to ~0.76 M, Ochs and Talerico 2004). Tightness with regard to CO₂ is relevant because CO₂ exchange influences porewater pH. Completely open/closed systems were considered in the data derivation and thus already included in the selected range of sorption parameters.

Salinities of groundwater up to seawater was considered in Ochs and Talerico (2004). Higher salinity may lead to lower K_d values, in particular for Cs/Sr/Ra. Increased chloride concentrations will lead to lower sorption of most radionuclides due to complexation, but this effect will, in most cases, be within the range already considered. Double layer effects will be decreased; therefore anion exclusion effects will be less important at high salinity. D_e could increase for anions at high salinity. The lowest porewater pH considered for sorption was 6.6 (Ochs and Talerico 2004). A lower porewater pH may lead to a different distribution of K_d values.

Need for studies of additional evolutions to rule out unfavourable conditions: A loss of buffer density or a change in montmorillonite content is not directly foreseen in the shear load scenario, but this issue is discussed further in the subsection immediately below. The evolution of pH and ionic strength of the groundwater is discussed in Section 13.5.5. The range of possible ionic strength is already considered in the data for diffusivities and K_d values in the **Data report**. However, as seen in the sensitivity study presented in Table 10-11, a combination of high groundwater flow, the MX-80 bentonite and a low groundwater pH could lead to a porewater with a pH that is slightly lower than the pH 6.6 that was used as the lower limit for the derivation of K_d values in the **Data report**. This means that there could be cases where the K_d values selected are inappropriate. This case requires a high flow, which is the case in the shear load scenario, but a high flow also means that the sorption in the buffer will contribute very little to the retardation of radionuclides. Also the limited additional consequences of this case are bounded by those of the combination of shear load and buffer advection, see below.

Buffer hydraulic conductivity and swelling pressure

To ensure that diffusion is the dominant transport mechanism in the buffer the safety function indicator criteria for hydraulic conductivity and swelling pressure should be upheld (see Section 8.3.2). The fulfilment of these criteria is basically dependent on the density and montmorillonite content in the buffer. Neither of these is expected to be directly affected by a shear failure of the canister. However, there may be indirect effects:

1. As described in Section 12.4 it cannot be excluded that metallic iron will have an effect on the montmorillonite. Currently, there is no reliable method to quantify this effect.
2. A combination of canister failure due to the shear load scenario and the buffer advection scenario would lead to a case with advective conditions in the deposition hole.

A severe transformation of the buffer caused by the metallic iron from the canister insert according to 1 above would lead to a similar situation as 2.

Need for studies of additional evolutions to rule out unfavourable conditions: A failed canister due to shear load in combination with advective conditions in the deposition hole needs to be considered. This can represent both cases described above. The consequences of such a case are presented in Section 13.6.3.

Rock data

Rock data are either stylised and pessimistic (applies to Q_{eq}) or irrelevant since geosphere retention is pessimistically neglected (applies to all other rock data).

Biosphere LDF factors

As for the corrosion scenario, all climate conditions emerging from the analyses of the evolution of the system are covered by the different LDF values available.

Overall conclusion regarding additional cases to analyse

The transport data provided in the **Data report** and used in the probabilistic base case calculation of the shear load scenario give a sufficient coverage of transport conditions for the shear load scenario.

13.6.5 Doses to biota, alternative safety indicators, analytical calculations and collective dose

Doses to biota

Releases for the shear load scenario have not been analysed with respect to doses to biota in SR-Site or the PSAR. However, since the releases are generally lower for this scenario than for the corrosion scenario, and since the margin to the reference value is, according to Section 13.5.7, several orders of magnitude in the latter, it is concluded that the effects on the environment for the shear load scenario are of no concern.

Alternative safety indicators

The same alternative safety indicators as for the corrosion scenario (Section 13.5.8) have been applied to the calculated releases for the shear load scenario (see further the **Radionuclide transport report**). Since the releases are generally lower for this scenario than for the corrosion scenario, the margins to the reference values are several orders of magnitude also for the shear load scenario.

Analytical calculations

The probabilistic case with shear failure with advective conditions in the deposition hole, for the period between 1 000 years and one million years (Figure 13-55), has been calculated also with the analytical models (see the **Radionuclide transport report**). The agreement is good and the peak dose, occurring at one million years is 0.36 μSv , compared to 0.34 μSv in Figure 13-55 for the numerical model.

Collective dose

SSMFS 2008:37 states the following: “The collective dose as a result of the expected outflow of radioactive substances during a period of 1 000 years after closure of a repository for spent nuclear fuel or nuclear waste shall be calculated as the sum, over 10 000 years, of the annual collective dose.”

In the shear load scenario, releases occur before 1 000 years and hence the collective dose is calculated for this scenario. The release during the first 1 000 years is dominated by C-14 and it is also the most important contributor to the collective dose. The complete, i.e. integrated over 50 000 years, collective dose commitment from C-14 releases during the first thousand years is estimated by multiplying the integrated release of C-14 during the initial 1 000 year period by a conversion factor of 109 000 manSv per PBq. This conversion factor has been recommended by the UNSCEAR (UNSCEAR 2000, Annex A) for estimating the complete collective dose commitment to the global population from releases of C-14 to the atmosphere. It has been calculated under the assumption that the future world population stabilises at 10^{10} people, and that the global inventory of stable carbon does not increase from its present value. Estimations of collective dose commitments from C-14 releases made with several different models have given very similar results (UNSCEAR 2000). This consistency between model predictions has been attributed to the long half-life of C-14, relative to its rate of environmental transport, which makes the estimated dose commitments insensitive to the detailed structure of the models or to the values of the parameters used in them. It is also concluded that doses following a release to soils or surface oceans are about the same as those for an atmospheric release (UNSCEAR 2000).

According to UNSCEAR (2000), 75 % of the complete dose commitment from a single release is delivered within 10 000 years. To estimate the incomplete collective dose commitment, i.e. the collective dose integrated over 10 000 years, the complete collective dose commitment is multiplied by 0.75.

The integrated release of C-14 during the initial 1 000 years is about 0.5 MBq. This yields a collective dose summed over 10 000 years for the shear load scenario of about 4×10^{-5} manSv.

13.7 Hypothetical, residual scenarios to illustrate barrier functions

In this section, hypothetical, residual scenarios to illustrate barrier functions are analysed. They encompass i) the scenario ‘canister failure due to isostatic load’, considered as residual according to the analysis in Section 12.7, ii) a failure mode where a hypothetical initial defect in the form of a penetrating pinhole in the copper shell grows into a larger defect in a single canister, iii) additional cases of hypothetical early failures in all canisters, and iv) a number of hypothetical cases where different barriers are assumed to be completely lost. The canister failure due to isostatic load scenario is analysed in Section 13.7.1. The pinhole case for a single canister is analysed in Section 13.7.2, using the COMP23 model for the near-field and both the FARF31 and MARFA codes for far-field transport. Additional cases of hypothetical early canister failures are analysed in Section 13.7.3, considering now failures in all canisters and also combinations with early buffer loss. Hypothetical cases illustrating consequences of assumed losses of barrier functions in all barriers, both one at a time and in combinations are analysed in Section 13.7.4.

13.7.1 Canister failure due to isostatic load

This section analyses the consequences of the scenario treating canister failure due to isostatic load, analysed in Section 12.7. This scenario was classified as residual in Section 12.7.6, since no routes to this failure mode were found. The following treatment is thus for a hypothetical, postulated failure mode.

For this failure mode, the canister (both the cast iron insert and the copper shell) is bypassed, whereas the buffer and the geosphere are assumed to have intact retention properties. Failure of the canister due to isostatic load would probably mean that the insert buckles slightly inwards, the copper shell follows and opens up near the lid. The dimensional changes are, however, expected to be small.

Three exits from the near-field are modelled: a fracture intersecting the deposition hole at the vertical position of the canister lid, denoted Q1, an excavation damaged zone, EDZ, in the floor of the deposition tunnel, Q2, and a fracture intersecting the deposition tunnel, Q3, see Figure 13-13 in Section 13.4.1. Geosphere transport data are from the base case of the semi-correlated hydrogeological DFN model. Thermally induced spalling is assumed to have occurred in the wall of the deposition hole meaning that the transport resistance at the interface Q1 is decreased.

The consequences of postulated failures of one canister due to isostatic collapse 10 000 years and 100 000 years after repository closure are shown in Figure 13-56. Since both hypothetical global causes (glacial load) and local causes (deficient material properties, higher than intended buffer density) for this failure mode can be envisaged, simultaneous failure of more than one canister needs to be considered and would yield consequences in proportion to the number of failed canisters, provided that all releases occur to the same biosphere object. If a large number of canisters fail, it is more appropriate to use the LDF values for a distributed release (Section 13.2.3) when converting release to dose, since the release can be expected to be distributed over several landscape objects. Illustrations of consequences of extreme cases where all canisters fail at 10 000 and 100 000 years are also shown in Figure 13-56. It is noted that the cases where one canister fails yield lower dose consequences at one million years compared to single canister failures due both to corrosion (where the buffer is eroded away, Figure 13-16), and to shearing (where geosphere retention is neglected, Figure 13-50). Additional cases are shown in the **Radionuclide transport report**.

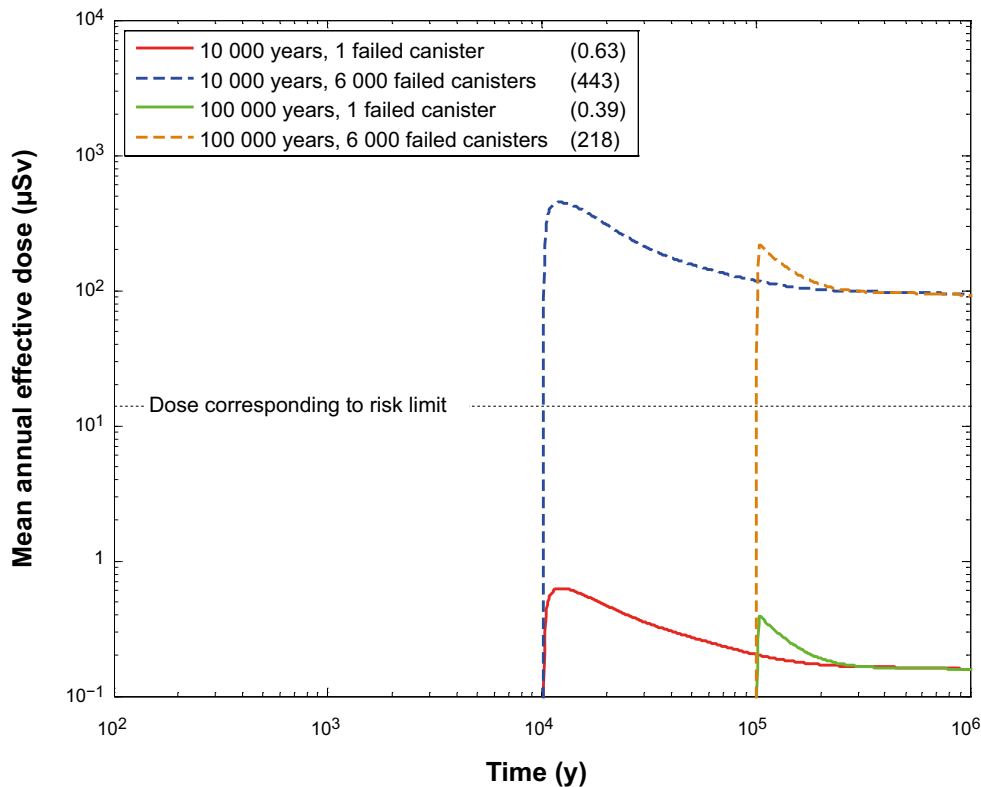


Figure 13-56. Postulated failures of one and of all 6 000 canisters at 10 000 years and at 100 000 years. The failed canisters are assumed to have no resistance to radionuclide transport. The single canister failures are calculated with the basic LDF values whereas for the global failures, LDF values for a distributed release are applied. Case not recalculated since SR-Site.

13.7.2 The growing pinhole failure in a single canister

As mentioned in the introduction, this failure mode is hypothetical since the initial state of the canisters implies that there will be no penetrating pinhole defects in the copper shell.

An analysis of this failure mode is, however, relevant in addressing important aspects of the internal evolution of the canister. For the pinhole failure mode, the pinhole in the canister wall initially offers a considerable transport resistance that is subsequently lost as the defect expands with time, whereas the buffer and the geosphere have intact retention properties. It is, therefore, also a convenient case for demonstrating the retarding capacity of the buffer and the geosphere and for exploring uncertainties relating to these components of the repository. Furthermore, the initially small defect is eventually expected to evolve into a large defect, which resembles the case of a failure caused by general corrosion of the canister, when the buffer is still intact. Although the likelihood of this latter failure mode was found negligible in the analysis of the corrosion scenario, Section 12.6, it is of interest to understand its consequences.

The evolution of the near-field (canister and buffer) after canister failure for the pinhole case and input data for the transport models, valid for the pinhole case, are described in the **Radionuclide transport report**, where also a number of calculation cases not shown here are found.

One canister is postulated to have an initial, penetrating defect. Water penetrates through the defect into the canister and the time to establish a continuous water pathway between the fuel and the canister exterior is pessimistically assumed to be 1 000 years. After an additional pessimistically estimated 9 000 years, the pinhole suddenly grows so large that all transport resistance is lost. (Cases with a continuous growth have been analysed in earlier assessments and shown to have the same general features in terms of consequences as cases with a sudden growth.) Three exits from the near-field are modelled: a fracture intersecting the deposition hole at the vertical position of the assumed pinhole defect (near the canister lid), denoted Q1, an excavation damaged zone, EDZ, in the floor

of the deposition tunnel, Q2, and a fracture intersecting the deposition tunnel, Q3, see Figure 13-13 in Section 13.4.1. Geosphere transport data are from the base case of the semi-correlated hydrogeological DFN model.

Calculations with COMP23 and FARF31

Figure 13-57 to Figure 13-60 show results for the near-field dose equivalent release and the far-field dose, as summed dose and decomposed into the three exit paths for a probabilistic base case calculation.

The near-field dose equivalent release is dominated by the non-sorbing nuclides C-14 and I-129, Figure 13-57. The peak values, occurring at 10 000 years when the canister is assumed to lose all its transport resistance, are due to the IRF and/or CRF of these nuclides. The release path Q1 dominates the initial releases and those immediately after 10 000 years, whereas the three release paths give more equal contributions longer after the failures, Figure 13-58.

The far-field peak total dose, Figure 13-59, is reduced by about a factor of 6 compared with that for the near-field. Non-sorbing nuclides dominate also the far-field dose. The reduction in dose between near-field and far-field is larger for sorbing species. The initial dominance of Q1 is less pronounced for the far-field, Figure 13-60, and here, the release paths Q2 and Q3 dominate in the long-term.

Several additional cases have been calculated to examine sensitivities to various transport conditions. The results are summarised in the text below and in Figure 13-61, and details are provided in the **Radionuclide transport report**.

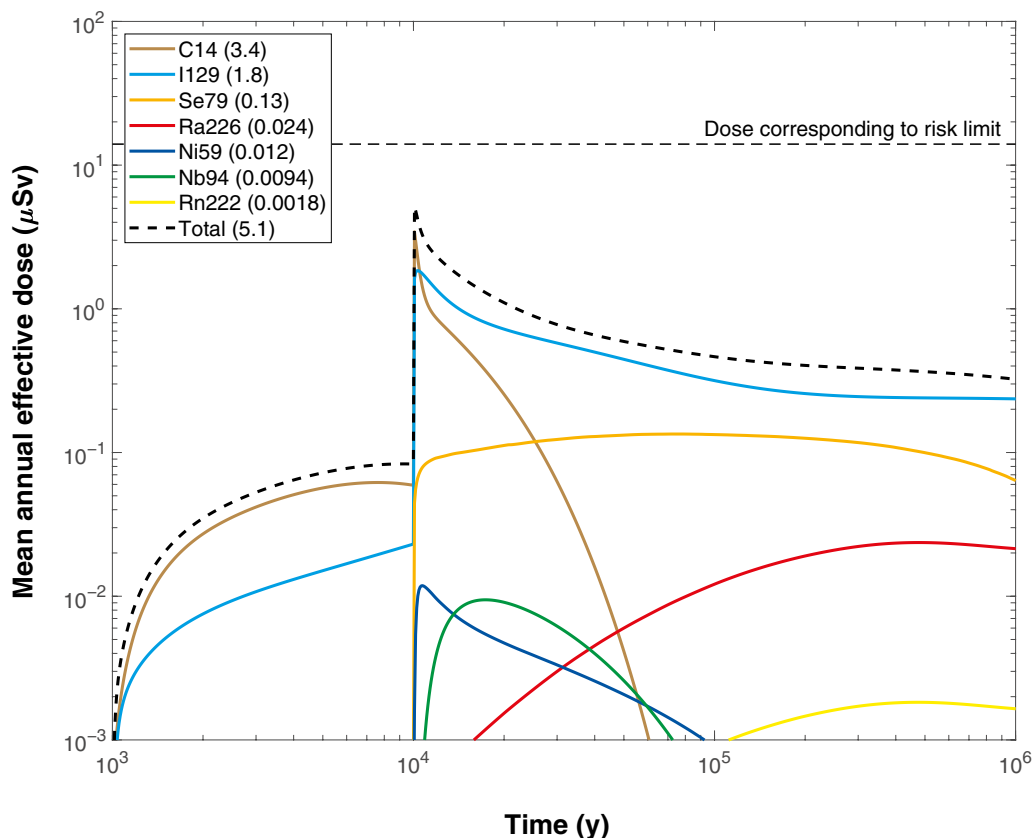


Figure 13-57. Near-field mean annual effective dose equivalent release for a probabilistic calculation for the base case for the pinhole failure mode. Summed doses for all release paths (Q1 + Q2 + Q3). The legends are sorted according to descending peak mean annual effective dose over one million years (given in brackets in µSv).

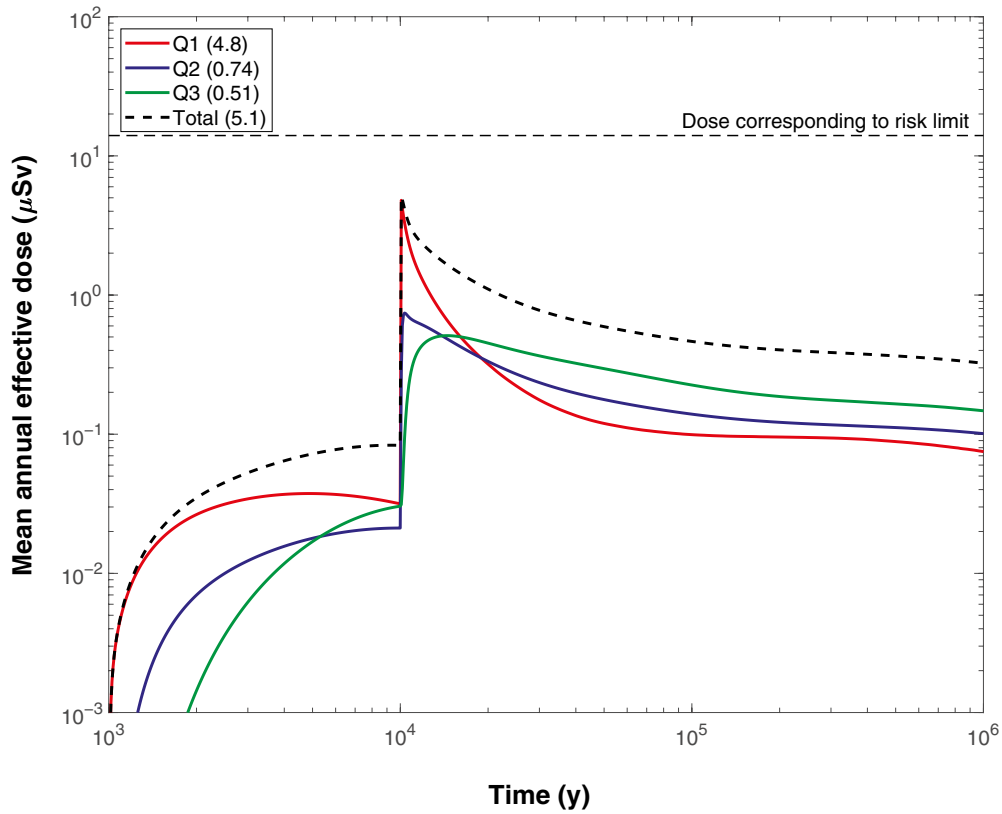


Figure 13-58. Near-field mean annual effective dose equivalent release for a probabilistic calculation for the base case for the pinhole failure mode. Doses decomposed into $Q1$, $Q2$ and $Q3$. The legends are sorted according to descending peak mean annual effective dose over one million years (given in brackets in μSv).

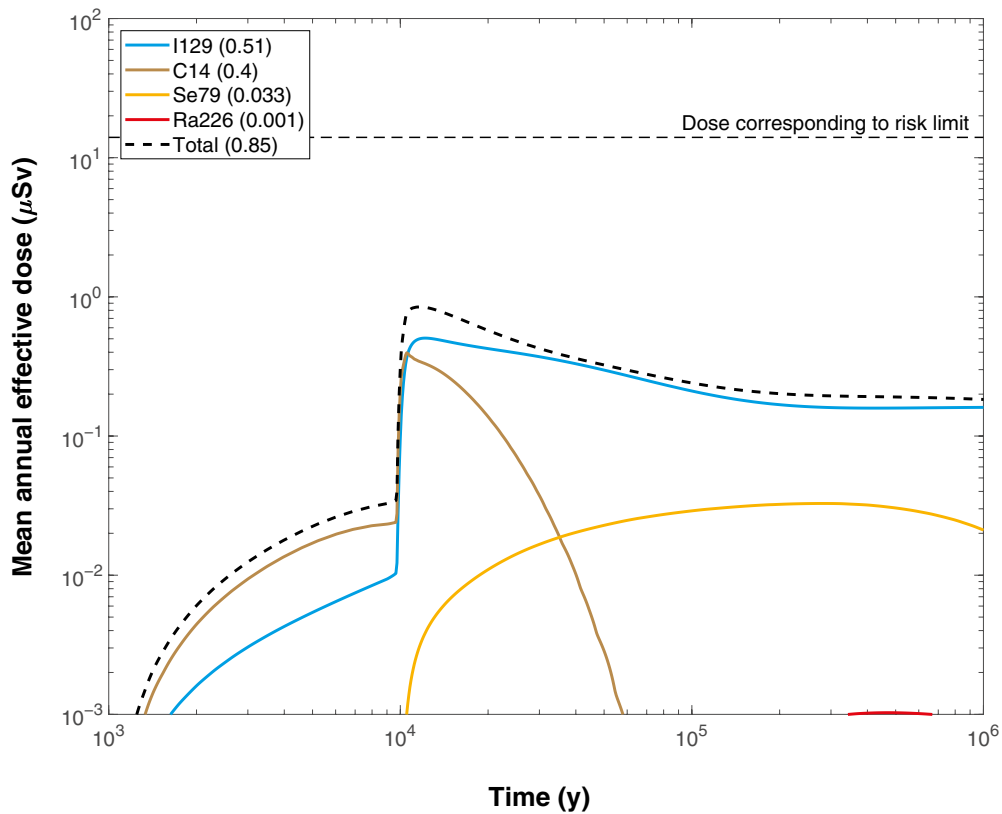


Figure 13-59. Far-field mean annual effective dose for a probabilistic calculation for the base case for the pinhole failure mode. Summed doses for all release paths ($Q1+Q1+Q3$). The legends are sorted according to descending peak mean annual effective dose over one million years (given in brackets in μSv).

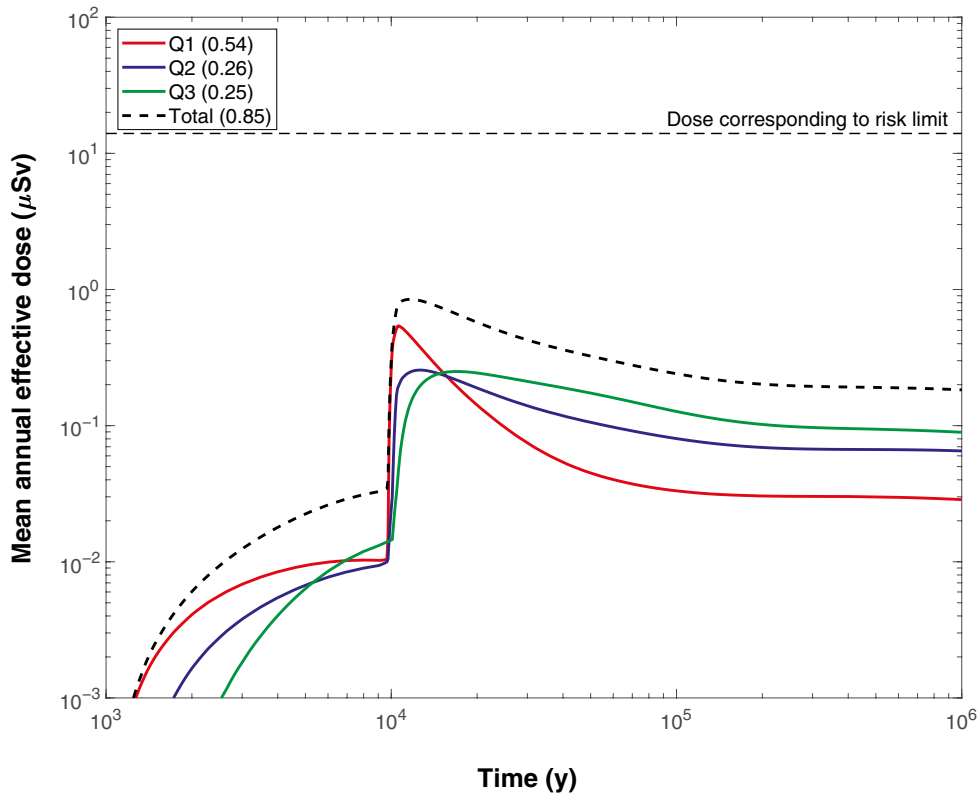


Figure 13-60. Far-field mean annual effective dose for a probabilistic calculation for the base case for the pinhole failure mode. Doses decomposed into $Q1$, $Q2$ and $Q3$. The legends are sorted according to descending peak mean annual effective dose over one million years (given in brackets in μSv).

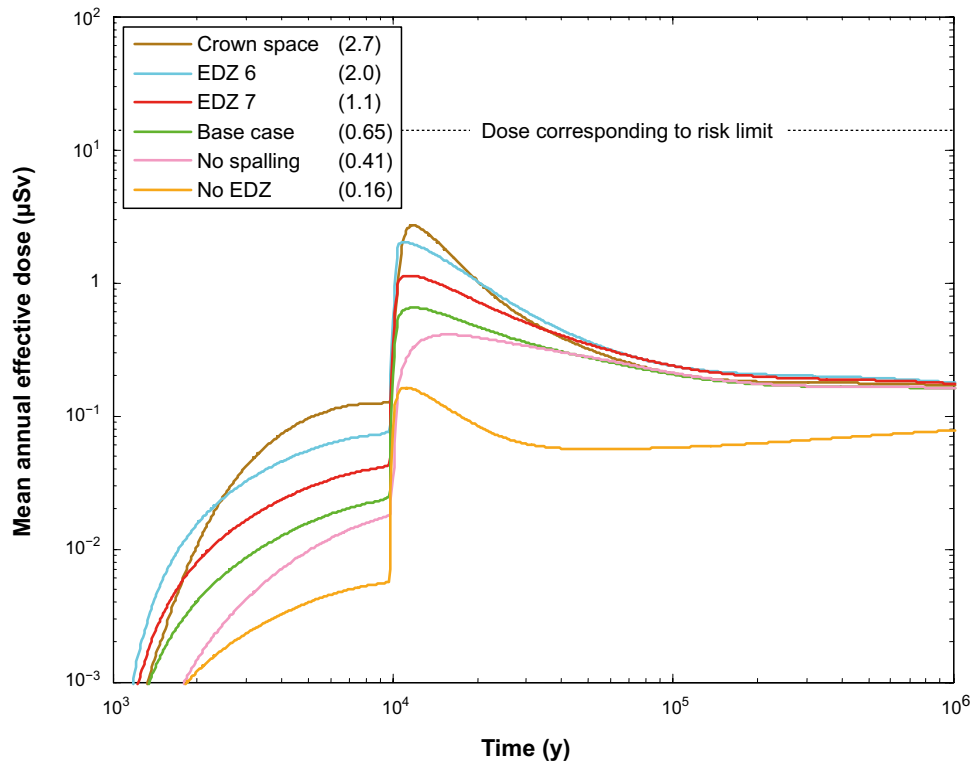


Figure 13-61. Far-field mean annual effective dose for the probabilistic calculations of the pinhole base case and cases with no spalling, with different assumptions regarding EDZ properties (EDZ6 and EDZ7 correspond to transmissivities of $10^{-6} \text{ m}^2/\text{s}$ and $10^{-7} \text{ m}^2/\text{s}$, respectively) and with a crown space in the deposition tunnel. Case not recalculated since SR-Site.

Thermally induced spalling may occur in the walls of the deposition holes and decrease the transport resistance in the interface between the buffer and the rock, see Section 10.3.5. For the base case calculation it is pessimistically assumed that all deposition holes experience spalling. An additional probabilistic case without spalling is, therefore, analysed. This yields a reduction of about a factor of 40 in total dose equivalent near-field release from Q1, whereas the effects on Q2 and Q3 are very limited. The total doses from the near-field and the far-field are reduced by factors of about 4 and 1.5, respectively. It is also noted that the occurrence of spalling does not affect the transport conditions in the corrosion and shear load scenarios.

The base case has an excavation damage zone (EDZ) transmissivity of 10^{-8} m²/s. The effects of different EDZ transmissivities are examined by considering probabilistic variant cases with no EDZ and EDZ transmissivities of 10^{-6} m²/s and 10^{-7} m²/s. The latter two cases are included to clarify what the effects would be of using a potentially more damaging technique than that of the reference method for tunnel excavation. Eliminating the EDZ has virtually no impact on the Q1 release, whereas the Q2 release by definition vanishes. The Q3 release is somewhat reduced and this is due to the fact that many escape routes from the deposition tunnel are minor fractures connecting the tunnel to the EDZ in the base case. Increasing EDZ transmissivity above the base case value of 10^{-8} m²/s does not increase the Q1 release. For Q2, each order of magnitude increase in transmissivity results in approximately a factor of 3 increases in near-field and far-field peak releases. Releases through Q3 are weakly affected. The increase in total far-field mean annual effective dose in going from the base case value of 10^{-8} m²/s to 10^{-6} m²/s is somewhat less than an order of magnitude, and the effect of assuming no EDZ is a reduction by somewhat less than an order of magnitude.

A flow model variant in which tunnel backfill has compacted with a resulting gap at the tunnel crown is also analysed, see Section 10.3.6. Early releases from the near-field of C-14 are about 3 times higher compared to the pinhole case with an intact tunnel backfill, and Q3 is the dominating release path. In the longer term Ra-226 contributes considerably to the total dose. For the far-field, early releases of C-14 are about 8 times higher compared to the pinhole case with an intact tunnel backfill, and also here Q3 is the dominating release mode. In the longer term, the total dose from the far-field is comparable to that of the pinhole base case.

Calculations with MARFA

Several variant cases of the growing pinhole failure mode have been investigated with MARFA to understand the sensitivity to various modelling assumptions, the potential for retention in engineered structures and soils, and the potential role of bentonite colloids in facilitating transport. MARFA was used for this assessment because it has capabilities to fully represent variability along pathways, including variability in the type of retention model. For example, MARFA can use an equilibrium sorption model for soils and tunnels in combination with matrix diffusion models for the fractured bedrock portions of the transport pathways. The analyses in this subsection have not been updated since the SR-Site assessment.

Because the focus here is in understanding modelling sensitivities, a simplified treatment of uncertainty is adopted. Preliminary deterministic values are used for initial radionuclide inventories, near-field transport parameters, and matrix parameters. Details can be found in the **Radionuclide transport report**. However, full pathway-to-pathway variability is included for flow-related transport parameters (the equivalent flow rate, advective travel time, and flow-related transport resistance). MARFA uses a segmented pathway representation in which advective travel time and flow-related transport resistance vary from segment to segment. Within the DFN regions, a segment is that part of a pathline contained within a single fracture. This detailed representation of spatial variability is in contrast to that of FARF31, which uses global values for advective travel time and flow-related transport resistance for each flow path. The results discussed below are for annual dose as expected values taking into account all deposition holes.

Reference case

The reference pinhole case analysed with MARFA differs from the above base case analysed with the COMP23 and FARF31 models in two significant ways: The parts of the pathway in tunnels and soil layers are included in the travel time (but no sorption is assumed), and deterministic values are used as described above. In particular the first of these factors yields a reduction in the calculated mean doses of about an order of magnitude compared to those obtained with the COMP23/FARF31 models. The far-field geosphere reduces peak total dose by a factor of approximately 20 for the Q1 path, approximately 5 for Q2, and approximately 2 for Q3. I-129, C-14 and Ra-226 account for almost all the far-field and near-field doses for all three release paths.

Sensitivity to flow and transport assumptions

The reference case includes soils and tunnel segments in the transport pathway, but assigns these segments zero equilibrium partitioning coefficients for all elements. Thus, the delay introduced by a non-zero groundwater travel time through soils and tunnels is accounted for, but retardation of sorbing elements is ignored. Effects of the soils and tunnels are summarised in Figure 13-62 for the Q1 release path. The blue curve is near-field release and the green curve is the reference case. The pink curve neglects the effect of transport in tunnels and soils. The black curve incorporates transport with sorption in tunnels and soil layers. There are two main conclusions to be drawn. First, the travel time in the tunnels and soil layers decreases the peak dose by a factor of approximately 5 (compare pink to green curves). This decrease is mostly due to the effect on the non-sorbing I-129 and C-14. Second, sorption in tunnels and soils has no significant effect on total dose. This lack of sensitivity is a consequence of the dominant role that the non-sorbing I-129 and C-14 play in determining the total dose. Indeed, examination of the far-field releases for individual nuclides (Figure 13-63) reveals that releases of sorbing radionuclides such as Ra-226 are significantly reduced by sorption in tunnels and soils.

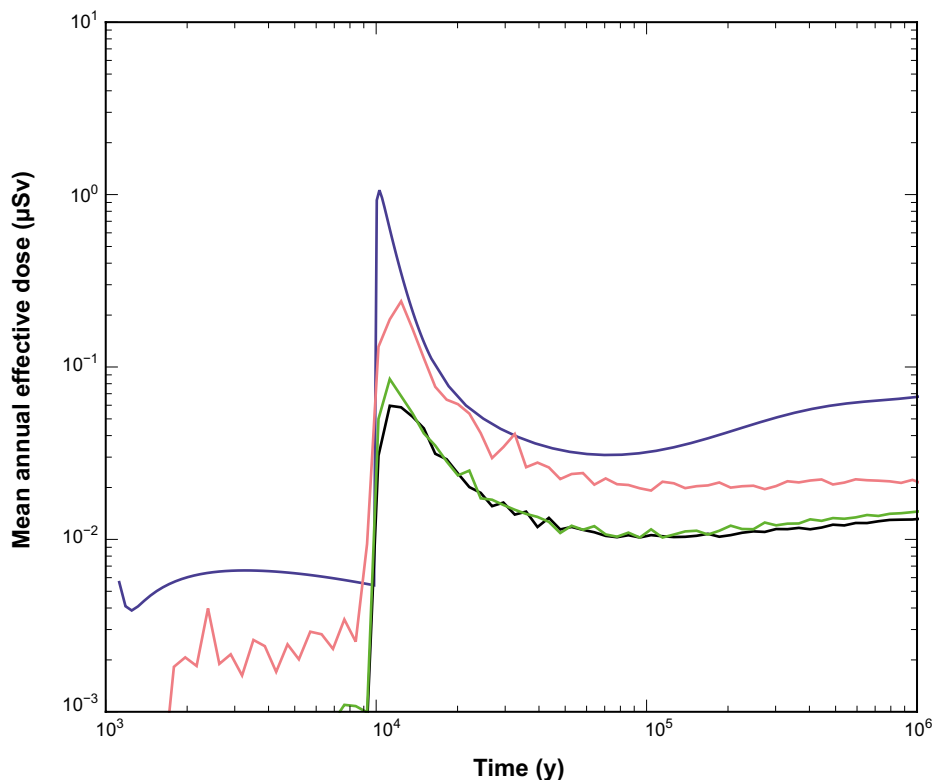


Figure 13-62. Expected values for all-nuclide releases for the Q1 pinhole release, expressed as equivalent doses. The blue curve is near-field release and the other curves are far-field releases as follows: pink neglects transport in tunnel and soil, green is the reference case (tunnels and soil layers included but with no sorption), black has sorption in tunnels and soils. Case not recalculated since SR-Site.

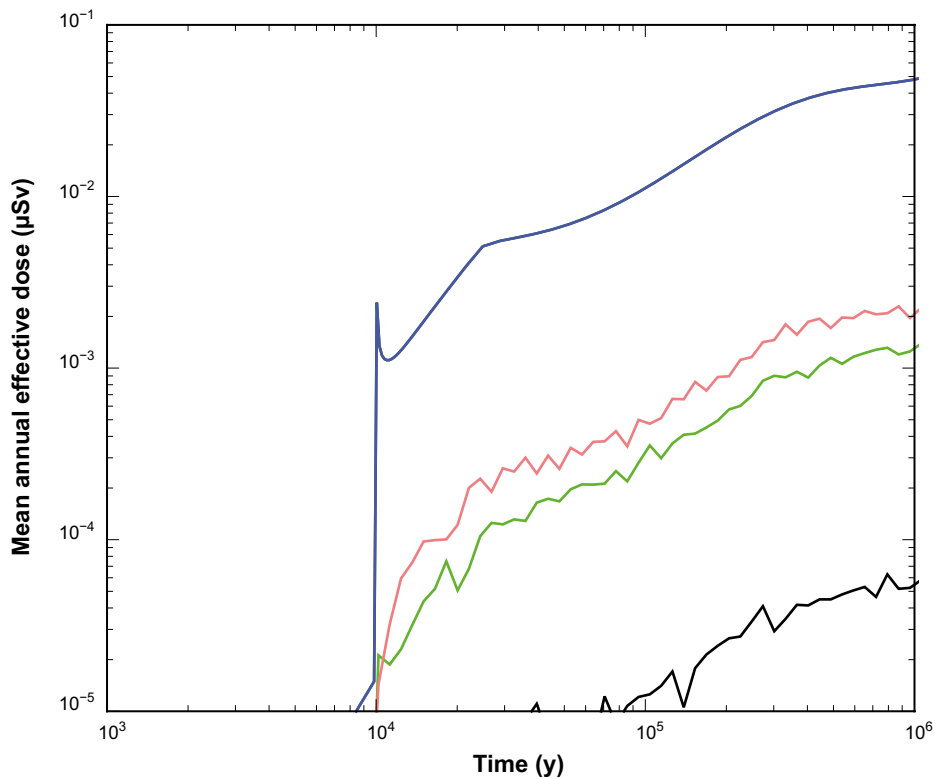


Figure 13-63. Expected Ra-226 release for pinhole Q1 release path and different assumptions about the role of tunnels and soils. The blue curve is near-field release and the other curves are far-field releases as follows: pink has no tunnel or soil segments in the pathway, green curve is the reference case (tunnels and soil layers included but with no sorption), black has sorption in tunnels and soils. Case not recalculated since SR-Site.

Cases with different assumptions regarding the EDZ transmissivity and with the assumption of a crown space in the deposition tunnel have also been analysed, with similar results to those reported above for the COMP23/FARF31 models (see the **Radionuclide transport report** for details).

The effect of releasing multiple tracer particles per deposition hole (see Section 10.3.6 for details of the flow case) is analysed in the **Radionuclide transport report**. Different tracer particles traverse different flow paths, which makes it possible to explore the dispersive effects of different flow paths diverging from a single source location. It is shown that the effect of multiple particles (ten) per release point relative to the case with a single particle implies very small differences in resulting doses. Thus, dispersion caused by having multiple flow paths connect a single source location to the biosphere is subordinate to other processes that spread radionuclide mass in time.

Colloid facilitated transport

Colloid facilitated transport may be represented in MARFA by replacing two transport parameter groups by apparent values, see Section 13.5.6, sub-section ‘Colloid facilitated transport’. The ratio of the colloid-free parameters and the apparent values in the presence of colloids depends only on the colloid mass density and the partitioning coefficient for sorption onto colloids, see the **Radionuclide transport report** for details. Assuming a colloid mass density of 10 mg/L (Wold 2010), sorption onto colloids is found to have a negligible effect, see the **Radionuclide transport report**. The main reason that colloids do not enhance transport significantly is that the radionuclides I-129, C-14 and Ra-226 dominate the near-field and far-field releases, and I, C and Ra do not have a strong affinity for bentonite, see the **Data report**. Elements that have a strong affinity for bentonite and could potentially be transported significantly by bentonite colloids are not released from the bentonite buffer in sufficient quantities to affect the total dose.

13.7.3 Additional cases of hypothetical, early canister failures

Purpose

The pinhole failure mode is an example of a hypothetical, early, in this case initial, canister failure. As discussed in section 11.3, it could be of value to provide a more general analysis of consequences of early canister failures. The analyses of containment in Chapter 12 led to the conclusion that early failures can be ruled out except in the case of shear load failures, where the estimated likelihood of failure is small but non-negligible during the initial 1 000 years. This case was analysed in Section 13.6.2.

In the following, early failures in *all* canisters are *postulated* and the consequences are analysed in order to elucidate the sensitivity of repository safety to such failure modes. Reasonably cautious assumptions are made for the performance of other parts of the repository system as base cases, and more pessimistic assumptions, for both the performance of the failed canisters and of other parts, are made in sensitivity cases. The analyses are probabilistic in order to address data uncertainties in various parts of the system.

Canister performance

Basis for early canister failures

Since no realistic early failure mode (except shear loads) has been identified, the nature and time of occurrence of the failure has to be postulated in a contra factual manner. The containment related safety functions of the canister (Section 8.3.1) imply that the canister can fail either due to chemical loads (corrosion) or due to mechanical loads. Combined loads are also conceivable; stress corrosion cracking (SCC) is an example of such a load although it was concluded in Sections 10.3.13, 12.6.2 and 12.6.3 that this particular form of failure is not expected in the repository environment.

According to Section 12.6, *corrosion failures* can be expected to occur in a time perspective of hundreds of thousands of years in a few highly exposed canisters following buffer loss. Localised corrosion is assessed not to contribute significantly to these failures, nor to the reduction of the corrosion barrier in general. To contrast these findings to an assumed early failure, consider a corrosion process that would cause a canister failure due to general corrosion in 100 000 years. It would then take a pitting factor of 100 to cause a failure in 1 000 years, and this factor would have to be applied throughout the corrosion process, without consideration of evening effects as a pit grows deeper and wider. A failure time of e.g. 1 000 years is thus in stark contrast to the assessment results based on the scientific understanding of copper corrosion and on the properties of the Forsmark site.

According to Section 12.8, mechanical failures can, based on pessimistic assumptions, not be ruled out due to *shear loads* in a million year perspective. The assessed probability is, however, only of the order of 10^{-5} per canister. Canister failures due to *isostatic loads* are ruled out according to Section 12.7, also when taking effects of long-term creep deformation into account. As mentioned above, also failure due to SCC is assessed as ruled out. A first prerequisite for any of the mechanical failure modes to be relevant is that the buffer is water saturated and has obtained its swelling pressure so that a mechanical load acts on the canister. As demonstrated in Section 10.3.8, this is expected to take at least hundreds of years for the majority of deposition positions at the Forsmark site, with a small fraction reaching this state within 100 years. The isostatic pressure of around 15 MPa (at most 10 MPa from buffer swelling and 4.5 MPa of hydrostatic pressure) is then far below the design load of 50 MPa. As regards strains in the copper shell that need to be considered in the analysis of creep deformation, these are considerably lower after buffer swelling than during a much later glacial load of up to 50 MPa, and also for this latter load, creep failures are not expected in the copper shell. Other creep-related potentially detrimental phenomena discussed in Section 12.7.4, like hydrogen embrittlement and time-dependent loss of ductility, are also more benign in a time perspective of a few thousand years. As for corrosion loads, failures due to isostatic loads in a 1 000 year perspective are hence not compatible with the scientific and technical bases on which the safety assessment is founded.

SCC during early, oxidising conditions was ruled out in Section 10.3.13 since maximum groundwater concentrations of SCC-assisting ions are too low, by 2-3 orders of magnitude for SCC to occur under these conditions. As regards SCC due to a combination of exposure to sulphide and mechanical stresses, it is seen in the **Fuel and canister process report** Section 3.5.4, that there is no viable scientific basis for this phenomenon occurring for sulphide concentrations and fluxes expected in the repository, even when high tensile stresses are applied in the laboratory. In a repository environment, the phenomenon,

if it existed, also requires tensile stresses that extend through the entire wall thickness of the copper, whereas generally the stresses on the canister, once established after buffer swelling, will be compressive. Penetrating tensile stresses can possibly occur in limited regions of the top and bottom parts of the canister, see Section 12.7.4.

Assumed failure time

Based on the above, it is not seen as reasonable to derive a time for early failures that is founded in the scientific and technical understanding of the canister in the repository environment. Therefore, for the analyses in this Section, it will simply be assumed that all canisters are failed initially.

Canister development after failure

As seen in the analysis of the pinhole failure in Section 13.7.2, the further development after the occurrence of a failure concerns two key questions:

1. What is the delay time between a canister failure and the establishing of a continuous water pathway between the fuel pellets and the canister exterior?
2. When will the further development of the canister interior have led to a situation where the transport resistance between the fuel pellets and the canister exterior is essentially lost?

To address the first question, an assumption regarding the geometrical nature of the failure is required, as this determines the rate at which water penetrates into the canister. A hypothetical, fast corrosion process involving pitting may be assumed to cause a failure of a canister in the form of one or several small holes in the copper shell. The 4 mm diameter hypothetical pinhole analysed in Section 13.7.2 may be taken as a representation of such a failure. The initial size of the failure is much larger than what could be caused by a pitting failure, whereas one could imagine more than a single hole for a hypothetical corrosion process. As seen in the discussion in the **Data report** Section 4.2.7, a reasonable estimate of the time to establish a continuous water path in this case is around 40 000 years, whereas pessimistic input data yields a time of around 10 000 years. The delay time for a hypothetical penetrating fracture in the copper shell is also discussed in the **Data report** Section 4.2.7, for the case of a one millimetre fracture extending around the entire circumference of the canister wall. For the hypothetical early mechanical failure modes due to an SCC like process or an early creep induced fracture, a fracture of these dimensions is seen as being too large a representation of the failure. The time to establish a continuous water path for the 1 mm fracture extending around the entire circumference of the canister wall is estimated in the **Data report** to around 250 years, when pessimistically neglecting the effect of the build-up of a hydrogen pressure in the canister interior counteracting the inflow of water. The modelled tensile stresses required to cause any of the types of mechanical failures considered above cover at most around $\frac{1}{4}$ of the canister circumference, suggesting that 4×250 years is a cautious estimate of the delay time. To encompass both types of defects (small holes and fracture), a delay time of 1 000 years will be assumed in the analyses in the present section.

To address the second question, it is noted that at early times, at least two factors contribute significantly to the transport resistance between the fuel pellets and the canister exterior: the geometrical limitation of the opening in the copper shell, if this is small, and the Zircaloy cladding of the fuel. In addition, the insert itself offers transport resistance both through physical constraints and by potentially sorbing diffusing species in the canister. These latter factors are, however, not considered in the following.

As regards the geometrical limitations of the failed copper shell, this was pessimistically assessed in the analysis of the growing pinhole failure in Section 13.7.2 to remain a significant transport hindrance for at least 10 000 years. During this time, the intruding water will cause the cast iron insert of the canister to corrode and the corrosion products are expected to exert a pressure on the canister parts. Based on extensive modelling (Bond et al. 1997), this is pessimistically assumed (the **Data report**, Section 4.2) to lead to a sudden widening of the initially small defect in the copper shell after 10 000 years. The widening is assumed to be such that neither the insert nor the copper shell offers any transport resistance for radionuclides after this point in time. In case of a fracture like defect, a 1 mm fracture that extends around the entire canister circumference is shown in the **Data report** to offer only a limited transport resistance.

Concerning the barrier effect of the Zircaloy cladding, it is assessed in the **Fuel and canister process report** Section 2.5.4, that it will take on the order of 100 000 years to cause cladding failure through general corrosion. As concerns pitting corrosion Evins (2020) notes that even a pessimistic pitting factor of 10 would yield cladding failure times of the order of 10 000 years. Delayed hydrogen cracking (DHC) is another failure mode that needs to be considered for the cladding. Evins (2020) considers that a pessimistic estimate of the fraction of fuel pins failing early due to this process in the repository is 12 percent. In spite of efforts to place fuel with failed cladding in isolating containers prior to encapsulation, it cannot be excluded that a small fraction of the fuel pins have a failed cladding initially, but this fraction is assessed as very small. The fraction of fuels for which one cannot exclude early cladding failure due to DHC occurring after deposition in the repository, is pessimistically estimated to 12 percent. Also a failed cladding would exhibit a transport resistance, but this is neglected in the following. Claddings that do not fail due to early DHC are expected to have an intact cladding for at least 10 000 years (Evins 2020).

In summary, for an initial failure in the form of a small hole, both the transport resistance of the hole itself and the barrier function of the cladding imply a time before the transport resistance in the canister is lost of 10 000 years. For a fracture like defect in the canister, the cladding is expected to limit the transport resistance for 10 000 years for 88 percent of the fuel, whereas for 12 percent it is pessimistically assumed that the transport resistance is lost as soon as a continuous water pathway is established, for both these fractions neglecting any transport resistance offered by the canister defect itself.

To encompass both pinhole like and crack like defects, it is assumed in the following that 10 percent of the canisters have lost their transport resistance already when the water pathway is established and the remaining 90 percent do so after 10 000 years. These order-of-magnitude fractions reflect the protective capacity of the Zircaloy cladding in the case of an initial, pessimistically large e.g. crack like failure and are a very pessimistic representation for an initial pinhole like failure. Before the transport resistance is lost in the 90 percent fraction, it is assumed to be the same as that in the growing pinhole failure mode analysed in Section 13.7.2. A sensitivity case where the transport resistance is completely lost in all canisters already when the water pathway is established is also analysed.

Fuel performance

The fuel, including the fuel matrix, the IRF and the fraction of the inventory embedded in metal parts of the fuel is assumed to perform as in all cases previously analysed, e.g. the single pinhole case analysed in Section 13.7.2.

Buffer performance

One role of the buffer, should the containment of the canister be breached, is to retard releases of radionuclides from the canister. The buffer is generally expected to maintain this function and this is the basic assumption also in the analyses in the present Section, the A cases in Table 13-9 below. However, according to the analyses in Section 12.2, buffer losses due to erosion/sedimentation cannot be ruled out in the long-term. In the assessment of the extent of buffer erosion/sedimentation for the buffer loss/corrosion scenario, two cases were considered: One where losses occur according to the PSAR model for buffer erosion and one where the buffer is lost initially. The latter is a pessimistic bound on uncertainties relating to the buffer loss process, in particular for sedimentation where the knowledge base is less developed than for the erosion process. The difference between the two in terms of canister failures is limited since canister corrosion essentially determines the canister failure times for the few canisters that fail in this scenario. In order to address buffer loss for cases where the canister is failed initially, a more differentiated treatment of the buffer loss processes is required. Therefore, buffer loss is calculated for a combination of erosion and sedimentation, where the buffer loss rate due to erosion is calculated with the PSAR model for erosion and where sedimentation is calculated for an experimental loss rate of 30 kg/m²/yr, see further Section 10.3.11. The upper bound on the number of deposition positions that could experience dilute condition (estimated at 5 % in Section 10.4.8, subsection “*Colloid release from buffer and backfill*”), is pessimistically disregarded. A sensitivity case where the buffer is completely lost in all deposition holes after 20 000 years is also considered.

Table 13-9. Cases of hypothetical early canister failure.

Case	A	B
Failure time	0 yr	
Delay between failure and onset of transport	1 000 yr	
Delay between failure and loss of transport resistance	Base case: 0 yr for 10 % of the canisters and 10 000 yr for 90 % of the canisters Sensitivity case: 0 yr for all canisters	0 yr for 10 % of the canisters and 10 000 yr for 90 % of the canisters
Buffer	Intact	Base case: Gradually lost due to erosion and sedimentation Sensitivity case: Buffer lost in all deposition holes after 20 000 years
Hydrogeology	Base case: Semi-correlated Sensitivity cases: Uncorrelated and fully correlated	Semi-correlated
Biosphere	Dynamic landscape model	

Hydrogeology

The semi-correlated hydrogeological model is used as the basis for the assessment of early canister failures. To cover variability and uncertainty as regards the hydrogeological conditions at the deposition holes and for the transport paths between the deposition positions and the biosphere, calculations are made for also the uncorrelated and fully correlated models, taking for each of these the ensemble of 6 000 deposition positions into account. It is noted that for these cases, as for the pinhole case in Section 13.7.2, all deposition positions are connected to the flow system. For positions that are not intersected by a water bearing fracture (no Q1 path), the connection occurs through the Q2 and Q3 transport paths, see further Section 13.4.1. The three model variants are applied also when analysing the extent of buffer loss.

Biosphere representation

As regards the biosphere representation, three possibilities are available, as mentioned in Section 13.2.3:

- Pessimistically derived constant landscape specific dose conversion factors (LDFs, used in most calculations in the previous sections) by which the geosphere release is multiplied to obtain a dose.
- Pessimistically derived distributed landscape specific dose conversion factors to be used when a large number of canisters fail.
- A less pessimistic biosphere model where the temporal development of the biosphere due to e.g. land-uplift is explicitly modelled in the consequence calculations. The release from the repository is distributed to the landscape objects according to the temporally developing release points of the transport paths in the geosphere. At each time step and for each nuclide the maximum total dose over all biosphere objects is used.

The pessimism of the two former biosphere representations accounts for uncertainties of the biosphere development in the far future. The latter dynamic biosphere is a less pessimistic representation of the more predictable near-future development of the biosphere for cases where early failures of a large number of canisters occur. The development covers the land-uplift during the present temperate climate period and then reaches an essentially steady state, under the assumption that the present interglacial climate persists during the entire assessment period of one million years. The dynamic approach will be used in the present Section. It is noted that this dynamic biosphere model, with the same input data, was used in some of the “what if” cases to illustrate postulated barrier losses in the SR-Site assessment, see Figure 13-68 in SKB (2011), reproduced as Figure 13-73 in Section 13.7.4 of the present report. In the supplementary information on canister integrity issues reported in SKB (2019c), the same model, but with updated input data was used. The altered data were to a larger extent based on site specific information and yielded lower doses than the SR-Site version for a couple of key radionuclides. This version has, however, not been qualified for use in the PSAR and is therefore not utilised in the following.

Cases

Two cases, A with an intact buffer and B with buffer loss due to erosion and sedimentation, are analysed, see Table 13-9. Failure characteristics and transport resistances are as discussed above. The semi-correlated hydrogeological model is used as a base case, and the two alternative models as sensitivity cases. The near-field and far-field models and other input data are the same as for the base case of the growing pinhole failure, Section 13.7.2.

Results

Base case A

Figure 13-64 shows the mean annual effective dose for base case A where all canisters have failed initially and the buffer is performing as intended. The peak annual dose is 32.8 μSv , i.e. slightly more than twice the dose corresponding to SSM's risk limit. The peak dose is completely dominated by I-129 and it occurs after around 15 000 years, reflecting the increased release from the canisters at 10 000 years, the point in time when the transport resistance in all canisters is assumed to have been completely lost. At earlier times, the sum dose is dominated by relatively rapid variations in C-14 dose. The C-14 dose is dominated by exposure through consumption of fish and the variations are caused by changes in the landscape due to land up-lift affecting the occurrence of lakes in the vicinity of the site. Beyond a few thousand years, the landscape is relatively unaffected by further land uplift.

Base case B

Figure 13-65 shows the mean annual effective dose for base case B where all canisters have failed initially and the buffer is gradually lost due to erosion and sedimentation. The peak annual dose is 32.8 μSv , the same as in base case A. The limited difference compared to case A occurs beyond 100 000 when the gradual loss of buffer leads to somewhat higher doses in case B.

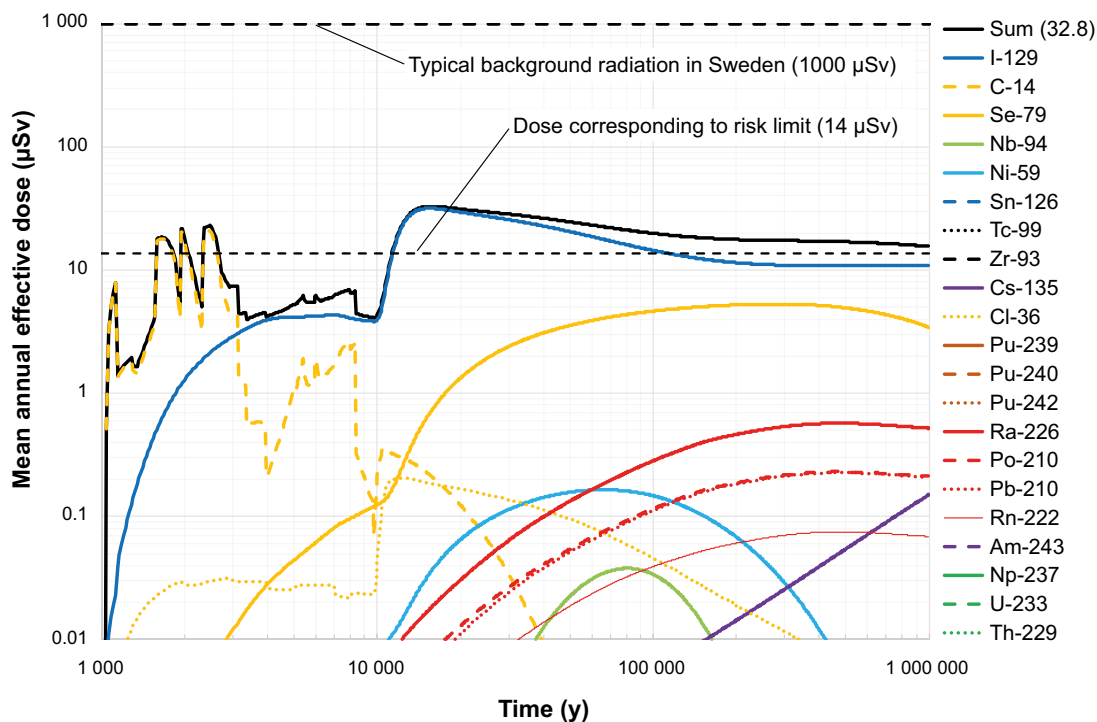


Figure 13-64. Results for the hypothetical early canister failure scenario, case A, with an initial failure in all canisters and where the buffer is performing as intended.

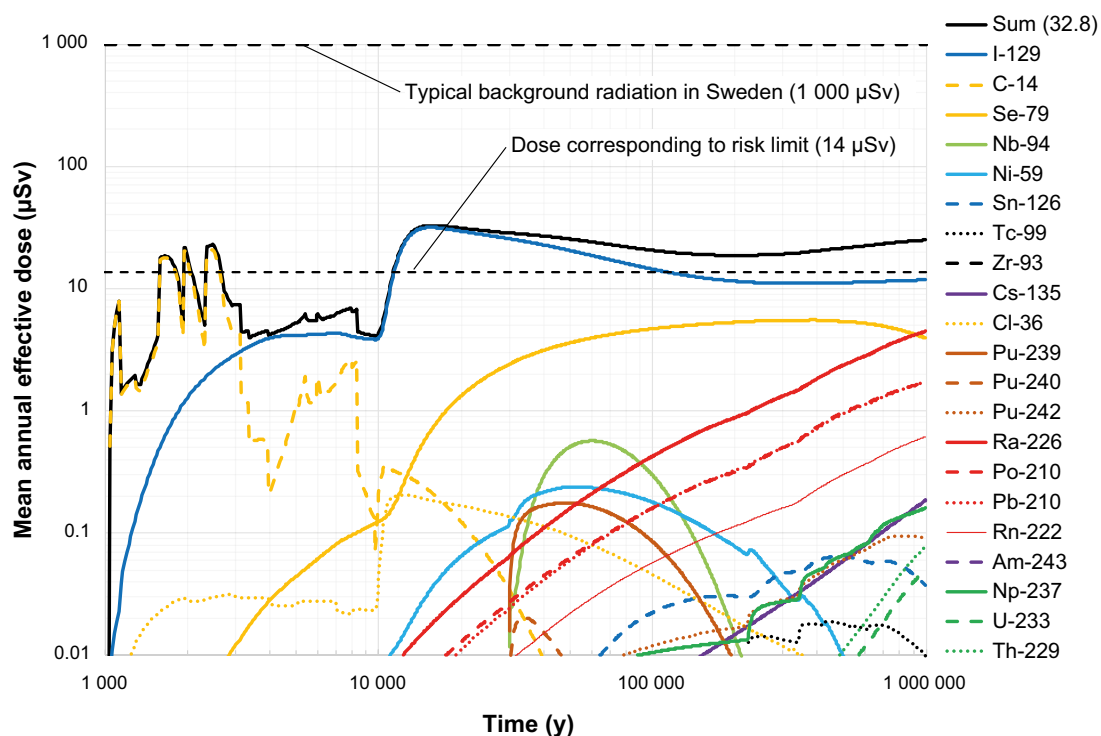


Figure 13-65. Results for the hypothetical early canister failure scenario, case B, with an initial failure in all canisters and where the buffer is gradually lost.

Sensitivity cases

Two cases to address the sensitivity to the choice of hydrogeological model have been calculated, using the uncorrelated and the fully correlated models instead of the semi-correlated model in the base cases. This yielded peak annual effective doses of 43 μSv and 53 μSv for the uncorrelated and fully correlated cases, respectively, i.e. less than a factor of 2 higher than in the base case. Again, the peak doses were the same and occurred after about 15 000 years for cases A and B, and the doses of the B cases are slightly higher than the A cases beyond 100 000 years.

Two additional, pessimistic sensitivity cases were calculated; one where all canisters, rather than 10 percent in the base case, are assumed to have no transport resistance as soon as a continuous water path is established and one where the buffer is completely lost in all deposition holes after 20 000 years.

The case with early loss of transport resistance results in a peak dose of 216 μSv after around 2 500 years, again completely dominated by C-14, with the peak lasting for a few hundred years (the same curve structure before 10 000 years as in Cases A and B, but elevated by a factor of 10).

The case with complete, early buffer loss yields slightly higher doses than the base case beyond 20 000 years, reaching at most 66 μSv at around 55 000 years after repository closure. The sum dose in this case is dominated by I-129 and Nb-94 and, at times beyond 200 000 years, by Ra-226.

Conclusions

This section discusses analyses of hypothetical, early canister failures, with reasonably cautious assumptions of other parts of the repository system in two base cases. The results of the base cases show that even when all canisters are assumed to be failed at deposition, the resulting doses are about twice as high as that corresponding to the regulatory risk limit and occur around 15 000 years after deposition.

Disregarding also the transport resistance in an initially failed canister leads to doses around 15 times the risk limit. Sensitivity cases with more pessimistic assumptions concerning buffer loss and the hydrogeological model yields doses of at most five times the risk limit dose.

These analyses demonstrate that the protective capacity of other parts of the system is considerable. The canisters are required to strictly demonstrate compliance with the regulatory risk criterion. The analyses presented in this Section imply, however, that even with completely hypothetical early failures in about half of the 6000 canisters, the risk criterion can be met for the base cases. The most pessimistic sensitivity case yields peak doses that are about 20 percent of that caused by the natural background radiation in Sweden and that last for about 1000 years.

13.7.4 Additional cases to illustrate barrier functions

Some conclusions regarding loss of barrier functions can be drawn from the analyses already presented. In order to provide a fuller treatment, the following cases of barrier deficiencies are postulated:

- A. An initial absence of enough buffer causing advective conditions in the deposition hole for all deposition holes.
- B. An initial pinhole in the copper shell for all canisters.
- C. An initial, large opening in the copper shell and in the cast iron insert for all canisters.
- D. A combination of cases A and C, i.e. an initial large opening in all canisters and advective conditions due to loss of buffer for all deposition holes.
- E. A combination of case C with an assumption of fast fuel dissolution and fast corrosion of metal parts. An initial, large opening in every canister is combined with the assumption of a complete fuel dissolution and metal corrosion in only 100 years.

A loss of the radionuclide retention capability of the rock is combined with each of the five cases, yielding a total of ten release situations. The cases without geosphere retention are denoted A* through E*.

In all cases it is assumed that the backfill and closure are installed and perform as expected. Also, all aspects of the rock other than those related to retention, e.g. the near-field groundwater flow, which is generally low and with only about one sixth of the deposition holes connected to water conducting fractures, as well as the stable and favourable groundwater composition in the near-field, are assumed to be present. Elemental solubilities are imposed on concentrations of radionuclides in the canister void volume only if the buffer is in place. This is the same approach as used in the analyses of the corrosion and shear load scenarios, Sections 13.5 and 13.6. The analyses in this Section have not been updated since the SR-Site assessment, with the exception of the treatment of Ag-108m in cases D and D*. The releases of Ag-108m dominated the early doses in these cases in SR-Site, where they were calculated very pessimistically due to lack of corrosion data for the alloy in the control rods that contains Ag. New data has allowed a more realistic treatment as reflected in the updated Figure 13-68 and Figure 13-69 (and the follow-on figures where all cases are summarised).

Table 13-10 gives an overview of the status of the retardation related safety functions, see Figure 8-4, for the cases.

The transport and dose calculations are probabilistic, since it is desirable to take into account both uncertainties due to lack-of-knowledge in general and the spatial variability of the properties of the deposition holes and their associated transport paths in the geosphere. The semi-correlated hydrogeological DFN model was used for these stylised calculations. Except for the case specific assumptions regarding failed barrier functions, all transport data are taken from the **Data report**. This applies to e.g. corrosion rates, fuel dissolution rate, sorption and diffusion data and LDF values.

Table 13-10. Status of safety functions for the ten release situations. In cases denoted with an asterisk also geosphere retention is absent.

Green: Safety function intact

Yellow: Safety function deteriorates over time

Red: Safety function absent initially

	A. Buffer missing	A*	B. Pinhole damage	B*	C. Large canister defect	C*	D. Large canister defect and buffer missing	D*	E. Large canister defect, rapid fuel and metal conversion	E*
Limited fuel dissolution rate	Green	Green	Green	Green	Green	Green	Green	Green	Red	Red
Limited corrosion rate of metal parts	Green	Green	Green	Green	Green	Green	Green	Green	Red	Red
Limited solubilities	Yellow	Yellow	Green	Green	Green	Green	Red	Red	Green	Green
High transport resistance in canister/ buffer interface	Yellow	Yellow	Yellow	Yellow	Red	Red	Red	Red	Red	Red
Retardation in buffer	Red	Red	Green	Green	Green	Green	Red	Red	Green	Green
High transport resistance in buffer/ rock interface ¹⁾	Red	Red	Green	Green	Green	Green	Red	Red	Green	Green
Geosphere retention	Green	Red	Green	Red	Green	Red	Green	Red	Green	Red

¹⁾ When this safety function is present, spalling is still pessimistically assumed in all deposition holes. When this safety function is not present, i.e. when the buffer is missing, the groundwater turnover in the deposition hole is still limited by the hydraulic properties of the rock.

The biosphere is here represented by the constant LDF values obtained when the release is distributed in the landscape according to the time dependent distribution of release locations from the repository during an interglacial. Furthermore, since the LDF values are suited primarily to handle releases that are constant over periods of time that are comparable to the duration of a typical Late Quaternary interglacial, i.e. around 10 000 years, the releases for these cases are, as a variant, also evaluated with fully time dependent modelling of the biosphere. Here, the releases are distributed in the landscape and the time dependent doses are presented, rather than a time dependent release converted to dose by a constant LDF value.

In the following, each case is discussed briefly using distributed, constant LDFs. The section is concluded with summarising accounts of all cases both with LDFs and with time dependent modelling of the biosphere.

Cases A and A*, initial absence of buffer

A 0.5 m high section of the bentonite buffer is assumed to be missing, leaving a void in the form of a hollow cylinder between the canister and the wall of the deposition hole. The Q1 fracture, if it exists, intersects the deposition hole at the location of the void (see Figure 13-13). The deposition hole is otherwise filled with buffer and the deposition tunnel backfill is assumed to be intact. This case is analysed in Section 13.5.6, as a variant of the central corrosion case. For most of the deposition holes, the groundwater flow and sulphide concentrations are not sufficient to cause canister failure during the one million year assessment period. The corrosion calculation takes both the natural variability of flow rates for the ensemble of 6000 deposition holes and the distribution of sulphide concentrations in the groundwater into account. This yields a calculated mean number of failed canisters of 0.17 at one million years, used also here. Only the deposition holes with the highest flow rates in the Q1 fracture contribute. This also means that releases to Q2 and Q3 release paths (Figure 13-13) are negligible for these positions. Canisters in positions without a Q1 fracture do not fail in this calculation case.

For a failed canister, radionuclide transport in the near-field and the far-field is modelled as follows.

- The instantaneous release fraction of the inventory dissolves in the water in the void volume of the canister and the void from the eroded buffer.
- Nuclides embedded in the metal parts of the fuel assemblies are released to the void water in congruence with the corrosion of the metals. This is pessimistically estimated to take on average 1 000 years.
- Nuclides embedded in the fuel matrix are released to the void water in congruence with the dissolution of the fuel matrix. This is estimated to take on average 10^7 years.
- No solubility limits are imposed since the buffer is not in place to act as a filter for fuel colloids required in order to uphold solubilities.
- Releases occur from the water filled volume to the Q1 fracture, assumed to intersect the deposition hole where the buffer is missing. Only the highest flow rates cause failures. This also means that the release to the geosphere for these positions is essentially controlled by the release of nuclides from the metal parts and the fuel matrix, since the groundwater flow is sufficiently high to carry all the released nuclides away.
- The far-field development is modelled as in all other cases (see case B below), but the retention in the far-field is generally poor since high flow rates at a deposition position are positively correlated with a low F values in the geosphere.

The consequences are similar to those presented in Section 13.5.6, see Figure 13-29 and Figure 13-30. The only differences is that the distributed LDF values are applied and the results are shown in Figure 13-72 later in this section. Many of the radionuclides have decayed to insignificance when the first failures occur after close to 50 000 years. Near-field release equivalent doses are dominated by Nb-94 from metal parts of the fuel and Ra-226, Pb-210 and Np-237 from the fuel matrix. Far-field doses are dominated by Nb-94, Se-79, Ra-226 and I-129.

Cases B and B*, initial, penetrating pinhole defect in all canisters

The canister defects are assumed to be the same as those modelled in the growing pinhole failure, Section 13.7.2, i.e. an initial, penetrating pinhole that grows into a large failure after 10 000 years, but now in all canisters. The deposition hole buffer and the deposition tunnel backfill are assumed to be intact. The dose consequences in the biosphere are calculated with the distributed LDF values since this is a more realistic approach when releases occur from all over the repository.

The near-field development for this case is modelled as follows.

- Every canister is postulated to have an initial, penetrating defect. Water penetrates through the defect into the canister and the delay time to establish a continuous water pathway between the fuel and the canister exterior is pessimistically assumed to be 1 000 years.
- The instantaneous release fraction of the inventory dissolves in the water in the void volume of the canister.
- Nuclides embedded in the metal parts of the fuel assemblies are released to the void water in congruence with the corrosion of the metals. This is pessimistically estimated to take on average 1 000 years.

- Nuclides embedded in the fuel matrix are released to the void water in congruence with the dissolution of the fuel matrix. This is estimated to take on average 10^7 years.
- Solubility limits are imposed since the buffer is in place and acts as a filter for fuel colloids.
- Releases from the canister to the buffer commence after the 1 000 years' delay time, but the small size of the pinhole defect suppresses the release rate considerably compared to the case with a large degree of damage. After an additional pessimistically estimated 9 000 years, the pinhole suddenly grows so large that all transport resistance from the canister is lost.
- The nuclides are sorbed with varying efficiency in the buffer and the diffusion and sorption properties determine the time for diffusion through the buffer. If this time is shorter than a few half-lives of the nuclide, it passes to the Q1 fracture in the rock. Thermally induced spalling is assumed to have occurred in all deposition holes, reducing the transport resistance in the buffer/rock interface considerably. The release rate is determined by the nuclide concentration in the outer part of the buffer and the flow rate in the deposition hole. The flow is obtained from the base case of the semi-correlated hydrogeological DFN model.
- The release rate is multiplied by the LDF value for a release distributed in the landscape to obtain a dose equivalent release rate from the near-field.

The far-field development for this case is modelled as for all cases:

- In the rock, the nuclide's sorption properties, together with the rock's transport properties, determine the time for transport through the rock to the biosphere. The half-life of the nuclide determines whether it passes through the geosphere before decaying to a substantial degree.
- This release rate is multiplied by the LDF value for a release distributed in the landscape to obtain a dose from the far-field.

The consequences are similar to those in the pinhole scenario, see Figure 13-57 and Figure 13-59 for the near-field and the far-field, respectively. The only difference is that all canisters are now assumed to have defects, meaning that the probabilistic single-canister results should be multiplied by 6 000 and that the distributed LDF values are applied, leading to a reduction of the consequences by typically one order of magnitude. The far-field results with all 6 000 canisters are shown in the summarising Figure 13-72 later in this section.

Cases C and C*, initial, large opening in all canisters

The canister defects are assumed to be in the form of a large opening in the copper shell and the cast iron insert. The deposition hole buffer and the deposition tunnel backfill are assumed to be intact.

In the reference evolution, some of the deposition holes are affected by buffer erosion to the extent that advective conditions occur in the hole. For the stylised case considered here, no such erosion is, however, assumed, in order to more clearly demonstrate the role of the canister if all other barriers are intact. Combinations of canister and buffer defects are analysed in one of the cases described below.

The calculation case is similar to the isostatic collapse probabilistic case for the semi-correlated DFN model, applied to all canisters in the repository, with the difference that the failure is assumed to exist at deposition. The near-field and far-field releases are calculated with the radionuclide transport models used for the isostatic load scenario.

The near-field and far-field developments for this case are identical to those for the above case with initial pinhole defects in all canisters, with the following exceptions.

- After 100 years, all canisters are assumed to be filled with water and a continuous water pathway is established between the fuel and the canister exterior. 100 years is a rough estimate, corresponding to an inflow rate of 0.1 L/yr through the buffer to the canister similar to that assumed for canister failures due to shear load in Section 13.6. The saturation time of the near-field is generally longer than 100 years at Forsmark.
- Releases from the canister to the buffer commence after the 100 years, and they are not suppressed by the canister due to the assumed, large degree of damage.

The dose equivalent release from the near-field is shown in Figure 13-66. The dose is dominated over the initial 10 000 years by C-14, Cs-137, Sr-90, Ag-108m, I-129 and Se-79. After about 10 000 years Se-79, C-14, Ra-226 and I-129 contribute most to the total dose. Releases of nuclides that sorb strongly in the buffer, e.g. Pu-238 and Pu-239, are strongly reduced compared to case D* below where the buffer is also assumed to be missing. There is a considerable reduction also of releases of Cs-137, Sr-90 and Ag-108m compared to the case in which the buffer is missing.

The dose from the far-field release is shown in Figure 13-67. The peak total dose is reduced by less than an order of magnitude compared to the near-field release, whereas doses from many of the short-lived or sorbing nuclides are considerably reduced.

It is noteworthy that this completely unrealistic case of initial loss of containment function for all canisters in the repository yields far-field releases, converted to doses, which never exceed the background radiation. However, the containment function is required for a majority of the canisters in order to fulfil the regulatory requirement on risk at Forsmark.

The long-term release rate of I-129 equals, to a good approximation, the release rate of this nuclide from the fuel matrix. This is caused by the assumed absence of sorption and long half-life of I-129. Regarding the calculated dose from I-129 for this and other hypothetical cases in this section, it is noted that the mitigating effect of mixing of I-129 with naturally occurring stable iodine is disregarded in the biosphere models.

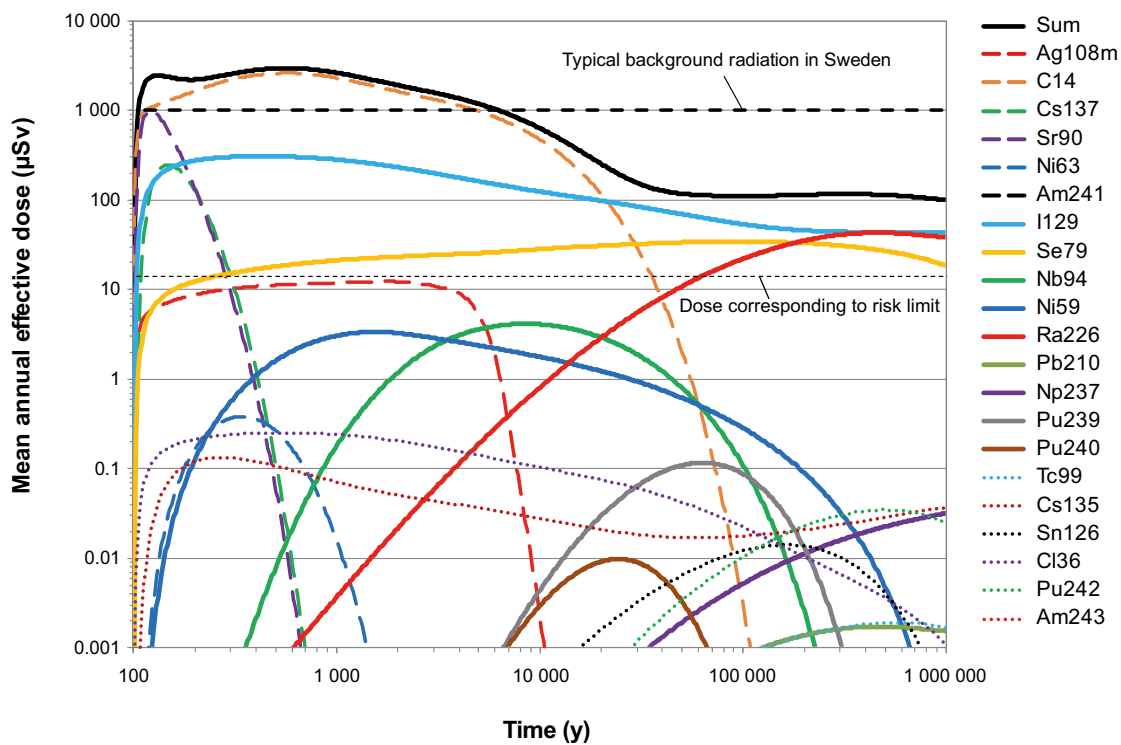


Figure 13-66. Near-field dose equivalent release for case C*, i.e. all canisters have an initial large defect and the buffer is intact.

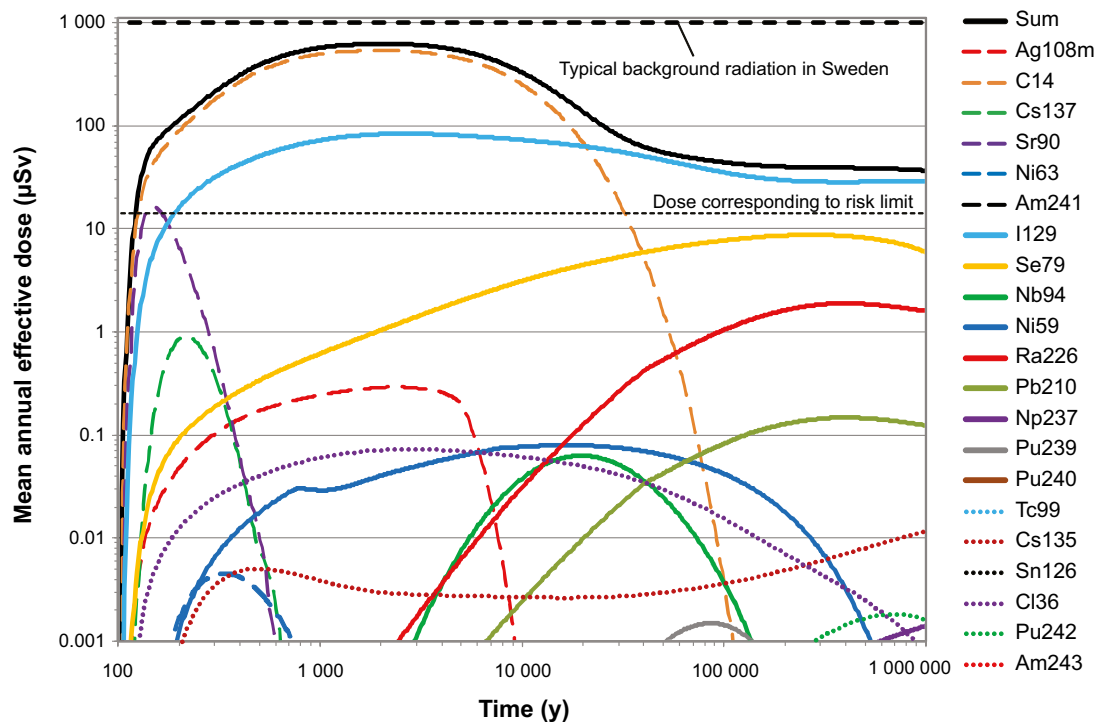


Figure 13-67. Far-field dose for case C, i.e. all canisters have an initial large defect and the buffer is intact.

Cases D and D*, initial large opening in all canisters and advective conditions due to loss of buffer for all deposition holes

The defects are assumed to be the same as those modelled in the corrosion scenario, i.e. a large opening in the copper shell and the cast iron insert and a section of the bentonite buffer is missing where the canister is damaged, leaving a void between the canister and the wall of the deposition hole in the form of a hollow cylinder. The deposition hole is otherwise filled with buffer and the deposition tunnel backfill is assumed to be intact. This means that releases occur predominantly to the Q1 fracture, if it exists. The near-field and far-field releases are calculated with the radionuclide transport models used for the corrosion scenario and applied to all deposition holes.

The near-field and far-field developments for this case are identical to those for the above case with initial pinhole defects in all canisters, with the following exceptions.

- After 100 years, all canisters are assumed to be filled with water and a continuous water pathway is established between the fuel and the canister exterior. 100 years is a rough estimate, corresponding to an inflow rate of 0.1 L/yr to the canister. The saturation time of the near-field is generally longer than 100 years at Forsmark.
- No solubility limits are imposed since the buffer is not in place to act as a filter for fuel colloids.
- For deposition holes that have a Q1 fracture, releases occur from the water filled volume to this fracture, assumed to intersect the deposition hole where the buffer is missing. The release rate is determined by the flow rate in the fracture and the size of its intersection with the deposition hole, taken to be equal to the deposition hole diameter. The flow is obtained from the semi-correlated hydrogeological DFN model, and multiplied by a factor of two to account for the locally increased flow due to the void from the missing buffer.

The dose equivalent release from the near-field is shown in Figure 13-68. The dose is dominated the initial 10 000 years by the IRF and/or CRF of Cs-137, Sr-90, C-14 and Nb-94. Note that only the generally low flow rates at Forsmark limit the releases for the IRF/CRF. After about 10 000 years Nb-94, Pu-239, Pu-240, Np-237, Ra-226, Pb-210 and I-129 contribute most to the total dose. The figure has been altered compared to the SR-Site version in that the Ag-108m curve has been multiplied by a factor of 3×10^{-4} , reflecting the reduction in IRF from 1 to 0.0003. This reduction is facilitated by the improved understanding of corrosion of the PWR control rods. The CRF yields a dose contribution comparable to that of the reduced IRF, but the CRF-contribution has not been quantified in detail in this simplified approach to demonstrating the insignificance of Ag-108m for the total dose. Ag-108m now gives a negligible contribution to the total dose at all times, whereas it was dose dominating during the initial several hundred years in SR-Site. Corrosion data for the control rods are discussed in the **Data report**, Section 3.2.7.

The dose from the far-field release is shown in Figure 13-69. The total dose is reduced by about a factor of 10 compared to the near-field release. For the earliest releases this is an effect of the travel time in the geosphere. In the long-term, strongly sorbing nuclides like Pu-239 and Pu-240 are retained in the geosphere. It is noteworthy that this completely unrealistic case of initial absence of all transport limitations in the engineered parts of the repository yields far-field releases, converted to doses, that are comparable to the background radiation during the initial 10 000 years and that in the long-term are less than a factor of ten above the risk limit. This figure has been altered in the same way as the near-field Figure 13-68 for Ag-108m.

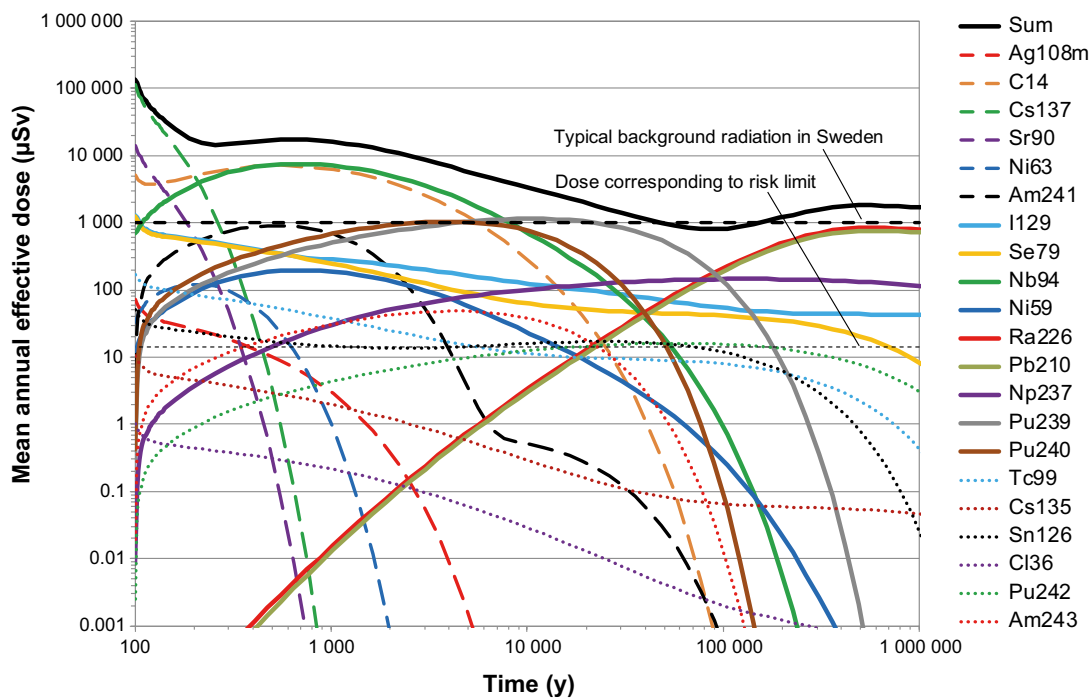


Figure 13-68. Near-field dose equivalent release for case D*, i.e. all canisters have an initial large defect and the buffer is missing between the defect in the canister and the wall of the deposition hole.

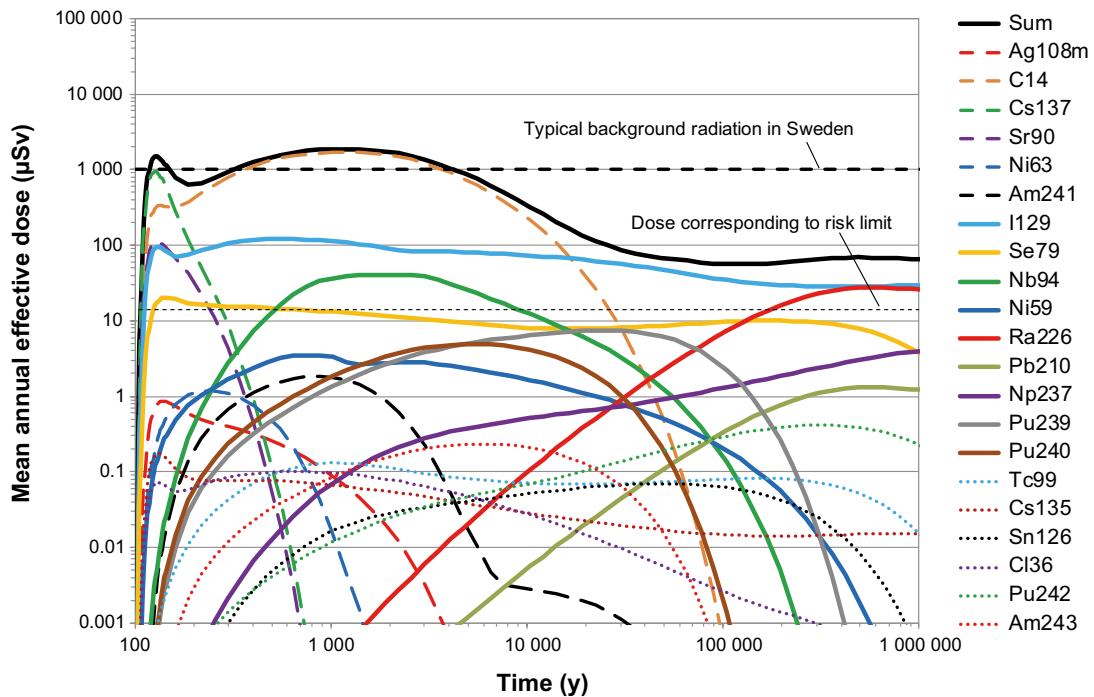


Figure 13-69. Far-field dose for case D, i.e. all canisters have an initial large defect and the buffer is missing between the defect in the canister and the wall of the deposition hole.

Cases E and E*, initial, large opening in all canisters and rapid fuel dissolution and metal corrosion

These cases are identical to cases C and C*, (all canisters have a large opening in the copper shell and the cast iron insert), except that for cases E and E* complete fuel dissolution and metal corrosion is assumed to occur in 100 years after water contacts the fuel. The containment function of not only the canister but also of the fuel matrix and the structural parts of the fuel is thus assumed to be absent. The deposition hole buffer and the deposition tunnel backfill are assumed to be intact.

The near-field and far-field developments for these cases are identical to those for cases C and C* with the exception of the fast fuel dissolution and metal corrosion.

The dose equivalent release from the near-field is shown in Figure 13-70. The dose is dominated by C-14, Cs-137, Sr-90 and I-129 for more than 10 000 years. In the longer term, Ra-226 and Se-79 together with I-129 contribute most to the total dose. Note that the release of Ag-108m is identical to that in case C* since this release is controlled by the solubility of Ag and not by corrosion in the model. The early releases of Sr-90, Cs-137 and I-129 have increased in inverse relation to the IRF values for these nuclides; cases E and E* are similar to assuming 100 % IRF for all nuclides. The decrease of I-129 at very long times is caused by depletion of I-129 from the repository and the host rock through outward transport and not through decay.

The dose from the far-field release is shown in Figure 13-71. The peak total dose is reduced by more than an order of magnitude compared to the near-field release, and doses from many of the short-lived or sorbing nuclides are considerably more reduced.

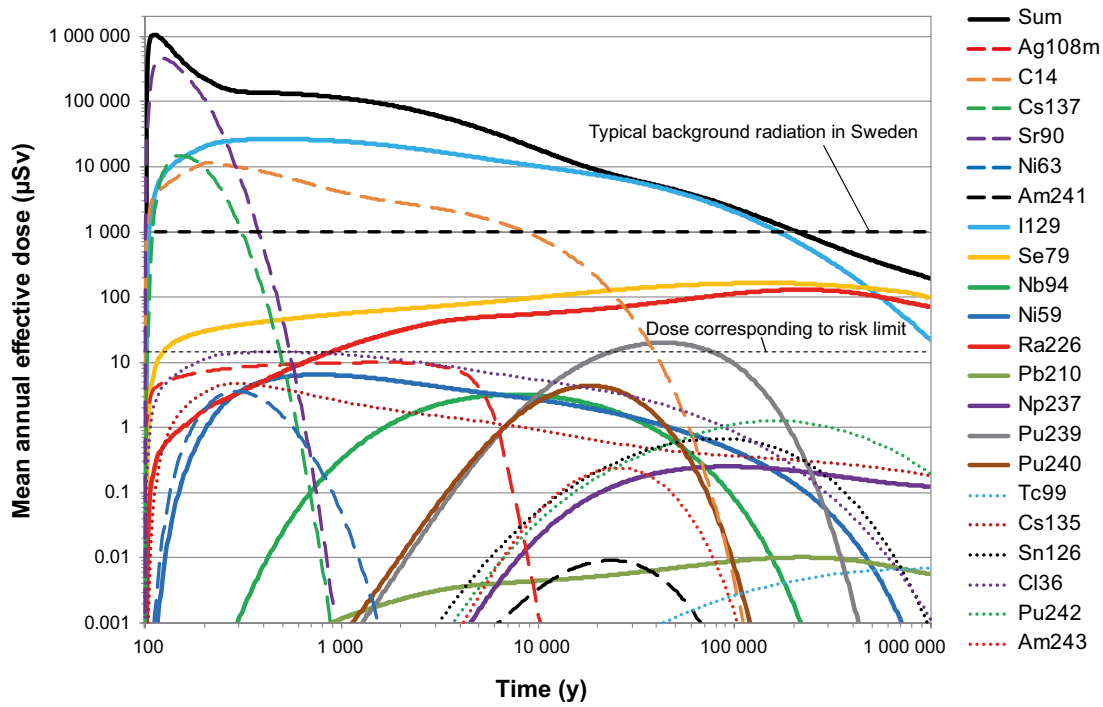


Figure 13-70. Near-field dose equivalent release for case E*, i.e. all canisters have an initial large defect in combination with a rapid fuel and metal conversion and the buffer is intact.

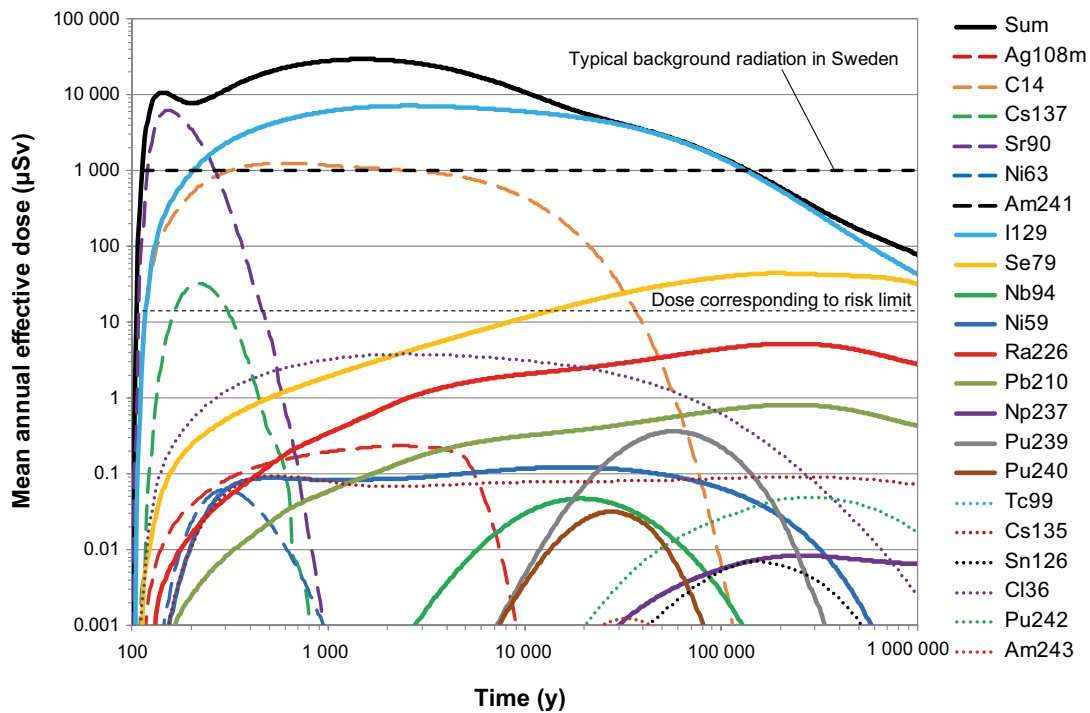


Figure 13-71. Far-field dose for case E, i.e. all canisters have an initial large defect in combination with a rapid fuel and metal conversion and the buffer is intact.

Summary of results with distributed LDF values

The summed dose for each case discussed above is given in Figure 13-72.

The following are noted.

After about 10 000 years, the doses for all cases are below the dose caused by typical background radiation in Sweden, except the case where retention properties of canisters, buffer and rock are all disregarded (case D*) and that with rapid fuel dissolution in combination with failed canisters (cases E and E*). The low flow and favourable groundwater chemistry of the rock and the presence of backfill and closure of the repository tunnel thus provide substantial protection from a fuel with unaltered dissolution rate.

If all canisters have large defects initially, but the barrier system is otherwise intact, case C, the peak annual dose to the most exposed individuals in the landscape does not exceed that caused by typical background radiation in Sweden, i.e. 1 mSv. Beyond 10 000 years this annual dose is less than an order of magnitude above the risk limit of 0.014 mSv.

If all canisters have large defects initially, and if also the buffer is assumed to be missing between the canister damage and the wall of the deposition hole, case D, the dose is comparable to the background radiation the first 10 000 years, and is thereafter quite similar to the case where the buffer is in place, case C. This suggests that the buffer is, from the point of view of total dose, not important as a retention barrier in this time perspective. However, a comparison between Figure 13-68 and Figure 13-66 shows that the buffer has a considerable impact on near-field releases of many sorbing nuclides that do not dominate the dose.

With a large degree of damage to the canisters, the buffer missing and retention in the rock disregarded, case D*, the calculation results suggest annual doses in the 0.1 Sievert range in the initial 1 000 years. This is a demonstration of the necessity of properly protecting man and the environment from the spent nuclear fuel, in particular in the 1 000 year time frame.

Beyond 10 000 years, the total dose is comparable to that caused by the background radiation even when neglecting the retention properties of all three barriers, case D*.

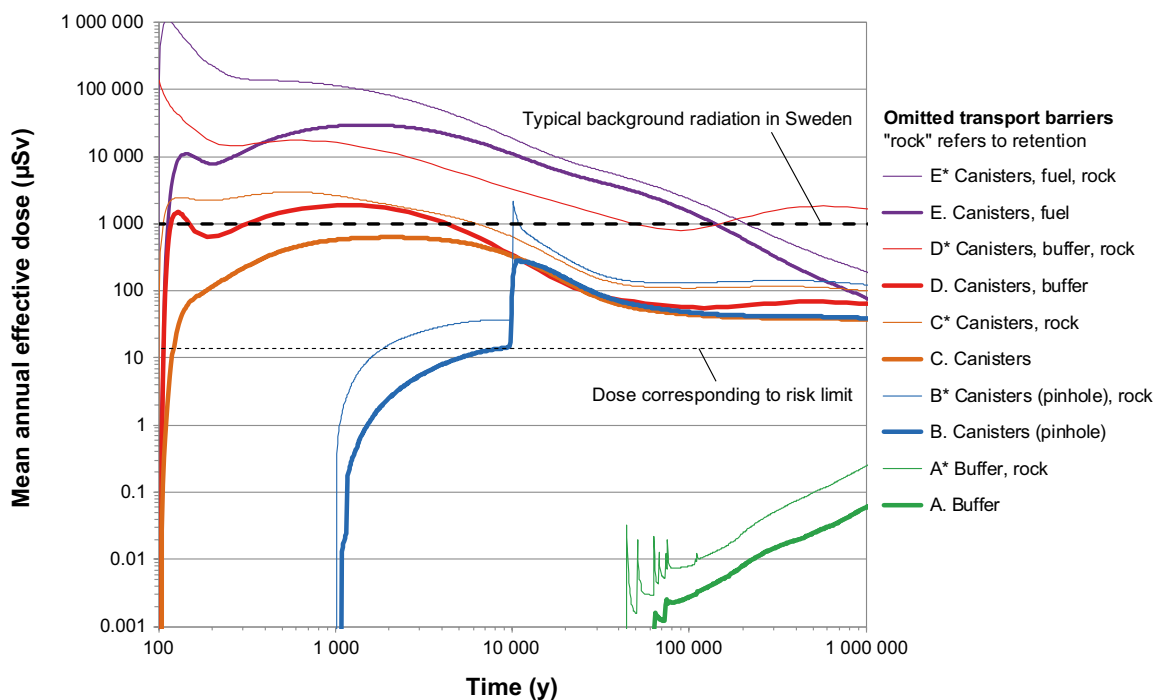


Figure 13-72. Results of stylised cases to illustrate loss of barrier functions. Note that an omission of the “rock” barrier in these cases refers to omission of retention of radionuclides in the rock fractures only, whereas the favourable, low flow rate at repository depth and the favourable geochemical conditions are still taken into account.

As expected, the case with initial pinhole defects, case B, and that with large initial defects, case C, are quite similar beyond 10 000 years, when the pinhole defects are assumed to have grown into large defects. It is also noted that neglect of rock retention does not affect the total dose much for these cases after about 1 000 years. However, a comparison between Figure 13-67 and Figure 13-66 shows that the rock has a considerable impact on far-field releases of many sorbing nuclides that do not dominate the dose.

A comparison of cases C and E shows the considerable containment function of the waste form for more than 100 000 years.

Summary of results with time dependent modelling of the biosphere

As mentioned in the introduction, the LDF values are suited primarily to handle releases that are constant over periods of time that are comparable to the duration of an interglacial, i.e. typically 10 000 years. Therefore, the releases for most of the above cases were also evaluated with a fully time dependent modelling of the biosphere. Here, the releases are distributed in the landscape according to the time dependent spatial distribution of release points from the repository and the time dependent doses are presented, rather than a time dependent release converted to dose by a constant LDF value. This modelling was performed for assumed temperate conditions over a period of 60 000 years. The results are given in Figure 13-73. The solid curves are doses obtained with distributed LDF values (i.e. the same curves as in Figure 13-72) and the dashed curves are the corresponding doses obtained with time dependent modelling of the biosphere.

The time dependent, dashed curves are generally within an order of magnitude of, but below, the curves obtained with LDF values. The one exception is the case where the retention properties of the canister, the buffer and the rock are all disregarded, case D*. Here, the time dependent dose from C-14 around 20 000 years slightly exceeds that obtained using the LDF. This is caused by accumulation and delay effects in the biosphere.

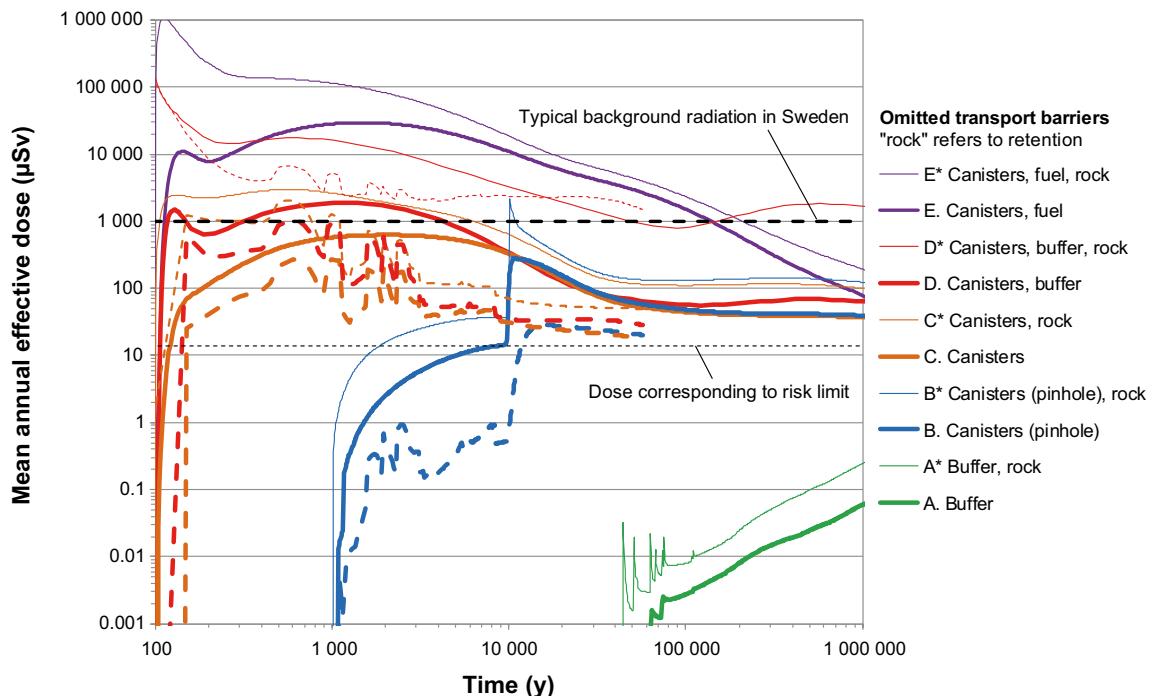


Figure 13-73. Results of stylised cases to illustrate loss of barrier functions. Solid lines: Same as in Figure 13-72 (dose conversion through distributed LDF). Dashed lines: Corresponding cases with time dependent dose modelling.

13.8 Radionuclide transport in the gas phase

Radionuclide transport in the gas phase, described by the processes Bu26, BfT22 and Ge25 for the buffer, the deposition tunnel backfill and the geosphere, is addressed in this section.

The formation of a gas phase is not possible for the corrosion scenario, since there is no buffer that can contain the gas in that case and the hydrogen is sufficiently soluble in water to be carried away by the advective flow i.e. gas can only accumulate if the buffer is intact. Hydrogen dissolution is a function of both the gas generation rate and water availability. The following description is valid for the shear load scenario, and the what-if cases treating the initial pinhole defect and the canister failure due to isostatic load.

The sealing properties of the buffer make it possible for a gas pressure to build up and a pulse of hydrogen gas to be released from a defective canister due to corrosion of the iron insert. Some radionuclides could potentially enter the gas phase and thereby be transported to the surface much more rapidly than would be the case for the aqueous pathway. In practice, only C-14 and Rn-222 are likely to enter the gas phase to any significant extent. (H-3 is expected to have decayed to insignificant levels before gas release could occur.)

It is assumed that if gas production exceeds the ability of the surrounding groundwater to take it into solution and transport it away from the canister that a pressure will build up within and adjacent to the canister. Based on experimental evidence (Harrington and Horseman 2003), the bentonite is assumed to ultimately open by fracturing and release gas when the internal pressure exceeds 20 MPa. A rapid outflow would be expected until the pressure fell to values below ~10 MPa when the buffer would seal and further gas transport would be by diffusion (however, see also below). This means that half of the gas generated from corrosion inside the canister would be released instantaneously together with the radionuclides contained in that amount of gas. Neither the buffer nor the geosphere is expected to significantly delay the transport to the biosphere.

After the initial breakthrough pulse, the pathway is expected to stay open as long as there is substantial gas production in the canister. After the breakthrough pulse, the gas is expected to be released at the same rate as it is produced by corrosion. The buffer will only close if the gas production falls to levels where the gas can dissolve and diffuse away. This means that either the pathway will stay open as long as there is a gas source or the pathway will open and close, causing repeated gas cycles.

Due to the uncertainties of the chemical form of carbon in the spent fuel, it is pessimistically assumed that the entire inventory of C-14 can enter the gaseous phase. The full inventory of Rn-222 is also assumed to be in the gaseous phase.

The time for gas breakthrough is determined by the failure time of the copper shell and the corrosion rate of the canister insert (see Section 13.5.2). At the time of breakthrough, half of the inventory of C-14 and Rn-222 is taken to be released immediately to the biosphere. The remaining gaseous inventory (and the Rn-222 that is produced) is then taken to be released together with the gas that is produced continuously. However, this release is neglected, since it will be insignificant in comparison with the pulse release. If the release occurs in the first 10000 years (unlikely) the release of C-14 would be about 10 GBq. A release of Rn-222 would be about 25 GBq if the release occurred after 100000 years.

In SKB (2006a, g) with clarifications and corrections in Hedin and Kautsky (2015), the calculated exposures from pulse releases of C-14 and Rn-222 are presented. C-14 may be released as methane (CH₄) or carbon dioxide (CO₂). It is assumed that if C-14 is released as methane from the repository, it will be oxidised to carbon dioxide by soil organisms. There are several alternatives regarding the fate of methane in its travel towards the surface:

1. Nothing happens and it will be released as gas to the atmosphere.
2. Microorganisms incorporate methane in the biosynthesis of other organic substances (i.e. not an oxidation). Eventually this organic carbon will be released by respiration to CO₂. This may occur in the rock as well as in the regolith.
3. Other microorganisms utilise the carbon source and produce CO₂ (i.e. an oxidation). This may occur in the rock as well as in the regolith.
4. The produced CO₂ will either degas to the atmosphere or be used in the photosynthesis by aquatic or terrestrial algae/plants. This may occur in surface ecosystems.

Thus, if a pessimistic approach is taken, the release as CO₂ will at least be handled in the biosphere model before it is released to the atmosphere. Methane released to the atmosphere is unlikely to be utilised. However, the potentially increased mobility of a gas in the geosphere is not considered.

Radon is a noble gas and will not undergo chemical transformations. Two exposure cases are considered for Rn-222 and C-14, one outdoors where radionuclides can be inhaled or consumed via uptake in plants in an area of 10 000 m², subject to a wind speed of 2 m/s and a mixing height of 20 m, the other inhalation of radionuclides indoors in a house with a volume of 1 000 m³ and a ventilation rate of 2 h⁻¹. For C-14, exposure may occur via inhalation or ingestion, for Rn-222 only inhalation of Rn-222 and its radioactive daughter products needs to be taken into account. A summary of the results is given in Table 13-11. It is noted that no account for decay in transit from the repository to the surface is taken, making the results for Rn-222, with a half-life of only 3.8 days, further pessimistic.

If the gas pressure is built up during a period of glaciation, the hydrostatic pressure from the ice has to be added to the gas breakthrough pressure. This may lead to internal pressures of about 50 MPa inside the canister. If the retreat of the ice is rapid, this could lead to pressure drops of around 40 MPa and consequently 80 % of the gaseous inventory would be instantaneously released.

The highest dose from a gas pulse of Rn-222 occurs in buildings. It is below the regulatory limits for an annual average life time risk for a repository, and it is considerably lower than the consequences of today's limit of 200 Bq/m³ for radon in buildings in Sweden, which gives about 2 mSv/y.

Table 13-11. Calculated annual mean life time risk from pulse releases of C-14 and Rn-222 for a single canister (SKB 2006a, g; clarifications and corrections in Hedin and Kautsky 2015).

Pathway	C-14 (μSv) (10 GBq release)	Rn-222 (μSv) (25 GBq release)
Ingestion	0.033	–
Inhalation outdoors	5.5 × 10 ⁻⁵	0.20
Inhalation indoors	0.0035	8.3

13.9 Risk summation

13.9.1 Introduction

The calculated risk as a function of time is an essential component of the compliance demonstration for the final repository. This section gives a summation of the risk contributions from the analysed scenarios.

According to the previous sections of this chapter, radiological consequences may arise for the scenarios in which canister failures due to copper corrosion and due to shear load occur. In the following, each of these is considered in isolation and then the total risk associated with the repository is discussed.

It is noted that the main scenario also gives rise to consequences, but that these are assessed as equal to the central corrosion case and subsumed under the corrosion scenario.

As a basis for the discussion, a number of dose curves calculated in the analyses of the corrosion and shear load scenarios are converted to risk and shown in Figure 13-74. The effective dose to risk conversion factor of 0.073 Sv⁻¹ has been used in accordance with SSM's regulations (Appendix A).

13.9.2 Risk associated with the corrosion scenario

Consequences have been calculated for the six corrosion variants identified in the corrosion scenario, each with base case transport data and conditions. For the central corrosion variant, five additional cases have been calculated exploring alternative transport conditions and data.

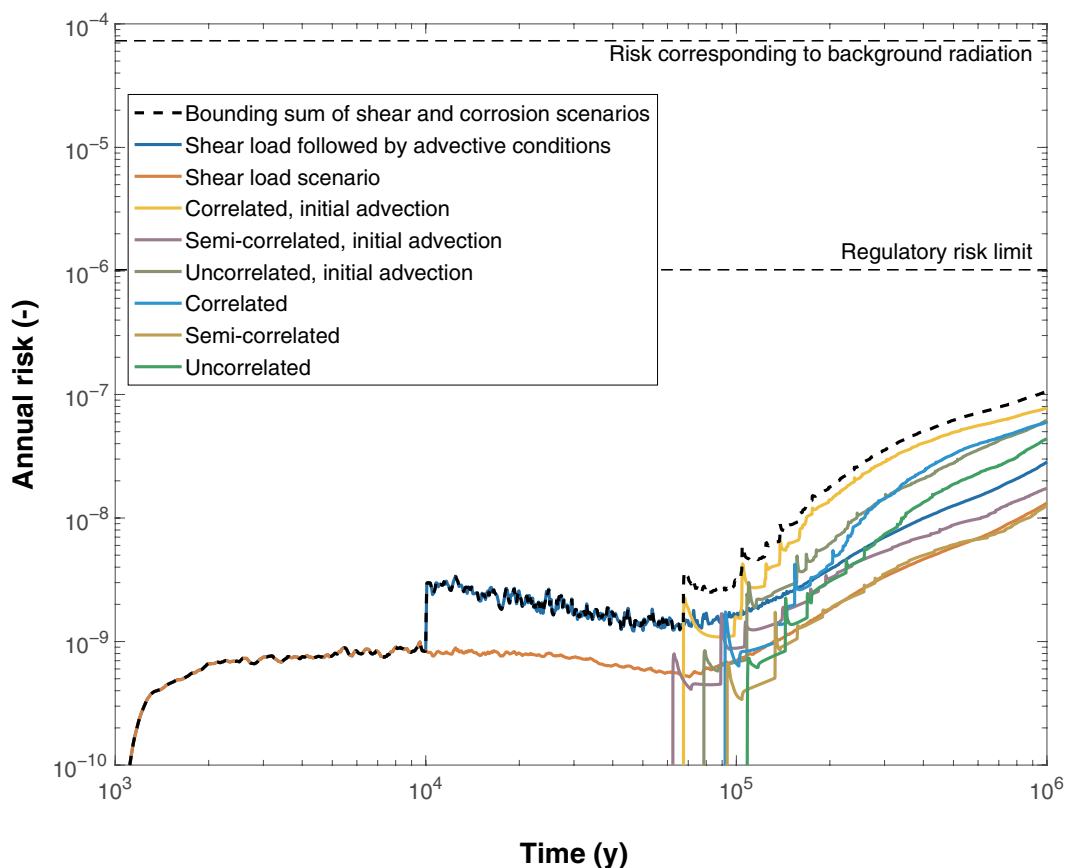


Figure 13-74. Risk curves, expressed as annual individual risk. Several alternatives for the corrosion scenario are shown, and two for the shear load scenario. The bounding, dashed curve is the sum of the curve for the shear load failure followed by advective conditions (dark blue) and the curve for the variant of the corrosion scenario yielding the highest risk (orange). The risk associated with the main scenario is subsumed under the corrosion scenario as it is equal to the semi-correlated case (brown).

Consideration of the six corrosion variants

The uncertainties associated with the erosion process are illustrated by the differences between the case with the PSAR erosion model and the case with the highly pessimistic assumption of initial advection, for a given hydrogeological DFN model. The initial advection cases put an upper bound on the possible consequences in terms of corrosion of the buffer erosion process. It bounds the impact on risk of uncertainties regarding the buffer erosion process, and covers impacts of gradually deteriorating functions of the buffer. It is, however, a highly pessimistic upper bound on the consequences. It is, therefore, argued that the central corrosion cases are reasonable and cautious representations of the risk associated with the corrosion scenario. However, since it is not possible to quantify several of the uncertainties associated with the erosion process, the pessimistically bounding cases of initial advection are also included as alternatives in the risk summation, noting that this case is clearly unrealistic as concerns the erosion process.

It is also noted that there are three corrosion variants where no advective conditions occur in deposition holes and where no canister failures due to corrosion occur. The risks associated with these variants are thus zero.

The uncertainties associated with the hydrogeological DFN model are illustrated by the differences between the cases with three different hydrogeological DFN models for a given assumption regarding buffer erosion. The semi-correlated DFN model is more compatible with the understanding of the water transmissive properties of fractures in crystalline rock. The uncorrelated and the fully correlated models are extreme variants of the correlation between fracture size and transmissivity, and are both seen as unrealistic. However, since the semi-correlated model gives the lowest consequences, and since it is not possible to quantify the degree of correlation in a strict sense, the uncorrelated and the fully correlated models are included as alternatives in the risk summation.

Consideration of the five alternative transport cases

Regarding alternative transport conditions, five alternatives to the central corrosion case have been calculated for the semi-correlated hydrogeological DFN model (not included in Figure 13-74). The two cases with mobile thorium in the near-field and inclusion of solubility limits yield somewhat lower dose consequences than the central corrosion case. The three calculations of time dependent flow and colloid facilitated transport in the geosphere suggest that the dose consequences are lowered if groundwater flow, rock K_d -values and LDF values are allowed to vary in accordance with a simplified climate development for the reference evolution. Furthermore, the dose consequences may temporarily be increased by a factor of less than three with colloid facilitated transport and for the highly pessimistic assumption that the colloid concentration is 10 g/L all along the geosphere transport path for 30 percent of both the temperate and the glacial climate domains, see Figure 13-35.

Based on these results, the central corrosion case, with base case transport conditions, is seen as a reasonable, cautious representation of the risk associated with the corrosion scenario for the semi-correlated hydrogeological DFN model, taking uncertainties in transport conditions into account. This also suggests that the other five corrosion variants, which have only been calculated for base case transport conditions, are appropriate representations with respect to assumptions regarding radionuclide transport.

Contribution from the IRF pulse

The annual risk associated with the IRF pulse contribution is obtained by multiplying the contribution of the IRF to the mean annual dose (calculated as for the central corrosion case, see Table 13-6 in Section 13.5.4) by 0.073 Sv^{-1} . The result of this procedure is shown for the case yielding the highest risk, i.e. that with the fully correlated hydrogeological DFN model and assuming initial advection in Table 13-12. The content of Table 13-12 is taken from the SR-Site assessment, since all input data to the calculations are quite close to those in the PSAR and since all calculated dose contributions in the table are negligible compared to the dose corresponding to the risk criterion. As seen in the table, the highest annual risk is 4.7×10^{-10} , i.e. more than three orders of magnitude below the risk limit. By comparing the pulse risk in each time interval to the risk curve, it is concluded that the pulse releases give negligible contributions to the calculated risk. They do, however, need to be considered in the account of risk dilution, see below. It is also noted that this treatment assumes that temperate conditions are prevailing. Including probabilities of periglacial and glacial climate conditions would reduce the calculated risk further.

Table 13-12. Risk associated with the pulse release for the case with the correlated hydrogeological model and initial advection. See Section 13.5.4 for further explanation. Results from the SR-Site assessment.

Time interval [yr]	p_{Fail}	p_{Expo}	$D_{\text{TotPulse}} [\mu\text{Sv}]$	Annual risk
0–100 000	4.3×10^{-2}	4.3×10^{-4}	6.3 ^a	2.0×10^{-10}
100 000–200 000	1.1×10^{-1}	1.1×10^{-3}	5.9	4.7×10^{-10}
200 000–300 000	1.2×10^{-1}	1.2×10^{-3}	5.5	4.7×10^{-10}
300 000–400 000	9.0×10^{-2}	9.0×10^{-4}	5.3	3.5×10^{-10}
400 000–500 000	8.2×10^{-2}	8.2×10^{-4}	5.0	3.0×10^{-10}
500 000–600 000	7.3×10^{-2}	7.3×10^{-4}	4.8	2.6×10^{-10}
600 000–700 000	6.0×10^{-2}	6.0×10^{-4}	4.6	2.0×10^{-10}
700 000–800 000	9.0×10^{-2}	9.0×10^{-4}	4.5	3.0×10^{-10}
800 000–900 000	1.2×10^{-1}	1.2×10^{-3}	4.4	3.7×10^{-10}
900 000–1 000 000	8.2×10^{-2}	8.2×10^{-4}	4.3	2.5×10^{-10}

^a This value determined for the time of the first canister failure, 48 000 years.

13.9.3 Risk associated with the shear load scenario

The two risk curves associated with the shear load scenario shown in Figure 13-74 are obtained from the calculated mean annual dose for the case with an intact buffer according to Figure 13-51 and the case with advective conditions in the deposition hole Figure 13-55, applied after a pessimistically chosen 10 000 years for reaching advective conditions through buffer erosion. These cases are both bounding with respect to the pessimistic treatment of the probability of earthquakes, of the transport conditions in the near-field and to the neglect of geosphere retention. Between the two, the case with advective conditions is bounding.

In addition, since the occurrence of earthquakes is a stochastic process, it cannot be entirely ruled out that a detrimental earthquake would occur during the initial 1 000 years. The probability that one out of the 6 000 canisters has failed at the end of the initial 1 000 year period is estimated at 2.4×10^{-5} , see Section 10.4.5, i.e. 40 000 repositories, each with 6 000 canisters would have to be constructed in order for there to be an expectation of one failure during the initial 1 000 years. Despite this extremely low probability, a risk contribution was calculated for the first 1 000 years, with the result that the expected dose rate is around $0.001 \mu\text{Sv}/\text{yr}$, see Figure 13-52 in Section 13.6. This corresponds to an annual risk of $10^{-10}/\text{yr}$, i.e. below the risk scale of Figure 13-74.

Regarding the risk contribution from the IRF pulse, a similar treatment to that above can be made, where only the p_{Fail} values would differ. Since these values are lower for the shear load scenario (the total failure probability over the entire one million year assessment period is 0.079) and since the risk for the corrosion scenario is very small, no such account is given.

13.9.4 Risk contributions from fuel residues and damaged fuel

As noted in Sections 5.3.2 and 5.3.4, containers with fuel residues and failed fuel rods will also be encapsulated and deposited. These fuel types represent a very small fraction of the total radionuclide inventory, but their risk contribution needs, nevertheless, to be assessed since their properties differ from those of the regular fuels, in particular since they are assumed to have a higher fuel dissolution rate. In Chapter 7 of the **Radionuclide transport report**, it is demonstrated that both these fuel types give negligible risk contributions also when considering the higher dissolution rates. The calculations were done for the canister failure case yielding the highest dose in the risk summation in Figure 13-74, i.e. the variant of the corrosion scenario where the buffer is assumed to be lost initially and where the fully correlated hydrogeological model is used.

13.9.5 Risk dilution

The results in this section are taken from the corresponding Section in the Main report of the SR-Site assessment (SKB 2011). The calculation cases that need to be considered in the PSAR are the same as in SR-Site and in Appendix M to the **Radionuclide transport report**, all these cases are demonstrated to yield results quite similar to the corresponding SR-Site cases. As regards in particular the input data for the results in Figure 13-75, the failure times and the pulse-LDF values are identical to those in the SR-Site assessment. The only factor that differs slightly is the IRF inventories for the contributing radionuclides.

The issue of risk dilution is discussed in the methodology Section 2.6.2 and needs to be addressed both for the corrosion scenario and for the shear load scenario. Doses in both these scenarios are accounted for as a continuous contribution and as relatively short pulse contributions.

The total doses from the continuous contributions have, for a fixed failure time, an initial peak of limited duration followed by an increasing curve that generally grows beyond the value of the initial peak. Since this means that the maximum dose occurs at the end of the one million year assessment time, risk dilution is not an issue for the continuous contributions; the maximum risk is experienced by the same hypothetical generation living at the end of the assessment period irrespective of failure time. This is verified by comparing the peak-of-the-mean value ($0.177 \mu\text{Sv}/\text{yr}$) to the mean-of-the-peaks value ($0.179 \mu\text{Sv}/\text{yr}$) for the central corrosion case (see Section 2.6.2 for an explanation of these concepts). For the shear load scenario, the peak-of-the-mean is $0.15 \mu\text{Sv}/\text{yr}$ and the mean-of-the-peaks is $0.28 \mu\text{Sv}/\text{yr}$. The cited annual dose values are taken from the SR-Site assessment and have not been re-calculated in the PSAR since changes of input data are insignificant with respect to the calculation endpoint. The calculation procedure is somewhat clarified in Hedin (2015).

Regarding the pulse contributions, the situation is different. Doses occur immediately after the canister failure and last short time intervals compared to the assessment time. The probabilistic treatment of the mean annual dose according to Table 13-12 leads to risk dilution as a consequence of the distribution of failure times. The peak doses given in Table 13-5 for the central corrosion case are an illustration of such doses. To address risk dilution for such short term releases, Appendix 1 to SSMFS 2008:37, reproduced in Appendix A of this report, suggests that risk dilution can be addressed by calculating an “accumulated short-term risk” (SKB’s terminology) as

$$D_{\text{TotPulse}}(T) \cdot \int_{T_0}^T f(\tau) d\tau \cdot 0.073 \text{ Sv}^{-1}$$

and comparing this entity to the risk limit. In this expression, T_0 is the time of closure of the repository, and f is the time dependent frequency of canister failures. The results of such a calculation for the corrosion (correlated case with initial advection) and shear load scenarios are shown in Figure 13-75, based on PSAR input data. The result shows the peak risk future individuals could be exposed to once during the one million year assessment period. The calculated entities in the figure are not comparable to the risk curves for the continuous releases and cannot be said to represent a true risk in the same sense as the continuous release. Rather, they represent a formal way of addressing the issue of risk dilution for short-term releases. The sum curves in Figure 13-75, and their total if they were to be added, are below the risk limit and hence the risk criterion is fulfilled also for this bounding way of addressing risk dilution.

It is also noted that both the LDF values used for the continuous releases and the pulse LDF values are derived by assuming that all of the release occurs to each biosphere object and the values obtained for the object giving the highest doses is then used for LDFs and pulse LDFs. There is hence no risk dilution due to uncertainty as to the biosphere object to which the release will occur.

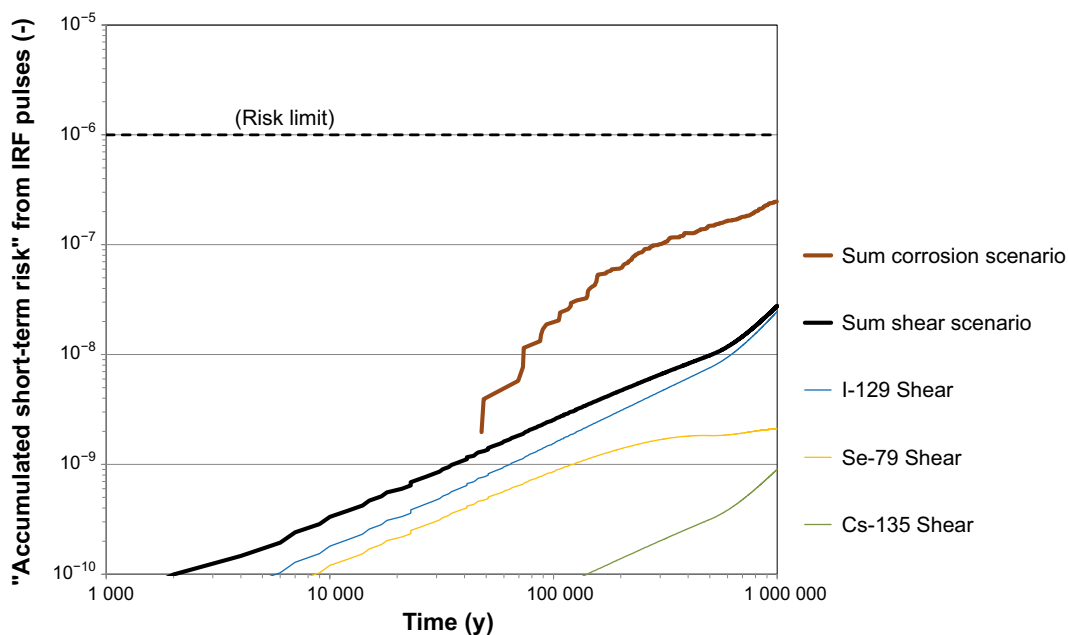


Figure 13-75. Accumulated short-term risk from IRF pulses in the corrosion (thick, brown curve) and shear (thick, black curve) scenarios. Also contributions from individual nuclides are shown for the shear scenario. The distribution of canister failure times for the corrosion scenario is taken from the fully correlated case assuming initial advection.

13.9.6 Extended discussion of risk for the initial 1 000 years

Introduction

According to SSMFS 2008:37, a more detailed account of the protective capability of the repository is required for the initial 1 000 years after closure. Since the radiological hazard of the waste is highest for this time period it is particularly important to account for repository evolution, safety functions and risk in this time frame. Such an account is provided in the following, largely based on material from previous parts of this main report.

Initial state

All canisters are assessed to be tight at deposition. The initial copper coverage is discussed in the account of the initial state of the canister in Section 5.4.3. The initial minimum copper thickness is given as 47.5 mm in Table 5-9. Taking also the occurrence of local internal defects in the copper shell into consideration, no canisters are assessed to have local reductions exceeding 20 mm. This is the manufactured and inspected thickness of the corrosion barrier after the final machining of the canister components.

Also, according to Section 5.5.3, the buffer is expected to be emplaced according to the reference design leading to an initial state where the buffer will acquire its post-closure safety related properties after water saturation.

Modelling of the general evolution of the repository

As required by SSM's regulations, many aspects of the repository evolution have been modelled in detail for the initial 1 000 years. This concerns the thermal, mechanical, hydraulic and chemical evolutions, as well as effects on the buffer and the canister. Detailed accounts are given in Sections 10.2 (the excavation and operational phases) and 10.3 (the initial period of temperate climate after closure). Also the biosphere development is modelled in detail during this time period.

According to Sections 10.2.5 and 10.3.13, no canister failures due to corrosion during the excavation/operational phase and during the initial 1 000 years of the reference evolution are expected. As concluded in Section 10.3.13 the total amount of copper corrosion during the excavation and operational phases and the first 1 000 year period can be estimated to be of the order of 1 mm, when taking into account the contributions from residual oxygen in the repository and possible microbial sulphate reduction as well as the contribution from sulphides in the bentonite and backfill. Given the initial state of the copper coverage above, the margin to failure due to corrosion is hence very large. No challenge to this conclusion was found in the analysis of the corrosion scenario in Section 12.6, see in particular Section 12.6.3.

The same applies to failures due to isostatic loads on the canisters, briefly treated in the reference evolution Section 10.3.13 and further in the scenario addressing this failure mode in Section 12.7. The isostatic pressures during the initial 1 000 years are considerably lower than those that may occur during later, glacial conditions, that the canister is designed to withstand. Pressures from uneven swelling of the bentonite buffer have been addressed in the design analysis of the canister (Section 5.4), with the conclusion that the probability that the canister will not withstand the loads is negligible.

Shear loads on the canister may occur as a consequence of large earthquake induced secondary shear movements in fractures intersecting deposition holes. Although the likelihood for large earthquakes is higher during glacial rebound, it cannot be entirely ruled out that a detrimental earthquake would occur during the initial 1 000 years.

The probability that one out of the 6 000 canisters has failed at the end of the initial 1 000 year period is estimated at 2.4×10^{-5} , see further Section 10.4.5, i.e. hypothetically 40 000 repositories, each with 6 000 canisters would have to be constructed in order for there to be an expectation of one failure during the initial 1 000 years.

Calculated risk for the initial 1 000 years

Of the three identified failure modes of the canister, i.e. failure due to corrosion, due to shear load and due to isostatic loads, corrosion and isostatic load induced failures can thus be ruled out with large margins for the first 1 000 years.

Failures due to shear load are extremely unlikely according to the above, and since no probability limit for excluding a risk is adopted in the PSAR, a risk contribution was calculated for the first 1 000 years, as reported in Section 13.6.2, with the result that the mean annual dose is at most around 0.001 $\mu\text{Sv}/\text{yr}$ corresponding to a risk of $10^{-10}/\text{yr}$, see Figure 13-52. This analysis builds on detailed modelling of the biosphere development and radionuclide transport in the developing landscape during the initial 1 000 years, as required by SSM's regulations.

It is noted that this calculation case is based on several pessimistic assumptions regarding the probability of shear failure, the modelling of the near-field and in the neglect of geosphere retention (Table 13-13). Additional pessimistic assumptions of relevance for the initial 1 000 years concern the time to establish water contact with the fuel, assumed pessimistically to be 100 years neglecting the build-up of a counter pressure in the canister interior as water enters the canister and neglect of the containment function of the Zircaloy cladding.

Based on the above, it is concluded that the analysed repository at Forsmark complies with the regulatory risk criterion during the initial 1 000 years after closure with a considerable margin.

Discussion of the barrier system for the initial 1 000 years

According to extensive analyses in the corrosion scenario, even a hypothetical initial absence of the buffer in all deposition holes does not lead to failure of canisters for tens of thousands of years. It is thus not relevant to discuss hypothetical buffer malfunction further in the 1 000 year perspective. For the same reason, the retention properties of the host rock are not further discussed here.

Regarding the canister, as mentioned above, all canisters are assessed to be tight at deposition. To discuss the barrier system in a 1 000 year perspective, a hypothetical case where a canister is not initially tight, may be considered. In such a case, there are several factors that contribute to safety according to the following.

- For the fuel:
 - The containment function of the fuel matrix.
 - The containment function of the structural parts of the fuel elements.
- For the canister:
 - The time required to fill the canister with water.
 - The containment function of the Zircaloy cladding.
- For the buffer:
 - Its contribution to delaying water saturation and limiting the rate at which the canister fills with water.
 - radionuclide retention.
- For the host rock:
 - Its favourable hydrogeological properties, contributing to slow water saturation and limited release rates.
 - Radionuclide retention.

In the following, each of these factors is briefly discussed.

The containment functions of the fuel matrix and of the structural parts of the fuel elements

These factors were discussed in the analyses of cases with assumed, complete losses of barrier functions in Section 13.7.4. There, it was concluded that the waste form has a considerable containment function for more than 100 000 years.

The time required to fill the canister with water

In the **Data report** it is shown that for a hypothetical, circular penetrating defect with a radius of 2 mm it will take more than 20 000 years to fill the canister with water. To cover any shape of the defect, the delay time is pessimistically estimated to be at least 1 000 years, used as the pessimistic delay time in the hypothetical pinhole case analysed in Section 13.7.2.

The derivations of all these delay times neglects the effect of gas generated by corrosion of the insert by the penetrating water, which could lead to substantially longer delay times (Bond et al. 1997).

The buffer's contribution to delaying water saturation and limiting the rate at which the canister is filled with water

A prerequisite for water to enter into the canister is a fully water saturated buffer. The saturation times for both backfill and buffer are likely to range from a few tens of years to several thousand years, as a consequence of the rock properties (matrix hydraulic conductivity and presence and characteristics of fractures) at Forsmark. Consequently, in many deposition hole positions, no water would be expected to come into contact with the waste during the first 1 000 years even if there were an initial defect in the canister.

The containment function of the Zircaloy cladding

According to the **Fuel and canister process report**, available data suggest a life of the cladding tubes of at least 100 000 years. Although Zircaloy is highly resistant to uniform corrosion, due to its potential susceptibility to local corrosion in groundwaters and to hydrogen induced cracking, cladding is generally not assumed to constitute a barrier to radionuclide release from the fuel in the PSAR, even though a more in-depth evaluation in Evins (2020) suggests that it would serve as a barrier for at least 10 000 years for the majority of fuel types in the repository. Furthermore, even a cladding with small cracks or corrosion defects would offer a large mass-transport resistance for water to get into contact with the fuel and for dissolved radionuclides to exit into the canister void.

Radionuclide retention in the buffer

The retention properties of the buffer are exemplified in the calculation cases with assumed complete losses of barrier functions in Section 13.7.4. A comparison between Figure 13-68 and Figure 13-66 shows that the buffer has a considerable impact on near-field releases of many sorbing nuclides.

The host rock's favourable hydrogeological properties

In addition to contributing to long saturation times mentioned above, the limited flow rates at the deposition positions limits the release rate of radionuclides from the near-field if releases occur from the canister.

Radionuclide retention in the rock

The retention properties of the rock are exemplified in the calculation cases with assumed complete losses of barrier functions in Section 13.7.4. A comparison between Figure 13-67 and Figure 13-66 shows that the rock has a considerable impact on far-field releases of many sorbing nuclides.

13.9.7 Conclusions

The bounding, dashed curve in Figure 13-74 is the sum of the risk associated with the shear load scenario and that associated with the corrosion scenario. The former is represented by the case with advective conditions and the latter by the correlated case with initial advection, both of which give the highest risks within their scenarios. (Within the scenarios the cases are mutually exclusive, meaning that only one from each scenario should be used in the summation. Since the main scenario is represented by the central corrosion variant, also the main scenario is included as subsumed under the bounding corrosion case.)

Other scenarios did not yield any contributions to the calculated risk. In the account of combinations of scenarios and phenomena in Section 12.9.3 it was concluded that the consequences of a shear load failure followed by buffer erosion needs to be assessed and this is done in the bounding case of the shear load scenario. All relevant risk contributions are, therefore, assessed to be included in Figure 13-74.

Since the bounding curve in Figure 13-74 is below the risk limit for the duration of the one million year assessment period, the analysed KBS-3 repository at the Forsmark site is assessed to fulfil the regulatory risk criterion. Risk dilution was shown not to challenge this conclusion.

It is furthermore concluded that a more realistic risk may be anywhere in the area below the bounding curve, down to zero risk based on the zero results of the three cases with no erosion and a situation where no canisters would fail due to shear movements induced by large earthquakes, which could be reached if somewhat less pessimistic assumptions could be defended for the shear load scenario.

It is also noted that through the use of LDF factors to transform releases to doses, it is in the risk assessment implicitly assumed that the landscape to which the releases occur is always fully populated, including the object where the highest dose is calculated to occur and at the time when this occurs. Furthermore, long periods of glacial and submerged conditions are expected where no doses to humans occur since the site is not habitable. This has not been taken into account in the risk summation. Rather, temperate conditions yielding the highest doses are assumed throughout.

Factors that have the greatest impact on overall risk are identified in the sensitivity analyses e.g. in Section 12.2.2 (buffer erosion), 12.6.2 (canister corrosion) and 13.5.11 (consequences for the corrosion scenario). These are summarised in the next section where also references to sections discussing steps that could be taken to reduce or mitigate these impacts are given.

It is also noted that the calculated risk is one of several indicators of repository safety for distant time frames. Four additional indicators have been applied in Section 13.5.8 with the result that the calculated consequences are well below the reference values to which they are compared. This is further discussed in the conclusions of the assessment, see Section 15.3.

A KBS-3 repository at Forsmark is assessed to fulfil the regulatory risk criterion for the initial 1 000 years with a considerable margin. The barrier system has a number of functions that contribute to safety in a hypothetical case where the canister is assumed to be initially defective. Several of the factors would, with cautious assumptions, alone prevent any releases during the initial 1 000 years for an initially defective canister. This relates particularly to the time required for water to get into contact with the fuel elements and the integrity of the Zircaloy cladding.

Finally, it is noted that the risks due to both the corrosion scenario and to the shear load scenario are increasing at one million years. This is primarily caused by the increasing probabilities for barrier failures for the later parts of the assessment period, whereas radioactive decay plays a minor role for the development since the dose dominating nuclides, in particular the parent nuclides of Ra-226, are very long-lived. It is not seen as meaningful to continue the calculations beyond one million years (see further Section 14.5), but an account of the consequences for a number of hypothetical cases where all canisters fail early in the assessment period is given in Section 13.7.4. For the hypothetical case where all canisters are failed, where the buffer is absent and where retention in the rock is disregarded, the calculated risk at one million years is comparable with that caused by the background radiation. This indicates a bound on the development of the risk curve beyond one million years, when the extent of barrier failures may be expected to increase.

13.10 Summary of uncertainties affecting the calculated risk

13.10.1 Summary of main uncertainties affecting the calculated risk

A number of issues relevant for post-closure safety are associated with considerable uncertainties. This is inevitable in an assessment of situations far into the future and where the parts of the system are not fully known. The following is an account of how main uncertainties affecting the calculated risk are handled in the PSAR with indications, through reference to the feedback Sections 15.4 to 15.7, of the potential of reducing them in later stages of the repository programme. The account deals with factors affecting the two scenarios contributing to the calculated risk, i.e. the corrosion scenario and the shear load scenario. A discussion of whether formal expert elicitations could be a means of reducing these uncertainties is provided in Section 13.10.2.

In the corrosion scenario, canister failures, and hence risk contributions, occur only in cases where the buffer has been eroded to the extent that advective conditions prevail in part of the deposition hole, leading to enhanced corrosion rates. In the sensitivity analyses of the extent of buffer erosion in Section 12.2.2, of canister corrosion for advective conditions in Section 12.6.2 and of dose consequences from canisters failed due to corrosion in Section 13.5.11, the main uncertain factors listed in Table 13-13 were identified. Means of reducing these uncertainties and the potential impact on risk this may have is also accounted for in the table. Regarding the shear load scenario, many of the uncertain factors are related to the assessment of the likelihood of earthquake induced shear failures in Section 10.4.5 and to the evaluation of consequences of such failures in Section 13.6. These are also listed in Table 13-13.

It is noted that, in addition to the factors mentioned in the table, more developed deposition position rejection criteria have a large potential of reducing risk. This is, however, a design issue rather than an uncertain factor in the risk calculations in the PSAR, see further Sections 14.3 and 15.3.5.

Table 13-13. Main uncertain factors affecting the calculated risk and future plans for their reduction.

Factor	Type of uncertainty	Handling in PSAR risk calculations	Means of reducing uncertainty	Potential impact on calculated risk	Plans in section
Mechanistic understanding of buffer erosion and sedimentation.	Conceptual.	Pessimistic. Use of state-of-the-art models as central case. Demonstration of low negative impact on corrosion for a bounding case of initial advection. Bounding case of initial advection included in risk summation and used to demonstrate risk compliance.	Further research.	Can only reduce risk, since bounding case is included in risk summation. Potential to lead to exclusion of buffer erosion and sedimentation in the corrosion scenario would result in exclusion of canister failures in the corrosion scenario according to analyses in the PSAR.	15.7.3
Groundwater salinity; low salinity required for buffer erosion to occur.	Site data, conceptual understanding.	Pessimistic. Cautious approach in modelling of salinity at high-flow deposition positions. Demonstration of limited negative impact on erosion and corrosion for a bounding case of dilute conditions 100 % of time. Cases with initial advective conditions bound impact of uncertainties regarding dilute conditions in risk calculation.	Additional groundwater sampling. See also groundwater flow as salinity evolution is strongly related to groundwater flow.	Can only reduce risk, since bounding case is included in risk summation. Potential to lead to exclusion of buffer erosion from the corrosion scenario would result in exclusion of canister failures in the corrosion scenario according to analyses in the PSAR.	15.6.9
Groundwater flow.	Conceptual as well as spatial and temporal variability.	Probabilistic modelling. Input data from comprehensive hydrogeological modelling of several concepts (correlation structures), in turn based on evaluation of conceptual uncertainty in site modelling. Each model generates an input data distribution covering spatial variability. Each distribution propagated to risk calculations. Distribution yielding highest risk used to demonstrate risk compliance.	Further development of models based on data from future underground characterisation. (Sensitivity to spatial variability difficult to reduce, other than by deposition hole rejection criteria.)	Limited, if developed model is within bounds of conceptual models used in the PSAR.	15.6.4 15.6.5
Flow at deposition positions affects erosion and corrosion.		Temporal variability addressed by stylised glaciation case. Simplified results used in variant case of risk calculation and shown to have limited impact on overall risk when considered together with biosphere alterations.			
Flow in host rock affects radionuclide transport.					
Sulphide concentrations over time; affect corrosion.	Incomplete understanding of causes for range in site data; both spatial variability and conceptual uncertainty. Incomplete understanding of temporal development.	Probabilistic. Use of measured range of values at the Forsmark site combined with distribution of groundwater flow at deposition positions to obtain mean number of failed canisters. Incomplete understanding of temporal development; pessimistically handled.	Additional site data. Further research.	Potentially considerable reduction in risk if spatial variability could be reduced and/or demonstrated to reflect temporal variability at deposition positions (see Section 12.6.2, subheading 'Groundwater concentrations of sulphide').	15.6.9 15.7.4
Probability of earthquake; affects probability of shear failure.	Conceptual; incomplete understanding.	Pessimistic. Frequency range, (several estimates) determined and upper bound of range chosen for risk calculations.	Further research.	May further reduce risk.	15.7.4
Probability that a zone hosts an earthquake; affects probability of shear failure.	Conceptual uncertainty.	Pessimistic. i) All zones affecting the repository assumed to host the largest earthquake compatible with their size. ii) Zone with largest impact chosen for risk calculation.	Further research.	May further reduce risk.	15.6.1 15.6.7 15.7.4

Factor	Type of uncertainty	Handling in PSAR risk calculations	Means of reducing uncertainty	Potential impact on calculated risk	Plans in section
Probability of a deposition position being intersected by a large fracture.	Conceptual uncertainty, spatial variability, insufficient information.	Pessimistic. All DFN models identified in site modelling evaluated. Variant yielding highest probability of intersection used in risk calculation.	Further research, methodology development, data from underground investigations.	May further reduce risk.	15.6.2 15.6.3 15.7.4
Efficiency in deposition hole acceptance criteria.	Measurement techniques not sufficiently tested for this context.	All EFPC fractures assumed to be found. No credit taken for additional signatures of large fractures; these may potentially be more efficient than EFPC in identifying deposition holes to reject.	Further development of methods to identify critical structures.	May further reduce risk.	15.6.2
Potential for damage if shear is larger than 5 cm; affects probability of shear damage.	Conceptual as well as spatial and temporal variability.	Pessimistic. i) Case with angle of intersection and point of impact yielding maximum impact on canister used as basis for risk calculation. ii) Upper bound on buffer density in technical design requirement used; no credit for demonstrated lower maximum density in reference design, nor of distribution of densities.	Additional mechanical analyses to cover cases where the angle and the buffer density are more beneficial. Probabilistic handling of impact location, angle of intersection and buffer density. Revised technical design requirements for buffer density.	Would further reduce risk.	15.7.2 15.5.3, 15.5.7
Failure criteria in assessment of canister response to shear loads; affects probability of shear damage.	Conceptual.	Pessimistic. i) Pessimistically chosen, local, failure criterion for cast iron insert in design analysis of canister used as criterion for global failure. ii) No allocation of containment potential to copper shell when insert fails locally.	Further development of criteria for global failure of canister. Further development of models for copper creep behaviour. Implementation in shear response modelling.	Would further reduce risk.	15.7.2
Hydraulic properties of shearing fracture and retention in migration pathway; affects retention.	Incomplete understanding of hydraulic properties resulting from shearing of a fracture.	Pessimistic. Near-field: i) Canister failure location assumed to fully coincide with location of shearing fracture; ii) Shear assumed to increase transmissivity of intersecting fracture such that its Qeq value is too high to contribute to transport resistance in the near-field; iii) Geometric transport resistance of fracture/buffer intersection neglected. Far-field: No credit taken for radionuclide retention in the geosphere.	Analyses of the impact on the flow system if only the shearing fractures were affected.	Potentially reduction in risk since only the shearing fracture, and not the fractures it connects to, would be affected. A local increase of transmissivity in a fracture network would not necessarily increase flow or reduce retention.	
Fuel dissolution rate.	Incomplete knowledge.	Probabilistic. Pessimistically derived distribution of rates from experiments.	Further research.	Reduction in risk if more favourable distribution can be defended.	15.7.1
Flow related transport parameters.	See groundwater flow. (Uncertainties in transport parameters are mainly due to uncertainties in flow. Conceptual understanding of channelling is an additional uncertain factor.)	See groundwater flow.	See groundwater flow. (Further data has impact on flow that influences transport parameters.)	Limited, if developed model is within bounds of conceptual models used in the PSAR.	15.7.4
Landscape specific dose conversion factors.	Conceptual.	Deterministic values, with pessimistic handling of several uncertainties, see further Section 13.2.6.	Further research and model development.	Potential to reduce risk by several orders of magnitude for specific nuclides.	15.7.5

13.10.2 Candidate issues for formal expert elicitations

In planning the SR-Site assessment, an evaluation of candidate issues for expert elicitations was made and the following criteria were used to determine whether an issue could be considered for an elicitation.

- The issue should be associated with large uncertainties that have a considerable impact on the assessed level of safety.
- A formal expert elicitation can be deemed to contribute to the reduction of these uncertainties in addition to what is achievable through other means established in the methodology for the assessment (evaluation of conceptual uncertainties in the **Process reports**, of data uncertainty in the **Data report**, through quality assured modelling, etc all of these leading to a well-motivated and often pessimistic handling of the issue in the assessment).

As pointed out in Section 2.8.5 the conclusion of the evaluation was that, although a number of uncertainties could in principle be amenable to a formal expert elicitation, no issue was identified for which both the above criteria apply. Based on the sensitivity analyses of the calculated risk in SR-Site, (similar to those presented in this chapter), the evaluation of candidate issues for expert elicitation was updated. This update is revisited below, based on the results of the PSAR. Since only the corrosion and the shear load scenarios contributed to risk, it would only be uncertainties related to these scenarios that would be of interest for formal expert elicitations. In particular, the issues listed in Table 13-13 are of interest to evaluate. The contents of Table 13-13 is similar to those of the corresponding table in SR-Site.

Candidate issues for the corrosion scenario

According to Table 13-13 issues related to the corrosion scenario mainly concern mechanistic understanding of the buffer erosion and sedimentation processes, groundwater flow, evolution of groundwater salinity and sulphide levels, releases rates from the spent fuel and the flow related transport parameters. These are assessed in the following.

Mechanistic understanding of the buffer erosion and sedimentation processes: This issue has been the target for intense research since it was identified as crucial for the safety evaluation in the SR-Can project. Building knowledge for the SR-Site project, a group of experts recruited internationally has studied the process experimentally and theoretically. Several expert reports and a summary report have been produced in the project and regular seminars where the entire expert group has discussed intermediate results and possible ways forward have been held. The project reports have also been reviewed internationally. It is difficult to conceive of an additional group of experts that could, in a limited time, evaluate these findings in such a way that the years of efforts by this expert group could be further refined or qualified for the safety assessment. Research has continued in a similar manner after the SR-Site project, addressing then also the sedimentation issue. Although this is an important issue for safety, it is, on the above grounds, not deemed as suitable for an expert elicitation.

Neither uncertainties related to the fraction of a glacial cycle during which erosion is active nor the buffer mass loss required to reach advective conditions in a deposition hole, nor the strongly related corrosion geometry are sufficiently important for the overall safety evaluation to qualify these issues as candidates for a formal expert elicitation. Furthermore, they are both evaluated by cautious interpretation of results of direct modelling and are thus addressable through the standard methodology for the assessment. Similar arguments can be put forward regarding the concentration of canister corroding agents over a glacial cycle.

The distributions of the equivalent flow rate, of the Darcy flux and of the flow related transport parameters for the ensemble of deposition holes are affected by both conceptual uncertainties and spatial variability. In particular the Darcy flux has a considerable impact on the safety evaluation through its importance for the erosion and corrosion processes. These factors have been evaluated in several steps including the collection of site data, comprehensive modelling of the hydraulic properties of the site including the consideration of several conceptual models and data uncertainties, modelling of the hydraulic evolution within the safety assessment, and a thorough evaluation of the resulting distributions in the **Data report**. All these steps have been carried out by several expert

groups with overlapping membership. The results have been externally reviewed. It is not deemed fruitful to attempt to further substantiate these findings, achieved through years of reviewed efforts, by a formal expert elicitation.

All data relating to the calculation of radionuclide transport and dose for the failed canisters are thoroughly evaluated in the **Data report**. A dominating factor, the fuel alteration rate, is evaluated in a dedicated report by a group of international experts forming the most important input to the evaluation in the **Data report**. The expert report has also been subject to peer review. It is difficult to conceive of an additional group of experts that would, in a limited time, reach better founded conclusions.

Candidate issues for the shear load scenario

According to Table 13-13 issues related to the shear load scenario mainly concern the probability of earthquakes; the probability that a zone hosts an earthquake; the probability of a deposition position being intersected by a large fracture, the efficiency of deposition hole acceptance criteria, the potential for canister failure if the shear is larger than 5 cm, the failure criteria in assessment of canister response to shear loads and the hydraulic properties of shearing fracture and retention in the migration pathway. As is clear from the table, these issues are generally handled by making pessimistic assumptions, combined with or evaluated by cautious interpretation of results of direct modelling and are thus accessible through the standard methodology for the assessment. For example:

- The probability of earthquake is handled by adopting a pessimistic frequency range based on estimates by a wide range of experts and input where an upper bound of range is chosen for the risk calculations.
- The probability that a zone hosts an earthquake and the resulting secondary movements in large fractures has been assessed by extensive modelling and final estimates and the zone with largest impact is chosen for risk calculations.
- The probability of a deposition position being intersected by a large fracture is handled by using the variant yielding the highest probability of intersection in the risk calculation and a pessimistic assessment on the possibility of finding large fractures during detailed investigations.
- The potential for damage if the shear is larger than 5 cm has been assessed by extensive modelling and further modelling efforts appears a viable approach in case current pessimistic assumptions on failure need to be replaced by a more differentiated approach.

In short, the impact of remaining uncertainties on risk is bounded, and if there is a requirement to reduce the estimated risk by more knowledge, other means than formal expert elicitation appear more promising. This has indeed proved to be an important approach considering the advances since SR-Site in earthquake analyses summarised by Hökmark et al. (2019) and the revised mechanical analyses by Jonsson et al. (2018).

Conclusions

In conclusion, although a number of uncertainties could in principle be amenable to a formal expert elicitation, no issue has, in this evaluation, been identified for which both i) the calculated risk is highly sensitive to the uncertainty and ii) the uncertainty can be expected to be significantly reduced through a formal expert elicitation.

The procedures established for the qualification of processes and data in SR-Site and the PSAR, the considerable and concerted research activities on critical issues, the comprehensive site modelling by expert groups including thorough evaluation of uncertainties and the formulation of a confidence statement, the reviewing by external experts, and the pessimistic handling of many factors in the assessment all contribute to this conclusion. Also, the fact that the pessimistically calculated total risk in the PSAR is well below the regulatory limit for the entire one million year assessment period has influenced the view on the absence of a need for further reduction of uncertainties through expert elicitations.

13.11 Conclusions

The analyses of the retardation potential of the repository reported in this chapter have led to the following conclusions.

For the corrosion scenario, the calculated mean doses are at least one order of magnitude below the dose corresponding to the regulatory risk limit. In the most pessimistic variants of this scenario, the first canister failures and hence the first releases occur after around 50 000 years. In these variants, the mean dose is about two orders of magnitude below the regulatory limit at 100 000 years and about one order of magnitude below the limit at one million years.

Different numbers of canister failures in the corrosion scenario propagated from the analysis of containment potential led to variations in calculated mean doses within one order of magnitude. Also uncertainties in the conceptualisation of the near-field transport conditions have a similarly limited impact on the calculation results.

For the shear load scenario, the calculated mean dose for the initial 1 000 years is negligible in comparison to the dose corresponding to the regulatory risk limit. Between 1 000 and 100 000 years, the calculated mean dose is about three orders of magnitude below the limit and then increases to become about two orders of magnitude below the limit at one million years.

The overall risk summation shows that a KBS-3 repository at Forsmark is assessed to comply with the regulatory risk criterion over the entire one million year assessment period. The margin to compliance is about one order of magnitude when pessimistically bounding a number of uncertainties in the risk calculation. Risk dilution has been analysed and found to not challenge the conclusion regarding compliance.

In the corrosion scenario, the geosphere provides only a modest attenuation of the dose-equivalent release from the near-field. The safety relevant role of the geosphere is here rather i) its contribution to the containment function of the repository through favourable geochemical and hydrological conditions limiting the number of failed canisters and ii) through its contribution to limiting the releases from the near-field by providing reducing conditions and hence limiting the fuel dissolution rate. In the shear load scenario the geosphere contributes to containment through favourable mechanical conditions and, as in the corrosion scenario, to limiting the fuel dissolution rate by providing reducing conditions.

Sensitivity analyses of the probabilistic calculation results show that input uncertainties for the fuel dissolution rate, the failure time of the canister and the flow related transport resistance in the geosphere account for most of the uncertainty in the calculated dose. Additional uncertainties are addressed through the formulation of variant calculation cases regarding e.g. different conceptual hydrogeological models or through pessimistic assumptions regarding, e.g. the likelihood of canister failure due to shear load. The influences of all important uncertainties on the calculated risk are evaluated based on the outcome of the risk summation, and possibilities of reducing the uncertainties are discussed as feedback from the assessment.

Application of four alternative indicators to risk show, for the central corrosion case, that release rates are about three orders of magnitude below the activity constraints issued by the Finnish regulator STUK, that the calculated concentrations in ecosystems at Forsmark from repository releases of Ra-226 are about three orders of magnitude below measured concentrations of naturally occurring Ra-226 at Forsmark and that geosphere fluxes caused by Ra-226 releases from the repository are about two orders of magnitude below naturally occurring fluxes of Ra-226 at the site, as estimated from site data. Similar conclusions are drawn for other relevant calculation cases.

Dose rates to non-human biota are well below the screening dose rate recommended in the ERICA Integrated Approach, meaning that the calculated radionuclide releases are not expected to lead to any detrimental biological effects on individuals of species found, or likely to be found, at the site. Hence, populations, communities and ecosystems are assured an adequate degree of protection.

Simplified analytical models applied to key variants of the corrosion and shear load scenarios are in good agreement with the numerical results. This enhances confidence in the calculation results i) by providing a quality assurance check on the numerical modelling of dose equivalent releases and ii) by demonstrating that releases for the cases in question are controlled by relatively simple processes that are straightforward to understand and model.

14 Additional analyses and supporting arguments

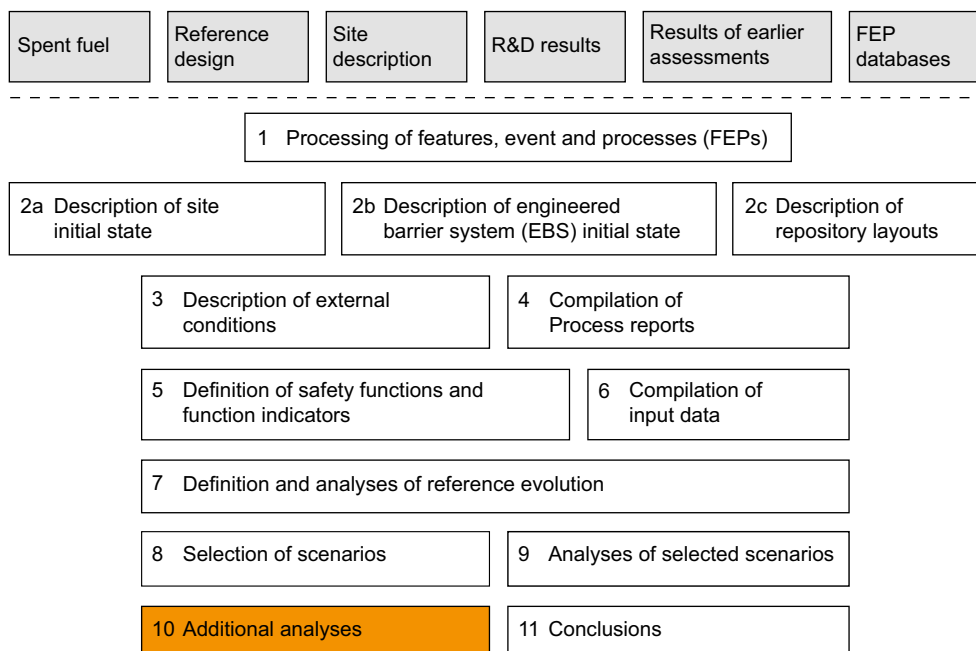


Figure 14-1. The PSAR methodology in eleven steps (Section 2.5), with the present step highlighted.

14.1 Introduction

In this chapter, additional analyses required to complete the safety assessment according to the methodology described in Chapter 2 are documented. The contents of the chapter are as follows.

Section 14.2 gives an account of the methodology used for the analysis of scenarios related to future human actions, followed by a summary of the analyses and their results. Sections 14.2.9 and 14.2.10 as well as parts of Section 14.2.1 describe developments and updates since the SR-Site assessment.

An account of the additional analyses required in order to demonstrate optimisation and the use of best available technique is given in Section 14.3. The calculations have been updated, with results quite similar to those in the SR-Site assessment. The conclusions are to some extent updated to reflect developments since the SR-Site assessment.

In Section 14.4, verification that FEPs omitted in earlier parts of the assessment are negligible in the light of the completed scenario and risk analysis is undertaken. Minor updates, reflecting updates in other parts of the report, have been made relative to the SR-Site version.

Section 14.5 gives a brief account of the time period beyond one million years. The text on denudation has been updated since the SR-Site assessment.

Finally, Section 14.6 gives an account of how natural analogues support the analyses and conclusions in the safety assessment. A study in Cyprus of long-term interactions between bentonite and alkaline groundwater has been added in Section 14.6.2. A study in Greenland of glacial subsurface conditions has been added in Section 14.6.3.

14.2 Scenarios related to future human actions

14.2.1 Introduction

The selected scenarios related to future human actions and analysis of the representative cases are the same as in the SR-Site assessment. New knowledge obtained after the previous assessment, and the potential impacts on the assessment of future human actions of this knowledge, are addressed in Section 14.2.9 and 14.2.10. In addition, as mentioned in Section 10.3.13, and discussed in further detail in Section 3.5.6 of the **Fuel and canister process report**, future anthropogenic earth currents have been further analysed since the SR-Site assessment. The extent of copper corrosion was found in a very pessimistic case to be limited to about 2 mm for the most exposed canister position in the repository. This phenomenon is, therefore, not further treated among scenarios related to future human actions.

According to the scenario selection described in Section 2.5.8 and Table 11-1, two main categories of scenarios related to future human actions, FHA, were distinguished, scenarios related to a sealed repository and scenarios related to an unsealed or incompletely sealed repository. These categories of FHA scenarios were previously identified in SR-Can (SKB 2006a), but only the former category was further analysed. In SR-Site, both categories are addressed and the analyses are provided in the **FHA report** and summarised in the following subsections.

The potential exposure to large quantities of radiotoxic material is an inescapable consequence of the deposition of spent nuclear fuel in a final repository, and consequently intrusion into the repository needs to be considered in repository design and safety assessment. To reduce the probability of inadvertent intrusion and resulting exposure to the spent fuel, in line with international recommendations (IAEA 2011, 2012, ICRP 2000, 2013, NEA 2012b), the following countermeasures have been applied in the repository siting and design.

- The repository is to be located at a site not containing exploitable natural resources.
- The repository depth is selected to be substantially greater than the depth of interest for water supply and more generally occurring sub-surface facilities.
- The repository will be sealed so as to make subsequent entry difficult.
- Measures will be taken to preserve institutional control, and records, knowledge and memory of the repository for as long as possible.

Intrusion in the post-closure phase of institutional control and beyond is primarily prevented through the design of the repository. In addition to that there will presumably continue to be safeguards measures, preservation of information (record keeping) and possibly some sort of markers placed at the site. During the institutional control period, activities at the site have to be restricted or directed if they have the potential to interfere with or hinder surveillance of the site, but this does not necessarily rule out all forms of access to the area. Measures and land use restrictions during the period of institutional control are exemplified and further discussed in the **FHA report**.

The fact that the repository contains fissile materials is an important aspect. Regarding today's situation, control of safeguards measures will most likely be upheld by national as well as international agencies (SSM, IAEA and Euroatom) (Fritzell 2006, pp 11–14). According to recent legislation in Sweden, the long-term responsibility for a geological repository for spent nuclear fuel or radioactive waste, after it has been sealed, rests with the state. The starting point of the ultimate responsibility of the state is when a geological repository is finally closed. Any measures needed to be taken after that time will be the responsibility of the state, and the practical implementation of these may be delegated to an authority or authorities that the government has appointed. The proposed changes have been incorporated in the Act (1984:3) on Nuclear Activities, and entered into force 1 November 2020.

14.2.2 Principles and method for handling FHA scenarios

Man is dependent on, and influences, the environment in which he lives. After closure of the repository, future generations should be able to utilise the repository site according to their needs without jeopardising their health. In the case of a final repository of the KBS-3 type, there are, however, inevitably examples of activities that, if carried out carelessly or without knowledge of the repository, could result

in exposure to radiotoxic elements. Examples of such activities are drilling of deep boreholes and construction of tunnels, shafts or rock caverns to great depth within the repository area. Globally occurring human activities, such as the emission of greenhouse gases or pollution, may also affect the repository. There is, therefore, an international consensus that future human activities shall be considered in safety assessments of deep geological repositories (NEA 1995, 2012, IAEA 2012, ICRP 2000, 2013).

Human actions of concern are those with a potential impact on the repository's safety functions. Human actions can be divided into different categories e.g. "recent and ongoing" or "future"; "global" or "local" (Wilmot et al. 1999) and "inadvertent" or "intentional" (NEA 1995, ICRP 2000). Recent and ongoing, local, intentional activities are considered in the description of the local ecosystems (see Sections 4.10 and 10.3.3). Mishaps can be regarded as local, inadvertent activities and the ones occurring during the excavation and operational phases are considered in the general handling of uncertainties in the main and additional scenarios. The global, recent and ongoing emissions of greenhouse gases, have no direct impact on the repository, but may affect the climate and are considered in the global warming variant of the reference evolution (Section 10.6), as well as in the analysis of the extended global warming climate case (Section 12.1.3). That leaves global pollution other than the emission of greenhouse gases and local, future activities for further analysis.

If people in the future for some reason deliberately enter the repository, they are responsible for the consequences of their actions. Society today cannot protect future societies from their own actions if the latter are aware of the consequences (NEA 1995, 2012, ICRP 2000, 2013). However, in developing a system for final disposal of spent fuel, as much consideration as reasonable should be given to future generations. Based on these generally accepted principles and the Swedish Radiation Safety Authority's, SSM's, regulations concerning safety in connection with the disposal of nuclear material and nuclear waste (SSM 2008a) and on the protection of human health and the environment in connection with the final management of spent nuclear fuel and nuclear waste (SSM 2008b), the future human actions considered in this part of the safety assessment are restricted to global pollution and actions that:

- Are carried out after the sealing of the repository.
- Take place at or close to the repository site.
- Are unintentional, i.e. are carried out when the location of the repository is unknown, its purpose forgotten or the consequences of the action are unknown.
- Impair the safety functions of the repository's barriers.

A problem when discussing future human actions is that the future of man and society cannot be predicted. On time spans of tens of years or more, the best we can do is to identify some important parameters or factors and combine them to explore possible outcomes. On time spans of hundreds of years and longer the future of man and society is, however, unpredictable and the uncertainties are indeterminate or unspecified, i.e. the outcome space is not known and cannot be described. It is for instance impossible to determine what scientific discoveries will be made the next 1 000 years. One commonly applied approach to handle this and to avoid speculation as to the future is to assume that the future conditions of society and technical practice are essentially the same as today (NEA 1995). This provides a practical and comprehensible procedure to illustrate the potential hazards related to future human actions at the repository site which is applied in this assessment.

In the General Guidance to their Regulations, SSM recommends the inclusion of direct intrusion by means of drilling as well as examples of activities that indirectly may affect the safety functions in the safety assessment (SSM 2008b). They also recommend basing the future human activity scenarios on current habits and technical practise.

Finally, in line with SSM's General Guidance (SSM 2008a), future human actions and their impact on the repository are evaluated separately, and are not included in the reference evolution or the risk summation.

Method

Human actions can affect the repository in different ways. The impact of the action on the repository as well as its consequences is the result of a combination of technical and societal factors. Examples of such factors are the level of technology and knowledge, existence of institutional control, infrastructure and settlement pattern and food supply system. For the purpose of providing as comprehensive a picture as possible of different human actions that may impact the deep repository as well as their background and purpose, the following approach has been used (see the **FHA report**).

- **Technical analysis:**
Identifies human actions that may impact the safety functions of the repository, describes such actions and, in technical terms, justifies that they may occur.
- **Analysis of societal factors:**
Identifies framework scenarios (framework conditions) that describe feasible societal contexts for future human actions that can affect the radiological safety of a deep repository.
- **Choice of representative cases:**
The results of the technical and societal analyses are put together and one or several illustrative cases of future human activities are chosen.
- **Scenario description and consequence analysis of the chosen cases.**

The three first steps are mainly based on work carried out in conjunction with the safety assessment SR 97 (SKB 1999a). Results from the development of the SKB FEP database, Chapter 3, and a review of some relevant literature published after SR 97 are also considered, as well as the authorities review of SR-Can (Dverstorp and Strömberg 2008). The last step is an update and extension of the work conducted for SR-Can, also here considering the authorities review of SR-Can (Dverstorp and Strömberg 2008). A summary of the work is provided in the following subsections.

14.2.3 Technical and societal background

Technical analysis

The technical analysis was based on the results from a workshop carried out within the framework of SR 97 (Morén et al. 1998). For SR-Can, the relevance of the results from the workshop regarding recent technical developments was reviewed based on consultation with technical experts within SKB. Furthermore, an audit against the NEA FEP database and linked national projects resulted in some minor amendments and the addition of the action “subsurface bomb or blast” (SKB 2006e). The complementary FEP work conducted for SR-Site (see Chapter 3) did not result in any modifications to the list of human actions developed for SR-Can and is considered applicable also for the PSAR.

The human actions identified for SR-Can and also applicable for SR-Site are listed in Table 14-1. Based on their principal impacts, the actions are divided into the categories human actions with thermal (T), hydraulic (H), mechanical (M) or chemical (C) impact. From the technical analysis it was concluded that actions that include drilling and/or construction in rock are those with the greatest potential influence on the repository. Furthermore, the repository site was regarded as more favourable than other places for building a heat store or heat pump plant, due to the heat generated by the spent fuel. For the other actions, the repository site was considered to be equivalent to, or less favourable than, other places with similar bedrock.

Table 14-1. Human actions that may impact repository safety.

Category	Action
Thermal impact	T1: Build heat store* T2: Build heat pump system* T3: Extract geothermal energy (geothermics)* T4: Build plant that generates heating/cooling on the surface above the repository
Hydrological impact	H1: Construct well* H2: Build dam H3: Change the course or extent of surface water bodies (streams, lakes, sea) and their connections with other surface water bodies H4: Build hydropower plant* H5: Build drainage system H6: Build infiltration system H7: Build irrigation system* H8: Change conditions for groundwater recharge by changes in land use
Mechanical impact	M1: Drill in the rock* M2: Build rock cavern, tunnel, shaft, etc* M3: Excavate open-cast mine or quarry* M4: Construct dump or landfill M5: Bomb or blast on the surface above the repository M6: Subsurface bomb or blast*
Chemical impact	C1: Store/dispose hazardous waste in the rock* C2: Construct sanitary landfill (refuse tip) C3: Acidify air, soil and bedrock C4: Sterilise soil C5: Cause accident resulting in chemical contamination

* Includes or may include drilling and/or construction of rock cavern.

Analysis of societal factors

Prevailing societal conditions are of importance both for the possible occurrence of inadvertent human actions impairing repository safety and for evaluation of their consequences. Important issues are why the disruptive action is being carried out and contemporary societal conditions such as general knowledge and regulations. These primarily humanistic and socio-economic questions were analysed at a workshop for SR 97 (see the **FHA report** and SKB 2006e, Morén et al. 1998, SKB 1999a). Experts in the fields of cultural geography, history of science and technology and systems analysis participated in this workshop. So called framework scenarios that describe plausible societal contexts for future human actions with an influence on the radiological safety of the deep repository were formulated. The framework scenarios were developed by means of morphological field analysis (Morén et al. 1998, Ritchey 1997), a group- and process-oriented interactive method for structuring and analysing complex problem fields that are non-quantifiable, contain non-determinable uncertainties and require a judgmental approach.

From the study of societal aspects, it was concluded that it is difficult to imagine inadvertent intrusion, given a continuous development of society and knowledge. Owing to the long time horizon, however, it is not possible to rule out the possibility that the repository and its purpose will be forgotten, even if both society and knowledge make gradual progress. Nor is it possible to guarantee that institutional control over the repository site will be retained in a long time perspective. With a discontinuous development of society, where the development of society and technology contains a sudden, large change, it seems likely that knowledge will be lost and institutions will break down. It is also reasonable to assume that knowledge is lost if society degenerates.

14.2.4 Choice of representative cases

Sealed repository

It is probable that the repository site will be used by people in the future. Human actions that influence radiological safety and are carried out without knowledge of the repository and/or its purpose cannot be ruled out. Actions that influence the containment or the function indicators for containment are the most severe, followed by actions that influence retardation or the function indicators for retardation. Changes in the biosphere may result in an increase in the doses to which human beings may be exposed if the containment has been violated and there are leaking canisters in the repository.

A KBS-3 repository will be situated at a minimum depth of 400 metres in the rock, and the suggested repository depth is below 450 m at Forsmark. One reason for this is the wish to locate the repository in an environment where the containment of the fuel will be retained even in the event of extensive changes on the surface. Changes considered in the determination of the depth for a KBS-3 repository are natural changes and changes caused by man. Examples of natural changes are change of the repository's location in relation to the sea, and the development of permafrost and ice sheets, see further Sections 5.2.2 and 14.3.4. These natural changes will also influence factors of importance for future human actions at the site e.g. settlement, society and man's opportunities to use the repository site.

Large uncertainties are associated with the development of technology and society. To reduce speculation, the NEA working group on assessment of future human actions (NEA 1995) as well as SSM in the general guidelines to their regulations (SSM 2008b) suggested an approach based on present-day knowledge and experience. However, applying this approach literally or with consistency there would be no inadvertent human actions yielding radiological consequences. The current activities at the repository site will not impact the safety. Drilling to great depth is solely performed to investigate the site for repository construction. If this were to result in hazardous conditions or circumstances, measures to avoid or minimise consequences for man and environment would be taken. There is another dilemma in the assessment of future human actions. In order to quantify the consequences, detailed descriptions of the human actions are required. Such descriptions will inevitably include speculations as to the course of actions which always can be questioned. However, both the technical and societal analyses can, even if they do not depict conditions that exist today, be said to be based on current practise and their results can be used for the selection of representative cases. When describing scenarios based on the selected cases, speculation is avoided by assuming the most severe among simplified and plausible alternatives.

All actions in Table 14-1 influence the migration of radionuclides in the biosphere. However, actions that are performed on or near the surface, down to a depth of a few tens of metres, are judged not to be able to directly affect the technical barriers and the containment of the fuel. This applies to the actions T4, H2, H3, H4, H5, H6, H7, H8, M3, M4, C2, C3, C4 and C5 (though some of them could include drilling of relatively deep wells). Activities near the surface that belong to categories M and H are deemed to have less influence on the repository than natural changes in conjunction with future climate change. Of the actions that entail a chemical influence (C2–C5), acidification of air and land (C3) has been studied in most detail. In realistic cases of acidification by atmospheric sulphur and carbon dioxide, the environment at repository depth is not affected (Nebot and Bruno 1991, Wersin et al. 1994). Soil layers and bedrock are judged to work efficiently as both a filter and buffer against other chemical compounds as well.

Bombing or blasting on the ground surface above the repository (M5) cannot affect the containment of the spent fuel, except if blasting is done with a powerful nuclear weapon. Such an event implies a nuclear war and the consequences of the war and the blast itself would be much greater than the consequence of the hypothetical leakage from the repository. However, sub-surface testing of nuclear bombs (M6) close to the repository may violate the containment in a similar way to an earthquake. The test would need to be carried out close to the deposited canisters. Testing of bombs could be combined with identified societal contexts to form a plausible scenario. However, tests of nuclear bombs require knowledge of nuclear fission and its associated risks and are carried out below the surface to avoid environmental impact. Since measurements are carried out in connection with the tests it is plausible that if a detectable leakage from the repository exists, it would be distinguished from the releases from the bomb and handled by a society performing sub-surface weapon tests.

Some of the actions in Table 14-1 can, besides influencing radionuclide transport, indirectly influence the containment of the spent fuel if they affect the capability of the geosphere to provide favourable hydrological or chemical conditions. Such actions would have to be performed directly above or very close to the repository and include drilling and/or construction in the rock (M1, M2). These categories include actions that have to do with heat extraction (T1, T2, T3), well drilling (H1) and disposal of hazardous waste in the rock (C1). Hydropower plants (H5) and open-cast mines and quarries (M3) may also involve drilling or rock works at great depth. Before a rock facility is built, drilling is carried out to investigate the rock. Therefore, if present day technology is applied, all these cases involve drilling in the rock.

Large rock facilities adjacent to the repository are deemed to be out of the question in a short time perspective, i.e. within a few hundred years, for several reasons. For example, the repository is itself a large rock facility, the only one of its kind in Sweden that is very unlikely to be forgotten over such a short time span. Institutional control can be expected to endure on this time scale. The enumerated actions that encompass major rock works are less likely at the repository site, based on current technology and economics. In a slightly longer time perspective, i.e. a few or several hundred years or more, it is difficult to predict how knowledge, technology and society will develop, and thereby how, where and why rock facilities will be built. Based on current practice, rock facilities at depth down to around 50 metres may very well occur and actually exist at Forsmark (the SFR facility, a repository for low- and intermediate-level radioactive waste). In the far future, the potential ore resources to the southwest of the investigated area in Forsmark may be exploited.

Of the actions in Table 14-1, "Drill in the rock" is judged to be the only one that can directly lead to penetration of the copper canister and breach of waste containment, while at the same time being inadvertent, technically possible, practically feasible and plausible. "Drill in the rock" is furthermore a conceivable action in the light of the results of the societal analysis. Even if it is possible to build a rock cavern, tunnel or shaft or to excavate an open-cast mine which leads to penetration of the copper canister, doing so without having investigated the rock in such a way that the repository is discovered, i.e. without knowledge of the repository, is not considered to be technically plausible. However, the construction of a rock facility at shallow depth or a mine in the vicinity of the Forsmark site may occur in the future. Therefore, the cases "Canister penetration by drilling" and "Rock facility in the vicinity of the repository" and "Mine in the vicinity of the Forsmark site" were selected as representative cases for scenarios related to a sealed repository, and which should be further described and analysed.

Unsealed or incompletely sealed repository

According to regulations, it is also necessary to define and analyse a case that illustrates the consequences of an unsealed repository (SSM 2008a). Since the repository is gradually excavated and operated, the case selected for analysis represents an incompletely sealed repository rather than an unsealed repository. The strategy for deposition of canisters implies that deposition tunnels are successively filled with canisters and then backfilled and sealed as soon they are filled. Abandoning the repository in the middle of this process is judged as rather unlikely because this would mean that canisters are left at the surface where they would constitute a larger risk than if emplaced in the repository. It is judged more plausible that the repository is abandoned when all canisters are deposited and all deposition tunnels backfilled and sealed, but all other repository volumes are still open due to, for example, political decisions not to seal the repository completely. Therefore, this is the basic assumption in the case selected as representative for scenarios related to an unsealed or incompletely sealed repository.

14.2.5 Assessment of the drilling case

Introduction and specification of the case analysed

Only drilling done without knowledge of the location and purpose of the repository is considered. Various countermeasures to reduce the likelihood of inadvertent intrusion into the repository have been discussed (NEA 1995, Eng et al. 1996). When the repository is sealed the countermeasures then deemed to be most efficient will be implemented. Examples of such countermeasures are conservation of information in archives, marking the site and various types of institutional control, for example physical surveillance, ownership restrictions and restrictions on land use. All these countermeasures are assumed to have lost their preventive and warning effect at the time for the drilling.

As discussed in Section 14.2.3, it is hard to imagine a societal evolution resulting in the loss of knowledge of the repository, its purpose and content in combination with preservation or development of knowledge, technology and society. It is likely that a society having the technical capability to drill to great depth also has the knowledge to analyse the findings and possibly will act to prevent harmful effects on man and the environment. In the drilling scenario, it is assumed that technology to drill to great depth is available, that the knowledge of the location and purpose of the repository is lost, that the intruders are incapable of analysing and understanding what they have found and that no societal regulations on drilling exist. It is assumed that an evolution rendering this situation will require some time. Countermeasures to prevent inadvertent intrusion are generally assumed to be preserved for between 100 and 500 years, whereas physical markers may be effective on a longer time perspective of up to a couple of thousand years (NEA 1995, Wilmot et al. 1999). A KBS-3 repository is a large industrial establishment that will be under operation for several decades and this type of facility has been debated, investigated and analysed since the first nuclear power plants commenced operation in Sweden. It is plausible that it will take some time before the knowledge about the repository is lost and also for society and land owners to give up the control of activities such as drilling at the repository site. Based on this, it is assumed that the drilling will take place 300 years or longer after repository closure.

The technical practise is assumed to be similar to that at present. Today, drilling is done to sink wells, for the extraction of heat from the ground, and for exploratory purposes. Rock wells are normally drilled to a depth of between 50 and 100 metres, but occasionally wells are drilled down to 130–150 metres. Deeper wells are more uncommon. The reason is that it is expensive to drill and the probability of finding potable water in sufficient quantity declines with depth. For extracting heat, deeper drilling may occur. Even though drilling to depths down to 500 m or more for the extraction of heat is performed today and may become more common in the near future, drilling to great depth is generally done for exploratory purposes, most often prospecting.

Prospecting generally involves surface-based investigations prior to drilling. Results from modelling of the geophysical response of a spent fuel repository at Forsmark indicate that the repository will comprise an anomaly that could be detected by reflection seismics, but not with the other geophysical methods studied (magnetics, gravity, induced polarisation, resistivity, transient electromagnetics) (Isaksson et al. 2010). The seismic response is due to the contrasts in velocity between the bentonite and the surrounding rock. Most likely, this type of anomaly would not be interpreted as a mineralisation, but it cannot be ruled out that the anomaly would be further investigated. Therefore, it is assumed that drilling through the repository is done for exploratory purposes.

Diamond (core) drilling is normally employed for exploratory drilling. The drill core is retrieved, placed in boxes and inspected by a geologist. Selected samples may be analysed more thoroughly. The cuttings (the pulverised rock mixed with the drill's cooling water) are normally removed with water, which also cools the drill. The water with cuttings is usually spread on the ground around the borehole. When the drilling is finished, the cores are sent to core mapping and the borehole is abandoned. If the hole has passed a zone with high water flow, so that a great deal of water is brought up to the surface, the borehole may be backfilled. This is generally only done if the flow entails a problem for local residents.

The direction of the borehole varies depending on the purpose and what is known about the rock volume to be investigated. In general the drill is inclined; the angle with the ground plane is usually 60–85 degrees. If there are no known obstacles or underground facilities, the drillers always try to continue the drilling even if they run into problems. If the drill reaches the buffer and the canister these may very well be penetrated and the drilling continued and not stopped until the drill core is inspected, or the agreed depth is reached. If penetration of the backfilled deposition tunnel occurs, the water cooling the drill and bringing the cuttings to the surface will be glutted with fine-grained material. The usual procedure is then to try to flush the fine grained material away. If this does not succeed, which is plausible if trying to drill through the backfill, the borehole is frequently grouted and the drilling continued through the concrete.

It is assumed that the purpose of the drilling is to reach great depth and that the drill rig therefore is placed at a low point in the terrain. The drilling angle is assumed to be 85° and the cuttings are assumed to be spread on the ground. When the backfilled tunnel is reached the borehole is assumed

to be grouted and the drilling continued. The buffer is assumed to be grouted as well, the drilling continued and the canister penetrated. When the drill core containing canister material and spent fuel is brought to the surface the anomalous situation is taken to be recognised and the drilling is stopped.

Since the assessment should not only consider the impact to the intruder, but also assess how the safety functions of the repository may be impaired, the following additional assumptions are made: The site and the borehole are abandoned without further measures. About a month later, a family moves to the site and operates a domestic production farm there. The abandoned borehole is used as a well by the family. The consequences for the repository and the annual effective doses to the family as well as the dose to the drilling personnel are assessed.

Function indicator(s) considered

Because this drilling case presumes that one canister as well as the buffer and backfill above the canister are penetrated by a borehole, function indicators related both to containment and retardation properties of the canister, buffer and deposition tunnel backfill are affected. In addition, the function indicators related to the capacity of the geosphere to provide favourable hydraulic and chemical conditions may be affected. Therefore, the following function indicators are considered in this drilling case:

- Can1, Provide corrosion barrier; ensure containment.
- Buff1, Limit advective transport in buffer; ensure tightness and self-sealing.
- BF1, Counteract buffer expansion; high density and self-sealing of backfill.
- R1, Provide favourable chemical conditions; ensure reducing conditions.
- R2, Provide favourable hydrologic and transport conditions; ensure high transport resistance in fractures and low equivalent flow rate at buffer/rock interface.

Further, the safety function Buff 5, Prevent canister sinking may be affected if sufficiently much buffer material is lost. However, if this occurs, the other buffer safety functions will have already been violated.

Qualitative description of the consequences of unintentionally penetrating a canister when drilling

It is assumed that one canister has been penetrated by core drilling. The borehole above the penetrated canister is assumed to be grouted and the buffer's capability to prevent advective transport, self-seal and prevent colloid transport are lost in the grouted area. Some buffer and backfill material is lost, but excluding the grouted parts both backfill and buffer are assumed to retain their safety functions. The water containing the cuttings from the drilling is brought the surface and spread on the ground on a circular area.

The grouted borehole has left an open pipe from the penetrated canister to the surface. As long as the grout remains intact, the tunnel backfill in the deposition tunnel and the buffer in the remainder of the deposition holes in the deposition tunnels are not directly affected by the presence of the borehole. However, the open borehole may, at least locally, affect the groundwater flow pattern. This, in turn, may affect the chemical conditions in and around the repository. Therefore, the impact on the groundwater flow field of an open borehole from the surface through the backfill into a deposition hole has been analysed.

With time, it is likely that the grout is degraded and that the buffer and backfill above the penetrated canister expands to fill the empty volume of the borehole in these barriers. Considering the self-sealing capacity of the buffer and backfill (Section 10.2.4) and the quite large amounts of buffer and backfill materials that can be lost before advective conditions occur (see Sections 10.3.9 and 10.3.11) it seems likely that this expansion will re-establish favourable hydraulic and mechanical conditions in the buffer in the deposition hole with the penetrated canister and the backfill above this deposition hole. However, even if this is not the case, the borehole will most likely not affect the backfill in other parts of the deposition tunnel. This implies that the buffer in other deposition holes in the tunnel also should be unaffected by the borehole.

Quantitative assessment of the radionuclide release and dose consequences of a penetrated canister when drilling

In the analysis of the dose consequences of this drilling case, the dose to the drilling personnel as well as to a family settled on the site are analysed. The analysis is provided in the **FHA report** (Section 6.3), and summarised below. The data used in the analysis are compiled in Table 14-2.

Table 14-2. Compilation of data used in the analysis of dose consequences of unintentionally penetrating a canister when drilling.

Parameter	Value/assumption	Comment/reference
Time of drilling	300 years after closure of the repository or later	
Time the exposed individual in the family spends in the middle of the contaminated area	365 hours	One hour per day every day of the year
Radionuclide inventory	Average canister	Data report , Section 3.1
IRF	Included in the inventory left on the ground	Median values according to Data report , Section 3.2
Portion of fuel in the canister brought to surface	0.03	FHA report , Appendix B
Fuel alteration rate	10^{-7} per year	Data report , Section 3.3
Corrosion rate of metal parts in fuel	10^{-3} per year	Data report , Section 3.2
Water flow through deposition hole	0.1 m^3 per year	FHA report , Appendix B
Elemental solubility limits	Representative for site conditions in the period 2000 to 3000 AD	FHA report , Section 6.3.
Volume of initially contaminated soil	2.8 m^3 (radius 3 m, thickness 0.1 m)	–
Dose conversion factors for contaminated ground	Dose factors for external irradiation, inhalation and ingestion of food cultivated at the site	Nordén et al. 2010
Sorption coefficients	Element specific sorption coefficients for soil in the irrigated area	Nordén et al. 2010
Density of agricultural soil	$323 \text{ kg dry weight/m}^3$	Löfgren 2010
Area of land used to grow vegetables	102 m^2	Large enough to produce vegetables for 5 persons, assuming a fraction of 2.5 % vegetables in the diet.
Productivity of vegetables on irrigated land	$0.135 \text{ kgC per m}^2$ and year	Löfgren 2010
Productivity of root crops on irrigated land	$0.127 \text{ kgC per m}^2$ and year	Löfgren 2010
Productivity of cereals on irrigated land	$0.114 \text{ kgC per m}^2$ and year	Löfgren 2010
Dust concentration in the air	$5 \cdot 10^{-8} \text{ kg dry weight/m}^3$	Nordén et al. 2010
Inhalation rate	1 m^3 per hour	Nordén et al. 2010
Yearly intake of carbon	110 kg carbon per year	Nordén et al. 2010
Yearly intake of water	0.6 m^3 /year	Nordén et al. 2010
Volume of irrigation water used each year	$0.15 \text{ m}^3/(\text{m}^2 \text{ y})$	Nordén et al. 2010
Number of irrigation events per year	5	Nordén et al. 2010
Runoff	0.186 m/y	Löfgren 2010
Well capacity	82502 m^3 /year	Löfgren 2010

Since the previous assessment, which the results in the **FHA report** is based on, the radionuclide inventory has been updated. The potential impact of this inventory on the assessment of future human actions is addressed in this report, Section 14.2.10.

It is assumed that one canister is penetrated by drilling and that this takes place at the earliest 300 years after repository closure. The water containing the cuttings from the drilling is brought to the surface together with the drill core comprising damaged or undamaged fuel. The fuel is contained as fuel rods in fuel assemblies in the cast iron insert in the copper canisters. Based on the geometry and arrangement of the fuel rods in the canister and assuming a diameter of the borehole of 0.056 m, the portion of the fuel in the canister that is brought to the surface is set to 3 %. It is further pessimistically assumed that all fuel brought to the surface remains at the site, and that radionuclides in this fuel, as well as the instantaneous release fraction of the inventory in the penetrated canister are spread on the ground. This is assumed to occur over a circular area with a radius of the contaminated area of 3 m and a thickness of the contaminated soil layer of 0.1 m. The drilling personnel receives dose from these radionuclides spread on the ground.

In this drilling case it is further assumed that a family settles on the site one month after the site is abandoned by the drillers. The grouted borehole has left an open pipe from the penetrated canister to the surface and the family uses the borehole as a well. In addition, the contaminated soil is used for cultivation purposes. The family receives dose from radionuclides in the borehole water as well as from radionuclides in agricultural products and air, the latter originating from radionuclides in the contaminated soil. The assumptions in the calculations of the dose obtained from using the abandoned borehole as a well are the same as those in the dose calculations for other scenarios analysed in SR-Site (Avila et al. 2010). It is assumed that the water from the borehole is used for irrigation and as drinking water for the family and for cattle. In the calculation of dose from radionuclides spread on the ground, it is assumed that the family uses the contaminated soil to establish a domestic garden for cultivation of vegetables. This garden is assumed to be large enough to produce vegetables for five persons, which implies that the radionuclides brought to the surface are spread over a larger area. The members of the family are also exposed to external radiation and through inhalation of dust when spending time in the garden.

The release of radionuclides from the fuel to the water in the penetrated canister is determined by the fuel alteration rate and the corrosion rate of the metal components. However, elemental solubility limits may govern the release of some radionuclides, depending on the magnitude of the water flow in the deposition hole containing the penetrated canister. Based on results of the hydrogeological modelling (Joyce et al. 2010), the water flow in the deposition hole is set to 0.1 m³/year. With this water flow and elemental solubility limits representative of groundwater chemical conditions between 2000 and 3000 AD, the release of ²³⁷Np, ⁹⁹Tc, ⁹³Zr and the uranium isotopes from the spent fuel becomes solubility limited.

Dose to drilling personnel

The dose to the drilling personnel originates from the radionuclides in cuttings, drilling water and fuel pieces spread on the ground around the borehole. The dose rate that a member of the drilling personnel would be exposed to while working in the highly contaminated area 300 years after repository closure is calculated to be 130 mSv/hour and the dose rate is totally dominated by exposure to Ag-108m (see the **FHA report**). If drilling occurs at ca 5 000 years after repository closure, the dose rate has decreased to values below 1 mSv/hour and is dominated by exposure to Nb-94 and Sn-126.

These calculated dose rates are very high. This is primarily a result of the cautious assumption regarding the amount of Ag-108m brought to the surface when drilling. In the spent fuel, Ag-108m is contained in the Ag-In-Cd alloy of the control rods, but in the calculations is assumed to be part of the radionuclides that are instantly released when a canister is penetrated and therefore the entire amount is taken to be brought to the surface. In the case of drilling intrusion Ag-108m would not be instantaneously released, so 3 % instead of 100 % of the inventory of Ag-108m would be brought to the surface when drilling. Due to the total dominance of Ag-108m in determining the dose rate, this would reduce the dose rate to workers to 3 % of the value, i.e. the dose rate 300 years after repository closure would be about 4 mSv/hour.

Dose to family settled on the site

The doses to the family that settles on the site originates from two sources. The abandoned borehole used as a well by the family and the cuttings containing the instant release fraction and the fuel particles spread on the ground. The calculated annual effective doses from using the abandoned borehole as a well and from the radionuclides spread on the ground are shown in Figure 14-2 and Figure 14-3, respectively. The calculated annual effective dose is that which an adult member of the family would be exposed to during the first year at the site.

The total dose rate from using the borehole as a well 300 years after repository closure is 0.31 mSv/year (Figure 14-2) and is dominated by the contribution from Am-241. This dose rate is above 0.014 mSv/year, the annual dose rate corresponding to the regulatory risk limit, but below the dose rate of 1 mSv/year from background radiation. Furthermore, the IAEA states that if inadvertent human intrusion after closure is expected to lead to an annual dose of less than 1 mSv to those living around the site, then efforts to reduce the probability of intrusion or to limit its consequences are not warranted (IAEA 2011). At 2000 years after repository closure, the dose is dominated by Pu-240 and if drilling takes place at still later times, Pu-239 and Nb-94 becomes more significant.

The maximum total annual effective dose rate from the use of the contaminated soil for agricultural purposes is about 10 Sv/year and this dose is obtained 300 years after repository closure. The dose is dominated by ingestion of vegetables contaminated with Tc-99 and there is also a significant dose contribution due to external radiation from Ag-108m. The calculated annual dose is very high, but it should be noted that there are a number of simplified, cautious assumptions made in the calculations (see further section on uncertainties below).

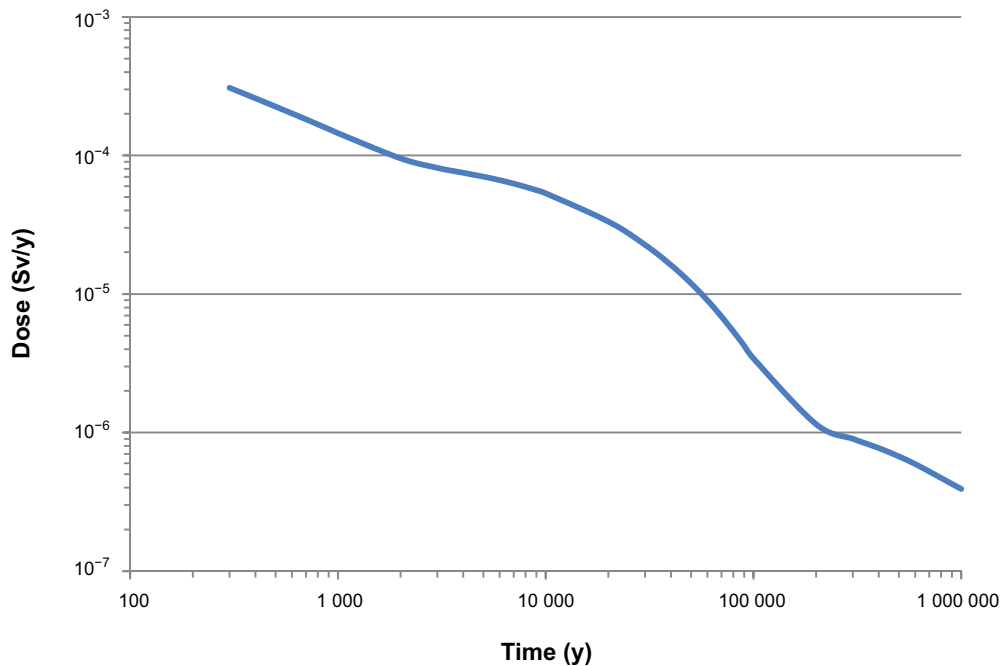


Figure 14-2. Calculated annual effective doses from using the borehole as a well for drinking water and irrigation at Forsmark. The dose is that which an adult member of the family would be exposed to during the first year at the site and the time is the year after repository closure when drilling takes place and the family settles on the site. This means that the only loss of radionuclides accounted for is that through radioactive decay (Figure 6-2 in the FHA report).

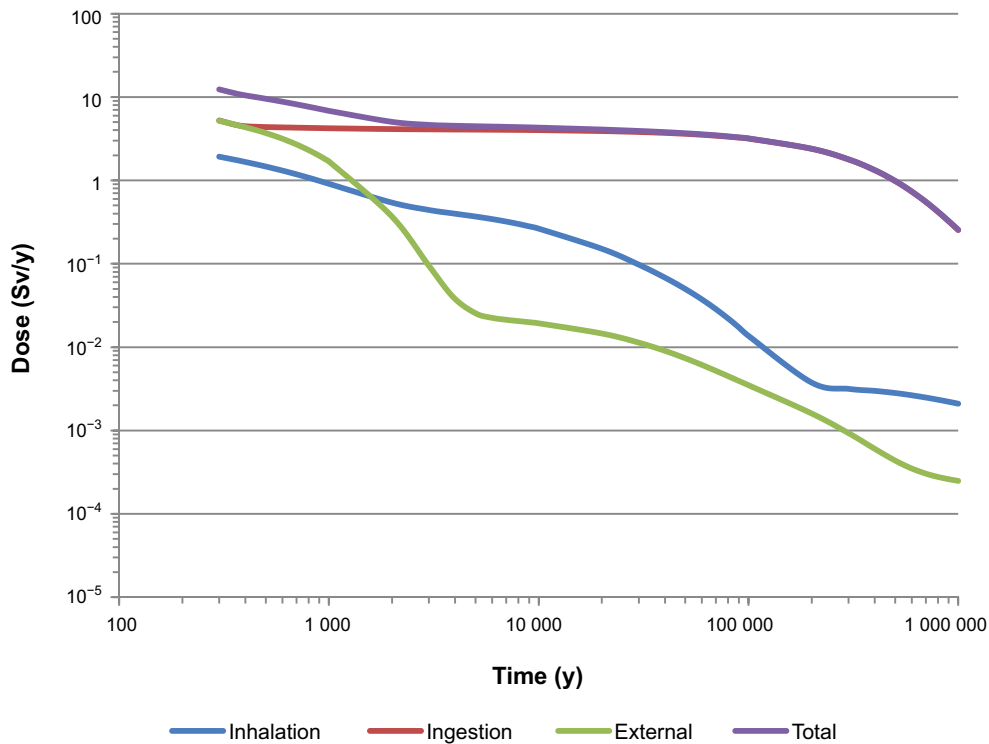


Figure 14-3. Calculated annual effective doses from exposure to the radionuclides brought to the surface as drill cuttings and fuel pieces (3 % of the inventory in a canister) via the use of the contaminated soil for domestic farming and through spending time in the contaminated area. The dose is that which an adult member of the family would be exposed to the first year at the site and the time is the year after repository closure when drilling takes place and the family settles on the site. This means that the only loss of radionuclides accounted for is that through radioactive decay (Figure 6-3 in the FHA report).

Quantitative assessment of the effects on the repository of unintentionally penetrating a canister when drilling

The impact of an open borehole on the groundwater flow in the repository and the surrounding rock has been studied by introducing boreholes at various locations in the hydrogeological base case model applied for analyses of the initial temperate period in SR-Site (Joyce et al. 2010, Section 5.6). The results show that a borehole through the backfill and buffer above a canister will act as a sink for many flow paths and that the water flow in the borehole is directed upwards. Although the flow paths are affected by the borehole, the results indicate only small effects of the borehole on the performance measures as compared with the hydrogeological base case model (see Section 10.3.6). This indicates that the flow paths established by the presence of the borehole have similar transport characteristics to the flow paths without a borehole. Furthermore, the upward directed flow in the borehole implies that reducing conditions prevail inside the penetrated canister. The modelling results do not show explicitly where the flow paths continue from the borehole, but the interpretation is that the water in the borehole exits into the highly transmissive fractures in the upper part of the bedrock and continues towards low points in the terrain.

Uncertainties

As stated in the **FHA report**, there are a number of uncertainties in the assumed drilling case regarding the impact on the deposition hole hit by the drilling and in the calculations of the doses that this action gives rise to. One major uncertainty concerns the amount of the inventory brought to surface by the drilling, and especially the amount of the dose-dominating radionuclide Ag-108m. In the calculations it is assumed that the whole inventory of Ag-108m is instantaneously released from the spent fuel and brought to the surface by the drilling. This is a pessimistic assumption, since Ag-108m is contained in metal parts of the fuel and would thus be brought to the surface in a quantity proportional to the amount of fuel brought to the surface. Furthermore, Ag-108m comes from control rods. These only exist in canisters with PWR fuel, i.e. in about 25 % of all canisters. The assumed radius of the borehole will also affect the amount of radionuclides brought to the surface, and the handling of the fuel and cuttings will affect their spreading and dilution in the biosphere. For example, unbroken fuel rods may be removed from the site for further inspection instead of left on the ground as it is assumed in the calculations. All these factors will affect the calculated doses from the fuel and cuttings left on the ground.

Another major uncertainty relates to the availability in, and loss of, radionuclides from the contaminated soil. The whole radionuclide inventory in the contaminated area is assumed to be instantaneously available for transfer to the agricultural production and air with contaminated dust. This assumption leads to a pessimistic value of the annual effective dose, since most likely only a fraction of the inventory will be available from the beginning. Further, it is assumed that there are no losses of radionuclides from the contaminated area other than by radioactive decay. However, in reality, other loss processes, such as leaching in percolating waters, are likely to be of importance. Note that the calculated annual effective dose from the radionuclides brought to the surface is valid only for the first year after the intrusion given these assumptions and that the land is assumed to be cultivated during that year.

It is not certain that the family finds the borehole and uses it as a well. Current practice is to place the pump just above the borehole for the well. Non-manual pumps are most often covered and some space is left around them to allow maintenance. Manual pumps require some space for pumping. The combination of using the borehole as a well and the contaminated soil from the area around it for cultivation therefore seems unlikely. Based on current practice the most likely situation seems to be that the contaminated area will either be used for cultivation or the borehole will be used as a well. Consequently, the person can be assumed to either receive the dose from the use of the contaminated area for agricultural purposes or from using the borehole as a well.

Uncertainties in the analyses of the impact of the borehole on parts of the repository other than the deposition hole directly affected by the borehole are judged as small compared to those associated with the calculations of dose from the canister penetrated by the drilling. The conclusion that a borehole through the backfill above, and buffer in, the deposition hole hit by drilling does not affect the backfill and the buffer in a neighbouring deposition hole, is based on results of analyses reported by Åkesson et al. (2010a, Appendix F). These analyses addressed loss of backfill above a deposition hole or in the middle between two deposition holes. Although the results reported by Åkesson et al. (2010a) are associated with uncertainties, their results in combination with the situation in this case, where a potential loss of backfill occurs still further away from a deposition hole, seem firm enough for the conclusion drawn. There are also uncertainties in the analyses of the impact of open boreholes on the groundwater flow in and around the repository, but these uncertainties are judged to not significantly affect the results (see the **FHA report**).

Conclusions

If a canister is penetrated and the borehole is used as a well for drinking and irrigation, the annual effective doses to representative members of critical groups will exceed the individual limit on annual effective dose for members of the public but not the annual effective dose due to background radiation. Assuming the site-specific median water yield of percussion holes drilled in the repository rock at Forsmark, the dose corresponding to the regulatory risk limit is exceeded if the intrusion occurs during the first ca 35 000 years after repository closure, see Figure 14-2.

If the instant release fraction and crushed material, pieces, and even unbroken fuel rods, from the fuel elements are brought to the surface by drilling, the persons executing the drilling will receive very high doses. After about eight hours of exposure, the threshold of 1 Sv for suffering from radiation

sickness is exceeded. Further, if the contaminated soil surrounding the borehole is used for agricultural purposes, the exposed persons in the case illustrated may be severely injured. However, as discussed above, the case analysed involves a number of simplified and cautious assumptions. Therefore, the calculated annual effective doses should be seen as illustrations of possible consequences rather than estimations of what the consequences would be. Furthermore, high doses from FHA calculation cases for a geological repository are expected; this hazard is inherent to the spent fuel to be disposed of in combination with repository concepts aiming at containment. Decreasing the potential for these radiological consequences to occur has been an important argument for selecting disposal deep down in the bedrock in the first place.

An open borehole might affect the long-term properties of the backfill in the deposition tunnel in the vicinity of the borehole but the effect on the backfill above neighbouring deposition holes is assessed as negligible. This implies that the buffer surrounding canisters in neighbouring deposition holes in the deposition tunnel is also unaffected by the borehole. An open borehole through the backfill will also change the pattern of flow paths in the rock beneath the highly transmissive fractures in the upper part of the bedrock. However, the new paths established have similar transport characteristics as those prevailing without an open borehole through the backfill. Therefore, it is judged that even though drilling a borehole that penetrates a canister will severely affect the deposition hole hit by drilling, the impact of the borehole on the containment potential of other parts of the repository as well as on the retardation potential of the geosphere is negligible. No significant additional doses would be incurred by people other than those directly using the contaminated borehole water or the land affected by contaminated drill core.

14.2.6 Assessment of the rock excavation or tunnel case

Introduction and specification of the case analysed

As discussed in Section 14.2.3 and in the **FHA report**, there are several plausible reasons for constructing tunnels or other types of underground excavations in the bedrock. Today, existing and planned underground excavations constructed to repository depth of 400 metres or deeper include mines, hard rock laboratories and deep geological repositories for radioactive material. These kinds of facilities are considered unrealistic at or close to the repository site. Mines are excluded, since sites including exploitable natural resources are excluded in the site selection. Hard rock laboratories and deep geological repositories are excluded, since it is probable that societies planning the construction of these kinds of facilities will discover and understand that the site is already used for a similar purpose and either construct their facility so that it does not intrude on the existing one or chose another site. For the other kinds of facilities mentioned in Table 14-1 the depth is generally as shallow as possible with regard to the geology and purpose of the facility. Generally, tunnels are constructed down to a depth of 50 metres, which is considered to be plausible also at Forsmark. This is, for instance, the depth of the final repository for low- and intermediate-level waste (SFR), located close to the planned final repository for spent fuel.

For most purposes, tunnels or rock excavations are sealed to prevent water inflow and reinforced to mechanically stabilise the tunnel and to avoid the fallout of rock blocks when they are in operation. In many cases, the tunnel walls are lined with concrete. If the tunnel is used for final storage, it is assumed that measures are taken to prevent hazardous quantities of the unknown stored material from escaping from the tunnel.

The size of a tunnel or rock excavation depends on its purpose. Tunnels can have cross sections from about four up to 100–200 m² and excavations can have volumes from 10 000 to 100 000 m³ or more.

Based on these considerations, the following case is analysed.

- A tunnel constructed at 50 metres depth with a cross section of 100 m² and with a length corresponding to the whole repository footprint along the centre line of the deposition areas is considered. The justification for this assumption is that it is plausible in relation to current practice and does not underestimate the possible impact on the repository.
- The purpose of the tunnel or rock excavation is not specified.

- The operational phase of the tunnel and the designed working life of sealing and reinforcement is assumed to be a couple of hundred years. After operation, it is assumed that the tunnel is abandoned and becomes saturated with groundwater.
- As in the drilling case, it is assumed that the existence of the repository is forgotten and that the technical standards for making underground constructions are similar to those used at the present. Further, it is assumed that the construction of the rock excavation (tunnel) is not initiated before 300 years after repository closure.

Function indicator(s) considered

The function indicator relevant for this case is:

- R2, Provide favourable hydrologic and transport conditions.

During operation of the tunnel, the hydraulic gradients in its vicinity may be affected. Indirectly, if the impact on the hydrologic conditions is substantial, the function indicator R1, Provide favourable chemical conditions, could be affected.

Assessment of the consequences of the construction of a tunnel above the repository

At Forsmark, the bedrock selected for hosting the final repository for spent fuel (the target volume) comprises the northwesternmost part of a tectonic lens (Section 4.3). The upper part of the bedrock (down to about 150 metres depth) in the target volume is recognised for its large horizontal fractures/sheet joints (SKB 2008a). Due to these structures and the high fracture frequency close to the rock surface, the upper part of the bedrock is much more water conductive than the lower part, especially below 400 metres depth. A measure of the hydraulic importance of these sheet joints in the upper part of the bedrock is provided by the exceptionally high water yields in the percussion boreholes drilled during the site investigation. The median yield of the first 22 percussion-drilled boreholes is ca 12 000 L/h (SKB 2008a, Section 8.4.4). This is ca 20 times higher than the median yield of the domestic water wells drilled outside the tectonic lens, which is no different from the median yield of all bedrock wells registered at the Geological Survey of Sweden (SKB 2008a, Section 8.4.4). The high water yield at shallow depth in the target volume of the bedrock inside the tectonic lens is not only due to these large horizontal structures in the upper part of the bedrock and the high fracture frequency close to the rock surface, but also due to the closeness to the sea, which acts as an endless source of water (positive hydraulic boundary).

If a tunnel is constructed at 50 metres depth, despite the high conductivity in the upper part of the bedrock in the target volume, this would place limitations on constructability and require extensive grouting. Grouting would, in turn, considerably limit the impact of the tunnel on the hydrogeology in the surrounding superficial rock. There is no reason to expect that an open tunnel at 50 metres depth located above the repository should result in up-coning of groundwater that significantly affects the hydrogeology in the repository bedrock at 450 metres depth. This conclusion is supported by the significant decrease in the frequency of water-conducting fractures with depth observed in the site investigations. It is noted that not even the spent fuel repository is expected to give noticeable up-coning during the construction and operational phase, as shown by modelling results for an open repository reported in Svensson and Follin (2010, Section 5.2).

The future isostatic uplift at Forsmark during the next 1 000 years is on the order of 7 m, whereas the resulting relative sea level change is around 4 m (if assuming no acceleration in sea level rise), see the **Climate report**. This decrease in shoreline elevation is not expected to change the importance of the horizontal fractures/sheet joints in the upper part of the bedrock for the hydrogeological system in the target volume of the rock as the horizontal fractures/sheet joints in the upper part of the bedrock occur also at greater depths than 7 m. The potential construction and operation of a tunnel above the repository during the next 1 000 years would then not negatively impact the performance of the repository. Abandoning the tunnel during this period would imply that the tunnel becomes filled with water as the grout in the tunnel degrades. The abandoned tunnel might act as a conductor for near-surface flows, but no significant impacts on the magnitude of the water flow in the rock surrounding the deposition holes in the repository is expected. This is based on the results from hydrogeological analyses of an abandoned, partially open repository (Bockgård 2010), which show very small changes

in the magnitude of Darcy flux at deposition hole positions if it is assumed that all excavations in the repository except deposition tunnels and deposition holes are open, as compared with the expected case that the repository is completely backfilled and sealed, see also Section 14.2.8. Consequently, there is little reason to expect that an abandoned open tunnel restricted to 50 m depth should impact the magnitude of the water flow at repository depth. Furthermore, similar arguments could be made for tunnels located down to at least the 150 m level.

Conclusions

The above assessment indicates that the upper 150 m of the bedrock above the repository is an unfavourable location for a tunnel from an engineering point of view, due to the exceptionally high water yield in this part of the bedrock. These conditions also imply that a tunnel constructed in this part of the bedrock would not affect the groundwater flow at repository depth such that the presence of the tunnel violates the safety functions of the deep repository. The design consideration to locate the repository to a depth that allows utilisation of the site for generally occurring future human activities should, therefore, be fulfilled at Forsmark.

14.2.7 Assessment of a mine in the vicinity of the Forsmark site

Introduction and specification of the case analysed

The ore potential at Forsmark has been analysed within the site investigations. In an area southwest of the Forsmark site a felsitic to metavolcanic rock, judged to have a potential for iron oxide mineralisation, has been identified (Lindroos et al. 2004) (see Section 4.3.2 and Figure 14-4). The mineral deposits have been assessed to be of no economic value. Nevertheless, as this judgement may be revised in the future due to economic reasons, the potential exploitation of this mineralisation is addressed.

Since the mineralisation at present is judged to be of no value, it is impossible to describe the design of a mine exploiting the mineralisation based on current mining standards. It could be a quarry or a mine and the depth could be from tens to hundreds of metres or for mines a thousand metres or even deeper.

Function indicator(s) considered

The function indicator relevant for this case is:

- R2, Provide favourable hydrologic and transport conditions.

During operation of the mine, the hydraulic gradients in its vicinity may be affected. Indirectly, if the impact on the hydrologic conditions is substantial, the function indicator R1, Provide favourable chemical conditions, could be affected.

Assessment of the consequences of a mine in vicinity of the Forsmark candidate area

If a mine, or other sub-surface rock excavation, were to be constructed in the vicinity of the Forsmark site, it may be assumed that the greatest influence on the repository for spent nuclear fuel would occur if the construction took place at the same depth and in close proximity to the repository for spent nuclear fuel. Since the southwesternmost part of the repository is located west of Lake Bolundsfjärden (Figure 14-4), the closest distance between the repository and a hypothetical mine in the potential area for mineralisation (Figure 14-4) would be on the order of 1 to 1.5 km.

In order to assess the potential influence on the repository, results from analyses of the hydraulic impact of an open repository are used. Calculations of the effects of water inflow to an open repository show that the drawdown of the hydraulic head is large in the rock close to the repository at a depth of 450 m (Mårtensson and Gustafsson 2010, Figure 7-20 lower insert). However, the drawdown decreases rapidly with distance from the open repository in a westerly direction to about 50 m within tens of metres from the repository and at distance of ca 1 km from the repository, the drawdown at 450 m depth is negligibly small. The reason for the small radius of influence is the low hydraulic conductivity of the rock mass volumes at depth in proximity to the repository. This constraining hydraulic condition is valid also for a potential future mine outside the tectonic lens. Therefore, it is reasonable to expect a very limited hydraulic impact from the mine on the repository because of the low-conductive bedrock in the target volume.

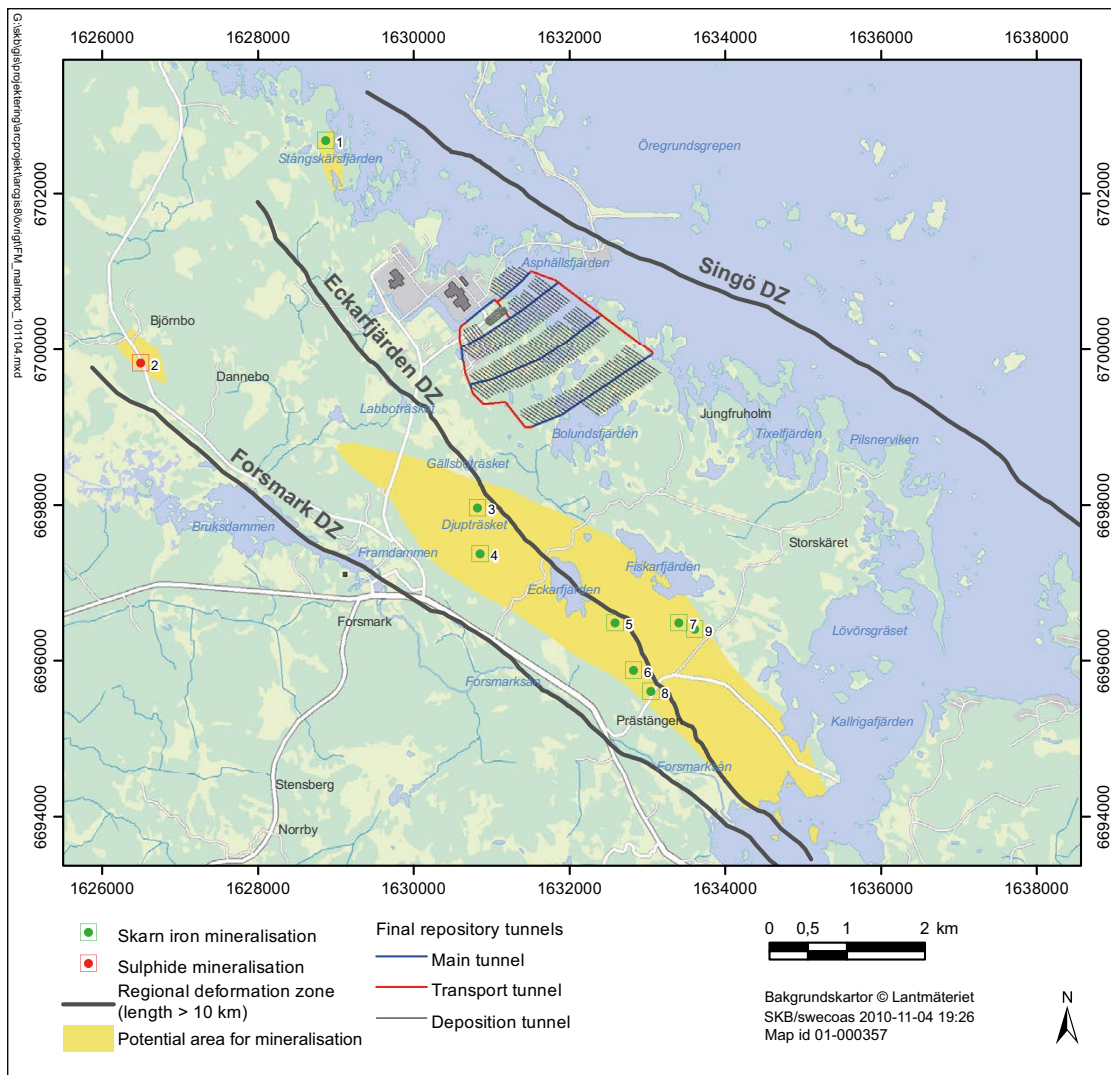


Figure 14-4. Map showing the areas on the surface that are judged to have some exploration potential for mineral deposits (Figure 6-5 in the FHA report).

Conclusions

The assessment indicates that exploitation of the potential mineral resources in the vicinity of the Forsmark site would not impact the safety functions of the repository. The design consideration to locate the repository at a site without natural resources is, therefore, considered to be fulfilled.

14.2.8 Incompletely sealed repository

Introduction and specification of the case analysed

According to regulations, it is also necessary to define and analyse a case that illustrates the consequences of an unsealed repository (SSM 2008a). The basic assumption in the case selected as representative for scenarios related to an unsealed or incompletely sealed repository is that the repository is abandoned when all canisters are deposited and all deposition tunnels backfilled and sealed, but the main and transport tunnels as well as the central area, repository access (ramp and shafts) and the ventilation shafts in the deposition area (see Figure 10-6) are still open due to, for example, political decisions not to seal completely. This assumption is based on the strategy for deposition of canisters, which implies that deposition tunnels are successively filled with canisters and then backfilled and sealed as soon they are filled. Abandoning the repository in the middle of this process is judged as rather unlikely because this would mean that canisters are left at the surface where they would constitute a larger risk than if emplaced in the repository.

Function indicator(s) considered

This case relates to the following function indicators:

- Can1, Provide corrosion barrier; ensure containment.
- Buff1, Limit advective transport in buffer; ensure tightness and self-sealing.
- Buff2, Reduce microbial activity.
- BF1, Counteract buffer expansion; high density and self-sealing of backfill.
- R1, Provide favourable chemical conditions; ensure reducing conditions.
- R2, Provide favourable hydrologic and transport conditions.

Qualitative description of the consequences of an incompletely sealed repository

If the repository is abandoned when the main and transport tunnels, central area, repository access and ventilation shafts in the deposition area are still open, these open volumes will successively be water filled. Water will flow through the open volumes with a magnitude and direction dependent on the magnitude and direction of the hydraulic gradient. In addition, the open volumes may affect the groundwater flow pattern in the repository bedrock.

All deposition tunnels will be plugged towards the main tunnels when the repository is abandoned. When the main tunnels have become filled with water, the cement and other components in the concrete plugs may be dissolved in the water and transported away. At some point in time the plugs will lose their function and the backfill in the deposition tunnel will swell out into the main tunnels. This swelling out into the main tunnels will decrease the density of the backfill in the deposition tunnels. How far into the deposition tunnel the decrease in density reach depends on the amount of backfill material that is lost from the deposition tunnel. If the density in the backfill above a deposition hole is significantly reduced, the buffer in the deposition hole may expand into the backfill above with the consequence that the density of the buffer also decreases.

Abandoning the repository without sealing the access from the surface may facilitate recharge of oxygenated water from the surface down to the central area and the main tunnels. In addition, the unsealed parts of the repository will contain air which will dissolve in the water that successively intrudes into the empty, unfilled parts of the repository. If dissolved oxygen reaches the canisters via the backfill in the deposition tunnels and the bentonite buffer or via fractures in the rock that intersect the deposition tunnel and further through the bentonite buffer, the oxygen will corrode the copper canisters. This may lead to corrosion breakthrough in the canisters and release of radionuclides from the spent fuel.

If and when corrosion breakthrough occurs depends on the supply of oxygen to the canister surface. Groundwater recharging from fractures and fracture zones intersecting the unfilled volumes deeper down in the rock will most likely not contain dissolved oxygen due to the large reduction capacity of both the rock and the overburden through which this water has infiltrated, see Section 10.2.5. The major supply of oxygen from the surface down into the open volumes of the repository will likely occur during glacial periods when glacial meltwater can be forced down due to the high hydraulic gradients established by the ice sheet. However, oxygen dissolved in the water in the empty volumes of the repository may also be consumed by both biotic and abiotic processes. For example, biological degradation of organic materials, already present in the empty volumes as well as supplied with incoming water, will continue until either the oxygen or the biodegradable organic material is depleted, and oxygen may react chemically with reducing minerals in the rock such as chlorite, biotite and pyrite (Sidborn et al. 2010), as well as be consumed by aerobic corrosion of iron construction materials left in the unfilled volumes of the repository.

Further transport of dissolved oxygen from the unfilled main tunnels in the repository to the canisters in the deposition holes will take place by advection or diffusion in the backfill in the deposition tunnels and in the bentonite surrounding the canisters, depending on the properties of these barriers. Alternatively, transport of dissolved oxygen may take place with groundwater flowing in fractures that intersect the deposition holes and are connected to either the unfilled main tunnel or to the deposition tunnel at a location close to the intersection with the main tunnel (see e.g. Figure 5-18). Both in the

backfill and the buffer, oxygen consumption may take place by chemical reactions with accessory minerals in the bentonite. In addition, microbial activity in the backfill is expected to consume oxygen (Section 10.2.5).

As described in Section 10.2.5, the bentonite contains organic materials that under anoxic conditions potentially could be utilised for microbial reduction of sulphate to sulphide. As long as the backfill above a deposition hole does not lose density to the extent that the buffer in the deposition hole can expand upwards into the backfill, microbial sulphate reduction in the bentonite buffer is not expected to take place to any extent (Section 10.2.5). If the backfill density is reduced to such extent that the buffer expands into the backfill, the buffer density may become too low to rule out microbial activity in the buffer. However, as noted in Section 10.2.5, although the amount of organic material in the bentonite accessible for microbial degradation is highly uncertain, it consists mainly of humic and fulvic acids that have molecules that are too large to be used by bacteria as a carbon source.

Quantitative assessment of the containment potential of an incompletely sealed repository

The assessment of the containment potential is based on analysis of expansion of deposition tunnel backfill into open main tunnels, on results from groundwater flow modelling of the effects of open tunnels and on simple estimates of oxygen supply and canister corrosion (see the **FHA report**, Section 6.6.3).

Expansion of deposition tunnel backfill

The expansion of deposition tunnel backfill into the main tunnels after degradation of the plug has been analysed by Åkesson et al. (2010a, Chapter 22). With the assumption that the entire plug is lost and that the backfill may freely swell out into the main tunnel, the results indicate that deposition holes located closer than 25 to 35 m from the degraded plug/backfill interface will experience a backfill with a dry density that is below the acceptance criterion of 1 240 kg/m³. Since no deposition hole will be located closer than 20.6 m from the deposition tunnel entrance (SKB 2009b), this implies that the loss of backfill from deposition tunnels could lead to density reduction of the buffer in at most four to five deposition holes located closest to the tunnel entrance.

The case analysed presumes that the plug is lost from neighbouring deposition tunnels and that the swelling is similar from all these tunnels, which implies that the backfill at most can expand 20 metres along the main tunnel since the distance between two deposition tunnels is 40 metres. The consequences of free swelling of the backfill in a deposition tunnel for a case where the plug in a neighbouring deposition tunnel is intact and the backfill in this tunnel remains in place have not been analysed quantitatively. Clearly, more backfill will expand out into the main tunnel and it is envisaged that a few additional deposition holes will experience a backfill with a density below the acceptance criteria, as compared with the case with expansion of tunnel backfill in two neighbouring deposition tunnels. However, the exact number of such deposition holes is not important for the approach selected for analysis of the dose consequences of this case.

Hydrogeological impact

In order to investigate the hydraulic influence of an abandoned, partially open repository, as compared to the reference closure of the repository, the effects of open tunnels have been studied for two situations with different boundary conditions; a temperate climate situation with present-day boundary conditions and a generic future glacial situation with an ice sheet covering the repository (Bockgård 2010). The boundary conditions in the glacial simulation represent a case with an advancing ice margin, but without permafrost, where the ice front is located above the repository at ice front location IFL II, as defined in Figure 10-135.

The results from the calculations imply that the open tunnels will cause a drawdown in the surrounding rock during temperate climate conditions, meaning that the tunnels will capture many flow paths from canister positions and thereby act as a conductor for flow to the surface. The general flow direction in the tunnels is recharge through the ventilation shafts in the deposition area and discharge through the ramp and shafts above the central area (see Figure 10-6 for locations of the repository features).

The water flow in the open system amounts to 0.42 L/s (13 230 m³/year) of which ca 60 % (0.26 L/s) is recharge from the transmissive surface layer and sheet joints above elevation -40 m. The impact of open tunnels on the Darcy flux at deposition hole positions is, however, small, with an increase of about 10 % in the median value compared with the reference closure case. The open tunnels decrease the median transport resistance to about 30 % of the reference value.

The consequences of open tunnels for the glacial conditions assumed in the calculations are, on the other hand, considerable. The high hydraulic head established by the ice sheet may cause a significant flow, about 250 m³/s, through the tunnel system, with recharge through the ramp and shafts above the central area and discharge through the ventilation shafts in the deposition area. The high hydraulic gradient will be transmitted by the tunnels to repository depth and water will be injected into the rock. The Darcy flux at deposition hole positions will in general increase and at certain deposition hole positions, a considerable increase in Darcy flux is indicated, but the open tunnels decrease the median transport resistance in the rock by only about 50 %.

Oxygen supply and canister corrosion

To illustrate the potential consequences for canister corrosion by oxygen dissolved in the water in the open tunnels in the repository, some simple calculations have been carried out (see the **FHA report**, Section 6.6.3 and Appendix B). In the calculations it is assumed that the water in the backfilled deposition tunnels above a deposition hole is saturated with dissolved oxygen and that oxygen is further transported to the canister lid by diffusion through the 1.5 m thick bentonite buffer above the lid (see Figure 5-13). For temperate climate conditions, the concentration of oxygen at the upper boundary of the buffer is set to 0.3 mol/m³, i.e. in equilibrium with atmospheric oxygen, and a concentration of 1.5 mol/m³ is assumed for glacial conditions, i.e. corresponding to the concentration in glacial meltwater (Sidborn et al. 2010).

With an effective diffusivity of 1×10^{-10} m²/s for dissolved oxygen, an approximate value representative for uncharged species (see the **Data report**) and assuming 1D-diffusion through the entire cross-sectional area of the buffer (diameter 1.75 m, Figure 5-13), the flux of oxygen after diffusion through 1.5 m buffer is calculated to 1.5×10^{-3} mol/year. If it is further assumed that this oxygen instantly reacts with the copper according to the stoichiometry 4 mol Cu/mol O₂, it would take 1 million years before corrosion breakthrough occurs in the 50 mm thick copper lid. If diffusion through the bentonite occurs through a cross-sectional area corresponding to the area of the canister lid, the time for corrosion breakthrough will be approximately three times longer. With a ten times higher diffusivity, representative of diffusion in unconfined water, it would still take on the order of 100 000 to 300 000 years before breakthrough occurs. With the higher concentration of dissolved oxygen, corresponding to glacial conditions, it would take on the order of 200 000 to 600 000 years for corrosion breakthrough provided that the buffer has retained its properties and about 20 000 to 60 000 years if the buffer above the canister is lost and diffusion of oxygen occurs through water only.

Sulphide as a corrosion agent is neglected in this scenario, since the corrosion breakthrough times are expected to be significantly longer than those estimated for oxygen. The main reasons for this are that the natural concentrations expected are at most in the order of 10⁻⁵ M (Tullborg et al. 2010), which is orders of magnitudes lower than the concentration of oxygen assumed in the simplified calculations, and that the stoichiometry of the corrosion reaction imply that less copper is consumed per mol sulphide (2 mol) compared with the consumption by oxygen (4 mol). The organic material contained in the bentonite material in buffer and backfill (see Section 10.2.5) is not expected to be utilised for microbial reduction of sulphate in the groundwater to sulphide as long as oxygen is present, if indeed they are at all susceptible to biodegradation.

Conclusion regarding containment potential

According to the reference glacial cycle evolution described in Section 10.4.1 and displayed in Figure 10-111, extensive glacial conditions are not established within the next c 58 000 years. Even if the density of the buffer in deposition holes close to the intersection between the deposition tunnel and the main tunnel significantly decreases, the calculations carried out indicate that no corrosion breakthrough occurs within the next ca 58 000 years in the reference evolution. Furthermore, the results of the hydrogeological analysis indicate that the hydraulic gradients during temperate climate conditions are directed towards the open tunnels and, hence, would act against oxygen transport from the

open tunnels to the deposition holes. The hydrogeological results for temperate conditions also indicate only small effects of the open tunnels on the Darcy flux at deposition hole positions. Although the open tunnels change the flow paths with somewhat reduced flow related transport resistances in the rock as a result, these resistances are still high. The fact that flow paths are captured by the open tunnels and discharge through the shafts and ramp above the central area is also considered as insignificant, since discharge points occur close to the repository also in the reference evolution and also because periglacial conditions with permafrost in the upper parts of the ramp and shafts prevails for large parts of the 58 000 year time period. This implies that the impact of the open tunnels for deposition holes other than those directly affected by the expanding tunnel backfill is small. Therefore, no analyses of radionuclide release and dose consequences are carried out for the period prior to the next reference evolution glaciation.

At the onset of the glacial period at Forsmark (c 58 000 years after present), the hydrogeology at the site is expected to change and high groundwater flows in the open tunnels cannot be excluded. According to the reference evolution, Figure 10-111, this glacial period lasts for ca 8 000 years. No corrosion breakthrough in canisters is expected during an 8 000 year long period with glacial conditions as long as diffusion is the dominating transport process in the buffer for corrosive agents in the groundwater. However, backfill that has expanded out into the main tunnels may be carried away during periods of high groundwater flow in the open tunnels. This may, in turn, result in further expansion of deposition tunnel backfill out into the main tunnels, exposing the buffer in deposition holes close to the intersection with the main tunnel to less and less counter pressure from the remaining backfill in the deposition tunnels. This may lead to expansion of the buffer upwards into the deposition tunnel, leading to a decrease in buffer density. Furthermore, if the deposition hole is intersected by a fracture large enough to carry substantial flow, buffer and backfill material could be carried away by groundwater flowing through the deposition hole and the deposition tunnel. Whether this situation is likely to occur during the 8 000 year long glacial period has not been quantitatively assessed. However, here it is assumed that it does and that this also implies that the groundwater flow through the deposition hole is large enough to supply the amount of corrosive species needed for corrosion breakthrough in the canister to occur before the end of this glacial period. This should be a cautious assumption, since permafrost prevails in the upper part of the bedrock, at least down to c 70 m depth, during the whole period (Figure 10-111), which should limit the water turnover in the open tunnels in the repository.

Quantitative assessment of the radionuclide release and dose consequences of an incompletely sealed repository.

According to the reference glacial cycle evolution (Figure 10-111), deglaciation at the site occurs at 66 200 AP after which the site is submerged during the following ca 8 000 years before periods with alternating periglacial and temperate conditions occur. In the analysis of the radionuclide release and dose consequences of this case (see the **FHA report**), the sequence of submerged and alternating periglacial and temperate conditions is not considered. Instead it is for simplicity assumed that temperate conditions prevail when calculating the radionuclide release from the repository and the subsequent dose impact. Further assumptions made in the calculations are listed below and data used in the calculations are the same as those provided in Table 14-2, except for the water flow through the deposition hole, which is set to the value of high water flow in the analyses of the scenario “canister failure due to corrosion (0.73 m³/year).

- No corrosion breakthrough in canisters occurs during the first period of temperate climate conditions lasting until ca 58 000 years after present.
- During the subsequent glacial period lasting until 66 200 years after present, corrosion breakthrough occurs in a canister in a deposition hole that is intersected by a fracture with high groundwater flow and which is located close to the intersection between a deposition tunnel and an open main tunnel.
- At year 66 200 after present, radionuclides are released from the spent fuel in the failed canister at a rate determined by the advective flow in the fracture intersecting the deposition hole. The released radionuclides are transported with the flowing water from the deposition hole to the central area and the access ramp and shafts above the central area via the deposition tunnel and open main and transport tunnels. The concentration of radionuclides in the water in the open system is determined by the groundwater turnover in the open tunnels as estimated for temperate conditions.
- The water in the access ramp and shafts is utilised by humans for agricultural purposes and as drinking water.

The calculated total annual effective dose (Figure 14-5) during the first 1 000 years after canister failure is 56 μSv and the dose is dominated by the intake of food and water contaminated by Pu-239 and by external radiation from Nb-94. Thereafter, the annual effective dose remains at a fairly constant level of about 25 μSv for the remaining period until the start of glacial conditions about 90 thousand years after present. During this period, the dose is dominated by the intake of food and water contaminated with Pu-239 and Ra-226.

The calculated annual effective dose is above 14 μSv , the annual dose corresponding to the regulatory risk limit, during the whole time period analysed, but below the annual dose of 1 mSv from background radiation. The calculated annual effective dose is obtained for a postulated failure of one canister in the repository during the glacial period prior to 66 200 years after present. In order to receive an annual effective dose that is comparable to that received from background radiation, approximately 20 canisters have to fail during this period.

Uncertainties

The uncertainties in the analyses of expansion of deposition tunnel backfill are rather large. The friction angle is a function of the swelling pressure and increases with decreasing swelling pressure. The values at low swelling pressure are not well known, but laboratory measurements indicate that the friction angle is higher than 20 degrees at low density and that the lateral stresses (corresponding to the normal stresses towards the rock surface) are higher than the stress in the swelling direction. This means that the resisting force from friction is probably larger than that modelled, which implies that the results are probably pessimistic in the sense that the swelling and thus density loss would be smaller than modelled (Åkesson et al. 2010a).

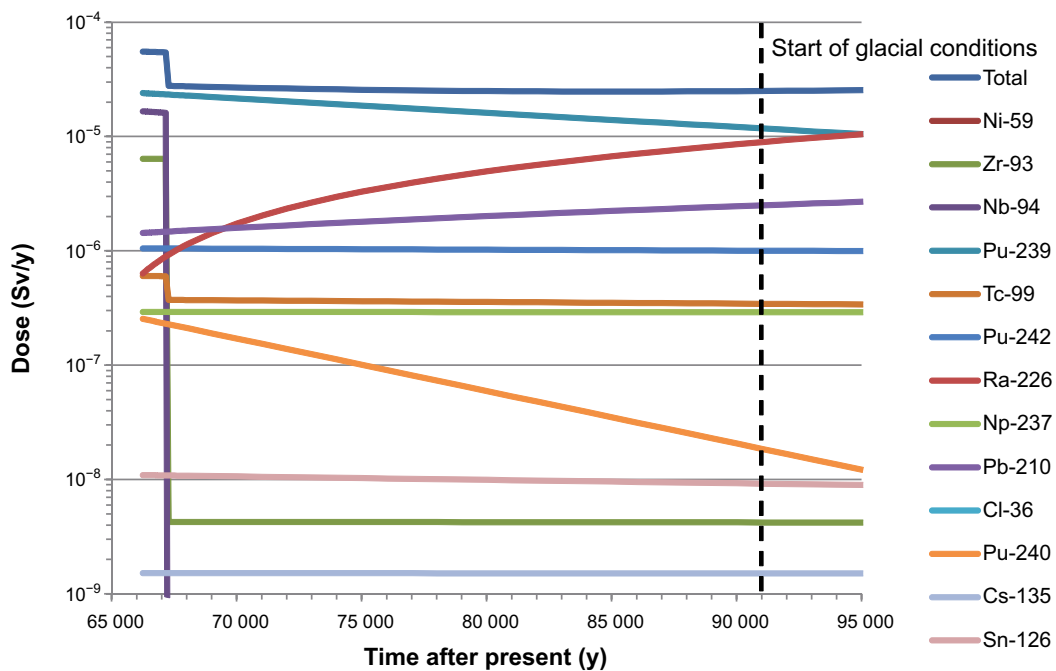


Figure 14-5. Calculated annual effective dose from using water in the open shafts and ramp as drinking water and for irrigation (Figure 6-19 in the FHA report).

There are a number of uncertainties in the analyses of the impact on groundwater flow of open tunnels in the repository, especially for the simulations with glacial conditions. One important uncertainty relates to the accessibility of water. In reality the flow in an open tunnel below the ice front will probably be limited by the supply of subglacial melt water in the transmissive subglacial layer at the ice-subsurface interface. If the supply of water is insufficient, there will be a drawdown of the pressure and the flow will decrease. In order to give such a high flow as adopted above, the tunnel entrances have to coincide with a major melt water tunnel under the ice. It should also be noted that the calculations assume a worst case location of the ice front in terms of hydraulic gradient. The hydraulic gradient below the ice sheet when the repository is completely covered by ice may be even lower than during the temperate conditions (Vidstrand et al. 2010).

Several simplified assumptions are made in the calculations of oxygen supply to the canister surface. The only transport resistance accounted for is that in the buffer surrounding the canister, whereas transport resistances in the backfill on top of the buffer in the deposition hole and in the deposition tunnel as well as in fractures in the rock are neglected. This is judged as very pessimistic, at least for temperate conditions. Even if the tunnel backfill expands out into the main tunnel and the density of the backfill above a deposition hole is significantly reduced, the transport resistance in the deposition tunnel should still be significant. This is supported by the results of the hydrogeological modelling that indicate that the hydraulic gradients are directed towards the open tunnels in the repository. Any oxygen transport from the open tunnels to the deposition holes then has to take place in a direction opposite to the hydraulic gradient. Other pessimistic assumptions concern the oxygen concentration and that it remains constant over a long time period. There are both biotic and abiotic processes that may consume oxygen in the repository environment.

The assumption that the tunnels will remain open after the advance and retreat of an ice sheet is also uncertain. Although the surface denudation is restricted at Forsmark (see Sections 3.5 and 4.5 in the **Climate report**), it seems very likely that eroded materials will fall down and fill in at least parts of the open tunnels.

The assumption that one canister fails due to corrosion during the next glacial period is not backed-up by any quantitative assessments, but is postulated based on cautious assumptions and therefore associated with large uncertainties. For example, it is assumed that the water flow in a fracture intersecting a deposition hole is large enough to carry away buffer in the deposition hole and backfill material above the deposition hole and to supply enough corrosive species for corrosion breakthrough to occur within an 8 000 year long glacial period. Considering that in the technical design requirements for the final repository there are limits on the water inflow to a deposition hole that will be accepted for hosting a canister (SKB 2009a), the potential for deposition holes that have intersecting fractures with high flow rates should be low.

Conclusions

From the simplified analyses carried out it can be concluded that abandoning the repository without backfilling and sealing all parts of the repository may imply that backfill in the deposition tunnels is lost and that the safety functions for containment are violated for deposition holes located close to the entrance of the deposition tunnels. Therefore, the general conclusion is that the repository should not be abandoned prior to complete backfilling and sealing.

The analyses of a not completely sealed repository further demonstrate that the repository system adapted to the Forsmark site is robust over a long period of time. Even without backfill in parts of the system, no canister failures are expected as long as diffusion dominates the transport of corrosive species in the backfill in deposition tunnels and buffer in deposition holes. The hydrogeological results for temperate conditions also indicate only small effects of the open tunnels on the Darcy flux at deposition hole positions. Although the open tunnels change the flow paths with somewhat reduced flow related transport resistances in the rock as a result, these resistances are still high. The fact that flow paths are captured by the open tunnels and discharge through the shafts and ramp above the central area is also considered as insignificant, since discharge points occur close to the repository also in the reference evolution and also because periglacial conditions with permafrost in the upper parts of the ramp and shafts prevails for large parts of the 58 000 year time period. This implies that the impact of the open tunnels for deposition holes other than those directly affected by the expanding tunnel backfill is small.

If corrosion breakthrough in canisters occurs during the next period with glacial conditions, i.e. from 58 000 years to 66 200 years after present according to the reference evolution, the annual effective dose from radionuclides in the failed canisters will exceed the annual effective dose corresponding to the regulatory risk limit. However, as long as the number of failed canisters is limited to less than ca 20, the dose from radionuclides in these canisters will be lower than the dose obtained from background radiation. Considering the large uncertainties and cautious assumptions made in the analysis, the calculated dose should be seen as an illustration of possible consequences rather than an estimation of what the consequence would be if the repository is not completely backfilled and sealed.

14.2.9 New knowledge since SR-Site assessment

This section discusses new knowledge related to future human actions since the above presented assessment of future human actions was conducted. The new knowledge is related to comments given by SSM (2018) and recent international development related to future human actions considerations.

Comments received from SSM related to future human actions in SR-Site

The material presented above in Sections 14.2.1 to 14.2.8 is essentially the same text as presented in SR-Site (SKB 2011). In the regulatory review of SR-Site, comments were given related to the residual scenarios for future human actions (SSM 2018, Section 8). Overall, SSM judged that the scenarios for human handling and human intrusion were handled in accordance with the regulations, and that the choice of representative cases was reasonable. However, there were a few comments regarding inconsistencies in data used for the assessment of the drilling case (**FHA report**, Section 6.3).

SSM pointed out that there were inconsistencies between the radionuclide inventory presented in the **FHA report** and the inventory presented elsewhere, especially in the SR-Site version of the **Radionuclide transport report** and the **Data report**. SSM also commented on potential small inconsistencies in 1) the estimated amounts of some of the radionuclides brought to the surface and the radionuclide inventory in the canisters, 2) the calculated radionuclide release rates from the fuel and activity concentrations in canister water compared with the reported radionuclide inventory, and 3) the calculated dose rate to drilling personnel in respect to the reported activity concentration and dose coefficients for external exposure.

These comments from SSM have been addressed by SKB in Hjerpe (2021). The key findings and conclusions from the evaluation can be summarised as follows:

- The reported radionuclide inventory in the **FHA report** was somewhat higher than in the Radionuclide transport report for two radionuclides: Th-229 (8 % higher) and Ag-108m (5 % higher). The effect of this is that the dose consequences derived in the FHA report were higher, although not much, than they would have been using the correct inventory from the Radionuclide transport report.
- The reported radionuclide inventory in the **FHA report** was significantly lower than in the Radionuclide transport report for two radionuclides: Se-79 (67 % lower) and Mo-93 (12.5 % lower), and somewhat lower, ca 1 %, for Sr-90, Eu-152 and Ni-59. However, the effect on the dose consequences derived in the FHA report of these discrepancies is insignificant since these radionuclides contributed insignificantly to maximum doses for the FHA calculation cases.
- The reported fractions of the Se-79 inventory in various fuel parts (**FHA report**, Table 6-1) are incorrect in the **FHA report**, but it is not these fractions that in the end were used for deriving the release rate. It was concluded that the reported release rate of Se-79 from the fuel and the corresponding concentration in the water in the canister 300 years after repository closure (**FHA report**, Table 6-3) were correct, and consistent with the radionuclide inventory in an average canister 300 years after repository closure given in the **FHA report**, Table 6-1.
- It was concluded that there was no inconsistency between the calculate dose rate to drilling personnel from Am-242m (**FHA report**, Table 6-5), the reported concentration in the water in the canister (**FHA report**, Table 6-1) and the dose coefficient for external exposure used to derive the dose.

Development of international recommendations and guidance

The strategy and methodology to handle FHA in SR-site is described in Chapter 3. During the development, considerations were taken to be in line with national regulations (SSM 2008a, b) as well as international recommendations and guidance from especially ICRP (2000) and NEA (1995). There have been no new national regulations issued since then, but there has been international development related to future human actions. This section gives a brief summary of the international development related to future human actions since the **FHA report** was published.

The IAEA have published two Specific Safety Guides including information relevant for future human actions considerations in a safety case for geological disposal (IAEA 2011, 2012). In ICRP Publication 122 (ICRP 2013), dealing with the radiological protection of humans and the environment following the disposal of long-lived solid radioactive waste in geological disposal facilities, considerations of future human actions are addressed. The NEA have published the report on the MeSA initiative (Methods for Safety Assessment for Geological Disposal Facilities for Radioactive Waste) (NEA 2012b). The joint positions, relevant for future human actions considerations, by the IAEA, ICRP and NEA can briefly be summarised as follows:

- An inadvertent action is to be understood as an action where the repository location is unknown, its purpose is forgotten, or the consequences of the actions are unknown; all other actions are advertent.
- Inadvertent human intrusion needs to be considered, in some form, in safety assessments of radioactive waste disposal to address the robustness of the disposal facility. Advertent intrusion does not need to be considered.
- When considering scenarios for inadvertent human intrusion, one or more stylised scenario based on present-day technological and societal conditions relevant for the disposal site should be used, rather than speculating about the potential behaviour of humans in the future.
- When making assumptions regarding the timing of the intrusion event, periods of institutional control (or periods of oversight) can be taken credit for.
- Measures to preserve the memory of the disposal facility might help to reduce the probability of inadvertent human intrusion.
- Consequences from inadvertent intrusion, into geological disposal facilities, are considered in the context of optimisation rather than being compared with a regulatory dose constraint. In general, the intent is to demonstrate and enhance the robustness of the disposal system by considering opportunities to reduce the potential for and/or consequences of inadvertent intrusion.

In addition, there has been one project conducted directly related to inadvertent human intrusion – the IAEA project HIDRA.³⁰ The topic of HIDRA was to address human intrusion in the context of disposal of radioactive waste. SKB participated actively in this project and also took the lead in the group considering inadvertent human intrusion into geological disposal facilities. The HIDRA project considered how to counter potential future human actions that could disturb areas occupied by radioactive waste disposal facilities, and how such actions could affect the integrity of the disposal facilities and potentially give rise to radiological consequences. As part of the HIDRA project, Member States developed an approach for identifying and selecting scenarios to be assessed, and protective measures to reduce the potential for and consequences of inadvertent human intrusions. The first phase of the project focused on potential scenarios, societal factors and protective measures, and was completed in 2015. Guidance on how to assess the consequences of potential future inadvertent human intrusions and incorporate them in the safety case for a radioactive waste disposal facility was developed. The second phase of the project focused on practical implementation of the HIDRA approach and documentation of country-specific examples, and was completed in 2018. Key conclusions, relevant for the current assessment, from the HIDRA project are:

- Especially for geological disposal facilities, it may not be required to demonstrate compliance with any dose constraints for the human intrusion scenarios. Rather, the potential consequences arising from human intrusion are considered in the context of identifying opportunities to reduce the potential for and/or consequences of human intrusion and, where appropriate, for opportunities to enhance the robustness of the disposal facility.

³⁰ Draft IAEA report available: <https://www-ns.iaea.org/downloads/rw/projects/hidra/hidra-draft-report.pdf>

- The use of stylised scenarios provides a basis for the identification of potential measures that could be considered necessary.
- A framework to consider the benefits of potential protective measures to mitigate against the potential impacts of human intrusion was identified. Measures must not obviously compromise the safety of the disposal facility (i.e. they must not compromise the primary safety targets for the disposal facility), must not lead to other undue hazards to people and the environment, and have to follow the principle of proportionality regarding benefits, efforts and costs, which will be considered as part of the overall optimisation of the disposal facility.
- In particular, when considering a potential protective measure against human intrusion it should be considered whether it would cause any negative impacts on ‘normal evolution scenarios’ (sensu IAEA); in all cases, the primary focus of the safety case is on the normal evolution scenarios, and the optimisation with regard to human intrusion impacts is considered secondary to optimising the safety of the normal evolution of the facility.

It is worth noting that the work by IAEA, ICRP and NEA is heavily focused on human intrusion, hence not covering all human actions identified as FHA FEPs. The international development conducted since the **FHA report** was published has better clarified how future human actions should be considered in the safety assessment, but there have been no fundamental changes made in the role they play in the safety assessment. It is concluded that the strategy and methodology to handle FHA applied in SR-Site still is in line with international recommendations and guidance, as well as national regulations.

14.2.10 Assessment of potential impact of updated information

A decade has passed since the analysis of future human actions were done (**FHA report**). In many fields the technology has developed immensely, new technical solutions have been invented and what may be seen as ‘present-day practice’ has changed. However, for scenarios related to future human actions, although technology has been advancing, the types of human actions that may impact repository safety (Table 14-1) are considered to be valid. In addition, what was considered ‘present-day practices’ a decade ago are still applicable today. Hence, it is judged that the conclusions drawn in the technical and societal analyses, and the choice of illustrative cases for future human actions (Section 14.2.4) are applicable for SR-Site (PSAR).

The key new information that is related to the assessment of the representative cases is the updated radionuclide inventory (see the **Data report**). The inventory does not affect the representative cases related to rock excavation or a tunnel, or a mine in the vicinity of the Forsmark site. Hence, the assessments of these cases are still valid (Section 14.2.6 and Section 14.2.7).

Two cases use the radionuclide inventory as input data: the drilling case (Section 14.2.5) and the case related to an incompletely sealed repository (14.2.8). As stated in previous sections, the doses from FHA calculation cases are as expectedly high, and international recommendations are to consider the doses in the context of optimisation rather than being compared with a regulatory dose constraint. Thus, it was not deemed necessary to perform new simulations for these cases using the updated inventory. Instead, the potential impact the updated inventory may have on the dose consequences is discussed from a more qualitative perspective. The impact on the doses is evaluated by simply scaling the radionuclide specific doses with the difference in the updated and previously used inventory. All radionuclides were included in the comparison, but the discussion below is limited to the radionuclides most contributing to the doses.

Potential impact on the drilling case – dose to the drilling personnel

In the assessment of the drilling case (Section 14.2.5), doses to the drilling personnel were calculated. The highest dose rate to drilling personnel from radionuclides brought to the surface is 300 years after repository closure was reported to be 500 mSv/hour. The dose rate is to almost 100 % due to exposure from Ag-108m, Cs-137, Am-241, Nb-94 and Sn-126 (**FHA report**, Table 6-5). Ag-108m is the main contributor, responsible for about 96 % of the total dose rate. By scaling the dose rates with updated radionuclide inventory, results in that the same five radionuclides contribute with almost 100 %, in the same order, to the dose rate. Ag-108m dominating the dose rate with about a 97 % contribution.

The activities of Ag-108m, Cs-137, Am-241, Nb-94 and Sn-126 are about 41 %, 17 %, 0 %, 39 % and 15 % higher, respectively, in the updated inventory compared with the inventory applied in SR-Site. This results in that the total dose rate to drilling personnel from radionuclides brought to the surface 300 years after repository closure potentially is about 40 % higher, hence in the order of 700 mSv/hour.

If drilling occurs about 5 000 years after repository closure the dose rate, with the old radionuclide inventory, decreased to values below 1 mSv/hour (0.5 mSv) and was dominated by exposure to Nb-94 and Sn-126 (Section 14.2.5). The activities of these two radionuclides are about 39 % and 15 % higher in the updated inventory, hence, the total dose rate to drilling personnel from radionuclides brought to the surface about 5 000 years after repository closure increases but is still below 1 mSv.

Potential impact on the drilling case – dose to a family

In the assessment of the drilling case (Section 14.2.5), dose to a family that settles on the site was also calculated. The dose to a family that settles on the site originates from using the abandoned borehole as a well and from radionuclides in cuttings and spent fuel spread on the ground.

The highest total dose rate from using the borehole as a well 300 years after repository closure was calculated to be 0.31 mSv/year with the old radionuclide inventory, and was dominated by the contribution from Am-241 (Section 14.2.5). Since the activity of Am-241 in the updated inventory is about the same as in the inventory applied in SR-Site, the update does not have any significant impact on the dose rate maximum from using the abandoned borehole as a well. At 2 000 years after repository closure, the dose rate due to using a well is dominated by Pu-240 and if drilling takes place at still later times, Pu-239 and Nb-94 become more significant. The activities of these three radionuclides are about 14 % (Pu-240), 9 % (Pu-239) and 39 % (Nb-94) higher in the updated inventory. The total dose rates at 2 000 years after repository closure and beyond are then expected to be about 10 to 40 % percent higher, but below the dose rate at 300 years after closure.

The highest total annual effective dose from the use of the contaminated soil for agricultural purposes was about 10 Sv/year, obtained 300 years after repository closure (Section 14.2.5). The dose was dominated by ingestion of vegetables contaminated with Tc-99 and there was also a significant dose contribution due to external radiation from Ag-108m. The activities of these two radionuclides are about 11 % (Tc-99) and 41 % (Ag-108m) higher in the updated inventory. The total annual effective dose 300 years after repository closure potentially is about ten to a few tens of percent higher. Changes in the inventory for other radionuclides than these dominating two had no significant effect on the resulting dose maximum.

Conclusions

Based on the discussions above, it is concluded that the updated radionuclide inventory may result in somewhat higher calculated doses in the representative cases for future human actions. However, no doses change significantly much to warrant any changes of the overall conclusion from the FHA analysis. Many of the calculation cases have several cautious assumptions which if altered would have a larger impact than the somewhat altered inventory.

Radiological consequences from FHA, especially direct inadvertent human intrusion, can be high. This is however expected, since the hazard of the spent fuel to be disposed of is inevitable for any disposal concept based on concentration and isolation of radioactive high-level waste. The main conclusion from the FHA analysis is that it is important to consider FHA in the safety assessment and take measures aiming at isolating the spent fuel from man. Selecting a disposal concept based on a deep geological repository is the most important measure taken in order to decrease the potential for radiological consequences related to future human actions to occur.

14.3 Analyses required to demonstrate optimisation and use of best available technique

14.3.1 Introduction

As stated in Section 2.7 some aspects of the demonstration of best available technique (BAT) need to be addressed in the assessment of post-closure safety supporting the PSAR. While a general account of the use of BAT is a broad issue spanning from the selection of method for the management of nuclear waste to fine details of the selected method, a limited part of this issue can and should be addressed in the safety assessment of the preferred method. Here, the account of BAT is, therefore, confined to the KBS-3 method with vertical deposition, using copper/cast iron canisters, buffer and backfill at the selected site.

Within the PSAR final judgements on BAT cannot be made, but a basis for such judgements can be provided. As stated in the introduction, Section 1.2, the PSAR is based on a reference design of the engineered parts of the repository, including reference methods to achieve the specified design, taking into account methods of controlling that the specifications of the reference design have been achieved. Feedback can be given as to whether alterations in relation to this reference design could lead to reductions in risk or in reduction in uncertainties that potentially could affect risk. For aspects of the design where no such reduction in risk or uncertainty in fulfilment of safety functions can be seen to be realistically obtainable, the solution will be claimed to be optimal and BAT. However, the PSAR is not an assessment of all conceivable technical solutions. SKB will continue technical development of several aspects of the design in order to further simplify construction and implementation.

The BAT related assessment focuses on the scenarios, with their related safety functions, contributing to risk, i.e. the scenarios treating canister corrosion failure and canister shear failure. For these scenarios aspects of the design influencing the occurrence of the scenario and its calculated risk are assessed considering whether realistic alterations of the design would significantly reduce risk. In addition, also the main features of the design, such as backfill, sealing or repository depth, that do not directly contribute to risk are assessed, in order to clarify whether there are aspects of these features that could be detrimental to any safety functions and whether changes to these features could enhance safety.

The analysis of the containment potential for the relevant scenarios presented in Chapter 12 and the analyses of retardation potential and risk, presented in Chapter 13, with associated sensitivity analyses, are the bases of the BAT related assessment presented in the following subsections, since they point to the most important issues to consider in the BAT discussion. Furthermore, in order to evaluate the calculated risk results in the assessment of post-closure safety from the point of view of BAT and optimisation, some additional analyses of the sensitivity of the risk with respect to important barrier dimensions and layout rules have been carried out and are presented below. The overall assessment of whether the current reference design is in compliance with this aspect of BAT is left to Section 15.3.5.

14.3.2 Potential for corrosion failure

For canister failure due to corrosion, i.e. violation of safety function criterion Can 1, copper shell thickness, according to Figure 8-4, is the main contributor to calculated risk. According to the corrosion scenario assessed in Section 12.6, corrosion failure could only occur if advective conditions develop in the buffer. Factors of the design influencing the potential for advective conditions in the buffer are (Section 12.2):

- Buffer density – amount of dry mass deposited.
- Backfill density – amount of dry mass deposited above the deposition hole.
- Type of buffer material used.
- Geosphere conditions yielding very high or very low ionic strengths of groundwater.
- Geosphere conditions leading to increased flow.

Factors of the design affecting the potential for corrosion failure in case of an eroded buffer are (see Section 12.6):

- Copper shell thickness.
- Deposition hole acceptance criteria – since these may affect the Darcy flux of the groundwater around the deposition hole.

In the following it is assessed, based on results already presented in this report complemented by some additional sensitivity analyses, whether realistic changes of the current reference design would lead to reduced risk.

Copper shell thickness

The mean number of failed canisters at one million years in the corrosion scenario has been calculated for cases where the reference design copper thickness of 5 cm is changed to 10 cm and to 2.5 cm. All other input data are as for the central corrosion variant, see Section 12.6.4, meaning e.g. that the result is based on a weighted mean of all semi-correlated hydrogeological DFN realisations. The results show that increasing the copper thickness to 10 cm reduces the mean number of failed canisters at one million years by a factor of about 3 while halving the thickness to 2.5 cm increases the number by about a factor of 2, see Figure 14-6.

The maximum dose and hence the risk depends on the canister thickness in a similar way to the mean number of failed canisters at one million years (see the **Radionuclide transport report**).

Since the calculated risk with the reference design is below the regulatory limit, the selected copper thickness is deemed adequate from the point of view of BAT. Potential problems of manufacturing and sealing a thicker canister have not been considered in this analysis.

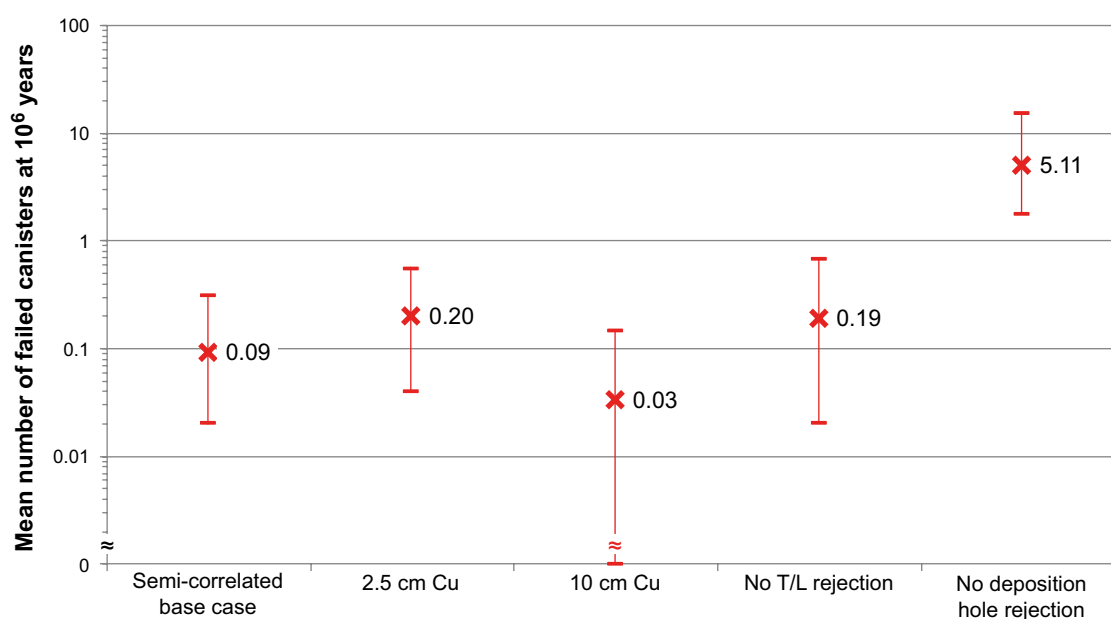


Figure 14-6. Sensitivity cases relating to BAT for the corrosion scenario. Cases with 2.5 and 10 cm copper thickness are shown as are two cases where the rejection criteria for deposition holes are eased and omitted, respectively. The crosses denote mean values and the bars denote the variability over the several realisations of the hydrogeological DFN models. Documentation of all calculations of buffer loss and subsequent canister corrosion under advective conditions is given in Hedin (2021).

Buffer material – potential for avoiding buffer erosion

The assessment of buffer erosion/colloid release, summarised in Section 10.3.11, demonstrates that the phenomenon cannot be ruled out in the assessment of post-closure safety. There is still uncertainty with regard to modelling of colloid formation and subsequent erosion of the buffer material and the modelling approach thus tends to be pessimistic. It also seems clear that it cannot with current understanding be defensibly mitigated by e.g. selection of another buffer material. A continued R&D program is needed.

Furthermore, it is possible that the erosion process will be hindered, from an early stage, by accessory material in the eroded buffer filling up the fractures in which the erosion process occurs (Neretnieks et al. 2009). Continued R&D is required before such a phenomenon could be taken credit for in the safety assessment.

Buffer mass and thickness

A thicker buffer and hence a larger deposition hole diameter, would to a limited extent mitigate the effects of buffer erosion, since an increased buffer mass would allow more buffer to be lost without advective conditions arising. This is however counteracted by the increased deposition hole diameter, which to some extent would increase the erosion rate (Moreno et al. 2010) and also increase the probability of having a water-conducting fracture intersecting the deposition hole.

In conclusion, a larger buffer mass is not seen as a practical means of mitigating the effects of buffer erosion. A larger buffer mass may offer a slightly longer time before advective conditions are encountered in the deposition hole, but this is not seen as a solution to the issue. It is also concluded that continued R&D on the erosion process is required. It may also be noted that changing the buffer thickness would also imply a need for revising the thermal design of the repository.

Backfill density – Amount of dry mass deposited above the deposition hole

According to Section 10.3.9 a maximum backfill material loss of 220 tonnes in a deposition tunnel section can be allowed before advective conditions have to be considered in the deposition hole below. As concluded in Section 10.3.11 none of the tunnel intersecting single fractures will cause erosion of the backfill to this extent. For a few positions where the tunnel is intersected by a transmissive deformation zone, potentially more than 220 tonnes could be lost, but this is not relevant from the point of view of canister integrity. Such local loss of backfill by erosion does not mean that the hydraulic conductivity of the entire tunnel will be affected and these occurrences are not judged to impair safety. In conclusion, the amount of dry mass deposited above the deposition hole according to current design is deemed appropriate.

Deposition hole acceptance criteria

The groundwater flow around and through deposition holes has a large impact on both the loss of bentonite which may potentially lead to advective conditions and on the rate of corrosion by sulphide in the groundwater as illustrated by Figure 10-81 and Figure 10-164. These figures also show the large impact of applying EFPC as a means to avoid deposition holes with high groundwater flow. As described in Section 5.2.3, in addition to the 'pure' EFPC criterion, also an additional deposition hole rejection criterion related to the combination of a high transmissivity and length of the intersecting fracture (T/L filtering) is assumed in the reference design of the repository and in the analyses carried out in the PSAR.

In order to further investigate the importance of the deposition hole acceptance criteria some additional cases have been studied.

The mean number of failed canisters at one million years in the corrosion scenario has been calculated for cases where i) the transmissivity-fracture length (T/L) filter is omitted and ii) no rejection is applied, i.e. neither the T/L-filter nor the 'pure' EFPC criterion are applied. All other input data are as for the central corrosion variant, see Section 12.6.4. The results show that omitting the T/L-filter increases the mean number of failed canisters at one million years by a factor of about 2 while the omission of all rejection criteria increases the number by about a factor of 50, see Figure 14-6. In particular the latter of these two results demonstrate the necessity of applying appropriate rejection criteria.

The maximum dose and hence the risk depends on the rejection criteria in a similar way to the mean number of failed canisters at one million years (see the **Radionuclide transport report**).

Furthermore, with the assumptions used in the corrosion calculations for advective conditions in the PSAR, in a deposition hole with a Darcy flux of 0.001 m/yr it takes more than 900 000 years to corrode through a canister after the buffer has been eroded away, even with the highest sulphide concentration considered in the corrosion calculations (0.00012 M). Also, the time to erode the buffer is of the order of 100 000 years for such a hole if the aperture of the fracture to which buffer is lost is 10^{-3} m and assuming dilute conditions 25 % of the time. This means that if deposition positions with long-term Darcy fluxes of 0.001 m/yr or more could be identified and rejected, then the risk over the one million year assessment time associated with the corrosion scenario should vanish. It is also noteworthy that a Darcy flux limit of 0.01 m/yr would not reduce the risk much compared to what is obtained with the EPFC criterion, since almost all of the few positions with such Darcy fluxes are already avoided. Typically less than one percent of the deposition positions have Darcy fluxes above 0.001 m/yr and around one in a thousand have fluxes above 0.01 m/yr without any rejection, meaning that if an efficient criterion more directly related to the Darcy flux could be formulated, the potential losses of deposition positions would be small.

It should be noted that since the PSAR considers the application of the EFPC (including the T/L criterion), in practise also a hydraulic consideration is applied. Since there is a correlation, although uncertain, between fracture size and transmissivity, application of the EFPC in fact reduces the number of high Darcy flux deposition holes significantly. This observation highlights the fact that it is not the EFPC as such that is important, but the finding of an observable property that would identify potentially flowing fractures. Based on the findings above, which were noted already in SR-Site, new technical design requirements have been formulated for the underground openings in PSAR, see Section 5.2. Specifically, in Section 5.2.3 the hydraulic conditions around deposition holes are discussed, and tentative hydraulic acceptance and rejection criteria are presented. It is noted that additional work and site-specific data and knowledge are needed before quantitative limits on such criteria can be formulated. In short the procedure is to obtain specific capacity (as a proxy for transmissivity) from pilot holes for deposition holes under open repository conditions, and utilising the correlation between specific capacity and Darcy flux for post-closure conditions, acceptance criteria for the deposition hole positions may be formulated.

Deposition tunnel acceptance criteria – including the EDZ

According to current technical design requirements, excavation induced damage in deposition tunnels should be limited and not result in a connected effective transmissivity, along a significant part (i.e. at least 20–30 m) of the disposal tunnel and averaged across the tunnel floor, higher than 10^{-8} m²/s. Evidence presented in the **Underground openings construction report** and further elaborated in the **Data report** and in Section 10.2.2 suggests there is ample evidence that a potential EDZ formed during excavation will be kept below the maximum allowed transmissivity as set out by the technical design requirements and data suggests that a continuous EDZ would not develop at all. Furthermore, the EDZ can be mitigated by floor levelling or direct mechanical excavation.

As shown in Table 14-3 the number of corroded canisters is identical between cases without an EDZ and with the basic assumption of an EDZ transmissivity of 10^{-8} m²/s.

The table also shows that a more transmissive EDZ could affect risk since the number of failed canisters starts to increase, although moderately when the transmissivity is increased. It is thus concluded that the transmissivity limit of 10^{-8} m²/s is adequate.

The EDZ appears even less important for radionuclide transport. For the pin-hole scenario, see Section 13.7.2, the presence of an EDZ with a transmissivity of 10^{-8} m²/s increases the dose only marginally compared with the case without an EDZ, and making the EDZ transmissivity larger does not further increase the dose.

Table 14-3. Calculated mean number of failed canisters at one million years for various assumptions regarding the properties of the EDZ and the existence of a crown space. Results from the SR-Site assessment.

	Mean number of failed canisters at one million years
Semi-correlated base case realisation without EDZ	0.083
Semi-correlated base case realisation (includes EDZ with $T = 10^{-8} \text{ m}^2/\text{s}$)	0.083
Semi-correlated base case realisation with $T = 10^{-7} \text{ m}^2/\text{s}$ EDZ	0.19
Semi-correlated base case realisation with $T = 10^{-6} \text{ m}^2/\text{s}$ EDZ	0.33
Semi-correlated base case realisation with crown space (includes EDZ with $T = 10^{-8} \text{ m}^2/\text{s}$)	0.25

14.3.3 Potential for shear failure

Canister failure due to shear, i.e. violating safety function criterion Can 3 “Withstand shear load”, according to Figure 8-3, is a contributor to calculated risk, even if the contribution is small. As concluded in Section 10.4.5, pessimistic estimates of canister failure due to rock shear indicate that the probability that one out of the 6000 canisters has failed at Forsmark at the end of the one million year assessment period is 0.079. This leads to a peak mean dose of 0.15 μSv , occurring at one million years, Section 13.6. It could well be argued that further reductions of this very low risk contribution are not very meaningful, but it is nevertheless worthwhile to consider what factors of the design influence the potential for shear failure. According to the assessment of the canister shear scenario (Section 12.8) these factors are:

- Insert strength and the occurrence of defects.
- Copper shell mechanical properties.
- Buffer shear strength.
- Efficiency in the implementation of deposition hole rejection.

These factors are assessed in the following, mainly using the findings of the studies by Jonsson et al. (2018) of the canister-buffer system response to shear loads within the canister design analysis, forming an important basis for the **Canister production report**. As stated in Section 10.4.5 the current technical design requirements are the result of a balance between achievable requirements on the canister and on the layout of the repository, given the understanding of earthquakes and secondary shear movements on the one hand and of the response of the buffer-canister system on the other. A lower technical design requirement shear displacement would give a higher probability for shear with given layout rules, but lower requirements on the canister design and material (especially the non-destructive testing of the insert) and vice versa. Furthermore, the cited analyses of the response of the buffer-canister system to a shear load also suggest that if the real variability in buffer density, fracture orientation and impact location on the canister were to be taken into account, then in many cases not even a 10 cm shear movement would jeopardise the integrity of the canister. This conclusion is further corroborated by the fact that the criteria used to evaluate the modelling results relate to local properties, and the violating of these criteria would not, in many cases, lead to loss of the integrity of the copper shell.

Insert strength and the occurrence of defects

The capability of the insert to withstand shear load depends mainly on the occurrence of surface defects in the cast iron. According to the damage tolerance analyses (Jonsson et al. 2018), discussed in Sections 10.4.5 and 5.4.3, the maximum acceptable crack-like defect size on the BWR cylinder surface is 9.0 mm deep, 22.5 mm long defect and circumferentially oriented. Larger shear displacement will lessen the acceptable depth, while decreasing the buffer density will increase it.

While the **Canister production report** concludes that the current canister reference design conforms to the stated technical design requirements, it is also noted that rigorous requirements on manufacturing and NDT capability are needed for the insert. Revising the design of the canister/buffer system such that the loads in the insert decrease, e.g. by reducing buffer density and thereby reducing the buffer shear strength, would thus allow relaxation of the manufacturing and NDT capability requirements relating to the insert.

Copper shell mechanical properties

The results from inspections of manufactured canister components, presented in the **Canister production report**, show that the specified values for elongation and creep ductility in the copper shells conform to the reference design. These design values are used in the subsequent damage tolerance analysis (Jonsson et al. 2018) and are found appropriate. While formal sensitivity analyses of the importance of the copper shell mechanical properties are not made, it is judged that there is little prospect that changing these properties would enable the canister to withstand even larger loads.

Buffer density and buffer material properties

Alteration of the buffer material due to cementation yields small effects in the shear analyses. In the shear calculation made for SR-Can (Börgesson and Hernelind 2006) an 8.75 cm thick zone of the buffer material around the canister was assumed to be converted to cement like material, with no swelling pressure, with an E-modulus increased by a factor of 100 and a shear strength increased by a factor of 5 compared to the unaltered buffer. No new calculations of this case have been done for the PSAR since such large changes of bentonite properties are unrealistic; the properties of converted material are unknown and the effect rather small. Conversely it is not judged feasible to change the buffer composition such that the E-modulus and shear strength are reduced considerably, while keeping the needed swelling pressure.

Efficiency in the implementation of deposition hole rejection

As stated in Section 12.8.2, the number of canisters that may fail due to shear load during the assessment period depends on the success of detecting and avoiding large fractures in deposition holes. The EFPC deposition hole rejection criteria have been shown to be effective in finding critical structures and enable the detection of > 97 % of the critical canister positions irrespective of DFN model (Munier 2010). The remaining positions are propagated to the assessment of seismic impact (Section 10.4.5), pessimistically disregarding findings in Hökmark et al. (2019) that suggest that the number of positions is overestimated by at least a factor of 4. However, the EFPC simulations are based on idealisations of fractures as being perfectly planar, infinitesimally thin discs for computational convenience. Most real fractures are not anonymous and, rather, display many properties that can be used as proxies for size (Cosgrove et al. 2006). It is therefore, as argued in Munier (2010), likely that critical fractures that escaped detection in the simulations used as input for this assessment will indeed be detected by a carefully designed investigation programme (SKB 2010b). Hence, it is likely that the number of potentially damaged canisters will be lower than predicted in this assessment. From the viewpoint of BAT it may thus be argued that while the current EFPC provides adequate protection against shear failure, there is reason to continue the efforts envisaged in the detailed investigation programme to be able to find critically large fractures by other means. Such efforts are also likely to be economically attractive, since application of EFPC implies that many deposition holes are rejected, even if they are not intersected by sufficiently large fractures to be of any concern.

14.3.4 Design related factors that do not contribute to risk

Failure due to isostatic overpressure

The assessment of the scenario “Canister failure due to isostatic load”, presented in Section 12.7.6, concludes that a maximum swelling pressure of 10 MPa could occur in the buffer, the groundwater pressure is around 4.5 MPa at Forsmark for ice-free conditions and an additional ground water pressure of at most 36 MPa could occur as a result of a maximum glacial load supported by geological evidence. The sum of these loads is 50.5 MPa. However, considering that the combined impact of swelling pressure and hydrostatic load is somewhat smaller than this sum, this, as suggested in Section 12.7.6, results in a total pressure of around 47.3 MPa.

The assessment of canister strength concludes that local collapse is avoided with substantial margin for a load of 50 MPa and the margin to total collapse (90 MPa), i.e. the criterion for canister failure, is considerable. For the given reference design there is ample margin to prevent canister failure due to isostatic load, even for the most extreme load situations and there seems to be no need to change the design in order to increase this margin.

Dimensions and material properties of the deposition tunnel backfill

The backfill safety functions BF1, according to Figure 8-4, are to keep the buffer in place and to have sufficiently low hydraulic conductivity. These safety functions are achieved and maintained with the current backfill design.

It is concluded in Section 10.3.9 that the swelling pressure of the buffer and the associated safety functions will be maintained during the expansion of the buffer into the backfill for all possible combinations of buffer and backfill conditions. Furthermore, several likely pessimistic assumptions are made in this analysis including assuming the buffer to be completely water saturated and homogenised from the start, assuming weak mechanical contacts between the backfill blocks, not including the local crushing of the blocks that may occur close to the floor and assumed that the backfill blocks are not overlapping.

It is also important that the backfill maintains its swelling pressure, thereby avoiding e.g. the formation of a water conductive crown space immediately beneath the tunnel ceiling. As demonstrated by the last row of Table 14-3, such a crown space could alter the flow situation e.g. such that it affects canister failures due to corrosion negatively. The swelling pressure is indeed assessed to be maintained with the current design.

- According to Section 10.3.9, there will be a remaining density gradient in the backfill after saturation. The calculations were done for the reference backfill in SR-Site and cannot directly be adapted to the design and material in PSAR. The difference is however small and the conclusion about the sufficient backfill self-sealing ability is still valid.
- As seen in Section 10.3.9, erosion of backfill in a tunnel intersected by a highly conductive fracture is important for the properties of the buffer in the deposition hole, but is not expected to have any significant importance for the transport properties itself. There will be a local volume with low swelling pressure and high hydraulic conductivity. However, the main part of the tunnel volume will be unaffected.
- Since the temperature is low under all conditions, montmorillonite alteration, in the form of illitization can be neglected in the backfill. It is also assumed that the cement in the repository will be of the “low-pH” type and will have insignificant impact on the properties of the backfill (see the **Buffer, backfill and closure process report**, Section 4.4.7).
- In Sections 10.4.8 it is shown that future changes in temperature and groundwater chemistry will have limited or no effect on the hydromechanical properties of the backfill material.

For the case when backfill material is lost, a maximum loss of 220 tonnes in a deposition tunnel section can be allowed before advective conditions have to be considered in a deposition hole. As found in Section 10.3.11 none of the tunnel intersecting single fractures will cause erosion of the backfill to the extent that it loses so much swelling pressure that advective conditions must be assumed in underlying deposition holes. For a few positions where the tunnel is intersected by a very transmissive deformation zone, potentially more than 220 tonnes could be lost, but this is not relevant from the point of view of canister integrity. Such local loss of backfill by erosion does not mean that the hydraulic conductivity of the entire tunnel will be affected and these occurrences are not judged to impair safety.

In conclusion, while there possibly could be improvements in the backfill design from an installation point of view, there does not seem to be a need to change the design to further improve its safety functions.

Dimensions and material properties of the closure

There are no direct safety functions connected to the closure of the repository, but its impact has been assessed in the PSAR. The reference design presented in the **Underground openings construction report** and in the **Closure production report** conforms to these technical design requirements and the analyses in the PSAR show that a design following these rules would be appropriate. Furthermore, based on the findings from varying the transmissivity of the EDZ, discussed in Section 14.3.2 it is not obvious that these rules can be relaxed. However, it is likely that the direct impact on risk would only apply to the EDZ in the deposition tunnels, whereas a higher transmissivity probably could be accepted in the other tunnels. Such a situation has, however, not been analysed in the PSAR.

Repository depth

As explained in the **Underground openings construction report** and further discussed in Section 5.2.2, the repository depth has mainly been decided by considering the hydraulic conditions of the Forsmark site, i.e. frequency and occurrence of transmissive fractures and their dependence on depth, while the constructability is mainly related to rock mechanical issues, e.g. the likelihood and extent of spalling in deposition holes prior to emplacement. It is judged that remaining uncertainties in the geological description can be sufficiently resolved using methods and techniques that were implemented during the site investigations and would only require minor re-adjustments of the available areas. Uncertainties in the orientation of maximum horizontal stress can only be significantly reduced by in situ tests at depth during access construction. The finding may necessitate a re-orientation of the deposition tunnels, but would not affect the overall suitability of the designated depth and repository areas. The PSAR version of the **Underground openings construction report** discusses how the currently selected reference depth will be potentially adjusted and verified during the course of repository construction and associated detailed investigations. The post closure safety implications of repository depth reported below are essentially the same as those listed in SR-Site, but updated with new findings on erosion depths. In addition, since the SR-Site assessment, it has been further demonstrated that the contribution to canister corrosion by natural and anthropogenic earth currents is expected to be negligible for both the selected repository depth and for a depth of 700 m (SKB 2012).

Chemical stability – Salinity, redox and sulphide

Factors relating to the chemical stability safety function R1 “Provide chemically favourable conditions” are generally favourable at the selected depth. The only remaining chemical stability issues of concern for repository safety relate to the potential for a few deposition holes to experience groundwater with too low ionic strength and presence of sulphide. The other R1 safety function indicator criteria regarding favourable chemically favourable conditions are upheld for the entire assessment period.

As already concluded in Section 14.3.2, the ionic strength of the groundwater; $\Sigma q[M^{q+}]$, will fall below 4 mM charge equivalent i.e. violating safety indicator criterion R1c, for some deposition holes during some time of the glacial cycle. This may, in turn, lead to loss of buffer in a few deposition holes and that a few (between 0 and 2) canisters would fail due to corrosion by the end of the 10^6 year assessment period. As already discussed this latter problem could probably be further mitigated by applying more strict inflow rejection criteria when selecting deposition holes. Generally, the risk of penetration of dilute waters would also decrease with increased repository depth. However, the few occurrences of such potential penetration are related to the scarce occurrence of highly transmissive migration paths in the generally very tight rock. There is no evidence that a practically realistic increase of the depth (i.e. in the order of a 100 m) would dramatically reduce the occurrence of such isolated paths – and it seems a better strategy to try to avoid them locally.

The sulphide contents of groundwaters at Forsmark have been examined in Tullborg et al. (2010). The data show that there is no indication that sulphide concentrations should be correlated with depth. No dependence has been found between the sulphide concentrations and the transmissivity of the fractures where the groundwaters were sampled. Other parameters that could be involved in the process of bacterial sulphate reduction are concentrations of dissolved organic carbon (DOC), methane and hydrogen. Organic carbon concentrations are higher in the upper 100 m of the rock, but at depth the values are low, less than 2×10^{-4} mol/L, and no depth trend can be discerned. The data on methane and hydrogen are scarce and show no depth dependency either. The conclusion is therefore that a change in the repository depth would not affect the number of failed canisters due to corrosion by sulphide.

Lengths and transport resistances of hydraulic travel paths to and from the repository

Safety function R2a “Transport resistance in fractures, F” is affected by repository depth. The length of the travel paths of solutes in the groundwater will increase with increasing depth, but the resulting impact on the transport resistance would only be marginal, i.e. increasing depth by 100 m would only imply an increase in path length by about 25 %. More importantly, the transport resistances offered by these paths would increase with depth if the hydraulic conductivity decreases with depth at the site, see further below.

Fracture frequency and fracture transmissivity

Both safety functions R2a “Transport resistance in fractures, F” and R2b “Equivalent flow rate in buffer/rock interface, Q_{eq} ” are affected by repository depth, since fracture frequency and fracture transmissivity show depth dependence. However, the selected repository depth is well below the depth at about 400 m where the already low frequency of water conducting fractures drops dramatically. Nothing in the data suggests that this extremely low frequency would drop further at realistically reachable greater depths. In summary, the chosen repository depth below 450 m is sufficient to reach the low fracture frequency and low permeability volumes of Forsmark, and there does not seem to be any advantage in going deeper.

Groundwater pressure

Groundwater pressure, safety function R3a, contributing to the isostatic load on the canister, increases with depth. However, compared with the buffer swelling pressure and hydrostatic pressures from a glacial overburden, the increased pressures are of marginal importance. An increased pressure will also increase the inflow to the repository during construction, unless this is counteracted by grouting – this is however mainly an issue for repository engineering. Furthermore, there will only be limited needs for grouting at depth in Forsmark, since the frequency of water conducting fractures and deformations zones is very low.

Rock stress

Rock stress indirectly affects safety function R2b “Equivalent flow rate in buffer/rock interface, Q_{eq} ”, since the *in situ* stress determines the potential for spalling. Stress in general increases with depth, but as concluded in the **Underground openings construction report** (and its underlying references), below 300 m depth, there appears to be little evidence that the horizontal stress magnitudes in fracture domain FFM01 increase significantly with depth. Hence placing the repository at 400 m or 500 m depth does not significantly increase the risk for spalling in the deposition holes.

Initial temperature

The *in situ* temperature, relates to safety function R4 “Provide favourable thermal conditions”. Temperature increases with depth, although the thermal gradient is relatively low in the considered depth range. This needs to be considered in the repository layout, when determining the necessary canister spacing that would ensure that the peak buffer temperature lies below stipulated limits, and this means that the canister spacing needs to increase with depth, leading to a larger footprint for a deeper location. However, given that this is considered in the repository design, there are no other detrimental effects of the elevated *in situ* temperature with depth.

Freezing

A colder future climate may lead to freezing and relates to safety function R4 “Provide favourable thermal conditions, of the buffer and the deposition tunnel backfill”. Such freezing could in turn have detrimental effects on the canister and the near-field rock. The likelihood of freezing decreases with increasing depth. The analyses in the PSAR have, however, demonstrated that buffer freezing with detrimental effects can be considered as a residual scenario, i.e. no reasonable way that this could occur has been identified for a depth of 450 m at Forsmark. For an eroded buffer, the freezing point is higher than for an intact buffer. At the current depth it is unlikely but cannot be fully ruled out. The effects are, however, not assessed to threaten the integrity of the canister. As demonstrated in Section 12.3 detrimental freezing of the deposition tunnel backfill at these depths can also be ruled out.

Surface erosion

Surface erosion of the host rock will occur, in particular by glacial erosion. This means that the repository depth will decrease somewhat for each glacial phase. For glacial cycles corresponding to the reference glacial cycle, the extent has been estimated to 1.6–3.5 m per glacial cycle for the Forsmark site (see the **Climate report**, Sections 3.5 and 4.5), when considering the repository site located in bedrock without major valleys and deformation zones. Also, the total future bedrock denudation over a one million year time perspective has been estimated to be less than 50 m for the Forsmark site (see the **Climate report**, Section 3.5). Therefore, erosion does not have to be considered when determining repository depth within the reference interval 400–700 metres.

Inadvertent human intrusion

The probability of inadvertent human intrusion into the repository decreases with increasing depth. Intrusion may have consequences both for the intruders and for the long-term performance of the repository after the intrusion. Intrusion scenarios are evaluated separately from other scenarios in the safety assessment, in accordance with Swedish regulations. Therefore, it is not straight-forward to assign this factor an importance measure in a sense comparable to the other factors discussed here. In general, intrusion to several hundred metres is considered unlikely in resource poor rock.

Other layout issues

In SR-Site and the PSAR a specific repository layout adapted to the Forsmark site and fulfilling the technical design requirements stated for layout adaptation has been assessed. The analyses show that for the scenarios contributing to risk (corrosion and shear failure) it is essentially the details of the layout, like the exact position of deposition holes and what deposition holes would be accepted that is important. These details can only be finalised during repository construction and operation and by application of the observational method using findings from the underground based detailed investigations and applying the technical design requirements for accepting deposition holes discussed in previous sections. Thus, the question whether the repository layout is BAT can at this stage only be assessed based on these technical design requirements. More specific feedback on these premises is given in Section 15.5.

14.4 Verification that FEPs omitted in earlier parts of the assessment are negligible in light of the completed scenario and risk analysis

14.4.1 Introduction

FEPs are omitted at various stages in the assessment. In establishing the SR-Can FEP catalogue, and the update of this to the SR-Site FEP catalogue, audits of FEPs in the NEA FEP databases were carried out (see Chapter 3). The first step in this process was to screen out Project FEPs in the NEA FEP database assessed as not relevant for SR-Can, SR-Site and the PSAR using some pre-defined screening criteria (see the **FEP report**). A FEP could be screened out if one or more of the criteria listed below are fulfilled.

- The FEP is not appropriate to the actual waste, canister design, repository design, geological or geographical setting.
- The FEP is defined by a heading without any description of what is meant by the heading, but from the interpretation of the heading it is judged that the FEP is covered by other NEA Project FEPs.
- The FEP is very general and covered by other more specific NEA Project FEPs.

The outcome of this first screening of FEPs is documented in the SKB FEP database and is not further addressed here. It should be noted that the general strategy in the screening of FEP relevance was to judge FEPs as relevant rather than to screen them out at this stage, unless it is clearly obvious that they are irrelevant.

As described in Section 3.3 and in the **FEP report**, all NEA Project FEPs remaining after the initial relevance screening were mapped to FEPs in the SR-Can and SR-Site FEP catalogues. The result was used to create check lists for updating process descriptions and for the descriptions of the initial states of the repository system components. In addition, FEP lists from the audit were used as checklists for the selected handling of external factors as described in the SR-Site Climate report (SKB 2010g), the PSAR **Climate report**, the SR-Can FHA report (SKB 2006e) and the SR-Site **FHA report**, as well as for the establishment of SKB FEPs for further consideration in the selection of scenarios. In this process, additional NEA Project FEPs were omitted by the various experts involved and the reason for omitting each FEP was documented together with the handling of NEA Project FEPs assessed as relevant. A common justification provided for not considering a NEA Project FEP, or an aspect of it, is that it is not relevant for a KBS-3 repository in Swedish crystalline rock, i.e. corresponding to the first screening criterion listed above. This documentation is included in the SKB FEP database, linked to the SR-Can and SR-Site FEP catalogues, and also as appendices in the **FEP report**, and is not further addressed here.

Since the SR-Site FEP catalogue, which is an update of the SR-Can version, is the compilation of FEPs assessed as relevant for a KBS-3 repository located at Forsmark, the remainder of this section is devoted to verification of the legitimacy of omission of FEPs included in the SR-Site FEP catalogue. FEPs considered are processes relevant for the reference evolution, whereas methodology-FEPs are excluded (see Section 3.3).

In the following subsections, the process tables in Section 7.4 are revisited and the legitimacy of omission of all processes assigned as “not relevant” or “neglected” is verified in the light of the completed scenario and risk analysis. The verification of the omission of process FEPs is restricted to the system components of primary concern for repository safety, i.e. the fuel, the canister, the buffer, the backfill and the geosphere. Process FEPs for the remainder of the engineered barrier system are generally judged as of secondary importance for safety and are, therefore, not considered. In particular, the following considerations are identified as being of secondary importance.

- Disintegration of tunnel plugs will only have a local impact around the plug. As assessed in Section 10.3.12, there will be no effect on the backfill above the nearest deposition hole.
- The only function of the closure of the cavities in the central area is to occupy the space with no other technical design requirement than to prevent substantial convergence and subsidence of the surrounding rock. The only purposes of the backfill in the upper part of the ramp and shaft are to hinder unintentional intrusion into the repository and to keep the lower backfill in place. Both these areas are filled with crushed rock with an assumed high hydraulic conductivity.
- To ensure that they do not act as preferential transport paths, a number of investigation boreholes, holes drilled both from the surface and from underground openings have to be sealed, at the closure of the deep repository. As concluded in Section 10.3.6, the impact of improper sealing of the boreholes is very moderate. Furthermore, according to the assessment presented in Section 10.3.14, the reference design of the borehole seals will perform as intended.

Climate FEPs of importance to the safety of a geological repository are those affecting biosphere and geosphere conditions. Climate issues, corresponding to the climate FEPs in the SR-Site FEP catalogue, and their impact on geosphere conditions as well as their handling in the assessment are documented in Chapter 3 in the **Climate report**. All these issues are considered in the assessment as well as couplings between them. One exception is the impact of surface denudation on the estimated depth of permafrost and frozen conditions. However, as discussed in Section 6.1, surface denudation (erosion and weathering) of the host rock has been estimated to generally be limited to a few metres or less per glacial cycle for the Forsmark repository site and up to < 50 m for 1 million years. This is of minor importance for repository safety considering that the assessment of permafrost depth (see Sections 10.4.1 and 10.4.3) shows that detrimental freezing can be excluded at the repository level. In addition, an illustrative theoretical case with a 10 times larger denudation has been analysed in terms of freezing depths (**Climate report** Section 5.5). No further treatment of climate issues of relevance to geosphere conditions is made here.

Climate issues of relevance to biosphere conditions as well as biosphere processes are described and handled in the Biosphere process report (SKB 2010c) and Ecosystem reports (Andersson 2010, Aquilonius 2010, Löfgren 2010). These are not further addressed here, since the LDF's used in the assessment are bounding values over the full range of climatic conditions of relevance and high utilisation of discharge areas has been assumed. Therefore, most biosphere FEPs will tend to mitigate rather than augment assessed doses.

14.4.2 Fuel

According to Table 7-2, the following fuel processes are omitted from the assessment for parts or a whole glacial cycle:

- F3 Induced fission (criticality).
- F7 Structural evolution of the fuel matrix (failed canister).
- F9 Residual gas radiolysis/acid formation (intact canister).
- F10 Water radiolysis (except for fuel dissolution).
- F15 Helium production (intact canister).
- F16 Chemical alteration of fuel matrix (failed canister).

F3 Induced fission (criticality)

Acceptance criteria for encapsulation of fuel assemblies in canisters are defined to ensure that intact canisters are sub-critical (see Section 5.3.4). Furthermore, analyses of the potential for criticality in failed canisters as well as outside failed canisters indicate that this is highly unlikely (see Section 13.2.7). Therefore, omission of this process is considered justified as long as the acceptance criteria for fuel encapsulation are met.

F7 Structural evolution of the fuel matrix

Structural evolution of the fuel matrix due to radioactive decay, mainly alpha decay, could possibly affect the distribution of radionuclides in the fuel matrix. The main impact of this process would be on the segregation of fission products to the grain boundaries of the fuel matrix. However, reported results indicate that radiation-enhanced diffusion in the fuel matrix is too limited to have any effects in the time scale of interest in the safety assessment. Therefore, the judgement in the **Fuel and canister process report** is that this process is negligible for the fuel types and burnup relevant for the PSAR. There are no results of the complete scenario and risk analyses that challenge this neglect, although there are some uncertainties in the gap inventory for future BWR and PWR fuel with higher burnup than the fuel produced so far. However, the cautious handling of the instantly released fractions of the radionuclide inventory (Section 13.5.2) in the assessment calculations is judged to cover remaining uncertainties in this respect. No other coupling than to the instantly released fraction is identified as relevant for this process.

F9 Residual gas radiolysis/acid formation

There are restrictions on the maximum amount of water and air that the canister shall contain at sealing (Section 5.3.1). With these amounts of oxidants available, the depth of insert penetration by general corrosion is of the order of ten micrometres (see the **Fuel and canister process report**). In addition, the restrictions on water and air (nitrogen) content (more than 90 % argon in the canister is required) constrains the formation of corrosive gases, such as nitric and nitrous acids and ammonium, implying that stress corrosion cracking of the insert or the canister shell is not likely (see the **Fuel and canister process report** and further Section 14.4.3). It is also noted that this argument is further strengthened if the technical design requirement regarding initial argon content is updated, see further Section 15.5.5.

F10 Water radiolysis

Any water initially present in the canister, at most 600 g according to the technical design requirements, is expected to be consumed by nitric acid formation or cast iron corrosion (see above). Radiolysis of water intruding into a failed canister will lead to the formation of oxidants and hydrogen. The contribution to hydrogen formation is negligibly small compared with hydrogen formation due to corrosion of the cast iron insert and therefore neglected (see the **Fuel and canister process report**). The formation of oxidants by radiolysis of water is considered in determining the range of fuel dissolution rates explored in the assessment.

In the assessment calculations, it is assumed that the spent fuel is accessible to intruding groundwater once the copper shell has failed and no credit is taken for any transport resistances in the canister interior. These cautious assumptions thus implicitly cover effects of build-up of hydrogen gas that would mechanically impact the cast iron insert and the fuel assemblies and disregard any beneficial effects of build-up of hydrogen that could counteract ingress of groundwater. These assumptions also justify the omission of the small contribution from radiolysis of water to hydrogen formation.

F15 Helium production

Helium is produced in the spent fuel due to alpha decay of actinides. This could lead to a pressure build-up inside the fuel rods, which, in turn, could lead to mechanical rupture of the rods. Based on estimates of the amount of helium that can be generated and the assumption that all generated helium is released to the canister interior, the pressure increase in the canister interior has been calculated and found to be considerably lower than the pressure external to the canister. Based on these results, reported in the **Fuel and canister process report**, the consequence of helium production for the mechanical stability of the canister is neglected. There is nothing in the completed scenario- and risk assessment that questions this neglect, since the reference design conforms to the technical design requirements for the fuel and canister. Concerning the fuel rods, the assumption in the assessment calculations is that they all are ruptured and therefore provide no resistance to release or transport of radionuclides from the fuel once the canister has failed. Concerning the impact of helium build-up on the mechanical stability of the fuel matrix and thus the gap inventory, it is concluded in the **Fuel and canister process report** that there are no detrimental effects, but that there are remaining uncertainties on this point relating to future fuel with a potential higher burn-up level than produced so far. However, as stated above for FEP *F7 Structural evolution of the fuel*, the cautious handling of the instantly released fractions of the radionuclide inventory (Section 13.5.2) in the assessment calculations is judged to cover remaining uncertainties in this respect.

F16 Chemical alteration of the fuel matrix

Chemical alteration of the fuel matrix refers to the alteration of the uranium dioxide matrix through the formation of coffinite in contact with silica-rich groundwater in a failed canister. According to the **Fuel and canister process report**, this will most likely occur through a dissolution and re-precipitation process where radionuclides in the fuel matrix are released during dissolution of the uranium dioxide. Therefore, assuming that the dissolution rate of uranium dioxide is determining the release of matrix-bound radionuclides in the assessment calculations should be appropriate even if this process is disregarded.

14.4.3 Canister

According to Table 7-3, the following canister processes are omitted from the assessment for parts or a whole glacial cycle:

- C4 Deformation of copper canister from external pressure in the case of a failed canister.
- C5 Thermal expansion (both cast iron insert and copper canister).
- C7 Radiation effects.
- C9 Galvanic corrosion (failed canister).
- C10 Stress corrosion cracking of cast iron insert.
- C14 Deposition of salts on canister surface.

C4 Deformation of copper canister from external pressure (failed canister)

Deformation of a failed copper canister from external pressure, such as the groundwater pressure and the buffer swelling pressure, as well as the load from rock shear, is neglected in the assessment. The assessment results show that failure of a canister by corrosion requires that advective conditions prevail in the buffer, i.e. the buffer is eroded. Therefore, pessimistic assumptions are made in the calculations of dose impact from a corrosion failure, implying that no transport resistance in the failed canister is accounted for (Section 13.5). In the consequence analyses of canister failure due to shear load (Section 13.6), the same pessimistic assumption concerning the state of the failed canister is made, i.e. that the failure is massive and, therefore, no transport resistance in the canister is accounted for. The assumptions made in the consequence calculations thus cover the effects of any subsequent deformation of a failed canister by external impact.

C5 Thermal expansion (both cast iron insert and copper canister)

This process concern the effects of differences in thermal expansion of the copper canister and cast iron insert. During temperature decrease in the repository, the shrinking of the copper canister is larger than that of the iron insert, which causes tensile stresses in the copper. These effects are neglected based on calculations provided in the **Fuel and canister process report** showing that the change in tensile strain in the copper is negligible compared to the creep ductility of copper. This is valid for temperatures up to the maximum temperature expected in the canister materials given by the design criteria for maximum temperature in the buffer and the canister. Since these technical design requirements are conformed to in the reference design, and also verified in the thermal analyses, see Section 10.3.4, the neglect of these effects is considered justified.

C7 Radiation effects

This process refers to changes in material properties of the cast iron insert and copper canister due to neutron and gamma radiation from the fuel. In order to avoid irradiation-induced hardening and embrittlement of the cast iron insert, a technical design requirement is set on the upper limit on Cu content in the cast iron insert. Since this technical design requirement is considered to be conformed to in the reference design of the canister with its content of fuel, the omission of these effects is justified.

C9 Galvanic corrosion (failed canister)

This process refers to the galvanic corrosion of the cast iron insert when the copper canister has failed. In the **Fuel and canister process report**, it is concluded that this process does not need any specific treatment since the influence of galvanic corrosion under oxygen-free, reducing conditions lies within the margins of error for the corrosion rate of the iron insert. Furthermore, no credit is taken for the cast iron insert either as a corrosion barrier or as providing any resistance to the release of radionuclides from a failed canister in the scenario- and risk assessment. Consequently, the omission of a specific treatment of galvanic corrosion of the cast iron insert is considered justified.

C10 Stress corrosion cracking of the cast iron insert

Stress corrosion cracking of the cast iron insert requires a combination of static tensile stresses, a corrosive environment and a susceptibility of the material. In the **Fuel and canister process report**, stress corrosion cracking is considered as unlikely and even if it occurred it would have no consequences for stability of the insert. A corrosive environment can be established by the radiolysis of water and air in the canister. In order to prevent this, a technical design requirement is set on the maximum allowable water (600 g) and air (nitrogen) content in the canister (see Sections 14.4.2, process F9, and 5.3.1). Since this technical design requirement is considered to be conformed to in the reference design, the neglect of this process is considered justified. Related to the above, strain ageing is assessed in Section 3.4.2 of the **Fuel and canister process report** not to occur in the cast iron insert, based on the limited temperature in the repository. The analyses in the thermal evolution of the canisters in Section 10.3.4 confirm that the canister temperature is well below those where strain ageing could occur.

C14 Deposition of salts on canister surface

According to the **Fuel and canister process report**, Section 3.5.7, it is possible that salts in the bentonite will be redistributed, enriched and deposited on the canister surface. The salts that may be of concern are chlorides and sulphates from the groundwater and sulphates and carbonates from the impurities in the bentonite. Of these, the chlorides are most important since the presence of high chloride concentrations may have an effect on the corrosion properties of copper. Sulphate and carbonate deposits are not electrically conductive, so they are not expected to increase the risk of pitting corrosion. An increase in the chloride concentration would, however, lower the susceptibility of copper to pitting corrosion, since it would favour general corrosion (King et al. 2010).

Section 12.6 demonstrates that the groundwater pH is always expected to be slightly alkaline. The water reaching the canister will be influenced by the reactions with the bentonite, but the pH would not be below 6, even for a groundwater pH of 6 (see Section 10.3.10), and the chloride concentration would not be changed to any large extent. A high chloride concentration will, consequently, not lead to increased general corrosion, and the extent of the corrosion will be determined by the amount of available oxygen (and sulphide). The process can thus be neglected.

14.4.4 Buffer

According to Table 7-4, the following buffer processes are omitted from the assessment for parts or a whole glacial cycle:

- Bu1 Radiation attenuation/heat generation (intact canister).
- Bu3 Freezing (resaturation/thermal phase and intact canister).
- Bu6 Gas transport/dissolution (gas phase transport) (intact canister).
- Bu9 Liquefaction (intact canister).
- Bu17 Iron-bentonite interactions (resaturation/thermal phase and intact canister).
- Bu19 Radiation-induced transformations (intact canister).
- Bu20 Radiolysis of porewater (intact canister).
- Bu21 Microbial processes (unsaturated conditions and intact canister).

In addition, processes related to radionuclide transport, e.g. diffusion, sorption, speciation and colloid transport are neglected for the excavation/operational period based on the assumption that no canister failure occurs over this period. This is confirmed by the analyses of the reference evolution for the excavation/operational phase as summarised in Section 10.2.7.

Bu1 Radiation attenuation/heat generation (intact canister)

Radiation attenuation and the resulting heat generation in the buffer is neglected in the **Buffer, backfill and closure process report** since quantifications have shown that the dose rate from an intact canister is too low to be of importance for the properties of the buffer (see processes Bu19 and Bu20 below). This is at least true if the dose rate is below 1 Gy/h, which is the limit stated as a technical design requirement, see Section 5.4.1. Furthermore, the highest obtained radiation dose rate stated in SKB (2010g) is 0.18 Gy/h. Therefore, the neglect of this process is considered justified.

Bu3 Freezing (resaturation/thermal phase and intact canister)

Detrimental effects of buffer freezing is ruled out during the resaturation and thermal phase since this requires a temperature of -6 °C at repository depth, which does not occur during this phase of repository evolution (or any later phase).

Bu6 Gas transport/ dissolution (intact canister)

As described in the **Buffer, backfill and closure process report**, any gas present in the buffer surrounding an intact canister is expected to be dissolved in the buffer porewater. Air that is trapped in the buffer during resaturation of the buffer is considered in THM-modelling of the resaturation phase. As long as the copper canister is intact, there are no processes occurring in the canister or buffer that are expected to produce gases in such amounts that the solubility of the gas in the buffer porewater is exceeded. Radiolysis of porewater in the buffer can produce hydrogen and oxygen, but the radiation level outside the canister is too low for this process to produce significant amounts (see Bu20 below). Furthermore, oxidants are expected to be consumed by copper corrosion. Microbial processes may also lead to formation of gaseous species, but as long as the high swelling pressure in the buffer is maintained, microbial activity in the buffer is expected to be low.

Bu9 Liquefaction

A process that could affect the canister significantly is liquefaction of the buffer. According to the **Buffer, backfill and closure process report**, liquefaction is a process implying that a stiff material (e.g. soil) turns into liquid due to an effect with short duration (see e.g. Lambe and Whitman 1969). It may take place in a loose sand when the porewater pressure is increased either due to a vibration that makes the sand particles float in the porewater (since they tend to go into a higher degree of compaction, but the water temporarily prevents this) or due to a strong upward water flow that releases the effective stresses between the particles (quicksand). It may also take place in clay that has been settled in salty water (forming an open structure with a high water ratio). If the salt is partly washed out by fresh water, the clay structure cannot hold the high amount of water at moulding or when subject to vibrations, meaning that the structure collapses when exposed to vibrations.

These two types of liquefaction cannot take place in a bentonite with high density, since the effective stress that holds the clay together is high due to the swelling pressure. This conclusion was also made by Pusch (2000b). However, a similar phenomenon has been observed during compaction of bentonite blocks at very high water ratios. If the bentonite is compacted at a very high stress to a state where the bentonite is completely water saturated, all further increases in stress will be taken up by the water and the bentonite will behave like a liquid. This phenomenon has been observed during uniaxial compaction when liquid bentonite has squirted from the mould.

The process requires a very strong impact of pressure and is rather unlikely to occur in a deposition hole. It can probably only result from an earthquake and requires a reduction in the volume of the deposition hole due to an increase in rock stress. A combination of factors may lead to an increase in rock stress of about 15 MPa (Bäckblom et al. 2004). Estimation according to Kirsch (Brady and Brown 1994) of the convergence of a deposition hole at such an increase in rock stress yields a convergence of the hole of about 1 mm. This is not sufficient for liquefaction to occur.

Neither earthquakes nor high hydrostatic pressure during a glacial event are expected to lead to a loss in effective stress in the buffer sufficient for liquefaction (see also Section 10.4.8).

Bu17 Iron-bentonite interaction

Reactions between metallic iron and montmorillonite in the buffer may lead to breakdown of the montmorillonite structure. As long as the copper canister is not breached, the iron insert will not be in contact with the bentonite buffer. Furthermore, the installation procedure of the buffer requires that the deposition hole is cleaned prior to the emplacement of bentonite blocks and pellets (see the **Buffer production report**, Section 5.4.3). Therefore, omitting this process for intact copper canisters is considered justified.

The scenario- and risk analysis shows that corrosion failure of the copper canister requires that advective conditions in the buffer have been established. In this case, the subsequent contact between the iron insert and the buffer is no longer significant, since the diffusion barrier is already lost. If canister failure occurs due to shear movements in a fracture intersecting the deposition hole, the buffer surrounding the canister will still be a diffusion barrier at the time of the shear failure. However, the analysis of a combination of the shear load and corrosion scenarios (Section 13.6) shows that both the retardation in the buffer and the limited solubility of the dose determining Ra-226, which requires an intact buffer,

are of limited importance for the result. A loss of the buffer as a diffusion barrier subsequent to a shear failure of the canister is therefore not of significance for the dose impact, and the omission of a specific analysis of the consequences of iron-bentonite interaction is considered justified.

Bu19 Radiation-induced transformations

This process refers to the direct breakdown of montmorillonite in the buffer by radiation from the spent fuel in the canister. The process is neglected in the **Buffer, backfill and closure process report** for intact canisters based on experimental results that show no effect for absorbed dose rates from γ -radiation well above 1 Gy/h. Consequently, as long as the copper canister is intact, the design requirement of 1 Gy/h on the canister surface will ensure that the dose rate outside the canister is too low to have any effect on the buffer properties.

If a canister fails, radionuclides that are released from the canister and sorbed in the buffer may expose the montmorillonite in the buffer to α -radiation. Based on results from radionuclide calculations for the safety assessment SR 97 (SKB 1999a) on the concentration of α -emitters in the buffer and the total dose they would give during one million years in case of an early canister failure, it is concluded in the **Buffer, backfill and closure process report** that the consequences can be neglected. Considering that these results are for an early failure of the canister, which is not expected to occur, and that there is a large margin to absorbed dose rates where impact on buffer occurs, these results justify the omission of this process. Furthermore, corrosion failure in the PSAR implies that advective conditions are established in the buffer prior to failure and that no credit is taken for retardation in the buffer in the assessment calculations. Therefore any consequences of radiation-induced changes of buffer properties after corrosion failure of the canister are of no concern. This is also the case for canister failure due to shear movements in a fracture intersecting the deposition hole for the same reasons as given above for the potential consequences of iron-bentonite interactions (see Bu17).

Bu20 Radiolysis of porewater

Radiolysis of porewater in the buffer by γ -radiation penetrating the canister leads to the formation of oxidants and hydrogen. This process is of primary concern for the corrosion of the copper canister and is neglected in the **Buffer, backfill and closure process report** as well as in the **Fuel and canister process report** based on an estimate of the maximum possible amounts of oxidised copper that can be produced before the γ dose rate has substantially declined and on available experimental information that shows no evidence for enhanced corrosion rates caused by γ -radiation (see Section 10.3.13).

Bu21 Microbial processes (unsaturated conditions)

Microbial processes are neglected during the initial period of unsaturated conditions in the buffer. The reason for this is that the extent of aqueous reactions during this period is limited (see the **Buffer, backfill and closure process report**). This is further substantiated in Section 10.3.10 subsection “*Unsaturated phase and period of elevated temperatures*” and Section 10.3.13, subsection “*Corrosion during not fully saturated conditions*”.

14.4.5 Backfill

According to Table 7-5, the following backfill processes are omitted from the assessment for parts or a whole glacial cycle:

- BfT2 Freezing (resaturation/thermal period, intact canister).
- BfT5 Gas transport/dissolution (long-term for intact canister, failed canister).
- BfT8 Liquefaction.
- BfT10 Diffusive transport of species (early stage, intact canister).
- BfT11 Sorption (including ion-exchange) (early stage, intact canister).
- BfT13 Aqueous speciation and reactions (early stage, intact canister).
- BfT17 Radiation-induced transformations.

In addition, processes related to radionuclide transport, e.g. diffusion, sorption, speciation and colloid transport are neglected for the excavation/operational period based on the assumption that no canister failure occurs at this period. This is confirmed by the analyses of the reference evolution for the excavation/operational phase as summarised in Section 10.2.7.

BfT2 Freezing (resaturation/thermal period, intact canister)

Freezing of the backfill in deposition tunnels is ruled out during the resaturation and thermal phase. Freezing will only have an impact on the repository if the stress from the backfill exceeds the crack propagation stress of the rock. This requires a temperature of lower than $-6\text{ }^{\circ}\text{C}$ at repository depth, which does not occur during this phase of repository evolution.

BfT5 Gas transport/ dissolution (long-term for intact canister, failed canister)

Corrosion of the cast iron insert in a failed canister would lead to the formation of hydrogen gas. This gas could potentially escape through the backfill in the deposition tunnel above the failed canister as could radionuclides in the gaseous phase released from the canister. This transport route for gas is neglected in the assessment because the impact on the saturation conditions in the backfill is assessed as small (see the **Buffer, backfill and closure process report**, Section 4.2.3). Furthermore, an instant transfer of the radionuclides in the gas phase to the biosphere after gas breakthrough through the bentonite is assumed. Neither the buffer nor the geosphere is expected to significantly delay the transport to the biosphere. Also, it is not certain that gas generated by corrosion of the iron insert will reach the tunnel. An alternative escape route is through fractures in the rock intersecting the deposition hole. This is related to FEP Ge4 and is further discussed in Section 14.4.6.

BfT8 Liquefaction

Liquefaction in the backfill is discarded using the same arguments as for the buffer, see Section 14.4.4, subheading “Bu9 Liquefaction”.

BfT10 Diffusive transport of species (early stage, intact canister)

Diffusion is suggested to be neglected in the **Buffer, backfill and closure process report** for the period before saturation of the backfill since advection is the dominating process during resaturation. However, the process is considered in the coupled hydrogeochemical analyses reported by Sena et al. (2010b).

BfT11 Sorption (including ion-exchange) (early stage, intact canister)

The argument in the **Buffer, backfill and closure process report** for neglecting sorption before saturation is that there are no continuous water paths available prior to water saturation of the backfill. However, the process is considered in the coupled hydrogeochemical analyses reported by Sena et al. (2010b).

BfT13 Aqueous speciation and reactions (early stage, intact canister)

Aqueous speciation and reactions are suggested to be neglected for the period prior to saturation since the geochemical processes are expected to be the same before and after saturation, see the **Buffer, backfill and closure process report**. However, consumption of oxygen by reactions with minerals in the backfill is addressed by Sena et al. (2010b) as discussed in Section 10.2.5 also for the resaturation phase.

BfT17 Radiation-induced transformations

Radiation-induced transformations of the backfill are neglected in the **Buffer, backfill and closure process report** since the dose rate in the backfill is too low to have any effect. Since the dose rate in the buffer is too low to have any effect because the technical design requirement on the maximum dose rate on the canister surface is conformed to (Section 14.4.4, FEP Bu19), it is considered verified also that the dose rate in the backfill, which is more shielded than the buffer, is too low to have any effect.

14.4.6 Geosphere

According to Table 7-6, the following geosphere processes are omitted from the assessment for parts or a whole glacial cycle:

- Ge1 Heat transport (excavation/operational period).
- Ge4 Gas flow/dissolution.
- Ge6 Reactivation – displacement along existing discontinuities (excavation/operational period).
- Ge8 Creep.
- Ge10 Erosion/sedimentation in fractures.
- Ge14 Reactions groundwater/rock matrix (excavation/operational period, temperate- and periglacial climate domains).
- Ge18 Colloid processes.
- Ge20 Methane hydrate formation.
- Ge22 Radiation effects (rock and grout).
- Ge23 Earth currents.

In addition, processes related to radionuclide transport, e.g. diffusion, sorption and speciation, are neglected for the excavation/operational period based on the assumption that no canister failure occurs during this period. This is confirmed by the analyses of the reference evolution for the excavation/operational phase as summarised in Section 10.2.7.

Ge1 Heat transport (excavation/operational period)

According to the **Geosphere process report**, Section 2.17, it is concluded that the thermal dimensioning of the repository neglects heat transport in the rock for the excavation/operational period in the sense that all canisters are assumed to be deposited simultaneously. This is based on calculations that show that the peak temperature in the buffer, which is the safety relevant issue (safety function indicator Buff4), is underestimated by less than 0.2 °C if simultaneous canister deposition is assumed, compared to a case where canisters are deposited in an orderly fashion (i.e. panel by panel) at a rate of 2 or 4 days per canister (Section 10.2.1 and Hökmark et al. 2009). However, as discussed in Section 10.2.1 there are deposition sequences for which this simplification does not apply, but these could be avoided by proper management of the disposal sequence. Therefore, it is judged that the legitimacy of omission of the disposal sequence in the evaluation of heat transport and the buffer peak temperature is verified.

Since the treatment of heat transport for the excavation/operational period is a simplification of the deposition sequence rather than an omission of the process, all relevant couplings to other processes are considered.

Ge4 Gas flow/dissolution

According to the **Geosphere process report**, an unsaturated region may be induced in the vicinity of the tunnels and an unsaturated zone above the repository during repository pre-closure operations, but that these unsaturated zones only have a marginal effect on inflows to the tunnels. Therefore, details of gas flow and dissolution during the excavation and operational period are neglected and the effect of gas flow is taken into account in a simplified manner in the calculations of the resaturation of the tunnels after repository closure.

Concerning repository generated gas, the main source is hydrogen produced by anaerobic corrosion of the cast iron insert in a failed canister. Calculations conducted for SR-Can (Hartley et al. 2006) showed that gas generated in the repository and released through the buffer can rapidly escape through the geosphere without causing a pressure build-up. Based on this result and the small change in bedrock properties between the hydrogeological models in SR-Can and SR-Site, the impact on geosphere performance is neglected in the **Geosphere process report**. Substantial localised gas generation in the repository implies that a canister has failed so that corrosion of the iron insert can occur. The assess-

ment shows that failure by corrosion requires advective conditions in the buffer which in turn implies that the deposition hole is intersected by a highly transmissive fracture. Since there is no buffer to contain the gas, hydrogen formed will dissolve and be carried away by water flowing in the intersecting fracture. This supports the neglect of impact of gas flow in case of corrosion failure of a canister.

In the case of canister failure by shear movement, the buffer is still acting as a barrier and gas pressure build-up inside the buffer will have to occur before gas is released to the geosphere. In the assessment, this scenario with build-up of gas pressure inside the buffer is addressed to analyse the dose consequences of the release of radionuclides in the gas phase (see Section 13.8). Since it cannot be excluded that the fracture causing the shear failure of the canister is transmissive or becomes transmissive after the shear movement, no credit is taken for any radionuclide retention in the geosphere in the analysis of the dose consequences in the shear failure scenario (Section 13.6) or in the scenario for release of radionuclides in the gas phase (13.8). Any potential impact of build-up of gas pressure or gas flow in the geosphere on the dose impact is then implicitly covered in the analyses and there is no need for a specific treatment of this process.

Ge6 Reactivation – displacement along existing discontinuities (excavation period)

Construction-induced seismicity is neglected based on an assessment in the **Geosphere process report**. It is concluded that in order for a fault slip larger than 0.05 m to be triggered by the excavation activities, an induced earthquake of approximately magnitude 5 is required. To host such an earthquake, the structure must have a rupture area exceeding a square kilometre. It is unlikely that such a structure would remain undetected after tunnel mapping, which makes it possible to avoid the structure during deposition. In addition, there is no evidence that present-day deviatoric stresses in Swedish bedrock at repository depth are sufficient to power seismic events of magnitude 5. Furthermore, the largest seismic events recorded in very deep mines in South Africa, for instance, where stresses are high and where the rate of excavation is much higher than it will be in the deep repository, are less than magnitude 5. In the light of the completed scenario- and risk assessment, there is no reason for modification of this conclusion.

Ge8 Creep

Creep along fractures and in intact rock is neglected in the **Geosphere process report** and is also discussed in Section 10.3.5. For the Forsmark fractures, creep displacements are likely to be insignificant compared to displacements caused by the direct changes in load and pore pressure projected for the different phases of the assessment period. Concerning creep in intact rock, it is concluded in the **Geosphere process report** that this requires stresses that will be found only in small volumes of the rock around the walls of the openings. These effects are accounted for in the assessment of thermally-induced spalling. Therefore, the neglect of this process is considered justified.

These conclusions are further justified by the assessment presented in Section 10.3.5. A study by Damjanac and Fairhurst (2010) assessing whether there is a lower bound to the long-term strength of rocks demonstrates that there is always a stress threshold for confined conditions, because confinement acts to suppress the tension stresses associated with crack growth. If spalling is encountered and a notch forms, the stress adjustments that can occur at the notch tip may cause additional time-dependent/creep deformations. The monitoring of the unconfined open notch in the APSE Experiment showed that the majority of the new displacements occurred in the existing notch (Andersson 2007). When the spalled notch is confined, any time-dependent deformations are expected to be insignificant, compared to the deformations that formed the notch. It can also be noted that the effects of fracture creep, in terms of fracture displacement under constant shear load because of time-dependent material strength properties, can be estimated using the modelling approach for fracture reactivation described in Hökmark et al. (2010). Even if the strength is reduced to zero over the entire fracture plane, only very minor fracture displacements would occur. Creep deformation and related issues like “sub-critical crack growth” are, therefore, not further considered in the PSAR.

Ge10 Erosion/sedimentation in fractures

Erosion and sedimentation in fractures is neglected for the excavation/operational phase because high-transmissive fractures in the repository rock will be grouted and the flow rates in non-grouted fractures are expected to be too low to cause significant erosion. After closure of the repository, the hydraulic gradients during the temperate period will be so low that the potential for erosion is negligible. During glacial advance and retreat, the hydraulic gradient will dramatically increase, but the shear stresses will still be low.

As noted in Section 10.4.8, Birgersson et al. (2009) found that the shear strength of MX-80 at a water ratio of 100 ($\phi = 0.0037$) for sodium concentration of 10 and 100 mM is larger than 5 Pa. The hydro-geological modelling of the “expanding ice front” case in the PSAR shows that the calculated shear stresses are always below 5 Pa and much lower most of the time. It can thus be concluded that the loss of bentonite from shearing of particles can be neglected for all reasonable conditions.

As mentioned in Section 10.4.8, effects on groundwater flow of potential clogging of fractures by bentonite particles eroded/sedimented for low groundwater charge concentrations are pessimistically disregarded.

Ge14 Reactions groundwater/rock matrix

Chemical reactions between groundwater and rock matrix minerals are neglected in the **Geosphere process report** since they are judged not to cause appreciable changes in groundwater composition or matrix porosity for the whole time period during which the function of the repository must be considered. The primary effects are expected to be caused by reactions between groundwater and fracture-filling minerals. This standpoint is based on observations of drill cores from the repository volume at Forsmark which show very little alteration of the rock matrix surrounding fractures (see also Section 4.4.4). These observations justify the neglect of reactions between groundwater and the rock matrix in comparison with reactions between groundwater and fracture filling minerals.

Ge18 Colloid processes

In the **Geosphere process report**, the impact of colloids on the geochemical conditions of the geosphere is judged as negligible. However, colloids may act as carriers for radionuclides. It is further noted that the current salinities of the groundwater at Forsmark are higher than that required to keep the concentration of colloids suspended in groundwaters to a low level. During the excavation and operational phases, substantial amounts of colloids may be formed, but the colloid concentrations will quickly resume the natural values under the saline water conditions that will be re-established (see also Section 10.2.5). Since the assessment shows that no canister failures occur during this period, the neglect of colloid processes for the excavation and operational period is considered justified.

Ge20 Methane hydrate formation

The potential for formation of methane hydrate during periglacial conditions at Forsmark is neglected in the **Geosphere process report**, Section 5.11, based on a modelling simulation. The conclusion from that study is that methane hydrate formation is unlikely at the methane concentrations and water salinities reported for Forsmark. This conclusion is also brought forward in Section 10.4.7, where estimates of maximum fluxes and production of methane are used to support this conclusion. Hence, the neglect of this process is considered justified.

Ge22 Radiation effects (rock and grout)

Radiation effects on ground supporting material are ruled out in the **Geosphere process report** based on findings from the Yucca Mountain project. According to the **Geosphere process report**, Section 5.13.4 no degradation of the mechanical properties of cement have been observed for a fast neutron fluence as high as 8.2×10^{19} n/cm², i.e. no change in dimension, weight, compressive strength, bending strength, or Young's Modulus of cement paste due to irradiation alone. This neutron fluence can be compared with e.g. the flux for a PWR element with a burn-up of 42.2 MWd/kgU after 34.1 years given in Section 5.3.4 as 1.2×10^8 /s. Assuming all this flux to be concentrated on

one cm², without considering radioactive decay and the moderation due to the water in the bentonite and the rock it would take in the order of 10¹¹ seconds, i.e. some thousands of years to reach these high fluence levels. In reality the neutron flux will be dispersed, decrease due to radioactive decay and it will also be absorbed, which implies that the omission of the process is clearly justified.

Ge23 Earth currents

The impact of earth currents, both natural and anthropogenically induced, are neglected in the **Geosphere process report** since expected electrical potential fields are too small to affect groundwater flow or solute transport. There are a number of reasons behind this conclusion. The main ones are that the fields usually are weak or become weak at repository level for geometrical reasons and that most of the fields are alternating and the effects, therefore, are reversible. There is nothing in the light of the completed scenario- and risk analysis that questions the neglect of this impact of earth currents. For corrosion issues see Section 14.2.1 and 14.3.4, sub heading “**Repository depth**”.

14.5 A brief account of the time period beyond one million years

For the time beyond one million years, no risk calculation is required. SSM’s General Recommendations related to SSMFS 2008:21 suggest that an account of the evolution of radiotoxicity may be the only meaningful way of illustrating the further development of the repository. Such an account is given in Figure 2-1 in Section 2.4. It is obvious from the figure that the radiotoxicity of the spent nuclear fuel decreases somewhat between 10⁶ and 10⁷ years. The radiotoxicity then stays constant for very long times beyond 10⁷ years. The following is a brief, qualitative discussion of the development of the site for the time period beyond one million years, based essentially on general tectonic considerations and indications from natural analogues.

Tectonics and bedrock surface denudation

Although geological processes are generally slow, the evolution of the site over a period larger than the one million year time frame is difficult to predict. The analysis in, for example, Section 10.4.5 regarding earthquakes cannot readily be extended to larger timeframes without taking into account additional effects that are beyond the scope of the PSAR. For instance, although it can be assumed that the Fennoscandian shield will remain a tectonically stable craton with most of its deformation localised at its margins, it cannot be assumed that pattern and properties of the deformation zones and fractures within the site will remain sufficiently constant over this time frame for enabling an earthquake hazard assessment.

The major part of the site is expected to experience a bedrock surface denudation of around a few m up to ~30 m in 10⁶ years, whereas parts of the site may experience a larger denudation of up to ~50 m in 10⁶ years (cf Section 6.1). Most of this denudation constitute glacial erosion. This means that in around 10 to 100 Ma, it cannot be fully excluded that parts of the site have experienced a bedrock lowering equal to the initial repository depth. In the multi-million year time perspective, the site is also expected to occasionally be loaded by sediment originating from the denudation of elevated terrain elsewhere, imposing mechanical effects that counteract, and delays, parts of the erosional effects of repeated glaciations.

On the other hand, the rocks, the ductile deformation and the brittle deformation zones at Forsmark all formed at least one billion years ago, and have experienced numerous past episodes of burial, both by sediments and glaciations. The effects of such events have been extensively studied during site investigations and it appears as if the pattern of localised strains, manifested as deformation zones of various orientations, has remained fairly constant for much longer than 10 million years. It is reasonable, therefore, to assume that essentially the same deformation zones will act as planes of weakness, thereby enabling release of accumulated stress in a manner similar to the past 10 million years or so. It is also reasonable to assume that the fracture intensity will increase, but reach an unknown level of intensity saturation beyond which jostling (reactivation) of the blocks within the brittle upper crust will largely dominate over fragmentation (creation of new fractures). Due to the power law nature of fracture sizes, fractures able to host slip exceeding 5 cm will still be rare even if both the intensity and the mean fracture size are increased.

Qualitative discussion of canister failures and releases

The above means that the probability of intersection of a fracture able to host slip exceeding 5 cm with an individual deposition hole will remain low even in the time beyond one million years from now, indicating that the extent of canister failures due to shear load would be limited also in a ten million year perspective.

Likewise, if geochemical and flow conditions were, when averaged over very long time periods, similar to those today, the extent of canister failures due to corrosion would be limited to a few failed canisters, compared to, e.g. on average 0.12 at one million years for the central corrosion variant (Section 12.6.2).

It is also noted that radioactive decay plays a minor role for the development of release curves beyond one million years since the dose dominating nuclides, in particular the mother nuclides of Ra-226, are very long-lived. Related to this, the scientific understanding of the fuel dissolution process suggests that the longevity of the spent fuel matrix is several million years in the repository environment (see Section 13.5.5).

Finally, the hypothetical case in Section 13.7.4, where all canisters are failed, where the buffer is absent and where retention in the rock is disregarded, yields releases that correspond to dose consequences that are comparable to the natural background radiation after one million years. The releases are in that case controlled by the groundwater flow at repository depth and the inventory of radionuclides, the latter of which decreases with time.

Indications from natural analogues

In the time beyond one million years from now, the radiotoxicity of the spent nuclear fuel in the repository will be comparable to a concentrated uranium deposit, as indicated in Figure 2-1, Section 2.4. The performance of the engineered barriers after one million years becomes increasingly uncertain. The further discussion regarding the evolution of the repository during the time beyond the one million years may, however, draw on existing knowledge of natural uranium ores and the behaviour of uranium in a geological environment.

One undisputable fact that emerges from geological observation is the existence of uranium ores that are many millions and even billions of years old. Studies of, for example, Cigar Lake in Canada, reveal a uranium ore body found today at a depth of 450 m, which has persisted for 1 300 million years (e.g. Ruiz López et al. 2004, Miller et al. 2000). There are today no geochemical indications of the Cigar Lake uranium ore body on the surface, indicating the possibility for a reducing, uranium rich environment with low hydraulic permeability to retain a majority of the elements associated with the ore for a time period well in excess of one million years.

Pockets of rich uranium ore at Oklo (Gabon) reached critical mass nearly two billion years ago. The natural spent fuel which was formed during this criticality has, to a large extent, been retained in the deposit for the almost two billion years that followed (Gauthier-Lafaye et al. 1996). This can be explained partly by the low mobility of uranium in a reducing environment, and partly by the relatively stable geology of the area. This does not mean that there has been a complete lack of tectonic events; one example is an episode of regional extension, ca 860 million years ago, which caused the intrusion of mafic magma in the sedimentary basin which hosts the uranium. The magma cooled and solidified and is now found as a network of dolerite dykes in the area. One of these dykes, ca 20 m wide, is found cutting across the Oklo deposit. The intrusion and regional extension caused elevated heat and circulation of hydrothermal fluids that have affected the Oklo deposit. In spite of this event, and the solid-fluid interactions that were associated with it, the uraninite in the natural fossil fission reactors is remarkably well preserved and has even retained fission-related impurities within the uraninite grains (Evins et al. 2005).

From the above, it seems clear that, in the case of stable tectonics and maintained reducing conditions in the repository, the uranium oxide which constitutes the fuel matrix can be stable for many millions of years. Another observation is that dissolution experiments in the laboratory yield faster dissolution rates than are estimated from observations of minerals in natural settings. This has been observed and discussed in the literature and may, in part, be explained by evolution of the surface of the dissolving mineral which occurs on a time scale that cannot be studied in a normal laboratory experiment (White and Brantley 2003).

Further discussion regarding knowledge gained from natural analogue studies is found in the next Section 14.6.

14.6 Natural analogues

Natural systems provide two things that cannot be achieved in the laboratory: The full complexity of the natural environment, and very long time scales. By making comparisons with natural systems in which some feature, event or process is deemed similar to what is expected in the repository system, the response of the repository to the natural environment in which it will evolve for such a long time can be assessed with better confidence.

There are different parts of the repository system – spent fuel, copper canister, bentonite buffer – for which comparisons with natural analogues have proven useful. Knowledge about many processes occurring in the geosphere, for example transport of uranium and other elements, has been enhanced by studies at natural analogue sites.

14.6.1 The role of natural analogue studies in safety assessments

Since the concept of natural analogues first started to take form in the 1980's (Chapman et al. 1984), the relationship between natural analogue studies and safety assessments of high-level waste repositories has changed. The quantification necessary in a safety assessment is difficult to extract from the natural analogue studies; however, these studies have a significant qualitative value in that it can be shown that a feature or process does exist in nature and that it has persisted in a natural environment for a very long time. This is an important aspect, especially for raising public awareness and understanding. Much of what is needed in order to understand safety assessment falls outside the realm of common knowledge. Here, analogues and demonstration experiments can, to some extent, provide also the general public with insights into conditions and processes of importance for post-closure safety. Material analogues, especially, have been useful for that purpose.

It is now clear that the two main reasons natural analogue studies are interesting, namely the exposure to natural complexity and long time scales, introduce uncertainties which render them difficult to use in a systematic safety analysis. For natural analogues, one limitation is often a lack of information about boundary conditions. The need for well-known initial conditions for quantitative evaluations of effects of processes is one example of where difficulties arise. In addition, analogues are never perfect: The difference between an analogue and the actual component under investigation will always be a source of doubt. Therefore, most natural analogue studies do not lead to quantitative data that can be used in safety assessment models. However, in spite of these limitations, these studies have significantly enhanced the understanding of natural processes relevant to those considered in safety assessments. The role natural analogue studies play in identifying relevant processes, and also in verifying that all relevant processes have been incorporated in the models, is significant. Examples to illustrate this role are given by Miller et al. (2000).

A different aspect of the natural analogue studies has been the opportunities these studies have provided to drive development of equipment and methods intended for investigation of repository sites. For the comprehensive studies of ore bodies, mainly uranium, site investigation methods had to be applied. In this case, the differences between individual analogues and typical repository sites present an opportunity rather than a difficulty. The differences make it possible to better test the methods used to interpret measurements of, for example, redox conditions in groundwater, pH, colloids, and microbial activity.

Many studies of natural analogues have been performed as international projects. These projects have gathered scientists from different fields and contributed to discussions generating valuable critiques of the hypotheses being tested. Post-closure safety, like science in general, ultimately rests on the combination of openness and critique.

The following is a short review of main outcomes from some of the analogue studies performed in the last three decades. These have been more extensively reviewed by Miller et al. (2000) and Ruiz López et al. (2004). Preference has been given to the ones recognised as relevant to the KBS-3 concept. Other groups of experts have also found these analogues to be of interest in this context (Apted et al. 2009, pp 23–24, Bath and Hermansson 2009, pp 58–68, Neall et al. 2008, pp 35–42).

14.6.2 Analogues of repository materials and processes affecting them

Natural materials and archaeological objects found in nature have been studied as analogues of repository materials. These materials have been subjected to the complex variety of natural processes for different amounts of time, and what we see today is the result of this “natural experiment”.

Spent nuclear fuel

The natural mineral uraninite (uranium dioxide) has many similarities with UO₂-based spent nuclear fuel. These materials are uranium oxides with the same crystallographic structure (fluorite structure), they form solid solutions with oxides of Th, Ca and REE, they are resistant to radiation damage (self-annealing), and they are similarly affected by oxidation (Janeczek et al. 1996). However, this does not mean that these materials are identical – there are many important differences. Examples of major differences are the amount of oxidized uranium, which is higher in uraninite, and the amount of radiogenic Pb, which can be almost 20 wt.% PbO in 2 billion year old uraninite, but is very low in spent nuclear fuel even after 10 000 years (0.00014 wt.% Pb, Janeczek et al. 1996).

Many natural analogue sites, for example Oklo (Gabon), Cigar Lake (Canada), Poços de Caldas (Brazil) and Palmottu (Finland), are centred on uranium deposits which formed many millions of years ago. The sites have been chosen partly due to the opportunity they provide to study how uraninite, as an analogue to spent nuclear fuel, behaves in different geological environments.

At *Cigar Lake*, the ore body is found at ca 450 m depth in a reducing environment, and dissolution of uranium oxide in the ore has been extensively discussed (Bruno et al. 1997). However, in spite of the reducing environment, the oxidation state of uraninite is somewhat higher in Cigar Lake uraninite than in uranium dioxide in spent fuel, which makes it difficult to draw parallels to dissolution of spent nuclear fuel in the KBS-3 repository. However, it is noteworthy that all natural processes that have affected this ore body since its formation, c 1 300 million years ago, have not resulted in any geochemical indications of its existence at the ground surface.

Another feature of importance for spent fuel dissolution that has been studied in Cigar Lake is radiolysis. Ionising radiation causes chemical reactions and the total energy deposited by radioactive decay is considerable. Therefore, early pessimistic evaluations of this effect on spent fuel dissolution tended to be grossly exaggerated. Observations of ferric iron precipitations in the clay nearest to the ore in Cigar Lake were, to begin with, interpreted as a result of oxidation by radiolysis. However, it could be demonstrated that the likely origin was hydrothermal alterations during ore formation. This and other observations stimulated the development of more realistic models (Smellie and Karlsson 1996).

As stated before, natural uraninite contains elements other than uranium and oxygen, for example Th and REE. Many of these elements also form in the nuclear fuel during reactor operation, or they can function as so-called “chemical analogues” for the elements in spent fuel. These chemical analogues are abundant in the *Poços de Caldas* ore deposits, and played an important role in the natural analogue studies performed at this site (Chapman et al. 1993).

The most striking natural analogue of spent nuclear fuel is the uraninite in the 2 billion year old *Oklo* natural fossil fission reactors, which is, in fact, a natural spent nuclear fuel (Neuilly et al. 1972, Naudet 1991, Gauthier-Lafaye et al. 1996). These fossil reactors are found in a uranium ore bearing formation in Gabon, western Africa, where they form reactor zones shaped by nuclear criticality. Some sixteen of these reactor zones were discovered in the mines at Oklo, at nearby Okélobondo and during prospecting in Bangombé, which is situated about 20 kilometres to the south. The nuclear reactions occurred some 2 000 million years ago when the U-235 content was still high enough for a sustained nuclear fission reaction. Geological studies involving Precambrian rocks elsewhere have failed to locate any sign of a similar fossil reactor. This is likely due to the many coincidences that allowed nuclear chain reactions to start naturally: High uranium concentration, the right isotopic composition of uranium, the presence of a neutron moderator (water) due to high porosity, and the unusually low abundance of neutron poisons (e.g. vanadium and manganese), which capture neutrons (Naudet 1991). In addition, the sedimentary formation that hosts these natural reactors is essentially unaffected by tectonic processes, despite 2 billion years of existence.

The Oklo uraninite and spent nuclear fuel have many striking similarities, but also important differences. These differences stem partly from the very different operating histories of the natural reactors and man-made power producing reactors. The nuclear reactions in Oklo uraninite proceeded at a very low rate and at low power, intermittently for some hundreds of thousands of years (Naudet 1991). Spent fuel from power producing reactors has a much more intense thermal history, a higher burn-up and contains higher concentrations of fission products. Another notable difference is the presence of hydrocarbons in Oklo which might have helped to keep the conditions reducing.

Knowledge regarding the requirements for criticality at Oklo was used in the evaluation of the possibility of achieving criticality in a spent fuel repository. There is still fissile material left in the spent fuel. A model based on Oklo conditions was therefore applied to the KBS-3 repository case (Oversby 1998). The result was negative in so far that no criticality was to be expected in the repository.

One aspect which makes Oklo uraninite unique among analogues for spent nuclear fuel is that reactor zone uraninite contains elements formed during the fission reactions (fission products). The reactor zones are also remarkably well preserved considering their age, so that few of the components have been lost to mass transport which would otherwise have complicated the evaluation of the nuclear reactions. For example, rare earth elements generated by fission are well preserved and contained in the uraninite, but volatile elements such as Cs have been lost. Analogues of the metallic aggregates, in spent nuclear fuel called ϵ -particles, are also found in the Oklo reactor zones. In spent nuclear fuel these $\sim 1 \mu\text{m}$ sized ϵ -particles consist of alloys of Mo, Tc, Ru, Rh, and Pd. There are also observations of the fission product Te associated with these particles (Cui et al. 2004). In the Oklo reactors, similar segregations of metallic fission products also occur, as evidenced by records of Ru-, Pd- and Pb-containing particles (Gauthier-Lafaye et al. 1996). These particles are up to $\sim 100 \mu\text{m}$ diameter and are not metallic alloys but are aggregates of different sulphide phases. Interestingly these aggregates are also associated with Te and Se, illustrating the chemical affinity between the noble metals and these chalcogenic metalloids.

Cast iron

A waterlogged archaeological site at Nydam Mose in Denmark contains buried iron objects of military equipment, sacrificed in the period 200–500 AD. Here, siderite was identified as a main corrosion product, which indicates an oxygen-free, carbonate-rich (10^{-2} M) corrosion environment (Matthiesen et al. 2003, 2004). The estimated corrosion rates range from an upper limit of $5 \mu\text{m}/\text{year}$ down to $0.03 \mu\text{m}/\text{year}$ or less. The average corrosion rate for 151 analysed lances is about $0.2 \mu\text{m}/\text{year}$.

Corrosion of archaeological cast iron artefacts has been studied by Neff et al. (2003, 2005), who analysed the corrosion products on artefacts from the 2nd century AD to the 16th century AD. Also low carbon steel objects, buried for long periods (Neff et al. 2006), were analysed to determine the average corrosion rate. The presence of oxygen in the corrosion process was indicated by the corrosion products. It was found that the measured or estimated corrosion rates varied over a relatively large range, but that the estimated average corrosion rates do not exceed $4 \mu\text{m}/\text{year}$.

Copper

Finds of native copper in geochemical environments relevant to repository conditions are illustrative examples of the long-term stability of copper canisters. Ore bodies containing native copper have therefore been investigated and particularly the processes corroding or potentially corroding copper. Archaeological copper objects have been used for the same purpose (Johnson and Francis 1980, Miller et al. 2000).

The world's largest deposit of native copper occurred on the *Keweenaw Peninsula* in Northern Michigan, USA. The native copper lodes, which are associated with conglomerate sediments interbedded in the host basalt, formed about 1.1 billion years ago (Brown 2006). About five million tonnes of native copper has reportedly been mined (Johnson and Francis 1980). Some native copper has been transported by glaciers from primary copper deposits in upper Michigan, like Keweenaw Peninsula. Sizes ranges from small pebbles to blocks of more than one tonne, such as the famous Ontonagon copper boulder. This is referred to as "float copper". Well preserved pieces of float copper have been found in banks of sand and gravel left by the glaciers. Two such pieces with evidence of glacial abra-

sion were investigated (Johnson and Francis 1980). The last glacier receded 8 000 to 11 000 years ago. Still, the pieces are well preserved with relatively thin layers of corrosion products identified as cuprite (Cu_2O) and malachite ($\text{Cu}_2\text{CO}_3(\text{OH})_2$). The abraded areas had a maximum oxide thickness of only 0.6 mm. One of the pieces was reportedly found at less than a metre depth (about two feet).

The *Hyrkkölä* copper-uranium mineralisation in Finland is situated in a geologic setting similar to the sites considered for disposal of spent nuclear fuel in Finland and Sweden. Native copper and uraninite in *Hyrkkölä* are hosted in granite pegmatite veins. The age of the mineralisations is estimated to about 1 700 million years. Native copper together with copper sulphide and secondary uranium minerals occur in open fractures at several depth intervals in these pegmatites. One interval with altered granite pegmatite contains native copper together with cupric oxide and the fracture surfaces were coated with smectite with adsorbed uranium and copper (Marcos et al. 1999). Investigations have been made by core drilling down to depths of about one hundred metres. Groundwater compositions related to the mineralised fractures were analysed using the SKB mobile field laboratory. Native copper in *Hyrkkölä* has evidently persisted despite exposure to sulphide-containing water as well as current oxidising conditions. Uranium series studies corroborate the exposure to groundwater and indicate together with other observations that sulphidation ceased a few hundred thousand years ago to be later replaced by oxidation. Native copper grains as large as one millimetre were found with thin rims of cuprite. Some of the smallest grains were totally oxidised. Some well-preserved grains of native copper were found embedded in smectite (Marcos et al. 1999).

Native copper in *Hyrkkölä* is one of many examples where copper found in nature has survived geochemical conditions similar to those expected in a repository for geologic time periods (Marcos 1989). However, native copper deposits in general are mainly associated with basalts, such as the Keweenaw Peninsula case, or supergene weathering of copper sulphide deposits (Amcoff 1998). *Hyrkkölä* is valuable in comparison because the geochemical setting is so close to that of a potential repository in Finland or Sweden.

Sheets of native copper, about 1–2 millimetres thick and up to more than ten centimetres across, have been found in outcrops of Permian mudstone at *Littleham Cove* in the UK (Milodowski et al. 2002). Apart from some signs of corrosion the copper is remarkably well preserved despite the indicated age of more than 176 million years. The copper sheets are associated with uranium containing nodules, formed within a halo caused by contemporaneous reduction of ferric iron in the mudstone. These uraniferous concretions and the native copper were formed early, before compaction of the mudstone, by mineral deposition from fluids. Then, for most of their history, the mudstone host rocks have been well below the present water table and remained saturated with water. Both the native copper and the uranium nodules have been evaluated as analogues to spent fuel disposal in copper canisters buried in compacted clay (Milodowski et al. 2002).

At *Littleham Cove*, copper precipitated along bedding lamina and thin fractures in the mudstone. A narrow, less than a millimetre, diffusive halo of copper has been measured in the mudstone next to the copper. This could be the result of either enhancement during formation or loss of copper later. Either way it indicates that diffusion occurred over distances of only a few hundreds of micrometres. Some early partial alteration to cuprite has been identified but, apart from that, the native copper remained relatively inert until the sequence was uplifted and exposed to surface erosion and oxidative weathering in the present-day environment. The radioactivity of the uranium-containing nodules has been used for evaluation of the effects of radiolysis. Methods used to calculate the production of hydrogen peroxide due to radiolysis of water by alpha particles from spent nuclear fuel were applied to a typical nodule. The calculated maximum production of peroxide was enough to oxidise over a gram of pyrite. However, there were no observations or measurements to indicate that radiolysis had been a significant process for inducing oxidation of ferrous iron or other reduced species in the water-saturated clay matrix of the mudstone (Milodowski et al. 2002).

The man-of-war *Kronan* exploded and sank south east of Öland in 1676, and its cannons scattered on the sea floor. One cannon made of bronze was chosen for investigations of corrosion. It was almost entirely buried, near vertically with its muzzle down in shallow marine clay. The copper content of the bronze was as high as 96.3 % and the surrounding relatively compact marine clay consisted partly of montmorillonite (Hallberg et al. 1988). Known boundary conditions such as age of the burial and the composition of the environment made it valuable as an analogue for a copper canister in a saturated clay buffer, despite the comparatively short time of burial. The surface of the cannon was analysed

together with the surrounding clay. Cuprite (Cu_2O) and some malachite ($\text{Cu}_2\text{CO}_3(\text{OH})_2$) were found on the surface, and slag inclusions of tenorite (CuO) in the bronze matrix below the surface. Diffusion of copper was traced four centimetres into the clay. The slag inclusions, and the fact that the cannon must have been covered with a layer of corrosion products before the ship sank, complicated the investigation. The facts at hand were carefully evaluated and a maximum corrosion of less than ten micrometres per hundred years was reported (Hallberg et al. 1988).

This study was later revisited and reassessed with reference to a corrosion mechanism developed for copper nuclear waste containers in a Canadian concept (King 1995). This mechanism included the formation of soluble copper species and the so called disproportionation reaction. The latter implies that divalent copper, for example from the tenorite slag inclusions, together with copper metal produces monovalent copper. The developed mechanism was able to satisfactorily explain the earlier reported observations and refine the conclusions (King 1995).

Three *lightning conductor plates*, located at separate places in middle and southern Sweden, were excavated after having spent more than fifty years in the ground (Hallberg et al. 1984). The three plates had been buried at depths ranging from 1.2 to 3.3 metres in soil of clay and/or silt. The corrosion of the plates was studied in relation to the chemical properties of the soil. Two of the plates were affected by pitting corrosion with a pitting factor of five, while the third and deepest plate showed no such signs. Copper oxides were found on the two former plates and copper sulphides on the latter. *Copper water pipes* also provided useful information about pitting.

Later evaluations of copper canister corrosion regarding pitting have had more benefit of experiments and theoretical considerations which were previously not available (King et al. 2010, Section 5.3).

Bentonite

Bentonite clay used in the buffer and backfill are usually taken from natural deposits with very little further processing, apart from drying, crushing and sieving. The deposits themselves and other occurrences of bentonite in different geological settings have been studied as analogues for buffer and backfill in a repository. Processes of interest are, for example, thermal and chemical influences, resistance to hydraulic flow and diffusion of dissolved substances.

Alteration of smectite to illite (illitization) is the most common transformation of smectite observed in natural sediments, and it has been reproduced under laboratory conditions. One of the requirements for illite to form is availability of potassium. Potassium is found both dissolved in groundwater and in rock-forming minerals. For kinetic considerations relating to smectite-illite alteration, the initial potassium concentration in groundwater and the dissolution rate of surrounding potassium-bearing minerals are of importance. Any other mineral formation that may compete with illite for the potassium may also be important.

The conditions for transformation of smectite to illite have been investigated in *deep wells in sedimentary basins* (Velde and Vasseur 1992). These studies of illitization in natural systems are not connected to any specific natural analogue site but have instead been performed in a variety of sedimentary basins in order to better describe the time and temperature relations of smectite-illite mineral changes. Samples from wells from the Texas Gulf Coast (USA), the Niigata basin (Japan), Los Angeles basin (USA), and the Paris Basin (France) were studied by Velde and Vasseur (1992). These wells, drilled in sedimentary basins of varying age (4.5 to 210 Ma), provide data on an almost complete burial sequence. The resulting model shows that the reaction rate at repository relevant temperatures is very slow in relation to the time scale considered for a repository (~1 Ma).

Thermal effects on bentonite have been studied at *Kinneulle* in Sweden, where a two m thick bed of bentonite clay formed from volcanic ash deposits ca 450 million years ago. Samples from the bentonite clay, situated about 95 metres below a cap of a ca 300 million year old diabase, were investigated (Pusch et al. 1998). The diabase formed when molten lava penetrated laterally into the sediment series. This magmatic event exposed the sediments to heat that reached down to the bentonite layers. The bentonite layers at Kinneulle have been known for some time and they were studied early as analogues to compacted bentonite clay buffers to test current understanding of heat effects (Pusch 1983). These early studies were later supplemented by investigations of samples from *Gotland* and *Sardinia* where episodes of lava flows have likewise heated smectite clay minerals but with different time-temperature profiles (Pusch and Karnland 1988).

Due to the magmatic intrusion, the centre of the bentonite layer reached a peak temperature of 140 °C after about 200 years, stayed above 100 °C for another 600 years and slowly decreased towards ambient for more than one thousand years (Pusch et al. 1998). Cementation of the clay by silica (SiO₂) and occurrence of the clay mineral illite have been interpreted as caused by the heating. Both of these processes, cementation by precipitation of silica and production of illite from smectite, can lower the swelling capacity of bentonite which is essential for its function as a buffer. Early observations (Pusch 1983, Pusch and Karnland 1988) confirmed the view that compacted bentonite will retain its swelling capacity providing the heat pulse is limited in temperature and time, and provided that the geochemical environment is not aggressive to smectite in any other aspect. Later investigations of Kinnekulle used a simplified one-dimensional diffusion-reaction model to simulate the observed development of the clay (Pusch et al. 1998). Sea water composition was assumed and two different options for the reaction were tested: Solid state conversion of smectite to illite versus dissolution of smectite followed by precipitation of illite. The second option was the better one and an even better agreement was reached by assuming that illite formation is non-reversible. Potassium, as expected, proved to be an essential component for the production of illite. Silica produced by the reaction was, according to the calculations, consumed by diffusion into the surrounding sediments and precipitation of quartz.

A number of bentonite deposits in the Cabo de Gata region in *Almería*, Spain, were selected for sampling and studies of different long-term buffer aspects (Barra project) (Villar et al. 2006). After a first phase, the studies were narrowed to three deposits and two processes: Morrón de Mateo for thermal effects; Cala del Tomate and Cortijo de Archidona for the effect of salinity. The thermal effect in Morrón de Mateo had been caused by a volcanic dome. Bentonite near the volcano was shown to be iron- and magnesium-rich smectite compared to normal aluminium smectite in more distant samples, but properties such as cation exchange capacity and specific surface were found to be the same. The presence of iron and magnesium in the smectite mineral structure was explained as due to a reaction of smectites with contaminants present near the volcanic dome at moderate temperatures (below 100 °C). Conditions may not have been extreme enough to transform the smectite to other minerals. The bentonite clays at Cala del Tomate and Cortijo de Archidona have evidently experienced changes in water composition. Sodium and magnesium are the dominating exchangeable cations in smectites at depth in Cala del Tomate as compared to magnesium and calcium near the surface. Observations from Cortijo de Archidona indicate a sea water intrusion later followed by infiltration of meteoric water, rich in calcium and magnesium. The ionic strength of porewater had varied between 0.02 and 0.23 moles per litre but the clay minerals had seemingly remained stable.

In *Wyoming*, USA, bentonite was formed by alteration of volcanic ash that fell over the shallow, now relict, Mowry Sea. The ashes formed thin but widespread layers on the sea floor and were subsequently altered to bentonite (Smellie 2001). These bentonite layers were formed about 100 million years ago and their remains are mined in some locations for their content of high grade sodium bentonite. The brand MX-80 has long been used by SKB as reference buffer material. Scientific studies support the view that the bentonite formed under shallow, brackish and partially reducing conditions, and that no further alteration occurred. However, isolation by subsequent depositions of mud and silt may have served to protect the bentonite clay. Consequently, it was not possible to address the question of what would happen under conditions more open to saline groundwater.

The protective and preserving potential of a clay buffer is demonstrated by clay deposits in *Dunarobba*, Italy, which contain a fossil forest (Valentini et al. 1997). Tree trunks were identified as *Taxodioxylon gypsaceum* which became extinct during the Pliocene indicating that they have been preserved by the clay deposits for more than one million years. The deposit hosting the trees was regarded as dense, consolidated clay with some cementation by calcium carbonate (hydraulic conductivity less than 2×10^{-10} m/s and yield pressure 1.5–9 MPa). The original cover was supposedly 80 metres before erosion took place. The tree wood is remarkably well preserved. Very little alteration has taken place and the material is still in all aspects wood, with a cellulose content not far from modern wood. Evaluation of the site suggested that the clay formation had acted on a local scale to protect the fossil trees from unsuitable conditions. The low hydraulic conductivity of the clay has prevented the ingress of oxygenated water which could otherwise have caused aerobic decomposition of the wood. More surprisingly the clay seems to have protected from anaerobic decomposition as well. Anaerobic bacteria are known to decompose organic and in particular cellulosic material. It is also known from archaeological excavations that clay can help to preserve such materials where conditions are generally anaerobic, for example in lake sediments. The *Dunarobba* fossil forest is in line with these examples

but more striking due to its great age. The usual assumption in safety assessments of radioactive waste disposal, that organic material will always become degraded by anaerobic bacteria, which thereby generate gas, is probably pessimistic in many cases where clay is used as buffer and backfill. One possible explanation as to why the clay so efficiently has hindered anaerobic degradation is that essential nutrients were kept out by the clay (Valentini et al. 1997, p 216).

At the *Cigar Lake* uranium deposit, in Canada, clay (mainly illite and kaolinite) surrounds the uranium ore body. The ore is situated at ca 450 m depth and the ore cannot be geochemically detected on the surface. This isolation of the ore, and the elements related to it, for many millions of years, is partly due to the low hydraulic permeability of the surrounding clay (Cramer and Smellie 1994). Results from the *Cigar Lake* studies also illustrate the colloid filtering capacity of clay (Vilks, pp 219–241 in Cramer and Smellie 1994). Sorption of radionuclides on sheet silicates, mainly chlorite and illite, in the natural fission reactor zones at *Oklo*, have also been shown to have played an important role in limiting the dispersion of these elements around the reactor zones (Bros et al. 2003).

Bentonite alteration is expected in environments where bentonite is not stable, such as in highly alkaline groundwater influenced by degrading Ordinary Portland Cement. Cements with lower pH (9-11) are considered as alternatives, however, the need to know more about the reaction between bentonite and alkaline groundwater triggered a natural analogue study in *Cyprus*, where long-term interactions between bentonite and alkaline groundwater were investigated. In *Cyprus*, bentonite is found in association with mafic to ultramafic rocks in an ophiolite sequence (the main components of oceanic plates that underlie sediments on the seafloor). Groundwaters that have interacted with the ophiolite are alkaline, similar to leachates of low alkali cements. Bentonite in contact with the ophiolite has thus been exposed to alkaline groundwaters for at least 100 000 years, maybe up to 1 million years. The results from *Cyprus* show that even after all this time of interaction with alkaline groundwater, only minimal reaction of bentonite has occurred: the reaction front has proceeded only a few mm into the bentonite (Milodowski et al. 2016).

14.6.3 Transport and retardation processes in the geosphere

Scientific investigations aimed at enhancing our knowledge about transport and retardation of radionuclides in the geosphere is based on studies of the geochemical behaviour of these elements (or their chemical analogues).

Subsurface conditions

The uranium ore zone at *Lake Palmottu* in Finland forms a steeply dipping zone that extends down to a depth of about 300 metres. Geology, hydrogeology, groundwater chemistry, climate, and landscape are similar to those of investigated potential repository sites in Finland and Sweden. It was therefore investigated as an analogue for disposal of spent fuel in crystalline rock (Blomqvist et al. 2000). At *Palmottu*, the conditions at depth are generally oxygen-free and reducing, whereas oxidising groundwater conditions were typically encountered in the topmost 100 metres. Reducing conditions at depth are also found at *Forsmark*. The 1 700 million year old uranium deposit at *Palmottu* has experienced several periods of glaciations, which may have temporarily subjected the ore to oxidising conditions; however, if so, reducing conditions were efficiently restored. Despite the low grade of ore (0.1 %), uranium was found to be abundant enough to be an additional sink for reduction of infiltrating oxygen. The observations in *Palmottu* illustrate the capacity of the rock to remain stable and maintain reducing conditions despite a long geologic history including periods of permafrost and glaciations.

Freezing conditions, causing salt exclusion, may have caused the unusual groundwater chemistry observed at *Palmotto*, with elevated sodium and sulphate. Freezing and subsequent dissolution of NaSO_4 minerals may lie behind this; however, this is still an open question (Blomqvist et al. 2000). Another aspect of subsurface conditions during permafrost and glaciations is the possible formation of methane gas hydrates. This has been studied mainly in Canada, where gas-hydrate bearing core samples were collected from the sediments in the present natural permafrost environment of the *Mallik* sea, Canada (e.g. Clark et al. 1999). Gas hydrates were also one aspect of the studies at the *Lupin* Mine, Canada; no methane hydrates were found during the studies, but there are indications of their presence in the past (Stotler et al. 2009a). The studies of natural permafrost environments support the conclusion that hydrate formation is unlikely at expected repository conditions.

Reducing conditions are prevailing at *Cigar Lake* in Canada, where a 1 300 million year old uranium deposit is situated at ca 450 m depth. The uraninite at Cigar Lake has interacted with groundwater at different times in the geological history of the ore, as is evidenced by oxygen isotopic composition as well as the presence of secondary uranium minerals; however, the conditions were still such that this has caused only minor disturbances to the uraninite chemical composition and texture, and limited actinide migration (Fayek et al. 2002).

Surface weathering processes and groundwater conditions at shallow depth are affecting the *Bangombé* natural fission reactor zone in Gabon. The Bangombé reactor is located at 12 m depth in a subtropical, variably oxidizing environment. Thus, the effects of such groundwater conditions on the reactor zone have been studied. The groundwater redox potential at Bangombé was found to be more sensitive to lithological variations than to depth and confinement. The interaction between reactor zone and oxygen-rich groundwater has been in progress for at least c 70 000 years (and probably much longer), as evidenced by the age of the secondary uranyl-mineral torbernite encountered at Bangombé (Gauthier-Lafaye et al. 2000). The concentration of colloids in the Bangombé groundwater was found to be low (less than 0.3 ppm), in spite of the dynamic subtropical conditions (Gauthier Lafaye et al. 2000, pp 55–56).

Glacial hydrological processes and their influence on subsurface environments were studied in the Greenland Analogue Project (GAP) and the ICE project, both carried out in the Kangerlussuaq region, western *Greenland*. The study region covered a 12 000 km² area of which approximately 70 % is occupied by the Greenland Ice Sheet. The present-day ice sheet, in its crystalline bedrock setting, serves as a natural analogue for future conditions expected for suggested and planned repository sites in previously glaciated terrain, such as for the Forsmark site in Sweden. At the Greenland study area, permafrost extends down to 350–400 m at the ice sheet margin. The proglacial area is characterised by numerous lakes, many of which are expected to overlay through taliks. The findings from the GAP study are presented in Harper et al. (2016) and Claesson Liljedahl et al. (2016), whereas the findings from the ICE study are given in Harper et al. (2019). The results are briefly summarised below.

From the hydraulic measurements and analyses of ice borehole data it is implied, for current Greenland ice sheet conditions, that the ice overburden hydraulic pressure provides an appropriate description of the basal hydraulic pressure when expressed as an average value for the entire ice sheet over a year. The hydraulic head then corresponds to 92 % of the ice thickness. Studies of a proglacial lake that was expected to overlay a through talik showed that this was indeed the case. The initial hypothesis suggested that discharging conditions prevailed at the lake location. This proved invalid, since stable isotopic conditions of the talik water indicated ongoing recharging conditions (Claesson Liljedahl et al. 2016), and modelling results showed that recharge and discharge conditions in the lake (talik) can shift in time and space (Johansson et al. 2015, Vidstrand 2017). Characteristics of glacial meltwater end-member showed depleted isotopic signatures, consistent with cold climate conditions and a very low total dissolved solid content, with solute concentrations ranging from practically zero to approximately 1 mM for the main solutes, such as Ca²⁺. Groundwater sampled in the deep (600 m) bedrock borehole (DH-GAP04) at the very ice sheet margin indicate a glacial meltwater origin. A preliminary interpretation of dissolved He concentrations suggests that the deep groundwaters may have residence times exceeding hundreds of thousands of years. Together with the extensive persistence of gypsum (hydrothermal origin) below 300 m, this suggests stable conditions with limited groundwater flow at depths below 300 m at the borehole location. Reducing conditions are interpreted to prevail below the permafrost in the study area. Past penetration into the bedrock of dissolved oxygen in meltwaters has been limited in depth, as indicated by the presence of pyrite in fractures below approximately 50 m; iron oxyhydroxides are found in fractures only in the upper parts of the rock (down to 60 m). In conclusion, the hydrogeochemical information from the GAP shows that oxygenated waters do not penetrate to larger depths close to the ice sheet margin, even though dilute waters do penetrate into the bedrock, i.e. the redox potential is effectively buffered by the rock, thus providing evidence that confirms the results from modelling (Sidborn and Neretnieks 2008, Sidborn et al. 2010, Spiessl et al. 2008).

The results from the GAP study has provided significant and important information within the fields of hydrogeology and hydrogeochemistry under glacial and proglacial conditions, whereas the GAP and ICE studies have provided a significantly increased process understanding within the field of glacial hydrology (see a summary in the **Climate report**, Section 3.2 and Section 10.4.1 in the present report (under the headings *Glacial hydrological conceptual model*, *Amount of water produced by melting*, *Spatial perspective on the subglacial hydrological system*, and *Temporal perspective on*

the subglacial hydrological system)). In the safety assessments, uncertainties related to e.g. process understanding are typically handled by making pessimistic assumptions. The increased understanding obtained from the Greenland studies, and associated reduction of uncertainties, makes it possible to reduce the need for pessimistic assumptions in certain areas, and also allows a re-evaluation of the degree of pessimism in some of the assumptions made in previous safety assessments and modelling work, the latter was the case for the assumption of using a head value that corresponds to 92 % of the overlying ice thickness. Based on the natural analogue results, it has been shown that this may not be a pessimistic assumption, as described in SR-Site, but rather a realistic one, at least for ice sheet conditions similar to present-day conditions at the GAP site (Jaquet et al. 2019). Natural analogue data on bedrock temperatures and geothermal heat flow obtained from the GAP study are also used in Hartikainen et al. (2022) for evaluating the permafrost model that simulated the depths of permafrost and perennially frozen ground used in the PSAR (see the **Climate report**, Sections 3.4, 4.5, 5.5 and the present report Sections 10.4.1 (heading *Permafrost development and modelling*) and 12.3).

All in all, the results from the GAP and ICE studies concerning sub-glacial hydrology (constituting the upper boundary conditions for groundwater modelling under glaciated conditions), groundwater mobility, and groundwater chemistry in the Greenland study area, support the handling of these processes in the PSAR safety assessment. The results of the GAP and ICE studies are planned to be used further in the SAR safety assessment.

Radionuclide transport and retardation

One important aspect of natural analogue projects is investigation of geochemical behaviour and geochemical reactions of elements of interest for nuclear waste disposal. This was a significant part of the studies at the *Poços de Caldas* natural analogue site in Brazil (Chapman et al. 1993). In this project, it was shown that the redox front played a significant role in retarding many trace elements, even those considered non-redox sensitive. In this study, colloids were not found to contribute to the transport; rather it was shown that particulate material and colloids in deep groundwater were immobile. Microbes in the system at *Poços de Caldas* were found to catalyse specific redox reactions, thereby affecting the redox front. Results of the *Poços de Caldas* project indicate that large-scale, rapid transport of radionuclides and trace elements has not occurred at this site (Chapman et al. 1993).

The *Cigar Lake* studies indicate a similar absence of large-scale transport since there are no geochemical indications of the 1 300 million year old uranium ore body on the surface. This apparent immobility of relevant elements may be due to the clay that surrounds the ore; the low hydraulic permeability of the clay may have been a contributing factor. This property has been simulated by mass-transport models of the kind that are used for performance assessment of repositories (Cramer and Smellie 1994). Observations at *Cigar Lake* also supported conclusions on the role of colloids in the transport of radionuclides. Filtering of colloids by the clay was indicated. There were also examples of irreversible sorption of radionuclides on colloids which is a mechanism that may enhance radionuclide transport (Vilks, pp 219–241 in Cramer and Smellie 1994). However, as was noted in the *Poços de Caldas* project, particles and colloids may be more or less immobile, in which case irreversible sorption on these particles and colloids will act as a sink, and work in favour of retardation (Chapman et al. 1993).

The natural fission reactors in Gabon, *Oklo*, *Okélobondo* and *Bangombé*, provide unique opportunities to study the dispersion of fission products and actinides in the geosphere as a result of 2 billion years of exposure to a natural geological environment. Despite the great age few of the components have been transported out of the zones. However, volatile elements, such as Cs, have been lost (Gauthier-Lafaye et al. 1996). Retention of plutonium is traced in some locations by anomalous concentrations of the U-235 that has been generated by the decay of Pu-239 (Bros et al. 1996).

The first and possibly most important episode of mobilization of radionuclides in and around the reactor zones relates to the thermal influence of nuclear reactions. The nuclear reactions themselves heated the groundwater which caused geochemical reactions and rearrangements of matter close to the zones. The clay halo surrounding the core of the reactors formed as a result of this episode of hydrothermal alteration. Transport of rare earth elements in the near-field of an *Oklo* reactor by circulation of heated water has been calculated. The near-field models were reasonably successful in simulating the pattern of rare earth elements distributed in the few metres above the reactor. No fissiogenic rare earth elements were detected further away from the reactor zones (Gauthier-Lafaye

et al. 2000, pp 77–79). The hydrothermal clay in and around the reactor zones has been shown to effectively retain U, REE, Zr and, to some degree, Mo through sorption on the sheet silicates (illite and chlorite) (Bros et al. 2003).

After the reactor zones cooled down followed ca 1 000 million years during which no major geological event affected the reactor zones. Around 860 million years ago, the Franceville sedimentary basin, which hosts the reactor zones, was subjected to regional extension associated with mafic magmatic dike intrusions. This event caused uraninite recrystallisation and lead loss. During this time radiogenic lead, expelled from the uraninite, precipitated as galena (PbS) crystals in and around the reactor zones (Evins et al. 2005). The association between galena, fissiogenic platinum metals (Ru, Rh, Pd), and chalcogens (Se, Te) found in aggregates in or near the uraninite grain boundaries, suggest the mobilisation and redistribution within the reactor zones of these elements during the main episode of galena crystallisation (Gauthier-Lafaye et al. 2000, p 16).

Transport and redistribution of actinides and radionuclides occur today in the reactor zones. This is most clearly demonstrated by studies performed at Bangombé, where oxidative alteration and dissolution of uraninite is observed as different varieties of secondary uranyl-minerals that have precipitated in and around the reactor zone, and by the uranium isotopic composition measured 50 m downflow from the reactor zone (Gauthier-Lafaye et al. 2000, p 53). Studies of the migration behaviour of REE have showed that only very small amounts of REE's have left the reactor zone, and the groundwater samples from the reactor zone are depleted in REE's. It was indicated that the uraninite and secondary uranium phases (including coffinite, $USiO_4 \cdot nH_2O$) played an important role in retaining the REE (Gauthier-Lafaye et al. 2000, p 51).

Uranium transport has been studied also at *Palmottu*, in Finland, where the groundwater conditions are similar to those at the Forsmark site. At Palmottu, groundwater facilitated uranium transport was only found to be significant in the oxidizing uppermost hundred metres. Colloids were also carefully analysed at Palmottu but found to be unimportant as carriers of uranium in this case (Blomqvist et al. 2000). The importance of redox conditions was also observed at the *Koongarra* uranium deposit in the Alligator Rivers Region (Australia), where transport and retention mechanisms are to a large extent connected to oxidising weathering of minerals or the presence of unique constituents such as phosphates (Duerden et al. 1992).

Transport of radionuclides has also been studied at the *Nevada Test Site* (USA), where groundwater samples from packed off sections in deep drilled wells contained detectable amounts of radionuclides from the nuclear tests (Kersting et al. 1999). Underground nuclear tests melt the wall of the rock cavity that forms as a result of the explosion. Most of the actinides and rare earth elements produced in the explosion are incorporated in the molten glass that coalesces into a “puddle” at the bottom of the collapsing cavity. Plutonium found in the well had the same isotopic signature as samples from the melt glass of the “Benham” test, which had been performed under the groundwater table, 1.3 kilometres away, 29 years prior to sampling. Moreover, the plutonium and some other radionuclides were found to be associated with colloidal particles. This is probably the best indication so far that radionuclides can in fact be transported in the form of colloids, over substantial distances in a relatively short time.

14.6.4 Model testing and method development

A major part of many natural analogue projects concerns validation and testing of geochemical models used in performance assessment and safety analysis of radioactive waste repositories. In addition, the methods and equipment developed for use in natural analogue studies are important for detailed site investigations.

In the *Koongarra* (Alligator Rivers, Australia) project, a total of 13 different mass transport models were tested to see how well they were able to reproduce the observed dispersion fan of uranium-238 and some of its daughter nuclides using the large amount of information and data gathered through extensive investigations at the site (Golian and Lever 1992). The age of the dispersion fan, according to these calculations, was in the range 0.5–3 million years which compared reasonably well with the 1–6 million years obtained from geomorphologic observations. However, none of the models were ruled out which implies that the test was not a very severe one for the models, probably due to the complexity of the analogue and a lack of well-defined boundary conditions. Also, loss of a small fraction travelling further than the measured dispersion fan could not be ruled out. Such an observation could have been important and possibly discriminated the models.

A unique approach for the Koongarra project was to test the scenario analysis method, originally developed as a safety analysis tool. It proved itself valuable in stimulating the evaluations, and also served to illustrate the complexity of the analogue (Skagius and Wingefors 1992).

At *Poços de Caldas* (Brazil), mass-transport models and reaction models were tested, for example by simulating redox front development and hydrothermal transport (Chapman et al. 1993). The models used in the predictive modelling were generally able to mimic the observed features, which involved transport of oxidized iron and uranium by rainwater followed by precipitation of pitchblende by reduction when the uranium-bearing water encountered reducing conditions. The pattern confirmed the assumptions of mass-transport in fractured crystalline rock where features such as channelling and matrix diffusion play an important role and where continuum models are no longer adequate (Romero et al. pp 471–502 in Chapman et al. 1993).

In the *Poços de Caldas* project different geochemical codes and databases for speciation and solubilities were tested and compared. It was observed that, for example, calculated solubilities tended to be on the pessimistic (over-estimated) side but not always. These exercises led to recommendations for amendments and improvements to the models and databases (Bruno et al. pp 451–470 in Chapman et al. 1993).

In studies of the *Bangombé* natural fossil fission reactor (Gabon), comparisons were made between two codes used for geochemical evaluation: A statistical approach of principal component analysis and a deterministic approach simulating coupled transport and chemical reactions along groundwater flow lines. Both were able to distinguish chemical reactions from mixing and both independently identified an increase in alkalinity around the *Bangombé* reactor zone (Gurban et al. 1998). This observation was explained by microbial analysis of iron reducing bacteria, capable of decomposing organic matter and generating carbon dioxide causing the alkalinity to increase. The code (M3) for principal component analysis has been used since for geochemical evaluations of results from investigations of potential repository sites in Sweden. The fact that availability of reliable and relevant thermodynamic data is a requirement for adequate modelling is illustrated by the improvements made in calculated predictions of mineral assemblages at *Bangombé*, which after an update of the thermodynamic database reached a much better agreement with observed mineralogy (Jensen et al. 2002).

Blind predictive modelling was used in studies of the *Palmottu* natural analogue site in Finland, where a flow path in the “Eastern Flow System” was covered by boreholes with packed-off sections for groundwater sampling. Mass transport models were applied to explain the measured concentrations and isotope ratios of uranium along the flow path (Blomqvist et al. 2000). The first attempts were made “blind”, based on a limited amount of data. These first simplified approaches were not adequate to explain the observations. In the second phase, additional data on groundwater chemistry were distributed and two advanced models were applied, one fully coupled reaction-transport model and another model incorporating matrix diffusion. Both of them were successfully used to explain the development of uranium concentrations. The coupled model closely explained the measurements of groundwater composition in the boreholes. The assumption of matrix diffusion in the second model, to explain uranium dissolution by gradual oxidation of the rock matrix, was supported by independent measurements of uranium series disequilibrium.

In addition to model testing, both the *Palmottu* project and the GAP project provided opportunities to test equipments developed for investigation of repository sites, such as flow-logging devices, borehole video camera, borehole radar, mobile groundwater chemistry laboratory, down-hole chemistry probes etc. Measuring and sampling in boreholes were thoroughly exercised and the results used to describe the site, for example, the distribution of fractures and composition of the rock, as well as flow and chemistry of the groundwater. Much of this approach was later repeated during investigations of potential repository sites.

14.6.5 Concluding remarks

An important contribution from natural analogue studies to post-closure safety assessments is to provide qualitative information on which processes and features to include in the assessments. The relevant processes are not limited to the well-known natural analogue sites, but can be studied in many natural systems. However, by focussing research efforts in these international projects, much site specific information has been made available, and researchers from different disciplines have been brought together to discuss the results.

Natural analogues can be considered experiments that have run for vast time periods in a complex, natural environment. Thus, observations of the results of these “experiments” can be made, from which hypotheses regarding processes that have affected the investigated feature can be formulated. These hypotheses can be tested with various methods. In this way, information from natural analogue studies can be used in development of conceptual models.

A central issue for many natural analogue projects has been to test the adequacy of the geochemical tools, and the mathematical models incorporated in them, that are used in analyses of post-closure safety. In practice this has resulted in an assessment of the applicability of associated databases used in geochemical models under natural conditions, and has helped to establish some of the uncertainties associated with these models.

There are, however, aspects of natural analogue studies that limit the use of the results acquired. The difficulty in extracting the quantitative data necessary for the safety analyses is the main limitation. Information regarding the initial state of the feature as well as details regarding events and processes affecting the feature through all of its history is normally not fully available. This is often a result of the long time scales involved and the complexity of the systems, which is inherent in the concept of a natural analogue.

In conclusion, the outcome of the natural analogue studies has been of a more qualitative than quantitative nature. The gathering of scientists and modellers in these international projects has focussed the research efforts and method development, so that enough information is available for identifying processes and scenarios relevant to safety assessments. Also, many natural analogues provide support to post-closure safety analyses by improving general perception and understanding of the concept of a deep repository.

Table 14-4. Selected references for some natural analogue studies with relevance for the KBS-3V safety assessment. This list is not exhaustive. Large and interesting overviews of analogue studies are given in Miller et al. (2000) and Ruiz López et al. (2004).

Spent nuclear fuel, subsurface conditions, transport and retardation in the geosphere, method development and model testing	
Oklo, Gabon	Gauthier-Lafaye et al. 2000
Cigar Lake, Canada	Cramer and Smellie 1994
Poços de Caldas, Brazil	Chapman et al. 1993
Palmottu, Finland	Blomqvist et al. 2000
Koongarra (Alligator Rivers), Australia	Duerden et al. 1992
Nevada Test Site, USA	Kersting et al. 1999
Greenland	Claesson Liljedahl et al. 2016
Copper canister	
Keweenaw Peninsula, USA	Johnson and Francis 1980
Hyrkkölä, Finland	Marcos et al. 1999
Littleham Cove, UK	Milodowski et al. 2002
Kronan cannon, Sweden	Hallberg et al. 1988
Lightning plates, Sweden	Hallberg et al. 1984
Buffer and backfill	
Deep wells in sedimentary basins	Velde and Vasseur 1992
Kinnekulle, Sweden	Pusch et al. 1998
Wyoming, USA	Smellie 2001
Almería, Spain	Villar et al. 2006
Dunarobba, Italy	Valentini et al. 1997
Cyprus	Milodowski et al. 2016

15 Conclusions

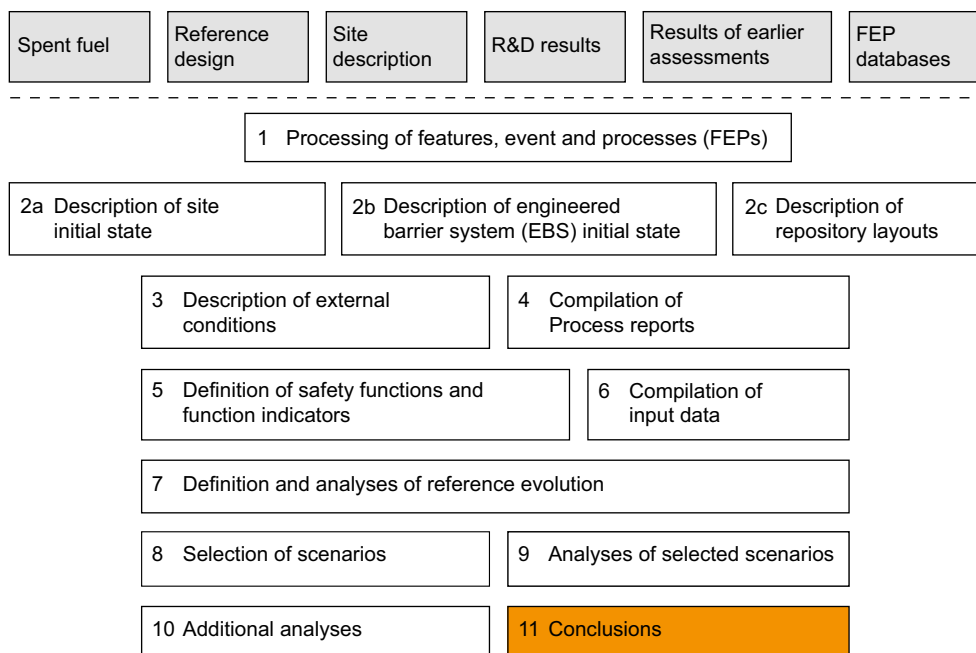


Figure 15-1. The PSAR methodology in eleven steps (Section 2.5), with the present step highlighted.

15.1 Introduction

The central conclusion of the post-closure safety assessment in the PSAR is that a KBS-3 repository built at the Forsmark site according to the specifications in the PSAR can be expected to fulfil the requirements of post-closure safety expressed in SSM's relevant regulations.

This conclusion is reached because the favourable properties of the Forsmark site ensure the required long-term durability of the barriers of the KBS-3 repository. In particular, the copper canisters with their cast iron insert have been demonstrated to provide a sufficient resistance to the mechanical and chemical loads to which they may be subjected in the repository environment.

The conclusion is underpinned by the following considerations.

- The reliance of the KBS-3 repository on i) a geological environment that has long-term stability with respect to properties of importance for post-closure safety, i.e. mechanical stability, low groundwater flow rates and the absence of high concentrations of detrimental components in the groundwater, and ii) the choice of naturally occurring materials (copper and bentonite clay) for the engineered barriers that are sufficiently durable in the repository environment to provide the barrier longevity required for safety.
- The understanding, through decades of research at SKB and in international collaboration, of the phenomena that affect post-closure safety, resulting in a mature knowledge base for the safety assessment.
- The understanding of the characteristics of the site through several years of surface-based investigations of the conditions at depth and of scientific interpretation of the data emerging from the investigations, resulting in a mature model of the site, adequate for use in the safety assessment.
- The detailed specifications of the engineered parts of the repository and the demonstration of how components fulfilling the specifications are to be produced in a quality assured manner, thereby providing a quality assured initial state for the safety assessment.

The detailed analyses, performed systematically according to a well-defined methodology, demonstrate that canister failures in a one million year perspective are rare. Even with a number of pessimistic assumptions regarding detrimental phenomena affecting the buffer and the canister, they are sufficiently rare that their cautiously modelled radiological consequences are well below one percent of the natural background radiation, meaning that they are also well below the Swedish regulatory risk criterion.

As a background to the discussion of conclusions in this chapter, the main features of the KBS-3 safety concept are repeated.

- The waste is isolated from the human and near-surface environment by placing the repository at depth in a long-term stable geological environment. This means that the repository is not strongly affected by either societal changes or by the direct effects of long-term climate change at the ground surface.
- The risk of human intrusion is reduced by locating the repository at a site where the host rock can be assumed to be of no economic interest to future generations.
- The spent fuel is surrounded by several engineered and natural safety barriers.
- The primary safety function of the barriers is to contain the fuel within a canister.
- Should containment be breached, the secondary safety function of the barriers is to retard a potential release from the repository.
- The engineered barriers are made of naturally occurring materials that are stable in the long-term in the repository environment.
- The repository is designed and constructed so that temperatures that could have significant detrimental effects on the long-term properties of the barriers are avoided.
- The repository is designed and constructed so that radiation-induced processes that could have significant detrimental effects on the long-term behaviour of the engineered barriers or of the rock are avoided.
- The barriers function passively, i.e. without human intervention and without artificial supply of matter or energy.

This chapter presents the detailed conclusions from the assessment of post-closure safety in the PSAR.

Two major roles for the presentation of these conclusions can be distinguished:

1. To demonstrate compliance with applicable Swedish regulations for a KBS-3 repository at the Forsmark site.
2. To provide feedback to design development, to SKB's RD&D Programme, to detailed site investigations and to future safety assessment projects.

The first purpose is addressed in Section 15.3 and the second in Sections 15.4 through 15.8. Before the formal discussion of compliance-related issues and the detailed feedback, an overview of the results of the analyses is given in Section 15.2 immediately below.

The central conclusions stated above are unaltered since the SR-Site assessment. Some details in Sections 15.2 (Overview of results), 15.3 (Demonstration of compliance) and 15.4 (Design basis cases) have been updated to reflect updates in other parts of the assessment. The Sections 15.5 to 15.8 providing feedback to the reference design, to detailed site investigations, to RD&D needs and to assessment methodology have been thoroughly updated, reflecting both updated results of the post-closure safety assessment and progress since the publication of the SR-Site assessment in the areas to which feedback is given.

15.2 Overview of results

This section gives a summary of the most important findings in the assessment of post-closure safety in the PSAR. The conclusions are further discussed and substantiated in the following sections of this chapter.

15.2.1 Compliance with regulatory risk criterion

A repository at Forsmark is assessed to comply with the regulatory risk criterion

The analyses carried out in the PSAR show that a KBS-3 repository at Forsmark constructed in accordance with the current reference design will comply with the regulatory risk criterion issued by SSM.

The likelihood of canister failures during the initial one thousand years, is assessed as negligible

The pessimistically calculated mean number of canisters failing due to earthquakes during the initial one thousand years is of the order of one in a hundred thousand. All other failure types are assessed as ruled out for this period. Furthermore, the evaluations of the canister sealing procedure, have led to the conclusion that all canisters will be tight at deposition.

In a one million year time perspective, there is a small risk contribution from canister failures due to enhanced corrosion following buffer erosion and sedimentation

Loss of buffer may occur from exposure to low ionic strength waters but the extent is uncertain. The Forsmark site has a large potential to maintain a sufficient ionic strength at repository depth over a glacial cycle. Loss of buffer mass due to erosion, to the extent that advective conditions arise in the deposition hole, may, however, occur in a 100 000 year perspective for typically less than ten deposition positions with high flow rates. Estimates of buffer loss due to sedimentation, based on pessimistic extrapolation to repository conditions of early experimental results, suggest that this process may lead to similar, or at most an order of magnitude higher, losses.

Advective conditions in a deposition hole will enhance the canister corrosion rate. In a one million year time perspective, this may lead to failures of a few canisters when applying the most pessimistic of the hydraulic interpretations made of the Forsmark site, with cautious assumptions regarding concentrations of corrosive agents and deposition hole acceptance rules.

With pessimistic assumptions regarding buffer erosion, buffer sedimentation, copper corrosion and radionuclide transport conditions, the radiological risk from such canister failures is pessimistically calculated to be around 1/100 of the regulatory limit in a 100 000 year perspective and around 1/10 of the regulatory limit in a one million year time perspective.

In a one million year time perspective, there is a small risk contribution from canister failures due to earthquakes

Canister failures due to large earthquakes cannot be categorically ruled out. However, the probabilistic analyses imply that, on average, it would take considerably more than one million years for even one such canister failure to occur.

The contribution to radiological risk from earthquakes is pessimistically calculated to be less than 1/100 of the regulatory limit in a 100 000 year perspective and less than 1/10 of the regulatory limit in a one million year time perspective. Studies performed since the SR-Site assessment within the PSAR further substantiate the pessimistic nature of this calculation as regards the likelihood of detrimental rock shear movements.

15.2.2 Issues related to altered climate conditions

Several issues of importance for post-closure safety are related to future glacial, periglacial or warmer climate conditions. A number of conclusions regarding effects of such conditions can be drawn.

Detrimental freezing of the buffer is ruled out – even for very pessimistically chosen climate conditions

According to the analyses, detrimental freezing of the buffer clay is ruled out, even for the most pessimistic periglacial climate conditions considered, which includes the large uncertainties related to future climate development. Also freezing of a deposition tunnel backfill material or of a water-filled cavity in an eroded buffer is ruled out for the most pessimistic climate development at Forsmark. The temperature at which a frozen buffer could cause detrimental effects on a canister is assessed to be $-6\text{ }^{\circ}\text{C}$ in the PSAR, giving even higher safety margins than for the $-4\text{ }^{\circ}\text{C}$ freezing criterion applied in the SR-Site assessment.

Canister failure due to isostatic load is ruled out – even for very pessimistically chosen climate conditions

According to the analyses, canister failure due to isostatic load is ruled out for the most severe future glacial conditions considered based on the glacial development of the past two million years. New studies conducted since the SR-Site assessment imply that the pessimistically estimated peak glacial load at the Forsmark site may be almost 20 % higher than assessed in SR-Site. Updated design requirements, however, imply a lowered maximum buffer swelling pressure and an increased canister resilience to isostatic loads. The updated design analysis of the canister suggests that the current design will sustain the estimated peak load at Forsmark with a considerable margin. This applies to both the static load on the insert and to long-term creep in the copper shell.

Oxygen penetration is very unlikely – even for very pessimistically chosen climate conditions – and the consequences are small

Oxygen penetration to canister positions is ruled out, except for enhanced flow situations occurring during the unlikely event when an ice sheet margin is temporarily stationary above the repository in combination with several other pessimistic assumptions. Even in such a case, the consequences in terms of canister corrosion are small.

Repository safety for a prolonged period of warm climate before the next glacial period is assessed as comparable to safety for a climate unperturbed by enhanced global warming

A prolonged period of warm climate (global warming due to an enhanced greenhouse effect) at the expense of the duration of glacial conditions is expected to lead to decreased exposure to dilute groundwater of a repository at Forsmark and hence to decreased buffer erosion and sedimentation.

The occurrence of large earthquakes is likely to increase during deglaciation, and this effect is thus delayed by a prolonged initial period of warm climate.

15.2.3 Other issues related to barrier performance and design

The reference design, forming the basis for the assessed initial state in the PSAR, yields a safe repository when implemented at the Forsmark site

Since the analyses in the PSAR show that the regulatory risk criterion is fulfilled, it is concluded that the assessed reference design implemented through the selected production and control procedures will yield a safe repository. The design requirements, the reference design and the production and control procedures have been substantially updated since the SR-Site assessment. Conclusions regarding design issues important for post-closure safety yielding feedback to future refinement of the design have been drawn.

It is crucial to avoid deposition positions intersected by large or highly water conductive fractures and the low frequency of water conducting fractures allows efficient application of such rejection criteria

The risk contributors are related to the occurrence of large and/or highly conductive fractures intersecting deposition holes. This applies to the buffer erosion process and the impact of major earthquakes in the vicinity of the repository. These two phenomena are related to canister failures due to canister corrosion and to secondary rock shear movements, respectively. As also the retention in large, highly transmissive fractures is small, such failures are in general associated with high consequences. Accordingly, such fractures need to be avoided once identified.

Cautious assumptions regarding the likelihood of occurrence of such fractures and regarding deposition hole rejection criteria are adopted in the PSAR. The results of the analysis are sensitive to these assumptions. It is important to continue the development of acceptance criteria for deposition holes as a basis for future assessments. This needs to be studied both by simulation of the effects of applying potential criteria and by exploring the practicability of applying the criteria.

The heat from the canister will likely fracture the rock in the deposition hole wall, which would enhance the in- and outward transport of dissolved substances, but this has little impact on risk

Thermally induced spalling around deposition holes at Forsmark cannot be ruled out and may have a considerable impact on mass exchange between the flowing groundwater and the buffer as long as diffusion is the dominant transport mechanism in the buffer. For diffusive conditions, there is, however, a considerable margin to canister failures even when spalling is pessimistically assumed in all deposition positions at Forsmark. If advective conditions prevail in the buffer, the effects of spalling are much less pronounced because it adds little to the already increased flow rate. In consequence, the overall effect on the calculated risk is small.

The importance of the excavation damaged zone in the rock around the deposition tunnels as a transport path for radionuclides is limited

The importance of the excavation damaged zone (EDZ) around deposition tunnels is limited in comparison to other transport routes for radionuclides. Very pessimistic assumptions about the EDZ in relation to the reference excavation method could affect the extent of canister corrosion for advective conditions.

This confirms the suitability of the cautious reference excavation methods adopted in the reference design of the repository.

In most deposition holes groundwater will not reach the canister for thousands of years due to the favourable rock properties at Forsmark

The saturation times for both backfill and buffer are likely to range from a few tens of years to several thousand years, as a consequence of the rock properties (matrix hydraulic conductivity and presence and characteristics of fractures) at Forsmark. The majority of deposition holes are not intersected by water conducting fractures, yielding slow saturation (with water from the deposition tunnel backfill) and slow inflow of e.g. corrosive agents in the groundwater both during unsaturated and saturated conditions. Transport of corrosive agents within the bentonite will be very limited and diffusion-dominated also during the unsaturated phase. Since the groundwater flow during saturation is towards the deposition holes, no erosion of the bentonite can occur during the unsaturated period. The effects of the unsaturated period on the geochemical, mineralogical and thermal property changes in the buffer have been investigated. They are found to be small and without any significant impact on long-term performance. Compared to the SR-Site assessment, considerable additional attention has been paid to the early conditions with particular focus on canister integrity.

15.2.4 Confidence

In summary, the elements contributing to the overall confidence in the assessment results are as follows.

- The knowledge of the Forsmark site from the completed, surface based investigations is sufficient for the assessment of post-closure safety. The site has favourable conditions for safety and no site-related issues requiring resolution in order to demonstrate safety have been identified.
- There is a well-established reference design with specified and achievable production and control procedures yielding an initial state of the repository system with properties favourable for post-closure safety at the Forsmark site. There is potential for additional optimisation when this reference design is developed and implemented, as is further discussed in Sections 15.3.5 and 15.5.
- The scientific understanding of issues relevant for post-closure safety is sufficiently mature for the purpose of the analysis of post-closure safety, as a result of decades of research both within the Swedish and other national programmes and in international collaboration projects.
- A complete analysis of issues identified as relevant to post-closure safety has been carried out in the PSAR according to an established assessment methodology comprising e.g. cautious approaches when addressing uncertainties.
- Documented quality assurance routines, including peer reviewing, have been applied in the assessment of the initial state, in the development of the site description and in the analysis of post-closure safety.

The discussion of confidence is further developed in Section 15.3.6.

15.3 Demonstration of compliance

15.3.1 Introduction

From applicable regulations from SSM and general recommendations and guidance associated with these regulations, a number of requirements on presentation of a compliance evaluation can be derived. The requirements are here categorised and addressed as follows:

1. Account of calculated risk to individuals, Section 15.3.3.
2. Account of effects on the environment from release of radionuclides, Section 15.3.4.
3. Demonstration of use of best available technique, BAT, Section 15.3.5.
4. A discussion of confidence, Section 15.3.6.
5. Other, general requirements on the system, e.g. demonstration of a multi-barrier system, Section 15.3.7.
6. General requirements on the safety assessment (adequate handling of uncertainties, quality assurance, etc), Section 15.3.8.

The above structure does not, however, address all aspects of the regulations. For a complete account of how the PSAR post-closure safety report meets these requirements, the reader is referred to Appendix A, where the regulations are reproduced and where references are given to sections in this report where each issue is addressed.

The analyses and conclusions in the PSAR are based on an established reference design with specified and achievable production and control procedures yielding an initial state of the repository system with properties favourable for post-closure safety at the Forsmark site. The engineered parts of the repository system are based on demonstrated technology and established quality assurance procedures to achieve the initial state of the system, including the construction of the repository facility. This is systematically documented in the **Production reports** and their underlying references as summarised in Chapter 5.

As an introduction to the discussion of compliance, a brief account of the safety concept, evaluated by results from the PSAR is given in Section 15.3.2 immediately below.

15.3.2 The safety concept and allocation of safety

The main safety function of the KBS-3 concept is containment and the secondary safety function, mobilised if the containment function is not upheld, is retardation.

Containment

The containment function is provided by an intact copper shell of the canister. The extent to which this function is upheld is dependent on the buffer's function of limiting advective transport between the host rock and the canister and on favourable mechanical, hydrogeological and geochemical properties of the host rock: i) limited flow rates and a minimum charge concentration of the groundwater to avoid erosion of the buffer ii) limited flow rates and low groundwater concentrations of sulphide to limit corrosion, in particular if the buffer has been eroded, and iii) a low probability of large fractures intersecting deposition holes in order to limit the potential impact on the canister of large earthquakes in the vicinity of the repository.

The analyses in the PSAR indicate that containment is maintained even in the one million year perspective for a vast majority of canisters. Deterioration of the barrier system to the extent that containment is lost is assessed to only occur, as a statistical average, for less than one canister due to buffer erosion leading to advective conditions and enhanced corrosion. The other failure mode that could not be ruled out, that due to earthquake-induced secondary shear movements in fractures intersecting deposition holes, is even less likely and affects on average considerably less than one canister when this failure mode is evaluated statistically with a number of pessimistic assumptions. This means that containment is assessed to be maintained for the vast majority of the 6 000 canisters throughout the assessment period.

All safety functions related to containment are shown in Figure 8-3. Many of these, like the canister's ability to withstand isostatic loads or the "ability" of the host rock to provide a favourable rock temperature, are assessed as upheld throughout the assessment period.

It is also noted that the consequences of a postulated, complete loss of containment for all canisters decrease with time, and are about a factor of 3 higher than the regulatory risk limit at the end of the assessment period (hypothetical case C in Figure 13-72).

Retardation

Both the failure mechanisms that could not be ruled out are of the common mode type, i.e. the canister, the buffer and the rock are all affected, either through a detrimental shear movement or through a high flow rate in the geosphere, affecting both erosion and corrosion. The causes of the failures affect also the retention properties through high flow rates and, in the case of erosion, through the absence of the buffer after failure. Hence the retarding potential of the repository is limited in these particular cases, for the canisters that have failed. Instead, safety is to a considerable extent achieved through the slow dissolution of the fuel and, to a lesser extent, through the limited corrosion rate of radionuclide-containing metallic structural parts of the fuel elements.

For the canisters that maintain their containment potential, retardation is a latent safety function throughout the assessment period. A more general view of the retarding potential of the buffer and the host rock is obtained from the analyses of hypothetical, complete losses of barrier functions in Section 13.7.4.

Retention in the buffer is important for the initial 1 000 years and limited in longer time frames (compare cases C and D in Figure 13-72). The latter is due to the fact that the total dose in the long-term is dominated by non-sorbing or very long lived nuclides. However, a nuclide specific comparison (Figure 13-68 and Figure 13-66) reveals that the buffer has a considerable retention function for sorbing nuclides also in the long-term, masked in the total dose by the dominance of the non-sorbing species.

The role of retention in the rock is similar; it is important for the initial 1 000 years and limited in longer time frames (compare cases C and C* in Figure 13-72) as concerns total dose, again since total dose is then dominated by nuclides that do not sorb in the rock. A nuclide specific comparison (Figure 13-67 and Figure 13-66) reveals that the rock has a considerable retention function for sorbing

nuclides also in the long-term, masked in the total dose by the dominance of the non-sorbing species. The low flow rates at repository depth also play an important role in limiting the release rate of radionuclides to the rock.

Summary

In summary, containment is the primary safety function of the KBS-3 repository and it is demonstrated to be efficiently upheld at the Forsmark site throughout the assessment period, directly through the properties of the canister and indirectly by the favourable hydrogeological and geochemical properties of the host rock. For the rare failures of containment, retardation is of limited importance due to the common mode nature of the failure mechanisms in question and since only very long-lived nuclides remain when these failures occur. As a latent function, retardation is significant for hypothetical releases of, in particular, sorbing species throughout the assessment period. For hypothetical failure modes affecting the canister only, retardation of sorbing nuclides is significant in the buffer and in the host rock.

15.3.3 Compliance with SSM's risk criterion

This section contains a discussion of the compliance with SSM's risk criterion in different time frames. A discussion of confidence in the results, e.g. that the assumed initial state or site properties in the assessment are justified, is given in Section 15.3.6.

Regulatory requirements

The primary compliance criterion in Swedish regulations is SSM's risk criterion. An account of the calculated risk is, therefore, an essential component of a compliance demonstration for the first 1 000 years. This is also explicitly stated in SSM's General Guidance, where a reporting of contributions to risk from each analysed scenario is also requested.

Also for the initial 100 000 years, approximately corresponding to the length of one glacial cycle, a risk calculation is required. SSM states the following regarding this period in its General Guidance:

“Reporting should be based on a quantitative risk analysis in accordance with the guidelines to Sections 5–7. Supplementary indicators of the repository's protective capability, such as barrier functions, flow of radionuclides and concentrations in the environment should be used to strengthen the confidence in the calculated risks. The given period of time of one hundred thousand years is approximate and should be selected in such a way that the effect of expected large climate changes, for instance, a glaciation cycle, on the protective capability of the repository and consequences to the surroundings can be illustrated.”

Regarding the time beyond the initial 100 000 years, SSM states the following in its General Guidance:

“The risk analysis should illustrate the long-term development of the repository's barrier functions and the importance of major external disturbances on the repository such as earthquakes and glaciations. Taking into consideration the increasing uncertainties over time, the calculation of doses to people and the environment should be made in a simplified way with respect to climate development, biosphere conditions and exposure pathways. Climate development can be simplified by being described as a repetition of identical glaciation cycles.

A strict quantitative comparison of calculated risk in relation to the criterion for individual risk in the regulations is not meaningful. The assessment of the protective capability of the repository should instead be based on reasoning on the calculated risk together with several supplementary indicators of the protective capability of the repository such as barrier functions, flows of radionuclides and concentrations in the environment. If the calculated risk exceeds the criterion of the regulations for individual risk or if there are other indications of substantial disruptions of the protective capability of the repository, the underlying causes of this should be reported on as well as possible measures to improve the protective capability of the repository.”

Calculated individual risk in the PSAR

A detailed summary account of the calculated individual risk for a repository at Forsmark is given in Section 13.9. The details are not repeated here, but the numerical result of the risk summation of the two contributing scenarios, the corrosion scenario and the shear load scenario is reproduced in Figure 15-2, as a background to the discussion below.

Compliance for the first 1000 years

All canisters are assessed to be tight at deposition. The initial copper coverage is discussed in the account of the initial state of the canister in Section 5.4.3. The initial minimum copper thickness is given as 47.5 mm in Table 5-9. Taking also the occurrence of local internal defects in the copper shell into consideration, no canisters are assessed to have local reductions exceeding 10 mm. This is the manufactured and inspected thickness of the corrosion barrier after the final machining of the canister components.

As required by SSM's regulations, many aspects of the repository evolution have been modelled in detail for the initial 1000 years. This concerns the thermal, mechanical, hydraulic and chemical evolution, as well as effects on the buffer and the canister. Detailed accounts are given in Sections 10.2 (the excavation and operational phases) and 10.3 (the initial period of temperate climate after closure). Also the biosphere development is modelled in detail during this time period.

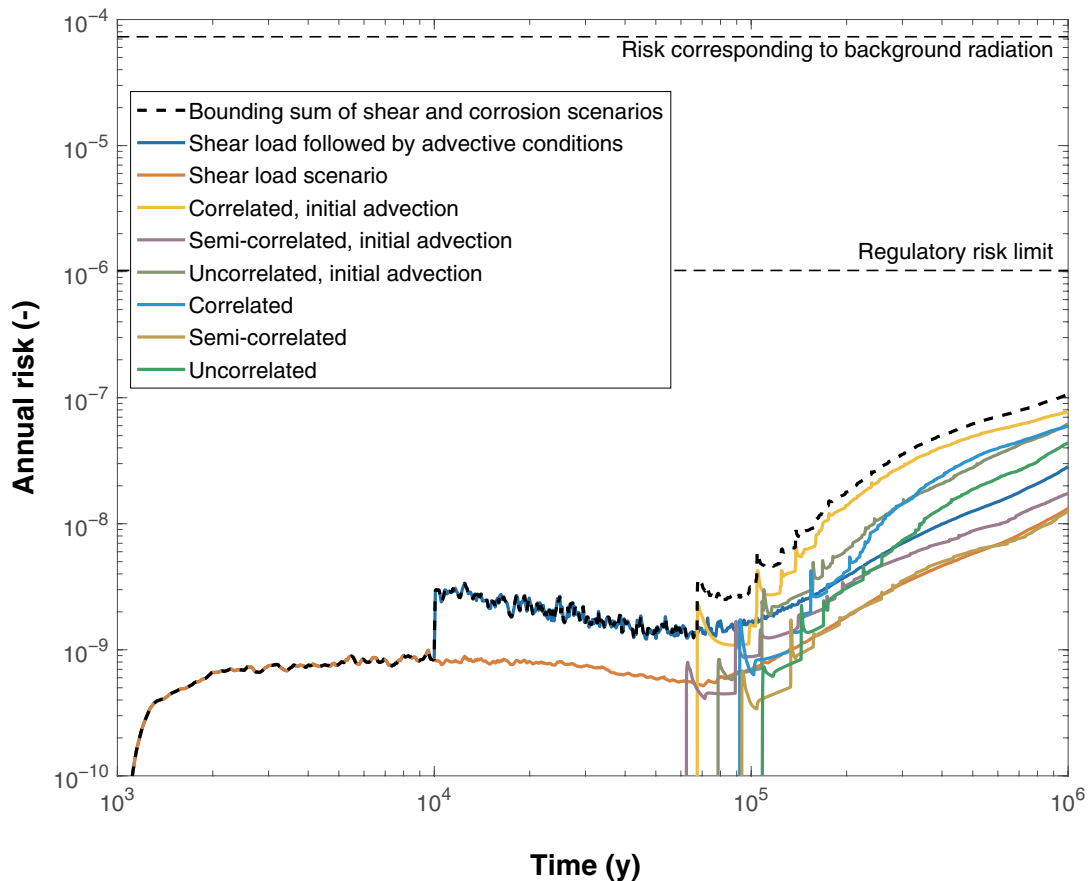


Figure 15-2. Risk curves, expressed as annual individual risk. Several alternatives for the corrosion scenario are shown, and two for the shear load scenario. The bounding, dashed curve is the sum of the curve for the shear load failure followed by advective conditions (dark green) and the curve for the variant of the corrosion scenario yielding the highest risk (brown). The risk associated with the main scenario is subsumed under the corrosion scenario as it is equal to the semi-correlated case (blue).

Of the three identified failure modes of the canister, i.e. failure due to corrosion, due to shear load and due to isostatic loads, corrosion and isostatic load induced failures can be ruled out with large margins for the first 1 000 years, as demonstrated in the reference evolution (Chapter 10) and the analyses of the corrosion and isostatic load scenarios (Sections 12.6 and 12.7, respectively). It is noted that the discussion on early canister failures has been extended substantially, in particular for the corrosion scenario (see Section 12.6.3), compared to the SR-Site assessment.

Shear loads on the canister may occur as a consequence of large earthquake induced secondary shear movements in fractures intersecting deposition holes. Although the likelihood for large earthquakes is higher during periods of increased tectonic stress, for example during glacial rebound, it cannot be entirely ruled out that a detrimental earthquake would occur during the initial 1 000 years.

The probability that one out of the 6 000 canisters has failed at the end of the initial 1 000 year period is pessimistically estimated at 2.4×10^{-5} , see further Section 10.4.5, i.e. hypothetically 40 000 repositories, each with 6 000 canisters would have to be constructed in order for there to be an expectation of one failure during the initial 1 000 years. Despite this extremely low probability, a risk contribution was calculated for the first 1 000 years, with the result that the mean annual dose is at most around $0.001 \mu\text{Sv/yr}$ corresponding to a risk of $10^{-10}/\text{yr}$, see Figure 13-52 in Section 13.6. This analysis builds on a detailed modelling of the biosphere development and radionuclide transport in the developing landscape during the initial 1 000 years, as required by SSM's Regulations.

It is, therefore, concluded that the analysed repository at Forsmark complies with the regulatory risk criterion during the initial 1 000 years after closure.

In hypothetical cases of initially defective canisters, there are several properties of the barrier system that provide protection, some of which are not important, or more difficult to claim, in longer time frames. As discussed in Section 13.9.6, some of these would, with cautious assumptions, alone prevent any releases during the initial 1 000 years for an initially defective canister. This relates particularly to the time required for water to get into contact with the fuel elements and the integrity of the Zircaloy cladding.

Compliance for the initial glacial cycle

As reported in Section 13.9 and reproduced in Figure 15-2, the calculated, pessimistically bounded risk during the initial 120 000 year glacial cycle is at most about $10^{-8}/\text{yr}$, i.e. about two orders of magnitude below the regulatory limit.

Only the shear load scenario contributes to risk for the first tens of thousands of years. Consequences in the corrosion scenario occur after about 50 000 years for the highly pessimistic and bounding case where initial advection in all deposition holes is assumed. With cautious estimates of the extent of buffer erosion, the first consequences of the corrosion scenario occur at the earliest after around 100 000 years.

Repository performance for the time beyond the initial glacial cycle up to one million years

As reported in Section 13.9 and reproduced in Figure 15-2, the calculated, pessimistically bounded risk beyond the first 120 000 year glacial cycle up to one million years is at most about $10^{-7}/\text{yr}$, i.e. about one order of magnitude below the regulatory limit.

In this time frame, both the shear load scenario and the corrosion scenario contribute to the calculated risk. The contributions are comparable in magnitude. However, since both are represented by pessimistic bounding cases, and because the pessimistic assumptions differ between the scenarios, the two risk contributions cannot be directly compared.

Alternative safety indicators for this time period are discussed below.

Risk dilution

Risk dilution was analysed in connection with the risk summation in Section 13.9 and found not to challenge the conclusion regarding compliance with the risk criterion in any of the time frames.

Alternative safety indicators

In particular for times far into the future, the calculated risk becomes less useful as an indicator of repository safety, and SSM's Regulations suggest that alternative indicators should, therefore, also be evaluated. Four alternative indicators to risk are used in the PSAR, as described in Section 13.5.8.

The following results emerged for the central corrosion case.

- Peak releases of activity from the geosphere are about three orders magnitude below the activity constraints issued by the Finnish regulator STUK.
- The peak radiotoxicity flux from the geosphere is more than three orders of magnitude lower than the reference value for radiotoxicity flux from the geosphere suggested by the EU SPIN project.
- Calculated radionuclide peak concentrations in ecosystems at Forsmark from repository releases of Ra-226 are about three orders of magnitude below measured concentrations of naturally occurring Ra-226 at Forsmark.
- Peak geosphere fluxes caused by Ra-226 releases from the repository are about two orders of magnitude below naturally occurring fluxes of Ra-226 at the site, as estimated from site data; the difference is larger for U-234 and U-238. The total release of all repository derived nuclides converted to dose is also around two orders of magnitude lower than the summed dose from fluxes of the three mentioned naturally occurring nuclides.

The results are readily applicable to other corrosion cases, for most indicators by simply scaling by the release of Ra-226, which is, at most, one order of magnitude higher than that for the central corrosion case.

Similar conclusions are reached for the shear load scenario, as accounted for in the **Radionuclide transport report**.

In summary, the application of alternative indicators shows that releases from the repository are orders of magnitude below the adopted reference values for the indicators. This suggests that the future radiological consequences on man and on the environment of releases from the repository are negligible, independent of assumptions in the biosphere model.

The time beyond one million years

The evolution of the repository after 1 million years is discussed in Section 14.5.

An account of the development of the radiotoxicity of the spent nuclear fuel up to ten million years is given in Figure 2-1 in Section 2.4.

Although the rocks, the ductile deformation and the brittle deformation zones at Forsmark all formed at least one billion years ago, the increasing uncertainties regarding the external conditions makes it not meaningful to predict the development of the site and of the repository for time periods beyond one million years.

It is noted that the hypothetical case in Section 13.7.4, where all canisters are failed, where the buffer is absent and where retention in the rock is disregarded, yields releases that correspond to dose consequences that are comparable to the natural background radiation after one million years. The releases are in that case controlled by the groundwater flow at repository depth and the inventory of radionuclides, the latter of which decreases with time and is dominated by radionuclides that also occur in natural ore bodies.

Finally, the scientific understanding of the fuel dissolution process suggests that the longevity of the spent fuel matrix is several million years in the repository environment (see Section 13.5.5). Furthermore, uranium ores that are many millions and even billions of years old are known through geological observations. This indicates that, in the case of stable tectonics and maintained reducing conditions in the repository, the uranium oxide which constitutes the fuel matrix can be stable for many millions of years.

Uncertainties linked to the risk calculation for different time periods

Uncertainties that have a significant influence on the calculated risk are discussed in Section 13.10, Table 13-13, where the handling of the uncertain factors in the PSAR is summarised together with references to plans for the reduction of these uncertainties. As seen in the table, most of the uncertain factors have been treated pessimistically, whereas some have been included as probability distributions in the risk calculations, where their full uncertainty range is used in the determination of mean annual doses, the relevant metric for determining the calculated risk.

The combination of pessimistic handling of uncertainties for which probability distributions could not be determined with the probabilistic handling of quantified uncertainties means that the total risk as determined in the risk summation in Section 13.9 is claimed to represent an upper bound on risk. Since this upper bound is below the risk limit throughout the one million year assessment period, there are no uncertainties of critical importance to resolve with respect to risk.

15.3.4 Effects on the environment from release of radionuclides

Doses to non-human biota for the central corrosion case have been calculated according to the methodology described in Section 13.2.5. The results are presented in Section 13.5.7. The highest dose rates to organisms in marine, freshwater and terrestrial ecosystems in Forsmark, both in total and for the dose-dominating radionuclides are well below the screening dose rate ($10 \mu\text{Gy h}^{-1}$) recommended in the ERICA Integrated Approach. It is therefore concluded that radionuclide releases predicted for this case will not lead to significant detrimental biological effects on individuals of species found, or projected to occur in future, at the site. In consequence, there will be no detrimental impact on populations, communities or ecosystems.

The results are readily applicable to other corrosion cases, by scaling the releases of the nuclides in question, which are at most about one order of magnitude higher than that for the central corrosion case. This means that the conclusion for the central corrosion case holds also for all other corrosion cases considered in the PSAR.

Releases for the shear load scenario have not been analysed with respect to doses to biota in the PSAR. However, since the releases are generally lower for this scenario than for the corrosion scenario, and since the margin to the reference value is several orders of magnitude in the latter, it is concluded that the effects on the environment for the shear load scenario are of no concern.

15.3.5 Optimisation and best available technique, BAT

The basis for the contribution to the demonstration of optimisation and best available technique (BAT) from the PSAR post-closure safety assessment, as well as existing regulatory requirements and general guidance is provided in Section 2.7. While, a general account of the use of BAT is a broad issue spanning from the selection of method for the management of nuclear waste to fine details of the selected method, a limited part of this broad issue can and should be addressed in the safety assessment of the preferred method.

Based on the findings from the PSAR, and especially the specific assessment presented in Section 14.3, feedback can be given whether alterations in relation to the analysed reference design could lead to reductions in risk or in reduction in uncertainties that potentially could affect risk. For aspects of the design where no such reduction in risk or uncertainty in fulfilment of safety functions can be seen to be realistically obtainable, the PSAR claims the solution to be optimal and BAT. However, the PSAR is not an assessment of all conceivable technical solutions. SKB will continue technical development of several aspects of the design in order to further simplify construction and implementation, adopting these developments provided that they comply with all other requirements on post-closure safety.

The canister

The assessment presented in Section 14.3 shows the following.

- Increasing the copper thickness to 10 cm reduces the mean number of failed canisters at one million years by a factor of about 3 while halving the thickness to 2.5 cm increases the number by about a factor of 2. However, since the calculated risk with the reference design is below the regulatory limit, the risk reduction obtained by increasing the thickness is moderate. Furthermore, considering the added problems of manufacturing and sealing a thicker canister, the selected copper thickness is deemed adequate from the point of view of BAT. An increase to, e.g., 10 cm would also imply a substantial and unmotivated increase in cost.
- The specified values for elongation and creep ductility in the copper shells are found appropriate and it is judged that there is little prospect that changing these properties would enable the canister to withstand even larger shear loads.
- The ability of the cast iron insert to withstand shear load depends mainly on the occurrence of surface defects in the insert. While it is concluded in the **Canister production report** that the current canister reference design conforms to the stated design premises, it is also noted that rigorous requirements are placed on manufacturing and NDT (non-destructive testing) capability.
- For the given reference design, there is ample margin to prevent canister failure due to isostatic load, even for the most extreme load situations and there seems to be no need to change the design in order to increase this margin. This applies to both the static load on the insert and long-term creep in the copper shell.

In conclusion, there seems to be little need to alter the canister design from a safety perspective.

The buffer

The assessment presented in Section 14.3 shows the following.

- A larger buffer mass, e.g. by increasing buffer thickness or buffer density, is not seen as a practical means of mitigating the effects of buffer erosion. A larger buffer mass may offer a slightly longer time before advective conditions are created in the deposition hole, but this is not seen as a solution to the buffer erosion issue.
- The assessment of buffer erosion/sedimentation/colloid release, summarised in Section 10.3.11, demonstrates that the phenomenon cannot be ruled out in the assessment of post-closure safety. Furthermore, there is still uncertainty with regard to modelling of colloid formation and subsequent erosion and sedimentation of the buffer material and the modelling approach thus tends to be pessimistic. It also seems clear that it cannot, with the current understanding, be defensibly mitigated by e.g. selection of another buffer material. A continued R&D programme on buffer erosion and sedimentation mechanisms is needed and is being implemented, see further Section 15.7.3.

The deposition tunnel backfill

The assessment presented in Section 14.3 shows that the buffer and the associated safety functions will be maintained during the expansion of the buffer into the backfill for all possible combinations of buffer and backfill conditions. For the case when backfill material is lost, a maximum loss of 220 tonnes in a deposition tunnel section can be allowed before advective conditions have to be considered in the deposition hole. However, none of the single fractures intersecting the tunnel close to deposition holes will cause loss of the backfill to the extent that it loses so much swelling pressure that advective conditions must be assumed in underlying deposition holes. For a few positions, where the tunnel is intersected by a very transmissive deformation zone, potentially more than 220 tonnes could be lost, but since these positions are far away from deposition holes, this is judged not to impair safety. In conclusion, while there possibly could be improvements in the backfill design from an installation point of view, there does not seem to be a need to change the design to further improve its safety functions.

Repository layout and acceptance criteria for deposition tunnels and deposition holes

As demonstrated in Section 14.3, the application of deposition acceptance criteria in the form of EFPC is important for limiting risk, both directly for mitigating the potential for canister shear failure due to earthquakes and indirectly for limiting the future high flows affecting the potential for advective conditions in the buffer and the potential for subsequent canister failure by corrosion.

With regard to shear failure, it is, as argued in Munier (2010) likely that critical fractures that escaped detection by strict application of EFPC will indeed be detected by a carefully designed investigation programme and that it is likely that the number of potentially damaged canisters will be lower than predicted in this assessment.

Regarding corrosion failure, application of EFPC significantly reduces the number of deposition holes with high Darcy flux, since there is a correlation, of uncertain magnitude, between fracture size and transmissivity. However, it can also be concluded that if it would be possible to even better identify the few deposition hole positions having the largest Darcy flux during saturated conditions before canister emplacement, this could contribute to a more efficient use of the rock volume.

From the viewpoint of BAT, the current EFPC provides adequate protection against shear failure, but there is reason to continue the efforts envisaged in the detailed investigation programme to be able to find critically large fractures by other means, since such efforts are also likely to result in criteria where fewer deposition holes would need to be rejected, contributing to a more efficient repository design.

Application of EFPC is also important for protection against corrosion failures, but criteria directly connected to the flow properties are preferable to such indirect criteria as discussed in Section 5.2.3. Specifically, there is a potential for enhancing safety by adopting technical design requirements for deposition hole positions using hydraulic injection tests in the pilot holes of the deposition holes. Even if the correlation between specific capacities obtained from the injection tests during the operational phase and long-term flow characteristics is not one-to-one given differences in boundary condition, the rejection of deposition hole locations failing the technical design requirement will (statistically) improve safety. Furthermore, deposition holes intersected by fractures showing visible grout also should be rejected, since the presence of grout suggests that the fracture was quite transmissive before grouting.

The assessment in Section 14.3 also shows that the number of failed canisters due to corrosion would increase if there is an EDZ that is much more transmissive than the currently stipulated limit of 10^{-8} m²/s, but the assessment also shows that there is no need to apply a more restrictive limit, i.e. the number of failed canisters would not decrease even if there was no EDZ at all.

In conclusion, the analyses show that for the scenarios contributing to risk (corrosion and shear failure) it is essentially the details of the layout, like the exact position of deposition holes and what deposition holes would be accepted that is important. These details can only be finalised during repository construction and operation and by application of the observational method using findings from the underground based detailed investigations and by applying the technical design requirements for accepting deposition holes, as discussed above. Thus, the question as to whether the repository layout is BAT can at this stage only be assessed based on these technical design requirements. More specific feedback on these is given in Section 15.5.

Repository depth

As concluded from the assessment of the adequacy of the selected repository depth, presented in Section 14.3.4, the depth has mainly been decided by considering the hydraulic conditions at the Forsmark site, i.e. frequency and occurrence of transmissive fractures and their dependence on depth, whereas the constructability is mainly related to rock mechanical issues, e.g. the likelihood and extent of spalling in deposition holes prior to emplacement. More detailed conclusions are given below.

- Factors relating to the chemical stability safety function R1, “Provide chemically favourable conditions”, are generally favourable at the selected depth. The only remaining chemical stability issues of concern for repository safety relate to the potential for a few deposition holes to experience groundwater with too low an ionic strength and to the presence of sulphide. Generally, the risk of penetration of dilute waters would decrease with increased repository depth. However, the few

occurrences of such potential penetration are related to the scarce occurrence of highly transmissive migration paths in the generally very tight rock. There is no evidence that a practically realistic increase of the depth (i.e. in the order of a 100 m) would dramatically reduce the occurrence of such isolated paths – and it seems a better strategy to try to avoid them locally. Furthermore, there is no indication that the occurrence of sulphide is correlated to depth.

- Safety function R2a “Transport resistance in fractures, F” is affected by repository depth. The length of the travel paths of solutes in the groundwater will increase with increasing depth, but the resulting impact on the transport resistance would only be marginal.
- Both safety functions R2a “Transport resistance in fractures, F” and R2b “Equivalent flow rate in buffer/rock interface, Q_{eq} ” are affected by repository depth, since fracture frequency and fracture transmissivity show depth dependence. However, the chosen repository depth below 450 m is sufficient to reach the low fracture frequency and low permeability rock volumes at Forsmark, and there does not seem to be any advantage in going deeper.
- Groundwater pressure, safety function R3a, increases with depth. However, compared with the buffer swelling pressure and hydrostatic pressures from a glacial overburden, the increased pressures are of marginal importance.
- Rock stress indirectly affects safety function R2b “Equivalent flow rate in buffer/rock interface, Q_{eq} ”, since the in situ stress determines the potential for spalling. Stress in general increases with depth, but placing the repository at 400 m or 500 m depth does not significantly alter the risk for spalling in the deposition holes.
- The in situ temperature relates to safety function R4 “Provide favourable thermal conditions”. The temperature increases with depth and this needs to be considered in the repository layout. However, given that this is considered in the repository design, there are no other detrimental effects of the elevated in situ temperature with depth.
- The likelihood of freezing, safety function R4, decreases with increasing depth. The analyses in the PSAR have, however, demonstrated that freezing of the buffer can be considered as a residual scenario and also freezing of the deposition tunnel backfill at these depths can be ruled out.
- Surface denudation (erosion and weathering) of the host rock has been estimated to generally be limited to a few metres or less per glacial cycle for the Forsmark repository site and less than 50 m for the coming 1 million years. Therefore, surface denudation does not have to be considered when determining repository depth within the reference interval 400–700 metres.
- The probability of inadvertent human intrusion into the repository decreases with increasing depth. In general, intrusion to several hundred metres is considered unlikely in rock poor in resources.

In conclusion, the selected repository depth is adequate and changing the depth is not deemed to significantly reduce the calculated risk. Furthermore, a shallower location, e.g. above the 400 m level, might increase the risk, since the frequency of water conducting fractures is higher there. Placing the repository some 100 m deeper would probably result in a risk contribution similar to the one obtained from the selected depth, whereas much deeper locations would imply that additional factors, such as very high stress levels, might need to be considered. Repository depth will finally be decided and verified during repository access construction with associated detailed investigations as further described in the **Underground openings construction report**.

15.3.6 Confidence

The assessment of post-closure safety is a key part of the PSAR. An approval of the PSAR by SSM is required for SKB to start construction of the final repository. The PSAR thus forms an important basis for a major decision point in SKB’s programme for the management of spent nuclear fuel. A statement on the confidence in the results obtained in the PSAR is, therefore, appropriate. The confidence in the results obtained is assessed as sufficient for the decision at hand based on the following.

- The knowledge of the Forsmark site from the completed, surface based investigations is sufficient for the assessment of post-closure safety. The site has favourable conditions for safety and no site-related issues requiring resolution in order to demonstrate safety have been identified. Confidence in the site-descriptive model and in the understanding of the site is obtained by a systematic and

quality assured programme for site investigations and site modelling. The confidence in the site model is assessed in detail and documented in the **Site description Forsmark**. Key properties of the site are documented in Chapter 4 of this main report.

- There is a well-established reference design with specified and achievable production and control procedures yielding an initial state of the repository system with properties favourable for post-closure safety at the Forsmark site. The engineered parts of the repository system are to a large extent based on demonstrated technology and established quality assurance procedures to achieve the initial state of the system. This is systematically documented in the **Production reports** and their underlying references as summarised in Chapter 5. Examples of important aspects of the initial state of the engineered barriers include:
 - a. The copper canister sealing quality.
 - b. The cast iron insert casting quality.
 - c. Buffer characteristics such as installed mass and material properties.
 - d. Backfill properties ensuring its ability to keep the buffer in place and to swell.
 - e. The approach to adapt the repository to the detailed conditions found underground and the quality of the excavation technique.
 - f. The quality of the deposition technique.

There is potential for additional optimisation when this reference design is developed and implemented, as is further discussed in Sections 15.3.5 and 15.5.

- The scientific understanding of issues relevant for post-closure safety is mature as a result of decades of research both within the Swedish and other national programmes and in international collaboration projects. The R&D efforts to understand repository evolution and safety have led to the understanding of key processes like copper corrosion, shearing of canisters and other potential canister failure causes, and of key phenomena controlling retardation. This knowledge is, in the PSAR, systematically documented in several reports in a format suitable for use in the safety assessment, see further Chapters 6 and 7.
- The present PSAR post-closure safety report and its supporting documents have undergone comprehensive peer reviewing. In particular the scientific basis of the safety assessment has undergone review by recognised experts in the relevant fields of science.
- A complete analysis of issues identified as relevant to post-closure safety has been carried out in the PSAR according to an established assessment methodology, described in Chapter 2 and comprising e.g. cautious approaches when addressing uncertainties.
 - The understanding of safety is built on a systematic identification of safety functions and criteria for the safety functions, see Chapter 8.
 - Repository evolution is analysed with a structured approach in several time frames, addressing in each of these the processes that have been identified as relevant and with the safety of the system, as expressed by the safety functions, as a focus, see Chapter 10. Data uncertainties and data quality are assessed and documented according to a pre-established template, described in Chapter 9. Quality assurance of models and modelling is achieved by following procedures documented in the **Model summary report**. The assessment is then broken down into a set of scenarios to exhaustively scrutinise all possible ways in which the identified safety functions could be impaired and the consequences of such situations, see further Chapters 11, 12 and 13.
 - Confidence in the key results of radionuclide transport and risk calculations is enhanced by the fact that they can often be closely reproduced with simple, analytical models, using the same input data as the fully qualified numerical models.
 - The key results of radionuclide transport and risk calculations are overestimates since a number of pessimistic assumptions were made in the analyses, both regarding the extent of canister failures and regarding their consequences.
- Documented quality assurance routines have been applied in the assessment of the initial state, in the development of the site description and in the analysis of post-closure safety. This is part of the overall methodology followed in the assessment, as documented in Chapter 2.

Completeness, comprehensiveness

Also relevant for the confidence discussion is the issue of completeness or comprehensiveness of the assessment. This issue may be formulated through the following questions.

1. Have all factors relevant for post-closure safety been identified?
2. Have all identified factors been adequately treated in the assessment?

The following two points summarise the efforts made to ensure that all relevant factors have been identified, see also Section 2.8.3, in particular the subheading 'System uncertainty'.

- Decades of systematic and documented R&D, in international collaboration has been performed to achieve a sufficient knowledge of the repository system and its evolution. New phenomena have only rarely been identified in recent years, indicating that the scientific and technical foundation is mature. Several safety assessments have been performed throughout the years to obtain an integrated evaluation of the knowledge base and to provide feedback to the research programme.
- Systematic and documented studies of factors identified by other organisations have been made, e.g. by comparisons to internationally available FEP databases.

The question of whether all identified issues have been adequately handled in the assessment is partly addressed in the confidence discussion above. A more complete answer is provided by the description of the methodology for the assessment described in Chapter 2. Of particular relevance is the systematic handling of uncertainties described in Section 2.8.3. The scenario selection and analysis is claimed to be comprehensive based on the systematic focussing of the scenario selection on safety functions and a systematic handling of factors that could impair safety functions, followed by a handling of combinations of scenarios. A formal check whether FEPs omitted in earlier parts of the assessment are of negligible importance to safety in light of the completed scenario and risk analysis has also been made and is reported in Section 14.4.

The above points support the claim that the PSAR assessment is comprehensive, whereas completeness in a strict sense can never be proved. In this context it is, therefore, relevant to discuss possible consequences if completeness has not been achieved, for example if an important detrimental process remains unidentified despite all efforts to ensure the opposite. In its most extreme form, such a discussion may take the form of the consequences of complete, early loss of safety functions. As evidenced by the section below, even very extreme and completely unrealistic assumptions regarding early barrier losses yield calculated doses that are comparable with those caused by natural background radiation.

Based on the above reasoning, it is concluded that the PSAR assessment is sufficiently comprehensive for its purposes.

15.3.7 Bounding cases, robustness

In Section 13.7.4, a number of stylised, bounding cases illustrating complete, initial loss of important safety functions are analysed. The analyses led to the following conclusions.

- A highly hypothetical calculation case with an initial, large defect in all 6 000 canisters would yield peak dose consequences to the most exposed individuals in a fully populated landscape of about 700 $\mu\text{Sv}/\text{yr}$, corresponding to a risk of about $5 \times 10^{-5}/\text{yr}$, occurring in the 10 000 year time frame. After about 100 000 years, the calculated risk is about a factor of two above the risk limit of $10^{-6}/\text{yr}$. Somewhat less pessimistic cases analysed in Section 13.7.3 indicate doses up to around 200 $\mu\text{Sv}/\text{yr}$.
- An even more hypothetical case with a large defect in all 6 000 canisters and with no buffer barrier present would yield peak dose consequences to the most exposed individuals in a fully populated landscape of about 4 000 $\mu\text{Sv}/\text{yr}$, corresponding to a risk of about $10^{-4}/\text{yr}$, occurring in the 10 000 year time frame. After about 100 000 years, the calculated risk is about a factor of two above the risk limit of $10^{-6}/\text{yr}$.

Several pessimistic assumptions, in addition to the completely fictitious losses of barrier functions, were made in the calculations of these cases.

The results reported in Section 13.7.4 indicate that the calculated doses are comparable to or below the natural background radiation also for very severe losses of safety functions. For example, an initial total loss of the canister and buffer in all deposition holes yields, for the Forsmark site, doses that are comparable to those arising from background radiation.

The bounding analyses also demonstrate the multi-barrier character of the KBS-3 system, which may be less evident from results of other analyses. For example, with intact canister and buffer properties the rock appears relatively unimportant, since most nuclides are retained already in these barriers. However, for the unrealistic case of complete initial failure of the canister and buffer barrier, the results in Figure 13-72 and Figure 13-73 indicate that retention in the rock reduces the doses by about two orders of magnitude, clearly illustrating the importance of the rock. Furthermore, the rock is always important in providing a low groundwater flow, suitable chemical conditions and stable mechanical conditions.

15.3.8 Additional, general requirements on the safety assessment

Use of natural analogues

An account of natural analogues as a support for a safety assessment of a KBS-3 repository is given in Section 14.6. Both the role of natural analogues in safety assessments and the actual supporting arguments for specific repository materials and processes affecting them are discussed.

In Section 14.6.5 it is concluded that the outcome of the natural analogue studies has been of a more qualitative than quantitative nature. The gathering of scientists and modellers in the international projects studying natural analogues has focussed the research efforts and method development, so that enough information is available for identifying processes and scenarios relevant to safety assessments. Also, many natural analogues provide support to post-closure safety analyses by improving general perception and understanding of the concept of a deep repository.

Furthermore, in cases where natural analogues provide useful information for the understanding of specific processes, this information is given in the **Process reports**, under a dedicated heading.

Quality assurance

Quality assurance routines have been developed and implemented, as described in Section 2.9. They encompass e.g. the reviewing of central documents, quality assured FEP management and the following of pre-established templates when documenting essential information regarding e.g. process understanding and input data in the safety assessment. A description of quality assurance relating to models and modelling is given in the **Model summary report**.

Handling of uncertainties

A systematic handling of uncertainties, addressing system uncertainty, conceptual/model uncertainty and data uncertainty has been applied. The systematic handling of FEPs, as documented in the **FEP report** is a key component in assuring that all relevant factors are considered in the assessment. Uncertainties regarding the understanding and modelling of processes of importance for post-closure safety are addressed in the **Process reports**, according to the template for process documentation. Data and data uncertainties for modelling are qualified in the **Data report**, according to the template for data qualification.

The analyses in the reference evolution aim at reducing the number of uncertainties requiring further consideration and at identifying and quantifying uncertainties that need to be propagated to subsequent parts of the assessment. These latter uncertainties are addressed in later parts of the reference evolution and/or in the subsequent analyses of additional scenarios.

Further details regarding the integrated handling of uncertainties in the PSAR are provided in Section 2.8.4.

15.4 Design basis cases

Feedback from assessments of post-closure safety is a key input to the refinement of the design of the KBS-3 repository and is also recommended by regulations. The recommendations to the regulation SSMFS 2008:21 state the following: “Based on scenarios that can be shown to be especially important from the standpoint of risk, a number of design basis cases should be identified. Together with other information, such as on manufacturing method and controllability, these cases should be used to substantiate the design basis³¹ such as requirements on barrier properties.”

A first set of design basis cases was formulated in the SR-Can main report (SKB 2006a, Section 13.4) and feedback to canister and repository design was given in Sections 13.5–13.6 of the SR-Can main report (SKB 2006a). This was further developed into requirements termed *design premises* in a report entitled “Design premises for a KBS-3V repository based on results from the safety assessment SR-Can and some subsequent analyses” (SKB 2009a). Design premises typically concern specification on what mechanical loads the barriers must withstand, restrictions on the composition of barrier materials or acceptance criteria for the various underground excavations.

The feedback on the assessed reference design and related design requirements given in the SR-Site main report (SKB 2011, Section 15.5), was further developed through a compilation of Posiva’s and SKB’s joint specification of technical design requirements (Posiva SKB 2017). As further described in Chapter 5, and in the **Production reports**, these design requirements formed the basis for establishing and justifying the reference design being assessed in the PSAR, although most of the design was developed before these design requirements were formally established.

As already envisaged when the design basis cases and the design premises were first presented in SKB (2009a), the design premises may be modified in future stages of SKB’s programme, e.g. after major updates of the safety assessment or as a result of reviews of the safety assessment. Reasons for such modifications include results of analyses based on more detailed site data and a more developed understanding of processes of importance for post-closure safety. Based on the findings of the PSAR, feedback to a potential update of the design basis cases is provided in this section, whereas detailed feedback to the technical design requirements is provided in Section 15.5.

15.4.1 General

The approach for arriving at design basis cases was outlined in the SR-Can main report (SKB 2006a), Section 13.4, and was further elaborated in SKB (2009a) and subsequently in the SR-Site Main report (SKB 2011, Section 15.4). This approach is judged adequate, but is for completeness repeated here.

As stated in SSM’s recommendations, the purpose of identifying design basis cases is to provide input to the formulation of requirements on barrier properties. This process is *iterative* and contains several elements.

1. Establishment of a repository reference design, i.e. a barrier system *with a chosen set of properties* (see the **Production reports** and Chapter 5 of this report).
2. Identification of the safety functions the system should fulfil over time, see Chapter 8.
3. Identification of the stresses the system will be subject to over time, potentially jeopardising safety. This is done in Chapter 10 (the reference evolution) and further in the scenario analyses in Chapter 12.
4. A quantitative analysis of how the identified stresses affect safety for the established design. This analysis is provided in Chapters 10, 12 and 13. The load situations occurring in the scenarios that are particularly important from the standpoint of risk, i.e. a set of design basis cases, are briefly summarised below in this section. These provide important input to the formulation of the technical design requirements.
5. Conclusions regarding the sufficiency of the chosen set of properties or recommendations regarding possible improvements. This is important feedback to the design process.

³¹ The cited text is from the current SSM, unofficial, translation of the regulation. In the official Swedish version, the word “design basis” is “konstruktionsförutsättningar”, which in most other cases, including the SKB usage, is translated into “design premises” or “technical design requirements”.

6. The derivation of modified requirements on barrier properties based on step 5, leading, with other adequate aspects taken into account, to a modified design for which the above steps can be repeated.

For a particular safety assessment, a certain repository design, step 1, is hence provided. Steps 2, 3, 4 and 5 essentially constitute the safety assessment. Step 6 is, however, not formally within the scope of the safety assessment, see further below.

Scenarios

It is clear from the analyses in the PSAR, as it was in the SR-Site assessment, that scenarios related to canister corrosion for an eroded buffer and to shear movements are most important from the standpoint of risk. In addition to these most important scenarios from the standpoint of risk, canister failure scenarios that did not contribute to risk, since the assumed design was sufficient to prevent failures, have also been considered among the design basis cases, although this is not a strict requirement in the nuclear safety regulations. The only such scenario identified in The PSAR, as in the SR-Site assessment is canister failures due to isostatic loads. Although such failures do not contribute to the calculated risk, the canister's resistance to isostatic loads is an important component of the design basis. Other scenarios than those leading to canister failures are not considered, since such scenarios do not, by definition, cause any risk. However, the canister failure scenarios encompass a number of other scenarios relating to the buffer and to the host rock and these are thus included in the design basis cases.

Time scale

The design basis cases also depend on the time scale considered. For times longer than 100 000 years the recommendations to the regulation SSMFS 2008:37 state that: "A strict quantitative comparison of calculated risk in relation to the criterion for individual risk in the regulations is not meaningful. The assessment of the protective capability of the repository should instead be based on reasoning on the calculated risk together with several supplementary indicators of the protective capability of the repository such as barrier functions, radionuclide fluxes and concentrations in the environment."

The likelihood that detrimental events, like large earthquakes, would occur increases with time. The detrimental effects of some continuous processes, like canister corrosion, also increase with time. Following the recommendation, a strict application of the risk criterion is relevant in a 100 000 year time scale and since the design basis cases are to be derived from scenarios that are important from the standpoint of risk, this could be taken as an indication that the design basis should also be developed for this time frame. However, the principle of best available technique (BAT) applies over the one million year assessment time. It does not seem reasonable to develop the technical design requirements for the time scale of 100 000 years and then use the one million year time scale when the principle of BAT is applied. Therefore, the one million year time scale is considered also when the technical design requirements are developed.

This does not, however, mean that the repository must be designed to withstand all loads identified in the safety assessment in a one million year perspective. The design must be such that the requirements on risk and BAT are met and this may well be compatible with the occurrence of some detrimental effects on the barriers during the assessment period.

Integrated approach

There is a considerable amount of information in the PSAR that can be used to evaluate the current technical design requirements for a KBS-3 repository, but as concluded also in the SR-Site assessment, there are few, if any, load cases *on individual barriers* that can be directly derived from the external conditions alone. For example, the isostatic load on the canister will depend not only on the external conditions like the size of a future glacial load and associated groundwater pressure, but also on the depth of the repository and the design of the buffer, that determines its maximum swelling pressure. The situation regarding shear movements on the canister is even more complex: This depends on external factors like probabilities of future large earthquakes, but also on the fracture distribution in the rock in the deposition area, how the layout of the deposition area and deposition holes is adapted to the site conditions, and the material properties of the buffer.

The load on one barrier will thus depend on the design of other barriers and on the site properties, meaning that the technical design requirements must be determined for the entire barrier system in an integrated manner, and in some respects also site specifically. It also means that there is a range of different combinations of barrier and site properties that could provide a similar performance of the repository. The role of the safety assessment in this context is to provide input to the derivation of technical design requirements, in the form of external loads the barrier system should sustain, informed by the calculated risk and, later, to audit the specific design and construction outcomes. It is, however, beyond the scope of the safety assessment report to develop the specific design, albeit safety assessment competence is required for the appropriate formulation of the technical design requirements.

The following is a summary of the most important results, *concerning the external loads the barrier system will be exposed to*, that need to be considered when the technical design requirements are developed. It furthermore serves as an introduction to the more detailed discussion on feedback to canister and repository design in Section 15.5.

15.4.2 Canister – Isostatic load

The isostatic load on the canister depends on groundwater pressure and on the swelling pressure of the buffer. It is pessimistically assumed that the combined effect of these two pressures determines the isostatic load. The detailed assessment of the isostatic collapse load scenario in Section 12.7 concludes that a maximum swelling pressure of 10 MPa could occur in the buffer, the groundwater pressure is around 4.5 MPa at Forsmark for ice-free conditions and an additional ground water pressure of at most 36 MPa could occur as a result of a maximum glacial load supported by geological palaeo-ice-sheet evidence. The sum of these loads is 50.5 MPa. However, considering that the combined impact of swelling pressure and hydrostatic load is somewhat smaller than this sum, this, as suggested in Section 12.7.6, results in a total pressure of around 47.3 MPa. The assessment of canister strength concludes that the margin to total collapse (90 MPa), i.e. the criterion for canister failure, is considerable. In the isostatic load scenario, also the copper shell's resilience to long-term creep is evaluated and it is found that the copper is resilient to the creep deformation resulting from an isostatic pressure of 50 MPa.

In the SR-Site assessment it was concluded that the design requirement concerning isostatic load needed to be revised and subsequently a requirement on resilience to an isostatic load of 50 MPa, both as concerns instant loads on the insert and creep deformation of the copper shell, was formulated (Posiva SKB 2017) and cited in Section 5.4.1. The assessments in the PSAR summarised above suggest that this is an adequate design requirement.

From the standpoint of risk, it is important to realise that the isostatic loads mentioned above, at least the (dominating) contribution from the groundwater pressure at repository depth, is likely to affect *all canisters simultaneously*. If the canisters are not designed to sustain these loads, a substantial number of canisters could potentially fail simultaneously. This is different from cases where the natural variability of the host rock affects the load situation, e.g. as concerns the likelihood of a large fracture intersecting a deposition hole.

The canister may be subjected to asymmetric loads during different phases in the repository evolution. This could temporarily occur due to uneven water saturation in the buffer and lack of straightness of the deposition hole. Permanent asymmetric loads may occur due to an uneven buffer density distribution after water saturation in combination with lack of straightness of the deposition hole. However, as seen in Section 10.3.9, the swelling pressure around the canister is expected to be homogenised and significant asymmetric loads are expected to be rare and thus to affect only a small fraction, if any, of the deposition positions. Such cases are useful to consider when assessing the isostatic load case but have too low a probability to be considered to coincide with the low probability shear load case discussed in the next section.

15.4.3 Canister – Shear movements

In rare cases, detrimental shear movements may occur as a consequence of earthquakes that could induce secondary movements in fractures intersecting deposition holes. As elaborated in Section 10.4.5, the response of the canister to shear loads depends on a number of factors. The most important ones are:

- The magnitude and location of the earthquake.

- The length over which the intersecting fracture is sheared.
- The velocity of the fracture shear movement.
- The angle of intersection of the fracture and its position in relation to the main axis of the canister.
- The buffer mechanical properties, many of which depend strongly on the density of the selected buffer material.
- The canister geometry and properties of the canister materials like Young's modulus and fracture toughness.
- The temperature of the canister and buffer at the time of the event.

The combined effect of all these factors determines if the canister will withstand a shear load.

The following design requirement is formulated in Posiva SKB (2017) with respect to shear movements (cited also in Section 5.4.1):

“The copper shell shall remain tight and the canister shall maintain its ability to resist loads for 5 cm rock displacements at all angles and a rate of 1 m/s, exerted on the canister by a buffer with an unconfined compressive strength at failure lower than 4 MPa at a deformation rate of 0.8 %/min”

The **Canister production report**, see also Section 5.4, demonstrates that the current canister reference design fulfils these requirements. However, in order to meet these requirements rigorous demands on manufacturing and NDT capability (especially of the insert) need to be imposed.

The potential for shearing was assessed in Section 10.4.5 and in Section 12.8, and it is found that on average less than one deposition hole will experience shear movements larger than 0.05 m over 10⁶ years, resulting in canister failure if it is assumed that the canister will actually fail if the load exceeds that of the design basis value. In reality, there will be even fewer failures, since i) the buffer in most deposition holes will have lower density than the maximally allowed value, ii) there are only a few fracture angles and locations that would lead to failure at 5 cm shear, iii) recent model studies demonstrate that several aspects of the assessment of the extent of secondary shear movements are pessimistic and iv) the copper shell elongation and creep ductility achieved in the pilot production implies there is a margin between the now assumed direct failure of the copper shell when the acceptable defect size in the insert is exceeded and the actual performance of the copper shell during a shear movement.

Furthermore, only few canisters would potentially be subject to shear movements of a detrimental magnitude. The majority of the canisters would be expected to experience only negligible shear movements, since their deposition holes would be intersected by only small fractures, if any. It is thus only a small fraction of the deposition holes that are expected to have properties that require the canisters to withstand a 5 cm shear movement. To the extent that a distribution of shear movement resilience can be determined for the ensemble of canisters, taking into account e.g. manufacturing flaws, the potential part of the distribution not fulfilling the design requirements should be evaluated against the distribution of deposition hole properties in order to estimate the likelihood that a canister will experience shear failure.

Generally, the canister's resilience to a shear movement decreases with decreasing temperature. The thermal analyses in Sections 10.4.3 and 12.3 show that extreme and unrealistic climate conditions are required to obtain temperatures below 0 °C at repository depth. Therefore, temperatures below 0 °C are not considered for the shear case.

As described in Section 10.3.10 there is no reason to believe that there would be mineralogical changes in the buffer that would lead to substantial changes of the mechanical or hydraulic properties over the assessment time scale. However, there are experimental results showing that the mechanical properties of bentonite can be altered if the material is exposed to an elevated temperature in a saturated state (Dueck 2010). On the other hand, assuming that buffer material around the canister is converted to a cement-like material with no swelling pressure, an increased E-modulus and shear strength, yields small effects in the shear analyses. It is thus considered that cementation of buffer material does not need to be included in the design basis case for shear movement.

The following are concluded.

- The risk contribution from canister failures due to shear movement is considerably lower than the regulatory risk limit, meaning that the current design basis case is sufficiently restrictive.
- The design basis case constitutes a balance between requirements on the canister, on the buffer and on the repository layout, the latter through the requirement on a maximum shear magnitude of 5 cm. In a revision of this design basis case, for example the following may be considered, provided that the resulting calculated risk from shear movements is comparable to or smaller than that in the PSAR:
 - Given the technical challenges in meeting the rigorous requirements on manufacturing and NDT capability, it might be appropriate to relax the requirement on the canister, e.g. by requiring resilience to a smaller allowed shear movement.
 - The maximum shear movement may be reconsidered. However, increasing the limit beyond 5 cm would mean increased demands on the canister design given the current capability of analysing the response of the canister/buffer system to shear movements. Decreasing the limit would mean an increased calculated risk with the current repository design and assessment of occurrence of secondary shear movements. However, as demonstrated in Section 10.4.5, several aspects of this assessment are pessimistic, meaning that the future calculations with current repository layout should lead to a lower assessed risk due to shear failures. The new findings would also feed into a potential revision of the repository layout.

15.4.4 Canister – Corrosion load

One of the three post-closure safety functions of the canister is to provide a corrosion barrier and a discussion of design basis cases as regards corrosion is, thus, required. The role of the safety assessment regarding corrosion loads is not merely to specify the loads, but also to calculate the resulting corrosion depths. A more direct feedback can therefore be given in terms of the sufficiency of the canister thickness assumed in the safety assessment and sensitivities to variations in that thickness.

The PSAR assessment generally shows that a requirement on nominal thickness of 5 cm, with allowances for local defects as given in Table 5-9, provides an adequate corrosion barrier, as elaborated in the following. It is, furthermore, noted that the assessed initial state provided essentially in Table 5-9 and on which the analyses are based, is more beneficial from the point of view of post-closure safety than the design requirement of a general thickness of at least 40 mm and with reductions down to 35 mm on at most 10 % of the canister surface given Section 5.4.1.

In Sections 10.2.5 and 10.3.13, the resulting corrosion depths for various corrosion processes are shown to be in the order of a few mm for an intact buffer, with its intended swelling pressure and transport properties.

In Section 10.4.9, the corrosion for a case with a partially eroded buffer is assessed, and the sensitivity is further analysed in the corrosion scenario (Section 12.6.2). The results show that the calculated mean number of failed canisters in one million years is between 0 and 2. This span of number of failed canisters covers uncertainties regarding the buffer erosion process, the variability in the hydrogeological DFN models and uncertainties in the sulphide concentration distribution, as well as uncertainties in the conceptual model of corrosion geometry (part of the copper surface that is corroded by the sulphide transported to the canister).

When assessing BAT, see Section 14.3.2, copper thicknesses of 2.5 and 10 cm have been evaluated. The results show that increasing the copper thickness to 10 cm reduces the mean number of failed canisters at one million years by a factor of about 3 while halving the thickness to 2.5 cm increases the number by about a factor of 2, see Figure 14-6. Potential problems of manufacturing and sealing a thicker canister have not been considered in this analysis.

In the evaluation of the corrosion, the copper thickness achieved for the reference design with current production and QA procedures is used. For the shell and the bottom and lid, the manufactured thickness is considered not to be less than 45 mm, which can be taken as a lower limit for the manufactured thickness. To evaluate the significance of the occurrence of small areas with lesser copper thickness (weld area, or surface defects from transportation and handling) probability aspects (small areas for a few canisters to coincide with a few deposition holes with high flow) are considered in the assessment.

In conclusion, corrosion in the case of a partially eroded buffer is the only risk contribution from canister failures due to corrosion. The design basis case relevant for the assessed repository at Forsmark should be the one assessed in the PSAR, considering uncertainties regarding the buffer erosion process, the variability in the hydrogeological DFN models and uncertainties in the sulphide concentration distribution, as well as uncertainties in the conceptual model of corrosion geometry. Furthermore, given the relative insensitivity of the number of failed canisters to the copper thickness it is clear that technical design requirements derived from this design basis case cannot be given in the same detail as the production specification and thus specifying the thickness in the centimetre scale is seen as a more appropriate output.

15.4.5 Buffer

The listed external loads that may affect the buffer are based on a thorough understanding of the safety-related functions of the buffer in the repository, i.e. on the role of the buffer in the safety concept and the expected variations in the chemical environment of the buffer, see Chapter 10. Based on this, the following chemical and thermal environment for the buffer should be considered as concerns design requirements.

- Generally, most deposition holes will experience a salinity with ionic strength $\Sigma q[M^{q+}] > 8$ mM charge equivalent. However, up to a few percent of all deposition holes may experience salinities below this value at some time in the overall glacial cycle.
- Groundwaters with a TDS up to 20 g/L may occur in the scenarios analysed in the PSAR. This should not pose a threat to the buffer functions.
- The pH may, at least for short periods be up to pH 11. Specifically, an initial, short term high pH load cannot be excluded and should also be acceptable, based on mass balance arguments. Consequently, the buffer should sustain such conditions, as indeed is shown to be the case for the reference buffer design assessed in the PSAR (see Section 10.3).
- The buffer may also be exposed to isostatic pressures up to 40.5 MPa. As was concluded in SR-Site, the buffer materials analysed are not negatively affected by such pressures, see Section 10.4.8, sub-heading Liquefaction.
- Regarding shear movements, see the discussion of this issue for the canister above.
- The function indicator criterion for detrimental effects from buffer freezing is pessimistically assessed to be -6 °C, see Section 8.3.2. As seen in Section 12.3.3, the groundwater at repository depth will never reach such low temperatures, which means that the -6 °C criterion for the buffer material is an achievable technical design requirement for the buffer.

The design requirements on the buffer are given in Section 5.5.1.

15.5 Feedback to assessed reference design and related technical design requirements

15.5.1 Introduction

In the PSAR a specific reference design based on specific technical design requirements has been assessed. In this feedback section, the safety aspects of the reference design are addressed and feedback given as to whether there is reason to consider revisions of the reference design and/or of the technical design requirements as they are formulated in the **Production reports**. These technical design requirements are equal to or based on a co-operative work on this issue between Posiva and SKB, as reported in Posiva SKB (2017).

The reassessment of the design basis cases, as well as other conclusions reached within the PSAR, can also be used as input for revising the specific technical design requirements.

Since the PSAR demonstrates a sufficient level of safety for a repository at Forsmark constructed in accordance with the reference design, conforming to the technical design requirements, the remaining reasons to revise these requirements are:

- Considering whether a refined formulation or requirement could significantly enhance the resulting safety, while considering if such a change is realistically achievable.
- Feedback from the design and production (**Production reports**) including possibilities to verify the technical design requirements both in design and production.
- Adjustment of premises proven to be unnecessary or providing no or little enhancement of safety.
- Clarification of wording, corrections and other minor modifications in order to enhance clarity.

Reasons to revise the reference design include:

- Challenges, e.g. complex or less well founded demonstrations verifying that the reference design will conform to given technical design requirements.
- Proposed changes in technical design requirements.
- Further refinement and development of methods for production, installation and inspection promoting improvements within the framework of the reference design.
- Research and development resulting in alternative designs that are e.g. easier to implement and with potential to maintain the barrier functions and safety.

Based on these general principles most of the already stated technical design requirements and associated reference designs are judged adequate as they are, whereas some can usefully be modified or elaborated. A more detailed assessment is presented in the following subsections.

A document describing general aspects of the plans for further development of the production of the repository components has been developed³², partly based on the feedback given below. More detailed plans for the further development of the design and manufacturing of the fuel and canister,³³ of the buffer, backfill, plug and closure,³⁴ and of the underground openings³⁵ have also been developed.

15.5.2 Canister mechanical stability – withstand isostatic load

In Posiva SKB (2017) and the **Canister production report** it is stated that: The copper shell shall remain leak tight and the canister shall maintain its ability to resist loads for an isostatic load of 50 MPa.

As stated in Section 5.4.15, and shown in the **Canister production report**, canisters can be designed and manufactured in conformity to the stated technical design requirement with respect to isostatic load. The detailed assessment of the isostatic collapse load scenario in Section 12.7 shows that such canisters will not fail due to any foreseeable isostatic load during the assessment period. The analyses in Section 12.7 are based on the updated canister design analysis cited in Chapter 5, on the updated maximum swelling pressure from the buffer and on updated estimates of maximum ice sheet thicknesses. Both the insert's ability to withstand instantaneous isostatic loads and the copper canister's ability to withstand long-term creep has been assessed.

Feedback to technical design requirements

The current technical design requirement is judged adequate.

Feedback to reference design

The current reference design is judged adequate.

³² "Plan för SAR Kärnbränsleförvaret – Utveckling av produktionslinjer", SKBdoc 1900846 (In Swedish) (Internal document.) *In prep.*

³³ "Plan för SAR Kärnbränsleförvaret – Bränsle och kapsel", SKBdoc 1895133 (In Swedish) (Internal document.) *In prep.*

³⁴ "Plan för SAR Kärnbränsleförvaret – Buffert, återfyllning, valvplugg och förslutning", SKBdoc 1889223 (In Swedish) (Internal document.) *In prep.*

³⁵ "Plan för SAR Kärnbränsleförvaret – Bergutrymmen", SKBdoc 1889493 (In Swedish) (Internal document.) *In prep.*

15.5.3 Canister mechanical stability – withstand shear movement

In Posiva SKB (2017) and in the **Canister production report** the following is stated: The copper shell shall remain tight and the canister maintain its ability to resist loads for 5 cm rock displacements at all angles and a rate of 1 m/s, exerted on the canister by a buffer with an unconfined compressive strength at failure lower than 4 MPa at a deformation rate of 0.8 %/min.

The 5 cm rock displacement and the 1 m/s rate are based on assessment of the post-closure evolution of the repository. The shear load applies for all locations and angles of the shearing fracture in the deposition hole. The technical design requirement for the shear load includes the characteristics of the buffer that affect how the shear movements in the rock are transmitted via the buffer to the canister. Further it can be noted that in general the material models used in the design and tolerance analysis are valid in the temperature interval 0–125 °C. The canister shall remain leak tight and maintain its ability to resist loads after being exposed to the shear load.

As already concluded in Section 15.4.3, a canister in conformity to the stated technical design requirements would on average result in less than one failed canister over 10⁶ years, even if it is assumed that the canister will fail directly if the load exceeds the design value. In reality, there will be even fewer failures, since i) the buffer in most deposition holes will have lower density than the maximally allowed value, ii) there are only a few fracture angles and locations that would lead to failure at 5 cm shear, and iii) there are several pessimistic assumptions in the geosphere analyses, Section 10.4.5.

As stated in Section 5.4, and shown in the **Canister production report**, the current canister reference design conforms to the stated technical design requirements, but it is also noted that this implies that rigorous requirements on manufacturing and NDT capability need to be imposed.

In addition to the shear load case, the canister may be subjected to asymmetric loads during different phases of the repository evolution (see technical design requirement in Section 5.4.1). This could temporarily occur due to uneven water saturation in the buffer or due to permanent asymmetric loads that may occur due to an uneven density distribution of the saturated buffer. These asymmetric loads lead to considerably less stress and deformation than caused by the shear load case.

Feedback to technical design requirements

The current technical design requirements have been demonstrated to yield a very low likelihood of shear load failures in a KBS-3 repository at the Forsmark site and the requirements are in this sense adequate. However, the result depends in a complex way on a number of factors related to the canister, the buffer and the host rock. These have been evaluated with varying degree of pessimism in the PSAR and an optimisation including all the concerned design requirements could be of value, in order to achieve a balanced set of requirements on a system level, thereby facilitating the further design development. For example, it could be examined if a somewhat lower requirement on the shearing magnitude the canister needs to sustain could be adopted, when considering the number of deposition holes that could experience such a magnitude in the light of emerging knowledge from the earthquake assessments.

Feedback to reference design

The current reference design is judged adequate. However, the comment regarding system optimisation immediately above concerns also the reference design.

As noted in Section 5.4, with reference to Section 7.1.2 of the **Canister production report**, development work remains in demonstrating that the manufacturing requirements of the insert can be achieved in an industrial production of canisters. One such aspect concerns non-destructive testing of inserts and here it is noted in Section 5.4 *i*) that the probabilistic analysis of the canisters' resilience to isostatic and shear loads do not take any credit for NDT and *ii*) that relatively large defects are acceptable between the channel tubes, i.e. in the volumes where it is more difficult to apply an efficient NDT. It is essential that the development work of the reference design of the insert and of its manufacturing and testing procedures is continued, to yield robust results for coming stages of the licensing of the KBS-3 method.

15.5.4 Provide corrosion barrier – Copper thickness

In Posiva SKB (2017) and the **Canister production report** it is stated that the copper thickness shall be ≥ 40 mm at deposition. Local reductions to a thickness of 35 mm is acceptable for 10 % of the copper shell.

The reference design of the canister has margins compared to the requirement with regard to the copper thickness. The copper shell thickness according to the reference design has minimum drawing dimensions that are 47.8 mm in the welds, 48.15 mm in the tube and 49 mm in the bottom and lid. In the lid, this dimension will be reduced to 48 mm due to canister markings.

As already concluded in Section 15.4.4, the current reference design provides an adequate corrosion barrier.

Feedback on technical design requirements

The corrosion calculations are based on the current reference design, rather than on the technical design requirements. The latter have not been evaluated in a strict sense, although it is implied by the result in Section 14.3.2 that the outcome of the corrosion calculations is not particularly sensitive to variations even as high as by a factor of two in the copper thickness.

Feedback on reference design

Current reference design is considered adequate, but it would be beneficial if a lower limit for the manufactured thickness for the shell, the bottom and the lid, were established. The results of the PSAR suggest that a suitable limit, including tolerances, is 45 mm.

15.5.5 Canister material etc

Posiva SKB (2017) and the **Canister production report** provides technical design requirements regarding the copper content in the cast iron, limits on other elements in the copper shell, the maximum amount of water left in the insert and allowed radiation levels. The analyses in the PSAR do not provide any direct feedback on these technical design requirements, but the further analyses made and presented in e.g. the **Fuel and canister process report** may allow some further elaboration of these technical design requirements, by enhancing the foundations for the limits given and for adjustment of some limits also to address allowable tolerances.

As discussed in Section 10.2.5, preliminary and pessimistic modelling results suggest that small amounts of ammonium could be formed in the canister interior as a consequence of radiolysis of residual water and air in the canister. The potential extent of this phenomenon would be considerably reduced if the technical design requirement of 90 % argon in the canister would be increased to be closer to the requirement on the production system, stating that the initial content should be at least 99 % argon (Ljungberg 2021).

15.5.6 Durability of the hydromechanical properties of the buffer material

In Posiva SKB (2017) and the **Buffer production report** it is stated that the buffer is assigned to limit advective mass transfer, limit microbial activity and keep the canister in place. Therefor the buffer should after swelling uphold the minimum swelling pressure 2 MPa and the hydraulic conductivity should not exceed 10^{-12} m/s. To protect the canister from detrimental mechanical loads, the swelling pressure is limited to 10 MPa. After swelling, the shear strength of the buffer must not result in a load larger than the load the canister can withstand for the shear movements. In addition, a dry density larger than 1 000 kg/m³ ensures filtering of colloids. Related to this, the maximum and minimum dry densities of the selected buffer material need to be determined to ensure the properties of the saturated buffer can fulfil the above in the long-term.

These conditions apply for temperatures down to 0 °C and temperatures up to 100 °C.

The design basis concerning the external chemical, mechanical and thermal loads that the buffer will be subjected to during the 10⁶ years, is considered in the technical design requirements related to material specific dry density, see section 5.5.1.

The assessment in Chapter 10 shows that the buffer safety function indicator criteria are upheld for all conceivable chemical and thermal conditions during the assessment period, as long as not too much buffer mass is lost, initially or due to erosion. The initial state is to be ensured by the procedures described in the **Buffer production report**. Mitigating loss of buffer due to piping erosion can be handled by selecting deposition holes where the potential for excessive piping erosion is avoided (see further Section 15.5.13).

It is concluded in Section 10.3.9 that when large amounts of bentonite are lost or missing from start, the bentonite swells and fills the empty space but the density and resulting swelling pressure is locally rather low due to the friction in the buffer and the friction against the rock surface. In such cases, the swelling pressure may at least locally fall below 1 MPa, depending on internal friction in the material and the smoothness (friction) of the rock wall. Advective conditions in the buffer can occur if the hydraulic conductivity is sufficiently high. The buffer function indicators prescribe a hydraulic conductivity of 10^{-12} m/s and a swelling pressure of 1 MPa to rule out advection in the buffer. These values do, however, have some safety margins included in them.

In the discussion about margins for the safety function indicator criteria, in Section 8.3.5, it is stated that, for the hydraulic conductivity, the margin is related to the hydraulic gradient and the diffusivity of the species in question, and that the margin is considerable. In practice, the hydraulic conductivity of the buffer will rarely determine whether diffusion will prevail as the dominating mechanism for transport. As the swelling pressure drops, the possibility for pathway formation in the buffer increases. There is an effect of the hydraulic gradient and possibly of salinity. Laboratory samples show piping at ~ 60 kPa. In a situation with piping, the bulk hydraulic conductivity becomes irrelevant. According to the analysis a minimum dry density of $1\ 000\ \text{kg/m}^3$ is required, corresponding to a void ratio of 1.75. This requirement is still met across almost the entire buffer diameter when two whole bentonite rings are omitted, corresponding to a dry mass loss of 2 400 kg. It should be noted that even though the margin for the safety function indicator criterion for the swelling pressure is more than an order of magnitude, the margin for mass (density) loss is only about a factor of two.

For the case when the buffer erodes by colloid formation, the mass loss may be quite local and it is appropriate to consider the limit for losses over typically half the circumference, i.e. a loss of 1 200 kg, which also would cover the situation when the loss occurs closer to the centre of the canister. This value still includes some pessimism, since homogenisation in the horizontal direction is neglected.

As concluded in Section 10.4.7, the ionic strength of the groundwater; $\Sigma q[M^{q+}]$, will fall below 8 mM charge equivalent i.e. violating safety indicator criterion R1c, for some deposition holes during some part of the glacial cycle. This means that colloid release may occur from these holes and from sections of the backfill. More specifically, it is concluded in Section 10.4.7 that less than two percent of the deposition hole positions may be assumed to experience dilute conditions during a glacial cycle, and they will only experience these conditions during a fraction of the time. While there still is uncertainty with respect to modelling of colloid formation and subsequent erosion and sedimentation of the buffer material and the modelling approach thus tends to be pessimistic, as discussed in Section 10.3.11, it seems clear that the process as such is real and that it cannot with current understanding be defensibly mitigated by e.g. selection of another buffer material.

It is concluded in Section 10.3.10 that an increased temperature may have an effect on the mechanical properties of the bentonite, but the effect is not very pronounced even at $150\ ^\circ\text{C}$ and does not seem to progress with time. However, this effect is discussed in the evaluation of shear load on the canister, see Section 10.4.5. In Sections 10.3.10 and 12.4 it is concluded that the increased temperature will have no significant effect on the mineralogical properties of the buffer.

As demonstrated in Sections 10.4.3 and 12.3, detrimental effects from buffer freezing can be excluded also for the case of a partially eroded buffer.

Feedback to technical design requirements

The analyses in the PSAR show that safety is maintained, even if a fraction of deposition holes loses the buffer due to a groundwater composition with the ionic strength $\Sigma q[M^{q+}]$ below 8 mM charge equivalent and since the impact of such conditions cannot be dramatically mitigated by e.g. selection of another buffer material, the technical design requirement would not need to consider groundwaters with ionic strength $\Sigma q[M^{q+}]$ below 8 mM charge equivalent.

Feedback to reference design

Currently analysed example of buffer material is judged adequate.

15.5.7 Installed buffer mass

In Posiva SKB (2017) and in the **Buffer production report** it is stated that the installed buffer material mass shall in average in the buffer volume result in a dry density interval from the lowest to the highest allowable material-specific dry density determined for the specific buffer material. The installed dry density of a MX-80 buffer may vary between 1 453–1 558 kg/m³ to fulfil the governing design requirements.

As shown in Sections 5.5.2 and 5.5.3, the installed average buffer density in a deposition hole will be well within the desired range. The final distribution of buffer density is dependent on:

- Homogenisation of blocks and pellets.
- Material loss from piping/erosion during the early period after emplacement.
- Expansion of buffer into the backfill.

In the long-term, loss due to colloid release may also affect the density in a deposition hole.

The initial state of the buffer after emplacement is unsaturated bentonite blocks and rings with a much higher density than the average density for the entire hole and one empty slot at the canister surface and a pellet filled slot with very low density at the rock surface. As shown in Section 10.3.9, the homogenisation process leads to residual density gradients in the material, mainly due to internal friction. This means that the density in the original pellet volume may be slightly below the target value for the entire buffer mass, but the safety function indicators will still be upheld.

Piping followed by erosion during the water saturation may lead to a local loss of buffer mass in some deposition holes (Section 10.2.4). For the allowed water flows in deposition holes, according to Section 5.2.1, the density may drop locally below the target value, but the safety function criteria will still remain upheld.

Expansion of buffer into the backfill and the interaction between the buffer blocks and pellets are discussed in Section 10.3.8. The expansion into the backfill will lead to a drop in the installed density, but the effect is limited even for unfavourable calculation cases.

The colloid release from buffer and backfill case, presented in Section 10.3.8, may lead to a substantial drop in buffer density.

As a result of a loss of buffer mass/density, sulphide may be formed as a result of microbial activity in the highly compacted bentonite, see Section 10.3.13. Though the factors limiting the activity are not fully understood, experimental results indicate that a minimum saturated density of 1 850 kg/m³ for the MX-80 material is required to keep the copper corrosion caused by microbial activity to a negligible level (see Section 10.3.10).

Feedback to technical design requirements

A buffer consisting of bentonite with a dry density yielding a swelling pressure in the range of 3–10 MPa will have good margins to the safety functions. However, this technical design requirement refers to the average installed density in a cross-section of the deposition hole and may not be upheld at all locations within the volume. While it is shown that there is a margin to ensure a safe function of the buffer, it is nevertheless suggested to keep 3 MPa lower limit as a technical design requirement in order to ensure a sufficient margin to buffer loss by piping/erosion etc. The technical design requirement was therefore clarified such that when assessing its fulfilment, buffer losses, e.g. due to piping erosion and homogenisation, need not be considered, since the potential for and significance of such losses are addressed in the safety assessment.

Furthermore, additional assessments should be performed to increase the understanding of the significance of limited local volumes of the buffer with a lower density than the main volume. This relates both to the mechanical properties and the possibility for significant microbial activity.

The findings from SR-Site suggested that the risk contribution from shear loads on the canister would be further reduced if the buffer density was lower than the maximum value of 2 050 kg/m³. Based on this the specification for the maximum buffer density was changed to the dry density that would correspond to a swelling pressure of 10 MPa for the material in question (Posiva SKB 2017). At the same time a technical design requirement for the shear strength was formulated. This is expressed as the maximum dry density yielding an unconfined compressive strength at failure < 4 MPa at a deformation rate of 0.8 %/min when determined with a specific specified laboratory test procedure, and for material specimens in contact with waters with less favourable characteristics than site-specific groundwater.

The new technical design requirements are directly related to parameters that affects the isostatic and shear loads on the canister. This makes the assessment of these cases clearer and more transparent, compared to the situation in SR-Site.

Feedback to reference design

The manufacturing method presented in Section 5.5.2 produces a buffer with a much narrower density interval than allowed in the technical design requirements. From the point of view of long-term performance, this strengthens the confidence in the assessment. The main reason for this is the strong dependence of swelling pressure on density. A narrowed range of initial density means that a smaller range of swelling pressures needs to be considered.

If the technical design requirement regarding initial buffer density are revised, the buffer reference design and quality control procedures for deposition hole geometry and buffer installation will need to be revised accordingly.

15.5.8 Buffer thickness

In Posiva SKB (2017) and in the **Buffer production report** it is stated that the distance between the canister and the deposition hole wall, i.e. the buffer thickness shall be at least 30 cm around the canister and at least 50 cm below and above the canister. These buffer dimensions has, in previous post-closure assessments (SR-Site) been shown to be sufficient for assuring safety.

As concluded in Section 14.3 a larger buffer mass is not seen as a practical means of mitigating the effects of buffer erosion. A larger buffer mass may offer a slightly longer time before advective conditions occur in the deposition hole, but it is not seen as a solution to the issue. It is also concluded that continued R&D on the erosion process is required.

Feedback to technical design requirements

The current technical design requirement is judged adequate.

Feedback to reference design

The current reference design is judged adequate.

15.5.9 Content of impurities in the buffer

In the **Buffer production report** it is stated that: The content of organic carbon should be less than 1 wt-%. The sulphide content should be less than 0.5 wt-% of the total mass, corresponding to approximately 1 wt-% of pyrite. The total content of sulphur, including sulphide, should be less than 1 wt-%.

The requirements on carbon, sulphide and sulphur concern the impact of these materials on the copper. As shown in Chapter 10, as long as the buffer is intact copper corrosion by contaminants in the buffer, backfill or groundwater does not pose a threat to canister integrity for the initial temperate period and even during the one million year overall assessment period the expected corrosion of the canister for an assumed temperate climate would cause corrosion depths of the order of a few millimetres, even for the most unfavourable deposition positions at Forsmark.

Feedback to technical design requirements

The current technical design requirements are judged adequate.

Feedback to reference design

The current reference design is judged adequate.

15.5.10 Deposition hole bottom plate

A plate of copper is installed in the bottom of the deposition hole, both as a base for the buffer block stack and to prevent groundwater uptake in the bottom bentonite block. In Posiva SKB (2017) there are no specific technical design requirements related to the bottom plate. However, since this plate is part of the current reference design, feedback on its adequacy is required.

In Section 10.2.4 it is concluded that additional assessments and possibly development work is needed for the bottom plate. There are uncertainties regarding the current design that are unresolved. These are connected to the possibility for a lifting of the buffer/canister package before the backfill is in place.

Feedback to technical design requirements

There is no reason to add technical design requirements directly addressing the bottom plate. Its presence does not affect risk.

Feedback to reference design

The current design, a copper plate, is judged fully acceptable.

15.5.11 Deposition tunnel backfill

In Posiva SKB (2017) and in the **Backfill production** report it is stated that the backfill shall keep the buffer in place and restrict groundwater flow through the deposition tunnels. Therefore, the minimum dry density installed in the deposition tunnel shall yield a:

- hydraulic conductivity $< 10^{-10}$ m/s.
- swelling pressure > 1 MPa.
- The overall deformation of the installed backfill both in dry and saturated state shall resist the swelling pressure from the buffer and maintain the buffer swelling pressure > 3 MPa on average over the buffer volume.

Further, the backfill shall not significantly impair the other barriers and it shall maintain its barrier function during long times.

It is concluded in Section 10.3.9 that the swelling pressure of the buffer and the associated safety functions will be maintained during the expansion of the buffer into the backfill for many possible combinations of buffer and backfill conditions. Furthermore, several likely pessimistic assumptions are made in this analysis, including assuming the buffer to be completely water saturated and homogenised from the start, assuming weak mechanical contacts between the backfill blocks, not including the local crushing of the blocks that may occur close to the floor and assuming that the backfill blocks are not stacked overlapping each other.

For the case when backfill material is lost, a maximum loss of 220 tonnes in a deposition tunnel section can be allowed before advective conditions have to be considered in the deposition hole. As concluded in Section 10.3.11, advective conditions may not be excluded in some very few deposition hole closest to the tunnel intersecting fracture but the contribution of loss of deposition tunnel backfill to the possible generation of advective conditions in deposition holes is considered negligible. For a few positions where the tunnel is intersected by a very transmissive deformation zone, potentially more than 220 tonnes could be lost, but this is not relevant from the point of view of canister integrity. Such local loss of backfill by erosion does not mean that the hydraulic conductivity of the entire tunnel will be affected and these occurrences are not judged to impair safety.

Generally, a requirement on the bulk hydraulic conductivity of the backfill has very little practical meaning and could probably be removed, whereas the requirement on swelling pressure is important to ensure a sufficiently tight contact between the backfill and the rock wall.

Feedback to technical design requirements

The technical design requirements regarding the deposition tunnel backfill are in most respects adequate. The requirement regarding compressibility needs however to be further elaborated. There may also be a need to better define the maximum content of potentially harmful impurities. The requirements should also be refined to reflect that backfill properties need not be retained where the deposition tunnel intersects very transmissive fractures (that would certainly not be allowed to intersect deposition holes).

Feedback to reference design

The current reference design appears adequate. There are very few identified uncertainties regarding the long-term performance of the current backfill design. However, the ongoing detailed design and testing of the tunnel plug needs to verify that it will be sufficiently tight to ensure that the inflow to deposition holes will be below the values that would lead to unacceptable piping and erosion of the buffer.

15.5.12 Selecting deposition holes – mechanically stable conditions

In Posiva SKB (2017) and the **Underground openings construction** report it is stated that the host rock shall provide mechanically stable conditions, therefore deposition holes must not be placed within critical volumes of class 1, 2 or 3 (CS1/CV1, CS2/CV2, CS3/CV3), see also Section 5.2.1. As stated in Section 5.2.3, the selection of positions for the deposition holes in the PSAR is, however, based in the same EFPC criterion as used in the SR-Site assessment, since there is currently no underground data available for the implementation of the new design requirement. Feedback from the SR-Site assessment was considered when defining the new design requirement. As the new requirement has not been implemented, there is no new feedback from the PSAR regarding this requirement.

15.5.13 Selecting deposition holes – hydrological and transport conditions

Large fractures and fractures with high flow rates intersecting deposition holes are common factors for many identified safety related issues. Flow in fractures intersecting deposition holes affects:

- Piping.
- Colloid release.
- Oxygen penetration.
- Inflow of corrodents, potentially leading to canister failure.
- Outflow of radionuclides (in both the corrosion and shear displacement cases, in particular for eroded buffer).

High flow rates in deposition holes are also generally associated with low F -values in the geosphere for both recharge and discharge flow paths.

In Posiva SKB (2017) and the **Underground openings construction report** it is stated that:

- Deposition holes must not be placed within critical volumes of class 1, 2 or 3 (CS1/CV1, CS2/CV2, CS3/CV3).
- Deposition holes shall be placed where the transmissivity of the pilot hole drilled in deposition hole position is less than a value that will be determined in connection with data being obtained on site underground (m^2/s).

Piping erosion

It is concluded in Section 10.2.4 that piping followed by erosion cannot be ruled out. Up to about 100 kg of dry bentonite may be lost due to erosion without jeopardising the function of the buffer. As seen in Section 10.2.4 this value may be exceeded in very few deposition holes. The inflow deposition hole inflow criteria of 0.1 L/min will further lower the probability of mass loss.

Furthermore, the stated rule on a maximum allowed total volume of inflow to a deposition hole is judged of limited practicality by designers and also is related to how much water would pass the deposition tunnel plug before saturation.

Correlation to Darcy flux and far-field transport resistance

In Section 5.2.1 it is stated that deposition holes shall be placed where the transmissivity of the pilot hole drilled in deposition hole position is less than a limit that will be selected when data from repository level has been obtained. This criterion reflects the correlation between Darcy flux and far-field transport resistance observed in SR-Site and discussed in Section 5.2.3 of the present report. There is no additional feedback from the PSAR on the reference design and related design premises since no new hydrogeological simulations are carried out as part of the PSAR.

Feedback to technical design requirements

There is no feedback from PSAR to the technical design requirements based on hydrogeological and transport conditions since no new hydrogeological simulations have been performed as part of PSAR. The feedback from SR-Site is incorporated in the current design requirements as discussed in Section 5.2.1.

Feedback to reference design

There is no feedback from PSAR to the reference design based on hydrogeological and transport conditions since no new hydrogeological simulations have been performed as part of PSAR. The feedback from SR-Site is incorporated in the current reference design as discussed in Section 5.2.2.

15.5.14 Hydraulic properties in deposition hole wall

The excavation damage zone around the deposition holes bored has been observed to be so minimal that currently no requirements in addition to the excavation method to be used are practical to define (Posiva SKB 2017). However, the investigations on the properties of the excavation damage zone and methods to verify it are continuing.

These damage zones are from excavation and new fracturing due to spalling. The conformity with the technical design requirement is demonstrated in the **Underground openings construction report** and there is no reason to revise the technical design requirement based on the PSAR findings. However, since spalling may also result from the thermal load it is worthwhile to consider its importance.

The rock mechanics assessment, see Section 10.3.5, concludes that thermally induced spalling, is likely to occur but the counter pressure exerted by bentonite pellets in the slot between buffer and rock wall, may suppress the spalling, or at least keep the spalled slabs in place and minimise the hydraulic transmissivity of the spalled damage zone.

The assessment of the impact of spalling, Section 10.3.6, demonstrates that spalling may increase the mass transfer (the equivalent flow rate Q_{eq}) for the Q1 path by more than an order of magnitude, but the other paths are not affected. However, this increase has essentially no impact on risk, since spalling will not affect the local Darcy flux in the case of advective conditions in the deposition hole or if the canister is damaged by a shearing fracture.

Feedback to technical design requirements

Since thermally induced spalling has a minor impact on risk, it is suggested not specify any design rule connected to its occurrence.

Feedback to reference design

While occurrence of thermally induced spalling has a minor impact on risk, efforts to handle and mitigate thermally induced spalling should continue.

15.5.15 Canister positions – adapted to the thermal conditions

According to current technical design requirements the minimum distance between deposition holes in a deposition tunnel and to deposition holes in adjacent tunnels shall be sufficient to maintain a temperature in the buffer ($T_{\text{buffer}} < 100 \text{ }^{\circ}\text{C}$).

As discussed in Section 10.3.10, the temperature requirement is adequate to protect the buffer, but possibly too strict at least if the temperature evolution is considered. It is found that an increased temperature will have an effect on the mechanical properties of the bentonite, but the effect is not very pronounced even at $150 \text{ }^{\circ}\text{C}$ and does not seem to progress with time.

The thermal analysis, see Section 10.3.4 demonstrates that with the current repository design, with its deposition hole spacing, buffer geometry and maximum residual power, there is an adequate margin to the peak temperature criterion for the buffer, even when the spatial variability of the rock thermal properties is taken into account and with other data essential for computing the result chosen pessimistically. However, it is possible to envisage deposition sequences, e.g. when a canister is deposited centrally in a deposition area where nearby positions were deposited several years before, where the resulting temperature in the buffer would exceed the maximum allowed. Such situations could always be avoided, but this possibility highlights the need for careful thermal management of the disposal sequence.

Feedback to technical design requirements

The current technical design requirement is judged adequate.

Feedback to reference design

The current reference design, stating maximum residual power, buffer geometry and minimum deposition hole spacing, appears appropriate, but may of course be revised if the technical design requirements are revised. However, restrictions regarding the canister emplacement sequence should be added to ensure that temperature requirement would not be violated during the operational period. Such assessments are judged meaningful only after repository excavation has reached repository depth. At that time the thermal dimensioning of the repository will be revisited and rules concerning deposition sequence will be developed based on this revised dimensioning.

15.5.16 Controlling the Excavation Damage Zone (EDZ)

Excavation works will result in mechanical alterations in the rock surrounding the excavated underground openings. In order not to cause a groundwater flow in the axial direction of the deposition tunnel which could jeopardize the safety function of the rock it is stated in Posiva SKB (2017) that the specific capacity $Q/\Delta p$ in EDZ (where Q is the flow in EDZ (m^2/s) and Δp is the draw down), measured in the pilot hole for the deposition holes, shall not exceed a transmissivity of, on average, 10^{-8} m^2 . The quantitative value is given in the **Underground openings construction report**.

The sufficiency of the upper transmissivity limit of $10^{-8} \text{ m}^2/\text{s}$ is indeed demonstrated in the PSAR. As further assessed in Section 14.3.2, the number of corroded canisters is virtually unaffected comparing a case without an EDZ with the basic assumption of an EDZ transmissivity of $10^{-8} \text{ m}^2/\text{s}$. However, the analysis also shows that a more transmissive EDZ could affect risk since the number of failed canisters starts to increase, although moderately, when the transmissivity is increased. The EDZ seem to be even less important for radionuclide transport. For the pin-hole scenario, see Section 13.7.2 the presence of an EDZ at $10^{-8} \text{ m}^2/\text{s}$ increases the dose compared to a case without an EDZ, but only marginally, and making the EDZ transmissivity larger does not further increase the dose.

Evidence presented in the **Underground openings construction report** and further elaborated in the **Data report**, see also Section 10.2.2, suggests that there is ample evidence that a potential EDZ formed during excavation will be kept below the maximum allowed transmissivity as set out by the technical design requirements and the data further suggests that a continuous EDZ would not develop at all.

Feedback to technical design requirements

The variation cases analysed in the PSAR can confirm that a connected EDZ transmissivity of 10^{-8} m²/s is adequate and need not to be decreased. However, connected EDZ transmissivity above this value will start to affect risk and needs to be avoided.

Feedback to reference design

No new analyses were made on this matter since SR-Site, therefore no feedback can be given beyond what has already been considered.

15.5.17 Engineered and residual materials

The use of engineered materials and residual materials must be limited and their compositions, quantities and location documented. According to the **Underground openings construction report** the following restrictions apply in deposition tunnels

- Only materials having leach products with a pH < 11 are permitted in deposition tunnels.
- There shall be no grouting of deposition holes.
- Deposition holes shall not be emplaced along tunnel sections where grouting or other measures to control inflow are applied, if these measures may even locally impair the backfill performance above the deposition hole.
- Rock surfaces in deposition tunnels must not be covered by construction or residual material on such large surfaces that the materials in the event of degradation leave voids that negatively affect the flow in the axial direction of the tunnel or the density of the backfill.

According to the **Underground openings construction report**, the reference design contains low pH cement that is used in shotcrete support, for embedding various rock support elements and in grout mixes used for sealing purposes. Various recipes that would generate porewater with pH < 11 have been developed for the purpose of grouting in rock types with potential for unacceptable inflows as well as for rock support elements that need to be embedded in cement. Furthermore, the assessment of repository evolution presented in Chapter 10 confirms that the currently estimated amounts of engineered and residual materials left at deposition, backfill or closure of the underground openings would have negligible impact on the safety functions.

Feedback to technical design requirements

Current technical design requirements are judged adequate. Furthermore, it should be clarified that a short duration pulse above pH 11 when the concrete is setting may be acceptable.

Feedback to reference design

The current reference design is judged appropriate, although it is recognised that the practical applicability of the suggested materials needs to be further tested and that final recipes may be modified. While the amounts of engineered and residual materials presented in the **Underground openings construction report** would not jeopardise safety and that probably even larger amounts and more alkaline materials would be acceptable, it is also noted that it will be important to keep a careful record of all materials that are brought into (and taken out of) the repository, allowing for updated assessments of whether the amounts would come close to detrimental levels.

15.5.18 Repository depth

In Posiva SKB (2017) and the **Underground openings construction report** it is stated that the repository shall be placed at the depth of several hundreds of meters to isolate it from the surface environment. The depth shall provide mechanically stable conditions, favourable thermal and chemical conditions, and favourable hydrogeological conditions to limit transport of solutes. The repository depth shall be:

- 400 m < repository depth < 700 m.

At the Forsmark site, permafrost (0 °C isotherm) and more importantly, freezing of ground water, cannot reach repository depth under typical future cold climate conditions (cf the reference glacial cycle used in SR-Site), whereas under the most pessimistic assumptions made in SR-Site and the PSAR, freezing of groundwater at repository depth cannot be excluded (e.g. SKB 2011, Section 12.3). However, freezing of the buffer clay and back-fill material at repository depth can be excluded also given the most pessimistic assumptions regarding e.g. low air temperatures under future cold climate periods (SKB 2011, Section 12.3).

The analyses in the PSAR corroborate the adequacy of the selected repository depth. A more detailed assessment is given in Section 14.3.4.

Feedback to technical design requirements

Current technical design requirements are adequate.

Feedback to reference design

There is no reason to revise the selected repository depth based on the findings from the PSAR.

15.5.19 Closure of main tunnels, transport tunnels, access tunnels, shafts and central area

In Posiva SKB (2017) and in the **Closure production report** it is stated that:

- The integrated effective connected hydraulic conductivity of the backfill in main and transport tunnels, in the lower part (–470 to –370 m) of ramp and shafts must be less than 10^{-8} m/s. This value need not be upheld in sections where e.g. the tunnel or ramp passes highly transmissive zones.
- There is no restriction on the hydraulic conductivity in the central area, upper part (–370 to –50 m) of the ramp and shafts and in the top seal. These shall, however, be backfilled.
- Only low³⁶ pH (< 11) materials are allowed below the level of –200 m.

The reference design presented in the **Closure production report** and in the **Underground openings construction report** conforms to these technical design requirements and the analyses in the PSAR show that a design following these rules would be appropriate. Furthermore, based on the findings from varying the transmissivity of the EDZ, discussed in Section 15.5.16, it is not obvious that these rules can be further relaxed. However, it is likely that the direct impact on risk would only apply for the EDZ in the deposition tunnels, whereas a higher transmissivity probably could be accepted in the other tunnels. Such a situation has, however, not been analysed in the PSAR.

Feedback to technical design requirements

Current technical design requirements are adequate. To further relax the demands would require additional sensitivity analyses focusing on the hydraulic properties of the access, main and transport tunnels.

Feedback to reference design

The current reference design, based on the deposition tunnel concept, could likely be simplified without violating current technical design requirements. Furthermore, additional simplifications could probably be made if the technical design requirements could be revised as discussed above.

15.5.20 Sealing of boreholes

In the **Closure production report** it is stated that: Boreholes must be sealed such that they do not unduly impair containment or retention properties of the repository. For boreholes in hydraulic contact with the repository this is achieved if the hydraulic conductivity of the borehole seal $< 10^{-8}$ m/s, which is ensured if the swelling pressure of the seal is > 0.1 MPa. This value needs not be upheld in sections where e.g. hole passes highly transmissive zones. The hydraulic conductivity shall be $< 10^{-6}$ m/s in the

³⁶ While pH 11 is not “low” in the general sense it is low with respect to cement based materials. *In prep.*

other boreholes. The reference design for borehole seals has been developed since SR-Site. The seal concept is a Sandwich-concept, which means that the main part of a borehole is filled with granular material (sand), while sealing sections of highly compacted bentonite, are positioned in sections with good rock quality (see Section 5.7.2).

The impact of an open borehole on the groundwater flow in the repository and the surrounding rock has been studied by introducing boreholes at various locations in the hydrogeological model applied for analyses of the temperate period in PSAR (Joyce et al. 2010). As concluded there and in Section 10.3.6, the impact of improper seals of the boreholes is very moderate. Furthermore, according to the assessment presented in Section 10.3.14, the reference design of the borehole seals will perform as intended. Clearly, the bentonite may be lost in sections intersecting highly flowing fractures, but in the reference design there is no bentonite in such sections. The only problem with the seals is to demonstrate their performance. The key issue is that it is difficult to inspect the quality of the seals after installation. A loss of bentonite in the range of a few metres in the seals will lead to a total loss of performance in that section, but the rest of the seal will be virtually unaffected. The function of the seal is not to hinder flow in the intersecting fractures, but to hinder flow along the borehole, so loss of function over a few metres is not a significant consideration.

Feedback to technical design requirements

Current technical design requirements appear adequate. However, it may be argued that current technical design requirements for the borehole seals are too strict, since even open boreholes seem to have a limited impact on the flow. Since it might be difficult to inspect the outcome of the current design of the sealing, it could be of interest to assess whether a solution that may result in higher effective permeability of the borehole seals, but that would be more robust to control, would provide sufficiently good protection. However, relaxing the technical design requirements in this way would require additional sensitivity analyses.

Feedback to reference design

The assessment in the PSAR indicates that the reference design is appropriate for the purpose. However, if technical design requirements are relaxed, more robust designs might be worth investigating.

15.6 Feedback to detailed investigations and site modelling

Previous chapters have demonstrated that several site-specific conditions have a large impact on repository evolution and also, in some cases, on individual risk. While, the confidence in the site understanding is judged adequate and remaining uncertainties are sufficiently well constrained to allow upper bound risk estimates to be made, the repository might still be further optimised with respect to efficiency and risk reduction. Furthermore, as should be clear from the assessment of the technical design requirements in the previous section, most of such potential improvements concern possibilities for local adaptation of the deposition tunnels and deposition holes to the conditions found in the rock. In addition, some issues remain concerning the properties of the rock mass outside the immediate vicinity of the deposition areas. Feedback to the detailed site investigations and site modelling can thus be given, considering the confidence and uncertainty in the **Site description Forsmark** as outlined in Chapter 4.

Programmes for the detailed investigations and associated site descriptive modelling have been developed for the shaft, ramp and central area³⁷ and for the deposition areas,³⁸ based, among other things, on the feedback presented below. Since the PSAR is based on the same SDM as SR-Site and since most of the geosphere analyses are essentially the same, the feedback provided below for host rock related issues is essentially the same as in the corresponding section in the SR-Site main report.

³⁷ "Kärnbränsleförvaret – Detaljundersökningsprogram för tillfarter och centralområde" SKBdoc 1862104 (In Swedish). (Internal document.) *In prep.*

³⁸ "Kärnbränsleförvaret – Preliminärt detaljundersökningsprogram för deponeringsområden" SKBdoc 1600833 (In Swedish). (Internal document.) *In prep.*

15.6.1 Further characterisation of the deformation zones with potential to generate large earthquakes

In order to ensure mechanical stability of deposition holes, it is a necessary condition that deposition holes are located with appropriate respect distances to deformation zones with the potential to host larger earthquakes, see Section 15.5.12. According to the **Site description Forsmark**, there is a very high confidence that only the few such zones already identified exist at the site and that even fewer of them intersect the repository volume in such a way that respect distances need to be considered.

It will also be important to locally establish the adequacy of applied respect distances in relation to observed occurrences (e.g. as mapped in transport tunnels) of the few zones able to host larger earthquakes that exist in the immediate vicinity of the repository. The detailed investigation programme needs thus spend further efforts in:

- Determining the extent of the damage zone for the few deformation zones able to host larger earthquakes at the Forsmark site.
- Identifying and characterising splays from these deformation zones.

15.6.2 Further develop the means to bound the size of fractures intersecting deposition holes

The mechanical stability of canisters also requires that the canisters are not intersected by fractures sufficiently large to cause shear failures of the canister in case of an earthquake. As noted in Section 15.5.12, the currently applied criterion, the EFPC, is only a proxy for avoiding such large fractures. Application of EFPC implies that several deposition positions might be rejected, even if the fracture intersecting them is not large enough to represent a problem as regards shear movements. Furthermore, the efficiency of EFPC, i.e. the risk of not identifying the problematic fracture, to some extent depends on the statistical distribution of fracture sizes. Consequently, it is of high interest to further develop the means for bounding the size of fractures intersecting deposition holes. Other properties of the fractures, like their undulation and orientation are also important in this context as demonstrated e.g. by the updated modelling reported in Section 10.4.5.

The ramp is the part of the underground facility that first reaches the planned reference depth, data gathered and assessments needs to be used to identify significant deviations in critical structures and volumes from site descriptive models.

15.6.3 Reduce the uncertainty of DFN models

The risk contribution from large earthquakes partly depends on the applied statistical description of the fractures, although the uncertainty in this description to a large extent is mitigated by applying the design rule that large fractures are not allowed to intersect the canister. Uncertainty in the geological DFN models is still an issue. Furthermore, reducing the uncertainty in the geological DFN model would also be of importance for reducing uncertainty in the hydrogeological DFN model, see Section 15.6.5.

The DFN model of the site is still quite uncertain and several alternatives are presented and assessed in the PSAR, see Section 10.4.5. The assessment of earthquake risk thus considers this wide range of uncertainty and even considering this, the risk contribution is very small. However, further efforts in reducing uncertainties are warranted.

In the **Site description Forsmark** it was concluded that the uncertainties in the geological DFN model can only be significantly reduced by data from underground. Such data include tunnel mapping and evaluations from boreholes (such as pilot holes drilled during the underground excavation work).

15.6.4 Identifying connected transmissive fractures

The analyses in the PSAR suggest that if it was possible to identify the few deposition hole positions having the largest Darcy flux during saturated conditions, this would dramatically reduce risk, without any significant loss of useful canister positions, see Section 15.5.13. Means of finding (and then avoiding) connected transmissive fractures capable of producing higher inflows and high Darcy fluxes into and around deposition holes should thus be a priority task of the detailed investigations.

15.6.5 Hydraulic properties of the repository volume

The hydraulic properties of the repository volume, expressed as the hydrogeological DFN model, together with the hydraulic description of the deformation zones, has a large impact on repository performance, even if some of the importance may be reduced by introducing more efficient deposition hole acceptance criteria, as discussed previously.

While confidence is high with regard to the very low frequency of connected transmissive fractures, there are still large uncertainties in the actual distribution of hydraulic properties within these fractures. This is expressed by formulating and propagating different variants concerning the correlation between fracture size and transmissivity. As shown in Chapters 10, 12 and 13, the selection of this correlation has an impact both on the number of failed canisters, due to corrosion for advective conditions in the buffer, and on the resulting migration of released radionuclides. It is thus concluded that better bounds, especially on the size versus transmissivity correlation, on the hydrogeological DFN model would be beneficial. Uncertainties in the flow-related transport resistance, due to the fact that individual fractures are treated as having homogeneous properties, are considered to be small based on the arguments provided in Section 10.3.6.

As for the geological DFN model, it is concluded in the **Site description Forsmark** that the uncertainties in the hydrogeological DFN model can only be significantly reduced by data from the underground characterisation. Combining hydraulic data obtained from underground, e.g. by hydraulic tests in boreholes (such as pilot holes drilled during the underground excavation work) with the geological characterisation of the fractures responsible for the measured flow will allow further integration between the geological and hydrogeological modelling.

15.6.6 Verifying the conformity to the EDZ technical design requirement

According to Section 15.5.16, the current technical design requirement requiring that excavation induced damage should be limited and not result in a connected effective transmissivity higher than 10^{-8} m²/s along a significant part (i.e. at least 20–30 m) of the disposal tunnel and averaged across the tunnel floor, is adequate. It was also concluded that a more transmissive EDZ starts to affect risk, even though the impact is moderate.

As already discussed, there is ample evidence that a potential EDZ formed during excavation will be kept below the maximum allowed transmissivity as set out by the technical design requirements, and data suggest that a continuous EDZ would not develop at all. It is also clear that further development of the methods to control the EDZ as well as demonstration of the reliability of these methods is needed.

The methods to control the development of an EDZ are to a large extent connected to the quality of the drill and blast operation, but some aspects of confirming that these measures actually result in an EDZ in conformity with the technical design requirements belong to the underground openings construction and need thus to be developed therein.

15.6.7 Rock mechanics

As discussed in Section 15.5.14, the *in situ* rock stress and the properties of the intact rock are such that thermally induced spalling is likely to occur. The hydraulic assessment of the impact of spalling, Section 10.3.6, demonstrates that spalling may increase the equivalent flow rate for the Q1 path by more than an order of magnitude, whereas the other paths are not affected. However, this increase has essentially no impact on risk, since spalling will not affect the local Darcy flux in the case of advective conditions in the deposition hole or if the canister is damaged by a shearing fracture.

According to the **Site description Forsmark**, there are remaining uncertainties with regard to the stress magnitude at Forsmark. There is also uncertainty in the spalling strength. While resolving these uncertainties is important for the design and layout of the repository, especially since the occurrence and amount of spalling affects the number of usable deposition positions, these uncertainties are of somewhat less importance for safety. Nevertheless, the potential for thermally induced spalling is evident considering the current uncertainty range and, since spalling affects one of the safety functions, although not risk itself, further efforts in finding methods to mitigate the spalling are warranted. This also includes a need for further characterisation of both the rock stress and the spalling strength of the rock.

15.6.8 Thermal properties

For a specific residual power in the canister the thermal conductivity and in situ temperature determine, together with the repository layout and the thermal properties and geometry of the buffer, the buffer peak temperature. The thermal analyses, see Section 10.3.4, demonstrate that the suggested layouts would conform to the thermal technical design requirements by a substantial margin, even considering remaining uncertainties in the thermal data. In fact, most deposition holes will have a temperature much below the allowed maximum. From a strictly safety point of view, further detailed investigations and modelling of thermal properties is only needed if SKB decides to aim for a more compact design, with adaptation of deposition hole distances and/or residual power in the canisters to the local thermal conditions in the tunnel.

15.6.9 Hydrogeochemistry

The chemical environment directly controls the evolution of the repository. The most important parameters are redox properties, salinity and ionic strength, which directly affect the canister and buffer safety functions, but also other factors are important, including the groundwater content of potassium, sulphide and iron(II), as they might affect the chemical stability of the buffer and the canister. In particular, as shown in Chapter 10 and Chapter 12, the levels of sulphide affect risk, since these levels control the canister corrosion rate and thus the number of canister failures due to corrosion in the case of advective conditions in the buffer.

Available hydrogeochemical data are clearly sufficient to prove that suitable conditions prevail at the Forsmark site today and also during the temperate period that should persist for at least the next few thousand years. Estimating possible changes in the groundwater composition for longer times and during a glacial cycle are more challenging and this has been done pessimistically in the PSAR. As shown in Section 10.4.7, upconing during glaciation will not result in excessively high salinity values, whereas intrusion of dilute glacial melt water, which may result in buffer erosion, cannot be excluded. Furthermore, for the case of an eroded buffer, the sulphide content becomes important, since excessively high values may lead to corrosion failure of the copper canister (see Section 10.4.9).

In order to enhance the confidence in these important evaluations and potentially also to be able to exclude the possibility of intruding dilute glacial melt water, more information would be valuable. Groundwater sampling data on sulphide, as well as dissolved organic carbon, microbial populations, hydrogen and methane, giving their concentrations and isotopic ratios would improve the possibility of estimating the future sulphide content. Isotope data on noble gases would also improve the understanding of diffusion of gaseous species. Also more uranium and radium analyses are needed in order to understand the heterogeneous distribution of these elements in Forsmark.

15.6.10 Surface ecosystems

The assessment of long-term effects on humans and the environment is based on two main foundations: i) a conceptual understanding of ecosystem function today, in the near and in the far future, and during different climate regimes, and ii) input data to assessment models, synthesised from the Forsmark site description and analogue sites, from the literature and from models describing the landscape development.

The two major groups of important parameters affecting dose are those related to the geometry of the landscape and those that affect radionuclide sorption and uptake. The geometry which affects basin and biosphere object areas, type of ecosystem and regolith type and layer thickness, is to a large extent determined by the site. From the site investigations a fairly good overall picture is available, but details in discharge areas are lacking. Moreover, a good understanding of the natural variation and alternative geometries due to long-term development is limited and requires further studies. It is necessary to obtain more data and understanding of sediment accumulation and erosion, mire development and a detailed stratigraphy of discharge areas. The geometries also affect hydrology and residence times. The hydrological models for the site are relatively complex and dependent on site parameters that are difficult to generalise over a longer timeframes, but still lacking resolution to resolve discharge patterns from the bedrock to critical parts at the surface. It is necessary to improve

the understanding of discharge positions, patterns and natural variation by measurements at the site and at analogue sites. This requires more studies on water fluxes in discharge areas as well as tracers of discharges of deep groundwater.

Since SR-Site, more site data have been collected for important input parameters to the biosphere radionuclide model, like partitioning coefficients (K_d values) and concentration ratios (CR) describing sorption and biological uptake, respectively. The understanding of uncertainty and model precision will increase further by collection of additional data on element concentrations in different media. Elemental concentrations in true paired samples for K_d and CR estimation and supporting data (pH, organic content and additional chemistry) is planned to be measured in relevant environments. Such environments include areas of deep groundwater discharge and agricultural land, in Forsmark and at analogue sites representing future environmental conditions and climate at the Forsmark site. It is important to evaluate the long-term changes of the chemistry due to the shore line displacement, leaching and oxidation. Moreover, alternative methods to estimate uptake (plant production, transpiration) and sorption (chemical speciation and association to organic matter) can further reduce uncertainties or constrain possible ranges for accumulation and uptake.

15.7 Feedback to RD&D Programme

In accordance with a proper safety culture, general research on processes of importance for safety should continue even if the current view is that existing knowledge is sufficient to demonstrate post-closure safety. More specifically, there are some issues which the outcome of the PSAR shows to contribute to risk and where the basis for the assessment can be improved through more R&D. A programme for further research related to the post-closure safety of the final repository has been developed³⁹, based, among other things, on the feedback presented below.

15.7.1 Spent fuel

Gap and grain boundary inventory

Since the gap release is important in relation to risk, see Section 13.5.11, the dependence of the gap and grain boundary inventories on burn-up and linear power needs to be further studied. The estimates of fission gas release from high-burnup fuel in the PSAR should be complemented with actual measurements of fission gas release and releases in solution of mobile elements such as Cs and I. A few radionuclides in the instant release fraction originate mainly from deposits on the fuel cladding (crud). An improved model for the crud inventory could reduce the uncertainties concerning the size of this fraction.

Spent fuel dissolution

Given the importance of the spent fuel dissolution for the amount of radionuclides released, see Section 13.5.11, research on fuel dissolution should continue. New fuel types with additives, such as Cr, need further study. Continued research should focus on improved process understanding, which together with data collected over the years, could be used to develop of a mechanistic model describing fuel dissolution in the repository environment over time. Such a model could reduce the calculated risk further.

A few irregular fuel types that represent a very small fraction of the volume of spent fuel, such as fuel with failed cladding, have to be included in the risk calculation, as done in the PSAR. Characterisation of such irregular fuels, combined with research concerning its dissolution behaviour, is therefore suggested to better quantify the risk contribution from these fuel types.

³⁹ ”Plan för SAR Kärnbränsleförvaret – Vetenskaplig fördjupning” SKBdoc 1884515 (In Swedish.) (Internal document.) *In prep.*

15.7.2 Canister

Corrosion of copper canister

Understanding copper corrosion is fundamental for the safety concept. While confidence is judged high it is still essential to continue ongoing research. Such research includes studies of the formation and properties of copper sulphide films, prerequisites for different forms of localised corrosion (in both oxidising and sulphide environments), corrosion behaviour during transient conditions as well as further assessing several aspects of the role of the buffer and the backfill in determining corrosion rates. The processes during the saturation of the bentonite need special attention, such as gas phase reactions.

Stress corrosion cracking of copper canister

Conditions for stress corrosion cracking under oxidising conditions are not judged to occur in the repository but the basic research focusing on the mechanisms and necessary conditions needed for stress corrosion cracking to occur should continue in order to reduce any uncertainties concerning the margins for SCC under repository conditions. The superficial cracking observed in some laboratory experiments with harsher sulphide conditions (interpreted as intergranular corrosion or possibly stress corrosion cracking) needs further research to gain a better understanding of the mechanisms and an improved assessment of the applicability to repository conditions.

Deformation of cast iron

Understanding the deformation of cast iron is essential for the confidence in the assessment of the impact of mechanical load on the canister. While confidence is judged high for the design analyses presented in the **Canister production report**, further work is warranted since this is a key issue and since pessimisms regarding e.g. failure criteria applied in the design analysis could be reduced. The ongoing development work on the design, manufacturing and testing of cast iron inserts, needs to continue in order to determine material requirements and specifications, and to ensure that all quality requirements can be fulfilled.

Deformation of copper shell from external pressure

Also the understanding of copper deformation under external pressure is essential for the confidence in the assessment of the impact of mechanical load on the canister. While confidence is judged high for the design analyses presented in the **Canister production report**, further work is warranted since this is a key issue. The ongoing work on assessing creep properties of copper should continue, with focus on theoretical understanding and its application in creep modelling. The role of the added phosphorus to increase the ductility of the copper would benefit from a better understanding on the atomic scale to ascertain the long-term properties.

Hydrogen embrittlement in copper

The potential for hydrogen to enter the copper material to any substantial extent is regarded as very limited, but hydrogen liberated in the corrosion of copper by sulphide is a process that will proceed during the whole assessment period. It is thus warranted to further study the mechanism for hydrogen ingress and possible influence on mechanical properties, including development of the laboratory experiments and techniques to measure hydrogen content.

15.7.3 Buffer and backfill

Water transport

As shown in Chapter 10, there is sufficient understanding of water transport in the buffer and backfill material to make adequate predictions with respect to post-closure safety. However, uncertainties remain, which when resolved might enhance current designs. Laboratory and field tests of different materials and calibration of models in order to optimise parameter values in the models to enhance knowledge of water transport in both dry and wet conditions are thus warranted.

Gas transport

Available experimental results show that gas can migrate through a highly-compacted buffer without jeopardising the continued function of the engineered barrier. Results from the final test in the Lasgit experiment at Äspö showed that this is the case even if the pressurised gas volume is equivalent to the entire canister void ($\sim 1 \text{ m}^3$). There are still uncertainties about the processes that controls gas migration in compacted bentonite, but the details are of minor importance since the results from the experiments are clear.

Composition of the gas in an unsaturated bentonite

The composition of the gas in an unsaturated bentonite has a negligible effect on the performance of the bentonite barrier itself. It may, however, have effects on canister corrosion. Initial experiments have given ambiguous results regarding the rate of oxygen consumption in unsaturated bentonite and further tests are therefore warranted and planned.

Piping/erosion

The understanding of piping/erosion is much advanced since SR-Site and has allowed formulation of technical design requirements with regard to inflow into deposition holes as documented in the updated **Buffer, backfill and sealing process report**. For fine tuning these technical design requirements and for developing the designs, further understanding of the importance of geometry, enhanced knowledge of when piping does not occur, the applicability of the erosion model, self-sealing of cracks and enhanced ability to quantify the process would be valuable. Such studies should consider the processes occurring during water saturation with a focus on homogenisation.

Mechanical processes

Homogenisation and self-sealing are important processes for the evolution of the buffer and the backfill. Ongoing research should continue.

Integrated THM development

The understanding of the THM development in the buffer and backfill has progressed considerably since SR-Site as documented in the updated **Buffer, backfill and sealing process report**. The ongoing development of the integrated coupled buffer THM model should continue. This should be facilitated by assessing different projects at Äspö, further development of the codes used and by new experiments on a smaller scale for studying hydromechanical processes. Effort should be focused on processes occurring during water saturation: Piping, erosion, water saturation, self-sealing, and homogenisation of both buffer and backfill.

Montmorillonite alteration

Buffer and backfill performance depends on understanding montmorillonite alteration. The impact from potential construction and grouting materials, such as low alkalinity cements and silica sol should continue to be studied, especially to further specify restrictions on their use in the repository.

Cementation

The studies on rheological effects of cementation should be continued.

Buffer erosion/Sedimentation/Colloid release

From the studies of buffer erosion/colloid release conducted since SR-Site, it has been concluded that the process cannot be ruled out in the assessment of post-closure safety and that a continued R&D programme is needed. The transport model basically considers a pure sodium system and the loss of bentonite is most likely overestimated. Further studies could reduce the pessimism. Some areas of interest are:

- The effect of gravity.
- Flocculation of generated colloids.
- The effect of calcium and mixed Ca/Na systems on swelling/colloid formation behaviour.
- Erosion in fractures or slots (both smooth and rough fractures).
- The effect of flow and water velocity on the erosion.
- The effect of different bentonite types.
- Detailed effects of the water composition.
- Sealing of erosion damage.

These studies are already progressing.

15.7.4 Geosphere

Much of the R&D related to the geosphere is covered by the detailed investigation programme, but research on some processes should also continue.

Spalling

Before SR-Site, several efforts were made to enhance the understanding of the conditions under which thermal spalling will occur, as well as the extent of the spalled zone. As already concluded, thermally induced spalling is likely to occur, but the counter pressure exerted by bentonite pellets in the slot between buffer and rock wall may suppress the spalling, or at least keep the spalled slabs in place and minimise the hydraulic transmissivity of the spalled damage zone. New efforts in terms of theoretical, numerical and laboratory studies have been initiated since SR-Site to increase the fundamental knowledge about the spalling process and the capability to predict it (see Section 6.5.2 in the **Data report**). Furthermore, the assessment of the impact of spalling demonstrates that spalling may increase the equivalent flow rate for the Q1 path by more than an order of magnitude and that this increase has essentially no impact on risk, since spalling will not affect the local Darcy flux in the case of advective conditions in the deposition hole or if the canister is damaged by a shearing fracture. Other exit paths than Q1 are not affected by spalling. Consequently, further progress in the actions to assess spalling is not critical to safety, but efforts to handle and mitigate thermally induced spalling should continue as this affects one of the safety functions.

THM assessment of the geosphere

The assessment of coupled thermo-hydro-mechanical processes presented in Chapter 10 clearly demonstrates that such processes have limited impact on safety. Continued research on the underlying processes is still warranted, although possibly primarily for input to the rock engineering design of the repository. In particular, efforts will be made to study the effect of more realistic assumptions regarding excavation induced changes on transmissivity around tunnels by incorporating hydro-mechanical coupling in the analysis. With respect to post-closure safety issues, those worth further assessment include revisiting the current assumptions on stress-transmissivity couplings for fractures and deformation zones and revisiting current assumptions on excess porewater pressure during the glacial cycle. Current assumptions are judged to overstate the importance of these effects.

Glacially induced stresses and earthquake simulations

There have been major advances regarding the potential for earthquakes and their implications for safety since SR-Site. Potentially, there is some risk contribution from this mechanism, but it is low. Furthermore, the adaptation of the repository to deformation zones and fractures is handled within the detailed investigation programme, see Section 15.6. Considering that mechanical stability is fundamental, research on the prerequisites (e.g. state of stress) for glacially induced fault triggering should still continue. Further development of the earthquake simulation tools and approaches is also considered worthwhile.

DFN methodology

A better knowledge of the fracture network in crystalline bedrock is essential for gaining a more realistic understanding, decreasing the uncertainty of models representing geological, mechanical, and hydrological aspects of the rock. Thus, efforts have been initiated to develop a unified DFN methodology for geological, hydrogeological and rock mechanical applications such that hydraulically active fractures are a true subset of all geological fractures. Also, hydro-mechanical couplings will be introduced, and means to describe fracture aperture variability and the distribution of open/closed fractures. Furthermore, alternative methods for generating fracture networks, e.g. genetic methods based on mechanical principles for fracture initiation, growth and truncation, are currently being developed. Efforts are also planned to investigate how estimated fracture intensity depends on measuring methods, to identify what extra data are needed for limiting values for input parameters that would limit the possible range of model outputs, to develop an efficient method in order to evaluate differences between different models, to further investigate the distribution of fracture apertures over the fracture surface, and to study effects of connectivity of fractures, for example through channelling, truncation, or alternative methods for generating fracture networks.

Groundwater chemistry – sulphide

As shown in Section 13.6, the future sulphide levels in the groundwater have a strong influence on risk. The sulphide distribution applied in the PSAR is judged to pessimistically overestimate the consequences of future sulphide concentrations, especially since it is assumed that locations with high sulphide levels will remain at high levels throughout the assessment period. Further research to better bound the expected evolution of sulphide and the processes affecting this evolution at the Forsmark site is thus warranted. Experimental and modelling efforts involving microbial processes, dissolved organic matter, hydrogen, and ferrous iron could also help to predict the expected evolution of the sulphide concentration. Such research would include further assessments of errors introduced by the sampling and monitoring equipment.

Microbial processes

Redox conditions and sulphide levels directly affect risk. Since these conditions are strongly affected by microbial activity, the ability of microbes to maintain a low and stable redox potential in the near-field and the far-field and their role for sulphide formation and oxygen consumption warrants further research.

Penetration of dilute water

The calculations in Sections 10.3.6 and 10.4.6 on penetration of dilute water have been up-dated relative to the corresponding calculations in SR-Site. Specifically, the previously approximate handling of matrix diffusion has been dealt with by using a model which explicitly accounts for a finite matrix depth, and the assumption of zero concentration infiltrating water has been relaxed. Furthermore, the effects of diffusion into stagnant water in the fracture plane with subsequent diffusion into the matrix have been illustrated, albeit not accounted for in the compliance calculations. However, the calculations are still based on one-dimensional recharge pathways assuming no interaction, i.e., mixing, between pathways. This is a likely very pessimistic approach which has been adopted since corresponding calculations based on the up-scaled continuum model drastically may over estimate mixing effects due to limitations in spatial resolution implying numerical dispersion effects. Thus, efforts should be made in future assessment to describe transport of solutes directly in the explicit DFN model, hence avoiding both the numerical dispersion of the ECPM approach and the limitations of the non-branching, one-dimensional flow path approximation of the current approach. Furthermore, efforts should be made to better conceptualise and parameterise the stagnant water volume within fracture planes.

Concerning the concentration of infiltrating water and weathering reactions in both soil and bedrock, further collection of surface samples, as well as laboratory investigations of weathering processes that can take place in the regolith should be performed in preparation for a future assessment. Efforts towards incorporating chemical weathering reactions in explicit DFN models that also include matrix diffusion will be undertaken as well.

Radionuclide migration

In Section 10.3.6 it is argued that the calculated flow-related transport resistance values do not need to be reduced due to channelling effects. This argument is based on motivations provided in the **Radionuclide transport report** and also summarised in the **Data report**. In short, the argument is based on calculations showing that channelling leads to stagnant water in the fracture planes (between the channels) enhancing the potential for matrix diffusion due to the fast diffusion from the flowing channels into the stagnant parts of the fracture. Furthermore, supporting calculations using the alternative conceptual model CHAN3D (Liu et al. 2010) indicate that broadly consistent flow-related transport resistance values to those presented in Joyce et al. (2010) are obtained, see Section 10.3.6 for details. This further supports the assumption made on channelling.

However, in order to shed additional light on the assumptions made in the PSAR, continuing research in the field of channelling should be pursued. Specifically, high resolution numerical simulations of fractures with spatially variable apertures will be continued. The objective is to study the effects of channelling within fractures, and between fractures in a network, with variable apertures. Preliminary studies focussing on advective travel time behaviour in simple networks with internal fracture variability indicate that internal aperture variability with strong connectivity implies earlier mass arrival for limited ranges of correlation length and domain size relative to cases with weak connectivity (Frampton et al. 2019). With a more detailed understanding of channelling phenomena and the relative importance of internal fracture variability relative to other network characteristics, more conclusive statements concerning the assumptions made in the PSAR can be drawn.

15.7.5 Biosphere

Since SR-Site, SKB has advanced the biosphere research within the RD&D program and developed the biosphere assessment further, mainly within the SR-PSU and SE-SFL safety assessment projects. Important results include improved exposure and dose calculations, more site specific data and updated K_d and CR estimates, detailed studies on some dose contributing radionuclides (e.g. Cl-36, C-14), development of the model for C-14 within an international cooperation framework, and development of the surface hydrological modelling. It also includes derivation of biosphere object specific hydrological parameters, accounting for variation in object properties and improvements of the biosphere assessment model, for example increased discretisation of deeper regolith layers. Relevant results will be used and implemented for the spent nuclear fuel repository assessment, and will contribute to increase confidence and reduce uncertainty, and possibly also decrease the level of pessimism, in future safety assessments.

Moreover, there are research questions and method development identified either by SKB or by reviewers during the reviews of SR-Site (SSM 2018), SR-PSU (SSM 2019) or the RD&D Programmes (SSM 2014, 2017, 2020), that will improve the assessment further. The RD&D Programme (SKB 2019b) describes future research plans, assessment development and data requirements for all three repositories, and many of those plans are relevant for the spent fuel repository. The plans include collection of additional data on element concentrations in different media and other environmental measures from relevant environments (see Section 15.6.10) in order to reduce uncertainties in assessment parameters describing radionuclide retention (K_d) and biological uptake (CR). Deepened analysis of existing and new data will improve the understanding of transport and uptake processes, and enable development of transport and uptake models to simulate also future conditions. When possible, existing and new data will be used in efforts to validate supporting models and sub models of the biosphere assessment.

Supporting models, describing e.g. landscape development, biosphere object properties and surface hydrology, provide input to the biosphere assessment, and these supporting models need updated input data from the site investigation (Section 15.6.10) for parametrisation and validation. Moreover, the supporting models can provide input to the biosphere assessment that account for variation and uncertainty in biosphere object properties and hydrology, both in a short and a long-term perspective. SKB has started and will continue to investigate how the supporting models used in SR-Site (RLDM and Mike-SHE) can be complemented by alternative models like the Untamo and Comsol models, or by other, simpler models.

The biosphere assessment is in the current calculation chain for the corrosion and shear load scenarios (Section 13.5 and Section 13.6) implemented by the concept of maximum LDFs (*Landscape dose conversion factors*) for a unit release (1 Bq/y), i.e. the maximum LDF is taken across all biosphere objects and all times, separately for each radionuclide. This means a simplifying decoupling between the LDFs on the one hand and the space and time dimensions on the other, and will most likely result in overestimated maximum doses if more than one radionuclide contribute significantly to total doses. However, for early releases, i.e. in the hypothetical what-if scenarios (Section 13.7.3) and early failures due to shear load (Section 13.6.2, subsection “*Distribution of failures up to 1 000 years*”), more integrated geosphere-biosphere modelling, where time-dependent releases to the biosphere were used as input to the biosphere model, generally results in lower doses. Both alternatives have their advantages, and more simple models are planned to be used for benchmarking and to increase the understanding of the modelled processes. Comparisons between the different modelling concepts and an awareness of how uncertainties generally increase with time will guide the choice of modelling strategy in future assessments.

15.7.6 Climate

Apart from the work of identifying and describing extremes within which climate- and climate-related processes may vary, the work within the PSAR also focussed on describing climate and climate-related processes within each of the climate domains, and during some of the transitions between domains. Future research should include further description and analysis of the temporal evolution of climate domains. This includes a more detailed analysis of transitions between climate domains and potential changes in processes that may relate specifically to such transition phases. This work should preferably include a representation of a realistic climate variability over the full 1 Ma assessment period. This realistic representation can be used to further assess the degree of pessimism in the methodology used in the PSAR which is based on repetitions of a reference glacial cycle accompanied by additional bounding cases. This work should also include the coupling to the representation of processes and features in e.g. the biosphere-, hydrogeology- and geochemistry programmes.

15.8 Conclusions regarding the safety assessment methodology

The assessment methodology is outlined in Chapter 2. Amendments to the methodology based on SSM’s review of the SR-Site assessment are essentially summarised in Section 11.3. The methodology has been found adequate for analysing post-closure safety of a KBS-3 repository according to requirements in applicable Swedish regulations. It is also in line with international practice for safety assessments. Much of the technical feedback given in the above sections is expected to lead to updated input to future assessments and will influence the approach used when addressing the issues in such future assessments. A plan for the further refinement of the safety assessment methodology has been developed.⁴⁰ Issues in the plan include the further development of the scenario methodology, a more consistent handling of uncertainties and sensitivities and an integrated handling of pulse and continuous releases in the radionuclide transport calculations.

⁴⁰ ”Plan för SAR Kärnbränsleförvaret – Analys av säkerhet efter förslutning”, SKBdoc 1877726 (In Swedish.) (Internal document.) *In prep.*

References

SKB's (Svensk Kärnbränslehantering AB) publications can be found at www.skb.com/publications. SKBdoc documents will be submitted upon request to document@skb.se, with the exception of internal documents.

References with abbreviated names

Backfill production report, 2022. Produktionsrapport Återfyllning. SKBdoc 1525864 ver 4.0, Svensk Kärnbränslehantering AB. (In Swedish.) (Internal document.)

Biosphere synthesis report, 2010. Biosphere analyses for the safety assessment SR-Site – synthesis and summary of results. SKB TR-10-09, Svensk Kärnbränslehantering AB.

Buffer, backfill and closure process report, 2022. Post-closure safety for the final repository for spent nuclear fuel at Forsmark – Buffer, backfill and closure process report, PSAR version. SKB TR-21-03, Svensk Kärnbränslehantering AB.

Buffer production report, 2022. Produktionsrapport Buffert. SKBdoc 1392269 ver 5.0, Svensk Kärnbränslehantering AB. (In Swedish.) (Internal document.)

Canister production report, 2022. Produktionsrapport Kapsel. SKBdoc 1407944 ver 2.0, Svensk Kärnbränslehantering AB. (In Swedish.) (Internal document.)

Climate report, 2020. Post-closure safety for the final repository for spent nuclear fuel at Forsmark – Climate and climate related issues, PSAR version. SKB TR-20-12, Svensk Kärnbränslehantering AB.

Closure production report, 2022. Produktionsrapport Förslutning. SKBdoc 1387771 ver 3.0, Svensk Kärnbränslehantering AB. (In Swedish.) (Internal document.)

Data report, 2022. Post-closure safety for the final repository for spent nuclear fuel at Forsmark – Data report, PSAR version. SKB TR-21-06, Svensk Kärnbränslehantering AB.

Deposition tunnel plug production report, 2022. Produktionsrapport Valvplugg. SKBdoc 1562518 ver 3.0, Svensk Kärnbränslehantering AB. (In Swedish.) (Internal document.)

FEP report, 2010. FEP report for the safety assessment SR-Site. SKB TR-10-45, Svensk Kärnbränslehantering AB.

FHA report, 2010. Handling of future human actions in the safety assessment SR-Site. SKB TR-10-53, Svensk Kärnbränslehantering AB.

Fuel and canister process report, 2022. Post-closure safety for the final repository for spent nuclear fuel at Forsmark – Fuel and canister process report, PSAR version. SKB TR-21-02, Svensk Kärnbränslehantering AB.

Geosphere process report, 2022. Post-closure safety for the final repository for spent nuclear fuel at Forsmark – Geosphere process report, PSAR version. SKB TR-21-04, Svensk Kärnbränslehantering AB.

Model summary report, 2022. Post-closure safety for the final repository for spent nuclear fuel at Forsmark – Model summary report, PSAR version. SKB TR-21-05, Svensk Kärnbränslehantering AB.

Radionuclide transport report, 2022. Post-closure safety for the final repository for spent nuclear fuel at Forsmark – Radionuclide transport report, PSAR version. SKB TR-21-07, Svensk Kärnbränslehantering AB.

Site description Forsmark, 2008. Site description of Forsmark at completion of the site investigation phase – SDM-Site Forsmark. SKB TR-08-05, Svensk Kärnbränslehantering AB.

Spent fuel report, 2021. Använt kärnbränsle att hantera i KBS-3-systemet. SKBdoc 1380282 ver 3.0, Svensk Kärnbränslehantering AB. (In Swedish.) (Internal document.)

Underground openings construction report, 2021. Produktionsrapport Bergutrymmen. (In Swedish.) (Internal document.) *In prep.*

Regular references

- Aastrup M, 1981.** Naturligt förekommande uran-, radium- och radonaktiviteter i grundvatten. SKBF/KBS TR 81-08, Svensk Kärnbränsleförsörjning AB. (In Swedish.)
- Agrenius L, 2010.** Criticality safety calculations of disposal canisters. SKBdoc 1193244 ver 4.0, Svensk Kärnbränslehantering AB.
- Agrenius L, Spahiu K, 2016.** Criticality effects of long-term changes in material compositions and geometry in disposal canisters. SKB TR-16-06, Svensk Kärnbränslehantering AB.
- Ahokas H, Hellä P, Ahokas T, Hansen J, Koskinen K, Lehtinen A, Koskinen L, Löfman J, Mészáros F, Partamies S, Pitkänen P, Sievänen U, Marcos N, Snellman M, Vieno T, 2006.** Control of water inflow and use of cement in ONKALO after penetration of fracture zone R19. Posiva Working Report 2006-45, Posiva Oy, Finland.
- Ahonen L, Vieno T, 1994.** Effects of glacial meltwater on corrosion of copper canisters. Report YJT-94-13, Nuclear Waste Commission of Finnish Power Companies.
- Allard B, Banwart S, Bruno J, Ephraim J, Grauer R, Grenthe I, Hadermann J, Hummel W, Jakob A, Karapiperis T, Plyasunov A, Puigdomenech I, Rard J, Saxena S, Spahiu K, 1997.** Modelling in aquatic chemistry. Paris: Nuclear Energy Agency, OECD.
- Alonso U, Missana T, García Gutiérrez M, Morejón J, Mingarro M, Fernández A M, 2019.** CIEMAT studies within POSKBAR project. Bentonite expansion, sedimentation and erosion in artificial fractures. SKB TR-19-08, Svensk Kärnbränslehantering AB.
- Amcoff Ö, 1998.** Mineral formation on metallic copper in a “future repository site environment”: textural considerations based on natural analogs. SKI Report 98:7, Swedish Nuclear Power Inspectorate.
- Andersson C, Johansson Å, 2002.** Boring of full scale deposition holes at the Äspö Hard Rock Laboratory. Operational experiences including boring performance and a work time analysis. SKB TR-02-26, Svensk Kärnbränslehantering AB.
- Andersson J, 2013.** Svar till SSM på begäran om komplettering rörande buffert och återfyllning under driften av slutförvarsanläggningen. SKBdoc 1371890 ver 2.0, Svensk Kärnbränslehantering AB. (In Swedish.)
- Anderson J G, 1986.** Seismic strain rates in the central and eastern United States. Bulletin of the Seismological Society of America 76, 273–290.
- Andersson E (ed), 2010.** The limnic ecosystems at Forsmark and Laxemar-Simpevarp. SR-Site Biosphere. SKB TR-10-02, Svensk Kärnbränslehantering AB.
- Andersson J, 1999.** Data and data uncertainties. Compilation of data and data uncertainties for radionuclide transport calculations. SKB TR-99-09, Svensk Kärnbränslehantering AB.
- Andersson J C, 2007.** Rock mass response to coupled mechanical thermal loading: Äspö pillar stability experiment. PhD thesis. Royal Institute of Technology, Stockholm, Sweden.
- Andersson J, Ström A, Svemar C, Almén K-E, Ericsson L O, 2000.** What requirements does the KBS-3 repository make on the host rock? Geoscientific suitability indicators and criteria for siting and site evaluation. SKB TR-00-12, Svensk Kärnbränslehantering AB.
- Andersson P, Garnier-Laplace J, Beresford N A, Copplestone D, Howard B J, Howe P, Oughton D, Whitehouse P, 2009.** Protection of the environment from ionising radiation in a regulatory context (protect): proposed numerical benchmark values. Journal of Environmental Radioactivity 100, 1100–1108.
- Andersson-Östling H C M, 2020.** Creep testing of copper intended for nuclear waste disposal – overview of studies from 1985 to 2018. SKB TR-20-06, Svensk Kärnbränslehantering AB.
- Andra, 2005.** Dossier 2005 Argile. Safety evaluation of a geological repository. Châtenay-Malabry: Andra.
- Appleyard P, Jackson P, Joyce S, Hartley L, 2018.** Conditioning discrete fracture network models on intersection, connectivity and flow data. SKB R-17-11, Svensk Kärnbränslehantering AB.

- Apted M J, Bennett D G, Saario T, 2009.** A review of evidence for corrosion of copper by water. Report 2009:30, Swedish Radiation Safety Authority.
- Aquilonius K (ed), 2010.** The marine ecosystems at Forsmark and Laxemar-Simpevarp. SR-Site Biosphere. SKB TR-10-03, Svensk Kärnbränslehantering AB.
- Arcos D, Grandia H, Domènech C, 2006.** Geochemical evolution of the near-field of a KBS-3 repository. SKB TR-06-16, Svensk Kärnbränslehantering AB.
- Arenius M, Hansen J, Juhola P, Karttunen P, Koskinen K, Lehtinen A, Lyytinen T, Mattila J, Partamies S, Pitkänen P, Raivio P, Sievänen U, Vuorinen U, Vuorio M, 2008.** R20 summary report: The groundwater inflow management in ONKALO – the future strategy. Posiva Working Report 2008-44, Posiva Oy, Finland.
- Arilahti E, Lehtikuusi T, Olin M, Saario T, Varis P, 2011.** Evidence for internal diffusion of sulphide from groundwater into grain boundaries ahead of crack tip in Cu OFP copper. Corrosion Engineering, Science and Technology 46, 134–137.
- Arvidsson A, Josefsson P, Eriksson P, Sandén T, Ojala M, 2015.** System design of backfill. Project results. SKB TR-14-20, Svensk Kärnbränslehantering AB.
- Arvidsson R, 1996.** Fennoscandian earthquakes: whole crustal rupturing related to postglacial rebound. Science 274, 744–746.
- Auqué L F, Gimeno M J, Gómez J B, Puigdomenech I, Smellie J, Tullborg E-L, 2006.** Groundwater chemistry around a repository for spent nuclear fuel over a glacial cycle. Evaluation for SR-Can. SKB TR-06-31, Svensk Kärnbränslehantering AB.
- Auqué L F, Acero P, Gimeno M J, Gómez J, Puigdomenech I, 2013.** Effects of weathering of silicate minerals and cation-exchange on the geochemical safety indicators during the hydrogeochemical evolution at Forsmark. SKBdoc 1417006 ver 1.0, Svensk Kärnbränslehantering AB.
- Avila R, 2013.** Derivation of a dose factor for Rn-222 release to a well. SKBdoc 1418460 ver 1.0, Svensk Kärnbränslehantering AB.
- Avila R, Bergström U, 2006.** Methodology for calculation of doses to man and implementation in Pandora. SKB R-06-68, Svensk Kärnbränslehantering AB.
- Avila R, Pröhl G, 2008.** Models used in the SFR 1 SAR-08 and KBS-3H safety assessments for calculation of ¹⁴C doses. SKB R-08-16, Svensk Kärnbränslehantering AB.
- Avila R, Ekström P-A, Åstrand P-G, 2010.** Landscape dose conversion factors used in the safety assessment SR-Site. SKB TR-10-06, Svensk Kärnbränslehantering AB.
- Aydan Ö, Ohta Y, Geniş M, Tokashiki N, Ohkubo K, 2010.** Response and stability of underground structures in rock mass during earthquakes. Rock Mechanics and Rock Engineering 43, 857–875.
- Bai X, Guo R, Mao F, Macdonald D M, 2023.** Effect of microalloying element P on the pitting behavior of copper. Corrosion Science 211, 110858.
- Banwart S A, 1999.** Reduction of iron(III) minerals by natural organic matter in groundwater. Geochimica Cosmochimica Acta 63, 2919–2928.
- Banwart S A, Gustafsson E, Laaksharju M, 1999.** Hydrological and reactive processes during rapid recharge to fracture zones: the Äspö large scale redox experiment. Applied Geochemistry 14, 873–892.
- Barton N, Chryssanthakis P, 1989.** Distinct element modelling of the influence of glaciation and deglaciation on the behaviour of a faulted rock mass. SKB AR 89-19, Svensk Kärnbränslehantering AB.
- Bath A, Hermansson H-P, 2009.** Biogeochemistry of redox at repository depth and implications for the canister. Report 2009:28, Swedish Radiation Safety Authority.
- Bath A, Lalieux P, 1999.** Technical summary of the SEDE Workshop on the use of hydrogeochemical information in testing groundwater flow models. In Use of hydrogeochemical information in testing groundwater flow models: proceedings of an NEA Workshop, Borgholm, Sweden, 1–3 September 1997. Paris: Nuclear Energy Agency, OECD, 13–30.

- Baxter S, Appleyard P, Hartley L, Hoek J, Williams T, 2018.** Exploring conditioned simulations of discrete fracture networks in support of hydraulic acceptance of deposition holes. Application to the ONKALO demonstration area. Posiva SKB Report 07, Posiva Oy, Svensk Kärnbränslehantering AB.
- Becker D-A, Buhmann D, Storck R, Alonso J, Cormenzana J-L, Hugli M, van Gemert F, O’Sullivan P, Laciok A, Marivoet J, Sillen X, Nordman H, Vieno T, Niemeyer M, 2002.** Testing of safety and performance indicators (SPIN). EUR 19965 EN, European Commission.
- Becker R, Öijerholm J, 2017.** Slow strain rate testing of copper in sulfide rich chloride containing deoxygenated water at 90 °C. Report 2017:02, Swedish Radiation Safety Authority.
- Becker R Forsström A, Yagodzinskyy Y, Heikkilä M, Hänninen H, 2020.** Sulphide-induced stress corrosion cracking and hydrogen absorption in copper exposed to sulphide and chloride containing deoxygenated water at 90 °C. Report 2020:01, Swedish Radiation Safety Authority.
- Behrenz P, Hannerz K, 1978.** Criticality in a spent fuel repository in wet crystalline rock. KBS TR 108, Svensk Kärnbränslehantering AB.
- Bengtsson A, Blom A, Hallbeck B, Heed C, Johansson L, Stahlén J, Pedersen K, 2017a.** Microbial sulphide-producing activity in water saturated MX-80, Asha and Calcigel bentonite at wet densities from 1 500 to 2 000 kg m⁻³. SKB TR-16-09, Svensk Kärnbränslehantering AB.
- Bengtsson A, Blom A, Johansson L, Taborowski T, Eriksson L, Pedersen K, 2017b.** Bacterial sulphide-producing activity in water saturated iron-rich Rokle and iron-poor Gaomiaozi bentonite at wet densities from 1 750 to 1 950 kg m⁻³. SKB TR-17-05, Svensk Kärnbränslehantering AB.
- Bengtsson A, Blom A, Taborowski T Schippers A, Edlund J, Kalinowski B, Pedersen K, 2017c.** FEBEX-DP: Microbiological report. Nagra Arbeitsbericht NAB 16-15, Nagra, Switzerland.
- Bengtsson A, Blom A, Hallbeck B, Taborowski T, Johansson L, Morsing J J, Chukharkina A, Pedersen K, 2019.** The effects of biofilm formation on deep groundwater chemistry and microbial sulphide production. Summary report. SKB R-19-19, Svensk Kärnbränslehantering AB.
- Benjamin L A, Hardie D, Parkins R N, 1988.** Stress corrosion resistance of pure coppers in ground waters and sodium nitrite solutions. British Corrosion Journal 23, 89–95.
- Beresford N, Brown J, Coplestone D, Garnier-Laplace J, Howard B J, Larsson C-M, Oughton O, Pröhl G, Zinger I (eds), 2007.** D-ERICA: An integrated approach to the assessment and management of environmental risks from ionising radiation. Description of purpose, methodology and application. ERICA Project, contract number FI6R-CT-2004-508847, European Commission.
- Berger A, 1978.** Long-term variations of daily insolation and Quaternary climatic changes. Journal of the Atmospheric Sciences 35, 2362–2367.
- Berger A, Loutre M F, 2002.** An exceptionally long interglacial ahead? Science 297, 1287–1288.
- Berglund S, Lindborg T, Kautsky U, Saetre P, 2015.** Reply to SSM question regarding homogeneous biosphere objects. SKBdoc 1480681 ver 1.0, Svensk Kärnbränslehantering AB.
- Beverkog B., Puigdomenech I., 1997.** Revised Pourbaix diagrams for copper at 25 to 300 °C. Journal of the Electrochemical Society 144, 3476–3483.
- Bhaskaran G, Carcea A, Ulaganathan J, Wang S, Huang Y, Newman R C, 2013.** Fundamental aspects of stress corrosion cracking of copper relevant to the Swedish deep geologic repository concept. SKB TR-12-06, Svensk Kärnbränslehantering AB.
- Birgersson M, Goudarzi R, 2013.** Studies of vapor transport from buffer to tunnel backfill (Sauna effects). SKB R-13-42, Svensk Kärnbränslehantering AB.
- Birgersson M, Goudarzi R, 2016.** Vapor transport and sealing capacity of buffer slots (“sauna” effects). SKB TR-15-09, Svensk Kärnbränslehantering AB.
- Birgersson M, Goudarzi R, 2017.** Summary report on “sauna” effects. SKB TR-17-07, Svensk Kärnbränslehantering AB.
- Birgersson M, Goudarzi R, 2018.** Investigations of gas evolution in an unsaturated KBS-3 repository. SKB TR-18-11, Svensk Kärnbränslehantering AB.

- Birgersson M, Johannesson L-E, 2006.** Prototype Repository. Statistical evaluation of buffer density. SKB IPR-06-15, Svensk Kärnbränslehantering AB.
- Birgersson M, Karnland O, 2009.** Ion equilibrium between montmorillonite interlayer space and an external solution – Consequences for diffusional transport. *Geochimica et Cosmochimica Acta* 73, 1908–1923.
- Birgersson M, Börgesson L, Hedström M, Karnland O, Nilsson U, 2009.** Bentonite erosion. Final report. SKB TR-09-34, Svensk Kärnbränslehantering AB.
- Birgersson M, Karnland O, Nilsson U, 2010.** Freezing of bentonite. Experimental studies and theoretical considerations. SKB TR-10-40, Svensk Kärnbränslehantering AB.
- Björck M, Tigerström M, Cederqvist L, Pehkonen H, Vouri L, Lahtonen K, Valden M, Purhonen T, 2017.** Evaluation of a gas shield for friction stir welding of copper canisters. Posiva SKB Report 02, Posiva Oy, Svensk Kärnbränslehantering AB.
- Björkblad A, Faleskog J, 2018.** Evaluation of Cu-OFP creep crack growth and theoretical fracture models for Cu-OFP. Swerea KIMAB. Posiva SKB Report 03, Posiva Oy, Svensk Kärnbränslehantering AB.
- Blomqvist R, Ruskeeniemi T, Kaija J, Ahonen L, Paananen M, Smellie J, Grundfelt B, Pedersen K, Bruno J, Pérez del Villar L, Cera E, Rasilainen K, Pitkänen P, Suksi J, Casanova J, Read D S, Frape S, 2000.** The Palmottu natural analogue project Phase II: Transport of radionuclides in a natural flow system at Palmottu. Project Report EUR 1961, European Commission.
- Bockgård N, 2010.** Groundwater flow modelling of an abandoned partially open repository. SR-Site Forsmark. SKB R-10-41, Svensk Kärnbränslehantering AB.
- Bond A E, Hoch A R, Jones G D, Tomczyk A J, Wiggin R W, Worraker W J, 1997.** Assessment of a spent fuel disposal canister. Assessment studies for a copper canister with cast steel inner component. SKB TR 97-19, Svensk Kärnbränslehantering AB.
- Bosson E, Sassner M, Sabel U, Gustafsson L-G, 2010.** Modelling of present and future hydrology and solute transport at Forsmark. SR-Site Biosphere. SKB R-10-02, Svensk Kärnbränslehantering AB.
- Boulton G S, Kautsky U, Morén L, Wallroth T, 2001.** Impact of long-term climate change on a geological repository for spent nuclear waste. SKB TR-99-05, Svensk Kärnbränslehantering AB.
- Bowman C D, Venneri F, 1994.** Underground supercriticality from plutonium and other fissile material. LA-UR-94-4022A, Los Alamos National Laboratory. (Also published in *Science and Global Security* 1996, 5, 279–302.)
- Bradbury M H, Baeyens B, 2005.** Modelling the sorption of Mn(II), Co(II), Ni(II), Zn(II), Cd(II), Eu(III), Am(III), Sn(IV), Th(IV), Np(V), and U(VI) on montmorillonite: Linear free energy relationships and estimates of surface binding constants for some selected heavy metals and actinides. *Geochimica et Cosmochimica Acta* 69, 875–892.
- Brady B H G, Brown E T, 1994.** *Rock mechanics for underground mining*. 2nd ed. London: Chapman & Hall.
- Brandefelt J, Otto-Bliesner B L, 2009.** Equilibration and variability in a Last Glacial Maximum climate simulation with CCSM3. *Geophysical Research Letters* 36, L19712. doi:10.1029/2009GL040364
- Brandefelt J, Zhang Q, Hartikainen J, Näslund J-O, 2013.** The potential for cold climate conditions and permafrost in Forsmark in the next 60 000 years. SKB TR-13-04, Svensk Kärnbränslehantering AB.
- Brantberger M, Janson T, 2009.** Underground Design Forsmark, Layout D2. Grouting. SKB R-08-114, Svensk Kärnbränslehantering AB.
- Briggs S, Lilja C, King F, 2021.** Probabilistic model for pitting of copper canisters. *Materials and Corrosion* 72, 308–316.
- Bros R, Carpéne J, Sere V, Beltritti A, 1996.** Occurrence of Pu and fissiogenic REE in hydrothermal apatites from the fossil nuclear reactor 16 at Oklo (Gabon). *Radiochimica Acta* 74, 277–282.

- Bros R, Hidaka H, Kamei G, Ohnuki T, 2003.** Mobilization and mechanisms of retardation in the Oklo natural reactor zone 2 (Gabon) – inferences from U, REE, Zr, Mo and Se isotopes. *Applied Geochemistry* 18, 1807–1824.
- Brown A C, 2006.** Genesis of native copper lodes in the Keweenaw District, northern Michigan: a hybrid evolved meteoric and metamorphogenic model. *Economic Geology* 101, 1437–1444.
- Brown G H, 2002.** Glacier meltwater hydrochemistry. *Applied Geochemistry* 17, 855–883.
- Brown J E, Alfonso B, Avila R, Beresford N A, Coppleson D, Pröhl G, Ulanovsky A, 2008.** The ERICA Tool. *Journal of Environmental Radioactivity* 99, 1371–1383.
- Bruno J, Casas I, Cera E, Duro L, 1997.** Development and application of a model for the long-term alteration of UO₂ spent nuclear fuel: test of equilibrium and kinetic mass transfer models in the Cigar Lake ore deposit. *Journal of Contaminant Hydrology* 26, 19–26.
- Brydsten L, 2004.** A mathematical model for lake ontogeny in terms of filling with sediments and macrophyte vegetation. SKB TR-04-09, Svensk Kärnbränslehantering AB.
- Brydsten L, 2009.** Sediment dynamics in the coastal areas of Forsmark and Laxemar during an interglacial. SKB TR-09-07, Svensk Kärnbränslehantering AB.
- Brydsten L, Strömberg M, 2010.** A coupled regolith-lake development model applied to the Forsmark site. SKB TR-10-56, Svensk Kärnbränslehantering AB.
- BSC, 2003.** Total system performance assessment – license application methods and approach. TDR-WIS-PA-000006 REV 00, Bechtel SAIC Company, Las Vegas, Nevada.
- Bungum H, Olesen O, Pascal C, Gibbons S, Lindholm C, Vestøl O, 2010.** To what extent is the present seismicity of Norway driven by post-glacial rebound? *Journal of the Geological Society* 167, 373–384.
- Bäckblom G, 2009.** Excavation damage and disturbance in crystalline rock – results from experiments and analyses. SKB TR-08-08, Svensk Kärnbränslehantering AB.
- Bäckblom G, Munier R, 2002.** Effects of earthquakes on the deep repository for spent fuel in Sweden based on case studies and preliminary model results. SKB TR-02-24, Svensk Kärnbränslehantering AB.
- Bäckblom G, Stanfors R, 1989.** Interdisciplinary study of post-glacial faulting in the Lansjärv area Northern Sweden 1986–1988. SKB TR 89-31, Svensk Kärnbränslehantering AB.
- Bäckblom G, Munier R, Hökmark H, 2004.** Earthquake data and modelling to study the effects of future earthquakes on a final repository of spent nuclear fuel in Sweden. Paper 3238. 13th World Conference on Earthquake Engineering, Vancouver, Canada, 1–6 August 2004.
- Bäckblom G, Munier R, Hökmark H, 2004.** Earthquake data and modelling to study the effects of Future earthquakes on a final repository of spent nuclear fuel in Sweden. 13th World Conference on Earthquake Engineering Vancouver, Canada, 1–6 August 2004, Paper 3238.
- Böðvarsson R, 2002.** Swedish National Seismic Network (SNSN). A short report on recorded earthquakes during the third quarter of the year 2002. SKB P-02-04, Svensk Kärnbränslehantering AB.
- Böðvarsson R, 2002–2009.** Swedish National Seismic Network (SNSN). Series of short reports on recorded earthquakes during the period 2002–2009. Svensk Kärnbränslehantering AB.
- Böðvarsson R, 2009.** Swedish National Seismic Network (SNSN). A short report on recorded earthquakes during the fourth quarter of the year 2008. SKB P-09-03, Svensk Kärnbränslehantering AB.
- Böðvarsson R, Lund B, Roberts R, Slunga R, 2006.** Earthquake activity in Sweden. Study in connection with a proposed nuclear waste repository in Forsmark or Oskarshamn. SKB R-06-67, Svensk Kärnbränslehantering AB.
- Börgesson L, Hernelind J, 2006.** Earthquake induced rock shear through a deposition hole. Influence of shear plane inclination and location as well as buffer properties on the damage caused to the canister. SKB TR-06-43, Svensk Kärnbränslehantering AB.

- Börgesson L, Hernelind J, 2009.** Mechanical interaction buffer/backfill. Finite element calculations of the upward swelling of the buffer against both dry and saturated backfill. SKB R-09-42, Svensk Kärnbränslehantering AB.
- Börgesson L, Hernelind J, 2017.** Modelling of the mechanical interaction between the buffer and the backfill in KBS-3V. Modelling results 2015. SKB TR-16-08, Svensk Kärnbränslehantering AB.
- Börgesson L, Sandén T, 2006.** Piping and erosion in buffer and backfill materials. Current knowledge. SKB R-06-80, Svensk Kärnbränslehantering AB.
- Börgesson L, Johannesson L-E, Sandén T, Hernelind J, 1995.** Modelling of the physical behaviour of water saturated clay barriers. Laboratory tests, material models and finite element application. SKB TR 95-20, Svensk Kärnbränslehantering AB.
- Börgesson L, Hedström M, Birgesson M, Karnland O, 2018.** Bentonite swelling into fractures at conditions above the critical coagulation concentration. SKB TR-17-11, Svensk Kärnbränslehantering AB.
- Cai M, Kaiser P K, Tasaka Y, Maejuma T, Morioka H, Minami M, 2004.** Generalized crack initiation and crack damage stress thresholds of brittle rock masses near underground excavations. *International Journal of Rock Mechanics and Mining Sciences* 41, 833–847.
- Calais E, Mattioli G, DeMets C, Nocquet J-M, Stein S, Newman A, Rydelek P, 2005.** Tectonic strain in plate interiors? *Nature* 438, E9–E10. doi:10.1038/nature04428
- Calais E, Han J Y, DeMets C, Nocquet J M, 2006.** Deformation of the North American plate interior from a decade of continuous GPS measurements. *Journal of Geophysical Research* 111, B06402. doi:10.1029/2005JB004253
- Carlsten S, Stråhle A, 2000.** Borehole radar and BIPS investigations in boreholes at the Boda area. SKB TR-01-02, Svensk Kärnbränslehantering AB.
- Cederqvist L, Garpinger O, Nielsen I, 2018.** Evaluation of depth controller for friction stir welding of copper canisters. Posiva SKB Report 08, Posiva Oy, Svensk Kärnbränslehantering AB.
- Chapman N A, McKinley I G, Smellie J A T, 1984.** The potential of natural analogues in assessing systems for deep disposal of high-level radioactive waste. SKB TR 84-16, Svensk Kärnbränslehantering AB.
- Chapman N A, McKinley I G, Shea M E, Smellie J A T (eds), 1993.** The Poços de Caldas project: natural analogues of processes in a radioactive waste repository. Amsterdam: Elsevier. (Reprinted from the *Journal of Geochemical Exploration* 45, 1992.)
- Chen J, Qin Z, Shoesmith D W, 2014.** Key parameters determining structure and properties of sulphide films formed on copper corroding in anoxic sulphide solutions. *Corrosion Engineering, Science and Technology* 49, 415–419.
- Chen J, Qin Z, Martino T, Shoesmith D W, 2017.** Effect of chloride on Cu corrosion in anaerobic sulphide solutions. *Corrosion Engineering, Science and Technology* 52, 40–44.
- Choi J-H, Edwards P, Ko K, Kim Y-S, 2016.** Definition and classification of fault damage zones: A review and a new methodological approach. *Earth-Science Reviews* 152, 70–87.
- Chukharkina A, Blom A, Pedersen K, 2016.** Release of H₂ and organic compounds from metallic and polymeric materials used to construct stationary borehole equipment. SKB R-16-01, Svensk Kärnbränslehantering AB.
- Chukharkina A, Blom A, Pedersen K, 2017.** Microbial sulphide production during consumption of H₂ and organic compounds released from stationary borehole equipment. SKB R-16-17, Svensk Kärnbränslehantering AB.
- Claesson Liljedahl L, Munier R, Sandström B, Drake H, Tullborg E-L, 2010.** Assessment of fractures classified as non-mineralised in the SICADA database. SKB R-11-02, Svensk Kärnbränslehantering AB.

- Claesson Liljedahl L, Lehtinen A, Harper J, Näslund J-O, Selroos J-O, Pitkänen P, Puigdomenech I, Hobbs M, Follin S, Hirschorn S, Jansson P, Kennell L, Marcos N, Ruskeenieniemi T, Tullborg E-L, Vidstrand P, 2016.** Greenland Analogue Project: Final report. SKB TR-14-13, Svensk Kärnbränslehantering AB.
- Clark I D, Matsumoto R, Dallimore S R, Lowe B, Loop J, 1999.** Isotope constraints on the origin of pore waters and salinity in the permafrost and gas-hydrate core intervals of the JAPEX/JNOC/GSC Mallik 2L-38 gas-hydrate research well. Geological Survey of Canada Bulletin 544, 177–188.
- Clark P U, Shakun J D, Marcott S A, Mix A C, Eby M, Kulp S, Levermann A, Milne G A, Pfister P L, Santer B D, Schrag D P, Solomon S, Stocker T F, Strauss B H, Weaver A J, Winkelmann R, Archer D, Bard E, Goldner A, Lambeck K, Pierrehumbert R T, Plattner G-K, 2016.** Consequences of twenty-first-century policy for multi-millennial climate and sea-level change. *Nature Climate Change* 6, 360–369.
- Cliffe K A, Kelly M, 2006.** COMP23 version 1.2.2 user's manual. SKB R-04-64, Svensk Kärnbränslehantering AB.
- Colleoni F, Krinner G, Jakobsson M, Peyaud V, Ritz C, 2009.** Influence of regional parameters on the surface mass balance of the Eurasian ice sheet during the peak Saalian (140 kya). *Global and Planetary Change* 68, 132–148.
- Colleoni F, Wekerle C, Masina S, 2014.** Long-term safety of a planned geological repository for spent nuclear fuel in Forsmark – estimate of maximum ice sheet thicknesses. SKB TR-14-21, Svensk Kärnbränslehantering AB.
- Collins G S, Melosh H J, Marcus R A, 2005.** Earth Impact Effects Program: a web-based computer program for calculating the regional environmental consequences of a meteoroid impact on Earth. *Meteoritics & Planetary Science* 40, 817–840.
- Cooke R M, 1995.** UNICORN: Methods and code for uncertainty analysis. Cheshire, UK: AEA Technology.
- Cooper R J, Wadham J L, Tranter M, Hodgkins R, Peters N E, 2002.** Groundwater hydrochemistry in the active layer of the proglacial zone, Finsterwalderbreen, Svalbard. *Journal of Hydrology* 269, 208–223.
- Cosgrove J, Stanfors R, Röshoff K, 2006.** Geological characteristics of deformation zones and a strategy for their detection in a repository. SKB R-06-39, Svensk Kärnbränslehantering AB.
- Couture R A, 1985.** Steam rapidly reduces the swelling capacity of bentonite. *Nature* 318, 50–52.
- Cowie P A, Scholz C H, 1992a.** Growth of faults by accumulation of seismic slip. *Journal of Geophysical Research* 97, 11085–11095.
- Cowie P A, Scholz C H, 1992b.** Displacement-length scaling relationship for faults: data synthesis and discussion. *Journal of Structural Geology* 14, 1149–1156.
- Cramer J J, Smellie J A T (eds), 1994.** Final report of the AECL/SKB Cigar Lake Analogue Study. SKB TR 94-04, Svensk Kärnbränslehantering AB. (Also published as AECL-10851, COG-93-147.)
- Cuadros J, Linares J, 1996.** Experimental kinetic study of the smectite-to-illite transformation. *Geochimica et Cosmochimica Acta* 60, 439–453.
- Cui D, Low J, Sjöstedt C J, Spahiu K, 2004.** On Mo-Ru-Tc-Pd-Rh-Te alloy particles extracted from spent fuel and their leaching behaviour under Ar and H₂ atmospheres. *Radiochimica Acta* 92, 551–555.
- Damjanac B, Fairhurst C, 2010.** Evidence for a long-term strength threshold in crystalline rock. *Rock Mechanics and Rock Engineering* 43, 513–531.
- Dansgaard W, Johnsen S J, Clausen H B, Dahl-Jensen D, Gundestrup N S, Hammer C U, Hvidberg C S, Steffensen J P, Sveinbjörnsdóttir A E, Jouzel J, Bond G, 1993.** Evidence for general instability of past climate from a 250-kyr ice-core record. *Nature* 364, 218–220.
- Dawers, N H, Anders M H, Scholz C H, 1993.** Growth of normal faults: displacement-length scaling. *Geology* 21, 1107–1110.

- Degueldre C, Baeyens B, Goerlich W, Riga J, Verbist J, Stadelmann P, 1989.** Colloids in water from a subsurface fracture in granitic rock, Grimsel Test Site, Switzerland. *Geochimica et Cosmochimica Acta* 53, 603–610.
- Degueldre C, Grauer R, Laube A, Oess A, Silby H, 1996.** Colloid properties in granitic groundwater systems. II: Stability and transport study. *Applied Geochemistry* 11, 697–710.
- Delos A, Trincherio P, Richard L, Molinero J, Dentz M, Pitkänen P, 2010.** Quantitative assessment of deep gas migration in Fennoscandian sites. SKB R-10-61, Svensk Kärnbränslehantering AB.
- Dillström P, 2009.** Updated probabilistic analysis of canister inserts for spent nuclear fuel. 50006980-2, Rev. 1, Inspecta Technology AB. SKBdoc 1207426 ver 1.0, Svensk Kärnbränslehantering AB.
- Dillström P, 2014.** Probabilistic analysis of BWR canister inserts for spent nuclear fuel in the case of an earthquake induced rock shear load. Report 50014130-1, Revision 5, Inspecta Technology AB. SKBdoc 1412158 ver 1.0, Svensk Kärnbränslehantering AB.
- Dillström P, 2015a.** Damage tolerance analysis of BWR-canister inserts for spent nuclear fuel in the case of an earthquake induced rock shear load – Influence of using more detailed models. Report 5000264-1, Revision 2, Inspecta Technology AB. SKBdoc 1450913 ver 1.0, Svensk Kärnbränslehantering AB.
- Dillström P, 2015b.** Damage tolerance analysis of PWR-canister inserts for spent nuclear fuel in the case of an earthquake induced rock shear load – Influence of using more detailed models. Report 5000264-2, Revision 1, Inspecta Technology AB. SKBdoc 1459222 ver 1.0, Svensk Kärnbränslehantering AB.
- Dillström P, 2019.** Probabilistic analysis of BWR canister inserts for spent nuclear fuel in the case of an isostatic pressure load. Kiwa Inspecta Technical Report 5001090-1, Revision 5. SKBdoc 1585534 ver 1.0, Svensk Kärnbränslehantering AB.
- Dillström P, Bolinder T, 2010.** Damage tolerance analysis of canister inserts for spent nuclear fuel in the case of an earthquake induced rock shear load. SKB TR-10-29, Svensk Kärnbränslehantering AB.
- Domènech C, Arcos D, Duro L, Grandia F, 2006.** Effect of the mineral precipitation-dissolution at tunnel walls during the operational and post-operational phases. SKB R-06-108, Svensk Kärnbränslehantering AB.
- Dong C, Mao F, Gao S, Sharifi-Asl S, Lu P, Macdonald D D, 2016.** Passivity breakdown on copper: influence of temperature. *Journal of The Electrochemical Society* 163, C707–C717.
- Dou W, Jia R, Jin P, Liu J, Chen S, Gu T, 2018.** Investigation of the mechanism and characteristics of copper corrosion by sulfate reducing bacteria. *Corrosion Science* 144, 237–248.
- Dowding C H, Rozan A, 1978.** Damage to rock tunnels from earthquake shaking. *Journal of the Geotechnical Engineering Division* 104, 175–191.
- Drake H, Suksi J, Tullborg E-L, Lahaye Y, 2017.** Quaternary redox transitions in deep crystalline rock fractures at the western margin of the Greenland ice sheet. *Applied Geochemistry* 76, 196–209.
- Drew M C, 1983.** Plant injury and adaptation to oxygen deficiency in the root environment: a review. *Plant and Soil* 75, 179–199.
- Du Rietz T, 1937.** Recenta förkastningar eller sprickbildningar i Västerbottensfjällen. *Geologiska Föreningens i Stockholm Förhandlingar* 59, 112–114. (In Swedish.)
- Dueck A, 2010.** Thermo-mechanical cementation effects in bentonite investigated by unconfined compression tests. SKB TR-10-41, Svensk Kärnbränslehantering AB.
- Duerden P, Lever D A, Sverjensky D A, Townley L R, 1992.** Summary of findings. Alligator Rivers Analogue Project, final report. Vol. 1. An OECD/NEA International Project Managed by ANSTO. SKI Report 92:20-1, Swedish Nuclear Power Inspectorate.
- Duro L, Grivé M, Cera E, Gaona X, Domènech C, Bruno J, 2006.** Determination and assessment of the concentration limits to be used in SR-Can. SKB TR-06-32, Svensk Kärnbränslehantering AB.
- Dverstorp B, Strömberg B, 2008.** SKI's and SSI's review of SKB's safety report SR-Can. SKI Report 2008:23, Swedish Nuclear Power Inspectorate, SSI Report 2008:04 E, Swedish Radiation Protection Authority.

- Ekeroth E, Granfors M, Schild D, Spahiu K, 2020.** The effect of temperature and fuel surface area on spent nuclear fuel dissolution kinetics under H₂ atmosphere. *Journal of Nuclear Materials* 531, 151981. doi:10.1016/j.jnucmat.2019.151981
- Ekman M, 1996.** A consistent map of the postglacial uplift of Fennoscandia. *Terra Nova* 8, 158–165.
- Ekström P-A, 2011.** Pandora – a simulation tool for safety assessments. Technical description and user's guide. SR-Site Biosphere. SKB R-11-01, Svensk Kärnbränslehantering AB.
- Elert M, Gylling B, Lindgren M, 2004.** Assessment model validity document FARF31. SKB R-04-51, Svensk Kärnbränslehantering AB.
- Eng T, Norberg E, Torbacke J, Jensen M, 1996.** Information, conservation and retrieval. SKB TR 96-18, Svensk Kärnbränslehantering AB.
- Engqvist A, Andrejev O, 2000.** Sensitivity analysis with regard to variations of physical forcing including two possible future hydrographic regimes for the Öregrundsgrepen. A follow-up baroclinic 3D-model study. SKB TR-00-01, Svensk Kärnbränslehantering AB.
- Enssle C P, Poppei J, 2010.** Implementation and testing of an improved methodology to simulate resaturation processes with DarcyTools. SKB R-09-54, Svensk Kärnbränslehantering AB.
- Ericsson L O, Stanfors R (eds), 1993.** Supplementary investigations of postglacial faulting in the Lansjärv area, northern Sweden, 1990–1992. SKB AR 93-18, Svensk Kärnbränslehantering AB.
- Ericsson L O, Brinkhoff P, Gustafson G, Kvartsberg S, 2009.** Hydraulic features of the Excavation Disturbed Zone. Laboratory investigations of samples taken from the Q- and S-tunnels at Äspö HRL. SKB R-09-45, Svensk Kärnbränslehantering AB.
- Ericsson L O, Thörn J, Christiansson R, Lehtimäki T, Ittner H, Hansson K, Butron C, Sigurdsson O, Kinnbom P, 2015.** A demonstration project on controlling and verifying the excavation-damaged zone. Experience from the Äspö Hard Rock Laboratory. SKB R-14-30, Svensk Kärnbränslehantering AB.
- Eriksson P, Hedin A, 2019.** Modelling of sulphide fluxes in unsaturated buffer and backfill for a KBS-3 repository. SKBdoc 1696975 ver 2.0, Svensk Kärnbränslehantering AB.
- Eriksson S, 2007.** Äspö Hard Rock Laboratory. Prototype repository. Analysis of microorganisms, gases and water chemistry in buffer and backfill, 2004–2007. SKB IPR-08-01, Svensk Kärnbränslehantering AB.
- Eriksson P, 2020.** Hållfasthetskrav på återfyllnadsblock för att klara buffertuppsvällning. SKBdoc 1906167 ver 1.0, Svensk Kärnbränslehantering AB. (In Swedish.)
- Eshelby J D, 1957.** The determination of the elastic field of an ellipsoidal inclusion, and related problems. *Proceedings of the Royal Society of London. Series A, Mathematical and Physical Sciences* 241, 376–396.
- Evans D F, Wennerström H, 1999.** *The colloidal domain: where physics, chemistry, biology, and technology meet.* 2nd ed. New York: Wiley-VCH.
- Evins L Z, 2020.** On the barrier function of spent fuel cladding. SKBdoc 1912057 ver 1.0. Svensk Kärnbränslehantering AB.
- Evins L Z, Jensen K A, Ewing R C, 2005.** Uraninite recrystallization and Pb loss in the Oklo and Bangombé natural fission reactors, Gabon. *Geochimica et Cosmochimica Acta* 69, 1589–1606.
- Evins L Z, Juhola P, Vähänen M, 2014.** REDUPP Final report. Posiva Working Report 2014-12, Posiva Oy, Finland.
- Fagerbakke K M, Heldal M, Norland S, 1996.** Content of carbon, nitrogen, oxygen, sulfur and phosphorus in native aquatic and cultured bacteria. *Aquatic Microbial Ecology* 10, 15–27.
- FASSET, 2004.** FASSET – Framework for Assessment of Environmental Impact. Final report. A project within the EC 5th Framework Programme, Contract No FIGE-CT-2000-00102, project co-ordinator: Swedish Radiation Protection Authority.
- Fastook J L, 1994.** Modelling the Ice Age: the finite-element method in glaciology. *Computational Science and Engineering* 1, 55–67.

- Fastook J L, Chapman J E, 1989.** A map plane finite-element model: three modelling experiments. *Journal of Glaciology* 35, 48–52.
- Fastook J L, Holmlund P, 1994.** A glaciological model of the Younger Dryas event in Scandinavia. *Journal of Glaciology* 40, 125–131.
- Fayek M, Harrison M T, Ewing R C, Grove M, Coath C D, 2002.** O and Pb isotopic analyses of uranium minerals by ion microprobe and U–Pb ages from the Cigar Lake deposit. *Chemical Geology* 185, 205–225.
- FENCAT, 2007.** Historical earthquakes in northern Europe. [Online]. Available at: http://www.seismo.helsinki.fi/english/bulletins/catalog_northeurope.html. Institute of Seismology, University of Helsinki, Finland.
- Fenton C, Adams J, Halchuk S, 2006.** Seismic hazards assessment for radioactive waste disposal sites in regions of low seismic activity. *Geotechnical and Geological Engineering* 24, 579–592.
- Fernández A M, Sánchez-Ledesma D M, Melón A, Robredo L M, Rey J J, Labajo M, Clavero M A, Carretero S, González A E, 2018.** Thermo-hydro-geochemical behaviour of a Spanish bentonite after dismantling of the FEBEX *in situ* test at the Grimsel Test Site. FEBEX-DP Project. Nagra Arbeitsbericht NAB 16-25, Nagra, Switzerland.
- Follin S, 2008.** Bedrock hydrogeology Forsmark. Site descriptive modeling, SDM-Site Forsmark. SKB R-08-95, Svensk Kärnbränslehantering AB.
- Follin S (ed), 2019.** Multidisciplinary description of the access area of the planned spent nuclear fuel repository in Forsmark prior to construction. SKB R-17-13, Svensk Kärnbränslehantering AB.
- Follin S, Johansson P-O, Hartley L, Jackson P, Roberts D, Marsic N, 2007a.** Hydrogeological conceptual model development and numerical modelling using CONNECTFLOW, Forsmark modelling stage 2.2. SKB R-07-49, Svensk Kärnbränslehantering AB.
- Follin S, Levén J, Hartley L, Jackson P, Joyce S, Roberts D, Swift B, 2007b.** Hydrogeological characterisation and modelling of deformation zones and fracture domains, Forsmark modelling stage 2.2. SKB R-07-48, Svensk Kärnbränslehantering AB.
- Forsström A, Becker R, Öijerholm J, Yagodzinskyy Y, Hänninen H, Linder J, 2017.** Hydrogen absorption in copper as a result of corrosion reactions in sulphide and chloride containing deoxygenated water at 90 °C in simulated spent nuclear fuel repository conditions. In Proceedings of EUROCORR, 2017: The Annual Congress of the European Federation of Corrosion, 20th International Corrosion Congress and Process Safety Congress, Prague, 3–7 September 2017.
- Forsström A, Becker R, Hänninen H, Yagodzinskyy Y, Heikkilä M, 2021.** Sulphide-induced stress corrosion cracking and hydrogen absorption of copper in deoxygenated water at 90 °C. *Materials and Corrosion* 72, 317–332.
- Forsyth R, 1997.** The SKB Spent Fuel Corrosion Programme. An evaluation of results from the experimental programme performed in the Studsvik Hot Cell laboratory. SKB TR 97-25, Svensk Kärnbränslehantering AB.
- Forsyth R S, Werme L O, 1992.** Spent fuel corrosion and dissolution. *Journal of Nuclear Materials* 190, 3–19.
- Fox A, La Pointe P, Hermanson J, Öhman J, 2007.** Statistical geological discrete fracture network model. Forsmark modelling stage 2.2. SKB R-07-46, Svensk Kärnbränslehantering AB.
- Frampton A, Hyman J D, Zou L, 2019.** Advective transport in discrete fracture networks with connected and disconnected textures representing internal aperture variability. *Water Resources Research* 55, 5487–5501.
- Frape S K, Stotler R L, Ruskeeniemi T, Ahonen L, Paananen M, Hobbs M Y, 2004.** Hydrogeochemistry of groundwaters at and below the base of the permafrost at Lupin: Report of phase II. Report 06819-REP-01300-10047-R00, Ontario Power Generation, Nuclear Waste Management Division, Canada.
- Fredén C (ed), 2002.** Sveriges nationalatlas. Berg och jord. Stockholm: SNA publishing. (In Swedish.)
- French H M, 2007.** The periglacial environment. 3rd ed. Chichester: Wiley.

- Fritz B, Kam M, Tardy Y, 1984.** Geochemical simulation of the evolution of granitic rocks and clay minerals submitted to a temperature increase in the vicinity of a repository for spent nuclear fuel. SKB/KBS TR 84-10, Svensk Kärnbränslehantering AB.
- Fritzell A, 2006.** Concerns when designing a safeguards approach for the back-end of the Swedish nuclear fuel cycle. SKI Report 2008:18, Swedish Nuclear Power Inspectorate.
- Fritzell A, 2017.** KBP1012 Verifiering av återfyllningens utformning avseende funktion i KBS-3-förvaret. SKBdoc 1531424 ver 1.0, Svensk Kärnbränslehantering AB. (In Swedish.)
- Funehag J, Emmelin A, 2011.** Injekteringen av TASS-tunneln. Design, genomförande och resultat från förinjekteringen. SKB R-10-39, Svensk Kärnbränslehantering AB. (In Swedish.)
- Fälth B, 2018.** Simulating earthquake rupture and near-fault fracture response. PhD thesis. Uppsala University, Sweden.
- Fälth B, Hökmark H, 2006.** Seismically induced slip on rock fractures. Results from dynamic discrete fracture modeling. SKB R-06-48, Svensk Kärnbränslehantering AB.
- Fälth B, Hökmark H, 2007.** Mechanical and thermo-mechanical discrete fracture near-field analyses based on preliminary data from the Forsmark, Simpevarp and Laxemar sites. SKB R-06-89, Svensk Kärnbränslehantering AB.
- Fälth B, Hökmark H, Munier R, 2007.** Seismically induced shear displacements in repository host rock fractures. In Proceedings of the 9th Canadian Conference on Earthquake Engineering, Ottawa, Canada, 26–29 June 2007.
- Fälth B, Hökmark H, Munier R, 2008.** Seismically induced slip on rock fractures – expanded study with particular account of large earthquakes. In Yale D, Holtz S, Breeds C, Ozbay U (eds). Proceedings of the 42nd U.S. Rock Mechanics Symposium, San Fransisco, 29 June – 2 July 2008.
- Fälth B, Hökmark H, Munier R, 2010.** Effects of large earthquakes on a KBS-3 repository. Evaluation of modelling results and their implications for layout and design. SKB TR-08-11, Svensk Kärnbränslehantering AB.
- Galíndez J M, Molinero J, 2010.** Assessment of the long-term stability of cementitious barriers of radioactive waste repositories by using digital-image-based microstructure generation and reactive transport modeling. Cement and Concrete Research 40, 1278–1289.
- Gascoyne M, 1999.** Long-term maintenance of reducing conditions in a spent nuclear fuel repository. A re-examination of critical factors. SKB R-99-41, Svensk Kärnbränslehantering AB.
- Gauthier-Lafaye F, Holliger P, Blanc P-L, 1996.** Natural fission reactors in the Franceville basin, Gabon: a review of the conditions and results of a “critical event” in a geologic system. *Geochimica et Cosmochimica Acta* 60, 4831–4852.
- Gauthier-Lafaye F, Ledoux E, Smellie J, Louvat D, Michaud V, Pérez del Villar, Oversby V, Bruno J, 2000.** OKLO – natural analogue Phase II. Behaviour of nuclear reaction products in a natural environment: final report. EUR 19139, European Commission.
- Gierszewski P, Avis J, Calder N, D’Andrea A, Garisto F, Kitson C, Melnyk T, Wei K, Wojciechowski L, 2004.** Third case study – postclosure safety assessment. Report 06819-REP-01200-10109-R00, Ontario Power Generation, Nuclear Waste Management Division, Canada.
- Giroud N, 2014.** FEBEX – assessment of redox conditions in phase 2 before dismantling. Nagra Arbeitsbericht NAB 14-55, Nagra, Switzerland.
- Giroud N, Tomonaga Y, Wersin P, Briggs S, King F, Vogt T, Diomidis N, 2018.** On the fate of oxygen in a spent fuel emplacement drift in Opalinus Clay. *Applied Geochemistry* 97, 270–278.
- Glamheden R, Fredriksson A, Röshoff K, Karlsson J, Hakami H, Christiansson R, 2007.** Rock mechanics Forsmark. Site descriptive modelling Forsmark stage 2.2. SKB R-07-31, Svensk Kärnbränslehantering AB.
- Glamheden R, Fälth B, Jacobsson L, Harrström J, Berglund J, Bergkvist L, 2010.** Counterforce applied to prevent spalling. SKB TR-10-37, Svensk Kärnbränslehantering AB.

- Glombitza C, Jaussi M, Røy H, Seidenkrantz M-S, Lomstein B A, Jörgensen B B, 2015.** Formate, acetate, and propionate as substrates for sulfate reduction in sub-arctic sediments of Southwest Greenland. *Frontiers in Microbiology* 6. doi:10.3389/fmicb.2015.00846
- Golian C, Lever D A, 1992.** Radionuclide transport. Alligator Rivers Analogue Project. Final report. Vol. 14. An OECD/NEA International Project Managed by ANSTO. SKI Report 92:20-14, Swedish Nuclear Power Inspectorate.
- Grambow B, Duro L, Spahiu K, Kulik D, Brandt F, 2014.** Final synthesis report. SKIN Deliverable 5.5., European Commission Collaborative Project Grant nr FP7-269688.
- Grandia F, Domènech C, Arcos D, Duro L, 2006.** Assessment of the oxygen consumption in the backfill. Geochemical modelling in a saturated backfill. SKB R-06-106, Svensk Kärnbränslehantering AB.
- Grandia F, Galíndez J-M, Arcos D, Molinero J, 2010a.** Quantitative modelling of the degradation processes of cement grout. Project CEMMOD. SKB TR-10-25, Svensk Kärnbränslehantering AB.
- Grandia F, Galíndez J-M, Molinero J, Arcos D, 2010b.** Evaluation of low-pH cement degradation in tunnel plugs and bottom plate systems in the frame of SR-Site. SKB TR-10-62, Svensk Kärnbränslehantering AB.
- Grigull S, Peterson G, Hyberg J, Öhrling C, 2019.** Phanerozoic faulting of Precambrian basement in Uppland. SKB R-19-22, Svensk Kärnbränslehantering AB.
- Grivé M, Domènech C, Montoya V, Garcia D, Duro L, 2010.** Determination and assessment of the concentration limits to be used in SR-Can. Supplement to TR-06-32. SKB R-10-50, Svensk Kärnbränslehantering AB.
- Gubner R, Andersson U, 2007.** Corrosion resistance of copper canister weld material. SKB TR-07-07, Svensk Kärnbränslehantering AB.
- Guimerà J, Duro L, Jordana S, Bruno J, 1999.** Effects of ice melting and redox front migration in fractured rocks of low permeability. SKB TR-99-19, Svensk Kärnbränslehantering AB.
- Guo M, Chen J, Martino T, Biesinger M, Noël J J, Shoesmith D W, 2019.** The susceptibility of copper to pitting corrosion in borate-buffered aqueous solutions containing chloride and sulfide. *Journal of The Electrochemical Society* 166, C550–C558.
- Guo M, Chen J, Lilja C, Dehnavi V, Behazin M, Noël J J, Shoesmith D W, 2020.** The anodic formation of sulfide and oxide films on copper in borate-buffered aqueous chloride solutions containing sulphide. *Electrochimica Acta* 362, 137087. doi:10.1016/j.electacta.2020.137087
- Gurban I, Laaksoharju M, Ledoux E, Made B, Salignac A L, 1998.** Indications of uranium transport around the reactor zone at Bagombé (Oklo). SKB TR 98-06, Svensk Kärnbränslehantering AB.
- Gustafsson B, 2004.** Millennial changes of the Baltic Sea salinity. Studies of the sensitivity of the salinity to climate change. SKB TR-04-12, Svensk Kärnbränslehantering AB.
- Hall A M, Ebert K, Goodfellow B W, Hättestrand C, Heyman J, Krabbendam M, Moon S, Stroeven A P, 2019.** Past and future impact of glacial erosion in Forsmark and Uppland. Final report. SKB TR-19-07, Svensk Kärnbränslehantering AB.
- Hallbeck L, 2009.** Microbial processes in glaciers and permafrost. A literature study on microbiology affecting groundwater at ice sheet melting. SKB R-09-37, Svensk Kärnbränslehantering AB.
- Hallbeck L, 2010.** Principal organic materials in a repository for spent nuclear fuel. SKB TR-10-19, Svensk Kärnbränslehantering AB.
- Hallbeck L, Pedersen K, 2008.** Explorative analysis of microbes, colloids and gases. SDM-Site Forsmark. SKB R-08-85, Svensk Kärnbränslehantering AB.
- Hallberg R, Engvall A-G, Wadsten T, 1984.** Corrosion of copper lightning conductor plates. *British Corrosion Journal* 19, 85–88.
- Hallberg R, Östlund P, Wadsten T, 1988.** Inferences from a corrosion study of a bronze cannon, applied to high level nuclear waste disposal. *Applied Geochemistry* 3, 273–280.

- Hamby D M, 1994.** A review of techniques for parameter sensitivity analysis of environmental models. *Environmental Monitoring and Assessment* 32, 135–154.
- Harper J, Hubbard A, Ruskeeniemi T, Claesson Liljedahl L, Kontula A, Brown J, Dirkson A, Dow C, Doyle S, Drake H, Engström J, Fitzpatrick A, Follin S, Frape S, Graly J, Hansson K, Harrington J, Henkemans E, Hirschorn S, Hobbs M, Humphrey N, Jansson P, Johnson J, Jones G, Kinnbom P, Kennell L, Klint K E S, Liimatainen J, Lindbäck K, Meierbachtol T, Pere T, Pettersson R, Tullborg E-L, van As D, 2016.** The Greenland Analogue Project: Data and processes. SKB R-14-13, Svensk Kärnbränslehantering AB.
- Harper J, Meierbachtol T, Humphrey N, 2019.** Greenland ICE Project. Final report. SKB R-18-06, Svensk Kärnbränslehantering AB.
- Harrington J F, Birchall D J, 2007.** Sensitivity of total stress to changes in externally applied water pressure in KBS-3 buffer bentonite. SKB TR-06-38, Svensk Kärnbränslehantering AB.
- Harrington J F, Horseman S T, 2003.** Gas migration in KBS-3 buffer bentonite. Sensitivity of test parameters to experimental boundary conditions. SKB TR-03-02, Svensk Kärnbränslehantering AB.
- Hartikainen J, 2004.** Permafrost modeling in DECOVALEX III for BMT3. In: Eloranta E (ed). DECOVALEX III, 1999–2003. An international project for the modelling of coupled thermo-hydro-mechanical processes for spent fuel disposal. Finnish national contributions. STUK-YTO-TR 209, Finnish Centre for Radiation and Nuclear Safety (STUK), Helsinki.
- Hartikainen J, Kouhia R, Wallroth T, 2010.** Permafrost simulations at Forsmark using a numerical 2D thermo-hydro-chemical model. SKB TR-09-17, Svensk Kärnbränslehantering AB.
- Hartikainen J, Näslund J O, Liakka J, Claesson Liljedahl L, Kolisoja P, Kouhia R, 2022.** Evaluation of the SR-Site and SR-PSU permafrost models against GAP site bedrock temperatures. SKB TR-21-08, Svensk Kärnbränslehantering AB.
- Hartley L, Roberts D, 2013.** Summary of discrete fracture network modelling as applied to hydrogeology of the Forsmark and Laxemar sites. SKB R-12-04, Svensk Kärnbränslehantering AB.
- Hartley L, Hoch A, Jackson P, Joyce S, McCarthy R, Rodwell W, Swift B, Marsic N, 2006.** Groundwater flow and transport modelling during the temperate period for the SR-Can assessment. Forsmark area – version 1.2. SKB R-06-98, Svensk Kärnbränslehantering AB.
- Hartley L, Hek J, Swan D, Baxter S, Woollard H, 2014.** Hydrogeological discrete fracture modelling to support Rock Suitability Classification. Posiva Working Report 2012-48, Posiva Oy, Finland.
- Hartley L, Appleyard P, Baxter S, Hoek J, Joyce S, Mosley K, Williams T, Fox A, Cottrell M, La Pointe P, Gehör S, Darcel C, Le Goc R, Aaltonen I, Vanhanarkaus O, Löfman J, Poteri A, 2018.** Discrete Fracture Network Modelling (Version 3) in Support of Olkiluoto Site Description 2018, Posiva Working Report 2017-32, Posiva Oy, Finland.
- Hartmann W K, 1965.** Terrestrial and lunar flux of large meteorites in the last two billion years. *Icarus* 4, 157–165.
- Haynes H M, Nixon S, Lloyd J R, Birgersson M 2019.** Verification of microbial sulfideproducing activity in Calcigel bentonite at saturated densities of 1 750 and 1 900 kg m⁻³. SKB P-19-07, Svensk Kärnbränslehantering AB.
- Hedenström A, Risberg J, 2003.** Shore displacement in northern Uppland during the last 6 500 calendar years. SKB TR-03-17, Svensk Kärnbränslehantering AB.
- Hedin A, 1997.** Spent nuclear fuel – how dangerous is it? A report from the project “Description of risk”. SKB TR 97-13, Svensk Kärnbränslehantering AB.
- Hedin A, 2002a.** Safety assessment of a spent nuclear fuel repository: sensitivity analyses for prioritisation of research. In Bonano E J, Camp A L, Majors M J, Thomson R A (eds). Proceedings of the 6th International Conference on Probabilistic Safety Assessment and Management, PSAM6, San Juan, Puerto Rico, 23–28 June 2002. Oxford: Elsevier.
- Hedin A, 2002b.** Integrated analytic radionuclide transport model for a spent nuclear fuel repository in saturated fractured rock. *Nuclear Technology* 138, 179–205.

- Hedin A, 2003.** Probabilistic dose calculations and sensitivity analyses using analytic models. *Reliability Engineering & System Safety* 79, 195–204.
- Hedin A, 2004a.** Methodology for risk assessment of an SNF repository in Sweden. In Spitzer C, Schmocker U, Dang V N (eds). *Proceedings of the 7th International Conference on Probabilistic Safety Assessment and Management, PSAM7*, Berlin, 14–18 June 2004. London: Springer-Verlag.
- Hedin A, 2004b.** Integrated near-field evolution model for a KBS-3 repository. SKB R-04-36, Svensk Kärnbränslehantering AB.
- Hedin A, 2008a.** Risk, uncertainty and sensitivity analyses in a recent safety assessment of a spent nuclear fuel repository in Sweden. In Kao T M, Zio E, Ho V (eds). *Proceedings of the 9th International Conference on Probabilistic Safety Assessment and Management, PSAM9*, Hong Kong, 18–23 May 2008. Hong Kong: Edge Publication Group.
- Hedin A, 2008b.** Semi-analytic stereological analysis of waste package/fracture intersections in a granitic rock nuclear waste repository. *Mathematical Geosciences* 40, 619–637.
- Hedin A, 2011.** Stereological method for reducing probability of earthquake-induced damage in a nuclear waste repository. *Mathematical Geosciences* 43, 1–21.
- Hedin A, 2013.** Sensitivity analysis of probabilistic dose results in SKB's license application. *Proceedings of the 14th International High-Level Radioactive Waste Management Conference*, Albuquerque, NM, 28 April – 2 May 2013. American Nuclear Society.
- Hedin A, 2015.** Svar till SSM på begäran om förtydligande om the mean-of-the-peaks. SKBdoc 1475753 ver 1.0, Svensk Kärnbränslehantering AB. (In Swedish.)
- Hedin A, 2021.** Models, input data and results for analytical erosion, sedimentation and corrosion calculations. SKBdoc 1927770 ver 1.0, Svensk Kärnbränslehantering AB.
- Hedin A, Kautsky U, 2015.** Svar till SSM på begäran daterad 2013-02-14 om komplettering rörande radionuklidtransport och dos. SKBdoc 1418468 ver 2.0, Svensk Kärnbränslehantering AB.
- Hedin A, Evins L Z, Spahiu K, 2013.** What if criticality in the final repository? SKBdoc 1417199 ver 1.0, Svensk Kärnbränslehantering AB.
- Helton J C, 1993.** Uncertainty and sensitivity analysis techniques for use in performance assessment for radioactive waste disposal. *Reliability Engineering & System Safety* 42, 327–367.
- Henderson P J, Sandström R, 1998.** Low temperature creep ductility of OFHC copper. *Material Science and Engineering A* 246, 143–150.
- Henkel L, Hult K, Eriksson L, Johansson L, 1983.** Neotectonics in northern Sweden – geophysical investigations. SKBF/KBS TR 83-57, Svensk Kärnbränslehantering AB.
- Henshaw J, Spahiu K, 2021.** Radiolysis calculations of air, argon and water mixtures in a KBS-3 canister. SKB TR-21-11, Svensk Kärnbränslehantering AB.
- Hernelind J, 2010.** Modelling and analysis of canister and buffer for earthquake induced rock shear and glacial load. SKB TR-10-34, Svensk Kärnbränslehantering AB.
- Hernelind J, 2014.** Detailed models for BWR-canisters for earthquake induced rock shearing. SKBdoc 1439722 ver 1.0, Svensk Kärnbränslehantering AB.
- Hernelind J, 2015.** Analysis of creep in the KBS-3 copper canister due to internal and external loads. SKBdoc 1399768 ver 2.0, Svensk Kärnbränslehantering AB.
- Hernelind J, 2017a.** Additional analyses of eccentric insert inside the copper shell and sensitivity analyses of creep. SKBdoc 1551711 ver 1.0, Svensk Kärnbränslehantering AB.
- Hernelind J, 2019a.** Extended canister analyses with emphasis on tensile stresses and uneven swelling pressure. SKBdoc 1614038 ver 1.0, Svensk Kärnbränslehantering AB.
- Hernelind J, 2019b.** Design parameters effect on tensile stresses for the copper shell. SKBdoc 1707582 ver 2.0, Svensk Kärnbränslehantering AB.

- Hernelind J, Börjesson L, 2019.** Global analyses to validate buffer properties corresponding to swelling pressures of 3–10 MPa and sensitivity analyses of buffer and steel tube properties. SKBdoc 1550977 ver 1.0, Svensk Kärnbränslehantering AB.
- Hjerpe T, 2021.** Utredning om frågor relaterade till FHA-rapporten. SKBdoc 1875060 ver 1.0, Svensk Kärnbränslehantering AB. (In Swedish.) (Internal document.)
- Holden B, Stotler R L, Frappe S K, Ruskeeniemi T, Talikka M, Freifeld B M, 2009.** High Lake permafrost comparison site: permafrost phase IV. NWMO TR-2009-11, Nuclear Waste Management Organization, Canada.
- Homma T, Saltelli A, 1996.** Importance measures in global sensitivity analysis of nonlinear models. *Reliability Engineering & System Safety* 52, 1–17.
- Honeycombe R W K, 1968.** The plastic deformation of metals. London: Arnold.
- Hora S, Jensen M, 2005.** Expert panel elicitation of seismicity following glaciation in Sweden. SSI Report 2005:20, Swedish Radiation Protection Authority.
- Howard B J, Beresford N A, Andersson P, Brown J E, Copplestone D, Beaugelin-Seiller K, Garnier-Laplace J, Howe P D, Oughton D, Whitehouse P, 2010.** Protection of the environment from ionizing radiation in a regulatory context – an overview of the PROTECT coordinated action project. *Journal of Radiological Protection* 30, 191–194.
- Huang W-L, Longo J M, Pevear D R, 1993.** An experimentally derived kinetic model for smectite-to-illite conversion and its use as a geothermometer. *Clays and Clay Minerals* 41, 162–177.
- Huertas F J, Rozalen M L, Garcia-Palma S, Iriarte, Linares J, 2005.** Dissolution kinetics of bentonite under alkaline conditions. In: *Ecoclay II: effects of cement on clay barrier performance – Phase II. Final report.* EUR 21921, European Commission, 132–142.
- Humlum O, Houmark-Nielsen M, 1994.** High deglaciation rates in Denmark during the late Weichselian – implications for the palaeoenvironment. *Geografisk Tidsskrift* 94, 26–37.
- Huotilainen C, Saario T, Toivonen A, 2018.** Review of the Aaltonen-mechanism. SKB R-18-03, Svensk Kärnbränslehantering AB.
- Huttunen-Saarivirta E, Ghanbari E, Mao F, Rajala P, Carpén L, Macdonald D, 2018.** Kinetic properties of the passive film on copper in the presence of sulfate-reducing bacteria. *Journal of The Electrochemical Society* 165, C450–C460.
- Huttunen-Saarivirta E, Rajala P, Carpén L, Wang J, Liu F, Ghanbari E, Mao F, Dong C, Yang J, Sarifi-Asl S, Macdonald D D, 2019a.** Response to Comments on E. Huttunen-Saarivirta et al. “Kinetic Properties of the Passive Film on Copper in the Presence of Sulfate-Reducing Bacteria” [*J. Electrochem. Soc.*, 165, C450 (2018)]. *Journal of The Electrochemical Society* 166, Y17–Y26.
- Huttunen-Saarivirta E, Ghanbari E, Mao F, Rajala P, Carpén L, Macdonald D D, 2019b.** Erratum: Kinetic Properties of the Passive Film on Copper in the Presence of Sulfate-Reducing Bacteria” [*J. Electrochem. Soc.*, 165, C450 (2018)]. *Journal of The Electrochemical Society* 166, X5–X5.
- Håkansson K, 2016.** Kvävehalter i berg. Kunskapsammanställning bakgrundshalter. Fallstudie och vattenprovtagningar TASS, Äspö. SKB R-10-32, Svensk Kärnbränslehantering AB. (In Swedish.)
- Hökmark H, Karnland O, Pusch R, 1997.** A technique for modeling transport/conversion processes applied to smectite-to-illite conversion in HLW buffers. *Engineering Geology* 47, 367–378.
- Hökmark H, Fälth B, Wallroth T, 2006.** T-H-M couplings in rock. Overview of results of importance to the SR-Can safety assessment. SKB R-06-88, Svensk Kärnbränslehantering AB.
- Hökmark H, Lönnqvist M, Kristensson O, Sundberg J, Hellström G, 2009.** Strategy for thermal dimensioning of the final repository for spent nuclear fuel. SKB R-09-04, Svensk Kärnbränslehantering AB.
- Hökmark H, Lönnqvist M, Fälth B, 2010.** THM-issues in repository rock. Thermal, mechanical, thermo-mechanical and hydromechanical evolution of the rock at the Forsmark and Laxemar sites. SKB TR-10-23, Svensk Kärnbränslehantering AB.

- Hökmark H, Fälth B, Lönnqvist M, Munier R, 2019.** Earthquake simulations performed to assess the long-term safety of a KBS-3 repository. Overview and evaluation of results produced after SR-Site. SKB TR-19-19, Svensk Kärnbränslehantering AB.
- IAEA, 1994.** Safety indicators in different time frames for the safety assessment of underground radioactive waste repositories. First report of the INWAC Subgroup on Principles and Criteria for Radioactive Waste Disposal. IAEA-TECDOC-767, International Atomic Energy Agency.
- IAEA, 2005.** Natural activity concentrations and fluxes as indicators for the safety assessment of radioactive waste disposal. Results of a coordinated research project. IAEA-TECDOC-1464, International Atomic Energy Agency.
- IAEA, 2011.** Disposal of radioactive waste. Vienna: International Atomic Energy Agency. (IAEA Safety Standards Series SSR-5.)
- IAEA, 2012.** The safety case and safety assessment for the disposal of radioactive waste. Vienna: International Atomic Energy Agency. (Specific Safety Guide SSG-23.)
- ICRP, 2000.** Radiation protection recommendations as applied to the disposal of long-lived solid radioactive waste. Oxford: Pergamon. (ICRP Publication 81; Annals of the ICRP 28.)
- ICRP, 2007.** The 2007 recommendations of the International Commission on Radiological Protection. Oxford: Pergamon. (ICRP Publication 103; Annals of the ICRP 37.)
- ICRP, 2013.** Radiological protection in geological disposal of long-lived solid radioactive waste. Oxford: Pergamon. (ICRP Publication 122; Annals of the ICRP 42(3).)
- Ikäläinen T, Jäppinen E, Saario T, 2021.** Susceptibility of Cu-OFP to SCC by acetate under aerated conditions. Posiva Working Report 2020-21, Posiva Oy, Finland.
- Iman R L, Conover W J, 1979.** The use of the rank transform in regression. *Technometrics* 21, 499–509.
- Imbrie J, Hays J D, Martinson D G, McIntyre A, Mix A C, Morley J J, Pisias N G, Prell W L, Shackleton N J, 1984.** The orbital theory of Pleistocene climate: support from a revised chronology of the marine $\delta^{18}\text{O}$ record. In Berger A L, Imbrie J, Hays J D, Kukla G, Saltzman B (eds). *Milankovitch and climate: understanding the response to astronomical forcing*. Dordrecht: Reidel, 269–305.
- IPCC, 2013.** *Climate Change 2013: the physical science basis*. Contribution of Working Group I to the fifth assessment report of the Intergovernmental Panel on Climate Change. Cambridge: Cambridge University Press.
- IPCC, 2018.** *Global Warming of 1.5 °C*. An IPCC Special Report on the impacts of global warming of 1.5 °C above pre-industrial levels and related global greenhouse gas emission pathways, in the context of strengthening the global response to the threat of climate change, sustainable development, and efforts to eradicate poverty [Masson-Delmotte V, Zhai P, Pörtner H-O, Roberts D, Skea J, Shukla P R, Pirani A, Moufouma-Okia W, Péan C, Pidcock R, Connors S, Matthews J B R, Chen Y, Zhou X, Gomis M I, Lonnoy E, Maycock T, Tignor M, Waterfield T (eds)]. Geneva: World Meteorological Organization.
- Isaksson H, Keisu M, Lindholm T, Martinson O, Mattsson H, Thunehed H, Triumf C-A, 2010.** The geophysical response from a KBS-3 repository for spent nuclear fuel. Theoretical modelling based on physical properties of underground constructions at Forsmark. SKB P-10-39, Svensk Kärnbränslehantering AB.
- Itasca, 2007.** 3 DEC – 3-Dimensional Distinct Element Code. Version 4.1. User’s guide. Minneapolis: Itasca Consulting Group.
- Jaeschke B, Smith K, Nordén S, Alfonso B, 2013.** Assessment of the risk to non-human biota from a repository for the disposal of spent nuclear fuel at Forsmark. Supplementary information. SKB TR-13-23, Svensk Kärnbränslehantering AB.
- Janeczek J, Ewing R C, Oversby V M, Werme L O, 1996.** Uraninite and UO_2 in spent nuclear fuel: a comparison. *Journal of Nuclear Materials* 238, 121–130.
- Jaquet O, Namar R, Siegel P, Harper J, Jansson P, 2019.** Groundwater flow modelling under transient ice sheet conditions in Greenland. SKB R-19-17, Svensk Kärnbränslehantering AB.

- Jensen K A, Palenik C S, Ewing R C, 2002.** U⁶⁺ phases in the weathering zone of the Bangombé U-deposit: observed and predicted mineralogy. *Radiochimica Acta* 90, 761–769.
- Jin L-Z, Sandström R, 2008.** Creep of copper canisters in power-law breakdown. *Computational Materials Science* 43, 403–416.
- JNC, 2000.** H12 – Project to establish the scientific and technical basis for HLW disposal in Japan main report and four supplementary reports. JNC Technical Report TN1410 2000-001, JNC TN1410 2000-002 – 005, Japan Nuclear Fuel Cycle Development Institute.
- Jockwer N, Wieczorek K, 2003.** Gas generation measurements in the FEBEX project (Abstract). In: *Clays in natural and engineered barriers for radioactive waste confinement: proceeding from the international meeting held in Reims, 9–12 December 2002*. Châtenay-Malabry: Andra, 108–117.
- Johannesson L-E, 2007.** Äspö Hard Rock Laboratory. Canister Retrieval Test. Dismantling and sampling of the buffer and determination of density and water ratio. SKB IPR-07-16, Svensk Kärnbränslehantering AB.
- Johannesson L-E, 2014.** KBS-3H. Manufacturing of buffer and filling components for the Multi Purpose Test. SKB P-14-07, Svensk Kärnbränslehantering AB.
- Johansson A J, 2019.** Surface examination of a copper heater used for investigations of gas evolution in an unsaturated KBS-3 repository. SKBdoc 1696574 ver 1.0, Svensk Kärnbränslehantering AB.
- Johansson A J, Svensson D, Gordon A, Pahverk H, Karlsson O, Brask J, Lundholm M, Malmström D, Gustavsson F, 2020.** Corrosion of copper after 20 years exposure in the bentonite field tests LOT S2 and A3. SKB TR-20-14, Svensk Kärnbränslehantering AB.
- Johansson E, Stenberg L, Olofsson I, Karlzén R, 2013.** Utbyggnad av Äspölaboratoriet 2011–2012. Karakterisering, projektering och tunneldrivning. SKB R-13-28, Svensk Kärnbränslehantering AB. (In Swedish.)
- Johansson E, Gustafsson L-G, Berglund S, Lindborg T, Selroos J-O, Claesson Liljedahl L, Destouni G, 2015.** Data evaluation and numerical modeling of hydrological interactions between active layer, lake and talik in a permafrost catchment, Western Greenland. *Journal of Hydrology* 527, 688–703.
- Johansson F, Kierkegaard J, Zetterström P, 2019.** Kriticitetsanalys för slutförvaring av använt kärnbränsle. SKBdoc 1605532 ver 1.0, Svensk Kärnbränslehantering AB. (In Swedish.) (Internal document.)
- Johnson A B, Francis B, 1980.** Durability of metals from archeological objects, metal meteorites, and native metals. Report PNL-3198, UC-70, Pacific Northwest Laboratory, U.S. Department of Energy, Richland, Washington.
- Johnson J, 1994.** A basal water model for ice-sheets. PhD thesis. University of Minnesota.
- Johnston A C, 1987.** Suppression of earthquakes by large continental ice sheets. *Nature* 330, 467–469.
- Johnston A C, 1996.** A wave in the Earth. *Science* 274, 735.
- Jonsson M, Hakami H, Ekneligoda T, 2009.** Analysis of the effect of vibrations on the bentonite buffer in the canister hole. SKB R-09-40, Svensk Kärnbränslehantering AB.
- Jonsson M, Emilsson G, Emilsson L, 2018.** Mechanical design analysis for the canister. Posiva SKB Report 04, Posiva Oy, Svensk Kärnbränslehantering AB.
- Jonsson M, Sarnet J, Holst L, 2019.** Statistisk värdering av kopparkomponenternas geometriska kvalitet. SKB R-18-11, Svensk Kärnbränslehantering AB. (In Swedish.)
- Joyce S, Applegate D, Hartley L, Hoek J, Swan D, Marsic N, Follin S, 2010.** Groundwater flow modelling of periods with temperate climate conditions – Forsmark. SKB R-09-20, Svensk Kärnbränslehantering AB.
- Joyce S, Simpson T, Hartley L, Applegate D, Hoek J, Jackson P, Swan D, Marsic N, Follin S, 2010c.** Groundwater flow modelling of periods with temperate climate conditions – Forsmark. SKB R-09-20, Svensk Kärnbränslehantering AB.

- Joyce S, Swan D, Harley L, 2013.** Calculation of open repository inflows for Forsmark. SKB R-13-21, Svensk Kärnbränslehantering AB.
- Joyce S, Woollard H, Marsic N, Sidborn M, 2015.** Future evolution of groundwater composition at Forsmark during an extended temperate period. SKB R-14-26, Svensk Kärnbränslehantering AB.
- Kalinowski B, 2013.** Betydelsen av mikrobiell sulfatreduktion med organiskt upplöst material (DOC). SKBdoc 1396704 ver 1.0, Svensk Kärnbränslehantering AB. (In Swedish.)
- Karlsson A, Eriksson C, Borell Lövstedt C, Liungman O, Engqvist A, 2010.** High-resolution hydrodynamic modelling of the marine environment at Forsmark between 6500 BC and 9000 AD. SKB R-10-09, Svensk Kärnbränslehantering AB.
- Karlzén R, Johansson E, 2010.** Slutrapport från drivningen av TASS-tunneln. SKB R-10-31, Svensk Kärnbränslehantering AB. (In Swedish.)
- Karnland O, Birgersson M, 2006.** Montmorillonite stability with special respect to KBS-3 conditions. SKB TR-06-11, Svensk Kärnbränslehantering AB.
- Karnland O, Sandén T, Johannesson L-E, Eriksen T E, Jansson M, Wold S, Pedersen K, Motamedi M, Rosborg B, 2000.** Long-term test of buffer material. Final report on the pilot parcels. SKB TR-00-22, Svensk Kärnbränslehantering AB.
- Karnland O, Olsson S, Nilsson U, 2006.** Mineralogy and sealing properties of various bentonites and smectite-rich clay materials. SKB TR-06-30, Svensk Kärnbränslehantering AB.
- Karnland O, Olsson S, Dueck A, Birgersson M, Nilsson U, Heman-Håkansson T, Pedersen K, Nilsson S, Eriksen T, Rosborg B, 2009.** Long-term test of buffer material at the Äspö Hard Rock Laboratory, LOT project. Final report on the A2 test parcel. SKB TR-09-29, Svensk Kärnbränslehantering AB.
- Kautsky U (ed), 2001.** The biosphere today and tomorrow in the SFR area. SKB R-01-27, Svensk Kärnbränslehantering AB.
- Kautsky U, 2012.** Svar till SSM på begäran om förtydligande information angående ”Distributed LDF”. SKBdoc 1339994 ver 1.0, Svensk Kärnbränslehantering AB. (In Swedish.)
- Kavanaugh J L, 2009.** Exploring glacier dynamics with subglacial water pressure pulses: evidence for self-organized criticality? *Journal Of Geophysical Research* 114, F01021. doi:10.1029/2008JF001036
- Kavanaugh J L, Moore P L, Dow C F, Sanders J W, 2010.** Using pressure pulse seismology to examine basal criticality and the influence of sticky spots on glacial flow. *Journal Of Geophysical Research* 115, F04025. doi:10.1029/2010JF001666
- Kellner E, 2003.** Wetlands – different types, their properties and functions. SKB TR-04-08, Svensk Kärnbränslehantering AB.
- Kelly M, Cliffe K A, 2006.** Validity document for COMP23. SKB R-06-76, Svensk Kärnbränslehantering AB.
- Kersting A B, Efurud D W, Finnegan D L, Rokop D J, Smith D K, Thompson J L, 1999.** Migration of plutonium in ground water at the Nevada Test Site. *Nature* 397, 56–59.
- Kim Y-S, Sanderson D J, 2008.** Earthquake and fault propagation, displacement and damage zones. In Landowe S J, Hammler G M (eds). *Structural geology: new research*. New York: Nova Science.
- Kim Y-S, Peacock D C P, Sanderson D J, 2004.** Fault damage zones. *Journal of Structural Geology* 26, 503–517.
- King F, 1995.** A natural analogue for the long-term corrosion of copper nuclear waste containers – reanalysis of a study of a bronze cannon. *Applied Geochemistry* 10, 477–487.
- King F, 2013.** A review of the properties of pyrite and the implications for corrosion of the copper canister. SKB TR-13-19, Svensk Kärnbränslehantering AB.
- King F, Kolář M, 2019.** Copper Sulfide Model (CSM). model improvements, sensitivity analyses, and results from the Integrated Sulfide Project inter-model comparison exercise. SKB TR-18-08, Svensk Kärnbränslehantering AB.

- King F, Lilja C, Pedersen K, Pitkänen P, Vähänen M, 2010.** An update of the state-of-the-art report on the corrosion of copper under expected conditions in a deep geologic repository. SKB TR-10-67, Svensk Kärnbränslehantering AB.
- King F, Chen J, Qin Z, Shoemith D, Lilja C, 2017.** Sulphide-transport control of the corrosion of copper canisters. *Corrosion Engineering, Science and Technology* 52, 210–216.
- King-Clayton L, Chapman N, Ericsson L O, Kautsky F (eds), 1997.** Glaciation and hydrogeology. Proceedings of the workshop on the impact of climate change & glaciations on rock stresses, groundwater flow and hydrochemistry: past, present and future. Hässelby, Sweden, 17–19 April 1996. SKI Report 97:13, Swedish Nuclear Power Inspectorate.
- Kinnunen P, Varis P, 2011.** Stress corrosion cracking investigation of copper in groundwater with ammonium under potential polarisation. Posiva Working Report 2011-05, Posiva Oy, Finland.
- Kjellander R, Marčelja S, Quirk J P, 1988.** Attractive double-layer interactions between calcium clay particles. *Journal of Colloid and Interface Science* 126, 194–211.
- Kjellström E, Strandberg G, Brandefelt J, Näslund J-O, Smith B, Wohlfarth B, 2009.** Climate conditions in Sweden in a 100 000 year time perspective. SKB TR-09-04, Svensk Kärnbränslehantering AB.
- Kong D, Dong C, Zhao M, Ni X, Man C, Li X, 2018.** Effect of chloride concentration on passive film properties on copper. *Corrosion Engineering, Science and Technology* 53, 122–130.
- Koistinen T, Stephens M, Bogatchev V, Nordgulen Ø, Wennerstrom M, Korhonen J V, 2004.** Geological map of the Fennoscandian Shield 1:2 000 000. Espoo: Geological Survey of Finland, Trondheim: Geological Survey of Norway, Uppsala: Geological Survey of Sweden, Moscow: Ministry of Natural Resources of Russia.
- Kopp R, Baldner K-R, Ji W, Nieschwitz P-J, 1988.** Einfluss des Sattelkantenradius beim Recken. *Stahl und Eisen* 108, 901–905. (In German.)
- Krall L, Sandström B, Tullborg E-L, Evins L Z, 2015.** Natural uranium in Forsmark, Sweden: The solid phase. *Applied Geochemistry* 59, 178–188.
- Krall L, Evins L Z, Kooijman E, Whitehouse M, Tullborg E-L, 2019.** Tracing the palaeoredox conditions at Forsmark, Sweden, using uranium mineral geochronology. *Chemical Geology* 506, 68–78.
- Krall L, Auqué-Sanz L, Garcia-Orellana J, Trezzi G, Tullborg E-L, Suksi J, Andersson P, 2020.** Radium isotopes to trace uranium redox anomalies in anoxic groundwater. *Chemical Geology* 531, 119296. doi:10.1016/j.chemgeo.2019.119296
- Kujansuu R, 1964.** Nuorista siirroksista Lapissa (Recent faulting in Lapland). *Geologi* 16, 30–36. (In Finnish.)
- Laaksoharju M, Gimeno M, Auqué L, Gómez J, Smellie J, Tullborg E-L, Gurban I, 2004.** Hydrogeochemical Evaluation of the Forsmark Site, Model Version, 1.1. SKB R-04-05, Svensk Kärnbränslehantering AB
- Laaksoharju M, Smellie J, Tullborg E-L, Gimeno M, Hallbeck L, Molinero J, Waber N, 2008.** Bedrock hydrogeochemistry Forsmark. Site descriptive modelling, SDM-Site Forsmark. SKB R-08-47, Svensk Kärnbränslehantering AB.
- Lagerbäck R, 1979.** Neotectonic structures in northern Sweden. *Geologiska Föreningens i Stockholm Förhandlingar* 100, 263–269.
- Lagerbäck R, 1992.** Dating of Late Quaternary faulting in northern Sweden. *Journal of the Geological Society* 149, 285–291.
- Lagerbäck R, Sundh M, 2008.** Early Holocene faulting and paleoseismicity in northern Sweden. Uppsala: Sveriges Geologiska Undersökning. (Research Paper C 836.)
- Lagerbäck R, Sundh M, Svedlund J-O, Johansson H, 2005.** Forsmark site investigation. Searching for evidence of late- or postglacial faulting in the Forsmark region. Results from 2002–2004. SKB R-05-51, Svensk Kärnbränslehantering AB.

- Lagerbäck R, Sundh M, Svantesson S-I, 2006.** Oskarshamn site investigation. Searching for evidence of late- or postglacial faulting in the Oskarshamn region. Results from 2005. SKB P-06-160, Svensk Kärnbränslehantering AB.
- Lambe T W, Whitman R V, 1969.** Soil mechanics. New York: Wiley.
- Lambeck K, Purcell A, Funder S, Kjær K H, Larsen E, Möller P, 2006.** Constraints on the Late Saalian to early Middle Weichselian ice sheet of Eurasia from field data and rebound modelling. *Boreas* 35, 539–575.
- Lambeck K, Purcell A, Zhao J, Svensson N-O, 2010.** The Scandinavian Ice Sheet: from MIS 4 to the end of the Last Glacial Maximum. *Boreas* 39, 410–435.
- Lantenois S, Lanson B, Muller F, Bauer A, Jullien M, Plançon A, 2005.** Experimental study of smectite interaction with metal Fe at low temperature: 1. Smectite destabilization. *Clays and Clay Minerals* 6, 597–612.
- La Pointe P, Wallmann P, Thomas A, Follin S, 1997.** A methodology to estimate earthquake effects on fractures intersecting canister holes. SKB TR 97-07, Svensk Kärnbränslehantering AB.
- La Pointe P R, Cladouhos T, Follin S, 1999.** Calculation of displacement on fractures intersecting Canisters induced by earthquakes: Aberg, Beberg and Ceberg examples. SKB TR-99-03, Svensk Kärnbränslehantering AB.
- La Pointe P R, Cladouhos T T, Outters N, Follin S, 2000.** Evaluation of the conservativeness of the methodology for estimating earthquake-induced movements of fractures intersecting canisters. SKB TR-00-08, Svensk Kärnbränslehantering AB.
- La Pointe P R, Cladouhos T, Follin S, 2002.** Development, application, and evaluation of a methodology to estimate distributed slip on fractures due to future earthquakes for nuclear waste repository performance assessment. *Bulletin of the Seismological Society of America* 92, 923–944.
- Leskinen N, Ronneteg U, 2013.** Tillverkning av kapselkomponenter. SKBdoc 1175208 ver 8.0, Svensk Kärnbränslehantering AB. (In Swedish.)
- Leupin O X (ed), Birgersson M, Karnland O, Korkeakoski P, Sellin P, Mäder U, Wersin P, 2014.** Montmorillonite stability under near-field conditions. Nagra Technical Report 14-12, Nagra, Switzerland.
- Levermann A, Clark P U, Marzeion B, Milne G A, Pollard D, Radic V, Robinson A, 2013.** The multimillennial sea-level commitment of global warming. *Proceedings of the National Academy of Sciences* 110, 13745–13750.
- Liakka J, Näslund J-O, Brandefelt J, 2021.** Timing of future glacial inception. In Haeberli W, Whiteman C (eds). *Snow and ice-related hazards, risks and disasters*. 2nd ed. Oxford, Elsevier, Chapter 11.2.
- Lidmar-Bergström K, Näslund J-O, 2002.** Landforms and uplift in Scandinavia. In Doré A G, Cartwright J A, Stoker M S, Turner J P, White N (eds). *Exhumation of the North Atlantic margin: timing, mechanisms, and implications for petroleum exploration*. London: Geological Society. (Special publication 196), 103–116.
- Lilja C, Puigdomenech I, 2012.** Förtydligande information om hantering av sulfidhalter och sulfatreduktion. SKBdoc 1346686 ver 1.0, Svensk Kärnbränslehantering AB. (In Swedish.)
- Lilja C, Sellin P, Hedin A, 2014.** Svar till SSM på begäran om komplettering rörande grundvattenkemi på kort och medellång sikt. SKBdoc 1437441 ver 1.0, Svensk Kärnbränslehantering AB. (In Swedish.)
- Lilja C, King F, Puigdomenech I, Pastina B, 2021.** Speciation of copper in high chloride concentrations, in the context of corrosion of copper canisters. *Materials and Corrosion* 72, 293–299.
- Lindblom E, Lund B, Tryggvason A, Uski M, Bödvarsson R, Juhlin C, Roberts R, 2015.** Microearthquakes illuminate the deep structure of the endglacial Parvie fault, northern Sweden. *Geophysical Journal International* 201, 1704–1716.
- Lindborg T (ed), 2008.** Surface system Forsmark. Site descriptive modelling, SDM-Site Forsmark. SKB R-08-11, Svensk Kärnbränslehantering AB.

- Lindborg T (ed), 2010.** Landscape Forsmark – data, methodology and results for SR-Site. SKB TR-10-05, Svensk Kärnbränslehantering AB.
- Lindroos H, Isaksson H, Thunehed H, 2004.** The potential for ore and industrial minerals in the Forsmark area. SKB R-04-18, Svensk Kärnbränslehantering AB.
- Liu L, Moreno L, Neretnieks I, 2009.** A dynamic force balance model for colloidal expansion and its DLVO-based application. *Langmuir* 25, 679–687.
- Liu L, Moreno L, Neretnieks I, Gylling B, 2010.** A safety assessment approach using coupled NEAR3D and CHAN3D – Forsmark. SKB R-10-69, Svensk Kärnbränslehantering AB.
- Ljungberg J, 2021.** Teknikbeslut Kärnbränsleförvaret – Tillåten mängd vatten och luft i kapseln. SKBdoc 1953875 ver 1.0, Svensk Kärnbränslehantering AB. (In Swedish.) (Internal document.)
- Lokrantz H, Sohlenius G, 2006.** Ice marginal fluctuations during the Weichselian glaciation in Fennoscandia, a literature review. SKB TR-06-36, Svensk Kärnbränslehantering AB.
- Lord N S, Lunt D, Thorne M, 2019.** Modelling changes in climate over the next 1 million years. SKB TR-19-09, Svensk Kärnbränslehantering AB.
- Lousada C M, Korzhavyi P A, 2020.** Hydrogen sorption capacity of crystal lattice defects and low Miller index surfaces of copper. *Journal of Materials Science* 55, 6623–6636.
- Loutre M F, Berger A, 2000.** Future climatic changes: are we entering an exceptionally long interglacial? *Climatic Change* 46, 61–90.
- Ludvigson J-E, 2002.** Brunnsinventering i Forsmark. SKB R-02-17, Svensk Kärnbränslehantering AB. (In Swedish.)
- Luna M, Arcos D, Duro L, 2006.** Effects of grouting, shotcreting and concrete leachates on backfill geochemistry. SKB R-06-107, Svensk Kärnbränslehantering AB.
- Lund B, 2005.** Effects of deglaciation on the crustal stress field and implications for endglacial faulting: a parametric study of simple Earth and ice models. SKB TR-05-04, Svensk Kärnbränslehantering AB.
- Lund B, 2006.** Stress variations during a glacial cycle at 500 m depth in Forsmark and Oskarshamn: Earth model effects. SKB R-06-95, Svensk Kärnbränslehantering AB.
- Lund B, Näslund J-O, 2009.** Glacial isostatic adjustment: implications for glacially induced faulting and nuclear waste repositories. In Connor C B, Chapman N A, Connor L J (eds). *Volcanic and tectonic hazard assessment for nuclear facilities*. Cambridge: Cambridge University Press, 142–155.
- Lund B, Schmidt P, Hieronymus C, 2009.** Stress evolution and fault stability during the Weichselian glacial cycle. SKB TR-09-15, Svensk Kärnbränslehantering AB.
- Lundquist J, Lagerbäck R, 1976.** The Pärve Fault: a late-glacial fault in the Precambrian of Swedish Lapland. *Geologiska Föreningens i Stockholm Förhandlingar* 98, 45–51.
- Luterkort D, Johannesson L-E, Eriksson P, 2017.** Buffer design and installation method. SKB TR-17-06, Svensk Kärnbränslehantering AB.
- Luukkonen A, 2008.** Äspö Hard Rock Laboratory. Prototype repository. Inverse modelling of a prototype repository using near-field groundwater samples from July 1998 – March 2004. SKB IPR-08-06, Svensk Kärnbränslehantering AB.
- Löfgren A (ed), 2010.** The terrestrial ecosystems at Forsmark and Laxemar-Simpevarp. SR-Site Biosphere. SKB TR-10-01, Svensk Kärnbränslehantering AB.
- Lönnqvist M, Hökmark H, 2010.** Assessment of potential for glacially induced hydraulic jacking at different depths. SKB R-09-35, Svensk Kärnbränslehantering AB.
- Maanoja S, Lakaniemi A-M, Lehtinen L, Salminen L, Auvinen H, Kokko M, Palmroth M, Muuri E, Rintala J, 2020.** Compacted bentonite as a source of substrates for sulfate-reducing microorganisms in a simulated excavation-damaged zone of a spent nuclear fuel repository. *Applied Clay Science* 196, 105746. doi:10.1016/j.clay.2020.105746

- Machel H G, 2001.** Bacterial and thermochemical sulfate reduction in diagenetic settings – Old and new insights. *Sedimentary Geology* 140, 143–175.
- Manson S S, Haferd A M, 1953.** A linear time-temperature relation for extrapolation of creep and stress-rupture data. Technical note 2890. Washington: National Advisory Committee For Aeronautics.
- Malehmir A, Andersson M, Mehta S, Brodic B, Munier R, Place J, Maries G, Smith C, Kamm J, Bastan M, Mikko H, Lund B, 2016.** Post-glacial reactivation of the Bollnäs fault, central Sweden – a multidisciplinary geophysical investigation. *Solid Earth* 7, 509–527.
- Malmberg D, Åkesson M, 2020.** Relative-humidity evolution near the canister in models: Analysis of SR-Site and Prototype Repository models. SKBdoc 1885367 ver 1.0, Svensk Kärnbränslehantering AB.
- Mao F, Dong C, Sharifi-Asl S, Lu P, Macdonald D D, 2014.** Passivity breakdown on copper: influence of chloride ion. *Electrochimica Acta* 144, 391–399.
- Marcos N, 1989.** Native copper as a natural analogue for copper canisters. Report YJT-89-18, Nuclear Waste Commission of Finnish Power Companies.
- Marcos N, Ahonen L, Bros R, Roos P, Suksi J, Oversby V, 1999.** New data on the Hyrkkölä native copper mineralization: a natural analogue for the long-term corrosion of copper canisters. In Wronkiewicz D J, Lee J H (eds). *Scientific basis for nuclear waste management XXII: symposium held in Boston, Massachusetts, 30 November – 4 December 1998*. Warrendale, PA: Materials Research Society. (Materials Research Society Symposium Proceedings 556), 825–832.
- Marrett R, Allmendinger R W, 1990.** Kinematic analysis of fault-slip data. *Journal of Structural Geology* 12, 973–986.
- Marshall M H M, McKelvie J R, Simpson A J, Simpson M J, 2015.** Characterization of natural organic matter in bentonite clays for potential use in deep geological repositories for used nuclear fuel. *Applied Geochemistry* 54, 43–53.
- Marsic N, Hjerpe T, Lindgren M, 2020.** Mapping of NEA IFEP List Version 3.0 to PSAR–SFK FEP catalogue. Post-closure safety for the final repository for spent nuclear fuel at Forsmark – PSAR version. SKBdoc 1911712 ver 1.0, Svensk Kärnbränslehantering AB.
- Martin C D, 2005.** Preliminary assessment of potential underground stability (wedge and spalling) at Forsmark, Simpevarp and Laxemar sites. SKB R-05-71, Svensk Kärnbränslehantering AB.
- Martin C D, Kaiser P K, 1996.** Mine-by Experiment Committee Report, Phase 1: excavation response, summary and implications. AECL Report AECL-11382, Atomic Energy of Canada Limited.
- Martin O, Nilsson K-F, Jakšić N, 2009.** Numerical simulation of plastic collapse of copper-cast iron canister for spent nuclear fuel. *Engineering Failure Analysis* 16, 225–241.
- Martinerie P, Raynaud D, Etheridge D M, Barnola J-M, Mazaudier D, 1992.** Physical and climatic parameters which influence the air content in polar ice. *Earth and Planetary Science Letters* 112, 1–13.
- Martino T, Chen J, Qin Z, Shoesmith D W, 2017.** The kinetics of film growth and their influence on the susceptibility to pitting of copper in aqueous sulphide solutions. *Corrosion Engineering, Science and Technology* 52, 61–64.
- Martino T, Smith J, Chen J, Quin Z, Noël J J, Shoesmith D W, 2019a.** The properties of electrochemically-grown copper sulphide films. *Journal of The Electrochemical Society* 166, C9–C18.
- Martino T, Chen J, Guo M, Ramamurthy S, Shoesmith D W, Noël J J, 2019b.** Comments on E. Huttunen-Saarivirta et al. “Kinetic Properties of the Passive Film on Copper in the Presence of Sulfate-Reducing Bacteria” [J. Electrochem. Soc., 165, C450 (2018)]. *Journal of The Electrochemical Society* 166, Y13–Y16.
- Martino T, Chen J, Noël J J, Shoesmith D W, 2020.** The effect of anions on the anodic formation of copper sulphide films on copper. *Electrochimica Acta* 331, 135319. doi:10.1016/j.electacta.2019.135319
- Martinsson Å, Sandström R, 2012.** Hydrogen depth profile in phosphorus-doped, oxygen-free copper after cathodic charging. *Journal of Materials Science* 47, 6768–6776.

- Masurat P A, 2006.** Potential for corrosion in disposal systems for high level radioactive waste by *Meiothermus* and *Desulfovibrio*. PhD thesis. Göteborg University.
- Masurat P, Eriksson S, Pedersen K, 2010.** Evidence of indigenous sulphate-reducing bacteria in commercial Wyoming bentonite MX-80. *Applied Clay Science* 47, 51–57.
- Mathurin F, 2018.** Nitrogen compounds in groundwater – Assessment of the influence of blasting during tunnel expansion of the Äspö Hard Rock Laboratory. SKB TR-17-09, Svensk Kärnbränslehantering AB.
- Matthiesen H, Hilbert L R, Gregory D J, 2003.** Siderite as a corrosion product on archaeological iron from a waterlogged environment. *Studies in Conservation* 48, 183–194.
- Matthiesen H, Hilbert L R, Gregory D, Sørensen B, 2004.** Corrosion of archaeological iron artefacts compared to modern iron at the waterlogged site Nydam, Denmark. Prediction of long-term corrosion behaviour in nuclear waste system. In Andra (ed). Long-term prediction and modelling of corrosion: proceedings of the 2nd International Workshop organized by the Working Party on nuclear corrosion (WP4) of the European Federation of Corrosion (EFC), Nice, 12–16 September 2004 (Eurocorr 2004), 114–127.
- Mazotti S, James T S, Henton J, Adams J, 2005.** GPS crustal strain, postglacial rebound, and seismic hazard in eastern North America: the Saint Lawrence valley example. *Journal of Geophysical Research*, 110, B11301. doi:10.1029/2004JB003590
- Melosh H J, 1989.** Impact cratering: a geologic process. New York: Oxford University Press.
- Mikko H, Smith C, Lund B, Ask M, Munier R, 2014.** Neotectonic faulting in Sweden: Surface expression from a LiDAR based digital elevation model. 31 Nordic Geologic Winter Meeting, Lund, Sweden, 2014. Geologiska Föreningen.
- Mikko H, Smith C A, Lund B, Ask M, Munier R, 2015.** LiDAR-derived inventory of post-glacial fault scarps in Sweden. *GFF* 137, 334–338.
- Miller B, Lind A, Savage D, Maul P, Robinson P, 2002.** Natural elemental concentrations and fluxes: their use as indicators of repository safety. SKI Report 02:3, Swedish Nuclear Power Inspectorate, SSI report 2002:02, Swedish Radiation Protection Authority.
- Miller W, Alexander R, Chapman N, McKinley I, Smellie J, 2000.** Geological disposal of radioactive wastes and natural analogues: lessons from nature and archaeology. Amsterdam: Pergamon. (Waste Management Series 2.)
- Milne, G A, Gehrels W R, Hughes C W, Tamisiea M E, 2009.** Identifying the causes of sea-level change. *Nature Geoscience* 2, 471–478.
- Milodowski A E, Styles M T, Horstwood M S A, Kemp S J, 2002.** Alteration of uraniferous and native copper concretions in the Permian mudrocks of south Devon, United Kingdom. A natural analogue study of the corrosion of copper canisters and radiolysis effects in a repository for spent nuclear fuel. SKB TR-02-09, Svensk Kärnbränslehantering AB.
- Mitrovica J X, Milne G A, 2003.** On post-glacial sea level: I. General theory. *Geophysical Journal International* 154, 253–267.
- Milodowski A E, Norris S, Alexander W R, 2016.** Minimal alteration of montmorillonite following long-term interaction with natural alkaline groundwater: implications for geological disposal of radioactive waste. *Applied Geochemistry* 66, 184–197.
- Moberg A, Sonechkin D M, Holmgren K, Datsenko N M, Karlén W, 2005.** Highly variable Northern Hemisphere temperatures reconstructed from low- and high-resolution proxy data. *Nature* 433, 613–617.
- Moberg A, Gouirand I, Wohlfarth B, Schoning K, Kjellström E, Rummukainen M, de Jong R, Linderholm H, Zorita E, 2006.** Climate in Sweden during the past millennium – Evidence from proxy data, instrumental data and model simulations. SKB TR-06-35, Svensk Kärnbränslehantering AB.
- Molinero-Huguet J, Samper-Calvete F J, Zhang G, Yang C, 2004.** Biogeochemical reactive transport model of the Redox Zone experiment of the Äspö Hard Rock Laboratory in Sweden. *Nuclear Technology* 148, 151–165.

- Moon S, Perron J T, Martel S J, Goodfellow B W, Mas Ivars D, Hall A, Heyman J, Munier R, Näslund J O, Simeonov A, Stroeven A P, 2020.** Present-day stress field influences bedrock fracture openness deep into the subsurface. *Geophysical Research Letters* 47. doi:10.1029/2020GL090581
- Morbidelli A, Bottke W F, Froeschlé C, Michel P, 2002.** Origin and evolution of near-Earth objects. In Bottke W F, Cellino P, Paolicchi P, Binzel R P (eds). *Asteroids III*. Tucson: University of Arizona Press, 409–422.
- Morén L, Ritchey T, Stenström M, 1998.** Scenarier baserade på mänskliga handlingar. Tre arbetsmöten om metod- och säkerhetsanalysfrågor (Scenarios based on human actions. Three workshops on issues related to method and safety assessment). SKB R-98-54, Svensk Kärnbränslehantering AB. (In Swedish.)
- Moreno L, Neretnieks I, Liu L, 2010.** Modelling of erosion of bentonite gel by gel/sol flow. SKB TR-10-64, Svensk Kärnbränslehantering AB.
- Muir Wood R, 1993.** A review of the seismotectonics of Sweden. SKB TR 93-13, Svensk Kärnbränslehantering AB.
- Muir Wood R, 1995.** Reconstructing the tectonic history of Fennoscandia from its margins: The past 100 million years. SKB TR 95-36, Svensk Kärnbränslehantering AB.
- Muir Wood R, 2000.** Deglaciation seismotectonics: a principal influence on intraplate seismogenesis at high latitudes. *Quaternary Science Reviews* 19, 1399–1411.
- Muir-Wood R, King G C P, 1993.** Hydrological signatures of earthquake strain. *Journal of Geophysical Research* 98, 22035–22068.
- Muir Wood R, Gregersen S, Basham P W, 1989.** Extraordinary deglaciation reverse faulting in northern Fennoscandia. In Gregersen S, Basham P W (eds). *Earthquakes at North-Atlantic passive margins: neotectonics and postglacial rebound*. Boston: Kluwer Academic Publishers. (NATO Advanced Study Institutes Series C, Mathematical and Physical Sciences 266), 141–173.
- Munier R, 2006.** Using observations in deposition tunnels to avoid intersections with critical fractures in deposition holes. SKB R-06-54, Svensk Kärnbränslehantering AB.
- Munier R, 2007.** Demonstrating the efficiency of the EFPC criterion by means of sensitivity analyses. SKB R-06-115, Svensk Kärnbränslehantering AB.
- Munier R, 2010.** Full perimeter intersection criteria. Definitions and implementations in SR-Site. SKB TR-10-21, Svensk Kärnbränslehantering AB.
- Munier R, Hökmark H, 2004.** Respect distances. Rationale and means of computation. SKB R-04-17, Svensk Kärnbränslehantering AB.
- Munier R, Mattila J, 2015.** Memo on terminology. POS-021685, ver 1.0. Posiva Oy, Finland.
- Munier R, Stenberg L, Stanfors R, Milnes A G, Hermanson J, Triumf C-A, 2003.** Geological site descriptive model. A strategy for the model development during site investigations. SKB R-03-07, Svensk Kärnbränslehantering AB.
- Munier R, Hökmark H, Fälth B, 2008.** Respect distances: rationale and means of computation. In Ahlbom K, Stephens M (eds). *Investigations of potential repository sites for spent nuclear fuel at Forsmark and Laxemar-Simpevarp, Sweden*. Abstracts, 33rd International Geological Congress, Oslo. SKB R-08-97, Svensk Kärnbränslehantering AB, 57.
- Muzeau B, Jégou C, Delaunay F, Broudic V, Brevet A, Catalette H, Simoni E, Corbel C, 2009.** Radiolytic oxidation of UO₂ pellets doped with alpha emitters (^{238/239}Pu). *Journal of Alloys and Compounds* 467, 578–589.
- Mårtensson E, Gustafsson L-G, 2010.** Hydrological and hydrogeological effects of an open repository in Forsmark. Final MIKE SHE flow modelling results for the Environmental Impact Assessment. SKB R-10-18, Svensk Kärnbränslehantering AB.
- Mörner N-A, 1978.** Faulting, fracturing, and seismicity as functions of glacio-isostasy in Fennoscandia. *Geology* 6, 41–45.

- Mörner N-A, 1989.** Postglacial faults and fractures on Äspö. SKB HRL Progress Report 25-89-24, Svensk Kärnbränslehantering AB.
- Mörner N-A, 2003.** Paleoseismicity of Sweden: a novel paradigm. Stockholm: N.-A. Mörner.
- Mörner N-A, 2004.** Active faults and paleoseismicity in Fennoscandia, especially Sweden: primary structures and secondary effects. *Tectonophysics* 380, 139–157.
- Nagra, 2002.** Project Opalinus Clay. Safety report. Demonstration of disposal feasibility of spent fuel, vitrified high-level waste and long-lived intermediate-level waste (Entsorgungsnachweis). Nagra Technical Report NTB 02-05, Nagra, Switzerland.
- Naudet R, 1991.** Oklo: des réacteurs nucléaires fossiles, étude physique. Paris: Commissariat à l’Energie Atomique. (In French.)
- NEA, 1991.** Disposal of radioactive waste: review of safety assessment methods: a report of the Performance Assessment Advisory Group of the Radioactive Waste Management Committee, OECD Nuclear Energy Agency. Paris: Nuclear Energy Agency, OECD.
- NEA, 1993.** Palaeohydrogeological methods and their application: proceedings of a NEA workshop, Paris, 9–10 November 1992. Paris: Nuclear Energy Agency, OECD.
- NEA, 1995.** Future human actions at disposal sites: a report from the NEA Working Group on Assessment of Future Human Actions at Radioactive Waste Disposal Sites. Paris: Nuclear Energy Agency, OECD.
- NEA, 1997a.** Lessons learnt from ten performance assessment studies. Paris: Nuclear Energy Agency, OECD.
- NEA, 1997b.** The Probabilistic System Assessment Group: history and achievements 1985–1994. Paris: Nuclear Energy Agency, OECD. (Disposal of radioactive waste.)
- NEA, 1999a.** Confidence in the long-term safety of deep geological repositories: its development and communication. Paris: Nuclear Energy Agency, OECD.
- NEA, 1999b.** Safety assessment of radioactive waste repositories – An international database of Features, Events and Processes. A report of the NEA working group on development of a database of Features, events and Processes relevant to the assessment of post-closure safety of radioactive waste repositories. Nuclear Agency of the Organisation for Economic Cooperation and Development (OECD/NEA), Paris, France. Electronic version 1.2 of the NEA FEP database developed on behalf of the Nuclear Energy Agency by Safety Assessment Management Ltd with support of Quintessa Ltd.
- NEA, 2000.** Features, Events and Processes (FEPs) for geologic disposal of radioactive waste. An international database. Paris: OECD Publishing.
- NEA, 2001.** Scenario development methods and practices: an evaluation based on the NEA Workshop on Scenario Development, Madrid, Spain, May 1999. Paris: Nuclear Energy Agency, OECD.
- NEA, 2004a.** The handling of time scales in assessing post-closure safety: lessons learnt from the April 2002 Workshop in Paris, France. Paris: Nuclear Energy Agency, OECD.
- NEA, 2004b.** Post-closure safety case for geological repositories: nature and purpose. Paris: Nuclear Energy Agency, OECD.
- NEA, 2005.** Management of uncertainty in safety cases and the role of risk: workshop proceedings. Paris: Nuclear Energy Agency, OECD.
- NEA, 2006.** Electronic version 2.1 of the NEA FEP database developed on behalf of the Nuclear Energy Agency by Safety Assessment Management Ltd.
- NEA, 2009.** International Experiences in Safety Cases for Geological Repositories (INTESC): Outcomes of the INTESC Project. Paris: Nuclear Energy Agency, OECD.
- NEA, 2012a.** The post-closure radiological safety case for a spent fuel repository in Sweden: An international peer review of the SKB license-application study of March 2011. Paris: Nuclear Energy Agency, OECD.
- NEA, 2012b.** Methods for safety assessment of geological disposal facilities – Outcomes of the NEA MeSA initiative. NEA 6923. Paris: Nuclear Energy Agency, OECD.

- NEA, 2013.** The Safety Case for Deep Geological Disposal of Radioactive Waste: 2013 State of the Art. Paris: Nuclear Energy Agency, OECD.
- NEA, 2019.** International Features, Events and Processes (IFEP) list for the deep geological disposal of radioactive waste. Version 3.0. NEA/RWM/R(2019)1. Paris: Nuclear Energy Agency, OECD.
- NEA, 2022.** IGSC Safety Case Symposium 2018: Current Understanding and Future Direction for the Geological Disposal of Radioactive Waste. Paris: Nuclear Energy Agency, OECD.
- Neall F, Pastina B, Snellman M, Smith P, Gribo P, Johnson L, 2008.** Safety assessment of a KBS-3H spent nuclear fuel repository at Olkiluoto. Complementary evaluation of safety. SKB R-08-35, Svensk Kärnbränslehantering AB.
- Nebot J, Bruno J, 1991.** The implications of soil acidification on a future HLNW repository. Part I: The effects of increased weathering, erosion and deforestation. SKB TR 91-45, Svensk Kärnbränslehantering AB.
- Neff D, Dillmann P, Beranger G, 2003.** An analytical study of corrosion products formed on buried ferrous archaeological artefacts. In Féron D, Macdonald D D (eds). Prediction of long-term corrosion behaviour in nuclear waste systems (EFC 36). Leeds: Maney Publishing, 295–315.
- Neff D, Dillmann P, Bellot-Gurlet L, Beranger G, 2005.** Corrosion of iron archaeological artefacts in soil: characterisation of the corrosion system. *Corrosion Science* 47, 515–535.
- Neff D, Dillmann P, Descostes M, Beranger G, 2006.** Corrosion of iron archaeological artefacts in soil: estimation of the average corrosion rates involving analytical techniques and thermodynamic calculations. *Corrosion Science* 48, 2947–2970.
- Neretnieks I, 1986.** Some uses for natural analogues in assessing the function of a HLW repository. *Chemical Geology* 55, 175–188.
- Neretnieks I, 2006a.** Flow and solute transport in a zone damaged due to spalling. SKB R-06-91, Svensk Kärnbränslehantering AB.
- Neretnieks I, 2006b.** Flow and transport through a damaged buffer – exploration of the impact of a cemented and an eroded buffer. SKB TR-06-33, Svensk Kärnbränslehantering AB.
- Neretnieks I, Liu L, Moreno L, 2009.** Mechanisms and models for bentonite erosion. SKB TR-09-35, Svensk Kärnbränslehantering AB.
- Neretnieks I, Liu L, Moreno L, 2010.** Mass transfer between waste canister and water seeping in rock fractures. Revisiting the Q-equivalent model. SKB TR-10-42, Svensk Kärnbränslehantering AB.
- Neretnieks I, Moreno L, Liu L, 2017.** Clay erosion – impact of flocculation and gravitation. SKB TR-16-11, Svensk Kärnbränslehantering AB.
- Neully M, Bussac J, Frejacques C, Nief G, Vendreys G, Yvon J, 1972.** Sur l'existence dans un passé reculé d'une réaction en chaîne naturelle de fission, dans le gisement d'uranium d'Oklo (Gabon). *Comptes rendus Hebdomadaires des Séances de l'Académie des Sciences, Série D: Sciences Naturelles* 275, 1847–1849. (In French.)
- Nicot J-P, 2008.** Methodology for bounding calculations of nuclear criticality of fissile material accumulations external to a waste container at Yucca Mountain, Nevada. *Applied Geochemistry* 23, 2065–2081.
- Nilsson A-C, Sandberg B, 2017.** Elevated pH values in groundwater. Observations from SKB investigations 1976–2014 and possible causes. SKB R-16-04, Svensk Kärnbränslehantering AB.
- Nilsson A-C, Pedersen K, Hallbeck B, Johansson J, Tullborg E-L, 2017.** Development and testing of gas samplers in tunnel environments. SKB R-16-16, Svensk Kärnbränslehantering AB.
- Nilsson K-F, Lofaj F, Burström M, Andersson C-G, 2005.** Pressure tests of two KBS-3 canister mock-ups. SKB TR-05-18, Svensk Kärnbränslehantering AB.
- Nilsson K-F, Burström M, Lofaj F, Andersson C-G, 2006.** Failure of spent nuclear fuel canister mock-ups at isostatic pressure. *Engineering Failure Analysis* 14, 47–62.
- Nilsson L, Widerlund A, 2017.** Tracing nitrogen cycling in mining waters using stable nitrogen isotope analysis. *Applied Geochemistry* 84, 41–51.

- Nordbäck N, Mattila J, 2018.** Brittle fault systems of the ONKALO underground research facility. Posiva Working Report 2018-20, Posiva Oy, Finland.
- Nordén S, 2013.** Svar till SSM på begäran om komplettering rörande effekter på andra organismer än människa. SKBdoc 1417654 ver 1.0, Svensk Kärnbränslehantering AB. (In Swedish.)
- Nordén S, Avila R, de la Cruz I, Stenberg K, Grolander S, 2010.** Element-specific and constant parameters used for dose calculations in SR-Site. SKB TR-10-07, Svensk Kärnbränslehantering AB.
- Nordstrom D K, Ball J W, Donahoe R J, Whittemore D, 1989.** Groundwater chemistry and water-rock interactions at Stripa. *Geochimica et Cosmochimica Acta* 53, 1727–1740.
- Norman S, Kjellbert N, 1990.** FARF31 – A far-field radionuclide migration code for use with the PROPER package. SKB TR 90-01, Svensk Kärnbränslehantering AB.
- Nummi O, Kyllönen J, Eurajoki T, 2012.** Long-term safety of the maintenance and decommissioning waste of the encapsulation plant. Posiva 2012-37, Posiva Oy, Finland.
- NWMO, 2011.** Postclosure safety assessment: Features, events and processes. NWMO DGR-TR-2011-29, Nuclear Waste Management Organization, Canada.
- Näslund J-O, Jansson P, Fastook J L, Johnson J, Andersson L, 2005.** Detailed spatially distributed geothermal heat-flow data for modelling of basal temperatures and meltwater production beneath the Fennoscandian ice sheet. *Annals of Glaciology* 40, 95–101.
- Ochs M, Talerico C, 2004.** SR-Can. Data and uncertainty assessment. Migration parameters for the bentonite buffer in the KBS-3 concept. SKB TR-04-18, Svensk Kärnbränslehantering AB.
- Olesen O, 1985.** Postglacial faulting at Masi, Finnmark, Northern Norway. In Proceedings of the 15th Meeting of the Nordic Association for Applied Geophysics, Espoo, Finland, 15–17 January 1985.
- Olesen O, Dehls J, Bungum H, Riis F, Hicks E, Lindholm C, Blikra L H, Fjeldskaar W, Olsen L, Longva O, Faleide J I, Bockmann L, Rise L, Roberts D, Braathen A, Brekke H, 2000.** Neotectonics in Norway. Final report. NGU Report 2000.002, Geological Survey of Norway.
- Olsson M, Niklasson B, Wilson L, Andersson C, Christiansson R, 2004.** Äspö HRL. Experiences of blasting of the TASQ tunnel. SKB R-04-73, Svensk Kärnbränslehantering AB.
- Olsson M, Markström I, Pettersson A, Sträng M, 2009.** Examination of the Excavation Damaged Zone in the TASS tunnel, Äspö HRL. SKB R-09-39, Svensk Kärnbränslehantering AB.
- Olsson S, Jensen V, Johannesson L-E, Hansen E, Karnland O, Kumpulainen S, Svensson D, Hansen S, Lindén J, 2013.** Prototype Repository. Hydromechanical, chemical and mineralogical characterization of the buffer and backfill material from the outer section of the Prototype Repository. SKB TR-13-21, Svensk Kärnbränslehantering AB.
- ONDRAF/NIRAS, 2001.** SAFIR:2 Safety Assessment and Feasibility Interim Report 2. NIROND 2001-06E, ONDRAF/NIRAS, Belgium.
- Osterholtz H, Turner S, Alakangas L J, Tullborg E-L, Dittmar T, Kalinowski B E, Dopson M, 2022.** Terrigenous dissolved organic matter persists in the energy limited deep groundwaters of the Fennoscandian Shield. *Nature communications* 13:4837 <https://doi.org/10.1038/s41467-022-32457-z>
- Oversby V M, 1996.** Criticality in a high level waste repository. A review of some important factors and an assessment of the lessons that can be learned from the Oklo reactors. SKB TR 96-07, Svensk Kärnbränslehantering AB.
- Oversby V M, 1998.** Criticality in a repository for spent fuel: lessons from Oklo. In McKinley I G, McCombie C (eds). *Scientific basis for nuclear waste management XXI: symposium held in Davos, Switzerland, 23 September – 3 October 1997*. Warrendale, PA: Materials Research Society. (Materials Research Society Symposium Proceedings 506), 781.
- Painter S, Mancillas J, 2009.** MARFA version 3.2.2 user's manual: migration analysis of radionuclides in the far-field. SKB R-09-56, Svensk Kärnbränslehantering AB.
- Painter S, Cvetkovic V, Mancillas J, Pensado O, 2008.** Time domain particle tracking methods for simulating transport with retention and first-order transformation. *Water Resources Research* 44, W01406. doi:10.1029/2007WR005944

- Parkhurst D L, Appelo C A J, 1999.** User's guide to PHREEQC (version 2): a computer program for speciation, batch-reaction, one-dimensional transport, and inverse geochemical calculations. Denver, CO: U.S. Geological Survey. (Water-resources investigations report 99-4259.)
- Parkhurst D L, Kipp K L, Engesgaard P, Charlton S R, 2004.** PHAST: a program for simulating groundwater flow, solute transport, and multicomponent geochemical reactions. U.S. Geological Survey Techniques and Methods 6-A8. Denver, CO: U.S. Geological Survey.
- Paterson W S B, 1994.** The physics of glaciers. 3rd ed. Oxford: Pergamon.
- Pattyn F, De Smedt B, Souchez R, 2004.** Influence of subglacial Vostok lake on the regional dynamics of the Antarctic ice sheet: a model study. *Journal of Glaciology* 50, 583–589.
- Payne A J, Huybrechts P, Abe-Ouchi A, Calov R, Fastook J L, Greve R, Marshall S J, Marsiat I, Ritz C, Tarasov L, Thomassen M P A, 2000.** Results from the EISMINT model intercomparison: the effects of thermomechanical coupling. *Journal of Glaciology* 46, 227–238.
- Pedersen K, 2006.** Microbiology of transitional groundwater of the porous overburden and underlying fractured bedrock aquifers in Olkiluoto, Finland. Posiva Working Report 2006-09, Posiva Oy, Finland.
- Pedersen K, 2010.** Analysis of copper corrosion in compacted bentonite clay as a function of clay density and growth conditions for sulfate-reducing bacteria. *Journal of Applied Microbiology* 108, 1094–1104.
- Pedersen K, 2012.** Subterranean microbial populations metabolize hydrogen and acetate under *in situ* conditions in granitic groundwater at 450 m depth in the Äspö Hard Rock Laboratory, Sweden. *FEMS Microbiology Ecology* 81, 217–229.
- Pedersen K, Kennedy C, Nederfeldt K-G, Bergelin A, 2004.** Äspö Hard Rock Laboratory. Prototype repository. Chemical measurements in buffer and backfill; sampling and analyses of gases. SKB IPR-04-26, Svensk Kärnbränslehantering AB.
- Pellikka H, Särkkää J, Johansson M, Pettersson H, 2020.** Probability distributions for mean sea level and storm contribution up to 2100 AD at Forsmark. SKB TR-19-23, Svensk Kärnbränslehantering AB.
- Penny R K, Marriott D L, 1995.** Design for creep. 2nd ed. London: Chapman & Hall.
- Pers K, Skagius K, Södergren S, Wiborgh M, Hedin A, Morén L, Sellin P, Ström A, Pusch R, Bruno J, 1999.** SR 97 – Identification and structuring of process. SKB TR-99-20, Svensk Kärnbränslehantering AB.
- Persson J, Lydmark S, Edlund J, Pääjärvi A, Pedersen K, 2011.** Microbial incidence on copper and titanium embedded in compacted bentonite clay. SKB R-11-22, Svensk Kärnbränslehantering AB.
- Pettersson K, 2016.** An updated review of the creep ductility of copper including the effect of phosphorus. Report 2016:02, Swedish Radiation Safety Authority.
- Pont A, Coene E, Idiart A, 2020.** Bentonite erosion project Preliminary study for the numerical simulation of bentonite erosion SKB P-20-16, Svensk Kärnbränslehantering AB.
- Porcelli D, Andersson P S, Baskaran M, Wasserburg G J, 2001.** Transport of U- and Th-series in a Baltic shield watershed and the Baltic Sea. *Geochimica et Cosmochimica Acta* 65, 2439–2459.
- Pourbaix M, 1974.** Atlas of electrochemical equilibria in aqueous solutions. 2nd ed. Houston, TX: NACE International.
- Posiva, 2012.** Safety case for the disposal of spent nuclear fuel at Olkiluoto – Description of the disposal system 2012. Posiva 2012-05, Posiva Oy, Finland.
- Posiva, 2021.** Operating Licence Application, Spent Nuclear Fuel Encapsulation Plant and Disposal Facility. Posiva Oy, Finland. Formal licence application presented to the Ministry of Economic Affairs and Employment (TEM) in Finland. Accessible via the following: Application for operating licence – Ministry of Economic Affairs and Employment (tem.fi).
- Posiva SKB, 2017.** Safety functions, performance targets and technical design requirements for a KBS-3V repository. Conclusions and recommendations from a joint SKB and Posiva working group. Posiva SKB Report 01, Posiva Oy, Svensk Kärnbränslehantering AB.

- Puidgomenech I, 2013.** Jämförelser av beräknade haltintervall som funktion av djup i berget med kocationern som uppmätts under platsundersökningarna. SKBdoc 1396705 ver 1.0, Svensk Kärnbränslehantering AB. (In Swedish.)
- Puidgomenech I, Ambrosi J-P, Eisenlohr L, Lartigue J-E, Banwart S A, Bateman K, Milodowski A E, West J M, Griffault L, Gustafsson E, Hama K, Yoshida H, Kotelnikova S, Pedersen K, Michaud V, Trotignon L, Rivas Perez J, Tullborg E-L, 2001.** O₂ depletion in granitic media. The REX project. SKB TR-01-05, Svensk Kärnbränslehantering AB.
- Pusch R, 1983.** Stability of deep-sited smectite minerals in crystalline rock – chemical aspects. SKBF/KBS TR 83-16, Svensk Kärnbränsleförsörjning AB.
- Pusch R, 2000a.** On the effect of hot water vapor on MX-80 clay. SKB TR-00-16, Svensk Kärnbränslehantering AB.
- Pusch R, 2000b.** On the risk of liquefaction of buffer and backfill. SKB TR-00-18, Svensk Kärnbränslehantering AB.
- Pusch R, Karnland O, 1988.** Geological evidence of smectite longevity. The Sardinian and Gotland cases. SKB TR 88-26, Svensk Kärnbränslehantering AB.
- Pusch R, Hiroyasu T, Steven B, 1998.** Chemical processes causing cementation in heat-affected smectite – the Kinnekulle bentonite. SKB TR-98-25, Svensk Kärnbränslehantering AB.
- Påsse T, Daniels J, 2015.** Past shore-level and sea-level displacements. Uppsala: Sveriges geologiska undersökning. (Rapporter och meddelanden 137.)
- Quiquet A, Colleoni F, Masina S, 2016.** Long-term safety of a planned geological repository for spent nuclear fuel in Forsmark, Sweden and Olkiluoto, Finland. Phase 2: impact of ice sheet dynamics, climate forcing and multi-variate sensitivity analysis on maximum ice sheet thickness. SKB TR-16-02, Svensk Kärnbränslehantering AB.
- Raiko H, Sandström R, Rydén H, Johansson M, 2010.** Design analysis report for the canister. SKB TR-10-28, Svensk Kärnbränslehantering AB.
- Railo A, Laitinen I (ed), Mustonen S, Kosunen P, Joutsen A, Ikonen A, Hollmen K, Nuijten G, 2016.** Design and construction of equipment and experimental deposition holes, in ONKALO Demonstration Tunnel 2. Posiva Working Report 2016-27, Posiva Oy, Finland.
- Railo A, Laitinen I (eds), Mustonen S, Kosunen P, Joutsen A, Mellanen S, Ikonen A, Nuijten G, 2017.** Design and construction of equipment and experimental deposition holes, in ONKALO Demonstration Tunnel 1. Posiva Working Report 2015-25, Posiva Oy, Finland.
- RETROCK, 2005.** Treatment of radionuclide transport in geosphere within safety assessments. Final report of the RETROCK Concerted Action. EUR 21230, European Commission.
- Ritchey T, 1997.** Scenario development and risk management using morphological field analysis. In Proceedings of the 5th European Conference on Information Systems. Cork: Cork Publishing Company, Vol 3, 1053–1059.
- Roberts M J, Russell A J, Tweed F S, Knudsen O, 2000.** Ice fracturing during jökulhlaups: implications for englacial floodwater routing and outlet development. *Earth Surface Processes and Landforms* 25, 1429–1446.
- Romero A L, 1995.** The near-field transport in a repository for high-level nuclear waste. PhD thesis. Department of Chemical Engineering and Technology, Royal Institute of Technology, Stockholm, Sweden.
- Romero L, Thompson A, Moreno L, Neretnieks I, Widén H, Boghammar A, 1999.** Comp23/ Nucltran user's guide. Proper version 1.1.6. SKB R-99-64, Svensk Kärnbränslehantering AB.
- Rosborg B, 2013.** Post-test examination of a copper electrode from deposition hole 5 in the Prototype Repository. SKB R-13-14, Svensk Kärnbränslehantering AB.
- Ruiz López C, Rodríguez J, Hernán P, Recreo F, Ruiz C, Prado P, Gimeno M J, Auqué L F, Gómez J, Acero P, González Á, Samper J, Montenegro L, Molinero J, Delgado J, Criado A, Martínez J A, Ruiz S, 2004.** Analogue application to safety assessment and communication of radioactive geological disposal. Illustrative synthesis. Colección Documentos I+D 11.2004, Consejo de Seguridad Nuclear, Madrid.

- Ruskeeniemi T, Ahonen L, Paananen M, Frapé S, Stotler R, Hobbs M, Kaija J, Degnan P, Blomqvist R, Jensen M, Lehto K, Moren L, Puigdomenech I, Snellman M, 2004.** Permafrost at Lupin: report of Phase II. Report YST-119, Geological Survey of Finland, Nuclear Waste Disposal Research.
- Salas J, Gimeno M J, Auqué L F, Molinero J, Gómez J, Juárez I, 2010.** SR-Site – hydrogeochemical evolution of the Forsmark site. SKB TR-10-58, Svensk Kärnbränslehantering AB.
- Saltelli A, Andres T H, Homma T, 1993.** Sensitivity analysis of model output: an investigation of new techniques. *Computational Statistics & Data Analysis* 15, 211–238.
- Saltelli A, Chan K, Scott E M (eds), 2000.** Sensitivity analysis. Chichester: Wiley.
- Sánchez M, Gens A, 2006.** FEBEX Project, Final report, Final report on thermo-hydro-mechanical modelling. ENRESA publicación técnica 05-2/2006, ENRESA, Spain.
- Sandén T, Börgesson L, 2010.** Early effect of water inflow into a deposition hole. Laboratory test results. SKB R-10-70, Svensk Kärnbränslehantering AB.
- Sandén T, Börgesson L, Dueck A, Goudarzi R, Lönnqvist M, 2008.** Deep repository-Engineered barrier system. Erosion and sealing processes in tunnel backfill materials investigated in laboratory. SKB R-08-135, Svensk Kärnbränslehantering AB.
- Sandén T, Olsson S, Andersson L, Dueck A, Jensen V, Hansen E, Johnsson A, 2014.** Investigation of backfill candidate materials. SKB R-13-08, Svensk Kärnbränslehantering AB.
- Sandén T, Andersson L, Jensen V, 2015.** System design of backfill. Full scale production test of backfill blocks. SKB P-14-24, Svensk Kärnbränslehantering AB.
- Sandén T, Nilsson U, Andersson L, 2016.** Investigations of parameters influencing bentonite block quality. Laboratory investigation. SKB P-16-06, Svensk Kärnbränslehantering AB.
- Sandén T, Börgesson L, Nilsson U, Dueck A, 2017.** Full scale buffer swelling test at dry backfill conditions in Äspö HRL. In situ test and related laboratory tests. SKB TR-16-07, Svensk Kärnbränslehantering AB.
- Sandén T, Nilsson U, Johannesson L-E, Hagman P, Nilsson G, 2018a.** Sealing of investigation boreholes. Full scale field test and large-scale laboratory tests. SKB TR-18-18, Svensk Kärnbränslehantering AB.
- Sandén T, Marjavaara P, Fritzell A, 2018b.** Water handling during backfilling. Development report. Posiva SKB Report 05, Posiva Oy, Svensk Kärnbränslehantering AB.
- Sandén T, Kristensson O, Lönnqvist, Börgesson L, Nilsson U, Goudarzi R, 2020.** Buffer swelling. Laboratory tests and modelling. SKB TR-20-04, Svensk Kärnbränslehantering AB.
- Sandiford M, Wallace M, Coblentz D, 2004.** Origin of the *in situ* stress field in southeastern Australia. *Basin Research* 16, 325–338.
- Sandström B, Stephens M B, 2009.** Mineralogy, geochemistry, porosity and redox properties of rocks from Forsmark. Compilation of data from the regional model volume for SR-Site. SKB R-09-51, Svensk Kärnbränslehantering AB.
- Sandström B, Tullborg E-L, Smellie J, MacKenzie A B, Suksi J, 2008.** Fracture mineralogy of the Forsmark site. SDM-Site Forsmark. SKB R-08-102, Svensk Kärnbränslehantering AB.
- Sandström B, Tullborg E-L, Larsson S Å, Page L, 2009.** Brittle tectonothermal evolution in the Forsmark area, central Fennoscandian Shield, recorded by paragenesis, orientation and $^{40}\text{Ar}/^{39}\text{Ar}$ geochronology of fracture minerals. *Tectonophysics* 478, 158–174.
- Sandström, R, 1999.** Extrapolation of creep strain data for pure copper. *Journal of Testing and Evaluation* 27, 31–35.
- Sandström R, 2012.** Basic model for primary and secondary creep in copper. *Acta Materialia* 60, 314–322.
- Sandström R, 2016.** The role of cell structure during creep of cold worked copper. *Materials Science and Engineering: A* 674, 318–327.

- Sandström R, 2017.** Fundamental models for the creep of metals. In Tanski T (ed). Creep. InTech.
- Sandström R, Wu R, 2013.** Influence of phosphorus on creep ductility of copper. *Journal of Nuclear Materials* 441, 364–371.
- Sandström R, Wu R, Hagström J, 2016.** Grain boundary sliding in copper and its relation to cavity formation during creep. *Materials Science and Engineering: A* 65, 259–268.
- Sandström R, Lousada C M, 2021.** The role of binding energies for phosphorus and sulphur at grain boundaries in copper. *Journal of Nuclear Materials* 544, 152682. doi:10.1016/j.jnucmat.2020.152682
- Schatz T, Akhanoba N, 2017.** Buffer erosion in sloped fracture environments. Posiva 2016-13, Posiva Oy, Finland.
- Schatz T, Kanerva N, Martikainen J, Sane P, Olin M, Seppälä A, Koskinen K, 2013.** Buffer erosion in dilute groundwater. Posiva 2012-44, Posiva Oy, Finland.
- Scherneck H-G, Lidberg M, Haas R, Johansson J M, Milne G A, 2010.** Fennoscandian strain rates from BIFROST GPS: a gravitating, thick-plate approach. *Journal of Geodynamics* 50, 19–26.
- Scholz C H, 2002.** The mechanics of earthquakes and faulting. 2nd ed. Cambridge: Cambridge University Press.
- Sellin P, 2013a.** Interaktion mellan kopparkorrosionsprodukter och bentonit. SKBdoc 1416862 ver 1.0, Svensk Kärnbränslehantering AB. (In Swedish.)
- Sellin P, 2013b.** Svar till SSM på begäran om komplettering rörande kemisk erosion av buffert. SKBdoc 1385068 ver 1.0, Svensk Kärnbränslehantering AB. (In Swedish.)
- Sellin P, Hedin A, 2013.** Svar till SSM på begärna om komplettering rörande vätagstransport i slutförvaret. SKBdoc 1385070 ver 1.0, Svensk Kärnbränslehantering AB. (In Swedish.)
- Sellin P (ed), Åkesson M, Kristensson O, Malmberg D, Börgesson L, Birgersson M, Dueck A, Karnland O, Hernelind J, 2017.** Long re-saturation phase of a final repository. Additional supplementary information. SKB TR-17-15, Svensk Kärnbränslehantering AB.
- Selroos J-O, Follin S, 2010.** Groundwater flow modelling methodology, setup and results. SKB R-09-22, Svensk Kärnbränslehantering AB.
- Selroos J-O, Walker D D, Ström A, Gylling B, Follin S, 2002.** Comparison of alternative modelling approaches for groundwater flow in fractured rock. *Journal of Hydrology* 257, 174–188.
- Sena C, Salas J, Arcos D, 2010a.** Thermo-hydro-geochemical modelling of the bentonite buffer. LOT-A2 experiment. SKB TR-10-65, Svensk Kärnbränslehantering AB.
- Sena C, Salas J, Arcos D, 2010b.** Aspects of geochemical evolution of the SKB near-field in the frame of SR-Site. SKB TR-10-59, Svensk Kärnbränslehantering AB.
- Sipilä K, Arilahti E, Lehtikuusi T, Saario T, 2014.** Effect of sulphide exposure on mechanical properties of CuOFP. *Corrosion Engineering, Science and Technology* 49, 410–414.
- Shen Y, Chapelle F H, Strom E W, Benner R, 2015.** Origins and bioavailability of dissolved organic matter in groundwater. *Biogeochemistry* 122, 61–78.
- Sidborn M, Neretnieks I, 2003.** Modelling of biochemical processes in rocks: Oxygen depletion by pyrite oxidation: model development and exploratory simulations. In Finch R J, Bullen D B (eds). *Scientific basis for nuclear waste management XXVI*. Warrendale, PA: Materials Research Society. (Materials Research Society Symposium Proceedings 757), 553–558.
- Sidborn M, Neretnieks I, 2004.** Modelling biochemical processes in rocks: Analysis and exploratory simulationsof competition of different processes important for ferrous mineral oxidation and oxygen depletion. In Oversby V M, Werme L O (eds). *Scientific basis for nuclear waste management XXVII: symposium held in Kalmar, Sweden, 15–19 June 2003*. Warrendale, PA: Materials Research Society. (Materials Research Society Symposium Proceedings 807), 829–834.
- Sidborn M, Neretnieks I, 2008.** Long-term oxygen depletion from infiltrating groundwaters: model development and application to intra-glaciation and glaciation conditions. *Journal of Contaminant Hydrology* 100, 72–89.

- Sidborn M, Sandström B, Tullborg E-L, Delos A, Molinero J, Hallbeck L, Pedersen K, 2010.** SR-Site: Oxygen ingress in the rock at Forsmark during a glacial cycle. SKB TR-10-57, Svensk Kärnbränslehantering AB.
- Sidborn M, Marsic N, Crawford J, Joyce S, Hartley L, Idiart A, de Vries L M, Maia F, Molinero J, Svensson U, Vidstrand P, Alexander R, 2014.** Potential alkaline conditions for deposition holes of a repository in Forsmark as a consequence of OPC grouting. Revised final report after review. SKB-R-12-17, Svensk Kärnbränslehantering AB.
- Silver W L, Lugo A E, Keller M, 1999.** Soil oxygen availability and biogeochemistry along rainfall and topographic gradients in upland wet tropical forest soils. *Biogeochemistry* 44, 301–328.
- Skagius K, Wingefors S, 1992.** Scenarios. Application of scenario development methods in evaluation of the Koongarra analogue. Alligator Rivers Analogue Project, final report. Vol. 16. An OECD/NEA International Project Managed by ANSTO. SKI Report 92:20-16, Swedish Nuclear Power Inspectorate.
- Skagius K, Ström A, Wiborgh M, 1995.** The use of interaction matrices for identification, structuring and ranking of FEPs in a repository system. Application on the far-field of a deep geological repository for spent fuel. SKB TR 95-22, Svensk Kärnbränslehantering AB.
- SKB, 1990.** Granskning av Nils-Axel Mörnerns arbeten avseende postglaciala strukturer på Äspö. SKB AR 90-18, Svensk Kärnbränslehantering AB. (In Swedish.)
- SKB, 1992.** SKB 91 – Final disposal of spent nuclear fuel. Importance of the bedrock for safety. SKB TR 92-20, Svensk Kärnbränslehantering AB.
- SKB, 1995.** SR 95. Template for safety reports with descriptive example. SKB TR 96-05, Svensk Kärnbränslehantering AB.
- SKB, 1999a.** Deep repository for spent nuclear fuel. SR 97 – Post-closure safety. Main report – Vol I, Vol II and Summary. SKB TR-99-06, Svensk Kärnbränslehantering AB.
- SKB, 1999b.** SR 97 – Processes in the repository evolution. Background report to SR 97. SKB TR-99-07, Svensk Kärnbränslehantering AB.
- SKB, 2001.** RD&D-Programme 2001 Programme for research, development and demonstration of methods for the management and disposal of nuclear waste. SKB TR-01-30, Svensk Kärnbränslehantering AB.
- SKB, 2004a.** Interim main report of the safety assessment SR-Can. SKB TR-04-11, Svensk Kärnbränslehantering AB.
- SKB, 2004b.** RD&D-Programme 2004. Programme for research, development and demonstration of methods for the management and disposal of nuclear waste, including social science research. SKB TR-04-21, Svensk Kärnbränslehantering AB.
- SKB, 2006a.** Long-term safety for KBS-3 repositories at Forsmark and Laxemar – a first evaluation. Main report of the SR-Can project. SKB TR-06-09, Svensk Kärnbränslehantering AB.
- SKB, 2006b.** FEP report for the safety assessment SR-Can. SKB TR-06-20, Svensk Kärnbränslehantering AB.
- SKB, 2006c.** Climate and climate-related issues for the safety assessment SR-Can. SKB TR-06-23, Svensk Kärnbränslehantering AB.
- SKB, 2006d.** Geosphere process report for the safety assessment SR-Can. SKB TR-06-19, Svensk Kärnbränslehantering AB.
- SKB, 2006e.** Handling of future human actions in the safety assessment SR-Can. SKB TR-06-24, Svensk Kärnbränslehantering AB.
- SKB 2006f.** Buffer and backfill process report for the safety assessment SR-Can. SKB TR-06-18, Svensk Kärnbränslehantering AB.
- SKB, 2006g.** The biosphere at Forsmark. Data assumptions and models used in the SR-Can assessment. SKB R-06-82, Svensk Kärnbränslehantering AB.
- SKB, 2008a.** Site description of Forsmark at completion of the site investigation phase. SDM-Site Forsmark. SKB TR-08-05, Svensk Kärnbränslehantering AB.

SKB, 2008b. Confidence assessment. Site descriptive modeling, SDM-Site Forsmark. SKB R-08-82, Svensk Kärnbränslehantering AB.

SKB, 2009a. Design premises for a KBS-3V repository based on the results from the safety assessment SR-Can and some subsequent analyses. SKB TR-09-22, Svensk Kärnbränslehantering AB.

SKB, 2009b. Underground design Forsmark. Layout D2. SKB R-08-116, Svensk Kärnbränslehantering AB.

SKB, 2009c. Site engineering report Forsmark. Guidelines for underground design. Step D2. SKB R-08-83, Svensk Kärnbränslehantering AB.

SKB, 2010a. Miljökonsekvensbeskrivning (MKB). Mellanlagring, inkapsling och slutförvaring av använt kärnbränsle. Svensk Kärnbränslehantering AB. (In Swedish.)

SKB, 2010b. Ramprogram för detaljundersökningar vid uppförande och drift av slutförvar för använt kärnbränsle. SKB R-10-08, Svensk Kärnbränslehantering AB. (In Swedish.)

SKB, 2010c. Components, processes and interactions in the biosphere. SR-Site Biosphere. SKB R-10-37, Svensk Kärnbränslehantering AB.

SKB, 2010d. Corrosion calculations report for the safety assessment SR-Site. SKB TR-10-66, Svensk Kärnbränslehantering AB.

SKB, 2010e. Spent nuclear fuel for disposal in the KBS-3 repository. SKB TR-10-13, Svensk Kärnbränslehantering AB.

SKB, 2010f. Radionuclide transport report for the safety assessment SR-Site. SKB TR-10-50, Svensk Kärnbränslehantering AB.

SKB, 2010g. Climate and climate-related issues for the safety assessment SR-Site. SKB TR-10-49, Svensk Kärnbränslehantering AB.

SKB, 2010h. Data report for the safety assessment SR-Site. SKB TR-10-52, Svensk Kärnbränslehantering AB.

SKB, 2011. Long-term safety for the final repository for spent nuclear fuel at Forsmark. Main report of the SR-Site project. SKB TR-11-01, Svensk Kärnbränslehantering AB.

SKB, 2012. Svar till SSM på begäran om komplettering avseende degraderingsprocesser för kapseln. SKBdoc 1398013 ver 4.0, Svensk Kärnbränslehantering AB. (In Swedish.)

SKB, 2013a. Responses to SSM on hydrogeology. SKBdoc 1396325 ver 1.0. Svensk Kärnbränslehantering AB.

SKB, 2013b. Svar till SSM på begäran om komplettering rörande osäkerheter i hydro-geologiska beräkningar. SKBdoc 1396324 ver 2.0, Svensk Kärnbränslehantering AB. (In Swedish.)

SKB, 2013c. Responses to SSM on uncertainties in hydro-geological calculations, Question 1. SKBdoc 1416510 ver 1.0, Svensk Kärnbränslehantering AB.

SKB, 2013d. Response to SSM on Hydrogeological conditions during glacial effects. SKBdoc 1416954 ver 1.0, Svensk Kärnbränslehantering AB.

SKB, 2014a. Svar till SSM på begäran om komplettering rörande grundvattenkemi på kort och medellång sikt. SKBdoc 1437441 ver 1.0, Svensk Kärnbränslehantering AB. (In Swedish.)

SKB, 2014b. Climate and climate-related issues for the safety assessment SR-PSU. SKB TR-13-05, Svensk Kärnbränslehantering AB.

SKB, 2014c. Svar till SSM på begäran om förtydligande om nedträngning av utspädda vatten. SKBdoc 1448717 ver 1.0, Svensk Kärnbränslehantering AB. (In Swedish.)

SKB, 2014d. Biosphere synthesis report for the safety assessment SR-PSU. SKB TR-14-06, Svensk Kärnbränslehantering AB.

SKB, 2018. Kärnbränsleförvaret – Referensutformning PSAR. SKBdoc 1178459 ver 5.0, Svensk Kärnbränslehantering AB. (In Swedish.) (Internal document.)

- SKB, 2019a.** Biosphere synthesis for the safety evaluation SE-SFL. SKB TR-19-05, Svensk Kärnbränslehantering AB.
- SKB, 2019b.** RD&D Programme 2019. Programme for research, development and demonstration of methods for the management and disposal of nuclear waste. SKB TR-19-24, Svensk Kärnbränslehantering AB.
- SKB, 2019c.** Supplementary information on canister integrity issues. SKB TR-19-15, Svensk Kärnbränslehantering AB.
- SKB, 2020a.** Post-closure safety for the final repository for spent nuclear fuel at Forsmark – Climate and climate-related issues, PSAR version. SKB TR-20-12, Svensk Kärnbränslehantering AB.
- SKB, 2020b.** Säkerhet i program Kärnbränsleförvaret (SIP-K). SKBdoc 1698455 ver 1.0, Svensk Kärnbränslehantering AB. (In Swedish.) (Internal document.)
- SKB, 2021a.** Hantering av använt kärnbränsle inom KBS-3-systemet. SKBdoc 1380283 ver 2.0, Svensk Kärnbränslehantering AB. (In Swedish.) (Internal document.)
- SKB, 2021b.** Kärnbränsleförvaret PSAR – Konstruktionsförutsättningar för barriärer efter förslutning och koppling till säkerhetsfunktioner efter förslutning. SKBdoc 1931046 ver 1.0, Svensk Kärnbränslehantering AB. (In Swedish.) (Internal document.)
- SKBF/KBS, 1977.** KBS 1 – Kärnbränslecykelns slutsteg. Förglasat avfall från upparbetning, II Geologi. Svensk Kärnbränsleförsörjning AB. (In Swedish.)
- SKBF/KBS, 1983a.** Kärnbränslecykelns slutsteg. Använt kärnbränsle – KBS-3. Del I–IV. Svensk Kärnbränsleförsörjning AB. (In Swedish.)
- SKBF/KBS, 1983b.** KBS 3 – Final storage of spent nuclear fuel – KBS-3, II Geology. Svensk Kärnbränsleförsörjning AB.
- Slunga R S, 1991.** The Baltic Shield earthquakes. *Tectonophysics* 189, 323–331.
- Smellie J, 2001.** Wyoming bentonites. Evidence from the geological record to evaluate the suitability of bentonite as a buffer material during the long-term underground containment of radioactive wastes. SKB TR-01-26, Svensk Kärnbränslehantering AB.
- Smellie J, Karlsson F (eds), 1996.** A reappraisal of some Cigar Lake issues of importance to performance assessment. SKB TR 96-08, Svensk Kärnbränslehantering AB.
- Smith P, Johnson L, Snellman M, Pastina B, Gripi P, 2008.** Safety assessment for a KBS-3H spent nuclear fuel repository at Olkiluoto. Evolution report. SKB R-08-37, Svensk Kärnbränslehantering AB.
- Sobol' I, 1993.** Sensitivity analysis for non-linear mathematical models. *Mathematical Modeling & Computational Experiment (Engl. Transl.)* 1, 407–414.
- Spießl S M, MacQuarrie K T B, Mayer K U, 2008.** Identification of key parameters controlling dissolved oxygen migration and attenuation in fractured crystalline rocks. *Journal of Contaminant Hydrology* 95, 141–153.
- SSI, 2007.** Strålmiljön i Sverige. SSI Rapport 2007:02, Swedish Radiation Protection Authority. (In Swedish.)
- SSM, 2008a.** Strålsäkerhetsmyndighetens föreskrifter och allmänna råd om säkerhet vid slutförvaring av kärnämne och kärnavfall (The Swedish Radiation Safety Authority's Regulations concerning Safety in connection with the Disposal of Nuclear Material and Nuclear Waste). Stockholm: Swedish Radiation Safety Authority. (SSMFS 2008:21) (In Swedish.)
- SSM, 2008b.** Strålsäkerhetsmyndighetens föreskrifter och allmänna råd om skydd av människors hälsa och miljön vid slutligt omhändertagande av använt kärnbränsle och kärnavfall (The Swedish Radiation Safety Authority's Regulations on the Protection of Human Health and the Environment in connection with the Final Management of Spent Nuclear Fuel and Nuclear Waste). Stockholm: Swedish Radiation Safety Authority. (SSMFS 2008:37) (In Swedish.)
- SSM, 2014.** Granskning och utvärdering av SKB:s redovisning av Fud-program 2013. Report 2014:12, Swedish Radiation Safety Authority. (In Swedish.)

- SSM, 2017.** Granskning och utvärdering av SKB:s redovisning av Fud-program 2016. Report 2017:17, Swedish Radiation Safety Authority. (In Swedish.)
- SSM, 2018.** Strålsäkerhet efter slutförvarets förslutning. Beredning inför regeringens prövning. Report 2018:07, Swedish Radiation Safety Authority. (In Swedish.)
- SSM, 2019.** Granskningsrapport – Utbyggnad och fortsatt drift av SFR. Report 2019:18, Swedish Radiation Safety Authority. (In Swedish.)
- SSM, 2020.** Granskning och utvärdering av Fud-program 2019. SSM2018-5179-9, Swedish Radiation Safety Authority. (In Swedish.)
- Stahlén J, 2018.** Exposure of copper to sulphate reducing bacteria and verification of a biofilm. Batch 1. SKBdoc 1701925 ver 1.0, Svensk Kärnbränslehantering AB.
- Stanfors R, Ericsson L O, 1993.** Post-glacial faulting in the Lansjärv area, Northern Sweden. Comments from the expert group on a field visit at the Molberget post-glacial fault area, 1991. SKB TR 93-11, Svensk Kärnbränslehantering AB
- Stephens M B, Fox A, La Pointe P, Simeonov A, Isaksson H, Hermanson J, Öhman J, 2007.** Geology Forsmark. Site descriptive modelling Forsmark stage 2.2. SKB R-07-45, Svensk Kärnbränslehantering AB.
- Stephens M B, Bergman T, Isaksson H, Petersson J, 2008a.** Bedrock geology Forsmark. Modelling stage 2.3. Description of the bedrock geological map at the ground surface. SKB R-08-128, Svensk Kärnbränslehantering AB.
- Stephens M B, Simeonov A, Isaksson H, 2008b.** Bedrock geology Forsmark. Modelling stage 2.3. Implications for and verification of the deterministic geological models based on complementary data. SKB R-08-64, Svensk Kärnbränslehantering AB.
- Stotler R L, Frappe S K, Ruskeeniemi T, Ahonen L, Onstott T C, Hobbs M Y, 2009a.** Hydrogeochemistry of groundwaters in and below the base of thick permafrost at Lupin, Nunavut, Canada. *Journal of Hydrology* 373, 80–95.
- Stotler R L, Frappe S K, Ruskeeniemi T, Ahonen L, Paananen M, Hobbs M Y, Lambie K E, Zhang M, 2009b.** Hydrochemistry of groundwaters at and below the base of the permafrost at Lupin: report of Phase III. NWMO TR-2009-10, Nuclear Waste Management Organisation, Canada.
- Strömngren M, Brydsten L, 2008.** Digital elevation models of Forsmark. Site descriptive modelling, SDM-Site Forsmark. SKB R-08-62, Svensk Kärnbränslehantering AB.
- Sui F, Sandström R, 2018.** Basic modelling of tertiary creep of copper. *Journal of Materials Science* 53, 6850–6863.
- STUK, 2014.** Disposal of nuclear waste. Guide YVL D5. STUK (Radiation and Nuclear Safety Authority), Finland.
- Svendsen J I, Astakhov V I, Bolshiyarov D Y, Demidov I, Dowdeswell J A, Gataullin V, Hjort C, Hubberten H W, Larsen E, Mangerud J, Melles M, Möller P, Saarnisto M, Siegert M J, 1999.** Maximum extent of the Eurasian ice sheets in the Barents and Kara Sea region during the Weichselian. *Boreas* 28, 234–242.
- Svendsen J I, Alexanderson H, Astakhov V I, Demidov I, Dowdeswell J A, Funder S, Gataullin V, Henriksen M, Hjort C, Houmark-Nielsen M, Hubberten H W, Ingólfsson O, Jakobsson M, Kjær K H, Larsen E, Lokrantz H, Lunkka J P, Lyså A, Mangerud J, Matiouchkov A, Murray A, Moller P, Niessen F, Nikolskaya O, Polyak L, Saarnisto M, Siegert C, Siegert M J, Spielhagen R F, Stein R, 2004.** Late Quaternary ice sheet history of northern Eurasia. *Quaternary Science Reviews* 23, 1229–1271.
- Svensson D, Dueck A, Nilsson U, Olsson S, Sandén T, Lydmark S, Jägerwall S, Pedersen K, Hansen S, 2011.** Alternative buffer material. Status of the ongoing laboratory investigation of reference materials and test package 1. SKB TR-11-06, Svensk Kärnbränslehantering AB.
- Svensson D, Lundgren C, Johannesson L-E, Norrfors K, 2017.** Developing strategies for acquisition and control of bentonite for a high level radioactive waste repository. SKB TR-16-14, Svensk Kärnbränslehantering AB.

- Svensson D, Eriksson P, Johannesson, L-E, Lundgren C, Bladström T, 2019.** Development and testing of methods suitable for quality control of bentonites as KBS-3 buffer and backfill. SKB TR-19-25, Svensk Kärnbränslehantering AB.
- Svensson D, Kalinowski B, Turner S, Dopson M, 2020.** Activity of sulphate reducing bacteria in bentonite as a function of water availability. SKB TR-20-08, Svensk Kärnbränslehantering AB.
- Svensson U, Follin S, 2010.** Groundwater flow modelling of the excavation and operation phases – SR-Site Forsmark. SKB R-09-19, Svensk Kärnbränslehantering AB.
- Svensson U, Ferry M, Kuylenstierna H-O, 2010.** DarcyTools, Version 3.4. Concepts, methods and equations. SKB R-07-38, Svensk Kärnbränslehantering AB.
- Söderbäck B (ed), 2008.** Geological evolution, palaeoclimate and historical development of the Forsmark and Laxemar-Simpevarp areas. Site descriptive modelling. SDM-Site. SKB R-08-19, Svensk Kärnbränslehantering AB.
- Talbot C J, 1999.** Ice ages and nuclear waste isolation. *Engineering Geology* 52, 177–192.
- Taniguchi N, Kawasaki M, 2008.** Influence of sulfide concentration on the corrosion behavior of pure copper in synthetic seawater. *Journal of Nuclear Materials* 379, 154–161.
- Taxén C, Sparr M, 2014.** Corrosion properties of copper materials. SKB R-14-15, Svensk Kärnbränslehantering AB.
- Taxén, C, Flyg J, Bergqvist H, 2018.** Stress corrosion testing of copper in sulfide solutions. SKB TR-17-16, Svensk Kärnbränslehantering AB.
- Taxén C, Flyg J, Bergqvist H, 2019.** Stress corrosion testing of copper in near neutral sulfide solutions. SKB TR-19-13, Svensk Kärnbränslehantering AB.
- Terzaghi R D, 1965.** Sources of error in joint surveys. *Géotechnique* 15, 287–304.
- Tohidi B, Chapoy A, Smellie J, Puigdomenech I, 2010.** The potential for methane hydrate formation in deep repositories of spent nuclear fuel in granitic rocks. SKB R-10-58, Svensk Kärnbränslehantering AB.
- Torudd J, 2010.** Long-term radiological effects on plants and animals of a deep geological repository. SR-Site Biosphere. SKB TR-10-08, Svensk Kärnbränslehantering AB.
- Tröjbom M, Grolander S, 2010.** Chemical conditions in present and future ecosystems in Forsmark. Implications for selected radionuclides in the safety assessment SR-Site. SKB R-10-27, Svensk Kärnbränslehantering AB.
- Tullborg E-L, Smellie J, Nilsson A-C, Gimeno M J, Auqué L F, Brüchert V, Molinero J, 2010.** SR-Site – sulphide content in the groundwater at Forsmark. SKB TR-10-39, Svensk Kärnbränslehantering AB.
- Tushingham A M, Peltier W R, 1991.** ICE-3G: a new global model of late Pleistocene deglaciation based on geophysical predictions of post-glacial relative sea-level change. *Journal of Geophysical Research* 96, 4497–4523.
- Unosson, M, 2016.** Numerical simulation of earthquake induced rock shear through a deposition hole – Crack initiation and propagation in an insert with pre-existing intertubular and edge crack planes. SKBdoc 1474363 ver 1.0, Svensk Kärnbränslehantering AB.
- UNSCEAR, 2000.** Sources and effects of ionizing radiation: UNSCEAR 2000 report to the General Assembly with scientific annexes. Vol. I. Annex A: Dose assessment methodologies: New York: United Nations Scientific Committee on the Effects of Atomic Radiation.
- UNSCEAR, 2008.** Sources and effects of ionizing radiation: UNSCEAR 2008 report to the General Assembly with scientific annexes. Vol. I. Sources. New York: United Nations Scientific Committee on the Effects of Atomic Radiation.
- Vahlund F, Hermansson H, 2006.** Compulink. Implementing the COMP23 model in Simulink. SKB R-06-86, Svensk Kärnbränslehantering AB.

- Valentini G, Lombardi S, Bozzano F, Scarascia Mugnozza G (eds), 1997.** Analysis of the geo-environmental conditions as morphological evolution factors of the sand-clay series of the Tiber valley and Dunarobba forest preservation. EUR 17479, European Commission.
- van den Bos B, 2018.** Pre study of eddy current testing to detect forging laps on copper lids. SKBdoc 1531045 ver 1.0, Svensk Kärnbränslehantering AB.
- Van Konynenburg R A, 1995.** Comments on the draft paper “Underground supercriticality from plutonium and other fissile material” written by C. D. Bowman and F. Venneri (LANL). Report UCRL-ID-120990 COM, University of California.
- Velde B, Vasseur G, 1992.** Estimation of the diagenetic smectite to illite transformation in time-temperature space. *American Mineralogist* 77, 967–976.
- Vidstrand P, 2017.** Concept testing and site-scale groundwater flow modelling of the ice sheet marginal-area of the Kangerlussuaq region, Western Greenland. SKB R-15-01, Svensk Kärnbränslehantering AB.
- Vidstrand P, Svensson U, Follin S, 2006.** Simulation of hydrodynamic effects of salt rejection due to permafrost. Hydrogeological numerical model of density-driven mixing, at a regional scale, due to a high salinity pulse. SKB R-06-101, Svensk Kärnbränslehantering AB.
- Vidstrand P, Follin S, Zugec N, 2010.** Groundwater flow modelling of periods with periglacial and glacial climate conditions – Forsmark. SKB R-09-21, Svensk Kärnbränslehantering AB.
- Vieno T, Nordman H, 1999.** Safety assessment of spent fuel disposal in Hästholmen, Kivetty, Olkiluoto and Romuvaara TILA-99. Posiva 99-07, Posiva Oy, Finland.
- Vilks P, 2007.** Forsmark site investigation. Rock matrix permeability measurements on core samples from borehole KFM01D. SKB P-07-162, Svensk Kärnbränslehantering AB.
- Villar M V, Pérez del Villar L, Martín P L, Pelayo M, Fernández A M, Garralón A, Cuevas J, Leguey S, Caballero E, Huertas F J, Jiménez de Cisneros C, Linares J, Reyes E, Delgado A, Fernández-Soler J M, Astudillo J, 2006.** The study of Spanish clays for their use as sealing materials in nuclear waste repositories: 20 years of progress. *Journal of Iberian Geology* 32, 15–36.
- Waber H N, Gimmi T, Smellie J A T, 2009.** Porewater in the rock matrix. Site descriptive modelling, SDM-Site Forsmark. SKB R-08-105, Svensk Kärnbränslehantering AB.
- Waddington E D, 1987.** Geothermal heat flux beneath ice sheets. In Waddington E D, Walder J S (eds). *The physical basis of ice sheet modelling*. Wallingford, Oxfordshire: International Association of Hydrological Sciences. (IAHS Publication 170), 217–226.
- Wadham J L, Tranter M, Skidmore M, Hodson A J, Prisco J, Lyons W B, Sharp M, Wynn P, Jackson M, 2010.** Biogeochemical weathering under ice: size matters. *Global Biogeochemical Cycles* 24, GB3025. doi:10.1029/2009GB003688
- Walsh J J, Watterson J, 1987.** Distributions of cumulative displacement and seismic slip on a single normal fault surface. *Journal of Structural Geology* 9, 1039–1046.
- Walsh J J, Watterson J, 1989.** Displacement gradients on fault surfaces. *Journal of Structural Geology* 11, 307–316.
- Washburn A L, 1979.** *Geocryology: a survey of periglacial processes and environments*. 2nd ed. London: Arnold.
- Weertman J, 1957.** On the sliding of glaciers. *Journal of Glaciology* 3, 33–38.
- Werme L O, Johnson L H, Oversby V M, King F, Spahiu K, Grambow B, Shoesmith D W, 2004.** Spent fuel performance under repository conditions: a model for use in SR-Can. SKB TR-04-19, Svensk Kärnbränslehantering AB.
- Werner K, Hamrén U, Collinder P, 2010.** Vattenverksamhet i Forsmark (del I). Bortledning av grundvatten från slutförvarsanläggningen för använt kärnbränsle. SKB R-10-14, Svensk Kärnbränslehantering AB. (In Swedish.)
- Wersin P, Bruno J, Laaksoharju M, 1994.** The implications of soil acidification on a future HLW repository. Part II: Influence on deep granitic groundwater. The Klipperås study site as test case. SKB TR 94-31, Svensk Kärnbränslehantering AB.

- Wersin P, Alt-Epping P, Pitkänen P, Román-Ross G, Trincherro P, Molinero J, Smith P, Snellman M, Filby A, Kiczka M, 2014.** Sulphide fluxes and concentrations in the spent nuclear fuel repository at Olkiluoto. Posiva 2014-01, Posiva Oy, Finland.
- White A F, Brantley S L, 2003.** The effect of time on the weathering of silicate minerals: why do weathering rates differ in the laboratory and field? *Chemical Geology* 202, 479–506.
- White M, Scourfield S (eds), 2019.** Deliverable D6.5: Modern2020 Project synthesis. repository monitoring: strategies, technologies and implementation. Contract number: 622177. European Commission.
- Whitehouse P, 2009.** Glacial isostatic adjustment and sea-level change. State of the art report. SKB TR-09-11, Svensk Kärnbränslehantering AB.
- Wilmot R D, Wickham S M, Galson D A, 1999.** Elements of a regulatory strategy for the consideration of future human actions in safety assessments. SKI Report 99:46, Swedish Nuclear Power Inspectorate.
- Witt A, Schumann A Y, 2005.** Holocene climate variability on millennial scales recorded in Greenland ice cores. *Nonlinear Processes in Geophysics* 12, 345–352.
- Wold S, 2010.** Sorption of prioritized elements on montmorillonite colloids and their potential to transport radionuclides. SKB TR-10-20, Svensk Kärnbränslehantering AB.
- Wu R, Sandström R, 2018.** Influence of cold work and notches on creep failure of Cu-OFB. SKB R-15-04, Svensk Kärnbränslehantering AB.
- Wänstedt S, 2000.** Geophysical and geological investigations of the Boda area. SKB R-00-23, Svensk Kärnbränslehantering AB.
- Yang C, Samper J, Molinero J, Bonilla M, 2007.** Modelling geochemical and microbial consumption of dissolved oxygen after backfilling a high level radioactive waste repository. *Journal of Contaminant Hydrology* 93, 130–148.
- Yershov E D, 1998.** General geocryology. Cambridge: Cambridge University Press.
- Zheng L, Samper J, 2008.** A coupled THMC model of FEBEX mock-up test. *Physics and Chemistry of the Earth, Parts A/B/C* 33, 508–515.
- Zou L, Cvetkovic V, 2020.** Impact of normal stress-induced closure on laboratory-scale solute transport in a natural rock fracture. *Journal of Rock Mechanics and Geotechnical Engineering* 12, 732–741.
- Zou L, Jing L, Cvetkovic V, 2017.** Modeling of solute transport in a 3D rough-walled fracture-matrix system. *Transport in Porous Media* 116, 1005–1029.
- Åkesson M, Kristensson O, Börgesson L, Dueck A, Hernelind J, 2010a.** THM modelling of buffer, backfill and other system components. Critical processes and scenarios. SKB TR-10-11, Svensk Kärnbränslehantering AB.
- Åkesson M, Börgesson L, Kristensson O, 2010b.** SR-Site Data report. THM modelling of buffer, backfill and other system components. SKB TR-10-44, Svensk Kärnbränslehantering AB.
- Åstrand P-G, Broed R, Jones J, 2005.** Pandora technical description and user guide. Posiva Working Report 2005-64, Posiva Oy, Finland.
- Öhman J, Follin S, 2010.** Site investigation SFR. Hydrogeological modelling of SFR. Model version 0.2. SKB R-10-03, Svensk Kärnbränslehantering AB.
- Öhring C, Peterson G, Mikko H, 2018.** Detailed geomorphological analysis of LiDAR derived Elevation data, Forsmark. SKB R-18-10, Svensk Kärnbränslehantering AB.

Applicable regulations relating to post-closure and SKB's implementation of these in the PSAR

This Appendix contains regulatory texts issued by SSM applicable to a safety assessment for a nuclear waste repository. References to SKB's plan for complying with the regulations have been inserted in italics at relevant places in Sections A1.1 (SSMFS 2008:21) and A2.1 (SSMFS 2008:37).

A1 SSMFS 2008:21

SSM has issued Regulations concerning Safety in connection with the Disposal of Nuclear Material and Nuclear Waste and General Recommendations concerning the application of those Regulations, both in SSMFS 2008:21.

Whereas the Regulations have a clear legal status, General Recommendations are described in 1 § Ordinance on Regulatory Codes (1976:725) as: Such general recommendations on the application of regulations that stipulate how someone can or should act in a certain respect.

A1.1 Regulations in SSMFS 2008:21

The Swedish Radiation Safety Authority's Regulations concerning Safety in connection with the Disposal of Nuclear Material and Nuclear Waste decided on December 19, 2008.

On the basis of 20 a and 21 §§ of the Ordinance (1984:14) on Nuclear Activities, the Swedish Radiation Safety Authority has issued the following regulations and decided on the following general recommendations.

Application

1 § These regulations apply to facilities for the disposal of spent nuclear fuel and waste (repositories). The regulations do not apply to facilities for landfill disposal of low-level nuclear waste in accordance with 19 § of the Ordinance (1984:14) on Nuclear Activities.

The regulations contain supplementary provisions to the Swedish Radiation Safety Authority's regulations (SSMFS 2008:1) concerning Safety in Certain Nuclear Facilities.

Barriers and their Functions

2 § Safety after the closure of a repository shall be maintained through a system of passive barriers.

3 § The function of each barrier shall be to, in one or several ways, contribute to the containment, prevention or retardation of dispersion of radioactive substances, either directly, or indirectly by protecting other barriers in the barrier system.

Handling in the PSAR: The ways in which the barriers contribute to safety is discussed in detail in Chapter 8. The calculation cases in Section 13.7.4 address this issue directly. In general, most of the safety assessment is aimed at demonstrating barrier safety.

4 § A deficiency in any of the repository's barrier functions that is detected during the construction or operational surveillance of the repository and that can lead to a deterioration in safety after closure in addition to that anticipated in the safety report⁴¹, shall be reported to the Swedish Radiation Safety Authority without delay⁴². The same applies if such a deficiency is suspected to occur or if the possibility that such a deficiency can occur in the future is suspected.

⁴¹ Cf Chapter 4, Section 2 of the Swedish Radiation Protection Authority's regulations (SSMFS 2008:1) concerning Safety in Certain Nuclear Facilities.

⁴² Cf Chapter 2, Section 2 of the Swedish Radiation Protection Authority's regulations (SSMFS 2008:1) concerning Safety in Certain Nuclear Facilities.

Design and Construction

5 § The barrier system shall be able to withstand such features, events and processes that can affect the post-closure performance of the barriers.

Handling in the PSAR: The overall purpose of the safety assessment can be said to demonstrate this point.

6 § The barrier system shall be designed and constructed taking into account the best available technique⁴³.

Handling in the PSAR: The issue of BAT is addressed in Sections 2.7, 14.3 and 15.3.5.

7 § The barrier system shall comprise several barriers so that, as far as possible, the necessary safety is maintained in spite of a single deficiency in a barrier.

Handling in the PSAR: This issue is addressed in many of the analyses. In particular, a set of calculation cases to illustrate this issue is presented in Section 13.7.4.

8 § The impact on safety of such measures that are adopted to facilitate the monitoring or retrieval of disposed nuclear material or nuclear waste from the repository, or to make access to the repository difficult, shall be analysed and reported to the Swedish Radiation Safety Authority.

Safety Assessment

9 § In addition to the provisions of Chapter 4. 1 § of the Swedish Radiation Safety Authority's Regulations (SSMFS 2008:1) concerning the Safety in Certain Nuclear Facilities, the safety assessments shall also comprise features, events and processes which can lead to the dispersion of radioactive substances after closure, and such analyses shall be made before repository construction, before repository operation and before repository closure.

*Handling in the PSAR: The systematic management in a database of the mentioned features, events and processes in the PSAR is discussed in Chapter 3 and in the **FEP report**. The detailed management of many of these factors is discussed throughout the report. Verification that FEPs omitted in earlier parts of the assessment are of negligible significance in light of the completed scenario and risk analysis is provided in Section 14.4.*

10 § A safety assessment shall comprise as long time as barrier functions are required, but at least ten thousand years.

Handling in the PSAR: The time scales of relevance for the PSAR are discussed in Section 2.4.

Safety Report

11 § The safety report for a repository shall, in addition what is required in Chapter 4 2 § of the Swedish Radiation Safety Authority's Regulations (SSMFS 2008:1) concerning Safety in Certain Nuclear Facilities, contain the information required in Appendix 1 of these regulations and which concerns the time after closure.

Prior to repository closure, the final safety assessment must be renewed and subjected to a safety review in accordance with Chapter 4. 3 § of the Swedish Radiation Safety Authority's regulations (SSMFS 2008:1) Concerning Safety in Certain Nuclear Facilities and must be reviewed and approved by the Swedish Radiation Safety Authority.

Exceptions

12 § The Swedish Radiation Safety Authority may grant exceptions, if particular grounds exist, from these regulations if this can be achieved without departing from the purpose of the regulations and on condition that safety can be maintained.

⁴³ Cf Chapter 2, Section 3 of the Swedish Environmental Code.

Appendix 1

The following shall be reported with regard to analysis methods:

– how one or several methods have been used to describe the passive system of barriers in the repository, its performance and evolution over time; the method or methods shall contribute to providing a clear view of the features, events and processes that can affect the performance of the barriers and the links between these features, events and processes,

Handling in the PSAR: The format for system description is discussed in Chapter 5 (initial state), Chapter 6 (external conditions) and Chapter 7 (processes). The description of system evolution is related to the entire assessment and is analysed in detail as a reference evolution in Chapter 10. Variants of this evolution are analysed for a number of scenarios in Chapter 12.

– how one or several methods have been used to identify and describe relevant scenarios for sequences of events and conditions that can affect the future evolution of the repository; the scenarios shall include a main scenario that takes into account the most probable changes in the repository and its environment,

Handling in the PSAR: The scenario selection method for the PSAR is described in Section 2.5.8 and its implementation in Chapter 11.

– the applicability of models, parameter values and other conditions used for the description and quantification of repository performance as far as reasonably achievable,

Handling in the PSAR: This is done in the **Model summary report**, see e.g. Section 7.5 and the **Data report**, see Chapter 9.

– how uncertainties in the description of the functions, scenarios, calculation models and calculation parameters used in the description as well as variations in barrier properties have been handled in the safety assessment, including the reporting of a sensitivity analysis which shows how the uncertainties affect the description of barrier performance and the analysis of consequences to human health and the environment.

Handling in SR-Site: The management of uncertainties permeates the safety assessment. A plan for the management of uncertainties is given in Section 2.8.3. Sensitivity analyses occur in a number of places in the reference evolution and the analyses of different scenarios, see e.g. Sections 12.2.2, 12.6.2, 13.5.11 and 13.6.2. Sensitivity of the main risk contributors to various conceptual uncertainties is analysed in Section 13.10.

The following shall be reported with respect to the analysis of post-closure conditions:

– the safety assessment in accordance with 9 § comprising descriptions of the evolution in the biosphere, geosphere and repository for selected scenarios; the environmental impact of the repository for selected scenarios, including the main scenario, with respect to defects in engineered barriers and other identified uncertainties.

Handling in the PSAR: This is essentially the reporting of the analyses of the reference evolution in Chapter 10 and of the selected scenarios in Chapter 12.

A1.2 Excerpts from the General Recommendations in SSMFS 2008:21

The Swedish Radiation Safety Authority's General Recommendations concerning the Application of the Regulations concerning Safety in connection with the Disposal of Nuclear Material and Nuclear Waste (SSMFS 2008:21).

The following is the unabbreviated Recommendations relevant to 9 and 10 § and Appendix of SSMFS 2008:21, i.e. those sections that concern the safety assessment.

On 9 § and Appendix

The safety of a repository after closure is analysed quantitatively, primarily by estimating the possible dispersion of radioactive substances and how it is distributed in time for a relevant selection of future possible sequences of events (scenarios). The purpose of the safety assessment is to show, *inter alia*, that the risks from these scenarios are acceptable in relation to the requirements on the protection of human health and the environment issued by the Swedish Radiation Safety Authority (SSMFS 2008:37). The safety assessment should also aim at providing a basic understanding of the repository performance on different time-periods and at identifying requirements regarding the performance and design of different repository components.

A *scenario* in the safety assessment comprises a description of how a given combination of external and internal conditions affect repository performance. Two groups of such conditions are:

- External conditions in the form of features, events and processes which occur outside repository barriers; this includes climate changes and their consequential impact on the repository environment, such as permafrost, glaciation, land subsidence and elevation as well as the impact of human activities,
- Internal conditions in the form of features, events and processes which occur inside the repository; this includes properties, including defects, of nuclear material, nuclear waste and engineered barriers and related processes as well as properties of the surrounding geological formation and related processes.

Based on an analysis of the probability of occurrence of different types of scenarios in different time-periods, scenarios with a significant impact on repository performance should be divided into different categories:

- main scenario,
- less probable scenarios,
- other scenarios or residual scenarios.

The main scenario should be based on the probable evolution of external conditions and realistic, or where justified, pessimistic assumptions with respect to the internal conditions. It should comprise future external events which have a significant probability of occurrence or which cannot be shown to have a low probability of occurrence during the time covered in the safety assessment. Furthermore, it should be based, as far as possible, on credible assumptions with respect to internal conditions, including substantiated assumptions concerning the occurrence of manufacturing defects and other imperfections, and which allow for an analysis of the repository barrier functions (it is, for example, not sufficient to always base the analysis on leak-tight waste containers, even if this can be shown to be the most probable case). The main scenario should be used as the starting point for an analysis of the impact of uncertainties (see below), which means that the analysis of the main scenario also includes a number of calculation cases.

Less probable scenarios should be prepared for the evaluation of scenario uncertainty (see also below). This includes variations on the main scenario with alternative sequences of events as well as scenarios that take into account the impact of future human activities such as damage inflicted on barriers. (Damage to humans intruding into the repository is illustrated by residual scenarios, see below). The analysis of less probable scenarios should include analyses of such uncertainties that are not evaluated within the framework of the main scenario.

Residual scenarios should include sequences of events and conditions that are selected and studied independently of probabilities in order to, *inter alia*, illustrate the significance of individual barriers and barrier functions. The residual scenarios should also include cases to illustrate damage to humans intruding into the repository as well as cases to illustrate the consequences of an unclosed repository that is not monitored.

Handling in the PSAR: The methodology for selection of scenarios is described in Section 2.5.8 and its implementation is described in Chapter 11.

The lack of knowledge and other uncertainties in the calculation conditions (assumptions, models, data) is denoted in this context as uncertainties⁴⁴. These uncertainties can be classified as follows:

- scenario uncertainty: uncertainty with respect to external and internal conditions in terms of type, degree and time sequence,
- system uncertainty: uncertainty as to the comprehensiveness of the description of the system of features, events and processes used in the analysis of both individual barrier performance and the performance of repository as a whole,
- model uncertainty: uncertainty in the calculation models used in the analysis,
- parameter uncertainty: uncertainty in the parameter values (input data) used in the calculations,
- spatial variation in the parameters used to describe the barrier performance of the rock (primarily with respect to hydraulic, mechanical and chemical conditions).

There are often no clear boundaries between the different types of uncertainties. The most important requirement is that the uncertainties should be described and handled in a consistent and structured manner.

The evaluation of uncertainties is an important part of the safety assessment. This means that uncertainties should be discussed and examined in depth when selecting calculation cases, calculation models and parameter values as well as when evaluating calculation results.

Handling in the PSAR: *The management of uncertainties permeates the safety assessment. A plan for the management of uncertainties is given in Section 2.8.3.*

The assumptions and calculation models used should be carefully selected with respect to the principle that the application and the selection should be justified through a discussion of alternatives and with reference to scientific data. In cases where there is doubt as to a suitable model, several models should be used to illustrate the impact of the uncertainty involved in the choice of model.

Handling in the PSAR: *This matter is mainly addressed in the **Process reports** and, for external influences, in the **Climate report**, see further Chapters 7 and 6, respectively. A structured account of important selected models is given in the **Model summary report**.*

Both deterministic and probabilistic methods should be used so that they complement each other and, consequently, provide as comprehensive a picture of the risks as possible.

Handling in the PSAR: *Most of the calculations in the PSAR are deterministic. Probabilistic calculations are used essentially as a means of handling data uncertainty and spatial variability in modelling radionuclide transport and dose, in particular in Chapter 13.*

The probabilities that the scenarios and calculation cases will actually occur should be estimated as far as possible in order to calculate risk. Such estimates cannot be exact. Consequently, the estimates should be substantiated through the use of several methods, for example, assessments by several independent experts. This can be done, for example, through estimates of when different events can be expected to have occurred.

Handling in the PSAR: *Probabilities of scenarios that are not excluded from the risk summation as being “residual” are derived pessimistically. This is a component of the general approach to risk estimates, see Section 2.6.2. Of relevance is also the method for scenario selection described in Section 2.5.8 and implemented as described in Chapter 11. The analyses leading to the categorisation of the selected scenarios is provided in Chapter 12.*

Based on scenarios that can be shown to be especially important from the standpoint of risk, a number of **design basis cases** should be identified. Together with other information, such as on manufacturing method and controllability, these cases should be used to substantiate the design basis such as requirements on barrier properties.

⁴⁴ This explanation of the term uncertainty only makes sense in Swedish where the same word (säkerhet) is used to denote both certainty and safety.

Handling in the PSAR: See Section 15.4.

Particularly in the case of disposal of nuclear material, for example spent nuclear fuel, it should be shown that criticality cannot occur in the initial configuration of the nuclear material. With respect to the redistribution of the nuclear material through physical and chemical processes, which can lead to criticality, it should be shown that such a redistribution is very improbable.

Handling in the PSAR: See Section 13.3 and further the **Fuel and canister process report**, Section 2.1.3.

The result of calculations in the safety assessment should contain such information and should be presented in such a way that an overall judgement of safety compliance with the requirements can be made.

Handling in the PSAR: This is an overall requirement on the quality of the safety reporting, which has governed the compilation of the PSAR report. Compliance is discussed in Section 15.3.

The validity of assumptions used, such as models and parameter values, should be supported, for example through the citing of references to scientific literature, special investigations and research results, laboratory experiments on different scales, field experiments and studies of natural phenomena (natural analogues).

Handling in the PSAR: Justification of models, on the bases mentioned, is done in the **Process reports**, and for external influences, in the **Climate report**. A structured account of all important models is given in the **Model summary report**. Parameter values are justified in the **Data report**.

Scientific background material and expert assessments should be documented in a traceable manner by thoroughly referring to scientific literature and other material.

Handling in the PSAR: This is addressed in much of the documentation of the PSAR, in particular the three **Process reports**, the **Climate report** and the **Data report**.

On 10 §

The time-period for which safety has to be maintained and demonstrated should be a starting point for the safety assessment. One way of discussing and justifying the establishment of such a time period is to start from a comparison of the hazard of the radioactive inventory of the repository with the hazard of radioactive substances occurring in nature. However, it should also be possible to take into consideration the difficulties of conducting meaningful analyses for extremely long time-periods, beyond one million years, in any other way than through showing how the hazard of the radioactive substances in the repository declines with time.

In the case of a repository for long-lived waste, the safety assessment may have to include scenarios which take into account greater expected climate changes, primarily in the form of future glaciations. For example, the next complete glacial cycle which is currently estimated to be on the order of 100 000 years, should be particularly taken into account.

Handling in the PSAR: The time scale for the PSAR is discussed in Section 2.4.

In the case of periods up to 1 000 years after closure, in accordance with the regulations of SSIFS 1998:1, the dose and risk calculated for current conditions in the biosphere constitute the basis for the assessment of repository safety and its protective capabilities.

Furthermore, in the case of longer periods, the assessment can be made using dose as one of several safety indicators. This should be taken into account in connection with the calculations as well as the presentation of analysis results. Examples of such supplementary safety indicators are the concentrations of radioactive substances from the repository which can build up in soils and near-surface groundwater or the calculated flow of radioactive substances to the biosphere.

(Compare the regulations in SSMFS 2008:37 and SSM's comments on those regulations).

Handling in the PSAR: Alternative safety indicators are selected in Section 2.6.3 and applied in Section 13.5.8 and further in the **Radionuclide transport report**.

A2 SSMFS 2008:37

SSI has in SSMFS 2008:37 issued Regulations concerning the Protection of Human Health and the Environment in connection with the Final Management of Spent Nuclear Fuel or Nuclear Waste, and General Guidance concerning the application of these regulations.

Whereas the Regulations have a clear legal status, General Recommendations are described in 1 § Ordinance on Regulatory Codes (1976:725) as: Such general recommendations on the application of regulations that stipulate how someone can or should act in a certain respect.

A2.1 SSMFS 2008:37

The Swedish Radiation Safety Authority's Regulations concerning the Protection of Human Health and the Environment in connection with the Final Management of Spent Nuclear Fuel or Nuclear Waste; decided on December 19, 2008.

On the basis of 7 and 8 §§ of the Radiation Protection Ordinance (1988:293), the Swedish Radiation Protection Institute stipulates the following.

1 § These regulations are to be applied to the final management of spent nuclear fuel or nuclear waste. The regulations do not apply to landfills for low-level nuclear waste in accordance with 19 § of the Ordinance (1984:14) on Nuclear Activities.

Definitions

2 § In these regulations, concepts are defined as follows:

- *best available technique*: the most effective measure available to limit the release of radioactive substances and the harmful effects of the releases on human health and the environment which does not entail unreasonable costs,
- *intrusion*: human intrusion into a repository which can affect its protective capability,
- *optimisation*: keeping the radiation doses to mankind as low as reasonably achievable, economic and social factors taken into account,
- *harmful effects*: cancer (fatal and non-fatal) as well as hereditary defects in humans caused by ionising radiation in accordance with paragraphs 47–51 of the International Radiation Protection Commission's Publication 60, 1990,
- *protective capability*: the capability to protect human health and the environment from the harmful effects of ionising radiation,
- *final management*: handling, treatment, transportation, interim storage prior to, and in connection with final disposal as well as the final disposal,
- *risk*: the product of the probability of receiving a radiation dose and the harmful effects of the radiation dose.

Terms and concepts used in the Radiation Protection Act (1988:220) and the Act (1984:3) on Nuclear Activities have the same meanings in these regulations.

Holistic Approach etc

3 § Human health and the environment shall be protected from the harmful effects of ionising radiation, during the time when the various stages of the final management of spent nuclear fuel or nuclear waste are being implemented as well as in the future. The final management may not cause impacts on human health and the environment outside Sweden's borders that are more severe than those accepted inside Sweden.

4 § Optimisation must be achieved and the best available technique shall be taken into consideration in the final management of spent nuclear fuel or nuclear waste.

The collective dose, as a result of the expected outflow of radioactive substances during a period of 1 000 years after closure of a repository for spent nuclear fuel or nuclear waste shall be estimated as the sum, over 10 000 years, of the annual collective dose. The estimate shall be reported in accordance with 10–12 §§.

Handling in SR-Site: *The aspects of optimisation and best available technique that can be addressed in the safety assessment are addressed in Sections 2.7, 0 and 15.3.5. Collective dose is addressed in Section 13.6.5.*

Protection of human health

5 § A repository for spent nuclear fuel or nuclear waste shall be designed so that the annual risk of harmful effects after closure does not exceed 10^{-6} for a representative individual in the group exposed to the greatest risk⁴⁵.

The probability of harmful effects as a result of a radiation dose shall be calculated using the probability coefficients provided in the International Radiation Protection Commission's Publication 60, 1990.

Handling in the PSAR: *Estimation of risk and assessing compliance with the above criterion is one of the main purposes of the PSAR. Much of the methodology outlined in Chapter 2 is aimed at achieving this end-point. Issues directly related to the calculation of risk are discussed in Section 2.6. A summation of the calculated risk contributions from relevant scenarios is given in Section 13.9 and a discussion of compliance is given in Section 15.2.1.*

Environmental Protection

6 § The final management of spent nuclear fuel or nuclear waste shall be implemented so that biodiversity and the sustainable use of biological resources are protected against the harmful effects of ionising radiation.

7 § Biological effects of ionising radiation in living environments and ecosystems concerned shall be described. The report shall be based on available knowledge concerning the ecosystems concerned and shall take particular account of the existence of genetically distinctive populations such as isolated populations, endemic species and species threatened with extinction) and in general any organisms worth protecting.

Handling in the PSAR: *This issue is addressed in Chapter 13, Sections 13.2.5 and 13.5.7. Conclusions are provided in Section 15.3.4.*

Intrusion and Access

8 § A repository shall be primarily designed with respect to its protective capability. If measures are adopted to make access easier or to make intrusion difficult, the effects on the protective capability of the repository shall be reported.

9 § The consequences of intrusion into a repository shall be reported for the different time periods specified in 11–12 §§.

The protective capability of the repository after intrusion shall be described.

Handling in the PSAR: *Intrusion issues are discussed in Section 6.2.1 and analysed in Section 14.2 as further documented in the **FHA report**.*

⁴⁵ With respect to facilities in operation, the limitations and instructions that apply are provided in the Swedish Radiation Protection Institute's regulations (SSI FS 1991:5, amended 1997:2) concerning the limitation of releases of radioactive substances from nuclear power plants and the Swedish Radiation Protection Institute's regulations (SSI FS 1994:2, amended 1997:3) concerning health physics for activities involving ionising radiation at nuclear facilities.

Time Periods

10 § An assessment of a repository's protective capability shall be reported for two time periods of orders of magnitude specified in 11–12 §§. The description shall include a case, which is based on the assumption that the biospheric conditions which exist at the time that an application for a licence to operate the repository is submitted will not change. Uncertainties in the assumptions made shall be described and taken into account in the assessment of the protective capability.

The first thousand years following repository closure

11 § For the first thousand years following repository closure, the assessment of the repository's protective capability shall be based on quantitative analyses of the impact on human health and the environment.

Period after the first thousand years following repository closure

12 § For the period after the first thousand years following repository closure, the assessment of the repository's protective capability shall be based on various possible sequences for the development of the repository's properties, its environment and the biosphere.

Handling in the PSAR (11 § and 12 §): This is mainly addressed in the reference evolution, Chapter 10, which is divided into several time frames. The first 1 000 years are treated as part of the initial temperate period. Particular attention is given to the canister evolution during the initial period of unsaturated conditions as the Forsmark site, see, e.g., Sections 12.6.3 and 13.7.3. A number of scenarios are analysed (Chapters 12 and 13), covering various possibilities for the repository evolution.

Exceptions

13 § If special grounds exist, the Swedish Radiation Safety Authority may announce exceptions from these regulations.

A2.2 General Guidance on SSMFS 2008:37

The Swedish Radiation Safety Authority's guidelines on the application of the regulations (SSMFS 2008:37) concerning protection of human health and the environment in connection with the final management of spent nuclear fuel and nuclear waste; decided upon on 19 December 2008.

Unofficial translation

Guidelines concerning geological disposal of spent nuclear fuel and nuclear waste

On Section 1 – Area of application

These guidelines are applicable to final geological disposal of spent nuclear fuel and nuclear waste. The guidelines cover measures undertaken with a view to develop, site, construct, operate and close a repository, which can affect the protective capability of the repository and environmental consequences after closure.

The guidelines are also applicable to measures that are to be undertaken with spent nuclear fuel and nuclear waste before final disposal and which can affect the protective capability of the repository and environmental consequences after closure. This includes activities at other installations such as the conditioning of waste that takes place by casting waste in concrete and by encapsulation of spent nuclear fuel, as well as transportation between installations and steering of waste to different repositories, including shallow land burials for low-level nuclear waste that are licenced in accordance with Section 19 of the Ordinance (1984:14) on Nuclear Activities. However, the guidelines, like the regulations, are not applicable to the land burial itself.

On Section 2 – Definitions

Terms used in the Radiation Protection Act (1988:220), the Act (1984:3) on Nuclear Activities and SSM's Regulations on protection of human health and the environment in connection with final management of spent nuclear fuel and nuclear waste have the same meaning in these guidelines. In addition, the following definitions are used:

Scenario	A description of the development of the repository given an initial state and specified conditions in the environment and their development.
Exposure pathway	The migration of the radioactive substances from a repository to a place where human beings or an organism covered by the environmental protection regulations are present. This includes dispersion in the geological barrier, transport with water and air flows, migration in ecosystems and uptake in human beings or organisms in the environment.
Risk analysis	An analysis with the aim to clarify the protective capability of a repository and its consequences with regard to the environmental impact and the risk for human beings.

On Sections 4, 8 and 9 – Holistic approach etc intrusion and access

Optimisation and Best Available Technique

The regulations require that optimisation must be performed and that best available technique should be taken into account. Optimisation and best available technique should be applied in parallel with a view to improving the protective capability of the repository.

Measures for optimisation of a repository should be evaluated on the basis of calculated risks.

Application of best available technique in connection with final disposal means that the siting, design, construction, operation and closure of the repository and appurtenant system components should be carried out so as to prevent, limit and delay releases from both engineered and geological barriers as far as is reasonably possible. When striking balances between different measures, an overall assessment should be made of their impact on the protective capability of the repository.

In cases where considerable uncertainty is attached to the calculated risks, for instance, in analyses of the repository a long time after closure, or analyses made at an early stage of the development work with the repository system, greater weight should be placed on best available technique.

In the event of any conflicts between application of optimisation and best available technique, priority should be given to best available technique.

Experience from recurrent risk analyses and the successive development work with the repository should be used in the application of optimisation and best available technique.

Handling in the PSAR: *The aspects of optimisation and best available technique that can be addressed in the safety assessment are treated in Sections 2.7, 14.3 and 15.3.5.*

Collective dose

The regulations require an account of the collective dose from releases that take place during the first thousand years after closure. For final disposal the collective dose should also be used in comparisons between alternative repository concepts and sites. The collective dose need not be reported if the repository concept entails a complete isolation of the spent nuclear fuel or the nuclear waste in engineered barriers during the first thousand years after closure.

Handling in the PSAR: *An estimate of the collective dose is provided in Section 13.6.5.*

Occupational radiation protection

An account should be given of measures undertaken for radiation protection of workers that may have a negative impact on the protective capability of the repository or make it more difficult to assess.

Handling in the PSAR: *No such measures have been identified in the PSAR.*

Future human action and the preservation of information

When applying best available technique, consideration should also be given to the possibility to reduce the probability and consequences of inadvertent future human impact on the repository, for instance, inadvertent intrusion. Increased repository depth and avoidance of sites with extractable mineral assets may, for instance, be considered to decrease the probability of unintentional human intrusion.

Handling in the PSAR: Ore potential is evaluated for the site, see Section 4.3.2. This information is propagated to the analyses of FHA-scenarios in Section 14.2. Inadvertent intrusion is discussed as one of many factors when feedback is given to the selection of repository depth in Section 14.3.4 and 15.5.18.

Preservation of knowledge about the repository could reduce the risk of future human impact. A strategy for preservation of information should be produced so that measures can be undertaken before closure of the repository. Examples of information that should be taken into consideration are information about the location of the repository, its content of radioactive substances and design.

Handling in the PSAR: The production of such a strategy is not an issue for the safety assessment. As documented elsewhere in the PSAR, information about the repository will be collected and stored during construction, operation and closure of the repository according to applicable legal requirements. A strategy for preservation of information after closure will be developed by SKB, to some extent as part of international cooperation on this subject, in reasonable time before closure.

On Sections 5–7 – Protection of human health and the environment

Risk for the individual from the general public

The relationship between dose and risk

According to the regulations, the recommendations of the International Commission on Radiological Protection (ICRP) are to be used for calculation of the harmful effects of ionizing radiation. According to ICRP Publication No. 60, 1990, the factor for conversion of effective dose to risk is 7.3 percent per sievert.

The regulation's criterion for individual risk

According to the regulations, the risk for harmful effects for a representative individual in the group exposed to the greatest risk (the most exposed group) shall not exceed 10^{-6} per year. Since the most exposed group cannot be described in an unambiguous way, the group should be regarded as a way of quantifying the protective capability of the repository.

One way of defining the most exposed group is to include the individuals that receive a risk in the interval from the highest risk down to a tenth of this risk. If a larger number of individuals can be considered to be included in such a group, the arithmetic average of individual risks in the group can be used for demonstrating compliance with the criterion for individual risk in the regulations. One example of such exposure situation is a release of radioactive substances into a large lake that can be used as a source of drinking water and for fishing.

If the exposed group only consists of a few individuals, the criterion of the regulations for individual risk can be considered as being complied with if the highest calculated individual risk does not exceed 10^{-5} per year. An example of a situation of this kind might be if consumption of drinking water from a drilled well is the dominant exposure path. In such a calculation example, the choice of individuals with the highest risk load should be justified by information about the spread in calculated individual risks with respect to assumed living habits and places of stay.

Handling in the PSAR: The most exposed group is defined as the group of individuals that receives the highest exposure across all potential release areas (i.e. biosphere objects) in the landscape, including exposure from well water (see further Section 13.2.3 and the **Biosphere synthesis report**).

Averaging risk over a lifetime

The individual risk should be calculated as an annual average on the basis of an estimate of the lifetime risk for all relevant exposure pathways for every individual. The lifetime risk can be calculated as the accumulated lifetime dose multiplied by the conversion factor of 7.3 percent per sievert.

Handling in the PSAR: *This approach is used in the PSAR, see Section 13.2.3 and the **Biosphere synthesis report**.*

Averaging risk between generations

Deterministic and probabilistic calculations can both be used to illustrate how risk from the repository develops over time. A probabilistic analysis can, however, in certain cases give an insufficient picture of how an individual detrimental event, for instance, a major earthquake, would affect the risk for a particular generation. The probabilistic calculations should in this case be supplemented as specified in Appendix 1.

Handling in SR-Site: *This so called risk dilution phenomenon is addressed in general terms in Section 2.6.2, subheading “Risk dilution” and analysed in Section 13.9.5.*

Selection of scenarios

The assessment of the protective capability of the repository and the environmental consequences should be based on a set of scenarios that together illustrate the most important courses of development of the repository, its surroundings and the biosphere.

Handling of climate evolution

Taking into consideration the great uncertainties associated with the assumptions on climate evolution in a remote future and to facilitate the interpretation of the risk to be calculated, the risk analysis should be simplified to include a few possible climate evolutions.

A realistic set of biosphere conditions should be associated with each climate evolution. The different climate evolutions should be selected so that they together illustrate the most important and reasonably foreseeable sequences of future climate states and their impact on the protective capability of the repository and the environmental consequences. The choice of the climate evolutions that serve as the basis for the analysis should be based on a combination of sensitivity analyses and expert judgements. Additional guidance is provided in the section with guidelines on Sections 10–12.

The risk from the repository should be calculated for each assumed climate evolution by summing the risk contributions from a number of scenarios that together illustrate how the more or less probable courses of development in the repository and the surrounding rock affects the repository’s protective capability and environmental consequences. The calculated risk should be reported and evaluated in relation to the criterion of the regulations for individual risk, separately for each climate evolution. The repository should thus be able to be shown to comply with the risk criterion for the alternative climate evolutions. If a lower probability than one (1) is stated for a particular climate evolution, this should be justified, for instance, by expert judgements.

Handling in the PSAR: *The method for selection of scenarios is described in Section 2.5.8. A reference climate evolution is used in the definition of a base case of the main scenario. In a global warming variant of the main scenario, a climate perturbed by the effects of anthropogenic greenhouse gas emissions is assumed. In the analyses of each of the additional scenarios in Chapter 12, both these variants are considered. In addition, for each scenario, the impact of uncertainties regarding the climate related factors of concern in that particular scenario, are analysed. The results of all these scenarios are considered in the risk summation.*

Future human action

A number of scenarios for inadvertent human impact on the repository should be presented. The scenarios should include a case of direct intrusion in connection with drilling in the repository and some examples of other activities that indirectly lead to a deterioration in the protective capability

of the repository, for example by changing groundwater chemistry or the hydrological conditions in the repository or its surroundings. The selection of intrusion scenarios should be based on present living habits and technical prerequisites and take into consideration the repository's properties.

The consequences of the disturbance of the repository's protective capability should be illustrated by calculations of the doses for individuals in the most exposed group, and reported separately apart from the risk analysis for the undisturbed repository. The results should be used to illustrate conceivable countermeasures and to provide a basis for the application of best available technique (see guidelines on optimisation and best available technique).

An account need not be given of the direct consequences for the individuals intruding into the repository.

Handling in the PSAR: *The above approach is used in the PSAR, see Section 14.2. Regarding countermeasures, the depth and location (away from ore potential) of the repository have been selected with the aim of minimising the risk of inadvertent human intrusion among several other considerations, see Section 14.3.4.*

Special scenarios

For repositories primarily based on isolation of the spent nuclear fuel or nuclear waste, an analysis of a conceivable loss, during the first thousand years after closure, of one or more barrier functions of key importance for the protective capability should be made separately from the risk analysis. The intention of this analysis should be to clarify how the different barriers contribute to the protective capability of the repository.

Handling in the PSAR: *Such an analysis is provided in Sections 13.7.3 and 13.7.4.*

Biosphere conditions and exposure pathways

The future biosphere conditions for calculations of consequences on human beings and the environment should be selected in agreement with the assumed climate state. Unless it is clearly unreasonable, however, today's biosphere conditions at the repository and its surroundings should be evaluated, i.e. agricultural land, forest, wetland (mire), lake, sea or other relevant ecosystems. Furthermore, consideration should be given to land uplift (or subsidence) and other predictable changes.

The risk analysis can include a limited selection of exposure paths, although the selection of these should be based on an analysis of the diversity of human use of environmental and natural resources which can occur in Sweden today. Consideration should also be given to the possibility of individuals being exposed to combinations of exposure pathways within and between different ecosystems.

Handling in the PSAR: *The above approach is used in the PSAR, see Section 13.2.*

Environmental protection

The description of exposure pathways should also include exposure pathways to certain organisms in the ecosystems that should be included in the risk analysis. The concentration of radioactive substances in soil, sediment and water should be accounted for where this is relevant for the respective ecosystem.

When a biological effect for the identified organisms can be presumed, a valuation should be made of the consequence this may have for the affected ecosystems, with the view to facilitating an assessment of impact on biological diversity and a sustainable use of the environment.

The analysis of consequences for organisms in "today's biosphere", carried out as above, should be used for the assessment of environmental consequences in a long-term perspective. For assumed climates, where the present biosphere conditions are evidently unreasonable, for instance, a colder climate with permafrost, it is sufficient to make a survey based on knowledge currently available about applicable ecosystems. Additional guidelines are contained in Appendix 2.

Handling in the PSAR: *The approach used in the PSAR is explained in Section 13.2.5.*

Reporting of uncertainties

Identification and assessment of uncertainties in for instance, site-specific and generic data and models should take place in accordance with the instructions given in general recommendations from the Swedish Nuclear Power Inspectorate. The different categories of uncertainties, which are specified there, should be evaluated and reported on in a systematic way and evaluated on the basis of their importance for the result of the risk analysis. The report should also include a motivation of the methods selected for handling different types of uncertainties, for instance, in connection with the selection of scenarios, models and data. All calculation steps with appurtenant uncertainties should be reported on.

Peer review and expert panel elicitation can, in the cases where the basic data is insufficient, be used to strengthen the credibility of assessments of uncertainties in matters of great importance for the assessment of the protective capability of the repository.

Handling in the PSAR: *The approach to handling of uncertainties is described in Section 2.8.*

On Sections 10–12 – Time periods

Two time periods are defined in the regulations: the period up to a thousand years after closure and the subsequent period.

For longer time periods, the result of the risk analysis should be successively regarded more as an illustration of the protective capability of the repository given certain assumptions.

Limitation of the risk analysis in time

The following principles should provide guidance for the limitation of the risk analysis in time:

- For a repository for spent nuclear fuel, or other long-lived nuclear waste, the risk analysis should at least include approximately one hundred thousand years or the period for a glaciation cycle to illustrate reasonably predictable external strains on the repository. The risk analysis should thereafter be extended in time as long as it provides important information about the possibility of improving the protective capability of the repository, although at the longest for a time period of up to one million years.
- For other repositories for nuclear waste, than those referred to in point 1, the risk analysis should at least cover the time until the expected maximum consequences in terms of risk and environmental impact have taken place, although at the longest for a period of time up to one hundred thousand years.

The arguments for the selected limitations of the risk analysis should be presented.

Handling in the PSAR: *The assessment period in the PSAR is one million years, see Section 2.4.*

Reporting on the first thousand years after closure

The period of time of a thousand years should be regarded as the approximate time period for which a risk analysis can be carried out with high credibility with regard to factors such as climate and biosphere conditions. For this time period, available measurement data and other knowledge about the initial conditions should be used for a detailed analysis and reporting on the development of the protective capability of the repository and its surroundings.

The conditions and processes during the early development of the repository, which can affect its long-term protective capability, should be described in as much detail as possible. Examples of such conditions and processes are the resaturation of the repository, stabilisation of hydrogeological and geochemical conditions, thermal evolution and other transient events.

Biosphere conditions and known trends in the surroundings of the repository should also be described in detail, partly to be able to characterise “today’s biosphere” (see guidelines to Section 5), and partly to be able to characterise the conditions applicable to a conceivable early release from the repository.

Known trends here refer, for instance, to land uplift (or subsidence), any trends in climate evolution and appurtenant changes in use of land and water.

Handling in the PSAR: *The above approaches are used in the PSAR, in particular in the analysis of the reference evolution, where the first thousand years after closure are included in the detailed evaluation of the excavation/operational phase, Section 10.2, and of the initial temperate period, Section 10.3. Particular attention is given to the canister evolution during the initial period of unsaturated conditions as the Forsmark site, see, e.g., Sections 12.6.3 and 13.7.3.*

Reporting on very long time periods

Up to one hundred thousand years

Reporting should be based on a quantitative risk analysis in accordance with the guidelines to Sections 5–7. Supplementary indicators of the repository’s protective capability, such as barrier functions, radionuclide fluxes and concentrations in the environment, should be used to strengthen the confidence in the calculated risks.

The given period of time of one hundred thousand years is approximate and should be selected in such a way that the effect of expected large climate changes, for instance, a glaciation cycle, on the protective capability of the repository and consequences to the surroundings can be illustrated.

Handling in the PSAR: *The above approach is used in the PSAR, in particular in the analysis of the first glacial cycle after closure, as part of the reference evolution, see Section 10.4. See also the discussion of compliance for this time period in Section 15.3.3.*

Beyond one hundred thousand years

The risk analysis should illustrate the long-term development of the repository’s barrier functions and the importance of major external disturbances on the repository such as earthquakes and glaciations. Taking into consideration the increasing uncertainties over time, the calculation of doses to people and the environment should be made in a simplified way with respect to climate development, biosphere conditions and exposure pathways. Climate development can be simplified by being described as a repetition of identical glaciation cycles.

A strict quantitative comparison of calculated risk in relation to the criterion for individual risk in the regulations is not meaningful. The assessment of the protective capability of the repository should instead be based on reasoning on the calculated risk together with several supplementary indicators of the protective capability of the repository such as barrier functions, radionuclide fluxes and concentrations in the environment. If the calculated risk exceeds the criterion of the regulations for individual risk or if there are other indications of substantial disruptions of the protective capability of the repository, the underlying causes of this should be reported on as well as possible measures to improve the protective capability of the repository.

Handling in the PSAR: *The above approach is used in the PSAR, in particular in the analysis of the period after the first glacial cycle up to one million years, as part of the reference evolution, see Section 10.5. See also the discussion of compliance for this time period in Section 15.3.3.*

Summary of arguments for demonstrating compliance with the requirements of the regulations

The reporting should include an account of how the principles for optimisation and the best possible technique have been applied in the siting and design of the repository and appurtenant system components and how quality assurance has been used in the work with the repository and appurtenant risk analyses.

Handling in the PSAR: *Regarding the account of optimisation and BAT in the safety assessment, see above and Section 15.3.5. Quality assurance for the safety assessment is described in Section 2.9.*

The arguments for the protective capability of a repository should be evaluated and reported on in a systematic way. The reporting should include a logically structured argument for the protective capability of the repository with information on calculated risks, uncertainties in the calculations made and the credibility of the assumptions made. To provide a good understanding of the results of the risk analysis, it should be evident how individual scenarios contribute to the risk from the repository.

Handling in the PSAR: *The arguments for the protective capability of the repository are provided in the discussion of compliance in Section 15.3, and in the various parts of the analysis that support the conclusions in that section.*

Appendix 1 – Guidelines on the averaging of risk between generations

For certain exposure situations an annual risk, calculated as an average of all conceivable outcomes of a probabilistic risk assessment, provides an insufficient picture of how risk is allocated between future generations. This applies in particular to events which:

- can be assessed as leading to doses during a limited period of time in relation to the time period covered by the risk analysis, and
- if they arise, can be assessed as giving rise to a conditional individual risk exceeding the criterion in the regulations for individual risk, and
- can be assessed as having such a high probability of occurring during the time period covered by the risk analysis that the product of this probability and the calculated conditional risk is of the same order of magnitude as, or larger than, the criterion for individual risk in the regulations.

For exposure situations of this kind, a probabilistic calculation of risk should be supplemented by calculating the risk for the individuals who are assumed to live after the event has taken place and who are affected by its calculated maximum consequence. The calculation can be made for instance by illustrating the importance of an event occurring at different times ($T_1, T_2 \dots, T_n$), taking into consideration the probability of the event occurring during the respective time interval (T_0 to T_1, T_0 to T_2, \dots, T_0 to T_n , where T_0 corresponds to the time of closure of the repository). The results from these, or similar calculations, can in this way be expected to provide an illustration of the effects of the spreading of risk between future generations and should, together with other risk calculations, be reported on and evaluated in relation to the regulation's criterion for individual risk.

Handling in SR-Site: *This approach is used in the handling of risk dilution in Section 13.9.5.*

Appendix 2 – Guidelines on the evaluation of environmental protection

The organisms included in the analysis of the environmental impact should be selected on the basis of their importance in the ecosystems, but also according to their protection value according to other biological, economic or conservation criteria. Other biological criteria refers, among other things, to genetic distinctiveness and isolation (for example, presently known endemic species), economic criteria refers to the importance of the organisms for different kinds of obtaining a livelihood (for instance, hunting and fishing), and conservation criteria if they are protected by current legislation and local regulations. Other aspects, for instance, cultural history, should also be taken into consideration in the identification of such organisms.

The assessment of effects of ionising radiation in selected organisms, deriving from radioactive substances from a repository, can be made on the basis of the General Guidance provided in the International Committee for Radiation Protection's (ICRP) Publication 91⁴⁶. The applicability of the knowledge and databases used for the analyses of dispersion and transfer of radioactive substances in ecosystems and for analysing the effects of radiation on different organisms should be assessed and reported on.

Handling in the PSAR: *The approach used in the PSAR is explained in Section 13.2.5.*

⁴⁶ A Framework for Assessing the Impact of Ionising Radiation on Non-human Species, ICRP Publication 91, Annals of the ICRP 33:3, 2003.

Glossary of abbreviations and specialised terms used in this report

The glossary is intended to explain all acronyms, SKB-specific terms, and technical terms that occur often in this report. It is not intended to contain all technical terms found in the report. Chemical formulae and units are usually not included in the glossary. In the glossary, the letters *x*, found in for example KFMxxx, have replaced the numbers/letters in the name of for instance the specific deformation zone KFM01D.

It is noted that some of the explanations differ slightly from the corresponding explanations in other, less specialised reports. The more technical explanations given below are appropriate for the context of this report.

1-D/1D	One-dimensional.
2-D/2D	Two-dimensional.
3-D/3D	Three-dimensional.
3DEC	A discrete element modelling code for analysis of rock and structural support in three dimensions, used to simulate the response of fractured rock that is subject to either static or dynamic loading.
ABAQUS	Finite element computer code used for the analysis of buffer homogenisation, canister sinking and earthquake induced shear loads on the canister-buffer system.
albedo	The ratio of the intensity of light reflected from Earth to that of the light it receives from the sun.
AMF	Assessment Model Flow chart.
APSE	Äspö Pillar Stability Experiment.
Asha	The reference backfill material studied by SKB.
backfill	The material used as filling in the deposition tunnels.
BAT	Best Available Technique.
biosphere object	An area in the landscape that potentially will receive radionuclides released from a future repository (instead of Landscape object).
boundary condition	The set of conditions specified for behaviour of the solution to a set of differential equations at the boundary of its domain.
BP	Before Present.
buffer	One of the barriers in the KBS-3 concept, consisting of bentonite clay that surrounds the canister.
burnup	Energy extracted from fuel due to fission, normally given in MWd/kgU.
BWR	Boiling Water Reactor.
CBI	Cement och BetongInstitutet (Swedish Cement and Concrete Research Institute).
CCC	Critical Coagulation Concentration.
CDF	Cumulative Distribution Function.
CEC	Cation exchange capacity. A measure of sites available for ion-exchange.
CFT	Colloid-facilitated transport.
CHAN3D	Computer code for simulation of groundwater flow.
Clab	Central interim storage facility for spent nuclear fuel in Oskarshamn.
climate domain	A climatically determined environment with a specific set of characteristic processes of importance for repository safety.
Clink	Central interim storage and encapsulation plant. Clab and the encapsulation plant as an integrated unit.
CMH	Canister Mid-Height.
Code-Bright	Computer code for thermal-hydraulic-mechanical calculations.
colloids	Finely divided particles, approximately 10 to 10000 angstroms in size, dispersed within a continuous medium in a manner that prevents them from being filtered easily or settled rapidly.
COMP23	Near-field model calculating the release rate of radionuclides into the geosphere far-field.
ConnectFlow	Computer code for simulation of groundwater flow.
copper ingot	A piece of copper cast into a shape suitable for further processing.
CPM	Continuous Porous Medium.

CPU	Central Processing Unit
craton	A large portion of a continental plate that has been relatively undisturbed since the Precambrian era and includes both shield and platform layers.
CRF	Corrosion Release Fraction. The fraction of the radionuclide inventory released by corrosion of metal parts in the fuel assemblies.
crown space	Space under the tunnel ceiling resulting from consolidation of the backfill material.
CRR	Corrosion Release Rate.
CRT	Canister Retrieval Test. Experiment at Äspö HRL.
CSH	Calcium silicate Hydrates.
D2	The repository design and layout assessed in SR-Site.
Darcy flux	Specific discharge, or flux[L/T], is the groundwater flow rate [L ³ /T] per unit area [L ²].
DarcyTools	Computer code for simulation of groundwater flow.
D _e	Effective diffusion coefficient.
deformation zone	An essentially 2-dimensional structure (a sub planar structure with a small thickness relative to its lateral extent) in which deformation (strain) has been concentrated (or, in the case of active faults, is being concentrated).
denudation	Surface weathering and erosion.
Deponit CA-N	A brand name of a bentonite clay, used as one of the reference materials for the buffer in SR-Can.
Design basis case	A calculation case formulated on the basis of a scenario that is shown to be especially important from the standpoint of risk. The result of the calculation of a design basis case is used as input to the formulation of requirements on barriers.
DFN	Discrete Fracture Network.
DLVO	Derjaguin and Landau, Verwey and Overbeek. Theory used in modelling of processes in bentonite.
DOC	Dissolved Organic Carbon.
drawdown	Change in groundwater level due to pumping in a well or underground excavation.
DZ	Deformation Zone.
EBS	Engineered Barrier System.
Ecologo	Calculation code for probabilistic radionuclide transport calculations.
ECPM	Equivalent Continuous Porous Medium.
EDPM	Equivalent Discontinuous Porous Medium.
EDZ	Excavation Damaged Zone.
Eemian	The penultimate interglacial (Marine Isotope Stage 5e) that preceded the Weichselian glaciation.
EFPC	Extended Full Perimeter intersection Criterion.
E-modulus	Elastic modulus. The mathematical description of an object or substance's tendency to be deformed elastically (i.e. non-permanently) when a force is applied to it
ERICA tool	Computer software used to obtain activity concentrations and radiological effects on different types of non-human biota.
eustatic change	Changes in the sea level due to water mass added to or removed from the oceans.
external conditions	Conditions occurring exterior to the final repository that are considered in the safety assessment and may impact the safety functions of the repository.
F	Flow-related transport resistance [T/L], an entity integrated along a flow path, that quantifies the flow-related aspects of the possible retention of a solute transported in a fractured medium.
FARF31	Far-field model for calculation of radionuclide transport in geosphere.
FEM	Finite Element Method.
Fennoscandian Shield	The exposed Precambrian northwest segment of the East European Craton.
FEP	Features, Events and Processes.
FFMxx	Fracture domain in Forsmark.
FGR	Fission Gas Release.
FHA	Future Human Actions.
flow channelling	Heterogeneously distributed flow along preferential flow paths within fractures and deformation zones.
forebulge	Flexural bulge in front of e.g. an ice-sheet load on the lithosphere.

FPC	Full Perimeter intersection Criterion.
FPI	Full Perimeter Intersection.
FSW	Friction Stir Welding.
fuel assembly	A group of fuel rods handled as a unit in the reactor.
fuel rod	Zirconium alloy tubes filled with cylindrical fuel pellets.
GIA	Glacial Isostatic Adjustment.
glacial	Cold period typically associated with ice sheet growth and decay. An alternative word is glaciation.
glacial climate domain	Regions that are covered by ice sheets.
glacial cycle	A period of ca 100 000 years that includes both a glacial (e.g. the Weichselian) and an interglacial (e.g. the Holocene).
glacial domain	See Glacial climate domain.
Global warming variant	A warm variant of the Main Scenario in which the future climate and hence external conditions are assumed to be substantially influenced by human-induced global warming, i.e. a situation with an increased greenhouse effect.
GRIP	European Greenland Ice Core Project.
HCD	Hydraulic Conductor Domain.
HM	Heavy Metal (but see also next).
HM	Hydro-Mechanical.
Holocene	Current interglacial period that began around 11 500 years ago.
HRD	Hydraulic Rock Domain.
HSD	Hydraulic Soil Domain.
Ibeco RWC	Possible material for backfill and pellet fill (called Deponit C-AN in SR-Can).
ICE3G	A global ice sheet reconstruction by W.R. Peltier.
ICRP	International Commission on Radiological Protection.
IFL	Ice Front Location.
illitization	Alteration of smectite (swelling sheet silicate) to illite (non-swelling sheet silicate).
initial state	The state at the beginning of an analysis, e.g. the time of deposition of the canister and buffer and backfilling and sealing of deposition tunnels.
interglacial	A warm period between two glacials. In SR-Site an interglacial is defined as the time from when the ice sheet retreats from the site (time of deglaciation) to the time for the first occurrence of permafrost.
internal processes	Processes occurring within the final repository that are considered in the safety assessment and may impact the safety functions of the repository.
interstadial	A warm period during a glacial, sometimes with ice-free conditions.
IPCC	Intergovernmental Panel on Climate Change.
IRF	Instant Release Fraction. The instantaneously accessible fraction of radionuclides assumed to be rapidly dissolved in the water entering a failed canister.
isostatic changes	Vertical movements of the Earth's crust due to changes in e.g. ice sheet loading.
ka	Kilo-annum or kiloyear, a unit of time.
K_d	Partitioning coefficient for sorption [L^3/T].
K_{eff}	Effective neutron multiplication factor. The design-basis requirement with a view to criticality is that k_{eff} , including uncertainties, shall be less than 0.95 during handling and disposal of canisters.
KFMxxx	Core drilled borehole in Forsmark.
ky	kilo year, a unit of time.
Landscape development model	A model at landscape level that describes the long-term development of a landscape. The model is used to describe time-dependent properties of the biosphere objects that are input parameters to the Radionuclide model.
Lasgit	Large Scale Gas Injection Test. Experiment at Äspö HRL.
LDF	Landscape Dose conversion Factor. LDF is a radionuclide specific dose conversion factor, expressed in Sv/y per Bq/y. The LDF relates a unit release rate to dose.
LGM	Last Glacial Maximum.
liquefaction	A process by which a stiff material (soil) turns into liquid.

lithosphere	The rigid outer layer of the earth, having an average thickness of about 75 km and comprising the earth's crust and the solid part of the mantle above the asthenosphere.
loss on ignition	Measure of amount of volatile substances (mainly water) in a sample.
low pH materials	Cementitious materials that when in contact with water do not elevate the pH of that water to values above 11.
Ma	Million years, a unit of time.
MARFA	Migration Analysis for Radionuclides in the Far-Field. Computer code for calculation of radionuclide transport in the far-field.
Matlab	Numerical computing environment and fourth-generation programming language.
MIKE SHE	Computer code for surface hydrogeological modelling.
Milos backfill	Bentonite corresponding to reference backfill material.
montmorillonite	Swelling phyllosilicate; key component of bentonite.
MOX fuel	Mixed Oxide fuel, blend of plutonium and natural or depleted uranium.
MX-80	A brand name of bentonite clay, used as one of the reference materials for the buffer in SR-Site.
Myr	Million years, a unit of time.
natural analogues	A natural system studied in order to investigate processes that have proceeded for a much longer time than can normally be followed by experiments in the laboratory or in the field.
NDT	Non-Destructive Testing.
NWMO	Nuclear Waste Management Organization, Canada.
Observational Method	A risk-based approach to underground design and construction that employs adaptive management, including advanced monitoring and measurement techniques.
Pandora	SKB's and Posiva's modelling tool for dose calculations in the biosphere.
Peneplain	A low-relief bedrock plain representing the final stage of surface denudation during times of extended tectonic stability.
periglacial climate domain	Regions with permafrost.
PhreeqC	Computer code for chemical speciation, batch-reaction, one-dimensional transport, and inverse geochemical calculations.
piping	Formation of hydraulically conductive channels in the buffer clay by erosion.
Pleistocene	The penultimate geological epoch. The Pleistocene and ongoing Holocene epochs together constitute the Quaternary period.
Posiva	Short for Posiva Oy, the organisation responsible for the final disposal of spent nuclear fuel in Finland.
Precambrian	The span of time before the beginning of the Cambrian Period.
PWR	Pressurized Water Reactor.
Q1 path	Release path from the near-field radionuclide transport model. The Q1 path represents transport into a fracture intersecting the deposition hole. The Q2 path represents transport into the excavation damaged zone (EDZ) located below the floor of the deposition tunnel. The Q3 path represents transport in the backfilled tunnel and into a fracture intersecting the deposition tunnel.
Q2 path	See Q1 path.
Q3 path	See Q1 path.
QA	Quality Assurance.
Q _{eq}	Equivalent flow rate used in e.g. COMP23.
Quaternary	The Quaternary Period (between 1.6 Ma and the present) is the most recent period of the Cenozoic Era in the geologic time scale. The Quaternary includes two geologic epochs: the Pleistocene and the Holocene.
R&D	Research and Development
radionuclide model	Model used to calculate radionuclide inventories in different compartments of the biosphere, radionuclide fluxes between the compartments and radionuclide concentrations in environmental media (soil, water, air and biota). Exposure calculations for humans to estimate LDF's is included in the radionuclide model, whereas exposure of non-human biota is calculated separately.
RD&D	Research, Development and Demonstration.
rebound	Uplift of the continental crust as a response to deglaciation.
regolith	In this report the term is used to designate all deposits on bedrock, including Quaternary deposits, soils, sediments, peat, organic debris, surface of rock outcrops and man-made structures.
repository layout	The layout in space of the repository components such as deposition tunnels, central area and access.

respect distance	The perpendicular distance from a deformation zone that defines the volume within which deposition of canisters is prohibited, due to anticipated, future seismic effects on canister integrity.
RFMxxx	Rock domain in Forsmark.
RH	Relative Humidity.
ridge push	Tectonic horizontal compression of continental plates due to seafloor spreading.
risk criterion	A regulatory criterion to which a calculated risk is compared.
risk dilution	The seemingly paradoxical situation where less knowledge about e.g. a detrimental phenomenon leads to lower calculated individual risks.
RN	Radionuclide.
Saalian	The penultimate glacial, preceding the Eemian interglacial.
SAFE	The renewed safety assessment of the low level waste repository (SFR) at Forsmark.
safety function	A role through which a repository component contributes to safety.
safety function indicator	A measurable or calculable property of a repository component that indicates the extent to which a safety function is fulfilled.
safety function indicator criterion	A quantitative limit such that if the safety function indicator to which it relates fulfils the criterion, the corresponding safety function is achieved.
SCC	Stress Corrosion Cracking.
SDM	Site Descriptive Model. A synthesis of geology, rock mechanics, thermal properties, hydrogeology, hydrogeochemistry, bedrock transport properties and surface system properties of the site for the planned spent nuclear fuel repository.
SDM-Site	Short name for the Site Descriptive Model resulting from the completed surface based investigations.
SFR	Repository in Forsmark for low-and intermediate-level radioactive waste.
sheet joints	Fractures that are oriented sub-parallel to the topographic surface at the time of unloading and lack alteration associated with hydrothermal alteration, i.e. sheet joints.
Silica sol	A suspension of nano-sized silica particles that may be converted into a gel by adding a concentrated salt solution. Silica sol may be used as an injection grout that has near-neutral pH.
site description	A model of the site providing descriptions of the present geosphere and biosphere conditions. It is the same as site descriptive model (SDM).
SKI	Swedish Nuclear Power Inspectorate. SKI and SSI were merged into the Swedish Radiation Safety Authority (SSM) 1 July 2008.
skin effect	Disturbance of the flow conditions of the interface between the formation (fractured rock) and the tunnel. It is described by the skin factor, which may be positive or negative depending on whether the permeability of the interface is reduced (positive skin factor) or increased (negative skin factor) in relation to the initial permeability of the formation.
SMOW	Standard Mean Ocean Water, a water standard defining the isotopic composition of water.
sorption	In this report the term is used to designate all processes by which a dissolved species is retained at a solid surface.
spalling	Rock surface failure in which rock chips are shed from the rock wall.
SR 97	Safety Report 97. The previous safety assessment to SR-Can.
SRB	Sulphate-reducing bacteria.
SR-Can	The preliminary safety assessment for the planned spent nuclear fuel repository, published in 2006.
SSI	Swedish Radiation Protection Authority. SSI and SKI were merged into the Swedish Radiation Safety Authority (SSM) 1 July 2008.
SSM	Swedish Radiation Safety Authority. SSI and SKI were merged into the Swedish Radiation Safety Authority 1 July 2008.
SSMFS	Regulations of the Swedish Radiation Safety Authority.
STUK	Finnish Radiation and Nuclear Safety Authority.
sub-catchment	The drainage area of a biosphere object minus the drainage area of the inlet(-s) to the object.
talik	A layer or body of unfrozen ground occurring in a permafrost area due to a local anomaly in thermal, hydrological, hydrogeological, or hydrochemical conditions.
TASQ-tunnel	Tunnel at the Äspö Hard Rock Laboratory.
TASS-tunnel	Tunnel at the Äspö Hard Rock Laboratory.
TDS	Total Dissolved Solids.
technical design requirements	Requirements – usually stated as “specification on what mechanical loads the barriers must withstand, restrictions on the composition of barrier materials or acceptance criteria for the various underground excavations.”

temperate domain	Regions without permafrost or ice sheet conditions. It is dominated by a temperate climate in a broad sense. Within the temperate domain, a site may also at times be submerged by the sea or by an ice dammed lake.
Tertiary	Geologic period 65 million to 2.6 million years ago.
thermally induced spalling	Spalling induced by the stresses resulting from the added thermal load from the canister heat.
THM	Thermo-Hydro-Mechanical.
till	Dominantly unsorted and unstratified material, generally unconsolidated, deposited directly by a glacier or an ice sheet.
t_w	Advective travel time.
UCS	Uniaxial Compressive Strength.
upconing	Raising of the interface between fresh water and saline water due to a drawdown of the groundwater level, e.g. due to pumping in a well or in and underground excavation. In SR-Site, upconing is also used to describe the significant changes in the position of this interface associated with the advance/retreat of an ice sheet margin.
Weichselian	Name of the last glacial in northeastern Europe.
Weichselian glacial cycle	The last glacial cycle, defined as comprising the Weichselian glacial and the Holocene interglacial periods.
XRD	X-ray diffraction.
ZFMxx	Gently dipping zone in Forsmark.
ZFMXXXxxxxx	Steeply dipping zone in Forsmark (XXX replaces letters for geographical direction, i.e. ENE).
Zircaloy	Name for a group of high-zirconium alloys commonly used as cladding for nuclear fuel rods.
Äspö HRL	Äspö Hard Rock Laboratory.
$\delta^{18}\text{O}$	Notation used for reporting oxygen isotope ratios, often used as a proxy for temperature in atmosphere or ocean.
